TAILINGS AND MINE WASTE 2019

Proceedings of Tailings and Mine Waste 2019

Vancouver, British Columbia, Canada
November 17–20, 2019

TAILINGS AND MINE WASTE 2019

Proceedings of Tailings and Mine Waste 2019

November 17–20, 2019 • Vancouver, Canada

Editors

Joe Goodwill, Vancouver, BC, Canada
Dirk Van Zyl, Norman B. Keevil Institute of Mining Engineering,
University of British Columbia, Canada
Michael Davies, Teck Resources Ltd.

ORGANIZED BY:

NORMAN B. KEEVIL INSTITUTE OF MINING ENGINEERING
THE UNIVERSITY OF BRITISH COLUMBIA

C3 ALLIANCE CORP
Community, Commitment, Cooperation

Disclaimer

Any views and opinions expressed in the articles published in these proceedings are solely those of the authors and do not necessarily represent those of the University of British Columbia (UBC), C3 Alliance Corp. (C3) or of the panel of editors. The authors take full and exclusive responsibility for technical content and accuracy of the information published herein. This information is not intended nor implied to be a substitute for professional advice. UBC, C3, and the panel of editors are not responsible for any damage to property or persons that may occur as a result of the use of the information contained in this volume.

CONTENTS

ORGANIZERS

Norman B. Keevil Institute of Mining Engineering, University of British Columbia (UBC)

UBC's Department of Mining Engineering has faculty that teaches and mentors graduate students and staff to undertake research in all aspects of mining in order to study and improve the industry for future generations. Known for being a small, close-knit family, the department is exemplified by the dedication of the faculty and staff who provide a dynamic, hands-on learning experience for both undergraduate and graduate students.

Gifts from alumni, corporations, foundations, students, parents and other friends assist the Keevil Institute in conducting leading edge research, providing outstanding education and contributing to social and economic development.

For more information, visit the website at http://mining.ubc.ca

C3 Alliance Corp.

At **C3 Alliance Corp**. we understand that the sharing of information and ideas is vital to gaining insights and developing relationships which, in turn, leads to successful natural resource development. Community members, business people, and government representatives can all benefit from meeting to share stories and knowledge. C3 employs an expert team of event planners who specialize in conferences and networking opportunities. We benefit from a vast network of professional contacts to organize exciting events that connect people and knowledge across resources sectors, communities and government.

For more information, visit the website at http://www.c3alliancecorp.ca/

COMMITTEES

Organizing Committee

Chairs

Dirk Van Zyl, Conference Co-Chair, University of British Columbia
Michael Davies, Conference Co-Chair, Teck Resources Ltd.

Other Organizing Committee members

Andy Haynes, Golder
Ben Wickland, Golder
Bradley Zaworski, Hayward Baker Wick Drains
Brant Jackson, Gregg Drilling and Testing
Carlo Cooper, MineBridge Software
Cassandra Hall, Freeport-McMoRan
Chris Anderson, Teck Resources Ltd.
Chris Johns, Tetra Tech
Clint Logue, BGC Engineering
Dan Friedman, Knight Piesold
Daniel Servigna, Wood
Jack Caldwell, Robertson GeoConsultants
Jason Hilgers, AECOM
Jessica Naus, SNF Mining
Kate Patterson, Klohn Crippen Berger
Kurt Schimpke, Barr Engineering
Louise Whitham, SNF Mining
Peter Kimball, Stantec
Pascal Saunier, AFITEX-Texel Geosynthetics
Rick Friedel, Klohn Crippen Berger
Scott Davidson, New Gold
Shane Kelly, Gregg Drilling and Testing Canada
Stewart Bodtker, Paterson & Cooke

Conference Secretariat

Agathe Deacon-Erasmus, C3 Alliance Corp.
Amrita Budhwar, C3 Alliance Corp.
Sarah Weber, C3 Alliance Corp.

Technical and Review Committee

The Organizing Committee expresses its appreciation and sincere gratitude to the following reviewers of the technical content, who helped to ensure the high quality of this publication.

Ali Hooshiar, Ausenco
Andre Zerwer, BGC Engineering

Andrea Lougheed, BGC Engineering
Andy Haynes, Golder
Ben Schmidt, Golder
Ben Wickland, Golder
Bradley Zaworski, Hayward Baker Wick Drains
Brant Jackson, Gregg Drilling and Testing
Carlo Cooper, MineBridge Software
Cassandra Hall, Freeport McMoran
Charles Dumaresq, Mining Association of Canada
Chris Anderson, Teck Resources Ltd.
Chris Johns, Tetra Tech
Chris McKane, BGC Engineering
Clint Logue, BGC Engineering
Daniel Friedman, Knight Piésold
Daniel Servigna, Wood
Dave Sego, University of Alberta
Dawit Abraha, Thurber
Gilles Tremblay, Natural Resources Canada
Iain Gidley, Thurber
Irwin Wislesky, Golder
Jason Hilgers, AECOM
Jeff Ubl, Barr Engineering
Jeremy Boswell, Thurber
Kate Patterson, Klohn Crippen Berger
Kristin Salzsauler, Golder
Kurt Schimpke, Barr Engineering Co.
Louise Whitham, SNF Mining
Maria Sanin, Golder
Mike Belfry, BGC Engineering
Pascal Saunier, AFITEX-Texel
Peter Kimball, Stantec
Randal Osicki, Thurber
Rick Friedel, Klohn Crippen Berger
Rob Hui, National Research Council of Canada
Song Jeerawvipoolvarn, Thurber
Stephen Adkins, SNF Mining
Stewart Bodtker, Paterson & Cooke

ACKNOWLEDGEMENTS

The Organizing Committee acknowledges with gratitude the contributions of authors for their high quality, detailed and innovative papers. The papers submitted for the *Tailings and Mine Waste 2019* conference reflect ingenious and proactive solutions to challenging mining conditions around the world.

We would also like to thank the technical reviewers and all those involved in the organization of this conference and the preparation and production of these proceedings. The support of the committees is invaluable and greatly appreciated.

The Organizing Committee also wishes to thank all of our exhibitors, sponsors, institutional partners and media partners.

Finally, we would like to thank all the delegates who attended the conference to exchange their valuable knowledge and expertise, thus contributing to the great success of *Tailings and Mine Waste 2019*.

We look forward to seeing you all again at the next conference in this international series.

Organizing Committee
Tailings and Mine Waste 2019

THE ORGANIZERS PROUDLY ACKNOWLEDGE THE FOLLOWING CONFERENCE SPONSORS AND EXHIBITORS:

Sponsors

Exhibitors

3V Geomatics

ACZ Laboratories

AECOM

Afitex Texel

AGAT Laboratories

AGRU America / Watershed Geo

Alfa Laval

Aqseptence Group SRL

Atarfil

Barr Engineering Co.

BGC Engineering

Canadian Induracoat Corporation

Carl Data Solutions

Carpi Tech BV

CGG Services (UK) Ltd.

ConeTec Investigations Ltd.

Copperstone Technologies Ltd.

DeWind One Pass Trenching, LLC

Eco-Mister Evaporator

Flottweg Separation Technology, Inc.

Freeport-McMoRan

Gannett Fleming Inc.

Geosyntec

Geotech and Gregg Drilling

GKM Consultants

Golder

GoldSim Technology Group LLC

Graymont

Ground Probe

Hoskin Scientific Ltd.

HUESKER Inc.

ICD Group

Keller

Klohn Crippen Berger

Knight Piesold and Co.

Layfield Group

Matec America Inc.

Measurand Inc.

Metso Minerals Industries Inc.

MineBridge Software Inc.

Mud Bay Drilling 2015 Ltd.

New Gold Inc.

Oil States

Paterson & Cooke Canada Inc.

PhotoSat – Satellite Surveying

Putzmeister Solid Pumps GmbH

Robertson GeoConsultants Inc.

RST Instruments Ltd

Sensemetrics Inc.

Sixense Group

SNF Mining

Solmax International Inc.

SRK Consulting

Stantec

Teck Resources Ltd.

TenCate Geosynthetics

Tervita

Tetra Tech

Titan Environmental Containment

Tre Altamira Inc.

Willowstick Technologies

Wood PLC

Worldsensing

Chapter 1:
Case Histories

Proceedings of Tailings and Mine Waste 2019
November 17–20, 2019, Vancouver, Canada
Published by the University of British Columbia, 2019

Design for Transition from Down-Valley Discharge of Tailings to Partial Perimeter Discharge

David Accadia, Golder Associates Pty Ltd, Australia
Peter Chapman, Golder Associates Pty Ltd, Australia
Mark Longbottom, OZ Minerals, Australia

Abstract

Down-valley discharge of tailings in a valley storage, where practical, can provide a cost benefit through minimizing the size of the containment embankment. However, down-valley discharge results in water pooling against the containment embankment and the collection of finer, saturated material that can be subject to rapid strength loss. These factors limit the potential for upstream raise construction and can also present a long-term dam break risk if the embankment is not appropriately designed. A down-valley layout can also present an erosion and sediment release risk at closure. The Carrapateena project in South Australia required the design of a new tailings storage facility (TSF) in a broad valley with a large drainage catchment.

Carrapateena represents one of Australia's largest undeveloped copper deposits, with the project on schedule for first concentrate production in Quarter 4 of 2019. To reduce start-up costs, a down-valley arrangement was adopted for the initial stage of the TSF. A staged design was then developed to address dam break and closure risks, transitioning the tailings storage method from down-valley discharge to up-valley discharge during the second stage of operation and then to partial perimeter discharge. Partial perimeter discharge was selected to trans-locate the supernatant pond to a location some distance from the cross-valley embankment, but near the ultimate closure spillway.

The staged design strategy considers up to six stages of development, for the cross-valley storage, with a transition from the downstream raise construction method to the upstream raise method. Although the site climate is arid, historical records show large rainfall events do occur. Gravity decant systems were developed for the life of mine design, with an inclined chute system during the down-valley discharge phase (for Stage 1) and a series of temporary towers for the transition phase and permanent towers for the long-term partial perimeter discharge arrangement.

Introduction

Tailings Storage Facilities (TSFs) are typically designed with one operational configuration for the life of mine. However, modifications to the layout are often made during operation and subsequent stages to account for unexpected tailings deposition performance, increases in mine production and/or address environmental and dam break risks. Dam failure case histories have shown that the original design concept is sometimes overlooked, with failure to account for an earlier design feature. The original design concept may not have considered an important characteristic of the site (e.g., weak foundations), an increase in the rate of rise (due to increased rate of production) or the tailings beach profile may not have conformed to the design expectation. Or the geometry of the embankment may have failed to account for potential changes to the strength of foundations and/or fill strength.

The design of a new TSF for the Carrapateena project in South Australia provided an opportunity to develop a life of mine raise and closure strategy, with utilization of a range of discharge arrangements and design controls that address failure modes while also maintaining relatively low start-up costs through deferment of capital expenditure to subsequent stages when mine production cash flow is established.

In addition to the design controls, a leading practice governance and independent auditing and technical review framework was developed to provide continued confidence to stakeholders of the geotechnical and environmental performance of the TSF through public reporting of compliance with design criteria.

Project background

Carrapateena is a copper-gold project located approximately 160 km north of Port Augusta in South Australia's highly prospective Gawler Craton. The deposit will be mined using sub-level caving. Using this method, the deposit is blasted in 25 metre sections and then collected by loaders. From there it will be crushed and loaded onto a conveyer belt that transports the ore up the decline to the surface. The ore will be processed onsite to produce a copper concentrate containing copper and gold minerals. The flotation tailings resulting from the concentration process will be stored entirely at surface.

The project site is an arid part of South Australia, where mean annual rainfall is approximately 200 mm and evaporation exceeds it by a factor of approximately 17. Seismicity for the region is relatively low, with publicly available data and a site-specific seismic hazard assessment indicating a peak ground acceleration of approximately 0.04g for a 1 in 1,000 Annual Exceedance Probability (AEP) earthquake event.

The tailings slurry will be thickened by high-rate thickener to a target solids concentration of 65% by weight, with a lower slurry density expected in the initial years of operation. Thickened tailings will be

delivered from the minerals processing plant to the TSF over approximately 6 km via pipeline. Other tailings dewatering strategies are under consideration for a potential expansion of the project. Key physical properties of the tailings are:

- Specific gravity: Average 3.5 (varies between 3.2 and 3.8, subject to zone of orebody)
- P_{80} particle size (particle size at which 80% is finer): 75 microns
- Settled and consolidated dry density: Approximately 1.7 and 2.0 t/m^3, respectively

Site and layout selection

Selection of the TSF site and design layout is critical in managing project costs, environmental and cultural heritage constraints, and technical risks. Where favourable valley terrain exists in suitable proximity to the mine site, opportunities present for construction of cross-valley embankments that minimize the quantity of construction materials.

Terrain at the site is characterized by a series of ephemeral watercourses and associated valleys. In the area around the mine, the valleys drain towards an ephemeral lake, located some 15 km to the north. A siting assessment identified valley storages to be the most cost effective means of forming a TSF. A site was selected near the head of a valley system to keep the drainage catchment of the facility as small as possible, minimizing the size of water management structures and limiting the reduction of flows to the downstream environment. The selected site allowed for construction of a main cross-valley embankment for tailings storage and a smaller embankment further downstream to form a decant dam, closing approximately 1,500 ha of drainage catchment. Within the tailings storage area of the selected site, two converging valleys exist, and the gradient of the watercourses varied between approximately 1% and 5% from the embankment to the head of the storage; a key consideration in discharge arrangement selection.

Tailings discharge arrangement considerations

The tailings discharge configuration influences the size of a containment embankment and the supernatant pond location. The pond location in turn informs how water is removed from the facility and implicitly how dam break risks are managed. A cross-valley embankment with suitable valley gradients presents opportunities for discharge of tailings down-valley towards the embankment and up-valley away from the embankment. Where the valley is wide, and a broad basin is formed, discharge from locations around the perimeter of the facility may be possible, providing opportunities to control the pond location. Central discharge may also be possible, however, would typically result in multiple and potentially problematic ponds around the perimeter of the facility.

Based on beaching performance of tailings at mines in the region with similar tailings characteristics, an average beach slope gradient of 0.7% was selected for design. Variability in the beaching performance of the tailings is expected and refinements to the design layout are expected during operation to account for the actual beach profile.

The applicability of discharge arrangements varies on a site by site basis and selection can aid the management of both storage efficiency and dam break risks. For the Carrapateena site, the gradient of the valley watercourse and expected average beach slope provided an opportunity to consider a range of discharge arrangements. Summary points and risk considerations for each discharge arrangement style are provided in Table 1.

Table 1: TSF discharge arrangements and advantages and disadvantages

Discharge layout	Description	Advantages	Disadvantages
Down-valley	Tailings are discharged from the head of the valley towards a cross-valley embankment	Large proportion of tailings above embankment crest, resulting in a relatively small embankment. Most favourable tailings storage to embankment fill ratio	Relatively small pond capacity adjacent to embankment. Requirement for relatively large spillway. Greater potential for seepage through embankment due to pond location. Not suitable for upstream raise construction
Up-valley	Tailings are discharged from the embankment, resulting in a depression at the upstream end of the storage	Relative largest distance between embankment and supernatant pond location	Relatively largest embankment required as pond is located at upstream end of valley. Least favourable tailings to embankment fill ratio. Not suitable for upstream raise construction due to discharge from the embankment
Perimeter discharge	Discharge from all sides of the impoundment, including from the embankment and valley reaches, results in a centrally located pond	Relatively large central pond provides significant flood storage capacity. Suitable for upstream raise construction due to flexibility to rotate discharge areas	Relatively large embankment fill quantity due to central depression. Large central pond, although providing significant flood storage capacity, results in saturation of a large proportion of the tailings deposit Problematic discharge of water at closure
Partial perimeter discharge	Discharge from selected sides of the facility, including from the embankment, to keep the pond on one side of the facility	Pond can be controlled at reasonable large distance from the embankment. Suitable for upstream raise construction due to flexibility to change between discharge areas	Relatively large embankment fill quantity due to pond located away from the embankment
Central discharge	Discharge from a central point, array of points or from a central spine, resulting in pond(s) at the perimeter	Relatively small embankment (but larger than for down-valley discharge). Water is shedded from a large proportion of the tailings beach, provided ponds can be efficiently decanted	Multiple ponds develop around the perimeter of the storage area

Storage selection assessment

Overview

Assessment of the storage layout for the life of mine tailings was undertaken using three-dimensional modelling software. Central discharge was excluded from the modelling assessment as it was identified that the valley system was not suited to this method; it would result in multiple ponds and water management inefficiencies. The down-valley, partial perimeter and perimeter discharge arrangements were shortlisted for the life of mine layout at the selected TSF site.

Life of mine concept layouts for the shortlist, including up-valley discharge, are presented in Figures 1a to 1d. Although up-valley was ruled out for the life of mine layout, it was adopted in the strategy for transitioning between discharge arrangements, discussed below.

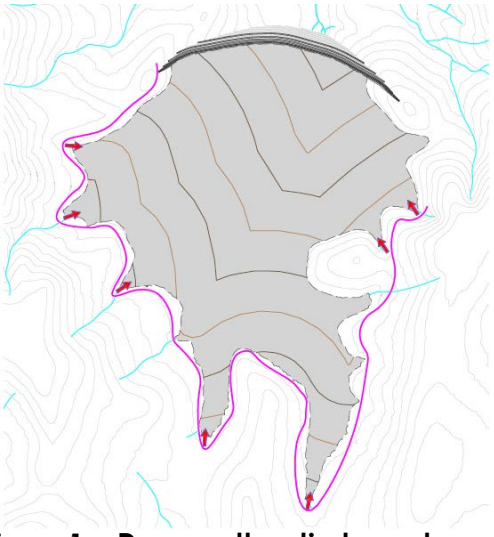

Figure 1a: Down-valley discharge layout

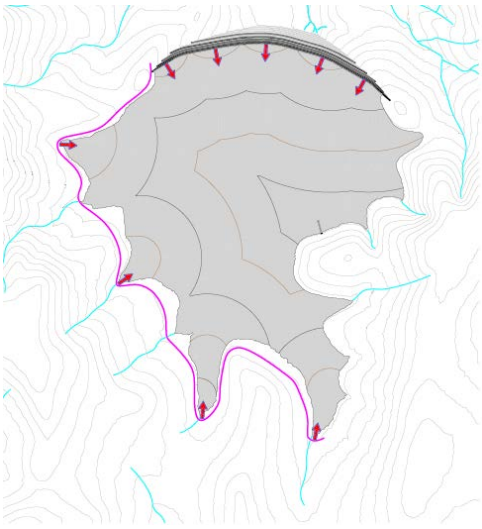

Figure 1b: Partial perimeter discharge layout

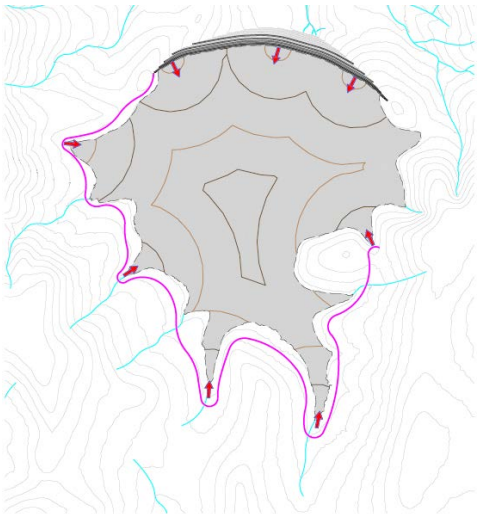

Figure 1c: Perimeter discharge layout

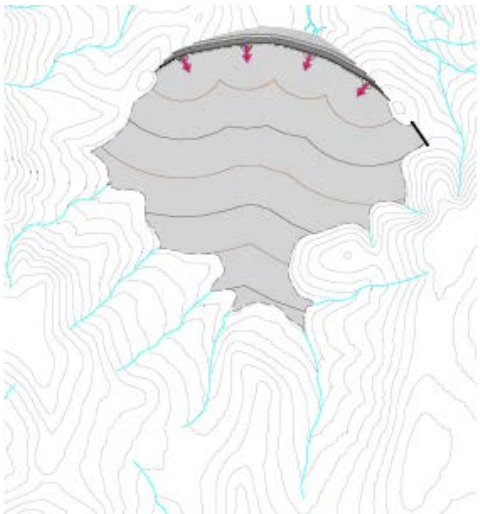

Figure 1d: Up-valley discharge layout

Embankment volume economy

For the life of mine layout and assuming downstream raise construction, the down-valley discharge arrangement presented favourably for keeping construction costs down. It resulted in the smallest embankment for tailings containment, with increasing embankment size (in order of the above shortlist) through to perimeter discharge. Approximately 40% less embankment fill would be required for the down-valley discharge layout compared to the perimeter discharge arrangement, assuming a downstream raise section. The partial perimeter discharge layout represented an embankment with 20% less fill than the perimeter discharge layout.

Due to a pond adjacent to the embankment and the requirement for drying of the tailings surface for strength gain, down-valley discharge did not provide suitable conditions for upstream raise construction. Coupled with environmental considerations related to rainfall runoff, scour erosion and discharge of tailings sediment, both during operation and at closure, it was ruled out as a life of mine solution. With suitable controls, however, it was favourable for the Stage 1 starter layout to minimize capital expenditure. Additional design controls, summarized below, were adopted to manage risks associated the expected lower tailings slurry density in the early years of operation and the relatively high rate of rise due to filling of the small basin adjacent to the embankment.

Water management

A perimeter discharge layout was identified as providing the largest flood storage capacity within the tailings storage area, however, would result in a potentially large pond over the tailings surface. Down-valley discharge on the other hand would provide practically negligible flood storage capacity and therefore require a larger spillway. With perimeter discharge, a central pond would develop which would require either a central gravity decant tower or a pump off system for removing water from the tailings storage. Although this layout presented some favourable aspects, it was ruled out due to the higher costs for construction. It would have also required alternative discharge arrangements during the early stages of the operation to account for the watercourse branches of the valley system.

A life of mine layout with up-valley discharge was assessed to be not practical due to terrain constraints and the requirement to construct a very large cross-valley embankment to accommodate the total forecast tailings. The method would, however, be used for part of the second stage of the TSF development strategy.

Partial perimeter discharge was selected as providing the most favourable life of mine layout. It would provide an opportunity to keep the pond a significant distance from the TSF embankment, as well as allow for utilization of a gravity decant system to remove flood water from the tailings surface due to the relatively

large catchment. A pump out system was not considered practical or economical as very large pumps would be required to remove water within a suitable timeframe.

Transition strategy

Considering the alternative discharge arrangements and associated costs and risks a staged strategy was developed that utilizes multiple layout types and embankment raise methods. A summary of the staging strategy and key factors for layout and raise method selection is provided in Table 2. A cross section showing the embankment staging is presented in Figure 2.

Table 2: Proposed TSF staging strategy to manage cost and technical risks

Stage and layout	Tailings discharge method, water management system	Key factors
Stage 1 – Starter embankment	Down-valley discharge, Inclined Gravity Decant System (chute against on embankment slope)	Relative low-density tailings slurry, relatively high rate of rise (progressively declining to 1.5 m/year by end of stage)
Stage 2 – Downstream raise (first phase of operation)	Up-valley discharge for initial years of Stage 2, Gravity Decant Tower System (series of towers in the impoundment accessed by a causeway	Expected strength of Stage 1 tailings not adequate for upstream raise construction
Stage 2 (second phase of operation)	Down-valley discharge for final year of Stage 2, continued use of tower decant system	Average rate of rise of less than 1 m/year Allows tailings beach adjacent to embankment to gain strength for geotechnical investigation and upstream raise
Stages 3 to 6 – Upstream raises	Partial perimeter discharge, with down-valley discharge only in the final year of each stage, leading up to raise construction	Average rate of rise approaches 0.5 m/year

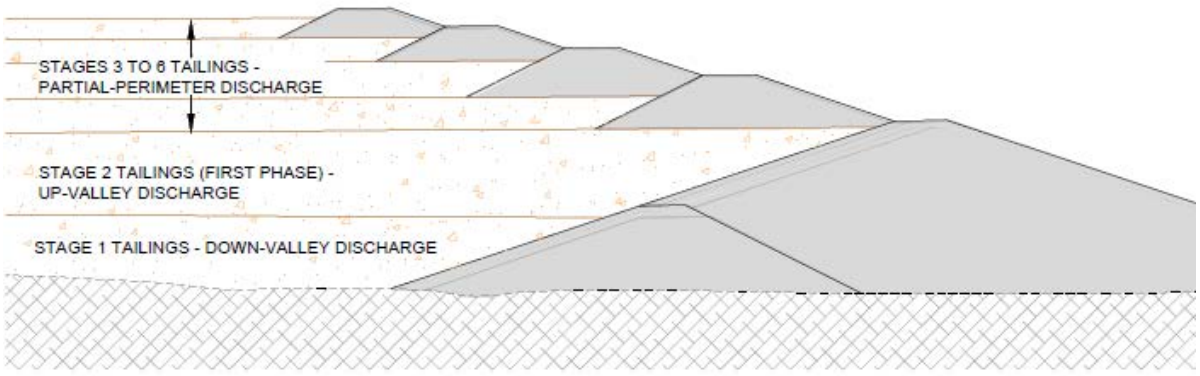

Figure 2: Embankment cross section showing transition between discharge arrangements

Failure modes and design controls

Dam break failure modes were reviewed to aid selection and implementation of design controls. A summary of selected dam break modes identified and how these are addressed by selection of the tailings discharge arrangement is presented in Table 3.

Table 3: TSF failure modes and discharge arrangement selection by development stage

Failure mode	Design controls, including discharge arrangement
Foundations and upstream raises	
Potentially weak or weakened foundations or loss of foundation strength during the life of the TSF	Development of geological model based on site investigations. Strong foundation conditions identified for Stage 1 starter embankment and Stage 2 downstream raise. Robust rockfill embankment for Stages 1 and 2, with 3H:1V downstream slope to account for potentially weak or weakened foundations. Foundation strength for upstream raises for Stage 3 onwards to be achieved by a period of down-valley discharge only, during which time the pond will shift marginally towards but still approximately 800 m away from the embankment. Gravity decant and seepage collection systems to limit head at upstream toe of embankment.
Embankment slope failure due to liquefaction of tailings	Saturated and potentially liquefiable tailings is expected to accumulate adjacent to the embankment during Stage 1. The starter embankment and Stage 2 downstream raise does not rely on tailings strength for slope stability. The partial perimeter discharge arrangement of Stages 2 to 6 results in a significant distance between the pond and the embankment, reducing the risk of saturated tailings adjacent to the embankment. By the end of Stage 2, when upstream raise construction is scheduled, the average rate of rise is below approximately 1 m/year Phreatic surface and strength of tailings deposit to be verified through piezocone penetration tests and vibrating wire piezometers.
Surface water and seepage	
Embankment slope failure in the downstream direction due to a high phreatic surface	Bituminous geomembrane liner on the upstream slope of the Stage 1 embankment, during down-valley discharge, to limit seepage through embankment. Up-valley discharge for the first phase of Stage 2 and partial perimeter discharge there afterwards will maintain pond at a significant distance from the embankment. Embankment design conservatively that a phreatic surface develops.
Embankment failure due to piping erosion	Transition zone between compacted clay and compacted weathered rockfill zones of embankment for Stages 1 and 2. Beyond Stage 3, by which time the pond will have been translocated away from the embankment, as part of the transition to partial perimeter discharge.
Embankment failure due to piping erosion around buried conduits	Concrete encasement around pipes and compaction of fill against side slopes of concrete encasement. Reduced risk after Stage 2, i.e. once the pond is shifted away from the embankment.
Embankment failure in the downstream direction due to overtopping	Down-valley discharge and the relatively small starter embankment for Stage 1 will result in negligible flood storage capacity. Water will be removed by a gravity decant chute and an emergency spillway for backup. Large flood storage capacity, a gravity decant tower system and emergency spillway provided for the partial perimeter discharge layout of Stages 2 to 6.

Starter layout construction

Construction of the Stage 1 starter layout of the TSF was completed in mid-2019. The embankments were formed with materials sourced from shallow borrow pits outside of the TSF impoundment. The key features of the starter layout are shown in Figure 3.

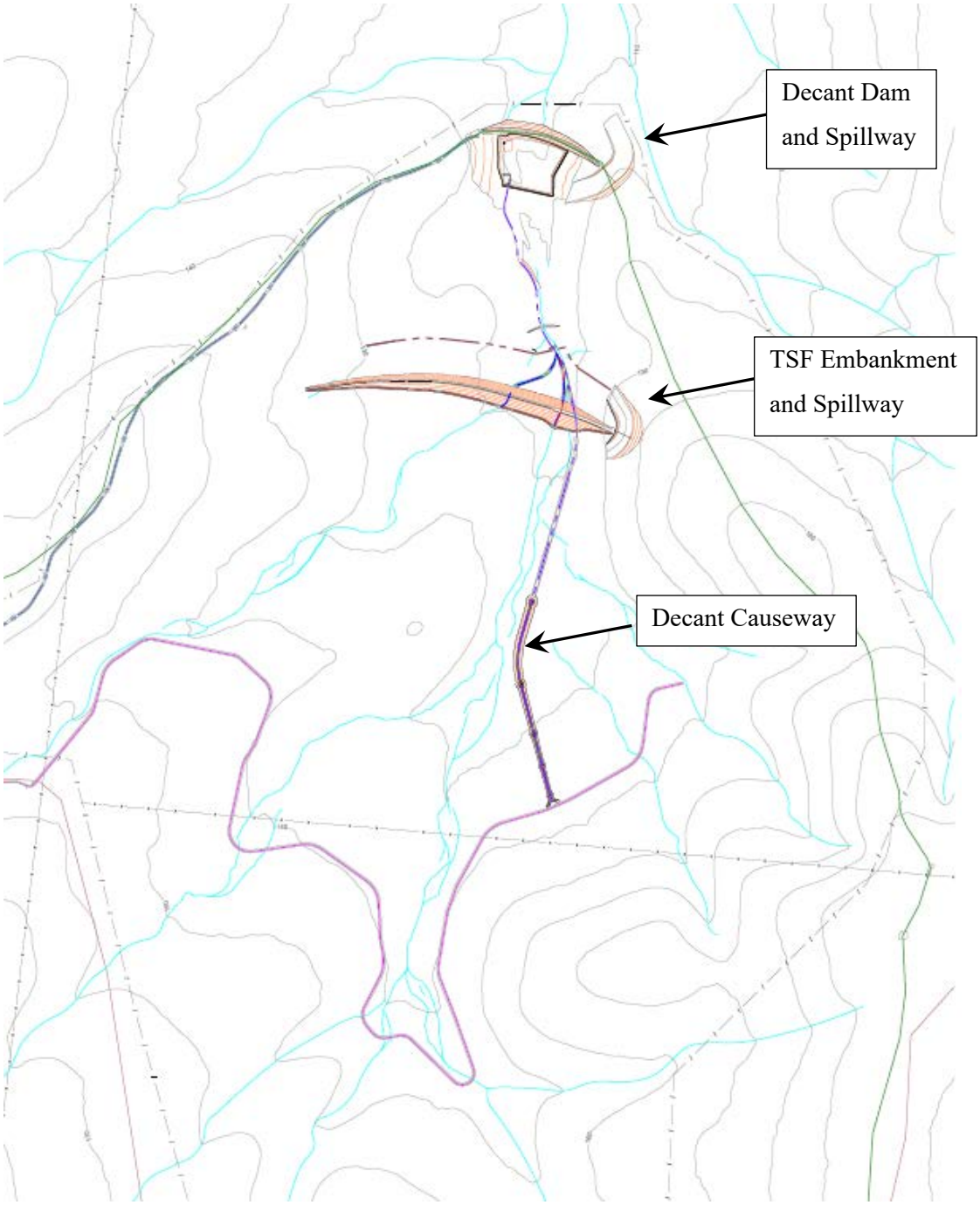

Figure 3: Starter layout of the tailings storage facility

The starter layout is expected to provide tailings storage for at least three years of operation by which time the Stage 2 downstream raise will be complete to allow for ongoing deposition. Key features of the starter layout are noted below.

- A starter embankment with maximum 16 m height, providing an end of filling storage area of approximately 160 ha. For the forecast production rate, this equates to a rate of rise of approximately 1.5 m/year by the end of Stage 1 filling. The rate of rise will progressively diminish thereafter for the scheduled discharge rate.
- An inclined chute on the upstream face of the embankment for gravity discharge of supernatant water and rainfall runoff from the valley catchment. Lids to be progressively placed on the chute to maintain the inlet above the tailings beach.
- A decant tower system comprising a system of slotted concrete rings and internal riser pipes, accessed via a decant access causeway, that discharge via an outfall pipe installed within the impoundment area and extends through the foundation of the starter embankment. Towers to be progressively decommissioned as the supernatant pond is shifted away from the embankment to the south, along the causeway alignment.
- A seepage collection drain along the upstream toe of the starter embankment to aid the drain down of tailings adjacent to the embankment, particularly for Stage 1, when the rate of rise is relatively high.
- A Decant Dam downstream of the TSF to receive water discharged from the seepage and decant systems. Impoundment formed by a cross-valley embankment with maximum height of approximately 10 m, providing for both operational and flood storage capacity.
- A bituminous geomembrane lined cell within the Decant Dam storage area to maximize retention of water prior to return to the Minerals Processing Plant.
- Spillways excavated into the hill slope adjacent to the TSF and Decant Dam embankments, should the decant and pumping capacity be exceeded respectively.

Monitoring design parameters during operation

The proposed strategy for transitioning between down-valley discharge to partial perimeter discharge and the success of upstream raise construction requires a sequence of changes to the locations of tailings discharge during operation and regular monitoring duration operation to update the timing of the sequence steps. In addition to a conventional program of dam safety monitoring, outlined in an Operations, Maintenance and Surveillance (OMS) Manual, the following program of deposition and pond performance monitoring is proposed during operation:

- Periodic assessment of the tailings beach performance, dry density and storage capacity during the Stage 1 of operation, to allow for adjustments to the tailings discharge strategy and updates to the timing to switch between down-valley and up-valley discharge.
- Assessment of tailings beach performance during Stage 2 to determine the timing of the switch from up-valley to a temporary resumption of down-valley discharge to allow for drying of the tailings within the Stage 3 upstream raise footprint. Monitoring of the supernatant pond location to verify that it does not encroach on the embankment during this temporary period in the last year of Stage 2.
- Review of the tailings beach slope performance with respect to the life of mine storage strategy to verify that the capacity can be achieved. Design refinements to the storage layout and discharge system to accommodate a different beach profile.
- Review of potential increases to the rate of tailings discharge and the implication to the rate of rise.
- Continuous monitoring of the overall effectiveness of thickened tailings discharge and consideration of alternative dewatering methods, either in conjunction with thickened tailings or as an entire replacement. Develop design controls to address risks associated with transitioning between tailings dewatering methods.
- Piezocone penetration test investigations and liquefaction assessment in late Stage 2, following the temporary resumption of down-valley discharge, to test the pore pressure and strength profile of the tailings deposit, particularly in the area of proposed upstream raise construction. Assessments for subsequent stages and/or designated increments in tailings surface elevation.
- Review of the supernatant pond size and location during each stage of operation to verify that other than during Stage 1 and the early years of Stage 2 when the pond is adjacent to the embankment, that the pond is at least 800 m away from the embankment and is maintained around the respective decant inlets.

The project has been approved by the South Australian government with a series of conditions relating to the TSF. These include the requirement for quarterly design engineer inspections and review, and annual independent inspections and review to verify that the TSF is being operated in according to the design and the OMS Manual.

Conclusion

The Carrapateena project provides an opportunity to strategically develop a greenfield TSF for a series of stages over a relatively extended timeframe. A staging strategy was developed for the valley storage of thickened tailings that utilizes a range of discharge arrangements, to reduce capital expenditure at start-up

while also managing dam break risks. A process of failure mode identification was undertaken to provide robust design controls at each stage, in conjunction with the transitioning between discharge arrangements.

Construction of the starter layout for the TSF was completed in mid-2019, and an operating strategy and monitoring program has been developed for the implementation of the life of mine raise and transition strategy. The monitoring program requires ongoing assessment of tailings beach performance and supernatant pond control, to allow for adjustments to the deposition strategy and sequence timing for transitioning between discharge layouts, required for implementation of upstream raises.

Upstream raises are proposed following a Stage 2 downstream raise, by which time tailings will beach away from the embankment and the average rate of rise will be relatively low. The discharge layout and sequencing strategy between discharge locations leading up to Stage 3 results in a supernatant pond some 800 m away from the embankment. The storage area progressively increases during operation, up to approximately 540 ha (from a Stage 1 area of 160 ha), and the rate of rise for the facility, for the forecast tailings schedule, will be below 1 m/year following Stage 2 operation, and as low as 0.5 m/year by the end of the final stage. These are favourable conditions for managing the dam safety risks associated with upstream raised tailings facilities, particularly in an area of arid climate and very low seismicity.

The Carrapateena project has a leading practice independent auditing and technical review framework that will provide continued confidence to stakeholders through public reporting of compliance with design criteria. The use of independent auditing and review is intended to provide confidence that the design will result in a geotechnically stable, non-polluting, and safe landform during operations and post-mine completion.

Acknowledgements

The authors acknowledge permission from OZ Minerals to publish this article.

Proceedings of Tailings and Mine Waste 2019
November 17–20, 2019, Vancouver, Canada
Published by the University of British Columbia, 2019

Large-Scale Tailings Filtration and Dry Stacking at Karara Magnetite Iron Ore Operation

N. Amoah, Karara Mining Ltd, Australia

Abstract

Karara Mining Limited in Western Australia owns one of the largest tailings filtration and dry stacking operations in the world, producing and stacking around 30,000 t/day of filtered tailings. This paper summarizes Karara's experience of the filtration process, operational performance of filters, dry stack TSF design concepts, operational control requirements and costs, in-situ behaviour of unsaturated tailings, and other aspects of the tailings production chain at this large-scale operation. The experience indicates that large-scale tailings filtration is feasible, but requires intensive operational management. Filter selection, sizing, throughputs, and component design should ensure that adequate redundancies are allowed in order to achieve the design production levels during operation.

For multiple filter operation, planning for good balance between availability, utilization, and maintenance is critical for operational performance. While optimal water recovery is usually a key factor in filter design, the target filtered moisture content and variations around the target value are more important in ensuring the engineering performance of the dry stack TSF, and these should always be related to the tailings geotechnical properties tested over a wide range. Unsaturated tailings properties that define the saturation and desaturation characteristics and water storage or retention behaviour give a good indication of dry stack TSF performance for the particular climatic condition. In dry and hot climatic areas, matric suction plays a significant role in dry stack TSF hydrology, shear strength development, and overall long-term stability.

Although tails filtration and dry stacking require intensive operational management, they are cost effective, especially for large-scale operations, and the operation costs depend on good balance between effective utilization and proactive maintenance planning optimized through continuous improvement programs.

Introduction

General background

Conventional slurry tailings that are deposited into purpose built impoundments involve very high water demand and management, engineering, operational, and environmental risks, as well as long-term closure liabilities. Improved methods such as paste and thickened tailings with higher solids contents between 60% and 70% have been successfully used in some operations, albeit still deposited in a fully saturated state. However, in many situations, storing tailings in a partially saturated or unsaturated state, commonly termed dry stacking, provides numerous benefits over conventional slurry (fully saturated) tailings. Filtered tailings and dry stacking have therefore attracted significant attention in recent years, due to factors such as improved filtration technology, shortage of water, regulatory requirements, and recognition of life cycle cost benefits. Recent failures of slurry deposited tailings facilities have also led to an accelerated interest in tailings filtration and dry stacking for safety and environmental risk mitigation, but unfortunately significant knowledge gaps exist in the engineering and operation of large-scale filtered tailings and dry stacks, due to the limited number of such operations to learn from. Consequently, numerous uncertainties and misunderstandings exist on the issues and benefits of filtered tailings and dry stacking in terms of factors that include feasibility, scale of operation, and cost effectiveness.

Crystal et al. (2018) prepared an inventory of 19 known dry stack TSF operations around the world, and showed that most operations are on a very small scale – below 10,000 t/day. It is not surprising that significant knowledge gaps exist in this area. This is sometimes reflected in the conflicting use of dry stacking terminology, which in itself is a misnomer, as the material being stacked is not dry but is in unsaturated or partially saturated state.

Karara Mining Limited (KML) in Western Australia owns one of the largest tails filtration and dry stack TSF operations in the world, producing and stacking about 30,000 t/day of filtered tailings since 2013. The experience obtained from dry stack TSF design concepts and the operation of various aspects of the tailings production chain is presented in this paper as a case study. Some key learnings about filtration process, filter performance, in-situ behaviour of the unsaturated tailings, dry stack TSF operational control requirements, and cost effectiveness obtained from this large-scale operation are presented.

Overview of Karara iron ore operation

Project location and key drivers for filtration

KML is a joint venture between Ansteel (China) and Gindalbie Ltd (Australia). KML owns a magnetite iron ore operation in the mid-west region of Western Australia, approximately 400 km from Perth and 230 km from the port of Geraldton. The site is located in a highly net positive evaporation area, with an average

annual precipitation of 310 mm and evaporation rates up to 3,000 mm. The main industry in the area is agriculture, predominantly commercial grain farming and animal husbandry, which are always given preference for water allocation by the government.

The magnetite processing plant was commissioned in late 2012, followed by production ramp-up in 2013 to name plate production of 8Mtpa (magnetite concentrate) in 2016. A unique feature of Karara's operation is the production of filtered tailings and operation of a dry stack TSF, which are not common in the Australian mining industry. The major constraint in the development of the Karara Magnetite project was the lack of water to meet the high water demand for magnetite processing. The maximum water allocation from the government for the operation was 5 GL/yr to be extracted from an aquifer over 200 km away from the plant site. No sustainable water source exists around the project area, except for some low yielding bores. Figure 1 shows estimates of wet tailings water demand at different solids contents and production levels for magnetite concentrate, which clearly indicate that the constraints imposed by water make the entire operation unviable. Using filtration to minimize water demand and maximize water recovery was the only viable alternative, and consequently was adopted by Karara.

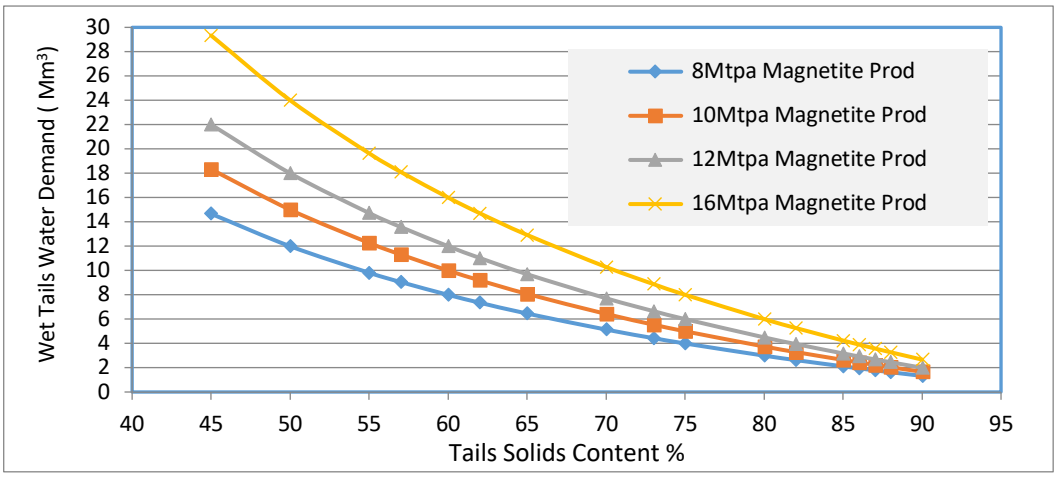

Figure 1: Estimated wet tails water demand at different solids contents and magnetite production levels

Magnetite production process

The production of magnetite concentrate and associated tailings generally involves conventional ore crushing, screening, milling, and a series of magnetic separation steps and reverse flotation, followed by thickening and filtration. First, the ore is crushed to a product size of <60 mm and then transferred to parallel trains of two high-pressure grinding rolls (HPGRs), which grind the ore to a maximum size of 4 mm. Then it is pumped in a slurry to the first stage of magnetic separation (raw magnetic separation – RMS). The non-magnetic material is rejected to the tailings stream, and the magnetic material is transferred to the primary grinding plant. There, the ore is ground into fine particle sizes of <50 µm, before the second stage of

magnetic separation (intermediate magnetic separation – IMS) to produce material with an elevated iron (Fe) grade. The process moves to the flotation circuit, where the product is upgraded through another stage of magnetic separation (cleaner magnetic separation – CMS). The final magnetite concentrate with a design grade greater than 65% Fe is filtered to a moisture content less than 10% (w/w), stockpiled, and later transported by rail to the port of Geraldton-Western Australia for export.

The non-magnetic tailings from the first stage of magnetic separation process is dewatered to around 15% (w/w) moisture content for disposal. The tails from the subsequent magnetic separation steps and reverse flotation process are combined in a common thickener for water recovery, followed by pressure filtration using Outotec vertical plate filters to recover the remaining recoverable free water, leaving a "filter cake" containing around 15% moisture (w/w). The filtered tailings are then transported via overland conveyors to a dedicated dry stack TSF, where they are stacked in a radial pattern called "sweeps" using mechanical conveyors and stackers.

Historical challenges at Karara magnetite operation

The Karara operation encountered many challenges in the early stages in 2013, which resulted in several years of production ramp-up until 2016, when it achieved name plate production rate of 8 MTPA. The poor performance of the crushing circuit due to the higher than design ore hardness resulted in increased wear and failure rates. However, the major issues at early stages related to the wet plant due to several factors, including the following.

Firstly, Karara was the first large-scale magnetite iron ore processing operation in Australia at the time, and hence there were several unknowns regarding the actual performance of the major areas of the process flow sheet. Most of the process depended on the success of the series of magnetic separation steps that progressively reject the non-magnetic materials into the tailings stream in order to produce the magnetite concentrate and associated tailings to design specifications and quantities. The problems with magnetic separation were recognized at an early stage, when the RMS that was designed to reject 27% of total plant feed material to the tailings stream could not even achieve 10% rejection rates. The immediate consequence was that all the downstream operating equipment was overloaded. Tails thickening and filtration became bottlenecks to production as their design capacities were exceeded up to 50%. A number of measures were taken, including the construction of a wet TSF in 2014 and a 55 m diameter thickener in 2016 to remove the bottlenecks. Karara therefore operates two TSFs, the dry stack TSF receiving between 70% and 75% of tailings, and the wet TSF receiving the remaining 25% to 30%.

Secondly, there were several unknowns regarding the operation and performance of the filters in achieving the design quantities and moisture contents for both the magnetite concentrate and tailings in such a large scale. Being the first major filtration operation in Australia and among the largest in the world

at the time, lack of knowledge and experience in filter operation became a major problem, and numerous operational processes were done through trial and error and correction of mistakes. This resulted in numerous issues, including frequent changes in filter cloths, plate damage, lower than design cycles and inconsistent cycle times, low percentage run times (low filter availability/utilization rates), and inconsistent filtration moisture contents for dry stacking. These required numerous trials, learnings, observational programs, and persistence over three years to achieve name plate production rates in 2016 and above name plate in 2017. Although many of the challenges remain, the experience derived from several years of operation has helped to develop continuous improvement programs to ensure filters operate at design and stable production levels.

Operational performance factors for tails filters

Filter type and components

The Karara operation uses the Outotec Larox fast-opening filter press (FFPs, Figure 2), which was selected based on its size and ability to filter the large quantities of tailings and magnetite concentrate materials. The processing plant was designed for 7 tails filter units and 4 concentrate filter units, based on the expected performance of the upstream equipment including the magnetic separators. The arrangement consists of recessed-plate membrane filters in which the chambers or plates are arranged vertically in a pack located between two rigid plates that are opened and closed using hydraulic cylinders. Each filter unit consists of filter press, plate pack (60 plates with nominal size 2.5 m × 2.5 m), filter cloths, cloth shaking system, head and end piece piping, process valves, swivel plates, hydraulic unit, weighing system, PLC control system, pull wires, splash curtains, feeder conveyors, and other ancillary and auxiliary equipment.

The tails filter feed density is 55%–60% solids (w/w/), the concentrate filter feed density is >70% solids (w/w), the design filter availability is 83%, and the cycle time is 9.75 minutes. Slurry is fed into filter chambers through a top feed channel. Slurry inlet, filtrate collecting, and drying air supply are all integrated into the polypropylene filter plate.

Several factors affect the performance of filters in operation, but some key ones to be given proper consideration at design and early stages of operation include:

1. filtration moisture content;
2. filter production rate and quantities;
3. filter cycle times;
4. filter availability and maintenance requirements; and
5. plant input factors, including variable feed densities and characteristics.

These are very important for determining the number of filters, sizes, and design of component parts, such as cloths and plates and the ancillary equipment for the type of filter selected. The importance of all these factors was noticed at the early stages of Karara's operation, and the sections below discuss how some of these affect filter performance.

Figure 2: Outotec Larox fast-opening filter press

Filter performance based on tailings filtration rates and quantities

The ability of the filters to operate and filter the large quantities of tailings and the magnetite concentrate was one of the major uncertainties in the entire production chain. Due to numerous factors, including the poor performance of filters and intensive maintenance requirements of the filter components parts at the early stages, tailings and magnetite concentrate production were severely hampered until a good understanding and experience led to gradual improvements and an increase in production to name plate. Figure 3 shows filtered tailings production rates between 2015 and 2019. Tailings filtration levels were around 30,000 t/day and are up to 35,000 t/day. This was achieved when all upstream equipment was in full operation. The numerous gaps reflect plant planned and unplanned down times, some of which relate to the filters, but in recent times relate to stability in filter operation. Many of the gaps are due to the unavailability of upstream equipment, predominantly a crushing circuit.

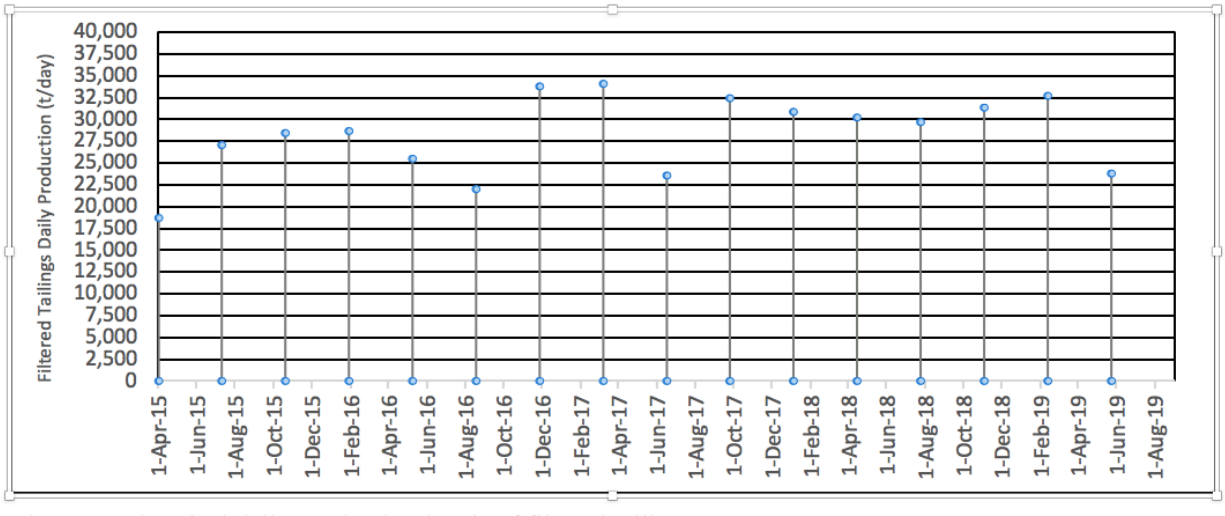

Figure 3: Historical daily production levels of filtered tailings

Filter performance based on achieved cycles times and percent run times

The cycle times, total number of cycles, and percentage run times are important measures of filter performance for such a large-scale operation. Figure 4 shows typical total daily cycles achieved for each of the 7 filters for the month of January 2019, which gives an average of 115 cycles per filter per day. It is important to note the significant variations in the number of cycles achieved by each filter. Many factors affect filter availability, with the major one being filter cloth performance. Different cloths perform differently, and it required several trials to achieve the most suitable to minimize the frequency of cloth change. The intensive maintenance required for the numerous filter components demand careful consideration in designing for throughputs and number of filters.

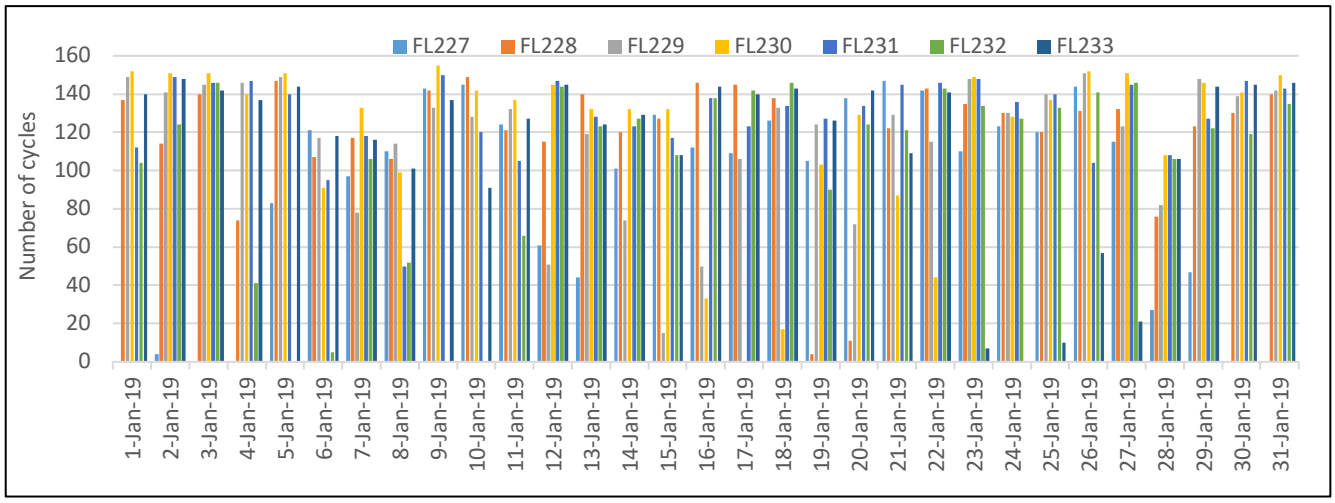

Figure 4: Typical daily filter cycles achieved for January 2019

The percentage run times for the various filters is important for assessing the utilization rates. Figure 5 shows typical percentage run times for each of the filters for the month of January 2019, which gives an average around 75% per filter for the period. Again, significant variations exist between the different filters in their utilization. A realistic balance between maintenance and utilization across multiple filters is critical for ensuring availability, and this should be properly managed to compensate for unplanned down times.

A proactive program has been implemented whereby one filter is taken offline for maintenance each week, and this has improved filter availability and stability. But in recent times, filter utilization has been highly influenced by upstream plant feed.

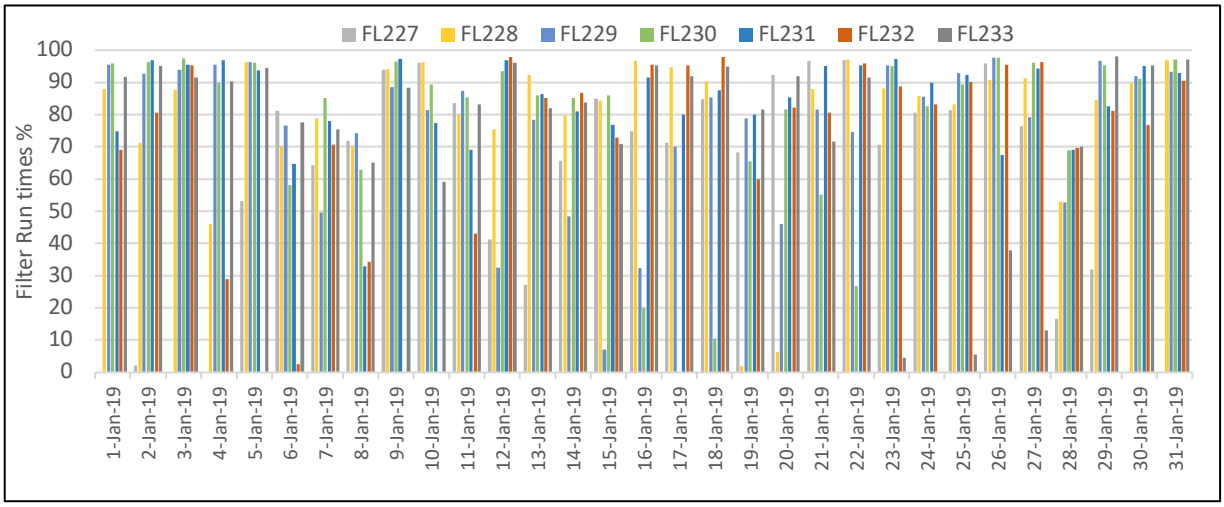

Figure 5: Typical daily percentage filter run times for January 2019

Filter performance based on filtered tailings moisture content

A critical performance parameter for a filter press is the moisture content achieved and the range of variations. It is important to note that moisture content is expressed differently by different scientific disciplines, therefore the terminology must always be defined. There is a significant difference between gravimetric and volumetric moisture content, which are therefore not interchangeable. The term moisture content in this paper refers to gravimetric moisture content, defined as the weight of water divided by the weight of soil solids (w/w) and expressed as a percentage.

For the Karara operation, a target moisture content of 15% (w/w) was selected as part of the filter design, mainly driven by the desire to achieve an optimal amount of water recovery. No upper limit was imposed, and no range of moisture variation was clearly defined at the early stages of the operation. The initial way of monitoring the filter moisture content was to ensure the average value was around 15%. The selection of target moisture content without direct relation to the geotechnical performance of the tailings in the dry stack TSF is very common in filter selection, and poses a significant problem in predicting dry stack TSF operational performance. In 2014, a number of geotechnical tests were undertaken, and an

operational range of moisture variation around the target 15% was determined with an upper limit of 18%. A non-stacking limit of 20% was imposed as a performance measure for filters.

Filtered tailings moisture content is measured at the processing plant as well as the dry stack TSF, where a minimum of 4 tests per day are conducted. Figure 6 shows the historical moisture content of the filtered tailings between April 2013 and June 2019. It is evident from the graph that a single average value or a target value of moisture content alone does not provide a meaningful measure of filter performance, as significant variations occur due to many factors including filter feed characteristics, filtration limits, changes in filter efficiencies and stages in cloth performance, operational experience, changes in ore characteristics, etc. It also shows how the early years were characterized by significant moisture variations around the target value, which had adverse effects on dry stacking. Although the long-term average is 14% (w/w), which is below the target moisture, variations around the average value still occur regardless of improvements in operational experience and/or efficiency.

The important factor is to ensure that such filtered moisture variations are within the limits acceptable for geotechnical performance. The adverse effects of significant variations in moisture content on dry stack TSF operation have been experienced at the Karara operation, when changes in ore characteristics combined with poor operational monitoring resulted in stacking issues involving surface trafficability and instability of outer faces. High moisture content materials deposited over long periods have the potential to create saturated zones in the dry stack TSF. Such materials also have high compressibility, and significant changes in void ratio may lead to increases in the degree of saturation.

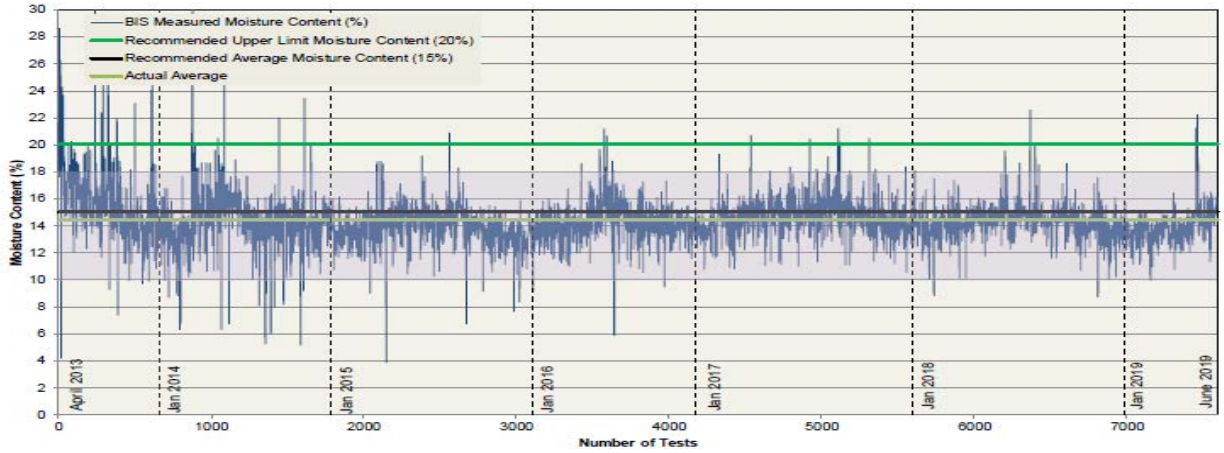

Figure 6: Historical filtered tailings moisture content (updated from Amoah et al., 2018)

Dry stacking of filtered tailings

Dry stack TSF design concepts

Karara was faced with the option of either trucking or using mechanized conveying and stacking of the

tailings when filtration was selected. The initial design concept for dry stacking was based on trucking as a means of conveying the filtered tailings to the dry stack TSF. Conceptual design was undertaken by SRK Consulting Perth in 2009 to assess geotechnical stability, seepage, water management, and other TSF infrastructure. The SRK conceptual dry stack TSF design report outlined the feasibility of stacking the tailings via truck dumping in a paddock style storage facility in three major lifts. The maximum height was set by the regulator to be at RL 450 m (AHD), hence the dry stack TSF would vary between 90 m and 100 m at the deepest side, due to surface topography.

In 2011, KML engaged Bis Industries to operate and manage the dry stack TSF and explore other alternative forms of tailings conveying and stacking. Bis Industries partnered with FLSmidth and proposed a radial stacking approach using mechanized tailings transport and stacking system. In this approach a mobile conveyor unit receives material from an overland conveyor, and then stacks it uniformly in a radial form using a series of conveyors, as shown in the layout plan in Figure 7A. The filtered tails from the processing plant conveyor (CV041), which is equipped with a telescopic radial stacker at the end, discharges into a chute (CH099), from which material is conveyed via a ramp conveyor (CV101-Figure 7B), which connects to a series of extendable conveyors (Figure 7C) in the dry stack TSF area for stacking (Figure 7D). If a problem occurs with CH099, or the conveyors, or moisture content is unacceptable, tailings are stockpiled in a temporary bay using the telescopic stacker and later re-loaded or conveyed by trucks to the dry stack TSF. Bis Industries and FLSmidth developed a conceptual radial stacking layout plan (sweep plan – Figure 7E) for the approved tailings storage area. The initial sweep plan consisted of 12 sweeps, and was later revised to 10 sweeps for the first lift, with each sweep showing the arc the mobile conveyor will cover and the next extension arrangement. Figure 7F shows the progress of radial stacking in Sweep #1.

The change from truck dumping to radial stacking resulted in a significant engineering review of the dry stack TSF. The first lift was set at RL 354 m to provide an average lift height of 20 m, based on geotechnical stability analyses by SRK at the initial stages, which also looked at safe stacker distance from the edge, seepage characteristics, surface traffic, etc. as discussed in Hore and Luppnow (2014). The tenement conditions demanded a full geotechnical design to reflect the new radial stacking concept, and to ensure that all future storage developments are structurally and operationally sound and consistent with regulatory requirements. It was also important to assess the impact of the new concept on the overall storage capacities and closure landform design.

Geotechnical assessment for radial stacking

A number of geotechnical tests were undertaken to supplement the previous tests by SRK. The historical moisture contents at the early stages of the operations provided a good understanding of the potential extent of moisture variations of the filtered tailings, and necessitated the various tests to be undertaken over a wide

range of moisture contents. The aim of the geotechnical assessment was to obtain an engineering understanding of the dry stack TSF, and to develop predictive performance measure criteria. The target moisture content of 15% and the variability of up to 25% were to be assessed against the geotechnical index properties of the tailings, and to determine the range that would provide a geotechnical stable stacking angle, safe and stable lift heights, and the ultimate heights that the radial stacking concept allows. Other factors included developing monitoring factors for dry stack TSF operating manual and setting the basis for proper engineering monitoring for the dry stack TSF when in full operation.

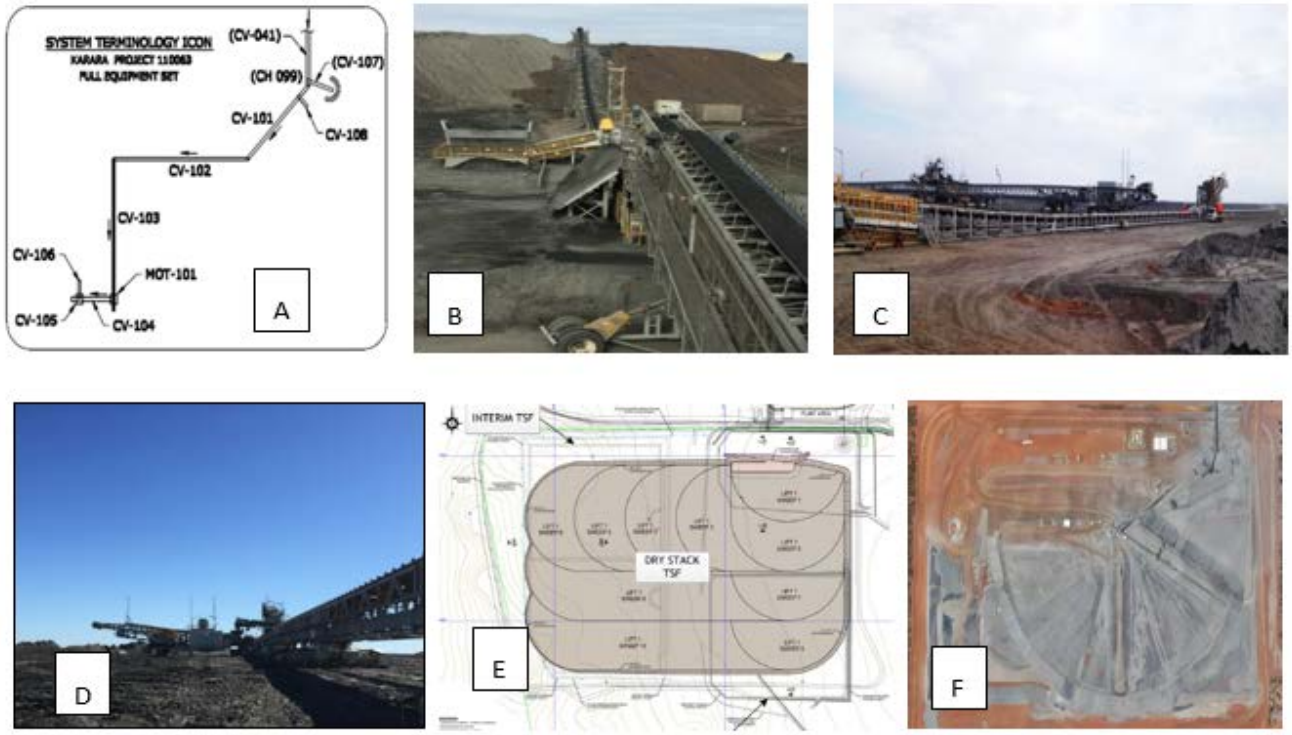

Figure 7: Components of tailings conveying and stacking system. (A) Layout of conveying and stacking system. (B) Ramp conveyor. (C) Extendable conveyors. (D) Mobile stacker. (E) Sweep plan. (F) Sweep #1 in progress

Geotechnical properties of filtered magnetite tailings

A review of previous geotechnical tests and analyses was undertaken to understand the site conditions and also to obtain the base parameters for assessing changes where necessary. Cone penetration testing with pore pressure measurement (CPTu) was undertaken at the early sections of the dry stack TSF in Sweep #1 to obtain actual in-situ strength profile and strength development. Laboratory tests included PSDs, Atterberg

limits, strength, and compressibility tests (direct shear, triaxial, I-D consolidation settlement, Rowe cell etc.).

The laboratory PSD tests indicated no significant difference between PSDs obtained from historical tests and those from the early stages of operation. They also confirmed that the tailings material is predominantly silt size, with a plastic limit varying between 18% and 20%, a plasticity index between 4 and 7, and standard Proctor optimum moisture between 12% and 16%. The tailings material compacts to high density for moistures under the plastic limit. A summary of geotechnical properties is provided in Amoah et al. (2018), but some are shown in Table 1, and typical PSD curves are shown in Figure 8.

Table 1: Some geotechnical properties of filtered tailings

Tailings property	Typical values	Range of values
Particle density (Gs)	3.0	2.9–3.2
Standard optimum moisture (%)	14	12.0–16
Standard maximum dry density (t/m^3)	2.05	1.9–2.1
Triaxial – cohesion (kPa)	12.5	12.0–14
Triaxial – friction angle (o)	36	34–38
Direct shear – cohesion (kPa)	8	5–9.5
Direct shear – friction angle (o)	35.5	35–38
Hydraulic conductivity (m/s)	1 × 10–7	>1 × 10–8

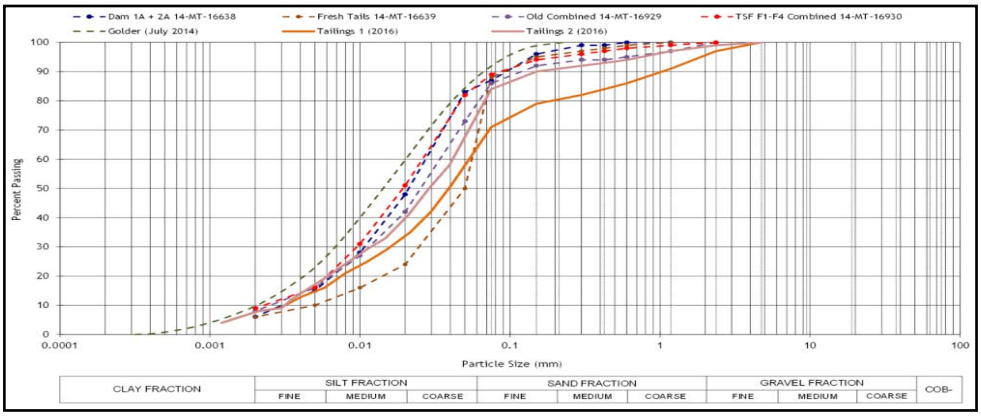

Figure 8: Example of particle size distribution curves for filtered tailings

Design analyses

Stability analyses were conducted for various heights using results from geotechnical tests obtained from different tailings moisture contents. Given that the dry tailings are stacked progressively with the stacker at its angle of repose, it was important to assess the optimal stacking height in relation to the first lift at RL 354 m, where the site topography will result in a maximum lift height of 27 m at the deepest side, and also

verify the stacker distance from the edge as initially proposed by SRK. This will also be used to determine the maximum number of lifts to the ultimate height imposed by the regulators. Several assumptions and limits were imposed as part of design. Filtered tails material above 25% moisture (liquid limit) was considered to be not stackable and would be disposed at the wet TSF, therefore all assessments were undertaken within a moisture range under 25%. Very large areas with saturated material would be managed as moisture content and will be monitored, and will not be allowed to be stacked for several weeks unnoticed. The management contract of the dry stack TSF included an allowance for trucking with a small fleet of trucks on site to respond to immediate situations and avoid long periods of wet tailings stacking.

The analyses were conducted within the practical operational conditions for acceptable moisture limits to evaluate dry stack TSF performance under static and seismic loading conditions. Total and effective stress analyses were performed for various stacking (lift) heights between 20 m and 35 m using conventional Limit equilibrium, Mohr-Coulomb failure criteria, and pseudo static for seismic. For each lift height considered, a zone at the outer face was assigned a very low shear strength to reflect the low density material at the angle of repose.

Summary of results of stability analyses for design and operation

The results of the stability analyses provided the following information:

- Global stability of the dry stack TSF structure was satisfactory for stacking heights up to 35 m.
- Local instability of the outer faces appeared to be the limiting factor in stacking height.
- Lift heights above 30 m result in local instability on the outer faces for moisture contents >18%.
- Moisture contents >20% result in local instability on the outer faces even for lift heights <30 m.
- For lift heights up to 30 m and material within 18% moisture, the minimum safe stacker distance from edge was 11 m, which confirmed the 12 m distance proposed by SRK.
- Maximum stacking angles of 38^{o} were achievable without stability issues if moisture control measures were adopted, although the achieved stacking angle on site at the time was around 35^{o}.

The stability of the outer faces was critical for the safety of the constantly advancing stacker. An operational stacking moisture content range was imposed with a maximum of 18% and non-stackable moisture of 20%, to guide both filter and dry stack TSF operation as moisture variations posed significant risk. Materials with moisture above 18% are placed in the temporary holding bay and later re-loaded for stacking or trucked to dry stack area.

Overall the dry stack TSF was divided into four stacking lifts with a nominal lift height of 26 m (maximum of 30 m). The overall outer slope was designed for closure landform to achieve a 17^{o} angle, as required by regulators. Figure 9 shows the dry stack TSF lifts to acceptable maximum height. Engineering

performance monitoring criteria were developed, which included annual CPTu and material testing to monitor strength development.

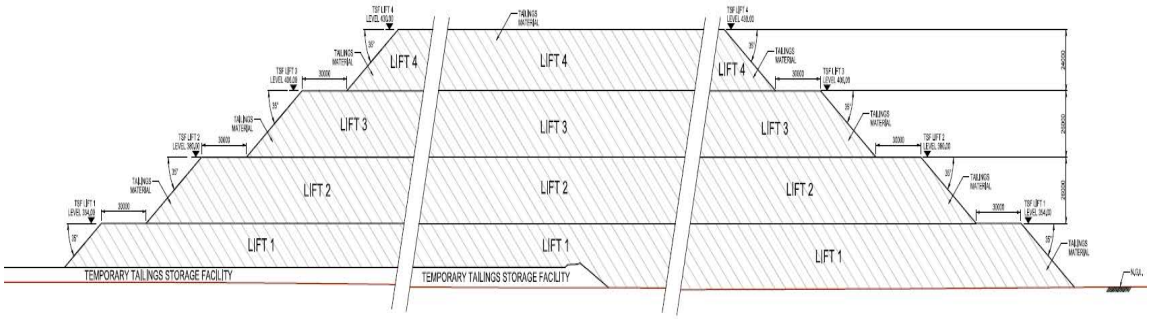

Figure 9: Dry stack concept design for radial stacking – cross section showing different lifts

Dry stack operational concepts

The operational requirements for a dry stack TSF are more intensive than conventional wet TSFs due to the significant number of activities and equipment involved. It demands operational discipline to meet all requirements for a conventional wet TSF in addition to the management of a large mechanical conveyor system. A comprehensive maintenance plan that ensures satisfactory equipment availability and utilization is critical for operational reliability. The maintenance plan should be guided by a good asset management plan that sets the framework for proactive management for conditioning monitoring, assessment, and documentation of equipment wear rates, wear patterns, failure modes, inventory of critical equipment spares, and a structured, well-resourced operations team.

For large-scale dry stacking such as in Karara, operational issues always require an allowance be made for the trucking of tailings, even in a fully functional mechanized system, in order to mitigate the risk of unplanned down times due to equipment or unsuitable material, e.g., high moisture. The Karara operation has experienced adverse situations resulting from all the above; therefore, effective systems and procedures should always be in place.

A major part of the Karara dry stack operation involves the regular extension of conveyors as the sweeps develop. This requires adequate planning to cover all aspects from procurement, engineering, construction, and commissioning in a timely manner; hence, dry stacking involves intensive operational planning and management.

Dry stack TSF performance monitoring

Dry stack TSF operation and engineering monitoring

Dry stacking at very high throughputs as at Karara is not common, therefore an observational method combined with engineering testing were considered to be critical. Stacking angles, stability of outer faces,

surface water infiltration, seepage, dust etc. were monitored. In addition, engineering monitoring was established for strength and pore pressure development. The observations from monitoring include the following:

- Very low infiltration rate through the dry stack TSF, with most of it occurring through surface cracks.
- Surface water ponding mainly disappears due to evaporation. Test pits after heavy rains show wetting front advance to within the upper layers, or to the extent of cracks, and with less moisture variations at depth.
- No signs of seepage around the dry stack TSF toe were observed, even after above average rainfall.
- Very steep stacking angles up to 44° were achieved on site, without any signs of instability.
- CPTu results between 2014 and 2019 indicate high strength and progressive increase in strength.
- Negative pore pressures along the vertical profile were observed. However, underneath parts of Sweeps 1 and 2, where slurry tailings were stored prior to dry stacking, show positive pressures from CPTu tests.
- In-situ tests in excavations to 14 m depths in areas around Sweeps 1 and 2 give densities between 91% and 94% of standard Proctor maximum dry density and moisture contents between 11% and 16%.

Unsaturated geotechnical properties of filtered tailings

To further understand the above observations and the full behaviour of the dry stack TSF in such a highly net positive evaporation area, it was important to characterize the unsaturated properties of the filtered tailings and the effect of the high matric suctions on the water storage and shear strength functions, which conventional saturated soil mechanics theories alone do not explain. The effects of matric suction on shear strength and the hydraulic behaviour of soils are very well documented in the geotechnical literature, although not very much in the tailings area.

Saturated and unsaturated laboratory tests were undertaken to understand how quickly the tailings material de-saturates in summer or saturates in winter, and whether the tailings characteristics support permanency of matric suction to maintain unsaturated conditions. Soil water characteristic curves (SWCCs) were developed from tailings water retention tests. Direct shear and triaxial shear tests were also undertaken for a wide range of matric suctions. Details of tests and results are presented in Amoah et al. (2018). The SWCCs are shown in Figure 10, which indicates that the air entry value (AEV) of the tailings is very low at around 15 kPa to 18 kPa. The tailings start to de-saturate at low matric suctions and reach residual suctions after 100 kPa. With such low AEV and high matric suction over long dry summers, large negative

pore-water pressures will develop and will not easily dissipate under the short winters and low rainfall regime, and supports the low infiltration rates due to very low hydraulic conductivity.

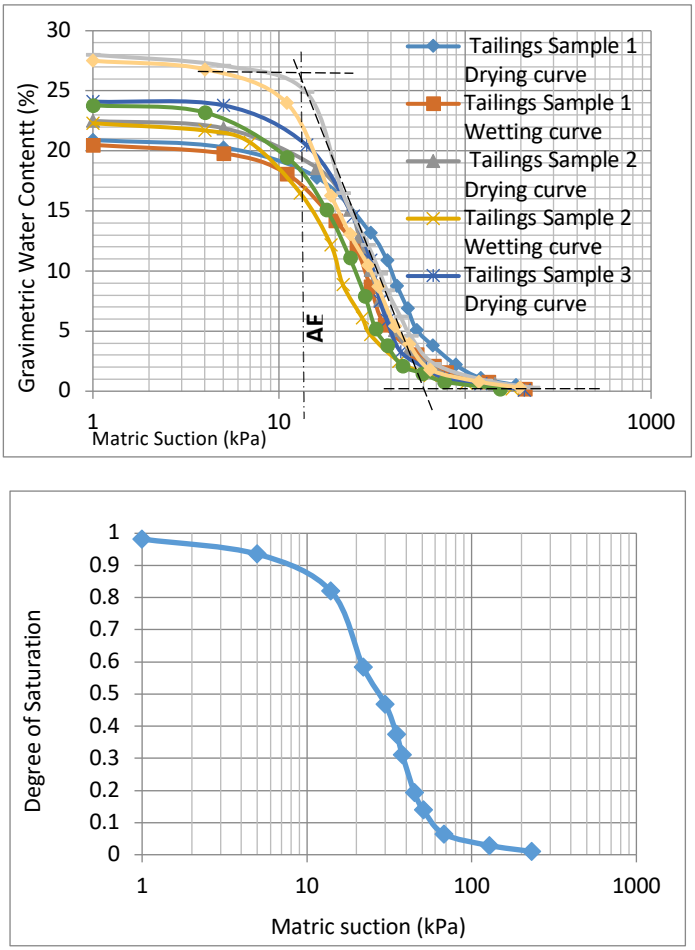

Figure 10: Soil water characteristics curves for magnetite tailings (Amoah et. al, 2018)

Operational costs for tails filtration and disposal

Tailings filtration and dry stack TSF operating costs will vary according to how cost elements are assigned to different cost centres in different organizations. Therefore it is important to understand the components when comparing costs from different mining operations. For the Karara operation, filtration cost includes all costs associated with operation and maintenance of the filtration facility, including conveyor systems to the discharge stacker near the dry stack TSF. Tailings disposal cost includes all costs for the day-to-day operational management and maintenance, and all costs for procurement and installation of conveyor extensions as the sweeps expand.

Figure 11 shows the unit costs (Australian dollar – A$) for the past four years, expressed as cost per tonne of tailings filtered and disposed, and are very sensitive to production levels. Lower unit costs were obtained in 2017 when production exceeded name plate, while the subsequent years' production levels are

slightly lower. The unit cost in 2019 (up to July) is slightly higher due to an increase in maintenance cost and lower production levels. Although tails filtration and dry stacking involve intensive operational management, the unit operating costs are reasonable compared with the potential water cost for operation and life cycle costs (including risk) of a typical wet TSF.

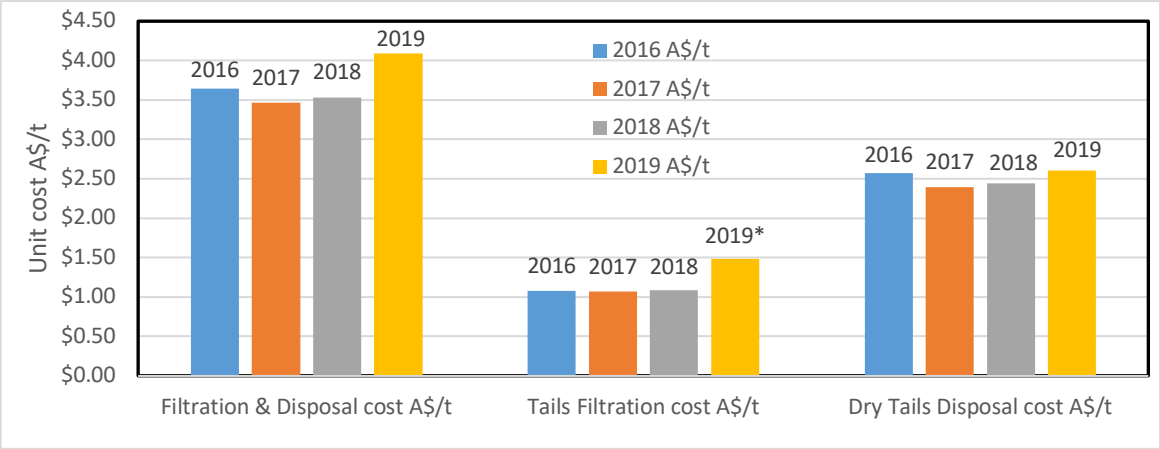

Figure 11: Tailings filtration and disposal costs

Conclusion

The Karara experience indicates that large-scale tailings filtration and dry stacking is feasible, but requires intensive operational management. A good balance between filter availability, utilization, and maintenance is key to achieving design production levels. The target filtered tailings moisture content and variations around the target value are very important in filter design, and should always be related to tailings geotechnical properties to ensure satisfactory dry stack operational performance. Unsaturated properties of the filtered tailings provide a good indication of dry stack performance for the particular climatic condition. Although tailings filtration and dry stacking require intensive operational management, they are cost effective, especially for large-scale operations.

References

Amoah, N., W. Dressel and A.B. Fourie. 2018. Characterisation of unsaturated geotechnical properties of filtered tailings in dry stack facility. In *Proceedings of Paste 2018.* Australian Centre for Geomechanics, Perth, 11–13 April, 2018.

Crystal, C., C. Hore and I. Ezama. 2018. Filter-pressed dry stacking: Design considerations based on practical experience. In *Proceedings of Tailings and Mine Waste*. Keystone, Colorado, USA, 30 September–2 October, 2018.

Hore, C. and D. Luppnow. 2014. Karara iron ore TSF – Design considerations for a unique large-scale dry stack facility. In *Proceedings of Tailings and Mine Waste 2014,* Colorado State University.

Proceedings of Tailings and Mine Waste 2019
November 17–20, 2019, Vancouver, Canada
Published by the University of British Columbia, 2019

Processes for the Closure Design of Greenfield and Brownfield Overburden Dump Sites

Monica Ansah-Sam, Canadian Natural, Canada
Julian McGreevy, BGC Engineering, Canada
Gord McKenna, McKenna Geotechnical, Canada

Abstract

In the Athabasca Oil Sands region of northeastern Alberta Canada, large open pit mines have been developed over the last 60 years to extract bitumen. Overburden (Pleistocene glacial materials and Cretaceous sands and shales) and interburden (low-grade Cretaceous oil sands) are excavated and placed into in-pit and out-of-pit dumps. The dumps are large mine structures, often encompassing hundreds of hectares and exceeding 60 m in height. At mine closure, the dumps are reclaimed to support the development of a locally common boreal forest ecosystem. To support meeting this goal, oil sands companies have undertaken applied research projects to identify grading, drainage, reclamation, revegetation, and wildlife habitat strategies that can be incorporated into closure designs to support the development of this ecosystem.

At greenfield dumps, where dump placement has not yet begun, closure designs that incorporate these closure strategies are incorporated into the initial designs of the dumps. Early incorporation of a closure design allows the dumps to be constructed to a configuration that limits the need for regrading and material movement at closure. At brownfield dumps, the initial dump design and construction frequently did not include these strategies and the dump configurations are updated to meet closure objectives – designs are prepared to retrofit the dump to meet the closure objectives, while limiting the amount of regrading and material movement. As a result, the design processes required to integrate closure designs at greenfield and brownfield sites vary and require the active participation of a variety of stakeholders. This paper presents processes used for developing closure designs for greenfield and brownfield dumps. The paper compares the design processes and identifies key design considerations for designers for both cases. The recent detailed design for closure of the brownfield Northeast Dump and the adjacent greenfield Dump 2C at the Canadian Natural Upgrading Limited (Canadian Natural) Muskeg River Mine is used as a case study. Using these processes, designers can effectively implement closure designs for either greenfield or brownfield dumps.

Introduction

The Canadian Natural Muskeg River Mine (MRM) is an open pit oil sands mine located approximately 75 km north of Fort McMurray, Alberta that has been in continuous operation since 2003. Mining is planned to continue through several decades. At MRM, to access the ore, overburden and interburden waste soils are stripped and placed into out-of-pit and in-pit waste dumps. These dumps are large structures covering hundreds of hectares and usually exceeding sixty metres in height. These mining landforms have been constructed over the life of MRM and as a result there are both greenfield and brownfield dumps. By way of definition, greenfield waste dumps are those that have not been constructed or are in early stages of construction. Brownfield waste dumps are already largely constructed and some are partially reclaimed.

In Alberta, each mine is required to submit a Life of Mine Closure Plan to the regulator every ten years. These plans present the conceptual closure design for the mine and indicate how the mine will meet the overall objective of providing a landscape at closure that supports the development of the locally common boreal forest ecosystem. Accordingly, MRM's Life of Mine Closure Plan lists the goals and objectives for the closure landscape and its component mining landforms, and provides a conceptual closure and reclamation design for each landform (Shell, 2016).

For each brownfield dump, a detailed landform design is prepared that involves retrofitting the dump to meet the closure objectives, while limiting the amount of regrading and material movement. Prior to constructing greenfield dumps, a detailed geotechnical design is prepared, followed by a detailed landform design to incorporate closure objectives. This paper presents the design processes for integrating a detailed closure design into as-built brownfield sites, and into the greenfield planning-level designs. The recent designs of the MRM Northeast Dump (NED) and Dump 2C are used to showcase the design process in action.

Background

North East Dump (NED) and Dump 2C are out-of-pit interburden/overburden waste dumps at MRM. They are located east of the mine pit (which is being actively infilled with tailings), south of the Syncrude Aurora North mine site, and immediately west of the Muskeg River (see Figure 1).

Construction of NED began in November 2004 and was substantially completed in 2007, with minor additions completed in 2008 and 2011. A reclamation material stockpile is located on the dump plateau which will be removed before final regrading and reclamation. The southeast face was previously regraded and permanently reclaimed. NED is a brownfield site for closure design, requiring some retrofitting.

Construction of Dump 2C began in 2017 and is planned to continue until 2020 when the dump reaches its planned design elevation of 360 m. Dump 2C is contiguous with NED and is being built over the north face of NED. Dump 2C is a greenfield site for closure design.

Dumps in the oil sands predominantly store interburden and overburden waste materials (predominantly lean oil sands fill at MRM). Some dumps at MRM (notably Dump 2C) also store atmospheric fines drying tailings which is placed in "polders" in the dump as non-trafficable slop zones that are contained by trafficable waste zones and dump shell zones. The materials are allotted to specific zones based on the material geotechnical properties and on the season during which the materials are placed. Waste dump landform designs consider the constructability of each zone and the resulting long-term landscape performance.

Detailed landform design process

At MRM a design process has been developed for integrating the closure-planning conceptual designs, the geotechnical designs, and the planning-level landform designs. At the start of the design process, management assembles the design team and identifies internal stakeholders. Roles and responsibilities are assigned. An initial closure strategy document (a roadmap for the closure plan and landform design and construction) is signed off by senior management. It sets the stage for both business and technical goals, and expectations of the design. This strategy document guides all closure designs within the mine site and is updated with each landform.

The landform design process for NED and Dump 2C involved the following steps (each of which is described in greater detail below):

- desktop review
- site visit
- constraints map development
- design basis preparation
- alignment and collaboration between disciplines
- landform design
- design concordance
- opportunities and risks identification
- stages of construction and design packages
- collaboration and alignment with internal and external stakeholders.

The landform design process involves the following teams:

- mine planning team

- geotechnical team
- engineer of record
- environmental team
- reclamation and closure team
- closure designer
- regulators
- stakeholders.

The following sections describe the key steps and identify how the key parties contribute to the overall design, differences in the design process for greenfield and brownfield sites are highlighted.

Desktop review

A review of the site wide Life of Mine Closure Plan and design basis is the first step of the landform design process for each dump. This step ensures integration and alignment of the landform design with the overall site design, especially the goals and design objectives, and the details of the adjacent landforms (as-built or planned). A desktop review of the existing information for the dumps is the next step to identify the key constraints and items that will need to be considered for the landform design. For greenfield sites, the information reviewed to support the closure design process will typically include:

- geotechnical and planning design reports and material placement plans
- site investigation reports
- proposed construction schedule
- life of mine closure plan conceptual design for the landform
- stakeholder commitments for the landform.

For brownfield sites the information to review to support the closure design process is slightly different:

- geotechnical and planning design reports
- as-built reports
- site observations
- site investigation reports
- life of mine closure plan conceptual design for the landform
- stakeholder commitments for the landform.

The desktop review for NED and Dump 2C highlighted several key constraints for the landform design: the need to avoid the establishment of a drainage channel within the footprint of a historical slump at NED,

and the need to accommodate future settlement at Dump 2C caused by the consolidation of atmospheric fines drying tailings in polders.

Site visit

Following the desktop review, a formal site visit provides an opportunity to collect site information, and an opportunity for the Engineer of Record and the closure designer to become aligned on design restrictions and potential design modifications required for the implementation of the landform design. For greenfield sites, the site visit focusses on identifying constraints at the proposed dump perimeter, and on examining adjacent as-built structures and natural features that will influence design. For brownfield sites, the site visit focusses on issues reported in as-built reports, examining the as-built dump for erosion and slumping, on examining the performance of as-built reclamation, and on examining transition zones where the dump landform design will connect with adjacent mining and natural landforms.

For NED and Dump 2C, a site visit was undertaken by the Canadian Natural Engineer of Record for the structure and the BGC Engineering landform designer. At the brownfield NED, slumping and erosion gullies were identified on the southeast and western slopes of the dump. These observations informed the proposed construction timing and identified specific areas of focus for the NED design. Specific recommendations were provided for the design which included the removal of berms, and the flattening of slopes that were observed to impede drainage or have significant rills and gullies. In addition, lessons from these site observations, including requirements for sloping and geometry of installation of toe ditches were used to support the design of the greenfield Dump 2C. For Dump 2C, site visit observations focussed on examining how the dump would tie into the Muskeg River valley and the surrounding mining landforms. Observations from the site visit supported the development of the integrated drainage plan between NED and Dump 2C where some drainage from NED's plateau is drained across Dump 2C.

Constraints map development

Based on the information collected during the desktop review and the site visit, a map is developed to highlight key constraints for the design. Constraints maps include the following types of constraints:

- boundary constraints, including neighboring landform tie in requirements and lease boundaries
- life of mine closure plan commitments, including watershed boundaries and landform drainage outlet points
- construction and material supply timing
- maximum or minimum design elevations
- stakeholder commitments for the landform
- regulatory commitments.

The constraints map is used as a key guide for the overall design process, as design decisions can be easily compared to spatial constraints. The constraints map is submitted along with the design basis for review by internal stakeholders as discussed in the following section.

Figure 1 shows the constraint map developed for NED and Dump 2C. Key constraints that were included on the constraints map and that influenced the design for NED and Dump 2C included: watershed boundary restrictions, offset requirements along lease boundaries, schedule and material supply constraints, and tie-in requirements with surrounding structures.

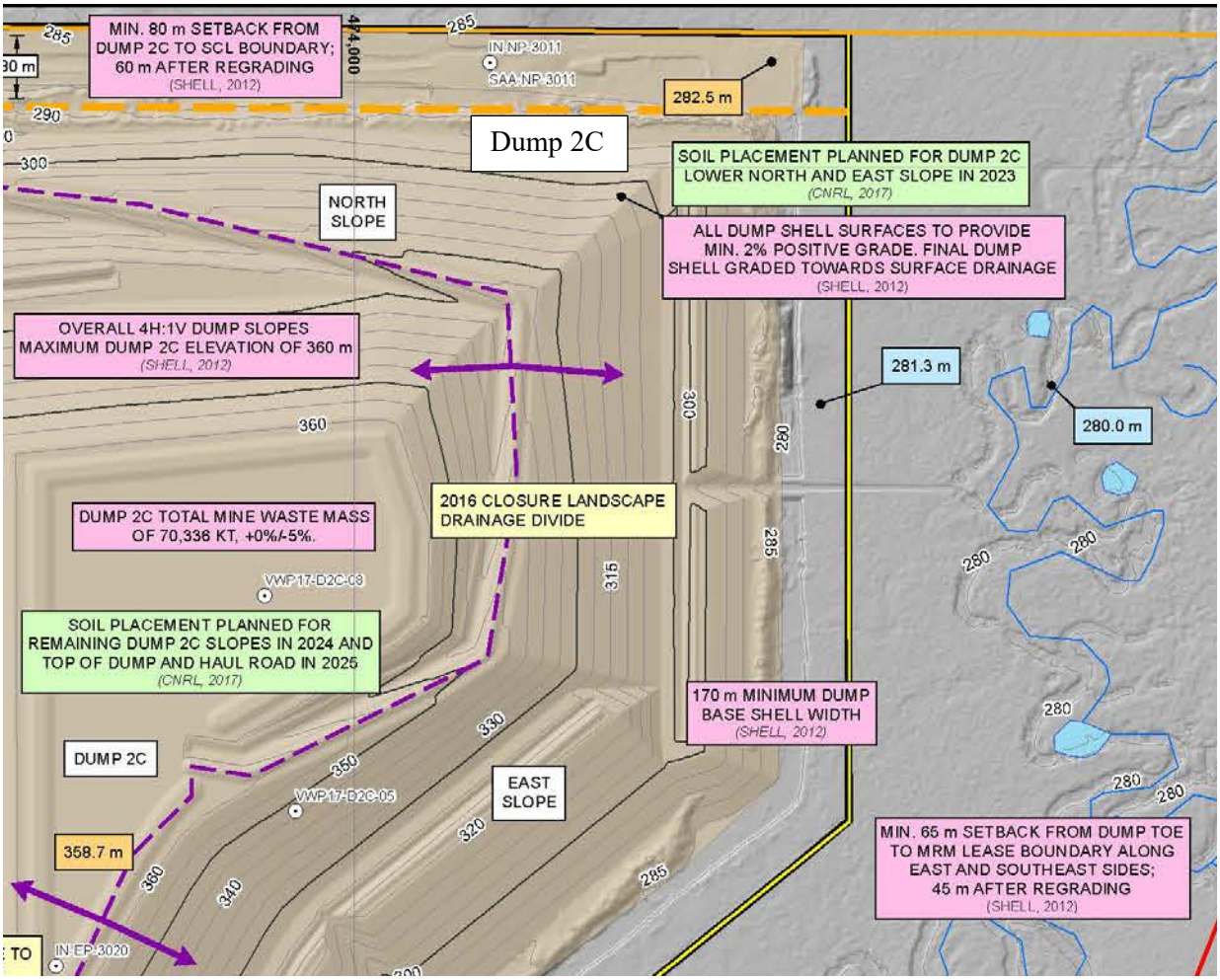

Figure 1: MRM NED and Dump 2C constraints mapping subset example

Design basis preparation

To align the closure design of individual landforms with the closure design for the overall landscape, the design basis approach described by Ansah-Sam et al. (2016) is used. The landform design basis compliments the overall landscape-scale design basis prepared for the life of mine closure plan. The design basis for the landform is aligned with the landscape-scale document, but is specific to the landform and has

more detail (for example, it includes specific design criteria germane to the specific landform).

Preparing the landform design basis involves filtering items in the landscape-scale design basis, keeping only the design bases that apply to the specific landform being designed. This step is followed by refining the design criteria to reflect the specifics of the landform with enough detail to allow final construction and reclamation to take place. For the design of NED and Dump 2C, the design basis included 15 design bases with 27 specific and measurable design criteria. By comparison, the MRM Life of Mine Closure Plan design basis included 29 design bases with 76 design criteria. Table 1 shows example design bases and criteria for NED and Dump 2C.

Table 1: Example NED and Dump 2C design bases

Design basis	Design criteria	Comment
Avoid ponded water near slope crests	• Ponded water on plateau and slope area shall be limited to <100 m diameter • Slope benches and plateau at a gradient >2% to provide positive surface water drainage.	Ponded water near slope crests can cause gullying and geotechnical instability. Ponded water can increase the consequence of slope movement by increasing mobility. Plateau mesotopography and channels will minimize the aerial extent that can be flooded.
Accommodate gully erosion and fan deposition	• Offset toe creeks >50 m to avoid blockage by erosional fans.	Gullies form as a result of surface water erosion on slopes and result in small alluvial fans at the slope toe. It is anticipated that some gullies and alluvial fans will form in the closure landscape (McKenna, 2002).

Alignment and collaboration between disciplines

Alignment is aided by presenting the design basis memorandum for review comments and sign-off by the teams before proceeding with the design. For brownfield sites the design basis alignment process may take longer than for greenfield sites since economic, reputational, and technical risks need to be balanced to create the design basis memorandum. For example, a brownfield site may require that a part of the reclaimed area be stripped to accommodate a new channel – getting buy-in to re-disturb reclaimed land takes extra consideration and time.

Landform design

This section highlights key differences between the design process for brownfield and greenfield dumps. For greenfield sites, the design process focuses on adapting the existing designs, which are geotechnically based. Before construction starts, there is considerable flexibility to change the design, and it is easier to get buy in from key stakeholders. Designs are able to be optimized to limit the cost of construction while also providing the required closure performance and meeting the landform analogues within the region.

For brownfield sites the design process focusses on identifying gaps in the current performance of the dump that need to be addressed for closure. There may be significant costs to retrofit an as-built dump; the

earthwork volumes for such work are minimized, and the design attempts a cut-and-fill balance to avoid hauling waste material on or off landform. For some brownfield sites, decisions will need to be made regarding the need to re-disturb already reclaimed areas, a difficult choice given that reclaimed areas usually have several years of good vegetation growth. For brownfield sites there are limited opportunities to redesign the dump to be more like natural analogues in the region (a typical design objective) due to the large rework that may be required.

For NED and Dump 2C the landform design differed in a few key ways. The NED landform design focussed on repairing and regrading areas of slumping and erosion mapped during the site visit, and on incorporating drainage channels into already reclaimed areas. The Dump 2C design focused on adjusting the overall geometry and grading to the meet the new design criteria. Despite the differing design approaches, both designs met the design criteria set out in the design basis memorandum. Figure 2 below provides an overview of the NED and Dump 2C landform design.

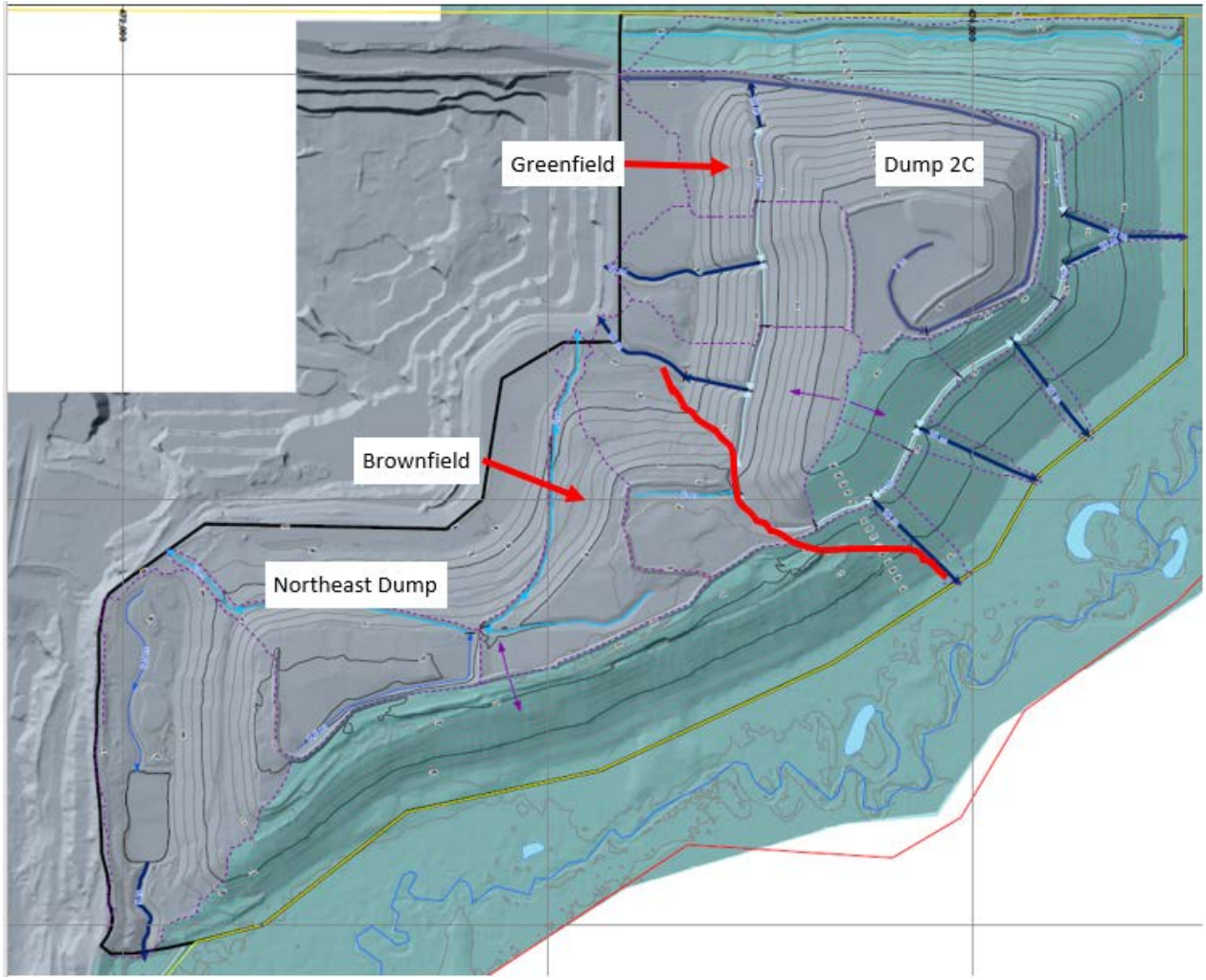

Figure 2: NED and Dump 2C closure design

Design concordance

As the landform design is completed, the design is assessed against the design basis to confirm that the design meets the requirements. Explicitly tracking the concordance with the design basis allows the designer to identify where certain design criteria may not be met due to competing requirements. In cases where design criteria are not met, there is risk of unacceptable long-term landscape performance and increased monitoring and maintenance requirements. In some cases, the design criteria may be adjusted after agreement with stakeholders.

Both the NED and Dump 2C designs were able to achieve the criteria in the design basis memorandum. An example design concordance table is provided in Table 2 below.

Table 2: Example NED and Dump 2C design concordance

Design basis	Design meets design basis	Comment
Avoid ponded water near slope crests	Yes	A minimum 2% grade is provided for surface drainage on benches. Channels on the plateaus are designed to limit areas of potential ponding to less than 100 m in diameter.
Accommodate gully erosion and fan deposition	Yes	Most toe channels are designed greater than 50 m from the toe of slopes to allow the formation of fans. Where channels are within 50 m of the toe of slopes, channels are designed to be wider and deeper to accommodate fan formation and sedimentation.

Opportunities and risks identification

Following the completion of the draft design, opportunities and risks are identified, under the broad categories of planning, construction, geotechnical, environmental, and cost. The design is then updated to reflect the identified opportunities, risks and contingency plans put in place. Residual risks related to long-term landscape performance are addressed with a long-term monitoring and maintenance plan (Fair et al., 2014) to address these risks in the closure landscape. Owners maintain a site-wide risk register and update it as risks are mitigated.

Opportunities identified for Dump 2C included the potential to reduce re-work by incorporating closure geometries into the operational designs, and opportunities for the expansion of the western portion of the dump to accommodate more waste volume. Risks for NED and Dump 2C are related to uncertainty regarding regulatory acceptance of eventual runoff water release from the reclaimed land directly to the Muskeg River and also time to obtain reclamation certification from regulators.

Stages of construction and design packages

For greenfield sites, major earthworks for closure will be predominantly completed by the mining fleet as a part of the operational construction of the dump whereas for brownfield sites, this work will typically be

completed by contractors. For both greenfield and brownfield sites the construction of channels and the implementation of bioengineering and revegetation will typically require specialized contractors. The design identifies the stages of construction for each landform logically sequenced to minimize re-work or negative impacts to the surrounding area. An example construction staging design for NED and Dump 2C is provided in Figure 3 below.

As a result of the several design stages, and the multiple contractors required to implement the work scope, several design packages are typically required – often with the simpler, larger volume work going to the mine fleet and more specialized / detailed work going to contractors. The level of detail in these issued for construction (IFC) packages varies accordingly.

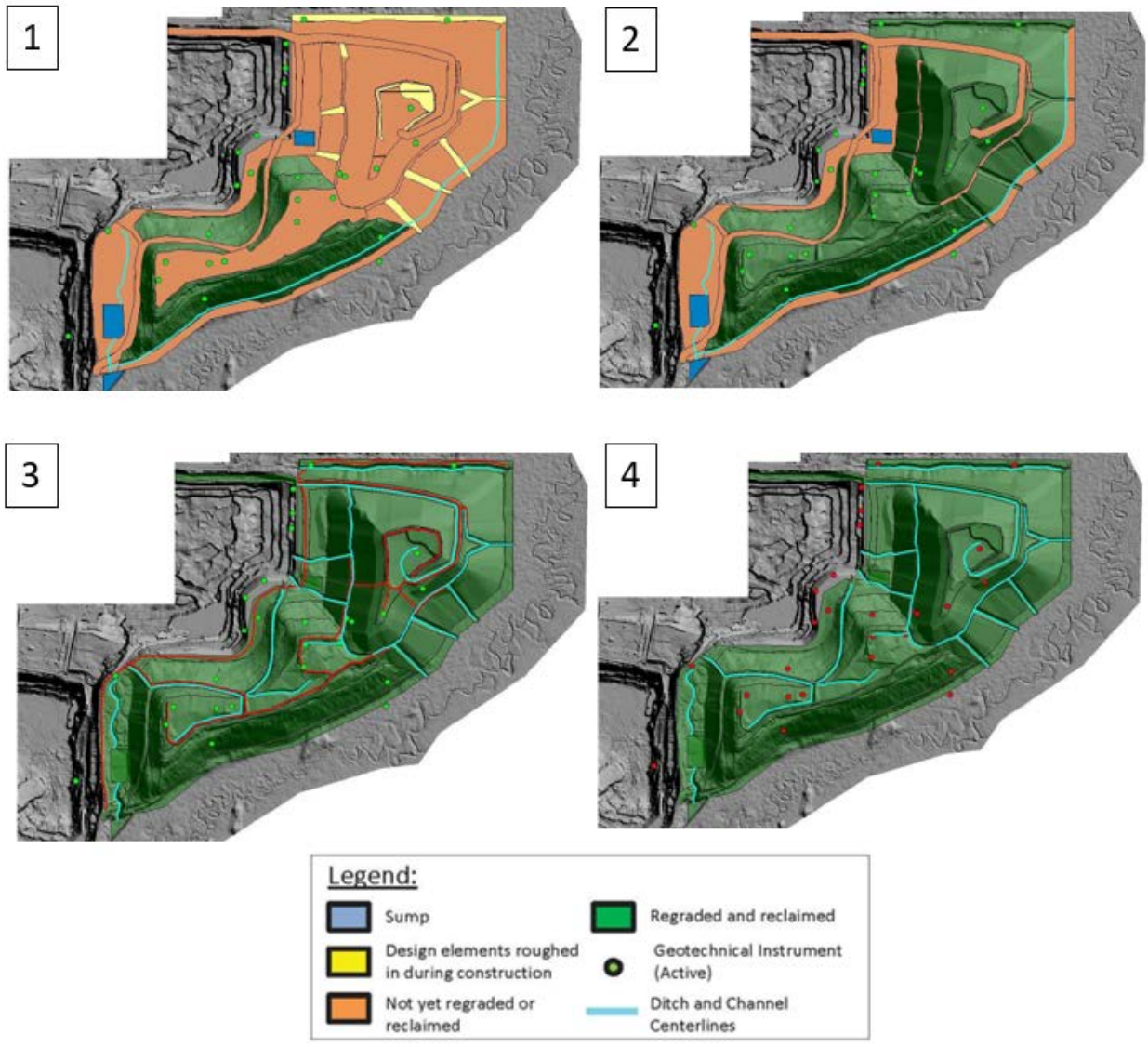

Figure 3: Example construction staging

Collaboration and alignment with internal and external stakeholders

The landform design package with the supporting design report is submitted to internal stakeholders for sign off on the overall design. This is done by providing an issued for review (IFR) package prior to the final submission of IFC packages. The IFR drawings are rolled out to all stakeholders including those who will be executing the design. Landform designs may be submitted to the regulator as an update to the permitted geotechnical and planning level designs for the landform. It is recommended that the details of the landform design be presented to the regulator prior to submission of the design update. This provides an opportunity to obtain feedback prior to submission.

Adaptive management

An adaptive management model is used to guide construction, monitoring, and maintenance of the landform (CEMA, 2014). The adaptive management model includes an iterative approach to planning by applying learnings from experience and new information (e.g., traditional ecological knowledge). Current landform designs are based on applied research, natural allegories, and the performance of a few already reclaimed landforms. As more landforms are constructed and closed, additional experience and information will become available that will allow for the modification and adaptation of closure designs to better meet the overall closure objectives. As the design is being constructed, learnings can be incorporated and traditional ecological knowledge can be incorporated as design changes. Most revisions should be documented, and changes managed to minimise unforeseen risks.

More specifically, the adaptive management model examines the risks, develops a supporting monitoring program, and allows the owner to enact pre-planned contingencies should the landscape performance fail to meet the objectives (CEMA, 2012).

Conclusion

The design process presented in this paper provides a method for integrating landform designs into detailed geotechnical and planning designs for dumps. The process requires the active participation of a number of key parties both within and outside of the mining organization. When implemented along with the design basis approach described by Ansah-Sam et al. (2016), the process allows for integration and alignment with the overall landscape scale design provided by the life of mine closure plan. This limits the risk of unaligned closure designs resulting in orphaned areas or non-workable designs that require expensive fixes. The process has been successfully demonstrated and implemented with the design of NED and Dump 2C.

Acknowledgements

Tianquan Hu of Canadian Natural and Brent Mooder of BGC Engineering are acknowledged for their support on this project.

References

Ansah-Sam, M., L. Hachey, G. McKenna and B. Mooder. 2016. The DBM approach for setting engineering design criteria for an oil sands mine closure plan. In *Proceedings of the 5th International Oil Sands Tailings Conference,* Lake Louise, Alberta, Canada.

Cumulative Environmental Management Association (CEMA). 2012. Oil sands end pit lakes guidance document. CEMA. Fort McMurray. 494 pp.

Cumulative Environmental Management Association (CEMA). 2014. *Guidelines for Wetlands Establishment on Reclaimed Oil Sands Leases,* third edition.

Fair, J.M., J. Pollard and G.T. McKenna. 2014. *Reclaimed closure landscapes: The importance and benefits of operations maintenance and monitoring*. 38th BCTRCR Annual British Columbia Mine Reclamation Symposium, 22–25 September, Prince George, British Columbia, Canada.

McKenna, G.T. 2002. *Landscape engineering and sustainable mine reclamation*. PhD Thesis. Department of Civil and Environmental Engineering. University of Alberta. 660p.

Shell Canada Limited. 2016. *Muskeg River Mine Life of Mine Closure Plan.*

Proceedings of Tailings and Mine Waste 2019
November 17–20, 2019, Vancouver, Canada
Published by the University of British Columbia, 2019

Responsible Design and Other Defences against Static Liquefaction of Tailings Structures

Jeremy Boswell, Thurber Engineering Ltd, Canada
John Sobkowicz, Thurber Engineering Ltd, Canada
Iain Gidley, Thurber Engineering Ltd, Canada
Amy Rentz, Thurber Engineering Ltd, Canada
Colin Schmidt, Thurber Engineering Ltd, Canada

Abstract

Static liquefaction is a failure mode contributing to some of the most devastating tailings failures in the last few decades, including those at Samarco (Fundão) in Brazil in 2015, and at Merriespruit and Bafokeng in 1994 and 1974 in South Africa, and many others. While other mechanisms may have also contributed to these failures, the role of static liquefaction is now inarguable.

Static liquefaction occurs when a saturated or partially saturated material experiences a rapid loss of strength due to an undrained loading response resulting from a trigger such as excessive rainfall, rapid loading as a result of high rate of rise, or loss of resistance as a result of excavation or erosion of the downstream toe. Even though static liquefaction is a known and credible factor in the failure of many tailings structures, this type of failure continues to occur. Many of the above failures could have been prevented if more responsible design approaches and better defences were adopted.

Methods for characterizing tailings deposits, in situ and in the laboratory, as well as methods for assessing their liquefaction potential using cone penetration testing have been published recently, summarizing leading practices for characterizing and assessing the liquefaction potential of tailings deposits. However, the authors have found very little published guidance on how to design, build, or operate structures to avoid the risk of static liquefaction.

The purpose of this paper is to provide guiding principles for the responsible design, construction, and operation of tailings structures such that static liquefaction can be avoided or minimized as a failure risk. This emphasis is now more relevant than ever, if future static liquefaction failures are to be avoided.

Importance of the static liquefaction phenomenon in tailings

Flow liquefaction resulting from a static trigger, herein termed static liquefaction, is the sudden loss of strength when the shear stress exceeds the undrained shear strength of a loose, cohesionless soil. Static liquefaction poses a significant risk to tailings storage facilities as many designs rely upon developing resistance within the impounded tailings for stability. It is of keen interest because it is a brittle failure mode that can occur with little warning, with seemingly small events causing catastrophic results. The "observational method", widely used in the tailings industry and responsibly applied with considerable merit in the oil sands, provides little to no protection for brittle failure, and for static liquefaction in particular.

There are a wide variety of potential triggers for static liquefaction, including a rising water table, beach loading, dyke raises, removal of confinement, slope steepening and others. These triggers can act on their own or in conjunction with other triggers to cause a liquefaction event. Undrained failures can occur in materials that are permeable and that have, up to a certain point, been following a drained loading path.

It is most challenging to design away the potential triggers of liquefaction and with the brittle (rapid) nature of the transition, there is insufficient time to mount a response. These risks must be properly accounted for in the design process as, by definition, failure will happen too quickly to enact mitigation measures.

The assessment of static liquefaction

Identification of liquefiable tailings

Methods for characterizing tailings deposits, in situ and in the laboratory, as well as methods for assessing their liquefaction potential through the use of cone penetration test (CPT)-based relationships have been well published recently, summarizing leading practice for characterizing and assessing the liquefaction potential of tailings deposits (see the references listed in the essential reading section below). Robertson and others (2017; 2018; 2019) and Fourie and Reid (2018; 2019) have presented comprehensive training courses on the assessment of static liquefaction. Annual courses at the University of Alberta and the University of British Columbia also traverse the topic.

In brief, the most common methods to assess liquefaction susceptibility are based on the measured resistance to either the standard penetration test (SPT) or the CPT. In recent years with the increased availability of cone testing rigs and the increased confidence in the results of the assessment methodologies, liquefactions assessments are more commonly performed using CPT. The assessment of liquefaction susceptibility defines the liquefiable boundary in terms of an offset to the critical state line of –0.05 in terms of void ratio or using a clean sand equivalent normalized cone resistance ($Q_{tn,cs}$) value of 70, which yields

a similar boundary (Robertson, 2010). Materials with a state parameter of > –0.05 are considered potentially liquefiable (see Figure 1).

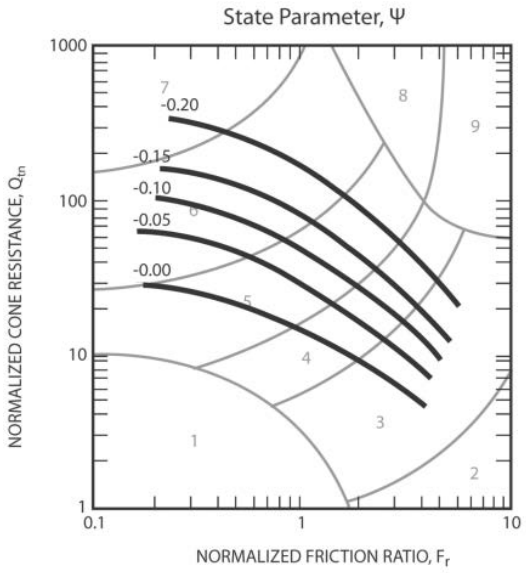

Figure 1: Approximate state boundary lines superimposed upon SBT chart (Robertson, 2009)

Strength of liquefiable tailings

Similar to the identification of liquefiable tailings, several methods exist that attempt to quantify the tailings post-liquefied residual strength (Olson and Stark, 2003; Robertson, 2010; Sadrekarimi, 2014). These methods are all based on the results of CPT soundings with pore pressure measurement. Using case histories of flow liquefaction failures, slope stability back analyses were conducted to estimate the strength of the material at the time of failure that would result in the final post-failure configuration.

The assessments by Olson and Stark (2003) and Robertson (2010) are based upon available in-situ test data, split into classes of reliability. Class A and B results are most commonly used in the assessment which comprise CPT measurements taken prior to the failure. The back analyses require simplifications to the stratigraphy and estimates of the momentum effect on the final slope configuration. The assessments were also conducted in two-dimensions. Sadrekarimi (2014) measured the post-liquefied strength ratio through a series of triaxial and direct simple shear tests. These results were compared against a re-analysis of the case histories presented by Olson and Stark (2003) using updated assessment methodologies. These methodologies can be used to assign the residual strength for use in a limit equilibrium-based assessment.

Application of the assessment methodology

The tools discussed in the previous sections are intended for the preliminary evaluation of tailings deposits, to address their susceptibility to liquefaction and to estimate the strength parameters that should be used in a stability evaluation of the facility.

Judgement is required in the application of the methods to design, and care needs to be exercised in understanding the assumptions within the analyses. Caution should be used when applying the strengths as the back analyses considered certain layer thicknesses, employed two-dimensional analysis, assumed that strengths were mobilized across the entire failure plane and also made other limit equilibrium assumptions.

The assessment of liquefaction susceptibility is intended to be used for cohesionless and low plasticity soils that experience a rapid loss in strength at small shear strains (Robertson, 2010). Current practice is to consider that liquefiable materials will liquefy, and that residual strengths should be used in analysis – essentially designing the containment structure to hold a heavy fluid. High plasticity clays also tend to experience strength loss. However, the loss of strength in these materials tends to occur much more gradually than for silty sands and the initiation of strength loss tends to occur at high shear strains. For these materials, peak shear strengths, with consideration for the imposed stress regime in light of the materials' stress history, are typically used in design, for example in the design of subsequent post-failure raises at Mount Polley (Golder, 2016).

The question arises as to what strength should be selected for intermediate materials that fall in between these two extremes. At a screening level, these materials could be addressed assuming residual strengths and peak strengths. The variance in the required design measures could then be used to justify a laboratory investigation into establishing the in-situ stress conditions and the stress-strain behaviour of the materials. Characterization of these materials can also be complicated by pore fluid chemistry, the presence of polymers (that usually degrade with time) and the presence of bitumen or other organic materials.

In special situations, more sophisticated analysis using numerical tools such as FLAC and the NorSand constitutive model can be considered in a stress-deformation analysis. This requires a thorough investigation of the material behaviour, the stratigraphy, the in-situ stress state and potential stress paths that the material could experience. The benefit of these types of analyses is that failures occur organically. However, the results are heavily dependent on assumptions that the user is obliged to make, especially for a partially constructed facility. These types of analyses are typically undertaken in failure investigations rather than as a design tool used in isolation.

Essential reading on liquefaction assessment

There are a number of useful references that provide information and background for undertaking a liquefaction assessment. In the authors' experience, the following references are essential reading for any engineer undertaking liquefaction assessment:

- Fear and Robertson (1995) – Estimating the undrained strength of sand: a theoretical framework.
- Jefferies and Been (2016) – Soil liquefaction: a critical state approach.

- Jefferies et al. (2019) – Report on NTSF Embankment Failure: Cadia Valley Operations for Ashurst Australia.
- Morgenstern et al. (2016) – Report on immediate causes of the failure of the Fundão Dam.
- Olson and Stark (2003) – Yield strength ratio and liquefaction analysis of slopes and embankments.
- Sadrekarimi (2014) – Static liquefaction-triggering analysis considering soil dilatancy.
- Robertson (2010) – Evaluation of flow liquefaction and liquefied strength using Cone Penetration Test.
- Sadrekarimi (2016) – Static liquefaction analysis considering principal stress directions and anisotropy.

Rationale for precaution and defence

Liquefaction is a brittle failure mode. The observational method, widely used in the tailings industry and responsibly applied with considerable merit in the oil sands and elsewhere, provides little to no protection for brittle failure, and for static liquefaction in particular. Defences must be provided through other means.

The numerical tools that are currently available are valuable, but they have several limitations as discussed above. Properly accounting for the combinations of events that could lead to failure also promotes a precautionary design approach.

The guidance provided below focusses on what precautionary steps can be taken during design, construction and operation, to mount a defence against liquefaction failure.

Precautionary principles for responsible design

Decide to not store water or fluid tailings behind tailings dams

Mount Polley, Fundão, and other recent tailings failures are reiterating the lessons of the past 50 years: do not store water behind tailings dams. Instead, store water behind water dams and aim at a zero-pond approach for tailings containment. A new corollary is now being added: aim for the storage of tailings which are inherently stable behind tailings dams and store liquefiable tailings against more conventional dams. Boswell and Sobkowicz (2015) list this as a Best Available Technology (BAT).

The ravages of time, climate change and other factors have shown in cold and northern climates how difficult it is to maintain water storage and thermal stability at the same time (Proskin et al., 2017).

The message is abundantly clear: if possible, avoid storage of water or liquefiable tailings behind tailings dams.

Identify all potential triggers for liquefaction

Identify all weak zones in the foundation, anticipated short and long term groundwater conditions, and other factors about the foundation, the dyke and the pond contents that could lead to a triggering mechanism for static liquefaction. Design to avoid those factors, as much as possible, and where not possible, provide several layers of mitigation.

Wherever possible, eliminate strain softening as a trigger

It is important to understand the variability of the foundation and dyke construction materials, and incorporate that into design. In particular, the complexity of the foundation for a large structure may demand much more than a single site investigation, in order to fully characterize and understand its behaviour. Instead, an iterative and integrated campaign approach is recommended, that evolves as new understandings are gleaned from previous test results, as early performance becomes evident, and as design changes occur. Good design and economic design are both derived from a full understanding of the hazards that are facing the structure. Typically, an increased investment in ground investigation results in a more cost effective design and at worst it may have cost a little more to gain a more reaffirmed understanding. Contrast this with an under-scoped investigation that fails to adequately capture the complexities of the foundation materials, resulting in increased cost, delay, increased potential for failure, or at worst, another failure such as occurred at Mount Polley.

Design the dam with a robust size of non-liquefiable zone

This will depend on the height of the dam, the dyke slope (heavily dependent on foundation conditions), and the strength of the contained tailings. The proposed dyke section should be plotted up in natural scale (never, ever visualize a dam using exaggerated scale drawings). The non-liquefiable zone should then not look like a “shell” or a “skin” or a “wall"; it should clearly be a significant structural component of the dyke. There is no hard number for this, but to start, size the non-liquefiable zone to be 5 to 10 times as wide at its base as the dyke is high, and either staying with that width or narrowing slightly towards the top of the dyke. The flatter the dyke slope, the wider (horizontally) the non-liquefiable zone should be. This is just for preliminary sizing during the concept stage; the width of this zone should be adjusted as the design progresses and is subject to various analyses.

DO NOT design on the basis of avoiding triggering liquefaction

Design on the basis that if a loose sandy zone can liquefy, it will. The dyke must be designed and built to perform adequately if that happens.

Incorporate substantial drainage in the design

Provide as many drains as possible for the dyke and beached materials (including at, or in the foundation). The better the drainage, the better the density will be when the dyke is constructed (if performed hydraulically) and when the beaches are poured.

Characterize material upstream of the non-liquefied zone

Determine the most likely case (MLC) and reasonable worst case (RWC) strengths for the material upstream of the non-liquefied zone. The MLC strength might be drained but representative of a loose sand (or silty sand); the RWC strength would of course be the liquefied case. Avoid being overly optimistic about these strengths during the initial design phases.

Characterize material in the non-liquefied zone

Likewise, determine MLC and RWC strengths for the material in the non-liquefied zone that are compatible with the identified failure modes and expected strain in the dyke and foundation.

Employ strain compatible and reliable downstream berm support

If downstream berms are required, use material that can be placed and compacted to a known condition, with well-understood material properties. These outside dyke zones and berms should have a ductile stress-strain response and be strain-compatible with whatever failure mechanisms are anticipated, so that this portion of the dyke can be instrumented, and all credible failure modes properly monitored. In particular, if the material in these zones is too soft or too loose, so that large deformations are required to develop their peak strengths, other portions of the dyke (such as the foundation under the upstream and middle portion of the dyke) may reach and pass peak strength. Large deformations and high deformation rates are to be avoided to prevent triggering liquefaction.

Use deformation analysis to identify zones of weakness

Since limiting deformations is such an important part of the design, reliance should not be placed on limit equilibrium stability analyses alone. Also, deformation analyses should be completed to identify areas where deformations might be significant and trigger liquefaction of overlying tailings. Again, design these areas to keep any potentially liquefiable material well away from the structural part of the dyke.

Pursue Best Available Technology (BAT) and Best Applicable Practice (BAP)

Process and tailings engineering technologies which serve to reduce liquefaction risk include:

- Substantial reduction in water content of the tailings prior to or during disposal.

- Avoidance of storage of water within tailings facilities, and storage within dedicated reservoirs or recycle water dams instead.
- Deposition of tailings stabilized by chemical or other means.
- Reduction of risk by compartmentalization (to reduce consequences), while also being careful to avoid the risk of cascading failures.
- Pursuit of in-pit or underground disposal (backfill), which potentially reduces the consequences of a failure.
- Adoption of an appropriate level of (extreme) precaution, in dealing with very high or extreme consequences and risks.

Further detail is provided by Boswell and Sobkowicz (2015) in listing and describing Best Available Technology (BAT) for reducing consequences, offering a context for Best Applicable Practice (BAP), and suggesting the key differences between the application of BAT versus BAP.

Perform a comprehensive FMEA and formally reduce liquefaction risk

Carry out a Failure Modes and Effects Analysis (FMEA) to identify all design, construction and operational conditions that could contribute to liquefaction of dyke zones (and other failure modes). In addition, build multiple layers of mitigation into the design, construction and operations of the dyke to deal with those conditions. The intimate involvement of groups that will construct and later operate the dyke is critical.

A formal process for evaluating tailings designs to fundamentally reduce liquefaction risk should be employed. While processes such as Failure Modes and Effects Analysis (FMEA) are useful, they cannot be allowed to merely develop a register of risks and mitigation measures for an existing design. The risk reduction requirements should address all aspects from early scoping through technology selection, and possible redesign, to closure.

Specific monitoring and surveillance precautions and actions required for mitigation of static liquefaction risk, should be systematically documented in an updated OMS manual.

Update this exercise every few years to attune new staff in the organization to the sensitivities of the design, and to identify any new design, construction and operational conditions that could contribute to liquefaction of dyke zones, and build multiple layers of mitigation into the design, construction and operations of the dyke to deal with those conditions.

Precautionary principles for responsible construction

Develop appropriate and relevant specifications

Work out specifications for dyke and non-liquefied zone density. Determine how these will be achieved and both the QC and QA controls that will be employed to confirm them.

Employ advanced laboratory testing to confirm material properties

Determination of MLC and RWC properties for both potentially liquefiable and non-liquefiable zones will require advanced laboratory testing of material covering the full gamut of fines content, grain size distributions, etc.

Appoint an Engineer of Record and define responsibilities

It is now accepted practice that a designated Engineer of Record be appointed to take responsibility for the construction and performance of the dyke. This responsibility is not however, in isolation. Boswell and Martens (2017) describe in detail the role of the Engineer of Record and summarize the other roles and requirements required of key personnel within an integrated dam safety management system.

Specify and build structural portions of the dyke accordingly

Ensure that portions of the dyke that need to be "structural" are actually specified as such, and built that way:

- All tailings that need to meet certain density specifications actually do, and are discharged in areas that are well-drained and/or track-packed.
- Upstream and downstream berms and ramps meet sufficient density specifications and are not just dumped waste. Material in these zones does not just provide weight; it must also provide strength and limit deformation.

Provide continuity for the operations phase

Consider what group will be responsible for the early/starter dyke construction. Their key engineers and construction staff should be involved in the FMEA (previous point). They should also have a designated Engineer of Record who takes responsibility for the construction and performance of the dyke. Proper transition of this responsibility to a different person during Operations should also be considered and implemented.

Precautionary principles for responsible operation

Among many important considerations, some of the primary operational defences against static liquefaction are preventive, rather than curative: these important defences are quite mundane and are often overlooked. These defences are described below.

Develop multiple precautions for the initial deposition, or start-up phase

Examine the initial behaviour of discharge into the pond – where will the tailings flow and where will the initial pond form? Design dyke elements that are robust in this area and keep any potentially liquefiable

material, e.g., beach below water (BBW), well away from the dyke structural zones. Precautions and additional preparation may include:

- Build the starter dyke in the area where the initial pond will form out of structural material, to a sufficient elevation and geometry to preclude potentially liquefiable material from close proximity to the dyke, where it might otherwise introduce risk and fragility.
- Include extra berms or ramps on the upstream side of the dyke to generate the requisite geometry. These should be constructed of compacted fill, not waste, as they will need to meet a certain strength specification.
- Consider an "engineered pond bottom", essentially reversing the natural slope of the ground, to force the initial pond well away from the dyke.
- This approach is particularly useful when the designer anticipates a lot of "off spec" tailings in the start-up phase of the plant and/or the need to store water in the tailings pond before start-up.

Design and operate the pond to be at a minimum size

This requires careful thought and much interaction with Operations staff so that they understand how important it is, and so they themselves design and build robust systems for removing water from the pond (e.g., using suction dredges rather than pumps when high sediment water is expected). Precautionary actions in regard to pond size might include:

- Minimizing the need for raw water import and maximizing water recycling opportunities.
- Anticipating any need to store water in the tailings area prior to start-up, i.e. during the initial construction phase.
- Anticipating the need to import additional water during high flow times in adjacent rivers so that water importation during low flow times or scarcity is avoided. There must be an allowance in the water inventory to store this extra water without impacting the dyke and beach operations (for example, through off-channel storage).
- If it becomes necessary to store water from other sources (e.g. groundwater) in the tailings pond, make allowance for this in the tailings plan as well, without compromising beach length and dyke design requirements.

Provide sufficient tailings contingency storage capacity

In addition to anticipating water storage needs, provide a tailings storage contingency within the tailings plan (6 months is typical) so that under minor upsets beach lengths can still be maintained. This is a critical aspect of tailings planning – as important as providing sufficient pond freeboard – and should not be ignored nor compromised. It should be formally recognized as a part of the tailings plan.

Design for specific beach above water (BAW) lengths

Assiduously monitor BAW lengths during Operations. Short-term tailings plans should project pond levels and beach lengths, and immediately implement plan changes to avoid encroachments. It is unacceptable to violate beach length/density requirements and then later "recover". This builds potentially liquefiable zones into what should be consistently a structural, non-liquefiable material.

Confirm that Beach Above Water (BAW) is truly non-liquefiable

Regularly confirm that BAW zones are non-liquefiable and adjust operations (e.g., by increasing deposition area, reducing rates of rise, or through implementing or increasing track-packing) where necessary.

Assiduously develop and preserve beach freeboard

A distinction should be made at the outset, between total freeboard and beach freeboard. As the name implies, beach freeboard is the amount of freeboard provided by the beach alone.

As illustrated in Figure 2, total freeboard provides the (as-measured) overall defence against overtopping, and may be rapidly improved by elevating the crest of the dam.

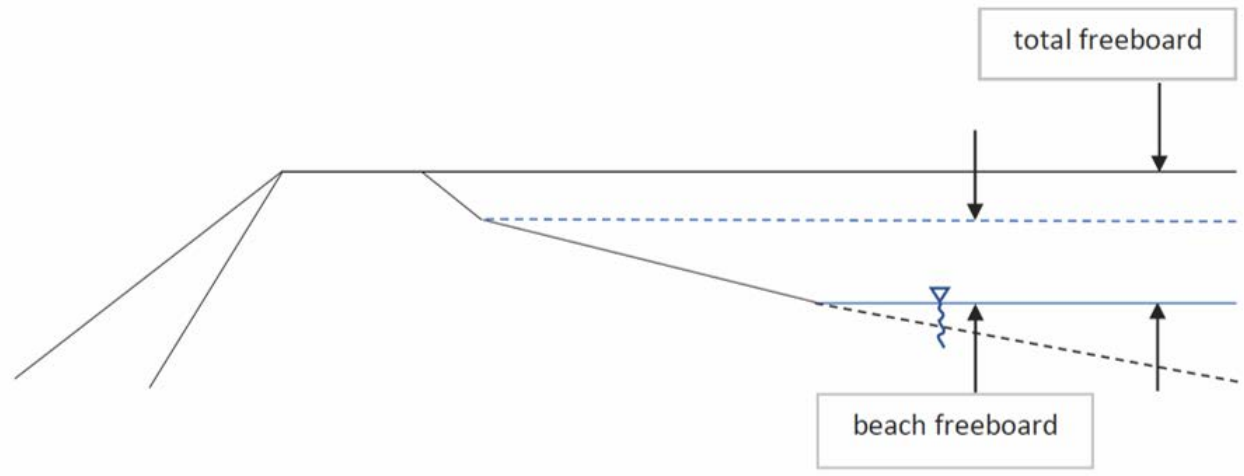

Figure 2: An illustration of the meaning of beach freeboard, vertical scale exaggerated (Boswell and Sobkowicz, 2018)

Beach freeboard is much harder won but provides a number of additional benefits including:

An additional defense against liquefaction

Tailings deposited on a subaerial beach, or beach above water (BAW), is usually not liquefiable, whereas tailings deposited sub-aqueously or beach below water (BBW) is usually liquefiable. There are exceptions to this rule, depending on climate, mineral type, particle size distribution, slurry specific gravity, mechanical compaction, but the trend is valid.

Improved slope stability

Existence of a long beach provides greater separation between the outer embankment and the pond, and consequently improved control of phreatic surface within the tailings and resulting embankment slope stability.

Beware of negligent and indiscriminate cost cutting measures which escalate the risk of liquefaction failure

Such measures may include:

- Delaying buttressing and remedial measures.
- Delaying the development of extension areas which are needed to reduce rate of rise.
- Storing water rather than treating or releasing water from inventory.
- Allowing contingency storage capacity to be reduced or consumed.

Boswell (2016) provides a more detailed list of cost cutting errors as summarized from interviews with 15 leading tailings practitioners worldwide.

Understand the critical role of deposition history in determining tailings behaviour

Even for tailings deposits constructed very recently, available records of deposition are often unrecorded, unavailable or not suitable to fully reconstruct the deposition history. Improvements in aerial photography and the use of drone photography have provided some insight into the general history of the deposition and rate of rise. However, if the tailings deposit has demonstrated large and unexpected material variability, or shows the presence of weak layers within the deposit, the deposition history should be determined in greater detail.

The selection and stability/deformation analysis of critical cross sections requires significant interpolation of field data, construction and operational records, phreatic surfaces, and the use of engineering judgement in order to determine the extent of liquefiable tailings, the extent and character of weak clay layers, and the likely pore pressure response to triggering.

In the event that the actual geometry and performance of key weak layers within the structure is markedly different from that which has been inferred, the design may be too conservative, or worse still, non-conservative.

A series of telephone and site interviews using questionnaires may be useful to amplify the understanding of the scheme deposition history, and in order to more accurately predict the structure behaviour. In addition, historical aerial or satellite photography (if possible, at monthly intervals) may be examined in order to establish deposition in which supernatant was not decanted, the largest pond size,

extent of accumulation of clay, bitumen, frozen ground and other interruptions of effective beaching, on the deposit, and degree of continuity between potential weak layers.

Rigidly apply limits to rate of rise as a critical operational precaution

Pollock et al. (2014) show that oil sands tailings beach above water (BAW) deposition at annual rates of rise in excess of 10 metres per year, which is not track-packed, is liquefiable. One of the reasons for this is insufficient time for drainage of new tailings beach.

Exceeding the established safe rate of rise limits will increase the risk of creating weak or liquefiable layers in beach above water (BAW), or subaerial deposition, and may limit the future tailings storage capacity. Mitigation of problem layers after the fact is time consuming, expensive and of limited effect.

It is usually preferable, but typically unachievable in practice, for deposition rates of rise to be slowing down rather than accelerating, as the dyke rises. Within reasonable norms, the slower the structure is built, the higher its maximum potential final safe height is likely to be.

It is recommended that a safe rate of rise be established for a structure, and that instantaneous and monthly rates of rise be measured, and recorded, as well as lift thickness. Widely differing rates of rise in different areas of the structure should also be avoided and replaced with consistent, scheduled, rotated and regular deposition across the entire surface.

One of the authors of this paper showed in a series of papers at Tailings and Mine Waste conferences (Boswell, 2009; Boswell and Sobkowicz, 2011; Boswell and Sobkowicz, 2015; Boswell and Gidley, 2017), the benefits which accrue from consistent adherence to rate of rise controls and limits in tailings deposition practice. Advice included the following:

- Calculation of allowable rates of rise for each deposit and each material.
- Establishment of allowable limits for rate of rise, and maximum height, based on the dewatering and consolidation characteristics of the tailings material.
- Measurement of incremental and average rates of rise.
- Strict compliance with seasonal, annual and overall rate of rise limitations.
- Adjustment of trigger levels and limits to cater for unseasonal or extreme precipitation.

Monitor closely

Monitor the dyke for movement, particularly in the foundation, and continually evaluate the implications of that movement in regard to the potential for triggering liquefaction in the dyke (in addition to other failure modes). Monitoring of changes in pore water pressure is just as critical and may, in some cases, provide an earlier warning (than deformation) of a developing problem.

Ensure continuity of responsibility through to Closure

Consider what group will be responsible for Operations, subsequent phases of Construction, and Closure. Their key engineers and construction staff should be involved in updating the FMEAs. At all times, there must be a designated Engineer of Record who takes responsibility for the construction and performance of the dyke. This requirement stands until the tailings facility is decommissioned or closed/reclaimed. Proper transition of this responsibility to a different person from Operations to Closure should also be considered and implemented where necessary.

Conclusion

Many practising engineers should now be familiar with the risk of static liquefaction. However, there appear to be too many who are still unaware of the extreme gravity of this risk. Hopefully, the many courses and papers now focussed on the subject (notably also at this conference) should help to remedy this industry weakness.

In regard to design and remediation however, reliable and published guidance has been wanting. Perhaps we are still digesting the urgency and importance of the problem.

The intention of this paper has been to present remedies and defences for three areas: design, construction, and operation. This is not the step-wise detail necessarily needed, but at the very least represents an initial list of guiding principles to alert the practising engineer to the tools that are now available, while also providing a 30-point checklist of precautions against static liquefaction.

Acknowledgements

We wish to express our thanks to our clients, our associates in the industry, and our colleagues at Thurber Engineering for their support, and to Dawit Abraha and Mauricio Pinheiro in particular, for the collaboration and insight they contributed to this paper.

References

Boswell, J.E.S. 2009. Strategies for dealing with fine fluid tailings and suspended fines: Some international perspectives. *Proceedings of the 2009 Tailings and Mine Waste Conference*, Banff, Alberta, November, 2009.

Boswell, J.E.S. and J.C. Sobkowicz. 2011. Duty of care applied to tailings operations. Plenary Paper, *Proceedings of the 2011 Tailings and Mine Waste Conference,* Vancouver, British Columbia, November, 2011.

Boswell, J.E.S. and J.C. Sobkowicz. 2015. International tailings failures and best available technology. *Proceedings of the 2015 Tailings and Mine Waste Conference,* Vancouver, British Columbia, October, 2015.

Boswell, J.E.S. 2016. Cost effective and responsible tailings management. *Proceedings of the 2016 Tailings and Mine Waste Conference*, Lake Louise, Alberta, December 2016.

Boswell, J.E.S. and I.D.C. Gidley. 2017. Strategic developments in the next decade for tailings. *Proceedings of the 2017 Tailings and Mine Waste Conference*, Banff, Alberta, November 2017.

Boswell J.E.S. and S. Martens. 2017. The role of the Engineer of Record in an integrated dam safety management system for tailings dams: Recent perspectives from the Alberta Dam Safety Community. *Proceedings of the 2017 Canadian Dam Association Annual Conference*, Kelowna, British Columbia, October, 2017.

Boswell J.E.S. and J.C. Sobkowicz. 2018. Leading versus lagging indicators of tailings dam integrity. *Proceedings of the 2018 Tailings and Mine Waste Conference,* Keystone, Colorado, September, 2018.

Fear, C.E. and P.K. Robertson. 1995. Estimating the undrained strength of sand: A theoretical framework. *Can Geotech J.* 32: 859–870.

Fourie, A. and D. Reid. 2018. Static liquefaction workshop. Workshop sponsored by CSIRO and The University of Western Australia (Australian Centre for Geomechanics). Melbourne and Brisbane.

Fourie A. and D. Reid. 2019. Static liquefaction workshop. Workshop sponsored by ConeTec. Calgary, Alberta, July 2019.

Golder. 2016. *Mount Polley Rehabilitation and Remediation Strategy: Detailed Site Investigation, Mount Polley Tailings Dam Failure, Mount Polley, BC*. Report prepared for Mount Polley Mining Corporation.

Jefferies, M. and K. Been. 2016. *Soil Liquefaction: A Critical State Approach*, second edition. London and New York: Taylor and Francis Group.

Jefferies, M., N.R. Morgenstern, D. Van Zyl and J. Wates. 2019. *Report on NTSF Embankment Failure: Cadia Valley Operations for Ashurst Australia*. Report prepared for Ashurst Australia.

Morgenstern, N.R., S.G. Vick, V.B. Viotti and B.D. Watts. 2016. *Report on the Immediate Causes of the Failure of the Fundão Dam: Fundão Tailings Dam Review Panel*. Report prepared for Cleary Gottlieb Steen and Hamilton LLP.

Olson, S.M. and T.D. Stark. 2003. Yield strength ratio and liquefaction analysis of slopes and embankments. *J of Geotech and Geoenviro Eng.* 129(8): 727–737.

Pollock, G.W., D.C.A. Mettananda and T. MacGowan. 2014. Suncor's new approach to tailings containment – Sand Dump 8. *Proceedings of 2014 Canadian Dam Association Annual Conference*, Banff, Alberta, October, 2014.

Proskin, S.A., J.E.S. Boswell and N. Sims. 2017. General guidance for the design of tailings dams in northern regions. *Proceedings of the 2017 Tailings and Mine Waste Conference,* Banff, Alberta, November, 2017.

Robertson, P.K. 2009. Interpretation of cone penetration tests – a unified approach. *Can Geotech J.* 8(158): 1–48.

Robertson, P.K. 2010. Evaluation of flow liquefaction and liquefied strength using the cone penetration test. *J of Geotech and Geoenviro Eng.* 136(6): 842–853.

Robertson, P.K. 2017. Evaluation of flow liquefaction: Influence of high stresses. *Proceedings of the 3rd International Conference on Performance Based Design in Earthquake Geotechnical Engineering,* Vancouver, British Columbia, July, 2017.

Robertson, P.K. 2018. Evaluation of liquefaction in tailings and mine waste: An update. *Proceedings of the 2018 Tailings and Mine Waste Conference,* Keystone, Colorado. October, 2018.

Robertson, P.K. 2019. *Geo-characterization using cone penetration test*. Workshop sponsored by Canadian Geotechnical Society – Southern Ontario Section. Richmond, Ontario, August, 2019.

Sadrekarimi, A. 2014. Effect of the mode of shear on static liquefaction analysis. *J of Geotech and Geoenviro Eng.* 140(12): 1–12.

Sadrekarimi, A. 2016. Static liquefaction analysis considering principal stress directions and anisotropy. *Geotech and Geol Eng.* 34(4): 1135–1154.

Proceedings of Tailings and Mine Waste 2019
November 17–20, 2019, Vancouver, Canada
Published by the University of British Columbia, 2019

Uranium Ore Treatment Tailings Pond Remediation – A Case Study

Laura Carbone, Huesker Synthetic GmbH, Germany
Ole Syllwasschy, Huesker Synthetic GmbH, Germany
Lilma Schimmel, Huesker Inc., USA
Melchior Briers, Huesker Inc., USA

Abstract

In the past, the eastern part of Germany (the former German Democratic Republic) was the world's third largest producer of uranium. After 1990, uranium excavation was no longer permitted in Germany; however, the existing uranium ore open-pit sites and tailings remained as old polluted sites. The Pond 4 tailings impoundment in Freital was built in 1957 as a settling basin for residues produced from the uranium ore treatment facility of the Wismut company. In 2006, the authority of water management declared Pond 4 as a contaminated site that needed to be rehabilitated. The main aim was to reduce the contamination risk and to improve the concentration values to the minimum acceptable for public health.

The solution proposed for the rehabilitation consisted of an impermeable capping that mainly aimed to:

1. isolate the residues and therefore reduce the exposure of uranium radiation; and
2. prevent new leakage formation by limiting the infiltration of water into the pond.

The restoration also included the geotechnical stabilization of the entire area and the management of rainfall water.

The remediation concept consists of an impermeable capping with the dual purpose of long-term reduction of contaminant release and providing the basis for subsequent landscaping. The construction of a cover system can be challenging due to the very soft subgrade. The use of geosynthetics provides the most economic and feasible solution and can be easily combined with other methods, as for example in this project, with vertical drains.

In this paper, the case study of Pond 4 in Freital is presented. Particular attention is given to the use of geosynthetics in the system. The stability analysis, the selection of the materials, and the installation phases are fully described, and can be used for reference for alternative solutions in similar projects.

Introduction

After 1990, mining of uranium ore was no longer permitted in Germany. Previously the former GDR, together with the Czech Republic, exported around 231,000 tonnes of uranium annually.

In particular, the Soviet-German stock company Wismut carried out an intensive uranium mining operation, resulting in large amounts of polluted tailings that were released into the so-called industrial sediment ponds. Pond 4 was built in 1957 as a settling basin for residues produced from the uranium ore treatment facility. Residues from the processing factory were released into the basin from January 1958 to December 1960, but due to its particular morphology the pond also acted as a rainwater retention dam. In 2006, the authority of water management declared Pond 4 a contaminated site that had to be remediated.

Generally, the management of tailings ponds consists of three main steps: solid-liquid separation, sludge dewatering, and disposal (Zinck, 2005). One of the main concerns is about rainfall infiltration, the material inside the impoundment never reaches a completely solid state, so with the lining system, a dam failure can potentially cause the uncontrolled release of toxic sludge (Syllwasschy and Wilke, 2014). For the IAA[1] Pond 4 in Freital, the remediation concept consisted of an impermeable capping to isolate the residues and to reduce exposure to nuclear radiation.

However, the construction of a cover system on top of a weak and heterogeneous tailings can be a challenge. Generally speaking, the placement of the cap on soft tailings can be done mainly mechanically or hydraulically. Depending on the site-specific conditions, the solution may include the combination of the two methods and/or the use of complementary materials and technologies (Langseth et al., 2015). For example, Wells et al. (2010) and Abusaid et al. (2011) described the conception, design, and the final construction of a cover system on a very soft oil sand tailings pond, which was achieved by using a 2-m thick layer of low density fill (coke), with geosynthetics (geotextile and geogrids) placed on the frozen tailings during the winter time, and vertical strip drains to accelerate the consolidation process.

The mechanical placement of the cover system uses light earthwork equipment working from the edges of the tailings basin, pushing a lift of fill material over the tailings. The use of geosynthetics plays a key role in such systems to enable a safe access surface for machinery.

In this paper, the remediation work for Pond 4 in Freital from its initial concept to the design and execution is fully described.

Capping system with geosynthetics

General background

The design of the cover system of a tailings pond normally depends on the requirements of the customer or

[1] Note: IAA is a German acronym for industrial sediment ponds.

the appropriate authority and the intended use after capping. In the design of such systems, the use of geosynthetics stabilizes the soft subsoil and therefore enables workers and construction machinery to work carefully on the tailings pond without treating the tailings further.

Generally speaking, the cover system may consist of a simple geosynthetic layer for reinforcement and fill material, or a multi-layer system with geosynthetics, soils, and qualified liner system with gas and water drainage.

According to the tailing's characteristics, the regulations in force in the specific lands, and the final use of the site after remediation, the thickness of the different layers may vary, but in general they are not less than 1.5 m – 2 m. The main challenge in designing such a structure is the construction of the system on top of a very soft and extremely heterogeneous soil. In fact, according to the deposition history, dewatering, and weather conditions, the hydraulic and mechanical characteristics of the tailings may differ in depth and across the area. In this case, geosynthetics for reinforcement, for example geogrids or woven geotextiles with adapted design strength, might be used.

For the technical design of the capping system an intensive investigation of in-situ soils is required. The following data are required:

- geotechnical parameters of tailings/fill material;
- stratification of the subsoil;
- tailings pond size;
- free water level; and
- live load of construction machinery.

Settlement estimation of the tailings

Settlement due to consolidation may be significant in these subgrade conditions. Therefore, conditions should be assessed, and should be consistent with the allowable deformation of the sealing system of the capping.

Soil investigation should include consolidation tests to specify settlement during and after construction period. If no data is available, a settlement assumption has to be made based on experience with similar soils, and the prediction should be verified during the construction phase; for example, by means of measuring points on the surface.

Geosynthetic reinforcement design

Typically in the design of capping systems, woven fabric or geogrids, or combinations thereof like woven/geogrid or geogrid/non-woven, are selected. The main function of woven fabrics and geogrids is to transfer tensile stresses resulting from the construction of the cover system, i.e., soil and traffic load, into

the anchor trench. In addition, non-wovens can also work as separators and filters to keep sludge in place below the geotextile. As tailings can have different origins such as mining, heap leaching, harbour or river sediments, and wastewater treatment sludges, they can have very diverse chemical properties. Depending on the chemical characteristics of the sludge, different raw materials should be selected. Normally polypropylene (PP), polyester (PET, PES), polyethylene (PE) and polyvinyl alcohol (PVA) can be used in a normal pH range from 4 to 9.5. In areas with a pH of 2–4 or 10–13, it is best to use PP and PVA if long-term stability is important.

The required tensile strength of the geosynthetic reinforcement should verify the stability of the system. Currently there is no established method available to design the geosynthetic reinforcement according to these membrane-like loading effects. Edil and Aydilek (2001) described a design procedure and Espinoza et al. (2012) presented a case history and a more sophisticated design method. These designs are based on bearing capacity (rutting) analyses, the latter in combination with a membrane contribution to the reinforcement. In addition, Bishop's method can be used for the stability analysis where mud waving at the edge of the geosynthetic during the filling process is considered. It is worth pointing out that the stability of the system, the stratification of the cover layers, and their soil parameters, have to be checked carefully during each stage of the filling process. The first soil layers of 0.3 m up to 1.0 m may be the most critical, due to the shear resistance of the weak sludge as well as the counter pressure activated by the surcharge, which is negligibly small to prevent ground failure.

Another key aspect during the design is the installation of the geosynthetic layers. This depends on the size of the pond and on the tailings characteristics. It can be done by sewing together a large panel that can be pulled by winches from the edge into the pond (Figure 1a), or by unrolling and overlapping them (Figure 1b).

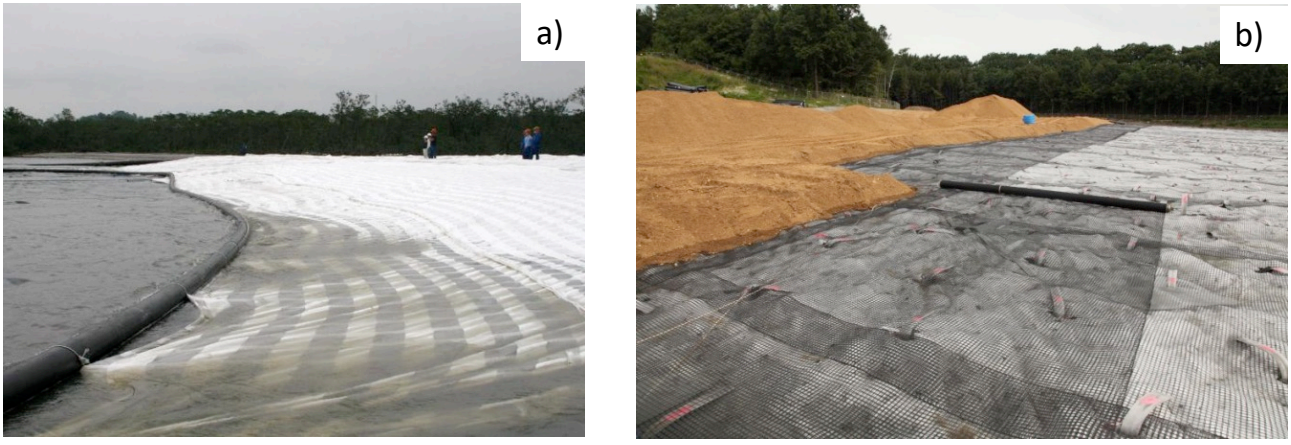

Figure 1: Examples of installation methods of geosynthetics in tailings ponds: a) assembling of large panels; b) unroll and overlap geosynthetic reinforcement elements

IAA "Pond 4" case study

The cover system of the IAA Pond 4 is aimed at isolating the residues and therefore reducing the exposure of nuclear radiation and preventing new leakage formation by limiting the infiltration of water into the pond. The remediation of the site also includes the geotechnical stabilization of the entire area and the management of the rainfall water.

In the case study of Pond 4, three main different areas could be identified depending on the tailings characteristics (Figure 2). Tailings deposited in the outer edge and middle region could be considered as partially dewatered and partially consolidated, while the tailings located in the central area under the free water level could be considered in saturated and unconsolidated state.

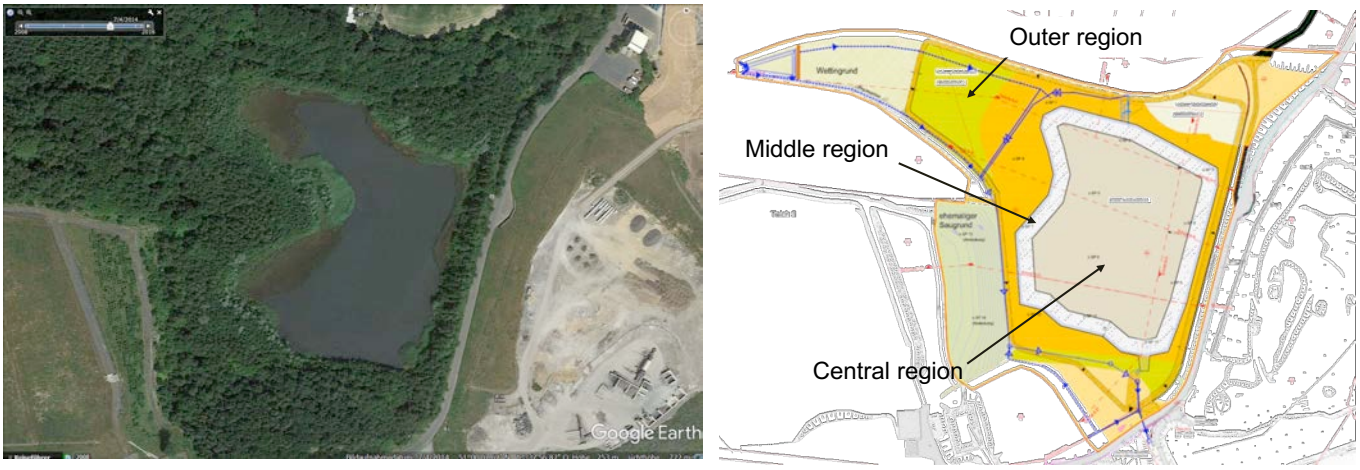

Figure 2: Pond 4: a) aerial view (Google Earth – April, 2014); b) top view – characterization according to the tailings properties

The cover system consisted of the succession of mineral soils and geosynthetics designed according to the storage and evaporation principle, with a total thickness of about 2.0 m. It is composed of the following layers (from the bottom to the top):

- 0.5 m drainage layer and base course;
- 0.5 m mineral sealing layer ensuring hydraulic conductivity $k \leq 1 \cdot 10^{-9}$ m/s; and
- 1.0 m vegetative cover soil.

In order to be able to build the mineral layer on a very soft subgrade (i.e., saturated tailings) vertical drains have been included in the system, a non-woven geotextile was used as a separation and filtration layer, and two perpendicularly placed geogrids were introduced into the system as a reinforcement element.

Therefore, the final cover contained the following layers (from the bottom to the top):

- tailings;
- non-woven geotextile;
- 2 layers of geogrid (installed perpendicularly to each other – T-shape);
- vertical drains (middle and central region);
- woven geotextile (central region);
- mineral drainage and bearing layer;
- mineral sealing layer ensuring hydraulic conductivity $k \leq 1 \cdot 10^{-9}$ m/s; and
- soil cover.

As a first step, the removal of the surficial water was carried out. The area was prepared by extracting the existing free water (~2.0 m, i.e., around 15,600 m^3) from the central part of the Pond 4 (Figure 3).

Figure 3: a) Preparation of the area (~50,000 m² – Google Earth – April, 2016)

It is worth noting that the water generated as part of the clean-up of former uranium mining and processing had to be treated prior to being discharged into receiving streams. For filtration purposes, as an alternative to a lamella separator, a geotextile dewatering tube was used. In this case, flocculants were added into the water-tailings mixture, and the fine sediments could be retained in the geotextile tube and afterwards easily transported to the treatment plant. The woven fabric of the geotextile tube served as filtration and was designed to withstand the forces acting during the operational filling.

Afterwards, the construction of the cover system proceeded with the installation of the materials in the outer regions. Here, subsoil material outside the water profile in the bank zone could be considered as dry. In this area, favourable conditions with regard to load bearing capacity could be assumed. Therefore, in this area the trenches to anchor the geogrid were constructed as follows. First, the non-woven fabric (E 250 K4) was rolled out as a filter and separation layer. Subsequently, the first geogrid layer (Base 40) was

rotated through 90° to the non-woven direction. The overlap between the different geogrid panels was a minimum of 0.50 m. The next step was the installation of the second geogrid layer (Base 40) for the load distribution, rotated by 90° to the first geogrid position and parallel to the bottom nonwoven layer (Figure 4). This method ensured that the forces from construction equipment are transferred in a longitudinal and transversal direction in an excavated area, so that the overlap between the panels will not be overstressed.

Figure 4: Geogrid T-shape installation

The installation was carried out by placing the layers of soil with a thickness of approximately 0.3 m, which acted as a load-distributing working surface. The use of light machinery was recommended for this purpose.

The middle cover area was free of surface water. This means that the same installation procedure as for the outer cover area could be used; but in addition, vertical drains in the triangular grid of 1.5 m were introduced into the system to enhance the consolidation process and expel pore water, followed by the placement of the drainage mineral layer. The vertical drains were installed through the first geogrid, and the nonwoven geotextile and then the second layer of geogrid were installed on top (Figure 5).

The central area of the pond was characterized by fine-graded sludge with a low bearing capacity. Due to the extremely soft soil conditions, large deformations were expected. In this case it was necessary to use an additional reinforcement layer. For this purpose, a woven geotextile (Sefitec PP 80), which has a longitudinal and transversal tensile strength of 80 kN/m, was placed on top of the other geosynthetic layers to provide additional support to the bearing capacity. Here, the woven geotextile was installed as one single large panel sewn in situ, and then pulled over the defined area to the outer region, where it was fixed.

The construction of the cover system proceeded with the installation of the top soil (Figure 6) on the whole surface and ended in June, 2019.

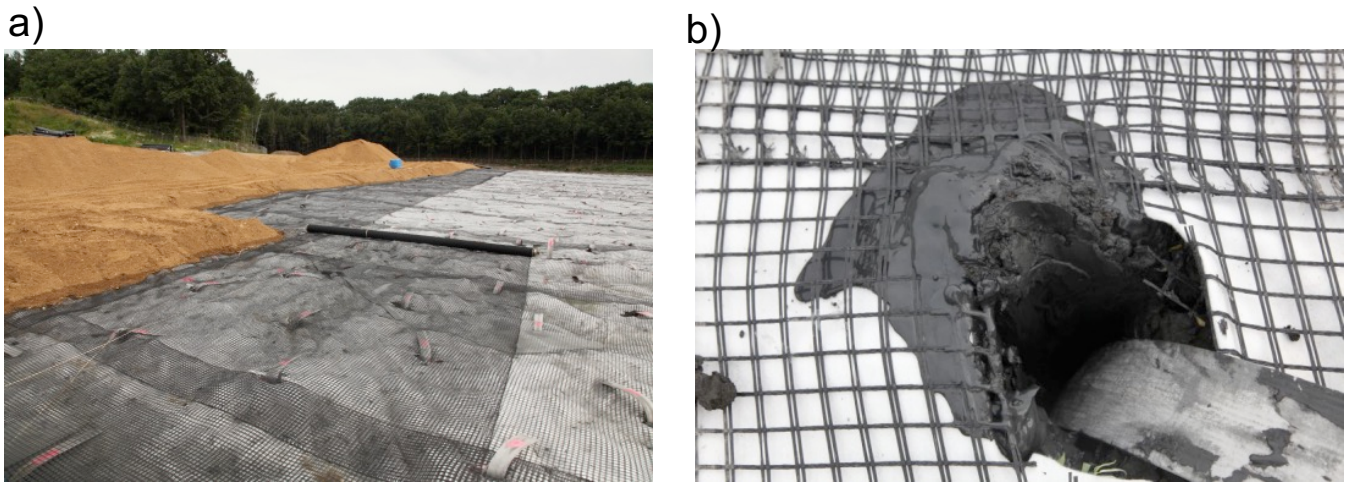

Figure 5: a) Installation of the cover system in the middle region: strip drain installed between the geogrid layers; b) Zoomed-in view showing the strip drain area after installation

Figure 6: Installation of the top soil

The remediated area works now as a rainwater retention basin as further flood protection.

Dimensioning of the geosynthetic reinforcement in "IAA-Pond 4" cover system

The tensile strength of the geosynthetic reinforcement was determined by carrying out a stability analysis of the system. The design took into account the verification of the bearing capacity of the combined system

(soft subgrade and geosynthetics). The analysis enabled us to determine the design tensile strength of the bearing layers, while the actual tensile strength of the reinforcement (i.e., geogrids or woven geotextile) was determined by applying reduction factors that take into account creep, installation damage, joints and connections, environmental chemical impacts, and dynamic effects if present. The service life of the geosynthetics was calculated to be 25 years, since its use is supposed to be limited to the construction period.

The static calculation was performed by using the GGU-stability program, applying the Bishop method. The stability calculations took into account seven main construction steps corresponding to different loading conditions. The traffic loads were set to p = 8 kN/m², and the soil thickness varied from 0.3 m in the first, up to 2.0 m in the last design phase. The design was performed according to the Eurocode 7 for a temporary load case.

Since the tailings varied significantly according to the region of the pond, a very low undrained shear strength equal to c_u = 3 kN/m^2 was chosen to characterize the tailings behaviour in the whole pond.

Once the stability calculation was carried out, the dimensions of the anchor trench were determined by verifying the analysis against the pull-out and/or sliding of the geosynthetic reinforcement.

Conclusion

As tailings ponds are built for various ore processing facilities, construction of a cover system on top of a weak and heterogeneous subgrade can be challenging. Project-specific solutions are required to remediate the contaminated sites. The use of geosynthetics has proven to be a safe and viable solution for a variety of projects.

In this paper we presented the remediation case study of Pond 4 in Freital, built in 1957 as a settling basin for residues of the uranium ore treatment of the Wismut company. Here, the remediation concept foresaw the placement of an impermeable cover with the dual purpose of long-term reduction of contaminant release and of providing the basis for a subsequent rainwater retention basin for flood protection.

The construction of the cover system in a very soft subgrade was made possible by the introduction of geosynthetics into the system. The selected geosynthetics separated and reinforced the weak subgrade, creating a safe and workable surface for the installation of the cover system. In this paper, overviews on the design, the selection of the materials, and the installation phases were fully described and can be used for reference for alternative solutions in similar projects.

References

Abusaid, A., C. Fear, E. McRobert and S. Wells. 2011. An update to the construction of the Suncor oil sands tailings pond 5 cover. In *Proceedings of Tailings and Mine Waste 2011.* Vancouver, Canada, 6–9 November, 2011.

Edil, T.B. and A.H. Aydilek. 2001. Geotechnics of capping very soft wastes. In *Proceedings of the 13th International Conference on Soil Mechanics and Geotechnical Engineering*, Istanbul, Turkey, August 2001, Vol. 3: 1903–1906.

Espinoza, R.D., W.M. Steier and M. Steiner. 2012. Construction of cover soil over soft sludge lagoons. In *Proceedings of Geoamericas 2012, the 2nd Panamerican Geosynthetics Conference*, Lima, Peru, 1–4 May, 2012.

Langseth, J., D. Luger, W. Jacobs, R. Sisson, E. Hedblom and T. Greenleaf. 2015. Placement of caps on soft and fluid tailings. *Proceedings Tailings and Mine Waste 2015.* Vancouver, Canada, 26–28 October, 2015.

Syllwasschy, O. and M. Wilke. 2014. Sludge treatment and tailings pond cappings by the use of geosynthetics, In *Proceedings of 7th International Congress on Environmental Geotechnics* (*7 ICEG*). Melbourne, Australia.

Wells, P.S., J. Caldwell and J. Fournier. 2010. Suncor Pond 5 Coke Cap – The story of its conceptions, testing, and advance to full-scale construction. In *Proceedings of Tailings and Mine Waste '10 Conference*, Vail, Colorado, October, 2010.

Wismut GmbH website. 2019. Retrieved from http://www.wismut.de/en

Zinck, J. 2005. *Review of Disposal, Reprocessing and Reuse Options for Acidic Drainage Treatment Sludge.* Canmet Mining and Mineral Sciences Laboratories, Natural Resources Canada, MEND Report 3.42.3.

Proceedings of Tailings and Mine Waste 2019
November 17–20, 2019, Vancouver, Canada
Published by the University of British Columbia, 2019

Foundation Geotechnical Investigations at Two Gold Mine Tailings Storage Facilities in Western Australia

Brendan Cummins, Golder Associates Pty Ltd, Australia
Riccardo Fanni, Golder Associates Pty Ltd, Australia
Peter Chapman, Golder Associates Pty Ltd, Australia

Abstract

In the wake of recent tailings storage facility (TSF) failures, many mine owners are considering the implications of the findings by review boards. Among other key aspects such as developing a thorough understanding of the geology, it was noted in reviews that there is a potential for clayey material to transition from over-consolidated to normally consolidated due to increased loading (i.e., due to staged TSF construction), and then be subject to contractive undrained failure, rather than dilating under load. This has prompted an industry-wide review into foundation conditions for TSFs, particularly in cases where the TSFs have been raised beyond the originally anticipated height.

This paper presents the results from two geotechnical site investigations, at two gold mines in Western Australia. At the first site, the investigation was triggered by a decision to increase the height of a TSF to double the original design height (~30 m to ~60 m). At the second site, the investigation was undertaken to address concerns raised by an internal review board, which noted deficiencies in the investigation undertaken for the original design. Both designs were carried out in the 1990s, with little or no laboratory testing undertaken as part of the foundation characterization. Typical of the time, effective stress strength parameters were assumed for the fine-grained material beneath the TSF.

The foundation investigations were both undertaken with the primary objective of confirming the subsurface conditions and retrieving relatively undisturbed samples to support characterization through laboratory testing. The laboratory results and their implications are presented and discussed.

Introduction

Catastrophic dam failures at Mount Polley (Canada), Fundão (Brazil), Cadia (Australia) and Feijão (Brazil) resulted in detailed reviews of the factors that contributed to dam failure.

One of the factors that was identified to have contributed to the failures at Cadia and Mount Polley was the incorrect characterization of the foundation. The failure was established to have been caused by the

foundation material transitioning from an "over-consolidated" state to "normally consolidated" under the loads applied during the construction of the perimeter embankments. The transition of the material from over-consolidated to normally consolidated, and the associated strength loss, had not been considered in the design.

This paper outlines the results from two foundation site investigations to identify parameters for input into TSF design to address the findings from the Mount Polley and Cadia failure investigations.

Industry requirements

In response to the failures, professional practice guidelines for the characterization of dam foundations in British Columbia by the Association of Professional engineers and Geoscientists of British Columbia (APEGBC, 2016) were prepared. In addition to this guideline, ANCOLD (2012) requires the consolidated undrained shear strength to be estimated accounting for stress history (e.g., Ladd, 1991; Ladd and DeGroot, 2004). Both of these documents were consulted during the investigations presented in this paper.

TSF designs

TSF A background

TSF A is located in the goldfields of Western Australia, in a semi-arid environment. TSF A was recommissioned after a period of care and maintenance, and raises were designed to increase the height of the facility to ~45 m. Further extensions to the life of mine necessitated increased tailings storage requirements, and the design was modified to target a maximum height of ~60 m. The embankments of the facility are raised using the upstream wall raise construction method shown in Figure 1.

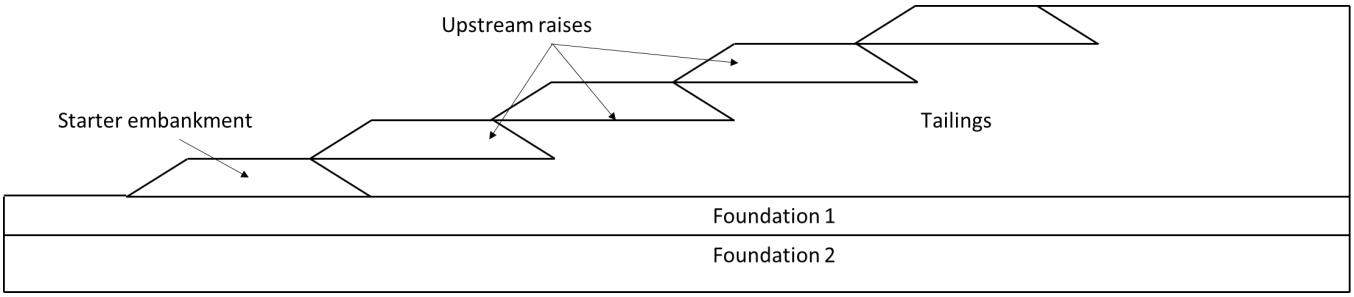

Figure 1: Schematic showing TSF A embankment configuration

TSF B background

TSF B is located in the Peel region of Western Australia, in a warm Mediterranean environment. The TSF was initially operated to receive oxide tailings before it was abandoned in the early 2000s. The TSF was then recommissioned and expanded to accept hard rock tailings. The storage requirements necessitated the

design height of the TSF to be increased to >70 m. The largest embankment is raised using a combination of downstream, centreline, and upstream wall raise construction methods, as shown in Figure 2.

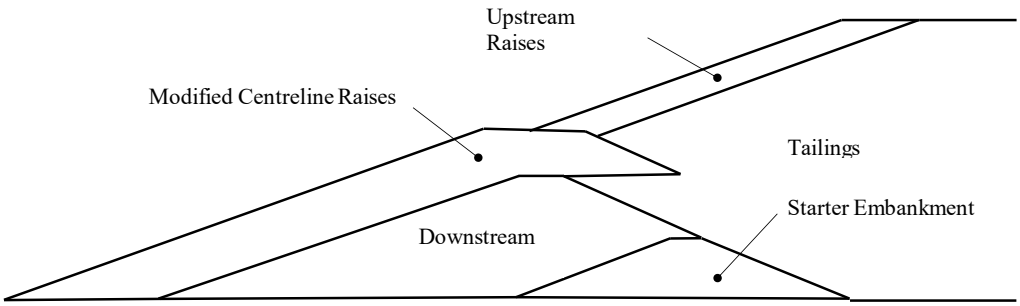

Figure 2: Schematic showing TSF B embankment configuration

Foundation conditions

The sub-surface beneath the TSFs was generally similar from a geological and geomorphological point of view. Both were originally characterized as primarily low to medium plasticity clay, overlying cap-rock at varying depths. The design assumed that due to over-consolidation and/or observed unsaturated conditions, the residual soils would exhibit dilative behaviour throughout depth under shear. However, the design did not consider the implications of the TSF expansions, and the possibility that the foundation soil would be loaded beyond its yield pressure, causing it to transition from an over-consolidated to a normally consolidated condition.

Proposed changes to design

Increased tailings storage requirements meant that the storage capacity at the two existing TSFs were re-evaluated, and the decision was made to increase the maximum expected heights of the embankments from ~30 to ≥60 m. During operation of the TSFs, several CPTu investigations were completed, vibrating wire piezometers installed, and stability reviews undertaken at regular intervals. However, recent reviews indicated that the design heights could not be achieved without slope stability improvement measures to address the possibility of a deep-seated slope failure of the TSF through the foundation causing static liquefaction of the tailings. As part of the ongoing stewardship review of the TSFs and slope improvement studies, foundation investigations were undertaken.

Foundation characterization studies

Desktop review

The typical soil profile at the TSFs is generally summarized as superficial alluvium/colluvium materials, generally loose and shallow to around 300 mm depth, becoming dense to very dense or very stiff to hard with depth, with ferricrete horizons occurring above the underlying clay. Bedrock consists typically of

banded meta-sedimentary rock or massive igneous rock, extensively weathered to depth and lateralized.

Variable depths of weathering and material types exist due to weathering of different sedimentary and volcanic parent rock types. The residual regolith material generally varies from sandy clay to ferruginous soils overlying saprolite.

Geotechnical investigations

Boreholes were completed in pairs in a section along the embankments at each TSF (one through the embankment and one at foundation level).

The subsurface conditions encountered during the drilling investigation were generally consistent with those presented in the geological series maps, and generally the subsurface encountered, excluding the tailings unit, included:

- Clay (CL-CH), medium to high plasticity, with some medium grained gravel. Firm transitioning to very stiff/cemented with depth.

Undisturbed samples were collected during the investigations for laboratory testing. The aim of the laboratory testing was to characterize the foundation materials in terms of geotechnical properties, including material type; estimate consolidation properties; and identify undrained and drained strength parameters. An overview of the laboratory testing completed is provided in Table 1.

Table 1: Laboratory testing program overview

TSF	Sample ID	Particle size distribution	Atterberg Limits	Particle density	Constant rate of strain (CRS) consolidation	Direct simple shear (DSS)	Consolidated drained triaxial
1	1					✓	
	2	✓	✓	✓	✓	✓	
	3						✓
	4						✓
	5					✓	
	6	✓	✓	✓	✓	✓	
2	1	✓	✓			✓	
	2	✓	✓	✓	✓	✓	
	3	✓	✓	✓		✓	
	4	✓	✓	✓		✓	
	5	✓	✓	✓	✓	✓	
	6	✓	✓	✓	✓	✓	
	7			✓	✓		

Laboratory results

Index testing

The results of the index testing are shown in Figure 3 (particle size distribution) and Figure 4 (Atterberg limits) below.

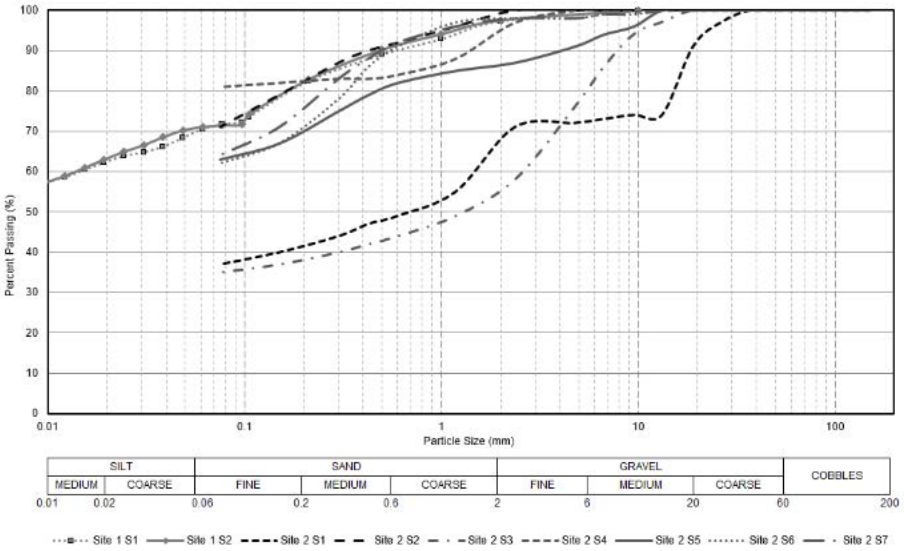

Figure 3: Summary of particle size distribution

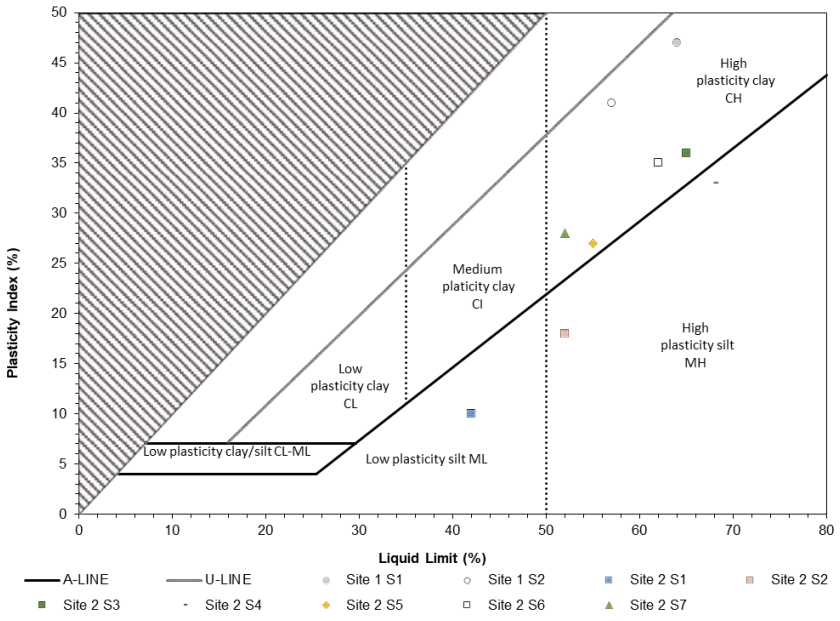

Figure 4: Results of Atterberg limits shown on the A-line plot

The result of the index testing indicate that the samples recovered are primarily high plasticity clay.

Consolidation testing

CRS testing was carried out to provide information on the compressibility and extent of over-consolidation of the materials, and to identify pre-consolidation/yield pressure if evident. The sample quality was assessed using the methods proposed by Terzaghi et al. (1996) and Lunne et al. (1997). A summary of the assessment is provided in Table 2. The void ratio versus the vertical effective stress plot of the tests undertaken in this study are shown in Figure 5. For comparison, the digitized consolidation tests undertaken during the Mount Polley failure investigation by the panel are also shown in Figure 5.

Table 2: Sample quality assessment

Sample ID	Terzaghi et al. (1996)		Lunne et al. (1997)	
	Strain at σ'_{v0} %	SQD*	$\Delta e/e_0$	Rating
Site 1 S1	1.5	B	0.038	Good
Site 1 S2	2.0	B	0.048	Good
Site 2 S1	3.8	C	0.070	Good to fair/Poor
Site 2 S2	5.9	D	0.120	Poor
Site 2 S3	6.6	D	0.140	Poor
Site 2 S4	1.8	B	0.040	Good to fair
Site 2 S5	5.4	D	0.10	Poor

*Sample quality designation

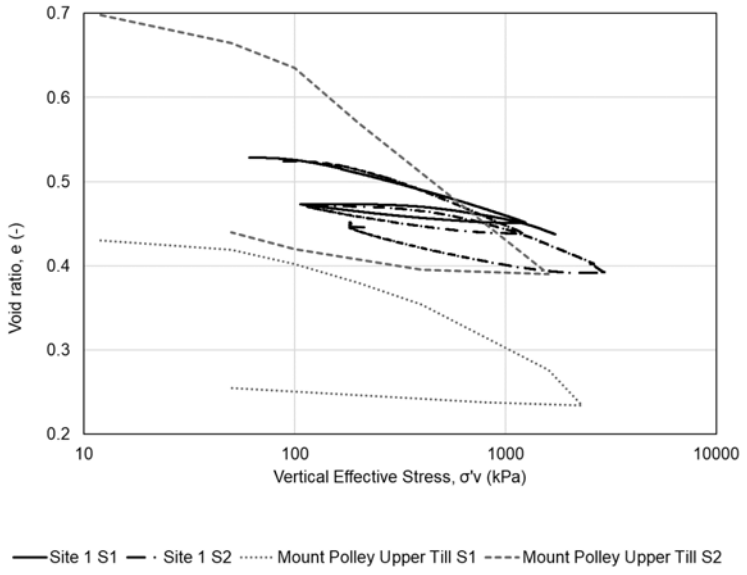

Figure 5: Void ratio versus vertical effective stress (log scale)

Site 1 results

Examining the void ratio against vertical effective stress using the linear plot rather than the semi-log plot (Figure 6), the compressibility of the material appears to initially decrease as the vertical effective stress

increases to a stress of approximately 200 kPa, and starts to increase again once this stress is overcome. The log plot appears to mask these trends, which are otherwise clear in examining both Figure 5 and Figure 6. The linear plot and constrained modulus show that the clay is strain hardening, consistent with the soil classification based on compressibility provided by Wesley (2013). This behaviour is not unexpected for residual soils.

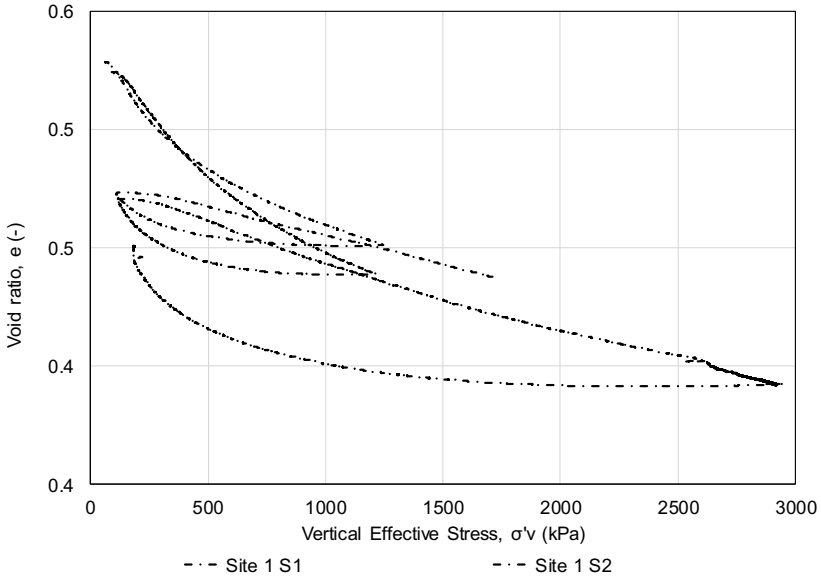

Figure 6: Void ratio versus vertical effective stress (linear scale)

Despite this trend, which may indicate that the material does not have a clear yield pressure if examined as a conventional soil, the Becker Work method, which estimates the yield pressure plotting strain energy and vertical effective stress in linear axis, indicates that the material yields to a stress higher than its in-situ vertical stress at a pressure ranging between 350 to 450 kPa. This outcome is not evident examining the compressibility behaviour of the material due to the strain hardening observed, which would otherwise indicate a significantly higher yield-pressure.

Site 2 results

Similarly to Site 1, the results of the testing undertaken at Site 2 do not show a typical behaviour of an over-consolidated sedimentary soil transitioning to normally consolidated (NC) behaviour, as the stiffness continues to increase with increased effective stress (Figure 7). A yield pressure of between 650 and 1,000 kPa was estimated using the Becker Work method.

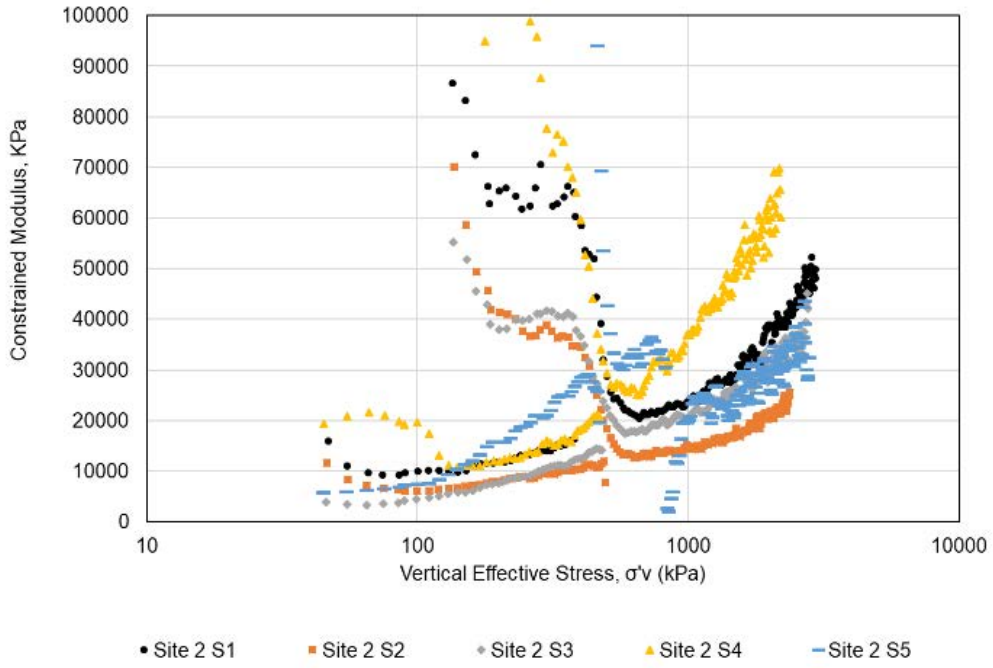

Figure 7: Constrained modulus M versus vertical effective stress

Direct simple shear testing

DSS testing was undertaken to provide information on the undrained shear strength of the samples. DSS testing was completed at varying stresses to capture the change in strength with the transition from over-consolidated (OC) to NC. Specimens were generally saturated over a minimum period of 24 hours in a water bath, under load at a pressure such as to avoid swelling.

The results of the DSS testing (Table 3 and Figure 8) were used to infer the undrained shear strength ratio versus the effective stress relationship for each site, and each material type was identified. The stress history and normalized engineering property model (SHANSEP) equation was used to infer the strength envelope, based on the testing using the recompression technique. As recommended by Ladd (1991), the SHANSEP technique of loading and unloading at different over-consolidation ratios (OCRs) is strictly applicable to truly mechanical over-consolidated and normally consolidated soils, or when the quality of the sample is poor. However, the technique is questionable in highly weathered clay crusts, in which mechanical over-consolidation does not represent the main mechanism for the over-consolidation of the clay. Therefore, acknowledging the residual nature of the clay investigated, the recompression technique was preferred to infer undrained strength parameters, with tests undertaken at a stress slightly higher than the in-situ stress, and at the maximum stress that the clay is expected to experience during the TSF life.

Table 3: Summary of DSS testing

Sample ID	Vertical stress (kPa)	s_u/σ'_v	Sample ID	Vertical stress (kPa)	s_u/σ'_v
Site 1 S1	1,000	0.76	Site 2 S1	1,450	**0.41**
Site 1 S1	1,000	0.47	Site 2 S1	1,200	0.35
Site 1 S2	1,000	0.25	Site 2 S1	800	0.50
Site 1 S2	400	0.33	Site 2 S1	250	0.70
Site 1 S5	250	0.91	Site 2 S2	1,500	0.26
Site 1 S6	1,000	0.27	Site 2 S2	800	0.30
Site 1 S6	500	0.31	Site 2 S2	550	0.26
Site 1 S6	400	0.38	Site 2 S2	1,000	0.27
			Site 2 S2	1,000	0.31
			Site 2 S3	500	0.35
			Site 2 S3	1,000	0.28

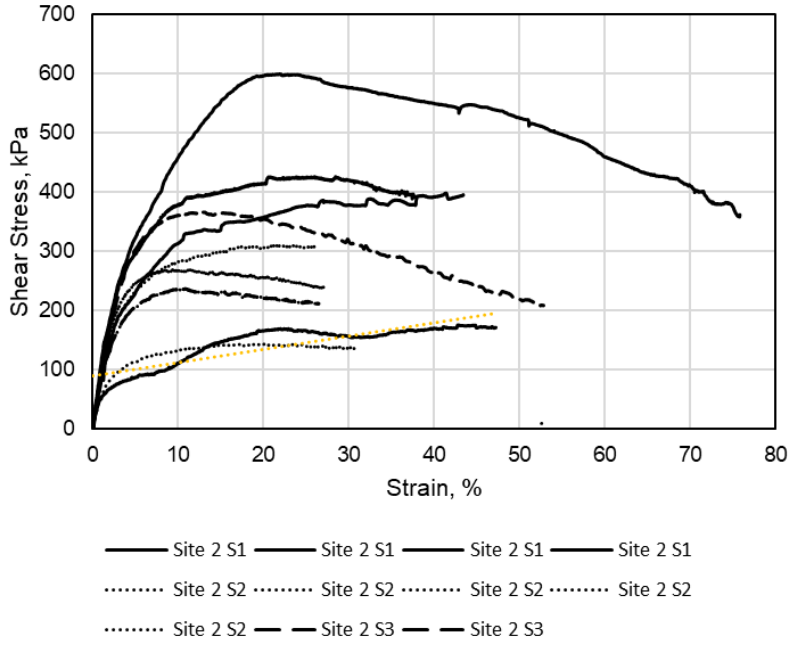

Figure 8: Stress strain curves site 2 DSS testing

The DSS results indicate that the materials exhibit a lower bound normally consolidated strength ratio of 0.25, which is typical of a CI-CH material in the DSS direction. The result is within the range of DSS strength reported by Ladd and DeGroot (2004) for materials of similar PI (see Figure 9).

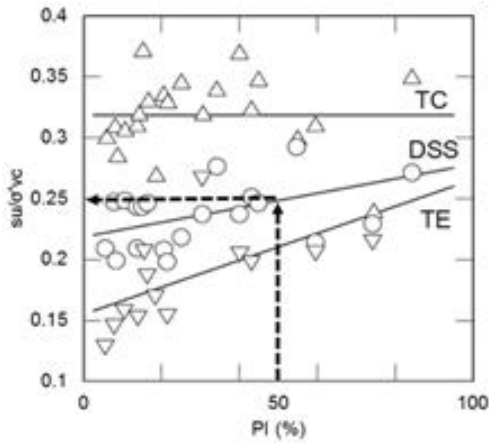

Figure 9: Expected undrained shear strength based on material PI (%) (Ladd and DeGroot, 2004)

The SHANSEP relationship is shown in Figure 10, and Table 3 provides a summary of the SHANSEP parameters indicated from the test results.

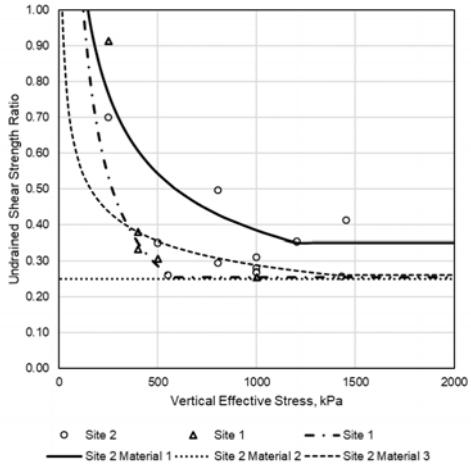

Figure 10: Strengths versus vertical effective stress (with SHANSEP relationship)

The yield pressure inferred from the DSS testing fitting the strength data to the SHANSEP equation indicates higher yield pressures than estimated from the CRS testing based on the Work method. Acknowledging the limitations of the conventional approach applied to residual soils to explain strength behaviour, which correlates yield pressure based on consolidation testing to strength, the DSS appears to provide a better estimate of the transitioning between the OC and NC range purely based on strength.

Several results show that materials may be cemented at a depth consistent with observations during the site investigations, and testing showing dilative behaviour. Dilative materials have been excluded from the SHANSEP relationship at Site 1, but acknowledged in the slope stability model as properties of Foundation Soil 2. Foundation 2 materials represent the increasing cementation of the material with depth that was observed during the site investigation.

Table 3: SHANSEP parameters

Material ID	s_u/σ'_v	*m*	σ'_{vy}[1]
Site 1 Material 1	0.25	0.9	570
Site 2 Material 1	0.35	0.5	1,200
Site 2 Material 2	0.25	N/A	N/A
Site 2 Material 3	0.25	0.3	1,400

Stability analyses

To inform the slope stability models for the TSFs, relationships were developed based on the results of the laboratory testing, which considered the in-situ state of the material and its stress history. The strength relationship accounts for the transition of the material from "dilative" conditions to "contractive" normally consolidated conditions at higher stresses. The relationship limits the strength of the material to the drained strength. This is determined from consolidated drained triaxial tests when the material is in a dilative state (i.e., stresses below the yield pressure) and the SHANSEP relationship described above. A summary of the strength profile developed for Site 1 is shown in Figure 10.

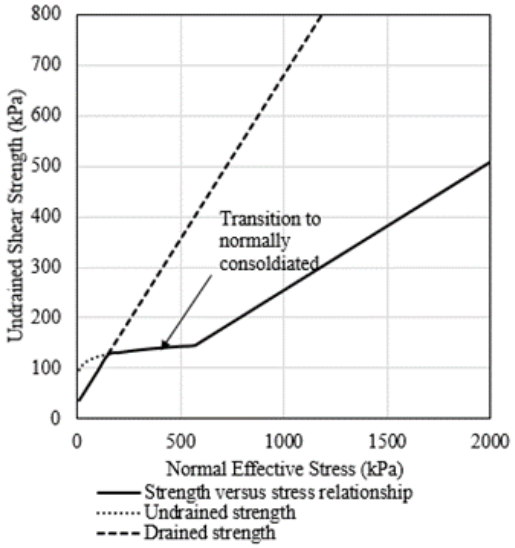

Figure 10: Site 1 strength relationship

The stability analyses were completed using limit equilibrium software. The results indicated that the global critical failure surface goes through the foundation when the facilities near their final heights. The stability analyses indicated that slope stability improvement measures (i.e., buttressing) will need to be implemented to allow the TSF to achieve the planned expanded heights.

[1] Yield pressure referred to in the SHANSEP framework as pre-consolidation pressure, σ'_p

Conclusion

Based on the field investigation and laboratory testing, the following summarizes the key findings:

- The results of the consolidation testing indicate increasing constrained modulus with increasing stress and do not demonstrate the typical strain softening compressibility behaviour (Wesley, 2013) that is typically seen in consolidation testing of truly mechanically over-consolidated sedimentary soils. This behaviour is however typical of residual soils. The yield pressure inferred using the Work method ranges between 350 and 450 kPa for site 1 and 650 and 1,000 kPa for site 2.
- The DSS results indicate that the material transitions from an over-consolidated to a normally consolidated state at a stress generally greater than 570 kPa and 1,200 kPa for site 1 and site 2 respectively. These pressures are higher than those inferred from the consolidation testing.
- The DSS strength data were fitted using the SHANSEP equation to provide relationships to use in limit equilibrium slope stability analysis. The results indicated that the global critical failure surface goes through the foundation when the facilities near their final heights.
- The results indicate that slope improvement in term of a buttress will be required to meet the minimum recommended factor of safety provided in relevant guidelines.

References

Association of Professional Engineers and Geologists of British Columbia (APEGBC). 2016. Site characterisation for dam foundations in BC. V1.2. Retrieved from https://www.egbc.ca/getmedia/13381165-a596-48c2-bc31-2c7f89966d0d/2016_Site-Characterization-for-Dam-Foundations_WEB_V1-2.aspx

ANCOLD. 2012. *Guidelines on Tailings Dams: Planning, Design, Construction, Operation and Closure.* Australian National Committee on Large Dams Incorporated.

Ladd, C. 1991. Stability evaluation during staged construction. 22nd Terzaghi Lecture, 540–615. JGE117.

Ladd, C. and D. DeGroot. 2004. Recommended practice for soft ground site characterization. Arthur Casagrande Lecture, 12th PanAmerican Conference on Soil Mechanics and Geotechnical Engineering.

Lunne, T., T. Berre and S. Strandvik. 1997. Sample disturbance effects in soft low plasticity Norwegian clay. In *Proceedings of Conference on Recent Developments in Soil and Pavement Mechanics*. Rio de Janeiro: 81–102.

Terzaghi, K., R.B. Peck and G. Mesri. 1996. *Soil Mechanics in Engineering Practice*. John Wiley & Sons.

Wesley, L.D. 2013. Residual soils and the teaching of soil mechanics. In *Proceedings of the 18th International Conference on Soil Mechanics and Geotechnical Engineering.* Paris.

Proceedings of Tailings and Mine Waste 2019
November 17–20, 2019, Vancouver, Canada
Published by the University of British Columbia, 2019

Case Study Using the Stability Rating and Hazard Classification System for Mine Waste Stockpiles

John Cunning, Golder Associates Ltd, Vancouver, Canada
Marielle Limoges, Golder Associés Ltée, Montreal, Canada
Matthew Brenner, Golder Associés Ltée, Montreal, Canada

Abstract

This paper presents a case study where the updated waste dump and stockpile stability rating and hazard classification (WSRHC) system was used to evaluate waste rock and overburden stockpiles at four existing mining operations. The updated WSRHC system was presented in the *Guidelines for Mine Waste Dump and Stockpile Design* (Hawley and Cunning, 2017). The current state of practice in managing mine waste dumps and stockpiles includes an understanding of the facility classification. Our case study will show an approach to apply the WSRHC system, which includes a global and holistic approach to quantifying and classifying the stability hazard. As part of design, planning, operation, and closure phases, at both existing and new development mine sites, a documented understanding of relative classifications with ranked hazards can support better mine waste management practices.

The results from applying the WSRHC system are planned to be used to feed into a risk assessment framework; however, undertaking the classification alone was found to allow stakeholders at each site to understand stability ratings on stockpile facilities relative to each other, with more critical facilities also being identified. The results were used to establish recommendations around documenting the operational performance and the geotechnical behaviour of the stockpiles at these mature mining operations. Through understanding of the WSRHC, the level of effort for investigating the foundation materials as well as the mine waste materials of stockpiles areas for future expansion designs can be better understood. The case study presented outlines the process and results for 21 stockpiles, ranging from 30 to over 250 m in height, with variable foundation conditions.

Introduction

The current state of practice in managing mine waste rock and overburden stockpiles includes an understanding of the facility classification. One approach to this is to follow the Waste Dump and Stockpile Stability Rating and Hazard Classification (WSRHC) system as described in Hawley and Cunning (2017),

which includes a global and holistic approach to quantifying and classifying the stability hazard. As part of design, planning, operation and closure phases, a documented understanding of the facility classification, can allow for better facility management and assist in controls which may prevent unwanted events. This case study presents the application of the WSRHC system used to classify the stability rating and hazard class of 21 selected stockpiles at four mine sites. This exercise was conducted with the objective of understanding the stability hazard associated with a number of stockpiles, relative to each other at each individual mine site, but also between mine sites within a similar regional setting. Some stockpiles are located next to important infrastructure and were built without documented engineering design or construction record documentation, leaving the owner without appropriate information to fully assess and understand the risks associated with each of the stockpiles. The WSRHC exercise was found to be a useful tool to identifying the more vulnerable stockpiles. Further, the results were used as a guide to define a recommended level of effort for foundation investigations, documentation, design, construction and monitoring for the waste rock and overburden stockpiles assessed at each site.

The WSRHC system can be used to feed into a risk assessment framework. Risk assessment and management are needed separate to hazard classification and can be used to develop required critical controls as part of an effective mine waste management system. Risk refers to the combination of the consequence of an event and its associated likelihood of occurrence. The scope of analysis and design required to effectively investigate and characterize an overburden or waste rock stockpile should be in balance with the associated stability rating hazard and should help better identifying the risks associated with each stockpile. It is considered a best practice, and often also legally and morally imperative that mines document hazards and risks, as a responsibility to both the shareholders and public stakeholders. The absence of this type of study and proper documentation can lead to important consequences, including economic, social and environmental, and in extreme cases this can even be life threatening. As mines grow bigger and faster than ever before, the need to reflect and classify hazards becomes imperative. While tailings storage facilities have received more attention from both the public and the industry in recent years due to recent failures such as Mount Polley in 2014, Samarco in 2015 and Feijao in 2019, the hazard associated with waste dumps and stockpiles should not be ignored and in some cases can be almost as significant as tailings. The spoil failure that occurred in Nachterstedt, Germany in 2009, where 3 fatalities were reported, reminds us of the possible consequences and highlights importance of understanding the behaviour of the material stockpiled (Niemann-Delius, 2014). The WSRHC helps defining the level of engineering required to develop safe designs.

Methodology of the WSRHC

Mark Hawley developed the updated classification system which is described in Chapter 3 of the 2017

Waste Dump Guidelines (Hawley and Cunning, 2017). The WSRHC system evaluates 22 key factors that are known to affect the stability rating. These factors have been divided into seven key groups, where the numerical rating of each factor is used to calculate the engineering geology index (EGI) and the design and performance index (DPI), with the sum providing a waste dump and stockpile stability rating (WSR). The numerical values assigned to each factor and group have been weighted to reflect their relative importance, as seen in Table 1, which also indicates the maximum possible rating for each rating factor. The WSRHC system attempts to strike a balance between complexity and utility. It should be noted that for certain factors, negative ratings exist and are meant to flag these factors as critical, which may require further evaluation.

Table 1: Waste dump and stockpile stability rating (WSR) breakdown

Engineering geology index (EGI)	Design and performance index (DPI)
Regional setting (max 10 pts.); Seismicity (0–2), Precipitation (0–8)	Geometry and mass (max 10 pts.); Height (0–4), Slope (0–4), Volume and mass (0–2)
Foundation conditions (max 20 pts); Foundation slope (0–5), Foundation shape (0–2), Overburden type (0–4), Overburden thickness (0–2), Undrained failure potential (–20–0), Foundation liquefaction potential (–20–0), Bedrock (0–4), Groundwater (0–3)	Stability Analysis (max 10 pts.); Static stability (0–7), Dynamic stability (0–3) Construction (max. 15 pts); Construction method (0–8), Loading rate (0–7)
Material quality (max 20 pts.); Gradation (0–7), Intact strength and durability (0–8), Material liquefaction potential (–20–0), Chemical stability (–5 to +5)	Performance (max. 15 pts); Stability performance (–15 to +15)

The WSR rating is on a scale of 0 to 100, with higher WSR indicating more stable conditions and a lower instability hazard, as seen in Table 2. This system is a major update from the previous system developed by Piteau in 1991 for the BC Mine Waste Rock Pile Research Committee called the 1991 dump stability rating (DSR) system, which used just 11 factors and provided an instability rating, as higher values indicated a less stable configuration (BCMWRPRC, 1991).

The WSRHC is more refined with double the contributing factors and with an increasing stability rating representing an increase in stability. The scale has a maximum possible rating of 100 which facilitates relative comparison between stockpiles, as compared to the 1991 DSR method which had a range of 0 to maximum rating of 1800 for the least stable configuration.

The rating is subdivided in five Waste Rock and Overburden Stockpile Hazard Classes that are organized by increments of 20 and associated with an Instability Hazard defined as Very Low, Low, Moderate, High and Very High. The completion of the WSRHC exercise leads to defining a class this can be used to inform in the level of effort required to build a future stockpile or to manage an existing one. A stockpile with a higher instability rating will require more investigative and design effort, with enhanced care and monitoring during construction, operations and closure phases.

Table 2: WSRHC – Stockpile stability rating, hazard class and instability hazard

Waste rock and overburden stockpile stability rating (WSR)	Waste rock and overburden stockpile hazard class (WHC)	Instability hazard
80–100	I	Very Low Hazard
60–80	II	Low Hazard
40–60	III	Moderate Hazard
20–40	IV	High Hazard
0–20	V	Very High Hazard

Site descriptions

The four sites are located in a similar regional setting and are characterized by the presence of relatively wide open pits that have been developed over the last 40 to 80 years. The long-term development of the open pits has led to the construction of broad overburden and waste rock stockpiles. At certain locations the operations allowed for in-pit disposal of the waste rock and overburden, while at other locations all stockpiles were developed adjacent to the open pit areas. The geometry of stockpiles at the four sites were found to be highly variable. Some stockpiles reached heights of up to 150 m, built on subsoils of unknown nature, and in a single lift with the face sitting at the angle of repose. Other stockpiles were only reaching 24 m high and were built on bedrock using placements of 12 m lifts, with set-backs between lifts resulting in an overall stockpile face at 2.5H:1V.

The mine sites are located in North America and are in a Low Seismicity and Humid Continental Climate region with an average rainfall of about 750 mm per year and average snowfall of 225 cm per year. The Peak Ground Acceleration for each of the site is less than 0.02*g*.

Stockpile descriptions

A brief description of the stockpiles evaluated at the four mine sites is presented to provide context to the results and discussion.

Site A

The long-term development of Site A with multiple open pits has led to the construction of broad overburden and waste rock stockpiles adjacent to the open pits. In some areas, the stockpiles reach heights of up to 150 m measured crest to toe. The Main pit recently undertook a pushback of the pit wall resulting in mining activities ongoing near the toe of stockpile A-5, and required an expansion of the A-3 stockpile. A-1 stockpile was identified as the most critical structure, as it was one of the few stockpiles that did not have benches, with the material sitting at the angle of repose of approximately 37°, over a height of 150 m. The adjacent stockpile A-2 has similar dimensions to A-1, however included benching to reduce the overall

slope angle. Downstream of both stockpiles A-1 and A-2 lies a series of infrastructure (railroad, power line, gas line, access road, pumping station, tailings pipeline) and during discussions with the mine it was identified that a stockpile failure in this area could lead to a major disruption to any or all of the downstream infrastructure.

A number of collection ponds were recently constructed downstream of the waste rock stockpiles for collecting site storm water drainage. The overburden was observed to generally consist of till material, some of which exhibits a cohesive behaviour. Some samples were collected during the site visit and tested in a local laboratory for grain-size distributions and Atterberg Limits. Prior to the study, foundation and pore water pressure conditions were largely undocumented, except for observed ponded water downstream adding to high groundwater conditions.

Site B

The current operations at Site B allow for in-pit disposal of the waste rock, along with continued advancement of overburden and waste rock stockpiles adjacent to the open pit mining area. In some areas adjacent to the pits, the waste rock stockpiles reach heights of up to 100 m and are progressively covered with soils from the stripping activities as part of reclamation efforts. Recent operations included a push back of the pit wall, which led to the interaction of the pit expansion with stockpile B-5, which was a closely regulated area inherited by the mine from previous owners. A detailed geotechnical study that included borehole investigations, instrumentation and slope stability verification for B-5 helped inform the desktop study and stability ratings.

The overburden was observed to generally consist of till material, some of which exhibits a cohesive behaviour, often overlaid by a peat layer of variable thickness, in some areas reaching 4–5 m. The observed stripping of the subsoil for the push back of the wall has triggered the need to develop a stockpile south of the open pit, named stockpile B-3 which is undergoing rapid expansion. Given the nature of the stripped soils at this site (low strength peat and glacio-lacustrine silts), some challenges have been experienced during the stockpiling activities and the WSRHC was expected to inform future action items for the expansion of this area.

Site C

Site C is smaller than the other sites in this review and started mining around 1965. The site history along with variable and undocumented conditions, created uncertainty in factors needed for the stability rating, particularly the foundations conditions which resulted in reduced ratings due to the potential for undrained failure. The current operations allow for in-pit disposal of the waste rock, along with continued advancement of overburden and waste rock stockpiles adjacent to the pit area to the east. Most of the stockpiles are in-pit, but in cases extend above the pit limits, with the large stockpile C-2 reaching 50 m

above the pit limits, for an overall height of 215 m measured from crest to toe.

Site D

The study of these four sites was initiated as a response to the stockpiling failure event that involved overburden stockpile D-5 in 2017 at Site D. The failure resulted in an environmental impact downstream of the stockpile and required investigation efforts to understand the failure mechanism and to document the event. Site D has been jointly operated since the early 1970s and is now an expansive mine site that runs over 16 kilometres linearly. Due to permit restrictions through the long history of production at the mine, land ownership by small block areas relative to the large mining area has presented challenges to the stockpiling plans and this has resulted in smaller-volume stockpiles over the implementation of a unified stockpiling layout.

Desktop review and methodology

The methodology for this study included a site visit to each of the four sites and discussion on each site with the teams responsible for mining and stockpile operations. Following the site visit, a desktop review of available and pertinent information was undertaken to inform the WSRHC. Complementary to the observations made during the site visits, existing plans, aerial photographs and site topography are key elements to the identification of the more critical areas. Available investigation reports as well as any geotechnical information, construction sequences, drawings or other information provided by the site team was used to inform the inputs to the WSRHC.

The WSRHC is highly dependent on the available information regarding the subsoil conditions and the geotechnical design of the waste rock and overburden stockpile. The WSRHC can also change as the stockpiles continue to develop through the life cycle of the mine. For this study, the current conditions of the stockpiles at the time of the site visit was used. Without detailed technical information, the engineer is left with site observations, assumptions and has to rely on professional experience, which may lead to non-representative results. For most of the waste rock and overburden stockpiles assessed during this specific study, few engineering geotechnical design reports were available and limited geotechnical investigation was provided. Given the lack of documentation, the assessment was based on observations made during the site visit, discussions with site personnel and general understanding of the geological context of the region. In some cases, some overburden material was sent for testing to allow a better understanding of the soil behaviour.

The pertinent information required to complete a detailed WSRHC is summarized below.

Table 3: WSRHC – Summary of pertinent documentation

Factors	Required data/test
Seismicity	Peak ground acceleration
Weather data – precipitation, snowfall	Historical annual precipitation totals, on site preferably
Foundation conditions	Ground LIDAR, boreholes, exploratory trenches, geologic reports, rock sample designation; piezometer, inclinometer and/or groundwater data
Material quality	Sieve analyses, Atterberg limits, permeability tests, SPT, CPT, shear strength tests, chemical acid-base accounting tests
Geometry and mass	Overall height, thickness, lift height, fill slope angle; survey data, as-built, and cross-sections; dry density, specific gravity, proctor tests
Construction	Average daily volume, annual volume, construction history plans, deposition plans, cross-sections

Detailed rating classification – Case study of Site A-5

The following presents a detailed rating classification for one of the stockpiles analyzed in this study, to illustrate the method, information required, decision making and subsequent discussions. A similar WSRHC procedure was applied to all 21 stockpiles analyzed in this study. A higher rating is more stable, however certain factors are negative to flag their hazard (e.g. undrained failure potential, liquefaction etc.).

The regional setting includes ratings for seismicity and precipitation. The WSRHC rating for seismicity is very low (rating 2) based on a PGA of less than 0.02g. The precipitation was rated moderate for rainfall and very high for snowfall (rating 2), based on reported annual values at the sites. The overall rating for the regional setting is the addition of these two factors, resulting in 4 points out of a maximum of 10.

The foundation conditions were observed at the toe of most stockpiles, but little historical documentation existed to quantify the foundation conditions below the older stockpiles, and there was no pore water pressure (PWP) monitoring in dump foundations at the time of the visit, so reasonable assumptions were made in the absence of site specific information. The average overall foundation slope was assumed to be 5–15° (rating 4) based on a provided section of the pit topography and was assumed to be planar or concave on gentle slopes (rating 1). The overburden was classified as Type IV (rating 3) typical of competent coarse-grained glacial till, and the stripped sections in the pit were observed to be of heights greater than 5 m (rating 0). The undrained failure potential was classified as low (rating –2.5) based on a mixed coarse-grained material that promotes drainage and moderate to low potential of excess PWP, however, at the time of the rating, this was largely unknown, and instrumentation was recommended to confirm this assumption. The foundation liquefaction potential was classified as negligible (rating 0) given the dense and low void ratio till combined with little seismicity. The bedrock was classified as Type D

(rating 3) bedrock which is typical of competent, hard, unweathered rock with GSI/RMR 60–80 and negligible potential for foundation failure. The groundwater was classified as moderate (rating 1.5) that sits just below the till surface level, which was confirmed by the observation of ponded water at the downstream toe of the stockpile. The overall rating for the foundation conditions is the addition of these eight factors, resulting in 10 points out of a maximum of 20.

The material quality was based on available gradation analysis and available borehole records. The gradation was classified coarse (rating 5), for material with 5–10% fines and little to no plasticity. The intact strength and durability was classified as Type 4 (rating 6), based on strong to very strong rocks with UCS 50–100 MPa, in line with Type D bedrock. The material liquefaction is negligible (rating 0) because of the nature of the well graded material with low regional seismicity. The chemical stability was classified neutral/moderate (rating 2.5) based on a low risk of ARD and limited precipitates; however, there was a potential for issues with water quality in runoff from the stockpile, which was not expected to significantly modify geotechnical strength properties. The overall rating for the material quality is the addition of these four factors, resulting in 13.5 points out of a maximum of 20.

The geometry and mass include factors related to the physical size and shape of the waste dump or stockpile. The height of this stockpile was 55 m measured from crest to toe and was classified as moderate (rating 2). The overall slope angle was based on the material sitting at its angle of repose of 37°, without any benching, resulting in a classification of steep (rating 1). The volume and mass were estimated to be 1×10^8 t based on the area and thickness of the stockpile, resulting in a classification of medium (rating 1). The overall rating for the geometry and mass is the addition of these three factors, resulting in 4 points out of a maximum of 10.

The stability analysis group is intended to directly capture and contrast the objective stability based on models and design criteria. A deterministic technique to calculate factor of safety (FoS) is the most commonly associated with limit equilibrium analysis techniques. In the case of this site and stockpile, no formal stability analysis existed at the initial WSRHC, so some preliminary models were produced to estimate the stability. These models assumed high PWP conditions, which given the lack of instrumentation to validate this assumption, was conservative. The critical section showed a static stability with a FoS of 1.1, which was classified as low (rating 1), while the dynamic stability was very high (rating 3). It was noted that the models were highly depended on PWP conditions, and variations in water table placement in the model had a sizable influence on stability. It was recommended to validate the model with high level stability analysis utilizing in-situ PWP conditions. The overall rating for the stability analysis is the addition of these two factors, resulting in 4 points out of a maximum of 10.

The construction rating is based on the method and loading rate. This stockpile was classified as Method IV (rating 6), built with an ascending sequence or bottom-up, with moderate lifts below 100 m and

overall foundation slopes between 15–25°. The loading rate was estimated as low (rating 5) based on limited operation and production reports for this stockpile. The overall rating for the construction is the addition of these two factors, resulting in 11 points out of a maximum of 15.

The performance rating is meant to capture the actual, documented stability performance of the existing waste dump or stockpile. The stockpile was classified very good (rating 15) based on the long-term stability of this stockpile, coupled with little signs of deformation or settlement and no operational closures or failures recorded. Only small surface erosion was noted on certain slopes siting at the angle of repose. The performance rating is based on only one factor, with a maximum of 15 points.

As shown in Table 4, the EGI for this site is the summation of regional setting, foundation conditions and material quality, resulting in 27.5, out of a maximum of 50. The DPI is the summation of geometry and mass, stability analysis, construction and performance resulting in 34, out of a maximum of 50. The total WSR is the addition of EGI and DPI, and for stockpile A-5 results in a WSR of 61.5 which is a low hazard class II instability hazard, just near the boundary with moderate hazard class III.

Table 4: Waste dump and stockpile stability rating (WSR) summary – Stockpile A-5

Engineering geology index (EGI)	Design and performance index (DPI)
Regional setting: 4 /(max 10 pts.)	Geometry and mass: 4/(max 10 pts.)
Foundation conditions: 10 /(max 20 pts.)	Stability analysis: 4/(max 10 pts.)
Material quality: 13.5 /(max 20 pts	Construction 11/(max 15 pts.)
	Performance 15/(max 15 pts)
EGI=27.5	DPI=34
WSR=EGI+DPI=61.5	Class II Low Hazard Class

Following the presentation of these study results, the mine was proactive in implementing our recommendations and investigated the foundation characterisation and proceeded to install piezometers to measure in-situ PWP conditions. This data was then used to update the stability analysis model with a more representative water table of the field conditions, as the preliminary model used an assumed conservative PWP condition given the lack of information at the time. After reducing the water table to the level indicated by the piezometers, the results of the static stability increased the FoS from 1.1 to 1.4, which placed the classification as high stability (rating 5), and increased the WSR by 4 remaining as a low hazard class II. This refined classification help improve accuracy, but more importantly the exercise provided a positive communication with the mine and a platform to discuss hazards and solutions based on industry best practice. The results of this WSRHC, and the other 20 stockpiles included in this study are summarized in the next section.

Results

Table 5 presents the result for the WSRHC across the 4 mine sites, here labelled A, B, C, and D. Along with the ratings, the location of in-pit and out-of-pit have been indicated. Figure 1 plots the results on an EGI vs. DPI coordinate system, with the hazard boundaries for Very Low Hazard Class I through Very High Class V also indicated on the plot. The 21 stockpiles studied plot in the moderate to very low range, with 6 moderate hazard stockpiles, three of which are out-of-pit stockpiles at site D. The lowest stability was observed at the out-of-pit stockpile D-5 with a WSR 45 placing it in the Moderate Hazard Class III; this was the stockpile that experienced a failure in 2017. The highest stability was observed at the in-pit stockpile C-1, with a WSR of 87 and strong ratings for both EGI and DPI and 6 stockpiles were squarely in the Very Low Hazard Class I.

Table 5: WSRHC – Summary results for 4 sites

Stockpile	In-pit/Out-of-pit	DPI	EGI	WSR	WHC
Stockpile A-1	Out-of-pit	34	25.5	59.5	III
Stockpile A-2	Out-of-pit	38.5	27.5	66	II
Stockpile A-3	Out-of-pit	39	25.5	64.5	II
Stockpile A-4	Out-of-pit	38.5	25	63.5	II
Stockpile A-5	Out-of-pit	38	27.5	65.5	II
Stockpile A-6	Out-of-pit	39.5	25	64.5	II
Stockpile B-1	In-pit	43.5	39	82.5	I
Stockpile B-2	In-pit	45	40	85	I
Stockpile B-3	Out-of-pit	27	21	48	III
Stockpile B-4	In-pit	42	37.5	79.5	II
Stockpile B-5	Out-of-pit	23.5	22	45.5	III
Stockpile B-6	In-pit	41.5	37.5	79	II
Stockpile C-1	In-pit	45	42	87	I
Stockpile C-2	Out-of-pit	43	39	82	I
Stockpile C-3	Out-of-pit	34.5	33.5	68	II
Stockpile D-1	In-pit	46	37	83	I
Stockpile D-2	In-pit	47	38	85	I
Stockpile D-3	Out-of-pit	37	19	56	III
Stockpile D-4	In-pit	35.5	32.5	68	II
Stockpile D-5	Out-of-pit	27.5	17.5	45	III
Stockpile D-6	Out-of-pit	31	19	50	III

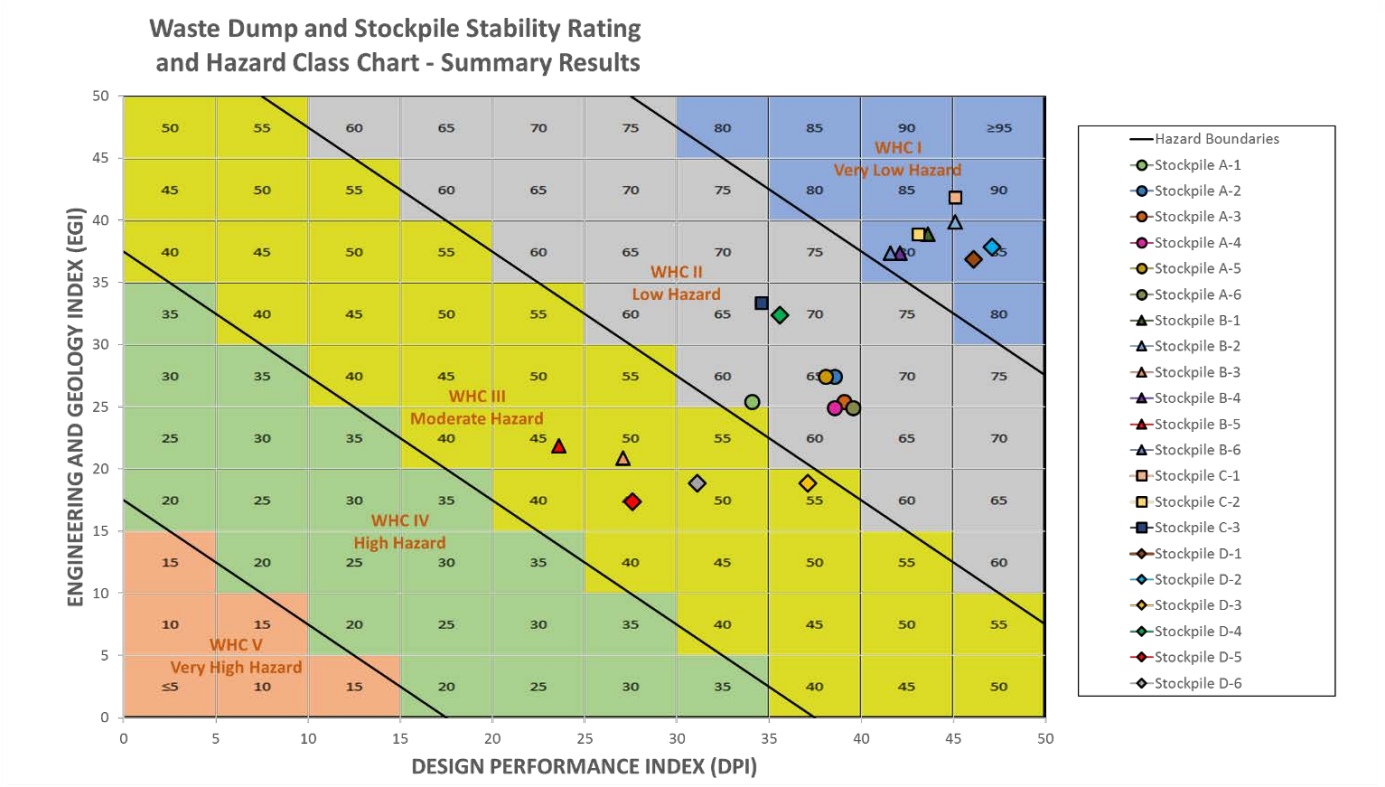

Figure 1: WSRHC summary results chart

Discussion

The results of applying the system to the four mine sites found a range of stability hazard conditions at each site and also showed some similarity between sites. Following the site visit and initial assessment, the results were presented to the teams at each site and during discussion of the results, stakeholders at each site gained a better insight and an understanding of stability ratings for stockpile facilities relative to each other. For these sites, a clear distinction between the in-pit stockpiles and the out-of-pit overburden stockpiles was noted. There is uncertainty associated with the factors considered in developing these ratings and this is especially applicable concerning the foundation conditions; the ratings for undrained failure potential have been reduced because of the presence of a variable and largely unknown thickness of glacial till primarily composed of approximately of silty sand and occasionally peat in the foundation. The results of the WSRHC closely follow the in-pit and out-of-pit divide. Stockpiles D-1 and D-2 are in-pit waste rock stockpile, while D-4 is an overburden in-pit stockpile. Stockpiles D-3, D-5 and D-6 are out-of-pit overburden stockpiles and all rated in Moderate Hazard Class III. This is visible in the cluster of moderate out-of-pit stockpiles. Moreover, the use of bottom up construction helps all the stockpile stability ratings.

While these ratings represent the associated hazard at the time of analysis, this process is variable with time and operational decisions and can be controlled by well informed, industry-best-practice decision making. As outlined in greater detail in the WSRHC system described in Hawley and Cunning (2017), the stability rating and hazard class helps inform the suggested level of investigative and design effort. With more information, the rating becomes more determinate and the hazard and associated risk can be better understood.

Based on the WSRHC, certain level of effort for each class is suggested and includes investigation and geotechnical characterization, analysis and design, and construction and operation guidelines. Very Low and Low Hazard Class waste rock and overburden stockpiles should be subject to investigation and characterization to confirm key assumptions made during the desktop study and plan limited supplementary field investigations with periodic inspections, while moderate-hazard waste rock and stockpiles should have a more detailed investigation. This could include in-situ instrumentation, material testing and shear strength testing to establish foundation and fill material properties that inform stability analysis.

Based on the results of the WSRHC, each site, and in some cases specific stockpiles, received recommendations and a priority sequence of action items. Our general recommendation included: design basis criteria to formalize stockpiling geotechnical procedures, material and foundation characterization, slope stability analysis, regular site inspection with third party inspections on moderate class hazard sites, and most importantly detailed documentation of site conditions and inspections. At certain sites, the recommendation of having a qualified employee that leads the management of the stockpile was encouraged to ensure uniformity and ease of information transfer. As outlined in the detailed case study of stockpile A-5, the implementation of the recommendations can increase the stability with the appropriate critical controls and serves to refine the WSRHC. Having mines that identify hazard and engage in the associated risk mitigation is responsible in the full life cycle of a mine and should be considered effective management practices.

Conclusion

This case study presented application of the updated waste dump and stockpile stability rating and hazard classification system to evaluate waste rock and overburden stockpiles at four existing mining operations. The WSRHC exercise was performed on 21 waste dumps and overburden stockpiles, with the resulting stability rating ranging from Moderate to Very Low Hazard Class. The mining teams at each site found the process to be a useful tool to help identify the more vulnerable stockpiles, and served as a guide to define the level of required effort to adequately investigate, document, design, construct, and monitor the waste rock and overburden stockpiles. Our recommendations identified certain critical controls, many of which were implemented to help better understand and manage these complex structures and sites.

Acknowledgements

Golder would like to thank the mines for allowing us to publish this case study. As the mining company was still implementing the recommendations from this study, they requested that it not be specifically identified in this paper. Thanks to Mark Hawley for development of the updated WSRHC system. The authors look forward to other published case study data using the updated WSRHC system.

References

British Columbia Mine Waste Rock Pile Research Committee (BCMWRPRC). 1991. *Investigation and Design Manual – Interim Guidelines*. *Mine Rock and Overburden Piles 1*. Prepared by Piteau Associates Engineering Ltd, May 1991.

Hawley, M. and J. Cunning. 2017. *Guidelines for Mine Waste Dump and Stockpile Design*. Australia: CSIRO Publishing; The Netherlands: CRC Press/Balkema.

Niemann-Delius, C. 2014. *Proceedings of the 12th International Symposium on Continuous Surface Mining.* Aachen: Springer Publishing.

Proceedings of Tailings and Mine Waste 2019
November 17–20, 2019, Vancouver, Canada
Published by the University of British Columbia, 2019

Rethinking Waste

Robyn Gaebel, Tailings Professional, Canada

Abstract

Through identification of by-products available and utilizing existing and emerging technologies, opportunities to manage and use waste to solve problems can be and have been developed. By examining synergies between by-products across different industries and within mining to reuse material by-products, the waste can be diverted from landfill or other long-term storage facilities, thereby reducing the industry environmental impacts.

The industries specifically discussed and identified in the case studies are forestry, water treatment, mining, and agriculture; however, the focus is on the mining industry. Each industry examined has by-products that have favourable material properties that solve problems or reduce issues. By evaluating alternate waste products that can be used in construction or co-disposed with, industry professionals can reduce the environmental impact and effective cost of waste management for the industries involved. Rebranding waste as a material by-product can change the perception that waste is only a burden; thereby turning waste into a viable material resource. While technology and innovation are available for responsible and environmentally aware material use, practices within the mining industry have remained the same. The case studies included outline some use of material by-products to demonstrate and support the concept of waste reuse, and ultimately waste as a resource.

This paper encourages awareness of the inconspicuous details of seemingly unconnected industries that are often overlooked. The mining industry and all industries need to respect natural resources, to use as much of the available materials, and waste as little as possible. With more public awareness around sustainability, the environment, impacts of industry on the environment and climate change, regulations are likely to start including social license into legislated requirements to operate. Industry practices are being closely examined in more detail, with a focus not only on the companies acting ethically, but also on the individual practitioners. To be socially acceptable and environmentally sustainable, the mining industry and industry professionals must practice better waste management.

Introduction

Statement of problem

The ideas surrounding sustainability and the environment have become more prominent, and there has been a push from the public for more responsibility and integrity in mining and other industries. Social license and the need for industry practitioners to be responsible and ethical is becoming more prominent (Heffron et al., 2018). It is likely that in the near future formal regulation will require aspects of social license to obtain approvals (Heffron et al., 2018). Specifically, when discussing the responsibility of industries, companies and practitioners, as demonstrated by the Mount Polley incident, even five years after the event only three individual engineers who worked on the dam, not the companies involved, are facing disciplinary hearings and fines (Hayward, 2018). The repercussions of the Mount Polley tailings dam failure go further to highlight that the industry practitioners have the responsibility to make ethical and technically sound decisions on behalf of industry.

The public, through social license, will force industries, and thereby individuals, to come up with better ways of operating, including managing waste to the betterment of the environment (Moffat and Zhang, 2014). Currently waste by-products are burdens, contributing to increasing overhead costs of production, are peripheral to optimum mining, and go to fill waste disposal facilities. The revenue is generated by mineral products, and the operational costs are dominated by the waste products. As such, waste is perceived by the industry as waste, a sunk cost and a by-product with no value. For example, managers in charge of tailings facilities receive additional renumeration for cutting the costs of operating tailings facilities, often to the detriment to the overall operation function (Leotaud, 2019).

In addition to the economic considerations, resources are starting to become increasingly scarce (Fixen, 2009). Using all the resources available, product or by-product, not only has an environmental benefit but a direct economic benefit. Waste products from one industry may have properties that another industry can benefit and take advantage of; when a by-product is used as a viable resource there is the added economic benefit of not having to store or treat the by-product in the long term.

By rebranding waste to a viable resource and utilizing the inherent properties, more sustainable solutions are available with leverage of creativity, information sharing, and scientific study.

Definitions

For clarity, Table 1 provides definitions for some jargon and industry terms used within this paper.

Table 1: Definitions

Term	Definition
Acid rock drainage	When by-product material that contains an abundance of sulphide minerals is exposed to water and air, a chemical reaction occurs where the material releases water that is more acidic than the natural surrounding environment. Often acid rock drainage also includes metals that have been leached from the rock.
Biosolids	By-product of the treatment of waste water that is soil like and can contain the contaminants as well as nutrients of the water cleaned, and will vary in quantity and chemically based on treatment process and inflow water quality.
By-product	A material produced as a result of industry processing of target material or main product, generally identified as a waste material.
Landfill	A storage facility for the long-term storage of various wastes, generally municipal. Facility can include both industrial and residential material. Facilities are required to be operated within the Environmental Compliance Approval conditions provided as part of licensing.
Mine waste	Includes both waste rock and tailings; however, this paper identifies mine waste as predominately waste rock. By-product of the mining process in the form of rock that does not contain the target mineral of the mine in sufficient concentration to be considered ore. The rock is still removed during the mining process to provide access to ore.
Residuals	By-products of the forestry milling industry that can include ash, pulp sludge, and other waste material from the mill or pulp and paper processing.
Slag	By-product of the mining mineral processing usually within the smelting process. Similar to sand, though uniform gradation and abrasive. Can be chemically inert but will depend on the specific process.
Tailings	By-product of mining mineral processing usually within the milling process, though in some industries tailings are a result of other processes as well as milling. Regardless of the type of mining, all have a tailings product. The product is a mix of rock, water, and residual chemicals left over after the milling process. Solid material in tailings is generally the size of sand or silt (smaller).
Tailings storage facility	A storage facility for the long-term storage of tailings. Facilities are required to be operated within the Environmental Compliance Approval conditions applied as part of licensing.

Hypothesis

Waste from industry can be managed more economically and environmentally consciously by leveraging new ideas and technology to minimize impact to the environment and decrease landfill or waste storage facility usage.

This paper aims to identify the need for and inspire creative concepts for practitioners for the management of by-products as material resources. Though use of waste is an old concept, more innovation is needed for more environmentally sound practices to be implemented by industry and specifically mining.

Scope

This paper includes a strategy to evaluate available by-product materials that are readily available and wasted within industries to encourage awareness of the inconspicuous details of seemingly unconnected industries. This paper also identifies, through case studies, emerging technologies and opportunities to manage and use waste to solve problems. By examining different synergies within mining and between industries to reuse material by-products, the waste is diverted from landfill or long-term storage facilities and in some cases made into a product. The industries specifically discussed and identified in the cases studies are forestry, water treatment, and mining; however, the focus is on the mining industry. Each industry examined has interesting by-products that have favourable material properties that solve problems or reduce issues in other industries. Case study examples provided within this paper are primarily in Canada, except for one example from the Netherlands.

The mining industry and industry practitioners need to respect the natural resources, to use as much of the available materials, and waste as little as possible to become sustainable.

How to identify opportunities for by-product uses

With the changing environmental landscape and climate change, the idea that all by-products are waste is a short-sighted understanding of the limited material resources available. Many decisions are due to a lack of understanding of outside industries and lack of communication between industry professionals (Witjes and Lozano, 2016). There are many strategies available to help solve the problems associated with waste management. To help understand how to bridge the gap between industries and repurpose wasted by-products, a three-step approach is proposed as a tool or framework that this author has found helpful.

Step 1: Understand the by-product available and the properties

Understanding the industries in the area and therefore the by-products available allows for development of a list of by-product materials readily available for possible use. The list will then provide a broad range of by-products that may or may not be useful to the targeted industry. However, the longer the list of ideas or materials, the more options that are available for aggregation, investigation, and development. Each

available by-product should be investigated and understood to ensure full acknowledgment of the material and handling problems associated with that material.

Detailed analysis of the chemical and physical properties is required to fully understand the material, how to properly manage it, long-term effects, and the life cycle. For example, using a material without understanding the reactive properties could have long-term detrimental effects on the environment or operation. Some material properties that might be useful include chemical analyses, moisture content, pH, reactivity, compaction, and strength. Due diligence must be exercised to ensure that risks are managed appropriately, and that a problem is being solved rather than pushed to another corporate entity. Companies and individual practitioners must act ethically, responsibly, and in good faith to foster cooperation and maintain good relationships.

Alternatively, the list described in Step 1 can be adapted to list multiple uses for one by-product. In the one by-product focus case, listing all the possible uses and material properties can be utilized in the same way as multiple materials. Some properties and use synergies would become apparent through simple comparison and listing.

Step 2: Communicate

Knowing what problems or issues and what by-products neighbouring industries have can increase opportunities and the ability to leverage industry professionals and materials not confined to one industry. To fully understand the by-product, information on how the product is produced, variations in material composition, current handling, and management strategies must be discussed. Communication with individuals that handle and work with the by-product can help to further refine and narrow the opportunities for the targeted industry or problem.

Moving forward with a one by-product focused list into Step 2 would lead to the specific specialists in each area providing more information on industry or material specifics that may support the by-product use.

Step 3: Creativity

Arguably the hardest of the steps is how to apply the knowledge of the by-products. However, once a good understanding of all the by-products that are available in an area is established the material properties by comparison to each other can show integrations and solutions. In some cases, it is as easy as listing the readily available by-products. For example, for tailings with an early acid onset, mixing in the mill with a caustic by-product that is otherwise chemically benign and low cost from the forestry industry rather than expensive slaked lime, can seem intuitive.

The act of tabulating the available materials or the problems can provide inspiration as well as reveal logical opportunities between industries. The case studies presented demonstrate how by-products and

knowledge can be leveraged to facilitate conservation and recycling. Communication and understanding of materials are critical to solving the problem without creating others.

Common by-product management practices

Ideally, by-products are managed in the most cost-effective manner to ensure the best rate on return of the main product. Unfortunately, in many scenarios the most cost-effective manner is not the best available technology (BAT) nor the most sustainable. Within the mining industry, many of the waste management practices are based on what was done in the past. Mining waste, specifically tailings storage facilities and waste rock piles, due to exposure over time, can cause environmental problems such as leaking or acid generation. The storage of the by-product is often the identified or used solution rather than long-term treatment or neutralization.

Storage facilities such as tailings storage facilities and landfills are often lined and isolated using a clay existing on site or a geosynthetic clay liner (GCL). GCLs are composite polypropylene plastic material and bentonite clay that has a low hydraulic conductivity. The polypropylene plastic materials are generally in the form of high-density polyethylene (HDPE) or linear low-density polyethylene (LLDPE). GCLs, HDPE and LLDPE are generally referred to as geotextiles. Clays and geotextiles are used in lining both the bottom, referred to as a liner and the top, referred to as a cover, of storage facilities. Due to the natural geology, availability of clay on site is variable and often the existing clay does not have favourable properties such as sand or granular inclusions or high plasticity. In the cases where native material is not available, facilities can be constructed using geotextiles.

Similar to a landfill, the by-product material is deposited from the process into the storage facility and covered to limit the exposure to the environment. After operations, a closure cover is installed over the by-product material to continue to isolate the material from the environment. Underneath the cover, the by-product material is allowed to sit and, due to the material properties, generally remains chemically and physically static. Unlike municipal wastes, most mining by-products do not decay while within storage facilities but remain in stasis until the cover material or lining material fails, and the internally stored by-product is once again exposed to the environment. When exposed to oxygen the by-product material will begin the oxidization process, produce acid drainage, and become a danger to the environment.

The rate at which mining by-products begin to oxidize is based on the properties inherent to the geology and milling process. Most by-product materials are stored untreated, deposited in the storage facility directly after production. A common long-term management strategy is chemical treatment. The treatment schedule is generally on an as-required basis determined through testing of surface water and internal mill processes.

In a similar circumstance in the forestry industry, residuals from the pulp and paper milling process are stored in piles on the mill property. The pile is usually left exposed to the elements, or placed in a landfill for long-term storage. Residuals are similar to municipal wastes rather than mining by-products in that the residuals are organic and will break down over time.

Waste from water treatment, biosolids, are also most commonly transported to landfills and used as cover material for the municipal wastes. Landfill or similar practices of storing material without treatment is common across industries.

Some by-products and properties

For discussion and highlighted in the case studies, Table 2 identifies at a high level some of the common by-products and properties of the forestry, water treatment, and mining industries. Properties provided are general and may not be indicative of every type of by-product produced from a specific facility. The by-products focused on are discussed further in the case studies in the next section.

Table 2: By-product details

By-product	Industry	Properties
Biosolids	Water treatment	- pressed soil like material - high in nutrients and moisture content - generally neutral
Residuals, ash	Forestry	- caustic - high phosphorus content
Residuals, sludges	Forestry	- high absorbency - low hydraulic conductivity when compacted - caustic
Residuals, wood chips	Forestry	- good thermal insulator - organic - flammable
Slag	Mining	- sand like, little variation in grain size/homogenous gradation - angular and abrasive
Tailings	Mining	- sand like, some variation in grain size within same facility - angular and abrasive - overtime with exposure can produce acid rock drainage, otherwise generally chemically benign

Existing practices/case studies of creative by-product use

The following section provides case studies of applications of by-product use that have been identified, selected for innovation and applicability to the concept of by-product use between industries. Each case study has the status of the concept, the type of industry the by-product is repurposed for, the source industry of the by-product, and the name of the by-product. Following each is a description of the process and repurpose of the by-product. At the end of each case study is a summary detailing the steps that were followed to identify opportunities for by-product uses.

"Slagpaper"

Status: Conceptual

Industry Use: Construction

Source Industry, By-Product: Mining, slag

References: Vale Thompson, 2019; Green and Permanand, 2019

Description: Slag is currently used consistently around the world as part of cement manufacturing. Due to a decrease in steel production, the demand for slag is greater than the supply internationally (Pro Global Media Ltd, 2019). In Canada, however, much of the slag produced from nickel processing is placed in piles as long-term storage facilities that require reclamation and closure as landforms. For example, at Vale's Thompson Manitoba Operations, slag produced is stored in a long-term storage facility pile, that contains most of the slag from the life of the mine. The slag pile is the source of dust into the neighbouring community and is a legacy issue for the site.

In an effort to use the slag to benefit the community, two young women started a school project to investigate three alternative uses for slag. One of the options they included was to use slag as the abrasive material for sandpaper. Instead of creating sand paper from other abrasive minerals such as aluminum oxide, garnet or silicon carbide (Whiteley, 1992), adhering slag to paper to create an abrasive paper for use in the construction industry and wherever sandpaper would be regularly used. Slag could also be used in similar scenarios for carpentry drill bits and sanding equipment in place of other abrasive natural materials, given the hardness of sand.

Slag could be used instead of a number of manufactured coarse materials in regular sandpaper. For example, replacement of slag instead of silicon carbide could allow for approximately 200,000 tonnes[1] of slag per year to be removed from long-term storage facilities, while reducing the volume of silicon carbide being manufactured. The manufacturing process of silicon carbide (Whiteley, 1992) is almost identical to the process by which slag is produced as a by-product. The reduction of volume from the storage facilities

[1] World consumption of silicon carbide is 700,000 tonnes per year with an estimated use for production of silicon carbide abrasives of up to 30% of the world consumption (Galevsky et al., 2018).

would ease the closure requirements on the facilities. Prior to closure this would reduce dust, improving air quality in the area. Production of the slag paper could be done locally as well, thereby reducing transportation and handling requirements.

Step 1: Focused on one readily available material that was causing long-term issues for the community and worked backwards to identify material properties and many possible uses.

Step 2: Identified stakeholders, company that owned the material, and contacted company specialists for information on the material.

Step 3: Conducted material and physical tests to verify, understand, and focus the list of possible uses to which uses were most functional and feasible.

Cement backfill

Status: Implemented

Industry Use: Underground mining

Source Industry, By-Product: Mining, tailings

Description: While normally stored in tailings storage facilities in the long-term, the process of cement backfill utilizes a portion of the tailings for filling of areas of the underground mine left open from ore extraction. The cemented tailings backfill provides additional structural stability within the underground mine. This can increase ore recovery and reduce cycle time (Palkovits, 2011), while reducing the volume of tailings to be stored above ground. In addition to diverting tailings from the storage facility, the addition of cement chemically isolates the tailings from oxygen and water, sufficiently encapsulating the tailings so as to inhibit oxidization and acidification.

The Vale Sudbury Operation is an example of backfill operations. Tailings material is separated by grain size, and a selection of the tailings grains are removed from the tailings circuit. The selected tailings are processed within a "sand plant" within the mill and mixed with cement. The resulting product is pumped underground into the mine and used to fill voids and selected parts of the mined area as backfill.

Cement backfill can account for a large volume of tailings diversion, utilizing approximately 65% of the total tailings produced and significantly reducing the volume of tailings stored above ground in tailings storage facilities. Many operations do not implement full optimization of this process due to cost, as the cement component for backfill could equate to as much as 5% of mine operating costs. Approximately 75% of mines in Canada use backfill of some kind, using an estimated 10% of the total volume of cement produced in Canada. (*Sudbury Mining Solutions Journal,* 2007).

Step 1: Tailings were identified as a readily available product that had similar material properties to the sand being mixed with cement as part of backfill operations.

Step 2: Each mine assessed the applicability and economic feasibility of using cement backfill in the operation through discussion with consultants and other qualified individuals in underground mining and mill operation.

Step 3: Conducted material and physical tests to verify that the specific tailings produced will function as estimated by industry professionals.

Biosolids in reclamation

Status: Implemented

Industry Use: Mining reclamation/Agriculture

Source Industry, By-Product: Water treatment, biosolids

Description: A by-product of the water treatment process, the residuals from the screening and the treatment process are called biosolids. The biosolids produced through this process have a high growth potential as they contain a high amount of nutrients. As a waste, most municipalities dispose of biosolids through landfill, often using the biosolids as a replacement day-to-day waste cover to prevent exposure and ensure containment of the municipal waste (Sylvis Environmental, 2017).

Within Ontario, the closure or reclamation requirements for a mine are prescriptive of growth rather than a depth of growth media or topsoil. Due to a lack of topsoil within the northwestern Ontario region, the use of biosolids to create a suitable growth media for remediation programs presents an opportunity to leverage a previously wasted by-product for use. Biosolids can be combined with local soils to provide physical, chemical, and biological benefits to poor quality soils typically found on mine sites (Van Ham et al., 2009). The properties of biosolids cause the material to be suitable to provide organic matter, water holding capacity, a biological medium for nutrient cycling, and a slow-release form of nutrients (Maltby, 2005). Biosolids generally contain the nutrients required by plants for growth, and can replace the addition of other expensive and synthetic fertilizers in many reclamation applications. The addition of biosolids has also been shown to accelerate seed germination and sustain plant growth for long-term reclamation. Fabricated growing media can be used in reclamation, slope stabilization, leachate treatment, and waste rock capping (Raghu et al., 1997).

The City of Calgary has been utilizing biosolids produced from wastewater treatment as a growth medium since 2013. Biosolids are blended with a mineral sand or local soil and a wood residual to create a fabricated growth media to meet the physical soil, water holding capacity, and organic matter requirements for healthy plant development. The specific formulation of the fabricated soil may be manipulated to achieve final goals for the blend (Sylvis Environmental, 2017).

The application of biosolids for reclamation has been employed successfully within the mining industry as well, at the Vale Sudbury Operations. Overall more than 176 ha of land has been rehabilitated

successfully, with more than 100,000 tons of biosolids diverted from landfill (Northern Ontario Business Staff, 2019). The operations have seen an increase in the quality of plant growth, species variety, and population. The biosolids reclamation projects have also been tied to the success of other projects, such as monarch butterflies and successful reintroduction of plant species (MAC TSM, 2018).

Step 1: Identification of several materials that could improve the growth potential of soils in the Northern Ontario region to aid in reclamation activities for mines.

Step 2: Discussion with industry professionals regarding the material produced, and with agriculture experts to determine material properties and performance of the various additives identified, including the biosolids.

Step 3: Consult with mining and agricultural industry experts to identify the best suited additive, application methods, mixing ratios, and maintenance requirements. Creatively combined agricultural procedures to mining reclamation activities.

Residuals landfill liner

Status: Implemented

Industry Use: Waste management

Source Industry, By-Product: Forestry, residuals

Description: Similar to biosolids, the residuals from pulp and paper, generally referred to as pulp and paper sludge (PPS), have successfully been used as an addition to improve soil quality with biosolids, as demonstrated in the previous case study. However, the material properties between PPS and biosolids differ distinctly in nutrient content, water absorption, and compaction. The material properties of PPS indicate that the material will act as a suitable landfill liner and cap for industrial wastes (Alrashed et al., 2016; Bolen et al., 2001).

When handled properly, including wetted to optimum moisture content and compacted, PPS acts as an effective barrier layer that inhibits leaching at rates similar to compacted clay liners and GCL (Van Ham et al., 2009). The difficulties in sourcing appropriate clay materials due to local geology and soil variability can cause significant problems, while many GCL replacements can be too expensive for waste management sites. As a waste by-product and a readily available material that would otherwise be landfilled, PPS is an economically feasible and locally sourced option for lining and covering facilities.

The use of PPS in landfills has been implemented and numerous studies have been conducted. One example was in 1991, when the town of Corinth, New York, successfully used PPS as an impermeable barrier. This demonstrated a use for the previously landfilled PPS material, as well as a significant cost savings for the town in landfill construction and closure (Moo-Young and Zimmie, 1997).

Step 1: Due to the high cost of GCL, the landfill professionals started with the target of finding an alternative material to GCL that was cheaper and readily available, but performed similarly. Assessment of a variety of by-products and other materials was conducted, with emphasis on a more natural alternative to plastics.

Step 2: Through discussion with various industry professionals, several materials were assessed for performance, and were identified as being available and cheaper.

Step 3: With multiple iterations and studies developed tests and treatment of the different materials to satisfy the requirements, by creatively applying soil analyses concepts and soil usage to material that is not soil, PPS was identified as a viable alternative.

Residuals tailings facility liner

Status: Conceptual

Industry Use: Mining

Source Industry, By-Product: Forestry, residuals

Description: Treasury Metals is developing a site as a gold mine. As part of the pre-feasibility stage of the project, Treasury Metals is assessing potential mechanisms for innovative waste management.

As previously established, the use of PPS waste material has had demonstrated success in providing an impermeable barrier for municipal waste management. Arguably, the design and function of municipal waste landfills and tailings storage facilities are similar, while the tailings storage facility maintains an equal scale to that of larger municipal landfills. Based on that idea, Treasury Metals commissioned Sylvis Environmental to perform material analysis and prefeasibility level assessment of the use of PPS as a liner for the tailings storage facility.

The results of the assessment were favourable and indicated the same results regarding the suitability of material properties of the numerous previous studies for PPS liner use. The study concluded that additional testing and permitting assessment would be required. However, at a prefeasibility study level, a PPS liner would perform at the same level as a GCL with the added benefit of additional buffering capacity. In addition, the study estimated that the PPS liner installation and material costs would be approximately half the cost of installation and material costs for a traditional GCL (Sylvis Environmental, 2019).

Treasury Metals is continuing with the development of the site and plans to continue the development of a PPS liner feasibility study, including field testing in 2020.

Step 1: With knowledge of both landfill and tailings management, and the high cost of GCL, the industry professional identified synergies between landfill and tailings facility design. By assessing locally available materials and knowledge of the previous case study, the PPS by-product was identified as a possible substitute for GCL.

Step 2: Through discussion with industry professionals who had worked on similar projects, identified the feasibility of the material performance and validity of the idea.

Step 3: Making the connection between landfill design and tailings facility design was the creative link for this case study.

Willow Energy Source

Status: Common use

Industry Use: Agriculture

Source Industry, By-Product: Forestry, residuals

Description: In an effort to find an energy source that is readily available and maintain energy availability, agriculture professionals identified a number of woody species that were examined to have sufficient growth rate. A specific genus of willow was identified to have a high enough growth rate and hardiness for the ease of energy production. The willows also have the added benefit of pulling contaminants, such as heavy metals, from the bedding soil. The willows for the process are grown, harvested, and then chipped or baled and left to dry. The chips or bales are then converted to energy or heat via high efficiency furnaces. To decrease fertilizer use and overall operating costs, commonly willow crops are grown in soil media partially consisting of previously discussed forestry and municipal wastes, PPS, and biosolids (Sylvis Environmental, 2017).

Since 2013, willow crops have been growing in New York State to provide biomass feedstock utilized to produce energy to power homes. In the first year only 100 acres of land were used to produce biomass to power 130 homes for a year. In 2015, 1,200 total acres in New York State were being used to grow willow biomass crops (Heavey and Volk, 2015).

In addition, Treasury Metals investigated the use of willow biomass for underground mine heating requirements. The prefeasibility level assessment indicated that the biomass grown near the mine project could provide approximately 25% of the heat requirements (Sylvis Environmental, 2019).

Step 1: Industry professionals were actively looking at better, more efficient biomass growth, and thereby identified several different plant species and growth mediums. The nutrient rich by-products from other industries including PPS and biosolids were identified as additives to enhance the growth mediums.

Step 2: Discussion with agriculture and forestry industry specialists to understand processing and growth of the different species.

Step 3: Application of forestry and agricultural practices to the energy production industry to find a carbon neutral, renewable, and consistent power source.

Zero Waste Mill Facility

Status: Implemented

Industry Use: Forestry

Source Industry, By-Product: Forestry, residuals

Description: The forestry industry creates several by-product residuals that are not currently used to their full potential. However, evolutions within the industry have seen developments in the technology to extract additional bioproducts, and make use of the residuals formerly disposed of in landfills.

An example of the technology developments is a mill in Finland that has identified multiple revenue streams from residuals to become a facility that produces no waste to landfill. The mill, Metsa-Aanekoski, is on a site where the old mill was demolished and replaced with a new facility. Through cooperation with other local industries such as chemical production, electricity generation, and agriculture, each residual has been turned into a source of revenue. The current revenue includes approximately 20% from bioproducts previously identified as waste. In addition, the mill itself produces enough energy for the operations and no fossil fuels are used in the mill operation. There is no need for a landfill or waste storage onsite as all the by-products are contained, used, or sold to other industries. Pulp is the main product; however, lignin, tall oil, turpentine, and advanced chemical fibres are also produced or extracted from the wood. Notably lignin and the advanced chemical fibres extracted are used as plastic replacements that are naturally biodegradable and have a smaller carbon footprint than the plastic equivalents. The bark and sludges are used for district heating and produce 550 GWh per year for local households, while 1.05 TWh per year of electricity is added to the electrical grid. Finally, the ash is provided to the local agriculture industry as a fertilizer component (Yuan, 2019)

Step 1: The industry professionals were specifically trying to find a use and repurpose for all the by-products produced. The target was to make each product a revenue stream.

Step 2: Discussion between agriculture, forestry, energy, and various other industries to identify gaps or solutions to each by-product.

Step 3: Application of different industry practices to creatively manage each by-product in a productive way and create a new revenue stream.

Conclusion

Environmental impacts of operations are becoming more of an issue, and sustainability is becoming an integrated part of licensing and regulation. The case studies prove that wastes can be managed in an economically and environmentally beneficial way. The concept of zero waste seems unachievable currently for some industries; however, the idea of managing by-products in innovative and better ways, leveraging across industries, is important to minimize the impacts of industry on the environment.

Effort should and can be made to minimize the volume of material stored in long-term storage facilities that do nothing to limit the reactivity or mitigate the risk of mining by-products. Where the volume of material cannot be mitigated, addition of other by-products should be examined and implemented for long-term environmentally responsible management.

Acknowledgements

The author would like to thank Lewis Kitchen for editing and general support, John Kitchen for his inspiration, and John Lavery of Sylvis Environmental for contributions to information on the case studies.

References

Alrashed, A., J. Atkinson, N. Alotaibi and X. Tan. 2016. Alternative landfill liner final report. SK Geotechnical Company.

Bolen, M., Arthur C. Roesler, C.H. Benson and W.H. Albright. 2001. Alternative cover assessment program: Phase II report. Madison: Dept. of Civil and Environmental Engineering.

Fixen, P.E. 2009. World fertilizer nutrient reserves – A view to the future. *Better Crops* 93: 8–11.

Galevsky, G.V., V.V. Rudneva1 and S.G. Galevsky. 2018. Microsilica in the production of silicon carbide: The results of testing and evaluation of technological challenges. *2018 IOP Conference Serial: Material Science Engineering* 411 012018. Novokuznetsk: Publishing house of SibSIU: 104–113.

Green, Samara and Anaya Permanand. 2019. Is it possible to repurpose slag from the nickel mining industry? Fredericton: 2019 Canada-Wide Science Fair.

Hayward, Jonathan. 2018. Three engineers to face disciplinary hearings in Mount Polley disaster. The Canadian Press, 26 September. Accessed July 15, 2019 from https://www.ctvnews.ca/mobile/business/three-engineers-to-face-disciplinary-hearings-in-mount-polley-disaster-1.4110941.

Heavey, J.P. and T.A. Volk. 2015. Shrub Willow fact sheet: Willow bioenergy in New York State. The Willow Project at SUNY-ESF. www.esf.edu/willow.

Heffron, Raphael J., Lauren Downes, Oscar M. Ramirez Rodriguez and Darren McCauley. 2018. The emergence of the "social license to operate" in the extractive industries? *Resources Policy*. In press.

Leotaud, Valentina Ruiz. 2019. Bonus schemes play a role in tailings dams failures – research. Mining.com, 5 June. Accessed June 6, 2019 from http://www.mining.com/bonus-schemes-play-role-tailings-dams-failures-research/.

MAC TSM. 2018. Towards sustainable mining progress report – TSM Environmental Excellence Award 2018 Winner: Vale. The Mining Association of Canada, 49.

Maltby, V. 2005. Compilation of alternative landfill cover experience using wastewater treatment plant residuals. Kalamazoo: National Council for Air and Stream Improvement Northern Regional Center.

Moffat, Kieren and Airong Zhang. 2014. The paths to social license to operate: An integrative model explaining community acceptance of mining. *Resources Policy* 39: 61–70.

Moo-Young, H.K and T.F. Zimmie. 1997. Utilizing a paper sludge barrier layer in a municipal landfill cover in New York. *Testing Soil Mixed with Waste or Recycled Materials,* ASTM STP 1275: 125–140.

Northern Ontario Business Staff. 2019. Vale, remediation company lauded for innovative Sudbury tailings rehab project. Retrieved from https://www.sudbury.com/local-news/vale-remediation-company-lauded-for-innovative-sudbury-tailings-rehab-project-1458570.

Palkovits, Frank. 2011. Paste thickening: Considerations for backfill vs. tailings management. November. Retrieved from https://www.e-mj.com/features/paste-thickening-considerations-for-backfill-vs-tailings-management/.

Pro Global Media Ltd. 2019. globalslag.com. March. Retrieved from https://www.globalslag.com/conferences/global-slag/review/global-slag-review-2019.

Raghu, D., H.N. Hsieh, S.C. Basin and M. Morgan. 1997. Physical characterization of water treatment plant residual and top soil mixtures. *Testing Soil Mixed with Waste or Recycled Materials,* ASTM STP 1275: 3–15.

Sudbury Mining Solutions Journal. 2007. Backfill basics: A Q& A with Paul Rantala. 1 June. Retrieved from sudburyminingsolutions.com/backfill-basics.html.

Sylvis Environmental. 2017. Calgary dewatered biosolids demonstration program: Annual Report. Calgary: City of Calgary Water Resources.

Sylvis Environmental. 2019. Pre-feasibility and costing options assessment for the use of organic residuals in mining operations. Dryden: Treasury Metals Inc. – Internal Document.

Vale Thompson. 2019. This slagpaper invention "could be big." 29 May. Retrieved from https://valenews.ca/this-slagpaper-invention-could-be-big/?

Van Ham, M, L. Dampier, K. Morton and S. Mullen. 2009. Pulp and paper sludge as a barrier layer in landfill closure: A new opportunity. *Pulp and Paper Canada* 110: 25–30.

Whiteley, Peter O. 1992. What you really need to know about sandpaper. *Sunset* October: 148.

Witjes, Sjors and Rodrigo Lozano. 2016. Towards a more circular economy: Proposing a framework linking sustainable public procurement and sustainable business models. *Resources, Conservation and Recycling* 112: 37–44.

Yuan, Zhirun. 2019. Cutting-edge technology meets forestry. In *Proceedings of the Prosperity Northwest Conference,* 5 June, Thunder Bay, Ontario.

Proceedings of Tailings and Mine Waste 2019
November 17–20, 2019, Vancouver, Canada
Published by the University of British Columbia, 2019

From Design to Operation: Filtered Tailings at the Meliadine Gold Mine, Nunavut, Canada

Nigel Goldup, Tetra Tech Canada Inc., Canada
Jennifer Pyliuk, Agnico Eagle Mines Ltd, Canada
Guangwen (Gordon) Zhang, Tetra Tech Canada Inc., Canada
Bill Horne, Tetra Tech Canada Inc., Canada
Thomas Lepine, Agnico Eagle Mines Ltd, Canada

Abstract

Agnico Eagle Mines Limited recently commenced gold production at the Meliadine Gold Mine, its newest mine in Nunavut, Canada. The mine is approximately 25 km north of Rankin Inlet in an area of continuous permafrost with a mean annual air temperature of –10°C. The mining operation had a designed mill throughput of 3,000 t per day in Year 1 to Year 3, and 5,000 t per day in Year 4 to Year 8.

On February 21, 2019, the Meliadine Gold Mine reached an important milestone: producing its first gold doré. Tailings from the process plant are filter pressed to produce a stackable filter cake at a design solids content of 85%. The filter cake is trucked to the tailings storage facility, where it is end-dumped, spread, and compacted in a sequence of layers. This case study paper presents a summary of the lessons learned to date in developing a filtered tailings facility through the design phases and into operations.

Project background

Project location and history

The Meliadine Gold Project is located in the Kivalliq District of Nunavut in northern Canada, approximately 25 km northwest of Rankin Inlet on the west coast of Hudson Bay. A private all-weather access road constructed by Agnico Eagle Mines Ltd (Agnico Eagle) connects Rankin Inlet to the Meliadine Project. The closest major city is Winnipeg, Manitoba, about 1,500 km south of the mine. Equipment, fuel, and dry goods depend on transportation by the annual warm-weather sealift by barge to Rankin Inlet via Hudson Bay, while personnel, perishables, and lighter goods arrive at the Rankin Inlet regional airport.

The Meliadine property contains the Tiriganiaq, Wesmeg, Normeg, Pump, F-Zone, Wolf, and Discovery deposits. Exploration activities on the Project were carried out by previous owners from 1987 to 2004. In July 2010, Agnico Eagle acquired Comaplex Minerals and gained 100% control of the Meliadine

Project. Since the acquisition, Agnico Eagle has conducted intensive drilling campaigns and updated Meliadine's mineral reserves and resources annually, incorporating the new drilling results. Figure 1 presents the Meliadine property location plan and regional geology map.

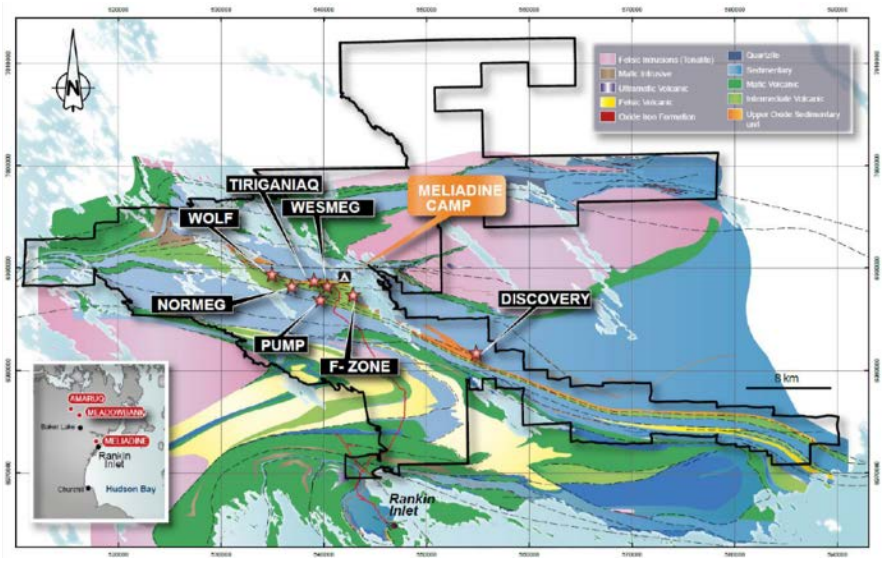

Figure 1: Meliadine property location plan and regional geology map (Agnico Eagle, 2015)

Climate and meteorology

The Meliadine Project site lies in the Southern Arctic Climatic Region where daylight reaches a minimum of 4 hours per day in winter and a maximum of 20 hours per day in summer. The monthly mean air temperature is typically above 0°C from June to September, and is below 0°C between October and May. July is typically the warmest month and January the coldest. The mean annual air temperature for the Canadian Climate Normals period of 1981 to 2010 was –10.5°C at Rankin Inlet.

Mean annual precipitation is estimated to be 412 mm, with approximately half of the precipitation occurring as rain and the other half as snow. Average annual evaporation for small waterbodies in the Project area is estimated to be 323 mm between June and September. The average annual loss of snowpack to sublimation and snow redistribution is estimated to vary between 46% and 52% of the total precipitation for the winter period and occurs between October and May.

The region is known for high winds, which are due in part to the broad, flat, uninterrupted expanses offered to moving air masses. The wind blows from the north and north-northwest more than 30% of the time. The mean values for wind speed show that the north-northwest winds, together with north and northwest winds, have the highest speeds and tend to be the strongest. Mean monthly wind speeds are typically between 19 km/h and 27 km/h.

Project and tailings management overall schedule

Figure 2 shows the key schedules for the Project and tailings management.

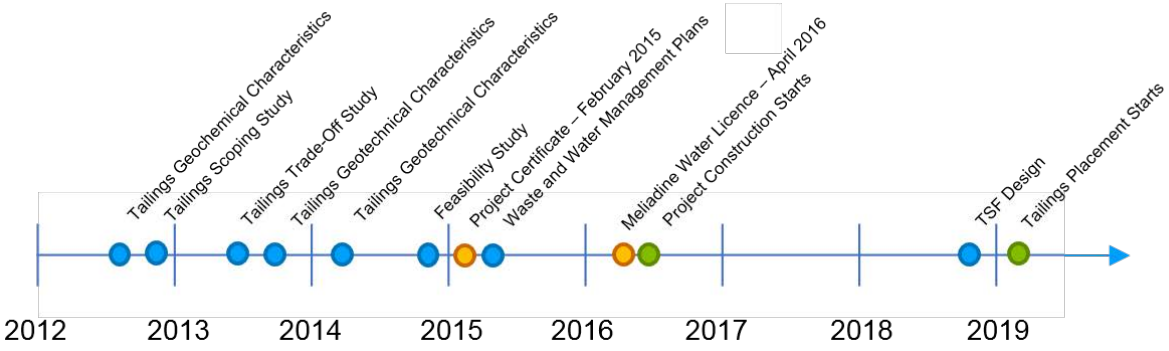

Figure 2: Project and tailings management key schedules

Past studies on tailings characteristics and management

Geochemical characterization of tailings

A series of waste geochemical characterization programs were carried out from 1998 to 2011. The principle testing results and findings of the geochemistry program were presented in Golder (2012). The methods used for testing the acid rock drainage (ARD) and metal leaching (ML) potential included mineralogical and chemical composition testing, acid base accounting, shake flask extraction testing, humidity cell tests, large column tests, and field cell tests. ARD potential was assessed following Guidelines for Acid Rock Drainage Prediction in the North (INAC, 1992) for waste rock and tailings and the Prediction Manual for Drainage Chemistry from Sulphidic Geologic Materials (MEND, 2009). From the available test results, tailings acid generation and long-term ML are not expected to occur.

Tailings scoping and trade-off studies

A scoping study of tailings management was carried out for the Meliadine Project in 2012. Scoping-level tailings management plans were developed for two tailings deposition options (thickened slurry and paste). Study Option 1 was designed to contain the thickened slurry tailings at a solid content of 57% and Option 2 was designed for paste tailings at a solid content of 75%. The proposed tailings storage facility (TSF) was located in an area covering an existing lake (Lake B7). Conceptual-level designs with construction cost estimates of the TSF were developed for the two options.

A trade-off study was undertaken by Agnico Eagle in 2013 to evaluate tailings management options including an additional option of filtered (dry stack) tailings. The trade-off focused on key considerations such as the tailings storage infrastructure, process equipment, and closure. A decision matrix was used to compare capital and operational costs, schedule, quality, and risks. At the end of this process, it was

determined that filtered tailings placed in a TSF constructed as a stack on land (not on a lakebed) could offer significant advantages at many levels. These benefits include no impact on fish-bearing lakes; no need to dewater a lake as a potential tailings basin; reduced environmental footprint; lower upfront capital costs for tailings containment structures; a lower risk tailing management strategy in terms of containment and stability; and opportunities to progressively reclaim the TSF during the mine life.

Geotechnical characterization of tailings

A laboratory test program on the tailings was conducted in 2013 for the slurry tailings option with solids contents of 65% and 72%. The test program included physical index testing and material characterization in terms of a gradation analysis, settling, thermal conductivity, strength, and consolidation characteristics. The index and gradation analysis tests indicated that the tailings would be of low plasticity and low compressibility and consist of 17% sand, 81% silt, and 2% clay size particles, as shown in Figure 3 (black dashed line).

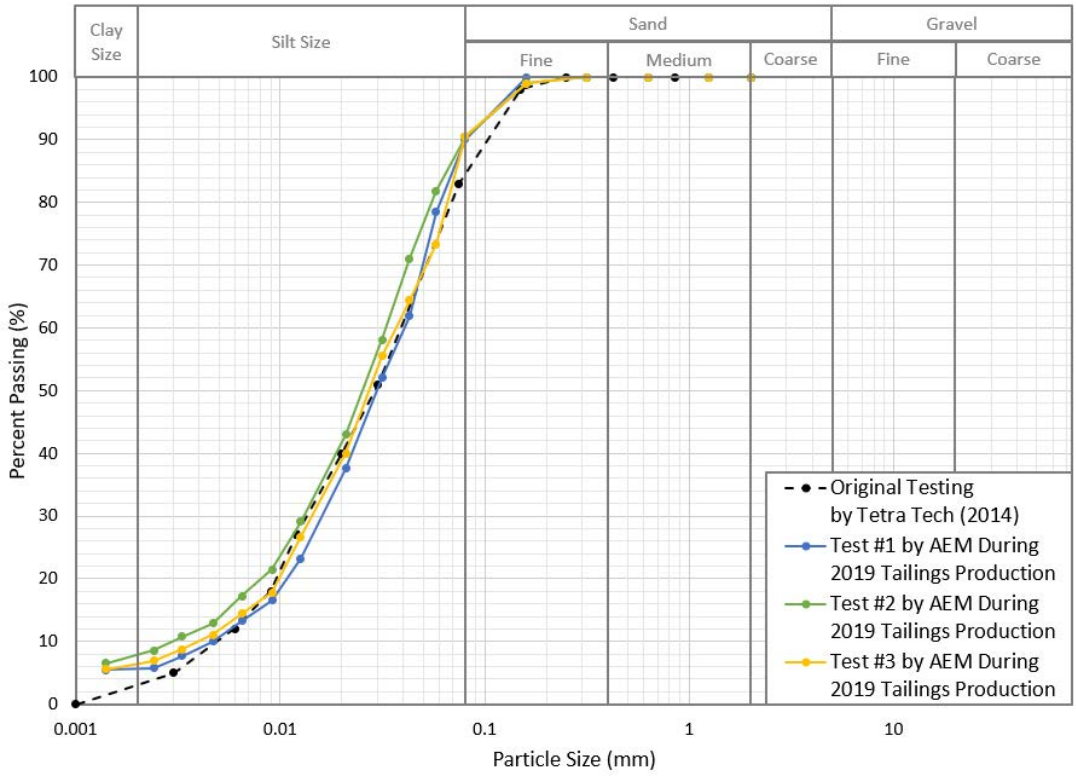

Figure 3: Tailings particle size distribution curve

Additional tailings laboratory geotechnical tests were carried out in 2014 for the dry stack tailings option with a tailings solid content of 85% at disposal. These tests included moisture-density relationship

(Standard Proctor), consolidation testing, soil water characteristic curve, direct shear testing, and hydraulic conductivity testing. The key finding from these test results are briefly summarized below:

- The moisture-density relationship (Standard Proctor, ASTM D698) test indicated that the maximum dry density of the tailings was 1.8 t/m^3 at an optimum gravimetric moisture content of 14.9%, as shown in Figure 4 (black dashed moisture-density line).
- The coefficient of consolidation (c_v) of the tailings ranged from 24.6 to 29.8 (m^2/year) under various pressures between 10 kPa and 1,600 kPa.
- The tailings had a soil water characteristic curve with an air entry value of 20 kPa and a residual suction of 900 kPa, as shown in Figure 5.
- The shear strength parameters were determined to be an inferred internal angle of friction of 33.5° and an apparent cohesion of 9.9 kPa for the tailings samples with a dry density of 1.7 t/m^3 which equates to approximately 94% of the maximum dry density.
- The saturated hydraulic conductivity of the tailings sample was 2.91E–07 m/s for the tailings sample with a dry density of 1.7 t/m^3.

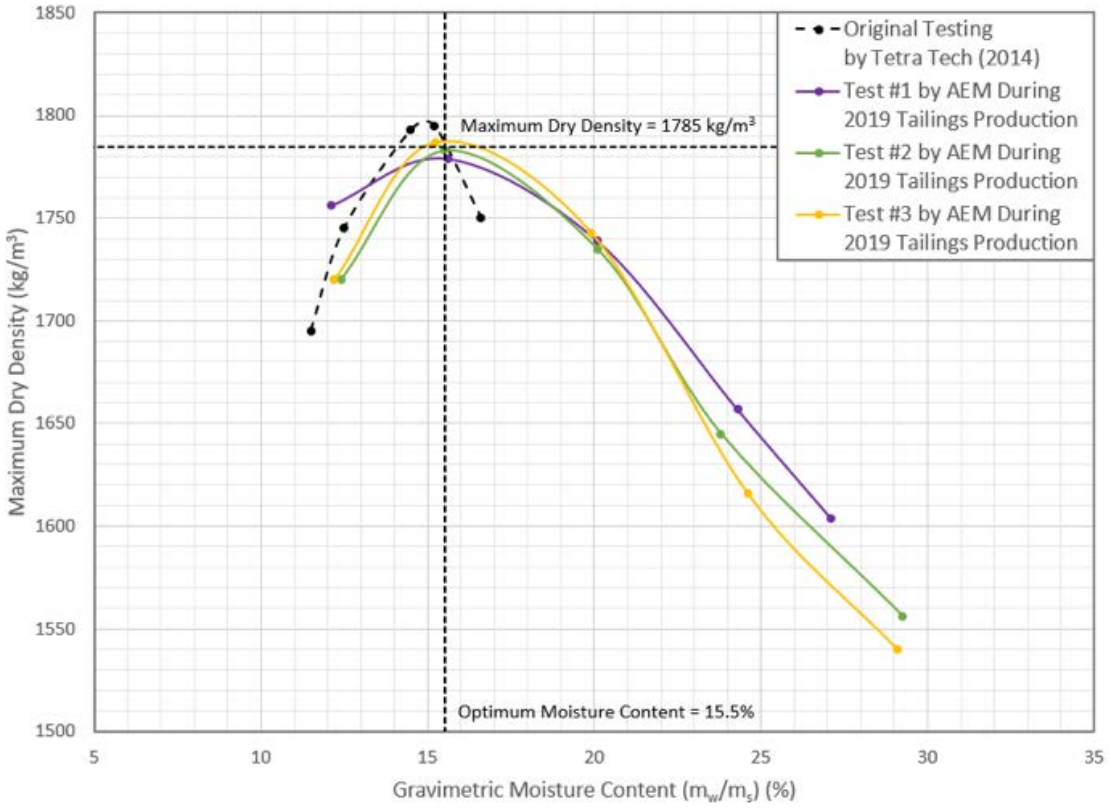

Figure 4: Tailings moisture-density relationship

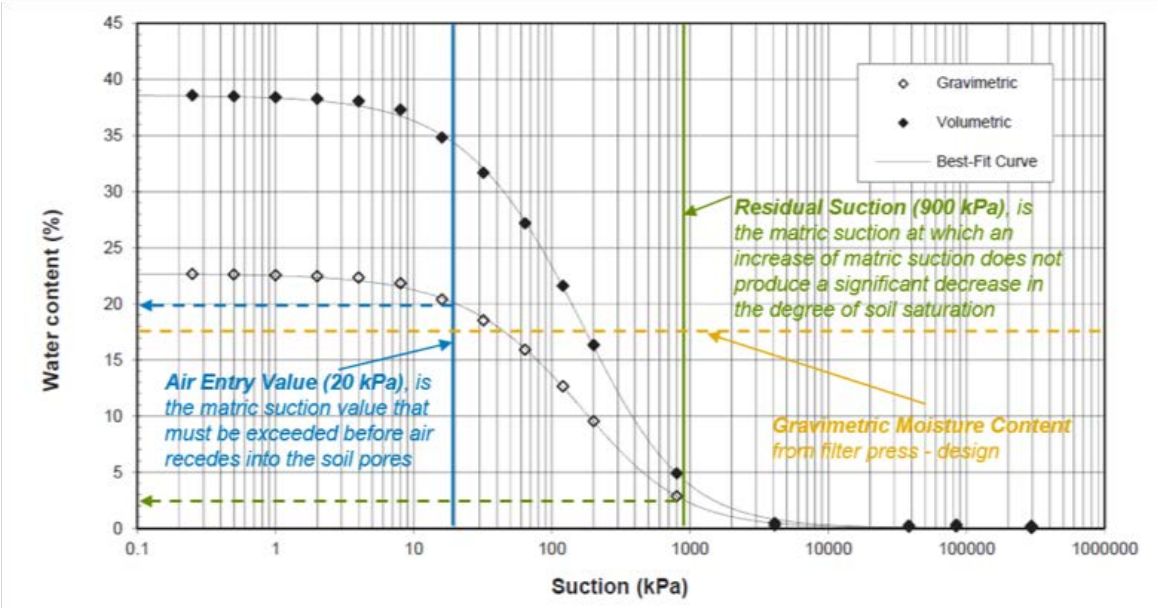

Figure 5: Tailings soil water characteristic curve

Tailings management feasibility study

A feasibility level study on tailings, waste, and water management for the Project was conducted in 2014. The mine plan for the study indicated that 12.1 Mt (million tonnes) of ore would be milled over a period of approximately 8 years at a milling rate of 3,000 tonnes per day (tpd) from October of Year 1 to Year 3 and 5,000 tpd from Years 4 to 8. The operation would produce 12.1 Mt of tailings: 2.4 Mt would be placed as backfill in the underground mine, and the balance of 9.7 Mt would be placed on surface in a dry stacked TSF. The tailings were proposed to be dewatered to a solids content of 85% for tailings disposal. With an estimated in-place density of 1.65 t/m³, the total volume required for the dry-stack TSF was approximately 5.9 million m³. During this stage, the slope stability and thermal analysis of TSF were evaluated. The TSF was designed to have three cells to facilitate stage tailings disposal and progressive closure cover placement during mine operation.

TSF design and operation

Filter press and tailings production

The tailings circuit incorporates three Outotec filter presses, Type Number FFP 2512 40/50 M50. Two of the units are used to filter press the tailings stream, and the additional unit is available as a backup/spare. The resulting filter cake is conveyed to an unheated storage building prior to being loaded and hauled to the TSF. The building has the capacity to store approximately three days of tailings production in the event that tailings cannot be placed on the TSF, for example, during winter whiteout conditions or caribou migration periods.

Detailed design

Detailed design of the TSF (Agnico Eagle, 2018) was advanced from the feasibility level study. To accommodate an anticipated additional 1.2 Mt of tailings in the facility, the height was increased and a two-cell design (Figure 6) adopted over the previous three-cell system to facilitate construction and enhance freeze-back potential. The facility dimensions are approximately 870 m (length) by 430 m (width) by 33 m (average height), with side slopes of 4H:1V for the bottom portion and 3H:1V for the upper portion of the facility. The final top surface will be sloped at 4% to promote lateral runoff from the facility during rain events and freshet. During operation, progressive closure of the facility will comprise waste rock placement on the side slopes (between 4.0 m and 4.5 m thickness), which also provides access and limits traffic on non-active placement areas, as well as reduces erosion and dust generation. Final capping of the top surface with overburden till fill (0.5 m thickness) and waste rock (2.5 m thickness) will occur once each cell has reached design height as shown in Figure 7. Runoff from the facility is captured by a series of berms and channels that are directed to collection ponds.

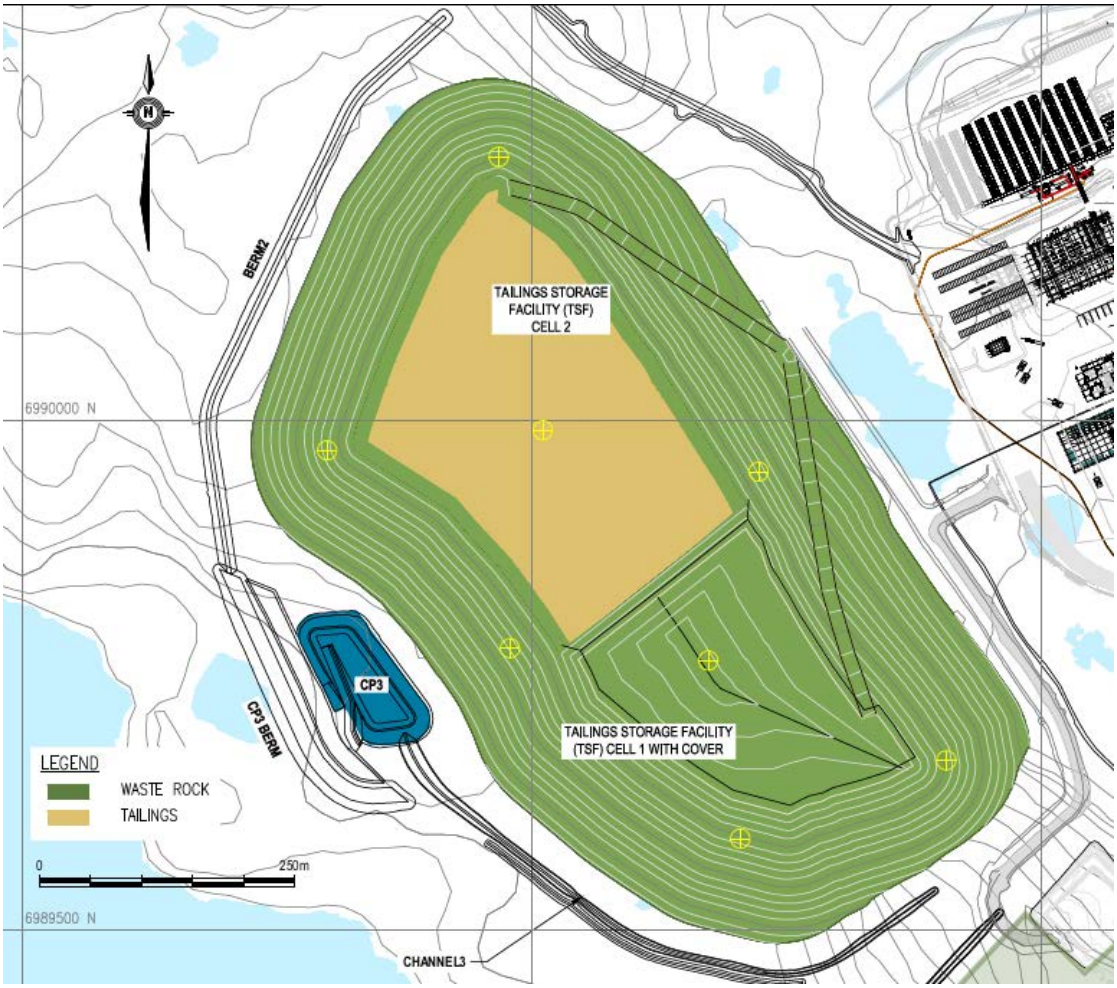

Figure 6: Plan of the TSF together with the water management infrastructure

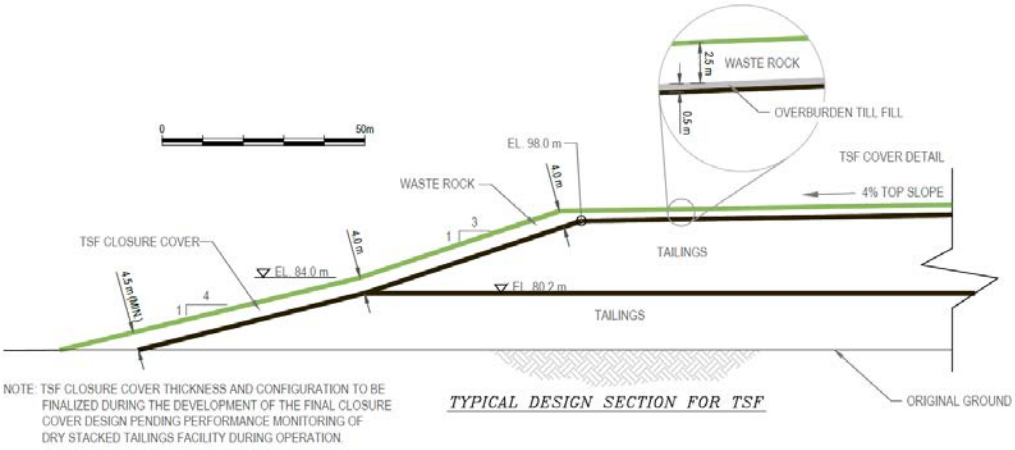

Figure 7: Typical cross-section through the TSF showing the progressive closure cover

Tailings and cover material placement

The tailings filter cake is hauled to the TSF from the unheated storage building using Volvo 40 t articulated haul trucks. The filter cake is end dumped from the haul trucks and spread in maximum 300 mm lifts using a CAT D6 bulldozer as shown in Figure 8. Compaction occurs with a CAT CS356 10 t vibratory smooth drum roller completing a specific number of passes at a specified speed and vibratory setting depending on weather conditions and moisture content. To aid placement and operations, the first main cell was divided in sub-cells that are generally operated on a rotational basis. Each lift of tailings is sloped approximately 1% towards the waste rock cover to direct run-off away and off the facility. Survey provides daily grade control, placement monitoring, and ongoing as-built records. Figure 9 shows an aerial view of the TSF.

As with the tailings, waste rock is hauled to the TSF with the Volvo 40 t haul trucks, end dumped, and spread with the D6 in lifts of maximum 1 m height before compaction occurs. The exterior slope is then shaped with a CAT 330 excavator. Cover material is increased after every 3 lifts of tailings and placed to the same elevation of the tailings at the interface to direct run-off from the facility and reduce erosion.

Figure 8: Tailings placement, spreading, and compaction

Figure 9: An aerial view of the TSF

In-situ measurements to date

Although commissioning of the filter presses is on-going, information to date indicates that the filter presses are generally performing well and producing a filter cake with an average gravimetric moisture content between 13% and 20% excluding obvious outliers as shown in Figure 10. Variability in the moisture contents is expected to decrease once the commissioning process has been completed.

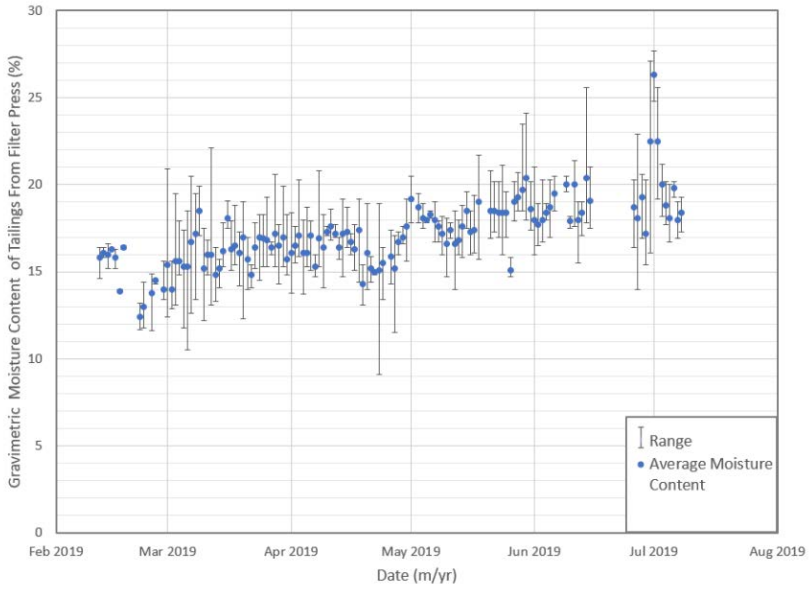

Figure 10: Filter press tailings moisture content against time

The actual tailings particle size distribution (Figure 3) is very similar to the original test sample provided in 2014. Nuclear density tests on the in-situ placed and compacted tailings indicate, for the most

part, that the filter cake is achieving dry densities in excess of the maximum dry density from the Standard Proctor test as shown in Figure 11. The placed tailings material shows very little signs of bleed water and are easily trafficable after placement and compaction. Measured in-situ gravimetric moisture contents range between approximately 8% and 21.5%.

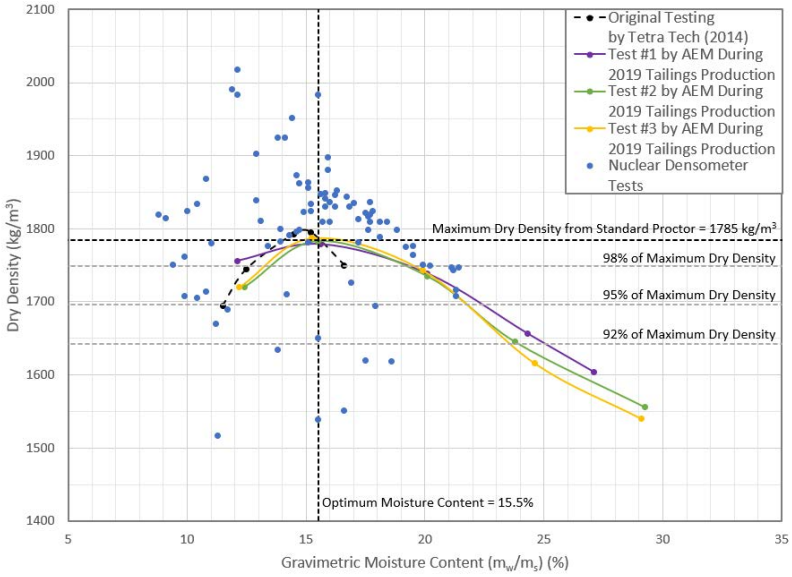

Figure 11: Tailings dry density against gravimetric moisture content.

Conclusions and lessons learned

After reflecting on the design process leading up to final design, permitting, construction, commissioning, and operational experience of the dry stacked storage facility, the following conclusions can be drawn from experiences to date:

- The Meliadine Gold Mine area has a large proportion of lakes in the area. Due to the self-supporting (stackability) characteristics of the tailings, the TSF could be located outside a lake bearing depression, thereby reducing the need to impact existing lakes.
- With the risks of using containment structures to impound slurry or thickened tailings, the plan of using dry stacked tailings for the Meliadine Gold Mine helped with streamlining the permitting approval process.
- Supply of a representative sample of tailings and process water to undertake the initial tailings characterization testing before the final design is important.
- Operation of a TSF often involves coordination between multiple departments and management levels (health and safety, mill, services, engineering, environment). Together with the involvement and collaboration of all team members through the different design phases, an operational risk

assessment process has been critical to creating a culture of commitment and investment in the Project.

- Moving from final design to operation needs special attention. Successful placement and compaction of the dry stacked tailings within the facility needs the commitment of dedicated equipment, a detailed operational plan, and staff training. The operators and supervisors (who may not be familiar with design drawings, for example) need training to understand what is required to achieve the design intent. During the initial stages of placement, this included daily tool box meetings, weekly operational meetings, daily and weekly inspections, monthly reporting, and continuous survey support.
- One of the keys to success is monitoring and providing feedback to the operators, as well as listening to their comments. Measuring and defining a moisture content target for the filter press cake is a must. Monitoring the moisture content of the press underflow is an early simple indicator of exceedances and upset conditions. These should also extend to the placement and compaction of tailings cake within the TSF, where a nuclear densometer can be used to rapidly determine the in-situ density and moisture content of the compacted layer.
- The definition of moisture content in the mining world is very different from the definition in the geotechnical world. The mining world defines gravimetric moisture content as (Mass of Water/Total Mass) whereas the geotechnical world defines gravimetric moisture content as (Mass of Water/Mass of Solids). We may think we are speaking the same language, but we are not. In terms of dry stacking, this could make the difference between a stackable and trafficable surface and an over wet non-trafficable surface. Therefore, be clear on the derivation of the design parameters being used for design and monitoring.
- Diverting surface water from running on to the dry stack area helps limit the volume of contact water the mine has to manage. In addition, it is important to manage the water falling on to the dry stack to maintain trafficability and avoid rework.

Acknowledgements

The authors would like to thank Agnico Eagle Mines Limited for the opportunity to publish this paper and to share the data contained within.

References

Agnico Eagle. 2015. Updated technical report on the Meliadine Gold Project, Nunavut, Canada. Prepared by J. Larouche, D. Caron, L. Connell, D. Laflamme, F. Robichaud, F. Petrucci and A. Proulx for Agnico Eagle Mines Limited, February 11, 2015.

Agnico Eagle. 2018. Tailings Storage Facility (TSF) Design report and drawings. Agnico Eagle Mines Limited, November, 2018.

Golder. 2012. SD 6-3 Geochemical characterization of waste rock, ore, tailings and overburden, Meliadine Gold Project, Nunavut, Canada. A technical report submitted to Agnico Eagle Mines Ltd by Golder Associates, October 10, 2012.

INAC. 1992. Guidelines for Acid Rock Drainage Prediction in the North. Department of Indian Affairs and Northern Development, Northern Mine Environment Neutral Drainage Studies No.1, Prepared by Steffen, Robertson and Kirsten (BC) Inc., 1992.

MEND. 2009. Prediction manual for drainage chemistry from sulphidic geologic materials. MEND Report 1.20.1. Mining Environment Neutral Drainage Program, Natural Resources Canada, December 2009.

Proceedings of Tailings and Mine Waste 2019
November 17–20, 2019, Vancouver, Canada
Published by the University of British Columbia, 2019

Mine Tailings and Fly Ash: More Alike than You May Think

Jeffrey Hill, Hayward Baker Inc., USA
Paul Schmall, Moretrench, USA
Josh Kolz, Hayward Baker Inc., USA

Abstract

Mine tailings have been an area of concern for mine owners and geotechnical engineers since the first recorded tailings impoundment failure in 1962. The study of mine waste has therefore been a focus of the engineering community since at least that time. However, there are still many questions that have not been answered about the geotechnical properties of mine tailings. The intent of this paper is to compare the geotechnical properties of mine tailings with those from other industries dealing with saturated waste products, such as coal combustion residuals (CCR) from coal-fired electricity generation. The authors will compare and contrast the geotechnical properties of the waste and then also discuss geotechnical treatment methods that have been utilized in both markets. This effort of comparison is intended to broaden the knowledge base of practitioners in both markets. The authors will use several actual case histories on projects in both market segments to illustrate the similarities and differences. Each case history will provide examples of the geotechnical properties of the materials and how these materials were treated.

CCR ponds and mine tailings facilities are both unwanted by-products of industrial processes. The environmental impact of failure of the facilities used to store these by-products has taken front stage after several high profile failures of ash and tailings facilities. Notably the most recent failures – the Vale mine tailings impoundment failure in Brazil, the TVA ash dike failure at Kingston, and the Duke failure at Dan River a few years ago – have resulted in the public becoming aware of the environmental and safety risks that can be associated with these facilities. The authors, from working on both types of facilities for decades, intend to provide lessons learned from each industry that may then be used by the other to increase safety and reduce the potential environmental impact of these facilities.

Overview

Coal Combustion Residual (CCR) ponds and mine tailings impoundments are both by-products of industrial processes. They are at the end of the revenue stream for either a mine or an electrical utility and are

essentially the facilities' "refuse piles" that do not provide any benefit, but sit there as eternal environmental liabilities.

The environmental impact of the pond facilities has taken front stage after several high profile failures of ash and tailings impoundments. Recent failures have released over one billion gallons of waste slurry into the surrounding area. As a result of these incidents, the public has become more aware of the environmental and safety risks that can be associated with these impoundments.

The impact of failures

While the frequency of failures in recent years has been reduced over the historical figures, the recent failures have resulted in much larger environmental impacts. The number of facilities and the failure rates must be understood to grasp the total potential impact that faces the industry (UN Report on Safety, 2016).

There are 427 fly ash impoundment facilities throughout the US whereas there is no public inventory of tailings impoundments. However, one earlier estimate that places the number of tailings impoundments at 3,500 worldwide could be a drastic underestimate since others have more recently estimated the number of active and abandoned industrial mine sites globally at more than 30,000 (Roche et al., 2017). The same report also notes that accidents with mine waste have killed 341 people since 2008. Meanwhile, loss of lives directly as a result of CCR has been dramatically less, perhaps a handful.

The failures in both industries have resulted in regulatory scrutiny as well as scrutiny from both internal and external stakeholders. This pressure is resulting in more transparent understanding of the risks associated with the facilities, and in the case of fly ash impoundments has resulted in enforceable regulatory statutes from State and Federal Governments.

Current regulatory requirements and waste administration

The two sources of this material face differing regulatory pressure. They also have historically been administered in very different manners. While power utilities are a product of the industrial age, often having a planned service area with expansion plans in mind during construction, mining ponds can be less of a planned, orchestrated event – often mining started as a small non-production mine only to expand dramatically once the dirt paid ("paydirt"). As the valuable minerals were discovered and expanded, the ponds also were expanded for the larger operations.

Ash ponds

Ash pond owners sell their electricity at rates controlled by the public utilities commission. It has thus been a direct avenue to impose regulatory pressure on these facilities, and current regulations require the initiation of capping or removal of all ponds by 2021. The power utility can ask for a rate increase to cover

remediation costs from their local regulations boards.

The recent failures and mass releases into the environment have put a lot of pressure to consider all of the possible environmental and health consequences of CCR. The individual states have been following up the EPA regulations with their own rulings.

The power companies have traditionally sought an aftermarket beneficial reuse of CCR; fly ash for use in concrete, gypsum for the manufacturing of wallboard, and bottom ash for a wide range of applications. However, thousands of yards of ash from the process of creating electrical power are still wet sluiced into ponds. Most of this material lies in ponds that were originally constructed decades ago. The ash is therefore a financial and environmental liability for the power utility.

Tailings impoundments

Mining companies vary widely in size and number of operations, from small private entities to large multinational corporations, but they all sell their ore at global market rates. Mining companies have not historically been under the same scrutiny as utility regulatory bodies and mine tailings ponds are currently not facing regulation to be closed. Additionally, mining operations are generally in more remote locations than power facilities which has resulted in an "out of site out of mind" mentality.

Often, tailings ponds are increased by upstream impoundment raises, i.e. building another dike on top of the impounded material. The evolution of these tailings facilities, that have often lacked an ongoing engineer of record throughout the evolution, is thought to have contributed to several of the global tailings failures.

While there are no actual closure requirements, the ponds are under increased scrutiny due to ongoing operational and safety concerns, environmental concerns, and stakeholder concerns. Similar to ash ponds, this material is a financial and environmental liability for the mining entity. The mining companies understand they have no way to pass the cost of tailings remediation onto the end-users of the mined materials, or to consumers in general, and are actively looking for ways to minimize any future costs.

Physical properties of the waste materials

Deposition

Each material is placed into an impoundment with water conveyance. Depositing by water leads to heavier material falling out of suspension first, forming deltas or "beaches" of more coarse-grained materials. During routine operations, the outlet pipe is moved to different locations in the pond, resulting in the distribution of coarser grained material at any possible location in the pond. The deposition history of most ponds is not well documented and the deposition within each pond can be complex, with corresponding

unpredictable hydrogeological behavior. The variable behavior translates to dangerous and somewhat unpredictable conditions for construction equipment and operations.

In general, both ash ponds and mine tailings impoundments were constructed historically without the use of modern lining systems. The lack of an impermeable layer below the ponds has resulted in concerns regarding the leaching of heavy metals and other contaminants into the groundwater.

Particle make-up and geotechnical properties

Both ash and mine tailings can be highly unstable. Because they are sluiced, the deposition within the pond tends to be very loose and uniform which promotes physical instability.

Fly Ash

Fly ash is typically composed of spherical, relatively uniform particles, like ball bearings or glass beads (Figure 1). The clean spherical particle shape has an obvious influence on the instability of the material, particularly when it is wet.

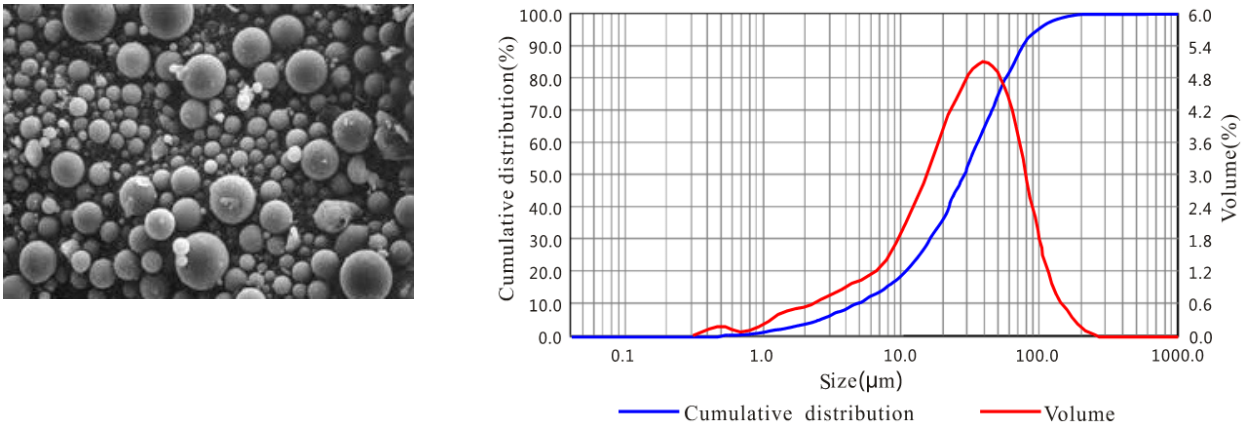

Figure 1: Magnified fly ash particles (left) and typical particle size distribution (right)

Although the particles are predominantly silt-sized, the material tends to behave more like a fine uniform sand than a silt. Ash does not consolidate like a natural silt or a clay. Typical fly ash, the main ingredient of the typical ash pond is approximately 80% silt-sized particles, and is absolutely non-cohesive.

All of the above properties of ash (loose, fine, uniform, non-cohesive) make this a material that is highly susceptible to liquefaction. Additionally, when liquefaction is initiated and the material is free to move, the material will flow like a chain reaction. The rearrangement of the particles upon movement generates enough free water to keep the material in motion. The term “static liquefaction” was coined at Kingston to describe how the initial movement occurred without known stimulus.

The presence or absence of water makes all the difference in the behavior of ash. When saturated, fly ash exhibits very little shear strength. When the “free” water is drained from the ash–what hydrogeologists

refer to as the specific yield-it exhibits significant apparent cohesion, significantly increased shear strength, and thus stability.

When saturated, the ash is a very dangerous material to work on with conventional construction equipment. Amphibious equipment is typically necessary when there is not a significantly thick dry crust to work from. There are countless incidents of equipment engulfed by ash when saturated (Figure 2). When the material is saturated, it will seek a very flat slope of say 10:1 or flatter, and even those slopes are unstable until they are drained.

Figure 2: Engulfed backhoe

Ponded CCR can be very mixed. It can consist of coarse-grained materials such as bottom ash and can include very fine-grained and difficult -to-handle materials such as gypsum which is also a by-product of the power generation process. Bottom ash comingled with fly ash can make the material more readily drainable. Gypsum comingled with fly ash has the opposite effect – it makes the material more difficult to drain and stabilize.

We are still learning about the complexities of fly ash behavior and the role the ash chemistry plays in its behaviour. Older and weathered ash exhibits different behaviour than younger and unweathered ash. It is believed that the unburnt carbon allows the ash to take on clay-like properties.

Mine tailings

The physical properties of mine tailings are more variable than ash and more difficult to generalize. They can vary by the type of mining and the ore used, and then of course the crushing and grinding process can

affect the physical make-up of the particle size. Mine tailings typically tend to be more angular in shape than the spherical fly ash particle. Again though, despite the angularity, they are still susceptible to flow and become unstable if agitated or otherwise disturbed. The unstable slopes and static liquefaction explained above in the fly ash section are also observed in the majority of tailings ponds. This can be attested to by the distance and liquid-like flow after failures such as at Vale, Brazil.

The very essence of the failures mentioned previously in the paper demonstrates the mine tailings material's ability to flow – generally in an unwanted and dangerous fashion. Once the material is mobilized and movement begins, the material will seek its natural angle of repose, which is nearly flat. The flowing of the material, whether ash or tailings, has been observed to fill bodies of water valleys or other downstream features and result in widespread damage to man-made structures or the natural environment.

The particle makeup and hydraulic deposition is in essence what makes these two materials from very different sources behave geotechnically in similar fashion. The authors would think of both fly ash and mine tailings as silt-like particles with a majority of the material passing the #100 sieve and with high water content. Because of the particle size and the moisture content, the material will exhibit little to no shear strength. Any shear strength that is available will soon be jeopardized with addition of vibration or other energy.

Historic treatment of materials – in-situ

Mine tailings

Tailings ponds have been remediated for a variety of reasons for the past 30+ years. Early successes in the use of pre-fabricated vertical drains, when installed with zero or low pressure ground equipment in wet ponds, have shown that water can be removed from this material. The reason for the water removal can be to allow mine process water to be recaptured, such as in arid regions where the mines need the water to produce and maintain the mine. In other ponds, the removal of pore water from the material has allowed for increased free board behind the impoundment. This can be beneficial to allow for increased fines storage containment. Lastly the removal of water from the tailings has been completed to increase the shear strength of the material, which in turn provides a significantly increased factor of safety for the impoundment or may also allow owners to cap the tailings in order to decommission the facility and move toward closure (Figure 3). Once the impoundment has been capped, the owner can begin the process of planting and reclamation of the site. Dewatering with wick drains requires an experienced contractor to complete the work safely from on top of the marginally stable pond. However if safety precautions are taken there are benefits of completing this work, as discussed above.

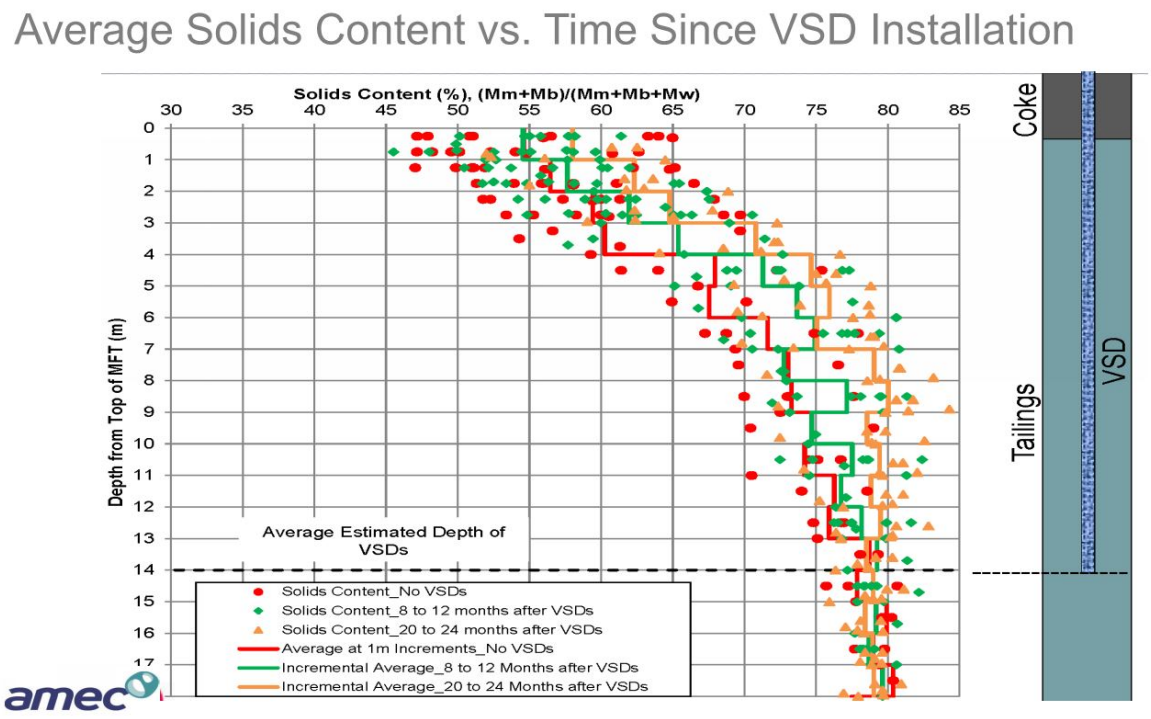

Figure 3: Increase in shear strength as a result if wick drain, SD installation

Fly ash

With regard to fly ash pond capping, decommissioning and reclamation, the industry is just at the beginning of this phase. For decades, the fly ash ponds have been the neglected part of every coal burning power plant, with no reason for attention prior to the EPA CCR ruling. In the uncommon instances where the ponds have seen excavation or earthwork, the material has been partially drained and stabilized by relatively crude and often dangerous open pumping drainage techniques referred to as rim ditching and sumping. The very few instances of pre-drainage dewatering with wellpoints in ash have been only slightly successful, as the techniques were never modified for the peculiar behaviour of fly ash until only recently. And even today, where dozens of ash ponds have been successfully pre-drained with dewatering techniques, the industry in general has been slow to accept the relatively new success of predrainage dewatering. Decades of the "this is how it has always been done" mentality are slow to change.

The authors have been involved in dozens of projects in which deep well or wellpoint dewatering systems were installed within the fly ash ponds. If properly filter-packed dewatering wells or wellpoints are constructed within the ash, the ash is surprisingly responsive to the application of dewatering when one considers the predominantly silt grain-size distribution. There are many theories and opinions why ash takes on its peculiar behaviors. However, what is undisputable is the significant difference in stability and behavior between saturated and drained ash. Once the ash has been dewatered, it can be traversed by conventional equipment, excavated, stacked, compacted or, in some cases, the material is then excavated

and disposed of at landfill facilities. Dewatering of the ash prior to removal from the pond allows for more efficient and less costly excavation. Dewatering can be accelerated if the dewatering devices are installed deep enough to intersect areas of higher permeability, particularly if these layers lie below areas of lower permeability and the lower "beach" layer of more coarse-grained material can be tapped into to effectively increase the radial influence of the dewatering devices.

One of the critical provisions of dewatering is that it provides for a much safer excavation process, with significantly reduced liquefaction potential, greater bearing capacity for construction equipment, and stand-up time of the material. Dewatering with wellpoints requires an experienced contractor to install the dewatering devices safely from on top of the marginally stable pond. However, if safety precautions are taken, there are benefits to completing this work, as discussed above. Dewatering can provide stable slope cuts in ash, appreciable stack heights (over 30.5 m [100 ft]), and high capacity haul roads for the safe operation of off road trucks. Dewatering can also be implemented to provide an engineered dry crust of more competent material. This crust can then be utilized in subsequent stages of construction to allow safe access of heavier equipment onto the pond. Dewatering can also be initiated from a flooded pond, which circumvents the demand for a dry workable crust for the system installation. This can be performed with floating installation equipment or amphibious equipment (Figure 4).

Where greater improvement of the ash is needed than can be provided by just drainage, ground improvement techniques such as soil mixing can be utilized.

Figure 4: Wellpoint installation from floating barge (left). Wick drain installation from customized pontoon (right)

Geotechnical information for remediation design

The amount of geotechnical information available to closure designers and contractors has increased in both quantity and quality in the last several years. Geotechnical information useful for dewatering and ground improvement design includes traditional SPT boring logs with soil/ash/tailings descriptions and

stratigraphy, CPT logs, grain size analysis, and pump test data.

In particular, the authors have observed that although most CCR/tailings materials are of low permeability, thin but highly permeable zones may exist at various depths in the subsurface column. These transmissive zones are generally only a small portion of the overall deposit thickness but represent most of the water transmitting capacity of the materials. These zones are likely a result of the discharge pipe location and water sluicing of material, resulting in heavier material dropping out of the sluice in zones. These zones may be identified by taking advantage of the near continuous data sampling ability of the CPT.

While it is possible to estimate the dewatering effort required based on SPT, CPT, and laboratory data, the best way to design a dewatering or ground improvement program is using real field data obtained from a pilot program or pump test (Figure 5). A ground improvement pilot test, for example, may evaluate the geometry, strength, permeability, or leachability of soil mixed columns. A pump test usually consists of either a pumped deep well or series of wellpoints and measurement of the resulting drawdown in strategically-placed instruments, typically at variable depths within the pond. Data obtainable from such tests may include traditional aquifer parameters such as transmissivity and storage coefficient. Possibly of greater importance, the test may provide an opportunity to measure the yield of a representative dewatering device or a device constructed and installed the way that production wells or wellpoints will be constructed and installed.

Figure 5: Typical wellpoint pilot test configuration

Oftentimes for the installation of wick drains in ponds we approach the pre-design work a bit differently. Because each wick drain is so cost effective to install there is relatively low costs in sticking wick drains on closer than needed spacing, and then monitoring the output of the wick drains and in turn

the removal of water from the tailings. This approach is often taken as the mine operators want to see the effectiveness of the drains more quickly. After the installation begins, the owner and contractor can then determine the spacing of the wick drains to achieve the desired results in terms of draw down and the time for consolidation to take effect.

Case histories of remediation of ash and tailings ponds

Dewatering of the ponds is one geotechnical approach to increasing the safety, reducing the environmental impact of the ponds, and moving toward closure. In some cases because of regulatory requirements, dewatering of the facility is not desirable. In these instances, a variety of other in-situ geotechnical construction methods have been utilized. The following are a few case histories in which specialty geotechnical construction techniques were utilized to meet regulatory or safety requirements for the owner.

Soil mixing-shear walls

A pond in the southern Midwest was reviewed for stability in the New Madrid Seismic area. As some of the impoundment dyke had been developed on ash material, which can liquefy as a result of seismic activity, there was a justified concern regarding the behavior of the ash beneath and behind the impoundment during an earthquake. A geotechnical solution was therefore required that would increase the seismic factor of safety for the impoundment to the current standard of care. Soil mix shear walls were installed at the toe of the embankment to increase the seismic factor of safety.

Soil mixing gravity wall

To achieve clean-closure of a south-eastern power plant's CCR pond/landfill complex, a temporary cellular gravity wall bisecting the pond was constructed using overlapping deep soil mixed (DSM) columns through an earthen berm/CCR/residual soil profile. This approach allowed excavation of one half while the other half remained operational in compliance with state permitting requirements.

Sheeting

There was a need at the same south-eastern power plant to provide excavation support within an ash backfilled drainage canal. CCR up to 9.1 m (30 ft) in depth required excavation and removal. An excavation support system consisting of driven sheet piles and tieback anchors was installed to retain the landfill while allowing vertical excavation of the exterior CCR. The excavation was required to install a drain below a portion of the landfill to collect potentially contaminated groundwater.

Dewatering

At a mid-Atlantic power station, CCR excavated from two smaller impoundments was to be placed on top

of existing CCR impounded by an earthen embankment in a former valley fill. However, adding mass to the top of the impounded ash while simultaneously excavating ash from near the bottom of the embankment would create an unsafe condition. A solution was developed whereby the phreatic surface in the CCR was lowered by deep dewatering well installation, improving the embankment stability so that it could withstand the additional load and increased toe resistance with an acceptable factor of safety. The well system was designed and constructed so that it could be raised as the CCR was placed in lifts.

Wick drains

At a mine facility's tailings pond that was approximately 1.6 km (1 mi) by 2.5 km (1.5 mi) in plan area and 39.6 m (130 ft) deep, wick drains were selected to dewater the saturated, low strength clay tailings and increase their shear strength to allow construction of a permanent cap. The existing working platform consisted of a floating coke cap, presenting a hazard to equipment and personnel. The geotechnical contractor developed purpose-built equipment and procedures that allowed safe installation of the 6.2 million LM (20 million LF) of wick drains from on top of the floating cover. The drains produced between 0.5 to 1.5 million gal/day (1.9 to 5.8 million L/day), rapidly accelerating an increase in shear strength to permit subsequent capping.

Conclusion

From working with waste tailings and CCR for decades, the respective authors have gained considerable experience in both areas. Sharing that information has highlighted that while there are a number of differences, the two types of materials also share a number of similar characteristics. Both materials will gain strength with dewatering, and dewatering is possible in nearly all cases with proper care, tools, and attention to safety. Dewatering devices, whether they are wells, wellpoints, or wick drains, can be installed from on top of the unstable material with specialty equipment.

Modern dewatering and geotechnical principles apply to both industries and both types of waste streams. Therefore, the experience from one industry can play a role in improving the results and outcome of work in the other. At the same time, each pond should be considered unique and will present different challenges, and must be addressed and evaluated as an independent project. Dewatering is specialized work. Close cooperation with an experienced and well-qualified contractor is considered critical to the successful and timely outcome of ash pond dewatering, and should be borne in mind for mine tailings remediation.

References

Roche, C., K. Thygesen and E. Baker. 2017. *Mine Tailings Storage: Safety is No Accident.* UN Environmental Programme and GRID-Arendal.

Proceedings of Tailings and Mine Waste 2019
November 17–20, 2019, Vancouver, Canada
Published by the University of British Columbia, 2019

Environmental Assessment of Residues from Multi-Step Passive Treatment of Fe-AMD: Field Case Study of the Lorraine Mine Site, Quebec, Canada

M. Jouini, University of Quebec in Abitibi-Témiscamingue, Canada
C.M. Neculita, University of Quebec in Abitibi-Témiscamingue, Canada
T. Genty, University of Quebec in Abitibi-Témiscamingue, Canada
M. Benzaazoua, University of Quebec in Abitibi-Témiscamingue, Canada

Abstract

Passive systems are often used for acid mine drainage (AMD) treatment in closed and abandoned mine sites. Depending on AMD loading and the technology used, passive treatment systems generate metal-rich residues with inconsistent stability. To ensure their proper management, these residues must be handled carefully to reduce the risk of further contamination. Therefore, an assessment of the potential leaching mobility of contaminants (e.g., metals and sulphates) is deemed necessary.

With this aim, six post-treatment solid residues were collected from a field operating an iron-rich AMD (Fe-AMD) treatment system implemented on the reclaimed Lorraine mine site in Quebec, Canada. Solid samples were collected from the inlet and outlet (In and Out) of a three-unit treatment system (PBR1, WA and PBR2). Three water samples (P1, P2, and P3) were also collected from piezometers installed in the outlet of each treatment unit. Geochemical equilibrium modelling was performed using the physicochemical quality of the water samples to evaluate the occurrence of metal precipitates. Physicochemical characterization and a pH-dependent leaching (pH_{stat}) test were carried out to assess the potential mobility of contaminants from solid residues. The pH_{stat} was also performed to determine the buffering capacity of the solids, to provide a better understanding of leaching behaviour of contaminants under different environmental conditions and to orientate the management of these residues. Results of elemental analysis showed that all residues had a high metal content. The geochemical modelling suggested that Fe, the metal with the highest concentration to be treated, was in the form of oxides, hydroxides, oxyhydroxides, hydroxysulphates, and sulphides. High residual neutralizing potential was found in WA residues. The results of the pH_{stat} test indicated that all residues were considered as leachable towards regulation limits of metal release once contacted with acidic medium (water and/or soil) or co-disposed

with alkaline wastes. Thus, contact with rainwater must be avoided to prevent metal mobility and dispersion. Landfill disposal at pH 7–8 could be a storage option for these residues.

Introduction

Acid mine drainage (AMD), generated by mine waste (e.g., sterile rocks, tailings and treatment process sludge), is characterized by low pH and a high concentration of metal(loid)s and sulphates. Because of its high toxicity potential, AMD is considered a serious environmental concern. In abandoned mine sites, passive treatment systems (PTSs) (chemical/biochemical) are usually used to treat AMD impacted-waters, particularly as multi-step systems (Skousen et al., 2017). They consist of either one unit, for low and average contamination, or multi-step units for high contamination treatment, including iron-rich AMD (Fe-AMD). Depending on the quality of the AMD to be treated and the technology employed, PTSs generate in the course of time metal-rich residues with inconsistent stability that have to be managed carefully after their renewing (Jouini et al., 2019). Indeed, it was reported that metal-rich (As, Cr and Se) residues from a passive biochemical reactor (PBR) were classified as non-hazardous waste (Simonton et al., 2000). However, Fe-rich residues from PBR are considered as potentially mobilizable and could be stored under water, at near neutral pH to limit their reactivity (Genty et al., 2012a). In the same time, metal-rich (Fe, Zn, Ni and Cu) residues from PBR were characterized as hazardous and inappropriate for landfilling without pre-treatment (Kousi et al., 2018). In addition, metal-rich (Fe, Al, and Zn) residues from dispersed alkaline substrate (DAS) systems should not be disposed in landfill and have to be stored in a dry environment to prevent the eventual metal release (Macías et al., 2012). Finally, for Fe-rich residues from a multi-step system using both PBR and DAS, it was found that contact with an acidic medium and alkaline waste should not be allowed (Jouini et al., 2019). Therefore, a case-by-case study and proper management of these metal-rich residues are deemed necessary to control and prevent the possible metals release.

Taking into account these concerns, the present study investigated the potential mobility of contaminants from residues generated during Fe-AMD passive treatment installed in the reclaimed Lorraine mine site, composed of two PBR units and one wood ash (WA) filter (Rakotonimaro et al., 2018). To this end, physicochemical characterization, geochemical equilibrium calculation, and pH-dependent leaching test (pH_{stat}), proposed by the US environmental regulations, have been investigated. Geochemical equilibrium modelling is commonly used to better understand the geochemical behaviour of tailings. In this study, thermodynamic geochemical equilibrium was used to determine the secondary mineral phases that were likely to precipitate during the treatment. In addition, the pH_{stat} was used to assess the potential release of contaminants under different pH to simulate various conditions of possible co-disposal of residues with waste (e.g., alkaline waste, mine waste, treatment sludge, incineration residues, sediments, cement and

concretes waste, etc.). At the same time, this test provides an estimation of the environmental availability of contaminants while comparing their concentrations to the threshold limits.

Materials and methods

Field study site

A tri-step field-pilot PTS was installed in 2011 on the reclaimed Lorraine mine site, located near the village of Latulipe in the region of Témiscamingue, Quebec, Canada (Figure 1a).

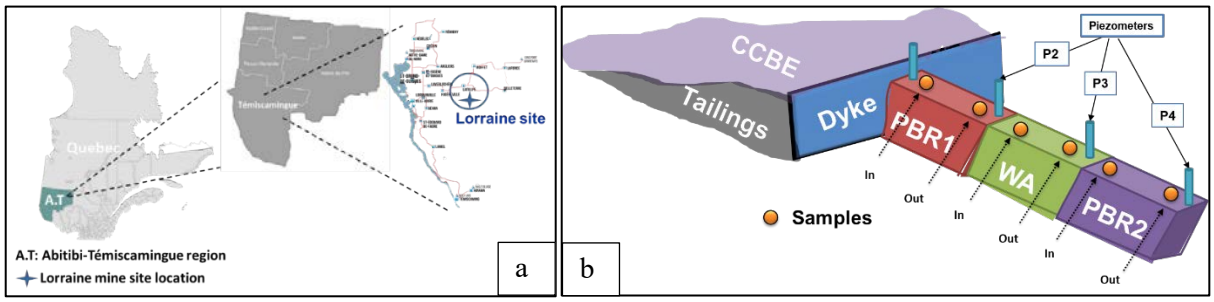

Figure 1: a) Location of the Lorraine mine site; b) Model of the tri-step treatment system

The mine operated from 1964 to 1968, extracting Cu, Ni, Au, and Ag. This produced about 600,000 t of acid-generating tailings, which were left without any reclamation for approximately 30 years in a pond of 15.5 ha and generated Fe-AMD. In 1998, the site was reclaimed with a 1.1 m of a multi-layer cover with capillary barrier effects (CCBE) that prevented oxygen from reaching the tailings and thus limited the production of AMD (Bussière et al., 2004). The CCBE proved effective since during the 19 years after restoration the pore water quality was significantly improved: pH<3, ~11,000 g/L of Fe, 8,100 g/L of sulphates versus pH~5.8 and 1,200 g/L of Fe, 3,636 g/L before and after the installation of the CCBE, respectively. Since Fe-rich interstitial pore water could take a few years before being completely discharged, a PTS consisted of a limestone drain and three anoxic dolomitic drains were installed in 1998 to treat the contaminated pore waters. In 2011, due to clogging problems, one of the dolomitic drains was replaced by a tri-unit treatment system composed of two PBRs separated by a WA filter (Figure 1b). Details concerning the design of this treatment system can be found in Genty et al. (2016) and Rakotonimaro et al. (2018).

The composition of the substrates is presented in Table 1. The first unit PBR1 was used to reduce the redox potential, to neutralize the acidity, and to partially remove metals. The second unit WA was used for Fe treatment. Finally, the last unit PBR2 acted as a polishing unit to remove the residual metals.

Table 1: Composition of the substrates (PBR1, WA, PBR2) used in the tri-step treatment system

Components	Wood chips	Chicken manure	Leaf compost	Sand	Calcite	Wood ash
PBR1(% w/w)	18	10	12	10	50	–
WA(% w/w)	–	–	–	–	–	100
PBR2(% w/w)	36	17	24	21	2	–

Sampling

Post-treatment residues were collected after six years of Fe-AMD treatment. Precisely, six solid samples from the inlet (In) and the outlet (Out) of each unit (PBR1-In, PBR1-Out, WA-In, WA-Out, PBR2-In and PBR2-Out) were collected (Figure 1b). Three water samples (P2, P3, and P4) were also sampled from piezometers installed in the outlet of each treatment unit (Figure 1b). Prior to their analysis, all samples were preserved in sealed containers (for residues) and bottles (for water samples) at T<4°C until analysis.

Physicochemical characterization of water samples and geochemical modelling

Based on ionic strengths and metal concentrations, geochemical modelling was used to predict the secondary mineral phases that are likely to precipitate during Fe-AMD treatment. Prior to the geochemical equilibrium calculations, samples P1, P2, and P3 were characterized for pH, Eh redox potential, electrical conductivity (EC), acidity, alkalinity, and total metal and sulphur concentrations. The elemental composition was analyzed on acidified (2% HNO_3) samples with Inductively Coupled Plasma-Atomic Emission Spectrometry (ICP-AES; relative precision of 5%) using a Perkin Elmer OPTIMA 3100 RL. The model PHREEQC V3 was performed using the aforementioned physicochemical parameters of water samples (P1, P2, and P3) to evaluate the possible mechanism of metal removal depending on ion activities and saturation indices of mineral phases. The WATEQ4F database was used during the PHREEQC geochemical modelling.

Physicochemical characterization of residues

The physicochemical characterization performed on solid samples consisted of determining: paste pH, elemental composition, total carbon (TC), inorganic carbon (IC), organic carbon (OC) total sulphur (TS), and acid volatile sulphide-simultaneously extracted metals (AVS-SEM). Paste pH was determined according to the method described in ASTM 1995 to provide preliminary information about the acid-generation or neutralization potential of residues. The chemical composition was analyzed on dried (60°C) and homogenized samples (150 µm) after their digestion (with HNO_3, Br_2, HCl, and HF). The digestate was analyzed by ICP-AES. The TC and TS were measured by combustion at 1,360°C in an induction furnace coupled to an infrared analyzer (ELTRA CS-2000). The IC was determined on calcined (375°C) solids for 16 h in a muffle furnace (Nabertherm HTCT 01/16) and then combustion in an induction furnace.

The OC was determined by the difference between TC and IC. For AVS-SEM, the AVS was converted into H_2S by hydrochloric acid at room temperature and trapped in an antioxidant buffer (2 M NaOH, 0.1 M ascorbic acid and 0.1 M EDTA; Brouwer and Murphy, 1994). The obtained solution was analyzed for sulphide concentration using a spectrophotometry HACH DR/890 kit and for metals using ICP-AES.

Leaching test

The pH-dependant leaching (pH_{stat}) test was carried out to evaluate the acid-neutralizing capacity (ANC) and the potential mobility of contaminants from solid samples. The test was performed according to the method 1313 (USEPA, 2012), and consisted of mixing the residues with water, diluted acid (HNO_3), or base (NaOH) to obtain leachate pH ranged from 2 to 13. The mixtures were then placed in rotated tumblers (S/L=1/10, speed of 28 ± 2 rpm, for 72 ± 2 hours at room temperature). Later, the pH was measured and the leachate was centrifuged and filtered (0.45 µm). Metal analysis was performed on acidified (2% HNO_3) leachates by ICP-AES. The dissolved organic carbon (DOC) was determined on acidified (1% HCl) leachates at 680°C using an infrared total organic C analyzer (SHIMAZU, Model TOCVcph). Results of metal concentrations were compared to:

1. threshold limits of Quebec's provincial regulation, Directive 019 (D019);
2. Canadian discharge limits as specified in the Metal and Diamond Mining Effluent Regulation (MDMER); and
3. the surface water quality criteria of Quebec province (SWQC) at a water hardness of 91.6 mg/L $CaCO_3$ (corresponding to the surface water hardness in Abitibi-Témiscamingue).

Results

Physicochemical characterization of water samples and geochemical modelling

Results showed that the evolution of pH during the 2-year monitoring period (2015–2017) varied slightly in P3 and P4 (Table 2). However, the pH in P2 decreased moderately from 6.8 to 6.3, but was still higher than the low discharge limit (pH=6) of the D019. Moreover, for all samples, Eh values were negative (–47 mV<) in 2015 whereas they largely increased to higher and positive values (324–344 mV) in 2017 as an indication of the evolution of pore water qualities from anoxic to oxic conditions, maybe because of the deterioration of the treatment system. On the contrary, EC significantly decreased between 2015 and 2017 for all water samples as an indication of the decrease of contaminant concentrations. Up to 63.4% and 57.5 % of acidity decreased in P2 and P4, respectively, whereas it remained similar in P3 (Table 2). Similar trends were observed for the alkalinity, since it largely decreased in P2 (88.0%) and P4 (51.7%), but no significant differences were found in P3 (~300 mg/L $CaCO_3$).

Table 2: Physical parameters (average) of pores water (P2, P3, and P4) between 2015 and 2017

Year	2015			2017		
Piezometers	P2	P3	P4	P2	P3	P4
pH	6.8	6.1	5.9	6.3	6.2	5.8
Eh (mV)	–181	–62	–47	334	324	344
Conductivity (mS/cm)	11.4	6.6	6.7	2.7	2.2	1.9
Acidity (mg/L $CaCO_3$)	1,065	1,210	1,502	390	1149	636
Alkalinity (mg/L $CaCO_3$)	3,800	306	373	455	339	180

Overall, saturation indices (SI; Figure 2) calculated with PHREEQC using water qualities in P2, P3, and P4 in 2015 and 2017 indicated the potential precipitation of metals (e.g., Fe and Al), following the dissolution of neutralizing agents (i.e., calcite) in the substrates, in the form of oxides, hydroxides, oxy-hydroxides, oxy-hydroxy-sulphates, and sulphides. These findings are in agreement with other results previously reported in the literature (Genty et al., 2012b). Likewise, between 2015 and 2017, the SI of oxy-hydroxide minerals tended to increase, whereas those for sulphides minerals tended to decrease, which was in agreement with the Eh increase.

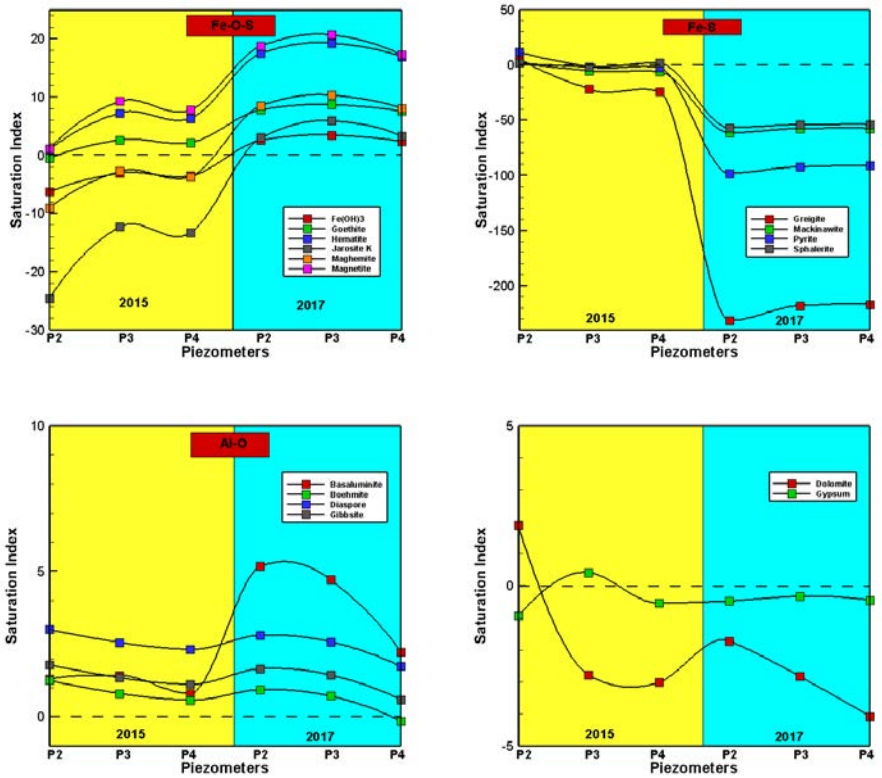

Figure 2: Evolution of saturation index in piezometers between 2015 and 2017

In 2015, Fe-oxy-hydroxide minerals such as magnetite (Fe_3O_4), hematite (α-Fe_2O_3), and goethite (α-FeOOH) were oversaturated (SI >0; Figure 2) in all the units. Moreover, Fe was also precipitated as greigite (Fe_3S_4), pyrite (FeS_2) and mackinawite ($FeS_{(1-x)}$) in the PBR1 unit as an indication of parallel treatment of both Fe and S. The same findings were also reported previously where Fe was found in the form of biogenic Fe-sulphide minerals in reductive media (Kousi et al., 2018). It is noteworthy that both greigite and mackinawite are precursors of the formation of pyrite (Goldhaber, 2003). However, Fe-sulphides were unlikely to precipitate in the WA unit. At the same time, sphalerite (ZnS) was oversaturated in PBR1 and PBR2 units. For Al, gibbsite [$Al(OH)_3$], diaspore (α-AlOOH), boehmite (γ-AlOOH), and basaluminite [$Al_4(OH)_{10}(SO_4)\cdot 4H_2O$)] were likely to precipitate in all units. Notably, precipitation of these Al-bearing minerals has also been reported during AMD treatment (Macías et al., 2012). In addition, S was likely to precipitate in the form of gypsum ($CaSO_4.2H_2O$) in the WA unit. Nonetheless, the SI of gypsum was very close to 0, indicating that its formation and dissolution rates are quasi-similar, suggesting a metastable phase. In addition, results showed that dolomite [($CaMg(CO_3)_2$] could also precipitate in the PBR1 unit. The presence of dolomite has been reported previously since it could precipitate under a high Mg^{+2}/Ca^{+2} ratio and high alkalinity, at a low temperature (25°C), through sulphate reducing bacteria activity (Vasconcelos et al., 1995).

In 2017, in addition to magnetite, hematite, and goethite, K-jarosite [($KFe_3(SO_4)_2(OH)_6$], $Fe(OH)_3$ and maghemite (γ-Fe_2O_3), Fe could precipitate in all units (Figure 2). Oxidation or weathering of magnetite at low temperatures may partially explain these results (McElhinny and McFadden, 2000). In addition, except for bohemite in P4, the same aforementioned Al-bearing minerals were also likely to be found in all the units. On the contrary, Fe-S precipitates were undersaturated (SI <0) in all units. This could probably be explained by the significant increase of Eh that destabilizes the sulphide minerals.

Physicochemical characterization of post-treatment residues

Overall, results showed that paste pH was circumneutral for all residues (Table 3). Indeed, during the treatment, the paste pH slightly decreased for PBR1 and PBR2, whereas it largely dropped in WA residues. A high acidity load in P3 (1,149 mg/L $CaCO_3$; Table 2) could probably explain these results. In addition, TC was high in WA and PBR2 compared to PBR1 residues. Likewise, significant OC was found in WA residues. However, OC decreased in the PBR1 (52.7%) and PBR2 (38.1%) residues, respectively, during the treatment. An advanced degradation of OC could explain these results. Moreover, WA had the highest IC content (~6.5%) among PBR1 and PBR2 residues, respectively. These findings indicated an important residual neutralization capacity of WA residues relative to PBR1 and PBR2 residues. Likewise, the high decrease of IC in PBR1 residues was probably due to the high acidity load of the AMD that directly feed the PBR1 unit. On the contrary, the TS content increased significantly in all the residues during treatment.

A retention of sulphur in all units as predicted by the geochemical modeling (e.g. Fe-sulphides or gypsum) could probably explain these observations. In addition, AVS from PBR1 was up to 12 times and 5 times higher relative to WA and PBR2, respectively. High AVS in PBR1 residues suggests the presence of metastable or acid-volatile Fe-sulphides (i.e., mackinawite and greigite predicted by geochemical equilibrium) that are soluble in HCl (Li and Schoonmaker, 2003). However, AVS/SEM molar ratios were low (<1) in all residues as an indication of the presence of low sulphide-bearing minerals relative to the other forms of metal precipitation (e.g., oxy-hydroxides and carbonates). Therefore, all residues exhibited a high potential mobility of metals.

Table 3: Physicochemical parameters and metal concentrations in the solids from the field tri-step treatment of AMD before and after treatment

	Initial (before treatment)			Final (post-treatment)		
				Physicochemical parameters		
	PBR1	WA	PBR2	PBR1	WA	PBR2
Paste pH	7.8	12.2	6.5	7.2–7.5	6.4–6.8	6.4–6.6
TC (%)	18.7	33.6	28.5	2.0–15.4	28.9–30.4	15.2–19.2
OC (%)	11.0	19.0	26.1	1.3–9.4	22.5–23.9	14.8–17.5
IC (%)	6.7	14.6	2.4	0.7–6.0	6.4–6.5	0.4–1.7
TS (%)	0.05	0.3	0.06	0.3–1.3	2.5–3.8	2.1–5.4
AVS (µmol/kg)	–	–	–	15.8–29.5	1.7–1.8	1.4–7.2
SEM (µmol/kg)	–	–	–	3.8 105 –9.1 105	4.5 105–7.4 105	4.7 105–5.3 105
AVS/SEM	–	–	–	<<1	<<1	<<1
				Metals (g/kg)		
Al	10.1	22.9	11.1	15.5–58.8	13.3–24.0	24.5–39.8
Ca	220.0	123.0	15.9	30.0–194.6	26.2–72.3	15.8–56.2
Fe	7.8	14.7	6.6	25.3–29.6	65.0–87.9	40.0–100.3
Mn	0.2	2.3	0.2	0.3–0.4	0.7–1.0	0.2–0.5
Ni	<DL	0.02	<DL	<DL	0.02–0.2	<DL
Zn	0.07	1.2	0.04	<DL	0.2–0.3	0.06–0.2

* DL: detection limit

Due to the increase of pH (3 vs 5.8) during Fe-AMD treatment, significant metal concentrations were found in all residues compared to their initial content (Table 3). High retention of Fe was also found in all residues. Indeed, an increase of ~90.6%, 80.8%, and 71.6% of Fe was found in PBR2, WA, and PBR1 compared to their initial concentrations, respectively. This was consistent with geochemical modelling, where Fe was precipitated in several forms. Likewise, up to 72.8% and 68.6% of Al was found in PBR1 and PBR2, respectively. The retention of Al is mainly due to the precipitation of amorphous Al-hydroxides at a pH greater than 5 (Vadapalli et al., 2008). Moreover, Ca concentrations largely decreased in PBR1 (~49%) and WA (56%) residues, respectively, as an indication of carbonates consumption (e.g. calcite) while neutralizing AMD acidity. However, an increase of ~126.4% of Ca was found estimated in PBR2; the transfer of Ca (after dissolution) from PBR1 and WA units and subsequent precipitation of Ca-bearing secondary minerals in PBR2 unit might partially explain these results.

Moreover, the Mn concentration decreased in WA (63%), whereas it increased in PBR1 (42.8%) and PBR2 (75%) residues, respectively. In addition, Ni was only found in WA residues. Furthermore, an increase of ~69% of Zn was found in PBR2. The presence of ZnS as predicted by the geochemical calculation could partially explain these findings, since it was previously found during AMD passive treatment (Kousi et al., 2018). The absence of Zn in the post-treatment PBR1 could probably be explained by its leaching during the treatment.

Assessment of the metal release potential from residues

To better understand the potential mobility of metals from residues, the ANC is a key property to be considered. Overall, the natural pH values (at 0 meq/g dry solid; Figure 3) were circumneutral to slightly basic for all residues. Indeed, results showed that, at pH=2, residues from PBR1-Out and WA-In had the highest ANC and could therefore resist against acid aggression (PBR1-Out> WA-In> WA-Out> PBR2-In> PBR2-Our> PBR1-In; Figure 3). These results confirm the chemical composition where IC content were high in WA residues (~6.5 %).

The solubility trends of all elements as a function of pH were similar for all residues. Indeed, the leaching of metals (As, Al, Fe, Mn, Ni, and Zn) increased significantly when the pH decreased below 7.0 or increased above 9.0. This shows the amphoteric characteristics (or V shape) of these metals since they exhibit high solubility at low and high pH. Non-negligible concentrations of these metals were also found in the alkaline pH-range.

In general, low dissolution of all elements was found at pH 7–8 (Figure 3). Regardless of the pH, Cd, Cr, Cu, and Pb concentrations (not presented) were below detection limits.

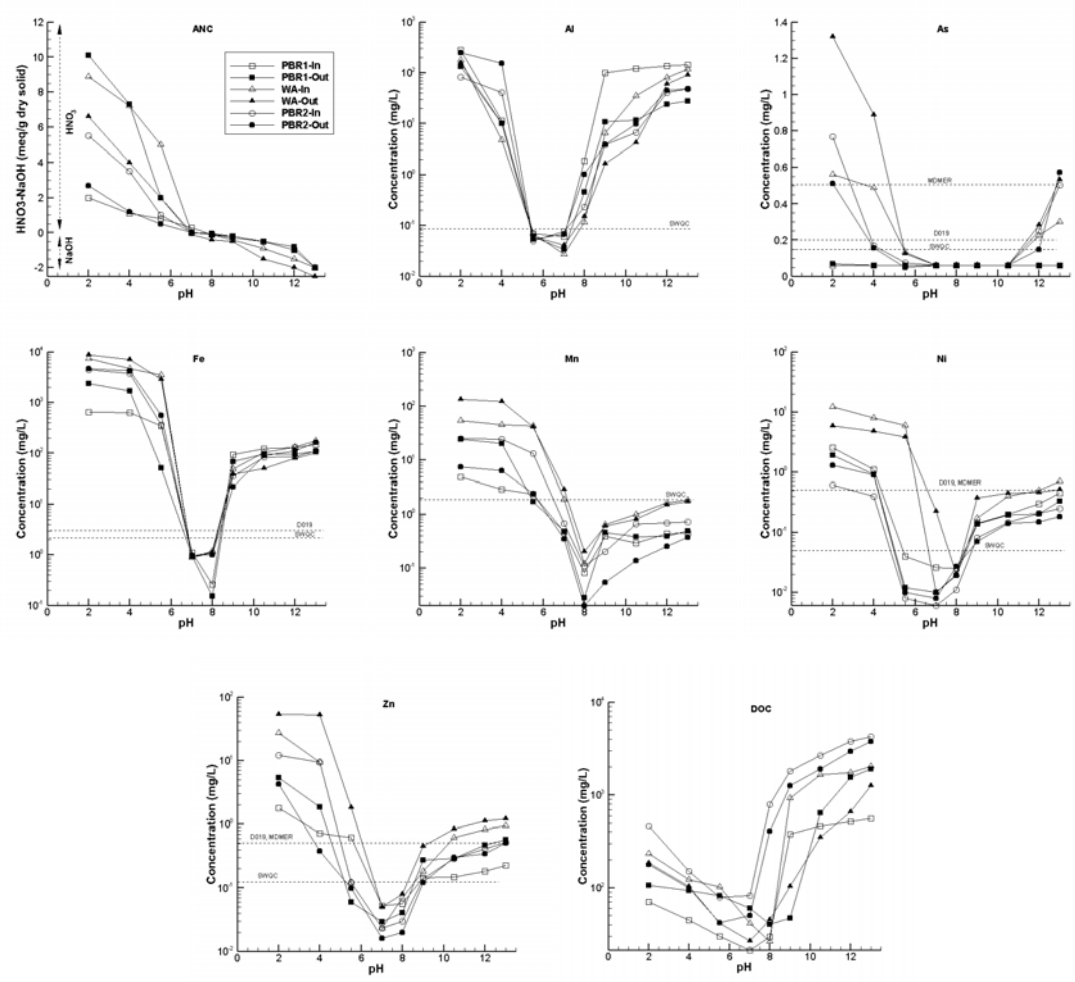

Figure 3: Buffering capacity and leaching of elements (Al, As, Fe, Mn, Ni, and Zn,) and DOC from PBR1-In, PBR1-Out, WA-In, WA-Out, PBR2-In and PBR2-Out residues as a function of pH

High Al concentrations occurred at pH<5.5 and pH>7.5, which exceeded the SWQC (0.087 mg/L) in leachates from all residues. The dissolution of poor crystalline Al-bearing minerals such as basaluminite at pH ~5.0 could probably explain this behaviour (Caraballo et al., 2010). In addition, Fe concentrations in the leachate from WA-In and WA-Out were higher comparing to other residues as the WA unit was used for Fe-treatment. At the same time, significant Fe concentrations from all residues were found at pH<6.5 and pH>8.5, which exceeded the D019 and SWQC limits. The high Fe leaching is probably due to the redissolution of poorly crystallized Fe-oxyhydroxides (Theng and Yuan, 2008) or desorption of Fe from organic matter and wood ash (Genty et al., 2012b). Moreover, regardless of the pH, As was weakly leached (<0.1 mg/L) from PBR1 (In and Out). Simultaneously, As concentrations from WA and PBR2 were low (0.15 mg/L) for pH 4.0–12.0. However, outside this pH range, significant As leaching was observed, especially from WA-Out (~1.3 mg/L> D019, MDMER and SWQC limits). The dissolution of poorly crystallized secondary Fe-oxy-hydroxide minerals, where As can co-precipitate and/or be absorbed, could

probably explain these findings (Gimenez et al., 2007). For Mn, it was lowly leached from all residues for pH>7.5 and respected the threshold limit (SWQC). Nonetheless, at lower pH, high Mn was found for all residues (especially WA-Out). Furthermore, significant Zn concentration (>D019 and MDMER limits) were leached from all residues at pH<4 and pH>9.5. In addition, taking into account the threshold limit of SWQC (0.11 mg/L), the stability range of Zn considerably decreased (pH 7.0–8.5). Likewise, the Ni concentration was stable (<0.5 mg/L; D019 and MDMER limits) for all residues at a wide range of pH (4.5–12.0) whereas, given the SWQC limits, the stability zone became narrower (pH 6.5–8.0). The significant Ni and Zn concentrations at near neutral pH from WA residues are explained by their high solubility at circumneutral pH (Stumm and Morgan, 1996). Besides, the DOC solubility had the same trends as metals, but greatly increased in the alkaline zone. Indeed, for high pH (pH>8.0), residues of PBR2 (In and Out) had the highest DOC concentrations (~5,000 mg/L). Organic carbon can bind metals and potentially increase their mobility. The dissolution of organic complexes could therefore influence the sorption and the release of metals (Bleam, 2017). Consequently, significant DOC concentration in an alkaline range could also control the high release of metals (e.g. Cu, Ni, Zn and Fe).

Preliminary classification of residues

Based on D019 and MDMER limits, except for Fe, metal concentrations in the leachates from residues of PBR1 and PBR2 units were low for a pH range of 4.5–12.0. However, considering the SWQC limits, the leaching of metals from these residues are stable only at a pH around 5.5–9.0. At the same time, if Fe is considered, the stability zone becomes narrower (pH 6.5–8.5 only). Moreover, for WA residues, because of their high metal content, their stability zone is limited for pH 7–8 only. Overall, for all residues, contact with rainwater (pH~5.5) is not recommended. Additionally, all residues could not be stored or co-disposed with municipal wastes (pH~5), acidic wastes (acidic soils and motor oil sludge), or alkaline wastes (concretes, red muds, flue gas desulphurization wastes, steelworks slags, coal combustion ashes, chromite ore processing residues, etc.). Therefore, to control the potential mobility of contaminants from all residues, their disposal in neutral to slightly basic pH is recommended. Outside that neutral pH range (~7–8), contaminants from all residues could be potentially mobilized towards regulation limits. However, since condition changes like absorption of carbon dioxide, contact with acid rain and alkali soil could happen in ordinary landfill (e.g., dumps), a pre-treatment is still mandatory before disposing of these residues.

Conclusion

The present study evaluated the leaching potential of contaminants from residues of a field tri-step PTS for Fe-AMD. The results showed that significant metal concentrations were present in all residues, especially in the Fe-treatment unit (WA). All residues were characterized by a residual neutralizing potential. The

results of the geochemical equilibrium also showed that Fe, the contaminant with the highest concentrations, is likely to precipitate in the form of oxides, hydroxides, oxy-hydroxides, hydroxysulphates, and/or sulphides. High ANC was found for residues from the WA unit. The results of the pH_{stat} test suggested that all solids should be stored in a neutral to slightly basic pH (7–8) environment in order to prevent metal release. Otherwise, a pre-treatment before disposal in landfill sites is deemed necessary to comply with the legal limits.

Mineralogical characterization is ongoing for a better understanding of metal removal mechanisms. Kinetic tests should be undertaken to assess the long-term stability of contaminants under weathering conditions for a better classification of residues and to anticipate their fate.

Acknowledgements

This study was funded by the NSERC (Natural Sciences and Engineering Research Council of Canada), Canada Research Chairs Program, Fonds de Recherche du Québec – Nature et Technologies (FRQNT, Québec's Research Funds – Nature and Technologies) and the industrial partners of RIME UQAT-Polytechnique Montreal.

References

American Society for Testing and Materials (ASTM). 1995. Standard test method for pH of soils. In *Annual Book of ASTM Standards D4972-95a,* Washington, DC, USA.

Bleam, William. 2017. Chapter 7 – Natural organic matter. In *Soil and Environmental Chemistry* (second edition), edited by Academic Press: 333–384.

Brouwer, H. and T.P. Murphy. 1994. Diffusion method for the determination of acid-volatile sulfides (AVS) in sediment. *Environ Toxicol Chem*. 13: 1273–1275.

Bussière, B., M. Benzaazoua, M. Aubertin and M. Mbonimpa. 2004. A laboratory study of covers made of low-sulphide tailings to prevent acid mine drainage. *Environ Geol*. 45(5): 609–622.

Caraballo, M.A., T.S. Rötting and S. Verónica. 2010. Implementation of an MgO-based metal removal step in the passive treatment system of Shilbottle, UK: Column experiments. *J Hazard Mater.* 181: 923–930.

Genty, T., C.M. Neculita, B. Bussière and G.J. Zagury. 2012a. Environmental behaviour of sulphate-reducing passive bioreactor mixture. *Proceedings of the 9th International Conference on Acid Rock Drainage,* Ottawa, Ontario, Canada, May 20–26.

Genty, T., B. Bussière, M. Benzaazoua and G.J. Zagury. 2012b. Capacity of wood ash filters to remove iron from acid mine drainage: Assessment of retention mechanism. *Mine Water Environ.* 31: 273–286.

Genty, T., B. Bussière, J. Dionne and C.M. Neculita. 2016. Passive biochemical treatment of ferriferous mine drainage: Lorraine mine site, Northern Quebec, Canada. *Proceedings of the International Mine Water Association,* Leipzig, Germany, July 11–15.

Gimenez, J., M. Martinez, J. Pablo, M. Rovira and L. Duro. 2007. Arsenic sorption onto natural hematite, magnetite, and goethite. *J Hazard Mater.* 141(3): 575–580.

Goldhaber, Martin B. 2003. Sulfur-rich sediments. In *Treatise on Geochemistry,* Volume 7, edited by Fred T. Mackenzie, Elsevier: 257–288.

Jouini, M., T.V. Rakotonimaro, C.M. Neculita, T. Genty and M. Benzaazoua. 2019. Stability of metal-rich residues from laboratory multi-step treatment system for ferriferous acid mine drainage. *Environ Sci Pollut Res*. Retrieved from https://doi.org/10.1007/s11356-019-04608-1

Kousi, P., E. Remoundaki, A. Hatzikioseyian, V. Korkovelou and M. Tsezos. 2018. Fractionation and leachability of Fe, Zn, Cu and Ni in the sludge from a sulphate-reducing bioreactor treating metal-bearing wastewater. *Environ Sci Pollut Res.* 25(36): 35883–35894.

Li, Y.H. and J.E. Schoonmaker. 2003. Chemical composition and mineralogy of marine sediments. In *Treatise on Geochemistry,* Volume 7, edited by Fred T. Mackenzie, Elsevier: 1–35.

Macías, F., M.A. Caraballo and J.M. Nieto. 2012. Environmental assessment and management of metal-rich wastes generated in acid mine drainage passive remediation systems. *J Hazard Mater.* 229–230: 107–114.

McElhinny, M.W. and P.L. McFadden. 2000. Chapter Two – Rock magnetism. In *Paleomagnetism: Continents and Oceans,* edited by Michael W. McElhinny and Phillip L. McFadden, International Geophysics, Academic Press, 73: 31–77.

Rakotonimaro TV, Neculita CM, Bussière B, Genty T, Zagury GJ, 2018. Performance assessment of laboratory and field-scale multi-step passive treatment of iron-rich acid mine drainage for design improvement. Environ Sci Pollut Res. 25(18):17575–17589.

Simonton, S., B. Thomson, L. Barton and M. Dimsha. 2000. Long-term stability of metals immobilized by in-situ bioremediation processes. *Proceedings of the Conference on Hazardous Waste Research,* Denver, Colorado, USA, May 23–25.

Skousen, J., C.E. Zipper, A. Rose, P.F. Ziemkiewicz, R. Nairn, L.M. Mcdonald and R.L. Kleinmann. 2017. Review of passive systems for acid mine drainage treatment. *Mine Water Environ.* 36(1): 133–153.

Stumm, W. and J.J. Morgan. 1996. *Aquatic Chemistry, Chemical Equilibria and Rates in Natural Waters* (third ed.), John Wiley & Sons, Inc, New York, USA.

Theng, B.K.G. and G.D. Yuan. 2008. Nanoparticles in the soil environment. *Elements* 4: 395–399.

US Environmental Protection Agency (USEPA). 2012. Method 1313: Liquid-solid partitioning as a function of extract pH using a parallel batch extraction procedure. Retrieved from https://www.epa.gov/sites/production/files/2015-12/documents/1313.pdf (last accessed 12.07.2019).

Vadapalli, K., M/ Klink, O. Etchebers, L. Petrik, W. Gitari, R. White, D. Key Dand E. Iwuoha. 2008. Neutralization of acid mine drainage using fly ash, and strength development of the resulting solid residues. *South African J Sei.* 104: 317–322.

Vasconcelos, C., J.A. McKenzie, S. Bernasconi, D. Grujic and A.J. Tiens. 1995. Microbial mediation as a possible mechanism for natural dolomite formation at low temperatures. *Nature* 377: 220–222.

Proceedings of Tailings and Mine Waste 2019
November 17–20, 2019, Vancouver, Canada
Published by the University of British Columbia, 2019

Impact of Climate Change on Surface Water Management at Tailings Storage Facilities

Pier-Luc Labonté-Raymond, Polytechnique Montreal, RIME, Canada
Thomas Pabst, Polytechnique Montreal, RIME, Canada
Bruno Bussière, UQAT, RIME, Canada
Émilie Bresson, UQAT, RIME, Canada

Abstract

Climate projections predict a significant increase in the intensity and frequency of extreme precipitation in Quebec, Canada, by the end of the current century, and especially in the Abitibi region, an important mining region. The most recent projections indicate an average rise in the intensity of the summer Probable Maximum Precipitation (PMP) from 10 to 16% by 2100 in this region. Greater PMP could pose major challenges for surface water management at tailings storage facilities. A significant rise of the PMP could affect the performance and integrity of mining infrastructure (berms, dams, spillways), and increase the risk of dike overtopping, which is a common mechanism for dike failure in the mining industry. Proper management of surface water is also necessary to limit the risks of uncontrolled discharge of contaminated water in the environment. The increase of the frequency and amplitude of extreme events should therefore be considered in the design to improve the long-term performance of mining infrastructure, so that it is more resilient to the future climate.

Precipitation and runoff data were collected at the Canadian Malartic Mine during the summer and fall of 2018 to characterize the rainfall-runoff characteristics of two watersheds in the tailings storage facility. Measurements were used to quantify the effect of temporal rainfall distribution, soil/tailings initial state, and catchment geometry on runoff. These results were then used to calibrate an integrated water flow model developed with Mike Hydro River (DHI) that simulates runoff, routing, and storage of surface water. The model was extrapolated using the most recent climate projections from Regional Climate Models, adapted for the site-specific conditions. This paper presents the methodological approach used in this project and the main field and simulation results. Practical recommendations are proposed to improve the integration of climate change into the design of surface water management infrastructure.

Introduction

Dam failures in mining operations occur about 10 times more often than for civil engineering applications (Davies et al., 2000). Tailings dam failures are often caused by intense precipitation events, as well as inadequate surface water management in tailings storage facilities (Lucas, 2001; Van Niekerk and Viljoen, 2005; Sammarco, 2004). A review of 221 incidents around the world carried out by ICOLD (2001) confirmed that overtopping was associated with the majority of tailings dam failures. Unusual rainfall events were responsible for about 25% of tailings dam ruptures around the world (Rico et al., 2008). Also, 90 % of tailings dam failures in Europe occurred during exploitation (Rico et al., 2008).

In accordance with the current regulations in Quebec (MDDEP 2012), mining companies have to design emergency weirs for retention structures based on the probable maximum flood (PMF). The PMF represents the largest flood theoretically possible for a watershed at any time of the year. It considers the worst combination of flood factors regarding maximum precipitation, initial soil state, and snowmelt (WMO, 2009). Probable Maximum Precipitation (PMP) must be used to calculate PMF. PMP is the maximum expected precipitation for a given duration, over a specific area of a given size and time of year (WMO, 2009). It can be calculated for small watersheds (<1,000 km^2) with a statistical approach using the Hershfield method (Hershfield, 1965). The generalized estimation method is another approach to calculate PMP. It is based on the principle of moisture maximization of high-efficiency storms, which determines the maximum rainfall that a storm could generate if all the moisture contained in the atmospheric column above a given area was to precipitate (Clavet-Gaumont et al., 2017).

PMP are directly affected by climate change. Global warming, and in particular the increase of ocean temperatures, contribute to accelerating and intensifying the water cycle (Kunkel et al., 2013; Huntington, 2006). The intensity and frequency of extreme precipitation events (including PMP) in the mid-latitudes is therefore expected to increase (IPCC, 2013). However, the changes in rainfall patterns are not homogeneous and show significant regional variations (IPCC, 2013).

In Quebec, it has been mandatory to take climate change into account in all construction projects since 2017 (Assemblée Nationale, 2017). However, the provincial regulations do not prescribe nor suggest any correction factor or methodological approach. In Europe, the European Commission (2007) adopted the 2007/60/EC Flood Directive in 2007 that also mandates consideration of climate change in construction projects, but does not propose a specific methodology to include climate change in the design of the infrastructure either. A few European countries have therefore set specific national correction factors for maximizing project floods, depending on the locality, the estimated return period, the season, and the size of the watersheds (Madsen et al., 2014). In practice, the integration of climate change into construction projects, and especially into mining operations, differs significantly from one project to another, even locally, and is not always based on a scientific methodology.

In this paper, a new approach is proposed to evaluate the effect of climate change on surface water management at tailings storage facilities. The climate scenarios for the investigated site, based on the available climate projections, are applied to a rainfall-runoff model calibrated on field monitoring. This article first describes the methodology used in this study, followed by an illustration of the methodological approach applied to the tailings storage facilities of the Canadian Malartic Mine, located in the mining region of Abitibi in the province of Quebec, Canada.

Methodology

Climate data

The methodology used in this paper consisted in using a set of climate models that combine simulations from different research centres (e.g., Beijing Normal University, Institute of Numerical Mathematics, Institut Pierre-Simon Laplace) to minimize the errors (Bresson et al., 2018). This method includes the most recent climate simulations in design, but it comes with a longer calculation cost, and it needs extensive field measurements for post treatment, since the output data of the climate models has to be debiased. Debiasing is necessary because local characteristics, such as the topography, the presence of a vast body of water or the vegetation cover, can have a significant impact on the climate (Dimri, 2009; Ma et al., 2008). Local climate data are therefore collected for a long time series and compared to simulated climate for the same period. The simulated climate is then corrected using a transfer function to represent this reference period. The transfer function is finally applied on projected climate simulations to correct the model bias (Charron, 2016). This method implicitly assumes, however, that the impacts of climate change observed globally will have a similar impact on the local climate of the studied site (ARCC, 2014).

A higher temporal definition of precipitation events was required to accurately simulate surface water behaviour since the temporal distribution of precipitation can have a significant impact on the observed maximum flood (Mácá and Torfs, 2009). Averaged daily precipitation data tend to minimize simulated discharge peaks (Bezak et al., 2018; Alfieri et al., 2008), while the largest runoffs on small watersheds are usually caused by brief, intense rain events (SCS, 1986). In this project, the Type II 24-hour synthetic rainfall distribution developed by the Natural Resources Conservation Service was used to distribute daily average data from climate models (NRCS, 2007).

Surface runoff

Rainfall-runoff models are commonly used to evaluate flood risks (Wheater et al., 2005; Brocca et al., 2011). Intensive field studies are usually required to accurately determine rainfall-runoff curves, even though empirical calculations can also be used to calculate expected peak flows (Dunne, 1983). Rainfall-runoff are also sensitive to rainfall input and therefore there is a need to ensure a representative model on

site measurements (Andréassian et al., 2001). Detailed models of each watershed are generally carried out, calibrated, and validated using field data to increase the precision of the predictions (Refsgaard, 1997). Once the model has been validated, the flow model can be extrapolated to simulate runoff for other rainfall events or longer time series.

Case study: Canadian Malartic mine site

Site description

The methodology proposed here was applied to the tailings storage facilities at Canadian Malartic Mine site, located in Western Quebec. This open-pit mine has been exploiting a gold deposit since 2011 and processes over 50,000 tons of ore daily. Over 40 Mt of waste rock and 20 Mt of tailings are produced annually (WSP, 2015). Water is collected on site through an extensive surface water collection system consisting of collecting ditches and basins of various sizes (Figure 1). The climate in this area is characterized by a cold temperate continental climate (MRNF, 2006). Summers are generally short and dry, while winters are long, cold and dry (MRNF, 2006). The average annual rainfall is 914 mm (Meteorological Services of Canada, 1971–2000). The Intensity-Duration-Frequency curves from the Val-d'Or Airport meteorological station estimate a 1:100-year recurrence rainfall around 75.2 mm. The most rain measured in one day since the installation of this station (in 1951) and before the present study was 68 mm (July 23, 1999, Meteorological Services of Canada, 1951–2019). The meteorological data used for water infrastructure design and bias correction in this project were obtained from the Environment Canada meteorological station installed at Val-d'Or Airport (VAL D'OR A, EC ID 7098600, coordinates 48°03'N, 77°47'W), about 23 km east of the mine.

Instrumentation

A meteorological station installed at the Canadian Malartic Mine, on top of the waste rock pile, was used to collect rainfall data directly on site. The rain gauge was exposed to winds, which could limit the accuracy of measurements. The station was equipped with a S-RGB-M002 rain gauge (ONSET) with an accuracy of +/– 1 % at up to 20 mm/h and which was calibrated on 2018, July 10, which is at the beginning of this study.

Two measuring stations were installed in ditches connected to different watersheds (Figure 1). Each station was instrumented with three Van Essen pressure sensors (DI261, DI501 and DI801, manufacturer) measuring the water head with an accuracy of +/– 0.5 cm. Two probes were placed along the stream to measure the hydraulic head at 8.3 m (north measuring station) and 5.1 m (south measuring station) interval every 15 minutes. A third probe was left in the open to measure atmospheric pressure and correct hydraulic head measurements (MEQ, 1999). Manual measurements were compared to pressure sensor measurements

for validation. The location of the two stations is shown in Figure 1. The measuring stations were installed on 2018, June 20th and removed on 2018, October 31st (total monitoring time of 133 days). The cross-sections of the ditches where the sensors were located were surveyed.

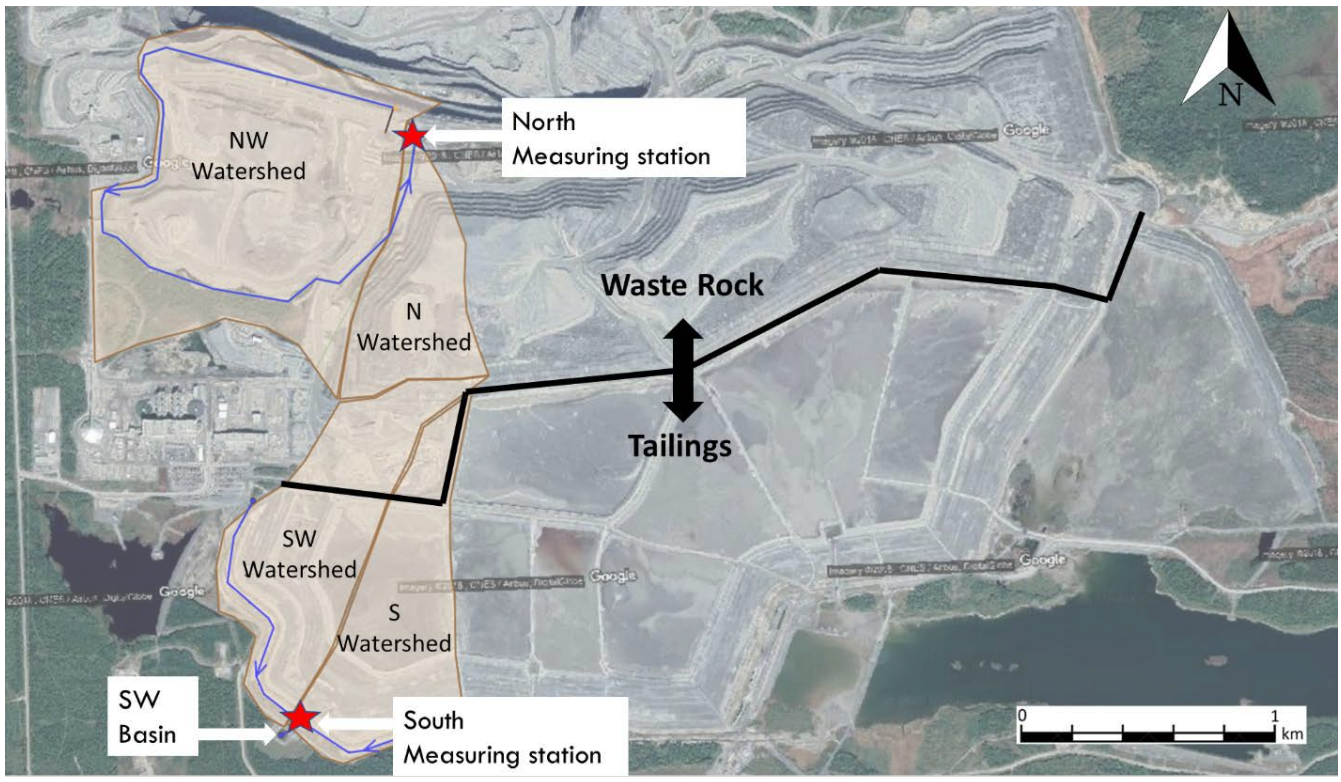

Figure 1: Waste rock pile and tailings storage facility at Canadian Malartic Mine with the location of the measuring stations. Watersheds are also shown

Numerical simulations

Surface flow at the Canadian Malartic mine site during summer 2018 was simulated using Mike Hydro River software (formerly MIKE 11), using the NAM rainfall-runoff model. The code is commonly used in climate change studies, in particular to assess the impact of climate change on expected flows in surface drainage system (Andersen et al., 2006) or flood risk analysis (Dinh et al., 2012).

The simulated area consisted of two sectors (north and south), with a measuring station at each outlet (Figure 1). The flow downstream of the south measuring station was directed to a pumping basin (SW Basin). The flow downstream of the north measuring station was a collector ditch. The north sector was divided in two watersheds of different topography: N watershed was steep and NW watershed was relatively flat. The south sector was also divided into two watersheds (SW and S; Figure 1). Cross-sections of ditches were available in a design report provided by the mine. The pumping station installed in the SW Basin was

also integrated in the model, using the manufacturer's pumping capacities and the mine's operation level to create an automated pumping station calibrated to represent the actual pumping observed during the instrumentation period.

The first calibration step was to analyze the main precipitation events individually to evaluate the time constant for routing (time between the peak rainfall and peak runoff). Subsequently, the runoff coefficient, interflow and baseflow calculation parameters were adjusted to represent the average water head in a realistic way. The calibration objective was, however, to simulate precisely the discharge peaks, which was the critical parameter for the dimensioning of ditches, basins and spillways. The calibration was carried out iteratively and the accuracy of the model was assessed by calculating the mean absolute error (MAE; Willmott and Matsuura, 2005).

$$MAE = [n^{-1} \sum_1^n |e_i|]$$

With n the number of observations and e the model error (e = predicted-observed). A MAE inferior to 15% of the observed difference in water levels between the peak and the initial level before the flood (Δh) was judged acceptable for peak water levels.

Results

Measured rainfall and runoff

The rainfall events that occurred during the 2018 summer were exceptionally high. Two recorded rainfall events were greater than a 5-year return period rainfall (i.e., >50.2 mm). Also, the 74.6 mm precipitation that was recorded over 9 hours on September 5th was the largest daily rainfall ever recorded at that station, and almost corresponds to a 100-year return period for a 24-h rainfall (75.2 mm; Meteorological Services of Canada, 1951–2019). The July 23rd and September 5th events were characterized by a few intense hourly rainfall rates interrupted by periods with little or no rain (Figure 2), while the September 1st and October 10th events were more evenly distributed in time and intensity, with the latter precipitating a total of 40.2 mm over 31 hours, never exceeding 4.4 mm/h (Table 1).

The water level, in metres above sea level (masl) measured in the ditches, rose rapidly following the larger precipitation events (>20 mm/d; Figure 3), while smaller events had a more limited impact (only a few cm for both stations; Figures 3 and 4). The decrease of water head was, however, significantly slower and lasted up to a few days at the north measuring station, while it was very fast (less than one day) for the south measuring station.

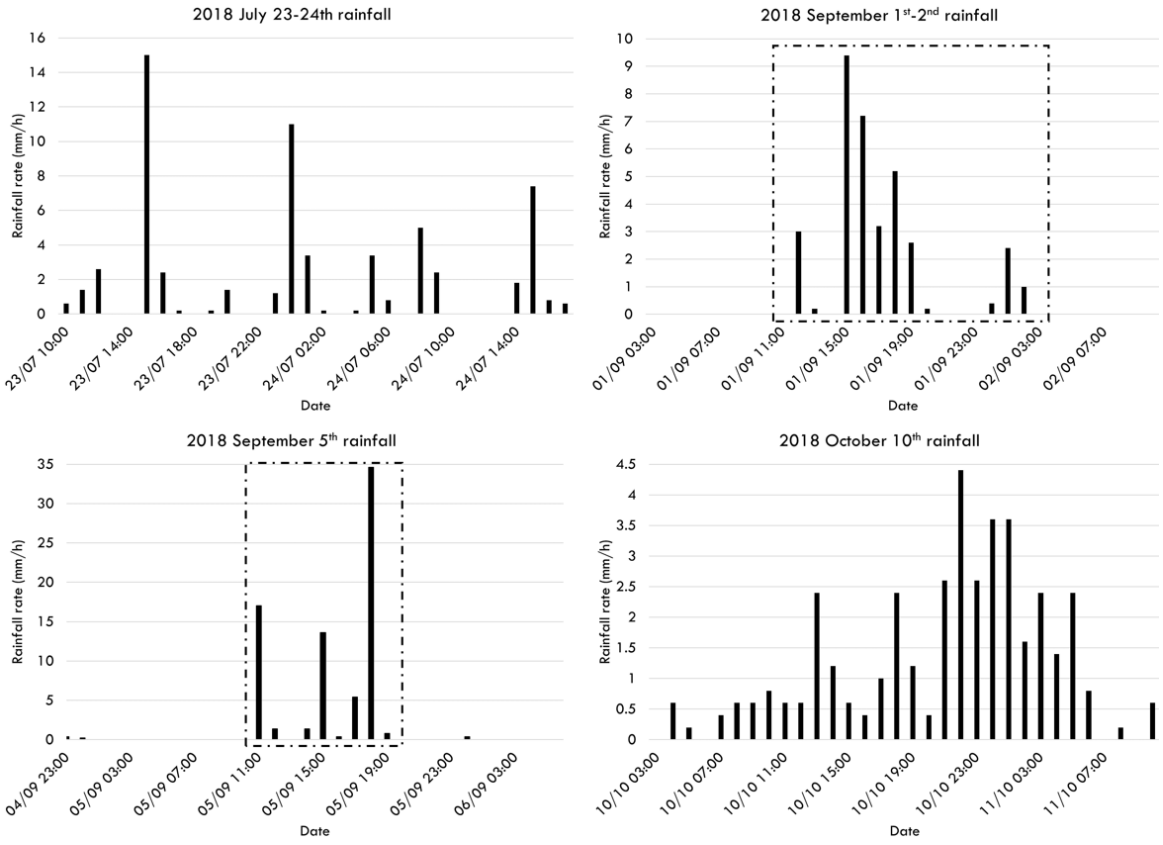

Figure 2: Time distribution of 4 major rainfall events measured during summer 2018 at the Canadian Malartic Mine. The horizontal scale is the same for all four rainfall events (33 hours)

Table 1: Major rainfall event measured during summer 2018 at the Canadian Malartic Mine characteristics

Rainfall event	Duration (h)	Total rainfall (mm)	Peak rainfall rate (mm/h)
2018 July 23	33	62.0	15.0
2018 September 1	15	34.8	9.4
2018 September 5	9	74.6	34.6
2018 October 10	31	40.2	4.4

Model calibration

Model parameters were calibrated iteratively to simulate as precisely as possible the field measurements (Table 2). The watersheds represented in this model had variable geometries and materials. The North sector was mostly composed of waste rock while the South sector was mostly made of tailings and dikes. Therefore, the watersheds had different runoff distributions with various storage, runoff and initial conditions (Table 2). The maximum water content parameter mainly controlled the initial infiltration as

well as the evaporation capacity. The storage in the root zone was reduced to a minimum (1 mm) in this case, because the study site was almost entirely free of vegetative cover. The overland flow runoff coefficient corresponded to the fraction of water directly flowing over the surface. Its value for the North region (0.62) was more than twice the value for the South region (0.27). The time constant for routing interflow determined the amount of interflow. A smaller value resulted in a greater contribution of interflow, as observed in the North sector (200 h) compared to the South sector (300 h). The time constant for routing overland flow indicated the time required for the water to flow overland to the outlet. A steep slope and a small catchment basin generally caused a lower value, such as for the South sector (2 h) in comparison to the NW (17 h) and the N (4 h) watershed

The simulated baseflow was well represented throughout the monitoring season, and the peaks of discharge simulated for the four main rainfall events were similar to those measured (Figures 3 and 4). Smaller simulated rain events (<20 mm/d) usually resulted in larger discharge peaks than observed. The event of October 10th was also excluded from the calibration process for the South measuring station since the observed water level rise was low compared to the North measuring station and other smaller rainfall events, and was considered not representative. The MAE at the two stations were 5 cm (North) and 4 cm (South), which represents 14% of relative error according to the mean observed Δh at the North measuring station and 4% at the South measuring station.

Parameter	NW watershed	N watershed	SW watershed	S watershed
Area (km^2)	2.66	0.64	0.815	0.541
Storage				
Maximum water content in surface storage (mm)	30	30	25	25
Maximum water content in root zone (mm)	1	1	1	1
Runoff				
Overland flow runoff coefficient	0.62	0.62	0.27	0.27
Time constant for routing interflow (h)	200	200	300	300
Time constant for routing overland flow (h)	17	4	2	2
Initial conditions				
Baseflow discharge (m^3/s)	0.015	0.005	0.01	0.01
Interflow discharge (m^3/s)	0.05	0.015	0.015	0.01

Table 1: Watershed properties used in the NAM rainfall-runoff model

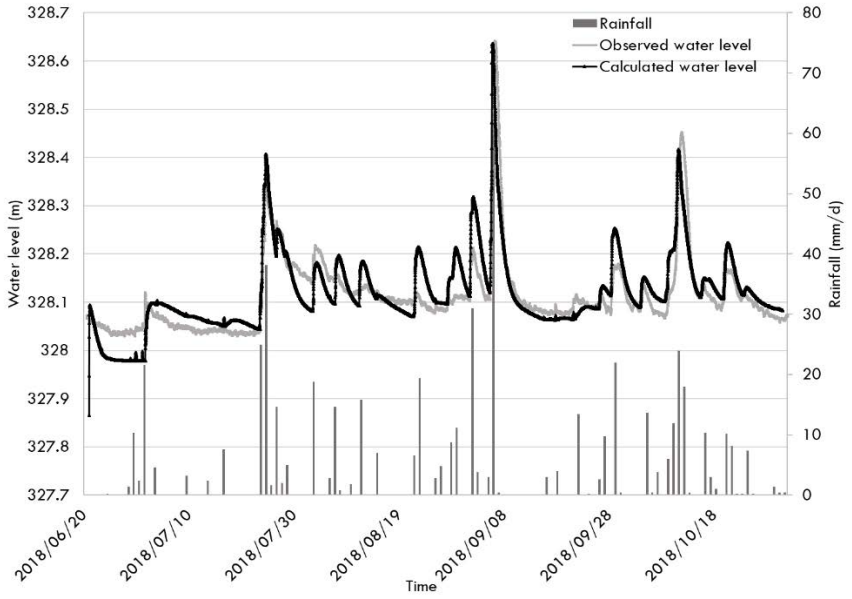

Figure 3: Observed (grey line) and simulated (black line) water levels (in masl) at North measuring station. Rainfall is also shown

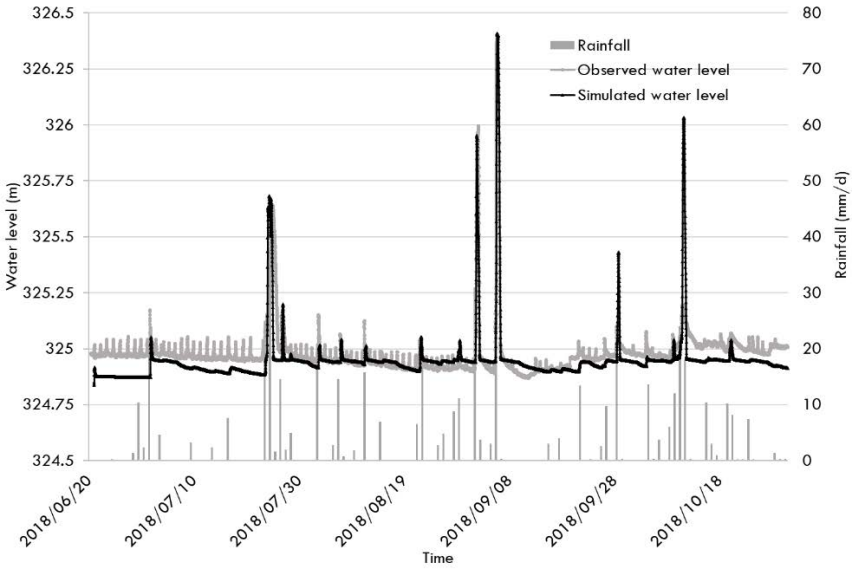

Figure 4: Observed (grey line) and simulated (black line) water levels (in masl) at South measuring station. Rainfall is also shown

PMP simulations

The calibrated model was then extrapolated to evaluate the consequence of a PMP. The runoff following the current PMP (1971–2000 reference period), was compared to the consequences of projected PMP for the 2041–2070 and 2071–2100 climates. PMP were calculated using the generalized estimation method and

were the mean values of 18 different climate simulations. The total 24-hour PMP were 120 mm (1971–2000), 150 mm (2041–2070) and 158 mm (2071–2100) for the three time periods considered. The PMP were then distributed according to a SCS type II rain (Figure 5), as generally recommended for Quebec (Rivard, 2011). PMP were then simulated to determine the maximum flow and water level in the surface ditch at North measuring station for each of the scenarios (Figure 6).

The total rainfall for the 2041–2070 and 2071–2100 PMP are expected to rise by 25 and 32 % compared to the 1971–2000 reference period at this site. The calculated peak discharge of the PMP for the 1971–2000 reference period is 2.82 m^3/s, 3.59 m^3/s for 2041–2070 (27% rise) and 3.89 m^3/s for 2071–2100 (38% rise) at the North measuring station (Figure 6).

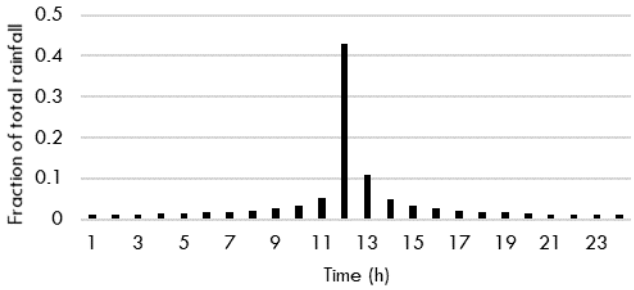

Figure 5: SCS Type II rainfall distribution of PMP simulated in this study

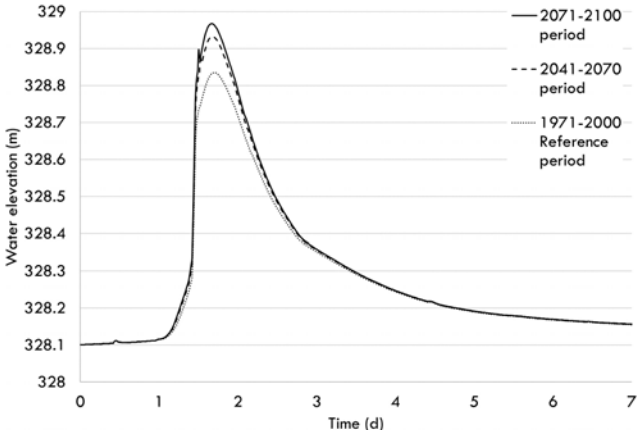

Figure 6: Simulated water levels (masl) for 1971–2000, 2041–2070 and 2071–2100 24-hour PMP at the North measuring station

Discussion and conclusion

The calibrated rainfall-runoff model was able to adequately simulate extreme rainfall events as well as baseflow throughout the instrumentation phase (133 days) at the Canadian Malartic Mine. The runoffs generated by smaller rainfall events were generally overestimated in the simulations.

The major rainfall events observed during summer 2018 were higher than usual, and the event recorded on September 5 was the largest precipitation ever recorded for a period under 24 hours at this station since its installation in 1951. The amplitude of these rain events facilitated the calibration of the simulations. However, the calibration was carried out only using the observed water levels at the measuring stations, and the discharge was not directly measured nor compared with the simulations. The precision of the calibration to estimate runoff may therefore be somewhat limited.

The simulation of the projected PMP (for 2050 and 2080 horizons) was just an example of possible outcomes of a calibrated rainfall-runoff model with climate projections. For this case, the model was able to determine the expected water level and peak discharge associated with the PMP, which could be used to design infrastructure. The projections provided by the climate models can also include time series of typical years for decades to better predict future water balance. It is also possible to determine the expected rainfall volumes according to the different return periods that may be associated with the level of risk of the surface water management infrastructure. The integration of future climate projections is a promising approach to design infrastructure based on realistic climate data rather than using overly conservative assumptions.

Acknowledgements

The authors thank the RIME UQAT-Polytechnique for providing funding for this project. We also acknowledge the financial support of the FRQNT. Additional support was also provided by the employees at URSTM-IRME who assisted with the field work and the Canadian Malartic Mine partner. The authors would also like to acknowledge MIKE Powered by DHI for the academic license that was used in this project.

References

Alfieri, Lorenzo, Francesco Laio and Pierluigi Claps. 2008. A simulation experiment for optimal design hyetograph selection. *Hydrological Processes: An International Journal* 22(6): 813–820.

Andréassian, Vazken, Charles Perrin, Claude Michel, Iolanda Usart-Sanchez and Jacques Lavabre. 2001. Impact of imperfect rainfall knowledge on the efficiency and the parameters of watershed models. *Journal of Hydrology* 250(1–4): 206–223.

ARCC. 2014. Review of downscaling methods for climate change projections.

Assemblée nationale. 2017. *Loi modifiant la Loi sur la qualité de l'environnement afin de moderniser le régime d'autorisation environnementale et modifiant d'autres dispositions législatives notamment pour réformer la gouvernance du Fonds vert. Éditeur officiel du Québec.*

Bezak, Nejc, Mojca Šraj, Simon Rusjan and Matjaž Mikoš. 2018. Impact of the rainfall duration and temporal rainfall distribution defined using the Huff curves on the hydraulic flood modelling results. *Geosciences* 8 (2): 69.

Bresson, Émilie, Marylin Gandonou, Gwendoline Hotton, Pier-Luc Labonté-Raymond, Élodie Lieber, Bruno Bussière, Isabelle Demers, Thomas Pabst and Philippe Roy. 2018. Quebec mining industry adapting to climate change. Canadian Meteorological and Oceanographic Society's 52nd Congress, Halifax, Canada.

Brocca, L., F. Melone and T. Moramarco. 2011. Distributed rainfall-runoff modelling for flood frequency estimation and flood forecasting. *Hydrological processes* 25 (18): 2801–2813.

Charron, I. 2016. *Guide sur les scénarios climatiques: utilisation de l'information climatique pour guider la recherche et la prise de décision en matière d'adaptation*. Montréal, Québec, Canada.

Clavet-Gaumont, Jacinthe, David Huard, Anne Frigon, Kristina Koenig, Phillip Slota, Alain Rousseau, Iris Klein, Nathalie Thiemonge, Fanny Houdré and John Perdikaris. 2017. Probable maximum flood in a changing climate: An overview for Canadian basins. *Journal of Hydrology: Regional Studies* 13: 11–25.

Davies, Michael, Todd Martin and Peter Lighthall. 2000. Mine tailings dams: When things go wrong. *Tailings Dams*: 261–273.

Dimri, A.P. 2009. Impact of subgrid scale scheme on topography and landuse for better regional scale simulation of meteorological variables over the western Himalayas. *Climate dynamics* 32 (4): 565–574.

Dunne, Thomas. 1983. Relation of field studies and modeling in the prediction of storm runoff. *Journal of Hydrology* 65 (1–3): 25–48.

Hershfield, David M. 1965. Method for estimating probable maximum rainfall. *Journal-American Water Works Association* 57 (8): 965–972.

Huntington, Thomas G. 2006. Evidence for intensification of the global water cycle: review and synthesis. *Journal of Hydrology* 319(1–4): 83–95.

ICOLD. 2001. Tailings dams – Risk of dangerous occurrences, lessons learnt from practical experiences (Bulletin 121). *Commission Internationale des Grands Barrages, Paris.*

IPCC. 2013. Summary for Policymakers in Climate Change 2013: The Physical Science Basis, Contribution of Working Group I to the Fifth Assessment Report of the Intergovernmental Panel on Climate Change. Cambridge University Press, Cambridge and New York, USA.

Kunkel, Kenneth E., Thomas R. Karl, David R. Easterling, Kelly Redmond, John Young, Xungang Yin and Paula Hennon. 2013. Probable maximum precipitation and climate change. *Geophysical Research Letters* 40(7): 1402–1408.

Lucas, Cédric. 2001. Baia Mare and Baia Borsa accidents: Cases of severe transboundary water pollution. *Envtl. Pol'y & L.* 31: 106.

Ma, Yaoming, Massimo Menenti, Reinder Feddes and Jiemin Wang. 2008. Analysis of the land surface heterogeneity and its impact on atmospheric variables and the aerodynamic and thermodynamic roughness lengths. *Journal of Geophysical Research: Atmospheres* 113 (D8).

Mácá, Petr and Paul Torfs. 2009. The influence of temporal rainfall distribution in the flood runoff modelling. *Soil & Water Research* 4(2): 102–S110.

Madsen, Henrik, Deborah Lawrence, Michel Lang, Marta Martinkova and T.R. Kjeldsen. 2014. Review of trend analysis and climate change projections of extreme precipitation and floods in Europe. *Journal of Hydrology* 519: 3634–3650.

MDDEP. 2012. *Directive 019 sur l'industrie minière.*

MEQ. 1999. *Guide des essais de pompage et leurs interprétations*. *Québec, Ministère de l'environnement.*

Meteorological Services of Canada. 1951–2019. Station results – Historical data. Val d'Or A, Climate Id: 7098600.

Meteorological Services of Canada. 1971–2000. Données des stations pour le calcul des normales climatiques au Canada de 1971 à 2000. Accessed 2019 July 1.

MRNF. 2006. Portrait territorial: Abitibi-Témiscamingue. Québec, Canada.

NRCS, USDA. 2007. *National Engineering Handbook: Part 630 – Hydrology.* USDA Soil Conservation Service: Washington, DC, USA.

Refsgaard, Jens Christian. 1997. Parameterisation, calibration and validation of distributed hydrological models. *Journal of Hydrology* 198(1–4): 69–97.

Rico, Mayte, Gerardo Benito, A.R. Salgueiro, Andrés Díez-Herrero and H.G. Pereira. 2008. Reported tailings dam failures: a review of the European incidents in the worldwide context. *Journal of Hazardous Materials* 152(2): 846–852.

Sammarco, Onofrio. 2004. A tragic disaster caused by the failure of tailings dams leads to the formation of the Stava 1985 Foundation. *Mine Water and the Environment* 23(2): 91–95.

SCS. 1986. Technical release: Urban hydrology for small watersheds. US Dept. of Agriculture, Soil Conservation Service, Engineering Division.

Van Niekerk, H. J. and M.J. Viljoen. 2005. Causes and consequences of the Merriespruit and other tailings-dam failures. *Land Degradation & Development* 16(2): 201–212. doi: 10.1002/ldr.681.

Wheater, H.S., R.E. Chandler, C.J. Onof, V.S. Isham, E. Bellone, C. Yang, D. Lekkas, G. Lourmas and M.-L. Segond. 2005. Spatial-temporal rainfall modelling for flood risk estimation. *Stochastic Environmental Research and Risk Assessment* 19(6): 403–416.

Willmott, Cort J. and Kenji Matsuura. 2005. Advantages of the mean absolute error (MAE) over the root mean square error (RMSE) in assessing average model performance. *Climate research* 30(1): 79–82.

WMO. 2009. *Manual on Estimation of Probable Maximum Precipitation (PMP)/World Meteorological Organization*, *WMO (Series) 1045.* Geneva: World Meteorological Organization.

WSP. 2015. *CMGP – Étude d'impact sur l'environnement.*

Proceedings of Tailings and Mine Waste 2019
November 17–20, 2019, Vancouver, Canada
Published by the University of British Columbia, 2019

Challenges Associated with Water Management and Embankment Raising of a Large Single-Cell Central Discharge Tailings Storage Facility in Australia

Gerrie Le Roux, Golder Associates Pty Ltd, Australia
Brett Mullen, BHP Nickel West, Australia
David Williams, Golder Associates Pty Ltd, Australia
Mahmud Safari, BHP Nickel West, Australia

Abstract

Surface water management is one of the most critical design aspects in maintaining the stability and safety of any tailings storage facility (TSF). Water management in TSFs often presents challenges, especially on a central discharge TSF (CDTSF), where water drains towards the perimeter embankment due to the deposition technique and the resulting configuration of the tailings beach. When this is combined with a requirement for perimeter embankment raises to provide on-going storage capacity, it becomes a bigger challenge.

The Mount Keith nickel concentrator (Mount Keith) in Western Australia has a CDTSF with a footprint area of approximately 1,600 ha (~4,000 acres). One of the largest risks associated with management and operation of the CDTSF is overtopping of the perimeter embankment during moderate to extreme rainfall events. Surface water management plays a significant role in controlling this risk. In addition to the challenge of managing water against the perimeter embankment, the embankment needs to be raised periodically, and must remain stable to ensure safe operation of the facility. At Mount Keith, the CDTSF embankment is upstream raised, using tailings borrowed from the nearby beach as the fill material. The CDTSF has been successfully operated and managed since its commissioning in 1996. A process of continuous improvement of surface water management and embankment construction has resulted in the implementation of additional controls to further strengthen safe operating practices.

The measures implemented to improve surface water management and maintain embankment stability include the installation of additional decant pipes at specified locations, the construction of cross-berms along the tailings beach to manage supernatant and stormwater, and the construction of a rock buttress along the downstream slope of the internal embankment.

Introduction and background

The Mount Keith Nickel Mine and Concentrator (Mount Keith), which is owned and operated by BHP Nickel West, is located approximately 750 km north-east of Perth, in a semi-arid region of Western Australia. Processing of ore from the open pit mine produces approximately 10 million tonnes of nickel tailings per annum (Mtpa). Tailings were initially deposited into two paddock-style TSFs, referred to as the TSF 1 East and West cells, for a period of approximately two years. The tailings production rate increased from an original design rate of approximately 6 Mtpa, to 8.5 Mtpa, and then to approximately 10 Mtpa, which resulted in excessive rates of rise for TSF 1, triggering the requirement for additional tailings storage area.

The CDTSF was constructed and commissioned in 1996, and has a footprint area of approximately 1,600 hectares (~4,000 acres). The CDTSF is near-circular, with a diameter of approximately 4.6 km and a perimeter length of approximately 14 km. Tailings are discharged into the CDTSF through vertical risers, comprising a central riser and eight perimeter/outer risers, four along the eastern half and four along the western half of the CDTSF. One of the eastern risers became inoperable in 2009, resulting in seven perimeter/outer risers currently (2019) being operational, in addition to the central riser.

The CDTSF was originally designed to receive tailings at a slurry solids concentration of approximately 45% by mass, for a design life of approximately 24 years, resulting in approximately 240 million tonnes of tailings to be stored. Pilot plant testing at the design solids concentration indicated that a beach slope of approximately 3% could be expected.

However, since commissioning of the CDTSF in 1996, the average slurry solids concentration has been 40%, and the overall beach slope is between 0.5% and 1%. The operations team has selected to discharge tailings at the lower than designed solids concentration to reduce the propensity for pipeline blockages and to reduce the risk of failure of the subsurface riser pipes due to excessive internal pipeline pressures. These changes, compared to the design criteria, resulted in modifications required to the design of the CDTSF during the early stages of operation in order to realize the anticipated storage capacity.

The design modifications comprised the construction of an internal perimeter embankment to confine the tailings to the designated footprint. The internal embankment is located between 80 m and 200 m inside the external embankment, and is used to retain tailings. The eastern flank of the internal embankment is referred to as the “Kidney Wall”, due to its shape. As a consequence of the beach slope that arises from the relatively low solids concentration, the internal embankment needs to be raised on a near continuous basis in order to provide the required storage capacity. The CDTSF therefore has both an external perimeter embankment, which was initially constructed to contain the tailings without having to be raised, and an internal embankment, which is used to contain the tailings.

A recent aerial view of the CDTSF is shown in Figure 1.

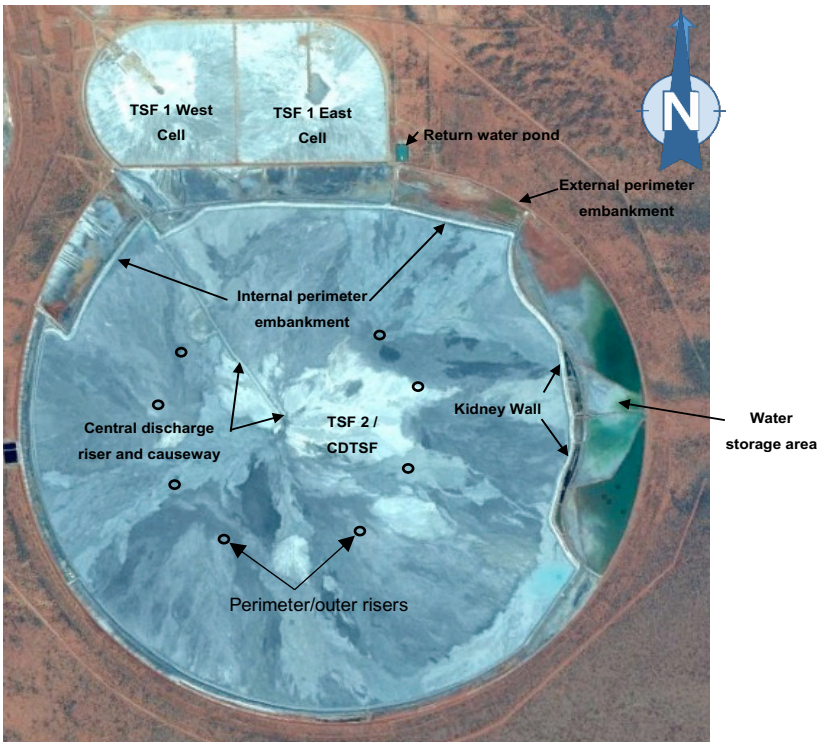

Figure 1: Recent aerial view of the Mount Keith CDTSF (2019)

The outer perimeter embankment was constructed from compacted earth fill and has never been raised. It is between 3 m high (western flank) and 5 m high (eastern flank). Due to sloping topography from west to east, the internal embankment varies in height between ~10 m along the western flank to ~15 m along the eastern flank, based on the 2019 aerial survey data. A typical cross-section through the southern flank of the CDTSF, showing the external and internal embankments, is provided in Figure 2.

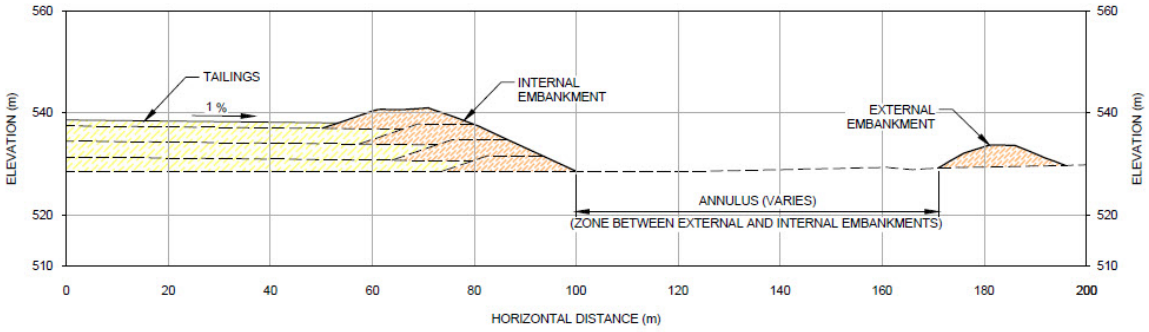

Figure 2: Cross-section through the CDTSF embankments

Supernatant water exuding from the tailings, as well as stormwater from the surface of the CDTSF, drains towards the internal perimeter embankment. The water is removed from the tailings beach through a series of decant pipes that are installed through the embankment at specific locations. The decant water flows in dedicated drains within the annulus (i.e., between the external perimeter embankment and the

internal embankment) towards the water storage area, located at the eastern flank of the CDTSF, from where it is pumped to the return water pond and from there back to the process plant for re-use.

Due to the large catchment area, stormwater management on the CDTSF presents some challenges. The tailings beach slopes from the centre of the facility to the internal embankment at an average beach slope of ~1%. Supernatant and stormwater therefore pond against the internal embankment, increasing the risk of overtopping and potential failure of the embankment. The location of water ponding largely depends on which of the riser pipes are operational, the topography of the CDTSF, and the location of cross berms that have been constructed across the beaches from the internal embankment.

Ponding against the internal embankment impacts the ability to construct wall raises by limiting the tailings drying time between deposition cycles. However, this is manageable, as the rate of rise of the facility is only about 1 m/year, which affords sufficient time to allow for evaporative drying of the tailings. A tailings deposition plan is implemented to manage deposition from the central riser and one of the perimeter/outer risers at any one time, or two perimeter risers if the central riser is under repair.

Due to the size of the facility, deposition can be rotated between the different perimeter/outer risers at a frequency that allows settled tailings to consolidate and dry out along the perimeter embankment, before it is excavated and used for embankment raising. The CDTSF can therefore be considered to effectively operate as a "multi-cell" facility, but without dividing embankments, in which some zones are used for tailings deposition, while other zones are left to desiccate to allow sections of the embankment to be raised. To ensure that the deposition and operation plan can be correctly executed, improved measures to deal with surface water have been implemented. The challenges associated with stormwater management and upstream raising of a central discharge TSF with water ponding against the upstream face of the embankment, and with tailings fines settling out in the perimeter beach area, are discussed in more detail later in this paper.

In addition to surface water management on the CDTSF, the stability of the internal embankment that is raised through upstream raising on a near-continuous basis, must be maintained.

Risk assessment

To check that the risks of the operating approach are appropriately managed, a quantified risk assessment and associated dam break study have been undertaken. The latest comprehensive risk-based dam break assessment of the CDTSF was undertaken in 2017. The approach followed was to use the technique of fault tree analysis to systematically combine potential faults in the system. The approach involves the identification of system faults that could potentially result in a dam break and the consequential release of liquefied tailings and/or water from the CDTSF. The fault tree technique represents the potential combination(s) of possible causes of a failure.

Probabilities were assigned to the appropriate faults in the fault trees through judgement, experience, data interpretation, modelling, analyses, and comparison with published literature. The likelihood of failure was assessed under sunny day as well as extreme weather conditions.

The results of the risk assessment indicated that a release from the Kidney Wall was the most likely cause of a flow failure from the CDTSF. It was also identified that failure of the Kidney Wall was most likely to result from overtopping following an extreme storm event, arising from the inadequate capacity of the decant pipes and marginal freeboard along the Kidney Wall. The likelihood of overtopping was estimated at approximately 1 in 3,500 per annum (~0.03% p.a.), while under sunny day conditions the probability of failure was estimated to be much lower (1 in ~70,000 per annum or ~0.001% p.a.).

Surface water management

Following the outcomes and recommendations from the risk assessment, a stormwater management model was developed to:

- Identify the potential consequences to the Mount Keith CDTSF as a result of a 1% annual exceedance probability (AEP) 72-hour storm event, classified as the design storm for a Significant consequence category TSF in accordance with the Australian National Commission on Large Dams (ANCOLD) guidelines.
- Provide a detailed assessment of the available freeboard, based on the most recent aerial survey data.
- Identify and recommend options to address deficiencies in the stormwater management capacity, where necessary.

Site-specific two-dimensional (2D) hydraulic modelling of the design storm and the inundation extent of the CDTSF surface was undertaken using TUFLOW, an advanced numerical engine for simulating free-surface water flow of urban waterways, rivers, floodplains, estuaries, and coastlines capable of solving all the necessary physical processes using 1D, 2D, and 3D solutions.

Several scenarios were modelled to establish the locations, and the minimum requirements for installation of additional decant pipes through the internal embankment to provide sufficient decant capacity. The modelling was also used to assess available freeboard (the vertical difference between the tailings beach and the embankment crest), to allow embankment raising to be focussed in the areas where minimum freeboard requirements were not met. The modelled scenarios included the following:

- Scenario 1 – model of conditions existing at the time (2016) without modifications – the base case.
- Scenario 2 – model of decant capacity through installation of additional decant pipes, as well as model of freeboard capacity with additional embankment raising in place.

- Scenario 3 – model with spillways installed at two locations along the Kidney Wall.

An output (flood map) of the model for Scenario 1 is shown in Figure 3. The flood map shows that, with all the existing decant pipes operational, water would pond along the south-eastern flank and in the north-western corner area to depths of approximately 2 m. Due to the natural fall in topography from west to east, and with the tailings beach surface following that natural trend, surface water generally drains from the centre of the CDTSF to the internal embankment and then flows along the inner toe of the embankment to the eastern flank (Kidney Wall) where it accumulates. Cross-berms are constructed on the tailings beach at locations downstream of the decant pipes to assist in controlling flow along the inner toe of the embankment, forcing the water to pond and to flow through the decant pipes. However, during large storm events the cross-berms are not effective, and flow bypasses the berms and surface water accumulates in the south-eastern corner of the CDTSF.

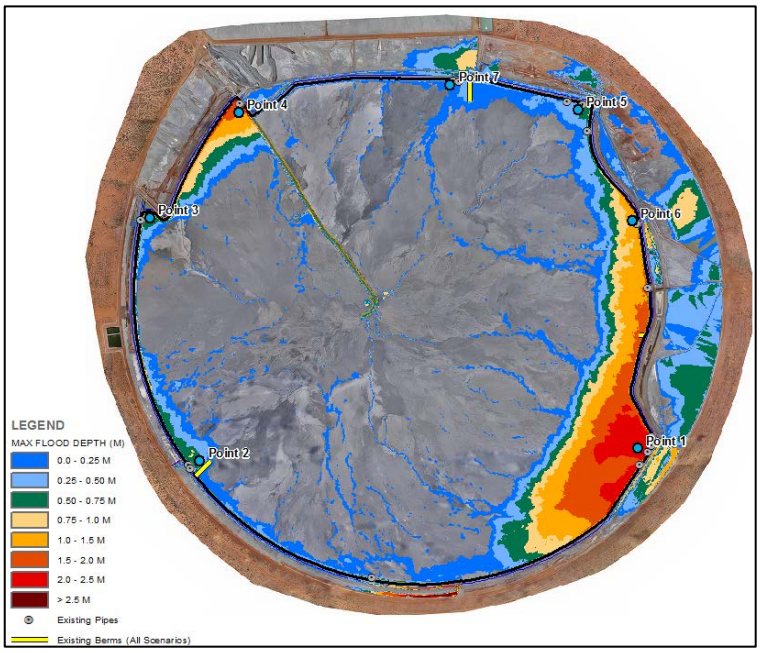

Figure 3: Maximum flood depth with existing (2016) decant pipes operational

Through the installation of additional decant pipes, as well as the construction of additional cross-berms on the tailings beach to assist in controlling run-off, the maximum flood depth has been reduced to approximately 1 m. The flood modelling was therefore effectively used to select locations where additional decant pipes and cross-berms had to be installed, and it also provided important data on where embankment raising was required to meet minimum freeboard requirements.

Decant system

Following the initial stormwater modelling in 2016, additional decant pipes have been installed – the

CDTSF currently (2019) has 11 operational decant and 22 stormwater pipes. In addition to the decant pipe system there are four cross-berm relief pipes, allowing drainage through the cross-berms, if required. The decant pipes are installed slightly lower than the stormwater pipes, with the decant pipe inlet aimed at decanting operational slurry water (supernatant). The stormwater pipes with elevated inlets are installed to remove stormwater. The typical installation arrangement is as follows:

- Operational water decant pipe – top of pipe located approximately 950 mm below the embankment crest.
- Stormwater decant pipe – top of pipe located approximately 500 mm below the embankment crest.

The operational and stormwater pipe arrangements are presented in Figure 4.

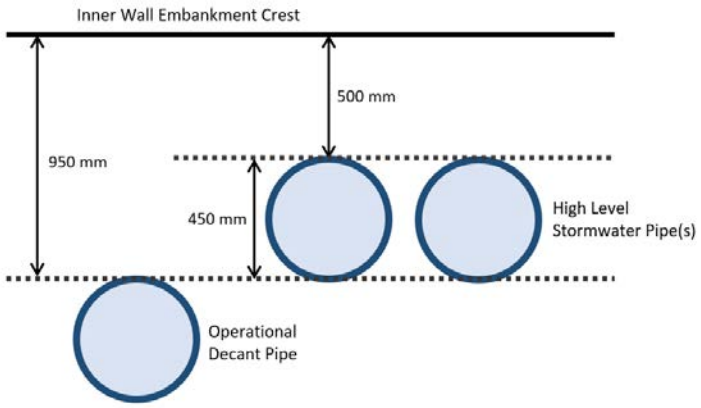

Figure 4: Typical operational and stormwater decant pipe arrangement

The additional stormwater pipes that were installed in 2017 effectively act as a spillway for the CDTSF. At full discharge capacity the pipes would be able to decant the design storm from the TSF without compromising freeboard.

In 2016, installation of a rock buttress along the downstream slope of the internal embankment necessitated modification of the decant and stormwater pipes arrangement to include a combination of temporary and permanent decant pipes along the downstream slope of the internal embankment. The permanent pipes comprise ~600 mm diameter corrugated high density polyethylene (HDPE) pipes, fixed along the downstream slope, with fabricated bends to allow discharge into a toe drain. The permanent pipes remain in place and are never moved, lifted or relocated. The temporary pipes are the pipes protruding through the tailings embankment, and these pipes are lifted and reinstalled during each embankment raise. The temporary pipes are ~450 mm diameter HDPE pipes and feed into the permanent pipes. Figure 5 shows details of the pipe arrangement along the downstream slope, where the temporary pipes feed into the permanent pipes. The pipe inlets at different elevations is also shown in Figure 5.

Figure 5: Decant pipe arrangement along the downstream slope (left) and at the inlet (right)

A procedure is in place to ensure that removal and replacement of the temporary pipes during embankment raising does not result in a weak point in the embankment that could lead to seepage and piping. The procedure identifies the zone to be excavated and the backfill and compaction requirements to maintain safe operation and long-term stability.

Embankment raising

The storage capacity of the CDTSF is increased through near-continuous raising of the internal embankment. The embankment is upstream raised using tailings as construction material. The tailings are excavated from the beach with long-reach excavators travelling along the embankment crest. The excavated material is stockpiled along the upstream slope of the embankment and left to dry to reach optimum moisture content (OMC) before it is spread along the crest and compacted in ~250 mm thick lifts to raise the internal embankment. This process is continued along the complete perimeter, and the embankment is raised at a rate of approximately 1 m per year at an average slope angle of 1(V) to 2(H). The deposition strategy directs tailings to be discharged into specific zones or quadrants via the central riser and one or two of the perimeter/outer risers, allowing the remaining beach enough time to consolidate and desiccate. The size of the CDTSF compared to the deposition rate makes this method of operation and embankment raising feasible, as the rate of rise on the CDTSF is less than 1 m/year, thus allowing sections along the perimeter to desiccate for several months before embankment raising is undertaken.

Figure 6 shows a typical excavation along the upstream toe of the internal embankment where tailings are excavated and stockpiled along the upstream slope of the internal embankment and left to dry out.

Figure 6: Tailing excavation and stockpiling along upstream toe of the internal embankment

A risk associated with borrowing tailings along the upstream toe is that it creates a drainage trench where surface water could get trapped, resulting in poor foundation conditions for further upstream raising. This issue is addressed through construction of cross-berms at intervals along the perimeter of the embankment. The berms are constructed perpendicular to the internal embankment and extend on to the tailings beach. Decant pipes through the embankment are installed on the upstream side of the cross-berms where the surface water ponds. It therefore allows sections of the inner toe to dry out sufficiently without water ponding against the embankment, thus facilitating upstream raising of the embankments.

Stability analyses and buttress construction

A preliminary buttress was constructed along the Kidney Wall in 2014 to improve its stability. Stabilizing measures were required due to the lower strength of the tailings along the upstream zone of the internal embankment and because the internal embankment had to be continuously raised to retain tailings. The tailings strength is lower in this zone due to fine-grained particles being transported across the beach and settling out along the perimeter embankment, as well as supernatant water ponding against the upstream slope compromising the potential for air drying, all resulting in a looser state, with lower shear strength. The buttress was constructed from a mixture of tailings and natural oxide materials, borrowed from the zone between the internal and external embankments of the CDTSF. The buttress dimensions were reviewed to accommodate ongoing embankment raising, and in 2015 it was extended to be approximately 8 m high and 10 m wide. The extended buttress was constructed with tailings, and a sand filter with outlet pipes was installed at the interface of the tailings embankment and the buttress to control the phreatic surface through the Kidney Wall.

In 2017, further stability analyses of the internal embankment were undertaken, which revealed the requirement to stabilize the complete length of the internal embankment. The stability analyses were based on material parameters of the tailings and foundation materials obtained from geotechnical investigations of the CDTSF (in-situ cone penetration testing and associated laboratory testwork) undertaken in 2010, 2014 and 2016. Pore pressure data were obtained from vibrating wire piezometers installed along the complete length of the internal embankment of the CDTSF.

Minimum buttress dimensions were established for the embankment slopes to maintain the minimum recommended factors of safety (FOS) as per the guidelines provided by ANCOLD (2012). Stability modelling of the internal embankment followed the approach recommended by the ANCOLD 2012 guidelines, comprising assessment of static equilibrium using effective stress and/or undrained strength parameters, as well as stability analyses under seismic loading through the adoption of post-seismic (residual) shear strengths.

The stability analyses were undertaken using the 2D limit equilibrium slope stability analysis software, SLIDE version 6.0 (Rocscience, 2010) using the Morgenstern-Price method. Model sections considered to represent the highest risk of instability for the embankment slopes were analysed. The buttress requirements were established for the existing (2018) slope geometry, but it was extended to establish ongoing requirements for the anticipated life of mine until 2040.

Foundation preparation for construction of the buttress along the remainder of the internal embankment commenced in October 2016. The near surface saturated soils were removed to caprock level, which was approximately 1 m below surface. Construction of the buttress using the mining fleet (Caterpillar 793D haul trucks and Caterpillar D11 dozers) to dump and spread waste rock along the toe of the internal embankment commenced in November 2016 – see Figure 7.

Figure 7: Waste rock buttress along the downstream slope of the CDTSF internal embankment

The buttress along the internal embankment, excluding the Kidney Wall, was completed in July 2017. In December 2017 the Kidney Wall buttress was raised to tie in with the rest of the perimeter buttress, and construction of the Kidney Wall buttress was completed in March 2018.

The minimum buttress width required for stability was approximately 14 m. However, to accommodate the available construction equipment the buttress was constructed with a crest width of 30 m. The buttress varies in height between 8 and 10 m. Ongoing raising of the buttress at the same rate as raising of the internal embankment is required for ongoing and long-term stability of the CDTSF.

Conclusion

The quantitative risk assessment undertaken to evaluate risks associated with operation of the CDTSF at Mount Keith identified that the largest risk to the safe operation of the facility was overtopping of the internal embankment. In order to address the overtopping risk, an assessment of the requirements for embankment raising to meet minimum freeboard, as well as an assessment of the total decant capacity of the CDTSF, were carried out. This included an aerial survey of the facility, which was used to model stormwater flow on the CDTSF surface. The modelling indicated where surface water would likely accumulate and where additional decant pipes would be required to allow discharge of surface water from the tailings beach. The modelling also indicated where embankment raising was required to meet freeboard requirements. Following implementation of the remedial measures, the risk of overtopping due to insufficient decant capacity has been reduced to approximately 1 in 43,000 per annum (~0.002% p.a.).

In addition to stormwater management on and from the CDTSF surface, embankment stability must be maintained to make sure the CDTSF operates in accordance with its design intent. Due to the potential for surface water to pond against the upstream crest, embankment raising is limited to zones along the perimeter where tailings have sufficiently air dried to allow construction to proceed. This is achieved by directing tailings discharge from the central and perimeter/outer risers to specific zones of the CDTSF, thereby allowing other areas to consolidate and dry out.

In order to ensure adequate factors of safety against instability of the embankment are maintained over the long term, a waste rock buttress was constructed along the complete length of the internal embankment. The rock buttress will be raised at the same rate that the embankment is raised to provide the required resistance. This effectively renders the embankment a much more substantial structure than the thin wedge provided by upstream raises, as shown in Figure 8. The CDTSF is therefore effectively developed as an integrated waste landform (IWL), where a substantial size rock mass, with a crest width of at least 30 m, is placed along the downstream slope of the complete perimeter of the internal embankment. The presence of the rock buttress significantly increases the factor of safety of the internal embankment,

and failure is now effectively only plausible through the section of tailings embankment above the rock buttress. This likelihood could be further reduced by buttressing the embankment to crest level.

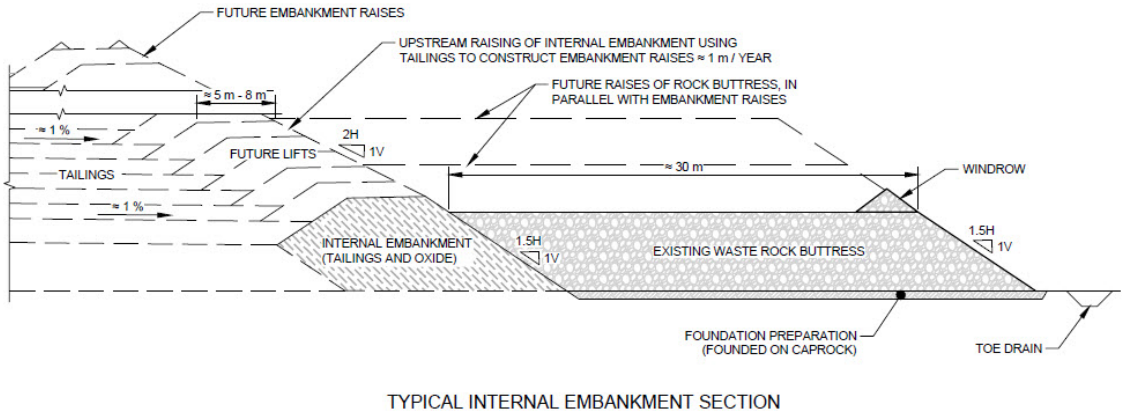

Figure 8: Indication of adjustment of upstream raised geometry provided by buttressing

To ensure long-term safety and stability of the Mount Keith CDTSF, the processes developed over the past three years, which include the following, will be maintained:

- Aerial surveys of the CDTSF at least twice per year.
- Updated stormwater modelling after each aerial survey to identify areas where minimum freeboard requirements are at risk of not being met or maintained.
- Stormwater modelling to evaluate whether additional decant capacity is required.
- Stability modelling to provide ongoing support and advice regarding buttress raising requirements.

Acknowledgements

The authors of this paper would like to acknowledge BHP Nickel West for its support and for providing permission to publish this work.

References

ANCOLD. 2012. Guidelines on tailings dams – Planning, design, construction, operation and closure.

Rocscience. 2010. See web site, https://www.rocscience.com

Proceedings of Tailings and Mine Waste 2019
November 17–20, 2019, Vancouver, Canada
Published by the University of British Columbia, 2019

Underground Mine Rehabilitation for Closure: A Uranium Case Study

Sue Longo, Golder Associates Ltd., Canada
Chloe Crossley, Golder Associates Ltd., Canada

Abstract

Historical mine sites pose multiple challenges for final closure. Environmental legacies are a common area of concern, but physical stability of the site is equally important for a long-term, walk-away solution. This paper will discuss the status of the underground workings of a decommissioned uranium mine and the paste backfill solution that was developed and implemented. Specifically, the physical hazards that are being addressed are near-surface hazards, e.g., empty underground stopes with thin crown pillars and surface openings to the underground, e.g., glory holes and raises. The consequence of not addressing these hazards is potential long-term failure, e.g., surface collapse, cracking, and subsidence which could have an impact on flora and fauna in the area as well as the nearby local population. In addition, the impact on the closure of the overall site and the lessons learned during the construction program will be discussed.

Introduction

Proper rehabilitation and closure of historical mine sites can be complex, expensive, and lengthy, often due to location (remote or adjacent to a community), era of mining (type of mining and when mining occurred), and availability of reliable and accurate as-built information. Historical mines often have several types of physical hazards, such as mine openings to the ground surface, near-surface mine workings, unreclaimed waste rock piles, and unreclaimed tailings storage facilities. If not mitigated, these physical hazards present risks to the environment and the general public. Therefore, the successful rehabilitation and closure of historical mines require an economical strategy that will work for the local conditions.

This case study summarizes the rehabilitation of a uranium mine (the site) that closed in the mid-1980s. Available mine plans show underground workings that comprise several horizontal development levels connected to the ground surface through a series of shafts, adits, and raises. The workings also include open vertical shafts extending to the ground surface. Some of the workings extend to areas near the ground surface, forming crown pillars between the surface and the void space. However, there was considerable uncertainty around the accuracy and completeness of the geometry and associated

geology of the workings. The incomplete and potentially inaccurate mine plans along with the physical constraints – e.g., no safe underground access – complicated the development of a suitable rehabilitation plan. In addition, temporary features, such as fencing around the vertical shafts and concrete caps over some openings, required consideration in regards to the long-term closure solution.

The closure goal at the site was the permanent elimination of the aforementioned physical hazards. This paper will discuss the application of paste backfill at the decommissioned uranium mine site and how the backfill system was developed and implemented to stabilize the underground workings.

Decommissioned mine rehabilitation strategy

Stability assessment and rehabilitation options evaluation

In this case study, a geotechnical investigation was completed for the site to evaluate the stability of the crown pillars over existing void spaces (some of which had existing concrete caps). The study identified 35 crown pillars, ten of which were assessed based on information from drilling and the rest through a desktop study. The results from drilling showed five stopes with crown pillars that were not long-term stable, and from the desktop study, five other stopes with crown pillars that were potentially not long-term stable. The remaining crown pillars were all considered to be low risk and not recommended for additional study. After a more detailed investigation, the ten identified crown pillars with stability concerns were reduced to seven. Regardless of the completeness of historical mine plans, a stability assessment should always be performed to determine and confirm which areas of the mine are stable and which are not. If this step is missed, there is a potential to incur significant and unnecessary project costs or worse, miss a problem area. Without completing the stability assessment in this case study, all 35 crown pillars could have potentially received rehabilitation efforts, which would have been expensive and unnecessary.

The next step was to determine the appropriate remediation methodology for the seven identified crown pillars with long-term stability concerns. Several options were identified for the rehabilitation of these crown pillars, including re-sloping, capping, and backfilling. Re-sloping refers to the process of blasting a crown pillar to effectively fill the void below with the rock settling at roughly a 45-degree angle. Capping is the process of constructing a concrete cap over the opening to surface and crown pillar. Backfilling refers to re-filling and eliminating the void space below the crown pillars to support the base of the crown pillar. Through a preliminary cost estimate and based on the nature of the site and the size of the openings, it was determined that backfilling would be technically feasible and cost-effective, and therefore the preferred option for stabilization.

Backfill system planning

Backfill selection

Once the preferred rehabilitation method was selected, in this case backfilling, the subsequent step was to choose the type of backfill. The typical types of backfill are as follows:

- rock fill;
- aggregate fill;
- hydraulic fill;
- paste fill;
- concrete; and
- grout.

The first four types of backfill can be applied as cemented or uncemented material. Since many of the stopes on the site were connected to other voids, any backfill application was required to be cemented to minimize the risk of liquefaction and movement of the fill material in the underground. To determine the most appropriate type for the site, backfill strength requirements, volume requirements, delivery locations, and other considerations, such as material availability, needed to be evaluated. The evaluation process involved the review of mine plans, previously completed surveys and drilling programs, and laboratory testing programs. It was known from the stability assessments that the total backfill volume requirement was approximately 85,000 m^3 and backfill strength requirements ranged from 200 kPa to 1,000 kPa. With this information in mind, the following backfill types were removed from consideration:

- Hydraulic fill was eliminated, as there was no underground access, and therefore no bulkheads could be built to contain the fill.
- Aggregate and rock fill were also eliminated since there were no on-site supply sources.
- Concrete and grout fill were eliminated, as site access could not support the delivery of concrete or grout fill directly to the underground.

Paste fill was therefore selected as the preferred backfill option. Paste backfill is an adaptable solution for filling voids, as it can quickly be modified for different recipes (strength requirements), as well as being able to use readily available material, such as tailings or overburden as a free source material.

Paste backfill design and sequence plan

For the site, two backfill recipes were required due to the geometry in the underground. Some stopes have multiple connection points to other areas in underground, such as raises or boxholes to the adit level or to other stopes. With stopes that are connected to other larger workings, it is necessary to plug those connection

points to limit the movement of the backfill and to ensure the fill stays where it is required to support the crown pillar. This is done with a paste barricade recipe. The other recipe is bulk paste fill. This is for bulk filling the voids once all connection points have been plugged.

The backfill sequence plan is the planned sequence for backfilling each stope, which includes: identifying the order of filling, the boreholes for fill delivery, required items to be completed prior to each pour, the monitoring plan, required strength parameters, and which paste recipe, barricade, or bulk is required.

Material sourcing and characterization

After paste backfill was established as the rehabilitation method of choice, volume and strength requirements were confirmed, and sequence plan developed, the backfill feed source material and its availability needed to be determined. This process generally involves finding a low cost, readily available material from a nearby source. On-site and off-site options are typically considered; however, cost and schedule can significantly be impacted if material needs to be sourced from off site. For this site, the tailings from the nearby tailings management area (TMA) were assessed and determined to be a viable feed source. It was identified that using the tailings would also assist with rehabilitation of the site's TMA because concurrent grading activities could occur during tailings excavation.

A laboratory testing program was then performed on the tailings to confirm material properties and develop a set of paste backfill recipes. Key considerations when making the paste recipes are the particle size distribution, moisture content, and minerology of the feed source. This has a direct impact on whether the paste will meet the strength, flow, and permeability targets of the backfill. The paste recipes comprised tailings, water from a local source, aggregate from an off-site source, and binder material (cement).

The two different paste recipes have different mixes but use the same source materials. The barricade fill is produced from a low slump paste, typically with a higher solids content, some aggregate and a higher binder content, while bulk fill is produced from a high slump paste with no aggregate and a lower binder content. The primary recipe mix designs and estimated binder usage rates for various design strengths are summarized in Table 1 and Table 2, respectively. One additional recipe was required to suit one stope that was flooded; this is shown below under sub-aqueous fill.

Table 1: Paste backfill recipes

Recipe	Slump (cm)	Tailings	Aggregate	Admixtures	Binder
Bulk fill	12.7–25.4	100%	0%	0%	Per the binder usage table below
Barricade fill	12.7–17.8	75–85%	15–25%	0%	Per the binder usage table below
Sub-aqueous fill	12.7–25.4	75–100%	0–25%	To be determined	Per the binder usage table below

Table 2: Estimated binder usage rates

Estimated binder usages							
Slump (cm)	**Agg wt%**	**Wt% Binder – 28 days**					
–	–	170 kPa	200 kPa	400 kPa	500 kPa	600 kPa	1,000 kPa
12.7	–	2.0%	2.5%	2.5%	3.9%	5.1%	8.3%
17.8	–	2%	2.5%	4.1%	5.5%	6.6%	9.9%
25.4	–	2%	2.5%	5.4%	7.8%	9.7%	15.2%
12.7	15%	2%	2.5%	2.5%	3.8%	4.9%	8.2%
17.8	15%	2%	2.5%	3.9%	5.4%	6.5%	9.8%
12.7	25%	2%	2.5%	2.5%	3.7%	4.8%	8.1%
17.8	25%	2%	2.5%	3.8%	5.2%	6.4%	9.6%

Once the testing program was complete, a targeted range of tailings properties were identified as being suitable for backfill. The TMA areas that contained the acceptable tailings were marked on site maps for selective excavation purposes.

Production planning

After the laboratory testing and material sourcing analysis, a paste production and delivery method needed to be determined. For this site, three different production options were assessed:

- Option 1: Use a volumetric mobile mixer located at the backfill site and direct pump/gravity discharge into the boreholes from surface.
- Option 2: Use a batch plant located at one of the TMA areas and pump all produced paste from this plant to the boreholes located around site.
- Option 3: Use a batch plant located at one of the TMA areas and use Redi-Mix trucks to deliver the paste to the boreholes.

To evaluate the three options, consideration was given to:

- Flexibility of the plant to change the paste recipe based on the feed properties of the tailings.
- Equipment required to handle the feed material from the tailings stockpiles.
- Radiation and other health and safety concerns.
- Ease of process control, including calibration, continuous versus batch mixing.
- Reliability of the plant type based on experience.
- Achievable production rates.

- Total approximate cost per cubic meter of backfill.

Based on these variables, Option 1 was chosen as the preferred production and delivery method. The general process description developed for the site is as follows:

- Excavate, transport, and stockpile tailings.
- Drill delivery boreholes for backfilling.
- Set-up mixing and pumping equipment.
- Deliver tailings from the stockpile to the production equipment.
- Produce a suitable paste and deliver it to the underground voids via boreholes.
- Observe the underground for monitoring and progress purposes.

Site planning

Once the production plan for the paste backfill was established, the site layouts and other site logistics were planned. At each production site, a pad needed to be developed for equipment and ancillary set-up, traffic turnaround areas, and areas for engineering staff to complete quality control and quality assurance (QC/QA) work, such as laboratory testing. A traffic management plan was required to assist with the safe operation of vehicles and heavy equipment during the program. Tailings stockpile areas also needed to be sized and built.

At the site it was determined that there would be three production areas set up at three different stope locations. Due to the distances between filling areas and site access restrictions, only two would operate at a time, but all three would be required over the course of the program. The layouts were designed to house all the equipment (excavators, mixer trucks, cement silos, water tanks, and temporary stockpiles), along with the areas for QC sampling and testing. Pipeline routings were also required to connect the production equipment to the various borehole locations around the site. Pressurized (pipeline) system safety requirements were also implemented during the design of the layouts, including allowable walkways, no go zones, and restricted access areas, along with related communication protocols. Additionally, consideration was given to the radiological hazards in designing the layouts. An example of the site layout drawings is shown in Figure 1.

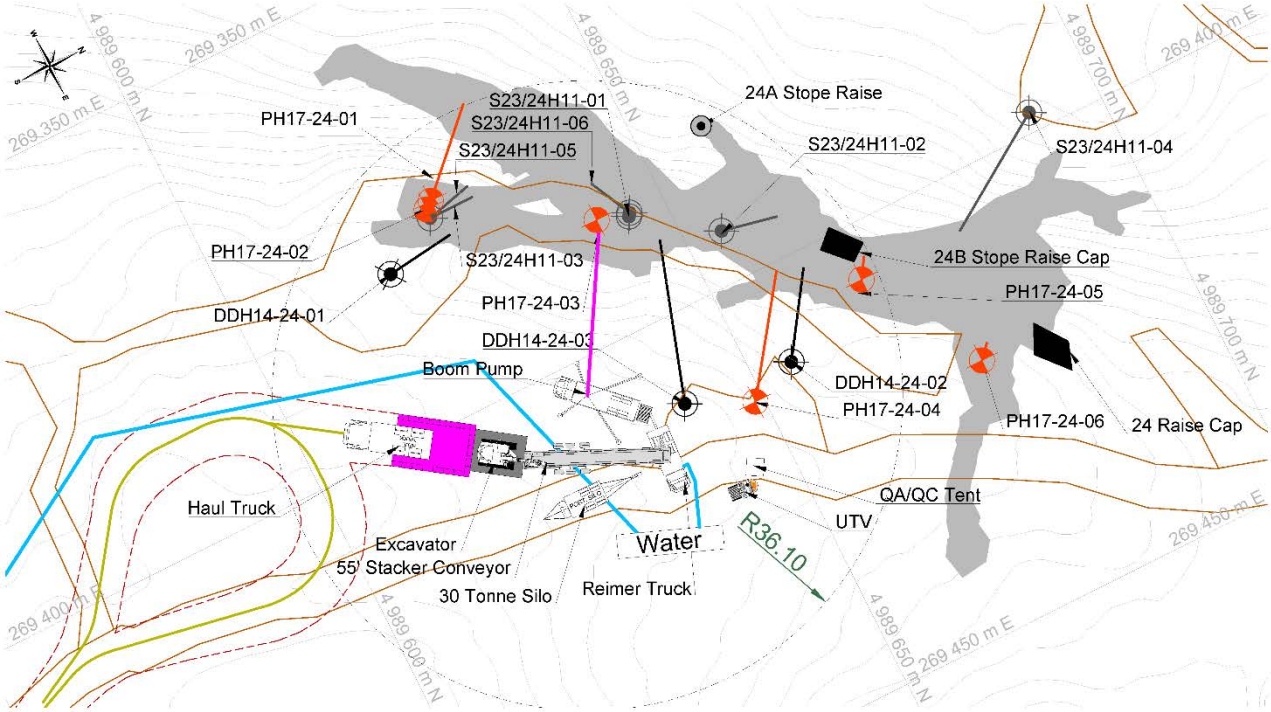

Figure 1: Site layout

Technical specification development

In tandem with production and site planning, the technical specifications for the scope of work were also developed. The specifications cover the targets required for each stope and crown pillar. The key performance targets for the site are the strength of the backfill and the fullness of the fill in the void space (how tightly filled it needs to be). Strength targets will be verified by laboratory testing, and monitoring during backfilling will be used to verify the placed backfill volumes and to confirm the void fullness design criteria. The void volume of each stope was estimated during the investigations using Cavity Monitor Survey (CMS) scans and historical data. Three volume types are to be measured and recorded during the work as part of the specifications:

- volume placed (volume produced and delivered into the underground, as measured by monitoring);
- volume gained (volume recognized by the CSM surveys and other void monitoring methods); and
- volume lost (difference between the two volumes which cannot be accounted for).

Another important specification is a technical definition of a rehabilitated stope. For this site, each stope is to be tightly filled such that the backfill is in contact with the base of the crown pillar (upper most part of the stope void). Tight fill is to be deemed successful when the backfill is in contact with the back of the stope for at least 50% of the stope back area; however, the goal is to have much higher than 50% contact

with the back of the stope. The preferred methods to confirm that the stope has been tightly filled is through existing drilled boreholes using borehole cameras, CMS scans, and sounding.

Quality management plan

A rigorous Quality Control/Quality Assurance (QC/QC) plan and program was undertaken to ensure the technical specifications were met. The requirements for this program needed to be established and well understood prior to execution. One key component of the quality management program is ongoing sampling and testing of the paste backfill to confirm that strength specifications are being met. Other specific tests included in the plan are particle size distribution, specific gravity, slump tests, and yield stress tests. To provide early and frequent feedback, all testing is done in the field or in the on-site laboratory. Table 3 provides some of the quality control testing requirements developed for the site.

Table 3: Quality control testing

Material type	Material name	Test name	Minimum frequency
Raw feedstock materials	Tailings	Specific gravity	2 times per week
		Particle size distribution	1 time per week
		Moisture content	1 time daily
		Temperature	1 time daily during summer or warm conditions; 3 times daily in colder weather
	Aggregate	Particle size distribution	Daily or every 500 m^3
		Moisture content	1 time daily
		Temperature	1 time daily during summer or warm conditions; 3 times daily in colder weather
	Binder	On-site lab binder certification	1 time for each binder type/supplier
	Water	Temperature	1 time daily during summer or warm conditions; 3 times daily in colder weather
Produced materials	Barricade, paste backfill, and grout	Slump test	1 every hour if running continuously, or every 100 m^3 if running intermittently or when recipe or delivery hole changes
		Unconfined compressive strength (UCS) Test	2 times daily (a.m. and p.m.) for each truck; or when recipe changes or when hole changes
		Temperature (in the pump hopper)	3 times daily
		Yield stress	1 time daily (only when pouring sub-aqueously)

Other requirements around equipment calibration and volume monitoring were also developed as part of the QC/QA plan. Paste production equipment calibration confirms that the system is operating within performance specifications. Third party off-site testing was also implemented as part of the QA activities to verify on-site results. Documentation systems were developed for on-site tracking for paste backfill volumes produced and placed underground. Documentation of the produced and placed volumes is critical, since it will be included in the final report that will be sent to the regulatory body.

Execution

Proof of concept

After the design and planning phase was complete, a trial was conducted in 2015 as a proof of concept. The proof of concept was to help mitigate the uncertainties around the performance of the production system and the underground. There were three goals for the trial:

- Confirm the on-site tailings materials were suitable for paste backfill production at a larger scale.
- Confirm the equipment proposed was suitable for consistent paste production and delivery.
- Confirm that the system performance could meet the production throughput targets to meet the overall rehabilitation schedule.

As part of the trial, test pits were dug and samples were retrieved from the source material, and sent to the on-site laboratory for moisture content, rheological, and strength property testing. On-site flow loops were also used to determine any delivery restrictions. Finally, one of the stopes was used as a production test. The backfill system was set up to run for a two-week period to produce and deliver paste backfill. The trial was a success, and 2,500 m^3 of backfill was delivered to the underground stope. A progressive scan of the underground stope showing the paste floor rising up during the trial can be see below in Figure 2.

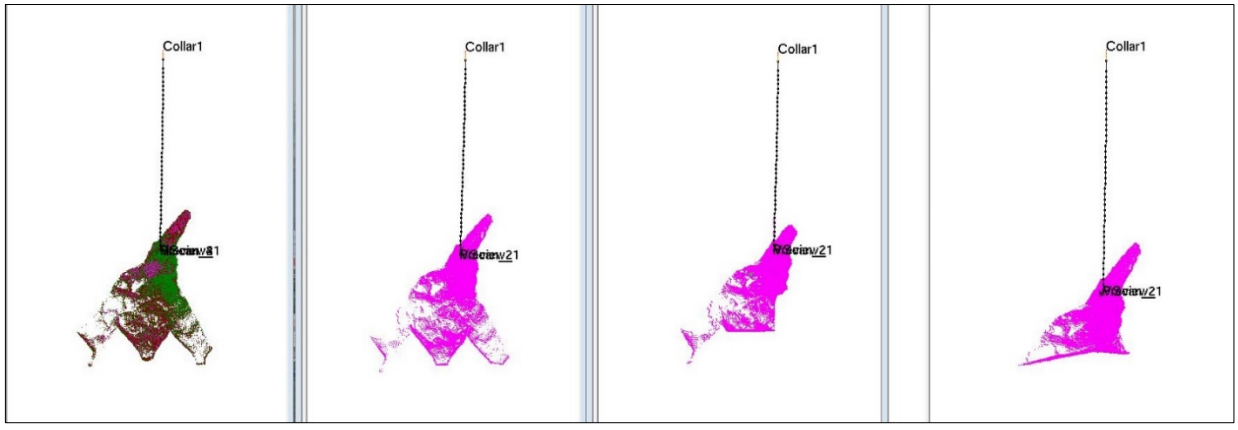

Figure 2: Progressive scan

Full-scale program planning

The learnings from the 2015 trial were incorporated into the final planning stages before the full execution program began in 2018.

Material sourcing and supply

Two stockpiles were created to manage the tailings materials (one for coarse material and one for fines). These two stockpiles were to be used as the source material for the full-scale backfilling program. It was noted during the 2015 trial program that the excavated tailings contained off-specification (off-spec) material, such as clay balls and organic materials like roots, branches, cobbles, and boulders. These off-spec materials could result in damage to the mixing equipment or plugs in the downstream pump and pipelines. To mitigate this risk, the stockpiles were screened prior to being delivered to the production sites. This had the added benefit of reducing the variation in the tailings moisture content. Prior to production start-up, samples were taken from the stockpiles to test the initial tailings parameters. Additionally, small paste batches were also produced for recipe testing to develop strength baselines and confirm binder contents. From the 2015 trial and during these batch tests, a 3:1 blend of coarse to fine material was determined to be the ideal ratio for bulk fill production. The addition of approximately 15% aggregate was added to this blend for barricade production.

Water and binder supply

Another learning from the 2015 trial was that a continuous water supply was required. In the trial, a water truck was used to feed the mixing operation, but there were too many stops and starts while waiting for the truck. In the design for the full-scale production, a water pumping scheme was implemented from the local lake to storage tanks at the stope sites. The storage tanks held enough water to supply the production equipment, and the pumping system was instrumented to control the tank level. With this system, the "permit to take water" requirements had to be monitored during production to make sure the daily limits were not exceeded.

Additionally, from the trial it was learned that the binder supply system needed modification to handle the full-scale binder quantity requirements. In the trial, the mixing truck drove to the main silo to fill up with cement powder, but this turnaround time would mean that production targets would not be met during full scale. A new system of a main silo near the entrance to site and remote silos at the production sites were implemented with an intermediate vehicle delivering from one to the other. This was required for two reasons: the site roads would not be able to accommodate a tanker from off-site, and the uranium tailings warranted keeping separation between highway vehicles and site vehicles.

Full-scale program results

The full-scale program began in April 2018 with mobilization and set-up taking approximately a month. Paste production began in May and finished for the season in October 2018. During the 2018 season, paste backfill was delivered to six stopes during the program with four being filled and completed and two being partially completed. Acceptable completion criteria for each stope was comprised of confirmation of tight filling of the void space and confirmation of the compressive strength of the backfill.

Production results

The on-site laboratory testing results for strength are shown below in Table 4, and the volume results for each stope are shown in Table 5. The 109 Stope was the flooded stope, and the data shows that the target strength took much longer to achieve in sub-aqueous deposition than in sub-aerial deposition.

Table 4: Laboratory results

Stope	No. of cylinders casted	Target strength (kPa)	Average actual strength (at 28 days)	No. of cylinders that missed target at 28 days	No. of cylinders that missed target at 56 days	Fail rate
3 Stope	70	500	813	1	0	0.0%
4 Stope	188	200/500	416/585	2	2	1.1%
5/5A Stope	510	500/1,000	604/2,412	10	7	1.4%
24 Stope	949	400	498	35	1	0.1%
42 Stope	333	500	716	4	2	0.6%
109 Stope	293	600	591	29	28	9.6%*

Table 5: Laboratory results

Stope	Target volume (m^3)	Actual volume (m^3)	Difference	Rehabilitation status
3 Stope	1,0951	816	10,135	Partially rehabilitated
4 Stope	3,203	3,078	126	Fully rehabilitated – hazards eliminated
5/5A Stope	15,463	17,412	–1,949	Fully rehabilitated – hazards eliminated
24 Stope	9,493	16,299	–6,806	Fully rehabilitated – hazards eliminated
42 Stope	19,126	15,235	3,891	Partially rehabilitated

During paste execution, progress figures were used as a visual tool to demonstrate progress and the tight filling of the stope. These progress figures are generated from the data produced from the cavity

monitoring scans. Figure 3 below is an example of a progress figure that shows one of the stopes that has been completed.

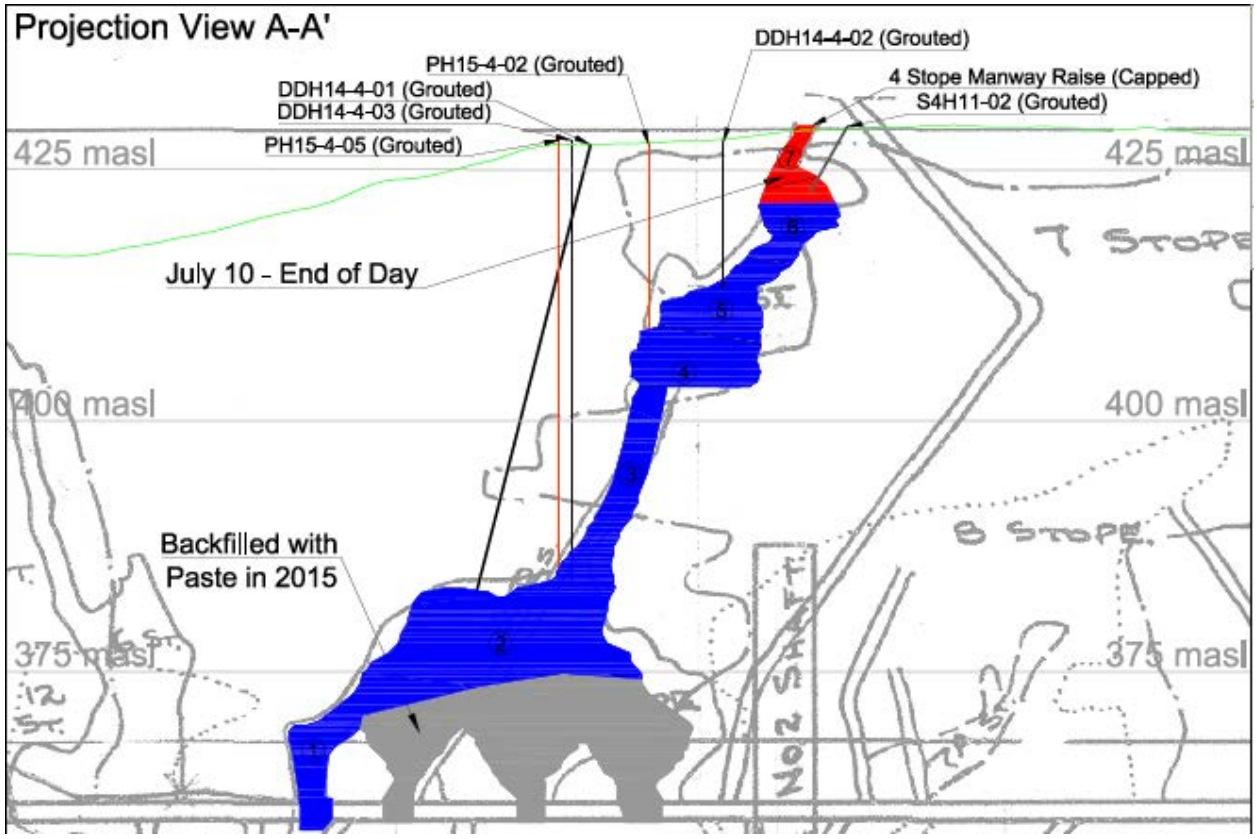

Figure 3: Progress figure

Production analysis

For the 2018 paste program, three independent methods of volume calculations were utilized. The first is based on the mixer truck calibrations, the second is based on the in-line flowmeter designed for this type of application, and the third is based on the delivery pump strokes. The data demonstrated that the truck counts and pump strokes were very consistent (within 3–4%) with the readings of the flowmeter. This gave confidence that volumes recorded over the program were accurate. Originally estimated stope volumes were also compared to actual volumes placed, which helped provide accuracy assessments on the CMS scans.

A pour profile was completed for each borehole that received paste during production. This analysis indicates the relative volumes of paste poured into each borehole in terms of the date of the pour and the recipe used. The pour profiles also display the laboratory strength data for the paste poured into each borehole.

Other production analysis included relating the volume of paste poured to the slump and binder content used, water consumption, solids content, production hours per day, and flow rate profile.

Learnings

During the execution plan there were several learnings that were identified. Where possible, the process was adjusted to incorporate the learning. The learnings can broadly be categorized into two main areas: material handling and underground.

The main learnings in material handling were around the blending and stockpiling of tailings. One example is that the tailings for backfill were stockpiled on unreclaimed tailings that still had the previous cover intact. The excavator operators had difficulty determining when they had reached the ground level of the stockpile, so would accidently dig down into the unreclaimed tailings, which resulted in off-spec material, including organics and oversized material being delivered to the system. The learning for the operators was to leave 1–2 m of stockpiled material as a base layer to avoid this problem.

In each stope there had been investigations to understand the void space and any connections to the rest of the workings. These were largely completed with the cavity monitoring survey (CMS) tool. This tool provides excellent information, but one learning was that the CMS does not always "see" or interpret everything. For example, the CMS cannot distinguish between rock and timber. In one stope, it was discovered that the floor the CMS had found was actually old timber platforms, not rock, and there were additional void spaces underneath the platforms. The CMS could not pick up these details, so additional borehole camera inspections were added to visually confirm features; e.g., floors, walls, and void spaces.

Conclusion

When considering the rehabilitation of underground workings at a historical mine, one of the main concerns is the uncertainty around the accuracy and availability of information about the site. The initial investigation is a key first step in understanding the limitations of the site. Rehabilitation options, development, and selection for physical hazards should take into consideration the site-specific circumstances, such as access, available laydown areas, material supply/delivery, and proximity of the openings/voids to sensitive receptors. Once the critical planning steps have been established, the execution of the rehabilitation option(s) begins. During backfill execution in particular, there is potential for changed condition events; therefore, the rehabilitation program needs to be planned out in sufficient detail and be flexible enough to respond to what is happening underground and on surface.

In spite of all the complexities around historical mine rehabilitation, with sufficient planning and a flexible solution, as is demonstrated by the case study, it is possible to eliminate historical physical hazards efficiently and effectively.

Proceedings of Tailings and Mine Waste 2019
November 17–20, 2019, Vancouver, Canada
Published by the University of British Columbia, 2019

Assessment of Different Reclamation Scenarios for the Abandoned Principale Mine Site (Quebec, Canada) Using Laboratory Column Tests

Abdelkabir Maqsoud, UQAT-RIME, Canada
Bruno Bussière, UQAT-RIME, Canada
Hassan Bouzehzah, University of Liège, Belgium
Sophie Turcotte, MERN, Canada

Abstract

The abandoned Principale mine site is located near Chibougamau, Quebec. During the mine's operation, tailings were produced and stored in three tailings storage facilities (TSFs): A, B, and C. These TSFs cover an area of approximately 170 hectares (ha) and have been identified as acid mine drainage (AMD) generating. The reclamation of this site has become necessary in order to limit the production of AMD.

Laboratory-based, instrumented experimental columns were used in this study in order to select an appropriate reclamation scenario for the Principale mine site. Three scenarios were tested:

1. a monolayer cover with a high elevated water table (EWT);
2. a monolayer cover with a low EWT; and
3. a cover with capillary barrier effects (CCBE).

The tailings used in these experimental columns were sampled from TSFs A, B, and C. Each column was submitted to wetting and drying cycles (>10 cycles) and, after each flush, leachates were collected from the base of the columns and analyzed for various physicochemical parameters.

Results showed that the monolayer cover with a high EWT effectively reduced AMD generation, and thus could be used in the remediation of the Principale mine site. The efficiency of this type of cover was equivalent to that of the CCBE, which is frequently regarded as the most appropriate reclamation technique for mine sites in humid climates. Finally, tailings from TSF C were found to be non-acid-generating and, therefore, could be recycled as cover materials.

Introduction

The Principale mine site is located on Merrill Island in Lac aux Dorés, about 5 km southeast of the city of

Chibougamau, Quebec, Canada (Gauthier et al., 2011.) Mining of the deposits began in the 1950s and generated approximately 26 million tonnes of ore (1.6% Cu and 0.3 g Au/t) from at least twelve separate deposits in the region. Tailings produced during mining activities were deposited in three tailings storage facilities (TSFs): A, B, and C. The total surface of these TSFs is about 170 ha (Figure 1).

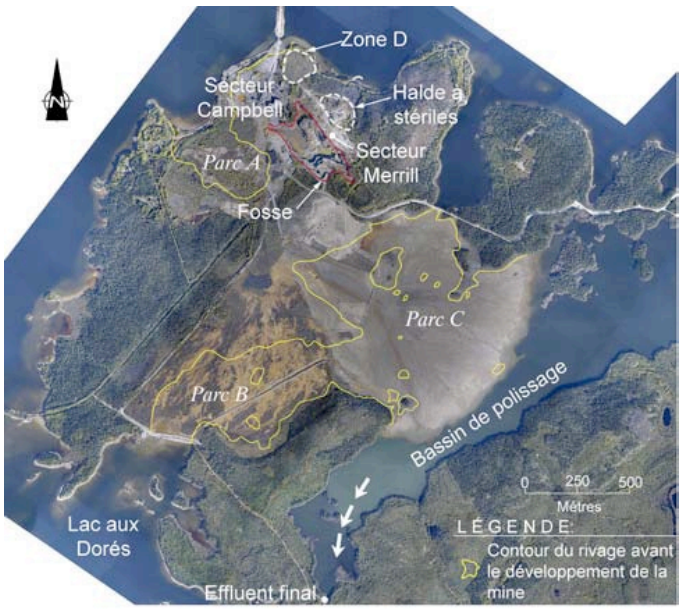

Figure 1: Site map of Principale mine; TSFs designated as Parc A (TSF A), Parc B (TSF B), and Parc C (TSF C)(after Gauthier et al., 2011)

After mining ceased, the Principale mine site was abandoned, due to the insolvency of Campbell Resources, and taken over by the Ministry of Natural Resources (MNR) in May 2010. Prior characterizations of the tailings suggested that they were potentially acid-generating (Golder, 2011; Gauthier et al., 2011). Given the problems associated with the production of acid mine drainage (AMD), the reclamation of this site has, therefore, become necessary in order to limit negative impacts on the environment.

Different management options and rehabilitation strategies are available to avoid the AMD production. Under the humid climate prevailing in most of the Canadian provinces, techniques to limit oxygen availability are considered the most viable option (e.g., SRK, 1989; MEND, 2001). Among these oxygen barriers one can find i) covers with capillary barrier effects (CCBE), and ii) monolayer covers combined with an elevated water table (EWT).

The CCBE (e.g., Nicholson et al., 1989; Aubertin et al., 1995; Bussière et al., 2006) relies on the water retention contrast between two superimposed materials (fine-grained over coarse-grained materials), to create a capillary barrier effect that limits the vertical flow of water at the interface. When overlapped by a coarse material layer, the CCBE maintains the fine-grained material layer near saturation.

The concept behind monolayer cover combined with an EWT is to raise or maintain the water table at a position that allow maintaining the reactive tailings at a sufficiently high degree of water saturation. This high degree of saturation will prevent tailings oxidation (more details can be found in Ouangrawa et al., 2009; Maqsoud et al., 2013; 2015; Demers et al., 2013; Ethier et al., 2018).

Physical models (i.e., laboratory-based, instrumented columns) were used to test and evaluate the performance of different scenarios proposed for the reclamation of the Principale mine site. In this article, configurations of the experimental columns are first presented following a characterization of physical, chemical and hydrogeological properties of used materials. Then, the results of the physicochemical analyses of the column leachates that simulate different scenarios are presented and a conclusion is offered. It is worth mentioning that performance evaluations of the different reclamation scenarios were performed in this study using hydrogeological behavior, oxygen fluxes and effluent qualities. Due to space constraints, only effluent quality results for the ten column configurations are presented in this paper.

Materials characterization

Small excavations were performed to reach the non-oxidized tailings in TSFs A, B, and C. The collected tailings were manually homogenized in the laboratory and subsamples were taken for various characterizations; the remaining materials were used in the construction of the instrumented columns. Two other materials, a sand and a silt, were also sampled and used as cover materials.

All materials, including the three tailings, the sand, and the silt, were characterized for the following parameters and properties:

1. Grain-size distribution – Malvern Mastersizer laser particle size analyzer (covering particle sizes between 0.05 μm and 900 μm – Merkus, 2009).
2. Specific surface area (SSA) – Micromeritics Gimini III 2375 surface area analyzer (ASTM C1069 – 09).
3. Specific gravity (G_s) – Micromeritics Accupyc 1330 helium pycnometer (ASTM D854 – 14).
4. Mineralogical composition – X-ray diffraction (XRD) and scanning electron microscopy (SEM).
5. Acid-base accounting (ABA) – acid-generating potential (AP) obtained from %S, neutralization potential (NP) obtained using the Sobek method modified by Lawrence and Wang (1997).
6. Saturated hydraulic conductivity (k_{sat}) obtained using rigid-wall permeameter test (ASTM D5084).
7. Water retention curves (WRCs) obtained using Tempe cell tests (ASTM D 5856-95).

More details on the methods used for material characterizations can be found in Pabst et al. (2010), Demers et al. (2013) and Bussière et al. (2011). The main results of these characterizations are presented in Table 1. Results show that tailings from TSF B were finer than tailings from TSF A and C, and thus had a slightly higher surface area (1.85 vs. 1.19 and 1.13 m^2/g, respectively). The k_{sat} values of tailings from TSF A and B were within the same order of magnitude (10^{-5} cm/s). However, the k_{sat} of the tailings from TSF C was approximately 10^{-4} cm/s. The air entry values (AEVs), i.e., the pressure at which the desaturation begins, obtained from the measured water retention curves, were between 10 and 12 kPa, 14 and 17 kPa and 7 and 8.5 kPa, for the tailings from TSF A, B and C respectively.

The tailings from TSF A contained much more sulphur (17.58%) than the tailings from TSF B (7.27%) and C (2.27%). Tailings from TSFs A and B were classified as acid-generating according to the net neutralization potential (NNP) criterion (NNP = –546 and –159 kg $CaCO_3$/t, respectively), whereas tailings from TSF C were non-acid generating (NNP = 27 kg $CaCO_3$/t; for more information on NNP criterion, see Miller et al., 1991).

Table 1: Material characterization

	Parameters	Tailings A	Tailings B	Tailings C	Sand	Silt
Physical	D_{10} (µm)	12.99	4.16	22	168.3	5
	D_{60} 9µm)	181.78	79.78	202	361.9	91
	C_u	14	19.2	9	2.15	18.3
	SG	3.32	3.72	2.89	2.75	2.73
	SSA (m^2/g)	1.19	1.85	1.13	1.18	1.42
Chemical	Sulphur (% p/p)	17.58	7.11	2.19		0.22
	AP	549.30	222.30	68.50	0.40	0.00
	NP	3	63	95	6	74
	NNP	–546	–159	27	5	74
Hydrogeological	Porosity	0.38	0.39 – 0.42	0.41 – 0.42	0.28 – 0.29	0.39 – 0.40
	k_{sat} (cm/s)	9.1×10^{-5} – 9.2×10^{-5}	1.5×10^{-5} – 2.9×10^{-5}	$2{,}0 \times 10^{-4}$ – 2.7×10^{-4}	2.7×10^{-3} – 3.6×10^{-3}	3.9×10^{-5} – 5.6×10^{-5}
	AEV (kPa)	10 – 12	14 – 17	7 – 8.5	4.8	12

Column configurations, instrumentation, and test procedures

To select the best reclamation technique for the Principale mine site, various configurations were tested. In these configurations, the following parameters were varied:

1. water table depth;
2. nature of tailings; and

3. type of cover (monolayer versus multilayer).

The scenarios tested were (Maqsoud et al., 2017):

1. control columns without any cover (1, 2, 3);
2. monolayer cover with a low elevated water table (EWT) (4, 5, 6,7, 8);
3. monolayer cover with a high EWT (9, 10, 11,12, 13); and
4. cover with capillary barrier effect (CCBE – 14).

In this paper, an emphasis was placed on the effects of the nature of tailings and the location of the EWT. These column configurations are described in more detail in Table 2. In the monolayer cover columns, the location of the EWT was set using the AEV as obtained from the WRCs for tailings from TSFs A, B, and C (Table 1). For the low EWT, the water surface was located at the AEV and, for the high EWT, the water table was located at ½ AEV. This last value was suggested by Ouangrawa et al. (2009) with the objective to reduce the risk of tailings desaturation.

Each column was submitted to wetting and drying cycles. Cycles began with a wetting period, at the start of which 2 L of deionized water was added to the top of each column. The water was left to percolate through the materials for approximately 7 days, then the leachate was collected from the base of the column. Subsequently, the columns were allowed to remain dry for four weeks. After each flush, the collected leachates were analyzed for: pH, Eh, and electrical conductivity (EC) using electrodes; total metal concentrations using inductively coupled plasma atomic emission spectrometry (ICP-AES); and acidity and alkalinity using titration with 0.02M NaOH and 0.02M H_2SO_4, respectively (method APHA 2310, 1995).

Table 2: Experimental column configurations

Column	Number#	Configuration
Controls	1	0.4 m of tailings from TSF A; water table maintained at 1.5 m
	2	0.4 m of tailings from TSF B; water table maintained at 1.5 m
	3	0.4 m of tailings from TSF C; water table maintained at 1.5 m
Monolayer + low EWT	4	0.4 m of tailings from TSF B; water table maintained at 1.4 m
	5	0.4 m of tailings from TSF C; water table maintained at 0.54 m
	8	0.4 m of tailings from TSF A; water table level is maintained at 0.66 m
Monolayer + high EWT	9	0.4 m of tailings from TSF B; water table maintained at 0.7 m
	10	0.4 m of tailings from TSF C; water table maintained at 0.27 m
	13	0.4 m of tailings from TSF A; water table level maintained at 0.33 m
CCBE	14	0.4 m of tailings from TSF B covered with a CCBE; the protective and capillary break layer were made of a sandy material and the moisture-retaining layer was made of a silty material; water table maintained at 1.5 m below the base of the column.

Results

Physical modeling for uncovered and covered materials from TSF A

The results of the column tests with tailings from TSF A, including the uncovered control (1) and two monolayer cover designs (8, 13), are presented in Figure 2.

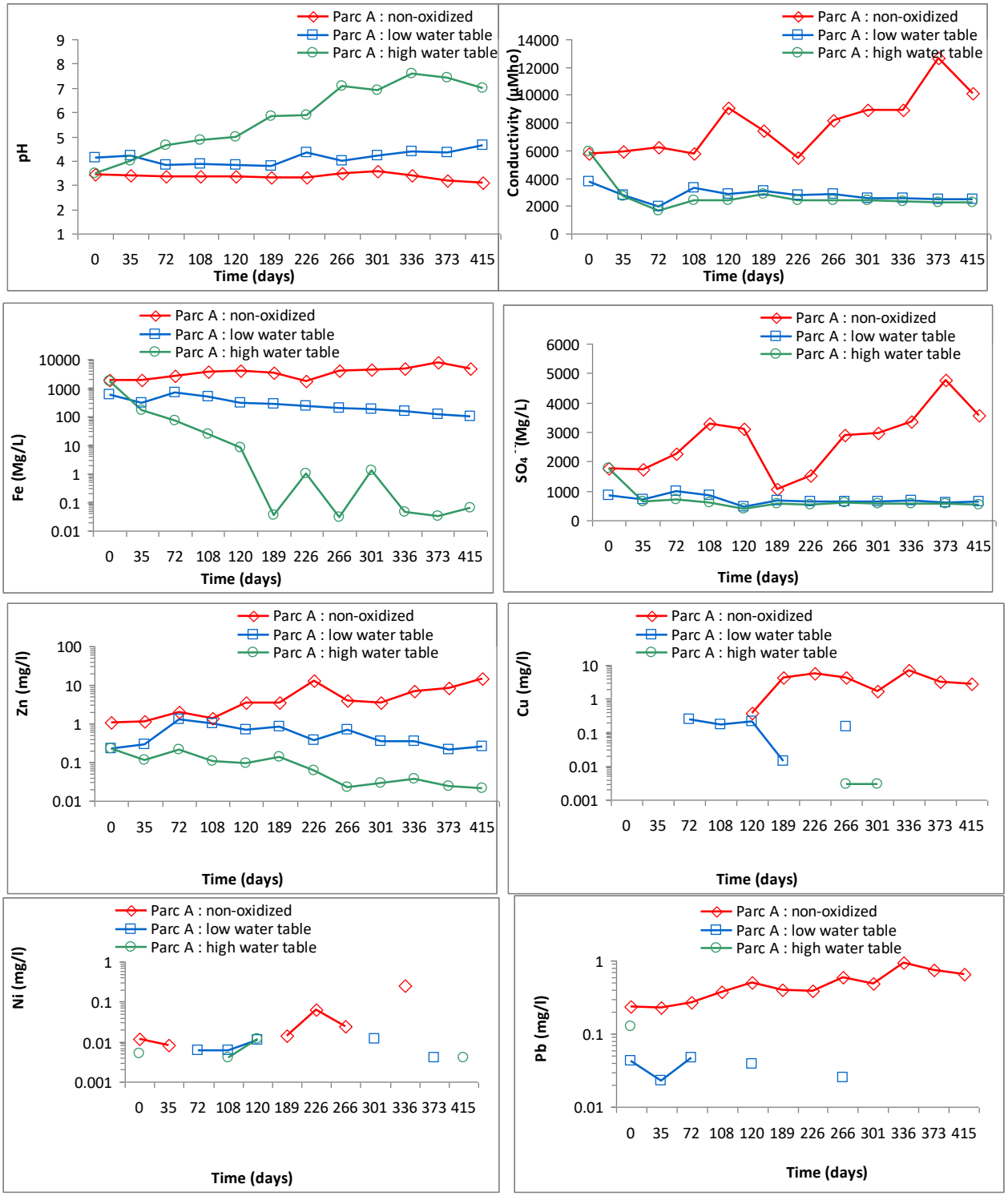

Figure 2: Physicochemical evolution of leachates for covered and uncovered tailings from TSF A

For the monolayer cover with the low EWT, the pH of the leachates ranged between 3.8 and 4.6. These values were slightly higher than the uncovered physical model (pH 3.1 to 3.6). However, for the configuration with high EWT, pH values ranged between 3.5 and 7.6. For this last configuration, the pH showed an upward trend from the beginning to the end of the tests. The EC of the leachates also showed the same behavior. For the monolayer cover with the low EWT, EC values ranged between 1,967 and 3,750 µS/cm, while values were between 1,682 and 2,400 µS/cm for the cover with the high EWT.

For the columns with monolayer + EWT covers, the concentrations of SO_4 and Fe generated by sulphide oxidation were lower than those generated by the uncovered tailings. More specifically, SO_4 concentrations were relatively stable and remained around 640 and 550 mg/L for the low and high EWT columns, respectively. The Fe concentrations showed a downward trend that was particularly notable in the column with high EWT. During the last flush, Fe concentrations remained around 110 mg/L for the low EWT, while they were below 1 mg/L for the high EWT.

For the monolayer cover with a low EWT, concentrations of Cu (0 and 0.244 mg/L), Ni (0 and 0.012 mg/L), and Pb (0 and 0.047 mg/L) remained below the regulation criteria in Quebec (MELCC, 2019). But, concentrations of Zn (0.22 and 1.32 mg/L) sometimes exceeded environmental standards (0.5 mg/L). For the monolayer cover with a high EWT, concentrations of Zn (0.022 to 0.224 mg/L), Cu (< 0.003 mg/L), Ni (0.004 to 0.012 mg/L) and Pb (0 to 0.127 mg/L) always remained below limits imposed by the regulator.

Physical modeling for uncovered and covered materials from TSF B

The results of the column tests with tailings from TSF B, including the uncovered control (2), two monolayer cover designs (4, 9), and CCBE (14), are presented in Figure 3. Leachate pH values ranged from 6.4 to 8.0 for the low EWT configuration, 6.6 to 8.1 for the high EWT configuration, and 7.1 to 7.8 for the CCBE configuration. These values were slightly higher than those obtained from the uncovered column (between 6.6 and 7.6); the implementation of the covers allowed a pH increase of approximately one unit.

The EC ranged between 1,845 and 3,970 µS/cm for the low EWT column, between 1,899 and 3,850 µS/cm for the high EWT column, and between 2,420 and 4,010 µS/cm for the CCBE configuration. These values were generally lower than those measured in the uncovered configuration (between 2,940 and 4,470 µS/cm). After the 4th cycle, a decreasing trend was observed in EC values, and by the 12th cycle (336 days) values were 2,440, 2,280, and 2,580 µS/cm, respectively, for the high EWT, low EWT, and CCBE configurations. In contrast, the EC in the uncovered column at 336 days was 3,080 µS/cm.

Sulphate concentrations decreased progressively over time, although, as early as the 7th cycle (196 days), values became relative stable. At the 12th cycle (336 days), concentrations were 556, 562, and 563 mg/L, respectively, for the high EWT, low EWT, and CCBE configurations. Thus, the covers reduced the

amount of sulphate in the leachates by 125, 119, and 118 mg/L, respectively, for the same columns as compared to the uncovered control (681 mg/L).

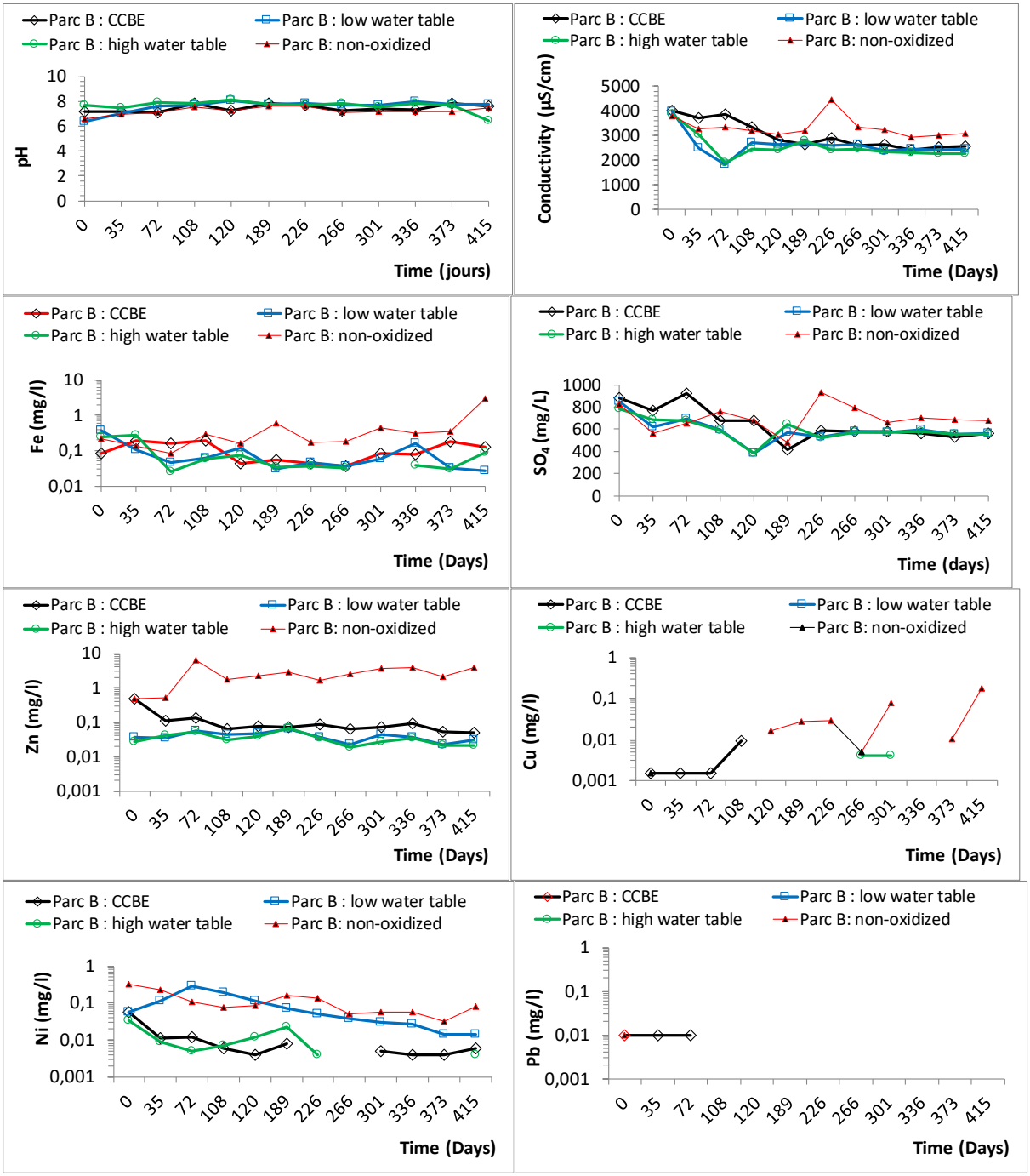

Figure 3: Physicochemical evolution of leachates for covered and uncovered tailings from TSF B

Iron concentrations were very low in the leachates from all columns, both with and without cover, likely due to the precipitation of Fe in the columns. Concentrations were between 0.031 and 0.28 mg/L for the low EWT, between 0.027 and 0.36 mg/L for the high EWT, and between 0.037 and 0.194 mg/L for the

CCBE. At the 12th cycle (336 days), concentrations remained below 0.2 mg/L for all columns (0.027 mg/L for the low EWT, 0.09 mg/L for the high EWT, and 0.128 mg/L for CCBE).

For the covered columns, Cu and Pb concentrations remained below the detection limit by ICP-AES. In contrast, Ni concentrations ranged from 0.014 to 0.286 mg/L for the low EWT, from 0.004 to 0.036 mg/L for the high EWT, and from 0.004 to 0.056 mg/L for the CCBE. Zinc concentrations were between 0.062 and 0.475 mg/L for the low EWT, between 0 and 0.069 mg/L for the high EWT, and between 0.022 and 0.065 mg/L for the CCBE. Nonetheless, the concentrations of these elements was below provincial regulatory requirements (Directive 019).

Physical modeling for uncovered and covered materials from TSF C

The results of the column tests with tailings from TSF C, including the uncovered control (3) and two monolayer cover designs (5, 10), are presented in Figure 4. Leachate pH values were between 7.1 and 8.0 for the monolayer cover with a low EWT and between 7.0 and 8.3 for the high EWT configuration. These values similar to those measured in the uncovered configuration (6.9 and 8.3), thus suggesting that the implementation of cover on tailings from TSF C did not have a significant influence on pH variation.

The EC values were between 1,378 and 4,820 µS/cm for the low EWT configuration and between 807 and 4,850 µS/cm for the high EWT configuration. The highest values were measured during the first flush and, by the final flush, EC values were 2,160 and 2,260 µS/cm, respectively, for the low and high EWT configurations.

Sulphate concentrations ranged from 347 to 878 mg/L for the low EWT configuration and from 87 to 894 mg/L for the high EWT configuration. At the 12th flush, the concentrations were 87 and 440 mg/L, respectively, for the high and low EWT configurations. This represents a reduction of 655 and 302 mg/L compared to concentrations in leachates from the uncovered tailings (742 mg/L).

Iron concentrations were very low in the leachates from all columns made with tailings from TSF C, both covered and uncovered. Concentrations were between 0.037 and 0.246 mg/L and between 0.009 and 0.394 mg/L, respectively, for the low and high EWT configurations. At the twelfth flush, Fe concentrations were 0.058 and 0.009 mg/L, respectively, for the same columns. For Pb, Cu, Ni, and Zn, concentrations remained below the provincial regulatory limits at all times (Directive 019).

Conclusion

For the uncovered configurations, pH values were close to 3.4 for tailings from TSF A, and greater than 6.5 for tailings from TSF B and C. Iron and sulphates concentrations and EC values were higher for tailings from TSF A than the other tailings. Based on these results, and those of the net neutralization potential tailings from TSF C can be considered as non-acid-generating and these materials could be used as

construction material for a CCBE. However, tailings from TSFs A and B are classified both as acid-generating or metal leaching tailings.

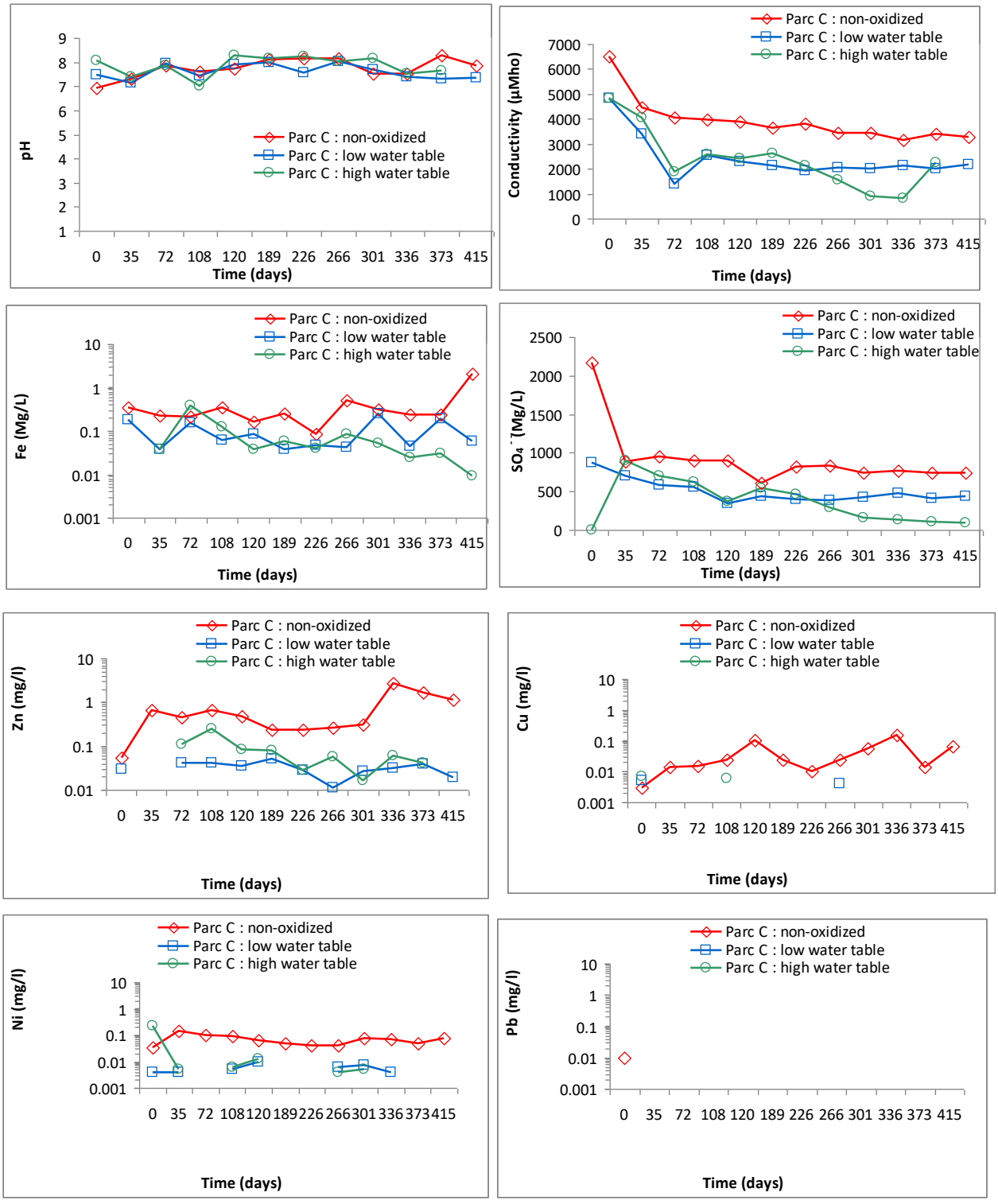

Figure 4: Physicochemical evolution of leachates for covered and uncovered tailings from TSF C

For the columns with EWTs, pH values were higher than 7, except for the column with tailings from TSF A and a low EWT. Iron and SO_4 concentrations and EC values decreased progressively and the concentrations of Zn, Cu, Ni, and Pb remained below the provincial regulatory limits (Directive 019). For tailings from TSF B, the performance of the high EWT was similar (or at times greater) than that of the CCBE. Tests showed that the height of the EWT played an important role in controlling sulphide oxidation and the release of contaminants. The sulphide oxidation was limited most when the EWT was located at ½ of the AEV, and this objective should be used as a minimum design criterion.

For the tailings from TSF A, results showed that the tailings could be reclaimed using a monolayer cover with a high EWT. Since the acid-generation potential of the tailings from TSF A was very high, it will be critical to ensure that, if an elevated EWT is used, the water table level is well controlled. Otherwise, the use of the CCBE technique would be more appropriate, since it would reduce the system's dependence on the location of the EWT (Bussière et al., 2006).

References

ASTM D 5856-95 2002. Standard test method for measurement of hydraulic conductivity of porous material using a rigid-wall, compaction-mold permeameter.

ASTM D6836-02. 2008. Standard test methods for determination of the soil water characteristic curve for desorption using a hanging column, pressure extractor, chilled mirror hygrometer, and\or centrifuge. *Annual Book of ASTM Standards* 04.08. 10.1520/D6836-02R08E02.

Aubertin, M., R.P. Chapuis, M. Aachib, B. Bussière, J-F. Ricard and L. Tremblay. 1995. *Évaluation en Laboratoire de Barrières Sèches Construites a Partir de Résidus Miniers, École Polytechnique de Montréal, Rapport NEDEM/MEND Projet 2.22.2a, p. 164*.

Bussière B., A. Maqsoud, M. Aubertin, J. Martschuk, J. McMullen and M. Julien. 2006. Performance of the oxygen limiting cover at the LTA site, Malartic, Québec. *Environmental Society of CIM* 99(1096), Paper 20: 1–11.

Bussière, B., A. Maqsoud, I. Demers, and M. Rousselle. 2011. *Modélisation physique de divers scénarios de recouvrement et étude du comportement hydrogéologique: site Manitou.* URSTM report presented to MRNF. Rouyn-Noranda.

Demers, I., B. Bussière, M. Aachib and M. Aubertin. 2011. Repeatability evaluation of instrumented column tests in cover efficiency evaluation for the prevention of acid mine drainage. *Water, Air and Soil Pollution*, 219: 113–128.

Demers, I., B. Bussière and M. Rousselle. 2013. Laboratory evaluation of reclamation scenarios for the spillage areas of the abandoned Manitou mine site using Goldex tailings. *Proceedings of the 23rd World Mining Congress*, Montreal.

Ethier, M.P., B. Bussière, M. Aubertin, A. Maqsoud, I. Demers and S. Broda. 2018. In-situ evaluation of the performance of the reclamation measures implemented on an abandoned reactive tailings disposal site. *Canadian Geotechnical Journal*, 55(12): 1742–1755.

Gauthier, M., M. Poulin and V. Bertrand. 2011. *Conditions hydrogéologiques et géochimie des résidus du site minier abandonné de la mine Principale à Chibougamau. GeoHydro, Québec du 28 au 31 Août 2011*

Golder Associates. 2011. *Caractérisation environnementale de la Mine Principale.* Report, presented to MERN, 009–10-1221-00811/3000&4000 Rev0.

Lawrence, R.W. and Y. Wang. 1997. Determination of neutralization potential in the prediction of acid rock drainage. *In Proceedings of 4th ICARD* 1: 451–464.

Maqsoud, A., B. Bussière and H. Bouzahzah. 2017. *Modélisation physique de divers scénarios de réhabilitation du site Mine Principale. Rapport final, URSTM-projet PU-2013-10-844, 794 pour le compte du MRNF.*

Maqsoud, A., M. Mbonimpa, B. Bussière and M. Benzaazoua. 2015. The hydrochemical behaviour of the Aldermac abandoned mine site after its rehabilitation. *Proceedings of the 68th Canadian Geotechnical Conference and the 13th Joint CGS/IAH-CNC Groundwater Conference,* Quebec City**.**

Maqsoud, A., M. Mbonimpa, B. Bussière, and J. Dionne. 2013. *Réhabilitation du site minier abandonné Aldermac, résultats préliminaires du suivi de la nappe surélevée***.** *Proceedings of the the 66th Canadian Geotechnical Conference and the 11th Joint CGS/IAH-CNC Groundwater Conference,* Montreal.

MELCC. 2019. Quebec. Retrieved from http://www.environnement.gouv.qc.ca/milieu_ind/directive019/.

MEND. 2001. *MEND Manual*, Report 5.4.2, Volume 4 – Prevention and Control, Secretariat CANMET.

Merkus, H.G. 2009. Particle size measurements: Fundamentals, practice, quality. Springer Particle Technology Series 17.

Miller, S.D., J.J. Jeffrey and J.W.C. Wong. 1991. Use and misuse of the acid-base account for AMD of acid generating tailings. 2nd International Conference, Abatement of Acidic Drainage, Montreal, Canada, 3: 489–506.

Nicholson, R.V., R.W. Gillham, J.A. Cherry and E.J. Reardon. 1989. Reduction of acid generation in mine tailings through the use of moisture-retaining cover layers as oxygen barriers. *Canadian Geotechnical Journal*, 26: 1–8.

Ouangrawa, M., J. Molson, M. Aubertin, B. Bussière and G.J. Zagury, G.J. 2009. Reactive transport modelling of mine tailings columns with capillarity-induced high water saturation for preventing sulphide oxidation. *Applied Geochemistry,* 24: 1312–1323.

Pabst, T., M. Aubertin, B. Bussière and J. Molson. 2010. Analysis of monolayer covers for the reclamation prediction. *Proceedings of 63rd Canadian Geotechnical Conference and 1st Joint CGS/CNC-IPA Permafrost Specialty Conference*, Calgary, Alberta: 1119–1127.

SRK (Steffen, Robertson, Kirsten). 1989. Draft acid rock technical guide. BC AMD Task Force, Vancouver, Canada.

Proceedings of Tailings and Mine Waste 2019
November 17–20, 2019, Vancouver, Canada
Published by the University of British Columbia, 2019

Challenges of Completing Dam Break Analyses on Large Copper Tailings Dams

Raúl Norambuena, SRK Consulting, Canada
Eloy Santos, Arcadis, Chile
José Campaña, Arcadis, Chile

Abstract

Recent cases of dam failures at Mount Polley (in Canada), as well as Fundão and Brumadinho (both in Brazil), demonstrate the catastrophic impacts of dam failures. These failures also highlight the importance of upholding high design, operation, and maintenance standards for large tailings dams. Various organizations, governing bodies, and public regulators around the globe now include requirements within their standards to analyze and estimate the potential consequences of hypothetical breaches in a dam. However, no unified and definite methodologies or procedures are currently available. The Canadian Dam Association (CDA) is in the process of putting together a technical bulletin on tailings dam break analysis that should be published later this year. However, in the absence of prescriptive guidelines, engineering practices internationally have adopted several custom procedures needed to complete dam break analyses.

As the trend in ore grades decreases and the processing capacity of mining facilities increases globally (Bowker and Chamber, 2015), the need for larger tailings storage facilities (TSFs) to be designed and operated grows. Dam heights are exceeding over 200 m and storage capacities are now exceeding 1,000 Mm^3 (million cubic meters). The work presented in this paper is based on the challenges found in dam break analysis, specifically on determining the breach parameters, on large Chilean copper TSFs. Through this work, issues were observed on the available methodologies currently used in various custom dam break analyses. Typically, these methodologies rely mostly on semi-empirical correlations (i.e., Rico et al., 2008; Small et al., 2017; Concha-Larrauri and Lall, 2018). Comments are also able to be made on the current state of the practice. Overall, these current semi-empirical relations were not seen as directly appropriate to be representative of large TSFs, such as for many Chilean TSFs. The challenge of determining the validity of the semi-empirical expressions for the breach parameters is discussed, followed by recommendations on what to look for when performing dam break studies on large TSFs.

Introduction: Current trend on high raise dams

The mining industry has experienced a great evolution in technology over the last century. This has resulted in increasing efficiency of metallurgical processes and is allowing for the reduction on the cut-off of what is an economically feasible ore grade. This is evidenced in the many tailings storage facilities (TSFs) and waste rock dumps that have been closed for many years but are now being reprocessed for significant economic returns. The increases of efficiency, together with the larger production capacity available today, is causing an increasing rate of waste generation. For example, the historical trend of copper mineral processing capacity (increasing total production with time) and copper ore grade (reduction with time) is depicted in Figure 1.

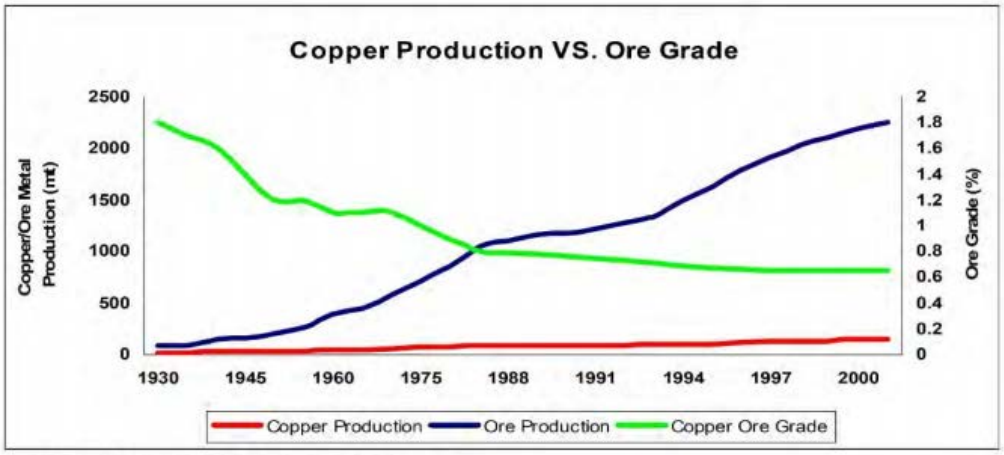

Figure 1: Evolution of copper production and the ore grade from the Raw Material Group of the World Bank (Bowker and Chambers, 2015)

The management of the increasing waste volumes has a direct impact on the overall size and magnitude of the TSFs and waste rock facilities. Mining companies are both developing greenfield projects and completing the expansion of operating facilities. Dam heights are now over 250 m, with storage capacities now exceeding 1.5 Bm^3 (billion cubic meters). Figure 2 summarizes a few examples of the evolution of copper TSFs' heights.

The International Commission on Large Dams (ICOLD), in its Bulletin 121, compiled several case studies on tailings dam failures. ICOLD has identified a decrease in the number of incidents in the past decades; potentially implying that risk assessment and safety management are improving. This is strong evidence of how mining companies and practitioners are developing more consciousness about the importance of safe practices for design, operation, and closure. Current practices and technologies for dam design and operation include strong characterization of the site foundation (e.g., site investigation and laboratory testing). Mining companies have been using more downstream and centreline construction methods (and less upstream methods), more thickening technologies, fines content limitation, compaction

control, redundant monitoring and instrumentation, robust drainage systems, optimization of the supernatant pond, freeboard management, and thorough closure planning.

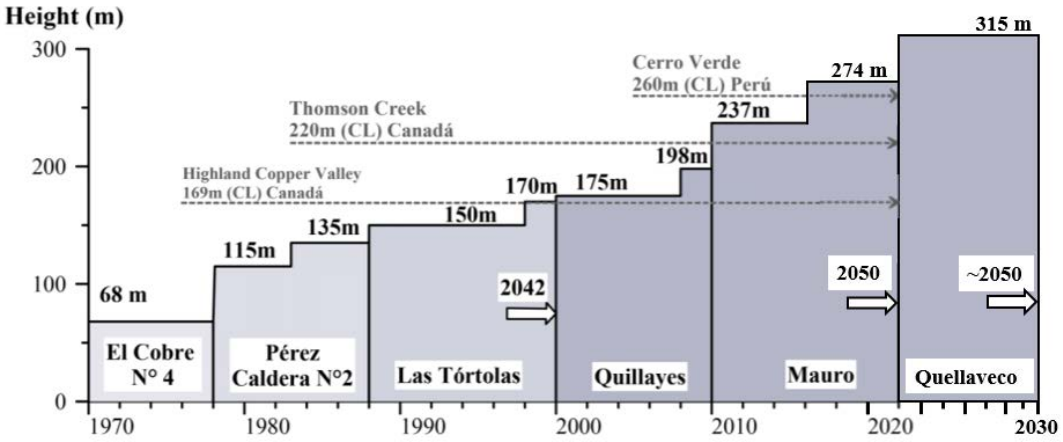

Figure 2: Evolution of the maximum height of tailings sands dams, modified from Valenzuela and Campaña, 2014

Bowker and Chambers (2015), a year after Mount Polley failure, revised and updated the ICOLD (2001) compilation, incorporating a risk approach. The cases studies were sorted by the magnitude of the consequences. This categorization demonstrated that while the numbers of cases during the past decades has been decreasing, the number of events with high severity consequences is on the rise. The increase in severe and very severe events could be attributed to the global need for larger and larger TSFs.

Technical reviews of the recent dam failures in Mount Polley (Canada), Fundão and Brumadinho (Brazil), and Cadia (Australia) show evidence that failure mechanism can be very complex, and even the highest standards of design, operation, and maintenance still contain inherent risk. This is why increasing focus on risk assessments is imperative. One component of the evaluation of the consequences should be carried out by a dam break analysis (DBA).

Some organizations and public regulators have included within their standards a requirement to analyze and estimate the potential consequences of a hypothetical breach in a dam. However, no methodologies or procedures are specified for this. Consequently, practitioners have adopted custom procedures to meet this requirement. These custom procedures are primarily based on historical data correlations and physical models developed for water-retaining dams.

Many advances have been developed in terms of the best practices in DBAs for tailings dams. In particular, many advances have been made since 2013, when the CDA formed a workgroup of experts and sponsored a series of workshops and conferences (James et al., 2017). The final objective of the CDA

workgroup was to consolidate the state of practice into guidelines for dam safety professionals (Martin et al., 2019).

The parameters for DBAs are difficult to define; moreover, the results are highly sensitive to the defined parameters (Martin and Akkerman, 2017). This difficulty is accentuated when the DBA is conducted for large copper dams, in which the geometry in terms of height and storage capacity is unprecedented, and the applicability of the recommended traditional empirical correlations and physical models developed for water dams is not clear.

Current practice on the dam break analyses on tailings dams

The practical use of the DBA in tailings dams is to develop emergency preparedness plans and consequence classification (CDA, 2007) and, depending on the stage of the assessed TSF, to revise the design or to provide mitigation measures. In particular, the Mining and Geological Service in Chile in Supreme Decree N°248 (Ministerio de Mineria, 2007) requires mining companies to estimate the distance reached by the released materials after a hypothetical breach in a dam. These results are usually presented as depth contours of the affected areas in the most likely inundation path. In addition, the decree requires the submission of an emergency preparedness manual for each tailings dam, in which the DBA is one of the main inputs. As in many other official documents, the requirement to perform a DBA is made explicit, but the procedure is not.

Several approaches to address this problem have been published by experts in the field, and lately many advances have been proposed towards establishing more standardized procedures using empirical correlations (Small et al., 2017). However, empirical correlations, as compared to methods based on first principals, can yield questionable results when applied to large tailings dams.

Large copper tailings dams

In Chile, one of the main copper producing countries in the world, there are currently at least seven copper tailings dams in operation, or in the process of ongoing construction or closure. The TSFs for these Chilean project sites have projected heights between 115 and 237 m, with 12 impoundments containing over 200 million cubic meters (Valenzuela, 2016).

Campaña et al. (2015) studied the Quillayes TSF. This TSF has been an example of successful design and operation, and is now in the process of closure, after ending operations almost 10 years ago. The Quillayes TSF was originally 175 m tall, but after great operational success, an expansion was carried out that resulted in this TSF reaching a height of 198 m, with an impoundment capacity of 360 million tons of dry tailings, approximately 250 Mm^3. The dam was constructed using the downstream method with a slope of 4:1 (H:V). The starter dam (cofferdam), was constructed using compacted earth, and its foundation

consisted of alluvial and colluvial deposits, underlain by a granodiorite that varied from weathered to moderately weathered with depth. The dam construction raises were then realized with hydraulic deposition of cycloned sand tailings (up to 18% fines content), which later were compacted to 95% standard proctor. Figure 3 shows a representative cross-section of the Quillayes TSF dam.

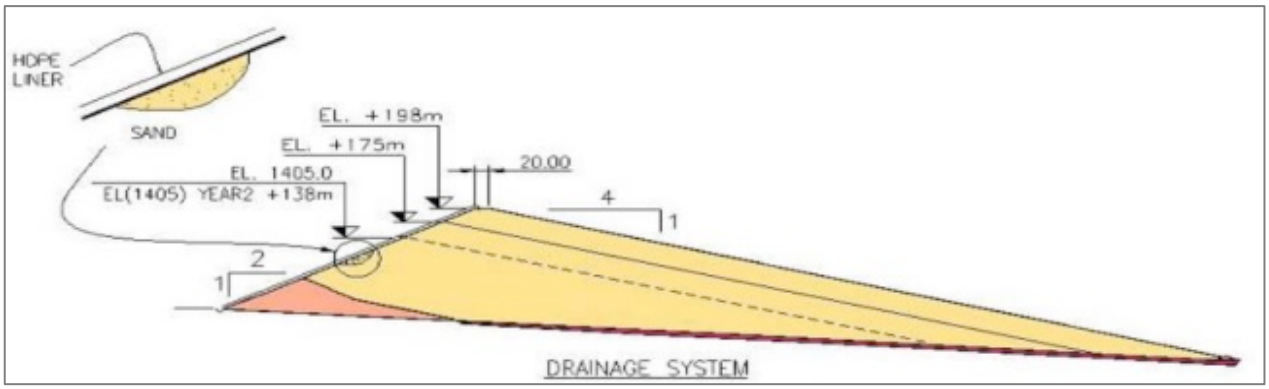

Figure 3: Quillayes tailings dam cross-section with elevations and slope details (Campaña et al., 2015)

Due to the success of the Quillayes TSF, and the need to keep up with the processing capacity of the mine, El Mauro TSF was designed and started to operate in 2009. The Quillayes TSF was designed with a maximum height of 237 m and a capacity of 1.7 billion tons (Antofagasta PLC, 2019). Quillayes and Mauro are two examples of large TSFs that required a DBA as part of the risk assessment and to fulfil Chilean regulatory standards.

The following subsections will provide some insights into the main breach parameters needed to perform a DBA on a large copper tailings dam, such as previously presented. Their applicability is discussed, and recommendations are provided.

Breach parameters for large copper tailings dam

Breach parameters allow for the determination of the geometry and distribution of the hydrograph, which represents a progressive breaching process in the retaining dam due to a specific mode of failure. The discharged volume, the breach formation time, and the peak outflow are the main parameters that determine a hydrograph. The breach hydrograph is one the most important elements in a DBA. Figure 4 presents a conventional hydrograph and its main elements. Hydrographs could be represented by simplified geometries such as a triangle or a Gaussian curve, where the height is the peak outflow, the width is the breach formation time, and the area below the curve is the discharged volume.

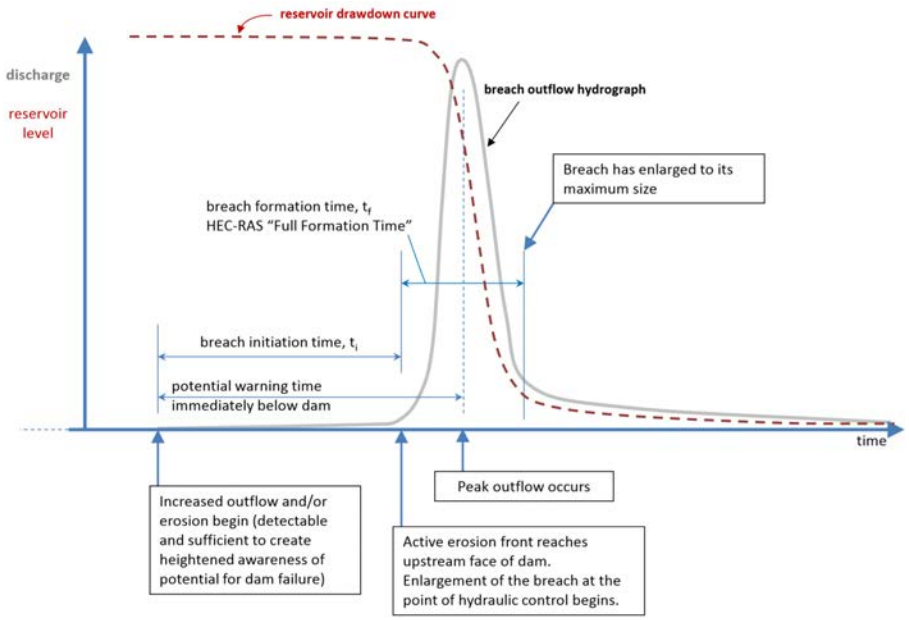

Figure 4: Identification of the preach parameters in a hydrograph (Wahl, 2014)

Discharged volume

One of the most important parameters to determine in a DBA in a TSF is the discharged volume. The discharge is difficult to define, but critical due to its significance for the DBA results. In contrast to water retention dams, the discharged volume from a TSF cannot be reasonably assumed as the total impounded tailings. This is unlike water tailings, which are classified as non-Newtonian fluids, i.e., they follow a visco-plastic behaviour in terms of stress and deformation. These fluids, at rest, can keep a residual angle of deposition, which has been a common observation in several case studies of past TSF failures.

Figure 5 presents two Chilean case studies, in which a terraced configuration resulted after failure, and the remaining tailings could be observed under the failure surface. The residual angle has been observed to be in the range of 2° and 9° for these cases.

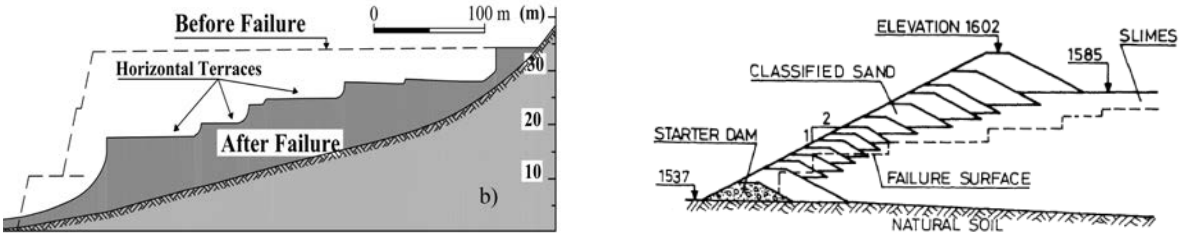

Figure 5: Residual angles after TSF failure, the left, Barahona N°1 TSF (Troncoso et al., 1993) and the right, El Cobre TSF (Dobry and Alvarez, 1967)

One approach to estimate potential discharged volumes is to use simple 3D models including the topography and the TSF geometry, together with the residual angles after failures presented previously.

Simple models such as that presented by McPhail (2015) using the residual angles obtained from case studies of failure surfaces.

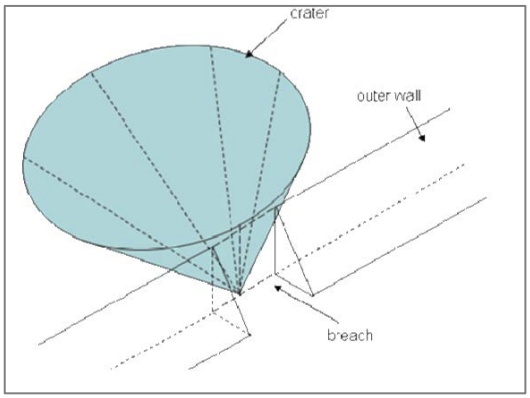

Figure 6: Simple conical geometry representing the mobilized tailings (McPhail, 2015)

Another more robust approach uses a statistical analysis. One of the most cited and used correlations between the impounded volume and the outflow volume, presented by Rico et al. (2008), is in Figure 5. The discharged volume is approximately 36% of the impounded volume. The Rico et al. study compiled several tailings case studies and generated some correlations to obtain breach parameters from the geometry of the assessed dam. Some of the case studies presented a discharged volume near 100% of the impoundment, and others below 10% of the impoundment, showing large variability. There are many other correlations with rigorous statistical analyses that provide robust expressions to obtain the discharged volume from the impounded volume (Concha-Larrauri and Lall, 2018). However, these expressions are not necessarily appropriate for extrapolation and application for dams over 200 m or with impounded volumes over 200 Mm^3.

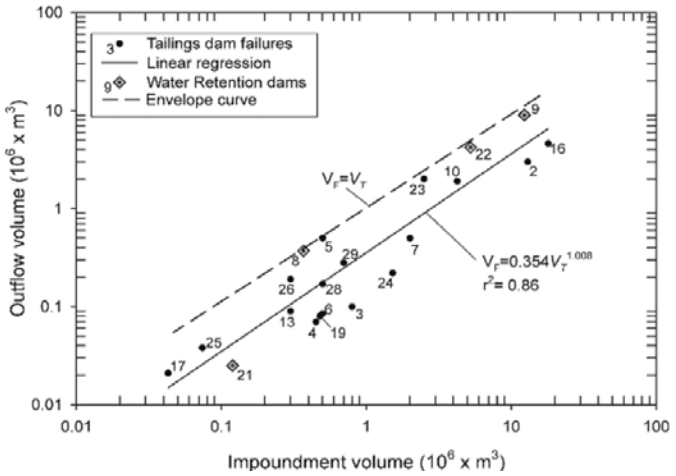

Figure 7: Outflow volume versus impoundment volume (Rico et al., 2008)

Alternative correlations were developed to estimate the discharge volume for large dams, such as in the CDA database, presented by Small et al. (2017). First, the database filters by mode of failure: slope seismic, slope static (seepage and static) and overtopping. It is reasonable to separate by failure mode, since the breaching mechanisms involved are different. The correlations obtain the discharged volumes by considering the dam height or the impounded volume. To consider the effect of large TSFs, for each mode of failure, sub-correlations were developed for short and tall dams and for small and large (containment volume) impoundments. These correlations are presented in the following figures (Figures 8, 9, and 10). The grey trend line represents the correlation for all the data available, while the blue trend includes the expression for the shorter/smaller TSFs, and the orange for the taller/larger TSFs.

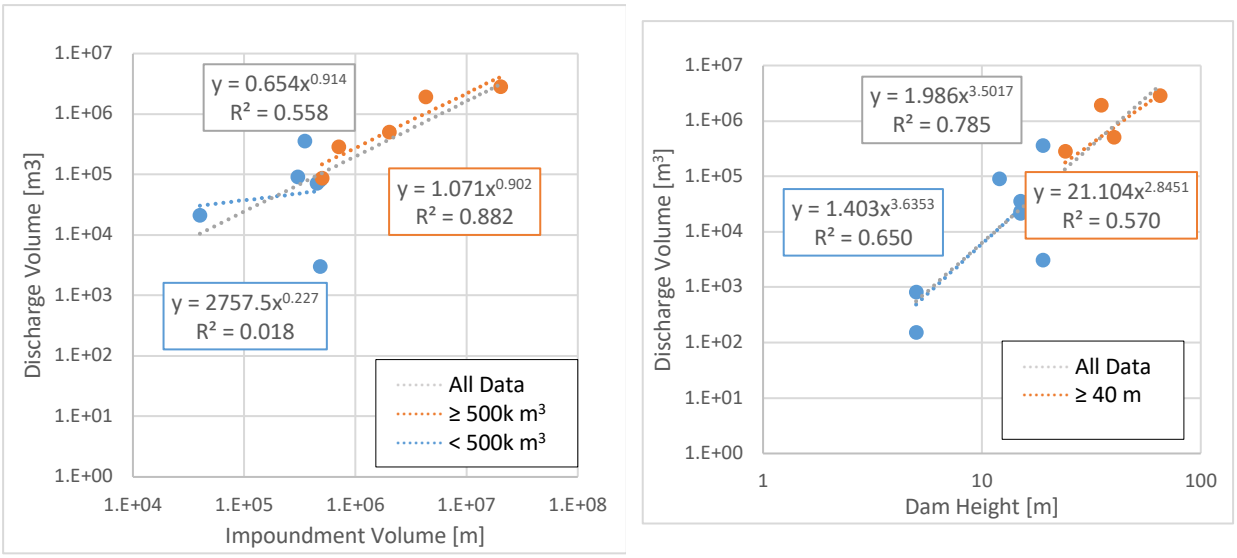

Figure 8: Correlations to obtain the discharged volume considering the seismic mode of failure

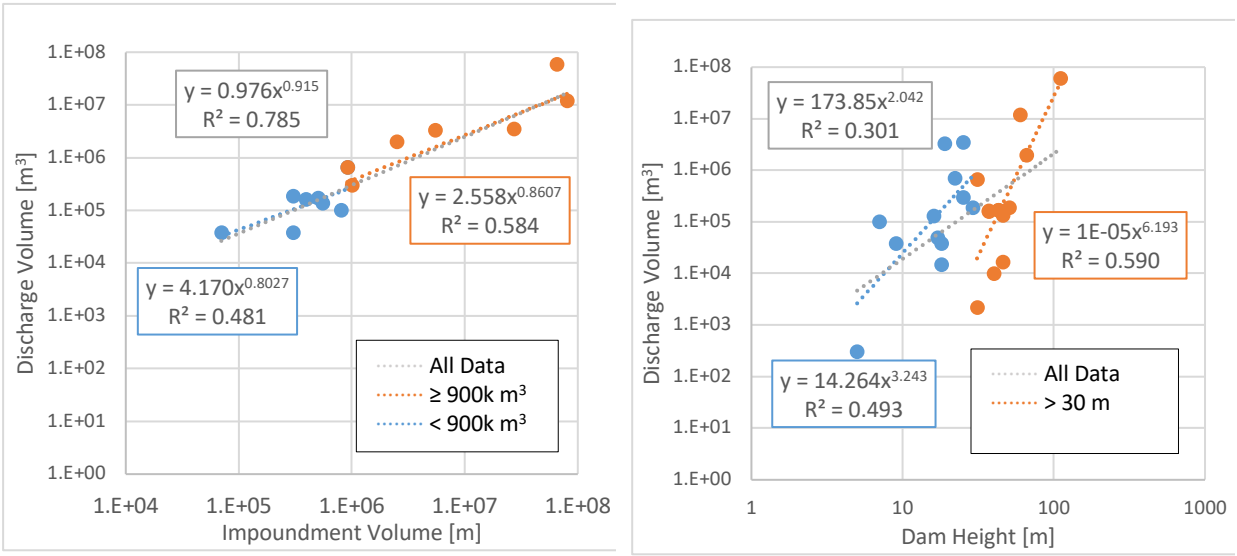

Figure 9: Correlations to obtain the discharged volume considering the static mode of failure

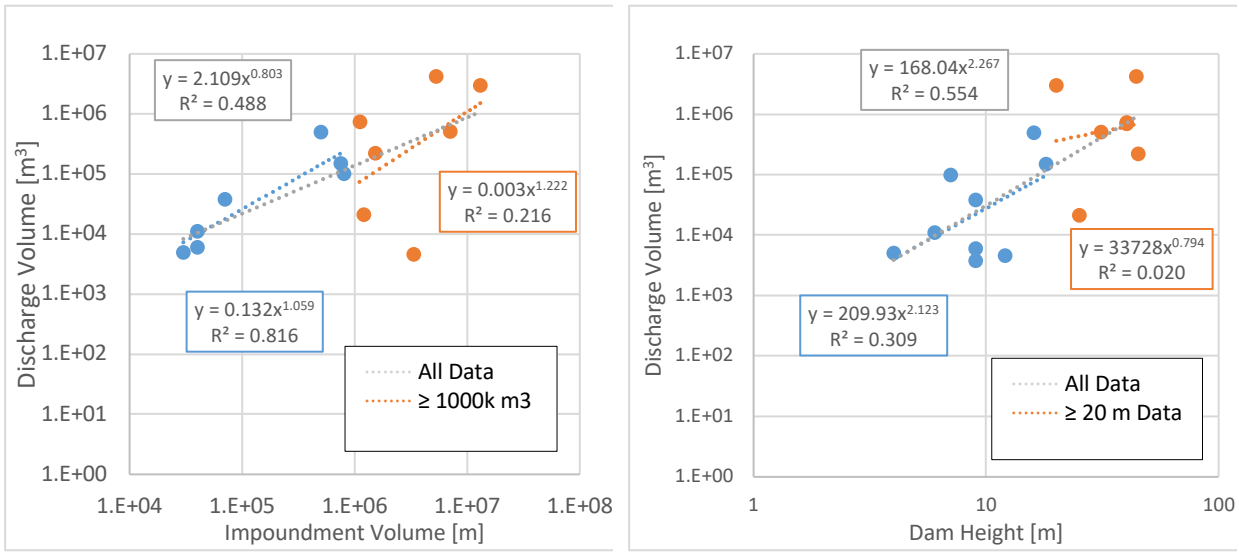

Figure 10: Correlations to obtain the discharged volume considering the overtopping mode of failure

The limit between short/tall and small/large was chosen to maximize the correlation square factor R^2. It can be observed that in some failure modes, the trend changes if it is subdivided. These trends therefore may be conservative or non-conservative, depending on the correlation used. For example, it is evident that for the static mode of failure, the correlation between the dam height and the discharge volume is not conservative; for taller dams the trend is steeper than the trend for all data, including the shorter dams' trend.

Breach formation time and peak outflow

The other two breach parameters, the peak outflow and the breach formation time, are not as clear and straightforward to determine. Most of the compiled TSF case studies, including the CDAs, do not provide this information. The most likely reason for this is that these two parameters are very difficult to interpret.

To face this problem, practitioners have relied on the available technical literature of water-retaining dams. Xu and Zhang (2009) updated the database of water retention dams, adding several Chinese case studies. A total of 1,443 case studies were compiled by Xu and Zhang, with information about peak outflow and breach formation time outlined for several cases. In Xu and Zhang's (2009) database, only a few cases coincide on the properties of a typical copper dam, such as Quillayes, in terms of height, storage capacity, and construction material. The peak discharge of the selected case studies is highly variable, with at least one order of magnitude between them. Nevertheless, when assuming a simplified geometry for the hydrograph, the breach parameters are dependent on each other, and as the discharge volume should already be constrained at this point, it becomes necessary to either define peak outflow or a breach formation time. Peng and Zhang (2012), using Xu and Zhang's (2009) database, found correlations for the breach formation

time, again using height, and/or the impoundment volume. Figure 11 presents these correlations. It can be inferred that the breach formation time is practically independent of the dam height and impounded volume. Further, it can be seen that the breach formation time for dams over 200 m in height, or over 1,000 Mm^3 in capacity, is between 4 and 8 hours. This is a reasonable range for sensitivity analysis.

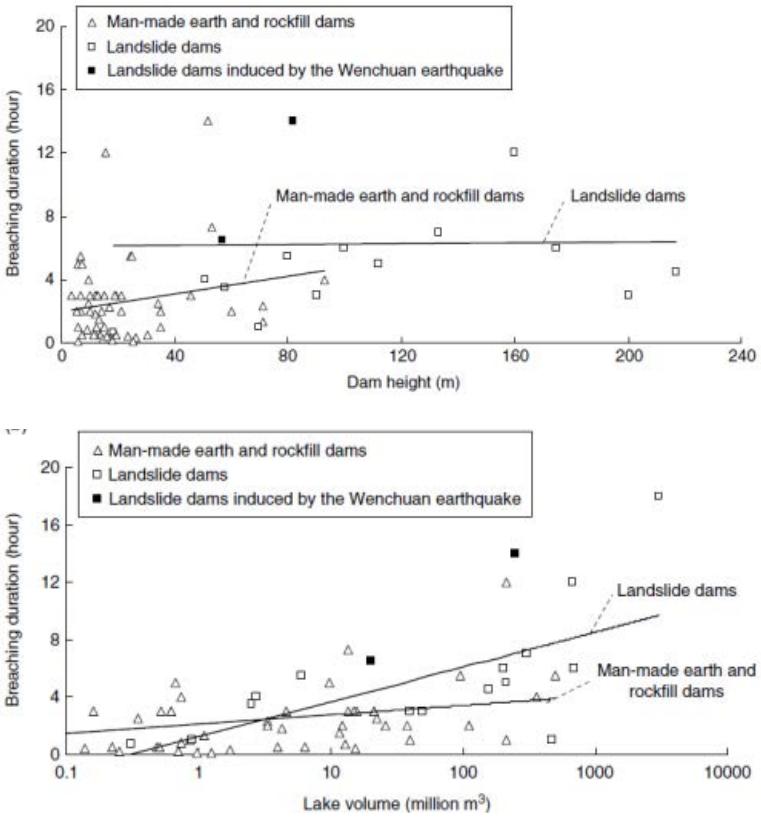

Figure 11: Breach formation time using the dam height and impoundment volume (Peng and Zhang, 2012)

Physical models have been shown to be a viable option to obtain hydrographs for DBA. One of the most common is BREACH developed by Fread (1988), validated by the National Weather Service. One downside is that these models were developed for water dams. It is not clear if the water-retaining case studies are expected to have more aggressive breach parameters, such as higher discharge peaks and shorter breach formation time. Further research should be conducted to benchmark tailings dams with the existing data of water dams and evaluate the applicability for TSFs.

Conclusion

For practitioners, DBAs have become an important challenge, especially during the current decade, in which the mining industry has been hit by some catastrophic failure events. In Chile, the authority has the ability to question or even deny a project if a DBA shows that the TSF represents a significant risk to the

communities and/or the environment.

This paper presented an issue that may gain importance during the upcoming years, as waste production increases, and with it the magnitude of tailings dam size and volumes increase. Some reasonable, primarily empirical based approaches were assessed to perform a reasonable and defensible DBA on larger copper tailings dams with unique characteristics. On this basis, when using semi-empirical correlations, sensitivity analyses should always be used. Further development and research on the DBA, specifically the derivation of breach analysis parameters, are required. The involvement of academia could be helpful, especially given the complex phenomena associated with the breaching process with hyperconcentrated (two-phase flowing) mixtures of sediment and water.

The state of practice on DBAs must be maintained as rigorously as possible. The custom procedures currently being used still rely mostly on professional judgement and loose criteria to tackle many aspects that are unknown, or largely unknown, when performing tailings dam break analysis.

The CDA guidelines to conduct tailings dam break analyses are about to be issued this year (Martin et al., 2019) and are expected to provide a first step in standardization that will help practitioners follow and further develop what is considered best practice for DBAs.

It is important to acknowledge that many mining companies are actively working towards the improvement of dam risk and management. This has resulted in helping to modify the governance structure and given more responsibility to dam-related roles such the dam owners, qualified persons, and the engineer of record within the mine/TSF hierarchy. This, along with the encouragement of active independent review boards and frequent dam safety reviews, are positive steps in advancing dam safety and design.

Acknowledgments

The authors would like to extend sincere thanks to Arcadis and to SRK Consulting for the assistance and resources provided, which contributed to the completion of this document. Thanks to Mr. John Kurylo for his technical comments, and to Mr. Aaron Fultz for his valuable style and editing assistance.

References

ANCOLD. 2012. Guidelines on the consequence categories for dams. Australian National Committee on Large Dams.

Antofagasta PLC. 2019. Tailings facility management. Retrieved from: https://www.antofagasta.co.uk/media/3556/antofagasta-tailings-facility-management-6-june-2019.pdf

Bowker, L.-N. and D. Chambers. 2015. *The Risk, Public Liability and Economics of Tailings Storage Facility Failures.* Bowker Associates Science and Research in The Public Interest and Center for Science in Public Participation.

Campaña, J., L. Valenzuela, A. Figueroa and J. Alarcon. 2015. The Quillayes sand tailings dam in Chile – Design and operation. In *Proceedings of Tailings and Mine Waste 2015 Conference.* Vancouver, Canada.

CDA, C.D. 2007. Technical Bulletins.

Concha-Larrauri, P. and U. Lall. 2018. Tailings dams failures: Updated statistical model for discharge volume and runout. *Environments* 5(28).

Dobry, R. and L. Alvarez. 1967. Seismic failure of Chilean tailings dams. *Journal of the Soil Mechanics and Foundation Division.* ASCE, SM6: 237−259.

Fread, Daniel. 1988. *BREACH: An Erosion Model for Earthen Dam Failures* (revised 1991). Silver Spring, Maryland: National Weather Service, National Oceanic and Atmospheric Administration (NOAA).

ICOLD. 2001. International Commission on Large Dams Bulletin 121: Tailings dams risk of dangerous occurrences: Lessons learnt from practical experience.

James, M., M. Al-Mamun and A. Small. 2017. Summary of the 2014 and 2015 Tailings Dam Breach Workshops of the Canadian Dam Association. CDA 2017 Annual Conference. Kelowna, Canada.

Martin, V. and A. Akkerman. 2017. Challenges with conducting tailings dam breach assessments. Prague, Czech Republic: 85th Annual Meeting of International Commission on Large Dams.

Martin, V., M. Al-Mamun and A. Small. 2019. CDA Technical bulletin on tailings dam breach analyses. 87th Annual Meeting of the International Commission on Large Dams. Ottawa.

McPhail, Gordon. 2015. Probabilistic dam break assessment and flow slide analysis for tailings storage facilities. *3rd International Seminar on Tailings Management, Tailings 2015.*

Ministerio de Mineria. 2007. *Decreto Supremo N° 248. Reglamento para la aprobación de proyectos de diseño, construcción, operación y cierre de los depósitos de relaves*. Santiago: Gobierno de Chile.

Peng, M. and L. Zhang. 2012. Breaching parameters of landslide dams. *Landslides* 9(1): 13−31.

Rico, M., G. Benito and A. Diez-Guerrero. 2008. Floods from tailings dam failures. *Journal of Hazard Management:* 79−87.

Small, A., M. James and M. Al-Mamun. 2017. Advancing the state of practice for tailings assessment using empirical correlations. In *Proceedings of the Canadian Dam Association 2017 Annual Conference*. Kelowna, Canada.

Troncoso, J., A. Vergara and A. Avendano. 1993. The seismic failure of Barahona tailings dams. *3rd International Conference on Case Histories in Geotechnical Engineering:* 1473−1479.

Valenzuela, Luis. 2016. Design, construction, operation and the effect of fines content and permeability on the seismic performance of tailings sand dams in Chile. *Obras y Proyectos:* 6−22.

Valenzuela, L. and J. Campaña. 2014. Sand tailings dams in Chile and its evolution since 1965. Tailings 2014. 2nd International Seminar on Tailings Management. Vancouver, Canada.

Wahl, Tony. 2014. Evaluation of erodibility-based embankment dam breach equations. Denver, USA: Interagency Agreement NRC-HQ-60-12-I-0013US Dept. of Interior. Bureau of Reclamation.

Xu, Y. and L. Zhang. 2009. Breaching parameters for earth and rockfill dams. *Journal of Geotechnical and Geoenvironmental Engineering* 135(12):1975−1970. ASCE.

Proceedings of Tailings and Mine Waste 2019
November 17–20, 2019, Vancouver, Canada
Published by the University of British Columbia, 2019

Quantitative Risk Prioritization of Tailings Dams

Franco Oboni, Oboni Riskope Associates Inc., Canada
Cesar Oboni, Oboni Riskope Associates Inc., Canada

Abstract

This paper assesses the quantitative risks of a portfolio of four dams. It is based on case histories and utilizes a predictive risk prioritization approach. Interdependencies between dams are explicitly considered as interdependent scenarios that significantly alter the portfolio risk prioritization. Stability analyses in static and pseudo-static conditions were performed by the engineers, using as input data observations/inspection reports. It was shown that the Factor of Safety is not a good discriminant to evaluate safety and thus risks. A documented and published symptom-based simplified probability of failure estimate was used to evaluate the probability of failure of each dam. Dams were benchmarked in relation to their world-wide historical performance. As well, the authors used theoretical dewatered and slurry state tailings dams' probabilities of failure. The consequences of the breach of dams were quantitatively evaluated using a multidimensional function. The potential for loss of lives was of course included and discussed, as well as reputational damage. A comprehensive risk metric is the cornerstone of risk communication, which is becoming a crucial part of any risk assessment. Enhanced transparency, sensible information, and better risk communication will help foster robust corporate social responsibility, social license to operate, and NI 43-101 (Canada's National Instrument 43-101). The risk portfolio was prioritized using various approaches, including a portfolio owner's risk tolerance threshold. A discussion of the impact on possible prioritizations and decision-making was introduced as well. The paper shows that gut-feeling risk prioritization may be misleading, and that multiple parameters must be carefully considered before a sensible and sustainable roadmap can be delivered and communicated to the stakeholders and the public. Finally, a roadmap to portfolio mitigation is defined.

Introduction

This paper describes the risk prioritization of a real-life dams' portfolio. The "map" of the system is schematically (no scale) displayed in Figure 1. The four dams used as an example are real dams from various owners. Their profiles and parameters have been altered to preserve confidentiality.

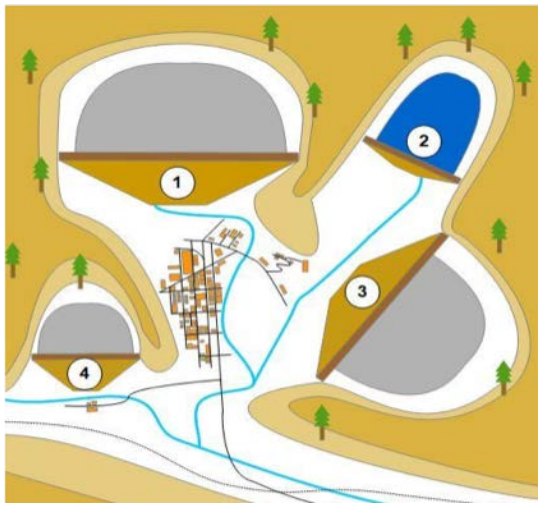

Figure 1: The system of dams constituting the portfolio

The map in Figure 1 helps to define the boundaries of the dam systems and the overarching portfolio. Tailings are depicted in grey, and the water of Dam 2 and the watercourses in blue. Some of the dams present internal and/or external interdependencies (possible concatenated failures). Valley bottoms are white and major residential and industrial structures are displayed as orange rectangles. Roads appear as single black lines, and a railroad, denoted by a dotted line, crosses the map from east to west at the south end of the map. The objective of examining the map is to allow a preliminary estimate of potential consequences by looking at the land-use downstream of each dam. It is very important to focus on the consequences, as engineering analyses often emphasize the hazard side of the risk equation and neglect the consequence side.

Due to space limitations, we will develop each case only to the level required for the discussion and the points we want to make. We use extant engineers' stability analyses and geotechnical characterization. For all the dams, the engineers declared the bedrock to be competent and free of weak layers and unfavourable discontinuities.

General descriptions of dams

Dam 1 is a rockfill downstream dam with a height of 162 m. Dam 1A is an intermediate situation, i.e. it is 100 m deep (Figure 2 left). Phreatic levels are at bedrock in Dams 1 and 2, and no significant deformations are detected. Note that Dam 1A and 1B are two stages of the same Dam 1. 1A is 100 m high. Dam 1B is the same dam as Figure 2 left, but has a final altitude of 162 m.

Dam 2 (Figure 2 right) is a water retention dam which displays an external interdependency with Dam 3. The external interdependency between Dam 2 and Dam 3 exists because a failure of Dam 2 would provoke an erosion at the toe of Dam 3, as we will describe later. Dam 3 is an upstream structure constituted

by a compacted till started berm on which upstream compacted waste rock berms have been built. Due to its construction, it has significant internal interdependencies.

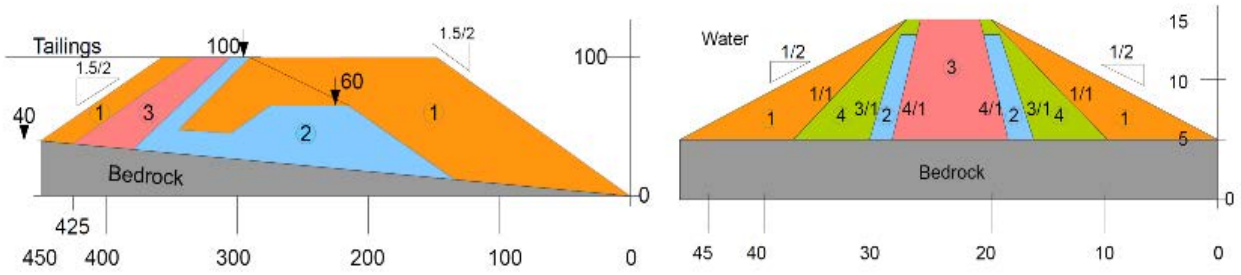

Figure 2: (Left) Dam 1A cross section: Raise at altitude 100 m of Dam 1 (final height 162 m). (Right) Cross-section of Dam 2, a water retention dam

Finally, Dam 4 is an upstream dam of obsolete design, with a penstock, similar to recently failed dams.

There are tailings pipelines at the crest of Dam 1A, 1B, and 3, while Dam 4 is in the process of deactivation, thus there are no active spigots at its crest. There is vehicular and subcontractors' traffic at the crest of all dams. The engineers defined the Factor of Safety (FoS) for the various dams under various conditions, i.e.: USA (undrained strength analysis), ESA (effective stress analysis), and pseudo-static as shown in Table 1, i.e., for Maximum Credible Earthquakes (MCE) and Operating-Basis Earthquake (OBE).

An exception is made for Dam 4 which is clearly a "bad apple." The FoS have very similar values in USA for Dams 2, 3, in ESA for Dams 1A, 1B, 2, and finally very similar FoS under pseudo-static conditions for Dams 1, 2, 3. We will see later that the image derived from the probability of failure is much more defined, with more evident variations from one dam to the next. This extra definition is very important when a risk prioritization of a large portfolio is sought. This will avoid falling into the trap of calling dams safe, when in fact they have a high probability of failure.

Table 1: Results of the engineers' stability analyses (FoS) for the various dams of the portfolio

Dam	USA	ESA	Pseudo-static
1A	n/a	1.61–1.68	1.18–1.23 for 1/475 Operating Base Earthquake (OBE) and 1:1,500 MCE
1B	n/a	1.59–1.65	1.15–1.26 for 1:475 OBE
2	1.63–1.76	1.59–1.68	1.28–1.33 for 1:1000 MCE
3	1.6	1.29–1.35	1.2 for 1:2,475 MCE
4	1 to 1.35, average 1.17		

Condition of dams since inception to the date of analysis (physical and governance)

The conditions over the known history of the dams, derived from extant reports and records, interviews and other classic means, were summarized. Table 2 displays such a summary for Dam 1A and 1B. Should modern hazard identification and monitoring data such as space or drone observation history be available (Oboni et al., 2018), then those results could be integrated into the descriptions of the dams. IoT (Internet of Things) and other data analyses would also complement this information. Of course, all the data and interpretations contained herein should be stored in a portfolio database (Hazard and Risk Register), allowing for easy retrieval when queries or updates are required

Table 2: Dam 1A, Dam 1B summary of conditions

Construction:
Centerline-rockfill tailings dam analyzed at two stages (100 m, 162 m). Non-erodible by assumed extreme meteorological conditions. Pipeline and traffic at crest. Supervision of the dam is excellent both in terms of frequency and of skills of the supervisor. No geometric divergences have been noted between the plans and the actual structures. Minor intermittent seepage is monitored at one location at the toe. There are no known errors and omission in this project, which has been third party reviewed by competent independent reviewers.
Geotechnical Investigations and testing:
Boreholes along the dam layout were regular, however they were less than 1/100 m (one borehole every 100 m), they were rather short, barely entering the bedrock. No continuous sampling was performed. Vane tests and cone tests were numerous but poorly distributed due to access reasons. Soil classification tests were performed in reasonable number and frequency. Geomechanical tests were numerous and distributed. A significant number of residual strength, oedometer and triaxal tests were performed.
Analyses and documentation:
The project is deemed of good quality by a competent engineering firm and a skilled team. The "as-built" plans display no significant imperfections and variations. The alteration plans have also been regularly updated.
Stability analyses:
As shown in Table 1 above, effective and pseudo-static stability analyses were performed by the engineers. Settlement analyses were performed. Liquefaction was dismissed by the engineers. Internal erosion analysis was estimated by the engineers as not being a problem.
Operations and monitoring:
Pore pressure is measured with numerous vibrating wire piezometers. Deformations are monitored by topographic observations and inclinometers. There is an active Independent Geotechnical Review Board (IGRB). There is an annual inspection ran by a reputable third party.
Maintenance and repairs:
Repairs are carried out in a timely manner when damage is pointed out by the inspectors.

Probability of failure of the portfolio's dams

Two approaches for the evaluation of the probability of failure of each dam were used. Table 3 displays the evaluation of the Category of dam (Dam 1A, 1B) using a method (Silva et al., 2008; Altarejos-García et al.,

2015) we call SLM, leading to the evaluation of the probability of failure. (The acronym is derived from the names of the authors of the paper in which the approach is described, that is, Silva, Lambe, and Marr [Silva et al., 2008; Oboni and Oboni, 2013]). The SLM methodology is general and of proven applicability, but should be used with caution for dams' slopes, where dam-specific hazards (e.g. water balance upsets, liquefaction, freeboard loss, etc.) are present.

Table 3: SLM results for Dam 1A,1B (Silva et al., 2008)

Investigation 0.2 to 0.3, Testing 0.2 to 0.3; Analysis and documentation 0.2: Best category I
Construction 0.4 Operations and monitoring 0.4: Above Average category II
Category min (best estimate) = 0.2+0.2+0.2+0.4+0.4= 1.4
Category max (worst estimate) = 0.3+0.3+0.2+0.4+0.4= 1.6

Thus, more tailings dam-specific approaches are to be preferred (Oboni and Oboni, 2019; Oboni et al. 2019) as they include those "missing" factors. As in SLM, the tailings dam specific approaches use "symptoms" or diagnostic points in the history of the dam from inception to the day of the evaluation. The 30 diagnostic points are summarized in Table 4. For each point the tailings specific methodology allows a pre-determined set of answers, and these are mathematically combined to deliver an estimate of the probability of failure, including uncertainties. Explicit consideration of uncertainties is indeed a fundamental step towards reasonable, transparent, and ethical risk assessments (Oboni, Oboni, 2017a 2017b, 2019).

Table 4: Summary of diagnostic points used in tailings specific approach (Oboni et al. 2019)

Physical aspects of the dam and its equipment (weirs, pipes, spigots, penstocks, etc.).
Construction: type of materials, cross section, supervision, berms and erosion, divergence from plans, etc.
Geotechnical investigations and testing.
Prior analyses and documentation of the project.
Various stability, deformation, erosion, liquefaction aspects:
◦ stability analyses (of various types, ESA, USA, pseudo-static, etc.),
◦ instability symptoms,
◦ settlements (actual and analyses),
◦ liquefaction, and
◦ internal erosion.
Operations, monitoring, maintenance and repairs.

Based on the list above, evaluations can be easily updated as they consider generally available or observable data (e.g. on site, monitoring, and satellite). The lack of knowledge (missing data) is explicitly entered in the evaluations.

The tailings specific approaches deliver, for dams 1A, 1B category 1.45 to 2.22, instead of 1.4 to 1.6, mainly because of the short, relatively far apart boreholes created during the investigations. The rockfill nature of the dam downstream body makes it insensitive to erosion, as pointed out by the engineers, and to a possible crest pipeline breach. Using the SLM categories together with the FoS (Table1) for the various dams of the portfolio, Table 5 can be created. Values are cut at the credibility threshold of one in a million or 10^{-6} (NUREG, 1990). For Dam 4 a simple evaluation of the probability of failure (p_f=p(FoS<=1)) delivers a probability of failure between 6% and 13%. Generally speaking, the SLM and dams-specific methodologies deliver similar values of the categories for the portfolio's dams. However, the application of the dam-specific application yields higher categories values because it considers the uncertainties, lack of monitoring, repairs and maintenance surrounding a dam, and the uncertainties of the geotechnical investigations that are not included in the FoS determination, as well as water balance, weirs and penstocks, and freeboard considerations.

That is to say that a probabilistic stability analysis based on the variability of the FoS is not sufficient to characterize a dam. The mere FoS is not sufficient either, of course. Indeed, SLM is a lot more deterministic in the sense that the range of probability of failure is narrower (Figure 3, left).

Table 5: Annual probabilities of failure for select dams (1A, 2, 3) in the portfolio using SLM

Dam	SLM Cat	Annual p_f USA/rapid draw down	Annual p_f ESA	Pseudo-static per event (to be divided by return)
1A	1.4	n/a	$\leq 10^{-6}$	$2.03*10^{-3}$ to $5.6*10^{-3}$
	1.6	n/a	$\leq 10^{-6}$ to $2*10^{-6}$	$4.83*10^{-3}$ to $1.16*10^{-2}$
2	2.2	$6.53*10^{-6}$ to $5.12*10^{-5}$	$2.32*10^{-5}$ to $9.65*10^{-5}$	$5.93*10^{-3}$ to $1.31*10^{-2}$
	2.4	$2.44*10^{-5}$ to $2.64*10^{-4}$	$7.49*10^{-5}$ to $2.64*10^{-4}$	$1.01*10^{-2}$ to $2.32*10^{-2}$
3	1.6	$3.32*10^{-6}$	$4.64*10^{-4}$ to $1.37*10^{-3}$	$7.84*10^{-3}$
	1.7	$6.74*10^{-6}$	$6.60*10^{-4}$ to $2.06*10^{-3}$	$1.14*10^{-2}$

Also, for a few cases the SLM gave completely different values as the SLM lacked critical data input specific to tailings dams. As can be seen from Table 5, short boreholes (Dam 1A) deliver higher probabilities of failure to an overall well-designed, built, maintained, and managed dam under constant FoS. This corresponds to observations in various recent catastrophic failures. The same occurs (Dam 3) if liquefaction is suspected, again in compliance with recent observations

To allow comparisons between SLM and the tailings specific approach, Figure 3 (left) includes ESA results with the probability of failure as a function of a FoS. The effect of ignoring dams' specific hazards

becomes evident, as the difference of probability of failure estimates is sometimes over an order of magnitude between the two approaches.

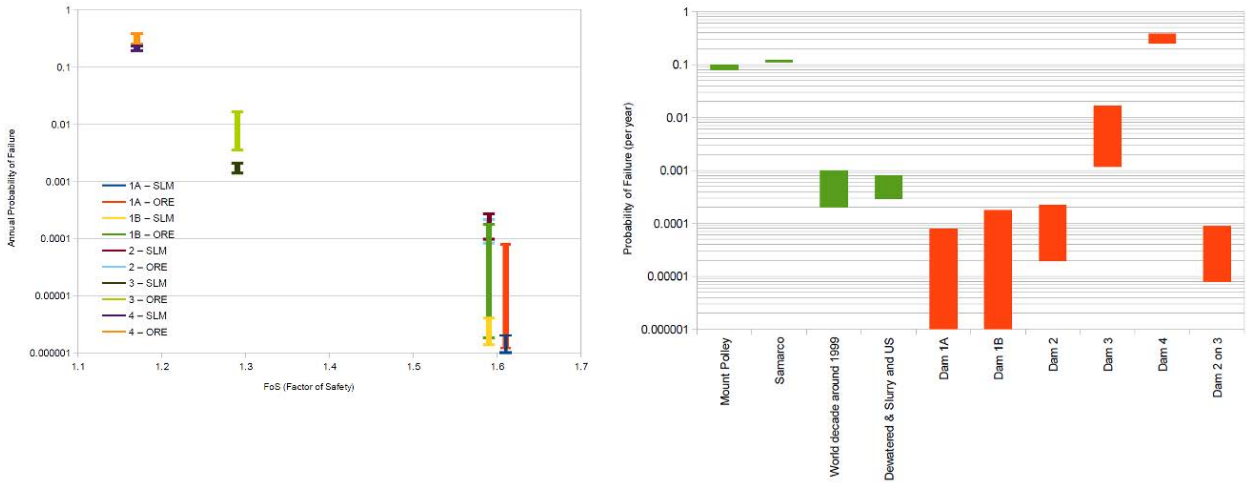

Figure 3: Left: SLM vs. dam specific methodology Optimum Risk Estimates (ORE). FoS vs Annual probability of failure for ESA. Right: Portfolio probabilities. In the vertical axis the annual probability of failure – PF – of various dams (horizontal axis) is shown as red vertical bars. The green bars are benchmarks

It is easy to see from Figure 3 (on the right) that the difference between an "optimistic" vs. a "pessimistic" category classification delivers probabilities of failure which lie within one or two orders of magnitude. That variation is compatible with extant uncertainty on the performance of the world-wide portfolio over the last hundred years, leading to the conclusion that the portfolio prioritization does not require systematic optimistic/pessimistic range evaluation, but more importantly requires consistency in the evaluation for each single item. In the case of Dam 2, where there are few tailings dam-specific features, the correspondence of SLM with the dam specific application is very good. As SLM does not consider liquefaction, in Dam 3 the divergence with the dam specific method is again significant, when the liquefaction hazard is included. For Dam 4, ORE emphasizes the probability of failure as it is characterized by a paucity of data and ignorance concerning many aspects of its history; SLM does not consider specific tailings dams' deficiencies. Similar conclusions can be derived from USA rapid draw down and pseudo-static.

If the failure criteria have been carefully selected, benchmarking becomes a powerful tool of comparison. Whereas risk comparison amounts to showing different activities of comparable risks, benchmarking rates a given activity's risk compared to other similar activities. Benchmarking of a tailings dams portfolio probability of failure can assume the aspect shown in Figure 3 (on the right) (Oboni et al., 2018). The extremes of the bars in Figure 3 (right) represent the minimum and maximum estimates of the

probability of failure for each dam. Hence, the length of the bars measures the uncertainty of the evaluation of the probability at the time of the assessment and with the data available at that time. The vertical axis shows four benchmark values described in prior publications (Oboni and Oboni, 2019; Oboni et al., 2019), namely the world-wide performance of the tailings dams' portfolio (around 1999 and following published theoretical approaches [Taguchi, 2014]), as well as Samarco and Mount Polley probability of failure evaluated using the symptom based methodology with data publicly available before the respective failures.

The portfolio benchmarking in terms of the probability of failure shows that in the considered case there are dams below the historical benchmark. Some dams overlap the benchmark limits, and some are above the upper limit; however, still significantly lower than the Mount Polley or Samarco estimates made with available pre-failure data. Additional studies and information would allow narrowing of the uncertainties (length of the orange bars).

Mitigation would push the bar down, an aspect we will discuss later. Long-term lack of maintenance and climate change effects will tend to push the bars up, as has already occurred with Dam 4.

Consequences

The Mackenzie Valley Review Board (MVRB, 2013: Appendix D, June 2013, see Section 5.2) defined what a modern risk assessment should include, based on public hearings. Thus, it becomes clear that partial components of the consequences such as biological impacts and land use, regulatory impacts and censure, public concern and image, health and safety, and direct and indirect costs have to be included in the analyses in an additive consequence function. Since risk data are often highly uncertain, ranges are strongly advisable with respect to "magic" single numbers.

Based on the system map (Figure 1) the following consequences were evaluated:

Dam 1A: Extensive damages to the town, town infrastructure, and tailings runout to the river stream with river transportation mechanism (i.e., 75% town full loss damage – if the dam fails, 75% of the town will be destroyed).

Dam 1B: Full loss of the town, town infrastructure, and tailings runout to the river stream with river transportation mechanism (i.e., 95% town full loss damage).

Dam 2: Inundation of the low areas of the town due to water flooding, damage to industries and loss of transport infrastructures (i.e., 35% town full loss damage).

Dam 3: Tailings runout blocks the valley, then floods the low areas of the town's industries and causes loss of transport infrastructures (i.e., 20% town full loss damage).

Dam 4: Damages to the mine perimeter, road failure, personnel safety, mining infrastructure (i.e., 60% mine full loss damage).

Interdependent failure of Dams 2 and 3: The combination of water and tailings flood makes the tailings more fluid, important scouring of the slope occurs, wider areas are impacted because of the combined volume and higher energy (compound damages to be carefully evaluated).

Risk tolerance or acceptability thresholds

In Figure 4 we display as an orange line the risk tolerance curve (Oboni and Oboni, 2014) selected by the owner of the portfolio. For this particular corporation, a $100 million loss event with a frequency of one out of ten years is intolerable. Also intolerable is an event generating a loss of $4,500 million with a probability at the limit of credibility (10^{-6}).

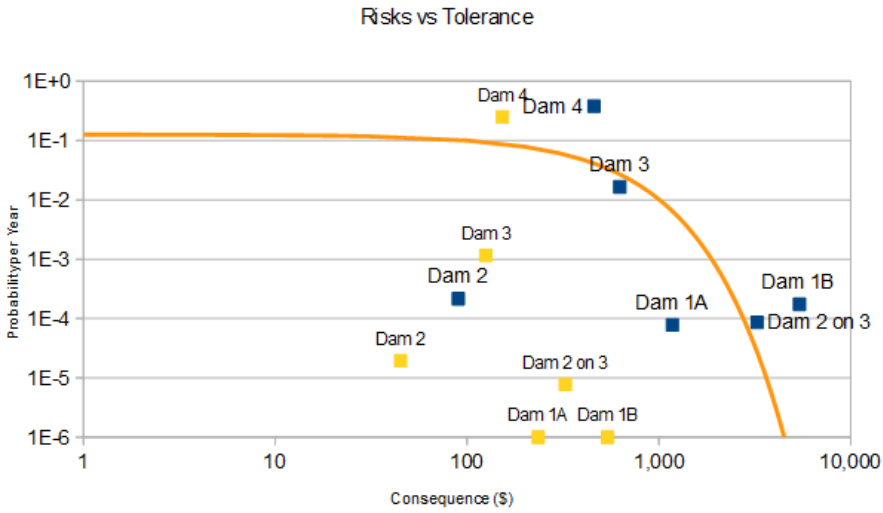

Figure 4: In blue p_{fMax} and C_{max} for each dam, and in yellow p_{fmin} and C_{min} for each dam. Risk tolerance is displayed in orange

In Figure 4 the yellow squares depict the C_{min} scenarios (i.e., without reputational damages [RD]) and the optimistic probability of failure (p_{fmin} and C_{min}) for each dam. Only Dam 4 is intolerable under these conditions. However, as history has demonstrated in various events, neglecting RDs is a flawed and unrealistic approach. Out of prudence, from this point on we will focus the discussion on the results, including RD.

Figure 4 shows that Dam 1A, Dam 2, and Dam 3 are below the selected corporate tolerance. Also, Dam 4, Dam 1B, and the dependency of Dam 2 on 3 are all above tolerance. Figure 5 displays the total risk for each structure as the sum of the tolerable part, i.e., the portion below tolerance (blue) and the intolerable portion (orange), i.e., the portion of the risk above the tolerance.

Common practice simplistic statements equating larger dams to bigger risks are to be left aside as they can easily be disproven, as clearly shown in Figure 5. Indeed, for example Dam 4, which is smaller than Dams 1A and 1B, generated significantly larger risks. Furthermore, Figure 5 shows that prioritizing a

portfolio mitigation plan based on total risk (blue + orange), i.e., without considering the corporate tolerance to risk would be far from optimal and could lead to squandering of mitigation capital because Dam 3 (tolerable) would be mitigated before Dam 1B, which has an intolerable portion of risk; and Dam 3 would also be mitigated before the interdependence of Dam 2 on 3 which has an intolerable portion of risk, despite its probability being two orders of magnitude lower.

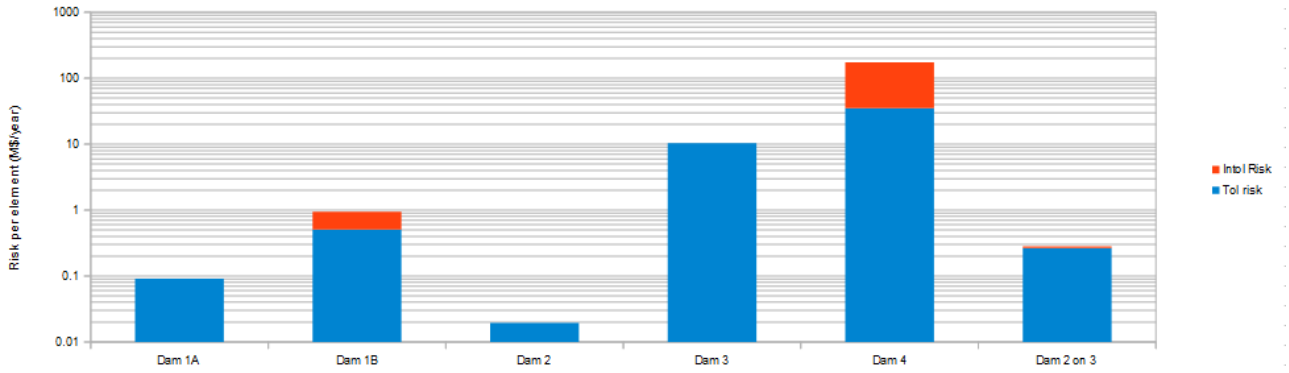

Figure 5: Total risk for each dam is equal to the sum of tolerable (blue) and intolerable (orange) risks

From the above we note that risks, and in particular risk prioritizations, cannot be ranked by gut feelings and intuition. The reason is simple: our human brain already has trouble understanding the simultaneous effect of two parameters, i.e., probability of failure and cost of consequences, and the introduction of a third vital one, which is the tolerance, certainly does not help the brain to make optimal decisions. Thus, it is paramount to use rational approaches to make decisions involving risks, even for simple portfolios of four dams like the one discussed here, where decisions might seem obvious!

Defining strategic tactical and operational risks

Risk Informed Decision Making (RIDM) is necessary to decide on priority of actions with dams, and which mitigations to implement. Risk Based Decision Making (RBDM) would be used to prioritize actions and select mitigations, but it would not be sufficient to evaluate the effectiveness of the mitigative investment in order to optimize it. When it comes to mitigation, actions need to be efficient, efficacious, and finally effective, i.e., producing the desired results (within clear financial goals, covered by RIDM). The idea is to develop effective risk reduction strategies implementation using Risk Informed Decision Making (RIDM). The first step of RIDM is to gain an understanding of which risks are operational, tactical, and strategic. This classification is paramount, is an important result of a modern risk assessment, and should not be the result of an arbitrary selection

Operational

Dam 4 can be mitigated, i.e., brought to a level of tolerance, with minimal effort at operational level. A reduction of the probability by only 1.5 order of magnitude would make it tolerable. In the case of Dam 4, two options could be attempted:

- reduce uncertainties and thus improve the appalling category of the structure, by implementing intensive monitoring, repairs, and possibly historical research and investigations (with care taken not to trigger a failure); and/or
- increase the FoS by building, if space and other conditions allow, a berm.

The final choice should be carefully examined using probabilistic cost estimates (Oboni et al., 2006).

Tactical

Interdependencies of Dam 2 on 3 can be lowered below tolerance by adding a mitigation on Dam 3 that would change the likelihood of failure of Dam 3 if Dam 2 failed. One example could be an armored toe, preventing erosion of Dam 3, after careful consideration of the liquefaction potential. Here again the portfolio risk assessment allows the allocation of resources, avoiding paralysis by analysis and feeling overwhelmed.

Strategic

Finally, Dam 1B is considered intolerable independently of possible implementable mitigations (the black arrow in Figure 6 remains above tolerance all the way down to the human credibility threshold).

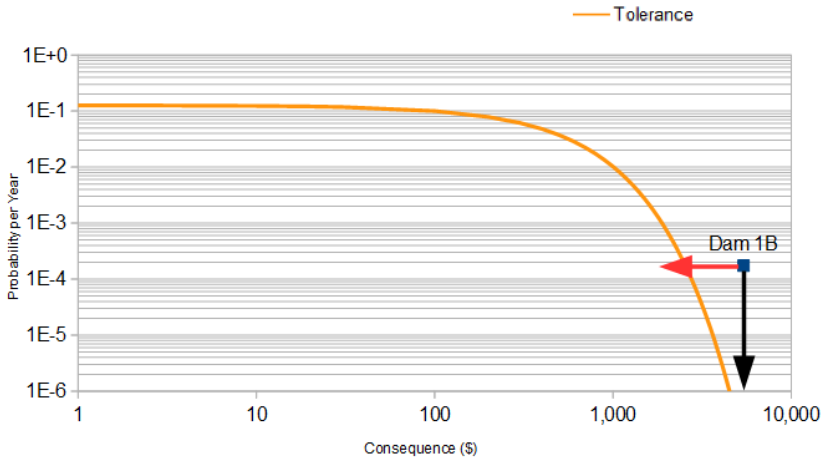

Figure 6: Mitigation of Dam 1B effects on risks

Dam 1B represents a strategic risk as only an alteration of the system would make it tolerable (red arrow). A solution could be moving the population, enhancing protection against environmental damages, lowering the dam etc. Thanks to the quantitative approach, strategic shifts can be evaluated.

Closing remarks

Simplistic statements equating larger dams to bigger risks are to be avoided as they can easily be disproven, as clearly shown in Figure 5, and do not facilitate constructive dialogue. Indeed, as structures become larger, their probability of failure should go down towards the values commonly accepted for major hydro-dams. That reduction necessitates acting on all aspects of the dam investigation, design, construction, monitoring, inspections, and management, as all contribute to the chance of failure. Increasing the FoS does not clearly reflect any of the above necessary improvements.

Population increase, land use shifts, and environmental constraints will increase the consequences of failures and therefore tend to increase risks. Again, the probability of failure will have to be lowered, especially considering that tailings dams have a long-life span during service and post-service, and, again, the FoS cannot help in measuring the changes. Predictive prioritization methodologies are the way to bring back credibility to the industry.

It is time for mining companies and governmental agencies to benefit from better understanding the risks they and the public are exposed to. Furthermore, we have to consider that:

1. Unless proper methodologies are used it will be very difficult to evaluate progress, as factors such as climate change, seismicity and increases in population will further complicate the situation.
2. Public outcry and hostility toward the mining industry, fuelled by the diffusion of information and communication technology, will likely increase.
3. The effects of any risk mitigation program will only become visible over long time spans, because any portfolio will contain mitigated and unmitigated (legacy) dams.
4. During that time the public, regulators, and legal authorities will perceive at best a status quo, with obvious negative consequences for the owners and operators.

References

Altarejos-García, L., F. Silva-Tulla, I. Escuder-Bueno and A. Morales-Torres. 2015. Practical risk assessment for embankments, dams, and slopes, *Risk and Reliability in Geotechnical Engineering* (eds Kok-Kwang Phoon and Jianye Ching), Taylor & Francis Group.

MacKenzie Valley Review Board (MVRB). 2013. Report of environmental assessment and reasons for decision Giant Mine Remediation Project. Retrieved from http://reviewboard.ca/upload/project_document/EA0809-001_Giant_Report_of_Environmental_Assessment_June_20_2013.PDF

NUREG/CP-0115 SAND90-2797. 1990. US Nuclear Regulatory Commission, CSNI Workshop on PSA Applications and Limitations Santa Fe, New Mexico, September 4–6, 1990.

Oboni, F. and C. Oboni. 2013. "Factual and Foreseeable Reliability of Tailings Dams and Nuclear Reactors: A Societal Acceptability Perspective," in *Proceedings 17th International Conference on Tailings and Mine Waste,* eds G.W. Wilson, D.C. Sego and N.A. Beier, 3–6 November 2013, Banff, Canada (Edmonton: University of Alberta Geotechnical Centre), 169–180.

Oboni, C. and F. Oboni. 2014. Aspects of risk tolerability, manageable vs. unmanageable risks in relation to governance and effective leadership, International Symposium on Business and Management, Nagoya, Aichi-ken, Japan.

Oboni, C. and F. Oboni. 2018. Geoethical consensus building through independent risk assessments. *Resources for Future Generations* 2018 (RFG2018), Vancouver, BC, June 16–21, 2018.

Oboni, F. 2006. Environmental restoration of a 60 m^3 dry asbestos tailings dump using risk based decision making, CLRA 2006 Reclamation and Remediation: Policy to Practice, 31st Annual Meeting and Conference, Ottawa.

Oboni, C. and F. Oboni. 2017a. Applying ORE to Balangero asbestos mine dumps environmental rehabilitation risk informed decision making, Tailings and Mine Waste 2017, Banff, Alberta.

Oboni, C. and F. Oboni. 2017b. Screening level risk assessment for a portfolio of tailings dams, *Canadian Dam Association (CDA, ACB)* Bulletin: 28(4).

Oboni, C. and F. Oboni. 2019. *Tailings Dam Management for the Twenty-First Century*. Springer. ISBN-10: 3030194469.

Oboni, F., C. Oboni and Morin, R., 2019. Innovation in dams screening level risk assessment, ICOLD 2019, Ottawa.

Oboni, F., C. Oboni, R. Morin, S. Brunke and C. Dacre. 2018. space observation, quantitative risk assessment synergy deliver value to mining operations and restoration, Rouyn-Noranda, Symposium on Mines and the Environment, Rouyn-Noranda, Québec.

Silva, F., T.W. Lambe and W.A. Marr. 2008. Probability and risk of slope failure, *Journal of Geotechnical and Geoenvironmental Engineering* 134(12).

Taguchi, G. 2014. Fault tree analyses of slurry and dewatered tailings management – a framework, Master's thesis, UBC.

Proceedings of Tailings and Mine Waste 2019
November 17–20, 2019, Vancouver, Canada
Published by the University of British Columbia, 2019

Tailings Storage Facility Embankment Reconstruction at Mount Polley Mine

Germán Pizarro-Sala, Golder Associates Ltd, Canada
Fernando Ascencio, Golder Associates Ltd, Canada
Adam Pfitzenmaier, Golder Associates Ltd, Canada

Abstract

On August 4, 2014, a breach of the perimeter embankment of the tailings storage facility occurred at the Mount Polley Mine in British Columbia (BC), Canada. At the time of the failure, the height of the perimeter embankment was about 40 m and damage occurred to approximately 400 m of the embankment. Construction of a rockfill and aggregates embankment, with a low-permeability cut-off wall, was selected as the preferred option to provide temporary containment of the 2015 freshet flows and prevent further release of tailings. Construction had to be completed in about four months under winter weather conditions.

Due to the urgent nature of this undertaking, construction had to be started with several uncertainties, including failure cause, foundation conditions, and internal configuration of the remaining embankment. Construction modifications were introduced to adjust to the encountered conditions, including water management and re-alignment of the cut-off wall. This paper presents key aspects of the flexibility of the design and large range of available construction equipment that allowed the design to be efficiently modified to the existing field conditions during construction. Construction of the cut-off wall was completed by April 2015, preventing the release of tailings and providing temporary containment for the 2015 freshet flows.

Introduction

The Mount Polley Mine is an open pit and underground copper and gold mine operated by Mount Polley Mining Corporation (MPMC). The mine is located approximately 56 km northeast of Williams Lake, BC, Canada. Since the start of production in 1997, the tailings generated from processing ore were deposited and stored in a tailings storage facility (TSF). Founded on glacially derived soils, the approximately 4.8 km long embankment of the TSF was constructed in stages utilizing modified centreline and centreline raises. The embankment is divided into three sections: main embankment, south embankment, and perimeter embankment.

On August 4, 2014, a breach of the perimeter embankment of the TSF occurred. At that time, the height of the perimeter embankment was about 40 m. The base width of the breach was about 100 m, although damage occurred to approximately 400 m of the embankment. An overview of environmental effects and remediation are provided in Nikl et al. (2016). Erosion control works in the scoured Hazeltine Creek channel are described in Bronsro et al. (2016).

On August 5, 2014, MPMC was issued a Pollution Abatement Order by the BC Ministry of Environment and Climate Change Strategy, which required MPMC to "Immediately take action, under the direction of a suitably qualified professional, to abate the discharge of mine-affected materials and sediments from the impoundment facility, and specifically into Polley Lake, Hazeltine Creek and Quesnel Lake" (BC Ministry of Environment and Climate Change Strategy, 2014). The development and implementation of plans to manage the impact of the 2015 freshet on the TSF began soon after the breach. Several options were developed to prevent the release of tailings and provide temporary containment of the 2015 freshet flows, and these options were presented to regulatory agencies (BC Ministry of Energy, Mines and Petroleum Resources and BC Ministry of Environment and Climate Change Strategy) in October and November 2014. Construction of a rockfill and aggregates embankment to an elevation of 950 m with a low-permeability cut-off wall, constructed using the cutter-soil mixing (CSM) technique at the location of the breach, was selected as the preferred option. The embankment is referred to as the 2015 freshet management embankment.

This paper presents key aspects of the flexibility of the design and large range of available construction equipment that allowed the design to be efficiently modified to the existing field conditions during construction. The experiences presented in this paper emphasize the importance of considering in the design the range of conditions that might be encountered and providing adequate flexibility to the design and construction to introduce geotechnically appropriate modifications during construction without extensive re-analysis, design and government permit amendment effort.

2015 Freshet management embankment design and existing perimeter embankment

Freshet occurs annually in March through May at the Mount Polley Mine area, with peak runoff in April (Golder, 2014). Therefore, to provide temporary containment of snow melt and direct precipitation within the TSF footprint and other inflows from the mine site that are pumped to the TSF, the 2015 freshet management embankment needed to be functional by April 2015.

Due to the schedule limitations for construction of the 2015 freshet management embankment, the design had to be advanced with several uncertainties. Only preliminary results of the forensic geotechnical investigations carried out to assess the failure mechanism that led to the breach were available at the time

of preparation of the design; as such, the design had to be capaPerimble of incorporating the findings of the investigation as they became available. Additionally, a review of the pre-breach as-built reports on the TSF identified discrepancies in information presented, and uncertainties existed regarding the exact location of material zones in the remaining perimeter embankment on either side of the breach area because only two as-built cross-sections, about 400 m apart on either side of the breach area, were available. Therefore, conservative assumptions were made and adequate flexibility was incorporated in the design so modifications to adjust the design to the encountered conditions could be incorporated during construction, if required.

The general zoning of the perimeter embankment is shown in Figure 1 and includes the following zones from downstream to upstream: rockfill, transition, filter, low permeability till core and upstream fill comprising sandy tailings, cycloned sand and coarse bearing layers (CBL) consisting of rockfill.

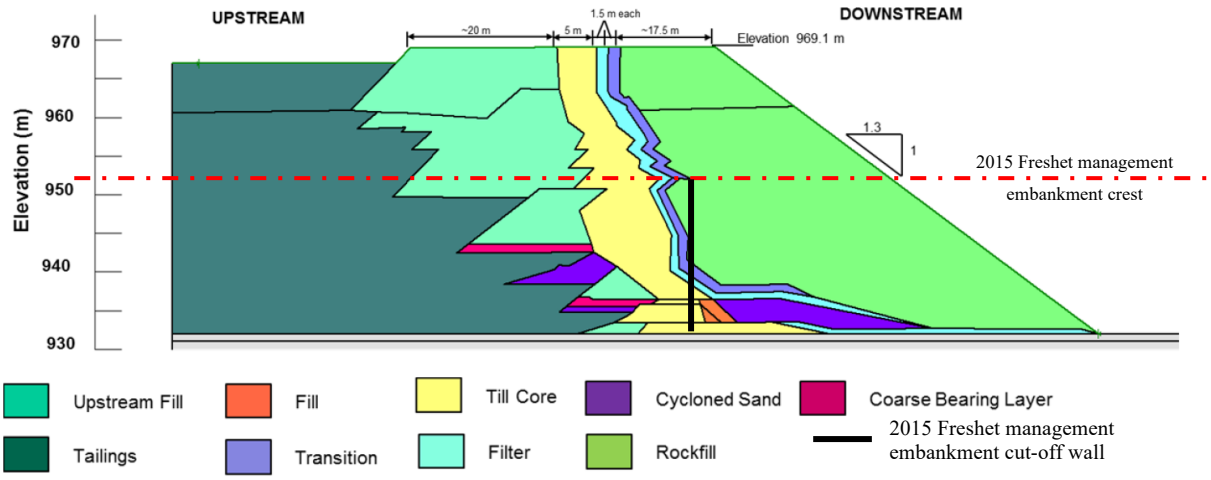

Figure 1: Perimeter embankment typical section and 2015 freshet management embankment cut-off wall approximate location

To facilitate coPerimnstruction during winter conditions, the design of the 2015 freshet management embankment comprised the use of granular materials and a cut-off wall constructed using the CSM technique. The use of moisture-sensitive materials (e.g., till) was not recommended as construction during prolonged periods of freezing temperatures (below 0°C), snow and rain events, and freeze-thaw cycles could have resulted in having to halt construction for long periods or potential large re-work. During winter, daily average temperatures at the Mount Polley Mine area vary between about –7 and –1 °C and the average precipitation (primarily in the form of snow) during December to March is estimated to be more than 200 mm (snow water equivalent) (Golder, 2014).

The design also included construction of a buttress along the perimeter embankment and re-sloping of the remaining perimeter embankment on either side of the breach to approximately 2.5 horizontal units to 1 vertical unit (2.5H:1V) and 3H:1V slopes, respectively. Re-sloping was required to remove cracked and damaged till core and filter materials from the breach event and to provide a safe working surface that would allow inspection of existing materials. The location and angle of re-slope were defined based on field observations and were to be confirmed during construction.

A plan, typical section and profile of the 2015 freshet management embankment as originally designed in November 2014 prior to the start of construction (Golder, 2014) are presented in Figures 2 to 4. From downstream to upstream, the embankment design consists of the following components:

- A wide rockfill embankment, with a 3H:1V downstream face, which serves to impose a low shear stress on the foundation soils and increase the length of potential slip surfaces through the foundation soils. The rockfill shell could be widened or the downstream slope flattened if the final data set of foundation soils strength deviated from the preliminary results of the forensic geotechnical investigations. The design included sensitivity analyses to assess the impact of potential deviations of strength.
- Filter and transition zones to prevent internal erosion and piping of foundation soils, existing till core and fills. At the base of the embankment, the filter and transition zones extend 25 m downstream of the cut-off wall to prevent piping of foundation soils.
- A central zone of aggregate material, referred to as cut-off wall aggregates, through which a low permeability cut-off wall would be constructed. The cut-off wall aggregate grain size distribution band was specified so it is filter compatible with the tailings. The 10 m wide cut-off wall aggregate zone allowed flexibility to modify the alignment of the cut-off wall if needed.
- A low permeability cut-off wall that forms the water-retaining element of the embankment. It extends from the crest of the embankment down through the existing till core on the remaining embankment on either side of the breach and into the till foundation at the base of the breach area. The cut-off wall was constructed using the CSM technique, which consists of sequentially penetrating the cut-off wall aggregates with rotating cutter wheels while injecting bentonite and then cement slurries. Each CSM panel was approximately 1.0 m wide (perpendicular to the alignment) and 2.8 m long (along the alignment).
- Upstream fill to provide support to the existing till core and for the cut-off wall and surrounding aggregates. The upstream fill material was allowed to be defined during construction based on availability of materials and constructability.

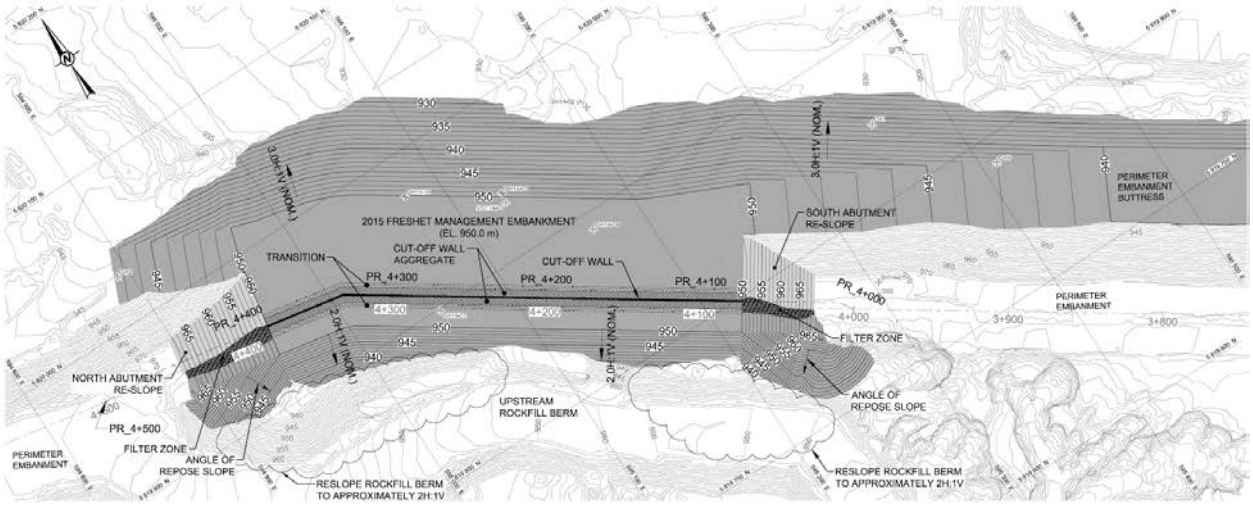

Figure 2: 2015 Freshet management embankment design plan

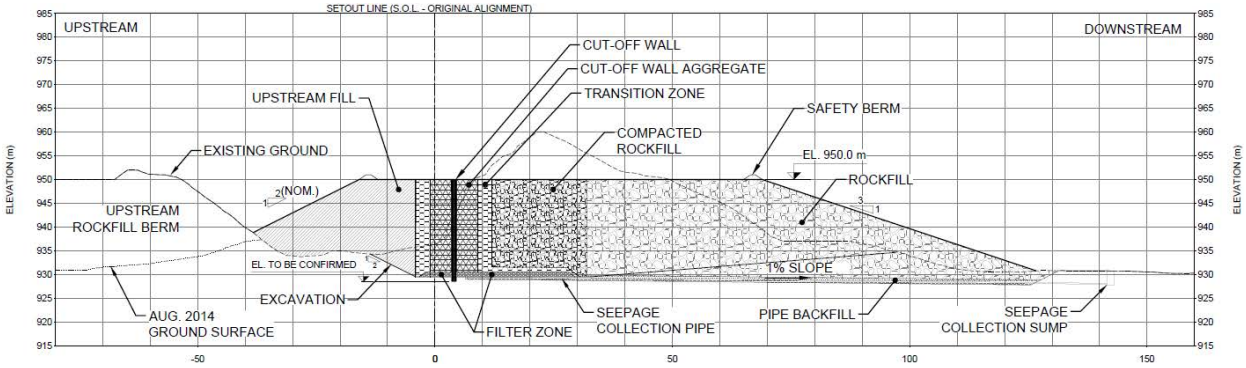

Figure 3: 2015 Freshet management embankment design typical section

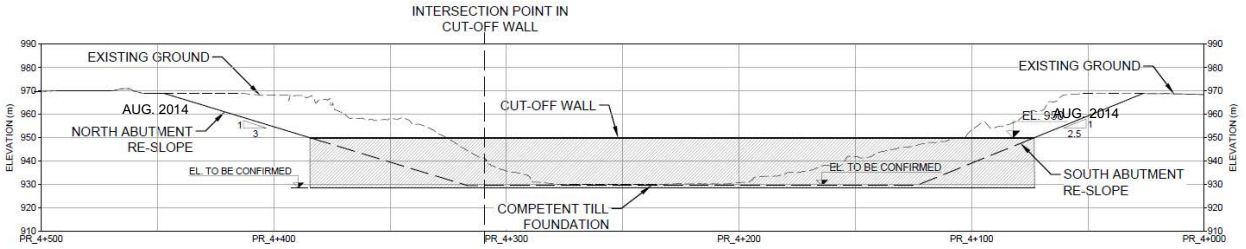

Figure 4: 2015 freshet management embankment design profile along cut-off wall alignment

An amendment to *Mines Act* Permit M-200 was issued bythe BC Ministry of Energy, Mines and Petroleum Resources on December 17, 2014 authorizing the construction of the 2015 freshet management embankment. The design of the 2015 freshet management embankment was revisited as modifications were introduced to the design during construction (Golder, 2015a, b).

Construction challenges and adjustments

Remaining perimeter embankment stabilization and bulk re-sloping

The breach eroded the upstream sides of the remaining perimeter embankment on both sides of the breach, leaving the embankment with unstable, steep faces. The left portion of the remaining perimeter embankment at the breach area (as seen from upstream to downstream) is referred to as the north abutment, and the right portion as the south abutment (Figure 2 and 4).

The abutments were stabilized by excavating the crest of the remaining embankment at the south and north abutments, mainly comprised of rockfill, and casting the material down the upstream face to form an angle of repose slope. During stabilization of the abutments, all other works at the breach and downstream areas were suspended and access was restricted for safety reasons. Re-sloping was started as part of the works to stabilize the abutments with a dozer pushing material from the crest of the abutments to the excavator casting material to the upstream side of the embankment. At this stage, re-sloping focused on the mass removal of any materials disturbed by the breach. Re-sloping continued until the north and south abutments were trimmed to about 3V:1H and 2.5V:1H slopes, respectively. Completion of bulk re-sloping made it possible to visually confirm the integrity of the till core and identify and survey the extents of the remaining embankment material zones (i.e. upstream fill, till core, filter).

The 2015 freshet management embankment cut-off wall had to connect to the existing till core on the north and south abutments; therefore, the survey of the exposed embankment material zones was used to validate the cut-off wall alignment. By end of December 2014, the alignment was adjusted to connect to the exposed till core on both abutments. The adjustment of the alignment was only possible due to the periodic survey, construction quality control and quality assurance and the timely updating of the three-dimensional as-constructed model.

Water management

The need to manage surface water flowing from the remaining tailings in the TSF towards the breach area was anticipated, and the pumps, ditches and sumps were planned early at the start of construction. Surface water had to be temporarily diverted and managed throughout construction of the 2015 freshet management embankment. Water coming from within the TSF was primarily managed by two sets of pumps installed upstream of a rockfill berm constructed upstream of the breach as an immediate action after the breach to prevent further large releases of tailings. The location of the two upstream sumps is shown in Figure 5.

After stabilization of the south and north abutments and prior to the start of foundation preparation at the breach area, a trench was excavated on the downstream side of the temporary rockfill berm, upstream of the construction area, to intersect any water not collected by the two sets of upstream sumps. The trench

extended from the north to the south abutments and directed water to a central sump upstream of the construction area. Water reporting to the upstream sumps and central sump was pumped to Springer Pit.

The implemented surface water management plan was effective in intercepting water flowing from the tailings within the TSF to the construction area; however, as re-sloping of the south and north abutments progressed, increasing water flow rates started to report to and freeze in the breach area. The increased water flow rates were identified to be surfacing from CBL on the south and north abutments near elevation 937 and 942 m. This condition had not been anticipated due to the uncertainties regarding the location and continuity of the upstream materials in the remaining perimeter embankment on either side of the breach area. The unanticipated water flows from the remaining embankment resulted in delays to the start of foundation preparation at the breach area. Temporary water management ditches were excavated on each abutment while re-sloping of the abutments was ongoing. After bulk re-sloping was completed, one water management ditch was left on each abutment to divert the water towards the upstream water management trench. The ditches were effective in directing water to the upstream trench, away from the construction area; however, foundation preparation at the breach area was delayed approximately two weeks and could only be started at the end of December.

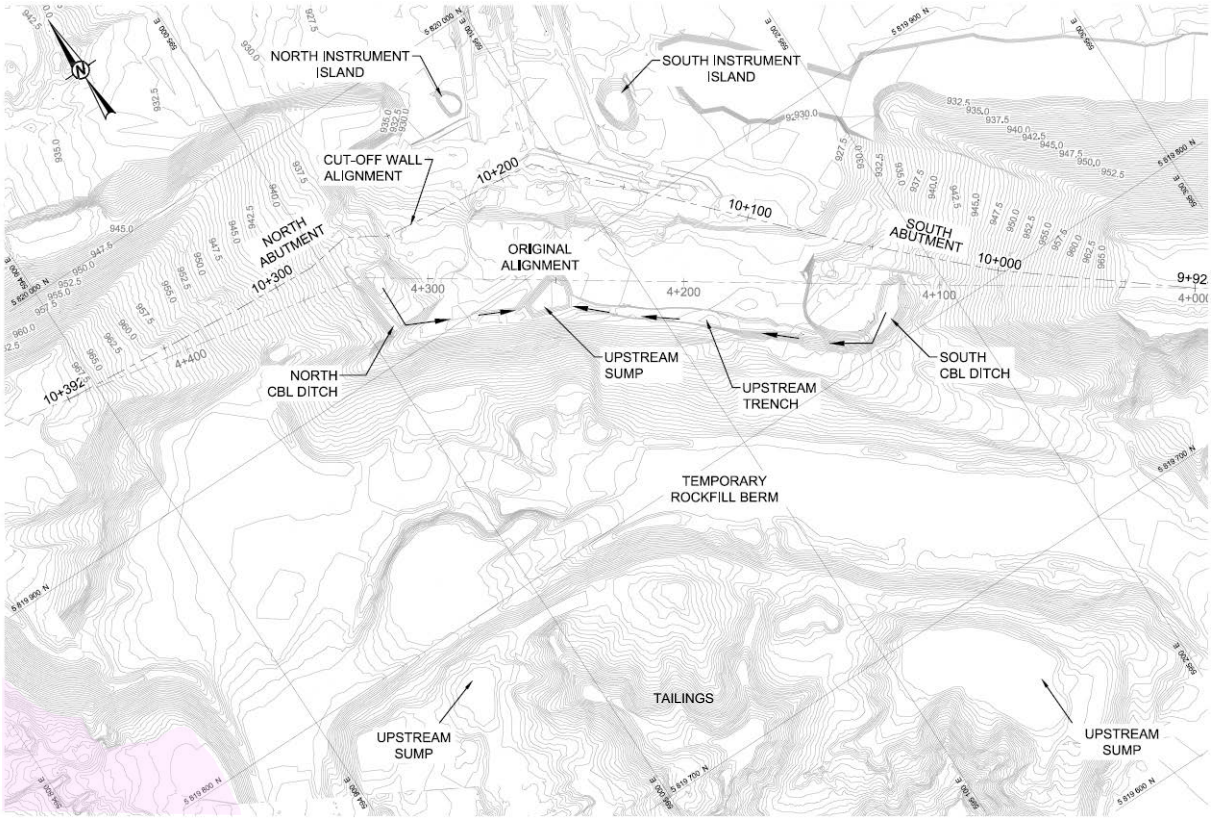

Figure 5: 2015 Freshet management embankment water management

Foundation preparation

Foundation preparation started after the north and south abutments were stabilized and water management had been implemented. Foundation preparation was carried out at the base of the breach area between the south and north abutments and downstream of the breach. The elevation of the prepared foundation of the perimeter embankment before the breach was estimated to be about 930 m based on the two as-built cross-sections available. The elevation of the existing ground surface at the base of the breach was also about 930 m; however, it was expected that the breach would have eroded the foundation, and loose tailings and embankment materials would have deposited at the breach area. At the time of the start of the foundation preparation, the thickness of tailings and deposited materials and the depth of erosion was unknown as access for heavy equipment to the base of the breach area was limited and only preliminary results of the forensic investigation were available.

Foundation preparation started with placement of rockfill on top of the loose tailings and debris to build a surface for heavy equipment to proceed with excavation of the loose tailings and debris deposited in the breach area. Tailings and embankment materials were removed until competent foundation, consisting of natural till, was confirmed. The elevation of the prepared foundation at the base of the breach ranged between 926 and 930 m with the exception of:

- material around two inclinometers that were used during construction to monitor the ground response; and
- a large test pit that had been excavated by the forensic investigation teams (the alignment of the cut-off wall had to be modified near the centre of the breach area to avoid the test pit) .

Foundation preparation progress in the area between the abutments allowed the start of placement and compaction of filter at the base of the 2015 freshet management embankment on January 8, 2015, about two weeks after the start of foundation preparation.

Detailed north and south abutments preparation

Detailed preparation of the till core and filter zones on the abutments was carried out as construction of the 2015 freshet management embankment progressed. The detailed preparation smoothened rough surfaces left during bulk re-sloping and removed snow and softened materials from snow melt and equipment traffic.

During detailed preparation of the north abutment, when construction was at about elevation 936 m in mid-February, the lower CBL at about elevation 937 m was identified to extend farther into the till core than the available as-built cross-sections showed, and than the bulk re-sloping had exposed. The exposed CBL was surveyed and confirmed to extend downstream of the cut-off wall alignment. The CSM equipment was likely not able to penetrate through the rockfill of the CBL and therefore the alignment of the cut-off wall needed to be revised. The wide cut-off wall aggregates zone used in the design allowed the alignment

of the cut-off wall to be moved about 4 m downstream to try to avoid the lower CBL; however, it was unknown if the lower CBL extended farther downstream into the till core in the remaining perimeter embankment at the north abutment. The revised and final alignment of the cut-off wall is presented in Figure 6.

After completion of placement and compaction of the fill materials to elevation 950 m near the north abutment, a sonic drill was used to assess the extent of the CBL. The drill core confirmed that some rockfill particles extended downstream to the revised cut-off wall alignment. The CSM equipment was unable to penetrate the lower CBL at two panels, and a second row of panels was installed immediately downstream that reached the till core foundation at the base of the remaining perimeter embankment.

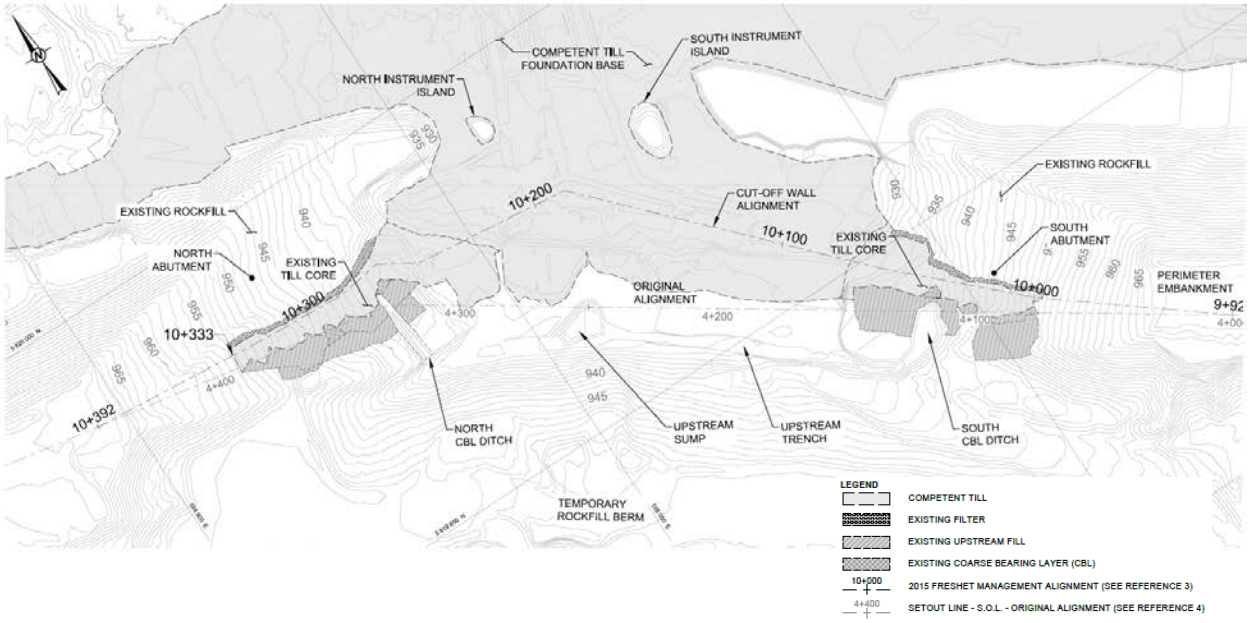

Figure 6: Exposed material zones on north and south abutments and as-constructed cut-off wall alignment

Equipment availability and construction flexibility

The construction schedule indicated that limited schedule flexibility was available, and therefore setbacks and unexpected conditions could result in the embankment not being ready for freshet. As such, the materials needed for construction of the embankment had to be available when required. MPMC operated the process plant to produce and make available filter, transition and cut-off wall aggregate materials that met the filter compatibility requirements.

The relatively small construction area (approximately 100 m long) and the limited access posed constraints that limited the efficiency of increasing the amount of construction equipment and manpower, if required. Instead, making available the most appropriate equipment for the specific tasks proved to be

the only means of increasing productivity of the construction. MPMC made available the mining fleet and personnel for the construction of the embankment. As such, a large range of equipment was available for construction and the most appropriate equipment was used for each task. For example, excavators with the greatest reach were used for the stabilization of the abutments and the electric shovel of the open pit was used to load material during re-sloping of the abutments. Similarly, haul trucks used for material placement were selected based on efficiencies identified during their full cycle times. Caterpillar 793F haul trucks were initially selected for use as the primary material haul vehicle, but loading times and constricted construction areas proved inefficient and the primary haul vehicle was changed to MPMC's fleet of Caterpillar 785 haul trucks.

In other cases where the available equipment on site was identified to not be the most efficient, MPMC brought to site additional equipment to improve efficiency of construction. For example, 18- and 20-tonne vibratory rollers were brought to site after construction had started to allow placement of thicker lifts for increased production. Similarly, an auger drill was brought to site to ease penetration of the cut-off wall aggregates by the CSM equipment and increase production.

Due to delays caused by unexpected conditions and as the construction area was increasing in size as the embankment was raised, it was recognized that flexibility in the construction sequencing would allow installation of the CSM panels to start on an earlier date. As such, when the construction of the embankment was at about elevation 942 m, fill placement and compaction were focused on the portion of the embankment near the north abutment to finish a section of the embankment to allow the CSM work to begin. Completing fill placement of this portion of the embankment allowed schedule gains to be realized by allowing additional construction tasks to take place concurrently (i.e. fill placement, abutment preparation and cut-off wall panels installation). Installation of the CSM panels started on March 1. Additionally, this allowed knowledge to be gained about the effort required to penetrate the cut-off wall aggregates by the CSM equipment, and construction of the other portion of the embankment was modified accordingly. As such, the ripper of a dozer was used during the rest of the construction to loosen up the cut-off wall aggregates along the cut-off wall alignment prior to placement of the next lift. This resulted in increased production during penetration of the cut-off wall aggregates by the CSM equipment.

Conclusion

Construction of the 2015 freshet management embankment had to be started with several uncertainties, including cause of the failure, foundation conditions at the breach area, and internal configuration of the remaining embankment. Therefore, the design and construction had to be flexible so that modifications could be incorporated as construction advanced. The cause of the failure and foundation conditions did not result in modifications to the design during construction; however, the circumstances of the breach

occurring between two cross-sections in the as-built documentation resulted in:

- delays to the construction due to unexpected relatively high water flows surfacing from the CBL on the north and south abutments; and
- a requirement to change the alignment of the embankment two times during construction.

Construction of the 2015 freshet management embankment cut-off wall was completed by April 2015, preventing the release of tailings and providing temporary containment for the 2015 freshet flows. The completion of the construction within the limited available schedule was possible due to:

- the imbedded design flexibility, including ample width of the material zones and ability to modify the cut-off wall alignment;
- effective construction quality control and quality assurance, including identification of material extents on the abutments;
- the ability to adjust construction as it progressed, including focussing on the construction of one side of the embankment to allow the start of installation of CSM panels; and
- the availability of the most appropriate equipment for the specific tasks, including mobilization of larger vibratory rollers to increase lift thicknesses and an auger drill to ease penetration of the CSM equipment through the cut-off wall aggregates.

The challenges and adjustments made during the construction of the 2015 freshet management embankment highlight the benefits of incorporating an adequate degree of flexibility to the design and construction of embankments that allow to introduce geotechnically appropriate modifications during construction without extensive re-analysis, design and government permit amendment effort.

Containment of flows from the TSF and return to treated water management provided the conditions necessary to proceed with the installation of habitat features onto the foundational Hazeltine Creek channel. In the rebuilt portions of Hazeltine Creek, there were approximately 4,890 adult spawning trout, and these produced 40,500 young-of-year trout, demonstrating that breach repair and environmental remediation is resulting in good ecological function.

Operation and deposition of tailings into the Mount Polley TSF was resumed in June 2016 and the 2015 freshet management embankment was raised in 2016, 2017 and 2018 using a centreline till core embankment to an elevation of 968 m.

References

BC Ministry of Environment and Climate Change Strategy. 2014. Pollution Abatement Order. File 107461. Dated August 5, 2014.

Bronsro, A., J. Ogilvie, L. Nikl and M. Adams. 2016. River rehabilitation following a tailings dam embankment breach and debris flow. In *Proceedings of Tailings and Mine Waste 2016*. October 2–5, Keystone, Colorado, USA.

Golder Associates Ltd. 2014. Mount Polley Mine 2015 freshet embankment design. Report revision 0 prepared for Mount Polley Mining Corporation. Dated November 28, 2014.

Golder Associates Ltd. 2015a. Mount Polley Mine 2015 Freshet management embankment design. Report revision 1 prepared for Mount Polley Mining Corporation. Dated March 30, 2015.

Golder Associates Ltd. 2015b. Mount Polley Mine 2015 freshet management embankment design. Report revision 3 prepared for Mount Polley Mining Corporation. Dated May 8, 2015.

Golder Associates Ltd. 2015c. Mount Polley Mine 2015 Freshet management embankment as-built construction. Report revision 0 prepared for Mount Polley Mining Corporation. Dated September 4, 2015.

Nikl, L., B. Wernick, J. Van Geest, C. Hughes, K. McMahen and L. Anglin. 2016. Mount Polley mine embankment breach: Overview of aquatic impacts and rehabilitation. In *Proceedings of Tailings and Mine Waste 2016,* October 2–5, Keystone, Colorado, USA.

Proceedings of Tailings and Mine Waste 2019
November 17–20, 2019, Vancouver, Canada
Published by the University of British Columbia, 2019

Liquefaction Assessment of a Thickened Tailings Deposit in an Arid Environment Using Empirical Approaches and Critical State Laboratory Testing to Calibrate Cone Penetration Tests

B. Tiver, Golder Associates Pty Ltd, Australia
H. Munoz, Golder Associates Pty Ltd, Australia
P. Chapman, Golder Associates Pty Ltd, Australia

Abstract

A case study of a liquefaction assessment undertaken on a thickened tailings deposit at a copper mine in an arid environment is presented. A program was undertaken that consisted of cone penetration tests with pore pressure measurement (CPTu), with variable rate penetration testing, and specialist critical state laboratory tests, with the objective of estimating undrained shear strengths and the potential for cyclic liquefaction to occur under the design earthquake. During the CPTu programme, the results were analyzed to assess zones where the tailings provided low penetration resistance, generally indicative of looser tailings than adjacent depth intervals. At these locations, multiple piston-tube tailings samples were collected for laboratory tests, allowing calibration of the field results. It was found that current available methods applied to the CPTu to infer the in-situ state parameter did not provide reasonable results, in particular for estimation of in-situ strength of the tailings, and hence they could not be applied to the tailings studied. Nevertheless, the testing gave insight into the behaviour of the tailings, and the estimates of the normalized dimensionless penetration rate of the cone indicated that undrained conditions controlled the shear behaviour of the tailings. Therefore, the method proposed by Robertson (2009) using the N_{kt} method was found to provide a reasonable estimate of the tailings undrained shear strength in the TSF, with comparisons to laboratory testing showing good agreement.

Introduction

The paper presents the results of analysis and interpretation of the CPTu, together with the results of advanced laboratory tests on the tailings to develop site-specific correlations to improve the estimation of the in-situ strength and cyclic liquefaction susceptibility of the tailings. The CPTu investigation was carried out in a tailings storage facility (TSF) located in an arid environment where evaporation far exceeds rainfall.

The TSF stores benign tailings that are transported to, and then discharged into, the TSF at a solids concentration of approximately 65% by mass. The tailings enter the TSF via sub-aerial spigot discharge points around the perimeter, facilitating the formation of a relatively uniform beach slope of approximately 1% and with a central decant pond.

Tailings samples were collected from the TSF during the CPTu investigation by a piston-tube sampling system. Laboratory tests were performed at Golder's Perth Laboratory. The results from the laboratory testing, including index tests and strength testing of the tailings, were used to improve estimates of the undrained strength of the tailings and its susceptibility to cyclic liquefaction.

Field investigation

A CPTu investigation was carried out at five locations within a TSF, i.e., locations CPTu01, CPTu02, SCPTu03, CPTu04 and SCPTu05, as shown in Figure 1a. The CPTu was performed at the standard penetration rate of 20 mm/s with a standard cone size (area of 10 cm^2), and with the pore pressure measurement sensor in the u_2 position. A photograph of the mobile rig in the TSF is presented in Figure 1b. Measurements of the cone tip resistance (q_c), sleeve friction (f_s), and dynamic pore pressures induced by the cone penetration (u_2) were recorded at continuous intervals of 20 mm during probing. In addition, the penetration was halted at three to four different depths per probe to allow the dissipation of the sustained increase of u_2 to equilibrium pore pressure (u_0) to infer the pore pressures within the TSF. Additional CPTu with a fast-rate (110 mm/s) and slow-rate (3 mm/s) penetration, referenced as FR-CPTu and SR-CPTu respectively, were also conducted at selected locations as shown on Figure 1a. The variable rate penetration testing was undertaken to examine the drainage response of the tailings under different rates of shearing.

A key feature of the field investigation was a sampling program in the TSF was to retrieve sufficient tailings samples to complete a series of laboratory testing. Testing included index properties, strength, and critical state testing of the tailings. A total of 28 tailings samples were collected from the TSF by thin stainless-steel piston tubes (60 mm diameter and 0.5 m long). At CPTu02, sampling by piston tubes from locations A to F (e.g., see A to F in the sketch in Figure 1 c) was as follows:

- Location A was sampled first along five different depths (i.e., a piston tube from 3 to 3.5 m, 8 to 8.5 m, 12 to 12.5 m, 16 to 16.5 m, and 20 m to 20.5 m), including the depth of interest (i.e., low penetration resistance zone) of 16 to 16.5 m.
- At locations B, C, D, E and F, only one piston tube sample was extracted from each one at the depth of interest of 16 to 16.5 m.

The depth of interest was selected in the field by observation where cone tip resistance was noticeably lower than adjacent intervals for a depth interval of at least 0.5 m to allow for the length of the tube sample. During the sampling program, six piston-tube samples were collected from the targeted layer.

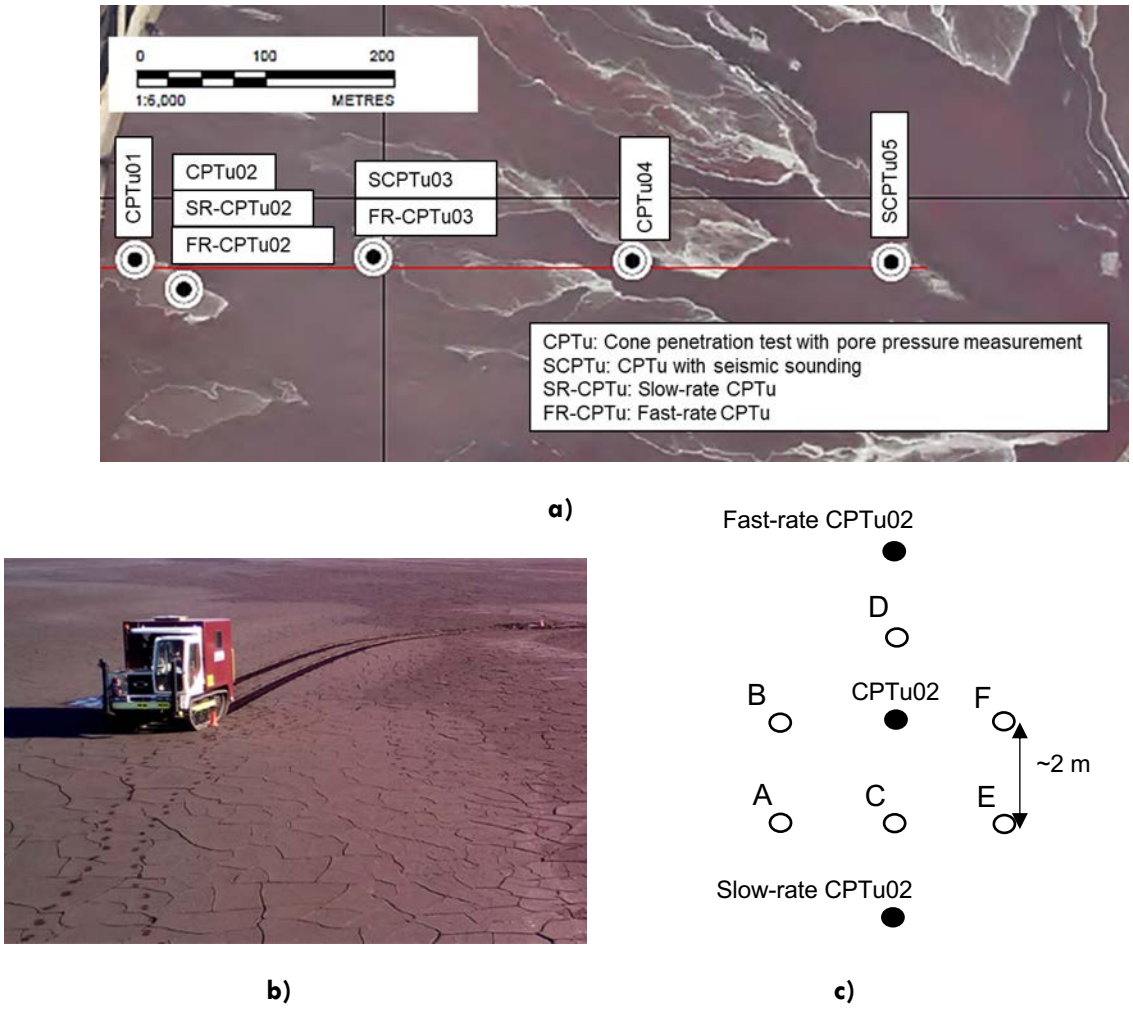

Figure 1: a) Location of the CPTu probes; b) mobile rig in the TSF; c) schematic of probing and sampling locations

A similar sampling arrangement was undertaken around SCPTu03. In this case, the low penetration layer was encountered between depths of 18.2 to 18.7 m, thus six piston-tubes samples were collected from this depth. The other piston-tubes samples were used to obtain and characterize the index properties of the tailings to assess spatial trends in these properties. Each retrieved tube was sealed at its top and bottom with nylon end caps, a waterproof sealant, and duct tape in an attempt to maintain the in-situ moisture content of the tailings which allowed for reasonable estimates of the in-situ void ratio of the tailings. A summary of the tests undertaken for CPTu02 and SCPTu03, at the depths of interest, is presented in Table 1.

Table 1: Laboratory tests on critical state and strength of the tailings

Test	No tests per CPTu probe	Purpose
Triaxial compression	4 (2 Consolidated isotropic undrained [CIU] and 2 Consolidated isotropic undrained [CID])	Critical state parameters estimation
Monotonic direct simple shear (MDSS)	3 (1 unbiased and 2 biased)	Undrained shear strength estimation
Cyclic direct simple shear (CDSS)	2	Cyclic resistance ratio (CRR) estimate

Laboratory characterization

Index properties

The index properties of the tailings were obtained in accordance with laboratory Australian testing standards (Methods of Testing Soils for Engineering Purposes AS1289) and are summarized in Table 2. The index properties of the tailings were consistent across the five CPTu carried out.

Table 2: Index properties of the tailings

Tailings property	Value
Unified Soil Classification System (USCS)	CL-ML to ML
Specific gravity	3.2 to 3.5
Dry density (kN/m^3)	21 to 23
Bulk density (kN/m^3)	24 to 26
In-situ moisture content (%)	14 to 17
Liquid limit (%)	16 to 17
Plasticity index (%)	3 to 4
Sand sized (>75 micron – <2 mm) (%)	25 to 35
Fines (<75 micron) (%)	65 to 77
Clay sized (<2 micron) (%)	10 to 14

Critical state locus and state parameter

The critical state locus (CSL) for the tailings was estimated after performing two CIU and two CID triaxial compression tests. The tailings specimens (63 mm diameter and 128 mm height) were prepared using the moist tamping method, to a loose density to target contractive behaviour. A photograph of a tailings specimen in the triaxial cell, before and after the monotonic triaxial compression, is presented in Figure 2a. The CSL and the state parameter (ψ) of the tailings of CPTu02 site is presented in in Figure 2b in the plot void ratio (e) versus mean effective stress (p'). The critical state intrinsic parameter (Γ) and compressibility parameter (λ_{10}) associated with the CSLs resulted in 0.65 and 0.09 for CPTu02 and 0.74 and 0.10 for

SCPTu03, respectively. These values are within a wide range of critical state properties for some cooper tailings presented elsewhere in the literature (Jefferies and Been 2015). The combination of the CIU and CID triaxial compression tests results provided consistency to define the CSL.

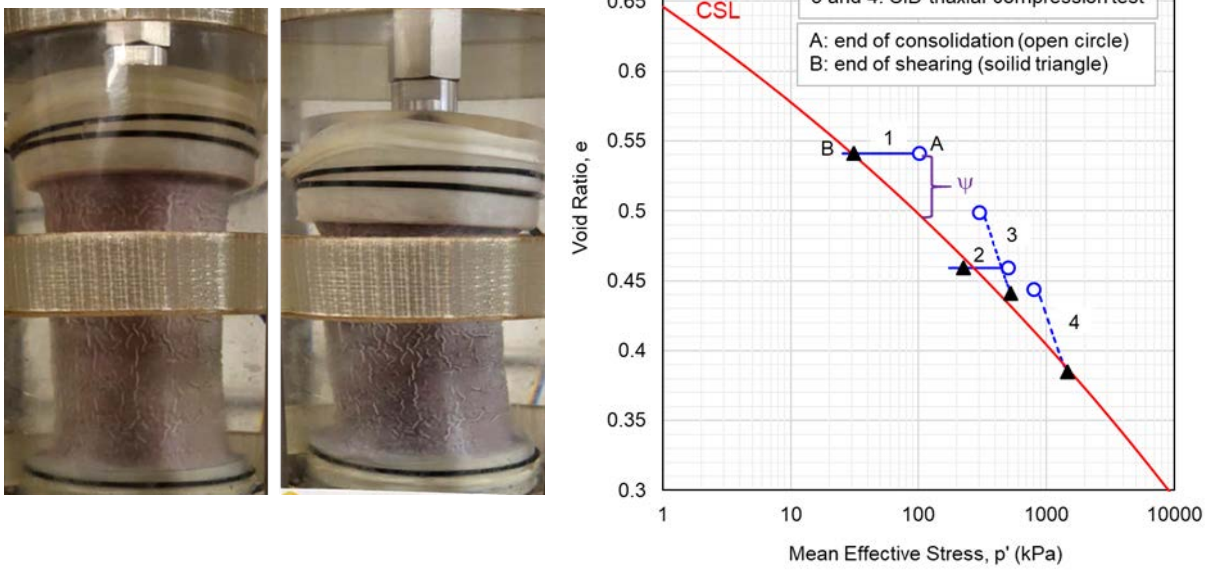

a) b)

Figure 2: a) Tailings specimen before and after triaxial compression and b) CSL for CPTu02

Undrained shear strength

The undrained shear strength (s_u) of the tailings was estimated from the shear stress-strain curves obtained from MDSS tests. The DSS tests were carried out on tailings specimens that were prepared close to the in-situ density of the tailings in the TSF (i.e., about 22 kN/m^3). The undrained shear strength ratio (s_u/σ'_{vo}) of the tailings, where σ'_{vo} is the pre-shear vertical effective stress, in six specimens with and without the application of initial static shear stresses (i.e., bias of 0 to 0.14) ranged from 0.19 to 0.22. A value for s_u/σ'_{vo} of 0.20 was adopted for stability modelling of the tailings. considered representative for the tailings.

Cyclic resistance ratio (CRR)

CDSS tests were conducted on four tailings specimens to estimate the CRR of the tailings. During the CDSS tests, the specimens were loaded to prescribed cyclic stress ratios (CSR) at a cyclic loading frequency of 1 Hz, considered representative of earthquake loading employed in current engineering practice. Adjustments to the cyclic strength to account for the effects of loading rate (e.g. when the loading frequency is different to 1 Hz) were therefore not needed (Boulanger and Idriss, 2007). A photograph of the tailings specimen at the end of the CDSS test is shown in Figure 3a. The CRR of the tailings, estimated as 0.12,

was defined as the CSR at 15 uniform loading cycles to trigger 3% single amplitude shear strain in the tailings (Seed et al., 2003), as shown in Figure 3b. A value of 15 uniform loading cycles was deemed comparable to the cycles demands of an earthquake event of moment magnitude M_w of 7.5, which was adopted for the TSF site.

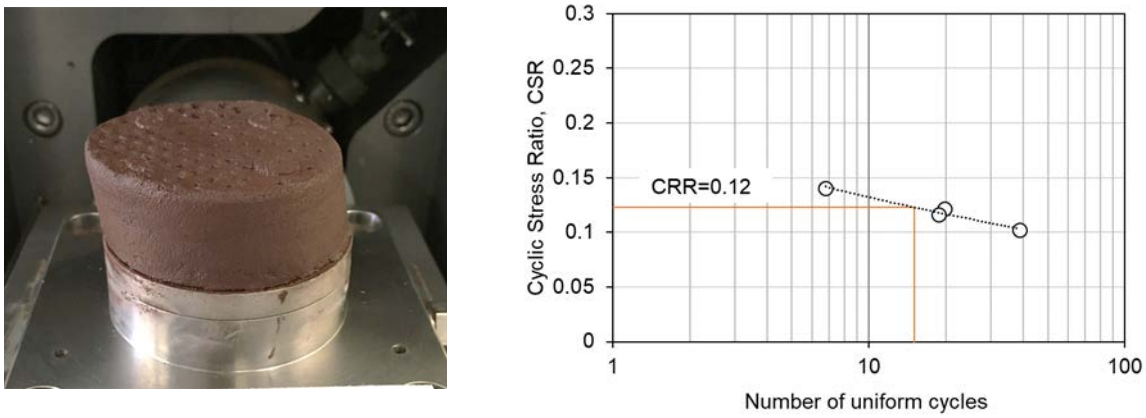

a) b)

Figure 3: a) Tailings sample at the end of cyclic shearing, and b) CSR versus uniform cycles

CPTu interpretation

CPTu parameter measurement

As cone penetration took place into the tailings in the TSF, the cone penetration resistance (q_c), sleeve friction (f_s), and induced pore pressure response (u_2) were recorded at 20 mm depth intervals throughout the exploration depth. In addition, three to four dissipation tests were undertaken to infer the pore pressures within the TSF. The CPTU data, including q_t (i.e., the corrected total cone resistance of q_c by pore pressure effects), f_s, u_o and u, and normalized pore pressure ratio (B_q), for CPTu02 probe are presented in Figure 4a to d respectively. The CPTu probes reached a depth about 20 m where a marked increase in q_t, f_s and F_r (i.e., F_r is the f_s normalized by net cone resistance) took place, which indicated that the cone encountered the interface between the tailings and the foundation.

In-situ pore pressure and tailings saturation conditions

With the tailings under study, the commencement of sustained positive pore pressures (u_2) during the cone penetration (indicative that the tailings were either at, or close to, saturation) took place in all the probes, from the surface of the tailings through-out the majority of the profile. An example of u_2 response in CPTu02 is shown in Figure 4c. Based on this, the tailings in the TSF was judged to be saturated or near-saturated. The results of the dissipation test of u_2 at selected depths (e.g., see the solid triangles in the u_2 profile in

Figure 4c in CPTu02 indicate that u_2 dissipated to zero kPa over time in all cases. Similar trends occurred in the rest of the CPTu probes. Therefore, it was inferred that there was no hydrostatic phreatic surface present in TSF at the time of investigation, despite it being saturated or near-saturated.

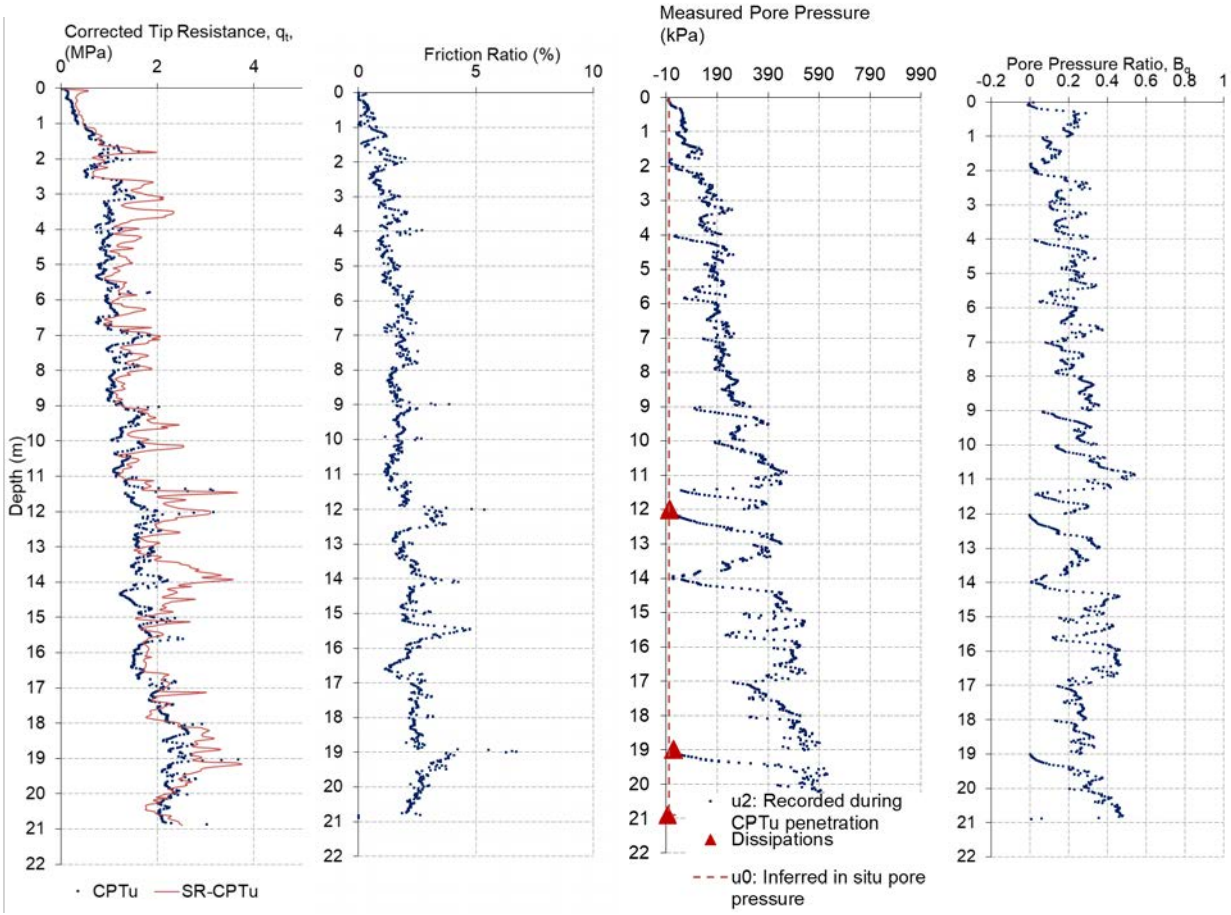

Figure 4: Profile of parameters a) q_t with standard and slow-rate penetration; b) f_s, c) u_2, u_o, and d) B_q in CPTu02

CPTu-based critical state parameters

Inferring the state parameter ψ from CPTu data requires estimates of both the friction ratio (i.e., F_r) and the slope of the CSL (i.e., λ_{10}). These parameters are not provided directly from the CPTu, and hence must be estimated through empirical correlations and (for the slope of the CSL) laboratory testing. The compressibility parameter of the tailings (λ_{10}) was initially assessed from empirical methods, e.g., Plewes et al. (1992) and Been and Jefferies (1992). The linear relationship by either $\lambda_{10} = F_r/10$ or $1/\lambda_{10} = 34–10\ I_{C,BJ}$, where and $I_{C,BJ}$ is the Soil Behaviour Type proposed by Been and Jefferies (1992), appears to be limited to capture the actual behaviour of the tailings in this study, as shown in Figure 5a and b. The results of the state parameter ψ of the tailings obtained from the CPTu probes by the above empirical methods was

considered to be limited in application as it did not entirely capture the compressibility behaviour of the tailings. Thus, the CPTu-based state parameter ψ was not be used in estimating the profile of shear strength ratios of the tailings (s_u/σ'_{v0}).

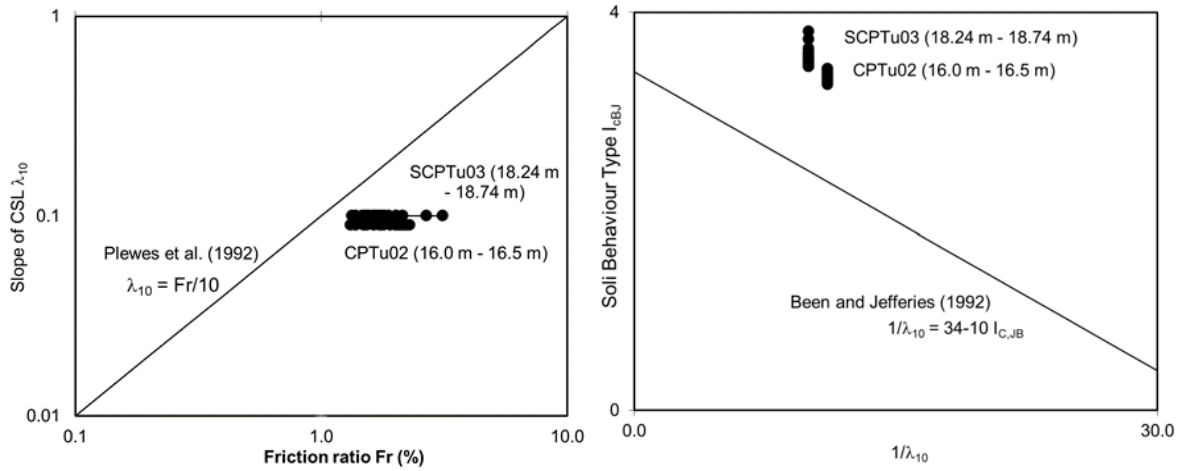

Figure 5: Performance of compressibility against empirical relationships

In-situ shear strength by the N_{kt} method

The drainage behaviour of the tailings around the cone tip is associated with the tailings' consolidation, drainage path lengths, and the cone penetration velocity. To account for these factors, a normalized, dimensionless penetration rate (V), as proposed by Finnie and Randolph (1994) has been used to identify the drainage conditions of the tailings during cone penetration. Undrained penetration is generally observed at V above 10 or 30 (Finnie and Randolph, 1994; Kim et al., 2008). V was higher than 30 in all the standard CPTu probes. Therefore, it was inferred that undrained conditions controlled the behaviour of the tailings during cone penetration. Under the fast-rate (110 mm/s) and slow-rate (3 mm/s) CPTu soundings, carried out at CPTu02 and SCPTu03, V values of about 370 and 10 were estimated, respectively, for a coefficient of consolidation of 300 m^2/year on average. This result indicates that partial drainage may have occurred at a slow-rate penetration. Of note, however, was that negligible differences in the measured tip penetration resistance of the cone were obtained with a standard and slow-rate penetration conditions, as can be seen by comparing q_t in Figure 4a.

On this basis, the N_{kt} method (Robertson, 2009) was applied to estimate the profile of undrained shear strength the tailings in the TSF. N_{kt} has been seen to vary from approximately 10 to 30 in a variety of soils within the geotechnical literature (Kulhawy and Mayne, 1990), which leaves uncertainty in an estimate of S_u/σ'_{v0} based solely on CPTu data. Therefore, the N_{kt} factor was selected by correlating the undrained shear strength ratio S_u/σ'_{v0} of the reconstituted tailings, prepared in the laboratory to about the same state (noting that there may have been fabric differences in the laboratory sample), which indicated a value of 0.2, and

that the S_u/σ'_{v0} for the field condition at the depth of interest of 16 to 16.5 m. A tailings specific N_{kt} factor of 14 was selected after calibration, well within the typical range. The calibrated s_u/σ'_{vo} profile for CPTu02 probe is shown in Figure 6a. A value of s_u/σ'_{vo} of approximately 0.20 was also estimated by the Sadrekarimi method (Sadrekarimi 2014), as seen in Figure 6a, although it is noted that there were some deviations of this estimate and the calibrated undrained strength with shallow depths (Sadrekarimi, 2014).

Liquefaction assessment

Tailings strength and earthquake demands

Following the Soil behaviour Type index (I_c) framework, Figure 6c suggested that the tailings would behave as sand-like soils (i.e., $I_c < 2.6$) in shallows depths (< 3 m) and as clay-like soils (i.e., $I_c > 2.6$) deeper than 3 m as shown in shown in Figure 6b (similar trend was observed in the rest of CPTu probes). The difference in I_c is unlikely due to different material properties (e.g. particle size distribution or plasticity) of the tailings and may be attributed to near surface changes due to suction. The surface of the tailings was slightly desiccated at the time of the investigation such that the CPT rig could be driven over the tailings. Hence, the CRR when $I_c < 2.6$ was estimated by the formulations proposed by Robertson (2009) and the profile of the clean-sand penetration resistance $(q_{c1N})_{cs}$ of the tailings, an example of this profile is shown in Figure 6c. On the other hand, when $I_c > 2.6$, the CRR of the tailings was estimated by applying a tailings-specific factor of about 60% to the undrained shear strength ratio of Figure 6a. This factor was estimated considering the following:

- tailings undrained shear strength;
- the ratio of cyclic shear stress to Su for a 15 uniform loading cycles to induce 3% single amplitude shear strain and a cyclic loading frequency of 1 Hz representative of earthquake loading;
- a magnitude scaling factor (MSF) of 1.0 for an earthquake of M_w= 7.5;
- a static shear stress ratio correction factor to account for sloping ground on cyclic strength of 1.0; and
- a correction factor for two-dimensional cyclic loading in the field (0.96) (Boulanger and Idriss, 2007).

An example of the CRR profile estimated for the tailings under study is shown in Figure 7a. The earthquake demands by the CSR on the tailings was estimated considering the horizontal acceleration demands of the site together with the stress reduction coefficient (r_d) (Youd and Idriss, 2001). The seismic setting of the site and the design and operational parameters of the TSF considered peak ground acceleration demands for the operational basis, maximum design, and maximum credible earthquakes (OBE, MDE and MCE) of 0.03g, 0.06g and 0.25g, respectively.

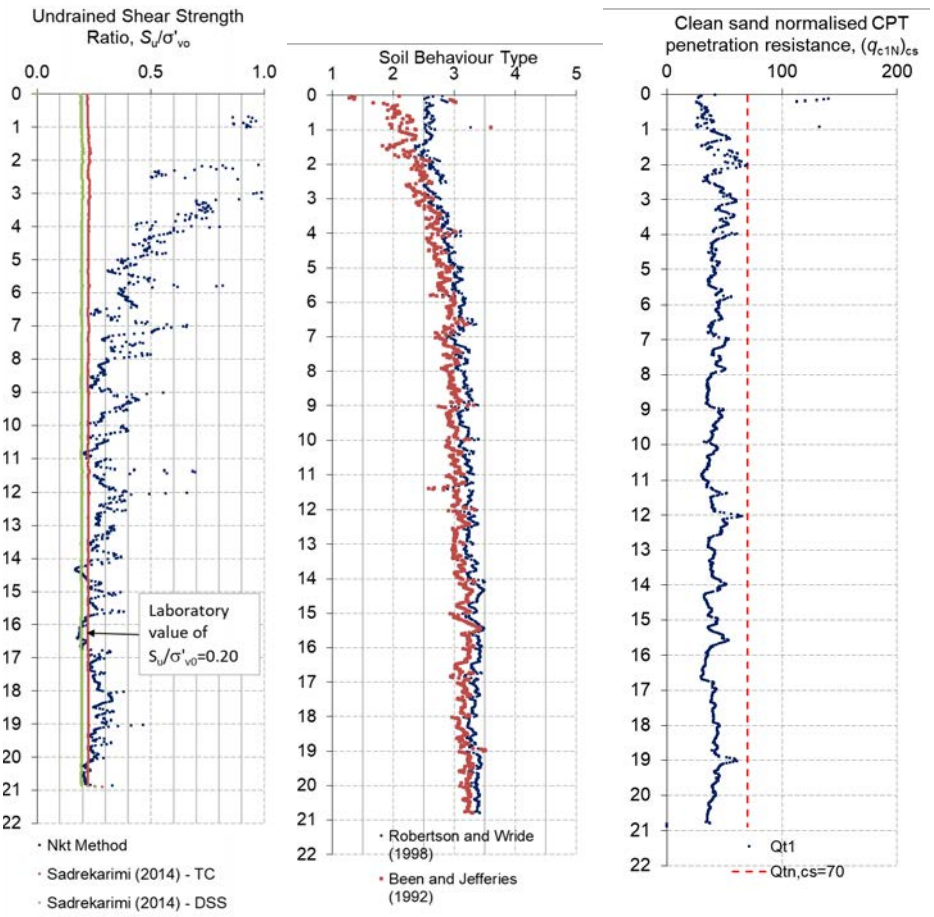

Figure 6: Profile of a) undrained shear strength; b) Soil behaviour type; and c) $(q_{c1N})_{cs}$ for CPTu02

Tailings liquefaction susceptibility

The cyclic liquefaction potential was assessed by a factor of safety (FoS) against liquefaction (Youd and Idriss 2001). The profile of FoS was consistent between the CPTu locations, thus only the FoS for CPTu02 is presented and discussed in the paper. The results indicate that the FoS was substantially higher than unity under OBE and MDE demands (not shown in Figure 7b). On the other hand, under the MCE event, the FoS suggests that the tailings could liquefy (i.e., FoS < 1) in shallow layers up to 3 m depth. Below the 3 m depth, the FoS is general higher than unity for depths up to 6 m from the tailings surface, suggesting that this zone of the tailings would not be susceptible to liquefaction. However, below 6 m from surface, the FoS suggested that these layers (which represent the bulk of the tailings) would liquefy in bands with variable thickness from few centimetres to meters (see Figure 7b). Despite the potential for liquefaction, the TSF is part of an integrated waste landform (IWL) and hence a satisfactory FoS against slope instability was indicated.

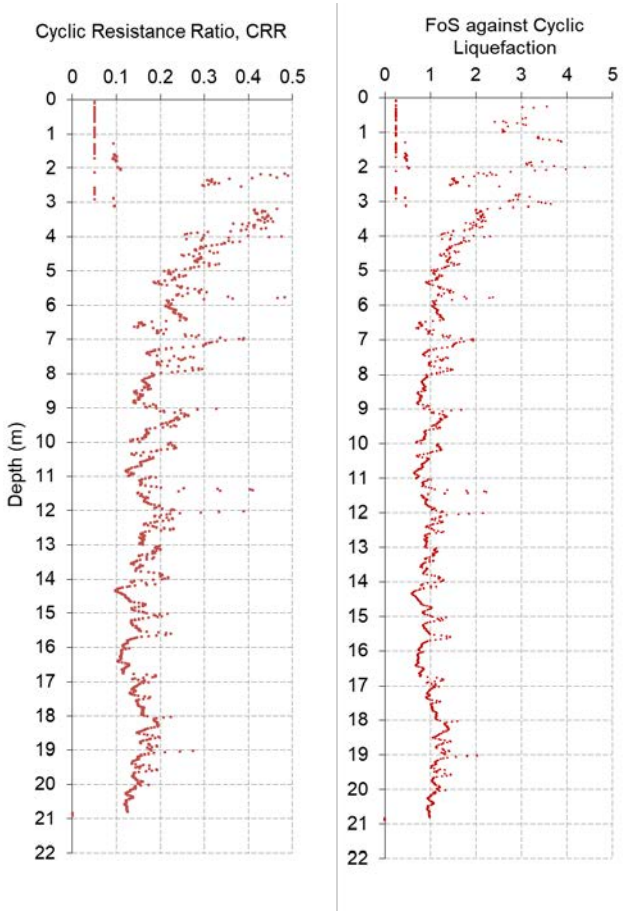

Figure 7: a) CRR; and b) FoS under a MCE demand for CPTu02

Conclusion

CPTu investigations were carried out at five locations within a TSF. The program included the collection of tailings samples for advanced laboratory tests. The laboratory test results on the strength of the tailings, in addition to the index properties of the tailings, were used to develop site-specific correlations utilized in the CPTu interpretation. The interpretation of the CPTu data demonstrated that a saturated, or near-saturated condition of the deposited tailings can be encountered in the TSF even if a phreatic surface was not present.

It was found that current available empirical methods (i.e., Plewes et al. [1992]; Been and Jefferies [1992]) applied to the CPTu to infer the in-situ state parameter and thus in-situ strength of the tailings are limited in capturing the behaviour of the tailings. However, dissipation testing indicated that the penetration occurred under undrained conditions and hence, the N_{kt} method was found to provide a reasonable approach for assessing the tailings undrained shear strength. A N_{kt} factor of 14 was selected after calibration between the undrained shear strength of the tailings from the CPTu and from independent laboratory measurements via testing of reconstituted tailings samples.

The potential for cyclic liquefaction of the tailings was assessed by estimating FoS as the ratio between the CSR and CRR. The results indicated that some layers of the tailings could be susceptible to liquefaction under a MCE event (0.25g). Despite the potential for liquefaction, the TSF is part of an IWL, and hence a satisfactory FoS against slope instability was indicated.

References

Been, K. and M.G. Jefferies. 1992. Towards systematic CPT interpretation. In *Predictive Soil Mechanics: Proceedings of the Wroth Memorial Symposium:* 121–134. 27–29 July 1992, St. Catherine's College, Oxford, UK.

Boulanger, R., and I.M. Idriss. 2007. Evaluation of cyclic softening in silts and clays. *Journal of Geotechnical and Geoenvironmental Engineering* 133(6): 641–652.

Finnie, I.M.S. and M.F. Randolph. 1994. Punch-through and liquefaction induced failure of shallow foundations on calcareous sediments. In *Proceedings of the 7th International Conference on the Behaviour of Offshore Structures,* 1, Cambridge; MA. In BOSS-CONFERENCE, Boston, MA, USA: 217–230.

Kim, K., M. Prezzi, R. Salgado, and W. Lee. 2008. Effect of penetration rate on cone penetration resistance in saturated clayey soils. *Journal of Geotechnical and Geoenvironmental Engineering* 134(8): 1142–1153.

Kulhawy, F.H. and P.H. Mayne. 1990. Manual on estimating soil properties for foundation design. EL-6800, Palo Alto, California: EPRI.

Plewes, H.D., M.P. Davies and M.G. Jefferies. 1992. CPT based screening procedure for evaluating liquefaction susceptibility. In *Proceedings of the 45th Canadian Geotechnical Conference.* Toronto, Ontario: 41–49.

Robertson, P.K. 2009. Evaluation of flow liquefaction and liquefied strength using the cone penetration test. *Canadian Geotechnical Journal* 46: 1337–1355.

Sadrekarimi, A. 2014. Effect of the mode of shear on static liquefaction analysis. *Journal of Geotechnical and Geoenvironmental Engineering* 140(12).

Seed, B.R., O.K. Cetin, R.E.S. Moss, A.M. Wu, J. Kamer, J.M. Pestana, R.B. Sancio, J.D. Bray, R.E. Kayen, M.F. Riemer and A. Faris. 2003. Recent advances in soil liquefaction engineering: A unified and consistent network. 26th Annual ASCE Los Angeles Geotechnical Spring Seminar. Keynote presentation, HMS Queen Mary. Long Beach, California.

Youd, T.L. and I.M. Idriss. 2001. Liquefaction resistance of soils: Summary report from the 1996 NCEER and 1998 NCEER/NSF workshops on evaluation of liquefaction resistance of soils. *Journal of Geotechnical and Geoenvironmental Engineering, ASCE.*

Bibliography

Jefferies, M.G. and K. Been. 2015. *Soil Liquefaction: A Critical State Approach,* second edition. CRC Press.

Proceedings of Tailings and Mine Waste 2019
November 17–20, 2019, Vancouver, Canada
Published by the University of British Columbia, 2019

An Alternative Tailings Deposition System for Uranium Tailings

Matt Treinen, Paterson & Cooke USA, Ltd, USA
Erik Ketilson, SRK Consulting (Canada) Inc., Canada
Jon Aydt, Orano Canada Inc., Canada
Justin Jacobs, Paterson & Cooke USA Ltd, USA

Abstract

Orano Canada Inc. (Orano) undertook a tailings deposition review for the JEB Pit Tailings Management Facility (TMF) at the McClean Lake uranium mill in northern Saskatchewan to optimize the utilization of available tailings storage capacity. After initial screening, two tailings deposition alternatives were advanced to the detailed review stage. The first option included continuing deposition using tremie injection, but with the implementation of satellite deposition barges placed radially from the existing barge. The second option utilized subaqueous rather than tremie deposition. Subaqueous deposition offered several advantages, but was a fundamental shift in the tailings deposition methodology and had to be investigated and proven suitable prior to implementation on site.

Computational fluid dynamics (CFD) was used to assess the expected suspended solids and relative impact on placed density during subaqueous deposition using different diffuser concepts. Deposition simulations assessed the accumulation of tailings during a short-term test.

Following concept development and computational optimization, a 25-day field trial was conducted to assess the full-scale behaviour of subaqueous deposition using a horizontal trumpet style diffuser. The results from this test were consistent with the predicted behaviour in both the CFD and deposition modelling. Following the successful field trial, Orano proceeded with full-scale, multi-deposition point implementation in 2018. This paper discusses the CFD analyses, field trial performance, and longer-term operation of the subaqueous deposition system.

Introduction

Uranium was originally mined from Orano Canada Inc's (Orano) JEB Pit in Northern Saskatchewan starting in 1995. The pit was then converted to a tailings management facility (TMF) in 1999 to receive tailings from the McClean Lake Mill. In 2016, Orano undertook a tailings deposition review for the JEB TMF to

optimize utilization of storage capacity. Prior to the study, the tailings were subaqueously deposited in the pit using a single tremie pipe injection point. The tremie pipe injected the tailings into the previously deposited tailings mass to minimize particle size segregation within the tailings mass, to minimize production of suspended solids within the water cover, and to attempt to maintain a high in-situ placed tailings density. Regular sampling campaigns indicated segregation occurred with the tremie method, so its effectiveness was questioned. The tailings must be deposited subaqueously with a minimum 1m water cover to shield from the radioactive tailings and to prevent ice lenses from forming and persisting between layers of deposited tailings.

The tremie pipe configuration is housed in a heated barge at the end of a rigid floating walkway. The barge can only be moved during summer. Moving the barge is a manpower intensive exercise due to the extensive floating walkway and barge anchoring system, and moving it is avoided. During winter the barge is frozen in place in an up to two meter thick ice cover.

Volumetric modelling indicated that as the tailings level in the pit increased over the next few years, it would be necessary to relocate the deposition barge as frequently as monthly to evenly distribute the tailings across the pit and prevent beaching of the barge. SRK Consulting (Canada) Inc. (SRK) and Paterson & Cooke, USA, Ltd. (P&C) were contracted by Orano to develop multiple conceptual options for more evenly and efficiently distributing the tailings placement within the pit.

Concept development

After initial screening, two tailings deposition alternatives were advanced to the detailed review stage. The first option was to continue deposition using tremie injection but with the implementation of multiple satellite deposition barges placed radially from the existing barge. The multiple barges and associated access walkways option was expensive and operationally complex.

The second option was to depart from the tremie deposition method and deposit the tailings subaqueously. Eliminating the tremie pipe eliminated the need for a heated barge at each location to periodically adjust the tremie pipe depth. By utilizing flexible walkways rather than their current rigid walkways, the subaqueous deposition point could also be swept over a wider area to spread out the deposition area.

The impact subaqueous deposition would have on the suspended solids within the pit and the placed tailings density was unknown. The authors first undertook materials characterization and rheology test work to define the tailings properties. Following this characterization, computational fluid dynamics (CFD) was used to evaluate the short-term deposition of three different subaqueous discharge diffuser configurations. Following promising modelling results, the concept was evaluated in a short duration field trial. Ultimately the field trial was successful, and a full-scale five discharge point subaqueous deposition system was

implemented. The deposition system was operated continuously over the first winter with no deleterious impact on reclaim water quality, or particle size segregation within the pit.

Tailings properties

Since 2015, Cigar Lake ore has been processed at McClean Lake and the resulting tailings are deposited within the JEB pit. Prior to 2015, JEB/SUE ore tailings were deposited within the JEB pit TMF. The JEB/SUE ore tailings typically had an average 50% of the particle sizes less than 0.075 mm. The tailings were typically transported to the JEB TMF at a solids content of approximately 32% to 34.5% solids by weight.

The current Cigar Lake ore tailings have approximately 80% of the particle sizes less than 0.050 mm. A plot of the current Cigar Lake ore tailings thickener underflow is presented in Figure 1. The solids specific gravity varied between 2.65 to 2.76 during the rheology test campaign.

The tailings are currently being transported to the JEB TMF at a solids content of 25% to 28% by weight. Rheology testing was completed on site in late April and early May and during a second campaign in June 2017 to measure the whole tailings and carrier fluid (minus 45 microns) fraction slurry rheology. Table 1 summarizes the measured whole tailings rheology parameters. Significant variability between samples was observed during the multiday testing campaign. This variability can be attributed to the clay content and grade variability in the ore feed into the mill.

CFD study

Of key concern in switching to a subaqueous deposition approach was understanding the flow behaviour of the tailings as it flowed out of the discharge, through the water column, and came to rest on the tailings surface within the TMF. Prior to the field trial, a computational fluid dynamics (CFD) study using Ansys Fluent (Ansys, 2018) was completed to gain a better understanding of the flow behaviour at discharge and to optimize the diffuser design for completing the subaqueous deposition test. Three discharge configurations were considered: a straight pipe discharge from the existing 3 inch HDPE pipeline, a trumpet diffuser to ensure that the flow was laminar at discharge, and a slotted pipe diffuser to further reduce the flow velocity. The primary objective of the analysis was to quantify the relative difference in suspended solids between the three different options.

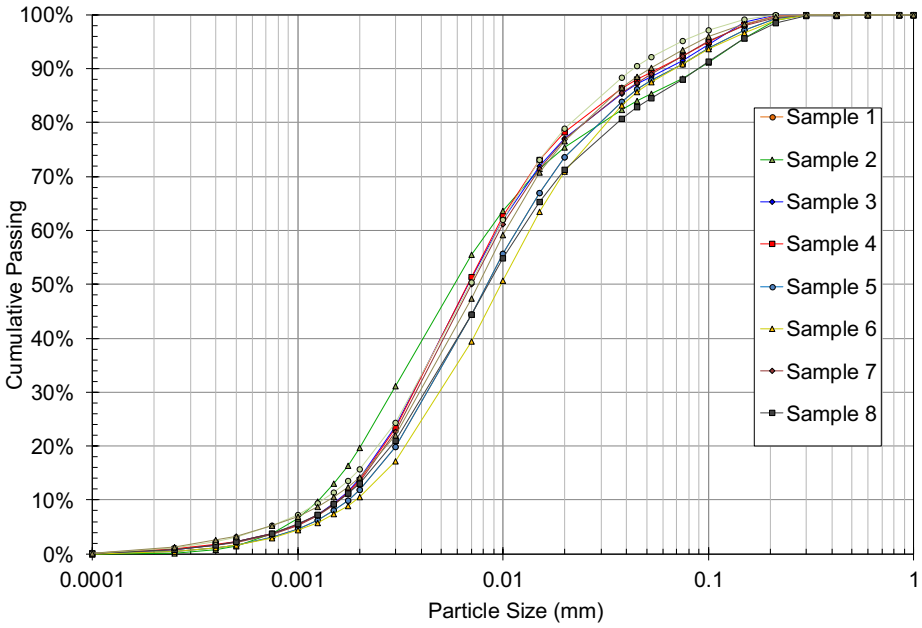

Figure 1: Particle size distribution – thickener underflow – November, 2017

Table 1: Typical Cigar Lake ore tailings underflow rheology parameters

Concentration %	Bingham Plastic yield stress Pa	Bingham Plastic Viscosity mPa.s
25%	2 Pa	5 to 10 mPa.s
30%	2 to 10 Pa	10 to 12 mPa.s
35%	2 to 10 Pa	12 to 35 mPa.s
40%	25 to 50 Pa	23 to 60 mPa.s

The discharge is modeled over a short duration timeframe simply to evaluate the initial flow behaviour and select the concept that produces the most favourable flow behaviour. It is not possible to efficiently quantify the suspended solids over long duration using CFD. The slurry was treated as a homogeneous slurry and the analysis did not predict physical segregation of the tailings solids as the tailings were deposited through the water column, or after the tailings solids contacted the tailings surface.

The CFD analysis showed that under laminar flow conditions for both the straight pipe and trumpet diffuser little mixing occurs between the tailings and water as the denser tailings flowed through the water column. Mixing only occurred at the outer extents of the tailings flow perimeter. As visually seen in Figure 2, this mixing was more pronounced in the straight pipe discharge than the trumpet diffuser. The tailings flow in all three concepts remained stable and intact through the water column. The trumpet diffuser had lower initial suspended solids, but the straight horizontal pipe discharge ultimately produced similar results after sufficient analysis time.

It was not advantageous to use a slotted pipe diffuser since the multiple discharges resulted in more contact area between the tailings flows and water column, resulting in significantly more suspended solids.

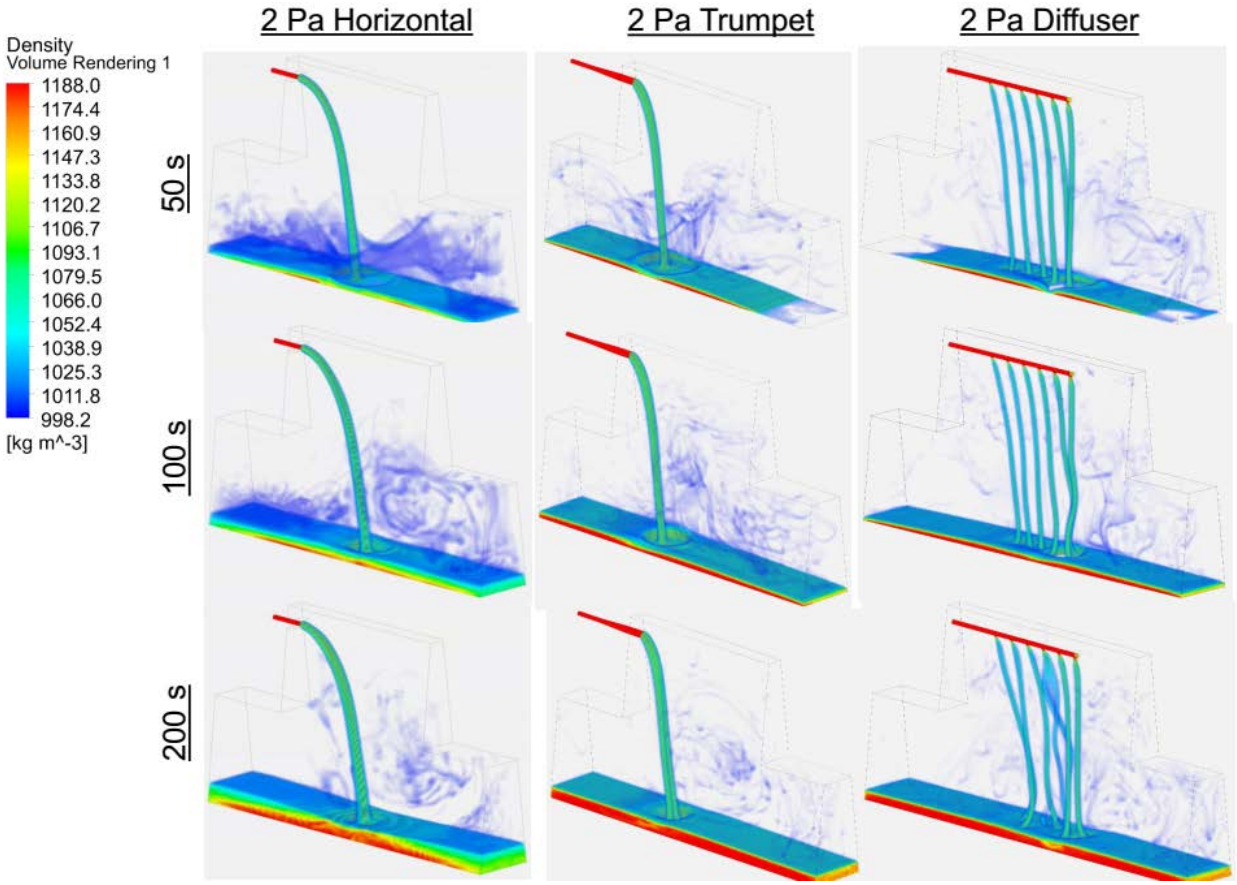

Figure 2: CFD Diffuser evaluation considering a solids content of ~25%

The CFD analysis was also used to investigate the impact the tailings rheology had on the flow behaviour and suspended solids within the water column. Figure 3 presents a comparison of adjusting the tailings yield stress between 0 Pa (Newtonian) and 100 Pa (paste tailings) regimes. The density of the tailings was kept constant to only evaluate the impact yield stress had on the flow behaviour.

Based on this analysis, it appears that increasing the yield stress to between 10 Pa and 20 Pa, which would correspond to approximately 30%m and 35%m underflow solids concentration, would reduce the suspended solids within the water column, but would result in a more mounded tailings surface. The relative impact this slope would have on the deposition behaviour cannot be evaluated during these short duration CFD simulations, but it is not expected to be substantially different relative to the current 2 Pa typical tailings yield stress.

At the high yield stress of 100 Pa, the deposition behaviour became unstable and the tailings showed a more significant mounding behaviour upon deposition. As with the other cases, the long-term deposition

slopes cannot be estimated based on these short-term simulations, but this instability raises some initial concern as to the flow behaviour of a paste type tailings subaqueous discharge. This deposition behaviour requires further evaluation, if paste deposition was to be advanced in the future.

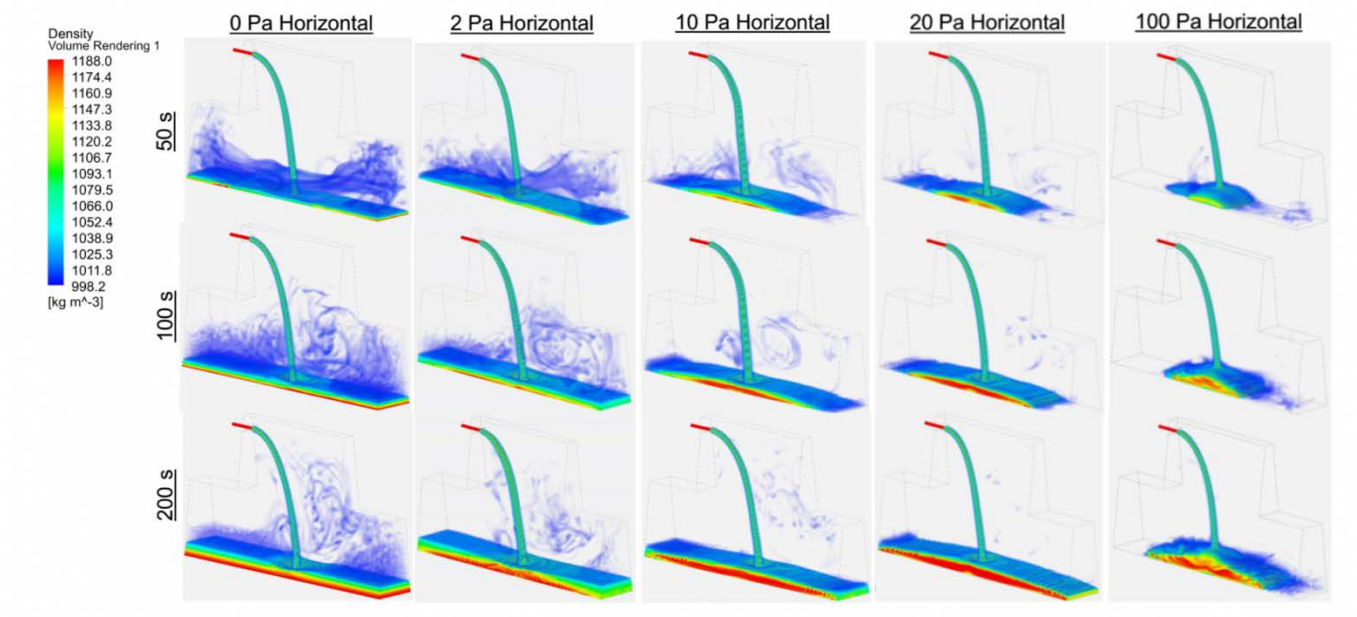

Figure 3: CFD evaluation of tailings yield stress (trumpet diffuser), 0 Pa to 100 Pa

Subaqueous deposition field trial

In order to prove the concept, and gain regulatory acceptance, Orano completed a 25-day trial of the subaqueous deposition between September 24 and October 18, 2017 with the assistance of SRK and P&C. During the trial, the deposition point was suspended from a barge connected perpendicular to the tremie barge walkway using segments of flexible walkway. Figure 4 provides a photograph of the field trial. A two-meter long, 150 mm nominal diameter DR 9 HDPE tremie pipe was used for the laminar flow diffuser. The two-meter length ensured that the flow had fully transitioned to laminar flow prior to discharge. The diffuser was suspended 3 m below the water level within the pit and approximately 10 m above the tailings bed.

The monitoring plan for the subaqueous test focused on monitoring the deposition through bathymetric surveys, measurement of the depth to tailings, collecting water samples for suspended solid and geochemistry analysis, visual aerial monitoring to monitor the deposition plume, and collecting tailings samples.

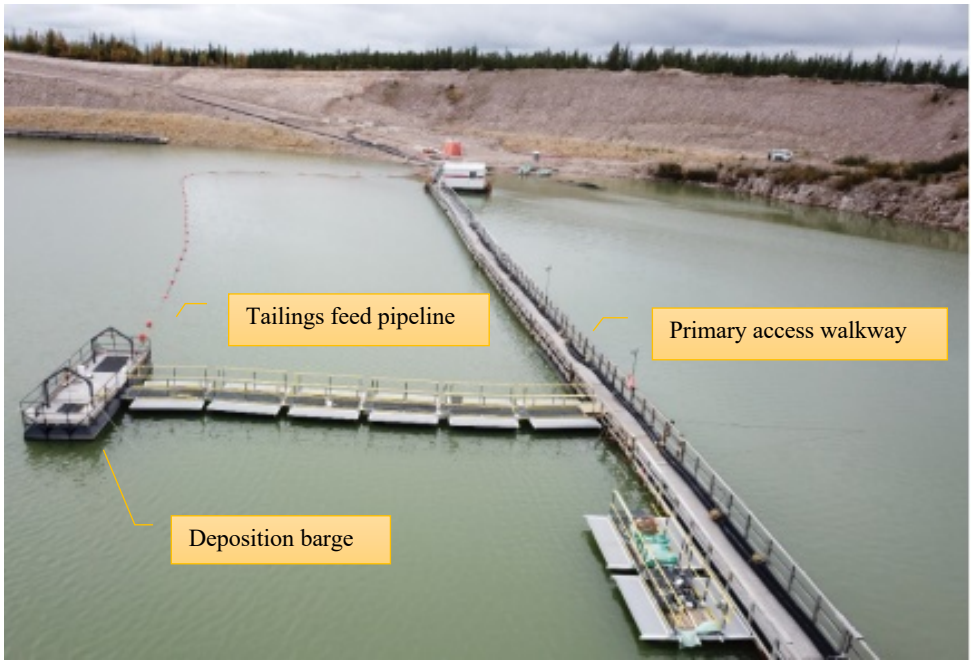

Figure 4: Subaqueous field trial configuration

Key findings

PSD segregation

The samples collected by dredge from the tailings surface after the trial show the tailings segregated between the discharge and at points between 5 m and 43 m from the deposition point. Figure 5 (a) presents a comparison of the PSD with distance. Based on PSD analysis, the coarse fraction of tailings deposits near the deposition point at the mound, while the fines are carried further away.

Beach profile

The beach profile surrounding the subaqueous deposition point was estimated based on the bathymetric survey completed at the end of the field trial. The profile indicates that a mound of coarse tailings is deposited near the deposition point, with finer material segregating and flowing away from the deposition point. This complex slope is compared to the slope from the tremie deposition in Figure 5(b). The subaqueous deposition results in a higher initial slope at the mounding area; however, the remaining profile is shallower. Due to this overall shallower slope, it is expected that over a long duration deposition, a larger volume of tailings can be placed at a single deposition location using the subaqueous deposition than with the tremie deposition.

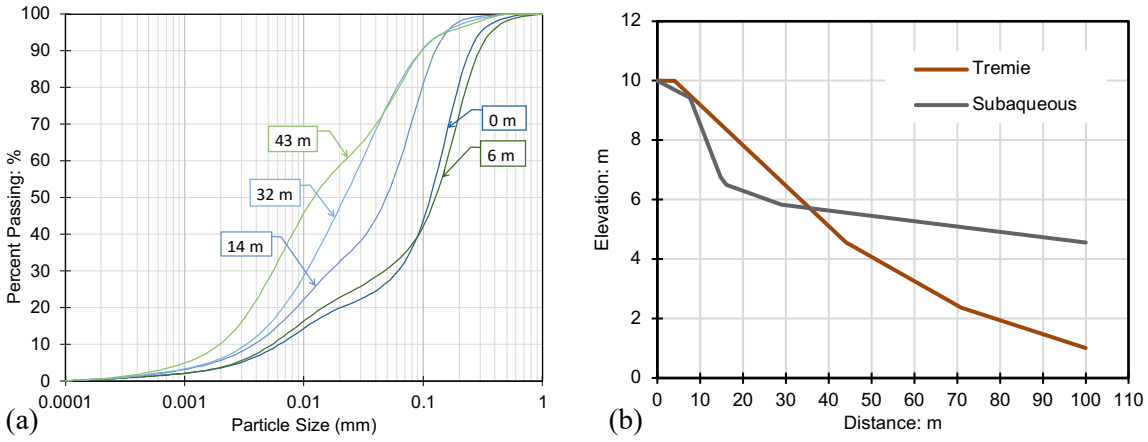

Figure 5: Subaqueous deposition (a) PSD (b) Beach profile

Suspended solids

Visual monitoring indicated that the tailings near the subaqueous discharge settled quickly and did not produce a significant plume of suspended solids around the deposition point. Water samples collected within the pit and at the reclaim water system inlet indicated no impact on the overall water quality or suspended solids.

Field trial summary

Ultimately the field trial indicated that subaqueous deposition did not adversely affect the tailings management facility operation. Segregation was observed, as was localized mounding, but both were within acceptable limits. Moving toward subaqueous deposition would greatly simplify the distribution of tailings through the pit.

Full-scale implementation results

Based on the successful performance of the field trial, Orano opted to implement full-scale subaqueous deposition beginning in the winter of 2018/2019 to monitor long term facility performance.

The key criterion for success of subaqueous deposition was the ability to deposit to multiple locations, therefore maximizing utilization of the available TMF volume without having to relocate the deposition system during winter months. This was accomplished by installing five subaqueous deposition points, where traditionally there had been one tremie deposition point. Tailings are transported from the tailings thickener to the TMF via two three-inch HDPE pipelines and then placed using two of the five subaqueous deposition points at any given time. Tailings are deposited in one location until the mound reaches a previously determined maximum allowable elevation, at which time tailings placement is moved to another

subaqueous deposition point. As shown in Figure 7, the subaqueous deposition points were installed on auxiliary floating walkways perpendicular to the primary tremie deposition walkway.

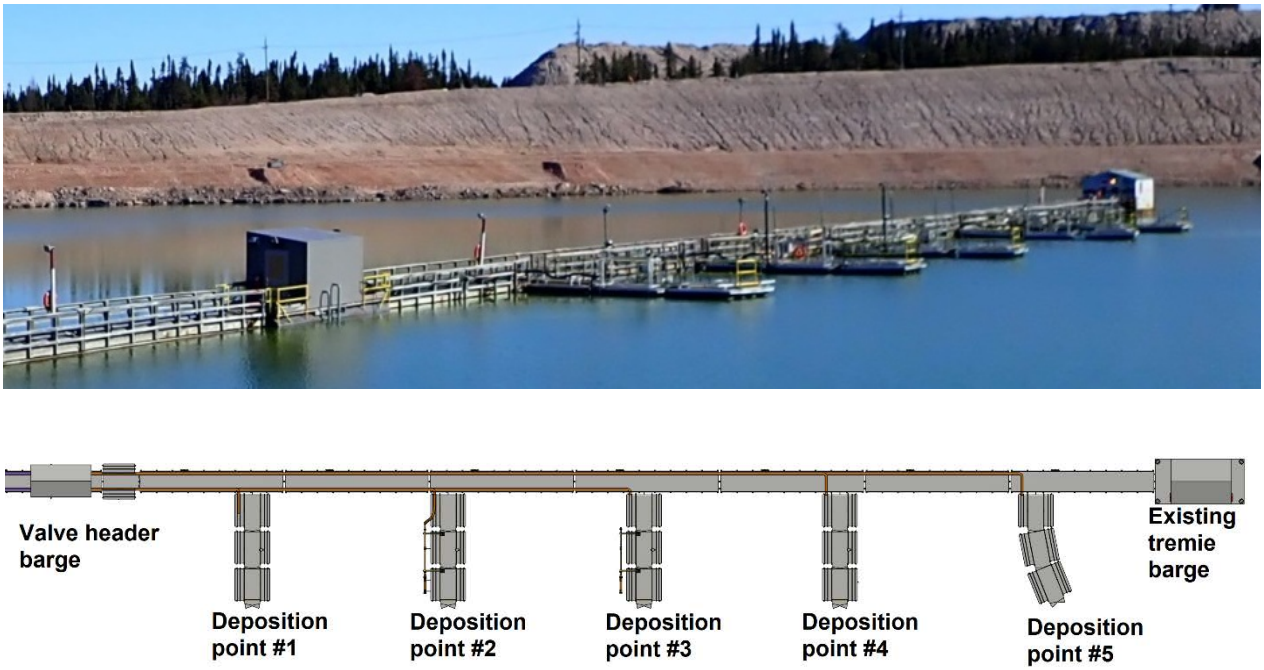

Figure 7: Subaqueous deposition installation

For added tailings placement flexibility, these auxiliary walkways are comprised of three floating sections that allow for ten degrees of articulation between each connection point. This results in the ability to sweep the deposition point up to approximately six meters, further maximizing use of existing TMF space.

The primary risk to operation of the subaqueous deposition system is freezing pipelines and valves during winter months. To mitigate this risk, various freeze protection options were reviewed including locally heated and insulated valve enclosures and complete insulation and heat tracing of pipelines and valves. Ultimately freeze protection of the deposition system is made up of two parts, a valve header barge and a diffuser lifting apparatus.

Valve header barge

To mitigate freezing valves and the dead legs associated with closed valves, the system was designed such that all redirection of flow activities occur within an enclosed and heated barge constructed specifically for this purpose. Tailings flow from the thickener through two three-inch HDPE pipelines that terminate at a valve header in this barge. As shown in Figure 8, using a series of valves and hoses, flow is directed from the tailings pipelines to the desired subaqueous deposition point.

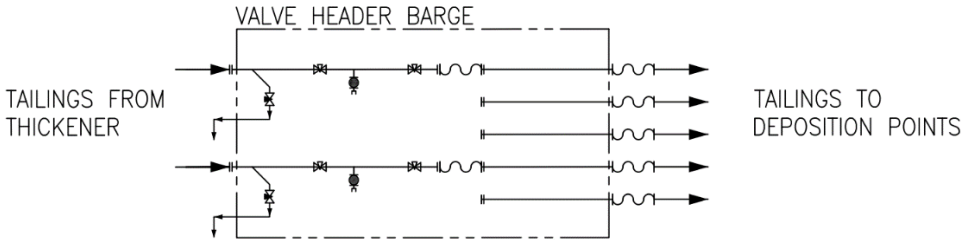

Figure 8: Flow redirection to deposition points

Each deposition point has independent piping with no valves or branches, reducing the potential to freeze dead legs and simplifying pipeline clearing activities when a deposition point is removed from service. Use of hoses versus valves to redirect flow is more labour intensive to operate but results in a simpler system that intrinsically protects from inadvertently filling and subsequently freezing an out-of-service pipeline due to a slurry valve passing or operator error.

Diffuser lifting apparatus and deicing

To prevent the out-of-service subaqueous deposition piping from freezing into to the surface of the tailings pond, two 0.75kW propeller style deicers per deposition point are installed. To prevent the still water in the water/pipe interface of the submerged piping from freezing, the subaqueous diffuser is lifted and secured above the surface of the TMF pond until it is placed into service. Figure 9 shows the lifting apparatus installed at each deposition point to facilitate raising and lowering the diffuser when it is placed into and removed from service.

Figure 9: Lifting apparatus shown in raised position

Lessons learned

The subaqueous deposition system has been in continuous operation for ten months (at the time of writing this paper) and has successfully placed approximately 260,000 tonnes of tailings. It has successfully operated through a winter season with completion of multiple changes in deposition point.

During operation, regular manual depth measurements are taken at each deposition point to monitor the elevation of the tailings mounds. At out-of-service deposition points directly adjacent to in-service deposition points a gradual increase in tailings elevation was observed over time. Referencing the beach profile shown in Figure 5b, it is believed that the finer tailings material flowing away from the deposition point is flowing into the adjacent deposition area. This behaviour was anticipated and suggests that increasing the distance between deposition points may result in longer periods of continuous deposition from any one point but with a higher degree of mounding. Alternatively, it suggests that shorter depositional durations from points placed closer together results in the maximized use of available TMF volume by minimizing mounding.

It has also been observed that the growth of the tailings mound, when plotted on a tailings elevation versus time curve, does not result in a continuous increasing mound. Shown in Figure 10, the mound grows at a continuous rate until such time the tailings elevation measurement abruptly decreases and the growth profile resets. This behaviour happens repeatedly at each in-service deposition point. It is assumed that coarser tailings sluff off of the peak of the mound resulting in this behaviour.

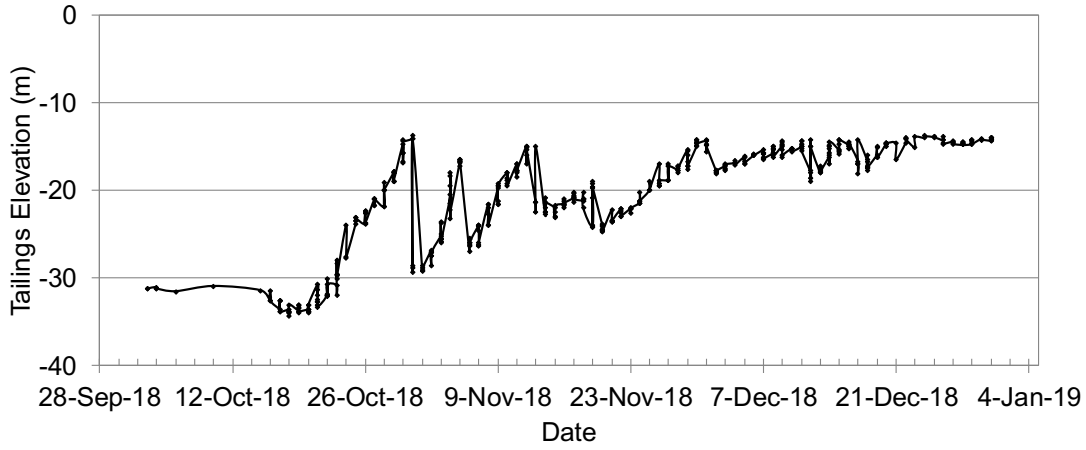

Figure 10: Deposition point #1 tailings elevation versus date plot

Additionally, at each deposition point it has been observed that as the tailings mound grows, the change in tailings elevation at the deposition point gradually decreases. This suggests that, as the volume of the tailings mound increases, the beach profile flattens out radially around the deposition point.

During a late winter 2017 field trial of the 0.75kW deicers, an unplanned power outage and the subsequent power restoration resulted in the deicers not restarting as they should. This resulted in the trial

section of floating walkway freezing into the TMF surface ice for the duration of the winter. This incident demonstrated a known risk with the subaqueous deposition system. As a result both engineered and administrative controls were added to the final design to mitigate freezing risks. Controls include providing power to the deicers from three circuits versus one such that a local circuit failure does not compromise the entire system. Additionally, each deicer has a run status indication light installed that from a distance shows there is current flow to the unit. A documented operational check, at a minimum of twice per 12hr shift, has been implemented to ensure deicers are operational and to minimize response time if they are not.

Conclusion

Ultimately moving away from a single tremie deposition point to multiple subaqueous deposition locations allowed Orano to better utilize the full capacity of the TMF, particularly over winter, with fewer major barge and walkway relocations. Prior to implementation, it was necessary to first characterize the tailings properties and rheology to provide inputs for modelling to evaluate the feasibility of subaqueous deposition. Volumetric deposition forecasting helped determine the deposition point sequencing to maximize tailings volume deposited with optimal switching between deposition points. CFD modelling indicated that little solids suspension would be observed during deposition provided the tailings flow was laminar at discharge into the water column.

Following the computational modeling, the full-scale field trial confirmed subaqueous deposition caused no water quality problems within the TMF. The trial also indicated that coarse particle segregation increased with subaqueous deposition, allowing the coarse particles to settle near the point of deposition, and allowing the finer fraction to flow towards the perimeter of the pit. The segregation was within acceptable limits considering the fine-grained Cigar Lake ore tailings being processed. Full-scale operation with five deposition points over the first winter season was successful. It also highlighted areas for improvement and greater understanding of the tailings deposition and sloughing behaviour.

Acknowledgements

The authors are grateful to the many people who assisted with the project within Orano, SRK, and P&C. We are also grateful to Ian Judd-Henry, formally of Orano, for managing the project from concept development through field trials.

References

Ansys Inc. 2018. Fluent version 19.2.

Proceedings of Tailings and Mine Waste 2019
November 17–20, 2019, Vancouver, Canada
Published by the University of British Columbia, 2019

Hazard Assessment of Tailing Dams Slope Instability by Finite Element Analyses with Stochastic Parameter Input

Stefano Utili, Newcastle University, UK
Marco Previtali, University of Milano Bicocca, Italy and Dundee University, UK
Riccardo Castellanza, University of Milano Bicocca and EG4 Risk Sr, Italy
Giovanni Crosta, University of Milano Bicocca, Italy

Abstract

The recent tragic case of the failure of the Brumadinho tailing dam in Brazil has highlighted yet again the great risk posed by static liquefaction to upstream tailing dams. At present, geotechnical assessment of tailing dams tends to be based on overly simplified mechanical models where each potential failure mechanism is considered in isolation. However, often different failure mechanisms appear concurrently. Also, the natural variability of the ground requires the analysis to be probabilistic with the ground parameters assigned as stochastic variables so that often, depending on the set of the ground parameters extracted from the stochastic distribution (the so called realization), a different failure mechanism may cause the dam collapse. The multiplicity of the failure mechanisms that may cause dam collapse and their mutual interaction requires the hazard assessment to be based on a rigorous geotechnical modelling accounting for all the possible failure mechanisms and their mutual influence.

In this paper, a novel approach based on Finite Element Method (FEM) analyses with strength reduction technique combined with a stochastic characterization of the geotechnical input parameters is showcased. These numerical analyses are superior to limit equilibrium methods in capturing the geomaterial behaviour since the identified failure mechanism is obtained as stemming from the FEM analyses and progressive failure is accounted for. Five different operational scenarios corresponding to a typical deterioration pattern of tailing dams subject to the slimes encroaching progressively into the sand zone were considered. For each scenario, a probability of failure was calculated based on several deterministic slope stability analyses of the statistical realization of the set of material parameters multivariate sampling was used to generate the input for deterministic analysis from which the Probability of Failure (PF) for the dam was calculated. The simulation results are then subdivided into failure and non-failure, with the PF being calculated as the ratio of the two.

Work is ongoing to include the simulation of static liquefaction within the same conceptual approach.

Introduction

The inherent risk for tailings storage facilities is the catastrophic failure of the embankment dam. Simplified 2D Limit equilibrium method (LEM) analysis is the standard for orienting short-medium term management decisions, through steady state probability of failure (PF) and Factor of Safety (FS). Finite Element Method (FEM) analyses can predict the system response to changes in operating conditions and be validated against field data.

In this paper we illustrate 2D FEM stochastic analyses with the Strength Reduction Method (SRM) of the progressively upstream raised TSF geometry typically found in literature. Five model conditions are discussed and compared against literature LEM results of Coffey and Susic (2019).

Method

A typical 2D geometry of an upstream tailing dam taken from Coffey and Susic (2019) was considered (see Figure 1). The tailing dam is made by six earthfill dykes laid in sequence on top of a high strength, low permeability foundation.

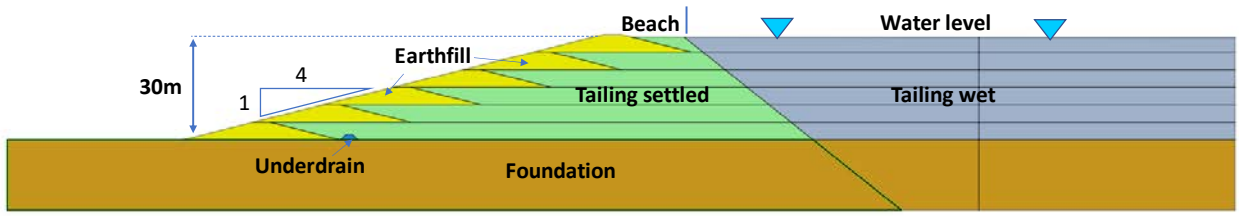

Figure 1: Tailings dam geometry and geomaterials

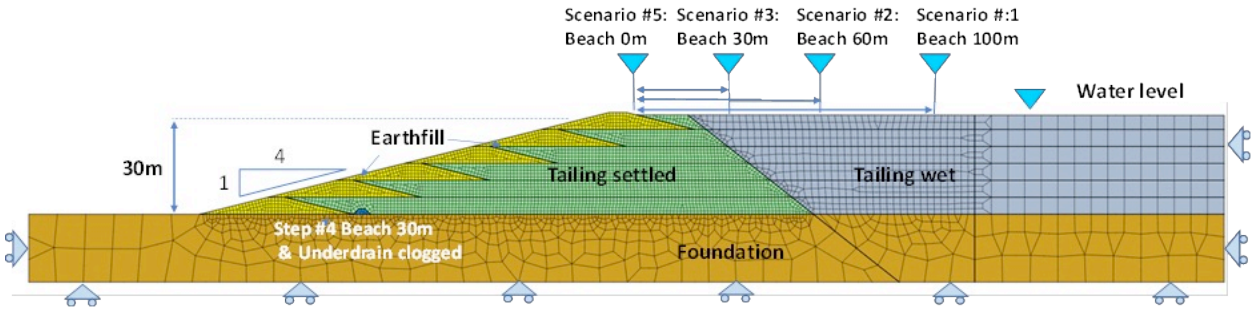

Figure 2: FEM mesh with boundary conditions for the scenarios considered

Following Coffey and Susic (2019), a set of five model scenarios were considered, corresponding to different operational conditions. The width of the dry beach between the dam and the wet decant pond is defined as the most important parameter in tailing dams by (ICOLD, 1994). Here we assumed that, after the sixth embankment is set in place, due to lack of suitable maintenance the dry beach width is progressively reduced. Underdrain clogging is also considered for the last two cases.

The five different conditions considered are the following (see Figure 2):

- **Scenario #1:** Design conditions, dry width of the beach equal to 100 m and drain active.
- **Scenario #2:** Dry width reduced to 60 m due to poor mining control or other causes.
- **Scenario #3:** Dry width reduced to 30 m.
- **Scenario #4:** Dry width reduced to 30 m and clogged underdrain.
- **Scenario #5:** Dry width reduced to 0 m and clogged underdrain.

Given a set of material parameters where the mean and standard deviation value is known or assumed, multivariate sampling was used to generate the input for deterministic analysis from which the Probability of Failure (PF) for the dam was calculated. The simulation results are then subdivided into failure and non-failure, with the PF being calculated as the ratio of the two.

The sampling technique employed to extract the parameter values for each FEM simulation is Latin Hypercube Sampling (LHS). This technique is well known to be the best way to sample the space of the problem parameters by minimizing the number of analyses required for a given target level of confidence sought. This method subdivides the parameter space in a k-dimensional set of bins and keeps track of those already sampled, preventing data redundancy. For further details, refer to McKay et al. (1979) and Olsson et al. (2003).

For slopes, the factor of safety is traditionally defined as the ratio of the actual soil shear strength to the minimum shear strength required to prevent failure (Bishop, 1955). Since it is defined as a shear strength reduction factor, an obvious way of computing FoS with a finite element program is simply to reduce the soil shear strength until collapse occurs. The resulting factor of safety is the ratio of the soil's actual shear strength to the reduced shear strength at failure (Dawson et al., 1999).

The domain was discretized using 4,150 8-node quadrilateral elements. This mesh was achieved after preliminary analyses to ensure negligible dependency of the results on the mesh size adopted. The constitutive model employed is elastic perfectly plastic with a Mohr-Coulomb yield surface. Generic boundary conditions (no displacement orthogonal to domain edges) were applied to the bottom and the sides of the model. Dirichlet hydraulic head conditions were used to define the dry beach width, while a review-type BC is applied to the dam slope and drain conditions to the underdrain nodes. One-way hydro-mechanical coupling accounts for water pressure (Figure 2).

The material parameters were chosen from literature data based on Morgenstern et al. (2016), Coffey and Susic (2019) and Alsharedah (2015). Vertical permeability is set to $1/10^{th}$ of horizontal. Vertical stress ratio K_0 was calculated using the Jaky's formula: $K_0 = 1 - \sin(\varphi)$. For the sake of simplicity, the foundation was considered linear elastic.

The reference model parameters are summarized in Table 1.

Table 1: Material parameters

Material	E $[kN \cdot m^2]$	v $[-]$	k_0 $[-]$	γ_{dry} $[kN \cdot 10^{-3}]$	γ_{sat} $[kN \cdot 10^{-3}]$	k $[m \cdot s^{-1}]$	c' $[kN \cdot m^{-2}]$	φ [°]
Earthfill	70,000	0.3	0.74	18	22	10^{-6}	5	26
Tailing settled	35,000	0.3	0.22	18	22	10^{-7}	0	25
Tailing wet	20,000	0.3	0.22	18	22	10^{-7}	0	15
Drain	50,000	0.3	0.44	18	22	10^{-6}	0	34
Foundation	100,000	0.3	0.53	18	22	10^{-9}	–	–

In the following figure the adopted scheme is summarized.

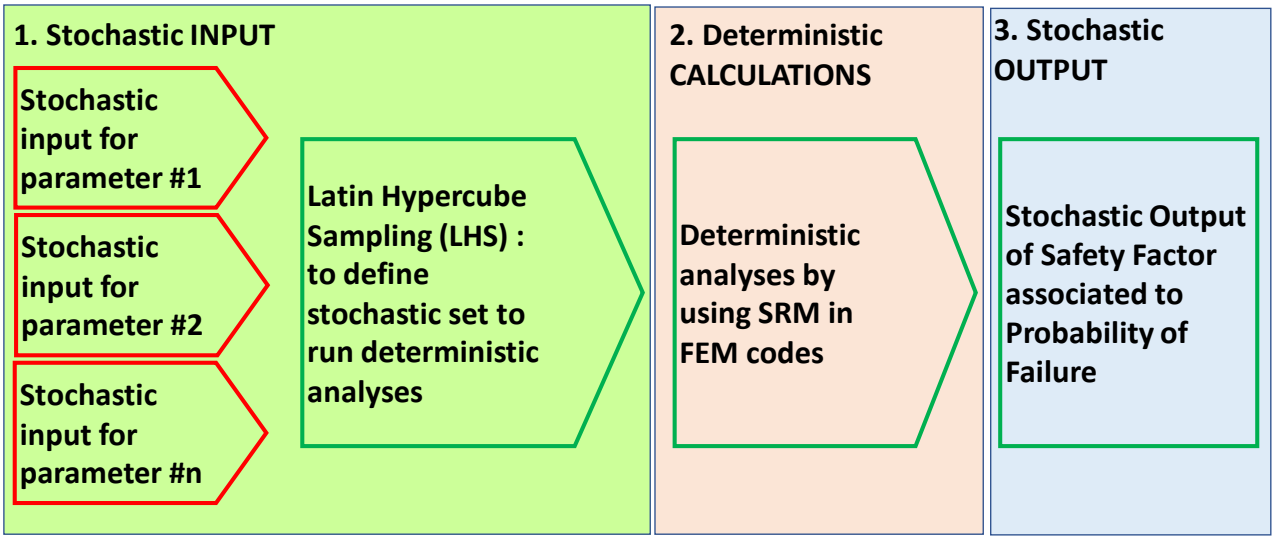

Figure 3: Schematic methodological approach

Stochastic input

We assumed the settled tailings have higher parametric variability than the compacted tailing as they are the result of a natural depositional process rather than the result of tailing management operations. Therefore, the parameter ratio standard deviation parameters associated to earthfill and tailing properties are 0.088 and 0.2, respectively. Parameter ratio is defined as the ratio between the input parameter and the reference parameter (i.e., $\text{Parameter Ratio} = \frac{\tan \varphi_{model}}{\tan \varphi_{ref}} = 1$ for the reference model). The materials parameters distribution is shown in Figure 5.

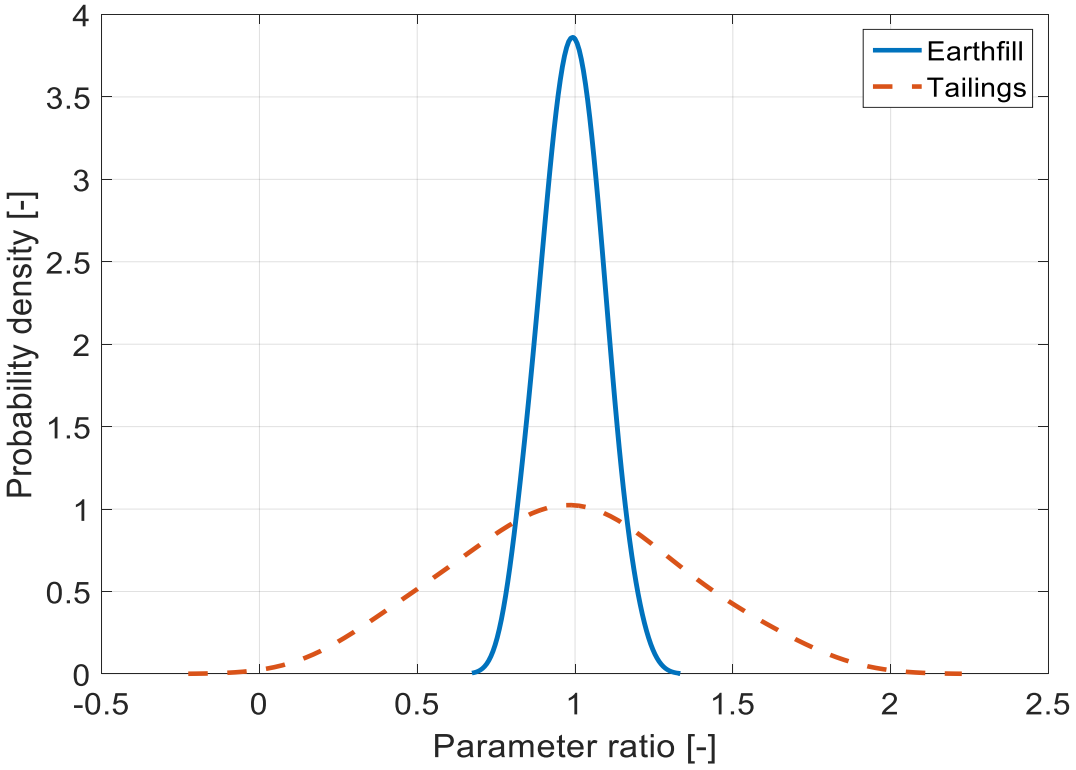

Figure 4: Normal distribution assumed for earthfill (better known) and for tailing settled (mode uncertainties)

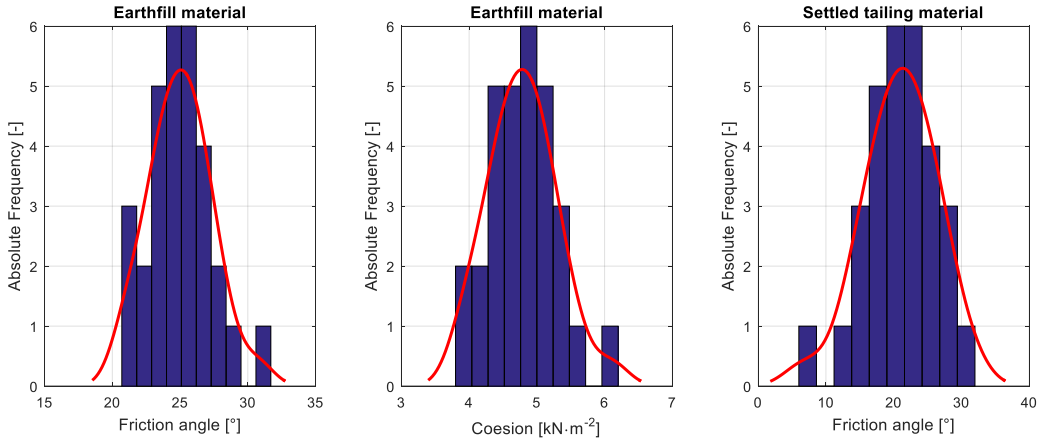

Figure 5: LHS stochastic set of data for the three input parameter

Table 2: Stochastic set for input in the deterministic analyses

Set #	φ_{earth} [°]	c' [kPa]	φ_{tail} [°]	$k0$ [−]
1	21.02	3.94	22.52	0.62
2	24.44	4.66	31.37	0.48
3	25.33	4.85	25.12	0.58
4	23.24	4.40	21.76	0.63
5	26.96	5.21	20.82	0.64
6	25.51	4.89	23.92	0.59
7	24.32	4.63	25.81	0.56
8	23.46	4.45	22.43	0.62
9	26.75	5.17	27.80	0.53
10	27.21	5.27	18.18	0.69
11	26.34	5.08	6.75	0.88
12	23.93	4.55	18.68	0.68
13	27.48	5.33	21.23	0.64
14	22.35	4.21	20.64	0.65
15	24.98	4.78	17.16	0.70
16	28.64	5.60	26.83	0.55
17	24.07	4.58	14.10	0.76
18	22.72	4.29	19.49	0.67
19	30.77	6.10	15.34	0.74
20	23.71	4.50	20.07	0.66
21	26.05	5.01	19.16	0.67
22	22.90	4.33	23.39	0.60
23	25.63	4.92	14.75	0.75
24	26.17	5.04	17.57	0.70
25	24.65	4.70	23.31	0.60
26	25.89	4.97	26.51	0.55
27	28.13	5.48	12.40	0.79
28	21.71	4.08	28.72	0.52
29	25.05	4.79	16.45	0.72
30	20.81	3.90	24.71	0.58

Deterministic FEM analyses

The advantage of this approach, compared to LEM, is the output of expected deformations and the possibility to capture more complex failure geometries and mechanisms (i.e., progressive creep, liquefaction). In the following pictures, a single simulation instance (Parameter Set #25) is presented. The failure surface geometries for the 100 m wide and 30 m wide beach cases (Figure 6 and 7, respectively, magnified displacements) are significantly different: in the former the active zone is much wider with low displacement values. As the model no longer converges after this stage, this can be interpreted the development of a tertiary creeping failure mechanism, typically found in Deep Seated Gravitational Slope Deformations (DSGSD) (Fukuzono, 1985). In the latter, the failure surface is well-defined and limited to the slope front, as typical of embankment failure cases.

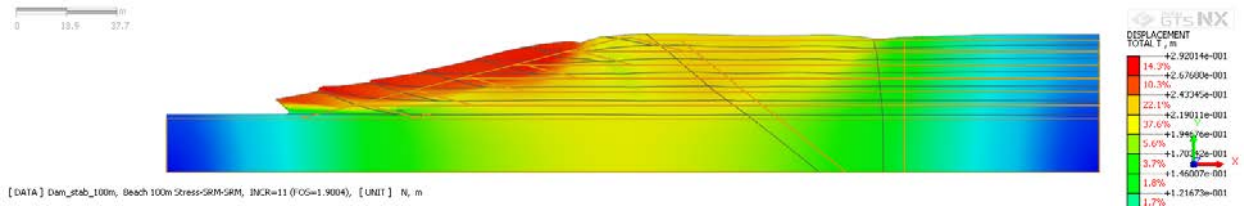

Figure 6: Total displacement at failure for Set #25 – Scenario #1

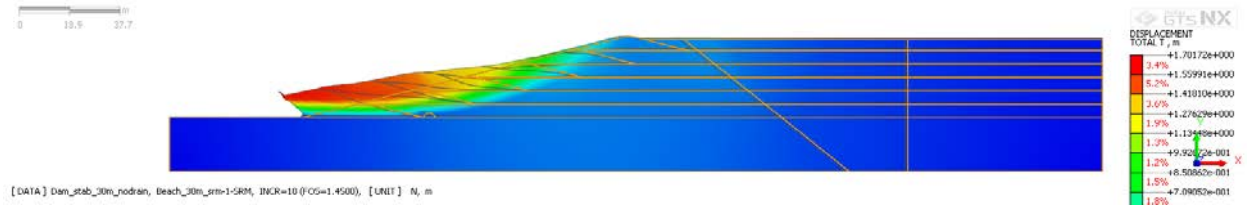

Figure 7: Total displacement at failure for Set #25 – Scenario #4

The Strength Reduction Method provides significant information about the development of the failure surface. In Figure 8, the plastic status of the material is shown at different FS values (FS = 1, FS = 1.4, FS = 1.45, final state before failure). The multiple potential surfaces shown at FS = 1 do not develop as the failure process progresses and the material plasticizes progressively from the bottom of the slope upward.

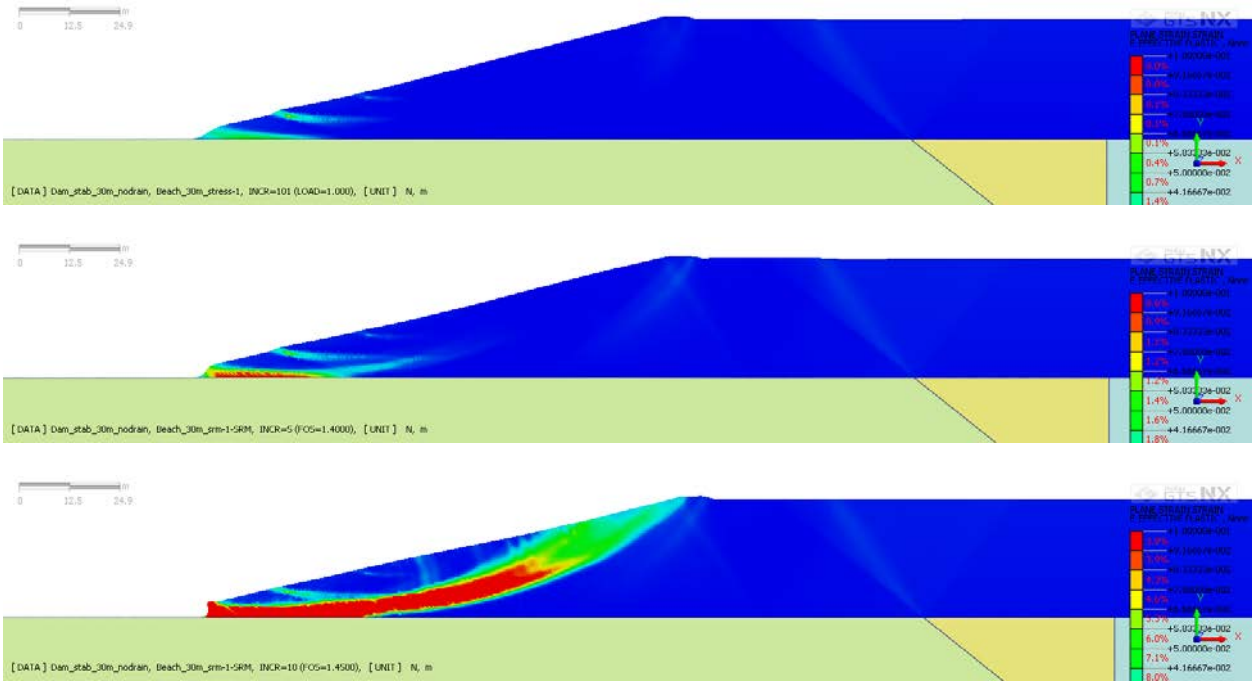

Figure 8: Progressive failure observed for Set #25 – Scenario #4 (from the top: SRF=1; SRF=1.4; SRF=1.45)

Figure 9 shows how this progressive mechanism is visible through discrete location monitoring (i.e., inclinometer data). As the failure surface develops the different portions of the material exhibit different displacement rates, which can be used to predict failure and guide short-term management decisions.

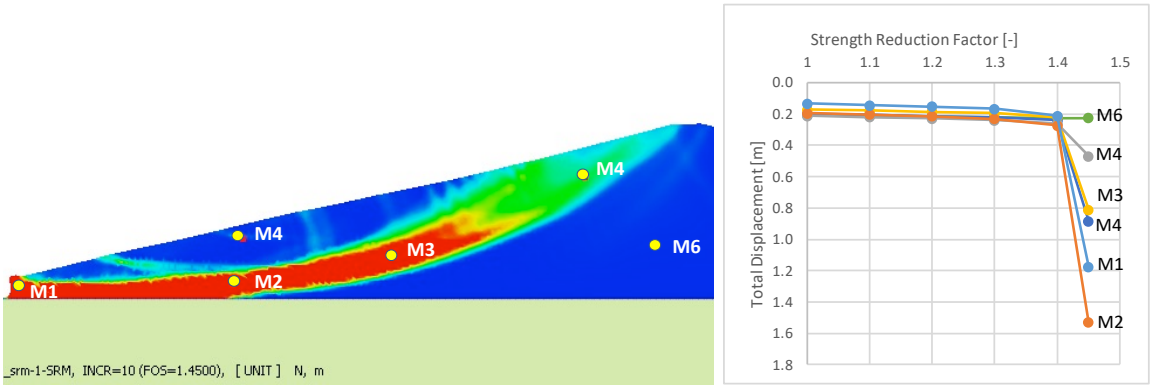

Figure 9: Progressive failure observed in specific monitoring point for Set #25 – Scenario #4 by increasing the Strength Reduction Factor (SRF)

Stochastic output

The results of the simulations are summarized in the following tables. Note that, as instability cannot be natively simulated with FEM, the lowest FS value is equal to 1 (Figure 10, scenario #5). The Probability of Failure PF is therefore obtained by numerical integration of the smoothed kernel function that fits simulation data (Bowman and Azzalini, 1997).

Table 3: Simulation output in term of Safety Factor FS for each input material set and scenarios

Set #	Scenario #1	Scenario #2	Scenario #3	Scenario #4	Scenario #5	Set #	Scenario #1	Scenario #2	Scenario #3	Scenario #4	Scenario #5
1	1.72	1.71	1.66	1.30	1.17	16	2.25	2.21	2.10	1.71	1.53
2	2.30	2.20	2.10	1.68	1.55	17	1.18	1.15	1.08	1.00	1.00
3	2.03	2.00	1.91	1.54	1.38	18	1.61	1.59	1.50	1.23	1.08
4	1.78	1.74	1.65	1.34	1.20	19	1.28	1.26	1.20	1.00	1.00
5	1.73	1.70	1.62	1.34	1.16	20	1.65	1.63	1.54	1.28	1.11
6	1.96	1.95	1.84	1.50	1.34	21	1.60	1.56	1.48	1.23	1.06
7	2.01	2.00	1.94	1.53	1.36	22	1.85	1.83	1.78	1.41	1.25
8	1.82	1.80	1.72	1.40	1.23	23	1.23	1.20	1.15	1.00	1.00
9	2.23	2.21	2.12	1.70	1.52	24	1.46	1.43	1.36	1.13	1.00
10	1.00	1.00	1.00	1.00	1.00	25	1.90	1.88	1.78	1.45	1.28
11	1.66	1.63	1.55	1.29	1.11	26	2.13	2.10	2.00	1.63	1.43
12	1.53	1.51	1.43	1.20	1.00	27	1.04	1.02	1.00	1.00	1.00
13	1.78	1.74	1.65	1.38	1.20	28	1.91	1.91	1.89	1.45	1.33
14	1.68	1.65	1.56	1.28	1.13	29	1.36	1.35	1.26	1.06	1.00
15	1.43	1.40	1.33	1.10	1.00	30	1.78	1.78	1.74	1.33	1.25

Table 4: FS mean value, standard deviation and Probability of Failure associated to the different Scenarios

	Scenario #1	Scenario #2	Scenario #3	Scenario #4	Scenario #5
FS – Mean value	1,71	1,69	1,61	1,32	1,18
Standard deviation	0,32	0,31	0,30	0,21	0,17
PF Probability of Failure	2.37	2.86	4.28	9.88	20.57

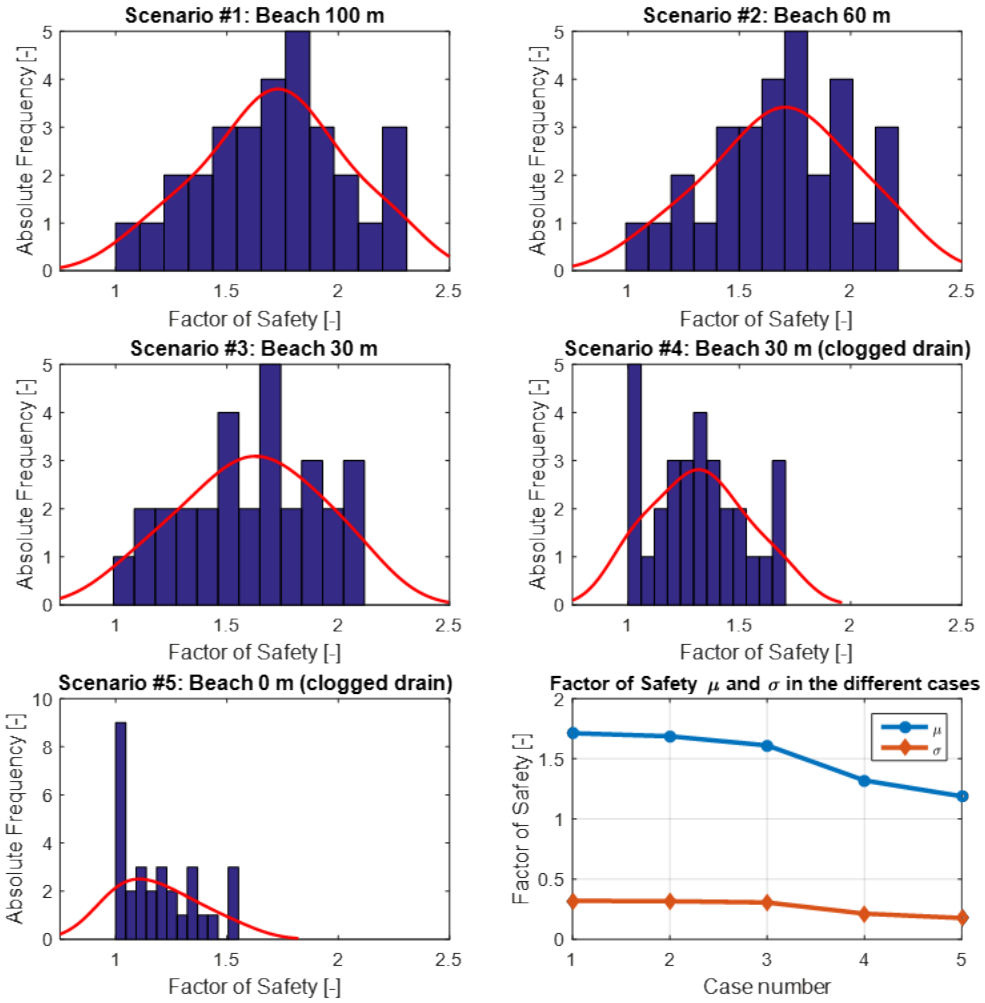

Figure 10: Stochastic distribution of Safety Factor (FS) and mean values and standard deviation for each scenario

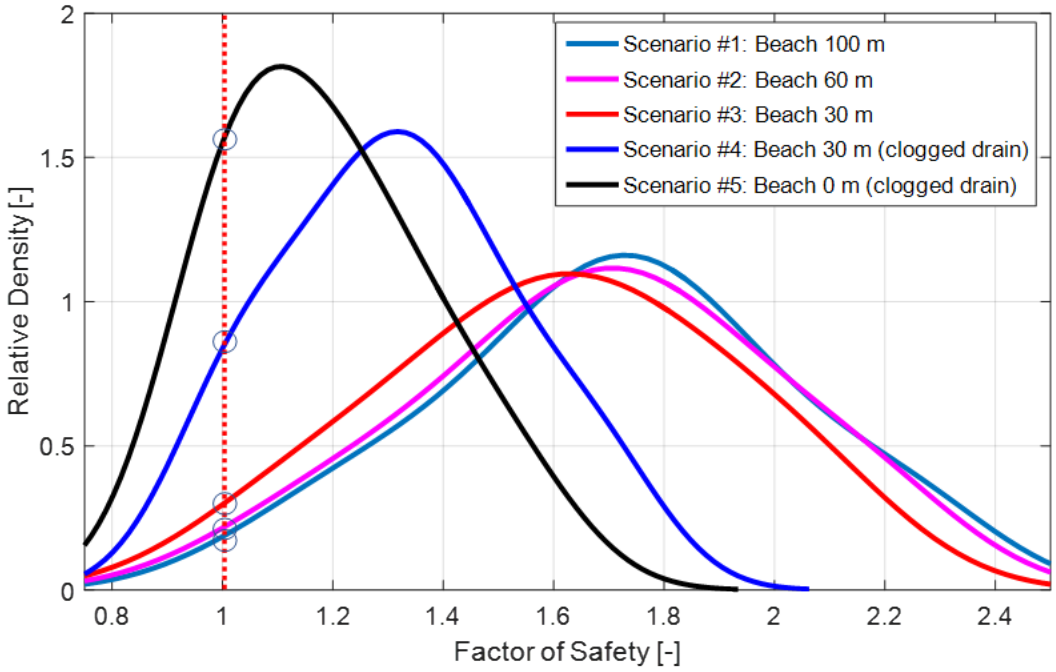

Figure 11: Density of probability for the normal distribution of Factor of Safety fitting the output data for each scenario;

Conclusion

A methodological approach to calculate the probability of failure for five different scenarios of a tailing dam via deterministic FEM analyses with SRT combined with a stochastic characterization of the key geotechnical parameters of the tailing materials was showcased. This approach allows capturing the natural variability of the tailing materials and provides a probability of failure for the structure that is a more valuable information to tailing managers than a deterministic value of the Factor of Safety. The FEM analyses of slope stability here presented provide a more sophisticated numerical tool than LEM since the failure surface is found as a result of the analyses and progressive failure is captured.

Here the approach was limited to considering one failure mechanism, namely a shear failure progressively developing in the dam. However, the same approach could be used to account for the development of failure by static liquefaction.

Bibliography

Alsharedah, Y.A. 2015. Slope stability enhancement of an upstream tailings dam: Laboratory testing and numerical modelling.

Bowman, A.W. and A. Azzalini. 1997. *Applied Smoothing Techniques for Data Analysis: The Kernel Approach with S-Plus Illustrations* (vol. 18). Oxford: Oxford University Press.

Coffey, J.P. and N. Susic. 2019. Getting back to basics: Risk fundamentals applied to the geotechnical engineering of tailings storage facilities. In J. Wesseloo (editor), *Proceedings of the First International Conference on Mining Geomechanical Risk*, Australian Centre for Geomechanics, Perth: 419–428.

Dawson, E.M., W.H. Roth and A. Drescher. 1999. Slope stability analysis by strength reduction. *Geotechnique*, 49(6): 835–840.

Fukuzono, T. 1985. A new method for predicting the failure time of a slope. In *Proceedings of 4th International Conference and Field Workshop on Landslides:* 145–150.

ICOLD. 1994. Tailings dams design of drainage. Review and recommendations. Bulletin 97.

McKay, M., R. Beckman and W. Conover. 1979. A comparison of three methods for selecting values of input variables in the analysis of output from a computer code. *Technometrics* 21(2): 239–245.

Morgenstern, N.R., S.G. Vick, C.B. Viotti and B.D. Watts. 2016. *Fundão Tailings Dam Review Panel Report on the Immediate Causes of the Failure of the Fundão Dam*. SAMARCO, SA, Vale, SA.

Olsson, A., G. Sandberg, and O. Dahlblom. 2003. On Latin hypercube sampling for structural reliability analysis. *Structural Safety* 25(1): 47–68.

Proceedings of Tailings and Mine Waste 2019
November 17–20, 2019, Vancouver, Canada
Published by the University of British Columbia, 2019

Baseline Investigations and Preliminary Design for an In-Pit Tailings Storage Facility, El Gallo Mine, Sinaloa

Patrick Williamson, INTERA Inc., USA
Hernan Beltran, Minera Pangea, Mexico
Chris Lane, L&MGSPL, Australia
Jim Willis, Tierra Group International, USA

Abstract

Minera Pangea recently completed a feasibility study (FS) for an in-pit tailing storage facility (IPTSF) that will receive tailings from the reprocessing of approximately 10 million tonnes of heap leach material (HLM). The HLM from the existing El Gallo heap leach pad would be reprocessed through a plant and then pumped to the IPTSF. The FS included a range of characterization and engineering design studies to determine the behaviour and potential environmental impacts associated with the IPTSF, including tailings deposition and consolidation; baseline hydrogeology and geochemistry; a groundwater control system; and closure design.

The El Gallo gold mine is located in the western foothills of the Cordillera Sierra Madre, east of the city of Guamuchil in the state of Sinaloa. The deposit is a low sulphidation epithermal vein system hosted in Late Cretaceous-Tertiary volcanic rocks, principally andesites. The climate is semi-arid with monsoonal rains during the wet season. Groundwater flow is controlled by fractures that run through and under the pit. The pit is currently a terminal sink, with evaporation exceeding groundwater inflow plus runoff into the pit. Geochemical characterization of the detoxified tailings indicate that are non-acid generating. Analysis of the tailings supernatant and leach solution indicate that neither would have a significant impact on groundwater quality.

A key aspect of the proposed IPTSF will be an underdrain system in the floor of the pit, which will reduce pore pressures and maintain the existing cone of depression in the groundwater surface around the pit during operation and closure, and aid in tailings consolidation by facilitating drainage (McDonald and Lane, 2010) . Tailings supernatant will be recovered using a floating pump on the surface of the tailings pond. Tailings solution recovered from the surface of the tailings as well as the mixture of groundwater and tailings solution captured by the pit's underdrain system will be reused in the process plant.

The El Gallo IPTSF presents an efficient and cost-effective engineered solution for tailings storage that benefits both Pangea and the community by:

1. Mitigating the potential impacts associated with the heap leach facility and evaporative groundwater consumption by the open pit.
2. Eliminating the potential impacts of a surface tailing storage facility (such as dam failures) and associated post closure management of a retention structure.
3. Providing an economical solution for the storage of process tailings to enable continued operation for Pangea.

Introduction

The El Gallo gold mine in Sinaloa, Mexico, provides an excellent example of the process of evaluation, testing, and design for an IPTSF. The mine has 10 million tonnes of HLM that is undergoing cyanide leaching, but the gold recovery is lower than expected (40%) due to the mineralogy of the ore and the method used to place the ore on the leach pad. Sufficient gold remains in the HLM to profitably reprocess the ore through a new 5,000 tonnes/day processing plant, which would include grinding, cyanide in leach, carbon sorption, and cyanide detoxification. Tailings from the plant would be discharged into the mined-out Samaniego pit in such a way as to maximize water reclaim and tailings consolidation. An underdrainage system would be installed to capture groundwater entering the base of the pit and water from tailings consolidation. Supernatant water liberated from the tailings slurry would be recovered at the surface of the IPTSF via a pontoon-mounted pump. The proposed IPTSF would have approximately 8.0 million cubic meters (Mm^3) of storage volume. This equates to a tailings storage capacity of 12 to 14.4 million tonnes, assuming a range of tailings in-situ dry densities between 1.5 and 1.8 tonnes per cubic meter (t/m^3).

As with any mine development project or significant change in mining operations, a wide range of tasks were performed to evaluate site conditions and develop the technical specifications of the IPTSF and support the permitting process, including:

- Design of a new processing plant.
- Hydrogeologic characterization of the Samaniego pit.
- Geochemical characterization of the tailings and pit walls.
- Design of the tailings fluid recovery and groundwater management system.
- Geotechnical testing of the tailings material.

Advantages of an IPTSF

Recent high-profile tailings dam failures in British Columbia (Mt. Polley), Bello Horizonte, Brazil (Córrego

de Feijão), and Chihuahua, Mexico (Cieneguitas) have raised the level of awareness of both mining professionals and the general public regarding the reputational, environmental, financial, and operational risks associated with traditional tailings storage facilities (TSF) that employ earthen retaining structures. Alternatives to traditional TSFs include disposal as a paste in underground workings and disposal in mined-out pits. The use of IPTSFs is not new, but is gaining increased acceptance for disposal of mine waste (tailings, waste rock and processing solutions), particularly if the material is acid generating. IPTSFs can be an attractive alternative to TSFs, within the following constraints (Arcadis, 2015; Lane, 2005):

- A locally available pit that will not cover or "sterilize" remaining mineral resources.
- Pit filling above active underground mines are considered unsafe.
- The amount of waste rock and tailings produced from a pit does not usually fit back into the pit, requiring dual disposal scenarios in some cases.
- Local hydrogeologic conditions are a critical factor in the selection and design of an IPTSF.
- The feasibility, cost and design of an IPTSF depends significantly on the leaching potential of mobile contaminants from the material placed in the pit.

Despite these constraints, an IPTSF can be an attractive engineering solution for tailings storage that can benefit the mine and community during operation and closure of the mine. These benefits include (ARCADIS, 2015):

- Isolate potential reactive mine waste in an anoxic environment, which inhibits the formation of acid and metal leaching.
- Reduce or eliminate the necessity of maintaining engineered structures.
- Improve social license and regulatory acceptance of the mining activity by restoring original landform and function.
- Create potential for reduced closure costs. In this case, the IPTSF will eliminate the need to close a heap leach facility (by reprocessing the ore) and minimize long-term closure costs.
- In some cases, return the pit site to its original use (e.g., grazing).

Site background

The El Gallo gold mine is owned and operated by Minera Pangea, the Mexican subsidiary of McEwen Mining. The mine is in the western foothills of the Sierra Madre Mountains in the state of Sinaloa (Figure 1). The mine operation consists of five open pits (Samaniego, San Rafael, Sagrado Corazón, Central, and Lupita), a heap leach pad, and a carbon adsorption, stripping, and electrowinning circuit. The proposed IPTSF would backfill the Samaniego pit, taking advantage of the gravity gradient from the proposed processing plant downhill to the pit.

Average annual rainfall is 865 millimetres (mm), occurring in well-defined wet and dry seasons. Precipitation during the wet season (June through October) averages 150 mm per month. During the dry season (February to May or June), rainfall averages 11 to 17 mm per month. The estimated average annual evaporation is 1,818 mm (Solum, 2018).

The El Gallo mine is hosted by Late Cretaceous-Early Tertiary volcanic rocks of the Lower Volcanic Series composed of andesitic flows and tuffs. The ground surface is covered with a thin veneer (1 to 3 m) of soil and alluvium, underlain by weathered andesite. The ore deposit is classified as a low sulphidation epithermal vein deposit (LSEVD). Mineralogical analysis of the ore from the Samaniego pit is characterized by quartz (56.3%), adularia (29.3%), kaolinite (7.9%), and minor hematite, chlorite, albite, and calcite. Gold mineralization in the El Gallo mine area occurs along two distinct structural trends, a northwest trend which hosted the San Rafael and Samaniego deposits and a northeast-striking structural trend that hosted the Sagrado Corazón, Central and Lupita deposits.

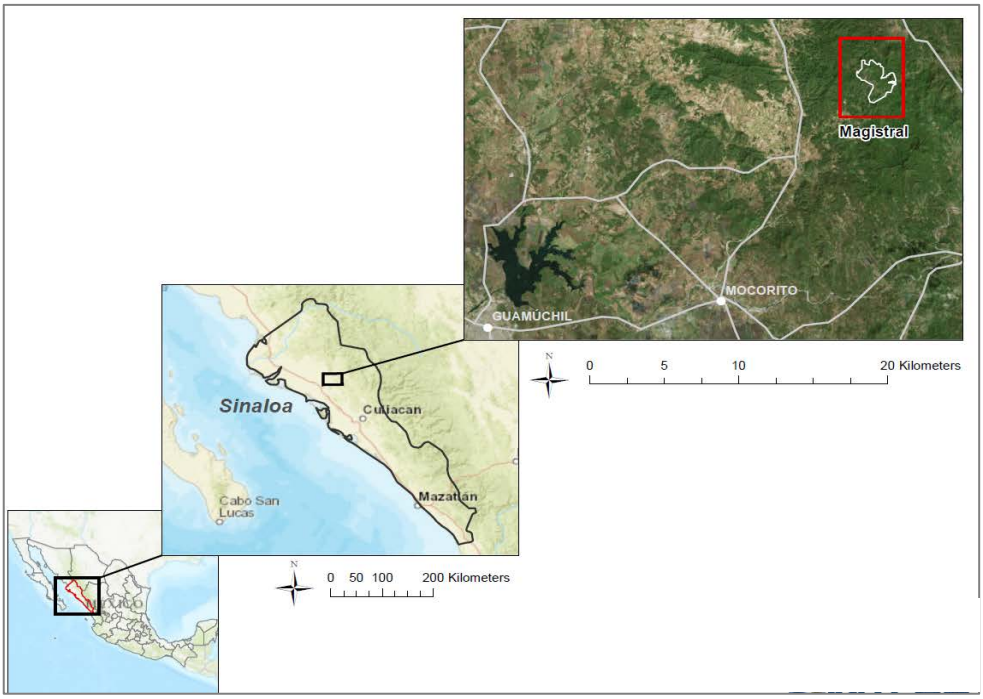

Figure 1: El Gallo Gold Mine location

The host rock presents extensive propylitic alteration and slight silicification near the margins of the principal structures. Multiple phases of hydrothermal activity deposited quartz with massive, banded, crustiform and colloform textures, which fills structures and produced stockwork zones in the dominant structures. The dominant alteration type directly associated with mineralization is silicification in the form of breccia cement, pervasively silicified breccia clasts, and, locally, pervasively silicified wall rock and quartz veining (PAH, 2011). Sulphide minerals occur at concentrations of less than 1% (by weight) but

have been observed at concentrations up to 3%. The main sulphide minerals are sphalerite, galena, pyrite, and chalcopyrite (PAH, 2011).

Groundwater flow in the vicinity of the Samaniego was measured by the mine operator using a network of shallow wells. Groundwater appears to flow to the west from the surface water divide approximately one kilometer east of the pit and follow topography to the west and northwest (Figure 2). Limited groundwater flow into the pit and the high evaporation rate produces a terminal pit lake approximately 120 m below the local groundwater surface with a steep cone of depression.

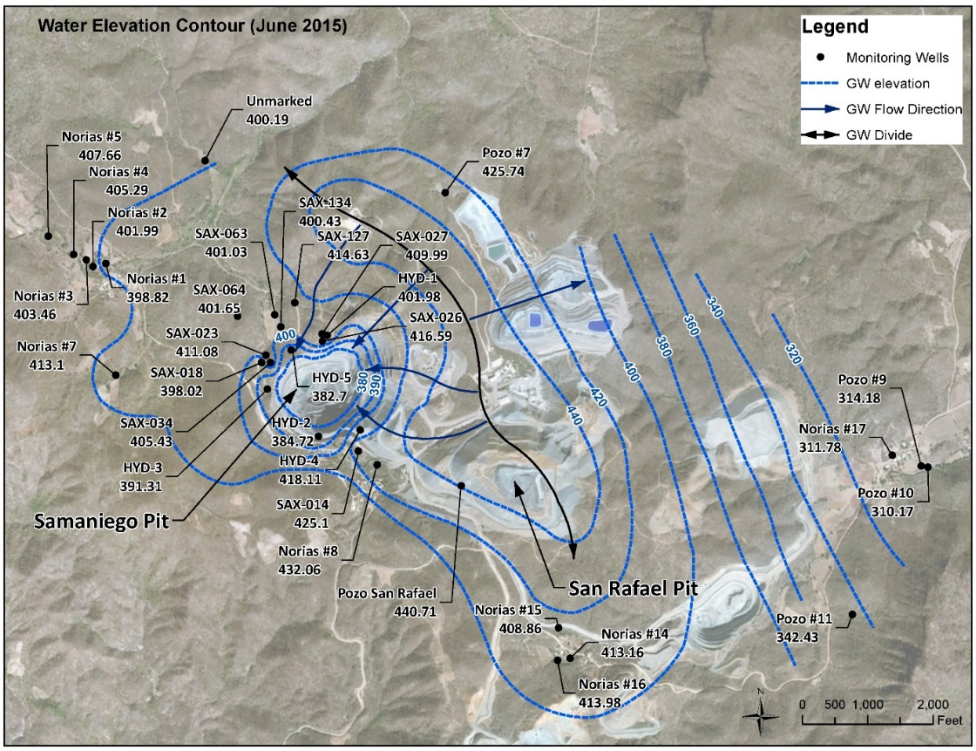

Figure 2: Regional groundwater flow map, El Gallo Mine

Methodology

Geochemical investigation

Two key geochemical elements were integrated into the engineering design of the IPTSF: the potential for acid generation and leaching of metals due to oxidation of sulphide minerals in the pit wall rock and tailings, and the chemistry of the tailings solutions that might leach from the pit into groundwater.

Six samples of the detoxified tailings samplers were generated from composited HLM material. The samplers were processed by Kemetco Research Inc. of Richmond, Canada, using a bench-scale version of the proposed cyanide leaching, carbon in pulp extraction and cyanide detoxification (SO_2/O_2 method). The cyanide destruction test was designed to achieve a proposed discharge limit of 20 mg/L WAD cyanide.

Samples at 40% solids were used for supernatant analysis. Tailings samples for geochemical analysis were filtered by Kemetco and then air dried prior to analysis.

The leaching potential of detoxified tailings in the IPTSF was evaluated by geochemical analysis of the solids (6 samples), the tailings supernatant solution (5 samples), and the leachate produced from interaction of the tailing solids with water (3 samples). Geochemical analysis of tailings solids included Acid-Base Accounting (ABA), paste pH, total elements, sulfur speciation, carbon speciation, mineralogy, and neutralization generation potential (NAG) tests. Leaching potential of the tailings was evaluated using the meteoric water mobility procedure (MPMP) specified in SERMARNAT NOM-157-2009 (NOM-157) and the modified ASTM D3987-85 (bottle roll) procedure specified in SERMARNAT-NOM-141-2003. Leachate samples and supernatant were analyzed for dissolved and total metals, major ions (chloride, fluoride and sulfate), cyanide species, acidity, ammonia, pH, and alkalinity. Samples were analyzed by SGS and ALS in British Columbia. Confirmation analysis of selected samples was performed by ALS Indequim in Monterrey, Mexico, to comply with requirements for data from a Mexican certified laboratory.

Geochemical evaluation of potentially reactive surfaces and weathering products in the pit wall was performed using paste pH of efflorescent salts (11 locations) and two samples of pit wall seeps.

Water recovery systems

The engineering design of the IPTSF underdrain collection system (UCS) was undertaken by Tierra Group International of Salt Lake City from conceptual designs provided by L&MGSPL (Cowaramup, Western Australia). The surface water recovery system is designed to remove up to 85% of the water from the slurry allowing self-weight consolidation of the tailings mass, thereby reducing the time required to achieve the highest density possible during the filling of the pit. The UCS serves the following purposes:

- Assist with consolidation through efficient water removal from the base of the pit.
- Reduce pore pressure in the base of the pit by maintaining the cone of depression around the pit, minimizing the migration of tailings solutions or weathering products into the surrounding aquifer.

Monitoring/recovery bores located around the pit's perimeter will provide secondary control on water movement from the pit via monitoring and pumping.

Hydrogeological investigation

The baseline hydrogeological study was carried out during May, June, and July of 2018. The study included an extensive field investigation carried out in and around the Samaniego pit, which included:

- Drilling five borings and performing packer (Lugeon) type permeability tests or tests at selected intervals where the borings intersected geologic structural features with potential hydraulic paths through or below the Samaniego pit.

- Injection (Lefranc) tests in six existing exploration boring.
- Completion of multi-level vibrating wire piezometers in three of the test holes.
- Observations in and around the pit of groundwater flow (locations, rates, and structural controls).
- A water balance for the Samaniego pit to estimate groundwater inflow.

The results of the hydraulic tests provided data to quantitatively calculate the in-situ permeability of the fractured rock mass. The packer data provided fracture specific measurements of K, while the injection test provided bulk rock values. The aquifer test data were analyzed using the nSIGHTS (n-dimensional Statistical Inverse Graphical Hydraulic Test Simulator) numerical code developed for Sandia National Laboratories (Geofirma and INTERA, 2011). The nSIGHTS code uses non-linear parameter estimation methods to find the optimal values of the model fitting parameters (typically hydraulic conductivity, specific storage, formation pressure, skin radius, and skin hydraulic conductivity) that provide the best match to the observed test data.

Geotechnical testing

An extensive geotechnical characterization program was undertaken to evaluate:

- the tailings storage capacity (a function of final density);
- the amount and timing of tailings dewatering;
- the total settlement of the tailings stack during operation; and
- the magnitude and time for the final settlement.

Testing on the final size distribution for tailings (60% smaller than 75 microns) was performed by the University of Alberta. A standard suite of geotechnical tests was performed on the tailings, including liquid limit, plasticity, density, and permeability. Specialized tests including large-strain consolidation and centrifuge testing were performed to generate data on the total settlement of the tailings stack during operation.

Permitting

The primary Mexican regulation governing the evaluation, construction, operation, and closure of a TSF is NOM-141. One of the challenges with the permitting of the El Gallo IPTSF is that NOM-141 was specifically written for traditional TSFs, so many of the NOM-141 requirements do not apply to an IPTSF. Only one other IPTSF had previously been permitted in Mexico, at the Agnico Eagle Pinos Altos mine, which will store paste tailings above an active underground mine. For the El Gallo IPTSF a highly collaborative permitting strategy was developed between Pangea staff and the Secretariat of Environment and Natural Resources (SEMARNAT) regulators that included presentations, site visits, and case studies of other IPTSFs. The permit was issued by the Sinaloa SEMARNAT office on August 25th, 2019.

Results

Geochemistry

The neutralization potential ratio (NPR) provides an indication of the acid-generation potential of a waste material based on the ratio of neutralization potential (NP) to acid potential (AP). The Mexican NPR criterion for potentially acid generating (PAG) tailings is 1.2. Material below this value is considered to be potentially hazardous, requiring additional characterization and a waste handing plan. Data from the ABA tests were also compared to NPR criteria recommended by MEND (2009), which specifies a NPR of 2 as the criterion for non-PAG material, and a range of NPR between 2 and 1 to define material that has uncertain acid-generating potential and might require additional characterization. Figure 3 shows the results for the El Gallo tailing samples. The average NPR for the tailings samples is 2.4, which is considered non-acid-generating. These results were confirmed by the NAG tests, which produced a NAG pH after reaction of 6.60 and 6.61. A NAG pH above 4.5 is considered non-acid-generating. The average concentration of sulphide minerals was 0.21% by weight (equivalent to an AP of 6.56 kg $CaCO_3$/ton).

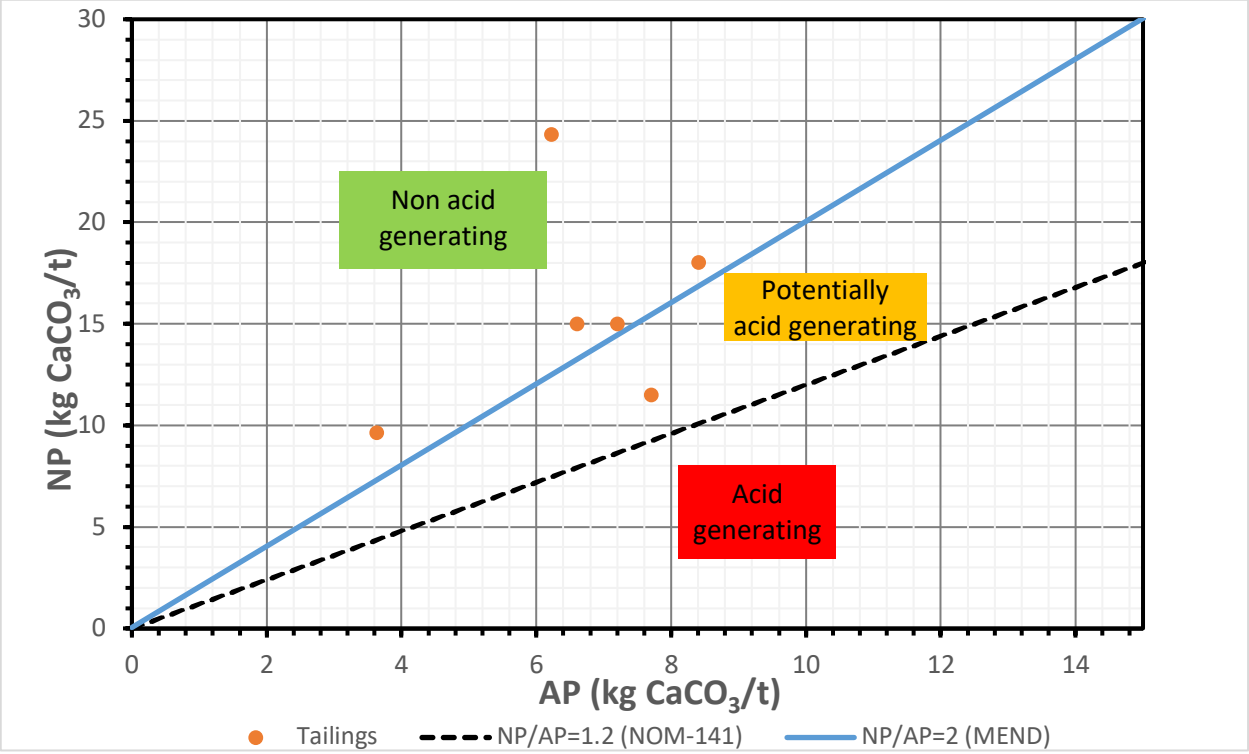

Figure 3: Neutralization potential vs. acid potential for El Gallo tailings samples

Additional results for the geochemical evaluation include:

- Geochemical evaluation of the paste pH of efflorescent salts in the pit wall at 11 locations resulted in one sample with low pH (2.83). The remaining 12 samples were all above 7.5.

- Concentrations of soluble metals in leachate samples did not exceed the NOM-141 criteria.
- Cyanide concentrations in the supernatant immediately after the detoxification procedure ranged from 0.5 to 4.4 mg/L. WAD cyanide ranged from 1.13 to 2.52 mg/L, while free cyanide was generally under 1 mg/L. The cyanide concentrations in the pore space of the tailings would be expected to be lower than the supernatant concentrations due to photochemical dissociation of iron cyanocomplexes and volatilization (Johnson, 2015).
- Cyanide concentrations in leachate samples were low, with total concentrations of 0.057 and 0.14 mg/L. WAD cyanide concentrations were below the reporting limits of 0.008 and 0.01 mg/L,

The available data indicates that the tailings would be non-acid-generating and unlikely to leach constituents that would impact the aquifer.

Hydrogeology

Results of the aquifer tests indicate that the majority of fractures present in the vicinity of the Samaniego pit have a low hydraulic conductivity (K), with most of the test intervals varying from 1E-06 to 1E-09 m/s. Higher transmissivity (K values <1E–04 m/s) correspond to the unit of conglomerate and weathered andesite near the surface and above the maximum planned level of the IPTSF. Higher values of K (up to 2.4E–2 m/s) were measured below the pit. Results of the pit water balance indicate that groundwater infiltration into the pit aquifer will range from 190 to 345 m^3/day (2.2 to 4 L/second).

The conceptual groundwater model envisions a fracture flow system with low hydraulic conductivity near a groundwater divide with a gentle gradient and limited recharge. Groundwater flow into the pit is primarily vertical from the higher K structures under the pit. The sum of groundwater flow into the pit and runoff during the rainy season is less than evaporation from the pit, resulting in a terminal pit lake with a surface more than 100 m below the local groundwater table.

Underdrain collection system

The proposed UCS is an industry standard in TSF design for tailings consolidation and seepage collection, and will consist of a blanket drain installed at multiple elevations within the pit's floor with a collection sump and pumps to return the mixture of supernatant and groundwater to the processing plant (Figure 4). The blanket drain will consist of a network of perforated high-density polyethylene (HDPE) pipes covered with gravel wrapped in high permeability, non-woven geotextile with a pore size of 0.15 mm or smaller. The mass of the geotextile will range from 400 to 800 g/m^2, depending on the required permeability and flow rate. Water collected by the UCS will be directed to a sump established in the pit's lowest point, where it will then be pumped to the processing plant for reuse.

From the pit's crest two solid wall HDPE reclaim sleeves will run along the pit wall and penetrate the sump, allowing reclaim pipes and pumps to be lowered into the sump from the crest of the facility through the sleeves. The two reclaim pipe sleeves also provide redundancy for the UCS should one of the lines become blocked or damaged. The reclaim sleeves will be installed along the pit's western wall using rock bolts and anchors.

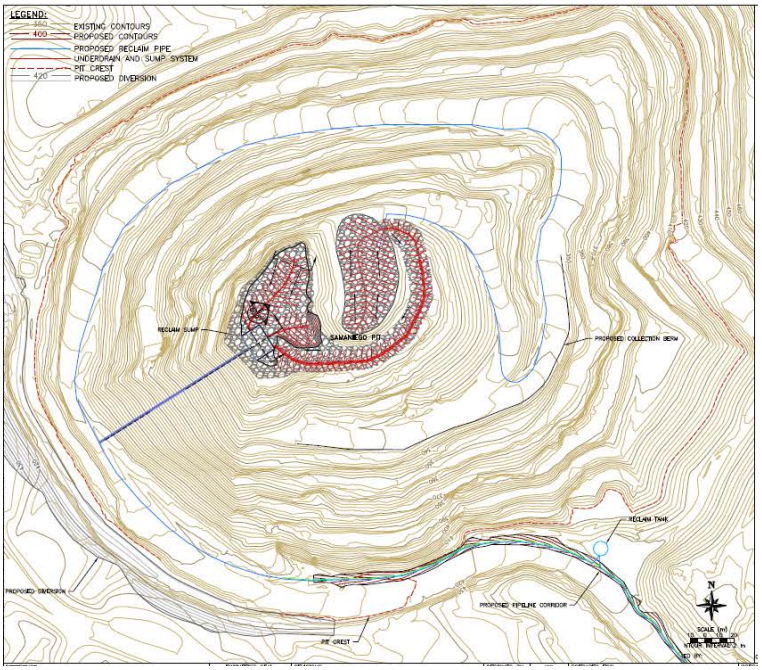

Figure 4: Proposed pit underdrain

Tailings consolidation

A summary of the various results obtained from the classification and density testing (with no loading applied) executed by the University of Alberta is presented in Table 1. Tests show low plasticity to no plasticity, so secondary settlement is not a consideration post closure. Creep settlement may occur over time post closure, but this settlement will be a small fraction of the total settlement during operation which the PLAXIS 2D model indicates as 8.45 m in Year 1 of Operation and 1.21 m in Year 8 of Operation.

The consolidation tests demonstrate that a low void ratio (high in-situ dry density and very low permeability) can be achieved during the operation of the IPTSF, provided water is continually removed from the facility. The centrifuge testing simulated a tailings depth of approximately 37 m, with final void ratio of 0.71, residual moisture content of less than 25% and dry density of 1.62 t/m^3. The actual pit depth to be filled with tailings is estimated to be between 127 m to 135 m. An extrapolation of the trend for the void ratio and dry density from 37 m to 120 m demonstrates that the void ratio would be less than 0.45 and the dry density would increase to at least 1.8 t/m^3. The implied permeability at this range of void ratios is 3.03×10^{-9} m/sec and 7.16×10^{-10} m/sec.

Table 1: Summary of geotechnical test results

Test	Results
Particle size distribution (% passing 75 microns)	60 (laser sizing)
Liquid limit (%)	Non-plastic
Plastic limit (%)	Non-plastic
Plasticity index (%)	Non-plastic
Soil particle density (t/m^3)	2.77
Estimated permeability (with 500 kPa loading) from large strain consolidation test (m/s)	5.12×10^{-7}
Initial dry density (t/m^3) at 50.4% solids with void ratio of 2.73	0.7
Settled dry density (t/m^3) from 500 kPa with void ratio of 1.04	1.4
Final average dry-density (t/m^3) effective stress 350 kPa with void ratio of 0.78	1.6
Implied permeability m/s below 37 m based on centrifuge test	10^{-9} to x 10^{-10}
Predicted post closure settlement (m) based on centrifuge test and PLAXIS 2D analysis	1.0
Estimated period for post closure consolidation (years)	8

Closure

Once the tailings have reached the maximum planned elevation within the IPTSF, the facility will be covered to prevent erosion as well as rainwater infiltration. The cover will consist of a compacted layer of material with low hydraulic conductivity overlain by a layer to promote the growth of vegetation. The cover will be domed (higher in the center) to facility drainage and account for final compaction. The UCS will continue to operate as long as the tailings continue to consolidate, to maintain the cone of depression around the pit.

Conclusion

Geochemical studies of the detoxified tailings that will be placed in the Samaniego pit indicate that they have a very low average sulphide content (0.21%) and will not be acid-generating or leach metals. Leaching tests and analysis of the supernatant indicate that residual solutions would not impact groundwater quality.

The limited groundwater flow into the pit via fractures (K less than 1E–7 m/s) and lower K of the consolidated tailings (10E–8 to 10E–9 m/s) will minimize potential groundwater flow through the mass of consolidated tailings. The contrast in Ks between the fractures and the tailings would lead to preferential flow around the tailings rather than through it (ARCADIS, 2015).

The geotechnical and hydrogeological testing clearly demonstrate that a key factor in the operation of the IPTSF is the water recovery system (pumps and piping), which will have sufficient capacity to remove water at a rate that will expedite the consolidation of the tailings and prevent migration of any tailings solutions from the pit by maintaining the cone of depression in the groundwater table. Emplacement of

fine-grained tailing in the pit would seal potentially reactive surfaces in the pit walls. The very low permeability of the tailings would limit oxygen diffusion and advection of water, two of the key components in the generation of acid drainage.

Acknowledgements

The author would like to acknowledge Minera Pangea for their enthusiasm in sharing this work with the mining community, specifically Hernan Beltran, Xavier Ochoa, Miguel Barahona, and Adrian Blanco. Thanks also to the project team members: Chris Lane, Ron Espell, Joel Carrasco, Mick Gavrilovic, Jim Willis, and Dominic Piscioneri .

References

ARCADIS. 2015. *In-Pit Disposal of Reactive Mine Wastes: Approaches, Update and Case Study Results.* MEND Report 2.36.1b. Prepared for the Mine Environmental Neutral Drainage (MEND).

Geofirma Engineering Ltd and INTERA Incorporated (Geofirma and INTERA). 2011. *N-dimensional Statistical Inverse Graphical Hydraulic Test Simulator (nSIGHTS).* Version 2.50.

Johnson, C. 2015. The fate of cyanide in leach wastes at gold mines: An environmental perspective. *Applied Geochemistry* 57: 194–205.

Lane, J.C. 2005. Use of completed open pits for tailings disposal. In *Handbook on Mine Fill*. Australian Centre for Geomechanics, Perth, Australia.

McDonald, L. and J.C. Lane. 2010. *Consolidation of inpit tailings.* In *Mine Waste 2010, Proceedings of the 1st International Seminar on Reduction of Risk in the Management of Tailings and Mine Waste,* Perth, Australia.

Mine Environment Neutral Drainage (MEND). 2009. *Prediction Manual for Drainage Chemistry from Sulphidic Geologic Materials. MEND Report 1.20.1.* Bill Price, editor. December 2009.

Pincock, Allen and Holt (PAH). 2011. Preliminary economic assessment for the El Gallo District, Sinaloa State, Mexico. Prepared for US Gold Corporation.

SEMARNAT. 2003. NOM-141-SEMARNAT-2003. *Que establece el procedimiento para caracterizar los jales, así como las especificaciones y criterios para la caracterización y preparación del sitio, proyecto, construcción, operación y postoperación de presas de jales. Diario Oficial de la Federación.*

SEMARNAT. 2011. NOM-157-SEMARNAT-2009. *Que establece los elementos y procedimientos para instrumentar planes de manejo de residuos mineros. Diario Oficial de la Federación.*

Solum Consulting Group (Solum). 2018. *Regional Climatology Study.* August 2018.

Proceedings of Tailings and Mine Waste 2019
November 17–20, 2019, Vancouver, Canada
Published by the University of British Columbia, 2019

Stability Buttress to Mitigate Observed Change in Design Conditions

Christina Winckler, AECOM, USA
Kanyembo Katapa, Freeport-McMoRan Inc., USA
Edwin Konrath, Freeport-McMoRan Sierrita Inc., USA
Tamara Johndrow, Freeport-McMoRan Inc., USA

Abstract

In 2017, Freeport-McMoRan Sierrita Inc. (Sierrita) learned of a potential localized structural slope instability at its upstream Sierrita Tailings Impoundment (STI). In 2018, Sierrita initiated a project to construct a precautionary stabilizing buttress. This paper discusses the field investigation, material characterization, and analyses that were performed to support the buttress design. It also highlights the cooperation between operator, regulator, and engineer of record (EoR) that resulted in the success of the design, permitting, and construction of the buttress.

The EoR updated the stability evaluation of the STI south slope in 2017, after increasing pore pressures were observed in the southeast embankment area. The most recent comprehensive geotechnical investigation of the STI was completed in 2014. The 2014 investigation identified a "lower resistance layer" at the interface between the tailings and alluvium. This layer ranges in thickness between one and 13 feet, primarily beneath the south embankment crest and downstream slope of the STI. Due to the pore pressure increase first observed in approximately mid-2017, the lower resistance layer was re-evaluated near the toe of the embankment downstream slope. The calculated factor of safety using the design shear strengths (not incorporating the lower resistance layer's fully softened shear strength) met internal criteria developed for consideration across the operational subsidiaries of Freeport-McMoRan Inc. (FCX) and met the minimum required factor of safety described in the Arizona mining guidance manual's *Best Available Demonstrated Control Technology (BADCT)* publication TB 04-01, published in January 2004 by the Arizona Department of Environmental Quality (ADEQ) .

As a lower bound sensitivity case, the lower resistance layer was modelled using fully softened shear strength to represent strength loss, i.e., strain weakening. The calculated factor of safety for this lower bound case did not meet the internal criteria and the BADCT minimum factor of safety. Therefore, the tailings engineers, EoR, and the STI Technical Review Board (TRB) recommended that Sierrita construct a precautionary buttress along the STI south slope to mitigate the risk associated with potential sudden strength loss of the lower resistance layer. The first phase of the buttress, designed to provide enhanced

stability for the current crest elevation was constructed between December 2018 and March 2019. Earthwork construction of the second phase of the buttress, designed to provide enhanced stability for the next ten years of operation, started in March 2019 and was completed in September 2019.

Introduction

Overview of Freeport-McMoRan Inc. tailings management and stewardship

Freeport-McMoRan Inc. (FCX) recognizes that the failure of a tailings storage facility (TSF) at their mining operations would affect employees, neighboring communities, and the environment and could, in certain circumstances, lead to loss of life, and severe or catastrophic property damage and environmental harm. As a result, FCX provides considerable resources to materially reduce the likelihood of such failures at their operations. FCX's Tailings Management and Stewardship Program was launched in 2004 and has evolved significantly over the past 15 years. Through the program, FCX provides financial and technical resources to its operations, including substantial engineering expertise and technological monitoring. FCX also provides corporate management oversight to tailings facility design, construction, operation and monitoring to minimize their risk. Tailings professionals are employed at the operational subsidiaries of FCX. FCX has a culture of communicating critical information upward so important matters at their operations are identified, evaluated and addressed.

Active mining operations have on-site, full-time, dedicated engineers who oversee the specialized work required to operate TSFs. Active mining sites also retain an Engineer of Record (EoR). The role of EoR is filled by a qualified external engineer and supported by a team from his or her company. The EoR is responsible for reviewing and approving all engineering and design, operating and monitoring procedures, and as-built drawings. The EoR also is responsible for facility inspections to confirm physical integrity, safety and confirm that TSF performance is within assumed design.

Technical Review Boards (TRBs) composed of internationally recognized independent experts provide advice regarding EoRs' designs and analyses, as well as management of TSF stability and water controls. The TRBs provide independent guidance on the physical integrity, safety, and performance of the TSFs and associated management systems.

Through the Tailings Management and Stewardship program, tailings professionals at FCX's operations regularly inspect and monitor phreatic level trends and adhere to deposition plans, good operational construction practices, water management controls, seepage management strategies, and other stability components. FCX's operations also periodically review as-built conditions through field and laboratory geotechnical testing programs under the EoR's guidance.

Overview of Freeport-McMoRan Sierrita Inc. tailings storage

The Sierrita tailings impoundment (STI) is the only active TSF at Freeport-McMoRan Sierrita Inc. (Sierrita). The STI has been an active upstream facility since 1970 and is raised approximately 6 to 8 feet per year. Initially, tailings were deposited behind a starter dam that was constructed along the eastern slope of the STI. The STI increased towards the west and the Esperanza tailings impoundment (ETI). The STI has an approximate height of 400 feet at the maximum section and abuts the inactive ETI on the west side, as shown on Figure 1. The ETI has a maximum height of approximately 130 feet and has been inactive since 1980. The STI has been raised over the downstream embankment of the ETI up to approximately 40 feet from the ETI crest.

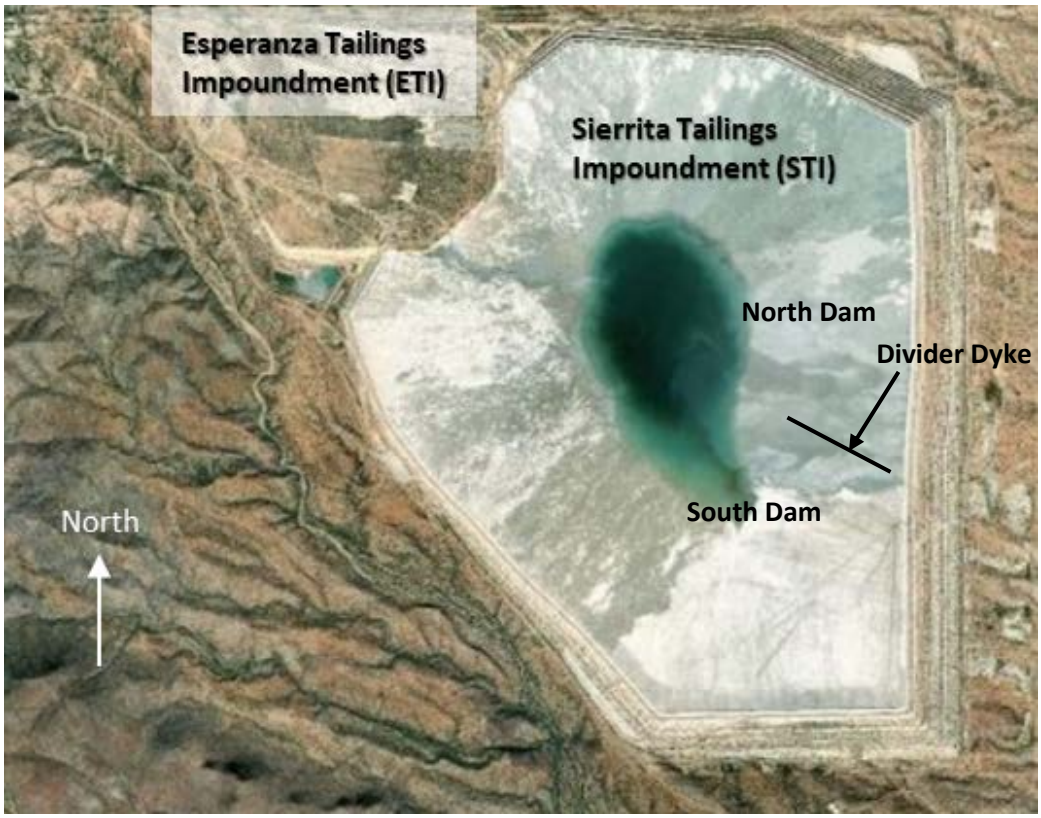

Figure 1: Esperanza and Sierrita tailings impoundments

The STI is operated by alternating deposition between the south and the north dams. The STI is constructed with an overall slope of approximately 3H:1V, with 50- to 80-foot wide benches every 40 feet in elevation. The inter-bench slope is between 1.3H:1V and 1.5H:1V. Sierrita currently constructs five approximately 8-foot high raise berms to construct an ultimate inter-bench height of approximately 40 feet. After the fifth raise, a 50- to 80-foot wide horizontal step-in is included. The step-in procedure requires relocating and raising the tailings delivery line (TDL).

In 2019, both the STI north and south dam crest elevations are 3,510 feet above mean sea level (amsl). For the south dam, the next raise is the berm raise to 3,518 feet amsl after the step-in and TDL relocation. The south dam TDL relocation and berm construction began in the first quarter of 2019 and will take approximately one year to complete. During construction, tailings mostly will be deposited on the north dam. For the north dam, the next raise is an 8-foot tall berm raise, which will begin in early 2020 and take approximately 4 to 6 months to complete. This raise will bring the north dam crest to elevation 3,518 feet amsl.

The observational method (Peck, 1969) is being implemented to monitor the pore pressures, saturation within the STI tailings, and the potential for any movement of the STI embankment. An updated comprehensive investigation and analysis is ongoing in 2019 (five years since the 2014 comprehensive).

Previous design conditions

FCX's operational subsidiaries perform regular comprehensive geotechnical investigations of the TSFs to update material and pore pressure characterizations. Sierrita's 2014 comprehensive geotechnical investigation included CPT soundings, drill holes, sample collection, laboratory testing, and geophysical suspension logging. The investigation also included interviews of past STI operators and review of historic aerial photos dating to the construction of the STI starter dam in 1969. The 2014 CPT locations plotted on the 1970 aerial photo are shown on Figure 2.

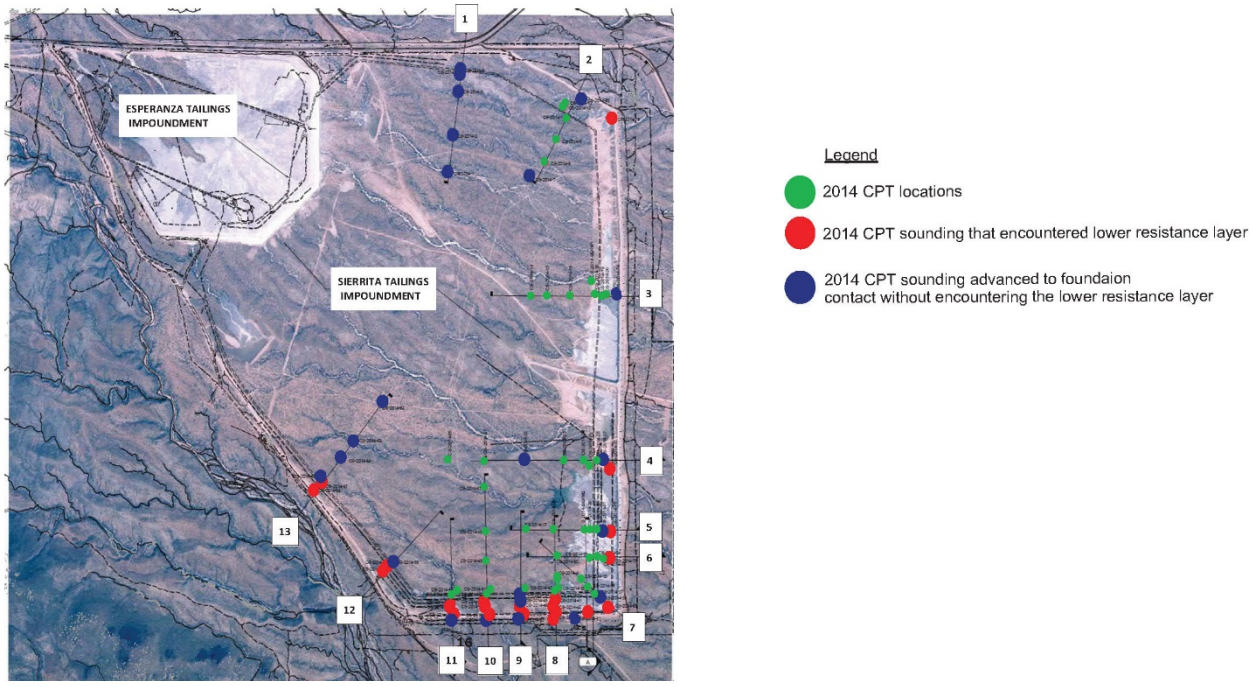

Figure 2: 2014 CPT locations and encountered extent of STI lower resistance layer

A lower resistance layer was encountered predominantly in the south area of the STI as shown on Figure 2. The lower resistance layer was indicated in CPT soundings by low tip resistance, low skin friction, and high dynamic pore pressures, as shown on Figure 3. The lower resistance layer has typical tip resistance between 20 and 100 tsf and skin friction between 0.2 and 1.0 tsf. The lower resistance layer is likely the result of the deposition of fine-grained tailings in topographic low spots and in borrow areas that were developed for the original starter dam construction. Historic photos of construction and the early operational period demonstrate this depositional pattern. Reviewing this history was recommended by the TRB and was key to understanding the STI construction from the early operational period.

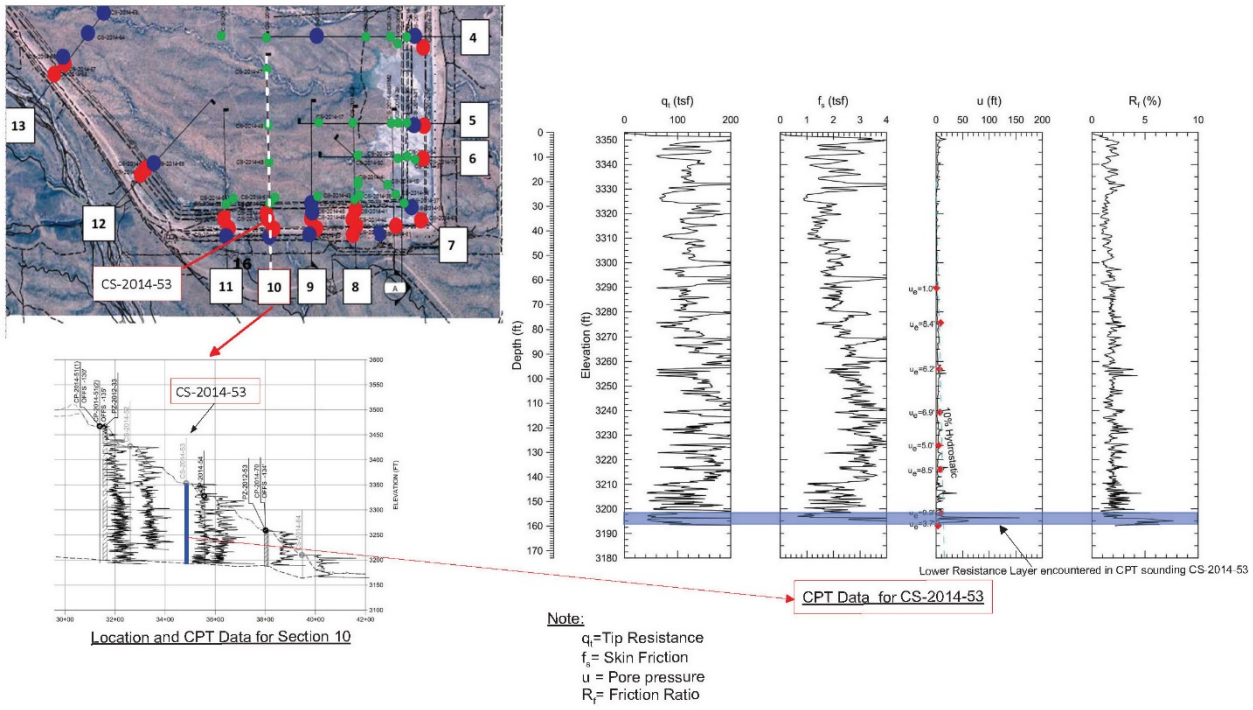

Figure 3: Typical CPT sounding characteristics for encountered STI lower resistance layer

In 2014, the analysis input parameters included a 1,000-foot thick shell consisting of partially saturated tailings using drained shear strength parameters and low pore pressures as had been observed in that year. This approach was endorsed by the TRB. There were no observed areas with increasing pore pressure, hence four study sections were evaluated for stability analysis to capture the range in internal geometries. These were Sections 3, 6, 8 and 10, as shown on Figure 2. Based on the 2014 selected design input parameters, the calculated factors of safety for the long-term drained, end-of-construction, and post-earthquake loading conditions were greater than 2.0 when the STI is raised to elevation 3,585 feet amsl. The critical failure surface was a non-circular global surface initiating near the crest, extending through the partially saturated tailings, and exiting near the downstream toe.

The 2014 investigation and analysis program concluded that the STI had good downward drainage and a wide shell of partially saturated tailings. The studies were performed using a liquefied residual shear strength for the lower resistance layer and increasing the percent hydrostatic pore pressures in the partially saturated tailings. Sensitivity studies showed that preventing the lower resistance layer from increasing pore pressures was critical for the STI stability.

Observed change in design conditions

In mid-2017, Sierrita observed increasing pore pressure in the southeast corner of the south dam. The increasing pore pressures presented a potential change to the 2014 design conditions. Sierrita and the EoR initiated an investigation program that included review of STI data, field investigations, laboratory tests, and installation of new instruments in the south area.

Revised design analysis

Seven design sections, both within and outside the buttress footprint, were evaluated for the south slope buttress design. Sections 8 and 10 are the critical design sections and are discussed in this paper. The locations are shown on Figure 2. Section 8 is near the southeast corner and Section 10 is at approximately 2,000 feet west of Section 8. The original starter dam was constructed in 1969 in a north south direction on the east side, with shorter extensions on the north and south sides. Hence, the starter dam is present at Section 8 but does not extend west to Section 10. The model geometries were developed using 2014 CPT soundings, 2014 drill hole information, 2018 topographic contours and topographic contours before the STI was constructed.

Material characterization

The lower resistance layer was encountered beneath the ETI in 2016 as part of a field investigation for a separate project. The 2016 ETI investigation program also included CPT sounding, drill holes, sample collection, laboratory testing, and geophysical suspension logging. Results from the 2016 ETI investigations were incorporated in the 2017 STI south area investigation. The CPT signatures from the ETI and STI lower resistance layers were compared, as shown on Figure 4. The CPT signatures for the STI and ETI lower resistance layers are similar. The ETI and STI lower resistance layers were also plotted on the soil behaviour type (SBTn) chart (Robertson, 2017), as shown on Figure 5, where they both plotted as contractive with positive state parameters.

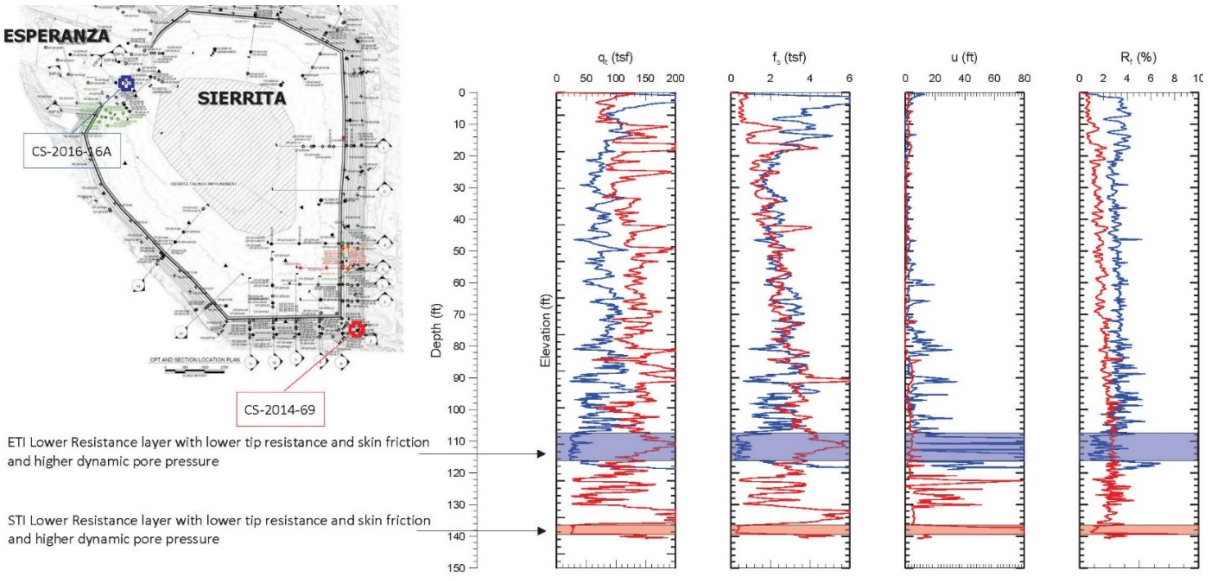

Figure 4: CPT sounding comparison of STI and ETI lower resistance layer

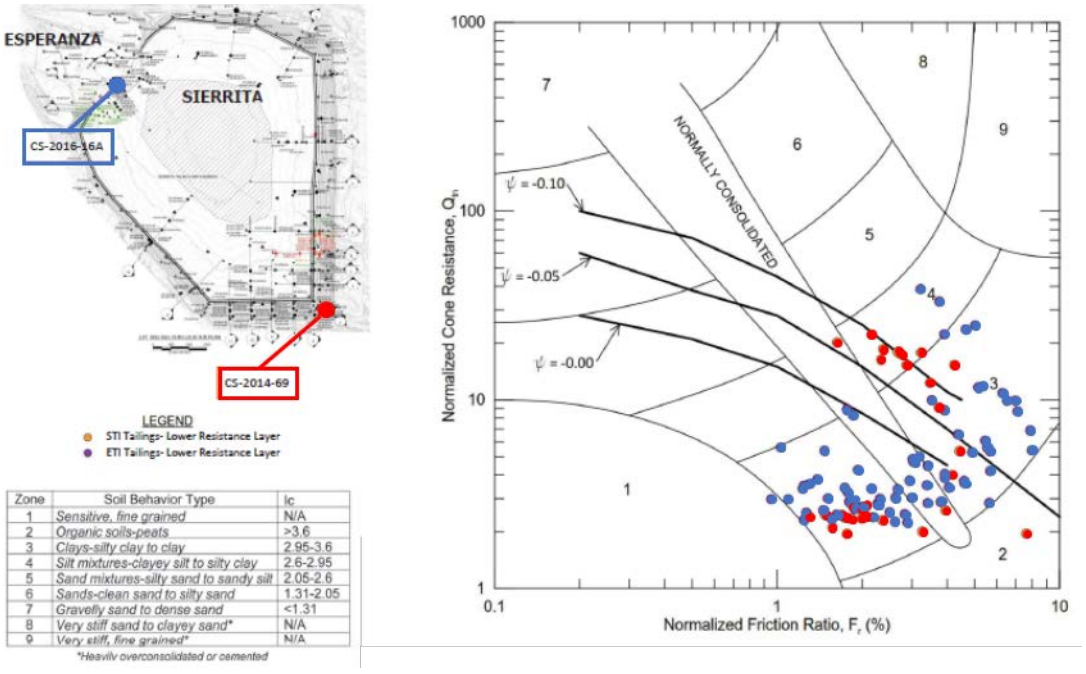

Zone	Soil Behavior Type	Ic
1	*Sensitive, fine grained*	N/A
2	*Organic soils-peats*	>3.6
3	*Clays-silty clay to clay*	2.95-3.6
4	*Silt mixtures-clayey silt to silty clay*	2.6-2.95
5	*Sand mixtures-silty sand to sandy silt*	2.05-2.6
6	*Sands-clean sand to silty sand*	1.31-2.05
7	*Gravelly sand to dense sand*	<1.31
8	*Very stiff sand to clayey sand**	N/A
9	*Very stiff, fine grained**	N/A

*Heavily overconsolidated or cemented

Figure 5: Soil behaviour type comparison of STI and ETI lower resistance layer

Direct simple shear, laboratory vane shear, and direct simple shear with strain reversal tests were performed on the STI and ETI lower resistance layer in 2014 and 2017. Static direct simple shear testing performed on the STI lower resistance layer in 2014 has shown that the lower resistance layer is contractive and exhibits peak and post-peak behaviour when in undrained conditions, as shown on Figure 6.

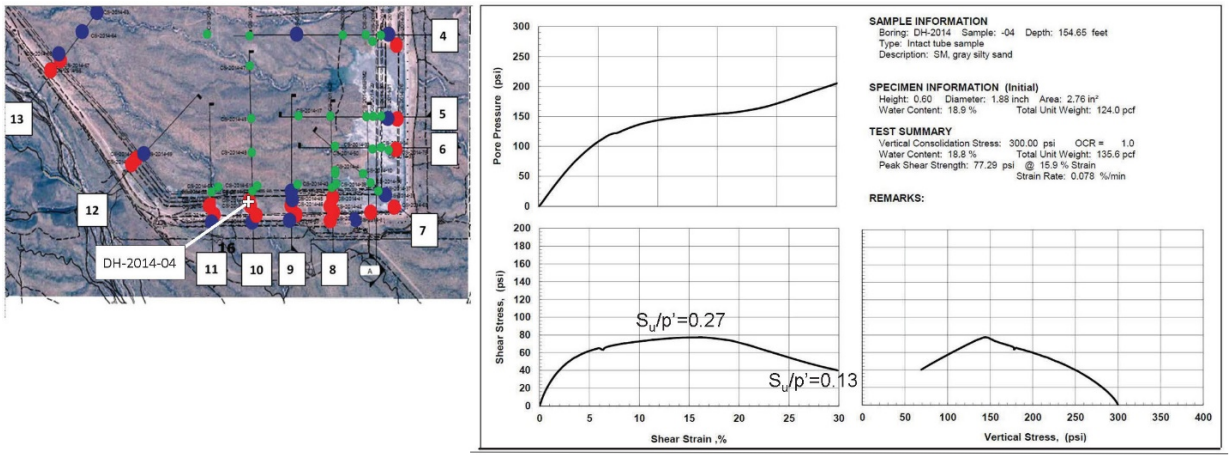

Figure 6: Direct simple shear testing results for STI lower resistance layer

The measured peak undrained shear strength ratio (S_u/p') was 0.27 with a residual undrained shear strength ratio of 0.13 (at 30% shear strain). Laboratory vane shear testing performed on the ETI lower resistance layer in 2017 shows a sensitivity of approximately 3 to 4, as shown on Figure 7, which would indicate a fully softened shear strength ratio between 0.07 and 0.09. The residual undrained shear strength ratio from direct simple shear testing with strain reversal performed on the ETI lower resistance layer indicated a fully softened strength ratio of 0.07, as shown in Figure 8. At lower strains the peak value would be mobilized, but if larger strains were to occur or collapse under low confining pressures, the fully softened or residual shear strength could be mobilized. Therefore, the buttress design analyses have been performed using a fully softened shear strength ratio value of 0.07 for the lower resistance layer in areas with lower confining pressure.

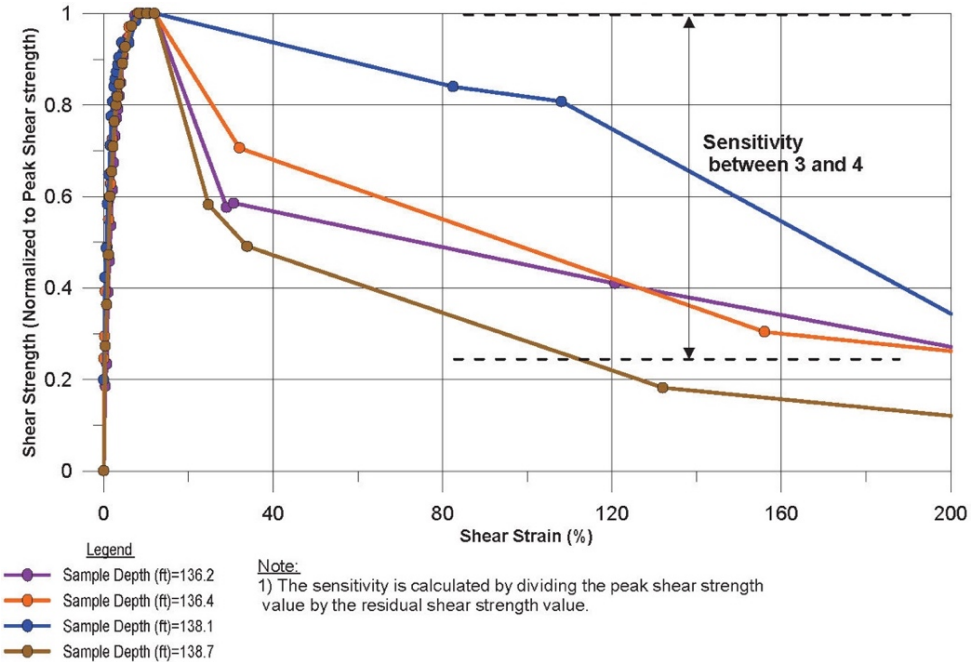

Figure 7: Laboratory vane shear test results of ETI lower resistance layer

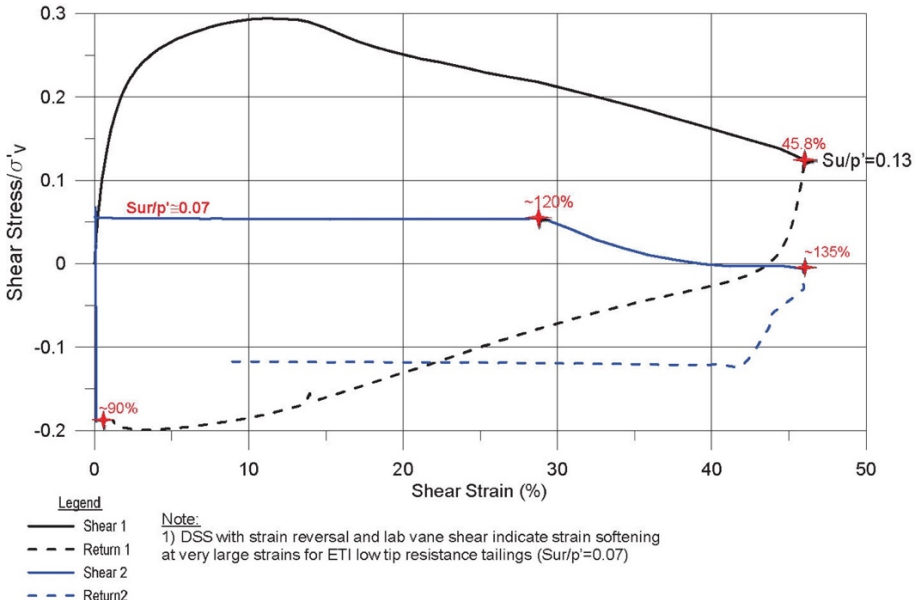

Figure 8: Direct simple shear test with strain reversal of ETI lower resistance layer

The potential for sudden strength loss is greater in areas with lower confining pressure, such as near the STI downstream toe. The ETI lower resistance layer has higher confining pressures due to the abutting STI dam. The compacted starter dam is present on the east side and provides stability for potential localized shear surfaces. Hence, analyses were focused on the STI, specifically on the south side with the identified critical Sections 8 and 10, as described further below. Analyses were performed to evaluate the mean effective stresses for Sections 8 and 10. A mean effective stress less than 5 atmospheres of pressure (atm) was selected to delineate the extent of the lower resistance layer that could potentially collapse, as shown on Figures 9 and 10. A typical value between 1 and 10 atm is commonly used to differentiate between ductile and brittle behaviour, where 10 atm is for rounded sand, 1 atm is for crushed sand with sharp edges, and a typical value for tailings is between 1 and 3 atm (Robertson, 2017).

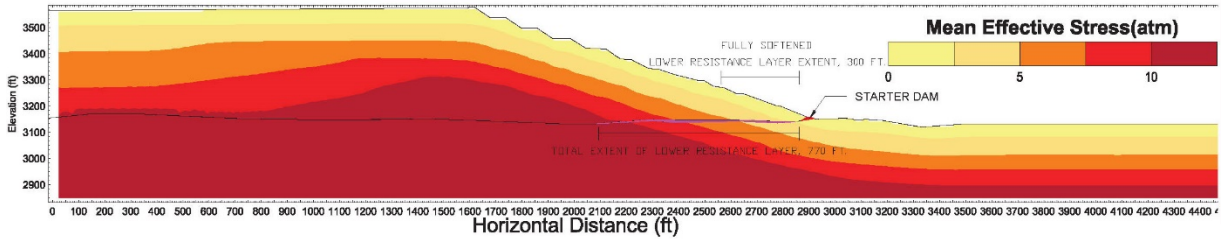

Figure 9: Calculated mean effective stresses for Section 8

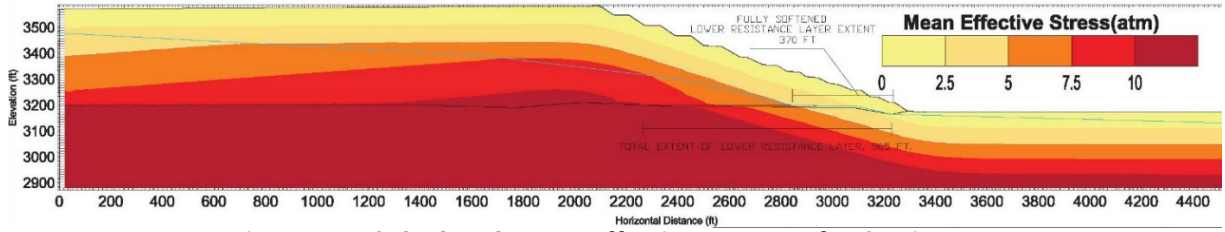

Figure 10: Calculated mean effective stresses for Section 10

Pore pressure conditions

For the design analysis for the Phase 1 buttress (corresponding to STI elevation of 3,510 feet amsl, which is the 2019 crest elevation), the pore pressure conditions within the tailings were established using piezometer data. The analyses were conservatively completed using 100% of hydrostatic pore pressure assumption below the phreatic surface. The intention was to move quickly with the design and be conservative while collecting more data.

For the future STI elevation of 3,585 feet amsl, approximately year 2029, the Phase 2 design analysis pore pressures were extrapolated based on the rate of increase observed in piezometers. An ongoing investigation showed that pore pressures within the tailings are less than 100% and could be as low as 40%. However, to be conservative a value of 70% hydrostatic pore pressure was used for the Phase 2 design analyses. The predicted percent of hydrostatic pore pressure when the STI is at elevation 3,585 feet amsl was calculated using a three-dimensional seepage model of the STI.

The pore pressure characterization is being further investigated by installing additional nested piezometers and performing geophysics suspension logging survey and CPT soundings with both pore pressure and seismic measurements.

CPT-based triggering

The lower resistance layer is susceptible to liquefaction in the areas with lower confining pressure for the design earthquake using a CPT-based triggering analysis. This zone is modelled with a fully softened undrained shear strength ratio of 0.07.

The CPT-based triggering analysis also shows that the remaining saturated STI tailings are not susceptible to liquefaction. However, to account for potential shear strength loss during and after shaking, a shear strength corresponding to 80% of the peak undrained shear strength was assigned to the saturated tailings for the post-earthquake loading condition.

Material properties

Four material types have been characterized: alluvium foundation material; the lower resistance layer at the contact between the STI tailings and the alluvial foundation; and saturated/unsaturated STI tailings. The proposed buttresses were modeled with properties representative of unsaturated tailings material. This assumption allowed Sierrita to construct the buttresses using either tailings or alluvium materials. The buttresses were constructed using alluvium. Hence, the analyses completed were conservative since the alluvial material has higher shear strength and unit weight. The material properties used in the slope stability analyses are summarized in Table 1.

Table 1: Summary of material properties used in the stability analysis

Material description	Total unit weight (pcf)	Drained shear strength		Undrained shear strength	Post-earthquake
		Friction angle (degrees)	Cohesion (psf)		
STI unsaturated tailings	120	35	0	Drained strength	Drained strength
STI saturated tailings	120	35	0	CIU: Su/p' = 0.35 DSS: Su/p' = 0.25	CIU: Su/p' = 0.28(1) DSS: Su/p' = 0.20(1)
Lower resistance layer	120	29	0	Su/p' = 0.25 Scs/p' = 0.07(2)	Supe/p' = 0.20(1) Scs/p' = 0.07(2)
Proposed tailings buttress	120	35	0	Drained strength	Drained strength
Alluvium	130	40	0	Drained strength	Drained strength

Notes:

(1) Assuming 20% reduction of the undrained shear strength.

(2) Denotes softened shear strength used when confining pressure is less than 5 atm.

Stability analysis

The Phase 1 and 2 buttresses were designed to meet the targeted factors of safety for the long-term drained, undrained, and post-earthquake analysis. The Arizona Department of Environmental Quality (ADEQ) has established that the Best Available Demonstrated Control Technology (BADCT) guidance manual (date published January, 2004) be followed as part of the Aquifer Protection Permit (APP) program. The document provides engineering design guidance that addresses minimum required factors of safety for various loading conditions. Guidelines established in the document provide minimum factor of safety requirements of 1.5, 1.3, and 1.1 for long-term drained, undrained, and post-earthquake loading conditions, respectively, for analyses performed using assumed shear strength parameters. FCX has established a minimum post-earthquake factor of safety of 1.2, unless deformation analyses are completed for slopes with calculated factors of safety of 1.1 and demonstrate tolerable deformations under the design earthquake event.

The calculated factor of safety for Sections 8 and 10 without the buttress is around 1.0 for the undrained loading, as shown on Figures 11 and 12, for a localized shear surface near the downstream toe. Runout distance of 260 feet was calculated for the identified shear surface with a factor of safety less than 1.0. A progressive failure analysis also was performed on the deformed slope geometry. The calculated factor of safety was greater than 1.0, indicating low potential for progressive failure.

NO.	MATERIAL DESCRIPTION	UNIT WEIGHT (pcf)	DRAINED STRENGTH		UNDRAINED STRENGTH
			COHESION (psf)	FRICTION ANGLE (degrees)	S_u/P'
1	UNSATURATED TAILINGS	120	0	35	–
2	SATURATED TAILINGS	120	0	–	0.35 CIU', 0.25 DSS
3	SATURATED LOWER RESISTANCE LAYER	120	0	–	0.25
4	SATURATED FULLY SOFTENED LOWER RESISTANCE LAYER	120	0	–	0.07
5	STARTER DAM	130	0	40	–
6	FOUNDATION	130	0	40	–

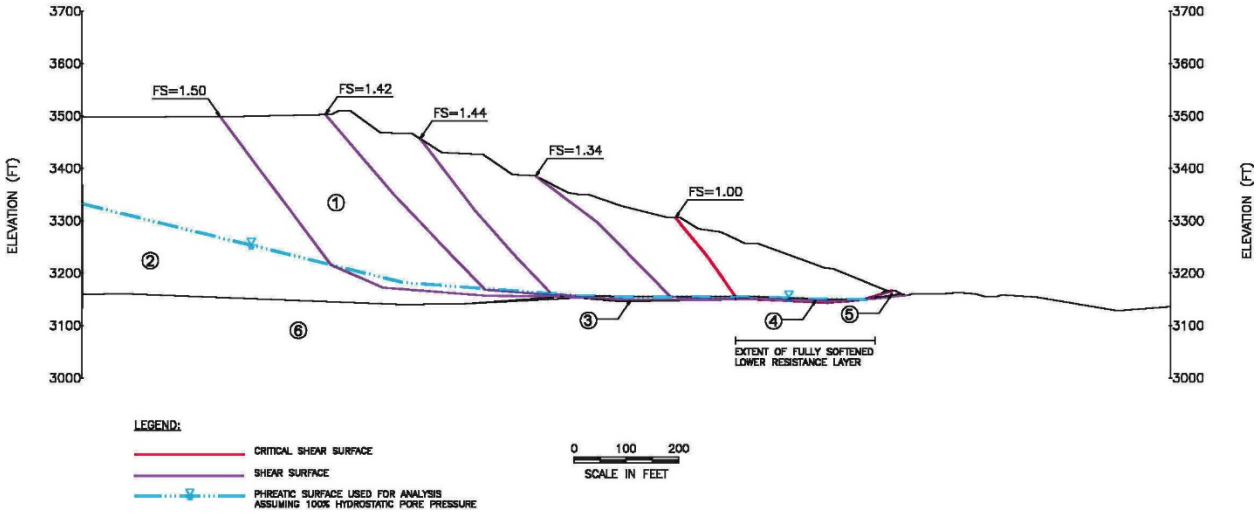

Figure 11: Section 8, STI elevation 3,510 feet amsl, undrained stability results without buttress

NO.	MATERIAL DESCRIPTION	UNIT WEIGHT (pcf)	DRAINED STRENGTH		UNDRAINED STRENGTH
			COHESION (psf)	FRICTION ANGLE (degrees)	S_u/P'
1	UNSATURATED TAILINGS	120	0	35	–
2	SATURATED TAILINGS	120	0	–	0.35 CIU', 0.25 DSS
3	SATURATED LOWER RESISTANCE LAYER	120	0	–	0.25
4	SATURATED FULLY SOFTENED LOWER RESISTANCE LAYER	120	0	–	0.07
5	FOUNDATION	130	0	40	–

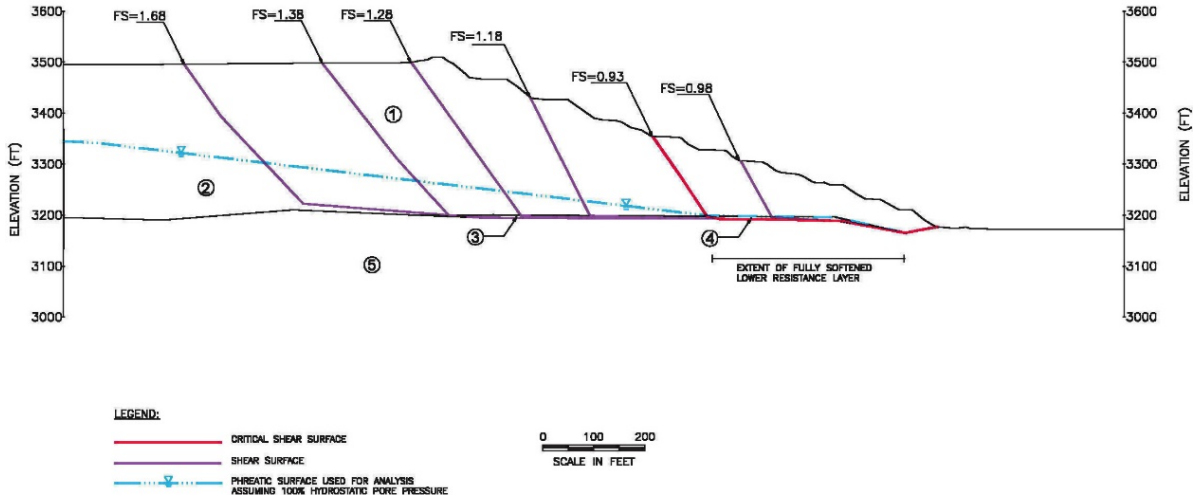

Figure 12: Section 10, STI elevation 3,510 feet amsl, undrained stability results without buttress

A Phase 1 buttress was analyzed to increase the calculated factor of safety for the identified localized shear surface, as shown on Figures 13 and 14 for the undrained loading condition. The post-earthquake calculated factor of safety is similar to the undrained loading condition since the critical shear surface is localized near the downstream toe and hence there would be minor contribution from cyclically softened tailings modeled with 20% shear strength reduction.

NO.	MATERIAL DESCRIPTION	UNIT WEIGHT (pcf)	DRAINED STRENGTH		UNDRAINED STRENGTH
			COHESION (psf)	FRICTION ANGLE (degrees)	S_u/P'
1	UNSATURATED TAILINGS	120	0	35	–
2	SATURATED TAILINGS	120	0	–	0.35 CIU', 0.25 DSS
3	SATURATED LOWER RESISTANCE LAYER	120	0	–	0.25
4	SATURATED FULLY SOFTENED LOWER RESISTANCE LAYER	120	0	–	0.07
5	STARTER DAM	130	0	40	–
6	FOUNDATION	130	0	40	–
7	PROPOSED SAND TAILINGS BUTTRESS	120	0	35	–

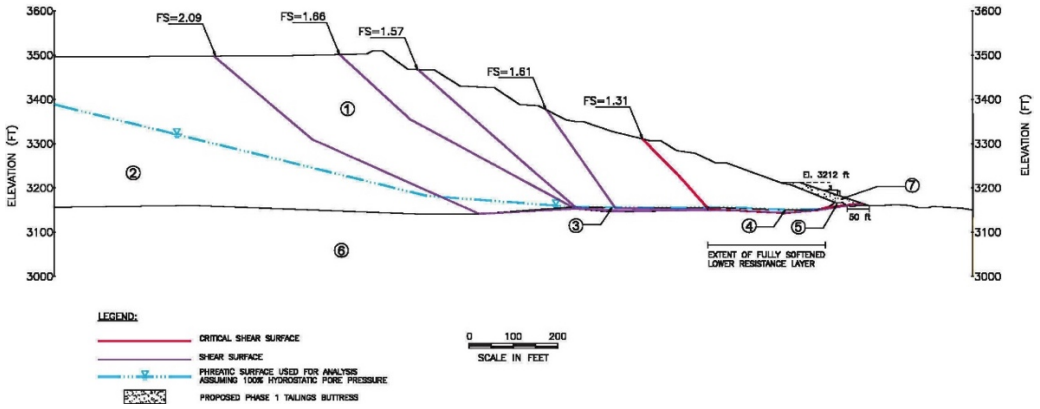

Figure 13: Section 8, STI elevation 3,510 feet amsl, undrained stability results with Phase 1 buttress

NO.	MATERIAL DESCRIPTION	UNIT WEIGHT (pcf)	DRAINED STRENGTH		UNDRAINED STRENGTH
			COHESION (psf)	FRICTION ANGLE (degrees)	S_u/P'
1	UNSATURATED TAILINGS	120	0	35	–
2	SATURATED TAILINGS	120	0	–	0.35 CIU', 0.25 DSS
3	SATURATED LOWER RESISTANCE LAYER	120	0	–	0.25
4	SATURATED FULLY SOFTENED LOWER RESISTANCE LAYER	120	0	–	0.07
5	FOUNDATION	130	0	40	–
6	PROPOSED SAND TAILINGS BUTTRESS	120	0	35	–

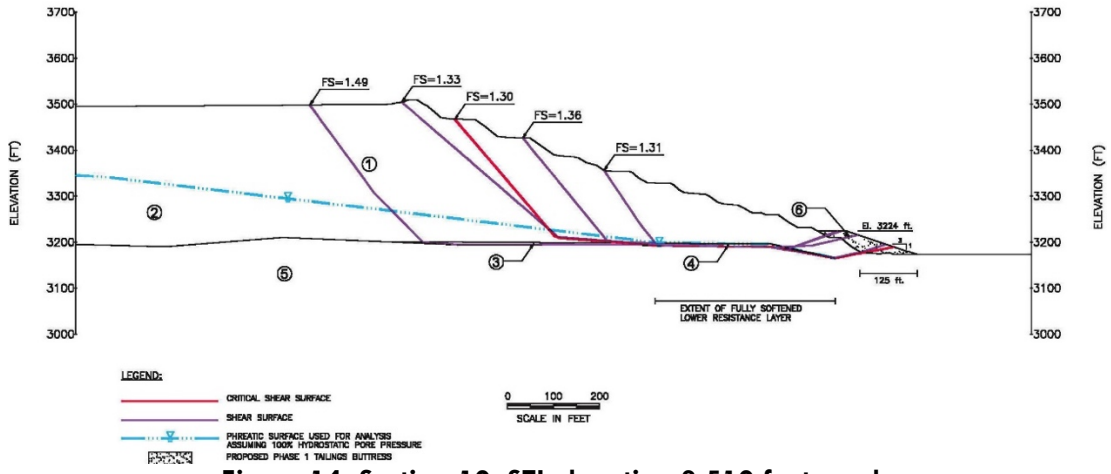

Figure 14: Section 10, STI elevation 3,510 feet amsl, undrained stability results with Phase 1 buttress

The design for the Phase 2 buttress, incorporates a potentially larger global shear surface for the future STI elevation of 3,585 feet amsl. The calculated factor of safety for the undrained loading condition is 1.3, as shown on Figures 15 and 16. The calculated factor of safety for the post-earthquake condition is 1.1, as shown on Figures 17 and 18. A deformation analysis was completed to meet the internal FCX criteria.

			DRAINED STRENGTH		UNDRAINED STRENGTH
NO.	MATERIAL DESCRIPTION	UNIT WEIGHT (pcf)	COHESION (psf)	FRICTION ANGLE (degrees)	S_u/P'
1	UNSATURATED TAILINGS	120	0	35	–
2	SATURATED TAILINGS	120	0	–	0.35 CIU', 0.25 DSS
3	SATURATED LOWER RESISTANCE LAYER	120	0	–	0.25
4	SATURATED FULLY SOFTENED LOWER RESISTANCE LAYER	120	0	–	0.07
5	STARTER DAM	130	0	40	–
6	FOUNDATION	130	0	40	–
7	PROPOSED BUTTRESS	120	0	35	–

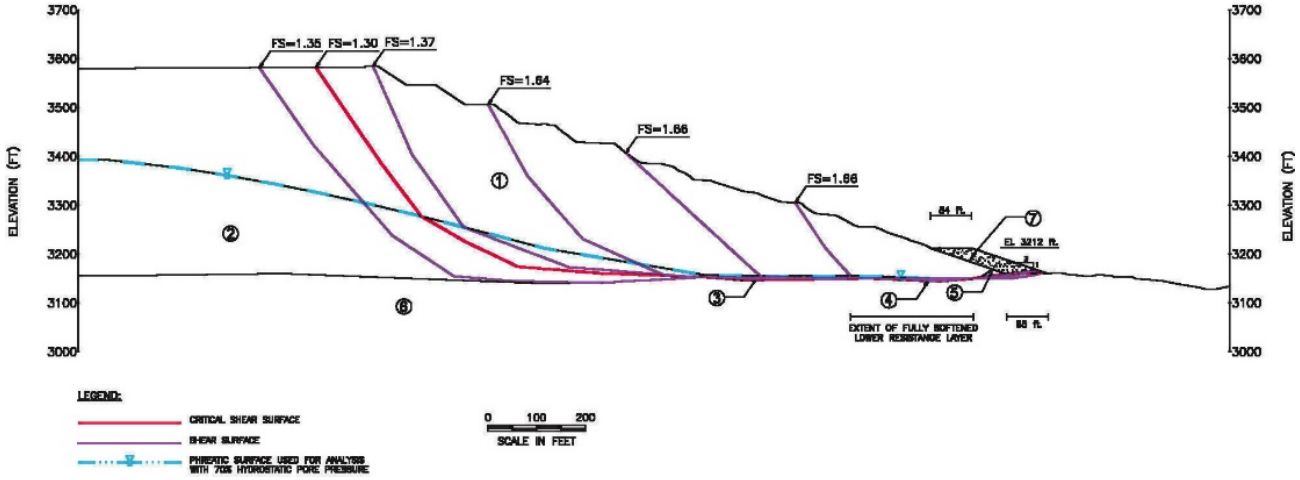

Figure 15: Section 8, STI elevation 3,585 feet amsl, undrained stability results with Phase 2 buttress

NO.	MATERIAL DESCRIPTION	UNIT WEIGHT (pcf)	DRAINED STRENGTH COHESION (psf)	DRAINED STRENGTH FRICTION ANGLE (degrees)	UNDRAINED STRENGTH S_u/P'
1	UNSATURATED TAILINGS	120	0	35	–
2	SATURATED TAILINGS	120	0	–	0.35 CIU', 0.25 DSS
3	SATURATED LOWER RESISTANCE LAYER	120	0	–	0.25
4	SATURATED FULLY SOFTENED LOWER RESISTANCE LAYER	120	0	–	0.07
5	FOUNDATION	130	0	40	–
6	PROPOSED BUTTRESS	120	0	35	–

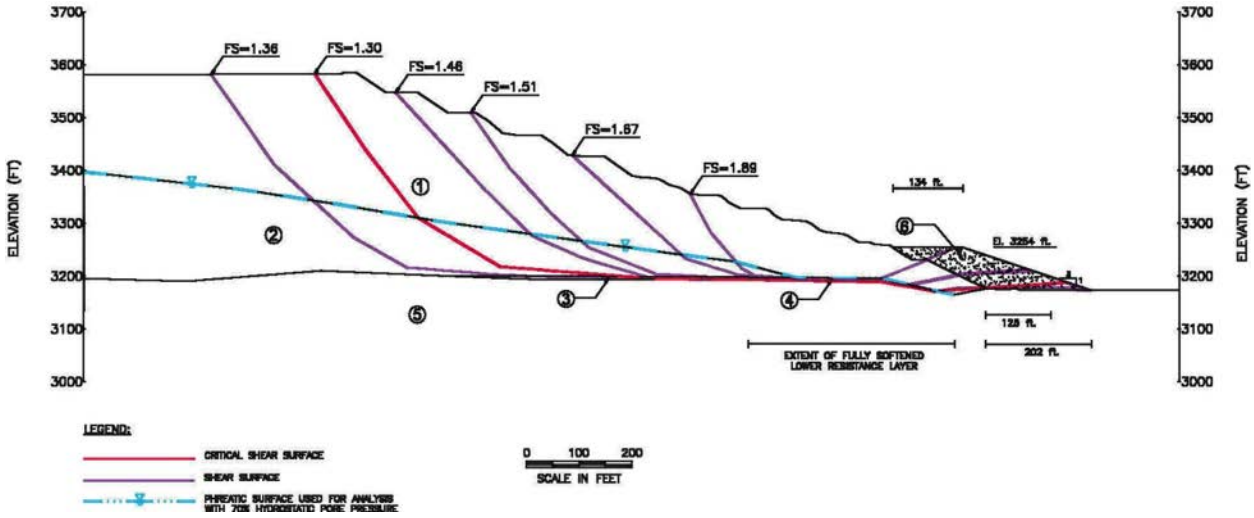

Figure 16: Section 10, STI elevation 3,585 feet amsl, undrained stability results with Phase 2 buttress

NO.	MATERIAL DESCRIPTION	UNIT WEIGHT (pcf)	DRAINED STRENGTH COHESION (psf)	DRAINED STRENGTH FRICTION ANGLE (degrees)	POST-EARTHQUAKE STRENGTH S_{UPE}/P'
1	UNSATURATED TAILINGS	120	0	35	–
2	SATURATED TAILINGS	120	0	–	0.28 CIU', 0.20 DSS
3	SATURATED LOWER RESISTANCE LAYER	120	0	–	0.20
4	SATURATED FULLY SOFTENED LOWER RESISTANCE LAYER	120	0	–	0.07
5	STARTER DAM	130	0	40	–
6	FOUNDATION	130	0	40	–
7	PROPOSED BUTTRESS	120	0	35	–

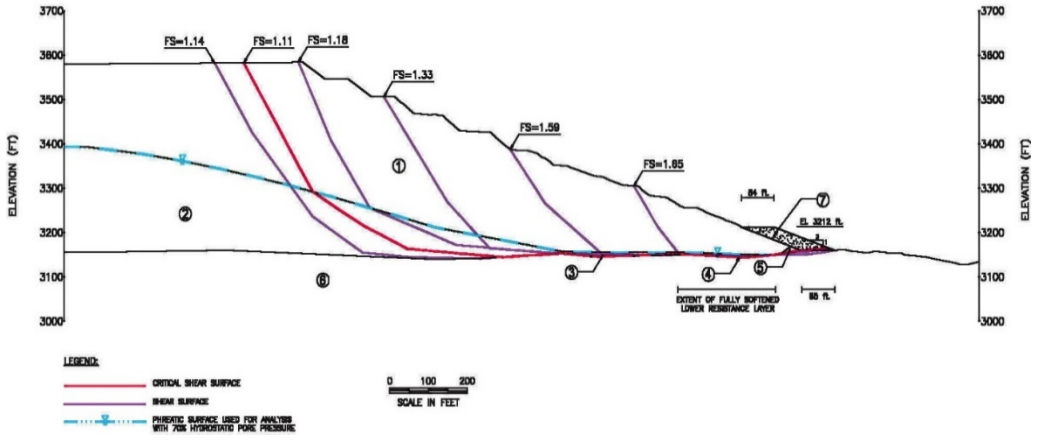

Figure 17: Section 8, STI elevation 3,585 feet amsl, post-earthquake stability results with Phase 2 buttress

NO.	MATERIAL DESCRIPTION	UNIT WEIGHT (pcf)	DRAINED STRENGTH COHESION (psf)	DRAINED STRENGTH FRICTION ANGLE (degrees)	POST–EARTHQUAKE STRENGTH S_{UPE}/P'
1	UNSATURATED TAILINGS	120	0	35	–
2	SATURATED TAILINGS	120	0	–	0.28 CIU*, 0.20 DSS
3	SATURATED LOWER RESISTANCE LAYER	120	0	–	0.20
4	SATURATED FULLY SOFTENED LOWER RESISTANCE LAYER	120	0	–	0.07
5	FOUNDATION	130	0	40	–
6	PROPOSED BUTTRESS	120	0	35	–

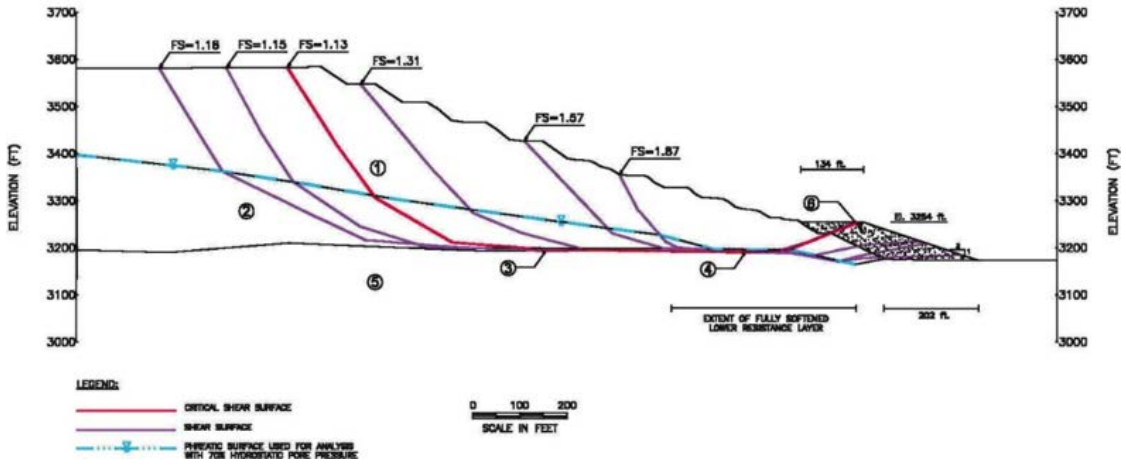

Figure 18: Section 10, STI elevation 3,585 feet amsl, post-earthquake stability results with Phase 2 buttress

Deformation analysis

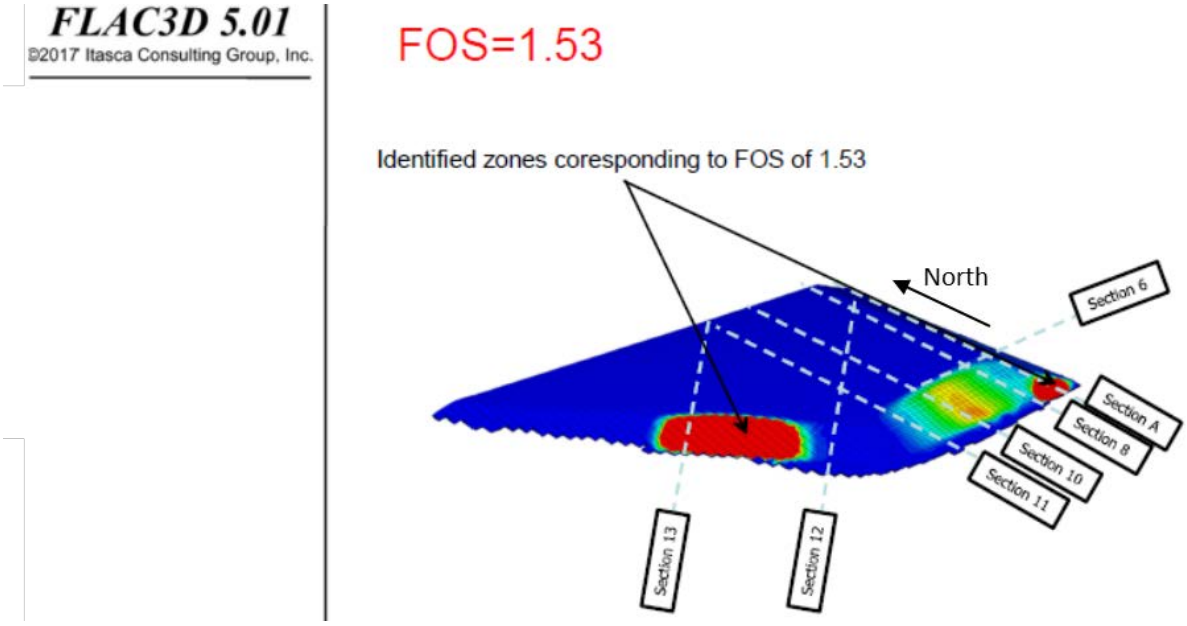

Figure 19: STI elevation 3,585 feet amsl, 3D post-earthquake stability results with Phase 2 buttress

Three-dimensional (3D) slope stability and dynamic deformation analyses were performed for the Phase 2 south slope buttress. The 3D model included the entire south slope and portions of the east and southwest

slopes to evaluate the extent of the buttress. The 3D slope stability analysis identified global shear surface, shown on Figure 19, similar to the two-dimensional stability analysis for the post-earthquake loading condition. This provided an independent verification of the identified critical shear surface.

The design earthquake is a 10,000-year event with a moment magnitude of 7.0. Seven time histories were generated and analyzed. The results presented herein correspond to motion with the highest Arias Intensity and duration. Each motion has two recorded components and both were applied in the model as north/south in the y-direction and as east/west in the x-direction. The calculated displacement magnitudes are less than 1 foot with a maximum crest settlement of 0.2 foot and maximum horizontal crest displacement of 0.5 foot, as shown on Figures 20 through 22. The movement stops and stabilizes at the end of the analysis, indicating tolerable deformation. Identified minor movements outside the buttress indicate a potential need for a future buttress beyond elevation 3,585 feet amsl if pore pressure continues to increase at the observed rate.

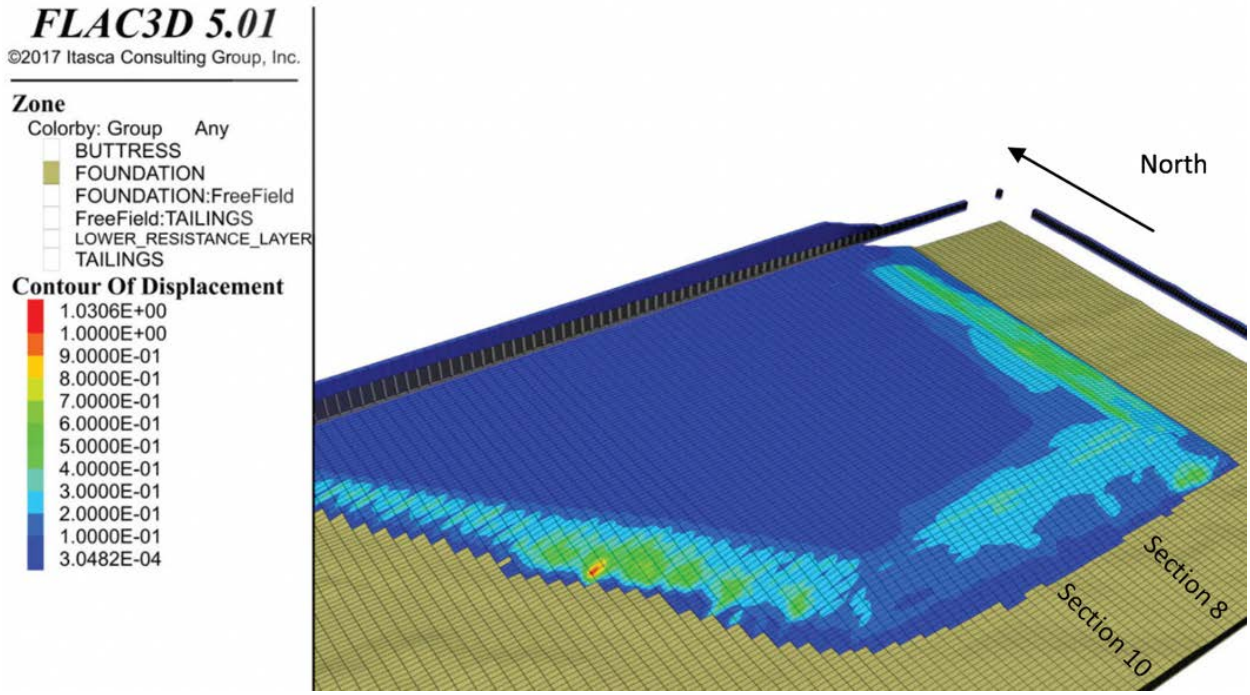

Figure 20: STI elevation 3,585 feet amsl, 3D dynamic deformation analysis results showing displacement contours (units in feet)

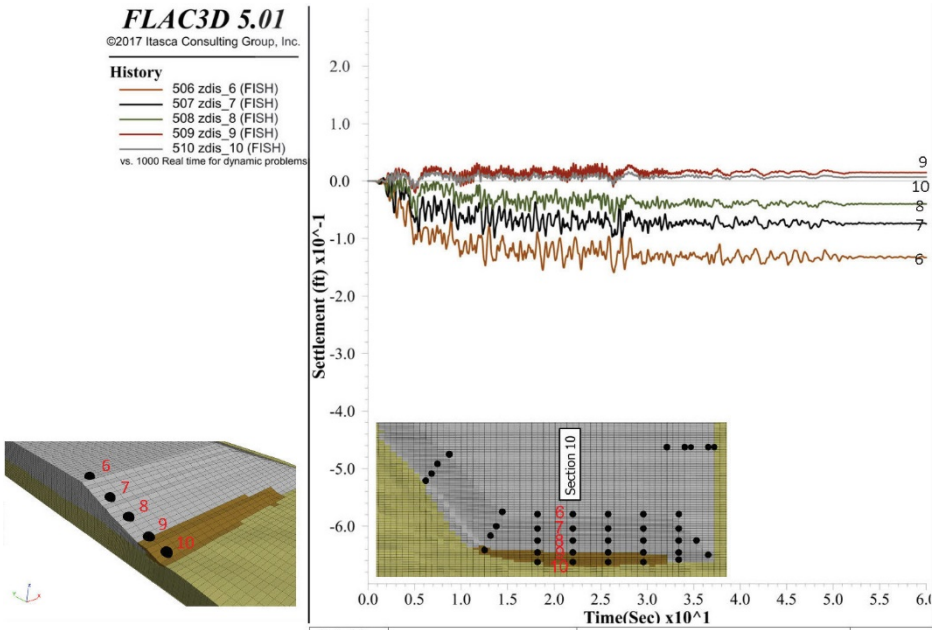

Figure 21: STI elevation 3,585 feet amsl, 3D dynamic deformation analysis results showing vertical displacements

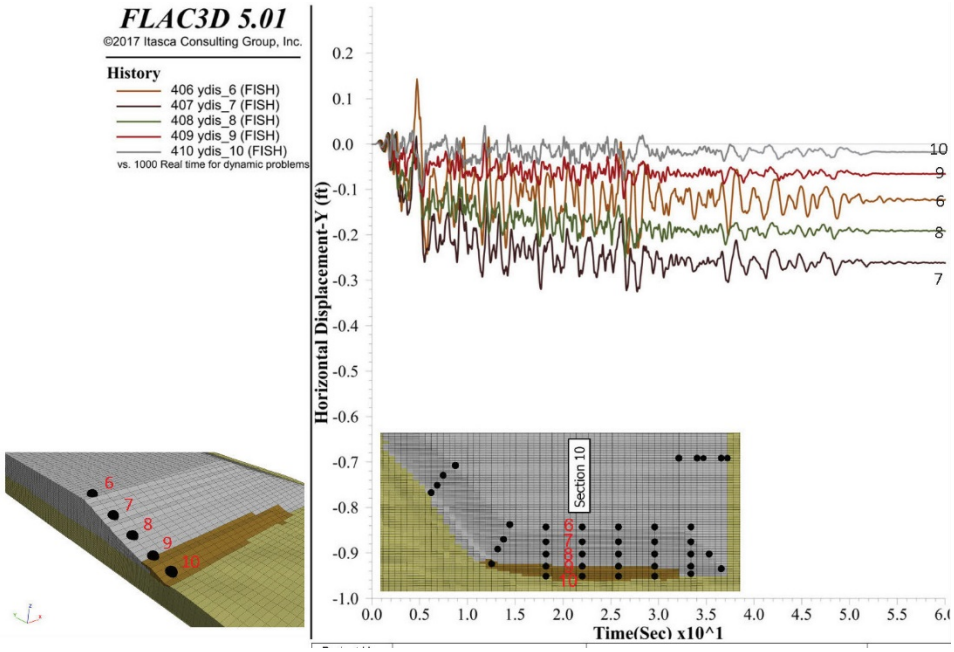

Figure 22: STI elevation 3,585 feet amsl, 3D dynamic deformation analysis results showing horizontal displacements

Stakeholder cooperation

In Arizona, tailings impoundments fall under the jurisdiction of the ADEQ. The STI is operated under an APP administered by ADEQ. Among other things, Sierrita's APP outlines monitoring, reporting, and stability requirements. The day after receiving the EoR's recommendation to construct the precautionary

buttress, representatives of Sierrita met with ADEQ to seek regulatory concurrence to allow construction in an expedient manner. Representatives of Sierrita briefed ADEQ on its tailings management and stewardship programs including how the issue was identified and the proposed action plan. Sierrita and ADEQ reviewed permitting options, with Sierrita agreeing to expeditiously construct a precautionary buttress while Sierrita provided ADEQ with the technical information on the STI and buttress required to amend the APP.

Sierrita assembled a project team that included the EoR, engineers from Sierrita and its parent company, community liaison officers from Sierrita and its parent company, Sierrita environmental specialists, and Sierrita tailings operators. The project team developed stakeholder engagement, permitting, and project execution plans. The plans were executed somewhat concurrently to construct the buttress in an expedient manner.

FCX is committed to the safety and sustainability of communities in which it operates and maintains positive relationships with those communities. Sierrita communicates with local stakeholders through regular meetings during which company representatives transparently discuss operational activities, encouraging questions and open dialogue. In addition, a dedicated Sierrita community liaison officer facilitates a range of other ongoing interactions between operations personnel and community stakeholders to ensure ongoing dialogue. Prior to construction initiation, Sierrita engaged local stakeholders to inform them about the precautionary buttress project and the tentative schedule. Communications with state and local stakeholders emphasized the commitment to responsible mining, transparency, and accountability across the operations of FCX. Sierrita management met with Sierrita employees and sent emails to explain the conditions at the STI and the action plan. Sierrita has maintained this rigorous level of engagement with stakeholders through participating in meetings whenever possible and practicable with appropriate government and community bodies, while also maintaining robust environmental stewardship and community benefit and development programs.

The precautionary buttress project was divided into two phases. Phase 1 addresses the current elevation of 3,510 feet amsl. Phase 2 addresses the future elevation of 3,585 feet amsl. At the current raise rate, elevation 3,585 feet amsl will be reached in approximately 10 years. Sierrita contracted an external construction contractor, Granite, to construct both phases of the project. Sierrita submitted the Phase 1 design package to ADEQ in November 2018. Construction was initiated in December 2018. Although the design submittal was required, it was not a prerequisite for construction. The Phase 1 design package included stability analyses and issued-for-construction drawings. Phase 1 was completed in March 2019. An approximate alluvium volume of 430,000 cubic yards was excavated from the undisturbed area, immediately south, and placed at the southern toe of the STI. Phase 2 earthwork construction was initiated in March 2019 and was completed in September 2019.

Conclusions

Stability analyses have been updated for sections located on the south slope where a lower resistance layer was encountered. Due to the increase in pore pressures, the material characteristics of the lower resistance layer were re-evaluated near the toe of the downstream STI south slope. At lower strains, the peak value would be mobilized, but if larger strains were to occur or collapse under low confining pressures, the fully softened shear strength could be mobilized. Therefore, the precautionary buttress design analyses were performed using a fully softened shear strength ratio value of 0.07. The calculated factors of safety for this case show values below the minimum required. Thus, a buttress was constructed along the STI south slope to mitigate the risk associated with potential strain softening of the lower resistance layer.

A buttress was designed in two phases: Phase 1 for STI elevation 3,510 feet amsl (up to mid-2020) and Phase 2 and for STI elevation 3,585 feet amsl (approximately year 2029). Stability analysis demonstrate factors of safety for the undrained and post-earthquake loading conditions that exceed the minimum required values for the Phases 1 and 2 buttress layouts. The buttresses will be constructed ahead of the targeted STI elevation. The Phase 1 buttress was completed in March 2019 and the Phase 2 buttress was completed in September 2019.

The observational method is being implemented to monitor the pore pressures, saturation within the STI tailings, and potential for any movement of the STI embankment. An updated comprehensive investigation and analysis is ongoing in 2019 (five years since 2014 comprehensive). If any unexpected changes in behaviour are observed, the proposed buttress layout would be re-evaluated and modified, if required.

References

Arizona Department of Environmental Quality (ADEQ). 2004. *Arizona Mining Guidance Manual's Best Available Demonstrated Control Technology (BADCT)*. Publication TB 04-01.

Peck, R.B. 1969. Advantages and limitations of the observational method in applied soil mechanics. *Géotechnique* 19(2): 171–187.

Robertson, P.K. 2017. Evaluation of flow liquefaction: Influence of high stresses. In *Proceedings of PBDIII Earthquake Geotechnical Engineering*, 16–19 July, Vancouver, Canada.

Proceedings of Tailings and Mine Waste 2019
November 17–20, 2019, Vancouver, Canada
Published by the University of British Columbia, 2019

Assessing Salt Migration from Compacted Bauxite Residual into Overlying Cover Using an Instrumented Column

Wenqiang Zhang, The University of Queensland, Australia
Chenming Zhang, The University of Queensland, Australia
Ximing Lei, The University of Queensland, Australia
Yuyang Zhu, The University of Queensland, Australia
Sebastian Quintero, The University of Queensland, Australia
David J. Williams, The University of Queensland, Australia
Mike O'Neill, Queensland Alumina Limited, Australia

Abstract

A cover of an inert growth medium is required over compacted, seawater-neutralized bauxite residue. The cover has to be revegetated, and it is necessary to demonstrate that the potential evaporation-driven uptake of salts from the seawater-neutralized residue will not impact the revegetation. An instrumented column was constructed to test the evaporation-driven uptake of salts from the compacted residue into an overlying cover material under natural weather conditions. The PVC column is 1.2 m in height, and 200 mm in diameter, and was filled with 600 mm of compacted residue overlain by 600 mm of loose cover material. It is instrumented down its length with ten sets of moisture, suction, salinity, and temperature sensors, designed and manufactured at the University of Queensland (UQ). Two pressure transducers are installed in the column to monitor the change of water level due to rainfall and evaporation. The instrumented column is installed on a roof of a building at UQ, alongside weather stations, and has been subjected to prevailing weather conditions for over one year, during which weather conditions and sensor responses have been continuously monitored. This paper reports on the instrumented column set-up and the first year of results obtained from the test.

Introduction

Covers are a vital aspect of the process of land rehabilitation and closure of tailings storage facilities (TSFs). Better design of covers would help in limiting infiltration, controlling air entry, resisting erosion by water and wind, reducing dust emissions, supporting vegetation, and remaining stable (Tordoff et al., 2000).

Seawater neutralizes the bauxite residual to a pH of about 8.5, sufficiently low to allow the bauxite residual to be stored safely, be suitable for re-use without further chemical treatment, and to improve soil chemistry and support plant growth. However, the salinity of seawater increases the salinity of neutralized bauxite residual 2 to 3-fold to an electrical conductivity of about 22 mS/cm, which is not suitable to be re-vegetated. A general soil cover is suggested to deposit above the bauxite residual tailings to lock the fresh rainwater and hence allow the vegetation to grow on top. With relatively coarse particle size and high permeability, the soil cover may have a shallow desiccation depth, and the capillary force may not be strong enough to uptake salt water from underneath bauxite residual tailings to the surface to disrupt the re-vegetation.

The idealized depths of the cover system may require an instrumented trial dump over a sufficiently long period to assess the salt migration and vegetation growth. However, a trial dump could be expensive, and results could be influenced heavily by the boundary of the trial pit. A cost-effective approach to assess the salt uptake is to carry out a large-scale instrumented column experiment under weather conditions with compacted bauxite residual overlaid by the general soil cover. With local weather conditions monitored by weather stations, and instrumented by both commercially available and in-house developed moisture, suction, temperature, and salinity sensors, the column experiment is expected to indicate how successfully the upper soil cover could seal the saline water from bauxite residual, hence providing valuable information to achieve successful mine capping.

Methodology

The schematic diagram of the instrumented column is shown in Figure 1. The PVC column has an internal diameter of 200 mm and a total height of 1,200 mm. A waterproof flange was designed in the middle of the column to ensure convenient installation and dismantling as compared to previous designed columns with only one section over the length (Shokouhi et al., 2017). The sensors were installed through the wall of the column at various depth intervals, with each set of sensors located at quarter points around the circumference of the column. The distances between neighbouring sensors was set to increase over the depths to the surface as the variations of temperature, soil moisture, suction and salinity due to weather occur more frequently near the surface. The column was enclosed by PVC panels to reduce the solar and wind influence on the side of the column body.

Five different types of soil sensors were installed in the column (Williams and Zhang, 2017). Ten in-house built dielectric moisture sensors measure the water content indirectly through acquiring the dielectric permittivity of the bulk soil, based on the principle that the dielectric permittivity of water (around 80 to 90 depending on salinity and temperature) is much higher than dry soils (around 10 to 15 depending on soil mineralogy and temperature). Although the readings from dielectric permittivity based moisture sensors are affected by salt and temperature, these impacts can be compensated by acquiring salinity and temperature

at the same location using other related sensors. Sensors based on this principle are found much more reliable to work in saline tailings than those based on time domain reflectometry method, which transmit high frequency waves in tailings and measure their reflections, as the incoming wave may get attenuated immediately by hypersaline water, resulting in the sensors becoming completely dysfunctional.

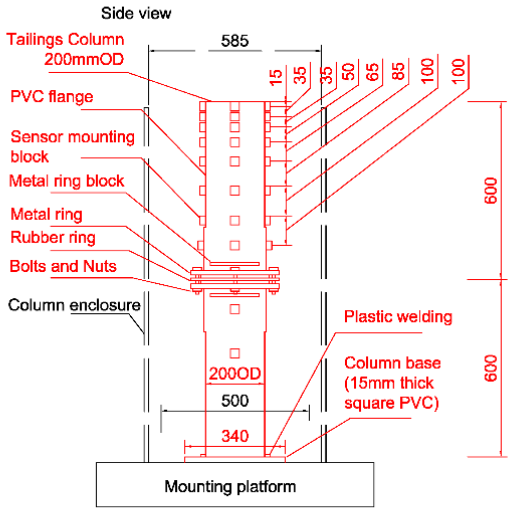

Figure 1: Schematic diagram of the instrumented column for bauxite residual

Ten thermal suction sensors were installed over the depth of the column, which measures the suction of the bulk tailings indirectly through acquiring their thermal conductivity, as well as ambient temperature. The advantage of this measuring principles is that the readings are not influenced by salinity, which varies significantly in TSFs. Two types of salinity sensors were installed. Two DECAGONTM GS3 sensors were installed to measure bulk salinity indirectly through electrical conductivity (EC), at a range of 0 to 30 mS/cm. Another five in-house salinity sensor were installed to indirectly measure soil salinity by acquiring the relatively humidity of the air adjacent to tailings. This is based on the principle that the solvent in the pore water would disrupt the exchange of water ions between liquid and gas phase.

As a result, the air humidity near the hypersaline pore water becomes less than saturation. This sensor is particular sensitive when tailings salinity becomes higher than seawater (from seawater salinity of 50 mS/cm to solubility limit of 300 mS/cm). Two pressure sensors were also installed in the column at 50 cm and 100 cm below the soil surface, to measure the location of the water table. Previous columns design employed load cells underneath the column to measure the change in weight due to evaporation/rainfall. However, due to significant fluctuation of temperature and wind, the monitored weight was found too noisy to identify the water balance in the column. Besides sensors in the columns, a weather station was installed next to the column to monitor in real time weather conditions, which can be correlated to the potential and actual evaporation. All these sensors were connected to an in-house manufactured data logger, which is powered by solar and sends monitored data instantaneously to internet for visualisation and analysis.

The packing of the tailings was carried out to emulate the field conditions (Figure 2). Bauxite residual was oven dried at 50°C over a period of 24 hours to minimize the chemical variations due to high temperature. The dried tailings were then grinded into powder using a pestle and mortar. Following that, the powder was compacted at standard maximum dry density (1.575 t/m^3) under standard optimum water content (28.9%) in the lower section of the column. This was achieved by repeatedly spreading 250 g of dry residual evenly into the column, spraying 100 g water above the bauxite residual, compacting the newly added bauxite residual down to 5 mm incremental thickness using a pestle and waiting for one hour with column top sealed before the next compacting cycle. As sensors were installed before the tailings compaction, care was taken especially at the layer where sensors present to minimize the risk of damaging sensor during the compacting processes. Once the lower column section was fully filled, the upper column section was installed through connecting the flange. Soil cover was poured into the top section slowly and carefully until the soil surface have reached the rim of the column.

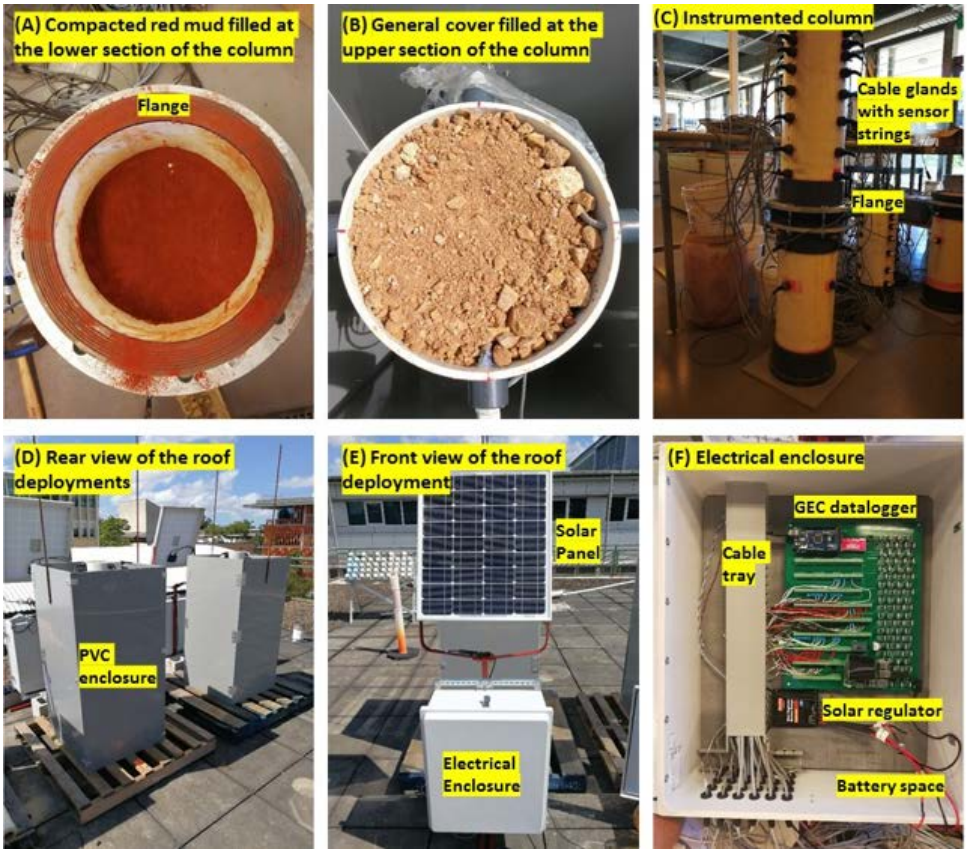

Figure 2: Images of column assembling processes. Compacted bauxite residual filled at the lower section of the column (A); soil cover deposited at the upper section of the column (B); assembled column with sensors installed (C); rear view of the roof deployment with column protected by a PVC enclosure (D); front view of the roof deployment with solar panels and electrical enclosure visible (E); setup in the electrical enclosure (F)

Data and results

The instrumented column test was commenced in February 2018 and has been running over 16 months to the time of reporting. As rainfall induced settlement was significant a few days after the test were started,

cover materials were topped up to reach the original height of the topsoil on 13th April. Since then, no settlement has been recorded. Figure 3 shows the monitored results from weather station. Rainfall occurred predominantly in the wet seasons, spanning from November to April next year. Although 2018 was a relatively dry year, occasional rainfall occurred during the dry seasons.

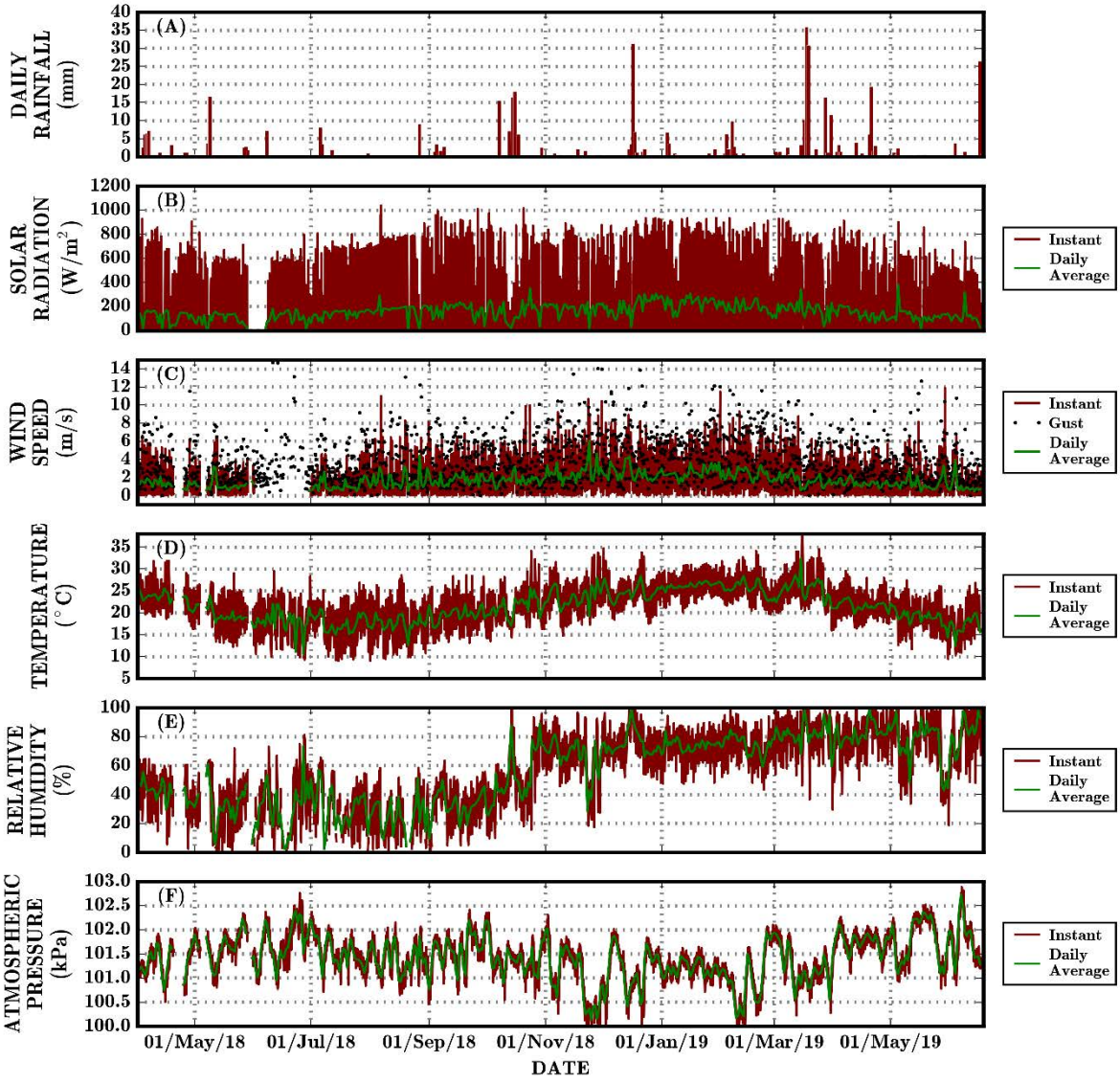

Figure 3: Monitored data from weather station, including: (A) daily accumulated rainfall, (B) solar radiation, (C) wind speed, (D) temperature, (E) relative humidity, and (F) atmospheric pressure. Brown lines are measured data and green lines are daily averages

As expected, the solar intensity and temperature were higher in summer. The average temperature was around 20°C during the dry season while 25°C during wet season, respectively, representing typical sub-tropical weather. The solar radiation remained high around 700 to 1,000 W/m^2 during most of the days

without rainfall, while became low during the rainy days. Similar to solar radiation, the daily average wind speed remained relatively high during the dry seasons which promotes evaporation. Meanwhile, after declining to the minimum at the end of wet season, the relative humidity rose gradually once rainy seasons arrives and remained average value of 75% at rainy seasons. At annual scale, the atmospheric pressure fluctuated with an average of 101 kPa over the monitoring periods.

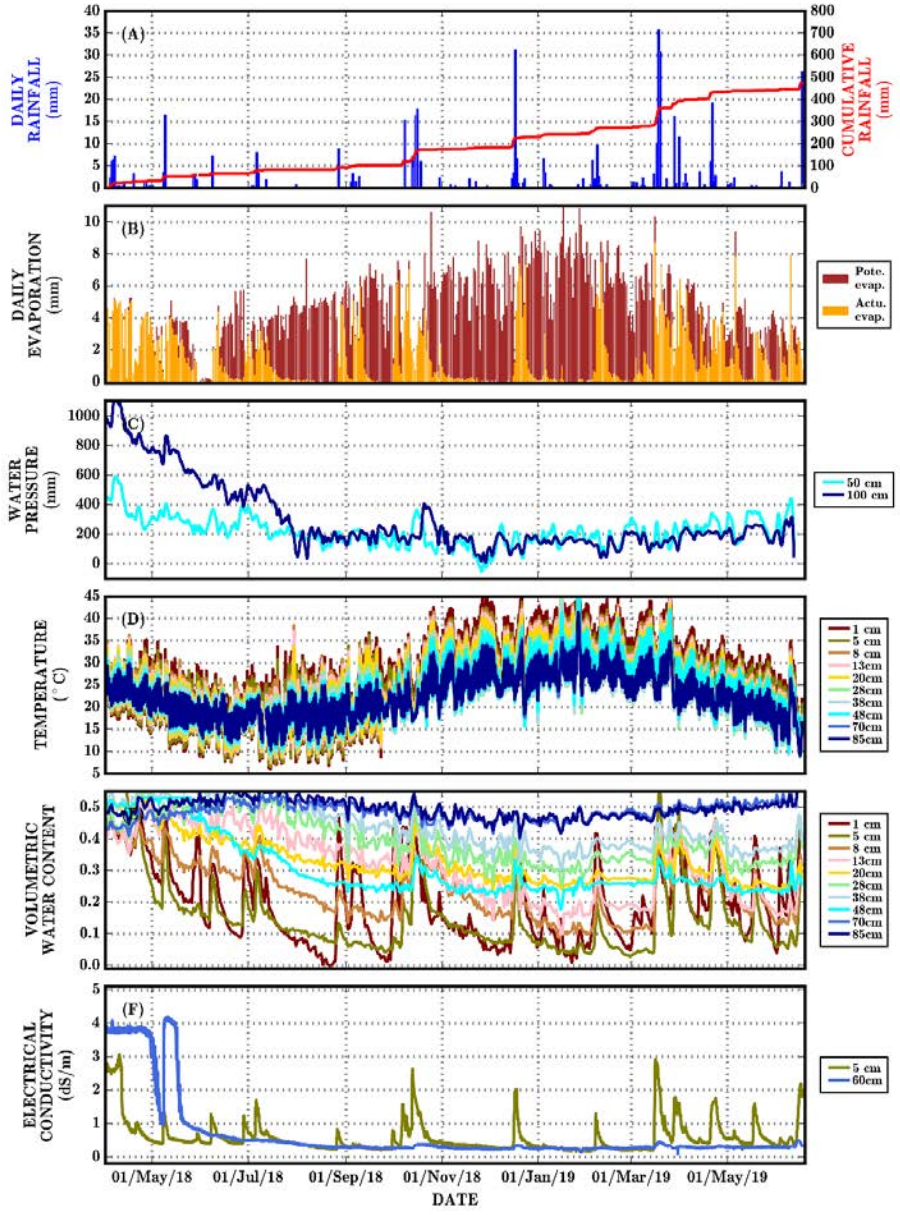

Figure 4: Monitored results including rainfall, potential evaporation derived from weather station data, water pressure, temperature, volumetric water content and EC over depths

Figure 4 shows the monitored data from the sensors inside the column as well as the water gain (from rainfall) and loss (from evaporation, which is derived from weather data using Penman-Monteith equation)

(Monteith, 1981). Figure 5 shows the images of the surface at different time. In the beginning, the overall water content in the soil cover (0 to 60 cm below the surface) was very low. The two moisture sensors at 70 and 85 cm below the surface were buried in the compacted bauxite residual, where the initial water content was high as compacting the bauxite residual to standard maximum dry density was achieved at optimized water content (gravimetric water content of 33.8%, or equivalently volumetric water content of 53.3%). With more rainwater filled in the column, the pressure sensors became responsive to the change of top boundaries. Similarly, the ECs monitored in dry soil cover remained low in the beginning as the cover was dry, while fluctuated according to evaporation and rainfall, after the cover became wet.

Based on the changes in volumetric water content (Figure 4E), and the comparison between the potential evaporation and actual evaporation (Figure 4B), the monitoring period can be divided into three wetting and drying periods. The first period is a short typical wetting period, spanning from early April to early May 2018. The period started with large amount of rainfall during the wet season in 2018, which completely saturated the column by water (Figure 5A). Although the actual evaporation rate was high at the sunny days, the rainfall is much higher than total evaporation during the wet seasons. The bulk salinity in the cover material increased with the rise of water content, the overall salinity was still relatively low, suggesting no porewater in the underneath bauxite residue has been transferring to the upper cover materials.

The second period cover the whole dry season of 2018, starting from the beginning of the May to the end of September. Intermittent rainfall took place during the dry season, with total amount less than 50 mm. Due to relatively high water content, and occasional rainfall supply at the beginning of the drying season, the actual evaporation is almost the same as potential evaporation. As the dry season continues, the water content on the surface became very dry, and hence evaporation was almost diminished. Although occasional rainfall can moisturize the top cover layer, the rainfall water is insufficient to saturate the entire soil cover, and hence evaporation decreased rapidly immediately after the rain. At the end of the dry season (30 September, Figure 6), the unsaturated soil thickness was found to be around 70 cm. This suggested that the unsaturated zone is predominantly located in the cover, and has partially stretched into the top of the compacted residue. The EC at the top of the soil cover is found to fluctuate accordingly with rainfall, again the rise of the intensity is rather limited, suggesting rain is the source of water. The bottom EC remained very low throughout the dry season, indicating no upward salt movement from residual to the cover.

The third period starts from early October 2018 to the time of reporting (mid-June 2019). Different from the wet season in 2018, where rainfall occurs consecutively in many days, the wet season in 2019 is featured by intensive rain over a short period. This has led to the sharp rise of water content at rainfall event and the presence of low actual evaporation rate at the sunny days in between the major rainfalls. Under

such repeated wetting and drying, the unsaturated zone maintained at 70 cm below the soil surface, and circulation of water is mostly from rainfall, not from the bauxite residue.

Figure 5: Images of column surface at different stages of the test

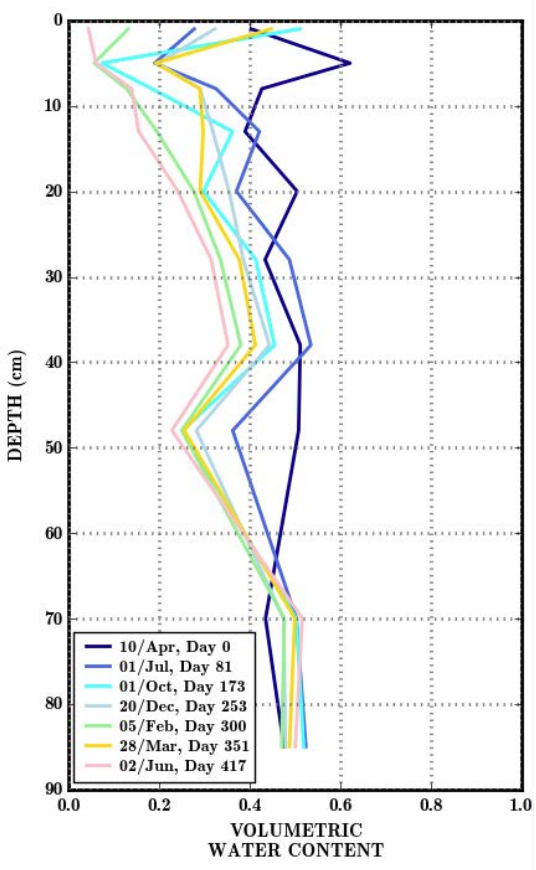

Figure 6: Monitored saturation profiles

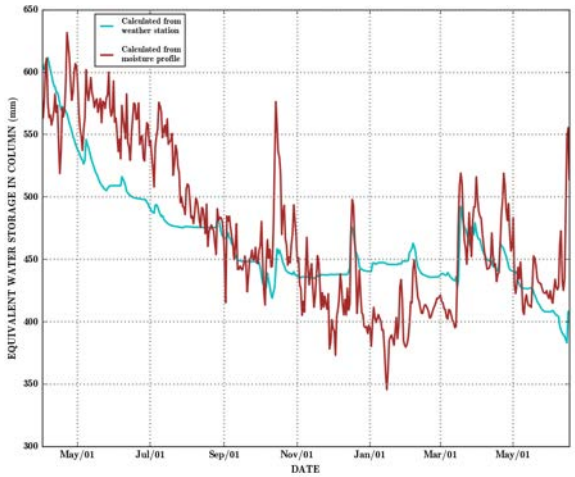

Figure 7: Water balance in the column

Figure 7 shows the water storage from the column calculated by using two methods:

1. through the net exchange from the column surface (e.g., actual evaporation and rainfall); and
2. through integrating water content in the column monitored by moisture sensors.

The water loss calculated by both methods follows almost similar patterns, suggesting that water balance is well captured during the monitoring period by the instrument deployed. However, note discrepancies are visible between the two lines, particularly that data estimated by moisture sensor varies more fluctuation than that obtained through net fluxes. This is probably due to the fact that moisture sensor experiences noise induced by temperature. The other reason on the oscillating water content curve is because data monitored by moisture sensor may not be representative to the water content at the depth as water infiltration and evaporation may be uneven over the depths. It is also worthy to note that during the intensive rainfall period (e.g., April, October 2018 and March 2019), water loss from water content profile were less than that estimated by net fluxes. This is very likely due to the fact that evaporation from ponded surface can be well monitored by weather station while not at all by moisture sensors.

Discussion

According to the salinity profile, the salinity uptake from red mud to soil cover was not evident during the monitoring stage. The uptake of the salt from bauxite residual to overlying soil cover is potentially induced by two transport processes:

1. advection driven by evaporation; and
2. solute diffusion driven by the concentration gradient between bauxite residual and soil cover.

Advection is mostly likely the process to lift the salinity level high enough in the soil cover to exert stress on the vegetation grown after rehabilitation, as root is expected to be accommodated in the soil cover.

Since evaporation induced advection occurs predominantly in unsaturated soils (Zhang et al., 2014), the optimized design of the soil cover to minimize the salt uptake into cover would be that the thickness of the unsaturated zone after a full desiccation (700 mm in this study) is less than the thickness of the soil cover layer. Under that design, a permanent fresh-water lens will develop and stabilize permanently at the lower soil cover layer, preventing hypersaline water in the bauxite residual from transporting upward to deteriorate the eco-environments in the upper soil cover. The upper soil cover layer lined by the fresh-water lens is suggested to be thick enough to accommodate the roots of shrubs and small trees, which stabilize the soils and maintain water content.

Conclusion

A column test was designed and deployed on the roof of a building at UQ under weather conditions to investigate the potential salt uptake from underneath compacted bauxite residual to the overlying general soil cover, a key process that can disrupt the revegetation after a mine closure. With 600 mm compacted bauxite residual tailings filled at the lower section and general soil cover at the 600 mm upper section, the column was instrumented with in-house and commercially available sensors measuring phreatic surface, as well as depth profiles of water content, suction, temperature, and salinity in both tailings and cover soil. The one-year monitoring results indicated that the unsaturated soil depth is about 70 cm below the surface. Rainwater recycles in the unsaturated zone through rainfall and evaporation, and so far, no salt uptake from underneath the bauxite residue to cover has been identified. The cover also shows no settlement after repeated rainfall and evaporation.

References

Monteith, J. 1981. Evaporation and surface temperature. *Quarterly Journal of the Royal Meteorological Society* 107(451): 1–27.

Shokouhi, A., C. Zhang and D.J. Williams. 2017. Settling, consolidation and desiccation behaviour of coal tailings slurry. *Mining Technology*. Taylor & Francis, 9009 (May): 1–11. doi: 10.1080/14749009.2017.1308691.

Tordoff, G.M., A.J.M. Baker and A.J. Willis. 2000. Current approaches to the revegetation and reclamation of metalliferous mine wastes. *Chemosphere* 41(1–2): 219–228. doi: 10.1016/S0045-6535(99)00414-2.

Williams, D.J. and C. Zhang. 2017. A suite of tests for designing slurried tailings deposition. In *Proceedings of the 4th International Seminar on Tailings Management.* Santiago De Chile, Chile.

Zhang C., L. Li and D. Lockington. 2014. Numerical study of evaporation induced salt accumulation and precipitation in bare saline soils: Mechanism and feedback. *Water Resources Research*: 1–23. doi: 10.1002/2013WR015127.

Chapter 2:
Management

Proceedings of Tailings and Mine Waste 2019
November 17–20, 2019, Vancouver, Canada
Published by the University of British Columbia, 2019

Running Downhill: An Adaptable Approach to Water Management Planning Used for Swift Creek Expansion

George Adom, Teck Coal Ltd, Canada
Daniel Hoover, Teck Coal Ltd, Canada
Jake Gentles, Wood, Canada
Monica Wagner, Wood, Canada
Matthew Graham, Wood, Canada

Abstract

Implementing water management structures at mine sites presents unique challenges to clients, engineers, and contractors related to the complexity of construction, potential disruption due to compressed construction schedules, and differing objectives of proponents and stakeholders. This includes the water management structures (designed by Wood) required for the multi-year Swift Creek Expansion (undertaken by Teck Coal Limited – Fording River Operations). As the project has progressed, Teck Coal and Wood has continuously evolved our team management strategies through trial and error, lessons learned, and value engineering sessions, as well as feedback from stakeholders.

This paper presents adaptable strategies that have proven successful in the context of a remote, high-elevation, and operational mine site. These strategies balanced the objectives of several internal and external stakeholders, and ensured that the project remained on schedule. The five main strategies that the authors recommend for similar projects are presented.

1. Begin with the end in mind: anticipate potential issues and develop solutions in advance by maintaining balanced "high altitude" and "ground level" perspectives and compiling a risk registry.
2. Gain alignment to ensure consistent delivery: align the project partners (Owner, Engineer, Contractor) through regular partnership meetings and observation of Tuckman's team development model (i.e., progressing the team through the "forming," "storming," "norming," and "performing" stages).
3. Obtain buy-in: ensure stakeholder support through the application of several stakeholder management best practices (e.g., stakeholder identification workshops, interviews, and stakeholder relationship building).

4. Develop practical solutions that are construction-ready: complete risk identification, lessons learned, and value engineering workshops, as well as independent design reviews so that the team's experience and site knowledge can be incorporated into the designs.
5. Build internal and external trust: build trust across organizations through the development of clear and transparent Quality Assurance/Quality Control procedures, operate in a fair and flexible manner, and ensure that the leadership is prepared to listen to their team as well as their partners.

Introduction

The objective of this paper is to distil the authors combined construction experience on the owner and engineering consultant sides of the equation to identify the recommended team management strategies to successfully progress a mine water management project through the planning, design, and construction phases. Key steps are:

1. begin with the end in mind;
2. gain alignment to ensure consistent delivery;
3. obtain buy-in;
4. develop practical solutions that are construction-ready; and
5. build internal and external trust.

Each of these areas are described below with supporting examples and solutions, as well as the benefits of implementation.

Begin with the end in mind

Although construction documents are ultimately used to implement a water management solution, development of the solution is an iterative process requiring refinement and revisions. A "high altitude" perspective is required to scan the project horizon, anticipate potential issues that may need to be addressed during the design phase, and develop solutions in advance.

This must also be balanced by a "ground level" perspective to understand the potential impacts of issues, which will inform the team's assumptions and decisions. These potential constraints and perspectives can be maintained in a risk registry and tracked during weekly progress meetings.

Table 1 presents some examples of anticipated construction challenges, and the corresponding adaptive planning solutions, that have been identified by "scanning the horizon" during the ongoing Swift Water Management System infrastructure project (Swift WMS Project).

Table 1: Identified construction challenges and adaptive solutions implemented on the Swift WMS Project

Anticipated construction challenge	Adaptive planning solution implemented
Potential scarcity of local construction materials that meet engineering design Technical Specifications	Conducted test pitting and material testing prior to construction to confirm material sources and suitability for construction
Lack of practical and effective erosion and sediment control and care of water during construction	Owner's engineer developed high-level Construction Environmental Management Plan, including Care of Water, that formed the basis for site-specific plans developed prior to start of construction. These plans were iterative and included input and consultation from the Teck Fording River Operations (FRO) Environment Team
Ambitious construction schedule (five month work window) prior to onset of winter could be upset if adverse field conditions are encountered	Identified presence of and depth to bedrock during design phase. This led to the early selection of a specialist blasting contractor and averted delays, which saved time and money Started design and tendering process early to allow for on-time mobilization of the contractor to site Completed pre-construction tasks, such as tree clearing and material source identification, to prevent delays during construction

These examples of implemented solutions provide an indication of the level of project planning required, how critical it is to have a clear understanding of the project goal (begin with the end in mind), and the role of project leaders in driving practical solutions.

Gain alignment to ensure consistent delivery

The Swift WMS Project leaders established a clear vision of the project goals and objectives at the project kick-off meeting; however, gaining alignment on shared goals and priorities during construction was difficult to maintain, as the Engineer, Owner, and Contractor were focused on construction, addressing Requests for Information (RFIs), and day-to-day construction actuals. It became clear that reconvening the wider construction and engineering teams at the mid-point of construction for a "partnership meeting" was critical to achieving a broader understanding of, and agreement to, the project goals. The objective of this meeting was to facilitate development of a high-performance construction team, which resulted in the team working collectively to resolve construction issues encountered in the field, ultimately yielding a more efficient delivery.

It is important to recognize project team dynamics and whether the team is in the "forming," "norming," "storming," or "performing" phase (Tuckman, 1965). Similarly, it is important to identify the techniques required to advance to a "performing" mindset. In terms of this project, this meant temporarily setting aside individual egos and organizational cultures to focus on the project's broader goals. Although the importance of team building or partnering meetings is sometimes overlooked, they can be transformative when implemented and adopted by the entire execution team. For the Swift WMS Project team, using the Tuckman team dynamic tool was useful to understand when we moved into the "storming" phase due to a particular issue or construction challenge. Similarly, it was useful to have a common understanding of how this tool could be leveraged to advance the team when stuck in a particular group phase.

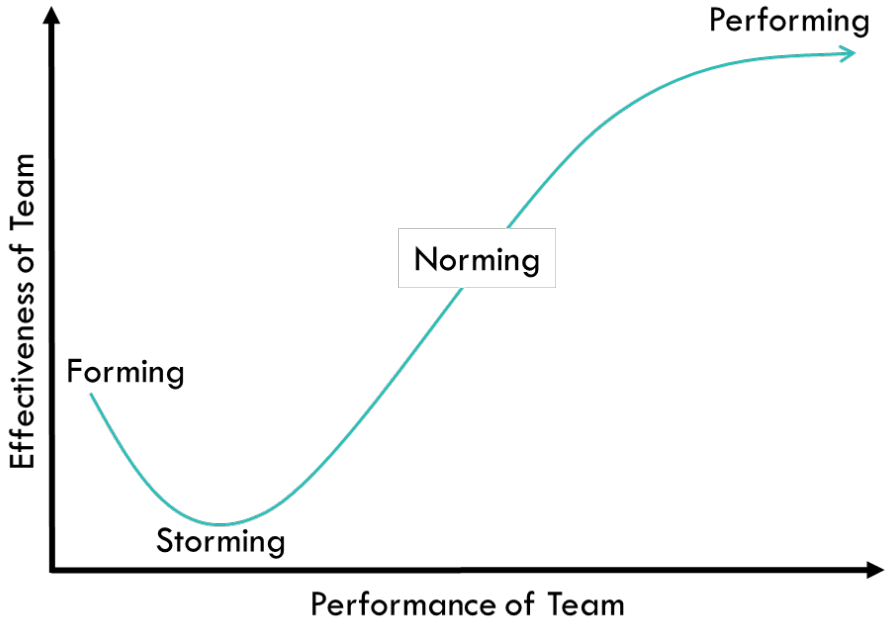

Figure 1: Tuckman's team and group development model

Obtain buy-in

Internal and external stakeholders have multiple objectives, plans, and strategies that may not align with each other or with the project. Early internal and external stakeholder input and buy-in have been critical to the ongoing construction of the Swift WMS Project, allowing Teck Fording River Operations (FRO) to meet its mine permit conditions.

Interfacing with multiple internal Teck departments has been required, since components of the Swift WMS Project directly influence other projects, as outlined in Table 2. Successful implementation of the Swift WMS Project is necessary for the internal departments to meet their projects' objectives.

Table 2: Internal stakeholders in relation to the Swift WMS Project

Internal stakeholder	Impacts from or relationship to Swift WMS Project
Active water treatment facility	Obtains its main feeder (water source) from Swift Secondary Pond, one of Swift WMS Project's ponds
Environmental group	Controls and manages the movement of water to ensure compliance. Eventually, FRO Environment will maintain the sediment ponds as part of operational activities
Water quality group	Provides FRO regional water quality models and manages water quality content for site-wide water quality analysis, effectiveness, and performance
Geotechnical and dam safety	Ensures ponds and dam specifications as detailed in drawings are compliant with dam safety classification as per regulatory requirements. FRO Geotechnical group ensures dam compliance (e.g. inspections, instrumentation, etc.)
Mine planning	Provides mine sequence maps and mining plans to show spoil and pit advancement to help plan water management system projects accordingly

The project also engages with external stakeholders that include First Nations and their partners such as Nupqu who are currently providing environmental monitoring for construction. The project leadership was intimately involved with discussions with local Regulators.

Table 3: External stakeholders in relation to the Swift WMS Project

External stakeholder	Parties	Impacts from or relationship to Swift WMS Project
Regulators	Department of Fisheries and Oceans Canada, British Columbia Ministry of Energy, Mines & Petroleum Resources; Forests, Lands, Natural Resource Operations and Rural Development; and Environment and Climate Change Strategy	Ensure designs and construction meet code, standards, specifications, and guidelines. Act on behalf of the public to protect public interest
First Nations	Ktunaxa Nation and others	Have land rights and mandate to partial ownership of landed property. Ensure First Nation and Indigenous Persons' interests are protected
Local community groups	Residents, locals of immediate property or mine operations' surroundings, and others	Ensure community interests, including water and air quality, are not compromised

Tools and techniques for complex stakeholder management

Concerted engagement at an early stage increases the likelihood that project objectives are identified and discussed, allowing a solution to be developed collaboratively that meets many, if not all, stakeholder needs. According to the Project Management Institute (2017), effective stakeholder involvement includes:

- stakeholder identification – finding the most effective ways to identify key stakeholders;
- list of stakeholders – ensuring major and important stakeholders are listed to help ascertain their needs; and
- stakeholder register – tracking stakeholders' involvements, engagement, and discussions.

The Swift WMS Project has implemented various optimized tools, described below, for effective engagement to meet the complex stakeholder involvement needs.

Expert judgement

As part of the stakeholder identification process, Subject Matter Experts (SMEs) with similar project experience were consulted for input on criteria to identify potential stakeholders. The project SMEs pointed out the importance of reviewing the business and project documents and performing impact analysis on which organizations and stakeholders the project may affect, both internally and externally.

Stakeholder identification workshop

At the early stages of the project, a stakeholder identification workshop was organized, with the list of organizations and invitees based on SME input. The workshop, which comprised functional leaders from various departments, enabled the development of a list of potential stakeholders by reviewing the scope of work and deliverables. The list was placed on a chart, which helped to group and assign stakeholders for each stage of the project during which engagements were to begin. A list of stakeholders and a register were developed from the chart and included in the project documents for future reference.

Interviews

To determine stakeholder expectations, the project team developed questions to ask selected stakeholders. The questions considered factors such as direct impact or influence of aspects of the project on each listed stakeholder. Stakeholders' roles and responsibilities, as well as their level of engagement, were gathered from the interviews. The outcomes were summarized in a comprehensive stakeholder management plan.

Leveraging lessons from previous design and construction projects

To expedite response to stakeholder needs and effectively manage requirements, the project team reviewed historic information and lessons learned from similar projects and consulted with a broad cross-section of project leaders and SMEs. One key point raised was the need to work closely with internal stakeholders who's input must be carefully considered and are therefore a fundamental component to the successful delivery of this project. Adopting a disciplined approach to learning from previous projects has resulted in benefits for streamlining the execution of this project. Stakeholder relationship building was highlighted as an important element on which to build a solid project foundation and to enable more informed decisions.

Hence, effort was made to develop stronger ties with project stakeholders and adopt a 'listen to learn' mindset to record their input.

Develop practical solutions that are construction-ready

While efforts to engage and collaborate are important to project success, these efforts can be undermined if designs call for difficult-to-source materials or do not fully consider existing site constraints. Solutions can be enhanced by getting input from the mine operations and the construction team to incorporate site and constructability knowledge at an early stage.

As a typical stage gate process (Project Management Institute, 2017), civil earthworks projects mostly go through various stages: design (prefeasibility, feasibility, and detailed); construction; and completion, including "As-Built report," Record Drawings, and Operations, Maintenance and Surveillance documentation. Although each stage has its unique challenges, the construction stage typically relies on the practicality of the design in terms of its constructability. Thus, a practical solution requires engineering designs that are easily constructible and "fit for purpose". These designs should incorporate the following principles.

Risk identification and lesson learned

Risk workshops are organized at each stage of the project to identify both threats (negative risks) and opportunities (positive risks) likely to be encountered during the execution of the project. A risk register developed at the feasibility stage is being updated throughout the project. Key project risks are grouped into threats and opportunities and ranked in order of magnitude. Mitigation measures are implemented to minimize threats, while steps to leverage opportunities are maximized. Risks are identified using brainstorming and white-boarding methods involving the project team and technical experts. Additional risk management techniques including risk ownership allocation, risk evaluation, risk plan mitigations and implementations were adopted on Swift WMS Project (Ana-Maria, 2012).

In progress meetings, lessons identified and documented during the project execution are reviewed on a bi-weekly basis to ensure that they are addressed in the design. The top five identified lessons are posted in selected project notice boards to serve as constant, visible reminders. In order to incorporate the lessons learned into other mine water management projects, Project Leads from similar projects are invited to participate in lessons learned workshops.

Independent reviews

As part of Teck's commitment to project excellence, a desktop study review of critical structural designs involving an outside engineering consultant was conducted at the feasibility stage in the design. Moreover,

a Third Party Review was performed at the detailed design stage to confirm conformance of design with industry standards (Canadian Dam Association, Engineers and Geoscientists BC, Canadian Standards Association) and mine regulatory (British Columbia Ministry of Energy, Mines & Petroleum Resources; and Forests, Lands, Natural Resource Operations and Rural Development) expectations. The report from the Third Party Review was shared with Wood engineering consultants to address comments and incorporate applicable inputs into the design.

Getting the most out of value engineering

Although most Value Engineering (VE) workshops focus primarily on cost savings, the project team used this Value Engineering workshop to provide an opportunity to address the constructability and practicality of the design. The Swift WMS Project VE workshop included participants from internal stakeholders, contractors, Third Party reviewers, and design engineers. To present an unbiased platform, an independent construction manager from a different mining company who has experience and exposure to similar projects facilitated the VE workshop. The Value Engineering comprised reviewing the technical specification, designed drawings, and quality of the drawings. Examples of suggestions that came from the Value Engineering meeting are:

- Where feasible, materials specifications such as pipes and granular materials will have alternatives specified as “or approved equal” in addition to the corresponding Technical Specification to make it easier for adjustment. This provides flexibility to “field-fit” or substitute items with the approval of the Resident Engineer for the project.
- Readily available local materials such as minus 3" mine crush will be incorporated in the design where feasible. This helps reduce the cost of importing numerous materials from far-and-wide places to remote mining locations.

Build internal and external trust

Due to the nature of the project’s demands, the key construction team comprised of the owner’s supervisors, contractor’s supervisors, consultant’s field engineers, and independent environmental monitors and safety representatives. Each of these supervisors or representatives has their own reporting criteria and sign-off procedures to ensure compliance with project requirements and documentation.

Swift WMS Project construction is occurring in two separate work fronts in the western portion of the mine, creating potential communication and delivery challenges. Thus, a Quality Assurance/Quality Control engineering strategy was developed to facilitate responses to RFIs, Field Instructions, Design Directives, and so on. Although the Design Engineer and Engineer of Record visit the site at a minimum once per week, during construction of critical structures (e.g. dams), the engineering field team are

empowered to approve preliminary design changes based on requests from the Owner or General Contractor. The field engineers involve the contractor's supervisors and owner's supervisors in field decision making by brainstorming the most practical solution prior to escalating to the Engineer of Record or Design Engineer, where necessary. This provides the opportunity for minor issues to be resolved on site, enabling the contractor to continue to focus on production and thereby reducing the potential for construction delays.

To set up field staff for success, efforts are made to build rapport and trust across teams prior to construction start up. Ultimately, construction field staff must be familiar with the key decisions and the design basis that supported the design development as well as risks that may be encountered in the field.

Fair and clearly stated procedures for incorporating alternative solutions into the design in response to emerging constraints and opportunities are vital to the implementation of a water management strategy that will meet the mine's needs now, and in the future, and also comply with standards. This requires championing by leadership to ensure that the design team adheres to these procedures and fairly considers practical solutions proposed by the contractor and field staff.

Team and relationship building meetings involving key construction team members have been organized to promote effective communication, motivate individuals, and enhance trust. Whether at these meetings or during day-to-day project execution, a critical component of assembling and maintaining a cohesive and adaptable team is the ability of project leadership to listen. This facilitates tapping into the team's collective knowledge and insight, which can be accomplished through establishment of clear and open lines of communication and engagement to make the team feel heard and to encourage collaboration on RFIs.

Conclusion

Project management processes, tools, and techniques are not innate or instinctive. Hence, the acquisition of project tools, practices, and support factors to facilitate effective teamwork required commitment from both Teck and Wood project leadership, as well as commitment at the employee-level.

The project framework developed for the execution of the Swift WMS project has proven effective in several ways:

- clear objectives have been developed;
- adequate resources have been assigned to the project;
- strong governance and commitment from both organizations' leadership teams are in place;
- a design philosophy was adopted that is flexible but sufficiently robust to garner permit approval and support from the construction team and third party reviewers;

- lines of communication, change approvals and process for issue escalation are understood and clear;
- the stakeholder engagement process is continuously being refined through adaptive management;
- value engineering, risk management processes, and lessons identification and learnings are been conducted as part of effective project improvements and documentation; and
- group troubleshooting was implemented to solve tough issues.

The organizational supports provided within the Teck and Wood engineering organizations are a contributing factor to the successful performance on this project. Knowing which management tools to apply and at what time has led to a significant positive improvement on project execution. Implementing these management tools has been critical to the success of the Swift WMS.

Acknowledgements

Teck Fording River Operations Swift Water Management Structures Project and Wood Design and Field teams express their profound appreciation to the support received from various individuals, parties, Teck and Wood managements through the execution of Swift WMS Project.

References

Dinu, Ana-Maria. 2012. Modern methods of risk identification in risk management. *International Journal of Academic Research in Economics and management Sciences 1(6).*

Project Management Institution. 2017. *A Guide to the Project Management Body of Knowledge*. Sixth edition.

Tuckman, Bruce W. 1965. Developmental sequence in small groups. *Psychological Bulletin* 63(6): 384–399.

Proceedings of Tailings and Mine Waste 2019
November 17–20, 2019, Vancouver, Canada
Published by the University of British Columbia, 2019

Approach and Considerations for Operation, Maintenance, and Surveillance Manual Development

Paul M. Bedell, Golder Associates Ltd, Canada

Abstract

This paper describes a recommended approach and key considerations for the development of an operation, maintenance, and surveillance (OMS) manual for tailings management facilities based on the guidelines of the Mining Association of Canada (MAC) and a case study. The OMS manual constitutes a foundational component for tailings management systems as recommended by recognized international best practice. Early development of an OMS manual ensures timely compliance during the operation, as well as more focused training and on-boarding for personnel. It also helps to align initial operations with the design intent of the tailings management facility.

Traditionally, a consultant who is usually the engineer of record, leads the development of the OMS manual. This is then handed over to the Owner for completion and use. This approach often leads to the Owner's personnel not internalizing and "owning" the document or making proper use of it. The new revision of the guideline for *Developing an Operation, Maintenance and Surveillance Manual for Tailings and Water Management Facilities*, published by MAC, advocates for Owner-led development; this approach was adopted as part of the operational readiness activities (MAC, 2019b). This paper discusses recommendations for an effective approach (such as using an earned value approach and Last Planner® system for the development planning) and key considerations to bear in mind based on the lessons learned through the development of the OMS manual. A practical overview of the development of the OMS manual will serve as the case study discussed in this paper.

Introduction

Catastrophic tailings facility failures occur as a result of, singularly or in combination with, misunderstanding technical issues, organizational culture weaknesses, and poor management practices. The series of major tailings facility failures over the past six years are no different from these three key issues still at the root of these undesirable events. Industry, public, and government views are aligned, in that catastrophic tailings facility failures are unacceptable and must be prevented. Therefore, a more holistic approach to tailings management is required; one in which technical issues, organizational culture, and

management practices are equally considered in the development of the tailings management system.

To fully embrace a holistic approach to tailings management, it is more important than ever that the correct implementation of responsible Ownership, the enforcement of best practices, use of the most appropriate technologies on a site specific basis, and a robust governance system that enables the Owner to ensure that the critical controls and surveillance are always in-place. The objective of a holistic approach is to prevent and avoid any unwanted event; namely, catastrophic failure (or any type of impactful failure for that matter). Voluntary compliance and self-regulation to satisfy the requirements of the Mining Association of Canada (MAC) is recognized by regulators and delivers confidence to the Owner on the governance and management standard of the facility. An operation that is aligned with the design intent, in combination with effective surveillance and maintenance programs, has the foundation to achieve the successful development of their tailings facility and its long-term sustainable management.

Keys to achieving the objective of a holistic approach include having an effective operation, maintenance, and surveillance (OMS) manual in-place (and used!) and an Owner´s team with a complete understanding of the OMS manual. These elements are critical in order to make good decisions in a timely manner. Best practice includes having the Owner's team fully responsible for leading the development of the OMS manual, rather than the classic, and often flawed, approach of "farm it out to a consultant". Owner team development of the OMS leads not only to a deeper knowledge of the facilities and the critical controls, but to better long-term effective use of the OMS manual. As Confucius said: "Tell me and I will forget; show me and I may remember; involve me and I will understand." The requirement to successful tailings management is to have knowledgeable, trained, and responsible personnel with appropriate levels of authority who understand the meaning within the OMS manual rather than having people who have memorized select aspects of the tailings management requirements. The latter case, unfortunately, is an all-too-often experienced reality that is reflected by a poor quality and under- to unused OMS manual.

Anecdotal experience of the author shows that in many instances the OMS manual is understood by select personnel to a certain degree, but not by the majority of those responsible for operating the tailings facility. The objective for all personnel involved in tailings management is to achieve a global understanding of the "why" behind the action and not only "doing the job". Parameters are not just numbers, critical controls are more than "things to be done and to have in-place"; each one has a meaning that needs to be understood, to the required level, by the personnel involved with the tailings management facility.

In this context, the Owner took the decision of an early development of the OMS manual for the tailings facility. The project is a large copper project in northern Chile that will start at approximately 140 ktpd in a facility with a dam that will be up to 310 m high at approximately year 25 of operation. This effort was led by the Owner´s Tailings Engineer, as part of the scope considered in the operational readiness activities. The early development preceded both full project sanction by several months and actual operation by

several years. The main objectives of this early effort are to raise awareness throughout the project development and early operations team by using the OMS manual for training purposes. The education of the importance of the tailings facility, through a focussed training and onboarding process for new personnel, generates a sense of ownership amongst the team, adopts early compliance with the international standards and best practices, and improves outcomes related to tailings planning, processes, and document traceability.

For the project, the desired deliverable is a best draft able to be produced with the current information, to be finished within a 16-month span, and to adjust according to time available and resources. This first draft would assist in refining the implementation of the design, identifying hiring requirements, instrumentation for dam surveillance, and give the Engineer of Record an ability to compare critical controls in the OMS manual with the design. Following the first revision, an update developed during Year 1 of operation will occur. An important target for this OMS manual is that it will be fully developed and assimilated and in-place before the start of operations.

Key considerations for the first draft development of the OMS manual are pre-operational activities, operational focus, and a scope the covers operation, risk, and change management using currently available information. A map concept was used in which information is summarized in the OMS manual and the information source is referenced.

The key reference documents used in the development included:

- Owner guidelines for tailings and water management;
- *A Guide to the Management of Tailings Facilities* (MAC, 2019a); and
- *Developing an Operation, Maintenance, and Surveillance Manual for Tailings and Water Management Facilities* (MAC, 2019b).

Methodology and tactics

The following process describes the approach for the development of the OMS manual: benchmarking of other Owner OMS manuals, review of the reference documents, defining the table of contents, and creating the structure of the sections of the OMS manual. Subsequently, in order to develop the work plan to prepare the OMS manual, each section was defined as a deliverable. A procedure was developed for section development management. This established all the guidelines for the process and included the development a preliminary responsible-accountable-supportive-consulted-informed (RASCI) matrix. A kick-off meeting with the group identified in the RASCI matrix, which included a presentation of the tailings facility and OMS manual concepts, was held. The expectations for each of the roles were discussed and agreed upon. The outcomes of these discussions were documented and distributed to the entire team identified on the

matrix. This development management approach defined roles with accountabilities that were developed in consultation with the team—fostering the Ownership of the OMS manual development.

For the OMS manual development schedule, major milestones were defined according to the proposed end date. Based on this, each section was prioritized according to a logical order of development. Review responsibilities, based on the RASCI matrix, and dates defined for every item was carried out to obtain agreement with each responsible party.

Implementation of the Last Planner® system to control the work plan formed the backbone of the OMS manual development system. The controls included defined key performance indicators (KPIs,) clear rules of progress, monthly plan look-ahead reports, which once confirmed by the support personnel, became the work plan for each week. This system was developed and put in-place before the start of the development of the OMS manual; it was also communicated to the team involved and enabled regular, clear, and action-oriented updates during the OMS manual development process.

Communication was by email and meetings as required and files were shared using the Owner's cloud system. An earned value system was developed and used to track "who had what section and action" and show progress. This process enabled traceability, allowing the status and activities tracking, as it kept record in writing of all comments and submittals, also ensuring the use of the most-current revisions of each available section.

Weekly reports were issued and distributed to the team and included progress for each deliverable milestone. Behind-schedule items required provision of a non-compliance reason and typically resulted in a schedule change. Non-compliance causes were assessed monthly in order to better understand the delays and to determine changes to the schedule or potential impacts to the development of the OMS manual (e.g., incomplete sections due to in-progress design components). Compilation and issue of the monthly reports occurred in the last week of the month. The Tailings Engineer controlled the program on a weekly basis. As an additional layer of control, the OMS manual program was uploaded weekly to the management system and was available to the entire operational readiness group. All changes to the schedule were transparent and reflected in the cumulative s-curve, where downward peaks in the forecasted progress would show when the schedule was modified. Reasons for modification were stated in the revision control notes of the document to track the changes performed in the document. This clear, concise, and rigorous system resulted in effective tracking and communication during the development of the OMS manual. Last Planner® use served to document the actual effort, schedule, and challenges to develop the OMS manual. This documentation will prove to be an invaluable reference for subsequent revisions to the OMS manual and the preparation of OMS manuals for other sites.

As information was received for the development of the OMS manual, metadata, such as the originator, revision, issue date, and reason for issue, was captured and confirmed. Once the Tailings

Engineer received the information, a quality assurance / quality control (QA/QC) review of the content was undertaken according to the requirements of the reference documents. If the quality of the information was acceptable, it was included in the OMS manual. Information that did not satisfy the QA/QC requirements resulted in a request for clarification. If clarification could not be provided according the development schedule, this information was noted for future updates and the associated section was issued noting that information was pending.

For the review process, sections developed were sent to a support group that provided the basic information as well as key personnel defined as stakeholders in the process. The support group comprised the corporate geotechnical manager, Plant Manager, TMF manager, and the Engineer of Record. Comments that were received were compiled and reviewed by the Tailings Engineer and incorporated in agreement with the TMF Manager. All review comments were documented and filed for record purposes.

A peer review process was used to execute a more comprehensive second review. This process was carried out when the OMS manual was completed in its first draft (to the extent of available information). This review involved personnel from the corporate office, other Owner mine sites, and external reviewers, as deemed necessary. After including these comments, the final draft was completed, and the OMS manual was ready for use. Training programs for personnel involved in the operation of the tailings facility will be developed based on the final draft of the OMS manual.

Results and discussion

Lessons Learned from OMS manual development

The following is a list of key lessons learned from the preparation of OMS manuals in general. The development of the OMS manual was managed to address, avoid, and improve upon many of the lessons.

- An Owner-led OMS manual development is a best practice. Input and involvement from the design engineers and the Engineer of Record are critical components to the development process. A common failure in OMS manuals, resulting in their non-use, occurs when Owners “farm out” their preparation by consultants as Owners, typically, do not fully complete and use the documents.
- It takes significant effort and attention to coordinate and produce a high-quality OMS manual. The under-budgeting of hours and underestimating of effort is a common mistake; make sure that adequate resourcing for Engineer of Record involvement is made. Allow enough time for reviews and delays, vacations, and other events. Earned value setup for progress rules, enabled the use of a predefined system to track, communicate, and document “who has what to do before the work may continue”.

- Having a clear procedure and defined roles and responsibilities goes a long way in smoothing the process. The importance of the communication of these to the team involved in the development of the OMS manual cannot be overstated.
- Including and getting all personnel to participate in the development of the OMS manual may be challenging, but involving the team early ensures proper alignment between the tailings facility and the other areas of the operation. Early involvement of the Engineer of Record during the OMS manual development is a recommended practice.
- The technical vocabulary may challenge the clear understanding of the message, especially to operators. It is recommended to engage a technical writer to improve style and to simplify the language making the OMS manual as easy to understand as possible.
- Understand the level of development of the draft. Accept there will be missing information that only exists once you start operation, and ensure these points are thoroughly detailed and documented for future updates. An OMS manual is a document that lives throughout the life of the tailings facility. The importance of having a fit-for-purpose OMS manual that is used, regularly reviewed, and updated (as required) cannot be over emphasized. Adoption of the "make it good now and better later" mindset is recommended – and OMS manual needs to be used to be improved.
- Drafts will evolve during the process. Proper documentation of updates and new/revised information must be stated in subsequent revisions.
- Make the most out of the design engineer's information. There is a lot of value in these documents; distilling the key components into the OMS manual, with complete references to the source information, is a recommended practice.
- Keeping track of the lessons learned during the development process, as well as documenting the development process, adds value to the company. Subsequent revisions to the OMS manual, as well as other OMS manuals to be developed at other sites, will do well to reference these lessons learned.
- Site visits are practical way of cross-referencing information and making the most out of experiences at other sites. Collaboration with other sites is very important to see the big picture and to give the OMS manual clarity and the appropriate context.
- Document control is an important system to have in place before the start of OMS manual development. Maintaining clear traceability of the information used in the process is imperative for future reference and subsequent updates.
- An action tracker to register agreements and pending items is a very useful tool, especially for meetings. Sharing these actions with the team is a good practice to keep all parties informed.

Key risks within OMS manual development

The key risks to be managed during the development of an OMS manual include:

- Not having sufficient detail on any of the "O", "M", or "S" areas. A common issue is to not provide sufficient detail in the maintenance (M) section.
- Inadequate quantity and quality of the information. Missing information that is crucial in order to control the operation in its early stages.
- Lack of experience of the team when it comes to the OMS manual development may produce a lesser quality document.
- Underestimating effort and resources.

Next steps in OMS manual development

As the OMS manual is completed and implemented, a key step will be to have the document accessible in digital format with user-friendly visual interfaces for monitoring, maintenance, and the like, via a mobile application. This digital format will provide a readily updatable format that will facilitate revisions to be made effectively.

Conclusion

The early development of an OMS manual is part of a well-planned and well-managed operation. Attention to detail, due diligence in the proper development of not only instructions and descriptions, but also potential issues, planned solutions and, contingency plans, constitute a solid basis for a successful start of the operational activities and a sustainable management through the life cycle of the facility. Involving multidisciplinary project and corporate teams ensures consistency in risk management and operations. Alignment with the Owner's corporate governance is critical to the successful operation of a tailings facility.

Ensuring a correct understanding and knowledge of the OMS manual at all levels of the organization is vital for a proper tailings management culture that thrives on Ownership, responsible tailings management, and continuous improvement in the pursuit of excellence. Key to achieving this is developing a training program based on the OMS manual for all personnel involved in the management of the tailings facility.

The development of the OMS manual constitutes the first key step towards the setup of a robust tailings management system. The Owner's internal requirement for the classification of tailings facilities is a to achieve a "Level AAA" rating according to the MAC's *Towards Sustainable Mining* program. The objective of this is that we, as professionals, need to commit to comply not only with the Owner's health, safety, and environmental compliance standards and applicable regulations, but also with the industry in

order to pursue excellence in all aspects of tailings management, so as to avoid unwanted events that endanger the environment, communities, facilities, and employees.

Acknowledgements

The author wishes to thank Ivette De Jesús for her collaboration in the development of the OMS manual and this paper.

References

Mining Association of Canada (MAC) 2019a. *A Guide to the Management of Tailings Facilities,* Version 3.1, Canada.

Mining Association of Canada (MAC). 2019b. *Developing an Operation, Maintenance and Surveillance Manual for Tailings and Water Management Facilities,* Second Edition, Canada.

Bibliography

Barrera, S. and H. Quelopana. 2017. Lessons learned about failures of Mount Polley and the Fundão tailings storage facilities. Tailings 2017, 4th International Seminar on Tailings Management, Gecamin, Chile: 1–11.

Proceedings of Tailings and Mine Waste 2019
November 17–20, 2019, Vancouver, Canada
Published by the University of British Columbia, 2019

The Benefits of a Quantitative Risk Assessment Approach to Assess the Risk of Catastrophic TSF Failure

Peter J. Chapman, Golder Associates Pty Ltd, Australia
David A. Williams, Golder Associates Pty Ltd, Australia

Abstract

Management of risk is a key aspect of tailings storage facility (TSF) design and stewardship. Recent catastrophic failures continue to highlight the need for identification of all potential contributory factors associated with TSF design and operation that could lead to failure. Unfortunately, this also highlights the inadequacy, in the view of the authors, of typical risk approaches to adequately characterize infrequent (very low likelihood), high consequence events such as the failure of a TSF. As described in the reports on the failures of the Mount Polley (Canada) and Fundão (Brazil) TSFs, loss of containment of tailings was not the result of a single cause, but rather a sequence of events that culminated in failure – that is, a systematic failure. In the authors' view, this has been the case for the majority of (if not all) TSF failures that have occurred.

A quantitative risk assessment (QRA), using the fault tree analysis technique to map both simple and complex interactions between contributory causes of failure can be applied to TSF design and/or operation. An integrated approach with the TSF owner and other stakeholders in selecting values used in the calculation of likelihood – a "team-based" approach – is essential, and is considered by the authors to be much more effective than typical qualitative approaches to identify, agree on, and mitigate risks.

A review of the risk tools that are typically adopted by mining companies is presented, along with a case study that adopted the QRA approach. The benefits of the QRA approach to identify the key contributors to the probability of catastrophic failure of a TSF, and candidate measures to mitigate the risks, are outlined. Adopting the QRA approach is a step that can be taken to move towards the industry goal of "zero catastrophic failures".

Introduction

The poor track record of the mining industry in relation to management of tailings storage facilities (TSFs) has recently been highlighted by a series of recent failures across the Americas. These are, however, only a few of the TSF failures that have occurred over the past 100 years or so. These recent tragedies have

highlighted the risk that TSFs pose, and they also demonstrate that conventional approaches to managing risk may not be applicable to effectively capture the causes and effects of high consequence, (relatively) infrequent/very low likelihood events. Risk has various meanings, but it is commonly accepted as being the combination of the likelihood of a negative event occurring and the consequence of the event. A normal risk assessment process would identify potential negative consequences, and then assign likelihoods of events occurring that would result in these consequences. Where risks are considered unacceptable, mitigation measures are put in place, either to reduce the likelihood or the consequence.

With respect to TSF failure (the event) resulting in loss of life or significant environmental damage (the consequence), there are few mitigation measures that can be put in place to reduce the consequences, and hence most risk mitigation measures seek to reduce the likelihood of "causes" that could result in the event. For infrequent events, therein lies the issue – many of these events are already rated as "unlikely" or "rare" under a typical qualitative matrix style risk assessment, and hence are already seen to be appropriately "managed". A case for using a more robust risk assessment process, adopting a quantitative risk assessment (QRA) is presented in this paper, along with commentary on other risk tools that the authors have observed in the industry.

It is also worthy of note that the recent catastrophic failures of TSFs have resulted in a significantly greater attention to tailings management on the world stage. Many industry and investment groups are posing more questions of mining companies and, in the authors' opinions, this is the beginning of the journey to zero catastrophic failures. The acceptance of even one catastrophic failure per decade, let alone the average of about two per annum in recent times, is unlikely. There will thus be an increasing focus on risk reduction over the coming decades, until a safety record is achieved that is socially acceptable, perhaps one similar to water retention dams, which are 100 times less likely to fail than TSFs (ICOLD, 2001). In our view, "zero catastrophic failures" is undoubtably going to be the target of the next decade.

Types of risk assessments

Overview

There is a variety of risk tools available across multiple industries, and the type of risk tool selected can dictate the level of confidence in the assessment, the types of risks that are identified and the mitigation measures that are proposed to address the risks. Many large mining companies have very sophisticated internal risk processes that are used to help manage the business, both from a financial and a safety perspective.

A few of the more common risk tools are discussed below, along with commentary on their applicability to assessing the risk of TSF failure resulting in loss of life or significant environmental damage

(the main consequence usually considered). In order to illustrate the various risk tools, two scenarios are considered, as follows:

1. An upstream-raised TSF containing highly brittle, contractive tailings, 40 m in height on a competent foundation, with a high phreatic surface.
2. An integrated waste landform (IWL), where the TSF containing highly brittle, contractive tailings, 40 m in height on a competent foundation, with a high phreatic surface, is contained by 30 m of waste rock for the full perimeter.

Both example facilities are located upstream of a permanent population presence, where the population at risk is greater than 10, and hence the consequences of a potential failure would be deemed "catastrophic". With these consequences in mind, under most (if not all) guidelines globally these two example TSFs would be assigned one of the highest consequence categories, requiring similar amounts of rigour in the design process despite the clearly different likelihoods of failure they pose due to their different construction techniques.

Risk assessment matrix

The risk assessment matrix is the most common tool adopted. It is widely used across many industries due to its simplicity. Most have a five-point scale for consequence on one axis, and a five-point scale for likelihood on the other axis, although some have as few as three and as many as seven. An example of a typical risk assessment matrix is shown in Figure 1.

		Consequence				
		Insignificant	Minor	Moderate	Major	Severe
Likelihood	Almost certain	Medium	High	High	Extreme	Extreme
	Likely	Medium	Medium	High	Extreme	Extreme
	Possible	Low	Medium	Medium	High	Extreme
	Unlikely	Low	Low	Medium	High	High
	Rare	Low	Low	Low	Medium	High

Figure 1: Risk rating calculation (University of Melbourne, 2019)

An example of values that would typically be assigned for each scenario outlined above, with reference to the example matrix included in Figure 1, is as follows:

- Scenario 1 – Upstream-raised TSF. Likelihood – Possible. Consequence – Severe. Risk = Extreme.
- Scenario 2 – IWL. Likelihood – Rare. Consequence – Severe. Risk = High.

As can be seen, if an event is categorized as "Severe", it will be considered as "Extreme" or "High" risk regardless of the likelihood. This means that mitigation measures that address likelihood will not allow the risk to be downgraded below "High", and there is a tendency to focus on the consequences. Whilst this has merit, as reducing the potential impacts to people or the environment is required on the journey to zero catastrophic failures, there are cases where the likelihood of failure of a TSF is so low, such as for an IWL (scenario 2), that it cannot even be calculated. Under this scenario, the IWL would still be "high risk" even though failure is considered implausible. Indeed, the extremely robust design of the IWL is not able to be demonstrated through the risk assessment matrix, potentially mis-leading people in to thinking that this approach to tailings management is just as "risky" as downstream construction (which would plot about the same), and only one level below upstream construction; an unjust comparison.

Bow-tie approach

As the name suggests, this approach has two clearly differentiated areas (the sides of a bow tie) with the risk event in the centre. On the left-hand side, the causes of failure are listed, with proactive mitigation measures identified that could address these causes. On the right-hand side, the consequences of failure are listed, with reactive mitigation measures identified. The reactive mitigation measures are items that seek to minimize these consequences after event occurs – e.g., protection bunds. The efficacy of each of these measures is assessed in a similar fashion to the risk assessment matrix outlined above.

The bow tie approach improves on the risk assessment matrix approach by providing visual clarity on what mitigation measures can be put in place to manage likelihood and consequences, and by outlining the critical risks to reduce the probability of specific events (e.g., fatalities), but the same commentary as noted for the risk assessment matrix approach still applies.

Failure mode and effects analysis (FMEA)

The FMEA approach is consistent with the Australian/New Zealand Standard on risk analysis of technological systems (AS/NZS 3931:1998). The FMEA technique can be adopted as a "screening" process to assess whether there is a need to carry out more rigorous analyses. It is more detailed than the risk assessment matrix approach, but values are still assigned qualitatively. It relies upon the subjective identification and assessment of potential failure mechanisms that could result in a catastrophic failure of the TSF. Some examples of potential failure mechanisms (however unlikely they may be) are as follows:

1. overtopping of a perimeter wall;
2. slope failure of an external embankment (under static loading conditions);
3. slope failure of an external embankment (under seismic loading conditions);
4. embankment erosion due to tailings delivery or return water pipeline breakage;

5. piping erosion failure through an external embankment;
6. progressive sloughing due to seepage; and
7. foundation failure.

The likelihood of occurrence of each event and the potential for the event to result in a catastrophic failure is typically estimated on a scale of 1 to 5 (low = 1, high = 5), similar to the risk assessment method. The risks of failure for each case is then computed as the product of these two assigned values, to provide an indication of which risks require further attention in the design. Examples of the FMEA approach for Scenarios 1 and 2 are shown in Tables 1 and 2, respectively.

Table 1: Example of FMEA – Scenario 1

Failure mechanism	Likelihood rating	Justification	Potential for catastrophic failure rating	Justification	Product
Uncontrolled overtopping of the external embankment	1	Significant capacity in basin for storm events	4	If overtopping occurs the likelihood of a flow failure is moderate to high due to the slopes being erodible	4
Slope failure of the external embankment (static conditions)	3	Moderate chance if there is a high phreatic surface and contractive materials	5	If slope instability were to occur, a flow failure is inevitable	15
Slope failure of the external embankment (seismic conditions)	2	Less likely to occur than under static conditions as a significant earthquake would be required	5	If slope instability were to occur, a flow failure is inevitable	10
Erosion of the embankment due to pipeline breakage	2	Pipeline failure possible but lines will be inspected on a frequent basis	2	Frequent inspections will limit duration of potential pipe failure	4
Progressive sloughing of embankment	2	Inspected on a frequent basis	2	Progressive sloughing unlikely to result in large scale failure due to 3(H):1(V) slopes	4
Piping erosion failure through the external embankment	2	Materials compacted and upstream toe drain in place	3	Localized piping erosion could result in large scale failure	6
Foundation failure	1	Competent foundation	4	Foundation movement, if it occurs, could result in large scale failure	4

Table 2: Example of FMEA– Scenario 2

Failure mechanism	Likelihood of occurrence rating	Justification	Potential to result in a catastrophic failure – rating	Justification	Product
Uncontrolled overtopping of the external embankment	1	Significant capacity in basin for storm events	1	If overtopping occurs the likelihood of a flow failure is very low due to the presence of waste rock	1
Slope failure of the external embankment (static conditions)	1	Very low due to presence of waste rock	1	Very unlikely given the thickness of the rock around the IWL	1
Slope failure of the external embankment (seismic conditions)	1	Very low due to presence of waste rock	1	Very unlikely given the thickness of the rock around the IWL	1
Erosion of the embankment due to pipeline breakage	2	Pipeline failure possible but lines will be inspected on a frequent basis	1	Waste rock will resist erosion	2
Progressive sloughing of embankment	1	Waste rock will be resistant to sloughing	1	Very unlikely given the thickness of the rock around the IWL	1
Piping erosion failure through the external embankment	2	Materials compacted and upstream toe drain in place	2	Waste rock would provide mitigation against piping and retain bulk of solids	4
Foundation failure	1	Competent foundation	1	Very unlikely given the thickness of the rock around the IWL	1

From Tables 1 to 2 above, it is evident that:

- The average score for Scenario 1 is above 6, with a maximum of 15.
- The average score for Scenario 2 is below 2, with a maximum of 4.

Based on these examples, while Scenario 2 (IWL) had a similar "risk" under the risk assessment matrix approach, the IWL is clearly of much lower overall risk when the FMEA approach is applied. The FMEA approach also demonstrates where some failure modes have been more clearly addressed, evidenced by the lower maximum score for the IWL and the prevalence of numerous scores of "1" that show that both the likelihood and potential to result in a flow failure have been addressed. The FMEA tool therefore provides a more robust approach to considering risk than the risk assessment matrix approach, but it still based on subjective scores being applied.

Failure mode, effects and criticality analysis (FMECA)

A variant of the typical FMEA approach is the FMECA, in which the criticality of the component/structure/facility being addressed is considered. This approach considers the timeframe under which the failure could occur, assuming no intervention, and hence can provide useful information on prioritization of resources, triggers and the regularity of inspections and other mitigation measures. For example, erosion of the outer slope of an upstream-raised TSF would occur much faster than erosion of the waste rock in an IWL, suggesting that more frequent inspections would be needed.

The approach includes an "engineering assessment," which involves reviewing all available design information, then identifying plausible damage mechanisms to the structure (consistent with the FMEA), the associated failure modes, consequence of failure, and required controls to prevent failure.

For the scenarios being considered, the frequency of inspections would be significantly less for the IWL (Scenario 2), and more for the upstream-raised TSF (Scenario 1), whereas the inspections based on a consequence category alone would be identical, due to the potential downstream impacts.

Quantitative risk assessment (QRA)

A quantitative risk assessment (QRA) draws upon the technique of fault/event analysis to systematically combine potential faults that could result in TSF failure, and to evaluate the possible consequences of such failure. This structured approach allows for modelling of the effects of physical events on the system (e.g., extreme rainfall, earthquakes), as well as allowing for incorporation of human interactions. It also allows for inclusion of uncertainties in design assumptions, or the expected outcomes of operating a TSF.

The method involves the identification of system faults that could potentially result in a "dam break" of the TSF and the subsequent catastrophic release of liquefied tailings and/or water to the downstream environment. The consideration of two or more failure events that individually and independently may have limited consequence, but in combination may result in a dam break is particularly relevant. A fault tree is developed to represent the potential combinations of plausible causes of such a failure, and an exposure assessment is undertaken to determine the population at risk (PAR) associated with a flow failure. This technique is consistent with the Australian/New Zealand standard 3931:1998 and ANCOLD's risk assessment guidelines (ANCOLD, 2003).

In reference to the scenarios outlined above, the QRA approach would be able to quantify the difference in likelihood of loss of life resulting from a catastrophic release of liquefied tailings and/or water between an IWL (Scenario 2) and an upstream-raised TSF (Scenario 1). If a QRA approach is adopted at the outset, it can also be used as a decision-making tool during design phases and as a risk mitigation tool during operations.

The QRA approach is discussed in more detail in the following sections.

Background and approach to QRAs

A QRA draws upon the fault tree analysis (FTA) approach, which was developed in 1962. Wikipedia describes FTA as a "top-down, deductive failure analysis in which an undesired state of a system is analyzed using Boolean logic to combine a series of lower-level events. This analysis method is mainly used in the fields of safety engineering and reliability engineering to understand how systems can fail, to identify the best ways to reduce risk" (Wikipedia, 2019). The approach has been used across a variety of industries to provide a greater understanding of why items/systems that rely on multiple inputs can fail, and hence how they can be improved (e.g., Yuan et al., 2018; Marchell, 2018; and many others).

A summary of the approach to undertake a QRA is described below (after Williams, 1998):

1. An intimate understanding of the TSF is required, gained through involvement/review of design studies, site inspections, dam safety reviews and other information relevant to the TSF.
2. Hazards (e.g., seepage, high precipitation, earthquakes) and mechanisms that could potentially result in catastrophic failure of the TSFs (release of tailings and/or water) are identified.
3. The "causes" (failure mechanisms, such as slope failure) of the potential release of material from the TSF are then derived from the identified hazards and an understanding of the operation and past behaviour is included, as well as other similar examples elsewhere.
4. The causes are logically combined through inter-linked "AND" gates and "OR" gates, which are used if the causes are statistically dependent or independent of each other, respectively. The causes are progressively subdivided into their contributory components through subsidiary AND gates and OR gates, until it is possible to assign a probability to an individual component cause with reasonable confidence.
5. Probabilities are assigned to the appropriate causes to yield a "fault tree". The probability of occurrence of the "top fault" is calculated by the fault tree according to the following formulae:
    a. for OR gates: $P_t = 1 - (1 - P_1) \times (1 - P_2) \times ..... \times (1 - P_n)$.
    b. for AND gates: $P_t = P_1 \times P_2 \times ..... \times P_n$.

    Where P_1, P_2 etc. are contributory components to P_t.
6. The potential consequences of a flow failure from the TSF have been identified and the probability of the "top consequence" (in this study – loss of life or serious injury due to a flow failure of the TSF) is estimated through "event analyses".

Probabilities are assigned to the appropriate faults in the fault tree through judgement, experience, data interpretation, modelling, analyses, and comparison with published literature. Where calculations or

model runs cannot be used, probabilities are assigned using the mapping provided in Table 3 as a guide, which has been adapted from a number of references (ANCOLD, 1998; Cole, 1993; Wellington, 1997).

Table 3: Mapping of assigned probabilities

Likelihood	Probability
Almost impossible/implausible (no published information on a similar case)	1 × 10-6 (1 in 1 million) to 1 × 10-7 (1 in 10 million)
Highly improbable (published information exists, but in a slightly different context)	1 × 10-5 (1 in 100,000)
Very unlikely (it has happened elsewhere)	1 × 10-4 (1 in 10,000)
Unlikely (recorded recently elsewhere)	1 × 10-3 (1 in 1,000)
Possible (could have occurred already without intervention)	1 × 10-2 (1 in 100)
Highly probable (a previous incident of a similar nature has occurred)	0.1 (1 in 10)
Nearly certain (one or more incidents of a similar nature have occurred recently)	0.2 to 0.9 (1 in 5 and greater)
Certain (or as near to, as makes no significant difference)	1 (or 0.999)

To reduce the potential for inaccuracy arising from the subjective opinion of an individual, the technique of "Expert Engineering Judgement" (ANCOLD, 2003) can be adopted, in which a group of knowledgeable persons discusses and assesses the likelihood of occurrence of an event. Each then individual assigns a probability to its expected occurrence. The (rounded) logarithmic average of the individually assigned probabilities is used in the fault tree.

After assignment of probabilities based on calculations, models or through "Expert Engineering Judgement", the probability of catastrophic release can be calculated. A typical outcome of a QRA is presented in Figure 2, representing Scenario 1 (upstream-raised TSF). The QRA shows that the probability of catastrophic release is 5.26×10^{-5}, and that slope failure is the biggest contributor to the potential release.

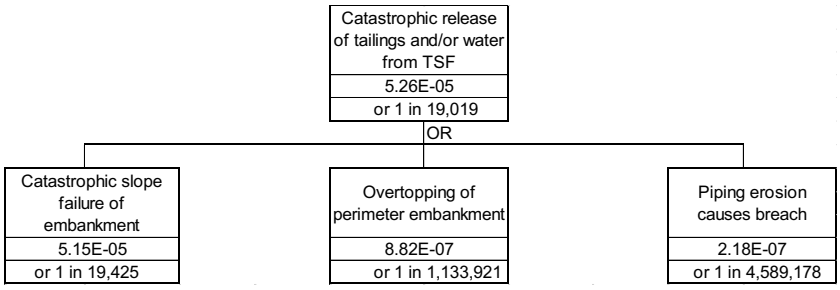

Figure 2: Example outcome of QRA – Scenario 1

If the same approach is taken for Scenario 2, adjusting slope failure only for the purposes of this paper (noting of course that the other failure modes would also have a lower probability of occurrence), the results would be 1.00×10^{-7} for Scenario 2 (two and a half orders of magnitude lower probability of catastrophic release), as shown in Figure 3. This is achieved in the QRA by reducing the probability of the factor of

safety (FoS) being less than unity under static and seismic conditions for each scenario, recognizing the lower probability of failure for an IWL.

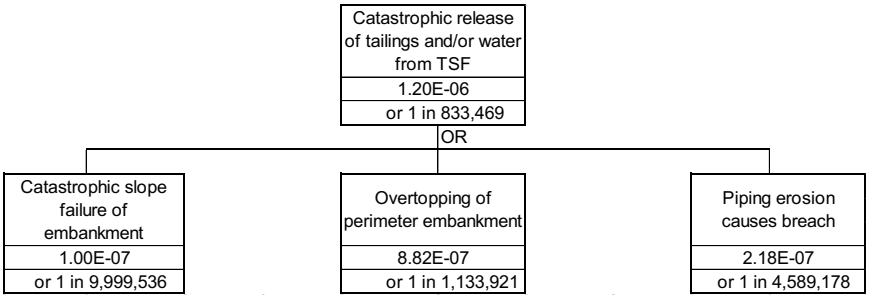

Figure 3: Example outcome of QRA – Scenario 2

The QRA results presented in Figures 2 and 3 indicate that, with reference to Table 3, the probability of catastrophic slope failure of the embankment reduces from "unlikely" for Scenario 1 to "almost impossible" for Scenario 2. Moreover, for Scenario 2, the probability is barely credible, providing confidence that this failure mechanism has all but been eliminated.

Using the QRA to mitigate risks

In the interests of moving to "almost impossible", or "implausible", the QRA can be interrogated to identify the key items that contribute to catastrophic release or directly link to fatalities (i.e., critical risks) and put in mitigation measures that specifically address these items, resulting in a quantifiable reduction in risk. When the QRA for Scenario 1 is interrogated, the top contributors to catastrophic failure are:

- FoS ≤1 under post-seismic conditions,
- FoS ≤1 under undrained conditions, and
- Undrained conditions prevail, which in turn has the following contributors:
    - Sufficient loose, saturated tailings through the presence of contractive tailings and sufficient zone(s) of saturation

This indicates to the designer that focussing on managing the phreatic surface, or implementing slope improvement measures, are needed to reduce the probability of catastrophic release. In a similar fashion, if overtopping were to be the biggest contributor, the QRA could be used to identify if the largest contributor is related to items such as poor pond management, inadequate freeboard management, construction activities, pipe bursts resulting in erosion, etc.

Summary

A summary of the advantages of each risk tool, and reasons for their selection, is presented in Table 4.

Table 4: Summary of risk tools

Risk tools	Advantages	Disadvantages	Possible reasons for use
Risk Assessment Matrix	Easy to use, intuitive Generally accepted (despite limitations – see disadvantages) Improved when more categories are in place (i.e., 7 rather than 5)	Qualitative only - poor characterization of high consequence, infrequent events (can never be less than high) and does not address systematic failure Does not provide clear framework for documenting detailed causes for risks Mitigation measures can focus on moving between levels and reducing category of risk rather than addressing the risk as far as practicable	Generally well accepted and understood, good for screening, quick to use and update Improved when more categories are in place (i.e., 7 rather than 4 or 5)
Bow Tie	Provides a clear distinction between proactive and reactive measures Relatively quick to develop	Qualitative only – does not address systematic failure Provides equal weighting on both proactive and reactive measures	Provides a clear distinction between proactive and reactive measures, so is favored when considering mitigation measures to reduce both aspects
FMEA	Provides clear framework for documenting detailed causes for risks Links failure modes to effects	Qualitative only More time consuming to develop – requires a detailed understanding of the structure and the possible failure mechanisms	Adopted when more detailed understanding of failure modes is required, allowing specific mitigation measures to be developed
FMECA	As for FMEA, but provides a framework to identify critical components Can be used to develop inspection timeframes, linked to failure of components	Qualitative only More time consuming to develop – requires a detailed understanding of the structure and the possible failure mechanisms	Adopted when more detailed understanding of timeframe of failure of components is required, allowing development of specific mitigation measures and inspection plans
QRA	Quantifies risk of catastrophic failure Provides a detailed approach and considers systematic failure Can be used to identify largest contributors to risk	Time consuming to develop Requires experience with FTA Requires a detailed understanding of the components of the structure and the possible failure mechanisms	Provides the most robust approach to risk identification, and can be used to develop specific mitigation measures The change in risk profile can be quantified allowing effective, defensible trade-off decisions to be made for mitigation measures

Conclusion

Many mining companies adopt the risk assessment matrix approach to catalogue risks associated with the failure of TSFs. However, this approach is considered to be too coarse to provide effective mitigation measures. If an event is categorized as "Severe", it will be considered as "Extreme" or "High" risk regardless of the likelihood. This means that mitigation measures that address likelihood will not allow the risk to be downgraded below "High", and there is then a tendency to focus on the consequences as the likelihood cannot be any lower, rather than focussing on credible failure mechanisms. Even the use of the FMEA method is considered to be inappropriate for very low likelihood, very high consequence risk analyses, such as evaluation of catastrophic failure of TSFs. In contrast, the use of a QRA can demonstrate not only that the likelihood of catastrophic failure is lower (and how low), but also provides the designer

with information on the largest contributions to failure, allowing effective mitigation measures to be put in place. If a QRA approach is adopted at the outset, it can also be used as a decision-making tool during design phases, and as a risk mitigation tool during operations.

In our view, the QRA approach provides the most robust approach to risk identification. It can be used to develop specific mitigation measures, and the change in risk profile can be quantified for each measure, allowing effective, defensible trade-off decisions to be made. Adopting the QRA approach is an effective step to move towards the industry goal of "zero catastrophic failures", particularly when the process includes input from a group of knowledgeable persons, including independent parties.

References

ANCOLD. 1998. *Guidelines for Design of Dams for Earthquake*.

ANCOLD. 2003. *Guidelines on Risk Assessment.*

Australian/New Zealand Standard, 1998. *Risk Analysis of Technological Systems – Application Guide,* published by Standards Australia and Standards New Zealand, 3931.

Cole, K. 1993. Considerations of risk and reliability, *Ground Engineering*: 14–30.

ICOLD. 2001. Tailings dams – Risk of dangerous occurrences, lessons learnt from practical experiences, Bulletin 121.

University of Melbourne. 2019. Incident reporting risk matrix, access date 5 July 2019, https://safety.unimelb.edu.au/incident-reporting/incident-reporting-risk-matrix

Wellington, N. 1997. *The Risk Assessment Process – Assignment of Probabilities*, Perth: Australian Centre for Geomechanics.

Wikipedia. 2019. Fault tree analysis, Wikipedia, access date 19 July 2019 https://en.wikipedia.org/wiki/Fault_tree_analysis

Williams, D.A. 1998. A suggested approach to conducting dam break studies of tailings storage facilities. In *Proceedings of AIC Tailings Disposal Management Summit,* 24 – 25 November, 1998, Brisbane, Australia. AIC Conferences.

Yuan, Changfeng, Hui Cui, Bin Tao and Siming Ma. 2018. Cause factors in emergency process of fire accident for oil–gas storage and transportation based on fault tree analysis and modified Bayesian network model, *Energy & Environment* 29(5): 802–821.

Bibliography

Marchello, Sara. 2018. Asbestos hazards analysis in construction projects with the fault tree analysis and the failure mode and effect analysis, *New Frontiers of Construction Management Workshop* 116–127: 2036–1602.

Proceedings of Tailings and Mine Waste 2019
November 17–20, 2019, Vancouver, Canada
Published by the University of British Columbia, 2019

Expanding Tailings Stewardship to Include Towards Sustainable Mining Verification

Melanie Davis, Stantec Consulting Services Inc., USA
Jason Cumbers, Stantec Consulting Services Inc., USA

Abstract

Tailings stewardship programs are increasingly common among major producers throughout the world. These programs serve as a third-party review to provide outside observation, recommendations, and unique insights to improving tailings management and reducing risks. The Mining Association of Canada (MAC) introduced its *Towards Sustainable Mining* (TSM) program in 2004 with the goals of stewardship, social license, encouraging excellence, and continuous improvement. One of the eight TSM protocols is Tailings Management. Operators can improve their tailings management practices while simultaneously accounting for the tailings management protocols and guidelines with the TSM framework. The aspects of a well-designed tailings stewardship program provide a framework for risk reduction and ongoing improvement, and by combining this process with a TSM review, operators can be recognized under the MAC framework for improving their tailings practices.

This paper provides a background on beneficial outcomes of tailings stewardship programs, explains how the TSM Tailings Management protocol can be evaluated by a tailings stewardship team, and discusses why tailings management practices can improve by incorporating TSM verification.

Introduction

Recent significant tailings failures emphasize the continued high risks associated with tailings management. Mining companies are receiving pressure from affected stakeholders to improve practices that reduce the number and severity of failures. Many mining companies have enacted tailings stewardship or tailings governance programs that promote responsible tailings management from design to closure. These programs are part of a multi-layered system of review that fosters safe and functional tailings operations.

The Mining Association of Canada (MAC) established the *Towards Sustainable Mining* (TSM) initiative in 2004 with the main objective of enabling mining companies to meet society's needs for miners, metals and energy products in the most socially, economically and environmentally responsible way (MAC, 2017a). This initiative was adopted by the Canadian mining industry and is becoming a globally recognized

sustainable mining standard. Focus areas include environmental stewardship, communities and people, and energy efficiency. Tailings management is a protocol assessed under environmental stewardship. Incorporating TSM review for tailings management into tailings stewardship promotes increased accountability and transparency for tailings management that encourages continued improvement.

This paper discusses aspects of a tailings stewardship program, presents an overview of the TSM program with emphasis on the Tailings Management Protocol assessment, and proposes benefits associated with adopting TSM into tailings stewardship.

Tailings stewardship

Tailings stewardship is responsible tailings management that promotes design, construction, operation, maintenance, monitoring, and closure of tailings facilities that minimizes risks to operators and stakeholders. Tailings stewardship programs typically include owner management oversight at the corporate and site level, and engagement of a third party individual or team that visits a site and provides a technical review of the current tailings facility and management conditions. The third-party stewardship team usually works with the site engineer of record (EOR), if one is assigned to the site, and the owner to provide recommendations for continued improvement. The team is often tasked with reviewing recent design documentation or technical reports prior to visiting the site. The team then conducts a site inspection, usually less comprehensive than an EOR's annual dam safety inspection. The stewardship team will often meet with the tailings and operations staff to gather information on current conditions and concerns. The team may also be tasked with performing a more comprehensive dam safety review of the facility.

The primary focus of tailings stewardship is risk reduction. Comprehensive risk assessment is used to identify as many tailings risks as possible, including environmental, regulatory, construction or design risks. The program includes developing plans to mitigate risks and their impacts.

Tailings stewardship compliments other activities that support responsible tailings management including EOR reviews and inspections, construction inspections, owner operation, maintenance, and surveillance processes, and dam safety inspections and reviews. For higher risk sites, an independent technical review board may be assigned.

MAC TSM initiative

The TSM initiative is MAC's commitment to promote responsible mining. Canadian MAC members are required to participate in TSM; several companies also apply TSM to their international operations. Some countries have voluntarily adopted the program, including Argentina, Botswana, Finland, the Philippines, and Spain. Adopting TSM allows operators to pledge in writing to apply sustainable practices and make continuous improvements in their operations.

TSM verification

Obtaining TSM verification comprises an internal assessment, an external third-party review, and a communities-of-interest (COI) review followed by a public report on the findings. The program's elements as outlined from MAC (2018b) are:

- Performance driven – A requirement to demonstrate measurable continual sustainability improvement.
- Accountability – Assessments are conducted at the facility level where mining activity takes place.
- Transparency – Annual reporting against 29 indicators with independent verification every three years.
- Credibility – Ongoing consultation with a national Community of Interest (COI) Advisory panel to improve industry performance and shape TSM for continual advancement. The COI Advisory Panel includes members from multi-interest groups, in addition to the MAC Board of Directors.

The TSM focus areas and protocols are below. The number of performance indicators required for evaluation are shown in parentheses for each protocol.

- Environmental stewardship
    - Tailings management (5)
    - Biodiversity conservation management (3)
    - Water stewardship (4)
- Communities and People
    - Aboriginal and community outreach (4)
    - Safety and health management (5)
    - Crisis management and communications planning (3)
    - Preventing child and forced labour (2)
- Energy efficiency
    - Energy use and greenhouse gas emissions (3)

Performance is rated on the five-level scale below (MAC, 2018b). Performance requirements increase from C to AAA. Level A to AAA are considered good to best practice, respectively, by MAC (2018b).

- AAA – Excellence and leadership
- AA – Integration into management decisions and business functions
- A – Systems/processes are developed and implemented

- B – Procedures exist, but are not fully consistent or documented; systems/processes planned and being developed
- C – No systems in place; activities tend to be reactive; procedures may exist, but they are not integrated into policies and management systems

Tailings Management Protocol

The Tailings Management Protocol provides guidance on assessing TSM performance indicators for tailings management. The protocol refers to and is supported by a Table of Conformance, A Guide to the Management of Tailings Facilities (the Tailings Guide), and Developing an Operation, Maintenance and Surveillance Manual for Tailings and Water Management Facilities (the OMS Guide). The documents associated with the TSM Tailings Management Protocol were updated in two stages as listed below.

- 2017
    - Tailings Management Protocol revised (MAC, 2017b)
    - The Tailings Guide, Third Edition (MAC, 2017a)
    - Table of Conformance introduced, replacing the 2011 Guide to Audit and Assessment of Tailings Facility Management (2017c)
- 2019
    - Tailings Management Protocol revised (MAC, 2019c)
    - The Tailings Guide, Version 3.1 (2019a)
    - The OMS Guide, Second Edition (2019b)
    - Table of Conformance revised (2019e)

For MAC members applying TSM, there is a transition period for implementation of the 2017 and 2019 versions of the Tailings Management Protocol as shown in Table 1.

Moving forward, 2019 TSM guidance will be required for internal and external reporting. The tailings management system criteria for the 2019 Table of Conformance adds quality management criteria. For 2019, a quality management plan or process is to be developed and implemented, including separate quality assurance and quality control plans or processes. The quality management plan must address construction, operation, maintenance, and surveillance practices throughout the facility life cycle.

Table 1: TSM Tailings Management Protocol reporting requirements (after MAC, 2019d)

Document to be used for reporting		2019 Reporting of 2018 performance		2020 Reporting of 2019 performance		2021 Reporting of 2020 performance	
		Internal reporting	External reporting	Internal reporting	External reporting	Internal reporting	External reporting
2011	Tailings Management Protocol		x				
	Tailings Guide		x				
	OMS Guide	x	x		x		
2017	Tailings Management Protocol	x			x		
	Table of Conformance	x			x		
	Tailings Guide	x			x		
2019	Tailings Management Protocol			x		x	x
	Table of Conformance			x		x	x
	Tailings Guide			x		x	x
	OMS Guide			x		x	x

The Table of Conformance is used to assess each indicator for the Tailings Management Protocol. Table 2 presents an overview of the 2019 Table of Conformance, listing the TSM performance indicators and corresponding criteria and applicable MAC guidance. For each criterion listed, questions (ranging from a few to about 30) must be answered to evaluate whether the criterion is met. Backup documentation must describe how the criterion is met and provide evidence (such as site references) to support the evaluation.

Results from completing the Table of Conformance are used to rank each indicator. Table 3 presents the assessment criteria for each indicator and rating. A performance level is met only when all assessment criteria are met; no partial scores are allowed. Members must publish action plans for sites that fail to meet a Level A performance and commit to reaching a Level A within 3 years (MAC, 2018b).

Table 2: TSM Tailings Management conformance criteria (MAC, 2019e)

Indicator	Criteria	Guidance document
1. Tailings management policy and commitment	Policy and commitment	Tailings Guide, Section 3
2. Tailings management system and emergency preparedness	Risk management	Tailings Guide, Section 4.1
	Independent review	Tailings Guide, Section 2.2.3
	Performance objectives	Tailings Guide, Section 4.2
	Conformance management	Tailings Guide, Section 4.4.1
	Managing change	Tailings Guide, Section 4.4.2
	Critical controls	Tailings Guide, Section 4.4.3
	Quality Management	NA
	Resources	Tailings Guide, Section 4.4.4
	Financial control	Tailings Guide, Section 4.4.4
	Document control	Tailings Guide, Section 4.4.4
	Training and competence	Tailings Guide, Section 4.4.4 and OMS Guide, Sections 2.5 and 3.1.6
	Communications	Tailings Guide, Section 4.4.4
	Performance evaluation	Tailings Guide, Section 6
	Addressing inundation risks	Tailings Guide, Section 5.2.3
	Testing the ERP and EPP	Tailings Guide, Section 5.2.4
3. Assigned accountability and responsibility	Accountability and responsibility	Tailings Guide, Section 4.3
4. Annual tailings management system review	Annual review	Tailings Guide, Section 7
5. OMS Manual	General requirements	OMS Guide, Section 2.1.2
	Linkage with other systems	OMS Guide, Section 2.4.3
	Implementation	OMS Guide, Sections 2.5 and 3.1.6
	Reviewing and updating	OMS Guide, Section 2.6
	Document control	OMS Guide, Section 2.7
	OMS governance	OMS Guide, Sections 3.1
	Tailings facility description	OMS Guide, Section 3.2
	Operation	OMS Guide, Section 3.3
	Maintenance	OMS Guide, Section 3.4
	Surveillance	OMS Guide, Section 3.5
	Linkages with ERP	OMS Guide, Section 4

Notes: ERP = Emergency Response Plan; EPP = Emergency Preparedness Plan; Tailings Guide (MAC, 2019a); OMS Guide (MAC, 2019b)

Table 3: TSM Tailings Management Protocol assessment criteria (MAC, 2019e)

Indicator	Level C	Level B	Level A	Level AA	Level AAA
1. Tailings management policy and commitment	Not at level B	Policy in place, action plan to meet level A	Mac-conforming policy with internal audit and approved by senior management	External audit of the policy to confirm level A	External audit with effectiveness evaluation
2. Tailings management system and emergency preparedness	Not at level B	Non-MAC conforming TMS, ERP, and EPP, action plan to meet level A	MAC conforming with internal audits, tested the ERP and EPP	External audits to confirm level A	External audits with effectiveness evaluation
3. Assigned accountability and responsibility	Not at level B	Documented accountability and responsibility, action plan to meet level A	Executive officer accountability, MAC-conforming delegation of responsibility to qualified person, internal audit	External audit to confirm level A	External audit with effectiveness evaluation
4. Annual tailings management system review	Not at level B	Non-MAC conforming periodic reviews, action plan to meet level A	MAC conforming with internal audit	External audit to confirm level A	External audit with effectiveness evaluation
5. OMS Manual	Not at level B	Non-MAC conforming manual, action plan to meet level A	MAC conforming with internal audit	External audit to confirm level A	External audit with effectiveness evaluation

Notes: TMS = Tailings Management System; ERP = Emergency Response Plan; EPP = Emergency Preparedness Plan

TSM benefits

Both tailings stewardship and TSM focus on continuous improvement and risk reduction. The TSM program benefits tailings stewardship by providing a framework to evaluate the tailings management system for a facility and ranking performance based on comprehensive criteria. TSM provides a more rigorous approach to tailings management system review and continuous improvement with the added benefit to stakeholders of public reporting. 2019 upgrades in the TSM Tailings Management Protocol add focus on more robust operation, maintenance, and surveillance activities, as well as emergency response and preparedness.

MAC's most recent progress report available, the 2018 TSM Progress Report (MAC, 2018a), assesses 67 mining facilities for 23 member companies. Many of the mining facilities are in Canada. Results show

92 percent have implemented tailings management systems that conform with MAC's tailings management guidance. The percentage of facilities with Level A or higher performance has increased on average for the five indicators from 50 to 85 percent since initial reporting in 2006. In 2006, there were 16 reporting companies and 35 facilities assessed (MAC, 2006). Reporting results show facilities increasing their assessment levels as they advance through the program.

The Investor Mining and Tailings Safety Initiative led by investors and initiated in 2018 emphasizes stakeholders' demands for information and transparency of tailings facilities and management practices. As part of this initiative, a disclosure request letter from investors was sent to mining companies to request data on tailings storage facilities and that this information be posted on the company website. The intent of this request was to better understand which companies are responsible for which facility and the scale of the risks associated with the facilities. TSM's transparent reporting compliments this investor led initiative.

Conclusion

Although many mining companies have tailings stewardship or governance programs, the current industry climate demands more rigorous checks. Incorporating TSM review and verification strengthens an existing tailings stewardship program and benefits the industry and affected stakeholders by elevating tailings management practices to a higher standard integrating executive-level accountability and best practices.

TSM also promotes responsible sourcing from mine to product. Sustainability has been a focus in the industry for several years, but due to recent devastating tailings dam failures stakeholders are pushing harder for increased improvements and transparency. Stakeholders want transparency to know more about the status of tailings dams and how mining companies are going to reduce the frequency and severity of tailings dam failures. In addition, consumer attitudes are driving companies to require that suppliers (e.g., mining companies) meet more stringent sustainability standards, with some adding a requirement to meet TSM standards (MAC, 2018).

Adopting TSM is not a cure-all for improving tailings management, but can be a driver for continuous improvement and can highlight key areas where more work is needed. The transparency of the program allows various stakeholders insight into company performance against the standard, as well as against other companies in the mining industry. TSM is a credible program that benefits a tailings stewardship or governance program by advancing measurement and promotion of sustainable tailings management.

References

Mining Association of Canada (MAC). 2006. *Towards Sustainable Mining Progress Report 2006.*

Mining Association of Canada (MAC). 2017a. *Towards Sustainable Mining 101: A Primer.*

Mining Association of Canada (MAC). 2017c. *Towards Sustainable Mining Tailings Management Protocol.*

Mining Association of Canada (MAC). 2017c. *Table of Conformance 2019.*

Mining Association of Canada (MAC). 2018a. *Towards Sustainable Mining Progress Report 2018.*

Mining Association of Canada (MAC). 2018b. *Towards Sustainable Mining Verification Service Provider's Training Workshop.*

Mining Association of Canada (MAC). 2019a. *A Guide to the Management of Tailings Facilities,* Version 3.1.

Mining Association of Canada (MAC). 2019b. *Developing an Operation, Maintenance, and Surveillance Manual for Tailings and Water Management Facilities*.

Mining Association of Canada (MAC). 2019c. *Towards Sustainable Mining Tailings Management Protocol.*

Mining Association of Canada (MAC). 2019d. *Description of Phase-in of Updates to the Tailings Management Component of TSM.*

Mining Association of Canada (MAC). 2019e. *Table of Conformance 2019.*

Proceedings of Tailings and Mine Waste 2019
November 17–20, 2019, Vancouver, Canada
Published by the University of British Columbia, 2019

The Role of Institutional Mining Investors in Driving Responsible Tailings Management

Sally Innis, University of British Columbia, Canada
Nadja Kunz, University of British Columbia, Canada

Abstract

Recent devastating tailings dam failures have led many investors to view mining projects as increasingly risky investments compared with other industrial projects. Recently, institutional investors worth US$12 trillion in assets have called for the development of an independent classification system for quantifying the safety risks associated with tailings storage facilities (TSF). Research and applied practices from the mine waste management community could be used to inform institutional investment risk criteria, and ultimately inform the development of risk communication tools for the investment community.

This research investigates if and how the mining investment community is evaluating TSF risk as an environmental, social, and governance (ESG) issue. In this paper, these concepts are explored through a literature review, which considers how institutional investors influence ESG performance. The non-technical causes of TSF failures are summarized. Results from qualitative research interviews with institutional mining investors are subsequently presented.

The research suggests that institutional investors have limited knowledge on tailings management, but that there is an emerging appetite for increased information on tailings risks. The majority of investors and investor stakeholders agree that they could play an important role in improved TSF management through managing and pressuring company boards. However, investors also feel limited in their ability to influence TSF management due to the lack of a global tailings standard and differing regulations across jurisdictions. Investors are already making efforts to contribute to improved tailings management by their creation and involvement in the Church of England's tailings disclosure request. However, despite this increased transparency, data accessibility and technical knowledge gap issues present challenges for investors to improve evaluation of the risks of TSF failures to investor portfolios. In addition, this paper outlines areas for future research to manage, assess, and communicate material and non-material risks associated with TSF failures.

Introduction

The gradual decline of average ore grades is requiring an increase in water, energy, and waste rock production per tonne of ore mined (Scott, 2018). Research has concluded that the increased cost of accessing lower grade ore and elevated prices of mineral resources may contribute to an increase in large-scale tailings failures (Bowker and Chambers, 2017). These and other factors have led to mining projects becoming an increasingly risky investment over other industrial projects (Kavakli, 2015). The consequence of a continued lack of initiative to invest in safer tailings storage facility design and management is evidenced by the most recent Brazilian tailings dam disaster in Brumadinho. The TSF failure left more than 250 people dead, caused irreversible environmental damage and resulted in a 16 billion dollar hit to investor portfolios (Freyman and Lall, 2019). Following this and other recent tailings failure events including Samarco and Mt Polley, there is a strong argument to drive a new level of accountability and transparency within the mining sector through sustainable investment (Church of England, 2019).

These failures show the potential financial benefit of long-term planning to avoid TSF failures (Larrauri and Lall, 2017). Although companies may be tempted by the most economical tailings management method, both stakeholders and shareholders will pay for the long-term liabilities associated with cost-cutting choices. Reaction to TSF failures by investors and other stakeholders may hold the key to stronger regulations with independent enforcement and better overall company stewardship (Freyman and Lall, 2019). Most recently, a tailings disclosure initiative spearheaded by the Church of England and the UN Principles of Responsible Investing suggests that institutional investors have a strong appetite for improved understanding of the mine waste risks within their portfolios. The disclosure asks mining companies to self-disclose various statistics about a range of features for each tailings dam such as dam location, height, volume and hazard rating. Based on the disclosure as of July 3, 2019, a total of 1,606 TSF sites had been identified and disclosed by 66 companies. Figure 1 shows a preliminary review of the data, which reveals that 52% of the disclosed dams are listed with a hazard rating of “High” or “Very High” or with equivalent classifications.

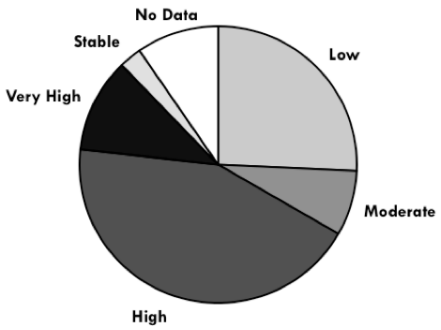

Figure 1: Frequency of hazard classification ratings from the Church of England tailings disclosure as of July 31, 2019

The primary research questions explored in this paper are:

1. Do institutional mining investors have a role to play in improved tailings management?
2. If so – what are the challenges they face in evaluating the financial and environmental, social and governance (ESG) risks that TSFs bring to their portfolio?

Literature review

In order to address the research questions, this section explores previous research on the non-technical threats to TSF risks and investor interest in ESG issues. This research defines non-technical risk as the root causes of TSF failures other than the physical attributes of tailings storage facilities that result in TSF failures. Bowker and Chambers (2017) go on to define these root causes as conditions that shape decision-making at mines. In recent years there has been a remarkable increase in research on the non-technical threats to tailings risks. However, there is a lack of research on the institutional investor's influence on the outlined non-technical threats. That withstanding, there is a recent body of research that encompasses how and if institutional investors influence the ESG performances of companies within an investor's portfolio, though not unequivocally focused on the extractive sector. We argue that it is important to consider how and if institutional investors influence TSF risks, as TSFs present enormous financial and ESG threats to both project stakeholders and investors.

Non-technical causes of TSF failures

Technical threats to tailings dams have been known for quite some time. Academia and industry are aligned on the technical causes of tailings containment wall failures causes being (Clarkson and Williams, 2019, Australian Government, 2007):

- slope instability;
- earthquake loading;
- overtopping;
- inadequate foundations; and
- seepage.

However, the importance of responsible engineering practices and management at TSFs has also been widely documented. Peck (1980) argued that companies have the technical capabilities to drastically reduce the number of annual tailings failures. Recent articles by Armstrong et al. (2019) and Rico et al. (2008) underline that TSF failures are more likely to occur due to a disregard of proper engineering practices or management rather than lack of technical knowledge on TSF risks. More specifically, both Armstrong (2019) and Bowker and Chambers (2015) argue that a doubling in TSF failures in the last two decades can

be explained by cost cutting measures concurrent with production increases and decreasing ore grades resulting in poor management choices. Furthering their research on cost cutting methods, Bowker and Chambers (2017) project 19 'Very Serious'[1] TSF failures by 2025. The proceedings from the class action lawsuit following the Samarco Fundão TSF failure in Brazil in 2015 also reveal that cost-cutting measures seriously impacted the stability of the Fundão TSF (Banco v. Samarco, 2018). Despite acknowledgement by the Samarco board that the Fundão TSF was a matter of concern, it was found that the board meeting decisions approved TSF designs that contradicted the original design, and that cost-cutting measures were implemented, such as a decision to expand the Fundão TSF to meet an increase in production rather than to build a new TSF.

Bowker and Chambers (2017) argue that the economics behind financing mining projects is inherently dysfunctional and encourages risky decision-making and unsafe TSFs. Armstrong (2019) extends this research by arguing that incentive packages linked to equity stock promote cost cutting measures, driving risk-taking with potentially catastrophic consequences. Regulatory bodies are also recognized as paramount. Morgenstern (2018) and Schoenberger (2016) underline the necessity of strict regulatory bodies in the management of tailings dams. Schoenberger's (2016) analysis of recent tailings disasters concluded that the successful integration of TSF within a mine's design required that there are strict regulatory standards in place.

Investor influence on ESG performance

ESG issues are becoming recognized as financially material to the investment community. Land conversion requirements and potential for contamination represent significant threats to ESG performance at mining companies and investment firms posed by TSFs (UNEPFI, 2010). Such threats are magnified in the event of a significant tailings release. Mining represents one of the lowest-performing industries in the Thomson Reuters ASSET4 ESG database, yet there has been limited research that considers how investors can create change specific within the mining industry (Dyck et al., 2019; Ernst and Young, 2015). This observation is not unique to the mining sector. Despite the surge in responsible investment that has occurred following the creation of the UN Principle of Responsible Investing, there remains a significant lack of understanding of how investors actually incorporate ESG issues into investment decisions (Sullivan, 2017). This does not necessarily mean that investors are not playing an important role in driving company practice. Both Sullivan (2017) and Mackenzie and Sullivan (2006) discuss that although there is a disconnect between company

[1] Bowker and Chambers (2015) define "Very Serious" failures "as having a release of at least 1 million cubic meters, and/or a release that travelled 20 km or more, and/or multiple deaths (generally ≥ 20)."

ESG reporting requirements and investor decisions-making, the simple engagement of investors in responsible investment strategies such as the UNPRI encourages companies to establish and maintain ESG management systems.

From the perspective of institutional investors, ESG investments have been proven to provide risk insurance and market differentiation. That withstanding, a positive relationship between ESG performance and returns to the average investor remains a contentious issue (Dyck et al., 2019). To the best of our knowledge, only one paper, Dyck et al. (2019) has studied if institutional investors are a driving-force behind improved ESG performance. Dyck et al. tested the relationship between institutional ownership and ESG performance and found that greater institutional ownership of companies resulted in a significant increase in ESG performances. Dyck et al.'s research opens the possibility for institutional investors to play a substantial role in transforming the ESG practices within the mining industry and the responsible management of TSF.

However, as highlighted by Sullivan (2017), there remains a requirement for mining companies to know how and if investors take into account ESG and tailings issues during decision-making before changes in the industry will be seen.

Research methodology: Interviews

Through this research over 40 institutional mining investors or investor stakeholders were approached to participate in a semi-structured interview. Responses to this invitation revealed that institutional mining investors are interested in understanding the risks TSFs present to their portfolios. However, several investors, especially those from firms with smaller assets under management, felt that they had too little knowledge on tailings dams or do not factor TSF risks into their analysis to feel adequately qualified to participate in this study. In total, 8 institutional mining investors or investor stakeholders were interviewed, all of whom had between 9 and 35 years of experience in the industry.

The mining investors interviewed all were aware of the Church of England tailings disclosure and 7 of the 8 participants were involved with the disclosure. Interview questions are summarized in Table 1. All interviews were completed in compliance with the requirements of the UBC Research Ethics Board (Certificate of Minimal Risk: *H19-01217*).

Table 1: Summary of interview questions with mining investors and investor stakeholders

Interview questions
• To the best of your knowledge, have any of the mines in your portfolio, current or past, been involved with a tailings incident?
• Are you seeing any evidence of increased shareholder activism in the extractive sector?
• What role do investors play in improving tailings management?
• How do you track risks related to tailings storage facilities of design stage mines?
• Does your firm have plans to assess the data from the Church of England tailings disclosure? If so, how?
• Will the Church of England tailings disclosure request cause any changes in your investment strategy? If so, how?

Results and discussion

The following section discusses the findings of two research questions from the qualitative interviews:

1. What role do institutional mining investors play in improved tailings management?
2. What are the challenges faced by mining investors in assessing financial and ESG TSF risks?

Investor role in tailings management

The research completed to date suggests that there is a promising community within institutional mining investment that strongly believes in their role to improve the state of TSF failures, globally. However, investors are not likely to actively track tailings risks within their portfolios, any tracking done is used with outsourced data from ESG research and rating companies such as Sustainalytics and MSCI. Interviewees that self-identified as impact-oriented investors[2] were attuned to taking into account ESG and TSF issues. A logical conclusion supported by interviews is that impact oriented investors prompt changes within their investment firm's policies and procedures for their current and future mining investments after tailings failures occur, regardless of whether these events arise within their portfolios. Conversely, non-impact oriented larger scale mining investors did not suggest they would change investment practices or policies when investing in mines. Moreover, one firm with significant shares in both Vale and BHP[2] stated that the tailings failures over the last five years within both companies did not affect their investment strategies. This interviewee further underlined the potential negative effects on the mining industry from exclusionary practices that may arise from investors divesting from mining projects. The interviewee extended research questions by Dyck et al. (2019) and supported by Bowker and Chambers (2017) discussing the role of

[2] Vale S.A. has been involved in both the Samarco Fundão TSF failure in November 2015 and the Brumadinho TSF failure in January, 2019. BHP Billiton Brazil LTD was involved in the Samarco Fundão failure through co-ownership of private mining company, Samarco Mineração S.A., with Vale (Banco v. Samarco, 2018).

negative or exclusionary screening[3] for ESG issues across all major industries. As the interviewee discussed:

> "Exclusionary screening … is like throwing in the towel, practically giving up on that particular company. It may help your portfolio, your portfolio will be cleaner as a result of that, but it may not change anything for the better on the ground. And that's what ultimately we should strive for."

Dyck et al. (2019) found that negative investing screening practices were unable to explain broad changes in firms ESG performances. Applying negative investment screening within the mining investment community may not necessarily improve overall TSF management, but could potentially have unintended consequences. The cash flow pressures from decreased investments could contribute to mismanagement of TSFs that Bowker and Chambers (2015) underline as an important contributor to the rise in failures. There is a need for further research to better understand these potential flow-on effects from divestment strategies, and to consider potential measures for mitigation as part of an overall transition plan.

All interviewees believe that they play some role in improved tailings management. Several investors and investor stakeholders highlighted that their role was limited to ensuring that the board of the invested company is competent and capable in overseeing management and that the company is compliant with regulations. Half of the investors interviewed underlined the limitations of their role due to the lack of a global tailings standard and government regulations. As one investor stakeholder noted:

> "When investors have issues like TSF that have different measurements and methodologies related to different regulations from jurisdiction to jurisdiction, it can be really challenging to find comparable metrics."

A large-scale institutional investor confirmed that:

> "One of the biggest issues I have is local regulations are wildly different by jurisdiction."

Given these responses, we believe the current work to create a global tailings standard will significantly improve the understanding and reach of investors on improving TSF management.

Challenges faced by investors

This research found that there is currently a lack of information on the financial and ESG risks of TSF presented to the investment community. Given the response from the Church of England tailings disclosure request, it is clear institutional mining investors can motivate companies to disclose tailings information.

[3] Negative or exclusionary screening is defined as avoiding (i.e., not investing in) companies on the basis of specified criteria, such as underperforming in certain ESG issues.

That being said, the role that investors involved in the Church of England request will play post-disclosure remains unclear. Until a database is publicly disclosed where company sites are listed in a single, functional database it is unlikely that investors or other stakeholders will devote time to acquiring data from the currently disclosed companies. A significant response from investor interviews outlined that the disclosure may not effect changes in investment practices, as shown by a very direct response from an institutional mining investor:

> "I'm not sure [how the Church of England disclosure request will] help me in my investment process."

How policy and procedural changes may affect investment in mining and TSF incident rates would require further research. The methodology used by Dyck et al (2019) to test the effect of institutional ownership on ESG performances after the 2010 BP Deepwater Horizon oil spill could be an interesting direction if recreated on ESG performances after a significant TSF failure such as at Brumadinho or Samarco. Dyck et al. (2019) argued the oil spill unveiled the financial risk of environmental disasters, which provoked firms with significant institutional investor ownership to bolster environmental policies.

The low response rate of investors could be attributed to several factors, including the recruitment method. However, the reasoning for several investors' decline to participate was that the investor had too little knowledge of tailings dams or did not factor TSF risks in their analysis to participate in this study. It may be of significance that the majority of the investors interviewed had technical mining or mining related background, whereas, the majority of the other investors contacted, to the best of the author's knowledge, had predominantly finance backgrounds. This correlation between technical experience with the mining industry and understanding of financial risk exposure of mining facilities is an area that should continue to be explored in future mining investment-related research.

As mentioned above, unreliable and differing regulations and standards present challenges to investors. As discussed by an institutional investor with a technical background:

> "For investors with a less technical background, in their questionnaire [on mine site visits]. All they can ask is are you managing your dam according to the regulations? Are you auditing it properly? The answer is always yes and yes."

In summary, a misalignment of regulations, standards and industry "best-safety practices" do not supply investors with the tools to properly compare and hold company boards accountable for unsafe TSF. As highlighted by the above quote, company self-reporting and bias presents a significant issue to investors. It is clear from interview responses that investors need global standards and easily digested data on TSF to inform investment decision-making. Communicating the risks of TSF failures to investors and other stakeholders while limiting self-reported bias presents ample opportunity for future research.

Conclusion

TSF failures present vast financial and ESG risks to investment portfolios. Fortunately, TSF failures are preventable and present a unique opportunity for investors to engage with companies to manage both economic and safety risks. In this paper, we address the role of institutional investors in improving mine waste management following the devastating tailings disasters at Mount Polley, Samarco, and Brumadinho. Drawing on the review of literature on non-technical causes of tailings failures and investor influence on ESG issues, we found that external financial influences on mines, such as cash flow into a mining operation, influence TSF management practices. Therefore, institutional mining investors have an important role to play in improved management of mine waste facilities. This conclusion is reflected by the Church of England tailings disclosure request; at the very least, investor involvement in the request revealed TSFs not previously publicly disclosed.

The Church of England disclosure is unlikely to be used by investors until it is compiled into a single, usable database. The qualitative research interviews with institutional mining investors reveal investors do play a role in improved tailings management through actively managing board members and decisions. However, investors are heavily limited and reliant on standards and regulations that reflect the "best safety practices". The lack of available information on mine management and TSF also presents a significant challenge to investors.

Areas for continued research on investor influence on ESG and TSF issues in the mining sector are numerous. Research such as an analysis using Dyck et al.'s (2019) methodology on the ESG performances of firms with institutional ownership involved in the TSF failures of Samarco, Mount Polley, or Brumadinho may validate this research with quantitative scope. This research will be continued by the authors in future to advance the preliminary findings in this paper. Specifically, the authors will confront the technical and communication gaps outlined in interviews and design risk assessment tools for investors and other stakeholders.

References

Armstrong, M., R. Petter and C. Petter. 2019. Why have so many tailings dams failed in recent years? *Resources Policy* 63: 101412.

Australian Government. 2007. Department of Industry Tourism and Resources, Tailings Management: Leading practice sustainable development program for the mining industry. Canberra.

Banco Safra S.A. v. Samarco Mineraco, BHP and Vale. 2018. 66 U.S. District Court. 2018. No. 01-16. Southern District of New York. March 2018

Bowker, L.N. and D. Chambers. 2015. The risk, public liability, and economics of tailings storage facility failures. *Earthwork Act*. 1–56.

Bowker, L.N. and D. Chambers. 2017. In the dark shadow of the supercycle tailings failure risk and public liability reach all time highs. *Environments* 4(4): 75.

Church of England. 2019. Investor mining and tailings safety initiative, The Church of England, 5 July, 2019. Retrieved from https://www.churchofengland.org/investor-mining-tailings-safety-initiative

Clarkson, L. and D. Williams. 2019. Critical review of tailings dam monitoring best practice. *International Journal of Mining, Reclamation and Environment:* 1–30.

Dyck, A., K.V. Lins, L. Roth and H.F. Wagner. 2019. Do institutional investors drive corporate social responsibility? International evidence. *Journal of Financial Economics* 131(3): 693–714.

Ernst and Young. 2015. Business risks facing mining and metals: 2015–2016. *Ernst and Young Global Limited.*

Freyman, M. and U. 2019. Lall U. Dammed if You don't, Reuters, 6 February 2019. Retrieved from www.breakingviews.com/features/guest-view-investors-can-shore-up-mining-risks/#.

Kavakli, Nevzat. 2015. Evaluation of mining investment projects with a new software. *Arabian Journal of Geosciences* 8(2): 6353–6362.

Larrauri, P.C. and U. Lall. 2017. *Assessing Risks of Mine Tailing Dam Failures.* Interim Report for Norges Bank Investment Management.

Mackenzie, C. and R. Sullivan. 2006. *Responsible Investment*. Routledge.

Morgenstern, N.R. 2018. Geotechnical risk, regulation, and public policy. *Soils and Rocks* 41(2) : 107–129.

Rico, M., G. Benito, A.R. Salgueiro, A. Díez-Herrero and H.G. Pereira. 2008. Reported tailings dam failures: A review of the European incidents in the worldwide context. *Journal of hazardous materials* 152(2): 846–852.

Schoenberger, Erica. 2016. Environmentally sustainable mining: The case of tailings storage facilities. *Resources Policy* (49): 119–128.

Scott, Michael. 2018. Reducing water, energy and emissions through grade engineering. *Mine Excellence 2018: Proceedings of the 3rd International Seminar on Operational Excellence in Mining.* March 2018, Chile.

Sullivan, Rory. 2017. *Valuing Corporate Responsibility: How Do Investors Really Use Corporate Responsibility Information?* Routledge, first edition: 9–20.

UNEPFI. 2010. *Translating ESG into Sustainable Business Value – Key Insights for Companies and Investors.*

Bibliography

Brest, P. and K. Born K. 2013. When can impact investing create real impact? *Stanford Social Innovation Review* 11(4): 22–31.

Proceedings of Tailings and Mine Waste 2019
November 17–20, 2019, Vancouver, Canada
Published by the University of British Columbia, 2019

Development of Tailings Management and Governance in a Mining Company in the People's Democratic Republic of Laos

Peter Jenner, Phu Bia Mining Ltd, People's Democratic Republic of Laos
Shaun Edwards, Phu Bia Mining Ltd, People's Democratic Republic of Laos

Abstract

Establishing appropriate management and governance structures for tailings storage facilities and waste rock is an issue for both junior and established mining companies across the world.

PanAust Limited acquired the Phu Bia Contract Area in Lao People's Democratic Republic in 2001. Following a period of exploration, it constructed Phu Bia Gold Heap Leach in 2005, and then completed the larger Phu Kham Copper-Gold operation in 2008. Construction of the nearby Ban Houayxai Gold-Silver operation was completed soon after, with operations commencing in 2012. The operations encountered challenges regarding tailings management due to their location, terrain, and climatic conditions.

While faced with a number of challenges with regard to the management and governance of its tailings storage facilities, PanAust constructed, developed, and now operates to the highest international standards two tailings storage facilities at its operations in Laos. Furthermore, the tailings governance processes that the company put in place in advance of the general TSF industry will continue through to each operation's life of mine, and into closure, and will provide a template for PanAust's future projects and operations. This paper presents how PanAust has developed and illustrates how improvements have been made to its tailings governance and stewardship program.

Introduction

PanAust Limited (PanAust) first started working in Laos in 2001 and owns a 90% interest in the Lao registered company Phu Bia Mining Limited (PBM). The government of Laos owns the remaining 10%. Geological drilling work for the Phu Bia Gold Project commenced in 2002. The project comprised four deposits: Ban Houayxai (BHX), Long Chen Track (LCT), Phu Kham (PKM), and Kham Tong Lai (KTL) (Figure 1). In 2004, PanAust initiated mine development and commenced construction of a gold heap leach operation to process the Phu Kham gold cap deposit, with the first gold poured in November, 2005.

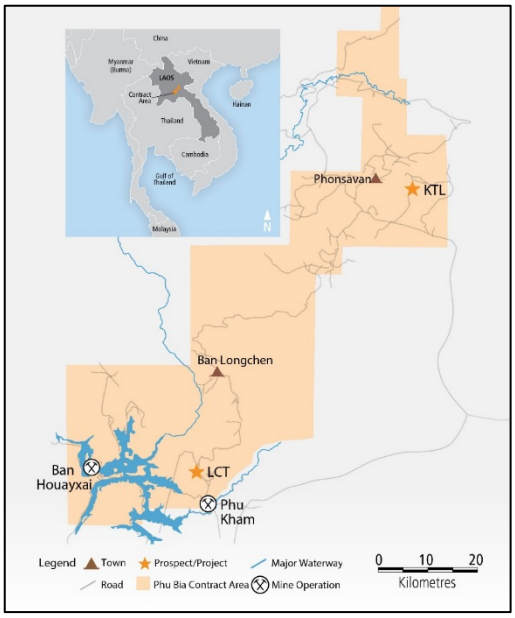

Figure 1: Phu Bia Mining Laos operations

Construction of the 12 Mtpa Phu Kham copper-gold project began in 2006 and was completed, with the first concentrate produced in 2008. The gold heap leach operation was decommissioned in 2010. Construction began on the 4 to 5 million tonne per annum (Mtpa) Ban Houayxai gold-silver project in 2011 and began to commercially produce gold and silver doré in June 2012. Following the construction of the Ban Houayxai project, PanAust completed the Phu Kham throughput upgrade project in early 2013, with the addition of a second ball mill and expanded flotation circuit increasing throughput rates to 16 Mtpa design capacity. Following the completion of the throughput project, the Increased Recovery Project targeting a 6% increase in copper and gold recovery was completed; subsequent operational and process control improvements have now seen the process plant milling between 18 and 20 Mtpa at significantly improved recovery.

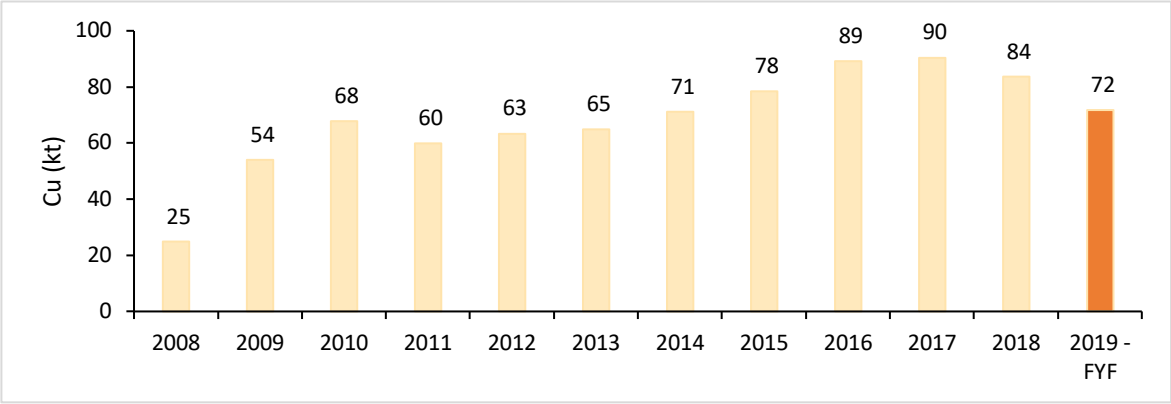

Figure 2: Annual copper concentrate production for PKM (kt)

In just over 10 years, PanAust grew from a junior exploration company to a respected mid-tier copper and gold mining company with annual metal production of 60,000 to 90,000 tonnes (t) of copper and 150,000 to 225,000 ounces (oz) of gold (Figures 2 and 3) produced in concentrate.

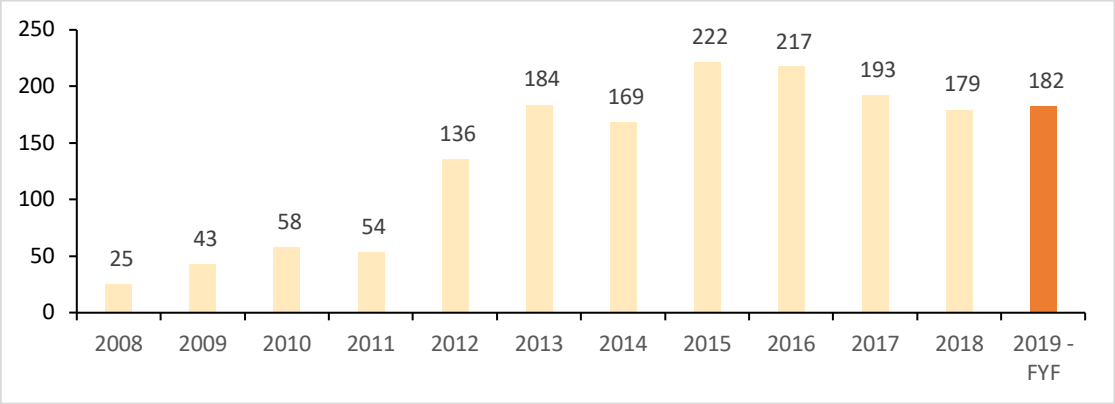

Figure 3: Annual gold production for PKM and BHX (koz)

Overview of PanAust's tailings storage facilities

PanAust operates two large tailing storage facilities (TSFs) for its operations in Laos. Both facilities utilize subaerial and subaqueous disposal of tailing and waste rock to manage deposition and encapsulate potential acid-forming materials.

The Ban Houayxai facility holds process tailings only, whereas the facility at Phu Kham has been designed to manage both process tailings and mine waste rock (Red Road Waste Dump) as an integrated storage facility. Waste at Ban Houayxai is housed within a separate clay-encapsulated waste dump remote from the TSF. Both facilities are designed to operate with a minimum water cover to prevent oxidization of tailings and to limit final embankment build height and construction costs. A passive spillway was incorporated into the design of the Ban Houayxai facility, while the Phu Kham facility has an emergency spillway only during operations. Salient features of each facility are listed in Table 1 below.

Both sites are located in similar geographic locations, with lower levels of infrastructure (communication and transport), as is usually found in developing country settings, mountainous terrain, and a tropical monsoon climate. Historical annual rainfall averages about 2,500 millimetres (mm) at both sites, although orographic effects occur, with high variations in total rainfall over short lateral distances. Between the mine sites located 25 km apart, annual rainfall can vary by as much as 1,500 mm and annual rainfall in excess of 4,500 mm has occurred on the Ban Houayxai site. Other significant issues to be dealt with during design and construction include availability and suitability of construction materials, and the potential for acid-forming conditions in the waste rock and tailings.

Table 1: Summary of PanAust tailings facilities

	Unit of measure	Phu Kham	Ban Houayxai
Year commissioned	Date	2008	2012
Surface area	ha	200	100
Catchment area	ha	500	2,000
Embankment height (current)	m	169	79
Embankment height (final)*	m	182	89
Crest length	m	1,880	286
Tails storage (current)	Mt	178.2	34.0
Tails storage (final)	Mt	240.0	50.0
Pond volume	Mm^3	4 – 14	1 – 6
Average settled tails density	t/m^3	1.43	1.41

PanAust's tailings storage facilities in Laos were designed by Knight Piésold Pty Ltd (KP) in accordance with ANCOLD/ICOLD guidelines and are constructed as zoned, earth, and rockfill structures. At Phu Kham, the facility's construction materials are sourced from local borrow pits and mining operations, whereas construction materials at Ban Houayxai are sourced from borrow pit operations only. Filter and crushed products are produced at both operations, using dedicated crushing plants. Contractors are used to conduct some earthworks and drainage works at both sites, although the Phu Kham mining fleet supplements construction by providing suitable waste materials from the pit.

Figure 4: Phu Kham tailings storage facility embankment

Mining is a developing industry in Laos and the regulatory framework for mining projects, and particularly tailings/waste management ,is not well developed. Consequently, PanAust has had to forge its own path with respect to following internationally accepted best practices regarding tailings and waste management. In 2018, draft guidelines for the management of tailings and mine dams in Lao PDR were developed. Following inspections of both mines by international consultants, PanAust was recognized as being "an in-country example of industry leading practice, which can be used as an example for other mining operations in Lao PDR." This finding shows the successful efforts PanAust has made as a company to ensure it is at the forefront of tailings management and stewardship.

Figure 5: Ban Houayxai tailing storage facility embankment and spillway

Tailings and waste management and stewardship

For many mining companies, tailings and waste rock management continues to be the most significant short- and long-term environmental risk. The quantity of tailings material, its mineral composition and fine sediment nature, and the requirement for long-term stable TSFs and waste dumps necessitate robust tailings management strategies and stewardship. The management of waste rock to prevent acid rock drainage (ARD) is comprehensive, because of the potential for ARD to induce acidity and dissolved metals into water, which can be harmful for receiving environments. Consequently, the design, construction, operation, and closure of tailings and waste at the operations is considered extremely important by the executive management team and the board of PanAust.

PanAust is committed to providing a level of stewardship that is commensurate with the risks associated with these facilities and that is consistent with leading global practice. This section presents

how the company developed its internationally recognized tailingsx and waste rock management and stewardship.

A timeline of improvement

PanAust has progressively developed significant capability in the construction and successful operation of its tailings storage facilities in a challenging environment, and has progressively enhanced its management and stewardship of the facilities. Figure 6 below illustrates the timeline for this development.

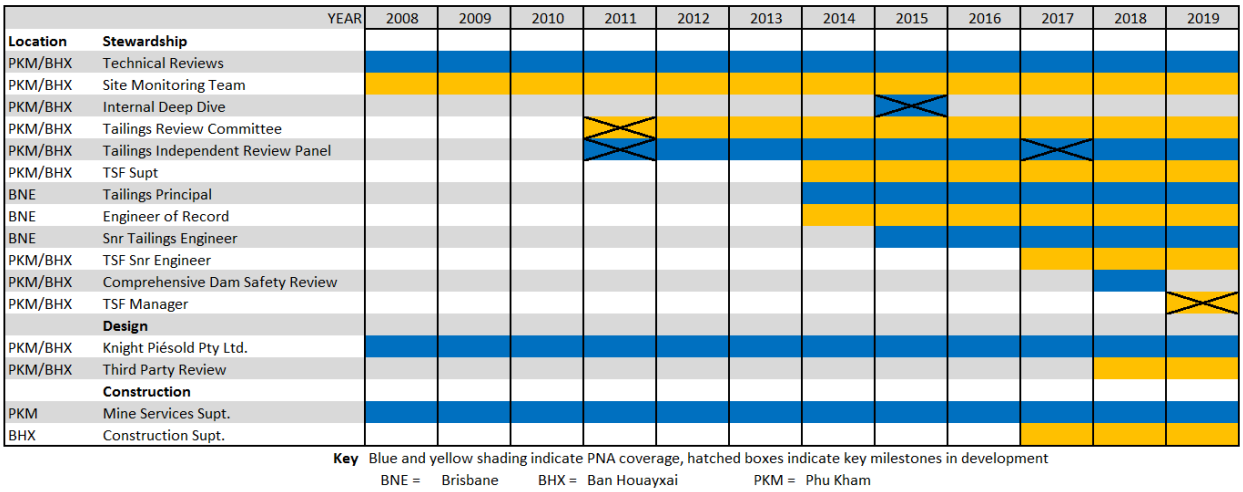

Figure 6: PanAust Tailings management and stewardship timeline

At the commencement of operations at Phu Kham, there were limited human resources with mining skills in Laos. Construction of the Phu Kham TSF commenced before the larger mine fleet arrived. Local earthworks contractors were contracted to undertake the majority of the embankment builds. Early construction of the facility was managed by the mine services superintendent, with technical support from KP.

During initial construction, a dedicated on-site soils laboratory was set up at both operations to provide quality control tests, with KP providing quality assurance. The laboratories were developed further with additional resources and personnel, and expanded to cover TSF inspections and monitoring. In 2009, PanAust hired a civil engineering superintendent with significant tailings experience to provide technical support to the growing on-site monitoring team. At that time, overall responsibility for the facilities fell under the responsibility of the then site process manager. During this time there was little in the way of an overriding governance system in place for the facilities, and stewardship was largely comprised of systems set up by KP in the original operations manual, with regular inspections and audits carried out by the KP design engineer.

Following the construction of Ban Hoauyxai and the expansion of the Phu Kham operation, PanAust identified a need for additional technical support and tailings stewardship. PanAust established a Tailings Independent Review Panel (TIRP) and a Tailings Review Committee (TRC) to meet this need. Comprised of internationally renowned specialists, the TIRP provided PanAust's former managing director and current executive chairman with an objective assessment of the company's tailings facilities stewardship performance and design standards. The TRC comprised key personnel and senior managers within the company, and was responsible for endorsing, managing, and executing decision making in relation to the TSFs.

The establishment of both the TRC and the TIRP provided a catalyst for the PanAust's tailings stewardship program. In 2014, a principal tailings engineer was hired to provide overall guidance and additional technical support to the site-based operational teams. The principal was also appointed as Engineer of Record (EOR). A TSF superintendent was also hired to manage and oversee construction, monitoring, and management of the facilities. The following year, a corporate senior tailings engineer was hired to provide to support the principal.

Following and prompted by the Samarco dam failure in 2015, PanAust conducted an internal deep dive safety audit on its tailings facilities in Laos. The audit identified several recommendations for how to improve stewardship of the facilities. This was followed by a TIRP visit to the facilities in April, 2016. The TIRP concluded that the company had insufficient resources to adequately complete a spillway weir raise at the Ban Houayxai facility and the embankment at Phu Kham prior to the wet season, which would add significant risk to the operations. The review findings and the deep dive audit were crucial to how the company addressed critical activities. Additional technical specialists in tailings management were mobilized to the site to provide continuous engineering support and enhance organizational construction capacity. As well as improving inspections, monitoring, and emergency preparedness, significant initiatives were undertaken to improve the aggregate crushing and concrete batch plant availability and productivity at both sites, as filter production was found to be a critical element in completing construction phases successfully.

A tailings senior engineer was appointed to the site at the beginning of 2017 to support the TSF superintendent at cover workload at both operations during design and construction phases. The use of third-party reviews for the most critical design work and a comprehensive dam safety review in 2018 enhanced designs and verified dam safety conditions. Most recently, a dedicated TSF department was established in May 2019. This final development (to date) in the evolution of PanAust's tailings governance and stewardship ensure that the facilities are discussed regularly at the highest level within the company during strategic and tactical meetings, facilitating continuous two-way communication between PanAust's corporate office and site-based operational personnel.

Increased tailings governance and stewardship has significantly improved risk management, operational efficiency, and PanAust's ability to execute its tailings facility construction projects on time and on budget. The increased costs of the governance and stewardship program, including additional studies, has been outweighed significantly by cost reductions brought about by more collaborative designs.

PanAust's current tailings management and stewardship framework

PanAust has dedicated considerable resources to tailings management and stewardship. The company's tailings governance and stewardship framework (Figure 7) enables PanAust to keep pace with developments around the world and implement strategic changes rapidly if required. It has proven to be a very proactive system, allowing for the strategic development of the facilities. The framework is supported by PanAust's tailings governance standard, which is reviewed annually and updated to reflect any changes considered best practice.

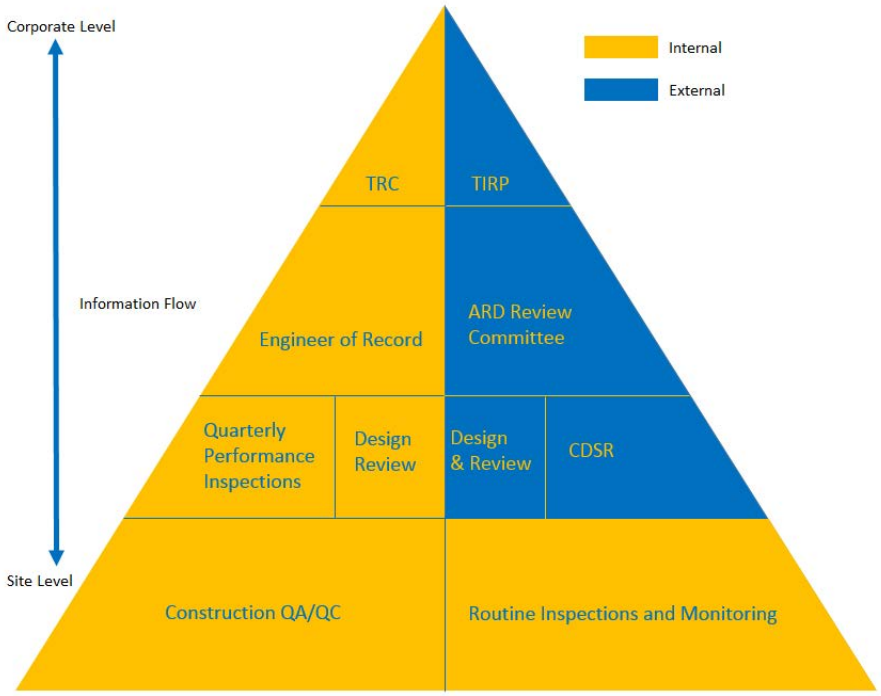

Figure 7: PanAust Tailings and waste rock governance framework

Tailings Review Committee (TRC)

The TRC is comprised of those with organizational accountability for the strategy, planning, design, construction, and operation of the company's facilities. This includes the executive chairman, general manager operations, general manager – technical services, principal tailings engineer and tailings storage facility manager. The TRC has been established to:

- inform the executive chairman of material risks associated with the facilities and the appropriateness and effectiveness of action plans intended to mitigate them;
- oversee the implementation of site actions regarding material risk management and continuous improvement;
- ensure that the TIRP completes annual reviews of the design, construction, operation, and closure of PanAust's facilities;
- provide executive management support and associated resources to close actions identified during TIRP reviews;
- evaluate plans proposed by operational management to action TIRP reviews to ensure they are appropriate, practical, and efficient; and
- update relevant risk registers annually for each facility.

Tailings Independent Review Panel (TIRP)

The TIRP comprises three eminent global experts in the disciplines of tailings, waste, geotechnical engineering, and water engineering. The TIRP annually reviews each facility and provides advice on material risks that may arise during the design, construction, operation, and closure of the company's facilities. Two of the panel's members have been involved with the project since 2011 and have a very good understanding of all aspects of the operation. The third member was recruited in 2017 to provide additional expertise on concrete spillway structures and hydrology aspects.

The panel reports the findings of annual reviews directly to the executive chairman. Recommendations arising from their reviews are transferred to action plans that are monitored by the TRC and the EOR. Responsibility for acceptance and implementation of the panel's advice lies with PanAust and its nominated design consultants and construction contractors. The TIRP also plays an important role in supporting PanAust's credibility for management of the company's facilities with the government of Laos, foreign government visitors, and the company's insurance providers.

ARD Review Committee

PanAust's acid rock drainage review committee comprises internal management and specialist external consultants. The committee verifies the effectiveness of strategies to limit the potential for acid rock drainage during operations, and will remain effective following mine closure. The committee:

- provides technical support to evaluate risks operation of tailings storage facilities using PanAust's Enterprise Risk Management framework;
- records new risks identified during the review period in site risk registers;

- provides guidance on procedures that ensure acid rock drainage management and closure planning are best international practice and standards, legal requirements and operating licenses;
- reviews the geochemical aspects of tailings, waste rock and construction material, particularly with respect to acid rock drainage and metals leaching potential;
- provide input on design, construction, operational, and closure activities that may have long-term stability or other critical performance implications; and
- review health, safety, environmental and social risks associated with the management of acid rock drainage and ensure they are appropriately addressed in accordance with design, construction, operation, and closure plans.

Consultant reviews of acid rock drainage management at Phu Kham and Ban Houayxai are performed routinely. These reviews confirm that the programs are highly developed and effective.

Engineer of Record

In 2014, PanAust appointed an EOR as the approver of all designs, as-built construction, operations, and performance monitoring of the company's facilities. The EOR works very closely with both the design engineer and the TSF manager to ensure that the highest standards of design are applied to any construction. PanAust's principal tailings engineer currently acts as the EOR for both the company's facilities.

Quarterly performance inspections

On a quarterly basis, the EOR inspects the facilities. Feedback is distributed to the corporate office, KP (the design engineer) and site-based teams. Action plans are then developed on the company's risk management software to address findings from the inspection, which are tracked by the TRC and the EOR.

Design

KP have been the design engineer for both facilities since initial construction. This has provided a level of continuity often difficult to achieve within a mining company. The designer typically visits both sites four to five times per year and provides feedback on all aspects of TSF construction, management, and operation. They are also updated regularly with performance information.

Facility designs are subject to a stage gated review and approval process. Designs are typically peer reviewed by a group of internal specialists and/or external independent experts (as required).

Designs are continually enhanced by new models and studies to ensure that data is current and of the highest quality. The following studies have been updated or conducted on both sites:

- Site specific seismic hazard assessment.
- Dynamic deformation analysis of embankments.
- 3D groundwater modelling.
- Dam break analysis.
- Computational fluid dynamics of spillway flows.

In addition, KP has recommended several site investigation/instrumentation programs to provide additional geotechnical/hydrogeological information for inclusion in updated ground and water models. This process ensures all designs are based on current data current. PanAust continually challenges its consultants to provide the highest level of technical design to meet or exceed international standards and employ best available techniques whenever possible.

Comprehensive dam safety review

In early 2018, a comprehensive dam safety review was held for both facilities to provide independent assessments of their operation. It is intended that another review will be conducted once life of mine plans have been finalized for closure.

Quality assurance and quality control

Site-based programs form the foundation of the tailings governance framework. Well-equipped site laboratories perform material testing for quality control and quality assurance of all construction materials. The site laboratories are audited every two years by an independent auditor. Independent testing activities are undertaken at an accredited external laboratory for validation of quality control activities and site investigation purposes. As well as internal QA processes, all test results are forwarded to the EOR and KP. Site construction adheres to signed issued for construction (IFC) drawings and technical specification documents and signed-off construction reports are required after each construction stage.

Routine inspection and monitoring

A comprehensive operation, maintenance and surveillance manual is available at both sites. This establishes monitoring and inspection requirements. Daily inspections and monitoring are performed by trained PanAust employees reporting to the TSF superintendent and TSF manager. Weekly inspections are conducted by the TSF superintendent or manager, with monthly performance reports provided to the EOR, design engineer, and senior management.

The company has an extensive instrumentation network installed on and around both the facilities that includes piezometers (VWP and standpipes), inclinometers, prisms, and extensometers. The latest technologies, such as site-wide InSAR deformation monitoring, are being implemented to supplement

traditional monitoring methods. PanAust is also planning to install remote monitoring technologies to improve data distribution and availability.

Conclusion

PanAust's tailings governance and stewardship program, systems, and processes have provided a strong, well-structured and supportive environment for the design, engineering, and construction of the company's tailings storage facilities. The program empowers and acknowledges the importance of, and PanAust's commitment to, its tailings storage facilities. The top-to-bottom approach to communication removes barriers between corporate expectations and operational functionality. Senior management is made aware of issues encountered on site rapidly, so that new strategies and expectations are communicated to site teams.

The tailings review committee allows issues to be discussed prior to implementation to ensure that they meet the overall established strategy. Expectations are established and clearly defined while governance recommendations and review actions enable appropriate physical and financial resources to be allocated for facility works. This approach protects PanAust's assets, people, the environment, and the communities who live close to the company's operations.

PanAust's tailings governance stewardship program is highly valued and enables and empowers employees. Its structure allows the company to critically review every stage of its facilities design and operations, resulting in significant cost savings to the facilities over the life of mine. Construction support has ensured that critical structures are completed on time and on budget, with no compromise to the integrity of the facilities. Significantly, cost savings and increased productivity have been achieved without any compromise to dam safety.

Acknowledgements

I would like to offer my sincere thanks to the following PanAust personnel for their contributions to this paper: General Manager Operations, David Reid; Ban Houayxai Mining Manager, Luke Morris; PanAust Principal Tailings Engineer, Edward Chong, and Mining Services Superintendent, Brian Authurs.

Proceedings of Tailings and Mine Waste 2019
November 17–20, 2019, Vancouver, Canada
Published by the University of British Columbia, 2019

Valorization of Phosphate Mine Wastes: The Challenge of Additional Resource Recovery from Phosphate Rock

Bernd G. Lottermoser, RWTH Aachen University, Germany

Abstract

Valorization of mineral resources is the process of exploiting resource ingredients with a view to optimizing the value of the geological ore deposits and creating added-value products for market applications. Thus, valorization of phosphate mine wastes aims: (a) to find alternative uses for wastes that accumulate during phosphate mining, mineral processing, and fertilizer manufacturing; and (b) to extract resource ingredients other than phosphate from phosphate rock (i.e., by-products like uranium, radium, or rare earth elements). This contribution reviews the different potential recovery techniques of additional resource ingredients from phosphate rock, providing some insights into valorization paths and critically describing their advantages and disadvantages.

Since the early 1900s, global annual phosphate rock production has steadily increased to a current peak of 270 Mt. Yet, the great majority (>90 %) of all phosphate rock material mined globally is wasted. In fact, the quantity of total solid waste produced can be high, but it varies significantly between mine sites and fertilizer plants – in general, for 1 tonne of phosphoric acid produced, 9.5 tonnes of phosphate ore are required and 21.8 tonnes of diverse wastes and 6.5 tonnes of tailings are produced. The growth in phosphate demand has caused an ever-increasing volume of wastes to accumulate during mining, mineral processing, and fertilizer production. Consequently, mining companies, fertilizer manufacturers, and government agencies face the challenge of managing the increasing load of mining, mineral processing, and metallurgical waste generated around the world at phosphate mines and fertilizer plants.

Reuse and recycling of wastes or reprocessing of resource ingredients from phosphate rock wastes could be an effective solution to this global challenge. Regardless, a "zero waste" concept is impossible to achieve in the current fertilizer production chain, because poor economics prevent the application of reuse, recycling, or recovery techniques in the real world. In the end, government authorities need to set legal limits not only for contaminants (e.g., Cd), but also for trace resource gradients (e.g., REE, U, Ra) in fertilizers, thereby enforcing the valorization of phosphate rock.

Introduction

Valorization of mineral resources is the process of exploiting resource ingredients with a view to optimizing the value of the geological ore deposits and creating added-value products for market applications. Valorization of fertilizer production aims: (a) to find alternative uses for wastes that accumulate during phosphate mining, mineral processing and fertilizer manufacturing; and (b) to extract resource ingredients other than phosphate from phosphate rock (i.e., by-products like uranium). Unfortunately, authors freely and inconsistently use the terms reprocessing, recycling, reuse, and resource recovery. Thus, the "R word" (i.e. reprocessing, recycling, reuse, resource recovery) has proliferated in the scientific literature covering aspects of valorization of fertilizer production.

In this paper, "reprocessing" is defined as the process that extracts valuable elements or compounds from existing waste piles. Similarly, "recycling" uses existing waste piles as feedstock, but it converts entire wastes into new valuable products or applications with limited reprocessing. "Reuse" is defined as the process that involves the new use or the application of waste in its original form for an identified purpose directly without any conversion or reprocessing. Finally, "resource recovery" is an approach that aims to use valuable resource ingredients from ores and waste streams, and therefore includes all forms of reprocessing, recycling, and reuse. This contribution reviews the recovery of additional resources during phosphate fertilizer production, provides insights into valorization paths of fertilizer production, and critically describes the major challenge of achieving valorization of fertilizer production.

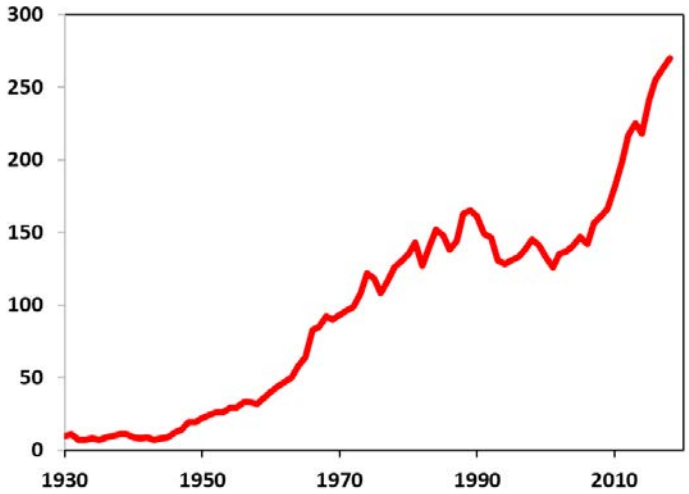

Figure 1: Global annual phosphate rock production (Mt) from 1930 to 2018 (USGS, 2019)

Valorization of mining wastes

Since the early 1900s, global annual mine production of phosphate rock has steadily increased to a current peak of 270 Mt (USGS, 2019) (Figure 1). The phosphate content of phosphate rock varies greatly from

~4% to ~20% P_2O_5 and some of the mined phosphate is lost during mining, mineral processing, and fertilizer manufacturing (Figure 2). Therefore, only a small proportion of the mined phosphate ore is used for phosphate fertilizer, whereas the great majority (~80 – 96 %) of the mined phosphate rock is presently discarded as waste throughout the whole fertilizer industry value chain. In fact, the quantity of total solid waste produced can be high, but it varies significantly between mine sites and fertilizer plants – one study reports findings where, for 1 t of phosphoric acid produced, 9.5 tonnes of phosphate ore are required and 21.8 tonnes of diverse wastes and 6.5 tonnes of tailings are produced (Villalba et al., 2008).

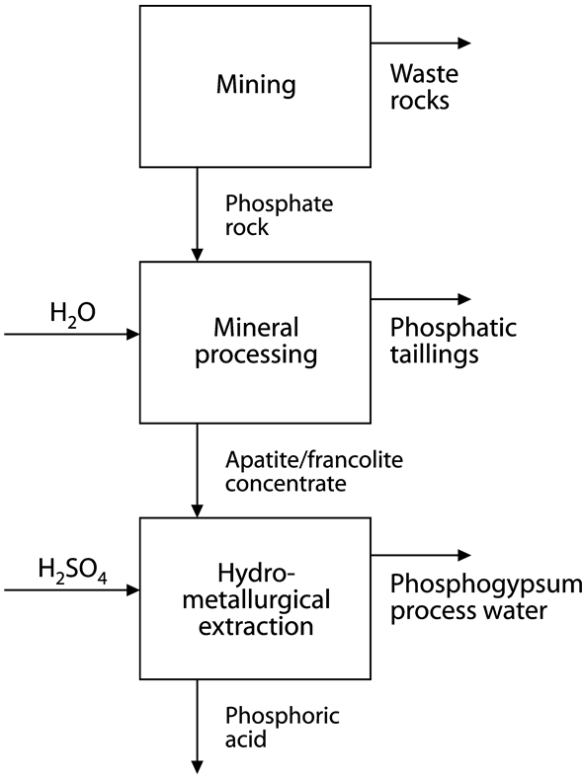

Figure 2: Simplified flow chart of a phosphate mine and phosphoric acid plant. Phosphate rock is mined, processed, and metallurgically treated to yield phosphoric acid and wastes

The growth in phosphate demand has caused an ever-increasing volume of wastes to accumulate during mining, mineral processing, and fertilizer production. At mine sites, significant overburden and waste rock volumes need to be removed to access the phosphate ore, and fine-grained tailings are generated during phosphate processing. These wastes are commonly placed into large engineered repositories. Such growing waste volumes and associated environmental concerns have stimulated much research into additional resource recovery at phosphate mines. Research around the valorization of phosphatic mine wastes have demonstrated that wastes can serve as: (i) dry covers in the capping and revegetation of mine waste repositories; (ii) additives in acid mine water treatment; (iii) feedstock for the ceramic industry; and (iv) resource materials in the building industry (e.g., Tayibi et al., 2009; Hascke et al., 2016; Hakkou et al.,

2016). Hence, phosphate mine wastes can be recycled and reused for a range of applications. Such activities would minimize potential environmental damage, reduce the footprint of phosphate mines, and lead to the development of other local industries.

Valorization of metallurgical wastes

Much larger waste volumes accumulate at fertilizer plants, with phosphogypsum (PG) being by far the major waste product, which accrues during the hydrometallurgical treatment of phosphate ores (Lottermoser, 2010). Global production of PG has been estimated to be as high as 300 Mt per year. PG largely comprises of calcium sulfate crystals, making it an attractive alternate to gypsum suitable for building and agricultural uses and as a source of valuable products (e.g. sulphuric acid, ammonium sulfate). Over the last few decades, different PG valorization routes have been developed in the agriculture, building, and environmental and energy sectors (e.g., Canovas et al., 2018). However, some PG may also contain residual phosphoric and hydrofluoric acid as well as metals (e.g., Cd, Pb), metalloids (e.g., As) and radionuclides (e.g., U-238, Th-232, Ra-226).

In the USA, the EPA has focussed on the presence of metals, metalloids and radionuclides in PG and has classified PG as "Technologically Enhanced Naturally Occurring Radioactive Material" (TENORM). This has prevented the large-scale reuse of PG (Wing, 2016). Hence in some countries like the USA, PG is stored in large stacks due to regulation of contaminant levels or because the alternatives (natural gypsum and flue gas gypsum) are more competitive. To be used for agricultural applications, PG needs to be very pure, or PG needs to reprocessed and purified from its contaminants. Otherwise, contaminants may be added to agricultural soils, become available to plants, and leach into ground and surface waters. Presently, only 15% of worldwide PG is recycled, whereas the remaining 85% is usually stacked, landfilled, or discharged to surface water (Zhang et al., 2017). Regardless, PG is increasingly utilized, with China, Brazil, Indonesia, and India leading the way and promoting its reuse, partly facilitated through supportive government policies and constructive regulation (Wing, 2016).

Valorization of by-products

Phosphate deposits may contain elevated concentrations of valuable elements, including uranium, radium, thorium, and rare earth elements (REE). Trace element concentrations of phosphate rock (e.g., U, Th, Ra, REE, As, B, Cr, Cu, Ga, Ni, Sc, Th, V, Zn) differ from region to region, with sedimentary phosphate ores containing in general higher trace element concentrations than igneous phosphate ores. Some uranium concentrations are high enough to be of commercial interest, and uranium has been recovered during fertilizer manufacturing at some locations (Haneklaus et al., 2017; Canovas et al., 2017). In the wet process, uranium and cadmium largely migrate into the phosphoric acid, whereas radium and thorium accumulate

in the PG. REE are present in both phosphoric acid and PG. Metal recovery is possible through acid leaching or the application of organic solvents and subsequent recovery of valuable constituents applying ion exchange technology (e.g., Valkov et al., 2014; Walawalkar et al., 2016; Cánovas et al., 2018; Wu et al., 2018). Thus, the extraction of by-products during fertilizer manufacturing is possible using established technologies. Such resource recovery would minimize potential environmental damage, reduce the environmental footprint of fertilizer plants, lead to the development of additional local industries, and generate added-value products for market applications.

Best practice examples in valorization

There are emerging best practice examples for the reprocessing of and the recovery of resources from PG and hence for the valorization of phosphate mine wastes. For example, patented radionuclide classification and separation systems are available to classify, sort, and separate non-radioactive PG material from radioactive, environmentally hazardous PG (raPHOSafe, 2019). This enables recycling of the non-radioactive PG into construction material (e.g., dry-walling gypsum boards, cement), whereas the radioactive (Ra-226) PG material provides a highly sought-after resource for further processing into radiopharmaceutical applications such as Ra-223 for cancer treatment (e.g., Xofigo, Bayer Pharmaceuticals; Haschke et al., 2016). Ra-223 is an isotope of radium with a 11.4-day half-life, and its principal use is as a radiopharmaceutical to treat metastatic cancers. The treatment takes advantage of the radionuclide's chemical similarity to calcium, and the short range of the alpha radiation it emits. The use of Ra-223, which originates from PG waste, is a best practice example for the valorization of phosphate rock. However, the demand for Ra-223 is miniscule compared to the gigantic volumes of PG available for reprocessing. In future, the push for the reprocessing of PG stacks may arise from the fact that in Europe the closure of coal power stations will lead to a dramatic decline of FGD (flue gas desulphurization) gypsum production (18–19 Mt pa), and availability. PG may arise as the alternative material to FGD gypsum.

Conclusions: Obstacles to the valorization of phosphate rock

Phosphate rock has diverse compositions and geological properties that control its site-specific characteristics and resultant opportunities for resource recovery and valorization. To date, scientists have identified diverse valorization pathways for phosphate rock. Unfortunately, many of the proposed reprocessing, reuse, and recycling routes have remained research outcomes that have not been taken up by industry. Consequently, much of the uranium, thorium, radium, and REE still end up in the waste stream or the fertilizer value chain, and agricultural soils and underlying drinking water aquifers become increasingly contaminated by uranium and other elements (Liesch et al., 2015).

Unfortunately, many research outcomes and concepts of resource recovery remain ideas that cannot be taken up in the real world, because existing government regulations do not allow such activities. In particular, legislation by government agencies in Europe and North America prevents the reprocessing and reuse of wastes. These authorities are obsessed with setting environmental risk limits for organic and inorganic substances. Changes in regulatory attitude are needed to ensure that regulations are based on scientific evidence and best practices. In particular, supportive government policies and constructive regulation are required (cf. Hilton et al., 2010), which will allow the safe use of pure phosphogypsum for suitable applications. Most of all, government authorities should not only set legal limits for contaminants in fertilizers (e.g., Cd, U) but also thresholds for resource ingredients that, when present above a certain concentration, have to be extracted from the mined ores. For phosphate rock in particular, thresholds for the compulsory recovery of by-products should be given (e.g., U, Ra, REE), enforcing the valorization of phosphate rock.

Financial incentives for industry such as subsidies for "cleaner fertilizers" may support the economic profitability of uranium and REE extraction from phosphate rock. However, such incentives would likely be ineffective and wasteful. Studies of incentives for other industries have established that most incentives only achieve temporary compliance, or give industry extra benefits to do things it would have done even without incentives. When it comes to producing lasting change, incentives are strikingly ineffective. In the end, government authorities need to be more proactive, legislate valorization of fertilizer production, and thereby enforce the manufacturing of added-value products for market applications.

References

Cánovas, C.R., R. Pérez-López, F. Macías, S. Chapron, J.M. Nieto and S. Pellet-Rostaing. 2017. Exploration of fertilizer industry wastes as potential source of critical raw materials. *J. Cleaner Prod.* 143: 497–505.

Cánovas, C.R., F. Macías, R. Pérez-López, M. Basallote and R. Millán-Becerro. 2018. Valorization of wastes from the fertilizer industry: Current status and future trends. *J. Cleaner Prod.* 174: 678–690.

Hakkou, R., M. Benzaazoua and B. Bussiere. 2016. Valorization of phosphate waste rocks and sludge from the Moroccan phosphate mines: Challenges and perspectives. *Procedia Eng.* 138: 110–118.

Haneklaus, N., Y. Sun, R. Bol, B.G. Lottermoser and E. Schnug. 2017. To extract, or not to extract uranium from phosphate rock, that is the question. *Environ. Sci. Technol.* 51: 753−754.

Haschke, M., B. Friedrich, S. Stopic, D. Panias, P. Schneider and C. Dittrich. 2016. Extraction of critical technology elements and radionuclides from phosphogypsum tailings. In Opportunities in Processing of Metal Resources (OPMR) Conference, Budapest.

Hilton, J., B. Birky and A.E. Johnston. 2010. The "constructive regulation" of phosphates and phosphogypsum. A new, evidence-based approach to regulating a NORM industry vital to the global community. In *Proceedings of IRPA12: 12. Congress of the International Radiation Protection Association: Strengthening Radiation Protection Worldwide – Highlights, Global Perspective and Future Trends*. International Atomic Energy Agency, Vienna.

Liesch, T., S. Hinrichsen and N. Goldscheider. 2015. Uranium in groundwater − fertilizers versus geogenic sources. *Sci. Total Environ.* 536: 981−995.

Lottermoser, B.G. 2010. *Mine Wastes: Characterisation, Treatment and Environmental Impacts*. Berlin Heidelberg: Springer-Verlag.

raPHOSafe. 2019. Retrieved from https://eitrawmaterials.eu/project/raphosafe/ Accessed 01.07.2019.

Tayibi, H., M. Choura, F.A. Lopez, F.J. Alguacil and A. Lopez-Delgado. 2009. Environmental impact and management of phosphogypsum. *J. Environ. Manag.* 90: 2377–2386.

USGS. 2019. Phosphate rock. US Geological Survey, Mineral Commodity Summaries, February 2019.

Valkov, A.V., V.A. Andreev, A.V. Anufrieva, Y.N. Makaseev, S.A. Bezrukova and N.V. Demyanenko. 2014. Phosphogypsum technology with the extraction of valuable components. *Procedia. Chem.* 11: 176–181.

Villalba, G., Y. Liu, H. Schroder and R. Ayres. 2008. Global phosphorus flows in the industrial economy from a production perspective. *J. Industrial Ecol.* 12: 557–569.

Walawalkar, M., C.K. Nichol and G. Azimi. 2016. Sustainable processing of phosphogypsum waste stream for the recovery of valuable rare earth elements. In R.E. Kirchain, et al. (editors) *REWAS 2016*. Springer: 107–112.

Wing, J. 2016. The phosphogypsum era – utilizing the phosphate industry's most abundant co-product. AIChE Clearwater Phosphate Conference, 11 June 2016, Clearwater Beach, Florida, USA.

Wu, S., L. Wang, L. Zhao, P. Zhang, H. El-Shall, B. Moudgil, X. Huang and L. Zhang. 2018. Recovery of rare earth elements from phosphate rock by hydrometallurgical processes – a critical review. *Chem. Eng. .J* 335: 774–800.

Zhang, F., Q. Wang, J. Hong, W. Chen, C. Qi and L. Ye. 2017. Life cycle assessment of diammonium- and monoammonium-phosphate fertilizer production in China. *J. Cleaner Prod.* 141: 1087–1094.

Proceedings of Tailings and Mine Waste 2019
November 17–20, 2019, Vancouver, Canada
Published by the University of British Columbia, 2019

Post-Córrego do Feijão: Continued Evolution of Tailings Dam Regulations in Brazil

Kimberly F. Morrison, Newmont Goldcorp, USA
Paulo C.R. Gomide, CMOC Brasil, Brazil

Abstract

The failure of Dam I at Vale's Córrego do Feijão iron ore mine near Brumandinho, Brazil, on January 25, 2019, was not only shocking and devastating, but raised the industry's radar with respect to so-called "inactive" tailings dams. With an anticipated death toll of approximately 270, this failure may be the worst industrial accident in Brazil's history. Mere days after the failure, new regulations were imposed in the state of Minas Gerais, while a couple of weeks later, stricter regulations were proposed for tailings management within the entirety of Brazil. The public's trust of the mining industry in Brazil has further degraded because of this failure, and hence the regulatory environment continues to evolve with a corresponding increase in regulatory controls. This paper is a sequel to a paper published in the *Proceedings of Tailings and Mine Waste '18,* titled "Changes to tailings dam regulation in Brazil in the aftermath of failures", which highlighted the post-Samarco regulatory changes.

Another failure in Brazil

On January 25, 2019, Dam I at Vale's Córrego do Feijão iron ore mine failed without warning. The failure occurred in the middle of the day, sending a mud wave through heavily occupied mine offices and a cafeteria into the downstream village of Brumandinho. As of July 10, 2019, 248 bodies have been identified, while another 22 people remain missing (Vale, 2019b; 2019c).

At a final height of 87 m, the tailings dam was initially constructed in 1976 and raised from 1982 to 2013 using the upstream construction method (Vale, 2016). Dam I had reportedly not received tailings since 2014 (BBC, 2019) and was considered inactive; however, at the time of failure, drill rigs were working on the dam attempting to repair failed horizontal drains. Also, shortly before the failure, on November 20, 2018, Vale had received approval from the State Secretary for Environmental and Sustainable Development ("SEMAD") that provided a 10-year license to expand the Córrego do Feijão Mine and the Jangada Mine, integrating what Vale called the Paraopeba Complex, including re-mining of tailings from Dams I and VI

to recover iron ore fines. The license application was fully approved on December 11 by the Chamber of Mining Activities of the State Environmental Policy Council ("CMI/COPAM") (Andrade, 2019).

The industry record on tailings dam performance, as measured by number of failures, remained generally unchanged over the last 50 to 60 years, with an average of about two failures per year. However, there is a disturbing trend of increased severity of the failures, with 63% of all incidents and failures since 1990 classifyied as Serious (i.e., large enough to cause significant impacts or loss of life) or Very Serious (i.e., catastrophic dam failures that released more than one million m^3 of tailings and, in some instances, resulted in multiple loss of life) (Bowkers and Chambers, 2015). The failure at Brumandinho was the second recent Very Serious tailings dam failure in Brazil, following the November 2015 Fundão tailings dam failure at the Samarco iron ore mine.

At least nine notable tailings dam failures have been documented in Brazil since 1986, many having severe consequences and the majority having occurred before the advent of Brazilian legislation applicable to tailings dams (Morrison et al., 2018). Figure 1 presents a timeline of major tailings dam failures in Brazil and implementation of key dam safety regulations.

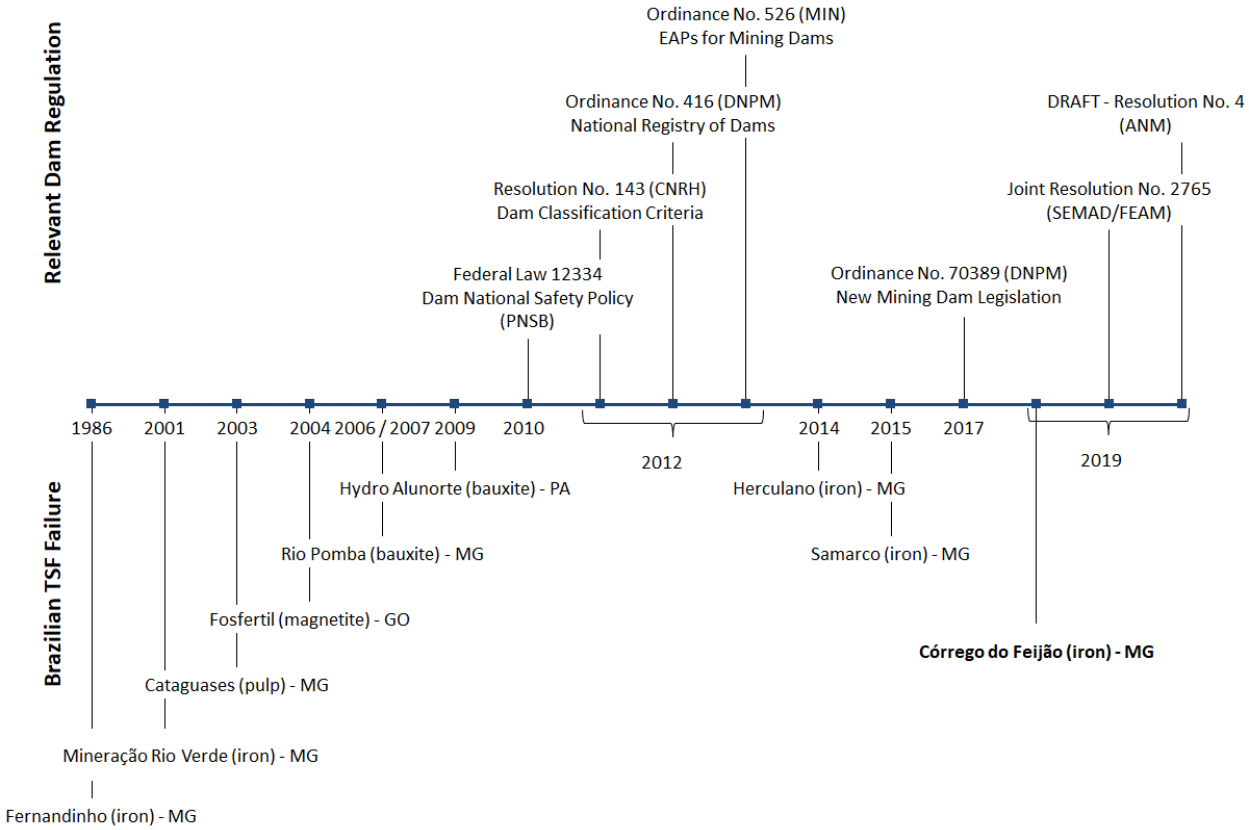

Figure 1: Chronological sequence of reported tailings dam failures in Brazil and notable changes in regulations (after Morrison et al., 2018)

Regulation in Brazil: A function of public trust?

At least seven tailings dam failures occurred in Brazil prior to the country publishing its first dam safety policy in 2010. Federal Law No. 12.334 (Presidência de República, 2010) established the Dam National Safety Policy ("PNSB"), which applies to any dam intended to accumulate water and/or waste for any use, which meets one or more of the following conditions:

1. dam height greater than or equal to 15 m;
2. reservoir capacity greater than or equal to three million m^3;
3. reservoir containing hazardous solids (according to Brazilian standards); and/or
4. classification of Medium or High with respect to associated potential damage ("DPA") (Morrison et al., 2018).

Law No. 12.334 set out general requirements for dam owners with respect to dam safety, including classifying dams based on risk, development of dam safety plans, and dam safety inspections and reviews (Morrison et al., 2018). As the law was general in nature, subsequent regulations were developed to provide necessary details.

The Samarco failure in November 2015 led to significant changes to the regulations and requirements surrounding tailings management in Brazil. Specifically, the National Mining Agency ("ANM", formerly known as the Department of Mineral Production, "DNPM") published Ordinance No. 70.389 in May 2017, which modified the National Mining Dams Registry; revised the classification criteria for tailings dams; overhauled the emergency action plan requirements; and established requirements for periodic dam safety reviews; among other requirements (Morrison et al., 2018). Operators had until May 2019 to comply fully with the new law. The dramatic video footage of the failure at Brumandinho was one of the results of this ordinance, as it required the installation of continuous (24-7) video monitoring of tailings dams. This ordinance also required the deployment of sirens and other appropriate mechanisms for warning the population in the self-rescue zone ("ZAS") downstream of the dam of imminent failure, whereby the ZAS is defined as the greater of:

1. the region downstream of the dam within 10 km; or
2. where the time of arrival of a flood wave based on a hypothetical dam breach analysis is equal to 30 minutes (Morrison et al., 2018).

However, this system was either not functioning, or was not triggered, to warn people downstream of Dam I on that fateful day in January 2019.

The failure of Dam I at the Córrego do Feijão mine has resulted in a further degradation of the public's trust in the mining industry, particularly in Brazil. The pyramid presented in Figure 2 shows how regulation

is largely a function of community trust. Specifically, when the public exhibits maximum trust, no regulation or guidelines are considered necessary. Conversely, when maximum public control is considered necessary, an activity is banned or prohibited.

Prior to 2010, some may argue that the public in Brazil exhibited significant trust in the mining industry, with no regulation of tailings and only generic guidance for dam safety (e.g., CRSB, 1999). With the advent of tailings regulation in Brazil in 2010 after a series of failures (refer to Figure 1), the public moved into the realm of general trust. The Samarco failure pushed the dial toward a higher level of control, while the failure at Brumandinho caused the public to desire a high level of control, with prescriptive regulations and banning of upstream dam construction.

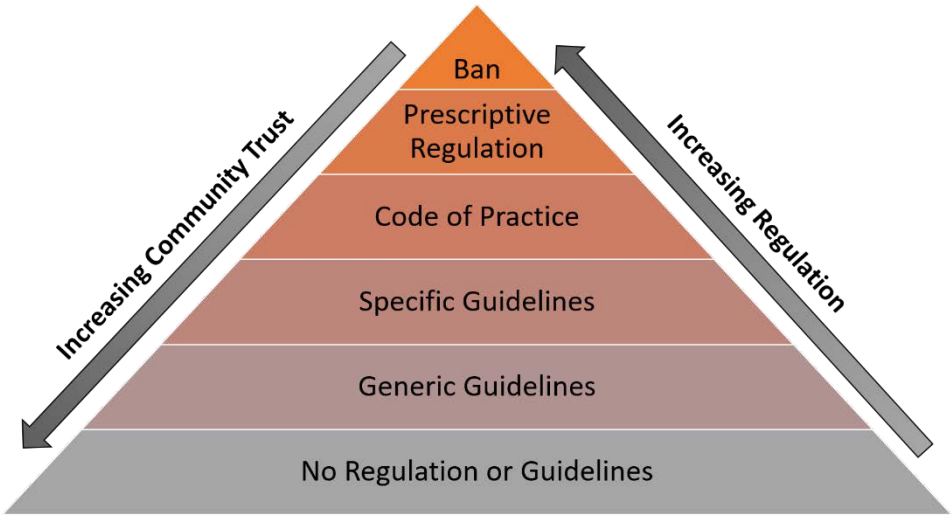

Figure 2: Trust-control regulatory relationship

Proposed new tailings dam regulations in Brazil

A mere five days after the failure of Dam I at Córrego do Feijão, SEMAD and the State Environmental Foundation ("FEAM") in Minas Gerais enacted new regulations, with ANM proposing new regulations for the entire country of Brazil a few weeks later. At the time of authoring this paper, the new regulations in Minas Gerais were in force; however, ANM's proposed regulatory changes for the remainder of Brazil had not been fully enacted. Many operators have started to work toward conformance with the new and proposed regulations to the extent feasible.

Joint Resolution No. 2.765 (SEMAD/FEAM)

On January 30, 2019, in response to the failure of Dam I and a mere five days later, Joint Resolution SEMAD/FEAM No. 2.765 ("Joint Resolution") was published in the Minas Gerais' Official Gazette (Antunes et al., 2019). The Joint Resolution requires de-characterization of all tailings dams constructed

using the upstream method or an unknown method in the state of Minas Gerais. De-characterization is defined as the process in which the dam no longer has the characteristics of a dam (i.e., does not operate as a tailings containment structure) and is destined for another purpose (Antunes et al., 2019). One day prior to publishing the Joint Resolution, on January 29, Vale (2019a) issued a press release stating that they had presented a plan to the Brazilian authorities to decommission all of its dams constructed via the upstream method (10 dams in total), with an aim to de-characterize the structures as tailings dams in order to reintegrate them into the environment.

Mining companies were required to develop a work plan for de-characterization of their upstream-constructed tailings dams. Article 5 of the Joint Resolution called for development of an expert committee to define the minimum content of the work plan and the maximum deadlines for implementation. For inactive upstream-constructed tailings dams, the mining companies were provided 180 days from the date of publication of the minimum work plan requirements to present their plan for de-characterization to the regulatory authority (i.e., FEAM), including deadlines and actions to achieve complete de-characterization. The Joint Resolution states that operators of upstream-constructed tailings dams that are currently in operation should promote migration to alternative technology, aiming to de-characterize the dam, and that the owner must, within 360 days of publication of the Joint Resolution, present the technology to be adopted with a work plan and schedule to FEAM. Owners of active dams then have a maximum of two years from presentation of the work plan to the regulatory authority to implement the strategy.

Draft Resolution No. 4 (ANM)

In mid-February 2019, ANM (2019a) published draft Resolution No. 4 ("Resolution") with new proposed regulations pertaining to tailings dams. Mining companies in Brazil were provided the opportunity to review the initial Resolution, and provide comments directly to ANM. The most significant comments pertained to the proposed schedule for completion of the various activities, with less aggressive schedules provided in the revised Resolution (ANM, 2019b). The proposed Resolution will establish regulatory measures targeted to all mining dams, and more specifically those that have been constructed or altered using the upstream method, or an unknown method.

First and foremost, the Resolution proposes to prohibit the use of the upstream construction methodology to raise mining dams throughout the national territory of Brazil. Both Dam I at Córrego do Feijão and the Fundão Dam at Samarco were constructed using the upstream method. In the case of the Fundão Dam failure, Samarco constructed upstream raises on previously-placed tailings at dangerously high rates of rise, averaging 1.1 to 1.5 m per month, with occasional months as high as 3 m per month (Morgenstern et al., 2016) in an effort to keep production levels high (Lombrana, 2019). After Samarco, at least one legislator previously attempted to pass legislation banning upstream dams in Brazil (Lombrana,

2019). Some countries have already banned upstream construction; for instance, Chile, a seismically-active country, issued a ban on upstream tailings dam construction in 1970 (Lombrana, 2019).

The Resolution proposes to prohibit mining companies from designing, constructing, maintaining, or operating any facilities intended for administration, accommodation, health, or recreation in the self-rescue zone (ZAS) downstream of any tailings dam, regardless of construction method. In addition, the Resolution proposes to ban the construction of dams or structures for storage of liquid effluents immediately downstream of a mining dam whose existence may compromise the safety of the dam, and any installation that uses or stores radioactive sources. The proposed Resolution provides timeframes for removal of existing facilities in the ZAS.

The Resolution provides factor of safety (FS) requirements for existing tailings dams, regardless of construction method adopted. The Resolution indicates that it is up to the dam designer, a professional who is legally qualified by the Regulatory Engineers Agency ("CONFEA/CREA"), to calculate the safety factors of mining dams using Brazilian regulatory requirements (NBR 13.028; ABNT, 2017), international standards and good engineering practices; and that values below 1.3 for peak resistance are prohibited for stability analyses and liquefaction susceptibility studies in the undrained condition. Though not in the proposed Resolution, some engineering firms in Brazil are assuming a minimum safety factor of 1.5 is required because the Brazilian regulatory requirements leave the definition open (NBR 13.028; ABNT, 2017). Also, internationally, mining companies are reacting to the failures by gradually requiring higher factors of safety, with static factors of safety less than 1.5 under undrained conditions becoming less accepted.

Further, the material parameters used in stability analyses must be defined from the analysis and interpretation of results of updated and representative geotechnical tests, as defined by the designer. In cases where the safety factor, under drained or undrained conditions, is momentarily below the minimum values established in the regulations (NBR 13.028; ABNT, 2017), the dam is immediately interdicted and the owner is obligated to suspend operations of the dam and notify ANM, as well as to implement mitigation actions to ensure the safety of the structure and to assess the need to evacuate the downstream area until the safety factors return to the acceptable minimum values. Notifications to ANM are to be done through SIGBM, which is a unique online database that provides ANM with access to key information on each registered tailings dam in the country (Morrison et al., 2018).

The factor of safety issue is highlighted by reportedly low factors of safety of Dam I at Córrego do Feijão. Approximately six years prior to the failure, Pirete and Gomes (2013) presented analyses of Dam I demonstrating that the tailings exhibited contractive behaviour during shear and were susceptible to liquefaction. However, they presented factors of safety of 1.14 to 1.36, stating that the tailings were unlikely to exhibit static liquefaction, whereby a factor of safety in excess of one was considered acceptable. The

last safety audit of Dam I submitted by TUV-SUD in September 2018, over four months prior to the failure, summarized several issues with the structure, including:

- lack of study of the dam foundation prior to dam construction;
- no internal drainage in the starter dike or the first dike (at a minimum) above the starter dam;
- damage to internal drainage tubes (due to cows or vegetation);
- muddy water and staining of the embankment indicative of internal erosion;
- seemingly unreliable piezometric data indicating water levels above the ground surface; and
- a factor of safety of only 1.09 in undrained conditions; among other issues (Emerman, 2019; TUV-SUD, 2018).

The classification system employed in Brazil for tailings dams considers two parameters, risk category ("CRI") and associated potential damage ("DPA"), each of which are scored separately. The classification by CRI considers the technical characteristics, and the state of conservation of the structure and compliance to the dam's safety plan, while the classification by DPA considers the potential of loss of human lives and economic, social, and environmental impacts arising from the possible dam failure (Petry et al., 2018). As shown in Table 1, Class A is the highest hazard and Class E is the lowest when considering both parameters.

Table 1: Brazilian classification matrix based on risk category and associated potential damage

	Associated potential damage (DPA)		
Risk category (CRI)	**High**	**Medium**	**Low**
High	A	B	C
Medium	B	C	D
Low	C	D	E

Article 6 of the Resolution states that owners of mining dams with a DPA of "High" are required to implement an automated monitoring system with real-time continuous monitoring following the criteria defined by the dam designer (by December 15, 2020). As a point of reference, Dam I at Córrego do Feijão was only classified as a Class C structure (or moderate risk), though the DPA was scored as "High" (Vale, 2016). Other dam hazard classification systems, such as that developed by the Canadian Dam Association (CDA, 2013), would have classified this structure as "Extreme" risk given the loss of life alone, highlighting the need for development of an international dam hazard classification system to more appropriately characterize a dam based on consequence as opposed to perceived likelihood of failure.

With the exception of conventional dams constructed in a single stage, the Resolution states that mining dams required to have an emergency action plan per Ordinance No. 70.389 (DNPM, 2017) must rely on automated systems for triggering of the early warning system (i.e., sirens) to warn of potential dam failure. Possibly an automated system for triggering sirens may have resulted in different consequences at

Brumandinho; however, the threshold level for establishing the alarm trigger is undefined (e.g., FS < 1.1, etc.) and would rely on definition by the engineer. A deadline for implementation of the automated system of August 15, 2020, is proposed.

Similar to Joint Resolution No. 2.765, the Resolution requires de-characterization of upstream-constructed tailings dams and dams constructed using an unknown method. Mining companies are required to complete development of a project that proposes works to reinforce the downstream dam, or construct a new containment structure downstream with a view of minimizing the risk of rupture by liquefaction or reducing the damage associated with a failure. Specifically, the Resolution proposes to change the wording of Ordinance No. 70.389 (DNPM, 2017) in Article 2, Part VIII, requiring de-characterization according to a technical project, including (but not limited to) the following steps:

- Decommissioning: Cease operations with the removal of associated infrastructure, except that intended to enhance the safety of the structure.
- Hydrological and hydrogeological control: Adopt effective measures to reduce or eliminate the supply of surface water and groundwater to the reservoir.
- Stabilization: Implement measures to ensure the long-term physical and chemical stability of the structure(s) that remains.
- Monitoring: Monitor for the period necessary to verify the effectiveness of stabilization measures.

A deadline for development of the work plan by December 15, 2019, was proposed, while construction of downstream reinforcement or a new containment structure downstream is proposed to be complete by September 15, 2021. A schedule for completion of the dam de-characterization process was proposed, with dams containing a volume of less than five million m^3 to be completed by September 1, 2022, and dams containing a volume larger than this by September 15, 2023.

The Resolution proposes additional modifications to the content of Ordinance 70.389 (DNPM, 2017), including promotion of alternative technologies for tailings management (e.g., dewatering), and the requirement for the statement of stability ("DCE") to be signed by both the technical representative responsible for dam safety, as well as an individual of greater authority in the hierarchy of the mining company. At the time of writing, the Resolution had not yet been voted into law in Brazil, and additional modifications should be expected to the final regulation.

Conclusion

Failures and incidents are often the catalyst for change. Brazil experienced significant re-design of regulations pertaining to tailings dams in response to the failure of the Fundão dam at Samarco, a joint

venture between Vale and BHP. However, further degradation of the public's trust of the mining industry in Brazil after the failure of Dam I at Vale's Córrego do Feijão in January 2019 will result in a push toward more prescriptive regulation, including an imminent ban on upstream-constructed tailings dams.

References

Agência Nacional de Mineração (ANM). 2019a. *Diário Oficial da União, Resolução Nº 4, de 15 de Fevereiro de 2019, GOV BR, 18 February, 2019.* Retrieved from http://www.in.gov.br/materia/-/asset_publisher/Kujrw0TZC2Mb/content/id/63799094/do1-2019-02-18-resolucao-n-4-de-15-de-fevereiro-de-2019-63799056.

Agência Nacional de Mineração (ANM). 2019b. Minuta Resolução Nº XX, DE XX DE XXXX DE 2019. Retrieved 28 July 2019 from http://www.anm.gov.br/assuntos/barragens/minuta.

Andrade, C. 2019. Estado concedeu licença de 10 anos para complexo de Vale no fim do ano, BHAZ. Retrieved 25 January 2019 from https://bhaz.com.br/2019/01/25/estado-concedeu-licenca-10-anos/.

Antunes, P.d.B., V. Gonçalves and B. Colaço. 2019. Brazil: Joint Resolution SEMAD/FEAM No. 2.765 /2019: De-characterization of upstream tailings dams in Minas Gerais, Mayer Brown. Retrieved 27 February 2019 from https://www.mayerbrown.com/en/perspectives-events/publications/2019/02/joint.

Associação Brasileira de Normas Técnicas (ABNT). 2017. Mining – Preparation and presentation of design of tailings, sediments and/or water dams – Requirements. ABNT NBR 13028:2017. 20 pp.

BBC News Brasil (BBC). 2019. *Brumadinho: O que se sabe sobre o rompimento de barragem que matou ao menos 115 pessoas em MG.* Retrieved 3 August 2019 from https://www.bbc.com/portuguese/brasil-47002609.

Bowker, L.N. and D.M. Chambers. 2015. The risk, public liability and economics of tailings storage facility failures. *Earthworks Action* 2015.

Canadian Dam Association (CDA). 2013. *Dam Safety Guidelines 2007*. 2013 edition. 88 pp.

Comissão Regional de Segurança de Barragens (CRSB). 1999. *Guia Básico de Segurança de Barragens.* Núcleo Regional de São Paulo.

Departmento Nacional de Produção Mineral (DNPM). 2017. Portaria No. 70.389, de 17 de Maio de 2017.

Emerman, S.H. 2019. English-language summary of the last safety audit of the failed dam at the Córrego do Feijão Mine. World Mine Tailings Failures, 5 February 2019. Retrieved from https://worldminetailingsfailures.org/wp-content/uploads/2019/02/Corrego_Feijao_Safety_Audit_Summary.pdf.

Lombrana, LM. 2019. Brazil's burst dam disasters blamed on cheap storage of mining waste. *Insurance Journal* 1 February 2019. Retrieved from https://www.insurancejournal.com/news/international/2019/02/01/516518.htm.

Morgenstern, N.R., S.G. Vick, C.B. Viotti and B.D. Watts. 2016. *Fundão Tailings Dam Review Panel: Report on the Immediate Causes of the Failure of the Fundão Dam*. 25 August 2016.

Morrison, K.F., H.G. Pedrosa, G.J.I. dos Santos, P.C.R. Gomide and A.M. Ferreira. 2018. Changes to tailings dam regulations in Brazil in the aftermath of failures. In Tailings and Mine Waste '18. *Proceedings of the 22nd International Conference on Tailings and Mine Waste*, Keystone, Colorado: Colorado State University: 27 –34.

Petry, A., M. Bomfim, L.F. Laus and A. Anderaos. 2018. Classification of dams by its hazard potential: The experience of the Brazilian National Water Agency. In *Dam World 2018. Third International Dam World Conference*, Iguazu Falls, Brazil.

Pirete, W. and R.C. Gomes. 2013. Tailings liquefaction analysis using strength ratios and SPT/CPT results. *Soil and Rocks* 36(1): 37–53.

Presidência de República. 2010. Lei No. 12.334, de 20 de Setembro de 2010.

TUV-SUD. 2018. Auditoria Técnica de Segurança 2o Ciclo 2018, Compexo Paraopeba – Mina Córrego Feijão Barragem I. 4 September 2018.

Vale, 2016. *Barragens de Mineração, Diretoria de Ferrosos Sul,* Vale, published 14 March 2016, https://www.slideshare.net/comcbhvelhas/barragens-de-mineracaovale.

Vale, 2019a. Vale announces the decommissioning of all its upstream tailings dams. Press Release, 29 January 2019. Retrieved from http://www.vale.com/EN/aboutvale/news/Pages/Vale-announces-the-decommissioning-of-all-its-upstream-tailings-dams.aspx.

Vale, 2019b. *Dams, Identified Bodies,* Vale, published 10 July 2019, http://www.vale.com/EN/aboutvale/reports/deaths-identified/Pages/default.aspx.

Vale, 2019c. Dams, uncontacted people until now, categorized as missing people, Vale, published 13 July 2019, http://www.vale.com/EN/aboutvale/reports/Missing_People/Pages/default.aspx.

Proceedings of Tailings and Mine Waste 2019
November 17–20, 2019, Vancouver, Canada
Published by the University of British Columbia, 2019

Transparent Online Monitoring System for Tailings Facilities through Meaningful Chilean Public-Private Collaboration

Angela Oblasser, Fundación Chile, Chile
Jorge Vargas, National Survey for Geology and Mining, Chile
Rodrigo Moya, Antofagasta Minerals, Chile
René Orellana, CODELCO, Chile
Cleve Lightfoot, BHP, Chile

Abstract

After the disaster in Brumadinho the mining industry has been the focus of attention. Beyond social, environmental, and technical considerations, the accident has affected mining from different angles with significant consequences for the industry if actions are not taken fast enough. The previous disasters of Samarco and Mount Polley underscored the issue of tailings management on an international level and in Chile. Today the Brumadinho disaster underscores the need to ensure significant progress in the short term.

In Chile, since 2015, a transparent and standardized online monitoring and early warning system for tailings facilities has been under development. The system will provide involved parties (authorities, mining companies, and communities) with better, reliable and timely information about the dams' behaviour in terms of physical (geotechnical) and chemical (environmental) stability. The ultimate goals are to strengthen preventative operational management and to improve communications and responses among the parties during emergency situations. The system is in the process of being fully implemented at El Mauro tailings facility at Los Pelambres Mine. It encompasses three interrelated subsystems: (1) a monitoring system that features methods and technologies for gathering relevant information for physical and chemical stability purposes (including data acquisition and data verification); (2) local (at the mine) and central (at a state agency) systems for collecting, processing, and analyzing the data gathered in order to measure dam performance (including data analysis and data integration tools); and (3) a communication model through which information is shared with the main parties (public entities, mining companies, and communities), including permanent, online disclosure of information and the generation of alerts in emergency situations. More than 180 professionals and 22 organizations and companies have collaborated in the development of the monitoring system over the last two and half years, making sure that it relevant and impartial. The whole

system, including the algorithms developed for data analysis and data intelligence, was developed using a free open source software stack and licensing scheme. All resulting products will be freely available to government agencies and mining companies. The aim is to provide local industry with highly specialized systems to reduce implementation costs and promote adoptability. This fully open architecture model is also focused on providing a framework for further data analysis modules development, and on enhancing interoperability with existing platforms.

In 2018, the Chilean government highlighted and recognized the results of the Transparent Tailings Initiative, announcing the inclusion of the system as part of the Chilean National Policy for Tailings to monitor the 104 active mine tailings in the country. During 2020 final adjustments to the system, based on the results of the implementation in the El Mauro and other tailings impoundments, will be carried out. The system will then be transferred to the National Geological and Mining Survey (SERNAGEOMIN).

Introduction – the shift from social to financial licence to operate

During 2015, mining companies in Chile faced important social risks to their tailings facilities. Obtaining a formal licence to operate from governments and meeting regulatory requirements was no longer enough. Instead, an increasing number of tailings projects were being delayed, interrupted, or even shut down (temporarily) due to public opposition.

This situation motivated three of the major mining companies, Antofagasta Minerals, BHP, and CODELCO to start the Transparent Tailings Initiative. This initiative aimed to generate transparent, on-line information regarding the performance of tailings, so as to improve confidence among downstream communities regarding this key operation for the mining industry. The initiative also aimed to generate on-line information for the operator (mining company) and the regulator (state) in order to improve the operational performance of the tailings and allow the operator to take early actions when an alert is triggered. The Transparent Tailings Initiative was co-designed and co-developed by Fundación Chile, the Chilean Mining Ministry, the National Geological and Mining Survey (SERNAGEOMIN), the National Office for Emergencies, the Superintendency of the Environment (SMA), the *Direccion General de Aguas* (DGA), the principal mining companies (Antofagasta Minerals, BHP, CODELCO), and actively involves communities and other local stakeholders. It pursues the development of a standardized monitoring and early-alert system applicable to tailings dams. This will create an information management platform that can provide the involved parties (authorities, mining companies, and communities) with good quality, reliable, and timely information about the dam's behaviour in terms of its physical stability and the potential changes to the surrounding natural water composition. The ultimate goal is to strengthen the preventative operational management, and improve communications and response among the parties when faced with unexpected emergency situations.

Today, three years after the initiative begun, and as a consequence of one of the worst tailings failure ever, another stakeholder has raised concerns about tailings management and tailings safety: the financial and insurance sector. Proof of this growing concern is the Investor Mining and Tailings Safety Initiative, an investor-led engagement assembling institutional investors who are active in the extractive industries, including major asset owners and asset managers. In April of 2019 this initiative requested more than 600 extractive companies to provide a specific disclosure regarding their tailings facilities, including information about the consequences of potential failure, such as loss of life and damage to the environment. This is just the first step in the important shift from social to financial licence to operate for mining sector.

Chilean mining authorities have also focused attention on tailings facilities, aiming to build a next-generation compliance monitoring system, based on electronic reporting to help make environmental reporting more accurate, complete, and efficient, and expanding transparency by making information more accessible to the public, while using innovative enforcement approaches such as data analytics and targeting to achieve more widespread compliance.

All three stakeholders, the communities, the financial and insurance sector, and mining authorities, are united by these objectives: transparency of tailings management; and sharing better, reliable, and timely information about the behaviour of dams in terms of geotechnical and environmental stability.

The Transparent Tailings Initiative is in line with these global requirements regarding tailings management. Beginning as a voluntary program in 2018, it was included in the Chilean National Policy for Tailings, in light of its potential mandatory application to all 104 active tailings facilities. Chile's Mining Minister highlighted that the:

> "Transparent Tailings Initiative will position Chile as a leader in the management of information on the performance of these tailings deposits, through online monitoring and accident prevention. All this through the delivery of timely information through the creation of the National Observatory of Tailings Deposits, administered and operated by SERNAGEOMIN."

This paper presents a detailed description of the monitoring systems, and their data analysis and early alerts components.

The Chilean monitoring and early warning system for tailings facilities

The system encompasses three interrelated subsystems and five basic components. These are the three subsystems:

1. The monitoring system features methods and technologies for capturing the relevant information for physical (geotechnical) and chemical (environmental) stability purposes (including data acquisition and data verification).

2. The local (at the mine) and central (at a state agency) monitoring systems responsible for collecting, processing, and analyzing the data in order to define dam performance (including data analysis and data integration tools).
3. The model through which information is disclosed to the main parties (public entities, mining companies and communities), including continuous online disclosure of information and the generation of alerts under emergency situations.

The system is designed to collect and process information with different degrees of complexity and frequency in different types and life cycles of deposits. These tools make up a system for monitoring and analyzing the performance of the deposit, based on the five basic components that are shown in Figure 1. The general process integrates sets of heterogeneous data such as visual inspection or instrument data, which are often massive, into models that can generate clear results to aid decision-making and remote control. This also helps to achieve a progressive knowledge of the behaviour of the structure, in order to facilitate clear and timely communication to different users.

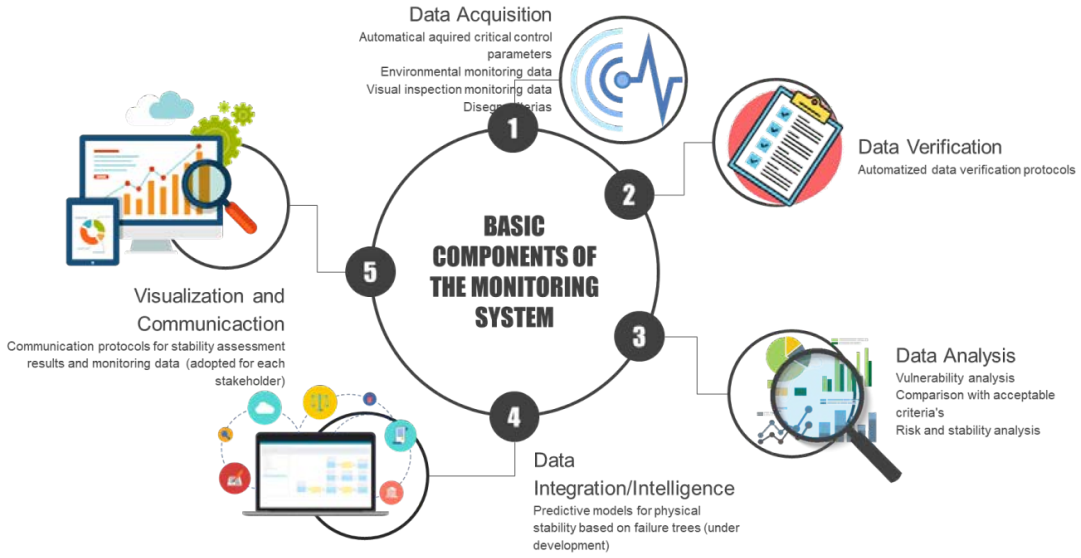

Figure 1: Basic components of the monitoring system

Local (mine) and central (authority) monitoring systems

Both mining companies and authorities will operate their own tailings monitoring systems, which are connected to each other and based on the same data analytics and intelligence modules: the local monitoring system (LMS), operated by the mining company and the central monitoring system (CMS) operated by SERNAGEOMIN. The LSM obtains monitoring information from multiple information sources: directly from monitoring sensors, indirectly from mining databases, and by manual data inputs provided by tailings operators. Simplified data verification processes are conducted in order to verify the truthfulness of the monitoring data, such as outlier detection, structural errors in sensors detected by calibration registers,

among others. Following, progressive data analysis processes, the information is analyzed in terms of tailings dams' vulnerability, critical controls, failure analysis, and environmental impacts. The information is presented through screen displays, co-designed for this purpose with mining operators and engineers of record.

The CMS in turn gathers the already processed monitoring data from the different local systems (having the right to directly access the detailed monitoring data of any local system), and connects with other systems operated by environmental or emergency agencies such as the SMA, the DGA, or the National Office for Emergencies. The CMS publishes accessible and comprehensive information for communities. It is important to highlight that the results of tailings monitoring are communicated simultaneously and online with mining authorities and communities, with different presentations and levels of details of information depending on each party's interests.

The devOps software and engineering was led by INRIA Chile, together with computer and software specialists from mining companies and authorities.

Physical (geotechnical) monitoring standard

Physical stability is defined by Chilean Law No. 20.551 on Closure of Mining Operations and Facilities (Chile, 2011) as a "structural safety situation that increases strength and reduces the destabilizing forces that may affect works or dams within mining operations. Different measures are applied with the purpose of preventing the occurrence of failures, collapses or removals". Within the framework of the Transparent Tailings Initiative, physical stability is defined as the dam have a structural state of equilibrium such that hydromechanical disturbances cannot trigger tailings failure, collapse, and removal or release phenomena. These are the three main types of failure capable of causing tailings release, collapse or removal from a dam:

1. Overtopping: Tailings are washed away and/or over the containment wall.
2. Internal erosion: Tailings water or fine material leak into the environment and seep under or through the dam.
3. Slope instability: Dam wall failure with tailings discharge.

The physical stability assessment tool is aimed at identifying and communicating the dam performance related to factors such as location site, selected design, and operation, in order to obtain a comprehensive panorama that can reinforce the preventative management applied to tailings dams.

Thirty critical geotechnical parameters are defined as key elements to determine the dams' stability, including properties of materials, water management, geometric elevations, piezometric level, moisture content, and compaction. Any deviation of these parameters from design considerations, together with the

existence of external determinants deemed as initiating events, can cause dams to fail. Table 1 details the critical parameters considered in the monitoring standard.

Table 1: Critical parameters for dam's physical stability

Recommended monitoring frequency	Parameter
15 days/Manual, Operator	Crest width and height; Slope inclination; Beach slope (filtered and pasted tailings);
Weekly/Manual	Minimum distance wall to clear-water pond; Soil foundation deformation; Wall displacement; Crest deformation
1 day/Automatic	Cracks observed in crest and wall; Tonnage; Operational status of emergency spillway; Integrity of the drainage system
1 day/Manual	Evidence of moisture and/or slope leaks downstream; Abutment integrity; Subsidence or caving in wall o in ditch, near the wall; Hydraulic freeboard; Operational freeboard
Threshold/Automatic, Manual	Wall and foundation soil pore pressures
Last year reports/Automatic	Heavy rain
Updated reports/Manual	Wall and dam phreatic level; Study of minimum required freeboard
Rain events/Automatic	Overflow potential
Verification after material placement/Manual	Wall compaction level; Wall material granulometry
Seismic records @ 200Hz/ Automatic	Wall seismic accelerations
Annual (Geotechnical campaign)/Manual	Tailing shear strength and rigidity (filtered and pasted tailings); Wall shear strength and rigidity; Foundation soil rigidity and strength
1 hour/Automatic	Turbidity of drain system water; Compliance of drain design criteria

In order to assess how a tailings dam is performing in terms of its physical stability, a tool has been developed that is capable of assessing the dam's condition based on the three main failure mechanisms likely to affect physical stability. Three sequential assessment blocks are proposed, differentiated by frequency, quantity, and complexity of information.

- B1: Qualitative assessment – a qualitative verification block that assesses vulnerability and aggravating factors, which verifies whether a specific event, or deviations from design, can trigger failure mechanisms.
- B2: Verification of critical parameters – verifies dam's condition by analyzing the monitoring system data, and provides alarms and/or alert signals based on predefined thresholds and control

parameter trends over time. If risk scenarios for any failure mechanism are encountered, it sends an emergency signal.

- B3: IEF – Fault trees – integration and predictive *R+i* tool that links data from blocks B1 and B2 in order to assess the dam's performance for each failure mechanism by means of models and analysis. Figure 2 details the dam stability assessment tool developed by the Transparent Tailings Initiative (Alamdari et al., 2012).

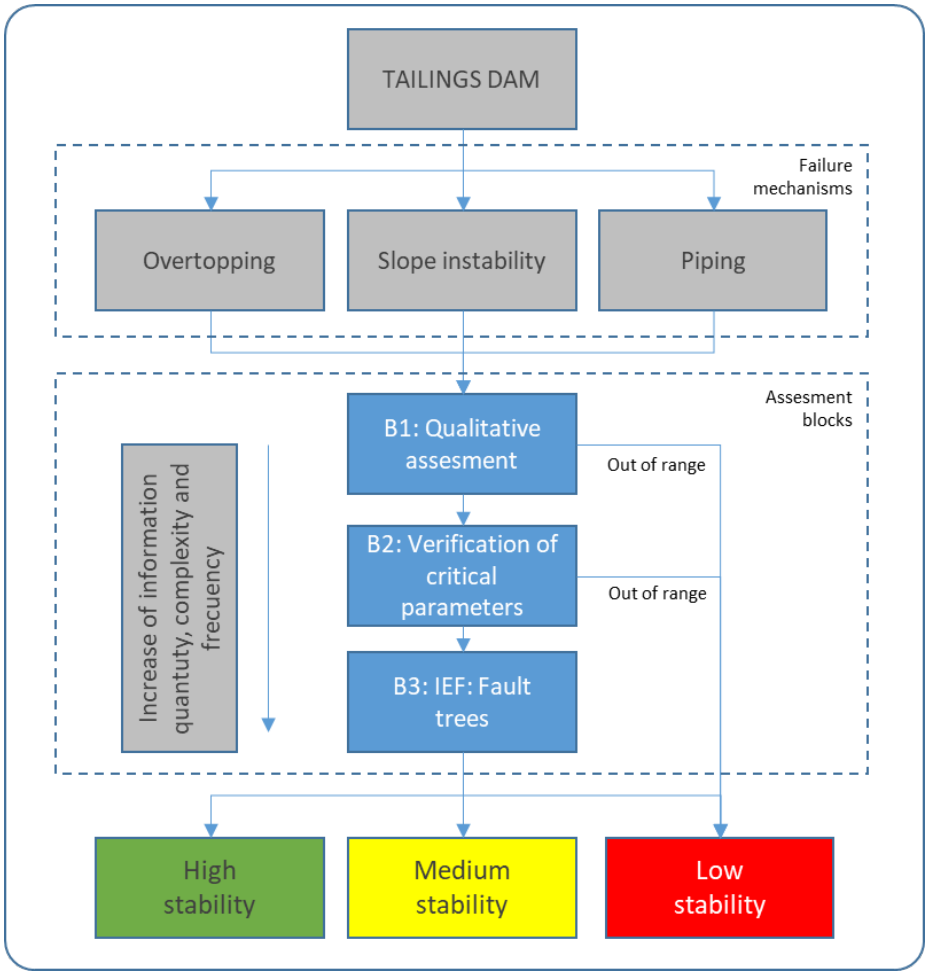

Figure 2: Dam's stability assessment tool

For each failure mechanism, specific scenarios to determine early warning and alert situations have been defined. As an example, the following scenario for the slope instability failure mechanism is presented. This scenario combines two critical parameters, in this case, the operational parameter *pore pressure* and the external event *earthquake.* In the event an intense VII[1] earthquake occurs, the operator must follow the procedure from B1; if previous to the earthquake there was evidence that more than one piezometric

[1] Mercalli Intensity: Difficult to stand or walk.

threshold had been exceeded (validation with redundancy instrument considered), a preventative *Early Alert Warning* is activated and simultaneously communicated to communities, mining company and mining authority. If, after the earthquake, an unfavourable trend in piezometer readings is detected, an *Emergency Alert* is activated, indicating the need for evacuation simultaneously to communities, the mining company, and the mining authority.

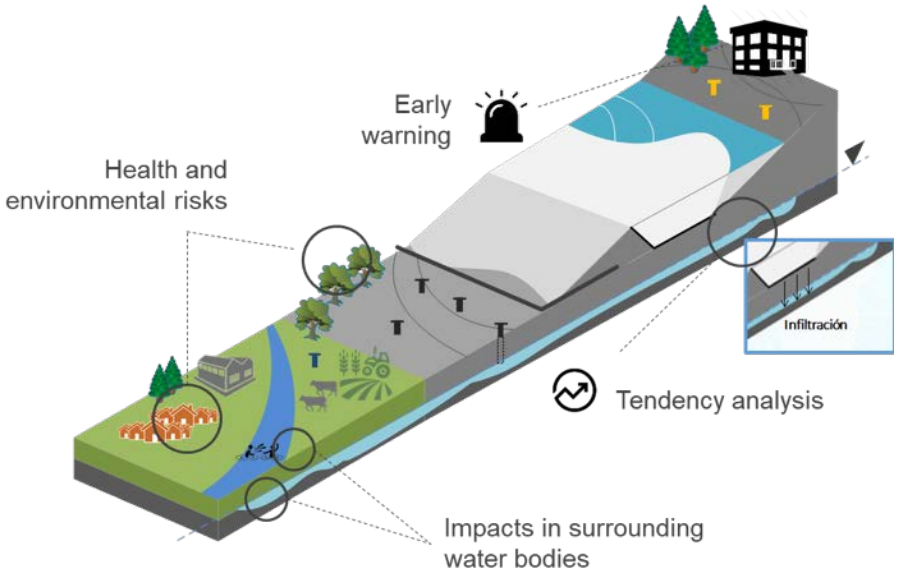

Figure 4: Example of slope instability failure mechanism

The geotechnical stability aspects were led by the University of Chile's Advanced Mining Technology Centre, together with Arcadis and BGC Engineering, and geotechnical, geomechanical and mining engineers, and other specialists, from mining companies and the authorities.

Chemical (environmental) monitoring standard

Chemical or environmental stability is defined by the methodological guide for the chemical stability of mining operations and facilities as follows: "Mining facilities are chemically stable when, in the course of their interaction with environmental factors, they do not generate impacts that pose significant risks to people's health and/or the environment" (SERNAGEOMIN, 2015). Within the Transparent Tailings Initiative framework, a tailings facility is considered to be chemically stable when such facility does not cause impacts on the surrounding waters or pose risks to people's health or the environment; nor are these expected to be impacted in the long term. Four different tools were developed for a timely assessment of the possible impacts a tailings dam might have on the adjacent waters, both underground as well as surface waters.

The monitoring standard considers both online measurement of physical-chemical variables and laboratory analysis of critical variables. Table 2 details the critical variables for chemical (environmental) tailings facility stability.

Table 2: Critical variables for chemical tailings stability

Recommended monitoring frequency	Parameter
Monthly	As; Al; B; Be; Cd; Cl-; Co; Cr; Cu; CN-; F-; Fe; Hg; Mn; Mo; Ni; Pb; Sb; Se; SO_4^{2-}; Zn
Daily (average measures)	Phreatic level; pH; Electric conductivity; ORP; Temperature

In order to assess how a tailings dam is performing in terms of its chemical (environmental) stability, four tools capable of assessing the tailings facility condition and its impact on natural surrounding water bodies have been developed.

- Early Management System (EMS): This conducts follow-up on the online-measured physical-chemical variables, allowing the early identification of deviations from the normal conditions of such variables.
- Trend Analysis (TA): Data is projected in order to capture the presence of trends, which will become significant if the 1 to 2 year projection exceeds the defined reference value (RV).
- Impact Index (II): The values of critical upstream (baseline) variables are compared against the downstream values. An impact is identified when downstream values are higher than upstream values (Roslan et al., 2007).
- Risk Index (RI): The values of critical variables downstream of the dam are compared against reference values (RV), compared to expected water use, i.e. irrigation, drinking water, etc. A risk is identified when at least one variable exceeds the reference values (RV) (Truett et al., 1975).

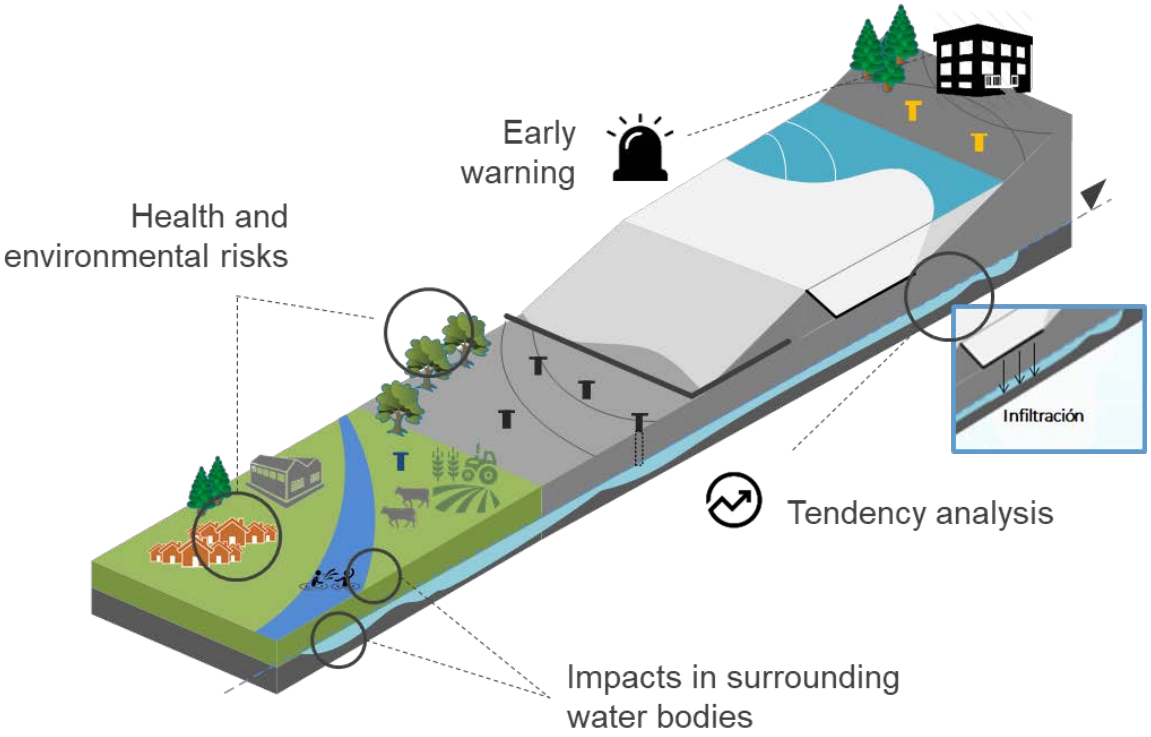

Figure 4: Chemical (environmental) tailings stability assessment tools

Figure 4 shows the four chemical (environmental) tailings stability assessment tools and their location in the surroundings of a tailings facility.

The environmental stability aspect was led by Fundación Chile, together with environmental, geological, and hydrogeological specialists from mining companies and authorities.

Screen displays and user interfaces

Different and specialized screen displays and user interfaces have been developed for mining companies users (tailings operator and engineer of record, amongst others), authorities, and communities. The construction was based on an intensive user experience (UX) process, an iterative method that helps continuously improve and polish the designs, involving relevant stakeholders in the process to make the end product highly efficient and usable. At this time more than 30 UX have been implemented with mine operators and 31 UX with representatives from five different mine related local communities. The preliminary results of this process are shown in Figures 5 and 6.

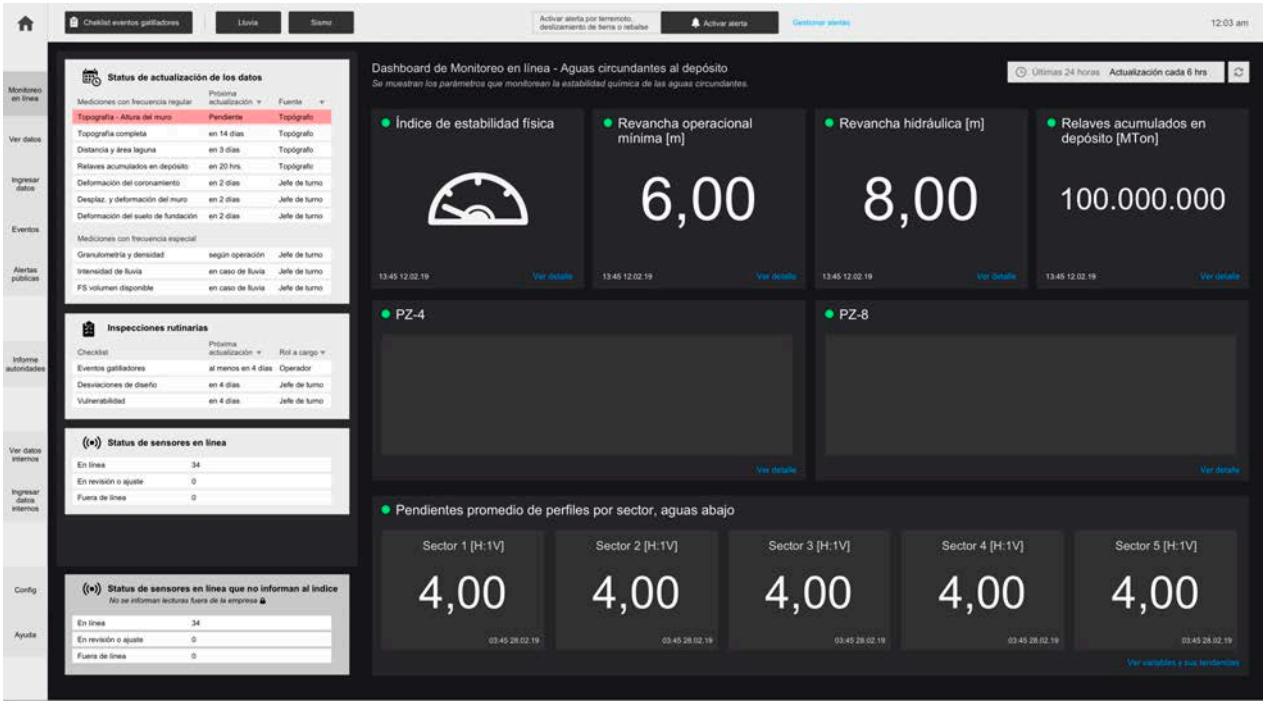

Figure 5: Mine operator interfaces (1)

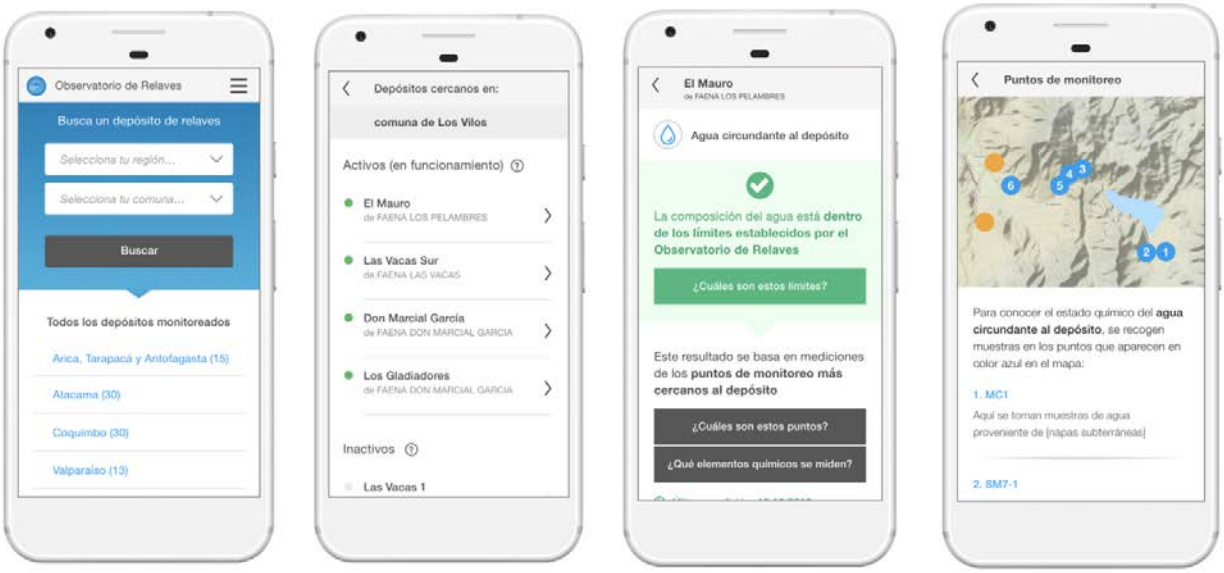

Figure 6: Community interfaces

Current stage of development

The system is currently being implemented at full scale at the El Mauro tailings facility belonging to Los Pelambres Mine owned by Antofagasta Minerals. It is also being considered as part of the design phase in the new SGO Spence and Laguna Seca tailings facility from BHP and Ovejería tailings facility from CODELCO.

In parallel, an intensive process to design the monitoring and control room for the central system has been implemented together with SERNAGEOMIN; as a result of this process a detailed technical and administrative process description, control room design, and estimation of operational and maintenance costs will be obtained during 2019. It is expected that the monitoring and control room will be implemented in the SERNAGEOMIN offices during 2020.

Full transparency to communities and authorities is expected to occur during 2020, once the data analysis tools have been validated with monitoring data from the three pilot tailings facilities.

Conclusion

Driven by a public private initiative composed of relevant representatives of the private and public mining sector and other related organizations, significant progress has been achieved in Chile towards transparent and preventative tailings management, ensuring both geotechnical and environmental stability. The system is under implementation at the El Mauro tailings dam at the Los Pelambres mine/Antofagasta Minerals (*local system).* It has also already been connected to the *central system* operated by SERNAGEOMIN. This system aims to provide authorities, mining companies, and surrounding communities with better, reliable and real-time information about the dams' behaviour in terms of physical (geotechnical) and chemical (environmental) stability. The ultimate goals are to strengthen preventative operational management, and to improve communications and response among the parties to unexpected emergency situations.

These achievements are the result of an innovative, collaborative, and voluntary effort made by mining companies and public agencies, in order to solve complex challenges and develop public goods and benefits.

Acknowledgements

The development of the Transparent Tailings Initiative has been possible thanks to Alta Ley Corporation and co-designed and implemented by FCH and its strategic partners, CORFO, Ministry of Mining, SERNAGEOMIN, ONEMI, SMA, DGA, Antofagasta Minerals, BHP, CODELCO, ENAMI, SONAMI, INRIA Chile, AMTC, and Valor Compartido.

References

Alamdari, N.Z., M. Banihashemi and A. Mirghasemi. 2012. A numerical modeling of piping phenomenon in earth dams, *Engineering and Technology* 6(1): 39–41.

Roslan, Mohamad M.K., Kamil Y. Mohd, S. Wan Nor Azmin and Mat Yusoff A. 2007. Creation of a ground water quality index for an open municipal landfill area. *Malaysian Journal of Mathematical Sciences* 1(2): 181 – 192.

ELK, Elasticsearch, Logstash and Kibana, https://www.elastic.co/pdf/arquitecture-best-practices.pdf

SERNAGEOMIN. 2015. *Guía Metodológica para la Estabilidad Química de Faenas e Instalaciones Mineras.* Retrieved from https://www.sernageomin.cl/wp-content/uploads/2017/11/GuiaMetodologicaQuimica.pdf

Truett, B., A.C. Johnson, W.D. Rowe, K.D. Feigner and L.J. Manning. 1975. Development of water quality management indices. J. *Water Resources Bulletin*. American Water Resources Association 11(3).

Bibliography

Alvarado, P., S. Barrientos, M. Saez, M. Astroza and S. Beck. 2009. Source study and tectonic implications of the historic 1958 Las Melosas crustal earthquake, Chile, compared to earthquake damage. *Phys Earth Planet Inter* 175(1–2): 26–36

Byrne, P.M. and M. Seid-Karbasi. 2003. Seismic stability of impoundments soil liquefaction Mochikoshi tailings dams. In *Proceedings, 17th VGS Symposium on Geotechnical Engineering for Geoenvironmental Applications,* Vancouver, British Columbia: 77–84.

Foster, M., R. Fell and M. Spannagle. 2000. A method for assessing the relative likelihood of failure of embankment dams by piping: Reply. *Canadian Geotechnical Journal* 3: 1025–1061. doi: 10.1139/t01-109.

Mattsson, H., J.G.I. Hellström and T.S. Lundström. 2008. Research report on internal erosion in embankment dams. *Geotechnical Engineering:* 1–70.

Psarropoulos, P.N. and Y. Tsompanakis. 2008. Stability of tailings dams under static and seismic loading. *Canadian Geotechnical Journal* 45(5): 663–675. doi: 10.1139/T08-014.

Walder, J.S. and J.E. O'Connor. 1997. Methods for predicting peak discharge of floods caused by failure of natural and constructed earthen dams. *Water Resources Research* 33(10): 2337. doi: 10.1029/97WR01616.

Wei, Z., Yin, G., Wang, J. G., Wan, L. and Li, G. 2013. Design, construction and management of tailings storage facilities for surface disposal in China: Case studies of failures, *Waste Management & Research*. 31(1): 106–112. doi: 10.1177/0734242X12462281.

Zandarín, M.T., L.A. Oldecop, R. Rodríguez and F. Zabala. 2009. The role of capillary water in the stability of tailing dams. *Engineering Geology.* Elsevier B.V., 105(1–2), pp. 108–118. doi:10.1016/j.enggeo. 2008.12.003.

Proceedings of Tailings and Mine Waste 2019
November 17–20, 2019, Vancouver, Canada
Published by the University of British Columbia, 2019

Static Liquefaction-Type Tailings Dam Failures: Understanding Options for Detecting Failures

Susanne Ouellet, BGC Engineering Inc., Canada
Naia Suszek, BGC Engineering Inc., Canada
Matt Lato, BGC Engineering Inc., Canada
Brad Russell, BGC Engineering Inc., Canada
Corey Froese, BGC Engineering Inc., Canada
Ed Carey, BGC Engineering Inc., Canada

Abstract

Recent tailings dam incidents have highlighted the need for near real-time methods capable of detecting static liquefaction-type failure. Based on experience with recent failures it is unclear whether any pre-failure deformation could have been observed with industry standard in-situ instrumentation or remote sensing monitoring methods. Jefferies and Been (2016) state the observational approach is inappropriate as it is not possible for conventional geotechnical monitoring to provide adequate notification of an imminent failure, which can occur in seconds to minutes. Thus, to detect a tailings dam failure and provide warning, the system must be capable of identifying a near instant change of state and reporting the change with high confidence. An event warning detection and notification system (EWDNS) is defined by the authors as a system capable of near real-time monitoring (i.e., the detection) of a tailings dam failure, with configuration into an alarm system to support the facility's emergency preparedness and response plan (EPRP). Warning systems to notify downstream stakeholders that would potentially be impacted in the event of a tailings dam breach are an important component of an overall risk management plan.

Several near real-time monitoring methods were assessed to determine if they were capable of detecting a tailings dam failure with no observable pre-cursory deformation, as a component of an EWDNS.

The methods were rated based on four primary factors: sampling rate, areal extent, frequency of false alarms, and maintenance requirements. The failure detection methods evaluated included in-situ instruments (downhole and linear on surface), ground-based remote sensing (lidar, radar and InSAR), and satellite-based methods. Following review, a linear fiber optics system was selected for installation at an upstream tailings dam facility.

This paper will present the method and rationale behind the selection of the monitoring method.

Introduction

Recent tailings dam incidents have highlighted the need for near real-time methods capable of detecting static liquefaction-type failure. Current understanding dictates these failures experience minimal pre-failure deformation.

Geotechnical site investigations, at an upstream tailings facility (the site) were carried out in 2017 and 2018. The site investigations encountered a wide areal extent of potentially liquefiable soils within the structures at the site. Due to the brittle nature of these soils, which can result in rapid failure of the structure, the observational approach is considered inappropriate for liquefiable materials as it is not possible for conventional monitoring to provide adequate notification of an imminent failure which can occur in seconds to minutes (Jefferies and Been, 2016).

Several near real-time monitoring options for implementation at the site as a component of an event warning detection and notification system (EWDNS) were reviewed. The purpose of the EWDNS is to provide near real-time monitoring (i.e., the detection) of a dam failure at multiple tailings dams, as well as be capable of configuration to an external alarm system to support the owner's emergency preparedness and response plan (EPRP).

Assessment factors

Several monitoring options were evaluated based on four assessment factors. These were developed based on the requirements of the EWDNS to provide adequate notification and timely detection of a dam failure.

Sampling rate

Based on the rapid nature of a brittle failure, a short response time is one of the most critical elements of the above system. The sampling rate of the chosen system should be capable at a minimum of one reading every five minutes, including transmission and processing of the data.

Areal extent

The chosen system must be capable of monitoring an area that covers the narrowest width of a dam breach that can reasonably be expected to occur at the structures. Because of the wide areal extent of the potentially liquefiable soils encountered at the site, a system that is capable of greater coverage is deemed advantageous over a system capable of lesser coverage. Systems that can provide continuous spatial coverage (i.e., 2 dimensional) are categorized as "Continuous". Systems that can provide lateral spatial coverage (i.e., 1 dimensional) along a structure are categorized as "Linear". Systems that cannot provide continuous or lateral spatial coverage (i.e., installed at discrete points) are categorized as "Discrete".

Frequency of false alarms

Due to the number of parties involved if a signal occurs indicating a dam failure (i.e., mine dispatch, first responders), the system should have a low probability for an erroneous reading that would trigger a false alarm. Erroneous readings that occur less than once per year and that can be recognized as a false reading are categorized as "Low", whereas erroneous readings that occur more frequently (i.e., once every few months) and that are difficult to recognize as a false reading are categorized as "Medium". Erroneous readings that occur more than once per month are categorized as "High".

Maintenance

The system should be capable of functioning year-round with minimal downtime given the environmental considerations at the site. "Low" maintenance was defined as requiring less than one site visit per year. "Medium" maintenance was defined as requiring approximately one site visit per year. "High" maintenance was defined as requiring more than one site visit per year.

Summary of monitoring methods

A thorough review of available monitoring technologies was undertaken based on the above factors. Table 1 presents a summary of the primary monitoring methods that were initially considered.

Table 1: Summary of monitoring methods assessed

Monitoring method	Sampling rate	Areal extent	Frequency of false alarms	Maintenance
DAS fiber optics	< 5 minutes	Linear	Unknown	Low
Brillouin fiber optics	Varies	Linear	Unknown	Low
Trip-wire / Slide detector fence	< 5 minutes	Linear	Unknown	Unknown
Seismic / Geophones	< 5 minutes	Continuous	Unknown	Low
Tiltmeter	< 5 minutes	Discrete	Medium	Low
Vibrating wire piezometers	< 5 minutes	Discrete	Medium	Low
Accelerometer	< 5 minutes	Discrete	High	Unknown
Time domain reflectometry	Unknown	Continuous	High	Unknown
Wireline extensometer	< 5 minutes	Linear	High	Unknown
Shape Accel Array (SAA)	> 5 minutes	Discrete	Medium	Low
Lidar	> 5 minutes	Continuous	High/Low (Climate)	Medium
Doppler radar	< 5 minutes	Continuous	High/Low (Climate)	Unknown
GB-InSAR / Terrestrial radar	< 5 minutes	Continuous	High/Low (Climate)	Medium
Differential GNSS	< 5 minutes	Discrete	Medium	Medium
Robotic Total Station (RTS)	< 5 minutes	Discrete	High/Low (Climate)	High

Many of the above monitoring methods, including lidar, GB-inSAR and RTS, are heavily influenced by climatic factors (frost or snow cover, or precipitation) and as such, would not function year-round without additional maintenance and/or data processing. As such, these methods were deemed inappropriate for use as the primary monitoring method in an EWDNS designed to detect a sudden static-liquefaction type failure. Although differential GNSS, accelerometers, SAAs, vibrating wire piezometers and tiltmeters were considered, the discrete point coverage was such that, alternative methods which provided linear coverage were considered more advantageous. In addition, the cost of a higher density coverage of a discrete point monitoring method, due to equipment, drilling and other installation factors, is generally much higher than the cost of a higher density coverage of linear or continuous monitoring methods.

Geophones and other seismic techniques were considered but ruled out due to uncertainties in the number of false alarms potentially generated at an active tailings and mine site, the lengthy calibration process, and the amount of pre-processing required.

Distributed fiber optics using Brillouin backscattering, traditionally used in geotechnical applications to measure strain, were deemed inappropriate due to the longer data acquisition time over longer lengths (Muanenda, 2018).

Monitoring methods deemed to meet the requirements of detection of a static liquefaction type failure from the above table are summarized below.

Doppler radar

Doppler radar calculates the velocity and direction of an object based on the shift in received frequency and can be applied to measure fast processes (few meters to few tens of meters per second) (Meier et al., 2016). Doppler radar has been used successfully in alpine settings to detect avalanches and automate closure of highways based on alarms across Europe. To the authors' knowledge, doppler radar has not yet been applied to detect tailings dam static liquefaction-type failures. As such, a period of calibration in the order of several months would be required before it could be implemented in either an event detection or early warning system.

Trip-wires or slide detector fences

Trip-wires (also referred to as wire sensors) and slide detector fences represent a simple concept of an alarm triggered by a break in a wire. To the author's knowledge, this type of system has not yet been applied in a tailings dam setting.

Trip-wires are more commonly used in geohazard applications to detect debris flows, landslides, and lahars (Keys and Green, 2008). Slide detector fences operate in a similar manner to trip-wires, consisting of a fence with a series of parallel wire sensors, and have been used to detect rock fall occurrences along railways (Pritchard et al., 2008).

Distributed acoustic sensing

Distributed fiber optic sensing systems provide a means of using a fiber optic cable as an array of sensors (Miah and Potter, 2017).

Distributed Acoustic Sensing (DAS) uses Rayleigh backscattering along a fiber optic cable to monitor multiple dynamic events in real time (Muanenda, 2018). This type of fiber optic method may consist of a standard telecommunications-grade fiber optic cable and a centrally-located signal processing module. The signal processing module transmits and receives beams of light through the fiber-optic cable. Vibrations or movement around the cable cause reflections in the beam of light to be sent back to the module, which are processed and configured to send an alarm at specific thresholds.

Rayleigh backscattering is considered advantageous over Brillouin backscattering in the EWDNS as it is capable of fast, distributed measurements over longer distances (Muanenda, 2018).

DAS has been used to monitor rockfall along long stretches of railway (Akkerman and Prahl, 2013).

Supplementary monitoring considerations

Where the notification of a dam failure extends to multiple stakeholders, it is critical to reduce the number of false alarms emitted to avoid desensitization of the different parties.

In addition, the following considerations are recommended for implementation of an EWDNS:

- Separate components of the systems should be duplicated for redundancy (i.e., if a cell modem goes offline there should be a separate radio network to connect to an adjacent modem and transmit the data. Additionally, a backup satellite communication system could be implemented for back-up coverage if a cell tower goes down).
- An infrared camera with weatherproof enclosure would provide the potential to view the tailings dams in near real-time and provide verification of the event of a dam breach.
- Existing instrumentation on site could be used to supplement the EWDNS. This may involve trenching piezometer cables directly to a datalogger to provide near real-time monitoring of pond levels.
- Seismic monitoring, such as geophones, could be implemented alongside the primary monitoring method to supplement the EWDNS. This could monitor for the potential of low seismic events that could act as pre-cursory triggers to a static liquefaction type failure, as well as detect vibrations associated with a ground disturbance caused by a dam breach event.
- dGPS/dGNSS sensors could be used as a supplementary system to detect surficial displacement of the structures.

- Parallel sensors should be integrated into the system to minimize the event of false alarms (i.e., multiple trip-wires installed in parallel).

Conclusion

Multiple monitoring methods were assessed to detect a static liquefaction-type failure of a tailings dam to be used as a component of an EWDNS. Following a thorough review of the assessment factors, the linear fiber optics system using DAS sensing was chosen as a primary monitoring method of the EWDNS.

Supplementary components, including redundant telemetry (i.e., a separate radio network), complementary sensors (i.e., geophones), dam breach verification (i.e., an infrared camera) were also considered for implementation to improve the robustness of the EWDNS. Research is currently ongoing to improve the understanding of the failure mechanisms of static liquefaction; this may lead to improvements in the prediction of tailings dam liquefaction failures in the future.

References

Akkerman, J. and F. Prahl. 2013. Fiber optic sensing for detecting rock falls on rail rights of way. AREMA 2013. In Proceedings of *American Railway Engineering and Maintenance-of-Way Association Annual Conference:* 1099–1113.

Jefferies, M. and K. Been. 2016. *Soil Liquefaction: A Critical State Approach*. Boca Raton: CRC Press.

Keys, H. and P. Green. 2008. Ruapehu Lahar New Zealand 18 March 2007: Lessons for hazard assessment and risk mitigation 1995–2007. *Journal of Disaster Research* 3(4): 284–296.

Meier, L., M. Jacequemart, B. Blattman, S. Wyssen, B. Arnold and M. Funk. 2016. Radar-based warning and alarm systems for Alpine mass movements. In *Conference Proceedings of Interpraevent,* Lucerne, Switzerland: 960–968.

Miah, Khalid and David Potter. 2017. A review of hybrid fiber-optic distributed simultaneous vibration and temperature sensing technology and its geophysical applications. Sensors MDPI. *Sensors* 17: 2511; doi:10.3390/s17112511.

Muanenda, Yonas. 2018. Recent advances in distributed acoustic sensing based on phase-sensitive optical time domain reflectometry. *Hindawi Journal of Sensors*. Article ID 3897873: 1–16.

Pritchard, M., T. Keegan, T. Edwards, A. Benson and S. Mumma. 2008. Use of rockfall nets on Canadian National Railway – Design constraints and solutions. Im *Proceedings of GeoEdmonton 2008*. Edmonton: 1018–1028.

Bibliography

Morgenstern, N.R. 2018. Geotechnical risk, regulations, and public policy. The Sixth Victor de Mello Lecture. Salvador, Brazil: 1–47.

Proceedings of Tailings and Mine Waste 2019
November 17–20, 2019, Vancouver, Canada
Published by the University of British Columbia, 2019

Human Factors: Can We Learn from Avalanche Incidents and Apply the Findings to Tailings and Mine Waste?

Lucy Philip, Stantec, Canada

Abstract

Year in, year out, experienced and qualified groups succumb to avalanche hazard, despite advances in equipment and technology. Unfortunately, and sometimes tragically, these groups learn lessons the hard way. What leads to the decisions that these groups make, that ultimately turn out to be poor decisions? Are there any lessons for tailings and waste management? How do our tailings and management systems stand up if we take those lessons learned into mine waste management? Perhaps, more importantly, can we avoid the same pitfalls and issues when it comes to making risk decisions for our facilities?

This paper presents several ideas and terms from avalanche incidents and learnings and places them in the context of tailings and mine waste. These ideas and terms include: judgement; group decision making; speaking up; accountability in group decision making, termed social facilitation; familiarity, which is a form of complacency; social pressures, such as acceptance; and the expert halo. Current guidelines for tailings management systems and roles and responsibilities are audited and evaluated against the learnings and findings from avalanche events and a reality check is presented. Finally, some thoughts and recommendations are provided.

This paper is intended to open eyes to learnings from other sorts of safety incidents and raise some ideas. The paper may pose more questions than provide answers.

Introduction

Experienced and qualified groups succumb to avalanche hazard, despite advances in equipment, technology and avalanche training (*Aspen Times,* 2019; Gunn, 2010; Schaerer, 1987) (see Figure 1). Two-thirds of the people who die each year – around 30 in the USA (*High Country News,* 2015) – have had avalanche training, and a higher level of avalanche education has been found be associated with a greater chance of dying in an avalanche (McCammon, 2004). The decisions groups make, and lessons learned post-incident, have sparked introspection within the avalanche community (*Powder Magazine,* 2018; *Colorado Sun,* 2019; *Backcountry Magazine,* 2018; *Revelstoke Mountaineer,* 2017; USFS, 2014).


13 people involved in another avalanche near Golden, B.C.

Avalanche Leaves 3 Presumed Dead In Alberta's Banff National Park

Those missing are highly-experienced climbers, Parks Canada says.

Canadian Press

BANFF, Alta. — Three renowned mountain climbers are presumed dead after an avalanche in Alberta's Banff National Park.

Death of 2 US ski team members in avalanche spurs changes

Colorado's avalanche season claimed 8 lives. Experts say there's much to learn from how they died.

The conditions during the historic 2018-2019 snow season left behind damage so mysterious that it's still being sorted through

Figure 1: Recent headlines

Unlike tailings and mine waste facility incidents, avalanches are typically triggered by the victims. However, despite the triggering differences, the incidents share some technical and planning similarities, such as: strength of materials, presence of weak planes, understanding of beneath-surface conditions, emergency preparedness and planning, and understanding that low risk doesn't mean no risk. Both avalanche incidents and tailings/mine waste incidents are also impacted by human factors. Human factors are well described in avalanche incidents and associated reporting and research; however, the author has rarely seen them described for tailings and mine waste incidents. On this basis, there may be learnings from human factors in avalanche research that can be applied to tailings and mine waste.

Human factors in avalanche incidents

McCammon (2002 and 2004) changed the way avalanche workers thought about avalanche incidents and introduced the concept of human factors. His work was triggered by the death of a friend in an incident and his drive to understand the causes. McCammon statistically analyzed 715 recreational accidents, and in doing so provided insight into the key question: "How do people come to believe that a slope is safe, even when they are faced with likely evidence that it isn't?". The same question can be adapted and similarly applied to tailings facilities.

McCammon (2002 and 2004) introduced the concept of heuristic traps in avalanche risk. In this context, heuristics are simple, efficient rules, learned or instilled by evolutionary processes, that explain how people make decisions, come to judgements, and typically solve problems when facing complex problems or incomplete information. These rules can work well under most circumstances, but also can lead to errors or cognitive biases, especially when using heuristic thinking instead of analytical evaluation

in unpredictable, high-risk environments. In this context, heuristic traps are mental shortcuts that can result in common decision-making flaws.

Heuristic traps have since been well discussed in avalanche research literature (McClung and Schaerer, 2006; Tremper, 2018) and are also described as human factors (Bright, 2010; Cierco and Debouck, 2013; Egbert, 2015; Furman et al., 2010; Tremper and Fedtson, 1994; Zajchowski et al., 2016). Another trap reported in avalanche literature is cognitive bias with reasoning and thinking about risk, called the *base rate fallacy*, wherein intuitive thinking about probabilities is off-target and can lead to serious misjudgments about the risk of certain events (Ebert, 2019).

Cultural communication issues contributed to an avalanche accident in which two US development ski team members died in the Alps in Jan 2015. The group failed to understand the differences in definitions and practices between US and Europe for description of patrolled and open, assumed safe, terrain. The team mistakenly believed the terrain they skied was safe, was open and evaluated as safe by ski patrol (BRASS Foundation, 2015).

The popular press has also covered human factors as a key driver for avalanche safety, replicating findings from research and discussing specific incidents in more detail (e.g., *The Spokesman Review,* 2019; *High Country News,* 2015; White Heat Project, 2017).

Tailings failures and/or waste dump failures are somewhat like avalanche incidents, in that they are *poor feedback* (*High Country News,* 2015), or *wicked learning* (*Powder Magazine,* 2018) environments. These are environments where there is no immediate feedback on the decision-making process.

> "If nothing bad happens on a day out *or on a tailing's facility,* or even during longer periods of time, we may evaluate our decisions as the right ones – not necessarily because those decisions were good, but because we didn't receive any feedback that they were bad. As such, we may inadvertently form inaccurate assessments or develop potentially dangerous habits based on poor decision-making." (*Powder Magazine,* 2018).

> "In back country trips, as unstable, snowy slopes remain intact about 95 percent of the time, terrible decisions are often rewarded with great skiing and a beer at the end of the day." (*High Country News,* 2015)

These environments are also known as *illusions of skill* (Tremper, 2018), where we mistake good luck for good decision making. Competence most often leads to success, but success itself does not indicate competence (Ebert, 2015). Significant avalanche events, like tailings or mine waste failures, produce major feedback, which feels pressing for skiers and engineering professionals to analyze and relate, but near misses and close calls also present educational opportunities that can be missed.

There is a wide range of heuristic traps. The six key heuristic traps (acronym FACETS) identified for avalanche incidents by McCammon (2002, 2004) are presented in Table 1.

Table 1: Six key heuristic traps identified for avalanche incidents

Heuristic trap	Trap detail	Example in avalanche incidents
Familiarity (complacency)	Doing what is familiar People believe a course of action is correct because it has been done before without incident (McClung and Schaerer, 2006).	The potential for hazards to go unnoticed when in terrain we know well (Mount Washington Avalanche Center, 2017). Avalanche incidents are around 4 times more likely in familiar terrain. Highly trained groups make riskier decisions in familiar terrain than in less familiar terrain.
Social acceptance	Following what others do to gain social acceptance (Tremper, 2018). Feeling uneasy with a situation but not speaking up (Mount Washington Avalanche Centre, 2017).	Some evidence of risk-taking behaviour by men in the presence of women. "The group that was caught [by an avalanche] — two guys and two girls — the girls were concerned but didn't speak up" (Pique News Magazine, 2016).
Commitment	People's preferences for future outcomes affects their forecasts, which can limit ability to realize safer options. Similar to *optimism* and *wishful thinking*. Parties that are highly committed take more risks than those who are less committed (McCammon, 2004). Similar to *goal blindness*.	Summit fever. Wanting to get lines, or tracks. Complicated by guide/client relationships and peer pressure. "We came here to film a great ski line."
Expert halo	Blind trust in a more experienced partner characterizes the *expert halo* effect. People perceived as experts can dominate decision making.	Unskilled parties with no leader take less risks than those with an unskilled leader, seemingly attributing more avalanche knowledge to their leader than to themselves, even when the leader has no such knowledge. Leaders make riskier decisions as the group size increases. Consensus decision is found to be better (McCammon, 2004).
Tracks (social facilitation and social proof)	Tendency for people to perform differently when in the presence of others than when alone – to show off if they have confidence or to get nervous or choke if they are unsure of themselves (Tremper, 2018). When some people are doing something, others tend to follow along, also called the *herding instinct* or *safety in numbers*. People believe their action is correct because other people are doing it (McClung and Schaerer, 2006). People feel safer when following the example of others, regardless of actual hazards present.	People have more confidence when they see previous tracks on the slope or meet other groups/parties out doing the same thing. Larger groups make riskier decisions. McCammon (2004) found groups of 6 to10, and solo skiers, were at increased hazard risk. Avalanche accidents are more likely to happen with groups that encounter other groups en route, presumably feeling more comfortable with the decision to be out. Exacerbated by social media (Tremper, 2018).
Scarcity	Competition for resources or among others.	Racing to get tracks or summit first.

Additional heuristic traps that are also are identified as contributing to avalanche incidents are presented in Table 2.

Table 2: Additional contributing heuristic traps identified for avalanche Incidents

Heuristic trap	Trap detail	Example in avalanche incidents
Search for supportive evidence	Willingness to gather facts that lead to certain conclusions and disregard facts that threaten them.	"The avalanche report said *Low Danger*, so that avalanche over there is a fluke" (Tremper, 2018).
Conservatism	Failure to change one's own mind in the light of new information or evidence (McClung and Schaerer, 2006). Similar to anchoring where predictions are unduly influenced by initial information. *Anchoring* can also result in acquiring information at one location and applying it to another. Similar to c*onfirmation bias,* in which our belief causes us to accept evidence that supports our belief and discount or rationalize away any contrary evidence (Tremper, 2018).	Failure to recognize and monitor changes in snowpack and instability. Dangerous when the desire to be consistent overrules critical new information.
Recency	The most recent events or data dominate those in the less recent past, which are downgraded or ignored (McClung and Shcaerer, 2006). Similar to a*vailability,* in which specific events are easily recalled from memory and *anchors*, where the last thing we heard is weighted disproportionality.	
Frequency	The most frequent events or data dominate those that are less frequent (McClung and Schaerer, 2006).	
Illusory correlations	Belief that patterns are evident, and/or variables are causally related when they aren't.	
Selective perception	People see problems in terms of their own background and experience.	Can be counter-acted by seeking a diverse team with collective opinions (McClung and Schaerer, 2006)
Rules of thumb	Using independent rules of thumb, which oversimplify problems.	May exist in engineering judgment.
Underestimating uncertainty	Caused by excessive optimism, illusory correlation, and a need to reduce anxiety; also, a poor understanding of probability.	Tendency to overestimate small events and underestimate large avalanche events.

Quotes from avalanche literature are presented in Figures 2 to 6.

"People don't think they are going into a problem area likely because they've been in similar situations before. It's not about thinking about what you might have experienced in the past. It's thinking about what you might experience today and how that's different than what you've experienced in the past." Dale Atkins.

Figure 2: Quote from *Colorado Sun* (2019)

"This experience, coupled with the group's willingness to share their story, ended up being a valuable combination of learning lessons from the day. As I skied onto the debris, I understood how they were fooled into thinking there were enough trees to inhibit an avalanche. There was no obvious avalanche path and there were many trees. A closer look showed that many of the trees were missing their uphill branches, a sign of past avalanche activity not obvious from where they entered the slope. If you believe you are not in avalanche terrain, as they did, then snowpack, weather, spacing and avalanche danger are all moot. Terrain trumps all, but as they found out you must be right in your assessment."

Figure 3: Quote from United States Forest Service (USFS, 2014)

"You can't ski the San Juans aggressively. You might get away with it for a while, based on dumb luck, but eventually you'll get caught. Ask many of the locals who've been buried numerous times. Pick your posse carefully – not one filled with Type A personalities, but a group with a variety of personalities. Beware of the 'Expert Halo' trail boss. No one wants to be the timid one, but you should always speak up and question a decision in a group if you are uncomfortable."

Figure 4: Quote from *Telluride News* (2019)

"This event, as with many avalanche incidents involving people, was not the result of one really bad decision. It was the cumulative effect of several smaller decisions and a lack of awareness to the subtle changes in conditions – both internal and external. We all felt fairly confident that we had done our research and investigated what we could. I had been given somewhat of an 'expert halo' as the one person who had been to the area before, even though it was only for an afternoon. I didn't want to feel as though people were relying on me to make decisions, but I failed to verbalize that and create more discussion about the decision making as a group. Instead I internalized my unease and just went with it. This led to a situation in which others were not as likely to voice their concerns and observations, and perhaps that could have made a difference in the decisions and outcomes of that day. We will never know."

Figure 5: Quote from *Revelstoke Mountaineer* (2017)

"I thought if you just give people the critical information, they'll automatically make the right decisions. But I found out it doesn't work that way." Bruce Tremper

"It's been almost an awakening for me, I realized I could spend the next 10 years researching how a particular snow crystal grows, and I'd help maybe two people make a better decision. Or I could spend the next 10 years really looking at how people interact with the landscape and how they make decisions, and I could make a much bigger impact." (Jordy Hendrikx)

Figure 6: Quotes from *High Country News* (2015)

Expert halo

Of the heuristic traps, expert halo is worth explaining in a little more detail, as we regularly rely on experts for safe management of tailings and mine waste. There are two main issues:

- Experts are subject to heuristic traps, like anybody else.
- Experts can sometimes be hard to spot.

The reason experts are hard to spot relates to confidence, which is not actually related to skills or experience and should not be used as an indication of expertise. The Dunning-Kruger effect (Kruger and Dunning, 1999) presented in Figure 7 demonstrates this. Kruger and Dunning (1999) found that people have a pattern of overlooking their own weaknesses and, in doing so, tend to overestimate themselves and their abilities. In other words, people really seem to believe they have expertise and value their own contributions in a biased way.

Initially, without experience, people are highly confident, they don't know what they don't know, which is referred to as the *peak of stupidity*. As people then realize what they don't know, they progress into a confidence crash, called *the trough of despair*, and then slowly gain confidence on *the slope of enlightenment*. People never re-achieve the confidence level they once had.

Migrating through the Dunning-Kruger effect is individual-specific, as migration through occurs at different rates. This is similar to the cycle of competence (Broadwell, 1969) shown in Figure 8. People who are not good at learning effectively spend longer in the early peak or the first box. For some, there is a potential for adverse incidents in the early career to lower confidence further, while also providing a deep learning experience.

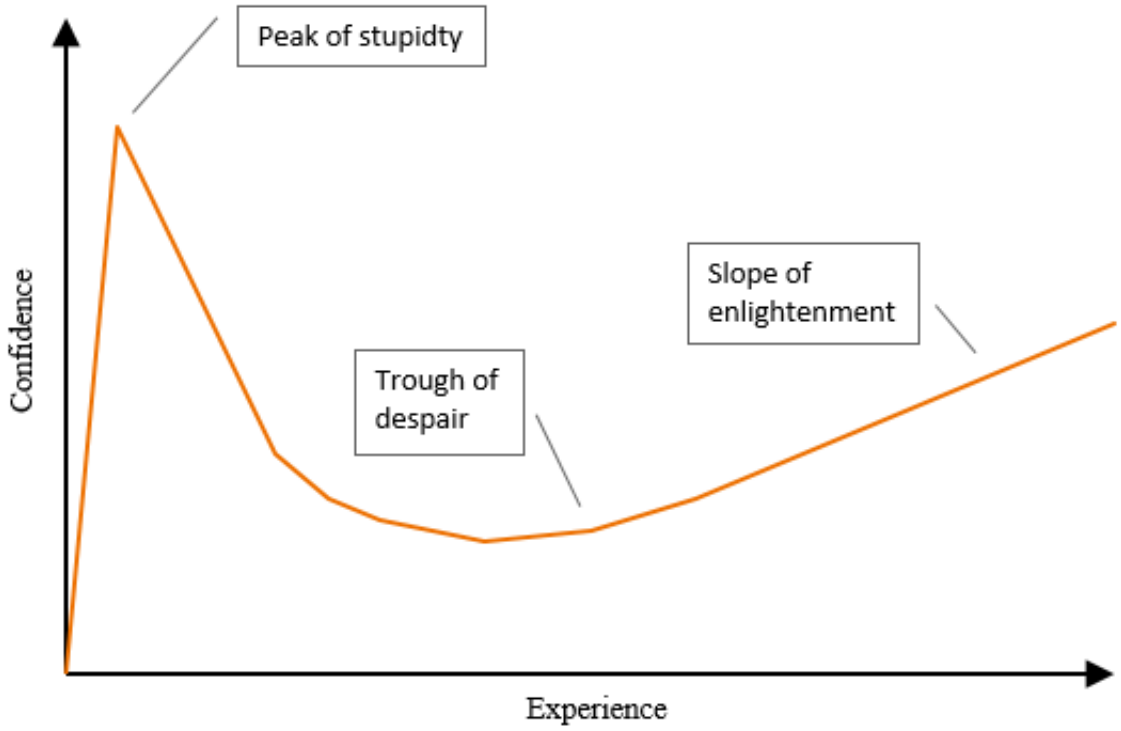

Figure 7: The Dunning-Kruger effect (Kruger and Dunning, 1999)

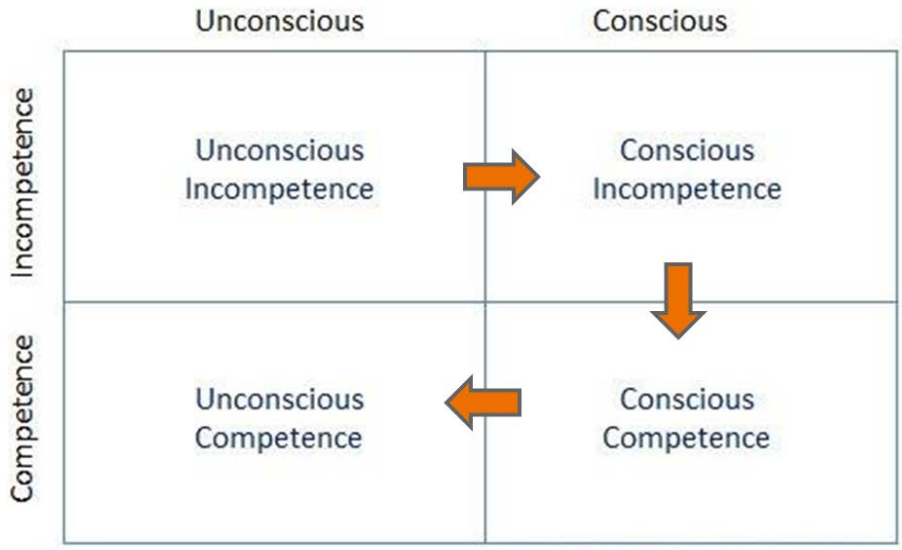

Figure 8: Cycle of learning competence (Broadwell, 1969)

Heuristic traps in tailings and mine waste

The heuristic traps presented for avalanche incidents are cross referenced to tailings and mine waste in Table 3. Most traps in avalanche incidents are also traps for tailings and mine waste projects, and the author has experienced or witnessed several of these during her career.

Audit against MAC Canada guidelines

In February 2019, the Mining Association of Canada (MAC) issued version 3.1 of the *Guide to the Management of Tailings Facilities* (MAC, 2019), and the industry seems to be trending towards stewarding tailings facilities to the MAC guidelines. The guidelines present responsibilities and concepts, which are audited against heuristic traps in Table 4. Most traps are applicable across all responsibilities and concepts and, overall, the author feels there is a system-wide tendency towards *Complacency/Familiarization, Expert Halo, Evidence review bias* and *Commitment*.

Conclusions and recommendations

Avalanche research has shown that people do not always make the right decisions, based on human factors. Engineers are human too, and human factors may also impact decisions made for tailings and mine waste. Knowledge, preparedness, and humility are keys to safety in avalanche country (Virtualmuseum.ca, 2015) and these can also be applied to tailings and mine waste safety.

Table 3: How heuristic traps can affect tailings and mine waste management

Heuristic trap	Author comment on applicability to tailings and mine waste
Familiarity (complacency)	The author has experienced complacency by all parts of the team; from instrument readers to experts. Fight complacency by educating about the risks.
Social acceptance	Grow a culture that encourages challenge and curiosity, rather than one offended by challenge with no room for curiosity.
Commitment	Commitment is a danger in tailings and mine waste as owners/clients/ operators are usually committed to a goal. Deviating from the goal has financial consequences, and disruptions to tailings plans can mean mine plans are not achieved. Consultants need to tell clients what they need to hear, not what they want to hear, and not react to commitment pressure.
Expert halo	We rely on experts and we need to know they are expert. An expert's work needs to be checked, as experts are also subject to heuristic traps.
Tracks (social facilitation and social proof)	*Heard and not Herd*. We may rely on others because of the multiple levels of involvement leading to carry-over error, e.g. the review board agreed with this approach, so it must be safe.
Scarcity	This is less applicable than for avalanche incidents as we are less likely to be competing blindly to be the first ones to use/do anything.
Search for supportive evidence	We need to view all evidence, and not select evidence to support theories. This heuristic relates to the way we select and review evidence.
Conservatism	We need to be comfortable with changing our mind, based on new evidence. This heuristic relates to the way we select and review evidence.
Recency	This heuristic relates to the way we select and review evidence.
Frequency	This heuristic relates to the way we select and review evidence.
Illusory correlations	We need to search for the right patterns and challenge any patterns we find. Review by others will help reduce susceptibility to this.

Selective perception	Create teams with technical diversity, e.g., geotechnical engineers, geological engineers engineering geologists, geohazard engineers, time-to-failure specialists, GIS and topography specialists, instrumentation specialists, etc. Embed people with ongoing experience outside tailings facilities, as we need cross-fertilization of ideas. Build Continuous Professional Development in non-mine problems as well as mine problems.
Rules of thumb	Using rules of thumb can be a form of complacency. Consider auditing against rules of thumb as a cross-check (LaChapelle, 1980), but be wary.
Underestimating uncertainty	Our understanding of the foundation geology is subject to a lot of uncertainty; we investigate a small % of the ground in volume terms. *What we know* is less than *what we realise we don't know* and less than *what we don't realise we don't know*. Try to understand the uncertainties and how these could affect design. Undertake sensitivity analyses and use results to optimize investigations targeted at proving (either way) the uncertainty is present or delineating the uncertain conditions that could impact safety. Produce robust, defensive designs. Consider geology in 3D rather than 2D slices.

Note that several traps relate to the way we review and weight evidence and are therefore linked:
Search for supportive evidence, Conservatism, Recency, Frequency.
Together the author terms these *Evidence Review Bias*.

Table 4: Audit of MAC guidelines for heuristic traps

MAC management concept	Top 3 heuristic traps (author's opinion)
Owners/Accountable Executive officer/Responsible person	Subject to Commitment, Social Facilitation, Complacency/Familiarity
Engineer-of-Record (EoR)	Subject to Expert Halo, Complacency, Underestimating Uncertainty
Independent reviewer (s) (IR)	Subject to Expert Halo, Complacency, Underestimating Uncertainty
Communities of interest (COI)	Selective Perception, Illusory Correlations, Evidence Review Bias
Best Available Technology (BAT)	Selective Perception, Conservatism, Expert Halo
Best Applicable Practices (BAP)	Selective Perception, Conservatism, Expert Halo
Critical controls	Selective Perception, Underestimating uncertainty, Evidence review bias
Operations, Maintenance and Surveillance Manual	Complacency/Familiarity, Illusory Correlations, Commitment
Emergency preparedness	Complacency/Familiarity, Frequency, Recency
Emergency response plan	Complacency/Familiarity, Frequency, Recency
Performance evaluation	Selective Perception, Illusory Correlations, Evidence Review Bias
Assurance	Subject to Commitment, Social Facilitation, Underestimating Uncertainty
Entire MAC tailings management system	Complacency/Familiarization, Expert Halo, Commitment

There are a few ways we can defend against human factors, specifically, heuristic traps:

- Be aware of heuristic traps and actively acknowledge and counter them (Mount Washington Avalanche Centre, 2017). Recognition of traps may help neutralize them.

- Improve communication. Communication is an important theme in overcoming human factors. Share questions, opinions, observations, and feelings (*Off-Piste,* 2017), and consider cultural differences.
- Grow teams that are curious and questioning and encourage speaking up (Ross, 2017).
- Create diverse teams that aren't reliant on the decisions of one person, or on very large groups. Collective decisions are usually better than those made by an individual (Makriddakis, 1990), but may be vulnerable to *social acceptance* and *facilitation*. Diversity may reduce *selective perception*.
- Make decisions using more than one method as cross-checks. Decisions made using single estimates may be less reliable than those based on more than one (LaChapelle, 1980).
- Be wary of using judgement based purely on experience, which may harbor evidence review biases. Use evidenced-based decision making. Good decision making requires good quality information.
- Consider and develop Plan Bs. This may reduce the *commitment* pressure.
- Use sensitivity analyses to indicate how changes in assumptions may impact results and projects.
- Share lessons and publish more near-misses, to help prevent *wicked learning*.

References

Aspen Times. 2019. Avalanches pose dangers even to back country experts. February 13, 2019. Retrieved from https://www.aspentimes.com/news/avalanches-pose-dangers-even-to-backcountry-experts/

Backcountry Magazine. 2018. Illusions of safety: After a friend's avalanche death, a lesson in intuition, April 12, 2018. Retrieved from https://backcountrymagazine.com/stories/illusions-safety-friends-avalanche-death-lesson-intuition/

Brad, R. 2017. Sharing critical control measures #2. Independent experts, black hats and sharing learnings, Rise to the Occasion Blog, March 30, 2017. Retrieved from https://risetotheoccasion.net/2017/03/sharing-critical-control/

BRASS Foundation. 2015. *Sölden Avalanche Accident Report, Austria — Sölden Ski Area*.

Bright, Leslie Shay. 2010. *Group dynamics and decision making: Backcountry recreationists in Avalanche terrain*. In partial fulfillment of the requirements for the Degree of Doctor of Philosophy, Colorado State University.

Broadwell, Martin M. 1969. *Teaching for learning (XVI*). Retrieved from wordsfitlyspoken.org. The Gospel Guardian.

Cierco, F.-X. and F. Debouck. 2013. Human factors in decision making in avalanche terrain. In *Proceedings: International Snow Science Workshop Grenoble – Chamonix Mont-Blanc,* October 7–11, 2013.

Colorado Sun. 2019. Colorado's avalanche season claimed 8 lives. Experts say there's much to learn from how they died. May 23, 2019. Retrieved from https://coloradosun.com/2019/05/23/colorado-2018-2019-avalanche-season-death-toll/

Ebert, PA. 2015. Conscious/ Unconscious decision making: Know Your Own Competence. *The Avalanche Review*, Vol. 33, No. 4 April 2015.

Ebert, P.A. 2019. Bayesian reasoning in avalanche terrain: A theoretical investigation, *Journal of Adventure Education and Outdoor Learning* 19(1): 84–95.

Furman, N., S. Schuman and W. Shooter. 2010. The roles of heuristics, avalanche forecast, and risk propensity in the decision making of backcountry skiers. *Leisure Sciences* 32(5): 453–469.

Gunn, M. 2010. *Out of bounds skiers and avalanche risk: High-risk cohort identification and characterization.* Master of Resource Management. Simon Fraser University.

High Country News. 2015. Can human judgement handle avalanches? July 20, 2015. Retrieved from https://www.hcn.org/issues/47.12/can-human-judgment-handle-avalanches

Kruger, J. and D. Dunning. 1999. Unskilled and unaware of it: How difficulties in recognizing one's own incompetence leads to inflated self-assessments. *Journal of Personality and Social Psychology* 77(6): 1121–1134.

LaChapelle, E.R. 1980. The fundamental processes in conventional avalanche forecasting. *Journal of Glaciology* 26(94): 75–84.

Makriddakis, S.G. 1990. *Forecasting, Planning and Strategy for the 21st Century.* New York: The Free Press.

McCammon, I. 2002. Evidence of heuristic traps in avalanche accidents. In *Proceedings of International Snow Science Workshop,* September 29 – October 4, 2002, Penticton, British Columbia: 244–251.

McCammon, I. 2004. Heuristic traps in recreational avalanche accidents: Evidence and implications. *Avalanche News* 68. Spring, 2004.

McClung, D. and P. Schaerer. 2006. *The Avalanche Handbook*, 3rd edition. Seattle: The Mountaineers Books.

Mining Association of Canada. 2019. *A Guide to the Management of Tailings Facilities,* 3(1), February, 2019.

Mount Washington Avalanche Center. 2017. Smarter, safer spring skiing: Part 6. May 19, 2017. Retrieved from https://www.mountwashingtonavalanchecenter.org/smarter-safer-spring-skiing-part-6/

Off-Piste. 2017. Avalanche safety – communication in the backcountry. December 10, 2017. Retrieved from https://offpistemag.com/communication/

Powder Magazine. 2018. How we learn from avalanche near misses. November 26, 2018. Retrieved from https://www.powder.com/stories/learning-from-avalanche-near-misses/

Revelstoke Mountaineer. 2017. It was a bluebird day, then all of a sudden. January 3, 2017. Retrieved from https://revelstokemountaineer.com/it-was-a-bluebird-day-then-all-of-a-sudden/

Schaerer, P.A.-V. 1987. *Avalanche accidents in Canada, III. A selection of case histories 1978–1984*. National Research Council of Canada, NRCC 279950.

Telluride News. 2019. Avalanche! Life and death by degrees. February, 2019. Retrieved from https://uexploreblog.wordpress.com/2016/02/01/human/

The Spokesman Review. 2019. With 90 percent of avalanches triggered by the victims, should meditation, mindfulness become backcountry tools? February 7, 2019. Retrieved from https://www.alpinedragons.com/mindfulness-in-helping-correct-heuristic-decision-making-while-in-avalanche-terrain/

Tremper, B. and J. Fredston. 1994. The human factor – lessons for avalanche education. In *Proceedings of the 1994 International Snow Science Workshop*, Snowbird, Utah.

Tremper, B. 2018. *Staying Alive in Avalanche Terrain*, 3rd edition. Seattle: Mountaineers Books.

USFS. 2019. An accident and a lesson. March 2014. Retrieved from https://www.mtavalanche.com/blog/accident-and-lesson

Virtualmuseum.ca. 2015. Remembering sad times for a safer tomorrow. 2015. Retrieved from http://www.landofthunderingsnow.ca/lecons_du_passe-lessons_from_the_past/index-eng.php

White Heat Project. 2017. A close encounter with human factors. March 15, 2017. Retrieved from https://whiteheatproject.com/2017/03/15/a-close-encounter-with-human-factors/

Zajchowski, C.A.B., M.T.J. Brownlee and N.M. Furman. 2016. The dialectical utility of heuristic processing in outdoor adventure education. *Journal of Outdoor Recreation, Education, and Leadership*, 8(2): 119–135.

Proceedings of Tailings and Mine Waste 2019
November 17–20, 2019, Vancouver, Canada
Published by the University of British Columbia, 2019

Effective Risk Management Controls for Tailings Storage Facilities

Zygi Zurakowski, Stantec, USA
Nicholas Brink, Stantec, USA
Lauren Meyer, Stantec, USA
Sam Abbaszadeh, Stantec, USA

Abstract

Recent failures have brought into focus the importance of the stability and safety of tailings storage facilities (TSFs), and the management of risks associated with operating a TSF. While the causal factors of the Brumadinho TSF failure continue to be evaluated, other recent TSF failures including those at Mount Polley, Fundão, and Cadia have been attributed to changing field conditions such as water pressures within the foundation and embankment, or unrecognized field conditions such as the strength of foundation and embankment materials.

This paper discusses effective risk management controls for TSFs during design, operation, and pre-closure. The specific role of geotechnical investigations, Quality Assurance and Quality Control (QA/QC) and instrumentation during design, construction, and operations are also discussed in the context of dam safety and risk management. Considerations for planning, executing, and interpreting these investigations are provided, along with lessons learned where risk mitigation controls have been implemented. There are other dam safety factors such as freeboard and water management that need to be continuously monitored on a TSF; however, the focus of this paper will be on providing suggestions for managing changing conditions and geotechnical risks within the embankment and foundation of a TSF.

Introduction

Tailings storage facilities (TSFs) are designed to meet a set of physical and chemical stability criteria intended to protect the safety of people (including site personnel and downstream communities) and the environment. The design intent of a TSF is based on a set of operating assumptions and design basis that are established prior to construction and operations. For physical stability, it is often assumed that conditions within a TSF embankment and foundation maintain a low phreatic level, low pore water pressure, and a homogenous material strength throughout the embankment. However, mines are dynamic facilities and therefore must be continually monitored and evaluated. Common changes in operating assumptions or

design basis can include variations in ore-characteristics, throughput rates, final storage capacity, operating life, weather and climate to name a few. Other factors that can affect the safety of a TSF, which should not be ignored, include changing ownership, operations personnel, and engineers or engineering companies. Changes of staff who have been involved in the design, construction and operation of a TSF results in a loss of institutional knowledge. This could include loss of design and operating philosophies, or loss of knowledge of foundation and embankment conditions which have long since been deeply buried and forgotten. These changing conditions at a TSF can result in deviations from the original design intent at many different points in time throughout the life of the facility which represents an ever present and changing safety risk which must be managed.

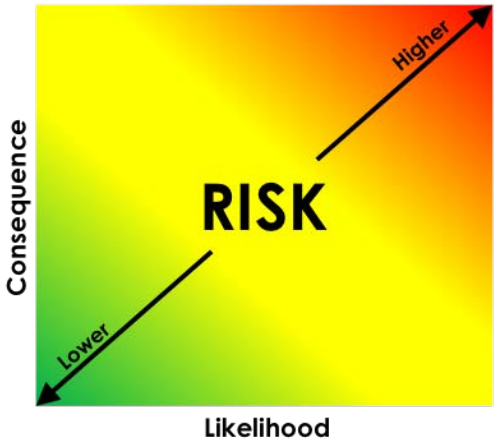

Figure 1: Typical risk matrix

Risk management

The risk management process often begins by determining a maximum foreseeable loss (MFL) of an asset if it were to fail and would include quantification of both financial and non-financial impacts. In the case of a TSF, the MFL is estimated based on a catastrophic failure scenario, assuming existing risk controls are ineffective. Residual risk of the failure event is then rated by assessing the severity (or consequence) and likelihood, assuming reasonable effectiveness of existing controls. The residual risk of an event is often presented on a probability-impact matrix as illustrated on Figure 1.

Once the residual risk is understood, the stakeholder(s) must then establish their level of risk tolerance and determine if additional controls or improvements to existing controls should be made to lower the residual risk to a tolerable level. At this point, controls that are considered more important for managing the risk should be identified and managed accordingly. It is preferable to have an Engineer of Record (EOR) and a single company that would support the owner with implementing these controls to provide consistency and preserve institutional knowledge.

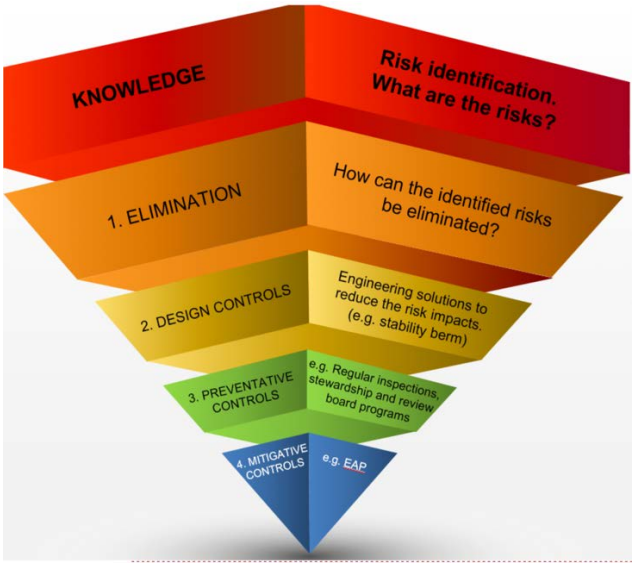

Figure 2: Simplified risk management for TSFs

Risk controls can be thought of in terms of a hierarchy based on their effectiveness, as shown on Figure 2. The most effective controls should be considered first (i.e. top of the hierarchy), followed by the next best control option and so-on. Knowledge is the foundation and the first step in proper risk identification and management of TSFs and is shown in the top tier of the hierarchy accordingly. At its core, this requires a comprehensive understanding of the TSF from various perspectives such as site geology, climate, construction material characterization, design, construction, operation, water management, potential failure modes, monitoring, and maintenance. Proper documentation of the design, construction, instrumentation and monitoring, and other activities are key to this step. Given the legal, social, technical, and physical complexities of a TSF, this tier of the hierarchy must by necessity involve a wide array of people with site-specific experience in order to capture the wide array of risks and failure modes which are potentially present. A Failure Modes and Effects Analysis (FMEA) workshop (Robertson and Shaw, 2013) has been used successfully by Stantec in many applications wherein owners, operators, contractors, engineers, and/or other stakeholders collectively identify risks and determine their likelihood and consequence. With risks appropriately identified, four levels of control should be considered: 1) Elimination, 2) Design Controls, 3) Preventative Controls, and 4) Mitigative Controls. The idea is not to suggest that one control should be used over another, but rather to think about how best to manage the risks. The different levels of risk controls are briefly explained below with some examples pertinent to TSFs.

Elimination: Elimination is the most effective risk mitigation measure, but also tends to be the most difficult to implement, particularly for an existing TSF that is already in operation. If the TSF is in the design or construction stage, elimination of a risk or potential failure mode could include excavation of foundation materials that are susceptible to liquefaction and/or strength loss, or removal of foundation

materials that are prone to piping risks. An example of elimination for an inactive TSF is planning and implementing a permanent closure plan that could include flattening the TSF slopes, placing appropriate cover materials and grading the landform with the goal of limiting surface water erosion and ponding. Complete elimination of the risk could be difficult and expensive to implement; therefore, design features to control or manage risks are more often considered as a feasible and acceptable alternative.

Design controls: Where complete elimination of the risk(s) is not practical or financially feasible, alternative engineering solutions can be designed to control a potential hazard or failure mode. The primary goal of the design control is to reduce the likelihood of the identified risk to a level tolerable to the risk owner (i.e. typically TSF owners). During design, a simple example would be to construct embankment filter zones to reduce the risk of a piping failure. During operations, conditions may arise that require additional design controls, for example a seep appearing in the foundation of an underdrain construction area would require a design modification to help with construction and minimize the risk of contamination of the drain. Another design control example would be to stabilize downstream slopes with stability berms and/or shear key trenches based on updated seismic hazard assessments and stability analyses.

Preventative controls: Not all risks can be eliminated during construction or isolated with design controls but rather need to be actively managed through the owner's risk management process. The next most effective control would be to implement preventative controls during operations. These can be thought of as controls that are implemented by the operator with the objective of proactively managing risk and reducing the likelihood of an event. Examples of Preventative Controls include instrumentation and monitoring, OMS plans, construction QA/QC programs, geotechnical investigations, short-term planning, external technical review boards, tailing stewardship programs, or regular tracking and reporting of key performance indicators. It is paramount that owners and operators understand and appreciate the importance of these controls. Obtaining operator approval to implement an unscheduled geotechnical investigation, for example, can often be difficult due to the unexpected costs and disruption to operations. In our experience, including a regularly scheduled geotechnical investigation and instrumentation installation program(s) as part of the OMS plan and overall QA programs helps owners and operators understand and plan for TSF investigation programs. The timely communication between the engineer, operator and owner are critical to the success of implementing these important risk controls.

Mitigative controls: Mitigative controls can be thought of as controls that would reduce the consequence of an event and are considered the least effective control as these are triggered after a failure has occurred. However, proper implementation of mitigative controls can help reduce loss of life and impact of an event and should still be taken seriously by owners, operators and engineers. Examples of Mitigative Controls include Emergency Action Plans (EAPs) and Crisis Management Plans which outline various failure modes and emergency levels and provide guidelines for responsive actions.

If the risk of certain elements of the TSF is perceived as high, key preventative or mitigative controls to manage the risk can be elevated to Critical Controls. Controls that are considered critical are subject to judgement and will likely differ from site to site based on TSF type and probable failure modes. An example of a critical control of a structure with a high hazard rating could include continuous on-site QA presence by the company of the EOR, or instrumentation with continuous data acquisition and regular monitoring by the EOR.

The following sections provide some guidelines and examples of risk controls, with the primary focus being QA/QC and field investigation programs at different stages of the TSF life, from design through construction, operations and end of operations.

Design

The design of a TSF evolves over several different phases from conceptual design to detailed engineering, and the TSF can continue to evolve and be modified throughout operations if an observational approach is adopted. Throughout the process, field investigation programs and testing are conducted, and knowledge of the site is continually improved. Note that risks and associated controls are specific to each embankment based on construction materials and method (i.e. upstream, centerline, or downstream) and therefore must be considered on a case-by-case basis for each TSF. TSF design is based on a set of criteria, basis, and operating assumptions; however, actual design features within the TSF are primarily incorporated to reduce risk elements based on hazards identified from site characteristics such as seismic setting, foundation conditions and embankment construction materials. These design controls are often made based on the engineers' judgement of potential failure modes and how best to effectively *and feasibly* control the risk. For example, at a TSF where we became the EOR, karst features were discovered in the flank of the impoundment and a low-permeability filter blanket was designed and constructed to reduce seepage and piping into the foundation. In addition, a granular drain and pumping system was constructed between the low-permeability blanket and karstic foundation to control head and provide seepage containment.

The first step to understand site hazards during the design of a TSF is to understand the general site conditions such as geology and the geologic setting, seismicity, and climate. If karst is present, design controls to limit seepage and piping from the impoundment will be costly, and a more prudent approach might be to eliminate the risk by selecting a more suitable site.

Once the site conditions are understood and associated risks are identified, field programs should be developed to investigate areas of concern and aid with the design of controls to mitigate the risks. As mentioned earlier, elimination of the risk is the most effective approach to managing risks associated with the different potential failure modes. In cases where elimination is not a feasible or practical option, risks

must be controlled through design elements and coupled with other preventative controls such as instrumentation and monitoring during operations.

Operations

The operational phase of a TSF requires close focus on preventative risk controls such as inspections, instrumentation, monitoring, and investigation programs. The purpose of monitoring and investigation during TSF operations is to either corroborate design assumptions or, if deviations to the design intent are uncovered, to understand and manage the risks in a timely manner. This observational approach helps to manage dam safety risks if it is applied correctly, diligently, and with enough frequency to capture the changing conditions within an operating TSF. Some example risk controls are discussed below.

Preventative risk controls

There are numerous preventative risk controls that can be adopted during the operation of a TSF, however the following sections will focus on the importance of OMS plans, quality assurance (QA) and quality control (QC) programs, instrumentation monitoring and installations, geotechnical investigations, advanced laboratory testing, with practical recommendations based on the authors' experiences.

Operations, maintenance and surveillance (OMS) plans

OMS plans are developed prior to construction and operation of a TSF and should be reviewed and updated on a regular basis during operations. The purpose of the OMS plan is to establish a comprehensive document that describes the required operating procedures for the facility, as well as roles and responsibilities of key staff. The OMS plan is intended to supplement, but not replace, the specific and comprehensive knowledge base of experienced operations personnel. The plan should cover procedures necessary for normal operating conditions and common upset conditions and provide a guideline for QA/QC of the facility including key performance indicators to be managed during operations such as deposition plan, freeboard and pond management. Inclusion of sustaining capital activities such as timing and general scope for future geotechnical investigations and instrumentation expansions can also be beneficial.

QA/QC program

A Quality Control and Quality Assurance (QC/QA) program is commonplace where construction of the TSF needs to meet a set of technical specifications. Quality Assurance (QA) programs are generally performed by a third party, and preferably by the company of the EOR. For high hazard TSFs, QA/QC programs can be considered a critical preventative control and represent the first opportunity for owners, operators, and engineers to detect and limit deviations from design assumptions.

The QA team should consist of engineers and technicians located at the site. The team's primary function is to check that the TSF is being constructed and operated in accordance with the design. A secondary function of the QA team is to provide a communication link between the EOR and the operator, which in our experience is critical to the timely identification and resolution of issues before they are buried deep in the TSF as an unknown risk and become difficult or impossible to correct later. When constructing high-risk facilities such as TSFs, there is one chance to build it properly, and rapid communication and response by the EOR is critical to minimizing construction defects.

Some of the key specific preventative controls performed by the QA team include the following:

Regular inspections: Regular inspections, accompanied by a photographic record and daily reporting, provide opportunity to detect deviations from design objectives and assumptions. QA/QC data, survey data, and detailed photo records provide important construction records that can be used later, if needed. For example, when a CPT investigation program revealed a zone of lower resistance within a TSF, photographic records from our QA program were reviewed and showed that construction crews were historically using the area for stockpiling construction materials. This resulted in an area where survey-control and QA/QC was extremely challenging, and an area of insufficient compaction was buried within the embankment and later identified by CPT. Other examples of construction defects that have been identified during field inspections include embankment cracking, inadequate foundation/abutment preparation, inadequate compaction of construction materials (particularly in tight areas where special compaction is required), erosion of constructed materials, development of new seeps or increased flow in existing seeps, and damages to instruments and/or signal cables.

Field testing: Field testing provides a second opportunity to detect construction defects. Sand cone density, nuclear densimeter, Guelph permeameter, and water replacement are examples of tests used to confirm whether construction materials have been placed according to design.

Sampling and index testing: TSF embankment construction materials must be regularly sampled and subjected to index testing as part of any QA/QC program. The ultimate objectives are to confirm that the in-place materials satisfy construction specifications and to maintain the design intent of the structure. Material from borrow or processing areas, stockpile areas, and in-place material should be tested to understand if and how the materials change with handling and placement.

Instrumentation data review: Another key aspect of a QA/QC program is regular review of instrumentation data. Instrumentation selection, installation, and design considerations are discussed below.

Instrumentation and monitoring

Failure to monitor necessary geotechnical parameters or conduct surveillance at an adequate frequency could result in a failure to identify potential risks or in-situ conditions requiring action (MAC, 2019). There

are three important questions to consider when developing an instrumentation plan: 1) what needs to be monitored; 2) what instrument or method is best suited for the site conditions and monitoring needs; and 3) where the instruments should be placed for optimal use. Properly planned and installed instrumentation can be used to identify unknowns and provide real time data to inform of changing conditions within an embankment. Ultimately, instrumentation provides a check on the design intent of a TSF.

The measurement of pore water pressure and phreatic level is important for understanding and recognizing risks associated with seepage and stability within a TSF. Vibrating wire and open standpipe piezometers are used to monitor saturated pore pressure and phreatic levels in key locations of the embankment including downstream of low-permeability features, within the foundation, near foundation contacts, and/or within or near engineered drainage features. Regular review of piezometer readings, and comparisons against threshold levels help provide an assessment of TSF performance and can be early indicators of potential problems. The engineer should also look holistically at piezometer data to gain an understanding of how seepage and gradients move through the TSF which could also help identify potential issues. Piezometric readings in the foundation could show head levels within the embankment; however, a piezometer located at the base of the embankment near a drain could show low or no head, which would indicate an upward gradient and that blanket filters/drains between the embankment and foundation are functioning as intended. Proper location, design and interpretation of piezometers is critical to a successful monitoring program.

Instrumentation such as inclinometers, survey monuments and shape arrays are useful for localized monitoring of slope movement. Monitoring of movement over large areas are most easily assessed using LiDAR or photogrammetry. Satellite surveys have also effectively been used for monitoring TSFs constructed by the upstream method. Aerial or satellite surveys can also be used for the monitoring of tailings beaches, including beach lengths, beach slope, and freeboard which is useful for managing risks associated with water management.

In the author's experience, a successful instrumentation plan is designed with long-term functionality in mind. As an example, the installation of redundant sensors is the most effective way of reducing the frequency of costly instrument replacements. For vibrating wire piezometers specifically, special care should be taken during installation of the instrument to ensure filter saturation is maintained (i.e. installing instrument with the tip and sensor facing upwards to prevent desaturation in partially saturated materials). Instrument cables are also a common source of instrument failure due to cable severing from trafficking of large construction equipment. Protection of the cables, either by burying or embedding them in stiff piping can aid in instrument longevity. Using thicker cables (e.g. 3/8" or thicker) and/or armoured cables can also increase instrument longevity.

While reviewing instrumentation and field data, it is paramount to think beyond the risks and potential failure modes identified in risk assessment and be open to the possibility that the information provided by surveillance is pointing to a potential risk that had not previously been identified or anticipated (MAC, 2019). Although instrumentation provides valuable data for the purpose of monitoring performance and safety of TSFs, it only fulfils one form of surveillance necessary for the safe monitoring and operation of a TSF. In tandem with QA/QC, monitoring, and instrumentation programs, regularly scheduled geotechnical investigations should be implemented to help characterize in-situ conditions and evaluate whether the TSF is performing in accordance with the design intent.

Investigations

Regularly scheduled geotechnical investigations conducted during TSF operations are important for the characterization of in-situ material properties, drain performance, seepage and stability, liquefaction triggering as well as the verification of instrumentation data.

The most common forms of geotechnical investigation are the advancement of Cone Penetration Tests (CPTs), drilling of bore holes accompanied by the collection of samples, and surface and downhole geophysics. Similar to the selection and installation of instrumentation, there are three important questions to ask when drafting a geotechnical investigation plan: 1) what key areas within the embankment should be investigated based on potential failure modes and identified risks (e.g., areas difficult to construct, areas with instrumentation showing unexpected conditions, etc.); 2) what investigation method is best suited for the site conditions and project needs; and 3) where should the investigation holes or geophysical surveys be placed for optimal value and information.

CPT allows for the general assessment of soil behaviour type, relative density, strength, and liquefaction triggering among other geotechnical parameters. Adequate spacing and depth of the CPT soundings is essential for exploring the extents of potential zones of concern, and to properly assess the entirety of the embankment. Based on the author's experience, it is recommended that CPT investigations be paired with pore pressure dissipation (PPD) tests, seismic compression (p-) wave and shear (s-) wave measurements, and resistivity modules, for the verification of in-situ saturation and material stiffness. Care should be taken when using relationships developed for CPT data, particularly for different material types (clay or sand) and relationships which are based on saturated or partially saturated materials. In tandem with laboratory testing, shear wave velocity data collected during seismic CPTs can also be used to estimate the in-place void ratio of penetrated materials. Empirical correlations based on Cunning et. al (1995) can then be applied for assessment of the critical state void ratio and in-situ conditions (i.e. dilative or contractive) of the material of concern. CPT rigs can also be used for the collection of samples, and the installation of vibrating wire piezometers.

For drill holes, consideration must be given to the appropriate drilling method based on site constraints and project needs. In-situ down-hole tests such as field vane tests (i.e., torvane, and vane shear), pressure meter tests, and permeability tests provide valuable information regarding in-situ resistance to shearing, material stiffness, and permeability. Sample collection is important for visual inspection and laboratory testing for confirmation of design parameters such as strength, permeability, and material gradation.

Performing more than one form of investigation method is recommended; supplementing CPT and geophysics with drill holes, where possible, allows for visual observation of the materials encountered and collection of samples for laboratory testing. For example, we had an experience at a TSF site where CPTu data was indicating positive dynamic and static pore pressures in an area designed to remain unsaturated. However, samples obtained from boreholes drilled adjacent to the CPT provided visual evidence that the embankment was indeed in an unsaturated condition. Upon further investigation, we concluded that the CPTs were generating positive pore pressures at locations where friction breaks were performed. Stantec recommended that piezometers be installed in the location where CPTs showed positive pore pressure to validate the result of the unsaturated borehole samples. Having additional instrumentation on hand, particularly piezometers, is recommended as it allows for quick installation and response to site conditions. Investigation programs need to be live and dynamic, allowing for changes to the investigation plan as it is conducted.

Laboratory testing and analyses

Laboratory testing is recommended alongside geotechnical investigation campaigns. Laboratory testing programs are used to confirm whether properties of the in-place materials conform to the assumptions used during design. The two most common properties to be evaluated are strength and permeability, as these properties generally control the facility behavior under normal operating conditions. Depending on the preliminary characterization of materials, additional testing may be warranted to evaluate if geotechnical properties have deviated from design assumptions and could include cyclic and/or residual shear strength, mineralogy and durability of construction materials, and the soil-water characteristic curve. Selection of samples for testing, as well as development of a testing program, should be informed by results from QA/QC records and results from instrumentation monitoring and geotechnical investigations to target areas where design deviations are suspected.

Results from investigation programs coupled with QA/QC data, laboratory test results, and instrumentation data provide additional understanding of actual conditions which can then be used to update appropriate engineering analyses.

Pre-closure

Upon reaching the ultimate storage capacity of a TSF, it is common to see migration of the operational and technical resources from the mine site to other active facilities. This transition typically occurs prior to establishing a comprehensive closure (remediation) plan. Most mines in the U.S. develop a monitoring and maintenance plan to monitor the performance and safety of the TSF during this pre-closure period which can last anywhere from a few years to multiple decades depending on many factors such as available funds, residual resources, commodity prices, and other ongoing activities at the mine site. Since these TSFs are non-operational, they are often classified as inactive, and thus tend to receive less attention in terms of safety and risk of failure. Justification may be based on assumptions regarding current TSF performance and the lack of physical changes to the TSF under non-operational conditions. However, it is important that the risks at inactive sites be managed with a similar level of thoroughness and evaluated for potential failure modes with risk ratings and appropriate controls similar to active sites. Potential failure modes at inactive sites could include failure of surface water management features, failure of decant structures, or blockage of drainage systems. The failure of the Brumadinho TSF is a recent example of how devastating the failure of an inactive TSF can be.

Conclusion

Tailings storage facilities are unique structures in that they continually grow and change over time, resulting in ever-changing risks. Coupled with this are possible changes in facility ownership, changes in management structure, and employee attrition resulting in the loss of institutional knowledge. Aggressive construction schedules tend to further exacerbate these risks, so that construction defects may go unnoticed. In this paper we have discussed in general terms the concept of risk management and have applied it by suggesting methods for managing risks specific to tailings dams. A concept involving a tiered hierarchy of effective risk controls was presented, beginning with risk identification (i.e., knowledge) and then continuing with 1) elimination of the risk, 2) design controls, 3) preventative controls, and 4) mitigative controls. Examples from the authors' experience in designing, constructing, and monitoring TSFs have been presented to demonstrate how these controls can be implemented at a site as part of an overall risk management strategy.

Preventative risk controls can be implemented during operations, and include a QA program with full-time, on-site engineering staff, frequent reviews of instrumentation data, regularly scheduled geotechnical investigations and corresponding instrumentation updates/installations, periodic laboratory testing of construction materials, and updates to engineering analyses to reflect changing conditions. Of importance is the appointment of an engineer of record (EOR) for each facility who ideally is involved in design,

construction, operation, and closure activities and can help the owner manage, document, and propagate institutional knowledge. Risk controls must be evaluated and applied on a case-by-case basis since every TSF is a unique structure. This framework has been used by the authors to successfully identify and mitigate risks during design, operations, and pre-closure phases.

References

Cunning, J.C., P.K. Robertson and D.C. Sego. 1995. Shear wave velocity to evaluate in situ state of cohesionless soils. *Canadian Geotechnical Journal* 32(5): 848–858.

Mining Association of Canada (MAC). 2019. A *Guide to Management of Tailings Facilities*. Version 3.1, February 2019.

Robertson, A.P. and S. Shaw. 2013. Risk management for major geotechnical structures on mines. In *Proceedings of the 4th International Conference on Computer Application in the Minerals Industries*. CD-ROM edition. Minerals Engineering International, Canada: n.p.

Bibliography

Jamiolkowski, M. 2012. Role of geophysical testing in geotechnical site characterization. *Soils and Rocks* 35(2): n.p.

Chapter 3
Geosynthetics

Proceedings of Tailings and Mine Waste 2019
November 17–20, 2019, Vancouver, Canada
Published by the University of British Columbia, 2019

Construction of a New Tailings Storage Facility with a Lined Basin in West Africa

Philip Addis, Golder Associates Ltd, Canada
Daniel Jones, Golder Associates Ltd, Canada
Brent Bronson, Golder Associates Inc., USA

Abstract

A two-year starter tailings storage facility (TSF) was recently constructed for a mine in west Africa. The facility was classified in terms of Canadian Dam Association guidelines as a "High" hazard facility. The TSF can be considered a co-disposal facility with the perimeter embankments constructed primarily with waste rock hauled directly from the open pit by the mining fleet. The starter embankment was constructed in two lifts to a nominal height of 10 m. The ultimate facility will have an embankment height of 44 m, which will be raised in a downstream direction.

The upstream slopes of the main embankments were reduced to design grade and covered with a cushion layer constructed of soft rock from a mine stockpile. The facility was lined with a 1.5 mm (60 mil) thick high-density polyethylene (HDPE) geomembrane to minimize seepage losses and prevent groundwater impacts. The base liner is a smooth and conductive geomembrane with a white upper surface to reduce folds and wrinkles from thermal expansion. The slopes were lined with a textured geomembrane overlying a cushion non-woven needle punched geotextile. The total lined area was approximately 130 hectares. The paper describes the embankment construction, challenges in preparing the base and slopes for lining installation, installation and welding difficulties in windy and hot conditions, and the post-installation leak detection.

Introduction

The precious metal mine's current operation consists of conventional open pit mining methods. Run-of-mine ore is processed by a three-stage crushing, ball mill, and carbon-in-leach circuit. Lower grade oxide ore is processed in run-of-mine dump leach facilities and an absorption, desorption, and refining plant. Construction of the first stage of a new tailings storage facility (TSF) was completed in 2017. The TSF can be considered a co-disposal facility, with the perimeter embankments constructed primarily with waste rock hauled from the open pit. The facility is lined with a high-density polyethylene (HDPE) geomembrane.

Site description

The site is in west Africa. The climate is classified as arid-desert under the Köppen climate classification system. The average temperature is 28.0° C with monthly average temperatures ranging from 20.4° C in December and January to 33.7° C in September. The minimum recorded temperature is 8.4° C, and maximum is 49.9° C. The mean annual precipitation is less than 100 mm. The estimated free water evaporation rate is 3,000 mm/year.

The prevailing wind direction at site is typically from the north and east. The average daily wind speed in the area is 14.5 km/hr but there are numerous occurrences of higher wind speeds. A daily maximum wind speed greater than 45 km/hr occurring on 31% of days. Wind-blown dust and sand are a frequent hazard to visibility.

The TSF site generally consists of a flat plain with elevations ranging between 121 and 125 m above mean sea level. It is covered by a gravel desert varnish lag deposit or by Aeolian dune sands, with sparse vegetation. Groundwater is unconfined in the mine area and the depth to groundwater varies from approximately 30 to 55 m with minimal seasonal variation.

Tailings storage facility

The TSF is a square shaped ring dyke with an internal footprint of approximately 1,000 m by 1,000 m. A two-year starter facility was constructed with a nominal embankment height of 10 m and a capacity of 8.6 million tonnes (Mt). The upstream composite slopes are 3.5H:1V, downstream slopes 1.4H:1V and the crest width is 38 m-wide crest. The ultimate TSF will have an embankment height of 44 m, raised in a downstream direction, with a capacity of 73 Mt.

The facility was classified in terms of Canadian Dam Association (CDA 2013) guidelines as a “High” hazard facility. The client standard, which is based on the CDA classification, was used to define the inflow design flood (IDF) and return period for the seismic design event. The TSF was designed without a spillway and must therefore store the IDF. The IDF was defined as the probable maximum flood (PMF). The PMF is the 30-day PMP (assuming underdrains, pumping, and evaporation losses are negligible) which was calculated as 666 mm. The site is located in a relatively low seismic area in the stable continental region of West Africa. A seismic hazard assessment defined the peak ground acceleration (PGA) parameter for a 1 in 10,000-year return period as 0.07g.

The facility is lined with a 1.5 mm HDPE geomembrane (60 mil). The base liner is a smooth and conductive geomembrane which has a white upper surface to reduce folds and wrinkles from thermal expansion. The white surface was also selected for constructability and worker safety in the hot conditions. The slopes are lined with a textured geomembrane overlying a cushion non-woven needle punched

geotextile (400 g/m^2). In some locations a sand bedding layer was placed below the geotextile if the surface was too angular.

A seepage collection system is provided at the base of the TSF above the liner, to facilitate drainage and for closure considerations. The drains have perforated pipes in minus 25 mm drainage stone, which was crushed on site, wrapped in a filtration geotextile and covered with a layer of Aeolian sand. The seepage collection system conveys seepage to an underdrain collection pond which is located outside the TSF footprint at a geographical low point. The underdrain pond is double lined, has an operating capacity of 5,000 m^3 and receives seepage via gravity and pressure gradient flow. Collected seepage is pumped back into the TSF.

Two decant pumps reclaim water from the tailings supernatant pond into the return water pond. The decant pumps are dri-prime skid mounted. The skid mounting allows the pumps to be moved up the access road on the internal dam slope as the pond elevation increases. The pumps are capable of handling solids up to 75 mm in diameter and can automatically prime to 8.5 m of suction lift. The return water pond is double lined with a 2 mm and 1.5 mm HDPE geomembrane (80 mil and 60 mil). It has an operating capacity of about 20,000 m^3 and two compartments. One compartment acts as a siltation trap and is protected by a geoweb with concrete infill of 150 mm-thick. This allows for machine access into the pond for silt removal. Water from the Return Water Pond is subsequently pumped to the process plant. See Figure 1 for a site layout.

Tailings are discharged into the TSF at approximately 60% to 65% solids (by mass) via perimeter spigots connected to a tailings header line. The tailings are typically 70% finer than 75 µm in size. From a geochemical perspective, there is little risk of acid rock drainage and the tailings have a low potential for metals leaching. The tailings delivery and return water lines from the process plant to the TSF are in a lined trench with an event pond to capture any tailings or water as a result of a pipe burst or leak.

Embankment construction

The use of mine rock sourced directly from the pit for TSF embankment construction was a new approach for the mine. A previous TSF at the mine was constructed by the mine's operations team with construction material sourced from a nearby rock dump. The "co-disposal" method requires the full commitment from the mine planning team. The haul distance to the new TSF was shorter compared to the mine's rock dumps. An additional dozer was purchased for material management.

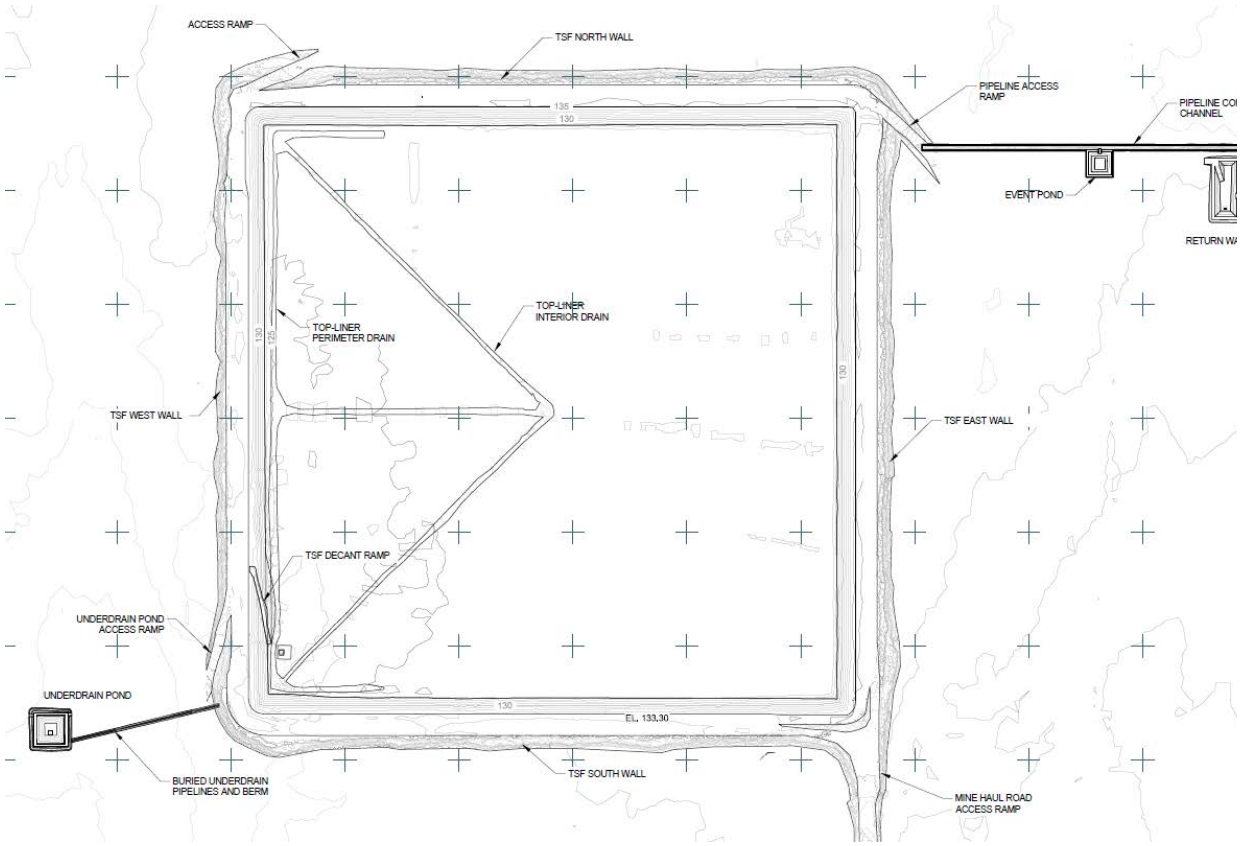

Figure 1: Site layout

The construction phase of the project began with the vegetation clearing, sand stripping and compaction of the TSF embankment footprint. The perimeter embankments were constructed with waste rock from the mine's open pit using mine's haul trucks (generally 220 t haul trucks). The rockfill had good fragmentation with minimal fines and particles sizes that generally ranged from approximately 50 to 600 mm in diameter. The rockfill was placed in controlled nominal 5 m-thick lifts with moisture applied to minimize future rockfill settlement. The reduced layer thickness, compared to the standard rock dump construction method, required more intensive spreading of dumped material. The dozer was used for spreading material and shaping the upstream slopes. Compaction was achieved by splitting the tracks of the loaded mine dump trucks along the crest of the placed fill when delivering material to site although this did result in additional tyre wear. In some locations, a layer of sand was provided on top of the waste rock to reduce tyre wear. Spreading with a dozer can create an uneven surface for traffic. A grader can provide a smoother finish but is not always practical with such large particle sizes.

An embankment crest width of 38 m allowed for two-way traffic and truck turning at the dumping points. The starter layer was initially constructed by employing the dump and doze approach. Two to three truck loads would be dumped before spreading. This in most cases resulted in somewhat thin layers, so the

paddy dumping approach was used for the final lifts to enhance efficiency. The internal and external embankment slopes were initially at the angle of repose. The upstream slope was formed by dozing down rock from the crest downward (Figure 2). The dozed-off material was stockpiled at the upstream toe and subsequently hauled mostly to waste along downstream edges of the main embankment or occasionally used for access ramp construction.

Figure 2: Forming of upstream slope

A liner bedding layer was placed on the upstream slope. The bedding layer consisted of weathered rock. This material was excavated and hauled to the TSF from a nearby stockpile by a civil contractor. On-site trials were completed in the pre-construction stage to determine the maximum upstream slope, the appropriate layer thickness for the cushion layer and to establish a method specification. The method specification consisted of moisture conditioning and compaction with 6 passes of a 15 ton vibratory smooth drum roller compactor. The upstream slopes were set to 3.5H:1V. On most of the upstream slope inclines, 5 layers were placed at 0.35 m thick and compacted to 0.3 m thick lifts. CQA personnel during construction observed and monitored the placement and compaction of the bedding layer to ensure lift thickness, moisture addition, and compaction procedures prescribed by the method specification was being adhered to. The quality of material was also monitored to ensure that it broke down to a soil like substance after compaction and moisture conditioning. A thin veneer of aeolian sand was generally spread to cover areas where the liner bedding fill had irregular finished surfaces. Any observed discrepancies were brought to the notice of the relevant construction management personnel for the appropriate corrective measures to be taken. A typical section of the north embankment is shown in Figure 3.

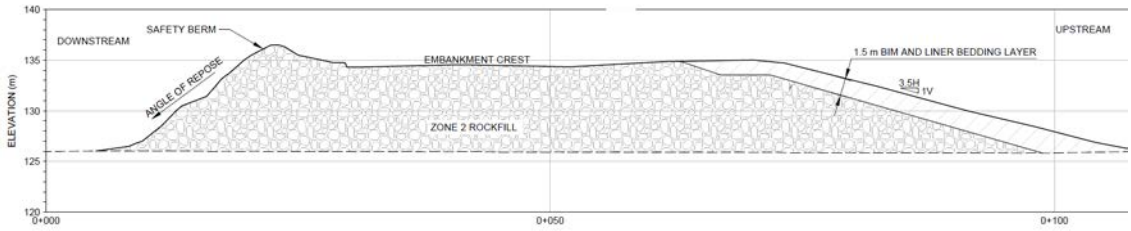

Figure 3: Typical embankment section prior to liner installation

Surface preparation

Surface preparation of the basin included scarifying, moisturizing, and smooth rolling to 98% of the maximum dry density, as determined by ASTM D698 (see Figure 4). Areas with very loose sandy/silty material was stripped off prior to compaction. Base preparation also included the grouting and closure of condemnation boreholes. Where holes had collapsed and could not be located for grout injection, a 4,000 g/m^2 geosynthetic clay liner was placed over the base surface, below the geomembrane, in the locations of the condemnation collapsed boreholes as an additional safeguard. Hand removal of roots, rock fragments, and all unsuitable material was also undertaken prior to HDPE liner deployment and installation.

Figure 4: Smooth rolling of the foundation immediately before geomembrane placement (rough grading by dozer in background)

Liners

Several different geomembrane types were specified and used for the various liner system components of the TSF and associated ponds as per the design. The different geomembranes used for the project are as listed below:

- 1.5-mm (60 mil) thick white conductive reflective smooth geomembrane was used primarily for lining the TSF basin. It was also used to along the embankment upstream slopes to supplement the 1.5 mm single side textured geomembrane. A white surface was selected to reduce folds and wrinkles from thermal expansion and improve worker safety in the hot conditions. The conductive liner was selected as an additional safeguard for leak detection.
- 1.5-mm (60 mil) thick single side textured black geomembrane was used for lining the TSF embankment upstream slopes. The textured surface was selected to improve worker safety on the slopes.
- 2.0-mm (80 mil) thick single side textured black geomembrane was installed as the upper primary geomembrane layer for the underdrain and return water ponds. It was also used to line the event pond and utilized as a protective rubsheet where required. The thicker liner was selected for the ponds due to the requirement for the placement of the concrete filled geoweb and subsequent machine access for silt removal from the pond.
- 1.5-mm (60 mil) thick smooth black geomembrane was installed as lower secondary liner for the underdrain and return water ponds.

Conformance testing and documentation

All the geomembrane panels used for the project were manufactured and supplied by a Canadian based liner supplier with material sourced from factories in Canada and Malaysia. The total quantity of geomembrane installed during the TSF construction, was approximately 1.3 million m^2. This consisted of approximately 2,000 m^2 for the Event Pond, 7,700 m^2 for the pipeline containment channel, 5,500 m^2 for the Underdrain pond double liner system and the remainder in the TSF.

The liner supplier contracted an independent third party to perform manufacturing quality assurance (MQA) sampling and testing. The MQA test results and the manufacturer's MQC certificates were reviewed by Golder and were found to be in compliance with the requirements of the technical specifications.

Installation

Intermediate anchors

The timing of the placement of waste rock meant that the floor of the basin had to be constructed before the sidewalls (which is not typical). To secure the geosynthetics a temporary anchor trench was constructed 20 m from the final upstream toe of each perimeter embankment (see Figure 5). A geotextile was needed to prevent puncture along the edges of the temporary anchor trenches. This was required because the loose soils of the anchor trench would not permit compaction near the edge without collapsing the trench.

Figure 5: Construction of temporary anchor trench in basin of TSF for liner installation, upstream embankment slope not yet formed

Wind issues

Wind was a factor that affected installation of the geomembrane. As the installation area of the basin was a large 1,000 m by 1,000 m square, full lengths of geomembrane (140 m long by 8 m wide) were deployed in an open area. There were no embankments to provide wind protection and wind uplift resulted in damage to about ten panels.

Liner ballast initially consisted of sandbags; however, the harsh sun exposure caused the sandbags to deteriorate quickly and it became clear that they would not last for the lifetime of the project. Additional ballast was provided by constructing single lane roads, approximately 1 m thick, within the basin, on the installed liner. The roads were constructed with fill sourced from a borrow source located west of the TSF. This material was a composite mixture of rounded sandy and silty gravels. A cushion geotextile was provided on the geomembrane at the access road locations. In addition to providing the required ballast the access roads also provided access to the center of the TSF to conduct installation and repairs (as truck traffic was not permitted directly on the geomembrane) (see Figure 6). A similar approach was also required for the embankment lining.

The subsurface preparation on the basin floor was also significantly hindered by high winds. The wind would scour prepared surfaces removing fine-grained materials, leaving behind angular stones which could damage the geomembrane. To combat this issue, smooth rolling was completed immediately before the geomembrane placement. It was not permitted to prepare an area that could not be covered by geomembrane in one day. A cushion geotextile was also used to cover areas which had been significantly eroded by wind and could not be recompacted in a timely manner.

Figure 6: Liner ballast access roads within the TSF basin

The wind also blew dust and sand, at times directly into the seaming equipment, causing defective welds that needed extensive repairs. This was exacerbated when the waste rock was being placed upwind of the liner construction as the dumping of fill material generated an excessive amount of dust. This resulted in fusion weld failures which required extensive repair work. Figure 7 demonstrates how close the waste rock was being placed to the geomembrane surface (although, in the photograph the wind is blowing in a favorable direction, which was not always the case).

Figure 7: Proximity of waste rock placement to geomembrane installation (note the dust generation)

Another effect of the co-disposal of waste rock was that the dust generated would create a thin film of dust on the top of the geomembrane, downwind of the tipping face. This meant that construction quality

control and quality assurance required labourers to sweep off the surface of the geomembrane to permit a thorough inspection.

Welding

A double fusion weld, as is typical for HDPE geomembrane installations, was used to bond geomembrane sheets. As the welding apparatus has drive-wheels which must pass underneath the geomembrane, the installation contractor opted to use a sacrificial rub sheet which was pulled along underneath the welding apparatus. The purpose of this rub sheet is to prevent the drive wheels from contacting the soil and bringing dirt and soil particles up into the weld (which would cause a poor -quality weld). While this was necessary, it is suspected that the use of a rub sheet above the very soft sand resulted in small stones being lifted and into the weld when the rub sheet was pulled forward. These small stones being lifted into the weld were repaired, although it did cause significant delays. It was only with very slow, gentle pulling of the rub sheet that welds were installed without defects.

The rub sheet remains the suspected cause of the stones being lifted into the weld (see Figure 8), as this phenomenon did not take place on the slopes (where a continuous geotextile was sewn in place directly underneath the geomembrane). The use of a rub sheet still introduced less deleterious material into the weld than when the installation contractor tried to forego the use of a rub sheet.

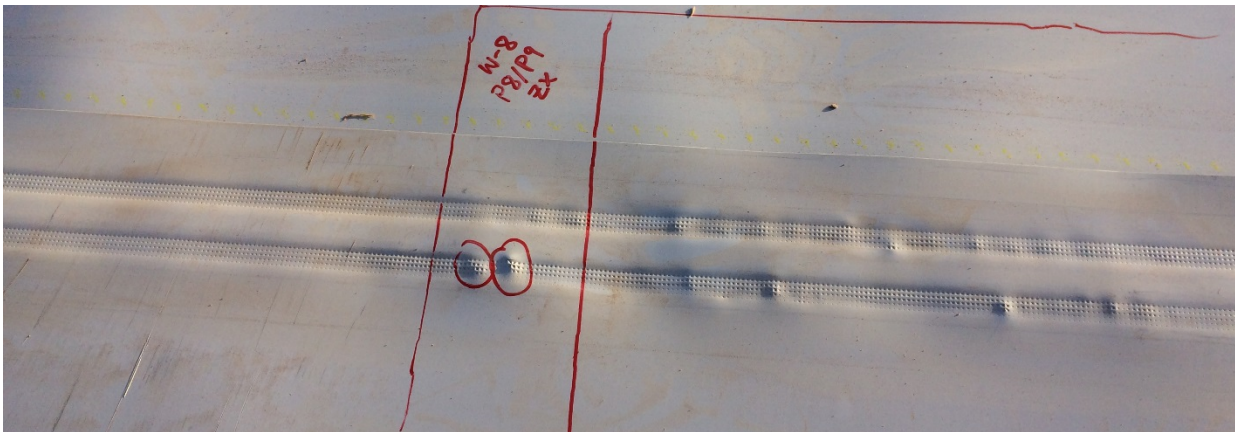

Figure 8: Small stones being picked up into the double fusion weld (presumably, resulting from the use of a rub sheet)

On the basin floor, a white conductive HDPE geomembrane was used, whereas on the slopes a textured black geomembrane was used. The conductive liner was placed on the underside to facilitate leak location surveys. The conductive backed geomembrane required higher welding pressures and slower welding speeds than a conventional geomembrane. It is hypothesized by the authors that some of the issues with the rub sheet, and dust generated by dam construction, may have been exacerbated by the higher welding pressures used to accommodate this conductive layer

The geomembrane manufacturer recommends no welding should take place on a geomembrane exceeding 70ºC. Field staff recorded temperatures of up to 65ºC on the white reflective HDPE and never had to cease welding. Temperatures of the textured black geomembrane routinely exceeding 70ºC in the afternoons (maximum recorded temperature was 89ºC on a geomembrane wrinkle) meaning that the installation was frequently halted in the afternoon.

Pipeline containment channel

The tailings delivery pipeline has a secondary containment channel and containment pond which were lined with 1.5 mm (60 mil) textured HDPE geomembrane. The liners were installed by a local installation crew. The field CQA staff worked closely with the local team to ensure that the CQC requirements were understood and that the standard of work was in line with the project requirements. Training a local contractor allowed work to commence in two different areas at the same time. While the main liner installation contractor worked inside the TSF, the local contractor could also make progress on the pipeline containment channel.

CQA – Weld testing

As is typical of all geomembrane installation, the liner installation contractor was required to perform trial (qualification) welds, at start of shift and mid-shift to demonstrate weld quality. For quick results, the contractor typically performed this testing on the back of a pickup truck in the field. The mid-shift trial welds consistently demonstrated marginally low yield strength. This caused some initial confusion and delays as the results from the start of shift did not demonstrate the same behavior. It was concluded that low yield strength results were due to the sample temperature from the extreme afternoon heat (for both black and white surfaced geomembranes). Samples that were cooled in the temperature-controlled site office for approximately thirty minutes had an acceptable yield strength. It should be noted that rapid cooling of specimens using water was not permitted, as it would have been less representative of the field conditions.

CQC – Leak detection testing

The use of a conductive geomembrane allowed the contractor to perform a leak location survey, using a Holiday detector. A CQA team member and the geomembrane installation foreman both received training on how to use the equipment from the geomembrane manufacturer. The leak location survey was conducted after a visual inspection of the geomembrane surface.

The leak location survey was significantly delayed due to accumulated dust on the geomembrane surface (resulting in false readings). This resulted in manual labour using brooms to sweep the geomembrane immediately before leak location testing. Once this issue was discovered, the leak location

survey was conducted immediate after the visual inspection to minimize the amount of sweeping required. Movable sand-filled bollards were then used to demarcate areas that were approved, so that no foot traffic took place over approved geomembrane surfaces. Field staff did not record the number of leaks found using this method, however it estimated it to be less than five leaks per hectare. Field staff, anecdotally, noted that many of the holes identified were knife cuts adjacent to patches. The CQA team members noted that the small knife cuts were difficult to locate visually, when compared to a typical tear or rip caused by handling or subgrade irregularities.

Visual inspection

The geomembrane was visually inspected by the CQA team and the contractor's CQC team for defects and to ensure that the repair methods were constant with best practices and the project specifications.

Conclusion

Constructing perimeter TSF embankments with waste rock hauled directly from the open pit by the mining fleet can be an economical method of construction. The process must be driven by the owner to ensure that there is buy-in from the on-site operators.

Lining installation in hot and dusty conditions present a number of challenges, but these can be overcome with good quality control and quality assurance measures. A summary of the lessons learned is presented below:

- Staging of the embankment construction should consider the effect of dust on geomembrane installation.
- The use of a geotextile underneath a geomembrane can prevent sand in the subgrade lifting into the weld (however, the authors note that in this location, a geotextile must be used with respect for interface transmissivity).
- Construction specifications for geomembrane installation in extreme heat conditions must consider the requirements for trial weld testing (not just the weld installation).
- Leak location testing should commence immediately after completion of all welding and visual inspection of geomembrane, as accumulated dust can lead to many false positives.

Proceedings of Tailings and Mine Waste 2019
November 17–20, 2019, Vancouver, Canada
Published by the University of British Columbia, 2019

Encapsulation of Mine Waste with Geomembrane as the Preferred Closure Option for Gordon Lake Sites in NWT

Kris Hojka, Stantec Consulting Ltd, Canada
Amy Allan, Crown Indigenous Relations and Northern Affairs, Canada
Giselle Cotta, Public Services and Procurement, Canada
Dave Bynski, DXB Projects, Canada
Allen MacGarvie, Stantec Consulting Ltd, Canada
Laya Bou-Karam, Stantec Consulting Ltd, Canada

Abstract

The Gordon Lake Group (GLG) consists of nine former mine and exploration sites located approximately 80 kilometers (km) northeast of Yellowknife, Northwest Territories (NWT). The GLG sites have been operated and abandoned in the last century by various owners leaving behind waste rock piles, impacted soil/tailings areas, and other mine-related debris and infrastructure (e.g., old cabins, metal debris, etc.). The closure project involved relocation of mine waste and consolidation at one location within the former Camlaren tailings area.

The former Camlaren tailings area was reengineered to accommodate additional waste to a new facility referred to as the Tailings and Soil Containment Area (TSCA). A protective composite cover and bituminous geomembrane (BGM) was selected as the preferred option for encapsulation of the mine waste. This paper focuses on engineering and logistical challenges to carry out the design and construction in a northern remote area including field investigation, embankment stabilization, design of the composite cover, and selection of geomembrane material. The main constraints of the project included lack of data; transportation including remote access by air or ice road; availability of coarse granular material; poor bedrock conditions; and a short construction period due to northern seasonal conditions.

The project design was carried out in phases from conceptual to detailed design, and updated as new data became available through various field programs. The final field investigation including test pits were carried out in the winter and spring of 2018, once heavy construction equipment was mobilized to the site. Immediate changes to the design were completed with updated information and in time to commence construction in July 2018. Design details were continually updated throughout construction, as new subsurface information became available. One of the main challenges during construction included difficult bedrock conditions. Once exposed, bedrock was observed to be highly fractured and weak, and in some

instances, too deep for the liner to be directly connected to the bedrock surface. Innovative solutions were developed to create a tight seal between the BGM and bedrock. This included encapsulation in a sand and bentonite mixture above the bedrock surface or in a "key-in" trench, depending on location-specific conditions along the perimeter of the TSCA liner system. Lined perimeter runoff ditches were also incorporated into the design to ensure that the ditch water could not percolate from underneath the liner. This paper will provide additional details on the project design conceptualization and actual implementation along with associated challenges, resolutions, and lessons learned.

Introduction

The Gordon Lake Group (GLG) consists of nine former mine and exploration sites located approximately 80 km northeast of Yellowknife, Northwest Territories. The GLG sites have been operated and abandoned in the last century by various owners and have consequently left behind waste rock piles; impacted soil/tailings areas; and other mine debris and infrastructure (e.g. old cabins, metal debris, etc.).

The Camlaren mine site operations included a small non-engineered tailings area, which was created by constructing perimeter dams approximately 3 to 5 meters (m) in height including the intermittent tailings pond area. Figure 1 shows the Camlaren tailings area prior to rehabilitation.

Figure 1: Camlaren Tailings Containment Area (2013)

Minimal information was available for the tailings area, but it was recognized that the dams could have been prone to failures, as documented by previous slump in the dam embankment. The challenge was to

characterize the dams and to design stabilization berms capable of withstanding additional loadings of mine waste.

The design and as-built records of the original dams were not available, however, based on surficial observations and test pits, it was determined that starter dams were constructed of alluvial sands and raised with coarse tailings. The dams were then covered by an erosion protection layer of fine rock-fill, which may have also been placed for stabilization. The actual thickness of the rock-fill layer was not known. The final slope of dams varied between 3H:1V (horizontal to vertical length) and 2H:1V.

The tailings were deposited within the impoundment by discharging from the west and south perimeter forming a tailings beach sloping towards the north-east. The overall thickness of the tailings varied between 1.5 and 3.5 (m), composed mostly of fine sand and silt. Based on the available field investigation results, the tailings were deposited over the existing natural bedrock or thin overburden (organics and colluvium).This primary objective of the project was to reengineer the former Camlaren tailings area to accommodate additional waste from identified impacted sites within the a newly developed facility referred to as the TSCA.

Project objectives

The GLG project area included abandoned mine sites scattered within approximately a 5 km radius. Part of the primary objective of the project was to remediate all identified mine sites to the appropriate mine rehabilitation protocols and relocate those mine wastes and debris into one engineered containment area.

Camlaren TSCA was selected as the containment area that would provide additional storage capacity to accommodate all additional mine waste for long term chemical and physical stability. Chemical stability of reactive waste was achieved by providing an impervious composite cover from atmospheric water and oxygen. Physical stability was achieved by the provision of additional engineered berms and regrading of slopes.

Site characterization

The original topography of the site is dominated by bedrock outcrops covered by a thin (0.1 to 0.3 m) layer of organics, and/or sand/gravel colluvium deposits within depressions typical of the Canadian Shield. Bedrock in the Gordon Lake Area lies within the Slave Province, an Archean granite-greenstone terrain (over 2.5 billion years old), dominated by metamorphosed turbidite sequences known to host quartz vein precious metal deposits. The bedrock surface is often highly fractured (frost shattered) and subject to extensive frost heave.

The original tailings containment located at Camlaren was constructed using a perimeter dam approximately 3 to 5 m in height. The design and as-built records of the dam were not available. Various

field investigations were carried out commencing in 2015 through to 2018. Based on the field inspection and test pit results, it was confirmed that initial dams on-site were constructed of medium to coarse sand material. The dams were constructed without foundation preparation and placed directly on organic soils or bedrock. The sand material seemed to be compact and competent, based on visual observations in test pits. The dams were covered by approximately 0.3 m of erosion protection layer consisting of fine rock-fill (mine rock) and sloped approximately 2H:1V.

Preferred solution

The Camlaren tailings, and the mine waste are both reactive to atmospheric conditions and required an engineered barrier to prevent water and oxygen from infiltrating. The "Cold Regions Cover System Design Technical Guidance Document" describes options applicable to northern regions and provides guidance for specific given site conditions (MEND, 2012). Among the barrier type options the most popular are:

- compacted clay layer (CCL);
- compacted sand-bentonite (CSB);
- permanent frozen layer; and
- cover systems with geosynthetic materials.

The CCL option was disqualified due to unavailability of clay locally. The CSB option would be cost prohibitive requiring significant importing of bentonite to the site and increased costs associated with the mixing process. In addition, the CCL and CSB options can be often prone to failure (cracking and increased permeability) due to frost action.

The Permanent Frozen Layer typically involves construction of a 2 to 3 m cover of rock-fill or sand and gravel. This involves construction of engineered permafrost within lower layers of the cover, with the top layer of the cover placed within the thermal active zone. The design is site specific, involving field tests of the cells across a few seasons. Due to schedule limitation, this option was disqualified. This option also required a significant amount of granular material, which local sourcing would be difficult. the composite cover system with geosynthetic membrane was selected as the most viable option. This would require limited amounts of granular material, which could be sourced locally.

Selected geomembrane

Cover systems with geosynthetic materials include:

- bituminous geomembrane (BGM);
- geosynthetic clay liners (GCL); and

- polyethylene geomembranes (high density polyethylene/linear low-density polyethylene [HDPE/LLDPE]).

The following design considerations were evaluated during selection of the geosynthetic material.

- The material had to be impermeable with no changing properties under severe weather arctic conditions.
- The material had to be flexible for installation in trenches, bends and curves.
- The material had to be resistant against potential settlements for elongation at failure and tear resistance.
- The material had to be resistant against puncture of sharp objects in the event of geomembrane exposure.
- The geomembrane should have a low temperature expansion coefficient to allow installation in a climate where high temperature fluctuations are possible during installation. The installation was intended to proceed in the summer, when temperature at the site may fluctuate between +30 to –10 degrees Celsius (deg. C).
- UV resistance and oxidation resistance – even though the geomembrane will be covered, exposure due to erosion of the cover may occur during catastrophic events. In such cases, the geomembrane shall possess superior properties to resist UV and oxidation weathering.
- High friction angle surface of the geosynthetic material.
- Sufficient friction resistance against sliding to ensure stability of the cover over the geomembrane, especially on the slopes during winter icy conditions.

From the above options, the following assertations were made for some of the considered materials. GCL was prone to cracking in dry climates due to desiccation of the thin clay layer in the liner, therefore this material was disqualified. HDPE in general is very durable but very stiff and less flexible than LLDPE, making it harder to install and prone to failure in areas that may undergo larger settlements. The final two products that were considered were LLDPE and BGM. The following table is a summary of the properties of the LLDPE material and the selected Coletanche ES 2 BGM detailed by their technical specifications by Layfield Environmental Containment (2017) and Axter Coletanche Inc. (2013).

Table 1: Mechanical properties of LLDPE and BGM liners

Mechanical properties	Unit	LLDPE		BGM
		Enviro 6060 smooth 60 mil	Enviro 6160 textured 57 mil	Coletanche ES2
Tear resistance	N	590	147	700–824
Puncture resistance	N	400	355	530
Elongation	%	1000	350	60–80
Tensile strength	kN/m	44	20	21–27
Tensile strength of the seam	kN/m	15.7	15.7	13–23
Water permeability	m/s	3 x 10–15	3x10–15	4x10–14
Friction angle	deg	18	26–28	36

Initially, LLDPE material was considered as it possesses superior tear resistance, flexibility and puncture resistance as compared to other materials. However, the LLDPE friction angle was not optimal in comparison with other materials. Smooth LLDPE had a friction of angle about 18 deg, and textured LDPE had friction of angle of about 28 deg. Textured LDPE seemed to have satisfactory friction angle, however, the tear resistance of the textured material was significantly lower and was not robust for long term closure conditions. A concern with additional loads of snow and ice on the slope surface could result in pulling and tear of the geomembrane in the long term.

The BGM was selected for the project as it showed superior strength properties and most importantly, a high friction angle of 36 to 38 deg. The sanded side of the BGM would provide a high shear resistance against sliding of the granular cover material on the slopes. The elongation and flexibility of the BGM is inferior to the LLDPE, and the risk of failure due to settlement was identified. This risk was mitigated by stockpiling additional material for future repairs, in the event of failure.

Design overview

The TSCA containment berms and waste material were covered with a composite geomembrane cover system to prevent infiltration, reduce acid rock drainage (ARD), and reduce the possibility of the release of contaminants. The cover system was designed as a composite layer including a BGM liner and 0.5 m sand fill cover and revegetation for erosion protection. The BGM cover was placed over the entire TSCA including slopes and perimeter ditches. In sloped areas, the cover was comprised of a 0.2m sand layer and 0.3 m of fine rock fill for erosion protection. The final TSCA surface formed a cone-like shape with a minimum slope of 3% draining the surface runoff away from the TSCA. The surface slope varied between 3 and 4%, to account for possible settlements and result in a minimum 2% slope after long term settlements.

Figure 2 illustrates typical design section of the cover on the slope and typical connection to bedrock.

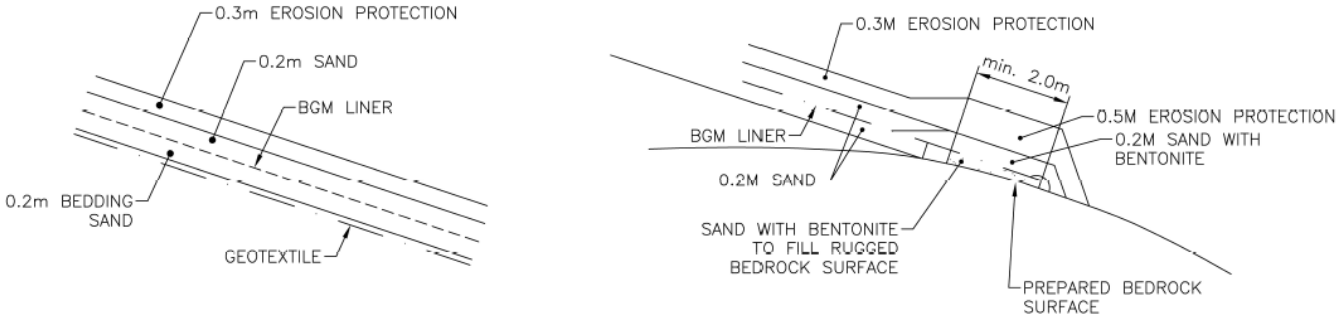

Figure 2: Typical design of cover and connection to bedrock

The BGM liner was anchored into the trench around the TSCA perimeter and backfilled with sand. The anchor provided additional resistance against liner sliding on the slope and against potential breakage. The top portion of the BGM was placed with about 1.5 m of overlap in the anchor trench area. This arrangement will allow BGM liner to move laterally in the case of the settlement. In the TSCA toe areas around the perimeter, except in low areas, the BGM liner was sealed into bedrock to prevent any surface water infiltrating into the TSCA. During construction, it was found that the bedrock was highly fractured in many areas and sometimes extending several feet in depth. In such cases, fractured bedrock was treated with a slush grout and larger cavities were filled with sand/bentonite mix. Due to irregular fracture surfaces within the bedrock, it was impractical to seal the BGM with batten bars or by fusion. Instead, the BGM liner was placed directly on the prepared bedrock surface and encapsulated or "sandwiched" in the sand/bentonite mixture zone (Figure 2).

Groundwater and toe drain

The BGM cover with perimeter key trenches was designed to prevent infiltration into the TSCA from the top and any surface water inflow from the perimeter sides. As a precaution, toe drains were installed in lower lying areas to relieve any pore pressure build-up. The toe drains were constructed of coarse granular material allowing any seepage, if present, out of the system.

Water management

The surface runoff is designed to be directed away from the TSCA by utilizing the natural topography and two perimeter ditches. The BGM cover restricts nearly 100% of infiltration over the TSCA. As a result, the surface runoff flows over the cover towards the TSCA perimeter. The surface runoff is then directed away from the TSCA on the north and east by the natural topography and away from the TSCA through ditches

located on the western and southern perimeter to be discharged safely into the Gordon Lake.

All ditches were fully lined with the BGM as a single unit to prevent water seeping back into the TSCA (Figure 3). The ditch sections show that the BGM extending from the TSCA into the ditch is one unit. In areas of deeper bedrock, the BGM was suspended over the bedrock and anchored in the trench downstream of the ditch or sealed to the bedrock within the key trench. The ditch was armoured with erosion-resistant material (riprap) to prevent erosion of the ditch and lining geotextile.

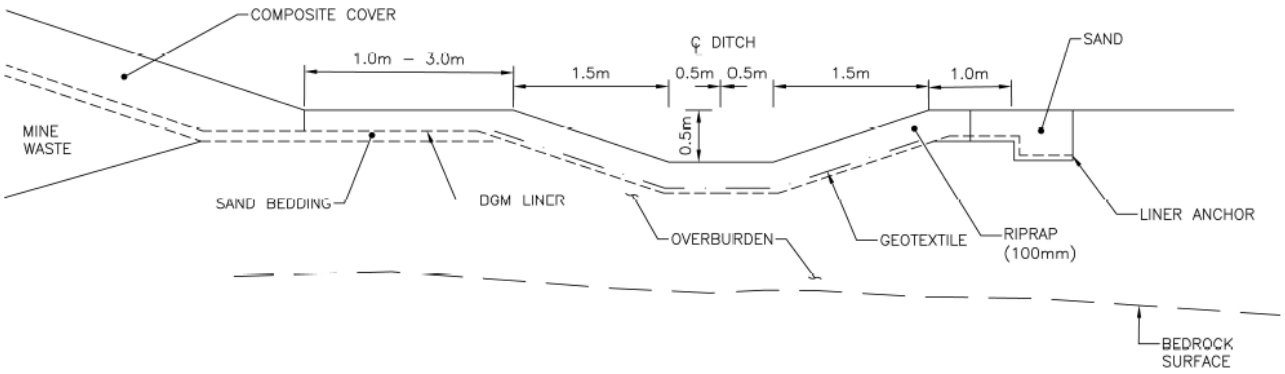

Figure 3: "One unit" BGM ditch section design

Construction

Major challenges for the reengineering, construction and project delivery included mobilization and transportation of materials to the site which is located on a remote island. Due to seasonal constraints, all material was brought to the site during the winter by using an ice road. This included all borrow materials used for cover construction and erosion protection.

The construction of the TSCA was performed in two phases. During Phase 1, mine waste was transported to the Camlaren TSCA during the winter of 2018, with the majority of earthwork conducted from February to March, 2018. Some of the waste was transported (flown by helicopter in bags) to the TSCA in the Summer of 2018. Approximately 23,400 cubic meters (m^3) of mining waste was brought into the TSCA. In addition, approximately 15,000 m^3 of sand and erosion protection material was brought from a borrow source (GD-37) located approximately 10 km to the south and stockpiled at the site. Figure 4 shows typical conditions for winter construction activities.

Figure 4: Placing mine waste in the TSCA (February 2018)

Phase 2 of construction took place from July to September, 2018 and involved the following:

- The slopes were stabilized by regrading perimeter embankments and slopes between 3.1H:1V to 4.3H:1V;
- Placement of the engineered composite cover with BGM;
- Construction of lined perimeter ditches; and
- Installation of instrumentation including monitoring wells, vibrating wire piezometers and thermistors.

During construction, the design was continuously adjusted to accommodate fractured bedrock and irregular undulating topography with deeper bedrock depressions. Where bedrock quality was poor, key trenches were excavated and a concrete mix was placed to fill deeper depressions to create smooth surfaces. A sand and bentonite mix was used to seal the BGM contact and to smooth the surface of bedrock to concrete. Figure 5 illustrates preparation of the key trench, and Figure 6 shows encapsulation of the BGM in the sand-bentonite mixture.

Figure 5: Preparation of bedrock surface in a key trench

Figure 6: Placement of sand-bentonite mixture on prepared foundation of BGM liner key trench

Another difficulty during construction was availability of borrow material for construction and erosion protection material. Due to availability of sand, the final cover was designed to include a 0.5 m sand layer on the top of the BGM. The sand material was sourced from alluvium sand with trace fines below 5%.

Some oversized material above the specified maximum 12 mm, was present at approximately 5 to 10% of the total material. Due to the short construction season, the decision was made to use this material as a cover without screening. It was recognized, that some gravel or cobble sized material could be in direct contact with the BGM after the sand cover placement.

As a due diligence, a trial test was performed testing the puncture strength of the BGM against sharp stones with simulated compaction to mimic actual conditions. The test involved placement of 0.4 m of cobble size stones directly over the BGM followed by driving over each area with heavy machinery. The results indicated that no punctures and only some denting was observed in the BGM. The dents were created by a Catepillar D6 bulldozer and no damage was observed when a Caterpillar D3 bulldozer was used. It was concluded that light compaction with bulldozers over 0.5 m cover would not cause any damage to the BGM. Figure 7 displays the BGM surface post trials.

Figure 7: The BGM surface after compaction with D3 dozer over 0.4 m of fill with cobbles

Conclusion

The rehabilitation project at the Camlaren tailings site was successful in meeting the primary objective. Nearly one year after completing the construction, the cover and slopes have performed as anticipated with no signs of distress, settlements, or seepage. Remote location, harsh subarctic climate and environment conditions necessitated a design that included geomembrane material that could effectively perform over long-term closure conditions and temperature extremes. The BGM and chosen geomembrane type provides sufficient properties able to resist various physical and chemical agents, and to perform in harsh environmental conditions. Due to the remote location of the site, the entire rehabilitation project is expected

to take several years from the initial investigation, through various design stages, through to the final construction. Proper planning and project management is essential for the successful completion of northern projects. Lessons learned included the need for allocating the required resources, and to properly characterize site conditions during the initial phases of the project, for efficient project planning and execution.

References

Axter Coletanche Inc. 2013. Product data sheet – Coletanche ES 2. Accessed July 23, 2019, from http://www.coletanche.com/assets/files/documentation/unites_si/en_2013-06-28-22-38-54_COLETANCHE-ES2-ASTM_SI_E.pdf

Layfield Environmental Containment. 2017. Enviro Liner 6000x – Technical data and specifications. Accessed July 23, 2019, from https://www.layfieldgroup.com/getmedia/c788ea73-8c2b-4b9f-98bc-591f9e3f087a/Enviro-Liner-6000x_Booklet_Low.pdf?ext=.pdf

Mine Environment Neutral Drainage (MEND). 2012. Cold regions cover system design technical guidance document. Prepared on behalf of Aboriginal Affairs and Northern Development Canada (AANDC), now Crown Indigenous Relations and Northern Affairs Canada (CIRNAC), accessed July 23, 2019 at http://mend-nedem.org/wp-content/uploads/2013/01/1.61.5c.pdf

Bibliography

Ecosystem Classification Group. 2008. Ecological Regions of the Northwest Territories – Taiga Shield. Department of Environment and Natural Resources, Government of the Northwest Territories, Yellowknife, NT, Canada. viii + 146 pp.

Proceedings of Tailings and Mine Waste 2019
November 17–20, 2019, Vancouver, Canada
Published by the University of British Columbia, 2019

Improved QA and QC of Double-Lined Ponds for Processed Water Containment

Heather D. McDaniel, Souder Miller & Associates, USA
Roman Belts, Groupe Alphard, CANADA
Pascal Saunier, AFITEX-Texel, CANADA

Abstract

Processed water storage is one of the main concerns for regulators and owners of operations in the shale gas and the oil sand industry, and for good cause: these extremely pollutant liquids concentrate all the toxic, organic, and chemical parts of the residues that are treated in the facilities. It is therefore necessary to be able to ensure storage under completely leakproof conditions – or at least, the most leakproof conditions we can achieve. Since assembled geomembranes are not 100% free of leaks, it is essential to consider the state of the art in quality assurance and quality control (QA/QC).

Experience all over the world shows that an average of 10 leaks per hectare can generally be found on a lined project where everyone is following the standard QA/QC guidelines (internal QC on site during installation, vacuum box, and basic visual inspection). However, several studies show that the application of additional control practices can lead to an almost zero-defect project to the level detectable. Among these practices is a strong third-party engineer dedicated to improving the quality on site during all stages of the project, from design to operation. The engineer's tasks will also include leak detection surveys during and after the installation of the geomembranes. These last methods, described by American Society for Testing and Materials (ASTM) standards, can be complicated – or even ineffective – depending on the materials used for the construction and the size of the defect.

Based on a recent case study that is currently occurring in a project related to the mining industry in the USA, this paper will present the importance of those complementary quality controls and the limits of traditional geosynthetic solutions, and will show how conductive multi-linear drainage geocomposites offer an effective solution to enhance the quality of storage ponds, reduce the construction time, and limit environmental risks.

Introduction

The project started in the southwestern United States in the oil and gas industry. The produced water pits are a direct result of the industry's usage of hydraulic fracturing since the 1940s, the by-products of these wells (produced water), and the long-standing drought that the southwest has been facing for nearly 15 years. When mass hydraulic fracturing started to become the norm in the southwest, with upwards of 6 to 10 horizontal wells per pad, the oil and gas industry started to acquire vast amounts of water rights to meet operational needs. With landowners, ranchers, and municipalities starting to struggle to maintain water usage demands, the public perception of oil and gas using upwards of 600 acre-feet of water per multi-well pad was not well received. The industry decided that instead of injecting the produced water into saltwater disposal wells, they could reduce trucking costs and improve neighbour relations by re-using a product that had been a nuisance of production.

Global quality

In this document, the global quality of a project is defined as the product of the quality levels of each of three principal components of a typical double lined pond project, which are:

- the design, or conception stage;
- the construction stage; and
- the operation stage.

Figure 1: The three components of the global quality of a project

The global quality of the entire project can be calculated as follows:

$$GQ = Q_{Design} \times Q_{Construction} \times Q_{Operations}$$

Design

Two important design criteria when determining the liner materials are:

1. the long-term operational requirements of the system, i.e., fresh water versus produced water, circulation versus non-circulation, types of pumping and piping being used within the system; and

2. the client's operational knowledge of liners, i.e., does the operator understand the fragility of liners?

In this example, it was assumed that the client understood the liner fragility and their operational requirements during design. This assumption led to many of the lessons learned throughout the project. Ultimately, the process led us to a design that included a secondary and primary liner system comprised of 45 Mil LLDPE scrim-reinforced liners, as shown in Figure 2.

The Client's design guidelines were clear: fit an operational treatment area within a small rig anchor pattern, supply ample room for operational vehicles, meet state design regulations, maximize the amount of produced water storage within the permitted federal boundary, and deliver a full set of construction plans from start to finish within 30 days. The Client started earthwork on the project five days before the plans were complete.

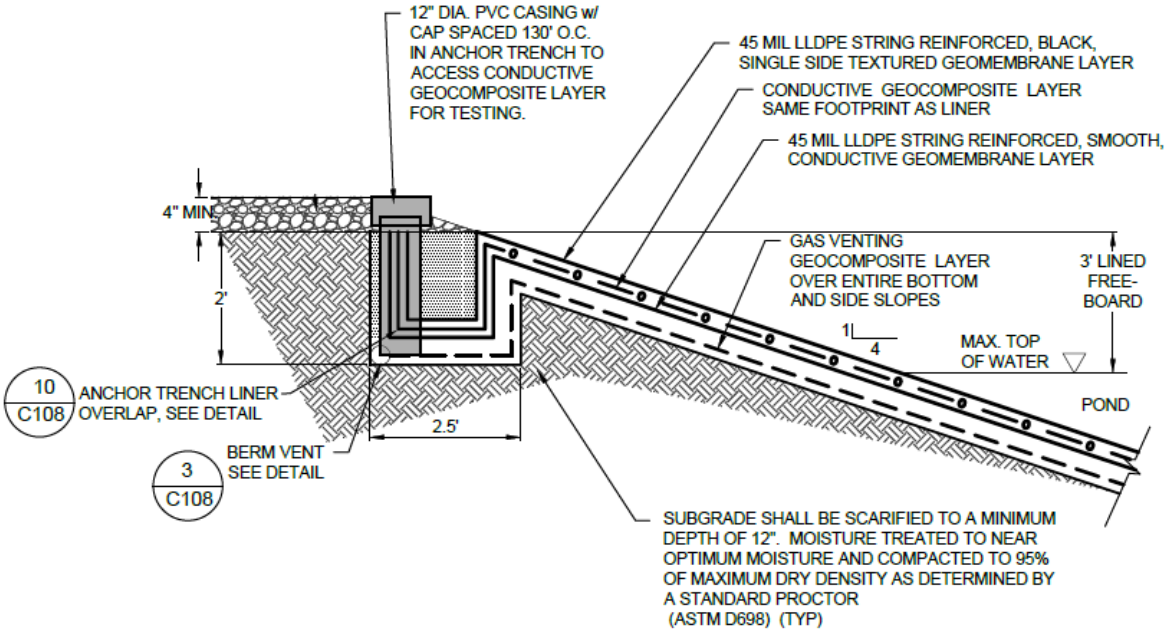

Figure 2: Typical cross-section on the slopes and anchor trench

Below the secondary liner, a multi-linear drainage geocomposite is used as a groundwater/gas venting system as well as a protection layer. Between the primary and the secondary liner, another multi-linear drainage geocomposite is installed for leak detection drainage. Both materials are comprised of 20 mm (¾ inch) corrugated polypropylene perforated pipes spaced on 1 m (40 inches) centres between two non-woven polypropylene geotextile layers (Figure 3). In addition to this, a conductive grid is inserted into the second product in order to make leak location surveys on the primary possible.

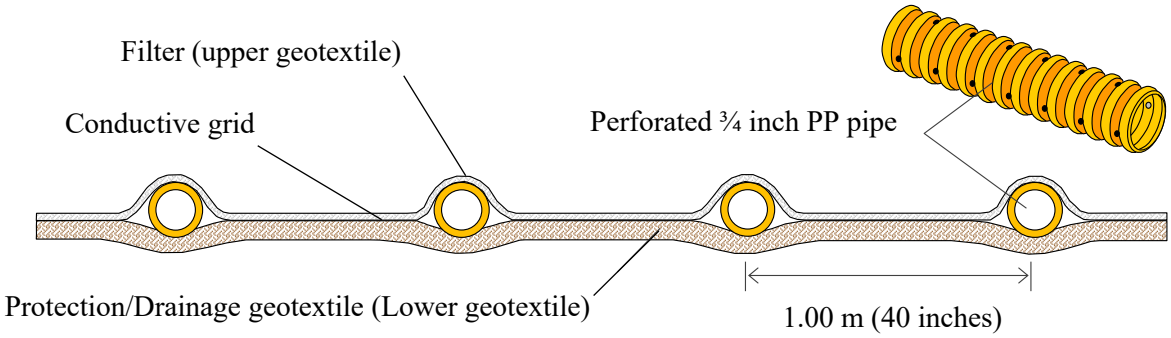

Figure 3: Conductive multi-linear drainage geocomposite description

Multi-linear drainage geocomposites have been used in landfill and mining (ponds) applications in Europe and Africa for 25 years. An important characteristic of those drainage geocomposites is that they maintain their transmissivity under significant normal stresses (Saunier et al., 2010) because they don't experience geotextile intrusion into the primary high-flow component (the primary flow being the drainage net in biaxial or triaxial geonet geocomposites type of products and the pipes in multi-linear drainage geocomposites). Therefore, for most of the applications, the applied combined reduction factors for multi-linear drainage geocomposite are almost half of those applied to standard biaxial/triaxial geonet geocomposites (Maier and Fourmont, 2013).

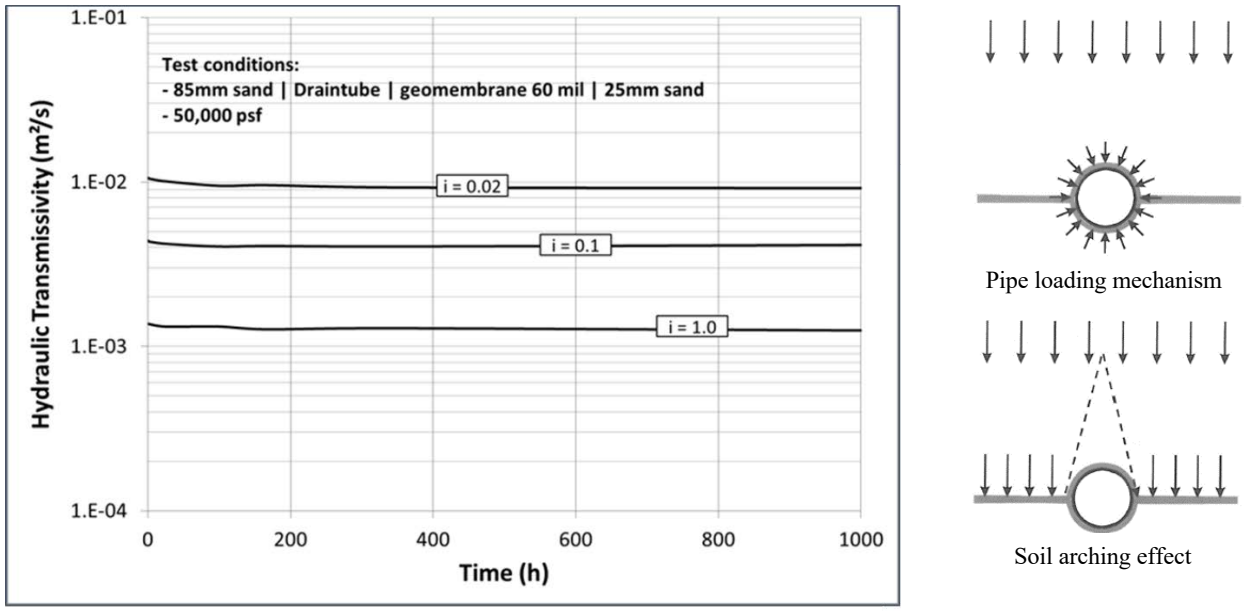

Figure 4: Measurement of transmissivity over time under high load

Construction

One of the major selling points of the design was using reinforced polyethylene (RPE) preassembled panels

and multi-linear drainage geocomposite for extremely high installation speed. The four-panel geosynthetics layers design allowed the owner to line their 6-acre pond within a week.

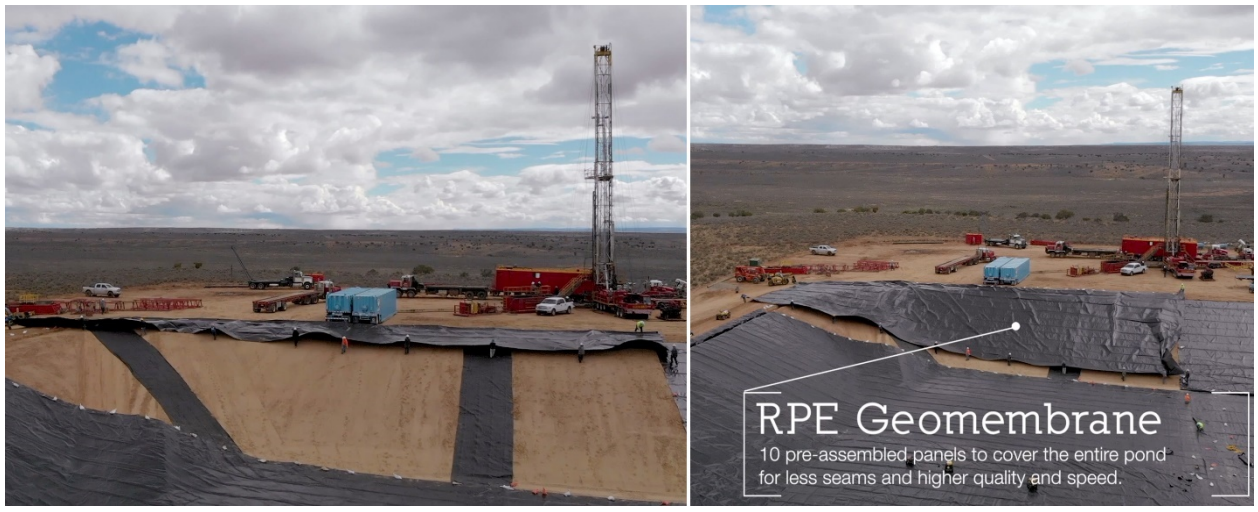

Figure 5: Deployment of a RPE panel in the slope

Figure 6: Deployment of the conductive multi-linear DRAINTUBE from the top of the slope

Figure 5 shows how to deploy each panel of RPE. Because larger panels can be pre-assembled at the factory, the installation allows for fewer seams in the field, reducing the risk of leaks at the joints compared to a traditional installation with narrow rolls. For this reason, the installation of the liner is faster and safer.

Figure 6 shows the lightness of the multi-linear drainage geocomposite. The rolls can be handled like geotextiles, unrolled from the top of the slope. Also, their structure is soft enough against the liner to avoid any risk of perforation due to heavy loads or harsh angles of plastic. Also, the installation is accelerated (in the order of 20 to 30% more productivity) and a lot safer for the crew than the installation of a geonet-type drainage geocomposite. Indeed, as most multi-linear drainage geocomposites products are made of

geotextiles and plastic pipes, they can be easily cut with traditional tools, whereas cutting a rigid heavy geonet might take longer and have increased risks of cuts to workers' hands.

Operations

As soon as the ponds are constructed, it is mandatory to control the access by external workers before filling with processed water. The operations are variable from site to site. In most cases, when the ponds are fully constructed they are immediately filled, without other human intervention. In this particular case, a lot of work was required after the primary layer was completed, i.e., equipment, pipes, pumps needed to be installed, and sometimes external works from sub-contracting companies.

Liners do leak

The simple act of using geosynthetics on a project does not guarantee imperviousness of the barrier layer. If fabrication practices are done properly, a geomembrane by itself is a fully impermeable material. However, every operation required to transform a manufactured geomembrane roll into an installed liner exposes the geomembrane to potential damage (mostly mechanical damage from impacts, but can also take the form of chemical degradation, resulting from improper storage, for instance).

Therefore, wherever a high level of uncompromised impermeability is demanded from the barrier layer, the use of third-party quality assurance and leak location services is imperative. We understand by third-party quality assurance an independent engineer hired by the owner to act as a global reviewer of the project including design, construction, and controls.

The relationship between third-party quality assurance (QA) and electrical leak location (ELL) is that of mutual dependency. The QA party is dependent on the ELL party for spotting breaches in geomembrane that have been overlooked, are invisible to the naked eye, or have occurred following the installation of subsequent system layers. Whereas the ELL party relies on the QA party for ensuring the adequacy and traceability of all installed materials, in addition to minimizing the number of geomembrane defects through oversight of the storage, handling, and installation phases of the work. Thus, ELL ensures that the geomembrane is uncompromised at the time of the inspection, while QA ensures that the geomembrane will continue to fulfil its function for the entire life expectancy of the project.

CQA third-party control

Internal quality control, which is conducted by the installer and controlled by the engineer representative, is typically a flawed process due to the inherent conflict of interest existing between the installation team and the quality team: both parties operate under an authority whose underlying interest is generally the fastest possible installation of geosynthetics on a given project. Thus, the employment of an independent

quality assurance party introduces an unbiased stakeholder whose underlying interest is the best possible installation of geosynthetics. More specifically: the mandate of a third-party QA inspector is to ensure the work is carried out as per project plans and specifications.

An expert third-party quality assurance inspector will oversee all aspects related to geocomposite materials on site: transport, handling and storage of geocomposite rolls; ensuring all material has undergone appropriate factory QC testing and is compliant with project specifications; subgrade approval, visual inspection of installed panels and seams; validation of welding machine calibration; non-destructive testing and intermittent destructive testing, including coordination with a testing laboratory.

In addition to collection and verification of all factory-issued documentation (factory QC testing, mill test certificates, datasheet, etc.), QA personnel also keep daily logs of panel installation sequence and the respective in-situ testing results, thus ensuring full traceability of geosynthetic material from the factory floor to their final resting place on the project site.

Additionally, much like the influence of a leak location operation, the very existence and on-site presence of an independent QA party has the effect of raising diligence and operational level of the internal QC personnel and the installation team.

Leak location survey

Most commonly, electrical leak location is carried out with two standardized methods: the water-puddle method and the dipole method.

Water-puddle is the more direct, more effective method of testing for breaches in the barrier layer, as it is carried out directly on top of the exposed geomembrane. The concept behind such methodology is that a continuous, fully impermeable assembly of geomembrane panels will not allow surface water to come into contact with the underlying substrate layer. When such contact is made (denoted by a signal from an electrical setup involving one electrode above the geomembrane and the other electrode in contact with the underlying layer), a breach in the geomembrane – either a hole or a tear – is thus located.

In order to successfully carry out the dipole leak location operation, the geomembrane must be covered by a single layer of homogenous, electrically-conducting material (e.g., wet granular material). The concept is identical to that of the water-puddle method: a continuous, impermeable assembly of geomembrane panels will not allow current propagation from above the geomembrane to the underlying substrate. The presence of a breach in the barrier layer is indicated by a typical leak signal in electrical current detected by the dipole apparatus.

When required, and when possible, both leak location methods are used on the same barrier layer. In addition to a redundancy check, this allows for separation of liability: holes detected via the water-puddle

methods are necessarily the responsibility of the geomembrane installer, whereas holes detected via the electrical dipole method are the responsibility of the civil-works contractor.

Average leakage per hectare

Typically, on a project in North America involving third-party QA oversight of geomembrane installation, a leak location operation will locate an average of 7 leaks/ha via the water-puddle method, and 1 to 4 leaks/ha via the dipole method (contingent upon whether a water-puddle survey had been first conducted). Unsupervised projects typically exhibit a much larger presence and range of breaches in the barrier layer. In some scenarios, the presence of breaches is so prevalent that it effectively nullifies the purpose of employing geomembrane panels in the first place (Forget et al., 2005).

Under favorable conditions, a thorough leak location survey will reduce the average presence of leaks down to 0 to 2 holes per hectare (it is important to keep in mind that the relationship between a hole and a leakage rate is dependent upon the size and the location of the hole within the containment basin).

In addition, in its history, the geomembrane system transformed from single- to double-lined (Peggs, 2009) because damage is unavoidable for a geomembrane during construction. The purpose of a double-lined system is that leakage through the primary geomembrane (with a constant hydraulic head on it) is collected by the secondary geomembrane and removed, so there is no head on the secondary. Therefore, the double-lining system doesn't leak – just as double-hulled ships do not sink.

Today, the most often applied primary Action Leak Rate (ALR) for water impoundments is 500 gallons per acre per day (gpad) as specified in *Recommended Standards for Wastewater Facilities* (Health Research Inc., 2004) by 10 northern states and in Canadian provinces for liners under 6 foot of water in waste water treatment plants. "Right sizing" the ALR to match the technical capabilities of the current leak-location methods is necessary (Darilek and Laine, 2011). Specifying a leakage rate that is too low can be a disaster if the source of the leakage cannot be located by current technology. If the source of the leakage cannot be located, then the only alternative is to reline the facility and hope that the new geomembrane does not also exceed the specified ALR.

According to the quality based action leakage (QBAL) method based on Giroud's equation for calculating flow through defects, with a good quality installation, a geomembrane could be expected to have 1 to 4 defects per acre and a poor-quality installation could have 10 to 20 defects per acre. This could equate to an ALR of 720 gpad to 3,600 gpad. Furthermore, according to Peggs (2009), a regulatory agency that holds to a zero-leakage policy is not being practical, which can lead to arguments, wasted time and efforts, and unnecessary expenses that benefit no one.

From theory to reality

Due to the limited understanding of lined pits, the state agency was expecting absolutely no leakage. The Required Global Quality was maximum.

The pit and liner stability started to be challenged directly at liner installation. Due to operational pressures, drill rig schedules, and lack of understanding of the fragility of the liner system, the Client decided to forgo electronic leak location surveys on the secondary and primary liner systems. To compound the situation, the drill rig crews utilized the completed pit as a drill cuttings pit that they later shovelled, then pressure washed at extreme pressures.

Shortly after the pit was put into its intended use, the Client started to report leakage through the primary liner. In January and February leakage pumping data resulted in 2,023 gallons per month and 1,685 gallons per month, respectively, for a 2.3 acre pit.

Following regulatory pressures, the Client shut down the operations of the pit, cleaned out the system, and brought in an electronic leak location survey specialist.

Leak location surveys

Leak location surveys have been conducted on each of the subsequent ponds based on lessons learned from the initial installation. Due to the liner surface type and slope the leak location surveys have been conducted depending on whether the survey was targeting the slopes or the bottom. The water puddle method (see Figure 7a) was selected by the client to control the integrity of the ponds in the bottom. The arc test method (see Figure 7b) was used in the slopes of each pond.

The results of the primary liner electronic leak location survey yielded 70 holes in the bottom of one of the pits and 8 in the second one. Additional issues were identified that were contributing to the leakage rate, such as the LLDPE material being damaged by the high-pressure cleaning, seams had been impacted during removal of drill cutting removal, and holes had been generated by inappropriate access to the liner (see Figure 8).

For each test, the conductive multi-linear drainage geocomposite offered an adequate sensitivity (arc test and water puddle) and permitted the detection of holes ranging in size from large (Figure 8) to very small holes (1 mm in diameter which was the size of the calibration hole; see Figure 7b).

Figure 7a: Water puddle method; Figure 7b: Arc test method

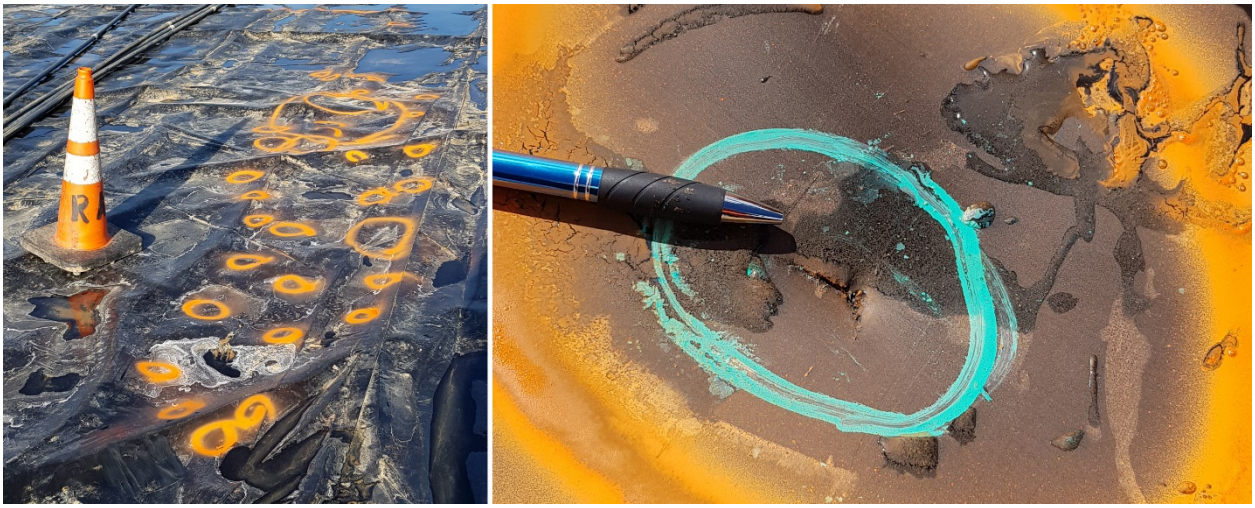

Figure 8: Example of leaks found on the primary liner at the bottom

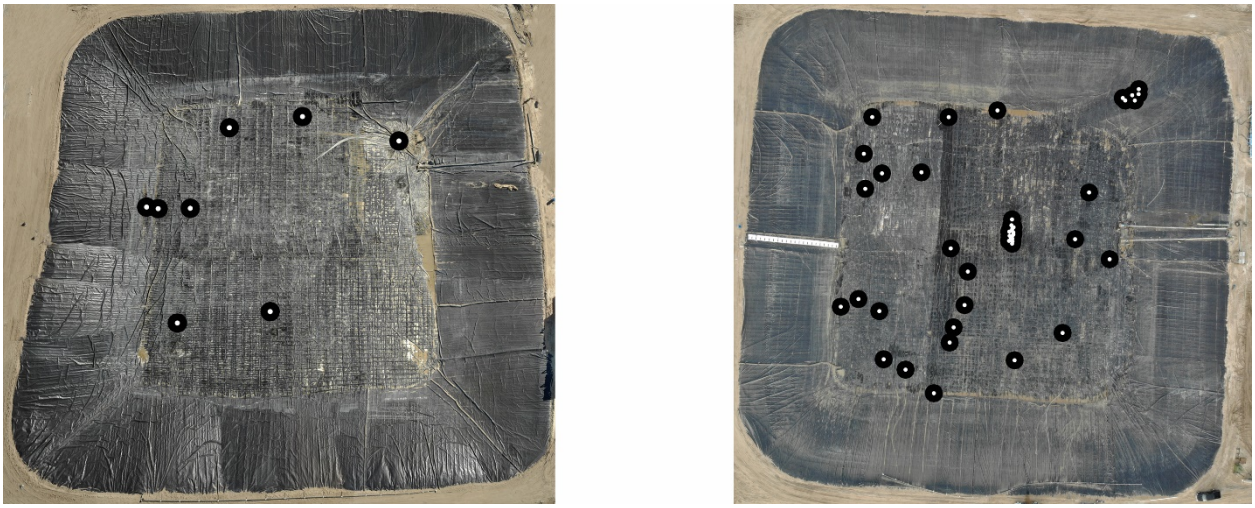

Figure 9a: Pond A (8 leaks); Figure 9b: Pond B (70 leaks)

Cost comparison

The costs have been compared, as is presented in Table 1. The scenario was as follows :

- Day 1: Pond filled up
- Day 1 + 1 month: Shut down the pond
- Day 1 + 2 months: Investigation, complete discharge of the pond, clean the bottom and run an ELL program
- Day 1 + 3 months: Relining of the primary liner, line a third layer and restart an ELL program
- Day 1 + 4 months: Pond filled up again and operated.

In this cost comparison, it is necessary to mention that every day of an active pond generating US$80,000 in revenue.

Good practices (ELL + 3rd Party QA/QC)		Bad Practices (no external QA/QC nor ELL)	
Leak location survey program	25 K$	720 k$	Pond shut down for 3 months
3rd Party QA/QC	25 k$	50 k$	Leak location survey program x 2
		50 k$	3rd Party QA/QC x 2
		250 k$	Relining the primary
Total Expected Costs 50 K$		**1,07 M$ Total Estimated Costs**	

Table 1: Comparison of costs between having a ELL campaign + 3rd party QA/QC or not

Table 1 shows that a non-quality approach can cost over 20 times what it would have cost to have a proper quality program, including ELL and third-party QA from the beginning of the project.

Lessons learned

Ultimately, the lessons learned from this costly exercise resulted in new operation and maintenance expectations within the company for lined pits. This includes:

- Slopes of 4:1 on smooth textured liners.
- Slopes of 3:1 on textured liners.
- Improved leak detection systems and grading methods.
- Suspension of LLDPE scrim reinforced liner as the primary liner.
- All approved access points are a differentiating colour of liner and have a minimum of two sacrificial layers to protect the primary liner.

- All entry into the pit is treated as a permitted entry through the company and is restricted to trained personnel only.
- All secondary and primary liners are electronically tested for leaks during construction to establish a base line.
- Leakage is monitored on a weekly basis and Action Leak Rates are calculated for every pit to establish operating parameters.

Conclusion

This case study shows that despite a good design and a normal construction, the Global Quality level of a project can be far away from the regulation expectations. Indeed, even with a 1.0 for the design and a not too bad 0.9 for construction, a poor of Operation 0.7 due to a high presence of uncontrolled workers on-site caused the GQL to rank as $1.0 \times 0.9 \times 0.7 = 0.63$. This is a little over half of the value targeted by the regulatory authority with a 1.0 condition in the operation permit. There is absolutely no way to meet that constraint in a geosynthetic work without having a strong QA program that includes a third-party QA and a complete electrical leak location survey campaign. Conductive multilinear drainage geocomposites have demonstrated their efficiency in this project by helping the operators to find an important amount of leaks of different sizes.

References

Darilek, G.T. and D.L. Laine. 2011. Specifying allowable leakage rates. *The Geosynthetics Magazine,* August 2011.

Forget, B., A.L. Rollin and T. Jacquelin. 2005. *Lessons Learned from 10 Years of Leak Detection Surveys on Geomembranes.*

Health Research Inc. 2004. Recommended standards for wastewater facilities. Accessed from https://www.broward.org/WaterServices/Documents/states_standards_wastewater.pdf

Maier, T.B. and S. Fourmont. 2013. How tubular drainage geocomposite was used in landfill final cover. *Geosynthetics* 31(3): 48–51.

Peggs, I.D. 2009. Geomembrane liner action leakage rates: What is practical and what is not? Retrieved from Geosynthetica.com.

Saunier, P., W. Ragen and E. Blond. 2010. Assessment of the resistance of drain tube planar drainage geocomposites to high compressive loads. 9th International Conference on Geosynthetics. Guarujá, Brazil. Vol. 3.

Chapter 4
Technologies

Proceedings of Tailings and Mine Waste 2019
November 17–20, 2019, Vancouver, Canada
Published by the University of British Columbia, 2019

Multi-Dimensional Tailings Deposition and Consolidation Modelling

Alessandro Amodio, Norwegian Geotechnical Institute (NGI), Australia
Hongjie Zhou, Norwegian Geotechnical Institute (NGI), Australia
Noel Boylan, Norwegian Geotechnical Institute (NGI), Australia

Abstract

Appropriate modelling of tailings gradual deposition and consolidation is required to predict the storage capacity of impoundments, the development of tailing consolidation settlement over time, the amount of water expressed during consolidation, and the required amount of backfilling material for reclaiming the mine site. This paper introduces a numerical modelling approach developed using the specialized geotechnical software FLAC (Itasca, 2016) to simulate the gradual deposition and large-strain consolidation of tailings in a multi-dimensional space.

Using an approach built on commercial software provides powerful flexibility in capturing a variety of modelling input conditions by utilizing built-in functions of the software. However, in order to model the tailings gradual deposition and consolidation with commercial software, specialized routines had to be developed in order to overcome key challenges associated with this process, such as the continuous change of hydraulic boundary conditions (corresponding to the top tailings surface), the extremely low effective stresses when the tailings are discharged in a slurry state, and the large variability of the tailings behaviour (i.e., compressibility and permeability) that can exist within a deposit.

In this paper, the developed approach is validated against the analytical solution developed by Gibson (1958), and benchmarked against commonly referenced cases. Case examples are also provided that demonstrate the flexibility of the calculation approach when applied to a full-scale model scenario.

Introduction

Large tailings impoundments are often required to store the vast amount of tailings (mining waste) generated at mines during operation. Estimation of the capacity of storage facilities and tailings consolidation settlements over time are key inputs for the management of an impoundment facility. The capacity of the impoundment needs to be estimated for planning purposes both prior to developing a facility and also during its operation. Mine management also requires a reliable estimate of the contaminated water

discharged over time during tailings consolidation (before and after the tailings deposition is concluded). The estimate of post-closure settlement is key information for determining the long-term condition and confirming post-closure conditions.

Tailings impoundments pose long-term environmental risks, for example due to insufficient capacity for treating expressed waste water. Reliable prediction of tailings consolidation is, therefore, central to the planning and management of the mine throughout its entire life.

The behaviour of fine-grained tailings material discharged in a semi-liquid state can be divided into three stages from the point of discharge: (i) flocculation; (ii) sedimentation; and (iii) consolidation (Imai, 1981). For the calculation of tailings settlements within the impoundments, this entire process is dominated by the consolidation stage and therefore in practice, consolidation typically is the only process analyzed (Znidarcic, 1999).

It is generally agreed that the consolidation settlements are influenced by two primary deformation mechanisms: i) volumetric strain due to changes of effective stress (often named "primary consolidation") and ii) time-dependent volumetric strain (i.e., creep). Although it is recognized that both of these mechanisms should be considered for a correct estimate of the consolidation settlements, the contribution of creep is often neglected in the settlement calculations performed on tailings. The main justification for this practice is that, for tailings, "primary settlements" are expected to be significantly larger than creep. However, it is also the case that laboratory measurements of tailings creep parameters as well as the prediction of settlement due to creep have not reached the same accuracy as has been achieved regarding the primary consolidation (Znidarcic, 2015). The modelling approach presented in this paper is generally used only to capture the component of consolidation settlements associated with change of effective stress; however, it has the capability to capture the effects of creep.

Due to the large compressibility of the tailings (especially when it is discharged in a semi-liquid condition) during consolidation, tailings undergo large-strain deformation, with compressibility and permeability changing with the void ratio; in turn, this behaviour influences the volumetric deformation.

Differing from many standard consolidation problems, where the same loading conditions are maintained constantly, during the tailings deposition, the loading (represented by the self-weight of the tailings) progresses during consolidation. The total stress in the tailings increases proportionally to the amount of tailings being discharged, while the excess pore pressure evolves based on the combined effect of the total stress variation and water flow conditions. When this process is combined with a slow pore pressure dissipation (associated with fine-grained material) the effective stresses can be close to zero in the proximity of the tailing top surface and then gradually increases with depth. Linked to this effective stress profile can be a large variability of tailings compressibility behaviour, with potentially three to four orders of magnitude difference in the constrained modulus (M) between the element at the top (next to the free

surface) and the bottom of the model (corresponding to the first material discharged). These conditions, coupled with the requirement of continuous updating of the tailing top free surface, represent significant numerical challenges.

In order to model this scenario, many numerical prediction models have been developed and used extensively by the industry. Due to many technical challenges, most of them use the 1D large-strain calculation approach, integrated in a 3D geometry (generally called "pseudo 3D" models).

The key value of the developed approach presented herein is that it is built on the commercial specialized geotechnical software, FLAC (and FLAC3D), which allows it to explicitly model complex multi-dimensional problems directly such as: accounting for irregular impoundment geometries, non-uniform distribution of the tailings across the impoundment, and complicated consolidation boundary conditions, e.g., under-drains, permeable/impermeable side walls, vertical and horizontal drains. As illustrated by the example application, this approach can be used to predict the development of tailings consolidation settlement over time, the amount of water expressed during consolidation, the capacity of the pit for tailings storage, and the required amount of rock for backfilling.

Benchmark examples and an analytical solution have been selected to validate the modelling approach: the gradual deposition modelling approach has been validated against the analytical solution developed by Gibson (1958), and the predictions presented in Townsend and McVay (1990) have been used to demonstrate the model performance under different scenarios.

State of the practice in tailings consolidation modelling

Tailings materials are often characterized by large compressibility and exhibit large-strain deformations with the development of effective stress. The equilibrium assumptions that regulate the large-strain deformations differ from those adopted for the conventional small-strain approach with the material properties (e.g., voids ratio, stiffness and permeability, which govern the consolidation response) continuously changing with accumulating deformation. Thus, large-strain consolidation theories have been developed (e.g., Gibson et al., 1967) and numerical models have been successfully applied to predict the consolidation behaviour of slurry materials including tailings (e.g., mine tailings, and dredged materials). Governing constitutive relationships include the void ratio – effective stress relationship (e-σ'_v, also known as compressibility) and the permeability – void ratio relationship (k-e). These are necessary to relate the coupled effects of increasing σ'_v on compressibility and permeability to solve the governing equations of large-strain consolidation (e.g., Gibson et al., 1967).

To date, many 1D large-strain consolidation computer programs have been developed, e.g., those presented in Townsend and McVay (1990), and are adopted in mining practice for assessing the consolidation settlement of tailing. For multi-dimensional problems, the "pseudo 3D" approach has been

developed by combining multiple 1D column consolidation models to approximate the multi-dimensional geometry (e.g., Gjerapic et al., 2008). Although most of these programs have been proven to work well for 1D problems, there are limited full-scale TSF case studies that evaluate the performance of the pseudo 3D approach. The pseudo 3D approach also has several intrinsic limitations that can be relevant when modelling impoundments with irregular geometries, non-uniform tailings distributions and complex (e.g., non-vertical) boundary conditions.

The main limitations of this modelling approach are related to the omission of the stress between the 1D columns, and the inability to model any non-vertical deformation and water flow. The latter can represent a key element when modelling scenarios where horizontal flow is significant (e.g., relatively deep impoundments with drained side walls boundaries); while the effect of shear stress between the 1D columns and the importance of horizontal tailings movements can be significant when the depth of the impoundment is not uniform and/or tailings properties vary spatially.

An evolution of the calculation technique toward realistic 2D/ 3D modelling is represented by the so-called "Quasi 2D/3D" approach, such as that developed by SoilVision Ltd (Fredlund et al., 2012). In the Quasi 2D/3D formulation, the water can flow in true 2D and 3D space, but the solid deformation is limited in the vertical direction (Jeeravipoolvarn, 2010); hence, this approach does not account for the effect of lateral tailings deformation.

The approach proposed in this paper is a full 2D/3D model, with both flow and deformation developed in a 2D/3D space, which allows consideration of the complexity of a 3D stress distribution, deformation, and water flow. One of the main strengths of the proposed approach is that it is built on the commercial specialized geotechnical software, FLAC (and FLAC3D). This provides great flexibility in the input geometry and boundary conditions. Complex model features like vertical and horizontal drains or geotextile installation can be explicitly modelled, and different geometry of waste rock to simulate capping process during mining closure can be applied.

Developed modelling approach

The proposed modelling approach is built on FLAC (Itasca, 2016) but it also includes various user defined routines developed to capture the key features of the tailings' behaviour during large-strain consolidation, and overcome the numerical challenges related to the modelling of the deposition process. These key aspects are discussed in more detail below.

Constitutive modelling of tailings material

The non-linear relationships between voids ratio (e) and vertical effective stress (σ'_v), and permeability (k) and *e* have been implemented by modifying the built-in Mohr-Coulomb model in FLAC (Itasca, 2016),

using the embedded programming language, FISH. The main variable for the adopted model is the void ratio (e) which is updated every step of the calculation for each element, according to the computed volumetric strain. Since the constitutive models in FLAC operate in incremental fashion, the elastic moduli (e.g., bulk and shear modulus) required in FLAC input are tangent moduli, and they are used to relate incremental stresses to incremental strains. Hence, at each calculation step, the tangent stiffness is updated based on the calculated void ratio, consistent with the input e-σ'_v relationship; a similar updating procedure is performed for the material density and permeability.

Materials with different constitutive relationships can be considered in the modelling to account for local variation.

Process modelling of coupled tailings deposition and consolidation

In order to simulate the gradual deposition of tailings, a staged-filling approach has been developed in combination with the built-in large-strain calculation model of FLAC (Itasca, 2016). Each deposition stage (i.e., activation of one new layer above the existing tailings in the impoundment) is performed in an undrained manner (i.e., no drainage occurs), and it is then followed by a period of consolidation.

Typically, the tailings are discharged in a semi-liquid state (i.e., slurry) maintaining a horizontal surface within the impoundment (assuming no shear strength for the slurry) during deposition. This condition is currently assumed in the proposed approach; however, additional complexity can be added by considering the tailings discharged predominantly at one side of the impoundment and maintaining a specific angle of deposition. If required, localized or distributed deposition of tailings with different properties can be also modelled explicitly.

For each newly activated layer, the top surface is purely horizontal while the bottom is deformed according to the consolidation settlements produced during the previous deposition stages. With this approach, different local deposition rates (i.e., deposition rate per unit area) are considered in the modelling, with more tailings material deposited in areas which experience more settlements (often corresponding to the deep part of the impoundment). A key capability of FLAC necessary to model this process is its capability to specify the geometry of newly activated elements prior to their activation. In this case the newly activated elements are shaped according to the settlements that have occurred prior to activation.

The consolidation time for each consolidation stage is computed according to the assumed deposition rate and the volume of the new layer. Two key challenges have been encountered in the modelling of the deposition process. The first one is related to the frequent update of the boundary conditions with the activation of new elements; in order to prevent numerical instability, a number of sub-steps have been introduced to activate each new element and update the total stress without compromising the stability and altering the excess pore pressure distribution.

A second challenge is represented by the large variability of the stiffness properties obtained by using the non-linear relationship of e-σ'. When the tailings consolidates only under its self-weight, large differences in the stiffness properties (of several orders of magnitude) can result from the effective stress distribution, with elements at the top of the model that experience only negligible effective stress compared to those at the bottom. In order to overcome this challenge several sub-routines have been developed within the user define constitutive model to regulate the water bulk modulus according to the calculated stiffness.

Approach validation

Various rigorous verifications and validations have been performed in the course of developing the modelling approach. For example, the user defined constitutive model has been tested at element scale in uncoupled and coupled analyses with small- and large-strain modes. The validation of the deposition modelling procedure against the analytical solution developed by Gibson (1958) is discussed in more detail below.

Gibson (1958) presents the results of the deposition of uniform material with a constant rate of deposition, *m*, and impermeable base boundary. The excess pore pressure profiles obtained by Gibson (1958) are presented in Figure 1 against the results obtained using the developed model for different time factors T, where:

$$T = \frac{m^2 \cdot t}{c_v} \qquad \text{(Equation 1)}$$

Where:

c_v= coefficient of consolidation (m^2/year)

t = total time for deposition (years)

m = deposition rate (m/year)

The results of the proposed modelling are presented in Figure 2, in comparison with the Gibson solution. The comparison indicates a good match between the results of the modelling and the analytical solution.

The scenarios presented by Townsend and McVay (1990) have been also used to demonstrate the model performance under different input conditions. Note that Townsend and McVay (1990) summarize results of a prediction competition where nine teams of modellers predicted the consolidation behaviour of four different waste clay disposal scenarios using 1D models, and the results are commonly used as a benchmark for the evaluation of numerical models of large-strain consolidation.

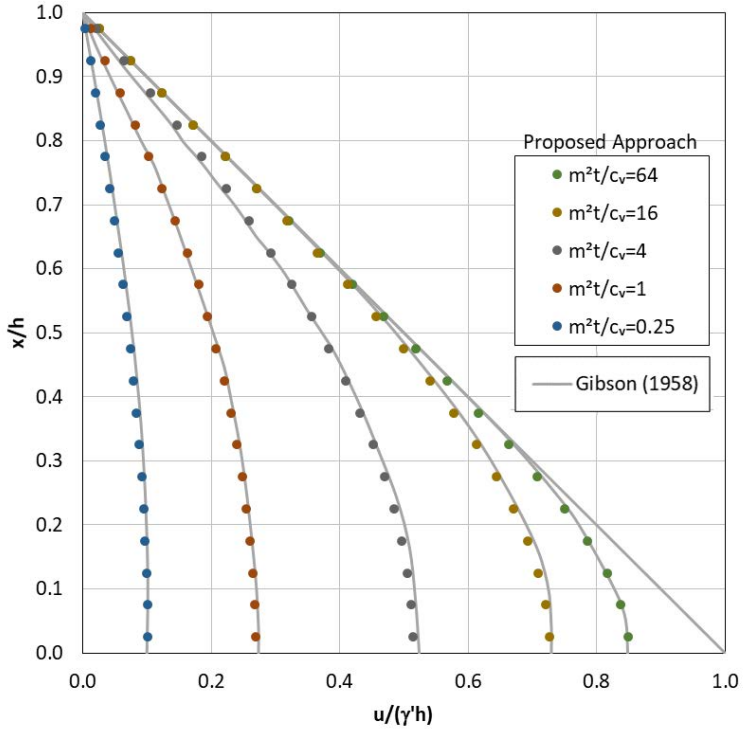

Figure 1: Validation against Gibson (1958)

Due to space limitations, only the results of two scenarios are reported in Figure 2. The two scenarios depicted in Figure 2 represent the most complex among those presented in Townsend and McVay (1990); this is underscored by the low number of modellers that managed to provide prediction for these scenarios (e.g., only three predictions out of nine modellers are reported for Scenario D). The results of the verification exercise against all the scenarios from Townsend and McVay (1990) are presented in Zhou et al. (2019).

In addition to the results of the modelling competition presented in Townsend and McVay (1990), the results obtained using the SVSolid/SFFlux software and presented in SoilVision (2018) are also compared in Figure 2.

As shown below, the developed modelling approach achieves excellent results in comparison with individual predictions made by the participants, and separately using the SVSolid/SFFlux software. Although there are some differences in results obtained using SVSolid/SFFlux for scenario D, where it seems to be providing a slightly different outcome from the other predictions. The "kinks" on the void ratio profile for the proposed approach and SVSolid/SFFlux can be understood by considering that the value of vertical pressure at these depths is less than the yield stress (Zhou et al., 2019).

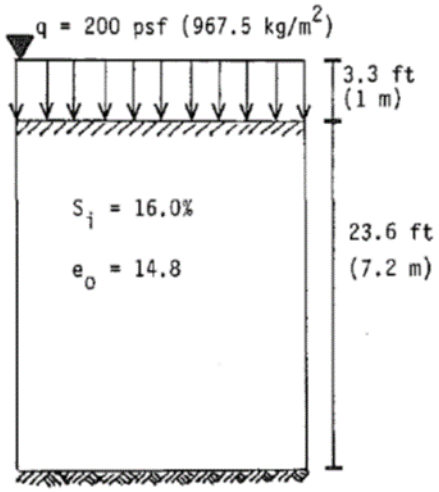

(a) Schematic of Scenario C

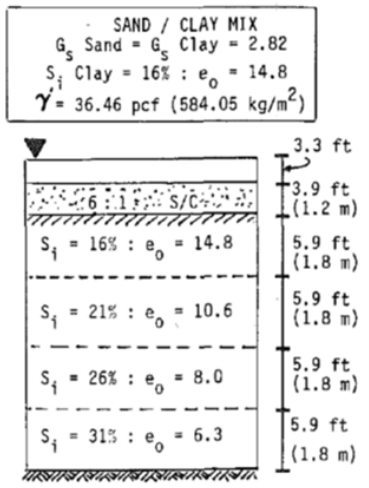

(b) Schematic of Scenario D

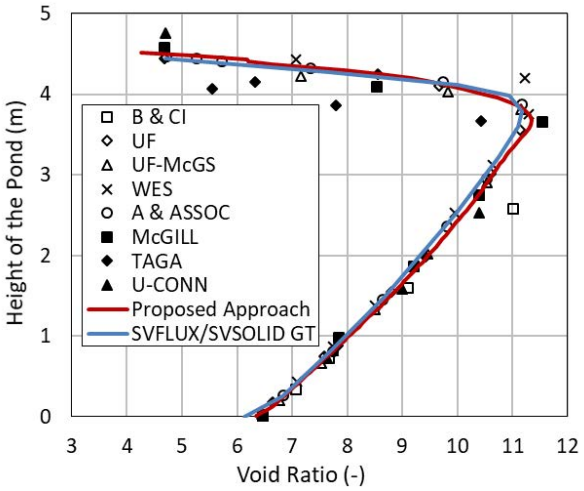

(c) Scenario C: void ratio after one year

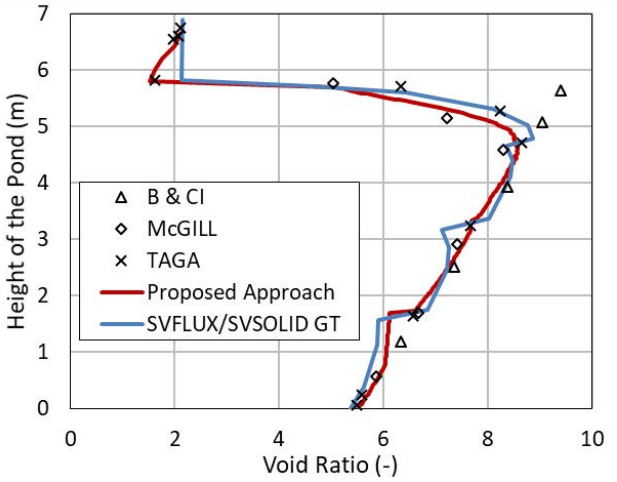

(d) Scenario D: void ratio after one year

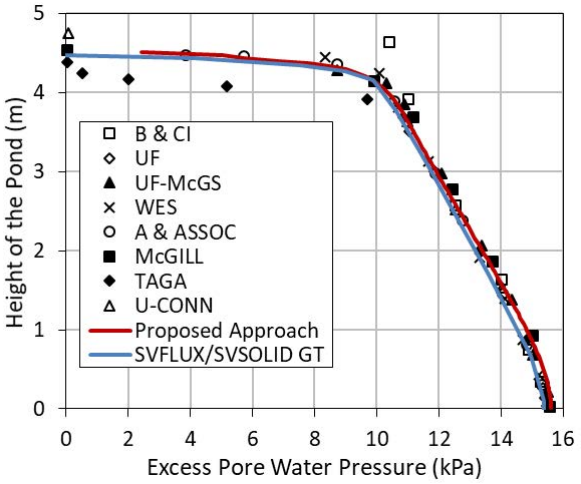

(e) Scenario C: pore pressure after one year

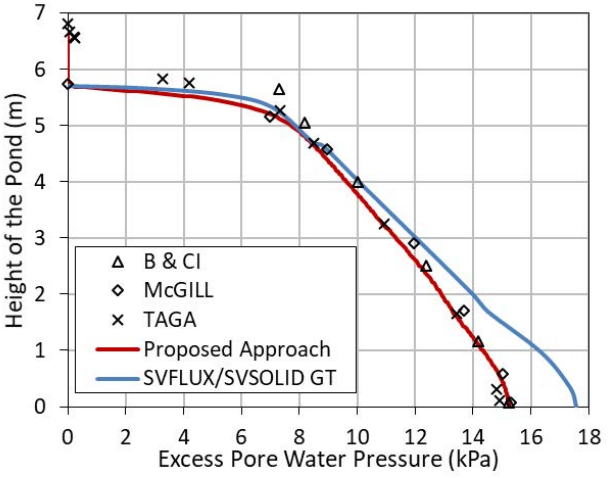

(f) Scenario D: pore pressure after one year

Figure 2: Predictions of Scenario C and Scenario D from Townsend and McVay (1990)

Example – Multi-dimensional modelling of tailings deposition

To further demonstrate the capability of the developed modelling approach, a full-scale example is presented in the following sections. A few analyses have been performed by changing the boundary conditions and the rate of deposition, to show how the model can perform under different input conditions and provide useful insights for the management of storage facilities. The results presented herein are focused on the tailings deposition stage, though other stages following deposition (e.g., quiescent consolidation with wick drains and dumped rock) can also be modelled, as presented in Zhou et al. (2019).

Modelling details

In this example, an axisymmetric impoundment is considered. The modelling procedure and discretized FLAC grid is shown in Figure 3. Wick drains, rock backfill, and the boundary of the impoundment are also presented in the figure; however, the effects of this modelling feature are not presented in this paper (the results of the example analysis post deposition are presented in Zhou et al., 2019). The grid shown in Figure 3 was pre-designed before the analysis actually started, so it does not show the deformed grid that develops during the analysis. The deposition (with the activated elements of the grid and the deformed geometry) is shown in Figure 4.

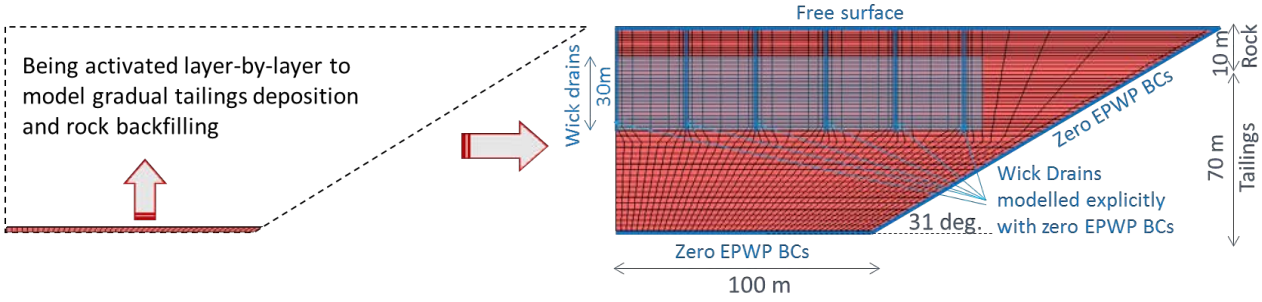

Figure 3: Modelling procedure: layer-by-layer activation of FLAC grid to model gradual deposition and consolidation of tailings and rock backfilling, inclusion of wick drains

Typical copper mine tailings material has been considered. Details on the material properties are reported in Zhou et al. (2019). A bonded interface is assumed between the tailings and side wall and base of the impoundment, though any intermediate interface conditions (between smooth and rough) can be modelled if necessary. During deposition, the water level is assumed to be flush with the tailing top. A constant tailings deposition rate is assumed in the simulations.

The main variation in the inputs of the example analyses are summarized in Table 1. The objective of performing these example analyses is to demonstrate how the proposed approach can be used to manage a storage facility and help to understand the consequence of project decisions, being able to capture most of the details of a 3D geometry.

Table 1: Key variation of the example analyses

Analysis	Bottom and side walls hydraulic boundary conditions	Deposition rate (t/month)
Base case	Permeable(1)	200,000
Sensitivity 1	Impermeable	200,000
Sensitivity 2	Permeable(1)	600,000
Sensitivity 3	Permeable(1)	67,000
Sensitivity 4	Permeable(1)	20,000

(1) Permeable boundaries are considered connected to the decant pond to maintain the hydrostatic pressure, modelled with zero excess pore pressures.

Results and discussion

The variation of tailings voids ratio with different deposition stages is plotted in Figure 4 for the base case analysis. This illustrates the modelling process of the gradual deposition of the tailings and changes in soil state over time.

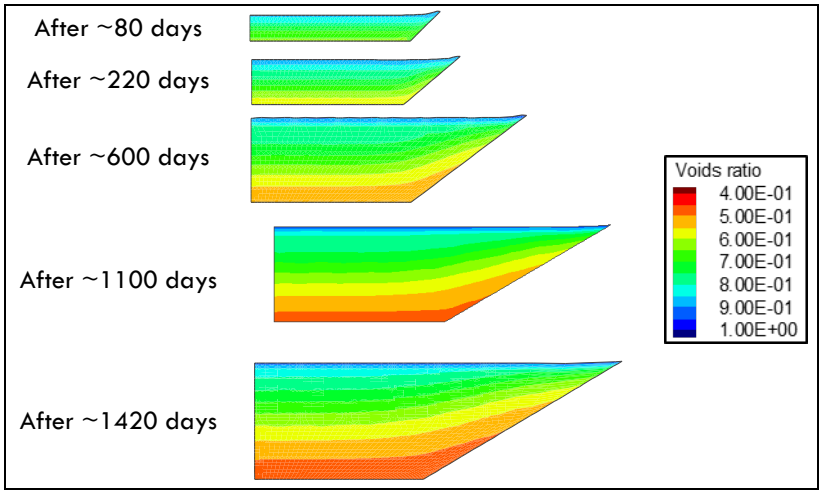

Figure 4: Contours of voids ratio with tailings deposition (base case)

The variation of the total dry weight of tailings stored in the facility with the logarithmic of time is compared in Figure 5 for all the analyzed cases. As shown, due to the consolidation occurring simultaneously with deposition, the actual capacity of the impoundment in terms of tailings dry weight is significantly greater than that corresponding to the geometric volume (assuming no expression of excess pore waters). However, the capacity of the impoundment does not seem to be greatly affected by the deposition rate and the boundary conditions considered. One of the reasons is that a large percentage of the volumetric reduction is completed at the very early stage of the consolidation due to the high nonlinear e-p relationship, when the permeability is also much higher. This observation may change for different tailings properties and impoundment geometry.

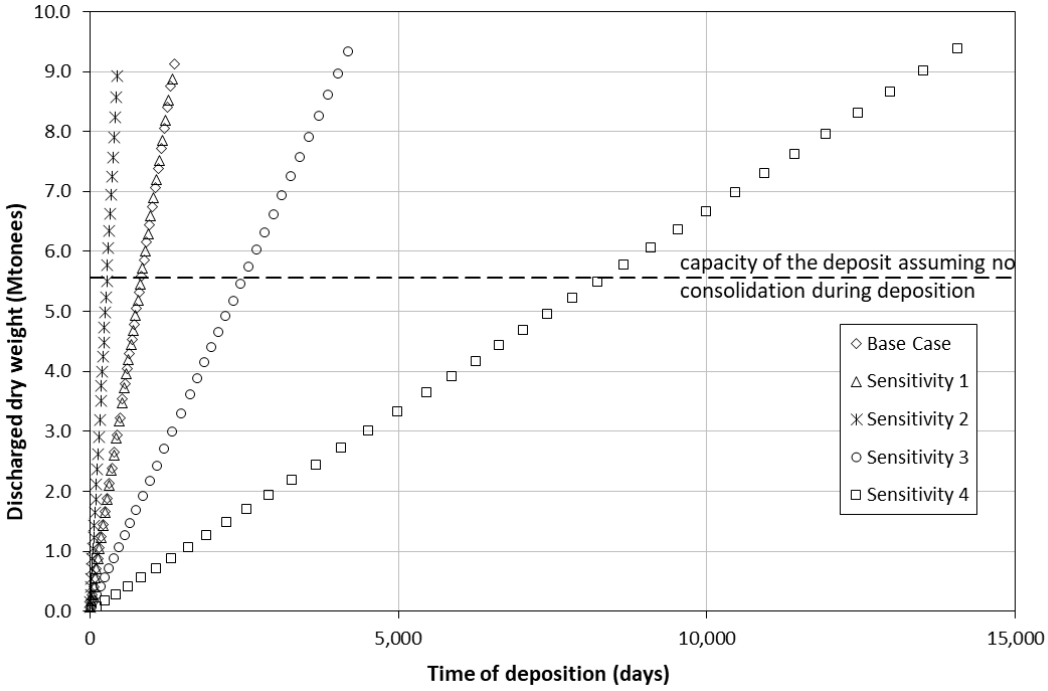

Figure 5: Capacity of the deposit in terms of tailings dry weight

Conclusion

Based on the foregoing discussion, comparisons, and example modelling, the following conclusions can be reached:

- The gradual deposition and large-strain consolidation of tailings is often performed using 1D models. Because of the intrinsic simplifications, 1D approaches may not be able to capture some key features of this complicated process.
- The modelling approach described in this paper accounts for both flow and deformation developed in a full 2D/3D space. The main strength of this approach is that it is built on the commercial specialized geotechnical software, FLAC (and FLAC3D). This provides considerable flexibility on the input geometry and boundary conditions; complex model features like vertical and horizontal drains or geotextile installation can be explicitly modelled; also, the different geometry of waste rock to simulate the capping process during mining closure can be applied.
- By modelling the problem in a real multi-dimensional space, the developed approach can be used to understand the relevance of specific project decisions and facilitate the management of the storage facilities.

- The developed model is shown to perform well when compared against analytical solutions and commonly referred-to benchmarks. These comparisons demonstrate the capability of the model to capture the realistic behaviour of tailings consolidation. A full-scale example case is provided to illustrate its application to a practical tailing consolidation scenario.
- Further development is ongoing in order to expand its modelling capability, e.g., including the effect of creep in the constitutive model, predicting the increase in tailings strength with consolidation, assessing the propensity to contract or dilate during shear deformation (using a state parameter based critical state approach), and so forth.

References

Fredlund, Murray, Jim Zhang and Dirk van Zyl. 2012. Multidimensional coupled sedimentation and consolidation theory. Accessed at www.semanticscholar.org

Gibson, R.E. 1958. The progress of consolidation in clay layer increasing in thickness with time, *Géotechnique*, 8(4): 171–182.

Gibson, R.E., G.L. England and M.J. Hussey. 1967. The theory of one-dimensional consolidation of saturated clays. *Géotechnique* 17(3): 261–273

Gjerapic, G., J. Johnson, J. Coffin and D. Znidarcic. 2008. Determination of tailings impoundment capacity via finite-strain consolidation models. *GeoCongress 2008*, ASCE: 798–805.

Imai, G. 1981. Experimental studies on sedimentation mechanism and sediment formation of clay materials. *Soils Found.* 21(1): 7–20.

Itasca. 2016. *FLAC 8.0. Fast Lagrangian Analysis of Continua, User Manual*.

Jeeravipoolvarn, S. 2010. Geotechnical behavior of in-line thickened oil sands tailings. PhD thesis, Faculty of Graduate Studies, University of Alberta, Edmonton.

SoilVision. 2018. *Consolidation Verification Manual.*

Townsend, F.C. and M.C. McVay. 1990. SOA: Large-strain consolidation predictions. *Journal of Geotechnical Engineering* 116(2): 222–243.

Znidarcic, D. 1999. Predicting the behavior of disposed dredging soils. *Geotechnical Engineering for Transportation Infrastructure.* Rotterdam: Balkema: 877–886.

Znidarcic, D. 2015. If it creeps, does it matter? In *Proceedings of Tailings and Mine Waste, 2015.* October 26 to 28, 2015, Vancouver, British Columbia, Canada.

Proceedings of Tailings and Mine Waste 2019
November 17–20, 2019, Vancouver, Canada
Published by the University of British Columbia, 2019

Using Technology to Identify Seepage Flow Paths Through, Under, and Around Tailings Impoundments

Ryan Blanchard, Willowstick Technologies, USA
Judson Kennedy, Willowstick Technologies, USA

Abstract

Tailings impoundments continue to undergo failures at an unacceptably high rate, including failures at operations owned by high profile mining companies, for example the Brumadinho Dam failure in Brazil. These failures are often the result of a combination of design, construction, and operation actions that are controlled by humans and must be better coordinated and managed in the future. The consequence of failure can be the discharge of tailings, environmental damage, and loss of life.

Any additional technology and information that enables an owner of a tailings impoundment to be more certain of its condition, and thereby reduce the risk of failure is of tremendous value to tailings and mine water management. The magnetometric resistivity (MMR) method can provide valuable information, and it involves the injection of a low frequency electrical current in the ground between two electrodes, generating a magnetic field that can be measured at the ground's surface with sensitive magnetic sensors. The map of the magnetic field, measured at the frequency of the injected current, can be used in turn to determine the position of the electric current paths in the ground. When the electric current is channelled in conductive paths, the MMR method can be used to identify the location of these paths. Conductive current paths are then interpreted as preferential seepage flow paths.

A case study from a recycle tailings pond (RTP) at a gold mine in Alaska, USA, is also presented. This dam had known seepage problems at the downstream toe of the dam. One grout curtain along the upstream toe of the dam and three smaller curtains that ran parallel to one another near the south abutment were installed to mitigate the seepage. Unfortunately, the seepage issues continued after the grout curtains were installed. A MMR investigation was performed on the tailings dam and the results showed the exact location of a preferential seepage flow path that bypassed the toe grout curtain and flowed through the dam. The remainder of the dam was performing as designed. With this information the client was able to make additional repairs and mitigate the seepage issues.

Introduction

Tailings impoundments continue to undergo failures at an unacceptably high rate, including failures at operations owned by high profile mining companies, for example the Brumadinho dam failure in Brazil. These failures are often the result of a combination of design, construction and operation actions that are controlled by humans and must be better coordinated and managed in the future. The consequence of failure can be the widespread flow of tailings, environmental damage, and loss of life.

Identifying the source and character of preferential seepage flow paths within tailings impoundments is notoriously difficult and faces numerous challenges. Engineers often drill holes in the structure by simply guessing the location of the seepage and hoping to intercept water flow paths. This method is expensive and has the potential of further impairing the integrity of the structure. Alternatively, the magnetometric resistivity (MMR) method can be used to identify the exact location of preferential seepage flow paths passing through, under or around the tailings impoundment. This method effectively and efficiently identifies groundwater flow in complex environments, at significant depths, and over large areas.

Methodology

The MMR method uses a low-voltage, low-amperage, alternating current to energize subsurface water by strategically placed electrodes (Jessop et al., 2018). At each study area one or more independent surveys are required. Each survey uses electrodes, connected by an insulated copper wire, and a power supply to energize the circuit (Figure 1).

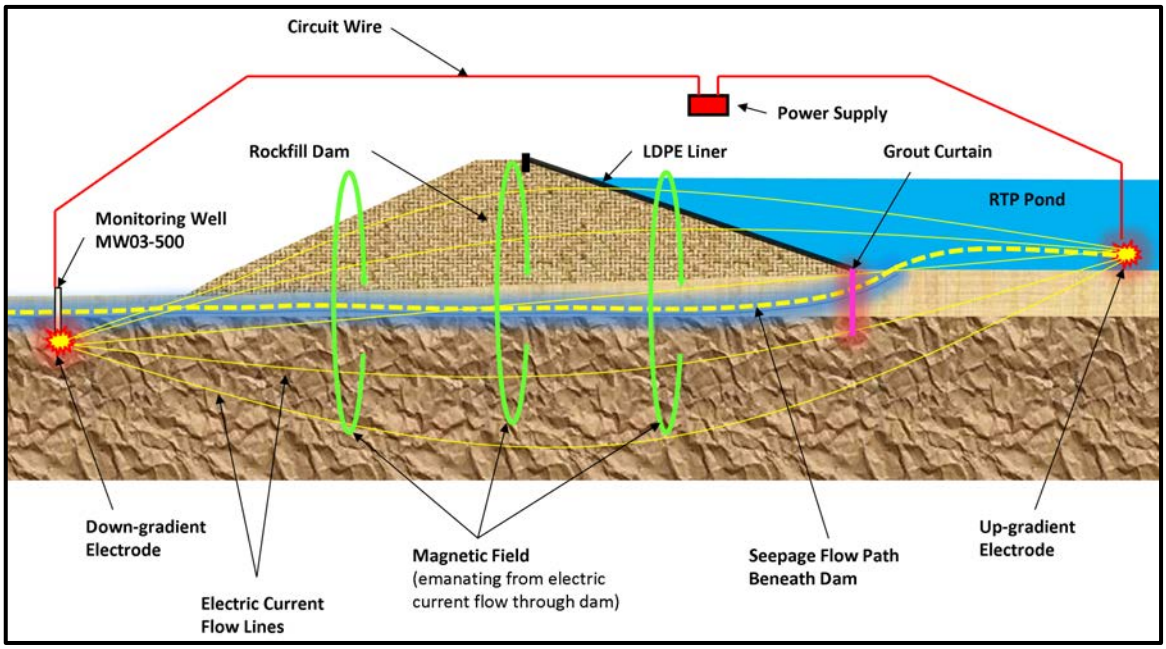

Figure 1: MMR survey setup

One electrode is placed in the upstream reservoir or tailings material and the other is placed downstream in contact with the water below the impoundment (in a well, pond or stream). The power supply uses between 150 to 300 V and 0.3 to 2.0 A. The exact voltage and amperage varies depending on the conductivity of the subsurface materials.

As with all alternating electrical currents, this circuit generates a magnetic field (Biot-Savart Law) that is measured and mapped from the surface using a Willowstick instrument. The instrument uses three magnetic sensors oriented in orthogonal directions (x-, y- and z-axes); an integrated digital signal processor is used to collect, filter and process the sensor data; a high resolution GPS is used to spatially define the measurement locations; and, a handheld computer with mapping software is used to couple the GPS data with the magnetic field data and store it for subsequent reduction and interpretation. All of this equipment is attached to a surveyor's pole and hand carried to each field measurement station, and each measurement is collected in eight seconds. All measurements are collected in free space without ground contact requirements. This collected data is used to create two- and three-dimensional (2D and 3D) maps and electric current distribution (ECD) models of seepage flow paths (Figure 2). The technology maps and models preferential groundwater flow paths similar to an angiogram that allows doctors "to see" blood vessels in a human body.

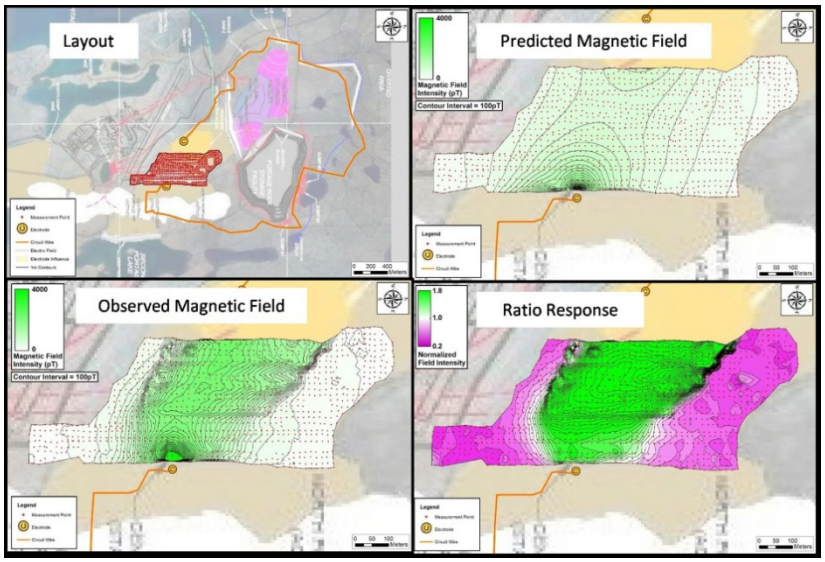

Figure 2: Steps to create data results and 2D maps

The application of the technology to tailings impoundments is based on the principle that water increases the conductivity of earthen materials through which it flows. As the signature electric current travels between electrodes strategically placed upstream and downstream of the impoundment, it concentrates in the more conductive zones, where water preferentially flows as seepage through, under and/or around the impoundment. An electric circuit is established in the study area of interest. Measuring the resultant

magnetic field at the surface reveals the electric current flow and distribution. Data is processed and compared to a predicted magnetic field from a theoretical homogenous earth model to highlight deviations from the "uniform" model. 2D maps and 3D models are generated and combined with known subsurface data to enhance preferential seepage path definitions. The purple shading in the ratio response map (Figure 2) shows actual flow that is less than flow predicted by the "uniform" model. Green shading shows actual flow that is more than flow predicted by the "uniform" model, so it likely represents a seepage path. Once seepage paths have been identified by the technology, sheet pile walls or grout curtains can be used to remediate them (Kofoed et al., 2011).

This technology has been applied to tailings impoundments all over the world, but has some limitations. One common limitation is conductive culture (man-made metal objects, metal fences, buried power lines) which can influence the magnetic field readings. Fortunately, the data can be filtered and the effects of the conductive culture can be modeled out to provide the needed results. Another limitation is that due to the dominant magnetic fields they generate, the circuit wire and electrodes must be placed far outside the study area. Occasionally – due to property boundaries/access – the circuit wire cannot be placed far enough outside the study area and the survey data can be compromised. And finally, at some sites the groundwater is not conductive enough to establish a good current.

This paper uses a RTP dam in Alaska for a case study. The method identified one preferential path of electric current that was interpreted as a preferential seepage flow path out of the dam through the grout curtain. This example is used to illustrate the procedures, findings and benefits of this technology.

Results and discussion

By way of background, the RTP dam consists of a rock filled embankment. To minimize seepage out of the dam a LDPE liner placed over the upstream face of the embankment and a grout curtain was installed beneath the upstream toe of the dam (see Figure 3). Despite these preventative efforts, shortly after filled seepage was observed at the downstream toe of the embankment. The primary grout curtain beneath the south abutment was designed to cut-off water below the dam's embankment but not necessarily around and through the dam's south abutment. Also, the grout curtain consists mostly of vertical grout holes that may not have adequately intercepted joints and fractures potentially existing in dam's foundation. As a result, three secondary grout curtains were constructed. These secondary grout curtains were located perpendicular to the primary grout curtain and installed in crisscrossing angular holes beneath the south abutment (see Figure 3). Unfortunately, after the additional grout curtains were installed the dam continued to seep.

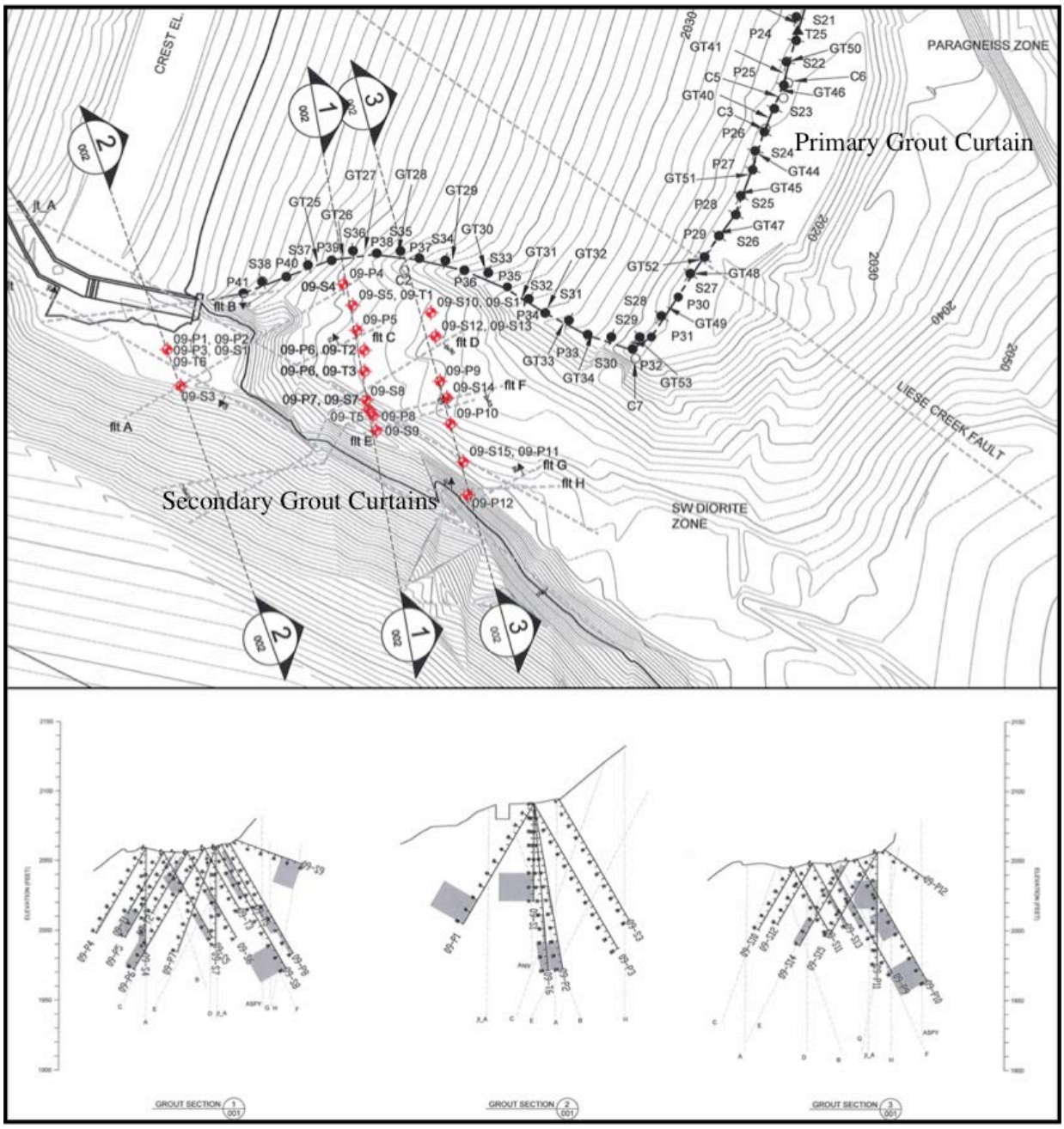

Figure 3: Plan and profile views of primary and secondary grout curtains

Using the MMR method Willowstick completed a seepage investigation of the dam. The survey had measurement stations on a 10 m by 10 m grid. The grid spacing was adequate to obtain sufficient details and resolution for identifying preferential electric current flow paths. The surveys required 306 measurement stations and 3600 m of wire. Figure 4 shows the survey layout and electrode configuration for the investigation. The fieldwork took one week to complete.

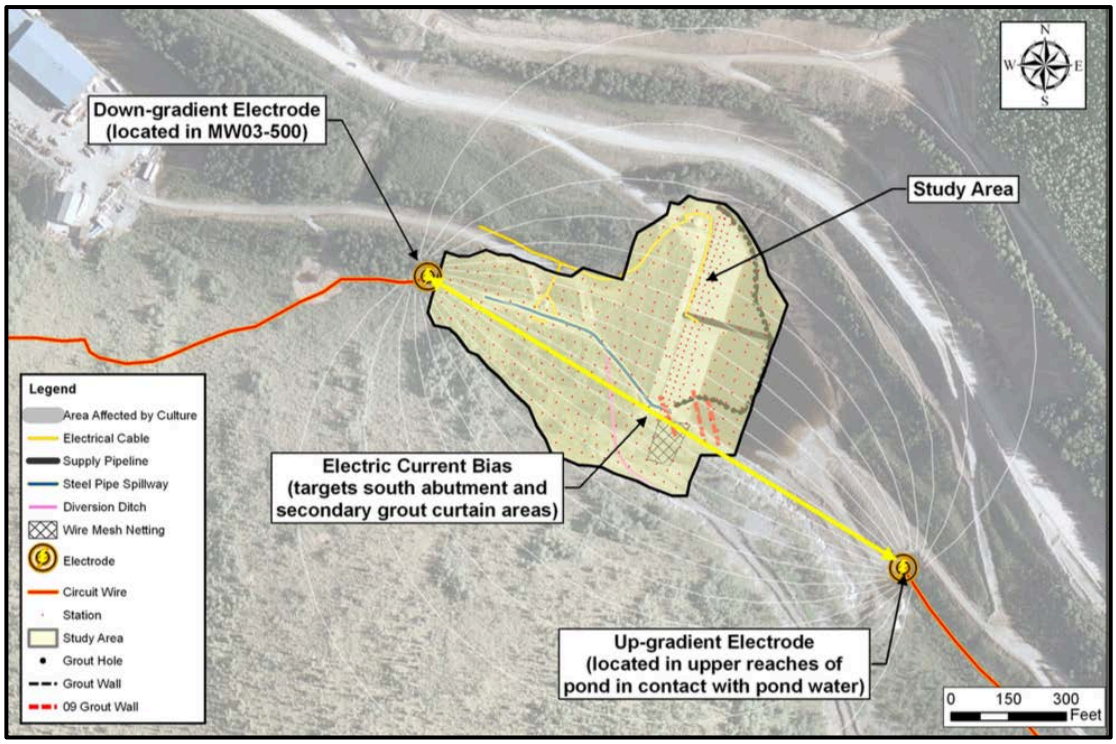

Figure 4: Survey layout and electrode configuration

Figure 5 presents a horizontal slice taken through the ECD model at elevation 2,000 feet (near the interface between fill material and native foundation soil and/or rock). The light-blue to dark-green shading (going up the scale) identified increasing levels of electric current density. The dark-blue to purple shading (going down the scale) indicated weak electric current flow. The yellow lines and arrows highlighted preferential electric current flow paths beneath the dam. The grey lines highlighted electric current that follows near-surface conductive culture.

Electric current flowed through and beneath the dam that bifurcated upstream of the embankment and flowed north and south around the dam rather than through and/or beneath the central part of the embankment. Due to the wire mesh netting and supply pipeline that ran down into the pond (coming in contact with the pond water), electric current flowed onto these conductive features and followed them up and over the embankment toward the return electrode which was located down-gradient of the dam. Electric current flowed through the subsurface, however, it clearly skirted around the dam's upstream toe and grout curtain to the south and north.

Electric current flowing to the south appeared to flow around the secondary grout curtains (shown as red dashed lines in the figure). However, electric current that flowed through the south abutment area rapidly weakened as evident by the rapidly fading dark green shaded flow path. This flow path was not continuous through the study area. This was likely a result of the secondary grout curtains which minimized seepage through the south abutment as was designed.

On the north side, electric current flowed along the upstream toe and grout curtain until it found a path beneath the grout curtain. This occurred between grout holes P7 and P12 as shown in Figure 5. This area was highlighted by a white dashed oval. After passing beneath the grout curtain at or about elevation 2,000 feet, seepage preferentially flowed beneath the north abutment area as was highlighted by the yellow lines and arrows shown in Figure 5. The thin dashed yellow lines were based on conjecture, and were drawn for visual purposes to create connectivity through the study area. These inferred flow paths were interpolated in the ECD model from measurement stations unaffected by near-surface conductive culture.

Near the dam's downstream toe, seepage appeared to flow beneath the spillway to the south for a short distance before turning west and following the alignment of the creek channel, which appeared to originate from the south abutment when in fact it originated from the north abutment. The flow path beneath the north abutment was interpreted to be the primary seepage flow path out of the RTP dam. This was because it was relatively strong and continuous through the study area. The flow path beneath the south abutment was secondary and not likely the primary source of seepage that was observed downstream in the collection system and monitoring wells. With this information the client was able to make additional repairs and mitigate the seepage issues.

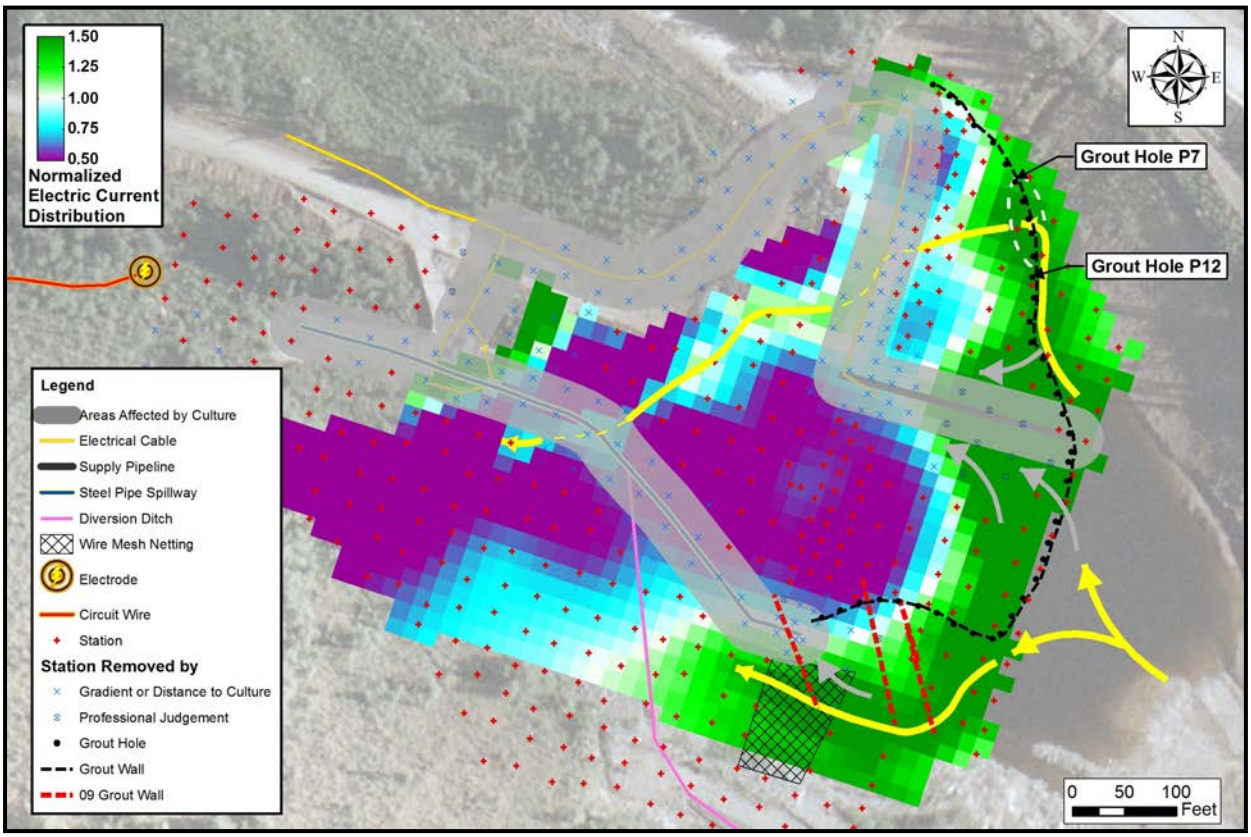

Figure 5: Preferential seepage flow beneath the dam (plan view)

Conclusion

The results from this dam investigation show how the MMR method can be used as a non-intrusive approach to supplement known information and identify preferential flow paths that were the cause of significant seepage. This information was used to target and cost-effectively support the design of dam remediation.

References

Jessop, M., A. Jardani, A. Revil and V.O. Kofoed. 2018. Magnetometric resistivity: A new approach and its application to the detection of preferential flow paths in mine waste rock dumps. *Geophysical Journal International* 215(1): 222–239.

Kofoed, V.O., M. Jessop, M.J. Wallace and W. Quan. 2011. Unique applications of MMR to track preferential groundwater flow paths in dams, mines, environmental sites, and leach fields. *The Leading Edge*, 30(2).

Proceedings of Tailings and Mine Waste 2019
November 17–20, 2019, Vancouver, Canada
Published by the University of British Columbia, 2019

A Computational Platform for the Quantification of the Seismic Demand in Mining Projects

Gabriel Candia, Universidad del Desarrollo, Chile
Jorge Macedo, Georgia Institute of Technology, USA
Miguel A. Jaimes, Instituto de Ingeniería UNAM, México
Carolina Magna-Verdugo, Universidad Adolfo Ibáñez

Abstract

This paper presents a computational platform for the quantification of the seismic demand in mining projects. The platform can be used to characterize the intensity and likelihood of ground motion scenarios and their consequences for civil systems and infrastructure in mining projects. The platform, developed as an object-oriented MATLAB GUI, allows the integration and convergence of different seismic zonation models, standard seismic hazard methodologies like probabilistic seismic hazard assessment (PSHA), and deterministic seismic hazard assessment (DSHA). The platform is also a hub for different developments in several branches of geotechnical/structural earthquake engineering, including depuration and declustering of seismic catalogs, generation of modified spectrum compatible ground motions, characterization of faulting mechanisms, ground motion prediction equations (GMPE), ground motion correlation models (GMC), and development of hazard maps, among others that are of great importance in the design of civil systems in mining projects. In addition, the epistemic uncertainty regarding the components of different hazard models is explicitly accounted for by the use of logic trees. The main goal of this tool is to aid engineers in the implementation of PEER's probabilistic risk equation in the context of mining projects. This paper shares sxamples of the platform application in characterizing the seismic hazard for mining projects in Peru and Chile.

Introduction

South America is located along the western edge of the convergent plate boundary between the Nazca plate in the west and the South American plate to the east. There are important features caused by the tectonic process that need to be considered for the proper estimation of seismic hazards in the context of the design of infrastructure in the context of mining projects (e.g., tailings dams, heap leach pads, stockpiles, open pits, etc.). For example, the eastern edge of the oceanic Nazca plate in Peru and Chile is marked by the deep

Peru-Chile Trench (PCT), located about 50 to 200 km offshore. The ongoing subduction of the Nazca plate beneath produces megathrust earthquakes (M>8.0) and strong ground shaking along the South American coast (i.e., Peru and Chile). The western edge of the continental South America plate is marked by the broad, high mountains of the Western and Eastern Cordillera of Peru, which preserve the numerous folds and faults that mark the eastern boundary of the Andes range. Important mining projects are located in both the western edge of South America and the Anders region, highlighting the importance of a proper seismic hazard assessment. The geometry of the Nazca plate dipping beneath the South America was modeled by Cahill and Isacks (1992) and by the USGS (2011). These models show that the subduction pattern of the Nazca plate (e.g., dip angle) increases with latitude, from about 15.5° near the Peru-Ecuador border up to 24° in South-Central Chile (Nuñez, 2014). Likewise, the convergence rate of the Nazca and South America varies geographically, from 60 mm/yr near the central Peruvian Andes up to 68–80 mm/yr in northern Chile (Dura et al., 2015), and occurs almost orthogonally to the PCT. The geometry of the subduction zone and its potential to produce large earthquakes in both the shallow regions (i.e., interface) offshore and the deeper regions (i.e., intraslab) are major inputs into the assessment of seismic hazard in South America, and need to be properly considered in a seismic hazard evaluation.

Over the last 15 years, several authors have developed seismic source geometry and parameters for South America (e.g., Nuñez [2014], Poulos et al. [2018], Alvarado [2012]), and either global or region-specific ground motion prediction equations (GMPEs). These efforts, collectively, have made probabilistic seismic hazard analysis (PSHA) a customary tool for researchers and engineering practitioners in the region. However, conducting a seismic hazard analysis remains cumbersome, and without proper validation of the computer codes used, the hazard assessment can be off by several orders of magnitude (Thomas et al., 2010).

The computational tool presented in this article is a state-of-the-art PSHA platform that can be used to perform site-specific and regional-based evaluations in the context of mining projects. The platform is presented in the format of a Graphical User Interface (GUI) developed in MATLAB (Guide, 1998). This modular platform includes built-in seismic models for South America, a library of ground motion models for subduction and crustal earthquakes, and more advanced features, such as the estimation of seismic source parameters from earthquake catalogs, seismic hazard desaggregation, and prediction of ground motion intensities based on earthquake scenarios. The architecture of the code enables the user to seamlessly incorporate epistemic uncertainty through logic trees, and to generate hazard compatible design spectra. To guarantee the accuracy and reliability of the results, the platform has been validated against rigorous independent solutions.

A new seismic hazard platform

The seismic hazard platform presented herein, similar to commercial PSHA codes, is based on the classical approach to PSHA developed by Esteva (1967) and Cornell (1968). Accordingly, the code allows users to estimate the annual rate of exceedance of ground motion intensities using a probabilistic framework, and also allows the prediction of ground motion intensities from earthquake scenarios. This article describes some of the features of the code and GUI characteristics. For a complete description of the code's capabilities and background information, refer to Candia et al (2019).

To compute the seismic hazard at a site, the user must input a seismicity model into the GUI through a plain text file. This file contains the site definition, the configuration of the logic tree, the geometry and parameters for seismic sources, and the GMPE data. This input file is processed by the platform to produce the desired outputs. An overview of the platform's calculation hierarchy and GUI layout are shown in Figure 1. For every site and every branch of the logic tree, the platform generates the earthquake scenarios (i.e., set of collectively exhaustive and mutually exclusive events) and computes their corresponding rates of occurrence. Then, the mean ($\underline{ln\ ln\ Y}$) and standard deviation ($\sigma_{lnln\ Y}$) of the ground motion intensity are obtained from standard GMPEs, and finally, the conditional probability of exceeding an intensity measure y is evaluated, summed for all scenarios, and multiplied by the earthquake rate to obtain the annual rate of exceedance, λ_Y. The user may take advantage of MATLAB´s Distributed Computing Toolbox (optional feature) to reduce the CPU-time and memory requirements.

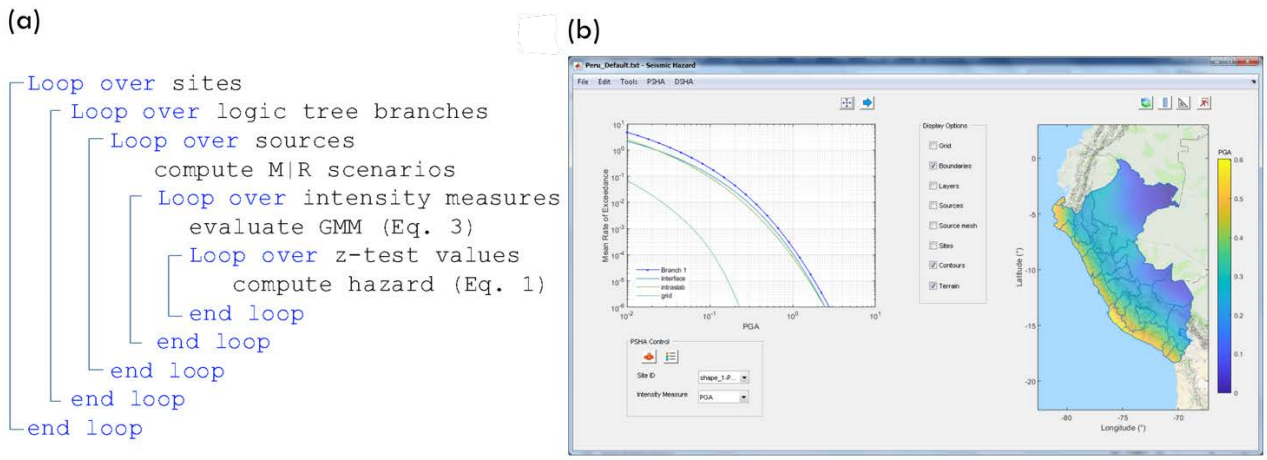

Figure 1: (a) Hierarchy of hazard computations used in the platform, and (b) Layout of the graphical user interface

Code features and capabilities

Graphical user interface

The improved user interface offers several components that enhance the user experience, making it a fertile ground for research, teaching, and engineering practice. The GUI has a clean and intuitive workspace with standard I/O capabilities, such as importing existing projects, saving, and re-loading a session. All results generated by the platform can be displayed graphically or exported to plain text files.

From the main window the user can import built-in or custom seismicity models, and modify/explore them through ad-hoc modules. These include a source geometry editor/viewer, a GMPE editor/viewer, and a site selection tool. After running the analysis, the hazard curves for all sites and hazard maps are automatically displayed in the main window. Separate modules allow the user to develop uniform hazard spectra (UHS), conditional mean spectra (CMS), and to deaggregate the seismic hazard, among other capabilities.

The site selection interface is a versatile tool that centralizes the definition of site coordinates used in the PSHA platform. It allows the user to select points on a map with a simple mouse click, or import sites from plain text files. For regional analyses consisting of several thousand sites, the platform allows the user to calculate a unique hazard curve for site clusters, significantly reducing computation times. The seismic sources and site locations may be specified in either WGS84 geodesic coordinates, Spherical Earth coordinates, or Cartesian (ECEF) coordinates. The source geometries and sites can be displayed in the main window. along with shape files (*.shp) for boundaries or landmarks, and background earth maps, which can be updated automatically using Google Static Map API (Esteva, 1967).

Seismic sources and rupture area models

The platform supports six types of seismic source, namely: point sources, lines sources, area sources, volume sources, grids, and faults. The platform also features background zones, which are used to model random earthquakes occurring off of known faults. A keyword describing the rupture mechanism of sources must be defined; for subduction zones the mechanism is either “interface” or “instraslab”, and in shallow crustal regions the rupture mechanism is “strike-slip”, “normal”, “normal-oblique”, “reverse”, “reverse-oblique” or “thrust”. Alternatively, the fault rupture mechanism can be defined in terms of the rake angle. Built-in seismic sources for Ecuador, Peru, Chile, and Mexico are available in the platform (Figure 2); alternatively, the user can specify seismic sources using the input text file.

The rupture area (RA) scaling with magnitude is defined from the model $log\ log\ A\ = aM - b$, where a and b are user specified parameters. Built-in coefficients are also available, e.g., Hanks and Bakun (2008); Wells and Coppersmith (1994); etc. Currently, two shapes of RA are available in the platform: circular RA

for area sources and background zones, and rectangular RA for fault sources. In both cases, the user controls the rupture behavior of the near the fault edges (e.g., tapered edges or "leaking" edges).

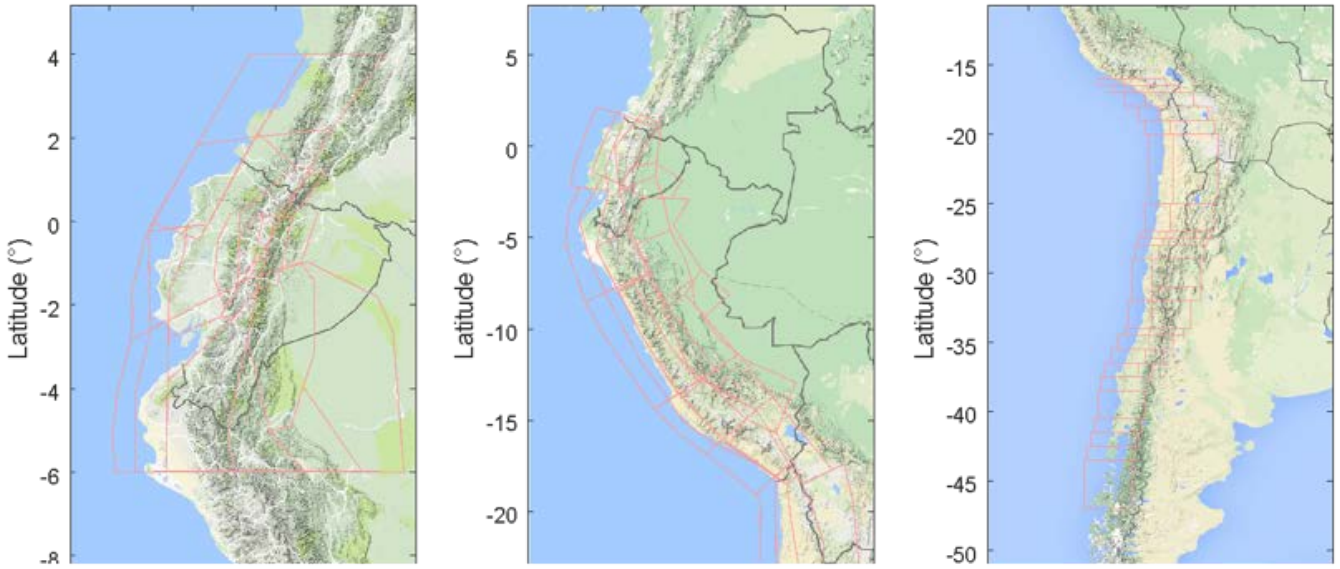

Figure 2: Schematic flow-diagram of seismic hazard computations in the platform

Ground motion prediction equations, GMPEs

The probability distribution of observed ground motion intensities associated with a given earthquake scenario and site conditions is obtained from Ground Motion Prediction Equations, formerly known as strong-motion attenuation relationships. The current platform has a library of 24 GMPEs for PGA and spectral accelerations (SA), and GMPS for other less common intensity measures: PGV, Arias Intensity, and PGD. Work is underway to expand this library to general ground motion prediction models.

Scenario-based ground motion assessment

To model the damage propagation through spatially distributed portfolios, a common approach is to use deterministic or stochastic earthquake scenarios. The current platform features "shakefield" (Pitilakis et al., 2014), which allows the user to generate scenario-based fields of spatially correlated and spectrally correlated ground motion intensities. These fields are realizations of the ground motion intensity that account for variability and spatial correlation. A shakefield for the Valparaiso and Metropolitan Regions in Central Chile is presented in Figure 3, for a hypothetical Mw 8.8 interface earthquake 26 km west of Valparaiso. The left plot shows the median pseudo-acceleration at 1s (Sa_1) based on the Youngs et al. (1997) GMPE for rock; the central plot shows a realization of Sa_1 taking into account the uncertainty term in the GMPE, and in the right plot the Goda and Atkinson (2009) correlation structure was used to develop a field spectrally correlated pseudo acceleration at T=0.2s ($Sa_{0.2}$), conditioned on the occurrence of Sa1, i.e. $Sa_{0.2|1.0}$.

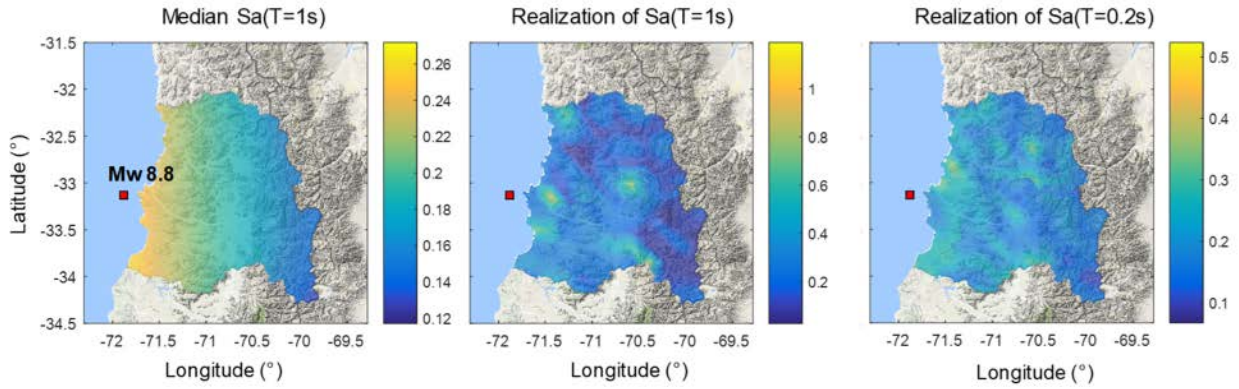

Figure 3: Strong ground motion fields for Valparaiso and Metropolitan regions in Chile due to a Mw 8.8 earthquake located 26 km offshore Valparaiso

Earthquake catalogs and seismic source parameters

The platform includes tools to perform the depuration of seismic catalogs (i.e., the elimination of event duplicates reported from different agencies), and to perform a catalog declustering based on the Reasenberg (1985) and Gardner and Knopoff (1974) algorithms. Additionally, the platform incorporates the Stepp (1972) algorithm to determine the catalog's magnitude completeness, and the Weichert (1980) algorithm to compute the seismic source parameters for a truncated exponential model. As an illustrative example Figure 4 shows the declustering results for a catalog compiled for Peru using the algorithms in Reasenberg (1985) and Gardner and Knopoff (1974).

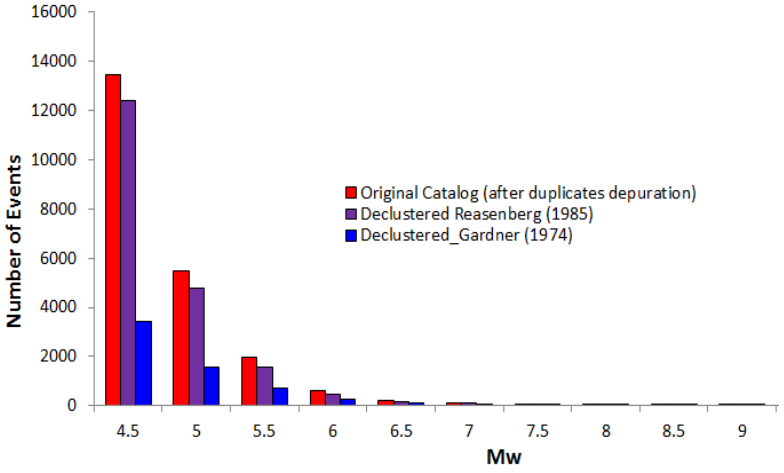

Figure 4: Depuration and declustering for a seismic catalog compiled for Peru (Latitude from 21°S to 2°N, Longitude from:65°W to 84°W)

Code validation

Verification of the platform results is a fundamental step to produce reliable hazard computations. To test the accuracy of results against standard and traceable solutions, the document "Verification of Probabilistic

Seismic Hazard Analysis Computer Programs" by the Pacific Earthquake Engineering Research Center (PEER – Hale et al., 2018) was adopted as a benchmark. The verification exercises consist of two sets of problems to test essential features of PSHA codes, referred to as "Set 1" and "Set 2" in Hale et al. (2018). Thus far, the platform has successfully reproduced the benchmark examples within a 1% error in most cases. This document provides an exact "hand (analytical) solution" for simple problems and approximate numerical solutions for the more sophisticated cases. In the latter, the hazard curves reported are the average hazard curves from 17 different PSHA codes.

The problems in Set 1 account for four types of source geometry, namely a vertical strike slip fault, a reverse fault dipping 60°W, an area source, and a volumetric source, shown schematically in Figure 5. The magnitude scaling relationships include the delta-function (Cases 1, 2, 3, 4, 8, 9), the truncated exponential model (Cases 5, 10, 11), the truncated normal model (Case 6), and the characteristic model (Case 7). The Sadigh et.al. (1997) ground motion model for rock is used, except in Cases 9b and 9c, which use the Abrahamson and Silva (1997) and Campbell (1997) models, respectively. Likewise, the Wells and Coppersmith (1994) model for magnitude-area scaling is used in fault sources, and a 1 km grid spacing of point sources is used to model the area and volume sources.

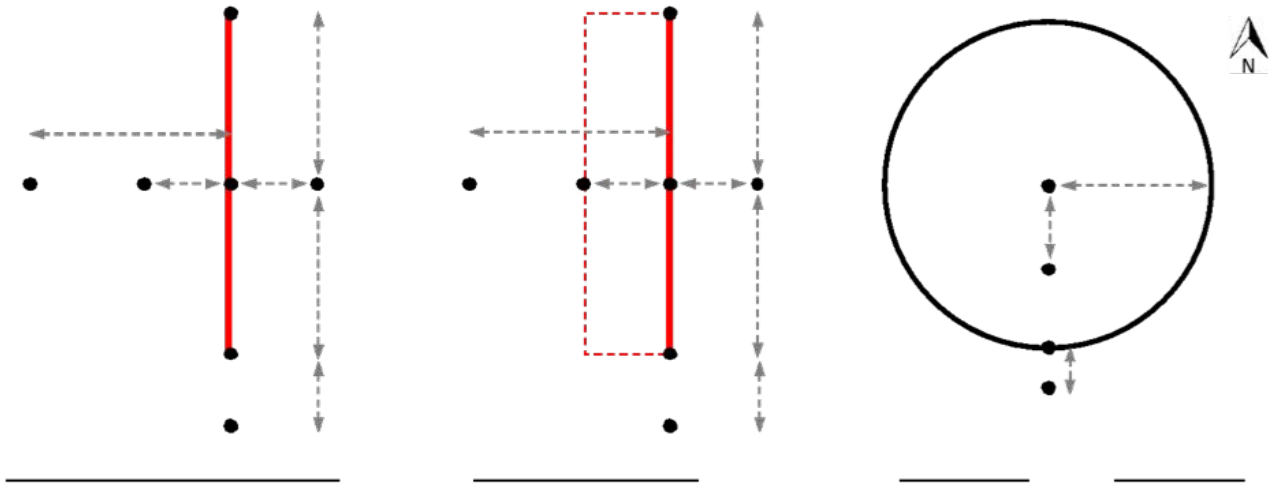

Figure 5: Source geometry for verification problems of Set 1, modified from Alvarado (2012)

A comparison of hazard curves for all sites in Cases 2, 7, 4, 9a, 10, and 11 is presented in Figure 6; again showing excellent agreement between the results.

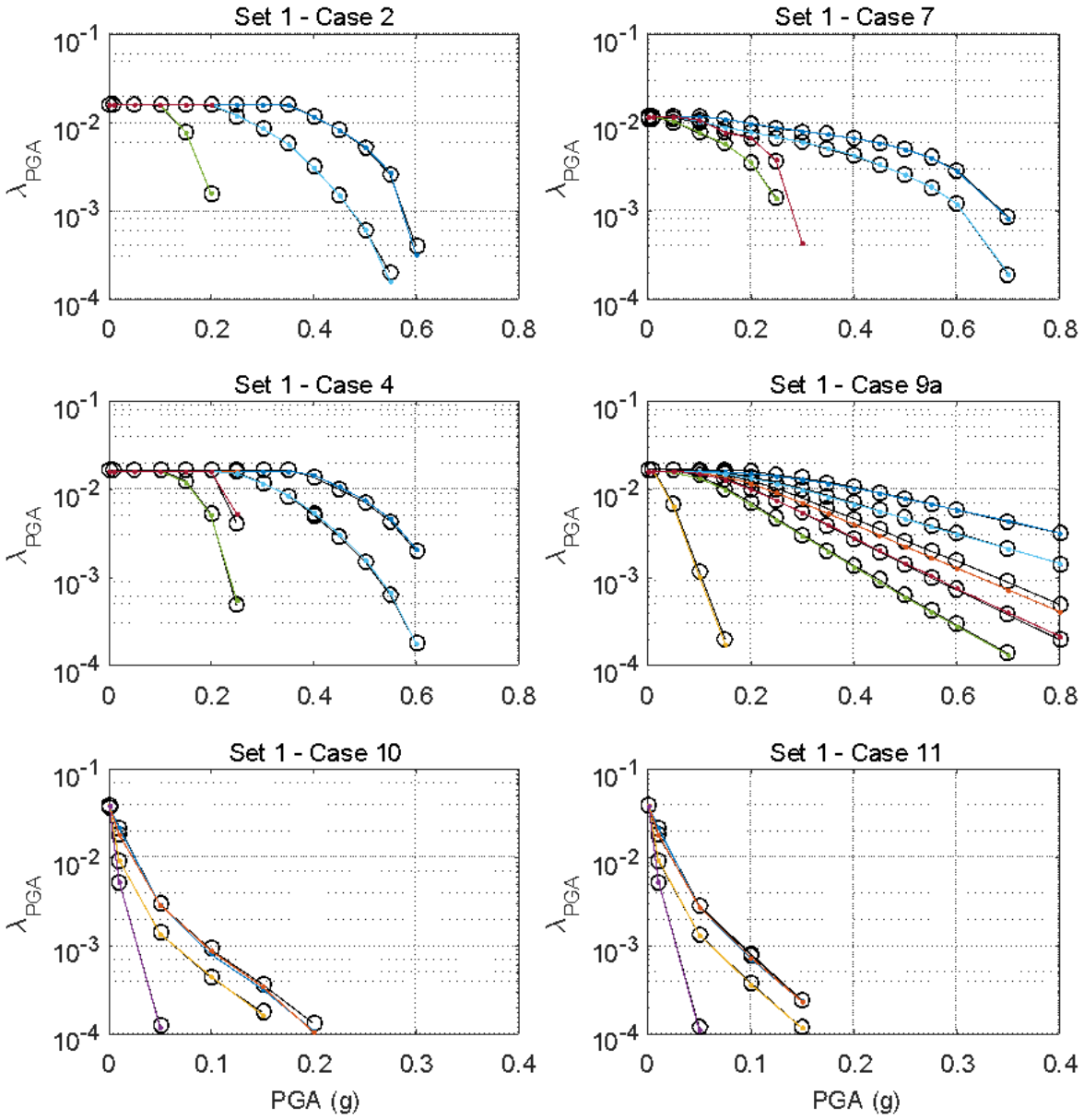

Figure 6: Comparison of seismic hazard curves for PGA. Current platform solutions (continuous lines) versus average results reported by PEER (Hale et al., 2018) (dots)

Illustrative examples

Here we consider two potential locations of mining projects in the Peru – one in the Peruvian Andes and the other on the Peruvian coast. With these locations, we illustrate some of the capabilities of the computational platform to perform seismic hazard evaluations. In the first case consider a mining project located in the Andes at coordinates: –11.92 (latitude), –76 (longitude). Figure 6a shows the seismic sources for Peru provided by Sencico (2016), the official agency for seismic hazard assessment, along with the

location of the evaluation point. The geometry of seismic sources and seismicity parameters for Peru are directly available in the implemented computational platform. Figure 7b shows the estimated hazard curve with the implemented computational platform for a spectral acceleration at T=0.5s.

In the case of a mining project on the Peruvian coast, we illustrate how a regional analysis can be performed with the implemented computational platform. First, we evaluate the PGA hazard on the Peruvian coast, considering a return period of 475 years. Figure 8a shows the results of such evaluation. In addition, in Figure 8b, we illustrate the generation of shaking fields (i.e., deterministic-based analyses in a region) for the Peruvian coast, considering an offshore Mw 8.3 earthquake with a circular surface projection. Results similar to those presented in Figures 7 and 8 are of primary importance for the evaluation the seismic performance of infrastructure in mining projects (i.e., tailings dams, heap leach pads, stockpiles, open pits, etc.).

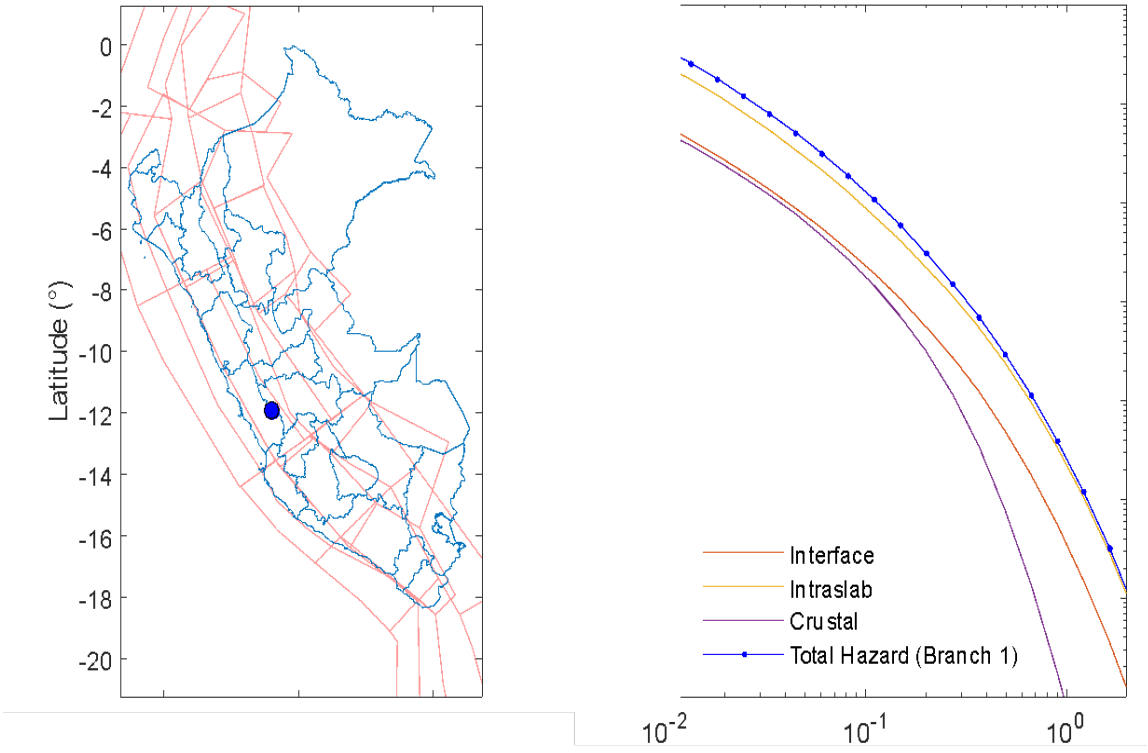

Figure 7: (a) SENCICO's (2016) seismic source model and site location; and (b) spectral acceleration hazard curves at a period of 0.5 s

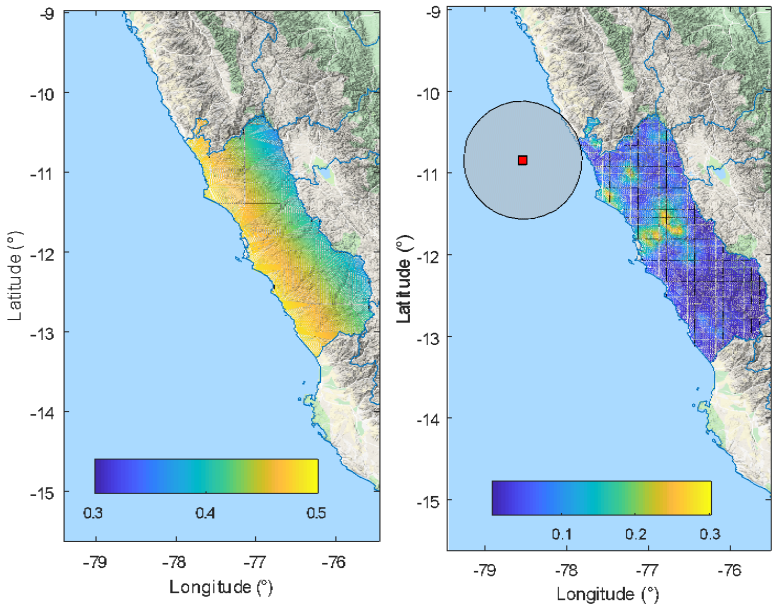

Figure 8: Example of seismic hazard analysis for mining projects on the Peruvian coast
(a) PGA with 10% probability of exceedance of 50 years;
(b) PGA field due to an offshore Mw 8.3 earthquake; surface projection of the rupture area and focus location are also shown in the figure

Conclusion

This work presents a new platform for probabilistic and deterministic seismic hazard assessment. The code takes into account the most recent developments in earthquake engineering, seismology, and geotechnical earthquake engineering to evaluate seismic hazard at a local or regional level. The platform offers several standard and innovative capabilities, which simplifies the computation of seismic hazard. Among the standard capabilities the code includes are the estimation of hazard curves, seismic hazard deaggregation, and the estimation of design spectra. Advanced capabilities, not commonly available in existing PSHA codes, include the computation of source parameters from earthquake catalogs and seismic sources geometry, vector-valued seismic hazard assessment, the use of conditional GMMs and user-defined GMMs, and uncertainty treatment in the median ground motions through continuous GMM distributions. The modular architecture and validated functionalities make the platform a powerful tool for evaluating seismic hazard in mining projects. The platform can be downloaded free of charge from https://github.com/gacandia/SeismicHazard.

References

Abrahamson, N.A. and W. J. Silva. 1997. Empirical response spectral attenuation relations for shallow crustal earthquakes. Seismol. Res. Lett. 68(1): 94–127.

Alvarado, Alexandra. 2012. *Néotectonique et cinématique de la déformation continentable en Equateur.* University of Grenoble.

Cahill, T. and B.L. Isacks. 1992. Seismicity and shape of the subducted Nazca plate. *Journal of Geophysical Research: Solid Earth* 97(B12): 17503–17529.

Campbell, K.W. 1997. Empirical near-source attenuation relationships for horizontal and vertical components of peak ground acceleration, peak ground velocity, and pseudo-absolute acceleration response spectra. Seismological Research Letters 68(1): 154–179.

Candia G., J. Macedo, M.A. Jaimes and C. Magna-Verdugo. 2019. A new state of the art platform for probabilistic and deterministic seismic hazard assessment. Accepted for publication at Seismological Research Letters.

Cornell, C.A. 1968. Engineering seismic risk analysis. *Bull. Seismol. Soc. Am.* 58(5): 583–1606.

Dura, T., M. Cisternas, B.P. Horton, L.L. Ely, A.R. Nelson, R.L. Wesson and J.E. Pilarczyk. 2015. Coastal evidence for Holocene subduction-zone earthquakes and tsunamis in central Chile. *Quaternary Science Reviews* V(113): 93–111.

Esteva, Luis. 1967. Criteria for the construction of spectra for seismic design. In *Proceedings of the 3rd Pan-American Symposium of Structures,* 3–8 July, Caracas, Venezuela (in Spanish).

Gardner, J.K. and L. Knopoff. 1974. Is the sequence of earthquakes in Southern California, with aftershocks removed, Poissonian? Bulletin of the Seismological Society of America 64(5): 1363–1367.

Guide, M.U.S. 1998. The Mathworks. Inc., Natick, MA. 5:333.

Hale, C., N. Abrahamson and Y. Bozorgnia. 2018. Probabilistic Seismic Hazard Analysis Code Verification. PEER Report No. 2018/03. Pacific Earthquake Engineering Research Center. Retrieved from https://peer.berkeley.edu/peer-reports.

Hanks, T.C. and W. Bakun. 2008. M-logA observations for recent large earthquakes. *Bulletin of the Seismological Society of America* 98(1): 490–494.

Nuñez, Ignacio. 2014. *Nuevo peligro sísmico para Chile.* Repositorio Académico de la universidad de Chile. Retrieved from ,http://www.repositorio.uchile.cl/handle/2250/116410.

Pitilakis, K., P. Franchin, B. Khazai and H. Wenzel. 2014. SYNER-G: Systemic seismic vulnerability and risk assessment of complex urban, utility, lifeline systems and critical facilities. Methodology and applications. Series: Geotechnical, Geological and Earthquake Eng. 31. Netherlands: Springer.

Poulos, A., M. Monsalve, N. Zamora and J.C. de la Llera. 2018. An updated recurrence model for Chilean subduction seismicity and statistical validation of its Poisson Nature. Bull. *Seismol. Soc. Am.* In press.

Reasenberg, P. 1985. Second-order moment of central California seismicity, 1969–82. Journal of Geophysical Research 90: 5479–5495.

Sadigh, K., C.Y. Chang, J.A. Egan, F. Makdisi and R.R. Youngs. 1997. Attenuation relationships for shallow crustal earthquakes based on California strong motion data. Seismol. Res. Lett. 68(1): 180–189.

Sencico. 2016. *Actualización del programa de Computo Orientado a la Determinación del Peligro Sísmico en el País.*

Stepp, J.C. 1972. Analysis of completeness of the earthquake sample in the Puget Sound area and its effects on statistical estimates of earthquake hazard. In Proceedings of the International Conference on Microzonation, Seattle, Washington, USA. Vol 2: 897–909.

Thomas, P., I. Wong and N. Abrahamson. 2010. Verification of probabilistic seismic hazard analysis computer programs. PEER-2010/106, Pacific Earthquake Engineering Research Center, University of California, Berkeley, 2010-05, PDF (400/P33/2010-106). Available online at http://peer.berkeley.

USGS. 2011. Slab model for subduction zones. Retrieved from http://earthquake.usgs.gov/research/data/slab/

Weichert, D.H. 1980. Estimation of the earthquake recurrence parameter for unequal observation periods for different magnitudes. Bull. Seismol. Soc. Am. 70(4): 1337–1346.

Wells, D.L. and K.J. Coppersmith. 1994. New empirical relationships among magnitude, rupture length, rupture width, rupture area, and surface displacement. Bull. Seismol. Soc. Am. 84(4): 974–1002.

Wells, D.L. and K.J. Coppersmith. 1994. New empirical relationships among magnitude, rupture length, rupture width, rupture area, and surface displacement. *Bulletin of the Seismological Society of America* 84(4): 974–1002.

Youngs, R.R., S.J. Chiou, W.J. Silva and J.R. Humphrey. 1997. Strong ground motion attenuation relationships for subduction zone earthquakes. *Seismological Research Letters* 68(1): 58–73.

Bibliography

Atkinson, G.M. and D.M. Boore. 2003. Empirical ground-motion relations for subduction-zone earthquakes and their application to Cascadia and other regions. *Bulletin of the Seismological Society of America* 93(4): 1703–1729.

Bender, B. and D.M. Perkins. 1982. SEISRISK II: A computer program for seismic hazard estimation (No. 82–293). US Geological Survey.

Chunga, K. 2010. *Terremoti crostali e zonazione sismica dell'Ecuador attraverso l'integrazione dei dati geologici, sismologici e morfostrutturali.* Università degli Studi dell'Insubria.

Field, E.H., T.H. Jordan and C.A. Cornell. 2003. OpenSHA: A developing community-modeling environment for seismic hazard analysis. *Seismological Research Letters* 74(4): 406–419.

Gamarra, C. and Z. Aguilar. 2009. *Nuevas fuentes sismogénicas para la evaluación del peligro sísmico y generación de espectros de peligro uniforme en el Perú.* Grade thesis. Civil Engineering faculty, National University of Engineering, Lima, Peru.

Goda, K. and G. M. Atkinson. 2009. Probabilistic characterization of spatially correlated response spectra for earthquakes in Japan. *Bull. Seismol. Soc. Am.* 99(5): 3003–3020.

Martín, A. 1990. *Hacia una nueva regionalización y cálculo del peligro sísmico en Chile.* Memoria de Título (Inédito), Universidad de Chile, Departamento de Ingeniería Civil: 132 pp.

McGuire, Robin. 1978. FRISK: Computer program for seismic risk analysis using faults as earthquake sources (no. 78-1007). US Geological Survey.

Taylor, Donald. 1948. *Fundamentals of Soil Mechanics*. New York: Chapman and Hall, Limited.

Proceedings of Tailings and Mine Waste 2019
November 17–20, 2019, Vancouver, Canada
Published by the University of British Columbia, 2019

Characterization of Oil Sands Tailings Using Hyperspectral Technology

Iman Entezari, ConeTec Investigations Ltd, Canada
James Sharp, ConeTec Investigations Ltd, Canada
Dallas McGowan, ConeTec Investigations Ltd, Canada

Abstract

A large volume of tailings result from the bitumen production conducted in the oil sands in northern Alberta, Canada. Oil sands operators need to characterize tailings for a number of reasons, such as to assess the tailings dewatering and consolidation performance, to control tailings treatment processes, to monitor the tailings state for reclamation, and to meet regulatory reporting requirements. Laboratory testing of the tailings samples is a common practice that provides measures of tailings properties including the contents of water, solids, residual bitumen, total fines (<44 μm size), and clays measured through methylene blue index (MBI) testing. However, it is a time consuming and costly process involving the collection and shipment of thousands of tailings samples to laboratories each year. Developing new technologies for quick in-situ or on-site characterization of tailings with sufficient accuracy is thus of interest to oil sands operators, and can significantly reduce the time and cost associated with laboratory testing.

This paper presents the results of our research and development program on the use of hyperspectral sensing for quick prediction of oil sands tailings properties. In order to investigate the potential and effectiveness of hyperspectral measurements for the estimation of tailings properties, hyperspectral data in the 350–2,500 nm spectral range were collected from 540 oil sands tailings samples from various tailings ponds of a major oil sands operator in Alberta during 2017 and 2018. An ensemble version of Neural Networks (NNs) was used to calibrate spectral data to the tailings properties measured in a commercial laboratory. The root mean squared error (RMSE) of the NN-based hyperspectral models was observed to be 4.22, 4.66, 1.01, and 4.87 wt% on the test set for the contents of water, solids, bitumen, and total fines, respectively. RMSE values of 1.36 meq/100g and 6.12 were also achieved for the MBI and clay to water ratio (CWR) models, respectively. Although the absolute accuracy of the hyperspectral models might generally be less than the laboratory measurements, it is sufficient for many applications and for investigating tailings behaviour. This technology can provide tailings engineers and planners with accurate and repeatable real-time information on the tailings constituents.

Introduction

Alberta's oil sands contain the third largest reserves of petroleum in the world (Alberta Energy, 2014). According to Kasperski (2001), oil sands are natural mixtures of minerals (55–80 wt%), water (2–15 wt%), and bitumen (4–18 wt%). The water intensive process of bitumen extraction through surface mining results in the production of large volumes of tailings. Consequently, tailings treatment and management are major challenges for the oil sands industry.

The development of efficient tailings treatment and processing technologies to reduce the tailings inventories requires fundamental knowledge of the tailings characteristics. Frequent characterization of the tailings is thus necessary to evaluate the tailings conditions and assess the effectiveness and operational performance of the tailings processing technologies. Several in-situ, on-site and off-site testing methods are employed to characterize tailings and provide information on tailings properties (e.g., AER, 2017; COSIA, 2015; Styler et al., 2018; Cabrera, 2008; Kaminsky, 2008). Laboratory-based analysis of the tailings samples is widely used for accurate measurement of tailings constituents. However, it is a time consuming and costly process normally taking weeks before the results are available and tailings constituents are known. Furthermore, the accuracy of many of the laboratory methods significantly depends on sample preparation and personnel expertise. Therefore, introducing cost-effective, rapid and repeatable methods for estimation of tailings characteristics with sufficient accuracy is of benefit for tailings management.

Hyperspectral sensing (or reflectance spectroscopy) is a technology used for acquiring qualitative and/or quantitative information about materials and has a broad range of applications in a variety of industries. It is defined as measuring the reflected light from a target material as a function of wavelength. Hyperspectral sensors divide the electromagnetic spectrum in hundreds of narrow continuous wavelength intervals (spectral bands) thus acquiring a detailed spectral response from the target under study. The spectral response from each target is largely controlled by the chemical composition and crystal structure of the materials within. Hyperspectral methods have become popular analysis tools as they are fast, cost-effective, non-destructive and can provide information on multiple characteristics of a sample in a single scan.

Spectral response of a material can potentially be used to estimate the concentration of its constituents. In order to use the spectral data for quantitative applications, it is required to correlate and calibrate the spectral features to desired information on the composition of the material using samples with known characteristics. This calibration process is normally done through regression analysis which is used to model the relationship between a dependent variable (e.g., tailings water content) and independent variables (e.g., spectral features).

Neural networks are also adoptable to regression problems (e.g., Dardenne et al., 2000; Geladi et al., 1996). In particular, neural networks are powerful tools when dealing with problems with nonlinear and

multidimensional dependencies in the data and can outperform traditional regression modelling. A weakness of neural networks is, however, that they are sensitive to the initial conditions, particularly in terms of the initial random weights and training set (Ukil et al., 2010). That means, each time a neural network model is trained, it can produce different prediction results depending on the initial conditions. A solution to this problem is to train multiple neural network models and combine their results (e.g., average the outputs). This is known as ensemble learning approach (Sollich and Krogh, 1996). It is proved that an ensemble of neural network models can significantly reduce the variance in the prediction results and have better generalization and robustness characteristics (Garcia-Pedrajas et al., 2005).

In this study we make use of hyperspectral measurements for the estimation of various oil sands tailings properties through the ensemble-based neural network modelling. In our previous study, we used partial least square regression to develop models for the estimation of MBI, water content, and bitumen content using hyperspectral data collected from 290 samples using one spectrometer (Entezari et al., 2018). Here, we expanded the dataset to include 540 samples and collected data using three spectrometers to be able to develop models robust against the variation in instrumentation. Furthermore, models were developed for the estimation of solids content, total fines content, and clay to water ratio of oil sands tailings. The remainder of this paper describes the sample suite used for calibration, the instrumentation used for spectral measurements, the neural network-based modelling, and the accuracy assessment of the models for the estimation of the oil sands tailings properties.

Materials and methods

Sample description

More than 3,000 samples were collected in the summers of 2017 and 2018 from various tailings ponds of a major oil sands operator in Alberta. These samples included a variety of tailings such as watery samples (more than 95 wt% water), fluid fine tailings (FFTs), thick FFTs and samples with high sand content. Samples with high bitumen concentration were also included in these samples (more than 10 wt% bitumen). These samples were sent to a commercial laboratory to measure the tailings properties including the contents of water, solids, bitumen, total fines (% <44 μm fines of total sample), clays measured through methylene blue index (MBI) testing, and clay to water ratio (CWR).

From these samples, a total of 540 samples were selected for spectral measurements and model development. The sample selection was done based on the laboratory data to ensure the selected samples represented the entire sample population and showed a wide range of variation in tailings characteristics. Table 1 summarizes the range of variation in tailings characteristics for the selected samples.

Table 1: Summary of the characteristics of the samples used for spectral measurement and model development

Bitumen content (wt%)	Solids content (wt%)	Water content (wt%)	Total fines content	MBI (meq/100g)	Clay to water ratio
0.05 to 10.63	2.7 to 84.74	13.78 to 95.75	2.8 to 61.23	0.42 to 20.56	7.63 to 118.5

Figure 1 shows a ternary diagram of the laboratory data showing the crescent-shaped property distribution in tailings. This figure shows that the tailings range from samples with high sand and low water content in the lower left corner to samples with high water and high fines along the top-right edge.

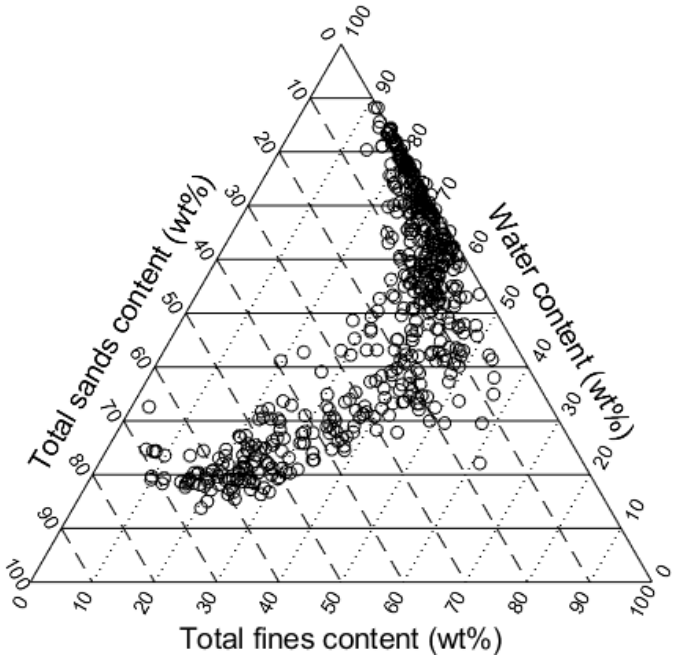

Figure 1: Ternary diagram of the samples selected for spectral measurement and model development. Note that not all samples are shown in this plot because there were samples with more than 90 wt% water content for which the laboratory could not measure fines content

Instruments and spectral measurements

The spectra of 290 of the selected samples were measured using one brand of spectrometer, while the spectrum of each of the remaining 250 samples was collected using two of a different brand of spectrometers (two spectral measurements per sample, thus 500 spectra). Consequently, our dataset included 790 spectra and associated laboratory results for the contents of bitumen, solids, water, and total fines as well as MBI and clay to water ratio. All three spectrometers employed for spectral measurements had identical spectral range and spectral resolution.

Prior to acquiring spectral measurements, each sample was stirred to create a homogenous mixture. The contact probe of the spectrometer was then pushed into the material so that the window of the probe

was in full contact with the sample and the spectrum was acquired. Employing different spectrometers and contact probes allowed for developing models that are robust against the variation in the instrumentation.

Neural network modelling and accuracy assessment

Neural Networks was used to develop the models and calibrate the spectral data to the laboratory results. A feed-forward backpropagation neural network structure with one hidden layer consisted of 10 neurons was implemented to develop models for each of the tailings properties of interest. Bootstrap aggregation technique (Bagging) was used to create the ensemble-based neural network models (Breiman, 1996). In Bagging method, several uniformly distributed training sets are randomly selected from the original training set and neural networks are trained using each of these training sets. All the outputs are then averaged to generate the final prediction results.

We first selected 10% of the dataset and put it aside as the test set. These samples were never used in the training phase and were kept to assess the final models performance. The remaining 90% of the dataset was used as the training set. To train the neural networks, a 100 bootstrapped training sets with a size equal to the size of the original training set were generated from the original training set. Due to replacement in bootstrap sampling, in each training set some of the samples were missing and some occurred several times. The final neural network model was thus an ensemble of 100 neural networks trained using each of the bootstrapped training set. The performance of the final models was assessed using the test set. R^2 and RMSE were calculated to evaluate the model's errors and goodness of fit. It is noted that any errors in the laboratory data will inherently introduce errors in the spectral model. Therefore, the performance of the models developed in this research can only be as good as the laboratory measurements. In other words, the laboratory data is incorrectly assumed to be perfect in order to determine model errors.

Results and discussions

Spectral properties of samples

The spectra of a subset of the tailings samples are shown in Figure 2. The absorption features at 1,450 and 1,900 nm are mostly attributed to the presence of water in the samples while the feature at 2,200 nm is the characteristic clay feature. Residual bitumen causes absorption features near 1,700 and 2,300 nm in the spectra. In addition to the variation in the depth of the absorption features, it is evident that the slope of the spectra in different wavelength regions also changes with a variation in tailings composition, in particular water content variations.

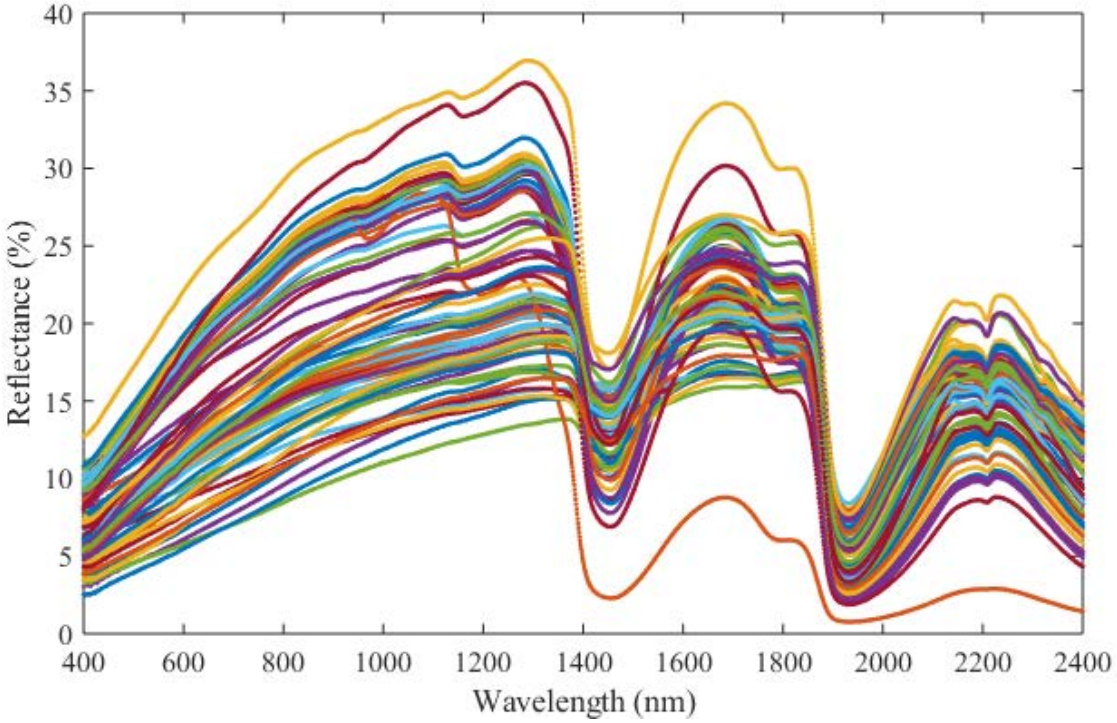

Figure 2: Reflectance spectra of some of the tailings samples

Tailings properties models

The relationship between the laboratory measured and hyperspectral-based predicted tailings properties are shown in Figure 3. The plots display both the training set (blue dots) and the test set (red hexagrams). Table 2 summarizes the RMSE and R^2 values of the neural network models for the estimation of various tailings properties examined during this work.

A strong correlation was observed between the predicted and measured tailings solids content (Figure 3a). The RMSE and R^2 were calculated to be 4.66 wt% and 0.95, respectively, on the test set. Similarly, as shown in Figure 3b, predicted and measured tailings water content were observed to be highly correlated with R^2 value of 0.96 and RMSE of 4.22 wt%. The high sensitivity of the samples spectra to the variation in water content explains this successful prediction performance.

Figure 3c shows the relationship between the measured and predicted residual bitumen content. Although the spectral model can predict the bitumen content with relatively small RMSE of 1.01 wt%, the goodness of fit of this model is not as good as the models for solids and water content (R^2 of 0.76 compared to R^2 of 0.95). This could be due to two main reasons. First, bitumen is the smallest component in the tailings mixture and is hard to homogenize into the sample during both laboratory testing and spectral measurement. Therefore, a higher discrepancy is expected between laboratory and spectral-based measurements of bitumen content (bitumen content measurement in the laboratory is not as repeatable as

for water and solids content). In addition, the distribution of the samples in terms of their bitumen content was observed to be non-uniform as 52% of samples had bitumen content of less than 2 wt% and 48% of the samples had bitumen content ranging from 2 to 10.63 wt%. This imbalanced distribution of data can cause the model to be biased towards the low bitumen regime. Adding samples with higher bitumen content to the dataset can likely improve the model performance.

The relationship between the laboratory measured total fines and the total fines predicted using the hyperspectral methods is shown in Figure 3d. Using the test set, the R^2 was observed to be 0.75 and the RMSE was 4.87 wt%. Accordingly, the total fines content of tailings samples can be predicted using the hypespectral measurements with sufficient accuracy.

Figure 3e shows the relationship between MBI measured in the laboratory and MBI predicted using the hyperspectral data and neural networks for both training and test sets. R^2 and RMSE were 0.91 and 1.36 (meq/100g), respectively, on the test set. The accuracy and repeatability of the laboratory-based MBI testing highly depends on the sample preparation and personnel expertise. We have observed errors higher than 3 meq/100g in MBI when laboratory testing has been repeated on the same sample. Therefore, when assessing the performance of the hyperspectral model for the estimation of MBI, the potential errors in the laboratory data used to train and test the models should be taken into account.

The measured and predicted clay to water ratio were observed to be highly correlated (Figure 3f). The R^2 and RMSE on the test set were calculated to be 0.91 and 6.12, respectively. The laboratory-based measurement of clay to water ratio needs measurement of tailings water content and clay content calculated through MBI using an empirical equation ($\%Clays = 7.14 \times MBI + 0.29$). The clay content obtained from this empirical equation and thus the clay to water ratio can be greater than 100%. It appears that hyperspectral methods can directly provide an estimate of clay to water ratio with an error of 6.12.

Table 2: RMSE and R^2 values for various neural network models developed for estimation of different tailings properties

Model	RMSE	R^2
Solids content	4.66 wt%	0.95
Water content	4.22 wt%	0.96
Bitumen content	1.01 wt%	0.76
Total fines content	4.87 wt%	0.75
Methylene blue index (MBI)	1.36 meq/100g	0.91
Clay to water ratio (CWR)	6.12	0.91

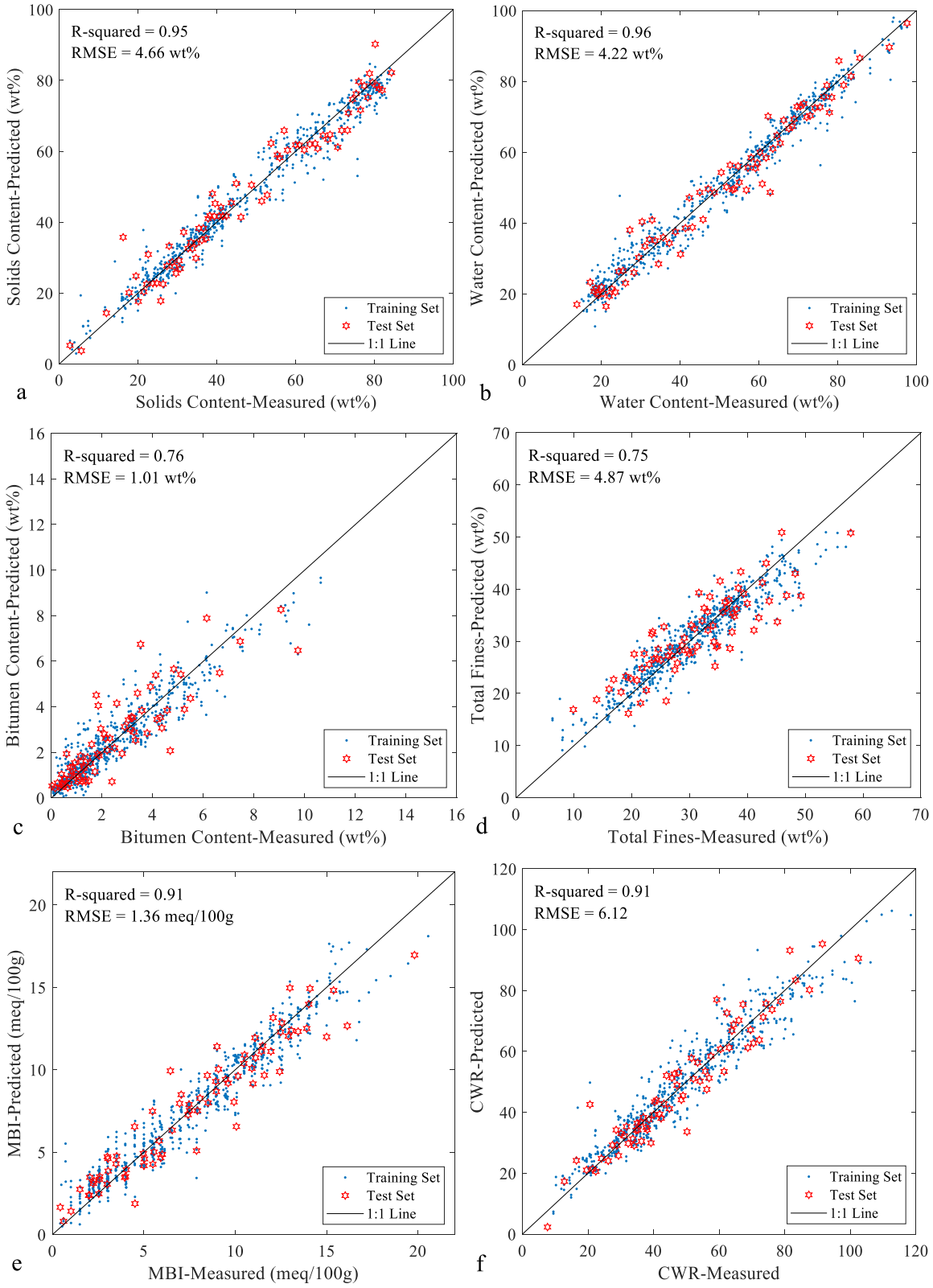

Figure 3: The relationship between the laboratory measured and hyperspectral-based predicted tailings properties: a) solids content, b) water content, c) bitumen content, d) total fines content, e) MBI, and f) clay to water ratio (CWR)

Conclusions

This research examined the use of hyperspectral sensing in the estimation of various tailings characteristics. Ensemble-based neural networks were employed to calibrate the spectral features to tailings characteristics. Different spectrometers and contact probes were used for spectral measurement of 540 tailings samples. This was done to minimize the impact of differences between the instrumentation on the prediction results and develop models that are robust against the variation in the instrumentation.

Generally, spectral models were observed to be successful in the estimation of the contents of solids, water, bitumen, and total fines as well as MBI and CWR. Although the errors of hyperspectral based predictions are generally higher than laboratory measurements, they are acceptable for many applications and for investigating tailings behaviour. Also, the key advantage of spectral models is that they provide rapid and consistent predictions that are less prone to human error. Consequently, the use of hyperspectral technology for tailings characterization can enable us to quickly analyze the tailings on-site and provide near real-time assessment of the tailings properties. Furthermore, this technology could eliminate the chain of custody and sample handling and disposal issues as samples can immediately be returned to the tailings pond after spectral measurement.

This is an on-going research and development project as we are currently carrying out hyperspectral testing on-site to continuously improve the performance and robustness of the models as we collect more data. It is also worth noting that the use of hyperspectral sensing and the methodology presented in this research for oil sands tailings characterization could potentially be expanded to other mine waste tailings.

References

Alberta Energy. 2014. Alberta's oil sands: the facts. Government of Alberta, Edmonton, Alberta.

Alberta Energy Regulator (AER). 2017. Directive 085: Fluid Tailings Management for Oil Sands Mining Projects.

Breiman, L. 1996. Bagging predictors. *Machine Learning:* 24(2): 123–140.

Cabrera, Sandra C. M. 2008. Characterization of oil sands tailings using low field nuclear magnetic resonance (NMR) Technique. MSC Thesis, Department of Chemical and Petroleum Engineering, University of Calgary.

Canada's Oil Sands Innovation Alliance (COSIA). 2015. *Measuring Undrained Shear Strength of Oil Sands Tailings Deposits.*

Dardenne, P., G. Sinnaeve and V. Baeten. 2000. Multivariate calibration and chemometrics for near infrared spectroscopy: Which method? *J. Near Infrared Spectrosc*. 8: 229–237.

Entezari, I., B. Rivard, J. Sharp, P.S. Wells and D. McGowan. 2018. Real-time prediction of oil sands tailings properties using hyperspectral observations. In *IOSTC 2018. Proceedings of the 6th International Oil Sands Tailings Conference*; Edmonton, Alberta, Canada: 102:106.

Garcia-Pedrajas, N., C. Hervas-Martinez and D. Ortiz-Boyer. 2005. Cooperative coevolution of artificial neural network ensembles for pattern classification. *IEEE T EVOLUT COMPUT*. 9(3): 271–302.

Geladi, P., H. Martens, L. Hadjiiski and P. Hopke. 1996. A calibration tutorial for spectral data. Part 2. Partial least squares regression using Matlab and some neural network results. *J. Near Infrared Spectrosc*. 4: 243–255.

Kaminsky, Heather. 2008. Characterization of an Athabasca oil sands ore and process streams. PhD Thesis, Department of Chemical and Materials Engineering, University of Alberta.

Kasperski, K.L. 2001. Review of research on aqueous extraction of bitumen from mined oil sands. (Division No. CWRC 01–17 [CF]). Natural Resources Canada, CANMET-WRC.

Sollich, P. and A. Krogh.1996. Learning with ensembles: How over-fitting can be useful. In D.S. Touretzky, Mozer M.C. Touretzky and M.E. Hasselmo, editors. *Advances in Neural Information Processing Systems*, MIT Press, Cambridge, MA: 8: 190–196.

Styler, M.A., D. McGowan and J. Sharp. 2018. Characterizing soft oil sand tailings by gamma cone penetration testing. In N.A. Beier, G.W. Wilson and D.C. Sego, editors. *IOSTC 2018. Proceedings of the 6th International Oil Sands Tailings Conference*; Edmonton, Alberta: 112:120.

Ukil, A., J. Bernasconi, H. Braendle, H. Buijs and S. Bonenfant. 2010. Improved calibration of near-infrared spectra by using ensembles of neural network models. *IEEE Sens. J.* 10(3): 578–584.

Proceedings of Tailings and Mine Waste 2019
November 17–20, 2019, Vancouver, Canada
Published by the University of British Columbia, 2019

InSAR as a Complementary Technology for Monitoring Programs of Tailings Storage Facilities and Waste Piles

Giacomo Falorni, TRE ALTAMIRA, Canada
Sara Del Conte, TRE ALTAMIRA, Canada
Nora Toro, TRE ALTAMIRA, Canada
Alain Boudreau, TRE ALTAMIRA, Canada

Abstract

Mine risk management programs require comprehensive knowledge of structural integrity within large assets such as tailings storage facilities and waste piles. Satellite InSAR is becoming increasingly popular as a surface deformation monitoring tool for mine sites due to its ability to cover an entire operation, without the need for any on-site equipment or support. Systematic coverage can be obtained every few days, depending on the revisit frequency of the satellite. New satellites with increasingly sophisticated SAR technology and shorter revisit times currently being launched lead to gaining momentum for InSAR as a reliable monitoring tool. Future satellite constellations could reduce the revisit time to daily or even hourly acquisitions over any site. Not only does InSAR provide millimetric precision of surface deformation, but new developments further exploit the InSAR outputs to provide acceleration profiles, algorithmic trend-variation detection, surface change detection, and tailings water position detection.

Two key features of InSAR are the ability 1) to detect early warnings of change in movement patterns over an entire mine site and 2) to provide an overview of ground deformation beyond the limits of localized instrumentation and capture the actual extent of the unstable area. From this vantage point, the use of satellite InSAR leads to a tactical deployment of other monitoring instrumentation and a more effective use of available resources in support of risk management. The integrated use of ground-based radar and InSAR has proven valuable for geomechanical analyses and modelling. InSAR is a digital product, which allows multi-asset monitoring directly from a central headquarter and distribution to collaborators and other interested parties. This paper will focus on the role of InSAR as a complementary technology for monitoring programs over active and closed mines. Case studies over different mine sites are presented, focussing on tailings storage facilities and waste piles.

Introduction

Monitoring the stability of tailings facilities, waste deposits and pit slopes is indispensable for sustainable mining development and risk management. The instrumentation used for monitoring surface deformation over mine sites is generally based on conventional survey techniques (total stations, levelling, GPS receivers, ground-based radars) but none of these usually offer the high density, bird's-eye view of the movement areas provided by satellite InSAR (Synthetic Aperture Radar Interferometry).

InSAR extracts high precision ground deformation information by exploiting satellite SAR images acquired over a site at different times (Gabriel et al., 1989; Massonnet and Feigl,1998; Rosen et al., 2000; Bamler and Hartl, 1998; Ferretti et al., 2000; 2001) and has been successfully applied over many mine sites (Carnec and Delacourt, 2000; Colesanti et al., 2005; Jung et al., 2007; Herrera et al., 2007; Herrera et al., 2010; Iannacone et al., 2015; Colombo and MacDonald, 2015; Sánchez et al., 2016; Carla et al., 2018). Beneficial features of InSAR for monitoring mine sites include:

- The provision of information without the requirement for ground instrumentation (no need to access remote or hazardous sites);
- The wide coverage and high density of information, not achievable with in-situ instrumentation;
- The capability to detect both slow and fast movement (from millimeters to meters) by integrating different InSAR techniques and satellites.

The existence of data archives going back to the 1990s make InSAR ideal for historical ground deformation analyses. However, in the last decade, advances in data processing algorithms and cloud computing have significantly reduced computational time. Furthermore, the advent of newer satellites, with increased spatial resolution and acquisition frequency have increased information density. Coverage of all mine assets can now be obtained every few days, depending on the revisit frequency of the satellite and the number of orbits used. Near-real time InSAR monitoring is currently integrated into operational monitoring plans at many mines to identify possible incipient movements in areas not visible to in-situ instrumentation.

Once a mine enters the closure phase, InSAR provides remote, automated monitoring with annual updates, with the option to increase monitoring frequency when issues are identified or at problematic sites. The recent launch of low-resolution satellites such as the Sentinel-1 constellation, offers free imagery covering large areas (250 × 250 km) and a high frequency of acquisitions (6 to 12 days), making InSAR a viable option for cost-effective and long-term monitoring of closed mines without year-round site access.

A new use of SAR imagery involves the identification and frequent updating of the water pond location within the tailings facilities. This is described briefly in the final section of the paper.

Operational InSAR tools for monitoring active mines

Operational monitoring programs over active mines require frequent updates of surface deformation over all assets, including tailings facilities, pits, infrastructure and waste piles. The timely identification of areas of movement and changes in deformation rates during operational activities is essential to ensure the safety and continuity of mining operations.

In the past, InSAR was often used to provide periodical updates or perform historical back-analyses, rather than to support real-time monitoring. However, the recent launch of satellites with shorter revisit times and the availability of cloud-computing solutions for InSAR processing have created opportunities for new InSAR applications that have progressed from static snapshots of deformation to a near real-time stream of information. These include:

- InSAR Bulletins, with a rapid delivery of surface information within hours of every new satellite acquisition. Bulletins provide a map of movement and surface changes larger than 0.5 cm that occur between the last two images (Figure 1). This product can be integrated with surface deformation information from real time in-situ instruments.
- Periodic and/or continuous advanced InSAR analyses complemented with trend change detection algorithms to automatically sift through large quantities of deformation time series for a detailed understanding of mm-scale up to metric-scale surface deformation. By analyzing archives of images, advanced InSAR techniques such as SqueeSAR (Ferretti et al., 2011) identify natural targets on the ground to detect millimetric deformation over entire mine sites and highlight changes in ground movement behaviour (Figure 3).

The combined use of these InSAR tools provides timely site-wide information of ground deformation and long-term movement trends, including potential precursors of slope failures.

Deformation trend change detection

Continuous Advanced, semi-autonomous InSAR processing algorithms have recently been applied by Raspini et al. (2018) to support the rapid identification of changes in deformation trends, which are often precursors of slope failures. The continuous processing allows deformation time series to be constantly updated and analyzed, with a frequency matching the revisit time of the satellite.

Continuous Advanced InSAR update millions of measurement points over a mine site every time a new image is acquired. This is a big data problem that requires an efficient approach to sieve through the stream of ground deformation information to highlight only those points containing useful data for early warning systems. Trend detection algorithms have been specifically developed to examine the time series of every single measurement point at every update for possible changes in trends, steps or accelerations.

An example of a trend changes analysis applied to Advanced InSAR monitoring data over tailings facilities is shown in Figure 4. In addition to the updated measurement point cloud, the processing automatically identifies points that have accelerated within the last three months.

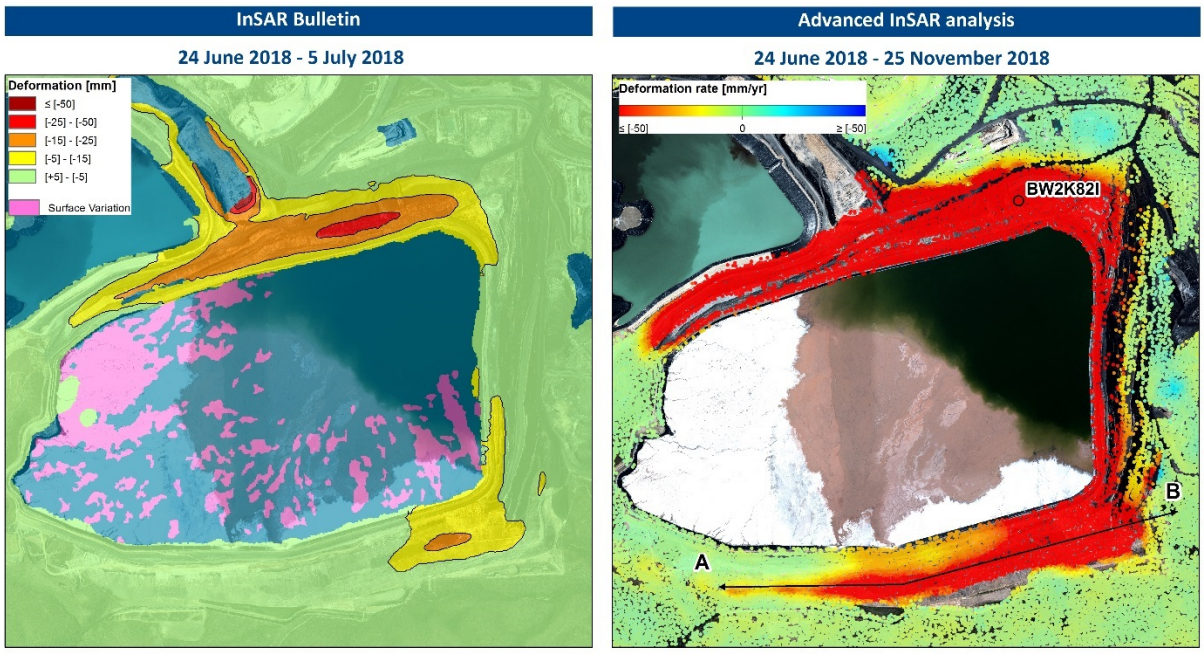

Figure 1: a) Sample InSAR bulletin over a tailings facility undergoing construction activities. The bulletin provides information over the last 11-day period, including areas within the ponds affected by surface reflectivity variations (generally induced by new slurry). b) Sample of Advanced InSAR results over tailings facilities. Each point corresponds to a natural radar reflector with an individual deformation time series covering a 6-month period (Figure 2)

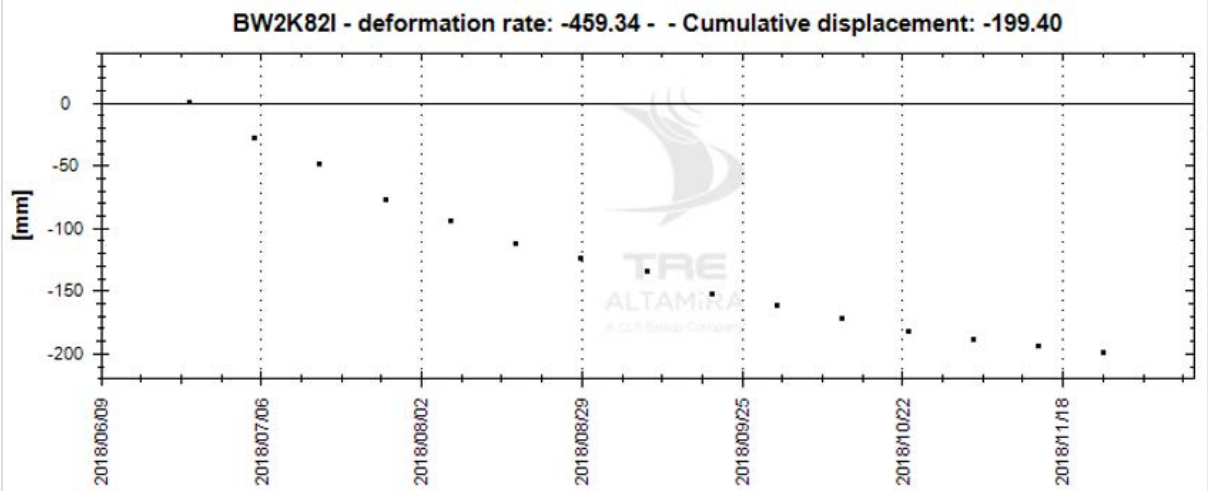

Figure 2: Deformation time series of an individual radar reflector (point BW2K821 in Figure 1. The deformation rate is reported in mm/year and cumulative deformation in mm. The time series highlights a deceleration

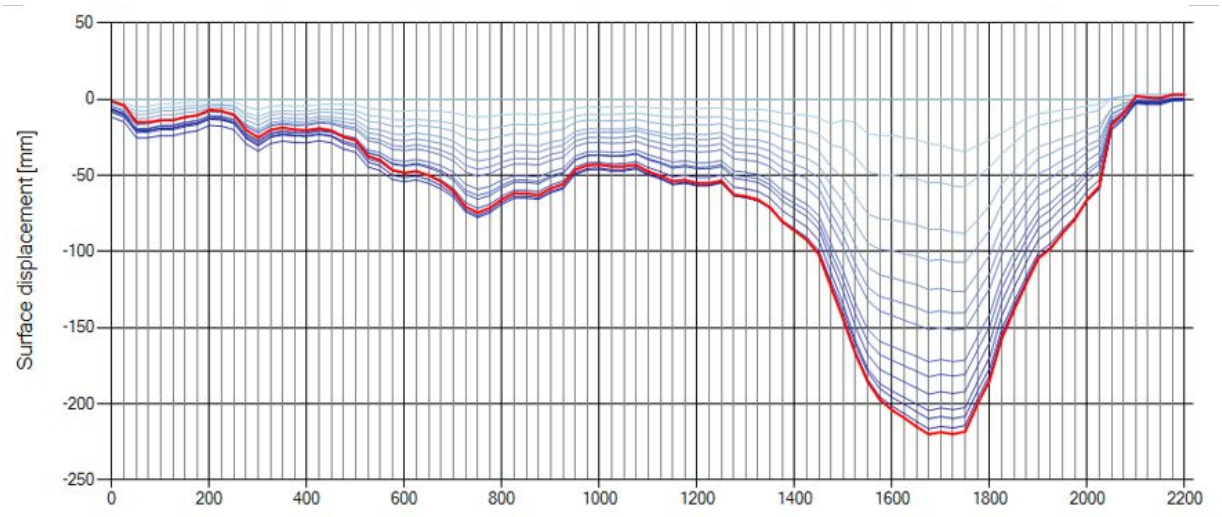

Figure 3: Cross-section A-B in Figure 1, showing the evolution of the surface profile though time. Each blue line corresponds to a satellite acquisition and reports the cumulative deformation compared to the first image (06 January 2018). The red line is the cumulative deformation on 12 July 2018. There are areas of differential deformation along the wall

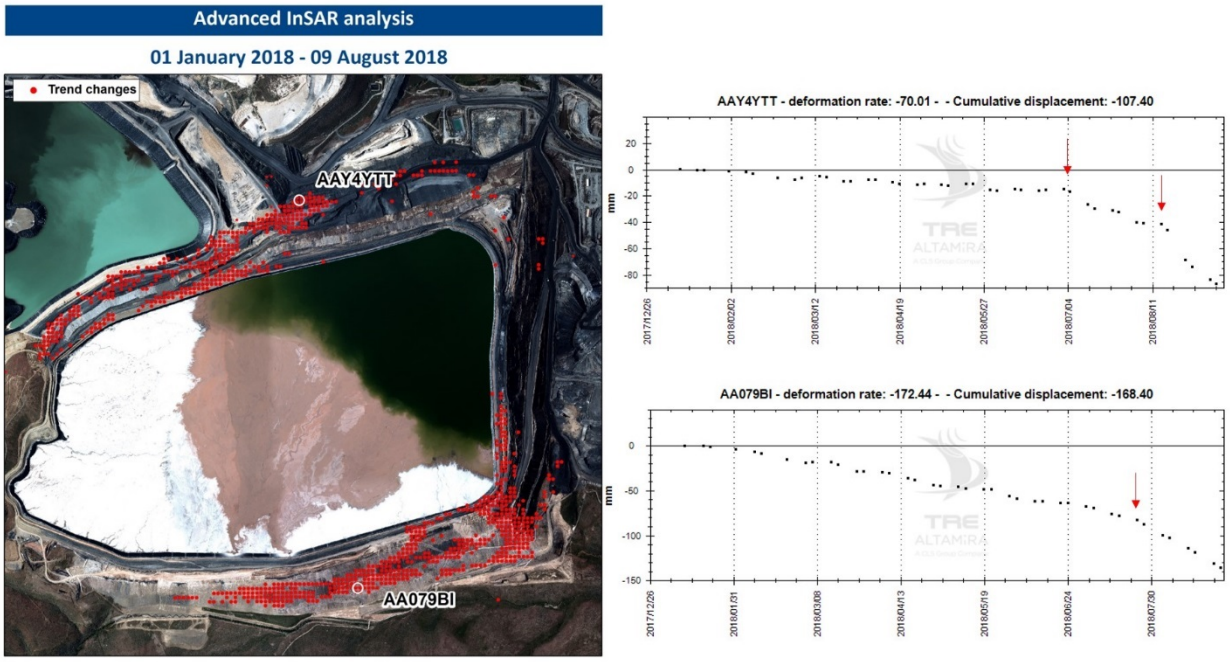

Figure 4: Advanced InSAR monitoring using trend change analysis over tailings facilities. The analysis automatically identifies accelerating points (red) in the last three months

Potential slope failure precursors

Satellite InSAR data can be used in conjunction with in-situ ground-based radars for the detection of slow accelerations and slope failure precursors. Satellites provide a comprehensive coverage and bird's eye view over the mine site that is not possible with in-situ instruments. Carlà et al. (2018) presented an excellent

example of the combined use of ground-based and satellite interferometry in the case of accelerating creep behaviour observed on an open-pit slope approaching catastrophic failure.

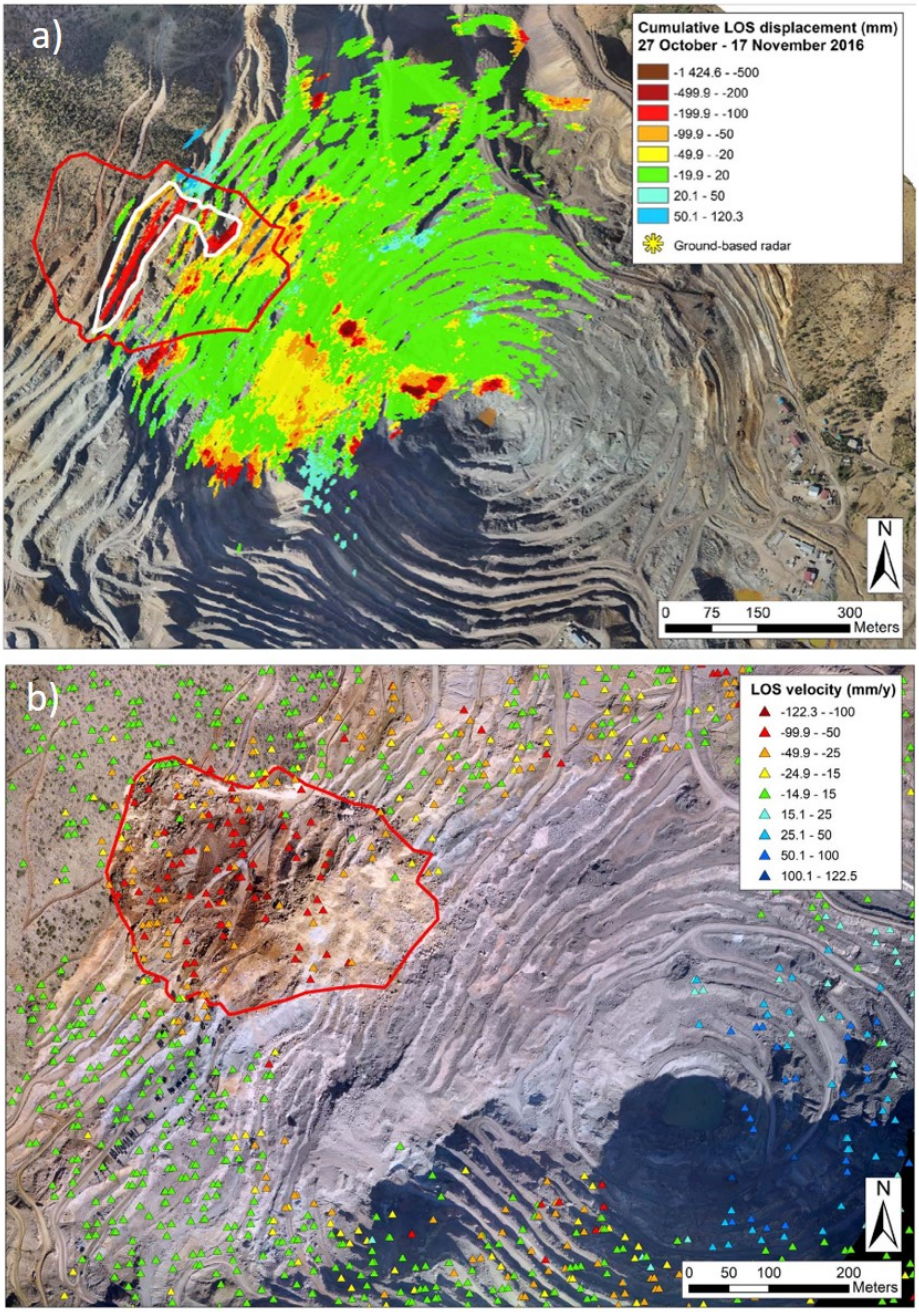

Figure 5: a) Cumulative deformation map (27 October to 17 November, 2016) from the ground-based radar. Red polygon indicates the failure area; white polygon indicates the area characterized by acceleration creep. The upper part of the slope is not visible to the ground-based radar. b) Average displacement rates (19 February to 21 November, 2016) produced by the SqueeSAR analysis. Movement in the slope above the crest is evident. Background aerial photo was captured after the event (modified from Carlà et al., 2018)

On 17 November 2016, an unexpected slope failure occurred in an undisclosed copper open pit mine (Figure 5), causing several fatalities. A ground-based interferometric radar was in use for measuring slope deformation at the time of the failure. The event was investigated through back-analysis in order to assess the size and temporal evolution of the slope failure and determine whether precursor signals were present. Satellite InSAR data spanning over 9 months before the failure were processed with the SqueeSAR approach and coupled to the ground-based radar data. Although progressive deformation of the two uppermost benches in the pit was observed by the ground-based radar, the satellite InSAR data revealed that the majority of the instability actually occurred in the natural slope above the mine crest (Figure 5). The predictability of the failure was investigated using the inverse velocity method (Fukuzono, 1985; Voight, 1989; Crosta and Agliardi, 2003; Sornette et al., 2004; Petley et al., 2005; Rose and Hungr, 2007) applied to both the ground-based and satellite data. The results indicate that a failure trend was evident in advance from both the satellite data (several weeks) and the ground radar data (approximately 10 days).

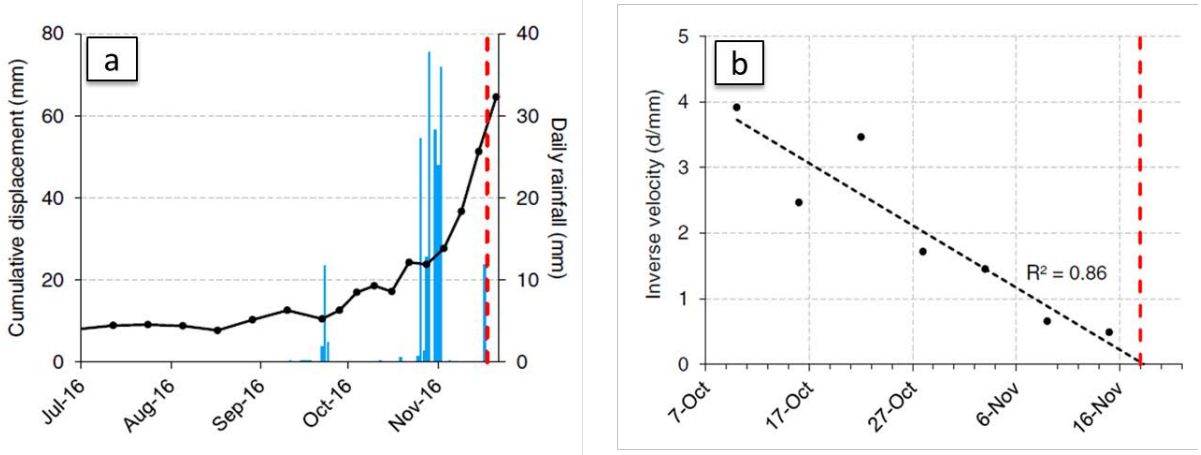

Figure 6: a) Average cumulative displacement of the area in accelerating creep captured by SqueeSAR from July to November, 2016, compared to daily rainfall. Accelerations occur after rainy days. (b) Inverse velocity analysis calculated from SqueeSAR data for October to November, 2016. Red line marks the failure date (17 November, 2016) (modified from Carlà et al., 2018)

Ground-based radar is widely considered essential for the timely detection of slope failures. However, this case study highlights that there are instances where constraints due to the limited field of view must be considered. The integration of satellite InSAR overcomes these limitations by providing a view over the crest of the pit as well as over all other mine assets.

InSAR monitoring for closed mines

As mines enter the closure phase, InSAR monitoring plans can be adapted and scaled back. Active mines require frequent updates with high resolution imagery to allow on-site geotechnical engineers to react quickly to changes in ground deformation. However, once a mine ceases operations, a decreased frequency

and lower resolution imagery is often sufficient for the monitoring program.

While both active and closed mine monitoring solutions are preventative, closed mines are monitored with a lower data processing frequency (e.g., annual). The satellite imagery used is often the publicly available Sentinel-1 (SNT) low-resolution data collected on a 12-day temporal interval. This solution is cost-effective while maintaining a high-temporal revisit frequency (12 days, or even 6 days in certain regions). The lower satellite resolution reduces the measurement point density (Figure 7) compared to high resolution commercial satellites but is often more than sufficient to characterize deformation trends. However, in particular cases it is necessary to continue with high-resolution monitoring during closure monitoring to identify localized deformation.

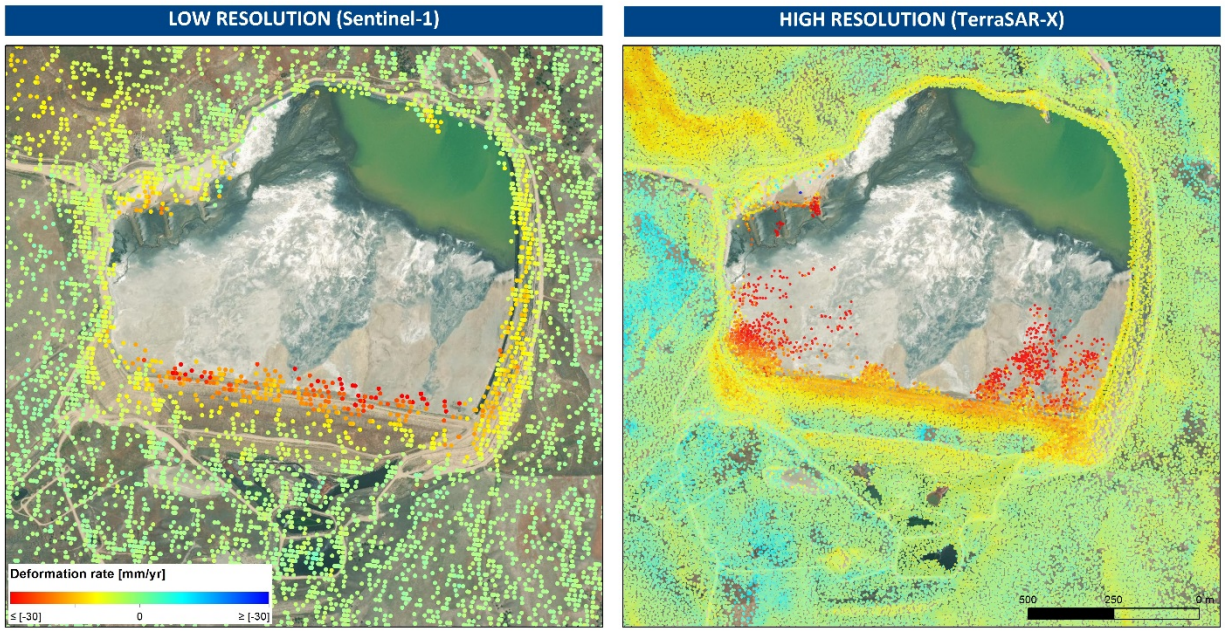

Figure 7: Comparison of measurement points obtained by the InSAR processing of low-resolution SNT (5 × 20 m) imagery (left) and high-resolution TSX (1 × 1 m) imagery over the tailings facilities of a closed mine

Clinton Creek Mine in Yukon, Canada, is remote and difficult to access during the lengthy winter period. Clinton Creek Mine is now transitioning from a manual survey method to an annual InSAR monitoring approach, and an initial four-year 2-D SNT baseline over the entire mine site identified several areas of deformation. While good coverage and density of the measurements was achieved with the low-resolution Sentinel data (Figure 8), localized drop structure features within the dam and Clinton Creek passageway could not be adequately monitored. As a result, Clinton Creek will transition to high-resolution TerraSAR-X (TSX) imagery for the annual monitoring program in order to increase measurement density and coverage in localized areas.

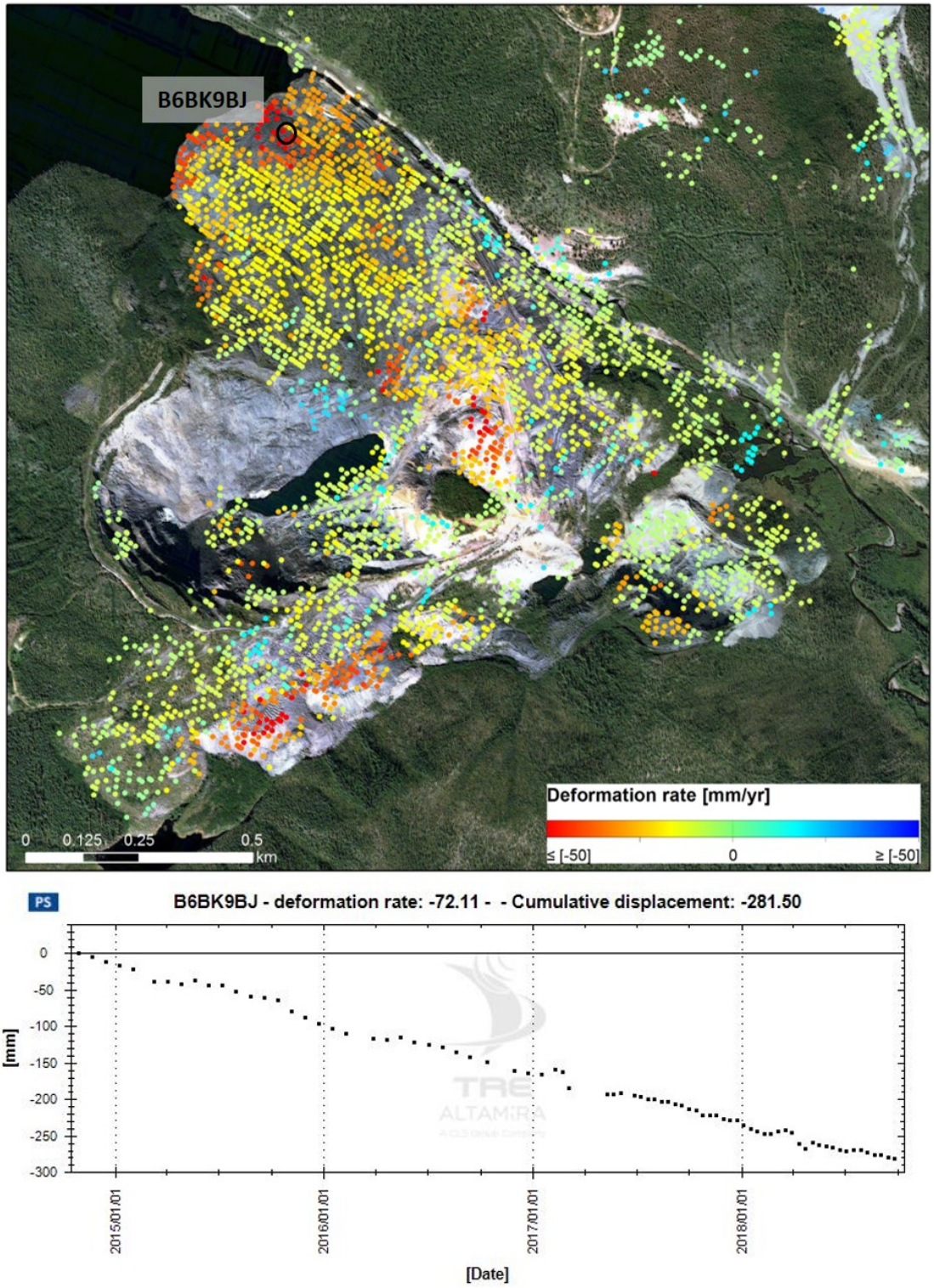

Figure 8: Clinton Creek Mine – Low-resolution Sentinel-1 InSAR results over the full mine site covering the period December, 2014 to December, 2018

Another option for monitoring specific areas is the use of Corner Reflectors (CRs). These are often installed through key areas on the mine site to allow precise year-round monitoring without having to access the site (Figure 9). CRs are passive aluminium trihedrals designed to reflect the satellite signal that do not require power supply. They are generally used over areas with dense vegetation and /or snow coverage to integrate the naturally occurring measurement points.

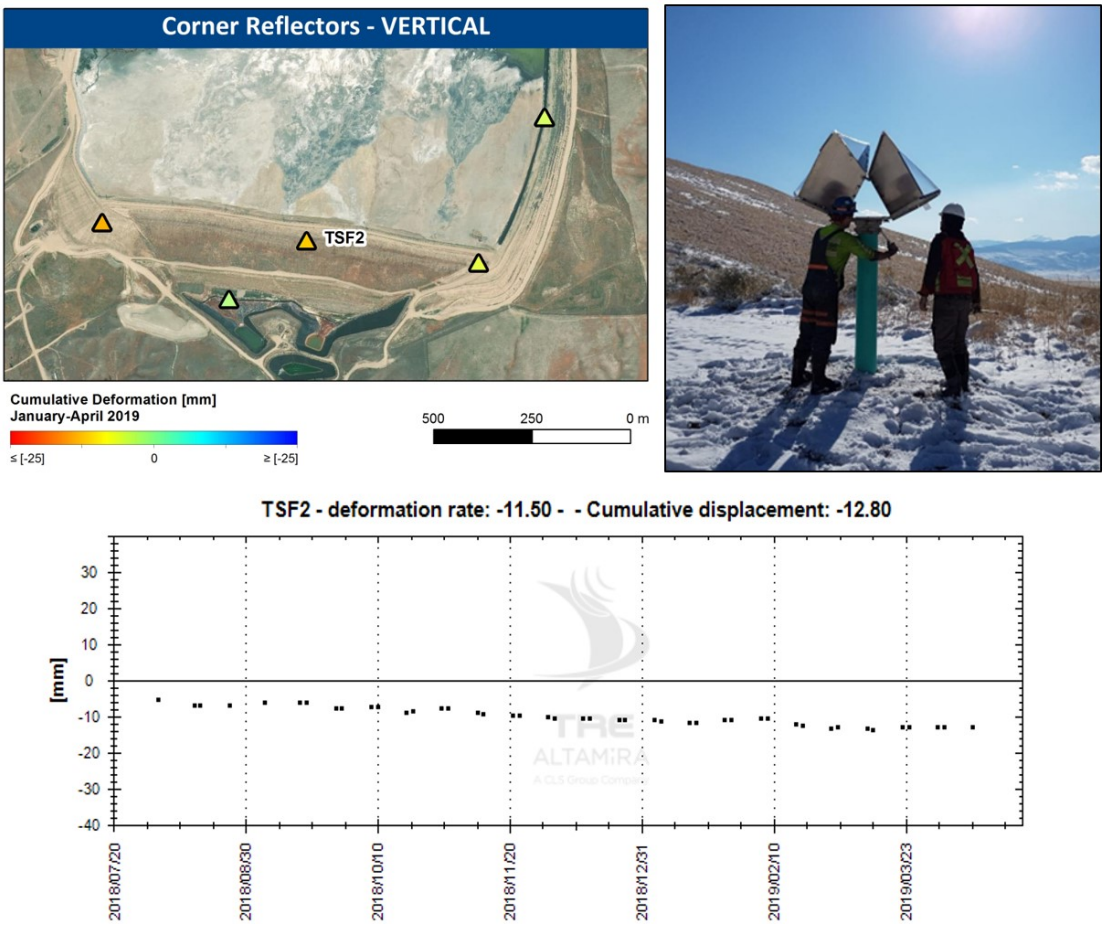

Figure 9: Corner reflectors at a mine entering the closure phase. For each CR the InSAR analysis provides high precision displacement time-series

Water pond tracking

SAR images contain another source of information that is directly related to the reflectivity of the ground surface: the signal amplitude. Amplitude represents the strength of the signal backscattered to the satellite (Figure 11a) and different surfaces exhibit different scattering characteristics. Generally, metallic and solid objects provide a stronger backscatter, while vegetation results in lower values. Standing water is usually a dark surface as the radar signal is specularly reflected away from satellite, unless there are waves.

The analysis of SAR amplitude data has been widely used in change detection investigations (White, 1991; Rignot and Van Zyl, 1993; Bazi et al., 2005; Meyer at al., 2015) and recently has been applied to detect variations in water content over tailings pond deposits (Figure 10) and to map standing water bodies (Figure 11). Image segmentation algorithms allow the classification of the SAR images into classes based on water content. The integration of different sources of satellite data with variable acquisition frequency and sensor characteristics can potentially provide a continuous water mapping service with weekly (or even higher frequency) updates.

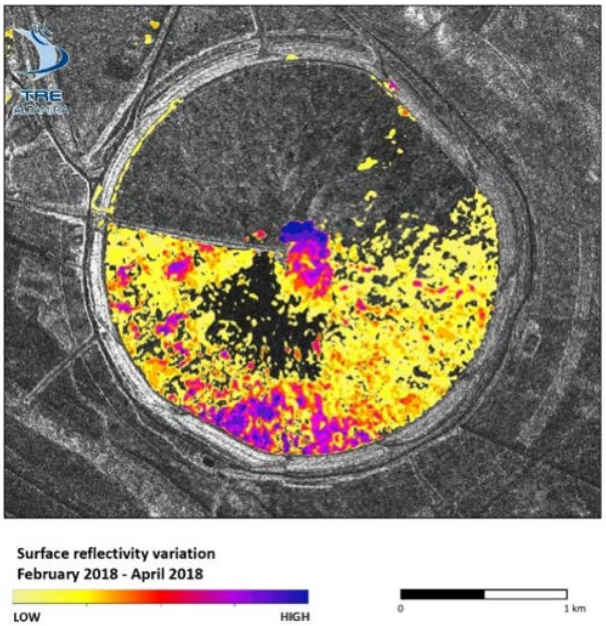

Figure 10: Change detection analysis of a data stack of TerraSAR-X images acquired over a tailings facility between February and April, 2018. The analysis provides an indication of areas affected by surface reflectivity variations, most likely related to the water content of the slurry deposits

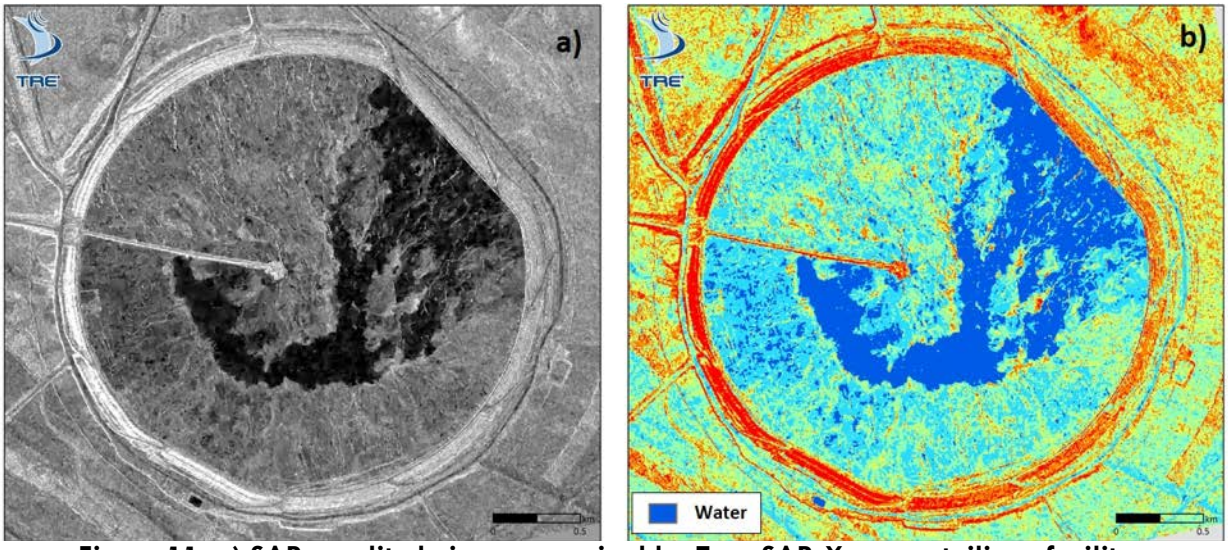

Figure 11: a) SAR amplitude image acquired by TerraSAR-X over a tailings facility. b) Image classification and identification of standing water

Conclusion

The benefits of InSAR as a complementary technology for monitoring programs over active and closed mine sites have been presented here through different case studies. The recent launch of satellites with a short revisit time and the developing of new processing algorithms and data analysis tools have progressively turned InSAR into a near real-time monitoring solution. Not only does InSAR provide millimetric precision of surface deformation over entire mine sites, but new developments further exploit the InSAR outputs to provide acceleration profiles, trend-variation detection, surface change detection, and tailings pond position detection. The output from all of these analyses allows multi-asset monitoring directly from a central headquarters, and facilitates distribution to collaborators and other stakeholders.

Finally, the availability of low-resolution public domain satellites makes InSAR a valuable solution for cost-effective and long-term monitoring solutions for closed mines without year-round site access.

Acknowledgements

The authors would like to acknowledge the Government of Yukon and the Government of Canada for funding the InSAR monitoring work carried out over the Clinton Creek Mine, as well as Tetra Tech for their involvement in the project.

References

Bamler, R. and P. Hartl. 1998. Synthetic aperture radar interferometry. *Inverse Problems* 14: R1–R54.

Bazi, Y., L. Bruzzone and F. Melgani. 2005. An unsupervised approach based on the generalized Gaussian model to automatic change detection in multitemporal SAR images. *IEEE Trans. Geosci. Remote Sens*. 43: 874–887.

Carlà, T., P. Farina, E. Intrieri, H. Ketizmen and N. Casagli. 2018. Integration of ground-based radar and satellite InSAR data for the analysis of an unexpected slope failure in an open-pit mine. *Engineering Geology* 235: 39–52.

Carnec, C. and C. Delacourt. 2000. Three years of mining subsidence monitored by SAR interferometry, near Gardanne, France. *Journal of Applied Geophysics* 43(1): 43–54.

Colesanti, C., S.L. Mouelic, M. Bennani, D. Raucoules, C. Carnec, C. and A. Ferretti. 2005. Detection of mining related ground instabilities using the Permanent Scatterers technique: A case study in the east of France. *International Journal of Remote Sensing* 26(1): 201–207.

Colombo, D. and B. MacDonald. 2015. Using advanced InSAR techniques as a remote tool for mine site monitoring. *Proceedings, Slope Stability Congress,* Cape Town, South Africa.

Crosta, G.B. and F. Agliardi. 2003. Failure forecast for large rock slides by surface displacement measurements. *Can. Geotech. J.* 40: 176–191.

Ferretti, A., C. Prati and F. Rocca. 2000. Nonlinear subsidence rate estimations using Permanent Scatterers in differential SAR interferometry. *IEEE Transactions on Geoscience and Remote Sensing* 38(5): 2202–2212.

Ferretti, A., Prati, C., and Rocca, F. 2001. Permanent Scatterers in SAR interferometry. *IEEE Transactions on Geoscience and Remote Sensing* 39(1): 8–20.

Fukuzono, T. 1985. A new method for predicting the failure time of a slope. In *Proceedings of the Fourth International Conference and field workshop on landslides*. Tokyo: Japan Landslide Society: 145–50.

Gabriel, A.K, R.M. Goldstein and H.A. Zebker. 1989. Mapping small elevation changes over large areas: Differential radar interferometry. *Journal of Geophysical Research* 94: 9183–9191.

Herrera, G., R. Tomás, J.M. Lopez-Sanchez, J. Delgado, J.J. Mallorqui, S. Duque and J. Mulas. 2007. Advanced DInSAR analysis on mining areas: La Union case study (Murcia, SE Spain). *Engineering Geology* 90: 148–159.

Herrera, G., R. Tomas, F. Vicente, J.M. Lopez-Sanches, J.J. Mallorquí and J. Mulas. 2010. Mapping ground movements in open pit mining areas using differential SAR interferometry. *International Journal of Rock Mechanics and Mining Sciences* 47: 1114–1125.

Iannacone, J.P., A. Corsini, M. Berti, J. Morgan and G. Falorni. 2015. Characterization of longwall mining induced subsidence by means of automated analysis of InSAR time-series. In *Engineering Geology for Society and Territory* 5, International Publishing.

Jung, H.C., S.W. Kim, H.S. Jung, K.D. Min, and J.S. Won. 2007. Satellite observation of coal mining subsidence by persistent scatterer analysis. *Engineering Geology* 92: 1–13.

Massonnet, D. and K.L. Feigl. 1998. Radar interferometry and its application to changes in the Earth's surface. *Reviews of geophysics* 36(4): 441–500.

Meyer, F.J., D.B. McAlpin, W. Gong, O. Ajadi, S. Arko, P.W. Webley and J. Dehn, J. 2015. Integrating SAR and derived products into operational volcano monitoring and decision support systems. I*SPRS J. Photogramm Remote Sens.* 100: 106–117.

Petley, D.N., F. Mantovani, M.H. Bulmer and A. Zannoni. 2005. The use of surface monitoring data for the interpretation of landslide movement patterns. *Geomorphology* 66: 133–147.

Raspini, F., S. Bianchini, A. Ciampalini, M.D. Soldato, L. Solari, F. Novali, S.D. Conte, A. Rucci, A. Ferretti and N. Casagli. 2018. Continuous, semi-automatic monitoring of ground deformation using Sentinel-1 satellites. *Scientific Reports* 8(7253).

Rignot, E.J.M. and J.J. Van Zyl. 1993. Change detection techniques for ERS-1 SAR data. *IEEE Transactions on Geoscience and Remote Sensing* 31(4): 896–906.

Rose N.D. and O. Hungr. 2007. Forecasting potential rock slope failure in open pit mines using the inverse velocity method. *Int. J. Rock Mech. Min. Sci*. 44: 308–320.

Rosen, P., S. Hensley, I. Joughin, F. Li, S.N. Madsen, E. Rodriguez and R. Goldstein. 2000. Synthetic aperture radar interferometry. *Proceedings of the IEEE*, 88(3): 333–382.

Sánchez, F., A. Conde, B. Salvá and D. Colombo. 2016. Use of SAR radar satellite data to measure ground deformation in underground and open pit mine sites, El Teniente case study, Chile. In *Proceedings of the First Asia Pacific Slope Stability in Mining (APSSIM) Conference 2016,* Brisbane, Australia, 6–8 September, 2016.

Sornette D., A. Helmstetter, J.V. Andersen, S. Gluzman, J.-R. Grasso and V. Pisarenko. 2004. Towards landslide predictions: Two case studies. *Physica A*. 338: 605–632.

Voight, B. 1989. A relation to describe rate-dependent material failure. *Science* 243: 200–203.

White, R.G. 1991. Change detection in SAR imagery. *International Journal of Remote Sensing* 12:2, 339–360,

Proceedings of Tailings and Mine Waste 2019
November 17–20, 2019, Vancouver, Canada
Published by the University of British Columbia, 2019

Static Liquefaction of Tailings: An Update on the Industry-Funded TAILLIQ Research Project

Andy Fourie, University of Western Australia, Australia
David Reid, University of Western Australia, Australia
Adrian Russell, University of New South Wales, Australia
Mizanur Rahman, University of South Australia, Australia
J. Vinod, University of Wollongong, Australia
Thanh Vo, University of New South Wales, Australia

Abstract

A major research project to investigate methods to determine the susceptibility of mine tailings to static liquefaction began in late 2017. The project is jointly funded by the Australian Research Council and six industry partners, and has four participating Australian universities.

This paper describes the key objectives of the project and the findings to date. Although the information is preliminary in nature, significant progress has already been made, as summarized in the paper. Field sampling has been completed at six sites designated by sponsoring partners, complemented by CPTu testing. The project includes extensive element testing, calibration chamber testing, and geotechnical centrifuge testing using tailings from the sponsor sites recovered during the field work. Additional work includes numerical modeling, focussing on the use of the Discrete Element Method for understanding the micro-mechanical behavior of material in both element tests.

A key feature of the project is to improve and validate the use of the CPTu for assessing the liquefaction susceptibility of tailings. A novel aspect of this project is the investigation of methods for interpretation of CPTu data obtained above the phreatic surface, i.e., within unsaturated material. Preliminary information on some calibration chamber tests on unsaturated tailings from one of the sponsor sites is also presented.

Introduction

There can be little doubt that the frequency and impacts of failures of tailings storage facilities (TSFs) have become totally unacceptable. Many people directly involved in the industry have long recognized this

reality. Of late, however, it has been brought to the attention of an extremely influential sector, namely the investment sector. No doubt there will be some discussion of the impact of investor concern and sensitivity at this conference. This paper focusses on a purely technical issue, recognizing that addressing technical concerns alone may no longer be sufficient. Deficiencies in the application of decades-old fundamental understanding of technical issues appear to have been a contributor to the majority of the recent TSF failures, most notably with respect to static liquefaction. This provided a compelling case to pursue work to confirm the long-standing fundamentals and investigate where meaningful increments in knowledge could be developed.

There are a myriad of potential failure mechanisms of a TSF, and many of these are well recognized and discussed in some detail in the literature, including overtopping, piping, and foundation failure, to name just a few. Unfortunately, less well-recognized (and indeed less well-acknowledged by some in the industry) is the failure mode that is often termed static liquefaction. While it is recognized that there are other terms currently in use to describe the same phenomenon, we retain static liquefaction in this paper as it neatly discriminates from failures induced by seismic or dynamic loading.

Although there have been references to static liquefaction of TSFs in the past (e.g., Smith, 1969; Carrier, 1991; Fourie et al., 2001; Davies et al., 2002), until the Fundão report appeared in 2016, this topic appears to have received relatively little attention from researchers in proportion to its contribution to failure case histories. The susceptibility of silty and sandy tailings to failure induced by static liquefaction appears to violate the commonly, but incorrectly, perceived wisdom (a wisdom that is transmitted by many undergraduate-level books on soil mechanics) that sands cannot fail in an undrained fashion, with the exception of seismically-induced liquefaction. What has been known by many for decades, but is now finally becoming increasingly accepted by the majority, is that if silty, sandy materials are loose enough, they are most certainly vulnerable to failure due to static liquefaction. A comprehensive understanding has been available for some time concerning the fragility of loose, saturated sand and silt deposits. For extensive coverage of this topic, see Jefferies and Been (2015), and the earlier version of that same book. It is exceedingly unfortunate this knowledge has not been more widely adopted, given the tragic results of the recent spate of incidents.

A research project was started in late 2017, jointly funded by the Australian Research Council and six large, multinational mining companies. For details about the sponsoring companies, kindly refer to the Acknowledgements section of this paper. It should be noted that although this project, conveniently referred to as TAILLIQ (see tailliq.com), started after the Fundão failure, it started well before the more recent failures in Australia, Mexico, Peru or, most notably, Brazil.

The project is led by the University of Western Australia (UWA), with collaborators from the University of New South Wales (UNSW), University of South Australia (UNISA), and the University of Wollongong (UoW).

Project objectives

The project has a number of discrete but complementary objectives that can be summarized as being to:

- Characterize tailings from a number of operational TSFs and determine the Critical State Line (CSL) of these tailings using laboratory element tests.
- Use the CSL characterization tests to determine target densities and conduct cone penetration tests in both a geotechnical centrifuge and a calibration chamber on tailings prepared in a contractive state, and model these tests using the Discrete Element Method (DEM).
- Investigate experimentally the susceptibility of tailings to static liquefaction under a range of stress paths corresponding to realistic field loading conditions.
- Develop an improved and practical method for evaluating susceptibility of mine tailings to static liquefaction using the results of the centrifuge, calibration chamber, and laboratory element tests, combined with DEM modeling, and to conduct in-situ cone penetration tests at operational TSFs to demonstrate and refine the method.
- Integrate the results from the above four aims to prepare a monograph for industry, describing a strategy and practical methodology to include results of in-situ testing in the evaluation and early identification of static liquefaction as a potential mechanism for failure of tailings storage facilities.
- Communicate these findings to industry through a series of workshops.

Components of the TAILLIQ project

There are a number of interlinking components to the project, and having multiple Australian universities involved in the work has enabled us to not only share the workload, but also leverage expertise that would otherwise not have been available at UWA. The nature of the project is best explained graphically, as shown in Figure 1.

All six of the sponsoring companies have nominated a site at which field tests (primarily CPT_u) will be carried out and samples retrieved. Although it may not prove achievable at all six sites, the intention is to retrieve a number of high-quality block samples, as well as a large volume (two bulker bags, each in excess of $1m^3$) of disturbed tailings from a location adjacent to where the CPT_u tests were carried out. The bulker bag samples are sent to both UWA and UNSW, primarily for calibration chamber tests at the latter,

and laboratory element tests, centrifuge tests, and calibration chamber tests at UWA. A small volume of tailings are sent to UNISA for laboratory element tests.

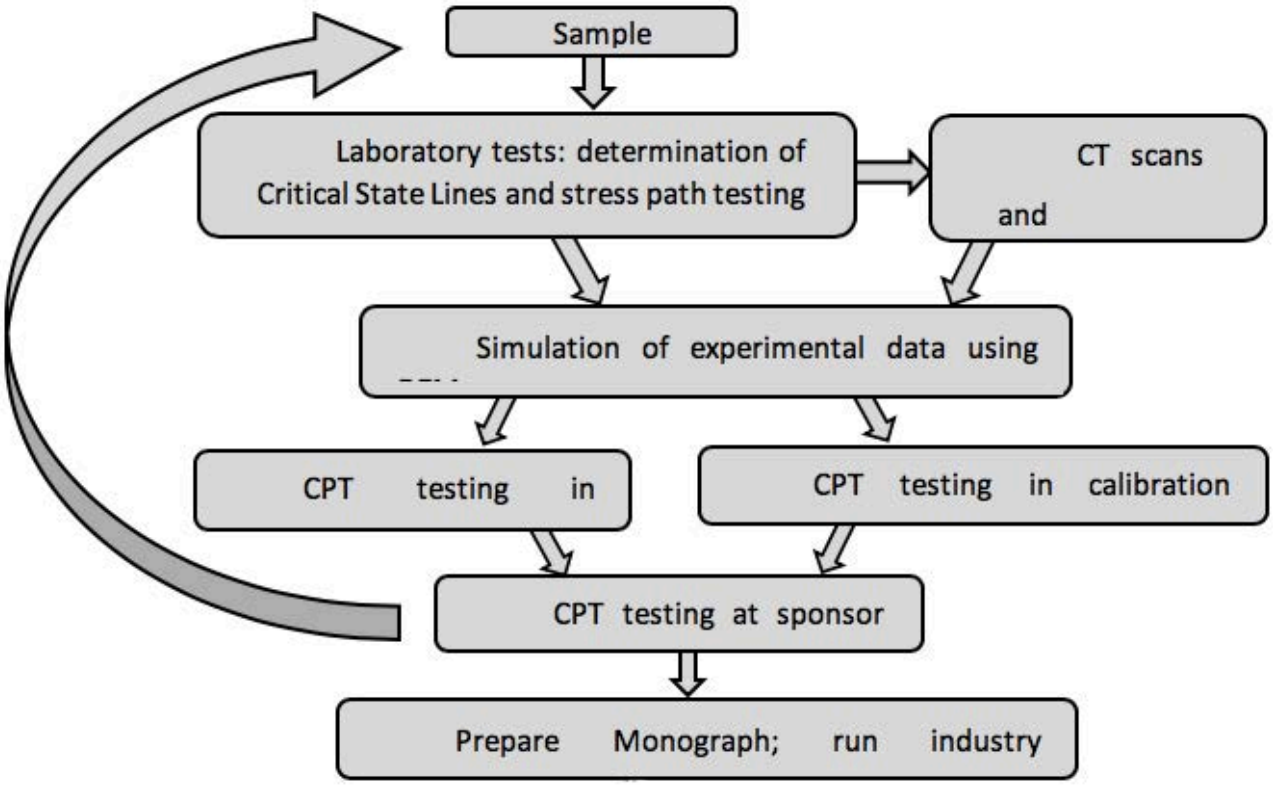

Figure 1: Project linkages for TAILLIQ

The laboratory element tests at UWA and UNISA focus on triaxial and simple shear tests, complemented of course by the usual suite of index tests. Although not originally planned for, UNSW are conducting a range of tests to determine the water retention curve(s) of tailings supplied to them. Testing at UWA will include the determination of the CSL of tailings from all six sites.

Using the CSL, target densities at a given confining pressure will be chosen for tests in the UNSW and UWA calibration chambers (once the latter is commissioned and operational). The intention is to prepare samples in a state such that they are contractive in nature, and then to probe these samples using the reduced-size piezocone in the laboratory calibration chambers. It is expected that a key challenge in these tests is preparing and maintaining large samples such as those used in the calibration chamber at a sufficiently loose density that they remain contractive in nature. To give some idea of the size of the calibration chambers to be used, Figure 2 shows the equipment that was manufactured and is currently operational at UNSW (see Pournaghiazar et al., 2011).

Figure 2: View of the calibration chamber at UNSW (the chamber itself has an outer diameter of approximately 0.7m)

Centrifuge tests will also be run using the large (5 m diameter, 240 g-tonne) beam centrifuge at UWA, preparing model tailings embankments from material that is targeted to be contractive. Various trigger mechanisms that may induce failure of contractive materials will be studied, such as a rising phreatic surface.

Finally, the above suite of field and laboratory work will be complemented by numerical modelling using the Discrete Element Method (DEM). Although DEM techniques are currently limited to relatively small applications, they are ideal for investigating fundamental aspects of micromechanical behaviour of materials during laboratory element tests such as triaxial and simple shear tests. A major challenge is modelling undrained element testing, and this is the focus of a PhD student at UoW.

Progress to date

At the time of writing, the project was less than 18 months old. Details of the six sites chosen for sampling are summarized in Table 1, together with some preliminary data. Specific details of each site have not been included, although once there has been an opportunity to socialize our results within each sponsoring organization, more specific information is likely to be published.

As is evident from Table 1, a range of different commodities are represented by the tailings tested, including low plasticity silts and somewhat more plastic iron ore tailings.

Figure 3 shows a battered excavation formed at one of the sites, enabling block samples to be recovered from depths of as much as 4 m below surface.

Table 1: Information on six sites at which sampling and testing were undertaken

Location	Primary product	Bulk samples obtained?	Block samples obtained?	CPTu testing completed?	Atterberg Limits		Specific gravity
					Liquid limit	Plastic limit	
Australia	Gold	Yes	Yes	Yes	22	17	2.78
Australia	Iron ore	Yes	Yes	Yes	39	21	3.76
Australia	Bauxite	Yes	Yes	Yes			
USA	Copper	Yes	Yes	Yes			
South Africa	Platinum	Yes	Yes	Yes			
Canada	Copper	Yes	Yes	Yes			

Figure 3: Battered excavation in tailings, enabling recovery of block samples and a large volume of disturbed material

Figure 4: Example of block sampling underway

Block samples of approximate dimensions 30 cm^3 were recovered at all sites, an example of which is shown in Figure 4. Between eight and twelve block samples have been obtained at each of the sites visited to date.

Now that the field sampling and testing is almost completed, attention has turned to completing index and characterization tests and updating Table 1, while simultaneously running laboratory element tests. Some results of the latter tests are discussed below.

Results from triaxial tests

Determination of Critical State Line (CSL)

There is now widespread acceptance within the tailings engineering community of the need to differentiate material that will likely behave in a dilative manner when sheared from potentially contractive material. Dilative behaviour results in the generation of negative pore water pressure increments when sheared, resulting in an increase in effective stress, meaning greater resistance to shear. The unfortunate aspect of contractive materials is the generation of positive pore water pressures during shearing, resulting in decreases in effective stresses and hence decreases in strength. The concept of the CSL is used to differentiate between potentially contractive and dilative materials, and is usually presented in void ratio versus (logarithm) vertical effective stress (or mean effective stress). The former definition is illustrated in Figure 5. The proximity of the in-situ void ratio to the void ratio on the CSL (at the same value of effective stress) is known as the state parameter, Ψ, as illustrated in Figure 5.

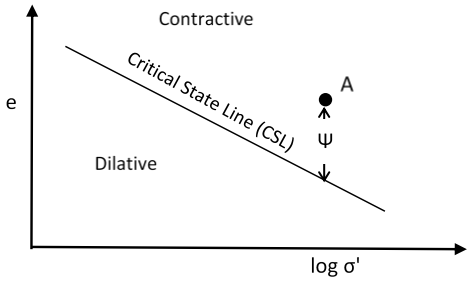

Figure 5: Illustration of critical state line concept, with a stress state at point A exhibiting a positive state parameter Ψ, which indicates contractive behaviour upon shearing

The concepts illustrated in Figure 5 will be well-known to most tailings engineers. What is perhaps less well-appreciated is the difficulties in accurately determining the CSL for a particular material. Variations in the slope and reference void ratio value (typically the void ratio value at a mean effective stress of unity) can occur due to differences in the testing technique used, as well as more obvious reasons such as operator variability. At the two-day short course on static liquefaction that was run in Melbourne

in March 2018, a great deal of discussion centred around this topic, i.e., how reliable are the CSLs obtained from a specific laboratory.

Given the importance of correctly determining the CSL for a given tailings in order to provide a reference value against which in-situ densities can be compared, TAILLIQ recently conducted a round-robin testing exercise in which identical (as near as possible) 15 kg samples of tailings from the Australian gold mine site were sent to 18 laboratories around the world. All participants in this study were asked to provide a CSL over the stress interval 50 kPa to 800 kPa. No instructions were given regarding how to prepare samples for testing, nor what testing procedure to use. The objective was to compare the possible range of CSLs that might result when a client sends material for testing to a laboratory.

Participants in this study were given the option to decide whether their company (or university) affiliation would be published or whether they preferred to remain anonymous; the requirement was that this decision be made before the results were made public. The majority of respondents chose the former option (not anonymous). Although the results of this study are not presented in this paper (because they are still being analyzed and prepared for publication), the study was certainly instructive. A number of laboratories produced CSLs that were very similar, with a range of void ratio offset values of within 0.03 (at a mean effective stress of 200 kPa, which is a value of relevance to most TSFs). However, perhaps quite predictably, there were also a number of results that deviated significantly from the clustered results. Of course, it is not possible to say what the "true" answer is, but it was notable that a number of CSLs were very close, whereas those that deviated from the clustered CSLs showed no consistent trend, some being above and some below the clustered data. All but one of the laboratory results within the "cluster" used end-of-testing soil freezing to determine void ratio.

Another issue that is being addressed in the project is how the CSL and state parameter are altered when the tailings becomes unsaturated. In some unsaturated geomaterials the presence of suction causes the isotropic compression line as well as the CSL to shift upwards in the void ratio versus (logarithm) effective stress plane, a phenomenon known as suction hardening (Loret and Khalili, 2002), which has consequences on the quantification of the state parameter. How to appropriately characterize the state of a tailings when unsaturated, and how to infer state changes when the tailings becomes saturated in the future, are ongoing research areas within the project.

Calibration chamber test results

Seven calibration chamber tests on unsaturated gold tailings have been completed to date, all at a confining stress of 100 kPa. The unsaturated samples were prepared to have uniform void ratios (ranging from 0.75 to 0.91) and moisture contents (ranging from 6.6% to 15.5%). The measured cone penetration resistances (q_c) and sleeve frictions (f_s) ranged from 2.6 to 8.9 MPa and 34 to 131 kPa, respectively.

A single calibration chamber test has also been completed on a saturated sample, the consolidation phase of which is shown in Figure 6. As indicated, to consolidate the sample to an effective confining stress of 100 kPa took around 10 days. Tests such as this, particularly on tailings having an appreciable fines content, can be lengthy.

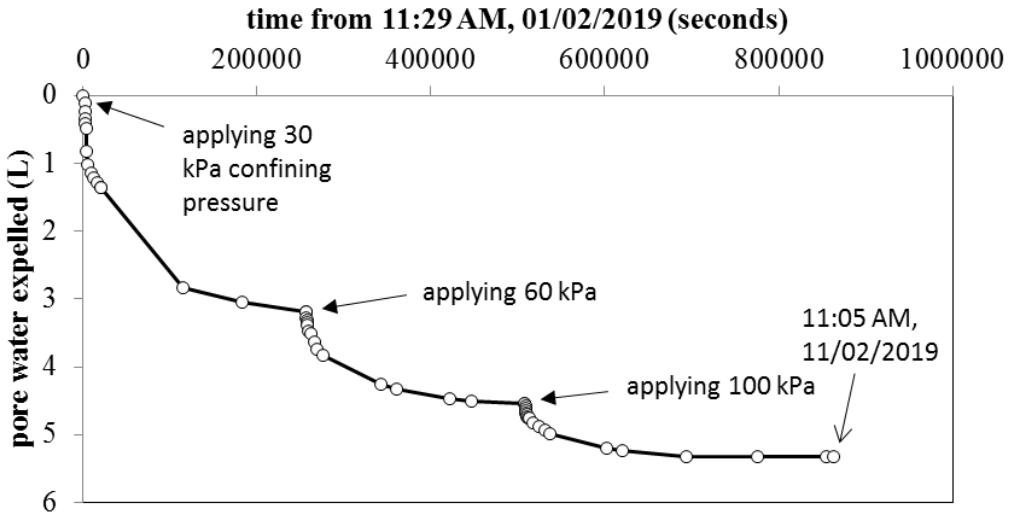

Figure 6: Consolidation of CPT sample for test on fully saturated sample

Immediately upon starting the penetration phase of this test, the cone misfunctioned. Some six months later the cone has yet to be repaired, but because a separate, near-identical calibration chamber is being set up at UWA, output in terms of calibration chamber tests is expected to increase rapidly in the second half of 2019.

Results from DEM studies

An important component of the TAILLIQ project is the incorporation of DEM modelling in a number of aspects, including modelling of laboratory element tests. Preliminary output from some of this modelling is demonstrated below.

DEM modelling is extremely demanding on computing time. To provide a proof of potential applicability, it was decided to focus on modelling a particle assembly that was relatively uniformly graded, with a fines content of zero. Once modelling approaches are refined, more realistic particle size distributions (PSD) will be modelled. In the example demonstrated in Figure 7, the target particle size distribution was modelled on that of Toyoura sand and the gold tailings sieved until it matched the Toyoura sand. The PSD used in the DEM model is also shown in Figure 7.

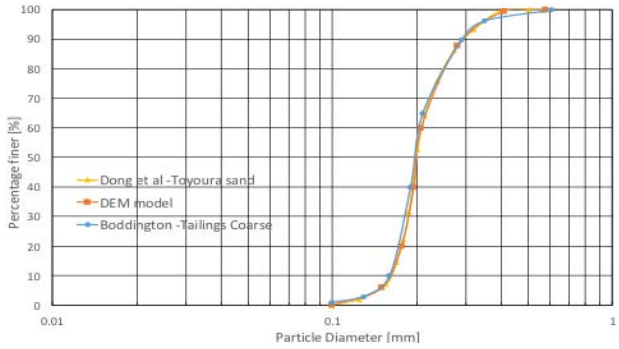

Figure 7: Particle size distribution used in DEM model compared with that of Toyoura Sand and sieved gold tailings

Initially the DEM "specimen" was consolidated with an isotropic confining stress of 200 kPa, after which the specimen was sheared at a constant strain rate, keeping the lateral stress constant during the test. The specimens were sheared under drained conditions with three deviatoric stress levels (q) of 120, 150, and 180 kPa, very similar to Dong et al. (2015). Then a CSD path with constant (q) was applied by reducing the confining stress at a rate of 1.0 kPa/2,500 cycles, until the specimen behaviour showed a marked decrease in deviator stress that finally led to a loss in controllability and the collapse of the assembly. The simulation results are shown in Figure 8 along with the experimental results.

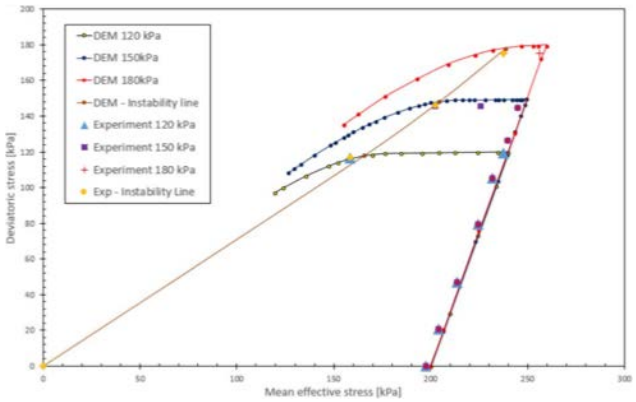

Figure 8: Deviatoric stress versus mean stress during CSD simulation

Centrifuge testing

The first TAILLIQ experiment using the recently commissioned 10 m diameter, 240 g-tonne geotechnical beam centrifuge at UWA was carried out in March 2019. It involved preparation of an embankment of Silica Fine (SF) sand in a loose, unsaturated state, and inducing a static liquefaction flow slide in the embankment with a rising phreatic surface (i.e., CSD path). The primary purpose of the first test was to assess the suitability of the strongbox insert developed for the project and gain feedback on refinements that might be necessary. However, although much was learned about successful operation of the strongbox insert, a

reasonable failure of the embankment was also achieved.

The system included mechanical and laser LVDTs to monitor displacement, allowance for CPT probing during flight prior to failure, and an ability to raise the upstream phreatic surface to trigger failure of the embankment. A clear acrylic plate covers the front of the box to allow imaging of embankment deformations leading up to and during failure.

Images of the centrifuge setup and the shallow failure induced in the first test are outlined in Figures 9 and 10. Additional information is provided in the project website blog. Back analysis of the embankment suggest a yield stress ratio (s_u / σ'_v) of about 0.3, which agrees well with back analyses of full scale failures and laboratory characterization of the SF sand.

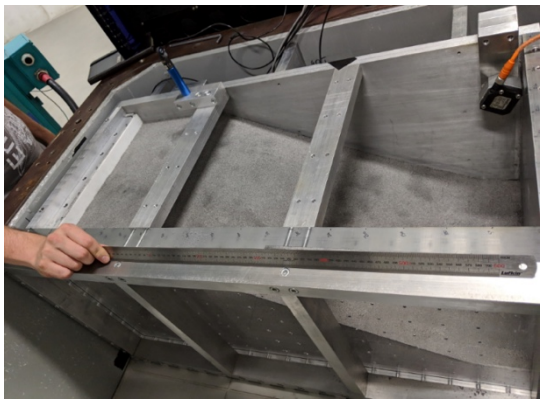

Figure 9: Embankment in centrifuge strongbox prior to testing

Figure 10: Shallow failure at the toe

Technology transfer

An important aspect of the TAILLIQ project is technology transfer. At the time of writing, five industry workshops have been run, three of them in Australia, and one each in the United States and Canada. The discussion sessions at these workshops have been immensely useful in fine tuning the activities being

undertaken as part of TAILLIQ. An example of this is the round-robin testing programme that emerged from discussions at the Melbourne workshop. Although provision for funding such a round-robin exercise was not made in the original TAILLIQ proposal, proceeds left over after the Melbourne workshop were used to fund this particular component of the project. Further, all of the industry partners have their own internal and external networks, and the work has and will continue to influence the "on the ground" practices used to assess for static liquefaction susceptibility where it can be a potential contributor to a failure mode(s) at existing or planned TSFs.

Acknowledgements

This work forms part of TAILLIQ (Tailings Liquefaction), which is an Australian Research Council (ARC) Linkage Project supported by financial and in-kind contributions from Anglo American, BHP, Freeport-McMoRan Inc., Rio Tinto, and Teck. The TAILLIQ project is being carried out at the University of New South Wales, The University of South Australia, The University of Western Australia (lead university), and the University of Wollongong. The assistance and co-operation of all six sponsors in getting access to their sites, in providing personnel to assist with the work, earthmoving equipment to excavate sampling pits and load bulker bags, and to ensure samples are shipped back to the receiving laboratories, is gratefully acknowledged.

References

Carrier, W.D. 1991. Stability of tailings dams. *XV Ciclo di Conferenze di Geotecnica di Torino*, Italy.

Davies, M., E. Roberts and T. Martin. 2002. Static liquefaction of tailings – fundamentals and case histories. In: *Proceedings Tailings Dams 2002*. ASDSO/USCOLD, Las Vegas.

Dong Q, Xu ., Y. Cai, H. Juan, J. Wang, Z. Yang and C. Gu. 2015. Drained instability in loose granular material. *International Journal of Geomechanics*, 16(2): 04015043.

Fourie, A.B., G. Papageorgiou and G.E. Blight. 2001. Static liquefaction as a possible explanation for the Merriespruit tailings dam failure. *Canadian Geotechnical Journal*, 38(4): 707–719.

Jefferies, M.G. and K. Been 2105. *Soil Liquefaction – A Critical State Approach,* 2nd edition, Taylor and Francis.

Loret, B. and N. Khalili. 2002. An effective stress elastic-plastic model for unsaturated porous media. *Mechanics of Materials:* 97–116.

Pournaghiazar, M., A. Russell and N. Khalili. 2011. Development of a new calibration chamber for conducting cone penetration tests in unsaturated soils. *Canadian Geotechnical Journal* 48(2): 314–321.

Smith, E.S. 1969. Tailings disposal and liquefaction. *Transactions, Society of Mining Engineers* 244.

Proceedings of Tailings and Mine Waste 2019
November 17–20, 2019, Vancouver, Canada
Published by the University of British Columbia, 2019

Introducing a Runout Zone Classification for the Analysis of Tailings Flows

N. Ghahramani, University of British Columbia, Canada
S. McDougall, University of British Columbia, Canada
A. Mitchell, University of British Columbia, Canada
S.G. Evans, University of Waterloo, Canada
W. A. Take, Queen's University, Canada
V. Cuervo, BGC Engineering, Canada

Abstract

Tailings-flows result from the breach of tailings dams; they can travel over substantial distances and impact large areas, and have caused significant loss of life and environmental damage in recent history. For example, the 1985 fluorite tailings dam breach at Stava, Italy, resulted in the release of a total volume of 0.19 million m^3 of muddy debris, which travelled 4.2 km and inundated an area of approximately 0.44 million m^2. In the very recent 2019 tailings dam breach at Feijão mine, Brumadinho, Brazil, the tailings flow travelled almost 9 km and inundated an area of approximately 3 million m^2 before reaching the Paraopeba River. The ability to understand and predict the behaviour and extent of tailings flows is a crucial step in protecting elements at risk in downstream areas.

We established a runout zone classification method in order to delineate the inundation area. Our analysis applies to the zone defined by the extent of the main solid tailings deposit, which is characterized by visible or field-confirmed sedimentation, above typical bankfull levels if extending into downstream river channels. We independently estimated the planimetric inundation area for 27 tailings dam breaches using satellite imagery, aerial photographs, and plan view sketches. Our results indicate that the scaling relation, $A = cV^{2/3}$, derived in previous studies to characterize the mobility of other types of mass flows, also characterizes the relationship between tailings release volume (V) and planimetric inundation area (A). Our analysis suggests that, for a given volume, tailings flows are, on average, less mobile than lahars (c = 200), but more mobile than non-volcanic debris flows (c = 17–20) and rock avalanches (c = 12–20).

Introduction

Tailings dams are a critical piece of mining infrastructure (Blight, 2009). These dams retain mine tailings, a waste product of mineral processing operations that includes finely ground rock and process water. Some of these wastes may classify as hazardous material (Vick, 1990). When a tailings dam breach occurs, a destructive flow of mine tailings can develop (e.g., Macías et al., 2015). These flows may travel over substantial distances and impact large areas (Rico et al., 2008). The ability to understand and predict the behaviour of flowing tailings is a crucial step in protecting people, infrastructure and the environment from these events.

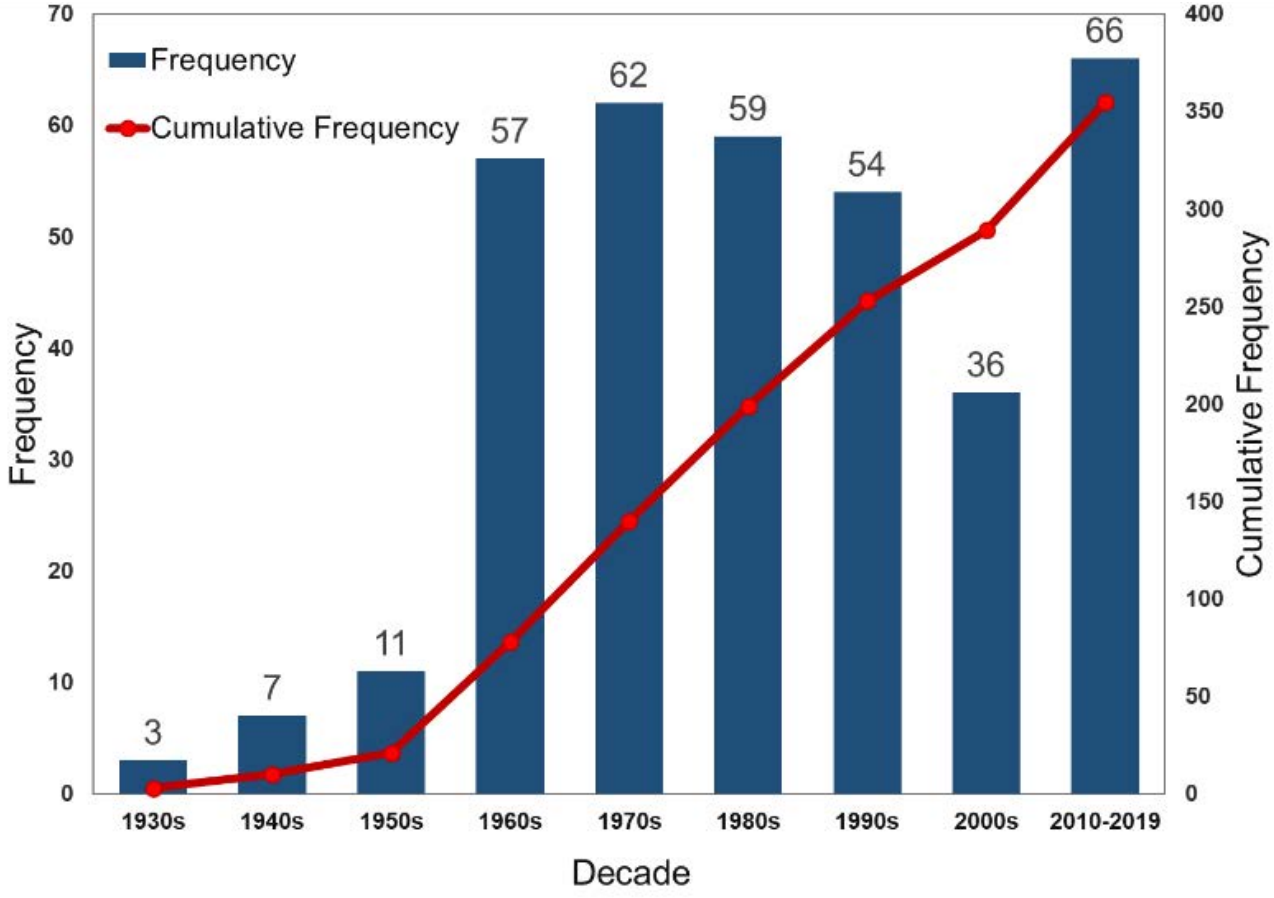

Figure 1: Frequency and cumulative frequency of tailings dam breaches worldwide between 1930 and 2019. (Data from ICOLD, 2001; WISE, 2019; Bowker, 2019)

More than 350 tailings dam breaches have been recorded worldwide since the early twentieth century (ICOLD, 2001; WISE, 2019; Bowker, 2019) (Figure 1). The records indicate that about one-third of the cases led to the loss of life and/or the release of more than 100,000 m^3 of tailings/water (Bowker, 2019). For example, in 1985, the failure of the fluorite tailings dam at Stava, Italy released a total volume of

185,000 m^3 of muddy debris. As a result, the villages of Stava and Tesero were destroyed and 243 people lost their lives (Chandler and Tosatti, 1996; Luino and De Graff, 2012; Pirulli et al., 2017). The 2015 Fundão tailings dam failure in Brazil resulted in the release of about 35 million m^3 of tailings materials. This event killed 19 people and caused long-lasting environmental damage to several water channels in the basin of the Doce River (Carmo et al., 2017; Hatje et al., 2017). More recently, in January 2019 another disastrous tailings dam breach occurred at the Feijão mine in Brumadinho, Brazil. Almost 12 million m^3 of tailings burst from the impoundment and the resulting tailings flow travelled for almost 9 km and inundated an area of approximately 3.0 million m^2 before reaching the Paraopeba River. At the time of writing, 243 people were reported killed and 27 were reported missing as a result of this failure (WISE, 2019).

Tailings dam breach runout analysis is the study of tailings flow behaviour. The term "tailings flow" refers to various forms of tailings outflow movement resulting from the breach of a tailings dam. This may include a partial or a total release of the stored tailings and associated water (Rico et al., 2008; Blight, 2009; Villavicencio et al., 2014). Tailings-flows exhibit different characteristics depending on various factors as listed by the Tailings Dam Breach Working Group (WG) of the Canadian Dam Association (CDA) Mining Dam Committee (e.g., sediment concentration, the presence of surface water, embankment configuration, failure mechanism, liquefaction potential, and downstream topography) (Small et al., 2017). As such, they can take various forms, ranging from a massive debris flood consisting of water and sediment, to a flowslide consisting of highly viscous slurry (Hungr et al., 2014). These flows can travel long distances at extremely rapid velocities (> 5 m/s) (Blight et al., 1981; Jeyapalan et al., 1983; Blight, 1997; Blight, 2009; Kossoff et al., 2014).

Runout modelling and inundation mapping of tailings dam breaches are essential steps for estimating the potential consequences of a tailings dam failure, determining appropriately stringent design criteria, and developing emergency response and preparedness plans (CDA, 2014; Knight Piésold, 2014; Martin et al., 2015). In recent years, there has been an increase in the study of the consequences of tailings dam breaches following several major disasters worldwide (Roche et al., 2017; Schoenberger, 2016). However, much engineering uncertainty still exists in this field. There are no standards for reporting data related to runout of tailings flows (e.g., runout distance). Furthermore, the number of available empirical-statistical runout models are very limited. Finally, most of the commonly used numerical models were developed primarily for either clear water flood analysis (e.g., Danish Hydraulic Institute [DHI], 2007; Brunner, 2016) or the analysis of flow-like landslides (e.g., Pastor et al., 2002; McDougall and Hungr, 2004; McDougall, 2017; Pirulli et al., 2017) and do not necessarily account for the compositional variety of tailings and its potential influence on the downstream flow behaviour (Pirulli et al., 2017; Martin et al., 2015). Due to these limitations, hazard maps delimiting potential inundation areas based on current techniques may not

adequately characterize the extent and intensity (e.g., flow depth and velocity) of possible tailings dam breach scenarios.

This paper:

1. introduces a runout zone classification method in an attempt to develop consistency in reporting runout distances and inundation areas of tailings flows; and
2. investigates the adaptability of a semi-physical area-volume relationship for tailings flow cases to help characterize the mobility and potential impacts of these type of failures.

Previous work

In a highly-cited paper, Rico et al. (2008) proposed a set of empirical correlations that relate tailings flow characteristics (e.g., released volume and runout distance) to the geometric characteristics of tailings dams (e.g., dam height and total impoundment volume). A database of 28 tailings dam breaches (from 1965 to 2000) containing information on the released volume and runout distance was used in their study. Rico et al. (2008) found positive correlations between i) the total volume of the tailings in the impoundment at the time of failure and the tailings released volume, and ii) the tailings released volume and the tailings runout distance. A parameter referred to as "dam factor" (the product of the dam height and tailings outflow volume, $H \times V_F$) was used to explore the correlations in their study.

The WG of the CDA Mining Dam Committee compiled a tailings dam breach database that includes the 28 cases presented by Rico et al. (2008), plus 51 additional cases (Small et al., 2017). Their study discussed the limited information provided in the Rico et al. (2008) database and listed additional factors that could influence the flow behaviour of tailings. The WG proposed a classification matrix based on two main factors: 1) the presence of free water in the area of the breach, and 2) tailings liquefaction potential. The empirical relationships of Rico et al. (2008) were re-examined based on the proposed classification (Small et al., 2017).

Larrauri and Lall (2018) updated the database presented in Rico et al. (2008) and re-examined their empirical correlations. They added a new element (V_F / V_T) to the dam factor parameter, called H_f ($H_f = H \times (V_F / V_T) \times V_F$), where V_T is the total volume of the tailings impoundment. Using the updated database, they concluded that the relationship between H_f and runout distance has a stronger correlation ($R^2 = 0.53$) than the relationship between dam factor and runout distance ($R^2 = 0.44$) (Larrauri and Lall, 2018). However, the physical basis of the H_f factor was not discussed in their study. Rico et al. (2008) and Larrauri and Lall (2018) noted that uncertainties in their database suggest that the results need to be treated with caution.

Several authors have investigated the relationship between inundation area (A) and flow volume (V) for different types of flow-type landslides (e.g., Hungr, 1981; Davies, 1982; Li, 1983; Hungr and Evans, 1993; Golder Associates Ltd., 1995; Iverson et al., 1998; Berti and Simoni, 2007; Griswold and Iverson, 2008; Delaney and Evans, 2014). Li (1983) presented an empirical relationship between rock avalanche deposit area and volume for 76 major European rock avalanches. The deposit area and volume were logarithmically transformed to apply a linear least-squares regression analysis (Li, 1983). Hungr and Evans (1993) applied a similar methodology to a different dataset of rock avalanches. However, they made an assumption that the deposits at various scales retain a similar geometry, which resulted in the following scaling relation for the area-volume relationship:

$$A = cV^{2/3} \tag{1}$$

where A is the inundation area, V is the total flow volume and c is a constant related to flow mobility.

Methodology

Data compilation

Tailings dam breaches have been recorded since the beginning of the twentieth century (ICOLD, 2001; Bowker, 2019). Several compilations and summaries of the characteristics of significant tailings dam breaches can be found in the literature (ICOLD, 2001; Rico et al., 2008; Small et al., 2017; WISE, 2019; Bowker, 2019). These summaries contain key information about the events, such as dates, causes and triggers of failure, dam heights and construction methods, and the volumes of released and retained tailings. However, most of them lack key data related to runout, including information related to some factors that may better characterize the tailings flows. In this study, a new database currently containing 27 tailings dam breaches was compiled. Data sources included existing literature on individual tailings dam breach events, existing databases, and remote sensing data obtained from satellite or aerial photograph images.

The new database contains 27 new, independently estimated measurements of runout distance and planimetric inundation area for each case. We classified the inundation areas into two zones (Figure 2). Zone 1 is the primary impact zone, defined as the extent of the main solid tailings deposit, which is characterized by remotely visible or field-confirmed sedimentation, above typical bankfull elevations if extending into downstream river channels. Zone 2 is the secondary impact zone, defined as the area downstream of Zone 1 that is further impacted by the tailings flow in some form. Such secondary impacts may include flood or displacement wave impacts (i.e., fluid impacts above typical downstream water levels) and sediment plume impacts (i.e., below typical downstream water levels).

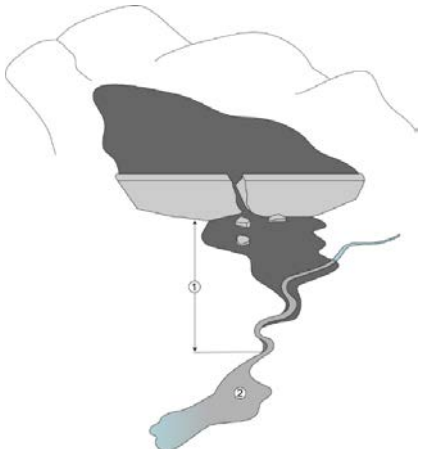

Figure 2: An idealized representation of a tailings flow showing the two runout zones proposed in this paper

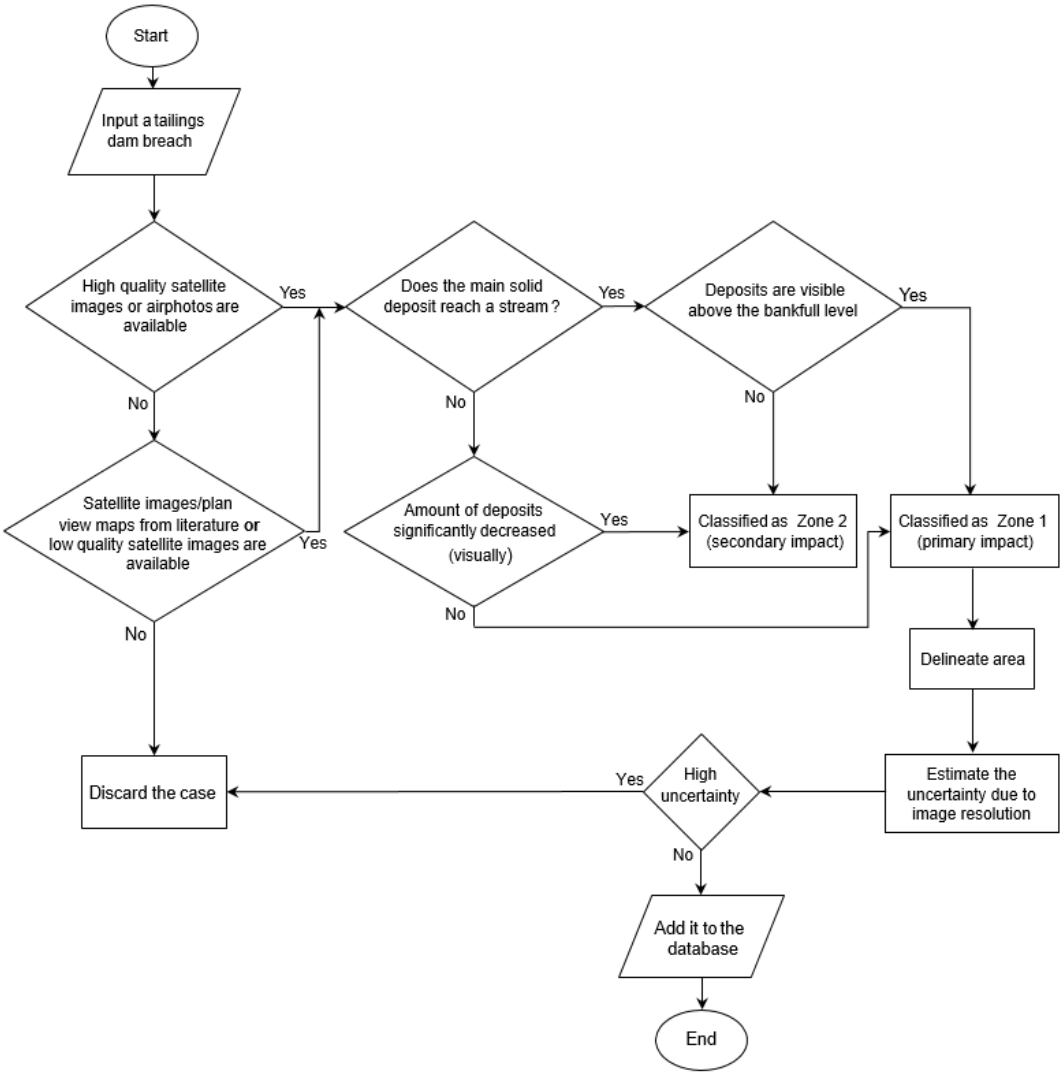

Figure 3: Schematic representation of the methodology applied to obtain data for tailings flows inundation area

Figure 3 shows a flowchart that summarizes the entire data compilation process, including the screening of data sources, the impact zone classification, the delineation of Zone 1, and the estimation of uncertainty due to image resolution. Figure 4 shows the extent of Zones 1 and 2 for the January 25, 2019 tailings dam breach at the Feijão mine, Brumadinho, Brazil.

Using satellite images from January 29, 2019, the red-dashed polygon in Figure 4 defines the primary impact zone (Zone 1). There is no visible sedimentation above the bankfull level of Paraopeba River (blue dashed-line in Figure 4), therefore, the extent of the flow along the river is considered as the secondary impact zone (Zone 2), in which the materials travelled for more than 100 km.

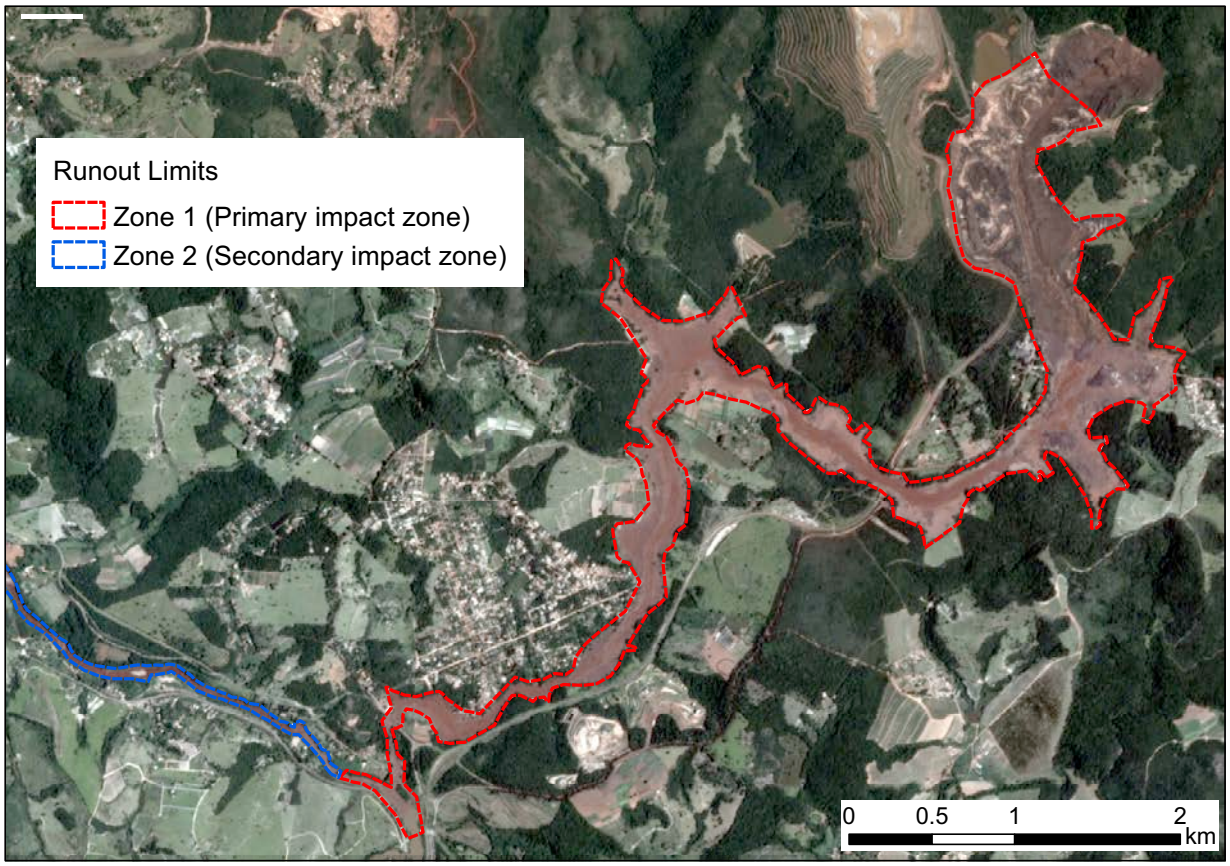

Figure 4: Aerial view of the tailings dam breach at the Feijão mine near Brumadinho, Brazil, January 25, 2019. Zone 1 is shown in the red dashed polygon. The portion of Zone 2 that is visible in this image is shown in the blue dashed polygon. Image courtesy of Planet Labs, Inc. (January 29, 2019)

The extent of Zone 2 is typically more challenging to estimate than the extent of Zone 1, due to the variability of downstream flow mixing conditions, the relatively transient nature of secondary impacts, and the inherent limitations (e.g., image resolution) of remote detection methods. Zone 2 is also arguably less

important to characterize than Zone 1 from a human safety standpoint; most fatalities occur within short distances of the tailings dam breach. The focus of this study was therefore on Zone 1.

Compared with the hundreds of tailings dam breach cases listed in previous databases, the relatively limited number of cases (27) in our new database reflects the limited availability of suitable imagery. We used a simple approach to quantitatively estimate the uncertainty due to image resolution limitations in our area measurements based on the pixel sizes of the images. The maximum uncertainty due to image resolution limitations was considered to be equal to the total area of the pixels intersected by the perimeter of Zone 1.

Additional attributes to characterize factors that may affect mobility are included in our database. We classified our cases using the CDA criteria (i.e., the presence of a water pond near the dam crest and the liquefaction potential) (Small et al., 2017). To classify the confinement of the travel path, we used the following two categories proposed by Golder Associates Ltd. (1995):

1. confined, in which the flow path is constrained by relatively steep side slopes of a gully or valley; and
2. unconfined, in which the flow path is on an open slope or relatively flat surface and the topography permits spreading of the tailings flow from an early stage.

Similarly, to classify the tailings type, we used the following two categories proposed by Small et al. (2017):

1. hard rock mine tailings, which includes lead-zinc, copper, gold-silver, molybdenum, nickel from sulphide deposits, and uranium; and
2. soft rock mine tailings, which includes coal, potash, fluorite, gypsum, and aluminium (Vick, 1990; Bussière, 2007; Small et al., 2017).

The dam height and released volume data were collected from existing databases or publications. We also included the volume of released water in our database, if available. However, for the empirical analysis, only the reported released tailings volume is considered. We note that there is no information on how the reported released volumes within the existing databases were obtained (including the distinction between the volume of released solid tailings, water, and the interstitial fluid).

Volume-dependency of Zone 1 inundation area

In this study, the scaling relationship shown in Equation 1 was applied to our database to relate the estimated Zone 1 inundation area to the reported released volume. We transformed the data into a log-log scale and applied the standard least-squares linear regression method with a specified slope of 2/3.

Results and discussion

Figure 5 shows the area-volume scatter plot for tailings flows (n = 27), alongside previously published data for lahars (n = 27), non-volcanic debris flows (n = 44), rock avalanches (n = 142), and flowslides resulting from the failure of mine waste dumps (n = 22). The tailings data points clearly show a positive linear correlation similar to the other data, although the scatter is relatively high, especially at higher volumes. The area-volume data for tailings flows also show considerable overlap with that of other flow processes, corresponding with the upper volume range for non-volcanic debris flows, and the lower to middle volume ranges for lahars and rock avalanches.

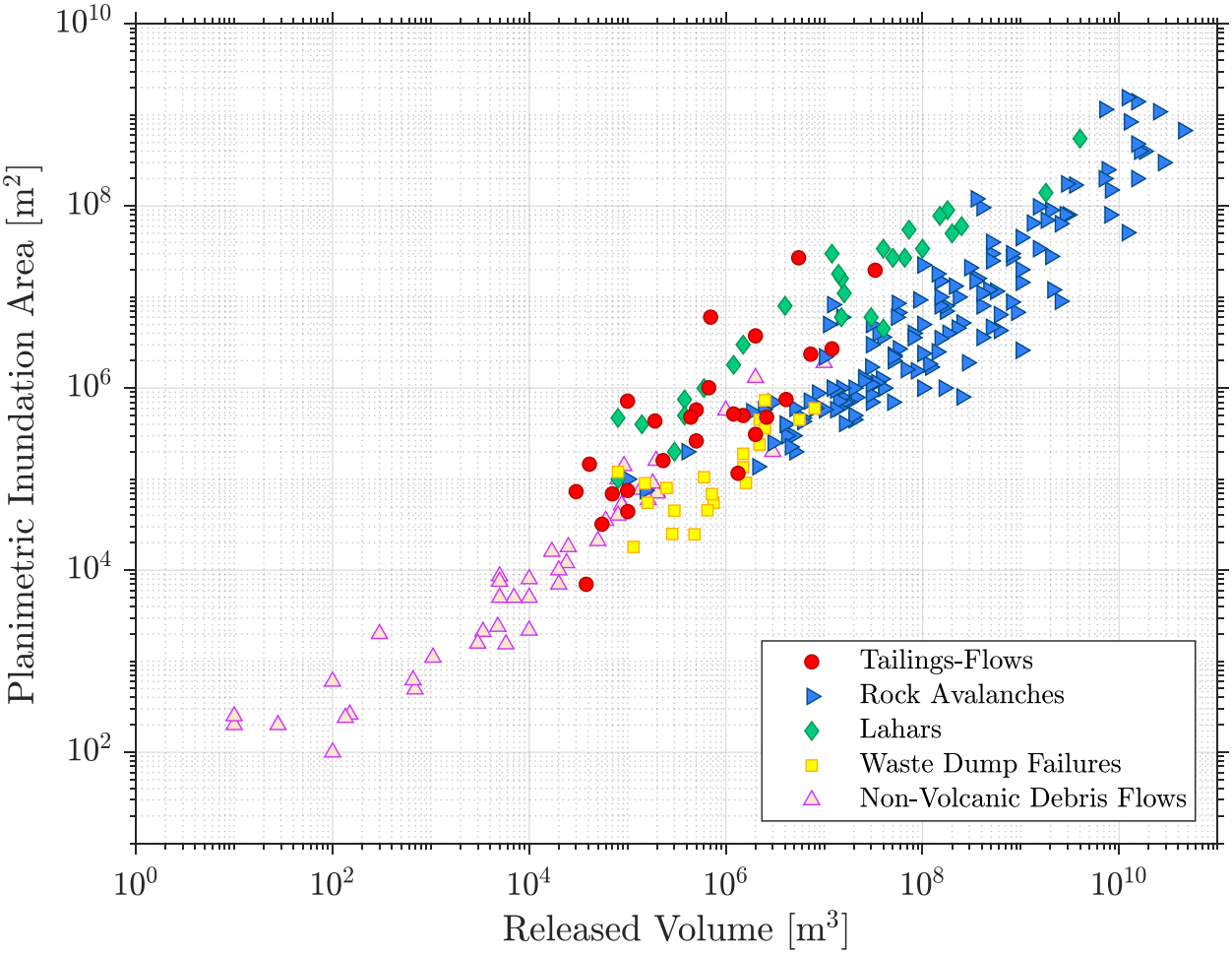

Figure 5: Comparison of the runout inundation area as a function of flow volume for tailings flows (red symbols; n = 27), waste dump failures (yellow symbols; n = 22), lahars (green symbols; n = 27), non-volcanic debris flows (pink symbols; n = 44) and rock avalanches (blue symbols; n = 142)

The differences between the *c* coefficient of Equation 1 indicate the relative mobility of the various flow processes, on average (Jakob, 2005; Griswold and Iverson, 2008; Berti and Simoni, 2007). A

comparison of published *c* coefficients for different types of flow processes is shown in Table 1. Our results suggest that, for a given volume, on average, tailings flows are less mobile than lahars but more mobile than mine waste dump failures, non-volcanic debris flows and rock avalanches of comparable volume.

A preliminary analysis of the residuals from the regression grouped by tailings type and flow path confinement indicates that these factors have an effect on the mobility of the tailings flows. For example, soft rock mine tailings tend to have greater mobility than hard rock mine tailings, and confined flow paths tend to enhance mobility relative to unconfined paths, but the uncertainty around the mobility of confined flow paths tends to be higher.

Table 1: Comparison of the c Coefficients in Equation 1 for different mass flow processes

Process Type	c Coefficient of Eq. 1	Source
Rock avalanches	12	(Hungr and Evans, 1993)
Rock avalanches	20	(Griswold and Iverson, 2008)
Debris flows	17	(Berti and Simoni, 2007)
Debris flows	20	(Griswold and Iverson, 2008)
Lahars	200	(Iverson et al., 1998)

Unlike natural hazards, tailings dams are human-made structures with significant impoundment volumes (ranging from 10^4 to 10^8 m^3) that increase over the course of mine operation. When a dam breach occurs, a portion or the entirety of the impounded material discharges. The empirical study by Rico et al. (2008) showed that, on average, 35% of the material is released during a failure. Nevertheless, the maximum volume that can be released in an extreme scenario equals the impoundment volume. Compared with some types of flow-like landslides, the source volume of a tailings dam breach is relatively well-constrained. The uncertainty associated with this input parameter can therefore be accounted for explicitly when using Equation 1 to make runout predictions.

Conclusion

Our empirical investigation of historical tailings dam breaches provides new insights into tailings flow processes and characteristics, and introduces new relationships that can potentially be used for risk analysis. In this study we established a data compilation methodology and introduced a runout zone classification system to reduce the uncertainties associated with previously reported data. Using our proposed methodology, we compiled a database of 27 tailings dam breach case studies. The degree of flow mobility of tailings flows was investigated using a well-established semi-physical area-volume relationship, and the

result was compared with other mass flow processes. Our analysis suggests that the relationship $A = cV^{2/3}$ is also valid for tailings flows, and that for a given volume, tailings flows are, on average, less mobile than lahars but more mobile than mine waste dump failures, non-volcanic debris flows, and rock avalanches. This paper is part of an ongoing project. We are currently building the database and investigating the effects of other attributes of the tailings and downstream topography, which could potentially be used to refine the area-volume empirical-statistical relationship.

Acknowledgements

This work was partly funded by a Fellowship from the University of British Columbia Department of Earth, Ocean and Atmospheric Sciences, as well as Discovery Grants from the Natural Sciences and Engineering Research Council of Canada. Special thanks are extended to the following five industrial partners who contributed funding and technical input to this work as part of the NSERC-supported CanBreach (Canadian Tailings Dam Breach Research) Project: Imperial Oil Resources Inc., Suncor Energy Inc., BGC Engineering Inc., Klohn Crippen Berger, and Golder Associates Ltd. NG also thanks Sophia Zubrycky for her help with the graphic design of Figure 2.

References

Berti, M. and A. Simoni. 2007. Prediction of debris flow inundation areas using empirical mobility relationships. *Geomorphology* 90(1–2): 144–61.

Blight, G.E. 1997. Destructive mudflows as a consequence of tailings dyke failures. *Proceedings of the Institution of Civil Engineers-Geotechnical Engineering* 125(1): 9–18.

Blight, G.E. 2009. *Geotechnical Engineering for Mine Waste Storage Facilities.* CRC Press.

Blight, G.E., M.J. Robinson and J.A.C. Diering. 1981. Flow of slurry from a breached tailings dam. *International Journal of Rock Mechanics and Mining Sciences & Geomechanics Abstracts* 18(5). Pergamon.

Bowker, L.N. 2019. World mine tailings failures (WMTF). Accessed July 10.

Brunner, G. 2016. *HEC-RAS River Analysis System – Hydraulic Reference Manual,* Version 5.0. Hydrologic Engineering Centre (HEC), US Army Corps of Engineers.

Bussière, B. 2007. Colloquium 2004: Hydrogeotechnical properties of hard rock tailings from metal mines and emerging geoenvironmental disposal approaches. *Canadian Geotechnical Journal* 44(9): 1019–52.

Canadian Dam Association (CDA). 2014. Technical bulletin: Application of dam safety guidelines to mining dams.

Carmo, F.F.D., L.H.Y. Kamino, R.T. Junior, I.C. de Campos, F.F. do Carmo, G. Silvino, K.J. da S.X. de Castro, et al. 2017. Fundão tailings dam failures: The environment tragedy of the largest technological disaster of Brazilian mining in global context. *Perspectives in Ecology and Conservation* 15(3): 145–51.

Chandler, R.J., and G. Tosatti. 1996. The Stava tailings dams failure, Italy, July 1985. *International Journal of Rock Mechanics and Mining Sciences and Geomechanics Abstracts* 33(1): A35.

Danish Hydraulic Institute (DHI). 2007. *MIKE Flood User Manual*. Copenhagen.

Davies, T.R.H. 1982. Spreading of rock avalanche debris by mechanical fluidization. Rock Mechanics Felsmechanik Mécanique Des Roches.

Delaney, K.B., and S.G. Evans. 2014. The 1997 Mount Munday landslide (British Columbia) and the behaviour of rock avalanches on glacier surfaces 11: 1019–36.

Golder Associates Ltd. 1995. Mined rock and overburden piles: Runout characteristics of debris from dump failures in mountainous terrain: Stage 2 : Analysis.

Griswold, J.P., and R.M. Iverson. 2008. Mobility statistics and automated hazard mapping for debris flows and rock avalanches scientific investigations report 2007 – 5276. USGS Scientific Investigations Report.

Hatje, V., R.M.A. Pedreira, C.E. De Rezende, C.A.F. Schettini, G.C. De Souza, D.C. Marin, and P.C. Hackspacher. 2017. The environmental impacts of one of the largest tailing dam failures worldwide. Scientific Reports 7 (1): 1–13.

Hungr, O., S. Leroueil, and L. Picarelli. 2014. The Varnes classification of landslide types, an update. Landslides 11 (2): 167–94.

Hungr, O. 1981. Dynamics of rock avalanches and other types of slope movements. University of Alberta, Edmonton.

Hungr, O., and S.G. Evans. 1993. The failure behaviour of large rockslides in mountainous regions. Geological Survey of Canada (Open File 2598).

International Commission on Large Dams (ICOLD). 2001. Tailings dams – risk of dangerous occurrences – lessons learnt from past experiences. Bulletin No. 121.

Iverson, R.M., S.P. Schilling, and J.W. Vallance. 1998. Objective delineation of Lahar-inundation hazard zones. *Geological Society of America Bulletin* 110 (8): 972–84.

Jakob, M. 2005. Debris-flow hazard analysis. In *Debris-Flow Hazards and Related Phenomena,* edited by Oldrich Jakob and Matthias Hungr, 411–43. Chichester: Springer Praxis.

Jeyapalan, J.K., H.B. Seed and J.M. Duncan. 1983. Investigation of flow failures of tailings dams. *Journal of Geotechnical Engineering* 109(2): 172–89.

Knight Piésold. 2014. Dam breach analyses and inundation studies for the Afton tailings storage facility.

Kossoff, D., W.E. Dubbin, M. Alfredsson, S.J. Edwards, M.G. Macklin and K.A. Hudson-Edwards. 2014. Mine tailings dams: Characteristics, failure, environmental impacts, and remediation. *Applied Geochemistry* 51 (December): 229–45.

Larrauri, P.C. and U. Lall. 2018. Tailings dams failures: Updated statistical model for discharge volume and runout. *Environments* 5(2): 28.

Li, T. 1983. A mathematical model for predicting the extent of a major rockfall. *Z. Geomorph. N.F* 27(4): 437–482.

Luino, F. and J.V. De Graff. 2012. The Stava mudflow of 19 July 1985 (northern Italy): A disaster that effective regulation might have prevented. *Natural Hazards and Earth System Science* 12(4): 1029–44.

Macías, J.L., P. Corona-Chávez, J.M. Sanchéz-Núñez, M. Martínez-Medina, V.H. Garduño-Monroy, L. Capra, F. García-Tenorio and G. Cisneros-Máximo. 2015. The 27 May 1937 catastrophic flow failure of gold tailings at Tlalpujahua, Michoacán, Mexico. *Natural Hazards and Earth System Sc*iences 15(5): 1069–85.

Martin, V., D. Fontaine and J. Cathcart. 2015. Challenges with conducting tailings dam breach assessments. In *Proceedings of Tailings and Mine Waste 2015*, 314–28. Vancouver, BC: University of British Columbia, Vancouver, Canada.

McDougall, S. 2017. 2014 Canadian Geotechnical Colloquium: Landslide runout analysis – Current practice and challenges. *Canadian Geotechnical Journal* 54(5): 605–20.

McDougall, S. and O. Hungr. 2004. A model for the analysis of rapid landslide motion across three-dimensional terrain. *Canadian Geotechnical Journal* 41(6): 1084–97.

Pastor, M., M. Quecedo, J.A.F. Merodo, M.I. Herrores, E. Gonzalez and P. Mira. 2002. Modelling tailings dams and mine waste dumps failures. *Geotechnique* 52(8): 579–91.

Pirulli, M., M. Barbero, M. Marchelli and C. Scavia. 2017. The failure of the Stava Valley tailings dams (northern Italy): Numerical analysis of the flow dynamics and rheological properties. *Geoenvironmental Disasters* 4(1): 1–15.

Rico, M., G. Benito, and A. Díez-Herrero. 2008. Floods from tailings dam failures. *Journal of Hazardous Materials* 154(1–3): 79–87.

Roche, C., K. Thygesen and E. Baker, eds. 2017. Mine Tailings Storage: Safety is No Accident. A UNEP Rapid Response Assessment. United Nations Environment Programme and GRID-Arendal, Nairobi and Arendal.

Schoenberger, E. 2016. Environmentally sustainable mining: The case of tailings storage facilities. *Resources Policy* 49: 119–28.

Small, A., M. James and M. Al-mamun. 2017. Advancing the state of practice for tailings dam breach assessment using empirical correlations. In Kelowna, BC, Canada: Canadian Dam Association, CDA 2017 Annual Conference.

Vick, S.G. 1990. *Planning, Design and Analysis of Tailings Dams.* Vancouver, BC: BiTech Publishers Ltd.

Villavicencio, G., R. Espinace, J. Palma, A. Fourie and P. Valenzuela. 2014. Failures of sand tailings dams in a highly seismic country. *Canadian Geotechnical Journal* 51(4): 449–64.

WISE. 2019. *Chronology of major tailings dam failures,* World Information Service on Energy.

Proceedings of Tailings and Mine Waste 2019
November 17–20, 2019, Vancouver, Canada
Published by the University of British Columbia, 2019

Micrometer-Scale Characterization of Solid Mine Waste Aids in Closure Due Diligence

Bryn E. Kimball, INTERA Incorporated, USA
Heather E. Jamieson, Queen's University, Canada
Robert R. Seal II, US Geological Survey, USA
Agatha Dobosz, Queen's University, Canada
Nadine M. Piatak, US Geological Survey, USA

Abstract

Precious- and base-metal mining often occurs in deposits with high acid-generating potential, resulting in mine waste that contains metals in forms of varying bioavailability, and therefore toxicity. The solids that host these metals are often noncrystalline, nanometer to micrometer in size, or undetectable by readily available analytical techniques (e.g., X-ray diffraction). This analytical shortcoming can pose a challenge when attempting to characterize sources and natural attenuation of metals at a given site, which is a best practice to satisfy closure due diligence. Numerous case studies have shown that efforts to characterize mine waste at multiple scales, particularly the micrometer scale, often lead to a better understanding of metal distribution and potential contamination risks.

This paper presents a case study that compares the use of both traditional and non-traditional techniques to identify and quantify metal hosts in sediments downstream of the abandoned mine waste piles at the Ely Copper Mine Superfund site in Vermont (USA). The contaminant present in the highest concentration in the sediments is copper, yet not all copper-bearing solids were detected with bulk X-ray diffraction (XRD). At the micrometer scale, a combination of synchrotron-based X-ray absorption spectroscopy (XAS) and an automated mineralogy (AM) system were used to identify the most abundant copper-bearing solids. Bulk XAS and AM also provided semi-quantitative abundances of these solids in the sediment.

At the Ely Copper Mine, copper in stream sediments was found to be predominantly hosted in sulphide minerals downstream of a major mine waste pile, whereas upstream copper was predominantly hosted in secondary iron and manganese (oxyhydr)oxides. These copper-bearing hosts were consistent with the expected bioavailability of copper in the sediments based on laboratory toxicity tests with aquatic organisms. When the bulk of copper was present in sulphides, aquatic organisms experienced greater

survival than when copper was mostly associated with secondary iron and manganese (oxyhydr)oxides. The information gained from probing the sediments at multiple scales can now be used to prioritize containment and remediation strategies.

While synchrotron-based analytical techniques have proven to be invaluable in many studies of mine waste, access to these techniques is limited. In contrast, access to a scanning electron microscope that can perform AM is becoming more common, primarily for the application in mining design and mineral processing operations. More recently, the successful use of AM to characterize mine waste suggests that this technique can be equally as valuable for mine closure plans. The resolution of information obtained may go beyond what is required from a regulatory perspective, but given that the results have the potential to be more conclusive than many traditional techniques, this level of characterization may save time and money in the long run.

Introduction

This paper presents a case study of mine waste characterization at the abandoned Ely Copper Mine in the Vermont Copper Belt (USA), now a USA Environmental Protection Agency Superfund site. Copper ore deposits in the area are stratabound within metasedimentary rocks (Howard, 1959); the sulphides are mostly massive and consist of pyrrhotite, chalcopyrite, sphalerite and pyrite (Slack et al., 1993). Gangue minerals are predominantly quartz, plagioclase, and muscovite, with minor calcite, tourmaline, and rutile (Slack et al., 1993). Copper was produced at this mine intermittently from 1820 to 1903 (Slack et al., 1993). Most of the ore was sorted by hand, crushed mechanically, roasted, and smelted (Kierstead, 2001). Further details on the historical mining, regional climate, and local surface water can be found elsewhere (Kimball et al., 2016, Seal et al., 2010). Copper sulphide minerals can now be found in solid mine waste piles (Piatak et al., 2004) and downstream sediments in Ely Brook (Kimball et al., 2016). Sediments in Ely Brook upstream of a major mine waste pile (Figure 1) contain fewer sulphides, and copper-bearing solid species are mostly secondary (e.g., copper sorbed to goethite). The latter are expected to be more mobile (Kimball et al., 2016) and are documented to be more toxic to aquatic organisms (Seal et al., 2010). The distribution of copper-bearing solid species in Ely Brook sediments has been quantified on a total copper basis (Kimball et al., 2016), but the solid-phase speciation of copper in the contaminated sediments as a whole is more challenging to quantify.

Traditional methods of identifying metal-bearing solids in soils and sediments have included examination of thin sections by petrographic microscopy, scanning electron microscopy (SEM), and electron probe microanalysis (EPMA). More recently, identification of hosts by synchrotron-based microanalysis (including X-ray absorption spectroscopy [XAS] and X-ray diffractometry [XRD]) has also been useful in characterizing metal-bearing particles by oxidation state, molecular structure, and

crystallinity (e.g., Hayes et al., 2012; Radkova et al., 2017). These grain-scale techniques are useful in identifying trace metal hosts, but do not provide reliable quantitative information about the abundance of these hosts when applied at the micrometer scale.

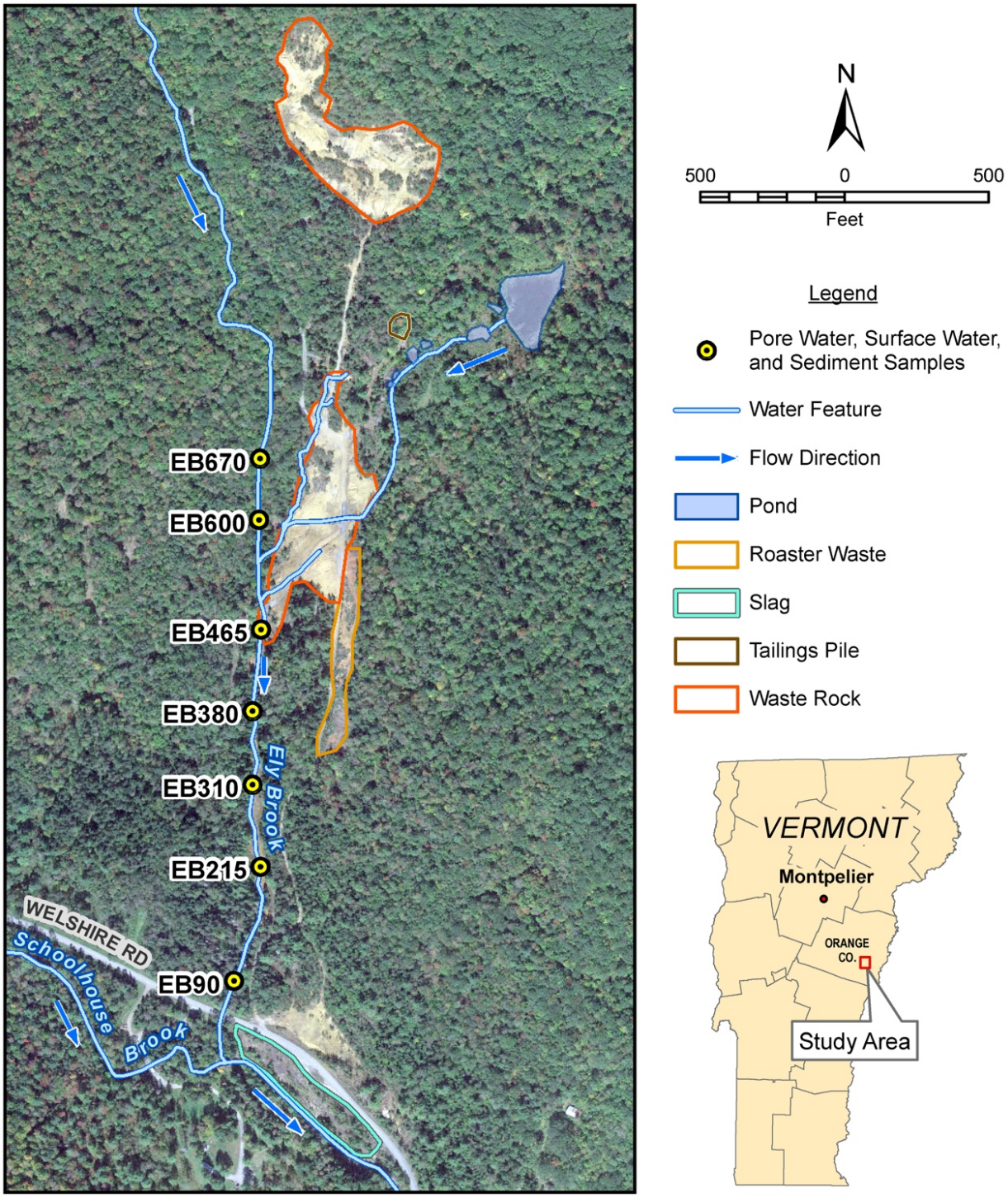

Figure 1: Sample location map for stream sediment samples of Ely Brook, a mining-impacted stream draining the abandoned Ely Copper Mine

Improved quantitative estimates of the abundance of trace metal hosts tend to include bulk techniques, such as sequential extractions (e.g., Dold, 2003b) and quantitative XRD (e.g., Dold, 2003a). Sequential extractions may target solid hosts to the level of mineral group (e.g., oxides, clays), but are operationally defined and otherwise nonspecific unless combined with other techniques. Quantitative XRD based on Rietveld refinement of bulk powder patterns has improved estimates of modal mineralogy (Mumme et al., 1996), but this technique does not accurately detect solids present below a few wt. % (Martin et al., 2012; Ryan et al., 2008). Furthermore, although quantitative XRD can be used to quantify the abundance of amorphous material in powdered samples (De La Torre et al., 2001), it does not provide chemical information about amorphous solids. Given these limitations, a technique that can both identify and quantify crystalline and amorphous material would be ideal.

Automated mineralogy is a technique that is based on SEM analysis of solids, and it has been increasingly applied in the mining industry to improve ore processing. Recently, this technique has also been used to characterize mine waste (e.g., Brough et al., 2017; Hudson-Edwards et al., 2019; Parbhakar-Fox et al., 2017). The most common SEM-software packages are MLA (Mineral Liberation Analysis) and QEMSCAN (Quantitative Evaluation of Minerals by SCANing electron microscopy). Details of the technique have been described previously (Fandrich et al., 2007; Gottlieb et al., 2000). The results include a backscattered electron (BSE) image of a region of interest, along with thousands of energy dispersive X-ray spectra (EDS) for points collected in the same region of interest. Minerals are classified based on distinct BSE intensities and an associated EDS spectrum, which is assigned to a matching spectrum in a reference mineral database. If the sample contains grains with unique EDS spectra, these unique spectra can be added to the reference mineral database. Because the method does not rely on crystal structure, both crystalline and amorphous solids can be characterized. Solids with similar EDS spectra are differentiated by distinct BSE intensities, whereas solids with similar EDS spectra and BSE values can be differentiated by element ratios (Gottlieb et al., 2000). When applied over an entire thin section, thousands of particles can be analyzed, and the generated data include chemical composition, modal mineralogy, grain size, liberation potential, and textural relationships.

Expanding upon previous analysis of the contaminated Ely Brook sediments described above, the purpose of this study was to identify and quantify the abundance of copper-bearing solids in the sediments, and to compare the abundance of these solids obtained from AM to other types of bulk and grain-scale analyses. Automated mineralogy offers an opportunity to identify solid metal hosts at the grain scale, and quantify these hosts at the bulk scale, thereby providing a better understanding of metal distribution and potential contamination risks. This study was motivated by the common difficulty in fully characterizing solid hosts of potentially toxic trace elements in mining environments, where trace elements often occur in

forms of varying bioavailability, and therefore toxicity. Efforts to characterize mine waste at multiple scales, using a technique such as AM, is a best practice to satisfy closure due diligence.

Methodology

Mine impacted stream sediment samples discussed in this study were collected in October 2009 following protocols described by Seal et al. (2010). Characteristics of the sediments and coexisting stream and pore water can be found in previous publications (Kimball et al., 2016; Seal et al., 2010). In this study we focused on seven sampling locations along Ely Brook. In the results and discussion that follow, the two sites located upstream (EB670 and EB600) and five sites located downstream (EB465, EB380, EB310, EB215, and EB90) of a major mine waste input into Ely Brook (Figure 1) are referred to as "upstream" and "downstream" samples, respectively.

Streambed samples were composites of the upper 10 cm of sediment collected from 5 to 10 subsamples located across the stream channel. Sediments were air dried, then sieved to < 2 mm. Samples for bulk-XRD were micronized for 3 minutes then back-loaded onto sample holders. Samples for optical and scanning electron microscopy were prepared as grain-mounted thin sections (30 μm thick) attached to quartz slides.

Bulk-XRD was carried out on an X'Pert Pro (PANalytical) diffractometer with Cu Kα and Co Kα radiation over the 2θ range of 3 to 80 degrees. Bulk-XRD patterns were analyzed with X'Pert HighScore Plus software combined with the Inorganic Crystal Structure Database and the Crystallography Open Database. To determine modal mineralogy from bulk-XRD results, Rietveld refinement was conducted by iteratively refining background, unit cell parameters, and peak parameters until the goodness of fit and weighted R indices could no longer be minimized. Estimates of the amorphous content was accomplished following the bulk-XRD method outlined by De La Torre et al. (2001).

Carbon-coated grain mounts were analyzed on a FEI MLA Quanta 650. Automated mineralogy analysis was based on numerous BSE and EDS points collected for each grain. These data were analyzed using MLA software. Inevitably, some BSE-EDS data will not match common rock-forming minerals in the mineral database, so the user must make an effort to identify the unknown solids. This can be accomplished with manual SEM-EDS, EPMA, or grain-scale XAS and/or XRD. Unknown grains that could not be identified with additional SEM-EDS analysis in this study were analyzed with EPMA using a JEOL JXA-8230. As unknowns are being identified, the user defines them in the reference mineral database. The goal is to reduce the number of unknowns as much as possible, and in the end, each project will have its own database of identified solids.

Results and discussion

Modal mineralogy based on XRD and Rietveld refinement (Figure 2) revealed that all stream sediment samples contained quartz (Qtz), albite (Ab), hornblende (Hbl), muscovite (Ms), and quantifiable amorphous material in upstream samples EB670 (13 wt. %) and EB600 (6 wt. %). Less abundant minerals detected in all samples included chlorite (Chl), garnet (Grt), goethite (Gt), jarosite (Jr), and chalcopyrite (Cpy, Figure 2). The values for some of these less abundant minerals are likely at or below the practical quantitation limit of XRD. Modal mineralogy from AM yielded abundances for the same nine minerals detected with XRD (Figure 2), plus at least 17 additional solids. These additional solids together made up 10 – 14 wt. % of the sediment samples. Of the additional solids detected by AM, the more abundant constituents included stilpnomelane (2 – 4 wt. %), orthoclase (1 – 4 wt. %), kyanite (0 – 2 wt. %), and ilmenite (0.5 – 1 wt. %). Two thin sections of sample EB600 were prepared and analyzed by AM. These duplicates (EB600 and EB600b in Figure 2) tested heterogeneity in the sample and reproducibility in the analysis. The mineral abundances determined to be greater than 0.1 wt. % were reproducible within 10% for quartz, albite, goethite, jarosite, stilpnomelane, orthoclase, ilmenite, and anorthite. Minerals determined to be less abundant showed poorer reproducibility.

Values for modal mineralogy in Ely Brook stream sediments based on XRD and AM rarely overlapped for each sample, but relative changes in mineral abundances were generally consistent between the two types of analyses (Figure 2). Quartz, albite, and muscovite abundances were relatively consistent from upstream to downstream, and XRD abundances were always higher than AM abundances for these minerals. Hornblende abundances based on XRD were also higher than those based on AM, and both analyses showed a sharp decrease between upstream sample EB600 and downstream sample EB465. Garnet, goethite, and jarosite abundances were generally greater with AM compared to XRD, and the changing trends in abundances were strikingly similar between the two analyses. Abundances of chlorite and chalcopyrite were relatively variable based on both types of analyses, apart from a clear decreasing trend from upstream to downstream for chlorite based on AM.

The disparity between XRD and AM modal mineralogy results was greater for the less abundant minerals, particularly chlorite and goethite. Variability in chlorite abundances from XRD analysis can be expected given the potential for preferred orientation of this sheet silicate. Greater variability in goethite abundances may also be expected given the common occurrence of goethite as a precipitate from solution that may form rims around other grains. This distribution of goethite may create challenges for both XRD and AM analysis. Furthermore, AM may have assigned poorly crystalline iron- and oxygen-bearing solids, such as ferrihydrite, to goethite. General disparities between XRD and AM modal mineralogy in this study could also be related to the different sample preparation methods, including smaller grain sizes used in bulk XRD (sieved to < 2 mm and micronized) compared to AM (sieved to < 2 mm).

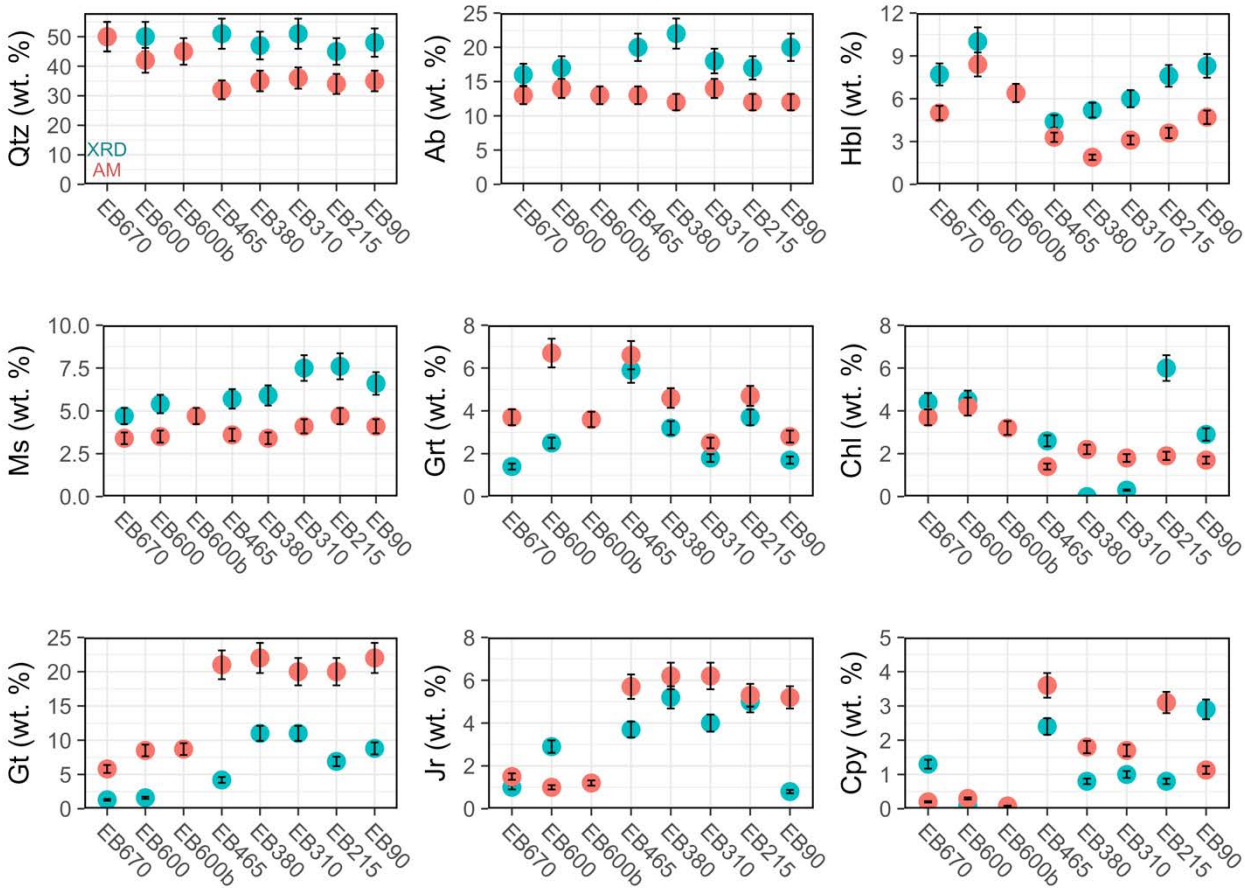

Figure 2: Modal mineralogy results from XRD (green) and AM (red) for Ely Brook sediments. Mineral abbreviations are defined in the text

Automated mineralogy results included several solids that needed to be added to the reference mineral database. This paper focuses on those added solids that contain copper. One is referred to as copper-manganese matrix (CuMnM), which was minimal in downstream samples (0.01 – 0.03 wt. %) and more abundant in upstream samples (0.32 – 0.48 wt. %). This solid locally occurred as rims on grains (Figure 3a, b, c). The EDS spectrum for CuMnM showed detectable copper and manganese, in addition to stronger peaks for iron, silicon, aluminium, and oxygen (Figure 3d). Zooming in on a grain of CuMnM (Figure 3b) shows that it is more of an agglomeration of fine particles rather than a single-phase grain, hence the term matrix in its name. Another copper-bearing solid is referred to as iron-manganese-copper oxide (FeMnCuOx). The abundance of FeMnCuOx was near 0.4 wt. % at all sites except the most upstream site EB670 (0.12 wt. %). Grains of FeMnCuOx were most often observed in association with goethite (Figure 4a, b), and occasionally with jarosite. The EDS spectrum for this solid is indicative of a metal oxide (Figure 4c). The occurrence of these copper-bearing solids on rims of grains and their common association with other secondary minerals suggests that they too are secondary solids in the sediments.

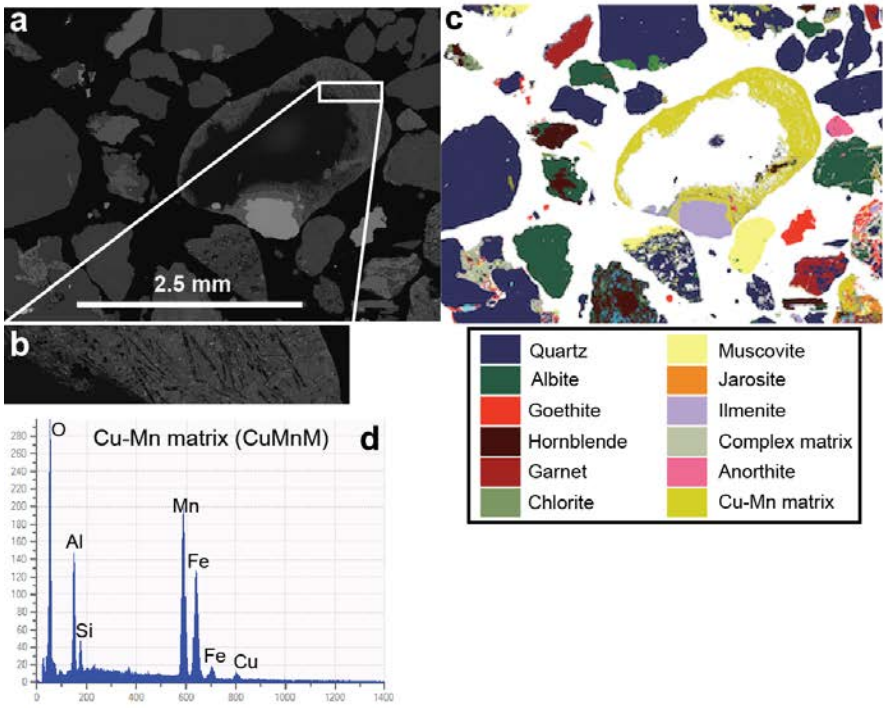

Figure 3: Results of AM analysis showing a lower resolution BSE image (a) and a higher resolution BSE image (b) of a CuMnM-bearing grain within EB600 sediments. The false-colour mineral map (c) shows the same area as (a), showing the CuMnM solid in mustard yellow colour. The EDS spectrum (d) is a typical example of the CuMnM solid

The AM results from this study are notably similar to previous results (Kimball et al., 2016) showing that all sites contained copper hosted by chalcopyrite and secondary iron and manganese (oxyhydr)oxides. For example, the CuMnM grain shown in Figure 3 was previously identified as copper associated with birnessite and jarosite using micro-XAS (Figure 2 in Kimball et al., 2016). Both studies also show the same trends in copper distribution amongst the possible copper hosts based on bulk-XAS and AM results. Upstream sites contained a greater proportion of copper associated with secondary iron and manganese (oxyhydr)oxides, whereas downstream sites contained a greater proportion of copper in chalcopyrite (Table 1). These results are consistent with sediment porewater pH values being near neutral at upstream sites and near 3.5 at downstream sites (Kimball et al., 2016). The lower pH values observed for downstream sites may create an environment where copper-bearing iron and manganese (oxyhydr)oxides would be unstable. Many iron and manganese (oxyhydr)oxides are expected to dissolve under acidic conditions, with the exception of jarosite. Jarosite is well known to be stable at low pH, and the higher abundance of jarosite in downstream sediments based on XRD and AM results in this study support this. Copper associated with jarosite does not appear to be as prevalent in downstream samples compared to upstream samples, however (Table 1). Considering that bulk XAS analyzes the samples as powders and AM analyzes the samples as grain mounts, the comparable results in Table 1 lend credibility to both the bulk XAS and AM results.

Table 1: Distribution of copper in Ely Brook sediment samples given in percent of possible hosts

Copper host	Study	EB670	EB600	EB465	EB380	EB310	EB215	EB90
Chalcopyrite	This study	25	24	89	82	78	87	75
Chalcopyrite	Kimball et al., 2016	18	23	94	79	87	95	88
Secondary	This study	75	76	11	18	22	13	25
Secondary	Kimball et al., 2016	81	76	6	21	13	5	12

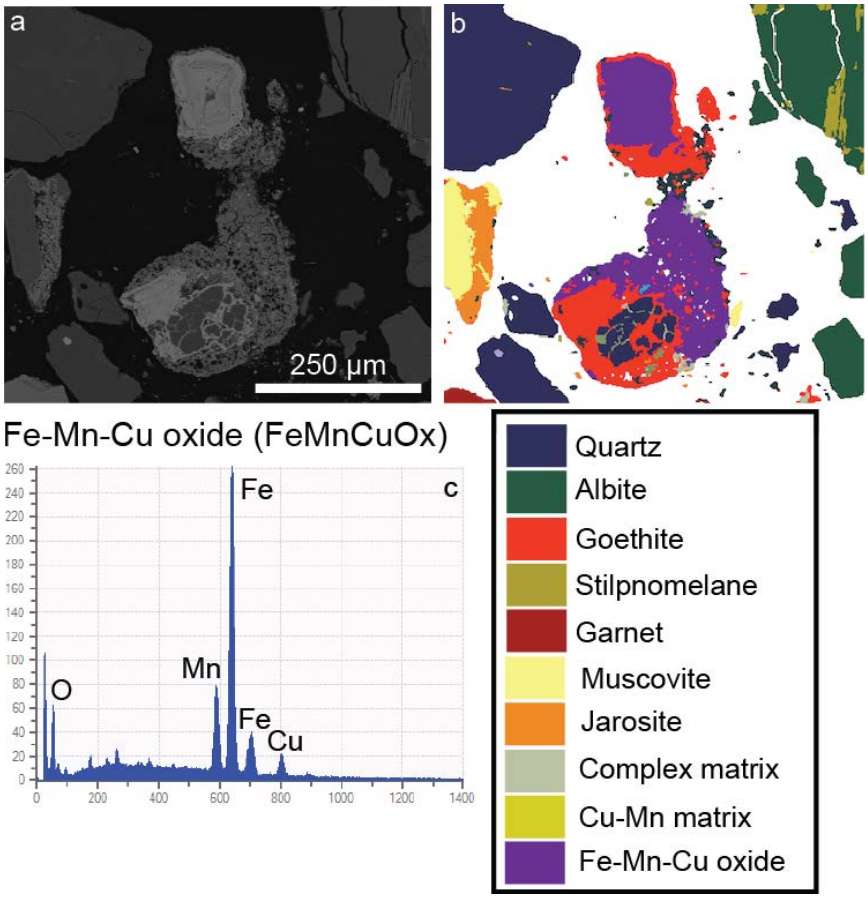

Figure 4: Results of AM analysis showing a BSE image (a) and a false-colour mineral map (b) of FeMnCuOx-bearing grains (purple) in sediments from downstream sample EB215. The EDS spectrum (c) is a typical example of the FeMnCuOx solid

Conclusion

The purpose of this study was to quantify the abundance of copper-bearing solids in contaminated stream sediments in an abandoned copper mining area, and to compare the abundance of these solids obtained from AM to other types of bulk and grain-scale analyses. The AM results in this study were similar to previous

results (Kimball et al., 2016) in terms of possible solid hosts and copper distribution amongst these hosts. The bulk XRD analysis with Rietveld refinement detected only chalcopyrite as a possible host of copper. The copper-bearing secondary solids were not identified with bulk XRD, and probing at the grain scale was necessary to identify them. The added benefit of the AM analysis was that these secondary solids could also be quantified.

Automated mineralogy has proven to be a tool for identifying and quantifying solids that are not easily identified with traditional techniques. As a relatively new technique, some unresolved challenges include the following:

- Thus far, the most common method to test the accuracy of modal mineralogy results is to compare element masses calculated from mineral masses to element masses determined by a chemical assay of the sample (e.g., Pooler and Dold, 2017). Utilizing both AM and chemical assays is reasonable for smaller numbers of samples, but for larger studies with many samples, this comparison could become time and cost prohibitive. An alternative method to test the accuracy of modal mineralogy results could involve analyzing well-characterized standard materials of similar composition, or synthetic mixtures of known mineral masses.
- The analytical reproducibility of modal mineralogy for major minerals has been shown to be acceptable (e.g., Lastra and Paktunc, 2016), but reproducibility for less abundant minerals is relatively poor (this study). Pooler and Dold (2017) showed that modal results from AM were highly dependent on sample preparation. Optimized and consistent sample preparation are likely to improve analytical reproducibility.
- Although AM can detect rare grains, the practical quantitation limits for modal mineralogy from AM are largely unknown. Furthermore, if the element of interest is present in solids at low concentration, the trace-element hosts may not be recognized as such. If elements of interest are hosted in solid solution, or as a sorbed species near the grain surface, AM should not necessarily be the sole analytical technique. In these cases, the AM analysis should be combined with higher chemical resolution techniques, such as EPMA or laser-ablation mass spectrometry.

The solids that host metals of interest in mine waste can be challenging to characterize. Efforts to characterize mine waste at multiple scales, including the micrometer scale, may lead to a better understanding of metal bioavailability and toxicity, distribution, and potential contamination risks. Automated mineralogy offers an opportunity to identify solid metal hosts at the grain scale, and quantify these hosts at the bulk scale, although routine use of AM for this purpose would benefit from further developments in method accuracy, precision, and reliable quantitation limits. Devoting the same analytical

resources to solid characterization of mine waste as is typical for ores may save time and money in the long run, and is recommended for mine closure due diligence.

References

Brough, C., J. Strongman, R. Bowell, R. Warrender, A. Prestia, A. Barnes and J. Fletcher 2017. Automated environmental mineralogy; the use of liberation analysis in humidity cell testwork. *Minerals Engineering* 107: 112–122.

De La Torre, A.G., S. Bruque and M.A.G. Aranda. 2001. Rietveld quantitative amorphous content analysis. *Journal of Applied Crystallography* 34: 196–202.

Dold, Bernhard. 2003a. Dissolution kinetics of schwertmannite and ferrihydrite in oxidized mine samples and their detection by differential X-Ray diffraction (DXRD). *Applied Geochemistry* 18(10): 1531–1540.

Dold, Bernhard. 2003b. Speciation of the most soluble phases in a sequential extraction procedure adapted for geochemical studies of copper sulfide mine waste. *Journal of Geochemical Exploration* 80(1): 55–68.

Fandrich, R., Y. Gu, D. Burrows and K. Moeller. 2007. Moderm SEM-based mineral liberation analysis. *International Journal of Mineral Processing* 84: 310–320.

Gottlieb, P., G. Wilkie, D. Sutherland, E. Ho-Tun, S. Suthers, K. Perera, B. Jenkins, S. Spencer, A. Butcher and J. Rayner. 2000. Using quantitative electron microscopy for process mineralogy applications. *JOM-Journal of the Minerals, Metals and Materials Society* 52(4): 24–25.

Hayes, S.M., S.M. Webb, J.R. Bargar, P.A. O'Day, R.M. Maier and J. Chorover. 2012. Geochemical weathering increases lead bioaccessibility in semi-arid mine tailings. *Environmental Science & Technology* 46(11): 5834–41.

Howard, Peter F. 1959. Structure and rock alteration at the Elizabeth Mine, Vermont. *Economic Geology* 54: 1214–1249.

Hudson-Edwards, K.A., P. Byrne, G. Bird, P.A. Brewer, I.T. Burke, H.E. Jamieson, M.G. Macklin and R.D. Williams. 2019. Origin and fate of vanadium in the Hazeltine Creek catchment following the 2014 Mount Polley Mine tailings spill in British Columbia, Canada. *Environmental Science & Technology* 53(8): 4088–4098.

Kierstead, Matthew A. 2001. History and historical resources of the Vermont Copper Belt. In *Environmental Geochemistry and Mining History of Massive Sulfide Deposits in the Vermont Copper Belt,* edited by Jane M. Hammarstrom and Robert R. Seal II, 35: 165–91. Society of Economic Geologists.

Kimball, B.E., A.L. Foster, R.R. Seal II, N.M. Piatak, S.M. Webb and J.M. Hammarstrom. 2016. Copper speciation in variably toxic sediments at the Ely Copper Mine, Vermont, United States. *Environmental Science & Technology* 50(3): 1126–1136.

Lastra. R. and D. Paktunc. 2016. An estimation of the variability in automated quantitative mineralogy measurements through inter-laboratory testing. *Minerals Engineering* 95: 138–145.

Mumme, W.G., G. Tsambourakis and L. Cranswick. 1996. Improved petrological modal analyses from X-ray and neutron powder diffraction data by use of the Rietveld method. 3. Selected massive sulphide ores. *Neues Jahrbuch Fur Mineralogie-Abhandlungen* 170(3): 231–55.

Parbhakar-Fox, A., B. Lottermoser, R. Hartner, R.F. Berry RF and T.L. Noble. 2017. Prediction of Acid Rock Drainage from Automated Mineralogy. In *Environmental Indicators in Metal Mining,* edited by Bernd Lottermoser: 139–156. Switzerland: Springer.

Piatak, N.M., J.M. Hammarstrom, R.R. Seal II, P.H. Briggs, A.L. Meier, T.L. Muzik and J.C. Jackson. 2004. Geochemical characterization of mine waste at the Ely Copper Mine Superfund Site, Orange County, Vermont. *US Geological Survey Open File Report:* 1248.

Pooler, R. and B. Dold. 2017. Optimization and quality control of automated quantitative mineralogy analysis for acid rock drainage prediction. *Minerals* 7:12.

Radkova, A.B., H.E. Jamieson, B. Lalinsk-Volekov, J. Majzlan, M. Stevko and M. Chovan. 2017. Mineralogical controls on antimony and arsenic mobility during tetrahedrite-tennantite weathering at historic mine sites Spania Dolina-Piesky and L'ubietova-Svatodusna, Slovakia. *American Mineralogist* 102(5): 1091–1100.

Ryan, P.C., S. Hillier and A.J. Wall. 2008. Stepwise effects of the BCR sequential chemical extraction procedure on dissolution and metal release from common ferromagnesian clay minerals: A combined solution chemistry and X-ray powder diffraction study. *Science of the Total Environment* 407(1): 603–14.

Seal, R.R. II, R.G. Kiah, N.M. Piatak, J.M. Besser, J.F. Coles, J.M. Hammarstrom, D.M. Argue, D.M. Levitan, J.R. Deacon and C.G. Ingersoll. 2010. Aquatic assessment of the Ely Copper Mine Superfund Site, Vershire, Vermont. *US Geological Survey Scientific Investigations Report:* 5084.

Slack, J.F., T.W. Offield, W.C. Shanks III and L.G. Woodruff. 1993. Besshi-type massive sulfide deposits of the Vermont Copper Belt. In *Besshi-Type Massive Sulfide Deposits of the Vermont Copper Belt,* edited by John F. Slack and Terry W. Offield, 17: 32–73. Society of Economic Geologists.

Proceedings of Tailings and Mine Waste 2019
November 17–20, 2019, Vancouver, Canada
Published by the University of British Columbia, 2019

A New Technique for Measuring the Reactivity of Sulphidic Ores and Wastes: The Application of Infrared Thermography

Marjan Knobloch, RWTH Aachen University, Germany
Bernd G. Lottermoser, RWTH Aachen University, Germany

Abstract

Presently, mine water testing techniques focus on the prediction and assessment of acid rock drainage (ARD). A plethora of laboratory- and field-based tests exists that evaluate readily leachable acid, metals and metalloids, and are able to predict the likelihood of sulphide oxidation and associated ARD development. By contrast, these existing tests are unable to forecast the presence of sulphides that could release metals, metalloids, and acid at near neutral to alkaline pH conditions. Therefore, a new rapid, field-based and easy feasible method was developed to detect and visualize the reactivity and presence of sulphides in ores and wastes, irrespective of likely pH conditions.

The test is based on the application of hydrogen peroxide to sulphidic samples and the subsequent detection of the thermal energy release upon exothermic sulphide oxidation using an infrared (IR) thermographic camera. Within the scope of this study, representative samples of the Podkozara Sb deposit (Bosnia-Herzegovina) were used and subjected to the newly designed test protocol. Sulphidic samples with significant sulphur (max. 9 wt%), metal and metalloid concentrations (max. 10 wt% As+Sb+Cu+Pb+Zn) as well as acid NAGpH values (–0.47 to 2.78) show comparatively high temperature increases (>10°C) during experimentation. Furthermore, the analyses show that samples with significant sulphur (>1 wt%) and metal contents (>2 wt% As+Sb+Cu+Pb+Zn) as well as detectable sulphide minerals (stibnite and pyrite), but with neutral or basic NAGpH values, also exhibit high temperature increases (>10°C). The results of the study have shown that the application of hydrogen peroxide to sample powders and subsequent visualization of the treated materials using a thermographic camera is a powerful technique in characterizing the presence of oxidizing sulphides. Moreover, compared to established field based tests, the new test protocol allows the recognition of sulphidic materials independent of pH, which is important for dissolved metalloids like Sb or As, which are also mobile under neutral pH conditions. Therefore, the presented testing method adds to the increasing array of field-based tests that provide important evidence for the prediction of mine water quality risks associated with metalliferous drainages.

Introduction

Today's mineral resource development requires best certainty in decision-making from the beginning of life-of-mine. Such well-informed decisions need to be based on total deposit knowledge that has been established using best practices. Total deposit knowledge is the solid understanding of all the pertinent characteristics of a mineral resource, including its environmental properties. Without this information, no meaningful Environmental Impact Assessment (EIA) can be carried out. This results in two essential requirements for the environmental test methods and analyses. On the one hand, the tests must provide quantitative data on a number of samples representative of the resource. Also, the test data should allow predictions on the likelihood of environmental risks. Presently, there are various geochemical static and kinetic testing procedures (e.g., Parbhakbar-Fox and Lottermoser, 2015), which help to identify and forecast acid rock drainage (ARD). However, these well-established geochemical tests suffer from inherent limitations. For example, kinetic tests take significant amounts of time to complete and these laboratory-based methods do not reflect actual site conditions. Furthermore, static tests often measure and analyze only the existing state of a particular sample (e.g., rinse pH test), without allowing predictive statements. Moreover, current ARD tests and tools do not consider the development of other drainage forms, for example, neutral pH metalliferous mine waters (e.g. As, Sb, U, Mo, Se). In particular, As and Sb are known for their mobility even under neutral pH conditions (Vink, 1996; Ashley et al., 2003; Wilson et al., 2010), and such As-Sb neutral mine drainage also occurs at the Podkozara Sb deposit (Bosnia-Herzegovina), which is the subject of this investigation. Finally, much of the established ARD testing protocol focuses on the use of geochemical analyses, whereas mineralogical investigations are limited to carbonate staining or time-consuming laboratory-based analyses (e.g., XRD). Hence, rapid mineralogical field tests, which can predict the presence of sulphide minerals and hence the likelihood of metalliferous drainage from mines and wastes, are still missing.

In order to close this gap, this paper presents the development of a cost-effective, rapid, field-based, easy-to-use method, which is based on the application of hydrogen peroxide and infrared thermography, for predicting the presence of sulphide minerals in sulphidic ores and wastes. The method essentially detected the presence and reactivity of sulphides as well as their likely oxidation within processed or unprocessed ore and waste samples. The method was developed, applied, and tested on samples from the Podkozara Sb deposit, Bosnia-Herzegovina. Therefore, this paper adds to our existing knowledge and the presented test complements existing ARD testing tools.

Materials and methodology

Deposit geology

Samples were obtained from the Podkozara Sb deposit (43°37'23.06"N; 19°01'12.61"E), Gorazde, Bosnia-Herzegovina. The Podkozara deposit was discovered in the 1920s and subsequently explored using underground levels and drives in the 1960s to 1980s. To date, the deposit remains an unexploited mineral resource. The deposit is hosted by graphitic to pelitic schists (phyllite) with a suite of parallel running discontinuous quartz lenses, strongly mylonitized carbonate rocks, primarily limestones, dolomites, and marble limestones of Carboniferous to Triassic age (Hrvatovic, 2006). The Sb-mineralization (stibnite) is hosted by quartz veins in the contact zone between schist and carbonate rocks.

Sampling and sample preparation

Drill cores (n: 34) with various diameters (2.5–8.2 cm) and lengths (35–100 cm) were extracted on four sundry levels by two different drilling campaigns. Individual samples were taken from the drill cores (length 8–10 cm), which were subsequently halved, dried, crushed, and milled using a vibration disc and tungsten carbide ring mill. Sample powders were used for portable X-ray fluorescence (pXRF), inductively coupled plasma mass spectrometry (ICP-MS), inductively coupled plasma atomic emission spectrometry (ICP-AES), Net Acid Generation pH (NAGpH), and X-ray diffraction (XRD) analyses as well as infrared thermographic (IR) tests.

Geochemical analyses

Portable XRF analysis were performed on all samples, using a Bruker S1 Titan 800 analyser with a 4 W, 50 kV Rh target X-ray tube, a fast drift silicon drift detector and an ultralene window in “Geochem Trace Mode”. Each single measurement is based on two different phases, one phase with TiAl filter (45 kV; 7.1 μA); as well, a second lower energy non-filter phase running with 15 kV and 17.45 μA. After warming up and checking the quality of the device, each individual sample was measured five times for 30 seconds per filter in a radiation protection chamber. Powdered samples were prepared in a synthetic cup, covered with an ultralene film. Subsequently, the mean ($\overline{x}$), standard deviation (σ_1) and difference between the mean pXRF and the reference values were calculated.

In addition, ten selected samples were geochemically analyzed using ICP-MS and ICP-AES at an external certified laboratory (ALS laboratory, Dublin, Ireland). Prior to elemental analysis, processed sample powders were digested using a four-acid digest of HNO_3, HF, $HClO_4$, and HCl.

The acid-generating potential of the powdered samples was established, using the single addition Net Acid Generation (NAG) pH test (Smart et al., 2002). Here, 2.5 g powdered sample was mixed with 250 ml of 15 % H_2O_2 in a beaker. After 18 hours of reaction, the NAG solutions were moderately heated until no

further reaction could be observed and the pH and Eh values were measured with a pH/ORP meter HI 991002 provided by Hanna Instruments Ltd. The instrument calibration was based on the manufacturer buffer solutions HI7007 (pH = 7) and HI7004 (pH = 4). Finally, the NAG solutions were filtered (0.45 µm), acidified with 1 ml HNO_3 followed by elemental analysis (As, Cr, Cu, Fe, Mn, Ni, Pb, Sb, Zn) using ICP-AES techniques.

Mineralogical analyses

The mineralogy of selected samples (n = 18) was determined using a STOE powder diffractometer (X-ray Laboratory Ermrich, Reinheim, Germany). The diffractometer was operated in Bragg-Brentano mode, reflection θ-θ configuration, running with a copper X-ray tube (40 kV, 35 mA) and 5 seconds counting steps. The results were evaluated both qualitatively, using the search-match software Crystallographica (ICDD PDF), and quantitatively, using the Rietveld method (SQ-ID), normalized to 100 % crystalline materials.

New test based on infrared thermography

The objective of the new test procedure was to visualize the oxidation of sulphide minerals in powdered sample materials due to exothermic sulphide oxidation, which was accelerated through the addition of hydrogen peroxide as an oxidizing agent, and measured using a thermographic camera (FLIR T650 sc) to visualize the resultant heat release. The thermal imaging camera uses an uncooled Vanadium Oxide microbolometer detector, and produces photos of 640 x 480 pixels with an infrared detector sensitivity of 0.03°C and accuracy of ±1°C (T <100°C) or 1 % (T >100°C) in a temperature range of –40 to 2,000 °C.

A pilot study on a limited number of samples led to the presented experimental protocol, in which powdered samples were mixed with hydrogen peroxide. Once the reaction had started, the temperature development and release were monitored using the FLIR T650sc thermal imaging camera until no further change in temperature was visible. The following parameters were recorded: initial temperature (T_{start}), maximum temperature (T_{max}), reaction time (t); time taken to maximum temperature (t_{max}). Such observations and recordings led to a visual inspection of individual samples, as well as to a temperature development curve for each individual sample. Interpretations about the possible presence and activity of sulphide minerals in the investigated samples were drawn due to the intensity, development, and duration of the recorded temperature curves.

Results

Geochemistry

The average, standard deviation, relative standard deviation, and the relative difference between the pXRF and ICP-MS averages were calculated to define the precision of the pXRF data. Based on these data, an error calculation was performed for the pXRF data presented below.

The pXRF data show that Sb is the most common metal in the samples and could be detected in dolomites, limestones, and quartz veins. The Sb values vary between 82 ppm and 76.52 wt% with an average of 9.72 wt% ($\sigma 1$ = 15.93 wt%, n = 29). However, no Sb concentrations could be detected in the marble limestones and phyllites. In contrast to Sb, the As concentrations are significantly lower, but could be detected in all lithotypes and ranged between 15 and 15,029 ppm, with an average of 745 ppm ($\sigma 1$= 2,636 ppm, n = 30). Other environmentally relevant metals with values above the limit of detection (LOD) are Pb, Cu, Fe, Mn and Zn (<1,905 ppm, <1,063 ppm, <39,196 ppm, <3,639 ppm, <2,720 ppm respectively).

The results of the NAGpH tests show a similar distribution of the metal concentrations in the eluates. Sb is also the main metal and ranges from 1 to 521 ppm. Apart from Sb, the majority of the other dissolved metal concentrations of interest (As, Co, Cu, Fe, Mn, Mo, Ni, and Zn) are below the LOD. In some solutions, concentrations up to 7 ppm could be detected for Fe, Mn, Pb, and Zn. The pH of the solutions varies in a wide range from –0.47 to 11.85. The E_h data show a similarly large variation and ranged from33 to 655, with the highest E_h values assigned to the lowest pH values and vice versa. By contrast, acid pH values are not always accompanied by high dissolved metal concentrations, and alkaline solutions do not always have low dissolved metal concentrations. The highest dissolved Sb value of 521 ppm was detected in an acid solution (pH = 0.87; E_h = 563). However, there are also samples with an acid pH and less than 3 ppm of dissolved Sb. In addition, increased Sb (>100 ppm) values could be found in alkaline solutions with pH more than 8.5.

Mineralogy

In total, eleven different mineralogical phases occur in different compositions and concentrations in the analyzed samples. Typically, ores (1 to 74 wt% Sb) contain variable amounts of pyrite (max. 1.4 wt%), siderite (max. 11.3 wt%), hydroxycalciоromeite ($(Ca,Sb)_2(Sb,Ti)_2O_6(OH)$, max. 35 wt%), and stibnite as the main ore mineral. Other gangue phases include quartz, dolomite, calcite, muscovite, kaolinite, microcline, and clinochlore.

Infrared thermographic tests

IR measurements show significant differences in exothermic reaction behaviour and associated heat release, as measured by the temperature profile of each tested sample. The temperature difference (T_{diff}) between

the initial (T_{start}) and maximum temperature (T_{max}) was calculated and is shown in Figure 1. The highest T_{diff} of 70.6 °C and T_{max} of 95 °C were reached after two minutes reaction time (Figure 2). Intense effervescent and gas release accompanied the reaction. By contrast, the lowest T_{diff} of 0.5 °C (T_{max} = 20.4°C) was recorded after three minutes. The time taken to reach the T_{max} varied from sample to sample, and was up to 90 minutes in the analyzed materials (Figures 1 and 2). The average time for all samples to reach the maximum temperature was 19.5 minutes with a T_{diff} average of 21.35°C. In general, the highest differential temperatures (>30°C) were reached in the first 20 minutes (Figure 1). After this time, only differences below 25°C have been recorded. For the majority of samples, the temperature decreases very rapidly after reaching T_{max} (Figure 2). Furthermore, some samples could be observed to exhibit a temperature plateau, keeping the maximum temperature constant for 5 to 15 minutes and not exceeding T_{diff} by 10°C compared to T_{start} (Figure 2). The longest time for a sample to react was 210 minutes; however, the majority of samples took between 120 and 150 minutes.

A comparison between IR test results, final NAGpH values, and the mineralogical data is presented in Figure 3. Sulphide-bearing samples with acid NAGpH values exhibit high temperature differences (T_{diff} >10°C). By contrast, samples with neutral and alkaline NAGpH values show lower T_{diff} values. However, there are samples with higher T_{diff} (>40 °C) but alkaline to strongly alkaline NAGpH values, in which sulphide minerals could be detected as well (Figure 3).

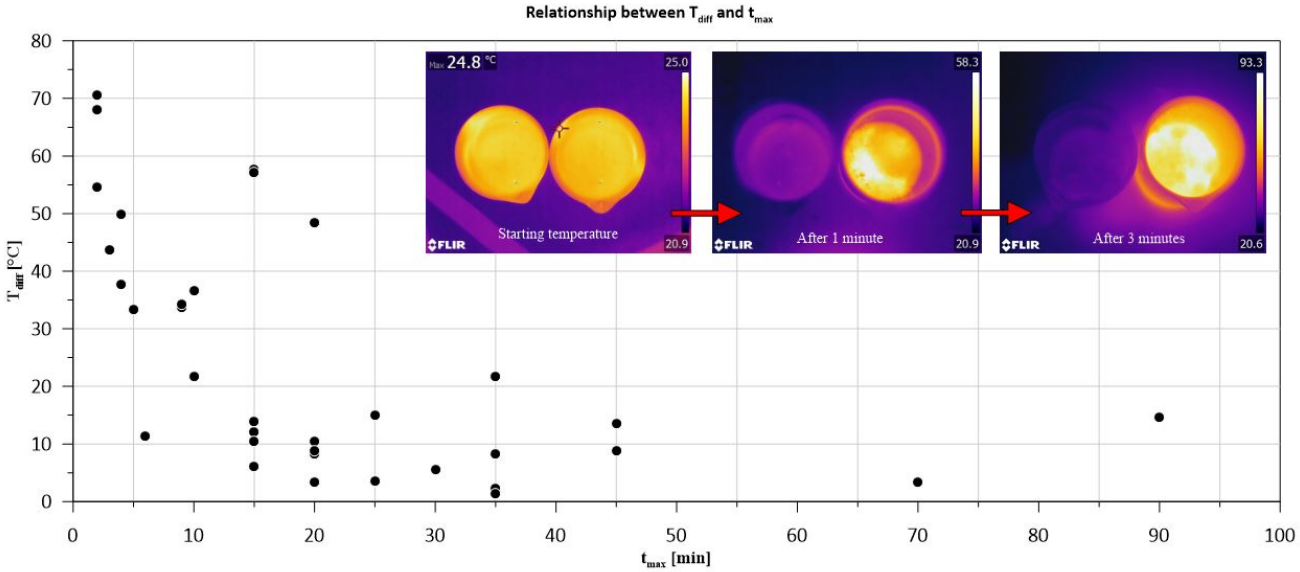

Figure 1: Time taken to reach the maximum temperature (t_{max}) versus temperature difference (T_{diff}) for sulphidic ore samples (n = 34) from the Podkozara Sb deposit as recorded by a FLIR T650sc thermal imaging camera

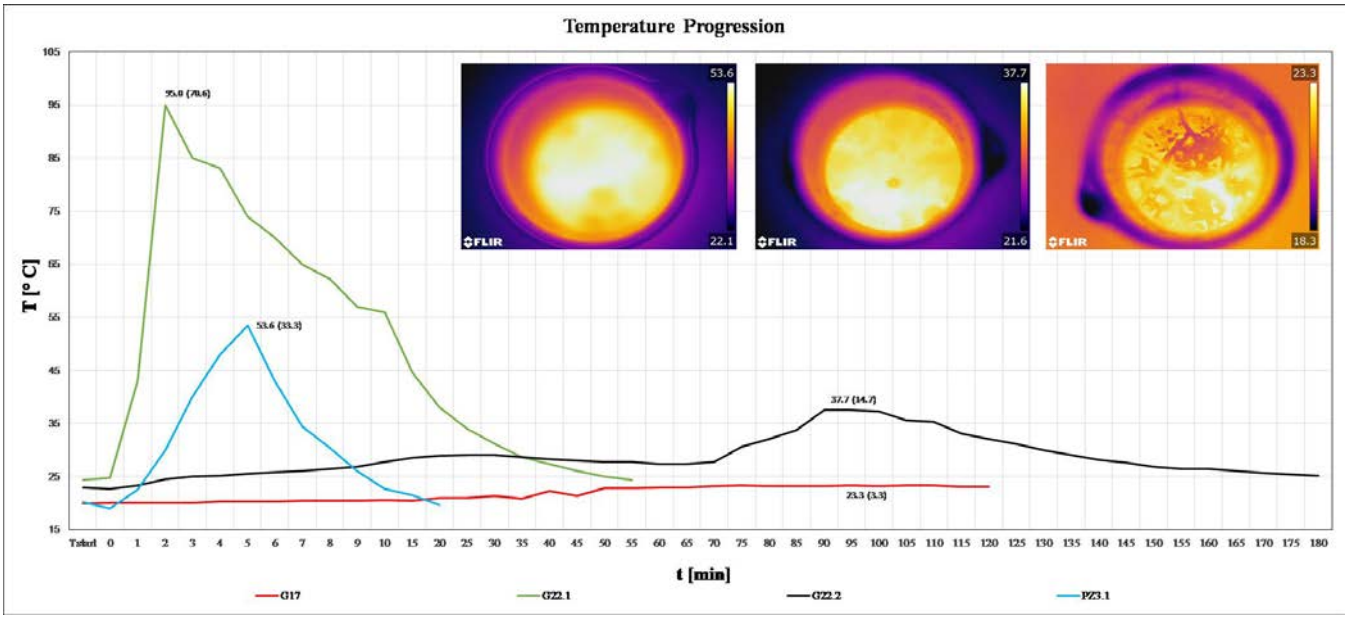

Figure 2: Temperature development curves for representative samples (n = 4) of the Podkozara Sb deposit as recorded by a FLIR T650sc thermal imaging camera. T_{max} and T_{diff} (brackets) are shown for each sample. Samples G22.1 and PZ3.1 reached the highest T_{diff} (>30°C) within the first 20 minutes of reaction time. Lower T_{max} (T_{diff}<30°C) and a longer reaction time were observed for sample G22.2. G17 formed a weak temperature plateau instead of a peak temperature

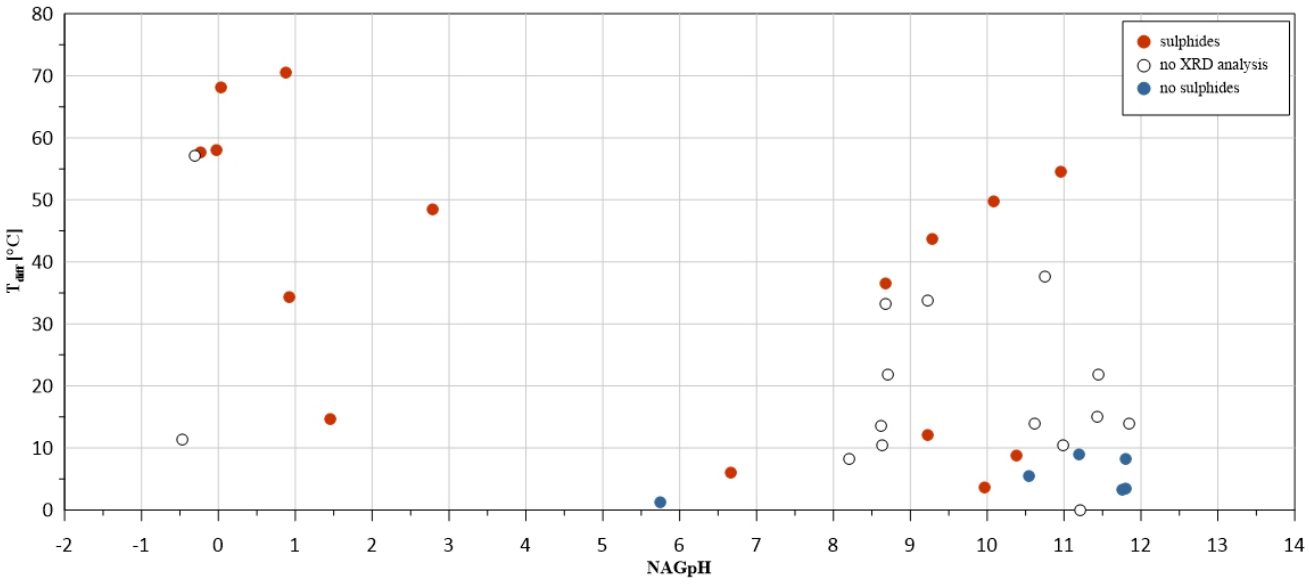

Figure 3: Relation between T_{diff} and NAGpH values. In general, sulphidic samples have elevated T_{diff} values but variable NAGpH values

Discussion

NAGpH tests

In general, NAGpH tests allow conclusions to be drawn about the reactivity of sulphides (oxidation) and the associated acid forming potential of samples. In this study, there is evidence of dissolved metals in acidic NAGpH eluates (pH <4.5), with Sb particularly elevated. Samples with NAGpH values <4.5 have Sb concentrations >10 wt% and abundant sulphide minerals like stibnite and pyrite, which are known to release sulphuric acid (H_2SO_4) based on their oxidation reactions (e.g., Kontopoulos, 1998; Perez-Lopez et al., 2007). By contrast, samples with Sb concentrations <1 wt% produce alkaline NAGpH solutions and occasionally contain a small amount of sulphide minerals. However, a simplistic relationship between NAGpH values, Sb concentrations in the NAG eluates, the abundance of sulphide minerals, and geochemical concentrations of Sb and Fe is not evident. For example, high dissolved Sb values were found in acidic as well as alkaline NAGpH solutions, and sulphidic samples produce both acid and alkaline NAGpH values. Alkaline NAGpH values (>7) are likely due to the neutralizing effect of alkalinity-generating materials such as carbonate minerals (cf. Gazea et al., 1996; Hammarstrom et al., 2003; Skousen et al. 2016; Dold, 2017). Moreover, some sulphidic samples of the Podkozara deposit show very high NAGpH values up to 11.85 (Figure 3). Such extraordinary pH values are likely due to siderite, calcite or dolomite dissolution during NAGpH testing and resultant $Ca(OH)_2$ formation (cf. Parbhakar-Fox and Lottermoser, 2015; Parbhakar-Fox et al., 2017). Consequently, NAGpH values cannot be used to predict the presence or absence of sulphide minerals within samples.

Infrared thermography test

The results from the IR test demonstrate that the presence and exothermic oxidation of sulphide minerals can be quantified and visualized using a thermographic camera (Figure 3). Such energy release may last several hours. Particularly reactive samples reach very high temperatures differences (>30 °C) within the first 20 minutes of the reaction (Figure 1). Poorly reactive samples are characterized by a temperature difference of less than 10 °C. In addition, some samples exhibit a temperature reaction profile with a distinct temperature plateau lasting up to 15 minutes (Figure 2). This likely reflects a constant energy release from an ongoing exothermic reaction without forming a temperature maximum peak. Samples with the highest temperature differences (T_{diff}) also have detectable sulphide minerals and acid NAGpH values. Thus, high temperature differences (T_{diff}) are related to the oxidation of sulphide minerals and the formation of acid solutions. In addition, there are also sulphidic, Sb enriched samples with T_{diff} values of >10 °C, which show neutral to extremely alkaline NAGpH values. This may due to buffering through carbonate dissolution and the formation of calcium hydroxides, which led to the very high alkaline pH values. Regardless, IR testing

allows the recognition of sulphide minerals within samples regardless of the NAGpH or the presence of acid buffering minerals like carbonates.

Conclusion

This study developed a rapid, easy-to-use technique to detect the presence and reactivity of sulphides in ores and wastes using hydrogen peroxide and infrared thermography. The major advantage of the developed test protocol is that it allows the rapid recognition of sulphide minerals within samples, regardless of the presence of carbonate minerals and regardless of pH.

Acknowledgements

We thank the Mineco Ltd team for supplying the sample materials, assisting with core sampling, and providing access to the mine site; N. Willing (RWTH Aachen) for help with sampling and preparation, and H. Bergstein (RWTH Aachen) for ICP-AES measurements. This study was financially supported by the European Union's Horizon 2020 research and innovation programme under grant agreement nº. 730411.

References

Ashley, P.M., D. Craw, B.P. Graham and D.A. Chappell. 2003. Environmental mobility of antimony around mesothermal stibnite deposits, New South Wales, Australia and southern New Zealand. *J Geochem Explor.* 77: 1–14.

Dold, Bernhard. 2017. Acid rock drainage prediction: A critical review. *J Geochem Explor.* 172:120–132.

Gazea, B., K. Adam and A. Kontopoulos. 1996. A review of passive systems for the treatment of acid mine drainage. *Miner Eng*. 9(1): 23–42.

Hammarstrom, J.M., P.L. Sibrell and E.B. Harvey. 2003. Characterization of limestone reacted with acid-mine drainage in a pulsed limestone bed treatment system at the Friendship Hill National Historical Site, Pennsylvania, USA. *Appl Geochem*. 18(11): 1705–1721.

Hrvatovic, Hazim. 2006. *Geological Guidebook through Bosnia and Herzegovina*. Sarajevo: Geological Survey of Bosnia and Herzegovina.

Kontopoulos, A. 1998. Acid mine drainage control. In *Effluent Treatment in the Mining Industry*, edited by S.H. Castro, F. Vergara and M.A. Sánchez: 57–118. Concepción: University of Concepción.

Parbhakar-Fox, A. and B.G. Lottermoser. 2015. A critical review of acid rock drainage prediction methods and practices. *Miner Eng*. 82: 107–124.

Parbhakar-Fox, Anita, John Aalders, Laura Jackson and Bernd Georg Lottermoser. 2017. Prediction of acid rock drainage using field-based testing tools. In *Environmental Indicators in Metal Mining*, edited by Bernd Georg Lottermoser: 115–138. Basel: Springer.

Perez-Lopez, R., J.M. Nieto and Ruiz de Almodovar. 2007. Utilization of fly ash to improve the quality of the acid mine drainage generated by oxidation of a sulphide-rich mining waste: Column experiments. *Chemosphere* 67: 1637–1646.

Skousen, J., C.E. Zipper, A. Rose, P.F. Ziemkiewicz, R. Nairn, L.M. McDonald and R.L. Kleinmann. 2016. Review of passive systems for acid mine drainage treatment. *Mine Water Environ.* 36: 133–153.

Smart, R., W.M. Skinner, G. Levay, A.R. Gerson, J.E. Thomas, H. Sobieraj, R. Schuhmann, C.G. Weisener, P.A. Weber, S.D. Miller and W.A. Stewart. 2002. *ARD Test Handbook: Project P387, A Prediction and Kinetic Control of Acid Mine Drainage.* Melbourne: AIMIRA International Ltd.

Vink, Bernard W. 1996. Stability relations of antimony and arsenic compounds in the light of revised and extended Eh-pH diagrams. *Chem Geol.* 130: 21–30.

Wilson, S.C., P.V. Lockwood, P.M. Ashley and M. Tighe. 2010. The chemistry and behaviour of antimony in the soil environment with comparisons to arsenic: A critical review. *Environ Pollut*. 158: 1169–1184.

Proceedings of Tailings and Mine Waste 2019
November 17–20, 2019, Vancouver, Canada
Published by the University of British Columbia, 2019

Creating Better Tailings Facilities Using Innovative Process Engineering

Christian Kujawa, Paterson & Cooke USA Ltd, USA
Jeff Winterton, Paterson & Cooke USA Ltd, USA
Rachel Jansen, Paterson & Cooke USA Ltd, USA
Robert Cooke, Paterson & Cooke USA Ltd, USA

Abstract

The mineral resources industry faces challenges as ore bodies become lower grade, more complex, and finely disseminated. The trend for the future is larger scale operations producing higher tonnages of tailings with finer, more problematic particle size distributions than past operations. This trend is combined with pressure to improve the stability and safety of tailings facilities, reduce environmental impacts and waste generation, ensure safe and secure mine closures, and operate with a social license while reducing mine energy and water consumption.

This paper explores technologies and approaches for tackling this future trend and creating better tailings facilities through innovative process engineering. The focus is on approaches which are novel, or which have not yet had wide implementation.

This paper explores how better tailings facilities can be created through innovative process engineering applied to both processes typically considered as part of the tailings system and to upstream processes which have generally not been considered in the past when developing tailings management strategies.

Apart from a drive to eliminate tailings altogether (e.g., in-situ mining) there are a range of technologies which have already been implemented to reduce the volume of tailings stored at the mine site. Increasingly in the future, the volume of tailings may be reduced further when tailings are viewed as a resource to generate commercially valuable by-products.

There are several approaches to enhance the tailings properties in the deposit. These include coarse grind processing, amendments to improve tailings dewatering and to sequester carbon.

The concept of engineered tailings has been developed to design flowsheets which optimize tailings dewatering, transport, and storage characteristics. The concept has wide application for improving tailings

management, including for existing operations looking to transition from conventional tailings. Classifying tailings and de-sulphurizing tailings to improve their properties are discussed.

Introduction

Historically the optimum tailings solution for a mining operation has largely been based on economics. With the recent tailings facility tragedies, there is increasing acceptance that storage facility stability and safety must take priority over cost. This change in emphasis will allow for the development and implementation of technologies previously considered cost prohibitive.

This paper focus on approaches which are novel, or which have not yet had wide implementation. Accordingly, the scope excludes:

- Conventional tailings approaches. In many cases conventional methods, such as a cyclone sand centerline or downstream construction, are well proven and safe and will continue to be used for tailings facilities in the future.
- Paste tailings (defined as tailings with minimal bleed water following deposition). While there have been several successful relatively small-scale implementations of surface paste technology, it has not scaled well to large tonnage operations. Due to the inherent technology limitations, we do not expect widespread implementation of paste tailings for large tonnage operations.
- The standard implementation of filtered tailings where the whole tailings stream is filtered. The approach is well proven for relatively small tonnage mining operations but has not been implemented yet for large scale operations. While we believe the challenges of equipment and operation scale-up will be overcome in the future, in this paper an alternative engineered tailings approach is offered which will allow for more effective implementation using currently available filtration technology.

The paper scope also excludes methods such as underground mine backfill and in-pit disposal to reduce the amount of tailings to be stored in the surface tailings facility. The Mount Polley Expert Panel (Morgenstern et al., 2015) consider these methods as “Best Available Technology” and they should always be considered as part of the tailings management plan where feasible.

The industry widely refers to the tailings continuum ranging from un-thickened through to filtered tailings with decreasing water content in the tailings. We note there is a discontinuity in this “continuum” where the water content results in tailings which are too concentrated for cost-effective pump and pipeline transport yet too wet to be transported mechanically using a belt conveyor and stacker system.

Process opportunities

Selective mining

Historically selective mining has been described as high-grading or 'robbing' the mine to process the highest grade possible. Increasingly, the term is being used to describe mining based on grade as well as other ore characteristics that affect recovery and processing performance. The resultant tailings properties are not always factored into the mine sequencing or economic models because of the perceived lower value compared to other key indicators such as mineral grade and deportment.

However, with the increasing emphasis on tailings facility stability, these techniques can be extended to allow mining operations to control tailings property variability for simplifying tailings dewatering, transport and deposition processes. Selectively excluding or scalping materials known to create challenges with the tailings system (e.g., high clay mineral content) from the mill feed could result in significant simplification of the tailings system. The viability of this approach needs to be assessed by weighing the benefits against the possible loss of recoverable minerals, but this practice will likely increase in importance as mine operations face increasing pressure to shift to lower water content tailings. The value and utility will depend on the scale of mineralogical variability in the ore body, mining scale and rate, as well as the alignment of long-and short-term operational goals.

Pre-concentration

Generally new ore deposits have lower grades requiring mining, moving and processing larger volumes of material per ton of mineral recovered. Rejection of liberated barren gangue from the feed by pre-concentration reduces the mass that needs to be processed (i.e., contacted with water) with the consequent reduction in the mass of tailings to be processed and stored.

The aim of pre-concentration is to remove barren material as early in the process as possible. The valuable minerals do not need to be fully-liberated and often it is only necessary for barren gangue to be available for rejection (Duffy et al., 2015). There are several technologies appropriate for pre-concentration including gravimetric, magnetic, optical, and radiographic techniques. The suitability in each case depends on the ore properties. Pre-concentration has the added advantage that it can complement selective mining at the bench or stope by determining grade or other mineral properties. More valuable metal may be extracted from the resource while the processing plant treats less tonnage at higher feed grade and generates less tailings for disposal.

Coarse grind processing

Traditionally, the optimum grind has been established by considering grinding costs (capital and energy) versus recovery (mining operational income). As comminution technology has advanced becoming more

cost effective and metal prices have increased with demand, this trade-off has generally led to finer grinding to increase recovery. This trend is further exacerbated by the fact that remaining ore reserves are of lower head grade and often more finely disseminated. Finer ground ores require more water for processing, the tailings are more difficult to dewater, and are more likely to remain in a "fluid" state within the tailings storage facility.

There is now recognition that in establishing the optimum grind consideration needs to be given to the implications for tailings dewatering, transport and storage. When these factors are included, it is probable that coarser grinds will result in an economic optimum for the mine life (and a safer tailings storage facility).

The difficulty of dewatering tailings is related to particle surface area, which increases exponentially with decreasing particle size:

- Water absorption and adsorption increases with finer particle size. Clay particles, which tend to accumulate in the ultra-fine –2 μm fraction with comminution, absorb and adsorb even more water because of their high surface activity.
- The interstitial flow paths between particles required for dewatering become narrower and more torturous as particles become finer.
- With finer grinds, it is more likely that minerals which have a negative impact on dewatering are liberated (e.g., clay minerals).
- The concentration of very fine particles has a direct impact on the tailings rheology with the concomitant impact on associated processes (e.g., effective flocculation).

Rather than simply selecting a coarser grind for the total ore stream, there are other options which may more effectively limit the fines generated by the extraction process while improving pay-mineral recovery:

- Designing flowsheets to facilitate early recovery of liberated mineral particles from the comminution circuit to minimize their exposure to grinding (for example flash flotation in the milling circuit). This prevents over grinding which may result in poor recoveries.
- Recovering middling (mixed mineral) particles early on for later selective grinding for liberation and recovery. This results in only a fraction of the feed being ground finer reducing the quantity of fines being generated. With this already common approach, the focus is generally flotation of middling particles that can be captured with traditional flotation technologies. However, the concept can be extended to even coarser middling particles using flotation technologies specifically suited to such coarser particles.

- Alternatively, utilization of technology requiring only partial mineral surface access to achieve full recovery (e.g., leaching), could be used.

Methods to engineer tailings

Paterson & Cooke have developed the engineered tailings concept, in which the tailings flowsheet is designed to optimize tailings characteristics for dewatering, transport, and storage. The concept has wide application to improving tailings management:

- For systems where delivery of consistent solids concentration (or rheology) tailings slurry is important, this can be achieved by blending thickener underflow with either thickener feed or filter cake.
- EcoTails™, developed by Goldcorp and FLSmidth, combines waste rock and filtered tailings to create a stable stack which is resistant to acid generation.
- For applications where it is important to chemically stabilize the tailings, improve dewatering or develop early strength, cementitious binder, chemicals or other waste streams can be mixed with the tailings slurry prior to deposition.

The following sections discuss two strategies for achieving an engineered tailings solution.

Classified tailings

Tailings can be classified to separate the fines fraction from the bulk tailings, which can then be treated separately to lower capital and operating costs. Desktop studies completed by Paterson & Cooke have shown potential savings up to 50% for capital and operation costs when dewatering classified tailings instead of whole tailings.

This is achieved by adding hydro-cyclones, hydro-separators or dewatering screens ahead of dewatering. Many tailings operators are already familiar with classification technologies as they operate cyclones to create construction sand from tailings for dam building. Paste backfill operations also often uses classification to de-slime tailings before using in backfill recipes to optimize binder consumption.

By splitting the tailings stream into two fractions, options such as filtered tailings become more attractive. The de-slimed coarse fraction has a smaller tonnage, coarser particle size distribution and minimal clays. This change in characteristics can significantly increase filtration rates and decrease the relatively high capital costs associated with filtration plants. In some instances, the classification step produces de-slimed tailings with a high enough solids concentration to feed directly to filtration, eliminating the need for thickening. Removal of fines and clays reduces filter cake compressibility which increases the filtration rate allowing simpler equipment to be used (such as recessed chamber filters). Stackable filtered

tailings are produced with less process variability, more consistent cake moisture content and at significantly lower cost than if the whole tailings stream was filtered.

Classifying tailings does not necessarily result in an increase in water recovery. The slimes fraction still needs to be handled, and this stream will have slower dewatering rates than the whole tailings. However, if this fraction is relatively small, technologies that were previously considered impractical due to low capacities become more feasible, such as screw press filters, centrifuges and geotubes.

The tailings storage strategy may be a combination of filtered tailings stacking and slurry tailings stored in separate facilities. Alternatively, filtered coarse tailings could be used to build "paddocks" and the thickened fines deposited within the interior.

The authors expect that classified tailings dewatering circuits will become a viable option for large tonnage, low grade operations, especially in conjunction with the development of filters with larger capacity to reduce the number of units required and thereby the costs.

Tailings desulphurization

Acid generating (AG) or potentially acid generating (PAG) tailings limit the options for storing tailings. Preventing oxidation and future acid mine drainage issues can significantly increase tailings storage costs. Substantial savings can be realized if tailings classified as non-acid generating (NAG) are separated from the main tailings stream.

Typically, the acid generating potential is due to the presence of pyrite and other sulphur bearing minerals. Generally, they are in either the coarser or the finer particle size fractions following flotation. In the coarser size fractions, only middling (mixed mineral) particles with some exposed sulphur bearing surfaces are of concern, as fully encapsulated sulphur bearing minerals are not exposed to oxygen and leaching. Sulphur bearing minerals in the finer size fractions are likely fully liberated.

Desulphurization is best achieved through flotation using tailored flotation equipment and conditions. Prior to flotation, the tailings are split into coarse and fine fractions using hydro-cyclones or hydro-sizers. Depending on the distribution of sulphur bearing minerals they are concentrated in either the fine or coarse size fractions. Size specific flotation is used to recover the sulphur bearing minerals:

- For coarse middling particles, typically hydro-cyclone underflow product, flotation technologies which can operate at high solids concentration and are capable of "lifting" coarse particles into the froth phase are employed.
- For the fine particle fraction, typically at lower solids concentration, flotation is done with flotation machines capable of high shear and therefore capable of capturing the fine particles.

With careful hydro-cyclone design, often both sulphur bearing particle categories can be concentrated in the cyclone underflow, simplifying the de-sulphurization.

Often additional valuable pay-minerals are recovered during desulphurization; the economic realizable benefit depends much on the proximity to the main plant, concentrate grade, other minerals recovered and how much additional processing is required.

Distributed tailings deposition systems

While thickened and paste tailings systems are most often implemented to achieve water savings as the prime objective, there are numerous applications where a key objective is the development of steeper tailings beaches to create a "stacked" deposit to maximize the tailings stored on the facility.

Early implementations of stacked hydraulically placed tailings were based on the Robinsky (1978) concept where the deposit is developed by depositing the tailings through one or more centrally located discharge points. These systems rely on the production of high solids concentration (i.e., high rheology) tailings to achieve the stacked deposit. The concept has achieved mixed success for smaller tonnage implementations (less than 30,000 tpd) but has not been successfully implemented for large tonnage systems.

McPhail (2018) developed a stream power methodology for predicting tailings beach slopes and recognized steep beach slopes could be achieved with low to moderate yield stress tailings if a distributed tailings distribution system is employed. Stowe et al. (2018) describes the process and hydraulic requirements for a distributed tailings deposition system comprising multiple simultaneously operating near equal flow rate discharges which are spaced sufficiently far apart to ensure the individual discharges do not combine on the tailings beach. The system must accommodate the inherent variability in process conditions and tailings properties (Martinson et al., 2015). Stowe et al. (2018) present two large tonnage (≈ 100,000 tpd) case studies showing how the implementation of distributed tailings systems increased beach slopes from 0.5% to above 2% for tailings with low (11 to 17 Pa) and moderate (35 to 55 Pa) yield stresses.

The development of the distributed tailings distribution system is a significant advancement as it allows high-rate or high-density thickeners to be used instead of paste thickeners which have not operated reliably for high-tonnage applications.

In-line flocculation

The high shear in centrifugal pumping of thickener underflow to the tailings storage facility generally destroys the flocculant chains so that little benefit remains of the initial flocculation to promote consolidation after deposition into the tailings storage facility. Yet flocculation after deposition will promote water disengagement and consolidation.

To promote dewatering and consolidation of tailings after deposition, specifically designed polymer is injected into the tailings pipeline before the discharge point. The turbulence in the pipeline is used to achieve contact and flocculation. The polymer chemistry creates large macro structures of polymer chains

combined with tailings particles in a loosely held matrix which stacks well. The solids concentration of the released water, generally well below half a percent of solids, is a function of the initial solids concentration and the polymer chemistry selected for the application. Because of the macro structure and the stacking, subsequent dewatering through self-weight consolidation is faster than for the same material not flocculated.

While flocculation is more effective at lower solids concentrations, in-line flocculation technology can be used for slurries with relatively high solids concentrations with the caveat generally, the higher the solids concentration, the higher the polymer dosage. In-line flocculation dosages tend to be higher than required for dewatering the same tailings in a thickener (with a dilute feed stream).

The macro structure created allows the tailings to be stacked which facilitates dewatering and consolidation of the tailings pile. This stacking characteristic of inline flocculated tailings may make it unsuitable where a long shallow tailings beach is required. The degree of stacking can be controlled by tailoring the polymer dosage.

The macro structure improves the dewatering rate allowing the tailings to become trafficable sooner than for conventional tailings. For small operations, the dewatering of an in-line flocculation facility and subsequent land reclamation can be within the span of a few months.

While the capital costs are low, the operating costs of an inline flocculation operation are typically higher than for tailings thickened to the same solids concentration due to the higher reagent costs and labor requirements for the operations. In-line flocculation is an ideal tool for use during times of emergency when the main dewatering process is unavailable. Further work is required to better understand and quantify the long-term impact of the polymer on tailings consolidation.

In-line tailings amendment

At the Horizon oil sand operation, Canadian Natural has developed a method for injecting CO_2 into their tailings pipelines to enhance the tailings settling rate. The addition of CO_2 reduces the tailings slurry pH, thereby reducing the tailings rheology and so increasing the settling and consolidation rate. This allows for quicker recycle of the process water reducing the volume of water stored on the tailings facility; Canadian Natural claim this process reduces the pond to half the size it would have been without CO_2 injection (Canadian Natural, 2019). Canadian Natural has installed a CO_2 recovery plant at Horizon's hydrogen plant with the capacity to capture 438,000 tonnes of CO_2 annually. Research is continuing to confirm that the CO_2 remains sequestrated within the tailings.

Carbon sequestration

Power et al. (2014) note that while the mining industry is a major greenhouse gas (GHG) emitter, due to their mineralogical composition and reactive surface area the tailings from some mines have potential to

mineralize carbon and so offset GHG emissions. Research has focussed on tailings from ultramafic and mafic ores which are amendable to carbon mineralization due to their high content of magnesium-silicate and hydroxide minerals. Felsic ores may also be suitable for carbonation reactions but due to their low reactivity little attention has been placed to date on these ores.

An investigation at the Mount Keith Nickel Mine in Western Australia has demonstrated that about 11% of the GHG emissions from the mine are currently being passively sequestrated by the tailings facility (Wilson et al., 2014). The tailings have the potential to sequestrate about ten times the mine's GHG emissions. The authors propose various strategies for accelerating carbon mineralization which include changing the current tailings management practice to extend tailings exposure to the atmosphere. This will require a larger surface area for the tailings facility and likely increase water losses. Despite these challenges it is evident there is significant potential to utilize tailings to offset not only the mine's GHG emissions but also potentially the emissions of other industries.

Emerging technologies

There are several technologies being developed to enhance tailings dewatering, these include microwave, microbial and electro-kinetic dewatering. While these technologies have not yet been implemented on a large scale, they will increasingly be considered for tailings projects where reducing water content is a key-driver. Their application appears promising for the dewatering of the fine tailings with engineered tailings.

There is opportunity to reduce the volume and/or improve the quality of tailings stored through additional processing to create commercially valuable by-products. This is done successfully with platinum and gold tailings (chromite and uranium) and possibly in the future with oil sand and phosphate tailings (heavy minerals and uranium).

Process technology selection

Clearly there is no single process solution for creating better tailings facilities, but rather a growing number of options in our "toolbox" from which to develop appropriate tailings systems. It is important that process, geotechnical, geochemistry, and environmental disciplines work together in an integrated team to ensure the best overall solution is identified for each unique operation. In assessing the available options, the following factors should be considered from a process perspective:

- Grind and mineralogy. These factors define not only which process options are suitable for dewatering and transporting the tailings, but also the geotechnical and geochemistry performance of the tailings in the deposit.

- Tonnage. Some technologies are too expensive or complex for implementation for large tonnage operations. Other technologies, such as paste thickening, have not scaled reliably to large tonnage applications.
- Water and energy. The quality, scarcity, and cost of water are key factors in assessing the degree of dewatering that is economically feasible. However, energy requirements increase with the degree of dewatering, and so water usage and energy consumption need to be appropriately balanced.
- Technology. There needs to be a recognition that implementation risk for new technologies can be high and that this risk generally increases with tonnage. When possible, the simplest solution is generally the best solution.

Conclusions

This paper has reviewed a range of technologies and approaches to create better tailings facilities in terms of stability, environmental impact, and societal acceptance. Specifically, the engineered tailings concept is seen as the way forward to optimize the tailings dewatering, transport, and storage characteristics. There is no doubt that these methods will continue to improve as the future of mining is dependent on how well we manage our tailings facilities.

References

Duffy, K., W. Valery, A. Jankovic and P. Holtham. 2015. Integrating bulk ore sorting into a mining operation to maximise profitability. In D. Pollard, G. Dunlop and P. Cameron, editors. *MetPlant 2015. Proceedings MetPlant 2015*, Perth, The Australasian Institute of Mining and Metallurgy, Melbourne: 273–287.

Canadian Natural. 2019. Managing tailings. Retrieved from https://www.cnrl.com/corporate-responsibility/advancements-in-technology/managing-tailings.

Martinson, R., J. Engels and G.I. McPhail. 2015. High density thickened tailings – new design challenges in transportation and deposition. In S. Barrera, editor, *Tailings 2015. Proceedings of the 3rd International Seminar on Tailings Management*, Santiago. Gecamin: 19–21.

McPhail, G.I. 2018. Beach prediction experience to date: further development and review of the stream power-entropy approach. In R.J. Jewell and A.B. Fourie, editors. *Paste 2018. Proceedings of the 21st International Seminar on Paste and Thickened Tailings*, Perth. Australian Centre for Geomechanics: 5–20.

Morgenstern, N.R., S.G. Vick and D. Van Zyl. 2015. *Independent Expert Engineering Investigation and Review Panel Report on Mount Polley Tailings Storage Facility Breach*. Province of British Columbia.

Power, I.M., J. McCutcheon, A.L. Harrison, S.A. Wilson, G.M. Dipple, S. Kelly, C. Southam and G. Southam. 2014. Strategizing carbon-neutral mines: A case for pilot projects. *Minerals 2014* 4(2): 399–436.

Robinsky, E.I. 1978. Tailings disposal by the thickened discharge method for improved economy and environmental control. In G. Argall, editor, *International Tailing Symposium 1978. Proceedings of the 2nd International Tailing Symposium*, Denver. Miller Freeman Publications Inc., San Francisco: 75–91.

Stowe, J.Q., R. Cooke, I. Farrell and R. Martinson. 2018. Design considerations for distributed tailings deposition systems. In *Tailings and Mine Waste 2018. Proceedings of the 22nd International Conference on Tailings and Mine Waste*, Keystone. Colorado State University: 35–42.

Wilson, S.A., A.L. Harrison, G.M. Dipple, I.M. Power, S.L.L. Barker, K.U. Mayer, S.J. Fallon, M. Raudsepp and G. Southam. 2014. Offsetting of CO^2 emissions by air capture in mine tailings at the Mount Keith Nickel Mine, Western Australia: Rates, controls and prospects for carbon neutral mining. *Int. J. of Greenhouse Gas Control* (25): 121–140.

Proceedings of Tailings and Mine Waste 2019
November 17–20, 2019, Vancouver, Canada
Published by the University of British Columbia, 2019

Utilizing Native Plants to Increase the Strength and Solids Content of Treated Oil Sands Tailings

Scott Laberge, University of Alberta, Canada
Nicholas Beier, University of Alberta, Canada
Amanda Schoonmaker, Northern Alberta Institute of Technology, Canada

Abstract

The oil sands of northern Alberta produce significant quantities of clay-rich tailings, containing clay particles less than 44 microns in size that can take centuries to settle. Determining ways to increase the rate at which ultra-soft deposits consolidate and strengthen is a key research area for the oil sands mining industry. Achieving an improved speed of reclamation and reducing the environmental impact of these tailings are essential desired outcomes of this study.

One technology being studied is the use of native plant species such as slender wheatgrass (*Elymus trachycaulus*), sandbar willow (*Salix interior*), and water sedge (*Carex aqualitis*) to speed the rate of dewatering that occurs in the deposits through evapotranspiration of the trapped water. These plants offer a sustainable method for increasing the rate of dewatering and therefore reclamation of tailings in the oilsands of Alberta.

This study examines the impacts these species have on the rate of dewatering, and the geotechnical characteristics of treated fine tailings. Plants were split into five plastic totes of approximately one cubic metre of volume of treated tailings, and data concerning water contents, shear strengths, water table drawdown, and matric suction were measured to compare the effects of these plants on the treatment of this tailings material. Four of the totes had a species planted or seeded in them, while one tote had no vegetation to allow for a comparison to a controlled, unmodified sample set. The totes were kept outside and open to the elements, and weather data including precipitation and temperature were also collected. The vegetation metrics of percentage cover, leaf area, and biomass were also collected to compare the viability of these plants in the treated tailings material. These metrics were contrasted with geotechnical data to determine if there were any correlations between these vegetation metrics and the solids content and strength of the tailings in these totes. This data was taken over an approximately four-month period at NAIT's Centre for Boreal Research in Peace River, Alberta. This paper will discuss the impacts of these plant species on the dewatering of the treated tailings.

Introduction

Mining operations in the Athabasca oil sands deposit of northern Alberta, Canada, produce significant quantities of clay-rich tailings as a result of extracting bitumen from oil-laden sands. One of the most significant challenges facing the industry is how to achieve more rapid dewatering of these fluid fine tailings (FFT). These tailings are known to have low strength and low consolidation rates due to their relatively low densities and permeability (Kasperski and Mikula, 2011). As of 2017, there was in excess of 1,240 Mm^3 of these tailings in storage across these oil sands mining sites (Alberta Energy Regulator, 2018).

The Government of Alberta and the Alberta Energy Regulator (AER) have replaced Directive 074 with the new Directive 085, which stipulates that these fine tailings deposits must reach a ready-to-reclaim state within 10 years (Alberta Energy Regulator, 2017). This has further pushed the industry to develop new ways to speed the rate at which strength gain can be achieved in these fine tailings deposits. One of these technologies is the use of plants to speed the dewatering of these tailings through evapotranspiration (Boswell et al., 2012).

Using plants to dewater tailings was first studied in the 1990s, with work by Johnson et al. (1993) and Silva (1999). Research has continued to demonstrate that plants could survive and assist in the dewatering of these tailings, as well as provide reinforcement as a result of their root systems developing at depth and near the surface (Renault et al., 2003; Renault et al., 2004; Wu, 2009; Schoonmaker et al., 2018; Smith et al., 2018).

The objective of this study was to determine the ability of three native boreal forest plant species to establish and persist in amended tailings. The study's key focus was to evaluate the potential for these plants to dewater the amended tailings material to a greater degree relative to evaporative drying. The study took place from June to October, 2018. Parameters including water content, shear strength, settlement, and matric suction were recorded to compare the dewatering and strength gain in each tote.

Materials and Methods

This study used five one cubic metre plastic totes, containing centrifuged cake tailings from an oil sands mine site in northern Alberta. The totes were placed outdoors and exposed to the elements at NAIT's Centre for Boreal Research in Peace River, Alberta. The totes were initially in storage and sampled at a lab at the University of Alberta in Edmonton, which led to some water release and pooling at the surface of the totes. After moving them to the study site in Peace River, most of the excess water was decanted using a bucket before planting, and the material was sampled to determine initial moisture content within the totes. The totes remained sealed on the bottom, representing a single drained consolidation process in this study.

The plant species used included slender wheatgrass (*Elymus trachycaulus*), sandbar willow (*Salix interior*), and water sedge (*Carex aqualitis*). The *Carex* (grown from seed) and *Salix* (grown from unrooted cutting) were both grown in a greenhouse prior to planting in the totes. Slender wheatgrass was introduced as seeds, and the initial seeding was 70 g per tote. After planting, a small quantity of fertilizer was added to the totes. These fertilizers included 15 g each of starter fertilizer (29-59-14) and urea (46-0-0), in addition to 500 g of alfalfa (Western Alfalfa Milling Co. Ltd, Norquay, Saskatchewan). These provided additional nutrients, nitrogen in particular, to better facilitate establishment and growth of the plants.

Each of the five totes contained a different selection of these species to allow for the comparison in dewatering and strength gain between each plant species. Tote A contained *Carex aqualitis*, which was transplanted from the greenhouse into the tailings. Tote C contained *Salix interior* plants that were also transplanted from the greenhouse. Tote D was seeded with an initial 70 g of *Elymus trachycaulus* seeds, and Tote E contained all three species. Tote B contained no plant species to provide a "control" tote for comparison with the vegetated totes.

Electronic sensors (Meter Group Inc., previously Decagon Devices Inc., 2016, 2017) were installed 25, 50, and 75 cm below the initial surface in each tote, and were connected to Decagon D50 data collectors (Meter Group Inc., previously Decagon Devices Inc., 2015). The data collected by these sensors included hourly measurements of matric suction, volumetric water content, temperature, and electric conductivity. The air entry value of the ceramic used in the MPS-6 sensors is equal to –9 kPa, therefore values equal or greater than this value was taken as reading between 0 kPa and –9 kPa.

Other metrics determined manually in the totes included height measurements, water table depth below surface, moisture content of the crust, and undrained shear strength. Settlement in the totes was measured by the change in surface height over time. This was determined as the distance between the bottom of a transect placed diagonally across the tote and the tailings surface. The transect was constructed from wooden survey stakes, and five measurements were taken along the length of the transect to give a mean settlement rate of the tailings in the totes. Water table measurements were collected using a piezometer, located in the centre of the tote, which was constructed from PVC pipe with holes drilled throughout its length and an open bottom wrapped in a fine mesh nylon material that allowed the movement of water but not solids. Both these measurements were taken on a weekly basis. Strain was also calculated from this settlement data by dividing the total settlement overtime by the initial thickness of the tailings in each tote.

The solids content of the crust was measured at three time intervals over the course of the growing season, using a 10 cm length auger to remove samples at depth intervals of 0–10 and 10–20 cm. The auger samples were placed in sample tins and dried for a minimum of 48 hours (or until weight constancy). The

change in mass was taken to be the quantity of water contained within the sample. Sampling was attempted at greater depth but was unsuccessful due to challenges recovering a sufficient quantity of sample.

Undrained shear strength was taken in situ using a handheld Geonor H60 (Geonor Inc., 2018) vane tester which was calibrated to an error of 10%. Three vane sizes were used to take these measurements based on the strength of the centrifuge cake: 16 mm diameter by 32 mm height, 20 mm diameter by 40 mm height, and 25.4 mm diameter by 50.8 mm height. Measurements were taken in September at 25, 50, and 75 cm below surface and compared against the initial strength of the centrifuged cake tailings of 345 Pa (Rima and Beier, 2018). The liquid and plastic limit of the tailings material was 57% and 26% respectively (Schafer and Beier, 2019).

Weather data was collected via a station located within ten m of the totes. This station collected precipitation (rainfall), air temperature, and wind speed and direction, with data recorded hourly.

Vegetation growth was measured in four surface quadrants (~0.25 m^2) in each tote. At each quadrant, the following was collected: percentage ground area covered and above ground biomass where all leaf tissue was harvested, dried, and weighed.

Results

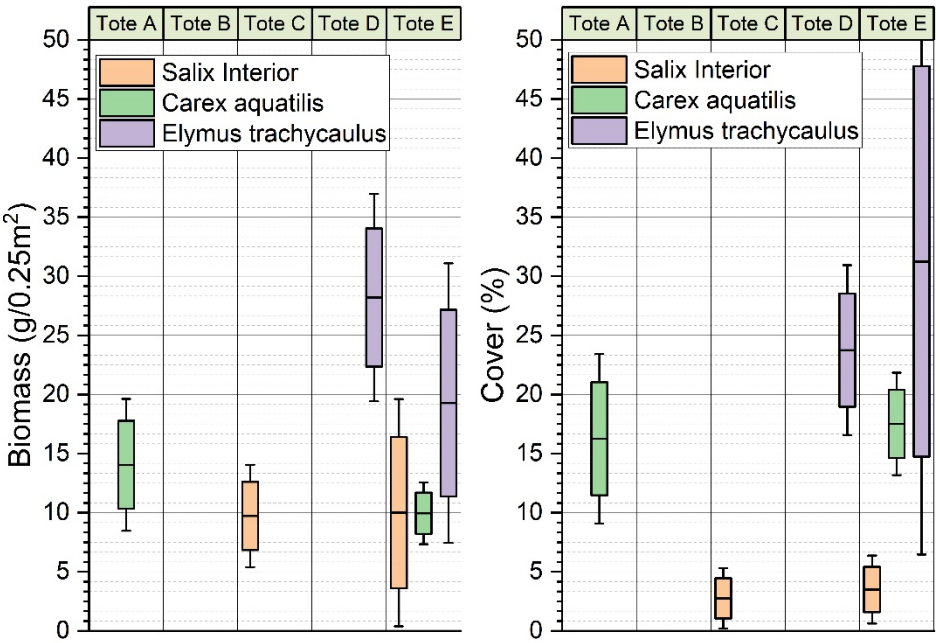

Figure 1: Percentage of cover (area covered by vegetation) and biomass (dry weight of above-surface plant biomass) of *Salix interior*, *Carex aquatilis*, and *Elymus trachycaulus* in each tote after one growing season (May – October, 2018). The mean is represented by the black horizontal line in each box of the plot, and the error bars represent one standard deviation from the box of each plot

All three species demonstrated observable growth in these tailings. *Elymus trachycaulus* had the greatest cover and biomass accumulation of the three species, while leaf biomass (though not cover) was similar between *Carex aquatilis* and *Salix interior* (Figure 1).

Figure 2: Image of (i) Tote B after decanting on day 0, (ii) Tote B after 91 days of drying, visible desiccation of surface (iii) Tote E after decanting and planting of all three plant species, (iv) Tote E after 91 days of drying, showing significant plant growth and desiccation of the surface

Development of an approximately 10 cm thick crust with significant desiccation and cracking was observed (Figure 2(ii)). Shrinkage resulted in pulling from the sides of the tote, and cracking was observed on the surface of all five totes; even after large precipitation events these cracks did not fully close.

There was a sustained drawdown of the water table over time in all five totes. There was a sudden rise in the water table after the major rain events around day 37 and day 78. Between these two events, all totes experience a prolonged period of drying that resulted in a drawdown of the water table in all five totes.

All totes recorded an initial volumetric water content of approximately 37% which reduced during drying cycles and increased during periods of rainfall. The sensor located 25 cm below the surface in Tote B, Tote C and Tote E reached maximum volumetric water contents of approximately 43%. Tote D and Tote A both reach an approximate peak volumetric water content of 35%. All totes except for tote A peaked after the first large rainfall event around day 40. Tote A reached its peak after the second significant rainfall around day 80 (Figure 3). The volumetric water content then continued to decrease in all totes until an apparent rewetting occurred around day 80. All totes experienced an increase in water content after this second rainfall, however; Tote D was the only tote that had sustained redrying after this rain event (Figure 3(ii)). Tote D had a minimum volumetric water content of less than 5%, reached around day 110 before rising again to approximately 13%, which was the lowest among all five totes.

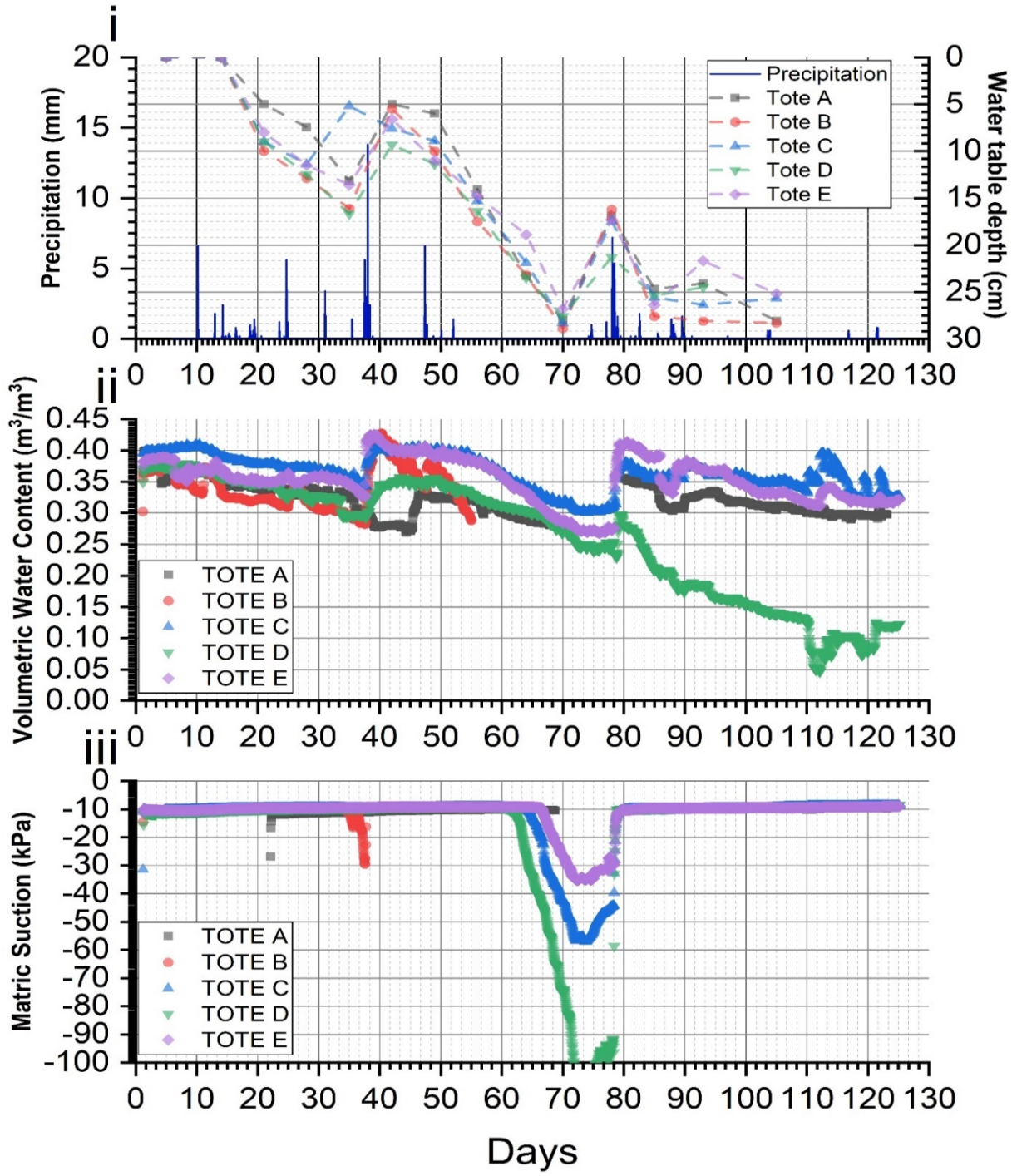

Figure 3: (i) Precipitation as recorded by weather station is plotted with the change in the depth of the water table below the tailings surface over time; (ii) The volumetric water content over time at 25 cm depths of each tote; (iii) Matric suction is plotted for all five totes over time at 25 cm depth. Tote B data after day 55 is excluded from (ii) and (iii) due to meaningless data likely due to development of a crack or air pocket. Tote A data at 25 cm depth was corrupted between day 68 and 80, explain the gap in plots (ii) and (ii). The sensors at 50 cm and 75 cm recorded no noteworthy data and were also excluded

An increase in matric suction was measured at the 25 cm depth after a long period of relative dryness. There was a steady increase in the magnitude of matric suction from day 68 to 75 in all totes until the second major rain event led to a decrease as the material became rewetted. The greatest suction was experienced in Tote D, which reached a maximum suction greater than 100 kPa on day 73. Totes C and E reached suctions of 55 kPa and 35 kPa respectively, after the second major rain event on day 78. All totes then returned to a matrix suction less than the air entry value of the instruments and could not be measured.

The initial gravimetric moisture content of the centrifuge cake at the beginning of the study was 56.9% and 56.8% for Totes B and E, respectively. There was a period of drying over the first 60 days of the study that reduced the moisture content in the top of the crust to less than 20% in both Totes B and E. The tailings at 10 cm to 20 cm depth had a minimum moisture content of less than 35% for all totes except Tote A (Figure 4). Tote A likely experienced an increased amount of drying relative to the other totes due to it being the smallest tote with the shallowest sample of tailings. All totes experienced rewetting and increases in moisture content after the large rain event on day 78 of the study.

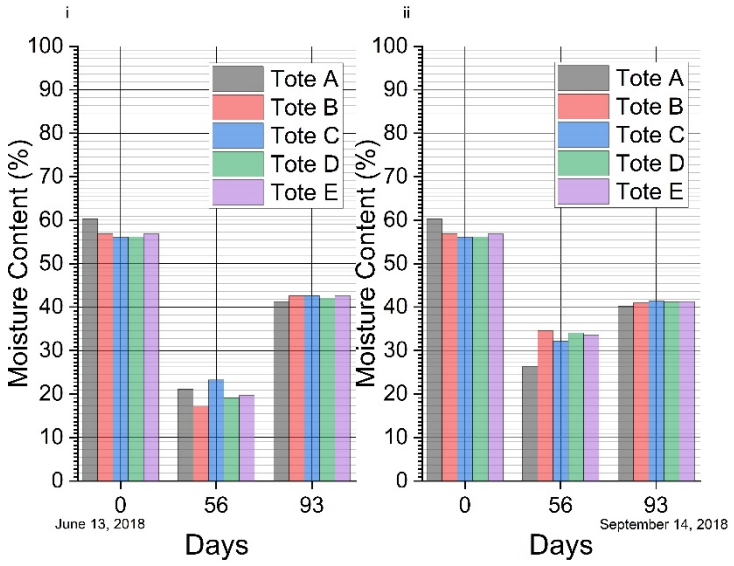

Figure 4: Moisture content (%) of totes at a depth of (i) 0–10 cm and (ii) 10–20 cm. Collected three times on June 13th (day 0), August 08th (day 56), and September 14th (day 93)

All totes experienced a maximum settlement of approximately 8 cm (Figure 5(i)). After the large rain event on day 38, all totes experienced very little swelling due to rewetting, except for the unvegetated Tote B. Tote B experienced a swelling of more than 1% and took a further 20 days to shrink again and return to a total settlement similar to the other four totes. The tailings in the other totes experienced little to no swelling after the major rain event compared to Tote B.

The shear strength of the totes near the end of the study (day 94), was compared to the initial strength of the centrifuge cake of 345 Pa (Rima and Beier, 2018). Shear strength measurements were taken at 25 cm,

50 cm, and 75 cm depths from the tailings' surface. The tailings in all totes experienced a strength gain from their original state, with Tote E showing the greatest overall strength gain, peaking at nearly 13 kPa (Figure 5). Higher relative strength near the bottom of the tote could be attributed to initial rapid settlement at the base of the totes that then consolidated and further strengthen over time. Based on a visual inspection of the crust and previous work by Beier (2015), we can conclude that the crust was over-consolidated while the remainder of the tailings sample below the crust was normally-consolidated. All totes experienced similar settlement of 8 cm, except for Tote A which was slightly less at 7 cm (Figure 5).

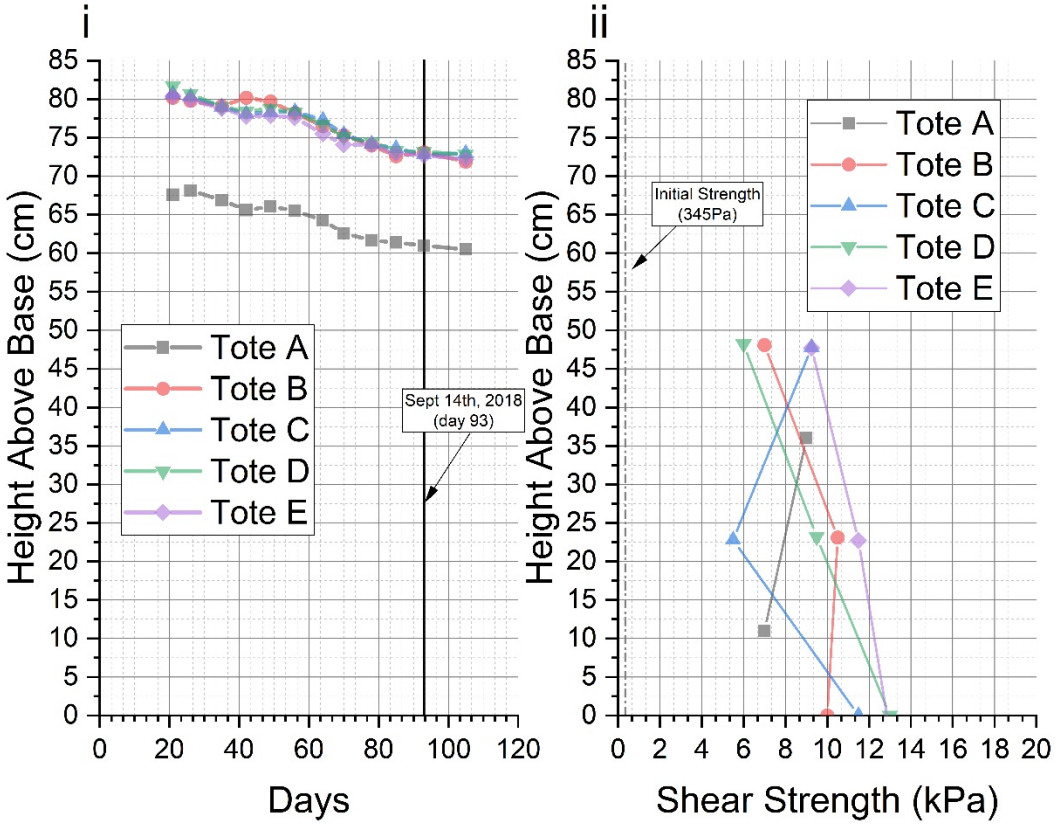

Figure 5: (i) Settlement of the tailings surface relative to the base of the tote demonstrating consolidation over time. Sept 14 (day 93) is highlighted for comparison to: (ii) Showing the shear strength at three depths (relative to tailings surface) in each tote. Tote A was too shallow for a third point at 75 cm depth. The initial strength of the tailings of 345kPa is also shown

The maximum and average shear strength was plotted against the vegetation biomass and cover to determine the existence of any relationship between plant growth and strength in the totes. A relationship was found to exist between peak shear strength and the plant metrics of biomass and cover, with an r-squared value of 0.23001 for peak shear vs. average biomass (Figure 6).

Tote A had poor strength gain relative to the biomass and cover, and had lower peak and average strength compared to Tote B which contained no plants. This suggests that *Carex aquatilis* was the least effective at dewatering and strength gain in this type of tailings material. Tote E, which contained all

species, consistently performed well with the greatest strength and the greatest plant growth. Tote D, which contained only *Elymus trachycaulus*, also performed well compared to the control and *Carex*-only totes.

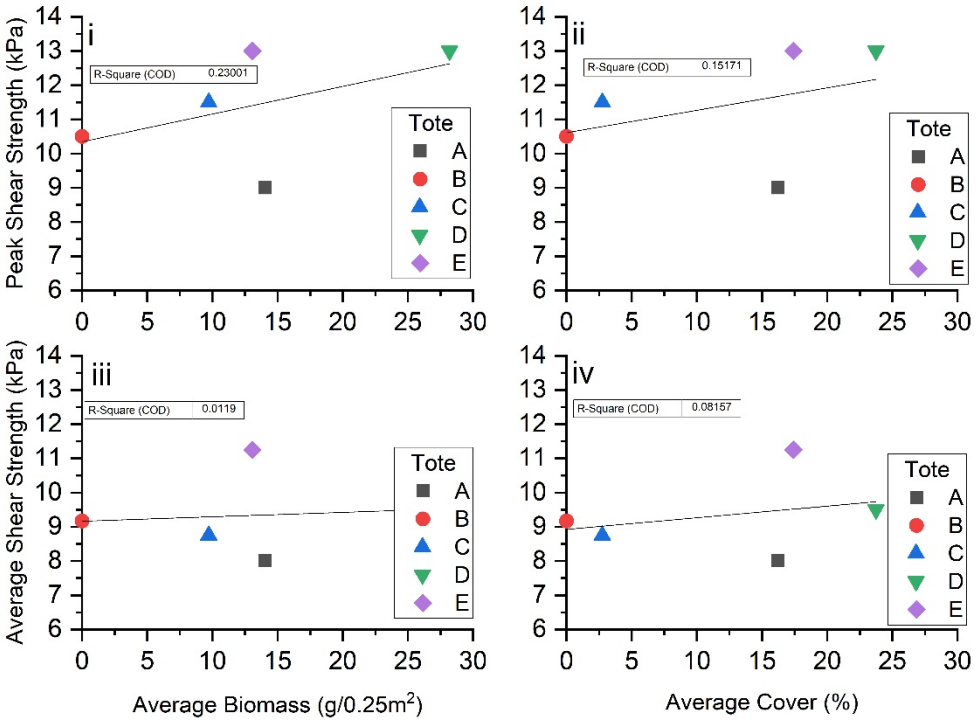

Figure 6: Average shear plotted against average biomass (iii) and average cover (iv). Peak shear strength was also plotted against average biomass (i) and average cover (ii). A linear trendline was calculated for each data set and the r-squared value is shown

Conclusion

This study demonstrated that these species can grow on centrifuge tailings cake material and, combined with evaporation, can contribute further to dewatering through evapotranspiration. A major contribution of the plant species in this study was their assistance in managing new water inputs during major rain events. Totes containing plant species were observed to swell significantly less relative to the tote containing no plants after rewetting. This suggests an uptake by the plants that prevented the same quantity of water being reabsorbed by the tailings. Totes containing plants still experienced water table rises after such a rain event, but to a lesser degree when compared with the control tote. This further indicates that the introduction of plants into a tailings cake material can improve the tailings material's ability to buffer the impacts of significant precipitation events.

The study also showed that, in general, the totes containing larger quantities of leaf mass (and therefore evapotranspiration potential) also had greater average and maximum shear strengths. Totes containing *Elymus trachycaulus* and *Salix interior* generally showed greater strength relative to the tote

planted with *Carex aquatilis* only. This may be attributed to the ability of the woody *Salix* and *Elymus* to quickly establish extensive fibrous root systems (Renault et al., 2004; Wani et al., 2011). This allows these species to be more adept at extracting moisture from tightly bound soils such as oil sands clays. In conclusion, *Elymus trachycaulus* and *Salix interior* are the more effective species at strength gain in the totes, and would be the best species to be included in future studies. This was also a conclusion reached by Smith et al. (2018).

Future research should aim to develop a complete strength and solids content profile throughout the depth of the totes. Biomass below the surface should also be collected to determine the impacts of deeper root depths on increasing solids content and strength, as well as contrast the potential difference between fine root species such as the *Salix* and *Elymus*, and wetland species with lesser root development such as the *Carex*.

Acknowledgements

The authors would like to acknowledge Kaela Walton-Sather, as well as other research assistants and laboratory technicians at NAIT and the University of Alberta, for their assistance in data collection and solids content determination in the totes.

References

Alberta Energy Regulator. 2017. Directive 085 – fluid tailings management for oil sands mining projects. Alberta Energy Regulator.

Alberta Energy Regulator. 2018. State of fluid tailings management for mineable oil sands, 2017. Calgary, Alberta, Canada.

Beier, Nicholas Alvin. 2015. Development of a tailings management simulation and technology evaluation tool. University of Alberta.

Boswell, Jeremy, Mickey Davachi and John Sobkowicz. 2012. Oil sands tailings technology deployment roadmap project report – Volume 22: 166. Retrieved from http://www.ai-ees.ca/media/7361/1906-component_1_report.pdf.

Decagon Devices Inc. 2015. Em50/Em50R/Em50G Em50 Series Data Collection System, Operator's Manual. Version: June 25, 2015 – 14:00:15. Pullman, Washington, 81 Pp. https://www.edaphic.com.au/wp-content/uploads/2018/02/Decagon-Em50-and-Em50G-Manual-June-2015.pdf.

Decagon Devices Inc. 2016. 5TE Water Content, EC and Temperature Sensor, Operator's Manual. Version: March 11, 2016 – 11:55:57. Pullman, Washington, 26 Pp. http://manuals.decagon.com/Retired and Discontinued/Manuals/13509_5TE_Web.pdf.

Decagon Devices Inc. 2017. MPS-2 & MPS-6 Diaelectric Water Potential Sensors, Operator's Manual. Version: July 10, 2017 - 16:08:16. Pullman, Washington, 30 pp. Retrieved from http://manuals.decagon.com/Retired and Discontinued/Manuals/13509_5TE_Web.pdf.

Geonor Inc. 2018. H-60 Hand-Held Vane Tester, Data Sheet. Augusta, New Jersey. 2 pp. Retrieved from http://geonor.com/live/products/geotechnical-test-equipment/h-60-hand-held-vane-tester/.

Johnson, R.L., P. Bork, E.A.D. Allen, W.H. James, L. Koverny and Alberta Environmental Centre. 1993. Oil sands sludge dewatering by freeze-thaw and evapostraspiration.

Kasperski, K.L., and R.J. Mikula. 2011. Waste streams of mined oil sands: Characteristics and remediation. *Elements* 7(6): 387–92. doi:10.2113/gselements.7.6.387.

Renault, Sylvie, Mike MacKinnon and Clara Qualizza. 2003. Barley, a potential species for initial reclamation of saline composite tailings of oil sands. *Journal of Environmental Quality* 32(6). *Madison: Am Soc Agronom:* 2245–53. Retrieved from http://jeq.scijournals.org/cgi/content/abstract/32/6/2245.

Renault, Sylvie, Clara Qualizza and Mike MacKinnon. 2004. Suitability of altai wildrye *(Elymus angustus)* and slender wheatgrass *(Agropyron trachycaulum)* for Initial reclamation of saline composite tailings of oil sands. *Environmental Pollution* 128(3): 339–49. doi:10.1016/j.envpol.2003.09.009.

Rima, Umme Salma and Nicholas Beier. 2018. Evaluation of temperature and multiple freeze-thaw effects on the strength properties of centrifuged tailings. In *GeoEdmonton* 2018, 71st Canadian Geotechnical Conference. Edmonton, Alberta, Canada.

Schafer, Haley L. and Nicholas A. Beier. 2019. Estimating the SWCC from the SFCC for mine waste tailings using TDR. *Canadian Geotechnical Journal* 1–52. doi:10.1139/cgj-2018-0145.

Schoonmaker, Amanda, Dani Degenhardt and Trevor Floreani. 2018. Evaluating the potential to establish plants to aid in dewatering of an atmospheric fine drying tailings deposit at Muskeg River Mine. In International Oil Sands Tailings Conference, 209–20. Edmonton, Alberta, Canada.

Silva, Marvin Jose. 1999. Plant dewatering and strengthening of mine waste tailings. University of Alberta.

Smith, William, Erin Olauson, Jack Seto, Amanda Schoonmaker, Reza Moussavi Nik, Gavin Freeman, and Gord McKenna. 2018. Evaluation of strength enhancement and dewatering technologies for a soft oil sands tailings deposit. In International Oil Sands Tailings Conference, 211–20. Edmonton, Alberta, Canada.

Wani, Bilal Ahmad, Amina Khan and R.H. Bodha. 2011. Salix: A Viable Option for Phytoremediation. doi:10.4314/ajest.v5i8.72048.

Wu, Shihong. 2009. A greenhouse study of selected native plant species for dewatering CT. University of Alberta.

Proceedings of Tailings and Mine Waste 2019
November 17–20, 2019, Vancouver, Canada
Published by the University of British Columbia, 2019

Stabilization of Copper Porphyry Tailings with Tailings-Glass Geopolymer Solidification

Donald Lake, Terra CO2 Technologies, Canada

Abstract

Recent high-profile tailings dam failures have highlighted the shortcomings of subaqueous tailings storage as a general solution. Viable alternatives are desperately needed; however, the most widely supported "dry" storage options (e.g., dry stacking, co-disposal of tailings and waste rock, lined/covered impoundments, etc.) also have vulnerabilities, limitations, and significant up-front costs. Nevertheless, most of these shortcomings can be overcome through the use of geopolymer binders to realize the long-term stabilization of mine tailings. Indeed, many previous studies have demonstrated the main advantages of geopolymer binders in this application: impermeability, acid-resistance, long-term chemical stability, pumpability, and more.

Low-cost geopolymer binder made from tailings could improve the effectiveness of dry methods for long-term tailings storage, and provide a permanent low-maintenance alternative to existing mine closure options. In this study, copper porphyry mill feed tailings from a deposit in Argentina were solidified using a synthetic glass-based geopolymer binder made from the tailings themselves. The tests used mix designs intended for a cemented paste tailings application. Compressive strength and static acid-leaching performance in acetic acid (pH ~2.4) were assessed. Geopolymer mix designs leached significantly lower values of metals (V, Fe, Co, Cu, Zn, As, Cd, Pb) than comparable Portland cement mixes. Results indicate tailings-glass geopolymer is a promising tailings solidification/stabilization method. Detailed techno-economic analysis and changes to process requirements imposed by this technique will need to be addressed.

Introduction

There is an urgent need to develop safe and permanent mine tailings storage methods that present little risk of long-term failure. Solidification and stabilization (SS) methods are one of the most promising tools that can potentially solve this problem (Malviya and Chaudary, 2006). Within the scope of SS, one may look to natural analogs such as the diagenesis of clastic sediments to provide inspiration for relatively cost-effective inorganic cements.

Ideally, mines could extract the valuable elements they seek without the need to finely grind a large proportion of waste rock at significant expense. In-situ leach processes may eventually provide such a solution, but the approach does not seem generally applicable for the foreseeable future (Sinclair and Thompson, 2015). Until such time, mines will continue to produce a lot of inconvenient finely ground rock tailings.

Storing tailings is problematic in the long term due to the incredible volumes of material, fine grain size, complex contaminants, and economic requirement for extremely low cost per tonne storage (typically $0.5–5 USD/tonne, Carneiro and Fourie, 2019). The most common solution that meets the minimum requirements in the short term has been subaqueous storage behind earthen dams (Davies, 2011).

Short-term subaqueous tailings storage is very practical, but as a permanent storage solution dams are generally inadequate (Roche et al., 2017). Many tailings dams contain tailings that exist in an unstable, or metastable state with respect to gravitational potential energy, and chemical potential energy. It is not surprising that over time nature attempts to find equilibrium, sometimes dramatically, and at the expense of human life (Morgenstern et al., 2016). If a typical impoundment fails at any time in the future, untreated tailings will discharge into the environment and potentially cause contamination (Fourie et al., 2012). Dewatering, lining and covering impoundments is possible and adequate in some cases (e.g., Power et al., 2017).

“Dry” stacking is an alternative tailings storage method that has been effective in certain environments and for certain tailings (Davies, 2011). Improved variations on dry stacking such as co-disposal with waste rock (Wickland et al., 2006) rely on optimized particle size distribution (much like optimized aggregate in concrete) to address deficiencies in previous methods. Co-disposal methods would best be considered complimentary to other solidification and stabilization methods; given the attention to particle size distribution in unconsolidated co-disposal approaches, adding a minimal amount of cement could create permanent, consolidated deposits.

Solidification reduces structural instability and reactivity of tailings by two methods. First, the tailings are stored in a “dry” (or more precisely, “not subaqueous”) structurally stable monolithic form with much higher compressive, tensile, and shear strengths than unconsolidated tailings. The second and most important mechanism: SS mitigates leaching by decreasing the reactive surface area of tailings by orders of magnitude. Other leaching mitigation mechanisms include reducing connected porosity.

Numerous studies have considered stabilizing mine tailings physically and chemically using geopolymerization approaches (Barrie et al., 2015; Caballero et al., 2014; Comrie, 2011; Davidovits, 1989; 1994; 2002; Paiva et al., 2019; Rao and Liu, 2015; Southam et al., 2007; Van Jaarsveld et al., 1997; 1999), and others have considered using mine tailings as a primary geopolymer feedstock with varying degrees of pre-processing to enhance reactivity (Ahmari and Zhang, 2013; Ahmari and Zhang, 2015; Allahverdi and

Mahinroosta, 2019; Capasso et al., 2019; Falah et al., 2019; Feng, 2015; Hart et al., 2006; Kinnunen et al., 2018; Kiventera et al., 2018; Misra et al., 1996; Pacheco-Torgal et al., 2008; Solismaa et al., 2018; Yu et al., 2017). Geopolymer cements could be useful for SS applications because they mitigate leaching of heavy metals and resist acids far better than ordinary Portland cement (Comrie et al., 1989; El-Eswed et al., 2015; Muhammad et al., 2018; Nikolic et al., 2014; Sato et al., 2019; Wang et al., 2018; Xia et al., 2019). Metakaolin-based geopolymer cements are a high-performance choice (Davidovits, 1994), but the cost of reagents is prohibitive except for low-volume, high-risk wastes (e.g., radioactive waste). If it is possible to make a cheaper geopolymer cement reagent from the local tailings, a solidification approach could reduce reactive surface area, and control drainage which would serve to decrease risk of environmental contamination over geologically-relevant time scales.

Tailings glass-based geopolymer stabilization of tailings

The approach to making a reactive mineral glass geopolymer reagent from tailings was to melt and quench aluminosilicate tailings minerals. This high-temperature route creates a reagent (similar to coal combustion fly ash, volcanic glass, etc.) that is reactive in a geopolymer binder system.

Methods

Sampling

A flotation tailings sample was generously provided from a copper porphyry project in Argentina. Copper porphyry tailings were used in this proof of concept due to their familiarity and global abundance.

Mineralogy

A sample of copper flotation tailings was reduced to the optimum grain-size range for quantitative X-ray analysis (<10 μm) by grinding under ethanol in a vibratory McCrone Micronizing Mill for 10 minutes. Continuous-scan X-ray powder-diffraction data were collected over a range 3 to 80°2θ with CoKα radiation on a Bruker D8 Advance Bragg-Brentano diffractometer equipped with an Fe monochromator foil, 0.6 mm (0.3°) divergence slit, incident- and diffracted-beam Soller slits and a LynxEye-XE detector. The long fine-focus Co X-ray tube was operated at 35 kV and 40 mA, using a take-off angle of 6°.

Tailings glass reagent preparation

Tailings were melted at approximately 1,200ºC using an oxy-fuel furnace built by Terra CO2 Technologies Ltd., then quenched. The resulting glassy tailings product was powdered in a ball mill until 95 wt.% passed a 45μm sieve (325 mesh).

Binder preparation

Binder mixes of several geopolymer systems were compared with Portland cement (commonly used for cemented backfill operations). Mix designs are given in Figure 1. Total water contents were designed at 20% (including binder water and tailings slurry together) and the final mixes have 15 to 20 wt.% water content which is much higher than is ideal for cements, but is at the margin of water content achievable using high-density thickeners for paste (20 to 25% moisture, Meggyes and Debreczeni, 2006). Using thickened tailings would be preferable to avoid the high cost of filter pressing. High binder dosages of 10 to 30% were used as a starting point. Further studies should aim to lower the dose.

Geopolymer mixes were prepared with tailings glass reagent, metakaolin (EPK Brand Georgia kaolinite calcined in a muffle furnace at 750ºC for 6 hours, with two-hour ramps and a two-hour hold), and a relatively user-friendly K-silicate solution (molar ratio = 1.45, water content considered part of total water content). Mix designs are divided by binder type (OPC or geopolymer). The sample naming convention provides weight percentages corresponding to the material abbreviations of the dry materials OPC – Portland cement, T – tailings, TG – glass made from tailings, and MK – Metakaolin. For example, OPC10-T90 consists of Portland cement and tailings at a 10:90 ratio.

Binders were mixed for 4 minutes and cast into sealed plastic cylinders. Portland cement samples should be cured for at least 28 days (and ideally for at least several months if pozzolanic effects aim to be considered) however due to time constraints of this study, the samples were cured for five days at 23ºC, then both the OPC samples and geopolymer samples were heat cured together (sealed) for 18 hr at 60ºC, followed by a final 1 hour at 80ºC.

Compressive strength

Compressive strength was measured using a cylinder compression test with a hydraulic pressure measurement platten in a hydraulic testing machine (Figure 2). Two specimens were evaluated for most samples (denoted by “A” and “B”).

Leaching procedure

A rapid leaching procedure was developed that is intended to simulate an aggressive long-term acidic tailings weathering case wherein the buffering capacity of excess alkalinity in solidified tailings is overwhelmed. The test was modified from the TCLP procedure (US EPA, 1992), which is not a suitable test for leaching of monolithic solidified tailings because it is performed on crushed material, and buffering capacity is not necessarily exceeded by the TCLP, which could cause misleading results. The modified procedure herein is only intended as a *relative* measure of metals leaching propensity under acidic pore fluid conditions. A better test, in future studies, would be the NEN 7375 Monolithic Leaching Test (EA NEN, 2005) that considers the effects of surface area and diffusion.

Figure 1: Mix designs (wt.%)

Other considerations that must be addressed in future are the potential for neutral leaching and effect on sulphate generation in sulphide-bearing tailings. One gram (1 g) of solidified tailings monolith left from the compressive strength test (passing 1 cm sieve, not passing 0.3 cm) was placed in Nalgene HDPE bottles with 20 g of pure lab-grade acetic acid (pH ~2.4). All samples were placed on a stir plate at 35 rpm for 18 h. The samples were decanted and filtered with a 1 µm filter and immediately sent for analysis. Leachate samples were analyzed for metals by (CRC) ICP-MS at ALS Environmental, Burnaby, Canada.

Results

The X-ray diffractograms were analyzed using the International Centre for Diffraction Database PDF-4 using Search-Match software by Bruker. X-ray powder-diffraction data of the samples were refined with Rietveld program Topas 4.2 (Bruker AXS). The results of quantitative phase analysis by Rietveld refinements are given in Table 1 and represent relative amounts of measured phases normalized to 100%. The estimated major element oxide chemistry of the sample was estimated from mineralogy (Table 2).

Table 1: Mineralogy of copper flotation tailings (qXRD)

Mineral	Ideal formula	Mill feed tailings
Calcite	$CaCO_3$	**0.7**
Clinochlore	$(Fe^{2+}, Mg)_5Al(Si_3Al)O_{10}(OH)_8$	**3.2**
Gypsum	$CaSO_4 \cdot 2H_2O$	**1.6**
Illite-Muscovite 2M1	$K_{0.65}Al_{2.0}Al_{0.65}Si_{3.35}O_{10}(OH)_2 – KAl_2AlSi_3O_{10}(OH)_2$	**23.7**
K-feldspar	$KAlSi_3O_8$	**10.6**
Plagioclase	$NaAlSi_3O_8 – CaAl_2Si_2O_8$	**24.0**
Pyrite	FeS_2	**0.1**
Quartz	SiO_2	**36.2**
	Total	**100.0**

Table 2: Major element oxide chemistry of tailings (est. from qXRD)

Element	Weight %
SiO_2	70
Al_2O_3	15
Fe_2O_3	0.5
MgO	2
CaO	5
Na_2O, K_2O	6

Compressive strength results are provided in Figure 2. OPC samples all cured acceptably, while the geopolymer mix designs in this study had relatively poor structural characteristics which can be explained by unoptimized reagent particle size, high water content of the mix design, and insufficient curing temperature/time. A heat-cured geopolymer mix design was used to expedite initial testing.

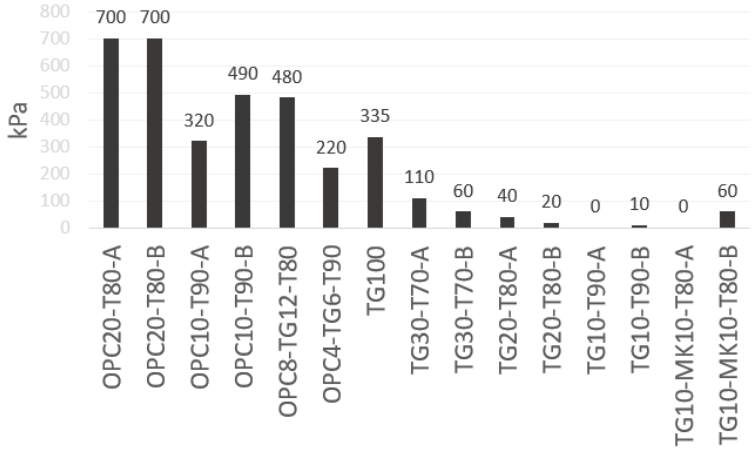

Figure 2: Compressive strength results (OPC = 7 day, GP = heat-cured, see text)

Acid "resistance" was qualitatively assessed by noting whether the sample lost structure or retained structure after the leaching procedure (Figure 3). Leaching in acetic acid for 18 h caused a complete loss of structure in all OPC cement samples, but some geopolymer mixes retained structure. Compressive strength was not measured post-leaching, but mixes TG100 and TG30 (Figure 3) were not visibly affected by the leaching test.

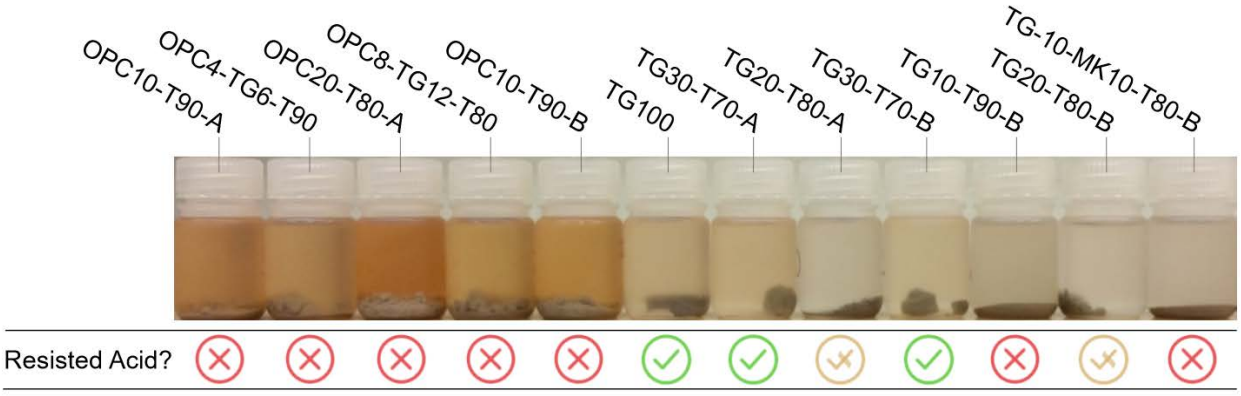

Figure 3: Acetic acid leaching test: several geopolymer samples did not degrade

Metals analyses of acid leachate are given in Figure 4. Tailings glass-based geopolymer mix designs returned lower metal values in leachate compared to all OPC mix designs. The leaching test was intended to rapidly estimate the long-term acid-leachable fraction of metals in a monolithic sample, and the results should only be considered relative to each other (no data on possible correlation with field leaching rates).

Discussion

Improvements to method

Future studies should improve upon the methods used in this work to achieve lower binder dosages, a more realistic curing procedure, and a more realistic long-term leaching test. In particular, a more realistic curing schedule would allow at least three months of ambient-temperature curing for both OPC and (ambient-cure) geopolymer mixes, prior to leaching tests. Similarly, a monolithic leaching test such as NEN 7375 (63-day duration) would provide a more accurate understanding of real-world leaching characteristics.

Leaching

The geopolymer mix designs all performed significantly better than OPC at containing heavy metals in an acidic environment. This was surprising because most of the geopolymer samples did not gain significant strength from the curing schedule prior to leaching, and it wasn't clear that curing was successful in some samples. Final pH measurements of the leachates were identical to initial pH measurements, as measured with a calibrated pH meter with accuracy of plus or minus pH 0.1. Having similarly low final pH for all samples was the intended consequence of using concentrated acid and a high acid to rock mass ratio (20:1).

It was expected that geopolymer mix designs with metakaolin would leach much less than a tailings glass-only geopolymer. However, the metakaolin-bearing geopolymer mixes in this study leached similarly low amounts for the elements considered – a result worth investigating further.

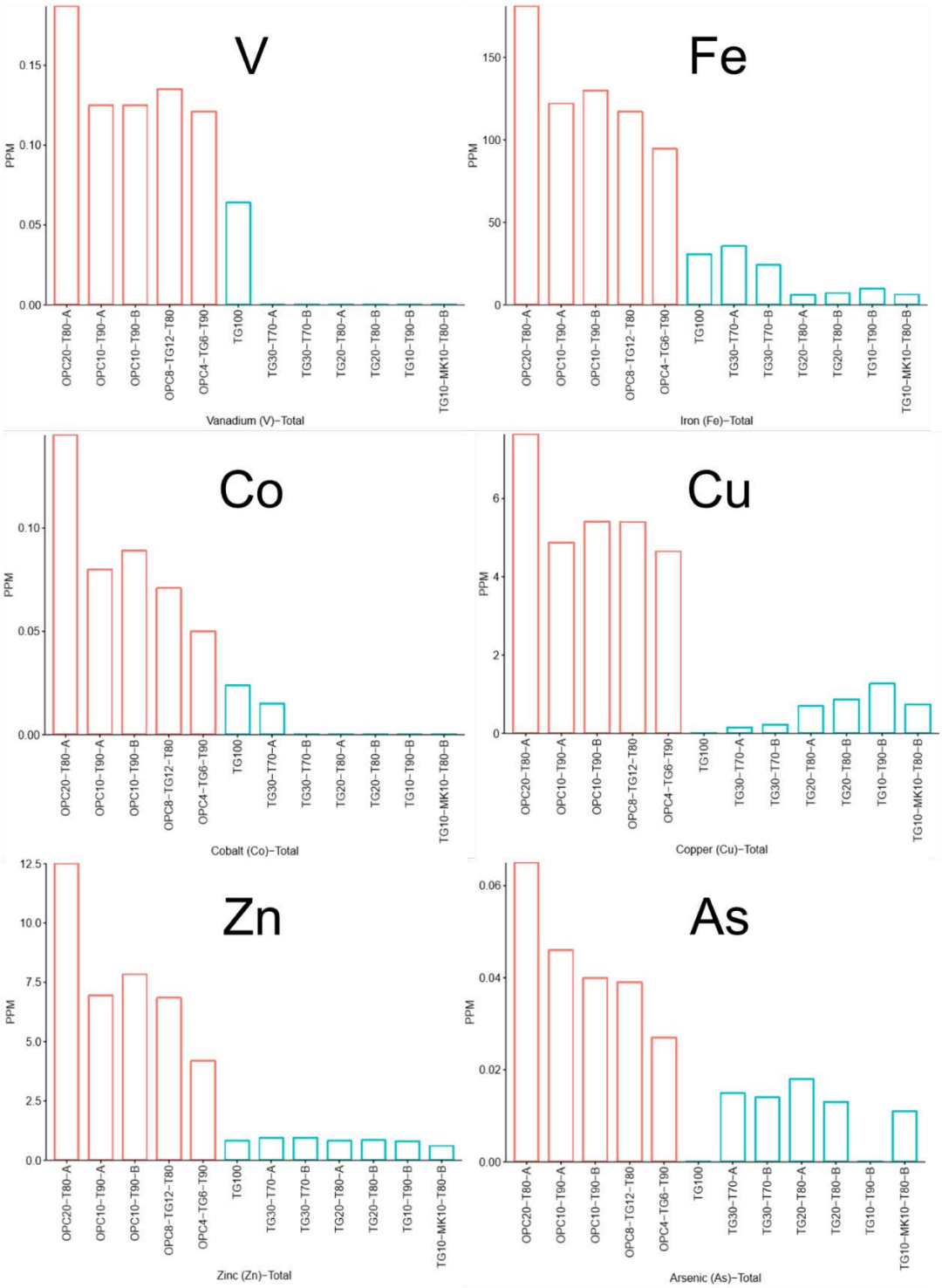

Figure 4: Acid leachate analyses for metals

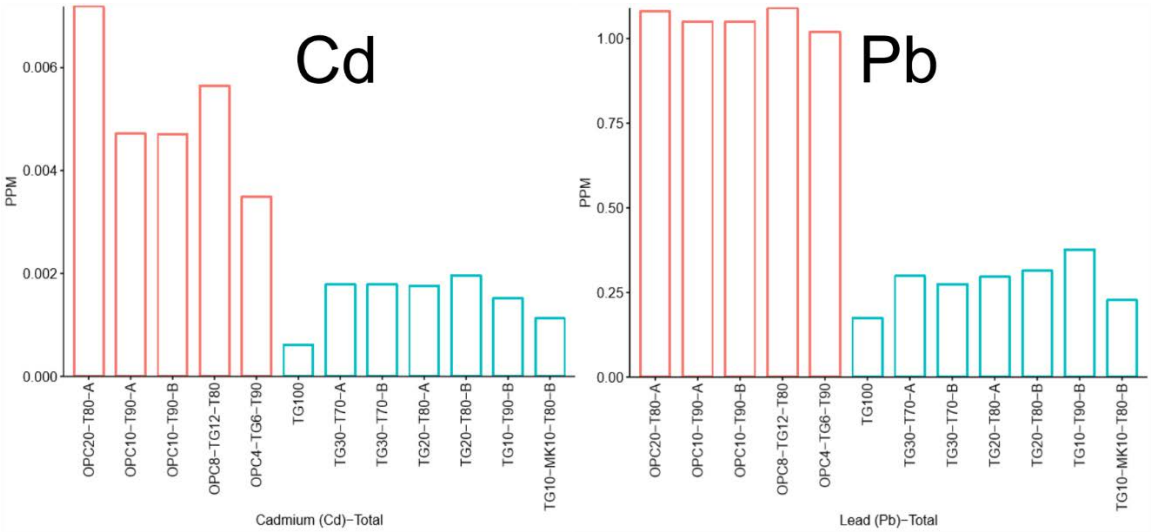

Figure 4, continued: Acid leachate analyses for metals

Potential drawbacks of geopolymer solidification

The most obvious drawback to geopolymer solidification approaches is cost. Under current methods, tailings must be dewatered to a large extent, and a relatively expensive binder must be added. Using a binder largely made from the local tailings themselves will still represent a significant operating cost, perhaps on the order of $50 to 100 USD/tonne to produce the binder, depending on many factors. At the binder dosages used in this study (10 to 30%), geopolymer solidification would cost on the order of ($5 to 30 USD/tonne) making most deposits uneconomic. However, if a binder dosage of 5% can be designed, it would equate to just $2.5 to 5.0 USD/tonne; a price that may be feasible in some locations, or with different deposit types. Existing processes at the mine site would also need to be modified to accommodate mixing equipment and storage of binder reagents used by the proposed method. Thickened tailings could be mixed and transported as paste (as in cemented paste backfill, e.g., Wu et al., 2015) at a cost, whereas filtered tailings could be mixed with binder, pelletized (e.g., Amaratunga, 1995), and transported by conveyor if water contents are too low for common pumping techniques.

Potential benefits and outlook

Geopolymer tailings solidification using tailings glass-based geopolymer can be tentatively interpreted to provide superior resistance to metal leaching compared to Portland cement. Other benefits of solidification (not restricted to geopolymer) are expected to include a much smaller impoundment footprint compared to subaqueous storage (similar to dry-stacking), no dust, and control over drainage. Unlike other potential tailings binders, this process would not require shipping the majority of cement reagents to the mine site.

Cost minimization of tailings treatment is a strict constraint considering the low grade and high tonnage of copper porphyry deposits in particular. However, curing time for cement in this context is almost

unlimited compared to other cement applications and the mix designs herein may be focused too heavily on expensive highly-reactive reagents. Short curing times enabled by common geopolymer reagents may be desirable in a cemented paste backfill application, but there may be an opportunity to decrease cost if tailings binders can be designed for 1 to 2 years of curing time. Future work should consider the possibility to promote slow in-situ solidification of subaqueous tailings at the lowest possible cost, ideally by some treatment of mill feed slurry with no dewatering step.

Conclusion

In this preliminary work, a tailings-glass geopolymer binder was made from Cu-porphyry tailings to assess its potential in tailings solidification/stabilization. The main findings were:

- Early strength was better in Portland cement solidified tailings samples using the materials, mix designs, and curing schedules in this study.
- Though weaker in compressive strength, the tailings glass geopolymer binders were not as prone to leaching of metals (V, Fe, Co, Cu, Zn, As, Cd, and Pb) by acetic acid as a Portland cement binder.
- Next steps include optimization of mix designs and reagents (e.g., for lower cost), and more comprehensive leaching tests on cured samples.

This new technique enables local production of geopolymers using tailings material and suggests that a geopolymer solidification/stabilization approach is worth pursuing further. This study used highly reactive reagents that are relatively expensive; however, cheaper and less reactive reagents curing over longer timescales may be a useful lever to bring costs down for tailings solidification/stabilization. Eventually, it may be possible to develop cost-effective geopolymerization additives to solidify and chemically stabilize co-deposited subaqueous tailings over long curing durations (i.e., years).

Acknowledgements

Support from Mitacs through an Accelerate Entrepreneur grant is gratefully acknowledged. Thank you to Tiera Naber for laboratory assistance and many thanks to Rick Friedel for his review that greatly improved the quality and clarity of this paper.

References

Ahmari, Saeed, Krishna Parameswaran and Lianyang Zhang. 2015. Alkali activation of copper mine tailings and low-calcium flash-furnace copper smelter slag. *Journal of Materials in Civil Engineering* 27(6): 04014193.

Ahmari, Saeed and Lianyang Zhang. 2013. Durability and leaching behavior of mine tailings-based geopolymer bricks. *Construction and Building Materials* 44 (July): 743–50.

Allahverdi, Ali and Mostafa Mahinroosta. 2019. Recycling aluminosilicate industrial wastes into geopolymer: A review." In *Reference Module in Materials Science and Materials Engineering,* B9780128035818115000. Elsevier.

Amaratunga, L.M. 1995. Cold-Bond Agglomeration of reactive pyrrhotite tailings for backfill using low cost binders: Gypsum β-hemihydrate and cement. *Minerals Engineering* 8(12): 1455–1465.

Barrie, E., V. Cappuyns, E. Vassilieva, R. Adriaens, S. Hollanders, D. Garcés, C. Paredes, Y. Pontikes, J. Elsen and L. Machiels. 2015. Potential of inorganic polymers (geopolymers) made of halloysite and volcanic glass for the immobilisation of tailings from gold extraction in Ecuador. *Applied Clay Science* 109–110 (June): 95–106.

Caballero, Erich, Wilson Sanchez and Carlos A. Rios. 2014. Synthesis of geopolymers from alkaline activation of gold mining wastes. *Ingenieria y Competitividad* 16: 317–30.

Capasso, I., S. Lirer, A. Flora, C. Ferone, R. Cioffi, D. Caputo and B. Liguori. 2019. Reuse of mining waste as aggregates in fly ash-based geopolymers. *Journal of Cleaner Production* 220 (May): 65–73.

Carneiro, A. and A.B. Fourie. 2019. An integrated approach to cost comparisons of different tailings management options. In *Proceedings of the 22nd International Seminar on Paste and Thickened Tailings,* Cape Town, South Africa: 115–126.

Comrie, D.C., J.H. Paterson and D.J. Ritcey. 1989. Applications of geopolymer technology to waste stabilization. In *Proceedings of 3rd International Conference of New Frontiers in Hazardous Waste Management.*

Comrie, Douglas C. 2011. Binder composition for waste materials. United States US7883576B2, filed January 29, 2007, and issued February 8, 2011.

Davidovits, Joseph. 2002. Environmentally driven geopolymer cement applications. In *Proceedings of 2002 Geopolymer Conference.* Melbourne, Australia, October 9.

Davidovits, Joseph. 1989. Waste solidification and disposal method. United States US4859367A, filed October 2, 1987, and issued August 22, 1989.

Davidovits, Joseph. 1994. Method for obtaining a geopolymeric binder allowing to stabilize, solidify and consolidate toxic or waste materials. United States US5349118A, filed July 13, 1993, and issued September 20, 1994.

Davies, Michael. 2011. Filtered dry stacked tailings – the fundamentals. In *Tailings and mine waste '11 : Proceedings of the 15th International Conference on Tailings and Mine Waste,* Vancouver BC, Canada, November 6 to 9, 2011.

EA NEN 7375. 2004. Leaching characteristics of moulded or monolithic building and waste materials: Determination of leaching of inorganic components with the diffusion test: 1– 32.

El-Eswed, B.I., R.I. Yousef, M. Alshaaer, I. Hamadneh, S.I. Al-Gharabli and F. Khalili. 2015. Stabilization/ solidification of heavy metals in kaolin/zeolite based geopolymers. *International Journal of Mineral Processing* 137: 34–42.

Falah, Mahroo, Robert Obenaus-Emler, Paivo Kinnunen and Mirja Illikainen. 2019. Effects of activator properties and curing conditions on alkali-activation of low-alumina mine tailings. *Waste and Biomass Valorization,* August.

Feng, Qingming. 2015. PhD Thesis: Applying mine tailings and fly ash as construction materials for a sustainable development. The University of Arizona. 139 pages.

Fourie, A.B., M. Tibbett and J. De Jong J. 2012. The fallacy of designing for in-perpetuity: geotechnical presumptions, ecosystem responses and concepts for managing inevitable change. In *Proceedings 7th International Conference on Mine Closure*. Mine Closure 2012, Brisbane, Australia. Edited by A.B. Fourie and M. Tibbett: 25-27.

Hart, R., J. Lowe, D. Southam, D. Perera, P. Walls, E. Vance, T. Gourley and K. Wright. 2006. Aluminosilicate inorganic polymers from waste materials. In *Proceedings of the Green Processing, Third International Conference on Sustainable Processing of Minerals and Metals,* Newcastle, Australia. Carlton (VIC): AusIMM: 5–6.

Kinnunen, Paivo, Arnold Ismailov, Soili Solismaa, Harisankar Sreenivasan, Marja-Liisa Räisänen, Erkki Levänen and Mirja Illikainen. 2018. Recycling mine tailings in chemically bonded ceramics – a review. *Journal of Cleaner Production* 174: 634–49.

Kiventerä, Jenni, Isabella Lancellotti, Michelina Catauro, Francesco Dal Poggetto, Cristina Leonelli and Mirja Illikainen. 2018. Alkali activation as new option for gold mine tailings inertization. *Journal of Cleaner Production* 187: 76–84.

Malviya, Rachana and Rubina Chaudhary. 2006. Factors affecting hazardous waste solidification/stabilization: A review. *Journal of Hazardous Materials* 137(1): 267–76.

Meggyes, T. and A. Debreczeni. 2006. Paste technology for tailings management. *Land Contamination and Reclamation* 14(4): 815.

Misra, M., K. Yang and R. K. Mehta. 1996. Application of fly ash in the agglomeration of reactive mine tailings. *Journal of Hazardous Materials* 5 (1–3): 181–192.

Morgenstern, N.R., S.G. Vick, C.B. Viotti and B.D. Watts. 2016. *Fundão Tailings Dam Review Panel Report on the Immediate Causes of the Failure of the Fundão Dam*. SAMARCO, SA, Vale, SA, eds.

Muhammad, Faheem, Xiao Huang, Shan Li, Ming Xia, Manli Zhang, Qiang Liu, Muhammad Arshad Shehzad Hassan, Binquan Jiao, Lin Yu and Dongwei Li. 2018. Strength evaluation by using polycarboxylate superplasticizer and solidification efficiency of Cr 6+ , Pb 2+ and Cd 2+ in composite based geopolymer. *Journal of Cleaner Production* 188: 807–15.

Nikolić, Violeta, Miroslav Komljenović, Nataša Marjanović, Zvezdana Baščarević and Rada Petrović. 2014. Lead immobilization by geopolymers based on mechanically activated fly ash. *Ceramics International* 40(6): 8479–88.

Pacheco-Torgal, Fernando, João Castro-Gomes and Said Jalali. 2008. Properties of tungsten mine waste geopolymeric binder. *Construction and Building Materials* 22(6): 1201–11.

Paiva, Helena, Juho Yliniemi, Mirja Illikainen, Fernando Rocha and Victor Ferreira. 2019. Mine tailings geopolymers as a waste management solution for a more sustainable habitat. *Sustainability* 11(4): 995.

Power, C., M. Ramasamy, D. MacAskill, J. Shea, J. MacPhee, D. Mayich, F. Baechler and M. Mkandawire. 2017. Five-year performance monitoring of a high-density polyethylene (HDPE) cover system at a reclaimed mine waste rock pile in the Sydney Coalfield (Nova Scotia, Canada). *Environmental Science and Pollution Research* 24(34): 26744-62.

Rao, Feng and Qi Liu. 2015. Geopolymerization and its potential application in mine tailings consolidation: A review. *Mineral Processing and Extractive Metallurgy Review* 36 (6): 399–409.

Roche, C., K. Thygesen and E. Baker. 2017. *Mine Tailings Storage: Safety Is No Accident*. UN Environment, GRID-Arendal.

Sato, Junya, Kenji Shiota and Masaki Takaoka. 2019. Stabilization of lead with amorphous solids synthesized from aluminosilicate gel. *Journal of Hazardous Materials*, 121109.

Sinclair, L. and J. Thompson. 2015. In-situ leaching of copper: Challenges and future prospects. *Hydrometallurgy* 157: 306–324.

Solismaa, S., A. Ismailov, M. Karhu, H. Sreenivasan, M. Lehtonen, P. Kinnunen, M. Illikainen and M.L. Räisänen. 2018. Valorization of Finnish mining tailings for use in the ceramics industry. *Bulletin of the Geological Society of Finland* 90 (1): 33–54.

Southam, D.C., G.F. Brent, F. Felipe, C. Carr, R.D. Hart and K. Wright. 2007. Towards more sustainable mine fills – replacement of ordinary Portland cement with geopolymer cements. In World Gold Conference, Cairns. Carlton (VIC): AusIMM:157–163

US EPA. 1992. Method 1311. Toxicity characteristic leaching procedure: 1–35.

Van Jaarsveld, J.G.S., J.S.J. Van Deventer and L. Lorenzen. 1997. The potential use of geopolymeric materials to immobilise toxic metals: Part I. Theory and applications. *Minerals Engineering* 10(7): 659–69.

Van Jaarsveld, J.G.S., J.S.J. Van Deventer and A. Schwartzman. 1999. The potential use of geopolymeric materials to immobilise toxic metals: Part II. Material and leaching characteristics. *Minerals Engineering* 12(1): 75–91.

Wang, Yaguang, Fenglan Han and Jingqiu Mu. 2018. Solidification/stabilization mechanism of Pb(II), Cd(II), Mn(II) and Cr(III) in *Fly Ash Based Geopolymers*. *Construction and Building Materials* 160: 818–27.

Wickland, B.E., G.W. Wilson, D. Wijewickreme and B. Klein. 2006. Design and evaluation of mixtures of mine waste rock and tailings. *Canadian Geotechnical Journal* (43)9: 928–945.

Wu, A.X., X.X. Miao, X.H. Liu, Y.M. Wang, C.L. Wang and J.J. Zhang. 2015. Paste backfill system design and commissioning at Chambishi Copper Mine. In *Proceedings of the 18th International Seminar on Paste and Thickened Tailings*. Australian Centre for Geomechanics: 301–308.

Xia, Ming, Faheem Muhammad, Linghao Zeng, Shan Li, Xiao Huang, Binquan Jiao, YanChyuan Shiau and Dongwei Li. 2019. Solidification/stabilization of lead-zinc smelting slag in composite based geopolymer. *Journal of Cleaner Production* 209: 1206–15.

Yu, Lin, Zhen Zhang, Xiao Huang, Binquan Jiao and Dongwei Li. 2017. Enhancement experiment on cementitious activity of copper-mine tailings in a geopolymer system. *Fibers* 5(4): 47.

Proceedings of Tailings and Mine Waste 2019
November 17–20, 2019, Vancouver, Canada
Published by the University of British Columbia, 2019

Pulsation Dampening in Tailings Handling with Piston Pumps

Tobias Lutz, Putzmeister, Germany

Abstract

During metallurgical mining, most of the mined material is of no use for the industry. Only a very small portion can be used to mine the desired precious metals. The waste material is called tailings and must be transported to surface dams or mixed with additives to become a backfill paste, which is transported back to the stopes. Hydraulic driven piston pumps are one solution to deliver this high volume over long distances in a safe and economical way. However, the design principle of a hydraulically driven piston pump leads to pulsation in a delivery pipeline, which is caused by the fact that the general design is based on a discontinuous working principle. The pumps are pumping one cylinder after another into the transportation pipeline. This results in flow fluctuations, and consequently in pressure losses.

For optimal performance of the system it is recommended to use a pulsation dampening system with the piston pump. The reason is to create an approximately continuous flow of the material, which prevents pressure peaks resulting from water-based high-density solids (the so-called water hammer effect) with a low air content being pumped at great speed against a high pressure. Furthermore, the limited variances in flow and pressure result in lower forces inside the pipeline system, which leads to lower operating costs and a safer working environment for the employees on the mine site.

This paper identifies and describes three major innovations and their different working principles of pulsation dampening of paste- and slurry systems, and discusses their application in detail.

The first system uses a hydraulic driven seat valve pump with a continuous flow system. The second possibility is the use of piston pumps with an hydraulically driven pulsation dampening system. The third option is the use of ventilated pulsation dampening systems.

Introduction

The working principle of hydraulic driven piston pumps

Pulsation in the delivery pipeline of a reciprocating pump is caused by the fact that the general design is based on a discontinuous working principle, as hydraulic-driven piston pumps are two-cylinder, single-acting, positive displacement pumps.

The pumping process can be described as follows: the hydraulic cylinder H1 is connected to the material piston P1, which moves backwards and forwards in the material cylinder M1. The same arrangement is applicable to the second hydraulic and material cylinder (Figure 1). During the pumping process, the hydraulic cylinder H1 moves backwards and sucks material into the material cylinder M1. At the same time hydraulic cylinder H2 does a counter movement and pushes the material in cylinder M2 into the delivery line. Both cylinders need to be connected to the delivery pipeline, which can be either a conical shaped pipeline that swivels in front of both cylinders (the so-called S-tube); or an arrangement of hydraulically operated seat valves (see Figure 1).

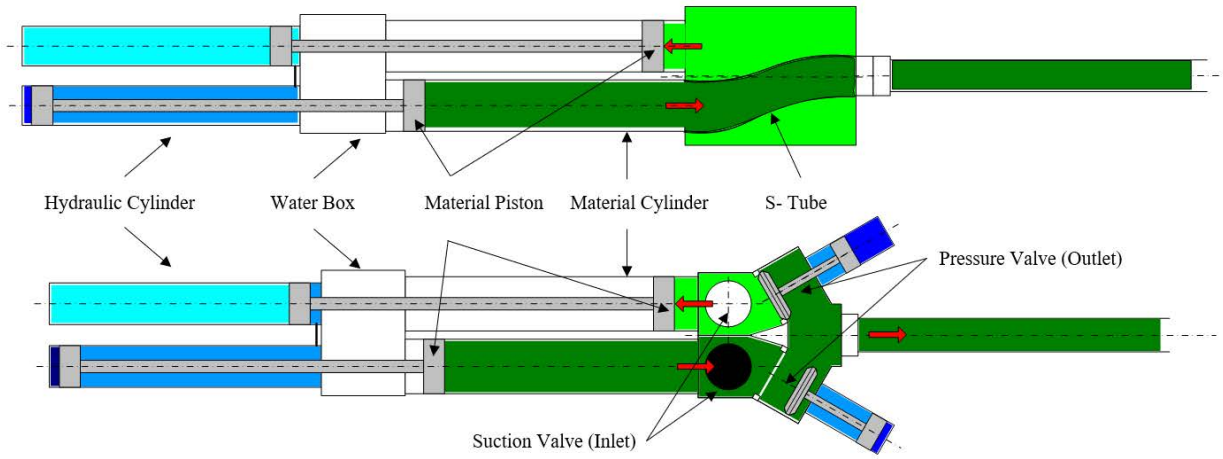

Figure 1: Schematic layout of an S-tube and seat valve piston pump

Depending on machine size and set up of the piston pump, the change-over of the S-tube or the seat valves is done within 0.5 to 1.0 second. Consequently, the material flow in the pipeline immediately drops, which is indicated in the pressure reading (Figure 2). Consequently, the static water column (along with the dissolved air) expands slightly from its compressed state. As soon as this pressure wave hits an upstream interference (valve, elbow, etc.), the wave will be reflected like an “echo” and can cause a water hammer. During this time, the velocity of the hydraulic drive cylinders is zero.

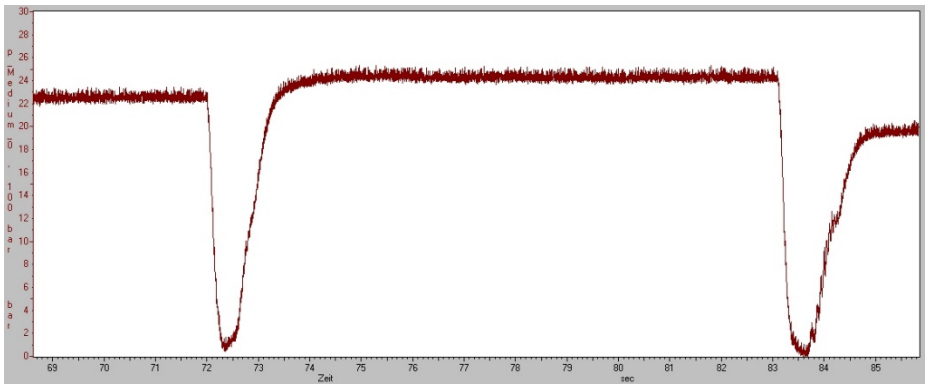

Figure 2: Typical pressure reading of a piston pump

Low volumes and/or low operating pressures of piston pumps can be operated easily with pulsations if the pipeline is designed with proper wall thickness and fixation. However, operating volumes and operating pressure in tailings handlings applications are increasing (Peschken, 2018, p. 308). This leads to the fact that pulsation damping is becoming an important factor for the economical evaluation of a tailings pipeline. Pump manufacturers for tailings handling systems have to provide solutions to prevent pressure peaks, especially those resulting from water-based high-density solids (the so-called water hammer effect) with a low air content being pumped at great speed against a high pressure. The savings in investment are substantial if the pipeline layout can be done with only a limited pulsation therein.

The water hammer effect

The water hammer effect is an example of conservation of energy, and results from the conversion of velocity energy into pressure energy (Bregman, 2017). It is created by stopping and/or starting a liquid flow (of a Newtonian fluid) suddenly, which creates shock waves that travel back and forth within the pumping material. A practical example of a water hammer is turning off the shower at home suddenly.

> "The hammer occurs because an entire train of water is being stopped so fast that the end of the train hits up against the front end and sends shock waves through the pipe. This is like a real train, instead of slowing to a stop, it hits into a mountain side. The back of the train continues forward even though the front cannot go anywhere. Since the water flow is restricted inside the pipe, a shock wave of incompressible water travels back down the pipe." (OMEGA Engineering, 2018)

This shock wave can be indicated as a variation in pressure (Dp). It creates a pressure wave almost like sound waves; traveling upstream the pipeline has "all of its kinetic energy of motion and that due to compression is converted into pressure energy" (Evans, 2011).

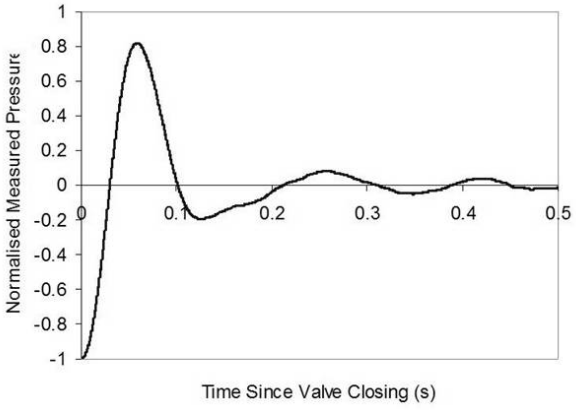

Figure 3: Normalized pressure reading of a water hammer (Donebythesecondlaw, 2009)

"The first person to describe this effect was the Russian scientist Joukowski. He showed both theoretically and experimentally that there is a maximum pressure that can be produced, known now as the "Joukowski head" or "Joukowski pressure," depending on the units of its expression (Ord, 2006).

It is given by the following formula:

$$h = \frac{v * c}{g}$$

where

c = speed of the sound wave in the pipe, known as the "wave celeric," (m/s[1])

v = initial velocity of the liquid, (m/s)

g = 9.81 (m/s²)

h = Joukowski head m

Thus, for water in a rigid pipe, where the speed of the sound wave in the pipe is (for example) 1,500 m/s, for an initial water velocity of 2,5 m/s, then suddenly stopping the flow with a rapid valve action will result in a head of about 380 m, or 38 bar. The maximum closure time that will give this head is given by:

$$t = \frac{2 * L}{c}$$

where

L = length of pipe in m

t = time, which is the time it takes for a pressure wave to travel the pipe length and back again (sec).

Hence if the pipe is 2,500 m long, the maximum closure time is about 3.33 seconds, i.e. a closure in this time or less produces a Joukowski head. "For closure times up to 10 times this (i.e., 33.3 s), the pressure is reduced in about inverse proportion which would result" (Ord, 2006, p. 4) in a pressure increase of 3.8 bar for the previous example.

Due to the pressure discontinuity, the passing of the wave front produces a force to the pipeline and its support at the next bend of the pipe. Thus, for a 150 mm diameter pipe, the passage of the 38-bar wave described above produces a force of

$$F = \frac{\pi}{4} * D^2 * P$$

where

F = force, (N)

P = the pressure equivalent of the Joukowski head (Pa)

[1] In water it is 1.484 m/s. However, for slurry or even paste the value is unknown and project-specific.

In our example, the pipeline would see a force of 6.7 kN, which is a significant force and could lead to damage of the pipeline, support, or even the pumping system.

> "Sadly, that's not the full story. The forces and pressures calculated above are for specific, fast events with water as medium and therefore for ideal Newtonian Fluids. There are lots of shades of grey between a Joukowski event and a gradual change in fluid speed that gives no perceptible surge forces. So, in many cases, a more complex analysis or even tests have to be done to ascertain if a pipe is at risk" (Ord, 2006: 2–5).

For different material characteristics such as different rheological behaviors (thixotropic pastes, slurries, cake pastes, etc.) it is even more difficult to predict whether the risk of a water hammer exists or not. Nevertheless, it can be stated that the more and the bigger the solids (by volume) are within the pumping media, the lower the risk of a water hammer as the speed of the sound wave in the pipe will be lower.

Consequences of pulsations in the pipeline

Pulsation in the pipeline is an unwanted circumstance for every designer and every operator of slurry- and paste systems. The reasons are clear. As described in the previous chapter, the pulsation may cause mechanical vibrations and fatigue failures, which can lead to serious damage to the pipeline and its related components, such as foundations and supports, due to the high level of fluctuating forces. The lifetime of valves, flanges, and other apertures will be shortened as they will be affected by the pulsations as well. If the pulsations are considered during the design phase, the entire pipeline becomes an even higher capital investment of the operator. Consequently, it is a calculation between adding a pulsation dampening system to the pump or additional supports to the pipeline. In addition to that, the pulsations in the pipeline lead to higher noise emissions to the environment of the pipeline, which can cause issues for surface pipelines (from tailings ponds and ash ponds).

Pulsation dampening systems for hydraulically driven piston pumps

Nitrogen charged diaphragm dampener

The first use of pulsation dampening systems was done with nitrogen charged diaphragm dampeners, as shown in Figure 4. Nitrogen charged diaphragm dampeners are commonly used in hydraulic fluid systems or other fluid pumping systems such as metering systems. The function of this pulsation dampener is based on the compression of a nitrogen gas diaphragm which is usually made of butyl- or fluoride rubber (Lutz-Jesco GmbH, 2018).

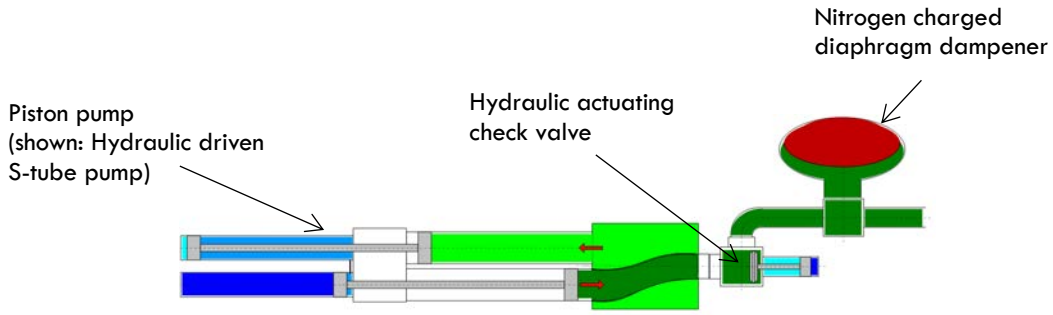

Figure 4: Schematic layout of a piston pump with nitrogen charged diaphragm dampener

During the discharge of the piston pump the pumping material is squeezed into the dampener and compresses the nitrogen diaphragm. During the changeover of the S-tube or seat valve, the material is pushed into the pipeline by the nitrogen pressure in the pulsation dampening diaphragm. As the volume of this bladder type pulsation dampeners is limited, the quantity of installed dampeners must be increased for high flow rates. Consequently, big tailing installations have to be equipped with more than ten of these diaphragm dampeners.

During the operation of various slurry systems with piston pumps, several issues have been reported (Hövemeyer and Zey, 2019). The main concern is that the entire diaphragm may be sucked into the pipeline due to the high velocity and rapid change-over of a piston pump. Furthermore, the system is very sensitive to foreign bodies such as stones or other spiky particles. These can harm the diaphragm, leading to excessive maintenance work on the dampeners. For this reason, this technology is not used for newly designed installations and plants. The industry has improved dampening methods by using three different working principles. First, the modification of the piston pump, which leads to an almost pulsation free operation. Second, utilizing a pulsation dampening system, which includes an additional delivery cylinder. Third, using a ventilated dampening system, which is a modification of the nitrogen charged diaphragm dampener.

Constant flow

The constant flow system is the best-in-class pulsation dampening system for seat valve or ball valve pumps, as it is a “no pulsation” dampening system. It is a pulsation avoidance system because it changes the way a piston pump operates, so pulsation is not even created. Consequently, no additional mechanical components need to be installed within the delivery pipeline. The only required equipment is a seat valve or ball valve piston pump equipped with a constant flow hydraulic power pack.

With this system the material flow is kept at an almost even level, which reduces the pressure peaks significantly. This continuous material flow is achieved as the connection between the hydraulic cylinders is eliminated. Every cylinder of the piston pump is connected to an independent hydraulic oil pump and acts as a single, independent piston pump. This enables the machine to perform the suction stroke faster

than the pressure stroke to pre-compress the material in the material cylinder before the pressure valve is opened. The constant flow system working principle is shown in Figure 5.

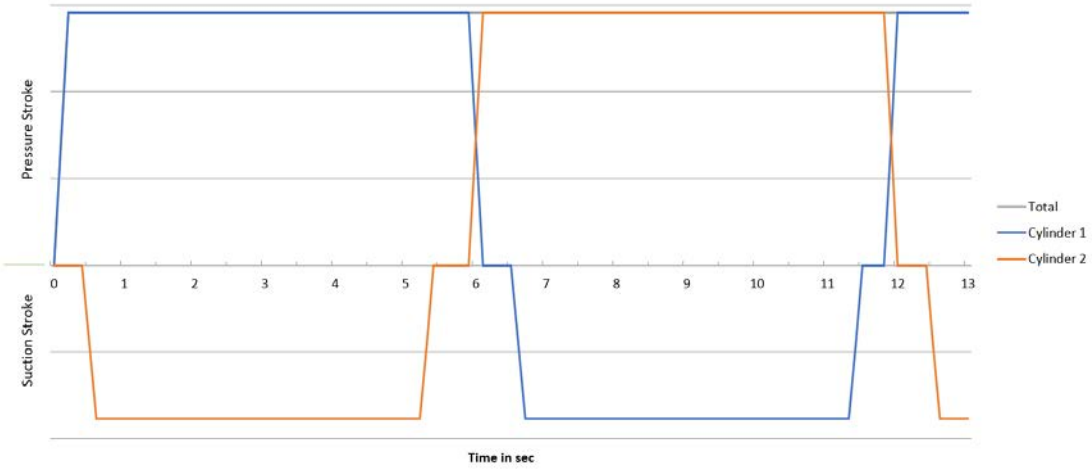

Figure 5: Constant flow system – working concept

Cylinder 1 performs its pumping stroke, and cylinder 2 starts compressing the material in the material cylinder. As piston 1 nearly reaches its end position, the speed is reduced and piston 2 softly takes over the load. At this moment the speed of both cylinders is equal. After reaching the end position, piston 1 moves quickly back and sucks paste into the delivery cylinder, while piston 2 pushes paste into the pipeline and performs its pumping stroke. The related pressure valve will close and now cylinder 1 does its pre-compression while cylinder 2 is finishing its cycle (Hövemeyer and Zey, 2019).

This control philosophy leads to an almost even flow and pressure curve of the pump, directly after the pressure outlet, as shown in Figure 6.

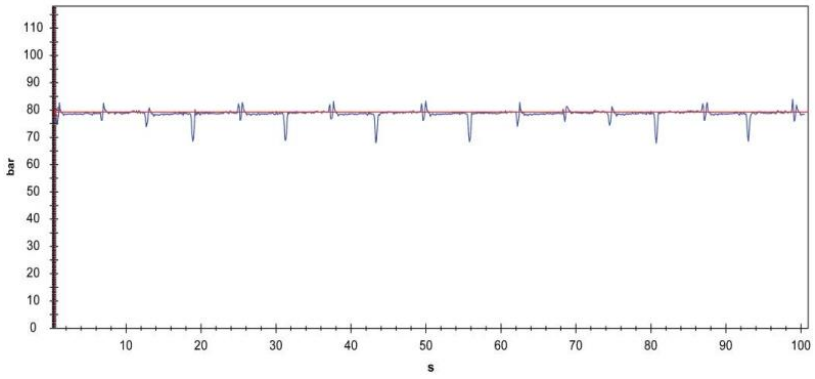

Figure 6: Constant flow pressure reading

Besides pulsation elimination, the constant flow system has additional benefits for the operator. The system doesn't need any additional mechanical or electrical components in the pipeline or in the pumping material. Consequently, no additional components must be maintained and operated. In addition to that, the

system can be used for various different materials with different flow rates up to a pipeline pressure of 150 bars without adjustment. It doesn't matter whether the paste or slurry contains cement and tends to harden as the constant flow system can be cleaned out completely. This has been proven by operators in multiple plants worldwide since the invention of the constant flow system. Due to the continuous flow of the material, the paste or slurry doesn't need to be accelerated with every stroke from 0 to full speed. This results in a lower pressure level in the pipeline compared to the operation with piston pumps without a constant flow system. Furthermore, the energy consumption of the electric motor(s) is homogenised as the load does not drop during the changeover (as is the case with pump systems without constant flow). This reduces the variations in the power grid and improves its reliability. Finally, the piston velocity during the pumping stroke is slower as compared to machines without constant flow control (due to the changeover). This results in a lower wear rate and a longer lifetime for the entire system.

Hydraulic pulsation dampening system

The hydraulic pulsation dampening system is the first real pulsation dampening system for any kind of piston pump application, and is used when slurry or paste contains sand or coarse material. The hydraulic pulsation dampening system literally acts as a third delivery cylinder, which is connected to the delivery pipeline by a T-flange immediately behind the pump outlet flange. It dampens the pulsation of the system as it delivers material into the pipeline during the changeover of the S-tube or the valves. It is either connected to the hydraulic power pack of the piston pump or is equipped with an independent one.

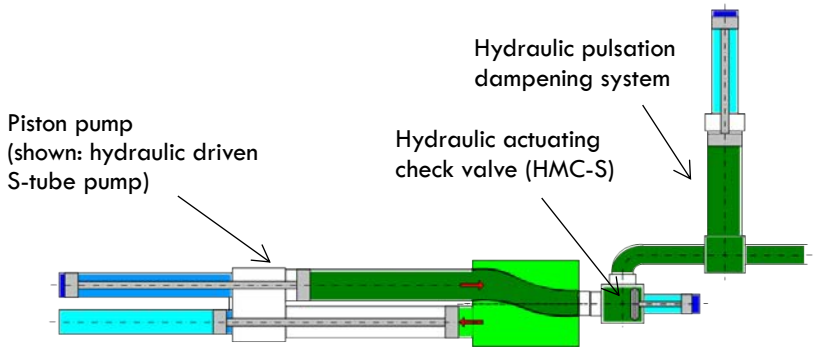

Figure 7: Schematic layout of a piston pump with an hydraulic pulsation dampening system

Tailings with a maximum grain size of <25 mm can be pumped with seat valve pumps or S-tube pumps. As soon as the grain size exceeds 25 mm, the material should be pumped only with S-tube piston pumps. If the hydraulic pulsation dampening system is used with a hydraulic driven S-tube piston pump, the pump has to be equipped with a hydraulic actuating check valve directly before the hydraulic pulsation dampening system to prevent any backflow of the material in the wrong direction in the pipeline (see Figure 7). The hydraulic pulsation dampening system is charged during each delivery stroke of the pump. The

content of this third cylinder is actively pushed into the delivery pipeline during the changeover of the piston pump. This closes the delivery gaps created by the change-over process and creates an almost even flow of material and consequently a much smoother pressure reading within the pipeline.

Figure 8: Hydraulic driven S-tube pump with an hydraulic pulsation dampening system

The hydraulic pulsation dampening system is designed as a stand-alone unit and driven by the common power pack of the piston pump, or driven by a dedicated, independent power pack. Hence it is of great interest for customers with existing paste plants, as it can be used for new installations or as a retrofit for existing pump lines. The working principle of a piston pump with the hydraulic pulsation dampening system pulsation dampening system can be described as follows. One material cylinder of the piston pump performs its pumping stroke. After reaching the end position, the hydraulic actuated check valve closes, and the hydraulic pulsation dampening cylinder extractings (and consequently pushes material into the delivery pipeline). As soon as the shift-over of the seat valve or the shift over of the S-tube is finished, the hydraulic actuated check valve is opened, and the material cylinder of the piston pump delivers material in the pipeline. At the same time the hydraulic pulsation dampening system stops extracting material into the pipeline and reverses its direction, so it is recharged for the next change-over. The pressure result can be seen in Figure 9:

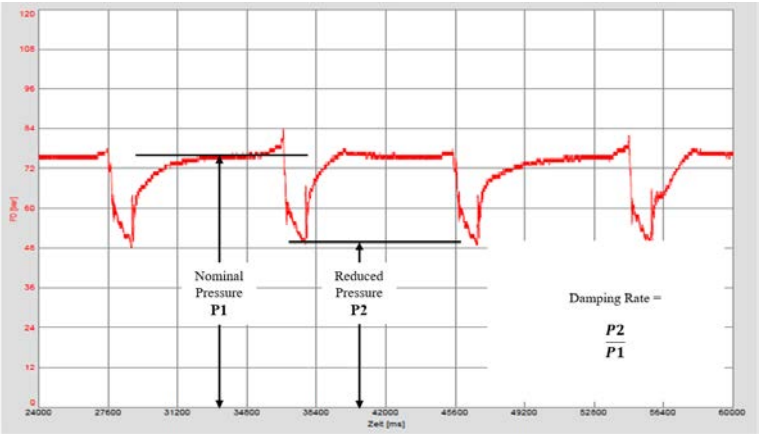

Figure 9: Pressure reading of a piston pump with hydraulic pulsation dampening system

Hydraulic pulsation dampening systems can achieve a dampening rate of approximately 60 to 70%. The dampening rate is calculated by the ratio between the nominal pressure and the pressure drop during the shift over, as indicated and described in Figure 9. This shows that the pulsation is not completely eliminated, but water hammers are not possible anymore. Consequently, the design forces for the pipeline and its supports are tremendously lower. The advantage of this system is that it is the best and most reliable pressure dampening solution for hardening material (like cemented paste or slurry) with coarse material (grain size above 25 mm). As it is designed for concrete material, the combination of S-tube piston pumps with a hydraulic pulsation dampening system is insensitive towards foreign bodies like stones. Consequently, it is the proven choice of operation for backfilling plants with coarse concrete and ash handling systems where bottom and fly ash are pumped as a mixture to the stope or ash pond. As it can be operated with an independent power pack, the hydraulic pulsation dampening system can be easily retrofitted to any piston pump system.

Ventilated pulsation dampening system

The ventilated pulsation dampener has been developed to reduce pressure drops in the pipeline with a maximum efficiency and a minimum required additional energy (Freitag, 2015). Like the hydraulic pulsation dampening system, the ventilated pulsation dampener literally acts as a third (or multiple) delivery cylinder(s), which is connected to the delivery pipeline by a T-flange immediately behind the pump outlet flange. It dampens the pulsation of the system using compressed air that acts as a spring.

The ventilated pulsation dampener consists of the actual dampening unit (which consists of multiple dampeners), an air accumulator and distribution unit, a high-pressure compressor, and the patented intelligent control unit (see Figure 10).

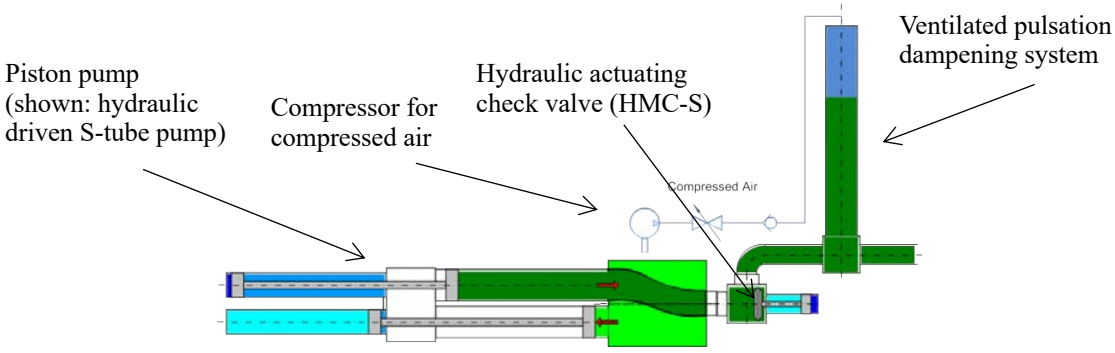

Figure 10: Schematic layout of a piston pump with ventilated pulsation dampening system

Important note: due to the design of the ventilated pulsation dampener it can be only used for non-hardening slurries and paste. Cemented paste must not be pumped through this system. Like the previously described hydraulic pulsation dampening system, the ventilated pulsation dampener is designed as a stand-

alone unit. Therefore, it can be used for new installations, or as a retrofit for existing pump lines, as shown in Figure 11.

Figure 11: Installed ventilated pulsation dampening system for tailings handling

During the pump stroke of the pump, the pre-compressed air in the dampeners is further compressed by the medium through which the medium rises in the dampeners. During the change-over of the seat valves or the S-tube, the compressed air presses the medium downwards into the conveying pipe, reducing the pressure collapse. The amount of air needed is detected by a pressure sensor in the dampening unit, calculated by the patented control system, generated from the compressor and provided from the accumulator and distribution unit (Freitag, 2015). As soon as the system is operating at a constant level, the compressor is automatically turned onto stand-by mode and no additional energy is consumed anymore. Small changes in variations are compensated by the accumulator and distribution unit. As soon as the flow/ pressure increases significantly, the compressor is turned on again and recharges the accumulator and distribution unit.

In regard to the dampening rate we can rely on the physical law, whereby more dampening volume will achieve higher dampening rates and consequently lower pressure drops during the change-over phase of the piston pump. From an economical point of view, the layout of the system should be done with a dampening rate of approximately 70% (see Figure 12).

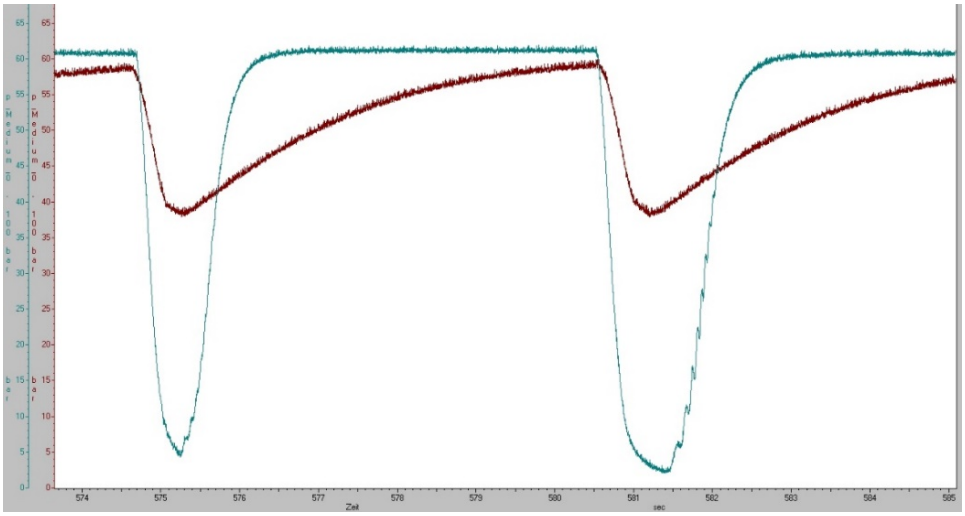

Figure 12: Pressure reading of a piston pump with and without ventilated pulsation dampener

The main advantage of the ventilated pipe dampener is the low consumption of energy combined with no additional wear on parts in the paste or tailings flow, as it uses compressed air as a spring that stores energy during continuous operation (the compressor is only needed if the output or the pressure change). With an intelligent control system, the ventilated pulsation dampener can be automatically operated at different pressure levels without any manual adjustment. Due to the proven technology, the system reliably eliminates water hammer in the pipeline. It is also easy to clean and maintain as no parts that could wear out (like membranes) are necessary. The ventilated pulsation dampener is a perfect pulsation dampening system for non-hardening pumping materials, and can be used in new installations, or else easily retrofitted into all kinds of existing pumps.

Conclusion

Pulsation dampening is an essential element for tailings handling and paste backfilling applications, and will become even more important for future projects. Due to increasing delivery volumes, distances, and pressures it is going to be crucial to install the right dampening solution to secure reliable and safe working conditions for the piston pump system. Furthermore, pulsation dampening systems help to reduce overall installation costs, as the wall thickness of the delivery pipeline and its safety factors can be optimised accordingly. This paper outlined three different pulsation dampening solutions to avoid or to reduce the shocks in the pipeline significantly.

The constant flow system is obviously not a dampening system as it avoids the pressure pulses in the pipeline due to its independent working cylinders. This system is the preferred solution for all new designed cemented paste and slurry systems and can be operated until 150 bar continuous delivery pressure. A ventilated pulsation dampening system is the economically friendly solution for tailings handling if the

material is not hardening. The additional benefit is that this system can be retrofitted to any existing piston pump station. Due to the patented intelligent control, the ventilated pulsation dampening system only consumes a minimum of energy during continuous operation.

Finally, the paper presented the hydraulic pulsation dampening system, which is the only solution for backfilling systems with coarse material that are operated with S-tube pumps. It can be supplied for new projects, and can also be retrofitted to existing pumping stations.

References

Bregman, A. 2017. Water hammer. Retrieved July 15, 2019, from valvemagazine.com: https://www.valvemagazine.com/magazine/sections/back-to-basics/8418-water-hammer.html

Donebythesecondlaw. 2009. *Wikipedia.* Retrieved February 27, 2018, from Water hammer pressure pulse: https://en.wikipedia.org/wiki/Water_hammer#/media/File:Water_hammer_pressure.jpg

Evans, J. 2011. *Pumps and systems.* Retrieved February 27, 2018, from The causes of water hammer (Part One): https://www.pumpsandsystems.com/topics/pumps/pumps/causes-water-hammer-part-one

Freitag, U. 2015. TI 151124 – Ventilated Pulsation Damper (VPD).

Hövemeyer, D. and W. Zey. 2019. *Industrial pump technology – Treatment, pipe transport and storage of high-density substances.*

Lutz-Jesco GmbH. 2018. *Pulsation damper PDM.* Retrieved from http://www.lutz-jescoasia.com/LJ-Pulsation_Dampener_PDM-EN-MB.pdf#targetText=A%20basic%20distinction%20is%20made,is%20compressed%20to%20damping%20volume.

OMEGA Engineering. 2018. *OMEGA Engineering*. Retrieved February 27, 2018, from https://www.omega.co.uk/techref/waterhammer.html

Ord, S.C. and Stopford Projects Ltd, UK. 2006. Water hammer – Do we need to protect against it? How to predict it and prevent it damaging pipelines and equipment. *IChemE*(SYMPOSIUM SERIES NO. 151), 1–20.

Peschken, P. 2018. Hydraulic driven piston pumps for the transport of pastes and slurries in the mining industry. *Mining Report Glückauf* 4: 306 – 317. Retrieved July 22, 2019, from https://mining-report.de/wp-content/uploads/2018/08/MRG_1804_KOSK_Peschken_180811.pdf

Bibliography

Hövemeyer, D. and A. Richter. 2014. Challenges of pump and process engineering for the transport of solids with hydraulic piston pumps. (B. Ernst and SohnVerlag für Architektur und technische Wissenschaften GmbH and Co. KG, editors) *Mining Report* 150(1/2). doi:https://doi.org/10.1002/mire.201400003

Putzmeister. 2014. *Putzmeister industrial technology in mining.* Retrieved April 25, 2019, from https://www.putzmeister.com

The Process Piping. 2017. Retrieved from https://www.theprocesspiping.com/water-hammer/

Proceedings of Tailings and Mine Waste 2019
November 17–20, 2019, Vancouver, Canada
Published by the University of British Columbia, 2019

Performance-Based Assessment of Seismically-Induced Slope Displacements in Tailings Dams

Jorge Macedo, Georgia Institute of Technology, USA
Gabriel Candia, Universidad del Desarrollo, Chile

Abstract

A computational platform for the performance-based probabilistic assessment (PBPA) of seismically-induced slope displacements (D) in tailings dams is presented in this paper. The platform is applicable to different tectonic settings, such as shallow crustal earthquakes and subduction zone earthquakes. This flexibility is important because many mining projects are located in sites with contributions from subduction and shallow crustal earthquake tectonic settings (e.g., South America). The procedures in the PBPA framework should be preferred in engineering practice, because they enable a hazard-consistent and rational seismic design. However, they are not commonly used in practice, because they are thought to be too cumbersome to be used in non-critical projects.

The computational platform is developed as an object-oriented MATLAB Graphical User Interface (GUI), and it features a variety of different slope displacement models typically used in the design of tailings dams. It provides novel implementations for the full treatment of existing uncertainties (i.e., epistemic and aleatory) in the estimation of D hazard curves. In addition, the platform is fully integrated with state-of-the-art probabilistic seismic hazard assessment tools for one or multiple intensity measures, which enables its direct application in engineering practice. An illustrative example for the application of the platform in the context of the evaluation of a tailings dam in a mining project is presented.

Introduction

Engineers use numerical or semi-empirical procedures for the estimation of seismically-induced displacements (D) to assess the seismic performance of tailings dams. Macedo et al. (2018) summarize the different approaches to estimating D, which are illustrated in Figure 1. These approaches rely on analytical models for D, which are typically defined in terms of intensity measures (IM) and the properties of the sliding mass; these procedures can be categorized as: a) deterministic, b) pseudo-probabilistic, and c) performance-based probabilistic (PBPA).

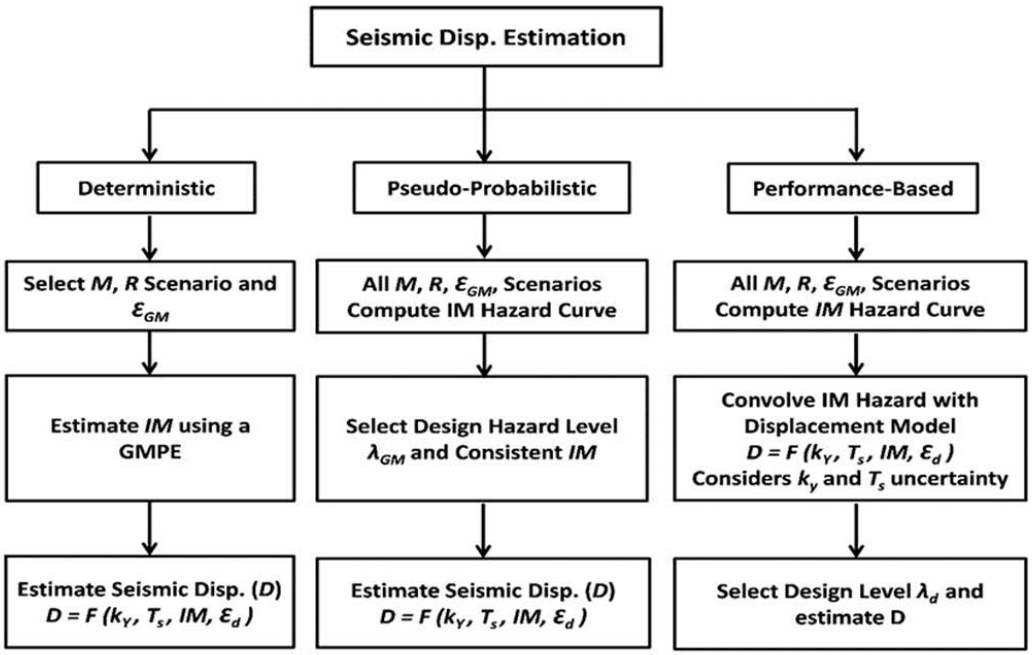

Figure 1: Different approaches for the estimation of D. Adapted from Macedo et al. (2018)

As discussed in Rathje and Saygili (2008) and Macedo et al. (2018), a deterministic approach first requires the selection of a design earthquake scenario, usually defined by the combination of the earthquake magnitude and site-to-source distance, among other parameters. This scenario may be the maximum magnitude event on the closest fault, or multiple scenarios may be specified. After selection of the earthquake scenario, the IM of interest is estimated based on a ground motion model (GMM) and a selected number of standard deviations above the median (usually set arbitrarily to 0 or 1). The presence of the standard deviation inherently introduces some probability into the analysis, despite it being considered deterministic. D is estimated using a D analytical model based on the IM previously evaluated and the sliding mass properties, which typically are the yield coefficient (ky) and the sliding mass fundamental period (Ts). The estimation of D can also consider the standard deviation of the D analytical model to incorporate uncertainty into the estimation. A pseudo-probabilistic assessment enables considering explicitly the IM variability, through a probabilistic seismic hazard assessment (PSHA). Here, the mean annual rate of exceedance for different ground motion levels (i.e., a hazard curve) is developed for the IM of interest. This IM hazard curve accounts for all potential earthquake/ground motion scenarios, the probability of occurrence of each scenario, and the probability that a ground motion level is exceeded given the scenario. The design IM is derived from the hazard curve through the selection of an acceptable hazard design level (or return period), and this IM is used in the estimation of D. However, the treatment of the variability in D remains ambiguous as in the deterministic case (i.e., it is accounted for only through the standard deviation in the analytical D model).

In a PBPA, the variability in IM and D can both be taken into account through a fully probabilistic analysis. This analysis convolves the full IM hazard curve, which includes all of the ground motion variability, with the analytical D model and all of its variability. The uncertainties in the properties of the sliding mass (e.g., ky and Ts) can also be incorporated. The result is a D curve that provides the mean annual rate of exceedance for different levels of D. This curve is well suited for making engineering decisions, as it provides the probability of exceedance for a damage measure of the tailings dam being designed, in this case the residual slope displacement, given all of the ground motion and the analytical D model variabilities (Rathje and Saygili, 2008). Within the PBPA framework the estimation of D hazard curves is typically performed using Equation 1 below. We present the simplest formulation for illustrative purposes; more complex formulations are possible.

$$\lambda_d = \sum_{i=1}^{nky} \sum_{j=1}^{nts} \int_0^{\infty} P\left(D > d \middle| IM, k_{yi}, T_{sj}\right) \left|\frac{d\lambda(IM)}{d(IM)}\right| d(IM)\, w_{kyi} w_{tsj} \quad (1)$$

In Equation 1, IM represents the intensity measure considered in the D model, k_{yi} and T_{sj} are realizations of the sliding mass properties, which are defined as the yield coefficient and the period of the sliding mass respectively (for a detailed explanation of these properties refer to Macedo et al., 2018). The term $P\left(D > d \middle| IM, k_{yi}, T_{sj}\right)$ in Equation 1 is the conditional probability that the displacement d level is exceeded given IM, k_{yi} and T_{sj}, and $\lambda(IM)$ is the annual rate of exceedance of IM. The uncertainties of k_y and T_s are treated as epistemic in a logic tree scheme, in which nky values for k_y are defined with weighting factors w_{kyi} ($i = 1 \cdots nky$) and nts values for T_s are defined with weighting factors w_{tsj} ($j = 1 \cdots nts$). The weighting factor for k_{yi} and T_{sj} may be obtained by adequate distribution functions.

The platform presented in this paper has been developed to perform PBPA assessments of tailings dams in a straightforward manner under different conditions typically found in mining projects.

In terms of existing implementations for the estimation of D hazard curves, Macedo et al. (2018) provide executables that can estimate DHC using the Bray and Travasarou (2007) and Bray et al. (2018) models. Saygili et al. (2018) provide implementations that can be used with the Rathje et al. (2014) models. The existing implementations require that the user inputs the information of IM hazard (e.g., the Saygili et al. 2018 implementation requires the external input of the PGV hazard curve for flexible sliding masses, and the Macedo et al., 2018, requires the spectral acceleration hazard information at the degraded period of the system), and they are not fully coupled with PSHA, preventing their straightforward use in engineering projects. In addition, the existing implementations do not allow the use of multiple D models since they have been developed for specific D models, they do not allow the user to account for multiple tectonic settings, and finally they do not allow a rigorous uncertainty quantification (epistemic and aleatory) on D hazard curves.

General description of the platform

The displacement platform introduced herein is a graphical user interface (GUI) developed in MATLAB, which simplifies the calculation of displacement hazard curves. The code allows the user to propagate the uncertainties developed at the different stages of the estimation of D hazard curves (i.e., ground motion level, displacement level, uncertainty in the system parameters, etc.).

The platform can be executed directly from MATLAB's workspace, and consists of two panels or windows. The main panel, shown in Figure 2(a), contains a summary of the logic tree components and the resulting D hazard curves and percentiles. All the input parameters are imported from a plain text file. The second panel, shown in Figure 2(b), allows the user to define the logic tree structure, i.e., alternative seismic hazard models, alternative model parameters, and displacement models.

(a)

(b)

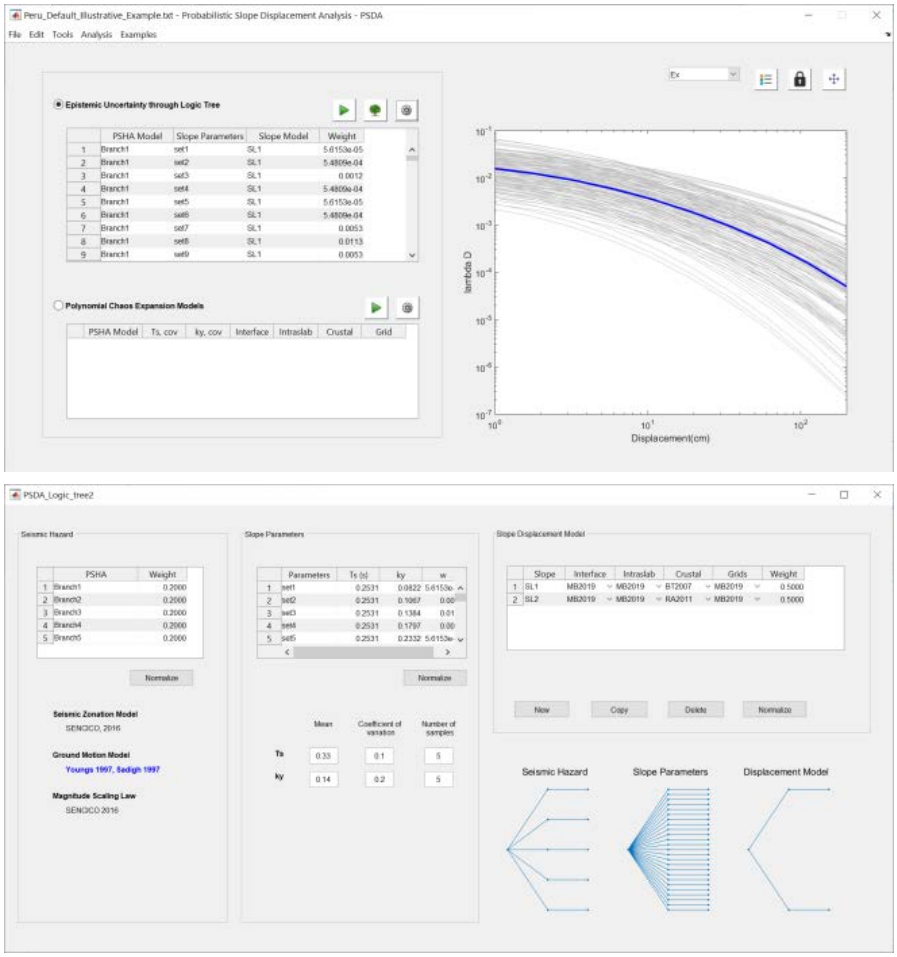

Figure 2: Displacement platform panels: (a) main window; (b) logic tree window

The main outputs from the platform are the displacement hazard curves, which can be shown graphically on the main window or exported to plain text files. A novel feature is that the platform allows the user to deaggregate the hazard by source and source mechanism, and to combine hazard curves using weights assigned in a logic tree, or computed average hazard curves using percentiles. Likewise, the platform allows the user to parallelize the computation of the logic tree branches, significantly improving the runtimes.

Platform capabilities

Embedded seismic hazard toolbox

The platform has embedded a state-of-the-art seismic hazard code to account for the ground motion variability, providing the necessary input to evaluate the D hazard curves in the context of a PBPA assessment. The embedded seismic hazard code (see full documentation in Candia et al., 2019a) includes built-in seismicity models for Peru, Chile, Ecuador, and Mexico, and provides a direct communication with the USGS website for evaluating IM hazard information in the United States. In addition, the platform allows the user to define custom seismic sources, seismicity parameters, and ground motion models, enabling the estimation of IM hazards and D hazards anywhere across the globe.

Automatic evaluation of D hazard curves with multiple IMs

Some models evaluate D in terms of jointly occurring IMs. Since IMs for a given scenario are actually correlated, a vector valued hazard analysis is needed (Bazzurro and Cornell, 2002). The present platform enables automatic evaluation of the vector hazard of multiple IMs and performs the convolution with the D model to produce D hazard curves. For instance, consider a rigid shallow sliding mass with a yield coefficient $k_y = 0.2$ located at S12.0469° and W77.1098° (i.e., the Peruvian coast), and the Saygili and Rathje (2008) slope displacement model, in which the median displacement takes the form.

$$\ln D = \mathrm{a}_0 + \mathrm{a}_1\left(\frac{\mathrm{k_y}}{\mathrm{PGA}}\right) + \mathrm{a}_2\left(\frac{\mathrm{k_y}}{\mathrm{PGA}}\right)^2 + a_3\left(\frac{k_y}{PGA}\right)^3 + a_4\left(\frac{k_y}{PGA}\right)^4 + a_5 \ln PGA + a_6 \ln PGV \quad (2)$$

Notice from Equation 2 that $\ln D$ is written in terms of both PGA and PGV values. Thus, using the seismic sources defined for Peru by SENCICO (2016), the SIBER-RISK ground motion model for PGV and PGA, and a correlation coefficient $\rho(PGA, PGV) = 0.87$ (Candia et al., 2019b), the resulting hazard surface is shown in Figure 3(a). Using the platform, this vector hazard is convoluted with the slope displacement model to produce the D hazard curve shown in Figure 3(b).

Estimation of D hazard curves considering multiple tectonic settings

In some cases, the performance-based evaluation of tailings dams needs to be performed considering the

contribution from different tectonic settings. For example, tailings dams in the Peruvian Andes may be affected by subduction type earthquakes as well as by shallow crustal earthquakes, a similar situation occurs for systems in other locations in the South America coast. The current platform incorporates D models for different tectonic settings, which can be used for the evaluations of displacement hazard in tectonic environments with contributions from different earthquake mechanisms. An example of this feature is provided in the next section.

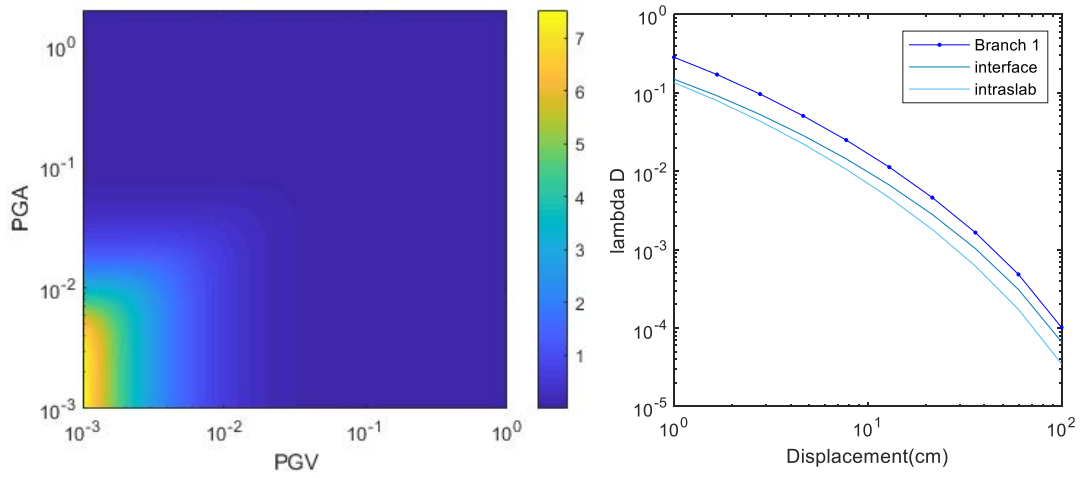

Figure 3: Example of D hazard estimation using with multiple IMs. a) Mean rate of exceedance of PGA and PGV for a site in the Peruvian coast; and b) estimation of the D hazard using the Saygili and Rathje (2008) model for a rigid shallow sliding mass with $k_y = 0.2$

Uncertainty treatment in D hazard curves

In the context of the estimation of D hazard curves, uncertainties are typically categorized as: I) aleatory variability, which is associated with the natural randomness in a process (i.e., D hazard realizations), and can be parametrized by probability density functions (PDF); and II) epistemic uncertainty, which is the scientific uncertainty in the model of the process. This uncertainty is due to limited data and knowledge, and it is typically characterized by alternative realizations for the properties of the sliding mass considered in the evaluation of a tailings dam as well as alternative D models. The proper treatment of the epistemic uncertainty is of primary importance for the estimation of D hazard percentiles. The aleatory uncertainty on the system properties is already accounted in Equation 1, through the inclusion of probability density functions (PDFs) for the random variables. However, in addition the epistemic uncertainties for alternative D models and sliding mass properties need also to be considered. To address this issue, the platform includes a logic tree option to account for the epistemic uncertainty in D models as well as the properties of the sliding mass. In a logic tree scheme, branches are populated by alternative models and weights assigned based on the appropriateness of the models for the specific application at hand. The logic tree must capture both the best estimates of what is known and the potential range of alternatives in light of what is currently

not known. The illustrative example in the next section shows the implementation of a logic tree in the platform (Figure 6), where alternative GMM, alternative properties for the system, and alternative D models are considered.

Illustrative example

Consider a tailings dam located in the Peruvian Andes at coordinates S11.92° W76.00°, near to the Peruvian-Chilean trench, an active subduction boundary. The geometry and properties of the dam are identical to the example used by Macedo et al. (2018). The maximum cross section of the 57 m-high rolled earth-fill dam, which is founded on rock, is shown in Figure 4. The displacement hazard is assessed for a deep slide through the dam, which in this case is considered as the critical sliding surface. The median estimates for T_s and k_y are 0.33 s and 0.14, respectively, and the coefficients of variation based on a lognormal distribution are $cov(T_s)$=0.1 and $cov(k_y)$=0.2, respectively.

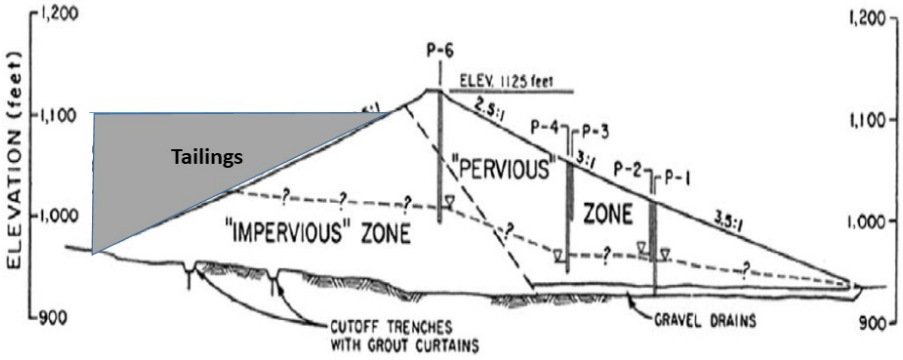

Figure 4: Cross section of dam used in illustrative example (adapted from Bray and Travasarou 2007 and Macedo et al., 2018)

Figure 5 shows SENCICO's (2016) seismic source model for Peru and the $Sa(T = 0.5s)$ hazard curve (i.e., the spectral acceleration at the degraded period of the system as required in the Bray et al. (2018) and Bray and Macedo (2019) slope displacement models). Notice from Figure 5(b) the contribution of different source mechanisms to the total hazard, which is dominated in this case by intermediate depth "intraslab" events.

We define a logic tree with five alternative seismic hazard models; each branch corresponds to a different combination of GMM. We adopted the logic tree defined by SENCICO (2016) for Peru, which considers five GMMs for subduction sources, and one GMM for shallow crustal sources; all branches have equal weights in the logic tree structure. For the parameters in the tailings dam's sliding mass, we consider five k_y values and five T_s values, sampled independently from their corresponding PDFs. Finally, we define two sets of alternative displacement models, with equal weights of 0.5: the first set uses the Bray et al.

(2018) D model for subduction earthquakes and the Bray and Travasarou (2007) D model for shallow crustal earthquakes, while the second set uses the Bray et al. (2018) D model for subduction earthquakes and Rathje and Antonakos (2011) D model for shallow crustal earthquakes. Notice that the Bray et al. (2018) D model is, to date, the only existing model developed for subduction sources. In summary, the resulting logic tree, shown in Figure 6, has 250 branches that combine five GMM models, 25 sets of sliding mass parameters, and two slope displacement models.

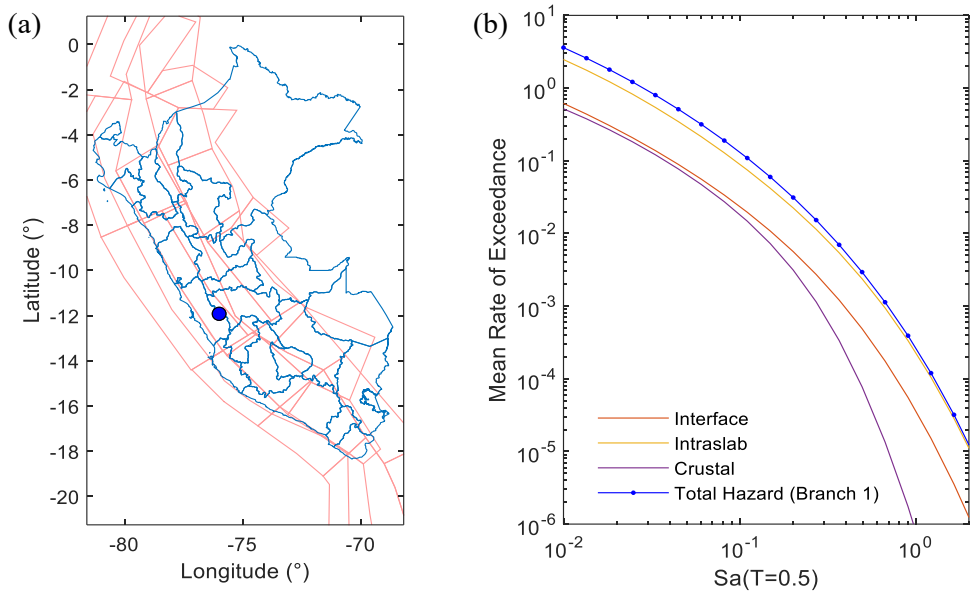

Figure 5: (a) SENCICO's (2016) seismic source model and site location; and (b) spectral acceleration hazard curves at the degraded period of 0.5 s based on one branch of the logic tree

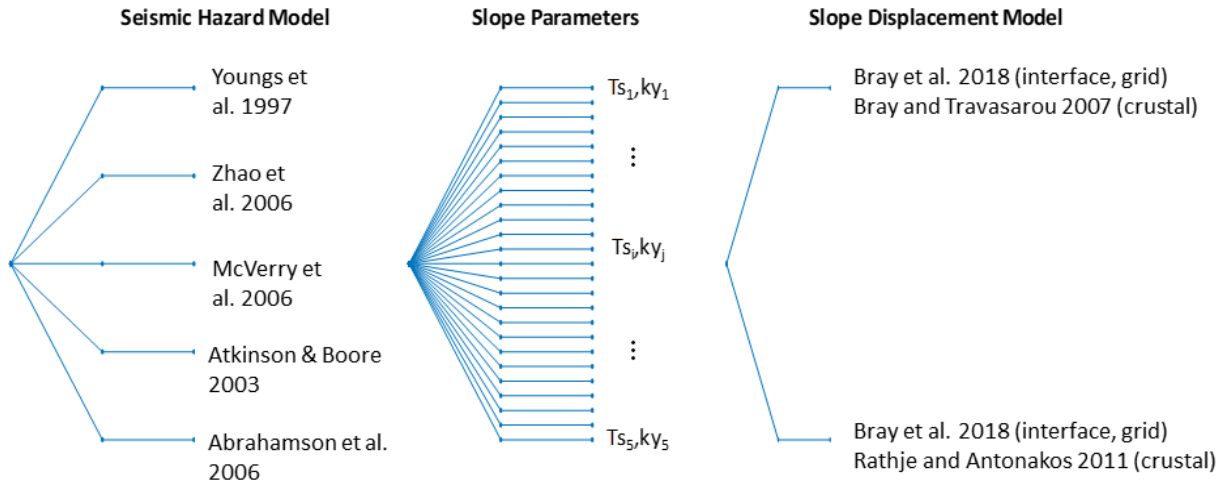

Figure 6: Logic tree definition within the proposed platform for the illustrative example

Using the inputs defined above, we perform the performance-based evaluation of D. The results shown in Figure 7 include the 250 individual D hazard curves from the logic tree (light gray lines), the median, and the 10th and 90th percentiles (thick blue lines). From these results, it can be observed that the median D estimate for a 475 year return period is 9.2 cm, whereas the median D for a 2,475 years return period is 37 cm. In addition, the 10th–90th D percentile range from 2 cm to 31 cm for a 475 year return period, and from 11 to 103 cm for a 2,475 year return period. Since D is an engineering demand parameter that relates to the seismic performance of the tailings dam, the D values presented herein, and their corresponding rate of occurrence enables designers to perform a hazard-consistent and risk-informed design.

Conclusion

Performance-based procedures for designing tailings dams provide a rational basis for design. However, these procedures are not popular among engineers because implementation is not straightforward; therefore, they are typically not used in non-critical projects. The present platform strives to advance the profession by demonstrating to engineers and researchers a tool that simplifies the performance-based assessment of a tailings dam in the context of a mining project. Thus, we present a new computationally efficient platform for the performance-based assessment of tailings dams in different tectonic settings, including shallow crustal earthquake zones, as well as subduction earthquake zones.

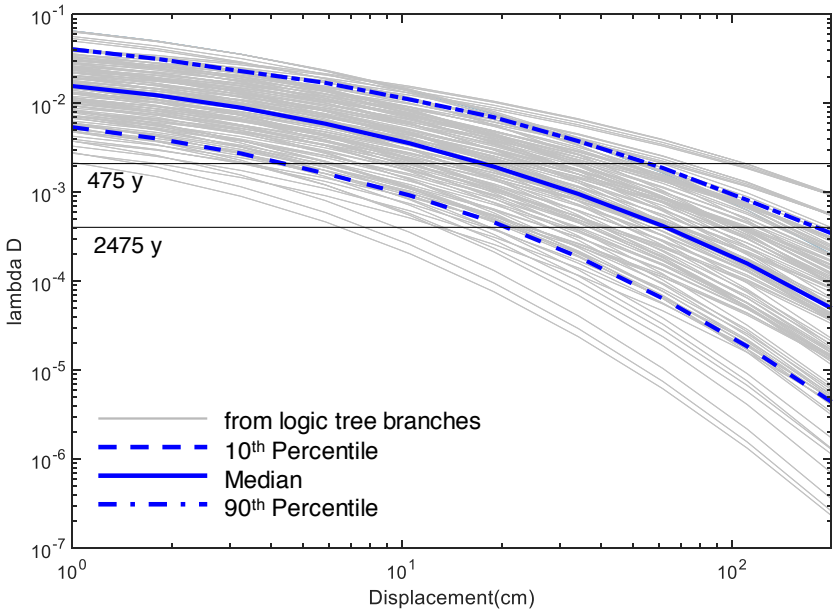

Figure 7: D hazard curves, median, and 10th and 90th percentiles

The platform is implemented as a Graphical User Interface in MATLAB and features several tools to conduct state-of-the-art evaluations of D hazard curves. The platform has several innovative capabilities,

such as an embedded state-of-the-art seismic hazard code, several built-in D models with one or multiple IMs, D models for different tectonic settings, and the quantification of aleatory and epistemic uncertainties. In the case of epistemic uncertainties, the platform allows the user to define logic trees for the ground motion intensity parameter(s), the properties of the sliding mass in the tailings dam, and alternative D models. The platform is publicly available at: https://github.com/gacandia/SeismicHazard.

References

Atkinson, G.M. and D.M. Boore. 2003. Empirical ground-motion relations for subduction-zone earthquakes and their application to Cascadia and other regions. *Bull. Seismol. Soc. Am.* 93(4): 1703–1729.

Bazzurro, P. and C.A. Cornell. 2002. Vector-valued probabilistic seismic hazard analysis (VPSHA). In *Proceedings of the 7th US National Conference on Earthquake Engineering*, Earthquake Engineering Research Institute, Boston, Massachusetts: 21–25.

Bray, J. and J. Macedo. 2019. Procedure for estimating shear-induced seismic slope displacement for shallow crustal earthquakes. *Journal of Geotechnical and Geoenvironmental Engineering.*

Bray, J.D. and T. Travasarou. 2007. Simplified procedure for estimating earthquake-induced deviatoric slope displacements. *Journal of Geotechnical and Geoenvironmental Engineering* 133(4): 381–392.

Bray, J.D., J.L. Macedo and T. Travasarou. 2018. Simplified procedure for estimating seismic slope deviatoric displacements in subduction zones. *Journal of Geotechnical and Geoenvironmental Engineering*, accepted for publication.

Candia, G., A. Poulos, J.C. de la Llera, J. Crempien and J. Macedo. 2019b. Correlations of spectral accelerations in the Chilean subduction zone. Submitted to *Earthquake Spectra*.

Candia, G., J. Macedo, M.A. Jaimes and C. Magna-Verdugo. 2019a. A new state of the art platform for probabilistic and deterministic seismic hazard assessment. Submitted to *Seismological Research Letters*.

Macedo, J., J. Bray, N. Abrahamson and T. Travasarou. 2018. Performance-based probabilistic seismic slope displacement procedure. *Earthquake Spectra* 34(2): 673–695.

Rathje, E.M. and G. Antonakos. 2011. A unified model for predicting earthquake-induced sliding displacements of rigid and flexible slopes. *Engineering Geology* 122(1): 51–60.

Rathje, E.M. and G. Saygili. 2008. Probabilistic seismic hazard analysis for the sliding displacement of slopes: Scalar and vector approaches. *Journal of Geotechnical and Geoenvironmental Engineering*, ASCE 134(6): 804–814.

Rathje, E.M., Y. Wang, P.J. Stafford, G. Antonakos and G. Saygili. 2014. Probabilistic assessment of the seismic performance of earth slopes. *Bulletin of Earthquake Engineering* 12(3): 1071–1090.

Saygili, G. and E.M. Rathje. 2008. Empirical predictive models for earthquake-induced sliding displacements of slopes. *Journal of Geotechnical and Geoenvironmental Engineering* 134(6): 790–803.

Saygili, G., E.M. Rathje, Y. Wang and M. El-Kishky. 2018. Cloud-based tools for the probabilistic assessment of the seismic performance of slopes. *Geotechnical Earthquake Engineering and Soil Dynamics V*, Geotechnical Special Publication 293. June 13–18, Austin, Texas. Retrieved from https://doi.org/10.1061/9780784481486.003.

SENCICO. 2016. *Actualización del programa de cómputo orientado a la determinación del Peligro Sísmico en el país. Servicio Nacional de Capacitación para la Industria de la Construcción*. Lima, Peru.

Bibliography

Abrahamson, N., N. Gregor and K. Addo. 2016. BC Hydro ground motion prediction equations for subduction earthquakes. *Earthquake Spectra.* 32(1): 23–44.

McVerry, G.H., J.X. Zhao, N.A. Abrahamson and P.G. Somerville. 2006. New Zealand acceleration response spectrum attenuation relations for crustal and subduction zone earthquakes. *Bull. New Zeal. Soc. Earthquake Eng.* 39(1): 1–58.

Youngs, R.R., S.J. Chiou, W.J. Silva and J.R. Humphrey. 1997. Strong ground motion attenuation relationships for subduction zone earthquakes. *Seismol. Res. Lett.*

Zhao, J.X., J. Zhang, A. Asano, Y. Ohno, T. Oouchi, T. Takahashi, H. Ogawa, K. Irikura, H.H. Thio, P. Somerville and Y. Fukushima. 2006. Attenuation relations of strong ground motion in Japan using site classification based on predominant period. *Bull. Seismol. Soc. Am.* 96(3): 898–913.

Proceedings of Tailings and Mine Waste 2019
November 17–20, 2019, Vancouver, Canada
Published by the University of British Columbia, 2019

CPT Approach to Evaluating Flow Liquefaction Using Yield Stress Ratio

Paul W. Mayne, Georgia Institute of Technology, USA
J. Sharp, ConeTec Group, Canada

Abstract

Cone penetration testing (CPT), specifically the piezocone test (CPTu), is a well-utilized tool for geotechnical studies by the mining industry to evaluate the state, strength, and stability of tailings and mine wastes. Of particular concern to tailings are the conditions prone to flow liquefaction, which consist of contractive geomaterials that are normally consolidated (NC) to lightly overconsolidated (LOC) silty to sandy soils. Using an established relationship for assessing yield stress (σ_p', or apparent preconsolidation stress) in terms of the net cone resistance and CPTu material index (I_c), the interpreted profile of yield stress with depth is used to discern the boundaries between contractive and dilative soils within the context of critical state soil mechanics. The methodology is analogous to the concept of state parameter (ψ) where the contractive-dilative demarcation is taken theoretically at $\psi = 0$. Alternatively, a critical threshold is defined in terms of yield stress ratio (YSR = σ_p'/σ_{vo}'), and contractive soils are identified when YSR is less than approximately 3, where σ_{vo}' = current effective overburden stress. The YSR method is applied to three case studies, including the recent tailings dam failure near Brumadinho, Brazil, in January 2019.

Introduction

Flow liquefaction is a phenomenon of rapid and brittle undrained loss of soil strength that must be analyzed for mine tailings dams and hydraulic fills, as well as natural sandy and silty deposits. Flow liquefaction may occur in saturated contractive soils on sloping ground, and may be triggered under static conditions such as a slow rise in the phreatic surface. Flow liquefaction and static liquefaction are terms often used interchangeably; however, flow liquefaction may also be triggered by cyclic earthquake loading. Soils prone to flow liquefaction are identified as exhibiting “contractive” soil behaviour, whereby volumetric strains decrease during shear, in contrast to “dilative” soil response, whereby volumetric strains are known to increase. In addition, these soils tend to be brittle; exhibiting a rapid loss of strength at low strain levels, resulting in rapid and progressive flow failures.

The identification of soil conditions susceptible to flow liquefaction can be made on the basis of conventional rotary drilling, high quality sampling, and careful laboratory testing, combined with in-situ testing and geophysical measurements; however, at great cost in terms of time and money (Robertson et al., 2000). This is particularly true for sands, silty sands, and silts because undisturbed sampling methods (e.g., freezing) are quite difficult and expensive. Therefore, screening approaches are preferred to facilitate an expedient and economic initial assessment of the potential for flow liquefaction, particularly in mine tailings storage facilities where screening is used during any stage of dam construction.

Existing CPT methodologies are available for screening and evaluating flow liquefaction potential of tailings and hydraulic fills. Been et al. (1986; 1987) establish a framework for the state parameter to describe initial state, soil behaviour, strength, and compressibility using a number of intermediate geoparameters that are correlated to CPT results. Full details are given in Jefferies and Been (2015). In another approach, Robertson (2010) relies on regions within CPT soil behaviour charts to identify potential soil layers that may be susceptible to flow liquefaction, and associates the state parameter boundary ($\psi = -0.05$) to a normalized cone resistance that is adjusted for fines content, designated $Q_{tn-cs}=70$.

Herein, an alternative screening scheme is presented to quantify contractive versus dilative soil behaviour via critical state concepts by assessing the in-situ soil stress history using an established CPT algorithm that profiles the effective yield stress with depth (Mayne et al., 2009). This approach is outlined here and supported by several case studies with supplemental cross-checking with the aforementioned methods. An advantage of the proposed new screening method is the ability to predict the future state of tailings with changes in effective stress.

Critical state soil mechanics

State parameter

The full form of critical state soil mechanics (CSSM) is defined with three- and four-dimensional spaces (x,y,z,t) using stress invariants such as octahedral stresses (e.g., Schofield and Wroth, 1968; Jefferies, 1993; Jefferies and Shuttle, 2005). A summary framework on the liquefaction behaviour of soils, including flow liquefaction, cyclic liquefaction, and cyclic softening is detailed by Idriss and Boulanger (2008). Within the context of CSSM, the utilization of a state parameter (ψ) helps explain the concepts of drained and undrained soil response, contractive versus dilative behaviour, and positive versus negative excess porewater pressures, as well as establishes the importance of initial state, often expressed in terms of void ratio (e_0), relative density (D_R), and effective stress (σ').

The state parameter is defined as the difference between the initial void ratio (e_0) and the critical state void ratio (e_{cs}) for shearing under constant normal effective stress, thus:

$$\psi = e_0 - e_{cs} \quad (1)$$

The state parameter concept is illustrated in Figure 1 and shows contractive soil behaviour occurs when $\psi > 0$, while dilative response is found for $\psi < 0$. In practical applications involving CPT interpretations, however, the boundary for contractive-dilative behaviour is empirically taken at $\psi = -0.05$, perhaps to allow for conservatism (Robertson, 2012; Been, 2016).

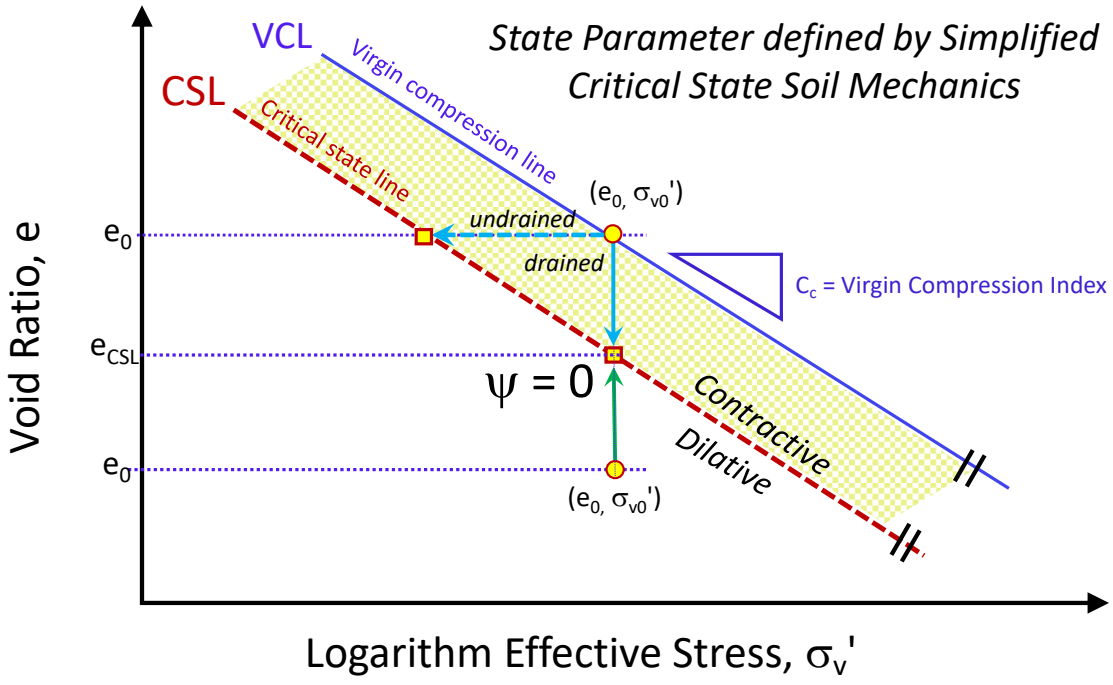

Figure 1: Concept of state parameter in terms of simplified critical state soil mechanics

Simplified critical state soil mechanics

A simplified form of critical state soil mechanics is available that uses more conventional tests and nomenclature, including (a) void ratio versus effective stress (e-logσ_v') from standard consolidation tests and (b) shear stress vs. effective stress (τ–σ_v') from direct simple shear (DSS) mode to convey the same concepts (Mayne, 2005; Mayne et al., 2009; Holtz et al., 2011).

For instance, Figure 2 illustrates that undrained stress paths can be utilized to separate contractive vs. dilatant response when shear-induced porewater pressures are zero: $\Delta u = 0$. In simple shear, the drained shear strength is given by:

$$\tau = \sigma_{vo}' \cdot \tan \phi'$$

where ϕ' = effective stress friction angle. The undrained shear strength is obtained for the special case when the stress path is maintained at constant volume ($\Delta V/V = 0$). For undrained simple shear of normally-consolidated soils, Wroth (1984) showed that the normalized undrained strength ratio is:

$$(s_u/\sigma_{vo}')_{NC} = \sin\phi'/2$$

where ϕ' = effective stress friction angle.

While the successful application of this is well-known for clays (e.g., Mayne et al., 2009), Figure 2 shows that it also successfully approximates the undrained shear strength ratio of sands. Data from simple shear (SS), torsional shear (TS), ring shear (RS), and hollow cylinder (HC) tests have been compiled in Table 1 with their corresponding reference sources. The observed range of strength ratios: $0.18 \leq s_u/\sigma_{vo}' \leq 0.36$ are in fact quite comparable to those back-calculated from field case studies of flow liquefaction (Olson and Stark, 2002; 2003). In lieu of ϕ', Robertson et al. (2000) related the ratio to relative density of the sand. Been (2016) also shows a similar range of s_u/σ_{vo}' for sands that is correlated with state parameter.

Table 1: List of sands and undrained shear strength ratios tested under laboratory conditions

Sand name	Test	ϕ' (deg)	s_u/σ_{vo}'	Reference
Ottawa 20/40	RS	31.0	0.23	Sadrekarimi and Olson, 2011
Illinois River	RS	32.2	0.24	Sadrekarimi and Olson, 2011
Mississippi River	RS	32.8	0.29	Sadrekarimi and Olson, 2011
Ham River	TS	36.0	0.36	Georgiannou and Tsomkos, 2008
Fontainebleu	TS	38.0	0.25	Georgiannou and Tsomkos, 2008
Fraser River	SS	30.0	0.20	Vaid and Sivathayalan, 1996
Toyoura sand	HC	33.6	0.24	Yoshimine et al., 1998
Silica sand #8	RS	36.8	0.33	Okada et al., 1999
Osaka Group	RS	37.5	0.38	Okada et al., 1999
Syncrude sand	SS	28.0	0.18	Sivathayalan, 1991

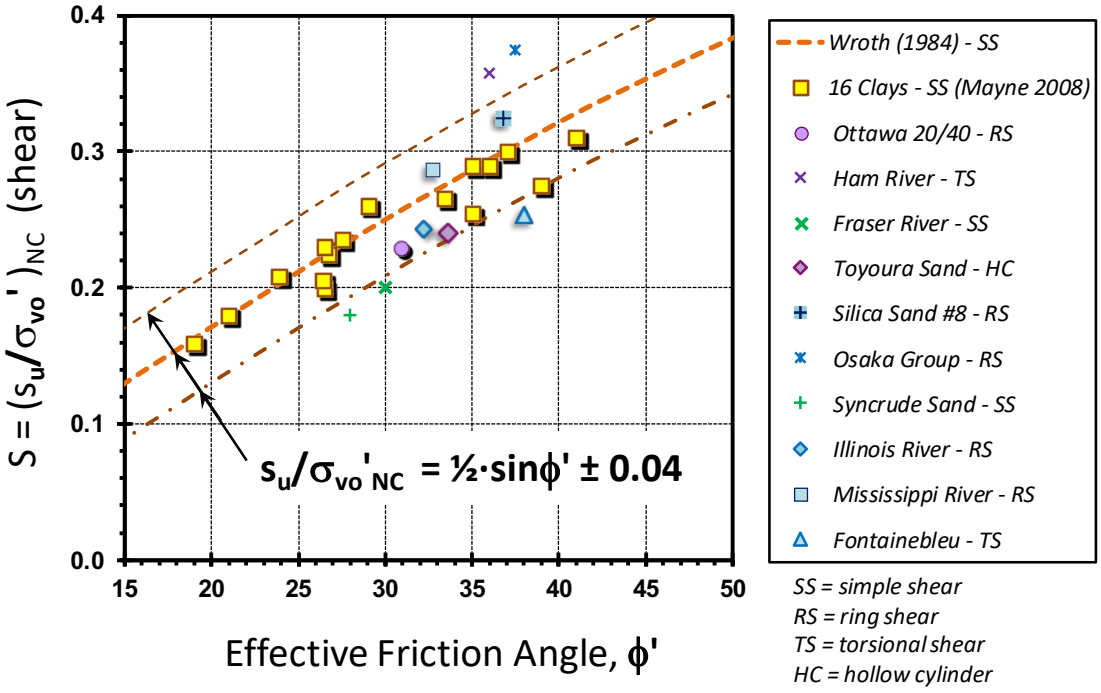

Figure 2: Undrained shear strength ratio with effective friction angle for sands and clays

For the undrained shear strength of overconsolidated soils in simple shear mode, the effect of yield stress ratio (YSR) becomes important (Ladd and DeGroot, 2003; Mayne et al., 2009):

$$s_u = ½ \sin\phi' \cdot YSR^{\Lambda} \cdot \sigma_{vo}'$$

where $\Lambda = 1 - C_s/C_c$ = plastic volumetric strain ratio, C_s = swelling or recompression index, and C_c = virgin compression index. For clays, the value of $\Lambda = 0.80$ is often adopted (Ladd and DeGroot, 2003). For sands, representative values of the index compressibility parameters for 6 sands at two different void ratios and two stress levels (n = 24) reported by Been et al. (1987) indicate a mean $\Lambda = 0.790$ with S.D. = 0.164.

The resulting excess porewater pressures obtained during undrained simple shear can then be expressed (Mayne et al., 2017):

$$\Delta u = (1 - ½ \cos\phi' \cdot YSR^{\Lambda}) \cdot \sigma_{vo}'$$

The contractive – dilative boundary is defined for undrained shear when $\Delta u = 0$, as depicted in Figure 3. From the aforementioned, the corresponding YSR at critical state is then calculated as:

$$YSR_{CSL} = (2/\cos\phi')^{1/\Lambda}$$

Taking the primary expected range of frictional angles of sands between $30° \le \phi' \le 45°$ and a representative value $\Lambda = 0.8$, the corresponding range of values falls: $2 < YSR_{CSL} < 4$, with a typical value $YSR_{CSL} \approx 3$.

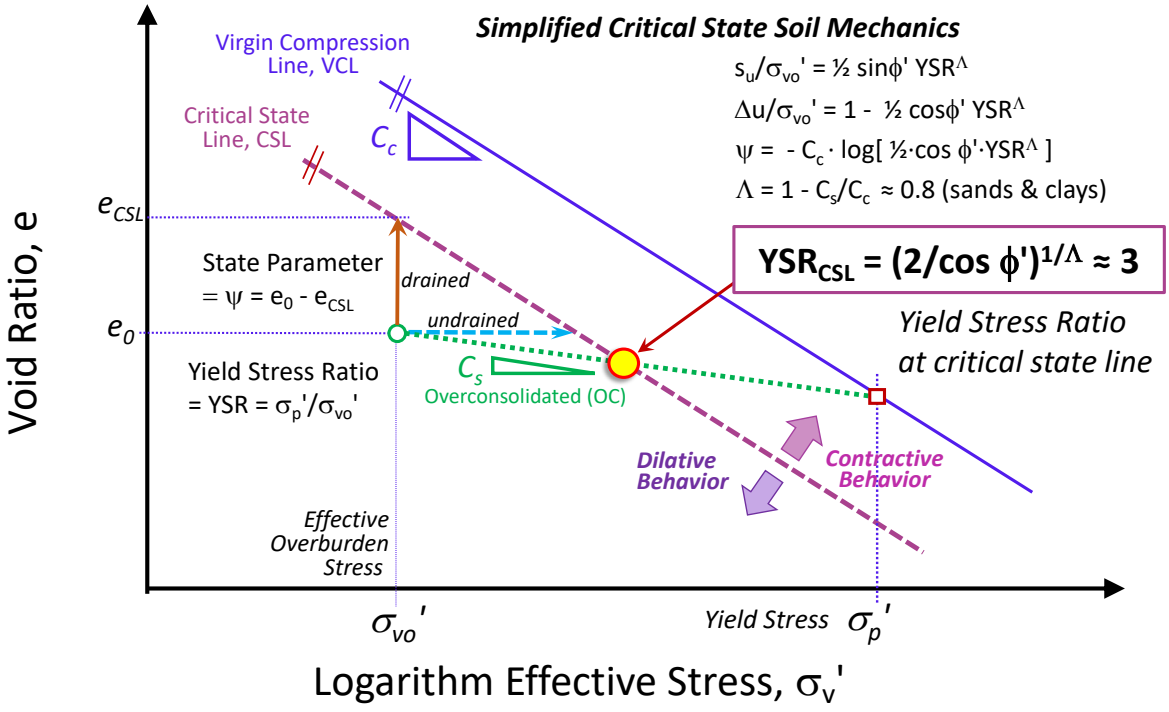

Figure 3: Yield stress ratio at critical state line (YSR_{CSL}) from simplified CSSM

Geoparameters from CPT

The cone penetration test (CPT) is an efficient and economical tool for geotechnical site characterization and establishing soil engineering parameters. Herein, specifically the use of CPT for evaluating soil type, unit weight (γ_t), yield stress (σ_p'), and effective stress friction angle (ϕ') are of interest.

The penetrometer readings provide the net cone resistance ($q_{net} = q_t - \sigma_{vo}$) and excess porewater pressure ($\Delta u = u_2 - u_0$). Dimensionless CPT parameters have been developed to give: (a) normalized cone tip resistance: $Q = q_{net}/\sigma_{vo}'$, (b) normalized sleeve friction: $F = 100 \cdot f_s/q_{net}$, and (c) normalized porewater pressure parameter: $B_q = \Delta u/q_{net}$. Also, an updated version of Q has been recognized that is designated Q_{tn} and utilized in the CPT material index (I_c) for soil behaviour type classification (Robertson, 2009).

Unit weight

The soil total unit weight (γ_t) is needed in the calculation of total and effective overburden stresses. For inorganic and non-cemented soils, an estimate of unit weight can be made from (Robertson and Cabal, 2010):

$$\gamma_t / \gamma_w = 1.776 + 0.27 \cdot \log(f_s / \sigma_{atm}) + 0.09 \cdot \log(q_t / \sigma_{atm})$$

where γ_w = unit weight of water (= 9.8 m/s2). Alternatively, an expression solely dependent on sleeve

friction is also available (Mayne, 2014):

$$\gamma_t / \gamma_w = 1.22 + 0.153 \cdot \ln(f_s / \sigma_{atm} + 0.01)$$

Soil type

The set of nine-zone soil behavioural type (SBT) charts based on Q, F, and B_q, termed SBTn, is one of the most popular means to discern soil types by CPTu (Lunne et al., 1997). Some updates to the SBTn system are given by Robertson (2009, 2012, 2016).

CPT material index

The CPT material index (I_c) is a convenient means for separating zones 2 through 7 in the SBTn system where:

$$I_c = \sqrt{(3.47 - \log Q_{tn})^2 + (1.22 + \log F_r)^2}$$

Full details are given elsewhere (Robertson, 2009; 2012). Using $Q = Q_{tn}$ initially in the evaluation of I_c, the upgraded value of normalized Q_{tn} is given by:

$$Q_{tn} = \frac{q_{net} / \sigma_{atm}}{(\sigma_{vo}' / \sigma_{atm})^n}$$

where the exponent "n" varies from 1 in intact clays to around 0.5 in sands. The exponent is specifically determined from Robertson (2009):

$$n = 0.381 \cdot I_c + 0.05 \cdot (\sigma_{vo}'/\sigma_{atm}) - 0.05 \quad \leq \quad 1.0$$

and the index I_c is recalculated. Iteration converges quickly and generally only 3 cycles are needed to secure the operational I_c at each depth.

Initial algorithms are available to cull the CPTu data for zone 1 (soft sensitive clays) and zones 8 and 9 (stiff over-consolidated clays and sands) from zones 2 to 7 (Mayne et al., 2014, 2017). Then, the remaining soil types are identified by the CPT material index: Zone 2 (organic soils: $I_c \geq 3.60$); Zone 3 (clays: $2.95 \leq I_c < 3.60$); Zone 4 (silt mixtures: $2.60 \leq I_c < 2.95$); Zone 5 (sand mixtures: $2.05 \leq I_c < 2.60$); Zone 6 (sands: $1.31 \leq I_c < 2.05$); and Zone 7 (gravelly to dense sands: $I_c \leq 1.31$).

Yield stress

The yield stress of inorganic, non-cemented, and insensitive soils can be evaluated from net cone resistance and soil type (Mayne et al., 2009). Figure 4 shows the general relationship between σ_p' and q_{net} for a variety of soils that can be expressed in dimensionless form:

$$\sigma_p' = 0.33\ (q_{net})^{m'} \cdot (\sigma_{atm}/100)^{1-m'}$$

where the exponent m' = 1 in intact clays and decreases with increasing grain size to m' = 0.72 in clean quartz-silica sands. The term σ_{atm} = reference stress equal to atmospheric pressure (1 atm ≈ 1 bar = 100 kPa). The exponent is directly a function of CPT material index where, for intact soils without fissures, the overall trend is expressed by (Mayne, 2017):

$$m' = 1 - \frac{0.28}{1 + (I_c / 2.65)^{25}}$$

Effective stress friction angle

The effective stress friction angle is one of the most important soil properties, as it represents the strength envelope for drained and undrained behaviour. It is required for stability analyses involving slopes, embankments, shallow and deep foundations, as well as lateral stress coefficient (K_0) and cyclic response.

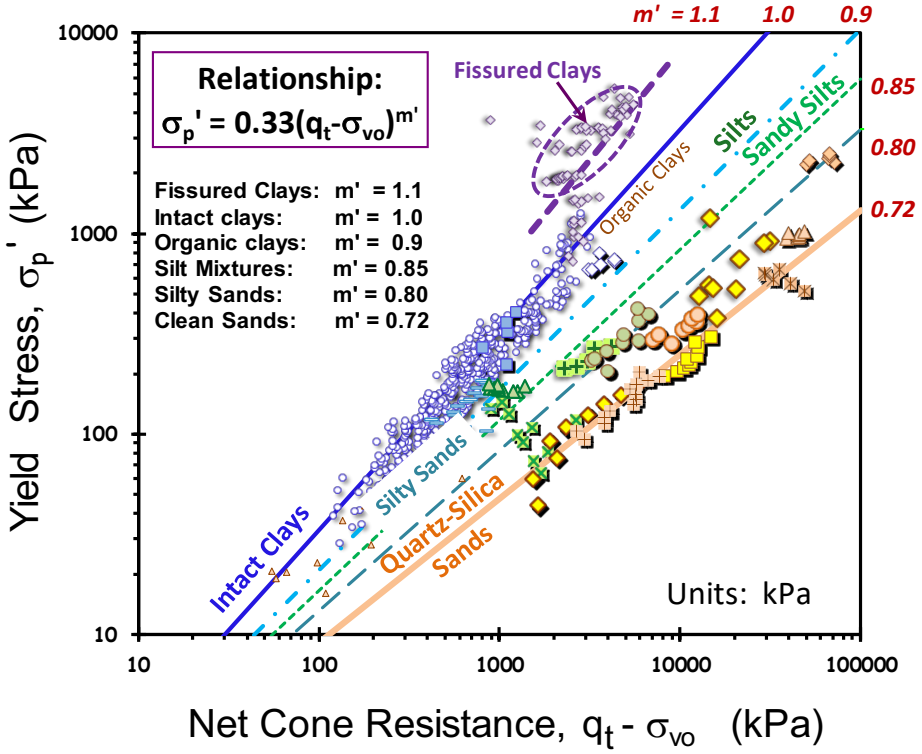

Figure 4: Yield stress relationship from CPT net cone resistance (after Mayne et al., 2009)

The results from laboratory triaxial compression tests conducted on undisturbed sand samples interrelated with CPT results have shown (Mayne, 2014):

$$\phi' = 17.6° + 11.0° \log Q_{tn}$$

For soft to firm intact clays with YSR <3, a limit plasticity solution can be approximated for the following restricted cases when $0.05 < B_q < 1.1$ and $20° < \phi' < 45°$ (Mayne, 2007):

$$\phi' = 29.5° \cdot B_q^{0.121} \cdot [0.256 + 0.336 \cdot B_q + \log Q]$$

For overconsolidated clays, a slight modification is required (Ouyang and Mayne, 2019).

As a guide, Robertson (2009) suggests that undrained penetration occurs when $I_c > 2.6$, while drained conditions prevail when $I_c \leq 2.6$. Alternatively, the normalized porewater parameter can be used, where drained response is taken when $B_q \leq 0.1$ and undrained behaviour governs when $B_q > 0.1$.

Equivalent cone resistance for clean sands

In the CPT flow liquefaction approach by Robertson (2010), the normalized cone resistance is adjusted to a value equivalent for clean sands, termed Q_{tn-cs}:

$$Qtn–cs = Kc \cdot Qtn$$

where the factor Kc has been related to estimated fines content and given in terms of material index, Ic:

(a) when $Ic \leq 1.64$: $Kc = 1.0$

(b) when $Ic > 1.64$: $Kc = –0.403 \cdot Ic4 + 5.58 \cdot Ic3 – 21.63 \cdot Ic2 + 33.75 \cdot Ic – 17.88$

Contractive soils occur when the magnitude of $Qtn–cs < 70$ and thus becomes the criterion to identify soils that are prone to flow liquefaction.

Application to flow liquefaction cases

A new and expedient approach for screening of flow liquefaction uses the CPT to evaluate the yield stress (or apparent pre-consolidation) and effective strength of soils. As shown from critical state soil mechanics, when the current YSR falls less than the critical value ($YSR_{CSL} < 3$), then the soils are identified as contractive and the potential for instability and possible flow liquefaction is heightened. In contrast, dilative soils exist when YSR >3. Moreover, when the current YSR <1, a higher risk of susceptibility to collapse is imminent since this is an indication of contractive soils that are underconsolidated. In this paper, three case studies have been selected to illustrate the application of the approach. Additional examples are presented

elsewhere (Mayne et al., 2017; Mayne, 2017; Styler et al., 2018). The method has also been applied to cases involving cyclic liquefaction (Mayne and Styler, 2018).

Dilative example: Western Canada tailings

A compacted tailings facility in western Canada is used as an example for the quantification of primarily dilative soils. Results from piezocone testing are shown in Figure 5 with the following profiles with depth: (a) cone resistance, (b) sleeve friction, (c) penetration porewater pressure, and (d) CPT material index. In terms of the SBTn system, the index (Ic) indicates mainly the presence of sands (zone 6) and gravelly sands (zone 7), excepting a limited layer of a sandy mixture (zone 5) at depths of 10 to 11 m.

Post-processing the CPT has been made using three different methods: (a) state parameter approach of Been (2016) and Jefferies and Been (2015); (b) normalized cone resistance for equivalent clean sand (Qtn-cs) method of Robertson (2010, 2012); and (c) yield stress ratio at critical state line, YSR_{CSL} (Mayne et al., 2017). The results of these analyses for the Western Canada tailings site are shown in Figure 5. All three methods clearly categorize that the majority of the soil profile consists of dilative geomaterials, excepting the layer at 10–11 m, which is identified as contractive.

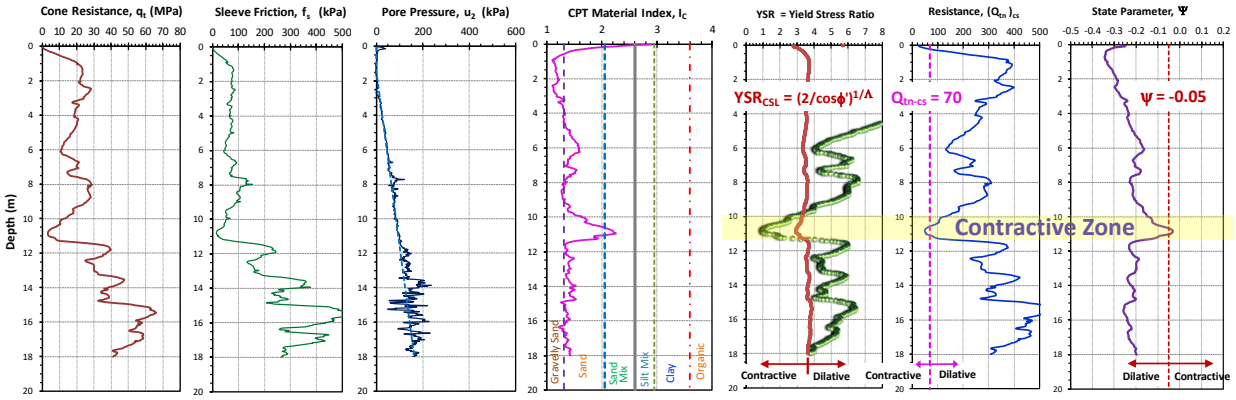

Figure 5: Profile in dense tailings at Western Canada Site X showing CPTu readings (q_t, f_s, u_2) with material index I_c and comparison of YSR_{CSL}, Q_{tn-cs}, and Ψ methods for screening flow liquefaction

Contractive example: Brumadinho tailings failure

On 24 January 2019, a large, apparently statically triggered, flow liquefaction failure occurred at the Brumadinho tailings dam operated by VALE for iron ore mining operations and located in State of Minas Gerais, Brazil. The 85 m high tailings dam completely collapsed in approximately 10 seconds, and released some 11.7 m^3 of tailings downstream, resulting in 324 deaths and/or missing people. A series of CPTu soundings was evaluated for the dam by Yassuda et al. (2018) as part of the periodic safety review and stability analyses. Both drained and undrained conditions were evaluated for the stability analyses using a commercial software package. The most critical case was found for undrained conditions and a slip circle

using the Spencer method with a calculated factor of safety FS = 1.09.

A representative CPTu sounding taken to 32 m depth (2016 CPT-03) is shown in Figure 6 (digitized here from Yassuda et al., 2018). The soil profile from material index shows complex layering with zones 2 to 6 indicative of clays, silts, sand mixtures, and sands. The three screening methods for flow liquefaction by CPT are applied to the data from Brumadinho dam. Post-processing to ascertain the potential for flow liquefaction show five soil layers identified as contractive zones in the profiles from both the Jefferies and Been (2015) procedure and Robertson (2012) approach. For the CPT YSR approach, two contractive zones are identified. In fact, the lower layer extends throughout most of the sounding profile from 5 m to the final 32 m depth.

Moreover, the yield stress ratio plots show five sublayers where YSR <1 which is indicative of underconsolidated soils. The very fragile nature and extreme brittle loss of stability at the Brumadinho dam site is well-documented in video capture of the event (New York Times, 2019).

It must be acknowledged that CPTu results in partially saturated soils and unsaturated geomaterials are still not fully understood. Most research and practical interpretations are based on soil tests for either completely dry or fully saturated conditions. At the Brumadinho site, results from piezocone dissipation testing showed residual excess porewater pressures (Yassuda et al., 2018). These indicated 33 <Δu <83 with a mean value of Δu = 51 kPa throughout the soil profile. The analyses reported above used this elevated condition of hydrostatic pore pressure. In addition, a completely hydrostatic case with shallow groundwater table (z_w = 0) and deep groundwater (z_w >32 m) were also explored, with similar findings concluded in the flow liquefaction assessment.

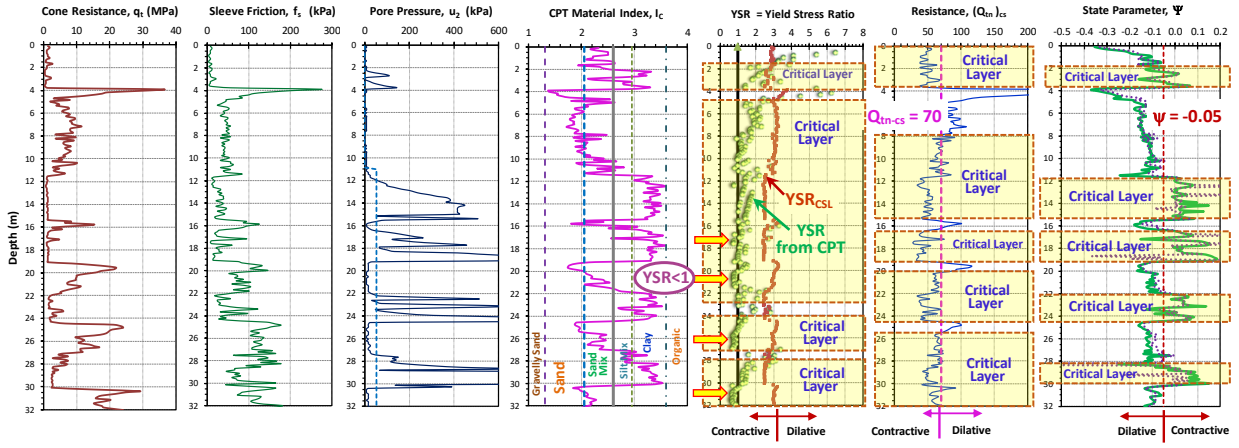

Figure 6: Profile in loose tailings at Brumadinho, Brazil showing CPTu readings (q_t, f_s, u_2) with material index I_c and comparison of YSR_{CSL}, Q_{tn-cs}, and Ψ methods for screening flow liquefaction

Contractive example: Sand Heads, Fraser River delta, BC

Sand Heads is an area located near the mouth of the Fraser River delta in British Columbia and comprised of natural young loose sands prone to flow liquefaction and instability issues. The site has been identified as one of the flow liquefaction case studies cited by Olson and Stark (2002) and Robertson (2010).

A series of soil borings, sampling, geophysics, and CPTs were established near the Sand Heads lighthouse to investigate this region (Christian et al., 1997). Alternating sequences of loose Holocene sediments were encountered that were subjected to tidal fluctuations and induced flow liquefaction. A representative CPTu sounding is shown in Figure 7. Post-processing of the CPT data presents the material index I_c and the three screening approaches for flow liquefaction: (1) yield stress ratio (YSR); (2) Q_{tn-cs} profile with depth; and (3) state parameter method. All three approaches indicate soils prone to flow liquefaction. While the Q_{tn-cs} <70 approach indicate contractive soils essentially over the full depth, the YSR solution indicates soils above 5 m are dilative while contractive soils are found from 5 to 30 m. In the state parameter approach, the calculated Ψ more or less hovers above and below the –0.05 demarcation.

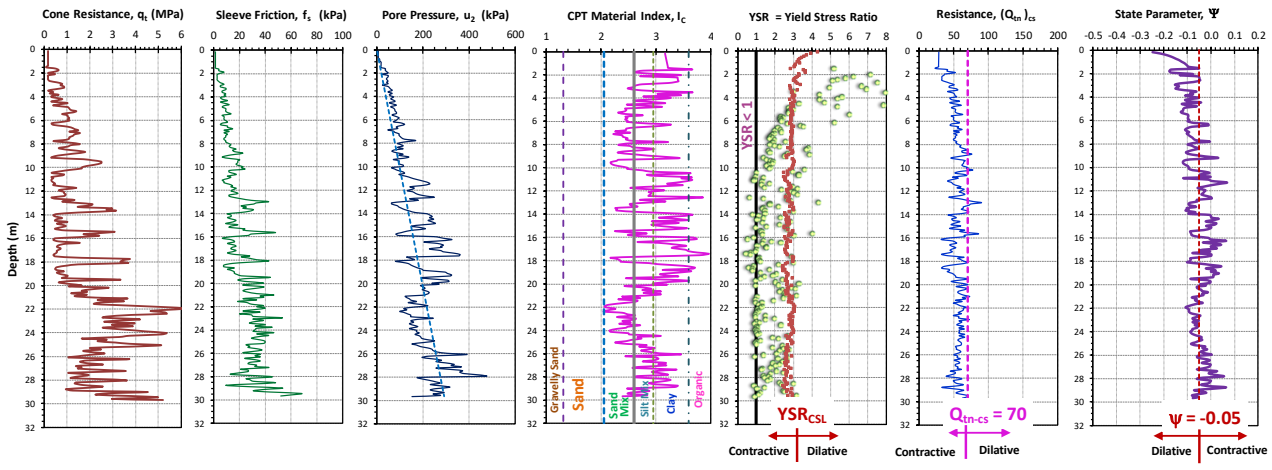

Figure 7: Profiles in loose natural silty and sandy soils at Sand Heads, BC, showing CPTu readings (q_t, f_s, u_2) with material index I_c and screening comparisons by YSR_{CSL}, Q_{tn-cs}, and Ψ methods

Increasing dam height

The evaluation of effective yield stress profiles facilitates an evaluation of the change in soil behaviour (i.e., dilative response to contractive behaviour) due to the heightening of tailings dams and embankments. Figure 8 depicts hypothetical changes due to the increase in fill corresponding to vertical stress increases of 0.5, 1, 2, and 4 atmospheres. Using a representative value $YSR_{csl} \approx 3$, Figure 8 shows that the initial soil profile is primarily categorized as dilative behaviour, since the calculated YSR >3. Later, due to the placement of additional fill above the working surface, the imposed loadings cause an increase in the

effective overburden stresses, thereby reducing the YSR = σ_p'/σ_{vo}' and changing the overall response from dilative to dilative/contractive, and eventually, to fully contractive.

Conclusions

Flow liquefaction occurs in loose tailings comprised of contractive sands, silts, and mixed soil types. Assessment of a state parameter (ψ) by CPT is a common means to evaluate flow liquefaction potential. The boundary separating contractive vs. dilative soils is established (theoretically) when $\psi = 0$. Alternatively, the contractive-dilative boundary can be formulated in terms of an apparent over-consolidation ratio, or yield stress ratio (YSR) at the critical state: $YSR_{CSL} = (2/\cos\phi')^{1.25}$, which approximately corresponds to a $YSR_{CSL} \approx 3$. The in-situ YSR can be profiled directly with depth using an established CPT methodology that relies on net cone resistance (q_{net}) and material index (I_c) to identify contractive soils where $YSR_{CSL}<3$. Moreover, when the CPT data show YSR <1, the screening provides a higher warning of soils in an underconsolidated state with more imminent risks of instability and failure. Three case studies involving loose natural soils in the Fraser River Delta, dense mine tailings from western Canada, and a spectacular tailings failure in Brazil are used to illustrate the approach and the results are compared to existing interpretation methodologies. In addition to assessing the current state of tailings, a particular utility of the method is to predict the future state due to changes in effective overburden stress incurred due to a rising phreatic surface or a dam height raise, for example.

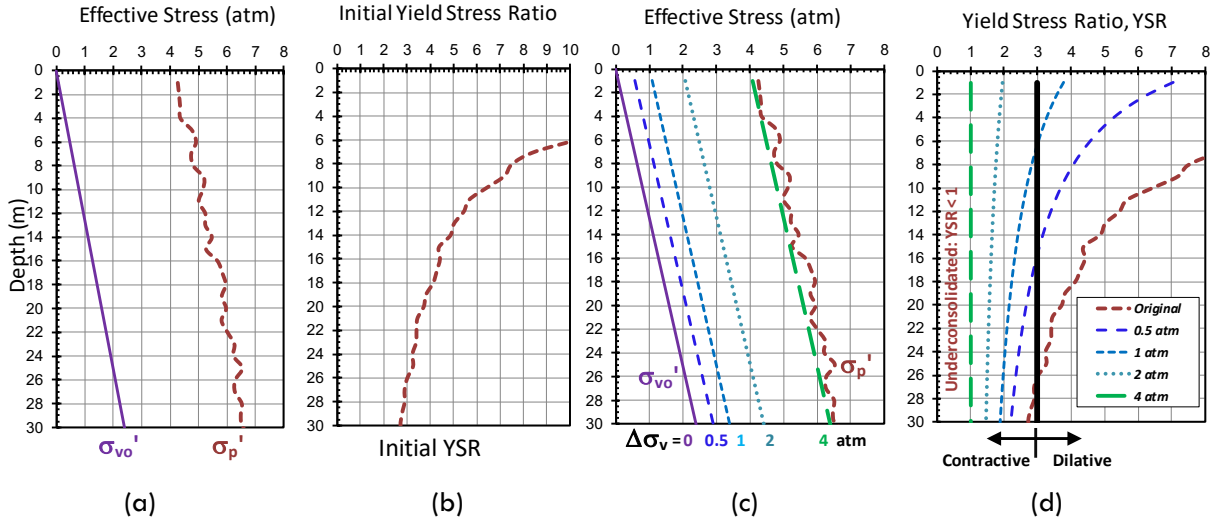

Figure 8: Predicted profiles due to raised embankment: (a) initial stresses, (b) initial YSR, (c) increased stresses due to heightened fill; (d) final YSRs showing change from dilative to contractive behaviour

References

Been, K., J.H.A. Crooks, D.E. Becker and M.G. Jefferies. 1986. The cone penetration test in sands: Part I: State parameter interpretation. *Geotechnique* 36(2): 239–249.

Been, K., M.G. Jefferies, J.H.A. Crooks and L. Rothenburg. 1987. The cone penetration test in sands: Part II, general inference of state. *Geotechnique* 37(3): 285–299.

Been, K. 2016. Characterizing mine tailings for geotechnical design. *Geotechnical and Geophysical Site Characterization 5,* vol. 1 In *Proceedings of ISC-5,* Gold Coast, Australian Geomechanics Society: 41–55.

Christian, H.A., D.J.Woeller, P.K. Robertson and R.C. Courtney. 1997. Site investigations to evaluate flow liquefaction slides at Sand Heads, Fraser River delta. *Canadian Geotechnical Journal* 34(3): 384–397.

Georgiannou, V.N. and A. Tsomokos. 2008. Comparison of two fine sands under torsional loading. *Canadian Geotechnical Journal* 45: 1659–1672.

Holtz, R.D., W.D. Kovacs and T.C. Sheahan. 2011. *An Introduction to Geotechnical Engineering,* 2nd edition, New Jersey: Pearson.

Idriss, I.M. and R.W. Boulanger. 2008. Soil liquefaction during earthquakes. Monograph MNO-12, Earthquake Engineering Research Institute, Oakland, CA. Retrieved from www.eeri.org

Jefferies, M. 1993. Nor-Sand: A simple critical state model for sand. *Geotechnique* 43(1): 91–103.

Jefferies, M. and D.A. Shuttle. 2005. Nor-Sand features, calibration, and use. In *Proceedings of GeoFrontiers: Soil Constitutive Models,* (GSP 128, Austin), ASCE, Reston, VA: 204–234.

Jefferies, M. and K. Been. 2015. *Soil Liquefaction: A Critical State Approach,* second edition, CRC Press/Taylor & Francis, London: 690 pages.

Ladd, C.C. and D.J. DeGroot. 2003. Recommended practice for soft ground site characterization. *Soil and Rock America 2003.* In *Proceedings of the 12th PCSMGE,* MIT, Essen: Verlag Glückauf: 3–57.

Lunne, T., P.K. Robertson and J.J.M. Powell. 1997. *The Cone Penetration Test in Geotechnical Practice,* EF Spon/Blackie Academic, Routledge Publishing, New York: 312 p.

Mayne, P.W. 2005. Practitioner/academic forum on geotechnical engineering. In *Proceeding of the 16th International Conference on Soil Mechanics and Geotechnical Engineering,* vol. 5 (issued 2006), Osaka, Millpress/Rotterdam: 2922 and 2931.

Mayne, P.W. 2007. *NCHRP Synthesis 368 on Cone Penetration Test*. National Cooperative Highway Research Program, Transportation Research Board, National Academies Press, Washington, D.C., 118 pp. Retrieved from: www.trb.org

Mayne, P.W., M.R. Coop, S. Springman, A.-B. Huang and J. Zornberg. 2009. SOA-1: Geomaterial behavior and testing. In *Proceedings of the 17th International Conference on Soil Mechanics and Geotechnical Engineering,* vol. 4 (ICSMGE, Alexandria), Millpress/IOS Press Rotterdam: 2777–2872. Retrieved from www.issmge.org

Mayne, P.W. 2014. Keynote: Interpretation of geotechnical parameters from seismic piezocone tests. In *Proceedings of the 3rd International Symposium on Cone Penetration Testing* (IS-CPT'14, Las Vegas): 47–73. Retrieved from www.cpt14.com

Mayne, P.W. 2017. Stress history of soils from cone penetration tests. 34th Manual Rocha Lecture. *Soils and Rocks* 40(3), Sept–Dec., Brazilian Society for Soil Mechanics, Saö Paulo: 203–218. Retrieved from www.soilsandrocks.com.br/

Mayne, P.W., M. Styler, D.J. Woeller and J. Sharp. 2017. Identifying contractive soils by CPT material index for flow liquefaction concerns. In *Proceedings of GeoOttawa 2017.* Canadian Geotechnical Society. Retrieved from www.cgs.ca

Mayne, P.W. and M. Styler. 2018. Soil Liquefaction Screening Using CPT Yield Stress Profiles. Geotechnical Earthquake Engineering and Soil Dynamics V: Liquefaction Triggering, Consequences, and Mitigation (GSP 290, Proc. GEESD-V, Austin), ASCE, Reston, VA: 605–616.

New York Times. 2019. Brumadinho dam collapse: A tidal wave of mud (9 February 2019): Retrieved from https://www .nytimes.com/interactive/2019/02/09/world/americas/brazil-dam-collapse.html

Okada, Y., K. Sassa and H. Fukuoka. 1999. Undrained shear behaviour of sands subjected to large shear displacement and estimation of excess pore pressure generation from drained ring shear tests. *Canadian Geotechnical Journal* 42: 787–803.

Olson, S.M. and T.D. Stark. 2002. Liquefied strength ratio from liquefaction flow failure case histories. *Canadian Geotechnical Journal* 39 (3): 629–647.

Olson, S.M. and T.D. Stark. 2003. Yield strength ratio and liquefaction analysis of slopes and embankments. *Journal of Geotechnical and Geoenvironmental Engineering* 129 (8): 727–737.

Ouyang, Z. and P.W. Mayne. 2019. Modified NTH method for assessing effective friction angle of normally consolidated and overconsolidated clays from piezocone tests. *Journal of Geotechnical and Geoenvironmental Engineering* 145(10), 04019067.

Robertson, P.K., C.E. Wride, B.R. List, U. Atukorala, K.W. Biggar, P.M. Byrne et al. 2000. The CANLEX project: Summary and conclusions. *Canadian Geotechnical Journal* 37(3): 563–591.

Robertson, P.K. 2009. Interpretation of cone penetration tests – a unified approach. *Canadian Geotechnical Journal* 46 (11): 1337–1355.

Robertson, P.K. 2010. Evaluation of flow liquefaction and liquefied strength using the cone penetration test. *Journal of Geotechnical and Geoenvironmental Engineering* 136 (6): 842–853.

Robertson, P.K. and Cabal, K.L. (2010). Estimating soil unit weight from CPT. In *Proceedings of the 2nd International Symposium on Cone Penetration Testing*, Vol. 2 (CPT'10, Huntingdon Beach, CA), Omnipress, Wisconsin: 447-454.

Robertson, P.K. 2012. Evaluating flow (static) liquefaction using the CPT: An update. In *Proceedings of Tailings and Mine Wastes '12,* Keystone, CO: Colorado State University: 11 pages.

Robertson, P.K. 2016. Cone penetration test-based soil behaviour type (SBT) classification system – an update. *Canadian Geotechnical Journal* 53: 1910–1927.

Sadrekarimi, A. and S.M. Olson. 2011. Critical state friction angle of sands. *Geotechnique* 61(9): 771–783.

Sivathayalan, S. 1991. Static, cyclic, and post liquefaction simple shear response of sands. Master of Applied Science Thesis, Dept. of Civil Engineering, University of British Columbia: 154 pages.

Schofield, A.N. and C.P. Wroth. 1968. *Critical State Soil Mechanics*. New York: Wiley & Sons. Retrieved from www.geotechnique.info

Styler, M.A., P.W. Mayne, D. McGowan and J.T. Sharp. 2018. Predicting changes in static liquefaction susceptibility using cone penetration tests. In *Proceedings of Mine Waste and Tailings Stewardship Conference,* Session 10, Paper 41, Brisbane: Retrieved from https://tailings.ausimm.com/

Vaid, Y.P. and S. Sivathayalan. 1996. Static and cyclic liquefaction potential of Fraser Delta sand in simple shear and triaxial tests. *Canadian Geotechnical Journal* 33: 281–289.

Wroth, C.P. 1984. The interpretation of in-situ soil tests (24th Rankine Lecture). *Geotechnique* 34(4): 449–489.

Yassuda, A.J., A. Black, N. Namba, M.O. Cecil, A.P. Ruiz and S. Ono. 2018. Periodic Review Dam Mine Safety Stream Bean – Dam Safety 1 Technical Report, Vale Paraopeba Complex in Brumadinho, State of Minas Gerais, Report SP-RC-117/17, prepared by TUV SÜD Technical Inspection Association, IBC Risk Management Geotechnical Bureau, São Paulo, Brazil: 265 pages.

Yoshimine, M., K. Ishihara and W. Vargas. 1998. Effects of principal stress direction and intermediate principal stress on undrained shear behavior of sand. *Soils and Foundations* 38(3): 179–188.

Proceedings of Tailings and Mine Waste 2019
November 17–20, 2019, Vancouver, Canada
Published by the University of British Columbia, 2019

High Performance Fine Tailings Dewatering with Hydrated Lime Slurry

Ben Mosher, Graymont, USA
Nikolas Romaniuk, Graymont, Canada
Jesse Fox, Graymont, USA
Narain Hariharan, Texas A&M, USA
Jared Leikam, Graymont, USA
Mike Tate, Graymont, USA

Abstract

Recent catastrophic fluid tailings containment failures in mining operations, such as Mount Polley and Brumadinho, have resulted in serious environmental damage, loss of human life, and immense cost to operators. To reduce the risk associated with fluid tailings, there is a growing interest in methods to produce tailings with significantly lower moisture content that can be stacked and which have the strength to be self-supporting without conventional containment. Development of dry stackable tailings requires high performance dewatering techniques, such as filtration, capable of providing gravimetric moisture contents below 30%. The challenges facing commercial tailings filtration are high capital costs and long cycle times, especially for fine tailings. Improving the dewatering characteristics of fine tailings, often dominated by clay minerals, is critical to improve filtration rates and reduce cycle times.

Investigations of hydrated lime's effect on both standard resistance to filtration (SRF) and benchtop pressure filtration of fine tailings and analogs (composed of silica and clay mineral blends) demonstrate significant improvements to dewatering rates and cycle times. Benefits of hydrated lime are not observed until a slurry pH of 11.8 is achieved, and are optimized at a slurry pH of approximately 12.4. SRF and benchtop pressure filtration studies of oil sands fluid fine tailings treated with hydrated lime slurry show remarkable improvements in water release rates and achieve lower moisture contents in the filter cakes within shorter cycle times. In addition, the hydrated lime treated filter cakes demonstrate significant increases in peak and residual shear strengths over time, resulting from both pozzolanic reactions and cation exchange. The benefits that hydrated lime provides to dewatering of both silica and clay minerals appear to be a result of chemical modifications of the mineral surfaces, which result in a near neutral zeta potential. The enhancements to dewatering and improvements in geotechnical properties provided by hydrated lime

slurry as an additive to fine tailings should improve the efficiency of commercial filtration processes to produce dry stackable tailings with improved geotechnical properties.

Introduction

Containment of fine tailings has become an ever-increasing concern for mining operations worldwide. Recent failures in Brumadinho, Mount Polley, and Fundão highlight the liability to the environment, human health and safety posed by fluid fine tailings (FFT) (Armstrong et al., 2019; Lyu et al., 2019). These recent failures have resulted in an increasing push by critics and regulators to move to dry-stackable tailings, away from traditional fluid tailings containment strategies.

Tailings produced by oil sands mining operations represent one of the largest inventories of FFT in the world, now exceeding 1.2 billion cubic meters, and represent an increasing environmental risk to the Athabasca region, as well as economic risk for the operators (AER, 2018). The fluid tailings inventories are mostly contained by large dams. While dam integrity is a high priority, with world-class dam construction and maintenance, the large quantities of fluid tailings nevertheless represent a substantial liability (Boswell and Cavanagh, 2018). The oil sands FFT is primarily composed of fine clays that are slow to settle and require centuries to consolidate beyond 30 to 40% solids (Kasperski, 1992; Scott et al., 1985), posing a serious dewatering challenge. Remediation to support an uplands ecosystem requires a shear strength greater than 20 kPa, which could require the FFT to be dewatered to above 70% solids content (McKenna et al., 2016). Achieving this high solids content in oil sands FFT is necessary to make dry stackable tailings, and may be possible using pressure filtration. CNRL and Teck are now reinvestigating pressure filtration as a method to achieve high solids content fine tailings, and recently commissioned a commercial trial at CNRL's Muskeg River operation.

High performance dewatering of fine tailings is necessary to achieve dry stackable tailings, where the optimal dewatering process is dependent on the tailings mineral properties and the climate of the operations. In dry climates, with easily dewatered tailings, thickeners can be used effectively with atmospheric drying to achieve a dry stackable product; however, many operations have tailings which contain troublesome clay minerals, or are in climates where atmospheric drying is not possible. Filtration, while more costly, is one of the few dewatering techniques capable of providing a dry-stackable product (Kaswalder et al., 2018). There are many types of filtration, but pressure filtration is increasingly being adopted as vendors produce larger and larger pressure filtration devices that can tolerate higher pressures (Chaponnel and Wisdom, 2018). The greatest downside to pressure filtration is the large upfront capital cost; however, these costs can be offset by water recovery in dry regions and by a lower cost of tailings containment. The economics of pressure filtration are largely driven by the cycle time of the process. Process additive chemistries, such

as coagulants and polymers, that can improve water release and filtration rates are critical for the viability of pressure filtration processes.

Role of hydrated lime in coagulant and pozzolanic modification of clay minerals

Inorganic coagulants, such as hydrated lime ($Ca(OH)_2$), provide calcium, a bivalent cation, in solution that can neutralize the negative surface charges of colloids that destabilize the inter-colloidal electrostatic repulsions and promote coagulation. In the case of fine inorganic particles, such as phyllosilicate clay minerals, cation exchange is a critical process whereby the bivalent calcium cation can replace a monovalent sodium cation on the mineral surface. The bivalent nature of the calcium cation promotes cationic bridging of the clay particles to form larger agglomerates (Little, 1995; Lane, 1983; Rogers and Glendinning, 1996). Several factors related to solution chemistry, including pH, alkalinity, ionic strength, and the concentration of other cations, can influence the effectiveness of the cation exchange (Tate et al., 2017).

Cation exchange reactions can modify the water film thickness of mineral surfaces. In aqueous solutions, water is coordinated with different cations in solution; therefore, a sodium or calcium ion bound to the clay surface will carry water with it. Sodium tends to form thick water films, while calcium cations form much thinner water films. This mechanism can considerably reduce the volume of water in slurries rich in clay minerals with high surface areas, such as FFT.

Unlike some acidic coagulants like gypsum, hydrated lime can also destabilize and permanently modify colloidal particles by chemically reacting with them. It is well established in soil stabilization applications that at a pH of 12.4, phyllosilicates dissolve into their aluminate and silicate constituents, which can react with soluble calcium and water to form pozzolanic products such as calcium aluminate hydrates (CAH) and calcium silicate hydrates (CSH) (Choquette et al., 1987; Little, 1995; Locat et al., 1996; Tran et al., 2014). Unlike cation exchange, which occurs quickly and is generally limited by diffusion, the pozzolanic reactions occur over several months and depend on temperature, soil chemistry, and soil mineralogy (Hunter, 1998; Wild et al., 1993). Under favourable conditions, the pozzolanic reactions promote remineralization, which is characterized by the formation of new mineral phases with significantly stronger and more resilient bonds.

Hydrated lime, applied as lime slurry to coagulate the fine clay minerals present in FFT, may improve the dewatering rate of the FFT during pressure filtration. An immediate textural modification of the clay minerals with hydrated lime is expected in the resulting filter cakes, which should provide further long-term benefits, such as the transformation of the clay minerals through pozzolanic reactions that are expected to permanently alter the fabric of the cake, and thereby develop resilient strength with time.

Experimental design

All experiments, unless otherwise indicated, were completed at Graymont's Central Laboratory in Sandy, Utah. Pressure filtration studies were performed by FLSmidth at their Salt Lake City laboratories as a component of a previous test program (Rahal et al., 2018).

Materials

The oil sands FFTs used in the experiments were analyzed for solids content, bitumen content, methylene blue index (MBI), and critical cations in the pore water, and sodium absorption ratio (SAR) as presented in Table 1. Note that FFT I is the same FFT used by the Northern Alberta Institute of Technology (NAIT) in their presentation at the Sixth International Oil Sands Tailings Conference (Li et al., 2018). The SAR measures of the Na^+ relative to the square root of the sum of the square of the Ca^{2+} and Mg^{2+}.

Table 1: Oil sand FFT properties

Sample ID	Gravimetric solids content	Dean-Stark Analysis			MBI	pH	Na^+	Ca^{2+}	Mg^{2+}	Sodium absorption ratio
		Bitumen	Minerals	Water	meq/100g solids		mg/L			
A	35.1%	2.9%	32.5%	61.6%	8.9	7.9	359	14	8	39
B	34.9%	1.3%	33.4%	64.4%	12.2	8.2	838	12	5	128
C	33.8%	1.5%	32.2%	66.3%	9.9	8.3	827	14	6	104
D	39.6%	1.5%	38.6%	59.9%	8.6	8.6	894	16	6	100
E	29.2%	n/a	n/a	n/a	9.3	8.6	739	20	8	64
F	28.8%	n/a	n/a	n/a	12.9	8.3	157	41	20	6
G	35.2%	n/a	n/a	n/a	7.2	8.4	354	16	9	33
H	25.9%	1.2%	24.7%	n/a	14.1	8.2	306	51	19	11
I	27.5%	1.5%	28.4%	70.3%	12.2	8.9	297	58	24	9
J	37.5%	n/a	n/a	n/a	7.9	8.8	404	31	14	22

The hydrated lime, $Ca(OH)_2$, used was high calcium from Graymont's Indian Creek quarry. The gypsum, CaSO4, was purchased from Hi Valley Chemical as a hemihydrate. The partially hydrolyzed polyacrylamide (HPAM) anionic polymer flocculants A3331 and A3338 were produced by SNF. The silica

gel was from BTC (Beantown chemical corporation) chemical. The kaolinite used was KGa-2 obtained from the clay minerals society source clay sample bank. The bentonite used was sodium bentonite from Fisher Chemical.

Methods

Coagulant and flocculant preparation

All coagulants (hydrated lime and gypsum) were prepared as 5% mixtures in distilled water by mass. The hydrated lime generates a lime slurry that must be resuspended before addition. Gypsum dissolved in solution without requiring remixing.

Model silica and clay slurry preparation

The desired mass of each was measured into a 1 L Nalgene jar. The appropriate mass of water was added and mixed thoroughly. Four mineral slurries were prepared: silica gel at 30% solids content by mass; kaolinite at 5% solids content by mass; bentonite at 5% solids content by mass; and a blend containing 20% silica gel, 5% kaolinite, and 5% bentonite for a total of 30% solids content by mass. The pH stick was calibrated to a pH of 7. After 30 minutes had passed the pH was measured and adjusted with either 5N NaOH or concentrated HCl until the pH was 8 ± 0.1.

Determination of standard resistance to filtration (SRF)

An OFITE filter press was used for the SRF measurement. The assembly consists of a stainless-steel cylinder that holds a Whatman 42 filter paper as a filtration media with calculated filtration area of 50.27 cm^2. 200 g samples of slurry were treated with lime slurry or gypsum to either a defined dose or to a specific pH with hand mixing for 2 minutes. The treated or untreated slurries were placed directly in the filtration apparatus. The apparatus was then pressurized to 100 PSI for FFT and 10 PSI for the model silica and clays slurries with nitrogen gas, and the filtrate was collected from the drain valve at the bottom of the cylinder. The mass of the filtrate and time elapsed was recorded. The SRF was calculated as reported by NAIT (Li et al., 2018).

Benchtop pressure filter for geotechnical analysis

An Outotec Labox 100 pressure filter was used to prepare the geotechnical samples. The goal was to achieve filter cakes with approximately 70% solids content. Using a double-sided filtration, an FFT I slurry was processed without treatment, and treated with lime slurry (4,000 ppm on total wet slurry), or with A3338 (1,500 ppm on a dry solids basis). The slurries were filtered at 6 bar using an air operated double diaphragm pump. After filtration ceased, the filter cake further dewatered with a membrane squeeze applied at 15 bar. The membrane squeeze was stopped once enough water was removed to produce a filter cake with

approximately 70% gravimetric solids content. The membrane was then relieved and an air blow of approximately 2 bar was applied for 2 minutes. The filter cake was then homogenized immediately, and transferred into specimen jars and sealed for strength and Atterberg limits measurements.

Strength measurements

The cakes generated in the pressure filter operations were carefully placed into jars in lifts to minimize the effect of air voids, and then levelled to obtain a smooth surface. The peak and residual shear strength of the cake samples were measured on a Brookfield RST-SST rheometer at a rotational speed of 0.1 RPM, using a VT-20-10 vane spindle for shear strengths less than 10 kPa or a VT-10-5 vane spindle for cakes with higher strength.

Results and discussion

Previous investigations of lime slurry as an additive to oil sand fine tailings have shown significant benefits in filtration processes (Tate et al., 2017; Rahal et al., 2018; Li et al., 2018). A method used to characterize and compare how different additives benefit filtration is to calculate the standard resistance to filtration (SRF). The SRF is a measure of filterability of a slurry containing incompressible mineral solids. As the calculated SRF should be directly proportional to the cycle time of a filter press, the lower the SRF the shorter the cycle time for the filter press.

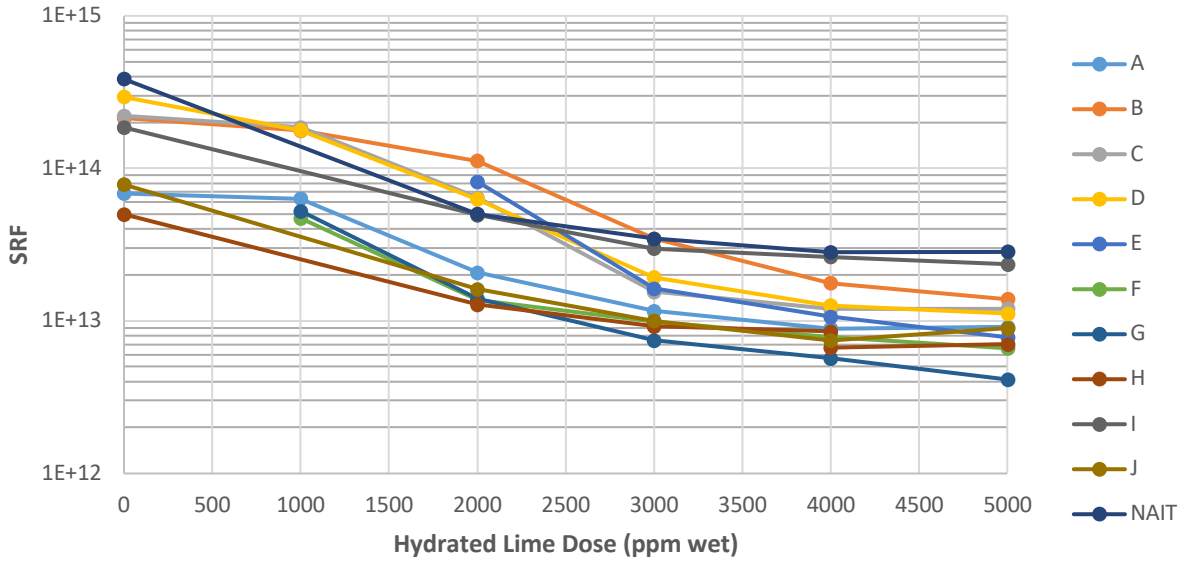

Figure 1: Response in standard resistance to filtration (SRF) of 11 different oil sands fluid fine tailings with 5% lime slurry treatments, reported as hydrated lime dose as ppm based on total wet tailings weight

Previous investigations of the effect of lime on the SRF, completed by NAIT, were completed with only one type of oil sands fluid fine tailing (FFT). To better assess the variability in oil sands fine tailings, ten FFTs across four operations demonstrating significantly differences in solids content, bitumen content, and MBI, as described in Table 1, were treated with lime slurry, and the SRF of the materials was determined using an air-driven filter press. This filter press system did not use the design modification developed in NAIT's experiments. The SRF values calculated from the filter press experiments are presented in Figure 1, along with the data report by NAIT for a 30-minute experiment using their modified design. The results show that the different FFTs initially had SRF values ranging from approximately 5×10^{13} to 8×10^{14}, which is expected considering they are composed of fine clay minerals. Treatment with lime slurry is demonstrated to significantly reduce the SRF, with the maximum benefit obtained generally at the 4,000 or 5,000 ppm doses, reducing the SRF values to between approximately 4.2×10^{12} and 5.5×10^{13}, an improvement in most cases of about an order of magnitude.

The entirety of the SRF data collected for FFTs A through J is presented in Figure 2(a) as a function of soluble calcium, or in Figure 2(b) as a function of pore water pH. Significant reductions in SRF are observed when there is no soluble calcium; however, in most of the analyzed FFTs, the SRF does not reduce until a pH above 11 is achieved and, in most FFTs, a pH above 12 is required to provide the greatest reduction. An interesting implication of this pH dependence is that the lime slurry dose can be applied based on an achieved slurry pH, rather than on the basis of a more complicated parameter such as MBI, which could provide a simple mechanism to control lime slurry dose as FFT properties change during operations.

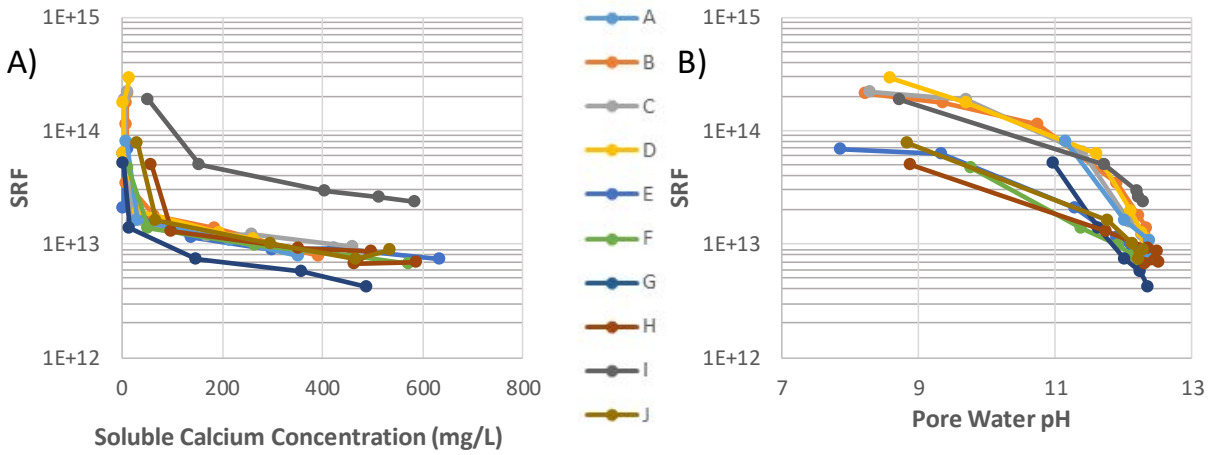

Figure 2: Response in standard resistance to filtration (SRF) of 11 different oil sands fluid fine tailings in properties measured in the filtrates; A) SRF as a function of soluble calcium concentration measured in filtrate water, and B) SRF as a function of pH measured in the filtrate

As FFT are known to be composed of a blend of clay minerals and fine silica, model systems composed of silica, clay minerals, or a blend of silica and clay minerals were analyzed to understand their

response to hydrated lime. Silica gel was selected due to its fine size and high purity and two clays were chosen, a high defect kaolinite and a bentonite, representing 1:1 and 2:1 clay minerals. Slurries buffered to pH 8 were prepared from the minerals, which were then treated with lime slurry to a pH of 9.5, 11.5, or 12.5. The treated minerals were then filtered to determine the SRF, which is presented in Figure 3 as a function of the pH achieved with the lime slurry treatment. The results demonstrate a clear dependency on pH for all mineral slurries, with significant benefits observed through all pHs for the silica gel, not until pH 12.5 for the clay minerals and at pH 11.5 for the silica gel and clay mineral blends. Much like what was observed in clay mineral rich FFT, a high pH of 12.5 was required to observe a reduction in SRF for the pure clay minerals. The results observed with silica are unlikely to be encountered in real world applications, as the silica gel is prepared to have a high surface area and it appears to dominate the behaviour of the blend; however, the responses seen in the individual clay minerals appear to confirm the decreases to SRF observed with FFT. These responses appear to track with observations made by Rehl on the effect of hydrated lime treatment of silica and kaolinite on colloid zeta potential develop (Rehl, 2019).

The work, reproduced in Figure 4, demonstrates that hydrated lime reduces the zeta-potential, i.e. surface neutralization, as pH increases for kaolinite. The reduction of the zeta-potential below –10 mV occurs at pH 12 for kaolinite, which follows the SFR trend observed where improvements to SRF were seen for clays at pH 12.5. The zeta-potentials shown in Figure 4 also demonstrate that the alkaline cation is critical, as sodium hydroxide further increases zeta-potentials, i.e., increases dispersion, as the pH increases. This principle component analysis would suggest that lime slurry at a high pH could be used to improve the filtration of any slimes or tailings that contain slow filtering clay minerals.

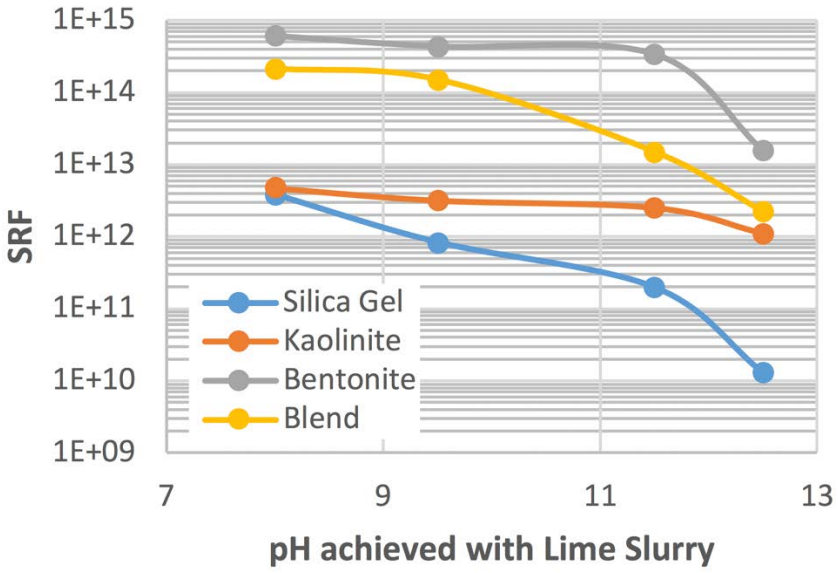

Figure 3: Response in standard resistance to filtration (SRF) of model silica gel, kaolinite, bentonite, and combined slurries to hydrated lime slurry treatment to pH 9.5, 11.5, and 12.5

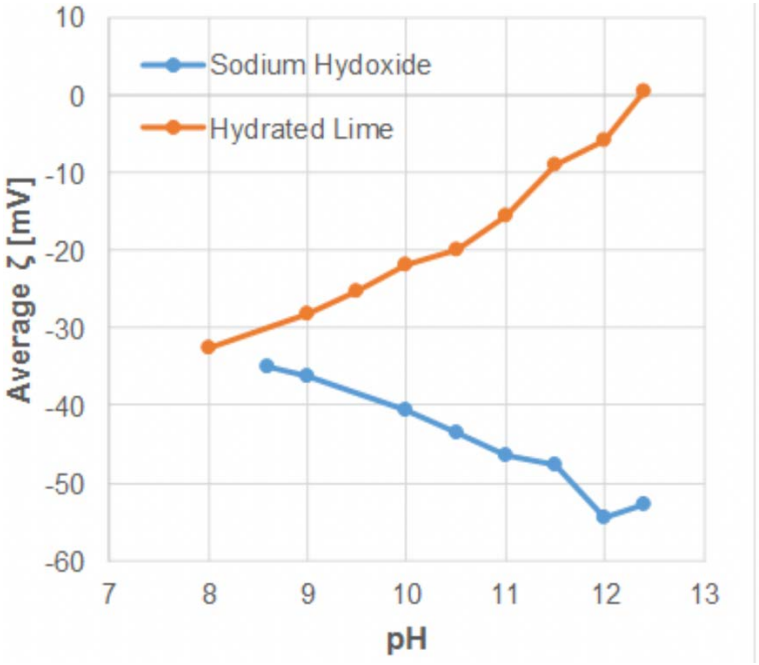

Figure 4: Response in zeta potential of kaolinite to hydrated lime or sodium hydroxide treatments based on pH achieved, reproduced from Rehl (2019)

Reduction in SRF

Hydrated lime provides a significant reduction to the SRF when it is added to oil sands FFT to achieve a critical pH above 12, with the greatest benefits observed around approximately 12.45, which is the pH defined as the lime fixation point for soil stabilization. In Figure 1, the reduction in SRF is plotted as a function of hydrated lime additive dose, based on the wet FFT weight, where the best reduction appears to be achieved at approximately 4,000 ppm.

The percentage reduction in SRF for the FFTs analyzed in this experiment with lime slurry and gypsum coagulants are compared to previous results presented by NAIT that investigated lime, gypsum, and anionic polymer in Figure 5. The result of the current study demonstrated a reduction in SRF for 6 FFTs treated with 4,000 ppm hydrated lime between 86 to 96% with an average of 90%. This is comparable to the 93% reduction using 4,000 ppm hydrated lime reported by NAIT. Gypsum provided a significantly smaller reduction in SRF in both this study's and NAIT's experiments, with 50 and 65% reductions respectively. The NAIT investigation found that the SRF using an anionic polymer (SNF A3338) provided an 88% reduction, which is only slightly lower than hydrated lime. However, the NAIT investigation noted that resulting filter cakes had significantly different properties, with the polymer filter cake appearing "sponge-like", unlike the solid cake provided by hydrated lime. These observations suggest that there are significant changes in the material properties of the cake developed by anionic polymer and hydrated lime treatments, which may affect how useful the SRF value is for predicting performance additive performance

in a filter press at high pressures. The most important aspect is the compressibility of the cake, as the SRF assumes the cake is incompressible. This assumption is likely accurate at low solids contents (such as below 40 to 50% solids in FFT); however, as the solids content of the cake increases it is also very likely, especially for the anionic polymer treated FFTs, that compressibility will affect the rate of filtration. The SRF experiments used to compare hydrated lime and polymer only achieve a maximum 55% solids in the hydrated lime cake and 40% solids in the polymer treated cake. However, long-term filtration performed by NAIT to produce a filter cake between 70 to 75% solids found that hydrated lime required only 3 to 4 hours versus 20 hours for polymer, suggesting that caution must be used when applying the SRF in high performance filtration, since the additives impacts the physical properties of the developing cake.

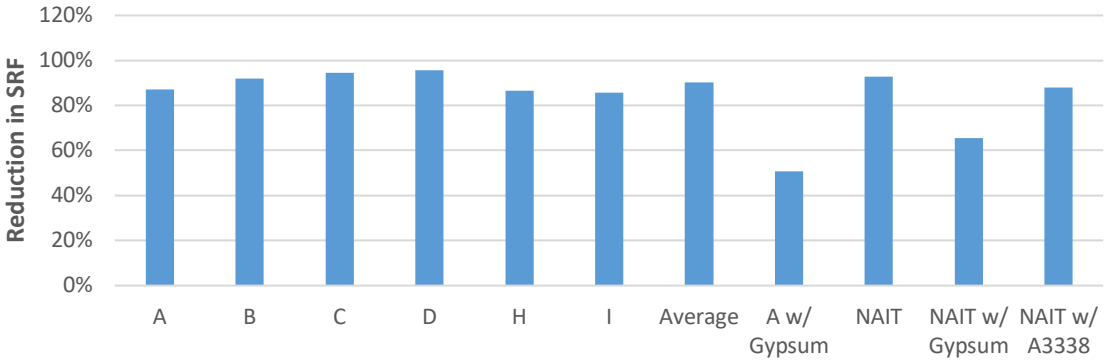

Figure 5: Reduction in SRF provided by lime slurry treatment using a 4,000 ppm dose of hydrated lime based on total wet tailings weight, unless additive is otherwise noted. Gypsum added as an equal calcium to the 4,000 ppm hydrated lime dose. NAIT data is reproduced from Li et al., 2018

A change in FFT properties likely explains why hydrated lime treated FFT outperformed an anionic polymer thickened FFT in pressure filter pilot experiments reported previously in a joint Graymont-FLSmidth study (Nowicki, 2018). In part of this study, FFT G was treated with either 4,000 ppm hydrated lime or an anionic polymer (A3331). The anionic polymer, as expected, readily releases free water, which was decanted, and reached 40% solids, at which point it was placed in the filter press, filtered at 140 PSI, and then a 225 PSI membrane press was performed. The hydrated lime treatment did not readily release water, so it was placed in the filter press at its native solids content of 34% solids and processed with the same pressure. The water release in the filter press as a function of time is shown in Figure 6(a), where the lime-treated FFT release water at a much more rapid rate and responds significantly faster when the membrane squeeze is applied. Figure 6(b) shows the calculated solids content versus time, and shows that the lime-treated FFT catches up to initial higher solids content polymer treated FFT after approximately 6 minutes of filtration time. The water release rates observed in the study generally support the conclusion that removal of water as the cake develops to 40% solids is quick for both lime slurry and anionic polymer

and likely reflect similar SRF, but the solids concentrates in the hydrated lime treatment maintain a clear advantage in dewatering, which suggests that the approximations made to calculate SRF are not valid.

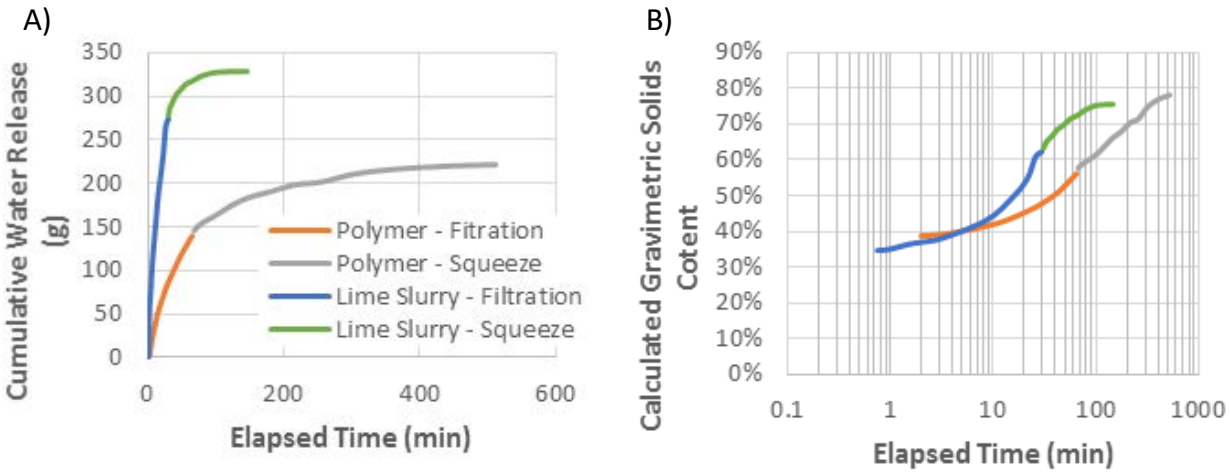

Figure 6: Comparison of lime slurry and anionic polymer (A3331) treatments of FFT G measuring water release rate (A) and gravimetric solids content (B) observed during pressure filtration at 140 PSI and membrane squeeze of the filter cake at 225 PSI, reproduced from Nowicki (2018)

Improvements to geotechnical properties of filter cakes

The treatment of FFT with lime slurry demonstrated significant benefits to the shear strength of the cakes that continues to increase with curing time, compared to both no additive and anionic flocculant, as shown in Figures 7(a) and 7(b). The initial peak shear strength of the lime slurry treated and polymer treated cakes were similar at 31 kPa and 26 kPa respectively, both outperforming no treatment at 11 kPA. However, the lime slurry treated cake continued to gain strength, reaching 39 kPa after 1 day and 49 kPa after 1 week, whereas both the polymer treated and no treatment cakes maintained the same strength over the same time period. The lime slurry treatment additionally demonstrated improvements to the residual shear strength that also increased with time, from 11 kPa immediately after treatment to 18 kPa after 1 week. Interestingly, the anionic flocculant treatment showed no benefit to residual shear strength compared to no additive, reporting values between 5 to 6 kPa that were insensitive to curing time.

The results demonstrate that treatment using lime slurry to a pH of 12.4 and above most likely allows for pozzolanic reactions to occur between the calcium ions and the aluminates and silicates released during partial dissolution of the clay minerals. This mechanism helps develop a durable inter-particle matrix resulting in strength gain with time, unlike the anionic flocculant that appears to develop a weak and shear-sensitive structure.

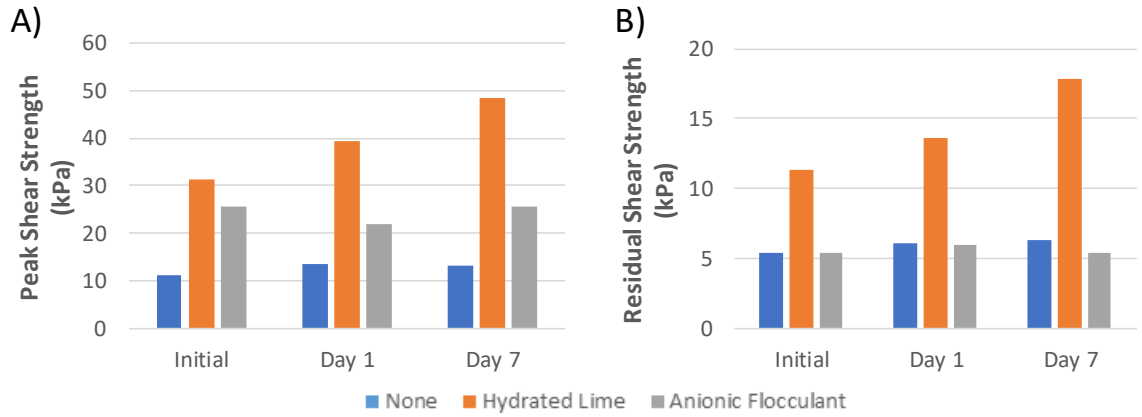

Figure 7: Effect of hydrated lime and anionic flocculant (A3338) treatments on peak shear strength (A), residual shear strength (B)

Conclusion

The effect of lime slurry as a coagulant for pressure filtration of FFT explored in this investigation suggests that there are significant benefits to dewatering based on reductions in SRF and increases in pressure filtration rates, and provides significant improvements to cake properties such as strength development that is beneficial for their use as dry-stackable tailings in landform development. The benefits to dewatering demonstrated in the SRF investigation appear to be due to cation exchange and pozzolanic reactions, which promote neutralization of clay surfaces, suggesting that lime slurry may enhance water release in the pressure filtration of other tailings or slimes that contain troublesome clay minerals or even highly active silicas, which could be beneficial by reducing pressure filter cycle times.

The benefits lime slurry provides to the geotechnical behaviour of FFT filter cakes suggests the formation of pozzolanic products. The mechanism for these reactions is dependent on the same pH target required for soil stabilization. The calcium aluminate and silicate hydrates formed in the pozzolanic reaction provide a transition of water from the liquid phase to a critical component of a structural mineral. This water requirement may be advantageous as filter cakes would need to be produced at slightly higher gravimetric water content, potentially providing a critical reduction in filtration or membrane squeeze times during a phase of the pressure filtration cycle where dewatering is hardest due to low hydraulic conductivity. The increase in strength may additionally allow for the material to be initially pliable and workable as the material will set and gain strength over weeks. Future study will continue to characterize the development of the geotechnical properties over extended timeframes.

References

Alberta Energy Regulator (AER). 2018. State of fluid tailings management for mineable oil sands, 2017.

Armstrong, M., R. Petter and C. Petter. 2019. Why have so many tailings dams failed in recent years? Resources Policy. In press.

Boswell, J. and P. Cavanagh. 2018. Stewarding dam safety in Alberta: The Dam Integrity Advisory Committee (DIAC). In *Proceedings of the Sixth International Oil Sands Tailings Conference,* Edmonton. Edmonton, Alberta: University of Alberta Geotechnical Centre: 246–251.

Chaponnel, J. and T. Wisdom. 2018. FLSmidth Colossal filter – demonstration plant. In *Proceedings of the 21st International Seminar on Paste and Thickened Tailings,* Cape Town. Perth, Western Australia: Australian Centre for Geomechanics: 53–62.

Choquette, M., M.A. Bérubé and J. Locat. 1987. Mineralogical and microtextural changes associated with lime stabilization of marine clays from eastern Canada. *Applied Clay Science* 2(3): 215–232.

Hunter, D. 1988. Lime induced heave in sulfate-bearing clay soils. *Journal of Geotechnical Engineering* 114(2): 150–167.

Kasperski, K. 1992. A review of properties and treatment of oil sands tailings. *AOSTRA Journal of Research* 8:11.

Kaswalder, F., D. Cavalli, A. Hawkey and A. Paglianti. 2018. Tailings dewatering by pressure filtration: Process optimisation and design criteria. In *Proceedings of the 21st International Seminar on Paste and Thickened Tailings,* Cape Town. Perth, Western Australia: Australian Centre for Geomechanics: 427–438.

Lane, S. 1983. Lime coagulation and stabilization of total oil sands tailings. Petroleum Society of Canada Annual Technical Meeting, May 10–13, Banff, Alberta, Canada.

Li, Y., H. Kaminsky, N. Romaniuk and M. Tate. 2018. Filter press modification to assess dewatering performance of fluid fine tailings. In *Proceedings of the 6th International Oil Sands Tailings Conference*, Edmonton. Edmonton, Alberta: University of Alberta Geotechnical Centre: 314–323.

Little, D.N. 1995. *Handbook for Stabilization of Pavement Subgrades and Base Courses with Lime*. The Lime Association of Texas.

Locat, J., H. Tremblay and S. Leroueil. 1996. Mechanical and hydraulic behaviour of a soft inorganic clay treated with lime. *Canadian Geotechnical Journal* 33(4): 654–669.

Lyu, Z., J. Chai, Z. Xu, Y. Qin and J. Cao. 2019. *A Comprehensive Review on Reasons for Tailings Dam Failures Based on Case History.* Advances in Civil Engineering. In press.

McKenna, G., B. Mooder, B. Buton and A. Jamieson. 2016. Shear strength and density of oil sands fine tailings for reclamation to a boreal forest landscape. In Proceedings of the 5th International Oil Sands Tailings Conference, Lake Louise. Edmonton, Alberta: University of Alberta Geotechnical Centre: 130–153.

Nowicki K. 2018. Graymont MFT – Thickening and pressure filtration work summary. Project Reference: P17093. Salt Lake City, Utah, USA.

Rahal, K., J. Fox, J. Leikam, M. Tate and N. Romaniuk. 2018. Impact of calcium hydroxide on the equipment and process of oil sands tailings treatment. In *Proceedings of the 22nd International Conference on Tailings and Mine Waste,* Keystone. Vancouver, British Columbia: UBS Studios: 387–397.

Rehl, B. Towards oil sand tailings reclamation through the use of lime observed by sum frequency generation spectroscopy. Presented at Prairie Environmental Chemistry Colloquium, Edmonton, Alberta, May 2019.

Rogers, C.D.F. and S. Glendinning. 1996. Modification of clay soils using lime. In *Lime Stabilisation,* edited by C.D.F. Rogers, S. Glendinning and N. Dixon: 99–114. London: Thomas Telford Publishing.

Scott, J., M. Dussealt and W. Carrier. 1985. Behaviour of the clay/bitumen/water sludge system from oil sands extraction plants. *Applied Clay Science* 1: 207–218.

Tate, M.J., J. Leikam, J. Fox and N. Romaniuk. 2017. Use of calcium hydroxide as a coagulant to improve oil sands tailings treatment. In *Proceedings of the 22nd International Conference on Tailings and Mine Waste,* Keystone. Edmonton, Alberta. University of Alberta Geotechnical Centre: 720–732.

Tran, T.D., Y.G. Cui, A.M. Tang, M. Audiguier and R. Cojean. 2014. Effects of lime treatment on the microstructure and hydraulic conductivity of Héricourt clay. *Journal of Rock Mechanics and Geotechnical Engineering* 6(5):399–404.

Wild, S., M.R. Arabi and G. Leng-Ward. 1993. Sulphate expansion of lime stabilized kaolinite II: Reaction products and expansion. *Clay Minerals* 28(4): 569–583.

Proceedings of Tailings and Mine Waste 2019
November 17–20, 2019, Vancouver, Canada
Published by the University of British Columbia, 2019

3D Simulations of Dam Breach and Deposition Using Viscosity Bifurcation Rheology

Étienne Parent, Carleton University, Canada
Paul Simms, Carleton University, Canada

Abstract

Simulations of tailings as they flow, whether for purposes of simulating beaching or dam breach, usually employ Bingham rheology. However, practical experience indicates that tailings manifest a different rheology at their initial rest state and after they have been sheared down. Recent studies have shown that this variable behaviour can be explained by viscosity bifurcation rheology (VBR), a rheology commonly used to explain non-Newtonian behaviour for different kinds of suspensions. This work describes the implementation of VBR into an open source material point method code, which is used to simulate tailings deposition and dam breach in 2D and full 3D simulations. The most striking observations are that VBR allows for simulation of realistic morphology during deposition, such as channel flow, and that the runout in dam breach simulations with VBR is substantially longer than when a Bingham rheology is employed. A 3D simulation of a recent tailings dam failure in China is presented.

Introduction

The flow behaviour of tailings is important to practice in at least two areas: controlling deposition for thickened or filtered tailings, and simulation of tailings flow out of a breached impoundment. Until quite recently, simulations of these flows have typically used Bingham or similar rheology (Pastor et al., 2014, 2002; Jeyapalan et al., 1983; Gao and Fourie, 2019; Mizani et al., 2013). However, the behaviour of many non-Newtonian suspensions under dam breach or other sudden failure conditions has been shown to be not well described by Bingham rheology (Coussot et al., 2002, Chanson et al., 2006), and better described by a "thixotropic" or "Viscosity Bifurcation" rheology (VBR). These latter type models describe the viscosity as a function of two competing processes, shearing and ageing. Shearing breaks down any network structure and reduces viscosity, whereas ageing describes the build-up of structure over time due to fine particle interactions. There are several such models, one of the first proposed by Coussot et al. (2002):

$$\frac{d\lambda}{dt} = \frac{1}{T} - \alpha \gamma \lambda \tag{1}$$

$$\mu = \mu_0(1+\lambda^n)$$

where α and T are material constants and γ is the strain rate. T is the characteristic time of evolution of the structure. The instantaneous viscosity μ to be a function of the instantaneous state of the material, where μ_0 is the fully sheared viscosity where structure is broken down (λ=0), and n is a parameter. The model predicts a critical shear rate or shear stress, which depends on the ratio of the ageing and shearing parameters (T and α) in Equation 1, and also the initial structure of the material. Below a critical shear stress or shear rate, the viscosity increases as ageing dominates, and the material comes to a stop. Above the critical shear stress or shear rate, the viscosity degrades the fully sheared value. The parameters can be obtained by fitting viscosity data obtained from controlled shear stress or controlled shear rate rheometry.

An example of such tests and the model fit for a clayey tailings are shown in Figure 1. Mizani and Simms (2016) show an example for a hard rock tailings. The consequence of this model is that the apparent yield stress required to initiate flow at a given density is much higher than the apparent yield stress required to stop flow at the same density, which is common practical observation for many types of tailings.

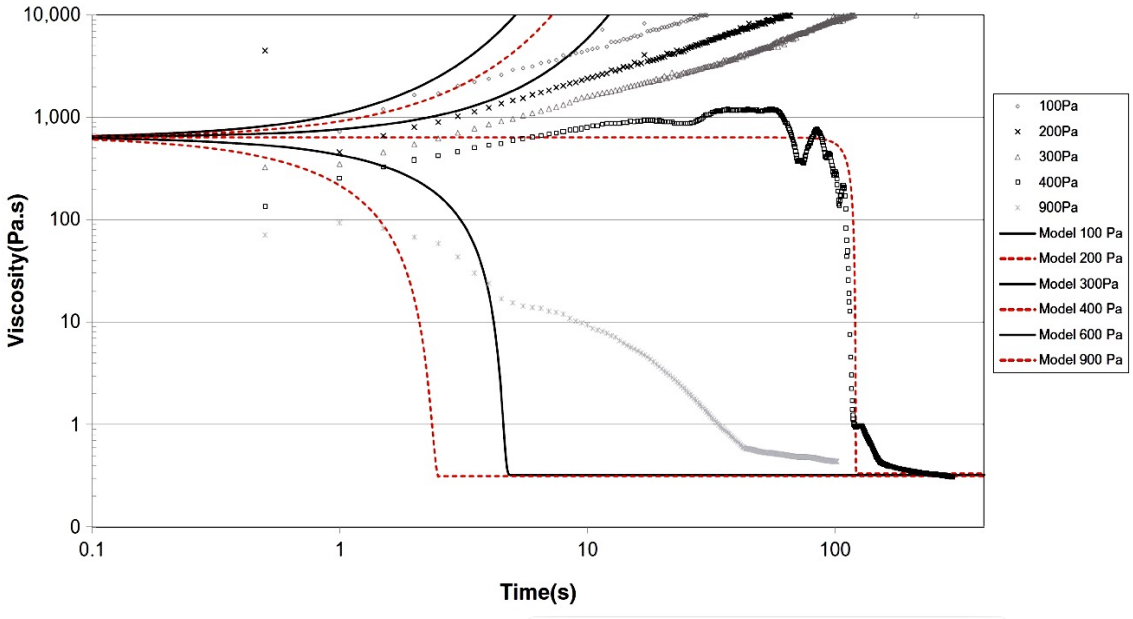

Figure 1: Equation 1 applied to viscosity measurements at different constant shear stresses in a clayey tailings (adapted from Mizani et al., 2017)

Methods

To simulate tailings flows, the authors implemented VBR into the open source material point method (MPM) solver Unitah-MPM. The Unitah code was created at the University of Utah and is available at http://www.sci.utah.edu/download/uintah/. To validate the implementation of VBR into UNITAH-MPM, a

number of test cases were modelled, extending from experiments of materials sloshing in a box (Cruchaga et al., 2007), to small-scale flume experiments of tailings either under constant rates of deposition or dam break simulation (Babaoglu and Simms, 2017; Mizani et al., 2013). These are described in detail in Parent (2019).

The baseline material parameters in the simulation are chosen to give identical predictions of runout for a small-scale flume test (2 m long in 2D). The *n* parameter (2.5 compared to 1) affects the rate of viscosity increase when ageing dominates, the effect of which is more pronounced at larger scales. The Coussot 2 material properties were originally obtained from rheometry on the clay-rich tailings (Mizani, 2017).

Table 1: Baseline material parameters used in the numerical simulations

Parameter	Bingham	Coussot 1	Coussot 2
Yield stress (Pa)	30	–	–
Viscosity (Pa*s)	0.05	–	–
α*T	–	0.36	0.36
n	–	2.5	1.0
Minimum viscosity (Pa*s)	–	1	1

The simulations shown in the paper include a 3D hypothetical simulation of thickened tailings deposition, 2D hypothetical simulations of dam breach, and a 3D simulation of the tailings dam breach from a bauxite mine in China is 2016.

Case 1

A pipe deposits the tailings at a rate of 100 L/s out of a 0.30 m diameter pipe onto an inclined plane with a slope of 3%. The flow lasts for a total of 180 seconds (three minutes) and then an extra 40 seconds is allocated to allow the material to fully age and reach static equilibrium conditions.

Coussot 1 was used for the material parameters, and a density of 1,500 kg /m^3. Coussot 1 was chosen as it has the higher *n* value, which allows ageing effects to appear quicker. The first 10 seconds of deposition are at an elevation of 0.3 m, after which the height of the end of the pipe is placed at 1 m elevation. This change in vertical elevation of the deposition point reduces splashing in the initial phase of the deposition. Since the mass represented by every point is rather small, dropping the particles from a large height will induce non-physical pressure oscillations of the material. The boundaries of the computational domain are located transversally 25 m on each side of the deposition point and 150 m in the longitudinal direction.

Case 2

Simulations of 2D dam break are conducted with an initially square domain of variable height and length (up to 100 m in length and height) for all three materials, on a flat domain. All three materials give near identical runouts for very small initial geometries (1 to 2 m runout).

Case 3

This case is a 3D simulation based upon what is known about the failure of the bauxite tailings impoundment in Xiangjiang Wanji Aluminum plant in Luoyang, Henan Province in China, which was breached in 2016. The impoundment contained 2 million m^3 of tailings at breach (az-china.com). Villages in the path of the flow slide had been evacuated due to problems detected in the dam. Google earth pictures of the site before and after the slide are shown in Figure 2. Figure 3 shows a picture of an impacted community.

This case was chosen as the geometry of the flow slide appears to be relatively simple. The tailings flowed in a valley of roughly triangular cross-section, approximately 200 m wide at the top. Open-source satellite imagery from Google Earth's archives has been used to determine the topography on site, which is shown in Figure 4. The initial height of the tailings is assumed to be uniform, and is calculated using the estimated footprint of the impoundment from google earth images and the reported volume of tailings (2 million m^3).

The tailings are bauxite, which typically contain substantial clay minerals and are deposited at low solids concentrations (30–40%). Therefore Coussot 2 was adopted, in the absence of other information. However, the sheared down viscosity and the density were varied, to explore the influence of consolidation of the tailings on the flow slide. This is discussed in the next section.

Figure 2: Google Earth images before and after the breach of the Luoyang TSF

Figure 3: Flow slide and an impacted community (az-china.com)

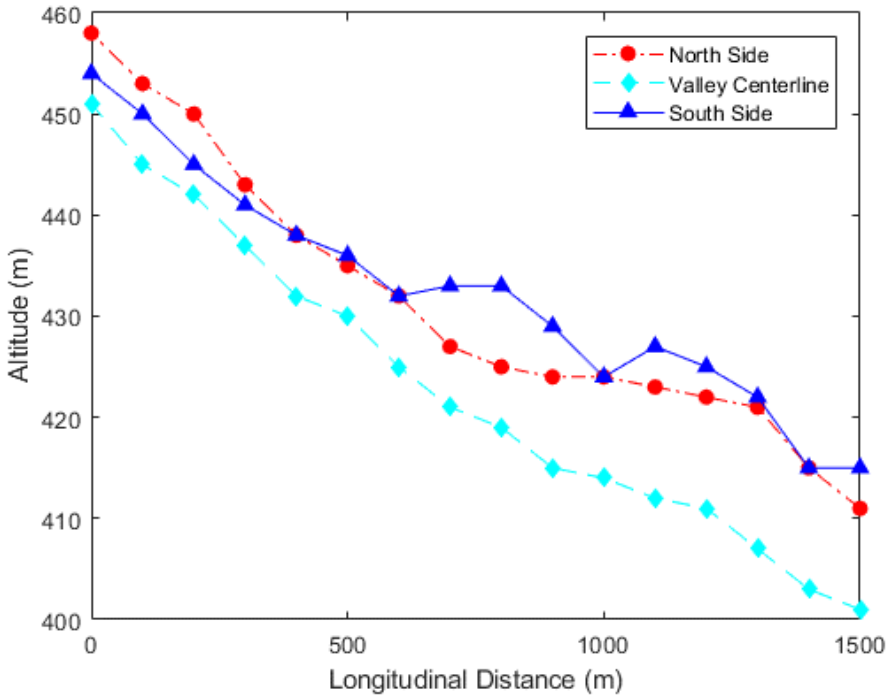

Figure 4: Topography of valley from Google Earth archives

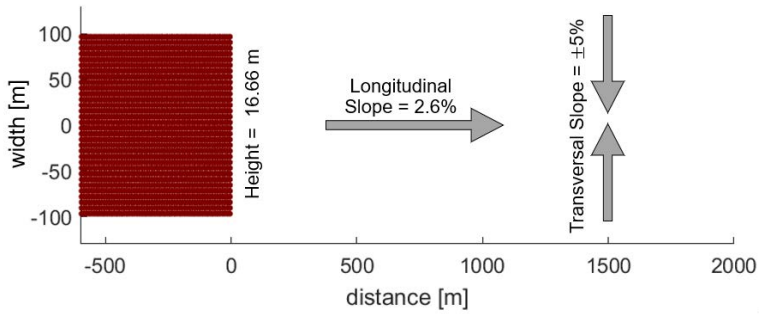

Figure 5: Assumed geometry for Case 3

Results

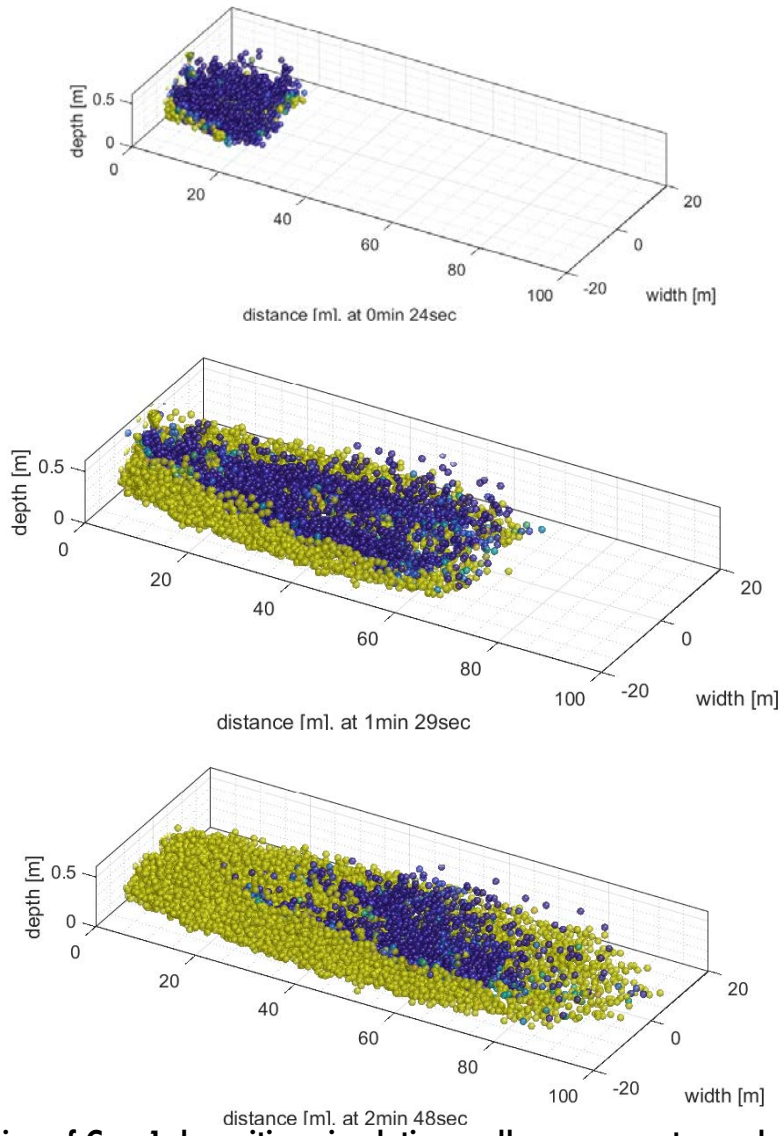

Figure 6: Rendering of Case1 deposition simulation, yellow represents aged material of high viscosity, blue represents material still flowing with low viscosity

Case 1

Visualization of the results of Case 1 are presented in Figure 6. The blue and yellow colours represent two extremes in viscosity, yellow representing aged material with very high viscosity that is effectively stopped, while blue representing viscosities that are low and near the fully sheared viscosity. This simulation produces two parallel channels that merge into one. The presence of two channels (as opposed to one) is an artefact of the change in deposition height mentioned in the methods section, as the raising of the pipe permits the ageing of some material immediately ahead of the pipe, which the tailings subsequently flow around. To the author's knowledge, this is the first instance where channel flow, a very well-known phenomenon in tailings flows, is successfully reproduced in a numerical simulation.

Case 2

Case 2 is used to show the influence of the different rheologies on predicted runout. As shown in Figure 7, the normalized runout (runout / height of tailings before breach) is substantially higher when the VBR is employed compared to a Bingham rheology. The reason mathematically for this difference is that when the simulated tailings become sufficiently slow for ageing to dominant, it takes a finite time for sufficient resistance (in the form of viscosity) to build up to resist the flow.

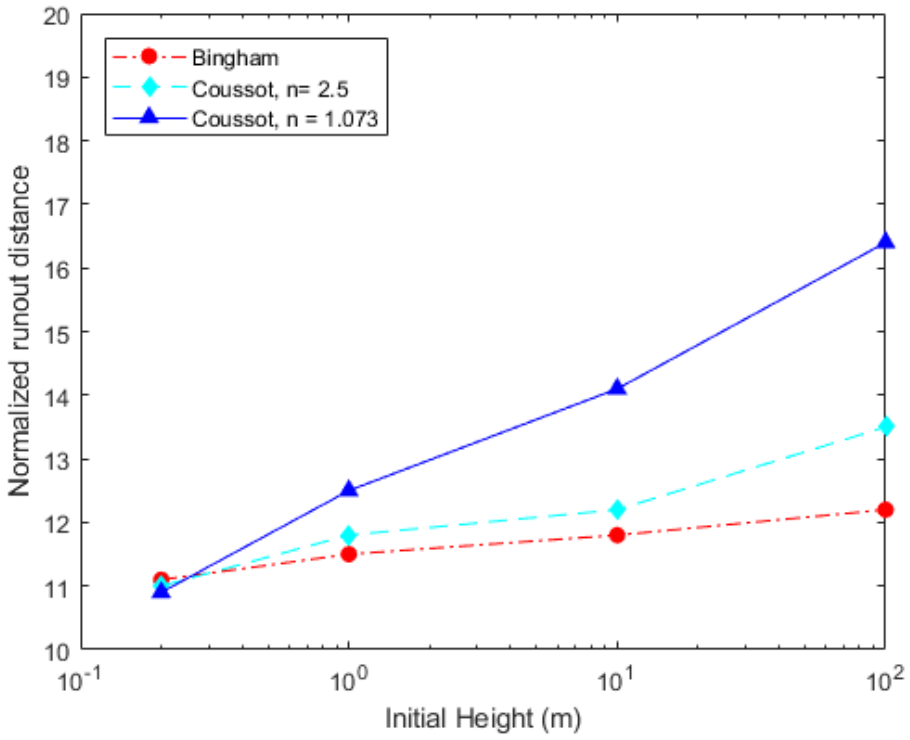

Figure 7: Normalized runout (runout / height) predicted for 2D dam break simulations with a flat slope and where initial height = initial length

For a Bingham rheology, the simulated tailings would come to rest near instantaneously once the shear stress drops below the yield stress. Note for a slope or the presence of a narrow valley to conduct the tailings, the differences between runouts using the different rheologies would be even greater.

Case 3

An example simulation is rendered in Figure 8. The flow develops into a pseudo-plug flow, with the aged material carried by the underlying sheared (blue) tailings.

With the default material parameters, the simulation predicts a runout of 2,700 m, almost double the observed runout. However, given the level of uncertainty, it is arguable that this is a conservative and useful estimate. It is also important to note that the parameters used are for a freshly deposited material, whereas the material in the impoundment, which had existed since 2005, has probably consolidated or otherwise dewatered to a degree. Increasing the density of the tailings will have a direct effect on the inertia of the flow, and an indirect effect on the fully sheared viscosity, which should increase with density. Figure 9 shows a sensitivity analysis to these two parameters: while the increase in density does increase the runout slightly over a probably range of densities (< 1,600 kg /m^3), the runout is more sensitive to the increase in fully sheared viscosity. For reference, 25 PaS is the viscosity of peanut butter.

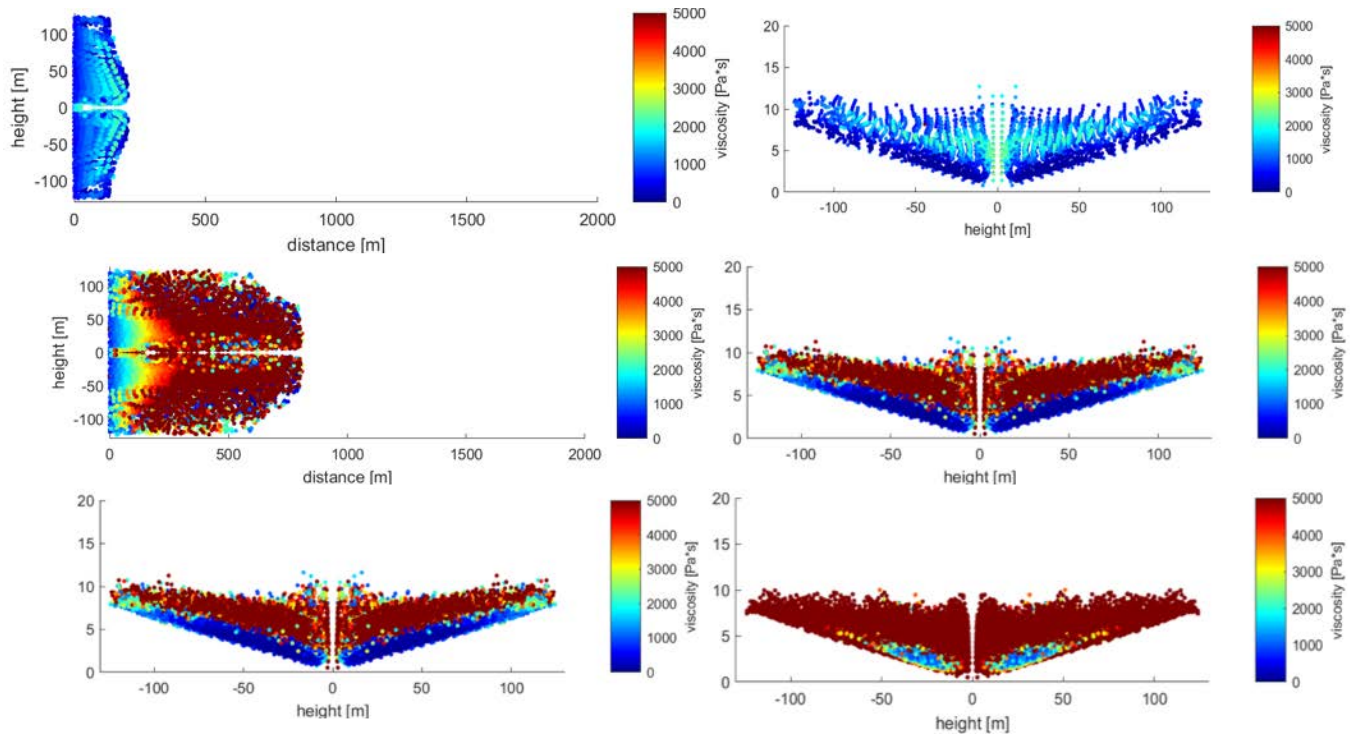

Figure 8: Top view and cross-section views (near the front) from 3D dam breach simulation

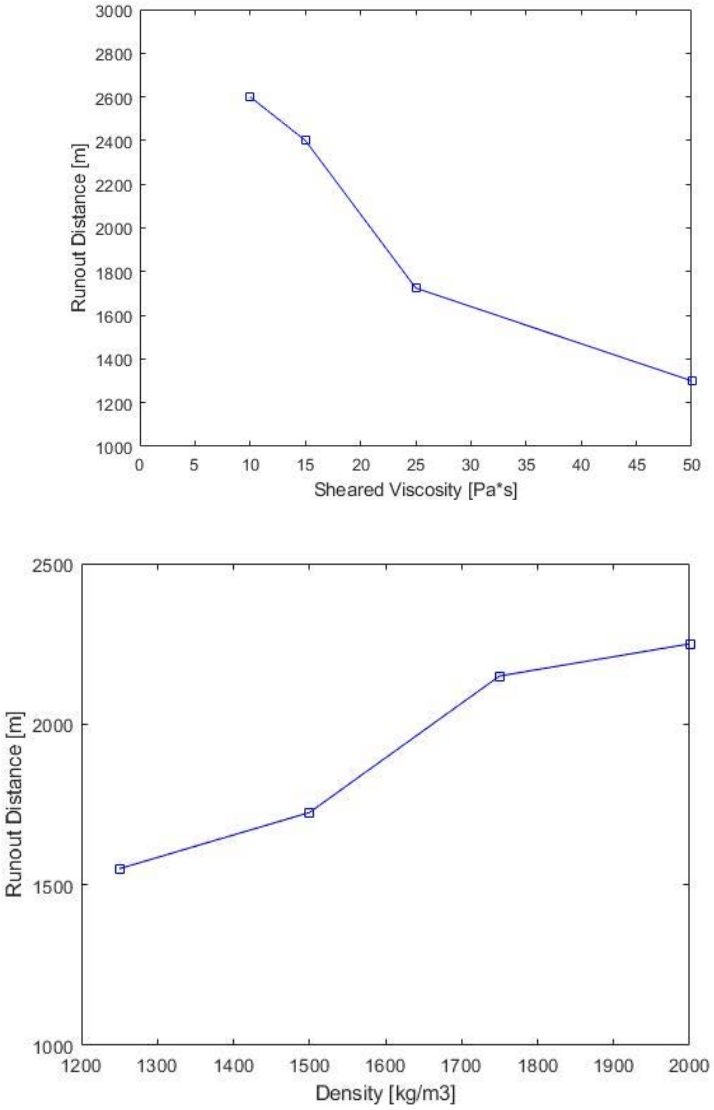

Figure 9: Sensitivity of predicted runout in 3D dam break simulation to assumed density and assumed fully sheared viscosity

Conclusion

VBR is implemented in a 3D MPM code and used to simulate 3D deposition and dam break cases. By allowing material to age, the implemented model can simulate realistic tailings morphology such as channels. In dam break analysis, VBR predicts longer runouts thea if a Bingham model is used, due to the fact that recovery of structure through ageing takes a finite time and is not implied to be instantaneous, as is the case with Bingham or similar yield stress model. The VBR-MPM code is able to reasonably simulate the flow slide from the failure of the Luoyang tailings impoundment, despite the large uncertainties as to material properties and the configuration of the tailings before the breach.

Acknowledgements

This research has been partially funded by combined grants from NSERC and COSIA (Canada's Oil Sands Innovation Alliance), and also in collaboration with research directed by Deltares, NL.

References

Babaoglu, Y. and P.H. Simms. 2017. Simulating deposition of high density tailings using smoothed particle hydrodynamics. *Korea-Australia Rheology Journal* 29: 229–237.

Coussot, T.P., Q.D. Nguyen, H.T. Huynh and D. Bonn. 2002. Avalanche behaviour in yield stress fluids. *Phys. Rev. Lett*. 88, article number 175501.

Chanson, H., S. Jarny and P. Coussot. 2006. Dam break wave of thixotropic fluid. *Journal of Hydraulic Engineering*, *ASCE* (March 2006),132(3): 280–285.

Cruchaga, M.A., D.J. Celentano and T.E. Tezduyar. 2007. Collapse of a liquid column: Numerical simulation and experimental validation. *Computational Mechanics 39*(4): 453–476.

Gao J. and A. Fourie. 2019. Studies on thickened tailings deposition in flume tests using the computational fluid dynamics (CFD) method. *Canadian Geotechnical Journal* 56: 249–262.

Jeyapalan, J., J. Duncan and H. Seed. 1983. Analyses of flow failures of mine tailings dams. *J. Geotech. Engrg.* 10.1061/(ASCE)0733-9410(1983)109:2(150): 150–171.

Mizani, S., P. Simms and W. Wilson. 2017. Rheology for deposition control of oil sands tailings. *Rheol Acta* 56: 623. Retrieved from https://doi.org/10.1007/s00397-017-1015-2

Mizani, S. 2017. experimental study and surface deposition modelling of amended oil sands tailings, PhD thesis, Carleton University, Ottawa.

Mizani, S. and P. Simms. 2016. Method dependent variation of yield stress in mine tailings explained using a structure based viscosity model. *Minerals Engineering* 98: 40–48.

Mizani, S., X. He and P. Simms. 2013. Application of lubrication theory to modeling stack geometry of high density mine tailings. *Journal of Non-Newtonian Fluid Mechanics* 198: 59–70.

Parent, E. 2019. Field-scale flow modeling of thixotropic mine tailings using the material point method. Draft Master's thesis, Carleton University, Ottawa.

Pastor, M., M. Quecedo, J.A. Fernández-Merodo, M.I. Herreros, E. González and P. Mira. 2002. Modelling tailings dams and mine waste dumps failures. *Géotechnique* 52(8): 579–591.

Pastor, M., T. Blanc and B. Haddad. 2014. Application of a SPH depth-integrated model to landslide run-out analysis, *Landslides* 11: 793. doi:10.1007/s10346-014-0484-y.

Proceedings of Tailings and Mine Waste 2019
November 17–20, 2019, Vancouver, Canada
Published by the University of British Columbia, 2019

Evaluation of a Split Stream Dewatering Flowsheet for Tailings

Kenneth Rahal, FLSmidth, USA
Todd Wisdom, FLSmidth, USA

Abstract

As interest continues to grow in tailings management strategies, FLSmidth (FLS) recommends that miners conduct tailings solutions technology trade-off studies to aid in determining the best solution for each property. These trade-off studies can help in both determining which tailings solution (thickened, paste, filtered, EcoTails™, etc.) is the most economic, and also can help to determine which flowsheet is optimal. The baseline in these tailings studies for filtered tailings is dewatering the entire tailings stream using pressure filters. One filtered tailings flowsheet option that FLS has investigated multiple times is called the split stream option. This flowsheet involves sending the entire tailings stream to cyclone clusters. The cyclone overflow is sent to a thickener, and the thickener underflow is sent to pressure filters. The cyclone underflow is sent to vacuum filters. The filter cake from both types of filters are then sent for stacking. This solution is usually included in trade-off studies for tailings that contain a significant portion of fines or clays. Either dewatering the whole tailings without separating the fines, or using the split stream for separating the fines, the stream containing the fines typically requires higher driving force for dewatering that can only be achieved in pressure filters. The philosophy behind this flowsheet is to separate the portion of the tails that contains fines or clays from the rest of the tails, reducing the flow that must be sent to pressure filters. This could potentially also reduce the size of the thickener required. The remaining tailings with coarser particles could be sent to vacuum filters, which are typically less expensive than pressure filtration. Vacuum filters are also continuous, which simplifies the material handling portion of the dewatering flowsheet. This paper will review two tailings studies that compared pressure filtration of the entire tailings stream against the split stream option. This comparison will include installed power, CAPEX, and OPEX.

Introduction

The mining industry has shown increased interest in filtered tailings in recent years due to notable tailings dam failures and increased water scarcity. As interest has grown, more companies are conducting studies

to determine costs associated with switching brownfields sites to filtered tailings, or using these costs to give direction on permitting for greenfield sites. As each mine site is different, it is important to understand the factors that can help guide the process to determine which solution is best. These factors include:

- water cost and availability;
- space requirements for waste (tailings and waste rock); and
- regulatory requirements.

If the above factors lead to a decision to use a high-performance dewatering unit operation on the tailings, there are multiple types of equipment that can be used to achieve low moisture content, including:

- dewatering screens;
- vacuum filters;
- centrifuges; and
- pressure filters.

These different technologies have different capacities, dewatering capabilities, capital costs, and operational costs.

Tailings processing, or dewatering of the tails, requires the site to specify typical feed and output conditions. Based on the specified conditions, the process for selecting the equipment can begin. Below are items for consideration that impact the rate at which the slurry will dewater and its impact on the cycle time or filtration area required to meet the specified conditions.

- **Feed solids** – The feed solids percentage by weight determines the hydraulic loading the filtration or dewatering equipment will process. As the feed solids increases, the amount of liquid to be removed decreases. Filtration rates will be increased as feeds solids are increased. In many flowsheets a high-density thickener will be installed to increase the feed solids to a high performance secondary dewatering device such as a filter or centrifuge. This is desirable, as the capital and operating costs for a thickener are typically an order of magnitude less than most filters or centrifuges.

- **PSD** – The particle size distribution (PSD) will provide insight into how the slurry will react to pressure filtration. A narrow band can impact cake formation by packing tightly, thereby limiting flow. Having a disproportionate number of fine particles smaller than 10 microns can cause poor cake formation, with the fines limiting the flow through the cake.

- **Particle shape** – The shape of the particle plays a role in the expected filtration. When the aspect ratio of the face to edge increases, the particles are more platelet in nature (clays, mica, etc.). This type of particle creates bridging and blinding, drastically reducing filtration rates and limiting the effectiveness of the air blow step.

- **Minerology** – Clay concentrations above 10%, especially swelling clays, will have a very negative impact on filtration rates.
- **Target moisture** – The target moisture for the product discharged from the filter determines the total amount of energy required by the equipment. As the target moisture, liquid remaining in the cake, decreases it typically requires a greater amount of energy and time. Low target moisture rates often result in the need for more filtration surface area.

As companies investigate filtered tailings the focus has largely been placed on the correct design of the tailings storage facility and required properties of the filtered material (Davies, 2011; Ulrich and Coffin, 2015). There are many filtration options for higher performance dewatering tailings prior to disposal. The four major categories of filtration equipment employed are screens, centrifuges, vacuum filters, and filter presses

Figure 1 shows the relationship between particle size and the driving force, f_D, needed to dewater the sample. Overlaid on this relationship are typical particle size ranges that can be treated with different dewatering technologies. The increased driving force needed for dewatering as particle size decreases is partly attributable to increased water adsorption on surfaces and smaller interstitial flow paths between particles (Kujawa et al., 2019).

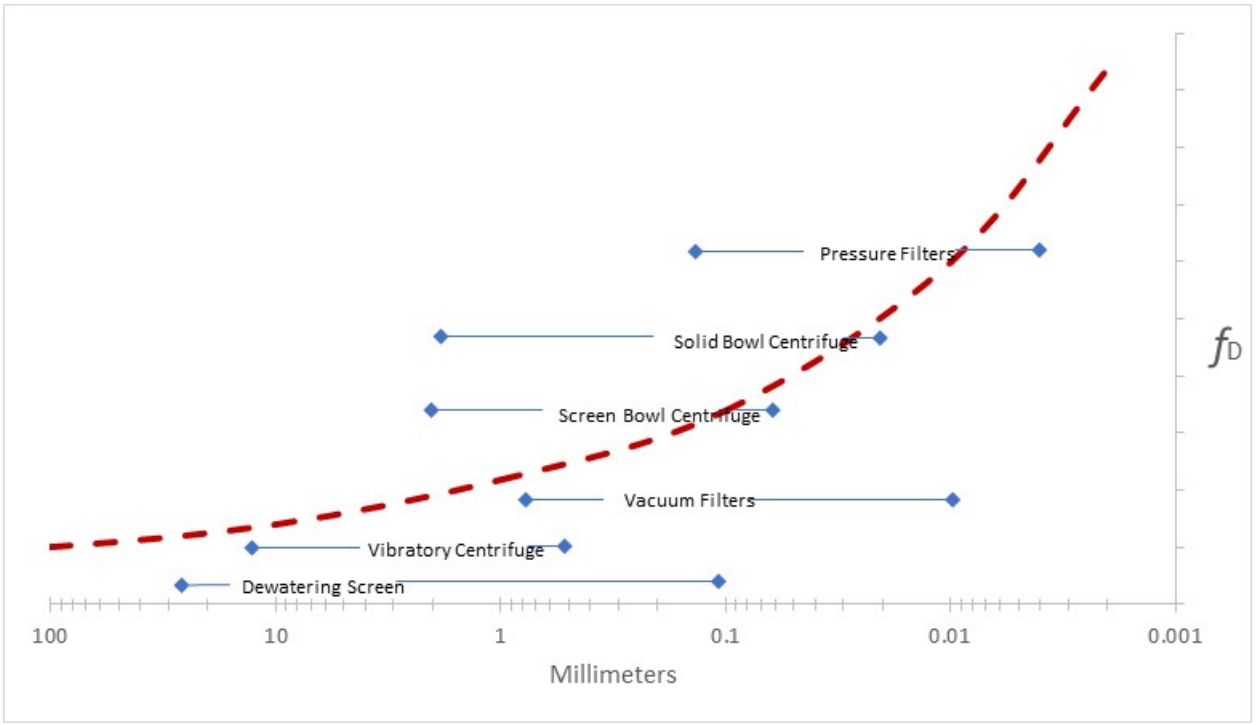

Figure 1: Particle size versus driving force

As can be seen in Figure 1, there is considerable overlap in the particle size ranges that each technology can dewater. This leads to comparing these different technologies in studies to determine the most economical solutions based on the total cost of ownership over the life of the mine. As these different technologies may have different maximum capacities, it is useful to look at different flowsheets to determine not only one type or the other, but if a combination of technologies could lead to the most economical solution. For large capacities, screens and centrifuges are typically too small in size. For over 5,000 tpd, vacuum filters and pressure filters are the equipment of choice.

FLS calls the flowsheet shown in Figure 2 the standard dewatering flowsheet for large tonnage mines, as all tailings passes through a thickener, and dewatering is completed using pressure filters (AFP). Another flowsheet option for filtered tailings, shown in Figure 3, involves classifying the tailings using hydrocyclones into coarse particle and fine particle streams and dewatering those streams separately. FLS calls this flowsheet a split stream dewatering flowsheet. Kujawa et al. (2019) have reported that studies have shown the potential for costs saving using this flowsheet. In the example for this paper, the split stream flowsheet uses a thickener and pressure filters to dewater the fines stream and uses horizontal belt filters (HBF) to dewater the coarse stream.

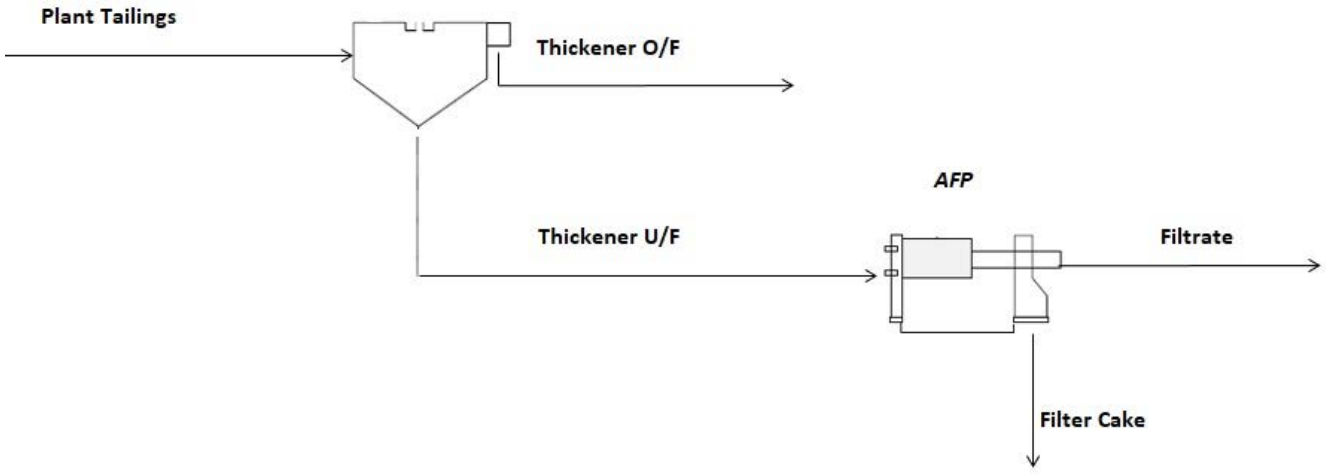

Figure 2: Standard dewatering flowsheet

The examples in Figure 2 and Figure 3 are to determine whether a less expansive vacuum filter, HBF, can be used to dewater the coarse material. This would in turn reduce the number of expensive pressure filters. More information on this comparison is given in the case studies below.

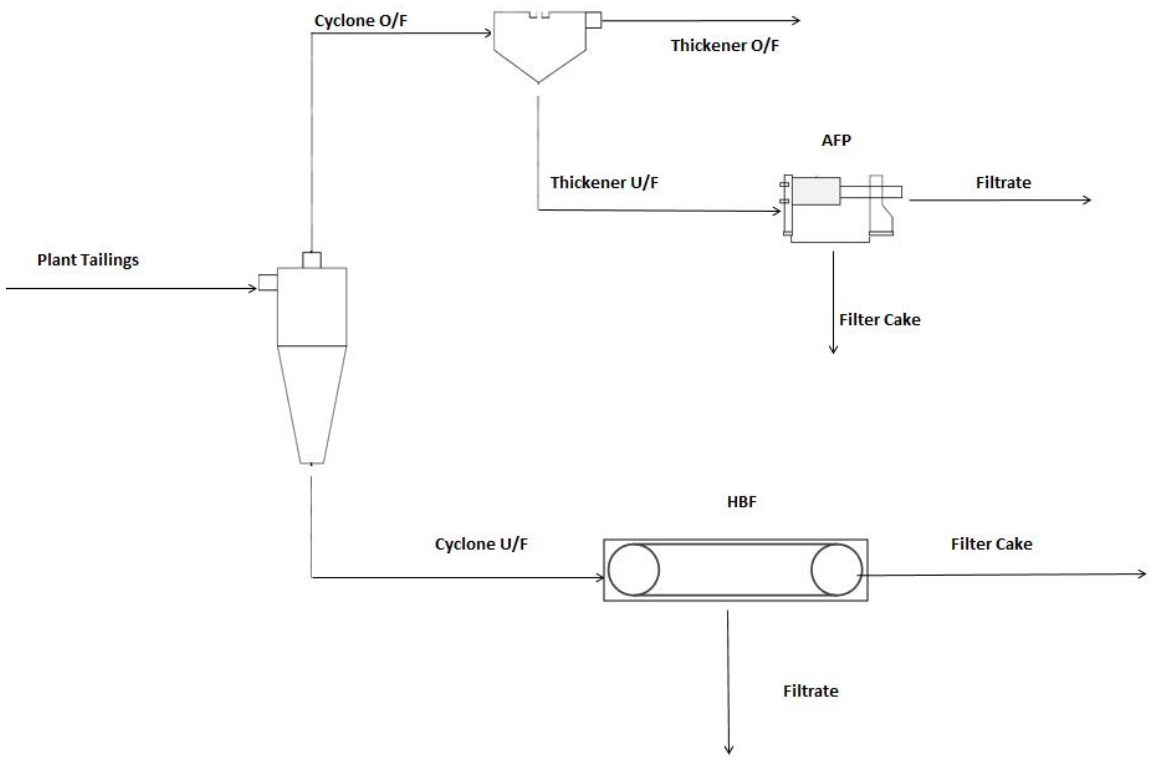

Figure 3: Split stream dewatering flowsheet

Case studies

These case studies are based on lab testing and are conceptual in nature with an accuracy of ±30%. Throughputs have been rounded to respect customer confidentiality. These case studies are based on obtaining the same moisture requirements for both the coarse and fines streams for the split stream flowsheet. This allows for straight comparison to the standard flowsheet. Due to this requirement, no consideration is taken of cost impacts of alternate storage facility designs that could alter the moisture requirements of the fines stream and hence the cost of dewatering.

Copper/Gold plant

The first case study is for a copper/gold plant that produces 3,750 tph of tailings at 35% solids. The target moisture of the filter cake was 15% w/w. The particle size distribution of the whole tailings is described in Table 1.

Table 1: Copper/gold tailings

P80 (µm)	125
% Passing 75 microns	62
% Passing 10 microns	23
Tailings, tph	3,750

The laboratory testing resulted in the following dewatering equipment list for the standard dewatering flowsheet:

- 70 m diameter high density thickener; and
- twelve AFP IV Colossal^{TM} pressure filters with 50 mm chambers and greater than 38 m^3 of total filtration volume (Chaponnel and Wisdom, 2018).

The installed power for the standard dewatering flowsheet, including tanks, pumps, air compressors and receivers, filter discharge feeders, instrumentation, and stacking system, is 25 mW. The consumed power will be lower due to the batch operation of the pressure filters.

FLSmidth performed cyclone simulations on a portion of the tailings to generate samples to analyze the potential for a split stream dewatering circuit. The d50c of the cyclone split was 75 microns and the water split to the underflow was assumed to be 70%. The particle size distributions for the cyclone overflow and cyclone underflow are shown in Table 2.

Table 2: Copper/gold cyclone split

	Cyclone O/F	Cyclone U/F
P80 (µm)	55	195
% Passing 10 microns	40	12
Tailings, tph	2,325	1,425

The laboratory testing resulted in the following dewatering equipment list for the split stream dewatering flowsheet:

- fourteen gMAX26 cyclones;
- 60 m diameter high density thickener for the fine stream;
- seven AFP IV Colossal^{TM} pressure filters with 50 mm chambers and greater than 38 m^3 of total filtration volume; and
- fourteen of 6.5m292.5 HBF for the coarse stream.

The installed power for the split stream dewatering flowsheet, including tanks, pumps, air compressors and receivers, filter discharge feeders, instrumentation, and stacking system, is 40 mW. The consumed power will be lower due to the batch operation of the pressure filters.

The reduction in tonnage going to pressure filtration in the split stream flowsheet reduces the thickener size by 10 m and reduces the number of pressure filters by 5. However, the need for 14 vacuum filters to dewater the coarse stream leads to 25% higher overall CAPEX. The split stream circuit has a higher installed power due to the vacuum pumps used on the horizontal belt filters, and the OPEX is 1% higher than the standard circuit. This OPEX includes labour, power, filter media, flocculent, and spares/consumables.

For this case study, the higher CAPEX of the split stream flowsheet is due to the large amount of fines found in the feed stream. Barrera et al. (2015) state a target of 60/40 split between coarse and fines for this flowsheet option to be viable. Table 1 showed that the split for the sample was 40/60 between coarse and fine streams, with over 20% of the particles below 10 microns. This case study shows agreement with the criteria proposed by Barrera et al. (2015).

The standard dewatering flowsheet proved to be the more economical solution for this mine site to achieve complete filtered tailings.

Base metal plant

The second case study is for a base metal plant that produces 5,000 tph of tailings at 30% solids. The target moisture of the filter cake was 17% w/w. The particle size distribution of the whole tailings is described in Table 3.

Table 3: Base metal tailings

P80 (µm)	95
% Passing 75 microns	75
% Passing 10 microns	35
Tailings, tph	5,000

The laboratory testing resulted in the following dewatering equipment list for the standard dewatering flowsheet:

- two of 60 m diameter high density thickener; and
- twelve AFP IV Colossal^{TM} pressure filters with 50 mm chambers and greater than 38 m^3 of total filtration volume.

The installed power for the standard dewatering flowsheet, including tanks, pumps, air compressors and receivers, filter discharge feeders, instrumentation, and stacking system, is 22 mW. The consumed power will be lower due to the batch operation of the pressure filters.

FLSmidth performed cyclone simulations on a portion of the tailings to generate samples to analyze the potential for a split stream dewatering circuit. The d50c of the cyclone split was 75 microns and the percent solids in the overflow and underflow were 20% and 60%, respectively. The particle size distributions for the cyclone overflow and cyclone underflow are shown in Table 4.

Table 4: Base metal cyclone split

	Cyclone O/F	Cyclone U/F
P80 (µm)	32	209
% Passing 10 microns	50	10
Tailings, tph	3,750	1,250

The laboratory testing resulted in the following dewatering equipment list for the split stream dewatering flowsheet:

- eighteen gMAX26 cyclones;
- one 75 m diameter high density thickener for the fines stream;
- eleven AFP IV Colossal^{TM} pressure filters with 32 mm chambers and greater than 31 m^3 of total filtration volume; and
- four of 6.5m292.5 HBF for the coarse stream.

The installed power for the split stream dewatering flowsheet, including tanks, pumps, air compressors and receivers, filter discharge feeders, instrumentation, and stacking system, is 24 mW. The consumed power will be lower due to the batch operation of the pressure filters.

The reduction in tonnage going to pressure filtration in the split stream flowsheet allowed 1 thickener to be used instead of 2. The coarse fraction could be processed with only 4 vacuum filters. However, only 1 pressure filter was removed. This is due to the quantity and poor settling of the fines fraction that resulted in low feed density, 50% solids, going to the pressure filters in the split stream flow sheet. This is opposed to the 65% solids that was achieved in the two thickeners in the standard dewatering flowsheet.

The CAPEX was 4% higher and the OPEX was 15% higher for the split stream flowsheet than the standard dewatering flowsheet. This OPEX includes labour, power, filter media, flocculent, and spares/consumables.

Due to the high fines content, this case study also showed that the standard dewatering flowsheet was more economical.

In summary, Table 5 shows the total cost of each solution, including all CAPX and OPEX, in terms of $/ton. This cost calculated at the 10th year of the mine life. No discounting or sustaining capital is included as these costs are for comparison only.

Table 5: Case study costs

Case study	Copper/gold	Base metal
Standard ($/ton)	2.17	1.71
Split stream ($/ton)	2.40	1.89

The primary drivers of the costs in Table 4 are dewatering rates, moisture targets, and ratio of fines. The high ratio of fines in these case studies causes a 10% increase in the cost. The difference in the two case studies is attributable to different moisture targets. The copper/gold plant has a lower moisture target, which causes higher costs due to an increase in required air compressors for cake blow.

Conclusion

FLSmidth is conducting an increased number of tailings dewatering studies as the industry becomes increasingly interested in methods of tailings storage that reduce risk for companiess. Two of these studies included comparing a split stream dewatering circuit to a standard dewatering circuit. The results of these studies indicated:

- Dewatering costs are impacted by the ratio of fines in the tailings.
- Support for the 60/40 guideline given by Barrera et al. (2015).

FLSmidth recommends the following:

- Studies should be conducted of material with coarser splits than 60/40 to investigate if the split stream flowsheet would be viable at lower fines ratios.
- Studies should be conducted that include different tailings storage designs that would allow for the fines fraction to have a higher moisture target, as this may improve the economic case for split stream dewatering.
- Research should be conducted into methods of pre-concentration (ore sorting, flash flotation, etc.) and the impact of their resulting coarser grinds on total costs, including the dewatering flowsheets.
- The impact of concentrate regrind technologies and flowsheets on tailings dewatering costs should be further studied.

References

Barrera, S., C. Cacciuttolo and J. Caldwell. 2015. Reassessment of best tailings management practices. In *Proceedings of Tailings and Mine Waste 2015*, Vancouver, British Columbia, Canada.

Chaponnel, J. and T. Wisdom. 2018. FLSmidth colossal filter – Demonstration plant. In *Proceedings of the 21st International Seminar on Paste and Thickened Tailings*, Perth, Western Australia.

Davies, Michael. 2011. Filtered dry stack tailings – The fundamentals. In *Proceedings of Tailings and Mine Waste 2011*, Vancouver, British Columbia, Canada.

Kujawa, C., J. Winterton, R. Jansen and R. Cooke. 2019. Innovative process engineering to create better tailings facilities. In *Proceedings of Tailings 2019*, Santiago, Chile.

Ulrich, B. and J. Coffin. 2015. Combined tailings and mine waste. In *Proceedings of Tailings and Mine Waste 2015*, Vancouver, British Columbia, Canada.

Proceedings of Tailings and Mine Waste 2019
November 17–20, 2019, Vancouver, Canada
Published by the University of British Columbia, 2019

Physical Modelling of Tailings Dam Breach

Andrea Walsh, Queen's University, Canada
W. Andy Take, Queen's University, Canada
Scott McDougall, University of British Columbia, Canada
Stephen G. Evans, University of Waterloo, Canada

Abstract

Tailings dams differ from conventional water retaining dams not only in materials retained (e.g., unconsolidated tailings slurry, water), but also with regards to construction methods and geometry. However, the dam breach relationships most often used in practice for breach analysis of tailings dams were developed for water storage dams and have not been fully calibrated for the simulation of a tailings dam case. Recent tailings dam failures have heightened public awareness and scrutiny of tailings dams, and have led to increased requirements to conduct tailings dam breach studies. Further, the geotechnical aspects related to dam breach are often oversimplified or neglected in available models. Physical modelling offers an attractive solution to further understand breach processes specific to tailings dams, allowing for modelling of simplified geometries and boundary conditions to test specific hypotheses. This paper describes the development of a new experimental study to investigate tailings dam breach behaviour, specifically, the difference in the outflow hydrograph between water storage dams and tailings dams. A two-stage experimental program was carried out in which eleven 1-meter-high dams were constructed in the large landslide flume facility at the Queen's University Coastal Engineering Laboratory and breached by overtopping. The first test series included six water retaining dams, and explored the sensitivity of the upstream slope angle on outflow. The second series of tests included the addition of a tailings-style beach into the dam reservoir to simulate geometries specific to the tailings dam case. This paper presents the development of the large-scale physical model testing program and preliminary results of test series one.

Introduction

Dam breach is a catastrophic type failure characterized by the sudden, rapid, and/or uncontrolled release of impounded materials. Tailings are by-products of mineral processing, and are typically comprised of sand, silt, and clay size particles. A tailings dam may retain water, mineral processing fluids, tailings and compacted dam construction materials. Tailing materials can also be utilized as dam construction materials.

Dam breach studies are conducted as part of the design process, and updated throughout the life of the dam. These studies aim to inform downstream flood inundation models, emergency preparedness planning, and help to quantify the risk level of a facility. However, the current models available for conducting breach analysis were developed for water storage dams (Martin et al., 2015). There are many differences between water and tailings storage dams, for example, construction methods, construction materials, retained materials, and life cycle of the structure. Empirical relations to adapt models to the tailings case do exist, however, there is limited data available from failure events to inform these relationships (Rico et al., 2008; Small et al., 2017).

Physical modelling is one method to build a robust dataset that can be utilized to calibrate numerical models, and help provide insight on data gaps in field based data. This technique allows researchers to construct models with precision, simplify boundary conditions, vary test geometry and complete a relatively large number of trials in a short time frame. Recent work on dam breach for water storage dams by the United States Geological Survey (USGS) at their debris-flow flume at the H.J. Andrews Experimental Forest has served as a base case study for this work (Walder et al., 2015). They described observations of an upstream erosional hydraulic control section during overtopping experiments of water retaining noncohesive earth dams on the order of 1 m in height, also observed by Coleman et al. (2002). This contrasts the trapezoidal 'gutter' analogy utilized in many current breach models (e.g., BREACH by Fread, 1988). In this research project, we aim to quantify the upstream weir hydraulic control structure in water retaining dams and contrast the difference in behaviour (if any) in the tailings dam case.

Methods

Experimental set up

Figure 1: Queen's University landslide flume (looking downstream)

An experimental program including eleven model dams on the order of 1 m in height was undertaken at the Queen's University Landslide Flume, located at the Coastal Engineering Laboratory. This flume is 2.09 m

wide, with a 36 m long horizontal reach. An additional 8.23 m sloped section exists at the south end, inclined at 30° from horizon tal (Figure 1). A 5.08 cm diameter drain is located at the north end of the flume, filtered with a piece of geotextile fabric. A 5.08 cm diameter water inlet tap is located at each of the north and south ends of the flume.

All dam structures were positioned at the midpoint of the horizontal reach, allowing for an approximately 15 m long reservoir to the south of the dam (upstream) and 15 m long inundation area north of the dam (downstream).

Test Series #1 included six dams and aimed to develop a relationship between the dam upstream slope angle and observed outflow. The upstream slope angle (α) ranged between 10° to 30° from horizontal, while the downstream slope angle remained constant at 18.43° (3H:1V). The dam crest measured 0.30 m in width in all tests (Figure 2).

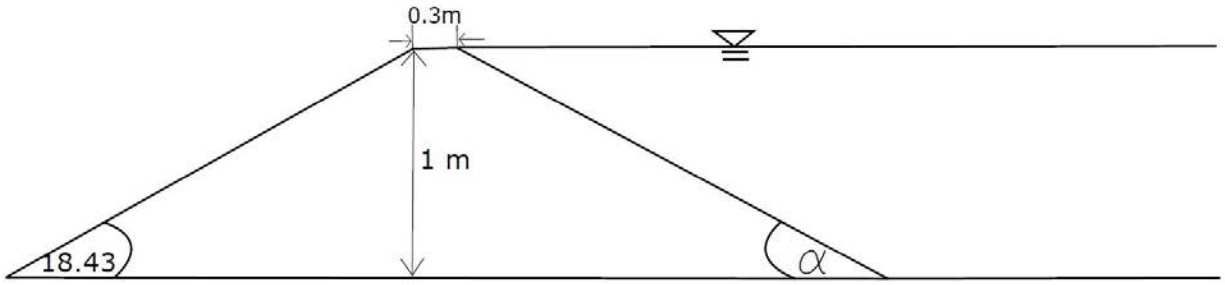

Figure 2: Test Series #1 – general cross-section (schematic, not to scale)

Test Series #2 comprised five dams and included the addition of a shallowly sloping 5% grade beach extending from the upstream slope down into the reservoir. The upstream and downstream slope angle of the dam structure was 18.43° (3H:1V) in all cases. The intersection height of the beach with the upstream slope of the dam ranged from 0.50 m to 0.90 m (h_w). The beach extended 3 m from the upstream toe of the dam into the reservoir and ended at a vertical cut-off wall equal to the height of the beach at the horizontal location of the cut-off wall (Figure 3).

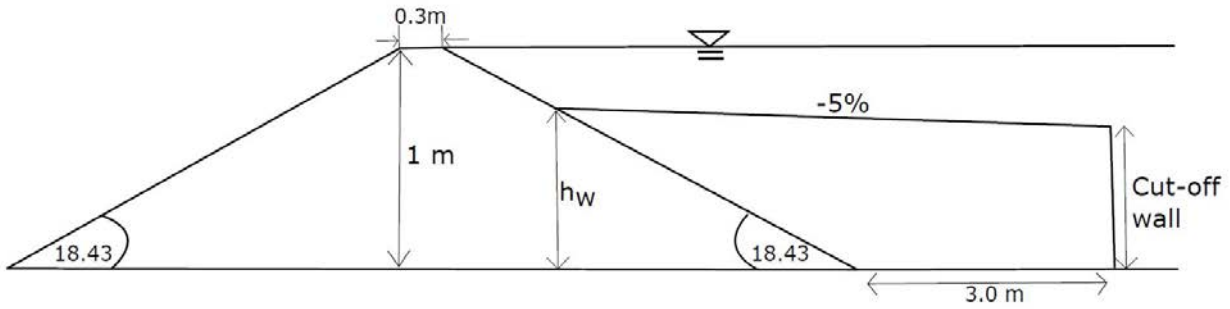

Figure 3: Test Series #2 – general cross-section (schematic, not to scale)

A toe drain was constructed utilizing a 10 cm diameter perforated flexible pipe wrapped in geotextile and anchored to the flume base at the horizontal location of the dam crest. A non-perforated section was attached with an L-connection to carry drain seepage downstream of the dam toe (Figure 4).

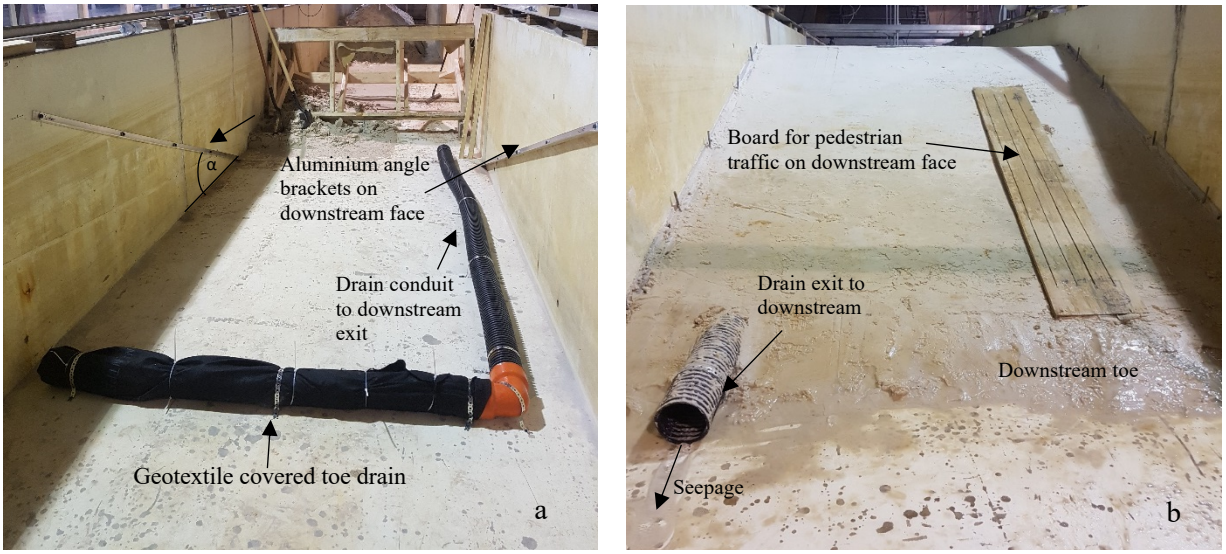

Figure 4: Dam toe drain. (a) Drain anchored to flume base; (b) Downstream view of drain outlet post dam construction

The reservoir surface elevation during breach was monitored with a series of six Akamina AWP-24 capacitance wave height gauges, with a reading frequency of 100 Hz. Five of the probes were distributed in the upstream reservoir, and one probe was placed 1 m downstream of the downstream toe of the dam.

To capture a plan view of the entire 2.09 m width and 6.30 m length of the dam, four Canon EOS Rebel T5 cameras Digital Single-Lens Reflex (DSLR) with 18–55 mm focal length lenses were mounted to a rotating support beam. The cameras each have an 18 megapixel APS-C 22.3 mm by 14.9 mm sensor. When the beam was in its upright position, the cameras were at a height of 2.0 m above the dam crest elevation (Figure 5).

These four cameras were synchronized and remotely triggered every 5 seconds during the test. Qualitative top-down video during the failure was captured with a Go-Pro Hero3 camera, also mounted to the support beam. Qualitative oblique video of the downstream dam face was recorded with a Canon EOS Rebel T5 camera, placed approximately 2 m downstream of the downstream dam toe.

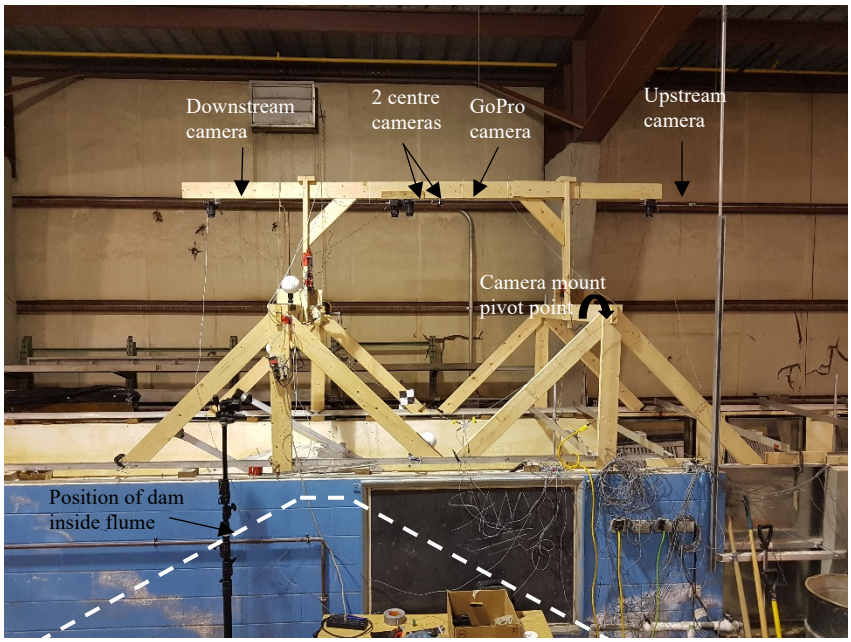

Figure 5: Camera mounting system

Materials

All dams were constructed with the uniform fine sand #730 Silica Sand by Weldon Company. The sand has a D_{50} of 0.12 mm. This sand is finer than the sand utilized in the experiments by Walder et al. (2015) which had a D_{50} of 0.21 mm. However, both sands are described as fine sand by the Wentworth grade chart. Sand was transported from an indoor storage area to the flume with a Bobcat skid steer loader. Following testing, several days were allowed for drainage of the flume and sand material. The deposited sand in the downstream area was then moved back to the former location of the dam downstream toe by shovelling and with a Bobcat 325 excavator for construction of the next dam.

Dams were constructed utilizing a combination of methods, including slurry pumping (hydraulic placement), shovelling and hand tamping. Sand slurry was created by water jetting sand with a high pressure 5.08 cm diameter hose, which provided both water and agitation necessary to liquefy the sand into a pumpable slurry form. The slurry was then pumped into place with a Tsurumi HSD 2.55S submersible single-phase portable slurry pump, equipped with a 5.08 cm diameter discharge hose. To contain the sand slurry in the desired dam shape, plywood formwork was constructed. 1.22 m wide by 2.08 m long by 0.019 m thick plywood sheets were saw cut and wrapped in geotextile fabric to allow for water drainage while retaining sand in place. 3.08 m long by 0.025 m wide aluminum angle brackets were anchored into the concrete side walls of the flume, inclined at 18.43° from horizontal on each of the downstream sidewalls and inclined at angles ranging from 10° to 30° from horizontal on each of the upstream sidewalls. The angle brackets served as a ledge to support plywood forms during construction (Figure 6). The plywood sections

were sequentially bolted in place as the dam height increased. A 186 W submersible puddle pump was also employed during slurry placement to evacuate ponded water. Following slurry pumping, dams were left to drain for several days prior to removing the formwork. The slurry's sand to water ratio generally ranged from 1:3 to 1:4 based on bottle samples taken during pumping.

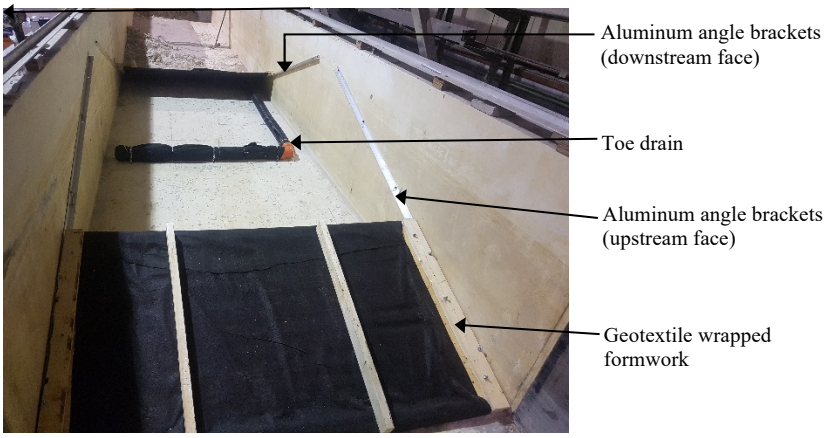

Figure 6: Plywood forms in place during dam construction

After the formwork was removed, the dam surface was smoothed with a trowel. Finally, a thin layer of sand dyed black with India ink was placed on the upstream slope. This provided contrast to the rest of the light coloured sand and aided in image analysis.

Test procedure

Upon completion of dam construction, the plan view cameras were connected to AC power, and the camera mount was raised into position over the dam. LiDAR scans of the as-constructed dam were captured with a Faro Laser Scanner Focus^s 150. Three scans were required to capture the upstream, downstream and crest of the dam due to occlusions.

A v-notch approximately 6 cm wide by 6 cm deep was incised into the centre of the dam crest with a piece of aluminum angle bracket prior to filling the flume reservoir. The upstream reservoir was then impounded at a rate of 0.0067 m^3/s. During reservoir filling, calibration of the capacitance wave height gauges was conducted. At the point that water began to enter the v-notch on the dam crest, the inlet water tap was turned off. As the first bead of water flowed through the notch and reached the downstream toe of the dam, data acquisition with the capacitance wave height gauges and plan view cameras was started simultaneously. The downstream oblique view camera began recording slightly after this time.

During several tests, sediment grab samples were taken downstream of the dam, around the time of peak outflow. The sand and water volumes of each sample were measured in a graduated cylinder and recorded.

Following the completion of the breach event, the flume was left undisturbed for several days to drain. LiDAR scanning was then repeated, capturing the downstream deposit surface and remaining post-breach dam structure.

Results and discussion

Sample test case details

The preliminary results presented below are from a dam failure test conducted on December 11, 2018. This dam is part of Test Series #1, and retained only water in the dam reservoir. The dam dimensions are shown in Table 1 below:

Table 1: Dam dimensions

Parameter	Dimensions
Dam height	1.00 m
Dam width	2.09 m
Crest width	0.30 m
Upstream slope	30°
Downstream slope	18.43°

Outflow observations

Figure 7: Downstream oblique view of a typical dam during breach. Times correspond to points on the outflow hydrograph in Figure 8 below. (a) Breach initiation through pre-cut centre crest notch, t=–61 s; (b) Breach reaches downstream toe, t=–55 s; (c) Undercutting of breach channel, t=–34 s; (d) Sideslope failures rapidly widen downstream breach channel, t=–5 s; (e) Breach headcut intercepts upstream side of crest, t=20 s; (f) Breach during peak outflow period, t=69 s; (g) Outflow slowing due to drainage limitation in downstream flume section, t=92 s; (h) End of breach, t=120 s

The images presented in Figure 7 display a typical failure evolution observed from the downstream oblique

perspective. Images (a) through (d) were captured during Stage 1 and Stage 2 of the breaching process, as described in Walder et al. (2015). Images (e) through (h) were captured during Stage 3 of failure, the main focus of this study, as this stage is marked by a dramatic increase in outflow volume commencing when the headcut intersects the upstream edge of the dam crest.

The outflow hydrograph was computed utilizing reservoir surface elevation data gathered from the upstream capacitance wave height gauges and the known upstream reservoir area. Time T=0 has been adjusted on the hydrograph to coincide with the start of breach Stage 3 (Figure 7).

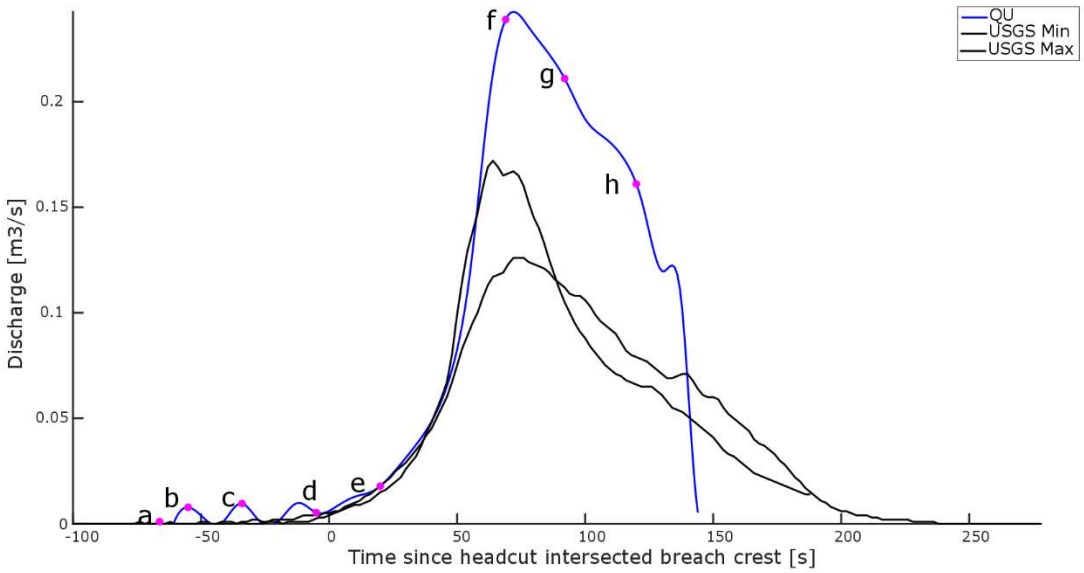

Figure 7: Outflow hydrograph; letter locations correspond to photos in Error! Reference source n ot found. above

Also plotted on Figure 7 are the maximum and minimum outflow results observed in the USGS baseline study (Walder et al., 2015). In the initial section of the exponential outflow increase period (see Point e), results from the Queen's University trial and the USGS trials agree quite well. This indicates that the Queen's University laboratory program results can be directly compared to published data from the USGS case, and that the breach evolution dynamics observed and described by Walder et al. (2015) are similar. The lower peak outflow values reported by Walder et al. (2015) can be attributed to the smaller reservoir capacity at their facility compared to the Queen's University flume, as shown in the storage function below (Figure 8).

A limitation of the Queen's University flume is downstream drainage. The 5.08 cm diameter drain at the end of the downstream runout area is insufficient to allow for immediate drainage of the downstream runout area during the breach event. As such, the downstream toe becomes impounded during later stages of the test, and the breach is attenuated as the downstream water level equilibrates with the upstream

reservoir. The USGS facility had an unconstrained toe, allowing the entire reservoir to drain freely. This is exemplified by the lower near-vertical part of the Queen's University hydrograph, beyond Point h. This abrupt halt to outflow is analogous to "turning off the tap", marked by the downstream runout area water level raising to a level that impeded outflow from the upstream reservoir.

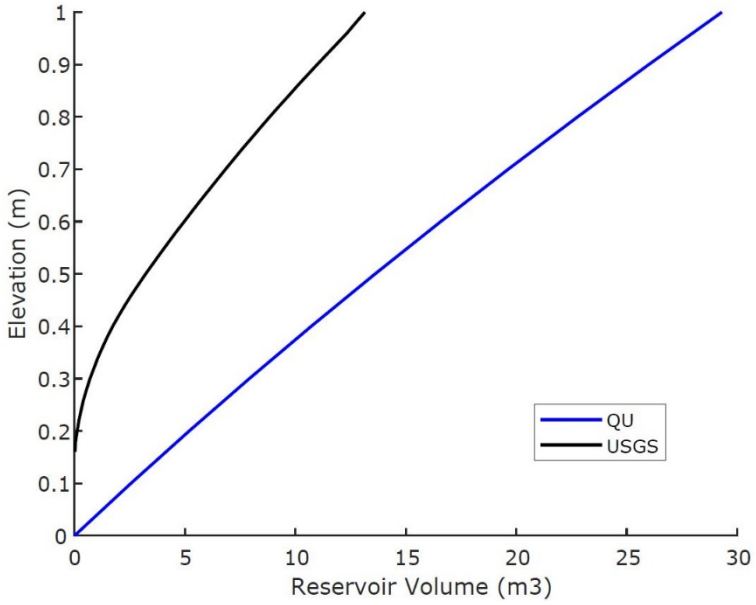

Figure 8: Reservoir storage function – comparing Queen's University flume to USGS facility

Conclusion

A series of 11 non-cohesive earth dam tests have been conducted to investigate the role of tailings dam geometry on breach behaviour; specifically, upstream slope angle and the presence of a tailing dam beach in the reservoir. Initial testing focused on replicating the experiment base case from the USGS. Good agreement between results by Queen's University and the USGS base case study was demonstrated during initial stages of breach, while variations later in the breaching process can be explained by differences in reservoir volume capacity and downstream drainage at each test facility. Work is currently underway on data analysis of remaining tests.

Acknowledgements

Support for this work was provided by the following five industrial partners who contributed funding and technical input as part of the NSERC-supported CanBreach (Canadian Tailings Dam Breach Research) Project: Imperial Oil Resources Inc., Suncor Energy Inc., BGC Engineering Inc., Klohn Crippen Berger, and Golder Associates Ltd.

References

Coleman, Stephan, Darryl Andrews and M. Grant Webby. 2002. Overtopping breaching of noncohesive homogeneous embankments. *Journal of Hydraulic Engineering* 128(9): 829–838.

Fread, D.L. 1988. Breach: *An Erosion Model for Earthen Dam Failures*. Silver Springs, Maryland: National Weather Service.

Martin, V., D. Fontaine and J. Cathcart. 2015. Challenges with conducting tailings dam breach studies. In *Proceedings of Tailings and Mine Waste 2015.* Vancouver, British Columbia: 314–328.

Rico, M., G. Benito and A. Diez-Herrero. 2008. Floods from tailings dam failures. *Journal of Hazardous Materials* (154): 79–87.

Small, Andy, Michael James and Mohammad Al-Mamun. 2017. Advancing the state of practice for tailings dam breach assessment using empirical correlations. In *Proceedings of Canadian Dam Association 2017 Annual Conference.* Kelowna, British Columbia, Canada.

Walder, Joseph S., Richard Iverson, Jonathan Godt, Matthew Logan and Stephen Solovitz. 2015. Controls on the breach geometry and flood hydrograph during overtopping of noncohesive earthen dams. *Water Resources Research* 51: 6701–6724.

Chapter 5
Environment

Proceedings of Tailings and Mine Waste 2019
November 17–20, 2019, Vancouver, Canada
Published by the University of British Columbia, 2019

Passive-Active Treatment of Arsenic in Mine Water Using Iron Hydroxide Sorption

Drummond Earley III, EA Engineering Science and Technology Inc. PBC, USA
Lee Becker, EA Engineering Science and Technology Inc. PBC, USA
Sheena Styger, EA Engineering Science and Technology Inc. PBC, USA
Jay Snyder, EA Engineering Science and Technology Inc. PBC, USA

Abstract

Natural and artificial iron hydroxide sorption media can be used to passively and aggressively treat arsenic in mine discharge water in flows ranging from less than 1 gallon per minute (gpm) to more than 10,000 gpm. This paper reviews the potential of iron hydroxide sorption spanning the range of application from passive treatment of mine water from abandoned tailings sites that are greater 100 years old to aggressive treatment of mega-scale dewatering flows at active mine sites. Geochemical modelling is used as a tool to design or augment iron coagulation treatment systems, as arsenic sorption is a function of iron oxidation and precipitation kinetics, pH, water composition and temperature, which vary from site to site. Engineered treatment systems usually focus on coagulant addition (usually iron chloride or iron sulphate), reaction tanks, settling ponds, and clarifiers, etc., whereas passive and aggressive systems can utilize natural and artificial channels. In some conditions, shallow and vegetated channels function as biofiltration swales to provide better aeration and iron hydroxide colloid filtering capacity than ponds. In addition, sludge management and activation can be facilitated by constructing multiple channel reaches that can be tiered, with alternating flow directions, and gated with alternative potential connections to control residence time, maintenance, and sludge removal. Bypass circuiting to lower channels can be used for cleaning out sludge buildup and to provide iron hydroxide sludge for activation of bacterially catalyzed iron oxidation in lower reaches. Open channels can be armored with riprap or covered with screens to prevent access by humans and wildlife.

Two case studies for arsenic treatment are presented: a passive system at a closed tailing facility in California, and aggressive system at active mines in Nevada. The passive system in California uses existing iron in drainage water to treat arsenic in contact water from 100-year-old plus closed tailing facility that has been stabilized by dam retrofitting. Here, passive treatment results in attainment of discharge water quality objectives for arsenic. At the active mine sites in Nevada, aggressive addition of iron coagulants in channels is used to remove naturally occurring arsenic from thousands of gallons per minute of water pumped from deep wells to dewater open pit mines. However, the water is naturally geothermally heated

and as the water cools along the treatment channels, flocculated iron hydroxide releases arsenic by exothermic desorption, resulting in arsenic concentration rebound in discharge water. Hence the dosage of iron added at the head of the channel must be increased to compensate for the rebound effect and meet arsenic discharge limits at the end of the channel.

In both cases geochemical, thermodynamic, and colloid transport modelling can be used for optimization of treatment system design to ensure water quality standards are met in discharge and within onsite sludge storage facilities. Because arsenic sorption onto iron hydroxide flocculant is reversible under changing physical and chemical conditions, predictive modelling can anticipate potential releases of arsenic from iron hydroxide sludge to pore water over time with increased depth of burial and repository chemistry and develop strategies for mitigation.

Introduction

Natural and mine influenced surface water and groundwater may contain elevated levels of arsenic that pose a risk to human health and the environment (Smith and Huyck, 1999). Arsenic in drinking water has been regulated in the USA since 1942 and the current standard in drinking water and groundwater aquifers is 10 parts per billion (ppb) (Southwest Hydrology, 2002a). Arsenic is one of the most commonly regulated and treated metals in mine effluents. Its sources include arsenopyrite, arsenic-bearing pyrite and other arsenic sulphide minerals in mill tailings and other mining wastes. Arsenopyrite and arsenic-bearing pyrite are commonly associated with gold ores. The arsenopyrite or arsenic-bearing pyrite oxidizes in the tailings as oxygenated water infiltrates into the pile and dissolves, releasing iron and arsenic. Arsenic is present in water as arsenate (As[V]) oxyanions (e.g. $HAsO_4^-$) under oxidizing and neutral to slightly alkaline pH, which is the predominant condition of surface water discharges and groundwater at mine sites (Figure 1).

Arsenic is most mobile in neutral to alkaline pH ranges and intermediate redox conditions (Figure 1) conducive to sulphide oxidation but not oxidizing enough to form iron hydroxides that sorb arsenic (Smith and Huyck, 1999). Arsenic is particularly mobile in variably saturated sediments or tailings where water levels rise and fall. In such environments, arsenic is released from sulphide minerals when water levels fall, creating oxidizing conditions, and can also be immobilized by iron hydroxides under these conditions. Conversely, it can also be remobilized from iron hydroxides when reducing conditions are generated by re-saturation of sediment and tailings and surface bound arsenic is released as the iron hydroxides dissolve. Eh conditions need to be oxidizing (0 volts or above) at circumneutral pH to ensure that arsenic is bound to iron hydroxides such as ferrihydrite ($Fe(OH)_3$) (Figure 1). Arsenic may be precipitated as sulphides at low Eh via sulphate reduction reactions, but this reaction is usually much slower than sorption onto iron hydroxides. Therefore, elevated arsenic concentrations may persist in reduced groundwater.

Arsenic sorption onto the iron hydroxide precipitate that forms after oxidation of pyrite is also a

significant natural attenuation mechanism and may be indicated by a correlated decrease in concentrations of dissolved iron and arsenic. The sorption effect is so strong, in fact, that iron precipitation is commonly used to remove arsenic in small municipal to large industrial water treatment facilities (Southwest Hydrology, 2002b). However, the sorption reaction is reversible, and even in oxidizing conditions, arsenic can be re-dissolved into surface and groundwater if pH increases significantly. This is because arsenic is an oxyanion and the surface charge of precipitated iron hydroxide particles becomes more negative as pH rises according to the generalized two-layer theory of sorption (Dzombak and Morel, 1990). Hence proper disposal of the treatment sludge is required to prevent release of arsenic back to the environment.

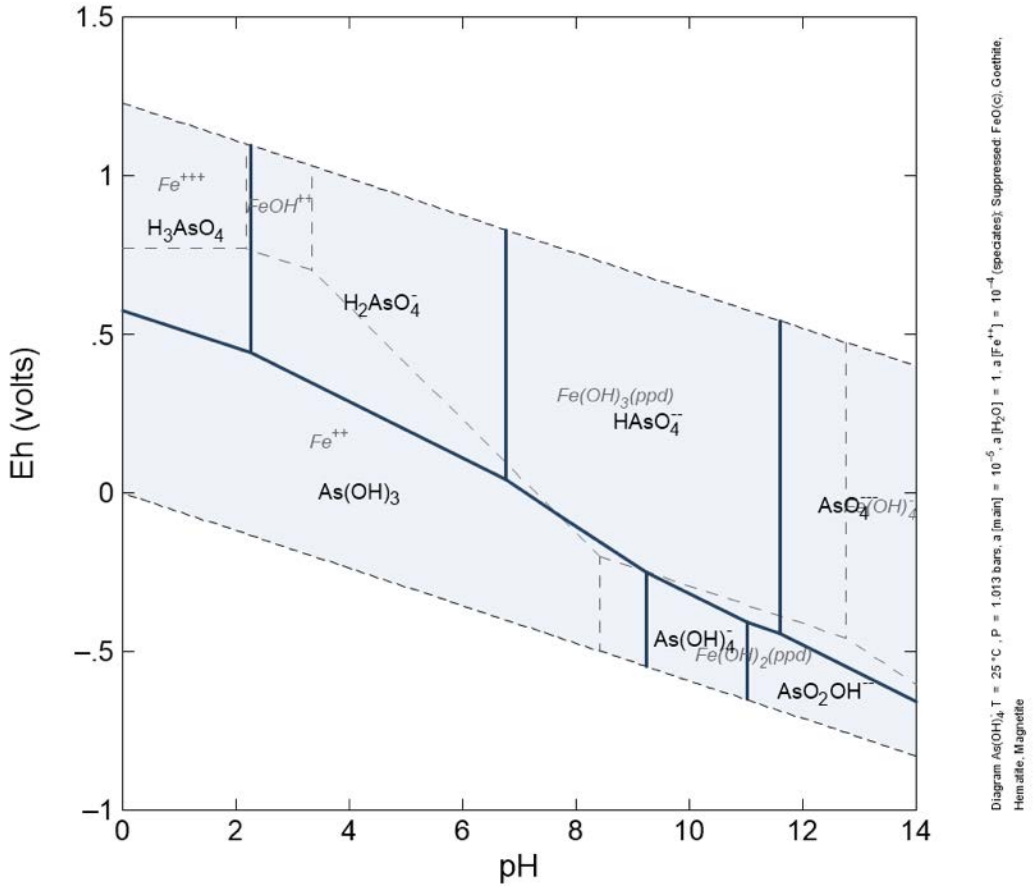

Figure 1: Eh-pH diagram for arsenic (black) and iron (gray) at 25°C and 1 bar

This paper describes two cases where geochemical modeling was used to optimize passive and aggressive treatment using natural and artificial iron coagulation and flocculation of arsenic, respectively. The generalized two-layer model of Dzombak and Morel (1990) is used in the modelling as a comprehensive database is available for arsenic sorption and potentially competing ions for specific iron hydroxide surface sites. Thermodynamic modelling can also be used to investigate arsenic sorption equilibrium in geothermal water discharges as there is some evidence that temperature can also affect

sorption (Stumm, 1992). A more detailed explanation of adsorption phenomena and the double layer model of sorption is provided in Stumm (1992).

Passive treatment of seepage from a historic tailings dam

Passive treatment is occurring at a historic underground gold mine and associated mineral processing and tailings storage facility is located in California, USA. The mine was developed in a quartz pyrite/arsenopyrite vein deposit hosted by slate and metamorphosed basaltic intrusive rocks (greenstone); calcite, chlorite and epidote are found in the propylitic alteration halos that envelope the veins. Therefore, the host rock provides some natural acid buffering capacity in the tailings along with the lime used for processing.

The tailings storage facility was initially constructed over 100 years ago and holds approximately 2 million tons of waste from a cyanide gold leaching operation. A concrete dam was constructed in the early 1900s to contain the accumulated tailings and wastewater generated by the mineral processing facility

Toe seepage contains high levels of iron, arsenic and sulphate. Sulphide oxidation generates dissolved ferrous iron, and the ferrous iron then oxidizes slowly to ferric iron, which is less soluble than ferrous iron and subsequently precipitates as ferric hydroxide. The oxidation reduction potential of the tailings pore water is consistently lower than that of the surface seeps below the dam, which indicates that oxidation of the seepage is occurring at the face of the dam and below the toe of the dam. The resulting near-neutral pH of the seepage is favorable for arsenic sorption to iron hydroxides that form near and below the toe of the dam.

Prior to stabilization and reclamation in 2018, the concrete dam had deteriorated over time, and numerous iron stained seeps occurred at the toe of the dam underflow and from cracks in the dam face itself. The seep water contains metals (arsenic, iron, and manganese) but was not acidic. Arsenic is the primary constituent of concern at the site and Figure 2 shows that, prior to dam rehabilitation, the mean concentrations in seepage below the dam were above the current drinking water standard of 10 ppb for arsenic.

In tailing pore water samples from the site prior to dam rehabilitation, total arsenic concentrations ranged from about 7 to 1,000 ppb with an average of approximately 500 ppb. In surface water, the total arsenic concentrations ranged from over 1,000 ppb to below the detection limit of 1 ppb, with an average of approximately 200 ppb. Total arsenic was positively correlated to total iron and high iron concentrations and formation of iron colloids affects the total and dissolved concentrations of arsenic and other constituents at the toe of the dam. On average, iron concentrations are more than an order of magnitude higher than the arsenic concentrations in both surface and groundwater.

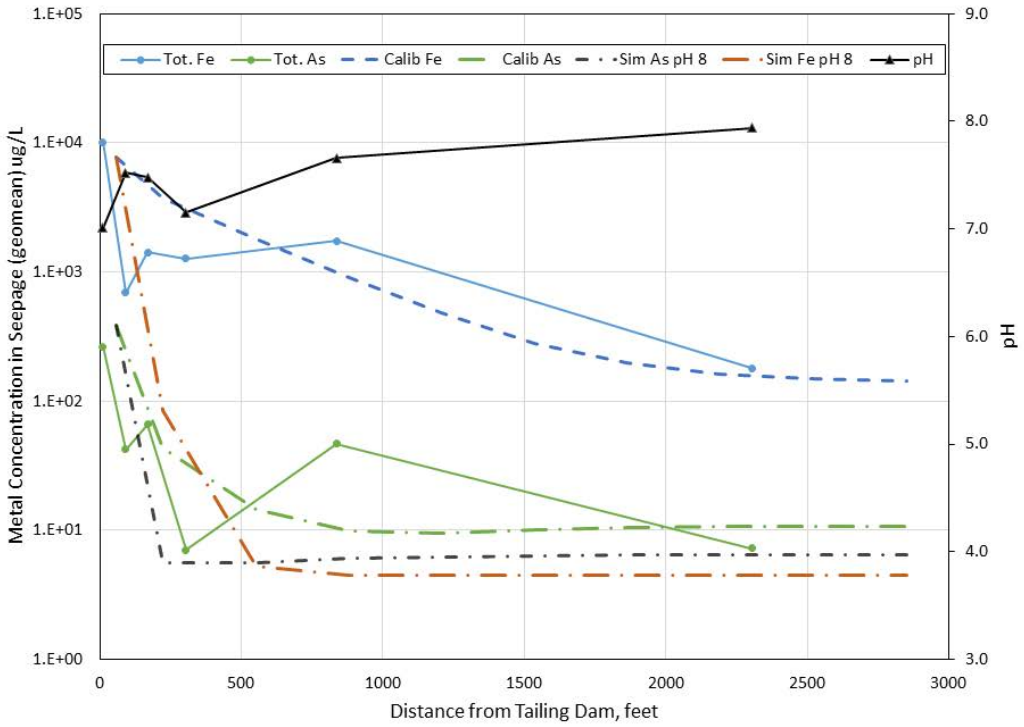

Figure 2: Seepage quality below tailing dam

Figure 2 shows that, prior to dam rehabilitation, total arsenic concentrations diminished from the tailings dam along the drainage channel until it fell below the drinking water standard of 10 ppb about a half mile below the dam. Some of this attenuation is a result of dilution and some is a result of the oxidation of ferrous iron in the reduced tailing pore water solutions and precipitation of ferric hydroxide as seepage is oxidized upon exposure and equilibration with the atmosphere. It was possible to use and accentuate these attenuation processes for passive treatment of arsenic and other constituents at the site after retrofitting. However, management of arsenic bearing iron hydroxide sludge deposits will be necessary to prevent direct contact, remobilization of arsenic.

Ferric iron (Fe^{+3}, the oxidized form of iron) is highly insoluble in neutral pH water and the pH of the surface water below the dam ranges from 7 to 8. The reduced or ferrous iron (Fe^{+2}) concentrations emanating from the seeps are lowered by with time and exposure to the atmosphere by Reaction 1:

$$Fe^{+2} + 0.25O_2 \text{ (dissolved gas)} + 2.5H_2O = Fe(OH)_3 + 2H^+ \quad (1)$$

This reaction generates the surface sites necessary for sorption of As[V], the primary arsenic species in oxygenated water with near-neutral pH, on the surface of precipitated ferric hydroxide (Dzombak and Morrel, 1990).

However, the oxidation reaction of ferrous iron to ferric is not instantaneous and is controlled by oxidation kinetics. Therefore, it takes a few minutes, hours, or even days to oxidize iron completely

depending on the chemical and physical state of the aqueous solution and the activity of iron oxidizing bacteria (Chapelle, 1993). The rate of iron oxidation has been measured experimentally under different conditions and a summary of these experiments is provided in Stumm and Morgan (1981). The kinetically controlled iron oxidation reaction can be expressed by the rate law equation:

$$\frac{dMFe^{+2}}{dt} = n_w k_+ mFe^{+2} mO_{2(aq)} a^2 OH^- (1 - \frac{Q}{K}) \quad (2)$$

The term on the left expresses the rate of change of moles of dissolved ferrous iron ($dMFe^{+2}$) per unit time (t) as a function of the moles of water (n_w), rate of iron oxidation (k_+), original molality of ferrous iron (mFe^{+2}), molality of dissolved oxygen ($mO_{2(aq)}$), square of the activity of hydroxyl ion (a^2OH^-) and the solubility product of iron hydroxide solids ($(1 - \frac{Q}{K})$). The rate of oxidation is affected by oxygen content, pH and the presence of iron oxidizing bacteria, which also increases the rate of reaction. Whereas ferrous iron oxidizes and precipitates fastest at neutral to alkaline pH, the favourability of arsenic sorption decreases under highly alkaline for pH conditions greater than 9 to 10 depending upon the arsenic species (Dzombak and Morrel, 1990).

Examination of water quality data from the site prior to dam rehabilitation shows that dissolved iron and arsenic were attenuating as a result of precipitation of iron hydroxide solids as water issued as seepage from the tailing dam (Figure 2). Figure 2 shows arsenic concentrations diminished downstream of the dam to less than the drinking water standard of 10 ppb in approximately 0.5 miles along the reach prior to entering the creek. Figure 2 also shows the predicted arsenic and iron concentrations using a calibrated geochemical sorption and reactive transport model constructed using the Geochemist's Workbench software (Bethke and Yekel, 2016). The model fits the decreasing iron and arsenic concentrations when the rate constant is adjusted accordingly. The model also predicts that raising the pH of the seepage slightly, to approximately 8, in the cement lined channel increased the rate of iron hydroxide precipitation and coprecipitation of arsenic (Figure 2).

Total iron includes both dissolved and particulate iron which can be sourced from suspended sediments. Therefore, sediment filtering is also critical to controlling total iron and arsenic concentrations. Sedimentation and filtration of iron precipitate, arsenic and other suspended solids in seepage can be enhanced with settling ponds or vegetated channels (Figure 3) in association with a water management and collection system constructed at the toe of the retrofitted dam where the new seepage exit point develops. Colloid filtering can occur in vegetated channels where biofilms adhere to aquatic grasses and reeds in the channel. This effect was simulated by adjusting colloid mobility in Geochemist's Workbench. Colloid mobility decreases rapidly with precipitation of biofilms and iron colloids on substrates by the action of filter ripening (O'Melia, 1990). Grasses and reeds accumulate iron colloid precipitate until sluffing off by gravity allowing the floc to settle to the bottom and freeing up the surface form more precipitation.

Alternatively, the stem or blade may collapse and become buried in the substrate and replaced with new growth. Excessive accumulation of organic matter is not desirable because it may create reducing conditions in the hyporheic zone and result in partial dissolution of the iron hydroxide sorbent and release of arsenic. After colloidal filtering and settling and accumulation in upstream reaches of the creek, additional attenuation results from natural or enhanced downstream dilution, which can be seen in decreasing concentrations of sulphate, a relatively conservative constituent.

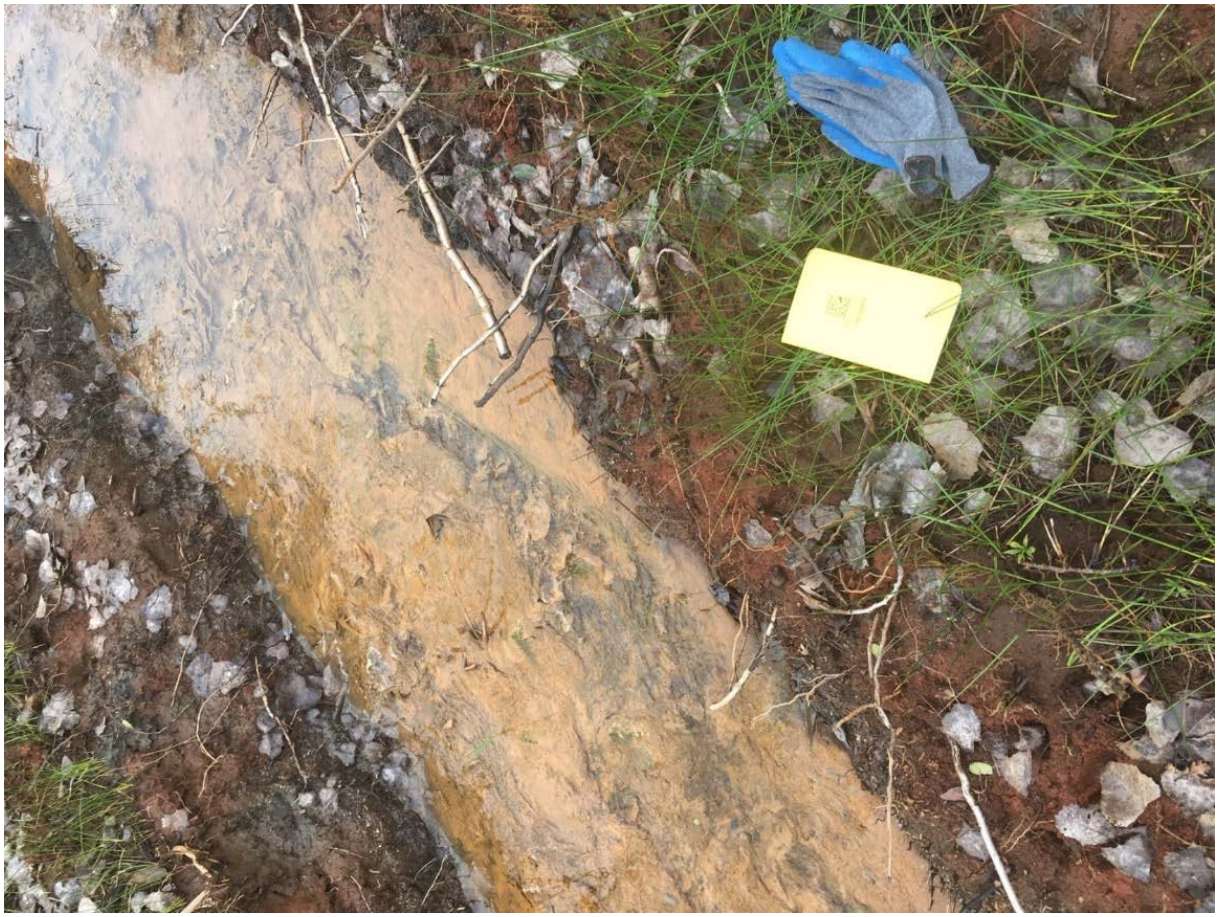

Figure 3: Iron hydroxide precipitation in tailing dam drainage channel

Iron precipitate in channels or ponds used for treatment must be managed to prevent desorption of arsenic and to minimize contact with and visual effects from the iron sludge itself. Periodic dredging or flushing and collection of sludge may be necessary to prevent the development of anoxic conditions that can release arsenic.

In some conditions, shallow and vegetated channels function as biofiltration swales to provide better aeration and iron hydroxide colloid filtering capacity than ponds. Table 1 illustrates how sludge management and activation can be facilitated by constructing multiple channel reaches that can be tiered, with alternating flow directions. The channel reaches are gated with bypasses to control residence time,

maintenance and sludge removal. Bypass circuiting to lower channels can be used for cleaning out sludge buildup and to provide iron hydroxide sludge for activation of bacterially catalyzed iron oxidation in lower reaches. Hydraulic flushing of the sludge to a depot at the end of the bypass channel may be more efficient than mechanical sludge removal with an excavator. Open channels can be armored with riprap or covered with screens to prevent access by humans and wildlife.

Table 1: Arsenic treatment channels, bypass gates and sludge depots

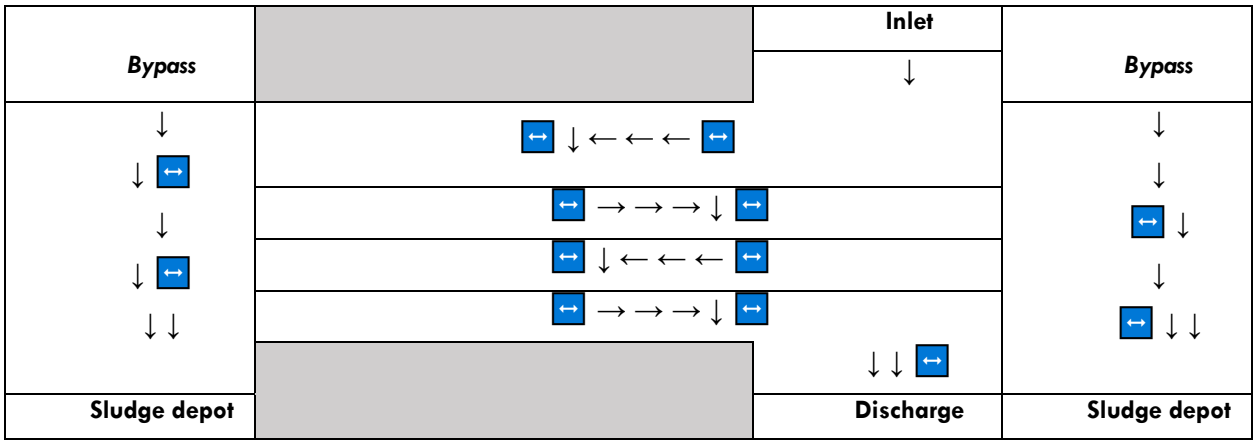

Aggressive treatment: Modern gold mine dewatering thermal flows

Large-scale open pit and underground gold mines in Nevada require mega-scale dewatering of thermal groundwater with pumping rates of tens of thousands of gallons per minute. Much of the groundwater in the Nevada mineralized districts contains moderate to high concentrations of naturally occurring arsenic and some concentrations are above the drinking water standard. Wetland treatment is used for some acidic mine drainage; however, according to Webster and Nordstrom (2003), the capacity of riparian zone plant attenuation of high flow geothermal arsenic water discharges along the Yellowstone river is only about 3 to 4 percent owing to finite plant production and uptake capacity. Based on these limitations, a large area would need to be devoted to wetland treatment in order for wetland plant promotion by itself to treat arsenic in discharge to the regulatory standard.

Pumped water from mines and some geothermal energy plants is typically treated with ferric salts that form iron hydroxides to lower arsenic concentrations below the drinking water standard prior to discharge. In some cases, the water is discharged into cooling channels to allow the water to cool to ambient temperatures prior to infiltration of discharge water to the subsurface for disposal. The senior author was involved in a treatment efficiency study of thermal discharge that was treated with ferric salts at the head of a cooling channel. Monitoring showed that the ferric treatment initially lowered natural arsenic levels to below the drinking water standard of 10 ppb in the treatment mixing zone where temperatures were highest. However, monitoring along the channel showed that the arsenic levels partially rebounded downstream as

the treated water cooled. The pH of the water was constant and slightly alkaline as a result of high alkalinity from the carbonate aquifer source, so rising pH was not causing arsenic desorption from the precipitated iron hydroxide sludge that had accumulated along the channel bed. However, laboratory studies by Banerjee (2008) and Feng et al. (2012) have shown that adsorption of arsenic onto iron hydroxide particles is endothermic and the equilibrium concentration of arsenic in water is lower at higher temperatures and higher at lower temperatures.

Sorption modelling using a Geochemist's Workbench software (Bethke and Yekel, 2016) and the sorption enthalpy calculated by Feng et al. (2012) was successful in matching the arsenic concentrations in the cooling channel as a function of temperature. However, because the arsenic treatment data described above is not publicly available, we used data from Yellowstone hot springs collected by the USGS (2010) to test the ability of sorption modelling to predict arsenic concentrations in spring discharges. Figure 4 shows the natural and computer simulated arsenic concentrations at the Rabbit Creek monitoring station, which increase downstream of the thermal spring (USGS, 2010). As[V] was simulated as it is the dominant form of arsenic at this site. The model also included slight increases in pH as the water flows downstream, as well as evapoconcentration of the heated water. Although the iron concentrations in the water are relatively low, iron and silica precipitates occur in the bed of the creek downstream of the thermal spring. Both iron and silica oxide surfaces sorb arsenic and other ions and the sorption can be modelled using double layer theory (Stumm, 1992). The equilibrium constants for the iron hydroxide sorption model database were altered to fit the data.

The best fit was achieved when the equilibrium constant (Kd) was varied with temperature, as isothermal Kd values were unable to simulate the slope and low As [V] concentrations at near boiling conditions. Model calibration to more reduced arsenite (As [III]) data for the Ojo Caliente site also required alteration of Kd with temperature to fit the field data (Figure 5). The heats of sorption (enthalpy) extracted from a linear fit of Kd with 1/T were endothermic and in the range of 11 to 64 kJ/mole for As[III] and As[V], respectively, which is in agreement with the reported enthalpies of sorption calculated by laboratory sorption test data (Banerjee et al., 2008; Feng et al., 2012).

Another field study conducted in the Altiplano region of Bolivia showed that arsenic concentrations are lower in water from high temperature geothermal springs as compared to lower temperature shallow aquifer samples (Munoz et al., 2015). Arsenic in sediments from the springs and aquifers was strongly correlated with iron, indicating that iron hydroxide sorption equilibria reactions were controlling arsenic concentrations in this area. These field findings also support the laboratory work of Banerjee et al. (2008) and Feng et al. (2012) indicating that arsenic sorption on iron hydroxide is endothermic.

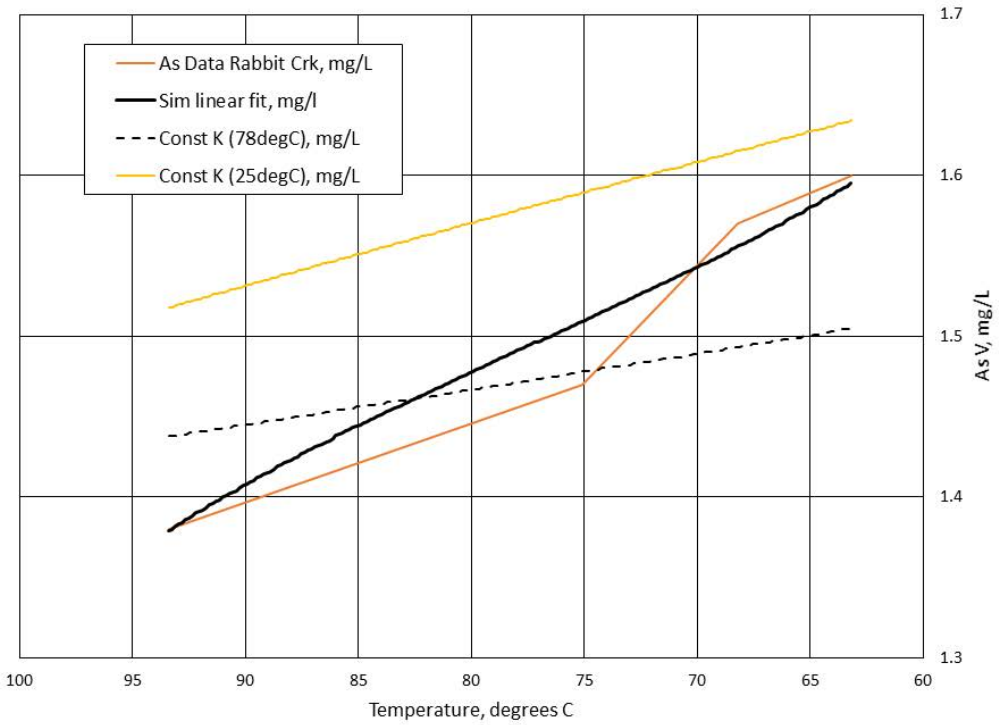

Figure 4: Simulated As concentrations for Rabbit Creek, Yellowstone National Park

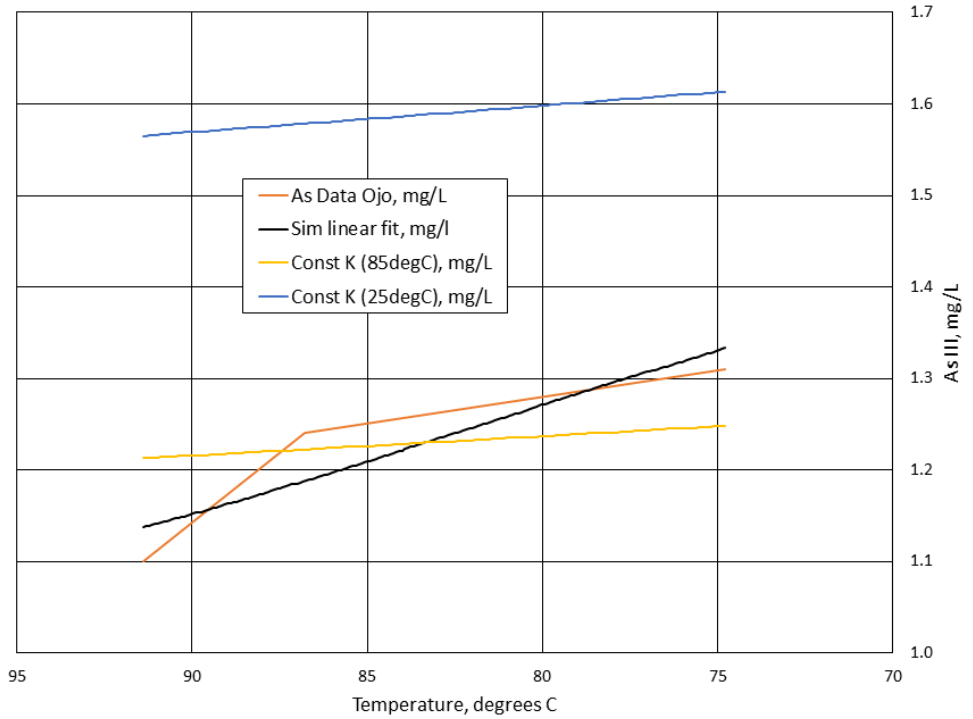

Figure 5: Simulated As concentrations for Ojo Caliente, Yellowstone National Park

Conclusion

The passive and aggressive arsenic treatment studies discussed in this paper illustrate that geochemical and thermodynamic modelling can be used as a tool in treatment system design, especially where site data are sufficient for model calibration. While not a replacement for bench-scale testing, geochemical and thermodynamic modelling can quickly narrow the scope of more expensive and time-consuming bench tests and guide the eventual scaling to pilot and full-scale treatment systems.

References

Banerjee, K., G.L. Amy, M. Prevost, S. Nour, M. Jekel, P.M. Gallagher and C.D. Blumenschein. 2008. Kinetic and thermodynamic aspects of adsorption of arsenic onto granular ferric hydroxide (GFH). *Water Research* 42: 3371–3378.

Bethke, C.M. and S. Yekel. 2016. *GWB Reaction Modeling Guide*. Champaign: Aqueous Solutions, LLC.

Chapelle, F.H. 1993. *Ground-Water Microbiology and Geochemistry*. New York: John Wiley & Sons.

Dzombak, D.A. and F.M.M. Morel. 1990. *Surface Complexation Modeling. Hydrous Ferric Oxide*. New York: John Wiley & Sons.

Feng, Q., Z. Zhang, Y. Ma, Y. He, Y. Zhao and Z. Chai. 2012. Adsorption and desorption characteristics of arsenic onto ceria nanoparticles. *Nanoscale Research Letters* 7(84): 8.

Munoz, M.O., P. Bhattacharya, O. Sracek, O.R. Ramos, J.Q. Aguirre, J. Bundschuh and J.P. Maity. 2015. Arsenic and other trace elements in thermal springs and in cold waters from drinking water wells on the Bolivian Altiplano. *Journal of South American Earth Sciences* 60: 10–20.

O'Melia, C.R. 1990. Kinetics of colloid chemical processes in aquatic systems. In *Aquatic Chemical Kinetics,* edited by Werner Stumm: 447–474. New York: John Wiley & Sons.

Smith, K.S. and H.L.O. Huyck. 1999. An overview of the abundance, relative mobility, bioavailability, and human toxicity of metals. In *The Environmental Geochemistry of Mineral Deposits Part A: Processes, Techniques and Health Issues,* edited by Geoffrey Plumlee and Mark Logsdon: 29–70. Littleton, CO: Society of Economic Geologists, Inc.

Southwest Hydrology. 2002a. The history of arsenic regulation. *Southwest Hydrology*, May/June: 16.

Southwest Hydrology, 2002b. Assessing arsenic removal technologies. *Southwest Hydrology*, May/June: 20–22.

Stumm, W. and J.J. Morgan. 1981. *Aquatic Chemistry*. New York: John Wiley & Sons.

Stumm, W. 1992. *Chemistry of the Solid-Water Interface*. New York: John Wiley & Sons.

USGS. 2010. *Water-Chemistry Data for Selected Springs, Geysers, and Streams in Yellowstone National Park, Wyoming, 2006-2008*. Open-File Report 2010-1192.

Webster J.G. and D.K. Nordstrom, 2003. Geothermal Arsenic. In *Arsenic in Groundwater,* edited by Andy Welch and Kenneth Stollenwerk: 101–125. Norwell, MA: Kluwer Academic Publishers Group.

Bibliography

Nordstrom, D.K. and A. Nicholson. 2017. *Geochemical Modeling for Mine Site Characterization and Remediation. Volume 4. Management Technologies of Metal Mining Influenced Water*. Englewood: Society of Mining, Metallurgy and Exploration.

Proceedings of Tailings and Mine Waste 2019
November 17–20, 2019, Vancouver, Canada
Published by the University of British Columbia, 2019

Current Acid Rock Drainage Impacts and Seepage Interception Strategies at the Myra Falls Mine Site

Paul Ferguson, Robertson GeoConsultants Inc., Canada
Mahmoud Hussein, Robertson GeoConsultants Inc., Canada
Christoph Wels, Robertson GeoConsultants Inc., Canada
Nicole Pesonen, Nyrstar Myra Falls, Canada

Abstract

This paper describes ongoing acid rock drainage (ARD) mitigation and management practices at the Myra Falls mine on Vancouver Island, British Columbia, Canada. The mine has operated for more than sixty years and is within the confines of the Strathcona Provincial Park. Cycloned fine tailings were originally deposited sub-aqueously in Buttle Lake and have been deposited sub-aerially in two tailings disposal facilities (TDFs) in Myra Valley since the early 1990s. Tailings in the TDFs are currently oxidizing and represent a large potential source of ARD to groundwater and nearby Myra Creek. Currently, however, sulphidic waste rock deposited at surface in historic waste rock dumps (WRDs) or used to construct the Lynx TDF embankment berm are the primary sources of ARD to groundwater.

ARD-impacted groundwater is actively managed by a site-wide seepage interception system (SIS) that consists of a series of gravity-fed under-drains beneath the original TDF and a fence of pumping wells downgradient of the Lynx TDF (referred to as the Phase I Lynx SIS). ARD-impacted mine water and contact water (runoff) from the tailings facilities are also managed via a system of decants and spillways. This paper describes the performance of the site-wide SIS during the first eighteen months that the Phase I Lynx SIS was operated and selected results that were incorporated into a numerical groundwater model, including the key inputs to a site-wide water and load balance model (WLBM) described in a companion paper, Hussein et al. (2019).

Introduction

Myra Falls is an underground zinc mine that has operated for more than sixty years and is within Strathcona Provincial Park on Vancouver Island, British Columbia, Canada. Myra Creek flows eastward through the mine site before discharging into Buttle Lake about 1.5 km downstream of the western site boundary. The creek is characterized by elevated concentrations of zinc (Zn) and other metals due to acid rock drainage

(ARD) that reports to the creek via groundwater in the Myra Valley Aquifer (MVA). Zn is the key parameter of interest at the site as Zn concentrations in Myra Creek can exceed provincial Water Quality Guidelines (WQGs).

Sulphidic waste rock in several historic Waste Rock Dumps (WRDs) and the waste rock used to construct the Lynx Tailings Disposal Facility (TDF) embankment berm are the key sources of ARD to groundwater. Potentially acid generating (PAG) tailings in the Lynx TDF and the original (or "Old") TDF are currently oxidizing and do not represent a substantial source of metals or other constituents to groundwater.

Most ARD-impacted groundwater is captured by a site-wide seepage interception system (SIS) to reduce contaminant loads to Myra Creek. The site-wide SIS consists of:

1. a series of gravity-fed under-drains beneath the Old TDF, including the Tailings Inner Drain along the buried toe of WRD#1 and the New Outer Drain (NOD); and
2. the Lynx SIS downgradient of the Lynx TDF and the mill area (see Table 1).

Table 1: Site-wide seepage interception system (sis) components

SIS component	Description
Tailings inner drain	• Gravity-fed drain along the buried toe of WRD#1 in 1984
Old outer drains	• Constructed between the Old TDF and Myra Creek in 1984 during dam construction
New outer drain (NOD)	• Electronically controlled sluice gates control flows to each section of NOD • NOD currently operated at settings of "10–0–10", which denotes 10% opening for Medium and Long Drain and 0% opening for Short Drain • NOD capacity is higher, but wider openings generally lead to larger inflows from Myra Creek and no significant improvement in seepage recovery
Phase I Lynx SIS	• Pumping wells PW14-01 and PW-14-04 downgradient of Lynx TDF • Pumping well PW14-03 in the mill area • Each well operated near-continuously since September 2017
PW18-01 to PW18-04	• Vacuum pumping system in four shallow pumping wells • Operated for 60 days in 2019

Groundwater captured by the site-wide SIS is directed to a low density sludge (LDS) water treatment system that consists of a primary treatment pond (the "Super Pond") and a series of polishing ponds. The

water treatment system also receives neutral mine drainage (NMD) pumped from the underground workings, gravity flows of mine water from several adits, and ARD-impacted precipitation runoff collected from the TDFs. Treated effluent is discharged to Myra Creek via a culvert about 50 m upstream of MC+400 m at station "11A Runoff" (see Figure 1).

Groundwater and surface water flows and contaminant loads to the water treatment system and Myra Creek are simulated by a site-wide water and load balance model (SWLBM). The model was developed in 2016 and updated in 2018 to:

- Simulate Zn loads and concentrations in Myra Creek and loads to the water treatment system during period(s) between January 2012 and October 2017 that are representative of steady-state conditions during the operation of the Old TDF under-drains.
- Predict future Zn loads in groundwater and in Myra Creek and flows and Zn loads to the water treatment system during operation of the Phase I Lynx SIS and during future mining operations and the post-closure mining phase.

This paper outlines key elements of Robertson GeoConsultants Inc.'s (RGC's) conceptual load balance model and groundwater and surface water quality observations for the site, including the key inputs and calibration targets for the updated SWLBM. Initial performance monitoring results for the Phase I Lynx SIS are also discussed as they pertain to model development and predictive runs from the SWLBM. Numerical modeling results and water quality predictions are provided in Mahmoud et al. (2019).

Results and discussion

Current ARD impacts to groundwater

Groundwater monitoring wells and pumping wells at the Myra Falls mine site are shown in Figure 1. Forty-one of these wells were installed in 2013 as part of RGC's environmental drilling program (i.e., the "MW13" and "TD13" well series). Other monitoring wells were installed during previous site investigations in 2011 or earlier (see RGC, 2014, for additional details) or as part of recent hydrogeological and geotechnical investigations of TDFs. Most of the wells are screened in the MVA, which is which is comprised of a complex mixture of colluvial, alluvial, glaciofluvial, and glaciolacustrine sediments. These sediments can be highly permeable and transmit substantial groundwater along the Myra valley thalweg. The MVA receives recharge from the surrounding hill sides (via creeks, springs, and groundwater) and surfaces within the mine site, e.g., WRDs, and is hydraulically connected to Myra Creek. Lesser flows occur in the underlying bedrock aquifer and in shallow colluvial and/or alluvial sediment that cover valley slopes, neither of which are simulated by the SWLBM.

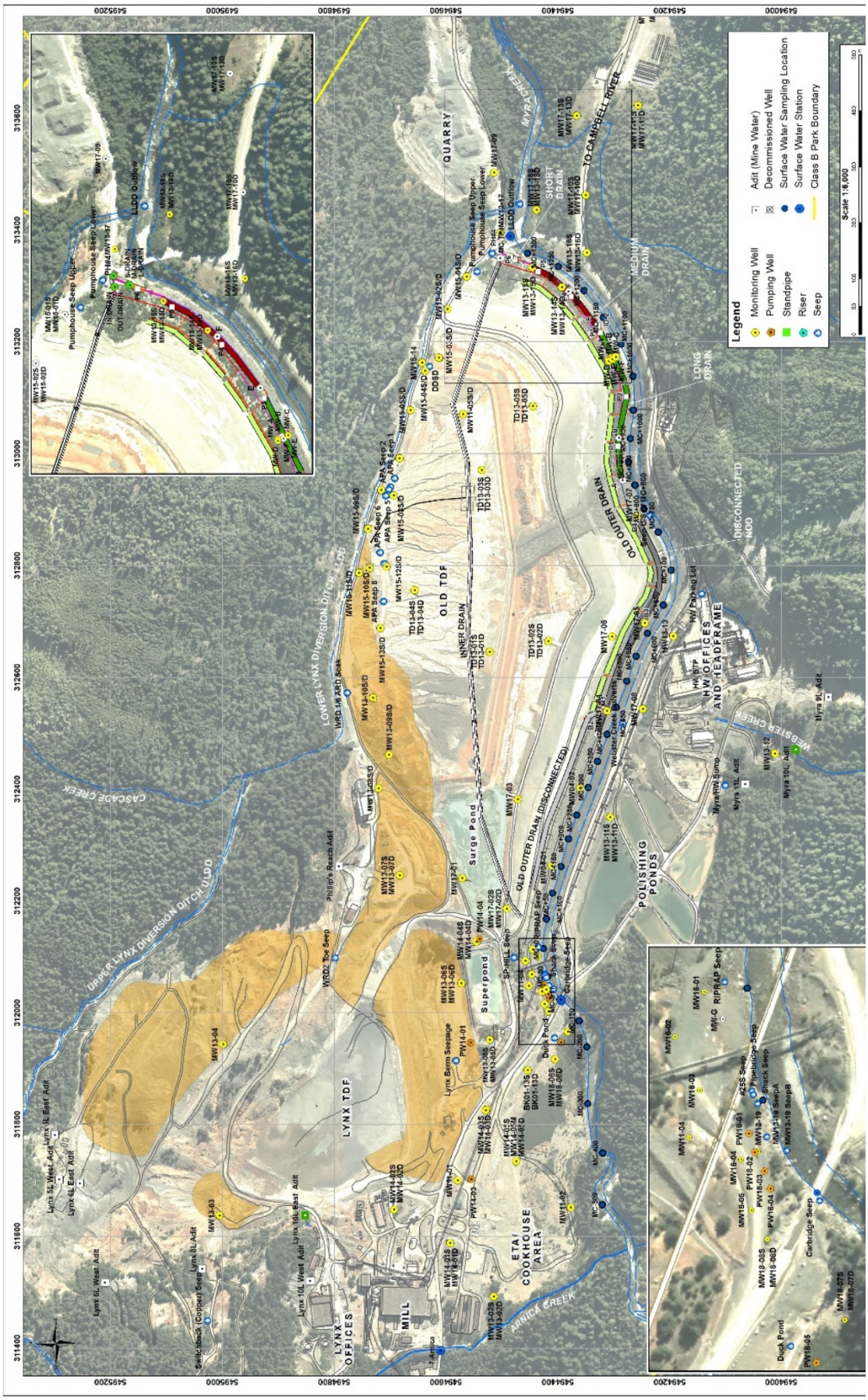

Figure 1: Location of the Myra Falls mine site on Vancouver Island. Key features included the access road from Campbell River, the Mill and office buildings, Lynx TDF (around the former open pit), the Old TDF and Seismic Upgrade Berm, the Lower Lynx Diversion Ditch (LLDD), the historic WRDs (WRDs 1 to 6), the former Emergency Tailings Area (ETA) and Cookhouse area, and the Super Pond and Polishing Ponds

Groundwater quality in the MVA is impacted primarily by seepage from the historic WRDs and the Lynx TDF embankment berm (Figure 2). Metal concentrations are highest in groundwater downgradient of Lynx TDF embankment berm and WRD#1. Approximately 37.4 t/year Zn reports to the MVA from all sources at surface. Together, WRD#1 and the Lynx TDF berm account for approximately 60% of this annual load. Seepage from waste rock in the mill area (and possibly WRD#4) accounts for an additional 20% of the annual Zn load and other sources, e.g., Seismic Upgrade Berm, seepage from the ETA/Cookhouse area account for the other 20% of the load to groundwater. Tailings account for less than 0.1% of the Zn load to groundwater in the MVA.

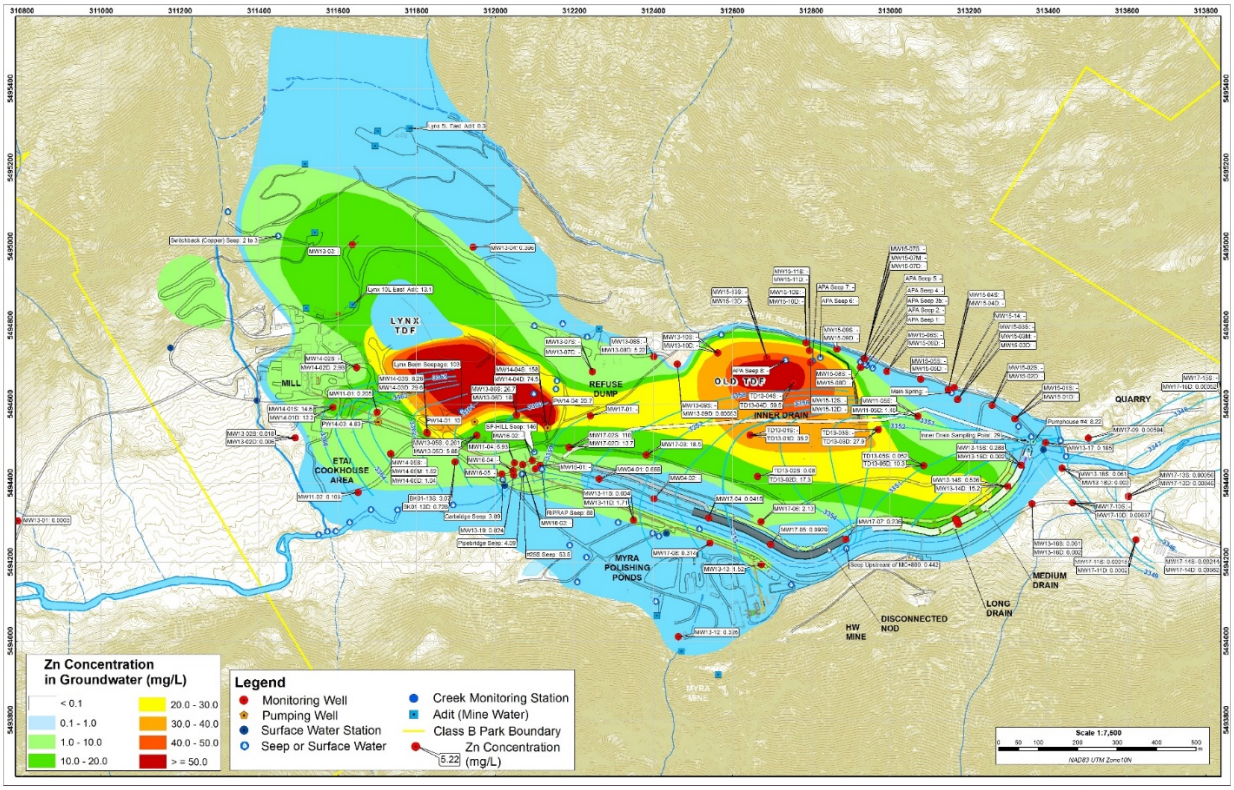

Figure 2: Observed Zn concentrations in groundwater and inferred Zn plume

Zn loads in Myra Creek

Key findings are summarized below:

- Zn loads from the Lynx Reach account for up to 50% of the Zn load in Myra Creek under high flow conditions and about 20% of the Zn load during low flow conditions. Higher Zn loads to Myra Creek during high flow periods are likely caused by (i) larger discharge of groundwater from the Lynx TDF area, the ETA/Cookhouse area, and the mill area due to an increase in groundwater levels and (ii) flows of impacted groundwater to Myra Creek from the Lynx TDF/Super Pond area.

During low flow conditions, the groundwater flow field shifts slightly and groundwater tends to flow down the valley towards the Old TDF under-drains.

- Zn loads from the Upper Old TDF Reach account for about 50% of the Zn load to Myra Creek during low flow conditions (see Figure 3). Higher loads to this area during low flow periods are likely related to impacted groundwater from the Lynx Reach that bypasses Myra Creek near the car bridge only to discharge to Myra Creek further downgradient. Differences in loads to Myra Creek at different times of the year are related to changes in the local flow field that affect the amount of impacted groundwater that discharges to Myra Creek.
- Zn loads from the Lower Old TDF Reach account for 10% or less of the Zn load to Myra Creek. This implies that the Old TDF under-drains capture the majority of the Zn load in this reach and that Zn bypass is small (i.e., ~1.4 t/year). Elevated Zn concentrations in groundwater between MC+1300 m and MC-TP4 (and near MC13-13S/D) suggest that most of this Zn load bypasses the Medium Drain.

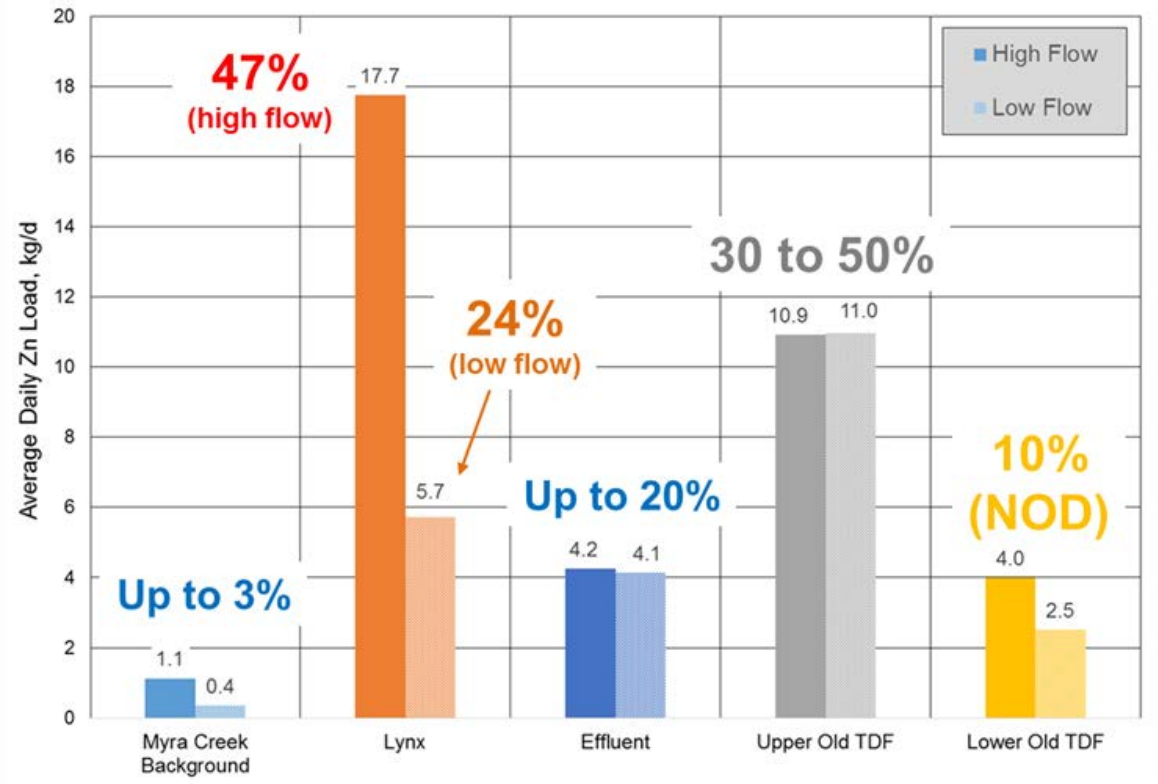

Figure 3: Average daily Zn loads in Myra Creek. High flow (left) and low flow (right)

From 2012 to 2016, the Old TDF under-drains recovered an estimated 43.7 t/year Zn from the groundwater system. The average Zn load in Myra Creek at MC-TP4 from 2012 to 2016 is estimated to be 14.0 t/year Zn. 2.2 t/year Zn is related to treated effluent and 11.8 t/year is estimated to enter Myra Creek

from the Lynx Reach, the Upper Old TDF Reach, and the Lower Old TDF Reach (combined). These loads imply that ~80% of the Zn load that enters the groundwater system is recovered by the Old TDF under-drains.

Zn loads in groundwater

Zn loads in groundwater within the Lynx Reach, Upper Old TDF Reach, and Lower Old TDF Reach were estimated to determine the contribution of source areas within these reaches. Estimating Zn loads involved the interpretation of local groundwater flow fields, hydrogeologic data from previous site investigations, and routine groundwater quality monitoring data. Estimated Zn loads to Myra Creek were calibrated to observed Zn loads in Myra Creek during 33 sampling campaigns undertaken from 2012 to mid-2016.

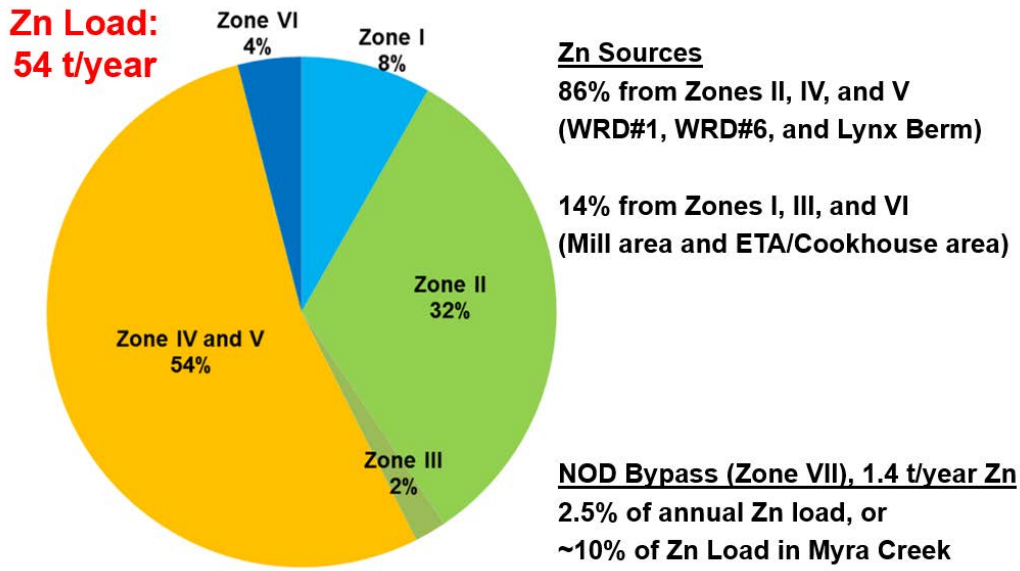

Figure 4: Zn Loads in Groundwater (By Reach). Zones I and II are in the Lynx Reach, Zones III and IV are in the Upper Old TDF Reach, and Zones V, VI, and VII are in the Lower Old TDF Reach (see Hussein et al., 2019, for further details)

Key findings of this conceptual load balance model are summarized here (see Figure 4):

- 53% (or 29.1 t/year Zn) of the estimated annual Zn load in groundwater originates from WRDs #1 and #6. The Lynx TDF and Super Pond area account for 32% (17.6 t /year Zn) of the annual Zn load in groundwater and other sources account for 15%.
- 68% of the Zn load captured by the Old TDF under-drains originates from WRDs #1 and #6. 23% originates from the Lynx TDF berm and the Super Pond area and 9% is from other sources (i.e., the mill area, ETA/Cookhouse area, etc.).

- NOD bypass is estimated to be 1.4 t/year Zn. This is 12% of the annual Zn load in Myra Creek. The other 10.2 t/year Zn reports to the creek from areas upstream of the NOD (namely the Lynx Reach, mill area, and ETA/Cookhouse area).

Zn loads captured by old TDF under-drains

Groundwater captured by the system of under-drains reports to the sump at Pumphouse #4 from where it is pumped to the Super Pond. Pumping rates for Pumphouse #4 represent the combined drain flow and no measurements of flow rates of the individual drains are possible. However, water quality is routinely sampled at the Short, Medium, Long, Old Outer, and Inner Drains, and percentage contributions by each drain can be inferred.

Key observations are summarized below:

- The Inner Drain is consistently characterized by ~30 mg/L of Zn and flows from this drain are inferred to be ~10 L/s. This represents 12 t/year Zn or 27% of the combined Zn load captured by the Old TDF under-drain system. Estimated flows from the NOD are estimated to capture around 90 L/s and a load of 11.2 t/yr.
- The Old TDF under-drains are estimated to capture 107 kg/day and 135 kg/day during low flow (< 4 m^3/s in Myra Creek) and high flow conditions (> 9 m^3/s in Myra Creek), respectively. The recommended calibration targets for the aggregated drain flows are 185 L/s during low flow conditions and 234 L/s during high flow conditions.

Zn loads captured by Lynx SIS

The Phase I Lynx SIS has operated near-continuously for 18 months (as of May 2019). The inferred capture zones for the Lynx SIS pumping wells extend throughout Lynx Reach and hydraulic testing suggests no well interference between PW14-03 and PW14-01. Some well interference was inferred between PW14-01 and PW14-04 beneath the Super Pond. However, this is required to maximize capture of the highly contaminated groundwater in that area.

The PW14 pumping wells operated an average combined pumping rate of 49.7 L/s from September 2017 to May 2019. Average pumping rates were 25.3 L/s for PW14-01, 13.2 L/s for PW14-03, and 16.8 L/s for PW14-04. Pumping rates increase in response to rainfall and slowly receded once rainfall ceased. The Phase I Lynx SIS was not operated for 17 to 59 days in starting December 4th, 2018 due to technical difficulties. Since PW14-01 resumed operation in February, pumping rates were about 8 L/s lower than previously observed and may suggest a deterioration in performance.

Pumping rates, pumped volumes, and Zn loads captured by each pumping well are summarized in Table 4. In total, the Phase I Lynx SIS captured an estimated 49.9 t of Zn during the first eighteen months

is was operated. This load is essentially equivalent to the Zn load captured by the Old TDF under-drains, despite the much lower flows to the pumping wells.

Groundwater quality effects downgradient

Zn concentrations in several key wells, e.g., MW17-02S and MW17-03, have decreased substantially during the operation of the Phase I Lynx SIS. After one year, for instance, Zn concentrations had decreased by 94% (from 13.7 to 0.951 mg/L) and 47% (from 18.5 mg/L to 9.76 mg/L) at MW17-02D and MW17-03, respectively. In 2019, Zn concentrations of around 40 mg/L were observed, with MW17-02D showing an increasing trend. The initial decreases in Zn concentrations downgradient of the Lynx SIS suggest the Phase I Lynx SIS was working as intended, thereby capturing ARD-impacted groundwater before it could migrate downgradient towards Myra Creek. Higher Zn concentrations in 2019 are therefore most likely related to system shutdown when impacted groundwater bypasses the SIS.

Water quality impacts to Myra Creek

No appreciable reduction in Zn concentrations was observed during the first eighteen months of SIS operation. Hussein et al. (2019) predicts reduced Zn concentrations within the next year once a new steady-state condition in the MVA has been achieved while the Lynx SIS is operating.

Table 4: Captured groundwater flows and Zn loads, September 2017 to May 2019

Drain	Zn, mg/L	Flow rate, L/s	Flow contribution	Zn load, t/year	Load contribution
Tailings inner drain	29.3	13	7%	12	27%
Old outer drain	6.3	107	51%	21	48%
NOD-short drain	1.7	5	2%	<0.5	1%
NOD-medium drain	6.2	30	14%	6	13%
NOD-long drain	2.9	55	26%	5	11%
Sub-total:	**–**	**210**	**100%**	**44**	**100%**
PW14-01	15.9	25	46%	15	30%
PW14-03	25.3	13	24%	17	31%
PW14-04	23.2	17	30%	18	39%
Sub-total:	**–**	**55**	**100%**	**50**	**100%**
Total:	**–**	**265**	**–**	**94**	**–**

Conclusion

Key findings from this paper are summarized below:

- Groundwater in the MVA is variably impacted by ARD, primarily from sulphidic waste rock in WRD#1 and the Lynx TDF embank berm. Other WRDs, e.g., WRD#2 and WRD#6, also contribution substantial Zn loads to groundwater. Mine water from the underground workings is a secondary source of NMD to local groundwater near the adits, as most groundwater flows from the underground are collected and directed to the water treatment system.
- The Old TDF under-drains are highly effective and have recovered ~80% of the Zn load in groundwater since the NOD was installed/optimized and before the Phase I Lynx SIS began operating in September, 2017. The Old TDF under-drains captured 44.3 t/year Zn, or approximately 50% of the total Zn load captured by the site-wide SIS. Drain bypass is minimal (<5% annually). Zn loads in Myra Creek are therefore related primarily to loads from impacted groundwater that discharges to the creek from the Lynx Reach and the Upper Old TDF Reach.
- The Phase I Lynx SIS (commissioned in late September 2017) captured approximately 2.5 Mm^3 of impacted groundwater and 50 t of Zn during the first eighteen months it was operated. This load is approximately equivalent to the load captured by the Old TDF under-drains, or about 50% of the total Zn load captured by site-wide SIS.
- The inferred capture zones of the Lynx SIS pumping wells extend throughout the mill area and the area downgradient of the Lynx TDF. After 12 months of operation, Zn concentrations in groundwater downgradient of the Lynx Reach had decreased significantly by about 94% and 47% at MW17-02D and MW17-03, respectively. Zn concentrations in groundwater have since increased due to temporary shutdown of the Phase I Lynx SIS in 2019.
- Zn concentrations in groundwater and Myra Creek are predicted to decrease within the next 6 to 12 months, assuming a new steady-state condition in the MVA is achieved. Further details are provided in Hussein et al. (2019).

References

Hussein, M., P. Ferguson, C. Wels and N. Pesonen. 2019. Numerical modelling of groundwater flow and contaminant transport at the Myra Falls Mine site. In *Proceedings of Tailings and Mine Waste, 2019.*

Robertson GeoConsultants Inc. 2014. Site hydrogeology report for Nyrstar Myra Falls, Report No. 212001/5, July.

Robertson GeoConsultants Inc. 2016. Contaminant load balance model for current and future conditions at Nyrstar Myra Falls, RGC Report No. 212010/1, December 2016.

Robertson GeoConsultants Inc. 2018. Updated contaminant load balance model and water quality predictions, RGC Report No. 212011/7, November 2018.

Proceedings of Tailings and Mine Waste 2019
November 17–20, 2019, Vancouver, Canada
Published by the University of British Columbia, 2019

Evolution of Landforms in Reclaimed Landscapes in the Surface Mineable Athabasca Oil Sands

Alexander Holden, BGC Engineering Inc., Canada
Heather Provost, BGC Engineering Inc., Canada
June Pollard, J Pollard Consulting, Canada
Gord McKenna, McKenna Geotechnical Inc., Canada
Patrick Sean Wells, Suncor Energy Inc., Canada

Abstract

A changing or evolving landscape is an inherent concept in sciences for natural environments. For example, soil settles, erodes, and accumulates, groundwater and surface water levels and flow patterns change, and wildlife and vegetative communities develop, diversify, or decline. In the mining industry, landform design draws from the science of natural landforms and applies this knowledge to the design, construction, and reclamation of mining landforms. While some landform evolution processes are considered, there is a need to provide clarity around the concept of landform evolution – its inclusion in prediction and design in the oil sands mining industry, and its communication to others.

In this paper, a definition for landform evolution in the context of mining has been created; creating this definition allows for clear communication of the concept. In addition, six categories of landform evolution processes and many specific processes have been identified as applicable to the oil sands mining post-closure landscape setting. The list can be used to set landform design goals and objectives as part of a design basis, as a checklist for landform design projects and/or adaptive management programs, and to guide risk assessments for long-term performance.

To better understand the impacts of the inevitable natural evolution of mining landforms on landform design, a literature review was conducted. It was found that the concept of landform evolution is not explicitly discussed in the technical guidance or regulatory documents that were reviewed, though several guidance and regulatory documents make reference to some aspect of long-term change. In addition, many publications were found that identify prediction tools or include some design guidance related to landform evolution processes.

Introduction

Mining and mine reclamation create new anthropogenic landforms and landscapes (Pollard and McKenna, 2018). Examples of mining landforms include:

- landfill;
- reclamation stockpile;
- overburden dump;
- tailings drainage basin or plateau;
- mined-out pit;
- tailings dyke;
- pit lake;
- waterways, streams, site drainage; and
- plant site.

No landforms, natural or anthropogenic, are static geomorphologically or ecologically – they inevitably evolve and evolve continually over time. This paper presents a concept review of landform evolution for reclaimed oil sands mining landscapes (landform evolution). It explores how mine operators can predict, design for, and/or manage the evolutionary changes to immature anthropogenic landforms. Focus is placed on the landform scale because much design work for mine reclamation and closure occurs at this scale for logistical reasons, though it is acknowledged that geomorphological processes are active at all scales, up to the earth's surface as a whole.

Oil sands mining companies already predict and design for selected, specific landform evolution processes. For example, consolidation of tailings has been researched extensively, and is carefully considered in landform design. Operating approvals for oil sands mines similarly speak to selected aspects of landform evolution (e.g., erosion). However, focus appears to be placed on individual landform evolution processes and not through the broader perspective of geomorphological change, which is an inherent part of natural systems and will affect landforms and landscapes in an extensive number and variety of ways. Consequently, mine operators are seeking to provide clarity around the concept of landform evolution and its inclusion in prediction and design for mining landforms in the reclaimed landscape.

This paper provides a concept review with the following objectives:

- Define the concept of landform evolution.
- Identify applicable landform evolution processes to the Athabasca Oil Sands.
- Explore how these processes can be predicted.

- Explore the concept of designing to accommodate and/or incorporate these evolutionary changes as part of design and identify where this is already being done (i.e., current state of practice).
- Explore how the concept of landform evolution is addressed is by regulators.

The concept of landform evolution was explored primarily through a review of publicly available literature, supplemented with professional experience.

Definition of landform evolution

Landform evolution is an established concept in the practice of earth sciences. For example, the term is defined within the *Encyclopedia Britannica* (n.d.) as follows:

> Landform evolution is an expression that implies progressive changes in topography from an initial designated morphology toward or to some altered form.

Adapting this definition to mining landforms, the authors have developed the following definition. Landform evolution in the context of mining reclamation is:

> Changes to the properties or performance of reclaimed landforms over time. These changes may occur quickly or slowly, may be triggered by events or the result of ongoing processes. These changes may have positive or negative effects on landscape performance and can occur over decades or centuries to come.

The life span of an oil sands mine may be subdivided into different stages:

1. pre-mining activities including exploration, infrastructure development;
2. mining operations including progressive reclamation;
3. final reclamation;
4. monitoring and maintenance; and
5. ongoing landform evolution.

Landform evolution begins and takes place within the context of the different stages of mining (Figure 1). While mining landforms undergo rapid changes during construction, for ease of communication, we propose that landform evolution begins once final reclamation is complete. Where progressive reclamation is practiced, this “time zero” will vary across the lease.

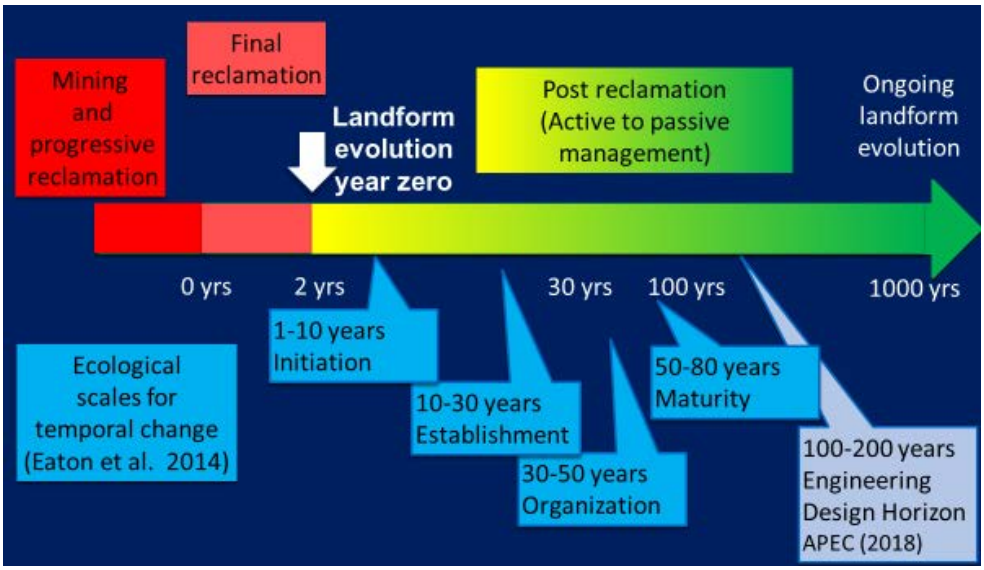

Figure 1: Landform evolution in the context of the oil sands mining life cycle and successional stages of forest stand development in the oil sands

Landform evolution processes

Landform evolution processes are those by which a mining landform in the post-closure mining landscape changes over time. Landform evolution processes are primarily geomorphological, but also include ecological succession, disturbance-driven changes such as changes induced by wildfire, and hydrological or climatic changes, such as changes to groundwater levels or flow directions. Accordingly, the landform evolution processes identified in this paper span multiple disciplines, including geotechnical engineering, geomorphology, hydrology, hydrogeology, water quality, and ecology (vegetation and wildlife).

Appendix A, Table 1, presents a list of landform evolution processes related to oil sands post-closure landforms. To create this list, the authors drew upon information from closure plans, landform designs, and related lists prepared for other applications (McKenna, 2002; MEND, 2012; CEMA, 2014). The list of processes are summarized within six broad categories of landform evolution processes: mass wasting (gravity induced deformation), erosion and deposition, weathering, disturbance, hydrologic and climatic, and ecological.

The list could be used to assist with closure planning in several ways:

- To set landform design goals and objectives as part of a design basis
- As a checklist during landform design or in the creation of adaptive management programs
- For clarity in discussing landform evolution with others
- To guide landscape performance risk assessments.

Literature review: Landform evolution

Methods

Publicly available scientific journal articles, conference papers, industry technical guidance documents and regulatory documents were reviewed to assess if, or how evolution of reclaimed mining landforms is being addressed. Sixty-nine publications were reviewed across several disciplines or focal areas including surface water, groundwater, climate change, geotechnical engineering, soils and covers, regulatory or technical guidance, vegetation, wildlife and pit lakes.

Results and findings

A selection of the findings from the literature review is presented below.

Finding #1

The concept of landform evolution is not explicitly discussed in the guidance or regulatory documents that were reviewed. However, several of the documents reviewed include mention or consideration of some aspects of long-term change pertaining to landforms.

Reviewed documents commonly speak to closure landforms needing to be geotechnically stable, geochemically non-polluting or stable, and ecologically sustainable. Several documents also identify using a risk-based approach for managing change. Documents that included some mention or consideration of long-term change in landforms are presented in Table 2 (Appendix A).

Finding #2

The concept of landform evolution is not explicitly presented in Alberta's Environment Protection and Enhancement Act (EPEA) operating approvals for oil sands mines. However, approvals provide direction concerning several landform evolution processes and identify selected activities useful for the prediction of landform evolution.

In the EPEA approvals reviewed, operators are directed to consider several kinds of long-term change through prescribed research and development programs, and through operational/progressive reclamation or reclamation and closure planning guidance. Landform evolution processes noted in EPEA approvals include:

- consolidation and settlement;
- erosion;
- retrogressing shorelines (pit lakes);
- migration of tailings release water and its potential effects on sediments, groundwater, or vegetation;

- long-term chemistry and mineralogy of tailings;
- long-term physical and chemical stability of tailings additives (coagulants and flocculants); and
- degradation of substances of concern in tailings release water or in pit lakes.

Reference to climate change was less common, though some approvals directed the consideration of climate change on the hydrologic sustainability assessment of aquatic closure features (i.e., lakes and wetlands) (AER, 2017; 2018; 2019).

Operating approvals commonly require the pre-disturbance landscape be used as a reference for mine reclamation and closure planning, for example, in the context of:

- the distribution of upland ecosite phases and wetland types;
- forest characteristics (equivalent areas, and potentially also: types of ecosystems, forest stand structure, forest growth, yield); and
- fish and wildlife habitats or habitat levels.

Operating approvals also regularly include mention of activities that will support landform evolution prediction, for example:

- construction and monitoring of pilot wetlands;
- use of benchmark sites in ecosystems that will be re-created in the reclaimed landscape, to evaluate and monitor biodiversity;
- use of natural undisturbed wetlands as reference sites for reclaimed wetlands; and
- use of fish and wildlife habitat suitability models.

Thus, EPEA approvals and regulations, which are based on a model of meeting locally common boreal forest ecosystems in the reclaimed landscape compared to that of pre-disturbance conditions, provide little guidance on how to manage landform evolution.

Finding #3

The literature identified many methods for predicting landform evolution processes. Examples of prediction methods or tools for prediction presented include:

Modelling

- Landform evolution and/or erosion models (e.g., SIBERIA, CAESAR-Lisflood, GeoFluv);
- climate change models;
- climate envelope models for species distribution;
- consolidation models;
- slope stability and deformation analyses;

- end pit lake models;
- habitat suitability index models;
- understory establishment conceptual models (i.e., initial floristics, relay floristics models); and
- forest growth-and-yield models.

Laboratory testing

- Consolidation testing;
- soil characterization for susceptibility to erosion;
- flume tests (erosion); and
- static and kinetic tests for metal leaching/acid rock drainage (ML/ARD).

Field tests

- Flume tests (erosion);
- test sites including progressive reclamation sites and demonstration pit lakes; and
- reference sites/natural analogs.

In the authors' experience, many of these methods are already part of the state-of-practice for design of earth structures.

Finding #4

Designing for landform evolution is being conducted (or guidance being provided) in some parts of the world, notably Australia, and in the Alberta oil sands.

In the authors' experience, designing for landform evolution is not commonplace in the mining industry. Where practiced, it is generally under the banner of "geomorphic design" and mostly relates to the design of channels and dump slopes, using natural analogues and stream hydrology patterns / modelling (e.g., Zeedyk and Clothier, 2014). Design guidance to accommodate landform evolutionary change was however found in the literature and covered the following processes:

- consolidation, settlement;
- landslides;
- erosion, sedimentation, bank scour, stream aggradation;
- retrograding shorelines;
- channel blockage (including caused by beaver activity);
- stream avulsion and flooding;
- wildlife succession/recolonization;

- vegetation succession;
- vegetative change due to wildfire;
- water level changes; and
- soil salinization, salt leaching, ML/ARD.

Additional tools presented in the literature that could be used to support design for evolutionary change include post-closure monitoring with some form of management plan (e.g., trigger action response plans) (e.g., Eaton et al., 2014; Environment Canada, 2009; Fair et al., 2014; Foster et al., 2017; Grant et al., 2016; Intergovernmental Forum on Mining, Minerals, Metals and Sustainable Development, 2013; Trites et al., 2012).

Landform design teams often design for landform evolution, but often the design reports are often not specific in this regard.

Finding #5

Landforms are non-static and instead experience change over a spectrum of timeframes.

Landforms experience change:

- on a seasonal basis (e.g., watercourse or groundwater levels);
- over decades (e.g., establishment of seedlings in reclamation plots (Cranston and Waterman, 2015);
- over centuries (e.g., flushing of salts from tailings [CEMA, 2012], consolidation of tailings); and
- potentially on an ongoing and continuous basis (e.g., changes resulting from a changing climate).

One type of change may stimulate another type of change. For example, climate change may influence vegetation and/or water temperatures, affecting permafrost, affecting stability of landforms or landform elements (AANDC and MVLWB, 2013). Thus, the concept of an equilibrated, static reclaimed landform or landscape is unrealistic.

Landform evolution processes as part of landform design

In the authors' experience state-of-the-art landform design includes addressing select processes. "Addressing" in this context means considering each process, and formally deciding whether or not to design or maintain the landform to deal with this change, whether to allow performance to change over. Designing to accommodate or manage these processes is complicated by differences in local conditions: different mines are located in different climatic zones (e.g., INAP, 2017), the properties of mine waste vary considerably from site to site, and the regulatory environment and expectations of local communities also vary. For some processes (e.g., tailings consolidation), there is a good understanding of the mechanisms, there are predictive tools for long-term performance, and there is available design guidance. But other landform evolution processes are not well understood (e.g., the rate and impacts of polymer treated tailings

strength changes with time) or there is limited experience with site-specific conditions and are thus more challenging to include in design.

In the authors' opinion, there is an opportunity to improve the state-of-practice by assessing each landform evolution process in Table 1, developing a better understanding of the process, creating better predictive tools, publishing design guidance, and compiling case histories and observations on long-term performance for a variety of climate conditions and mine waste properties. A focussed effort over the next decade would benefit the state-of-practice in landform design and allow design and construction of landforms and landscapes to more reliably meet agreed-upon goals and objectives, even as the landforms continue to evolve.

Addressing landform evolution in design and management

Landforms in the oil sands post-closure landscape will evolve over long timeframes – over hundreds or thousands of years. The impacts of landform evolution processes can be complex and there will be interactions between various processes (e.g., settlement leading to ponding leading to changes in vegetation that all affect water balance) adding to the complexity of net impacts. Inherent in this complexity is uncertainty in predictions that attempt to link landform evolution processes to landscape performance.

The use of a design basis memorandum (DBM) is one method for creating a common vision and understanding for landform design, construction, reclamation, monitoring and maintenance (Ansah-Sam et al., 2016). The landform evolution processes listed in Table 1 could be screened, and the key processes formally addressed in the DBM. For example, settlement of soft tailings can be evaluated and the design updated to accommodate the expected settlement. Similarly, inevitable ecological succession could be predicted and embraced by designers, regulators, and local communities.

Inclusion of landform evolution in a DBM is envisioned to include the following:

- Designing landforms with consideration and anticipation of landform evolution (e.g., inclusion of boulders buried in a shoreline, which can be exposed due to future erosion processes, self-armouring the shoreline).
- Defining landform performance objectives that consider landform evolution processes.
- Developing an adaptive management plan to accommodate situations where the performance fails to meet agreed-upon objectives.
- Developing and implementing a landform monitoring and maintenance plan to measure landform performance and correct deficiencies using pre-planned and funded contingencies.

Including landform evolution as part of the DBM could lead to a reclaimed landform that anticipates landform evolution, with better potential alignment between performance and design. In addition, a DBM

could create clarity for others (e.g., Indigenous Peoples, local communities, regulators) concerning the landform design process and the considerations inherent to that process.

Adaptive management, using the framework of pre-planned contingencies as outlined in the geotechnical observational method (Peck, 1969), is a central tool in landform design (CEMA, 2012). Best practice would see the landform design process follow an adaptive management approach of designing for the expected conditions, constructing the landform to adapt to potential evolution processes if they occur, developing contingency designs in advance, then monitoring the landform to allow timely implementation of the contingencies should they be necessary to meet agreed-upon landscape performance goals and objectives. If monitoring results over a sufficient period of time indicate observed behaviour within predicted ranges, that is, that the landform was largely evolving in the predicted and designed for manner, a case could be made for certification of that landform. If monitoring results indicate observed behaviour that deviates from predicted ranges, the prediction method itself might need to be re-assessed or active management used to restore the landform to the predicted trajectory with additional, follow-up monitoring. In some cases, goals and objectives might need be reframed.

Conclusion

The following conclusions are drawn from this concept review:

- The evolution of landscapes and landforms over time through geomorphic processes is an inherent part of natural systems. The landforms created by oil sands reclamation activities will become part of the natural systems and will evolve over time predominantly through these natural processes. The science discipline of geomorphology was consulted in this study to provide a framework to communicate the processes that will be active. Using natural process as a baseline will allow operators, designers, regulators, Indigenous Peoples, and local communities to evaluate performance over time.
- A definition for landform evolution, in the context of mining reclamation, has been created. Defining this term allows for clear communication of the concept of landform evolution.
- Six categories of landform evolution processes and many specific processes have been identified that are relevant to the oil sands mining post-closure landscape. The list of landform evolution processes can be used to set landform design goals and objectives as part of a design basis, as a checklist for landform design projects and/or adaptive management programs.
- A review of publicly available literature found that the concept of landform evolution is not explicitly discussed in technical guidance or regulatory documents, though several guidance and regulatory documents made reference to some aspect of long-term change.

- Many publications were found that identified prediction tools for landform evolution processes, including models and laboratory and field tests, or included some design guidance for addressing landform evolution processes.
- There are inherent limitations to prediction of complex environmental systems (such as reclaimed landforms and landscapes) supporting the need for a comprehensive adaptive management system as part of the design, construction, and monitoring/maintenance of reclaimed lands in the oil sands.

Acknowledgements

The authors gratefully acknowledge the funding and support provided by COSIA to complete this work.

References

Aboriginal Affairs and Northern Development Canada (AANDC) and Mackenzie Valley Land and Water Board (MVLWB). 2013. Guidelines for the closure and reclamation of advanced mineral exploration and mine sites in the Northwest Territories. Retrieved from https://mvlwb.com/sites/default/files/documents/wg/WLWB_5363_ Guidelines_Closure_Reclamation_WR.pdf

Alberta Energy Regulator (AER). 2017. *Amending Approval, Alberta Energy Regulator, Environmental Protection and Enhancement Act R.S.A. 2000 c.E-12, as amended.* Approval #94-02-18.

Alberta Energy Regulator (AER). 2018. *Approval, Alberta Energy Regulator, Environmental Protection and Enhancement Act R.S.A. 2000 c.E-12, as amended.* Approval #046586-01-00.

Alberta Energy Regulator (AER). 2019. *Amending Approval, Alberta Energy Regulator, Environmental Protection and Enhancement Act R.S.A. 2000 c.E-12, as amended.* Approval #151469-01-01.

Alberta Environment. 2010. *Guidelines for Reclamation to Forest Vegetation in the Athabasca Oil Sands Region,* second edition. Fort McMurray, Alberta, Canada: Terrestrial Subgroup of the Reclamation Working Group of the Cumulative Environmental Management Association. Retrieved from https://open.alberta.ca/publications/9780778588252.

Ansah-Sam, M., L. Hachey, G. McKenna and B. Mooder. 2016. The DBM approach for setting engineering design criteria for an oil sands mine closure plan. Fifth International Oil Sands Tailings Conference.

Cranston, B.H. and L.P. Waterman. 2015. Assessing the level of difficulty of vegetation establishment on reclaimed sites. In A.B. Fourie, D. Tibbett, L. Sawatsky and D. van Zyl, editors. *Mine Closure 2015. Proceedings of the 10th International Seminar on Mine Closure:* Vancouver, Canada: InfoMine Inc.: 1125–1136.

Creasey, R. 2012. *Professional Judgment in Mineable Oil Sands Reclamation Certification: Workshop Summary*. Edmonton, Alberta: Oil Sands Research and Information Network, University of Alberta, School of Energy and the Environment.

Cumulative Environmental Management Association (CEMA). 2012. *End pit lakes guidance document 2012*. Fort McMurray, Alberta, Canada: Cumulative Environmental Management Association.

Cumulative Environmental Management Association (CEMA). 2014. *Guidelines for wetlands establishment on reclaimed oil sands leases, third edition*. Fort McMurray, Alberta, Canada: Cumulative Environmental Management Association.

Eaton, B.R., J.T. Fisher, G.T. McKenna and J. Pollard J. 2014. *An ecological framework for wildlife habitat design for oil sands mine reclamation* (OSRIN Report No. TR-67). Edmonton, Alberta: Oil sands research and information network, University of Alberta, School of Energy and the Environment.

Encyclopedia Britannica. Landform evolution, *Encyclopedia Britannica,* June 28, 2019. Retrieved from https://www.britannica.com/science/landform-evolution

Environment Canada. 2009. *Environmental code of practice for metal mines.* Retrieved from https://www.ec.gc.ca/lcpe-cepa/documents/codes/mm/mm-eng.pdf

Fair, J.M., J. Pollard and G. McKenna. 2014. Reclaimed closure landscapes: The importance and benefits of operations maintenance and monitoring. British Columbia Mine Reclamation Symposium. doi:http://dx.doi.org/10.14288/1.0042668

Foster, K.R., C.M. Godwin, P. Pyle and J. Saracco. 2017. Reclamation and habitat-disturbance effects on landbird abundance and productivity indices in the oil sands region of northeastern Alberta, Canada. *Restoration Ecology (Open Access)* 25(4): 532–538.

Government of Alberta. 2018. Alberta issues first-ever oil sands land reclamation certificate, Government of Alberta. March 19, 2008, Retrieved from https://www.alberta.ca/release.cfm?xID=23196C8880E90-A0E1-9CE0-1B3799BC38A51E3E

Grant, C., N. McCaffrey, D. Doley, R.J. Loch and S. Anstee S. 2016. *Mine Rehabilitation: Leading Practice Sustainable Development Program for the Mining Industry.* Commonwealth of Australia. Retrieved from https://www.researchgate.net/profile/Nic_Mccaffrey2/publication/310560937_Mine_Rehabilitation_Leading_Practice_Sustainable_Development_Program_for_the_Mining_Industry/links/5831891408ae004f74c27651/Mine-Rehabilitation-Leading-Practice-Sustainable-Development-Program-for-the-Mining-Industry.pdf?origin=publication_detail

INAP. 2017. *Global cover system design – technical guidance document* (report). Retrieved from http://www.inap.com.au/wp-content/uploads/2018/05/global-cover-system-design.pdf

Intergovernmental Forum on Mining, Minerals, Metals and Sustainable Development (IGF). 2013. *IGF mining policy framework, mining and sustainable development.* Retrieved from https://www.igfmining.org/wp-content/uploads/2018/08/MPF-EN.pdf

McKenna, G. 2002. Sustainable mine reclamation and landscape engineering. PhD dissertation, University of Alberta.

MEND. 2012. *Cold regions cover system design technical guidance document* (report). Retrieved from https://mvlwb.com/sites/default/files/mvlwb/documents/Cold%20Regions%20Cover%20System%20Design%20Technical%20Guidance%20Document%20(MEND%20Report%201.16.5c).pdf

Peck, R.B. 1969. Advantages and limitation of the observation method in applied soil mechanics. *Geotechnique*. 19(2): 171–187.

Pollard, J.A. and G. McKenna. 2018. Design of landform elements for mine reclamation. British Columbia Mine Reclamation Symposium. doi:http://dx.doi.org/10.14288/1.0374933.

Slingerland, N.M. 2019. Geomorphic landform design and long-term assessment of tailings storage facilities in the Athabasca oil sands. PhD disseration, University of Alberta.

Trites, M., T. Charette, J. Hornung, G. Haekel and C. Wytrykush. 2012. *Oil Sands Marshes: A Knowledge Transfer*. Fort McMurray, Alberata: Cumulative Environmental Management Association.

Zeedyk, B. and V. Clothier. 2014. *Let the Water Do the Work: Induced Meandering, an Evolving Method for Restoring Incised Channels.* White River Junction, VT: Chelsea Green Publishing.

Appendix A

Table 1: Landform evolution processes in the oil sands

Process type	Causal factors	Processes
Mass wasting	Gravity	Dyke collapse/loss of containment
		Landsliding
		Slumping
		Flow-sliding
		Soil creep/solifluction
		Settlement of dumps and dykes
		Tailings consolidation
Erosion and deposition	Surface water	General erosion
		Sheet erosion
		Rill/gully erosion
		Channel degradation/scour
		Riprap degradation
		Channel avulsion
		Channel blockage
		Stream/wetland aggradation
		Fan deposition
		Flooding
	Wave-action	Shoreline erosion/regression
		Sediment deposition at lake/wetland inlets or shoreline
	Groundwater	Spring sapping
		Piping/tunnel erosion
		Spring emergence or loss
		Failure of internal dyke drains
	Aeolian	Wind erosion and deposition
Weathering	Chemical	Soil nutrient or carbon cycle changes
		Salt leaching
		Acid rock drainage (ARD) and metal leaching
		Tailings polymer degradation
		Coke oxidation/combustion
		Gas generation
		Contamination by oil sands process-affected water (OSPW) seepage
		Soil salinization/sodification
		Karst development

Table 2 continued: Landform evolution processes in the oil sands

Process type	Causal factors	Processes
	Biological	Soil formation
	Physical	Soil detrital layer accumulation or loss
		Frost action/freeze thaw
		Thawing of frozen fills or natural permafrost
Disturbance	Natural and anthropogenic	Wildfire
		Plant disease, pests
		Wildlife (grazing/browsing)
		Burrowing
		Invasive plant or wildlife species
		Human land use impacts
		Recreational land use
		Commercial land use
		Mining, re-mining, forestry, or other industrial activity
Hydrologic and climatic	Surface water and groundwater	Watershed hydrograph change
		Watershed water balance change
		Pit lake water balance change
		Lake overturning
		Lake meromixis
		Groundwater level change
		Groundwater flow direction change
Ecological	Vegetation and wildlife communities	Lake ecology change
		Ecological succession
		Wildlife succession/re-colonization
		Species re-introduction
		Appearance of invasive species
		Local extinction (extirpation)

Table 2: Guidance or regulatory documents that included some mention or consideration of long-term change in landforms

Document	Reference
Northern Mine Decommissioning and Reclamation Guidelines	Government of Saskatchewan, Ministry of Environment. 2008. *Northern mine decommissioning and reclamation guidelines.* http://publications.gov.sk.ca/documents/66/96788-Northern%20Mine%20Decomissioning%20and%20Reclamation%20Guidelines.pdf
Guidelines for the Closure and Reclamation of Advanced Mineral Exploration and Mine Sites in the Northwest Territories	AANDC and MVLWB (2013)
Environmental code of practice for metal mines	Environment Canada (2009)
Pit lakes guidance document 2012	CEMA (2012)
De-licensing of oil sands tailings dams – Technical guidance document	Oil Sands Tailings Dam Committee. 2014. *De-licensing of oil sands tailings dams – Technical guidance document*. https://doi.org/10.7939/R3QJ7811S
Guidelines on tailings dams, planning, design, construction, operation and closure	Australian National Committee on Large Dams Incorporated. 2012. *Guidelines on tailings dams. Planning, design, construction, operation and closure*. Australia: Australian National Committee on Large Dams Incorporated.
Guidelines for Preparing Mine Closure Plans	Government of Western Australia Department of Mines and Petroleum and Environmental Protection Authority. 2015. *Guidelines for preparing mine closure plans*. http://www.dmp.wa.gov.au/Documents/Environment/ENV-MEB-121.pdf
A Guide to the Management of Tailings Facilities	Mining Association of Canada. 2017. *A guide to the management of tailings facilities. Third edition*. http://mining.ca/sites/default/files/documents/MAC-Guide-to-the-Management-of-Tailings-Facilities-2017.pdf
Mine Closure, Checklist for Governments	Asia-Pacific Economic Corporation . 2018. *Mine closure, checklist for governments*. https://www.apec.org/Publications/2018/03/Mine-ClosureChecklist-for-Governments
Mine Rehabilitation: Leading Practice Sustainable Development Program for the Mining Industry	Grant et al. (2016)
Guidelines for Reclamation to Forest Vegetation in the Athabasca Oil Sands Region	Alberta Environment (2010)

Note: Abbreviated references are listed in the References section.

Proceedings of Tailings and Mine Waste 2019
November 17–20, 2019, Vancouver, Canada
Published by the University of British Columbia, 2019

Numerical Modelling of Groundwater Flow and Contaminant Transport at the Myra Falls Mine Site

Mahmoud Hussein, Robertson GeoConsultants Inc., Canada
Paul Ferguson, Robertson GeoConsultants Inc., Canada
Christoph Wels, Robertson GeoConsultants Inc., Canada
Nicole Pesonen, Nyrstar Myra Falls, Canada

Abstract

This paper describes a numerical groundwater flow and transport model developed using the software MODFLOW/MT3D to simulate the movement of groundwater and the transport of zinc (Zn) in the Myra Valley Aquifer (MVA). The groundwater model is a numerical representation of a hydrogeological conceptual site model described in a companion paper by Ferguson et al. (2019).

Groundwater conditions in the MVA during low-flow and high-flow periods are reproduced very well by the groundwater model. Key sources of Zn, and other constituents, are the Lynx TDF berm, sources in the Mill area, and WRDs #1 and #6. The calibrated Zn plume is reasonably representative of conditions prior to the operation of the Lynx Seepage Interception System (SIS) and suggests most impacted groundwater that reports to Myra Creek originates near the Lynx Tailings Disposal Facility (TDF) and in the Upper Old TDF reach.

Operating the Phase I Lynx SIS is predicted to substantially reduce Zn concentrations in groundwater and Zn load to the Old TDF under-drains. The Zn load to Myra Creek from groundwater is predicted to decrease by two orders of magnitude within 6 to 12 months. The Zn load intercepted by the Old TDF under-drains is predicted to decline more gradually and may reach new steady-state conditions within two to five years due to the larger travel distance.

Modelling objectives

The specific objectives of the numerical modelling work presented in this paper are:

- To develop a numerical groundwater flow and transport model that mathematically represents the conceptual hydrogeological model for the site.
- To simulate current groundwater flows and Zn concentrations in the MVA and Zn loading to Pumphouse No.4, the SIS and Myra Creek during low-flow and high-flow conditions.

- To predict groundwater flows and Zn loads in the MVA and to the SIS and Myra Creek during future operation of the Phase I Lynx SIS.

Model setup

Model domain

Boundaries of the numerical model domain are shown in Figure 1. The numerical model domain covers the valley floor and lower side slopes of Myra Valley with a total surface area of approximately 2.6 km^2. The model extends about 3.3 km in the east-west direction and 1.1 km in the north-south direction, up to a maximum elevation of 3,500 m mine datum on the valley side slopes.

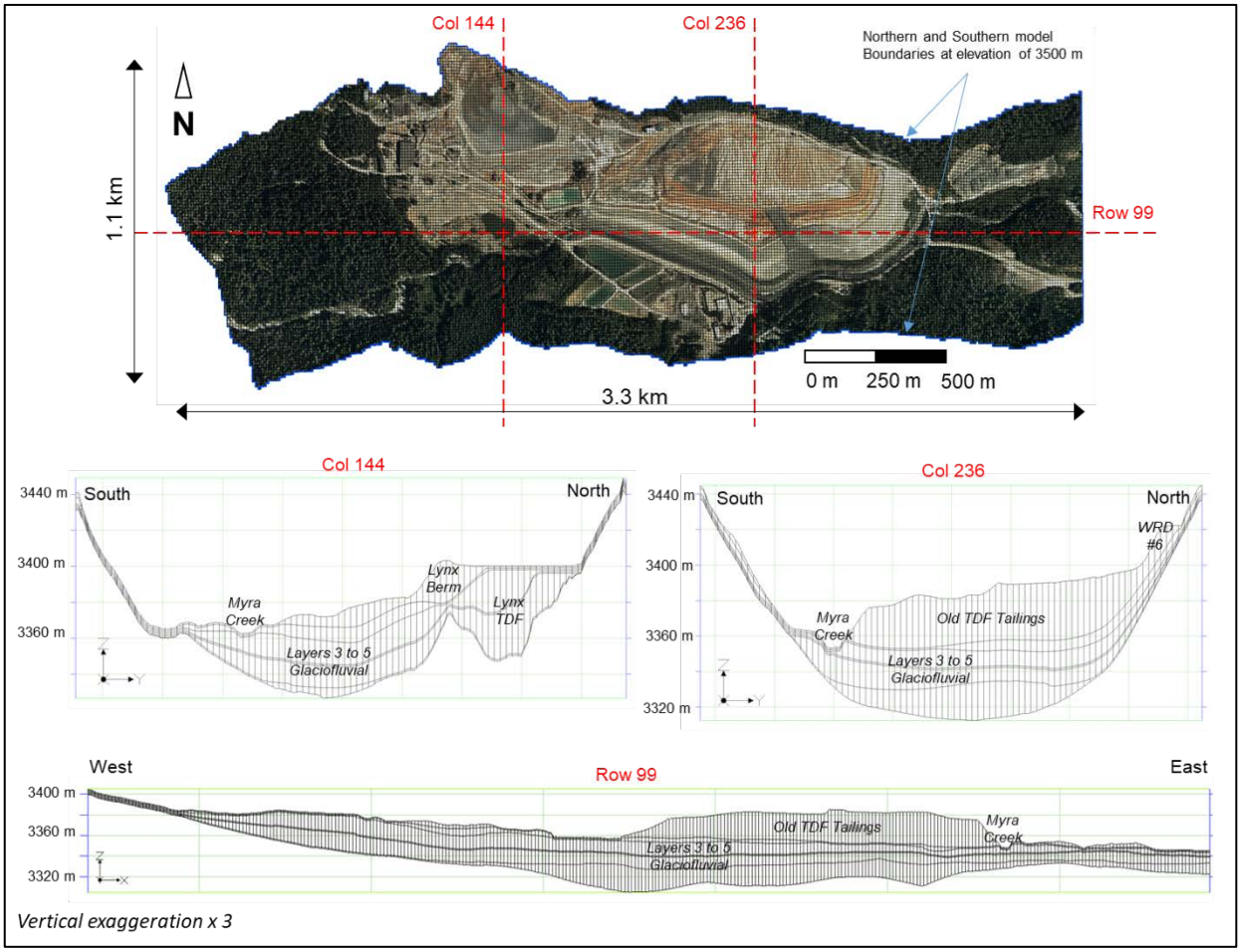

Figure 1: Model domain and 2D cross sections of finite difference grid

Grid design and spatial discretization

The model domain was discretized spatially into a uniform grid of 10 m by 10 m and vertically into 6 layers, with layer 1 representing mine waste units (tailings, waste rock, berms) and layers 2 to 6 representing valley and side hill sediments. Figure 1 shows 2D cross sections of the finite difference grid. Surface topography from a recent Lidar survey was used to define the top of Layer 1. The bottom surfaces for all model layers

were created to primarily align with observed elevations of defined hydrostratigraphic units derived from 148 borehole logs, which were integrated from different previous investigations.

Temporal discretization

Low-flow and high-flow conditions were simulated as steady-state snapshots in time and were calibrated to available heads and fluxes observed on March 30, 2018 and January 24, 2018, respectively. The transport model was set up to run transiently for the period from 2003 to March 2018 based on the validated low-flow field with the Lynx SIS wells not operating. In other words, the plume is numerically developed over 15 years assuming a fixed-flow field which represents low-flow conditions prior to the operation of the Lynx SIS wells.

Flow and transport boundary conditions

The numerical implementation of flow and transport boundary conditions along the perimeter of the model domain is illustrated in Figure 2. Groundwater recharge to the northern and southern model boundaries was simulated using specified flux boundary conditions (using the WEL package) across all model layers. Eastern and Western model boundaries were simulated using the specified head package (CHD).

Internal sources and sinks

Internal sources and sinks represent internal boundary conditions where water can enter or exit the groundwater model. The MVA model includes the following internal sources and sinks (see Figure 2):

- The river package (RIV) was used to simulate Myra Creek through the assignment of a riverbed conductance and stage head.
- The drain package (DRN) was used to represent the system of gravity-fed drains beneath the Old TDF by assigning drain cells with a drain conductance set high enough to not restrict flow, and at locations and head elevations as per design drawings.
- The Multi-Node-Well Package (MNW2) was used to simulate the disconnected Outer Drain as a horizontal well, or connected linear feature, with a pumping rate of zero.
- The MNW2 package was also used to simulate pumping of the Phase I Lynx SIS wells PW14-01, PW14-03 and PW14-04.
- The Specified Head package (CHD) was used to simulate the Lynx TDF assuming tailings are fully saturated at an elevation of 3,400 m.
- Specified flux boundary conditions (WEL) were used to simulate recharge from Arnica Creek and Lynx Ditch.
- The recharge package (RCH) was used to simulate recharge rates and source terms concentrations.

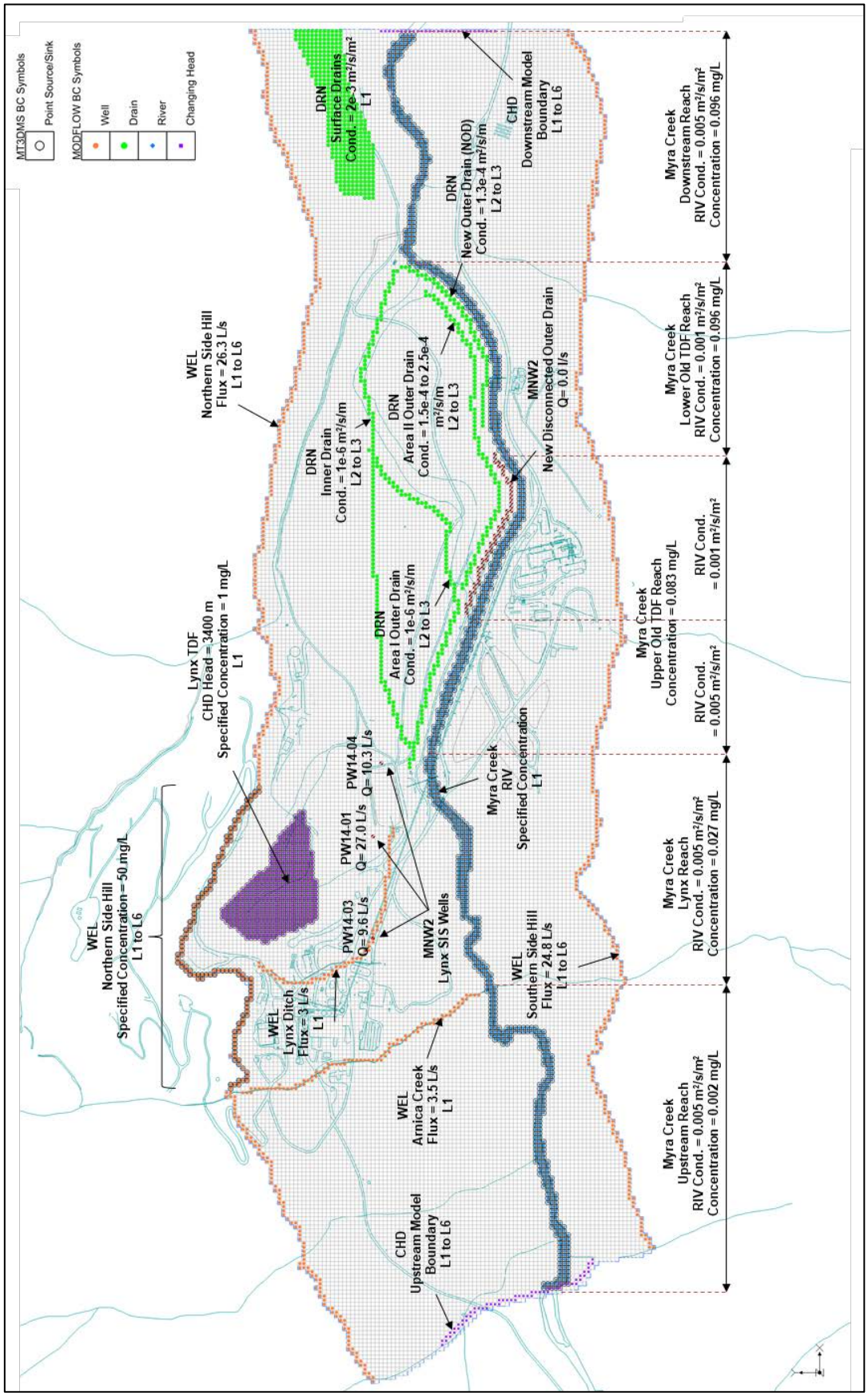

Figure 2: Boundary conditions and internal sources and sinks

Model calibration

Calibration targets

The numerical groundwater flow and transport model ("MODFLOW/MT3D model") was calibrated to:

- Observed groundwater levels on January 24, 2018 (high-flow conditions) and March 30, 2018 (low-flow conditions)
- Estimated flows and Zn loads collected by the Old TDF under-drains via Pumphouse No. 4 (Table 1)
- Zn concentrations in the MVA observed between 2015 and 2017, and
- Estimated Zn loads discharging from MVA to Myra Creek during high and low-flow periods (Table 1).

Table 1: Estimated versus simulated Zn loads intercepted in the old TDF under-drains and bypassing to Myra Creek

	Low-flow calibration				High-flow calibration			
	Flow (L/s)		(Zn) Load (t/year)		Flow (L/s)		(Zn) Load (t/year)	
	Estimated	Simulated	Estimated	Simulated	Estimated	Simulated	Estimated	Simulated
Discharge to Pumphouse No. 4								
Inner drain	6.6	5.6	5.8	6.5	11.8	12.5	10.4	14.5
Area II Outer D_Upper	36.5	20.6	2.3	3.0	64.9	46.7	4.1	6.0
Area II Outer D_Lower	36.5	50.0	13.8	10.9	64.9	90.3	24.6	29.2
NOD Long D	36.5	35.8	3.5	4.6	64.9	49.5	6.1	5.9
NOD Medium D	19.9	21.4	3.8	2.1	35.4	29.9	6.7	2.6
NOD Short D	3.3	4.7	0.1	0.1	5.9	6.4	0.3	0.2
Sub Total	139.3	137.9	29.3	27.1	247.7	235.2	52.2	58.3
Discharge to Myra Creek								
Upstream Reach	–	125.8	0.1	0.0	–	159.3	0.4	0.0
Lynx Reach	–	74.7	2.1	2.4	–	83.0	6.5	5.2
Upper Old TDF reach	–	44.0	4.0	4.0	–	22.2	4.0	7.7
Lower Old TDF reach	–	16.0	0.9	0.0	–	9.0	1.5	0.0
Sub total	–	260.6	7.1	6.5	–	273.5	12.4	12.9

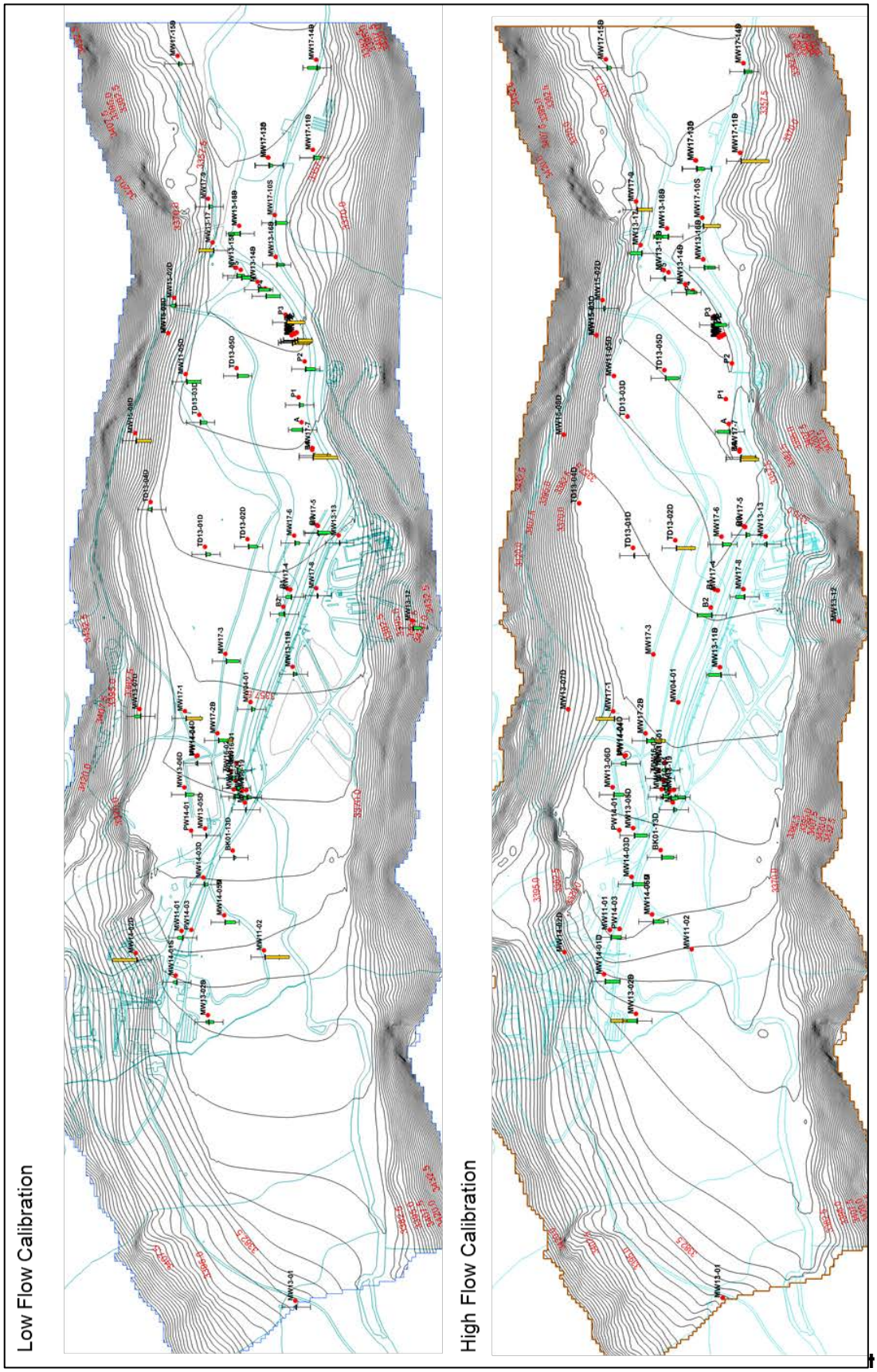

Figure 3: Spatial distribution of heads calibration error for low-flow and high-flow simulations

Calibration statistics

Overall, the calibration of the flow model (MODFLOW) is considered very good for both low-flow calibration and validation (Normalized root-mean-square error, NRSME <1.5%) and for high-flow calibration (NRSME of ~3%). Both calibrations have a consistent bias with a negative residual mean of ~0.3 m, which is largely dominated by the heads in the Old TDF area being somewhat underestimated in model simulations (Figure 3). This is partially due to the significant control on simulated heads in this area by the Old TDF under-drains (DRN cells) and moderation by Myra Creek head stage (RIV cells). In addition, the size of model grid cells (10 m × 10 m) limited the spatial resolution of the flow solution, particularly in the area between the New Outer Drain and Myra Creek where simulated heads at all drain risers are consistently underestimated.

Considering the scale and complexity of the transport problem and the simplified representation in the numerical model (cell size, equivalent porous medium approach and simplified conditions of the warmup period), calibration statistics (NRSME of <14%) are considered satisfactory.

Table 1 compares the simulated Zn loads intercepted in the Old TDF under-drains and bypassing to Myra Creek to target loads inferred for low-flow and high-flow conditions. The calibrated model matches the inferred target Zn loads reasonably well.

Calibrated recharge and material properties

Figure 4 shows calibrated recharge rates and source term concentrations. For low-flow conditions, the calibrated recharge rates ranged from a low of 140 mm/year for undisturbed areas to a maximum of 1436 mm/year for WRDs #1 and #6 and the Lynx berm. For high flow, the calibrated recharge rates ranged from a low of ~1 mm/day for undisturbed areas to a maximum of 17.7 mm/day for WRDs #1 and #6 and the Lynx berm. Note that units for recharge during low-flow periods was calculated as a percentage of annual precipitation as it is the more dominant condition. Recharge during high-flow periods is treated as a short term condition in which groundwater recharge was calculated as the percentage of a high precipitation event.

The calibrated K values for the various hydrostratigraphic units generally fall within the observed range of K values for those units. As expected, the glaciofluvial sediments comprise the most permeable aquifer unit in the MVA. The calibrated K for the glaciofluvial sediments in the shallow aquifer (model layer 3) ranges from 5×10^{-5} m/s to 5.5×10^{-4} m/s. The calibrated K for the glaciofluvial sediments in the deep aquifer (model layer 5) ranges from 5×10^{-5} m/s to 2×10^{-4}. On the hillsides, the calibrated K varies from a low of $\sim1\times10^{-7}$ m/s for basal till to a high of $\sim5\times10^{-4}$ m/s for sidehill colluvium. The lateral till unit has an intermediate K ranging from $\sim5\times10^{-6}$ m/s to $\sim2\times10^{-5}$ m/s.

Calibrated model results (current conditions)

Simulated heads and Zn plume

The simulated flow field and Zn plume of the MODFLOW/MT3D model layer 3 are shown in Figure 5a for the "base case", i.e. current conditions prior to start of pumping in the Lynx Reach. This plume approximates pseudo steady state conditions, assuming steady groundwater flow and constant Zn loading (for low-flow conditions) and continuous operation of the Old TDF under-drain system.

The simulated flow field and Zn plume compare reasonably well to the delineated flow field and Zn plume during conceptual modelling (Ferguson et al., 2019) and illustrates how the major Zn sources, i.e. WRDs #1 and #6, the Lynx TDF embankment berm, and sources in the mill area, contribute to groundwater quality impacts.

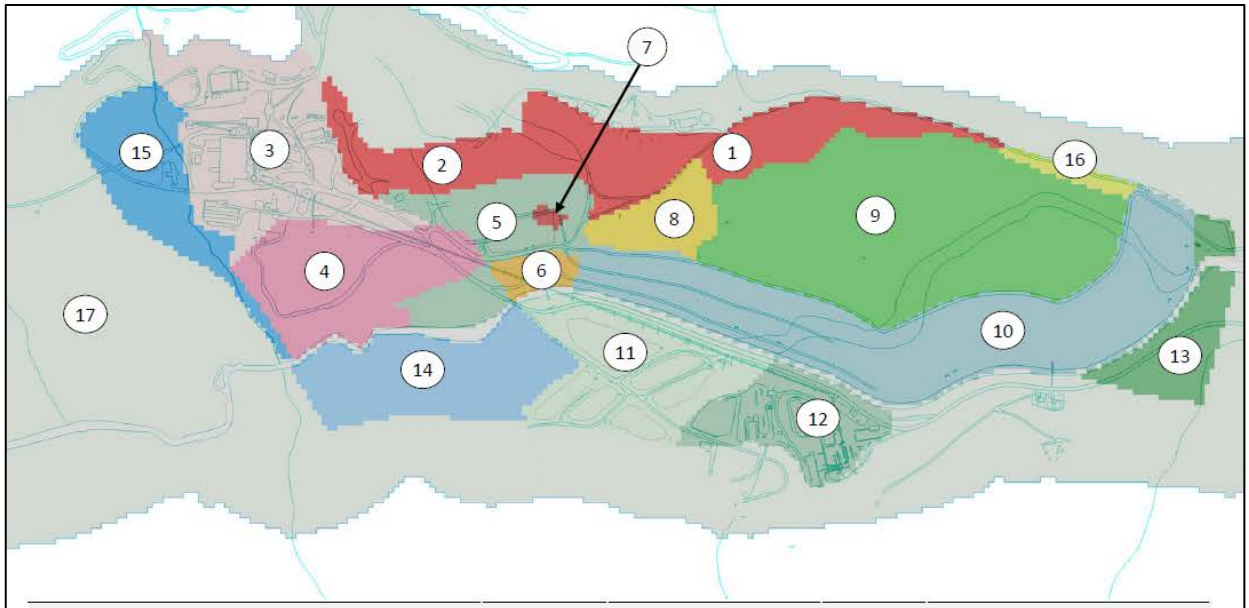

Zone #	Area	Recharge (Low Flow)			Recharge (High Flow)			Zn Conc (mg/L)
		m/s	mm/year	% of MAP	m/s	mm/day	% of 35 mm/day*	
1	WRD#1, WRD#6	4.55E-08	1435.9	57.9	2.05E-07	17.7	50.5	125
2	Lynx Berm	4.55E-08	1435.9	57.9	2.05E-07	17.7	50.5	110
3	Mill Area	2.73E-08	861.5	34.7	1.31E-07	11.3	32.2	15
4	Former ETA/Cookhouse	2.90E-08	915.2	36.9	1.31E-07	11.3	32.2	12
5	Super Pond	2.00E-08	631.2	25.4	1.31E-07	11.3	32.2	7
6	Super Pond South	2.50E-08	788.9	31.8	1.13E-07	9.7	27.8	7
7	Perched Zone	2.50E-07	-	-	3.00E-07	-	-	150
8	Former RSA	2.45E-08	773.2	31.2	1.10E-07	9.5	27.2	25
9	OLD TDF Tailings	9.51E-09	300.0	12.1	9.51E-09	0.8	2.3	0.03
10	Seismic Upgrade Berm	1.56E-08	492.4	19.9	1.56E-08	1.3	3.9	5
11	Polishing Ponds	8.35E-09	263.6	10.6	8.35E-09	0.7	2.1	0.004
12	HW Offices	2.00E-08	631.2	25.4	9.00E-08	7.8	22.2	12
13	Downstream of NOD	1.11E-08	350.4	14.1	1.07E-07	9.2	26.4	0.004
14	South of ETA and Myra Creek	1.58E-08	497.6	20.1	1.58E-08	1.4	3.9	0.004
15	West of Arnica Creek	1.75E-08	550.8	22.2	1.75E-08	1.5	4.3	0
16	PAG Rockfill	2.38E-08	750.0	30.2	3.50E-08	3.0	8.6	20
17	Other	4.50E-09	142.0	5.7	1.35E-08	1.2	3.3	0

** 35 mm/day is the average precipitation rate over the week prior to the high flow calibration date (24th January 2018)*

Figure 4: Recharge rates and specified Zn concentrations for low-flow and high-flow calibration

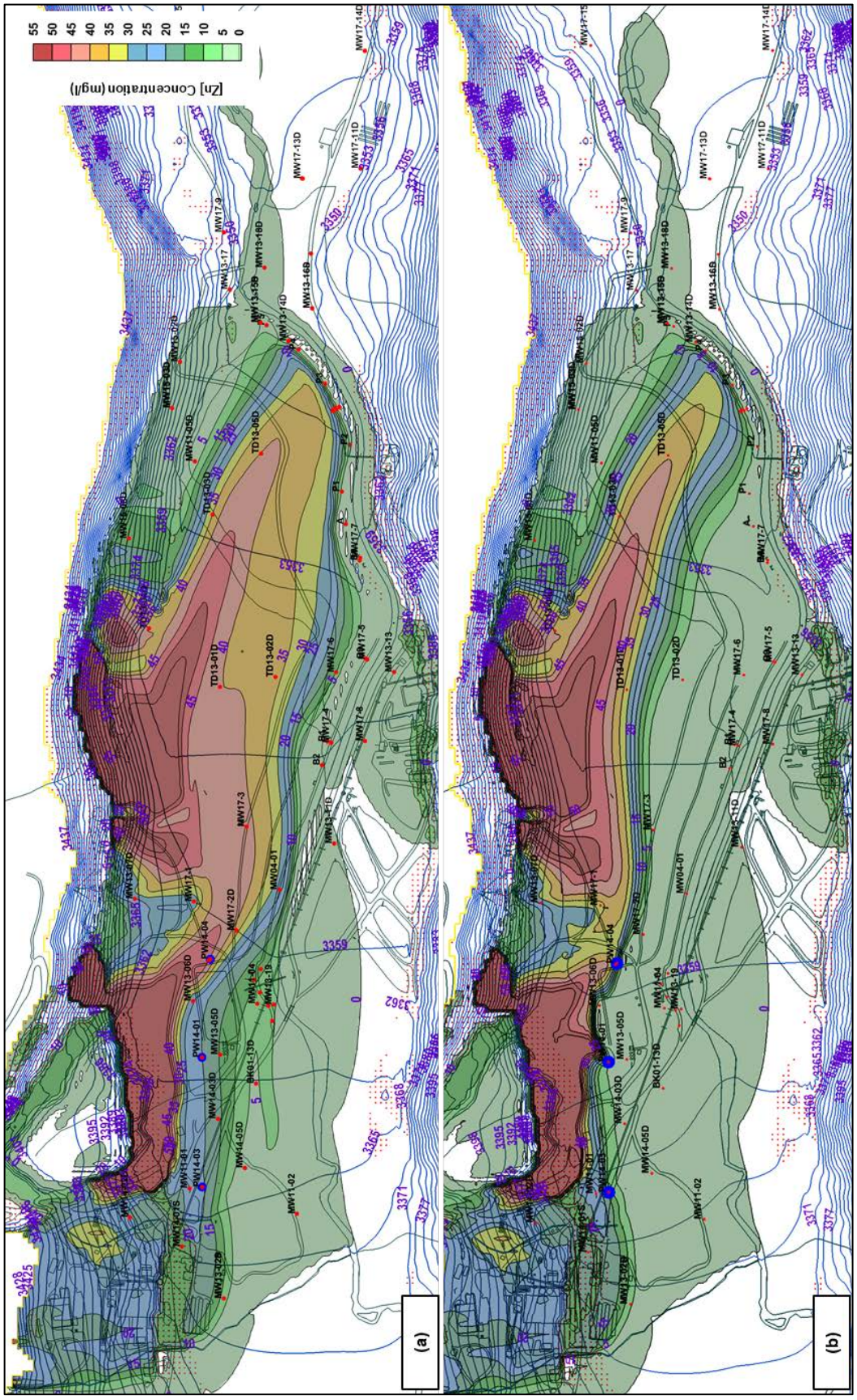

Figure 5: Simulated low-flow heads and Zn concentrations for (a) the Base Case and (b) Scenario 1 (Phase 1 Lynx SIS Operating)

Key findings for the "base case" during "low-flow" and "high-flow" conditions are summarized below:

- Overall, the calibrated transport model for the base case provides a good match to recently observed Zn concentrations in the MVA, except for the area south-east of the Super Pond (at MW17-02D, MW17-03 and MW04-01) where simulated concentrations tend to be higher than observed ranges.
- The model predicts that the zinc plume (with up to 45 mg/L Zn) extends to significant depth (down to model layer 6) beneath the mill area. This was required to match the observed extracted load at PW14-03 (10 to 15 t/year, with Zn concentration up to 35 mg/l) and observed average concentrations south of the Mill area (up to ~50 mg/L at MW11-01 and MW14-03D over the period 2015 to 2017).
- Impacted groundwater from the mill area and highly impacted groundwater from the Lynx berm area (>50 mg/L Zn) merge near the Super Pond and travels in an easterly direction into the Upper Old TDF reach, where it merges with the Zn plume from the WRD#1 and WRD#6.
- The model predicts background Zn concentrations in the MVA downstream of the Old TDF, indicating a very high efficiency of the Old TDF drain system. Note that slightly elevated Zn concentrations (up to 0.1 mg/L) are predicted in groundwater in proximity of Myra Creek downstream of the Old TDF. This is due to recharge of Myra Creek water (with slightly elevated Zn concentrations) to groundwater in this portion of the MVA.

Simulated load balance

Figure 6 shows predicted Zn loads to groundwater in the MVA for low-flow conditions. The upper chart shows simulated "low-flow" loads to groundwater in the MVA and the lower charts show the simulated Zn loads within the three site reaches. Table 2 provides a summary of calibrated zinc loads for all mine waste units grouped by the three site reaches.

Key findings with respect to sources of Zn loading to the MVA from the calibrated low-flow model are summarized below:

- The highest Zn loads are inferred to enter the MVA in the Lynx reach (20.8 t/year) and the Upper Old TDF Reach (16.0 t/year). Zn loading to the MVA in the Lower Old TDF reach are minor (0.6 t/year) by comparison.
- The mill area has been identified as a significant source of Zn loading (19.0%, 7.1 t/year). Potential sources of Zn loading in the mill area include (i) waste rock used for foundations and (ii) sidehill recharge from upgradient sources (primarily waste rock). Leakage from the Lynx Ditch is inferred to represent only a minor source of Zn loading (0.95 t/year).

- Aside from the mill area, the main sources of Zn loading to the MVA represent sulphide-bearing waste rock in the WRDs and the Lynx berm: WRD#1 (7.9 t/year Zn), WRD#6: (7.0 t/year Zn) and Lynx berm (6.6 t/year Zn).
- Secondary sources of Zn loading to the MVA include: Perched seepage in the Super Pond area (2.6 t/year), potentially originating from the Lynx berm and/or buried mine waste in this area. In addition to the Mine waste in the ETA/Cookhouse area (1.5 t/year).
- The calibrated Zn transport model for the base case provides a good match to observed Zn loads collected in the Pumphouse #4 and by-passing to Myra Creek (Table 1).
- Most of the Zn load in the Old TDF reach is intercepted in the Old TDF drain system, with the highest zinc loads intercepted by the lower Area II Outer Drain, Inner Drain and the Long section of the NOD. The simulated Zn load intercepted by the Old TDF drain system ranges from 27.1 t/year for low flow to 58.3 t/year for high flow.

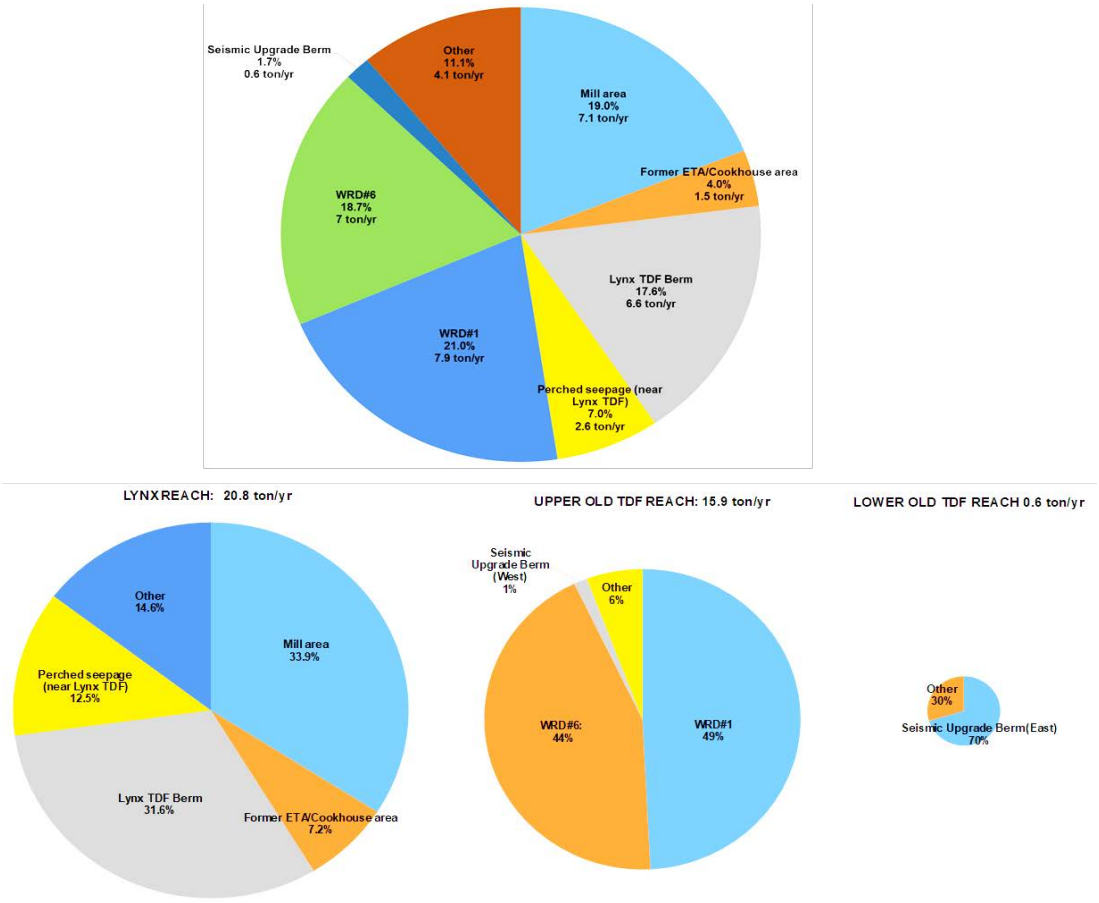

Figure 6: Low-flow simulated Zn loads in the MVA and within the major site reaches

- The simulated Zn load discharging to Myra Creek ranges from 6.5 t/year for low flow to 12.9 t/year for high flow, primarily in the Lynx and Upper Old TDF reaches. The model predicts that Zn load

to Myra Creek originates primarily from the Super Pond area with some secondary contributions from the ETA/Cookhouse area.

Table 2: Calibrated Zn loads for all mine waste units grouped by the three site reaches

Reach	Area (km^2)	Flux (L/s)	Recharge			Conc. (mg/L)	Load (t/year)	% of Load
			m/s	mm/year	% of MAP			
Lynx Reach								
Arnica creek	–	3.5	–	–	–	0.0	0.0	0.0%
Lynx ditch	–	3.0	–	–	–	10.0	0.9	2.5%
Mill area (side-hill)	–	3.5	–	–	–	50.0	5.5	14.8%
Mill area	0.122	3.3	2.7E-08	861.5	34.7	15.0	1.6	4.2%
North of Lynx pit	0.075	0.3	4.5E-09	142.0	5.7	20.0	0.2	0.6%
Lynx TDF berm	0.042	1.9	4.6E-08	1435.9	57.9	110.0	6.6	17.6%
Lynx side hill	–	1.0	–	–	–	50.0	1.6	4.2%
Former ETA/cookhouse area	0.171	3.8	1.6E-08 to 2.9E-08	631 to 915	20.1 to 36.9	77.0	1.5	4.0%
Surface waste near Super Pond	0.052	1.1	2.0E-08 to 2.5E-08	631 to 789	25.4 to 31.8	22.0	0.3	0.8%
Perched seepage (near Lynx TDF)	0.002	0.6	2.5E-07	–	–	150.0	2.6	7.0%
Sub total		22.0					20.8	55.7%
Upper Old TDF Reach								
WRD#1 (East):	0.030	1.4	4.6E-08	1435.9	57.9	125.0	5.4	14.4%
WRD#1 (West):	0.014	0.6	4.6E-08	1435.9	57.9	125.0	2.5	6.6%
WRD#6:	0.039	1.8	4.6E-08	1435.9	57.9	125.0	7.0	18.7%
Surge Pond	0.027	0.7	2.5E-08	773.2	31.2	25.0	0.5	1.4%
Seismic upgrade berm (West)	0.089	1.4	1.6E-08	492.4	19.9	5.0	0.2	0.6%
Polishing bonds area	0.082	0.7	8.4E-09	263.6	10.6	0.0	0.0	0.0%
HW office area	0.052	1.0	2.0E-08	631.2	25.4	12.0	0.4	1.0%
Sub total		7.5					16.0	42.7%
Lower Old TDF Reach								
PAG rockfill	0.008	0.2	2.4E-08	750.0	30.2	55.0	0.2	0.5%
Seismic upgrade berm (east)	0.088	1.4	1.6E-08	492.4	19.9	10.0	0.4	1.2%
Old TDF tailings	0.084	0.8	9.5E-09	300.0	12.1	0.0	0.0	0.0%
Strip Area	0.132	1.3	9.5E-09	300.0	12.1	0.0	0.0	0.0%
Sub total		3.6					0.6	1.6%
TOTAL		**33.2**					**37.4**	

Predictions for Scenario 1 "Phase I Lynx SIS Operating"

Scenario 1 represents future conditions during operation of the Phase I Lynx SIS pumping wells. In this scenario the three Lynx SIS wells (MNW2 package) were assigned to pump a combined total of 47 L/s and 75 L/s for low flow and high flow, respectively. Figure 5b shows the predicted groundwater flow field for low-flow conditions and the predicted Zn plume for Scenario 1 once the groundwater system has reached steady-state. Key findings for Scenario 1 are summarized below:

- Operation of the Lynx SIS wells is predicted to effectively intercept all the Zn load from the mill area and Lynx berm, resulting in a significant reduction in zinc concentrations in groundwater in the Super Pond area, and the southern portion of the upper and lower Old TDF reaches. This predicted reduction in Zn concentrations is consisten with recent observations of groundwater quality in the Lynx area.
- The model also predicts that the residual Zn plume in the northern portion of Old TDF reaches is sourced primarily by seepage from WRDs #1 and #6 and continues to be intercepted in the Old TDF under-drains. Groundwater discharging to Myra Creek in the Lynx and Upper Old TDF reaches is only marginally impacted (<0.3 mg/L Zn).
- Under steady-state low-flow conditions, the Lynx SIS wells are predicted to intercept the largest proportion of the Zn load in the MVA (19.4 t/year or 55.4% of the total zinc load), followed by the Old TDF under-drains (15.5 t/year or 44.4% of the total). Zn load by-passing the SIS and discharging to Myra Creek is predicted to be minor (<0.1 t/year or 0.2% of total). Thus, the Phase I Lynx SIS is predicted to reduce the Zn loads from groundwater to Myra Creek by a factor of 65 compared to simulated Zn loads for the base case (6.5 t/year).
- Under high-flow conditions, the Lynx SIS wells and Old TDF under-drains are predicted to intercept Zn load of 49.9% (33.5 t/year) with 0.2% (0.2 t/year) load by-pass to Myra Creek.
- Transient results from the MODFLOW/MT3D model suggest that Zn concentrations in the MVA would decline and approach steady-state conditions within two to five years of start of operation of the Lynx SIS.
- Zn loading to Myra Creek is predicted to decrease significantly faster (within about six to twelve months) because the travel distance from the Phase I Lynx SIS pumping wells to the main discharge areas along Myra Creek (Lynx reach and Upper Old TDF reach) is shorter.
- Zn loads collected in the Old TDF under-drains are predicted to decrease gradually within three to five years after start of pumping of the Lynx SIS wells as the groundwater system approaches the new steady-state condition.

References

Ferguson, P., M. Hussein, C. Wels and N. Pesonen. 2019. Current acid rock drainage (ARD) impacts and seepage interception strategies at the Myra Falls Mine Site. In *Proceedings of Tailings and Mine Waste, 2019.*

Bibliography

Robertson GeoConsultants Inc. 2018. Updated contaminant load balance model and water quality predictions, RGC Report No. 212011/7, November 2018.

Proceedings of Tailings and Mine Waste 2019
November 17–20, 2019, Vancouver, Canada
Published by the University of British Columbia, 2019

Hurricanes Harvey and Florence – Are Storms Changing, and How Does This Effect TSF and Dam Design?

Bill Kappel, Applied Weather Associates, USA

Abstract

Rainfall resulting from Hurricane Harvey reached historic levels over the coastal regions of Texas and Louisiana during the last week of August 2017, accumulating over 60 inches of rainfall in southeastern Texas. Although extreme rainfall from this type of landfalling tropical system is not uncommon in the region, Harvey was unique in that it persisted over the same general location for several days, producing volumes of rainfall not previously observed in the United States and most of the world. Devastating flooding and severe stress to infrastructure in the region was the result. Coincidentally, Applied Weather Associates (AWA) had recently completed an updated statewide probable maximum precipitation (PMP) study for Texas and is currently completing a regional PMP study for the states of Oklahoma, Arkansas, Louisiana, and Mississippi. This storm proved to be a real-time test of the adequacy of those values. AWA calculates PMP following a storm-based approach.

Just over a year later in September of 2018, Hurricane Florence produced a similar devasting rainfall event with unprecedented rainfall accumulations along the Carolina coastlines. The result was significant flooding and damage in both North and South Carolina. Like Harvey, this storm moved very slowly over the same region for several days, remaining in a favourable position to allow a continual supply of moisture to feed the storm. Florence produced more than 40 inches of rainfall, far surpassing any previous rainfall totals in the region. This presentation will compare the results of the Harvey and Florence rainfall accumulations in time, space, and magnitude against previous similar storms and provide comparisons of the rainfall against previous and current PMP depths. Discussion will be included regarding the implications of the storms on previous and future PMP estimates, dam safety design, and infrastructure vulnerable to extreme flooding. This will include a discussion on climate change and how it relates to these storms and past extreme events.

Introduction

Rainfall from Hurricane Harvey resulted in some of the greatest rainfall accumulation ever recorded in the

United States. Rainfall accumulations were most extreme at large area sizes (greater than 5,000 miles^2) and long durations (greater than 24 hours). However, even at smaller area sizes and shorter durations, the storm still produced record setting rainfall. This was extremely unusual and points to the fact that the storm was truly a probable maximum precipitation (PMP) event.

PMP is "theoretically, the greatest depth of precipitation for a given duration that is physically possible over a given storm area at a particular geographical location at a certain time of the year" (WMO, 2009). Therefore, PMP represents a theoretical upper limit of the greatest amount of rainfall that can accumulate, and the analysis of the Harvey rainfall confirms that it reached that level.

Devastating flooding was the result of the extreme rainfall, with the hardest hit region extending from the Houston metropolitan region through southwestern Louisiana. Fortunately, no high hazard structures failed during the vent. Coincidentally, Applied Weather Associates (AWA) had recently completed the statewide PMP study for Texas, updating the previous PMP values provided in the National Weather Service Hydrometeorological Report 51 (HMR 51, Schreiner and Riedel, 1978). Of course, this meant the timing of the Harvey rainfall was perfect for testing and comparing the newly developed values and Harvey's implications for the dam safety community. This storm was a PMP event and provided excellent data from which we were able to test the previously derived PMP depths and many of the assumptions that are inherent in PMP calculations and hydrologic analysis applied for design purposes against high hazard dams.

Harvey background

Texas is home to some of the most extreme rainfall events ever observed in the US and in some cases the world. Examples of US and world record rainfalls that have occurred in Texas include Galveston, TX June 1871; Thrall, TX September 1921; D'Hanis, TX May 1935; and Alvin, TX July 1979. Favoured locations in the state include the Balcones Escarpment and immediate coastal regions from Corpus Christi through Beaumont-Port Arthur and southern Louisiana. These regions are favoured because of topographic interactions with moisture flowing in from the Gulf of Mexico and interacting with the Balcones Escarpment and hurricane landfall interaction with coastal terrain. Along the coastal sections during hurricane season, atmospheric steering currents are very weak. This often results in slow movement of the landfalling tropical systems in this region, allowing heavy rain to accumulate over the same general region.

Given these favoured conditions, major rainfall events are expected every few years, and of course will happen again. Within recent history, similar storms in the area include Hearne 1899, Beulah 1967, Alvin 1979, and Allison 2001. So, what made Harvey different? Harvey was unique because it was fueled by near record Gulf of Mexico sea surface temperatures that provided exceptional amounts of moisture as it remained over the same general area for several days. In addition, Harvey stayed in a position close

enough to the coast that allowed extremely moist air to continue to feed into the storm, while it was able to retain its warm-core tropical characteristics that would normally be disrupted by interactions with land.

Several excellent analyses and discussions of the meteorological environment associated with Harvey's formation, track, and dissipation, as well as resulting flooding impacts have been completed. The focus of this paper is on the rainfall accumulation of the storm and how it compares to PMP and extreme storm analyses. The reader is referred to the following resources for more information on the synoptic meteorological environment associated with the storm:

- https://www.nhc.noaa.gov/data/tcr/AL092017_Harvey.pdf
- https://www.weather.gov/hgx/hurricaneharvey
- https://weather.com/storms/hurricane/news/tropical-storm-harvey-forecast-texas-louisiana-arkansas
- American Water Resources Association-Impact (January, 2018)

SPAS rainfall analysis

The rainfall produced by Hurricane Harvey was analyzed using AWA's Storm Precipitation Analysis System (SPAS). AWA has completed more than 700 similar rainfall analyses since 2002, with the results often used for PMP development. Each SPAS storm analysis is given a number to designate which storm is being evaluated. Hurricane Harvey's SPAS number was 1667. Results of these analyses have been primarily used as input for PMP development, model calibration, model validation, and forensic investigations.

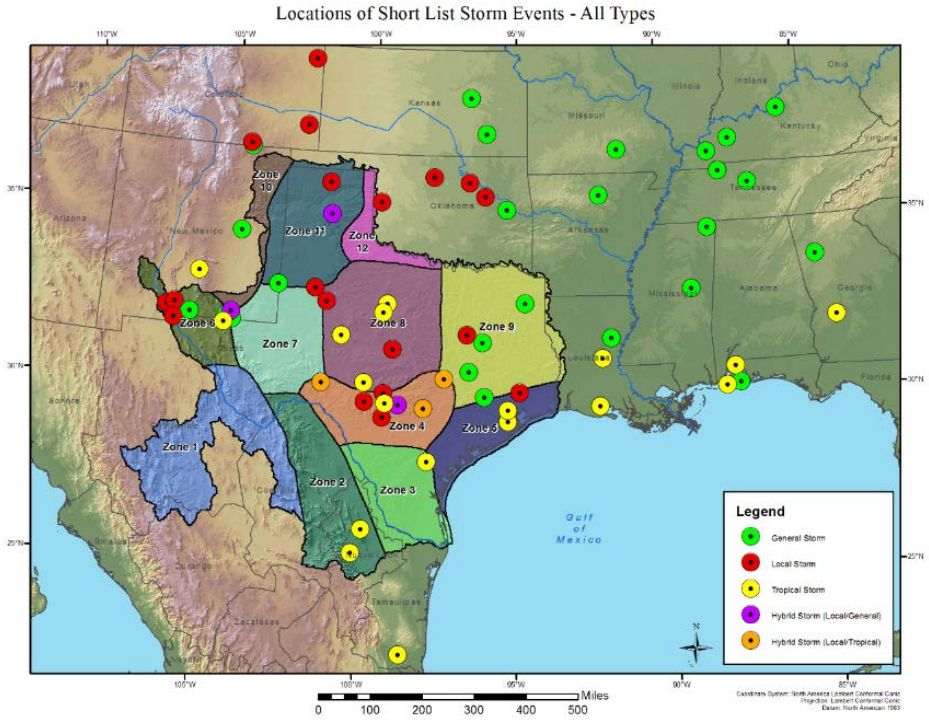

Figure 1: Storm locations used to calculate PMP in Texas

The SPAS process has been extensively reviewed and accepted for use in these types of analyses (NRC, 2017). SPAS produces several standard outputs including hourly gridded rainfall data, total storm isohyetal maps (lines of equal rainfall accumulation), depth-area-duration information, annual exceedance probability maps, and mass curve accumulations.

SPAS analyses were completed for all storms used during the Texas PMP study (Figure 1) and therefore provided a consistent and reliable data set from which to make comparisons of the forecast rainfall from Harvey, Harvey rainfall as it was occurring, and comparisons from the post-analysis investigations. The SPAS database was critical in understanding the severity of the potential rainfall from the storm before it occurred, and in communicating how this might compare to the recently updated PMP values, as well as understanding the hardest hit regions.

Forecast rainfall amounts were showing the potential for extreme rainfall as much as a week before landfall, as shown in Figure 2 (McMahan, 2017).

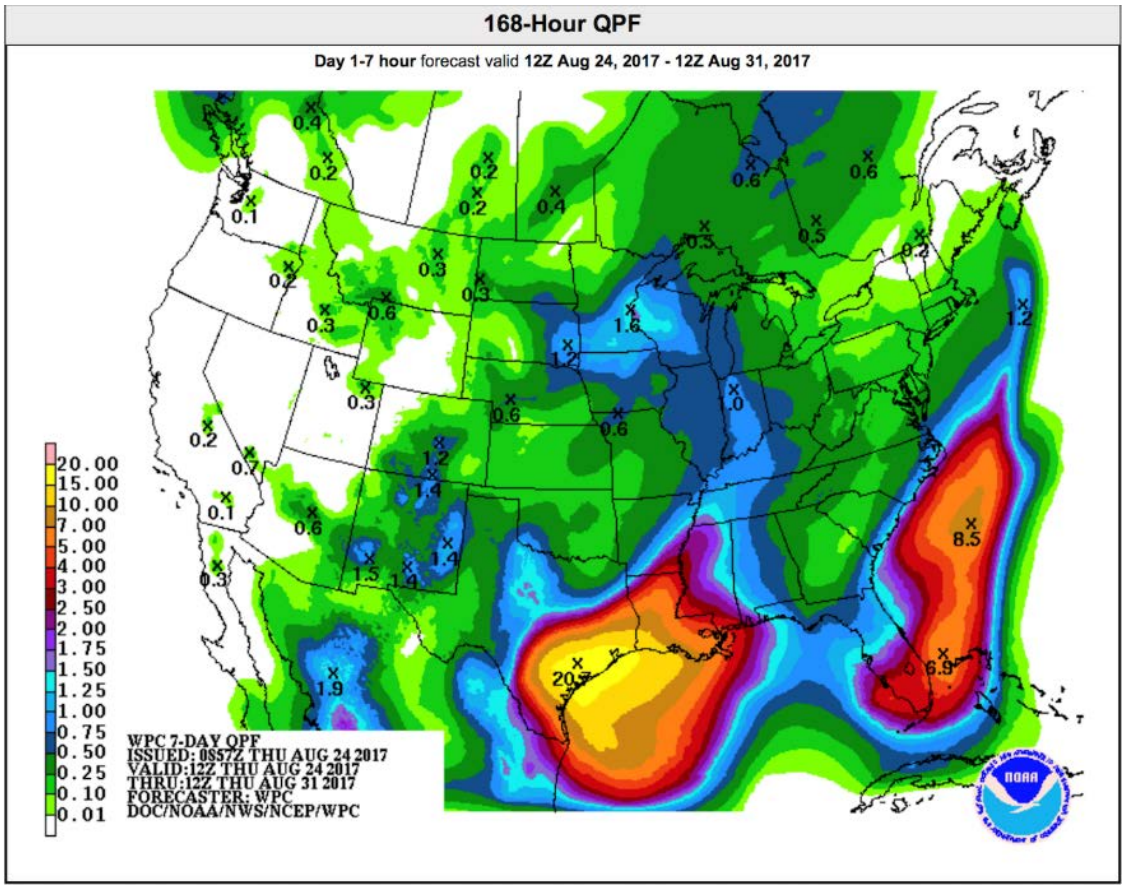

Figure 2: Quantitative precipitation forecast from the weather prediction center for the period August 24, 2017 through August 31, 2017

The possibility of extreme rainfall put the dam safety community on alert several days ahead of time. This was especially relevant in the context that updated PMP depths has just been developed and released

for public use earlier that year (Kappel et al., 2016). AWA was in contact with the Texas Commission of Environmental Quality (TCEQ) head of dam safety before the storm began to affect the region to help with situation awareness. While the storm was occurring, communications with TCEQ and others involved in monitoring and analyzing the rainfall continued (e.g., Dr. Nielson-Gammon, Texas State Climatologist and professor at Texas A&M University). AWA immediately began an analysis of the rainfall using the SPAS program, and worked with Dr. Nielson-Gammon to develop various comparisons of the Harvey rainfall versus previous similar events in order to put the rainfall accumulations in perspective.

The comparisons demonstrated that the Harvey rainfall far exceeded any other observed event, especially for durations greater than 24 hours and area sizes greater than 5,000 square miles, not only in Texas but also in the United States (Figure 3). Figure 4 provides the total storm accumulation pattern resulting from Harvey. Figure 5 provides the results of the SPAS rainfall analysis as a depth-area-duration table. This provides a 3-dimensional look at the rainfall accumulation both spatially and temporally. Unprecedented amounts of rainfall occurred, with over 60 inches at the storm center during the 5-day period. Even more amazing was the volume of rainfall, with over 20 inches spread over more than 20,000-square miles during the 5-day period. This would be equivalent to more than 25 times the average daily flow through the Mississippi River (Nielson-Gammon, 2017).

The fact that Harvey rainfall exceeded all other observed events in the United States demonstrated its importance for the dam safety community and hydrologic decision processes. This type of storm is exactly the type of event that is needed to validate the processes that are utilized to calculate PMP. Given the need to ensure that high hazard dams are appropriately designed, this analysis provided a real-time, well-observed event to validate the processes and assumptions. Specifically, the rainfall accumulation data was utilized as input for hydrological model validation, providing an example runoff scenario which was similar to a Probable Maximum Flood (PMF) event. This represented a rare opportunity where a PMF-type flood occurred in a highly gauged series of basins, and the output has been used to verify many of the assumptions in the PMP and PMF processes.

Harvey Rainfall: Percent Greater Than Previous Largest			
Area Size	**48-Hours**	**72-hours**	**120-hours**
5000-square miles	11%	22%	42%
10000-square miles	25%	27%	49%
20000-square miles	17%	29%	43%

Figure 3: Comparison of the Hurricane Harvey rainfall against similar previous storms

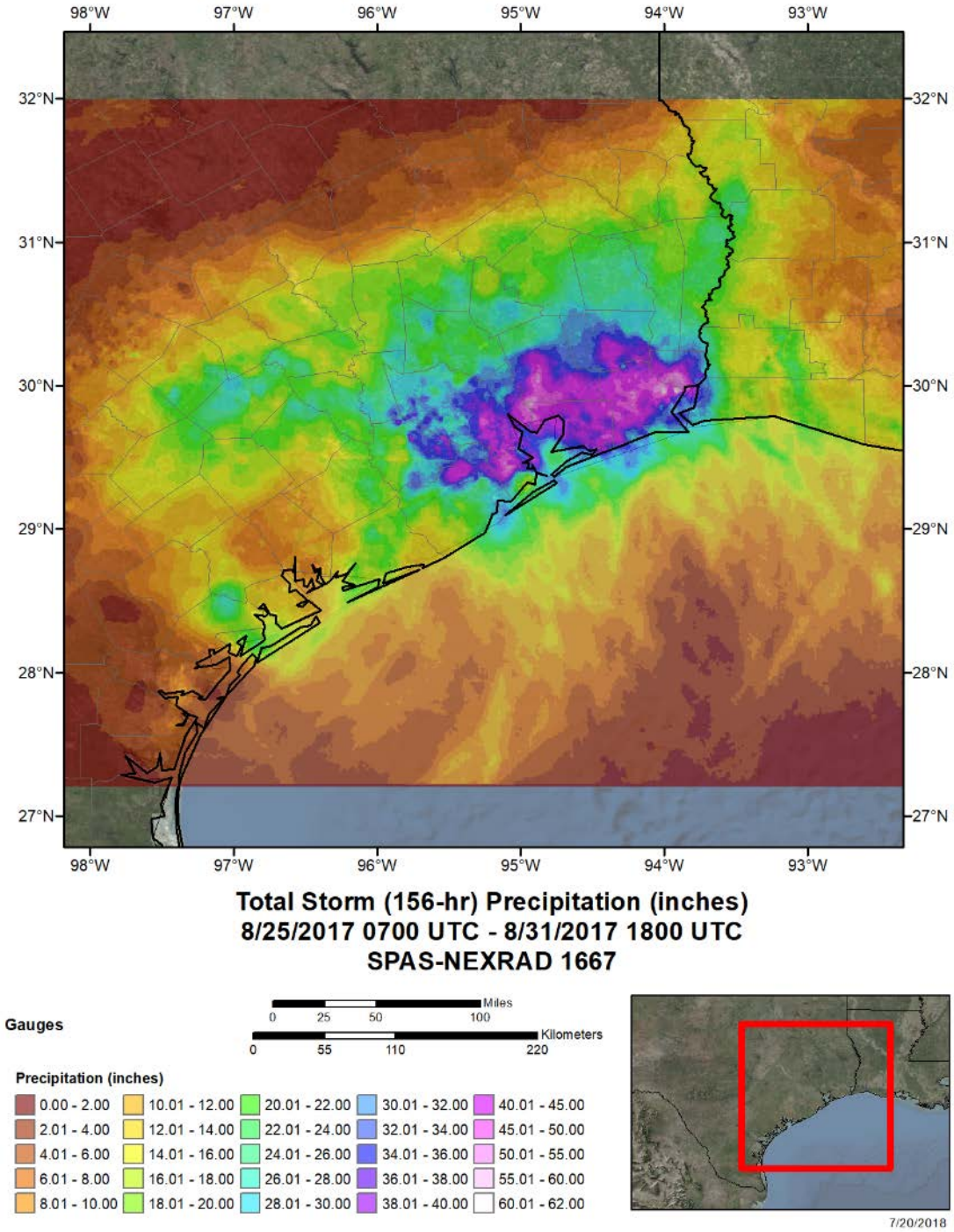

Figure 4: Hurricane Harvey SPAS 1667 total storm isohyetal

The rainfall accumulation pattern followed a similar footprint to that seen in other similar previous storms in the region. The heaviest rainfall was centred just inland from the coast, where coastal convergence processes maximized the rainfall production. Also noteworthy was the accumulation pattern through time

with the heavy rainfall occurring over long time periods covering several days. The extreme rainfall, which occurred over several days, resulted in daily rainfall records that were set at the Houston Intercontinental Airport official observation site (KIAH). At this location, Harvey produced the greatest daily amount on August 27, and the fifth greatest daily amount on August 26.

SPAS Storm 1667 - August 25 (0700 UTC) - August 31 (1800 UTC), 2017
MAXIMUM AVERAGE DEPTH OF PRECIPITATION (INCHES)

Area (mi^2)	Duration (hours)									
	1	6	12	18	24	36	48	72	96	Total
0.4	5.45	19.32	23.34	28.33	32.17	35.54	40.47	49.86	55.41	56.47
1.0	5.38	19.19	23.16	28.11	31.91	35.30	40.21	49.47	54.92	55.99
10.0	5.17	18.87	22.54	27.52	31.25	34.67	39.57	47.98	53.26	54.29
25.0	5.06	18.65	21.88	26.64	30.50	33.34	38.40	46.71	51.85	52.90
50.0	4.91	18.26	21.30	25.82	30.01	31.74	37.32	45.28	50.29	51.44
100.0	4.74	17.65	20.51	24.95	29.33	31.14	36.28	44.00	48.66	49.83
150.0	4.59	17.13	19.88	24.35	28.71	30.51	35.50	43.17	47.64	48.82
200.0	4.45	16.67	19.35	23.76	28.09	29.95	34.88	42.51	46.91	48.11
300.0	4.18	15.90	18.47	22.87	26.99	28.97	33.71	41.56	45.71	46.96
400.0	3.93	15.22	17.75	22.16	26.17	28.17	32.76	40.74	44.88	46.12
500.0	3.71	14.62	17.17	21.47	25.53	27.52	32.01	40.11	44.13	45.48
1000.0	2.99	12.21	15.20	19.09	22.68	25.11	29.36	37.56	41.67	43.29
2000.0	2.36	9.46	12.85	16.31	19.66	22.69	26.80	34.39	39.13	40.94
3500.0	1.85	7.58	11.03	14.23	17.41	20.76	24.79	31.35	36.49	38.41
5000.0	1.57	6.58	9.99	12.96	15.99	19.44	23.54	29.40	34.51	36.34
7500.0	1.29	5.58	8.83	11.66	14.39	17.97	21.90	26.99	31.83	33.88
10000.0	1.12	4.94	8.06	10.59	13.30	16.86	20.81	25.35	29.89	31.84
15000.0	0.89	4.17	6.95	9.24	11.55	15.18	18.66	22.84	26.83	28.93
20000.0	0.71	3.64	6.10	8.14	10.38	13.77	17.04	21.03	24.75	26.68
35000.0	0.52	2.71	4.65	6.27	7.83	10.67	13.40	17.10	20.12	22.11
50000.0	0.39	2.11	3.60	4.93	6.27	8.83	11.06	14.24	16.69	18.79
75000.0	0.29	1.53	2.69	3.68	4.62	6.61	8.37	11.33	13.32	15.06
100000.0	0.22	1.21	2.20	3.00	3.75	5.30	6.71	9.08	10.71	12.11
120162.0	0.18	1.05	1.91	2.59	3.22	4.59	5.83	7.88	9.31	10.53

Figure 5: Hurricane Harvey SPAS 1667 depth-area-duration values

Comparison to previous storms

During June 2001, Hurricane Allison produced devastating flooding in the Houston region, with over 40 inches of rainfall occurring in 24 hours. This storm spatial coverage was similar to Harvey. However, the rainfall from Allison only lasted a little over a day. This resulted in total storm rainfall amounts and volumes that were much smaller than Harvey (Figure 6). Previous to Allison was Alvin in July 1979. Again, this tropical system produced extreme rainfall over the Houston area, with more than 40 inches in 24 hours in some locations (Figure 7). Each of these storms were similar regarding storm type and location, but the total rainfall amounts and spatial coverage were limited by overall duration.

Maximization of Hurricane Harvey

Most important for TCEQ and the dam safety community in general was whether Harvey exceeded PMP estimates. This is because high hazard structures are designed in relation to the PMF. The PMF is a direct result of the PMP, therefore if PMP design values were exceeded, there is a possibility that high hazard structures could be compromised

Storm 1464 Zone 1 - June 5 (1200 UTC) - June 11 (1100 UTC), 2001													
MAXIMUM AVERAGE DEPTH OF PRECIPITATION (INCHES)													
	Duration (hours)												
areasqmi	1	3	6	12	18	24	36	48	72	96	120	144	Total
0.4	6.28	14.09	20.98	29.17	29.39	29.41	29.53	29.71	29.89	40.56	40.74	40.97	29.53
1	6.25	14.04	20.92	29.06	29.29	29.32	29.42	29.61	29.77	40.42	40.61	40.82	29.42
10	5.74	13.31	19.95	27.88	27.99	28.01	28.27	28.27	28.52	38.35	38.61	39.15	28.27
25	5.40	12.14	18.05	26.73	27.10	27.13	27.16	27.30	27.69	36.99	37.20	37.68	27.16
50	5.26	11.36	16.04	24.27	25.21	25.25	25.30	25.48	26.23	35.42	35.79	35.92	25.30
100	5.07	10.32	13.61	20.46	20.59	20.63	20.64	22.57	24.69	31.77	32.87	33.10	20.64
150	4.88	8.64	13.06	19.42	19.68	19.75	19.81	20.33	24.23	29.38	31.06	31.81	19.81
200	4.68	8.52	12.39	17.42	17.53	17.53	17.81	19.02	23.85	27.91	30.03	30.61	17.81
300	4.32	7.86	11.57	16.44	16.67	16.67	16.69	17.84	22.75	25.49	28.83	29.05	16.69
400	4.04	7.19	10.70	15.46	15.80	15.86	15.95	16.57	21.71	24.68	27.79	27.99	15.95
500	3.79	7.12	9.54	14.15	15.08	15.12	15.24	15.31	20.48	24.12	26.73	26.94	15.24
1,000	2.73	5.71	7.70	12.12	12.31	12.38	12.41	14.15	18.18	21.11	23.91	24.15	12.41
2,000	2.08	3.92	6.06	9.63	9.80	9.80	9.91	11.98	14.03	15.84	17.45	20.85	9.91
5,000	1.61	2.70	4.24	5.65	5.87	7.74	8.56	9.37	11.81	15.57	15.90	17.88	8.56
10,000	0.51	1.46	2.47	4.77	5.57	5.61	6.85	8.21	10.50	12.41	12.79	15.29	6.85
20,000	0.38	0.92	1.40	2.73	3.48	4.40	5.59	6.58	8.81	10.59	12.07	13.01	5.59
50,000	0.24	0.51	0.95	1.56	2.14	2.59	3.25	4.40	5.93	7.64	9.11	9.24	3.25
54,778	0.23	0.50	0.90	1.54	2.10	2.43	3.16	4.39	5.82	7.62	8.59	8.70	3.16

Figure 6: Allison, SPAS 1464 June 2001 depth-area-duration values

Storm 1463 Zone 1 - July 23 (0700 UTC) - July 28 (0600 UTC), 1979												
MAXIMUM AVERAGE DEPTH OF PRECIPITATION (INCHES)												
	Duration (hours)											
areasqmi	1	3	6	12	18	24	36	48	72	96	120	Total
0.4	6.46	13.79	20.52	32.51	39.79	43.08	45.46	45.47	45.48	45.49	45.49	45.49
1	6.45	13.75	20.47	32.37	39.61	42.88	45.24	45.24	45.27	45.28	45.28	45.28
10	6.26	13.36	19.88	30.47	36.90	40.15	42.25	42.31	42.39	42.39	42.44	42.44
25	6.09	12.97	19.41	27.97	33.82	35.34	37.29	37.61	37.61	38.37	38.54	38.54
50	5.89	12.75	18.87	25.26	31.40	32.67	34.06	34.06	34.06	35.59	35.78	35.78
100	5.60	12.24	18.06	23.89	28.14	30.20	31.27	31.30	31.57	32.81	35.23	35.23
150	5.40	11.82	17.46	22.77	27.53	28.61	28.61	29.89	30.69	30.71	34.68	34.68
200	5.22	11.44	16.92	21.72	26.10	27.27	27.80	27.85	30.01	30.41	34.13	34.13
300	4.89	10.70	15.85	20.55	24.89	25.60	26.56	26.99	29.39	30.26	33.03	33.03
400	4.58	9.99	14.65	18.73	22.62	22.62	22.62	26.21	28.92	30.12	31.94	31.94
500	4.28	9.38	13.53	17.75	21.71	22.08	22.41	25.41	28.48	29.97	30.84	30.84
1,000	3.52	7.61	9.64	14.52	17.83	20.48	21.95	23.89	26.35	27.69	27.85	27.85
2,000	2.48	5.87	8.09	11.33	13.74	16.14	19.00	19.18	22.03	24.35	24.51	24.51
5,000	1.71	2.65	5.10	7.63	9.24	12.10	14.33	15.27	15.40	19.07	19.16	19.16
10,000	0.51	1.33	2.22	5.06	7.06	8.95	10.55	10.69	11.55	14.87	14.95	14.95
20,000	0.30	0.77	1.61	2.31	2.82	4.82	4.82	5.62	9.71	10.62	10.81	10.81
50,000	0.24	0.51	0.87	1.54	2.08	2.56	3.60	4.29	4.74	5.72	5.77	5.77
54,778	0.24	0.50	0.82	1.51	2.04	2.55	3.47	3.98	4.72	5.10	5.15	5.15

Figure 7: Alvin, SPAS 1463 July 1979 depth-area-duration values

Remember that PMP is developed by analyzing actual storm events, then maximizing those storms, transpositioning those storms to your locations of interest, and combining the results to produce worst-case scenarios. Previous work by AWA during the Texas statewide PMP study provided a readily available data set to compare to the Harvey values (Figure 4). As soon as the preliminary SPAS analysis of Harvey was completed, AWA began the in-place maximization process. Not surprisingly, Harvey was nearly at the maximum amount of moisture that the atmosphere could provide, with a resulting in-place maximization factor of only 1.04. This demonstrates that the storm was already near the maximum that could occur, with the IPMF resulting in a 4% increase compared to what was observed.

Comparison to PMP values

Once Harvey was maximized, direct comparisons to the recently completed Texas statewide PMP and HMR 51 PMP depths were completed. The results of these comparisons demonstrated that Harvey was significantly larger than the previous tropical storm PMP values in the region (Figure 8). However, Harvey did not exceed the overall PMP values for the region when all storm types were considered, with two minor exceptions. At 96 hours, 20,000 square miles, and 120 hours, Harvey was 1.5% greater and 8.4% greater respectively (Figure 9). Unfortunately, HMR 51 PMP values only extend to 72 hours, so similar comparisons to those values were not possible. This also demonstrates one of the problems with HMR 51, in that it does not provide PMP values at all required area sizes and durations for regions of the country where storms last longer than 72 hours, like the Texas coastal region.

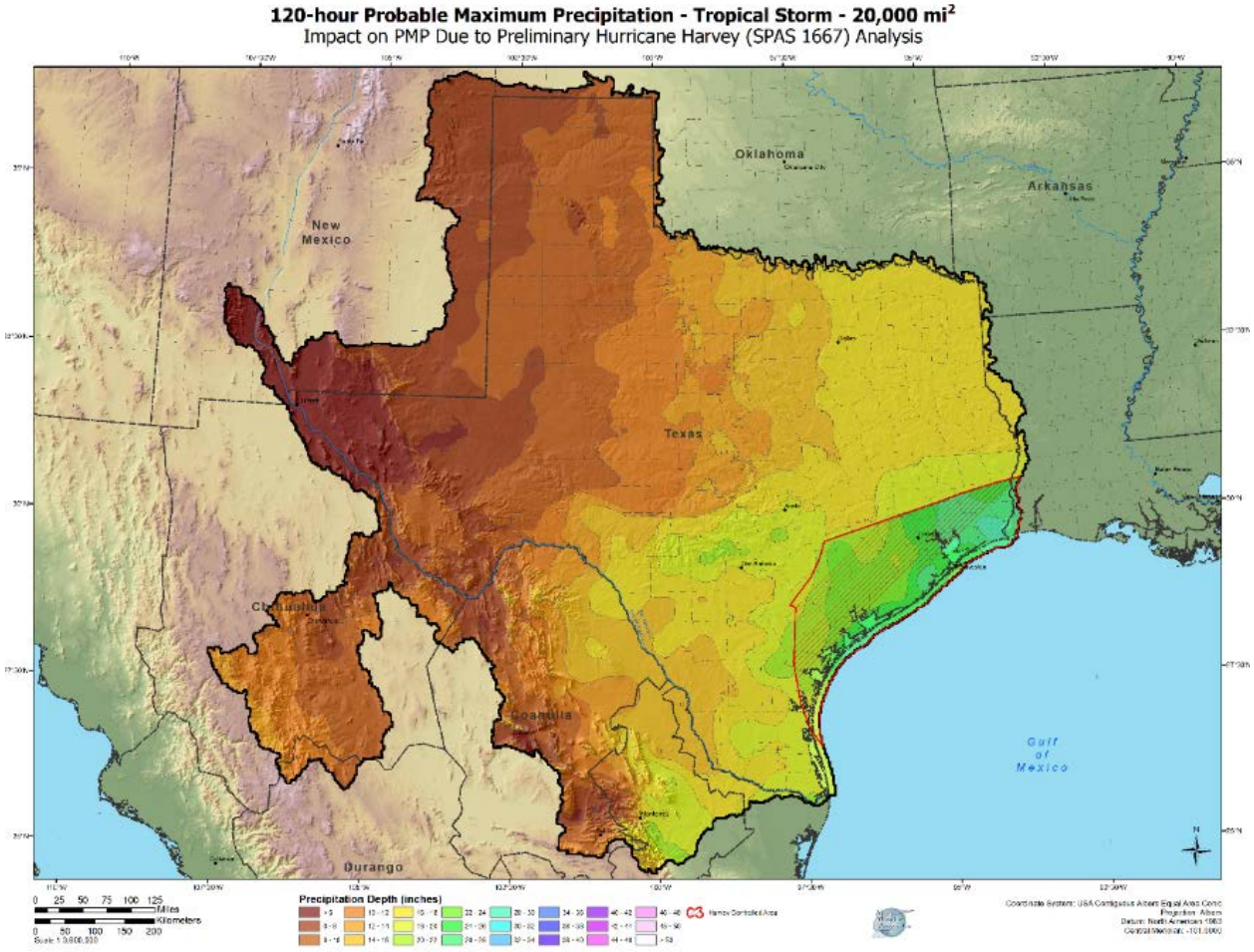

Figure 8: Region where tropical storm PMP values increased after Hurricane Harvey

Not surprisingly, the storm far exceeded the NOAA Atlas 14 precipitation frequency values, with a large region experiencing greater than a 1,000-year recurrence interval (Figure 10). AWA analysis of the

Annual Exceedance Probability of the storm show that is was likely somewhere between a 10^5 and 10^6 recurrence interval in and around the storm center location.

These comparisons against the previously calculated PMP depths, that did not include Harvey, provided a very beneficial real-time example that the PMP development process does appropriately envelope the processes which produce extreme rainfall. This was very important for the dam safety community, as it confirmed that the PMP depths developed in the region were reasonably rare when applied to high-hazard structures.

	# of Grid Points Controlled by Harvey	Average Tropical PMP (post-Harvey)	Average Tropical PMP (pre-Harvey)	Average % Increase	Average General PMP (pre-Harvey)	Average % Increase over General PMP	Average HMR 51 PMP	Average % Increase from HMR 51
5,000-sqmi 48-hour	485	25.8"	25.4"	1.6%	31.7"	No Increase	-	-
5,000-sqmi 72-hour	4,566	30.1"	27.4"	9.9%	35.3"	No Increase	31.1"	No Increase
10,000-sqmi 48-hour	1,668	22.0"	21.1"	4.0%	24.7"	No Increase	22.9"	No Increase
10,000-sqmi 72-hour	4,736	25.9"	23.4"	10.7%	29.1"	No Increase	26.8"	No Increase
10,000-sqmi 96-hour	9,785	27.3"	23.6"	15.7%	28.2"	No Increase	N/A	N/A
10,000-sqmi 120-hour	9,785	29.5"	23.8"	24.0%	28.4"	No Increase	N/A	N/A
20,000-sqmi 48-hour	4,009	17.4"	16.2"	7.3%	20.6"	No Increase	22.8"	No Increase
20,000-sqmi 72-hour	6,167	20.8"	18.4"	12.5%	22.0"	No Increase	26.8"	No Increase
20,000-sqmi 96-hour	7,714	23.4"	20.6"	13.8%	23.1"	1.5%	N/A	N/A
20,000-sqmi 120-hour	9,566	24.7"	20.7"	18.9%	22.8"	8.4%	N/A	N/A

Figure 9: Comparison of PMP to maximized Harvey rainfall

Conclusion

Harvey was a real-world example of a PMP-rainfall event and demonstrated that PMP can happen. One very important outcome for the dam safety community is that even with Harvey producing PMP level rainfall, no high hazard dam failed in Texas or Louisiana. This is likely the result of good dam safety practices and design, as well as luck. Therefore, it is extremely important that the dam safety community follows standard practice in design of structures, monitoring of structures, and applying the most up-to-date science and data. Harvey also demonstrates the need to continually update the storm database and PMP estimates as new storms occur and the understanding of extreme rainfall mechanisms increases.

Programs should be in place that allow for updating of these databases and PMP values in real time as events occur. TCEQ dam safety, National Weather Service, members of the academic community, and private consultants should all be commended for their monitoring, communication, and response prior to, during, and after Harvey occurred. This type of coordination and communication should become the standard for other state dam safety and Federal dam safety offices, because these types of events will occur again.

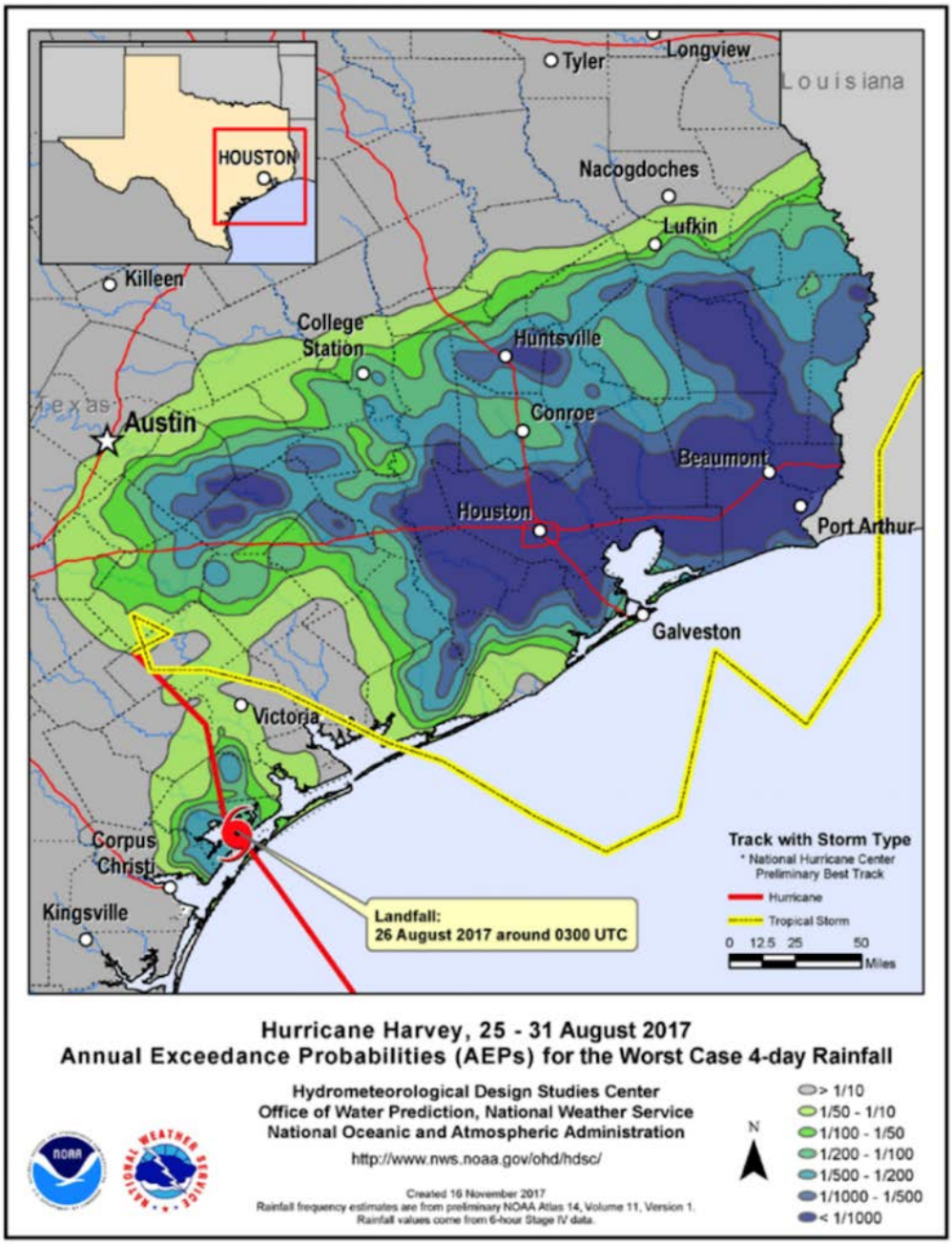

Figure 1: Annual exceedance probability of Harvey rainfall using NOAA Atlas 14 (downloaded from https://www.nws.noaa.gov/oh/hdsc/aep_storm_analysis/)

References

Kappel, W.D., D.M. Hultstrand, G.A. Muhlestein, K. Steinhilber, D. McGlone, T.W. Parzybok and B. Lawrence. 2016. Statewide Probable Maximum Precipitation for Texas. Prepared for the Texas Commission of Environmental Quality.

McMahan, Michael. 2017. Senior Hydrometeorologist with HDR. Personal communication, August 2017.

Nielson-Gammon, John. 2017. Personal communication, September 2017.

NOAA National Weather Service. 2017. Hydrometeorological Design Studies Center, Exceedance probability analysis for selected storm events, retrieved from https://www.nws.noaa.gov/oh/hdsc/aep_storm_analysis/

Nuclear Regulatory Commission (NRC). 2017. Commercial grade dedication and audit of SPAS, ENERCON appendix B program.

Schreiner, L.C. and J.T. Riedel. 1978. Probable Maximum Precipitation Estimates, United States east of the 105th Meridian. Hydrometeorological Report No. 51, National Weather Service, National Oceanic and Atmospheric Association, US Department of Commerce, Silver Spring, MD.

World Meteorological Organization (WMO). 2009. *Manual for Estimation of Probable Maximum Precipitation,* 1045, WMO, Geneva, 259.

Proceedings of Tailings and Mine Waste 2019
November 17–20, 2019, Vancouver, Canada
Published by the University of British Columbia, 2019

Developing a Sustainable Local Native Forb Seed Source to Maintain Biodiversity at an Arctic Mine

Alison Kelley, fuse & traverse, llc, USA
Peter Johnson, fuse & traverse, llc, USA
Johanna Salatas, Teck Alaska, Inc., USA

Abstract

Restoring the land at one of the largest zinc mines in the world is one of the cornerstones of an operating agreement between the Alaska Native NANA Regional Corporation ("NANA") and Teck Alaska, Inc. ("Teck"), the mine operator. Revegetation is necessary to stabilize disturbed lands and control erosion, but the lack of arctic-adapted native seed species, especially forbs, presents challenges to soil development and maintaining the local biodiversity. Additionally, the use of commercially available seed on reclaimed lands can introduce non-local and unintended species and result in poor viability in arctic conditions. Noatak is a remote community near the mine with similar climate and habitat conditions. NANA and Teck collaborated with the State of Alaska Plant Materials Center ("Plant Materials Center") to develop a program to identify and harvest native forbs in Noatak that could be used to reclaim disturbed lands at Red Dog Mine ("Red Dog"). The opportunity for community members to develop a seasonal seed harvest business presented an additional benefit. The team trained local adults and high school students to key the target plants, evaluate seed maturity, and harvest seed. Seed was harvested during two arctic growing seasons, including two harvest events in 2015 and two harvest events in 2016. Phenology data for species observed in 2015 and 2016 were used to develop a flowering calendar to identify potential future harvest periods. The seed was tested for purity and germination. The results confirmed high purity and germination in seed that was harvested from five species of forbs and one grass species.

In 2017, four species of the locally harvested forb seed were combined with a prescribed Alaska native grass seed mix (approximately 94% grasses and 6% forbs) that was applied to mulched and un-mulched test plots on a waste rock stockpile at Red Dog to evaluate potential seed viability for the challenging growing conditions on the waste rock. An additional plot was seeded with one forb species and no grasses. The plots were amended with 20-20-10 fertilizer. Mulch was selectively applied to test plots to enhance moisture and seed retention. Thereafter, the test plots received only local precipitation and were not otherwise treated during the growing season. Mulched and un-mulched plots were compared to evaluate

the benefits and cost-effectiveness of mulch. At least two of the Noatak seed forb species were observed in the first (2017) and second (2018) growing seasons. By the second growing season, forbs represented 1% of the total vegetation cover in at least one test plot. Monitoring is ongoing, but initial observations indicate that at least two native forb species may be viable options to effectively reclaim disturbed lands.

Introduction

Since 1982, NANA Regional Corporation, an Alaska Native Corporation, has maintained an agreement with Teck Alaska, Inc., to operate Red Dog, one of the world's largest zinc mines, located in remote northwest Alaska, USA. All materials that enter or leave Red Dog Operations are transported by air or sea. Teck's operating agreement with NANA stipulates that, "to the extent reasonably practicable," disturbed lands shall be restored "to a condition compatible with the surrounding land." State regulations specify that permittees shall reclaim lands to the standards established in *A Revegetation Manual for* Alaska (Wright, 2008). *The northwest A*rctic presents unique challenges to revegetation success, including temperature extremes, a short growing season, and periods of heavy precipitation alternating with very dry conditions. Commercial seed mixes suitable for reclamation in the region typically consist of grass species; arctic-adapted forbs are not available for purchase. To honour its agreement with NANA and its sustainability commitments, Teck sought local sources of native seed species, particularly forbs, that are adapted to climate conditions similar to those at Red Dog. In 2015, NANA developed the work plan and committed resources to implement the first year of the Noatak Seed Source Pilot Study, with financial support from Teck and technical support from the Plant Materials Center. Teck assumed full responsibility for the program in 2016.

Noatak is a village of approximately 500 Alaska Natives located approximately 60 km (37 miles), by air, from Red Dog, on the Noatak River, and approximately 75 km (45 miles) from the regional hub community of Kotzebue, Alaska. There are no roads connecting Noatak to other communities; the primary modes of transportation include two commercial regional airlines, overland travel by snow machine (winter only), and via boat on the Noatak River (summer only). The shallow river conditions do not support barge travel, so fuel and supplies are delivered by air. Noatak is governed by the local tribal council (Native Village of Noatak) and has a school, a clinic, a store, and a church. Most community members are employed by the tribe, school, clinic, etc., or at Red Dog.

Noatak exhibits similar climate, habitat, and plant communities as Red Dog. The community members practice traditional subsistence hunting and gathering for survival. Given the close geographical similarities and proximity between Red Dog and Noatak, combined with limited local employment opportunities, Noatak's subsistence culture, and the abundance of traditional knowledge in the community, Noatak was selected to implement the Seed Source Pilot Study. The goals of the pilot study were to:

1. identify native arctic forbs to improve soil health and maintain biodiversity;
2. determine if one or more target species was available to harvest in Noatak;
3. train community members to identify, harvest, and ultimately sell local native seed to Red Dog;
4. evaluate the quality and viability of the seed harvested from Noatak on reclaimed lands at Red Dog; and
5. develop a market price schedule for seed harvested in and purchased from Noatak.

The first three goals were addressed in the first phase of the study. The second phase of the pilot study (2017, ongoing) addressed the fourth goal and consisted of constructing revegetation test plots at Red Dog to evaluate the success of the seed harvested from Noatak in the reclamation conditions at the mine. The fifth goal, the market price analysis, is in progress and is not addressed in this paper.

Methodology

Community outreach

Beginning in the spring of 2015 and continuing through the summer of 2016, the study team hosted a series of community workshops to educate the community about the seed program and related job opportunities. The workshops consisted of plant identification, seed harvest and cleaning demonstrations and, depending on the weather and the level of interest, community plant walks.

The community plant walks provided an opportunity to:

- develop relationships between the study team and the community members;
- familiarize potential harvesters with the target plant species at different phenological stages;
- utilize traditional ecological knowledge to locate potential harvest areas; and
- demonstrate responsible harvest practices to sustain the long-term health of the target species.

The community plant walks were also effective in locating potential seed harvest sites within an approximately 15- to 30-minute walk from Noatak.

Plant identification and harvest site selection

Harvest site reconnaissance was conducted in June, July, and August of 2015 and July and August of 2016 to evaluate the growth phase of the plants identified for harvest. The potential harvest sites were qualitatively evaluated for abundance to ensure that sufficient seed was available to harvest without impacting the long-term health of the species or harvest location. The species' value to reclamation, such as nitrogen fixation or habitat biodiversity, and the economic factors for each species, were also considered. For example, *Deschampsia cespitosa* (tufted hairgrass) is available to harvest in Noatak but is also

commercially grown and has demonstrated viability in the northwest Arctic, so it is unlikely that local harvest can compete with the commercial seed market. Ultimately, six target species were selected for harvest in Noatak, including one grass: *Calamagrostis canadensis* (reed bluejoint); and five forbs: *Artemisia arctica* (lesser boreal sagebrush), *Astragalus aboriginum* (Indian milkvetch), *Chamerion latifolium* (dwarf fireweed), and *Eriophorum scheuchzeri* (Scheuchzer's cottongrass). The final harvest locations consisted of four sites within walking distance of Noatak and five river sites accessed by boat. Each of the river sites was located within approximately 3 km (2 miles) of Noatak. The observations from the site selection reconnaissance were used to estimate a flowering calendar for the target species that would be grown in Noatak.

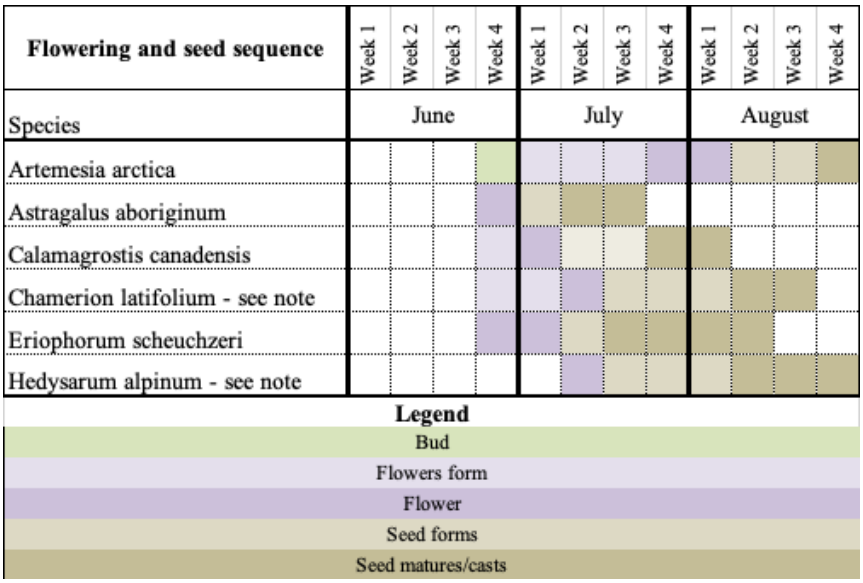

Figure 1: Estimated flowering calendar for Noatak species

Seed harvest

The study team utilized clean, breathable, cotton pillow cases or burlap sacks ("seed bags") provided by the Plant Materials Center[1] to collect seed. A sample of ten of each type of seed bag was weighed, and the average weight for each bag type was used as the tare weight for the empty seed bags. Each bag was labeled with the sample ID, harvester name, date, a three-letter abbreviation for the species' common name, and the harvest start and end times. This information was logged on a chain of custody for the Plant Materials Center.

The study team mobilized to the harvest site, documented the site coordinates, and spent approximately 15 minutes with the crew keying plants, locating harvestable quantities of seed, and checking for seed maturity. The study team reviewed clean harvest techniques to ensure only the target species were

[1] During this study, co-author Peter Johnson was employed by the PMC, a division of Alaska DNR, and this project was a collaboration between DNR, NANA, and Teck/Red Dog.

collected and to minimize debris and then proceeded to harvest. To ensure sustainable harvest practices, harvesters were directed to collect seed from no more than 75% of the individual plant (e.g., to collect seed from no more than 2 of 3, 3 of 4, 7 of 10, etc. seed-bearing stems from any one plant). The study team harvested alongside the harvesters to conduct occasional quality checks.

The harvest period ranged from approximately 15 to 60 minutes per site, or until the site was sufficiently harvested, whichever occurred first. The harvest duration was consistent with Plant Materials Center observations of other community harvest programs, such as invasive weed harvests, that demonstrated most workers can maintain interest for 45 to 60 minutes. When the harvest was complete, the group moved to a new harvest site.

C latifolium, *E scheuchzeri* and other species produce seeds inside seed dispersal structures, such as cotton-like seed heads (pappi). *C canadensis* seed is contained in a cluster-like panicle, or flower head. These seed dispersal structures were collected to minimize the loss of seed during harvest. Seed harvested in the field was defined as *pre-cleaned seed*, as it had been harvested to minimize debris and non-target species, but not the seed dispersal structure or flower head, and required mechanical cleaning at a later date. At the end of each harvest day, the study team weighed and recorded the mass of pre-cleaned seed collected by each harvester. The full bags of seed were placed into cardboard boxes to permit air circulation and then stored in a locked outdoor shed until they were hand-delivered to the Plant Materials Center.

Seed quality

The pre-cleaned seed was shipped to the Plant Materials Center for mechanical cleaning and purity and gemination tests. Prior to cleaning, the Plant Materials Center weighed each bag of pre-cleaned seed to confirm the field weight. The mechanical cleaning equipment is designed for farm-scale operations and requires a large mass of seed to operate. There was insufficient seed mass to mechanically clean each harvester's seed individually, so the total of all seed harvested for a single species, e.g., *C latifolium*, was combined into a single lot for cleaning and testing. For this reason, it was not possible to evaluate the quality of the seed for each individual harvester. The Plant Materials Center conducted purity and germination tests on the cleaned lots for each seed species.

To quantify the lot debris %, that is, the percentage of non-seed material, the lot weight of a single species of cleaned seed was subtracted from the lot weight of the pre-cleaned seed and divided by the lot weight of the pre-cleaned seed.

$$\text{Lot debris \%} = \frac{\text{weight of precleaned seed} - \text{weight of clean seed, grams}}{\text{weight of precleaned seed, grams}} \times 100$$

Commercial seed is typically sold as pure live seed (PLS), which is the weight of the cleaned seed multiplied by the % purity and the % germination.

$$PLS = weight\ of\ clean\ seed, grams \times Purity, \% \times Germination, \%$$

The percent yield compares the theoretical mass of pure, live seed that could be attained if the seed was 100% pure and 100% of the seed germinated, to the actual yield of pure, live seed.

$$\%\ \text{Yield} = \frac{(\text{actual yield of pure live seed, grams})}{(\text{theoretical mass of pure, live seed, grams})} \times 100$$

Revegetation test plots at Red Dog

The Main Waste Stockpile consists of waste rock that Red Dog generates from the mining process. It occupies approximately 77 hectares (190 acres) and is approximately 380 m (1,200 feet) above mean sea level at its top surface. As currently constructed, reclamation of the Main Waste Stockpile is expected to require approximately 5,300 kg (12,000 pounds) of grass seed, applied at a rate of 47.3 kg per hectare (kg/ha) (42.5 pounds per acre (lb/ac)), and approximately 310 kg (690 pounds) of forb seed, applied at a rate of 2.8 kg / ha (2.5 lb/ac), to complete revegetation.

The reclaimed surface of the Main Waste Stockpile is planned to consist of an approximately 45 to 60 centimeters (18 to 24 inches) thick cover of clean, non-mineralized Kivalina shale (SRK Consulting [US], Inc., 2016). The growing conditions on the Main Waste Stockpile present potentially significant challenges during the first one to three years of plant growth. Kivalina shale consists of gravel and cobble-sized particles with limited fines to retain moisture. Data from baseline soil samples indicated the material contained very low soil organic matter (mean, 0.35%), which is necessary to retain nutrients, and the estimated nitrogen release (range, 9 to 16 kg / ha (8 to 14 lb/ac)) was less than 20% of the amount recommended for cool season grasses (Spargo et al., 2013), which is insufficient to support plant growth without fertilizer. The Main Waste Stockpile is not equipped with power or water, so water to support plant growth is limited to natural precipitation. The flat, top surface ("top deck") of the Main Waste Stockpile is exposed to sustained high winds. Field observations in test pits at a similarly reclaimed stockpile at Red Dog demonstrate that, once vegetation has been established, Kivalina shale breaks down to support long-term plant growth. The test plots indicate that despite the conditions it is possible to attain first and second year plant growth on the Main Waste Stockpile.

In 2017, four revegetation test plots ("test plots") were constructed on the top deck of the Main Waste Stockpile to evaluate the success of both the forb seed harvested from Noatak and the prescribed grass seed mix, as well as how the application of commercial mulch affected the performance of the test plots. Each test plot was approximately 84 m^2 (900 ft^2) and was subdivided into two 42 m^2 (450 ft^2) sub-plots[2]. The plot grass and forb seed mixes and the fertilizer and mulch treatments are described in the following tables.

[2] The single forb plot, ASTR, was not subdivided.

All commercial grass seed was prepared to order by Alaska Garden and Pet Supply. One sub-plot in each of the test plots was treated with commercial mulch (Hydromulch1000® and Earthbound TerraNovo® tackifier) that was applied with a Finn T120 HydroSeeder®, at either 50% or 100% of the specified manufacturer's application rate ("MAR"). All test plots were treated by hand with an initial application of commercial fertilizer (United Agri Products 20-20-10 fertilizer) using a broadcast seed spreader. Only four of the Noatak species were used in the mix. The grass species, *C canadensis*, was excluded because it was not prescribed by the Plant Materials Center, and *E scheuchzeri*, a wetlands forb, was not suitable for use given the dry conditions of the main waste stockpile.

Table 1: Test plot parameters

Plot name	Seed type	Estimated area (square meter)	20-20-10 Fertilizer application rate, kg/ha	Mulch: % of manufacturer's application rate
G100	Grass	42	168	None applied
G100	Grass	42	168	100%
GF100	Grass + forb	42	168	None applied
GF100	Grass + forb	42	168	100%
GF50	Grass + forb	42	168	None applied
GF50	Grass + forb	42	168	50%
ASTR	*A aboriginum* only	84	168	None applied

Table 2: Test plot grass species mix

Common name	Species name	Maturity	Origin	Percent of mix	Germi-nation	PLS mass applied: g/plot	Applica-tion rate: kg ha
Nortran tufted hairgrass	*Deschampsia cespitosa*	Late season	AK	28.87%	83%	86	10
Boreal red fescue	*Festuca rubra*	Early to mid-season	CAN	19.67%	85%	59	7.3
Glaucous tundra bluegrass	*Poa glauca*	Late season	AK	23.87%	95%	82	9.9
Gruening alpine bluegrass	*Poa alpina*	Early season	AK	24.52%	94%	82	10
Wainwright slender wheatgrass	*Elymus trachycaulus*	Late season	AK	94.96%	80%	68	8.3

Table 3: Test plot forb species mix

Common name	Forb species name	Maturity	Origin	Percent of mix	Germi-nation	Purity	PLS mass applied: g/plot	Applic-ation rate: kg/ha
Indian milkvetch	*Astragalus aboriginum*	Late season	Noatak	25%	91%	98%	4.5	0.6
Lesser boreal sagebrush	*Artemisia arctica*	Late season	Noatak	25%	87%	100%	4.5	0.6
Dwarf fireweed	*Chamerion latifolium*	Late season	Noatak	25%	83%	99%	4.5	0.6
Masu (Eskimo potato)	*Hedysarum alpinum*	Late season	Noatak	25%	75%	96%	4.5	0.6

Data and discussion

Local seed harvest program

The long-term goal of the program is to develop local harvesters to collect and sell seed by weight (piece rate) to Red Dog, however the study team needed to pay local harvesters during the pilot study to generate baseline harvest rate and seed quality data. Due to the lack of a defined commercial demand for and supply of the target species, seed prices were not available to pay harvesters a piece rate, so the study team paid harvesters the minimum local labour rate ($15/hour) established by the Native Village of Noatak to attend training workshops, harvest seed, and travel to and from harvest sites.

Two harvest events were conducted in each year of 2015 and 2016. The number of harvesters, excluding the study team members, increased from four in 2015 to a maximum of 27 in 2016, with an average of six harvesters. The make-up of the harvest crew changed daily due to conflicts with subsistence activities, lack of interest, or the addition of new harvesters. Two of the 2015 harvesters returned to the program in 2016 and 11 of the harvesters who attended the July harvest in 2016 returned for the August harvest.

The study team hosted two additional workshops to train selected individuals to harvest unsupervised so they could sell the pre-cleaned at a suggested piece rate established from harvest rates and the market price study (in progress). An established piece rate would offer efficient harvesters the opportunity to earn

significantly more income than the hourly rate, and Teck has committed to buy all seed harvested from Noatak. The study team provided pre-weighed bags and a scale to the Native Village of Noatak to weigh and purchase seed from the harvesters and get reimbursed by Teck. Despite these efforts, no harvesters collected seed in 2017 or 2018. The study team explored this issue with community members but were unable to identify a root cause. One explanation is that, although community members are accustomed to selling consumable harvested resources, such as local berries, the concept of selling a cash crop such as seed, which cannot be eaten or used in another way to support survival, is not consistent with the subsistence culture.

The Noatak River is a vital transportation route that connects community members to the subsistence hunting, fishing, and plant resources. The study team originally planned to identify harvest sites near fish camps and hunting areas along the river to collocate seed harvest with these activities, but later learned that, during subsistence season, there is little opportunity to engage in other activities such as harvesting seed. Ultimately, the study team conducted reconnaissance by helicopter, river boat, and on foot to identify harvest locations that harvesters could easily access on foot or via boat on their own schedule.

The Noatak River is a braided river system and subject to significant flooding ("freshet") and erosion during the spring ("break-up"). The river had changed significantly between 2015 and 2016, so that some of the river sites that were harvested in 2015 were difficult to locate or had been washed away or naturally stripped of vegetation. Other conditions, such as heavy rains and breakup, appeared to have changed the plant communities at the 2015 river locations.

For example, plants in the prime *H alpinum* harvest sites harvested in 2015 produced very little seed, while the abundance of *A aboriginum* seed was significantly higher than in 2015. New river harvest sites were selected in 2016 based on accessibility, and access to the sites changed daily. Meltwater from the upriver mountains and storms contributed to high fluctuations in the river stage throughout the day, such that the study team had to pay attention to changing conditions throughout the day and change harvest sites accordingly.

Seed quality

Three measures were used to evaluate the quality of the seed harvested from Noatak: lot percentage of non-seed material (lot debris %), % purity, and % germination.

Table 4: Seed quality measures for seed lots harvested in 2016

Genus species	Pre-clean seed, grams	Clean seed, grams	Lot debris, %	Germination, %	Purity, %	Certified seed (g) (clean/pure/ germ)	% yield
Artemisia arctica	153	27	83	87%	100%	23	87%
Astragalus aboriginum	595	312	48	91%	98%	278	89%
Astragalus aboriginum	1673	822	51	91%	98%	733	89%
Calamagrostis canadensis	851	40	95	92%	98%	36	90%
Calamagrostis canadensis	110	2.8	97	92%	98%	2.5	90%
Chamerion latifolium	12531	765	94	83%	99%	628	82%
Eriophorum scheuchzeri	1470	510	65	37%	100%	189	37%
Eriophorum scheuchzeri	432	78	82	37%	100%	29	37%
Hedysarum alpinum	376	127	66	75%	96%	91	72%

The lot debris % was used as an indicator to infer the mass of pre-cleaned seed required to attain a target mass of clean seed. *A aboriginum* exhibited the lowest lot debris % (51%), which is consistent with the seed pod structure, which opens and sheds easily in the field. *C canadensis* (95% and 97%, per lot) and *C latifolium* (94%) exhibited the highest lot debris %, which is expected due to the seed dispersal structures.

The percent purity was high (range, 96 to 100%) and is consistent with seed obtained from trained hand harvesters, whereas mechanical harvesting collects all plant matter in the harvest path and thus results in a lower purity percentage. The high purity indicates the effectiveness of the field training effort and high performance of the harvesters. The percent germination was high (range, 75% to 92%), with the exception of *E scheuchzeri* (37% for both lots). Field verification indicated that the *E scheuchzeri* seed appeared mature. Although not ideal for upland reclamation, which was the focus of this particular study, the species is still recommended for harvest to revegetate wetlands habitats. With the exception of *E scheuchzeri*, the percent yield of all species collected was good (range, 72% to 90%).

Revegetation test plots

Monitoring data collected from the Main Waste Stockpile during the first growth year (2018) indicated that two of the Noatak species, *A arctica* and *A aboriginum*, represented 1% of the total vegetative cover on the test plots, which is consistent with the forb seed application rate and suggests they may be a viable revegetation option at this site going forward. Monitoring is ongoing.

Table 5: Test plot monitoring data, June 28, 2018

Plot name	Total cover	Increased cover, M v. U	Grass cover	*Poa glauca*	*Poa arctica*	*Deschampsia caespitosa*	*Festuca rubra*	*Elymus trachycaulus*	Forb cover	*Astragalus aboriginum*	*Hedysarum alpinum*	*Artemisia arctica*	*Chamerion latifolium*
G100-U	75%	20%	75%	DOM[3]	DOM	0%	0%	Trace	0%	0%	0%	0%	0%
G100-M	90%		90%	DOM	DOM	0%	0%	Trace	0%	0%	0%	0%	0%
GF100-U	80%	6%	79%	DOM	DOM	DOM	0%	trace	1%	Pos-sible	0%	1%	0%
GF100-M	85%		85%	DOM	DOM	0%	0%	trace	trace	0%	0%	trace	0%
ASTR-U	50%	20%	49%	0%	DOM	DOM	0%	trace	1%	0.5%	0%	0.5%	0%
ASTR-M	60%		59%	DOM	DOM	0%	0%	trace	1%	1%	0%	0%	0%
GF50-U	45%	89%	45%	DOM	DOM	0%	0%	trace	–	–	–	–	–
GF50-M	85%		85%	DOM	DOM	0%	0%	trace	trace	0%	0%	trace	0%

Conclusions

The study achieved four of the stated goals. Six species of arctic-adapted native plants were identified in the Noatak area in harvestable quantities, including five forb species and one grass species. Four of the forb species (*A arctica*, *A aboriginum*, *C latifolium*, and *H alpinum*) are suitable for uplands revegetation projects and one (*E scheuchzeri*) is suitable for wetlands revegetation. The commercial availability of *C canadensis* is in decline, which may increase the value of *C canadensis* harvested from Noatak in the future. *A aboriginum* and *H alpinum* are nitrogen fixing, which supports the goal of improving soil health. Further investigation may identify additional species to harvest in the Noatak area.

The purity and germination results demonstrated that high quality seed was attained for five of the six species. Despite the relatively low germination rate of *E scheuchzeri*, this wetlands species is not commercially available and provides value for tundra revegetation. The high quality of seed harvested in

[3] DOM = dominant

Noatak demonstrates the potential viability of a future local market for such seed; however, the success of the training program was somewhat limited due to lack of commercial interest from the local community.

Two of the forb species, *A arctica* and *A aboriginum*, have emerged in the test plots, indicating initial success on the Main Waste Stockpile. Continued monitoring is necessary to demonstrate long-term success for these species.

In addition to the stated goals, the study resulted in the strengthening of community relationships. The team stayed with a local family in Noatak, interacted and worked directly with the community, shared study results, and trained youths as well as adults. As a result, the community has begun to embrace the program. In addition, the program provided the study team with the opportunity to provide ad hoc workshops in the schools so that young people could learn more about the science underscoring the program. Recommendations going forward include a continued effort to develop a local seed sales business, identify additional forbs to harvest, and explore the application of grass and forb "mulches" (i.e., seed that has not been mechanically cleaned) to potentially improve moisture and seed retention, reduce the cost of seed processing, and offset or preclude the use of commercial mulch.

Acknowledgements

The study team wishes to acknowledge the community of Noatak and the Native Village of Noatak for their support of the project and welcoming the study team into the community, and Mrs. Rachel Sherman, an Inupiaq translator, for her assistance with local plant names.

References

Spargo, J., T. Allen and S. Kariuki. 2013. Interpreting your soil test results. Retrieved from The Center for Agriculture, Food, and the Environment at https://ag.umass.edu/soil-plant-nutrient-testing-laboratory/fact-sheets/interpreting-your-soil-results

SRK Consulting (US), Inc. 2016. Reclamation and Closure Plan Red Dog Mine, Alaska, USA. Anchorage, Alaska: Teck Alaska, Inc.

Wright, S.J. 2008. *A Revegetation Manual for Alaska* (edited by P. Hunt). Palmer, Alaska, USA: Alaska Plant Materials Center.

Proceedings of Tailings and Mine Waste 2019
November 17–20, 2019, Vancouver, Canada
Published by the University of British Columbia, 2019

Geochemical Assessment of Tailings, Soils, and Sediments along the Areas Affected by the Samarco Dam Breach

Kristin Salzsauler, Golder, Canada
Thais Moreira Amaral, Golder, Canada
Rens Verburg, Golder, USA
Cheryl Ross, Golder, USA
Antônio Freitas, Golder, Brazil
Luis H. Melges Figueiredo, Golder, Brazil
Pedro Ivo Diógenis, Fundação Renova, Brazil

Abstract

On November 5, 2015, the Fundão tailings dam at Samarco's Germano Mining Complex in Brazil failed, releasing approximately 43.8 million cubic meters (Mm^3) of iron ore tailings, dam construction materials, and other debris into the upper Rio Doce during the first two quarters after the collapse of the dam. These tailings and debris travelled for approximately 670 km along the river system until they reached the Atlantic Ocean, with some portion being deposited along river beds and flood plains.

An advanced geochemical characterization program was developed as part of the research to understand the environmental impacts of the dam breach and to support decision-making related to rehabilitation. The primary objective of the program was to determine the environmental stability of the tailings, soil, and sediment present in the various depositional environments. Over 300 samples were collected from affected and unaffected areas, the latter to establish reference conditions, in an area extending from the Fundão dam to the coastal zone in the Atlantic Ocean. A phased program was implemented, which included a wide range of industry-standard and custom-made static, kinetic, and mineralogical tests. Results were evaluated statistically and compared to available regulatory standards and regional reference databases. A robust field and laboratory quality assurance/quality control program was employed to ensure data quality objectives were achieved.

Tailings samples generally contained some of the lowest concentrations of trace metals and were the least reactive of the material types tested because they consisted of insoluble mineral phases (i.e., hematite and goethite) that effectively sequester the trace metals. In contrast, the samples of soils and sediments

collected from areas unaffected by the released tailings presented some of the highest trace metal concentrations and contained a greater proportion of soluble mineral phases (i.e., reducible Fe/Mn (hydr)oxides). Soil and sediment samples collected from affected areas are a physically and chemically heterogeneous mixture of soils and/or sediments and tailings. The chemical composition of soils and sediments from the areas affected and unaffected by the tailings dam failure is influenced by regional, naturally-occurring mineralization and anthropogenic activity.

Multiple lines of evidence contributed to the principal conclusion of this program: that the tailings generally contained some of the lowest concentrations of trace metals and were the least reactive of the material types tested. This study provided a robust basis for understanding and evaluating the potential chemical impacts to the environment resulting from the Fundão tailings dam breach. In addition, the geochemical data support other studies necessary to understand the full effect of the breach as well as the identification of appropriate rehabilitation measures.

Introduction

Samarco Mineração S.A. (Samarco) operates the Germano Industrial Unit, an iron ore mine located in Mariana Municipality, Minas Gerais State, Brazil. Coarse tailings and fine tailings were discharged as a slurry to the Germano and Fundão conventional tailings impoundments, which were constructed in a river valley with tailings dams constructed at the downstream ends. The Fundão tailings dam failed on November 5, 2015, releasing approximately 43.8 Mm^3 of iron ore tailings, dam construction materials and other debris into the upper Rio Doce river system during the first two quarters following the collapse of the dam (Fundação Renova, 2016).

A geochemical investigation was initiated after the Fundão tailings dam failure to support decision making with respect to management of the spilled tailings. This paper discusses the geochemical and mineralogical signature of the spilled tailings, soils and sediments within the drainages downstream of the Fundão tailings storage facility (TSF) affected by tailings deposition. The short-term and long-term environmental stability of the tailings, soils and sediments, including the potential for mobilization of metals (i.e., transfer from the solid to solution phase) was evaluated based on chemical composition, mineralogical characteristics, the results of short and long-term leach tests, and geochemical speciation modelling.

Fundão tailings dam failure

Following the failure of the Fundão tailings dam, tailings deposition extended from the Fundão TSF to the Atlantic coast (Figure 1). Located immediately downstream of the Fundão TSF is the Santarém dam, a water retention facility. Material released from the Fundão TSF overtopped the Santarém dam, resulting in

some erosion of this structure. The tailings slurry continued downstream from the Santarém dam through a small creek, Córrego Santarém, and subsequently entered the Rio Gualaxo do Norte, which discharges to the Rio do Carmo, which in turn flows into the upper Rio Doce. In the upper Rio Doce, when the debris flow entered the Candonga reservoir (Risoleta Neves hydropower plant) a large volume of material settled within the reservoir. Finer suspended materials exited the reservoir via the dam spillway. Some of these suspended materials settled out within the Rio Doce, between the Candonga dam and the next hydropower plant, the Baguari reservoir. Smaller particles remained in suspension along the mid and lower sections of the Rio Doce to its mouth.

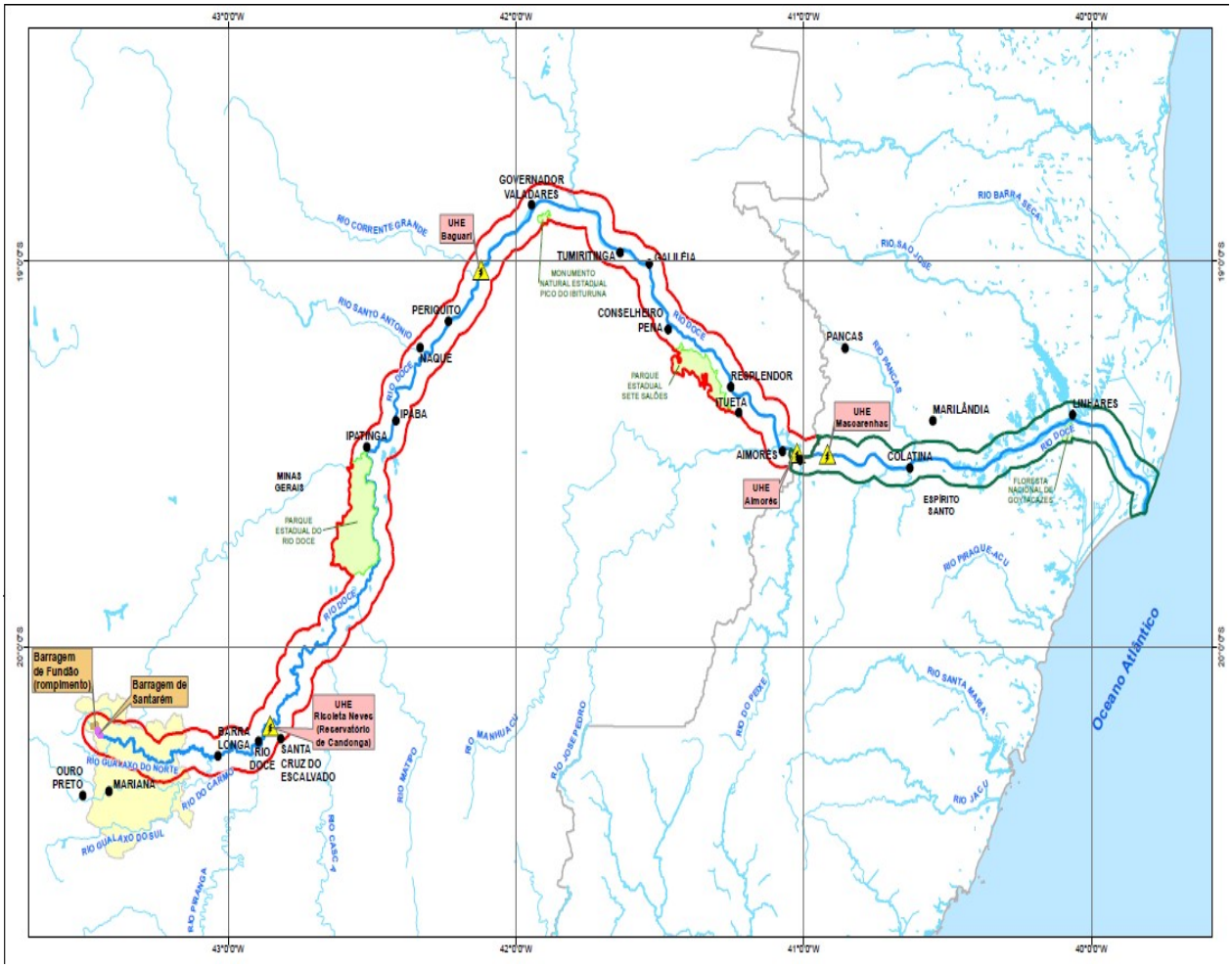

Figure 1: Overview of geochemical study area

Soils and sediments were scoured, and vegetation removed along the flowpath, resulting in a mix of tailings, soils, sediments, vegetation and other debris being deposited on the floodplains, in stream channels of the main rivers, and along edges and mouths of tributaries as the flood wave receded and/or flow velocities slowed in certain areas.

Sample collection and analysis

The geochemical dataset consists of a compilation of data collected for tailings from the Germano TSF (located adjacent to the Fundão TSF) prior to 2014, as well as data resulting from geochemical characterization of samples collected from areas downstream of the Fundão tailings dam, collected in 2016 and 2017, after the failure.

Tailings samples from the Germano TSF were obtained and analyzed by Samarco in 2013 and 2014 as part of a resource investigation.

Sample collection following the Fundão tailings dam failure took place in two stages. In 2016, over 300 samples of tailings, soil and sediment were obtained to evaluate the geochemical characteristics of areas affected by Fundão tailings ("Geochemical Characterization Program"). In 2017, additional samples were collected from areas directly downgradient of the Fundão tailings dam and from a sample location in Rio do Carmo to evaluate the geochemical composition of a "supernatant" (surficial layer of floating particulate matter) observed in the water column at these locations ("Colloid Investigation").

As part of the geochemical testing programs, samples were submitted for solid phase characterization including whole rock analysis, bulk elemental analysis, mineralogical analysis (including X-ray diffraction (XRD) with Rietveld refinement, mineral liberation analysis (MLA), and scanning electron microscopy (SEM)), grain size analysis and acid base accounting (ABA; including carbon and sulphur speciation). Samples underwent a variety of short-term leach tests, including acid leaching (AL) and deionized water dissolution (DWD) according to Brazilian methods ABNT NBR 10005/2004 (ABNT, 2004a) and ABNT NBR 10006/2004 (ABNT, 2004b), river and sea water leach tests using a method modified from USEPA (1998), and targeted pH leach tests (initial pH of 2, 4, 6, 8 and 9) using a method modified from USEPA (2012). Samples were submitted for sequential extraction using the method presented in Tessier et al. (1979). A subset of samples were submitted for humidity cell testing according to method ASTM 5744 (ASTM, 2013) and column tests using the method outlined in MEND (2009).

Geochemical characteristics of tailings from the Germano TSF

Tailings were discharged to the Germano TSF between 1977 and 2015. The Germano tailings are considered by Samarco to be very similar in chemical and physical composition to the Fundão tailings as they were produced from ore mined from the same three open pits.

Two tailings types were generated: sand (coarse) and fine tailings, each with distinct chemical characteristics. Chemically, the coarse tailings were characterized by a higher silica (SiO_2) content than the fine tailings (i.e., approximately 80 and 20 percentage by weight [wt. %] for the coarse and fine tailings, respectively). The iron content of the fine tailings (i.e., approximately 50 wt. %) was higher than that of the

coarse tailings (approximately 14 wt. %); metals and metalloids associated with iron in fine tailings included As, Mn, Mo, Pb and Zn. Pires et al. (2003) reported the mineralogical composition of the Germano tailings to be goethite (~60%), hematite (~25%), quartz (~10%) and kaolinite (~7%).

Four samples of tailings were collected from the Germano TSF following the Fundão tailings dam breach, for the purpose of comparison to samples collected from areas affected by released tailings. These tailings had D_{50} values ranging from 0.098 to 0.141 mm. As presented in Table 1, the Germano TSF samples had the lowest trace metal concentrations (including Sb, As, Ba, Co, Cu, Pb, Ni, Ag, V, and Zn) of all material types evaluated following the Fundão tailings dam breach.

Geochemical, mineralogical and physical characteristics of released tailings, soil and sediment downstream of the Fundão TSF

Several lines of evidence were used to attempt to distinguish the released tailings, and mixtures of tailings, soils and sediment downgradient of the Fundão tailings dam, including particle size, geochemical composition and mineralogical characteristics of samples collected from the flow path.

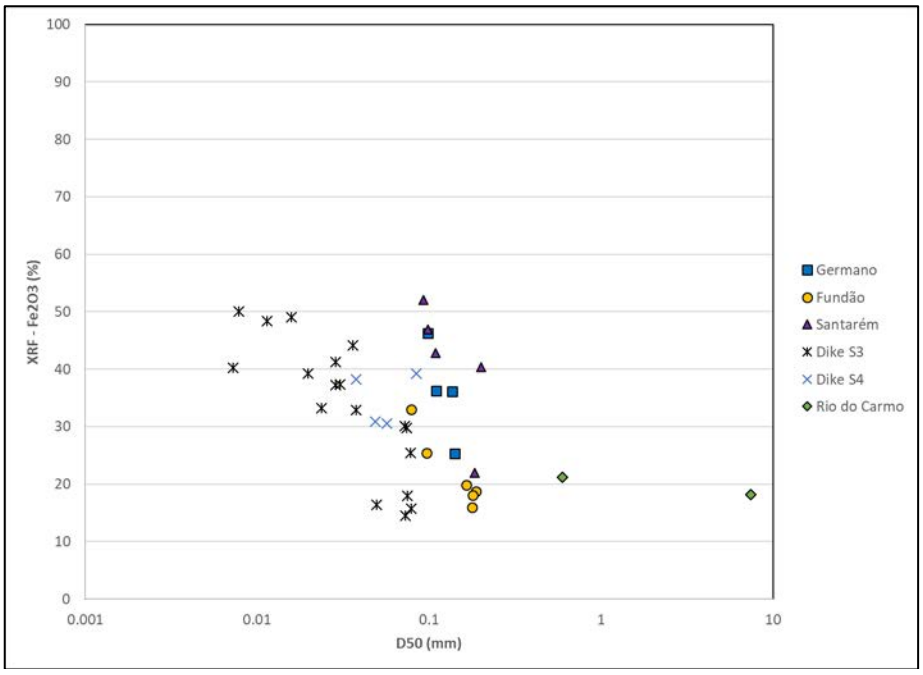

Figure 2: Median grain size of select samples from the Geochemical Characterization Program and Colloid Investigation Program compared to Fe_2O_3 content

Following the dam breach, turbulent mixing of tailings/soils/sediments modified some of the original textural characteristics of the materials, including the particle size distribution. As such, particle size distribution curves and D_{50} values were generated and used to compare the physical characteristics of samples of tailings, mixed soil/sediment, and unaffected soil/sediment. Figure 2 compares the median particle size (D_{50}) of a subset of tailings dominant samples (Germano TSF, Fundão TSF, Dike S3 and Dike

S4) to sediment dominant samples collected from Rio do Carmo. The D_{50} of samples collected from immediately downgradient of the dam breach ranged from 0.01 to 0.175 mm. The maximum particle size of samples collected from the tailings dam was approximately 1 mm. Therefore, any material with a particle size greater than 1 mm could be interpreted to be natural soil and sediments. Material with a particle size less than 1 mm could be tailings, natural soil and sediments, or their mixtures.

Table 1 compares the composition of mixed materials to that of Germano tailings, and unaffected soil and sediment. Like the physical morphology, the chemical and mineralogical composition of the soil and sediment samples affected by tailings deposition is controlled by the degree of mixing of the tailings with soils and/or sediments. While general trends in physical and chemical composition are evident, it is difficult to definitively identify, or "fingerprint" tailings affected materials using a distinct physical or chemical characteristic. In general, the tailings and tailings-rich mixed samples have higher concentrations of iron than unaffected soil and sediments. Unaffected soil and sediments are distinguished by higher aluminum and trace metal concentrations.

Table 1: Summary of solid phase composition of Germano tailings, unaffected soils and sediments, and soils and sediments affected by the Fundão tailings dam breach

Parameter		Al	As	Co	Cu	Cr	Fe	Ni
Unit		mg/kg	mg/kg	mg/kg	mg/kg	mg/kg	mg/kg	mg/kg
Germano tailings	# Results	4	4	4	4	4	4	4
	Minimum	1,433	1	8	4	10	72,047	3
	Average	2,213	4	8	6	18	107,170	3
	Maximum	2,670	7	8	8	37	171,294	3
Sediment-affected area	# Results	97	97	97	97	97	97	97
	Minimum	384	1	8	3	4	7,428	3
	Average	10,803	15	9	6	22	39,673	8
	Maximum	52,643	104	18	28	70	255,867	26
Sediment-unaffected area	# Results	18	18	18	18	18	18	18
	Minimum	2,051	1	8	3	8	9,285	3
	Average	12,684	38	9	7	28	47,759	10
	Maximum	32,308	161	18	27	76	249,436	24
Soil-affected area	# Results	154	154	154	154	154	154	154
	Minimum	360	1	8	3	3	10,925	3
	Average	16,603	10	11	13	36	72,992	12
	Maximum	49,728	63	54	44	79	283,483	36
Soil-unaffected area	# Results	33	33	33	33	33	33	33
	Minimum	1,575	1	8	3	4	6,098	3
	Average	31,550	6	13	17	49	47,548	15
	Maximum	77,693	40	60	102	173	216,529	49

Tailings-dominant materials collected immediately downgradient of the Fundão tailings dam consisted of a mixture of anhedral, angular, grains of quartz, iron oxide and mica. The dominant mineral was quartz, which occurred both as angular, free mineral grains and as intergrowths with Fe oxide minerals (Figure 3). The Fe oxide mineral textures identified in the tailings-dominant samples are typical of the regional laterite profile (Ramanaidou, 2009).

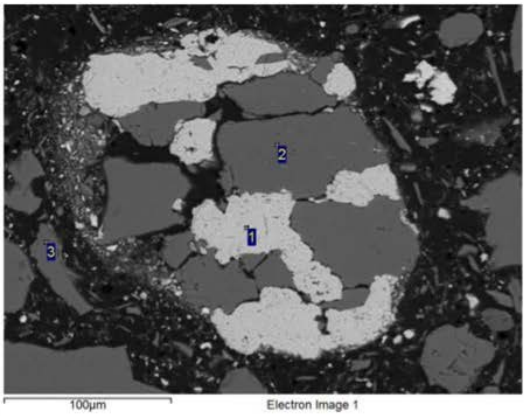

Grain of intergrown Fe-oxide (1) and quartz (2 and 3).

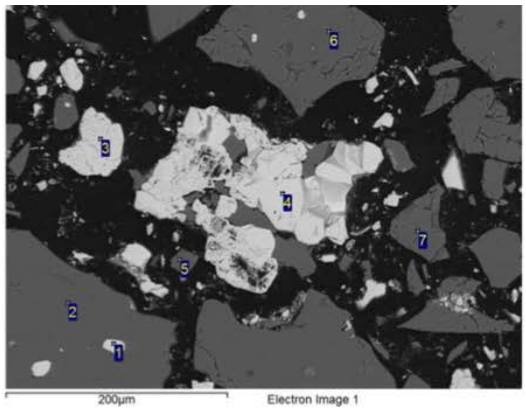

Iron oxide replacement textures in Dike S3 sediments (Fe oxide (goethite (1,3,4)), and quartz (2,5,6,7))

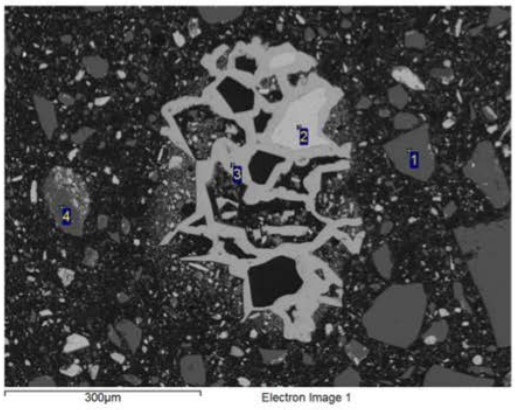

Goethite and hematite textures in Dike S4 sediments (Fe oxide (2,3), quartz (1) and Fe oxide and kaolinite (4))

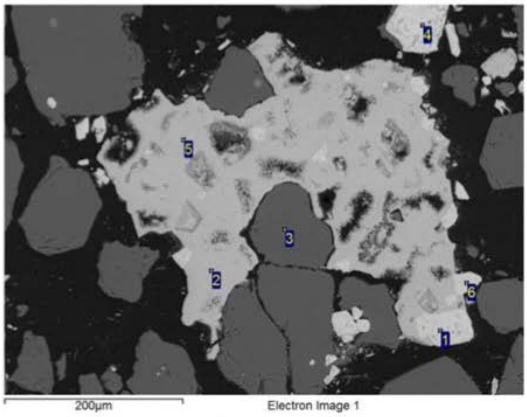

Pseudomorphic replacement texture (Fe oxide (hematite (1, 4, 6)), Fe oxide (goethite (2, 5)), quartz (3)).

Figure 3: Mineralogical textures observed in tailings affected sediments

As lateritic weathering occurs, aluminosilicates and primary iron oxide minerals (e.g., magnetite) in Banded Iron Formation (BIF, the ore unit) are replaced by goethite, hematite, and kaolinite. As observed by Ramanaidou (2009), secondary Fe oxide minerals contain trace concentrations of metals and metalloids incorporated into the mineral structure during mineral weathering and recrystallization; these were detected using EDS spectra (SEM analysis). The chemical analysis also confirmed the presence of secondary amorphous Fe oxide minerals, such as ferrihydrite, which cannot be identified by XRD.

The mineralogical composition of unaffected soil and sediment samples was more complex than that of the tailings' samples. Most unaffected soil and sediment samples were ferruginous soils typical of the

BIF terrains of the Iron Quadrangle. Minerals present in the soils included quartz, various silicate minerals, hematite, goethite and gibbsite. The presence of gibbsite (10 to 12 wt.%) was the main mineralogical difference relative to the Germano dam's tailings. Sequential extraction results for the tailings confirmed that iron was largely contained in the crystalline Fe minerals (i.e., hematite and goethite). In contrast to the tailings samples, up to 10% of the extractable iron in unaffected soil and sediments samples was found in association with the reducible Fe/Mn fraction, which are amorphous Fe-Mn (hydr)oxides. These amorphous minerals represent a mineralogical reservoir that effectively retains trace metals and restricts their release to the aqueous environment, albeit that they are typically more soluble than their crystalline counterparts. In further contrast to the tailings' samples, unaffected soils and sediments contained elevated concentrations of several trace metals. The unaffected soil and sediment samples had the highest concentrations of several parameters in the overall geochemical dataset, including Co, Cu, Cr, Pb, Mn, Ni, Ti, V, and Zn (some parameters shown in Table 1). SEM images of unaffected soils and sediments indicated that these materials were less angular than tailings, and were consistently coarser (Figure 4).

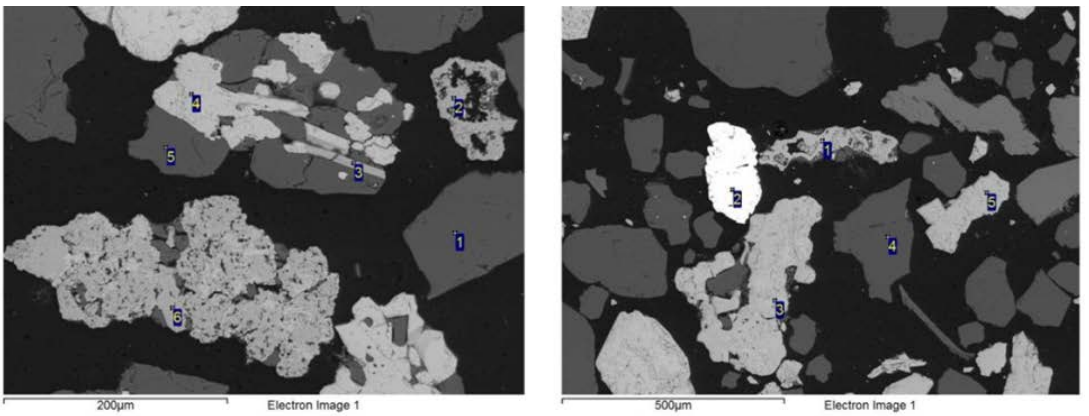

Rounded to sub-angular grains of quartz (1,5), ferrihydrite (2,3,6) and hematite / goethite (4) in unaffected sediments.

Rounded to sub-angular grains of hematite / goethite (1,3,5) and quartz (4) in unaffected sediments.

Figure 4: Mineralogical textures observed in unaffected sediments

Metal mobilization potential from tailings, soils and sediments

Several laboratory-scale leach tests were used to evaluate the potential for metal mobilization from tailings, soils and sediments. The short-term leach test results were used to perform speciation modeling using PHREEQC Version 3.3.5 (PHREEQC), an equilibrium speciation and mass-transfer code developed by the United States Geological Survey (USGS) (Parkhurst and Appelo, 1999). PHREEQC modelling was completed using the Minteq.V4 database. The speciation modelling results were used to evaluate mineral stability for geochemically-credible mineral phases that are known to be present in natural waters and mining environments (Nordstrom and Alpers, 1999).

Metal leaching was most pronounced for Al, Fe, and Mn. In general, metals concentrations in short-term and long-term leachates were low, indicating that the tailings, baseline soils and sediments have a low

potential for metals mobilization. Tailings had the lowest potential for metals mobilization observed in this study, while baseline soils and sediments presented higher leachability. Therefore, metals release to the aqueous environment from affected materials is governed by the natural soils and sediments present in any tailings/soil/sediment mixtures.

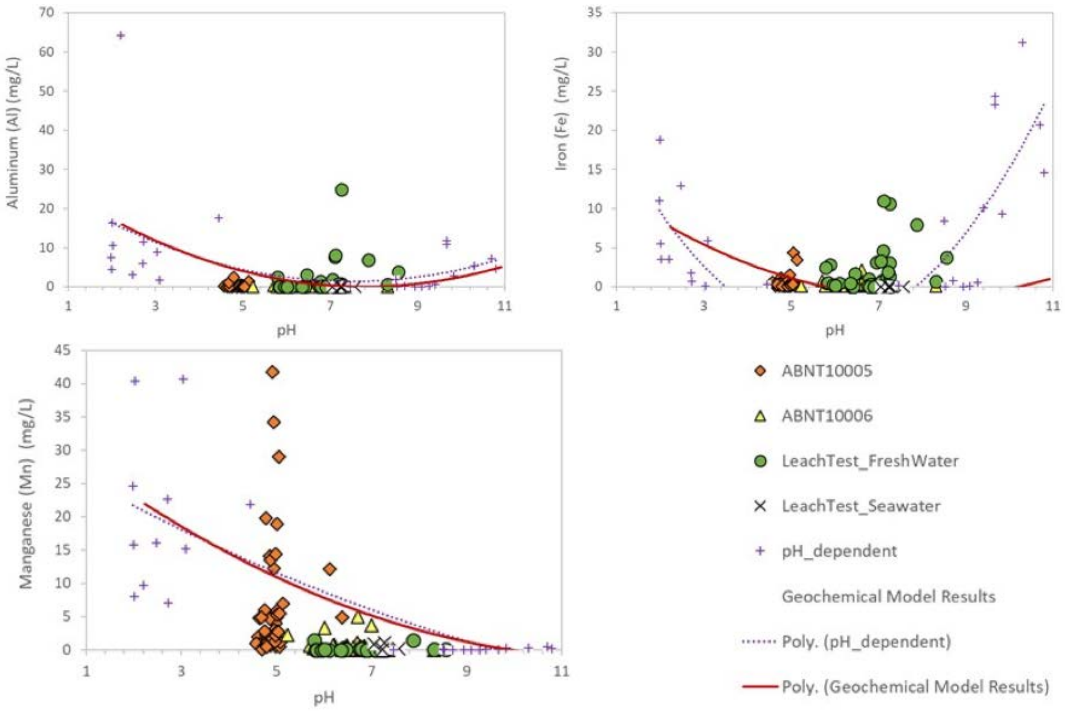

Figure 5: Solubility curves developed using short-term leach test data

As can be seen from the leach test results, the general concentration trend for Fe resembles a U-shape (Figure 5). The U-shaped curve labelled "pH_dependant" is a polynomial regression for the pH-dependant leach test results. This is a typical solubility profile for amorphous Fe (hydr)oxides, commonly captured under the term "ferrihydrite" [am-Fe$(OH)_3$]. Ferrihydrite is known for its significant capacity for retention of trace metals through sorption, and it is considered a very common control on trace metal mobility (e.g., Nordstrom and Alpers, 1999). Geochemical modelling also identified that the solubility profiles of selected trace metals/metalloids (e.g., As, Cu) were consistent with sorption onto ferrihydrite. Aluminum and manganese solubility was found to likely be controlled by gibbsite and manganite, respectively (demonstrated by the curves labelled "geochemical model results" on Figure 5).

Conclusion

In conclusion, tailings released from the Fundão TSF failure in November 2015 have the lowest reactivity, with some of the lowest trace metal concentrations, of the material collected as part of the geochemical characterization study. The tailings consist primarily of quartz and crystalline iron oxide minerals, which are insoluble in the pH conditions present in the river downstream of the TSF.

Baseline soils and sediments contain some of the highest trace metals/metalloids concentrations, while tailings contain some of the lowest. As such, in soils and sediments affected by tailings deposition, the elevated concentrations of these mixtures were derived from their soil/sediment component.

In addition to the higher trace metal/metalloid concentrations present in baseline soils and sediments, these constituents occur in more soluble form than in tailings. In contrast to the tailings' samples, soils and sediments contain amorphous iron hydroxide minerals, that are typically more soluble than their crystalline counterparts. Geochemical modelling confirmed that the solubility characteristics of ferrihydrite and sorption onto ferrihydrite governed release of iron and trace metal/metalloids to the aqueous environment.

References

ASTM Standard D5744-13. 2013. Standard test method for laboratory weathering of solid materials using a humidity cell. ASTM International, West Conshohocken, PA, 2013, DOI: 10.1520/D5744-1.

Associação Brasileira de Normas Técnicas (ABNT). 2004a. ABNT NBR 10005:2004: *Procedimento para obtenção de extrato lixiviado de resíduos sólidos.*

Associação Brasileira de Normas Técnicas (ABNT). 2004b. ABNT NBR 10006:2004: *Procedimento para obtenção de extrato solubilizado de resíduos sólidos.*

Fundação Renova. 2016. *Atualização do Plano de Recuperação Ambiental Integrado – PRAI. Fundação Renova, Belo Horizonte. Dezembro de 2016.* 121 pp.

Mine Environment Neutral Drainage (MEND). 2009. Prediction manual for drainage chemistry from sulphidic geologic materials. MEND Report 1.20.1. December 2009.

Nordstrom, D.K. and C.N. Alpers. 1999. Geochemistry of acid mine waters. The environmental geochemistry of mineral deposits. Part A: *Processes, Techniques, and Health Issues,* 6: 133–60.

Parkhurst, D.L. and C.A.J. Appelo. 1999. User's guide to PHREEQC (Version 2) – A computer program for speciation, batch-reaction, one-dimensional transport, and inverse geochemical calculations, US Geological Survey Water-Resources.

Pires, J.M.M., J.C. Lena, C.C. Machado and R.S. Pereira. 2003. *Potencial Poluidor de Resíduo Sólido da Samarco Mineração: Estudo de Caso da Barragem de Germano. Sociedade de Investigações Florestais. R. Árvore, Viçosa-MG* 27(3): 393–397.

Ramanaidou, E.R. 2009. Genesis of lateritic iron ore from banded iron formation in the Capanema mine (Minas Gerais, Brazil). *Australian Journal of Earth Sciences* 56(4): 605–620.

Tessier, A., P.G.C. Campbell and M. Bisson. 1979. Sequential extraction procedure for the speciation of particulate trace metals. *Analytical Chemistry* 51(7): 844–850.

United States Environmental Protection Agency (USEPA), USACE. 1998. Evaluation of dredged material proposed for discharge in waters of the US — Testing manual. Washington, DC: USEPA and Dept. of the Army, 1998.

United States Environmental Protection Agency (USEPA). 2012. Method 1313 – Liquid-solid partitioning as a function of extract pH using a parallel batch extraction procedure. Method 1313, 2012.

Proceedings of Tailings and Mine Waste 2019
November 17–20, 2019, Vancouver, Canada
Published by the University of British Columbia, 2019

The Effect of Arctic Conditions on the Geochemical Behaviour of Sulphidic Tailings

Gary Schudel, Université du Québec en Abitibi-Témiscamingue, Canada
Benoît Plante, Université du Québec en Abitibi-Témiscamingue, Canada
Bruno Bussière, Université du Québec en Abitibi-Témiscamingue, Canada
Joyce McBeth, University of Saskatchewan, Canada
Guy Dufour, Raglan Mine, Canada

Abstract

Acid mine drainage (AMD), which occurs when sulphide minerals are exposed to atmospheric oxygen and water, is one of the most significant environmental challenges in the mining industry. Given that the costs of reclaiming acid-generating wastes can be up to 100 times greater than for those of non-acid-generating wastes, it is critical to accurately predict the acid-generating potential of wastes as early as possible in the development of a mine. In mineralogical terms, the acid-generating potential of a waste is controlled by the balance between the rates of sulphide oxidation (i.e., acid production) and the rates of carbonate dissolution (i.e., acid neutralization). Although prior studies have shown that temperature and, to a lesser-known extent, salinity, exert influence over these reaction rates, these factors are not commonly considered in predictions of the geochemical behaviour of mine wastes.

Using laboratory-scale column tests, this project seeks to assess the influence of arctic conditions (i.e., low temperatures and high salinity) on the mineral weathering processes that affect the long-term geochemical behaviour of sulphidic mine wastes. Eight kinetic column tests were mounted, with four testing the effects of freeze/thaw cycles and four operated under ambient laboratory conditions. Within each set of four, two columns were rinsed with deionized water and two were rinsed with a KCl and NaCl solution (5 g/L each). The tailings used in this study were characterized before kinetic testing using various physical, mineralogical, and chemical analyses. Oxygen consumption tests were performed each month prior to flushing the columns in order to estimate rates of sulphide oxidation. Following each flush, leachates were collected and analyzed for pH, Eh, electrical conductivity, acidity, alkalinity, and metal concentrations, as well as concentrations of sulphate, thiosulphate, and tetrathionate. The results of this study will be used to better understand the long-term evolution of tailings in impoundments at arctic mine sites.

Introduction

One of the most significant and pervasive challenges in the mining industry today is the contamination of waters that drain from solid wastes such as waste rocks and tailings. Aquatic contamination usually occurs when such wastes are left exposed to atmospheric oxygen and water. Under these conditions, sulphide minerals, such as pyrite (FeS_2) and pyrrhotite ($Fe_{(1-x)}S$, x = 0 to 0.125), can oxidize and release protons (H^+, acid), metal(oid)s, and sulphate (SO_4^{2-}) or, in some cases, thiosalts (e.g., $S_2O_3^{2-}$, $S_4O_6^{2-}$) (Blowes et al., 2014).

Since the financial costs and environmental risks associated with the long-term management and/or treatment of contaminated drainages are usually high, preventing contamination is preferred in most cases (Lottermoser, 2011; Parbhakar-Fox and Lottermoser, 2015; Lottermoser, 2010). To accomplish this, laboratory-scale kinetic tests are often used to predict the long-term weathering and leaching behaviour of mine wastes. However, these tests rarely account for factors that may be critical in arctic environments, such as temperature or salinity. In fact, until relatively recently, the majority of research on the geochemical weathering behaviour of mine wastes has been oriented towards sites in humid, temperate climates (MEND, 2006).

Despite stark contrasts in the environmental conditions of Arctic and temperate regions, the geochemical behaviour of mine wastes in Arctic environments is still not well understood, particularly at a systems level. More specifically, the effects of temperature (and to a lesser extent, salinity) on sulphide oxidation have not yet been fully investigated in a broad range of actual mine wastes, either in laboratory experiments or in situ. Furthermore, most studies have focused primarily on wastes where pyrite was the main or only sulphide mineral present. Knowledge on the effects of temperature and salinity on the neutralizing minerals and secondary minerals in mine wastes is even sparser, with most of the current knowledge coming primarily from theoretical assumptions (MEND, 2006).

Given the current gaps in the literature, the overall goals of this study were to:

1. determine the effects of freeze/thaw cycles and salinity on sulphide oxidation rates; neutralization sources, pathways, and reaction rates; and the sequestration of metals and metalloids in secondary minerals; and
2. understand the sources and transformations of sulphur species in leachates.

Eight leached laboratory-scaled columns were set up to follow the geochemical evolution of tailings from Raglan Mine under ambient temperatures and freeze/thaw cycles, as well as using deionized water or saline leaching solutions. Results from the first ten cycles (318 days) are presented here.

Materials and methods

Study site

The Raglan property is comprised of a series of active, underground Ni-Cu-Co mines located in the Nunavik region of Québec (61°41′15″ºN, 73°40′41″W) approximately 70 km west of the Inuit village of Kangiqsujuaq and 110 km southeast of the Inuit village of Salluit (SNC-Lavalin 2015). The region exhibits typical polar, semi-arid climatic conditions, with a mean annual air temperature of around –10.3 °C (2010 to 2016) (Environment and Climate Change Canada, 2017) and an average annual rainfall of ~480 mm (1960 – 1990) (SNC-Lavalin, 2015; New et al., 2002). Permafrost at Raglan is continuous and can reach depths of up to ~586 m. The active layer, or upper portion of the soil that freezes and thaws each year, is approximately 1 m thick (Fortier, 2006).

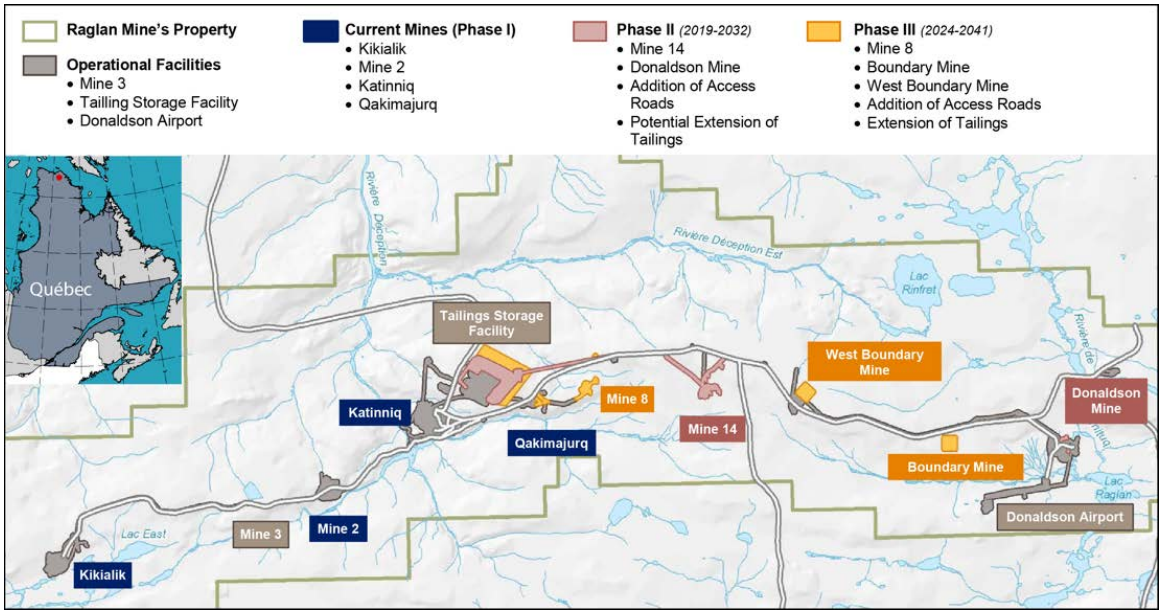

Figure 1: Map of current (Phase I) and future operations (Sivumut Project – Phase II and III) at the Raglan property. Location of Raglan represented by the red point on the inset map. The Raglan property (bounded by light green lines) spans ~70 km east to west and 10 km north to south, covering a total area of 50,457 ha. Adapted from SNC-Lavalin (2015)

The current tailings storage facility (TSF) at Raglan Mine was constructed at the beginning of operations in 1997 and continues to receive wastes from the neighboring ore concentrator (SNC-Lavalin, 2015). Four different underground mines provide feed to the concentrator (Figure 1). Prior to deposition, the concentrator wastes are thickened and filter-pressed, which results in tailings with a water content of around 15% (Garneau, 2012). The tailings are then transported by truck to the TSF and deposited by "dry stacking". After deposition, the tailings are leveled and left exposed to the cold climatic conditions (Bussière, 2007).

Column setup and leaching procedure

Eight leached column tests were constructed to study the weathering behaviour of the Raglan Mine tailings under various conditions. Tailings were sampled from an area of the Raglan Mine TSF with an estimated age of 3 to 5 years. The tailings were manually homogenized in the laboratory using a shovel prior to being installed in the columns. The tailings were not dried before installation.

Four columns were operated under ambient conditions (A1D, A2D, A1S, A2S), while the other four alternated between freezing and thawing (FT) with each leaching cycle (F1D, F2D, F1S, F2S). Within each set of columns, two were leached with deionized water (DI) and two were leached with a saline solution comprised of DI and 5 g/L each of KCl and NaCl. Leaching cycles lasted approximately 35 days each. At the beginning of each cycle, 1 L of solution was added at the top of each column and allowed to sit for 4 hours. The columns were subsequently drained over a 7-day period. Leachates were collected for chemical analyses and the columns were left for the remaining 28 days of the cycle.

Material characterizations

Prior to weathering in the kinetic column tests, representative portions of the initial tailings were submitted to various physical, chemical, and mineralogical analyses. The grain-size distribution (GSD) was determined using a laser particle size analyzer (Malvern Mastersizer 3000; ISO 2009; see Merkus, 2009, for details) and specific gravity (G_s) was measured with a helium pycnometer (Micromeritics Accupyc 1330; ASTM International 2014). The bulk chemistry of the solid sample was investigated by XRF and by ICP-AES (Perkin Elmer Optima 3100 RL) following a complete digestion ($HNO_3/Br_2/HF/HCl$) of a 500 mg pulverized aliquot (Potts, 1987). Total carbon and sulphur concentrations were determined by infrared absorption following combustion in an induction furnace (ELTRA CS-2000; e.g., Terashima, 2007). The quantitative mineralogical composition of the tailings was determined by QEMSCAN (SGS Canada Inc.), using XRF data to perform mineral abundance reconciliations (e.g., Edahbi et al., 2018).

Oxygen consumption tests

Oxygen fluxes were assessed using the oxygen consumption test (OCT) method developed by Elberling et al. (1994). In this method, decreases in the O_2 concentration in a sealed chamber are measured over time. To calculate O_2 flux at the surface, the method assumes that O_2 ingress into tailings is controlled by diffusion and can be resolved with a modified version of Fick's second law (Equation 1). When the boundary conditions $C(z) = C_0$ at $z = 0$ and $C(z) = 0$ as $z \rightarrow \infty$ are applied, the steady-state O_2 flux can be calculated as:

$$F_L = C_0\sqrt{k_r D_e} \quad (1)$$

Where F_L is the one-dimensional O_2 flux at the surface of the tailings, C_0 is the initial concentration of O_2 ($\approx$ 20.9%), k_r is the reaction rate constant for the material, and D_e is the effective diffusion coefficient of oxygen. When the area (A) and volume (V) of the chamber are known, the plot of ln $(\frac{C}{C_0})$ vs. time gives the value of $\sqrt{k_r D_e}$ (Equation 2).

$$\ln\left(\frac{C}{C_0}\right) = -t\sqrt{k_r D_e} \times \frac{A}{V} \quad (2)$$

In the present study, the columns were hermetically sealed with plumber's putty (Oatey®) and PVC caps. SO-110 oxygen sensors (Apogee Instruments) were used to monitor oxygen concentrations in the headspace over a period of 2 to 3 hours (precision = ± < 0.1% of mV output). All OCTs were performed approximately 1 to 2 weeks before the beginning of a new flush.

Leachate chemistry

Leachates were collected at the end of each cycle and analyzed for pH, Eh, electrical conductivity (EC), acidity, alkalinity, metal concentrations, and sulphur speciation. Acidity and alkalinity were measured on filtered samples (0.45 µm nylon membrane filter) using 0.02N NaOH and 0.02N H_2SO_4, respectively (Metrohm 848 Titrino Plus, ASTM International, 2000).

Metal concentrations were determined by inductively coupled plasma mass spectrometry (ICP-MS) (Agilent 7700 Series Quadrupole) and atomic emission spectrometry (ICP-AES). Concentrations of sulphur species (i.e., thiosulphate, tetrathionate, sulphate) were determined by ion chromatography ICP-MS (IC-ICP-MS). All (IC-)ICP-MS and -AES samples were filtered through nylon membrane filters (0.45 µm) prior to analysis. For metal samples, which required acidification to 2% HNO_3 (trace metal grade), samples were first treated with hydrogen peroxide (37% H_2O_2, reagent grade) in order to oxidize all sulphur species to sulphate and prevent unwanted precipitation upon acidification. These samples were gravimetrically diluted in a ~1:1 ratio with H_2O_2 and heated to 90 – 100°C for 10 to 15 minutes in a water bath. Samples were cooled to room temperature, then acidified and weighed.

Results

Material characterizations

The Raglan tailings had a G_s of 3.18 g.cm^{-3}. The tailings' GSD was typical of hard-rock tailings (Bussière, 2007), with 10%, 60%, and 90% of the material passing at grain sizes of 4.09 µm, 29.2 µm, and 99.5 µm, respectively. The coefficient of uniformity (C_u) was 7.14. The mineralogical composition of the initial sample (Figure 2) was dominated by serpentine minerals (34.0%) and pyrrhotite (27.9%). Minor amounts of pentlandite (0.73%) and chalcopyrite (0.14%) were also observed. The sample also had minor carbonates (0.48% calcite, 0.47% dolomite), with the balance being predominantly silicate and oxide gangue minerals.

The bulk chemical composition of the tailings is shown in Table 1. Nickel and copper concentrations were high in the initial material (0.32 wt.% and 631 ppm, respectively) compared to elemental concentrations in continental crust (Wedepohl, 1995). Prior work demonstrated that Ni concentrations were elevated in surface waters across the Raglan formation, even in areas where little to no mining had occurred; however, Ni concentrations were generally greatest in areas of active mining and exploration (Nicholson et al., 2003). Given the relationships between mining activities and Ni concentrations, Ni was identified as a potential contaminant.

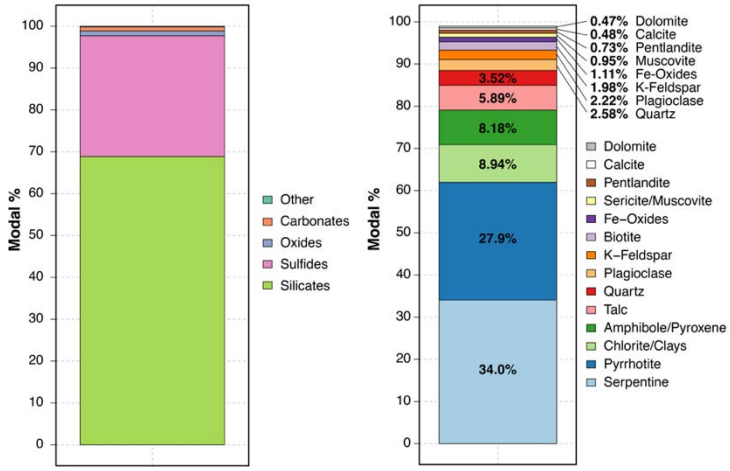

Figure 2: Quantitative mineralogy of the Raglan tailings as determined by QEMSCAN

Table 1: Bulk chemistry of the Raglan tailings as determined by ICP-AES (± 10%, 1SD)

Element	Al	C[1]	Ca	Cr	Fe	K	Mg	Na	Ni	S	S[1]	Ti
%	2.3	0.22	1.4	1.51	20.7	0.46	9.49	3.2	3.17	9.4	10.8	1.17
Element	**As**	**Ba**	**Be**	**Bi**	**Cd**	**Co**	**Cu**	**Li**	**Mn**	**Mo**	**Pb**	**Zn**
ppm	<5	114	<5	80	37	49	631	18	671	7.74	54	110

[1] Determined by infrared absorption

Oxygen consumption tests

Figure 3 shows the calculated oxygen fluxes for all columns over the first ten leaching cycles. During this period, oxygen fluxes into the tailings were between 250 and 2,000 mol $O_2.m^{-2}.yr^{-1}$ for the ambient temperature columns and 0 and 2250 mol $O_2.m^{-2}.yr^{-1}$ for the FT columns. For the ambient columns, O_2 fluxes increased over the first three OCTs, then remained stable until OCT 8 or 9. Subsequently, the columns leached with DI (A1D, A2D) appear to have stable or slightly increasing O_2 fluxes, whereas those leached with the saline solution (A1S, A2S) appear to have decreasing fluxes.

The FT columns showed similar initial O_2 fluxes as the ambient columns, however, fluxes were too low to be calculated during the frozen periods of the tests. Therefore, zero values were used to represent

negligible fluxes that could not be calculated using Fick's law ("valleys" in Figure 3B). Overall, the FT columns show alternating peaks and valleys, where successive peaks tend to decrease in magnitude relative to prior peaks; presently, the magnitude of the peaks has not stabilized at a specific value. No consistent differences have yet been observed between the columns rinsed with DI or saline solutions for the FT columns.

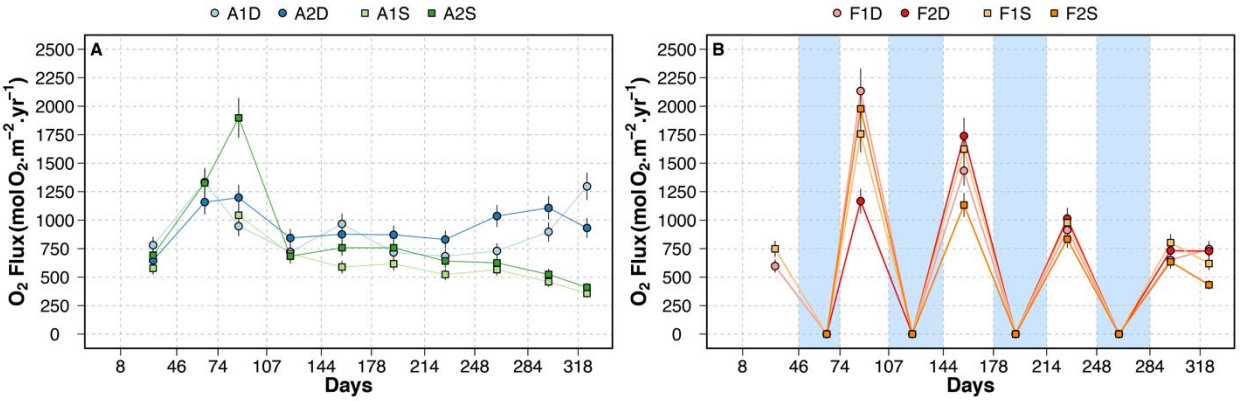

Figure 3: Oxygen fluxes for (A) ambient temperature columns and (B) FT columns. Zero values in the FT columns were used to represent points where the O_2 data did not allow for the resolution of Fick's law. Vertical gridlines indicate the final day of a leaching cycle. White sections indicate ambient temperatures and blue sections indicate freezing temperatures

Leachate chemistry

Figures 4, 5, 6, and 7 show preliminary data for pH values, and Ca, Mg, and Ni concentrations, respectively. In the FT columns, pH values appear to be largely circumneutral throughout the current duration of the tests. A decrease to more acidic pH values was observed in all samples but F1D around the tenth flush (318 days). In the ambient columns, pH values were more acidic at the beginning of the tests, likely reflecting the release of stored acidity and oxidation products. Presently, the ambient columns display circumneutral to slightly acidic values. In both sets of columns, no significant differences have yet been observed between the columns rinsed with DI and saline solutions.

Calcium (Figure 5) and magnesium concentrations (Figure 6) were relatively high in both sets of columns (ambient: Ca = 240 – 2,700 mg.L^{-1}, Mg = 350 – 5,600 mg.L^{-1}; FT: Ca = 240 – 4,500 mg.L^{-1}, Mg = 290 – 4,300 mg.L^{-1}). This suggests the dissolution of calcite ($CaCO_3$), dolomite ($CaMgCO_3$), and possibly serpentine phases (nominally $Mg_3Si_2O_5(OH)_4$). In the FT columns, Ca concentrations were relatively stable throughout the tests for the columns rinsed with saline water. However, concentrations increased slightly in the DI columns and diverged from the saline columns around 178 days. In the ambient columns, Ca concentrations in the columns rinsed with DI corresponded relatively well to those rinsed with the saline solution, however, concentrations were slightly higher in those rinsed with DI. Similar trends were observed for Mg concentrations.

Nickel concentrations (Figure 7) were relatively stable over the first ten leaching cycles for both the ambient temperature columns and FT columns. Concentrations generally varied between ~0.878 and 20.0 $mg.L^{-1}$. No consistent differences in Ni concentrations have been observed between the columns rinsed with DI and those rinsed with saline solution.

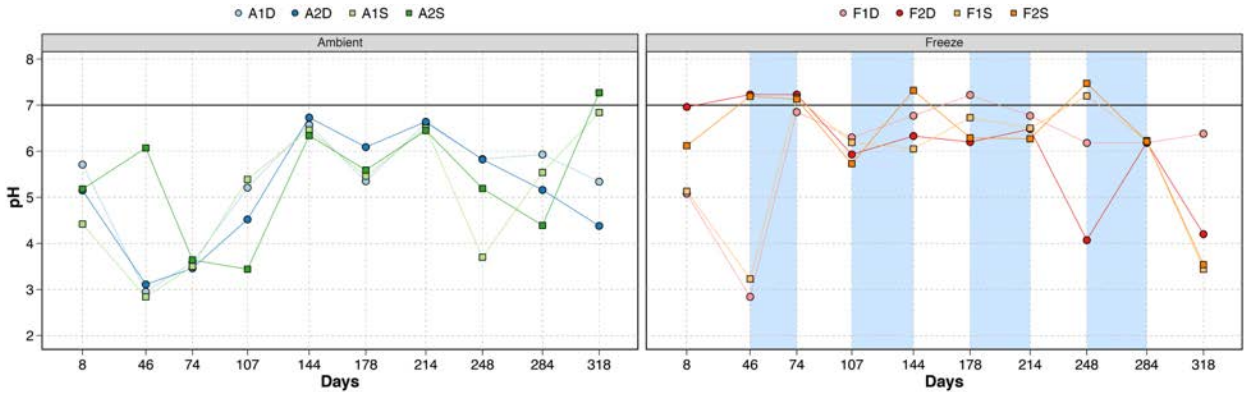

Figure 4: pH of the leachates over the first ten flushes. White sections indicate ambient temperatures and blue sections indicate freezing temperatures

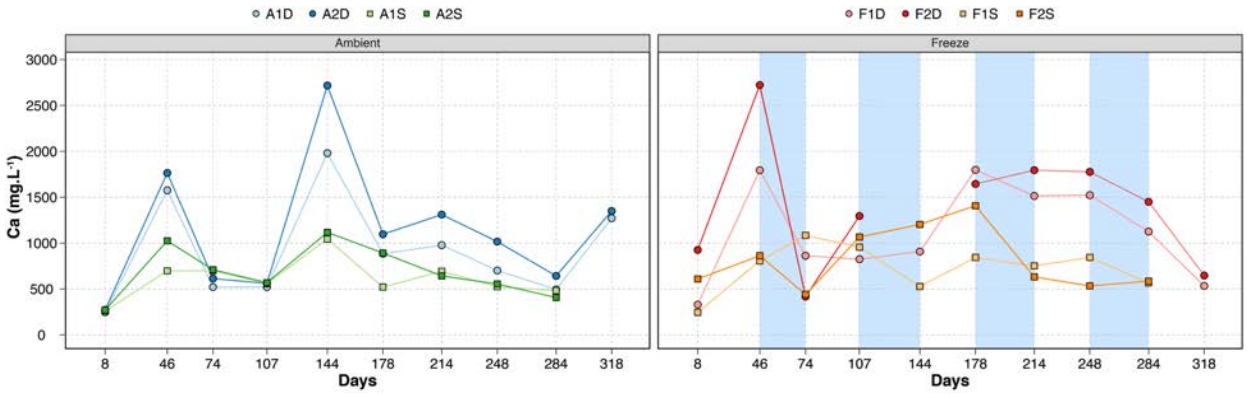

Figure 5: Ca ($mg.L^{-1}$) in the leachates over the first ten flushes. White sections indicate ambient temperatures and blue sections indicate freezing temperatures

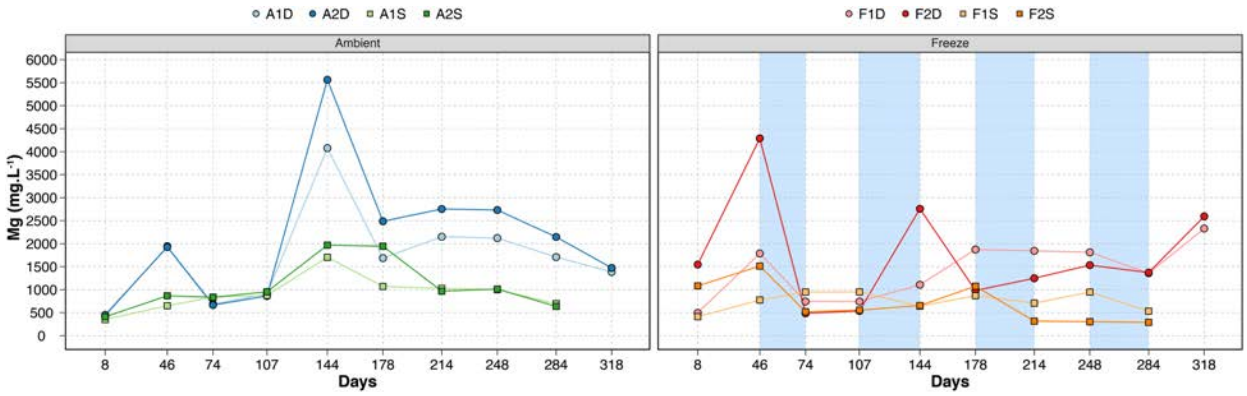

Figure 6: Mg ($mg.L^{-1}$) in the leachates over the first ten flushes. White sections indicate ambient temperatures and blue sections indicate freezing temperatures

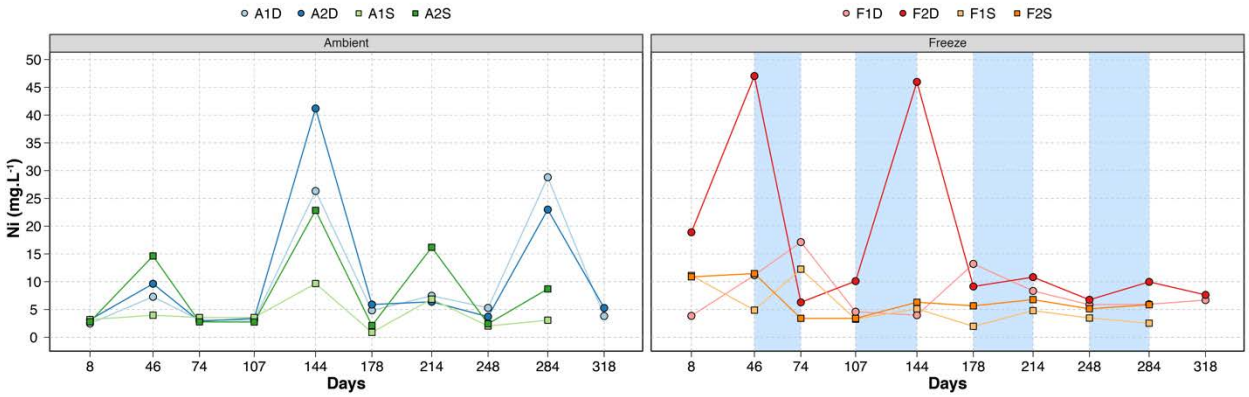

Figure 7: Ni (mg.L⁻¹) in the leachates over the first ten flushes. White sections indicate ambient temperatures and blue sections indicate freezing temperatures

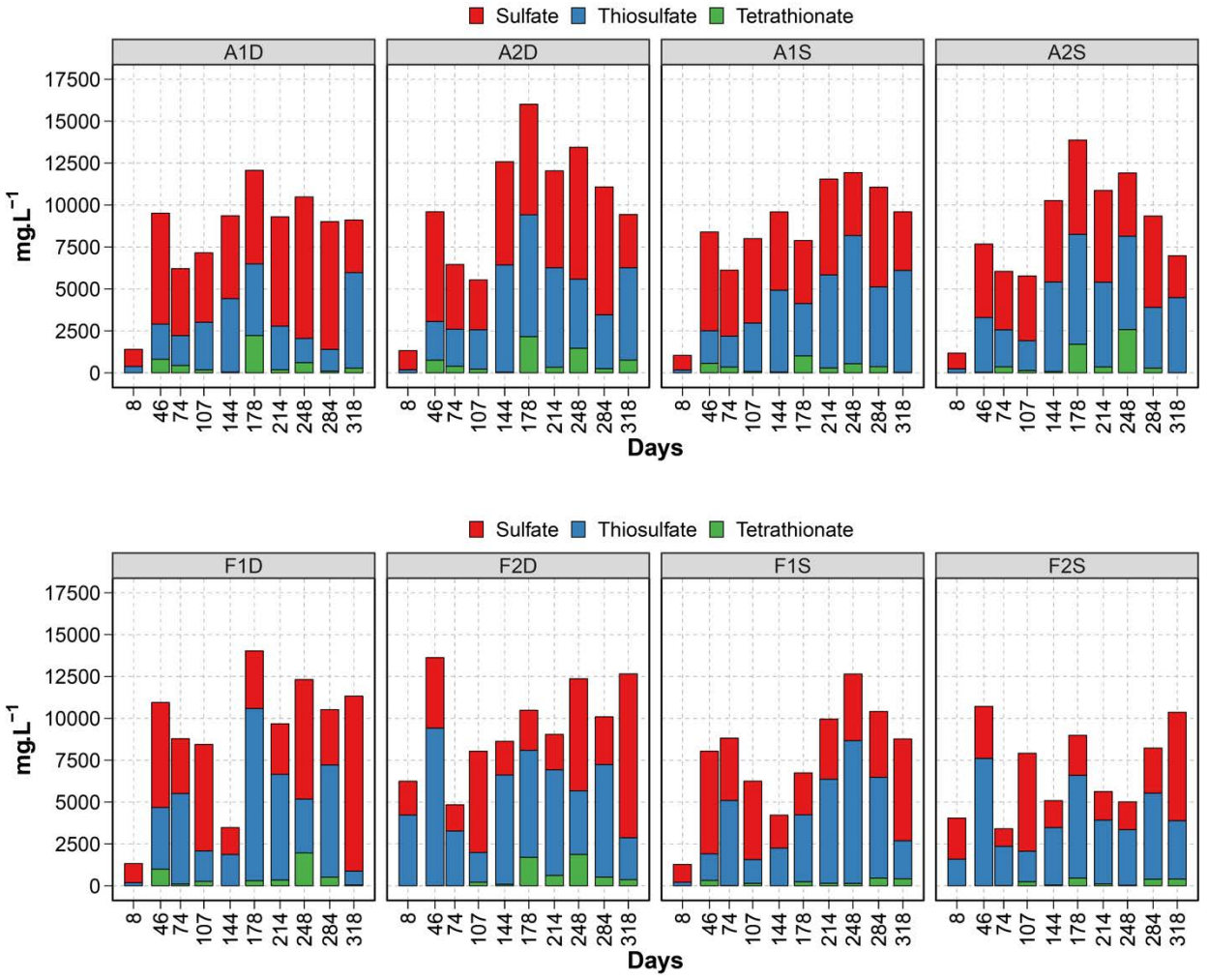

Figure 8: Stacked bar plots showing the concentrations of sulphate (red), thiosulphate (blue), and tetrathionate (green) in leachates from ambient (top) and freeze/thaw columns (bottom)

Leachates were also analyzed for thiosulphate ($S_2O_3^{2-}$), tetrathionate ($S_4O_6^{2}$), and sulphate (SO_4^{2-}) concentrations (Figure 8). Thiosulphate concentrations ranged from 170 to 7,200 mg.L^{-1} in the ambient columns and from 190 to 10,000 mg.L^{-1} in the FT columns; tetrathionate ranged from 8.5 to 2,200 mg.L^{-1} in the ambient columns and from 7.4 to 2,600 mg.L^{-1} in the FT columns; and sulphate ranged from 870 to 8,400 mg.L^{-1} in the ambient columns and from 1,000 to 10,000 mg.L^{-1} in the FT columns. Thiosulphate and tetrathionate are both intermediate sulphur species that result from the incomplete oxidation of sulphide minerals, and are considered metastable, with the significant dependencies on pH and temperature (Vongporm, 2008; Miranda-Trevino, 2013). Preliminary results suggest that the FT columns produce slightly higher proportions of thiosulphate than the ambient columns. No consistent differences have currently been noted between the DI and saline columns.

Conclusions and future work

Initial characterizations of the Raglan Mine tailings sample showed a material typical of hard rock tailings, with a mineralogical composition dominated by pyrrhotite and serpentine minerals. Trace amounts of calcite and dolomite were also identified as potential sources of alkalinity in the material. Oxygen consumption tests performed monthly on all columns suggested high sulphide oxidation rates in the early cycles of the column tests. In the ambient columns, oxidation rates appear to have achieved relative stability; however, in the FT columns, alternating between sub-zero and ambient temperatures appears to have delayed this behaviour.

In both sets of tests, pH values remain circumneutral to slightly acidic after 318 days of testing. Elevated Ca and Mg concentrations suggest that this may be due to the dissolution of calcite, dolomite, and possibly serpentine minerals. The similar concentrations of Ni in both the ambient and FT columns suggest that: 1) Ni remains soluble under the circumneutral to weakly acidic conditions observed in the leachates, and 2) following freezing periods, Ni is leached at levels similar to after ambient temperature periods. Therefore, as suggested by prior studies, Ni should be monitored closely.

Despite this preliminary data, further information will be needed to more completely understand the observed results. In particular, analyses performed upon column dismantlement (e.g., mineralogical and textural characterizations, microbiological assays, and thermodynamic equilibrium modeling) will be invaluable. More information is also needed to understand the speciation and oxidation dynamics of the sulphur species present in the leachates.

In addition to the tests presented in this article, CO_2 tests are being performed to investigate the carbonate system dynamics within the Raglan tailings. This is important because the tailings not only contain trace amounts of carbonate minerals that dissolve upon sulphide oxidation, but are also suspected of having a carbonation potential due to the high serpentine (Assima et al., 2014). The results of these tests

currently show a net production of CO_2 under ambient temperature conditions for all columns. Further development is required to refine the interpretation of these tests for the columns in this study.

Acknowledgements

Funding for this study was provided by an FRQNT grant awarded to Dr. Benoît Plante and Dr. Carmen Neculita (2015-MI-191491), the NSERC Industrial Research Chair on Mine Site Reclamation held by Dr. Bruno Bussière, and an NSERC Discovery Grant awarded to Dr. Benoît Plante. Additional funding was provided by the NSERC TERRE-CREATE program. The authors would like to thank the employees at Raglan Mine for assistance with sample collection, and the staff at the Unité de recherche et de service en technologie minérale for assistance in the laboratory.

References

Assima, Gnouyaro P., Faïçal Larachi, John Molson and Georges Beaudoin. 2014. Comparative study of five Québec Ultramafic mining residues for use in direct ambient carbon dioxide mineral sequestration. *Chemical Engineering Journal* 245 (June): 56–64. doi:10.1016/j.cej.2014.02.010.

ASTM International. 2000. D1067 – 16: Standard test methods for acidity or alkalinity of water.

ASTM International. 2014. D4892 − 14: Standard test method for density of solid pitch (helium pycnometer method). West Conshohocken, PA: ASTM International. doi:10.1520/D4892.

Blowes, David W., C.J. Ptacek, John L. Jambor, C.G. Weisener, D. Paktunc, W.D. Gould and D.B. Johnson. 2014. The geochemistry of acid mine drainage. In *Treatise on Geochemistry* (2nd edition), edited by Heinrich D. Holland and Karl K. Turekian, 2nd edition, 131–90. Oxford: Elsevier.

Bussière, Bruno. 2007. Colloquium 2004: Hydrogeotechnical properties of hard rock tailings from metal mines and emerging geoenvironmental disposal approaches. *Canadian Geotechnical Journal* 44 (9): 1019–52. doi:10.1139/T07-040.

Edahbi, M., M. Benzaazoua, B. Plante, S. Doire and L. Kormos. 2018. Mineralogical characterization using QEMSCAN® and leaching potential study of REE within silicate ores: A case study of the Matamec Project, Quebec, Canada. *Journal of Geochemical Exploration* 185 (February). Elsevier: 64–73. doi:10.1016/j.gexplo.2017.11.007.

Elberling, Bo, Ronald V. Nicholson, E.J. Reardon and R. Tibble. 1994. Evaluation of sulphide oxidation rates: A laboratory study comparing oxygen fluxes and rates of oxidation product release. *Canadian Geotechnical Journal* 31(3): 375–83. doi:10.1139/t94–045.

Environment and Climate Change Canada. 2017. Monthly climate summaries.

Fortier, R. 2006. *Étude Du Pergélisol De La Zone 5-8 Du Plateau Katinniq Au Nunavik (Québec) – Rapport Préliminaire Sur Les Travaux De Terrain Réalisés Depuis Le Mois D'août 2003*. *Département De Géologie Et Génie Géologique*. *Québec, Québec: Université de Laval.*

Garneau, Philippe. 2012. *Oxygen Consumption in a Northern Canada Tailings Storage Facility*. Edited by B. Bussière. School of Environment and Sustainability. Victoria, British Columbia: Royal Roads University.

Lottermoser, Bernd G. 2010. *Mine Wastes: Characterization, Treatment, and Environmental Impacts*. 3rd edition. Springer. doi:10.1007/978-3-642-12419-8.

Lottermoser, Bernd G. 2011. Recycling, reuse and rehabilitation of mine wastes. *Elements* 7(6): 405–10. doi:10.2113/gselements.7.6.405.

MEND. 2006. MEND Report 1.61.6: Update on cold temperature effects on geochemical weathering. 1st edition. Mine Environment Neutral Drainage Program.

Miranda-Trevino, Jorge Clemente. 2013. *The Importance of Thiosalt Speciation in the Management of Tailing Ponds.* Edited by Kelly Hawboldt. Memorial University of Newfoundland.

New, Mark, David Lister, Mike Hulme and Ian Makin. 2002. A high-resolution data set of surface climate over global land areas. *Climate Research* 21(1): 1–25.

Nicholson, Ronald V., M. Rinker, M.A. Venhuis, G. Williams and B. Swabrick. 2003. Implications of non-acidic metal leaching on mine rock management at a nickel mine in permafrost terrain: Environmental baseline investigation.

Parbhakar-Fox, Anita and Bernd G. Lottermoser. 2015. A critical review of acid rock drainage prediction methods and practices. *Minerals Engineering* 82(10/15/): 107–24. doi:10.1016/j.mineng.2015.03.015.

Potts, P.J. 1987. Classical and rapid methods of analysis. In *A Handbook of Silicate Rock Analysis*, 2nd edition, 36:47–76. Dordrecht: Springer Netherlands. doi:10.1007/978-94-015-3988-3_2.

SNC-Lavalin. 2015. The Raglan mine property beyond 2020 (phases II and III): Continuation of Mining operations east of Katinniq. Environmental and social impact assessment. Volume 1 – Main Report. 624572nd ed. Glencore.

Terashima, S. 2007. Determination of total carbon and sulfur in forty-two geochemical reference samples by combustion and infrared spectrometry. *Geostandards and Geoanalytical Research* 3(2). John Wiley & Sons, Ltd (10.1111): 195–98. doi:10.1111/j.1751-908X.1979.tb00256.x.

Vongporm, Y. 2008. *Thiosalt Behaviour in Aqueous Media.*

Wedepohl, K. Hans. 1995. The composition of the continental crust. *Geochimica Et Cosmochimica Acta* 59(7): 1217–32.

Proceedings of Tailings and Mine Waste 2019
November 17–20, 2019, Vancouver, Canada
Published by the University of British Columbia, 2019

Synthetic Water Calibration for Water Quality Parameters and Water Treatment Program Validation

Lynda Smithard, McCue Engineering Contractors, Canada

Abstract

To support the environmental assessment (EA) of a new gold mine project in British Columbia (BC), Canada, McCue Engineering Contractors (McCue) completed the preliminary design of a mine water treatment plant (WTP) using a water profile modeled by others for the future open pit sump water. The water profile is complex and the treatment plan includes heavy metals removal by chemical precipitation. Plant effluent quality was initially predicted largely based on published theoretical heavy metal solubility data.

To address uncertainty with the treatment process and improve the inputs for the impact assessment model (by others), McCue created a synthetic water sample from field leachate samples and laboratory-grade salts to match the modeled plant inlet water profile. The synthetic water sample was used to validate the water treatment process at a bench scale and provide effluent quality data for impact assessment modeling. The bench-scale test program also provided valuable data needed in the future to advance the design of the mine water treatment plant from preliminary to detailed.

Data from the bench-scale work reduced uncertainty as to what could be achieved with water treatment at the project site, and as to what impact the treated water would have on the local environment. This was important in satisfying both the regulators reviewing the EA and the project stakeholders, including local First Nations.

The bench-scale test results and data from an ensuing full-scale treatment plant at another project site have also contributed to the body of knowledge for heavy metals precipitation treatment performance. For instance, previously, literature indicated that no or negligible removal of copper could be achieved. McCue's work has provided valuable data about copper that could benefit EA work at other mine sites globally.

McCue will present the synthetic sample method, bench-scale test program results, and how they related to the detailed design and performance of a full-scale metals precipitation plant that offered an economical treatment program for complex water containing high levels of salts in addition to heavy metals.

Introduction

The future gold mine project is located in northern BC. An application for an environmental assessment certificate/environmental impact statement was submitted in December 2015 for this project, undergoing a coordinated environmental assessment under both the *British Columbia Environmental Assessment Act* and the *Canadian Environmental Assessment Act*. In October 2016, reviewers at the BC Ministry of Energy and Mines (MEM) provided comments indicating that the information provided to date on the proposed water treatment systems at post-closure was insufficient to support the surface water quality effects assessment. In response to these comments, additional work was undertaken related to the closure and post-closure water management plans and associated surface water quality model results.

In that context, McCue evaluated the active water treatment options for dissolved metals in mine affected water during closure and post mine closure of the future open pit mining project. McCue had previously completed a preliminary WTP design in early summer 2016 for the open pit sump water for the mine operation. At that preliminary stage, McCue made several assumptions since a bench-scale test program to validate the chemical treatment process had yet to be completed. The preliminary design was completed with the intention of using a two-stage chemical treatment program combined with settling for the removal of dissolved and total metals, respectively. The metals precipitation process was to be validated by a bench-scale test program at a later time when a representative water sample could be collected and used in the test program.

However, to support the evaluation of closure and post-closure water treatment options, McCue was asked by the environmental consultant who would complete the water quality effects assessment, to prepare a synthetic site water sample and complete a bench-scale test program to validate the predicted Pit Sump WTP effluent quality presented in the preliminary design report, issued in July 2016 by McCue.

The Pit Sump WTP preliminary design and the bench-scale test program results that followed were incorporated into the evaluation of active treatment options for mine affected water in closure and post-closure to reduce uncertainty as to what level of water treatment could be achieved.

This document summarizes the Pit Sump WTP preliminary design, the synthetic water sample and bench test program results, as well as an overview of the results of a full-scale metals precipitation plant employing a similar water treatment process at large infrastructure project in Lower Mainland BC. This work fills in many data gaps in the theoretical end points for water treatment by metals precipitation. It further establishes practical end points, which have been demonstrated to be lower than the theoretical ones.

Regulatory framework

Major projects in BC are assessed for potentially significant adverse environmental, social, economic, health and heritage effects by the Environmental Assessment Office (EAO). Descriptions of the BC Environmental Assessment Process and the Environmental Impact Assessment Process are provided in Appendix A. Applicable regulatory guidance for the design work is also summarized in Appendix A.

Stakeholder involvement

During the environmental assessment, the EAO seeks input from Scientific Professionals, Indigenous groups, the public, local governments, and federal and provincial agencies to help ensure that no adverse effects are missed. Therefore, Ministries of Environment (MOE) and Energy & Mines (MEM) as well as First Nations are involved in the EA process.

Project description

Project overview

The mine project is located in northern BC and is the future site of an open pit gold mining operation. The objective of the Pit Sump WTP is to treat mine affected water collected from the pit sump and pit perimeter groundwater dewatering wells to a quality suitable for discharge to a fish-bearing creek. The intent is to operate the WTP for approximately seven months of the year from March through September each year of the mine operation.

Design criteria – inlet water quality

The Pit Sump WTP design focused on treatment of nine target (identified by others) dissolved metal parameters; the inlet values provided for those parameters are shown below in Table 1.

Table 1: WTP inlet water quality – target parameters

Parameter	95th Percentile
Dissolved aluminum	0.179
Dissolved antimony	0.027
Dissolved arsenic	0.035
Dissolved cadmium	0.00736
Dissolved chromium	0.0009
Dissolved cobalt	0.0072
Dissolved copper	0.00395
Dissolved manganese	3.22
Dissolved zinc	1.357

Note: All data expressed in mg/L

In addition, the preliminary design incorporated the following assumptions:

- The inlet pH is near neutral to slightly acidic: an inlet pH range between six and seven was assumed.
- The total suspended solids (TSS) of the homogenized inlet water stream was assumed to be approximately 300 mg/L TSS.

Design criteria – discharge water quality

The discharge targets provided to McCue are summarized in Table 2 below. Some of the parameters are hardness or pH dependent and accordingly the targets for these parameters have been indicated as a range.

Table 2: End of pipe water treatment discharge targets

Parameter	Guideline (mg/L)
Dissolved aluminum	0.1
Dissolved antimony	0.018
Dissolved arsenic	0.01
Dissolved cadmium	0.0000352–0.000254
Dissolved chromium	0.002
Dissolved cobalt	0.008
Dissolved copper	0.004
Dissolved manganese	1.4 – 1.6
Dissolved zinc	0.0150

Notes:

1. It is assumed the 30-day average hardness is less than 50 mg/L as $CaCO_3$
2. It is assumed the maximum temperature of the water in the creek is 15°C

Design criteria – flow rate

The WTP design is based on a maximum flow rate of 285 litres per second (L/s).

Key technical issues

Key technical issues impacting the design of the WTP included:

- Representative water sample is not available for bench-scale test and design work. First, a water profile modeled by the consultant was used for the preliminary design, and then synthetic site water was prepared to validate that design.

- The mean temperature is below zero between November and March. Temperature is a key factor in the application and/or performance of some water treatment technologies.

Preliminary treatment process

The preliminary treatment process for the mine affected water consisted of a two-stage metals precipitation, coagulation, and flocculation chemical program followed by settling in ponds for solids removal. Following the second settling pond the water will be buffered (as necessary) to a suitable pH for discharge to the creek. The preliminary WTP process flow diagram is illustrated in Figure 1.

The preliminary chemical treatment program consisted of the following: pH adjustment and metal hydroxide precipitation; metal hydroxide precipitation or sulphide precipitation; coagulation; flocculation; and, pH neutralization.

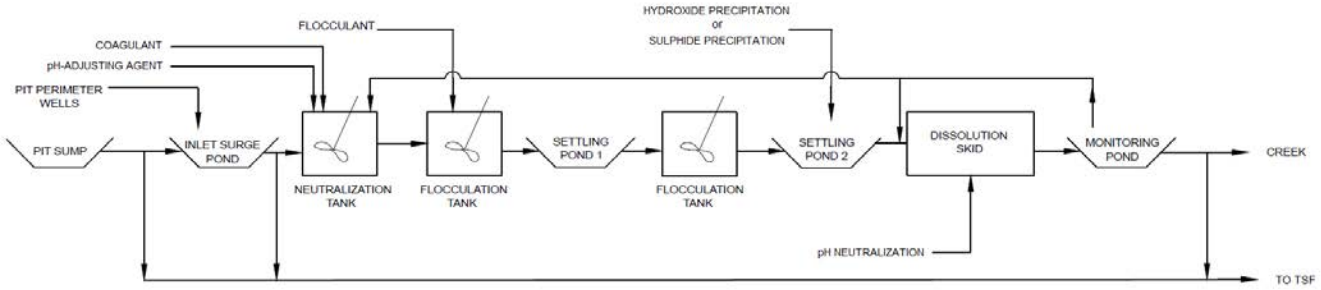

Figure 1: WTP preliminary design process flow diagram

Subsequent bench-scale tests helped determine whether the two-stage chemical treatment process should include hydroxide precipitation optimized at two target pH ranges or a hydroxide precipitation stage followed by sulphide precipitation (see "Bench-scale test program" section).

Literature findings on metals removal

Theoretical and predicted end points

A comparison between the theoretical and the predicted minimum effluent concentration attainable through the identified chemical program is presented in Table 3 below. The minimum predicted effluent concentration was based on the greater concentration of the theoretical percent removal and theoretical minimum effluent concentration from literature. This data is based on metal solubility data. Where this data was not available, the predicted minimum effluent concentrations were based on the results of a neutralization test previously completed for the project by others. Those results did not account for the addition of a coagulant and were, therefore, conservative.

Table 3: Theoretical versus predicted end points

	Single stage hydroxide		Two-stage hydroxide		Two-stage hydroxide/ sulphide	
	Minimum effluent concentration attainable					
Parameter	Theoretical (10.5 – 11.5)[1]	Predicted	Theoretical (8 – 9/10.5 – 11.5) [1]	Predicted	Theoretical (8 – 9) [1]	Predicted
Dissolved aluminum	–	0.103	0.05	0.1	0.05	0.05
Dissolved antimony	NR	NR	NR	NR	NR	NR
Dissolved arsenic	0.005	0.005	0.005	0.005	0.005	0.005
Dissolved cadmium	0.0005	0.0005	0.0005	0.0005	0.0005	0.0005
Dissolved chromium	NR	0.0007	NR	NR	NR	NR
Dissolved cobalt	–	0.0001	–	0.0001	–	0.0001
Dissolved copper	NR	NR	NR	NR	NR	NR
Dissolved manganese	–	0.0042	–	0.0042	0.01	0.01
Dissolved zinc	0.05	0.05	0.05	0.05	0.01	0.01

Notes:

1. All reported data expressed in mg/L
2. [1] pH set point for chemical precipitation reaction
3. "–" information unavailable for the specified pH range
4. NR – No or negligible estimated removal
5. Theoretical values based on: BioteQ Environmental Technologies, 2015; Eckenfelder, 2000: 38–156; Ersoz, 2013: 34; Scott, 1977; Peters et al., 1985: 165–196; Robinson et al., 2008.

Limitations based on solubility

- Removal of metals from mixed metal wastes by hydroxide precipitation may not be effective since the minimum solubilities for different metals occur at different pH conditions. The pH required to precipitate most metals from water ranges from 6 to 9; aluminum generally forms aluminum hydroxide that precipitates at pH >5.0 but the aluminum can re-enter solution again at pH 9.0; manganese precipitation is variable due to its many oxidation states, but will generally precipitate at a pH of 9.0 to 9.5. Sometimes, however, a pH of 10.5 is necessary for complete removal of manganese (Skousen, 2014).
- Insoluble sulphide precipitation does not treat manganese, as manganese sulphide has a higher solubility than ferrous sulphide (Department of Army, US Army Corps of Engineers, 2001).

Data gaps specific to contaminants of concern

Regarding theoretical end points of chemical programs, no information was available for:

- Aluminum, cobalt, and manganese, single stage hydroxide process, at pH = 10.5 – 11.5
- Cobalt and manganese, two-stage hydroxide process, at pH = 8 – 9 / 10.5 – 11.5

- Cobalt, two-stage hydroxide/sulphide process, at pH = 8 – 9 / 10.5 – 11.5
- No or negligible estimated removal for antimony, chromium and copper for all three processes

Synthetic water sample

Four iterations of synthetic water samples were prepared by McCue to fit the Pit Sump WTP inlet water profile modeled and provided by the consultant as part of the prior submission to the BC EAO.

McCue received nine leachate water samples from the mine. The water samples were mixed together to make one homogenized sample (Raw Water) at McCue's Delta facility. Once homogenized, samples were collected for total metals, dissolved metals, TSS, anions and nutrients analyses.

Based on the Raw Water analytical results, McCue diluted the homogenized leachate water sample using deionized water at a ratio of 1:4. The concentrations of dissolved antimony, arsenic, barium, chromium and iron were then increased or spiked using laboratory-grade metal salts.

The values for target parameters from the predicted inlet WTP water profile, and lab analysis for Raw Water and the synthetic sample used for bench testing are summarized in Table 4 below.

Table 4: Target parameters in predicted, raw and synthetic inlet water

Parameter	Predicted maximum inlet (95th percentile)	Raw water	Synthetic inlet water
Dissolved aluminum	0.179	7.970	2.21
Dissolved antimony	0.027	0.008	0.304
Dissolved arsenic	0.035	0.004	0.00864
Dissolved cadmium	0.00736	0.12900	0.0291
Dissolved chromium	0.0009	<0.0005	0.0017
Dissolved cobalt	0.0072	0.0375	0.0094
Dissolved copper	0.00395	0.14700	0.04
Dissolved manganese	3.22	6.10	1.37
Dissolved zinc	1.357	18.900	4.23

Note: All reported data expressed in mg/L

Bench-scale test program

Objectives

The bench-scale test program had the following objectives:

- Support the selection of the successful chemical program: investigate the efficacy of single stage hydroxide precipitation, two-stage hydroxide precipitation and two-stage hydroxide/sulphide precipitation process; each of them also incorporating a coagulant.
- Support the selection of a flocculant.
- Optimize hydraulic retention times for neutralization, coagulation, and flocculation.
- Verify the anticipated performance.
- Provide settling rate information to re-evaluate and optimize (i.e., minimize) the footprint of each settling pond.
- Characterize the sludge volume and quality at each step.

This documents focusses only on the first objective.

Methodology

Table 5 below shows the work completed to verify the metals precipitation process. The process verification was performed over a series of nine tests; three for each of the possible process configurations.

Table 5: Process verification/optimization summary

Process configuration	Stage	Test 1	Test 2	Test 3
Single stage hydroxide precipitation + coagulant	–	Vary pH / Constant coagulant dosage	Constant pH / Vary coagulant dosage	Vary pH and coagulant dosage based on Test 1 and 2
Two-stage hydroxide precipitation + coagulant	1	Constant pH / Constant coagulant dosage	Constant pH / Vary coagulant dosage	Vary pH and coagulant dosage based on Test 1 and 2
	2	Constant pH / No coagulant added	Constant pH / Vary coagulant dosage	
Two-stage hydroxide and sulphide precipitation + coagulant	1	Constant pH / Constant coagulant dosage	Constant pH / Constant coagulant dosage	Validate best performing chemical program from Test 1 and 2
	2	Constant pH / Vary sulphide dosage	Vary pH / Constant sulphide dosage	

Decision criteria

The performance of each metal precipitation process was evaluated by comparing the target dissolved metal concentrations in last-stage supernatant water samples of each test against the end of pipe treatment targets in Table 2.

Bench testing results

Table 6 and Table 7 below show the results corresponding to the best performing tests for each chemical program evaluated during the bench testing. The values for the Synthetic Inlet Water are also presented.

Table 6: Bench testing results – dissolved metal concentrations

Parameter	Synthetic inlet water	Single-stage hydroxide	Two-stage hydroxide	Two-stage hydroxide/ sulphide	Flocculated[1] two-stage hydroxide/sulphide
Dissolved aluminum	2.21	0.104	0.0578	0.0161	**0.119**
Dissolved antimony	0.304	0.00344	0.00168	0.0078	0.0129
Dissolved arsenic	0.00864	0.00037	0.00032	0.00043	0.00046
Dissolved cadmium	0.0291	**0.000239**	<0.000005	<0.0000050	<0.0000050
Dissolved chromium	0.0017	<0.0001	<0.0001	<0.00010	<0.00010
Dissolved cobalt	0.0094	0.00032	<0.0001	0.00094	0.00021
Dissolved copper	0.04	<0.0002	<0.0002	<0.00020	0.00029
Dissolved manganese	1.37	0.288	0.00077	0.624	0.226
Dissolved zinc	4.23	0.0043	<0.001	<0.0010	0.000059

Notes:

1. All reported data expressed in mg/L
2. Analytical results provided by an accredited third-party laboratory
3. "<" – Less than the reported detection limit
4. **bold** – indicates the reported concentration is over the end of pipe treatment target
5. [1] Pass/fail testing of several flocculants was performed on a qualitative basis, where "pass" was considered to be an instance where a visible flocculant formed. Afterwards, the short-listed flocculants, based on Pass/Fail and Settling velocity testing, were evaluated in terms of target dissolved metals concentrations.

Table 7: Bench testing results – removal percentage

Parameter	Single-stage hydroxide	Two-stage hydroxide	Two-stage hydroxide/ sulphide	Flocculated two-stage hydroxide/sulphide
Dissolved aluminum	95.29%	97.38%	99.27%	94.62%
Dissolved antimony	98.87%	99.45%	97.43%	95.76%
Dissolved arsenic	95.72%	96.30%	95.02%	94.68%
Dissolved cadmium	99.18%	>99.98%	>99.98%	>99.98%
Dissolved chromium	>94.12%	>94.12%	>94.12%	>94.12%
Dissolved cobalt	96.60%	>98.94%	90.00%	97.77%
Dissolved copper	>99.50%	>99.50%	>99.50%	99.28%
Dissolved manganese	78.98%	99.94%	54.45%	83.50%
Dissolved zinc	99.90%	>99.98%	>99.98%	>99.99%

Some highlights from these results are:

- Sufficient removal of multiple parameters, such as cadmium and aluminum, at a single process pH, is often unachievable due to the parameter-specific relationship between the optimal formation of hydroxides and pH.
- A single stage hydroxide precipitation process would not provide sufficient treatment because of the process pH having to vary to achieve sufficient removal of all target parameters. However, this should be investigated further on each case, considering each raw water composition.
- Although the bench testing demonstrated that the treatment targets could be achieved with either a two-stage hydroxide precipitation process or a two-stage hydroxide/sulphide precipitation process, the advantage of the latter is that the process pH would remain within the allowable pH range for discharge to the environment, and therefore neutralization would not be required prior to discharge. Neutralization could be needed to lower the effluent pH for discharge to the creek after a two-stage hydroxide treatment process.

Comparison to literature findings

The bench testing results demonstrated better metal removal rates and lower dissolved metals concentrations than the preliminary predicted discharge concentrations provided by McCue in the preliminary design, which are summarized in the "Theoretical and predicted end points" section of this document.

Stakeholder acceptance

Data from the bench-scale work reduced uncertainty as to what could be achieved with water treatment at the project site and what impact the treated water would have on the local environment. This was important in satisfying both the regulators reviewing the EA and the project stakeholders, including local First Nations.

Scaling up – full-scale WTP case study

Bench-scale tests on representative water samples

Bench tests were recently performed by McCue on metals contaminated water samples from a large infrastructure project currently under construction in the Port of Vancouver. The water discharge is required to meet both the Provincial and Federal Surface Water Quality standards for marine discharge. Strict standards, particularly for copper and zinc, the presence of salts (from seawater intrusion), and construction activities in the excavation have made the water treatment project technically challenging.

The bench-scale tests were modeled on the metals precipitation tests previously completed by McCue for the gold mine project.

Table 8 below compares the concentration of targeted parameters in inlet and treated water between previous bench tests with synthetic water and the current program on samples from the Port project.

Full-scale WTP performance

Following the bench-scale test program, McCue rapidly deployed a full-scale metals precipitation plant at the Port project site. The chemical precipitation program has consistently removed copper, zinc and other target metals from the construction water at a fraction of the cost of the other treatment methods considered by McCue's client. Typical results from the full-scale WTP operation are also provided in Table 8 for comparison. The results indicate better performance at a field scale than at a bench scale. Furthermore, the results prove that metals precipitation is a viable method for reducing heavy metals, including copper.

Table 8: Performance using representative water sample versus synthetic water sample

Parameter	Synthetic inlet water	Flocculated two-stage precipitation	Port project inlet water (bench-scale)	Port project bench-scale	Port project inlet water (operation)	Port project treated water
Dissolved aluminum	2.21	0.119	<0.010	NM	0.0100	<0.0060
Dissolved antimony	0.304	0.0129	<0.0010	NM	<0.00060	<0.00060
Dissolved arsenic	0.00864	0.00046	<0.0010	NM	<0.00060	<0.00060
Dissolved cadmium	0.0291	<0.0000050	<0.000513	<0.000010	0.000248	<0.000030
Dissolved chromium	0.0017	<0.00010	<0.0010	NM	<0.00060	<0.00060
Dissolved cobalt	0.0094	0.00021	0.0087	0.00423	0.00504	0.00075
Dissolved copper	0.04	0.00029	0.0168	0.00149	0.0158	<0.00090
Dissolved manganese	1.37	0.226	4.730	3.650	2.93	0.146
Dissolved zinc	4.23	0.000059	2.410	0.00529	0.0271	<0.0090

Notes:

1. All reported data expressed in mg/L
2. Analytical results provided by a third-party laboratory
3. "<" – Less than the reported detection limit
4. "NM" – Not measured

Conclusion

The work presented in this document could have both a local and global impact by:

- Filling gaps in literature on data for end points of chemical precipitation of aluminum, cobalt, and manganese at specific pH, which values were recorded for the bench tests performed.
- Filling gaps in literature on data for end points of chemical precipitation of antimony, chromium, and copper, which were found to decrease in the bench tests performed.
- Revising theoretical end points of chemical precipitation programs and establishing practical end points, which have been demonstrated to be lower than the theoretical ones.
- Establishing a detailed procedure and methodology to test and compare chemical precipitation programs.

Filling gaps in knowledge decreases uncertainty as to what level of water treatment and environmental protection can be achieved. Lowering uncertainty helps with gaining social (First Nations) and regulatory acceptance. Better data also helps advance engineering design work more efficiently. Combined, the work will lower both project risk and cost.

References

BioteQ Environmental Technologies. 2015. *Metals Removal from Kemess Pit Water Laboratory Testing Final Report.*

Department of Army, US Army Corps of Engineers. 2001. Engineering and design – precipitation/coagulation/ flocculation. *Manual No. 1110–1-4012*.

Eckenfelder, Jr., W.W. 2000. *Industrial Water Pollution Control*. New York: McGraw-Hill Series in Water Resources and Environmental Engineering.

Environmental Assessment Office. 2015. *Environmental Assessment Office USER GUIDE – An Overview of Environmental Assessment in British Columbia.*

Ersoz, M. 2013. *Best Practices Guide on Metals Removal by Treatment*. London: IWA Publishing.

Government of British Columbia. 2014. Environmental mitigation policy. Retrieved from https://www2.gov.bc.ca/gov/content/environment/natural-resource-stewardship/policy-legislation/environmental-mitigation-policy

Government of British Columbia. 2018. The Environmental Assessment Process. Retrieved from http://www.eao.gov.bc.ca/process.html

Peters, R.W., Y. Ku and D. Bhattacharyya. 1985. Evaluation of recent treatment techniques for removal of heavy metals from industrial wastewaters. In *AIChE Symposium Series* 81(243): 165–196.

Robinson, Alan K. and Joyce C. Sum. 1980. Sulfide precipitation of heavy metals. *EPA-600/2-80-139.*

Scott, Murray C. 1977. Sulfex™ – A new process technology for removal of heavy metals from waste streams. In *Proceedings of the 32nd Industrial Waste Conference.*

Skousen, Jeffrey. 2014. Overview of acid mine drainage treatment with chemicals. *Acid Mine Drainage, Rock Drainage, and Acid Sulfate Soils: Causes, Assessment, Prediction, Prevention, and Remediation*. West Virginia University. 325–337. 10.1002/9781118749197. Ch. 29.

Wang, Lawrence K., Yung-Tse Hung and Nazih K. Shammas. 2005. *Physicochemical Treatment Processes*, Vol. 3, *Handbook of Environmental Engineering*. New Jersey: Humana Press.

Xiao, F., B. Zhang and C. Lee. 2008. Effects of low temperature on aluminum (III) hydrolysis: Theoretical and experimental studies. *Journal of Environmental Sciences* 20(8): 907–914.

Bibliography

Ministry of Environment, Ecosystems Branch, Environmental Sustainability and Strategic Policy Division. 2014. Procedures for mitigating impacts on environmental values (environmental mitigation procedures). Version 1.0.

Appendix A – Regulatory framework

The preliminary design was completed in accordance with the following provincial regulatory guidance:

- Technical Guidance 1 of the Environmental Management Act – Environmental Impact Assessment and Technical Assessment Report (TG1), prepared by the British Columbia Ministry of the Environment (BC MOE).
- Technical Guidance 7 of the Environmental Management Act – Assessing the Design, Site, and Operation of Sediment Ponds Used in Mining (TG7), prepared by the BC MOE.

Environmental assessment process in BC

Major projects in BC are assessed for potentially significant adverse environmental, social, economic, health and heritage effects by the Environmental Assessment Office (EAO), as required by the *BC Environmental Assessment Act* (Government of British Columbia, 2017). The company building the project (the proponent) provides details on what they believe to be the potential adverse effects of the project, and how they mitigate those effects. Figure 2 below illustrates the process.

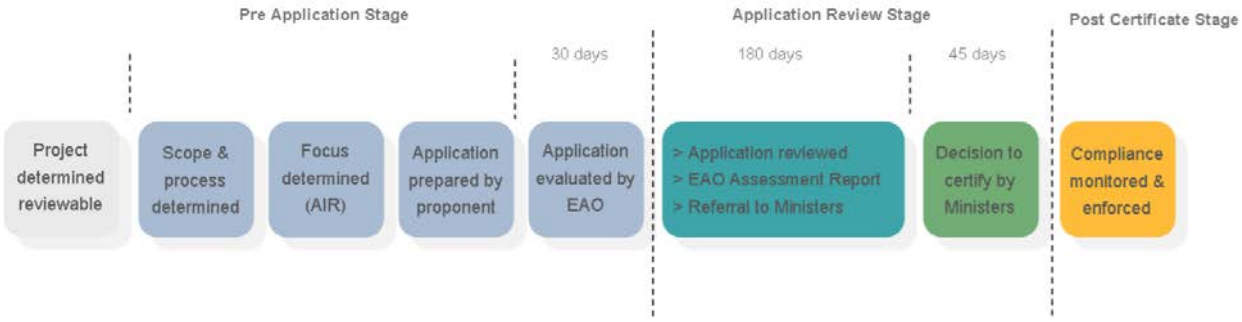

Figure 2: Environmental assessment process chart (Environmental Assessment Office, 2015)

Environmental impact assessment process in BC

An environmental impact assessment determines the nature and extent of environmental impacts from a proposed development and outlines what mitigation measures would be appropriate. This evidence is used to make informed and durable natural resource decisions (Government of British Columbia, 2014). The environmental impact assessment is included within the Environmental Mitigation Policy and supporting procedures; it is meant to be preceded by the "Identification of environmental values and components of concern" stage and to be followed by the "Consideration and application of mitigation".

Stakeholder Involvement

During the environmental assessment, the EAO seeks input from Scientific Professionals, Indigenous groups, the public, local governments, and federal and provincial agencies to help ensure that no adverse effects are missed. Therefore, Ministries of Environment (MOE) and Energy & Mines (MEM) as well as First Nations are involved in the EA process.

Proceedings of Tailings and Mine Waste 2019
November 17–20, 2019, Vancouver, Canada
Published by the University of British Columbia, 2019

Laboratory Methods Used to Design Effective Mine Tailings Dust Management Programs

Bryce Uytiepo, SUEZ Water Technologies Solutions, USA
Michael Raab, SUEZ Water Technologies Solutions, USA
Robert Greifzu, SUEZ Water Technologies Solutions, USA

Abstract

Most copper mines in the southwestern USA operate very large tailings storage facilities (TSF). In many cases, these facilities are partitioned such that the active areas receive continuous wet slurries from the mill or concentrator, while inactive sections are dry and exposed. These inactive portions of the TSF can be dry and exposed for several months, or even years, requiring treatment to reduce fugitive dust. In arid climates, using water alone provides limited but typically short-lived control of dust. To extend the control of fugitive dust, chemical binders are utilized. Various types of chemical sealants, glues, and other agglomerating agents can be applied to tailings to form a hard crust designed to prevent wind erosion. Over time, however, these chemically treated tailings surfaces can become more difficult to manage, leaving exposed surfaces that readily erode. Laboratory testing of the treated tailings was conducted to measure dust control efficiency of chemical binders. In addition, mechanical test methods were used to evaluate crust strength of various binders and dosages.

Finally, the dust management program that was designed using these laboratory methods was put into practice. The engineering considerations, equipment application, and the results of a 100-acre tailings surface stabilization project is presented.

Introduction

There are numerous mines in North America and other parts of the world that generate large volumes of mine tailings as a result of normal mineral processing operations. Since these tailings offer little or no economically recoverable value, they must be stored on site. Tailings storage facilities (TSF) are impoundments designed to receive and store tailings for the life of the mine and can occupy several hundreds of hectares. There has been significant work on the development of best practices related to design and construction of these TSFs. The following discussion focusses on evaluating chemical treatment technologies used to control fugitive dust from these impoundments. A well designed treatment

program offers financial benefits such as lower operating costs, as well as promoting safety and environmental stewardship.

Mechanical methods used to control dust generally involve containment, compaction, or collection. When using water sprays or chemical treatment, however, the specific mechanisms involved include particle knockdown, bulk agglomeration, and surface stabilization. While particle knockdown is an important dust control mechanism, its effects are often short-lived and are more important when evaluating belt-related material handling operations. For tailings impoundments, we will focus our discussion on bulk agglomeration and surface stabilization.

Bulk agglomeration

Bulk agglomeration occurs when small particles adhere to larger particles or vice versa. For materials that wet easily, agglomeration can be accomplished using water or moisture addition alone. This is the same phenomenon that allows the building of sand castles with wet sand. Unfortunately, these fragile structures eventually weaken when the water drains or evaporates. To agglomerate materials for longer durations, chemical binders are applied. Chemical binders used for bulk agglomeration include:

- salts;
- lignins or lignosulfonates;
- polymer emulsions;
- oils; and
- petroleum-based products.

The various chemistries employed offer distinct advantages and disadvantages when used on mine tailings. To maximize distribution most are diluted with water before being applied. To compare the effectiveness of various binders on specific tailings under a set of conditions, dustiness testing is conducted.

Relative dustiness testing

Dustiness can be evaluated qualitatively using simple visual methods. Treated and untreated materials can be transferred from one container to another while carefully observing the amount of dust generated. For more precise comparative analysis, however, laboratory instrumentation is required. A drop box or dust chamber provides a convenient way to measure relative dustiness of treated samples. An apparatus (Roe, 1991) used for measuring relative dustiness is shown in Figure 1.

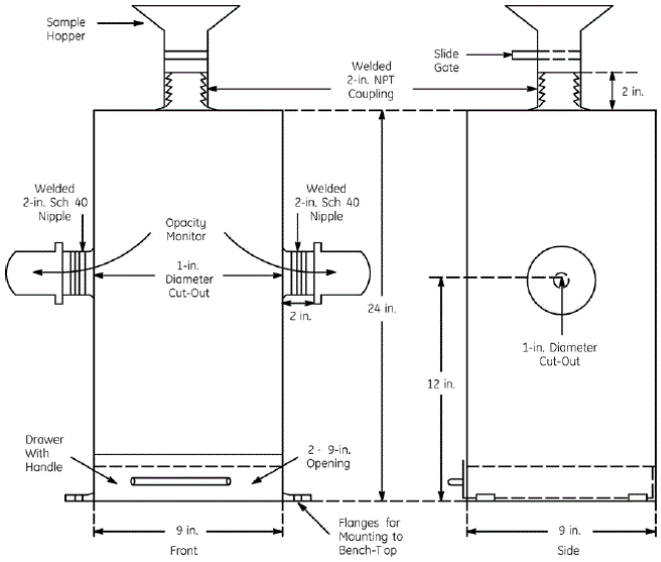

Figure 1: Dust chamber apparatus

When collecting and preparing samples, it is critical that test samples contain particles 75 microns or smaller to ensure that there is dust that can be measured (Jeglic, 1986). Sample sizes are generally 100 grams or less. Sample preparation steps include screening, weighing, treatment or moisture addition, mixing, and drying. Sample treatment is performed by adding the chemical solution to the tailings and mixing thoroughly. After drying, the treated (or untreated) sample is dropped through the chamber, where dust is measured and recorded with time. The dust chamber is equipped with a light source and sensor that will measure dust optically. Dust is measured in terms of light absorbance and recorded in percent (0% correlates to no dust). In general, a maximum dust reading is measured at the onset, and decays with time. The control sample produces the profile that constitutes the maximum amount of dust generation for the specific material. A sample dust profile is shown in Figure 2.

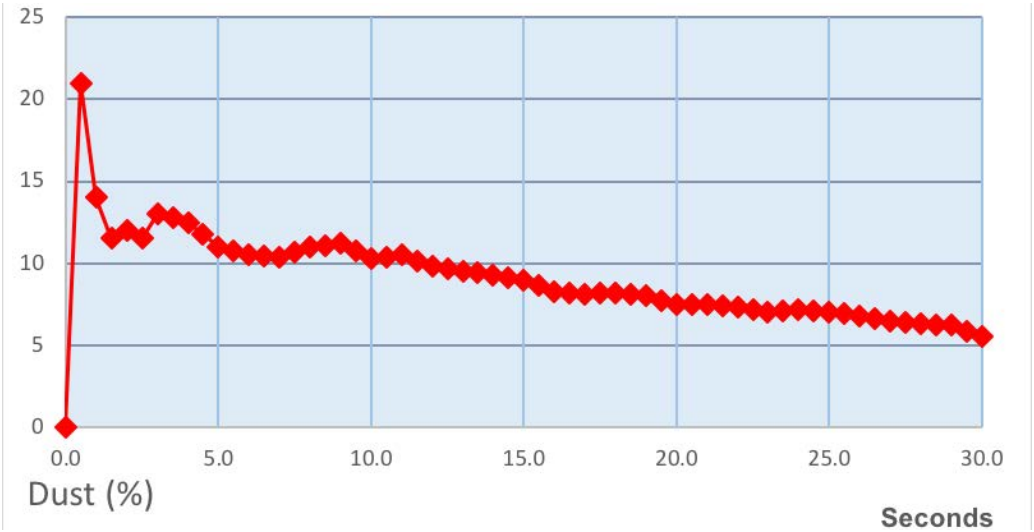

Figure 2: Dust chamber measurement profile (30s)

For the profile shown above, the initial or maximum dust reading was about 21% with a final reading of 5% after 30 seconds. The Relative Dust Number (RDN) for this sample is essentially the area under the curve, or approximately 13%. To normalize results from different samples, a Relative Dustiness Index (RDI) can be calculated. This is done by dividing a treated sample's RDN by the that of the untreated (or control) sample. When comparing treated sample results, a lower dust number or index for a given binder indicates more effective control of the tailings dust. Tailings were treated with several polymer products and then tested in the dust chamber to illustrate varying effectiveness with respect to chemistry and product concentration. Relative dustiness results are shown in Table 1.

Table 1: Polymer binders used on mine tailings

Binder	% conc	RDN(%)	RDI(%)
No treatment	NA	150	–
Polymer A	5%	48	32
Polymer A	10%	35	23
Polymer B	5%	40	27
Polymer B	10%	25	17

Surface stabilization

Another important property of chemical binders is their ability to create a crust on tailings surfaces. When sprayed on large surfaces like a tailings impoundment, the binder can form a crust that is intended to seal the material surface. When applied successfully, a chemical binder will effectively stabilize the surface such that weathering effects brought about by sun, wind and rain are minimized or virtually eliminated for the treatment duration. There are several factors that affect a binder's ability to create a strong crust. For example, binders that exhibit humectant qualities rely on the continued presence of water or moisture to be effective. Other types of chemical binders with more adhesives properties tend to create stronger crusts and maintain their strength long after water added during treatment has evaporated or dried. One of the best ways to evaluate surface stabilization is by measuring crust strength.

Crust strength test

A simple way to evaluate binder crust would include measuring the thickness of the crust formed or observing its appearance after drying. However, the most reliable way to evaluate crust strength is by measuring its resistance to an applied force. This is performed by measuring compressive strength. To properly compare and evaluate different binders, samples to be treated and tested should have a roughly even distribution of coarse and fine particles. Mine tailings particle size can range from 20μm to 2mm, but for measuring compressive strength, it is sufficient to have a –6/+30 distribution (between 30 and 6

mesh). Accordingly, it is best that treated samples undergo the equivalent or similar environmental conditions that the tailings are, or would be exposed to. In general, these conditions include storage time, low humidity and/or elevated temperatures. Major elements of a compressive strength analyzer are shown in Figure 3.

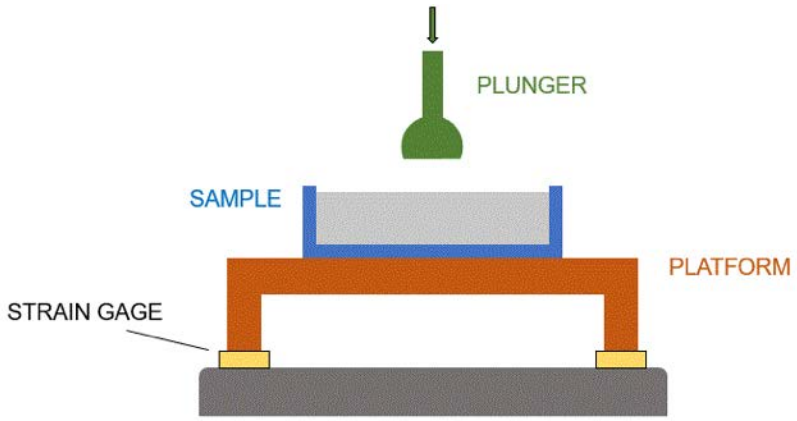

Figure 3: Compressive strength analyzer elements

As with any comparative testing or evaluation, proper sample preparation will reduce errors and provide reliable results. It's interesting to note that the manner of how samples are treated prior to testing can provide valuable insight on how application steps should be performed to achieve optimum results. Normally, the test samples are thoroughly mixed, transferred to a weighing dish and allowed to dry. During the test, the analyzer drives a probe toward the treated sample on a platform at slow controlled speed. Compressive force is steadily increased until the "crust breaks." The maximum or peak force is recorded as the strength of the crust.

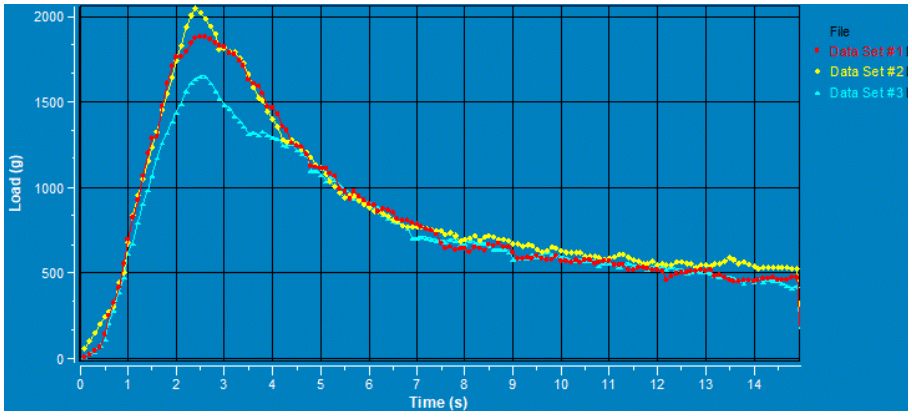

Figure 4: Compressive strength results

In many cases, compressive or crust strength increases with chemical binder dosage (or concentration). A lignosulfonate binder was applied to a sandy substrate (–6/+30) at three different

solution concentrations (5% light blue, 10% red, and 15% yellow). The comparative crust strength results from these tests are compiled in Figure 4.

Surface penetration

Many tailings impoundments have been exposed to the environment for years. It is not unusual for the tailings surface to have been chemically treated multiple times, travelled upon, mechanically groomed, or fresh tailings deposited. As mentioned earlier, an important factor that affects crust strength is its thickness. Crust thickness is directly related to treatment solution's ability to penetrate the tailings surface. On one hand, a high dosage of binder could produce a strong but thin crust, whereas a lower (or dilute) dosage of binder produces thicker, but slightly weaker crust.

An effective treatment program should define specific chemistry, dilution and application guidelines. It may be useful to conduct liquid penetration tests to ensure that the treatment targets can be achieved. These are visual tests that are easily done by pouring specific dilutions of a chemical binder over test columns. **Note**: this qualitative type of laboratory test involves small, uncompacted samples and should not be used to interpret permeability or other hydraulic properties of the tailings. Five different treatment solutions of equal volume were poured over 30 grams of tailings in a 50ml graduated cylinder. As shown in Figure 5, Test solutions 3, 4 and 5 were able to penetrate more than 50% of the depth, while Tests 1 and 2 did not.

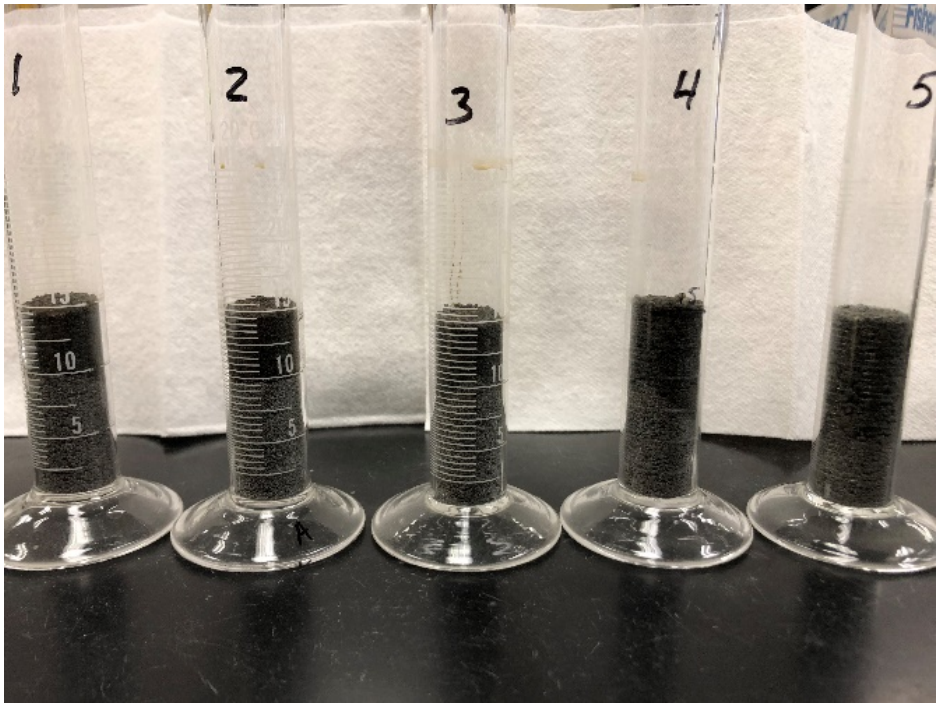

Figure 5: Penetration testing

Treatment program design

Once compatible chemistry options and dose performance analyses have been assessed, treatment program design can begin. The basic elements should include most or all the following:

- surface preparation requirements;
- moisture addition (dilution water);
- chemical binder formulation(s), concentration;
- spray application plan – frequency;
- required spray equipment, staging operations; and
- performance monitoring – visual and instrument.

Field application – case history

A copper mine in the southwestern region of the USA operates approximately 400 acres of tailings impoundments. Several large areas are exposed to the environment and require surface stabilization to control fugitive dust. Tailings from these exposed areas were collected and sent to Suez Water Technologies and Solutions laboratories to be evaluated. Multiple dustiness and compressive strength tests were conducted to define the most effective binder chemistry and target dosages. The specific treatment program design includes organic polymer formulation applied at 5–10%.

Unfortunately, field data and results were not available prior to final paper submission. Every effort will be made to present findings during the conference.

References

Jeglic, M.F. 1986. Laboratory device for evaluating dust control agents. *J. of Coal Quality* 5: 104–107.

Roe, D.C. 1991. Laboratory techniques for evaluating chemical dust control programs. EPRI Conference on Coal Handling Systems, Pensacola, Florida, USA, 1991.

Bibliography

American Society for Testing and Materials. 1980. *Annual Book of ASTM Standards*. Standard test method for index of dustiness of coal and coke, D: 547–41.

Chapter 6
Design

TAILINGS AND MINE WASTE 2019

Proceedings of Tailings and Mine Waste 2019
November 17–20, 2019, Vancouver, Canada
Published by the University of British Columbia, 2019

Long-Term Performance of Oil Sands Mine Reclamation Covers under High-Resolution Climate Change Projections

Md. Shahabul Alam, University of Saskatchewan, Canada
S. Lee Barbour, University of Saskatchewan, Canada
Mingbin Huang, University of Saskatchewan, Canada
Yanping Li, University of Saskatchewan, Canada

Abstract

Oil sands reclamation covers are typically evaluated using soil-vegetation-atmosphere-transfer (SVAT) models calibrated with short-term (~10 years) field monitoring, followed by simulation of long-term (~60 years) water balances based on historical climate records. Climate change impacts are commonly studied using climate change projections statistically downscaled from the global to the site-specific scale, based on the historical baseline period. The largest source of uncertainty is the choice of global climate models (GCM) followed by the choice of representative concentration pathways (RCP). The high-resolution climate change projections obtained from dynamical downscaling and their impacts on oil sands reclamation covers have not been studied to date.

This study explored the water balances of a reclamation cover (South Waste Sand Tailings Storage – SWSS) at Syncrude's Mildred Lake Mine in Alberta, Canada using: (a) meteorological data for a historical baseline period; and (b) climate change projections generated at two different resolutions (i.e. global and regional). The global scale (200-km) climate change projections (i.e. precipitation, temperature) were obtained from a GCM (e.g. CanESM2 and RCP8.5) for the period of 2070–2099 and the regional scale (4-km) projections were generated by the World Research and Forecasting (WRF) model for the period of 2086-2100, both representing the end of the 21st century. The projections of precipitation and temperature were statistically downscaled by a widely used stochastic weather generator (Long Ashton Research Station Weather Generator – LARS-WG), as well as dynamically downscaled with the WRF model. The temperature datasets for the baseline and future periods were used to calculate potential evapotranspiration (PET) using the Hargreaves-Samani method. The downscaled precipitation and calculated PET were utilized in a physically-based water balance model (i.e. Hydrus-1D) to simulate actual evapotranspiration (AET) and net percolation (NP) for a reclamation cover during the historical and future periods.

The results demonstrate that future temperature, PET, and precipitation increase as compared to the historical baseline with changes based on the LARS-WG show larger increases than the WRF. Both the

LARS-WG and the WRF show similar directional shifts in climate variables (temperature and precipitation) and water balance components (AET and NP) as compared to the baseline period. In future, the relative increase in NP is higher than AET for both climate models. The results suggest that the high-resolution (i.e. 4-km) climate change projections based on the WRF model would lead to increased and more variable NP with concomitant impacts on the release of chemical constituents from reclaimed mine waste, as well as a greater water yield from reclaimed watersheds.

Introduction

The economic contribution of oil sands mining to Canada also comes with an environmental cost. By law, the industry is obliged to return the disturbed land to an equivalent capability to what existed before mining (Cumulative Environmental Management Association [CEMA], 2006). The industry has based reclamation cover design on simulations of water balance components (e.g. actual evapotranspiration [AET] and net percolation [NP]) from calibrated soil-vegetation-atmosphere-transfer (SVAT) models. Historically, the SVAT models are calibrated against short-term (<~10 years) monitoring and then used to predict long-term (~60 years) water balance for historical climate (Boese, 2003; Huang et al., 2011a, b, c; Keshta et al., 2009; Price et al., 2010; Qualizza et al., 2004). However, given the expected future climate changes (IPCC, 2013) the industry recognizes that future climate impacts need to be included in cover design.

General circulation models (GCMs) have been used as the primary tool for the assessment of climate change impacts (Meehl et al., 2007). However, GCMs with coarse spatial resolution (typically 100–300 km) are not able to represent local and/or regional-scale climate changes. Therefore, downscaling methods (e.g. statistical and dynamical downscaling) are used to generate local and/or regional-scale climate variables based on GCM climate variables (Wilby and Wigley, 1997). While statistical downscaling is based on the relationships between local-scale predictands and global-scale predictors, dynamical downscaling is based on the regional climate models (RCMs) typically driven by the GCMs' outputs (Giorgi, 1990). Although statistical downscaling is computationally inexpensive, it assumes stationarity in the distribution of climate variables. RCMs, on the other hand, are computationally demanding but also explicitly represent small-scale characteristics and atmospheric processes by considering underlying local-scale circulation patterns (Gao et al., 2012). RCMs are still of relatively coarse resolutions that suffer from the misrepresentation of convection-dominated precipitation. One possible solution is the use of high resolution and convection-permitting RCMs (e.g. the Weather Research and Forecasting – WRF – model, Skamarock et al., 2008). The WRF model with a horizontal grid spacing of 4 km can represent the impact of small-scale surface topography on the convective processes. Despite high computational cost, WRF models have value as a dynamical downscaling method, particularly when assessing climate change impacts in western Canada where small-scale convections play a vital role (Li et al., 2019).

A few previous studies (Alam et al., 2017, 2018; Keshta et al., 2012) demonstrated the impact of climate changes on the long-term future water balance of reclamation covers and natural forest sites in northern Alberta, Canada, based on GCM predictions. No studies have used high-resolution WRF simulations of temperature and precipitation to assess changes in water balance for oil sands mine reclamation covers. The overall objective of this study was to compare the water balance components of a reclamation cover using climate change projections downscaled by a statistical downscaling method and a WRF model.

Methodology

Study area

The study area was a reclamation cover built on a sand tailings dyke (Southwest Sand Tailings Storage: SWSS) located near Fort McMurray in Alberta, Canada. The 45-cm reclamation cover consisted of a layer of salvaged peat/mineral soil mixture overlying salvaged glacial clay. The cover was placed directly on the tailings sand. The watershed of this site has been monitored since 2001.

Data used

The historical climate records (daily minimum [Tmin], maximum [Tmax], and mean [Tmean] temperature and daily precipitation) for 1976–2015 were obtained from the Environment and Climate Change Canada (ECCC) weather station at the Fort McMurray Airport. The daily Tmin, Tmax, Tmean, and precipitation projections were based on the Canadian GCM (CanESM2) and a representative concentration pathway (RCP8.5) for a historical (1976–2005) and future (2070–2099) period. CanESM2 was selected as an example in this study, while RCP8.5 was selected as it is the highest emission scenario. The source was the Coupled Model Intercomparison Project Phase 5 (CMIP5, https://esgf-node.llnl.gov).

Statistical and dynamical downscaling methods

The stochastic weather generator LARS-WG (Semenov and Barrow, 1997) was used to generate site-scale daily temperature and precipitation time series (100 realizations) for the historical (1976–2005) and future (2070–2099) periods using the global-scale temperature and precipitation projections from CanESM2: RCP8.5. The dynamical downscaling was conducted using a high-resolution (4-km) and convection-permitting WRF model (Li et al., 2019; Skamarock et al., 2008) to generate regional-scale hourly temperature and precipitation for the historical (CTL: 2001–2015) and future (Pseudo-Global Warming [PGW]: 2086–2100) periods. WRF-PGW simulations were obtained by perturbing climate variables of WRF-CTL using changes in 2070–2099 relative to 1976–2005 based on CMIP5 GCMs. For details on CTL and PGW experiments, please refer to Li et al. (2019).

Physically-based water dynamics modelling

The growing season water balance for the SWSS cover was simulated using Hydrus-1D (Simunek et al. 2013). This model was previously calibrated and validated by Alam et al. (2018). Details of the model domain, boundary conditions and material properties are described in detail in that paper. The daily precipitation for the unfrozen growing season (April–October) was calculated using the method of Carrera-Hernández et al. (2011) and the daily potential evapotranspiration (PET) was calculated using the Hargreaves-Samani method (Hargreaves and Samani, 1985).

Results and discussion

Performance of the downscaling methods

Key climate variables from the LARS-WG model were compared to those from the Environment Canada station for the historical period in order to test the reliability of the climate model. Table 1 shows a comparison between the percentiles of the observed and simulated daily precipitation, Tmin, Tmax and Tmean. Table 1 shows that both extreme and mean precipitation and temperature values were simulated reasonably well by LARS-WG (with relative error of <10% in most cases).

The performance of WRF in simulating climate information for the grid of Fort McMurray Airport station was evaluated by comparing the WRF simulated mean annual cycles of daily temperature and precipitation with those calculated from the measurements at Fort McMurray Airport station during the historical baseline period (2001–2015). The performance evaluation included daily minimum, maximum, and mean temperature and daily precipitation (Figure 1).

Overall, WRF reproduces the seasonal cycle reasonably well with respect to both temperature and precipitation despite the systematic biases in each month. Both WRF-CTL simulations and observed data show peaks in July for Tmin, Tmax, Tmean, and precipitation. The WRF-CTL simulated peak values of Tmin, Tmax, Tmean, and precipitation were 8.50ºC, 22.8ºC, 15.6ºC, and 77.7 mm, which were 10.7ºC, 24.5ºC, 17.6ºC, and 118 mm for the observed data, respectively. The difference in these values between the WRF-CTL and observed data has been originated from the cold biases (particularly between March and July) and wet biases for all seasons as explained by Li et al. (2019).

Table 1: Comparison of percentiles between the observed and simulated daily precipitation (mm/day⁻¹) and temperature (°C) by LARS-WG with relative error (%) at Fort McMurray Airport station during the historical period 1976–2005

		Percentile					
		5th	**25th**	**50th**	**75th**	**95th**	**99th**
Observed	***Precipitation***	0	0	0	0.70	6.41	17.2
	Tmin	–30.7	–14.7	–2.24	6.02	12.1	14.6
	Tmax	–19.5	–3.87	9.03	19.3	26.8	30.3
	Tmean	–24.7	–9.17	3.43	12.7	18.8	21.6
Simulated	***Precipitation***	0	0	0	0.61	6.37	17.5
	Tmin	–28.0	–14.9	–2.35	5.78	11.4	13.9
	Tmax	–16.8	–3.81	8.97	19.1	25.7	29.3
	Tmean	–21.9	–9.28	3.33	12.5	17.9	20.3
% error	***Precipitation***	0	0	0	12.3	0.68	2.23
	Tmin	8.97	1.30	4.96	4.00	6.23	4.80
	Tmax	13.9	1.75	0.72	0.96	3.95	3.34
	Tmean	11.00	1.13	2.81	1.26	4.80	5.99

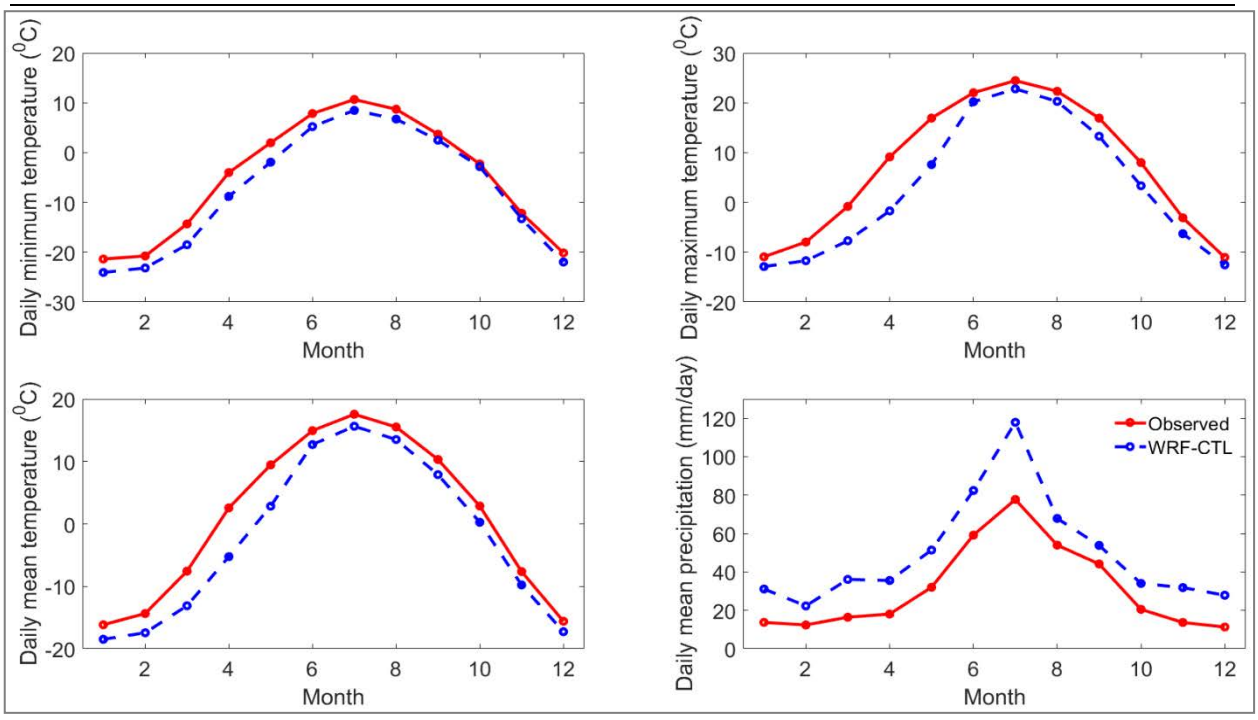

Figure 1: Comparison between the mean annual cycle of temperature (°C) and precipitation (mmday⁻¹) for the observed time series and the time series generated by WRF-CTL at Fort McMurray Airport station during the historical baseline period 2001–2015

Comparisons between statistical and dynamical downscaling methods

Projection of changes in temperature

The future LARS-WG median value of Tmean (7.20ºC) is 112% higher than the historical value of 3.40ºC, while WRF future median value of Tmean (3.10ºC) shows nearly a 300% increase over the historical value of –1.60ºC (Figure 2). While WRF underestimates the historical Tmean, both LARS-WG and WRF predict warmer future winters and summer periods. However, the magnitude of increases in winter, summer, and Tmedian are lower for the WRF simulations. The cold biases in WRF baseline simulations might play a role in lower intensification in future as compared to the GCM projections (which were downscaled by LARS-WG) although both LARS-WG and WRF downscaling methods show similar directions of change in future temperature. Both LARS-WG and WRF simulated daily temperatures show similar variability and skewness.

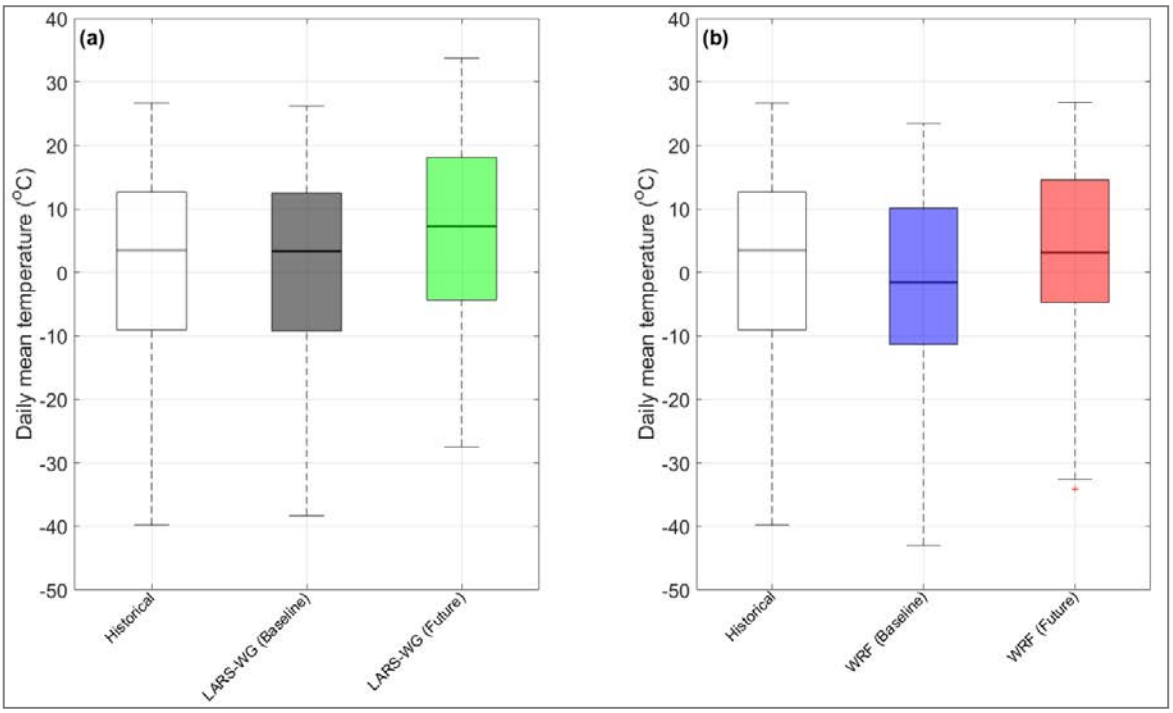

Figure 2: Distributions of daily mean temperature based on (a) 100 realizations from LARS-WG during baseline (1976–2005) and future (2070–2099) periods for CanESM2 (RCP8.5) and (b) WRF simulations for baseline (2001–2015) and future (2086–2100) periods as well as for the historical (1976–2005) observations at Fort McMurray Airport station. The boxplots represent the inter quartile range (IQR) values with median shown as black thick line for 100 realizations, with whiskers showing values within 1.5 IQR extending from both ends of the boxes and red markers outside the whiskers indicating outliers

Projection of changes in precipitation

The future LARS-WG median growing season (April–October) precipitation was 475 mm as compared to the historical value of 387 mm (i.e. a 22.7% increase), while the WRF simulated future median growing

season precipitation of 583 mm was 11.5% higher than the baseline value of 523 mm (Figure 3). WRF overestimates the historical growing season precipitation. Both LARS-WG and WRF predict more precipitation, but also more variability in future precipitation, as defined by minimum and maximum values of growing season precipitation. The magnitude of increases in median growing season precipitation is lower in the case of WRF than for LARS-WG, although both downscaling methods show similar directions of change in future growing season precipitation. Both methods predict a similar skewness in precipitation; however, WRF future predictions have more variability (larger box) suggesting higher uncertainty.

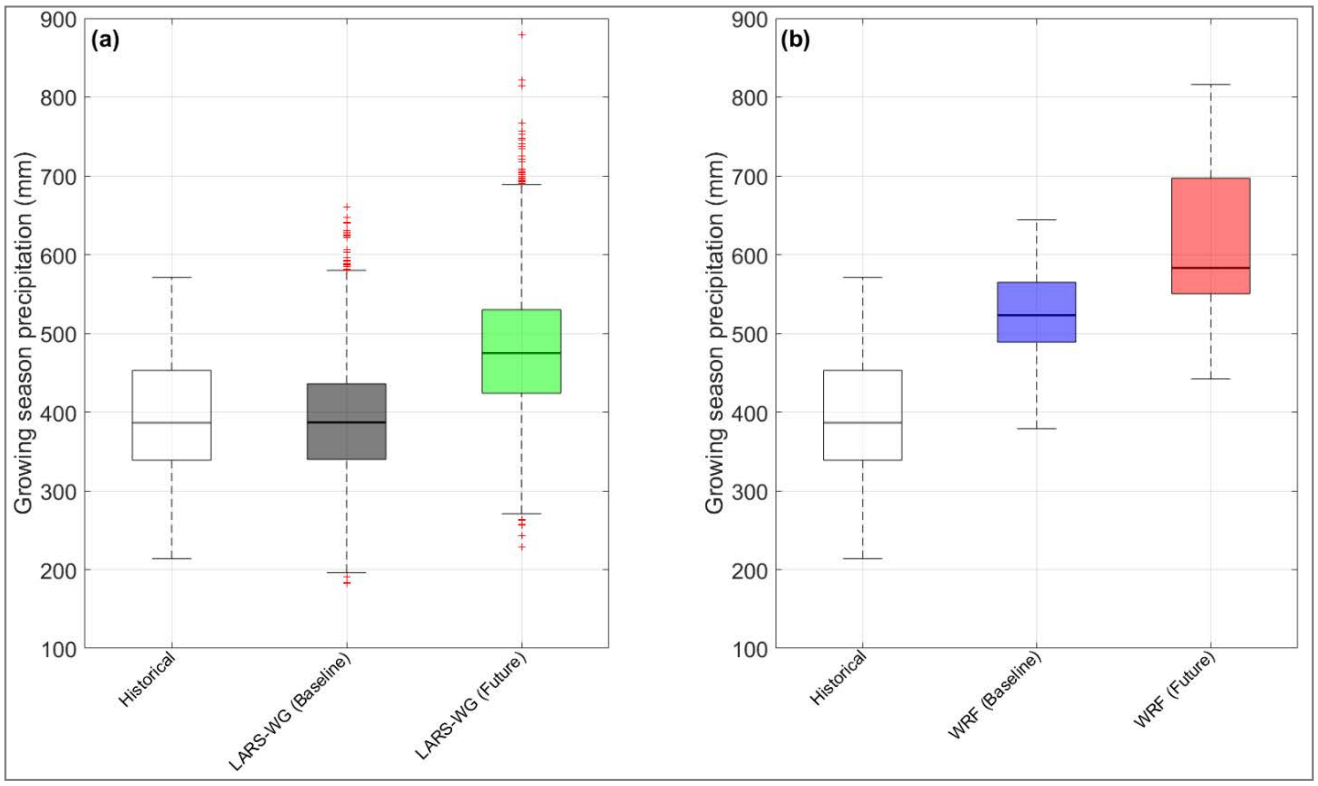

Figure 3: The same as Figure 2 but for growing season precipitation

Projection of changes in potential evapotranspiration (PET)

The calculated future growing season (April–October) median PET based on LARS-WG was 763 mm as compared to the predicted historical value of 638 mm (i.e. a 19.6% increase), while the future growing season median PET from WRF was 646 mm as compared to the predicted historical value of 541 mm (i.e. a 19.4% increase (Figure 4). While WRF underestimates historical growing season PET, both LARS-WG and WRF show increased future growing season median PET as well as increases in minimum and maximum values. The magnitude of increases in growing season median PET of WRF simulations is similar

to that of LARS-WG simulations, and both LARS-WG and WRF downscaling methods show similar directions of future change in PET. The WRF growing season PET is negatively skewed for the historical period and positively skewed for the future period. WRF simulations show more variability (larger boxes) in the growing season PET than the LARS-WG simulations, suggesting higher uncertainty in the case of WRF simulations.

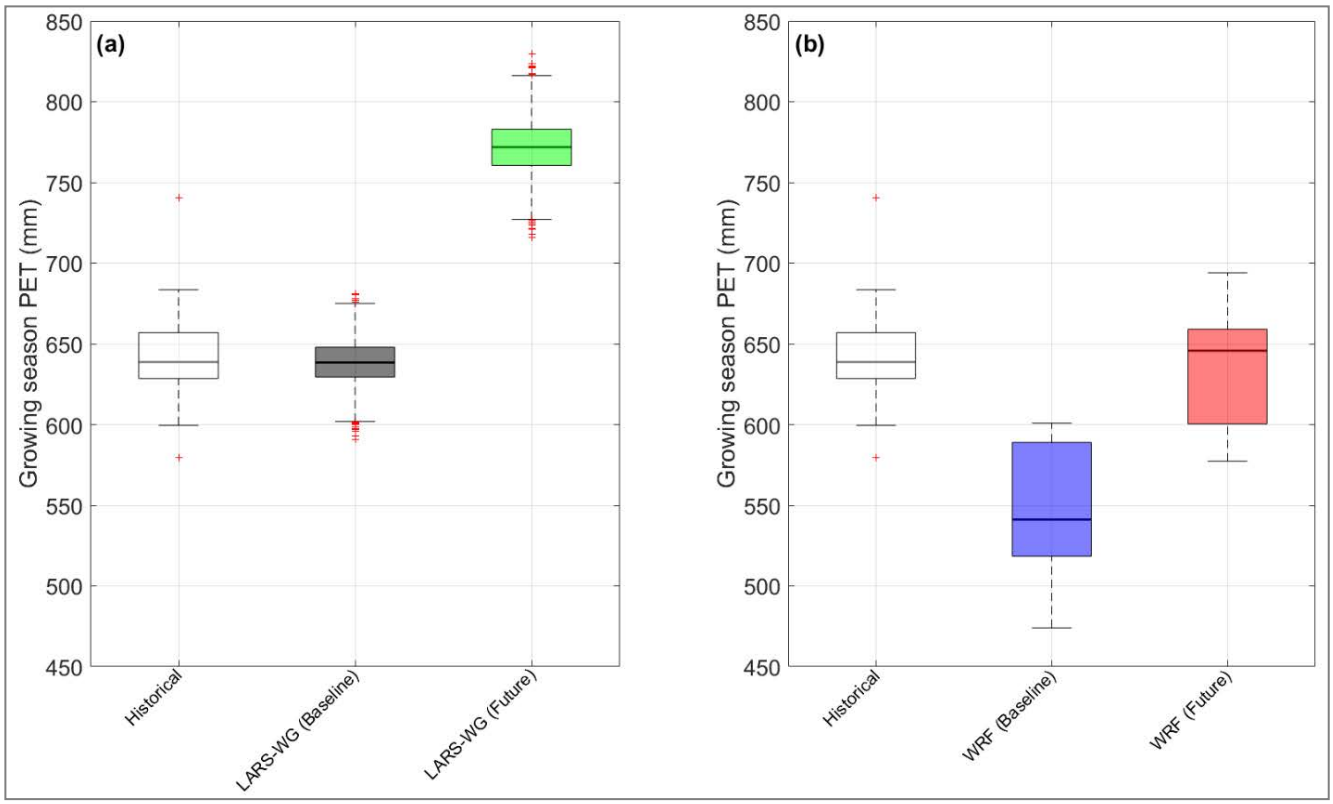

Figure 4: The same as Figure 2 but for growing season PET

Projection of changes in growing season water balance

The future growing season median AET for LARS-WG climate was 440 mm compared to the historical predicted value of 375 mm (i.e. a 17.3% increase), while comparable values for the future and historical simulations from WRF were 477 mm and 425 mm respectively (i.e. a 12.2% increase, Figure 5). While WRF overestimates historical growing season AET, both LARS-WG and WRF show increased growing season median AET in future, as well as an increase in extreme (i.e. minimum and maximum values) growing season AET. The magnitude of increases in growing season median AET of WRF simulations is lower than that of LARS-WG simulations; however, both LARS-WG and WRF downscaling methods show

similar directions of change in future growing season AET. Both LARS-WG and WRF simulated growing season AET show similar variability during baseline and future periods.

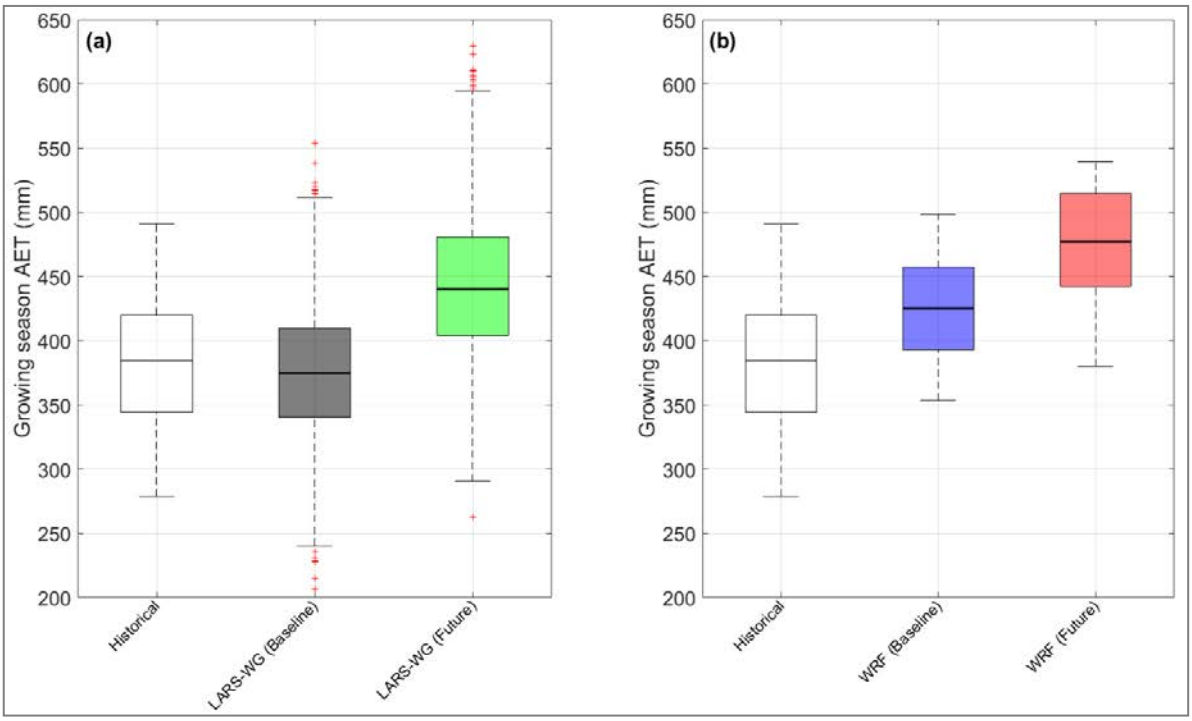

Figure 5: The same as Figure 2 but for growing season AET

The future growing season median NP from the LARS-WG climate was 29 mm, as compared to the predictions for the historical climate of 11.2 mm (i.e. a 158% increase), while WRF-PGW climate led to a future NP of 136 mm, as compared to the historical climate value of 92 mm (i.e. a 47.2% increase, Figure 6). While WRF overestimates historical growing season NP, both LARS-WG and WRF show an increased growing season median NP in future, as well as an increased extreme (i.e. minimum and maximum values) growing season NP. The magnitude of increases in growing season median NP of WRF simulations is lower than that of LARS-WG simulations; however, both LARS-WG and WRF downscaling methods show similar signs of change in future growing season NP.

The LARS-WG simulated growing season NP is positively skewed for both baseline and future periods, while WRF simulations show more variability (larger boxes) in growing season NP than the LARS-WG simulations, suggesting higher uncertainty in the case of WRF simulations than the LARS-WG simulations.

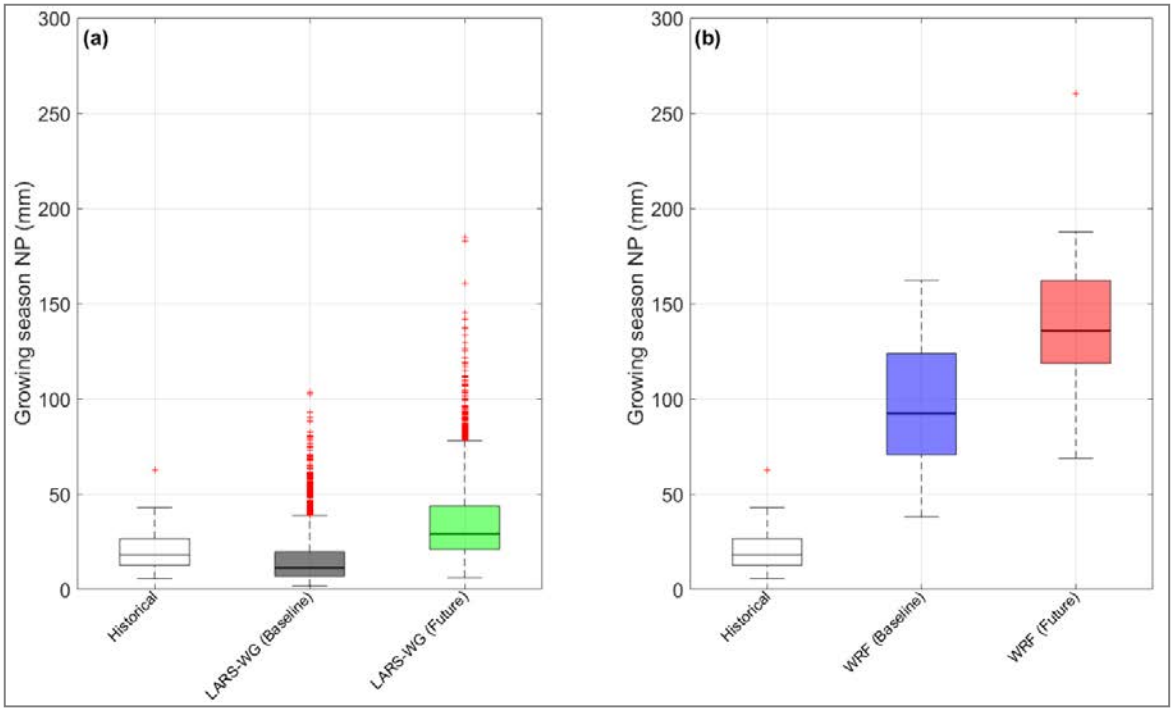

Figure 6: The same as Figure 2 but for growing season NP

Recommendations for reclamation cover designs

The design of reclamation covers in the face of climate change requires understanding the potential impact that climate change may have on cover performance, including the uncertainties in generating regional/local climate change projections. This study shows that the climate change projections in the oil sands region may result in increased rates of both AET and NP on reclaimed sites, regardless of the choice of downscaling methods. These shifts in water balance would be likely to accelerate vegetative re-establishment and possibly shift the vegetative regime on reclaimed sites. More importantly, the increase in NP could result in accelerated rates of water migration through reclaimed mine waste. The potential impact that these increases in NP may have on increased chemical loading to the environment will need to be evaluated. In some cases, improvements to surface water management practices or landscape design could also provide the opportunity to increase freshwater yields from reclaimed landscapes as precipitation levels increase.

It is also important to highlight that the increased variability associated with WRF climate predictions will also be reflected in a greater range in outputs for water balance components such as NP. Just as it has become common practice to utilize multiple models and methods (i.e. GCMs, downscaling techniques) to make decisions on the potential impact of climate changes, it may be prudent to also undertake an evaluation of reclamation cover and closure landform performance using a range of climate change predictions. While physically based WRF predictions highlight the potential variability associated with higher spatial and temporal resolutions, LARS-WG might provide a useful base case to evaluate shifts in overall expected

performance. Considering the computational costs of WRF, the statistical downscaling technique might offer a quick alternative to test different management policies and adaptation plans to tackle the impacts of climate change on the reclamation covers in the study region.

Conclusion

Based on the results of this study, both statistical (LARS-WG) and dynamical (WRF) downscaling methods demonstrated increased temperature, precipitation, and PET in future with associated increases in the future water balance components (i.e., AET and NP). Both LARS-WG and WRF showed similar directions of change in future AET and NP, although the magnitude of increase differed. For both downscaling methods, the increase in future NP relative to the historical period was higher than the corresponding increase in AET. The shifts in future precipitation for both LARS-WG and WRF were greater than the corresponding shifts in future AET relative to the historical cases, resulting in much higher shifts in the growing season NP.

The large differences in the simulated AET and NP based on the LARS-WG and WRF simulations seem to have originated from the large differences in the temperature and precipitation between the WRF simulations and historical observations. The biases in the WRF simulations relative to the historical observations need to be considered when making comparison with other downscaling methods. Use of a single GCM and RCM (which is WRF in this study) might lead to greater uncertainty in simulating water balance components (particularly NP), so the use of multiple GCMs and RCMs might lead to less uncertainty.

Acknowledgements

We would like to thank Dr. Zhenhua Li for providing WRF simulations. The first three authors would like to acknowledge funding from Syncrude Canada Ltd and the Natural Sciences and Engineering Research Council of Canada (NSERC) for this study, and the Department of Civil, Geological and Environmental Engineering, University of Saskatchewan, Canada. The fourth author acknowledges support from NSERC Discovery Grant.

References

Alam, M.S., S.L. Barbour, A. Elshorbagy and M. Huang. 2017. The impact of climate change on the performance of oil sands reclamation covers: A comparison of multiple general circulation models and representative concentration pathways. *Proceedings of 70th Canadian Geotechnical Society Conference;* GeoOttawa 2017, Ottawa, Ontario, October 2017.

Alam, M.S., S.L. Barbour, A. Elshorbagy and M. Huang. 2018. The impact of climate change on the water balance of oil sands reclamation covers and natural soil profiles. *J. Hydrometeorol.* 19(11): 1731–1752.

Boese, CD. 2003. The design and installation of a field instrumentation program for the evaluation of soil-atmosphere water fluxes in a vegetated cover over saline/sodic shale overburden. MSc Thesis, University of Saskatchewan.

Carrera-Hernández JJ, Mendoza CA, Devito KJ, Petrone RM, Smerdon BD. 2011. Effects of aspen harvesting on groundwater recharge and water table dynamics in a subhumid climate. *Water Resources Research* 47(5): 1–18.

Cumulative Environmental Management Association (CEMA). 2006. Land capability classification system for forest ecosystems in the oil sands, 3rd edition, Volume 1: Field manual for land capability determination. Alberta Environment.

Gao, Y., J.S. Fu, J.B. Drake, Y. Liu, and J.F. Lamarque. 2012. Projected changes of extreme weather events in the eastern United States based on a high resolution climate modeling system. *Environmental Research Letters* 7(4): 1–12.

Giorgi, F. 1990. Simulation of regional climate using a limited area model nested in a general circulation model. *Journal of Climate* 3(9): 941–963.

Hargreaves, G.H. and Z.A. Samani. 1985. Reference crop evapotranspiration from temperature. *Appl. Eng. Agric.* 1(2): 96–99.

Huang, M., A. Elshorbagy, S.L. Barbour, J. Zettl and B.C. Si. 2011a. System dynamics modeling of infiltration and drainage in layered coarse soil. *Canadian Journal of Soil Science* 91: 185–197.

Huang, M., S.L. Barbour, A. Elshorbagy, J. Zettl and B.C. Si. 2011b. Water availability and forest growth in coarse-textured soils. *Canadian Journal of Soil Science* 91: 199–210.

Huang, M., S.L. Barbour, A. Elshorbagy, J. Zettl and B.C. Si. 2011c. Infiltration and drainage processes in multi-layered coarse soils. *Canadian Journal of Soil Science* 91: 169–183.

IPCC. 2013. Climate change 2013: The physical science basis. In Stocker et al. (eds.), *Contribution of Working Group I to the Fifth Assessment Report of the Intergovernmental Panel on Climate Change.* Cambridge University Press, Cambridge, United Kingdom and New York.

Keshta. N., A. Elshorbagy and S. Carey. 2009. A generic system dynamics model for simulating and evaluating the hydrological performance of reconstructed watersheds. *Hydrology and Earth System Sciences* 13(6): 865–881.

Keshta, Nader, A. Elshorbagy and S. Carey. 2012. Impacts of climate change on soil moisture and evapotranspiration in reconstructed watersheds in northern Alberta, Canada. *Hydrological Processes* 26(9): 1321–1331.

Li,Y., Z. Li, Z. Zhang, L. Chen, S. Kurkute, L. Scaff and X. Pan. 2019. High-resolution regional climate modeling and projection over western Canada using a weather research forecasting model with a pseudo-global warming approach. *Hydrol. Earth Syst. Sci. Discuss.* 201: 1–38.

Meehl, G.A., C. Covey, T. Delworth, M. Latif, B. McAvaney, J.F.B. Mitchell, R.J. Stouffer and K.E. Taylor. 2007. The WCRP CMIP3 Multimodel Dataset: A new era in climate change research. *Bulletin of the American Meteorological Society* 88(9): 1383–1394.

Price, J.S., R.G. McLaren and D.L. Rudolph. 2010. Landscape restoration after oil sands mining: Conceptual design and hydrological modelling for fen reconstruction. *International Journal of Mining, Reclamation and Environment* 24(2): 109–123.

Qualizza, C., D. Chapman, S.L. Barbour and B. Purdy. 2004. Reclamation research at Syncrude Canada's mining operation in Alberta's Athabasca oil sands region. *Proceedings of the 16th International Conference on Ecological Restoration SER2004*, Victoria, BC, Canada, Society for Ecological Restoration.

Semenov, M.A. and E.M. Barrow. 1997. Use of a stochastic weather generator in the development of climate change scenarios. *Climatic Change* 35(4): 397–414.

Simunek, J., M. Sejna, H. Saito, M. Sakai and M.T. van Genuchten. 2013. The HYDRUS software package for simulating the two- and three- dimensional movement of water, heat, and multiple solutes in variably-saturated media, Technical manual version 2.0. University of California, Riverside, CA.

Skamarock, C., B. Klemp, J. Dudhia, O. Gill, D. Barker, G. Duda, X. Huang, Wang, W. and G. Powers. 2008. *A Description of the Advanced Research WRF Version 3.* NCAR Technical Note NCAR/TN-475+STR (2008).

Wilby, R.L. and T.M.L. Wigley. 1997. Downscaling general circulation model output: A review of methods and limitations. *Progress in Physical Geography* 21(4): 530–548.

Bibliography

Huang, M., S.L. Barbour and S.K. Carey. 2015. The impact of reclamation cover depth on the performance of reclaimed shale overburden at an oil sands mine in Northern Alberta, Canada. *Hydrological Processes* 29(12): 2840–2854.

Proceedings of Tailings and Mine Waste 2019
November 17–20, 2019, Vancouver, Canada
Published by the University of British Columbia, 2019

Detailed Geomorphic Design of a Waste Dump in the Mineable Oil Sands Region

Monica Ansah-Sam, Canadian Natural Resources Ltd, Canada
Dejiang Long, Golder Associates Ltd, Canada
Collen Middleton, Golder Associates Ltd, Canada
Matthew Knapik, O2 Planning + Design Ltd, Canada

Abstract

A detailed geomorphic landform and drainage design was prepared for the Jackpine Mine (JPM) Dump 3, which is approximately 20 km northeast of Fort McKay on Oil sands lease 13 in the Athabasca Oil Sands in northeastern Alberta. The design was based on the overall development and closure goals, objectives, and strategy of Canadian Natural Upgrading Ltd. (Canadian Natural) for JPM, the JPM closure landscape design basis, as well as pertinent studies, practices, and guidelines on oil sands mine closure landscape planning and design. The objectives of preparing a detailed geomorphic design for Dump 3 were to support its economic development and safe operation, to create a sustainable landform and drainage pattern requiring minimum maintenance post closure, and to integrate novel geomorphic landform and drainage design elements into its construction. Potential natural analogues in the region were identified to guide the design. A search of the available regional terrain data was conducted to identify natural landforms with comparable dimensions to Dump 3 (i.e., maximum length, maximum width, and local relief). For each of the three nearest analogues selected, the slope forms and gradients, convexities, localized relief, slope path lengths, and erosional features were analyzed to determine the tolerances of geomorphic parameters that could be used to guide the design.

The design of the landform was constrained by geotechnical and mining requirements. A procedural model was developed to iterate surface options within target volumes and geometric constraints. Modifications to the surface terrain were driven through a combination of manual and parametric control, informed by a range of real-time assessment metrics that indicated areas of the design that fell outside the acceptable range of constraints. Terrain roughening procedures were developed and applied to the final surface to achieve target meso-variability. This paper describes the incorporation and implementation of closure goals into the design, as well as incorporation of geotechnical constraints and existing

infrastructure at the end of dump placement into the final geomorphic design by a multidisciplinary team. The paper includes commentary on how the geomorphic design is aligned with the JPM closure plan.

Introduction

Historically waste dumps have been constructed based on geotechnical requirements and mining considerations. The geomorphic design of the dumps was typically considered after the final placement of waste on the facility. Some "older" dumps did not consider geomorphology if constraints did not allow for flattening or contouring of slopes to provide a natural appearance and to support sustainable drainage. The most efficient way to reduce rework and cost of dump construction is to construct the dump to its final geomorphic "shape" prior to reclamation placement or any progressive reclamation. Some dumps that have already been constructed can be retrofitted to a geomorphic "shape" if geotechnical, mining and reclamation constraints still provide that flexibility. The closure landscape plan is a building block to the closure plan, which develops closure topography based on the underlying mine plan (Ansah-Sam et al., 2016). The closure landscape plan is used to provide a realistic base or reclamation ready surface from which to develop plans for progressive reclamation, including placement of cover soil, revegetation, watercourse construction, and End Pit Lake (EPL) construction (Ansah-Sam et al., 2016). The geomorphic design of a specific structure becomes an integrated part of the site wide closure plan and should be aligned with the design basis of the closure plan.

There are examples of waste dumps that have been contoured and constructed to its geomorphic design in the oil sands region and these examples can be used as learnings as the strategic approach of constructing dumps to its final geomorphic shape during waste placement progresses. Unlike closure landform designs of large oil sands tailings facilities, geomorphic designs of dumps are less challenging and much easier to construct and every opportunity to do so is strongly recommended during the operational phase of the structure. This case history will highlight how Dump 3 Geomorphic design involves balancing key design criteria with long-term goals, volume placement, constraints, and long-term performance of the landform.

Background

Dump 3 is an external mine waste disposal facility which is located east of the JPM pit, outside of the maximum mine advance limit. It will permanently dispose mine waste materials deemed unsuitable for construction of other mine earth structures. Due to its location (east of In-pit Cell 1 [IPC1]), it interacts indirectly with the east pit wall and the future In-Pit Dyke 1 (see Figure 1).

Dump 3 is expected to be founded on original ground which varies between elevations 315 and 320 masl. The structure height is planned to reach a maximum of 50 m in the center and north areas of the

footprint (for a nominal crest at 370 masl) with an overall slope of 4H:1V. A maximum offset of 90 m from the pit wall crest is to be maintained around the west perimeter of the structure. Dump 3 has a footprint area of 0.47 km^2 and a maximum elevation of 370 masl. The construction of Dump 3 is currently ongoing and planned to be completed in 2021.

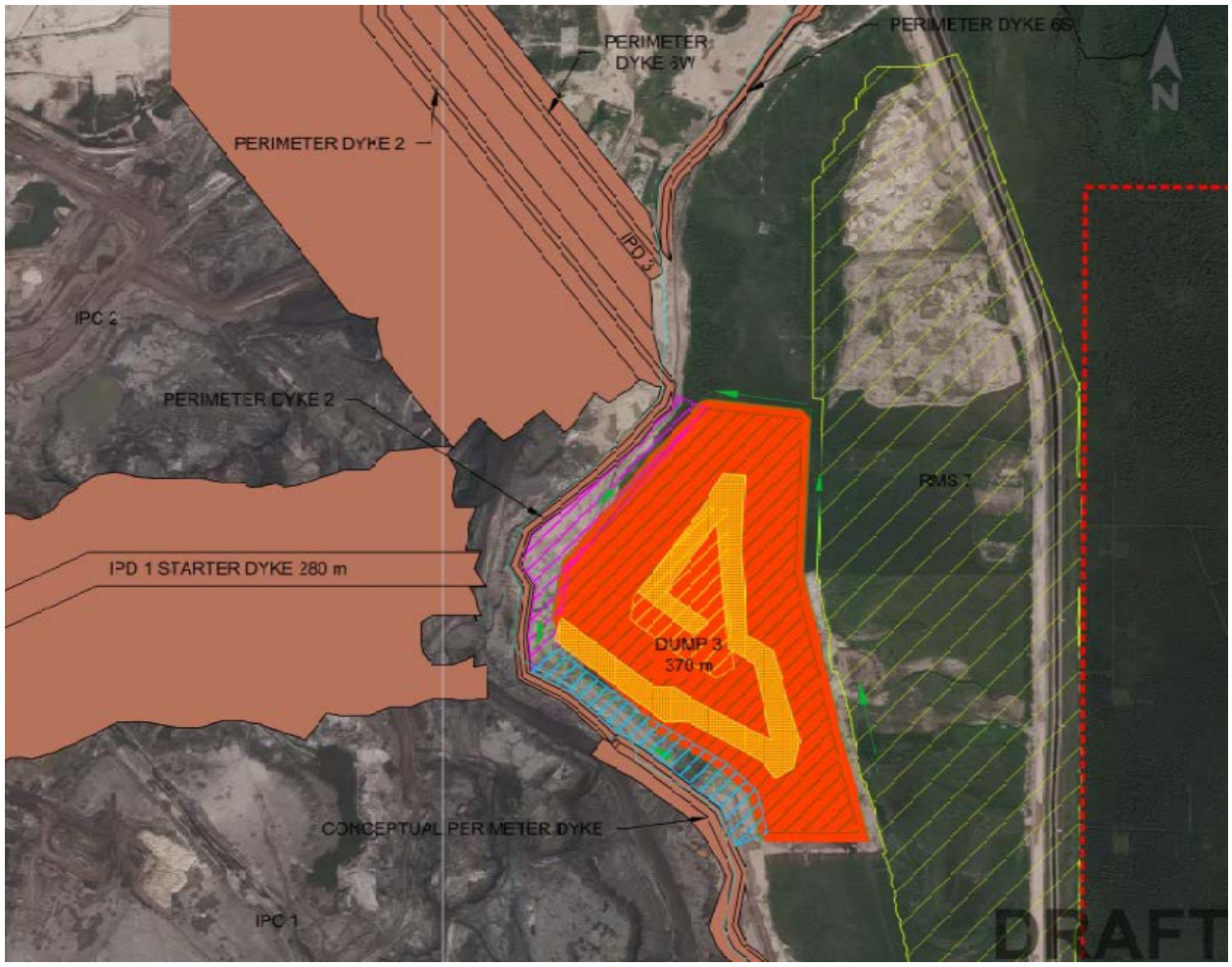

Figure 1: Location of Dump 3

Dump 3 was designed to accommodate 5 m high maximum local overbuilds for any operational requirements such as temporary surface water management, corridors, haul roads, safety berms, etc. Figure 1 shows the location of Dump 3 at the JPM site.

Canadian Natural required that elements of geomorphic landform design be integrated into construction and development of Dump 3, such that re-grading is optimized for final landform conformation at closure. Geomorphic landform design is an approach to the design of closure landforms and landscapes that mimics the appearance and performance of landforms that occur naturally on the pre-development landscape. The goals of geomorphic landform design are to minimize maintenance post

closure and to provide a stable surface for achieving end land use objectives on the closure landscape. Canadian Natural also required that the design output format be a Digital Elevation Model (DEM) surface for Dump 3 to enable use of vehicle-mounted GPS systems to guide sophisticated construction activities.

Design basis

The objectives of preparing the detailed geomorphic design for Dump 3 were to support economic development and safe operation of Dump 3 and the JPM, development of sustainable Dump 3 closure landform and drainage requiring minimum maintenance post closure, and integration of the geomorphic landform and drainage design elements into the construction and development of Dump 3. The applicable basis for the landform design included the following:

- Meet mine planning volume balance tolerance for the Dump 3 closure surface.
- Incorporate elements of natural appearance of comparable natural analogues including micro, meso and macro topographic variability and diversity.
- Provide geotechnically stable landform slopes.
- Allow geometry for placement of reclamation material to design thicknesses.
- Provide adequate trafficability to equipment for reclamation material placement and for end land uses.
- Provide access for monitoring and maintenance.
- Design topography to provide access for mining equipment during operation.
- Provide sufficient spatial resolution in designed surfaces to support closure planning activities.

The applicable basis for the drainage design included the following:

- Provide adequate drainage density, landscape stability and sediment yield characteristics similar to comparable natural analogues in the oil sands region.
- Provide vegetated waterways on steep slopes with long flow paths where required.
- Accommodate gully erosion and sediment deposition.
- Exclude any side hill channel that is not sustainable over the long term.

Selection of natural analogues

Potential natural analogues in north eastern Alberta were identified to provide regional landscape precedents to guide the geomorphic design of the final reclamation surface of Dump 3. An automated search of the available terrain data in the oil sands region was conducted in ArcGIS to identify natural landforms with comparable dimensions to Dump 3 (i.e., maximum length, maximum width, and local relief). This yielded a long list of about 20 landforms of variable geomorphic origins. Of these, a short list of five landforms that most closely resembled Dump 3 were manually selected.

The geomorphic origins of the short-listed landforms included basal till and ice-thrust features up to 100 km west of the JPM site on the lower slopes of the Birch Mountains and on the Cheecham Hills about 120 km south of the JPM site, a field of large drumlins about 80 km east-northeast of the JPM site, and ice-contact glaciofluvial deposits (i.e., localized kames) up to 250 km south-southwest of the JPM site. From this short list, 15 m LiDAR data was purchased for the three nearest matches to Dump 3. Figure 2 illustrates the natural appearance of these three analogues. For each of these three analogues, the slope forms and gradients, convexities, localized relief, slope path lengths and erosional features were analyzed to determine the tolerances of geomorphic parameters that could be used to guide the design of Dump 3. These analogues were used throughout the Dump 3 design process to incorporate variability of topography and slope shapes to create a visually appealing naturalized landform. See Figure 2 below for the three main natural analogues that were selected to guide the design.

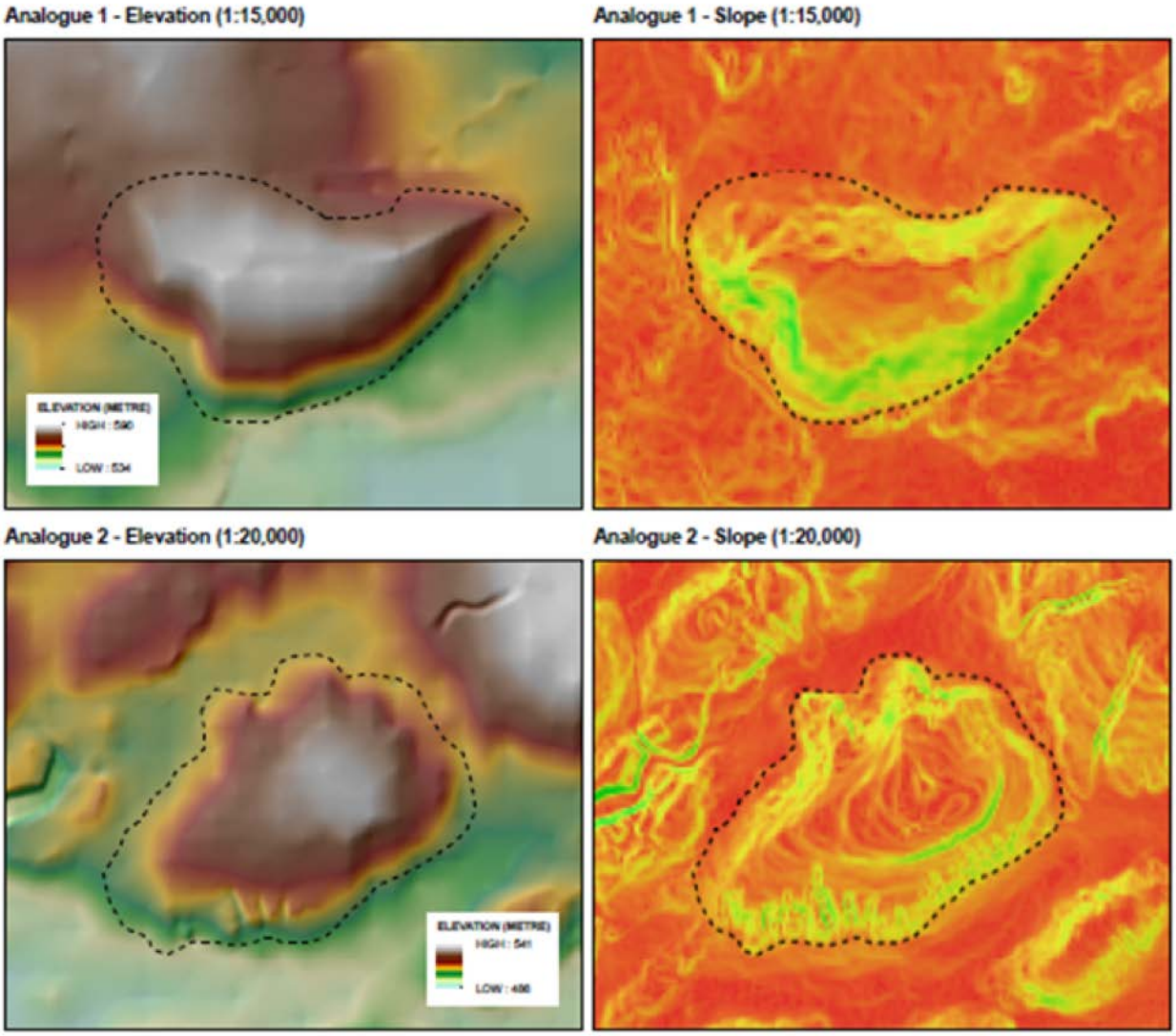

Figure 2 : Selected natural analogues to guide Dump 3 design

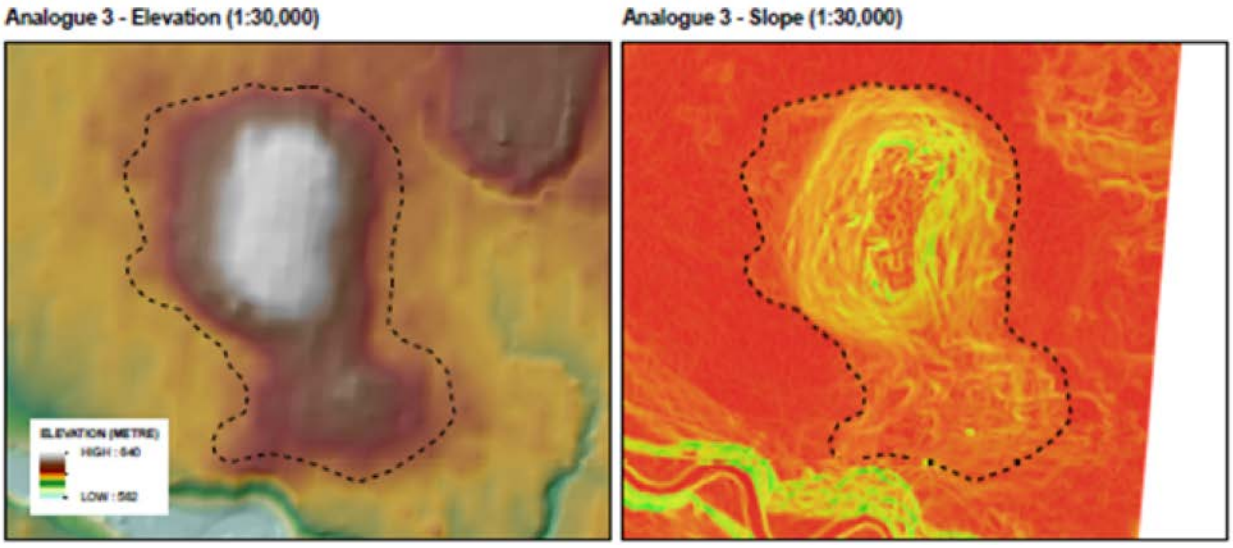

Figure 2 continued: Selected natural analogues to guide Dump 3 design

Geomorphic design process

Design requirements and constraints

Canadian Natural identified several requirements and constraints for the Dump 3 geomorphic design, including the following:

- maximum dump toe footprint in consideration of the required setbacks from the adjacent reclamation stockpile, mine pit crest, and pit wall design limits;
- maximum top-of-dump elevation of 370 masl;
- within ±5% of the target total overburden storage volume of 9.7 Mm^3, plus 0.5 m reclamation material placement;
- overall surface slopes of 4(H):1(V) or flatter; and
- a haul road of 50 m width and a maximum slope of 5%, which will be maintained until closure.

The final Dump 3 surface was designed to meet the requirements and constraints including those listed above.

Drainage concept evaluation and selection

Three options of closure drainage concepts for Dump 3 were identified and evaluated. Option 1 involved overland drainage only by minimizing overland flow path lengths and slopes. Option 2 was an overland drainage combined with one drainage channel situated along the access ramp to reduce the overland flow path lengths. Option 3 involved overland drainage combined with a number of vegetated waterways to reduce gully erosion risk in the areas with relatively long overland flow paths and/or steep slopes.

A design guide chart was used in evaluating the drainage design concepts. This chart was developed based on available geomorphic survey data collected in the oil sands region (Golder 2004). Based on the available regional data included in the design guide chart, most of the surface areas at Dump 3 are estimated to have small to negligible gully erosion risk (green zone), and the some of the surface areas at Dump 3 are estimated to have small to moderate gully erosion risk (yellow zone).

For Option 1, most of the Dump 3 design surface (about 80%) falls within the green zone of "no channel" in the design guide chart, and the remaining area (about 20%) falls in the yellow zone of "considering channel". To control and reduce the erosion risk of the surface areas in the yellow zone, select reclamation soils (i.e., peat-mineral mix) were planned to be placed in these areas. With implementation of this mitigation measure, the overall gully erosion risk at Dump 3 is estimated to be small, after mature vegetation is established post reclamation.

Option 1 was the selected drainage concept for detailed geomorphic design of Dump 3. Option 2 would require construction of a relatively long drainage channel along the access ramp. Incorporating such a side-hill channel at Dump 3 would increase the risk of gully erosion due to potential concentrated flow overtopping at unpredictable locations along the access ramp. This would also result in higher erosion risk than Option 1. Option 3 would incur additional cost for design, construction and initial maintenance of a number of vegetated waterways. Placement of select reclamation soils (i.e., peat-mineral mix as described above) in the areas of the yellow zone, was considered to be more cost effective than installing vegetated waterways in these areas. Therefore, Option 1 was preferred over Option 3.

Geomorphic surface design

Rhino 3D software and its associated Grasshopper programming environment were used alongside ArcGIS as the principal tools for the detailed design of the Dump 3 landform. The parametric capabilities of the Grasshopper software suite allowed for the iterative creation of 3D surfaces based on the design objectives and constraints. The tools were also used alongside manual modelling techniques to smooth the large-scale surface geometry and add roughness to mimic the mesovariability of comparable natural analogues. Modifications to the surface terrain were informed by a range of real-time assessment metrics, highlighting areas of the design which were outside the acceptable range of constraints.

Reproducing the initial Dump 3 geotechnical design within "Rhino" resulted in the creation of a geometric surface with slopes varying between 17% and 35%, and a storage volume of 10.45 Mm^3. This surface was subsequently modified to have slopes no greater than 25% (with temporary construction-phase slopes of up to 33%), and a total overburden storage volume of 9.22 Mm^3, including final adjustment to the toe locations.

The final geometric construction surface constrains the outer slopes (i.e., those beyond outer edge of the haul road surface) to be within 25%. The inner slopes (i.e., those above the road surface) are constrained to be within 33% during the construction phase. Figure 3 illustrates creation of the geometric construction surface. Figure 4 highlights the slope surfaces.

Following creation of the geometric construction surface, the top 10 m of the placed material in the constructed surface was designed to be pushed down to fill in the 50 m haul road. This was to ensure that all slopes on the final Dump 3 closure surface are within the target 25% maximum slope. This outer slope grade limit pushed the spiraling haul road inwards at a steady rate, providing a natural limit to the road's length, and the maximum height of the pile. An interim 5 m service road was planned to be maintained along the haul road prior to closure of Dump 3 to allow access during monitoring and final reclamation. Figure 5 highlights the "push-down" area.

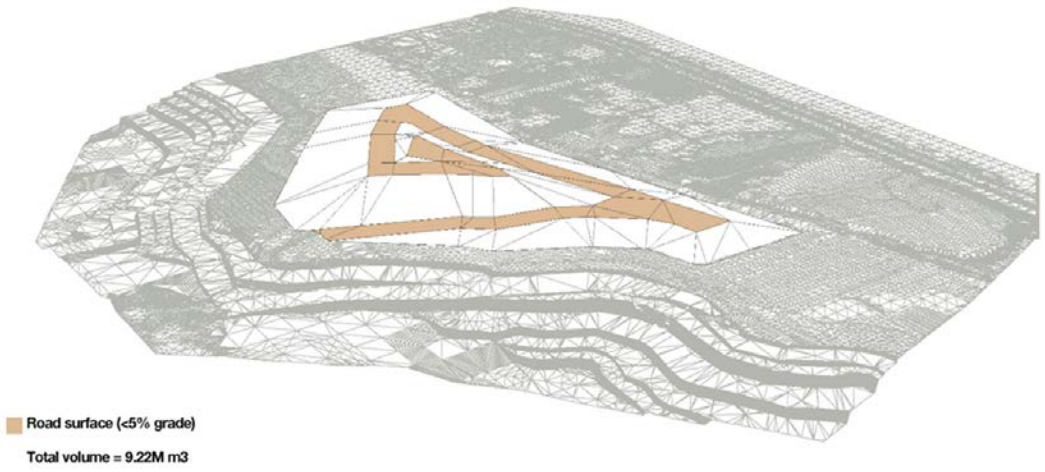

Figure 3: Oblique view of the complete geometric construction surface

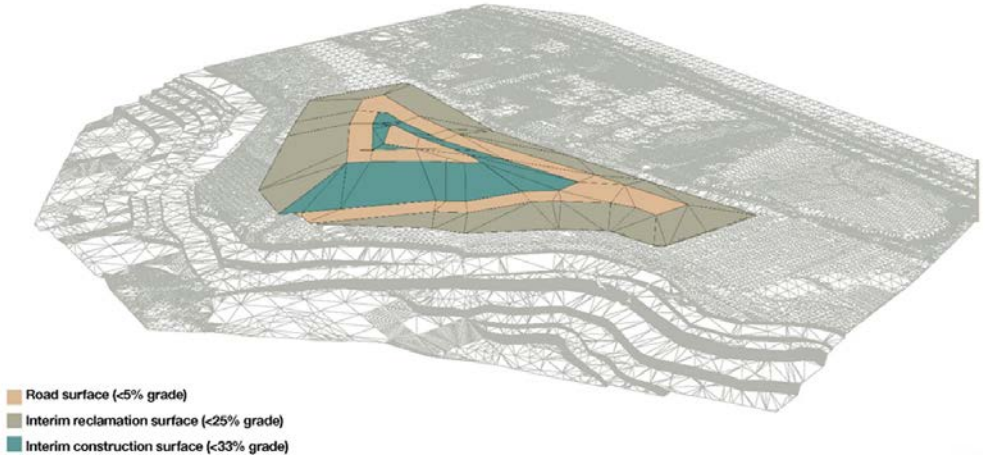

Figure 4: Oblique view highlighting the slope classes of the complete geometric construction surface

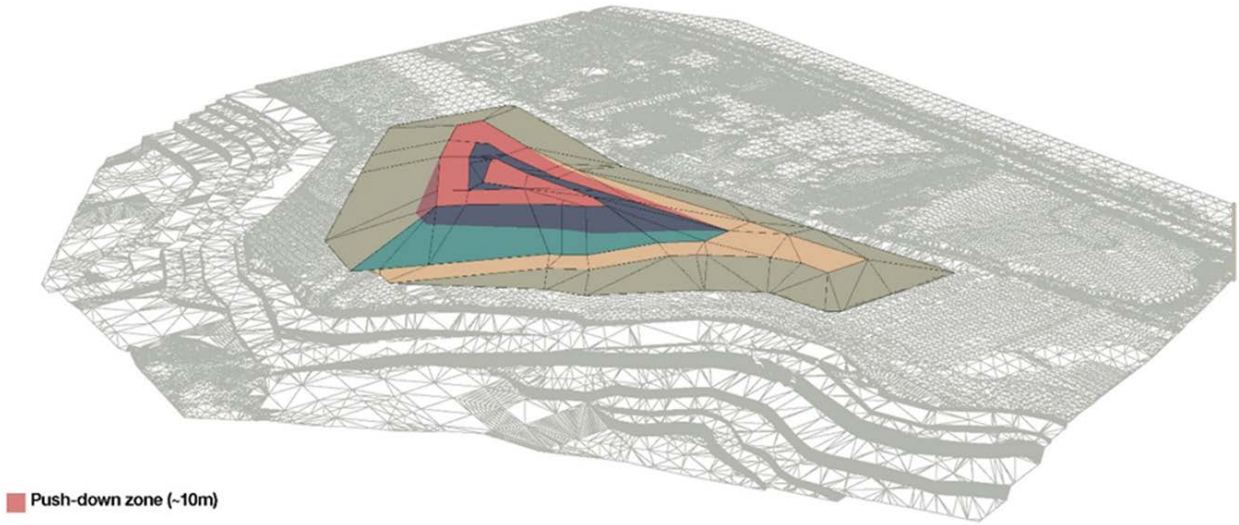

Figure 5: Oblique view highlighting the push-down areas of the complete geometric construction surface

Additional micro-topographic surface variation was introduced to the geomorphic design of final Dump 3 surface to mimic variation of the natural analogue terrain. The surface was subdivided into 10,000 scattered points, and these points were then randomly displaced between +0.5m and -0.5m. This process resulted in a non-uniform surface that had meso-variability comparable to the terrain measured in the natural analogues. The randomized location and displacement of the points (as compared to, for example, a regularized grid) was an important component of this process, as it created "noise" that resisted emergent patterns that may have increased risk of channel formation.

The Vector Ruggedness Measure (VRM) parameter measures terrain ruggedness as the variation in three-dimensional orientation of grid cells within an area. Vector analysis was used to calculate the dispersion of vectors normal (orthogonal) to grid cells within the specified area. This method effectively captures variability in slope and aspect into a single measure. Ruggedness values in the output raster can range from 0 (no terrain variation) to 1 (complete terrain variation). Typical values for natural terrains range between 0 and 0.4.

As shown in Table 1, the comparison between the final reclamation surface of Dump 3 and the three comparable natural analogues in the oil sands region suggests that the range, mean and standard deviation of the Dump 3 reclamation surface design fall in the middle of the values of the three analogue surfaces. Figure 6 illustrates the final reclamation surface.

Table 1: Statistics of vector ruggedness measure

Surface	Range	Mean	Standard deviation
Natural analogue 1	0.00918	0.00037	0.00060
Natural analogue 2	0.00404	0.00046	0.00051
Natural analogue 3	0.01410	0.00074	0.00126
Dump 3 reclamation surface	0.00768	0.00044	0.00034

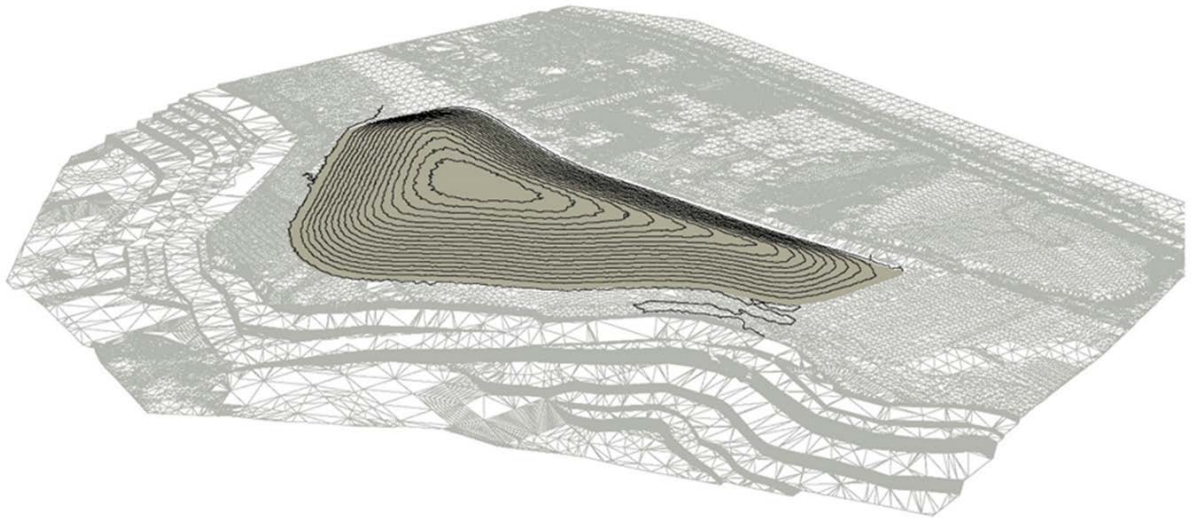

Figure 6: Oblique view of the final reclamation surface for closure

Table 2 presents a comparison of the major geometric parameters of the final Dump 3 reclamation surface and the three comparable natural analogues in the region. This table shows that Dump 3 is generally comparable to the three analogues, but it has higher maximum and overall overland slopes than the analogues due to the overburden disposal volume requirement in a constrained footprint. As described earlier, Dump 3 slopes were successfully controlled in the design to have most of its surface (i.e., about 80%) in the zone of negligible gully erosion risk, and the remaining surface area (i.e., about 20%) in the zone of small to moderate gully erosion risk which is mitigated by placement of select reclamation soils. Controlling these overland slopes while achieving the targeted overburden storage volume required by mining, was the primary consideration in the geomorphic design of the final Dump 3 landform.

Table 2: Comparison of Dump 3 design with natural analogues

Surface	Area (km^2)	Length (km)	Width (km)	Elevation range (relief) (m)	Overland slope (%)		
					Minimum	Maximum	Overall
Natural analogue 1	0.77	1.3	0.9	49	<1	16	6
Natural analogue 2	1.41	1.7	1.1	48	<1	14	4
Natural analogue 3	3.46	2.6	1.7	50	<1	15	3
Dump 3 reclamation surface	0.47	1.1	0.6	41	<1	25	18

A look back at the design process

The key success factors addressed during the process of the Dump 3 geomorphic design include the following:

- Setting clear goals and objectives for the closure landform design: The development of sustainable closure landform and drainage requiring minimum maintenance post closure was a clear objective that influenced the design approach and method, including selection and consideration of comparable natural landform analogues to guide the Dump 3 design.
- Using the Design Basis Memorandum (DBM) for the ongoing closure plan of the JPM site: This was to ensure integration and alignment of Dump 3 into the JPM closure plan and the final closure landscape plan, and application of consistent design basis, considerations and criteria.
- Challenging design constraints: The initial volumetric and geotechnical design of Dump 3 was modified to reduce the total volume of overburden disposal and the maximum overland slope, so that the final dump will have more sustainable slopes of 25%.
- Integrate technical inputs from multiple disciplines: Although Dump 3 is a relatively small structure in comparison to many other large structures of the JPM, closure geomorphic design of Dump 3 required many if not all of the considerations for large structures. The Dump 3 design involved technical inputs and close collaboration of mine planners, geotechnical engineers, geomorphologists, drainage designers, landscape designers, civil engineers, and reclamation specialists from Canadian Natural, Golder Associates and O2 planning + design.

Looking ahead

The construction of Dump 3 is scheduled to be completed in 2021 and built to the final geomorphic surface as much as practical. If any optimizations are identified during the construction, some adjustments will be made to accommodate these optimizations, while ensuring that the design goals and criteria are

still met. It is anticipated that the final grading and contouring to final geomorphic surface will be completed prior to reclamation placement. In addition, vegetation selection and cover soil design are expected to minimize erosion and allow for the long-term stability of the landform. Canadian Natural will monitor Dump 3 during construction and after vegetation placement to ensure that the dump's performance is aligned with the design intent.

The case history described above represents a geomorphic design practice successfully implemented in a particular time (i.e., at the beginning of construction of Dump 3 when a geomorphic design was developed before the dump construction and based on available information and past studies). The design process and practice will continue to evolve as more dumps in the region are constructed based on geomorphic designs. However, this case history highlights the benefits of developing geomorphic design before construction to reduce the cost of potential retrofit and to reduce potential long-term requirements for care and maintenance of a closure landform.

Acknowledgements

Thanks and appreciation to Canadian Natural's Geotechnical Engineering, Britany Skinner of the closure design team, the environment and mine planning teams, Golder Associates, and O2 Planning + Design for collaboration on the detailed geomorphic design of Dump 3. A large number of engineers, designers, and specialists from the three organizations participated in the design. Their contributions to the successful completion of the design are gratefully acknowledged.

References

Ansah-Sam, M., L. Hachey, G. McKenna and B. Mooder. 2016. The DBM approach for setting engineering design criteria for an oil sands mine closure plan. In *Proceedings of the 5th International Oil Sands Tailings Conference (IOSTC 2014).*

Bibliography

Canadian Natural Upgrading Ltd. 2018. Jackpine Mine Dump 3 detailed design report, July.

Proceedings of Tailings and Mine Waste 2019
November 17–20, 2019, Vancouver, Canada
Published by the University of British Columbia, 2019

Comparison of Oil Sand Tailings Consolidation Properties Derived from Beam Centrifuge and Large-Strain Consolidometer Testing

Monica Ansah-Sam, Canadian Natural Resources Ltd, Canada
Jason Stianson, Golder Associates Ltd, Canada
Karsten Rudolf, Canadian Natural Resources Ltd, Canada
Gonzalo Zambrano Narvaez, University of Alberta, Canada

Abstract

Closure landscape planning provides a basis for development of a ready-for-reclamation surface from which plans for subsequent activities such as the placement of the closure cap, water course construction, placement of reclamation material, and revegetation can be developed. One of the key components of closure landscape planning is the evaluation of settlement for tailings facilities. Tailings settlement can affect a significant portion of the landscape once mining is complete. Assessment of tailings settlement must take into consideration the different types of tailings planned to be deposited into a given facility, the volume distribution of tailings within a given deposit, the proposed deposition strategies, and the detailed consolidation properties of the different tailings materials.

The consolidation properties consist of two main functions; namely, the compressibility and the hydraulic conductivity functions of the tailings. Tailings compressibility is defined as a non-linear relationship between void ratio and effective stress and provides the basis for assessing the overall amount of tailings settlement. Tailings hydraulic conductivity is generally a function of void ratio and is used to assess the rate of tailings consolidation over time. Consolidation testing undertaken to measure the compressibility and hydraulic conductivity of tailings is time consuming and can take as long as one year to complete depending on the type of tailings and the test boundary conditions. The use of elevated gravitational forces in a beam centrifuge has been identified as a possible means of obtaining the required tailings consolidation properties at a much faster rate. This paper shows a comparison of tailings consolidation properties measured using conventional large-strain consolidation apparatus to the consolidation properties obtained from a 2 m radius 50 g-tonne beam centrifuge.

Introduction and background

An understanding of the consolidation behaviour of tailings deposits is required in order to develop a

closure plan that takes long term settlement into account. A testing program was undertaken to expand on Canadian Natural's understanding of the consolidation behaviour of tailings materials present at both the Muskeg River Mine's external tailings facility (MRM ETF) and the first in-pit cell (IPC1). Both facilities were deposition sites for MRM's froth treatment tailings. The final treatment step for the froth treatment tailings occurs in the tailings solvent recovery unit (TSRU). The froth treatment creates a tailings stream that can aggregate during deposition and produce a deposit with considerably higher than usual bitumen content. Regular TSRU tailings (as found in IPC1), can have bitumen contents greater than 20% by weight. When TSRU tailings are mixed with other tailings streams (e.g., thickened tailings and coarse sand tailings, as found in MRM-RTF, and known as the North Pool Deposit [NPD]), bitumen contents of 5 to 15% by weight are common. The present testing program was developed to assess the impact of variability in bitumen and fines content on the consolidation properties of the tailings. This testing program consisted of several samples in large-strain consolidation cells, which were paired with tests run in the beam centrifuge.

Large-strain consolidation (LSC) testing is used for the measurement of compressibility and hydraulic conductivity property functions. These material properties are then used for numerical modelling to predict settlement behaviour under a given set of boundary conditions. Testing for material properties requires considerable time for high fines materials. Beam centrifuge testing provides a faster alternative for the characterization of long-term settlement behaviour. A laboratory program was conducted on similar samples using LSC and centrifuge testing. Conducting tests on the same samples provided an opportunity to compare results between the two testing methods. This paper presents a comparison of the two laboratory testing methodologies. It also describes the numerical modelling procedure used to develop a predictive model for estimating settlements for a 20 m thick deposit. A similar set of paired tests that were performed on samples from a 10 m centrifuged deposit (CFFT) from the Jackpine Mine (JPM) is also discussed.

Approach to testing

Tailings properties and sample selection

The MRM ETF and MRM IPC1 facilities contain TSRU tailings that have significant variability in bitumen content. The TSRU tailings were the source selected for this test program. Samples were collected during the 2017 Annual Tailings Investigation. The samples were primarily used for characterization and index testing. The individual samples were of insufficient volume for the planned parallel testing program. To ensure that the desired variability in fines and bitumen content was maintained, multiple samples were identified (i.e., 3–4 per batch) which were then combined into one larger composite sample. The individual samples were from multiple locations and varying depths within

the deposit. The batch samples were prepared to create a distribution of bitumen contents, sands to fines ratios (SFRs) and age of samples. The paired testing program was performed on the JPM CFFT. The bulk batch samples were homogenized and split into two subsamples for subsequent LSC and beam centrifuge testing. The index properties of the composite batch samples selected for this paper are shown in Table 1.

Table 1: Sample index properties

Parameters	IPC1 shallow	IPC1 deep	NPD medium bitumen high SFR	JPM centrifuge deposit
Sample significance	Pure TSRU freshly deposited	Pure TSRU significantly aged in-situ	Mixed tailings with some bitumen and intermediate amount of fines	Baseline bitumen content and very high fines
Age	0–2years	4–6 years	NA	NA
USCS[1]	SM	ML	ML	CH
UOSTCS[2]	T–1	T-2	T-2	F-2
Solids (wt%)	43.8	46.6	58.3	44.6
Specific gravity	1.79	1.77	2.25	2.43
Bitumen (B) (wt%)	16.5	17.5	8.0	1.5
Water (wt%)	56.2	53.4	41.7	55.4
Fines content (*44 μm*)	36.6	48.2	38.8	98
SFR [3]	1.7	1.1	1.6	0.02
MBI[4]	2.7	2.9	1.6	14.5

Note[1]: Unified Soil Classification System
Note[2]: Unified Oil Sands Tailings Classification chart.
Note[3]: Sands to Fines ratio is based on non-dispersed sieve hydrometer.
Note[4]: Methane Blue Index.

Beam centrifuge test program

A geotechnical beam centrifuge can be used for modeling large-scale problems for which gravity is the primary driving force. This includes the self-weight consolidation of fine tailings materials. The fundamental principle of centrifuge modeling is based on the stress similarity between a prototype and a centrifuge model. Scaling laws for size and time are used to design the appropriate centrifuge operation (Sorta, 2015; Zambrano-Narvaez et al., 2018). Equations 1 and 2 illustrate the scaling laws for size and time in a geotechnical centrifuge model when modelling self-weight consolidation of tailings materials.

$$h_p = N * h_m \quad (1)$$

$$\mathrm{t_p} = \mathrm{N}^2 * \mathrm{t_m} \quad (2)$$

where, h_p is the height of the prototype being simulated, h_m is the height of the centrifuge model and N is the multiple of earth gravity that the centrifuge model is subject to in the forms of centrifugal force (N

times earth gravity), t_p is the duration of the prototype being simulated and t_m is the duration of the centrifuge experiment. The consolidation cells manufactured for this study were made from a transparent Plexiglas cylinder of 177 mm internal diameter, 300 mm height with a wall thickness of 13 mm. The supporting structure was built of aluminium. Rulers with millimetre graduations were glued with epoxy to the internal wall of the transparent cylinder. Settlement with respect to time was monitored using a high-resolution in-flight camera. All the tests were carried out under one-way drainage conditions, with drainage towards the top of the specimen. Each centrifuge model was equipped with 7 pore-pressure transducers located along the side of the consolidation cell. The relative elevations of the transducers were 4 cm, 6 cm, 8 cm, 10 cm, 12 cm, 14.3 cm, and 17.5 cm.

Towards the end of each centrifuge test, a T-bar penetration test was performed to determine the surface undrained shear strength of consolidation material. The T-bar was penetrated at a constant speed of 1 mm/s. Each beam centrifuge test was completed in about one week including sample preparation, spinning, and characterization.

Consolidation properties derived from modelling beam centrifuge results

The software was used to determine the compressibility and hydraulic conductivity functions that provides a reasonable simulation of the laboratory test measurements. In other words, both compressibility and hydraulic conductivity were determined from a back analysis of the measured settlement, pore-water pressure, and solids content. The following sections present the modelling approach and conditions, model calibration measurements, and the resulting consolidation properties.

Software

The beam centrifuge tests are exposed to an elevated "g" force which allows a relatively small sample of soil to be used to model a prototype that represents a condition closer to field conditions. Previous modelling studies conducted on behalf of Canadian Natural on high fines material have confirmed that one-dimension (1D) consolidation software can be used to simulate the beam centrifuge tests provided that the length and time measurements are converted to the prototype scale. Conversion from the model scale to the 80 g prototype scale means that the software is used to simulate an increased tailings thickness from about 15 cm to 20 m and increased time from a few days to about 35 years. The software simulations also needed to account for changes in g-force applied throughout the test. For example, the initial ramp-up period when the test is held at 50 g (to confirm the equipment is balanced) and then increased to a g-force of 80 g. Increases in g-force were modeled as an instantaneous tailings deposition event to increase the thickness of the tailings by the required amount depending on the increase in g force. The back analysis modelling results are presented in terms of prototype scale.

One-dimensional large-strain consolidation modelling was conducted using the *FSConsol* version 3.49 (GWP Geo Software Inc., 2011) developed based on the Gibson et al. (1967) finite-strain consolidation theory.

Modelling approach

The back analysis of a consolidation test involved an iterative procedure where software was used to determine the consolidation properties that provided a reasonable simulation of the test measurements. The consolidation properties consist of two main functions; namely, the compressibility and hydraulic conductivity functions of the tailings. The known test parameters were used to define a one-dimensional large-strain, non-linear (LSNL) consolidation model. A trial set of consolidation properties were input into the software, the model was run, and the model output was compared to the test measurements. The tailings compressibility and hydraulic conductivity properties were adjusted until a reasonable match was obtained between the measured and modelled settlement, pore-water pressure, and solids content/density records. The end result constitutes a set of consolidation properties that are considered to represent the tailings material properties.

Model conditions

A summary of the consolidation model conditions is provided in Table 2 including the governing tailings index properties, model geometry, model duration, and boundary conditions. The test conditions are further summarized below:

- The specific gravity was obtained from the characterization test results and the initial solids content was set to the average “settled” solids content estimated after the initial period of self-weight settlement.
- The “settled” solids contents correspond to conditions just prior to spinning the specimen.
- The tailings height is listed according to the prototype height for the maximum g-level applied during testing. Intermediate tailings heights were modelled as instantaneous tailings filling episodes corresponding to the ramp-up procedure used during the test.
- The top and bottom boundary conditions were set to model single drainage test conditions including the development of a water cap as a result of settlement during the test.

Table 2: Consolidation modelling conditions

Parameters	IPC 1 shallow	IPC1 deep	NPD medium bitumen/ high SFR
Sample no.	1b	2	5
SFR	1.7	1.1	1.6
Specific gravity	1.79	1.77	2.25
Initial (settled) solids content (%)[1]	43.7	48.9	60.3
Initial (settled) void ratio	2.31	1.85	1.48
Initial height (m)[2]	17.2	20.3	19.1
Model duration (yr.)	2	35	35
Top boundary condition	Constant hydraulic head equal to the initial tailings height (i.e., water cap maintained above the tailings surface)		
Bottom Boundary condition	Zero flux (i.e., single drainage to match the test conditions)		

Note[1]: Estimated values after 1-g settlement (before start of centrifuge test)
Note[2]: Converted to prototype conditions.

Derived consolidation properties

The calibrated compressibility functions are presented in Figure 1 and the calibrated hydraulic conductivity functions are presented in Figure 2.

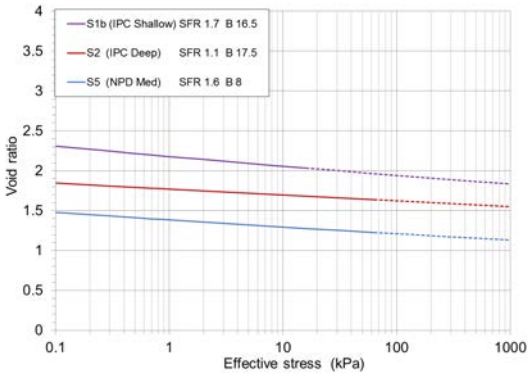

Figure 1: Beam centrifuge calibrated compressibility properties

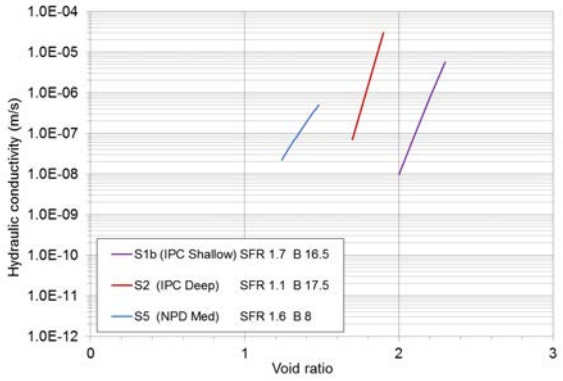

Figure 2: Beam centrifuge derived hydraulic conductivity properties

Large-strain consolidation test program

Large-strain consolidation testing was performed in parallel with the beam centrifuge testing. The LSC tests were performed using Canadian Natural's preferred approach and following the procedures and guidelines published by Scott et al. (2008). The tests started with self-weight settlement followed by the incremental increase of loading to result in a doubling of the effective stress in the tailings up to a final effective stress of 160 kPa. Hydraulic conductivity tests were performed at the end of each load increment once consolidation was observed to be complete based on the interpretation of load settlement data. Due

to the higher SFR in the TSRU tailings (compared to high fines material), consolidation testing took a total of two months for all specified load stages.

Results

Beam centrifuge results

A summary of the beam centrifuge test results is provided in Table 3 which includes the "settled" solids content, prototype settlement, final prototype height, segregation index, and degree of consolidation.

Table 3: Summary of beam centrifuge test results

Parameters	IPC 1 shallow	IPC1 deep	NPD medium bitumen/ high SFR
Sample no.	1b	2	5
Settled solids content (%)[1]	43.7	48.9	60.3
Settled void ratio	2.31	1.85	1.48
Prototype settlement (m)[2]	1.38	1.18	1.77
Final prototype height (m)	15.3	18.3	17.3
Segregation index[3]	2.5	0.53	6.2
Degree of consolidation	100%	100%	100%

Note[1]: Estimated values after 1-g settlement (before start of centrifuge tests)
Note[2]: Values at the end of centrifuge test
Note[3]: The segregation index (Is) was calculated based on a definition Scott (2003)

Settlement

The TSRU tailings samples tested were found to have low compressibility. The settlement ranged from 1.18 m to 1.38 m for a 20 m thick tailings layer. The shallower samples in IPC1 experienced more settlement than the deeper samples due to the lower initial solids content. Sample 5 had the least settlement since it started at the highest "settled" solids content.

Degree of consolidation

All the samples were fully consolidated by the end of the centrifuge tests both in terms of pore-water pressure dissipation and settlement. The pore-water pressure dissipated to hydrostatic conditions and there was no further settlement. The test results indicated that primary consolidation in a 20 m thick layer of TSRU tailings could be completed in 10 years or less.

Solids content, segregation, and SFR

The solids content generally increased with depth. Samples were considered to have segregated if the

segregation index was computed to be greater than 5. Out of the three samples listed above, Sample 5 had a measured segregation index to be greater than 5 and this impacted the settlement results.

Undrained shear strength

The lowest undrained shear was measured on Sample 1 and Sample 2 from IPC1. The shear strength increased to about 50 kPa at 6 m depth. The undrained shear strength at 6 m depth was about 110 kPa for Sample 5.

LSC results

The measurements taken when each load increment is applied were fitted with a best fit power law function, to produce compressibility and hydraulic conductivity functions. The measured values and fit functions are plotted on Figure 3 and Figure 4. The constants for the derived fit functions are presented in Table 4.

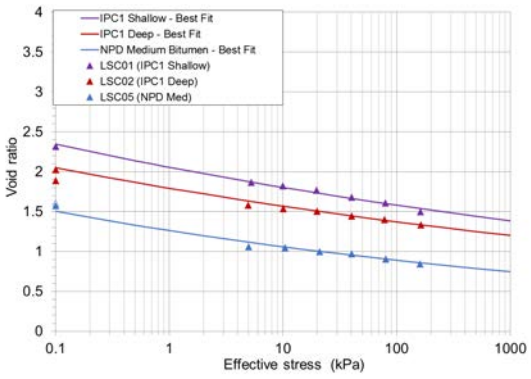

Figure 3: LSC derived compressibility

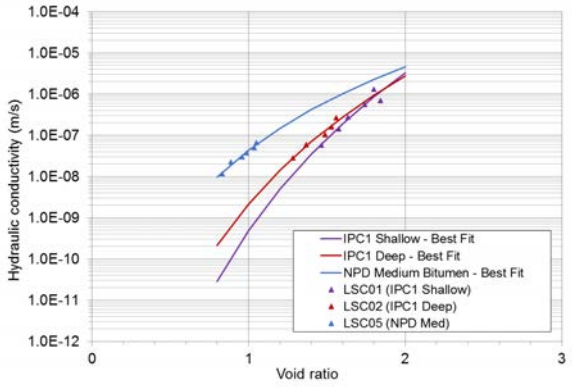

Figure 4: LSC derived hydraulic conductivity

Table 4: Compressibility and hydraulic conductivity functions

Sample	Gs	Compressibility, $e=A\sigma'^{B}$ (kPa)		Hydraulic conductivity, $k=Ce^{D}$ (m/s)	
		A	B	C	D
IPC1 shallow	1.79	2.057	–0.0570	4.900E-10	12.700
IPC1 deep	1.77	1.794	–0.0580	2.173E-09	10.320
NPD medium bitumen	2.25	1.264	–0.0763	4.348E-08	6.712

Comparison of beam centrifuge and LSC

Comparison of consolidation properties

The comparison between LSC properties and beam centrifuge modelling back analysis properties are shown on Figure 5 and Figure 6, respectively. The following observations can be made.

- The TSRU material was interpreted to have lower compressibility based on calibration models of the beam centrifuge tests with void ratio changes of about 0.3 to 0.5 up to an effective stress of approximately 200 kPa. The LSC testing results on the same TSRU tailings suggested the material had higher compressibility with void ratio changes of about 0.5 to 1 over a similar range of effective stress.
- The beam centrifuge model calibration results show the hydraulic conductivity to be generally between 1×10^{-5} m/s to 1×10^{-8} m/s for void ratios between 2 and about 1, respectively. For the LSC test, the hydraulic conductivity was generally between 1×10^{-6} m/s to 1×10^{-8} m/s for a void ratio between 2 and about 0.8, respectively. The hydraulic conductivity functions derived from the centrifuge calibration models showed a more significant decrease in hydraulic conductivity with decreasing void ratio compared to measurements from the LSC tests and the LSC tests did not always start at the same initial void resulting in a shift in the comparison. The model functions were considered representative of the general range of hydraulic conductivity but the shape of the functions were considered to be influenced by limitations in the power law fitting functions and the inability to model segregation that might have occurred during testing.

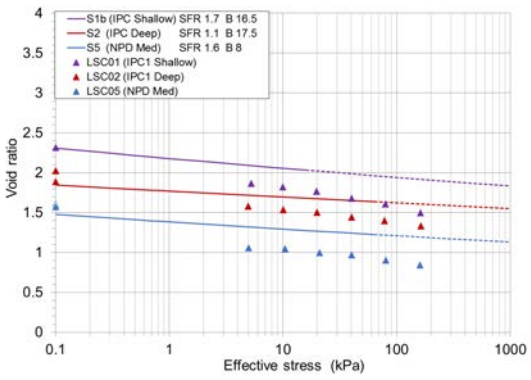

Figure 5: Beam centrifuge test vs. LSC compressibility properties

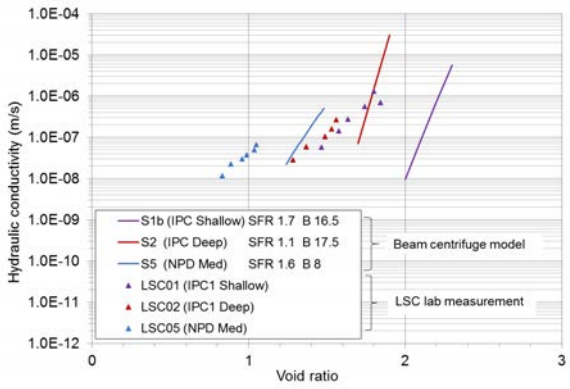

Figure 6: Beam centrifuge test vs. LSC hydraulic conductivity properties

Comparison of a 20 m deposit of TSRU tailings

The consolidation properties determined from the beam centrifuge test, and consolidation properties measured from LSC tests were used to predict the behaviour of a 20 m thick layer of TSRU tailings in a typical field deposit. The analysis provides a basis for observing potential differences in the consolidation behaviour that would be predicted using the different test measurements. Table 5 presents the ultimate settlement, final average solids content, T_{50} and T_{90} properties from the physical model (i.e., centrifuge), and numerical modelling.

The settlement predicted based on the LSC measurements is over double the amount predicted from the prototype beam centrifuge testing. The LSC results appeared to show some additional settlement due to creep behaviour (i.e., settlement that occurred after the excess pore-water pressure had dissipated) but the creep was not sufficient to account for the overall difference in settlement. The beam centrifuge results would indicate that the TSRU material borders on a small-strain material with strains in the order of 10% while the percent strain from LSC testing is in the order of 20%. The average predicted solids content was also about 5% higher from LSC test results. The higher solids content predicted from LSC testing is expected given the additional settlement. There is variability in the comparison of T_{50} and T_{90} but all the test results predict that the consolidation of a 20 m lift would be complete in less than one year. The results can be compared to the consolidation behaviour of a 20 m thick lift of material in the field for completeness.

Table 5: Consolidation properties of a 20 m thick lift of TSRU

Parameters	IPC 1 shallow			IPC1 deep			NPD medium bitumen/high SFR		
	Beam test	Beam model	LSC model	Beam test	Beam model	LSC model	Beam model	Beam test	LSC model
Sample no.	1b	1b	1b	2	2	2	5	5	5
Ultimate settlement (m)	1.38	1.39	2.82	1.18	1.19	2.57	1.77	1.79	4.01
Final average solids content (%)	49	47	50	53	51	54	67	64	70
t_{50} (days)[1]	13	30	10	10	12	50	37	46	87
t_{90} (days)[2]	167	177	37	153	167	150	237	202	315

Note[1]: time required to reach 50% settlement
Note[2]: time required to reach 90% settlement

Comparison of a 10 m casing deposit of CFFT tailings

Canadian Natural did a comparison of consolidation properties for treated FFT material (CFFT) which included measured LSC material properties, beam centrifuge modelling back analysis properties, and measured field data from a 10 m deep by 3 m diameter field casing experiment. Samples were obtained for this comparison from Canadian Natural's Tailings Consolidation Casing Experimental Pilot Project (TCCEPP). The results are shown on Figure 7 and Figure 8. The difference between using beam centrifuge test results and LSC test results for the finer treated material is less in comparison to the TSRU material when considering ultimate settlement, the final average solids content, and degree of consolidation. Similar outcomes were reported in a comparison of geotechnical beam centrifuge predictions of field data from 10 m deep FFT centrifuge cake columns (Dunmola et al., 2018).

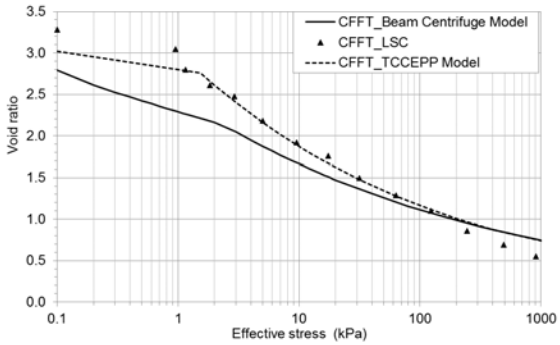

Figure 7: Beam centrifuge test model vs. LSC compressibility properties

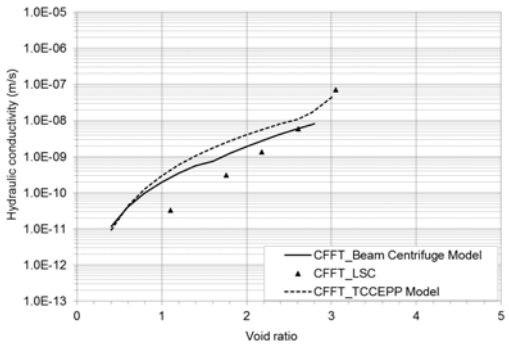

Figure 8: LSC vs. beam centrifuge model hydraulic conductivity properties

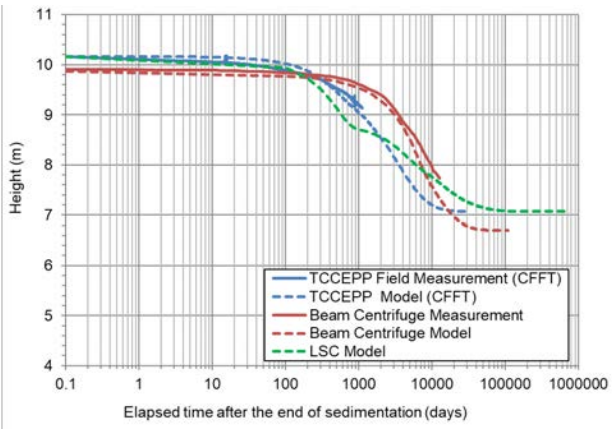

Figure 9: TCCEPP CFFT settlement comparison

Table 6: Consolidation behaviour of a 10 m thick lift of CFFT

Parameters	CFFT			
	Beam test	Beam model	LSC model	Field model
Ultimate settlement (m)	[1]	3.2	3.09	3.09
Final average solids content (%)	[1]	60.4	57.5	57.5
t_{50} (years)[2]	20	16	4	5
t_{90} (years)[3]	[1]	50	60	19

Note[1]: Beam centrifuge test was run for 35 years but did not reach the end of primary consolidation
Note[2]: time required to reach 50% settlement
Note[3]: time required to reach 90% settlement

The ultimate settlement was predicted to be 3.1 m to 3.2 m based on beam centrifuge, LSC, or field models as shown on Figure 9 and in Table 6. The T_{50} of LSC test and the field model were less than the beam centrifuge test and model. This was due to higher hydraulic conductivity values at the initial void ratio. The field model has the shortest T_{90} due to the overall higher hydraulic conductivity function.

Learnings

The following learnings were identified and will be used to guide the use of LSC beam centrifuge test methods for future consolidation characterization programs:

- The LSC test results were considered to govern when there was a discrepancy between beam and LSC testing. The LSC tests were found to be easier to control and have been found to align more closely with large scale field tests conducted at 1 g (e.g., 10 m high by 3 m diameter field casings).
- A key benefit from beam centrifuge testing is the ability to obtain consolidation data in a short period of time. The data can be used to guide early interpretation and decision making regarding deposit consolidation performance while additional field data and longer term tests are conducted to refine the understanding of consolidation behaviour.
- LSC testing is planned to be used for characterizing higher SFR material in a class similar to the TSRU material (e.g., SFR >1). Large Strain Consolidation testing (or traditional oedometer testing in some cases) will likely be used for tailings with relatively high SFR that approach small-strain consolidation behaviour.
- The time savings associated with beam centrifuge testing compared to LSC was found to be particularly valuable when characterizing the consolidation properties of finer more compressible material with lower hydraulic conductivity such as CFFT.

Summary and conclusion

- The beam centrifuge testing conducted on all three samples of tailings – two samples of TSRU tailings from MRM IPC1 and one sample from MRM ETF (within the NPD) – were determined to reach the end of primary consolidation.
- The beam centrifuge model calibrations were considered to provide a suitable representation of the tailings consolidation behaviour, except where beam centrifuge samples were considered to be influenced by segregation. The model calibration was more challenging and considered to be less reliable for materials that had segregated (e.g., Sample 5).
- The LSC tests on TSRU tailings showed some suspected “creep” behaviour where settlement continued after the excess pore-water pressure had dissipated. Similar behaviour was not observed in the beam centrifuge test results, partly because it would be more difficult to identify creep behaviour the way the testing is performed.
- The beam centrifuge test in fines enriched sand and sandy fines deposits tested seems to estimate lower values of ultimate settlement and higher values of hydraulic conductivity changes compared to the LSC measurement.

- The beam centrifuge calibration model results show the hydraulic conductivity to be generally between 1×10^{-5} m/s to 1×10^{-8} m/s for void ratios between 2 and about 1.1, respectively. For the LSC test, the hydraulic conductivity was generally between 1×10^{-6} m/s to 1×10^{-8} m/s for a void ratio between 2 and about 0.8, respectively. The hydraulic conductivity functions derived from the centrifuge calibration models were relatively "steep" compared to values measured from the LSC tests. The model functions were considered representative of the general range of hydraulic conductivity, but the shape of the functions were considered to be influenced by limits in the power law fitting functions and the inability to model segregation that might have occurred during testing. The hydraulic conductivity of the TSRU tailings (from the two tests), on average, fall within a similar range, which is about 1 to 2 orders of magnitude higher than a typical FFT material over a similar void ratio range.
- The ultimate settlement for CFFT was predicted to be 3.1 m to 3.2 m based on beam centrifuge, LSC, or field models. However, time to reach 90% settlement varied between models.

Acknowledgements

The authors would like to acknowledge the Canadian Natural closure design team and Josh Sun of Golder Associates, Thurber Engineering, and the research group of the Geotechnical Centrifuge Experimental Research Facility (GeoCERF) for their contributions to the paper.

References

Dunmola, A., N. Wang, J. Lorentz, G. Zambrano-Narvaez, R.J. Chalaturnyk and J. Song. 2018. Comparison of geotechnical bean centrifuge predictions to field data from 10 m deep FFT centrifuge cake columns. In *Proceedings of the 6th International Oil Sands Tailings Conference,* Edmonton, Alberta, Canada.

Gibson, R., G. England and M. Hussey. 1967. The theory of one-dimensional consolidation of saturated clays. Finite non-linear consolidation of thin homogeneous layers. *Geotechnique* 17(2): 261–273.

Scott, J.D. 2003. Definitions and conversion equations for oil sands tailings. Geotechnical Research Centre, University of Alberta, Canada.

Scott, J.D, S. Jeeravipoolvarn and R.J. Chalaturnyk. 2008. Tests for wide range of compressibility and hydraulic conductivity of flocculated tailings. In *Proceedings of the 61st Canadian Geotechnical Conference and 9th Joint CGS/IAH-CNC Groundwater Conference,* Edmonton, Alberta, Canada.

Sorta, A. R. 2015. Centrifugal modelling of oil sands tailings consolidation (Doctoral dissertation), University of Alberta, Canada.

Zambrano-Narvaez, G., Y. Wang and R. Chalaturnyk. 2018. Comparative study of consolidation behaviour of differently-treated mature fine tailings specimens through centrifuge modelling. In *Proceedings of 9th International Conference in Physical Modelling in Geotechnics,* London, UK: 1271–1276.

Bibliography

Stianson, J., R. Mahood, D. Thomas and J. Song. 2016. A Shell tailings consolidation casing experimental pilot project (TCCEPP). In *Proceedings of the 5th International Oil Sands Tailings Conference*, Lake Louis, Alberta, Canada.

Proceedings of Tailings and Mine Waste 2019
November 17–20, 2019, Vancouver, Canada
Published by the University of British Columbia, 2019

Tailings Dam Safety: Is Waste Rock Coming to the Rescue?

Anton Bain, Anglo American, South Africa
Moseli Motselebane, Anglo American, South Africa
Timothy Gardner, Anglo American, Chile
Caius Priscu, Anglo American, Canada

Abstract

Tailings dam safety has been a subject of intense discussion for the last several years, particularly in the light of recent catastrophic events associated with tailings storage facilities that have occurred around the world. One of the concepts that is being applied in many countries world-wide is the use of waste rock as a construction material for the outer wall of a tailings storage facility, in a co-deposition concept. This approach has been used by Anglo American at several tailings storage facilities, either from the beginning, or as a solution for reinforcement or expansion of existing facilities. The benefits are numerous and go well beyond the main focus of improved stability. The method also minimizes the overall mineral waste final footprint, provides competent construction material that is often scarce, and lowers closure costs. Moreover, it mitigates potential residual risks associated with the tailings dam design, such as the ability to accept more variable and finer tailings, as opposed to other construction methods using cycloned or spigotted systems.

This paper presents several applications located at the Venetia and Mogalakwena mines in South Africa, and the Collahuasi mine in Chile, and will discuss lessons learned, including embankment zoning, selection of interface versus low-permeability barrier, filters, and construction materials. While these concepts are not considered an ultimate or complete solution, the paper clearly notes that the benefits of co-deposition of two or more mineral waste streams to help minimize the potential for a catastrophic tailings dam failure and/or release of tailings slurry into the environment, far outweighs related challenges.

Introduction

The use of rockfill in tailings dams is not a new concept and has been reported in literature as far back as 1974 (Mittal and Morgenstern, 1976) and earlier references probably exist. The practice of using mine

waste rock in construction of tailings storage facilities has been published and noted multiple times in the past, for a variety of geometries, construction methods and material types (e.g., Klohn, 1981; Vick, 1990; Scognamillo and Barrera, 1999; Coarser et al., 2011; ICOLD, 2013; 2019).

The literature also reports failures of tailings dams constructed using waste rock. Los Frailes (Eriksson and Adamek, 2000) and Mount Polley (Morgenstern et al., 2015) are two well-known examples where foundation failure occurred. Piping failures causing a release of tailings at Bethlehem tailings dam (Klohn, 1979), as well as outer wall failure due to piping of Omai tailings dam is also reported (Vick, 1996).

These failures are a reminder that waste rock impounded tailings dams need rigorous site investigation, analysis and design, like any other engineering structure, in order to be successful.

Embankment construction and zoning

Venetia Mine, South Africa

At Venetia Mine the existing tailings dams are raised by placing open pit waste rock around the perimeter of the existing dams to provide space for future underground mining tailings deposition. The waste rock will extend up to 40 m above the current residue level to create the impoundment for future deposition. Waste rock is placed by the mining operations in horizontal lifts of 10 to 12 m high to create inner benches to facilitate access for deposition and outer benches to reduce the amount of reshaping to achieve final slopes suitable for closure purposes.

Figure 1 shows a general cross-section of the tailings dam. Note that underground waste rock, of a finer grading is used to construct the final lift that becomes too narrow for the mine fleet to access and place the material. The finer underground waste rock is also used to provide the final inner geometry to specified tolerances that are difficult for the mine fleet to obtain.

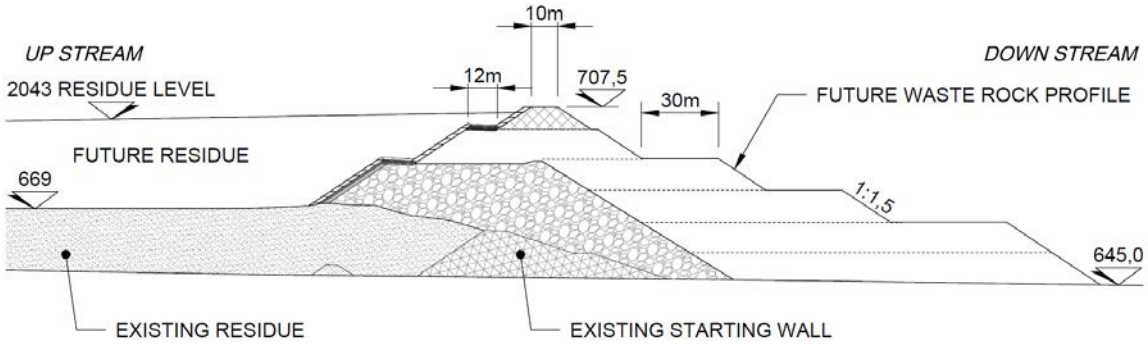

Figure 1: Venetia Mine tailings dam general cross-section

Collahuasi Mine, Chile

All tailings produced at Collahuasi since the start of the operation in 1999 are stored in the Pampa Pabellon dam, which is projected to continue operations for at least another 50 to 60 years. The dam currently has a maximum height of approximately 70 m and a crest width of 35 to 50 m, mainly to enable the safe passage of the mine haul trucks used for the construction of the dam. The main dam is over 5 km long, with a smaller saddle dam of some 500 m in length which entered operation in early 2018. The dam is built using selected mine waste from the nearby (5 km) mine and waste dumps, using the downstream construction method. The material is placed in 1.5 m thick lifts and compacted via the passage of the haul trucks and 20 tonne vibratory compactors to a minimum density of 1,900 kg/m^3.

During initial stages of construction, lacustrine materials present beneath the dam foundation at select locations were not removed. Subsequent analyses indicated that these may behave in an undrained manner during seismic events and may be susceptible to liquefaction. Hence these have been removed in subsequent dam raises and a 50 m wide buttress was constructed at the downstream toe to provide additional stability to the structure.

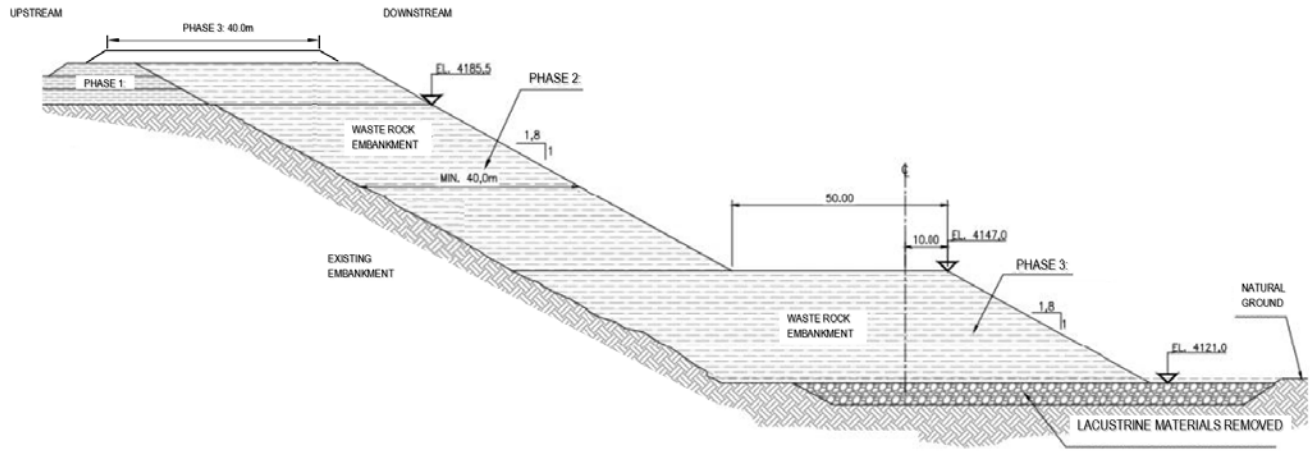

Figure 2: Pampa Pabellon tailings dam cross-section

Mogalakwena Mine, South Africa

The Blinkwater Tailings Dam is built in a downstream direction using stockpiled and future run of mine waste rock. The material is placed in 4 to 7 m thick lifts and are nominally compacted by the passage of the haul trucks. Figure 3 shows the proposed future development where waste rock is placed by a smaller fleet, offering more control in advance of the waste rock to be placed by the mine fleet.

The geotechnical investigation has identified a thin but weak clay layer that will be removed in part to ensure stability.

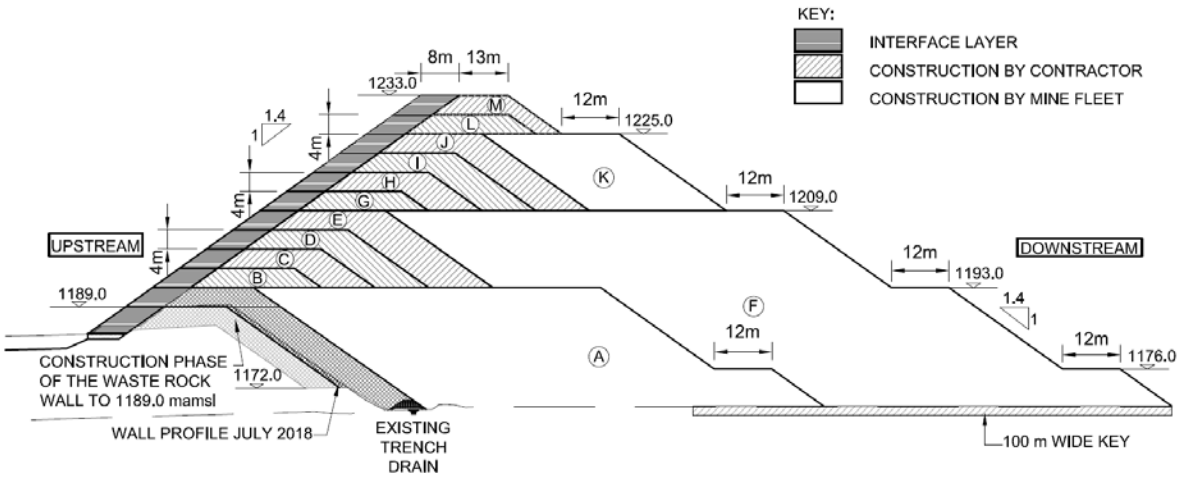

Figure 3: Blinkwater tailings dam cross-section

The interface structural element

Two fundamentally different approaches to the placement of an interface layer between the tailings and the waste rock outer shell are described below: namely a filter compatible system, and a compacted soil layer that is not filter compatible.

Filter compatible layer

This interface layer is designed with the aim of preventing piping though the waste rock where pockets of material exist that are similar to the open voided structure shown in Figure 4.

Venetia Mine

The interface zone consists of three layers that are progressively finer and essentially filter compatible. The first layer was specified as a 1 m wide nominal 53 mm particle size to be placed against the waste rock, followed by a 1 m wide, 8 mm particle size layer followed by a 5 m wide layer of compacted tailings harvested from the adjacent beach. The boulders and cobbles that form the matrix of the waste rock were observed to be approximately 300 mm even though much larger boulders are present throughout the waste rock as observed in Figure 4. The 53 mm aggregate and the 300 mm cobbles cannot be verified to be filter compatible, as the 300 mm cobbles is based on observation and there is no means to measure this in situ on an ongoing basis. The aggregate material will not be able to migrate though the cobbles as the aggregate will not be moved or transported by seepage flow and is expected to arch over the holes between the cobbles. The final design is depicted in Figure 6.

Trial placement of the 53 mm aggregate is shown in Figure 5. Early indications show that the angle of repose of the filter materials varies and is generally flatter than the waste rock. This was expected but the significance of these flatter slopes was undefined during the design phase. In order to obtain the specified layer thickness higher up the slopes, provision may need to be made to provide for additional future material placement as the tailings surface rises. The trials indicate that the material does not segregate significantly.

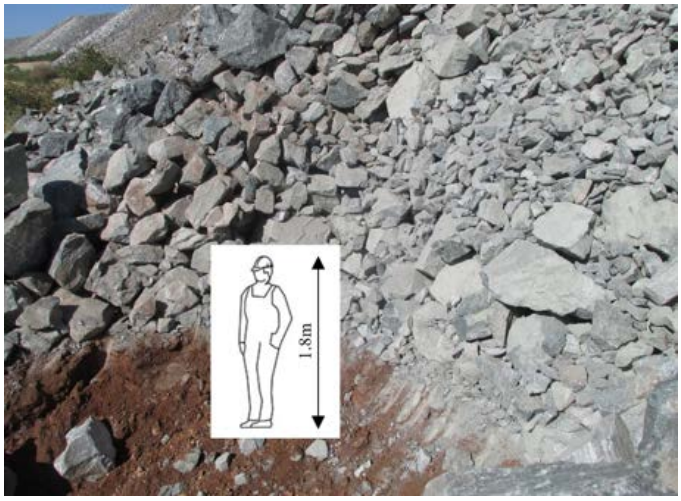

Figure 4: Open voided waste rock at Venetia mine

Figure 5: Venetia mine 53 mm aggregate

Compacted soil layer

The tailings material, interface material and waste rock are not filter compatible, and piping is theoretically possible.

The design basis for such a system is to manage seepage gradients by wide beaches, use of lower permeability soils to avoid high seepage gradients during transient conditions caused by floods and cyclical deposition.

It should be noted that the compacted soil layers described below have been observed to perform satisfactorily to date although it cannot be proven by accepted engine ing principles that piping will not occur.

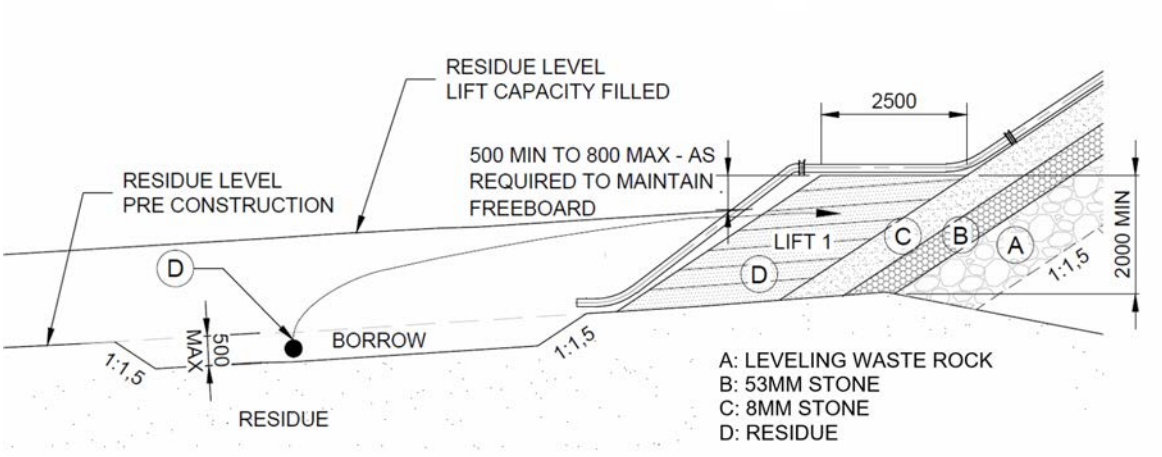

Figure 6: Venetia Mine tailings dam typical interface layer cross-section

Collahuasi Mine

At the Pampa Pabellon dam, the interface layer consists of a single 3 m wide layer of compacted soil which is placed on the upstream (inner) face of the rockfill dam. The material is placed in 0.5 m thick lifts and compacted to 95% of the maximum modified Proctor density. The relatively thin layer is achieved as the waste rock and interface are raised simultaneously. A typical section and as-built photo are shown in Figures 7 and 8 respectively.

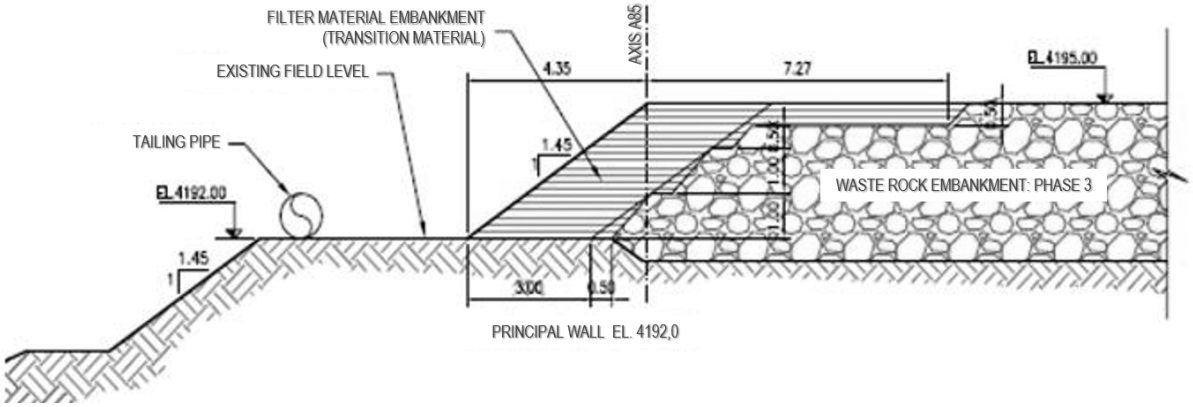

Figure 7: Pampa Pabellon tailings dam typical interface layer section

Figure 8: Pampa Pabellon tailings dam as-built interface layer

Mogalakwena Mine

At the Blinkwater tailings dam, the interface layer consists of a single 8 m wide soil layer compacted to 95% modified AASHTO at +/– 2% of optimum moisture content and constructed in 0.5 m lifts. The interface layer construction must not proceed to an elevation higher than 6 m above the tailings at the outer edge of the basin of the TSF at any time, as the interface layer could become unstable and internal slip failures could occur. The specified width allows safe vehicular access on the interface as the waste rock is placed at least 6 m in advance of the interface. A typical section and as-built photo are shown in Figures 3 and 9 respectively. The key function of the interface layer is a low permeability medium between the tailings and the waste rock.

Figure 9: Blinkwater tailings dam as-built interface layer

Advantages of waste rock dam construction

Opportunity for cost savings

The cost of a waste rock tailings dam may not be less than upstream constructed dams, but has a major advantage when compared to centreline or downstream constructed methods where material is imported to construct the outer walls. The advantage arises from the fact that the mining operations already pay for the loading, hauling and placing of waste rock on the waste rock dumps. The tailings dam must therefore only provide for the additional cost, which typically includes for additional hauling distance, efficiency reductions due to placement of waste rock in more confined spaces around the tailings dam, compaction and processing (if needed).

It is however possible that waste rock haulage to the tailings dam can result in a cost saving for the mining operations when the waste rock dump is much higher than the tailings dam and the tailings dam is only marginally further. This saving is often not apparent at the onset of studies but is realized when truck cycle times are compared between haulage to the waste rock dump and the tailings dam and could be reduced due to the increased truck speeds on flat ground to the tailings dam instead of to higher levels on the waste rock dump. Trade-off studies become critically important and need to cover life of asset scenarios.

Resilience and robustness

The resilience of a system is the opposite of risk and is the ability to adjust and sustain required operations under both expected and unexpected conditions. Robustness is the resilience prior to initiation of failure (Robertson, 2017).

The build-up of pore pressure and associated deterioration in stability is unlikely due to the relatively free draining nature of the waste rock. Changes in pond management, large rainstorms and possibly climate change can therefore be accommodated. The potential for liquefaction of waste rock is insignificant.

The relatively high erosion resistance of waste rock as compared to dams or outer shells constructed from fine tailings material, provides robustness when unwanted events such as pipe bursts and overtopping occur.

The deposited tailings material can vary more within the impoundment created by waste rock and its characteristics do not need to adhere to the stringent design specifications that are typically expected of spigoted or cycloned facilities. The mining operation is therefore allowed a bit more flexibility in terms of process changes and management of mills, thickeners and slurry deposition systems.

Reduced mine footprint

A greenfield open cast mine development has the opportunity, though integrated mineral deposition planning and design, to place waste rock as close as possible to the pit, followed by abutting tailings dams to provide a stable structure that does not introduce a risk of pit flooding. The additional cost for the waste rock operations will be to haul the material slightly further to create the tailings deposition space. This should in principle provide an optimised and consolidated mineral residue deposit but is subject to site specific constraints.

The waste rock is also used as opposed to being placed on a separate facility, and reduces further disturbance of the mine footprint by limiting the opening of borrow areas for competent fill.

Closure costs and robustness

Waste rock typically provides an improved erosion resistant material that can be shaped to provide aesthetically pleasing landforms that are more easily vegetated than exposed tailings surfaces. Waste rock slopes for final closure reduce the cost of importing additional erosion-resistant materials and provide a more robust long-term solution in a post-closure environment.

Key success factors and lessons learned

Uncontrolled material within an engineered structure

The tailings dam construction team must accept, in some cases, either accept the waste rock that the mine provides or must select as appropriate. Such processes remain a challenge. Sometimes the waste rock that the mining team provides is unsuitable as dam fill. In many situations, it is either very coarse, highly uniform, or gap-graded.

This aspect is addressed in part by placement of the unsuitable material in less critical zones in the embankment shell. Maximum boulder sizes should also be specified in critical areas and provision must be made to either remove oversize or provide for breakage. Areas such as the inner face of the waste rock where in contact with the filter and interface layers should be placed using smaller trucks in a much more controlled manner as opposed to using the mine fleet.

Geochemistry

It is important to define geochemical characterization of waste rock at the onset of the conceptual design. Waste rock that is potentially acid generating or metal leaching is typically deemed unsuitable for dam construction unless areas within the cross-section can be reserved where the material will remain relatively dry and can be capped, and where a detailed drainage and collection system is in place, designed for such a purpose.

Monitoring and trigger action response plans (TARPs)

Waste rock tailings dams should be provided with comprehensive monitoring systems and Trigger Action Response Plans (TARPs). Of critical importance is embankment settlement, phreatic surface location and foundation pore pressure monitoring to allow changes in the waste rock to be detected. The installation of piezometers to measure pore pressure is particularly problematic and must be designed to be installed with proper protection as part of the construction effort rather than being retrofitted, which is virtually impossible. It should be noted here that changes in the waste rock properties due to long term weathering and possibly tailings ingress are often not adequately considered during the design phase. Therefore, rockfill material testing for long term weathering is key at early stages of the project.

Use of large equipment of the mine fleet

The typical mine fleet consist of much larger trucks than conventional civil engineering construction equipment. The mine vehicles are less manoeuvrable, require wider access ways (i.e. typically 30 m one way and 40–50 m two way) and have difficulty ramping up or down, which must thus be avoided as far as possible. This is often not fully recognized during initial design and planning stages. Waste rock dam design and construction would need to allow for such traffic and haulage geometry parameters.

Integration of mine plan/schedule, dam design and dam raising schedule

Mine waste rock excavation and placement schedules should be flexible to allow the mining operation to remain viable. The waste rock tailings dam may sometimes not accommodate the flexibility needed by the mine and typical response is to start adjusting dam design and construction to accommodate mine plan changes. Unmanaged design changes often impact on reliability of performance, and dam safety becomes compromised. Changes can lead to uncertainty and conflicts in responsibilities/accountabilities/priorities.

The key drive to reduce operational costs ripples through to dam construction and the focus on production often impacts on the quality of dam construction and fulfilling the design intent. Construction practices can become more akin to uncontrolled waste dump practices than to a critical civil engineering structure.

These risks can be reduced by improving communication, maintaining regular planning sessions, and at times creating storage capacity via smaller equipment in critical upstream areas allowing the mining operations to complete the embankment when available.

Requirements for appropriately experienced and empowered personnel in the cross disciplines of mining and civil engineering applies to all the key stakeholders including the engineer, the operator and the owner team members. The Anglo American Mineral Residue Facilities Standard AA TS 602 001 (Anglo American, 2019) requires sign-off on specific documentation and verification, such as short and long term deposition plans, design and as built reports; furthermore, the Anglo American technical

standard requires the appointment of an Engineer of Record (EoR) and an independent Technical Review Panel (TRP) to provide the necessary continuous oversight. The risks are also greatly reduced by the introduction of independent experience and review from the TRP team as early as the concept phase.

Conclusion

This paper describes the key advantages, success factors, and some lessons learned which, although not considered exhaustive, are useful when considering waste rock as a construction material in tailings dams.

The paper has presented three case studies where waste rock was used for constructing tailings dam outer shells. In two of the three cases, weak material needed to be removed at foundation level to ensure stability. The paper also indicated how the critical risk of piping through waste rock can be addressed using interface layering.

While waste rock is not necessarily the perfect solution for constructing waste rock impoundments for tailings dams, such an alternative, when properly designed and implemented, does provide a more robust and safer solution for storage of tailings, and for co-deposition of waste rock and tailings.

A mine-wide (including waste rock storage), risk-based, and full life cycle approach needs to be adopted, including post-closure conditions, when comparing waste rock impoundment construction to alternative methods for tailings storage. When properly designed and built, waste rock impoundments provide a level of resilience and robustness that more traditional tailings dams often lack.

The integrated approach to residue management across an operation is one of the key success factors to implementation of co-deposition and building of such facilities.

Acknowledgements

This technical exchange could not have been possible without the full support of the technical teams at:

- Mogalakwena site and Anglo American Platinum personnel in Johannesburg, South Africa;
- Venetia operations site personnel and De Beers personnel in Johannesburg, South Africa;
- Compañía Minera Doña Inés de Collahuasi (CMDIC) personnel, Copper JV, Chile; and
- Consulting engineers SRK Consulting, Jones and Wagener and Wood.

References

Anglo American. 2019. Anglo American Technical Standard AA TS 602 001 mineral residue facilities and water management structures standard and technical specifications. Original version released February 2014. Retrieved from www.angloamerican.com/sustainability

Coarser, P., J. Rogers, J. Misiewicz, D. Ross-Watt and J. Gutierrez. 2011. Design, construction, and operation of a centerline rockfill tailing dam with low permeability core zone. In *Proceedings of Tailings and Mine Waste 2011*, November 6 to 9, 2011, Vancouver, British Columbia, Canada: 829–841.

Eriksson N. and P. Adamek. 2000. The tailings pond failure at the Aznalcollar mine, Spain. In Proceedings of the *6th International Symposium in Environmental Issues and Waste Management*. Calgary, Canada

ICOLD. 2013. Sustainable design and post-closure performance of tailings dams. *International Commission on Large Dams*. Bulletin 153.

ICOLD. 2019. Tailings dam design – technology update. *International Commission on Large Dams*. Bulletin 181 Pre-print.

Klohn, E.J. 1979. Seepage control for tailings dams. In *Mine Drainage. Proceedings of the First International Mine Drainage Symposium*. San Francisco: Freeman: 671–725.

Klohn, E.J. 1981. The development of current tailings dam design and construction methods. In *Seminar Proceedings, Design and Construction of Tailings Dams*. Colorado School of Mines, November 6–7, 1980.

Mittal, H.K. and N.R. Morgenstern. 1976. Seepage control in tailings dams. *Can. Geotech. J*. 13: 277–293.

Morgenstern, N., D. van Zyl and S. Vick. 2015. Independent expert engineering investigation and review panel. Report on Mount Polley tailings storage facility breach, January 30, 2015.

Robertson, A.M. 2017. Doing, checking and checking the checkers for tailings, water and waste management. Keynote presentation at the 2nd Seminar on Risk Management and Safety of Tailings Dams. Belo Horizonte, Brazil.

Scognamillo, C. and S. Barrera. 1999. Tailings deposits with waste dams. In *Proceedings of Tailings and Mines Waste '99*. Balkema, Rotterdam, pp. 217–226.

Vick, S. 1990. *Planning, Design and Analysis of Tailings Dams*. BiTech Publishers Ltd.

Vick, S. 1996. Failure of the Omai Tailings Dam. *Geotechnical News*, September 1996: 34–40.

Proceedings of Tailings and Mine Waste 2019
November 17–20, 2019, Vancouver, Canada
Published by the University of British Columbia, 2019

Tailings Dam Made Redundant Using Solid Bowl Centrifuge

Amol Chinchankar, Alfa Laval Lund AB, Sweden
Sunny Li, Alfa Laval Australia Pty Ltd, Australia

Abstract

A member of the Bloomfield Group of Companies, Rix's Creek South is an open-cut mining operation that produces both thermal coal and high quality semi-soft coking coal for overseas customers. Located 5 km northwest of Singleton in New South Wales, it is based in the heart of the Hunter Valley, one of Australia's largest coal mining regions.

Rix's Creek South had a vision to address their limited tailings dam capacity, and had recognized for some time that a suitable dry tailings disposal method had to be found. The existing tailings dam used on site was nearing capacity, and there were no suitable alternative sites for a replacement dam. Within this operational context, they set out to find the best solution for dewatering thickener tailings at Rix's Creek South. Rix's Creek South questioned if there was a dewatering technology that could handle tailings containing high levels of clays.

Four different technologies were trialled at pilot plant scale on-site for dewatering their thickener tailings from their Coal Handling and Preparation Plant (CHPP). Eventually the Alfa Laval solid bowl centrifuge was selected based on the outcomes of the trials.

Three Alfa Laval 720 mm solid bowl centrifuges were installed at Rix's Creek South to handle part of the tailings flow. In 2018, two more new, larger solid bowl centrifuges were installed to handle the total volume of thickener underflow. The new installation has made the existing tailings dam redundant, thereby removing the need to construct a new tailings dam.

This paper will outline the process results and decision making that drove Rix's Creek South over a period of a few years to install solid bowl centrifuges. These centrifuges are also known as decanter centrifuges.

Introduction

A member of the Bloomfield Group of Companies, Rix's Creek South is an open-cut mining operation that produces both thermal coal and high quality, semi-soft coking coal for overseas customers. Located 5

km northwest of Singleton in New South Wales, it is based in the heart of the Hunter Valley, one of Australia's largest coal mining regions. Rix's Creek South produces an estimated 2.58 M tonnes of raw coal and 1.49 M tonnes of saleable thermal and semi-soft coking coal each year for use in the steel and power industries. With the existing tailings dam nearing capacity, Rix's Creek decided to pursue a dry tailings management alternative.

Tailings background

Rix's Creek South has 29 different seams that contain hard-to-dewater fines, such as bentonite clay and volcanic sediments. For the life of the mine to date, the tailings from the CHPP have been deposited in several tailings emplacement facilities or tailings dams. This involves pumping the material to the dam, allowing natural settling of the solids to occur, and recycling water back to the CHPP.

By using solid bowl centrifuges (SBC) to dewater tailings at the CHPP, 62% to 70% of the water from the thickener underflow would be recoverable without it leaving the plant. It would contain the water within the CHPP processing circuit, reducing the cost of pumping tailings to the tailings dam and returning water back to the CHPP.

Rix's Creek South aimed to co-dispose the dewatered solids produced by the SBCs by placing them back in the mine, with the overburden as part of the rehabilitation of the site. Sometimes this is also mixed with coarse reject material. Typical samples of the thickener underflow material from the CHPP were taken to determine the particle size distribution (PSD) of the tailings, as shown in Table 1.

Table 1: Typical PSD of thickener underflow at Rix's Creek South (feed to SBC)

Size (microns)	Sieve (ASTM E11)	Mass (wt%)
less than 25	less than 500	59.23
25 – 38	500 – 400	3.53
38 – 63	400 – 230	7.60
63 – 125	230 – 120	11.23
125 – 250	120 – 60	11.53
250 – 500	60 – 35	5.73
500 – 710	35 – 25	0.50
710 – 1,000	25 – 18	0.27
Above 1,000	Above 18	0.37

Looking for a solution

Rix's Creek South identified the following key evaluation criteria for dry disposal of coal tailings:

- Spadeable cake (separated solids without any water dripping out of it) with approximately 60% dry solids by weight.
- Clean centrate (water coming out from the SBC after separation) for re-use in the coal washing process.
- Sound operating economy.

Based on the above criteria, they set out to find the best solution for dewatering thickener tailings. It was decided to evaluate various technologies by conducting a research program including:

- laboratory experiments;
- pilot plant testing; and
- preparing a comparative report.

Along with the technical feasibility assessment, an internal commercial assessment of the various options was conducted.

Four different technologies were considered or trialled on-site for dewatering the thickener tailings. After careful evaluation, Rix's Creek decided to go ahead with solid bowl centrifuge technology.

The Alfa Laval solid bowl centrifuge was selected due to its key benefits:

- reduction in tailings dam capacity requirement (if there is an existing tailings dam that the mine wishes to continue using);
- avoiding the necessity of having a tailings dam;
- reduced capital investment compared to various other dewatering technologies;
- dry solids in excess of 60% (by mass) contribute to open-cut rehabilitation;
- water savings and water re-use in the plant;
- continuous, enclosed, and clean operation;
- smaller footprint compared to other technologies;
- reduced operator intervention compared to other mechanical dewatering technologies; and
- lower life-cycle cost for the dewatering system using SBC.

Solid bowl centrifuges

Solid bowl centrifuges have for many years been known for their separation efficiency based on the enhancement of sedimentation in a high centrifugal field of 1,000 to 3,000 times the earth's gravity. Sedimentation velocities increase with a similar factor, and the footprint or area needed for a given

sedimentation task is greatly reduced. Dewatering of tailings will in most mining applications involve both sedimentation and dewatering. In recent years, we have seen an increased focus on water recovery and a push for dry stacking instead of tailings ponds. This has increased the demand for good dewatering, while maintaining high capacity and clean liquid.

The original solid bowl centrifuges used in the mining industry during the 1970s and 1980s relied on drainage of liquid from the solid particles to generate a high concentration of the discharged solids. Screen bowl centrifuges, where the solids are conveyed across a section with a perforated outer rotor wall, were also introduced to improve the drainage capacity to reach a high solids concentration. Drainage is a relatively slow process when the solid fraction contains significant amounts of fine particles. In many of these applications other technologies including plate and frame filter presses have been the preferred solution, presumably due to the low dewatering capacity of the drainage process in solid bowl centrifuges. In recent years, a new design of the solid bowl centrifuge coupled with a change of operating mode, where solids are compacted below the liquid surface in the decanter, have shown an impressive increase in solids handling capacity, to the extent that solid bowl centrifuges are once again becoming an attractive alternative to other dewatering solutions (Madsen, 2017).

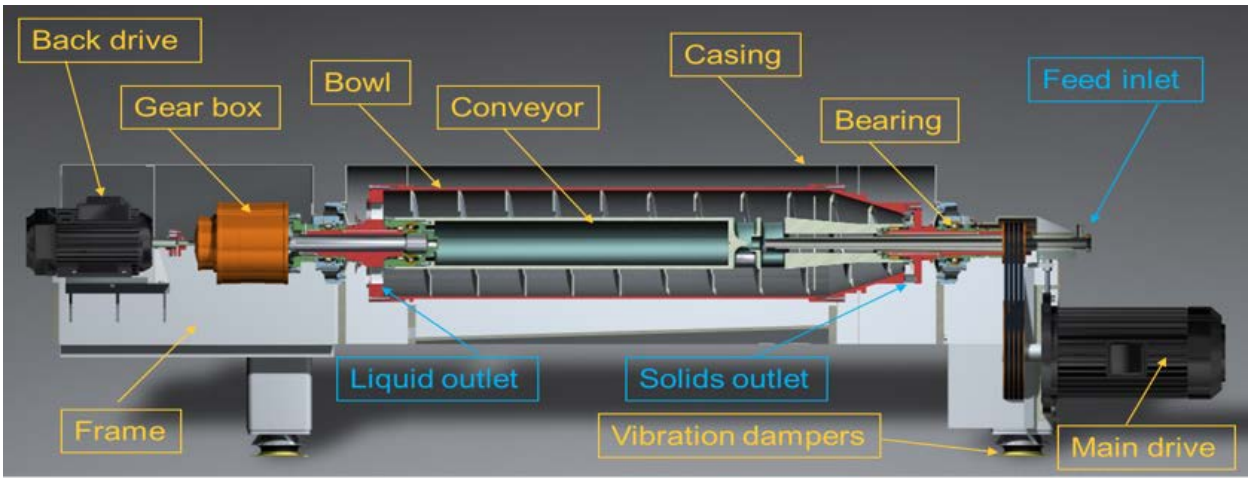

Figure 1: Schematic view of a solid bowl centrifuge

The horizontal centrifuge rotor (bowl) with a red cross-section is driven from the main motor on the right side to provide fast rotation where the feed suspension is accelerated to form a liquid ring inside the rotor after being pumped into the centrifuge through the stationary feed tube. The particles in the suspension will settle to the inside of the rotor, while the liquid flows through the centrifuge and leaves by overflowing weir plates at the end wall to the left. The decanter centrifuge has an internal conveyor (inner rotor with a helical flight), which is connected to the outer rotor through a high torque gear box (shown in orange). The central shaft of the gearbox is connected to the motor to the left, whereby it is possible to

establish and control a differential speed between the conveyor and the rotor. The differential speed of the conveyor will transport the separated solids towards the conical end, where it leaves the centrifuge at a radial position unreachable for the liquid (Madsen, 2017).

For a deeper understanding of the historic development of solid bowl centrifuge technology, please see Records and Sutherland (2001).

Solids consolidation/dewatering

In the original configuration of decanter centrifuges the solids (cake) were dewatered when the conveyor transported the solids out of the liquid pond on its way along the conical section towards the solids discharge openings and liquid could drain off and return to the pond. This situation is shown in the upper half of Figure 2. The pond depth was very shallow, allowing for a long drain zone. For large particles with high permeability the drainage is efficient, but capacity will be reduced if we have fine particles in the cake.

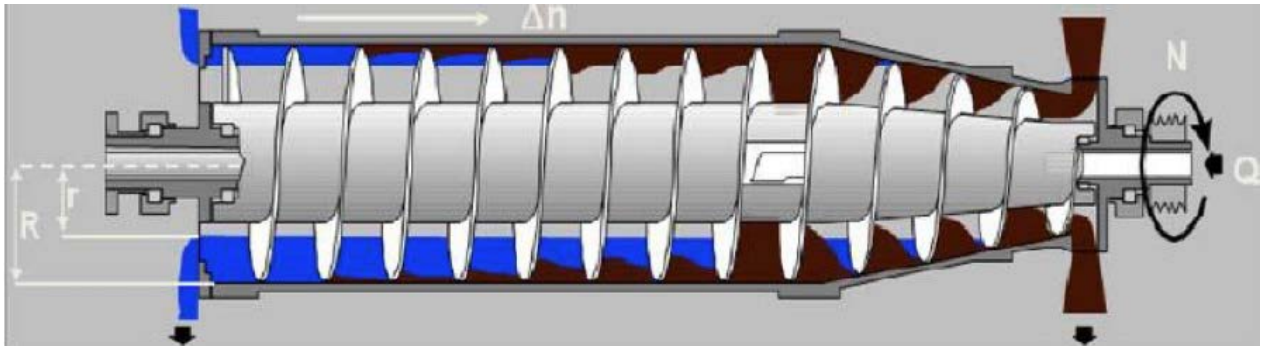

Figure 2: The upper half of the picture shows a shallow pond design used for mining applications. The lower half shows a deep pond configuration where the solids are compacted below the liquid surface by the load from the overburden of solids

For suspensions with a content of fine particles it is better to operate with a deeper pond, as shown in the lower half of Figure 2. With a deeper pond the load from the overburden of solids can be used to compact or consolidate the solids before they are conveyed into the conical section, and we no longer need the drainage to achieve a high solids concentration.

A further development of the deep pond operation is shown in Figure 3, where a baffle disk has been added to be able to operate with a liquid surface level radially inside of the solids discharge radius. In this way, we can stack the solids in an even thicker layer for more radial compaction, and in addition we get a hydraulic pressure supporting the mechanical conveying of the solids towards the solids discharge. This solution is particularly useful for cakes with a low permeability, and this is also the reason the liquid cannot pass through the cake and escape through the solids discharge openings.

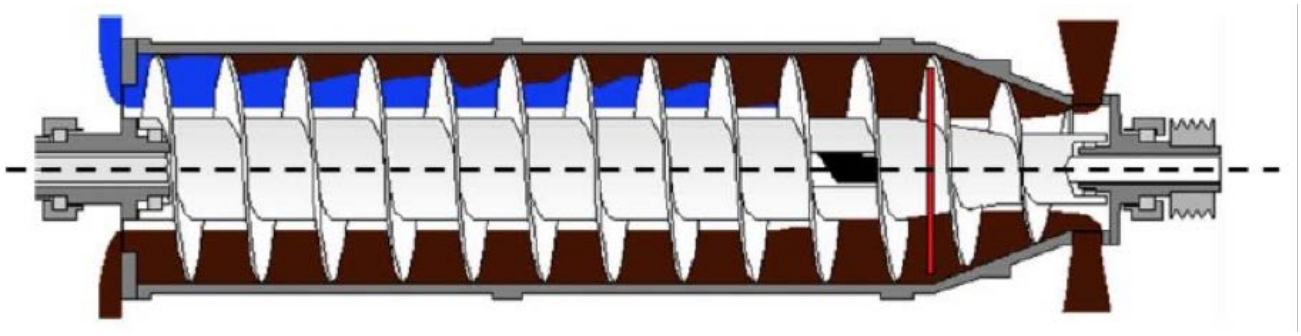

Figure 3: A circular disk, known as a baffle disk (shown in red), allows operation with a very deep pond

Robust design

Alfa Laval has designed and developed the solid bowl centrifuge for tough duties such as in mining. It has the most robust construction, suitable for handling erosive solids. Highly wear-resistant materials such as tungsten carbide are used as the materials of construction in the feed zone, the solids discharge, and the conveyor (shown below as a, b, and c, respectively). In addition to that, the bowl is protected from the inside by using Stellite strips.

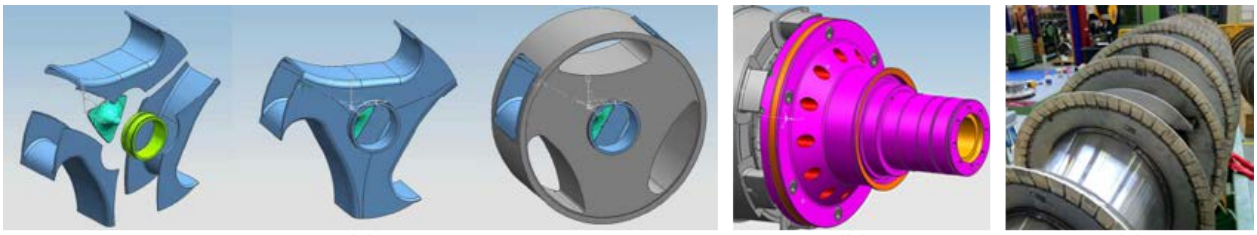

(a) (b) (c)

Moving forward

Three Alfa Laval 720 mm solid bowl centrifuges were installed at Rix's Creek South to handle part of the tailings flow.

Table 2: Typical mass balance for the 720 mm solid bowl decanter

PROJECT	DUTY	Alfa Laval Australia Pty Ltd
Rix's Creek	Coal Tailings Dewatering	P3 Mining Decanters
DATE 25/01/2018		

Mass Balance and Sizing — Data below is per decanter centrifuge

Feed (before floc addition)	
Total Dry Solids (mass%)	30
Dry solids mass flowrate (t/hr)	21.70
Solids Density (kg/m3)	1800
Liquid Density (kg/m3)	1000
Slurry Flowrate (m3/hr)	62.69
Slurry Density (kg/m3)	1154

Polymer (flocculant)	
Dose (kg/ T Dry Solids)	0.26
Concentration (%)	0.25
Flowrate Diluted (m3/hr)	2.26
Active polymer use (kg/hr)	6

Duty data shown is for each centrifuge

P3-8070 SBC (720 mm DIA)

Cake (Solid phase outlet)	
Total dry solids (mass %)	65.0
Cake Volume Flowrate (m3/hr)	23.3
Total Cake Mass Flowrate (T/hr)	32.7
Dry Susp. Solids Flowrate (T/hr)	21.3

Centrate (liquid phase outlet)	
Total dry solids (mass %)	1.00
Solids Recovery (%)	98.1%
Flowrate (m3/hr)	42
Mass Flow Rate (T/hr)	42

Figure 4: Solids cake discharged on the conveyor from solid bowl centrifuges at Rix's Creek South, close up

Figure 5: Solids cake discharged on the conveyor from solid bowl centrifuges at Rix's Creek South

Performance of the three SBCs has been closely monitored over a number of years by Rix's Creek South. Table 3 shows typical data. It will vary depending on which coal seam is being washed in the CHPP.

Table 3: Typical results obtained at Rix's Creek South

SG of the thickener underflow	1.1 to 1.32 (Average 1.22)
Particle size	D50 less than 25 microns (see a typical PSD in Table 1 of this paper)
Mass flow of dry solids	Throughput per 720 mm diameter machine of 20 – 25 dry tonnes/hr
Solids content of the thickener underflow	25 – 40% w/w
Product (cake) moisture	30 – 38% w/w
Product (cake) solids	62 – 70% w/w

New installation of large solid bowl centrifuges

In 2018, Rix's Creek South decided to dewater 100% of their coal tailings, rather than sending a portion of the wet tailings to the tailings dam. In order to achieve this, they decided to add two more new, larger-sized SBCs, each with a bowl diameter of 1,000 mm, to the existing SBC installation. The plan was to get

the new SBCs into operation in Quarter 4 of 2018, with the intention of removing the need for a new tailings dam as the existing dam's capacity runs out.

Table 4: Typical mass balance for the 1,000 mm solid bowl decanter

PROJECT	DUTY	Alfa Laval Australia Pty Ltd
Rix's Creek	Coal Tailings Dewatering	P3 Mining Decanters
DATE 25/01/2018		

Mass Balance and Sizing — Data below is per decanter centrifuge

Feed (before floc addition)	
Total Dry Solids (mass%)	30
Dry solids mass flowrate (t/hr)	60.00
Solids Density (kg/m3)	1800
Liquid Density (kg/m3)	1000
Slurry Flowrate (m3/hr)	173.33
Slurry Density (kg/m3)	1154

Polymer (flocculant)	
Dose (kg/ T Dry Solids)	0.3
Concentration (%)	0.25
Flowrate Diluted (m3/hr)	7.20
Active polymer use (kg/hr)	18

Duty data shown is for each centrifuge

P3-10070 SBC (1000 mm DIA)

Cake (Solid phase outlet)	
Total dry solids (mass %)	65.0
Cake Volume Flowrate (m3/hr)	64.4
Total Cake Mass Flowrate (T/hr)	90.5
Dry Susp. Solids Flowrate (T/hr)	58.9

Centrate (liquid phase outlet)	
Total dry solids (mass %)	1.00
Solids Recovery (%)	98.1%
Flowrate (m3/hr)	116
Mass Flow Rate (T/hr)	117

Figure 6: 1,000 mm solid bowl centrifuge supplied by Alfa Laval

Based on the operating data from the earlier SBCs, the typical performance of the two new 1,000 mm SBCs is outlined in the table below. It should be noted here that the performance will depend on the composition of the specific seam being processed through the CHPP.

Table 5: Expected performance from the 1,000 mm solid bowl centrifuges at Rix's Creek South

Performance of SBCs on coal tailings	Range
Product (cake) moisture	32% to 38% (w/w)
Solids capture	Above 95% (w/w)
Solids capacity (dry solids)	55 to 70 dry tonne/h
Feed solids	25 to 40 % (w/w)
Volumetric feed capacity	110 to 190 m3/hr

The two new 1,000 mm solid bowl centrifuges (model: P3-10070) were commissioned in Q4 2018. The results from the initial commissioning period are tabulated in Table 6 (on the next page). It may be noted that both the solid bowl centrifuges have been handed over for taking into regular operation at the end of 2018.

Conclusion

By utilizing a deep pond design coupled with robust materials of construction, solid bowl centrifuges can be utilized to deliver high cake concentration, even at high flow rates. A better understanding of scaling to high capacities will allow large diameter SBCs to be used for high capacity duties in mine tailings applications. While applying this technology it may be helpful to carry out field tests using pilot-scale SBCs, as the tailings characteristics including mineralogy, particle size distribution, etc., might affect the dewatering performance from one site to another.

It is expected that solid bowl centrifuges with their low hold-up volume, small foot-print, automated operation, reduced operator intervention, and lower CAPEX and OPEX as compared to some other mechanical dewatering technologies, will become an attractive choice for dewatering duties in mining applications in the future.

Table 6: Initial commissioning data with new 1,000 mm SBC at the CHPP

Date (dd/mm/yy)		24-10-18	24-10-18	25-10-18	26-10-18	26-10-18
Time (hh:mm)		10:13	13:27	10:59	10:30	13:36
Machine conditions						
N (Bowl speed)	**rpm**	1,100	1,100	1,100	1,100	1,100
n (Conv. diff.)	**rpm**	7,82	7,77	8,48	11,66	12,07
T (Conv. torq.)	**kNm**	39,70	42,37	35,31	25,40	24,99
Feed conditions						
Feed flow rate	**m3/h**	85,24	101,76	115,16	130,00	140,00
Solids conc (oven drying)	**%w/w**	32,10	26,76	25,86	27,58	31,37
Dry solid flow	**kg/h**	33,929	33,222	35,736	43,017	54,019
Density from density meter	**kg/m³**	1,240	1,220	1,200	1,200	1,230
Polymer conditions						
Floc solution flow	**m³/h**	7,80	9,50	10,20	7,20	7,20
Floc conc. (w/o dilution)	**%w/w**	0,25	0,25	0,25	0,25	0,25
Cake conditions						
Recovery	%	98,10	97,57	98,64	98,58	98,66
Solid concentration (oven drying)	**%w/w**	66,3	62,4	62,3	63,8	62,4
Dry solid flow	**kg/h**	33,302	32,438	35,275	42,425	53,314
Cake density	**kg/m³**	1,284	1,263	1,262	1,270	1,263
Cake volume	**m³/h**	39,13	41,17	44,85	52,36	67,63
Centrate conditions						
Solid concentration	**%w/w**	1,021	0,989	0,531	0,631	0,769
Solid flow	**kg/h**	645,96	807,65	487,35	610,19	722,88
Centrate flow	**ton/h**	63,27	81,66	91,78	96,70	94,00
Centrate density	**kg/m³**	1003	1003	1002	1002	1003
Centrate flow	**m³/h**	63,05	81,39	91,62	96,50	93,76

Acknowledgements

The authors of this paper acknowledge the assistance and co-operation of the CHPP and its management in preparing this paper.

References

Madsen, B. 2017. Re-introducing solid bowl decanter centrifuges for dewatering in the mining industry. Conference paper presented at SYMPHOS 2017, 4th International Symposium on Innovation and Technology in the Phosphate Industry. May 8 to 10, Benguerir, Morocco.

Records, A. and K. Sutherland. 2001. *Decanter Centrifuge Handbook*, first edition. New York: Elsevier.

Bibliography

Chinchankar, A., L. Sunny and D. Oyanadel. 2019. Tailings dam made redundant using solid bowl centrifuge. 6th International Seminar on Tailings Management, Tailings 2019. July 10 to 12, Chile.

Proceedings of Tailings and Mine Waste 2019
November 17–20, 2019, Vancouver, Canada
Published by the University of British Columbia, 2019

Effects of Microbial-Induced Calcium Carbonate Precipitation on Settling and Consolidation of Tailings

Hernan Cifuentes, The University of Queensland, Australia
David J. Williams, The University of Queensland, Australia

Abstract

There is increasing interest in biological applications in a range of fields of engineering. In geotechnical engineering, the use of microbes or bacteria to modify the parameters of soft soils or tailings, while not widespread, has huge potential. To date, there have been just a few attempts to improve soft soils and tailings using microbes. The approach makes use of naturally occurring bacteria that are fed urea and a calcium source to promote their selective exponential growth, leading to the precipitation of calcium carbonate or calcite cementation. This serves to improve the shear strength and stiffness of bacterially treated soft soils or tailings.

Microbial-induced calcium carbonate precipitation has the potential to improve the geotechnical parameters of tailings, to improve their settled density and shear strength, and to facilitate the closure of a tailings storage facility. In addition to improvements to the shear strength, compressibility, and permeability of tailings, microbes can be used to control dust generation.

This paper examines the effects of microbial-induced calcium carbonate precipitation on the settling and consolidation behaviour of a range of mine tailings. Interpretation and analysis of the results achieved at bench scale are presented, suggesting potential for large-scale application in tailings management.

Introduction

The increasing concern related to tailings management is driven by the recent, high profile catastrophic failures of tailings dams, such as at Corrego de Feijão iron ore mine in Brumadinho, Brazil, which caused the deaths of about 280 mine workers. The volume of tailings slurry to be stored is increasing as the demand for mineral commodities increases and ore grades decrease. Conventional technologies available to dewater tailings slurry have not proven to be cost-effective at high tailings production rates or for tailings with a high content of clay minerals. Most of the conventional dewatering technologies rely mainly on physical processes, with the addition of some chemical polymers to enhance them. There is potential for the biological enhancement of the dewatering of tailings and the improvement of tailings parameters during operations and at closure.

Microbes have been used for copper extraction for over 50 years following the patenting of copper extraction using *Thiobacillus ferroxidans* by Kennecott Copper Corporation. Biological solutions are attracting increasing interest from the mining industry. Ore grade reduction, environmental pollution, and a sharp increase in costs have enticed the mining sector to explore these alternatives. More recently, bioleaching and bioremediation have been developed, and microbial flotation has been studied at laboratory scale.

A few attempts have been made to use microbes for tailings management. Most of these were related to the control of dust, bioremediation, and the improvement of geotechnical parameters such as consolidation and undrained shear strength. Buikema et al. (2018) sought to increase the surface strength of iron ore tailings through the formation of a mineral crust using microbes to control dust. Govarthanan et al. (2013) sought to reduce active lead ions present in tailings through carbonate mineralization. Chen et al. (2017) attempted to immobilize heavy metals by the cementation of particles through bio-mineralization. Pan et al. (2017) attempted to isolate native bacteria from lead-zinc tailings to understand the mechanism involved in bio-mineralization, to study the potential for lead remediation. Kang et al. (2016) evaluated the potential use of bio-sequestration of copper from soil at abandoned mine sites.

To improve the geotechnical parameters of tailings, Liang et al. (2015) investigated the effect on undrained shear strength and consolidation behaviour of fluid fine tailings from the oil sands industry of bacteria, and demonstrated a significant increase in the undrained shear strength and the consolidation rate.

DeJong et al. (2010) and Dhami et al. (2013) described microbial-induced calcium carbonate precipitation (MICCP) as a natural phenomenon catalysed by microbes. MICCP can be enhanced by high microbe concentrations, the availability of nucleation sites, the presence of urea, and the presence of excess calcium ions. Some external conditions, such as the quality of the water, temperature and pH, are also required.

The volume occupied by tailings deposited as a slurry are a function of their settled density, their self-weight consolidation and desiccation if exposed to sun and wind. The tailings density achieved has very significant implications for the required tailings dam raises and the stability of the tailings dam.

In this paper, the effects of microbial-induced calcium carbonate precipitation on settling and consolidation of tailings is studied at laboratory scale. The use of bacteria to induce MICCP was measured in settling columns to evaluate the improvement in the final dry density or solids concentration, and the improvement in stiffness was measured in oedometer consolidation tests.

Characterization of tailings tested

Tailings and process waters from three different Australian mine sites were collected, including coal tailings and process waters from mines located in the Bowen Basin and Hunter Valley Coalfields, Australia, and

seawater-neutralized red mud and process water from the refining of bauxite to produce alumina from Queensland Alumina Limited (QAL) located in Gladstone, Australia. The results of geotechnical characterization testing of the tailings and chemical characterization testing of the process waters are summarized in Tables 1 and 2, respectively.

Table 1: Summary of tailings geotechnical characterization

Parameter	Bowen Basin coal tailings	Hunter Valley coal tailings	QAL bauxite residue
% Clay-sized particles by mass (<0.002 mm)	~0	32	13
% Silt-sized particles by mass (0.002 to 0.06 mm)	18	48	78
% Sand-sized particles by mass (>0.06 mm)	82	20	9
Specific gravity	1.90	1.72	2.93
Liquid Limit (%)	43.0	42.3	46.0
Plastic Limit (%)	29.0	27.6	30.1
Plasticity Index (%)	14.0	14.7	15.9
Unified Soil Classification	ML/CL	ML/CL	ML
Soil description	Low plasticity, Silty SAND	Low plasticity, Sandy Clayey SILT	Low plasticity, Sandy Clayey SILT

Table 2: Summary of process water chemical characterization

Parameter	Bowen Basin coal tailings	Hunter Valley coal tailings	QAL bauxite residue
Electrical conductivity (mS/cm)	4.2	6.0	52.0
pH	8.7	9.1	8.1
Calcium (mg/L)	29.4	7.0	56.1
Magnesium (mg/L)	72.1	21.4	0.1
Sodium (mg/L)	64.9	0	0
Potassium (mg/L)	9.8	11.7	289.8

Test methodology

Bacterial and cementation solutions

Sporosarcina pasteurii (DSM 33) bacteria were cultured in each of the process waters to a concentration of 30 g/L in a Tryptone Soya Broth medium (Oxoid CM0129), sterilized by autoclaving, and 20 g/L of filter sterilized urea solution was added. Urea, also known as carbamide, has the chemical formula

$CO(NH_2)_2$, and is an organic carbon compound containing 47% nitrogen. It is safe to handle and suitable for growing bacteria. Prior to culturing, the tailings process waters were vacuum filtered firstly using a Corning bottle-top with a pore size of 0.45 µm, and again using a pore size of 0.22 µm, to reduce the impedance against sterilization by autoclaving. The growth medium was aerobically incubated at 30°C for approximately 18 hours before harvesting the bacteria at a final optical density (OD_{600}) of 0.48 measured using a Shimadzu spectrophotometer (UV-3600 Plus UV-VIS-NIR, at 600 nm).

The capability of the bacteria to grow in the tailings process waters was demonstrated by a series of electrical conductivity, pH and optical density (OD_{600}) readings at 0 hours, 12 hours and 18 hours after inoculation of the process waters.

The cementation solution comprised urea and calcium chloride, to promote calcite precipitation after the tailings were inoculated with bacteria.

Tailings sample preparation

Settling column samples

The settling column tests were performed in graduated 250 ml cylinders. The tailings samples without or with treatment were made up to 250 mL at 38% solids concentration by mass for the Bowen Basin coal tailings, 35% for the Hunter Valley coal tailings, and 31% solids for the bauxite residue. The samples were homogenized using a mechanical stirrer operated at 1,200 rpm for 25 min, prior to being poured into the graduated cylinders. Two column tests were prepared for each tailings type; one as a control with 5 mL of make-up distilled water and no treatment, and the other with 5 mL of bacterial and cementation solutions.

All settling column samples were cured for 20 hours at room temperature to allow the bacteria to grow, followed by the addition of 15 mL of cementation solution to all samples. The filled cylinders were then shaken manually for 1 min to ensure good mixing of the bacterial solution with the tailings slurry, after which the columns were allowed to settle. The dosage rates for bacterial and cementation solutions added to the settling columns are summarized in Table 3. Figure 1 shows the settling columns after the application of the bacterial solution.

Table 3: Summary of dosage rates for bacterial and cementation solutions added to settling columns

Sample	Bacterial solution		Cementation solution	
	Tryptone Soya Broth (g/kg)	2% Urea (g/kg)	Urea (g/kg)	Calcium chloride (g/kg)
Bowen Basin coal tailings	1.30	0.87	0.78	14.5
Hunter Valley coal tailings	1.50	1.00	0.90	16.7
QAL bauxite residue	1.56	1.04	0.94	17.3

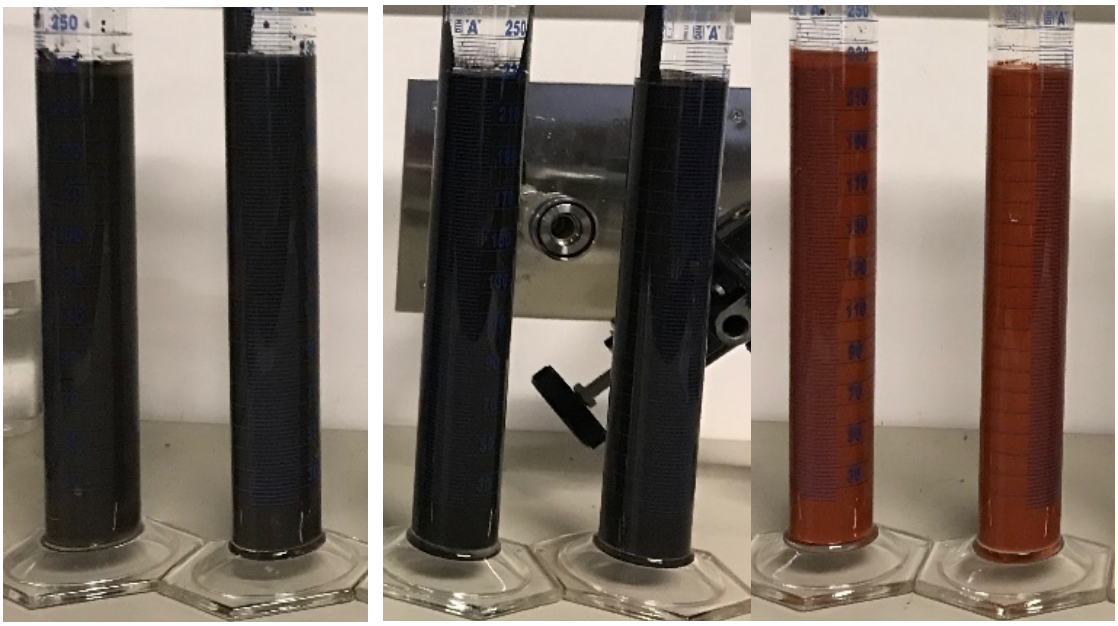

(a) (b) (c)

Figure 1: Settling column tests before cementation: (a) Bowen Basin coal tailings, (b) Hunter Valley coal tailings, and (c) QAL bauxite residue

Consolidation samples

Specimens for oedometer consolidation tests were formed in plastic containers measuring 150 mm × 100 mm × 50 mm. To allow drainage, 2 mm diameter holes were drilled in the base of each container, and a geotextile liner having 37 μm openings placed in the base to avoid the loss of fine-grained tailings particles. Two 8 mm diameter holes were drilled in the lids of the containers to allow controlled desiccation by evaporation during the curing. A similar sized container without holes was placed beneath each sample container to collect any drainage form the sample.

Two container samples were prepared for each tailings type; one as a control with make-up distilled water and no bacterial treatment, and the other with bacterial treatment. The container samples were prepared to 65% solids for the Bowen Basin coal tailings, 64% for the Hunter Valley coal tailings, and 54% solids for the bauxite residue. The tailings samples, without or with bacterial inoculation, were poured into the containers to a minimum height of about 40 mm, sufficient to allow oedometer ring specimens to be cut from the cured samples. About 600 mL of tailings was prepared for each container, before injecting 10 mL of distilled water by syringe (control samples) or 10 mL of bacterial solution (treated samples). The samples were then cured for 20 hours at room temperature with the lids on, to allow the bacteria to grow (Figure 2), followed by the injection by syringe of 10 mL of cementation solution to all samples. The dosage rates for

bacterial and cementation solutions added to the container samples are summarized in Table 4. Oedometer ring specimens were cut from the container samples, when the treated Bowen Basin coal tailings, Hunter Valley coal tailings and QAL bauxite residue samples had reached 74%, 71% and 64% solids, respectively. The treated samples had 3% higher solids than the control samples, indicating the effect of the treatment. Three load increments of 50 kPa, 100 kPa and 200 kPa were applied in the oedometer tests, which were carried out in water baths.

Figure 2: Coal tailings prepared in plastic containers

Table 4: Summary of dosage rates for bacterial and cementation solutions added to consolidation specimens

Sample	Bacterial solution		Cementation solution	
	Tryptone Soya Broth (g/kg)	2% Urea (g/kg)	Urea (g/kg)	Calcium chloride (g/kg)
Bowen Basin coal tailings	0.53	0.35	0.11	1.95
Hunter Valley coal tailings	0.57	0.38	0.11	1.95
QAL bauxite residue	0.58	0.39	0.12	2.16

Figure 3: Coal tailings specimens being cut for oedometer testing

Test results

Effect of bacterial treatment

Figure 4 shows the cell densities obtained on bacterial treatment of each tailings sample in their process water. The cell density (OD_{600}) increased with curing time for all tailings samples, indicating the increasing effect of treatment as the bacteria grew. The effect of curing time was more immediate and more marked for the coal tailings samples than for the bauxite residue. This is considered to be due to the high concentrations of calcium and potassium ions in the bauxite residue. Autoclaving gave a similar response to curing to that of the treated coal tailings samples, while control by sterilization gave a similar response to curing to that of the treated bauxite residue. Overall, the growth of the bacteria is not excessively impeded by the harsh chemistry of the process waters.

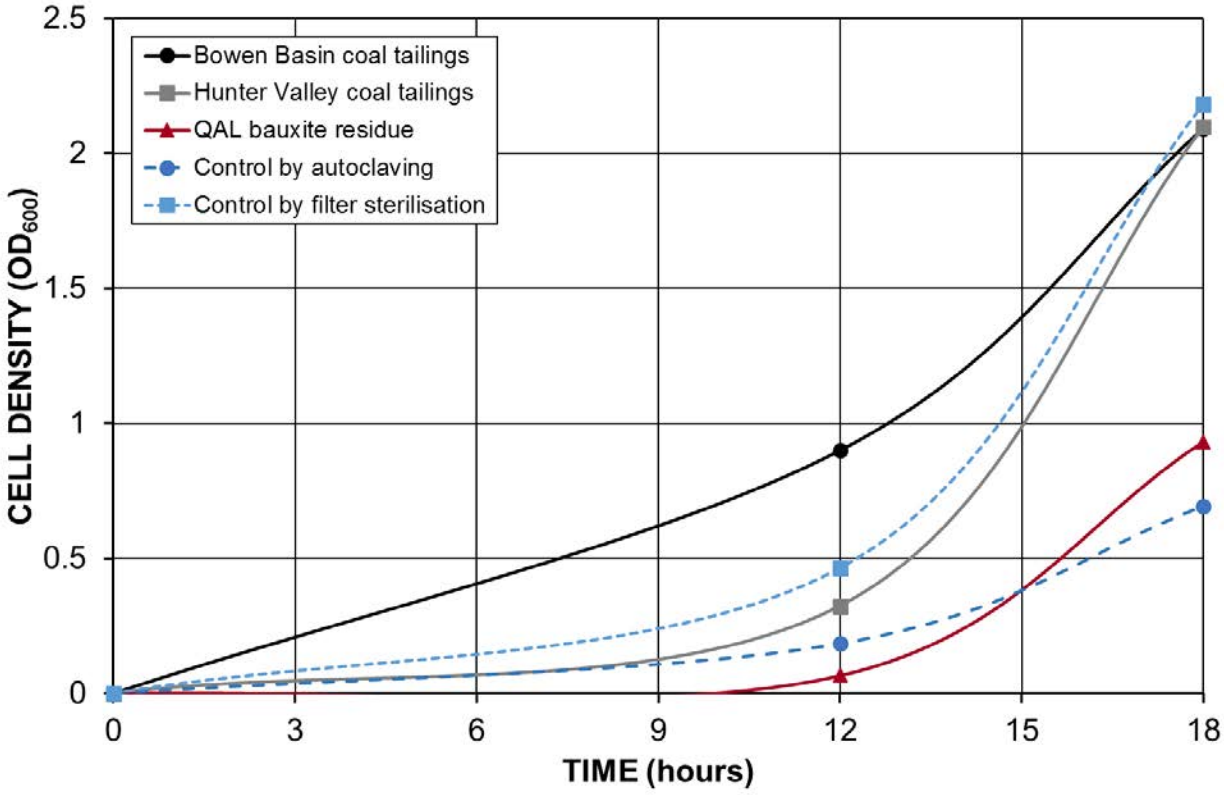

Figure 4: Bacterial growth with time for each tailings sample

Settling behaviour

The results of the settling tests are shown in Figure 5 and summarized in Table 5, which demonstrate distinct differences between the settling behaviours of the low plasticity, Silty SAND-sized Bowen Basin coal tailings compared to that of the much finer-grained, low plasticity, Sandy Clayey SILT-sized Hunter Valley coal tailings. The low plasticity, intermediate and modified, Sandy Clayey SILT-sized QAL bauxite residue showed intermediate settling behaviour between the two coal tailings samples. There was relatively little difference in the settling behaviour of the control and treated samples of the Bowen Basin coal tailings and QAL bauxite residue samples.

However, the problematic clay mineral-rich Hunter Valley coal tailings showed improved settling behaviour on bacterial treatment, compared with virtually no settling from 35% solids with no bacterial treatment. Figure 5 shows that the rate of settling for all tailings samples was highest from 12 to 24 hours, as highlighted in red in Figure 5.

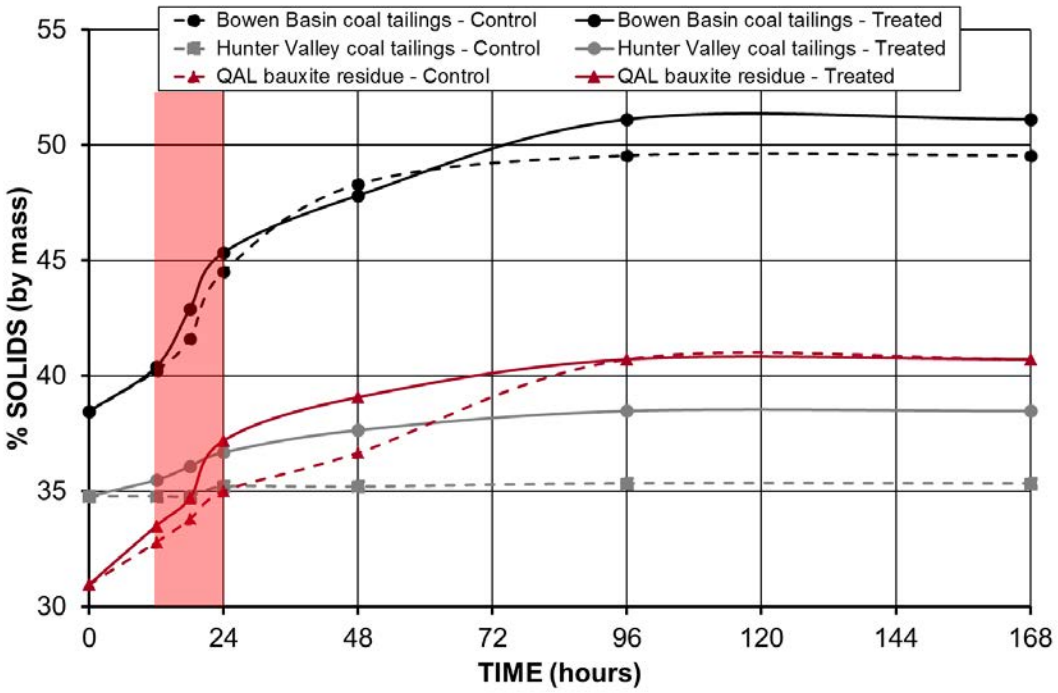

Figure 5: Settling test results

Table 5: Summary of settling column test results

Sample	Bacterial treatment	% Solids before testing	% Solids after testing
Bowen Basin coal tailings	Control	38	50
	Treated	38	51
Hunter Valley coal tailings	Control	35	35
	Treated	35	38
QAL bauxite residue	Control	31	41
	Treated	31	41

Consolidation behaviour

The results of the oedometer consolidation tests are shown in Figure 6 and summarized in Tables 6 and 7, which demonstrate that bacterial and cementation treatment resulted in a reduced initial void ratio and higher initial dry density, and less change in void ratio or dry density on consolidation. The low plasticity, Silty SAND-sized Bowen Basin coal tailings consolidated most, and the low plasticity, Sandy Clayey SILT-sized QAL bauxite residue hardly at all, with the Sandy Clayey SILT-sized Hunter Valley coal tailings

between the other two. The limited consolidation of the QAL bauxite residue is likely due to the high concentrations of calcium and potassium ions present.

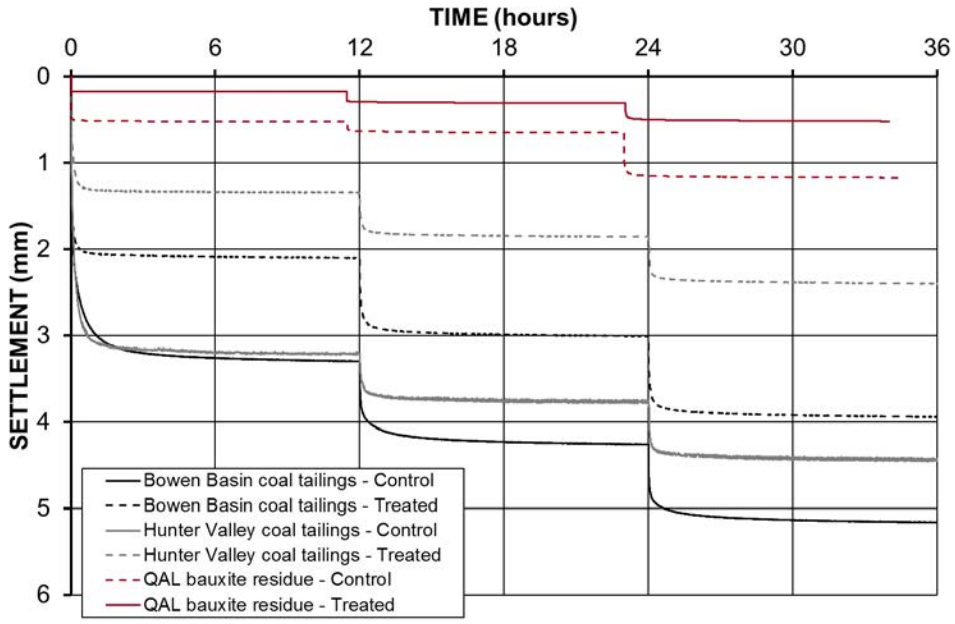

Figure 6: Consolidation test results

Table 6: Summary of consolidation test results – Void ratio

Sample	Bacterial treatment	Initial void ratio	Final void ratio	Change in void ratio
Bowen Basin coal tailings	Control	1.014	0.512	0.501
	Treated	0.928	0.561	0.368
Hunter Valley coal tailings	Control	1.098	0.643	0.455
	Treated	1.005	0.787	0.218
QAL bauxite residue	Control	2.152	1.944	0.208
	Treated	2.036	1.934	0.102

Table 7: Summary of consolidation test results – Dry density

Sample	Bacterial treatment	Initial dry density (t/m^3)	Final dry density (t/m^3)	Change in dry density (t/m^3)
Bowen Basin coal tailings	Control	0.944	1.257	0.313
	Treated	0.985	1.217	0.232
Hunter Valley coal tailings	Control	0.820	1.047	0.227
	Treated	0.859	0.963	0.104
QAL bauxite residue	Control	0.930	0.995	0.065
	Treated	0.965	0.999	0.034

Potential application at field scale

The reported results of laboratory-scale microbial-induced calcium carbonate precipitation on the settling and consolidation behaviour of a range of mine tailings demonstrated improved performance. Cifuentes and Williams (2018) similarly demonstrated improvements to the undrained shear strength of bacterially-treated mine tailings, as measured by a laboratory shear vane.

To extend these results to field scale, a bacterial pre-treatment system would be required. Such a system would comprise large mixing tanks with agitators, similar to those used for the addition of chemicals, in which the bacterial and cementation solutions would be cultured. Curing would require the control of temperature, pH and electrical conductivity. Once the bacteria achieved optimal concentration, they could be added to dewatered tailings, either in the plant or in the delivery pipeline, or possibly at the end of the delivery pipe, depending on where improvement of the tailings parameters and behaviour is best achieved.

Conclusion

Three types of tailings and process waters: (i) Bowen Basin coal tailings, (ii) Hunter Valley coal tailings, and (iii) QAL bauxite residue, were subjected to conventional laboratory physical and chemical characterization, settling, and consolidation testing. Each type of tailings was tested with and without bacterial treatment, with cementation solution added in both cases.

The results of the settling tests showed that while bacterial and cementation treatment had little effect on the settling behaviour of the Bowen Basin coal tailings and QAL bauxite residue samples, the problematic clay mineral-rich Hunter Valley coal tailings showed improved settling behaviour, compared with virtually no settling from 35% solids with no bacterial treatment.

The results of the consolidation sample preparation and testing showed that bacterial and cementation treatment resulted in a reduced initial void ratio and higher initial dry density, and less change in void ratio or dry density on consolidation. The low plasticity, Silty SAND-sized Bowen Basin coal tailings consolidated most, and the low plasticity, Sandy Clayey SILT-sized QAL bauxite residue hardly at all, with the Sandy Clayey SILT-sized Hunter Valley coal tailings between the other two. The limited consolidation of the QAL bauxite residue is likely due to the high concentrations of calcium and potassium ions present.

These findings need to be confirmed by testing other bacteria dosage rates, and suggest that bacterial and cementation treatment of tailings, in harsh process water, has potential for large-scale application in tailings management.

Acknowledgements

This paper is based on the PhD research of the first author, which is being funded by Minera Escondida-BHP, Chile. The authors acknowledge the suppliers of tailings samples for testing. The authors are also very grateful to Dr Emma Gagen, research fellow from the School of Earth and Environmental Sciences at The University of Queensland, for her assistance and guidance on the microbiology activities performed.

References

Buikema, N.D., B. Zwissler and E. Seagren. 2018. Stabilisation of iron mine tailings through biocalcification. *Environmental Geotechnics* 5(2): 94–106.

Chen, X., H. Guo and X. Cheng. 2017. Heavy metal immobilisation and particle cementation of tailings by biomineralisation. *Environmental Geotechnics* 5(2): 1–7.

Cifuentes, H. and D.J. Williams. 2018. Potential improvement of tailings geotechnical behaviour using bacteria. In *Proceedings of Mine Waste and Tailings Stewardship Conference 2018, July 23–24, Brisbane, Australia*.

DeJong, J.T., B.M. Mortensen, B.C. Martinez and D.C. Nelson DC. 2010. Bio-mediated soil improvement. *Ecological Engineering* 36(2): 197–210.

Dhami, N.K., M.S. Reddy and A. Mukherjee. 2013. Biomineralization of calcium carbonates and their engineered applications: A review. *Frontiers in Microbiology* 4(314): 1–13.

Govarthanan, M., K.J. Lee, M. Cho, J.S. Kim, S. Kamala-Kannan and B.T. Oh. 2013. Significance of *Autochthonous bacillus sp. KKL* on biomineralization of lead in mine tailings. *Chemosphere* 90(8): 2267–2272.

Kang, C.H., U.Y. Shin, P. Anbu, I.H. Nam and J.S. So. 2016. Biosequestration of copper by bacteria isolated from an abandoned mine by using microbially induced calcite precipitation. *J of General and Applied Microbiology* 62(4): 206–212.

Liang, J., Z. Guo, L. Deng and Y. Liu. 2015. Mature fine tailings consolidation through microbial induced calcium carbonate precipitation. *Canadian J of Civil Engineering* 42(11): 975–978.

Pan, X., Z. Chen, L. Li, W. Rao, Z. Xu and X. Guan. 2017. Microbial strategy for potential lead remediation: A review study. *World J of Microbiology and Biotechnology* 33: 2, 35.

Proceedings of Tailings and Mine Waste 2019
November 17–20, 2019, Vancouver, Canada
Published by the University of British Columbia, 2019

Liquefaction Susceptibility Evaluation of Mine Tailings Using Cone Penetration Tests

Iván A. Contreras, Barr Engineering Co., USA
Aaron Grosser, Barr Engineering Co., USA

Abstract

Saturated, fine-grained, low-plasticity materials are often characterized for liquefaction susceptibility using cone penetration tests (CPTs). Often the CPT soundings indicate that the tailings material is dilative and thus not susceptible to liquefaction. Two side-by-side CPT soundings were performed on a mine tailings deposit at a standard penetration rate (20 mm/s) and a fast penetration rate (200 mm/s). The data were used to assess liquefaction susceptibility of the deposit using commonly accepted methodologies. A change in the penetration rate suggests that some commonly used methodologies may incorrectly indicate dilative behaviour when, in fact, the actual behaviour is contractive. This paper presents the data, procedures to evaluate liquefaction susceptibility, and the differences encountered regarding susceptibility prediction between two penetration rates and considerations in assessing liquefaction susceptibility.

Introduction

Liquefaction is characterized by a sudden decrease of shear strength from the yield strength to the steady-state strength, which can be substantially lower under undrained conditions induced by static or dynamic loading (Poulos et al., 1985). The loss in shear strength during liquefaction is so significant that a sizeable portion of the soil mass, rather than just the soil along a sliding surface, temporarily assumes the consistency of a thick liquid. The consequences of liquefaction include flow slides of sloping ground, lateral displacement of retaining structures, tilting or sinking of foundations, ground rupture, formation of sand boils, and floating of light buried structures (Terzaghi et al., 1996). Liquefaction has been the mechanism responsible for many tailings basin failures around the world, including the failure of Samarco's Fundão tailings storage facility in Brazil (Morgenstern et al., 2016).

Olson and Stark (2002; 2003) suggested a detailed procedure for liquefaction analysis of earthen structures involving three basic steps: (1) liquefaction susceptibility evaluation; (2) liquefaction triggering analysis; and (3) post-triggering/flow-failure stability analysis.

- Liquefaction susceptibility evaluation: In the first step, foundation materials are evaluated to determine whether they are contractive (i.e., susceptible to strength loss due to strain-softening behaviour) or dilative (i.e., strain-hardening behaviour).
- Liquefaction triggering analysis: In the second step, the contractive materials are further evaluated to determine whether liquefaction will be triggered (i.e., whether the anticipated seismic or static shear stresses will exceed the yield shear strength). In the case of seismic triggering, a site-response analysis is completed. However, in the case of static triggering, the analysis is more complex due to the uncertainty of the loading mechanisms.
- Post-triggering/flow-failure stability analysis: In the third step, slope stability analyses are performed using the pre-failure geometry and the liquefied shear strength of the contractive materials that are anticipated to trigger. In this step, slope stability analyses determine whether the applied static shear forces are greater than the available shear resistance. The computed factor of safety is then used to assess the post-triggering stability and likelihood of flow liquefaction.

A detailed description of the liquefaction analysis procedure is provided by Olson and Stark (2003). A number of methods for assessing liquefaction susceptibility exist (i.e., the first step above), many of which rely on in-situ testing such as CPT or standard penetration testing (SPT). The methods that utilize CPT data are based on soundings performed at a standard penetration rate of 20 mm/s. However, comparison of side-by-side CPT soundings performed by the authors at a standard penetration rate (20 mm/s) and a fast penetration rate (200 mm/s) suggest that some commonly used methodologies may incorrectly indicate dilative behaviour, when, in fact, the actual behaviour is contractive. This paper presents details of the evaluation and discussion of the results for one CPT probe, as well as considerations for assessing liquefaction susceptibility of mine tailings using the CPT.

Background

The soils most susceptible to liquefaction are saturated, cohesionless (or fine-grained soils of low plasticity), loose enough to be contractive, and of sufficiently low permeability to experience no significant drainage during the period of undrained shearing or ground shaking. These characteristics are determined by the method of deposition, geologic age, and stress history of the deposit (Terzaghi et al., 1996).

Mine tailings comprise the uneconomical residue left from the mineral processing of the ore body to extract the desired mineral. Mineral processing generally involves size reduction and separation processes to achieve liberation and concentration of the desired mineral. The residue commonly known as tailings

consists of middling and gangue material with particle sizes ranging from coarse (i.e., sand size) to fine (i.e., clay size). In many instances, the size reduction can result in very fine material that can be clay size, which may or may not necessarily contain clay minerals. In the case of conventional tailings, these are typically deposited hydraulically from a slurry.

Mine tailings are typically considered highly susceptible to liquefaction because they are commonly composed of non-plastic or low-plasticity solids. Furthermore, the potential for mine tailings to liquefy in response to triggering events is related to the fact that these materials are hydraulically deposited; thus, the materials come to equilibrium under very loose conditions. Moreover, tailings are recent deposits of a very young geologic age, which is typically associated with greater potential for liquefaction. Furthermore, mine tailings do not undergo any additional loading other than the overburden stresses from continued tailings deposition and dam construction (resulting in nearly normally consolidated deposits). Thus, the saturation, very loose condition, stress history, and young geologic age of mine tailings generally results in contractive behaviour during undrained shearing and makes them highly susceptible to liquefaction.

In summary, mine tailing deposits typically display characteristics resulting from the method of deposition, geologic age, and stress history which make them highly susceptible to liquefaction. As a result, liquefaction is a relevant mode of failure that is commonly evaluated at tailings basins. When performing the liquefaction analyses of these deposits the first step, a liquefaction susceptibility assessment, is required.

Liquefaction susceptibility assessment in geotechnical practice

Multiple state-of-the-practice methodologies exist to assess liquefaction susceptibility of soils in geotechnical engineering practice. The majority of them utilize in-situ tests (i.e., SPT or CPT) to estimate the state of the deposit and assess susceptibility. Others, involving fine-grain soils, utilize index properties (Bray and Sancio, 2006). Commonly used methods that utilize CPT data include those by Olson and Stark (2003), Olson (2009), Robertson (2016), Jefferies and Been (2015), and Winckler et al. (2014). The following briefly describes each of these methods and how they are used to evaluate liquefaction susceptibility:

Olson and Stark (2003) and Olson (2009) – Tip resistance from CPT: This methodology is based on in-situ measured CPT data tip resistance. The methodology proposed by Olson (2009), supported by previous work by Olson and Stark (2003), uses a relationship between the normalized tip resistance (q_{t1}) and vertical effective stress (σ'_{vo}) to define the boundary that separates contractive from dilative soils based on material compressibility. The boundaries between contractive and dilative materials were

defined based on back-analyses of liquefaction case histories. The compressibility of the material is based on the slope of the critical state line, λ_{10}, measured in e-log σ'_{mean} space.

Winckler et al. (2014) – Dynamic pore-water pressure from CPT: This methodology, proposed by Winckler et al. (2014), is based on in-situ measured dynamic pore-water pressure from CPT data. It uses the relationship between the dynamic pore-water pressure (u_2) measured by the CPT and the in-situ pore-water pressure (u_0) to determine the normalized pore-water pressure (P). Positive P values are associated with contractive soils, and negative values are associated with dilative soils.

Jefferies and Been (2015) – Tip, sleeve resistance and dynamic pore-water pressure from CPT: This methodology is based on a dimensionless penetration Q_t $(1–B_q)+1$, which uses tip resistance and dynamic pore-water pressure (u_2) and the normalized sleeve friction ratio (F_r) plotted in a chart for several state parameter lines (ψ). It was postulated by Jefferies and Been (2015) that soils with a state parameter (ψ) lower than –0.05 are dilative, while soils with a ψ larger than –0.05 are contractive.

Robertson (2016) – Tip and sleeve resistance and dynamic pore-water pressure from CPT: This methodology proposed by Robertson (2016) is also based on in-situ measured CPT data, and represents a refinement (update) of prior work by Robertson (2010). It uses a relationship between the dimensionless normalized corrected tip resistance (Q_{tn}) and normalized friction ratio (F_r) plotted with respect to soil behaviour types (SBTs). This defines the boundary that separates contractive from dilative soils based on an equivalent clean sand dimensionless, normalized, corrected tip resistance (Q_{tn}) value of 70.

The four methodologies described above were used by the authors to assess liquefaction susceptibility of two side-by-side CPT soundings performed in a mine tailings deposit at a standard penetration rate (20 mm/s) and a fast penetration rate (200 mm/s).

Further details regarding each of these methodologies, as well as the results of the assessment, are provided in the following sections, with the objective of quantifying the liquefaction susceptibility of the mine tailings.

Data used in the susceptibility assessment

Method of deposition, geologic age, and stress history of the deposit are typical characteristics related to susceptibility to liquefaction. Data used in the assessment are associated with a mine tailings deposit where hydraulic deposition is used; thus, the tailings came to equilibrium under very loose conditions. Similarly, the tailings have been deposited within the last three decades, making them very young geologically. Finally, the stress history of the data presented in this paper corresponds to a normally consolidated soil (i.e., OCR equal to unity) since none of the mechanisms leading to over-consolidation are present. Since the tailings discussed herein have been hydraulically deposited and essentially normally

consolidated, they are generally in a fairly loose condition. As a result, they are expected to exhibit mostly contractive behaviour under undrained conditions, and thus are susceptible to liquefaction.

The tailings discussed herein correspond to silty material with 75 to 100 percent passing No. 200 US sieve and a low clay-size fraction (0 to 10 percent). Data used in the assessment were presented previously in a separate publication, and further details on the subsurface conditions and CPT equipment can be found in Contreras and Grosser (2009).

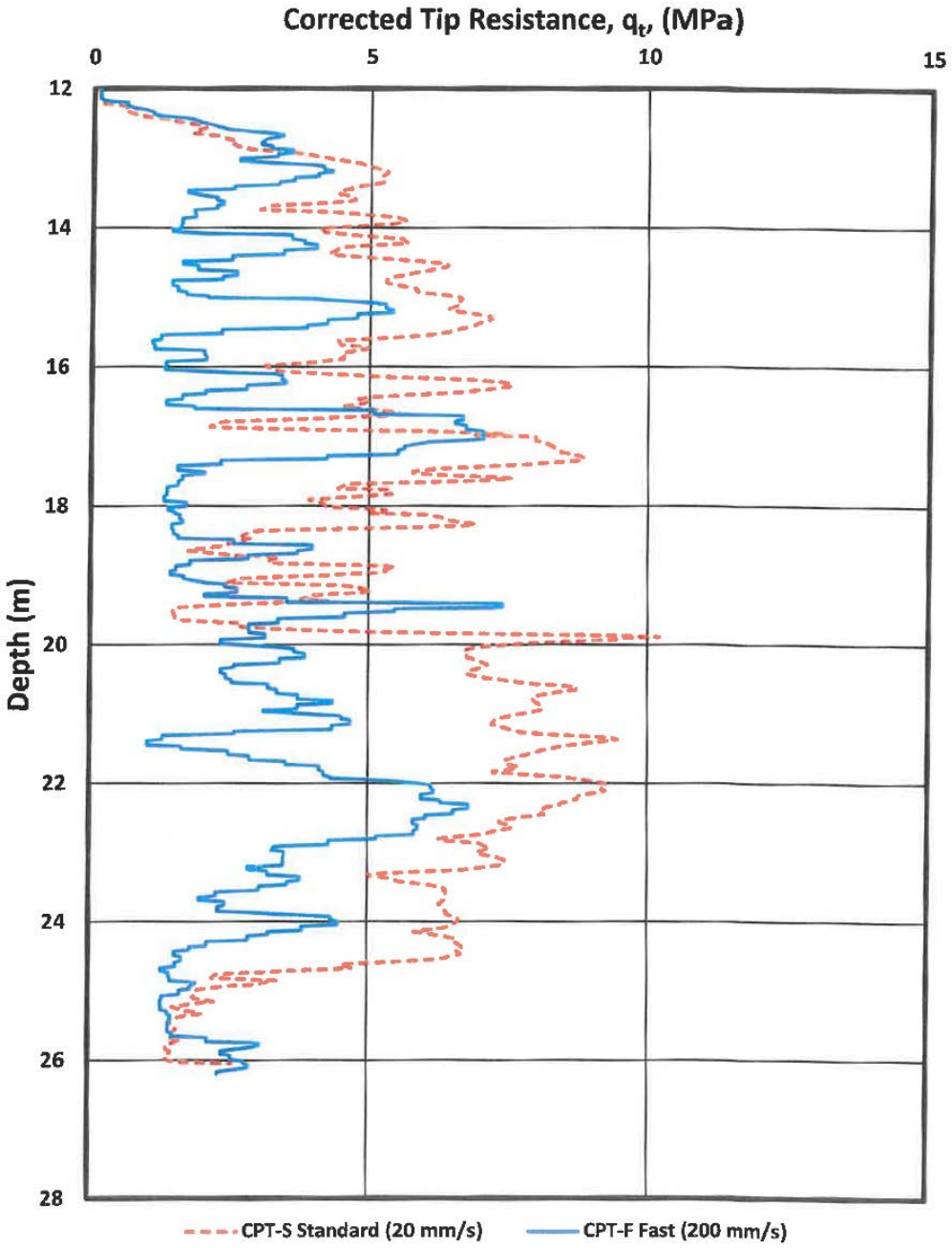

Figure 1: Corrected tip resistance versus depth for CPT-S and CPT-F

Figure 1 shows the typical results of two adjacent CPT soundings performed at the site but at different penetration rates. CPT-S represents the sounding performed at the standard rate of 20 mm/s (shown by the dashed line), whereas CPT-F represents the sounding performed at 200 mm/s (shown by the continuous line). The upper 12 m were predrilled due to the presence of a dense granular layer; this layer is not shown for clarity. In a few instances during the fast penetration, the depth measuring device slipped during cone advancement; thus, the depth in the fast sounding shifted slightly (i.e., greater than the standard sounding) and is not precisely correct. However, no attempts were made to correct for the slippage.

Figure 1 includes the plot of the corrected tip resistance (q_t) versus depth for both soundings CPT-S and CPT-F. It can be seen from Figure 1 that, in general, the corrected tip resistance for CPT-F (i.e., fast rate 200 mm/s) is lower than the corrected tip resistance for CPT-S (i.e., standard rate 20 mm/s). This lower corrected tip resistance is attributed to the associated increase of dynamic pore-water pressure due to the fast penetration rate. The couple of instances where the CPT-F tip is higher than the CPT-S are attributed to the slippage previously described. There are, however, general shape indicators in tip resistance that can be used to correlate with depths.

Figure 2 includes the plot of dynamic pore-water pressure (u_2) versus depth for CPT-S. The dynamic pore-water pressure for CPT-S is almost linear (except between depths of 17.8 to 19.8 m) and practically coincides with the in-situ pore-water pressure (u_0) distribution at this location (shown by the solid circles) based on the equilibrium pore-water pressures from dissipation tests. This behaviour indicates that cone penetration for sounding CPT-S mostly takes place under drained conditions.

Figure 3 includes the plot of dynamic pore-water pressure (u_2) versus depth for CPT-S and CPT-F. Figure 3 also includes a series of solid triangles on the ordinate axis which represent the depths where penetration stopped for CPT-F due to rod addition or other reasons. Figure 3 shows that pore-water pressures for CPT-F (fast penetration rate) increases significantly (in certain zones) from the pore-water pressures measured in sounding CPT-S (standard penetration rate). It is interesting to note that in the CPT-F sounding, the depths or zones where the pore-water pressure decreases to the in-situ pore-water pressure coincides with the depths at which cone penetration was stopped due to rod addition or other reasons, thereby dissipating pore-water pressure over a very short period of time. The process of rod changing and short stops has an effect on the overall dynamic pore-water pressure distribution.

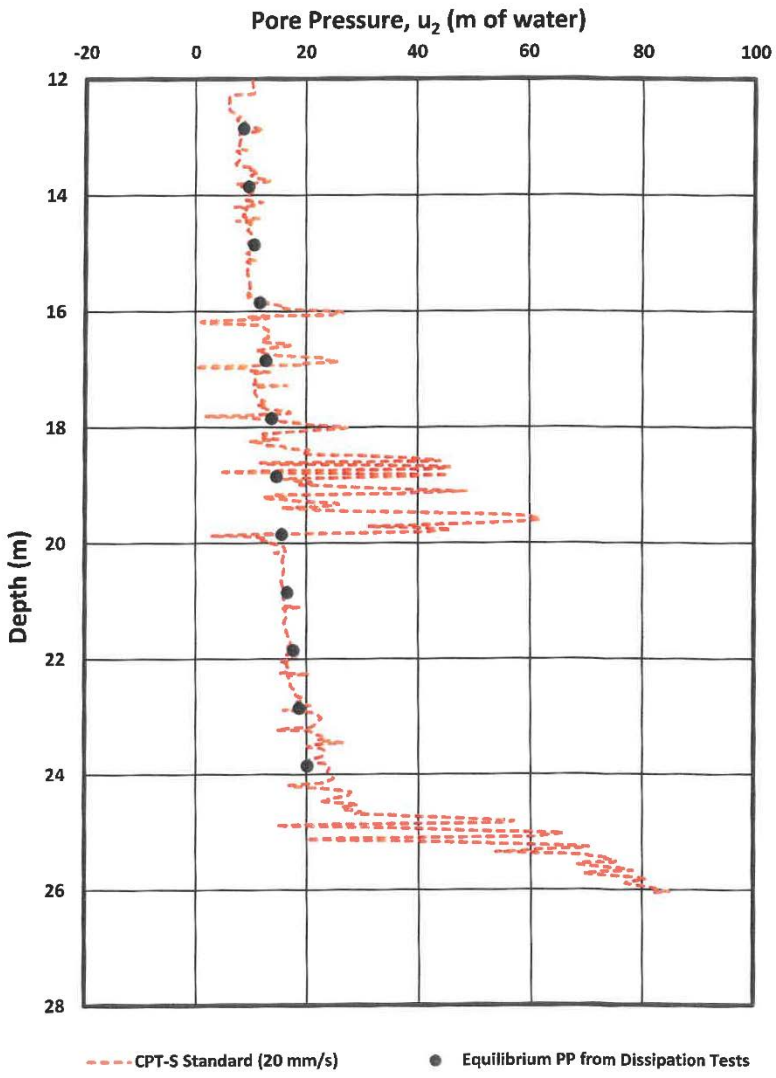

Figure 2: Dynamic and equilibrium pore-water pressure versus depth for CPT-S

In low permeability soils at the standard penetration rate, the effect of rod changing is not typically reflected in the dynamic pore-water pressure distribution results because this does not dissipate the pore-water pressure as fast as the tailings at the site. However, the tailings materials at the site have a relatively high permeability such that the pore-water pressure generated during the fast penetration dissipates fairly quickly.

The results shown in Figures 1 through 3 illustrate that the tailings at the site develop positive shear-induced pore-water pressures during fast loading and likely undrained shear. These results further support the hypothesis that the tailings at the site are likely contractive. To further assess the behaviour of the tailings at the site their susceptibility to liquefaction was evaluated.

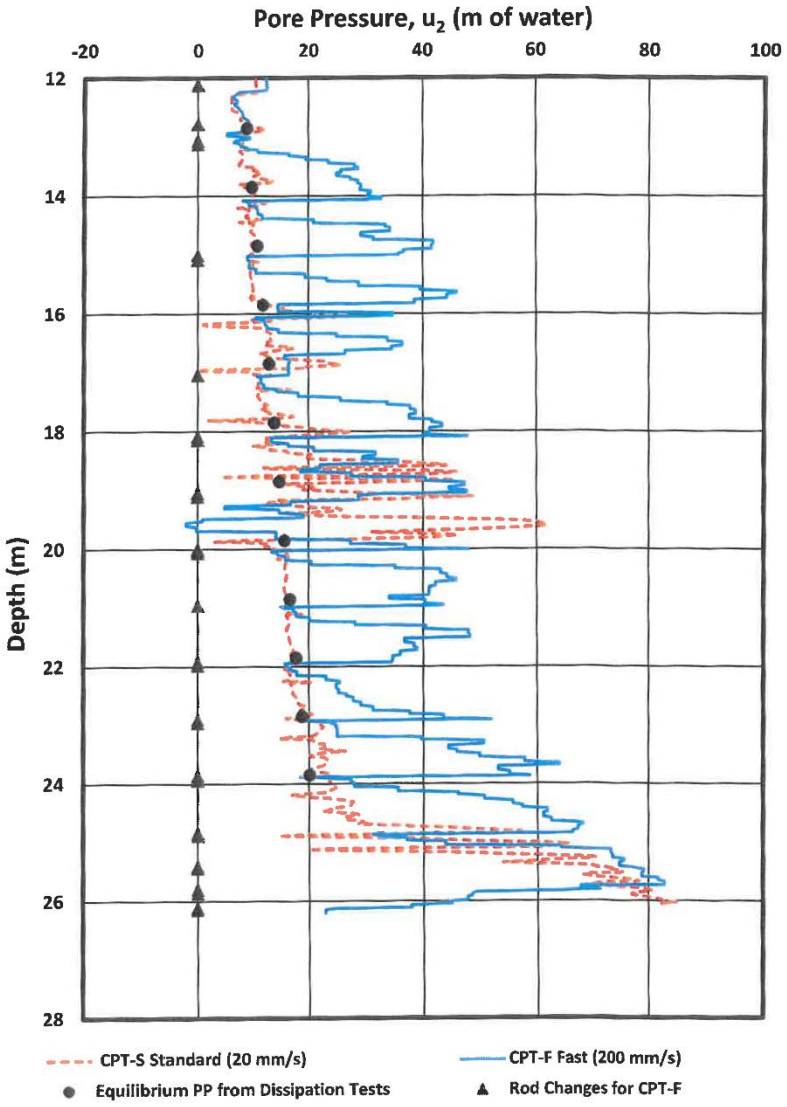

Figure 3: Dynamic pore-water pressure versus depth for CPT-S and CPT-F

Liquefaction susceptibility assessment

The following four methods that utilize CPT data were used in the liquefaction susceptibility assessment: Olson (2009), Robertson (2016), Jefferies and Been (2015), and Winckler et al. (2014).

Olson and Stark (2003) and Olson (2009)

Olson (2009) proposed an updated CPT-based relationship for liquefaction susceptibility consisting of three boundaries based on material compressibility. These boundaries were to apply in the case of compressible soils, including mine tailings. The three tentative boundaries proposed by Olson (2009)

include the original boundary from Olson and Stark (2003), based on Fear and Robertson (1995) for low compressible materials ($\lambda_{10} = 0.03$), a new boundary for medium compressibility materials ($\lambda_{10} = 0.06$), and a new boundary for high compressibility materials ($\lambda_{10} = 0.17$). Each of the three boundaries was based on the estimated compressibility of the material (Jefferies and Been, 2006) in terms of the slope of the critical state line (λ_{10}) associated with the liquefaction case histories contained within the database presented by Olson and Stark (2003).

Figure 4 shows the data from Figures 1 and 2 in the relationship between the normalized tip resistance (q_{t1}) and vertical effective stress (σ'_{vo}). Figure 4 includes three tentative boundary lines that separate contractive from dilative soils based on material compressibility. The material at the site is characterized with a critical state line of $\lambda_{10} \sim 0.17$ and thus is classified as high compressibility. It can be seen from Figure 4 that a large number of points associated with CPT-S fall to the right of the high compressibility boundary line, indicating dilative behaviour, whereas almost all the points associated with CPT-F fall to the left of the boundary line, indicating contractive behaviour. Therefore, based on the Olson and Stark (2003) correlation, CPT-F predicts that almost all of the tailings material in the sounding is contractive, while CPT-S predicts that only a portion of it is contractive with a significant portion exhibiting dilative behaviour.

Winckler et al. (2014)

Winckler et al. (2014) proposed this approach based on the observation that materials not susceptible to liquefaction will tend to increase in volume when sheared (i.e., dilative behaviour), inducing a reduction in dynamic pore-water pressure with respect to the in-situ pore-water pressure. Conversely, materials susceptible to liquefaction will tend to decrease in volume when sheared (i.e., contractive behaviour), thereby generating an increase in dynamic pore-water pressure. The contractive or dilative nature of the materials can then be characterized by CPT pore-water pressure measurements using the normalized pore-water pressure parameter (P) defined by the following equation:

$$P = \frac{u_2 - u_o}{\sigma'_{vo}} \tag{1}$$

The normalized pore-water pressure parameter (P) is the difference between dynamic pore-water pressure (u_2) measured from the CPT and the in-situ pore-water pressure (uo) normalized by the vertical effective stress (σ'vo). Positive values are associated with contractive behaviour (i.e., susceptible to strength loss due to strain-softening behaviour) and negative values are associated with dilative behaviour (i.e., strain-hardening behaviour).

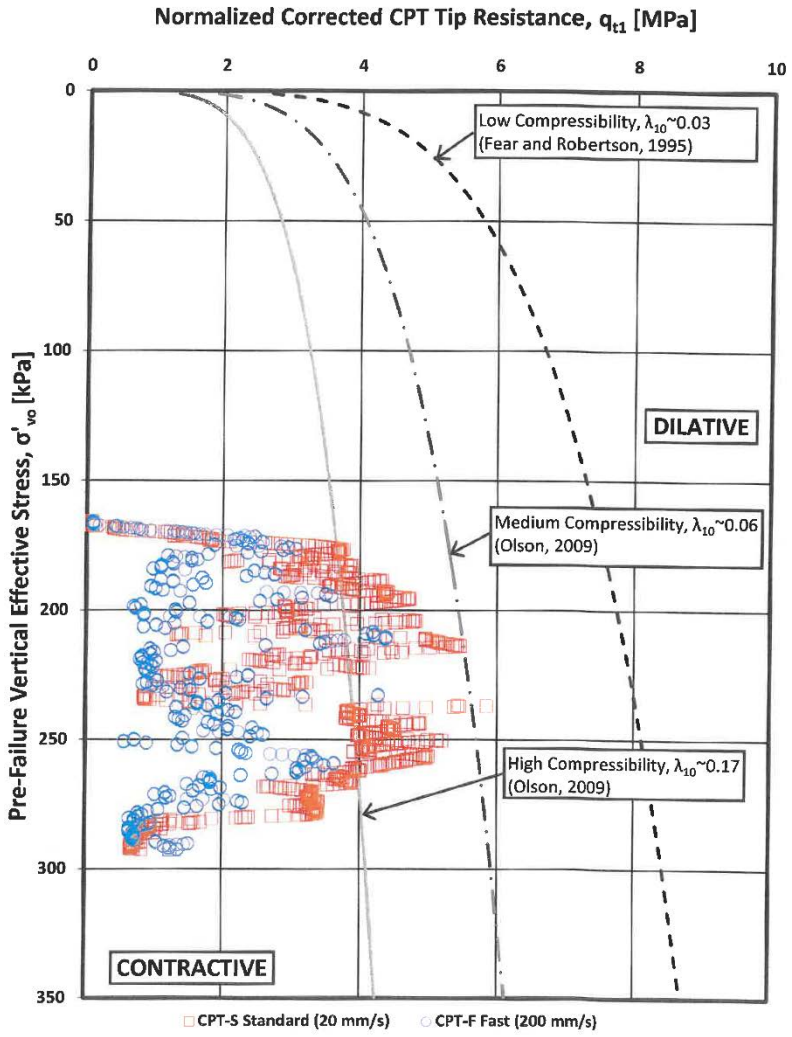

Figure 4: Liquefaction susceptibility assessment for CPT-S and CPT-F based on soil compressibility (Olson, 2009)

Figure 5 shows the data from Figures 1 and 2 in the relationship between the normalized pore-water pressure (P) and depth. Also in Figure 5 is the boundary presented by Winckler et al. (2014), separating positive and negative values associated with contractive and dilative behaviour, respectively. It can be seen in Figure 5 that the majority of the data associated with CPT-S fall to the left of the boundary line (i.e., P<0), indicating dilative behaviour of the tailings at the site. In fact, only a small portion of the points (i.e., at depths between 18–20 m and greater than 23 m) indicate contractive behaviour (i.e., P>0).

On the other hand, Figure 5 also shows that the majority of the points associated with CPT-F fall to the right of the boundary line (i.e., P>0), indicating contractive behaviour of the tailings at the site. In

fact, only a small portion of the points, mainly near the depths where penetration stopped for CPT-F due to rod addition or other reasons, indicate dilative behaviour (i.e., P<0).

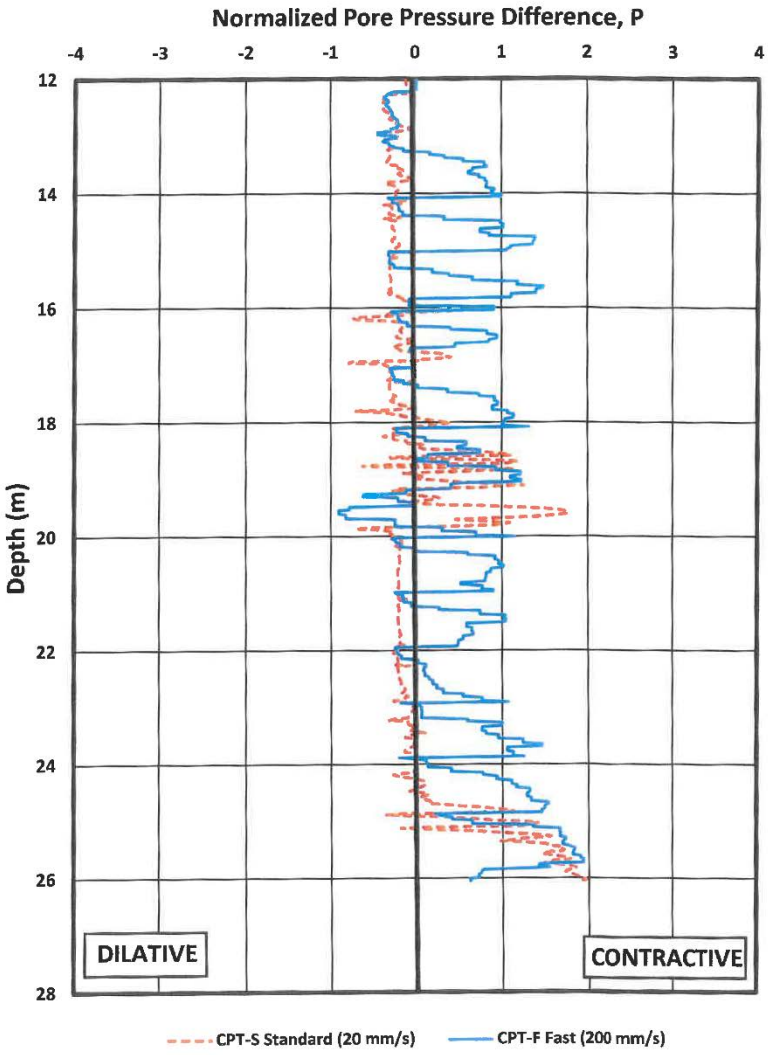

Figure 5: Liquefaction susceptibility assessment for CPT-S and CPT-F based on normalized pore-pressure parameter (P) (Winckler et al., 2014)

Jefferies and Been (2015)

Jefferies and Been (2015) proposed this methodology based on a dimensionless penetration parameter, Qt (1–Bq)+1, and the normalized sleeve friction ratio (Fr) plotted in a log-log chart. Several lines representing different state parameter lines (ψ) are incorporated in the chart. It was postulated by Jefferies and Been (2015) that the soils with a state parameter (ψ) lower than –0.05 are dilative while the soils with a ψ larger than –0.05 are contractive.

Figure 6 shows the data from Figures 1 and 2 (i.e., CPT-S and CPT-F) in the proposed chart using the dimensionless parameter, Qt (1–Bq)+1, and the normalized sleeve friction ratio (Fr). It can be seen in

Figure 6 that the majority of the points associated with CPT-S fall above the boundary line (i.e., $\psi < -0.05$), indicating dilative behaviour of the tailings at the site. In fact, only a small portion of the points indicate contractive behaviour (i.e., $\psi > -0.05$).

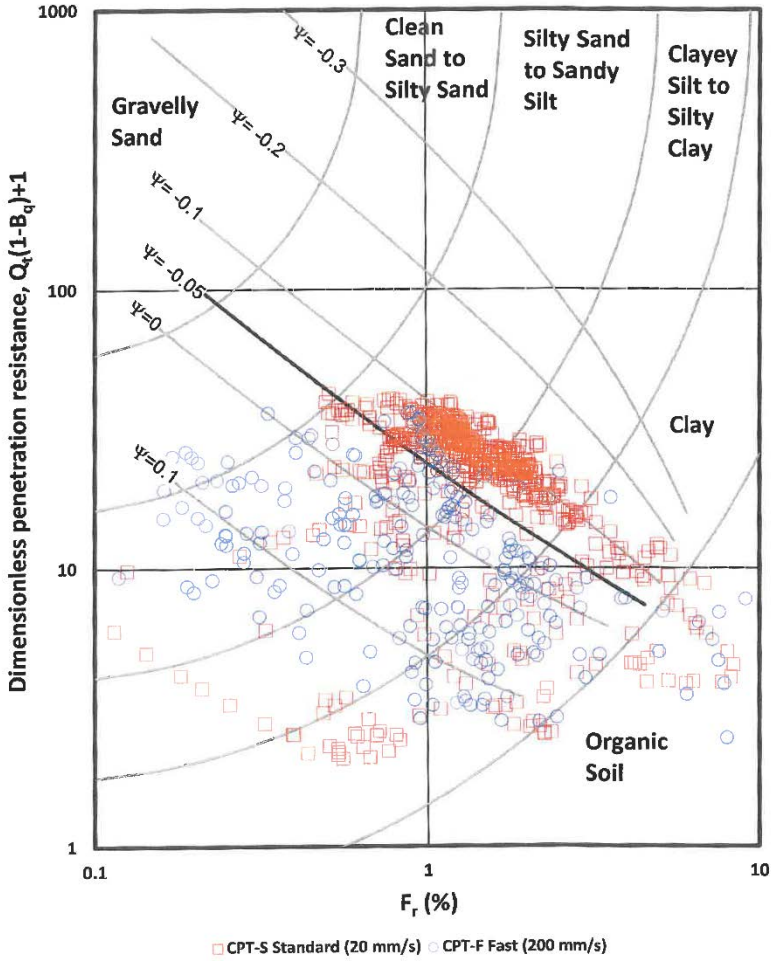

Figure 6: Liquefaction susceptibility assessment for CPT-S and CPT-F based on penetration parameter Q_t $(1-B_q)+1$, normalized sleeve friction ratio (F_r), and state parameter lines (ψ) (Jefferies and Been, 2015)

On the other hand, Figure 6 also shows that the majority of the points associated with CPT-F fall below the boundary line (i.e., $\psi > -0.05$), indicating contractive behaviour of the tailings at the site. In fact, only a small portion of the CPT-F points indicate dilative behaviour (i.e., $\psi < -0.05$).

Robertson (2016)

Robertson (2016) proposed this methodology based on the dimensionless normalized corrected tip resistance (Q_{tn}) and normalized friction ratio (Fr) plotted with respect to SBTs. This methodology represents a refinement (update) of a prior work by Robertson (2010). Robertson (2016) postulated that

the contour of the dimensionless normalized corrected tip resistance (Q_{tn}) equal to 70 separates contractive and dilative material response.

Figure 7 shows the data from Figures 1 and 2 (i.e., CPT-S and CPT-F) in the chart proposed by Robertson (2016) using the dimensionless normalized corrected tip resistance (Q_{tn}) and normalized friction ratio (Fr) plotted with respect to SBTs. It can be seen from Figure 7 that practically all data associated with CPT-F plots below the Q_{tn} line equal to 70, indicating contractive material behaviour. On the other hand, the data associated with CPT-S has a significant number of data points plotting above the Q_{tn} line equal to 70, indicating dilative material behaviour. Therefore, based on the Robertson (2016) chart, CPT-F predicts that almost all of the tailings material in the sounding is contractive, while CPT-S predicts that only a portion of it is contractive, with part of it exhibiting dilative behaviour.

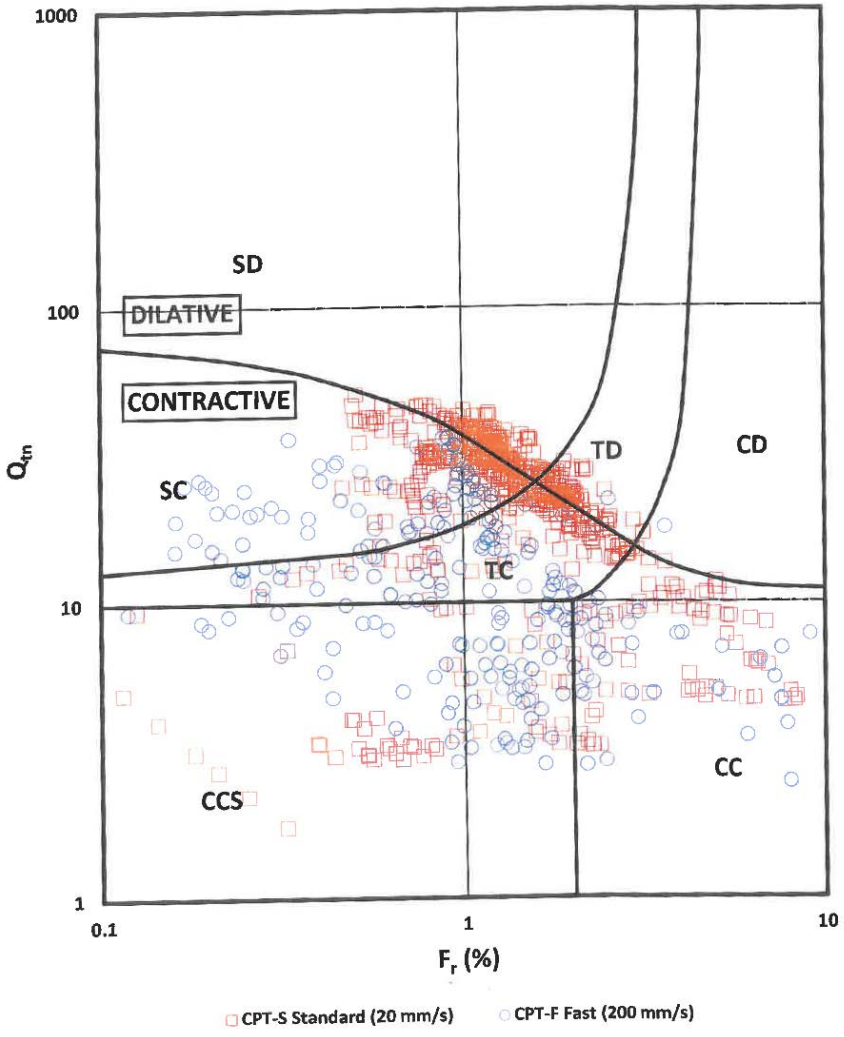

Figure 7: Liquefaction susceptibility assessment for CPT-S and CPT-F based on penetration parameter Q_{tn} and normalized sleeve friction ratio (F_r) (Robertson, 2016)

Conclusion

The first step in the procedure for liquefaction analysis of earthen structures involves the performance of a liquefaction susceptibility assessment. In this step, typically in-situ test data such as CPT are used to assess the state of the material. The most common methods for evaluation of liquefaction susceptibility that utilize CPT data include Olson and Stark (2003), Olson (2009), Robertson (2016), Jefferies and Been (2015), and Winckler et al. (2014). These methods are based on soundings performed at a standard penetration rate of 20 mm/s.

The authors collected data on CPT soundings performed at the standard rate (20 mm/s) and a fast penetration rate (200 mm/s). This comparison of side-by-side CPT soundings is presented and discussed in Figures 1 through 3. The data from the side-by-side CPT soundings were used to assess liquefaction susceptibility using the methods previously mentioned. It should be noted that this approach has not been used for assessment of strength parameters.

The following provides conclusions of the comparison of the side-by-side CPT soundings performed at standard (CPT-S) and fast rates (CPT-F), as well as the subsequent liquefaction susceptibility assessment of the tailings.

- CPT-S mostly takes place under drained conditions (i.e., little or no pore-pressure generation).
- CPT-F yields lower tip resistance attributed to the generation of excess pore-water pressure during cone penetration. These results indicate contractive behaviour of the tailings.
- Tailings at the site were hydraulically deposited and essentially normally consolidated, and thus generally in a fairly loose condition. Therefore, they are expected to exhibit mostly contractive behaviour under undrained conditions.
- When using Olson (2009) and Robertson (2016) methodologies for liquefaction susceptibility, CPT-F predicts that almost all of the tailings material in the sounding is contractive, while CPT-S predicts that only a portion is contractive – with a significant portion exhibiting dilative behaviour.
- When using Jefferies and Been (2015) and Winckler et al. (2014) methodologies for liquefaction susceptibility, CPT-F predicts that almost all of the tailings material in the sounding is contractive while CPT-S predicts that only a very small portion of it is contractive – with the largest portion exhibiting dilative behaviour.
- The results of the susceptibility assessment presented herein suggest that some commonly used methodologies may incorrectly indicate dilative behaviour when, in fact, the actual behaviour is contractive. Therefore, in some of these methodologies the boundary between dilative and contractive may be susceptible to adjustments.

- Mine tailings that have been hydraulically deposited, essentially normally consolidated, and encountered in the field in a fairly loose condition are expected to exhibit mostly contractive behaviour. Therefore, it is prudent to assume that mine tailings with such characteristics are contractive.

CPT is probably the best tool to assess liquefaction susceptibility of soils. The current methodologies can be improved and adjusted based on the results presented herein.

Acknowledgements

The help of Mr. Matt Walker in preparation of the figures for this paper is really appreciated. Review and comments provided by Dr. Gonzalo Castro during the preparation of this manuscript are greatly appreciated.

References

Bray, J.D. and R.B. Sancio. 2006. Assessment of the liquefaction susceptibility of fine-grained soils. *Journal of Geotechnical and Geoenvironmental Engineering*, ASCE, 132(9): 1165–1177.

Contreras, I.A. and A.T. Grosser. 2009. Evaluation of CPT response under fast penetration rate in silty soils. *Proceedings of the University of Minnesota 57th Annual Geotechnical Engineering Conference*, Minnesota Geotechnical Society, Minneapolis, MN.

Fear, C.E. and P.K. Robertson, 1995. Estimating the undrained strength of sand: A theoretical framework. *Canadian Geotechnical Journal*, 32(4): 859–870.

Jefferies, M. and K. Been. 2006. *Soil Liquefaction: A Critical State Approach*. New York: CRC Press, Taylor & Francis Group.

Jefferies, M. and K. Been. 2015. *Soil Liquefaction: A Critical State Approach*. Second Edition. New Ork: CRC Press, Taylor & Francis Group.

Morgenstern, N.R., S.G. Vick, C.B. Viotti and B.D. Watts. 2016. *Fundão Tailings Dam Review Panel, report on the immediate causes of the failure of the Fundão dam*. August 25, 2016.

Olson, S.M. 2009. Strength ratio approach for liquefaction analysis of tailings dams. In *Proceedings of University of Minnesota 57th Annual Geotechnical Engineering Conference*, Minnesota Geotechnical Society, Minneapolis, MN.

Olson, S.M. and T.D. Stark. 2002. Liquefied strength ratio from liquefaction flow failure case histories. *Canadian Geotechnical Journal* 39(3): 629–647.

Olson, S.M. and T.D. Stark. 2003. Yield strength ratio and liquefaction analysis of slopes and embankments. *Journal of Geotechnical and Geoenvironmental Engineering*, ASCE, 129(8): 727–737.

Poulos, S.J., E.I. Robinsky and T.O. Keller. 1985. Liquefaction resistance of thickened tailings. *Journal of Geotechnical Engineering* 111(12): 1380–94.

Robertson, P.K. 2010. Evaluation of flow liquefaction and liquefied strength using the cone penetration test. *Journal of Geotechnical and Geoenvironmental Engineering*, ASCE, 136(6): 842–853.

Robertson, P.K. 2016. Cone penetration test (CPT)-based soil behaviour type (SBT) classification system — an update. *Canadian Geotechnical Journal* 53(12): 1910–1927

Terzaghi, K., R.B. Peck and G. Mesri. 1996. *Soil Mechanics in Engineering Practice, Third Edition*. New York: John Wiley & Sons, Inc.

Winckler, C., R. Davidson, L. Yenne and J. Pilz. 2014. CPTu-based state characterization of tailings liquefaction susceptibility. In *Proceedings of Dams and Extreme Events, 34th Annual USSD Conference*, San Francisco, CA.

Proceedings of Tailings and Mine Waste 2019
November 17–20, 2019, Vancouver, Canada
Published by the University of British Columbia, 2019

Strategies for Climate Change Adaptation During Land Restoration and Mine Closure

Gabriel Castillo Devoto, University of British Columbia, Canada
Nadja Kunz, University of British Columbia, Canada

Abstract

Climate-related risks are growing for mining companies due to global warming and the associated changes in climate variability. At the end of 2018, the Intergovernmental Panel on Climate Change stated that the manifestation of climate risks depends on the magnitude and rate of warming, geographic location, levels of development and vulnerability, and on the choices and implementation of adaptation and mitigation options. In the last decade, the mining sector has improved energy efficiency and implemented new technologies in efforts to reduce the emission of greenhouse gases (GHG) and reduce costs. These mitigation activities will support the reduction of the impact generated from anthropogenic emissions. However, the design of mining operations and related activities should also be informed by models of projected future climate scenarios, to be able to understand, prevent, and plan risk management activities as adaptation strategies. Furthermore, when analytic modelling is limited, expert judgment can be used to inform decision makers.

Closure planning should likewise consider the impacts of a changing climate on closure design. A changing climate will result in environmental impacts that are potentially quite large, and this may require the reassessment of closure strategies at some mines and the management of associated ecosystem services. This paper examines, identifies, and characterizes the potential risks and opportunities that climate change could pose during mining closure stages, with a focus on mines located in mountainous watersheds. Through a Delphi survey, with a worldwide panel of experts in mine closure and mountain ecosystems, a group of practices and strategies were identified that could facilitate mining sector adaptation to climate risks, and promote resilience to climate change in the watersheds surrounding mining operations. The discussion emphasizes the relevance of ecosystem-based adaptation strategies for land restoration and mine closure design, in the context of mountainous watersheds.

Introduction

Worldwide changes in extreme weather and climate events have been observed since around the middle of

the previous century (Flato et al., 2013). It is now indisputable that anthropogenic activity is the main cause of climate change. Some of these changes include a decrease in cold temperature extremes, an increase in warm temperature extremes, an increase in extreme high sea levels, and an increase in the number of heavy precipitation events in a number of regions (IPCC, 2014). There is increasing concern that the impacts of climate change will pose a physical and investment risk to mining operations, local communities within the influence area, and the ecosystem in associated watersheds (ICMM, 2013).

For many existing mining operations, infrastructure was designed and built based on parameters that envisaged a constant climate, without any potential future changes (Ford et al., 2010). An increase in hazards related to extreme climate events would affect the feasibility of some mining operations, and possibly increase the management costs for logistic supplies, transport, water management, reclamation, infrastructure, and other costs. For example, as mining is an industry with a high water demand, an increase in water scarcity in some regions would complicate the production and processing activities of mining operations. Likewise, mine closure and restoration activities could be at risk under a changing climate, considering the vulnerability of the land disturbance.

The use of modelling and simulation techniques to assess and respond to the possible impacts of climate change requires access to reliable climate and weather data. Modelling is therefore needed to support our understanding of the ecosystem infrastructure and dynamic, through using the observational networks and monitor climate indicators available in each specific region (Sundaresan, 2014). However, anticipating the future impacts of climate change is always associated with uncertainties, and when analytical modelling is limited, experts can inform decision makers (Morgan and Keith, 1995) with their concrete knowledge and long-term expertise in a subject matter area (Haida et al., 2016). There is an urgent need for the mining industry, the general society, and academia, to work together to integrate concepts and look for consensus regarding immediate actions. According to the IPCC (2014), the process of integration should start with an assessment of the environment's sensitivity to climate change, followed by an identification and prioritization of adaptation requirements applicable locally.

In the context of future climate risk and hazards due to a changing climate, a comprehensive mine closure plan should include advice from climate risk experts that could contribute to strengthening knowledge and identifying innovative strategies as part of a proactive approach to managing these risks in the mining industry. Making use of the experts' high level of insight and aggregated knowledge allows for assessing climate change adaptation strategies in a resource-efficient, participatory, and consensus-building manner (Haida et al., 2017). The Delphi survey is a technique widely used to assemble experts' knowledge on economic, business, environmental, social, and other areas to assess the present or the future (Nguyen et al., 2017). The experts are individuals with specialized knowledge, in this case on topics relating to

climate change adaptation, with demonstrated experience and involvement in relevant projects and/or publications.

Methodology

The methodology used for this survey is called a Delphi technique. In a classical Delphi study, an anonymous panel of experts works to resolve a complex technical problem through consensus. The process enables researchers to obtain immediate access to professional information and solid knowledge without personal investigations (Baker, 2006). The process consists of two or more rounds (Gotay, 2013) of analysis and data interpretation regarding future developments and incidents. In a classical Delphi study, the questions are defined around a particular problem, and the first round of questions is used to facilitate brainstorming in order to obtain opinions from a panel of experts. This round of questions can be administered online (Gotay, 2013).

This method links together a group of experts who anonymously reply to a questionnaire and afterwards receive feedback in the form of a statistical representation of the group response. Subsequently, the process is repeated (Adekunle and Adeyinka, 2017). The objective is to focus on opinion building, to gain consensus from the panel in answering the research question. The process begins once the panel of experts agree to engage with the study, with a continuous focus on group communication between the panel of experts. The Delphi technique is a survey technique extensively used to gather data in the form of an anonymous, written, multi-stage survey process (Von der Gracht, 2012).

As climate change impacts multiple sectors, there is a need for a wide variety of experts and decision makers to cooperate towards solutions. The Delphi survey methodology is therefore an appropriate technique to engage climate change experts from academia, the mining industry, and public institutions. This study recruited a total of 30 experts to assess potential adaptation strategies that could be applied in the mining sector, specifically in land restoration and mine closure planning. Individuals were selected using the professional network LinkedIn search function.

The search function within LinkedIn was also utilized to identify persons with a specific skill, in a specific position within a company, or working at a specific location. The search function is extremely useful when one is conducting a people skills search and doing a good deal of outreach. The search function has an option to search for combinations of information. This type of search is also referred to as a Boolean search. A user can search on a host of keywords, people's names, job titles, company names, and locations. The data can be filtered by degree of relationship and multiple other options that will help target specific results.

All the participants received written explanations with an invitation to be interviewed. The academic participants were recruited from faculties and universities in North and South America, and Europe. The sampling criteria specified that the individuals must have a PhD and more than ten years' experience in climate change and/or adaptation strategies, with an interest in mountainous regions. The industry participants were recruited from mining companies and associations in North and South America, and Europe. The sampling criteria specified that the individuals must have at least ten years' experience in the environmental and/or sustainability areas. The participants from general society were recruited from global institutions or organizations related to climate change and adaptation management in North and South America, and Europe. For this group, the participants must have had at least ten years' experience in climate change and/or adaptation strategies.

The survey began with a group of general questions to identify the objectives and problems the study should address. The first round was implemented as an open questionnaire to define the importance of the selected problems. In the second round a closed questionnaire was used to re-assess the importance of the declarations based on the panel responses from the first round (Rowe and Wright, 1999). For this Delphi study, the online survey tool Qualtrics software was used. This software also supported the qualitative data analysis, organization, and reporting of the results.

The first question (Table 1) assessed the significance level of potential impacts on the watershed ecosystem that a mine infrastructure failure could generate as a consequence of extreme climate events. The Likert scale to measure significance are: Not significant; moderately significant; and, very significant.

Table 1: Significance impact level of potential infrastructure failure

Question	Mine infrastructure
To fully understand the potential impacts of climate change on the following mine infrastructure, define the Significance an infrastructure failure could generate on the watershed ecosystem. Consider extreme climate events for: precipitation, wind, periods of heat, flooding, warmer average temperatures (seasonal, annual), warm winter days (temperature >0°C), drought, and any examples of cumulative hazards.	Waste rock dumps Tailing management facilities Roads (paved/unpaved) Drainage channels Heap leaching pads Water management structures Train rails Power lines Pipelines

The second question (Table 2) assessed the degree of agreement regarding specific consequences of climate change impacts that could affect the process of land restoration or mine closure activities in mountainous regions. The Likert scale to measure statement of Agreement are: Strongly disagree; somewhat disagree; neither agree nor disagree; somewhat agree; and strongly agree.

Table 2: Impacts of climate change on land restoration or mine closure activities

Question	Potential consequences
Based on your knowledge, define your degree of Agreement with the following statements in respect to the impacts of climate change on land restoration or mine closure activities.	A – Long, dry periods can limit vegetation growth. B - Establishment of vegetation to stabilize disturbed areas may be slower. C - Tipping points will affect species ranges and ecosystem resilience. D - Water disposal and treatment will be more difficult. E - Increased rainfall can promote acid rock drainage (ARD). F - Wetter conditions will affect covers and revegetation stability. G - Hydraulic structures may need to be designed to manage more water. H - The selection of plant species for revegetation should be considering future change of climate, rather than choosing species based on historical presence in the area.

The third question (Table 3) assessed the degree of Importance for a group of adaptation strategies in reducing the adverse effects of climate change in mountainous watersheds. The Likert scale to measure a statement of Importance are: Not at all important; slightly important; moderately important; very important; and extremely important.

Table 3: Degree of Importance for adaptation strategies

Question	Mine infrastructure
Based on your knowledge, what is your opinion of the degree of Importance of the following adaptation strategies, in reducing the adverse effects of climate change in mountainous watersheds?	A - Design and implement future land use that can withstand extreme weather events. B - Execute climate risk assessment of physical and biological systems at watershed level. C - Improved management and conservation of ecosystems. D - Develop climate scenarios with local expert-based narratives. E - Design emergency response and evacuation plans. F - Integrate the management of the watershed and long-term plans. G – Manage, conserve and restore wetlands. H - Design infrastructure based on risk assessment for future climate scenarios and extreme weather events.

Results

Descriptive statistics were used to describe group responses to each statement in the three questions.

Consensus was defined as:

- >70% of participants choosing moderately significant/very significant or not significant for a statement in the first question;
- >70% of participants somewhat agreeing/strongly agreeing or somewhat disagreeing/strongly disagreeing with a statement for the second question;
- >70% of participants choosing very important/extremely important or slightly important/not at all important with a statement for the third question.

Analyses were conducted using Qualtrics software. Table 4 presents the group's responses to the first question, to fully understand the potential impacts of climate change on the mine infrastructure, defined by the significance an infrastructure failure would have for the watershed ecosystem. A complete consensus (100%) was achieved for three statements, that is, that the event would have a very significant impact on the potential failure of the water management structures and the tailing management facilities; and a moderately significant impact on the potential failure of the drainage channels. Responses to two statements, regarding waste rock dumps and heap leaching pads, achieved consensus (84.6%) as well. The statement about water management structures was considered the highest ranking for a very significant impact on the watershed ecosystem in a potential infrastructure failure as a consequence of climate change.

Table 4: Significance of impact level of potential infrastructure failure

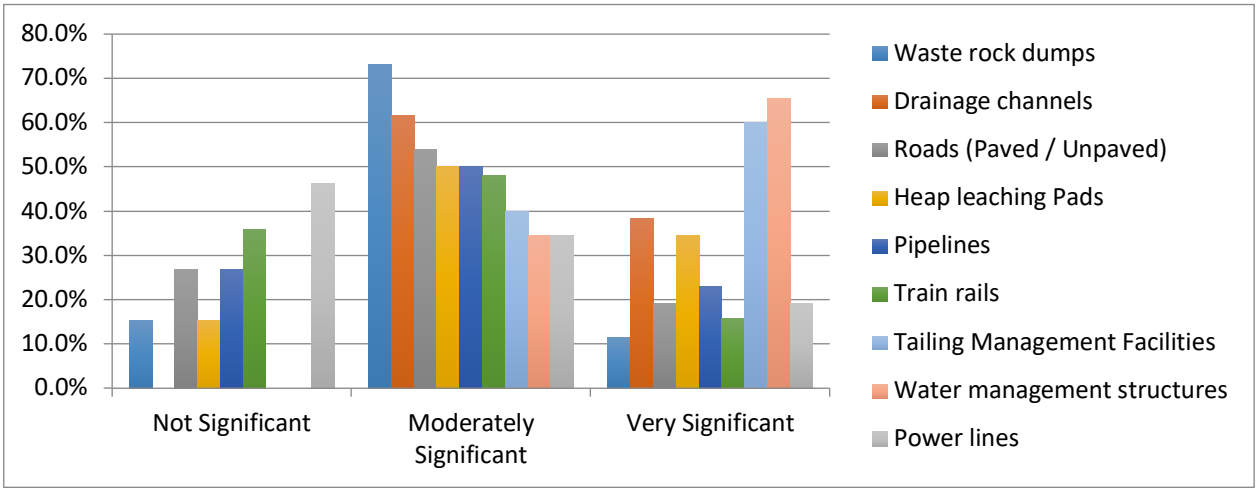

Table 5 presents the group's responses to the second question, defining the degree of agreement about the impacts of climate change in the process of land restoration or mine closure activities. Consensus (92.3%) was reached for the agreement that hydraulic structures may need to be designed to manage more water during the mine closure stage. At the same time, a consensus (80.8%) was achieved in agreeing that long dry periods can limit vegetation growth. Likewise, a consensus (73.1%) was reached that the selection

of plants species for revegetation should consider future climate change, rahter than choosing species based on historical presence in the area of interest.

Table 5: Impacts of climate change on the process of land restoration or mine closure activities

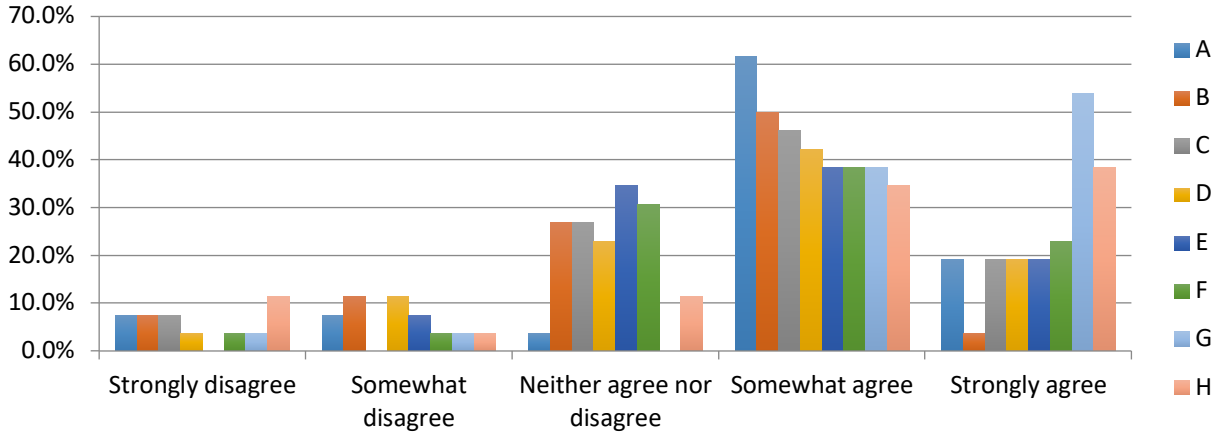

A. Long dry periods can limit vegetation growth.
B. Establishment of vegetation to stabilize disturbed areas may be slower.
C. Tipping points will affect species ranges and ecosystem resilience.
D. Water disposal and treatment will be more difficult;.
E. Increased rainfall can promote acid rock drainage (ARD).
F. Wetter conditions will affect covers and revegetation stability.
G. Hydraulic structures may need to be designed to manage more water.
H. The selection of plants species for revegetation should consider future climate change, rather than choosing species based on historical presence in the area of interest.

Table 6 presents the group's responses to the third question, defining the degree of importance for adaptation strategies in reducing the adverse effects of climate change in mountainous watersheds. A consensus (96.2%) was achieved about the importance of an integrated management approach within the watershed and the development of long-term plans for reducing the adverse effects of climate change in mountainous watersheds. The next consensus (88.5%) reached highlights the design and implementation of future land uses that can withstand extreme weather events as an adaptation strategy. The next consensus achieved, with the same degree of importance in total (84.6%), was about design infrastructure based on risk assessment for future climate scenarios and extreme weather events, and the design of emergency response and evacuation plans. From all the statements, 57.7% of respondents rating as extremely important the integrated management of the watershed and long-term plans. Regarding the statement about design infrastructure based on risk assessment for future climate scenarios and extreme weather events: 53.8% of respondents felt it was extremely important to develop adaptation strategies to reduce the adverse effects

of climate change in mountainous watersheds. In summary, from a total of 8 statements assessed, 7 achieved consensus.

Table 6: Degree of importance for adaptation strategies

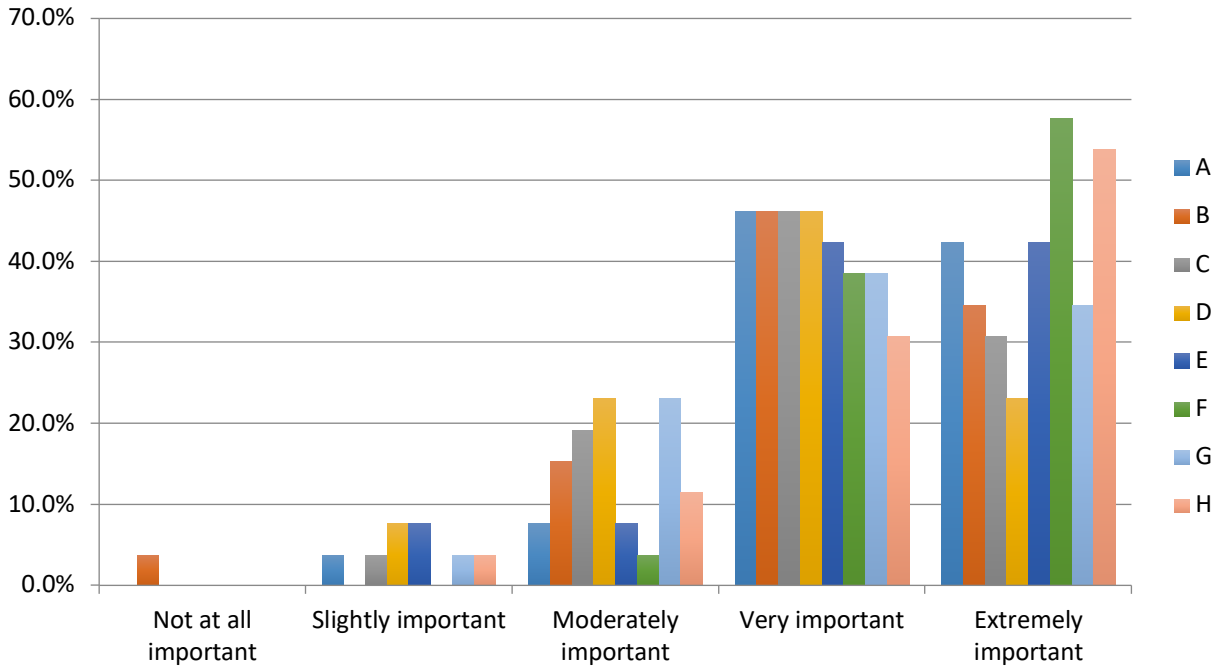

A. Design and implement future land use that can withstand extreme weather events.
B. Execute climate risk assessment of physical and biological systems at watershed level.
C. Improve the management and conservation of ecosystems.
D. Develop climate scenarios with local expert-based narratives.
E. Design emergency response and evacuation plans.
F. Integrate the management of the watershed and long-term plans.
G. Manage, conserve, and restore wetlands.
H. Design infrastructure based on risk assessment of future climate scenarios and extreme weather events.

Conclusion

Extreme events associated with climate variability are expected to result in potentially extensive impacts on the environment that will require the reassessment of mine closure strategies in some mining operations. The manifestations of these climate risks are related to warming magnitude, geographic location, local vulnerability, and the implementation of strategies for adaptation. Therefore, it is critical that the design of mining operations and associated mine closure planning should be informed by a framework of potential future climate scenarios. However, anticipating the future impacts of climate change is always associated with uncertainties, and when analytical modelling is limited, expert judgment can be used to inform decision makers.

The panel of experts in the present research considered that extreme climate events would have very significant impacts on the watershed ecosystem in the mine closure stage if a water management infrastructure were to fail. The highest impacts would be experienced by water management structures, tailings management facilities, and drainage channels. These risks will be associated with potential increases in precipitation, and landscape structure modifications at the sites. Therefore, hydraulic structures may need to be designed to manage more water during the mine closure stage.

On the other hand, droughts and long dry periods would limit vegetation growth in restoration areas. The removal of topsoil during mine development results in a loss of organic content and water retention capacity, requiring a structured restoration plan to recover the health ecosystem. Furthermore, vegetation pattern and growth rates and soil moisture levels would also be impacted. Therefore, the selection of plants species for revegetation should take into consideration future changes in climate, rather than focus on species historically present.

To reduce the adverse effects of climate change in mountainous watersheds it is extremely important to develop an integrated approach to management of the watershed and long-term plans. This will support an informed decision-making process, which incorporates understanding of cumulative effects and the implementation of future land uses that can withstand extreme weather events as an adaptation strategy. Moreover, it is very important that the mine infrastructure design is based on a risk assessment for future climate scenarios and extreme weather events, as well as the design of emergency response and evacuation plans. The incorporation of climate risk assessment practices combined with adaptation strategies will support an approach to designing sustainable mine operations, with more attention to the closure and land restoration plans.

A vulnerability assessment process is crucial to identify the areas and communities that are most at risk, as well as the key impacts of a changing climate. Risk and vulnerability assessment will help to establish resources where they are most needed, and to design monitoring plans. These risks are beyond the mine site area, because these industries are often located in challenging geographies and manage climate sensitive resources (i.e., water and energy) that are critical in the mountain ecosystem.

In this group of ideas, it is important to have a holistic approach and design adaptation strategies for climate change by promoting the use of ecosystem services and biodiversity during engineering design. A potential strategy entails an ecosystem-based adaptation approach, which is a process that involves restoration, conservation, and sustainable management of natural resources, the use of biodiversity, and ecosystem services to help people adapt to the adverse effects of climate change. When the mountain ecosystem is in good health, it will help to protect against natural hazards and the impacts of extreme events, particularly hydrological events such as floods and droughts; and will increase the resilience of communities to climate change effects.

References

Adekunle, Ayodele and Francis Adeyinka. 2017. Regional response to climate change and management: An analysis of Africa's capacity. Retrieved from https://doi.org/https://doi.org/10.1108/IJCCSM-02-2017-0033

Baker, John. 2006. How expert are the experts? An exploration of the concept of "expert" within Delphi Panel Techniques. *Nurse Researcher* 14(1): 59–70.

Flato, G., J. Marotzke, B. Abiodun, P. Braconnot, S.C. Chou, W. Collins, P. Cox et al. 2013. IPCC 2013 AR5 - Chapter 9: Evaluation of climate models. Climate change 2013: The physical science basis. Contribution of Working Group I to the Fifth Assessment Report of the Intergovernmental Panel on Climate Change: 741–866. Retrieved from https://doi.org/10.1017/CBO9781107415324

Ford, J.D., T. Pearce, J. Prno, F. Duerden, L.B. Ford, M. Beaumier and T. Smith. 2010. Perceptions of climate change risks in primary resource use industries: A survey of the Canadian mining sector. *Regional Environmental Change* 10(1): 65–81. Retrieved from https://doi.org/10.1007/s10113-009-0094-8

Gotay, Jose Antonio. 2013. A classical Delphi study to identify the barriers of pursuing green information and communication technologies. *ProQuest Dissertations and Theses:* 276.

Haida, Christin, Clemens Geitner, Michiko Hama, Richard Hastik, Karl-Michael Höferl and Katrin Schneider. 2017. Prioritizing adaptation needs for ecosystem services: A regional case study in the eastern Alps. In *Ecosystem Services of Headwater Catchments,* edited by J. Křeček. New Delhi, India: Capital Publishing Company. Retrieved from https://doi.org/10.1007/978-3-319-57946-7_15

Haida, Christin, Johannes Rüdisser and Ulrike Tappeiner. 2016. Ecosystem services in mountain regions: Experts' perceptions and research intensity. *Regional Environmental Change* 16(7): 1989–2004. Retrieved from https://doi.org/10.1007/s10113-015-0759-4

ICMM. 2013. Adapting to a changing climate: Implications for the mining and metals industry. Climate Adapt. Retrieved from https://climate-adapt.eea.europa.eu/metadata/publications/adapting-to-a-changing-climate-implications-for-the-mining-and-metals-industry

IPCC. 2014. Climate Change 2014 Synthesis Report Summary Chapter for Policymakers. Contribution of Working Groups I, II and III to the Fifth Assessment Report of the Intergovernmental Panel on Climate Change. Core Writing Team, R.K. Pachauri and L.A. Meyer (editors). IPCC, Geneva, Switzerland, 31. Retrieved from https://doi.org/10.1017/CBO9781107415324

Morgan, M. Grange and David W. Keith. 1995. Subjective judgments by climate experts. *Environmental Science and Technology* 29(10): 468A-476A. Retrieved from https://doi.org/10.1021/es00010a003

Nguyen, An Thinh, Anh Dung Vu, Giang T. H. Dang, Anh Huy Hoang and Luc Hens. 2017. How do local communities adapt to climate changes along heavily damaged coasts? A stakeholder Delphi study in Ky Anh (Central Vietnam). *Environment, Development and Sustainability* 20(2): 749–67. Retrieved from https://doi.org/10.1007/s10668-017-9908-x

Rowe, Gene and George Wright. 1999. The Delphi Technique as a forecasting tool . *Issues and Analysis* 15: 353–75.

Sundaresan, Janardhanan. 2014. Geospatial technologies and climate change. Retrieved from https://doi.org/10.1007/978-3-319-01689-4.

Von der Gracht, Heiko A. 2012. Consensus measurement in Delphi studies. *Technological Forecasting and Social Change* 79(8): 1525–36. Retrieved from https://doi.org/10.1016/j.techfore.2012.04.013

Proceedings of Tailings and Mine Waste 2019
November 17–20, 2019, Vancouver, Canada
Published by the University of British Columbia, 2019

Management of Geotechnical and Rheological Behaviour of Tailings to Produce Engineered Fill

Janis Drozdiak, Golder Associates Ltd, Canada
Eduardo Salfate, Golder Associates South America, Chile

Abstract

As the production tonnage of mines around the world continues to increase, the location, topography, and capacity of tailings storage facilities becomes an even greater challenge. Finding a site with enough capacity to store the life of mine (LOM) tailings production may be a limiting factor when evaluating the viability of a project or mine expansion. Identifying a storage site with a topography that is conducive to building a tailings dam with the capacity to store the LOM tailings production at a reasonable distance from the process plant can be difficult.

One option to help overcome these challenges is to process the tailings to produce a material with a specific range of rheological and geotechnical properties, which can then be placed into the tailings storage facility as an engineered fill. Engineered fill, in relation to tailings, is managing the material properties in a way that facilitates the implementation of the desired filling sequence and deposition strategy (i.e., maximize water recovery, increase density for desiccation, produce targeted beach slopes, consider stability, etc.). By clearly defining the desired geotechnical and rheological behaviour of the engineered fill at the start of a project, the process equipment needed to produce it can be defined in consistency with both mill production requirements and tailings management strategy. Thickening tailings to a desired yield stress in order to generate sloping beaches, rather than to a target solids concentration, is one such example being explored by various mining companies, particularly in South America. This paper discusses the use of the concept of engineered fill as a key element for selecting the processing equipment needed to adjust tailings properties to achieve increases in the LOM tailings storage capacity.

This paper further discusses the broader implications for best practices in tailings management of applying the concept of engineered fill in early project development stages, rather than relying on evaluation of the standard tailings management options.

Introduction

Development of mining projects around the world is a long and complicated process, particularly when the question of how to handle tailings storage is considered. In the past few years, societal awareness of tailings dams, their method of construction, what is contained within them, and the consequences of failure, have risen significantly with the failures of tailings facilities in Mount Polley, Samarco, and Brumadinho. With the increased scrutiny and regulations brought about by these failures, the question of how to safely manage the tailings and select a site with the ability to store the LOM tailings production can be crucial in determining a project's viability.

Over the past 100 years, storing conventional tailings in an impoundment using the natural topography (i.e., valley, creek, etc.) with a dam constructed from rock fill, sand, or other natural materials has been the most common method of tailings storage. Conventional tailings essentially means no processing of the tailings and deposition of the material occurs at low solids concentration by weight (C_w = 30% to 35% for copper tailings), which is the solids concentration produced by the process plant in the absence of thickeners. Storage of tailings at these concentrations requires more space and involves the storage of large volumes of water, which may or may not be reclaimed for use at the mine.

Finding a convenient valley that can be dammed with enough capacity to store the total volume of tailings over the mine life, and which is located at a reasonable distance from the mine or process plant, is often a daunting challenge. Storage of large volumes of water, such as with conventional tailings, in arid climates, where water is a valuable commodity to the local population and region is also problematic. Lastly, storage of large volumes of impounded water in tailings dams is often undesirable, as it may increase the likelihood and consequence of a failure, should it occur.

Due to these issues, there has been a progressive shift from storing conventional tailings (and the associated water), towards processing of the tailings in order to store thicker and thicker tailings material. Today, during the development stage of a mining project, the methods of tailings storage – conventional to thickened to paste to filtered – are evaluated and compared to determine which is the most appropriate for the project.

With the progression towards thicker tailings, there is often a disconnect between what is needed geotechnically in order to efficiently and effectively fill a storage area, and how the tailings are processed. For a conventional tailings storage facility this was not a consideration, as the facility was designed to handle whatever the tailings happened to be, and the main consideration was to control the pond to ensure it did not compromise the dam stability, and could allow for water recovery. For deposition and storage of thickened tailings, there needs to be a clear understanding and management of the geotechnical and rheological properties of the tailings in order to fill the selected site, achieve the defined storage capacity, ensure the stability of the impounded tailings if sloping beaches are created (especially in seismically active

areas), and avoid costly construction methods that need to be hastily enacted when contingency plans are not included.

Engineered fill, in relation to tailings, is managing the material properties in order to produce the desired geotechnical and rheological properties that facilitate the implementation of the desired filling sequence and deposition strategy (i.e., maximize water recovery, increase density for desiccation, produce targeted beach slopes, consider stability, etc.). Producing engineered fill – i.e., processing the tailings to a geotechnical and rheological specification – is a method that has started to gain traction within South America. This paper focusses on the use of tailings thickeners to produce a material within a target yield stress range to achieve a range of beach slopes to fit the topography, in order to store a larger quantity of tailings than would be possible with other methods of tailings storage.

Engineered fill

Traditional methods of storing tailings are changing. Building a rock-fill dam in a valley and then depositing wet slurry has become harder to permit, harder to secure financing for, and harder to gain societal approval of. Basically, mine tailings need to be managed in a better way if the mining industry is to survive and thrive.

For sites that may have constraints on LOM production if conventional deposition methods are used, evaluation of tailings processing (or technology) should be considered in a different way. In such cases, processing of the tailings should be worked backwards, with the objective of achieving the drivers needed to increase storage to the maximum extent feasible. The methodology generally follows this order:

- Evaluate the topography of the potential site (constraints and opportunities for increased storage).
- Determine the tailings tonnage to be stored over LOM.
- Identify how the tailings could be managed/processed to accommodate the ultimate LOM volume. That is, how can the tailings be processed to maximize water recovery, make a material that reduces or eliminates a reclaim pond, desiccates, densifies, and produces targeted beach slopes that help achieve the filling strategy for the impoundment.
- Produce a specification for engineered fill, and design a system to make it.

History of engineered fill

The concept of engineered fill is not a new one to the mining industry. Paste backfill, where the tailings are processed to produce underground structural backfill, has been commonly used for many years. Essentially, this is taking a waste product and using it for the underground mining plan by making a material that exhibits the strength properties to support the underground workings. Parameters such as yield stress (or slump), binder content, cure rate, placement, and fill sequence determine the performance criteria for both the short-

and long-term cure strength. An important learning from paste backfill is that proper selection of the paste plant equipment to make the engineered fill to satisfy the structural criteria is key to success.

Cyclone sand is another example of engineered fill, where the coarse fraction of the tailings is used as a dam construction material. The specification for the sand is set by the dam design engineer, who sets the maximum allowance of fines content in the material to meet both stability and drainage requirements. Typically, the fines content can be anywhere from 10% to 20%, with 15% as a common number. Too many fines prevent draining and can lead to permeability issues. Fines can also affect the sand deposition angle, resulting in flatter slopes as fines will carry the larger (i.e., coarser) particles further and decrease the slope.

Cyclones are designed for a specific cut to ensure the majority of the fines are removed with the overflow. Depending on the tailings material particle size distribution, two stages of cycloning may be necessary to achieve the sand specification for fines content.

Engineered fill – beach slope and yield stress

Thickening of tailings has been almost exclusively for water recovery, with a target solids concentrations for this recovery identified in the water balance for the process. Clarity of the overflow so that the recovered water can be re-used in the process plant is also a key component, with flocculent typically used to achieve the desired clarity.

To produce an engineered fill material by thickening, the focus needs to shift away from water recovery and towards producing a material that meets the geotechnical and rheological requirements of the chosen storage site (Drozdiak and Norwood, 2017). For thickened tailings, beach slope is a key parameter for filling and managing the storage area. If the beach slope of the deposited material is too steep, the impoundment area cannot be filled. If the beach slope is too flat, the storage capacity of the area is compromised.

Understanding of the beach slope of deposited material, and of the different methods to predict beach slope (McPhail, 2008; Simms et al., 2011; Li, 2011) have been the subject of much work over the past two decades. Beach slope is governed by the fully sheared yield stress of the deposited tailings material (Luppnow et al., 2009), and is determined by the tailings slurry parameters that contribute to the yield stress. For a given discharge flow, as the fully sheared yield stress of the material increases, the beach slope becomes steeper. When tailings deposition is modelled and storage capacity calculated for a tailings facility, the relationship between the beach slope and the point of discharge yield stress needs to be recognized. To produce engineered fill in order to achieve targeted beach slopes, the effects of shear thinning on the yield stress of the thickener underflow material during transport from the thickener to the deposition point need to be recognized and understood.

Shear thinning effects (or why a 50 Pa yield stress material does not give a 1% beach slope)

From a beach slope stability perspective, the tailings material deposited needs to have a yield stress which is fully sheared. Thickeners will produce a tailings material with an unsheared yield stress – which can be as much as ten times higher than the yield stress of the material at the point of deposition. Figure 1 is a yield stress decay curve that shows the effect of shear thinning on a tailings material whose thickener underflow yield stress is significantly higher before shear thinning occurs. This figure illustrates that although the tailings material has a yield stress of between 150 to 500 Pa upon exit from the thickener, once energy is applied to the tailings material, shear thinning occurs and the yield stress is reduced to the fully sheared value.

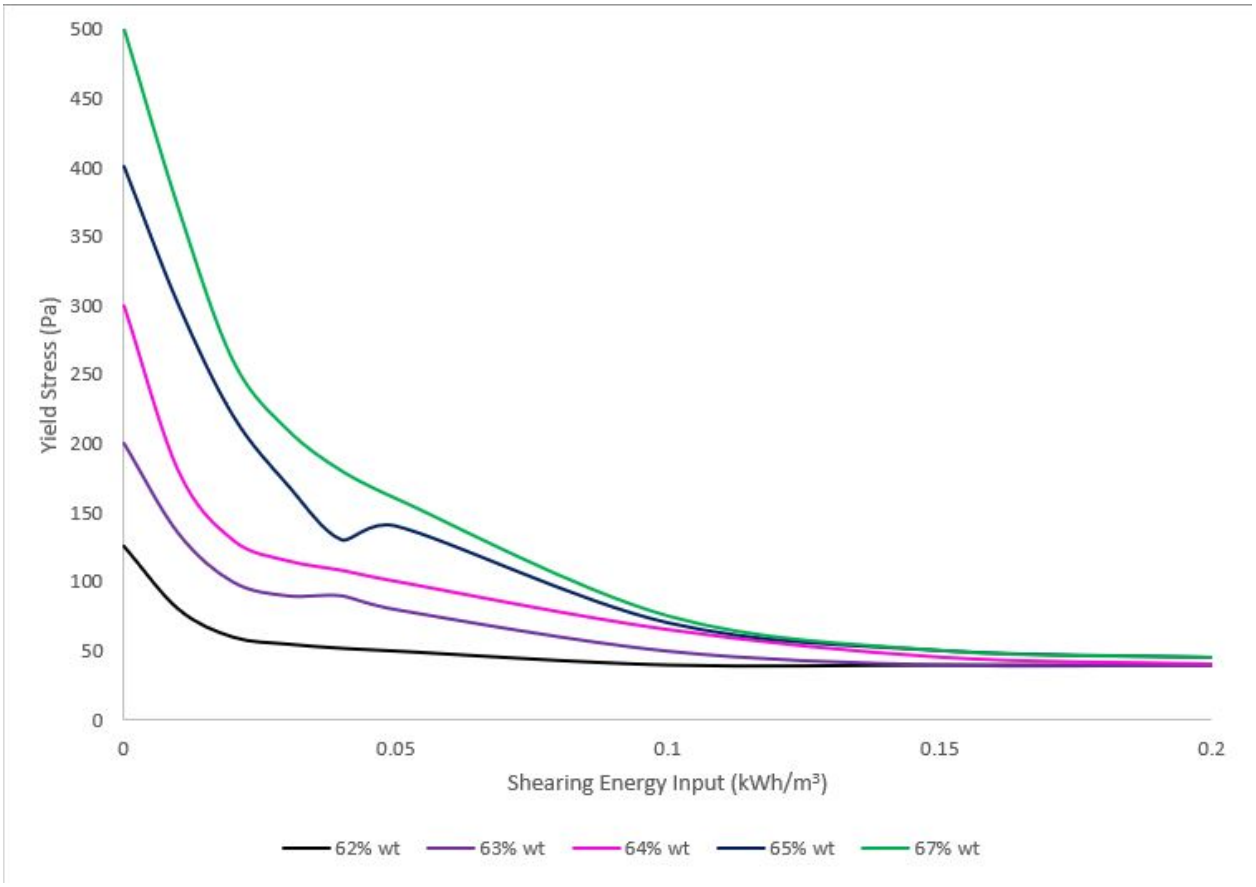

Figure 1: Yield stress decay curve

Once the thickener underflow material exits the thickener bottom, shear thinning can occur in the underflow pumps, in any tank or box the material flows through, and in any tailings distribution pumps and any pipeline to the deposition point, resulting in a lower yield stress value at the point of discharge than the discharge from the tailings thickeners. Measurement of the yield stress at the point of deposition after undergoing the shear thinning process is rarely a part of a tailings facility operation. Yield stress

measurements (if taken at all) are usually obtained by sampling from the thickener or thickener underflow and analyzing the material with a rheometer in a lab setting. These yield stress measurements are inevitably higher than the actual yield stress at the point of deposition, leading to the false conclusion that a material with a 50 Pa yield stress results in a 1% beach slope.

Tailings processing equipment selection

To produce an engineered fill material from tailings with a target yield stress, thickener selection is a critical component. Trying to achieve a dual purpose with the thickeners will not work for engineered fill. Either the thickeners are to produce an engineered material with a specific target yield stress, or they are to produce a specific solids concentration to achieve water recovery. Recognizing how one affects the other is key in order to achieve the primary objective. Target yield stresses can have varying solids concentrations, or target solids concentrations can have varying yield stresses.

Tailings thickeners in common use today fall into roughly four categories depending on the end use:

- Conventional thickeners – typically produce tailings with an unsheared yield stress between 0 Pa and 30 Pa.
- High rate thickeners – typically produce tailings with an unsheared yield stress between 30 Pa and 50 Pa.
- High density thickeners – typically produce tailings with an unsheared yield stress between 50 Pa and 120 Pa.
- Paste thickeners – typically produce tailings with an unsheared yield stress between 200 Pa and over 350 Pa.

For the thickener types which produce the higher yield stress tailings, the cone angle gets steeper. A high density thickener typically has a cone angle of 15^{o}, while a paste thickener has a steeper cone angle, starting at 30^{o}. To produce an engineered fill material with a target yield stress, the yield stress decay curve must be produced and understood in order to properly select a thickener that will consistently make the desired fill. A lab testing program centered on understanding the yield stress decay of representative samples of tailings that will be produced is vital to thickener selection. Because thickener technology has long been focussed on solids content, water recovery or the production of a paste material, it may be that the thickener required to consistently make the desired yield stress is a hybrid of thickener types (i.e., somewhere between a high density and a deep cone thickener with a custom cone angle). Purchasing a thickener based on the general type, rather than customized for producing tailings material that adheres to the fill specification, may result in extremely high capital costs that are unnecessary; for example, purchasing a deep cone thickener when a modified steeper cone angle on a high density thickener would work.

A word about thickener control

Control of the thickener to meet engineered fill needs to be based on the fill specification's yield stress range. Because yield stress cannot be directly measured, reliance for control has to be on indirect methods, a robust sampling program, an on-site rheology laboratory, and effective use of the start-up or commissioning period to learn to manage different operating scenarios.

Although a solids concentration target for water recovery is not the primary focus of thickener use for making engineered fill, the relationship between yield stress and solids concentration can be utilized for the control scheme. Increasing solids concentration without an understanding of the corresponding relationship to yield stress can push the thickener beyond the operating range (e.g., thickener rakes pushed beyond the operating range). Without this understanding, a proper control scheme to achieve a target yield stress range cannot be implemented.

Figure 2 illustrates the relationship between fully sheared yield stress and solids concentration for an expected range of copper tailings produced from various ore blends.

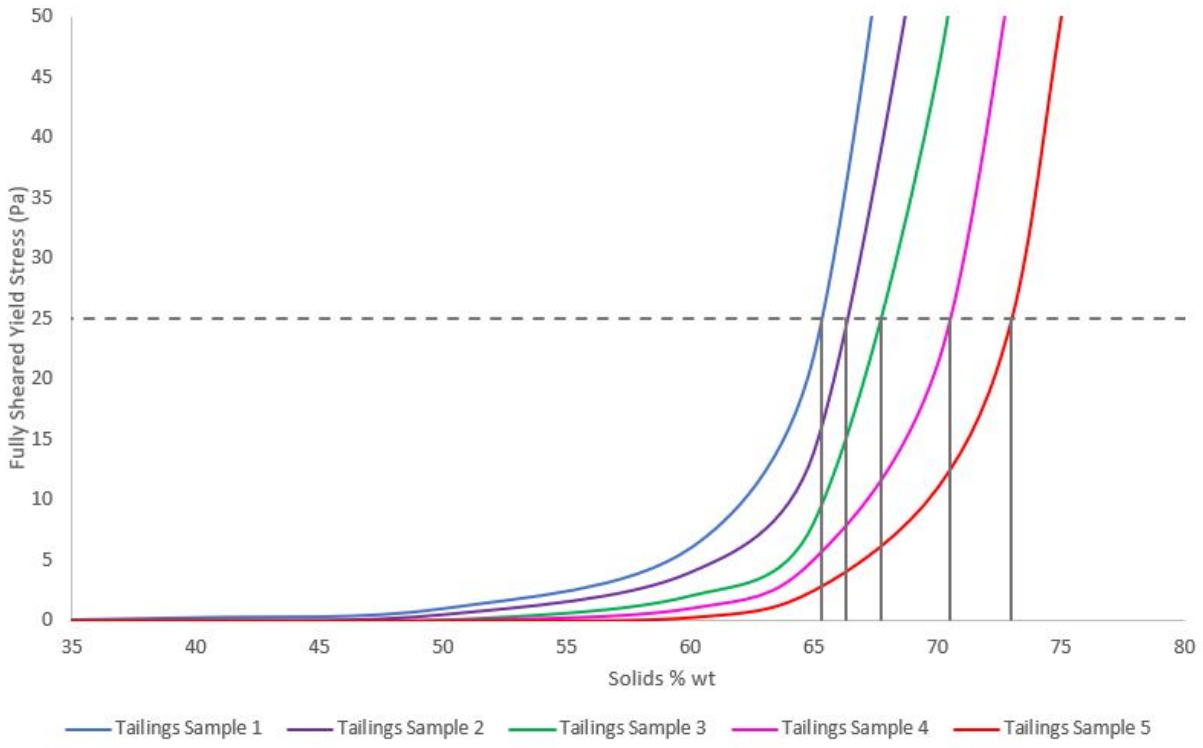

Figure 2: Fully sheared yield stress versus solids concentration

As can be seen from this figure, a solids concentration can have a range of yield stresses depending on the ore blend which produced the tailings. Through an expansive laboratory program during the project

phase, and from operating knowledge gained in the start-up period, the relationship between yield stress and solids concentration can be well understood and used to adjust the thickener operation to produce a material with the desired yield stress at various solids concentrations. Because solids concentration is a measurable value, this relationship can be used to fine-tune the operation of the thickeners to produce a consistent material that complies with the engineered fill specifications.

Geotechnical considerations for engineered fill

Development of the specifications for an engineered fill to be placed in a tailings storage facility relies on an understanding of the rheological characteristics of the tailings, a deposition strategy to achieve the optimal filling configuration to effectively use the site storage, and understanding that all scenarios cannot be designed for – therefore, pick a design criteria to work with, and plan for how to deal with outliers.

Deposition strategy

Although several methods exists to estimate beach slopes, the reality is that beach slopes achieved in the field are a direct result of the deposition strategies and operational procedures developed to manage the tailings at the discharge. In this regard, beach slopes model results should be used to guide the operating procedures required to achieve a target beach slope, and avoid those that would yield undesirable deposition mechanisms (e.g., gullying).

As an example, a material with a fully sheared yield stress of 30 Pa could deposit at slopes anywhere between 0.5% and 4%, should the operators use one or multiple spigots for discharge. One end of the range may significantly increase the rate of rise of the dam, while the other may allow significant reduction of dam size for the LOM. Both ends of the range are equally possible to achieve. The range of achieved beach slopes could also significantly vary depending on drying cycles used, convergence of flows, active deposition times, and other variables that can only be controlled during active deposition and by trained operators.

In this regard, as for any other engineered fill, the need for quality assurance and quality control (QA/QC) of the material properties and placement methods is key to the success of the concept. The need for proper QA/QC during active and inactive deposition becomes even more relevant when specific in-situ properties for the impounded tailings (density or void ratio, degree of saturation, limiting beach slope angle) are to be achieved to ensure slope stability under static and seismic conditions.

Conclusion

Engineered fill, in relation to tailings, is managing the material properties in a way that facilitates the implementation of the desired filling sequence and deposition strategy (i.e., maximize water recovery,

increase density for desiccation, produce targeted beach slopes, consider stability, etc.). By clearly defining the desired geotechnical and rheological behaviour of the engineered fill at the start of a project, the process equipment needed to produce it can be defined in consistency with both mill production requirements and tailings management strategy. Thickening tailings to a desired yield stress in order to generate sloping beaches, rather than to a target solids concentration, is one such example of engineered fill. Selecting processing equipment capable of producing tailings materials to specifications, and with the ability to adjust those tailings properties, can increase the storage capacity of an otherwise insufficient tailings storage site.

References

Drozdiak, J. and J. Norwood. 2017. Changing our thinking – from tailings processing to engineered fill. In *Proceedings of Tailings and Mine Waste 2017.* Banff, Alberta, Canada.

McPhail, G.I. 2008. Prediction of the beach profile of high-density thickened tailings from rheological and small-scale trial deposition data. In *Proceedings of Paste 2008*, Kasane, Botswana: 179–188.

Li, A.L. 2011. Prediction of beach slope and tailings flow properties. In *Proceedings of Paste 2011,* Perth Australia.

Luppnow, D., J. Moreno and M. Palape. 2009. Control and management of thickened tailings beach – a simplified approach*. Proceedings of Paste 2009*, Vina de Mar, Chile: 245–250.

Simms, P., M.P.A. Williams, T.G. Fitton and G. McPhail. 2011. Beaching angles and evolution of stack geometry for thickened tailings – A review. In *Proceedings of Paste 2011*, Perth Australia: 323–338.

Proceedings of Tailings and Mine Waste 2019
November 17–20, 2019, Vancouver, Canada
Published by the University of British Columbia, 2019

Assessment of Leach Ore Dry Unit Weight and Hydraulic Performance

Peter D. Duryea, Knight Piésold and Co, USA

Abstract

Proper design of a heap leach facility requires the development of a leach ore loading plan that can accommodate its ultimate capacity. The loading plan and associated capacity assessments will be more representative of actual field performance if they consider the variation in leach ore dry unit weight over time as the heap is loaded and the leach ore compresses under self-weight. That can be accomplished by careful evaluation of results from laboratory testing of representative samples of the leach ore.

Rigid wall permeability testing provides data about dry unit weight (and hence void ratio), saturated hydraulic conductivity, and vertical effective confining stress. These data can be fitted to relationships for compressibility (void ratio as a function of effective confining stress) and conductivity (saturated hydraulic conductivity as a function of void ratio) that were originally developed for self-weight consolidation of soft, fine-grained soils, e.g., tailings. The forms of those equations also typically fit laboratory test data from coarse-grained leach ore.

Once the compressibility and conductivity relationships are defined, incremental stress calculations with a spreadsheet allow for the development of: (1) profiles of dry unit weight and saturated hydraulic conductivity with depth in a unit area column of leach ore; and (2) the variation in depth-weighted average dry unit weight with average heap height. The average dry unit weight relationship may then be incorporated into heap loading plans and capacity assessments. Comparison of the planned leach application rate to the anticipated saturated hydraulic conductivity of the leach ore under the maximum heap height, assuming vertical percolation under unit hydraulic gradient, also provides a preliminary assessment of hydraulic performance.

Results for two case studies, including both a crushed and agglomerated copper heap and a run-of-mine gold heap, are presented. Actual results from mine production records compare well with predictions, although assessment of the run-of-mine gold heap required additional refinement to adjust for the effects of oversize material that could not be incorporated into the laboratory-scale testing.

Introduction

Proper design of a heap leach facility (HLF) requires development of a leach ore loading plan to include its ultimate capacity. The mine plan provides anticipated production in dry tonnes (or dry tons), while the assessment of the heap capacity is typically evaluated based on volume, which requires knowledge of the leach ore dry density (or dry unit weight) to relate the anticipated mine production to heap capacity. Often, the dry density (or dry unit weight) of the leach ore is assumed based on prior experience with similar projects, or estimated from the loose dumped dry density (or dry unit weight) achieved in bench-scale metallurgical column testing that may not consider the increase in density (or unit weight) resulting from an increasing depth of confinement. It is not uncommon for such initial assessments to significantly under- or over-predict the capacity of the associated HLF. The loading plan and associated capacity assessments will be more representative of actual field performance if they consider the variation in leach ore dry density (or dry unit weight) over time as the heap is loaded and the leach ore compresses under self-weight.

That can be accomplished by careful completion and evaluation of laboratory rigid wall permeability testing of representative samples of the leach ore. Testing conducted in accordance with standard procedures such as USBR 5600 or USBR 5605 (USBR, 1998; USBR, 1990) provides data relating dry density (or dry unit weight and, hence, void ratio), saturated hydraulic conductivity, and vertical effective confining stress. Abu-Hejleh and Znidarcic (1994) present relationships for compressibility (void ratio as a function of effective confining stress) and conductivity (saturated hydraulic conductivity as a function of void ratio) that were originally developed for self-weight consolidation of soft, fine-grained soils, e.g., tailings. The forms of those equations also typically fit laboratory test data from coarse-grained leach ore.

Once the compressibility and conductivity relationships are defined, incremental stress calculations with a spreadsheet allow the development of profiles of dry density (or dry unit weight) and saturated hydraulic conductivity with depth in a unit area column of leach ore and the variation in depth-weighted average dry density (or average dry unit weight) with average heap height. The average dry density (or average dry unit weight) relationship may then be incorporated into heap loading plans and capacity assessments, thereby enhancing the accuracy of those assessments by quantifying the variation in dry density (or dry unit weight) as the HLF is loaded to its capacity over time.

Comparison of the planned leach application rate to the anticipated saturated hydraulic conductivity of the leach ore under the maximum heap height, assuming vertical percolation under unit hydraulic gradient, also provides a preliminary assessment of hydraulic performance.

Analysis methodology

As noted, the detailed assessment of leach ore dry unit weight and hydraulic performance is conducted in

two distinct phases. These comprise: (1) the development of leach ore compressibility and conductivity relationships from rigid wall permeability test results; and (2) the evaluation of leach ore performance as indicated by the behaviour in a unit area column.

Compressibility and conductivity relationship development

In conducting laboratory rigid wall permeability testing of representative samples of a leach ore:

- Large-scale apparatus should be employed, e.g., 8-inch-diameter (USBR 5600) or 19-inch-diameter (USBR 5600) rigid wall permeameters, to permit inclusion of most, or all, of the material gradation, while maintaining an appropriate ratio of specimen diameter to maximum particle size, which is typically not less than 6:1.
- Plumbing that supplies water to the permeameter should be oversized such that hydraulic head losses in the apparatus are small relative to the hydraulic head losses in the specimen. If not possible, test results should be corrected for system head losses.
- Bead of hydrated bentonite should be placed at mid-height on the inside of the rigid wall permeameter to limit side wall leakage, i.e., preferential flow along the interface between the permeameter and the specimen, during permeability testing.
- Material should be placed loose in the rigid wall permeameter to simulate its initial condition in the field, and then subjected to a nominal seating load.
- Specimen should be inundated from the base to present a more uniform wetting front that moves upward through the specimen, and displaces more of the air from within the material.
- Initial saturated hydraulic conductivity of the material should then be measured via a constant head permeability test.
- Vertical effective confining stress on the specimen should thereafter be increased incrementally by means of a load frame and hydraulic jack with displacement measurements (from which dry density or dry unit weight are later calculated), and saturated hydraulic conductivity measurements should be taken at each load increment, once deformations are complete, to a maximum effective confining stress selected based on the anticipated maximum height of the HLF.

Resultant test data will include vertical effective confining stress, dry density (or dry unit weight and, hence, void ratio), and saturated hydraulic conductivity, from which the necessary compressibility and conductivity relationships can be developed.

Test data, compressibility (void ratio versus effective confining stress), and conductivity (void ratio versus saturated hydraulic conductivity) relationships can be developed using simplified curve fitting techniques proposed by John (1998) in accordance with the forms of the relationships suggested by Abu-Hejleh and Znidarcic (1994), which comprise:

Compressibility: $e = A(\sigma' + Z)^B$
Conductivity: $K = Ce^D$
where: e – void ratio
σ' – vertical effective confining stress
K – saturated hydraulic conductivity
A, B, Z, C and D – curve fitting parameters

with typical compressibility and conductivity relationships shown in Figure 1, along with their underlying laboratory test data.

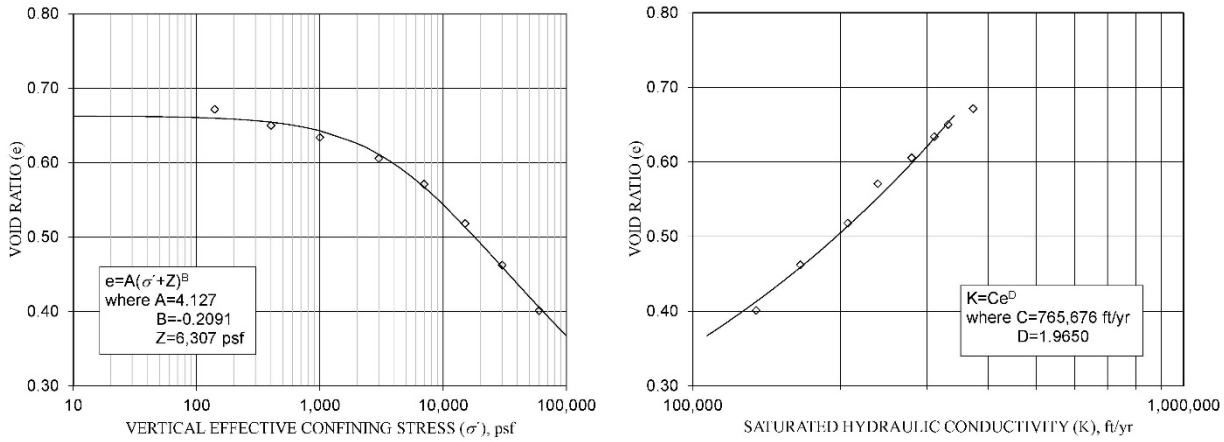

Figure 1: Typical leach ore compressibility and conductivity relationships

At the conclusion of the rigid wall permeability testing, it is also useful to establish: (1) the steady state, under leach moisture content at the project-specific target leach application rate; and (2) the draindown moisture content, i.e., the moisture content based on the water that will be held in the specimen against gravity, for use in later incremental stress calculations and/or HLF water balance assessments.

Leach ore performance evaluation without oversized material

Given the compressibility and conductivity relationships as defined above, incremental stress calculations can be completed with a spreadsheet to define the distributions of dry density (or dry unit weight) and saturated hydraulic conductivity versus depth in a typical unit area column of leach ore. As conceptually illustrated in Figure 2, the calculations involve a coordinate transformation.

1. Distribution of vertical effective stress is calculated as a function of depth in the "z" dimension, i.e., depth in a conceptual unit area column of leach ore solids with the volume of pore air and pore water removed, based on one of several assumptions regarding the influence of the pore water within the leach ore.
2. Distribution of void ratio with depth is then calculated from the vertical effective stress distribution and the previously established compressibility relationship.

3. Depths in the "x" dimension, i.e., actual depth in a unit area column of leach ore, are calculated from the depths in the "z" dimension and the associated void ratios.

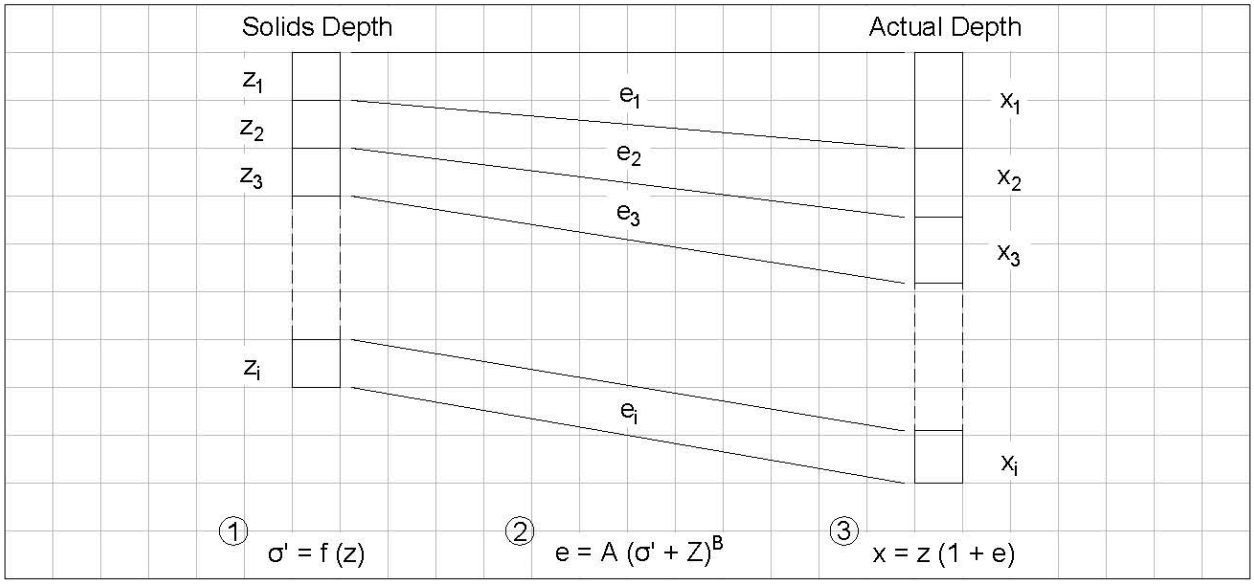

Figure 2: Coordinate transformation concept

The calculation of the vertical effective stress profile in the "z" dimension is dependent upon the effect of the pore water, if present. The simplest case comprises a dry unit area column without pore water, and, thus, with zero pore pressure throughout the unit area column. In that case:

Dry Material: $\Delta\sigma' = G_s * \gamma_w * \Delta z$

where: $\Delta\sigma'$ – vertical effective confining stress increment
G_s – particle specific gravity
γ_w – unit weight of water
Δz – solids depth increment

Another situation would comprise a saturated unit area column with hydrostatic pore pressures below a phreatic surface at the top of the unit area column. In that case:

Saturated Material: $\Delta\sigma' = (G_s*\gamma_w - \gamma_w) * \Delta z$

where: $\Delta\sigma'$ – vertical effective confining stress increment
G_s – particle specific gravity
γ_w – unit weight of water
Δz – solids depth increment

Most commonly, an HLF is operated with the leach ore in an unsaturated state under a fixed leach solution application rate. For these analyses, it has been assumed that the gravimetric moisture content of the leach ore is constant with depth. It should be noted that moisture content is defined herein as a percentage of the dry mass of the material present. This differs from the definition of moisture content commonly used in metallurgy, which is defined as the percentage of the total mass of the material present. Under the

assumption of unsaturated material (i.e., pore pressures are approximately zero) at a constant gravimetric moisture content with depth, vertical effective confining stresses can be defined as follows:

Moist material: $\Delta\sigma' = G_s * \gamma_w * \Delta z * (1 + w/100)$

where: $\Delta\sigma'$ – vertical effective confining stress increment
G_s – particle specific gravity
γ_w – unit weight of water
Δz – solids depth increment
w – gravimetric moisture content (percent by dry mass)

As noted previously, the gravimetric moisture content of the material under leach was assumed to be constant with depth. Although that may not be strictly correct, it is a reasonable assumption, because it results in slightly higher degrees of saturation deeper in the leach ore as the dry unit weight increases with depth and the void ratio decreases. That trend is to be expected, since the capillarity of the deeper, denser leach ore should be higher as well. Given the generally coarse, granular nature of most leach ores, these analyses have also assumed that self-weight compression of the leach ore occurs quickly such that time rate effects do not have to be considered, i.e., this behaviour comprises immediate compression and not time rate consolidation of a porous media.

Once the effective stress profile in the "z" dimension is established, the void ratio at each point within the unit area column of solids can then be calculated from the compressibility relationship defined previously, i.e., $e = A(\sigma' + Z)^B$, and the actual depth of each increment of material in the "x" dimension can be calculated as:

$\Delta x = \Delta z * (1 + e)$

where: Δx – actual depth increment
Δz – solids depth increment
e – void ratio

which completes the desired coordinate transformation. The actual depth at each point within the unit area column is then calculated by summing the overlying incremental actual depths. Note that it is often necessary for mass conservation to adjust the initial "z" dimension increments on an iterative basis to yield the correct actual depth of unit area column in the "x" dimension.

Once profiles of vertical effective confining stress and void ratio are established over the correct actual depth of the unit area column, dry density (or dry unit weight) can be calculated at each depth as follows:

$\rho_{dry} = G_s * \rho_w / (1 + e)$

where: ρ_{dry} – dry density
G_s – particle specific gravity
ρ_w – density of water
e – void ratio

$\gamma_{dry} = G_s * \gamma_w / (1 + e)$

where: γ_{dry} – dry unit weight
G_s – particle specific gravity
γ_w – unit weight of water
e – void ratio

The saturated hydraulic conductivity at each point within the unit area column can then also be calculated at its actual depth in the "x" dimension from the conductivity relationship defined previously, i.e., $K = Ce^D$.

Given the distribution of dry density (or dry unit weight) with actual depth in the "x" dimension within a unit area column of leach ore, the variation in overall average dry unit weight with increasing average heap height can be developed, which illustrates changes as the facility is loaded over time. For each average heap height considered, the corresponding overall average dry density (or average dry unit weight) comprises the depth weighted average value for the overlying leach ore from the dry density (or dry unit weight) profile in the "x" dimension as illustrated in the later case histories.

Under the assumption of vertical infiltration at unit hydraulic gradient, the saturated hydraulic conductivity of the leach ore may be compared to the planned leach application rate to assess the anticipated hydraulic performance of the leach ore. If the saturated hydraulic conductivity of the leach ore is expected to remain well above the planned leach application rate at the maximum depth of burial, the leach ore may be expected to remain freely drained throughout leach operations.

Leach ore performance evaluation with oversized material

Unadjusted results from laboratory-scale tests conducted on material from which an oversized fraction had been removed can under-predict the average dry density (or average dry unit weight) as compared to actual production-scale data. This is most likely due to the effect of the oversize particles that were excluded from the laboratory permeability testing.

Laboratory derived dry densities (or dry unit weights) developed as described above can subsequently be adjusted for the effect of the oversized fraction by application of a procedure (ASTM D4718), which is commonly used to rock correct Proctor compaction test results for the effect of oversized material, but can be applied to other, similar circumstances. The rock corrected dry unit weights are calculated as:

$$\gamma_{dry,c} = 100 * \gamma_{dry,f} * G_s * \gamma_w / (\gamma_{dry,f} * P_c + G_s * \gamma_w * P_f)$$

where: $\gamma_{dry,c}$ – rock corrected dry unit weight
$\gamma_{dry,f}$ – dry unit weight of the finer fraction
G_s – particle specific gravity
γ_w – unit weight of water
P_c – percent of oversize fraction by weight
P_f – percent of finer fraction by weight

The rock corrected laboratory-scale test results often match the production-scale data well. Updated void ratios can subsequently be calculated at each depth within the profile in the "x" dimension as follows:

$$e = G_s * \gamma_w / \gamma_{dry} - 1$$

where: e – void ratio
G_s – particle specific gravity
γ_w – unit weight of water
γ_{dry} – dry unit weight

with updated saturated hydraulic conductivity values then developed from the updated void ratios and the conductivity relationship defined previously, i.e., $K = Ce^D$.

Case history results

Although the author has applied this approach to numerous HLFs, two projects are presented herein as case histories because sufficient production data were available to provide some verification of the performance predicted based on laboratory-scale testing. These included: (1) a crushed and agglomerated copper heap; and (2) a run-of-mine gold heap.

As illustrated in Figure 3, the fresh and spent samples of the crushed and agglomerated copper ore comprise a well graded gravel with sand (GW) when sieved dry (i.e., agglomerates intact); however, the effect of agglomeration can be seen in comparing those to the wet sieved gradations (i.e., agglomerates destroyed) where the increased fines content shifts the classifications to a poorly graded gravel with silt and sand (GP-GM) and a silty gravel with sand (GM), respectively. It should also be noted that the fresh and spent gradations are similar, which would seem to indicate little or no decrepitation of the leach ore after one leach cycle, although those effects may be more pronounced after multiple cycles or a greater depth of burial under subsequent lifts of leach ore. Figure 3 further illustrates the gradation of the run-of-mine gold ore, i.e., a poorly graded gravel with silty clay and sand (GP-GC), before and after removal of the oversized fraction.

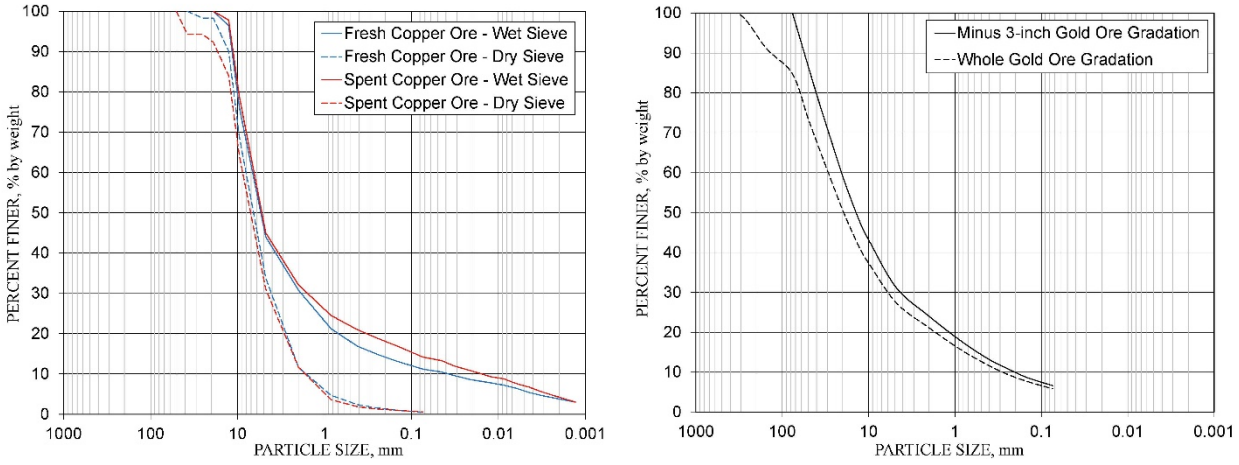

Figure 3: Copper and gold leach ore gradations

Figures 4 and 5 depict the compressibility and conductivity relationships for the copper and gold leach ores that were derived as described previously. The copper leach ore laboratory testing included rigid wall permeability testing of both fresh and spent ore specimens. Given that the results were not markedly different, they were interpreted together, which is further evidence of little or no decrepitation within that particular copper ore. The gold leach ore laboratory testing also includes results from two separate trials.

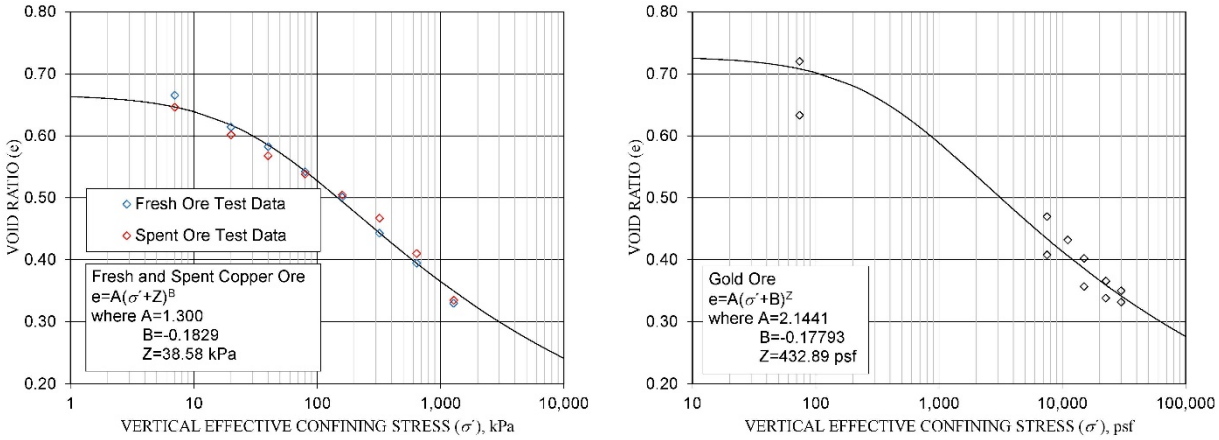

Figure 4: Copper and gold leach ore compressibility relationships

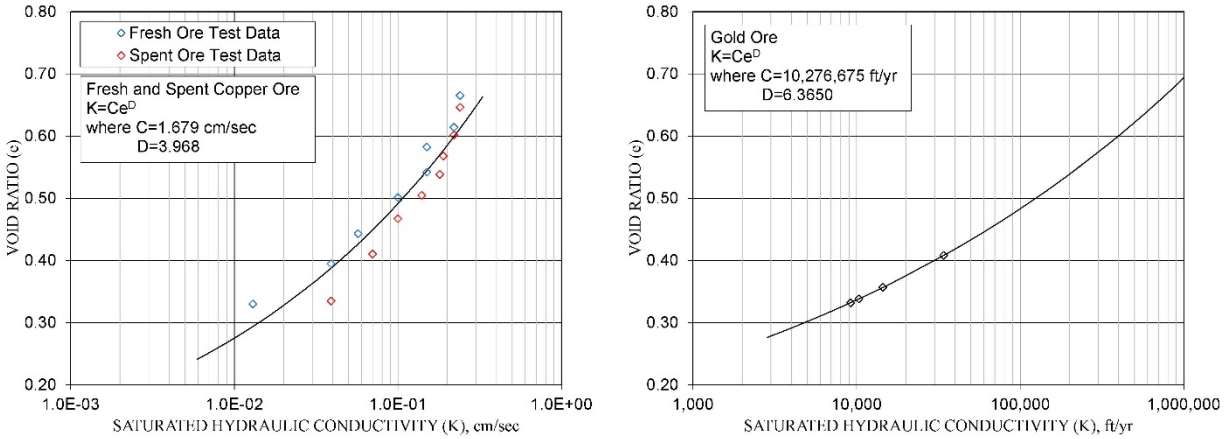

Figure 5: Copper and gold leach ore conductivity relationships

As a result of the incremental stress calculations described previously, Figure 6 depicts the variation in dry density (or dry unit weight) with actual depth within unit area columns of the copper and gold leach ores under their planned leach application rates. The results for the run-of-mine gold ore have been adjusted for the effects of the oversize material removed from the laboratory test specimens using the methodology described previously in this paper.

Figure 7 depicts the variation in leach ore average dry density (or dry unit weight) with average heap height for both the copper and gold HLFs that were developed from the density (or unit weight) profiles shown on Figure 6. To assess the accuracy of these predictions, dry densities (or dry unit weights) were calculated from production records at one or more different times during the operation of the copper and gold HLFs. Given three-dimensional topography of the heaps and their underlying liner systems, comparison of the two surfaces via AutoCAD Civil3D provided the volume and two-dimensional area of

the HLFs at the time of the heap surveys. Volume divided by area provided estimates of the average height of the heap, and average dry densities (or dry unit weights) were calculated by coupling the volumes with the known production (i.e., leach ore dry tonnage placed on the heap) as of the dates of the various surveys. Good agreement is noted between predicted average dry densities (or average dry unit weights) based on laboratory test results and values calculated from production records.

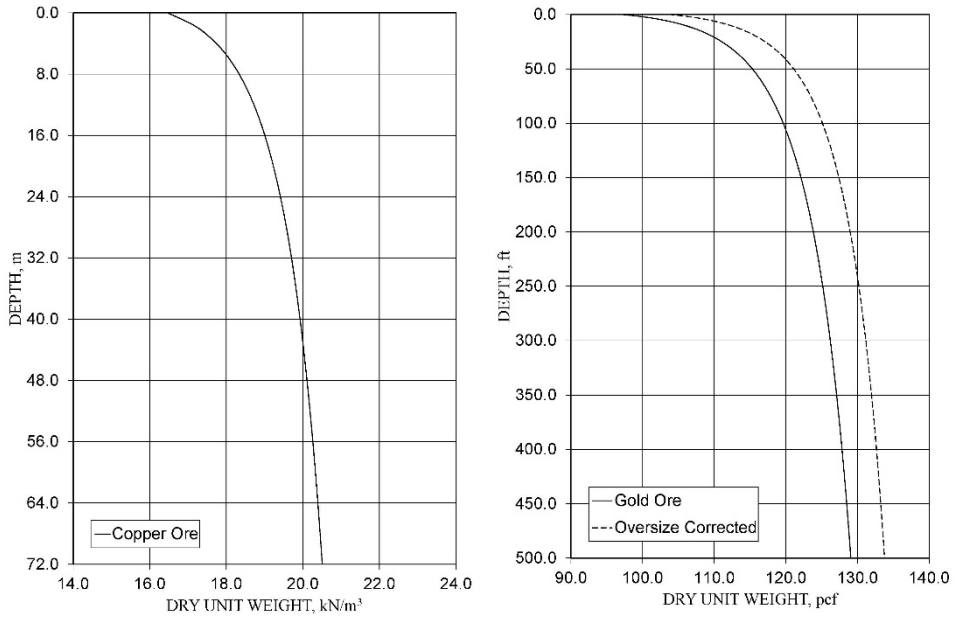

Figure 6: Copper and gold leach ore dry density (or dry unit weight) profiles

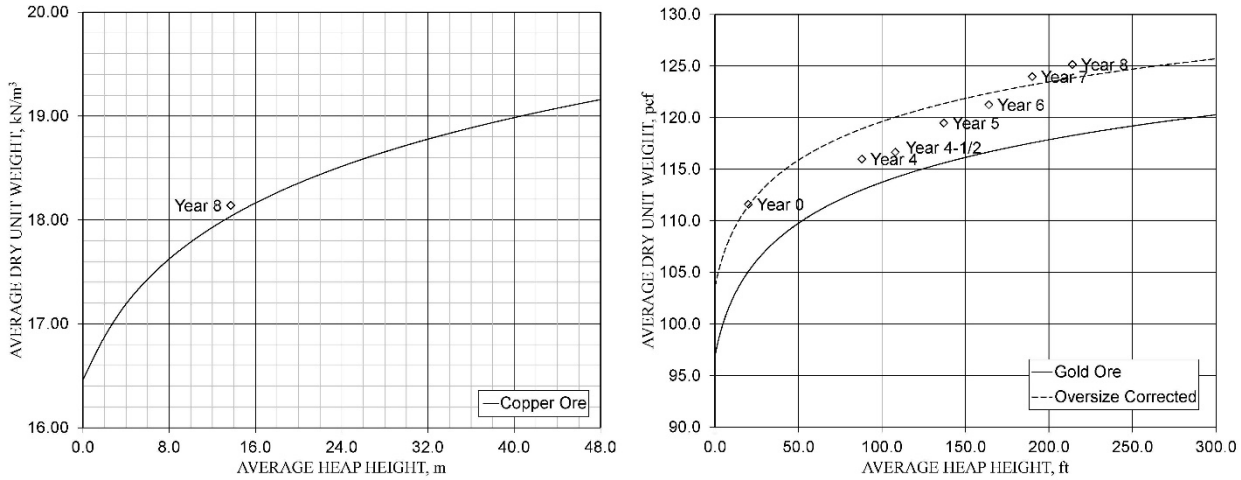

Figure 7: Average dry densities (or dry unit weights) with average heap height

Figure 8 presents comparisons of the saturated hydraulic conductivity profiles for the copper and gold leach ores with their respective planned leach application rates under the assumption of vertical infiltration at unit hydraulic gradient. Since the saturated hydraulic conductivities remain well above the planned leach

application rates at the maximum depth of burial, the copper and gold leach ores are expected to remain freely drained and perform well throughout leach operations. It should be noted that the copper HLF is an aerated facility with interlift liners, and while project assessments did evaluate the counter current flow of air upward from low pressure blowers and process solution downward from the drip irrigation system at the heap surface, discussion of those assessments is beyond the scope of this paper.

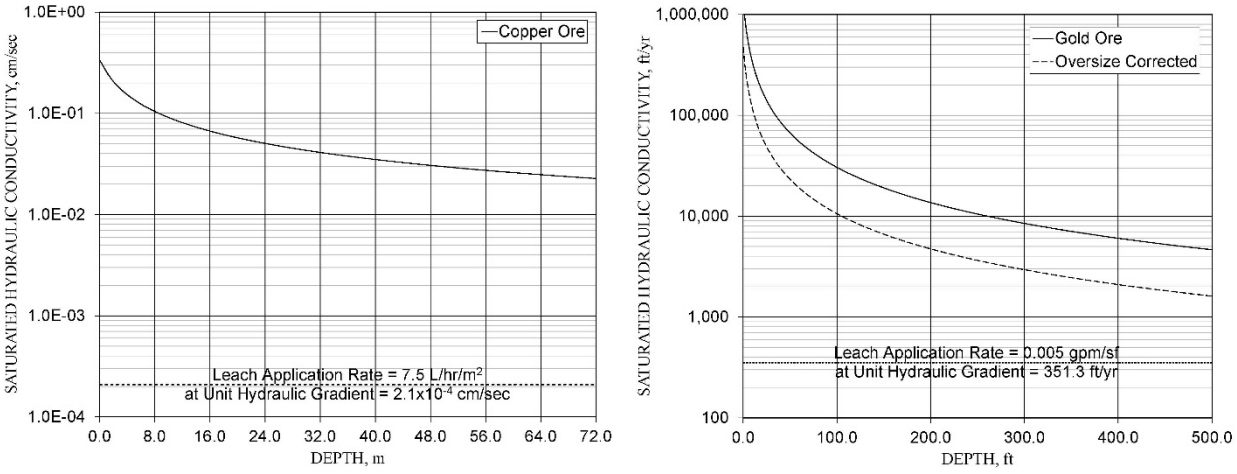

Figure 8: Copper and gold leach ore saturated hydraulic conductivity profiles

Conclusion

Rigid wall permeability test results typically include data relating dry unit weight (and hence void ratio), saturated hydraulic conductivity, and vertical effective confining stress. When carefully completed on representative samples of leach ore and adjusted for removal of oversize material if necessary, those test results can be fitted to relationships for compressibility (void ratio as a function of effective confining stress) and conductivity (saturated hydraulic conductivity as a function of void ratio) for leach ore that were originally developed for self-weight consolidation of soft, fine-grained soils, e.g., tailings.

Once the compressibility and conductivity relationships are defined for the leach ore, incremental stress calculations with a spreadsheet, with proper consideration of pore water conditions, allows the development of profiles of dry density (or dry unit weight) and saturated hydraulic conductivity with depth in a unit area column of leach ore and the variation in depth-weighted average dry unit weight with average heap height. Development of a HLF loading plan, to include its ultimate capacity, is enhanced by considering the variation in leach ore average dry density (or average dry unit weight) over time as the HLF is loaded and the leach ore compresses under self-weight. Furthermore, comparison of the planned leach application rate to the predicted saturated hydraulic conductivity of the leach ore under its maximum height, assuming vertical percolation of process solution under unit hydraulic gradient, provides an assessment of anticipated hydraulic performance.

Results were presented for two case studies including both a crushed and agglomerated copper heap and a run-of-mine gold heap. When rigid wall permeability test results on representative samples of the copper and gold leach ores were interpreted as described herein, the predicted variation in average dry density (or average dry unit weight) with average heap height compared well with actual results from mine production records. Hydraulic performance of both HLFs during production has been good, as predicted by the interpreted laboratory test results, based on observed conditions under the planned leach application rate, e.g., little or no ponding on the surface of the HLFs, no observed seepage on the sides of the HLFs, no phreatic surface development within the HLFs where solution levels could be monitored with installed instrumentation (e.g., vibrating wire piezometers), and process solution recovery in line with expectations.

Acknowledgements

The efforts of the combined Knight Piésold and client teams, who brought the projects presented herein as case histories into successful production, are gratefully acknowledged. In addition, the author would like to express his appreciation for the insightful comments and valuable critique of the draft manuscript provided by Dobroslav Znidarcic, Jeff Coffin, and Jordan Scheremeta.

References

Abu-Hejleh, A.N. and D. Znidarcic. 1994. Estimation of the consolidation constitutive relations. In H.J. Siriwardane and M.M. Zaman (editors), *Proceedings of the 8th International Conference on Computer Methods and Advances in Geomechanics*. Rotterdam: Balkema: 499–504.

ASTM. 2015a. *Annual Book of ASTM Standards Volume 04.08 Soil and Rock (I): D420 – D5876*. West Conshohocken, Pennsylvania: American Society for Testing and Materials.

ASTM. 2015b. *Annual Book of ASTM Standards Volume 04.09 Soil and Rock (II): D5877 – latest*. West Conshohocken, Pennsylvania: American Society for Testing and Materials.

John, E.G. 1998. Simplified Curve Fitting Using Spreadsheet Add-Ins. *International Journal of Engineering Education* 14(5): 375–380.

USBR. 1998. *Earth Manual, Part 1*, third edition. Washington, DC: United States Bureau of Reclamation, United States Department of the Interior.

USBR. 1990. *Earth Manual, Part 2*, third edition. Washington, DC: United States Bureau of Reclamation, United States Department of the Interior.

Proceedings of Tailings and Mine Waste 2019
November 17–20, 2019, Vancouver, Canada
Published by the University of British Columbia, 2019

On Some Considerations Related to Pore Fluid Chemistry in Tailings Critical State Testing

Riccardo Fanni, Golder Associates Pty Ltd, Australia
David Reid, The University of Western Australia, Australia
Kyle Smith, Golder Associates Pty Ltd, Australia

Abstract

The use of the critical state approach to assess tailings liquefaction susceptibility has increased dramatically in the past two decades – including, for example, implementation in prominent failure investigations. A key input to the critical state approach is accurate measurement of the critical state line (CSL). Techniques to measure the CSL have reached a near-consensus level across a number of tailings testing laboratories, including the use of moist tamping to prepare loose specimens, oversized lubricated end platens to promote sample uniformity during shear, and end-of-test soil freezing to enable accurate measurement of void ratio. These techniques were developed in the testing of sands in the 1980s and subsequently expanded to mine tailings.

An aspect of mine tailings that differs from sands is that tailings generally have a significant proportion of fines, including in some cases fines with appreciable plasticity. Further, the mineral processing is such that at deposition the pore fluid of a tailings slurry often contains appreciable quantities of total dissolved solids (TDS), most often salts. In Australia, hypersaline groundwater is often used in the ore processing, causing the concentration of TDS in the pore fluid to far exceed that found in ocean water. Moreover, in an arid climate, the concentration of TDS may increase further following deposition if air drying occurs on the tailings beach. The combination of tailings material with an appreciable percentage of fines, including potential plasticity (i.e., clay mineralogy) and pore fluid with significant TDS raises the important question of what effect pore fluid chemistry may have on the mechanical behaviour of the tailings. For example, there is ample evidence that pore fluid chemistry effects the mechanical behaviour of clays. Furthermore, it is currently unclear what is the best way to potentially incorporate pore fluid chemistry considerations into testing to measure the CSL. These are topics that have not been addressed sufficiently in tailings engineering practice.

This paper outlines available data on the effect of pore fluid chemistry on the CSL of tailings, and the development of techniques to incorporate pore fluids with significant TDS into CSL testing programs. This includes the measurement of TDS concentration on samples recovered from tailings deposits, and slight modifications to moist tamping test procedures to target the desired TDS concentration in triaxial specimens. Available evidence in the literature clearly suggests that in tailings, a plasticity index greater than about 10 and pore fluid with high TDS concentrations, have an effect on CSL elevation. For tailings with lower TDS and lower plasticity, the evidence is less clear.

Introduction

Effect of dissolved solids on tailings

Mineral processing activities rarely use deionized water for mineral processing. Instead, mines most often use readily available water sources. In the case of mines that are located within arid climate zones, such as those located within much of Western Australia, the available water source is often brackish or hypersaline. This often results in tailings containing an appreciable quantity of dissolved solids at deposition (Poulos et al., 1985; Fujiyasu and Fahey, 2000; Al-Tarhouni et al., 2011; Mundle et al., 2012; Gorakhki and Bareither, 2016), with salts most commonly making up a large proportion of the dissolved solids.

Significant evidence is available in the literature that highlights the effects of salinity on geotechnical properties, including Atterberg Limits, compressibility, brittleness and sensitivity, and CSL elevation. The effect that pore fluid chemistry and dissolved solids have on clay particles is well understood. The surface of clay particles is negatively charged and cations, which are positively charged, are attracted electrostatically to the particle surface. Depending on the clay minerals, the charge of the cations (single, double, or triple) and the concentration of cations in the pore fluid, the clay may disperse or flocculate. Clays with a high concentration of exchangeable cations, e.g., Na^+, disperse if the pore fluid solution contains a high concentration of Na^+, as the sodium tends to separate clay particles such that Van der Walls polarization intermolecular forces are not strong enough to bring particles close together. Clays that have a tendency to disperse are mobile within a soil, and their mobility is accentuated with the infiltration of rainwater, or any water with a low concentration of cations. This is particularly relevant for post-closure of tailings storage facilities that contain high TDS pore fluid and clay minerals with high concentrations of exchangeable cations, as the phreatic surface may be periodically recharged by the infiltration of rainwater. Even if the clay particles in the tailings mass do not have the tendency to disperse or to undergo significant internal erosion (due to its general low clay particle size content), the long-term effect that infiltration of a solution with a low concentration of TDS may have on the mechanical behaviour of tailings, in particular brittleness, is not well understood.

Moreover, while tailings are often of low plasticity, being derived primarily from crushed rock, it is not currently clear below what threshold of plasticity the salt content of the pore fluid would not affect mechanical behaviour. A recent study undertaken on low plasticity tailings indicated that dissolved solids may influence the CSL of tailings (Reid et al., 2019), with potential repercussions on how tailings facilities may be decommissioned. Therefore, it is important to carry out laboratory testing replicating the in-situ pore fluid at deposition and to account for the concentration of dissolved solids and the density of the liquor, in order to enable accurate measurement of the void ratio for CSL development during tailings deposition. It is also of particular importance to carry out studies on the long-term performance of tailings containing high TDS pore fluid subject to long-term leaching due to infiltration of a low TDS pore fluid.

Void ratio calculation accounting for TDS

To account for the presence of TDS in the tailings pore fluid, adjustments to the standard soil mechanics phase equations are required (Mundle et al., 2012). The following formulas are used in this paper to account for TDS in calculation of void ratio. The variables presented in the formulas form the basis for the laboratory testing procedure highlighted in this study.

- $e_c = \frac{w_l G_s}{\rho_{l,20} S}$ (equation 1)
- $w_l = \frac{w_u}{1 - w_u c_{TDS}} (1 + C_{TDS})$ (equation 2)
- $e_u = \frac{w_u G_s}{S}$ (equation 3)

Where:

- Salt corrected void ratio $= e_c$
- Salt corrected gravimetric moisture content expressed as $\left(\frac{M_w + M_{TDS}}{M_s}\right) = w_l$
- Salt corrected particle density $(\frac{g}{cm^3}) = G_s$
- Liquor density at 20^0C $(\frac{g}{cm^3}) = \rho_{l,20}$
- *S*aturation degree $= S$
- Uncorrected gravimetric moisture content $\left(\frac{M_w}{M_s + M_{TDS}}\right) = w_u$
- TDS concentration $(\frac{M_{TDS}}{M_w}) = C_{TDS}$
- Mass of solids $= M_s$
- Mass of water $= M_w$
- Mass of TDS $= M_{TDS}$

Liquor density of typical tailings pore fluids

Although NaCl is probably the most common dissolved solid that is encountered in tailings pore fluids, a number of other constituents are possible. Figure 1 and Figure 2 provide the relationship between liquor density and concentration of TDS (C_{TDS}) for two types of dissolved solids (sodium chloride – NaCl, and magnesium sulphate – $MgSO_4$). These relationships are benchmarked against the pore fluids of three

different tailings, namely Pore Fluid 1, Pore Fluid 2 and Pore Fluid 3. It is noted that in this paper TDS concentration is expressed as mass of TDS in mass of water, and not mass of solution as commonly adopted.

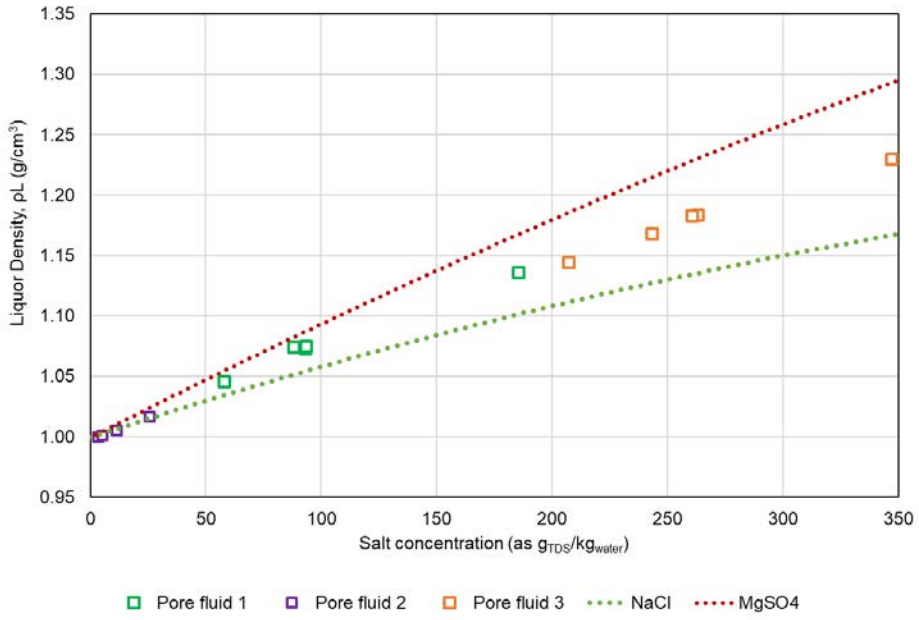

Figure 1: Liquor density relationships for NaCl, $MgSO_4$ and three tailings pore fluids

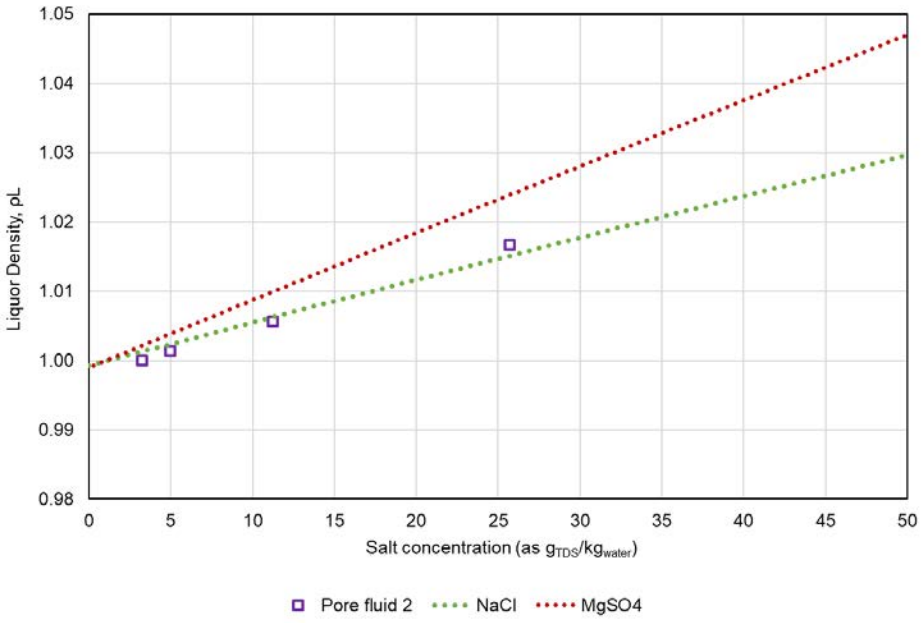

Figure 2: Liquor density relationships for NaCl, $MgSO_4$ and Pore Fluid 2 (C_{TDS} from 0 to 50 g_{TDS}/kg_{water})

It can be seen from Figure 1 and Figure 2 that Pore Fluid 2 is close to the NaCl curve within the range of C_{TDS} measured in the testing, while Pore Fluid 1 and Pore Fluid 3 lie in between the NaCl and $MgSO_4$

curves, with the latter indicating the presence of various constituents in solution.

Void ratio accuracy and error due to TDS

The error in void ratio if dissolved solids are not accounted for in calculations is provided in Figure 3, based on a tailings containing various concentrations of dissolved solids and pore fluid typical of Pore Fluid 1 or Pore Fluid 3, which lie between the NaCl and $MgSO_4$ curves:

- Case 1 = 25 g/kg
- Case 2 = 50 g/kg, and
- Case 3 = 150 g/kg.

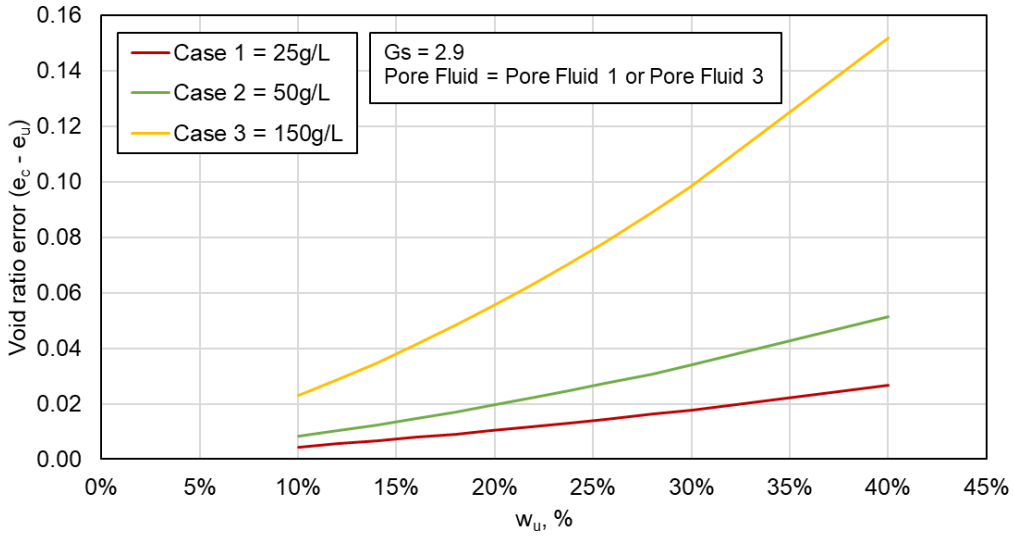

Figure 3: Void ratio error ($e_c - e_u$) versus uncorrected gravimetric water content for Case 1, Case 2 and Case 3

Figure 3 shows that the error in void ratio would be low for the case of low concentration of dissolved solids as in Case 1 (i.e., 0.01 to 0.02 void ratio within typical range of w_u) and would increase to a range considered important for a CSL estimate for Case 2 (i.e., 0.01 to 0.03 void ratio within typical range of w_u) and becomes quite significant for Case 3 (i.e., 0.03 to 0.10 void ratio at typical range of w_u).

While the typical error on the CSL for tailings having pore fluid with TDS concentrations similar to Case 1 would be likely minimal, the errors for Case 2 and particularly for Case 3 would be important and might influence estimation of the elevation and slope of the CSL. The magnitude of these errors is examined in this study for CSL testwork undertaken on three tailings, each having different pore fluid TDS concentrations.

Laboratory testing techniques

General

Prior to outlining the methods applied in this study to consider TDS in critical state testing, the authors emphasize that there is no established standard to guide the management of dissolved solids in tailings laboratory testing, including testing to measure the CSL. The methods outlined herein have been developed by the authors. However, it is emphasized that further development and refinement appears warranted. The procedures are described for triaxial specimens prepared using the moist tamping technique. However, with a few adjustments they could also be applied to other specimen preparation methods, i.e., slurry deposition or, if feasible, wet or dry pluviation.

Preparation of materials

Preparation of moist tamped samples of tailings implies that the material has likely been dried back either from a slurry or from a sample obtained from a TSF – either from the beach or from depth. The moisture content of the sample is generally adjusted to achieve an optimal value for moist tamping. Based on the authors' experience, the optimal gravimetric moisture content is generally 10 to 15% for silty tailings and 5 to 7% for sandy tailings.

It is important that such drying is either done at room temperature or in a "cool" oven, as there is evidence that drying at higher temperatures may affect the subsequent mechanical behaviour of soils or tailings that include an appreciable quantity of clay mineralogy.

The drying process (however it is carried out) results in a loss of water from the sample, while the dissolved solids remain with the tailings and/or the remaining water. Tracking of all three main constituents (solids, TDS, and water) from the as-received material is fundamental for the replication of in-situ pore fluid conditions.

Measuring TDS on the as-received tailings sample

Measuring of the TDS and gravimetric moisture content in the as-received material is undertaken on a small subsample of the parent material previously dried at room temperature or in a "cool" oven. Generally, 100 g should suffice; however, less material may be used if the sample quantity is limited. The drying of this subsample is done as per standard procedures in a hot oven. We have found the most practical means to achieve this is to dry the sample within a glass beaker, as this allows for salt correction of the dried specimen to be undertaken without transferring of masses between containers. Following removal of the subsample from the oven and recording of the dry mass, we undertake these steps:

1. Add a known mass of demineralized water to the subsample.

2. Stir thoroughly for a period of 15 minutes, to ensure thorough re-dissolution of the dissolved solids.
3. Seal the beaker with cling wrap and allow the sample to settle at least overnight.
4. Once the tailings have settled, measure the mass of the sample in order to capture the loss of water due to evaporation.
5. Remove most of the clear water with a syringe.
6. Filter the clear water into another beaker through a funnel.
7. Record the mass of the decanted solution and dry the solution in an oven at 110°C to determine the TDS.
8. The total dissolved solids in the bulk sample is calculated from the salt content of decanted solution, the amount of demineralized water added and the initial dry mass of the specimen.

Test procedures

General triaxial test procedures employed thus far have followed typical methods (e.g., Jefferies and Been, 2015) for the preparation of samples for CSL testing, i.e., moist tamping using the under-compaction techniques (Ladd, 1978), use of oversize lubricated end platens to promote greater sample uniformity, and end-of-test soils freezing to provide a more accurate measure of sample volume and density.

The primary difference when carrying out the previously listed procedures when managing pore fluid TDS lies in the flushing, back pressure saturation, and end-of-test measurement procedures. These are outlined as follows:

1. Undertake flushing of the specimen with a volume of demineralized water such that will result in an aggregate ratio of solids, water, and dissolved solids consistent with in-situ conditions. This is undertaken flushing a known volume of demineralized water equal to the amount that was removed though the process of sample drying required to target an optimal moisture content for moist tamping.
2. If deemed necessary, additional flushing is carried out using site water prepared to the same TDS as the target value for the sample. Alternatively, “synthetic” pore fluids prepared to the same TDS as the target in-situ value, but using NaCl dissolved in water, have been used with apparent success both in tailings CSL testing (Reid et al., 2019) and in testing of clays (e.g., Pineda et al., 2016). This representative pore fluid is applied by means of a toxic interface system chamber connected to the back pressure pump, so that subsequent flushing and back

pressure activities would not bring hypersaline pore fluid into contact with the pressure pump itself.

3. Once flushing is complete, back pressure saturation is carried out using standard triaxial procedures. Given the salt concentration being used, leaving the sample for an extended period under back pressure saturation may promote the dissolution of salt within the pore fluid.
4. After shearing, the sample is sealed and then frozen using typical end-of-test CSL testing procedures. The gravimetric moisture content of the sample is then measured by means of oven drying using standard laboratory procedures, except that the sample is dried within a beaker rather than a typical drying tin. The rationale for the use of a beaker is discussed subsequently.

While the above steps present the techniques that the authors have adopted on a number of test campaigns, we are of the view that there is the potential for some refinements. For example, it is unclear to what extent Step 1 to Step 3 will result in complete dissolution of salts, in particular when very high TDS is targeted (e.g., greater than 100 g/kg). Some discrepancy between the target TDS and the end of test TDS has been observed, which may be attributed to precipitation of salts within the triaxial apparatus and accumulation in subsequent specimens during the progression of the testing programme. This was addressed by thorough flushing with demineralized water of the triaxial piping system, and top and base caps prior to undertaking testing on consecutive specimens. Measuring TDS on triaxial specimens at end of test

Although the testing procedure outlined in the previous section was developed in order to target a particular TDS, it is generally unknown how accurately this will be reproduced. Therefore, measurement of the sample TDS after testing, is likely prudent as a check on the outcomes obtained. The same procedure described for measuring the TDS on the as received tailings is employed also to measure the TDS of the triaxial specimens at end of test.

Presentation of results

Tailings samples

Three laboratory testing programmes are summarized for the purpose of this paper:

1. Sample 1 – A tailings with low pore fluid TDS, ranging between 18 to 30 g/kg and average of 20 g/kg.
2. Sample 2 – A tailings with medium pore fluid TDS, ranging between 50 to 60 g/kg and average of 55 g/kg.

3. Sample 3 – A tailings with hypersaline pore fluid, with TDS ranging between 135 to 150 g/kg and average of 140 g/kg.

All tailings were sampled using multiple tubes taken at a depth of interest, generally characterized by loose and contractive tailings based on cone penetration testing with pore pressure measurement (CPTu) data interpretation using screening methods such as Plewes et al. (1992) and Been and Jefferies (1992). CSL testing was undertaken on reconstituted specimens. TDS correction of tube density tests was carried out following the procedure outlined in this paper to enable comparison of state parameter (ψ) from laboratory testing with the ψ from the screening methods (not included in this paper). Index testing of the three samples are provided in Table 1. The CSL results are presented in Figure 4 to Figure 6 and in the tables. CSL have been represented using conventional semi-log and power law idealizations.

Table 1: Index testing of Sample 1, Sample 2, and Sample 3

Sample ID	Gs	Particle size distribution		Atterberg limits		
		<75 µm	<38 µm	LL	PL	PI
1	2.90	99%	98%	36	25	11
2	2.85	64%	50%	22	20	2
3	2.91	59%	46%	Slip in base	Not determined	Non-plastic

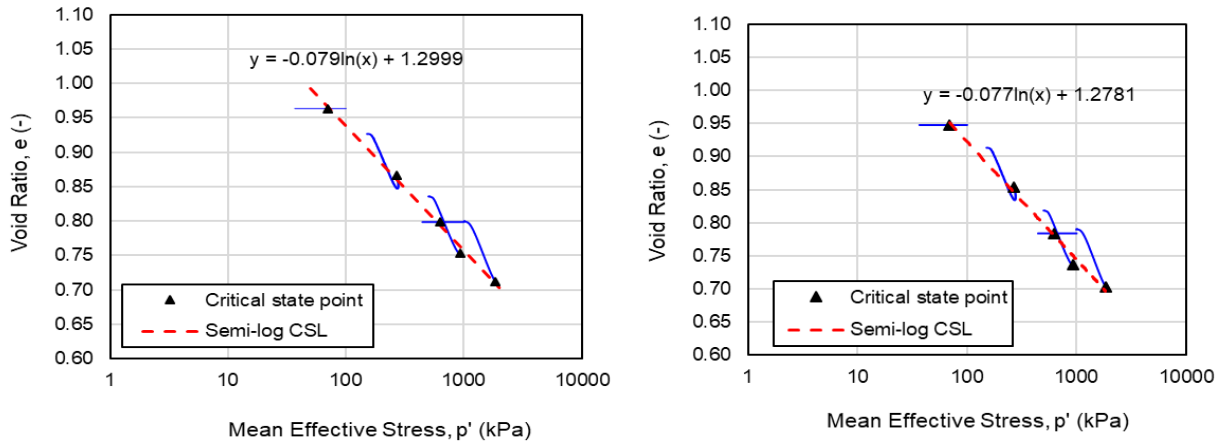

Figure 4: Sample 1 – Salt corrected (left) and uncorrected (right) CSLs

Table 2: Sample 1 – Salt corrected and uncorrected CSLs

Test number	C_{TDS} (g/kg)	Salt corrected CSL			Salt uncorrected CSL		
		e	ψ_0	CSL parameters	e_c	ψ_0	CSL parameters
1	28	0.75	0.02		0.74	0.02	
2	25	0.87	–0.11		0.85	–0.11	
3	27	0.80	0.04	$\lambda_e = 0.079$, $\Gamma = 1.30$	0.78	0.05	$\lambda_e = 0.077$, $\Gamma = 1.28$
4	33	0.87	0.02		0.85	0.02	
5	19	0.71	0.04		0.70	0.05	

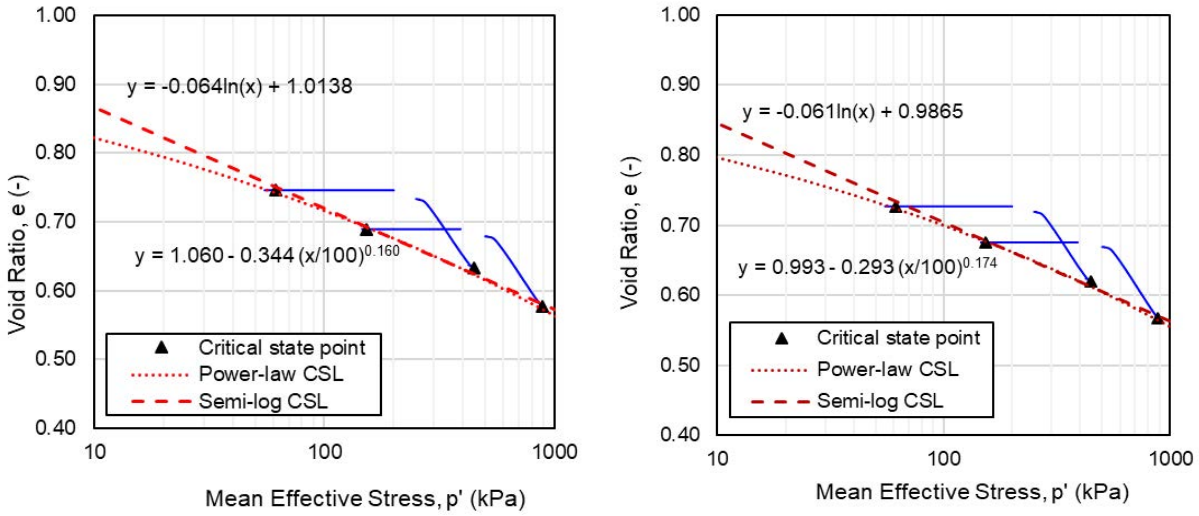

Figure 5: Sample 3 – Salt corrected (left) and uncorrected (right) CSLs

Table 3: Sample 2 – Salt corrected and uncorrected CSLs

Test number	C_{TDS} (g/kg)	Salt corrected CSL			Salt uncorrected CSL		
		e	ψ_0	CSL parameters	e_c	ψ_0	CSL parameters
1	51	0.75	0.07	$\lambda_e = 0.064$, $\Gamma = 1.01$	0.73	0.07	$\lambda_e = 0.061$, $\Gamma = 0.99$
2	35	0.58	0.06		0.57	0.06	
3	41	0.69	0.06	A = 1.060, B = 0.344, C = 0.160	0.68	0.05	A = 0.993, B = 0.293, C = 0.174
4	44	0.63	0.07		0.62	0.07	

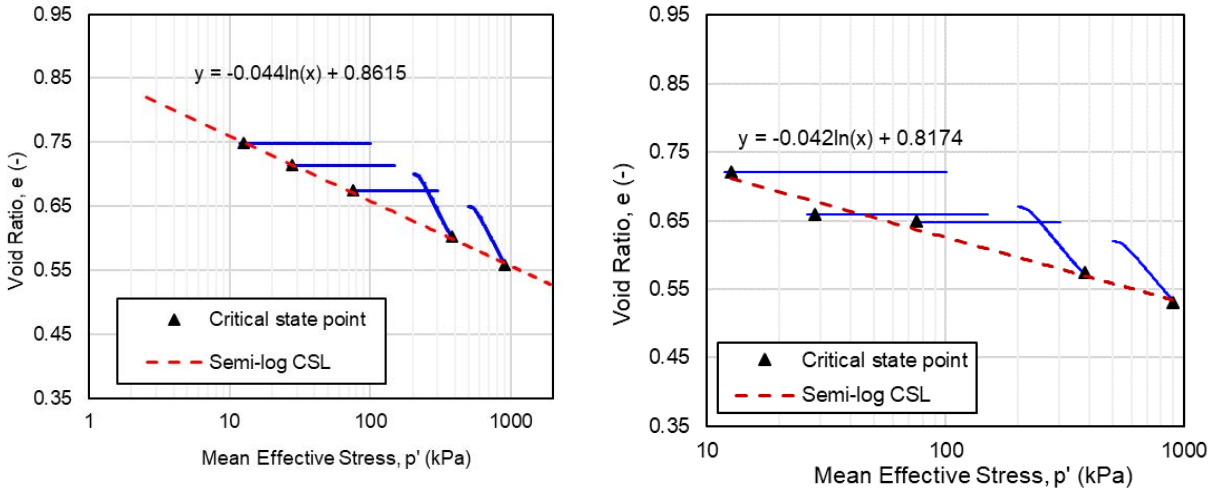

Figure 6: Sample 3 – Salt corrected (left) and uncorrected (right) CSLs

Table 4: Sample 4 – Salt corrected and uncorrected CSLs

Test number	C_{TDS} (g/kg)	Salt corrected CSL			Salt uncorrected CSL		
		e	ψ_0	CSL parameters	e_c	ψ_0	CSL parameters
1	80	0.67	0.06		0.65	0.07	
2	87	0.60	0.07		0.57	0.07	
3	60	0.75	0.09	$\lambda_e = 0.044$ $\Gamma = 0.86$	0.72	0.09	$\lambda_e = 0.042$ $\Gamma = 0.82$
4	57	0.56	0.06		0.53	0.06	
5	127	0.71	0.07		0.66	0.05	

The results of the CSL testing on salt corrected and uncorrected specimens indicate that the correction of void ratio for TDS concentration has an influence on the CSL elevation (Γ) more than on the CSL slope (λ_e). Significant differences between corrected and uncorrected CLSs are evident when the TDS exceeds values greater than 50 g/kg, whilst differences are minor at TDS of 20 g/kg. It is noted that testing on Sample 3 was undertaken prior to testing on Sample 1 and Sample 2. Therefore, the discrepancies seen in achieving the target TDS concentration of 140 g/kg is largely due to the refinement of the laboratory testing procedure during progression of the testing. The higher accuracy in achieving the target TDS concentration for Sample 1 and Sample 2 reflects improvement in the testing procedure.

The results also indicate that once correction for TDS is undertaken, the CSLs appear to not be dependent on TDS concentration (at the ranges of TDS concentrations tested), as indicated specifically in testing of Sample 3, where testing undertaken at TDS concentration ranging between approximately 60 g/kg and 130 g/kg shows a unique CSL. Although, it is important to acknowledge that Sample 3 was

non-plastic, indicating a lack of clay mineralogy and therefore being less likely to be affected by the pore fluid chemistry and charging of particle surfaces.

Conclusions

A laboratory testing procedure relevant to CSL estimation has been outlined in this paper. The procedure describes the steps for testing reconstituted specimens containing relevant quantities of TDS concentration and correction of void ratio for TDS concentration. The procedure has been developed by the authors. However, it is emphasized that further development and refinement appears warranted. The procedures are described for triaxial specimens prepared using the moist tamping technique. However, with few adjustments, these procedures could also be applied to other specimen preparation methods, i.e., slurry or, if feasible, wet or dry pluviation.

Three laboratory test programs on tailings containing different pore fluid TDS concentrations were outlined. The results of the CSL testing on salt corrected and uncorrected specimens indicate that the correction of void ratio for TDS concentration has an influence on the CSL elevation more than on the CSL slope. The results also indicate that once correction for TDS is undertaken, the CSLs appear to not be dependent on TDS concentration (at the ranges of TDS concentrations tested), as indicated specifically in testing of a sample at varying TDS concentration ranging between approximately 60 g/kg and 130 g/kg, which shows a unique CSL. However, it is important to acknowledge that this sample was non plastic and was therefore unlikely to be significantly affected by the pore fluid chemistry. As indicated in other studies, the effect of long-term leaching of TDS from plastic tailings is unclear and further studies should be undertaken. The laboratory testing procedure proposed in this paper could be used as the basis for these investigations.

References

Al-Tarhouni, M., P. Simms and S. Sivathayalan. 2011. Cyclic behaviour of reconstituted and desiccated-rewet thickened gold tailings in simple shear. *Canadian Geotechnical Journal* 48(7): 1044-1060. doi:10.1139/t11-022.

Been, K. and M.G. Jefferies. 1992. Towards systematic CPT interpretation. In Predictive soil mechanics: The Wroth Memorial Symposium, Oxford, UK: 121–134.

Fujiyasu, Y. and M. Fahey. 2000. Experimental study of evaporation from saline tailings. *Journal of Geotechnical and Geoenvironmental Engineering* 126(1): 18–27. doi: 10.1061/(ASCE) 1090-0241(2000)126:1(18).

Gorakhki, M. and C. Bareither. 2016. Effect of salinity on the geotechnical characterisation of fine-grained soils and mine tailings. *Geotechnical Testing Journal*, 39(1): 45–58.

Jefferies, M.G. and K. Been. 2015. Soil liquefaction – a critical state approach, second edition. Boca Raton: CRC Press.

Mundle, C., P. Chapman, D. Williams and D. Fredlund. 2012. The impact of high density liquors on standard soil mechanics calculations. *Proceedings of the 16th International Conference on Tailings and Mine Waste:* 281–290. Information Technology, Creative Media, Keystone, Colorado.

Pineda, J.A., L.P. Suwal, R.B. Kelly, L. Bates and S.W. Sloan. 2016. Characterisation of Ballina clay. *Geotèchnique*, 66(7):556–577. doi:10.1680/jgeot. 15.P.181.

Plewes, H.D., M.P. Davies and M.G. Jefferies. 1992. CPT based screening procedure for evaluation liquefaction susceptibility. *45th Canadian Geotechnical Conference*. Canadian Geotechnical Society, Toronto, Ontario: 41–49.

Poulos, S., E. Robinsky and T. Keller. 1985. Liquefaction resistance of thickened tailings. *Journal of Geotechnical Engineering* 111(12): 1380–1394. doi: 10.1061/(ASCE)0733-9410(1985)111:12(1380).

Reid, D., A. Fourie and S. Moggach. 2019. Characterisation of a gold tailings with hypersaline pore fluid. *Canadian Geotechnical Journal* doi: 10.1139/cgi-2018-0579.

Proceedings of Tailings and Mine Waste 2019
November 17–20, 2019, Vancouver, Canada
Published by the University of British Columbia, 2019

Interpretation Uncertainty within a Mechanics-Based Critical State Approach to Tailings Characterization

Andrew Fuggle, Golder Associates, USA
Jean Kugel, Golder Associates, USA

Abstract

Properly understanding and characterizing the potential for liquefaction is important for the design and operation of tailings impoundments. Liquefaction has often been viewed as a somewhat mysterious and difficult problem, but it is simply one aspect of tailings behavior that can be captured with good constitutive models. The critical state soil mechanics (CSSM) framework provides a mechanics-based tool for understanding and predicting liquefaction behavior.

One of the key components of the critical state framework is defining the critical state line (CSL). This is typically accomplished using a suite of consolidated drained and undrained triaxial compression tests on initially loose samples tested to a relatively large strain. Once the CSL is defined (usually by tailings property parameters Γ and λ) it can be used for a variety of purposes, from screening-level evaluations to detailed constitutive modelling. This paper focuses on estimating the tailings property parameters that define the CSL from measured laboratory data, and on an assessment of the variability in the interpretation of these parameters.

The authors provided triaxial data from 14 triaxial compression tests performed on a single tailings gradation to a group of practising consulting geotechnical and tailings engineers. The participants were asked to provide their interpretation of the critical state locus. The results of these interpretations were then compared, and an assessment of the interpretation uncertainty was made. No separate assessment was made of the uncertainty of the source laboratory data itself, since all of the interpretations were performed on the same data set. The paper also demonstrates the resulting variation in geotechnical design parameters that depend on the CSL interpretation.

The paper demonstrates that the CSL can be reliably estimated from a carefully planned and executed laboratory testing program. Resulting analyses that use the CSL provide valuable insights and the ability to quantitatively characterize tailings behaviour, including liquefaction.

Introduction

Properly understanding and characterizing the potential for liquefaction is important for the design and operation of tailings impoundments. Estimating the CSL for a given tailings gradation is an important step in this process. This paper focuses on uncertainty in interpreting the CSL from triaxial compression data, which is the most common way of obtaining the required information.

The critical state of a tailings material is the end state that the material reaches when it is sheared continuously. This state was defined by Roscoe et al. (1958) as the state at which a soil continues to deform at constant stress and constant void ratio. The CSL is the locus of void ratio-effective stress conditions achieved at this end state and is the boundary between contractant and dilative behavior. The CSL is commonly represented as semi-logarithmic, but curved or bilinear CSL representations are also used.

For the purposes of this paper, we have taken the approach that the CSL is a useful reference point. This is the case especially in regard to assessing static liquefaction where the density of the material, in relation to the critical state reference condition, is of paramount importance (more so than the permeability of the material). Recent practical applications of the CSL (and the CSSM framework in general) include the analyses by the technical review boards of the failures at both the Fundão tailings dam and the Cadia NTSF embankment.

We have also taken as a given the hypothesis that a unique CSL exists for a material with a given gradation, although the influence of sample preparation, pore fluid chemistry, and shearing mode on the CSL are acknowledged. Including any of these possible effects was not necessary for this work, as the goal was to assess interpretation uncertainty in current practice, not absolute accuracy of the CSL.

It should also be noted that reliable estimation of the CSL is one step in a larger task of characterizing tailings behaviour. How representative the tested sample is of the tailings mass in-situ, and the effects of layering and desiccation are important questions, amongst others, that also need to be considered when assessing tailings behaviour at field scale.

Methodology and material

The authors solicited volunteer participants from Golder who have some experience with CSSM and CSL interpretation. Each participant received a spreadsheet that included triaxial test data (ε_a, ε_v, σ'_3, σ'_1, p', q, Δu, and e) and basic summary plots (e-log(p'), p'-q, ε_a-q, ε_a- Δu, and ε_a-ε_v).

The participants were asked to parameterize the critical state locus and were not provided with direction as to how to fit the data or which type of fit to use. Participants were left to their own judgement as to which points to include in the fit and which, if any, to exclude. Table 1 presents a summary of the

participants and responses. Table 2 presents a summary of the basic properties of the molybdenum tailings beach material tested.

Table 1: Participation summary

Category	Value	CSL trend line type	Quantity
Number of unique participants	27	Semi-log	22
Total number of trend lines provided	32	Bi-Linear Semi-log	2
Average self-assessed level of CSSM expertise (1 = Novice to 5 = Expert)	2.9	Curved	8

Table 2: Tailings properties

Category	Value	Category	Value
USCS classification	SM to ML	Specific gravity	2.63
D_{50} (mm)	0.07	In-situ dry density (kN/m^3)	15.1
Fines (% <0.075mm)	51%	$V_{s,30}$ (m/s)	140
Grain shape	Angular to sub-angular		
Mineralogy	Quartz, some biotite and muscovite		

Triaxial testing performed to obtain provided data

Triaxial compression testing was performed on 14 reconstituted specimens prepared using the moist tamping method. The material was tamped into a vacuum mould using the under-compaction uniform-density procedure (Ladd, 1978). The triaxial equipment included oversized and lubricated end platens to reduce the sample distortion at large strains. Samples were soft-frozen at completion of shear, and the final void ratio was measured using the entire specimen. Undrained and drained shear rates were 5% and 1.25% axial strain per hour, respectively. Table 3 summarizes the tests performed.

Table 3: Summary of triaxial test data provided to participants

Drained test ID	e_o	σ'_3 (kPa)	e_f	Undrained test ID	e_o	σ'_3 (kPa)	e_f
CD T1	0.54	340	0.47	CU T5	0.56	240	0.56
CD T2	0.52	690	0.44	CU T6	0.54	290	0.54
CD T3	0.46	2760	0.35	CU T7	0.48	1020	0.48
CD T4	0.61	34	0.56	CU T9	0.54	510	0.54
CD T5	0.57	210	0.51	CU T10	0.49	1490	0.49
CD T6	0.61	55	0.54	CU T11	0.53	330	0.53
CD T7	0.45	240	0.47				
CD T8	0.48	70	0.51				

Of the 14 tests performed, eight were drained and six were undrained. Two of the drained tests were performed on initially dense samples, so the CSL was not expected to be able to be estimated from those two tests. None of the tested samples were able to be reconstituted to a dry density as low as the estimated in-situ dry density.

The conventional e-log p plot for the 14 tests is presented in Figure 1. There is variability in the post-shear data points from the undrained tests. When selecting a data set, the authors intentionally chose a data set that would require interpretation and insight into laboratory testing, tailings behavior, and CSSM.

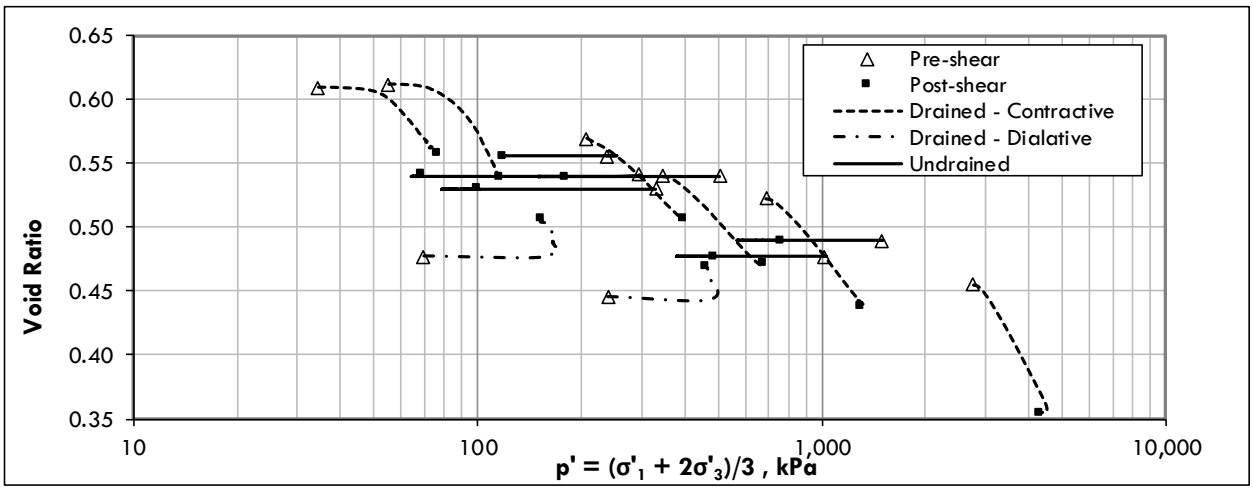

Figure 1: e-log(p') plot

Results and analysis

As shown in Table 1, 22 semi-log, eight curved, and two bilinear trends were provided by participants. The instruction given to participants was deliberately silent on the form of the CSL to use. The semi-log trend was the most common, likely due to its relative simplicity and widespread familiarity.

Semi-log CSL trend lines

The compiled response from participants who used a semi-log CSL trend line is shown in Figure 2. The variability in the CSL interpretation is clearly greater in the low stress (p'<100 kPa) and high stress (p'>1,000 kPa) regions, with the lowest variability seen at about p' of 350 kPa. Estimated property parameters (Γ and λ_{10}) for the semi-log CSL trend lines are presented in Table 4.

Table 5 and Figure 3 present statistical summaries of the Γ and λ_{10} values estimated for the semi-log CSLs. Of the 22 independent estimates, two possible outliers were identified using Tukey's Inner Fence criterion. No estimates fell into the probable outlier category (Tukey's Outer Fence). The two possible outliers were outliers both on Γ and λ_{10}, as may be expected given the relationship between the property parameters shown in Figure 3. Both of the possible outliers were included in the statistical summaries.

The range in Γ was 0.105, indicating the maximum altitude change (change in void ratio) based on this parameter. The quartile coefficient of dispersion, a dimensionless measure of variability, indicates that there is about three times more variability in λ_{10} as there is in Γ. Figure 3 shows that these two variables have a strong positive correlation. As the altitude (Γ) increases the slope (λ_{10}) also increases to match the data points.

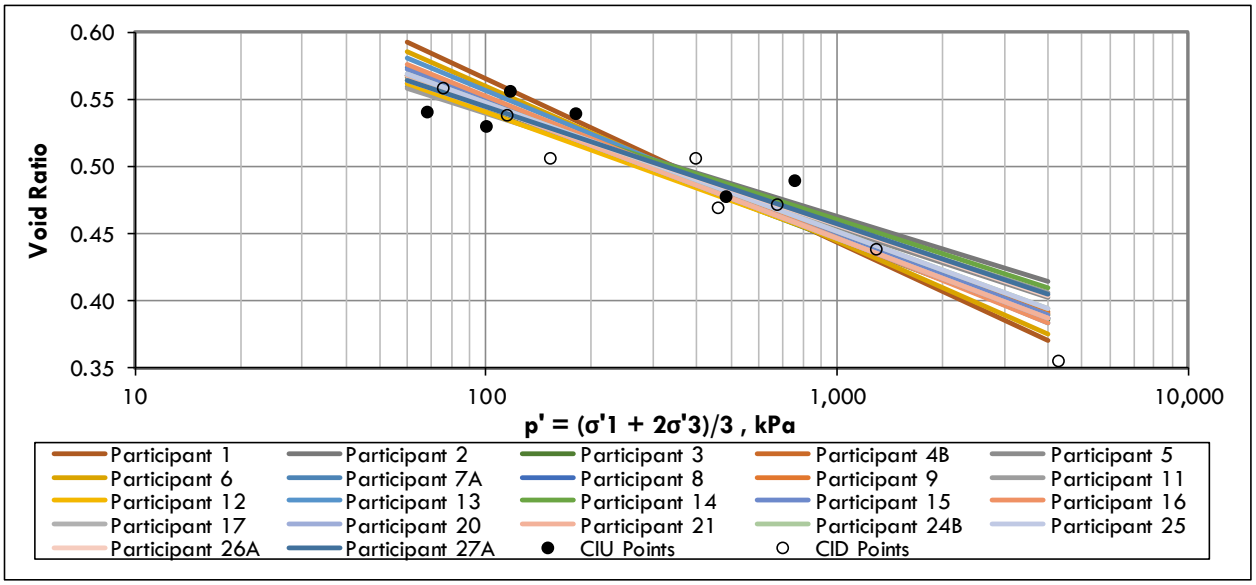

Figure 2: Semi-log trend lines

Table 4: Summary of results from semi-log CSL trend lines

Participant ID	Γ	λ_{10}	Participant ID	Γ	λ_{10}	Participant ID	Γ	λ_{10}
1	0.810	0.122	9	0.741	0.097	20	0.744	0.099
2	0.705	0.081	11	0.706	0.083	21	0.744	0.099
3	0.743	0.099	12	0.730	0.094	24	0.740	0.096
4	0.740	0.097	13	0.773	0.108	25	0.740	0.096
5	0.713	0.086	14	0.716	0.085	26	0.721	0.088
6	0.790	0.115	15	0.750	0.100	27	0.720	0.087
7	0.755	0.102	16	0.765	0.106			
8	0.744	0.099	17	0.744	0.099			

Curved versus semi-log CSL trend lines

The compiled responses from participants who used a curved CSL trend line is shown in Figure 4. When comparing the semi-log to curved fits (Figure 2 and Figure 4, respectively), the curved fit allows for a larger range of effective stresses to be matched by a single trend line.

Table 5: Statistical summary of results from semi-log CSL trend lines

Category	Γ	λ_{10}	Category	Γ	λ_{10}
Number of measurements	22	22	Mean	0.743	0.098
Minimum	0.705	0.081	Quartile coefficient of dispersion	0.017	0.054
Maximum	0.810	0.122	Possible outliers	2	2
Range	0.105	0.041			

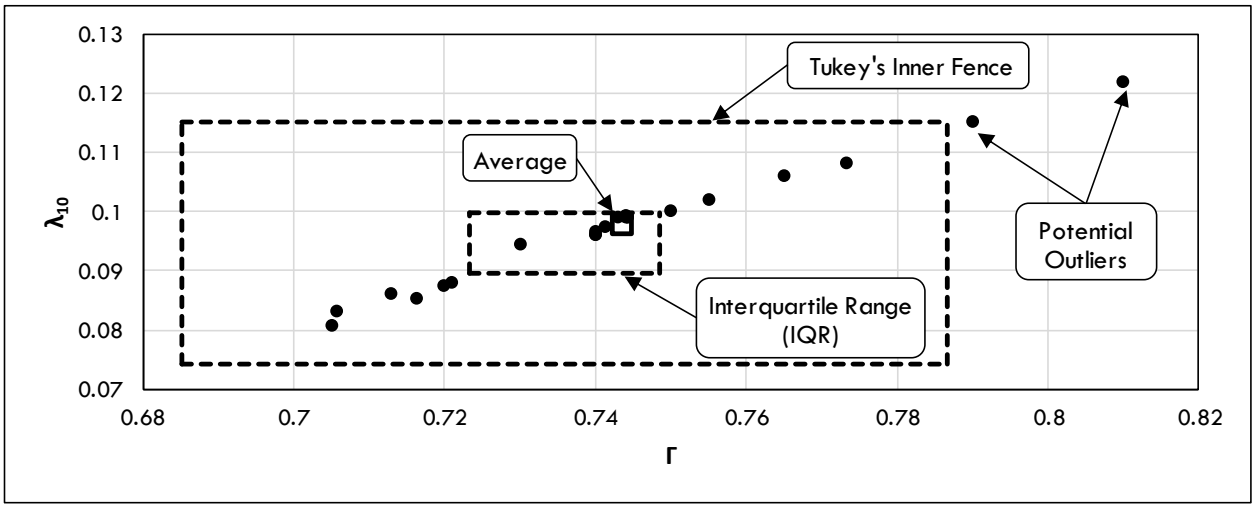

Figure 3: Graphical statistical summary of results from semi-log CSL trend lines

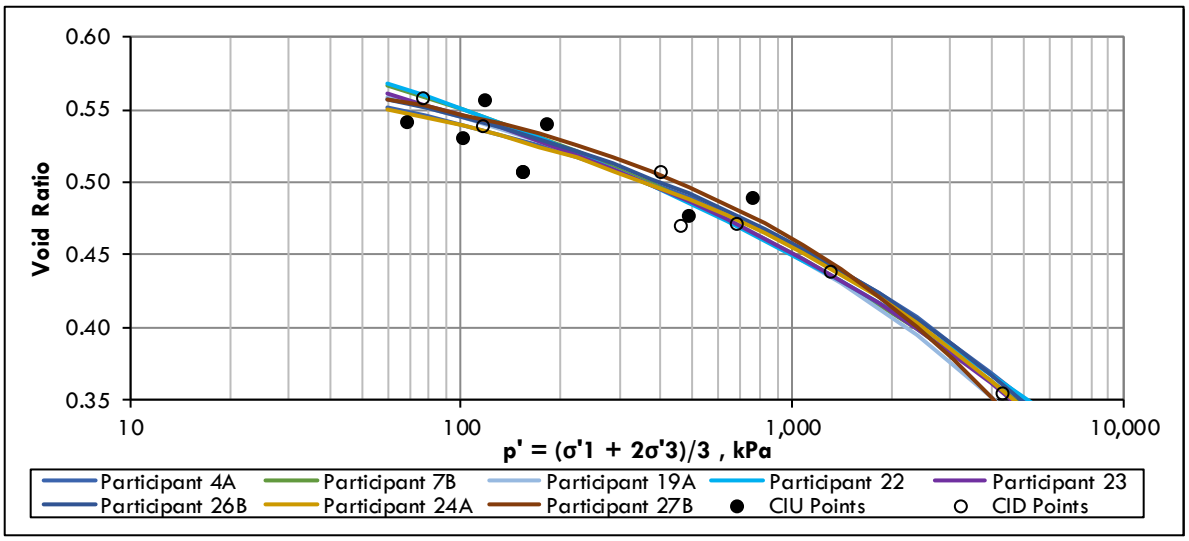

Figure 4: Curved CSL trend lines

Each set of CSL trend line parameters was used to estimate the void ratio at three discrete mean effective stresses across the range laboratory data (100, 350, and 1,000 kPa). The CSL-estimated void ratio ranges are presented in Table 6 for both semi-log and curved CSL trend lines. As expected, the void ratios

in the middle of the stress range (350 kPa) are relatively precise for both the semi-log and curved trend lines. The curved trend lines maintain a fairly consistent void ratio range across the full stress range of interest (100 to 1,000 kPa) while the semi-log void ratio range about doubles at the outer limits of the stress range.

A number of factors influence the lower variation in the curved trend lines, including: the smaller number of participants that submitted curved trend lines, the increased input it takes to fit the additional parameters, the likelihood that the more sophisticated trend lines came from the more advanced practitioners, and that the curved trend lines contain one more parameter than the semi-log trend lines (with an associated expectation of a superior fit). However, most participants that submitted a curved fit also submitted a semi-log fit, which discounts some of the issues mentioned above.

Assuming the influence of these factors does not overwhelm the general observed trend in Table 6, it appears that the curved CSL trend line provides for a more precise fit over a wider stress range without overfitting the data.

Table 6: Range of void ratio for semi-log and curved CSL trend lines

p' (kPa)	Minimum void ratio		Maximum void ratio		Void ratio range	
	Semi-log	Curved	Semi-log	Curved	Semi-log	Curved
100	0.540	0.539	0.566	0.550	0.026	0.011
350	0.490	0.501	0.500	0.510	0.010	0.009
1,000	0.444	0.450	0.463	0.461	0.019	0.011

Discussion

Void ratio variability

As shown Table 6, the variability in the critical void ratio changes with mean effective stress. In the range of most practical interest covered by this data, from 100 to 1,000 kPa, the variation in the critical void ratio is between 0.010 and 0.026 for the linear CSLs. How does this compare to the expected variation?

The resolution of the post-shear void ratio measurement in good commercial laboratories is about 0.01 (Jefferies and Been, 2016). This provides a reasonable lower limit to the expected variation in critical void ratio as a result solely of CSL interpretation.

A recent and ongoing study by the TAILLIQ project seeks to estimate the variation between different laboratories performing the same kinds of tests and interpreting the same kind of data as was used in this study. Preliminary results indicate that the variation in critical void ratio between different laboratories is approximately 0.03 over a similar stress range (50 to 800 kPa), provided that the laboratories used soil freezing at the end of the test to estimate void ratio, and that lubricated, oversized end platens were also

used. Both conditions were met for the data provided as part of this study. This provides a reasonable upper limit to the expected variation in critical void ratio as a result solely of CSL interpretation.

The variation in the critical void ratio due to CSL interpretation was observed to fall within the expected upper and lower limits. It may be expected that there would be less variation in interpretation if a more well-behaved data set had been used. However, the data set used is not atypical of data sets that the authors have worked with in practice.

Variation in the critical void ratio directly correlates to variation in the state parameter. Available evidence suggests that tailings exhibit ψ less than (denser than) about -0.05 to ensure a dilative response. The relative magnitude of the uncertainty appears significant relative to this dilative/contractive threshold.

Selection of void ratio-stress data points for CSL interpretation

Not all high-strain triaxial tests reach the critical state. It is imperative that practitioners use judgement as to which points to include and which to exclude while establishing a CSL. An important corollary to this imperative is that CSL triaxial testing programs should include more planned tests than is strictly necessary, as some tests will inevitably need to be excluded from the data set. For some triaxial tests, even if the test does not fully reach critical state, it can be assessed where the CSL would likely lie with respect to the final test data point. As discussed previously, the selected data set included some points that would need to be excluded to assess the techniques and processes of the participants.

Most participants used the triaxial strain-based data sets to select which points to include or exclude from their CSL trend line. The plots in Figure 5 show a particularly elegant way to evaluate whether or not a given test reached critical state by co-plotting p', q, and Δu or e. These plots create a simple visual cue as to whether the sample has reached a steady-state condition or whether it is still dilating/contracting, changing pore pressure, or otherwise changing. Although not shown in the plots in Figure 5, this type of plot can also readily identify suspicious data or test equipment errors (e.g. data continuing to record while unloading the sample) that a cursory pull-the-final-data-point summary would miss.

Implications for geotechnical design

This section discusses the implications of variability of CSL parameterization on design parameters and material characterization. Specifically, the effects of the λ_{10} variability were evaluated for theoretical design evaluations including residual strength estimation and screening-level liquefaction assessment.

Residual strength

The slope of the CSL (λ_{10}) can be used to estimate residual strength ratio (s_r/p'_o). This approach is only valid for undrained stress paths, relies on the undrained steady-state concepts of Poulos et al. (1985), and incorporates the critical state idealized definition of state parameter. Following the logic presented in

Jefferies and Been (2016), residual strength ratio during undrained liquefaction can be estimated as a function of M (M_{tc} = 1.44 for this data set), ψo, and λ_e ($\lambda_e = \lambda_{10} / 2.303$).

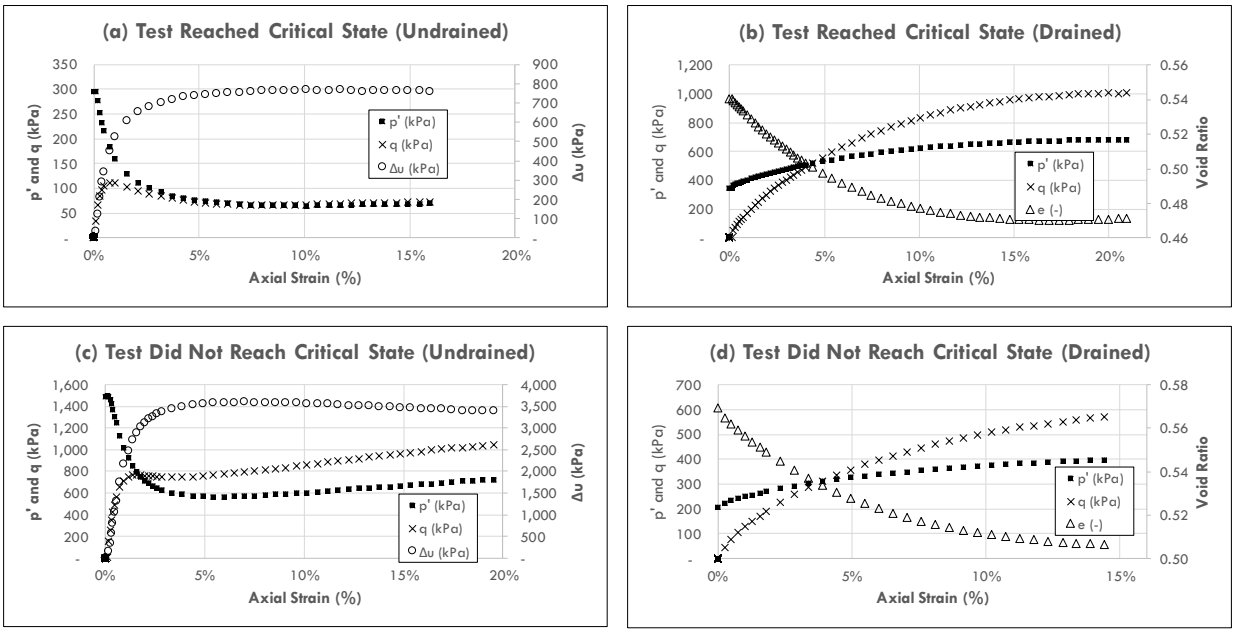

Figure 5: Assessment of triaxial test shear end state

Using the range of λ_{10} values gathered from participants during this study, a range of normalized residual strength values can be estimated. Assuming a fixed ψ_0 value of 0.05, the mean value for normalized residual strength is 0.22 with a range of 0.11 (maximum of 0.28 and minimum of 0.17). This range shows that the variability of input λ_{10} value can shift the estimate for normalized residual strength by about 20-25% in either direction. The uncertainty in the estimate of residual strength introduced by the variability in CSL interpretation indicates that the use of multiple methods for estimating residual strength should be employed in addition to this approach, including methods developed from case history back-analysis.

Screening-level liquefaction assessment

Two of the ways that the CSL trend line can influence the screening-level liquefaction assessment are through the Plewes relationship and the estimation of state parameter from CPT data.

The range of λ_{10} values submitted by the participants correlates well with the Plewes relationship as shown on Figure 6. Figure 6 overlays the range of λ_{10} values at a Friction Ratio (F) of 1% on top of the compiled plot from Jefferies and Been (2016) that includes Plewes et al. (1992), Reid (2012), and Jefferies and Been (2016) data. A constant value of F = 1% was selected because it matches the average F with depth from multiple CPT records. The λ_{10} values corroborate the λ_{10} = F/10 approximation and demonstrate a similar λ_{10} range as the base data sets included on the plot. As expected, all the λ_{10} values plot in the tailings range.

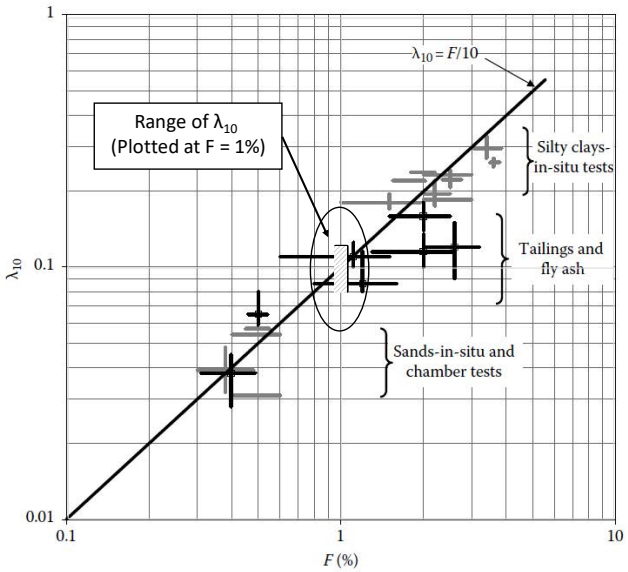

Figure 4.30 Relationship between λ_{10} and *F* suggested by Plewes et al. (1992) with additional data from Reid (2012) and authors' files.

Figure 6: Semi-log CSL λ_{10} range overlaid on Plewes (Figure 4.30, Jefferies and Been, 2016)

One of the CPTu records from the project files was used to investigate the influence of λ_{10} variability on the state parameter estimation using methodology presented in Been and Jefferies (2016). State parameter was calculated using the effective inversion parameters (m' and k'), which were based on the minimum and maximum λ_{10} values from this study. As shown in Figure 3, the maximum value is a possible outlier, and even including this possible outlier, a small average variation of +/- 0.027 is calculated for the state parameter along the CPTu profile plot. Selection of appropriately conservative characteristic state parameters from CPT data appears prudent.

Applicability of results

The results presented pertain to a single composite tailings material. The average CSL from the participants in this study is shown in Figure 7, along with a number of other CSLs from tailings materials (data obtained from Jefferies and Been [2016]). The data used in this study is clearly in the lower void ratio range compared to the other data (smaller Γ) but the slope (λ_{10}) is seen to be very similar to many other materials.

Since the variation in Γ was determined to be less than the variation in λ_{10}, this observation is encouraging in that the findings from this study are likely relevant across a broader range of materials than were include in this study.

Precision and accuracy

This work provides an assessment of the precision (closeness or variability) with which independent

analysts can estimate the CSL. It cannot provide an assessment of the accuracy (trueness or bias) of the interpreted CSL since the true CSL is not known. In this case, it seems reasonable to assume that a relatively precise grouping would indicate a relatively accurate grouping, barring a significant systematic error made by all participants.

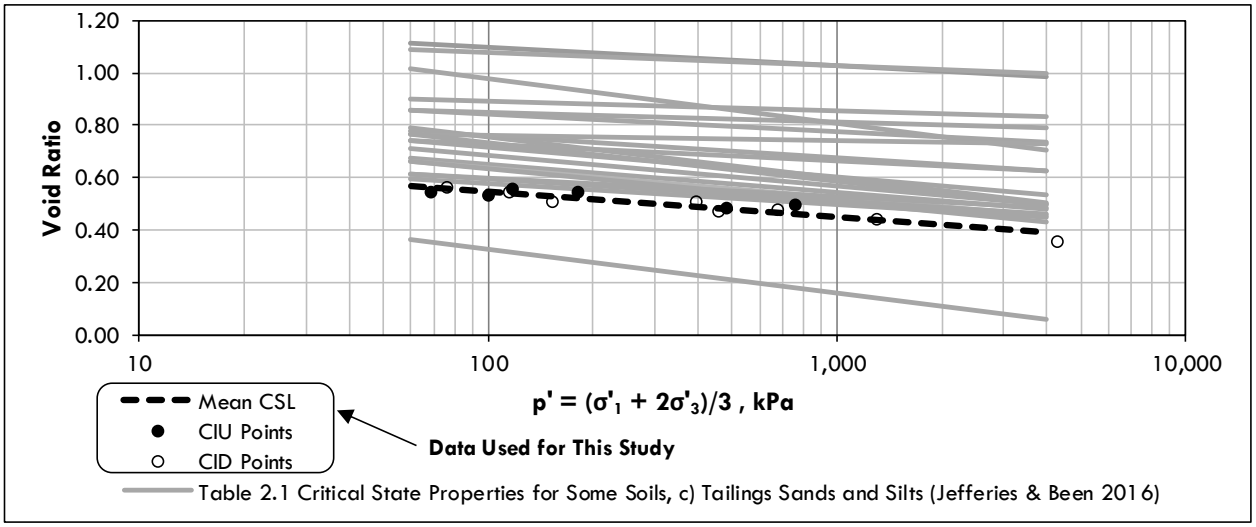

Figure 7: Semi-log CSL properties in relation to other tested tailings

Recommendations for CSL interpretation

Based on the findings of this study, we recommend the following to improve the reliability of CSL interpretation: (a) within the stress range of interest, perform sufficient (assume some tests results will not be used) tests that reach the critical state, (b) explicitly specify the stress range over which the CSL interpretation is valid, (c) use a curved CSL representation when appropriate, (d) record which tests were used for CSL interpretation, and reasons for excluding tests, (e) use staff familiar with laboratory testing to perform CSL interpretation, and (f) recognize that engineering judgement is a necessary part of good CSL interpretation.

Conclusion

Determining the CSL for a given tailings gradation is an important task when characterizing tailings for engineering purposes. This paper focused on estimating tailings property parameters that define the CSL from measured laboratory data, and an assessment of the variability in the interpretation of these parameters. Triaxial compression test data from 14 tests on a single composite sample was analyzed by 27 independent geotechnical and tailings engineers. The results were compiled and analyzed to assess variability in CSL interpretation. The semi-log representation of the CSL was most commonly used in this study, although a curved representation was shown to provide a more precise result over a broader range of mean effective stresses.

The variation in critical void ratio as a result of semi-log CSL interpretation falls within the expected limits, and ranges from about 0.010 to 0.026 over the stress range of interest. The impact of this variation on the estimation of engineering parameters, such as residual strength and state parameter, is noticeable, but is unlikely to be a determining factor when considering other sources of uncertainty in geotechnical parameterization and the application of prudent engineering judgement. Selection of which void ratio-stress points to use for interpreting the CSL is important. This aspect of CSL interpretation can be improved with experience, greater familiarity with laboratory testing, and improved data visualization approaches.

This study demonstrates that the CSL can be reliably estimated from a carefully planned, executed, and interpreted laboratory testing program, taking care to obtain sufficient data over the stress range of interest. Estimation of the CSL is one step in a larger task of characterizing tailings, and other sources of uncertainty should be considered.

Acknowledgements

We would like to thank Golder and our valued clients for the opportunity to work on challenging projects and to publish this paper. We would also like to thank our colleagues from around the world who generously participated in this study, in particular Riccardo Fanni, who provided the example of the visualizations used in Figure 5, and Mike Pegnam for his helpful comments. Lastly, we owe a debt of gratitude to Ken Been for his inspiration and encouragement.

References

Jefferies, M.G. and K. Been. 2016. *Soil Liquefaction: A Critical State Approach*. Taylor & Francis Group: CRC Press.

Ladd, R.S. 1978. Preparing test specimens using under-compaction. *ASTM Geotechnical Testing Journal* 1(1): 1–8.

Plewes, H.D., M.P. Davies and M.G. Jefferies. 1992. CPT based screening procedure for evaluating liquefaction susceptibility. In *Proceedings of the 45th Canadian Geotechnical Conference*, Toronto, Canada.

Poulos, S.J., G. Castro and J.W. France. 1985. Liquefaction evaluation procedure. *ASCE Journal of Geotechnical Engineering Division* 111(GT6): 772–792.

Reid, D. 2012. Update on the Plewes method for liquefaction screening. In *Proceedings of Tailings and Mine Waste 2012*, Keystone, CO. TMW12: 337–345.

Rosco, K.H., A.N. Schofield and C.P. Wroth. 1958. On the yielding of soils. *Géotechnique*. 8(1): 22–53.

Bibliography

Reid, David. 2019. Preliminary results of critical state testing round robin, The University of Western Australia TAILLIQ project, publication date March 13, 2019. Retrieved from https://www.linkedin.com/pulse/preliminary-results-critical-state-testing-round-robin-david-reid/?trackingId=Ptokccy5TVmdTdOQ2%2ByzGg%3D%3D

Proceedings of Tailings and Mine Waste 2019
November 17–20, 2019, Vancouver, Canada
Published by the University of British Columbia, 2019

Field Testing to Assess the Relative Evaporation Potential of Granular Cover Materials

Kristen Gault, Wood Environment & Infrastructure Solutions, Canada
David Bleiker, Wood Environment & Infrastructure Solutions, Canada
Xiaogang Hu, X.Hu Consulting Inc., Canada

Abstract

Developing effective oxygen limiting soil covers for mine waste generally requires maintaining a prescribed minimum degree of saturation of one or more soil layers. This requires an accurate water balance, often on a time scale of days, for the cover's soil layers and potentially the underlying mine waste. Evaporation is a key component and is often challenging to accurately quantify, particularly on a daily basis. Soil evaporation can be estimated theoretically through the surface energy balance method, or quantified using complex in-situ instrumentation to evaluate a cover's water balance in detail. However, the use of in-situ instrumentation can be costly, and the associated level of detail is not always necessary for screening-level mine closure assessments. Further, field data for evaporation from granular cover materials are limited in the literature. This represents a gap for screening-level mine closure studies considering the use of soil covers to limit evaporation. Therefore, simple field tests were constructed to support determination of the relative evaporative potential of various granular materials being considered for use in closure designs for a subaerial tailings facility in northern Ontario.

Seven field tests were constructed utilizing various granular cover materials ranging from fine-medium sand, uniformly graded gravel, and mine rock. The tests were conducted by constructing cells in plastic totes with a surface area of 1 m^2 (1 m × 1 m). Each cell included a 0.4 m thick layer of cover material. Six cells comprised monolayer covers and one cell comprised a composite cover with 0.3 m of sand overlain by 0.1 m of gravel. Five of the cells were initiated in the spring and monitored over a six-month period. Two of the cells were constructed in the autumn and monitored over the subsequent two months. The precipitation, runoff, and stored water were monitored and measured allowing a water balance approach to be used to estimate the relative water loss through evaporation. The field tests were designed to evaluate the relative evaporative potential of various granular materials being considered for use in closure designs, rather than an absolute measure of evaporation that would occur under field conditions.

Results indicated that the uniformly graded gravel had the lowest observed potential evaporation. This included the test comprising a single layer of uniformly graded gravel and the test with the composite cover of sand overlain by uniformly graded gravel. The highest observed potential evaporation occurred for the tests prepared with a single layer of sand. The differences in observed evaporation between the tested materials were inferred to be related to particle size-dependent factors associated with evaporation and were generally consistent with observations from the available literature. The test method will also be discussed and represents a simple and cost-effective approach for evaluating the relative potential evaporation of granular cover materials under field conditions, in support of screening-level analyses for cover design.

Introduction

The subaerial storage of tailings (e.g., dry stack) is becoming an increasingly attractive option for tailings management owing to the potential risks associated with tailings dam safety. However, the subaerial storage of potentially acid generating and/or metal leaching tailings can be problematic for water quality management and can incur significant costs and risks for mine closure. For example, sulphide mineral oxidation in subaerially deposited tailings is governed by gaseous oxygen diffusion which is strongly linked to the saturation level (moisture content) of the tailings and the overlying soil cover. Therefore, mine closure approaches that aim to maintain saturation of soil covers and/or the underlying tailings to limit the ingress of atmospheric oxygen and subsequent oxidation of sulphide minerals and the release of oxidation products can be considered. In theory, this objective could be achieved by using a soil cover to store water and limit evaporative water losses, thereby enhancing the saturation level of the underlying tailings.

Evaluating the potential performance of such covers requires an accurate water balance, often on a time scale of days, for the cover's soil layers and potentially the underlying mine waste. Evaporation is a key component and is often challenging to accurately quantify, particularly on a daily basis. Soil evaporation can be estimated theoretically through the surface energy balance method or quantified using complex in-situ instrumentation to evaluate a cover's water balance in detail. However, the use of in-situ instrumentation can be costly, and the associated level of detail is not always necessary for screening-level mine closure assessments, where many options for cover design and cover materials are being considered. Further, field data for evaporation from granular cover materials are limited in the literature. This represents a gap for screening-level mine closure studies considering the use of various materials to limit evaporation. Therefore, simple field tests were constructed to support determination of the relative evaporative potential of various granular materials being considered for use in closure designs for a subaerial tailings facility in northern Ontario. The test was intended to evaluate observed potential evaporation in a relative sense between the tested materials, rather than an absolute measure of evaporation that would occur under field conditions.

The approach for this study was to design and monitor evaporation test cells under field conditions, using six different materials in monolayer or composite cover configurations. Granular cover materials evaluated as part of this study ranged from fine to medium sand, uniformly graded gravel, and mine rock. To the authors' knowledge, screening-level field testing of relative evaporation potential from granular cover materials has not been previously documented in literature related to mine closure studies. Therefore, this paper focuses on the methodologies for the evaporation field tests, which represent a novel yet simple method for evaluating the relative performance of granular cover materials to minimize evaporative water losses. Results of the field tests are discussed in terms of material properties, to strengthen the available data on evaporative potential for granular materials for use in screening-level water balance analyses and mine closure designs.

Experimental method

Study site

The evaporation field tests were conducted at a northern Ontario tailings facility. The study site climate is cold and temperate. Regionally, the average annual temperature is approximately 1°C, although temperatures reach an average of approximately 17°C in summer months. Approximately 800 mm of precipitation falls annually. Annual lake evaporation and pan evaporation are on the order of 540 mm and 770 mm respectively for the region.

Closure concept and field test cell design

The field tests were developed to be simple tests in support of screening-level mine closure designs. The overall closure concept being considered included the use of a sand or rockfill cover to enhance saturation of subaerial tailings, by storing water and minimizing evaporative water losses. Engineering contingencies in the design included an irrigation system to supplement rainwater inputs to the cover during dry periods and maintain tailings saturation. The field tests were designed to be consistent with this overall approach and evaluate the relative evaporative potential of various granular materials being considered for use in closure designs. The simplistic approach for the test means that the results represent observed potential evaporation in a relative sense between the tested materials, rather than an absolute measure of evaporation that would occur under field conditions.

Field test vessels were prepared by constructing cells in leak proof plastic totes with a surface area of 1 m^2, as shown in Figure 1. 275 gallon plastic totes were used to construct the cells. The totes were cleaned, and side walls cut down to approximately 0.45 m. The totes were equipped with an overflow pipe, installed at 0.4 m from the base of the tote. A screen was placed on the overflow pipe to limit the erosion of test material during runoff periods. The overflow pipe drained to a plastic pail with a lid. All connections were

sealed with silicone to limit potential water loss due to leakage. The test cells were situated on 25 cm high pallets.

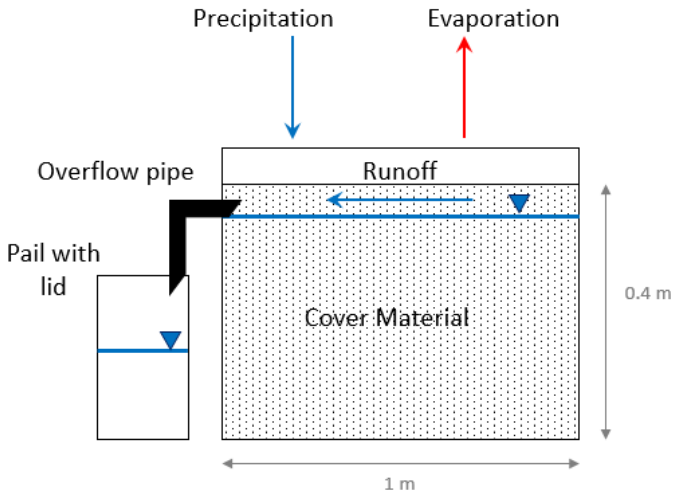

Figure 1: Configuration of field test cells

Seven field test vessels were prepared and placed in an open area. Granular materials were gently placed into each test cell to a height of 0.4 m using an excavator and/or hand shovel. In this configuration, the surface of the test materials was approximately 0.65 m above the ground surface and open to the atmosphere. Based on the design configuration, precipitation that was intercepted by the test cell surface (1 m^2 footprint area) could either runoff into the overflow pail, be stored in the cell, or evaporate from the cell.

The seven field tests and associated types of granular cover material in each test cell are summarized in Table 1. Six of the field tests comprised single-material tests, representing monolayer covers with a thickness of 0.4 m. One of the field tests was prepared with two types of material and represented a composite cover comprised of 0.3 m of sand overlain with 0.1 m of gravel. Test materials were locally sourced from aggregate areas and two mine sites, Mine A and Mine B. The tested materials included “fine sand” (sand with silt), “medium sand” (sand), “gravel” (uniformly graded fine gravel), “run-of-mine rock, Mine A” (poorly graded gravel with sand and silt), “run of mine rock, Mine B” (well graded gravel with sand and silt), and “screened mine rock, Mine B” (uniformly graded coarse gravel).

To initiate the tests, water was added to the test cells, to a height of approximately 0.375 m above the base of the tote, so approximately 2.5 cm of the test material was above the water surface. Water addition was guided by material properties (porosity) and visual observations of the water line in the cell (for coarser materials).

Table 1: Field tests cell summary

Test cell	Test configuration	Material description
Cell 1	0.4 m fine sand	Sand with silt
Cell 2	0.1 m gravel / 0.3 m fine sand	Uniformly graded fine gravel/sand with silt
Cell 3	0.4 m medium sand	Sand
Cell 4	0.4 m gravel	Uniformly graded fine gravel
Cell 5	0.4 m Run of mine rock, Mine A	Poorly graded gravel with sand and silt
Cell 6	0.4 m Run of mine rock, Mine B	Well graded gravel with sand and silt
Cell 7	0.4 m screened mine rock, Mine B	Uniformly graded coarse gravel

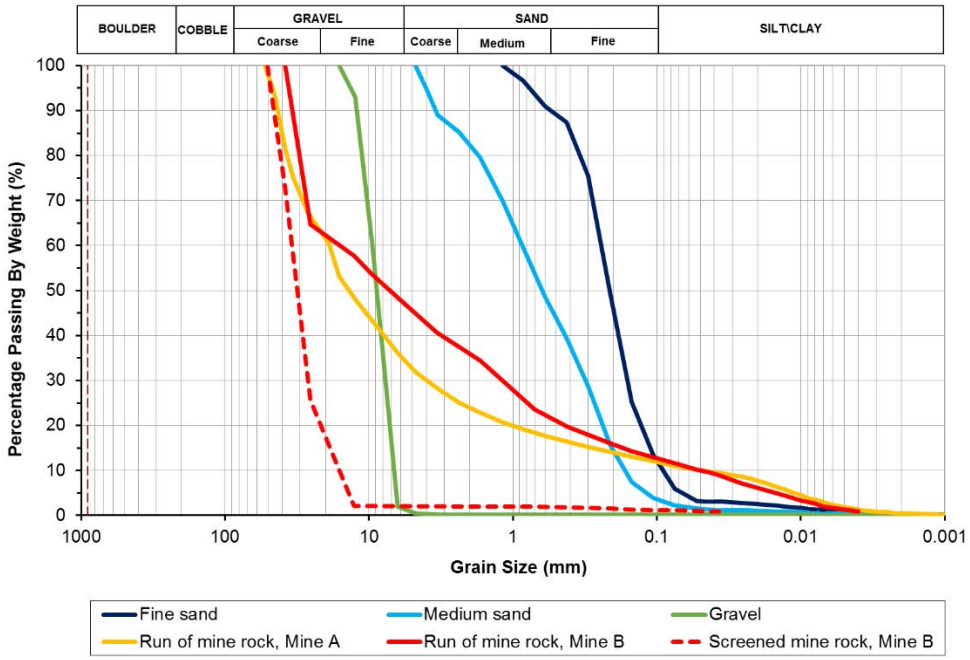

Figure 2: Particle size distribution of tested materials

Test operation, monitoring and data analysis

All field tests were conducted during the same year period. Cells 1 to 5 were initiated in June and Cells 6 and 7 were initiated in September. All tests operated until November; the tests had frozen in early December after which time freezing conditions precluded test operation.

After test initiation, the test cells were monitored every two weeks. Monitoring included measuring the water level in the cover materials in each cell by advancing several hand-dug holes in the cover material to measure the depth to free water and measuring the water level in the overflow pail for each cell. This was considered a conservative and reasonable means by which to measure the saturation of the material for this screening-level assessment. If no free water was observed, additional water was added to the cell to saturate the material to approximately 0.375 m above the bottom of the tote, and support continuation of

the test. Additional water was not added if free water was observed; however, on one occasion additional water was added to Cell 5 when water levels were observed to be nearly depleted and addition of water at the next monitoring period would not have been logistically possible. It is recognized that the addition of water to the test cells during the test period likely enhanced the observed potential evaporation relative to evaporation that could otherwise occur under field conditions. However, the intent of this analysis was to evaluate the relative evaporative potential between the tested materials, as opposed to an absolute evaporation rate that would occur under field conditions as they relate to construction of a granular cover over mine waste. Further, as previously discussed, closure designs included the potential use of an irrigation system to supplement rainwater inputs to the cover during dry periods, so the test approach was consistent with the closure design concept.

As previously described, based on the configuration of the test cells, precipitation could either runoff into the overflow pail, be stored in the cell, or evaporate from the cell. Therefore, a simple water balance was developed for the test cells, supported by monitoring data and site meteorological data. The goal of the water balance was to calculate the observed potential evaporation. Since the test materials have different characteristics and will store water differently, stage storage curves were developed for each of the test cells to support this analysis. Stage storage curves were prepared using known and assumed information for porosity and field capacity for the test materials, as shown in Table 2. Field capacities were based on engineering judgement and pore volumes were generally based on field measurements. The field capacity was integrated into the stage storage curves and represented the residual water volume unavailable for evaporation.

The observed potential evaporation in the field test cells was calculated by Equation 1 below, for each two-week monitoring period:

$$\text{Evaporation} = \text{precipitation} + \text{delta volume} - \text{overflow volume} \quad (1)$$

Where:

$$\text{Delta volume} = \text{water volume start of time period} - \text{water volume end of time period} \quad (2)$$

The change in volume over each two-week monitoring period was estimated using Equation 2. Stage storage curves developed for the cells were used to convert water levels to water volumes considering porosity. The water volume at the start of the two-week time period was based on the measured water level at the end of the previous monitoring event, and the water volume at the end of the time period was based on the measured water level at the end of the current two-week monitoring period. The overflow volume was the measured volume in the overflow pail at the end of each monitoring period. The overflow pail was emptied at the end of each period.

Table 2: Key material properties

Test cell	Material and configuration	Initial pore volume (L)	Field capacity (%)	Porosity	D_{50} (mm)	Specific surface area (m^2/kg)	Monitoring period
Cell 1	0.4 m fine sand	129	15	0.34	0.2	32.1	June to November
Cell 2	0.1 m gravel / 0.3 m fine sand	132	2.5	0.35	9/0.2	2.1/32.1	
Cell 3	0.4 m medium sand	94	8	0.25	0.6	14.7	
Cell 4	0.4 m gravel	144	2.5	0.38	9	2.1	
Cell 5	0.4 m Run of mine rock, Mine A	82	20	0.22	15	42.9	
Cell 6	0.4 m Run of mine rock, Mine B	67	20	0.18	7	24.7	September to November
Cell 7	0.4 m Screened mine rock, Mine B	126	2.5	0.34	32	1.0	

Notes: Initial pore volumes were measured directly during initial water addition for Cells 4 to 7 and calculated for Cells 1 and 3 based on the gravimetric moisture content of the fully saturated material. A combination of these approaches was used for Cell 2. Field capacity for Cell 2 is based on properties of the uniformly graded gravel as the underlying sand was saturated throughout the test period.

Results and discussion

The observed evaporation results for Cells 1 to 5 (June to November test period) and Cells 1 to 7 (September to November test period) are presented in Figures 3 and 4 below. Pond evaporation and pan evaporation are shown for reference, based on monthly averages for the region. All evaporation data are provided as cumulative values over the specific monitoring period identified. Observed evaporation results are tabulated in Table 3. The results are best used to interpret the relative performance of the various covers as opposed to an absolute evaporation rate that would occur under field conditions as they relate to placement of the cover.

Among the five cells that operated from June to November, the fine sand (Cell 1) and medium sand (Cell 3) had the highest observed potential evaporation, followed by the run of mine rock (Mine A, Cell 5). The gravel (Cell 4) and gravel/sand composite cell (Cell 2) performed the best in terms of minimizing evaporation overall. The water volume contained within the gravel cells remained relatively constant over time relative to the initial volume of water added during initiation of the test. In addition, the gravel (Cell 4) had a slightly higher observed evaporation than the gravel sand composite (Cell 2). This was unexpected as other studies have observed the thickness of a coarse layer to result in lower evaporative water losses (e.g., Diaz et al., 2005). However, the differences in observed evaporation between Cell 2 and Cell 4 were low and may be within the sensitivity of the test method which was designed to evaluate relative evaporative potential rather than absolute values. The observed potential evaporation from the fine sand (Cell 1) was

significantly higher than gravel/sand composite (Cell 2). This was expected due to capillary barrier effects. Overall it is noted that several cells (Cells 1, 3 and 5) were observed to be void of free water / dry at several monitoring events and as such, potential evaporation may have exceeded the observed evaporation for these cells for several periods during the test. Further, due to the observed dry condition of the cells, water was added to continue the test, consistent with the engineering concept being evaluated. This may have enhanced the observed evaporation relative to what would occur in the field. However, simplistically, the observed drying of these materials indicated they were less suitable for use in closure designs relative to the gravel, in terms of their potential to limit evaporative water losses.

Other than the fine sand, none of the tested materials were observed to be void of free water during the September to November monitoring period. Trends in the observed relative potential evaporation data for the test period from September to November, including the two tests initiated in September, were somewhat inconsistent with the five tests that operated from June to November, as shown in Table 3. In general, these differences are likely due to the sensitivity of this simple test during periods of generally low evaporation. As such, the data collected from September to November are considered inconclusive and a longer monitoring period would benefit interpretation of the performance of the run of mine rock (Mine B, Cell 7) and screened mine rock (Mine B, Cell 7).

Table 3: Observed potential evaporation results

Test cell	Material and configuration	Total inputs (mm)	Observed potential evaporation (mm)	Days compared
June to November				
Cell 1	0.4 m fine sand	932	786[A]	161
Cell 2	0.1 m gravel / 0.3 m fine sand	555	372	161
Cell 3	0.4 m medium sand	792	631[A]	161
Cell 4	0.4 m gravel	566	429	161
Cell 5	0.4 m Run of mine rock, Mine A	746	535[A]	161
September to November				
Cell 1	0.4 m fine sand	220	208[A]	56
Cell 2	0.1 m gravel / 0.3 m fine sand	223	82	56
Cell 3	0.4 m medium sand	185	146[A]	56
Cell 4	0.4 m gravel	234	103	56
Cell 5	0.4 m Run of mine rock, Mine A	174	87	56
Cell 6	0.4 m Run of mine rock, Mine B	158	84	56
Cell 7	0.4 m Screened mine rock, Mine B	216	101	56

Note: Total inputs = precipitation + water added upon initiation of cell + water added if no free water observed.

[A] Potential evaporation may have exceeded observed evaporation as cell was observed to be void of free water during the monitoring period.

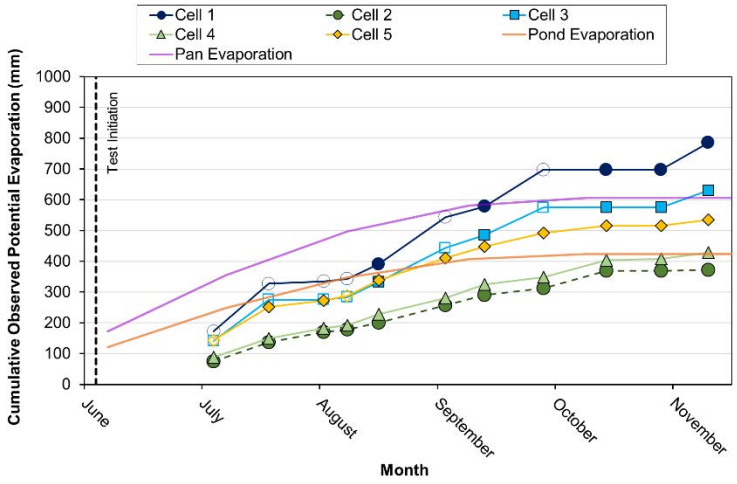

Figure 3: Observed potential evaporation (June to November)

Note: Cumulative monthly pond and pan evaporation are shown for reference based on long term monthly averages for the region. Open symbols indicate the cell was observed to be void of free water / dry and required supplemental water additions. Potential evaporation may have exceeded observed evaporation for these periods.

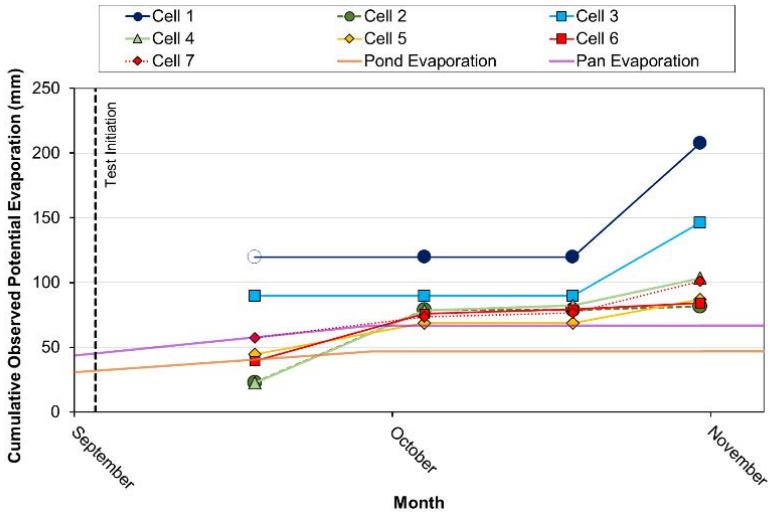

Figure 4: Observed potential evaporation (September to November)

Note: Cumulative monthly pond and pan evaporation are shown for reference based on long term monthly averages for the region. Open symbols indicate the cell was observed to be void of free water / dry and required supplemental water additions. Potential evaporation may have exceeded observed evaporation for these periods.

Climate plays a significant role in evaporation and observed potential evaporation data were compared to site meteorological data over the test period. However, only broad relationships with observed potential evaporation and temperature were evident: all cells showed higher to slightly higher evaporative water losses during the summer months when temperatures were higher, and evaporative water losses showed a downward trend into the autumn months as expected. The lack of other relationships with climate data is

likely related to the complex relationships between meteorological processes and evaporation, which cannot be defined in simple tests. Further, the time step on which the cells were monitored as part of this conceptual-level assessment was long relative to the rate at which climatic factors change, so the specific days which had the most evaporation between monitoring periods (two weeks) could not be determined.

Observed potential evaporation was evaluated with respect to the particle size of the materials in each test cell to evaluate the relationship between particle size and evaporation. Previous studies (e.g., Heinonen, 1985) conducted for soils (clods / clayey soil aggregates) observed a relationship between evaporation and particle size, whereby maximum evaporation was observed for particle sizes ranging from approximately 0.005 – 0.02 mm due to capillary transport of water to the surface of the material as it is heated, and for particle sizes greater than 50 mm, due to turbulent air flow (Heinonen, 1985). A minimum evaporation was observed for particle sizes of 2 mm, driven by gas diffusion. Although there are differences in material properties for clod soils and the granular materials tested herein, a similar overall trend was expected. This has been evaluated in other studies, but typically a wide range of particle sizes is not considered. For example, Modaihsh et al. (1985) showed that fine sand was not as effective at limiting evaporation compared to coarser sand and gravels. An et al. (2018) evaluated evaporation from sand and found that sand particle size had a limited effect on its potential for evaporation, although the particle sizes covered a narrow range (0.2 to 3 mm). Xie et al. (2006) evaluated evaporation from gravel mulch applied to soil. Increased evaporation was observed with increasing particle size, with the lowest evaporation for particle sizes on the order of 2–5 mm diameter, and increased evaporation for particle sizes on the order of 20–60 mm in diameter. This was attributed to air turbulence effects (Xie et al., 2006). Smaller grain sizes were not examined as part of that study. Qui et al. (2014) made similar observations, with higher evaporation noted from coarser gravel mulches (on the order of 40 mm) relative to finer gravel mulches (on the order of 3 mm). Hellwig (1973) identified that evaporation decreased with increasing coarseness of the sand, whereas Xu et al. (2016) observed slightly higher evaporation for coarser sand relative to finer sand.

The interplay between finer materials which can maintain high rates of evaporation through capillary action and coarser materials which have greater air turbulence between particles presents challenges for interpreting literature studies that describe average particle size, as evaporation is likely influenced by the grain size distribution (particularly the smaller particle sizes) as it relates to the size of the pore spaces.

The observed potential evaporation for the five cells (Cells 1 to 5) which operated from June to November was compared to the grain size of these materials (represented by their D_{50}) as shown in Figure 5. Cells 6 and 7, which operated from September to November, were excluded from this analysis due to their short operating period. This analysis indicated that the cells containing gravel, with a D_{50} value of 9 mm, had the lowest observed potential evaporation relative to the other tested materials (Cells 2 and 4). Higher observed potential evaporation was noted for the fine sand (Cell 1), medium sand (Cell 3) and run of mine

rock (Mine A, Cell 5) which were respectively composed of predominantly finer-grained and coarser-grained materials (with a significant fine fraction and lower porosity), relative to the gravel (Cells 2 and 4). Overall this is consistent with observations in Heinonen (1985) and other studies.

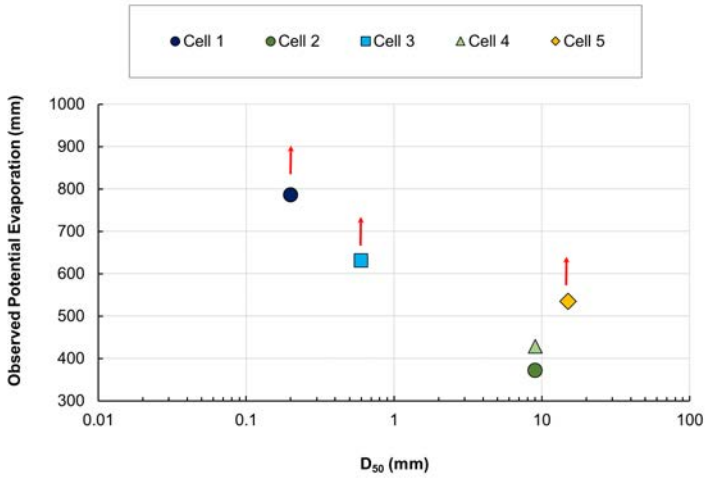

Figure 5: Observed potential evaporation and particle size

Note: Red arrow indicates that the test cell was observed to become dry during the test and potential evaporation may have exceeded the observed evaporation.

As previously described, the monitoring data collected from September to November for the run of mine rock (Mine B, Cell 6) and the screened mine rock (Mine B, Cell 7) was limited and may not represent the relative evaporative potential of these materials well, due to the overall low evaporative demand from September to November. However, results of the other tests could be used to extrapolate an expected test response for the run of mine rock (Mine B, Cell 6) and screened mine rock (Cell 7). Based on this extrapolation, it is expected the Cell 6 (run of mine rock, Mine B) would show higher potential evaporation than Cell 7 (screened mine rock, Mine B), likely consistent with the observations for Cell 5 (run of mine rock, Mine A) given their generally similar properties and textures. It is expected that Cell 7 (screened mine rock, Mine B) would show higher evaporation than Cell 4 (gravel) as both cells have a low fines content but Cell 7 has a greater pore size and may be more affected by turbulent airflow.

Conclusion

The foregoing method represents a simple and low-cost approach to evaluate the relative potential evaporation for granular cover materials as part of screening-level mine closure assessments. The results of this study indicated that the uniformly graded fine gravel would perform better in terms of minimizing evaporation relative to the other tested materials if used for the tailings closure design. The relative

relationships between observed potential evaporation and the textures of tested materials generally align with available information from other studies, in which a minimum evaporative potential was observed for uniformly graded fine gravel and a relatively higher evaporative potential was observed for sands and run of mine rock (gravel, sand, and silt). The observed differences are understood to reflect evaporative effects relative to particle size and pore size.

References

An, Ni, Chao-Sheng Tang, Shi-Kang Xu, Xue-Peng Gong, Bin Shi and Hilary Inyang. 2018. Effects of soil characteristics on moisture evaporation. *Engineering Geology* 239: 126–135.

Diaz, F., C.C. Jimenez and M. Tejedor. 2005. Influence of the thickness and grain size and texture of tephra mulch on soil water evaporation. *Agricultural Water Management* 74(1): 47–55.

Heinonen, R. 1985. Soil management and crop water supply. Department of Soil Sciences. Swedish University of Agricultural Sciences, Uppsala, Figure 26, p. 71.

Hellwig, D.H.R.1973. Evaporation of water from sand, 4: The influence of the depth of the water table and the particle size distribution of the sand. *J. Hydrology* 18: 317–327.

Modaihsh, Abdullah Saad, Robert Horton, and Don Kirkham. 1985. Soil water evaporation suppression by sand mulches. *Soil Science* 139: 357–361.

Xie, Z., Yajun Wang, Wenlan Jiang and Xinghu Wei. 2006. Evaporation and evapotranspiration in a watermelon field mulched with gravel of different sizes in northwest China. *Agricultural Water Management* 81: 173–184.

Qui, Yang, Zhongkui Xiea,Yajun Wanga, Jilong Rena and Sukhdev S. Malhib. 2014. Influence of gravel mulch stratum thickness and gravel grain size on evaporation resistance. *J. Hydrology* 519: 1908–1913.

Xu et al. 2016. Effect of grain size on soil moisture evaporation process. In *Unsaturated Soil Mechanics – From Theory to Practice*, edited by Cen et al. London: Taylor and Francis Group: 451–454.

Bibliography

Yanful, E.K. and Choo, L-P. 1997. Measurement of evaporative fluxes from candidate cover soils. *Can. Geotech. J.* 34: 447–459.

Proceedings of Tailings and Mine Waste 2019
November 17–20, 2019, Vancouver, Canada
Published by the University of British Columbia, 2019

Determination of Consolidation Parameters using Settling Column Tests

Gordan Gjerapic, Golder Associates Inc., USA
Murat Kaya, Golder Associates Inc., USA
Matt Barrett, Golder Associates Inc., USA
Dobroslav Znidarcic, University of Colorado at Boulder, USA

Abstract

The settling column test is commonly used to evaluate initial/settled tailings densities and the effectiveness of additives (flocculants and coagulants) for the thickener design. The test is also used by the tailings storage facility (TSF) designers to estimate the amount of water reporting to the tailings pool, to evaluate the potential for segregation, and to estimate the hydraulic conductivity of tailings at low effective stresses. The settling column data, however, are rarely used to determine tailings compressibility parameters for the TSF design due to limitations in the applied stress levels.

A conventional approach to determine tailings compressibility from settling column measurements involves collecting soil samples after cessation of the consolidation process, or measuring pore pressures and densities with depth. Historically, these measurements have been conducted using large tailings quantities, non-standard laboratory equipment, and employing relatively cumbersome measurement procedures. Methods that are commonly used in the industry to determine tailings compressibility parameters at low effective stresses include the use of slurry consolidometers using large-strain consolidation (LSC) and seepage induced consolidation (SIC) testing procedures. However, the tailings consolidation properties, i.e., hydraulic conductivity and compressibility parameters, can also be determined from settling column measurements by employing parameter-averaging methods or inverse problem solution techniques.

This paper discusses the method to determine compressibility and permeability parameters using settling column measurements. The proposed method is applicable to small-scale and large-scale settling column experiments and allows for the single-drained (impervious bottom) and the double-drained (pervious bottom) boundary conditions. Consolidation parameters are determined by using analytical solutions and inverse problem techniques to fit the predicted settling column behaviour to laboratory measurements. In this study, the consolidation parameters were determined for a 0.3-meter high settling

column experiment on elastic silt (MH) tailings. The model predictions based on the interpretation of settling column data were compared to model predictions based on compressibility and permeability measurements from the slurry consolidation test. A comparison between model results and the experimental measurements demonstrates the importance of determining consolidation properties by accounting for the initial discharge conditions and the stress range of interest. Presented results demonstrate that the proposed approach, based on analytical solutions for the initial and the steady-state conditions at the end of the settling column experiment, can be used to successfully determine tailings consolidation properties.

Introduction

Settling column measurements often rely on cumbersome analytical and laboratory procedures to determine consolidation parameters for tailings slurries. In the past, researchers have used x-ray techniques (see e.g., Been, 1980), sampling of the moisture content and pore pressure measurements with depth (see e.g., Jeeravipoolvarn et al., 2009), and inverse problem solution techniques based on Gibson et al.'s (1967) equation to determine consolidation properties (see e.g., Bartholomeeusen, 2003).

This paper discusses the approach to determine permeability and compressibility parameters based on the settling column experiments using analytical solutions for the single-drained (impervious bottom) and the double-drained (pervious bottom) boundary conditions. Therefore, the proposed method does not require periodic laboratory measurements to determine the density of the soil profile with depth nor the use of numerical tools to solve the large-strain consolidation equation (Gibson et al., 1967). The method is based on the following constitutive relationships (see e.g., Abu-Hejleh and Znidarcic, 1996) for the compressibility:

$$e = A\,(\sigma' + Z)^B \tag{1}$$

and the saturated hydraulic conductivity:

$$k = C\,e^D, \tag{2}$$

where e denotes the void ratio, σ' is the effective stress and k stands for the hydraulic conductivity. *A, B, C, D* and *Z* are material parameters typically determined from laboratory measurements. The parameter Z has units of stress and allows the void ratio at zero effective stress to be properly defined (Liu and Znidarcic, 1991). The proposed method allows for the non-linearity of material properties and is based on analytical expressions for the initial and the steady state conditions determined for a given set of boundary conditions using constitutive relationships defined by Equations (1) and (2). The method uses an inverse-solution approach to determine material parameters by fitting the measured height of the settling column (at the attained steady-state condition) with the analytical expression for the height of the soil column determined from:

$$H = \int [1+e(\lambda)]\, d\lambda, \quad 0 \le \lambda \le Hs \tag{3}$$

where H denotes the height of the settling column at the steady-state condition, $e(\lambda)$ is the void ratio profile with depth, $d\lambda$ is the increment in the height of solids and Hs is the total height of solids (i.e., the height of the tailings material at zero porosity). The proposed method is not recommended for the determination of consolidation properties for tailings that are exhibiting segregation during the settlement process because it assumes uniqueness of constitutive parameters with depth.

Theoretical background

The hydraulic conductivity determination at the initial stage of the settling column experiment is a relatively straightforward process because, at early times of the experiment, the void ratio profile is constant. Therefore, the hydraulic conductivity at early times of the settling column test can be determined by simply rearranging the expression for the increase in the effective stress with depth:

$$d\sigma' = \gamma_w [(Gs-1) + v/k\ (1+e_0)]\, d\lambda \tag{4}$$

At early times, $d\sigma'/d\lambda = 0$, where $d\sigma'$ denotes the effective stress increment and $d\lambda$ is the corresponding increase in the height of solids with depth; γ_w denotes the unit weight of water, Gs is the specific gravity of solids, v is the Darcy's velocity, k is the hydraulic conductivity and e_0 is the initial void ratio of the tailings slurry. Assuming the uniform void ratio profile at early stages of the settling column experiment and the unique relationship between the void ratio and the effective stress, Equation (4) can be rearranged to express the hydraulic conductivity of tailings as:

$$k = v\ (1+e_0)/(Gs-1) \tag{5}$$

where Darcy's velocity, v, is determined by measuring the amount of water accumulating at the surface of the tailings during the initial stages of the experiment with the impervious bottom boundary. The rate of water accumulation at the tailings surface is equal to the settlement velocity of the tailings-water interface. Equation (5) indicates that the dissipation of excess pore pressures at the start of the test results in an upward gradient equal to the critical gradient (i.e., the seepage gradient at the start of the settling column tests is assumed to correspond to the liquefied soil condition also known as the "quick" condition).

For the settling column experiment with the impervious bottom boundary, one can integrate Equation (3) to express the steady-state height of the settling column in the following form:

$$H = Hs + A\ \{\ [\ (Gs-1)\ \gamma_w\ Hs + Z\ ]^{B+1} - Z^{B+1}\ \}\ /\ [\ \gamma_w\ (Gs-1)\ (B+1)\ ] \tag{6}$$

Equation (6) allows for the determination of the final height of the settling column as a function of the total height of solids (i.e., the total amount of tailings material at zero porosity) and the compressibility parameters A, B and Z. Pore pressures at the end of the settling column test with the impervious bottom boundary are hydrostatic. Hence, the final height of the sample defined by Equation (6) does not depend on

the parameters defining hydraulic conductivity. Therefore, the process of determining constitutive parameters may be simplified in its initial stages by using independent determination of permeability and compressibility parameters, i.e., one can use Equation (6) to determine compressibility parameters from the experimental steady-state conditions for which the seepage forces are equal to zero.

For non-segregating slurries, one can use Equation (1) to determine the value of parameter Z at zero effective stress as:

$$Z=(e_0/A)^{1/B} \tag{7}$$

The initial void ratio e_0 in the above equation can be confirmed by sampling the material at the surface of the settling column at the end of the test.

The expression for the tailings height at the end of the settling column experiment with the pervious bottom can be determined analytically by solving Equation (3) for the steady-state conditions (i.e., for the conditions where the sample height and the Darcy's velocity remain constant at the end of the settling column experiment). Alternatively, the steady-state height at the end of the settling column test can be determined numerically using the procedure outlined in Figure 1.

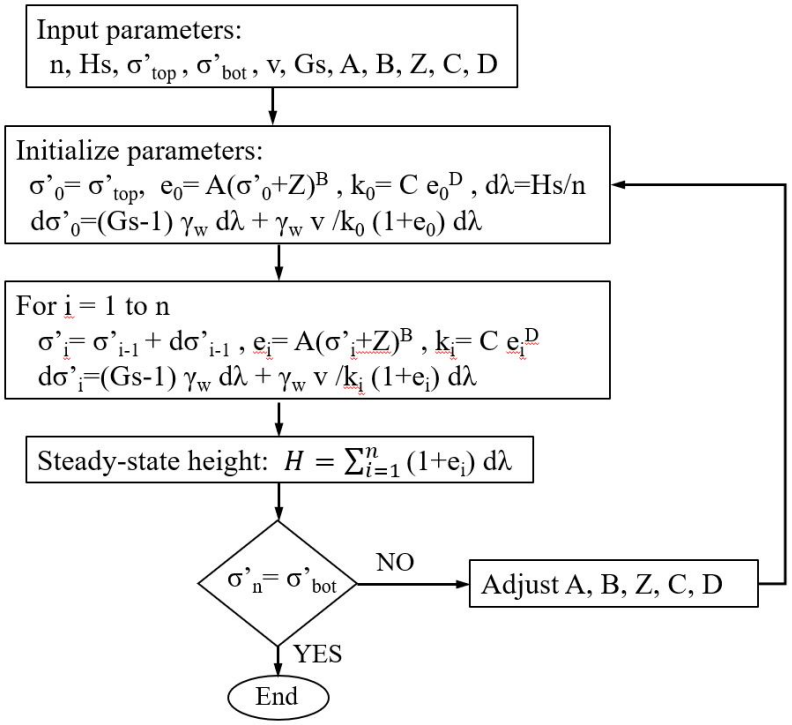

Figure 1: Algorithm for settling column steady-state with pervious bottom boundary

When fitting constitutive model parameters A, B, Z, C and D using data from the settling column test with the pervious bottom boundary, one should also satisfy conditions at the early and the final stages of

the corresponding test(s) with the impervious bottom boundary, see Equation (5), (6) and (7), if these tests were chosen to aid in the parameter estimation process.

To ensure steady-state conditions at the end of the experiment, and to allow for accurate determination of constitutive parameters, it is important to perform the settling column tests in accordance with the appropriate testing procedure.

Experimental procedure

The purpose of the proposed testing procedure is to collect data for the determination of constitutive parameters but also to validate engineering assumptions and to allow for the error-bound determination (accuracy and variability) of critical testing parameters. While the proposed inverse solution approach to determine consolidation parameters A, B, Z, C and D can be applied to settling columns of all sizes, the recommended experimental procedure allows for a relatively fast and inexpensive determination of consolidation parameters at low effective stresses using the initial settling column height between 0.3 and 1.0 m. The procedure consists of the following steps:

1. Prepare the settling column set-up by weighing all mechanical components (acrylic cylinder, stand, valves, pipes, porous stones, feed and drainage containers). If using funnel and mixing tools to prepare the sample, record the weights of this equipment (before and after use) to allow for the adjustments in the recorded mass, as necessary. The amount of water in the empty settling column cylinder (without the tailings sample) should be just enough to cover the bottom porous stone and the filter paper.
2. Collect samples to determine the initial moisture content of the tailings slurry. Carefully pour the slurry into the settling column to minimize air intrusion, avoid splashing and preserve uniformity of the sample. Record the initial mass, time and the height of the slurry at the start of the test.
3. Record the settlement of the slurry (height and time) with the intent to record elapsed time for every 1 to 2 mm of settlement in a column with a minimum initial height of approximately 30 cm. If conducting the test with the drained bottom boundary, record the outflow of water from the bottom of the settling column (to enable calculations of the Darcy's velocity). Also, record the inflow of water on top of the settling column if required to maintain the saturation and the constant head on top of the column while reaching the steady-state conditions. To ensure steady-state conditions at the end of the test, it is important to maintain constant pore pressures (water levels) at the bottom and the top of the settling column (effectively imposing

the constant head conditions at the end of the test to improve accuracy of the hydraulic conductivity parameters).

4. After reaching the steady-state conditions, decant the water on top of the column and place it in the oven at 60°C ("cool" oven) for a couple of days until the sample is firm enough for extrusion. Carefully extrude the sample and cut it into three sections (top, middle and bottom) while rinsing any remaining material into a separate container. Oven-dry the containers with the collected material but make sure to dry the tailings collected at the top and bottom sections of the column in the "cool" oven (e.g., in case the tailings contain gypsum) for the future particle size distribution testing to evaluate the segregation potential.
5. Compare the total dry mass determined by oven-drying at the end of the test, Msf, with the dry mass, Ms0, determined from the initial tailings mass in the settling column, M0, and the initial gravimetric moisture content, w0, of the tailings sample: Ms0=M0/(1+w0). Repeat the test if the absolute value of the relative mass error is larger than approximately 3 percent: $| Ms0 - Msf | / Msf > 3\%$.
6. Compare the initial volume measurement, V0, with the volume determined from the dry mass measurements, $V0m=Msf/(\rho_w Gs) + (Msf\ w0)/\rho_w$. Repeat the test if the absolute value of the relative volume error is larger than approximately 5 percent: $| V0m - V0 | / V0 > 5\%$.
7. Perform sieve analyses on the samples collected from the top and the bottom of the settling column. If there is evidence of segregation, repeat the settling column test using the sample with the higher initial solids content.

Example

A series of settling column tests was conducted on two mill samples collected at the end of the thickening process and reconstituted to 17.4 and 28.4 percent solids. The classification parameters for the two tailings samples are summarized in Table 1

Table 1: Classification parameters

Sample ID	Solids content	Gs	% Fines (<#200)	Liquid limit	Plastic limit	Plasticity index	USCS symbol
T1	17.4	3.04	75.5	67	52	15	MH
T2	28.4	3.11	78.2	69	53	16	MH

Particle size distribution (PSD) curves for T1 and T2 samples are presented in Figure 2. Considering that both samples originated from the same location in the mill and were collected at approximately the

same time, the observed variability in the PSD and the classification parameters is considered typical for this material. As with any laboratory measurement, some of the observed differences may be also due to the scatter in laboratory results (due to experimental errors).

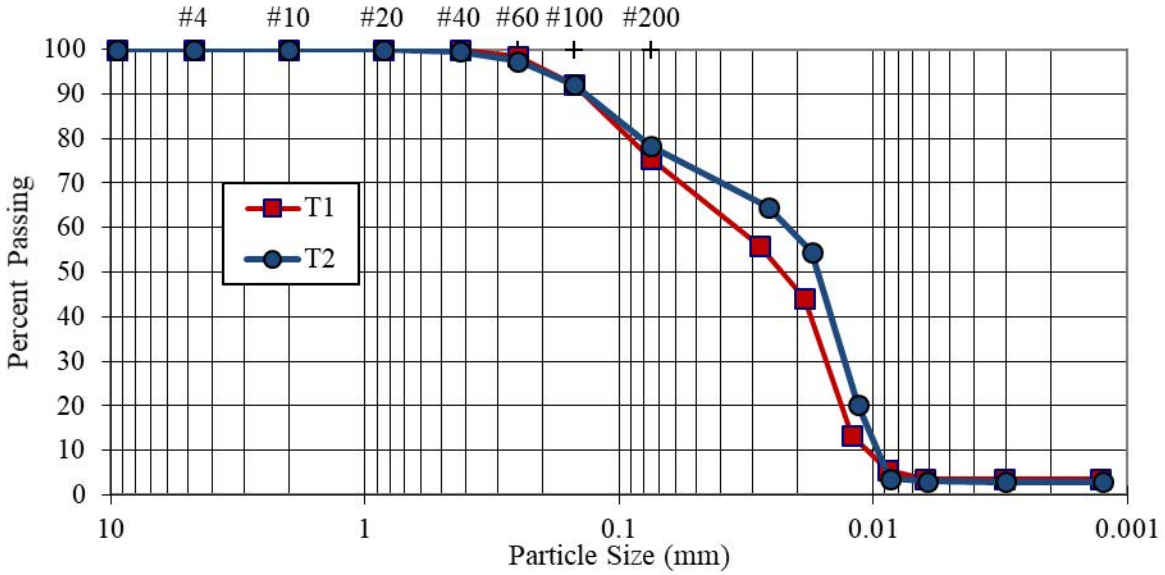

Figure 2: Particle size distribution – T1 and T2 samples

The PSD curves for the material sampled at the top and the bottom of the settling column at the end of the test on T1 sample, i.e., after reaching the steady state condition are shown in Figure 3.

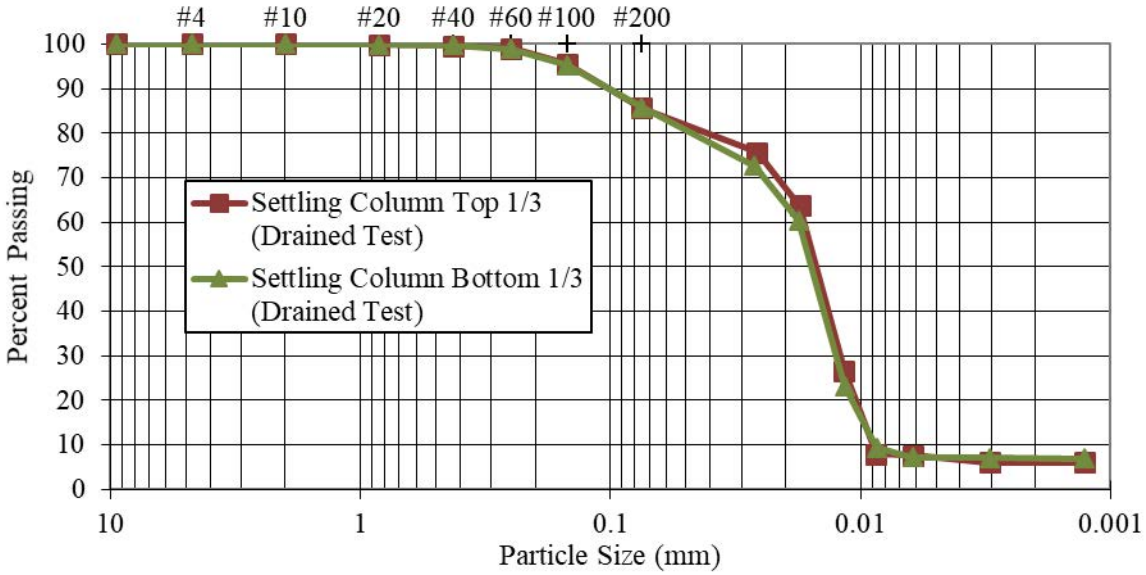

Figure 3: PSD for top and bottom of settling column material – T1 sample

Results in Figure 3 demonstrate a favourable agreement between the PSD curves for the top one-third and the bottom one-third of the settling column material indicating that the segregation effects on the

settling process are likely negligible. However, results in Figure 3 demonstrate that the T1 settling column sample was somewhat finer than the original T1 sample received from the mill (see Figure 2) indicating that some of the sand fraction was lost during the preparation of the sample for the settling column experiment.

Settling column tests

A series of settling column tests was conducted using impervious (undrained) and pervious (drained) bottom boundaries with the results presented in Table 2.

Table 2: Settling column testing – Results

Sample ID	Test	Height of solids (cm)	Initial height (cm)	Final height (cm)	Final dry density (t/m³)	Mass error (%)	Volume error (%)
T1	Undrained	2.227	33.70	19.10	0.35	–0.2	–2.3
	Drained	2.040	32.75	14.45	0.43	3.1	–5.5
T2	Undrained	3.406	30.25	26.35	0.39	–5.3	3.8
	Drained	3.161	28.20	19.90	0.49	–2.1	–2.9

The settling column tests with the impervious bottom boundary resulted in the average settled dry densities of 0.35 and 0.39 t/m^3 at the end of the test. Similarly, the settling column tests with the drained bottom boundary (with the bottom boundary exposed to the atmosphere) resulted in the average settled dry densities of 0.43 and 0.49 t/m^3 at steady-state conditions. Steady-state velocities of 6.76×10^{-5} and 5.95×10^{-5} cm/s were determined at the end of the settling column tests on T1 and T2 samples, respectively. The analyses indicate the maximum effective stresses of approximately 0.7 and 3 kPa at the bottom of the T2 column for the undrained and the drained bottom boundary conditions, respectively.

The fitting procedure using selected analytical solutions resulted in the determination of consolidation parameters summarized in Table 3

Table 3: Consolidation parameters based on settling column tests

Sample ID	A (kPa$^{1/B}$)	B (–)	Z (kPa)	C (cm/sec)	D (–)
T1	4.781	–0.2638	0.015	1.04×10^{-8}	4.86
T2	5.817	–0.2286	0.237	1.83×10^{-6}	2.09

Comparison with slurry consolidation testing

Consolidation relationships determined from the settling column tests were compared to compressibility and permeability curves determined using the slurry consolidometer apparatus for the range of vertical effective stresses between 7 and 690 kPa in Figure 4.

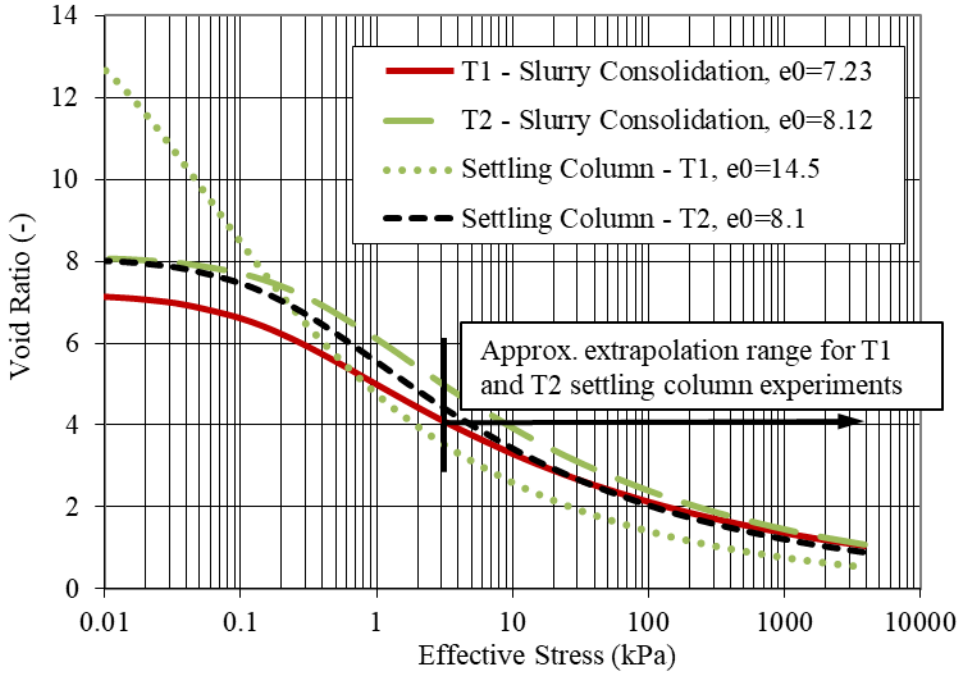

Figure 4: Compressibility relationships – settling column versus slurry consolidation testing

Hydraulic conductivity relationships determined from the settling column data and the slurry consolidation data are presented in Figure 5.

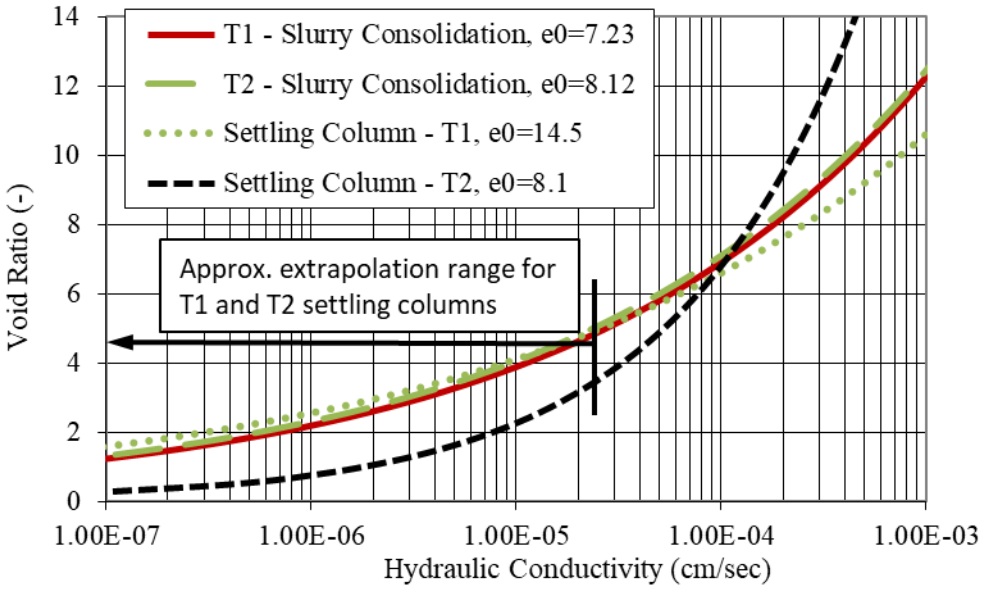

Figure 5: Hydraulic conductivity – settling column versus slurry consolidation testing

Predicted and measured settlement curves

Constitutive parameters determined from both the settling column data and the slurry consolidation tests were used to develop large-strain consolidation models for the conducted settling column experiment using the computer program CONDES (Yao and Znidarcic, 1997). A comparison between the measured and the predicted time-settlement curves for the T1 tailings sample is shown in Figure 6.

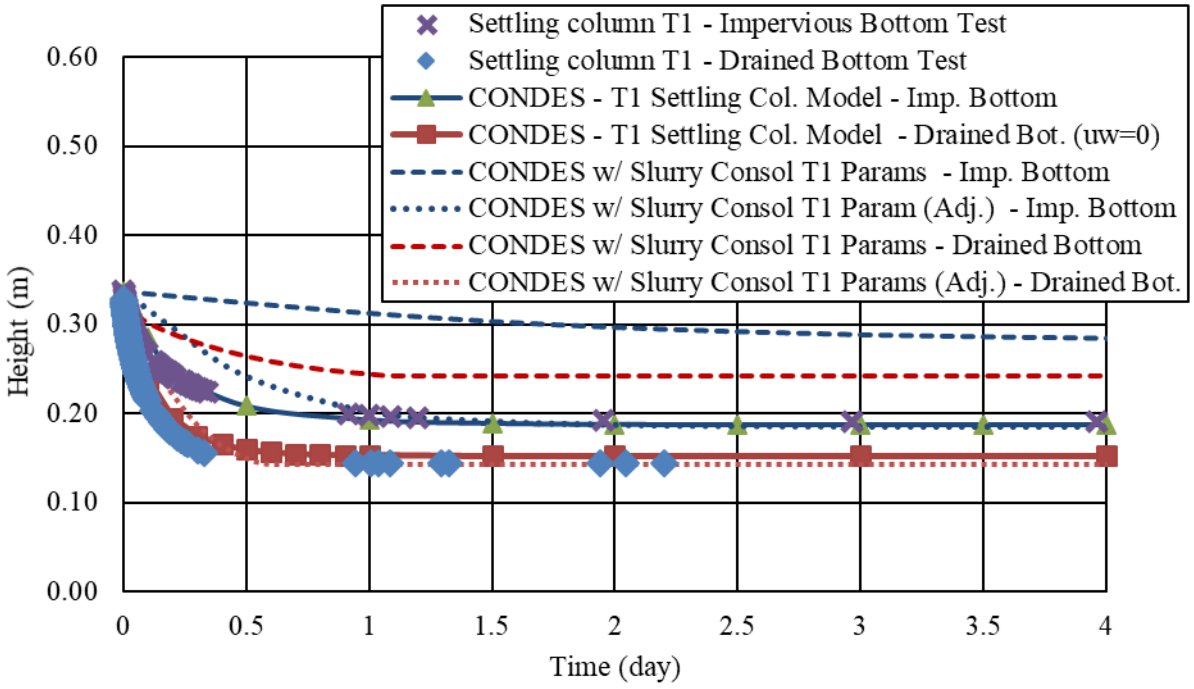

Figure 6: Predicted and measured settlements – T1 sample

The slurry consolidation test on the T1 sample (see Figure 4) was conducted with a significantly higher initial density than the settling column tests displayed in Figure 6. Consequently, the initial height of solids in the CONDES model based on the original T1 slurry consolidation parameters is approximately two times larger than the height of solids in the actual experiment resulting in the relative settlement error of approximately 50% between the calculated (using the original T1 slurry consolidation compressibility relationship) and the measured settlement for the T1 settling column sample. One can adjust the compressibility curve for the T1 slurry consolidation sample to enforce the same height of solids in the CONDES model and the settling column experiment (see dotted curves in Figure 6) resulting in an improved agreement between the calculated and the measured final heights. Numerical models that are employing constitutive parameters determined for the range of stresses, solid contents and flow rates observed in the experiment (e.g., the initial void ratio for the T2 slurry consolidation sample is approximately the same as the initial void ratio in the T2 settling column experiment) are expected to exhibit significantly better agreement with the measured data as demonstrated by results in Figure 7.

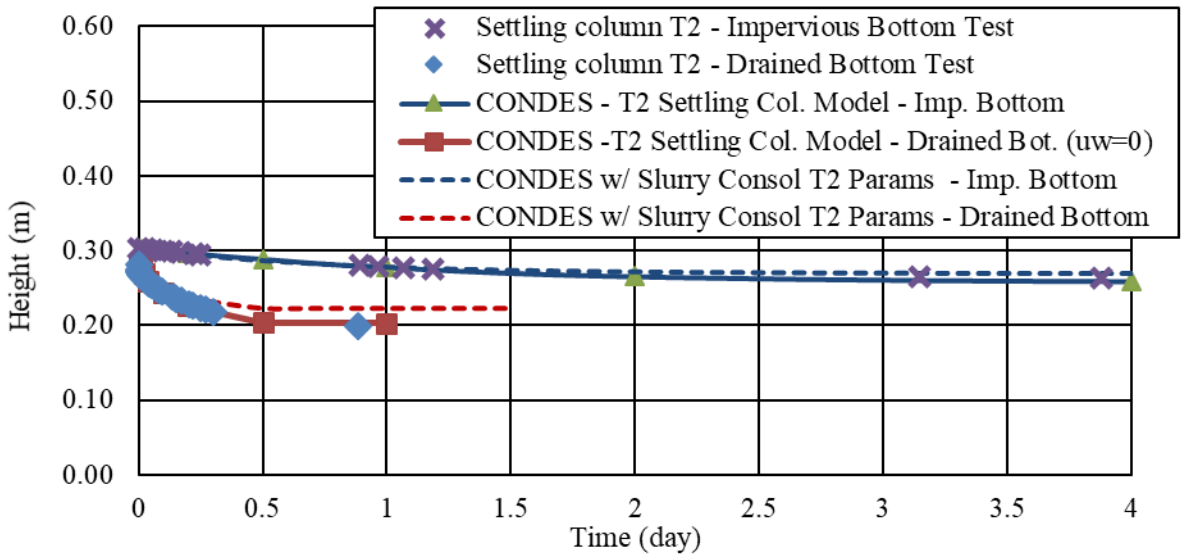

Figure 7: Predicted and measured settlements – T2 sample

Conclusion

This paper discusses a method to determine consolidation properties from the settling column experiments using analytical solutions for the initial and the steady-state laboratory conditions. To validate the proposed methodology, constitutive properties from the settling column tests were used to develop a numerical model and compare the predicted time-settlement curves with the measured data. In addition, consolidation parameters from the settling column tests were compared to parameters from the slurry consolidation tests.

The inverse solution approach (applied to determine consolidation parameters from settling column tests) indicates the need to consider potential variability of material properties, as well as the variability of imposed initial and boundary conditions, when interpreting laboratory data. To compare differences between tests on different tailings samples (assuming that these tests are conducted using the same or similar materials), one should consider:

- The variability in the particle size distribution between different materials.
- The error bounds for the reported mass and volume quantities.
- Potential variability in the initial and boundary conditions during the test on an individual sample and between different laboratory experiments.

The proposed methodology provides flexibility and redundancy to determine consolidation parameters for the range of effective stresses applicable to settling column experiments. A minimum of two settling column experiments are required to determine five consolidation parameters: A, B, Z, C, and D. Compressibility parameters A, B, and Z can be determined using analytical solutions for the final height of the sample and by using the constitutive equation for the initial void ratio at zero effective stress (i.e., by

determining the void ratio at the surface of the sample). Two permeability parameters C and D can be determined from data collected during the initial stage of the settling column experiment with impervious boundary. However, to provide permeability data over a wider range of tailings densities, it is recommended to use steady-state measurements from the settling column experiment with the pervious bottom boundary.

Consolidation parameters determined from the settling columns compare favourably to parameters from the slurry consolidation tests for slurries prepared at similar initial densities. The relative differences between measured and predicted final heights based on slurry consolidation measurements (for slurries with the initial solid content similar or corrected to the initial solid content of a settling column) range from 1 to 12 percent. Model predictions based on the interpretation of the settling column data resulted in the relative difference ranging from 2 to 5 percent considering both the single-drained and the double-drained conditions.

The proposed approach allows for rapid and inexpensive determination of consolidation parameters. Consequently, the method can be used as a screening tool in cases where conventional consolidation measurements are not available and to confirm the validity of consolidation measurements obtained from other methods.

References

Abu-Hejleh, A.N., D. Znidarcic and B.L. Barnes. 1996. Consolidation characteristics of phosphatic clays. *Journal of Geotechnical Engineering* ASCE, New York, 122(4): 295–301.

Bartholomeeusen, G. 2003. Compound shock waves and creep behaviour in sediment beds. Ph.D. thesis, Oxford University, UK.

Been, Ken. 1980. Stress strain behaviour of cohesive soil deposited under water. Ph.D. thesis, Oxford University, UK.

Gibson, R.E., G.L. England and M.J.L. Hussey. 1967. The theory of one-dimensional consolidation of saturated clays, *Geotechnique* 17: 261–273.

Jeeravipoolvarn, S., J.D. Scott and R.J. Chalaturnyk. 2009. 10 m standpipe tests on oil sands tailings: Long-term experimental results and prediction. *Canadian Geotechnical Journal* 46(8): 875–888.

Liu, J.C. and D. Znidarcic. 1991. Modeling one-dimensional compression characteristics of soils. *Journal of Geotechnical Engineering*, ASCE, 117(1): 164–171.

Yao, D.T.C. and D. Znidarcic. 1997. Crust formation and desiccation characteristics for phosphatic clays – Users' manual for computer program CONDES0, *Florida Institute of Phosphate Research (FIPR)* Publication No. 04-055-134.

Proceedings of Tailings and Mine Waste 2019
November 17–20, 2019, Vancouver, Canada
Published by the University of British Columbia, 2019

In-Situ Hydraulic Conductivity Testing of a Geowaste Test Pile

Mohammad H. Gorakhki, Colorado State University, USA
Christopher A. Bareither, Colorado State University, USA
Joseph Scalia, Colorado State University, USA
Manuel Aparacio, Newmont Goldcorp, Guatemala
Michael Jacobs, Newmont Goldcorp, Canada

Abstract

An in-situ hydraulic conductivity test was conducted on a GeoWaste pile using a sealed double ring infiltrometer (SDRI). GeoWaste is a mixture of fast-filtered tailings and waste rock blended such that waste rock particles exist as inclusions within a tailings matrix. The GeoWaste pile was a truncated 5-m tall pyramid with 25-m base sides and a flat 5-m × 5-m surface. The pile experiment was operated for 26 months, and the SDRI test was conducted during decommissioning. Tensiometers and water content sensors were used to measure progression of the wetting front, and the ultimate extent of the wetting front was identified during decommissioning. Hydraulic conductivity measured via the SDRI was compared to results from laboratory tests on specimens prepared to represent GeoWaste of the test pile. The average hydraulic conductivity of the GeoWaste pile was 1.4×10^{-6} m/s for the first two days of experiment and 9.0×10^{-7} m/s for the last three days of experiment. Hydraulic conductivity measured in-situ was approximately 50 to 100 times higher than hydraulic conductivity measured on laboratory-prepared specimens. Differences in hydraulic conductivity measured in-situ and on laboratory specimens were attributed to the presence of macropores from pedogenesis and/or inclusion of larger waste rock particles in the test pile.

Introduction

The increased consumption of raw materials combined with the ability to extract metals from lower-grade ore bodies has led the mining industry to generate larger volumes of waste that require innovative and sustainable approaches to waste management (Blight, 2009; Yilmaz, 2011). The main challenges facing waste rock management in piles are acid mine generation and mechanical stability. Management of slurry, thickened, or paste tailings commonly is within a tailings impoundment that requires retention via tailings dams, whereas filtered tailings can be deposited without the need for tailings dams (Bussière, 2007; Davies, 2011). Management of tailings impoundments and dams has presented challenges throughout the history of mining, and recent failures (Morgenstern et al., 2015; Morgenstern et al., 2016) have highlighted the

need to re-evaluate the existing methods of mine waste management to create alternative approaches that improve stability and decreasing potential risk to human health and the environment.

Mixing waste rock and tailings (WR&T) has been evaluated as an alternative mine waste management technique to address the following:

1. increase waste stability to reduce risk of failure;
2. improve water management to reduce contamination potential;
3. mitigate acid production from waste rock;
4. facilitate post closure and reclamation of mine waste facilities; and
5. eliminate tailings dams (e.g., Williams et al., 2003; Leduc et al., 2004; Wickland et al., 2006; Bussière, 2007; Bareither et al., 2018).

Hydraulic properties of WR&T, in particular hydraulic conductivity, control infiltration, seepage, and generation of leachate. Waste rock and tailings mixtures with low hydraulic conductivity can reduce infiltration from precipitation, the rate of seepage, and percolation at the base of a deposit.

An innovative WR&T mixture, referred to as GeoWaste, has been introduced as a potential mine-waste management solution to create geotechnically and geochemically stable deposits that do not require dams of embankments (Bareither et al., 2018). GeoWaste is a mixture of fast-filtered tailings and waste rock prepared in a tailings-dominated mixture. Recent research on GeoWaste has focused on shear strength (Burden et al., 2018; Borja, 2019), compressibility (Bareither et al., 2018), and hydraulic properties (Gorakhki et al., 2019). In addition, a field-scale test pile was constructed to evaluate the potential for GeoWaste to encapsulate potentially acid-generating waste rock within the tailings matrix and mitigate acid generation. This test pile was constructed at a mine in Central America and operated under natural climatic conditions for 26 months. In addition to assessing the ability of GeoWaste to mitigate acid generation, the field-scale test pile also provided an invaluable opportunity to measure in-situ hydraulic conductivity. The purpose of this study was to conduct an in-situ hydraulic conductivity test on a field-scale GeoWaste test pile after two years of operation. In-situ hydraulic conductivity was also compared to results from laboratory tests conducted on mine waste materials used to construct the test pile.

GeoWaste test pile

The pile was constructed in January 2017 at a mine in Central America. The pile was designed as a truncated 5-m tall pyramid with 25-m base sides and a flat 5 m × 5 m surface. The pile was constructed with GeoWaste prepared to a mixture ratio of 0.40 (total mass of waste rock/total mass of tailings). Potentially acid generating (PAG) waste rock was used in GeoWaste placed in the central core of the pile and non-PAG waste rock was used in GeoWaste placed on the side slopes. GeoWaste was prepared with filtered mine tailings and either PAG or non-PAG waste rock. All materials were mixed on site using an excavator prior

to placement. GeoWaste for the side slopes of the test pile, which included non-PAG waste rock, was placed using an excavator to create a 5 m × 5 m ring to form the central core. GeoWaste prepared with PAG waste rock was dropped from a height of 2 to 3 m using an excavator to form the central core of the pile. This deposition process for the central core simulated the anticipated full-scale GeoWaste final placement process via disposal at the end of a conveyor system. The in-situ hydraulic conductivity test was conducted within the central core of the GeoWaste pile.

Plan view and cross-section schematics of the GeoWaste pile central core are shown in Figure 1. The pile was instrumented with four layers of sensors, and each layer contained five sets of sensors: one set located in the center and four sets positioned approximately 2-m radially from the center on sides of the pile. The main sensors relevant to this study were TDR-315L Acclima sensors to measure volumetric water content. These sensors were connected to a CR-1000 Campbell Scientific datalogger. The instrumentation station had a solar panel that provided excitation voltage for sensors and energy to run the datalogger.

The GeoWaste pile experiment was operated for approximately 26 months. At the end of the experiment duration, a sealed double-ring infiltrometer (SDRI) test was conducted on the central core of the pile. Approximately 0.4 m of the surface of the GeoWaste test pile was removed prior to installation of the SDRI to clear the surface of vegetation and create a smooth, clean surface to construct the SDRI.

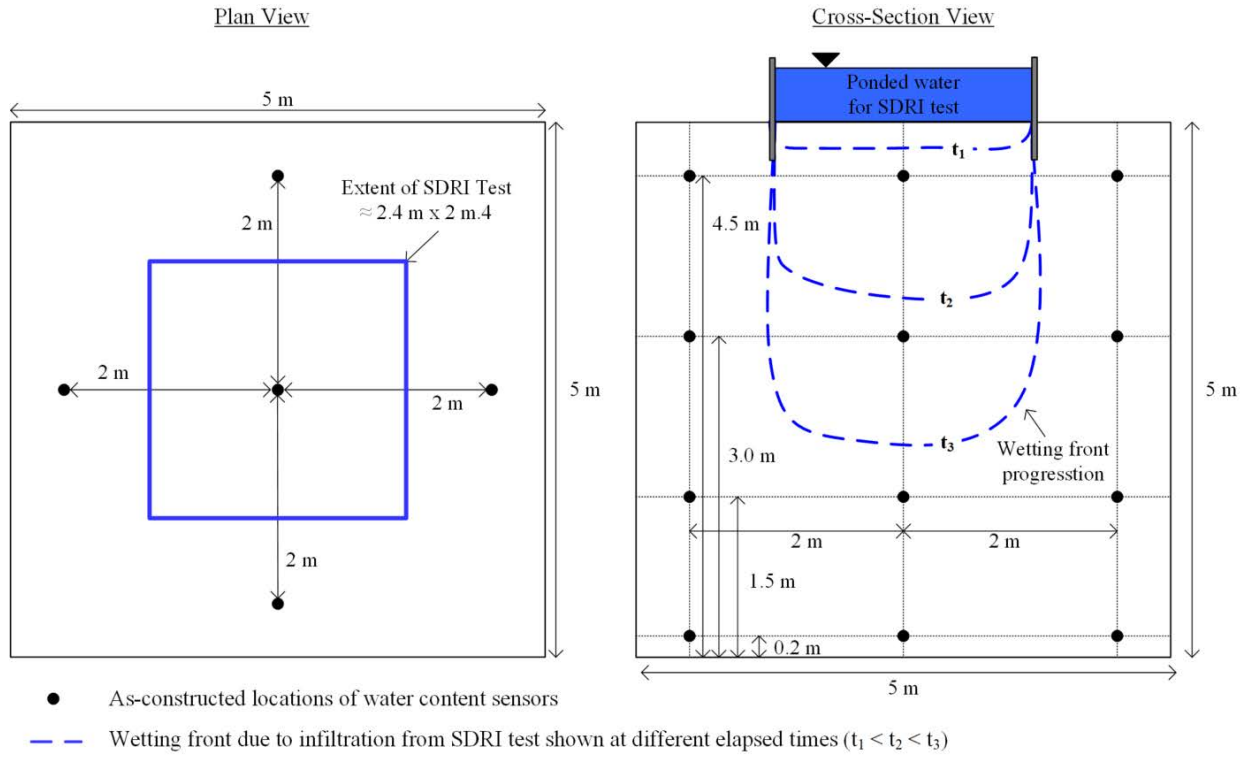

Figure 1: Plan view and cross-section schematics of the GeoWaste pile that identify approximate locations of water content sensors and the size, location, and anticipated wetting front at different elapsed times from the sealed double-ring infiltrometer (SDRI) test

Materials and methods

Materials

Geotechnical material characterization of mine tailings and waste rock included mechanical sieve and hydrometer (ASTM D422) and Atterberg limits (ASTM D4318). Material characteristics of the tailings and waste rock are summarized in Table 1. These characteristics were measured on samples representative of mine waste used to construct the GeoWaste pile. The liquid limit (LL) of tailings agreed with the reported range in literature (i.e., 18% <LL <40%). Jehring and Bareither (2016) presented an average, upper-bound, and lower-bound particle-size distributions for tailings and waste rock based on a compilation from literature. Tailings were comparable with average tailings properties reported by Jehring and Bareither (2016); however, waste rock was more well-graded and had a higher fines content (fine content >23%) compared to the average waste rock particle-size distribution compiled from literature (fines content <2%).

Table 1: Summary of physical characteristics and classification for tailings and waste rock

Material	*LL* (%)	*PI* (%)	USCS	Gravel content (%)	Sand content (%)	Fines content (%)	Clay-size content (%)
Tailings	30.1	9.2	CL	0	14.3	85.7	23.6
Waste rock	NA	NA	GM	45.0	31.7	23.3	NA

Notes: *LL* = liquid limit; *PI* = plasticity index; USCS = Unified Soil Classification System; and clay-size content taken as percent particles by mass <0.002 mm; NA = not applicable

Sealed-double ring infiltrometer (SDRI) test

The execution and data evaluation of the sealed-double ring infiltrometer test were conducted in accordance with ASTM 5093 and per recommendations in Daniel (1989). The SDRI outer ring had dimensions of 2.4 m × 2.4 m and was constructed from 13-mm-thick plywood, whereas the inner-ring had dimensions of 1 m × 1 m and was constructed of 3.2-mm-thick sheet metal. The outer ring and inner ring were centered on the surface of the test pile to focus infiltration in the central core of the pile (Figure 1). Plywood for the outer-ring was treated with polyurethane paint and sealed along the edges with wood glue and caulk to create a watertight structure. The level of water ponded within the outer ring was monitored via a meter stick adhered to the sidewall of the outer ring. Inflow in the sealed inner ring was monitored via connection to a 5-L flexible plastic bag.

Depth of the wetting front during infiltration was monitored via tensiometers, water content sensors (Figure 1), and observations post-testing made during decommissioning of the pile. Three tensiometers were installed between the outer and inner rings of the SDRI in the test pile at different depths from the surface. During the SDRI test, there were 10 water content sensors from the 20 originally installed in the GeoWaste pile that were functional and capable of monitoring progression of the wetting front.

The SDRI test in the GeoWaste pile was operated for 7 days and the ponded water depth was maintained between 0.11 m and 0.43 m. During SDRI testing, inflow measurements from the flexible plastic bag connected to the inner ring and measurements of ponded water height in the outer ring were recorded at a frequency of approximately once or twice per hour during the day (i.e., measurements were not recorded during the night). Hydraulic conductivity of the test pile was computed as

$$k = \frac{I}{i} \tag{1}$$

where I is infiltration rate and i is hydraulic gradient. Infiltration rate of the inner ring was computed as

$$I = \frac{V}{A_{ir}\,\mathrm{g}\Delta t} = \frac{\Delta W_{bag}}{\rho_w\,\mathrm{g} A_{ir}\,\mathrm{g}\Delta t} \tag{2}$$

where V is the volume of infiltrated water in the inner ring, A_{ir} is the area of inner ring, Δt is the elapsed time of inner ring infiltration, and ΔW_{bag} is the change in the weight of bag connected to the inner ring. The infiltration rate of the outer ring was computed based on the change in ponded water depth and area of the outer ring. The ponded water depth in the outer ring was corrected for evaporation based on pan evaporation recorded during the SDRI test. The hydraulic gradient was computed as

$$i = \frac{D_p + D_f + \Psi_f}{D_f} \tag{3}$$

where D_p is depth of water ponded in the outer ring, D_f is depth of the wetting front, and ψ_f is suction head at the wetting front. The same hydraulic gradient was computed for the outer and inner rings and used in Equation 1 to determine hydraulic conductivity.

Several suggestions are provided in literature to estimate ψ_f in Equation 3. Daniel (1989) reported that a conservative assessment of hydraulic conductivity can be obtained by assuming $\psi_f = 0$, which decreases the hydraulic gradient. Wang and Benson (1995) presented the following equation to estimate ψ_f:

$$\Psi_f = \frac{\Psi_a}{3}\left[1 - \frac{D_f}{L}\right] \tag{4}$$

where ψ_a is the air-entry pressure and L is the total thickness of the layer being evaluated during an SDRI test. In this study, ψ_a in Equation 4 was measured for GeoWaste via laboratory testing (Gorakhki et al., 2019). Laboratory pressure plate tests were conducted on 152-mm diameter by 76-mm-tall GeoWaste specimens prepared to the same mixture ratio as the pile test, but with a maximum particle size of 25 mm. Air-entry pressures of 2.5 m and 1.0 m were the maximum and minimum measured values for GeoWaste (Gorakhki et al., 2019), and were used in Equation 4 for calculating hydraulic conductivity.

Results

Wetting front assessment

Temporal trends of normalized tensiometer (T_n) readings in the GeoWaste pile during the first day of the SDRI test are shown in Figure 2a. The T_n was calculated as suction measured by a tensiometer during infiltration divided by the equilibrated suction of the same tensiometer measured prior to infiltration (i.e., at t = 0 d). Normalized tensiometer readings were used to assess wetting front progression because the actual soil suction was not used in the analysis. The change in soil suction relative to the equilibrated soil suction was used to identify the time at which the wetting front reached a given tensiometer. A modest increase in T_n above 1.0 at the onset of infiltration from the SDRI was observed in all tensiometers, which was subsequently followed by a sharp reduction in T_n that identified arrival of the wetting front. The sharp reduction in T_n corresponded to the wetting front reaching the installed depth of the tensiometers.

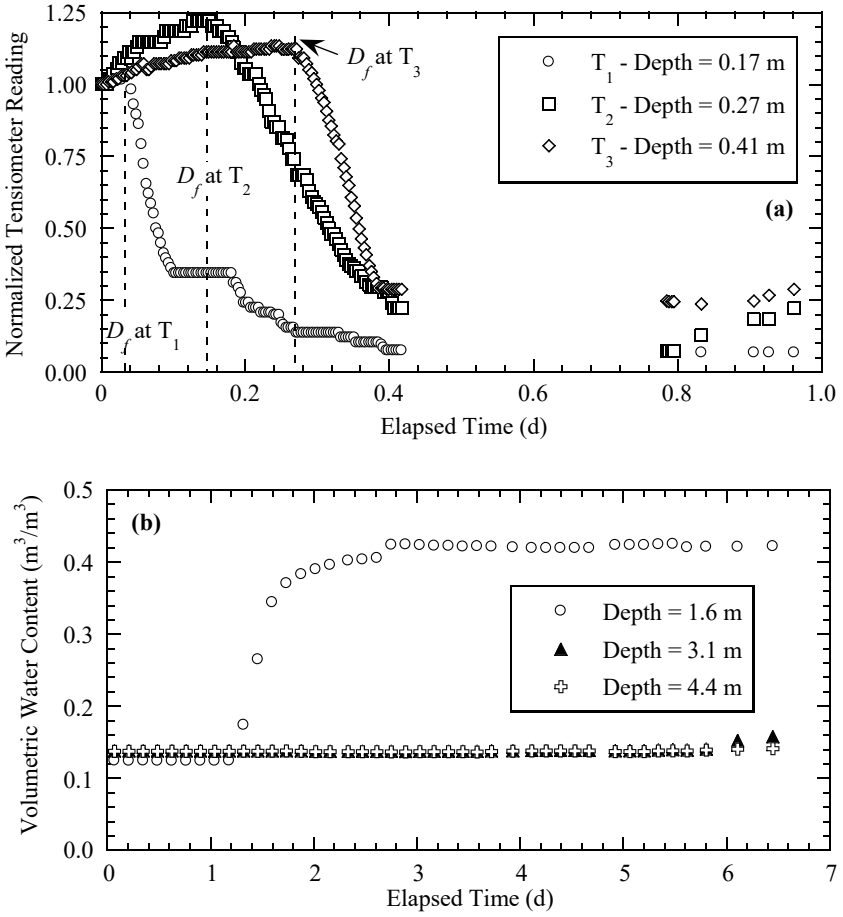

Figure 2: Temporal relationships of (a) normalized tensiometer readings (T_n) and (b) volumetric water content sensors in the GeoWaste pile during infiltration. Note: T_n was computed as tensiometer measurement at any time divided by measurement of tensiometer at t = 0 d

Volumetric water content was monitored in the GeoWaste pile during the SDRI test via sensors installed at different depths (Figure 1). During the SDRI test there were two sensors active in Layer 2 (depth = 1.6 m), three sensors active in Layer 3 (depth = 3.1 m), and five sensors active in Layer 4 (depth = 4.4 m). Average volumetric water contents for each of the three layers (Layer 2, 3, and 4) in the GW pile during the SDRI test are shown in Figure 2b. The average volumetric water content was similar in all three layers at the onset of the SDRI, and ranged between 0.12 and 0.14. The average water content in Layer 2 (depth = 1.6 m) exhibited a pronounced increased at t = 1.3 d, which correspond to the arrival of the wetting front. The average volumetric water content in Layer 3 exhibited a slight increase at t = 6.0 d.

The wetting front also was tracked during pile excavation. The wetting front was observed to just intersect sensors in Layer 3. Observations made during excavation were used to confirm that the small increase in volumetric water content observed in Layer 3 as the datalogger station was powered down corresponded to arrival of the wetting front. The average volumetric water content in Layer 4 (depth = 4.4 m) did not exhibit a marked change (Figure 2b), which correlated with observations made during excavation that the wetting front did not reach the deepest set of sensors.

The depth of the wetting front as a function of time during an SDRI test can be estimated via a wetting front-time relationship. The wetting front-time relationship for the GeoWaste pile is shown in Figure 3, which was developed using tensiometers at depths of 0.17, 0.27, and 0.41 m (Figure 2a) and water content sensors at depths of 1.60 and 3.10 m (Figure 2b). Least squares linear regression of the wetting depth versus square-root of time yielded the wetting front-time relationship to estimate D_f in Equation 5 at any time during operation of the SDRI in the GeoWaste pile.

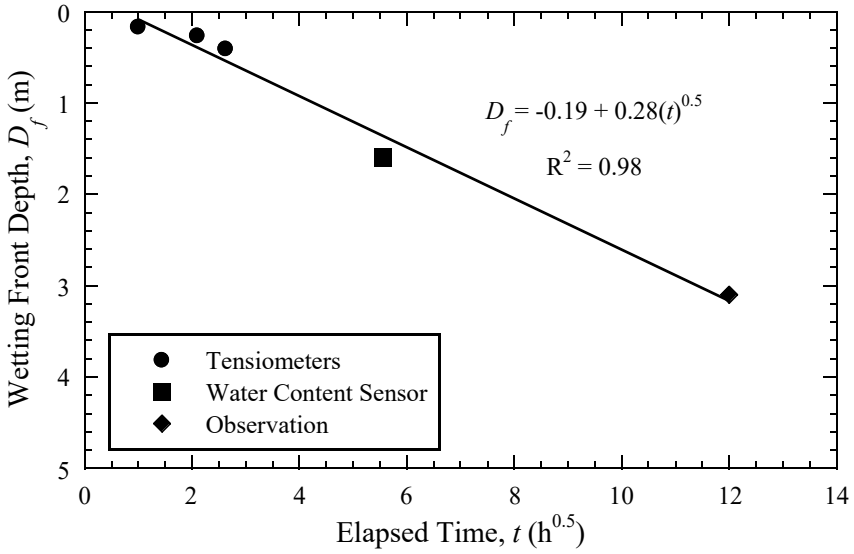

Figure 3: Wetting front-time relationship for the SDRI test conducted in the GeoWaste pile

Infiltration rate and hydraulic conductivity

Temporal trends of infiltration rate in the GeoWaste pile computed from fluctuations of ponded water depth in the outer ring and measurements of inflow via the flexible plastic bag connected to the inner ring are shown in Figure 4a. Readings of the water depth in the outer ring are also shown in Figure 4a. The target water depth in the outer ring was approximately 0.4 m. In general, the infiltration rate for the outer ring was faster than the infiltration rate for the inner ring during the first three days of the SDRI test. Subsequently, infiltration rates from both rings converged on Day 4 and remained similar until the end of the experiment. The initial faster infiltration rate for the outer ring was attributed to a more pronounced 2-dimensionsal (2D) flow path relative to the concentrated 1-dimensional (1D) flow path of the inner ring. As infiltration from the SDRI continued and the wetting front progressed deeper in the pile, infiltration rates from the outer and inner ring converged due to a reduced contribution of the horizontal component of flow to total infiltration in the outer ring.

The infiltration rates for the outer and inner rings decreased during the first three days and approached a constant value of approximately 10^{-6} m/s for the last four days of the SDRI test. The decrease in infiltration rate as a function of time may be a result of two mechanisms: (i) decrease in hydraulic gradient or (ii) decrease in hydraulic conductivity. The hydraulic gradient decreased from 2.6 (at t = 0.2 d) to 1.15 (at t = 6.0 d) as depth of the wetting front increased. Hydraulic conductivity is equal to the infiltration rate divided by the hydraulic gradient (Equation 1), which implies that for a constant hydraulic conductivity the infiltration would decrease by a factor of approximately two as the hydraulic gradient decreased. However, the infiltration rate decreased by a factor of four during the SDRI test (Figure 4a), which suggests that hydraulic conductivity also decreased with depth and/or time.

Temporal trends of hydraulic conductivity for the GeoWaste pile are shown in Figure 4b. Hydraulic conductivity was calculated based on three assumptions to calculate suction at the wetting front: (i) $\psi_f = 0$ m; (ii) $\psi_a = 2.5$ m; and (iii) $\psi_a = 1$ m. Air-entry pressures of 2.5 m and 1.0 m were the maximum and minimum measured values for GeoWaste based on laboratory specimens prepared to represent field conditions (Gorakhki et al., 2019). The three assumptions used to calculate ψ_f yielded hydraulic conductivities that varied no more than a factor of 1.6 (Figure 4b). Furthermore, differences in hydraulic conductivity between the three assumptions were a maximum at the beginning of the SDRI test and reduced as the wetting front progressed (i.e., increase in D_f in Equation 3). The average hydraulic conductivity of the GeoWaste pile was 1.4×10^{-6} m/s for the first two days of experiment and 9.0×10^{-7} m/s for the last three days of experiment using $\psi_a = 1.0$ m.

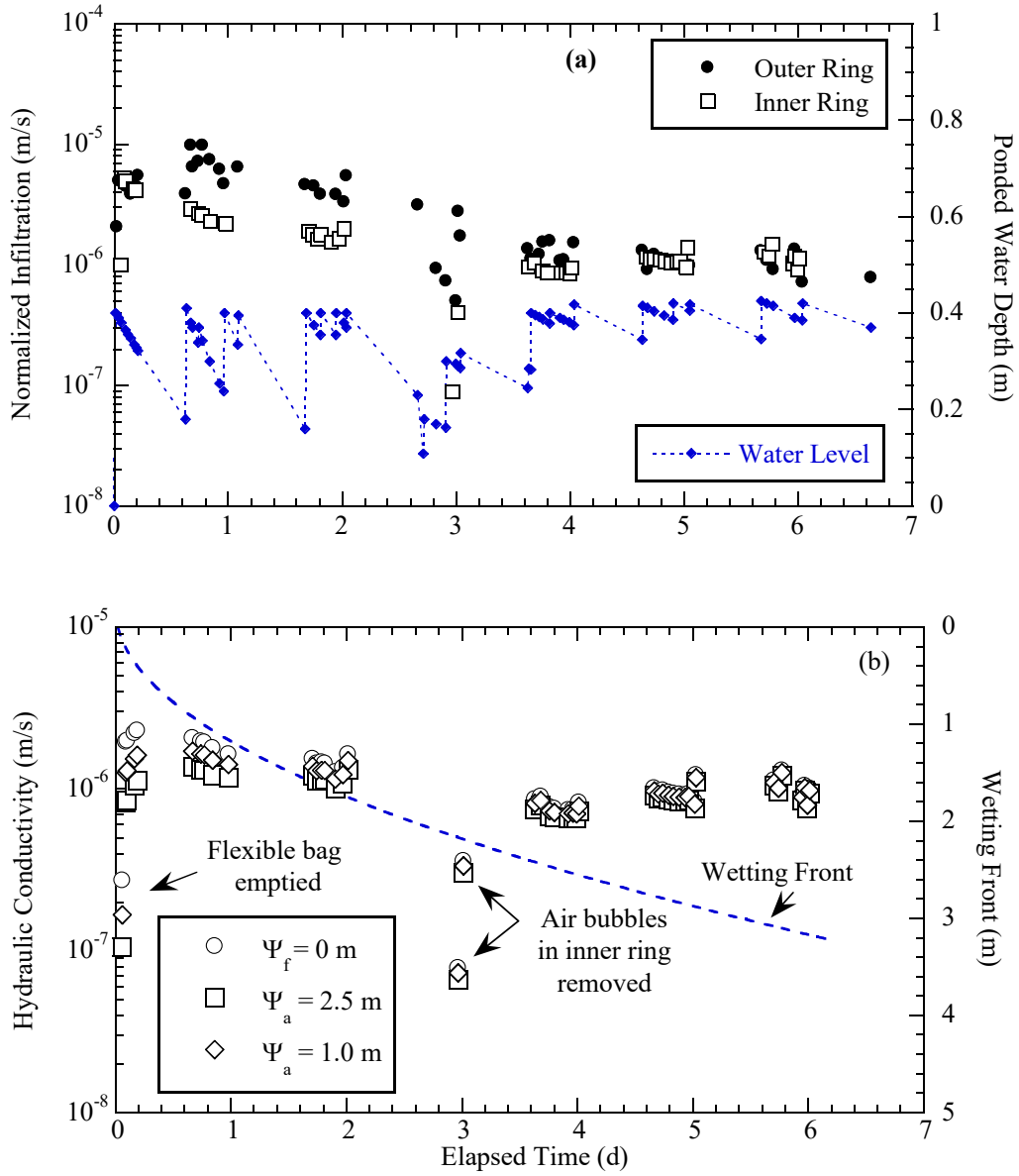

Figure 4: (a) Infiltration rate of the inner and outer ring and depth of ponding on the outer ring of SDRI, and (b) hydraulic conductivity measurements and depth of wetting front relationship with time for GeoWaste pile

Hydraulic conductivity of the GW pile reduced by a factor of approximately two from the start of the SDRI test until reaching a nearly constant value at the start of Day 4. This reduction in hydraulic conductivity was attributed to two mechanisms: (i) pedogenesis and/or (ii) settlement. Pedogenesis is a natural soil formation process could have created a macroporous structure near the surface of the pile due to wet/dry cycling and biological instruction (e.g., plant roots and animals). During excavation of the GeoWaste pile, a dense concentration of roots was observed up to 0.75 m below surface, which correlated with surface vegetation conditions observed for the GeoWaste pile. A macroporous structure in the surficial

GeoWaste may have resulted in a faster hydraulic conductivity during the first few days of the SDRI test when infiltration was controlled by the more surficial GeoWaste (Figure 4). Settlement of the GeoWaste pile surface occurred during the SDRI test, and was concentrated within the wetting zone. Settlement could have led to an increase in density and reduction in hydraulic conductivity. The two mechanisms of pedogenesis and surface settlement both support the measurements of a higher initial hydraulic conductivity in the GeoWaste pile followed by a reduction in hydraulic conductivity with time as wetting progressed.

A few minor issues were observed during the SDRI test that contributed to abnormally low infiltration rates and hydraulic conductivities (Figure 4). The flexible plastic bag completely emptied during the first few measurements due to a higher than anticipated infiltration rate. Towards the end of the third day, a small piping zone below the SDRI outer ring reduced the water level (i.e., ≈ 0.1 m at t = 2.8 d) and allowed air bubbles to enter the inner ring. The piping zone was mitigated, air-bubbles were removed from the inner ring, and the water depth in the outer ring was increased. Abnormally low hydraulic conductivities computed during these two events are identified in Figure 4b and were considered non-representative of the actual hydraulic conductivity of the GeoWaste pile.

Hydraulic conductivity comparison

Laboratory-scale experiments conducted on GeoWaste prepared to the same mixture ratio had a hydraulic conductivity of 1.7×10^{-8} m/s at an effective stress of 10 kPa (Gorakhki et al., 2019). The hydraulic conductivities measured for the GeoWaste pile were 1.4×10^{-6} m/s (first two days) and 9.0×10^{-7} m/s (last three days). Thus, hydraulic conductivity measured via the SDRI in the GeoWaste pile were approximately 50 to 100 times faster than hydraulic conductivity measured on laboratory-prepared specimens under a low effective stress of 10 kPa. This low effective stress is representative of conditions in the pile because:

1. GeoWaste was placed in a loose state, with compaction via dropping material from a height of 2 to 3 m; and
2. infiltration from the SDRI only penetrated the first couple meters of the pile.

The one to two orders of magnitude higher hydraulic conductivity measured in the laboratory relative to field agrees with observations made by Benson et al. (1999) and Benson et al. (2007) pertaining to hydraulic conductivity measured in laboratory- and field-scale tests. Benson et al. (1999) reported that heterogeneity and macropores existed in field-scale test sections, whereas hand-compacted laboratory-scale specimens were more uniform. On average, field-scale hydraulic conductivity was 11.2 times faster than the laboratory for material with $k > 10^{-9}$ m/s. Benson et al. (2007) compared laboratory hydraulic conductivity of field-scale test sections after multiple years in service to laboratory hydraulic conductivity representing the as-built conditions. Benson et al. (2007) reported an increase in hydraulic conductivity up

to four orders of magnitude following two to three years of test section operation. The data in this study suggest an increase in hydraulic conductivity in the same range as reported in Benson et al. (2007).

An additional factor that could have contributed to the difference in hydraulic conductivity measured in the test pile and on laboratory-scale specimens was the size of the waste rock particles. Waste rock used to prepare the GeoWaste specimens in the laboratory was screened on a 25.4-mm sieve to adhere to particle-size requirements for hydraulic conductivity testing. However, waste rock used in the test pile contained particles up to 300-mm diameter. Although the ratio of waste rock to tailings was similar between the GeoWaste pile and laboratory-prepared GeoWaste specimens, the influence of the larger-sized particles in the pile on hydraulic conductivity is uncertain. Additional laboratory-scale test specimens are required on GeoWaste prepared with larger particles to assess if the presence of larger particles contributes to increasing or decreasing the measured hydraulic conductivity.

Conclusion

In-situ hydraulic conductivity of a GeoWaste pile was measured using a sealed double ring infiltrometer. The in-situ hydraulic conductivity was 1.4×10^{-6} m/s during the first two days and 9.0×10^{-7} m/s during the last three days of the experiment. The decrease in hydraulic conductivity was attributed to settlement of pile during infiltration and/or pedogenesis that created a more macroporous zone near the surface of the pile. The in-situ hydraulic conductivity was approximately one to two orders of magnitude faster than laboratory measured hydraulic conductivity on GeoWaste specimens prepared to the same mixture ratio, but with smaller-size waste rock particles. The difference between laboratory- and field-scale measurements of hydraulic conductivity agrees with past research, and for this study may be attributed to differences in waste rock particle size and/or the presence of a macroporous structure in the GeoWaste pile.

Acknowledgements

Financial support for this study was provided by Newmont Goldcorp and the National Science Foundation (CMMI #1538344). The opinions, findings, and conclusions expressed herein are those of the authors and do not necessarily represent the views of the Newmont Goldcorp or the National Science Foundation.

References

Bareither, C.A., M.H. Gorakhki, J. Scalia and M. Jacobs. 2018. Compression behavior of filtered tailings and waste rock mixtures. In *Proceedings of Tailings and Mine Waste 2018*, UBC Studios, University of British Columbia, Vancouver, British Columbia: 163–173.

Benson, C.H., D.E. Daniel and G.P. Boutwell. 1999. Field performance of compacted clay liners. *Journal of Geotechnical and Geoenvironmental Engineering* 125(5): 390–403.

Benson, C.H., A. Sawangsuriya, B. Trzebiatowski and W.H. Albright. 2007. Postconstruction changes in the hydraulic properties of water balance cover soils. *Journal of geotechnical and geoenvironmental engineering* 133(4): 349–359.

Blight, G. 2009. Geotechnical engineering for mine waste storage facilities. Londom: CRC Press.

Borja, R.C. 2019. Undrained shear behavior and critical state analysis of mixed mine waste rock and tailings. M.S. Thesis, Civil and Environmental Engineering, Colorado State University, Fort Collins, Colorado, USA.

Burden, R., G.W. Wilson, D.J. Williams and M. Jacobs. 2018. The shear strength of filtered tailings and waste rock blends. In *Proceedings of Tailings and Mine Waste Conference 2018*, UBC Studios, University of British Columbia, Vancouver, British Columbia: 347–355.

Bussière, B. 2007. Hydro-geotechnical properties of hard rock tailings from metal mines and emerging geo-environmental disposal approaches. *Canadian Geotechnical Journal* 44(9): 1019–1052.

Daniel, D.E. 1989. In-situ hydraulic conductivity tests for compacted clay. *Journal of Geotechnical Engineering* 115(9): 1205–1226.

Davies, M. 2011. Filtered dry stacked tailings–the fundamentals. In *Proceedings of Tailings and Mine Waste Conference 2011*, British Columbia, Canada.

Gorakhki, M.H., C.A. Bareither, J. Scalia and M. Jacobs. 2019. Hydraulic conductivity and soil water retention of waste rock and tailings mixtures. *GeoCongress 2019 GSP 312,* ASCE: 41–50.

Jehring, M.M. and C.A. Bareither. 2016. Tailings composition effects on shear strength behavior of co-mixed mine waste rock and tailings. *Acta Geotechnica* 11(5): 1147–1166.

Leduc, M., M. Backens and M.E. Smith. 2004. Tailings co-disposal at the Esquel Gold Mine Patagonia, Argentina. SME Annual Meeting, Colorado, USA.

Morgenstern, N.R., S.G. Vick and D. Van Zyl. 2015. Report on Mount Polley tailings storage facility breach. Report of independent expert engineering investigation and review panel. Prepared on behalf of the British Columbia government and the Williams Lake and Soda Creek Indian Bands.

Morgenstern, N.R., S.G.Vick, C.B. Viotti and B.D. Watts. 2016. Fundão Tailings Dam Review Panel Report on the immediate causes of the failure of the Fundão Dam. SAMARCO, SA, Vale, SA, Eds: 76.

Wang, X. and C.H. Benson. 1995. Infiltration and saturated hydraulic conductivity of compacted clay. *Journal of geotechnical engineering* 121(10): 713–722.

Wickland, B.E., G.W. Wilson, D. Wijewickreme and B. Klein. 2006. Design and evaluation of mixtures of mine waste rock and tailings, *Canadian Geotechnical Journal* 43: 928–945.

Williams, D.J., G.W Wilson and C. Panidis. 2003. Waste rock and tailings mixtures as a possible seal for potentially acid forming waste rock, *Proceedings of the 6th International Conference on Acid Rock Drainage*, Cairns, QLD: 427–435.

Yilmaz, E. 2011. Advances in reducing large volumes of environmentally harmful mine waste rocks and tailings. *Gospodarka Surowcami Mineralnymi*, 27: 89–112.

Proceedings of Tailings and Mine Waste 2019
November 17–20, 2019, Vancouver, Canada
Published by the University of British Columbia, 2019

Variably-Saturated Flow Modelling of a Heap Leach Pad: Analysis of Saturation Mechanisms

Kelly Greaser, Golder Associates Inc., USA
Jean Kugel, Golder Associates Inc., USA
Arlen Striegl, Golder Associates Inc., USA

Abstract

A hybrid model was developed to directly simulate variably saturated flow within heap leach facilities through construction and operation, including the addition of new material lifts and applied leach cycles throughout the life of the facility. The hybrid model allows for dynamic and transient simulation of changing heap geometry and the associated changes in hydraulic properties. Time-varying material properties within the model are used to account for the decrease in hydraulic conductivity and changes to the soil water storage relationships resulting from compaction, compression, and decrepitation of heap materials. The hybrid model uses HYDRUS-1D and HYDRUS-2D software along with customized modules developed in FORTRAN and MATLAB to automate the processes of simulating time-varying material properties, changing heap geometry by adding lifts of fresh ore to the modelling grid, and interpolating moisture content between successive model grids.

The hybrid model enabled calibration to field conditions for an existing heap leach facility which required transient simulation throughout the life of the facility. This would not have been possible with commercially available software because of the large number of model runs required to manually simulate transient conditions. In addition, the hybrid model was used to evaluate mechanisms of saturation within the heap leach facility by evaluating a series of conditions. The evaluation revealed that saturated or near-saturated conditions could occur within and immediately above compacted layers that may form at the surface of each lift when placing the next lift, even when the saturated hydraulic conductivity of the compacted ore was greater than the raffinate application rate. In contrast, simulation of the facility using uniform material properties representing the compacted material did not result in the development of saturated conditions. This demonstrated that the contrast in material properties between the layers could result in discontinuity in flow, which could lead to saturated or near-saturated conditions.

Simulating the dynamic and transient conditions throughout the life of a heap leach facility can be critical in the design and operation of some heap leach facilities when:

1. The heterogeneity of ore over the life of a facility may lead to discontinuity in flow.
2. Compaction of ore during placement of lifts may be a concern.
3. Stability concerns are heightened in earthquake prone areas.
4. Leach cycles with long irrigation durations and short rest durations may not allow sufficient drainage, especially as the facility increases in height.

Although not specifically included herein, the hybrid model framework could be used to evaluate various options to limit development of saturated or near-saturated flow conditions such as the use of wick drains, finger or blanket drains at intermediate lifts, liners at intermediate lifts, modified leach cycles, or reduced leach rates. In addition, the hybrid model framework could be used to dynamically simulate a waste rock facility or dry stack tailings facility.

Introduction

A hybrid model was developed to directly simulate variably saturated flow within heap leach facilities through construction and operation. The hybrid model enables direct simulation of the addition of new ore lifts and applied leach cycles throughout the life of the facility. The hybrid model allows dynamic and transient simulation of changing heap geometry and the associated changes in hydraulic properties. Time-varying material properties within the model are used to account for the decrease in hydraulic conductivity and changes to the soil water storage relationships resulting from compression, compaction, and decrepitation of heap materials. The hybrid model uses HYDRUS-1D (Simunek et al., 2009) and HYDRUS-2D (Sejna et al., 2011) software in combination with customized modules developed in FORTRAN and MATLAB (2013) to automate the processes of simulating time-varying material properties, changing heap geometry by adding lifts of fresh ore to the modelling grid, and interpolating moisture content between successive model grids.

Currently, no commercial software is available which can simulate variably saturated flow within heap leach facilities throughout the life the facility without compromises or simplifications that are likely to impact the accuracy and utility of the model. Typical soil-atmosphere models cannot simulate changes in material properties and geometry within the heap through time. Other variably-saturated models (e.g., FEFLOW [DHI, 2015]) simplify simulation of the soil-atmosphere interface, which in areas with dynamic upper boundary conditions (e.g., high evaporation rates, snow accumulation/melting), it is critical to simulate directly. This paper describes the development of the hybrid model and application of the hybrid model with examples. In addition, other uses of the hybrid model are described.

Development and function of the hybrid model

The hybrid model was developed in one dimension (1D) using HYDRUS-1D and FORTRAN. HYDRUS-1D can be customized to simulate conditions unique to each project because it can be simulated in a DOS command-line environment and the input text files can be generated by an external code (e.g., FORTRAN). The implementation in 1D was performed using HYDRUS-1D version 4.08, which was the software version available at the time the modelling was completed for the example presented in this paper. However, the FORTRAN codes could be used with more recent versions of HYDRUS-1D with minor modifications.

In the example presented herein, the hybrid model consisted of a series of sub-models simulated in sequence to represent construction of a heap leach pad through time, while accounting for changes in material properties and compression of the lifts through time. Specifically, the time-varying material properties were implemented to account for the decrease in hydraulic conductivity, the change in the soil water storage relationship, the decrepitation of the ore, and compression of the buried ore as the heap was constructed.

FORTRAN codes were used to prepare input files for the various HYDRUS-1D sub-models, execute each sub-model, and manage output from the various sub-models. With this implementation, the code for HYDRUS-1D was not modified. Figure 1 demonstrates the changes in heap geometry and material properties through time during construction and interpolation of the initial conditions of one sub-model from the final conditions of the preceding sub-model. The interpolation was executed with non-equivalent grids and with varying material properties to account for compression and decrepitation of the ore. To conserve mass, the interpolation was completed using water content rather than soil suction. In addition, water mass balance error was tracked within each sub-model and evaluated for the full hybrid model to confirm appropriate convergence. In the event model convergence required adjustment, input for the FORTRAN codes enabled adjustment of convergence criteria within each HYDRUS-1D sub-model. For simplicity, one set of input and output files within the FORTRAN module was used define properties, such as model grids, material properties, and convergence criteria, for all sub-models, rather than requiring the user to manipulate the input and output files for each sub-model manually.

Once each sub-model was completed, results were extracted from each sub-model and compiled within one output file for each output type (e.g., mass balance error, water balance components, and data from observation nodes). Consequently, the FORTRAN codes enabled an automated process to:

1. implement the changing geometry and time-varying material properties of the heap with no user input or intervention required between simulation of each sub-model; and
2. seamlessly extract results from each sub-model.

This automated process across the sub-models was required to represent construction and operation of a heap leach facility with multiple lifts to facilitate calibration of time-varying material properties of the ore, which will be described in the next section. Additionally, the automated nature of the FORTRAN interface allowed for adjustment, modification, and calibration of the complete model to achieve project goals.

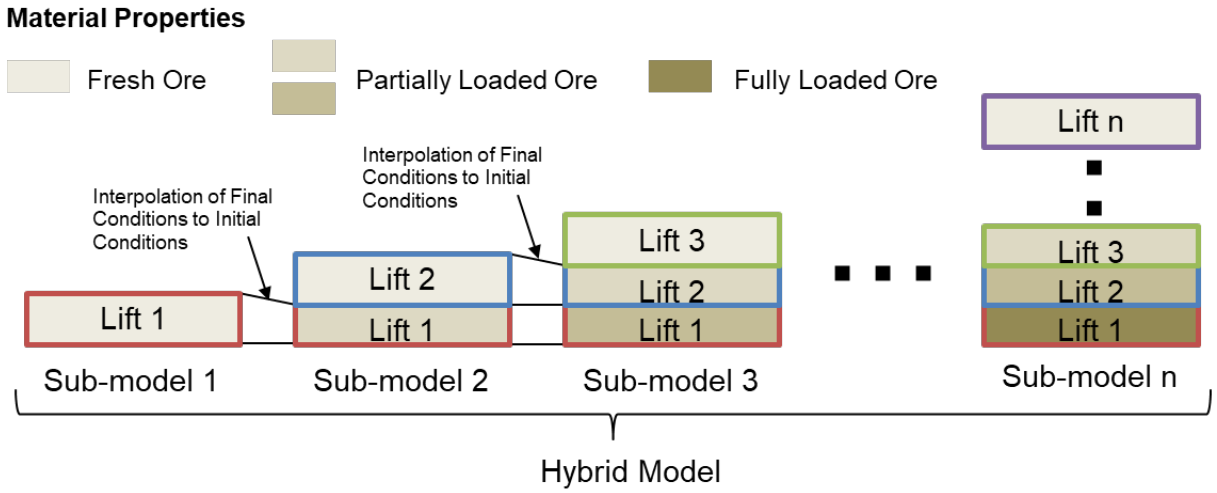

Figure 1: Schematic of hybrid model functions

Implementation in two dimensions (2D) was completed with HYDRUS-2D, version 2.01. In 2D, the implementation was less automated compared to 1D. FORTRAN modules and MATLAB were used to interpolate initial conditions of one sub-model from final conditions of the preceding sub-model. The interpolation was more complex in 2D than in 1D. The 2D interpolation was completed using the radial basis function, which required solvers in MATLAB for faster execution times compared to FORTRAN.

Application of the hybrid model

In 1D, the hybrid model was employed to simulate actual conditions in an existing heap and predict potential future conditions in a proposed heap. In 2D, the results from 1D were extrapolated in cross sections to evaluate conditions which may contribute to saturated or near-saturated flow conditions in a heap.

Simulating conditions in a heap in one dimension

Simulation of the actual conditions in a heap was designed to represent construction and conditions of the heap. The stacking history and raffinate application rate were input to the hybrid model. Climate was applied as a surface boundary condition and free-draining conditions were simulated at the base. The goal of the modelling effort was to calibrate material properties, investigate saturation mechanisms, provide a modelling framework to better understand variably saturated flow in heap leach pads, and predict future flow behaviour through the heap.

To simulate actual conditions in a heap, calibration of material properties was required in order for simulation results to show reasonable agreement with measured moisture conditions in the heap and measured outflow from the heap. Climate data, obtained from a local climate station, were used as model inputs for precipitation and estimated potential evaporation. The mine site provided details regarding the lift stacking activities and climate data used were consistent with the time period of construction of the heap. The actual leaching rate and schedule were used to amend the precipitation data to simulate flow through the heap resulting from both precipitation and raffinate application. For calibration of material properties, actual leach cycles were used.

To define initial material properties, saturated hydraulic conductivity data were obtained from stacking tests, porewater pressure dissipation tests from cone penetration investigations, consolidation and permeability testing on the ore, and in situ permeability tests conducted in the heap. The range of saturated hydraulic conductivity values estimated from the above testing are the result of heterogeneity of the ore, the effects of stacking and leaching the ore, and the inherent biases of the various test methods. To establish input parameters, the saturated hydraulic conductivity data were sorted into three material classifications based on relative particle size distributions. The effects of leaching and stacking were then included by reducing the saturated hydraulic conductivity; a series of decreasing saturated hydraulic conductivity values were assigned to each material classification to represent the progressing stages of aging ore properties.

Soil water characteristic curves (SWCC) were developed for the ore based on a combination of pedotransfer functions and open capillary rise tube tests. The particle size distributions (PSDs) of various ores for pre-leach and post-leach conditions were translated to SWCCs using the Modified-Kovacs method (Aubertin et al., 2003) pedotransfer function. The pedotransfer functions capture the changes in the SWCCs as stacking decreases the porosity of the material and leaching causes the material to break down into finer particles. A series of SWCCs were developed for each material classification based on the pre- and post-leach PSDs and the assumed porosity. Results from two column tests, also known as open capillary rise tube tests (Fredlund et al., 2012) were used to corroborate assumed air-entry values for the SWCC parameters used in the modelling. Finally, a series of decreasing porosity values were assigned to each material classification to represent the progressing compression of the ore. Total porosity values were estimated based on site-specific data.

Each new lift was assumed to be placed at a relatively low water content with a loose, permeable structure. Once buried under a subsequently placed lift, the lift was assumed to compress and change material properties due to leaching and compression as discussed above. Once the top lift has been loaded by the subsequent lift, compaction was assumed to occur instantaneously, with the lift compressing by 15% and no further compression occurring in subsequent placement of ore lifts.

Calibration of material properties was accomplished by matching flow measured from the heap through time and moisture conditions measured within the heap leach pad. More than 100 hybrid models were simulated to facilitate calibration. Manually preparing the input files and completing the simulations would not have been feasible due to the large number of simulations necessary to complete adequate calibration. In addition, relying on the FORTRAN modules to simplify manual inputs, automatically prepare all the input files for the sub-models, run the sub-models, and extract results from the sub-models avoided user errors that may occur if performing these tasks manually. Figure 2 shows an example of the calibrated material properties, which were developed to account for dynamic processes occurring throughout the operation of the heap leach pad. The calibrated saturated hydraulic conductivities shown in Figure 2, and those used in subsequent modelling, are greater than the raffinate application rate. The saturated hydraulic conductivities for the "average" and "coarse" ore are more than one order of magnitude greater than the raffinate application rate, while the saturated hydraulic conductivity of the leached "fine" ore is within an order of magnitude of the raffinate application rate.

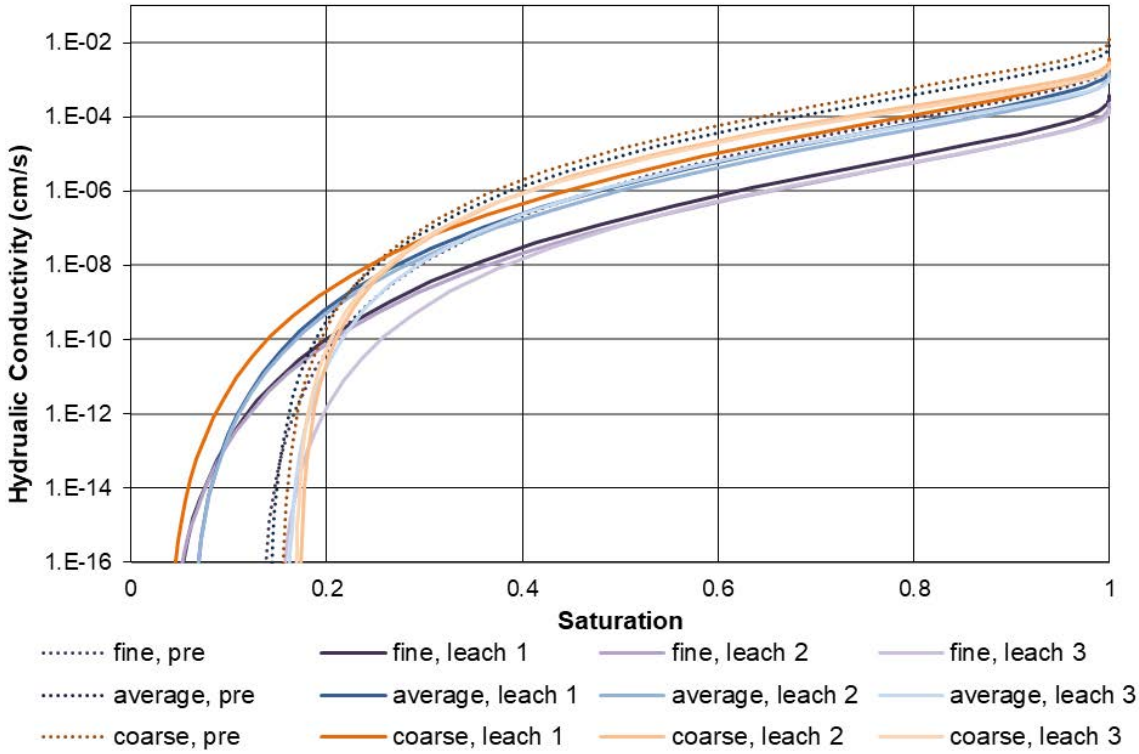

Figure 2: Calibrated material properties for various ores

Results

The hybrid model confirmed the presence of areas of near-saturation in the heap leach pad and demonstrated a lag between raffinate application and outflow from the pad. This lag time became greater with placement of each additional lift due to the increased distance to the bottom of the pad and the lower hydraulic

conductivity of the compressed ore material throughout lower layers in the pad. Figure 3 shows the results of the hybrid model with saturation increasing in critical layers with finer ore.

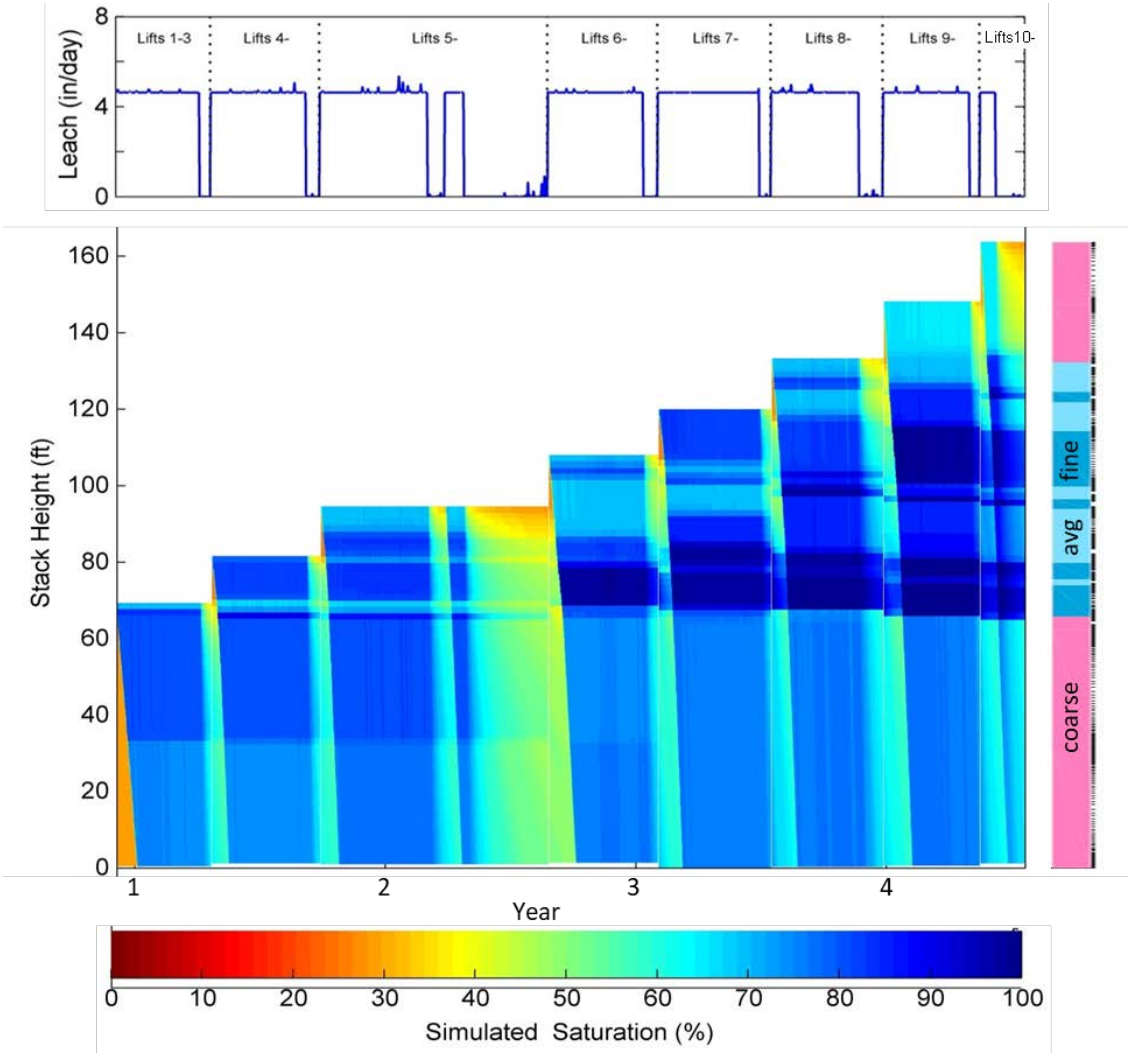

Figure 3: Simulated saturation in the 1D calibrated model with material properties (right)

Using the calibrated material properties, various simulations were completed to compare the hydraulic behaviour of ore types and evaluate saturation mechanisms. Two hybrid models were developed with homogenous material properties (one model with fine ore material properties and one model with coarse ore material properties) throughout the model grid. Results from model using the fine ore material properties indicate a longer lag time between raffinate application and outflow as compared to the results from the model using the coarse ore material properties. Predicted drain down between ore lifts from the fine ore model is also slower and less complete than drain down between ore lifts for the coarse ore model. Based on these results, a heap constructed from a finer ore blend is predicted to operate in a significantly wetter state compared to the coarser ore blend. However, saturated or near-saturated conditions were not simulated within either of the heaps with homogeneous material properties.

Additional simulations were completed in 1D to evaluate the potential effects of hard, compact crust layers formed at the top of each lift. These "interlift" layers were simulated simply as 2 feet of fine ore from the calibrated material properties while the remainder of each lift was simulated as the coarse ore. These simulations evaluated the flow patterns and storage within the heap. Figure 4 shows the results of the hybrid model incorporating interlift layers and the influence on saturation within the heap. The fine ore in the interlift layers results in greater average saturation and an increased lag between the start of raffinate application and resulting outflow in later lifts (outflow not shown in Figure 4). While the average saturation increases with decreasing hydraulic conductivity of the interlift layer, the increased saturation occurs primarily within and just above the interlift layers, rather than being distributed throughout the heap. Additionally, the thicknesses of predicted saturation extends farther above the interlift layers as more ore lifts are placed on the heap leach facility, which may be due to less effective drainage as the heap is constructed.

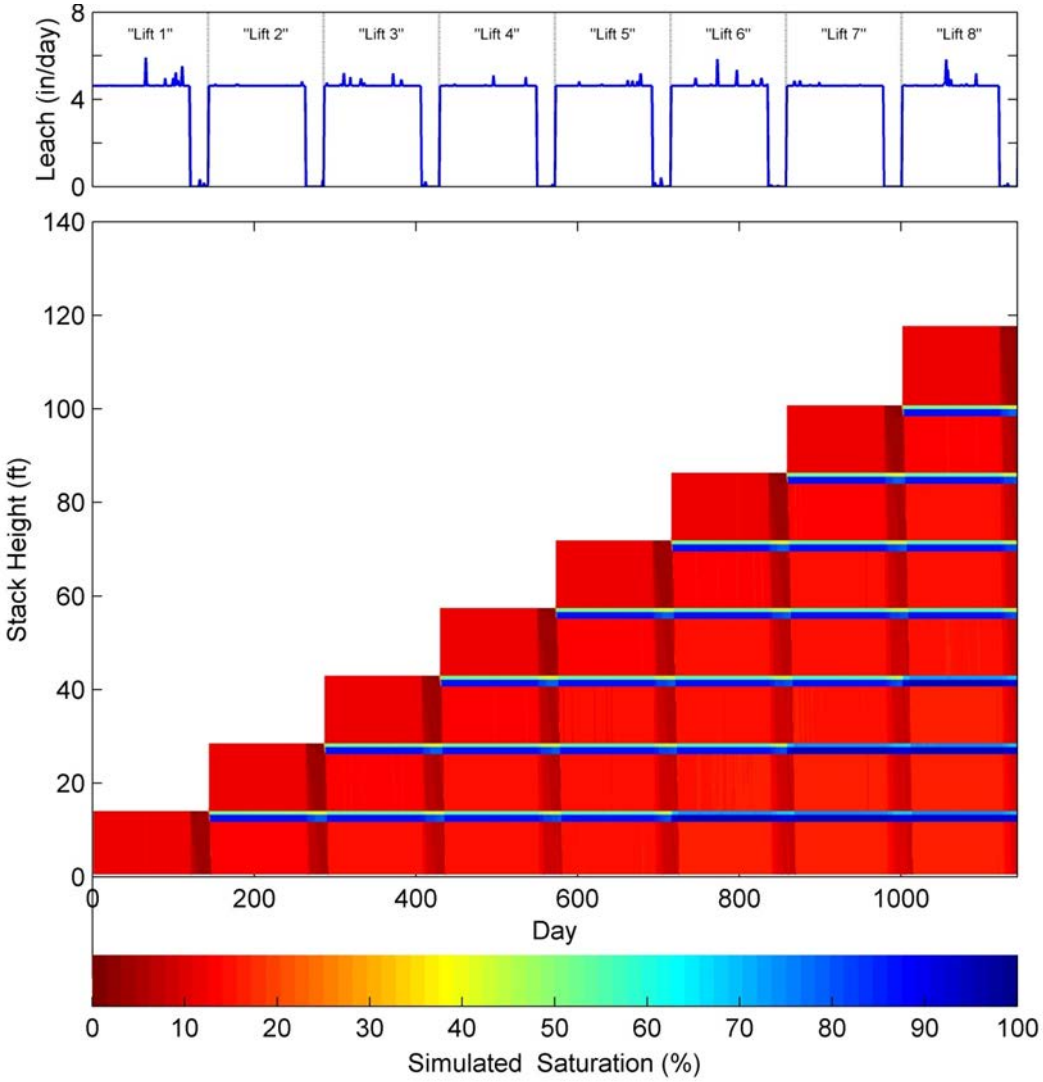

Figure 4: Simulated saturation in the 1D interlift model

Simulating conditions in a heap in two dimensions

The heap was simulated in 2D to evaluate the potential lateral flow behaviour within the heap given simulations in 1D cannot directly evaluate lateral flow. The 2D models reflect the variability in material properties which resulted from the 1D calibrated material properties and the range of data available for the ore. Fewer material properties were simulated in 2D compared to 1D due to the scale of the 2D simulations. In addition, due to the computational complexity of 2D modelling, efforts focused on the most recent three lifts stacked on the heap. The final conditions from the 1D model prior to the simulated period for the 2D models were used as initial conditions for the 2D models; the water contents were linearly interpolated based on material property and depth. Several cross sections were developed in 2D to evaluate configurations of ore and material property delineation was based on cone penetration logs. Simulations completed in 2D used similar inputs as 1D for stacking history, raffinate application, and surface and basal boundary conditions.

Results

Figure 5 shows predicted saturation levels in one of the cross sections simulated in 2D. Saturation levels are shown and in areas that are predicted to become fully saturated, porewater pressures are shown rather than saturation level. Saturation levels and porewater pressures vary with raffinate application rates, evaporation, and precipitation. The 2D model results show that saturated conditions can develop even in portions of the heap that are characterized by saturated hydraulic conductivity greater than the raffinate application rate. The heterogeneous conditions that develop in the heap create contrasts in hydraulic properties that can adversely affect solution flow. The 2D model indicates flow paths that are primarily vertical. The areas near the side slope of the heap are predicted to remain unsaturated.

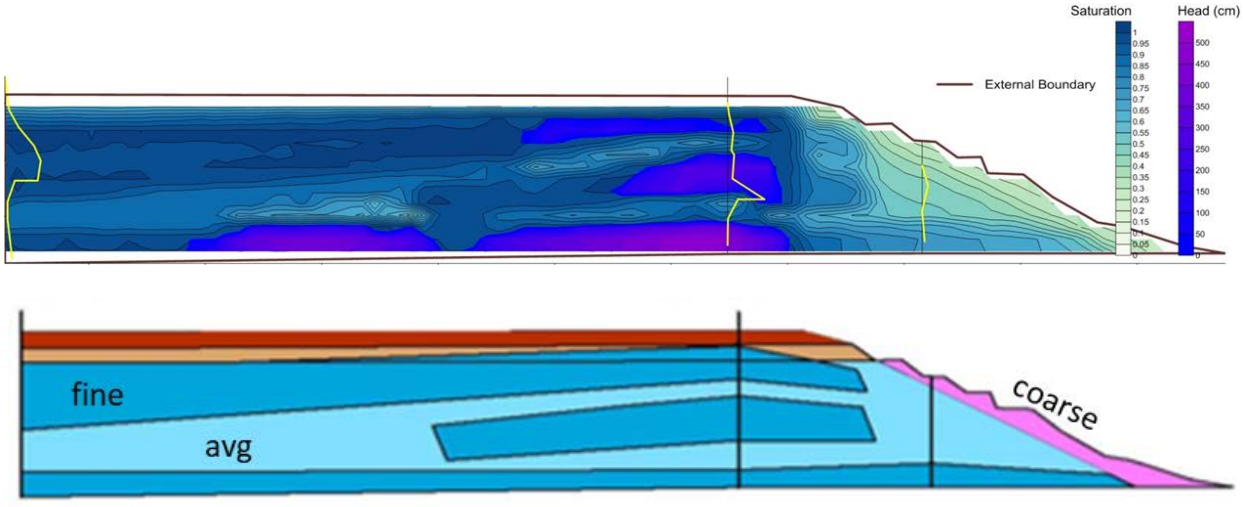

Figure 5: Simulated saturation in the 2D model (top) and material properties (bottom)

Two potential mechanisms were investigated that could result in higher saturation near the side slopes. The first mechanism was vertical anisotropy in hydraulic conductivity. Layered materials often exhibit hydraulic conductivity values that are lower in the vertical direction than horizontal. A set of models were constructed to evaluate this mechanism. Evaluation of these models indicated that reasonable values of vertical anisotropy did not result in significant increases in saturation in the side slopes of the heap. The second mechanism was the presence of interlift layers, similar to the 1D modelling. Compaction due to the movement of a radial stacker and other equipment on the surface of the heap can cause low hydraulic conductivity interlift layers to develop between successive lifts. The predicted saturation levels near the side slopes were more saturated compared to the results without this mechanism (shown in Figure 5). This indicates that the presence of interlift layers is a potential mechanism for moving pore fluid laterally toward the face of heap leach pads.

Conclusions and applications

A hybrid model was developed to directly simulate variably saturated flow within heap leach facilities through construction and operation. The hybrid model enables direct simulation of the addition of fresh ore lifts and applied leach cycles throughout the life of the facility. The hybrid model allows dynamic and transient simulation of changing heap geometry and the associated changes in hydraulic properties. The hybrid model uses HYDRUS-1D and HYDRUS-2D software along with customized modules developed in FORTRAN and MATLAB.

A series of 1D and 2D, variably saturated, transient flow simulations were completed using the hybrid model to investigate potential mechanisms for saturation in a heap leach pad. The effects of stacking, compression, and combined mechanical/chemical decrepitation were incorporated by varying material properties, lift thicknesses, and mesh geometry in the modelling process. Potential effects of variable ore characteristics, hydraulic conductivity anisotropy, and interlift layers were also evaluated.

The evaluation revealed that saturated or near-saturated conditions could occur within and immediately above compacted layers that may form at the surface of each lift when placing the next lift, even when the saturated hydraulic conductivity of the compacted ore was greater than the raffinate application rate. In contrast, simulation of the facility using uniform material properties representing the compacted material did not result in the development of saturated conditions. Using the calibrated material properties and the site-specific conditions simulated, this demonstrated that the contrast in material properties between the layers resulted in discontinuity in flow, which led to saturated or near-saturated conditions.

Simulating the dynamic and transient conditions throughout the life of a heap leach facility can be critical in the design and operation of some heap leach facilities when:

1. The heterogeneity of ore over the life of a facility may lead to discontinuity in flow.
2. Compaction of ore during placement of lifts may be a concern.
3. Stability concerns are heightened in earthquake prone areas.
4. Leach cycles with long irrigation durations and short rest durations may not allow sufficient drainage, especially as the facility increases in height.

Although not specifically reported herein, the hybrid model framework could be used to evaluate various options to limit development of saturated or near-saturated flow conditions such as the use of wick drains, finger, or blanket drains at intermediate lifts, liners at intermediate lifts, modified leach cycles, or reduced leach rates.

In addition, the hybrid model framework could be used to dynamically simulate a waste rock facility or dry stack tailings facility through the life of the facilities. The hybrid model structure has also been used to facilitate variable climate inputs between summer and winter seasons: hourly climate inputs in the summer to simulate storm intensity and daily climate inputs in the winter to simulate effective precipitation from snow melt (calculated) when data typically are not available to calculate hourly snow melt. For assistance in applying the hybrid model, please contact the authors.

Acknowledgements

The authors would like to acknowledge Walter Weinig and Nate Monnig for their assistance with developing the hybrid model.

References

Aubertin, M., M. Mbonimpa, B. Bussiere and R.P. Chapuis. 2003. A model to predict the water retention curve from basic geotechnical properties. *Canadian Geotechnical Journal* 40: 1104-1122.

DHI. 2015. *FEFLOW 7.0 User Guide*. November.

MATLAB. 2013. R2013a. Natick, Massachusetts: The MathWorks Inc.

Fredlund, D., H. Rahardjo and M.D. Fredlund. 2012. *Unsaturated Soil Mechanics in Engineering Practice*. John Wiley & Sons. Column tests described on pages 248-249, photo of apparatus on page 250.

Sejna, M., J. Simunek and M. Th. van Genuchten. 2011. *The HYDRUS Software Package for Simulating the Two- and Three-Dimensional Movement of Water, Heat, and Multiple Solutes in Variably-Saturated Media. User Manual. Version 2.* Prague, Czech Republic.: PC-Progress.

Simunek, J., M. Sejna, H. Saito, M. Sakai and M. Th. van Genuchten. 2009. *The HYDRUS-1D Software Package for Simulating the One-Dimensional Movement of Water, Heat, and Multiple Solutes in Variably-Saturated*

Media. Version 4.08. Department of Environmental Sciences, University of California Riverside: Riverside, California.

Proceedings of Tailings and Mine Waste 2019
November 17–20, 2019, Vancouver, Canada
Published by the University of British Columbia, 2019

Experimental and Numerical Analysis of a Slurry Consolidation Test on Tailings

Shriful Islam, The University of Queensland, Australia
David J. Williams, The University of Queensland, Australia
Marcelo A. Llano-Serna, The University of Queensland, Brisbane and KCB, Australia

Abstract

The deposition of fine-grained tailings as a somewhat thickened slurry remains the norm, and presents challenges in the assessment of their geotechnical parameters and the analysis of their settling and consolidation behaviour. The conventional oedometer and Rowe cell consolidometer are not suitable for testing tailings from a slurry state. In this paper, silty sand-sized gold tailings of low plasticity are tested in an instrumented slurry consolidometer and their consolidation is simulated numerically. The purpose-built slurry consolidometer measures 150 mm in diameter and 410 mm in height, and is instrumented with top and base load cells, seven pore water pressure (PWP) transducers starting from the base and spaced at 40 mm intervals spirally up the side of the consolidometer, and a displacement transducer. Up to 560 kPa stress can be applied to the top of the sample, equivalent to about 60 m depth of tailings. The tailings were placed in the slurry consolidometer in a series of layers at an initial 25% solids concentration by mass, and each layer was allowed to settle and the surpernatant water removed before the next layer was placed. Step-wise loading was then applied, since this is the conventional means of loading in a consolidation test, and is the basis of the available numerical analysis software. The difference with the slurry consolidometer over conventional consolidation testing is that the test can commence from a slurry state and follow the large-strain consolidation process.

The numerical simulation of a large-strain consolidation problem is challenging due to extreme mesh distortions during numerical calculations. The emerging and innovative material point method (MPM) was used to numerically simulate the consolidation of the tailings from a slurry state. The analysis was carried out using the code and software developed by the MPM Research Community, Anura3D, focussing on PWP dissipation and the resulting consolidation. This numerical approach captured the consolidation behaviour well and provided a reasonable match with the experimental results.

Introduction

Mining activities are significant contributors to the economy in many countries, including Australia. Fine-grained tailings are produced in slurry form from the crushing, grinding and processing the ore (Adazar and Zarco, 2013; Wang et al., 2014). Tailings slurry requires proper management during disposition and storage, typically in surface tailings storage facilities (TSFs). Gold tailings from hard rock ores are essentially a non-plastic ground rock flour (Vick, 1983; Vermeulen, 2001; Adajar and Zarco, 2013). Tailings consolidate under their self-weight and consolidation is slow due to their fine particle size and hence low hydraulic conductivity, which reduces considerably as they consolidate.

Consolidation of mine wastes is conventionally tested in the laboratory using an oedometer, and has been applied to coal tailings and coarse reject (Shokouhi et al., 2014), red mud (Newson et al., 2006; Gore, 2015), iron ore tailings (Hu et al., 2017), and gold tailings (Adazar and Zarco, 2013). However, the test material needs to have a "soil-like" consistency sufficient to support the initial loading applied in the oedometer test without loss of material between the consolidation ring and the porous stone. Hence, the oedometer test does not lend itself to testing tailings from an initial slurry state, and the settling and early consolidation of a slurry tailings is missed. For tailings that do not achieve a "soil-like" state in the TSF, the oedometer test gives unconservative results.

A Rowe cell (Rowe and Barden, 1966) can be used to test a slurry-like material, and to measure induced PWPs. Sheahan and Watters (1996), Bo et al. (2003) and Bo et al. (2010) used a Rowe cell to consolidate soft soil. However, the limited height of the cell, maintaining a level surface at the top of the sample during loading, and excessive extension of the rubber diaphragm used to apply stress to the sample present difficulties for using the Rowe cell to test slurries (Blewett et al., 2002). The seepage-induced consolidation test (SICT) has been used to consolidate soft dredged sediment and mine tailings (Berilgen et al., 2006; Znidarcic et al., 2011; Estepho, 2014). However, there are some challenges in measuring accurately the void ratio, due to sample rebound and non-steady-state conditions (Znidarcic et al., 1984).

Slurry consolidometers have successfully been used since the 1980s to test slurry-like materials undergoing large-strain consolidation (Roma, 1976; Barvenik, 1977). However, the slurry consolidometers used before 2006 did not determine the considerable friction that develops between the sample and the cell wall, which was identified by Sivrikaya and Togrol (2006). Wall friction is also an issue for oedometer and Rowe cell testing, but the generally smaller sample height makes it less significant than in the case of a high slurry consolidometer.

A large stress-controlled slurry consolidometer purpose-built for the Geotechnical Engineering Centre at The University of Queensland was successfully used to test coarse-grained coal tailings (Shokouhi and Williams, 2015; Shokouhi and Williams, 2017). The cell was modified to spiral the seven PWP transducers up the side of the cell, starting from the base and spaced at 40 mm intervals spirally up the side of the

consolidometer, and a stiffer piston seal was used to eliminate the loss of ultra-fines around the piston on loading. While the stiffer piston seal achieved the aim of eliminating the loss of ultra-fines, it caused significant friction with the cell wall that the applied stress had to overcome. The modified slurry consolidometer test was used by Islam and Williams (2018a), Islam and Williams (2018b) and for the test reported herein.

The numerical simulation of large-strain, slurry consolidation is challenging, requiring coupled interactions of solid and liquid phases and introducing a non-linear geometry (Spiezia et al., 2015). The conventional Finite Element Method (FEM) cannot cope with the severe element distortions involved. Alternative methods of analysis that accommodate large-strain include Smoothed Particle Hydrodynamics (SPH), the Material Point Method (MPM), and the Particle Finite Element Method (PFEM). The MPM is a particle-based method that uses a background mesh for computational purposes. The technique has been growing rapidly in simulating large deformations problems. This study uses the MPM formulation and code developed by the MPM Research Community, Anura3D (http://www.anura3d.com/) to simulate consolidation behaviour in a slurry consolidometer. The consolidation settlement and PWPs observed experimentally and in numerical simulations are analysed and compared.

Test material and procedure

The test material and procedure used are described in the following sections.

Test material and sample preparation

Gold tailings were collected from the thickener underflow of an Australian processing plant. The specific gravity of the tailings solids is 2.72, as determined using a helium pycnometer. The tailings solids consist of about 44% sand-sized, 45% silt-sized and 11% clay-sized particles. X-ray diffraction analysis showed that the tailings minerals include 33% albite (sodium feldspar), 24% quartz, 13% orthoclase (potassium feldspar), and 14% chlorite (clay minerals). The tailings water was found to have a pH of 7.98 and electrical conductivity of 3.13 mS/cm, indicating the presence of some salts, likely derived from the recycled process water.

The tailings sample was dried in the oven at 60°C, and sufficient dry tailings was collected to form three layers of slurry, each about 100 mm high, at a nominal solids concentration of 25% by mass, made up using process water. Each layer comprised 502 g of dry tailings and 1,507 g of process water, which were mixed for about 30 minutes using a mechanical stirrer at 900 rpm, prior to being poured into the slurry consolidometer cell. The first two layers of tailings slurry were allowed to settle for about 4 hours, before the supernatant water was removed using a syringe, and the next layer poured. The final layer was allowed to settle for 48 hours prior to the final supernatant water being removed using a syringe. The final height of

the sample was about 99 mm, having a corresponding solids concentration of 55.8% and a dry density of 861 kg/m^3.

Test procedure

The slurry consolidometer used in this study is shown in Figure 1. It comprises a confining cell, 150 mm in diameter and 410 mm in height, and seven PWP transducers, one at the base of the cell and six spaced at 40 mm intervals spirally up the side of the consolidometer, and a displacement transducer. The top piston applies stress via the top load cell, and a base load cell measures the stress transferred to the base of the sample, which enables the combined piston-cell wall and sample-cell wall frictions to be estimated. A 7-mm thick O-ring incorporated in the piston eliminates the loss of ultra-fine particles around the piston. The PWPs are calibrated prior to the start of each test by pressurising the cell with water.

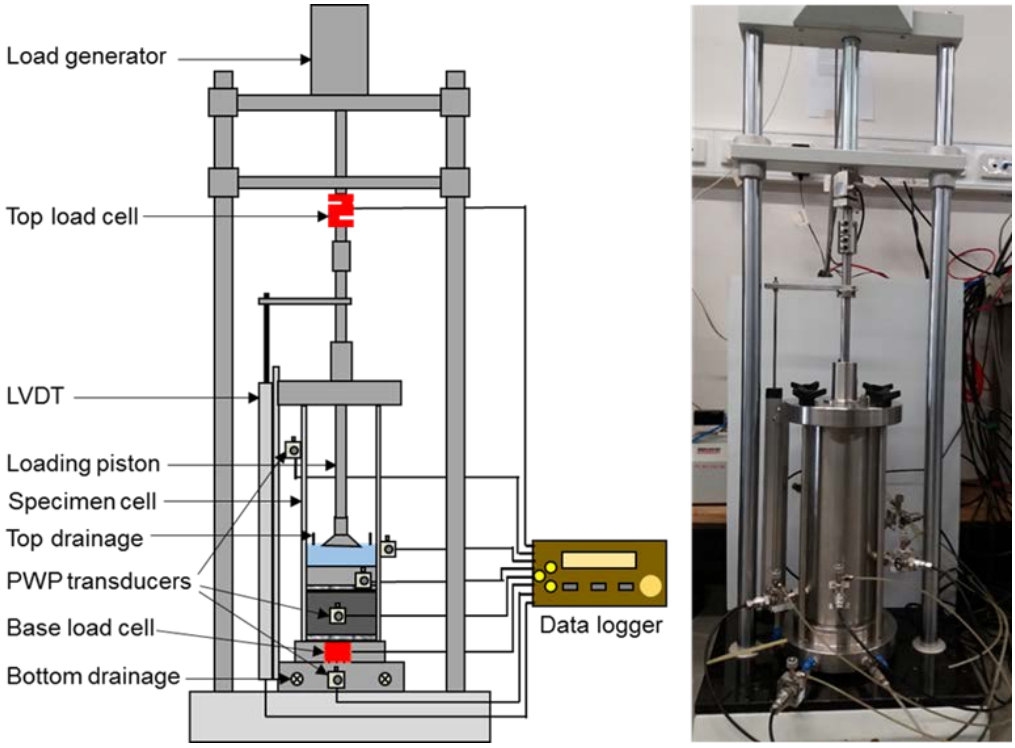

Figure 1: Schematic and photograph of slurry consolidometer

A saturated porous stone is placed on top of the sample before the piston is inserted in the cell, and only upward drainage was allowed, it being the dominate drainage direction in deposited tailings. The initially 99 mm high sample was loaded in two stages of 160 kPa and 320 kPa. Loading up to 160 kPa was applied at a rate of 20 kPa/min, after which the stress was maintained at 160 kPa until consolidation was complete, as indicated by hydrostatic PWP being achieved at the base of the cell. Loading up to 320 kPa was applied at a rate of 40 kPa/min, after which the stress was maintained at 320 kPa until consolidation was complete. The applied stress at the top, the stress at the base of the cell, the seven PWP responses, and

the settlement of the sample are recorded continuously via a data logger attached to a computer.

Experimental results and discussion

Figure 2 shows the experimental results of the slurry consolidometer test. During the establishment of each loading increment, the applied stress converted to excess PWP, with minor dissipation of PWP. The excess PWP dissipation in Stage 2 is faster than Stage 1 as the sample had attained a soil-like consistency with high contact between particles. The stress transferred to the base of the sample decreased with time as effective stress developed and the friction between the sample and the cell wall increased (Shokouhi et al., 2018).

The slurry consolidometer test was complete in 15 hours, and the total consolidation settlement in Stage 1 was 43.3 mm, while in Stage 2 the total consolidartion settlement was only 2.7 mm. The solids concentration and dry density of the sample at the end of Stage 1 were 77.8% and 1,530 kg/m^3, respectively, while the corresponding values at the end of Stage 2 were 80.5% and 1,640 kg/m^3.

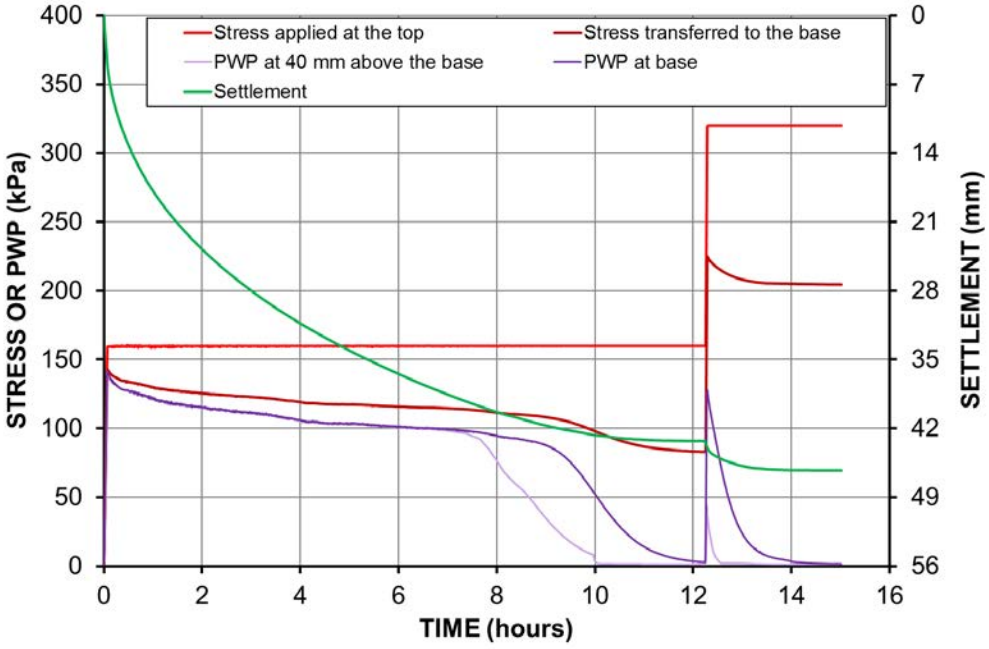

Figure 2: Experimental results of slurry consolidation test

Numerical analysis, results and discussion

An 18° slice of the slurry consolidometer cell was constructed in Anura3D platform using the pre-processing software GiD (Figure 3). The initial height of the sample for Steps 1 and 2 were 99.0 mm and 55.7 mm, respectively. The tailings solids are assumed fully saturated with water, and hence the material is considered as a saturated, fully coupled, two-phase system, and is assumed to be linear elastic. The

numerical analyses were in two parts: (i) N1 for Stage 1, and (ii) N2 for Stage 2. Four material points per element were assigned, and the loading was applied to the material points as uniformly distributed loads to capture the large deformations. MPM-mixed integration was chosen as the computation method in the Anura3D platform. Times for each calculation step of 0.05 s for N1 and 0.02 s for N2 ensured a stable result in each segment, with 30 and 120 total calculation steps for N1 and N2, respectively. The self-weight of the sample was neglected during the experimental procedure because the data logger starts to record the data from about 5 kPa applied stress, and hence the gravity was neglected in the numerical analysis. The stress at the top of the sample was applied instantaneously in both N1 and N2 and was maintained constant.

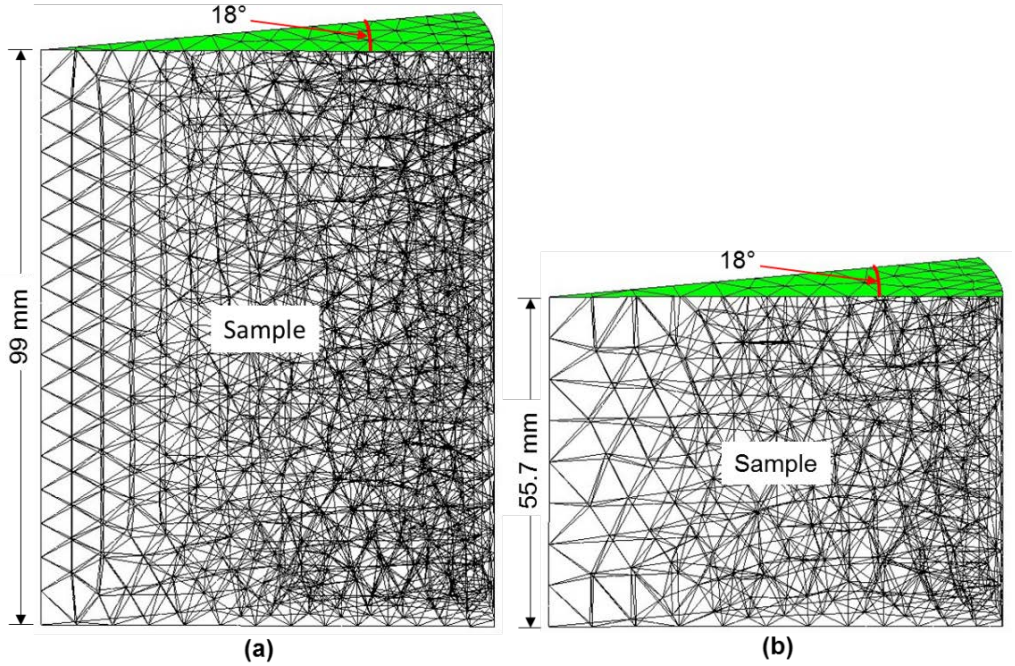

Figure 3: Geometry of numerical models with generated meshes and stresses applied to the top (in green): (a) N1, and (b) N2

Piston-cell wall and sample-cell wall friction, need to be considered in the analysis. However, the increasing sample-wall friction as the sample consolidates is quite difficult to simulate, and adjustments to the average applied stress were made based on the experimental results. The experimental average applied stress can be determined by assuming a triangular distribution of the stress over the height of the sample, following Shokouhi (2017), and including the piston-cell wall friction using:

$$\sigma_{av} = \left(\sigma_t - \sigma_p\right) - \frac{1}{2}\left(\sigma_t - \sigma_p - \sigma_b\right) \tag{1}$$

where $\boldsymbol{\sigma_{av}}$ is the average applied stress (kPa), σ_t and σ_b are the stresses at the top and base of the sample (kPa), respectively, and σ_p (kPa) is the friction between the piston and the cell wall.

In loading Stage 1, the average applied stress when a top applied stress of 160 kPa had been reached was about 147 kPa using Equation (1), with a piston of 8 kPa. In loading Stage 2, the average applied stress when a top applied stress of 320 kPa had been reached was about 259 kPa. Figure 3 shows the geometry of the numerical models developed, along with generated mesh and applied stresses on the top of the sample.

It is difficult to test for values of intrinsic permeability (K) and elastic modulus (E) for the initially slurry-like N1 sample. The permeability of the sample at a void ratio of 1.85, which is the highest for which an experimental result can be obtained (lower than the actual value of 2.16), was calculated using the falling head method (AS 1289.6.7.2, 2001), giving a corresponding intrinsic permeability of 2.5E–10 m^2. The intrinsic permeability should not change the final consolidation settlement, providing that all other parameters are constant and infinite computational time is allowed. Limiting the calculation time produces significant differences in average consolidation settlement with the changes in intrinsic permeability.

A sensitivity analysis was carried to estimate N1 parameters, the results of which are given in Table 1. Table 1 shows the variations of total consolidation settlement with changes in K, E and mesh size. During the sensitivity analysis for E, K was kept constant at 2.5E–8 m^2 to reduce computational time, while for the sensitivity analysis for K, E was kept constant at 400 kPa. The mesh size in both cases was kept constant at 0.014 mm, but was then varied with the optimised K and E held constant. Mesh size can have a significant effect on numerical results (Beuth et al., 2008; Fern and Soga 2016). A combination of a K value of 2.5E–8 m^2, an E value of 400 kPa, and a mesh size of 0.006 mm, with 4,087 tetrahedral elements and 6,769 nodes, provided the closest match to the experimental total consolidation settlement for N1.

The E value for N2 of 2,700 kPa was determined from an unconsolidated undrained triaxial test (Xu et al., 2018) under a confining stress of 10 kPa and a shearing rate of 1 mm/min. The K value for N2 of 1.6E–13 m^2 was based on the result of the falling head permeability test carried out on the sample at a representative void ratio. An optimal mesh size for N2 of 0.007 mm, with 1,496 tetrahedral elements and 2,630 nodes, provided the closest match to the experimental total consolidation settlement for N2. The values of all material parameters adopted in the numerical analyses are given in Table 2.

An Intel Core i7 CPU with 16 GB RAM was to run the numerical analyses, with a GiD pre-processor. A ParaView post-processor was to visualise the numerical results. Figure 4a shows the calculated consolidation settlements and PWPs for N1. The calculated total consolidation settlement of 38.7 mm is 90% of the experimental value of 43.3 mm, which is a reasonable match given the simplifications inherent in the selection of material parameters and the numerical analysis. The excess PWPs developed during the load application were generally fully dissipated at the end of the numerical analysis (Figure 4b).

Table 1: Sensitivity analysis for intrinsic permeability, elastic modulus and mesh size for N1

K (m^2)	E (kPa)	Mesh size (mm)	Consolidation (mm)
2.5E–12	400	0.014	14.5
2.5E–11			24.4
2.5E–10			24.1
2.5E–9			23.8
2.5E–8			35.6
2.5E–8	**400**	0.014	35.6
	600		24.6
	1,000		17.4
	1,500		10.9
	2,100		6.22
	2,700		4.92
2.5E–8	400	0.014	35.6
		0.012	35.7
		0.010	35.5
		0.008	37.5
		0.007	38.3
		0.006	**38.7**

Table 2: Material param

eters adopted in MPM analyses

Material parameter	Type/Values/Model
Initial porosity, n	0.69 (N1) and 0.44 (N2)
Specific gravity of solids	2.720
Density of pore water (kg/m^3)	1.000
Intrinsic permeability, K (m^2)	2.5E–8 (N1) and 1.6E–13 (N2)
Bulk modulus of pore water (kPa)	2.15E4
Dynamic viscosity of pore water (kPa/s)	1.002E–6
Young modulus, E (kPa)	400 (N1) and 2,700 (N2)
Poisons ratio	0.25

* The value is 100-times smaller than the physical one in order to increase the calculation time following Anura3D Tutorial Manual.

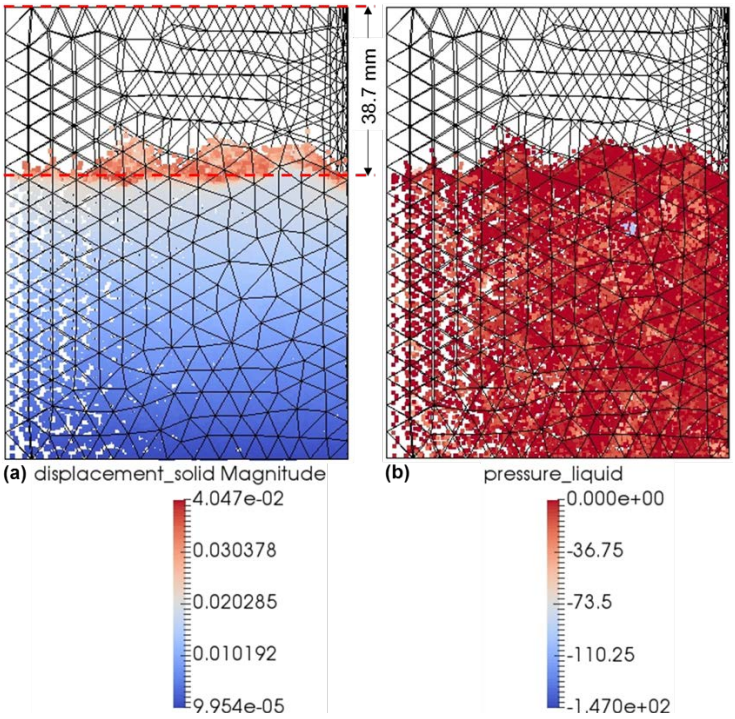

Figure 4: Numerical results for N1: (a) final consolidation settlements, and (b) final PWPs

Figure 5 shows the calculated consolidation settlements and PWPs for N2. The calculated total consolidation settlement of 2.6 mm is 96% of the experimental value of 2.7 mm, which is a good match. The excess PWPs developed during the load application were not fully dissipated in the lower part of the sample (furthest from the top drainage boundary) at the end of the numerical analysis (Figure 5b). The simulation took 21 days to complete. A larger number of time steps (say 200 steps or more) and a longer simulation time could lead to PWPs being fully dissipation. A higher K value would also speed up the dissipation of PWPs.

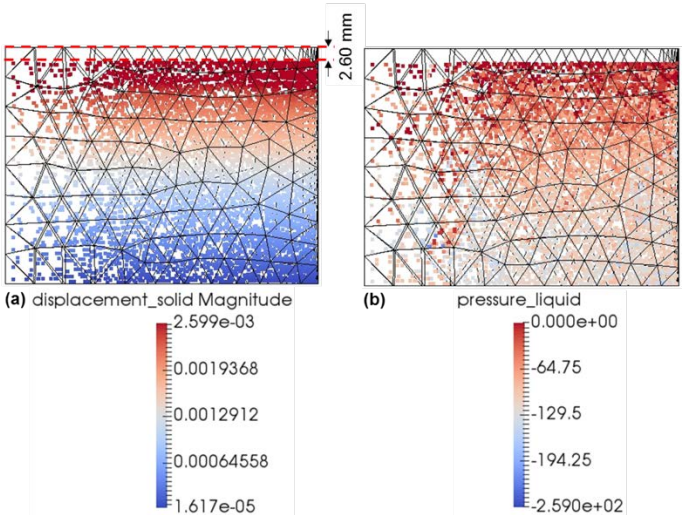

Figure 5: Numerical results for N2: (a) final consolidation settlements, and (b) final PWPs

Conclusion

A two-stage, incremental loading slurry consolidation test was carried out on a sample of silty sand-sized gold tailings of low plasticity, from a slurry consistency. The slurry consolidometer was instrumented with top and base load cells, seven PWP transducers up the side of the cell, and a displacement transducer. The initially 99 mm high sample was loaded in two stages of 160 kPa and 320 kPa. Loading up to 160 kPa was applied at a rate of 20 kPa/min, after which the stress was maintained at 160 kPa until consolidation was complete. Loading up to 320 kPa was applied at a rate of 40 kPa/min, after which the stress was maintained at 320 kPa until consolidation was complete.

The slurry consolidometer test was completed in 15 hours, and the total consolidation settlement in Stage 1 was 43.3 mm, while in Stage 2 the total consolidartion settlement was only 2.7 mm. The solids concentration and dry density of the sample at the end of Stage 1 were 77.8% and 1,530 kg/m^3, respectively, while the corresponding values at the end of Stage 2 were 80.5% and 1,640 kg/m^3.

Numerical simulations of the two stages of the slurry consolidometer test were carried out using the MPM-mixed integration method in the Anura3D platform. The self-weight of the sample was neglected, and allowance was made for piston-cell wall and sample-cell wall friction material parameters were selected based on laboratory testing for the soil-like Stage 2 sample, and sensitivity analyses for the more slurry-like Stage 1 sample.

For Stage 1, the calculated total consolidation settlement of 38.7 mm is 90% of the experimental value of 43.3 mm, which is a reasonable match given the simplifications inherent in the selection of material parameters and the numerical analysis. The excess PWPs developed during the load application were generally fully dissipated at the end of the numerical analysis.

For Stage 2, the calculated total consolidation settlement of 2.6 mm is 96% of the experimental value of 2.7 mm, which is a good match. The excess PWPs developed during the load application were not fully dissipated in the lower part of the sample (furthest from the top drainage boundary) at the end of the numerical analysis.

The paper demonstrates that the MPM can capture well the consolidation behaviour of a silty sand-sized gold tailings of low plasticity tested from a slurry consistency, and can provide a reasonable match with the experimental results.

References

Adajar, M.A.Q. and M.A.H. Zarco. 2013. Estimating hydrocompression settlement of mine tailings. *Philippine Eng J.* 34(1): 11–30.

AS 1289.6.7.2. 2001. Soil strength and consolidation tests – determination of permeability of a soil – falling head method for a remoulded sample. *Methods of Testing Soils for Engineering Purposes*, Standards Australia.

Barvenik, M.H.J. 1977. Generation of pore pressures in dredged material. MSc thesis, MIT, Massachusetts.

Berilgen, S.A., M.M. Berilgen and I.K. Ozaydin. 2006. Compression and permeability relationships in high water content clays. *Appl Clay Sci.* 31(3): 249–261.

Beuth, L., T. Benz, P.A. Vermeer and Z. Wieckowski. 2008. Large deformation analysis using a quasi-static material point method. *J Theor Appl Mech.* 38(1–2): 45–60.

Blewett, J., W.J. McCarter, T.M. Chrisp and G. Starrs G. 2002. An automated and improved laboratory consolidation system. *Can Geotech J.* 39(3): 738–743.

Bo, M.W., V. Choa and K.S. Wong. 2010. Constant rate of loading test on ultra-soft soil. *Geotech Test J.* 33(3): 192–200.

Bo, M.W., W.K. Sin, V. Choa and T.C. Ing. 2003. Compression tests of ultra-soft soil using a hydraulic consolidation cell. *Geotech Test J.* 26(3): 310–319.

Estepho, M. 2014. Seepage induces consolidation test: Characterization of mature fine tailings. MASc Thesis, University of British Columbia, Vancouver.

Fern, E.J. and K. Soga. 2016. The role of constitutive models in MPM simulations of granular column collapses. *Acta Geotech.* 11: 659–678.

Gore, M.S. 2015. Geotechnical characterization of bauxite residue. PhD thesis, The University of Texas at Austin, Texas.

Hu, L., H. Wu, L. Zhang, P. Zhang and Q. Wen. 2017. Geotechnical properties of mine tailings. *J Mater Civil Eng.* 29(2): 04016220.

Islam, S. and D.J. Williams. 2018a. Consolidation and shear strength of coal tailings slurries. In *Proceedings of Tailings and Mine Waste*, Brisbane, Australia: 62–71.

Islam, S. and D.J. Williams. 2018b. Optimisation of constant rate of loading slurry consolidometer testing of fine-grained coal tailings. In *Proceedings of Tailings and Mine Waste*; Brisbane, Australia: 72–82.

Newson, T., T. Dyer, C. Adam and S. Sharp S. 2006. Effect of structure on the geotechnical properties bauxite residue. *J Geotech Geoenviron Eng.* 132(2): 143–151.

Roma, J.R. 1976. Geotechnical properties of Florida phosphatic clays. MSc thesis, M.I.T, Massachusetts.

Rowe, P.W. and L. Barden L. 1966. A new consolidation cell. *Geotechnique* 16(2): 162–170.

Sheahan, T.C. and P.J. Watters. 1996. Using an automated Rowe cell for constant rate of strain consolidation testing. *Geotech Test J.* 19(4): 354–363.

Shokouhi, A. 2017. Experimental study of geotechnical behaviour and parameters of coal washery wastes. PhD thesis, University of Queensland, Brisbane, Australia.

Shokouhi, A., C. Zhang and D.J. Williams. 2018. Settling, consolidation and desiccation behaviour of coal tailings slurry. *Mining Technology Trans Inst Min Metal* 127(1): 1–11.

Shokouhi, A. and D.J. Williams. 2015. Settling and consolidation behaviour of coal tailings slurry under continuous loading. In *Proceedings of Tailings and Mine Waste*, 26–28 October, Vancouver, British Columbia.

Shokouhi, A. and D.J. Williams. 2017. Volume change behaviour of mixtures of coarse coal rejects and tailings. *Mining Technology Trans Inst Min Metal: Sec A.* 126(3): 163–176.

Shokouhi, A., D.J. Williams and A.K. Kho. 2014. Settlement and collapse behaviour of coal mine spoil and washery wastes. In *Proceedings of Tailings and Mine Waste*, Keystone, Colorado: 107–116.

Sivrikaya, O. and E. Togrol. 2006. Measurement of side friction between sample and consolidation ring with newly designed oedometer cell. *Geotech Test J.* 29(1): 87–94.

Spiezia, N., F. Ceccato and P. Simonini. 2015. Simulation of consolidation in large strains: a comparison between finite element method and material point method. In *Proceedings of the 6th International Conference on Computational Methods for Coupled problem in Science and Engineering,* Venice, Italy.

Vermeulen, N.J. 2001. The composition and state of gold tailings. PhD thesis, University of Pretoria, Pretoria, South Africa.

Vick, S.G. 1983. *Planning, design and analysis of tailings dam*. New York: Wiley.

Wang, C., D. Harbottle, Q. Liu and Z. Xu. 2014. Current state of fine mineral tailings treatment: A critical review on theory and practice. *Miner Eng.* 58: 113–131.

Xu, Y., S. Wu, D.J. Williams and M. Serati. 2018. Determination of peak and ultimate shear strength of parameters of compacted clay. *Eng Geol*, 243: 160–167.

Znidarcic, D., P. Croce, V. Pane, H.W. Olsen and R.L. Schiffman. 1984. The theory of one-dimensional consolidation of saturated clays. III: Existing testing procedures and analyses. *Geotech Test J.* 7(3): 123–134.

Znidarcic, D., R. Miller, D. Van Zyl, M. Fredlund and S. Wells. 2011. Consolidation testing of oil sand fine tailings. In *Proceedings of Tailings and Mine Waste*, November 6–9, Vancouver, British Columbia.

Proceedings of Tailings and Mine Waste 2019
November 17–20, 2019, Vancouver, Canada
Published by the University of British Columbia, 2019

Geotechnical and Unsaturated Properties of Metal Mines and Oil Sands Tailings

Louis K. Kabwe, University of Alberta, Canada
Ahlam Abdulnabi, University of Alberta, Canada
G. Ward Wilson, University of Alberta, Canada
Nicholas A. Beier, University of Alberta, Canada
J. Don Scott, University of Alberta, Canada

Abstract

Dedicated disposal areas for metal mines tailings are considerably different from those designed for oil sands mines. Oil sands tailings dams have a much larger footprint, averaging 4 km^2, and can reach up to about 15 km^2. Tailings from metal mines extraction plants usually contain between 65 to 70% solids; in contrast, fluid fine tailings from oil sands extraction plants contain approximately 8% solids. Geotechnical characterization tests on these two types of tailings are presented and evaluated. Unsaturated soil properties such as soil water characteristic curves (SWCC) are also discussed. A comparison of the geotechnical and unsaturated properties between the metal mines and oil sands tailings is made to investigate their unique properties and drying performance.

Introduction

Over the last century, the volumes of tailings being generated has grown dramatically as the demand for mineral and metals has increased, and also because lower grades of ore are being mined due to advances in extraction and processing technologies. In the 1960s, tens of thousands of tonnes of tailings were produced each day, and by the year 2000, this figure had increased to hundreds of thousands (Jakubick et al., 2003). Today, there are individual metal mines producing more than 200,000 tonnes of tailings per day. In surface mining, to produce one ton of copper, 350 tons of waste are generated, of which 147 tons are tailings (Festin et al., 2018; Kangwa, 2008). In Zambia, about 9,125 ha of land is estimated to contain 791 million tons of tailings (Sikaundi, 2013; Festin et al., 2018). At a global scale, between 5 to 7 billion tons of tailings dams are created annually (Edraki et al., 2014; Festin et al., 2018). Tailings characteristics may vary significantly and are dependent on the ore mineralogy together with the physical and chemical characteristics. Table 1 presents a summary to underscore some of the typical distinctions between oil sands and metal mines tailings.

Table 1: Comparison of conventional tailings at metal and oil sands mines

Factor	Typical metal mine	Typical oil sands mine
Tailings slurry properties Beaching	Crushed rock, little to no clay minerals Partially segregating, coarse near discharge, finer down the beach	Natural sands and dispersed clays with residual bitumen Highly segregating, coarse beaches, clay fines in the pond
Settling/consolidation	Fine tailings generally settle and consolidate within a few years	Consolidation of fine tailings takes decades to centuries
Trafficability	Upper beaches are fully trafficable, lower beaches with small equipment, fine require special soft tailings techniques	Beaches above water trafficable beaches with higher water table trafficable with good frost, fine tailings not trafficable
Pore water	Often higher metal contents, metals leaching, acid mine drainage	Elevated salts and naphthenic acids

Tailings from Canadian oil sands

About 20 percent of Canada's oil sands resources can be accessed using surface mining techniques (AER, 2018). Like other surface mining operations worldwide, oil sands mining operations generate a by-product (tailings) of the process used to extract bitumen from mined oil sands. The in-situ method of accessing oil sands resources does not produce tailings. As of 2017, there were 176 operating and approved oil sands projects in Alberta (AER, 2018). On average at the mining projects, approximately 1.5 barrels of tailings are produced for each barrel of bitumen produced. The tailings are made up of water, fine sand, silts and clays, residual bitumen, salts and soluble organic compounds. They also include solvents that are added to the oil sands during the separation process. Tailings ponds are managed within a closed-circuit drainage system, and no tailings or process-affected water are allowed off-site. As the tailings' solids are about 72% fine sand, the sand settles out upon deposition to form tailings dykes and beaches, and much of the water and residual bitumen and about half of the fines flow into the tailings pond. With the removal of the recycled water about one m^3 of sand and 0.25 m^3 of fluid fine tailings, FFT at a solids content of about 30 to 35% is created for every barrel of bitumen produced. This has led to the accumulation of approximately one billion m^3 of FFT, which require long-term storage in tailings ponds as the water cannot be released.

The total area covered by tailings ponds in 2010 was 176 km^2, and as 200 million litres per day continues to accumulate, the area is forecasted to increase to 250 km^2 by 2020. The reason for this massive accumulation is that the FFT consolidate exceptionally slowly (Table 1). The properties of the oil sands tailings depend on the ore properties and the extraction procedure to remove the bitumen from the ore. Ore properties over the oil sands mining area vary substantially and could reach maximum (minimum) content by mass values of 80 (55)% sands 34 (5)% fines, 18 (4)% bitumen, and 15 (2)% water. Typical deposits of

average grade oil sands contain 72% sand, 12% fines, 11% bitumen and 5% water. The objective of this paper is to assess the behavioural difference between metal mines and oil sands tailings in the final depositional scheme.

Geotechnical properties of tailings

A series of samples from oil sands and metal mines tailings were tested to determine their basic and advanced geotechnical properties. Both untreated fluid fine tailings (FFT) and thickened tailings (TT) from oil sands tailings were tested. Furthermore, copper (Cu) and gold (Au) tailings from metal mines were assessed. Tables 2 and Figures 1 to 5 summarize the basic and geotechnical properties measured for each type of tailings, including the initial solids content, specific gravity, particle-size distribution (PSD), Atterberg Limits, bitumen, and large strain consolidation (LSC). Tests to determine the PSD curves were conducted in accordance with ASTM D6913-04 and ASTM D4221-11.

The fines content by mass (particles smaller than 44 μm in diameter) of FFT and TT are about 96% and 55%, respectively (Table 2 and Figure 1). It should be noted that in the oil sands industry, the sand-silts boundary is defined as being at 0.044 mm but in metal mines industry the sand-silts boundary is defined as being at 0.075 mm as illustrated in Figure 1. The main difference between FFT and TT is in their sands contents; 4% for FFT and 45% for TT. The initial void ratio of FFT is 16, and that of TT is 2.74. Similarly, the solids contents of Cu and Au tailings are 59% and 50%, respectively. The fines content (particles smaller than 75 μm in diameter) for Cu and Au are 10% and 60%, respectively, and the sand's contents are 90% and 40% for Cu and Au, respectively as illustrated in Table 2 and Figure 1.

Table 2: Initial and geotechnical properties of oil sands and metal mines tailings

Sample ID	Solids content (%)	Fines content (%)	Sand content (%)	Void ratio	Specific gravity Gs	Liquid limit (%)	Plastic limit (%)	Plasticity index (%)	Bitumen content (%)
FFT	14	96	4	16	2.44	50	21	29	1.6
TT	49	55	45	2.74	2.63	25	14	11	0.6
Au	50.4	60	40	2.73	2.77	23	20	3	–
Cu	58.8	10	90	2.76	2.76	N/A	N/A	N/A	–

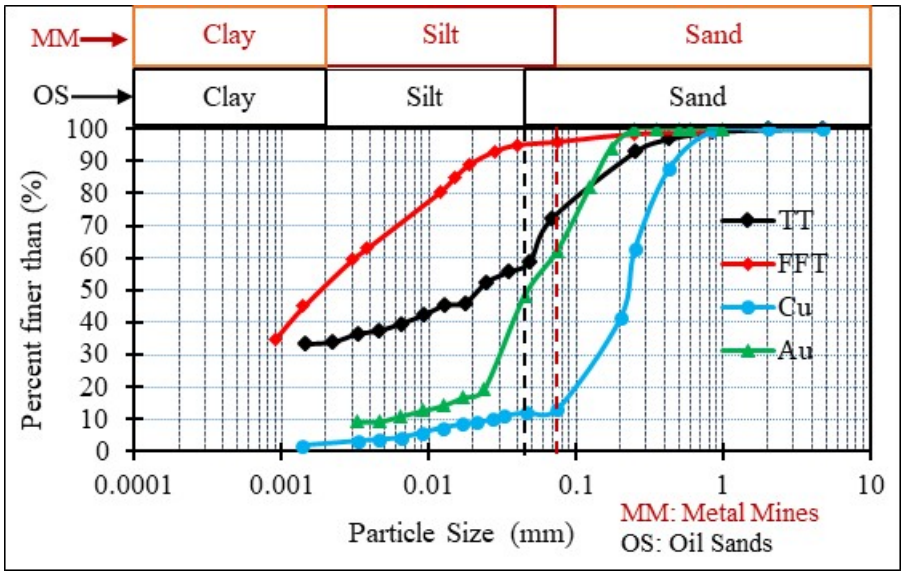

Figure 1: Particle-size distribution curves for the investigated tailings from the metal mines (MM) and oil sands (OS) industries

The FFT and TT have a bitumen content of 1.6% and 0.1%, respectively. These reported percentages are defined as the mass of bitumen divided by the mass of fines and bitumen. FFT that is bitumen-free generally shows lower liquid limit (w_L) than presented here (Scott et al., 2017).

Atterberg Limits for all tested tailings are presented on the plasticity chart, as illustrated in Figure 2. Atterberg Limits of Cu were not measured, as these tailings are mainly sand dominated.

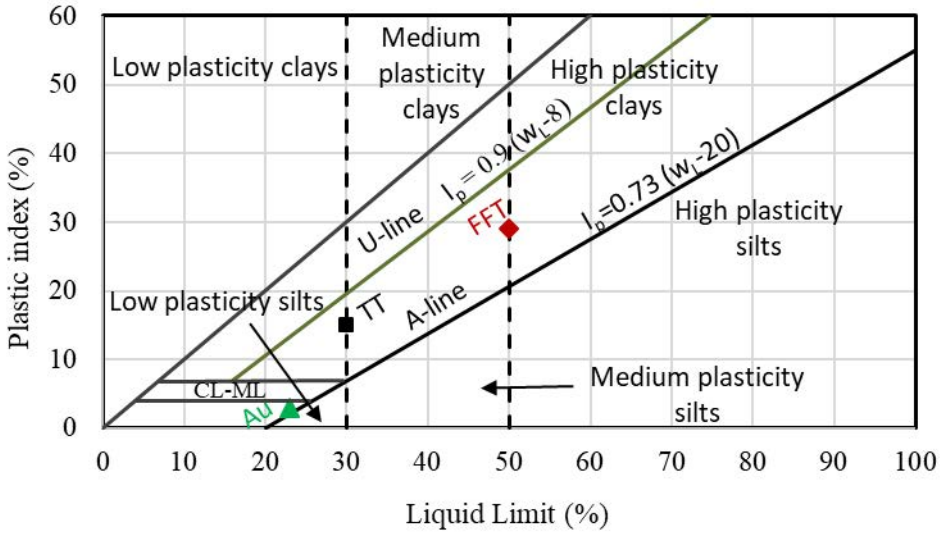

Figure 2: Plasticity classification chart showing the location of tested tailings

The FFT sits on the border between inorganic clays of medium plasticity and inorganic clays of high plasticity. FFT from different geological ores could have a higher w_L than presented here. The thickened

tailings (TT) exhibits a lower w_L (25%) due to their high sand content. The Au tailings also exhibit a lower w_L of 23%. The Atterberg Limits results on the plasticity chart shown in Figure 2 indicate that the oil sands tailings FFT and TT plot in a line approximately parallel to the A-line, indicating a similar origin and similar clay mineralogy (Wilson et al., 2017). However, Au does not align with the oil sands tailings indicating a different origin and clay mineralogy. Based on the Plasticity and Soil Classification Charts in Figures 2, TT is classified as low-plastic clays. As for the metal mines, Au tailings is classified as low-plastic silts and the copper tailings as sandy soil.

Consolidation properties

Tailings consolidation behaviour is typically evaluated through two essential relationships, namely compressibility (effective stress versus void ratio) and hydraulic conductivity-versus void ratio. These two relationships were determined by conducting a series of large strain consolidation tests (LSC) on each of the tailings samples.

Compressibility

Figure 3 shows the compressibility curves of all tested tailings. The compression index (swelling index) values for each type of tailings are: 1.5 (4.0) for FFT, 0.3 (0.5) for TT, 0.0 (0.1) for Au, and 0.0 (0.1) for Cu. The samples start at different initial void ratios, but both metal mining tailings exhibit similar compressibility. The FFT void ratio starts at 16 and rapidly decreases to 4 as effective stress is increased from 0.1 to 1.5 kPa, and after that, the void ratio starts to decrease gradually with increasing effective stress. The treated TT, which contain a large amount of sand, exhibit similar compression behaviour as the metal mines tailings.

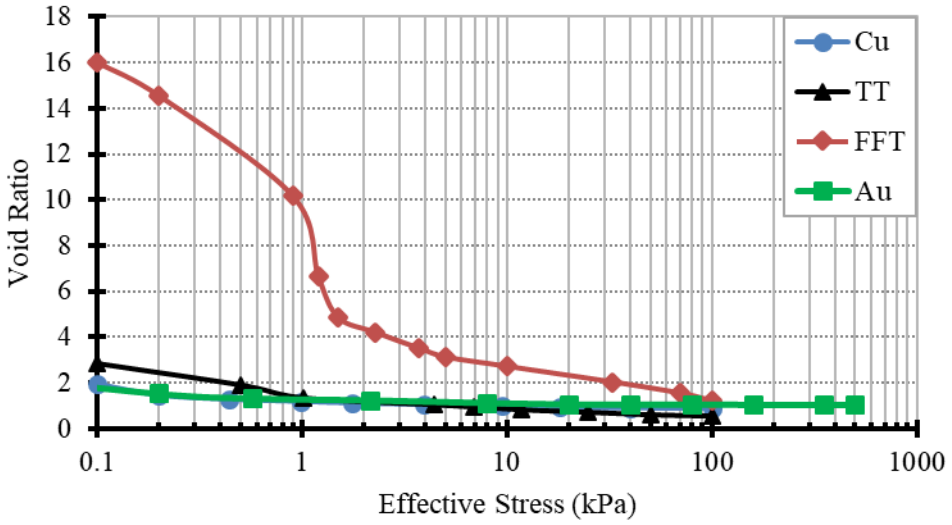

Figure 3: Combined compressibility curves of oil sands and metal mines tailings

Hydraulic conductivity

The relationship between hydraulic conductivity and the corresponding effective stress following loading are illustrated in Figure 4. In this section, the consolidation properties of the oil sands and metal mines tailings are first compared and evaluated individually, and then the two types of tailings are compared to each other.

The hydraulic conductivity of the TT sample is compared with that of the untreated FFT to evaluate the effect of thickening and sand addition. The data presented in Figure 4 show that the hydraulic conductivities of the treated TT sample are consistently much higher (about one order of magnitude) than that of the FFT at all effective stresses. The effect of the treatment processes is to change the hydraulic conductivity. An increase in hydraulic conductivity will result in the treated TT consolidating much faster.

The metal mines (Cu and Au) tailings have similar hydraulic conductivities at effective stresses lower than 1 kPa. At effective stresses greater than 1 kPa, the hydraulic conductivities of Cu tailings diverge. The difference in hydraulic conductivity increases as the effective stress is increasing. The conclusion from this observation is that the Au tailings will consolidate faster than Cu tailings when the effective stresses are greater than 1 kPa. This consolidation behaviour is due to the mineralogy and treatments of the two metal tailings. However, the mineralogy and treatments of the two metal mines tailings are outside the scope of this paper.

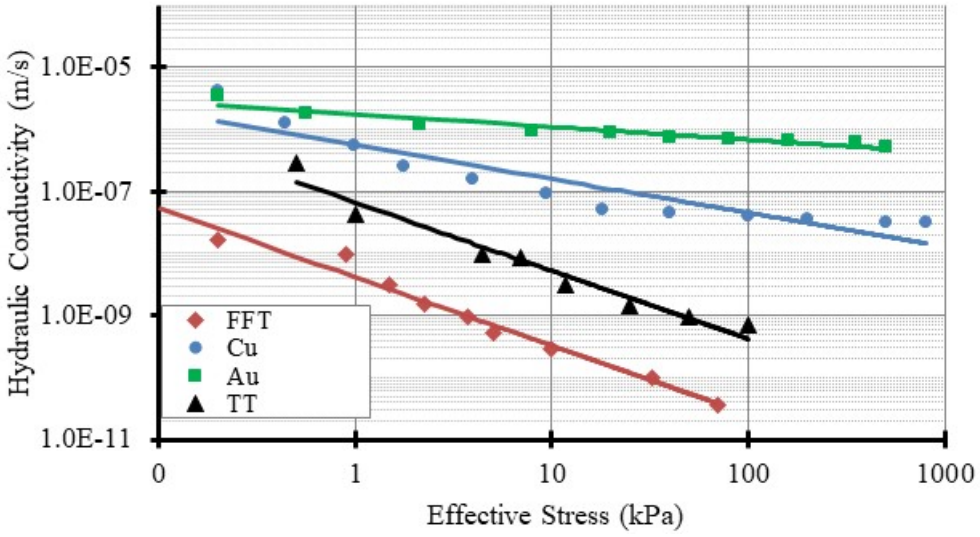

Figure 4: Hydraulic conductivity of tailings as a function of the applied effective stress

A comparison between the hydraulic conductivities of the oil sands and metal mines tailings indicates that the hydraulic conductivities of the metal mines tailings are considerably higher than those of oil sands tailings at effective stresses greater than 1 kPa. Therefore, the metal mines tailings will consolidate much faster than the oil sands tailings.

Shear strength

The development of shear strength upon loading was determined during the LSC test for the FFT and TT samples. The test was conducted using a mechanized, miniature vane apparatus as per the ASTM D 4648-05 Standard. The Au and Cu samples were mostly sand dominated, and their strength parameters were determined by conducting a direct shear test as per the ASTM D3080-04 Standard. Figure 5 illustrates the undrained shear strength development with the applied effective stress during the LSC tests for TT and FFT samples. The plots show that TT has a slightly higher shear strength at effective stresses greater than 30 kPa. The direct shear results for Cu and Au samples showed the values of shear strength parameter ϕ' (peak friction angles) of 41° and 33°, respectively. This indicates that Cu and Au behave as cohesionless sandy soils (Craig, 1992). Most mineral mine tailings are sandy tailings and have the potential for both static and cyclic liquefaction failures.

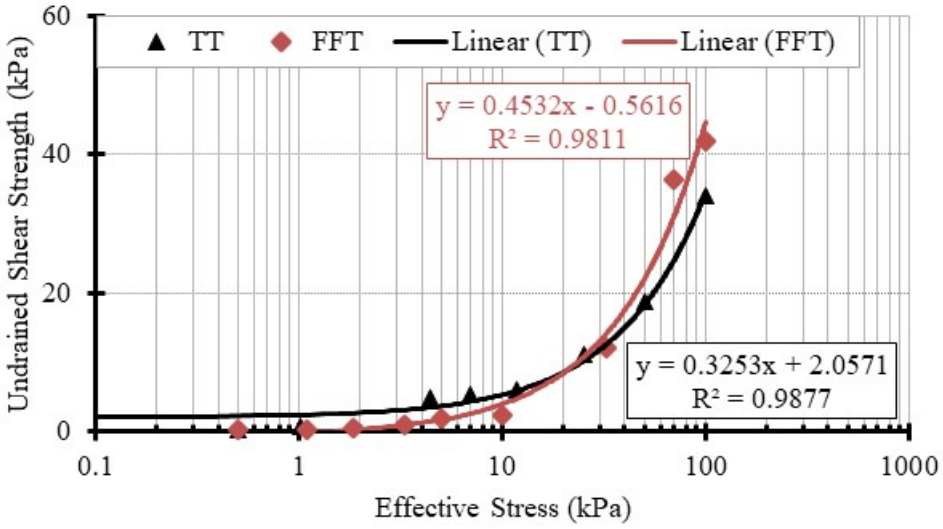

Figure 5: Undrained shear strength stress of oil sands tailings FFT and TT

Unsaturated soil properties of tailings

The unsaturated properties of the tailings help to understand their drying behaviour in the depositional scheme. The soil water characteristics curve (SWCC) is an indispensable tool that can be related to many unsaturated properties, including but not limited to, the unsaturated hydraulic conductivity.

Soil water characteristic curve

SWCC defines the relationship between water content (gravimetric, volumetric or degree of saturation) and the soil's matric suction. The choice of appropriate representation of water content depends on whether the soil undergoes significant volume change (Fredlund et al., 2013). For volume-changing tailings, the degree

of saturation should represent the water content. Furthermore, the shrinkage curve should be determined to evaluate the volume change response of said tailings. SWCC was measured using HYPROP® and PW40 devices for lower and higher suctions, respectively. Figures 6 illustrates the SWCCs of tested tailings as a function of the degree of saturation. The SWCC of TT was not determined. FFT sample was prone to volume change as soil suction is increased. Therefore, the air-entry values (AEV) could only be determined using the degree of saturation SWCC (Fredlund et al., 2013). AEV for FFT, Au, and Cu were determined graphically as 1,000, 200, and 20 kPa, respectively as seen in Table 3. The residual degree of saturation (θ_r) and the corresponding residual (suction) of FFT, Au, and Cu were also determined graphically as 20 (30,000), 5 (2,000), and 35% (200 kPa) (Table 3).

Table 3: Soil water characteristic curves properties

Parameter	FFT	Au	Cu
AEV (kPa)	1,000	200	20
θ_r (%)	20	5	35
Residual suction (kPa)	30,000	2,000	200

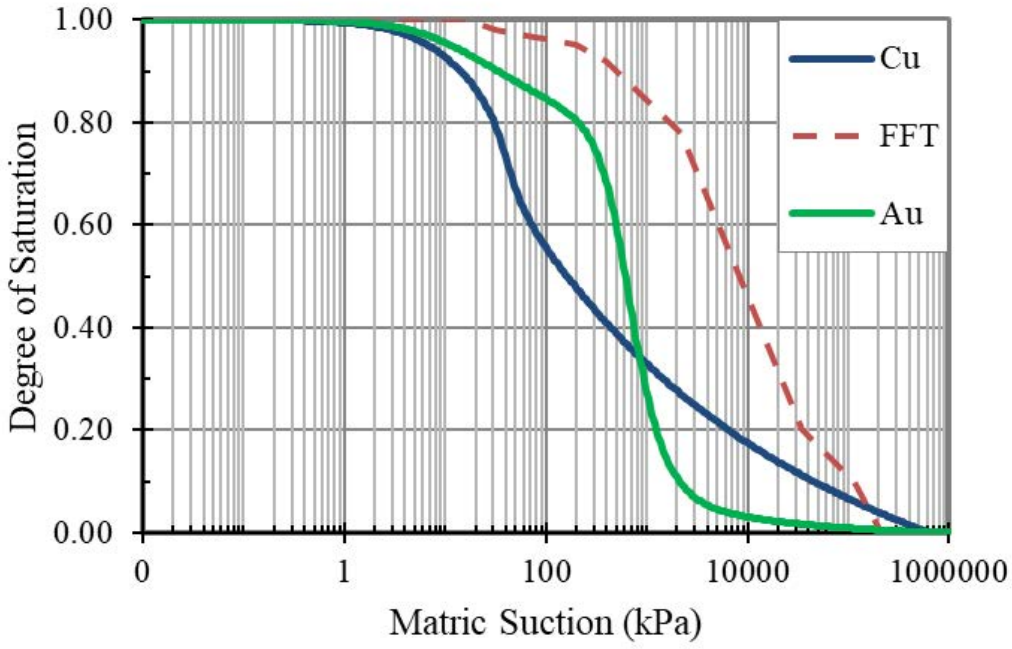

Figure 6: Soil water characteristic curves of tested tailings

Figure 7 indicates a positive exponential relationship between the AEV and the fines content of the tested tailings. This relationship ($AEV=9.57e^{0.049X}$, X=fine content) can help to predict the AEV of tailings from oil sands and other metal mines tailings.

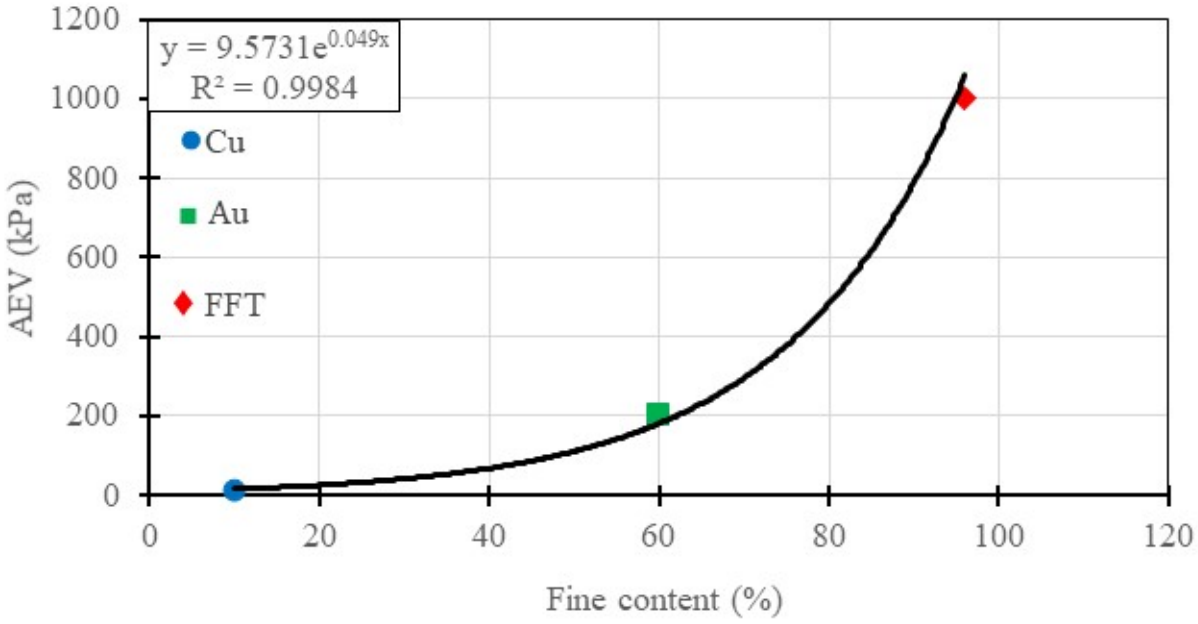

Figure 7: Relationships between air entry value AEV and fines content in various tested tailings

Shrinkage curve

Shrinkage curves were measured only on FFT and TT since they are both prone to volume change; results can be seen in Figure 8. The shrinkage curve is necessary to interpolate the SWCC data. The initial condition of each soil tested was saturated, and the shrinkage curves obtained for both samples were similar. The results show that the tailings start to de-saturate when the water content reaches about 25%. This point is generally quite close to the plastic limit of the tailings. There is an approximate correlation between the plastic limit of soil and its AEV. The average shrinkage limit of the two tailings samples is about 15%. The shrinkage limit is defined as the water content corresponding to the minimum volume that soil can attain upon drying to zero water content and generally falls slightly below the plastic limit of the soil (Fredlund et al., 2013. The true shrinkage limit was determined to be approximately correlated with residual soil conditions. The curves show that there is virtually no volume change at soil suction higher than the residual suctions. The measured values of the shrinkage curve are similar to those reported for oil sands tailings (Fredlund et al., 2013; Qiu and Sego, 2001).

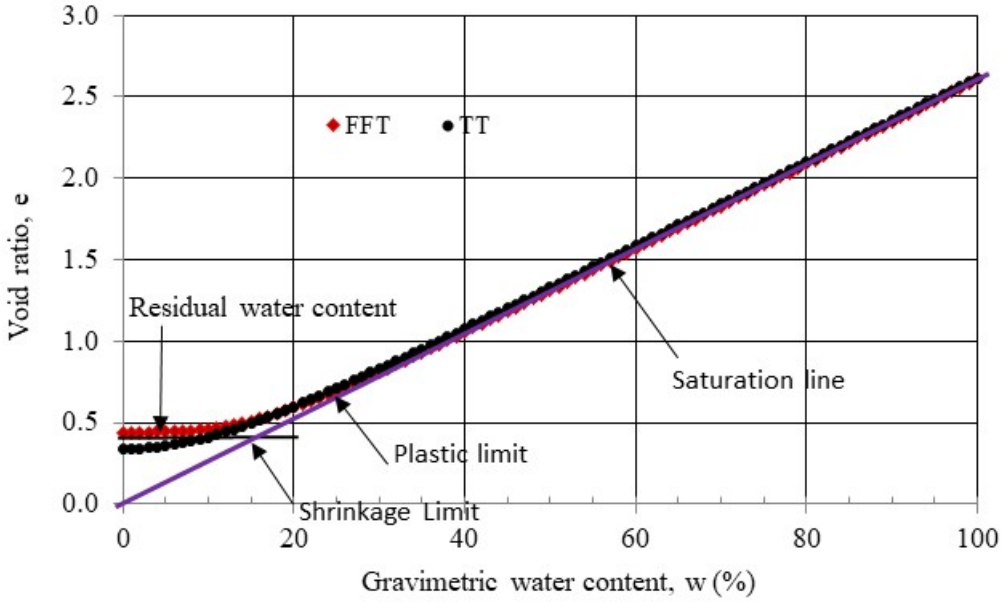

Figure 8: Shrinkage curves of oil sands fluid fine tailings and thickened tailings

Drying tests

The atmospheric drying test was performed on untreated oil sands tailings FFT and on metal mine Cu tailings in three identical containers 150 mm in diameter and 100 mm in height at room temperature (20 – 23° C). One vessel contained water to measure the potential evaporation (PE), and the two other pots contained the tailings samples to measure actual evaporation (AE). Figure 9 presents the drying test results of the FFT and Cu tailings samples plotted as the ratio AE/PE versus time. The surfaces of both FFT and Cu samples were initially wet or saturated (i.e., AE/PE = 1) and were allowed to evaporate under atmospheric conditions. The AE/PE ratio of both samples initially remained nearly constant and close to 0.9. During this period, evaporation is a function of the atmospheric conditions (such as temperature, relative humidity, wind speed, etc.) (Wilson, 1990; Wilson et al., 1997). As drying continues the AE/PE ratio for each sample begins to decline at different drying times as the availability of water decreases past a ratio of 0.8. It can be concluded that the AE/PE ratio of 0.8 represents the boundary between the saturated and unsaturated states of the two samples (Kabwe et al., 2014). The Cu tailings display a sharp drop in the AE/PE ratio on Day 7 while the FFT displays a gradual decrease in the AE/PE ratio from Day 10. The shapes of the drying slopes are similar to those of the SWCCs, as illustrated in Figure 6. The curvatures represent the AEVs of the tailings (the time when the tailings start to desaturate). The drying slopes are a function of the soil properties of the tailings, such as the PSDs as illustrated in Figure 2, and they are characteristic of sandy and clayed tailings. The Cu sample reached an AE/PE value of about zero on Day 10 and the FFT sample on Day 20. The results show that Cu tailings lost water at a rate twice as fast as the FFT sample.

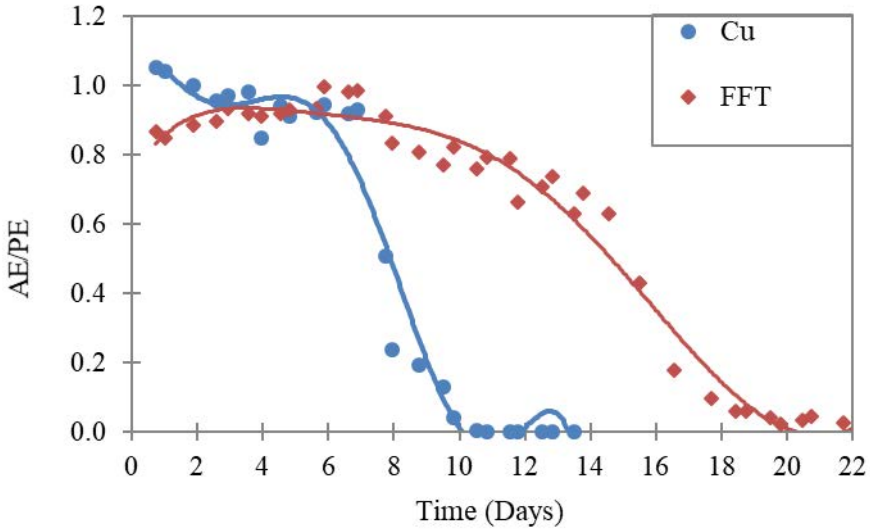

Figure 9: Drying curves of oil sands tailings FFT and Cu tailings

Conclusion

Metal mines and oil sands tailings were tested to evaluate the difference in their geotechnical behaviour. The tailings samples tested were classified as follows:

- The FFT sits on the border between inorganic clays of medium plasticity and inorganic clays of high plasticity.
- TT is classified as low-plastic clays.
- Au tailings are classified as low-plastic silts.
- The Cu tailings are nonplastic sandy soil.

Large-strain consolidation tests indicated similar compressibility behaviour in the metal mine tailings and TT. The compressibility index of FFT is five times higher than that of TT due to the dilution effect (both start at different void ratios).

Essential observations from the hydraulic conductivity versus effective stress relationships results include: the hydraulic conductivities of the treated TT sample are consistently higher (about one order of magnitude) than that of the FFT at all effective stresses, due to the effect of thickening and sand addition treatment. This will, therefore, result in the treated TT consolidating faster.

The metal mines (Cu and Au) tailings have similar hydraulic conductivities at effective stresses lower than 1 kPa. At effective stresses greater than 1-kPa, the hydraulic conductivities of Cu tailings are lower than that of Au tailings. The conclusion from this observation is that the Au tailings will consolidate faster than Cu tailings when the effective stresses are greater than 1 kPa.

A comparison between the hydraulic conductivities of the oil sands and metal mines tailings indicates that the hydraulic conductivities of the metal mines tailings are considerably higher than those of oil sands tailings at effective stresses greater than 1 kPa. Therefore, the metal mines tailings will consolidate much faster than the oil sands tailings.

The shear strength results indicate that TT has a slightly greater shear strength than FFT at effective stresses greater than 30 kPa. The values of peak friction angles ϕ' measured by direct shear for Cu and Au tailings are 41° and 33°, respectively. This indicates that Cu and Au behave as cohesionless sandy soils.

The AEV determined graphically for the FFT sample was about 1,000 kPa, while those of Au and Cu were 200 and 20 kPa, respectively. The AEV of the tested tailings exhibited a power function relationship to their fines content that can be used to predict the AEV of oil sands and other metal mines tailings.

The shrinkage limits and plastic limits determined for FFT and TT oil sands tailings samples tested were similar and were 15% and 25%, respectively. All the samples started with similar initial saturated conditions and desaturated at about 25% water content. The drying test results show that the metal mine Cu tailings (10% fines content) lost water at a rate twice as fast as the untreated oil sands tailings FFT (96% fines content).

Acknowledgements

The authors thank David Barsi for assisting in measuring the SWCCs and Elena Zabolotnii for conducting some of the LSC measurements on FFT. Thanks to Vivan Giang for proofreading the manuscript.

References

AER (Alberta Energy Regulator). 2018. State of Fluid Tailings Management for Mineable Oil Sands.

ASTM D 4318-05. 2008. Test methods for liquid limit, plastic limit, and plasticity index of soils. ASTM International, West Conshohocken, PA, USA. ASTM, 2008. Retrieved from https://doi.org/10.1520/4318-05

ASTM D6913-04. 2009. Standard Test Methods for Particle-Size Distribution (Gradation) of Soils Using Sieve Analysis, ASTM International, West Conshohocken, PA, 2009. Retrieved from https://doi.org/10.1520/D6913-04R09E01

ASTM D4221-11. 2011. Standard Test Method for Dispersive Characteristics of Clay Soil by Double Hydrometer, ASTM International, West Conshohocken, PA, 2011. Retrieved from https://doi.org/10.1520/D4221-11

ASTM D3080-11. 2014. Standard Test Method for Direct Shear of Solids under Consolidated Drained Conditions ASTM International, West Conshohocken, PA, 2014. Retrieved from http://doi.org/10.520/D3090M-11.

ASTM D6836-16. 2016. Standard Test Methods for Determination of the Soil Water Characteristic Curve for Desorption Using Hanging Column, Pressure Extractor, Chilled Mirror Hygrometer, or Centrifuge, ASTM

International, West Conshohocken, PA, 2016. Retrieved from https://doi.org/10.1520/D6836-16.

ASTM D 4648/D4648M. 2016. Test Method for Laboratory Miniature Vane Shear Test for Saturated Fine-Grained Clayey Soil ASTM International, West Conshohocken, PA, 2016. Retrieved from https://doi.org/10.1520/D4648/D4648M-16.

Craig, R.F. 1992. *Soil Mechanics,* fifth edition. London: Chapman & Hall.

Edraki, M., T. Baumgarti, E. Manlapig, D. Bradshaw, D.M. Franks and C.J. Moran. 2014. Designing mine tailings for better environmental, social and economic outcomes: A review of alternative approaches. *J. Clean Prod.* 84: 411–420.

Festin, E.S., M. Tigabu, M.N. Chilishe, S. Syampungani and Per Christer Oden. 2018. Progresses in restoration of post-mining landscape in Africa. J. For. Res. (2019) 30: 381. https://doi.org/10.1007/s11676-018-0621-x

Fredlund, D.G., J. Stone and J. Stanson. 2013. Determination of water storage and permeability functions for oil sands tailings. In *Proceedings of Tailings and Mine Waste Conference 2011,* Vancouver, British Columbia, Canada.

Kabwe, K.L., J.D. Scott, G.W. Wilson and A. Sorta. 2014. From fluid to solid: Oil sands fluid fine tailings. In *Proceedings of the 7ICEG Conference,* November 10–14, Melbourne, Australia.

Kangwa, K.P. 2008. An assessment of the economic, social and environmental impacts of the mining industry: A case study of copper mining in Zambia. Dissertation, Lund University, Sweden.

Jakubick, Alex. T., G. McKenna and A.M. Robertson. 2003. Stabilisation of tailings deposits: International experience. Mining and the Environment, Sudbury, Canada.

Qiu, Y. and D.C. Sego. 2001. Laboratory properties of mine tailings. *Can. Geotech. J.* 38: 183–190.

Scott, J.D., L.K. Kabwe, G.W. Wilson, A. Sorta and S. Jeeravipoolvarn. 2017. Properties which affect the consolidation behaviour of mature fine tailings. In *Proceedings of the Tailings and Mine Waste Conference,* Banff, Alberta.

Sikaundi, G. 2013. Copper mining industry in Zambia: Environmental challenges. Retrieved from http:/unstats.un.org/unsd/environt.

Wilson, G.W., L.K. Kabwe, N.A. Beier and J.D. Scott. 2017. Effect of various treatments on consolidation of oil sands fluid fine tailings. *Can. Geotech. J.* November 2017.

Wilson, G.W., D.G. Fredlund and S.L. Barbour. 1997. The effect of soil suction on evaporative fluxes from soil surfaces. *Can. Geotech. J.* 34: 145–155.

Wilson, G.W. 1990. Soil evaporative fluxes for geotechnical engineering problems. PhD thesis, Department of Civil Engineering, University of Saskatchewan, Saskatoon.

Bibliography

Fair, A.E. and N.A. Beier. 2012. Collaboration in Canada's oil sands: Fluid fine tailings management. In *Proceedings of the 3rd International Oil Sands Tailings Conference,* December 2–5, University of Alberta Geotechnical Centre, Edmonton, Alberta, Canada.

Fredlund, D.G. and S.L. Houston. 2013. Interpretation of soil-water characteristic curves when volume change occurs as soil suction is changed. Advances in Unsaturated Soils, Caicedo et al. (editors). London: Taylor & Francis Group. ISBN 978-0-415-62095-6.

Proceedings of Tailings and Mine Waste 2019
November 17–20, 2019, Vancouver, Canada
Published by the University of British Columbia, 2019

Calibration of Two Plasticity Models against the Static and Cyclic Response of Tailings Materials

Jorge Macedo, Georgia Institute of Technology, USA
Alexandros Petalas, Imperial College of London, UK

Abstract

This paper evaluates the performance of two different constitutive models against the response observed in static and cyclic laboratory tests for tailings materials, and examines the calibration procedures for the two models. The constitutive models considered in this study are the SANISAND model and the Norsand model. We use a complete laboratory dataset (i.e., critical state line tests, cyclic tests, bender element tests) to evaluate the robustness of the considered models in simulating the mechanical response of a silty tailings material. This offers an opportunity to examine the common assumption in engineering practice, for the design of mining geotechnical infrastructure, of using constitutive models formulated for clean sands to represent the response of tailings. This assumption has not been proven to be valid, and it will be explored in this study using the experimental results of the tested tailings material. Comparisons between the considered models are shared, highlighting advantages and disadvantages, and offering guidelines for their calibration.

Introduction

In moderate to high-risk tailings storage facility (TSF) projects, it is often necessary to perform advanced numerical analyses to gain a better understanding of the TSF's overall response. A geotechnical engineer is usually in charge of performing advanced numerical analyses to evaluate the TSF dam's response to static and dynamic loading events. In these analyses the adequate modelling of the tailing's mechanical response may be critical in some cases, depending on the dam configuration. For example, Figure 1 shows a case in which capturing the adequate response of the deposited tailings is critical in the evaluation of the tailings dam.

The current state of practice for the numerical analysis relies on continuum-based numerical models, implemented on finite element or finite difference computer codes. A critical component for this type of analysis is the proper selection of a constitutive model to realistically simulate the mechanical response of

the existing materials, including the deposited tailings. The parameters of the constitutive model are first selected based on laboratory tests and then adjusted based on field tests, if there is available information.

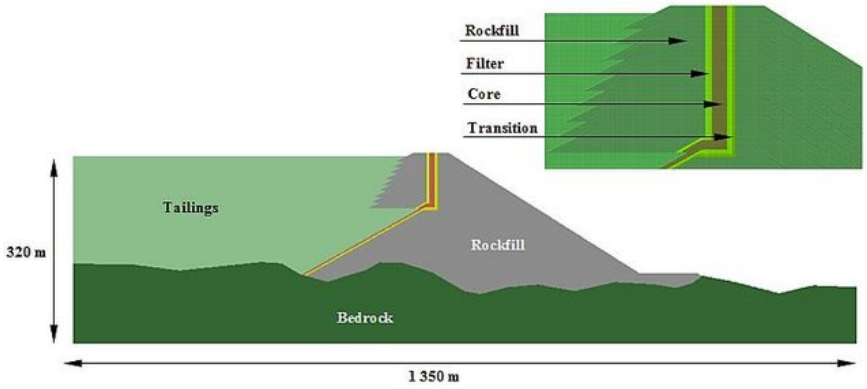

Figure 1: Example of a centreline tailings dam numerical model where the mechanical response of the deposited tailings is critical in the evaluation of the overall performance (after Pretell-Ductram and Dismuke, 2016)

The calibration of constitutive models is an essential step in any numerical analysis. The calibration process is usually performed in an iterative manner by comparing numerical simulations against the available experimental data at the element test level (e.g., monotonic and cyclic triaxial tests, etc.). This process is illustrated in Figure 2, which shows one of the calibrations performed for the numerical modelling of the well-known failure of the Fundao dam as part of the forensic studies after the Samarco dam disaster, which occurred in 2015 in Brazil. The failure of the Fundao dam has been described as the worst environmental disaster in Brazil's history. Around 60 million cubic meters of iron waste flowed into the Doce River, causing toxic brown mudflows to pollute the river and beaches near the mouth when they reached the Atlantic Ocean 17 days later (Wikipedia, 2019). The disaster created a humanitarian crisis as hundreds were displaced and cities along the Doce River suffered water shortages. The adequate characterization of the response of the tailings materials was critical in the case of the Fundao dam. This is a reminder of the importance of the adequate characterization of tailings materials and the subsequent conceptualization of this response through adequate constitutive models for evaluation purposes, especially in critical projects.

Most available constitutive models have been formulated within the framework of the plasticity theory. For example, the 2D-UBCSAND model (Beaty and Byrne, 1998; Park and Byrne, 2004) has been formulated under the classical plasticity theory. The Norsand model (Jefferies and Been, 2015) was also developed under the framework of classical plasticity, but it is also consistent with the critical state soil mechanics framework (i.e., Roscoe et al., 1958; Schofield and Wroth, 1968). The 3D-PDMY02 model (Elgamal et al., 2002; Yang et al., 2003) is formulated under the multisurface plasticity framework of

Prevost (1985). The model represents an elastic-plastic material response and simulates the essential response characteristics of pressure sensitive soil materials under general loading conditions.

The two-surface models within Bounding Surface (BS) plasticity by Manzari and Dafalias (1997) and Dafalias and Manzari (2004) are stress-ratio controlled, critical state compatible models, with a state dependent dilatancy formulation. Based on these works, a family of subsequent models for sands were introduced and called collectively SANISAND models (Dafalias et al., 2004; Taiebat and Dafalias, 2008; Dafalias and Taiebat, 2016). Boulanger and Ziotopoulou (2015) developed the 2D-PM4SAND model as extension of the two-surface bounding surface plasticity framework for sands (Manzari and Dafalias, 1997) and recently they proposed a similar model for silty materials, named the 2D-PM4Silt (Boulanger and Ziotopoulou, 2018). Both models are developed primarily for earthquake engineering applications. In addition, a number of fabric-based BS plasticity constitutive models have been recently proposed (Gao et al., 2014; Petalas et al., 2018; Papadimitriou et al., 2018), which are formulated within the Anisotropic Critical State Theory by Li and Dafalias (2014), to simulate the anisotropic response of granular soils.

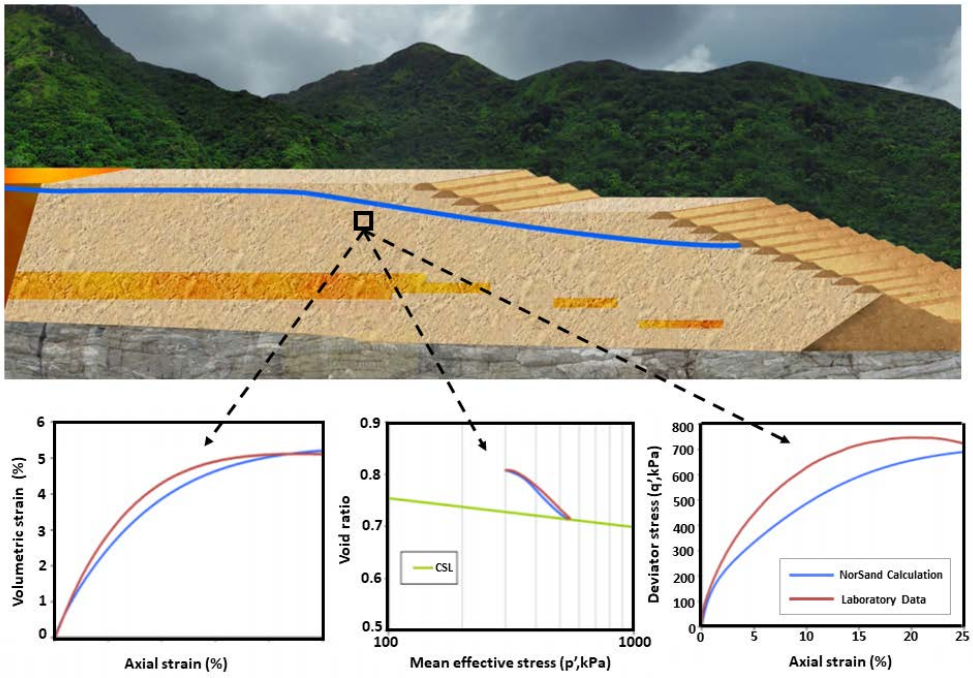

Figure 2: Illustration of the calibration of the Norsand model in the forensic analyses after the Samarco disaster (Morgenstern et al., 2016)

Finally, there have been recent developments that add a constitutive feature described as a memory surface, proposed by Corti et al. (2016), to the bounding plasticity framework to improve the simulation capabilities for the cyclic response of materials that are subjected to a large number of cyclic loadings (see Liu et al., 2018). The next section provides additional details for the constitutive models considered in this study.

Constitutive models considered in this study

We discuss in this sections the constitutive models considered for this study, which are the Norsand (Jefferies and Been, 2015), and the SANISAND (Dafalias and Manzari, 2004) models.

Norsand Constitutive model

Norsand (Jefferies and Been, 2015) is a plasticity-based model formulated within the critical state framework, which states that any particulate material, upon sufficient shearing, will ultimately reach a unique state called the critical state at which the particulate material undergoes a continued deformation without any volume change. Norsand captures the effect of density and pressure dependence on the behaviour of particulate materials, and it can be conceptualized as a generalization of the original Cam Clay model, which means that Cam Clay is a particular case of Norsand. The Norsand model overcomes some of the well-known issues with the Cam Clay model, such us for example the excessive dilation for dense sands (Jefferies and Been, 2015) observed in the Cam Clay model. The main advantage of Norsand over Cam Clay is that it decouples the critical state conditions from the yield surface by abandoning the assumption of a unique normally consolidation line, through the use of the state parameter defined by Been and Jefferies (1985). Following the idea of Taylor (1948) that the dimensionless plastic work done to the soil skeleton (strength) M is the sum of the stress ratio η and the plastic dilation D (particle interlocking), Roscoe et al. (1958) proposed a stress-dilatancy relation $D = M - \eta$, which is the base for the well-known Cam Clay model. The stress-dilatancy relation, also known as flow rule, was further modified by Nova and Wood (1982) to fit experimental data $D = (M - \eta)/(1-N)$, where N represents volumetric coupling between mean and deviatoric strain at peak strength. Based on Rowe's stress-dilatancy theory Manzari and Dafalias (1997) suggested a multiaxial dilatancy rule within the BS plasticity framework with a state parameter ψ (Been and Jefferies, 2015) dependent phase transformation line, following the idea of a state dependent peak stress by Wood et al. (1994). This dependence renders the dilatancy D function of ψ and resulted in the breakthrough unification of loose and dense sand response description for any pressure with same material constants. Shuttle and Jefferies (2010) followed the same idea and suggested the stress-dilatancy flow rule as:

$$D = M_i - \eta. \tag{1}$$

where the plastic dilation is defined as $D = d\varepsilon_v^p / d\varepsilon_d^p$, and the stress ratio is defined as $\eta = q/p$. Note the subscript i denotes image condition, which evolves with state parameters, and gradually reaches the critical state, $M_i \rightarrow M$. Following Drucker's normality rule, the yield surface of Norsand model is directly derived by the integration of the flow rule (Eq.1) as:

$$F = \eta - M_i\left(1 - ln(\frac{p}{p_i})\right) = 0 \tag{2}$$

.

where p_i denotes the image stress, which gives $\eta = M_i \leftrightarrow p = p_i$. Figure 3 sketches a typical yield surface for Norsand. The increment of stress as well as the increment of plastic strain is normal to the yield surface since plastic associative flow rule is adopted.

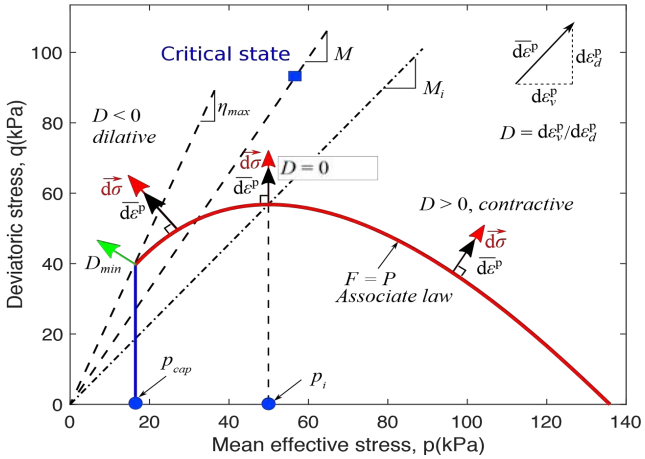

Figure 3: Sketch of Norsand yield surface

Figure 4 shows typical behaviours obtained with Norsand for the case with (a) loose particulate material and (b) a dense particulate material subjected to triaxial compression drained test. Loose materials show consistent hardening and contractive behaviour. Dense materials show contraction and hardening in the first stage until point A (Figure 4b), then it dilates with continued hardening to reach the peak strength (point B, where the minimum dilation D_{min} is reached), followed by softening behaviour with continuous dilation. Both samples will eventually reach the critical state (point A'), at which $D = 0$ and $D' = 0$. It is worth noting that the image condition in Figure 3 is the point (p_i, $M_i p_i$) on yield surface that gives zero dilatancy $D = 0$. However, it does not necessary indicate $D' = 0$, hence we name it image condition as only one condition for critical state is satisfied.

Dafalias and Manzari (2004) constitutive model

In this study, the two-surface bounding surface plasticity model proposed by Dafalias and Manzari (2004) is used and for simplicity is named DM04. The DM04 model builds upon the previous work by Manzari and Dafalias (1997) and introduces three new aspects. The first is a fabric-dilatancy state variable, scalar valued in the triaxial and tensor-valued in the generalized stress space, which is instrumental in modelling macroscopically the effect of fabric changes during the dilatant phase of deformation on the subsequent contractive response upon load increment reversals, and the ensuing realistic simulation of the sand behaviour under undrained cyclic loading. The second aspect is the Lode angle dependent plastic strain rate direction, a feature necessary to produce realistic stress-strain simulations in non-triaxial conditions.

The third aspect is a very systematic connection between the simple triaxial and the general multiaxial formulations, in order to use the model parameters of the former in the implementation of the latter.

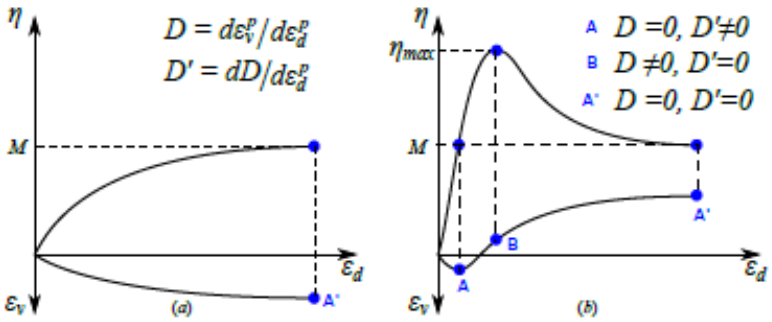

Figure 4: Sketch of stress/strain behaviour obtained with the Norsand model in a triaxial drained compression test of (a) loose particulate material and (b) dense particulate material.
Where n= q/p is the effective stress ratio. Dilatancy $\boldsymbol{D = d\varepsilon_v^p / d\varepsilon_d^p}$ is the ratio of volumetric strain over deviatoric strain. Note both the zero dilatancy $\boldsymbol{D} = 0$ and zero dilatancy rate $\boldsymbol{D'} = 0$ have to be satisfied to meet the critical state conditions

We will illustrate some aspects of the DM04 model by considering the simpler triaxial stress space. A detailed presentation of the model is presented in Dafalias and Manzari (2004). With σ_1, $\sigma_2 = \sigma_3$ the principal effective stresses, triaxial stress variables are defined as $q = \sigma_1 - \sigma_3$, and $p = 1/3(\sigma_1 + 2\sigma_3)$, and the stress ratio is defined as $\eta = q/p$. Since the DM04 considers only deviatoric plasticity, a yield surface according to Equation 3 is defined:

$$f=|\eta - \alpha| - m = 0 \tag{3}$$

As discussed in Dafalias and Manzari (2004) Figure 5 shows the representation of the yield, dilatancy and bounding lines in the p-q space. Equation 3 represents geometrically a ‘‘wedge’’ in the *p-q* space, shown by the shaded area in Figure 5, whose bisecting line has a slope α, and the wedge opening a value of $2mp$. The α and m are stress ratio quantities. For η inside the wedge only elastic strain is induced for small variations of η. When η satisfies Equation 3 and its derivative, $d\eta$, points ‘‘outward’’ from the wedge i.e., $d\eta$ >0 at the upper wedge boundary and $d\eta$ <0 at the lower wedge boundary, plasticity occurs. In this case the wedge changes orientation, α, in order to have η remaining on the yield surface in what can be called kinematic hardening plasticity, with α the corresponding back stress ratio in plasticity terminology (Dafalias and Manzari, 2004). The bounding line defined by the slope M^b determines the simulated peak stress ratio and the dilatancy line defined by the slope M^d determines the phase transformation from contractive to dilative response or vice versa.

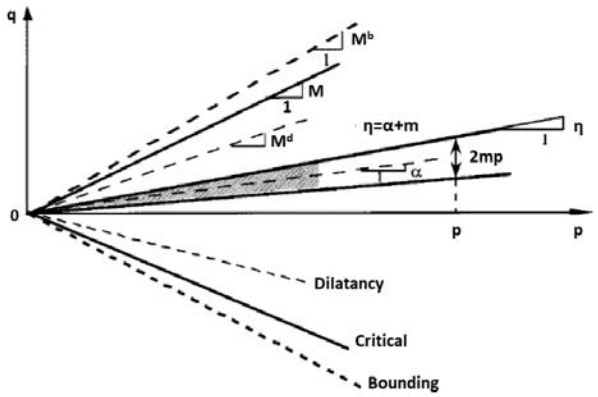

Figure 5: Sketch of the yield, critical, dilatancy, and bounding lines in the DM04 model

Experimental results

Figure 6 shows the particle size distribution for the tested material (denominated as T1), which correspond to a mine tailing with a plasticity index of 3 and with Atterberg limits that locate the material just above the "A-line" in a plasticity chart, classifying the material as ML, according to the unified soil classification system (USCS). As part of the experimental program 4 CD triaxial tests, 2CU triaxial tests, 6 bender elements and 3 cyclic shear tests were performed. Figure 7 shows the post-processing of the triaxial tests (Figures 7a, 7b, and 7c), to stablish the critical state line and stress-dilatancy relationships. Figure 7d shows the results from the bender element tests, and Figures 7e and 7f shows the results of two cyclic shear tests, that caused liquefaction (defined as 3% of single amplitude shear strains) in 15 and 6 cycles respectively.

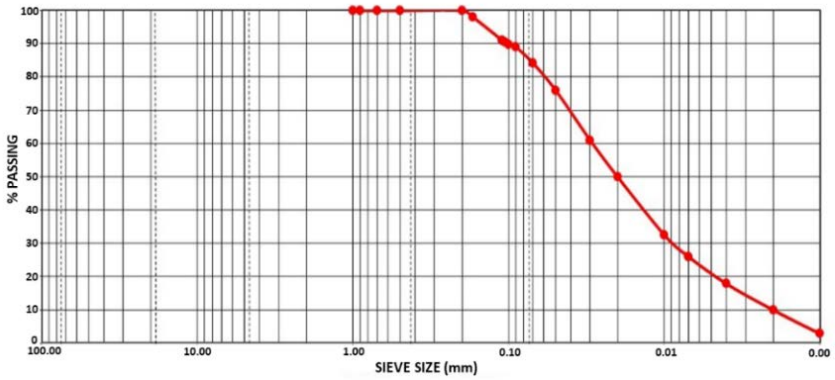

Figure 6: Particle size distribution for the tailings material

Calibration of constitutive models

Norsand

The following steps were used and can be considered as a guideline for the calibration of particulate materials using the Norsand model:

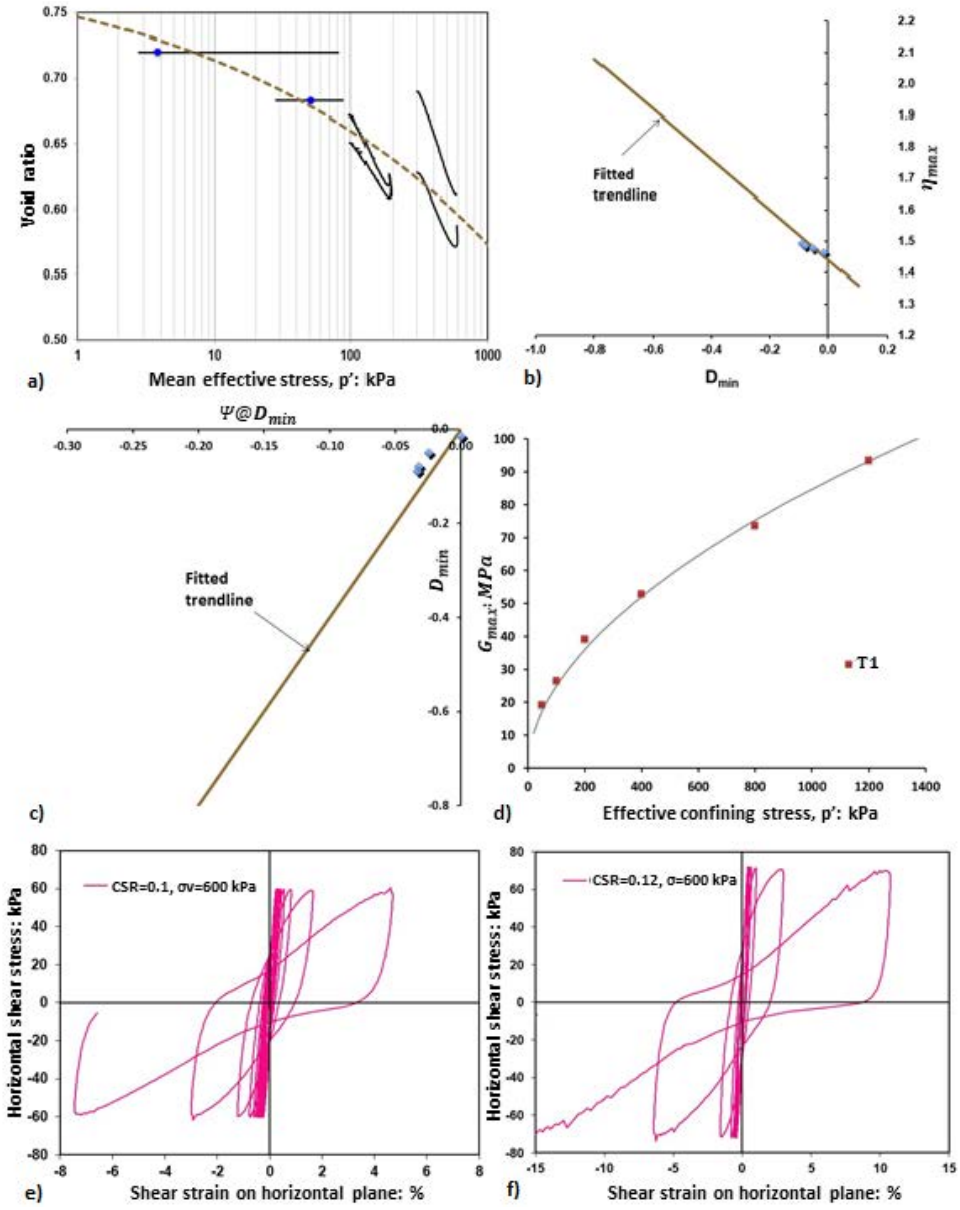

Figure 7: Experimental results: (a), (b) and (c) show the post-processing of 4 CD triaxial tests and 2 CU triaxial tests. η_{max} is the maximum stress ration, Dmin is the minimum dilatancy (i.e., the maximum of the absolute value), $\psi@D_{min}$ is the state parameter at minimum dilatancy. (d) shows the results of bender element tests, and (e) and (f) show results of two selected cyclic shear tests

1. The critical state line (CSL) in Figure 7a was fitted to an exponential law, providing the following relationship: $e_c = 0.8 - 0.14 * (\frac{p}{100})^{0.21}$. This equation is used in the Norsand model to define the CSL, from which the state parameter (ψ) can be defined.
2. Using Figure 7b, the Norsand M_{tc} parameter is estimated as 1.44, and N (the volumetric coupling) is estimated as 0.2. The Norsand χ parameter, is estimated as 4, using Figure 7c, and considering

that the relationship $D_{min} = \chi.\psi$ is valid, where D_{min} is the minimum dilatancy (i.e., the maximum of its absolute value).

3. The plastic modulus (H) in Norsand was estimated as H=30 using a forward iterative calibration (i.e., test and error). This value provided reasonable results for the triaxial tests simulations.
4. The elasticity for the Norsand the model was defined based on Figure 7d, through the relationship $G_{max}(Mpa) = 25(\frac{p}{100})^{0.53}$.
5. Finally, the Z parameter needed for cyclic simulations in the plane stress rotation formulation of Norsand (Jefferies and Been, 2015) was taken as Z=30. The coefficient of lateral stress at rest K_0 is unknown during the experimental tests, then we performed sensitivity analyses with K_0=0.5,0.7, and 0.9. These values were considered based on the range of values considered in Jefferies and Been (2015) for the calibration of the Fraser River sand.

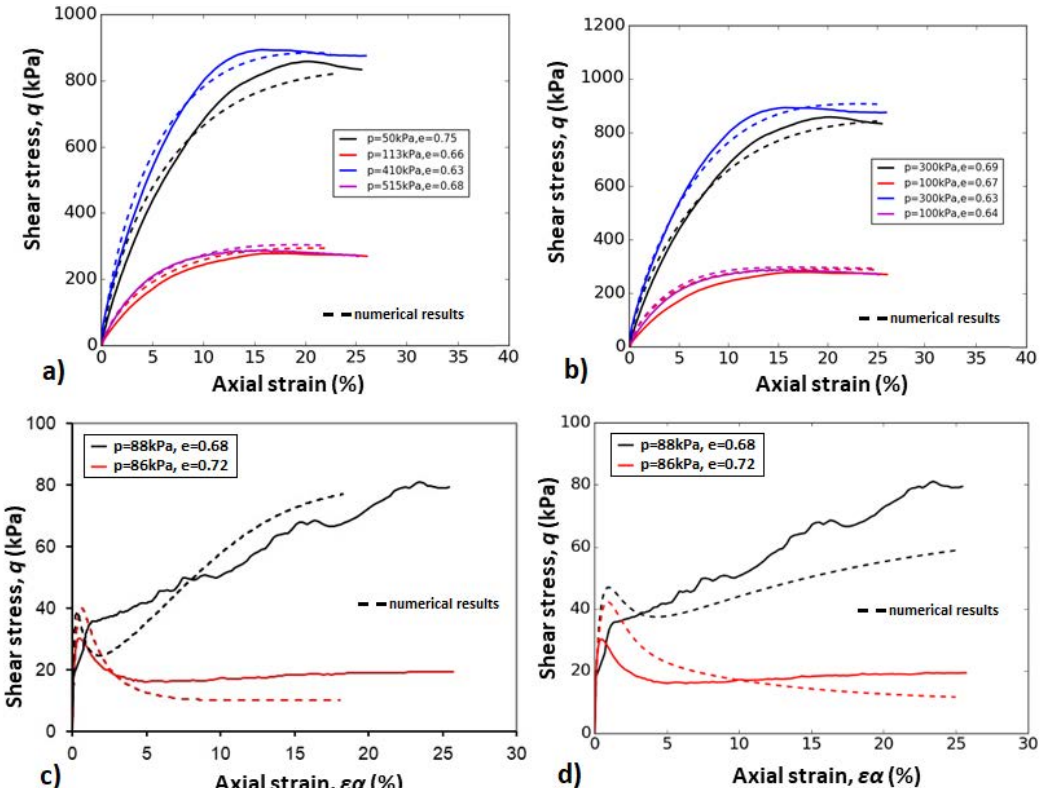

Figure 8: Calibration results triaxial static tests: (a) CD triaxial tests with the Norsand model, (b) CD triaxial tests with the DM04 model, (c) CU triaxial tests with the Norsand model, and (d) CU triaxial tests with the DM04 model

Figure 8 shows a comparison between the numerical simulations with the Norsand model and the experimental tests, considering both triaxial CD and triaxial CU tests. Figure 9 (a,b and c) shows similar comparisons considering the stress-strain response obtained from the cyclic shear tests and during the

numerical simulations with Norsand for the three cyclic shear tests, which have cyclic stress ratios (CSR) of CSR=0.08, 0.10, and 0.12. Figure 9d shows the sensitivity of the pore pressure development in the 3 cyclic shear tests, considering K_0 values of 0.5, 0.7, and 0.9.

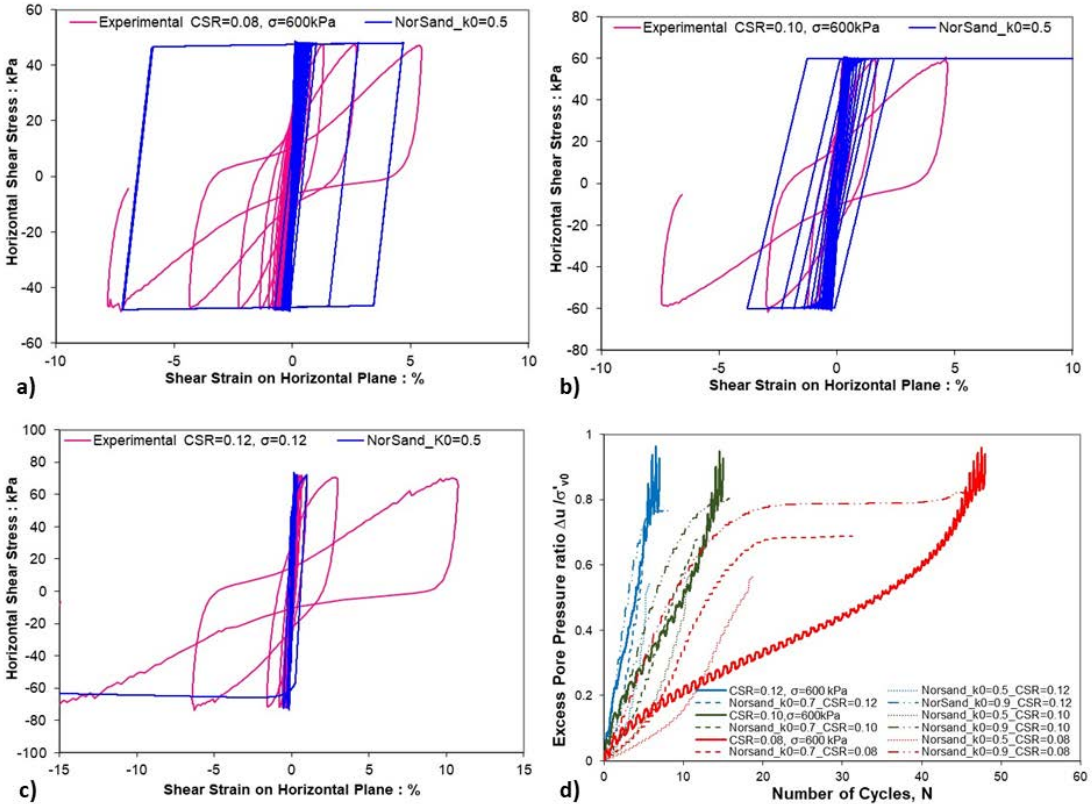

Figure 9: Norsand calibration results, cyclic shear tests: (a) stress strain curve CSR=0.08, σ=600 kPa, (b) stress strain curve CSR=0.10, σ=600 kPa, (c) Stress strain curve CSR=0.10, σ=600 kPa, and (d) pore pressure build up for different k_0 values

Dafalias and Manzari, 2004 (DM04)

The following steps were followed for the calibration of the DM04 model:

1. The CSL in the DM04 model is defined as, $e_c = e_{ref} - \lambda_c * \left(\frac{p}{p_{atm}}\right)^{\xi}$. This exponential equation introduces three material constants to the model, and by using e_{ref}=0.8, λ_c=0.14 and ξ=0.21, a consistent calibration with the Norsand model is achieved for the same tailing material. The critical state line is defined by the critical state slope in compression, M_c=1.44, and c=0.712, that means that the slope in triaxial extension is $M_e = cM_c$.

2. The n^b=1.3 and the n^d=0.40, and they are estimated by solving, $n_b = \frac{ln\left(\frac{M}{M^b}\right)}{\psi^b}$ and $n_d = \frac{ln\left(\frac{M^d}{M}\right)}{\psi^d}$, where M^b and M^d are the peak and phase transformation rations respectively, and ψ^b and ψ^d are

the values of the state parameter at peak and phase transformation respectively. These values are determined from the drained and undrained monotonic triaxial compression tests.

3. The plastic modulus parameters h_0= 6 and c_h=0.968 and the dilatancy parameter A_0=1.1. Those three parameters are determined by trial-and-error numerical simulations and comparison against the monotonic experimental data. Only the h_0 parameter had to be modified for the cyclic tests and becomes h_0=20 to partially overcome the tendency of the model for higher excess pore pressure generation that what is observed in the experimental results.
4. The elastic shear modulus in DM04 is defined as, $\frac{G}{p_{atm}} = G_0 \frac{(2.97-e)^2}{1+e}\left(\frac{p}{p_{atm}}\right)^{0.5}$, it introduced one material parameter, G_0, that is 25 kPa in this case. The Poisson's ratio is v=0.05.
5. Finally, the fabric-dilatancy parameters z_{max}=12 and c_z=800, and they are determined by trial-and-error numerical simulations and comparison against the cyclic undrained DSS tests.

Figure 8 shows a comparison between the numerical simulations with the DM04 model and the monotonic experimental tests, considering both triaxial CD and triaxial CU tests. Figure 10 (a, b and c) shows similar comparisons considering the stress-strain response obtained from the cyclic shear tests and during the numerical simulations with DM04 for the three cyclic shear tests, which have cyclic stress ratios (CSR) of CSR=0.08, 0.10, and 0.12. Figure 10d, shows the sensitivity of the pore pressure development in the 3 cyclic shear tests, considering K_0=0.5. In passing notice that the DM04 is much less sensitive to the change of K_0 than Norsand and this is why the estimated K_0=0.5 for the consolidation process in a DSS device is judged as sufficient to validate the model against the experimental data.

Discussion and closure

From Figure 8, it is observed that the Norsand constitutive model provides excellent results when it is calibrated to reproduce the experimental results in the triaxial CD tests, and it provides reasonable results for the calibrations against the CU triaxial tests. In the case of the CU tests, the model captures only partially the hardening observed in the CU test with initial conditions of p=88 kPa, and void ratio (e)=0.68 (which corresponds to a $\boldsymbol{\psi} = 0.01$). In addition it is observed that Norsand captures the transition to static liquefaction in the CU tests with initial conditions of p=88 kPa, and e=0.72 (which corresponds to $\boldsymbol{\psi} = 0.06$. In terms of the calibration of the cyclic shear tests, Norsand cannot capture the stress-strain response observed in the laboratory tests (see Figure 9), in particular only narrow hysteretic loops are observed before the shear strains increase dramatically. Interestingly K_0 has an important influence in the pore pressure generation (Figure 9d) and consequently in all other aspects of the cyclic response in the Norsand model. For example, when CSR=0.08, the pattern for the pore pressure

generation can change considerably for K_0 variations from 0.5 to 0.9. Likewise, the number of cycles for liquefaction can change from 18 (for K_0=0.5) to 48 (for K_0=0.9). For K_0=0.9, the number of cycles to reach initial liquefaction is close to the number of cycles in the experimental test, even though the experimental pattern of pore pressure generation is not captured.

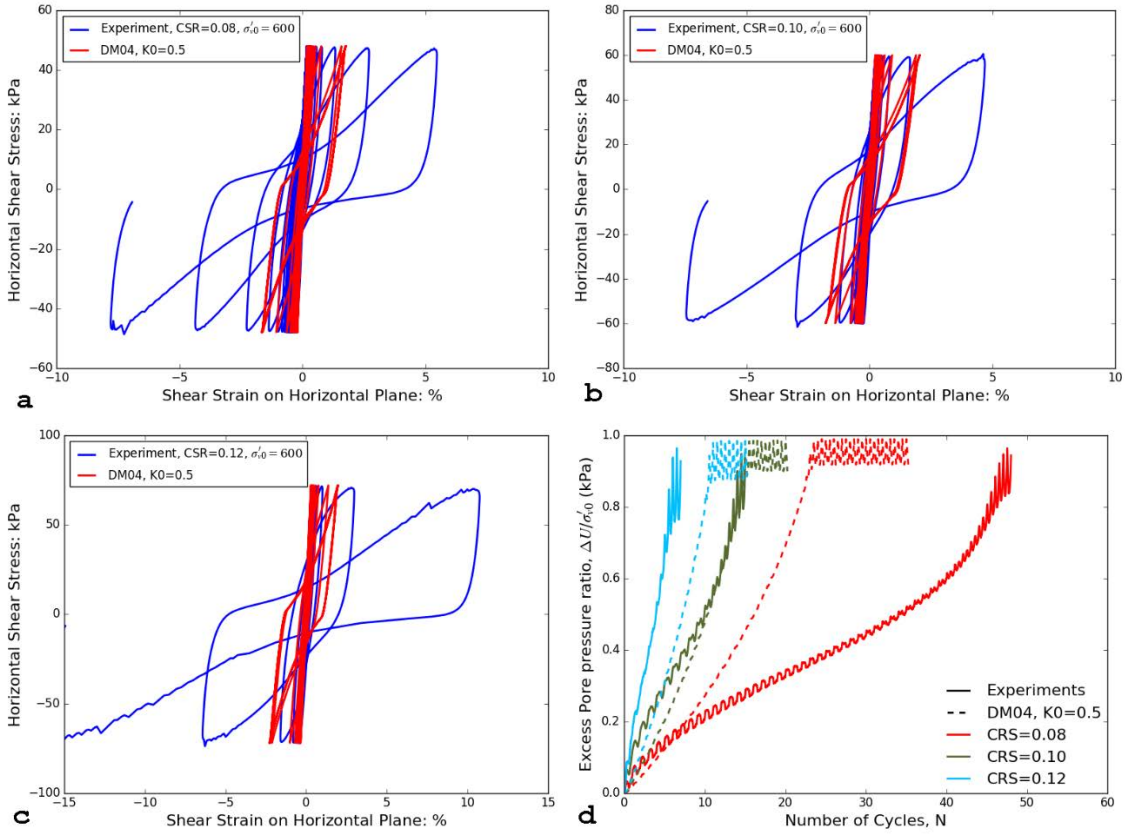

Figure 10: DM04 calibration results, cyclic shear tests: (a) stress strain curve CSR=0.08, σ=600 kPa, (b) stress strain curve CSR=0.10, σ=600 kPa, (c) Stress strain curve CSR=0.10, σ=600 kPa, and (d) pore pressure build up

Similarly, the DM04 provides a very accurate fit of the monotonic CD tests and reasonable results against the monotonic CU triaxial tests. It simulates accurately the undrained softening behaviour for the test with initial conditions of p=88 kPa, and void ratio (e)=0.68, that leads to static liquefaction. However, the model cannot reproduce accurately the response of the tailing material as far as cyclic loading is concerned. Even though the model simulates the non-linear stress-strain curves in a correct manner, the maximum simulated shear strains are consistently smaller than the ones observed in the three experiments. The number of cycles to reach liquefaction are very accurate for the case of CRS=0.10, slightly higher for the case of CRS=0.12 and significantly lower for the case of CRS=0.08. This proves that the model cannot consider the effect of CRS for this material, especially for low CRS values.

In summary, both the Norsand and the DM04 model can capture the response observed in the triaxial CD and CU tests well. However, they cannot capture the patterns observed in the experimental cyclic shear tests. Norsand is a model mainly used for static applications and the discrepancies in reproducing cyclic responses may be expected. The DM04 model was originally formulated for sand materials, however, for this tailing material the model suffers from the inability to simulate accurately the effect of CRS, especially for small values, when the densification of the soil due to cyclic loading plays a key role. Even though it is part of the state of the practice the use of sand-based constitutive models for tailings (typically classified as silts), the discrepancies in the observed responses suggest that a further examination of this issue is needed. Further there are more recent formulations of models in the SANISAND family that may help to clarify these issues. For example, the version that incorporates the memory surface (Liu et al., 2018) may improve the accuracy of the simulations with low CRS values. Moreover, the recently proposed fabric-based SANISAND-FN (Petalas et al., 2018) may improve the simulations of the cyclic DSS tests, due to the fact that it takes into account the effect of stress principal axis rotation. Future studies will be focused on this. In addition, we observed that K_0 can significantly affect the pore pressure generation in cyclic shear tests. Since K_0 is not measured in standard cyclic shear tests, this issue also deserves further exploration. This is particularly important because the cyclic shear test is the preferred test to characterize the cyclic response of tailings materials in the current state of practice.

References

Beaty, M. and P.M. Byrne. 1998. An effective stress model for predicting liquefaction behavior of sand. *Geotechnical Earthquake Engineering and Soil Dynamics III*, ASCE Spec. Pub. 75, Reston, Virginia, 1: 766-777.

Been, K. and M.G. Jefferies. 1985. A state parameter for sands. *Geotechnique* 35(2): 99–112.

Boulanger, R.W. and K. Ziotopoulou. 2015. A sand plasticity model for earthquake engineering applications: Version 3.0. Report No. UCD/CGM-15-01, Center for Geotechnical Modeling, Department of Civil and Environmental Engineering, University of California, Davis, CA, 113 pp.

Boulanger, R.W. and K. Ziotopoulou. 2018. PM4Silt (Version 1): A silt plasticity model for earthquake engineering applications. Report No. UCD/CGM-18/01, Center for Geotechnical Modeling, Department of Civil and Environmental Engineering, University of California, Davis, CA.

Corti, R., A. Diambra, D.M. Wood, D. E. Escribano and D.F.T. Nash. 2016. Memory surface hardening model for granular soils under repeated loading conditions. *Journal of Engineering Mechanics*, 142(12), 04016102. https://doi.org/10.1061/(asce)em.1943-7889.0001174

Dafalias, Y.F. and M.T. Manzari. 2004. Simple plasticity sand model accounting for fabric change effects. *Journal of Engineering Mechanics* 130(6): 622–634.

Dafalias, Y.F., A.G. Papadimitriou and X.S. Li. 2004. Sand plasticity model accounting for inherent fabric anisotropy. *Journal of Engineering Mechanics* 130(11): 1319–1333.

Elgamal, A., Z. Yang and E. Parra. 2002. Computational modeling of cyclic mobility and post liquefaction site response. *Soil Dyn. Earthq. Eng.* 22(4): 259–71.

Gao, Z., J. Zhao, X. Li and Y.F. Dafalias. 2014. A critical state sand plasticity model accounting for fabric evolution. *Int. J. for Numerical and Analytical Methods in Geomechanics* 38(4): 370–390.

Jefferies, M.G. and K. Been. 2015. *Soil Liquefaction: A Critical State Approach*, second edition, CRC Press. ISBN 9781482213683.

Li, X.S. and Y.F. Dafalias. 2000. Dilatancy for cohesionless soils. *G´eotechnique* 54(4): 449–460.

Li, X.S. and Y.F. Dafalias. 2012. Anisotropic critical state theory: Role of fabric. *Journal of Engineering Mechanics* 138(3).

Manzari, M.T. and Y.F. Dafalias. 1997. A critical state two-surface plasticity model for sands. *G´eotechnique* 47(2): 255–272.

Morgenstern, N.R., S.G. Vick, C.B. Viotti and B.D. Watts. 2016. Fundão Tailings Dam Review Panel: 541. Report on the immediate causes of the failure of the Fundão dam.

Nova, R. and D. Wood. 1982. A constitutive model for soil under monotonic and cyclic loading. In *Soil Mechanics – Transient and Cyclic Loading,* edited by G.N. Pande and C. Zienkiewicz: 343–373. Chichester: Wiley.

Papadimitriou, A.G., Y.K. Chaloulos and Y.F. Dafalias. 2018. A fabric-based sand plasticity model with reversal surfaces within anisotropic critical state theory. *Acta Geotechnica* 14(2): 253–277.

Park, S.S. and P.M. Byrne. 2004. Stress densification and its evaluation. *Canadian Geotechnical Journal* 41(1): 181–186.

Pretell-Ductram, R. and J. Dismuke. 2016. Comparison of simplified and detailed analyses for assessment of dynamic displacement of a centerline tailings dam. 4th Itasca Symposium*,* March 2016.

Prevost, Jean H. 1985. A simple plasticity theory for frictional cohesionless soils. *Journal of Soil Dynamics and Earthquake Engineering* 4(1): 9–17.

Roscoe, K.H., A.N. Schofield and C.P. Wroth. 1958. On the yielding of soils. *Géotechnique* 8(1): 22–53.

Schofield, A.N. and C.P. Wroth. 1968. *Critical State Soil Mechanics*. London: McGraw-Hill.

Shuttle, D. and M. Jefferies. 2010. Norsand: Description, calibration, validation and applications*.* Retrieved from http://itasca-udm.de/media/download/norsandm/NorSand_M.pdf

Taylor, Donald. 1948. *Fundamentals of Soil Mechanics.* New York: Chapman and Hall, Ltd.

Wikipedia. 2019. Mariana dam disaster. Retrieved from https://en.wikipedia.org/wiki/Mariana_dam_disaster

Wood, D.M. and K. Belkheir. 1994. Strain softening and state parameter for sand modelling*. Géotechnique* 44(2): 335–339.

Yang, Z., A. Elgamal and E. Parra. 2003. Computational model for cyclic mobility and associated shear deformation. *Journal of Geotechnical and Geoenvironmental Engineering* 129(12): 1119–27.

Proceedings of Tailings and Mine Waste 2019
November 17–20, 2019, Vancouver, Canada
Published by the University of British Columbia, 2019

Earthquake Ground Motion Selection Criteria for Analysis of Tailings and Mine-Waste Critical Facilities

Marcelo Martinez, Golder Associates, Chile
Alan Hull, Golder Associates, USA

Abstract

Site-specific probabilistic (PSHA) and deterministic (DSHA) seismic hazard analysis for different earthquake performance targets are typically used to select earthquake acceleration time histories (ATHs) as inputs for dynamic stability studies. However, although local and international guidelines for seismic analysis of critical facilities are widely cited by designers, the selection of earthquake ground motions can often appear arbitrary and inconsistent. This paper addresses this shortcoming and proposes unified criteria for the selection of earthquake ground motions used for analysis and design of tailings and mine-waste critical facilities.

In the initial stages of earthquake engineering analyses, the important elements for mine-waste critical facilities are the site-specific earthquake hazard, the use of probabilistic and/or deterministic approaches, and the seismic performance expectations based on the facility-failure consequence.

Modern international tailings guidelines typically recommend an operating basis earthquake (OBE), and a safety evaluation earthquake (SEE) performance level. These two performance levels specify post-earthquake functionality and readily repairable earthquake damage for the OBE, and acceptable damage but without collapse for the SEE. While the OBE is typically evaluated using PSHA, the SEE ground motions are evaluated from either the DSHA-based maximum credible earthquake (MCE), or the PSHA-based spectral accelerations at low annual exceedance probabilities (AEP) of up to 1 in 10,000 (1:10,000).

This paper describes how contemporary PSHA and DSHA approaches can be used together to define earthquake performance targets in different seismic hazard regions to establish the ground motion selection criteria for the analysis and design of tailings and mine-waste facilities.

Introduction

Critical mining facilities have unique features (i.e., height, size, capacity, material storage, etc.) that represent a potentially large hazard to communities, the environment, economy and property, during their life spans, which exceed ordinary engineered structures. Examples of critical mining facilities are tailings

storage facilities, heap leach pads, waste-rock dumps, water-reservoir dams, large ponds, and other complex engineered structures that support mining activities. The specific characteristics of these critical facilities typically exclude them from local seismic provisions developed for standard structures for human occupancy. Earthquake ground motions developed for local seismic building codes are, therefore, not applicable for the design and analysis of critical mining facilities because they are neither site-specific, nor useful beyond life-safety design for standard structures.

Available international guidelines

In the absence of specific code-base regulations, international dam organizations (e.g., ICOLD), local dam associations (e.g., CDA, NZSOLD, ANCOLD, etc.), and mining corporations provide general guidelines for the development of seismic design criteria for critical mining facilities. Typically, seismic criteria are based on risk-target levels defined as a function of the facility failure consequence. The earthquake selection criteria set out in these guidelines requires careful judgement when applied to seismic analysis and design of critical facilities.

Although international guidelines are widely cited by designers (e.g., ICOLD, 2010; 2016; CDA, 2014; NZSOLD, 2016; BAT, 2018; ANCOLD, 2019; etc.), the appropriate selection of earthquake ground motion outputs at a specified performance level often remains unclear and can result in the adoption of an arbitrary level for seismic design. To improve clarity and work toward a common approach to the development of seismic design criteria for mine facilities this paper aims to:

1. Show how the local tectonic setting is an important input into the analysis, and that local guidelines developed in one type of seismic region are not necessarily applicable in other regions. For example, guidelines developed for sites located in stable continental regions (i.e., Australia and eastern Canada) are not readily applicable for the development of design-level earthquake ground motions in regions with moderate-to-high seismicity like New Zealand, or the west coast of the USA, Canada, and South America.
2. Clarify a general misinterpretation where earthquake ground motions are developed for either a low or very-low annual exceedance probability (AEP), or for the deterministically based maximum credible earthquake (MCE) as the safety evaluation earthquake (SEE) performance level.
3. Specify when the median or median plus one standard deviation (84^{th}-percentile) ground motion should be used for the MCE when it is used as the SEE.

This paper does not propose a change in the application of existing international guidelines. Instead, we aim to clarify the use of the concepts involved by proposing an approach toward developing a unified

practice in the selection of earthquake ground motions for seismic stability analysis and the design of critical mining facilities. Consistent with most guidelines, the proposed approach uses both probabilistic seismic hazard analysis (PSHA) and deterministic seismic hazard analysis (DSHA), including ways to reconcile the different results derived from these two analysis methods.

The earthquake hazard curves presented here are mean horizontal spectral accelerations from site-specific seismic hazard studies undertaken by Golder Associates in low, moderate, and high seismic hazard regions worldwide. Earthquake ground motion values presented here are generalized and are not suitable for use in design at a specific site. A glossary and a list of acronyms are included in an appendix to assist the reader.

Site-specific seismic hazard

Seismic hazard arises from earthquake occurrences that are typically geographically defined and related to a geologic province and the present-day tectonic framework. The site's location with respect to tectonic plate boundaries, seismically active crustal faults, and historical earthquakes epicenters are key elements in the assessment of the site-specific seismic hazard.

Table 1 lists the key parameters used to classify a site into one of three general seismic hazard regions. These features account for the geological and seismic setting, the average slip rate on mapped faults, and the maximum expected earthquake magnitude. Table 1 also indicates the ease of defining the maximum credible earthquake (MCE) for conducting deterministic seismic hazard analysis (DSHA) based on data available in the region surrounding a site.

Earthquake hazard and return periods

Available international guidelines for earthquake ground motion selection of mine facility design are typically based on discrete annual exceedance probabilities (AEP, or their inverse of return period), and for a specified failure consequence. Understanding the interrelation between PSHA- and DSHA-based earthquake ground motions and their AEP is critical to the selection of earthquake design ground motions. Furthermore, the use of PSHA and/or DSHA to evaluate earthquake ground motions for design depends on the regional seismic hazard level where the critical facility is located. The influence of seismic region on the selection of ground motions is summarized in Table 1 and described further below.

Table 1: Key features used for classification of seismic hazard regions and selection of MCE ground motions for critical facilities

Seismic hazard	Seismotec-tonic framework	Expected maximum magnitude (M)	Crustal fault characteristics	Maximum credible earthquake (MCE)	Comments and observations
Very low to low	Stable continental regions (SCR) and continental craton geologic setting. Great distance (1,000+ km) from active plate boundaries.	Definition of maximum earthquake magnitude from fault dimensions (e.g., length and width), fault slip rates and paleo-seismic data is generally absent. Maximum instrumental earthquake typically less than about **M**6.0.	Surface fault ruptures generally absent or represent very long (10^5yrs) recurrence intervals for surface rupture and negligible generation of large earthquakes.	Definition of an MCE typically not possible.	1. Limited number of recorded earthquakes, or no historical record. 2. Seismically capable faults generally absent and difficult to identify and characterize. 3. A rational procedure to select the closest site-to-source distance is usually not available.
Moderate	Evidence of ongoing crustal deformation and intermediate -to-deep earthquakes at subduction source zones.	Major earthquakes (≥**M**7.0) are infrequent although possible, but moderate intraplate crustal earthquakes (≥**M**4.5) are known and well located.	Low-to-intermediate fault slip rates (e.g., ≤0.1 to 1mm/year) and readily defined uniform area source zones. Near-field ground motion effects considered when source-to-site distance is relatively close.	MCE can be defined with reasonable confidence.	1. Historical earthquake record available. 2. Rare large damaging earthquakes, and some geologic evidence for seismically active faults. 3. Seismic sources can usually be identified and characterized with good confidence.
Very high to high	Complex, geologically active regions close to convergent plate boundaries (interface and inslab source zones) and large slip rate crustal faults or fault segments.	Large magnitude earthquakes (**M**≥7.0) occur within the subduction interface (e.g., up to **M**9.0±0.5) or inslab (e.g., up to **M**8.0±0.2) source zones, or large slip rate crustal faults.	Crustal fault zones and fault segments have moderate to high slip rates (e.g., ≥1 to 5 mm/year). Earthquake near-field effects are important, if the source-to-site distance is ≤10 km.	MCE can be defined with high confidence.	1. Historical and instrumental record of multiple large and damaging earthquakes. 2. Annual occurrence of many moderate (**M**≥5.0) earthquakes. 3. Well mapped faults with well-documented average slip rates and paleo seismic evidence for repeated late-Quaternary and Holocene surface rupture (i.e., last 11,700 years).

Very low and low seismic hazard regions

Regions of very low to low historical earthquake activity are typically within the cratons of the major continents. Johnston (1994) considers a stable continental region (SCR) to be an area that has not experienced any major tectonism or orogenic activity (i.e., major crustal deformation and mountain building) younger than early Cretaceous (i.e., since about 70 million years [Ma] ago), and no rifting or major extension or trans-tension since Paleogene time (i.e., 66 to 56 Ma ago).

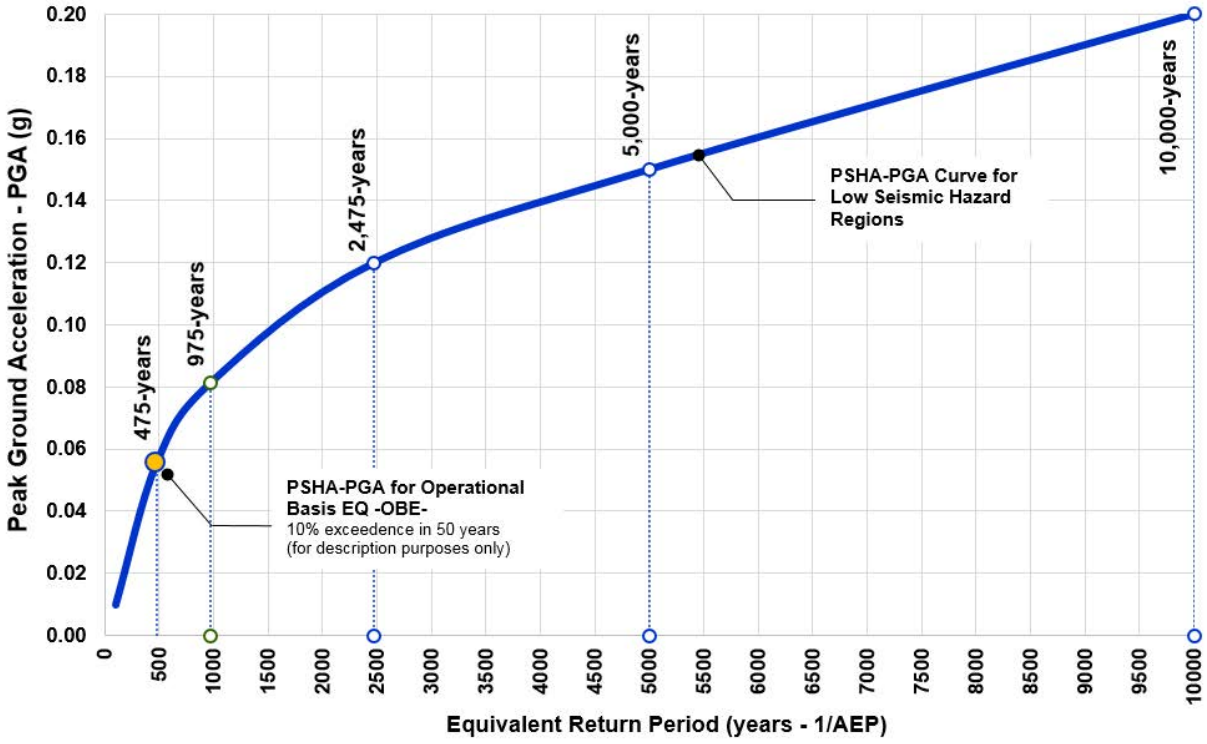

Figure 1: Characteristic peak ground acceleration (PGA) hazard curve in a very low to low seismic hazard region
(*Disclaimer*: ground motion values are referential and for description purposes only)

The relatively historical seismic quiescent in SCRs often makes it difficult to develop a robust estimate of the earthquake recurrence parameters needed for probabilistic analyses. Because the maximum horizontal compressive stress directions are relatively uniform within the SCRs (Johnson, 1994), the estimation of acceptable earthquake activity parameters is generally based on uniform-area crustal earthquake source zones that assume a uniform frequency of earthquake occurrence across a wide area (Cornell, 1968). The SCRs typically do not contain seismically active faults associated with large earthquakes in historical or Holocene times. Some exceptions to this general rule are, however, known from regions of the world including, for example, Australia (e.g., Quigley et al., 2006; 2010) and the Fennoscandia region of northern Europe (Olesen et al., 2004; Grigull et al., 2015; Korja, 2015; Landgraf et al., 2017).

In low seismic hazard regions, the identification and characterization of fault sources is typically very challenging because even when active faults are present, they are difficult to identify. Accordingly, finding the source of the maximum credible earthquake (MCE) needed to undertake a DSHA is not practical. The results from PSHA, therefore, are usually used to develop design earthquake ground motions for critical mine facilities.

In very-low to low seismic hazard regions, design-level earthquake ground motions are typically selected for low AEPs (e.g., from 1:2,500 to 1:10,000) depending on the facility failure consequence rating. However, earthquake ground motion values are typically low and may not control the design, even when the earthquake ground motions are selected for a low AEP (e.g., PGA ≈ 0.20 g for an AEP of 1:10,000). Figure 1 shows a typical probabilistic earthquake hazard curve for mean peak ground acceleration, (PGA expressed as a fraction of the acceleration of gravity, g) in a generic low seismic hazard region.

Moderate seismic hazard regions

Figure 2 shows a mean horizontal PGA hazard curve typical for a region with a moderate level of seismic hazard. Moderate seismic hazard regions are typically located away from present-day tectonic plate boundaries but not within the adjacent SCRs.

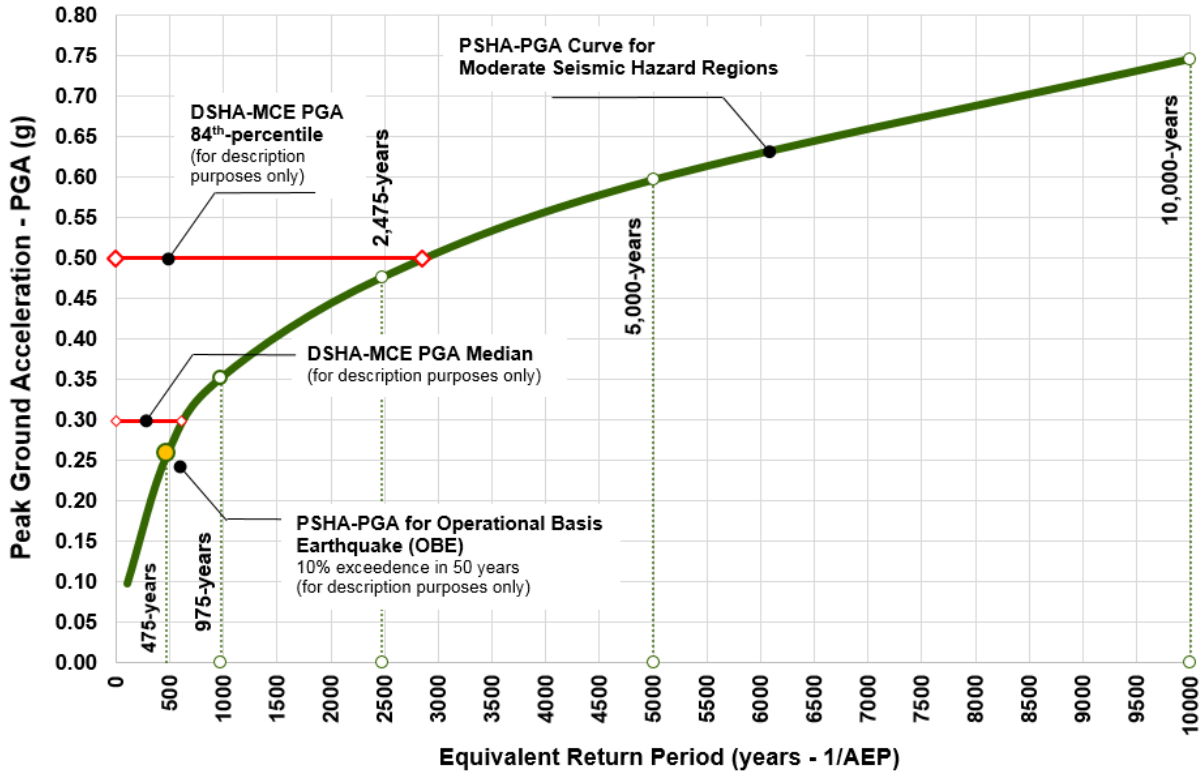

Figure 2: Characteristic seismic mean horizontal PGA-curve for moderate-earthquake hazard regions (*Disclaimer*: ground motion values are referential and for description purposes only)

At subduction zones, moderate seismic hazard regions are where subduction inslab earthquakes occur at depths ≥100 km below the surface as the subducting plates are extended and sink into the mantle. Crustal deformation is typically associated with faults away from the plate boundary with seismically active fault systems with lower (≤1 mm/yr) average slip rates and distributed earthquakes throughout the region with intermediate rates of occurrence. In moderate seismic hazard regions, earthquake recurrence parameters can be estimated based on historical and instrumental record of earthquakes. Evidence for the location and activity of any seismogenic faults is variable, so fault activity parameters often require estimation with wide ranges in uncertainty. Uniform or gridded-area crustal earthquake source zones based on earthquake catalogues are used to characterize regions with no obvious surface faults.

As indicated in Table 1, there are usually sufficient data available to define the source of the MCE and to estimate the median, or the 84th-percentile (median plus one standard deviation) ground motions originating from the MCE source. In moderate seismic-hazard regions, the MCE median ground motion values are generally closer to or greater than the 1:475 AEP, and the MCE 84th-percentile ground motions typically associated with an AEP of about 1:2,500 to 1:5,000 (Figure 2).

Very high and high seismic hazard regions

Figure 3 shows the probabilistic mean PGA hazard curve for a typical very high to high seismic hazard regions, usually located within or close to major present-day tectonic plate boundaries such as the margins of much the Pacific Ocean or the "Ring of Fire," the Mediterranean, and India-Asian.

In high to very high seismic hazard regions, earthquakes occur because of the ongoing active tectonics associated with plate boundaries, such as plate convergence at subduction zones and high slip rate seismogenic faults at transform boundaries. The major faults in these regions typically have evidence for repeated surface ruptures and near-field earthquake effects may be applicable.

In high seismic hazard regions, a robust analysis of earthquake recurrence parameters can usually be undertaken from the historical (i.e., pre-instrumental) and instrumental record of earthquakes; and good evidence of past surface fault rupture. Uniform or gridded-area crustal earthquake source zones based on earthquake catalogues can be included to characterize regions with no obvious surface faults.

Figure 3 shows that spectral accelerations (e.g., PGA) are generally much greater than those in low and moderate seismic hazard regions. The 84th-percentile MCE PGA acceleration is typically associated with AEPs from about 1:500 to 1:2,500 in very-high and high seismic hazard regions. In high seismic hazard regions, the median MCE accelerations are typically closer to or even below the 1:475 AEP. This is particularly evident in regions with (very) frequent large events where paleo seismic studies indicate greater subduction earthquakes and surface fault ruptures with short recurrence intervals (e.g., Chile-Peru Trench, Alaska, San Andreas and Sumatran faults).

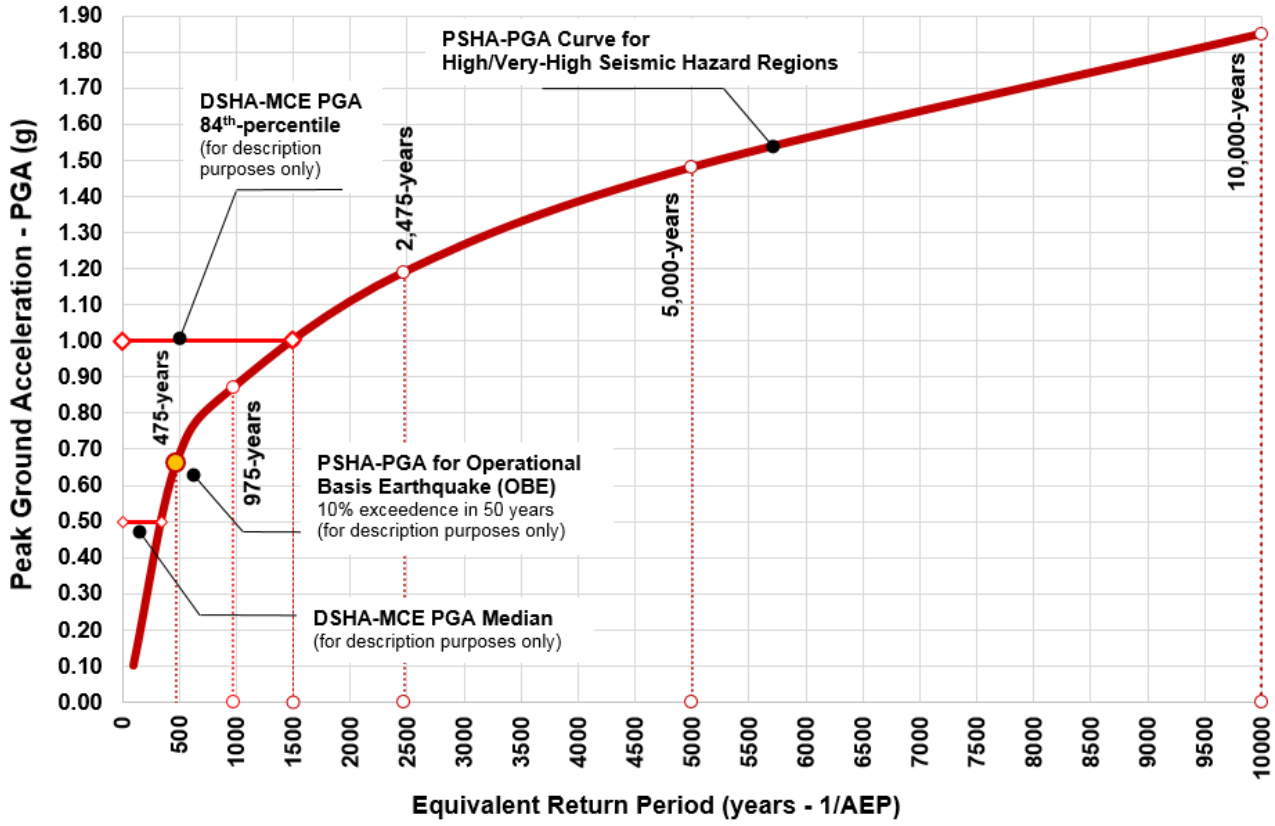

Figure 3: Characteristic seismic mean horizontal PGA-curve for very-high to high earthquake hazard regions (*Disclaimer*: ground motion values are referential for description purposes only)

Probabilistic versus deterministic earthquake ground motion severity

Figure 4 shows the relationship between mean horizontal PGA hazard curves developed from PSHA and the 84th-percentile MCE PGA values from the three seismic hazard regions above. By definition, the MCE scenario represents the "largest reasonably conceivable earthquake considered possible along a recognized fault, or within a tectonic province" (ICOLD, 2010; 2016).

If the earthquake ground accelerations estimated for the MCE are lower than those calculated from the PSHA approach (e.g., for an AEP of 1:10,000), then the "largest reasonably conceivable" MCE accelerations will likely control the seismic design of the critical facility. Otherwise, the probabilistically based earthquake ground motions for the appropriate AEP can be applied. The earthquake ground motion severity adopted will be the MCE ground motion (median or 84th-percentile), or the seismic ground motion for the selected AEP for the selected facility failure consequence, whichever is lower (Figure 4).

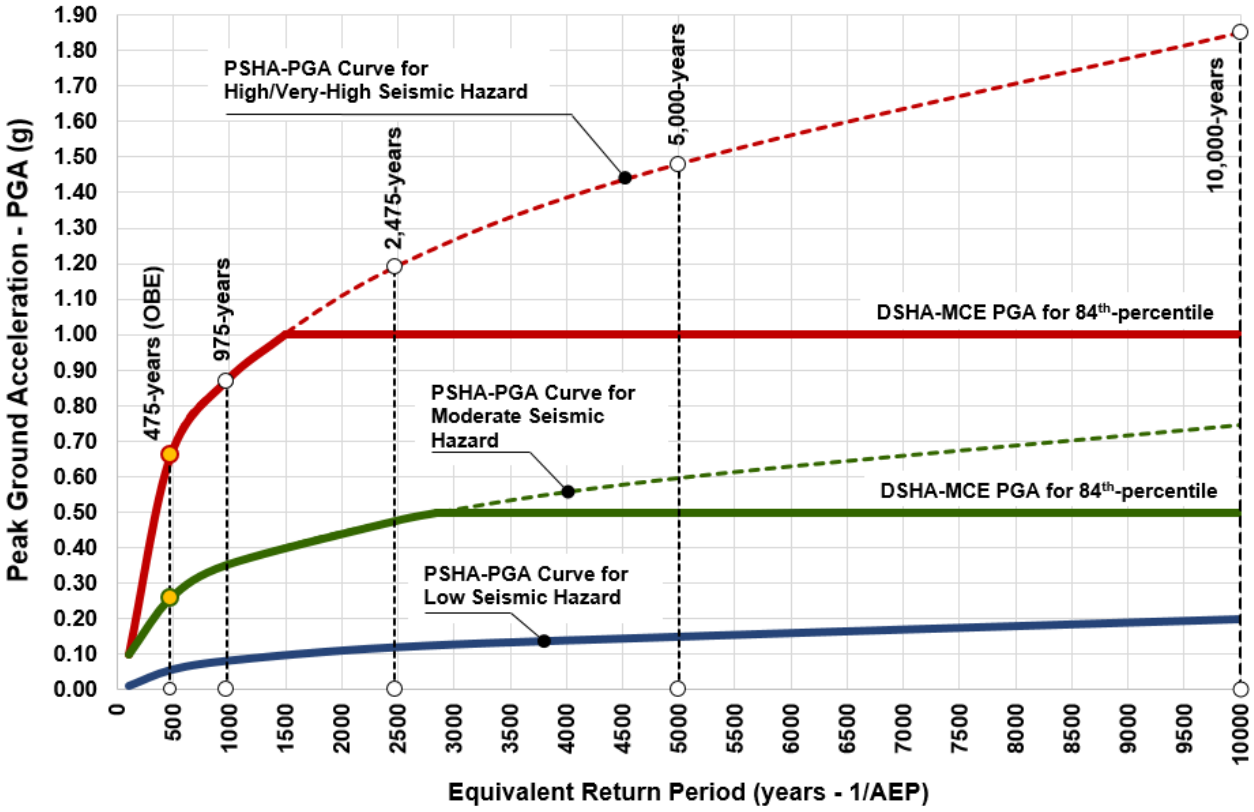

Figure 4: Typical PGA hazard curves for low, moderate and high earthquake hazard regions
(*Disclaimer*: ground motion values are referential and for description purposes only)

Design earthquake ground motions in very low and low hazard regions (where the MCE cannot be defined -Table 1, Figures 1 and 4-) can be estimated for low to very low AEPs (e.g., AEP of 1:2,500 to 1:10,000) depending on the facility's failure consequence rating.

In moderate seismic hazard regions, the MCE 84th-percentile accelerations typically have AEPs of 1:2,500 to 1:5,000, with relatively high earthquake ground motion values. Seismic ground motion values for lower AEPs (e.g., 1:5,000) appear feasibly for design of tailings dam and mine-waste facilities at moderate-hazard regions, as shown in Figures 2 and 4.

For high and very high seismic hazard regions, large earthquakes are typically very frequent, and the return periods for higher value earthquake ground motions are shorter than in low to moderate hazard regions. These strong earthquakes typically produce very high accelerations at the site (Figures 3 and 4).

In high seismic regions, the 84th-percentile MCE accelerations are typically bounded by accelerations with AEPs of about 1:500 to 1:2,500, and accelerations for AEPs lower than about 1:2,500 appear unnecessary for critical facilities' seismic design. As expected, MCE median (50th-percentile) accelerations generally have short equivalent return periods and may fall below the AEP of 1:475 (Figure 3).

Figure 4 shows that the adoption of low to very low AEPs (i.e., long earthquake recurrence intervals) to provide additional conservatism for the seismic design of critical facilities is unnecessary, particularly in moderate to high seismic hazard regions. The earthquake ground motions adopted for stability analysis and seismic design of critical facilities in moderate to high seismic hazard regions should be evaluated using both probabilistic and deterministic approaches with comparison of MCE ground motions (median and 84th-perentile) to ground motions with a range of AEPs, depending on the failure consequence rating.

Period range of interest for dynamic deformation analyses

Unlike the pseudo-static stability analysis that uses only PGA accelerations, earthquake ground motions used in dynamic stability analyses are generally developed for a period range of interest. For typical TSF embankment dams at modern mines, the period range of interest is typically in the range of about 0.2 s to 2.0 s (i.e., near the natural period of the dam structure). Figure 5 illustrates the probabilistic mean hazard curves and the 84th-percentile MCE accelerations for three spectral periods (i.e., PGA, 0.2 s and 1.0 s) and for the three seismic hazard regions (low, moderate and high). These hazard curves can be used to evaluate the impact on earthquake acceleration return period for spectral periods other than PGA.

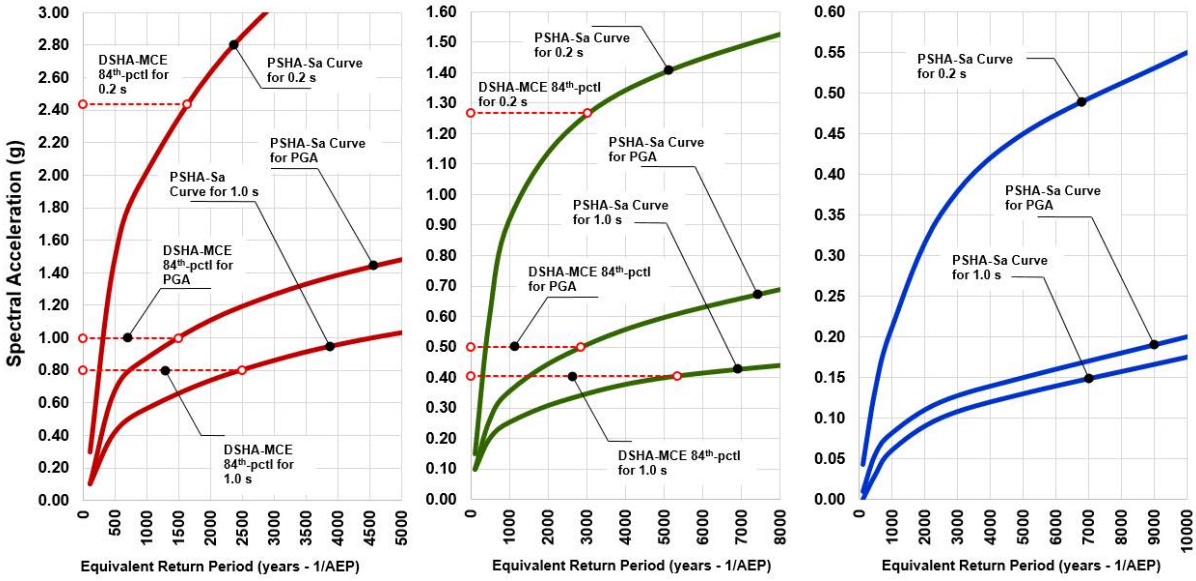

Figure 5: Typical mean hazard curves for PGA, 0.2 s and 1.0 s for high (left), moderate (centre) and low (right) seismic hazard regions.
(*Disclaimer*: ground motion values are for illustrative purposes only)

For 84th-percentile MCE accelerations, Figure 5 shows that similar AEPs (i.e., the reciprocal of return period) for PGA and 0.2 s and for both moderate and high seismic hazard regions have AEPs ranging from about 1:500 to 1:2,500 in high seismic regions, and 1:2,500 to 1:5,000 in moderate seismic hazard areas. For the 1.0 s spectral period, the 84th-percentile MCE accelerations typically have lower AEPs (i.e., longer earthquake-return periods).

Impact of uncertainties on earthquake ground motion return periods

Based on the current international standard of practice, probabilistic earthquake ground motions are provided as mean values (e.g., curves in Figures 4 and 5) estimated from one or more weighted ground motion models (GMMs) selected for their relevance to seismic sources included in a site-specific seismic model. Rather than using a single mean seismic hazard curve, hazard modellers are now recommending that designers consider a band of ground motions (e.g., between the 5th- and 95th-fractile around the mean values) to capture the uncertainties associated with the probabilistic analysis.

Figure 6 shows the correlation between the mean curve of earthquake ground motions and their equivalent return periods complemented by the upper- (95th-fractile) and lower-bound (5th-fractile) hazard curves developed for the identification, quantification and incorporation of uncertainties within the probabilistic analysis. Figure 6 illustrates lower-bound hazard curves (i.e., 5th-fractile) associated with longer return periods, while upper-bound hazard curves (i.e., 95th-fractile) are related to shorter return periods. As a corollary, the aleatory variability and the epistemic uncertainty that affect the mean ground motion values and their return period should be reviewed for seismic stability analysis and design of critical mine-waste facilities.

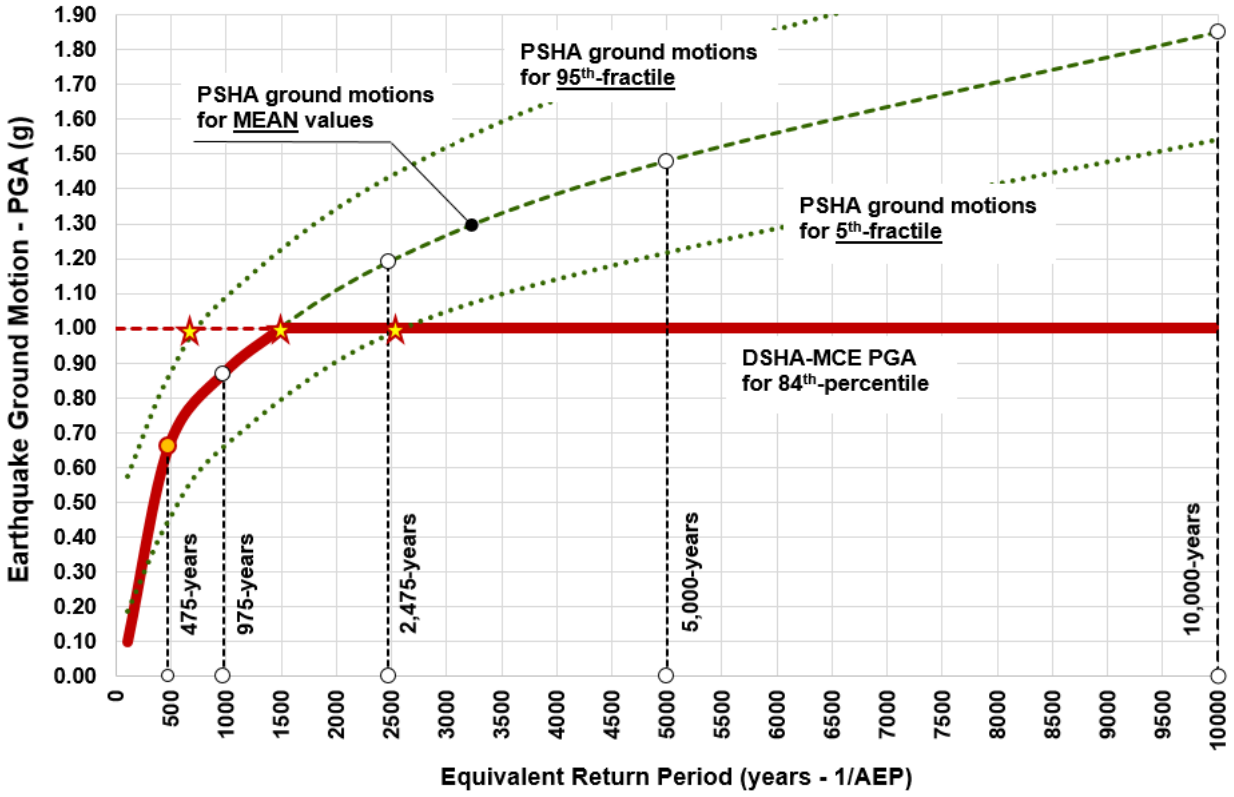

Figure 6: Typical 84th-percentile MCE Spectral Accelerations versus the mean hazard curve complemented by the probabilistic upper- (95th-fractile) and lower-bound (5th-fractile) curves that Incorporate the aleatory variability and the epistemic uncertainty for a seismic hazard region.
(*Disclaimer*: ground motion values are referential and for description purposes only)

Earthquake ground motions for tailings and mine-waste critical facilities

Current international guidelines emphasize the importance of safe, sustainable, and environmentally responsible operation management of critical mine-waste facilities using a risk-based approach. The earthquake ground motion selection criteria recommended for critical mining facilities should then be based on both the understanding of the specific seismic hazard at the site where the mine-waste facility is located, and the expected seismic performance target as indicated in international local or industry guidelines and standards. A significant number of earthquake performance targets are specified in different guidelines and industry standards. However, the operating basis earthquake (OBE) and the safety evaluation earthquake (SEE) are two common earthquake performance levels used in critical mining facilities.

Earthquake ground motions for the OBE performance level

The OBE is the ground motion level for which a TSF dam embankment and the mine-waste facilities are designed to remain operational, with any damage being minor and readily repairable following the OBE occurrence. OBE ground motions can reasonably be expected to occur during the facility's operating life.

The OBE performance level for tailings dams typically has an AEP of 1:475. An OBE performance level at a higher or lower AEP can be selected based on the needs of the owners, designers and local regulators. However, any change in the OBE ground motion AEP must still meet the performance requirement that the dam remain operational, with minimal, easily repairable damage (Wieland, 2012; 2016). An OBE performance level may not be necessary in low seismic hazard regions because the ground motion level is very low and has a minimal impact on dam stability.

Earthquake ground motions for the SEE performance level

Failure consequence

Existing international guidelines for the design of critical facilities recommend that the failure consequence be based on a qualitative and quantitative analysis of the consequence of a hypothetical collapse. Guidelines typically define a minimum of three main failure targets; *low*, *high* and *extreme*, with the ranking dependent on the human, environmental and economic consequences of the structure collapse (e.g., number of lives lost, long-term environmental consequences, economic and property losses, etc.).

SEE ground motion performance level

The SEE is the most severe earthquake ground motion that a critical facility must be able to endure, and for which the structure should be designed or analyze d (e.g., ICOLD, 2010; 2016). Under the SEE, mine-waste facilities can be damaged but must retain functionality.

Damage may be extensive, operation may be disrupted, or economic losses may be significant (Wieland, 2012; 2016). However, the facilities' structural integrity needs to be maintained and, for instance,

in the case of dam embankments, uncontrolled release of water and/or tailings must be prevented. Table 2 below lists common SEE earthquake ground motion selection criteria suggested in this paper for seismic stability design of critical facilities.

Table 2: Ground motion selection criteria for critical facilities and SEE performance Level

Failure consequence	Ground motion selection criteria	Earthquake ground motion AEP
Extreme	The lesser of MCE 84th-percentile and AEP	1:10,000 (≈0.5% probability of exceedance in 50 years)
High	The lesser of MCE 84th-percentile and AEP	1:5,000 (≈1% probability of exceedance in 50 years)
Low	The lesser of MCE 50th-percentile (Median) and AEP	1:2,500 (≈2% probability of exceedance in 50 years)

Note: the conventionally accepted MCE definition is used in this paper (see Glossary in Appendix to this chapter)

During the SEE, plastic deformations may occur in different sections of the mine-waste facility. As result, time-domain earthquake dynamic deformation stability analyses must be undertaken through the use of synthetic scaled or spectrally matched acceleration time histories (ATH).

The SEE is the performance target typically adopted for the long-term sustainable physical stability of critical mine-waste facilities for closure and post-closure (ICOLD, 2013). The SEE term replaces the Design Basis Earthquake and the Maximum Design Earthquake terms used in the earlier editions of ICOLD.

Conclusions

Current international guidelines provide earthquake ground motion selection criteria for the analysis and design of critical facilities in mining. While these guidelines show clear definitions of the expected earthquake performance levels, it often remains unclear which specific ground motions should be used, particularly for the safety evaluation earthquake (SEE).

This lack of clarity often leads to confusion, inconsistencies, and the arbitrary selection of earthquake ground motions for analysis. In many cases, the confusion arises because there is not always a good understanding of the nature and application of the probabilistic and deterministic approaches to the estimation of earthquake ground motions for design.

For the SEE performance level, the facility failure consequence should be assessed because it influences the ground motions recommended for design and closure. We suggest that the *lower* of the 84th-percentile MCE, or the earthquake ground motions for the AEP of 1:10,000 and 1:5,000 be used for analysis and design of extreme and high failure consequence, respectively. For facilities with a low failure consequence, the controlling ground motion can be the *lower* of the 50th-percentile (median) MCE, or the 1:2,500 AEP earthquake ground motions.

When the MCE ground motions are *lower* than the probabilistic values at the design AEP, then the controlling earthquake ground motions can be the MCE. Otherwise, the probabilistic ground motions should be used for earthquake stability analysis and design of critical mine-waste facilities. This approach is favoured because MCE represents the "largest conceivable earthquake possible to occur along a fault or within a seismogenic setting", while larger earthquake ground motions can be expected to be extremely rare. Consequently, lower AEP values (e.g., 1:10,000) do not apply.

As argued in this paper, an arbitrary adoption of low to very low AEPs (i.e., long return earthquakes periods) to provide conservatism for the design of critical facilities is unnecessary and may lead to a fallacy, when the MCE ground motion controls the design, particularly in moderate to high seismic hazard regions.

The earthquake ground motion suggested for stability analysis and design of critical mine-waste facilities in moderate to high seismic hazard regions should be evaluated from both PSHA and DSHA to compare earthquake ground motions estimated for discrete AEPs with the median or the 84^{th}-percentile ground motions for MCE at the site.

When DSHA is not possible because of the lack of identifiable fault sources in very low to low seismic hazard regions, then engineering judgment should be used to select the most appropriate probabilistic earthquake ground motion associated with a low AEP based on the assessed failure consequence.

In moderate and high seismic hazard regions, earthquake ground motion near-field effects developed near the crustal fault earthquake sources can generate high MCE ground motions for a low AEP (i.e., for long to very long earthquake return periods). If large magnitudes (e.g., $\mathbf{M} \geq 6.0$) are from a fault rupture and the source-to-site distance is relatively close (e.g., less than ±10 km), then the impact of earthquake near-field effects in the ground motion selection criteria may require engineering judgment based on the owner's risk-based decisions.

Although earthquake performance targets recommended in this paper are not necessarily the same as used in seismic design for different components of mine facilities (e.g., TSF dam embankment, heap leach pads, waste-rock dumps, ponds, and other complex engineered structures), the procedure proposed here can be similarly applied based on their failure consequence.

References

ANCOLD. 2019. Australian Guidelines for Design of Dams and Appurtenant Structures for Earthquake.

BAT. 2018. Best Available Techniques. Reference Document for the Management of Waste from Extractive Industries, in EUR 28963 EN, European Commission (2006/21/EC), Elena Garbarino, Glenn Orveillon, Hans G.M. Saveyn, Pascal Barthe, Peter Eder.

CDA – Canadian Dam Association. 2014. Bulletin: Application of Dam Safety Guidelines to Mining Dams.

Cornell, C.A. 1968. Engineering seismic risk analysis, Bulletin of Seismological Society of America. SSA 58(5): 1583–1606.

Grigull, S., R. Sutinen and E. Kosonen. 2015. Faults activity during the Quaternary period. In A. Korja and E. Kosonen (editors), Seismotectonic Framework and seismic source area models in Fennoscandia, Northern Europe. Institute of Seismology, University of Helsinki, Report S-63: 49-62.

ICOLD. 2010. Bulletin 72. Selecting seismic parameters for large dams. Guidelines. Committee on Seismic Aspects of Dam Design, International Commission on Large Dams.

ICOLD. 2013. Bulletin 153. Sustainable design and post-closure performance of tailings dams.

ICOLD. 2016. Bulletin 148. Selecting seismic parameters for large dams, guidelines. Committee on Seismic Aspects of Dam Design, International Commission on Large Dams.

Johnston, A.C. 1994. Seismotectonic interpretations and conclusions from the stable continental region seismicity database. In A.C. Johnston, K.J. Coppersmith, L.R. Kanter and C.A. Cornell (editors), The earthquakes of stable continental regions, c.1: Palo Alto, California, Electric Power Research Institute: 4-1 to 4-104.

Korja, A. 2015. Discussion in: A. Korja and E. Kosonen (editors), Seismotectonic Framework and Seismic Source Area Models in Fennoscandia, Northern Europe. Institute of Seismology, University of Helsinki, Report S-63: 212–215.

Landgraf, A., S. Kubler, E. Hintersberger and S. Stein. 2017. Seismicity, fault rupture and earthquake hazards in slowly deforming regions. Geological Society of London Special Publication, DOI: https://doi.org/10.1144/SP432.

NZSOLD. 2016. New Zealand Society of Large Dams. Dam Safety Guidelines.

Olesen, O., L. Blikra, A. Braathen, J. Dehls, L. Olsen, L. Rise, D. Roberts, F. Riis, J.I. Faleide and E. Anda. 2004. Neotectonic deformation in Norway and its implications: A review. *Norwegian Journal of Geology* 84: 3–34.

Quigley, M.C., M.L. Cupper and M. Sandiford. 2006. Quaternary faults of south-central Australia: Palaeoseismicity, slip rates and origin. *Australian Journal of Earth Sciences* 53: 285–301.

Quigley M., D. Clark and M. Sandiford. 2010. Tectonic geomorphology of Australia. In P. Bishop and B. Pillans (editors.) *Australian Landscapes*. Geological Society of London Special Publication 346: 243–265.

Wieland, M. 2012. Seismic design and performance criteria for large storage dams. In *Proceedings of 15 WCEE,* Lisbon 2012, Committee on Seismic Aspects of Dam Design, International Commission on Large Dams (ICOLD).

Wieland, M. 2016. Safety aspects of sustainable storage dams and earthquake safety of existing dams. *Engineering* 2 (2016): 325–331, Elsevier, Committee on Seismic Aspects of Dam Design, International Commission on Large Dams (ICOLD). Retrieved from http://dx.doi.org/10.1016/J.ENG.2016.03.011

Bibliography

ASCE 7-15. 2015. Minimum Design Loads for Buildings. American Society of Civil Engineers (in glossary).

IBC. 2015. International Building Code, International Code Council, including USA (in glossary).

Appendix

List of Acronyms

AEP	Annual Exceedance Probability
ANCOLD	Australian National Committee on Large Dams
ASCE	American Society of Civil Engineers
CDA	Canadian Dam Association
DSHA	Deterministic Seismic Hazard Analysis
g	Acceleration of gravity (9.805 m/s^2)
IBC	International Building Code
ICOLD	International Commission on Large Dams
PGA	Peak Ground Acceleration
PSHA	Probabilistic Seismic Hazard Analysis
MCE	Maximum Credible Earthquake
NZSOLD	New Zealand Society on Large Dams
OBE	Operating Basis Earthquake
SCR	Stable Continental Region
SEE	Safety Evaluation Earthquake
TSF	Tailings Storage Facility

Glossary

Annual Exceedance Probability (AEP): Estimated probability for an earthquake ground motion threshold to be equalled or exceeded in a given exposure time (e.g., 1 in 475, or 1:475, associated with a 10% probability of exceedance in 50 years).

Consequence of Failure: The effects resulting from a hypothetical critical facility failure or collapse. For instance, in the case of water reservoir or tailings storage facility dams, a potential failure is an uncontrolled release of water and/or the tailings.

Crustal Fault: Mappable geologic structure known to have produced earthquakes in the recent geological past, including faults with evidence for surface rupture in the Holocene (i.e., in the last 11,700 years), large faults with surface displacement in the Late Pleistocene (i.e., between 11,700 and 130,000 years

ago), and major faults which have moved repeatedly in Quaternary time (i.e., ~2.6 million years ago).

Earthquake: A sudden motion vibration in the earth caused by an abrupt release of energy due to a fault rupture or a subduction mechanism. Earthquakes produce a range of seismic waves (e.g., s-wave, p-wave, Love and Rayleigh) that travel through the Earth and along its surface.

Earthquake Ground Motions: Movement of the earth's surface or ground shaking (i.e., ground acceleration, velocity or displacement) produced by seismic waves during an earthquake. This concept is used to describe the probabilistic or deterministic seismic hazard acceleration response spectra and earthquake acceleration time histories. The acceleration is the more commonly parameter used for ground motions (e.g., peak ground acceleration [PGA], or spectral accelerations [S_a]). The term "*earthquake design ground motion*" refers to the parameters selected for the seismic stability analysis and seismic design or validation of a structure or facility.

Holocene: Geological Epoch of the Quaternary Period for the past 11,700 years. The Holocene includes most of the period since the end of the most recent ice age in most higher latitude regions. For engineering purposes, if a fault has ruptures to the ground surface in the Holocene, then the fault is commonly considered seismically "*active*".

Maximum Credible Earthquake (*MCE*): The MCE is used only in deterministic seismic hazard analysis (DSHA) to represent the "*largest reasonably conceivable earthquake that is considered possible along a recognized fault, or within a geographically defined tectonic province, under the presently known or presumed tectonic framework*" (ICOLD 2010; 2016). By definition, the MCE does <u>not</u> explicitly consider the earthquake return period. This MCE definition should not be confused with the "*Maximum Considered Earthquake*" defined in the USA standard ASCE 7 and the International Building Code (IBC) seismic provisions with an AEP of 1:2,475.

Earthquake Magnitude: Quantification of an earthquake's relative size. Earthquake magnitude is based on measurement of the instrumentally recorded amplitude (e.g., in a seismograph). Many magnitude scales have been defined, but the most commonly used are the local or Richter magnitude (ML), the surface-wave magnitude (Ms), the body-wave magnitude (Mb), and moment magnitude (**M** or Mw).

Moment Magnitude: Measure of the energy released at the earthquake source (i.e., hypocentre) its area (i.e., crustal faults or subduction source zones), and the average slip rate on the fault source.

Near-field effects: Impact typically produced by ruptured faults at a close site-to-source distance, and moderate-to-large magnitude earthquakes (e.g., M≥6.0). Although the site-to-source distance defined for near-field earthquakes not well defined, the range of interest can vary from 5 to 50 km. In the near-field zone, earthquake ground motions may be associated with one or multiple short-duration large pulses, distinctive directivity, residual displacements and high-frequency content.

Operating Basis Earthquake (*OBE*): Earthquake performance level for which a critical facility (components

and equipment also needed for its safety function and operation) is designed to remain operational, with any damage being minor and readily repairable following the event. For the OBE level the ground motion is expected to cause no structural damage (cracks, deformations, leakage, etc.), or limited damage and deformations repairable without significantly disrupting operations.

Pleistocene: Geologic Epoch of the Quaternary Period defined between about 11,700 years before present and about 2,600,000 years ago. Faults of Pleistocene age may show some level of seismogenic capacity though their average slip rates and earthquake recurrence intervals are usually lower than faults that have been active in the Holocene Epoch.

Recurrence Interval: Estimated average time between earthquakes within subduction source zones or faults in a specified seismotectonic region or in a specified fault zone.

Return Period: The return period is the average elapsed time between occurrences of earthquake ground motions that exceeding a specified ground motion threshold (e.g., spectral acceleration) for a defined exposure period. Return period is the inverse of the annual exceedance probability (i.e., 1/AEP).

Safety Evaluation Earthquake (*SEE*): An earthquake performance level that would result in the most severe ground motion which a critical facility must be analyze d and designed to avoid partial or total collapse (e.g., in the case of dams, no uncontrolled release of the reservoir). During the SEE, post-elastic deformations may occur in some facility's sections.

Seismic Hazard: Inherent natural occurrence of earthquakes within a geographically defined geologic province under a presently known or a presumed tectonic framework. Seismic hazard may also include surface faulting rupture, ground shaking, landslide, liquefaction, tectonic deformation, tsunamis, seiches, and other shaking-related phenomena.

Seismic Risk: Combined impact of the probability of occurrence (hazard) and the associated consequence (e.g., structural vulnerability) over all possible scenarios. Seismic risk is the product of the seismic hazard and the facility's structural vulnerability. Earthquake risk is the probable damage, including the number of people expected to be hurt or killed if a likely earthquake occurs and the economic losses expected. Important: earthquake hazard and earthquake risk are commonly incorrectly used as interchangeable.

Spectral Acceleration (*Sa*): Response acceleration of a facility modelled as a simplified single degree of freedom (SDOF) oscillator having the same structural natural period of vibration of the facility. In turn, the peak ground acceleration (PGA) is the maximum acceleration experienced by a soil-particle during an instrumentally recorded earthquake. Both parameters (PGA and Sa) are typically expressed as a fraction of the acceleration of gravity (g = 9.805 m/s2).

Tailings Storage Facility (*TSF*): Dam or embankment and complementary structures analyze d, designed and built to retain tailings or other waste materials from mining or industrial operations.

Proceedings of Tailings and Mine Waste 2019
November 17–20, 2019, Vancouver, Canada
Published by the University of British Columbia, 2019

Water Matters – Final Draindown Modelling for Mine Waste Facilities

Iozsef Miskolczi, SRK Consulting (Canada) Inc., Canada
Maritz Rykaart[1], SRK Consulting (Canada) Inc., Canada

Abstract

Excess water content in mine waste poses a particular set of challenges for closure of mine waste storage facilities. For well-designed and well-built structures high water content will not cause physical instability and catastrophic failure; however, managing the residual leachate is a complex technical challenge to be dealt with at significant cost to the operators. This is particularly true in the case of heap leach facilities, designed to be operated with relatively high water content while also retaining as little residual water as possible. The state-of-practice in developing leachate management plans for the closed facilities includes deterministic models such as the heap leach draindown estimator (HLDE) developed in the state of Nevada, USA. Such models rely on an approximation of the unit draindown rate using theoretical formulations of unsaturated flow, which is then extrapolated to a regular orthogonal geometry and a single defined date for cessation of irrigation. In SRK's experience this approach, if adopted with due care and validated through calibration, can be reasonably used on smaller heap leach piles; however, operators must often rely on the experience of their employees to "gut check" the validity of the draindown durations predicted by the HLDE.

An improved method is proposed in this paper, consisting of a combination of numerical modelling of unsaturated flow and analytical modelling to predict the time required to achieve passive water management. The heap leach pile is first discretized geometrically into domains, grouping areas of similar height. Then, in the second step, the unit draindown rate is determined for each domain through a rigorous finite element numerical modelling based on the physical and hydraulic properties of the leach material. The resulting draindown curve is then multiplied by the representative surface area to compute the expected volume of draindown from each of these areas. In the third step of the assessment, the individual draindown volumes are assembled in a time scale, taking into consideration the actual schedule of when irrigation has been completed in the various regions of the facility leading up to the final closure date.

1 Deceased on May 30, 2019.

Various complexities can be added, like recirculation to some areas and not others, or enhanced evaporation methods for portions of the recirculation.

A discussion will be provided about applying a similar method to predict the draindown duration and leachate volumes for tailings storage facilities and other mine waste facilities covered with impermeable liners.

Introduction

About heap leaching

To maximize the economic potential of marginal projects low cost processing methods are increasingly used, such as heap leaching. In heap leaching the ore is extracted using conventional mining techniques and placed in a heap in preparation for processing. A leach solution is then applied to the top of the heap to permeate the ore and dissolve the metal of interest, draining to the bottom from where it is directed to the processing plant to recover the metal of interest from solution.

Heap leach facilities vary widely in size and shape, with large solution inventories (often in the order of millions of cubic meters) being sometimes required to sustain economically viable operations. Leaching of the ore is typically achieved in pre-determined leach cycles, where the leach solution is recirculated onto the heap continuously for a number of weeks or months. Once the metal concentration in the leach solution reaches a lowest economic cut-off value, irrigation is moved onto a new leaching area and the process is repeated. The portion of the heap that ceased to be irrigated transitions into the draindown phase.

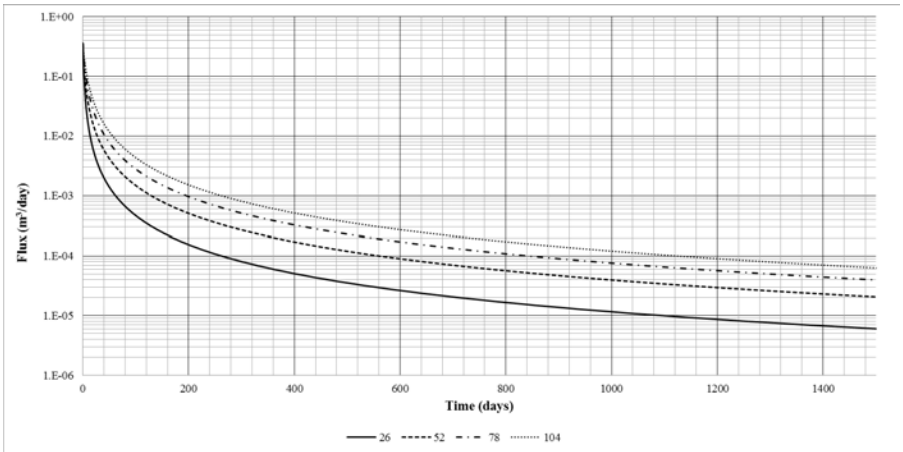

Figure 1: Typical draindown curves for various column heights (26 m, 52 m, 78 m, and 104 m)

Draindown is defined here as the period of time during which the flow rate is gradually reduced from the operational level to the residual steady-state value. Draindown is highly non-linear, with an initial quick reduction in flow rates followed by a gradual slowing down, as shown in Figure 1. The combination of the actively leached portions and portions of the heap in various degrees of draindown makes predicting the fluxes of leach solution that will need to be managed in closure difficult.

In closure, management of the leach solution inventory could be split into two distinct stages: active and passive. During the active stage, the inventory is managed by recirculating the solution to the heap to prevent the existing ponds from overflowing, coupled with inventory reduction methods such as treatment/discharge or enhanced evaporation. In the passive stage, recirculation is no longer necessary to prevent the ponds from overflowing. In most situations passive water management can only be achieved when the outflows from the leach pile consisting of draindown and net percolation from precipitation become less than the achievable evaporation flux.

Importance of predicting draindown

The fundamental question to be answered by the heap leach final draindown model revolves around how much water will need to be managed after the heap leach pad ceases to be economically viable and for how long. As the draindown rates are non-linear, large fluxes comparable to active operations period will have to be dealt with in the initial closure period. Consequently, active water management will likely be required to prevent the ponds from overflowing causing uncontrolled discharge to the environment. As the fluxes gradually decrease to a residual flux (theoretically equal to the long-term precipitation infiltration rate) active pumping may no longer be required, and the water management can be transitioned to a passive phase.

It is desirable to transition from the active water management phase to the passive phase as early as possible to reduce the costs. Accurate prediction of draindown rates allows for design and cost estimating of optimal water management solution and ideally, the passive water management would allow a "walk-away" closure scenario.

Significant owner's costs are typically part of the active water management stage. By way of example, at a mine SRK has recently worked at in South America, the cost of keeping the access road open alone exceeded $5millions per year. Therefore, being able to plan in advance may be crucial for the operation. Logistically, when the leach solution fluxes are predicted with a high level of certainty, various closure methods and scenarios can be evaluated that result in increased efficiency or even a reduction of the active draindown phase.

Challenges of draindown prediction

Accurately predicting final draindown of an entire heap is a process that must overcome challenges related to hydraulic properties of the heap material, geometry, heterogeneity of the heap leach ore, operational history of the heap, and lack of adequate calibration data. The following subsections provide details on these parameters.

Predicting draindown rates

Throughout the entire life cycle of the heap leach pile, the flow regime within the heap is unsaturated. Even during active leaching period, the irrigation rates are well below values that would cause saturation of the heap material. There are various practical reasons for this, not least being the need for air circulation for the lixiviation process to occur at reasonable efficiency. The flow rates required to efficiently leach the metal from the ore are determined in the laboratory based on column experiments where flow rates and extraction coefficients are observed. These column studies are the basis for successful operations, but it was noted in various studies that column studies tend to drain faster than the full-scale heaps (Kappes, 2002; Muller and Newton, 2008).

It is therefore just natural to approach the draindown as an unsaturated flow problem, where the moisture content of the pile changes continuously in time while it also varies spatially in the different regions of the heap.

To quantify the relationship between saturation levels and drainage quantities, the soil water characteristic curve (SWCC) is used. The SWCC, also referred to as the water retention curve, is a graphic expression of the relationship between the moisture content and the matric suction in a soil and provides an indication of the manner in which a soil gains and "gives up" the stored water. The SWCC is normally determined experimentally, but theoretical methods were also developed to estimate it when experimental results are not available (van Genuchten, 1980; Brooks and Corey, 1964; Fredlund and Xing, 1994).

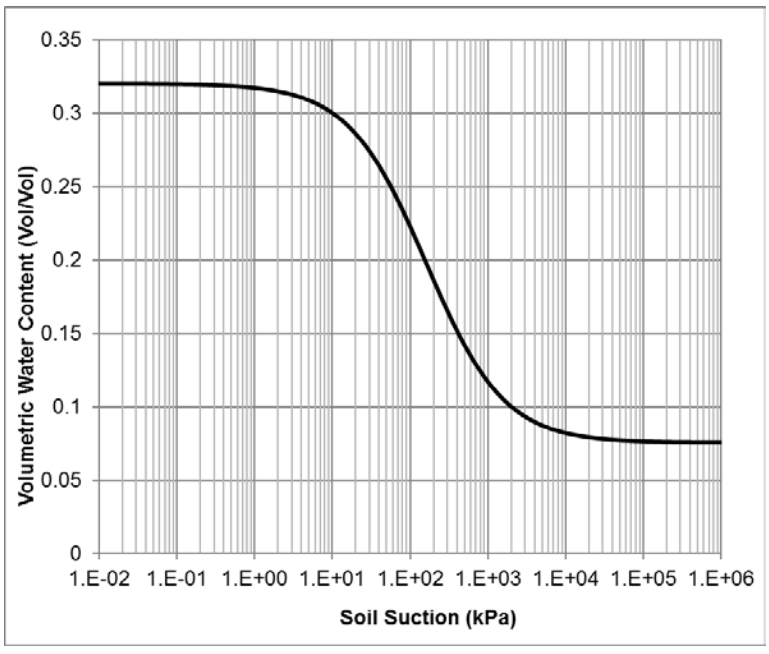

Figure 2: Typical SWCC for heap leach materials

As suction increases, smaller and smaller pores become empty. Conversely, larger and larger suction is required to remove less and less water until a residual water content is reached where essentially no more water can be removed through normal natural processes. When irrigation of the heap leach pile occurs, the infiltrating water first fills the smaller pores (having a higher suction applied to them) and then gradually larger pores are filling up as suction is reduced. Then, once irrigation stopped and draindown begins the largest pores start emptying of water first followed by successively smaller pores. The level of suction at which the largest pores begin to drain of water is called the air entry value (AEV).

Applying this model to the entire heap would require a complex 3D model of large dimensions and relatively small mesh size due to the non-linearity of the equations to be solved, making the model computationally very expensive. Simplifications are therefore made, where the heap geometry is discretized as described in the following section, while unit draindown curves are applied to each sub-domain. The unit draindown curves are determined a-priori, to be representative of the subdomains.

Heap geometry

The pre-mining topography dictates the shape and configuration of the heap. Some operations are located in areas where flat land is available for development, and therefore the shapes are regular. Other operations are located in difficult topography, where the constraints of the difficult terrain will produce complicated shapes as the heap will be developed using the available footprint, as shown in Figure 3. This will yield highly variable overall 3D shapes with sharply changing height, footprint and slope angles (on the base liner).

Overlaying the 3D shape, the internal geometry of the pile is an additional complicating factor, with the heaps typically built in layers and oftentimes in successive phases adjacent to each other. The larger the heap, the more opportunities for the shape to become more complicated, as oftentimes the heap size is expanded beyond the original design to accommodate increased ore quantities.

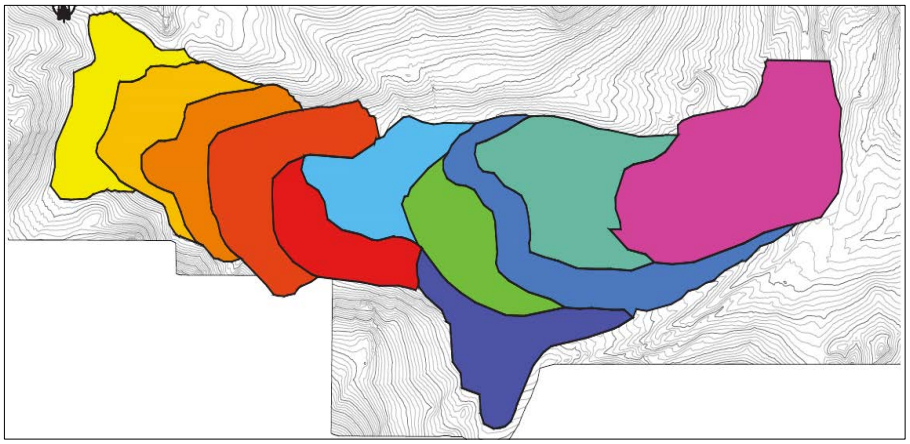

Figure 3: Plan view of a typical heap leach. Each color represents a different operational phase

Heterogeneity of heap leach ore material

Another challenge in predicting the heap draindown is heterogeneity in the physical and hydraulic properties of the heap ore material. While the heap in general is thought of as a unified extraction unit, the geology of the orebody results in leach ores with distinctly different properties. The mine plan resulting in ores with distinct properties being stacked on the heap will be the source of primary heterogeneity in properties. Then, stacking plans with distinct construction phases being built over time, will further increase heterogeneity. Layering during deposition will result in density gradients repeating at each layer, with a higher density trafficked layer near the surface with gradually increasing overall density increasing with depth.

Weathering characteristics of the various ore portions may also be different, resulting in changes in the properties after the material is placed on the heap. As these changes occur after placement, relatively similar initial properties may change in time, and become quite different by the time the heap is spent and final draindown can begin.

Density of the heap material will normally be increasing with depth due to self-weight compaction, influencing hydraulic properties in a relatively consistent continuum. However, changes due to the other phenomena described above may result in significant change in density with depth, as well as between the different regions of the heap.

Operational history

History of heap operations will have a direct influence on the saturation state of the various regions at the end of operations. Application rates of the leach solution will also influence the saturation state of the heap at the end of operations. During normal operations, various areas of the heap are irrigated in a pre-determined sequence but resulting overall in zones that were irrigated far in the past (sometimes years) compared to the most recently irrigated sections.

Calibration data

Another challenge in heap leach draindown modelling is scarcity of suitable calibration data. Typically, reliable calibration datasets are limited or more often not available (the typical metallurgical estimates do not honor unsaturated flow principles – mass balance approach). Heap drainage values typically available are normally limited to a small subset of the site (but this is better than nothing).

State of practice

The reality is that there really is no “Best Practice”. A multitude of models are used to predict draindown time, ranging from simplified empirical methods to computational fluid dynamics integrating leach solution flow and metallurgical recovery. All these models are suitable to provide information for specific

issues related to heap leach operations and closure.

A brief list would include the following methods:

- Simplified empirical methods, i.e., the heap leach draindown estimator (HLDE) based on the implementation of the Brooks and Corey equation.
- Numerical models of saturated flow, i.e., conventional groundwater flow models.
- Numerical models of unsaturated flow, some of the most common codes used being HYDRUS, Seep/W and SVFlux.
- Computational fluid dynamics (CFD) modeling, typically used for recovery modelling, with a flow component.

Arguably multidimensional (geometry and heterogeneity) unsaturated flow numerical modeling is the superior approach. However, complicated models requiring days or weeks to run often far exceed the need for information. It is therefore important to keep in mind the "fit for purpose" approach, where simplified and cruder models could provide the information needed to make the required decisions.

The SRK approach

Overall concept

Considering all the challenges presented in the sections above, SRK has developed an analytical model to predict the final draindown time of a heap leach pile. To overcome these challenges, the draindown analysis is conceptualized by breaking the heap into multiple smaller building blocks. Draindown analysis is conducted on each of these columns independently as if they have unit dimensions and then the separate draindown curves are combined to yield a single composite curve, as shown schematically in Figure 4.

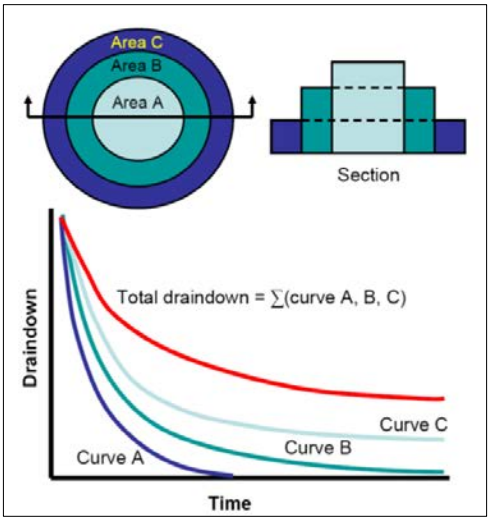

Figure 4: Conceptualized geometry used in draindown model

Each of these blocks represents a unique portion of the heap in the form of a column that extends from the base to the top of the heap, as illustrated in Figures 5 and 6. In this approach the dimensions (surface area and height), material properties, and draindown state (time passed since last production irrigation) of each column can be uniquely varied and the sequence in which they are summed can be set based on an understanding of the construction and operating (i.e., irrigation) sequence. In essence, this approach presents a simplified three-dimensional representation of the problem.

Conceptually, the model manages leach solution inventory as if the heap consists of two sections; (1) passively draining phases, and (2) an active recirculation phase. This is a crucial feature of the model, as it allows recirculation to be included in the calculations while keeping track of real-time inventory on a daily time step. If recirculation is selected, the drained inventory from the passive phase is recirculated as part of the active phase which means the passive phase reaches a drained state first.

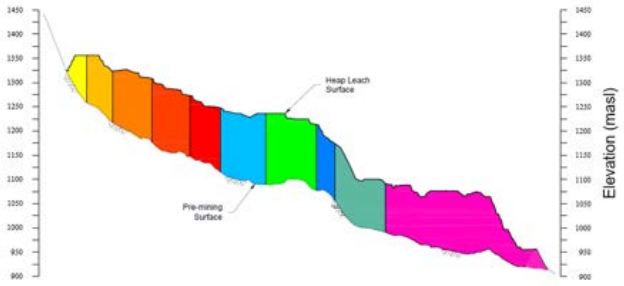

Figure 5: Elevation profile through a typical valley-fill type heap leach facility

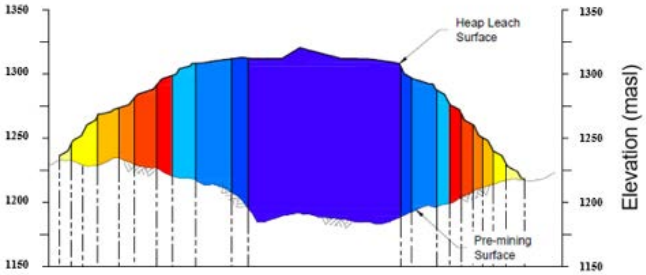

Figure 6: Typical cross-section of heap leach facility showing column discretization by height

The drainable inventory is calculated as the difference between the volume of water at the initial time in the model and the residual water expected to never drain. This takes into account the time passed since the last day of irrigation for each cell and computes the water content based on the draindown curves previously modelled (2). The inventory of leach solution is calculated on the initial model date based on the moisture content within each phase, which is a function of the time passed since the last irrigation of each particular phase was completed.

The chosen computation platform is Microsoft Excel, building on the wide distribution and familiarity of the software. Not least, the choice was guided by the desire of creating a tool that can be widely used by the site personnel of SRK's client corporations. The model includes four interconnected functional modules: draindown, inventory, recirculation, and evaporation. The computed water balance includes a series of intermediate terms dealing with assumed pond storage capacity.

Typical model inputs

Draindown curves

At its core, the model is based on the fact that assuming soil properties are homogeneous, height of the column will cause large differences in draindown flux from different areas of the pile. The draindown curves were therefore created for unit surface area which is then multiplied by the footprint of each column, phase by phase. This was done to avoid the need for creating a large matrix of curves for each height for each surface area and facilitate the update of the model when more refined heap leach configurations become available in the future.

The draindown unit curves can be created using various methods. Unsaturated flow modelling using Hydrus or Seep/W would yield the most accurate unit draindown curves, although spreadsheet models solving the Brooks and Corey equation could result in satisfactory curves.

Climate parameters

Precipitation and potential evaporation values can be included in the model, to allow quantification of the soil-atmosphere interaction and the long-term moisture regime in the heap. Site precipitation data is highly desirable, but synthetic rainfall data obtained through reanalysis methods are also routinely used by SRK. Potential evaporation (PE) values are typically computed based on a range of models, with the FAO model based on the Penman-Monteith equations (FAO, 1998) and Priestly-Taylor model (Priestley and Taylor, 1972) being the most common. A simple snow sublimation routine can also be included if appropriate.

Operational history

Operational history of a heap is captured by the final irrigation schedule included in the model. The idea is that the final irrigation schedule allows quantification of the time elapsed since the last active irrigation on any particular location on the heap. This will in turn allow the model to find the corresponding moisture content in that location and thus compute the inventory for the current time step. The fundamental assumption is that model time starts once the final irrigation is complete and continues until the outflow from the heap diminishes to a pre-determined value allowing long-term passive water management.

Ore volume isopach

Based on drawings (as-built or design schematics) and ore deposition schedules, an isopach is produced for the heap in an effort to obtain the characteristic footprint of the number of lifts placed within each phase. The isopach is developed into a matrix of reference values for each height and for each zone within the heap, which is them multiplied by the unit draindown flux to compute the overall flux for any particular time step.

Model results example

The heart of the model is the water balance sheet. On this sheet the inflow and outflow terms are brought together and the water balance for each time step is computed. The water management methods, such as treat and discharge or enhanced evaporation are accounted for in the water balance.

Pinpointing the date of transition from active to passive water management is a trial-and-error process. Although a goal seek function is available to direct the search, due to the many assumptions one must consider in such a complex system a graphical interface was found to be most useful.

An example of a modelled draindown scenario is shown in Figure 7. In this scenario active water management is required for the first 7 years, with the first four years of continuous recirculation followed by three years of seasonal recirculation. The available pond capacity is increasing as new ponds become available, although the pond volume (red curve) is shown to be well below the existing capacity.

Conclusion

The analytical model presented here can also be used to predict draindown from other mine waste facilities such as tailings deposits and waste rock dumps. Material heterogeneity is present in these other waste materials, although differences in particle size distribution and SWCC of tailings may range on a narrower scale. Geometry, as for heap leach facilities, is dictated by the original topography. The notable difference is the relatively uniform moisture content the tailings typically present at the end of active deposition. The time scale for tailings draindown is also expected to exceed the time scale of heap leach draindown by a wide margin, possible orders of magnitude, while waste rock draindown is likely to be similar.

The model can be implemented for any climate, from cold arid to wet moist, with the appropriate surface water management assumptions being included in the inputs. This flexibility is allowed by the fact that run-off and net percolation are dealt with as separate independent terms in the water balance. This fact is also one of the limitations of the model, where the direct effect of precipitation on the moisture content of the heap cannot be assessed.

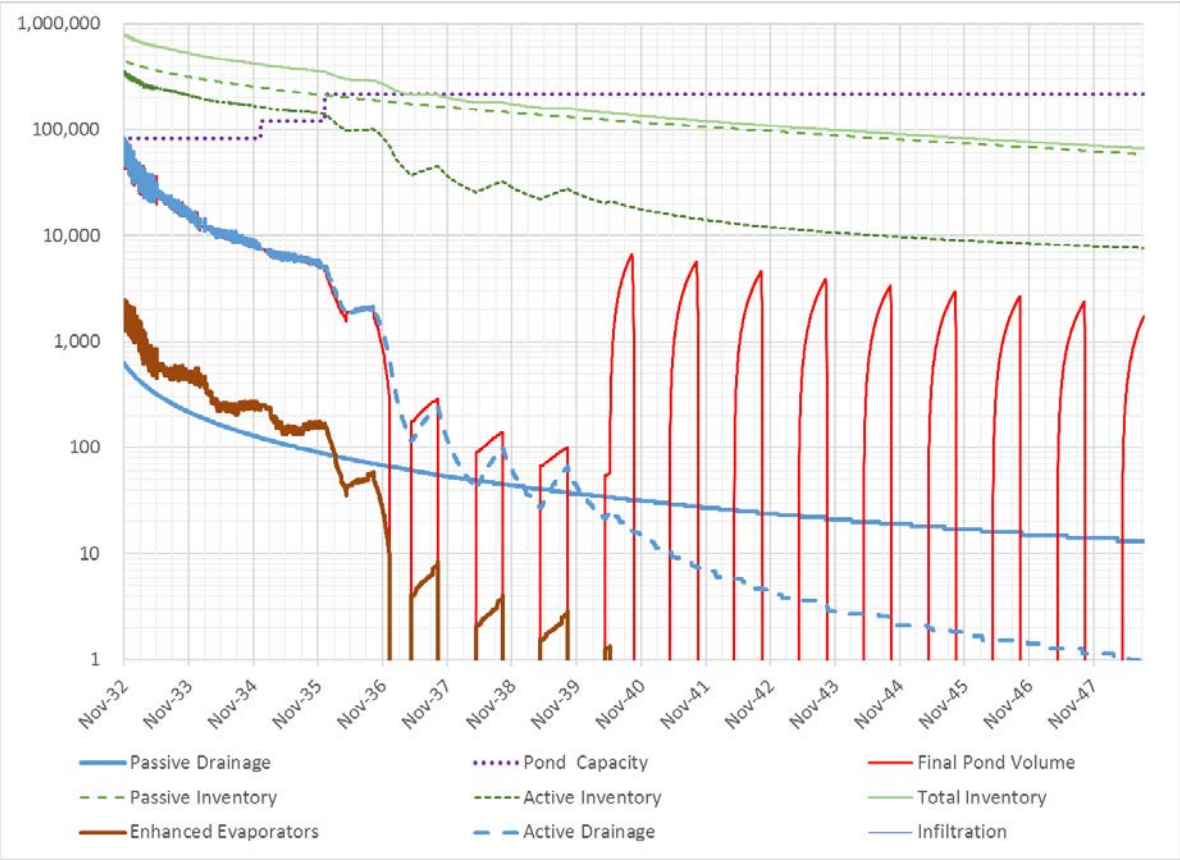

Figure 7: Example of draindown model results

When considering a facility covered with a geomembrane, the draindown problem becomes simplified by the fact that net percolation is nil. Passive draindown concept still applies, with all other challenges discussed above still present. However, as shown in the previous sections, the model is suitable to predict draindown for such facilities.

What sets the SRK model apart is the simplicity of the approach, using the Excel platform and computing a series of building blocks. No computational fudge factors such as constants or internal adjustment factors are used. The internal structure of the model is fully transparent to allow easy review and query of assumptions, although the large number of computations and referencing loops requires a thorough understanding of the working principles.

Acknowledgements

Maritz Rykaart died on May 30, 2019. This paper is dedicated to his memory.

References

Brooks, R.H. and A.T. Corey. 1964. Hydraulic properties of porous media. *Hydrology papers.* Colorado State University, Fort Collins, Colorado.

Food and Agriculture Organization of the United Nations (FAO). 1998. Crop evapotranspiration – guidelines for computing crop water requirements. *FAO Irrigation and Drainage Paper* 56.

Fredlund, D.G. and A. Xing. 1994. Equations for the soil-water characteristic curve. *Canadian Geotechnical Journal* 31: 521–532.

Kappes, Daniel. 2002. Precious metal heap leach design and practice. Retrieved from 911 Metalurgist.com.

Muller, B. and T. Newton. 2008. Look before you leach: Dynamic simulation of heap leach flowsheets. In *Proceedings of ALTA Copper Conference*, 2008.

Priestley, C.H.B. and R.J. Taylor. 1972. On the assessment of surface heat flux and evaporation using large-scale parameters. *Monthly Weather Review* 100: 81–92.

Van Genuchten, M. Th. 1980. Closed-form equation for predicting the hydraulic conductivity of unsaturated soils. *Soil Sciences Society of America Journal* 44: 892–-898.

Proceedings of Tailings and Mine Waste 2019
November 17–20, 2019, Vancouver, Canada
Published by the University of British Columbia, 2019

Field Shear Vane Testing in Tailings

Chad Mundle, Golder Associates Ltd, Canada
Fiona Esford, Golder Associates Ltd, Canada
Michel Julien, Agnico Eagle Mines Ltd, Canada

Abstract

The field shear vane test (FSVT) is an established method for measuring the undrained in-situ shear strength of clay. For silt, due to its relatively high hydraulic conductivity, it is a commonly held view that FSVTs are not applicable as undrained conditions cannot be achieved using standard test methods.

A series of FSVTs were carried out in non-plastic tailings consisting of silt- and sand-sized particles using vane rotation rates higher than are typically used for clay. Using results from FSVTs, pore pressure dissipation tests as part of cone penetration tests, and criteria from literature, it is believed that undrained conditions can be demonstrated in specific circumstances. Uncertainties do exist however, and lessons learned are discussed.

Introduction

The field shear vane test (FSVT) is an established method for measuring the undrained in-situ shear strength of clays (Craig, 2004; ASTM D2573; Skempton and Bishop, 1950). Due to low hydraulic conductivity, undrained testing conditions can be achieved in clays provided the standard vane rotation rate of 6° per minute is used (ASTM D2573). In contrast, application of the standard FSVT rates, which were developed for clays, to sandy soils and non-plastic silts, can result in drained to partially drained conditions during the test. This could also occur in clays with sand and silt laminations where FSVTs conducted at standard rates could measure higher strengths than if the laminations were not present (Terzaghi et al., 1996; Craig, 2004).

Consideration of drainage conditions during FSVTs have been investigated previously by several authors on tailings and natural soils (Blight, 1968; Chandler, 1988; Reid, 2016). These investigations found that undrained conditions were achieved provided the rate of vane rotation was suitably fast enough, between 12 to 240° per minute depending on the material, based on the material's coefficient of consolidation.

This paper presents result of FSVTs that were carried out as part of a geotechnical investigation of a Tailings Storage Facility at a gold mine. The tailings consist of non-plastic silt- and sand-sized particles,

and therefore understanding the drainage conditions during tests was important for interpreting the results. This paper will outline how, in some cases, undrained testing conditions were demonstrated, and thus reliable undrained shear strengths were determined.

Geotechnical investigation

Site description

The Kittilä Mine is located in Northern Finland, about 900 km north of the city of Helsinki and 150 km north of the Arctic Circle. Although north of the arctic circle, the climate is more comparable to eastern Canada: northern boreal vegetation zone, winter temperatures between –10 to –30° C, and summer temperatures between 10 to 25°C (Doucet et al., 2010).

The mine is operated by Agnico Eagle Mines Finland Oy, a subsidiary company of Agnico Eagle Mines Ltd. The mill processes approximately 4,500 tonnes of gold bearing ore per day from underground workings (Masengo et al., 2018). Two tailings streams are produced as a by-product of processing: neutralized flotation tailings (NP tailings) and carbon-in-leach tailings (CIL tailings). Since, 2011, NP tailings have been deposited into the NP3 tailings storage facility (NP3). The FSVTs results being presented in this paper were conducted within the NP3 facility as part of an overall geotechnical investigation program.

NP3, is a sidehill structure consisting of zoned earthfill starter embankments, with an upstream inclined compacted low permeability till layer, and downstream filters and rockfill. The basin of the facility has a bituminous geomembrane liner. Figure 1 presents aerial photographs of NP3 in 2014 and 2017. Initially, tailings were deposited via a single point discharge from the north embankment, with a solids content between 20 and 25%, by mass. In the 2014 photograph a sub-aerial tailings beach is visible in the north half of NP3, and subaqueous tailings and a supernatant pond within the southern portion of the facility. In late-2015, tailings discharge changed to a system using multiple spigots, rotating around the perimeter of the facility. As evident in the 2017 aerial photograph, the supernatant pond was moved to the eastern boundary where it is retained by topography, and beaches were established along embankments. In 2017 and 2018, gradual improvements to the operation were implemented to increase the solids content of the slurry to between 35% and 40%, at discharge.

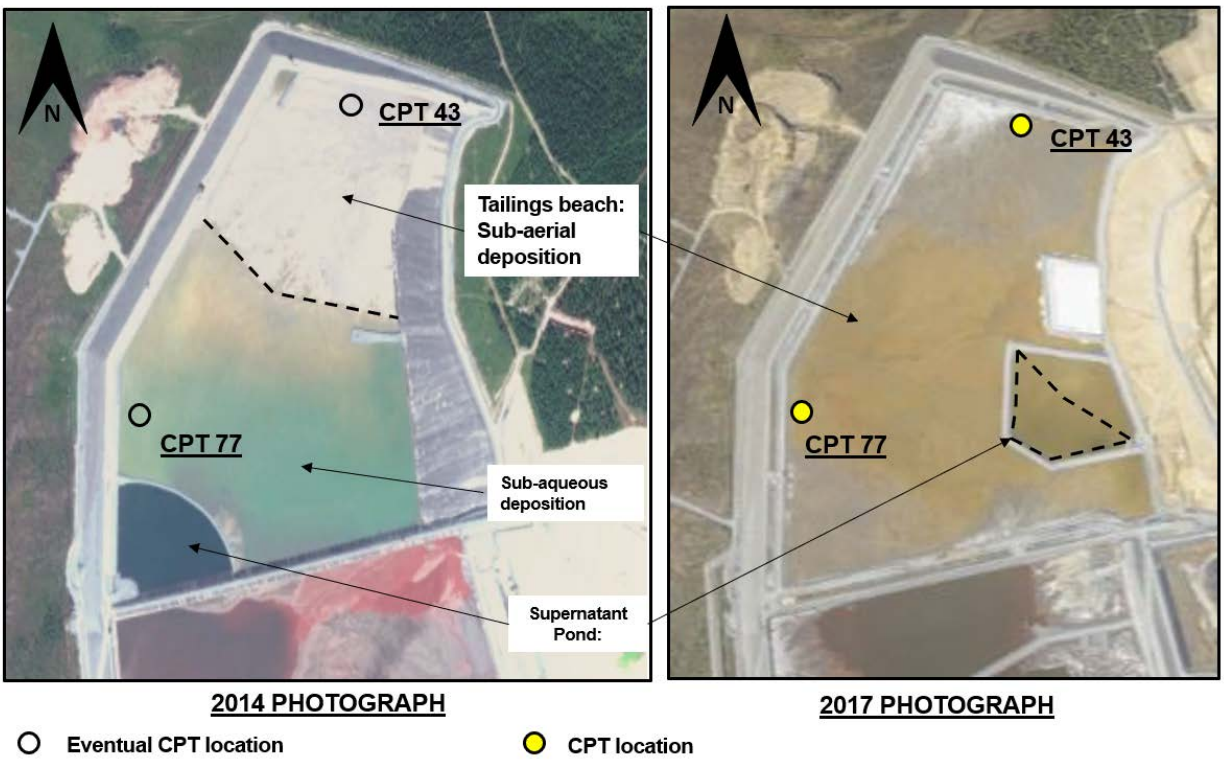

Figure 1: NP3 tailings facility layout – 2014 and 2017

Investigation locations

To expand the storage capacity of NP3, the design called for upstream raises to be constructed. Geotechnical investigations of the tailings that would become the foundation of the future raises were conducted. This included Cone Penetration Tests (CPTs), with Pore Pressure Dissipation Tests (PPDTs) and FSVTs, along with boreholes drilled adjacent to select CPT locations using a solid-stem auger to collect representative grab and tube samples, for laboratory testing.

Between March and December 2017, a total of 125 CPTs were completed, with 52 of those locations having PPDTs, and 51 locations had FSVT profiles collected. Typically, PPDTs were carried out at intervals of 2 m and FSVTs at intervals of 0.5 or 1 m. Two of the investigation locations with contrasting conditions, have been selected for presentation and discussion in this paper: CPT 43 and CPT 77, are shown in Figure 1. Both of these CPTs were completed from the surface of the tailings beach. CPT 77 was located where historic sub-aqueous deposition occurred and CPT 43 was located at the north in the vicinity of the historic single point discharge where sub-aerial deposition occurred.

Table 1 summarizes the investigation information available for CPT 43 and CPT 77. FSVTs and PPDTs were both completed at CPT 77 and a sample was collected nearby. At CPT 43, the PPDTs and sampling were completed at nearby locations.

Table 1: Testing completed at CPT 43 and CPT 77

Test type	CPT 43	CPT 77
Field shear vane	Yes	Yes
Pore pressure dissipation	25 m away	Yes
Sampling	28 m away	16 m away
• Material characterization	Yes	Yes
• Advanced	No	Slurry consolidation

Laboratory testing of the samples consisted of material characterization (particle size distribution, Atterberg limits, specific gravity of solids, semi-quantitative mineralogy by X-ray diffraction), and advanced testing.

Slurry consolidation testing was conducted in the laboratory to provide a coefficient of vertical consolidation (c_v) for the tailings based on a sample that was reconstituted from a slurry. This was to replicate tailings deposition in sub-aqueous conditions. The slurry used for the sample tested was prepared to a solids content of 44% (void ratio around 4.4) and when permitted to settle under self-weight, reached a void ratio of around 2.0, which set the initial condition for the test, upon which incremental loads were applied. Additional advanced testing to characterize the tailings was completed, but the results are not presented in this paper.

Cone penetration testing

CPTs were completed using a 10 cm^2 cone manufactured by Geomachine (Geomachine, 2018c). Rate of advancement of the cone was electronically controlled at the standard rate of 20 mm/s (ASTM D5778).

At locations where PPDTs were completed, cone advancement was typically stopped at intervals of 2 m for a duration of 10 minutes. The correlation shown in Equation 1 (Robertson, 2010), was used to calculate the coefficient of horizontal consolidation from the PPDT results using:

$$c_h = (1.67 \times 10^{-6})10^{(1-\log t_{50})}$$

Where: c_h = coefficient of horizontal consolidation (m^2 per second);

t_{50} = time to 50% dissipation of excess pore water pressure (minutes).

The relationship used in Equation 1 can vary with the rigidity index (I_r) of the material (Robertson et al., 1992). Correlations can be developed based on I_r, typically between 50 to 500, and for the work in this paper an intermediate I_r of roughly 300 was used. Also, to allow a systematic interpretation of t_{50} used in Equation 1, the equalization pressure for the PPDT was estimated using the hyperbolic curve fitting technique outlined by Chung et al. (2014).

Values calculated using Equation 1 provide a reasonable estimate of coefficient of horizontal consolidation, but uncertainty remains as it is a correlation. Based on a comparison of Equation 1 to results in Robertson et al. (1992), the coefficient of horizontal consolidation obtained from vertical measurements in the laboratory were up to one order of magnitude lower than estimated from PPDTs. Theoretically, the uncertainty may be reduced if the rigidity index of the tailings were known.

Field shear vane testing

All FSVTs presented in this paper were carried out using a vane measuring 80 mm in diameter, 160 mm in height, and a bottom taper of approximately 25°. Vanes were rotated at a rate of 120° per minute, the maximum possible with the equipment used (Geomachine, 2018a). Torque applied to the vane rods was electronically recorded (Geomachine, 2018b). Shear strengths were calculated in accordance with ASTM procedures (ASTM D2573).

To assess drainage conditions during the FSVTs a dimensionless time factor was calculated using Equation 2 (Blight, 1968):

$$T = \frac{c_v t_f}{D^2}$$

Where: T = time factor (dimensionless);

t_f = time to failure (seconds);

c_v = coefficient of vertical consolidation (m^2 per second);

D = vane diameter (m).

Time to failure is measured from the time when vane rotation began to when the maximum torque applied to the rods was measured. Values of c_v were from Equation 1 and assumed a coefficient of consolidation in the horizontal to vertical directions of 1.5 (i.e. c_h / c_v = 1.5). A value of 1.5 is reasonable for natural soils with an origin similar to sub-aerial and sub-aqueous tailings deposition (Mayne, 2011).

Results

Material characterization

Samples tested in the laboratory consisted of fine sand- and silt-sized particles (0.002 to 0.425 mm in size) with a specific gravity of solids of 2.9. Figure 2 presents the particle size distributions of the two samples considered in this paper. These samples coincide with intervals where PPDTs and FSVTs were carried out during the geotechnical investigation.

Mineralogy of samples at CPT 43 and CPT 77 were similar. On average the samples contained 28% dolomite, 29% plagioclase, and 29% quartz by weight. Although the clay mineral illite was present at

roughly 14%, it was bound to muscovite (illite-muscovite), a non-clay mineral silicate sheet (Kearey, 2001). The non-plastic behaviour indicated by Atterberg Limit testing is consistent with the mineralogy results.

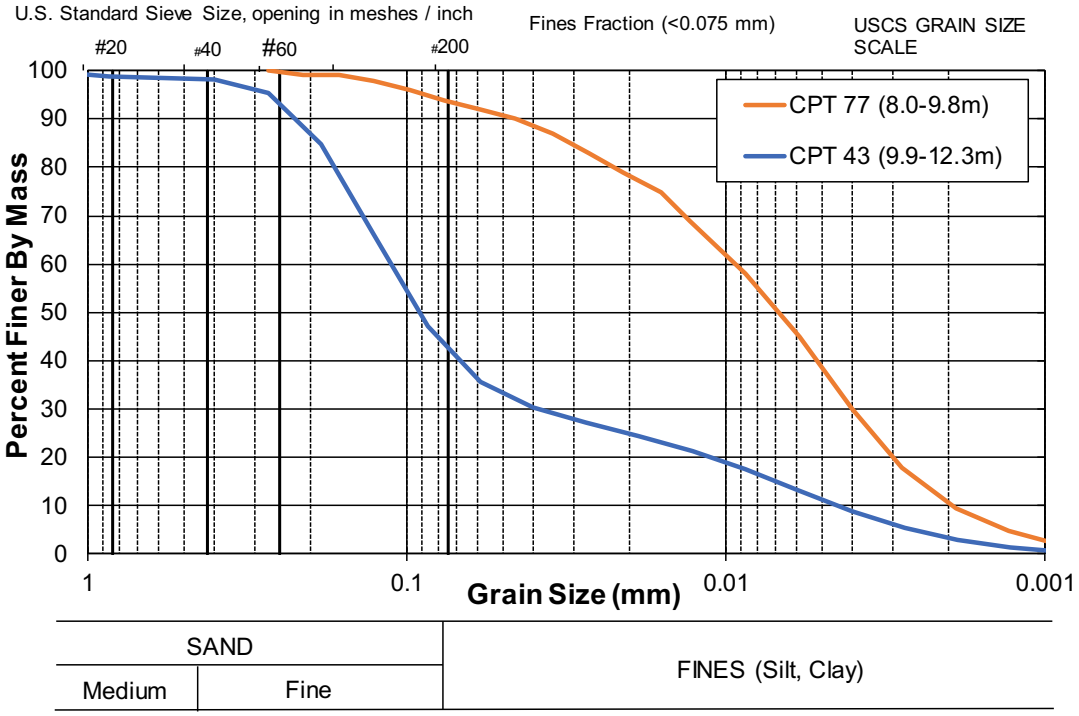

Figure 2: Particle size distribution results

Cone penetration test profiles

Figure 3 and Figure 4 present profiles of normalized CPT readings and soil-behaviour type with depth for CPT 77 and CPT 43, respectively. Dashed black lines indicate specific intervals that are analyzed in this paper, as they demonstrate the contrast in results. Soil-behaviour type is calculated based on Jefferies and Been (2006).

At CPT 77, located in the area of the supernatant pond prior to 2015, compressible fine-grained layers are identified in the analysis intervals (13.4 to 16.6 m). These are interpreted to represent sub-aqueously deposited tailings as the average soil-behaviour type is generally between 2.6 and 2.8 (average of 2.7), clayey silt to clay, with pore pressure ratios between 0.6 and 0.8. The particle size distribution of the sample, a silt, is consistent with the CPT result. At CPT 43, the analysis intervals have coarser and less compressible material than the intervals analyzed for CPT 77. In CPT 43 the average soil-behaviour type has a value of 2.3, silty sand to sandy silt, with a pore pressure ratio of less than 0.2. The sample tested at a similar depth was a sand and silt, which is aligned with the soil-behaviour type. The results are consistent with the depositional history, where single point discharge resulted in hydraulic segregation of particle sizes.

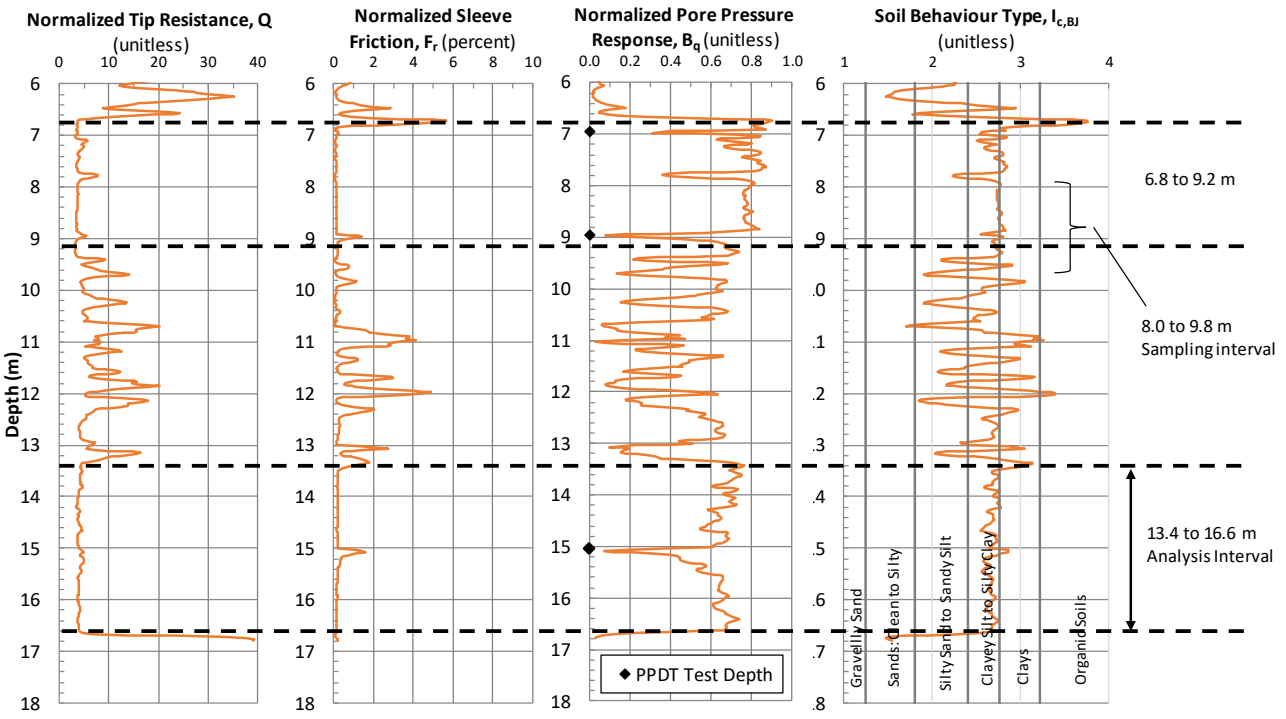

Figure 3: CPT 77 – Normalized readings and soil behaviour type with depth

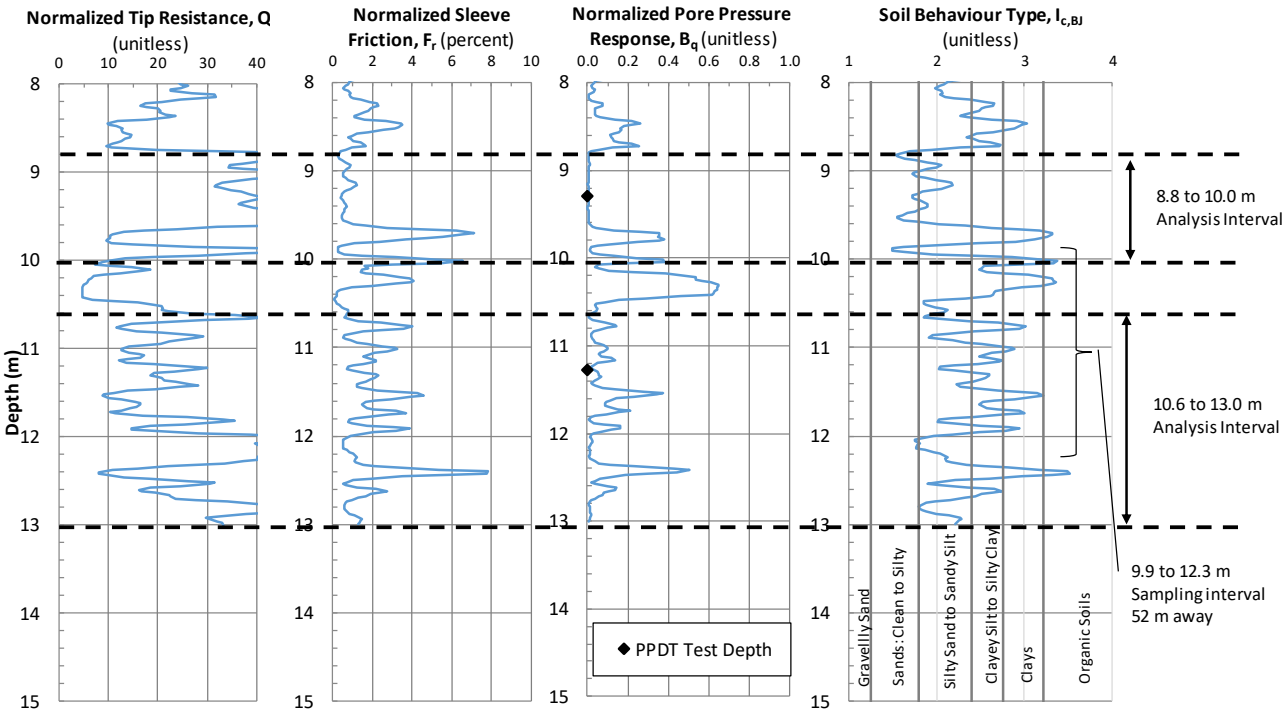

Figure 4: CPT 43 – Normalized readings and soil behaviour type with depth

Coefficient of consolidation

Within the analysis intervals shown in Figure 3 and Figure 4, five PPDTs were conducted and test depths are shown in the pore pressure ration profile as solid black markers. Figure 5 presents the horizontal coefficient of consolidation calculated from PPDT tests and vertical coefficients of consolidation measured in the laboratory. Results from CPT 77 are about one to one-half an order of magnitude lower than those from CPT 43. This difference is consistent with the differences in particle size distribution (for the intervals analyzed): tailings at CPT 77 are almost entirely silt-sized, whereas those at CPT 43 are a mixture of sand and silt.

From the slurry consolidometer test, using the sample obtained near CPT 77, the coefficient of vertical consolidation was between 100 and 150 m^2 per year. This is approximately one to half an order of magnitude lower than the PPDT results, which is an expected result.

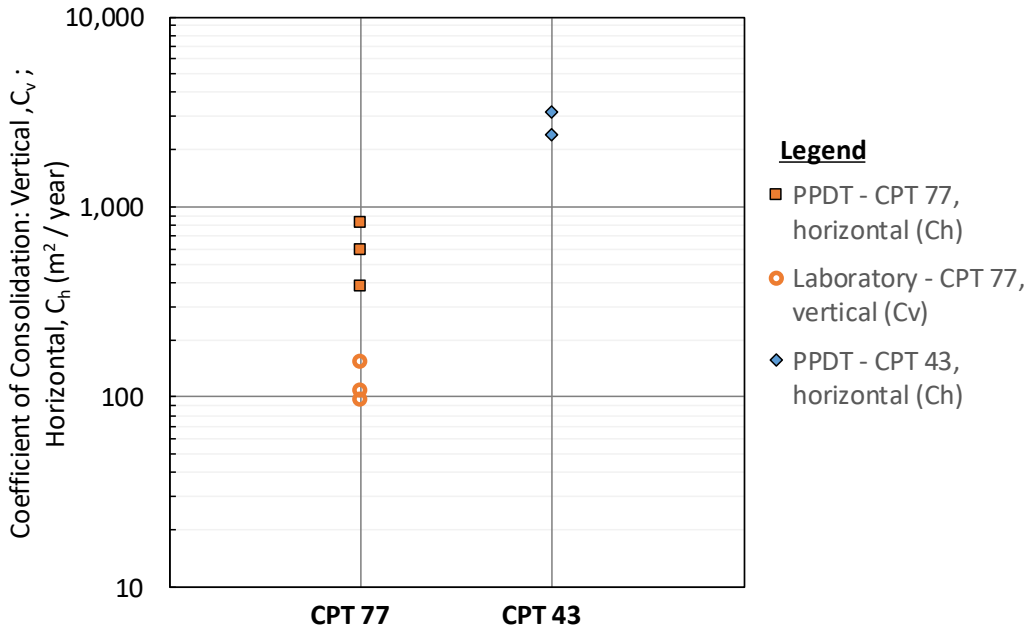

Figure 5: Coefficients of consolidation from PPDT and laboratory testing

Shear strength

Figure 6 presents the shear strength results with depth from CPT 77 and CPT 43 obtained from the cone's tip resistance compared with those measured during the FSVTs. Shear strengths from CPT were calculated using a cone bearing factor (Nkt) of 15.

At CPT 77, the average shear strength ratio from the FSVT over the two analysis intervals is 0.23 and there is good agreement with values estimated from the CPT for the 6.8 to 9.2 m interval. For the 13.4 to 16.6 m interval, the strength from the FSVT is slightly lower than that from the CPT.

At CPT 43, the average shear strength ratio is 0.67, with a minimum of 0.57 over the analysis intervals. These ratios are considered high for silt and sand mixture. FSVT values tend to coincide with minimum strengths estimated from the CPT. Although not a common practice to present FSVT results as friction angles, on average the strengths would be 34° and a minimum of 30°, as calculated by taking the arctangent of the shear strength ratio.

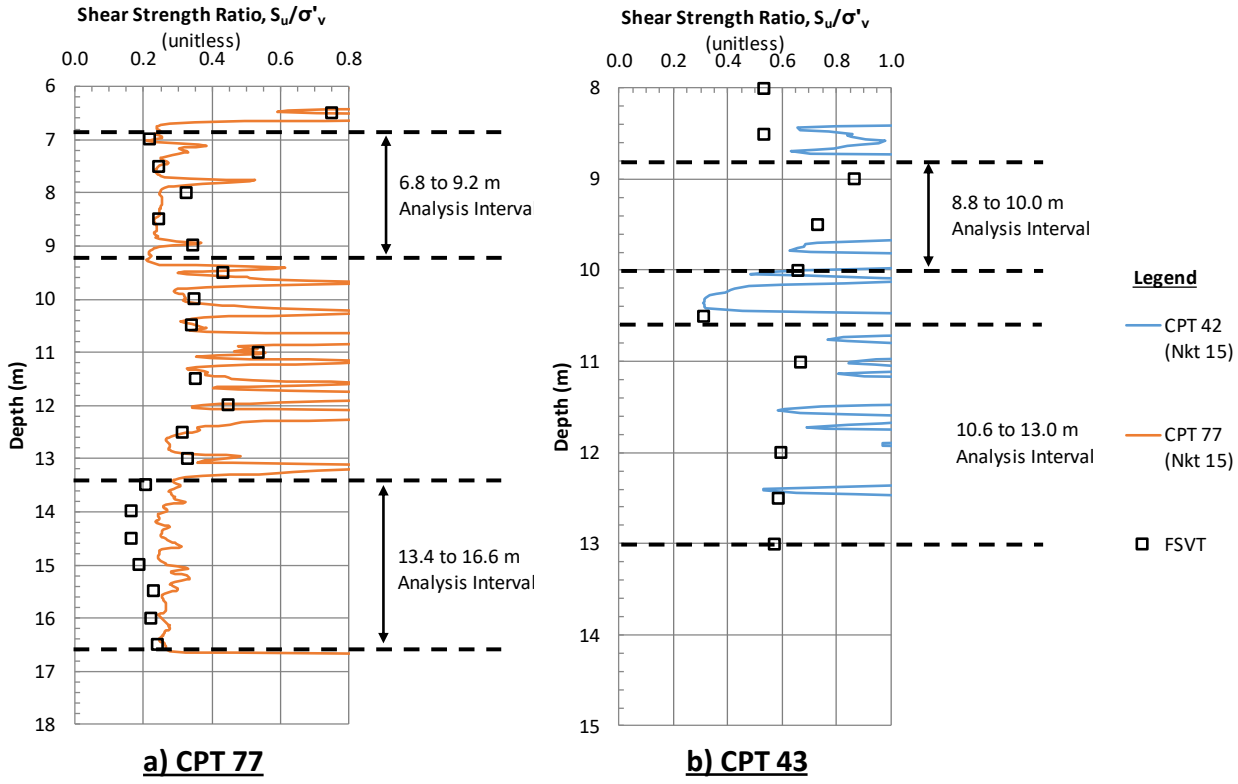

Figure 6: Shear strength with depth: (a) CPT 77 and (b) CPT 43

Time factor

In Figure 7 shear strengths measured from the FSVTs are plotted versus their corresponding dimensionless time factor calculated using a ratio of 1.5 for horizontal to vertical coefficient of consolidation. At CPT 77 the time factors are generally in the undrained range (T<0.05). The average shear strength ratio of 0.23 from the FSVT are within the range of 0.2 to 0.3, typical of normally consolidated low plasticity fine grained soil tested in undrained direct simple shear (Ladd, 1991). At CPT 43, time factors are 0.25 on average and all results are greater than 0.2, and thus indicate drained condition during the FSVTs.

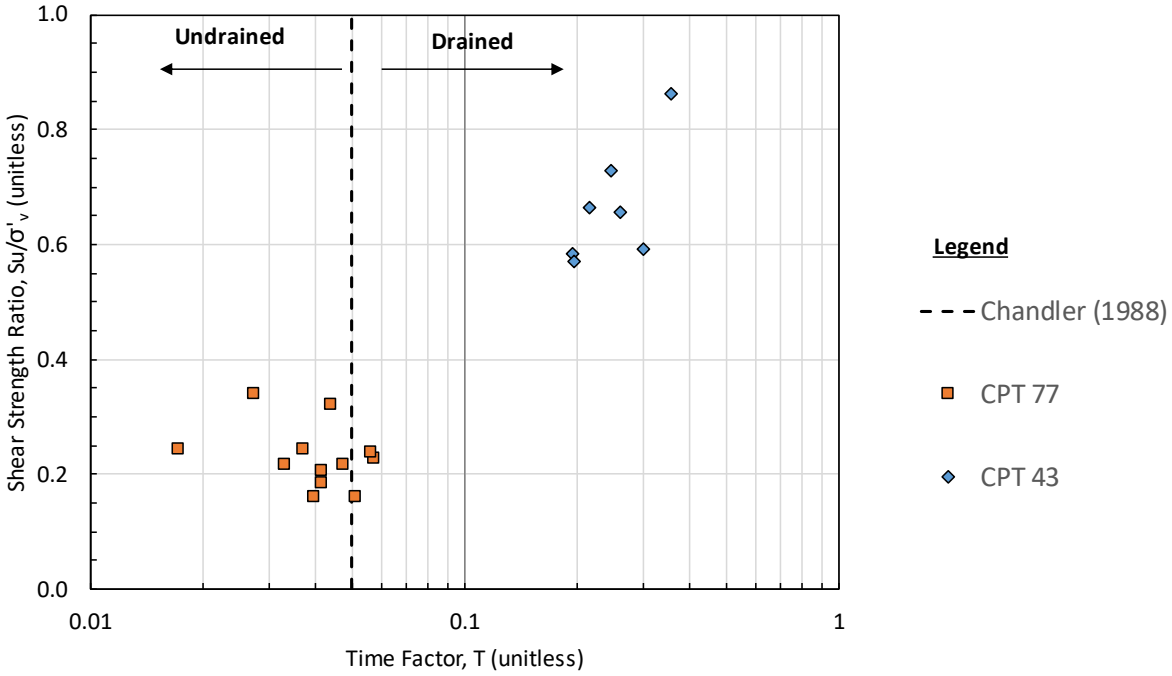

Figure 7: Shear strength ratio versus time factor

For CPT 77, interpretation of drainage conditions during the FSVTs is sensitive to the ratio of horizontal to vertical coefficient of consolidation. When a ratio of 1.5 or greater was used, the time factors indicate the testing was performed in undrained conditions. However, if a ratio of 1.0 was used, time factors would indicate testing was carried out under drained conditions. The selected ratio of 1.5 is considered reasonable for this material, and therefore the interpretation of undrained conditions. CPT 43 results are not sensitive to the ratio, as time factors are in the drained range using ratios of 1.0 to 5.0.

Discussion

Based on the analysis, FSVTs carried out in the silt tailings (CPT 77) were in undrained conditions and thus in-situ undrained shear strengths were measured. While the vane rotation rate was sufficiently fast to provide shear strength ratios in the range expected of fine grained soil in undrained conditions a good understanding of the range of coefficients of consolidation for the material was required to demonstrate undrained conditions. Although this paper focused on a select few FSVTs and PPDTs, similar results were obtained at different locations providing the authors with the confidence that undrained conditions with FSVT were being consistently achieved. Using CPTs and PPDTs, as part of the investigation provides in-situ measurements, is relatively quick, and can provide a larger dataset that can be analysed, in comparison to sampling and laboratory testing.

During the work described, two uncertainties were encountered and were related to the coefficient of consolidation. First, time factor calculations require the vertical coefficient of consolidation, but PPDTs provide this coefficient in the horizontal direction. Even though the conversion to vertical required an assumption, it was shown to be reasonable.

Secondly, an understanding of the rigidity index of the material appears to be one potential means of reducing the variation in estimates of horizontal coefficient of consolidation from PPDT results. Although indices can be obtained from seismic CPT testing, these were not carried out as part of this investigation. Nevertheless, the intermediate rigidity index used in this paper yielded reasonable results for coefficients of horizontal consolidation.

For the silt and sand tailings (CPT 43), FSVT were carried out in drained conditions and thus strength ratios are indicative of drained strength. When calculated as a friction angle, the values are comparable to those published for silty and sandy silts tested in drained conditions (Been, 2016). It is recognized that it is not common to present FSVT results as friction angles, and thus more formal investigation would be required to determine if such a convention is appropriate. A faster rate of rotation would have been required for undrained conditions.

Conclusion

The work presented demonstrates that undrained conditions can be achieved during FSVTs in non-plastic silt tailings. Although this was successful, the geotechnical investigation was not specifically designed to fully assess this approach. For projects with non-plastic silt tailings an understanding of in-situ undrained strengths are of importance. Lessons that can be learned from the work undertaken are as follows:

- Consideration should be given to performing FVSTs over a range of vane rotation rates in similar materials. This should produce results over a range of time factors, thus allowing for consideration of how sensitive strength results are to drainage.
- Frequent pairing of FSVT with PPDT locations. This is to reduce uncertainty in the application of representative drainage conditions to the FSVT result. In this case, due to the depositional history of NP3, the results of PPDTs and FSVTs completed 25 m apart were considered to be representative of one another.
- Complete seismic CPTs to estimate the rigidity index of materials, as this will refine the correlation of PPDT results to estimates of the horizontal coefficient of consolidation.

References

ASTM D2573. Standard Test Method for Field Vane Shear Test in Saturated Fine-Grained Soils. ASTM D2573/D2573-15. ASTM International: Pennsylvania.

Blight, G.E. 1968. A note on field vane testing of silty soils. *Canadian Geotechnical Journal* 5(3): 142–149.

Been, K. 2016. Characterizing mine tailings for geotechnical design. *Australian Geomechanics* 51(4): 59–78.

Chandler, R.J. 1998. The in-situ measurement of the undrained shear strength of clays using the field vane 1988. In *Vane Shear Strength Testing in Soils: Field and Laboratory Studies, ASTM STP 1014*, edited by A.F. Richards: 13–44. Philadelphia: American Society for Testing and Materials.

Chung, S.G., H.J. Kweon and W.Y. Jang. 2014. hyperbolic fit method for interpretation of piezocone dissipation tests. *Journal of Geotechnical and Geoenvironmental Engineering* 140(1): 251–254.

Craig, R.F. 2004. *Craig's Soil Mechanics,* seventh edition. New York: Spon Press, Taylor & Francis Group.

Doucet, D., D. Girard, L. Grondin and P. Matte. 2010. Technical Report on the December 31, 2009 Mineral Resource and Mineral Reserve Estimate and the Suuri Extension Project, Kittila Mine, Finland. Prepared for Agnico Eagle Mines Limited.

Geomachine. 2018a. GM 4W Vane test. Technical specification. Accessed on 29 October 2019 from http://geomachine.fi/_media_1094_/Wane%20test/GM_Technical_specification_GM_4W.pdf. Accessed

Geomachine. 2018b. RUFCO DL2 Field computer technical specifications. Accessed on 29 October 2019 from http://geomachine.fi/_media_1718_/PDF/RUFCO_DL2S-2x19P-G.pdf.

Geomachine. 2018c. GM CPT-U: Technical specification. Accessed on 29 October 2019 from http://geomachine.fi/_media_1098_/CPT-U/Technical_specification_GM_CPT-U.pdf.

Jefferies, M. and K. Been. 2006. *Soil Liquefaction: A Critical State Approach*. New York: Taylor & Francis Group.

Kearey, P. 2001. *Dictionary of Geology,* second edition. Toronto: Penguin Group.

Ladd, C. 1999. Stability evaluation during staged construction. The 22nd Karl Terzahi lecture. *Journal of Geotechnical Engineering* 117(4): 540–615.

Masengo, E., M.R. Julien, P. Lavoie, T. Lépine, T. Nousiainen, J. Saukkoriipi, M. Piekkari and J. Karvo. 2019. Enhancement of contractive tailings using deep soil mixing technique at Kitilä Mine. In *Proceedings of the ICOLD-CIGS* Ottawa 2019.

Mayne, P.W. 2011. *Engineering Design Using the Cone Penetration Test: Geotechnical Applications Guide* – third printing. ConeTec. September 2011.

Reid, D. 2016. Effect of rotation rate on shear vane results in silty tailings. In *Proceedings of Geotechnical and Geophysical Site Characterization 5.* Sydney. Australian Geomechanics Society.

Robertson, P.K. 2010. Estimating in-situ soil permeability from CPT & CPTu. In *Proceedings of the 2nd International Symposium on Cone Penetration Testing*. Las Vegas.

Robertson, P.K., J.P. Sully, D.J. Woeller, T. Lunne, J.J.M. Powell and D.G. Gillespie. 1992. Estimating coefficient of consolidation from piezocone tests. *Canadian Geotechnical Journal* 29: 539–550.

Skempton, A.W. and A.Q. Bishop. 1950. The measurement of the shear strength of soils. *Géotechnique* 2: 90–108.

Terzaghi, K., R.B. Peck and G. Mesri. 1996. *Soil Mechanics in Engineering Practice,* 3rd edition. New York: John Wiley & Sons.

Bibliography

World Weather and Climate Information (WWCI). 2019. Climate and average monthly weather in Kittilä (Lapland), Finland. Accessed on 26 July 2019 from https://weather-and-climate.com/average-monthly-Rainfall-Temperature-Sunshine,kittila-lapland-fi,Finland.

Proceedings of Tailings and Mine Waste 2019
November 17–20, 2019, Vancouver, Canada
Published by the University of British Columbia, 2019

Mine Tailings Consolidation Properties Derived from Beam Centrifuge

Gonzalo Zambrano Narvaez, University of Alberta, Canada
Rick Chalaturnyk, University of Alberta, Canada
Yazhao Wang, University of Alberta, Canada

Abstract

Disposal of mine tailings is an important aspect of the total process of mineral extraction. For proper management of a tailings disposal area, it is important to understand the mechanics that control the movement of water in the tailings, the rate and final amount of surface settlement (self-weight consolidation), and the changes of strength through the depth of the tailings. The work presented in this study focuses on the self-weight consolidation of mine tailings. It is possible to determine the tailings properties and to verify the numerical model by a combination of laboratory tests and observations of the performance of a full-scale disposal area. It is extremely time consuming to evaluate the long-term behaviour of mine tailings self-weight consolidation, especially for comparative purposes, as conventional settling column tests or field pilot tests take years to produce meaningful results. However, geotechnical centrifuge testing offers a more effective way of "calibrating" and verifying the model of large-scale nonlinear problems for which gravity is the primary driving force, including the self-weight consolidation of fine tailings materials. The Geotechnical Centrifuge Experimental Research Facility (GeoCERF) at the University of Alberta, operates a 2-m radius geotechnical beam centrifuge. The fundamental principle of centrifuge modelling is based on the stress similarity between a prototype and a centrifuge model. Scaling laws for size and time are used to design the appropriate centrifuge operation. To analyze the large-strain consolidation process, the numerical model requires the compressibility (void ratio – effective stress) and hydraulic conductivity relationships. The void ratio – effective stress (compressibility) relationship was derived from the solids content profile at the completion of the centrifuge tests. The permeability relationship was estimated using a back-analysis method that provided a best fit between numerical predictions and the observed behaviour in the centrifuge tests. The Finite Strain Consolidation Analysis (FSCA) software was used to predict and history match the measured consolidation curve of the physical model at the prototype scale. FSCA is based on the 1D finite strain consolidation theory.

Introduction

Mineral extraction operations generate large volumes of fine tailings. The proper management of a tailings-disposal area is critical in both economic and environmental terms. It is crucial to understand the consolidation processes occurring within tailings ponds, including the rate and degree of surface settlement.

The mechanism of large-strain self-weight consolidation of tailings can be numerically modelled with a continuum theory developed by Gibson et al. (1981). The theory is built on the continuity equations for the fluid and solid phase which are governed by Darcy's law and Terzaghi's effective stress theory. It is essential to obtain relationships regarding tailings compressibility and hydraulic conductivity with volume change in order to accurately construct a numerical model. The acquisition of these parameters is generally obtained with traditional laboratory methods, such as odometer test and hydraulic conductivity test. However, the laboratory environment differs from field conditions and validation through field-scale performance tests is time consuming. These issues can be alleviated through centrifuge or physical modelling which can provide an effective way to obtain the long-term consolidation behaviour of mine fine tailings (Toh, 1992; Sorta et al., 2016; Zambrano-Narvaez et al., 2018).

A geotechnical beam centrifuge can be used for modelling of large-scale nonlinear problems for which gravity is the primary driving force, including to the self-weight consolidation of mine tailings. The self-weight consolidation process can be modelled in a greatly reduced time frame while centrifuge model replicates stress and flow conditions that govern the in-situ consolidation process. The fundamental principle of centrifuge modelling is based on the stress similarity between a prototype and a centrifuge model. Scaling laws for size and time are used to design the appropriate centrifuge operation. Centrifuge scaling relationships for the consolidation process have been extensively described by several publications, for example Croce et al. (1984); Williams (1988); Balay et al. (1988); Taylor (1995); and Garnier et al. (2007). Equations 1 and 2 illustrate the scaling laws for size and time in a geotechnical centrifuge model when modelling large strain consolidation, such as the self-weight consolidation of tailings.

$$h_p = N * h_m \tag{1}$$

$$t_p = N^2 * t_m \tag{2}$$

where, h_p is the height of the prototype being simulated, h_m is the height of the centrifuge model and N is the multiple of earth gravity that the centrifuge model is subject to in the forms of centrifugal force (N times earth gravity), t_p is the duration of the prototype being simulated and t_m is the duration of the centrifuge experiment.

The Geotechnical Centrifuge Experimental Research Facility (GeoCERF) at the University of Alberta, operates a 2-m radius geotechnical beam centrifuge – the first of its kind in Western Canada. The facility can model high-gravity environment up to 150 time of earth gravity (Zambrano-Narvaez and Chalaturnyk,

2014). Since GeoCERF's inception, the need for safe, time- and cost-effective solutions to pond reclamation has been a primary directive for the research team. While other disciplines focus on recycling and managing risks associated with the water itself, the GeoCERF research group is investigating new treatment techniques developed to increase the dewatering rate of tailings. These treatments, including chemical flocculants, are intended to assist not only with reclamation efforts over the lifetime of the project, but also to expedite full reclamation upon completion.

Centrifuge test

The mine tailings used for this study was obtained from a gold mine. The measured unit weight of the material was 2.77. The initial solids content of the gold tailings was 65%. The specimen was tested under 100 time Earth's gravity acceleration in the geotechnical beam centrifuge, with an initial sample height of 47 cm and was spun for 9 hours at 100 g. Based on geotechnical centrifuge scaling laws, the model represented a prototype (field) height of 47 m and prototype time of 10 years. The centrifuge model adopted a surface discharge to reflect the one-way, upwards drainage condition of the field deposit. A surface dewatering system (GeoSDS) capable of operating under the 100 g conditions was developed for this study to allow for modelling of surface drainage conditions in-flight. The system comprises of a floating vacuum vehicle, in-flight vacuum and water collection tank. Table 1 summarizes the model and prototype conditions of the centrifuge test.

Table 1: Centrifuge test program

Testing sample	G-Level	Thickness		Time	
		Prototype	Model	Prototype	Model
Gold tailings	100	47 m	47 cm	10 yrs	9 hrs

Figure 1 shows the consolidation cell constructed for this study. It was made of a transparent Plexiglass cylinder of 177.8 mm internal diameter, 568.6 mm internal height and a wall thickness of 13 mm and a supporting aluminum structure. The transparent wall allows for readings of solids interface during the test. Rulers with millimeter graduations were glued with epoxy on the internal wall of the Plexiglass cylinder.

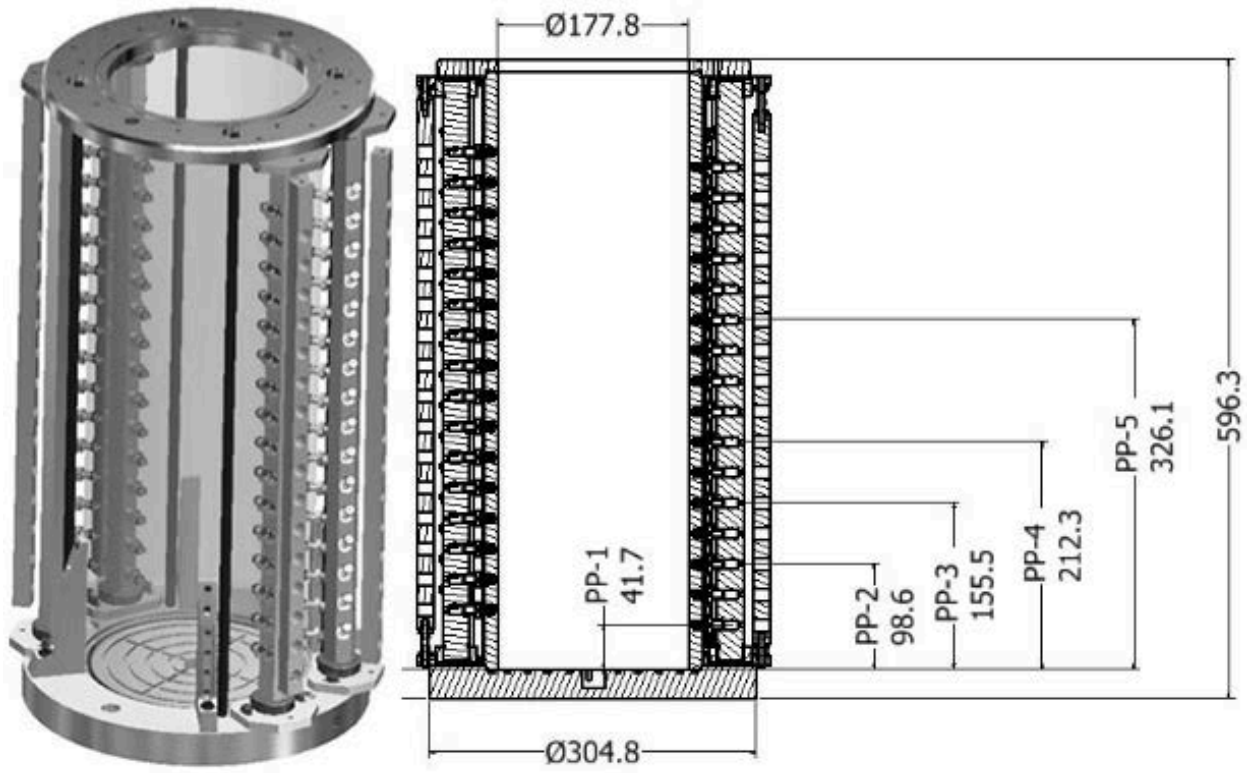

Figure 1: Consolidation cell and pore pressure sensors

Five pore pressure transducers (Model EPRB-1-15B) were attached to the consolidation cell after the filling of the materials. As shown in Figure 1, the transducers were located 41.7mm (PP-1), 98.6mm (PP-2), 155.5mm (PP-3), 326.1mm (PP-4) and 596.3mm (PP-5) above the base of the cell. Pore-water pressure was monitored during the consolidation and utilized to compute the effective vertical stress and excess pore-water pressure profiles.

A post-test analytical test was performed on the model to obtain geotechnical index properties after 10 years of consolidation. An aluminium tube with 35mm ID was slowly inserted into the sample to obtain a complete column of consolidated sample. The column was sliced into 19 layers of 2 cm thick sub-samples with a customized dispensing device (Figure 3).

Solids content, moisture content, bulk density and void ratio measurement were obtained from the sub-samples. The index property profiles with depth were constructed by integrating the sub-sample measurements.

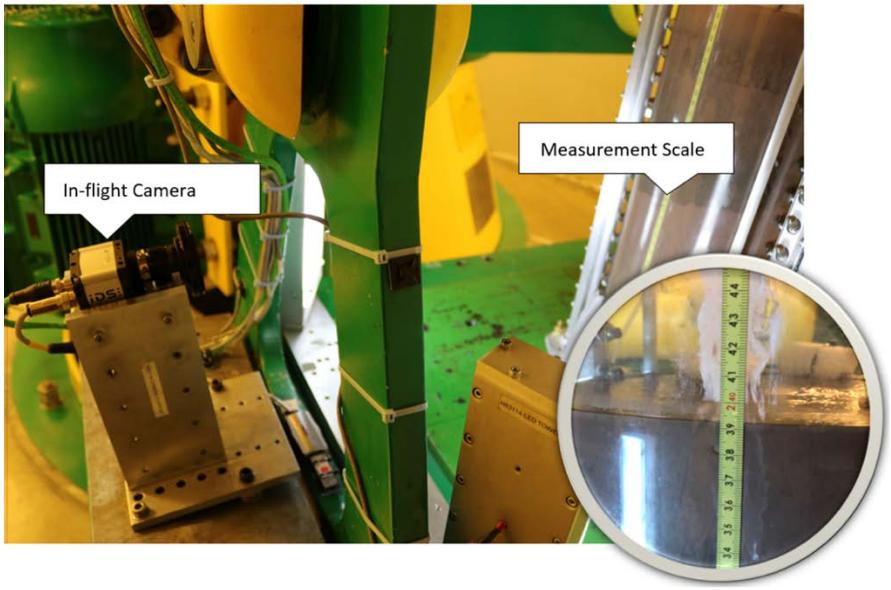

Figure 2: High-resolution in-flight camera measuring mudline interface

Figure 3: Post-test analysis of index properties

Centrifuge test results

The tailings settlement curve is a clear expression of the consolidation process. Ten years of self-weight consolidation behaviour of a 46.7 m thick prototype tailings deposit was successfully assessed with centrifuge modelling. Under one-way surface drainage condition, the deposit prototype settled 7.58 m, or 16.2% of the initial, resulting in a final height of 39.12 m. Figure 4 shows the prototype consolidation curves for the tailings centrifuge model.

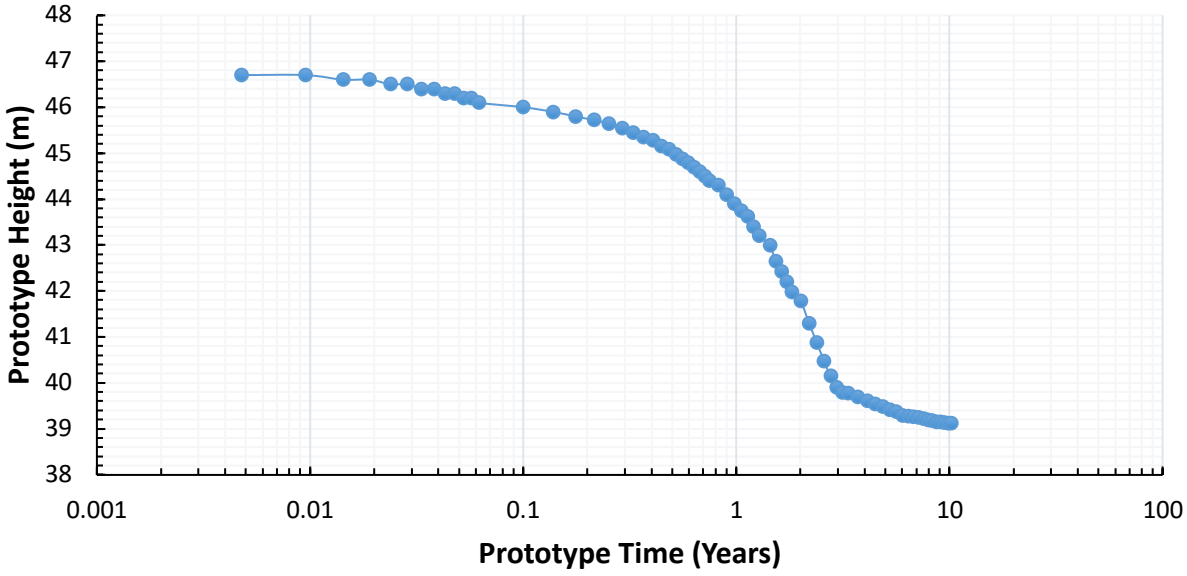

Figure 4: Prototype settlement curve

Figure 5 shows the measured index properties profiles, including solids content, void ratio, water content, dry unit weight and bulk density, of the tailings model after 10 years of prototype consolidation.

Pore pressure was measured at five locations during the test (see Figure 6). The pore pressure profile at the end of the consolidation test was estimated by interpolating the final pore pressure measurement.

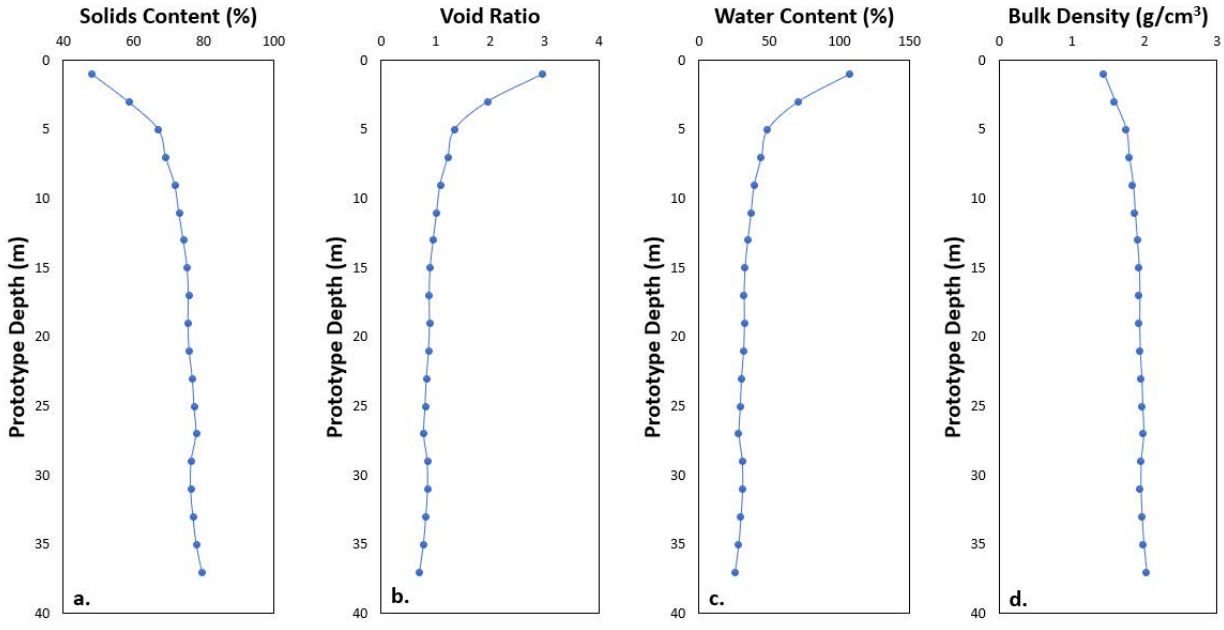

Figure 5: Index properties profile obtained after test:
a: Solids content, b. Void ratio, c. Water content, d. Bulk density

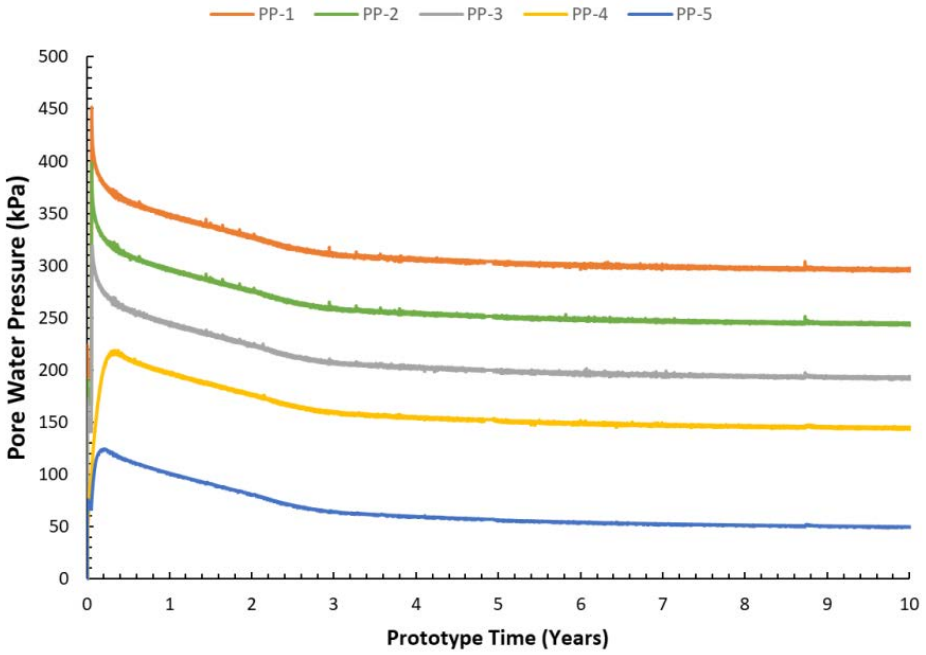

Figure 6: Pore pressure dissipation curves during the centrifuge test

Combining the bulk density profile, pore pressure profile and void ratio profile at the end of the centrifuge test, the effective stress (σ') versus void ratio (e) relationship was constructed at the end of the test and is shown in Figure 7. Consolidation parameters A and B were obtained by curve fitting the e-σ' curve. In the centrifuge model, A = 2.759 and B = –0.215.

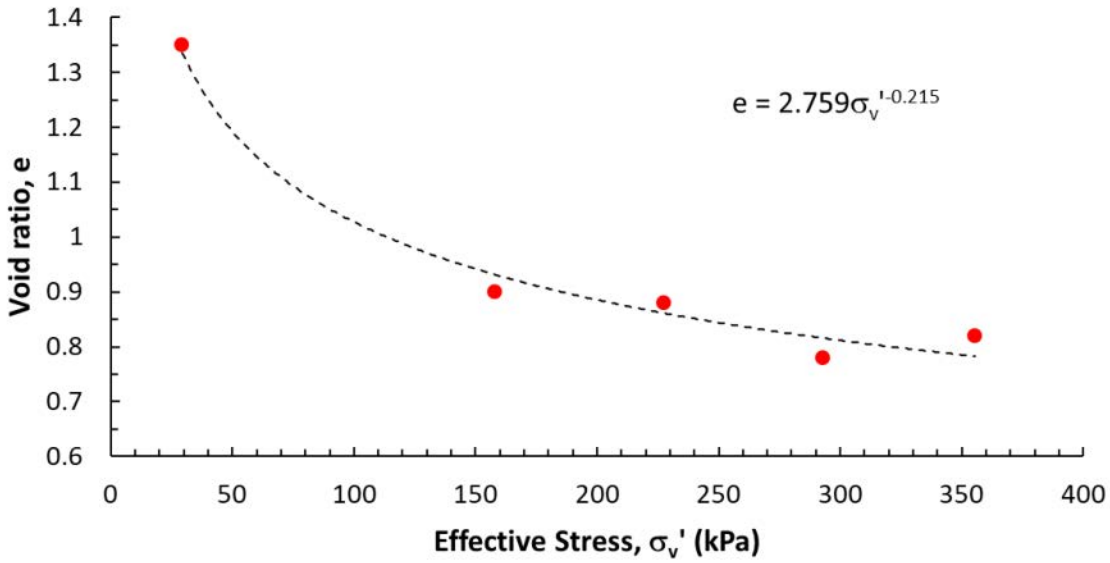

Figure 7: Void ratio versus effective stress relationship for the gold tailings

Numerical analysis

Finite Strain Consolidation Analysis Software (FSCA) was used for the numerical simulation of the same tailings model. FSCA is a 1D finite strain consolidation analysis software used to determine rate and amount of settlement for tailings, slurry and soft soils. FSCA is based on the finite strain consolidation theory. Material properties in terms of stress-strain, flow-strain are required for the solution. The governing equations for the properties are assumed to be monotonic functions relating void ratio to the effective stress and permeability.

Consolidation parameters

The governing equations of finite strain consolidation was solved using two important non-linear relationships: compressibility (e-σ') and hydraulic conductivity (k-e). These relationships, account for the dynamic values of the soil properties during the consolidation process.

The relationship between void ratio and effective stress is crucial as it governs the soil strain changes under self-weight loading. Mine tailings are usually deposited with very high void ratios and low effective stress, it is important that the e-σ' relationship covers a broad range of effective stresses. A power function (Equation 3) is used in FSCA. The curve-fitted consolidation parameters A and B can be obtained through odometer test but in a centrifuge test, the stress conditions represent the self-weight loading more accurately and consolidation parameters are derived through the sample profiling as mentioned in the previous section.

The relationship between hydraulic conductivity and void ratio can also be determined through standard laboratory tests such as large strain consolidation (LSC) tests. It can also be back analyzed though curve fitting with measured consolidation behaviour such as from centrifuge tests. The hydraulic conductivity relationship has been expressed in many forms and the power function (Equation 4) is used in FSCA.

$$\text{Compressibility: } e = A\sigma_v'^{B} \tag{3}$$

$$\text{Hydraulic conductivity: } k = Ce^{D} \tag{4}$$

where, σ_v' is the vertical effective stress (kPa), e is the void ratio, k is the hydraulic conductivity, and A, B, C and D are the empirical parameters.

The A and B parameters can be derived from the centrifuge test as presented in Figure 7. The C and D empirical parameters are estimated through back analysis method described in the following section.

Back analysis

A back-analysis procedure was used to estimate the (k-e) relationship. The workflow for this back-analysis employs the compressibility relationship shown in Figure 7 and varies the empirical hydraulic conductivity

parameters C and D of Equation 4 in the FSCA numerical analysis until the numerical results matched the time-settlement behaviour measured in the centrifuge. This procedure leads to an accurate (k-e) relationship because the back-analysis is very sensitive to variations of permeability. For the current test, Figure 8 shows a history match between the numerical and the centrifuge model settlement curve based on the hydraulic conductivity parameters C = 0.0028 and D = 5. Based on these parameters and Equation 4, Figure 9 illustrates the shape of the k-e relationship for the gold tailings material.

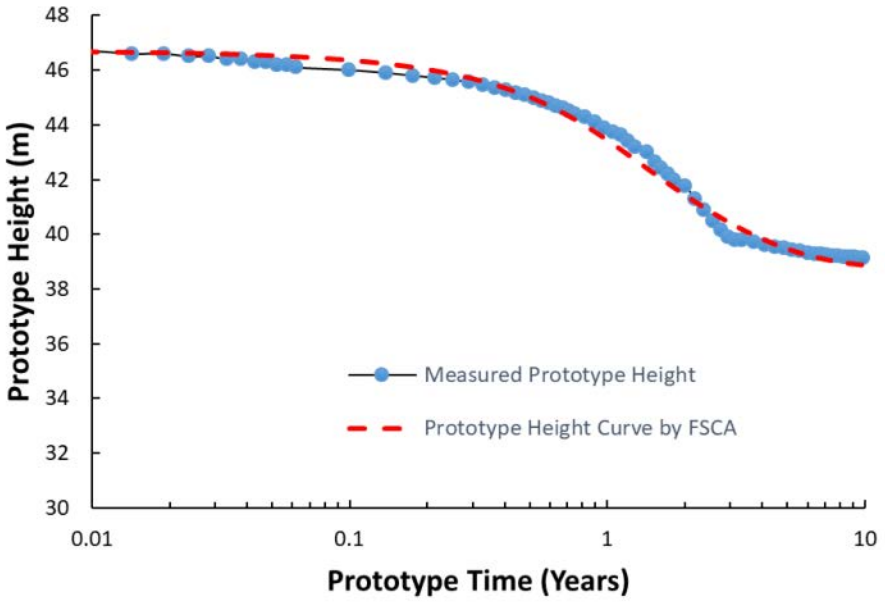

Figure 8: Measured consolidation curve and predicted curve by FSCA

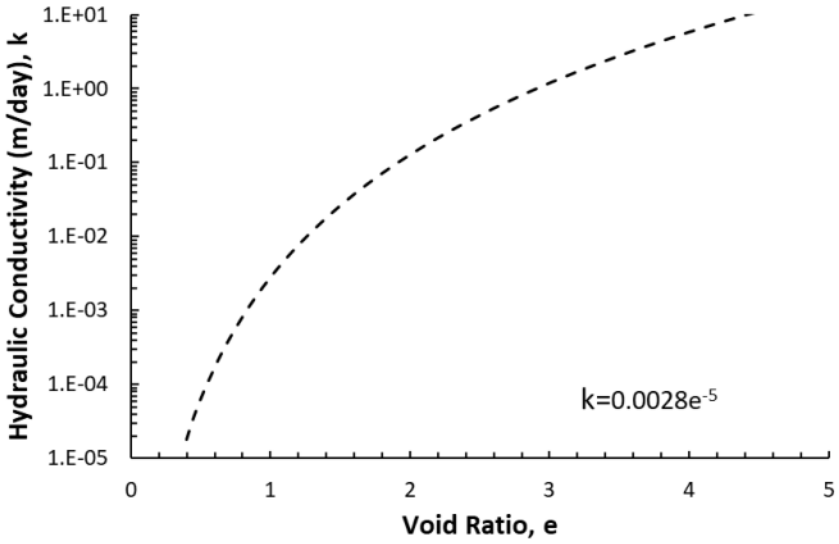

Figure 9: Hydraulic conductivity and void ratio relationship curve

Conclusion

As part of a commercial technical assessment of the behaviour of tailings from a gold mine in Central America, a centrifuge modelling test to simulate 10 years of self-weight consolidation behaviour was conducted in GeoCERF at the University of Alberta. The test duration was 9 hours under 100 times the Earth's gravity acceleration. The model simulates a one-way drainage, single-layer tailings deposit. A surface dewatering system (GeoSDS) developed for this testing allowed the removal of supernatant water in flight under the extreme 100 g conditions, demonstrating that complex boundary conditions can be achieved under the centrifuge environment. Unique test cells were developed by the GeoCERF research group that allow closely-spaced measurements of pore pressure change within tailings specimens, and permit unparalleled visualization of the settlement behaviour of the specimens.

The centrifuge model offers an effective method to assess tailings consolidation parameters. The void ratio and effective stress relationship were derived from the void ratio and pore-water pressure profile at the completion of the centrifuge tests. The permeability relationship was estimated by the back-analysis method, varying the relationship to obtain the best fit between numerical predictions and the observed behaviour in the centrifuge tests. The numerical model uses the compressibility parameters (void ratio – effective stress relationship) obtained from the centrifuge model and the best matched hydraulic conductivity parameters were determined.

This study has shown that combining numerical simulation and centrifuge simulation through the back-analysis approach is a powerful tool in obtaining tailings consolidation parameters and predicting tailings consolidation performance. The ability to "fail fast" offers obvious cost- and time-saving benefits that appeal to both industry and consumers, but by far the greatest and most important impact of research carried out in GeoCERF is risk mitigation. Knowledge being acquired through testing performed today will shape industry's ability to implement reclamation efforts both during and upon completion of projects, with the ultimate objective being to meet or exceed the mandates of the regulator.

Acknowledgements

The GeoCERF center was funded by Canadian Foundation for Innovation and Alberta Enterprise and Advanced Education.

References

Balay, J., R. Berdat and L. Harfouche. 1988. *Etude en centrifugeuse de la consolidation sous poids propre desols très laches.* In *Proceedings of International Conference Centrifuge 88*, Paris, Balkema: Rotterdam: 193–202.

Garnier, J., C. Gaudin, S.M. Springman, P.J. Culligan, D. Goddings, D. Konig, B. Kutter, R. Phillips, M.F. Randolph and L. Thorel. 2007. Catalogue of scaling laws and similitude questions in geotechnical centrifuge modelling. In *International Journal of Physical Modelling in Geotechnics* 7(3): 1–23.

Gibson, R.E., R.L. Schiffman and K.W. Cargill. 1981. The theory of one-dimensional consolidation of saturated clays. II. Finite nonlinear consolidation of thick homogeneous layers. *Can. Geotech. J.* 18(2): 280–293.

Sorta, A.R., D.C. Sego and W. Wilson. 2016. Physical modelling of oil sands tailings consolidation. *International Journal of Physical Modelling in Geotechnics* 16(2): 47–64.

Taylor, R.N. 1995. *Geotechnical Centrifuge Technology*. London: Blackie Academic.

Toh, Seng Huat. 1992. Numerical and centrifuge modeling of mine tailings consolidation. PhD dissertation, University of Western Australia.

Williams, D.J. 1988. Consolidation, crusting and loading of a soil slurry at 1 and 100 gravities. In *Proceedings of 5th Australia – New Zealand Conference on Geomechanics*, Sydney, Australia: 202–206.

Zambrano-Narvaez, G. and R.J. Chalaturnyk. 2014. The New GeoREF geotechnical beam centrifuge at the University of Alberta, Canada. In *Proceedings of the 8th International Conference on Physical Modelling in Geotechnics*, Perth, Australia: 163–167.

Zambrano-Narvaez, G., Y. Wang and R.J. Chalaturnyk. 2018. Comparative study of consolidation behaviour of differently-treated mature fine tailings specimens through centrifuge modelling. In *Proceedings of 9th International Conference on Physical Modelling in Geotechnics*, London, UK: 1271–1276.

Bibliography

Sorta, A.R. 2014. Centrifuge modelling of oils sands consolidation. PhD dissertation, University of Alberta.

Proceedings of Tailings and Mine Waste 2019
November 17–20, 2019, Vancouver, Canada
Published by the University of British Columbia, 2019

Applying Circulating Load in Thickeners Modifies Decantation of Fine Particles

Hossein Nematollahi, Asfalt Tous Company, Iran

Abstract

In some cases the overflow of thickener fed by a low solids content slurry is turbid, containing very fine particles. These particles do not settle, even after some days. In such cases, increasing the percentage of solids content of input slurry to more than a certain value modifies the condition of the slurry and produces a quite clear supernatant. By establishing a circulating load, the freed solid content can be adjusted to the desired value.

Introduction

Decantation of slurries containing fine particles at low solids content is very difficult. With sufficient time a significant proportion of the material may settle, but in some cases, the very fine particles remain dispersed. This condition can be modified using various methods, including coagulation (using multi-cation electrolyte), flocculation (using flocculants), centrifuges, etc.

If the concentration of solids exceeds a certain level – the critical solids concentration (CSC) level – then the sedimentation of coarser particles entrains the finer particles with them, and in consequence, the supernatant becomes quite clear.

In thickeners, under the condition of an acceptable area, by establishing a circulating load (CL), and transferring a part of the thickener underflow to its feed, the solid concentration of the feed can change to more than CSC and as a consequence, change the overflow to a clear water.

Decantation methods of fine particles

Sedimentation of fine particles can be accelerated by different methods:

Centrifugal forces

In normal conditions, the fine particles settle with a given speed, according to Stokes law:

$$v = \frac{(\sigma_s - \sigma_f)\, d^2\, g}{18\, \eta}$$

Where

v: terminal velocity of the particle ($m.s^{-1}$)

σ_s: particle density ($kg.m^{-3}$)

σ_f: fluid density ($kg.m^{-3}$)

d: particle diameter (m)

g: acceleration due to gravity ($m.s^{-2}$)

η: fluid viscosity ($N.s.m^{-2}$); (η = 0.001 $N.s.m^{-2}$ for water)

In centrifuges, acceleration could rise to several times the acceleration of gravity, as follows:

$$g_{cen} = r\, \omega^2$$

Where

g_{cen}: acceleration due to centrifuge ($m.s^{-2}$)

r: radius of rotation (m)

ω: angular velocity ($rad.s^{-1}$)

Therefore, the velocity of sedimentation can be obtained from the following equation:

$$v = \frac{(\sigma_s - \sigma_f)\, d^2\, \omega^2\, r}{18\, \eta}$$

Since the capacity of centrifuges is limited, compared with thickeners, this process is rarely used in mineral processing circuits for decantation aims.

Coagulation

The fine particles, due to the repulsion force raised from their electrical charge, get dispersed in slurry. The stability of dispersed particles depends on the magnitude of the charges. If the charge is decreased to less than a certain value, the repulsion force will be decreased too, so the particles can get closer together, and in consequence the attractive force of Van der Waals arises (Figure 1). So, aggregates of particles are formed and settle in the media. This phenomena is known as coagulation. To decrease the electrical charge of particles, the pH value of the media should be adjusted to near ZPC (zero point of charge). Another method to decrease the electrical charge is to add an electrolyte to media. This method is used widely in water refineries.

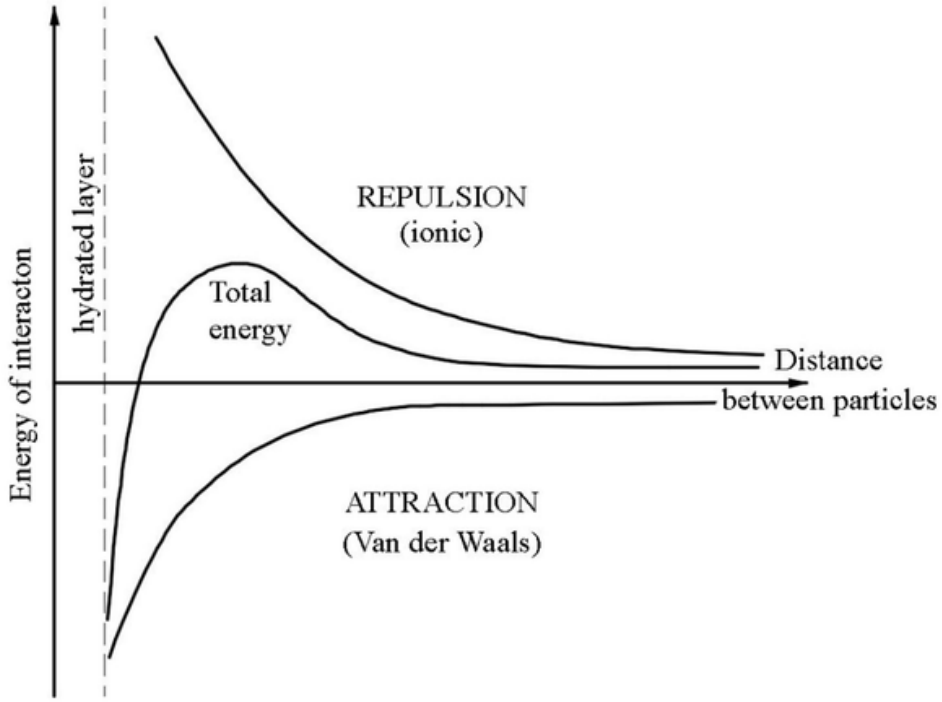

Figure 1: Impact of distance between particles on the energy of interaction

Flocculation

Flocculation is an effective method of decanting fine particles and clarifying water. In this method, the long chains of an adequate polymer join the fine particles by bridging between them and forming flocs that can settle in a short period of time, leaving clear water. This method is more effective than coagulation. This method is widely used as a sedimentation aid in thickeners.

Agglomeration

Another method of separation of fine particles from a liquid is agglomeration. That is the process of removing particles from liquid suspension by selective wetting and gathering with a second immiscible liquid.

This method is applied in cases such as:

- upgrading coking coals;
- separation of $CaSO_4$ precipitated from phosphoric acid;
- pelletization and sphere formation; and
- upgrading ores by liquid-liquid particle transfer,

But it is not also applicable (or feasible) as a sedimentation aid in tailings thickeners, because tailings are not valuable.

Increasing the input of solids content

Design and selection of a thickener is based on decantation tests, carried out in a laboratory. Unlike many other unit processes, the selection of a thickener does not need to include time consuming and expensive pilot tests. It can be done with high precision just by laboratory tests. One of the earlier methods is the one which was proposed by Coe and Clevenger in 1916. This method is a little time consuming but quite precise. Many other methods were subsequently suggested, most of them in an attempt to simplify the test, but with the same principles.

The method of Coe and Clevenger is based on preparing a series of pulp samples with different solids percentages and measuring the downward velocity of the mud line during sedimentation. Taking the linear part of the mud line height/time (velocity) of curves, the minimum flow is calculated.

When the material contains very fine particles, in a low solids percentage, the mud line can be performed, but the upper zone of the mud line is not clear, and in some cases can remain turbid for several days. Increasing the percentage of solids to a certain value named Critical Solids Concentration (CSC), causes the fine particles to be entrained by the media and precipitate with them. So, the upper zone becomes clear and the mud line becomes observable.

We can obtain some benefit from this phenomenon in thickeners. By installing a circulating load, from thickener underflow to its feed, the solids percentage of the thickener inlet can be increased to more than CSC, and in consequence, the overflow of the thickener will be clear. This method can be used when the thickener has sufficient capacity.

Experimental approach

Basic conditions

This study was carried out in a concentration plant of apatite by flotation method. For the decantation of 60 t/h of its tailings, it installed a lamella thickener (manufactured by Sala, Sweden) with a real surface area of 16 m^2 and a total settling area of 350 m^2.

The characterization of tailing is as follows:

- Feed to thickener: 60 t/h solid,
- Slurry: 126 m^3/h,
- Slurry density: 1,356 kg/m^3,
- Solid density: 4,000 kg/m^3,

Under normal conditions, the solids content of the overflow is 8 to 13% (on average, 9.85%). The particle size distribution of solid content of overflow is shown in Figure 2.

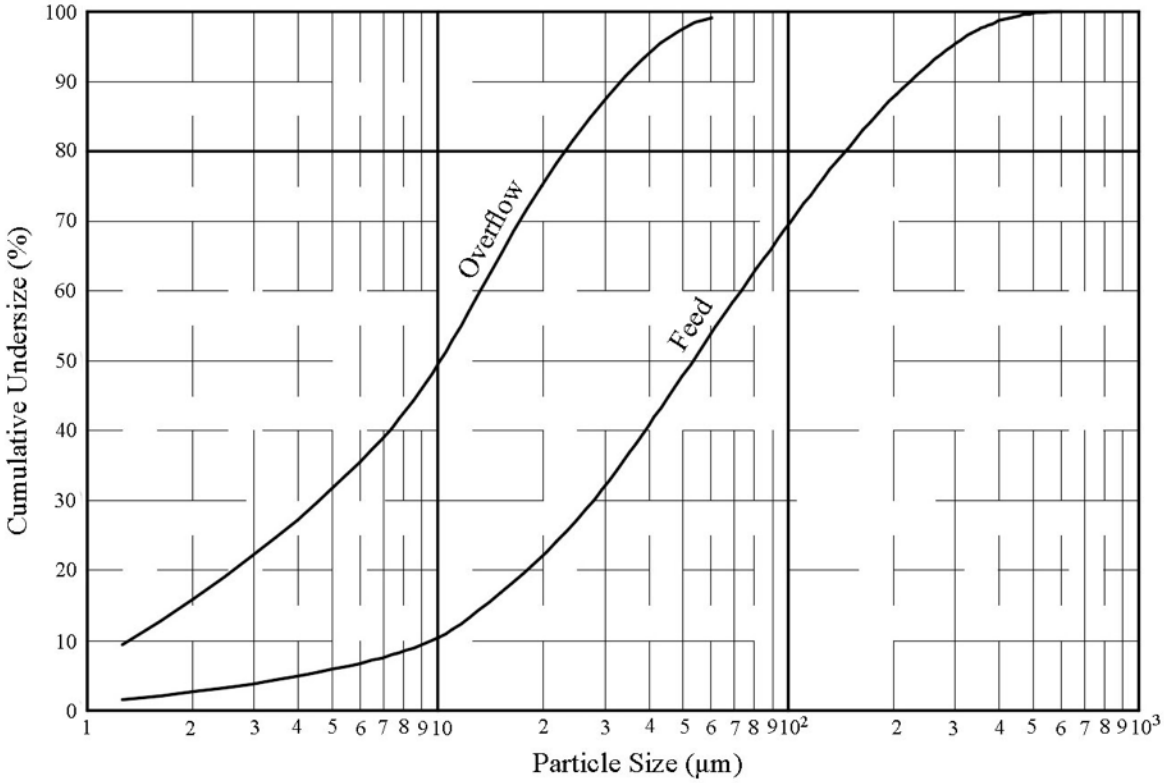

Figure 2: Particle size distribution of inlet and overflow of thickener

Flocculation test

A series of tests were carried out with different flocculants (anionic, cationic, non-ionic). The selected one was the cationic flocculant (C-567, Cytec).

The optimum quantity of flocculant is 20 g/m^3 of slurry (43 g/t of solids). Carrying out the decantation tests in this condition, the necessary area of thickener is 173 m^2. So, the present thickener with 350 m^2 area is quite adequate for this purpose.

Applying circulating load

In actual conditions, the solids percentage of apatite flotation tailing (feed to thickener) is 35% with a rate of 60 t/h. The solids percentage of underflow of thickener is 70%. The overflow is muddy and contains on average 9.85% of solid as fine particles.

On the basis of laboratory decantation tests, when the solids percentage of slurry is equal to or more than 45%, the decantation becomes visually perfect and the overflow is not muddy, but quite clear. The minimum flow obtained from decantation tests is 0.432 t/h.m^2.

A fraction of underflow is diverted to the thickener feed (circulating load), so that the solids content of the thickener inlet gets to about 45%. The calculation shows that a flow volume of underflow equal to 32.21 m^3/h (47.46 t/h dry solid, equivalent of 79.1% circulating load) should be directed to the inlet of thickener. The area necessary for this quantity of material is:

$$(47.46 + 60) : 0.432 = 250\ m^2$$

So, it seems that the existent 350 m^2 thickener is still adequate.

The above conditions are implemented in an existing plant. After about 24 hours, the modification of thickener operation is observed. During this period, the solid content of overflow gradually decreased and finally a clear water was obtained. The solids content of the overflow decreased to 700 ppm. It was recycled to the beginning of plant.

Conclusions

The results of this research project showed that in conditions where fine particles are not decanted in a thickener, if the area of thickener is sufficient, installing a circulating load to increase the solid concentration of thickener inlet to a certain level has the result that the fine particles can be decanted and clear overflow water can be obtained.

References

Coe, H. and G.H. Clevenger. 1916. Methods for determining the capacities of slime thickening tanks. *Trans. AIME,* 55: 365–384.

Bibliography

Hogg, R. 2000. Flocculation and dewatering. *International Journal of Mineral Processing,* 58: 223–236.

Hogg, R., T.W. Healy and D.W. Fuerstenau. 1966. Mutual coagulation of colloidal dispersions. *Trans. Faraday Society,* 62: 1638–1651.

Sirianni, A.F., C.E. Capes and I.E. Puddington. 1969. Recent experience with the spherical agglomeration process. *The Canadian Journal of Chemical Engineering,* 47: 167–170.

Proceedings of Tailings and Mine Waste 2019
November 17–20, 2019, Vancouver, Canada
Published by the University of British Columbia, 2019

The UNSATCON Model for Tailings Deposition

Shunchao Qi, Sichuan University, China
Paul Simms, Carleton University, Canada

Abstract

UNSATCON is a soft soil/tailings deposition model that couples large-strain consolidation with unsaturated flow in an elasto-plastic framework. Its formulation contains certain innovations that allow for accurate simulation of layered deposition techniques, such that it can be used as a tool to optimize deposition for liquefaction resistance and to manage risk of acid generation. The theoretical basis of the model has been published in Qi et al. (2017a; b; 2019). Developed with support from Canada's Oil Sands Innovation Alliance (COSIA), the model can also consider time-dependent effects such as creep and ageing, which are potentially relevant to certain high clay content tailings.

Here we show the application of the model to a field case at a thickened gold tailings mine, a field trial of flocculated oil sands fine tailings, and an evaluation of desiccation of tailings following a dam breach. The model simulates the relevant behaviours, and makes useful predictions of density and desaturation. The model appears suitable as a design aid to provide more confidence in the future performance of more complex deposition practices, such as thickened or filter cake tailings.

Introduction

Sub-aerially deposited tailings, whether by the intent of those running deposition operations or not, may experience desiccation before burial by fresh tailings. This desiccation may impart positive and negative consequences to the geotechnical and geoenvironmental performance of the tailings. Desiccation, in addition to providing additional volume reduction, is known to impart positive stress history effects. Tailings that are contractive may be rendered dilative under monotonic loading, even after the tailings are buried and subsequently re-saturated (Al-Tarhouni et al., 2011; Daliri et al., 2014; 2016; Simms, 2017). However, if desiccation results in surface tailings becoming desaturated, and exposed to the atmosphere for prolonged time periods (weeks to months), these tailings may oxidize and acid generation may occur, depending on mineral composition. The consideration of desiccation stress history is likely important to consider in forensic analysis of tailings impoundments failures, especially if the tailings have sat above the post-failure water table for some time before the investigation.

While previous models such as CONDES and MINTACO have been used by practitioners to simulate some aspects of desiccation, the UNSATCON model is an advance in terms of its ability to simulate actual desaturation and to simulate desiccation stress history effects. Additional complexity has its disadvantages, but it is the goal of this paper to show that the model can be applied to field problems without the burden of difficult parameter measurements or estimation.

Basic formulation of the model

To simulate multilayer deposition, any model needs to simulate the processes that occur, which include i) initial self-weight consolidation of the layer; ii) any subsequent drying once the evaporation rate exceeds the flux of consolidation produced water to the surface, which may induce desaturation at the surface concurrent with self-weight consolidation in the lower part of thick layers or deposits; iii) once a new layer is added, the immediate increase in total stress due to its weight; and iv) the interchange of water between the layers, which will re-saturate the bottom layer at the same time as accelerating consolidation in the new layer. These processes are shown in Figure 1.

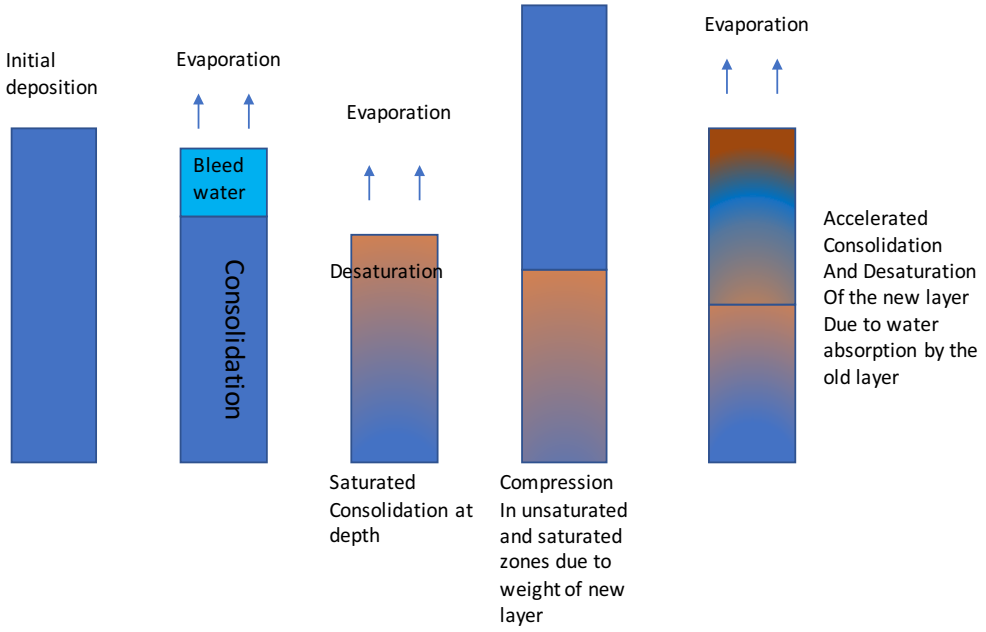

Figure 1: Conceptual model of dewatering processes in multilayer deposition

The full formation of this 1D model is described in three papers, (Qi et al., 2017 a and b; Qi et al., 2019), and is only briefly described here. The large consolidation part of the model is an extension of the piecewise linear formulation of Fox and Berles (1997), used in their model CS2. This approach gives identical results to more conventional large-strain consolidation formulations based on Gibson's equation

(Fox and Berles, 1997; Qi et al., 2017a). It has been recently shown that both formulations are theoretically equivalent, as Gibson's equation can be derived from the two basic continuity and stress equations used in CS2 and UNSATCON (Qi et al., 2019).

In UNSATCON the piecewise linear formulation is extended to unsaturated conditions, and a number of elasto-plastic constitutive models for unsaturated soils are implemented. These include a modified state surface model (MSSM), the Glasgow Coupled Model (GCM), and the Basic Barcelona model (BBM). All the simulations presented in this paper are performed using the MSSM.

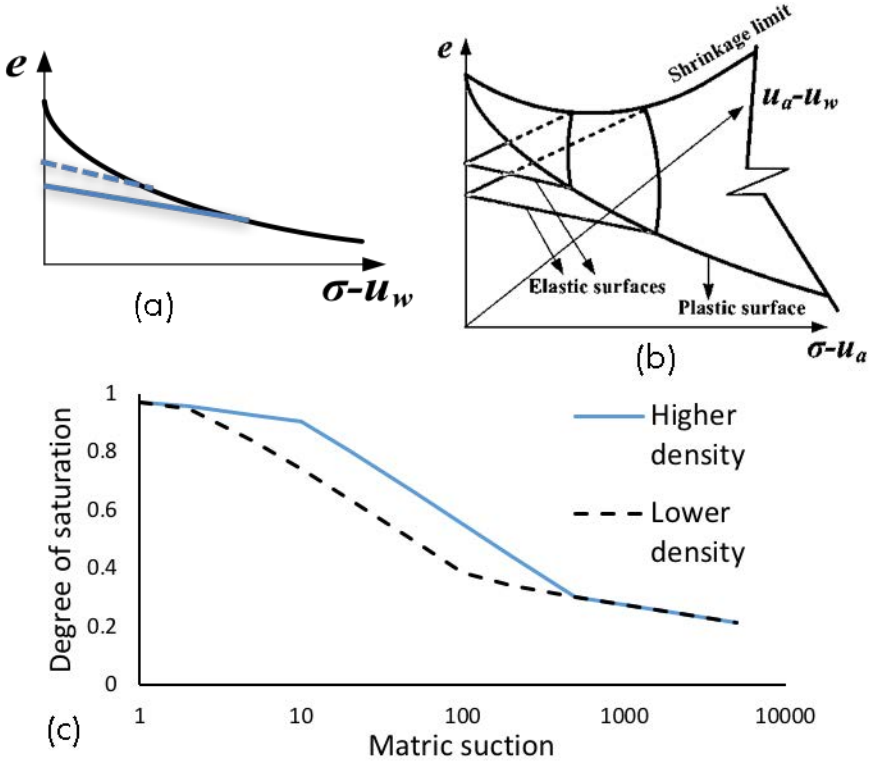

Figure 2: (a) Compressibility curve for saturated conditions with unload-reload line; (b) 3D constitutive surface to include unsaturated conditions; (c) Void ratio dependent water retention curve

The differences between UNSATCON and a conventional large-strain consolidation model can be explained using Figure 2. In saturated conditions, a compressibility function is required to relate vertical effective stress to density, or void ratio (e). To simulate irrecoverable volume change, the unload-reload line is also required. The position of the unload-reload line changes with the last past maximum stress. In unsaturated conditions, the compressibility function becomes a surface, also dependent on matric suction, while the unload-reload line becomes a plane. To simulate desaturation, a water retention curve is required. This water retention curve has a dependency on void ratio, as the air entry value increases as volume change decreases. To simulate elasto-plastic behaviour, the base variables, gravimetric water

content, and void ratio, are determined at every point by tracking its position on the 3D void ratio surface and the void ratio-dependent water retention curve. In addition, the permeability function (k-e) also becomes dependent on degree of saturation.

Despite the apparently more complex constitutive relationships, the only additional material property required, besides the standard compressibility and permeability functions, is the water retention curve. These properties are sufficient to define the 3D surface for void ratio as well as the void ratio dependent water retention curve. The authors have developed a spreadsheet for rapidly determining the constitutive surfaces from the compressibility curve and the water retention curve.

Example model output

Figure 3 (on the next page) presents model outputs for a simulation of two layer deposition of a clayey tailings over two years in a mildly arid climate. Each layer of 1.2 m thickness is deposited in the fall (October), and no evaporation is assumed to occur until early summer. Evaporation is zero until June, after which a uniform evaporation rate of 2 mm/day is imposed from June until the end of September. These tailings initially consolidate due to self-weight until the yellow line in the void ratio chart in Figure 3(a). Thereafter, evaporation is turned on, driving more consolidation and developing an evaporation front, which can be seen to progress through the degree of saturation plot. Eventually, the shrinkage limit is achieved near the surface, though not quite at depth.

Figure 2(b) shows the short-term interactions due to compression of the older tailings and water interchange after the placement of the new layer. The degree of compression of the older tailings is variable due to the different stress history with depth, the higher older tailings are less compressible due to the larger degree of desiccation experienced during drying of the first layer. The subsequent hydraulic interaction redistributes water both by accelerating the consolidation of the new layer, and by redistributing water in the old layer due to dissipation of suctions in the top part of the old layer. Over the course of the following year, a drying front eventually develops, even slightly progressing into the original layer of tailings, as seen in Figure 3(c).

Application to field cases

Two cases are presented where field data is available for comparison: a single layer deposit of 4 m of polymer amended FFT (oil sands fluid fine tailings), and multilayer deposition at a gold mine in Northern Ontario (Musselwhite Mine). These cases are also presented in Qi et al. (2017a) and Qi et al. (2017c), though some additional analyses are shown in this paper. An additional hypothetical case is presented: a hard rock tailings impoundment that loses its water cover and therefore undergoes evaporation.

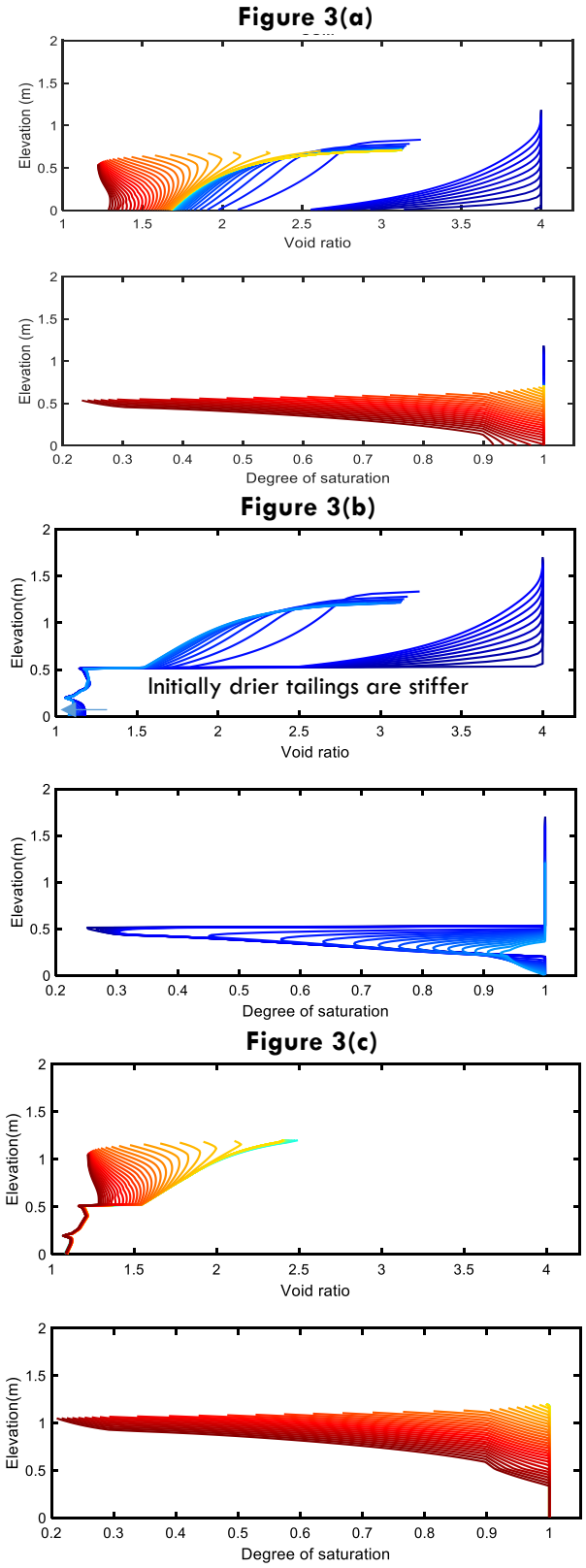

Figure 3: Example of UNSATCON outputs simulating deposition of two layers: a) Initial self-weight consolidation to yellow line; thereafter, drying once evaporation rate exceeds bleed water generation; b) initial compression and short-term interactions after placement of new layer; and (c) eventual second drying phase

In both field cases the saturated consolidation properties were determined using laboratory column tests, while the unsaturated properties were determined from a water-retention curve test with void ratio measurement for the unsaturated properties. An example of the column test used is shown in Figure 4.

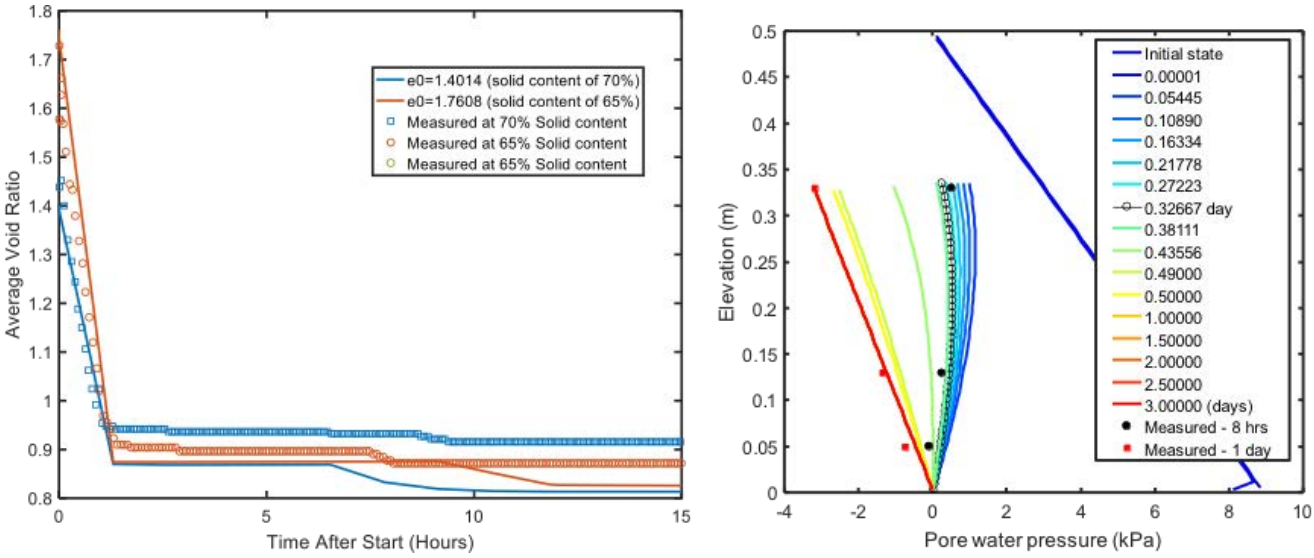

Figure 4: Example data from a 0.5 m tall, 0.15 m diameter column test used to calibrate large-strain consolidation properties

Case 1: Field trial 4 m deposit of polymer-amended oil sands tailings

This case is an initially ~4 m deposit of in-line flocculated oil sands tailings, part of the atmospheric fines drying field trials conducted by Shell, now CNRL (Dunmola et al., 2013). The deposit is a good test for UNSATCON as consolidation under saturated conditions continues to occur at depth during this year of data. The initial condition at October 15 is a void ratio of 2.6, which corresponds to the post-sedimentation void ratio, and also the average solids content of the tailing 48 hours after deposition. An evaporation rate of 2 mm/day is applied on May 1 and thereafter. Calibration of the parameters was done using a laboratory column experiment, similar to that described in Figure 4. Further details are presented in Qi et al. (2017b).

Figure 5 shows the model output compared to field data. Aside from the points near the bottom, the predicted profiles of solids content agree well with the measurements.

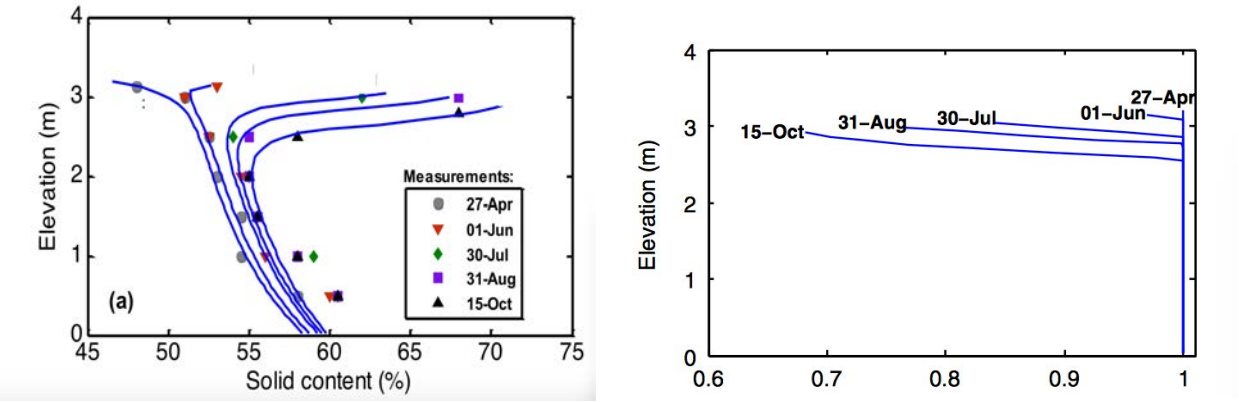

Figure 5: Model predictions for soilds content (left) and degree of saturation (right) in an oil sands talings dewatering test case

Case 2: Multilayer deposition at a mine in Northern Canada

This case is a small thickened tailings (Musselwhite Mine) site in Northern Canada, where deposition is cycled from different points in a U-shaped embankment. The rate of cycling is such that the whole circuit of the impoundment is completed in a year. The mine owners wanted to know if changing the rate of cycling would affect either geotechnical or geoenvironental performance. The measured rate of rise appears to be somewhere between 2 and 3 m a year, and the solids content at deposition 65 to 68%. However, water contents measured in the field indicate that the tailings rapidly lose water after deposition. Subsequently, the upper layers lose some additional water during the summer, but much less during the winter (Figure 6).

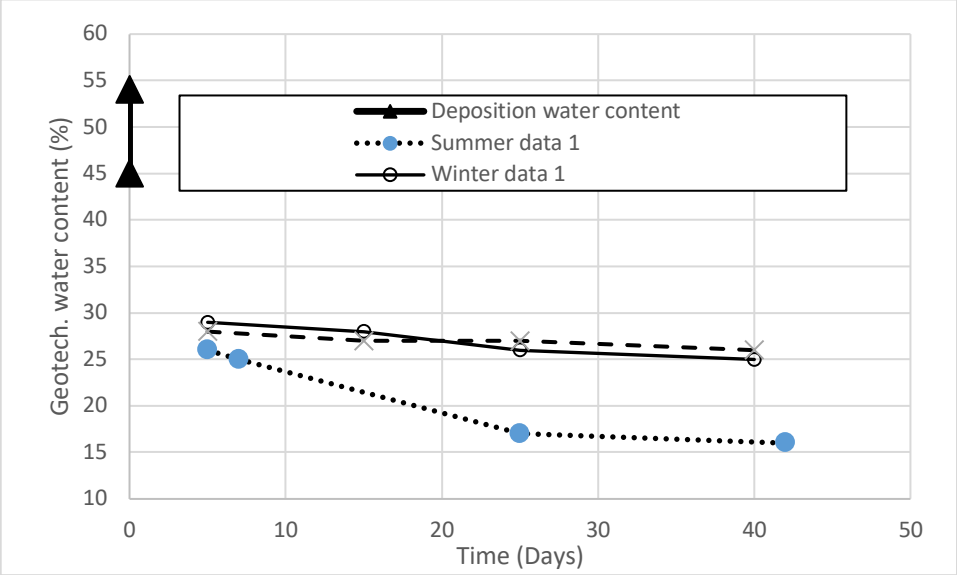

Figure 6: Measured variation in water content for case 2 in the last deposited layer (Kam et al., 2011)

The model was employed to simulate the evolution of the deposit over three years for different rates of rise. During summer (June to September 15), an average evaporation rate of 1.5 mm/day was applied based on site-specific potential evaporation data. Figure 7 shows the final state of the deposit for rates of rise: 2, 2.5, and 3 m per year, each layer deposited either at the beginning of winter or summer. The void ratio profile is relatively insensitive to the variation in the rates of rise; however, the degree of saturation is indeed sensitive to the rate of rise, which would potentially affect the risk of acid generation (though this is not an issue at Musselwhite). Figure 8 shows the predicted void ratio in the top layer for summer and winter – the same trends as the measurements presented in Figure 6. Figure 8 also explains why there is little difference between the summer and winter profiles and why the density predictions are relatively insensitive to variation in rate of rise – the initial consolidation in a fresh layer happens very quickly, and makes up most of the volume change. More details on this case are presented in Qi et al., 2017c.

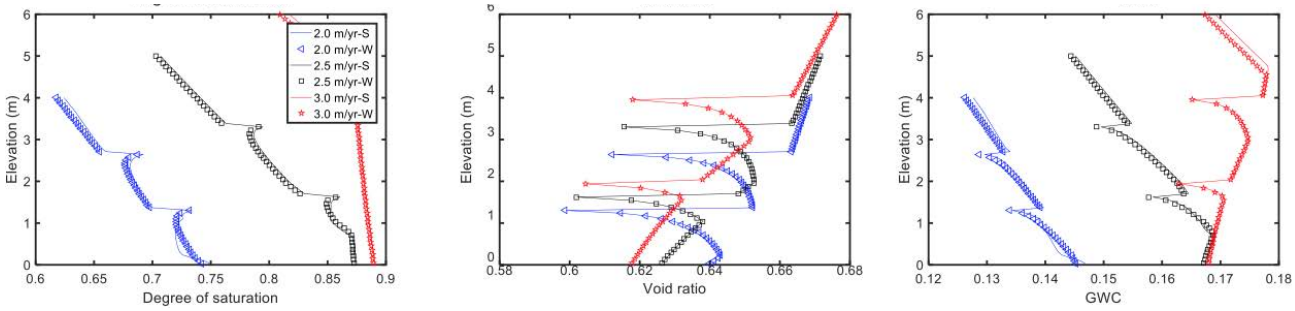

Figure 7: Final predicted profiles after 3 years of deposition for different rates of rise and timings of deposition

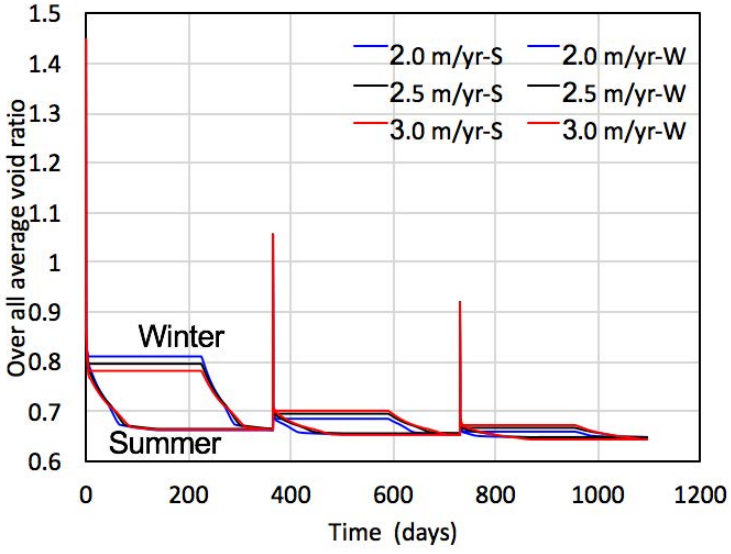

Figure 8: Overall void ratio predicted by the model over 3 years for different rates of rise

Case 3: Decantation and drying of a 10 m thick deposit of previously submerged tailings

This case is a hypothetical analysis of an initially 15 m thick deposit, deposited at 65% solids, which would consolidate to 10 m, with the void ratio profile shown in Figure 9. We then imagine that a dam breach occurs, the tailings become exposed, and the water table drops. In the simulation, the water is decanted and evaporation proceeds at 2 mm/day for 150 days, or 5 months. A substantial part of the deposit (the top 3 m) becomes unsaturated and develops substantial suctions, with corresponding strength and stiffness, even if subsequently re-saturated. This case may inform alternate ways to take advantage of desiccation to improve strength in tailings impoundments. It may also speak to forensic analysis of tailings dam failures.

Following most dam breaches, substantial volumes of tailings remain in the impoundment, but they are no longer submerged, and the water table may be at a quite a depth relative to the surface of the tailings. Depending on their properties, the climate, and the time before any field investigation (for example, CPT) was conducted, desiccation may have substantially changed the mechanical response of the tailings. Desiccation is known to substantially alter the mechanical properties of some tailings (Daliri et al., 2016; 2014).

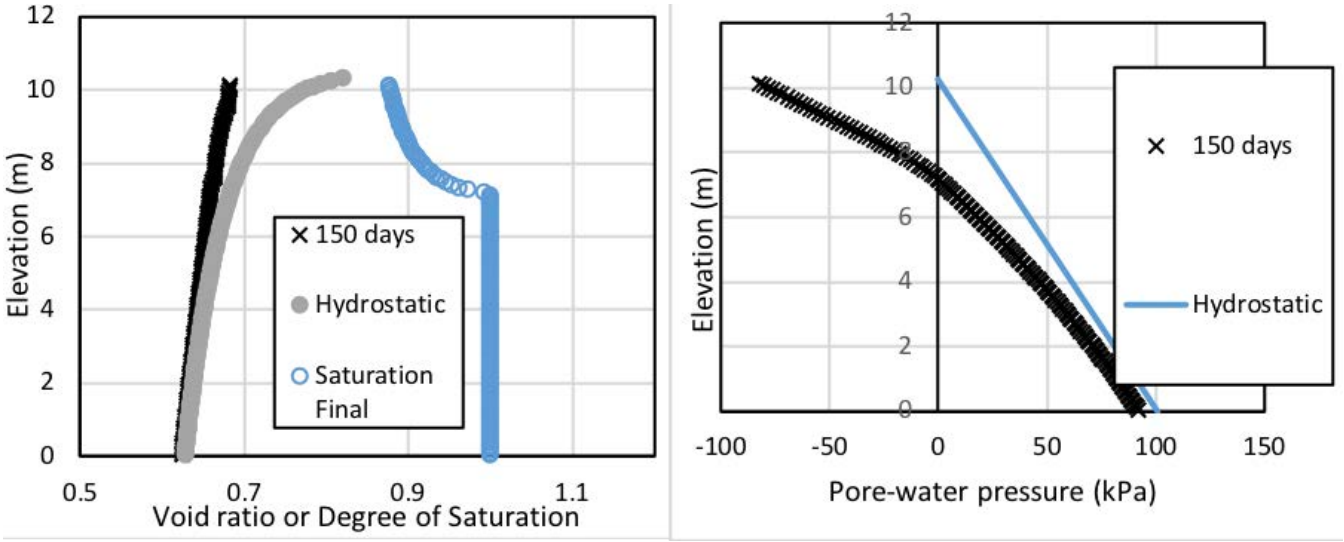

Figure 9: Void ratio, degree of saturation (left), and pore-water pressure (right) in a deposit of initially 15 m deposit of thickened gold tailings, left to consolidate, and then decanted and exposed to evaporation for 150 days

Conclusion

The formulation of the UNSATCON model is briefly reviewed. Its application is demonstrated in two field cases, one a thickened tailings gold mine, the other a field trial on oil sands tailings. A third case is presented, a hypothetical analysis of desiccation of previously sub-aqueously deposited tailings. The model is capable of reproducing real field data with minimal data requirements. As with all similar models, it is best used as an aid to deposition design, either in the exploratory phase, or when extrapolating pilot results or early field results to assist optimization of full-scale performance.

References

Al-Tarhouni, M., P. Simms and Sivathayalan, S. 2011. Cyclic behaviour of reconstituted and desiccated-rewet samples of thickened gold tailings in simple shear. *Canadian Geotechnical Journal* 48(7): 1044–1060.

Daliri, F., H. Kim, P. Simms and S. Sivathayalan. 2014. Impact of desiccation on monotonic and cyclic shear strength of thickened gold tailings. *ASCE J. Geotech. Geoenviron. Eng*. 140(9), 04014048.

Daliri, F., P. Simms and S. Sivathayalan. 2016. Shear and dewatering behaviour of high density gold tailings in a laboratory simulation of multi-layer deposition. *Canadian Geotechnical Journal* 53(8): 1246–1257.

Dunmola, A., C. Cote, G. Freeman, D. Kolstad, J. Song and S. Masala. 2013. Dewatering and shear strength performance of in-line flocculated mature fine tailings under different depositional schemes. In *Proceedings of Tailings and Mine Waste 2013,* University of Alberta Geotechnical Group, Edmonton, Canada.

Fox, P.J. and J.D. Berles. 1997. CS2: A piecewise-linear model for large strain consolidation. *Int. J. Numer. Anal. Methods Geomech*. 21(7): 453–475.

Kam, S., J. Girard, N. Hmidi, Y. Mao and S. Longo. 2011. Thickened tailings disposal at Musselwhite Mine. In *Proceedings of the 14th International Conference on Paste and Thickened Tailings*, April 1–7, Perth, Australia.

Simms, P. 2017. Colloquium paper of the Canadian Geotechnical Society: Geotechnical and geoenvironmental behaviour of high density tailings. *Canadian Geotechnical Journal* 54(4): 455–468, 10.1139/cgj-2015-0533

Qi, S., P. Simms, F. Daliri and S. Vanapalli. 2019. Coupling elasto-plastic behaviour of unsaturated soils to large strain consolidation. *Geotechnique*, published ahead of print, June 2019.

Qi, S., P. Simms and S. Vanapalli. 2017a. Piecewise-linear formulation of coupled large strain consolidation and unsaturated flow. I: Model development and implementation. *ASCE Journal of Geotechical and Geoenvironmental Engineering*. Published on the web March 2017. DOI: http://dx.doi.org/10.1061/(ASCE)GT.1943-5606.0001657

Qi, S., P. Simms, S.Vanapalli and S. Soleimani. 2017b. Piecewise-linear formulation of coupled large strain consolidation and unsaturated flow. II Model calibration and testing. *ASCE Journal of Geotechnical and Geoenvironmental Engineering.* Retrieved from http://dx.doi.org/10.1061/(ASCE)GT.1943-5606.0001658

Qi, S., P. Simms, W. Thomas and N. Hmidi. 2017c. Hydro-geotechnical analysis of a thickened tailings deposit in Northern Canada via UNSATCON. In *Proceedings of Tailings and Mine Waste*, Banff, Alberta, University of Alberta Geotechnical Group, Edmonton, Alberta, Canada.

Proceedings of Tailings and Mine Waste 2019
November 17–20, 2019, Vancouver, Canada
Published by the University of British Columbia, 2019

Cyclic and Post-Cyclic Response of Tailings under Direct Simple Shear Loading

Miguel Regalado, Anddes, Peru
Rolando Rojas, Anddes, Peru
Renzo Ayala, Anddes, Peru
Denys Parra, Anddes and National University of Engineering, Peru

Abstract

Due to declining grades of precious ore in the mining industry, mining operations had to grow larger in order to have a profitable production rate; therefore, their mine waste management infrastructure had to grow larger as well. This is of course the case with tailings storage facilities. Seismic analyses of these facilities located at highly active seismic zones need to be based on a comprehensive understanding of the cyclic and post-cyclic response of the tailings over a range of consolidation stresses and seismic demands, among other conditions. For this reason, it is necessary to conduct a wide range of laboratory tests that allow a proper characterization of the materials involved in tailings storage facilities, especially on those whose behaviour has not been largely reviewed, like tailings.

The current paper presents the results of different cyclic and post-cyclic direct simple shear tests performed on tailings storage facilities at Peruvian mining operations. To improve the dynamic characterization of these materials, the tests included the cyclic response over a range of stresses and relative density conditions. The paper also addresses the sensitivity of these conditions on the liquefaction potential considering cyclic loadings and a remoulding process in one case. Furthermore, the post cyclic undrained shear behaviour is analyzed and discussed, providing the undrained residual shear strength at different strain levels, which were compared to a processed seismic cone penetration test with pore pressure measurement (SCPTu) field data, and other literature sources.

Given the usual loose and saturated conditions of deposited tailings in the field and the active seismic conditions of the sites where these are placed, they are prone to be subjected to large pore pressure generation and shear strains. Their variation of fine-grained fraction may affect tailings behaviour, making it different from that expected in a typical sand; therefore, its compressibility could modify the potential for liquefaction, triggering a range of different stresses and density conditions. The improvement of knowledge

about tailings' responses will lead to better understanding of its behaviour, which in turn will lead to less uncertainty about the seismic design of tailings storage facilities.

Introduction

The current paper presents the result of 15 tests conducted to characterize the cyclic and post-cyclic response, plus 1 additional test on the cyclic behaviour, of 4 types of saturated tailings related to 3 mining projects located in Peru. All the testing was performed using a bidirectional cyclic simple shear at University of California, Berkeley; nevertheless, despite its capability of taking into account both directions, the loads were applied along one axis. The main goal of the tests was to determine the loading conditions to reach the liquefaction failure under undrained conditions, and to obtain the subsequent monotonic shear response avoiding reconsolidation, therefore the monotonic shear stress was applied immediately after the liquefaction state, given by a 5% shear strain in either direction.

Testing program

This section describes the materials, equipment, and preparation procedures used for the testing program.

Materials

The overflow tailings (a mix of coarse and fine tailings) of Site 1 are classified as non-plastic silty sand (SM), the underflow tailings of Site 2 are classified as non-plastic silty sand (SM), the underflow tailings of Site 3 are classified as non-plastic silty sand (SM), and the overflow tailings are classified as low plasticity silt (ML). The particle size distribution curves (PSDC) of all materials tested appear in Figure 1.

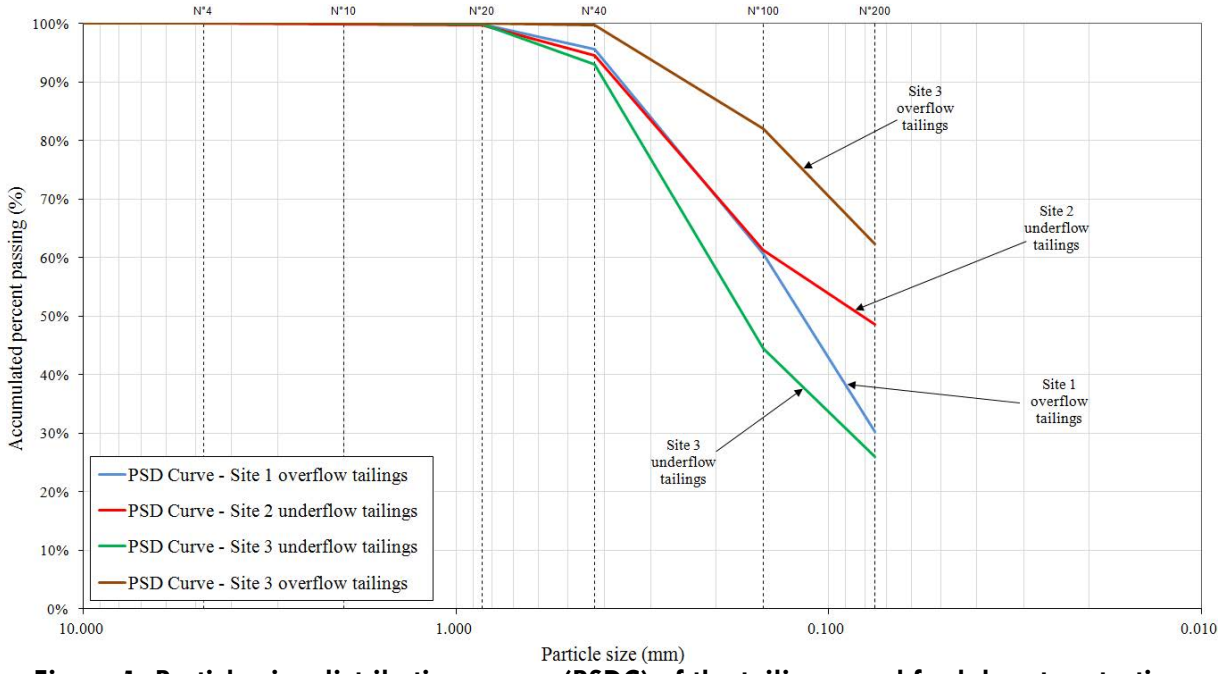

Figure 1: Particle size distribution curves (PSDC) of the tailings used for laboratory testing

Table 1 summarizes the results of the physical properties of all tailings specimens tested on the cyclic direct simple shear device; these results are separated by sites and their corresponding disposal location.

Table 1: Physical properties of tailings tested on the cyclic simple shear device

Material	G_s[1] –	D_{30}[2] (mm)	D_{50}[3] (mm)	D_{60}[4] (mm)	Fines (%)	WC[5] (%)	WC[6] (%)	γ_d[7] (kN/m³)	e[8] –	USCS[9] –
Site 1 overflow tailings	3.49	ND[10]	0.12	0.15	30.3	5.6	17.0	19.13	0.789	SM
Site 2 underflow tailings	2.63	ND[10]	0.08	0.14	48.6	11.0	11.0	15.18	0.700	SM
Site 3 underflow tailings	2.88	0.09	0.18	0.21	26.0	16.8	15.0	14.95	0.890	SM
Site 3 overflow tailings	2.79	ND[10]	ND[10]	NF[10]	62.3	10.0	25.0	15.98	0.713	ML

Notes: 1) Specific gravity. 2) Diameter corresponding to 30% finer. 3) Diameter corresponding to 50% finer. 4) Diameter corresponding to 60% finer. 5) Water content from the field tests. 6) Water content used for laboratory tests due to remolding issues. 7) Dry unit weight of field. 8) Void ratio before consolidation state. 9) Unified Soil Classification System (USCS) Symbol for Soil Type. 10) Not determined.

Equipment

The cyclic simple shear tests were performed with the University of California's Berkeley bidirectional device, developed initially by Boulanger et al. (1991). The membranes reinforced with wires for the simple shear tests were 10.1 cm in diameter and 2.4 cm in height. This device allows the user to simulate an undrained behaviour showing the consolidation of the specimen, by means of the application of a chamber and back pressure, and applying the subsequent normal and shear loads or displacements via the pneumatic pistons. This normal load is applied by a rigid system in order to minimize the rocking and the continuous non-uniformities in the stress conditions on the specimen. Moreover, the specimen is equipped with three large displacement transducers on the perimeter of the sample to quantify the variations in height and rotations that occur. Figure 2 shows the cyclic direct simple shear device, in which all tailings specimens were tested.

Figure 2: Bidirectional cyclic simple shear device (Kammerer et al., 2004)

Preparation procedures

Sites 1, 2, and the underflow and overflow tailings of Site 3 were reconstituted from bulk samples, by combining the tailings with deaired water to reach the target water content (17, 11, 15 and 25% for Sites 1, 2, and the underflow and overflow Site 3 tailings, respectively). The selected value permitted the generation of capillary tension that bulked up the material and prevented segregation of the fines from the coarser fraction. An adjustable height system enabled the tamping of the specimen to reach the correct moist mass of soil for each of the layers in which the specimen was divided in height. As part of the procedure, the wire-reinforced membrane was sealed to the base cap, and a split-mold was used in order to reach the target density. Because of some variations of volume generated by the device and specimen placement procedures, the actual density resulted in values lower than the designated (below 1.95, 1.5 and 1.7 g/cm^3 for Sites 1, 2 and 3, respectively). This last fact led to inherent and unavoidable variability in the density before the subsequent consolidation. After the specimens reached equilibrium under a lower level of vacuum confinement, the specimen was saturated by means of the vacuum and back pressures under a constant effective stress. After that, the specimens were ready to be tested. As expected, changes in dimensions were observed, due to the disappearance of capillary forces between the grains and the consequent rearrangement of particles.

Additional overflow tailings specimens of Site 3 (CSS-P3-1, CSS-P3-2, CSS-P3-P3 and CSS-P3-P4) were prepared, mixing the fines tailings with water to a consistency similar to the one of a thick slurry, and poured into the split mold. Then, a disk of a filter and a porous stone were placed on the surface to use the consolidation apparatus up to about a 25 kPa consolidation stress, in order to not deform the wire-reinforced membrane and specimens. Two layers more of the material were placed atop the specimen within the mold to reach the full height of the specimen. The initial height and volume were also obtained after equilibrium under a low level of internal vacuum, then the specimens were subjected to vacuum and back pressure for saturation under constant effective stress, before testing. The variations mentioned due to releases of capillary tension were also observed.

Results and discussion

As mentioned above, the vertical consolidation effective stresses were achieved by means of a combination of shear loading, and chamber and back pressures, so that the lateral effective stress would remain controlled by the K_0 value with respect to the vertical stress within the wire-reinforced membrane. The stresses applied to the specimen were controlled, basically by the amplitude of the cyclic stress ratio to which the specimens were subjected in the form of a sinusoidal loading. While the cyclic loading was applied, the conditions were undrained (the drainage valve on the saturated specimen remained closed), and height variations were not permitted (the vertical loading system remained locked).

Because of the imposed undrained condition during cyclic loading, there is a reduction in effective stress and the generation of pore pressures. Figures 3a and 3b show the time history of vertical effective stress, and the hysteresis loop for one of the Site 1 tests. For Site 1, the cyclic loading was applied at a frequency of 1Hz, while data on applied stress, deformations and pore pressures were recorded at 100 Hz, resulting in 100 sample points per cycle of loading.

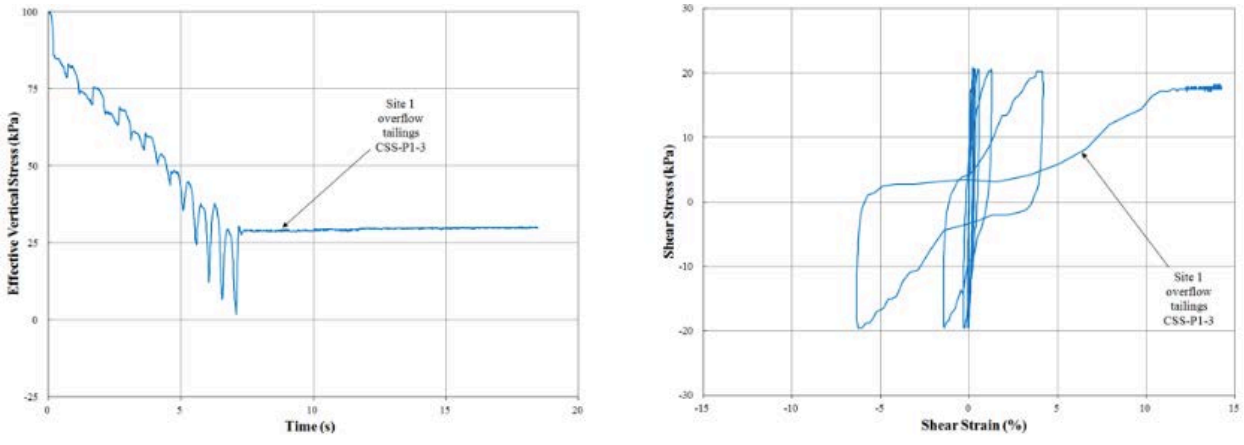

(a) (b)

Figure 3: (3a) Time history of vertical effective stress and (3b) resulting hysteresis loop stress-strain for CSS-P1-3 testing

The criterion to determine the number of cycles to failure (N) was defined as the N to reach 5% shear strain in either direction. Figure 4 shows the results for all the tests performed, and the tendency lines for the cyclic stress ratio versus the number of cycles. Also, this figure presents the fitting curves for cyclic stress ratios as a function of the number of cycles. Also, the figure shows the difference in the number of cycles for Site 3 at a consolidation stress at 100 kPa and the same cyclic stress ratio (0.145) for both slurry depositing (fewer number of cycles) and moist tamping preparation methods. It also should be highlighted that static shear stress during consolidation was not applied to the specimens, so that the effects of liquefaction triggered generated by this factor were not taken into account.

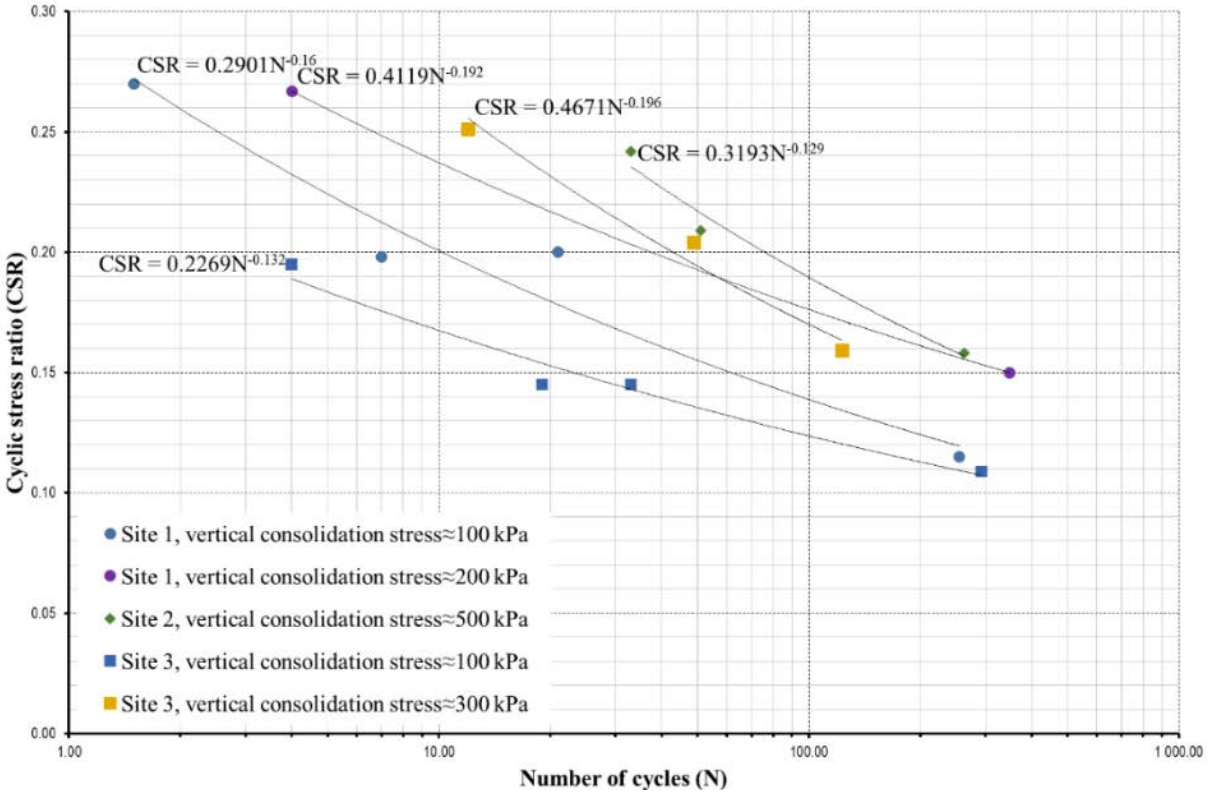

Figure 4: CSR versus N curves of tailings from all sites

On the other hand, Figure 5 shows the variation of dry density (γ_d) versus relative density (D_r) for all types of tailings tested. The dry density range of overflow tailings from Site 1 is larger than the dry density range from other tailings, as expected due to the larger specific gravity (see Table 1) and considering that the density range for overflow tailings from Site 3 is not found. Moreover, the underflow tailings from both Sites 2 and 3 are in substantial agreement with their dry density ranges.

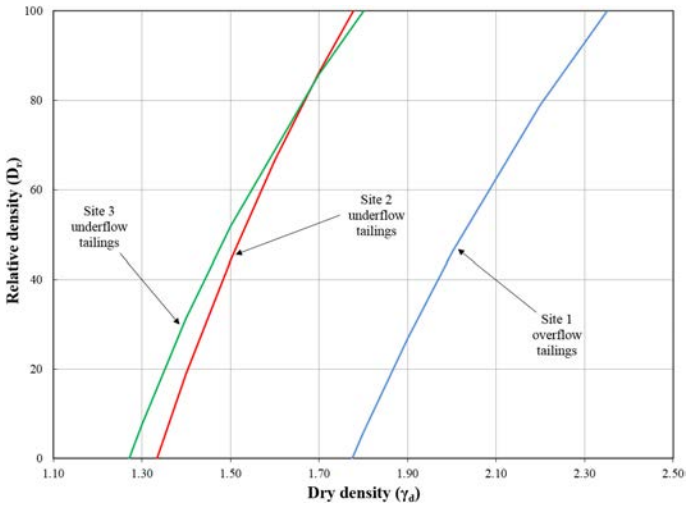

Figure 5: Dry density (γ_d) versus relative density (D_r) relationships of tailings from all sites

Table 2 summarizes the results for the cyclic response of the tailings specimens, showing the cyclic stress ratios used and their associated number of cycles to reach failure.

Table 2: Results from the cyclic direct simple shear tests

Site	Code	Vertical consolidation stress (kPa)	Dry density after consolidation (g/cm³)		Cyclic stress ratio (CSR)
1	CSS-P1-1	97	2.03	51	0.200
	CSS-P1-2	99	1.96	39	0.270
	CSS-P1-3	100	1.97	40	0.198
	CSS-P1-4	100	1.97	40	0.115
	CSS-P1-5	200	2.02	50	0.267
	CSS-P1-6	200	2.02	50	0.150
2	CSS-P2-1	489	1.51	47	0.242
	CSS-P2-2	503	1.51	47	0.209
	CSS-P2-3	489	1.48	40	0.242
3	CSS-P3-1	100	1.76	ND[1]	0.145
	CSS-P3-2	101	1.79	ND[1]	0.145
	CSS-P3-3	106	1.74	ND[1]	0.195
	CSS-P3-4	99	1.78	ND[1]	0.109
	CSS-P3-5	296	1.73	90	0.159
	CSS-P3-6	295	1.73	90	0.251
	CSS-P3-7	298	1.70	86	0.204

Note: 1) Not determined.

After a few cycles reaching failure, the specimen was returned to its original position under an original horizontal shear stress equal to zero. Once the strain level in the monotonic test exceeds that experienced

during cyclic loading, it is common for the excess pore pressures to dissipate somewhat, which leads to greater effective confining stresses and thus greater shear resistance. It should be remembered, however, that these element tests may not reflect the same degree of void ratio redistribution, and that other macro effects could alter the local shear resistance after liquefaction of a field deposit.

The results of the post-cyclic response of all the tailings specimens are better understood when considering their plots in conjunction with the cyclic hysteresis loops of the preceding tests; therefore, one post-cyclic response for tailings sample CSS-P3-1 and CSS-P3-4 is shown in Figures 6a and 6b, respectively.

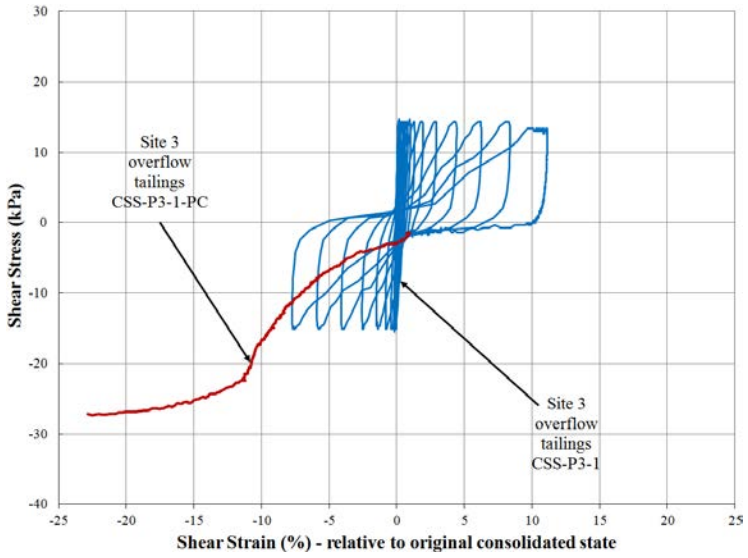

Figure 6a: Comparison of post-cyclic response with hysteresis loop cycle for (a) CSS-P3-1 and (b) CSS-P3-5 tests

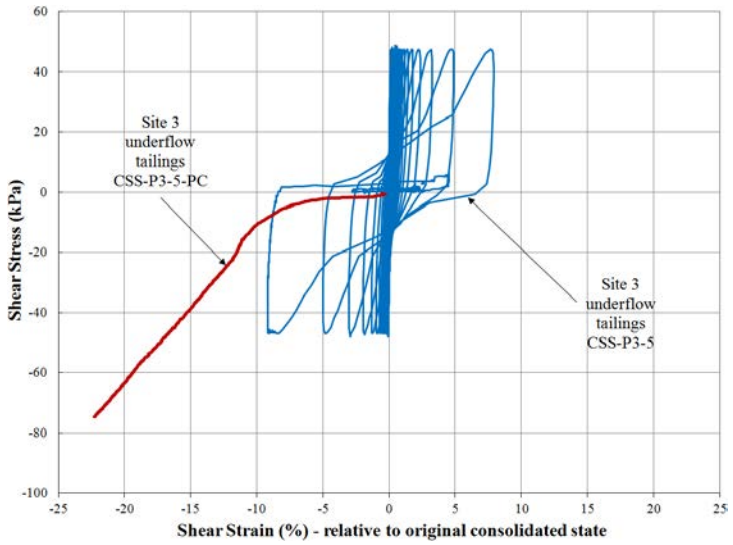

Figure 6b: Comparison of post-cyclic response with hysteresis loop cycle for (a) CSS-P3-1 and (b) CSS-P3-5 tests

Table 3 summarizes the results for the diverse specimens tested and their related shear strength at different strains of 5, 10, and 15%, respectively.

Table 3: Results from the monotonic post-cyclic direct simple shear tests

Site	Code	Vertical consolidation stress (kPa)	Cyclic stress ratio (CSR)	S_{ur}/σ'_n at 5% of shear strain	S_{ur}/σ'_n at 10% of shear strain	S_{ur}/σ'_n at 15% of shear strain	Maximum S_{ur}/σ'_n	Strain at maximum S_{ur}/σ'_n (%)
1	CSS-P1-2-PC	99	0.270	0.016	0.021	0.035	0.062	23.78
	CSS-P1-3-PC	100	0.198	0.034	0.068	0.114	0.177	21.68
	CSS-P1-4-PC	100	0.115	0.011	0.038	0.086	0.171	21.79
	CSS-P1-5-PC	200	0.15	0.247	0.291	0.295	0.296	24.31
	CSS-P1-6-PC	200	0.267	0.113	0.211	0.270	0.32	19.81
2	CSS-P2-1-PC	489	0.158	0.063	0.13	0.19	0.231	20.25
	CSS-P2-2-PC	503	0.209	0.108	0.22	0.306	0.408	20.88
	CSS-P2-3-PC	489	0.242	0.137	0.272	(note 1)	0.271	14.3
3	CSS-P3-1-PC	100	0.145	0.067	0.167	0.252	0.273	22.31
	CSS-P3-2-PC	101	0.145	0.067	0.166	0.25	0.271	26.24
	CSS-P3-3-PC	106	0.195	0.067	0.166	0.249	0.286	23.3
	CSS-P3-4-PC	99	0.109	0.079	0.194	(note 1)	0.259	13.08
	CSS-P3-5-PC	296	0.159	0.008	0.036	0.129	0.25	22.35
	CSS-P3-6-PC	295	0.251	0.011	0.102	0.245	0.352	22.19
	CSS-P3-7-PC	298	0.204	0.078	0.164	0.228	0.295	19.85

Note: 1) The undrained shear strength was not determined at this strain, because the test finished in a strain lower than 15%.

Considering the results of Table 3, it can be seen that regardless of the sample preparation method, the CSS-P3-1-PC and CSS-P3-2-PC reached almost the same resistances at the considered strains.

Comparison with other sources

Research has been conducted to set relationships between the residual shear strength and SPT blow count or CPT tip resistance, calculated at effective stresses prior to the earthquake. The Idriss and Boulanger (2008) and Robertson (2010) methods were used to determine ranges for the values of residual shear strength after liquefaction. These values were compared with the ones obtained by means of the direct simple shear apparatus. In Figures 7 to 9, the results indicate that the values obtained from the laboratory testing program at strain rates of 10% and 15% are higher than the ones obtained by the empirical methods, in agreement with Robertson (2010).

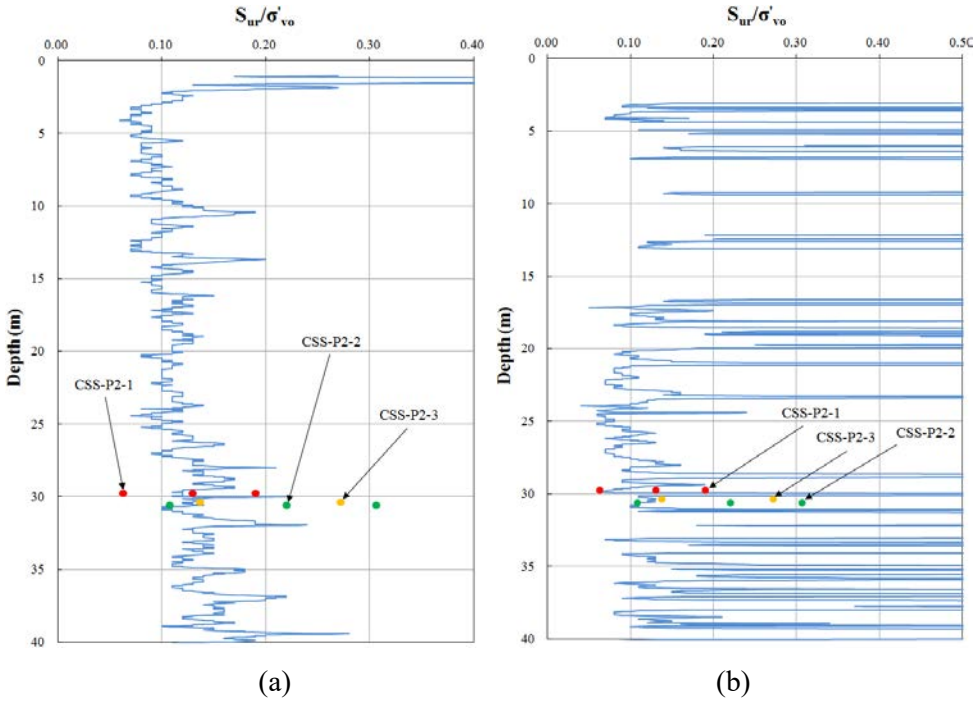

Figure 7: Liquefied residual strength obtained by empirical methods in blue continuous line: (8a) Idriss and Boulanger (2008) and (8b) Robertson (2010) compared to the post-cyclic undrained residual shear strength of underflow tailings from Site 2 as different coloured dots, the increment is due to the calculation of shear stress at different the strain levels (5%, 10% and 15%)

Clearly, both Figures 8(a) and (b) show a strength lower than underflow tailings from Site 2 for both cases. As can be seen, by means of the comparison between Figures 7(a) and 8(a), using the Idriss and Boulanger (2008) methodology for the second case, the strength decreases to half of the tailings along the depth of the tailings impoundment. In the case of Figure 9, the methodology of Robertson (2010) could not obtain the liquefied shear strength due to the high tip resistance values obtained by the SCPTu; therefore, t only the values of residual shear strength by the Idriss and Boulanger method are shown (2008).

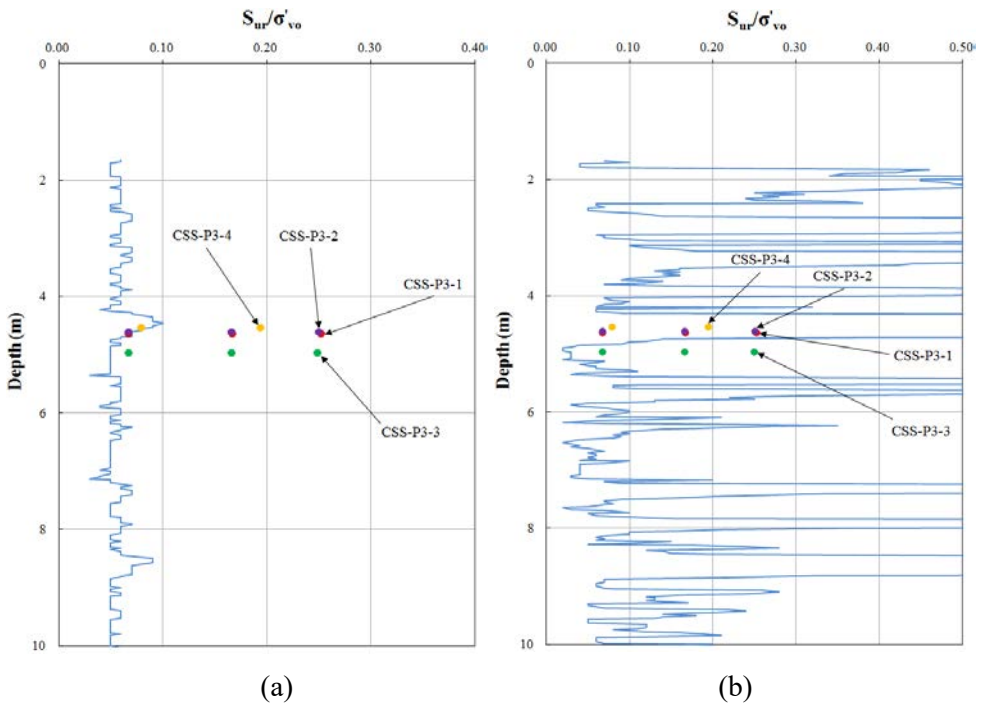

Figure 8: Liquefied residual strength obtained by empirical methods in blue continuous line. (8a) Idriss and Boulanger (2008) and (8b) Robertson (2010) compared to the post-cyclic undrained residual shear strength of overflow tailings from Site 3 as different coloured dots, the increment is due to the calculation of shear stress at different the strain levels (5%, 10% and 15%)

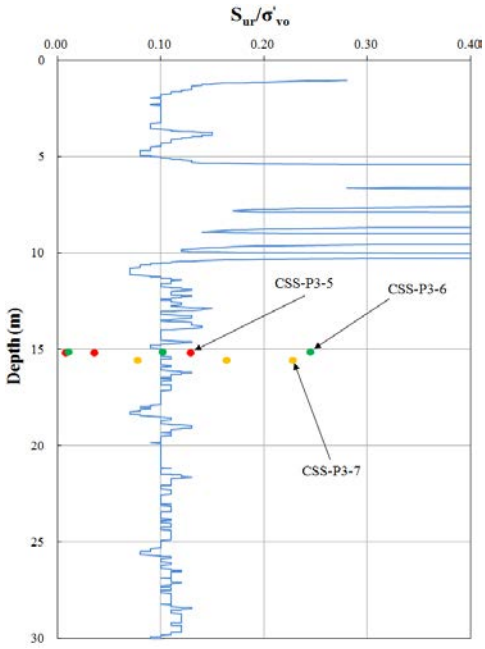

Figure 9: Liquefied residual strength obtained by Idriss and Boulanger (2008) (blue continuous line) compared to the post-cyclic undrained residual shear strength of underflow tailings from Site 3 (different coloured dots), the increment is due to the calculation of shear stress at different the strain levels (5%, 10% and 15%)

Conclusion

This laboratory testing program yielded valuable information about different types of tailings. For all of the sites, the cyclic direct simple shear tests yielded valuable information on the liquefaction triggering of the materials.

In regard to the cyclic response of tailings specimens, the following conclusions were reached:

At Sites 1 and 3, overflow tailings consolidated at 100 kPa and remoulded at the densities shown in this research, are less susceptible to liquefaction until a cyclic stress ratio below 0.15, approximately; for larger cyclic stress ratios, liquefaction is triggered in few cycles.

Site 1 overflow tailings consolidated at 200 kPa and at a density above the sample consolidated at 100 kPa, are less susceptible to liquefaction until a cyclic stress ratio below 0.2, approximately; for larger cyclic stress ratios, liquefaction is triggered in few cycles.

At Sites 2 and 3 underflow tailings consolidated at 500 and 300 kPa, respectively, and remoulded at the densities shown in this research, are less susceptible to liquefaction until a cyclic stress ratio below 0.2, approximately; for larger cyclic stress ratios, liquefaction is triggered in few cycles. As for the post-cyclic response of the tailings specimens, the following conclusions are inferred:

For all the sites the shear stiffness of the tailings were initially very low due to its softened behaviour and the very low effective confining stresses when subjected to shearing. Once the strain level in the monotonic test exceeds that experienced during cyclic loading, it is common for the excess pore pressures to dissipate somewhat, which leads to greater effective confining stresses and thus greater shear resistance. It should be remembered, however, that these element tests may not reflect the same degree of void ratio redistribution, and other macro effects that could alter the local shear resistance after liquefaction of a field deposit.

It is important to note that more research is needed in order to determine a proper residual shear strength of tailings, given that the values obtained by laboratory testing indicate higher resistances than using empirical methods. The results indicated that the values obtained by the direct simple shear device for undrained residual shear strengths at 5% shear strain are more conservative than the calculated ones by means of empirical methods.

All the results for the direct simple shear tests should be examined carefully, recognizing that this is an element test; therefore, it is unlikely to take into account the void ratio redistribution and other macro effects which could affect the post-liquefaction shear resistance in an actual tailings storage facility.

It is important to set appropriate densities according to the field values, because density plays an important role in tailings, which have a more compressible behaviour than standard sands (which do not have fines). From all of the above mentioned, an adequate characterization of the consolidation behaviour could allow greater understanding of their responses.

The cyclic and post-cyclic direct simple shear tests provide valuable information for numerical modelling of liquefaction because they facilitate a broader understanding of the materials' behaviour. Moreover, the most accurate representation of the rotation of the principal stresses makes the obtained information more appropriate for modelling purposes. The appropriate calibration of numerical models allows users to perform advanced and more realistic simulations of phenomena like liquefaction and its subsequent effects.

Acknowledgements

The authors would like to thank the Anddes professionals for their support, guidance, and collaboration with this research.

References

Boulanger, R.W., R.B. Seed, C.K. Chan, H.B. Seed and J.B. Sousa. 1991. Liquefaction behavior of saturated sands under uni-directional and bi-directional monotonic and cyclic simple shear loading. Geotechnical Engineering Report No. UCB/GT/91-08, University of California, Berkeley, 521 pp.

Idriss, I.M. and R.W. Boulanger. 2008. Soil liquefaction during earthquakes. Monograph MNO-12, Earth-quake Engineering Research Institute, Oakland, CA, 261 pp.

Kammerer, A., J. Wu, M. Riemer, J. Pestana and R. Seed. 2004. A new multi-directional simple shear testing database. In *Proceedings of the 13th World Conference on Earthquake Engineering*, Vancouver, No. 2083.

Robertson, P.K. 2010. Evaluation of flow liquefaction and liquefied strength using the cone penetration test. *Journal of Geotechnical and Geoenvironmental Engineering*. ASCE, 136(6): 842–853.

Bibliography

Olson, S.M. and T.D. Stark. 2002. Liquefied strength ratio from liquefaction flow failure case histories. *Canadian Geotechnical Journal* 39(3): 629–647.

Proceedings of Tailings and Mine Waste 2019
November 17–20, 2019, Vancouver, Canada
Published by the University of British Columbia, 2019

Resistance of Lead-Zinc Tailings to Cyclic Loading

Masoumeh Saiyar, Golder Associates Ltd, Canada
Dennis E. Becker, Golder Associates Ltd, Canada
Steven L. Anderson, Golder Associates Inc., USA

Abstract

The dynamic response and properties of lead-zinc tailings were evaluated using cyclic laboratory testing. Both relatively undisturbed tube and reconstituted samples were consolidated to vertical effective stresses of 50 and 75 kPa and subjected to constant volume cyclic direct simple shear (CV CDSS) testing with cyclic stress ratio (CSR) values between 0.08 and 0.15. The cyclic resistance ratio (CRR) (which reflects liquefaction resistance) of the samples was found to be fairly similar to non-plastic silt and other fine grained mine tailings. The shear modulus reduction of the tailings under cyclic loading was found to be smaller than that described for clean sands in the literature.

Introduction

Seismic induced liquefaction is one of the major geotechnical engineering concerns posed by mine tailings ponds. During the last 50 years, there are a number of cases where mine tailings dams have failed due to earthquake induced cyclic loading. Examples are: Las Palmas sand tailings dam failure in February 2010 in Chile (Villavicencio et al., 2013), Amatista tailings dam failure in November 1996 in Peru, and the flow of the impounded tailings slime during the January 14, 1978 earthquake near Izu-Ohshima (Ishihara, 1984).

The mechanical response of tailings under earthquake induced cyclic loading is required for seismic analysis of the tailings dams. This response can be determined from laboratory tests, such as cyclic direct simple shear (CDSS) test or cyclic triaxial test. Natural soil units (such as sand and clay) have had their dynamic response studied extensively by researchers, while relatively less effort has been placed to study the response of fine-grained tailings to seismic loading (Moriwaki et al., 1982; Poulos et al., 1985; Vick, 1990; Wijewickreme et al., 2005).

This paper presents the results of a laboratory investigation of the dynamic properties of tailings from the tailings impoundment of a lead-zinc mine in the United States. The objective of the work was to evaluate the properties of the lead-zinc tailings and compare them to other types of mine tailings and natural soils and add to the knowledge and database of tailings response to seismic events.

Materials tested

Tailings samples were obtained from the impoundment at a lead-zinc mine. In this mine, the tailings are deposited as a slurry from the perimeter of the impoundment. Two boreholes to depths of about 20 m below ground surface (bgs) were advanced along the beach of the tailings impoundment. Soil sampling was performed through the hollow stem augers using Large Penetration Testing (LPT) or thin-walled "Shelby" tubes. Samples taken with LPT methods were collected in a 3.0-inch outer diameter split-barrel sampler driven by a 300-pound automatic hammer with a drop height of 30 inches. The samples were driven approximately 24 inches beyond the drilled depth or previously sampled depth. Shelby tube samples were taken both with a conventional ball-check Shelby head and with a "piston" sampler. The piston sampler reduced the sample length from 36 to 30 inches.

Shelby tube samples collected were measured for recovery, plugged, capped, and stored upright (end of tube highest in the hole denoted as top) to strive to preserve the 'undisturbed' integrity of the sample for shipment and testing. Shelby tube samples were measured, weighed, and then sealed in paraffin wax to maintain integrity of the in-situ water content and reduce disturbance effects while in transport to testing facilities.

Tailings physical properties and classification

The tailings were classified in the field as sandy silt (except for a single interval, 7.6 to 8.2 m bgs where it was logged as silty sand), grey, and dry to wet. Plasticity of the samples varied from non-plastic to high plastic (mostly low to medium plasticity except for a single interval at 10.7 to 11.3 m bgs where plasticity index, PI, of 19 was measured). Minor, localized variation in color, oxidation, and stratification was observed in the borehole samples. Frozen tailings were encountered in the top 0.6 m of the borings and classified as having less than 5% ice by volume. Saturation increased with depth as groundwater was encountered at approximately 7.6 to 10.2 m. According to the Unified Soil Classification System (ASTM, 2006), the tailings are classified as sandy silt (ML). The geotechnical water content of the samples varied between 6% to 62% with an average of about 20%. An average bulk unit weight of 18.8 kN/m^3 and specific gravity of 3.18 was measured for the tailings.

Gradation

The grain-size distributions of six bulk samples of the tailings were evaluated using ASTM standard D6913 (ASTM, 2017). The range of particle size distributions of the tailings are shown in Figure 1.

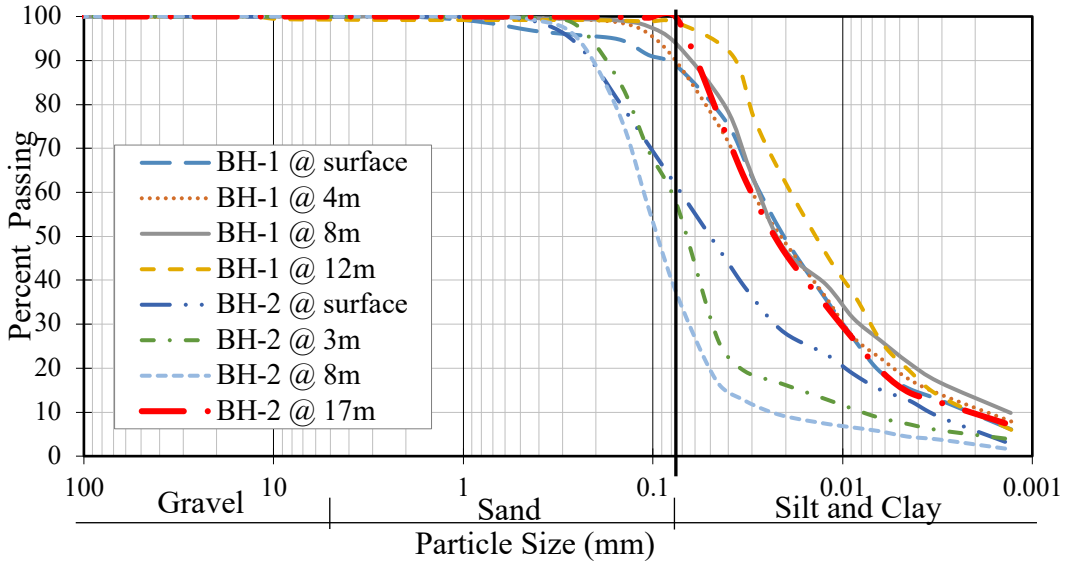

Figure 1: Particle size distribution of the tailings

Equivalent SPT penetration resistance

The large penetration test (LPT) results were recorded as number of hammer blows per 6-inch penetration intervals. The penetration resistance was characterized with "N values," which represent the blow counts required to drive the sampler from 6 to 18 inches below the start of the sampling interval. The equivalent standard penetration testing (SPT) "$(N_1)_{60}$" values were calculated after applying overburden correction, energy correction, rod length correction, and borehole diameter correction on field N values per Idriss and Boulanger (2008). The $(N_1)_{60}$ values are presented in Figure 2.

The $(N_1)_{60}$ values vary between 0 (weight of rods) to 14 with an average of about 3 blows per foot penetration. The tailings are mostly very loose to loose, except for an interval in one of the boreholes at depth of about 3 m bgs where the tailings were compact.

Cyclic shear testing

The constant-volume cyclic simple shear (CV CDSS) test data used herein had been obtained using the GDS electromechanical dynamic cyclic simple shear (EMDCSS) device at the geotechnical laboratory of Golder Associates Ltd in Burnaby, British Columbia, Canada. In this apparatus, the cylindrical soil specimen is laterally confined by Teflon coated low friction retaining rings and an alternative wire-reinforced membrane maintains a constant cross-sectional area. Vertical displacement is prevented thereby achieving constant volume conditions. A shear force loading is then applied to the bottom of the sample allowing it to deform in simple shear. The constant volume condition is achieved by controlling the external boundaries, and porewater does not participate in volume control. Hence, there is no need for measurement of porewater pressure because the vertical effective stress on the specimen at any given time is directly

obtained from the measured load at the vertical stress boundary. The tested specimens had a height of about 71 mm and a diameter of about 24 mm. The tested specimens were initially consolidated to a desired vertical effective stress (σ'_{vc}) prior to cyclic loading as indicated in Table 1.

During the cyclic loading phase, symmetrical sinusoidal shear pulses were applied at constant cyclic stress ratio τ_{cy}/σ'_{vc} amplitudes, at a frequency of 0.1 Hz, where τ_{cy} is the cyclic shear stress.

The monitored test variables in CV CDSS tests consisted of full time-histories of horizontal shear stress (τ), decrease in vertical stress (taken to be equal to an equivalent increase in excess porewater pressure, Δu in undrained condition), and horizontal shear strain (γ). The cyclic loading phase was continued until excess porewater pressures reached a point approximately equal to the value of the initial consolidation vertical effective stress (r_u=1). A total of 12 CV CDSS tests were conducted at σ'_{vc} values of 50 kPa and 75 kPa and cyclic stress ratio (CSR=τ_{cyc}/σ'_v) values of 0.08, 0.10, 0.12, and 0.15.

Upon completion of the cyclic loading phase, the post cyclic monotonic shear response was investigated by testing the specimens at a shear strain rate of about 10% per hour.

Relatively undisturbed tube versus reconstituted samples

Considering the very loose to loose and fine-grained nature of the tailings, obtaining undisturbed samples is a difficult task. Shelby tube sampling, despite its potential for sample disturbance, is still used as the common practical and cost-effective sampling tool. The source of disturbance for Shelby tube samples can be potential water content loss and resulting densification due to potential vibrations and shaking during transportation, and compression of the outer portion of the sample caused by pushing the tube and when extruding/removing the sample from the tube.

Borehole	Depth (m)	$(N_1)_{60}$
BH-1	2.4	0
BH-1	4.0	3
BH-1	5.5	3
BH-1	7.6	1
BH-1	10.7	0
BH-1	12.2	2
BH-2	1.5	0
BH-2	3.0	14
BH-2	7.6	6
BH-2	10.7	3
BH-2	13.7	7
BH-2	16.8	0

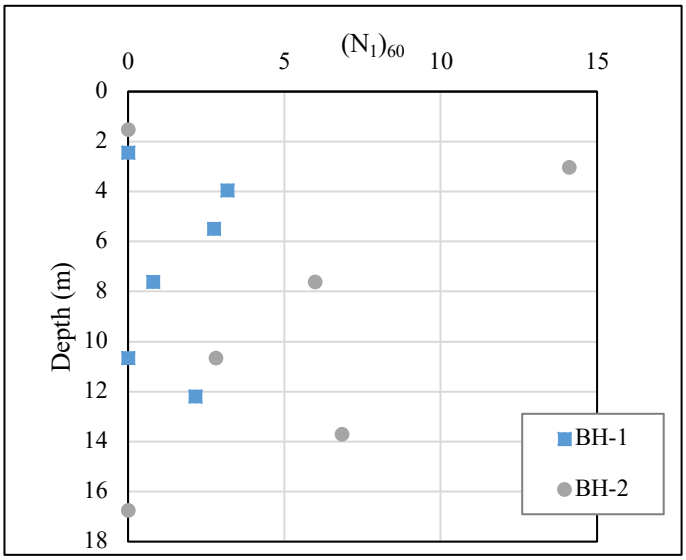

Figure 2: SPT $(N_1)_{60}$ values versus depth

Table 1: Summary of cyclic simple shear (CV CDSS) testing

Test series σ'_v (kPa)	Test	Sample type	CSR τ_{cyc}/σ'_v	Dry unit weight (kN/m³)	Water content (%)	Number of cycles to γ=3.75 %	Number of cycles to r_u=1	Post cyclic strength (kPa)	Post cyclic strength ratio
50	BH-1a	Tube	0.08	16.8	13.8	169	178	31	0.62
	BH-1b	Tube	0.10	15.4	17.1	18	21	49	0.98
	BH-1c	Tube	0.12	17.1	18.0	170	200	68	1.36
	BH-1d	Tube	0.15	15.7	11.8	13	17	47	0.94
75	BH-2a	Tube	0.08	19.8	11.4	178	188	47	0.63
	BH-2b	Tube	0.10	18.0	7.3	28	29	13	0.18
	BH-2c	Tube	0.12	18.1	16.0	132	150	67	0.90
	BH-2c'	Tube	0.12	16.7	9.0	32	36	45	0.59
	BH-2d	Tube	0.15	15.9	7.4	3	3	14	0.18
	BH-2aR	Reconstituted	0.08	15.6	20.0	61	61	–	–
	BH-2bR	Reconstituted	0.10	15.6	20.0	12	12	–	–
	BH-2cR	Reconstituted	0.12	15.6	20.0	4	4	–	–

The ability of samplers such as the Sherbrooke sampler (Lefebvre and Poulin, 1979) and the Laval sampler (La Rochelle et al., 1981) to retrieve higher quality "undisturbed" samples of fine-grained soil, in comparison to those from conventional tube sampling, is well known. The use of these samplers is not practical and cost-effective; however, they are becoming more popular techniques for sampling tailings, especially for advanced measurements such as tailings critical state parameters in the laboratory. Although, the tube samples obtained using piston sampler, used in the tests reported herein had been shipped with cautionary measures in place, the samples might not be representative of the field conditions; therefore, they have been called "relatively undisturbed" samples. The samples were removed from Shelby tubes using a piston extruder; then cut into smaller specimens and trimmed to fit exactly into the test equipment.

Although obtaining an "undisturbed" sample is ideal for most laboratory testing programs, relying on limited number of laboratory tests on undisturbed samples of tailings might not be the best approach. Considering the variability of tailings components including stratigraphy, gradation, and density within the impoundment, enough samples must be tested for accurate and representative characterisation. Accordingly, three samples from the test program were reconstituted to the tailings average unit weight of 18.8 kN/m^3 and water content of 20%, and their measured responses compared to those from Shelby tube samples.

Cyclic shear testing results

Figure 3 shows the typical stress path and stress–strain relationships obtained from the CV CDSS tests conducted on a Shelby tube sample (BH-2c); consolidated to vertical stress of 75 kPa and sheared at CSR of 0.12. The response of a reconstituted sample (BH-2cR) at the same conditions (σ'_{vc}=75 kPa and CSR=0.12) is presented in Figure 4. The responses of the other samples were similar to those presented in Figures 3 and 4.

The summary of the number of uniform cycles to reach shear strain (γ) of 3.75% (liquefaction triggering criteria) and the total number of uniform cycles to reach r_u of about 1 are provided in Table 1. As shown, the number of cycles to produce r_u=1 varied inversely with the magnitude of the applied CSR for reconstituted samples, while there is no correlation between the number of cycles and applied CSR for Shelby tube samples. This is considered to be due to the variation in initial density and void ratio of the samples taken from even the same Shelby tube. Overall, the Shelby tube samples show a stronger and stiffer response than the reconstituted samples, which might be due to the effect of soil fabric and structure, and densification during sampling and extrusion operations.

All the specimens show a predominantly contractive response during the first quarter cycle of loading. With an increasing number of load cycles, the specimens experience a cumulative increase in equivalent excess porewater pressure with associated progressive degradation of shear stiffness.

Cyclic resistance ratio (CRR)

The cyclic shear resistance of the tailings based on a single amplitude shear strain, γ, of 3.75% (liquefaction triggering as defined by NRC, 1985) are shown in Figure 5 and summarized in Table 1. As seen in Figure 5, the reconstituted samples show consistent results in terms of increasing the number of cycles by decreasing the applied stress ratio, while the results from the tube samples are scattered. This might be due to non-homogeneous nature of tailings. Figure 5 also compares the measured cyclic resistance ratio of the tailings to those reported by others: McKee et. al. (1978) on lead-zinc-silver tailings (liquefaction triggering criteria of r_u=1), Sanin et. al. (2005) on silt, and Seidalinova (2014) on gold tailings (liquefaction triggering criteria of γ=3.75%). The Fraser River Delta silt studied by Sanin (2005) was classified as ML with water content of about 35% to 40%, specific gravity of 2.68 and plasticity index of 4. The gold tailings (Seidalinova, 2014) was classified as sandy silt (ML) with water content of about 19% to 26% and specific gravity of 2.89 and is similar to lead-zinc tailings reported in this paper. As seen, the cyclic resistance ratio of Fraser River Delta silt and lead-zinc-silver tailings are comparable with those measured for lead-zinc tailings within this study.

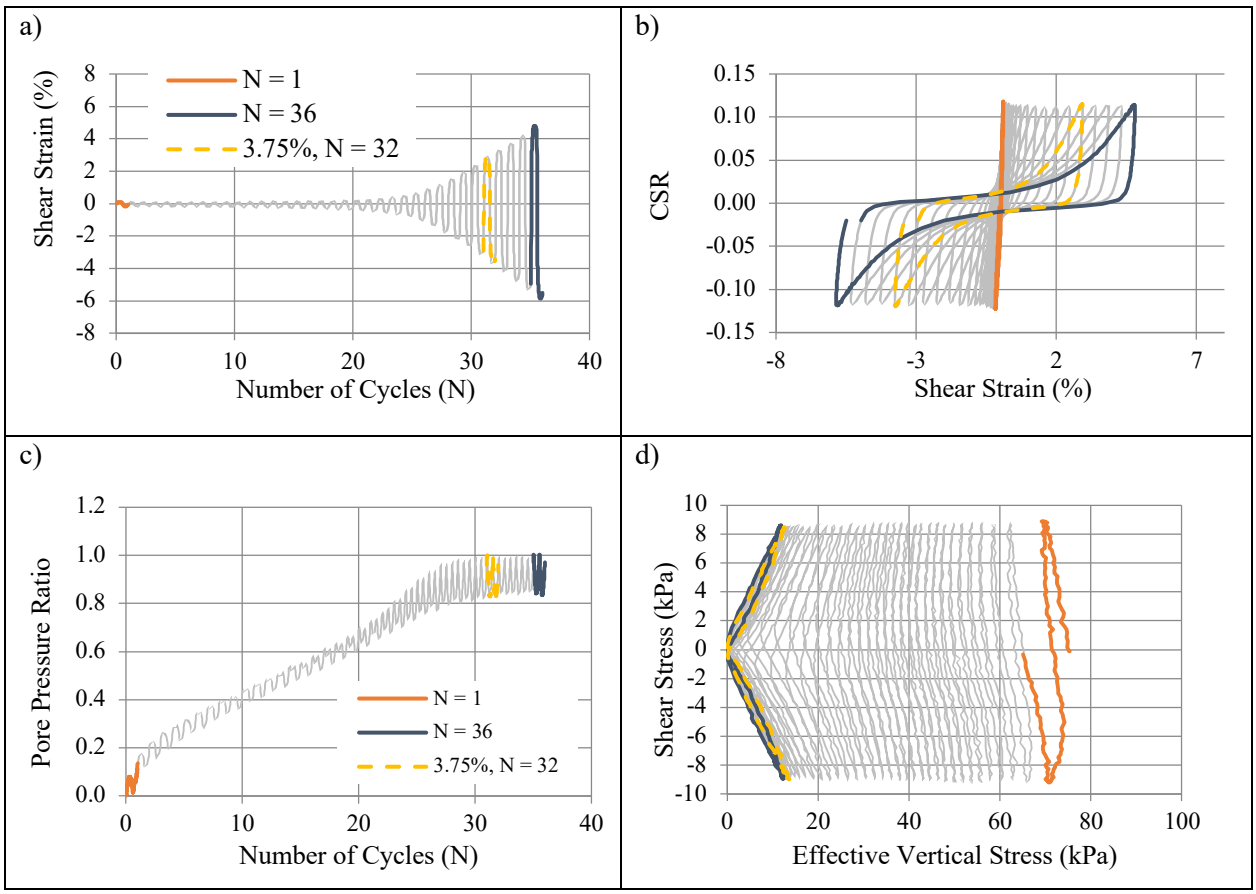

Figure 3: Typical response of relatively undisturbed tube tailings in constant-volume CDSS loading (σ'vc = 75 kPa, CSR = 0.12): (a) shear strain versus number of cycles; (b) Cyclic stress ratio versus Number of cycles; (c) equivalent excess porewater pressure ratio versus number of cycles; (d) stress path response

Figure 6 compares the relationship between CRR and $(N_1)_{60}$ values proposed by the 1996 NCEER workshop (Youd and Idriss, 1997) with data from this study and the Canadian Liquefaction Experiment (CANLEX) project (Robertson et al., 2000). The data are shown in terms of average values plus and minus one standard deviation. The CANLEX project involved the investigation of six sites in Western Canada containing loose tailings sand deposits. The results from J-Pit site of Syncrude Canada Ltd. (oil sand tailings) located north of Fort McMurray, Alberta, and LL and Highmont (HM) Dams (copper tailings) of the High Valley Copper mine site south of Kamloops, British Columbia, are compared with the results from this study due to similarity of these tailings in terms of fines content. As shown in Figure 6, the results from this study are comparable to those from copper tailings.

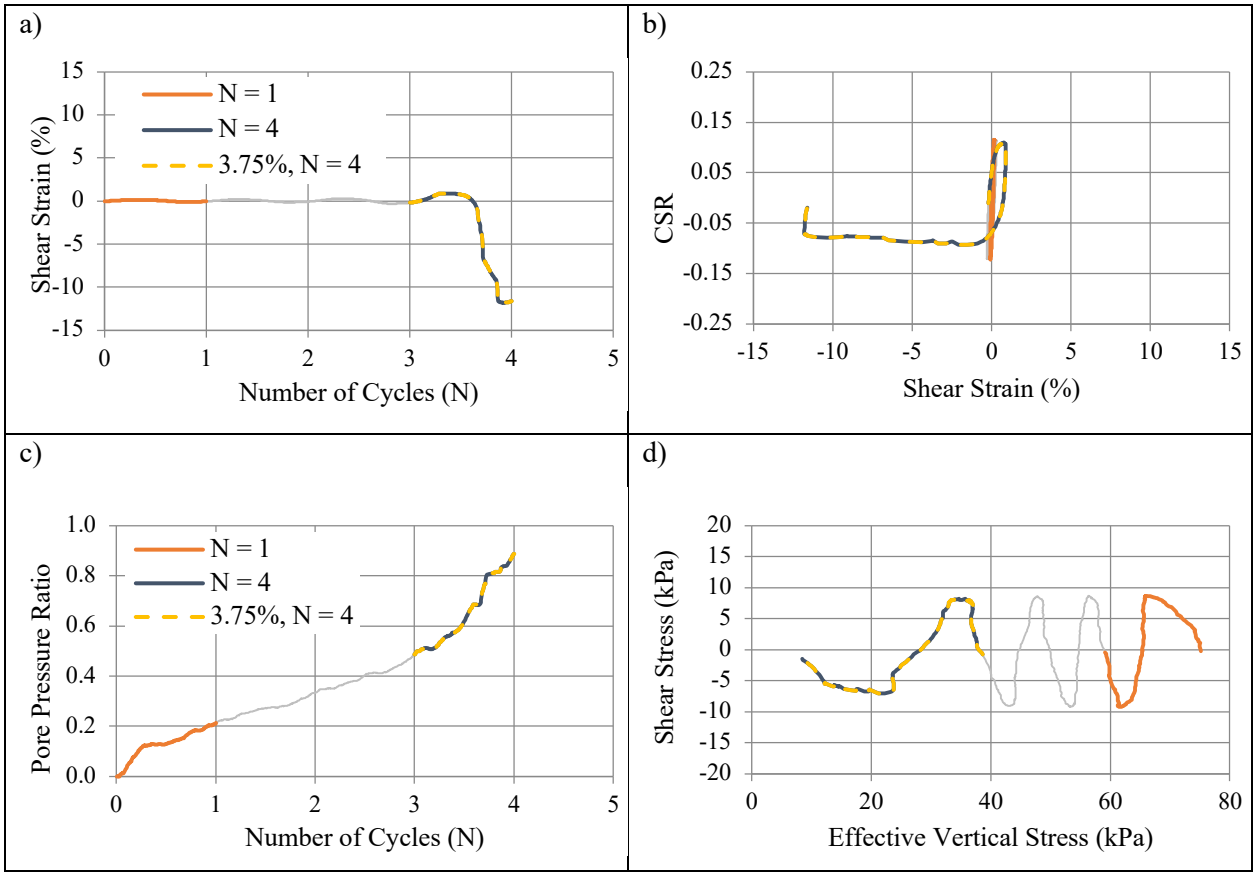

Figure 4: Typical response of reconstituted tailings in constant-volume CDSS loading (σ'_{vc} = 75 kPa, CSR = 0.1): (a) shear strain versus number of cycles; (b) Cyclic stress ratio versus number of cycles; (c) equivalent excess porewater pressure ratio versus number of cycles; (d) stress path response

Post cyclic strength

Post-cyclic testing was conducted on all tube samples and consisted of monotonic shear testing at a shear strain rate of 10% per hour to a maximum shear strain of 20%. The results of testing are shown in Figure 7. The post-cyclic undrained shear strengths, s_{u_PC}, varied from 13 to 68 kPa, and the liquified strength ratio s_{u_PC}/σ'_{vc} varied from 0.18 to 0.96. The range of liquified strength ratios are within the range reported by Wijewickreme et al. (2005) based on a series of post cyclic monotonic shear tests conducted on 20 undisturbed samples of copper–gold–zinc tailings (low plastic silt), (0.13 to 1.07, with an average value of 0.34).

Shear modulus

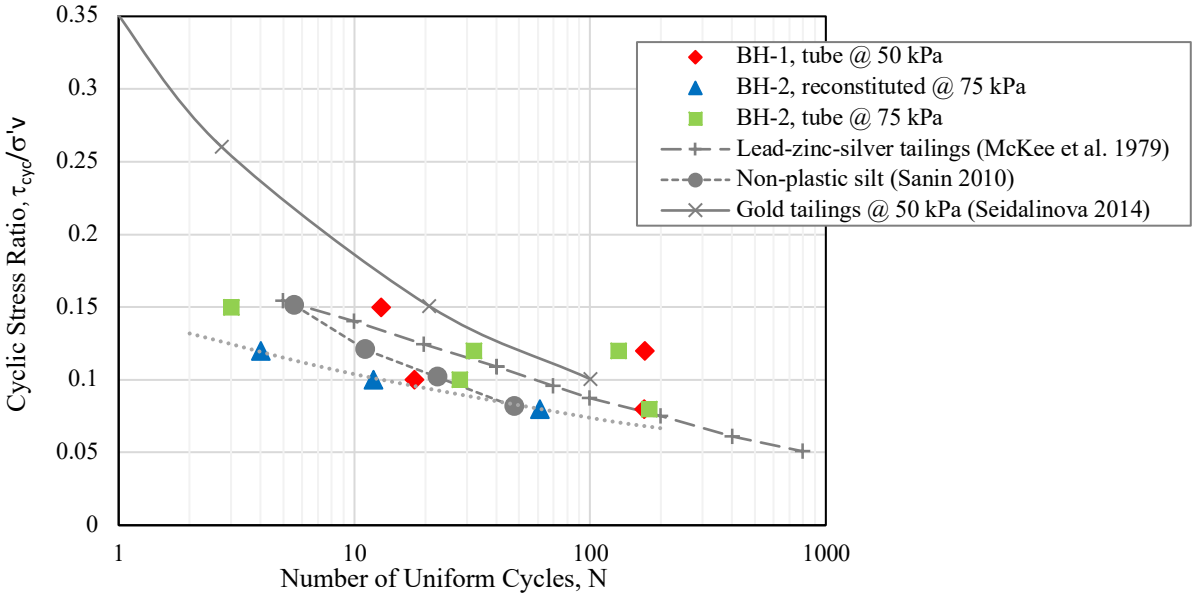

Figure 5: CSR of lead-zinc tailings from CV CDSS testing

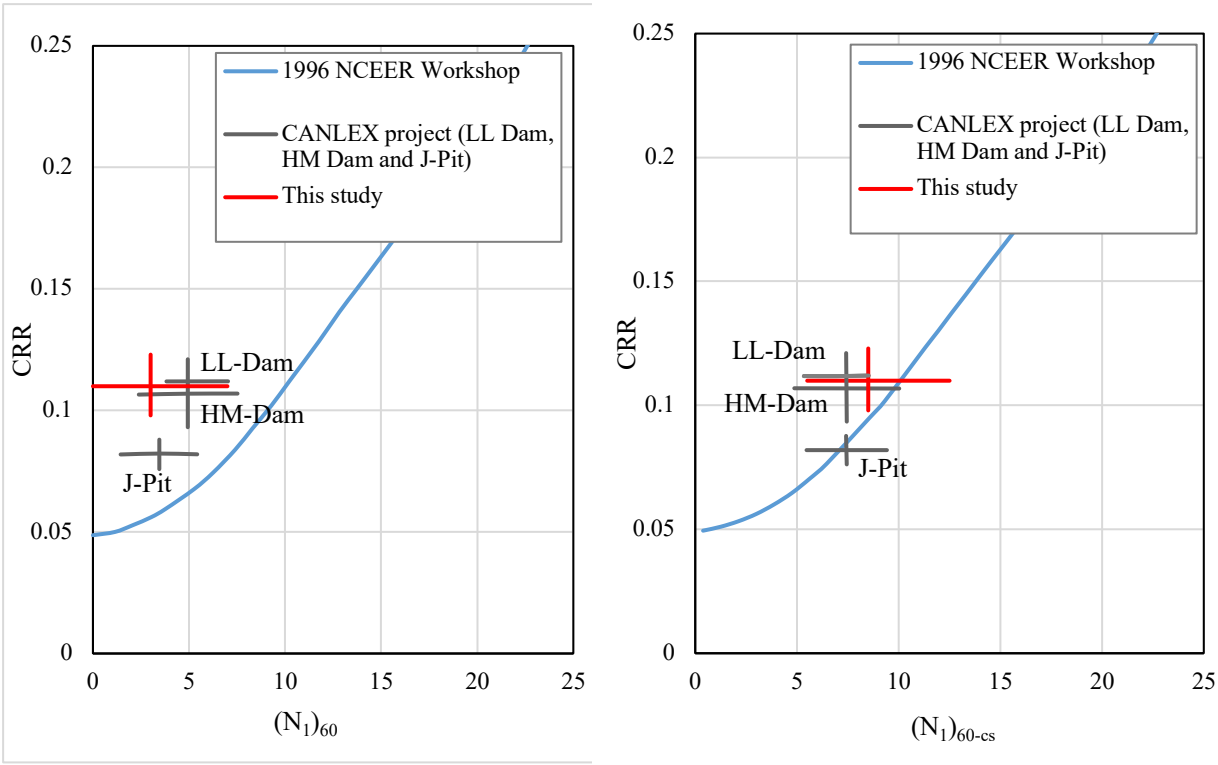

Figure 6: a) Laboratory CRR versus SPT $(N_1)_{60}$, b) Laboratory CRR versus SPT $(N_1)_{60-cs}$

The secant shear modulus, G, was calculated at the shear strains corresponding to the first quarter of the first load cycle. These values are presented in Figure 8. The degradation of the G with increasing shear strain (γ) for sand under mean principal effective stresses, σ'_m, of 25, 50, and 100 kPa derived from G/G_{max} empirical relationships proposed by Seed et al. (1984) are also shown in Figure 8, where $\sigma'_m=(\sigma'_x+\sigma'_y+\sigma'_z)/3$ and σ'_x, σ'_y, and σ'_z are the effective stresses in three dimensions, and G_{max} is the maximum shear modulus (the shear modulus at strain levels less than about 10^{-4}%).

To estimate the mean principal effective stress, the theoretical at-rest pressure coefficient, K_0 was approximated using the expression suggested by Jaky (1948).

$K_0=1-\sin\phi$

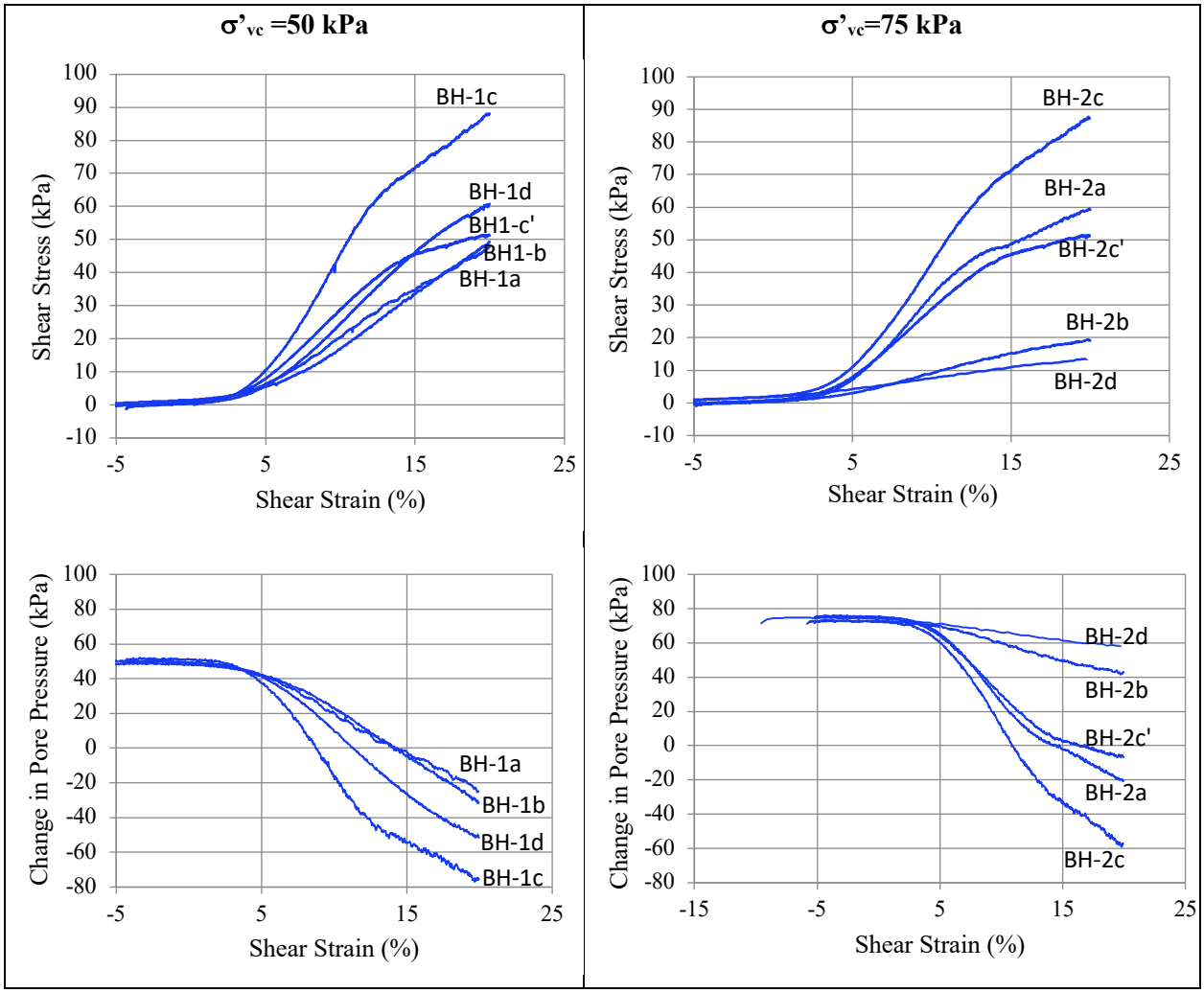

Figure 7: Post-cyclic monotonic shear stress versus shear strain

A friction angle of 30 degrees was assigned for tailings using the previous Cone Penetration Test (CPT) and SPT data (not presented in this paper due to lack of available space). Assuming this condition

in the specimens prior to cyclic loading, the mean effective principal stress, σ'_m, within the sample was approximately 0.6 of σ'_v. Thus, the CV CDSS test results at 50 and 75 kPa are comparable to the Seed et al. (1984) curve for σ'_m of 25 and 50 kPa, respectively. As shown, the modulus reduction response of tailings is smaller than that of sands, as described by Seed et al. (1984).

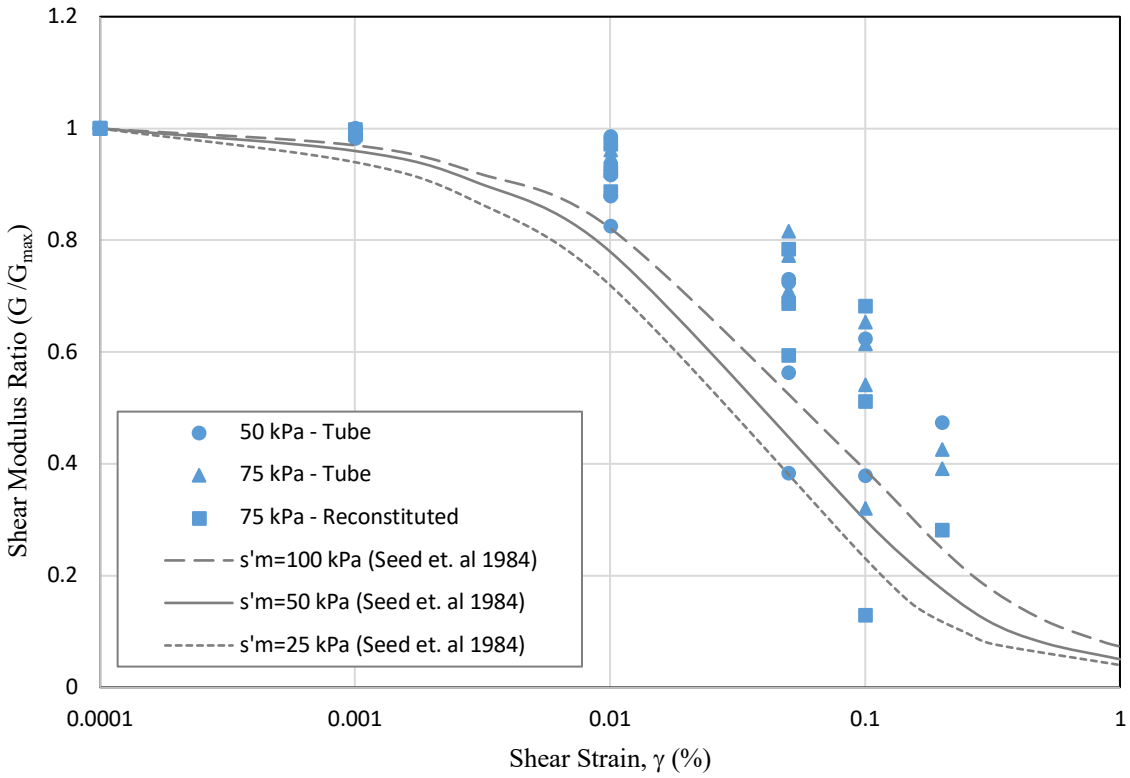

Figure 8: Shear moduli from CV CDSS testing

Conclusion

The properties of tailings from a lead-zinc mine in the United States were investigated using dynamic laboratory tests conducted on both relatively undisturbed tube and reconstituted samples. The tailings are classified as low to medium plastic sandy silt. The reconstituted samples showed consistent results in terms of expected behaviour with increasing cyclic stress ratio, while the relatively undisturbed tube samples had scattered results. Considering the difficulties associated with obtaining undisturbed tailings samples as well as the heterogeneity within tailings, reconstituted tailings samples may be required for determining the dynamic behaviour of tailings. The cyclic resistance ratio of the studied tailings was found to be fairly similar to those from silts, lead-zinc-silver tailings, and copper tailings, and generally lower than gold tailings. The shear modulus reduction response of tailings was also found to be smaller than that of natural sands.

References

Idriss, I.M. and R.W. Boulanger. 2008. Soil liquefaction during earthquakes. Earthquake Engineering Research Institute, Monograph MNO 12.

Ishihara, K. 1984. Post-earthquake failure of a tailings dam due to liquefaction of the pond deposit. In *Proceedings of the International Conference on Case Histories in Geotechnical Engineering,* Rolla, Missouri, 6–11 May, 3: 1129–1143.

La Rochelle, P., J. Sarrailh, F. Tavenas, M. Roy and S. Leroueil. 1981. Causes of sampling disturbance and design of a new sampler for sensitive soils. *Canadian Geotechnical Journal* 18(1): 52–66.

Lefebvre, G. and C. Poulin. 1979. A new method of sampling in sensitive clay. *Canadian Geotechnical Journal* 16(1): 226–233.

Moriwaki, Y., M.R. Akky, A.M. Ebeling, I.M. Idriss and R.S. Ladd. 1982. *Cyclic Strength and Properties of Tailings Slimes:* 82–539. New York.

National Research Council (NRC). 1985. Liquefaction of soils during earthquakes. National Academy Press, Washington, DC Report.

Poulos, S. J., E.I. Robinsky and T.O. Keller. 1985. Liquefaction resistance of thickened tailings. *Journal of Geotechnical Engineering* 111(12): 1380–1394.

Robertson, P.K., C.E. (Fear) Wride, B.R. List, U. Atukorala, K.W Biggar, P.M. Byrne, R.G. Campanella, D.C. Cathro, et al. 2000. The CANLEX Project: Summary and conclusions. *Canadian Geotechnical Journal* 37: 563–591.

Sanin, M.V. 2005. Cyclic shear loading response of Fraser River delta silt. Masters Thesis, University of British Columbia.

Seed, H.B., R.T. Wong, I.M. Idriss and K. Tokimatsu. 1984. Dynamic moduli and damping factors for dynamic analysis of cohesionless soils. Earthquake Engineering Research Center, Berkeley, Calif. Report No. UCB/EERC-84/14.

Seidalinova, A. 2014. Monotonic and cyclic shear loading response of fine-grained gold tailings. Masters thesis, University of British Columbia.

Vick, S.G. 1990. *Planning, Design, and Analysis of Tailings Dams*. New York: John Wiley & Sons. Retrieved from http://www.amazon.com/Planning-Design-Analysis-Tailings- Dams/dp/0921095120.

Villavicencio, G., R. Espinace, J. Palma, A. Fourie and P. Valenzuela. 2013. Failures of sand tailings dam in a highly seismic country. *Canadian Geotechnical Journal*, 2014, 51(4): 449-464.

Wijewickreme, D., M.V. Sanin and G.R. Greenaway. 2005. Cyclic shear response of fine grained mine tailings. *Canadian Geotechnical Journal* 42(5): 1408–1421. doi:10.1139/T05-058

Youd, T.L. and I.M. Idriss. 1997. *Proceedings of the National Center for Earthquake Engineering Research (NCEER) Workshop on Evaluation of Liquefaction Resistance of Soils,* Salt Lake City, Utah, January 1996.

Bibliography

James, M., M. Aubertin, D. Wijewickreme and G.W. Wilson. 2011. A laboratory investigation of the dynamic properties of tailings. *Canadian Geotechnical Journal* 48(11): 1587–600.

National Center for Earthquake Engineering Research, Report NCEER-97-0022.

Proceedings of Tailings and Mine Waste 2019
November 17–20, 2019, Vancouver, Canada
Published by the University of British Columbia, 2019

Critical State Testing of Tailings: Comparison between Various Tailings and Implications for Design

Kyle Smith, Golder Associates Pty Ltd, Australia
Riccardo Fanni, Golder Associates Pty Ltd, Australia
Peter Chapman, Golder Associates Pty Ltd, Australia
David Reid, The University of Western Australia, Australia

Abstract

The design of tailings storage facilities (TSFs) informed by a critical state soil mechanics (CSSM) framework is rapidly gaining acceptance within the consulting industry for TSF designs of all levels of complexity. The critical state locus (CSL), which represents a practical means to assess the strength-deformation behaviour of stored tailings and therefore the stability of TSFs, is a key component of applying critical state soil mechanics to TSF design. However, information relating to CSLs for tailings is sparse, with the majority of available CSL data being on research sands, natural sands, and natural silty sands. Tailings, which are predominantly silt-sized geomaterials of young origin from mineral processing or beneficiation, often present markedly different CSL parameters than the aforementioned geomaterials. The CSL parameters inferred from testing various tailings are presented, with trends identified between CSL parameters and fines content (FC, % <75 μm), Atterberg limits, and associated commodity (the commodity separated during processing, which generated the tailings).

The CSL of a tailings is key to understanding its potential behaviour, including the onset of flow liquefaction, as well as the potential strength loss from liquefaction. Established relationships between the slope of the CSL (λ_e), initial state parameter (Ψ_0), and post-peak strength loss (i.e., material brittleness) are compared to the presented CSL parameters and are found to be in general agreement. These relationships can enable the identification of high-risk, highly-brittle tailings, which are susceptible to significant post-peak strength loss (flow liquefaction), often with disastrous consequences.

The use of CSL testing early in the design of a TSF is almost always overlooked. As CSL testing requires only a relatively small tailings sample (generally <5 kg), undertaking CSL testing using pilot or batch plant samples, at the design phase of new mining project, is often feasible. Additionally, CSL testing can be undertaken at a relatively low cost (<US$10,000 per sample), and therefore cost should not represent a significant impediment to it being undertaken. The understanding gained from CSL testing can greatly

inform the design of a TSF as it can be used to characterize the likely behaviour of the tailings in situ, and support identification of high-risk tailings.

Introduction

Critical state soil mechanics

CSSM is a theory that links a soils mechanical behaviour to its void ratio; it is presently the only theory to do this (Jefferies, 2018). Soil and other granular materials, if continuously distorted until they flow as a frictional fluid, will come to a critical state (Schofield and Wroth, 1968). In more specific terms, the critical state is attained during shear when the rate of change of each of mean effective stress, deviatoric stress, and volumetric strain, with distortional strain is equal to zero and maintains so (Jefferies and Been, 2015). The critical state varies with mean stress to form a unique CSL (Jefferies and Been, 2015). As such, the CSL forms a base of reference for soil behaviour during shear (Schofield and Wroth, 1968).

Critical state locus

The CSL of a geomaterial is usually inferred through the use of a combination of undrained and drained triaxial tests, to infer the location of the CSL at stresses generally above and below 300 kPa, respectively. CSLs are generally represented by a semi-log CSL idealization $e = \Gamma - \lambda_e \ln(p')$, where Γ represents the CSL intercept at 1 kPa mean effective stress (p') and λ_e represents the slope of the CSL (analogous to compressibility). In some cases when the CSL of a geomaterial is found to be "curved" in e-log(p') space, a power law function, $e = A - B(p'_{cs}/p'_{ref})^C$ can be used to represent the CSL , where p'_{ref} is a reference stress (usually 100 kPa), A is analogous to Γ, and B and C control the "curvature" of the CSL. It is generally accepted that the semi-log CSL idealization is not appropriate at "high stresses" where the CSL becomes "curved" in e-log(p') space (i.e., the material does not exhibit a lower limit to compressibility), the cause of which is often attributed to particle crushing, although this is not necessarily supported by testing (Carerra et al., 2011).

The CSL of a geomaterial is influenced by particle size gradation (Been and Jefferies, 1985; Zlatovic and Ishihara, 1995: Olsson and Stark, 2003: Carerra et al., 2011), particle angularity and roughness (Poulos et al., 1985; Hird and Hassona, 1990; Olsson and Stark, 2003; Yang and Wei, 2012), soil plasticity index (PI)(Schofield and Wroth, 1968; Jefferies and Been, 2015), and particle hardness (Jefferies and Been, 2015). However, although the aforementioned material properties are widely accepted to influence the CSL of geomaterials, published information relating material properties to CSL parameters for tailings is sparse, with the majority of available CSL data being on research sands, natural sands, and natural silty sands. Tailings, which are predominantly silt-sized, highly angular, geomaterials of young origin from mineral

processing or beneficiation, often present markedly different CSL parameters than the aforementioned geomaterials.

State parameter

The state parameter (Ψ), as proposed by Been and Jefferies (1985), defines the difference between the void ratio of an element of soil, and the void ratio on the CSL at the same mean effective stress. This concept is demonstrated schematically in Figure 1. Since the proposal of this state parameter, it has gained widespread use in characterizing natural soils and tailings, as it provides a useful normalization of the density and behaviour of geomaterials. Generally, geomaterials with $\Psi < -0.06$ exhibit undrained strengths greater than drained strengths during rapid shearing, while for geomaterials with $\Psi > -0.06$ exhibit undrained strengths less than drained strengths and the risk of brittle strength loss under rapid or cyclic shearing exists (Jefferies 2018). The likelihood of brittle strength loss, and the severity of strength loss, increase with increasing Ψ (Jefferies and Been, 2015).

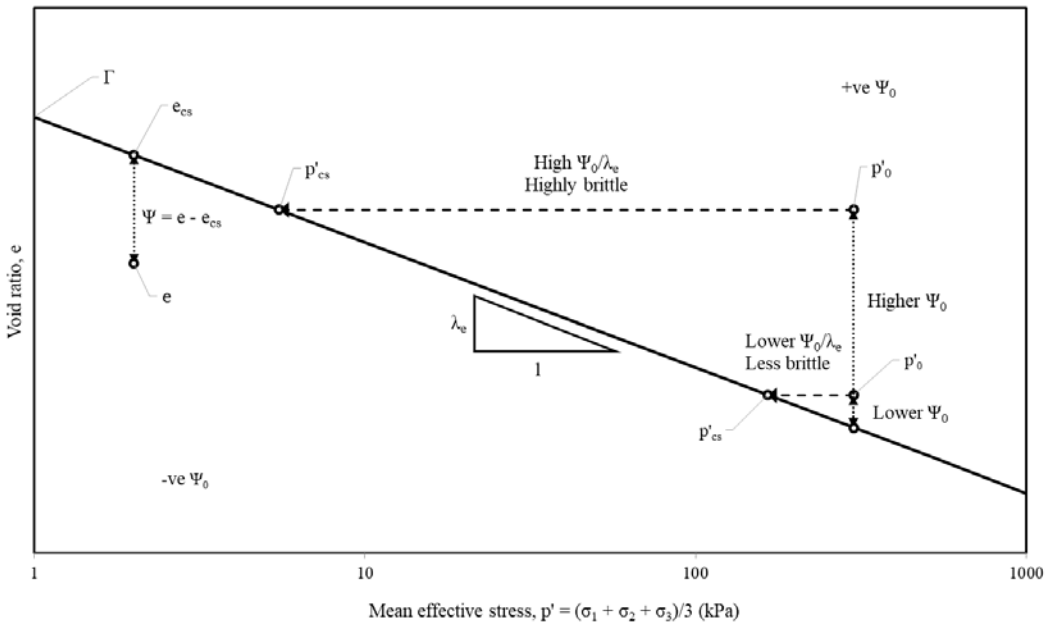

Figure 1: CSL and brittleness schematic

Brittleness

The degree of post-peak strength loss, between peak undrained and critical state undrained strengths, is commonly characterized in terms of the brittleness index $I_B = (s_{u,p} - s_{u'r})/s_{u,p}$ (Bishop, 1971) (herein referred to as brittleness). The parameter coupling Ψ_0/λ provides normalization of geomaterial brittleness (Hird and Hassona, 1990) with $s_{u'r}/p'_0 = 0.5\ M / \exp(-\Psi_0/\lambda_e)$ resulting from the semi-log CSL idealization (Jefferies and Been, 2015). Alternatively stated, for an undrained triaxial test or soil element undergoing undrained shearing, the brittleness is proportional to the reduction in mean effective stress (or pore pressure

generation) along the undrained stress path, as captured by the initial stress ratio ($p'_0/p'_{cs} = 10^{(\Psi_0/\lambda_e)}$) as defined by Robertson (2017), and as shown in Figure 1. Robertson (2017) further states that laboratory data show that for very loose contractive "sand-like" soils, brittleness decreases, and soil become progressively more ductile with increasing stress level due to non-linear CSLs at "high stresses", which act to reduce the possible initial stress ratio. Jefferies (2018) suggest that such CSL "curvature", which represents constant compressibility, may occur above 800 kPa.

Research and experience indicate that the higher the proportion of low plasticity fines in a geomaterial, the greater the opportunity for the geomaterial to exist in the field in a contractive state with high Ψ_0 (Verdugo and Ishihara, 1996; Reid and Jefferies, 2017). Furthermore, low energy deposition environments have been observed to result in decreased stored density and increased Ψ values (Reid and Jefferies, 2017).

Testing undertaken

This paper presents the CSLs inferred from triaxial testing of 35 tailings and four other geomaterials at Golder's Perth Laboratory between 2015 and 2019. The tailings were obtained from 15 separate mines, located throughout Australia and Asia, which produce six general commodity groupings. The testing program for each tailings sample involved undertaking index testing (fines content [FC], particle density and Atterberg limits) and a series triaxial compression tests for inferral of the CSL.

Testing methods

Fines content (FC) was measured by sieving at 75 μm following AS 1289.3.6.1. Particle density (G_s) was measured by helium pycnometry following ASTM D5550 and weighing in water following AS 1289.3.5.1. Liquid limit (LL) was measured following AS 1289.3.1.1 and AS 1289.3.9.9. Plastic limit (LL) was measured following AS 1289.3.2.1. Triaxial testing used to infer the CSLs of the various geomaterials followed the recommendations of Jefferies and Been (2015), with void ratio determined from gravimetric water content (based on end of test freezing) and particle density, predominantly moist tamping "loose" sample preparation (always employing under-compaction), and use of lubricated oversized end platens. Salt correction of void ratio as outlined by Reid and Fanni (2019) was undertaken on tailings containing appreciable concentrations of dissolved solids. Testing standards such as ASTM D4767 and ASTM D7181 and AS 1289.6.4.2 were generally followed to undertake the triaxial testing.

Results

The CSL parameters λ_e, Γ, and M_{tc} (critical friction ratio) are presented in Table 1 and Table 2, along with index test results (FC and Atterberg limits) of the tailings. CSLs with minor "curvature" (void ratio deviation less than 0.02 over p' = 30 – 900 kPa) have been represented using the conventional semi-log

CSL idealization for purposes of comparison. The CSLs for 4 of the 39 geomaterials tested were assigned power law idealizations due to greater "curvature". The median range over which CSLs were defined was 30 – 900 kPa, which is generally suitable to characterize tailings storage facilities (TSFs) up to 60 m height, or alternatively, the upper 45 m of higher TSFs.

Plots comparing both CSL parameters Γ and λ_e to index test results (FC, normalized LL and PI) are presented in Figures 2 to 5. CSL data of tailings from Been and Jefferies (2015) and Reid (2015) are also presented in order to supplement the presented data at lower FC, as the majority of the tailings presented in this paper contain between 45 and 90% fines. However, the best-fit lines provided in this study to identify correlations between CSL parameters and index test results include only the tailings presented in this paper. This was done to avoid potential variations resulting from testing procedures, which have been shown to influence estimation of Γ (Reid, 2019) and in the hope that this exclusion will also somewhat remove the influence of particle angularity on the CSL parameters, as tailings particles are generally highly angular.

Table 1: CSL parameters and index test results for tailings and other geomaterials (1 of 2)

Name	Associated commodity	G_S	FC (%)	LL (%)	PL (%)	PI (%)	Γ	λ_e	M_{tc}
Tailings 1	Iron ore	2.99	87	27	22	5	0.900	0.043	1.47
Tailings 2	Iron ore	3.23	93	26	22	4	1.035	0.053	1.33
Tailings 3	Gold	2.85	64	22	20	2	1.014	0.064	1.32
Tailings 4	Copper, gold	2.73	63	24	16	8	0.737	0.048	1.31
Tailings 5	Copper, gold	2.63	45	25	0	–	A = 0.823, B = 0.089, C = 0.420		1.51
Tailings 6	Copper, gold	2.69	55	19	17	2	0.803	0.049	1.33
Tailings 7	Copper, gold	2.74	56	19	16	3	0.745	0.044	1.34
Tailings 8	Copper, gold	2.68	55	23	19	4	0.772	0.045	1.48
Tailings 9	Silver, lead, zinc	2.90	97	36	25	11	1.300	0.079	1.38
Tailings 10	Gold	2.74	45	NO	NO	NP	0.815	0.036	1.39
Tailings 11	Gold	2.74	68	NO	NO	NP	0.865	0.045	1.46
Tailings 12	Gold	2.91	59	NO	NO	NP	0.857	0.042	1.44
Tailings 13	Gold	2.78	54	23	17	6	A = 0.735, B = 0.117, C = 0.271		1.44
Tailings 14	Manganese ore	3.40	3	–	–	–	A = 1.184, B = 0.078, C = 0.615		1.37
Tailings 15	Copper, gold	3.39	70	16	13	3	0.677	0.039	1.42
Tailings 16	Copper, gold	3.46	72	16	13	3	0.741	0.044	1.47
Tailings 17	Bauxite	2.58	15	–	–	–	A = 0.904, B = 0.115, C = 0.365		1.48
Tailings 18	Bauxite	2.86	76	36	20	16	1.257	0.098	1.49

NO: not obtainable

NP: non-plastic

Table 2: CSL parameters and index test results for tailings and other geomaterials (2 of 2)

Name	Associated commodity	G_s	FC (%)	LL (%)	PL (%)	PI (%)	Γ	λ_e	M_{tc}
Tailings 19	Silver, lead	3.37	59	37	NO	NP	0.827	0.036	1.50
Tailings 20	Lead, zinc	2.82	45	22	NO	NP	0.947	0.044	1.36
Tailings 21	Lead, zinc	3.01	91	29	24	5	1.077	0.049	1.29
Tailings 22	Silver, lead, zinc	3.99	81	22	16	6	1.195	0.089	1.32
Tailings 23	Copper, gold	2.81	56	22	14	8	0.749	0.051	1.34
Tailings 24	Copper, gold	2.85	34	20	15	5	0.761	0.053	1.40
Tailings 25	Copper, gold	2.82	58	20	15	5	0.828	0.058	1.41
Tailings 26	Copper, gold	2.82	86	33	17	16	1.119	0.094	1.15
Tailings 27	Iron ore	2.96	87	NO	NO	NP	0.925	0.045	1.42
Tailings 28	Gold	2.94	86	–	–	–	1.164	0.070	1.50
Tailings 29	Gold	2.93	54	–	–	–	0.784	0.037	1.40
Tailings 30	Gold	2.93	85	–	–	–	1.045	0.054	1.33
Tailings 31	Gold	2.54	82	29	18	11	1.013	0.053	1.30
Tailings 32	Gold	2.63	86	32	19	13	0.947	0.045	1.34
Tailings 33	Gold	2.57	80	27	18	9	0.919	0.045	1.33
Tailings 34	Iron ore	3.75	78	37	18	19	1.427	0.109	1.47
Tailings 35	Iron ore	3.46	84	32	18	14	1.160	0.075	1.33
Geomaterial 1	Fly ash	2.09	96	–	–	–	0.900	0.026	1.13
Geomaterial 2	Fly ash	2.10	88	–	–	–	0.980	0.033	1.35
Geomaterial 3	Coal rejects	1.49	50	30	23	7	0.873	0.086	1.59
Geomaterial 4	Coal rejects	1.89	46	35	23	12	0.727	0.059	1.52

NO, not obtainable

NP, non-plastic

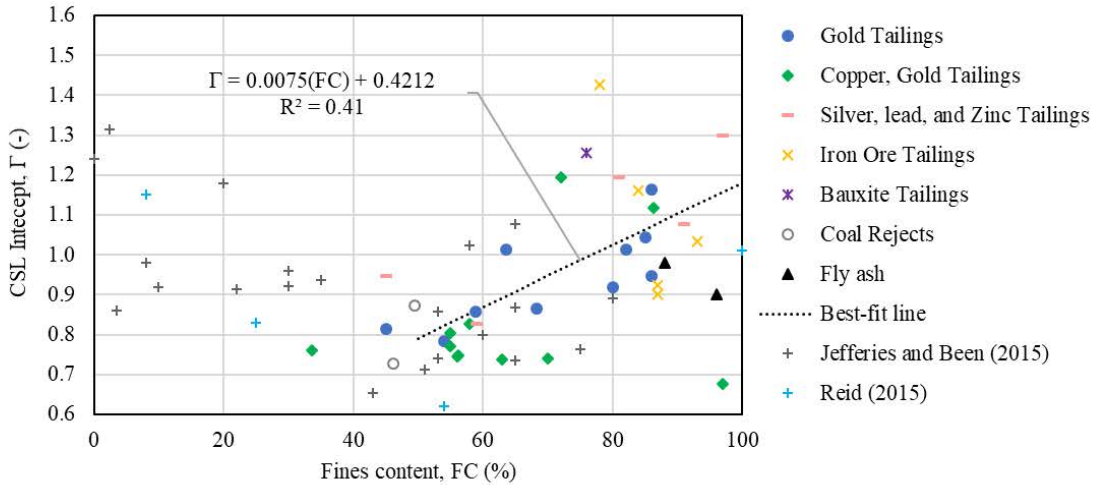

Figure 2: CSL intercept versus FC

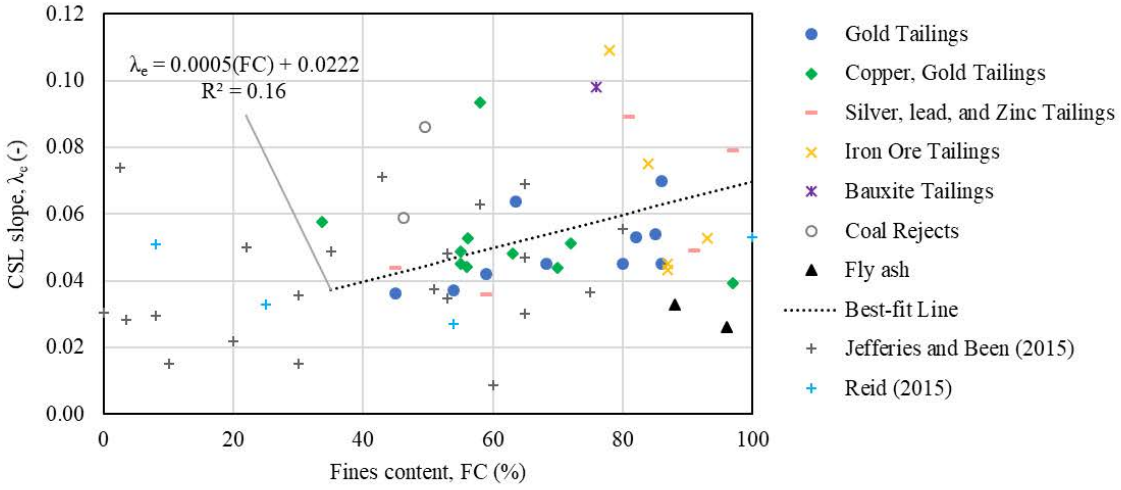

Figure 3: CSL slope versus FC

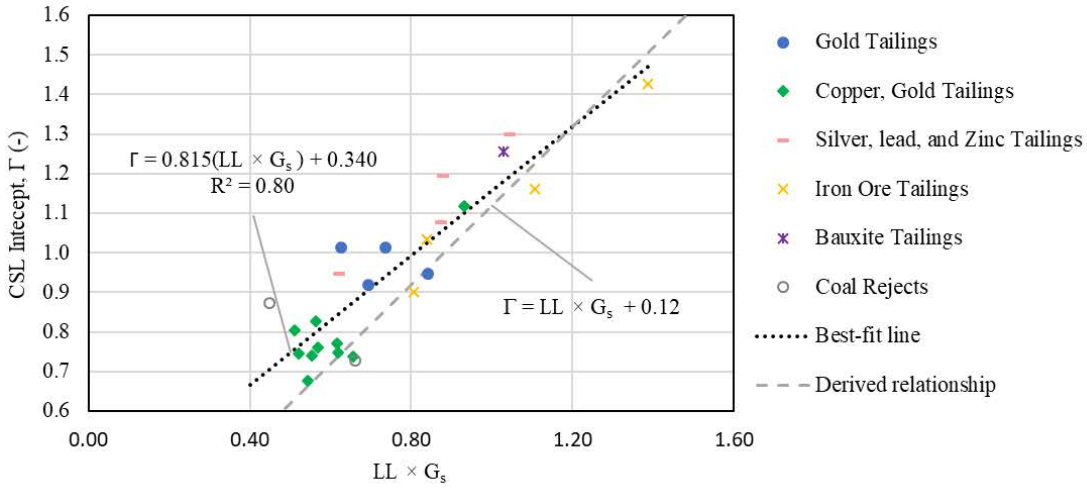

Figure 4: CSL intercept versus normalized LL

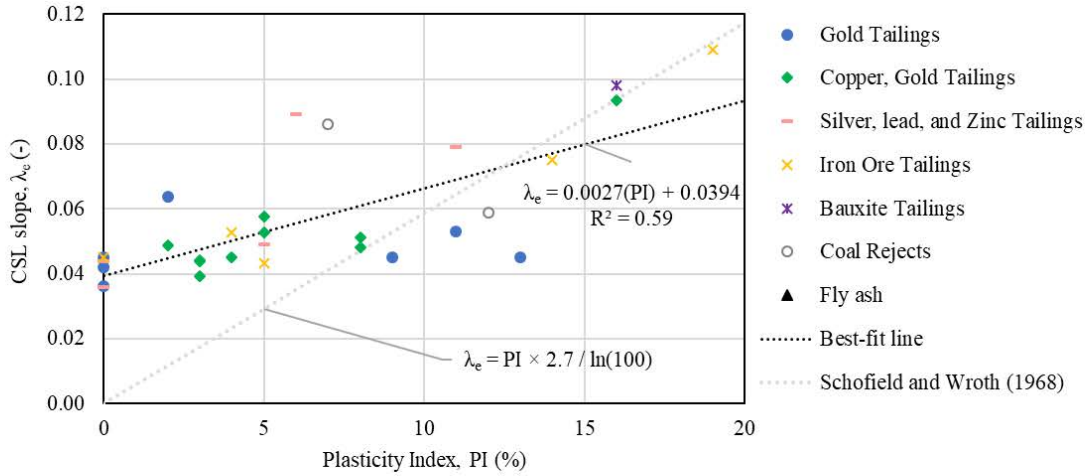

Figure 5: CSL slope versus PI

Discussion

CSL parameters – index test results correlations

The data presented in Figure 2 indicates that Γ has a weak to moderate correlation to FC, with Γ decreasing with increasing FC until approximately 50% fines, and increasing thereafter, consistent with findings of Carrera et al. (2011). This may indicate that at FC below 50% the grain contacts at the critical state are predominantly influenced by sand-sized particles, while at FC greater than 50% grain contacts are predominantly influenced by silt and clay sized particles, a concept previously proposed by Zlatovic and Ishihara (1995) as well as Polito and Martin (2001) and Jefferies and Been (2015).

The data presented in Figure 3 indicates that λ_e has a very weak correlation to FC, with λ_e generally increasing with increasing FC for the tailings tested (approx. FC > 35%). This is generally consistent with the findings of Olson and Stark (2003) who note that although the addition of fines to a given sand may increase the slope of the steady state line, no general trend was observed between slope of steady state line and increasing FC. However, research has shown strong correlation between FC and both of λ_e and Γ for a single TSF or processing plant (Carerra et al., 2011; Reid 2015). Jefferies and Been (2015) note that consideration of particle size gradation may provide a better indication of λ_e than FC alone.

The data presented in Figure 4 indicates that Γ has a strong correlation to LL when normalized by particle density as LL × G_S. This is expected as LL is a measure of the moisture content of a soil at approximately s_u = 2 kPa (Wood, 1990). By assuming a universal peak undrained shear strength ratio for loose, isotropically consolidated tailings of $s_{u,p}/p' = 0.2$, the LL should approximate the altitude of the CSL at p' = 10 kPa. Further, adopting the median λ_e from the data presented ($\lambda_e = 0.05$), the relationship $\Gamma = LL \times G_s + 0.12$ is derived. However, this relationship appears to underpredict Γ, in particular for tailings with low LL, potentially as a result of saline pore fluid, which has been shown to reduce reported LL in low plasticity silts (Jang and Santamarina, 2016), or failure to follow test procedure by sampling from the vicinity of the cone where moisture content may not be representative following cone penetration. Regardless, the correlation between Γ and LL is limited by the accuracy of methods used to determine the LL.

The data presented in Figure 5 indicates a moderate correlation between λ_e and PI, with λ_e increasing with increasing PI. The data is in general agreement with the theoretical correlation proposed by Schofield and Wroth (1968) $\lambda_e = 2.7\ PI / \ln(100)$ (based on the plastic limit representing an approximate measure of the moisture content of a soil at $_{u,PL} = 100 \times s_{u,LL}$) at PI greater than 7, with improved agreement at PI greater than 15. Tailings with PI less than 7 have λ_e values above the correlation proposed by Schofield and Wroth (1968); normalization by the LL or clay activity may improve the correlation.

The data presented in each of Figures 2 to 5 indicate that different ore properties and mineral processing methods may have an important influence on CSL parameters, as seen through slightly different

trends observed for various associated commodities. Whether this is a result of the different mineral processing and beneficiation processes adopted for different commodities or of the varying geology of the ore properties is not speculated upon. Additional CSLs for each associated commodity are likely required to further investigate any potential correlation. Regardless, significant variation in CSL parameters is observed within each associated commodity grouping.

No correlation was observed between M_{tc} and any of FC, Atterberg limits, or associated commodity.

Brittleness

Figure 6 presents a plot of I_B against Ψ_0/λ_e for the undrained triaxial tests used to infer the CSLs of the tailings presented herein. The data are overlaid over data presented by Jefferies and Been (2015) for sands, in order to show trends at values of I_B greater than 0.7, which were not generally observed during testing of the tailings. For "curved" CSLs an equivalent lambda value of $\lambda_{e,eq} = \Psi_0/\ln(p'_0/p'_{cs})$ was adopted.

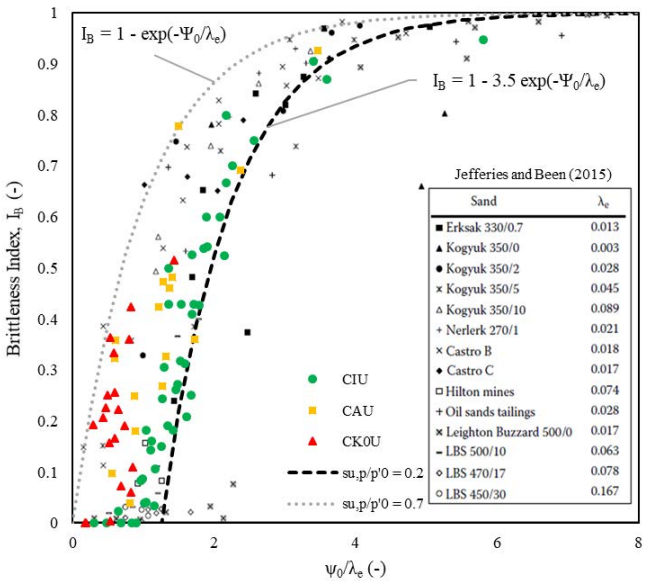

Figure 6: Brittleness Index vs. Ψ_0/λ_e

Functions representing peak undrained shear strength ratios of $s_{u,p}/p' = 0.7$ and 0.2 are also presented in Figure 6. The functions are derived from the semi-log CSL idealization assuming $M_{tc} = 1.4$ (median value for CSLs presented). The $s_{u,p}/p' = 0.2$ function is observed to provide a reasonable lower bound for the isotropically consolidated, undrained (CIU) triaxial tests, whilst the $s_{u,p}/p' = 0.7$ function is observed to provide a reasonable upper bound for the K_0 consolidated, undrained (CK_0U) triaxial tests. The CK_0U and anisotropically consolidated, undrained (CAU) tests are observed to be significantly more brittle than the CIU tests, confirming that stress path has a significant impact on brittleness. This is expected, as I_B contains a ratio of critical state undrained shear strengths, which are mobilized at high strains at the CSL and are

therefore independent of stress path and initial sample fabric (Been et al., 1991), and peak undrained strengths, which are mobilized at low strains and are dependent on stress path and initial sample fabric.

CSL "curvature"

It should be noted that for each tailings for which a semi-log CSL idealization was adopted (31 of 35 tailings CSLs), CSL "curvature" was not observed over the range of stresses tested. As the median range over which CSLs were defined was 30 – 900 kPa, it is reasonable to suggest that transition to "ductile" behaviour with CSL "curvature" (Robertson, 2017) occurs at stresses above 900 kPa for most tailings, which is generally consistent with the suggestion of Jefferies (2018). It should also be noted that of the tailings requiring a power law CSL idealization due to "curvature", "curvature" was greater for tailings with lower FC.

Design implications

Testing

For tailings, CSL parameters (particularly λ_e) cannot reliably be inferred from either FC or Atterberg limits, nor from experience with "similar" tailings (i.e., concepts such as associated commodity or similar). Triaxial testing is required to reliably define a CSL. An accurate CSL is important as it forms a base of reference for soil behaviour and can reveal the potential brittleness of a tailings. Thankfully, CSL testing requires only a relatively small tailings sample (generally <5 kg). Therefore, undertaking CSL testing using pilot or batch plant samples, at the design phase of new mining project, is often feasible. Additionally, CSL testing can be undertaken at a relatively low cost (<US$10,000 per sample), and therefore cost should not represent a significant impediment to it being undertaken at early study levels. As CSL parameters vary with material gradation, a range of gradations representative of that expected in the TSF can be tested to estimate the range of λ_e and Γ for the tailings in situ.

Resilient design principles

Regardless of whether design of a TSF is informed by CSSM and CSL testing, several resilient design principles can be taken from the CSL data presented in this paper (which are generally a reiteration of existing principles and heuristics). Firstly, preclude attainment of high Ψ values (i.e. "loose" tailings) in zones of tailings relied upon for TSF stability. Practically, this can be achieved by avoiding each of the following near TSF embankments: sub-aqueous deposition of tailings, deposition of fine-fraction tailings, high rates-of-rise, zones of loosely placed fill, and supernatant ponds. Furthermore, embankment setbacks or step-ins which may encroach the embankment onto "loose" tailings that were once remote from the embankment should be avoided. A resilient design approach would also include provision of compaction in zones of tailings relied upon for TSF stability. Secondly, avoid development of a high phreatic surface

or zones of near saturated tailings that may be susceptible to liquefaction, in zones of tailings relied upon for TSF stability. Provision of adequate underdrainage and potentially additional elevated drainage features (i.e. beach drains) is required. Lastly, be cautious of highly brittle tailings, which exhibit low λ_e (λ_e <0.04), as well as high FC (particularly low plasticity fines). Reliance on such tailings for TSF stability is not recommended unless adequate underdrainage and/or compacted zones are provided.

Conclusion

This paper has presented CSLs inferred for 35 tailings and four other geomaterials. The correlations between index test results (FC and Atterberg limits) and CSL parameters (λ_e and Γ) have been shown to be unreliable for the useful application of CSSM to TSF design. Additionally, experience with "similar" tailings (i.e., associated commodity) has been shown to be unreliable. Two resilient design principles can be taken from the CSL data presented in this paper, namely: preclude attainment of high Ψ values and high phreatic surfaces in zones of tailings relied upon for TSF stability, and be cautious of highly brittle tailings.

References

Been, K. and M.G. Jefferies. 1985. A state parameter for sands. *Géotechnique* 35(2): 99–112.

Been, K., M.G. Jefferies and J. Hachey. 1991. The critical state of sands. *Géotechnique* 41(3): 365–381.

Bishop, A.W. 1971. Shear strength parameters for undisturbed and remoulded soil specimens. *Proceedings of the Roscoe Memorial Symposium*, Cambridge: 3–58.

Carerra, A., M. Coop and R. Lancellotta. 2011. Influence of grading on the mechanical behaviour of Stava tailing. *Géotechnique* 61(11): 935–946.

Hird, C.C. and F.A.K. Hassona. 1990. Some factors affecting the liquefaction and flow of saturated sands in laboratory tests. *Eng. Geology* 28: 149–170.

Jang, J. and J.C. Santamarina. 2016. Fines classification based on sensitivity to pore-fluid chemistry. *J. Geotech. and Geoenviro. Eng.* 142(4): 06015018.

Jefferies, M.G. 2018. Critical state soil mechanics: 125 years of history to current use. South African Institution of Civil Engineering – 16th Jennings Memorial Lecture.

Jefferies, M.G. and K. Been. 2015. *Soil liquefaction – A critical state approach*, 2nd edition. Boca Raton: CRC Press.

Olsson, S.M. and T.D. Stark. 2003. Use of laboratory data to confirm yield and liquefied strength ratio concepts. *Can. Geotech. J*. 40: 1164–1184.

Poulos, S.J. G. Castro, G. and J.W. France. 1985. Liquefaction evaluation procedure. *J. Geotech. Eng*. 111(6).

Reid, D. 2015. Observations on the behaviour of a gold tailings with hypersaline pore fluid. *Proceedings of Tailings and Mine Waste Management for the 21st Century*, Sydney: 191–200.

Reid, D. 2019. Preliminary results of critical state testing round robin. LinkedIn, posted March 13, 2019.

Reid, D. and M.G. Jefferies. 2017. State parameter as a geological principle in tailings. In *Proceedings of the Twenty-first International Conference on Tailings and Mine Waste*, Banff, Alberta: 305–314.

Reid, D. and R. Fanni. 2019. Critical state testing of tailings: considerations related to pore fluid chemistry. *Proceedings of Tailings and Mine Waste 2019*. Vancouver, Canada.

Robertson, PK. 2017. Evaluation of flow liquefaction: Influence of high stresses. *Proceedings of the Third International Conference on Performance-based Design in Earthquake Geotechnical Engineering*, Vancouver.

Schofield, A. and C.P. Wroth. 1968. *Critical State Soil Mechanics*. London: McGraw Hill.

Verdugo, R. and K. Ishihara. 1996. The steady state of sandy soils. *Soils and Foundations* 36(2): 81–91.

Wood, D. 1990. *Soil behaviour and critical state soil mechanics*. Cambridge: Cambridge University Press.

Yang, J. and L.M. Wei. 2012. Collapse of loose sand with the addition of fines: The role of particle shape. *Géotechnique* 62(12): 1111–1125.

Zlatovic, S. and K. Ishihara. 1995. On the influence of nonplastic fines on residual strength. In *Proceedings of The First International Conference on Earthquake Geotechnical Engineering,* Tokyo: 239–244.

Bibliography

ASTM. 2014. Standard test method for specific gravity of soil solids by gas pycnometer, ASTM D5550-14. West Conshohocken, PA.

ASTM. 2011a. Standard test method for consolidated undrained triaxial compression test for cohesive soils, ASTM D4767-11. West Conshohocken, PA.

ASTM. 2011b. Method for consolidated drained triaxial compression test for soils, ASTM D7181-11. West Conshohocken, PA.

Standards Australia. 2006. Methods of testing soils for engineering purposes. Method 3.5.1: Soil classification tests – Determination of the soil particle density of a soil – Standard method. Sydney, Australia.

Standards Australia. 2009b. Methods of testing soils for engineering purposes. *Method 3.2.1: Soil classification tests – Determination of the plastic limit of a soil* – Standard method. Sydney, Australia.

Standards Australia. 2009a. Methods of testing soils for engineering purposes. *Method 3.1.1: Soil classification tests – Determination of the liquid limit of a soil* – Four point Casagrande method. Sydney, Australia.

Standards Australia. 2009c. Methods of testing soils for engineering purposes. *Method 3.6.1: Soil classification tests – Determination of the particle size distribution of a soil* – Standard method of analysis by sieving. Sydney, Australia.

Standards Australia. 2015. Methods of testing soils for engineering purposes. Method 3.9.1: Soil classification tests – Determination of the cone liquid limit of a soil. Sydney, Australia.

Standards Australia. 2016. Methods of testing soils for engineering purposes. Method 6.4.2: Soil strength and consolidation tests – Determination of compressive strength of a soil – Compressive strength of a saturated specimen tested in undrained triaxial compression with measurement of pore water pressure. Sydney, Australia.

Proceedings of Tailings and Mine Waste 2019
November 17–20, 2019, Vancouver, Canada
Published by University of British Columbia Press, 2019

Normalized Shear Modulus Reduction and Damping Ratio Curve of Mine Waste and Leached Ore

Eder Tapia, Anddes and National University of Engineering, Peru
Renzo Ayala, Anddes and National University of Engineering, Peru
Denys Parra, Anddes and National University of Engineering, Peru

Abstract

The seismic analysis and design of mining geotechnical facilities, such as mine waste dumps and heap leach pads, located in the Andes mountain range or close to it (Peru and Chile), require a proper determination of the dynamic properties of the materials that will be stacked on them, such us mine waste and leached ore. However, despite the seismic design importance of those facilities, the references about dynamic properties of these materials are very limited or non-existent, due to lack of research and laboratory testing on those materials.

Shear modulus and damping ratio are two essential soil dynamic parameters in seismic response analysis of geotechnical structures; moreover, many authors agree that these properties are nonlinear and strain-dependent. Therefore, degradation curves of normalized shear modulus and increments of damping ratio with shear strain are commonly used to model these features.

This paper presents laboratory research of the strain-dependent dynamic properties of mine waste and leached ore of current Peruvian mining operations. Mine waste and leached ore samples were reconstituted in a laboratory using the parallel or homothetic gradation technique (Marachi et al., 1972; Varadarajan et al., 2003; Verdugo and De la Hoz, 2006; Dorador, 2010; Besio, 2012). The materials were evaluated at the University of Texas at Austin using a combined resonant column and torsional shear (RCTS) device in all cases and cyclic-triaxial equipment for some of them; thus, the normalized shear modulus and damping ratio as a function of the shear strain amplitude were obtained. Based on the laboratory investigation on mine waste and leached ore, and statistical regression analysis, the hyperbolic model proposed by Darendeli (2001) and the model proposed by Zhang et al. (2005) were modified for the representation of the normalized shear modulus degradation and the damping ratio increment. Based on these results, the authors propose normalized shear modulus and damping ratio curves of mine waste and leached ore materials, which can be used in seismic response analysis of mine waste dumps and heap leach pads.

Introduction

Facilities such as heap leach pads and mine waste dumps are formed by stacking precious or base metal ore materials and mine waste rock materials, respectively. Currently, these facilities can be higher than 100 m due to area and environmental impact constraints; a failure of these massive facilities would generate substantial damage (environmental, economic, and human lives). Therefore, proper static and seismic slope stability performance is essential for safe operation and closure.

The seismic design of South America's mining projects has significant importance due to the assessment of seismic response analysis. This assessment is used to calculate the seismic coefficient and seismic-induced permanent displacement. For these reasons, a proper determination of the dynamic properties of leach ore (LO) and mine waste rock (MW) is necessary. This paper studies LO and MW as similar materials, since the samples used were obtained as run-of-mine (ROM).

There are several empirical curves for dynamic properties in the technical literature for soils, such as Seed and Idriss's (1970) sand model, Seed et al.'s (1986) and Rollins et al.'s (1998) gravel model, Vucetic and Dobry's (1991) clay model, Darendeli's (2001) fine-grained soils model, Menq's (2003) sand and gravel model, and Senetakis et al.'s (2013) model for quartz and volcanic sands. Beyond the empirical curves for LO and MW, presented by Parra et al. (2016), based on a database of vibration and cyclic test. However, there are no databases available for dynamic behaviour characterization of LO and MW, due to the maximum particle size incompatibility allowed by standard testing devices.

The laboratory tested a total of 9 samples; 2 LO and 7 MW were used, which were taken from different mines located in the Peruvian Andes.

Materials and methodology

Materials used

The materials presented by Parra et al. (2016) were complemented with 3 MW samples, making a total of 2 LO and 7 MW samples, which were reconstituted in the laboratory using the parallel-gradation technique or homothetic technique (Marachi et al., 1972; Varadarajan et al., 2003; Verdugo and De la Hoz, 2006; Dorador, 2010; Besio, 2012). The homothetic technique scales the field particle-size distribution curve to a parallel one considering the maximum particle size allowed by a commercial testing device; for LO and MW samples tested its size was 10 to 15 times smaller than the maximum particle size found in the field. The homothetic gradation curve of the materials tested in the laboratory maintained a similar coefficient of uniformity (C_u), shape, and dry density as the materials in the field, but limiting the fines content to a maximum of 10%. Figure 1 shows the contrast between the field and laboratory samples. Table 1 summarizes the index properties of the materials, and Figure 3(a) shows the global and homothetic grain-

size curve of all materials. It must be said that these materials are typical for MW and LO, as shown in Figure 3(b), when compared to typical mine waste from Hawley and Cunning (2017).

According to Table 1 the field LO matrix was classified as well-graded gravel (GW) according to the Unified Soil Classification System (USCS), and the LO reconstituted for laboratory testing was classified as well-graded sand (SW) according to the USCS. The field MW matrix was classified as poor-graded clayey gravel, well-graded gravel, and well-graded silty gravel (GP-GC, GW and GW-GM) according to the USCS. The MW reconstituted for laboratory testing was classified as well-graded silty sand, well-graded sand, and poorly graded silty sand (SW-SM, SW and SP-SM) according to the USCS.

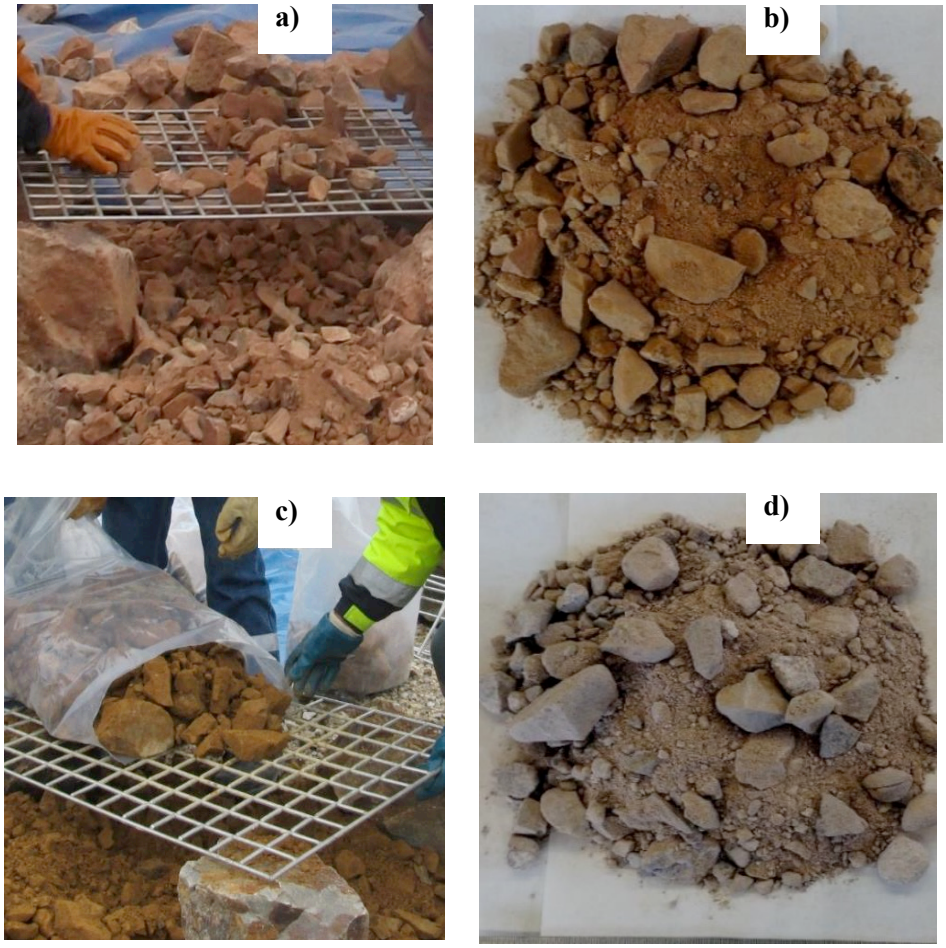

Figure 1: LO tested in the (a) field and (b) laboratory.
MW tested in the (c) field and (d) laboratory (Parra et al., 2016)

Table 1: Index properties of field and laboratory specimens

Material	Sample	Location	Dynamic test	USCS[1]	G_s[2]	W[3] (%)	γ_T[4] (kN/m³)	e[5]	C_u[6]	D_{50}[5] (mm)
Leached ore	LO_01	Field	RCTS and CTX	GW	2.61	2.17 – 2.23	20.0 – 21.4	0.15 – 0.214	28	90
		Laboratory		SW	2.61	2.96	26.1	0.299	28	3,1
	LO_02	Field	RCTS and CTX	GW	2.61	2.17 – 2.23	20.0 – 21.4	0.15 – 0.214	28	90
		Laboratory		SW	2.61	2.94	20.1	0.299	28	3,1
Mine waste	MW_01	Field	RCTS	GP-GC	2.5	1 – 12.7	–	–	12	32,6
		Laboratory		SW-SM	2.5	8.8	15.8	0.712	12	3,2
	MW_02	Field	RCTS and CTX	GW	2.67	0.4 – 4.5	20.8 – 23.8	0.111 – 0.265	21	111
		Laboratory		SW	2.67	4.76	22.1	0.265	26	3
	MW_03	Field	RCTS and CTX	GW	2.67	0.4 – 4.5	20.8 – 23.8	0.111 – 0.265	21	111
		Laboratory		SW	2.67	4.24	21.0	0.265	26	3
	MW_04	Field	RCTS	GW-GM	3.23	1.9 – 2.8	23.4 – 24.5	0.166 – 0.607	220	25,4
		Laboratory		SP-SM	3.23	3.23	24.7	0.35	24	1
	MW_05	Field	RCTS	GW-GM	3.23	1.9 – 2.8	23.4 – 24.5	0.166 – 0.607	220	25,4
		Laboratory		SP-SM	3.23	3.13	25.2	0.32	24	1
	MW_06	Field	RCTS	GW-GM	3.23	1.9 – 2.8	23.4 – 24.5	0.166 – 0.607	220	25,4
		Laboratory		SP-SM	3.23	3.39	23.9	0.39	24	1
	MW_07	Field	RCTS	GW-GM	3.23	1.9 – 2.8	23.4 – 24.5	0.166 – 0.607	220	25,4
		Laboratory		SP-SM	3.23	2.60	24.2	0.37	24	1

Notes:
1) Unified Soil Classification System, 2) Specific gravity, 3) Water content, 4) Total unit weight, 5) Void ratio at 1 atmosphere of confining pressure, 6) Coefficient of uniformity and 7) Average diameter by mass.

Abbreviation:
RCTS: Resonant column and torsional shear test.
CTX: Triaxial cyclic test.

Experimental equipment and sample preparation

Using a combined resonant column (RC) and torsional shear (TS) device and a triaxial cyclic (CTX) device, the G/G_{max}-log(γ) and $D\text{-}D_{min}$-log(γ) curves of LO and MW were assessed at the University of Texas at Austin. Figure 2 shows a schematic of the RCTS device used for the laboratory program. The characteristics of the devices used in this study have been thoroughly presented by Parra et al. (2016).

The laboratory program used the homothetic grain-size distribution (Figure 2) to reconstitute and match in-situ density and water content (Table 1).

RCTS tests were performed using a range of confining pressures from 69 to 1,379 kPa over a shearing strain (γ) ranging from 10^{-7}% to 0.1% to samples LO_01, LO_02, MW_01, MW_02, MW_03, MW_04, MW_05, MW_06 and MW_07. A CTX test was performed using a range of confining pressures from 303 to 700 kPa over a shearing strain (γ) ranging from 0.01% to 1.4% with a load control (stress) and displacement control (strain) to samples LO_01, LO_02, MW_02 and MW_03. These confining pressures represent the different heights of the heap leach pads and mine waste dumps.

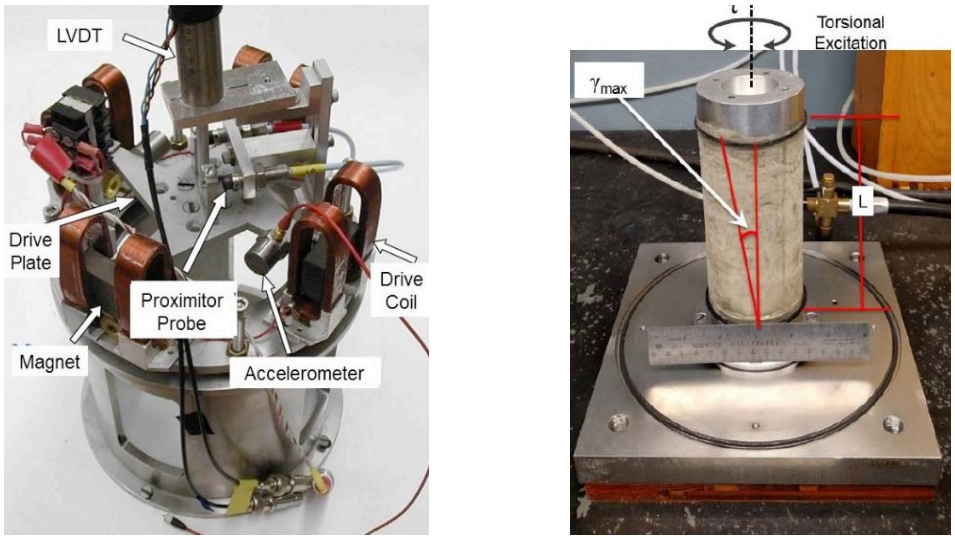

Figure 2: Resonant column torsional shear (RCTS) test device of The University of Texas at Austin

Experimental results

Representative RCTS and CTX tests results of LO and MW are plotted in Figures 4 to 5. In the same figures, the G/G_{max}-log(γ) and D-D_{min}-log(γ) curves proposed by Menq (2003), Darendeli (2001) and Senetakis et al. (2013) are also shown for comparison purposes.

It must be mentioned that the curves proposed by Darendeli (2001) are oriented to fine-grained soils; however, for this comparison, we only take into account the hyperbolic model proposed by Darendeli (2001).

Based on the comparison in Figures 4 to 5, we can conclude that:

- In Figure 4 the G/G_{max}-log(γ) curves by Darendeli (2001) and D-D_{min}-log(γ) curves by Menq (2003) and Darendeli (2001) have the best agreement with the RCTS and CTX test results of LO, while Senetakis et al. (2013) do agree with the RCTS and CTX tests.
- In Figure 5 the G/G_{max}-log(γ) and D-D_{min}-log(γ) curves by Darendeli (2001) show the best agreement with the RCTS and CTX test results of MW, while Menq (2003) and Senetakis et al. (2013) do not agree with the RCTS and CTX tests.

We can conclude that the G/G_{max}-log(γ) and D–D_{min}-log(γ) curves by Darendeli (2001) and Menq (2003) have better agreement with the RCTS and CTX test results of LO ore and MW, respectively. For this reason, the same hyperbolic model employed by Darendeli (2001) and Menq (2003) was used to represent the dynamic behaviour of those materials.

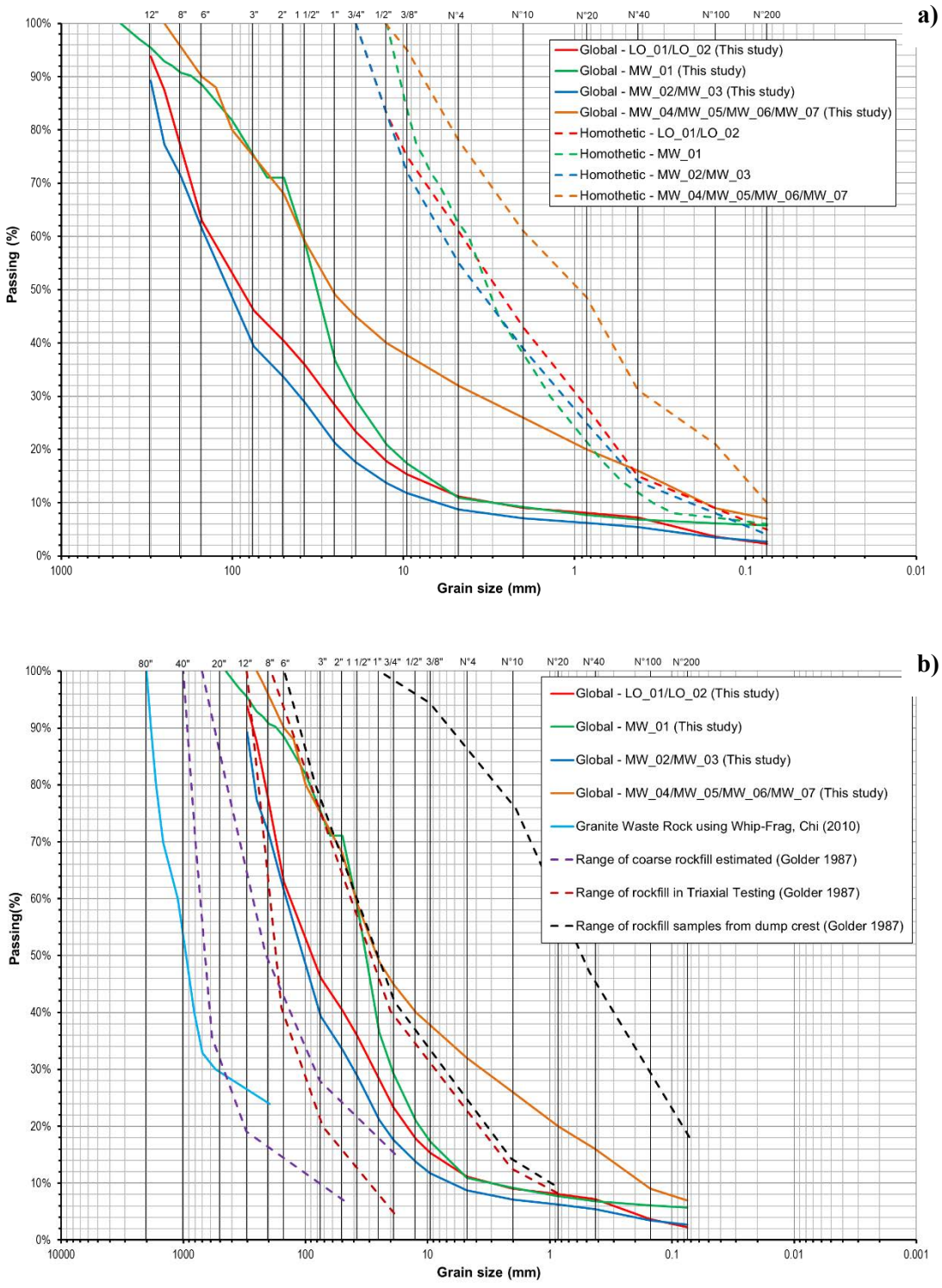

Figure 3: (a) Grain-size distribution of LO and MW used (global and homothetic); and (b) grain-size distribution contrast between waste dump rockfill materials (Hawley and Cunning, 2017) and LO and MW (this study)

Proposed relationships

G/G_{max}-log(γ) curves

In order to describe the behaviour of normalized shear modulus, the hyperbolic model proposed by Darendeli (2001) was used with equations (1) and (2). Unlike Hardin and Drnevich (1972), this model adds a curvature coefficient (a), which allows a better modelling of the nonlinear range of G/G_{max}-log(γ) curve. Based on the RCTS and CTX tests, Table 2 summarizes the experimental values of curvature coefficient (a), reference shear strain at 1 atm (A_y), and the slope of log(γ_r)-log(σ_m) curve (n_y).

Table 2 shows that the experimental curvature coefficient (a) is between 0.75 and 1.2, with an average value equal to 0.925. In this paper, 0.925 was used. Figure 6 shows that the coefficient of uniformity (C_u) and mean grain size (D_{50}) do not influence experimental A_y and n_y values. Therefore, mean values for both, 0.017 to A_y and 0.486 to n_y, were used.

$$\frac{G}{G_{max}} = \frac{1}{1 + \left(\frac{\gamma}{\gamma_r}\right)^a} \quad (1)$$

$$\gamma_r = A_y \sigma_m^{n_y} \quad (2)$$

Where:

G/G_{max}	=	Normalized shear modulus
γ	=	Shear strain
γ_r	=	Reference shear strain
a	=	Curvature coefficient
A_y	=	Reference shear strain at 1 atm
n_y	=	Slope of log(γ_r)-log(σ_m) curve
σ_m	=	Mean effective confining pressure

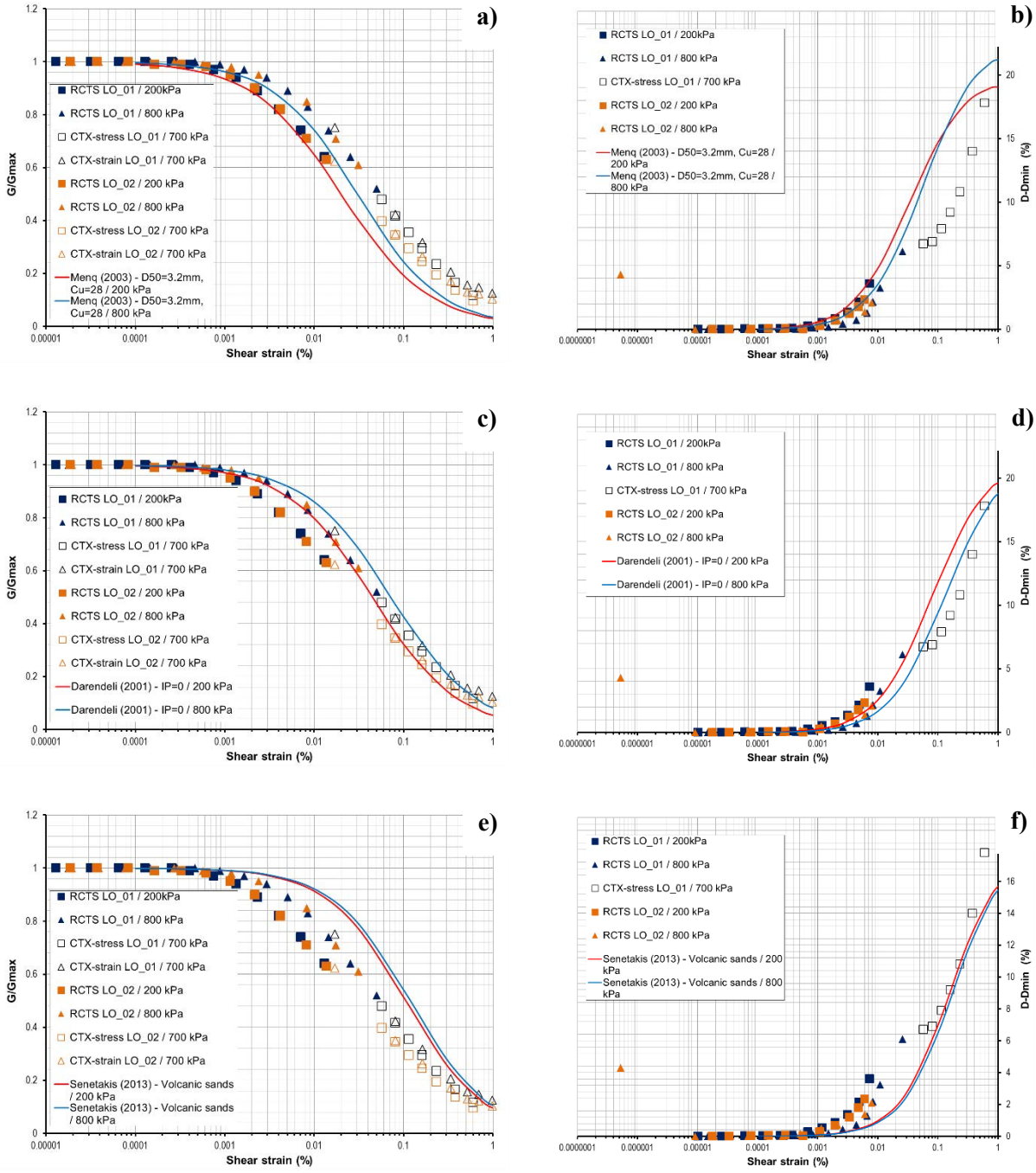

Figure 4: Experimental versus analytically derived G/G_{max}-log(γ) and $(D-D_{min})$-log(γ) curves of leached ore (LO_01 and LO_02). Representative result

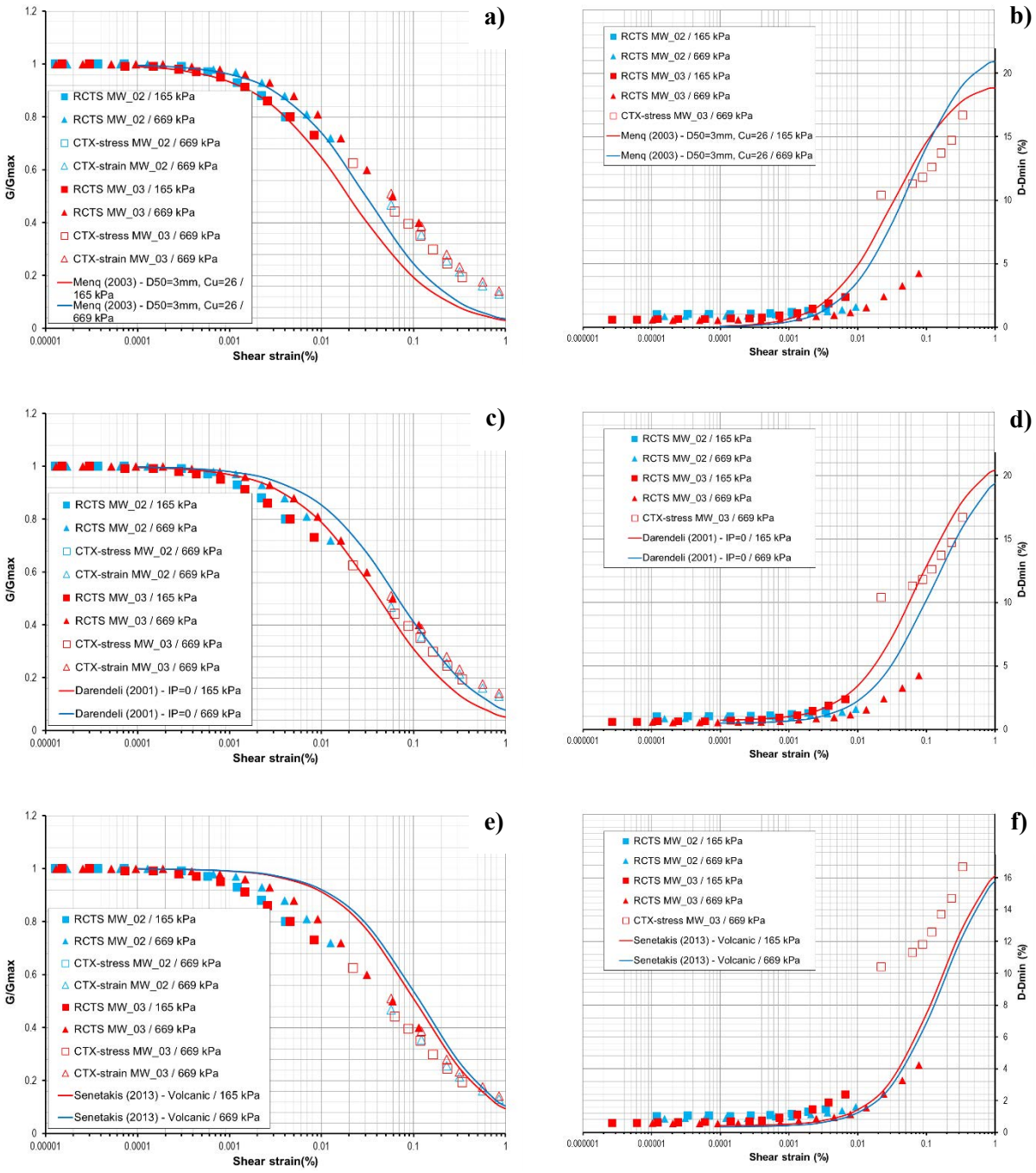

Figure 5: Experimental versus analytically derived G/G_{max}-log(γ) and $(D-D_{min})$-log(γ) curves of mine waste (MW_02 and MW_03). Representative results

Table 2: Curvature coefficient and reference strain parameters (A_y, n_y) of specimens of this study

Sample	σ_m[1] (kPa)	α[2]	γ_r[3] (%)	A_y[4] (%)	n_y[5]	R^2[6]
LO_01	200	0.93	0.023	0.0008	0.0629	1.00
	800	0.86	0.055			
LO_02	200	0.85	0.026	0.0021	0.472	1.00
	800	0.95	0.050			
MW_01	69	0.84	0.020	0.0029	0.464	0.99
	138	0.73	0.030			
	276	0.85	0.038			
	551	0.84	0.053			
	1103	0.80	0.075			
MW_02	165	0.88	0.021	0.0017	0.495	1.00
	669	0.85	0.042			
MW_03	165	0.75	0.031	0.0023	0.506	1.00
	669	0.82	0.063			
MW_04	345	1.20	0.014	0.0007	0.516	1.00
	689	1.10	0.020			
MW_05	345	1.00	0.025	0.0054	0.264	1.00
	689	1.05	0.030			
MW_06	345	1.15	0.018	0.0007	0.576	0.82
	689	0.95	0.037			
MW_07	1,379	1.00	0.040	–	–	–
	689	0.90	0.050			

Notes:

1) Mean effective confining pressure, 2) Curvature coefficient, 3) Reference shear strain, 4) Reference shear strain at 1 atm, 5) Slope of log (γ_r)-log (σ_m) curve and 6) Coefficient of correlation to γ_r with Ay and n_y

According to the RCTS and CTX test results and after analyzing the normalized modulus degradation curves through the hyperbolic model (equation 1), the experimental values of G/G_{max} and γ_r may be expressed as a function of mean effective confining pressure (σ_m) through equation (3) and (4).

$$\frac{G}{G_{max}} = \frac{1}{1 + \left(\frac{\gamma}{\gamma_r}\right)^{0.925}} \quad (3)$$

$$\gamma_r = 0.017\sigma_m^{0.486} \quad (4)$$

Where:

G/G_{max} = Normalized shear modulus

γ = Shear strain

γ_r = Reference shear strain

σ_m = Mean effective confining pressure

Figure 7 shows the measured against the analytically derived G/G_{max} values from this study, which is satisfactory for practical geotechnical purposes.

D-log(γ) curves

An average two-order polynomial curve (equation 5) was used to represent the behaviour of damping ratio ($D-D_{min}$) as a function of normalized shear modulus (G/G_{max}). This equation has also been used to correlate the damping increase as a function of the degradation of the normalized shear modulus of granular and cohesive soils (e.g., Senetakis et al., 2013; Zhang et al., 2005).

$$D - D_{min} = f\left(\frac{G}{G_{max}}\right) = a_1\left(\frac{G}{G_{max}}\right)^2 + a_2\left(\frac{G}{G_{max}}\right) + a_3 \quad (5)$$

Where:

$f(G/G_{max})$ = Function of the normalized shear modulus

D = Damping ratio

D_{min} = Small strain damping ratio

G/G_{max} = Normalized modulus degradation

a_1, a_2 y a_3 = Fitting parameters

Figure 8 shows $D-D_{min}$ against the corresponding G/G_{max} values of all samples tested. Considering the experimental results of Figure 7, equation (5) may be written as equation (6).

$$D - D_{min} = f\left(\frac{G}{G_{max}}\right) = 19.36\left(\frac{G}{G_{max}}\right)^2 - 40.28\left(\frac{G}{G_{max}}\right) + 20.98 \quad (6)$$

Where:

D = Damping ratio

D_{min} = Small strain damping ratio

G/G_{max} = Normalized shear modulus

In Figure 9, the measured against the analytically derived D-D_{min} values from this study were plotted; the comparison between measured and estimated D-D_{min} is acceptable for geotechnical purposes. In addition, Figure 8 shows that from $G/G_{max} < 0.6$ a better fitting than $G/G_{max} > 0.6$ is obtained. This is because there are more RCTS tests than CTX tests.

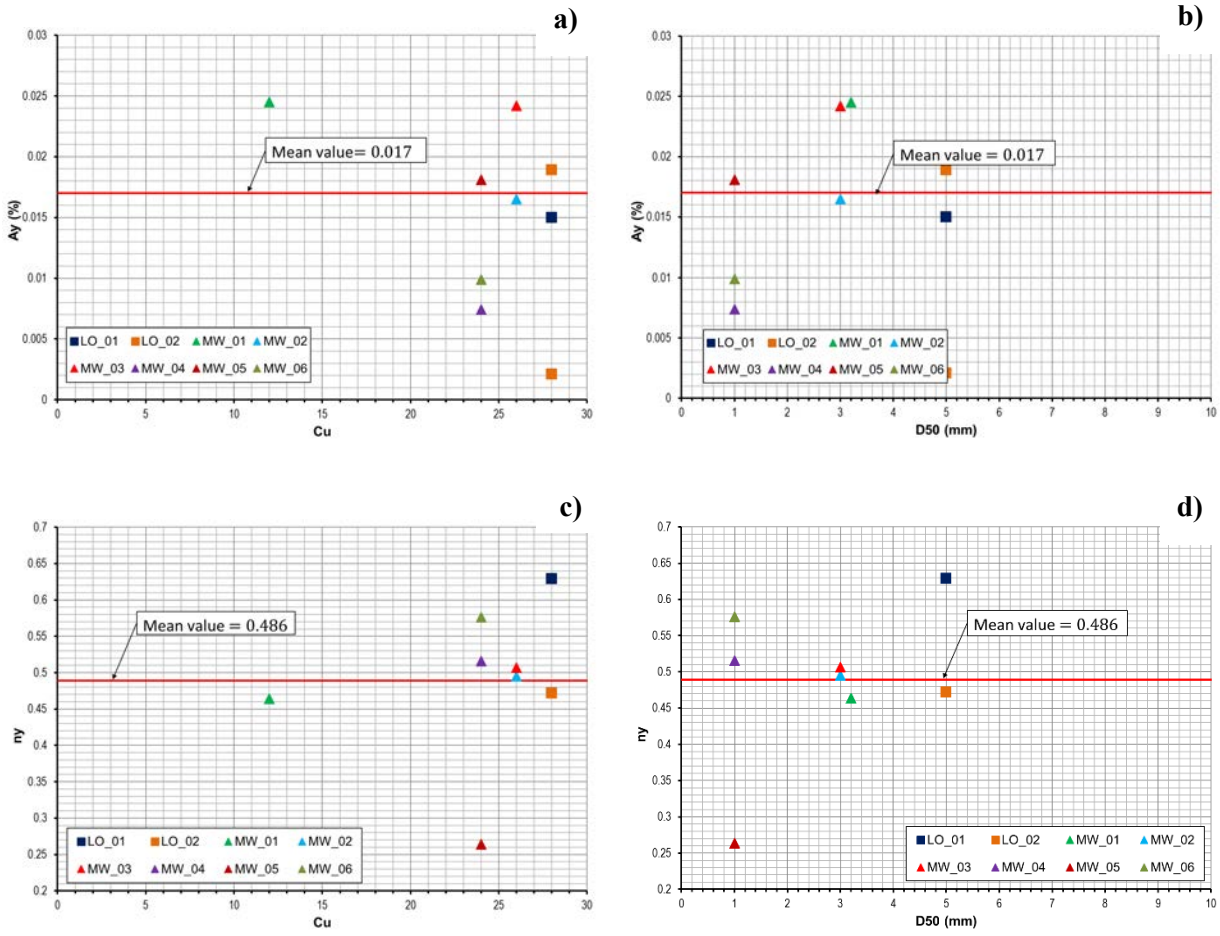

Figure 6: Effect of coefficient of uniformity (C_u) and mean grain size (D_{50}) on parameter A_y (a and b) and n_y (c and d)

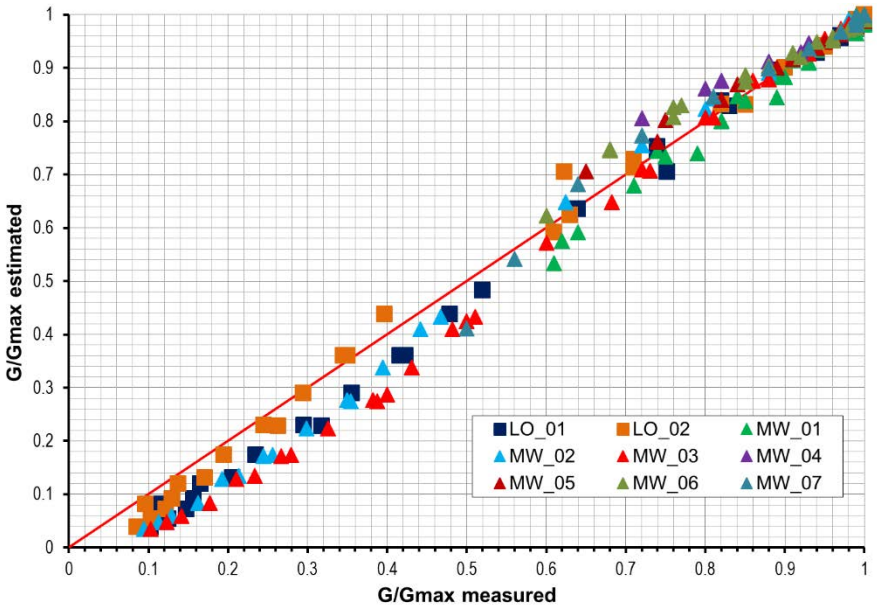

Figure 7: Experimental against analytically derived values of normalized shear modulus (G/G_{max}) of samples tested in this study

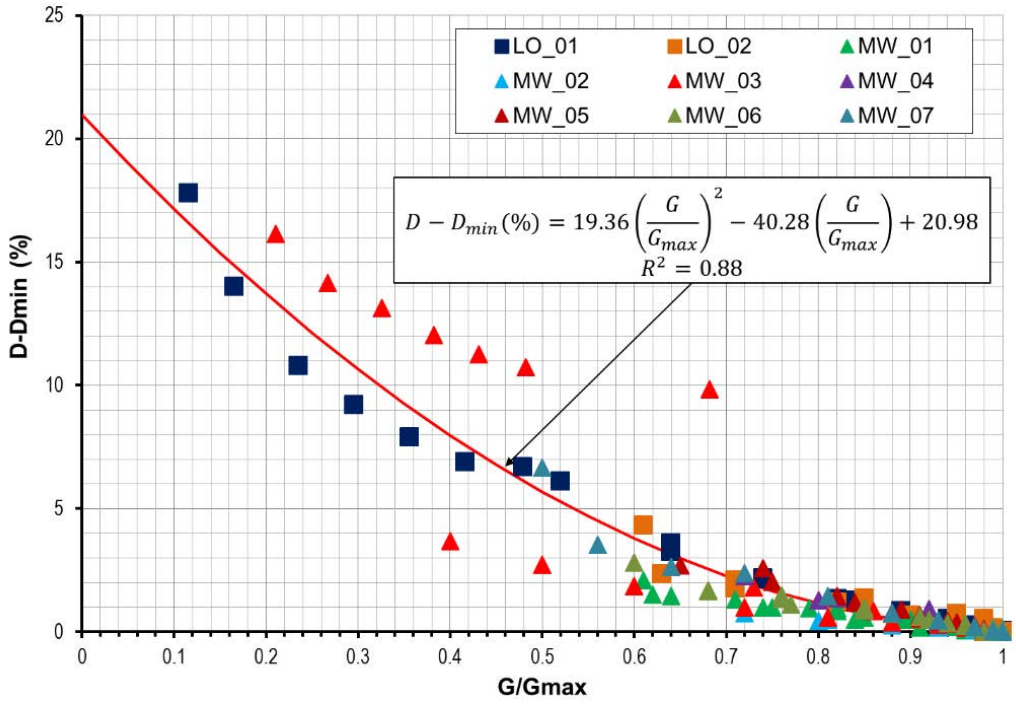

Figure 8: Damping ratio $D\text{-}D_{min}$ against G/G_{max}

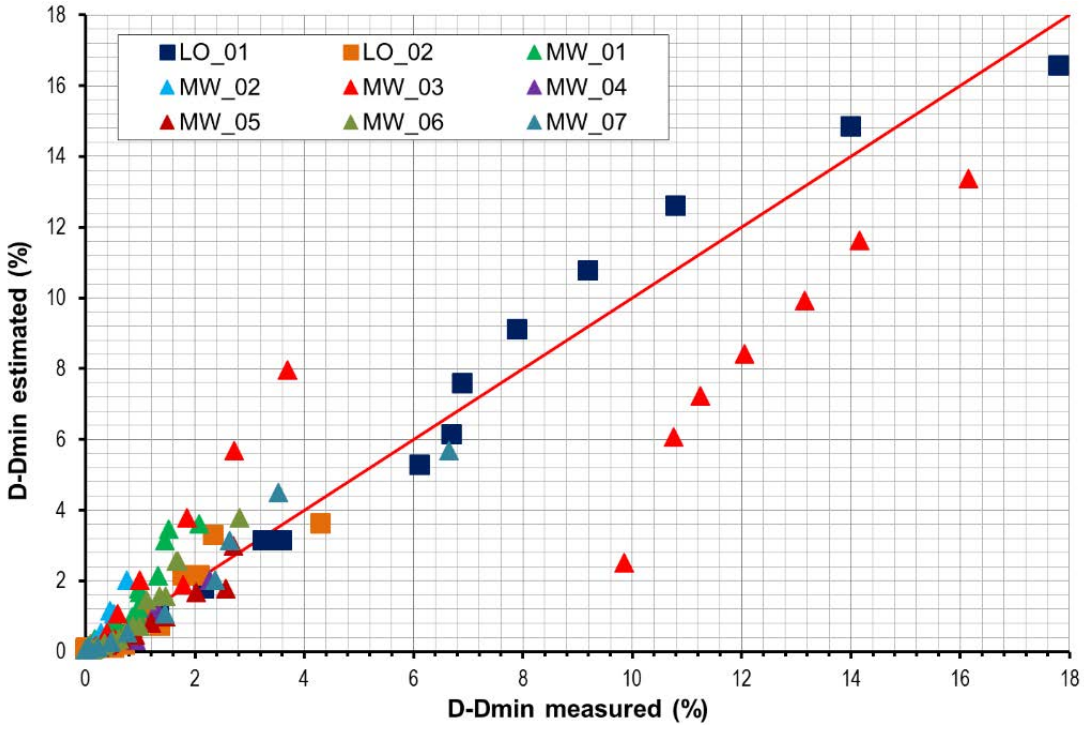

Figure 9: Experimental against analytically derived values of damping ratio (D-D_{min}) of specimens of this study

Overall, the sample MW_03 shows greater deviation from estimated values to D-D_{min}> 2%. This is because RCTS test results are better than CTX test results. However, it is acceptable for geotechnical purposes.

Comparison

Comparison of this investigation and literature curves

Using the analytical relationship developed in this paper (equations 3, 4, and 6), in Figure 10 G/G_{max}-log(γ) and D-D_{min}-log(γ) curves for LO and MW to 500, 1,000 and 1,500 kPa are presented. In the same figure the corresponding curves proposed by Darendeli (2001), Menq (2003), and Senetakis et al. (2013) are plotted. As expected, the design G/G_{max}-log(γ) curves proposed in this paper are in good agreement with the corresponding curves proposed by Menq (2003) at low confining pressure (500 kPa), but at high confining pressures (1,000 and 1,500 kPa) they are not.

On the other hand, the design D-D_{min}-log(γ) curves proposed in this paper are in good agreement with the corresponding curves proposed by Darendeli (2001); although Darendeli's (2001) curves are not proposed for granular soil. We can conclude that the curves presented in this paper accurately represent the dynamic properties of these materials.

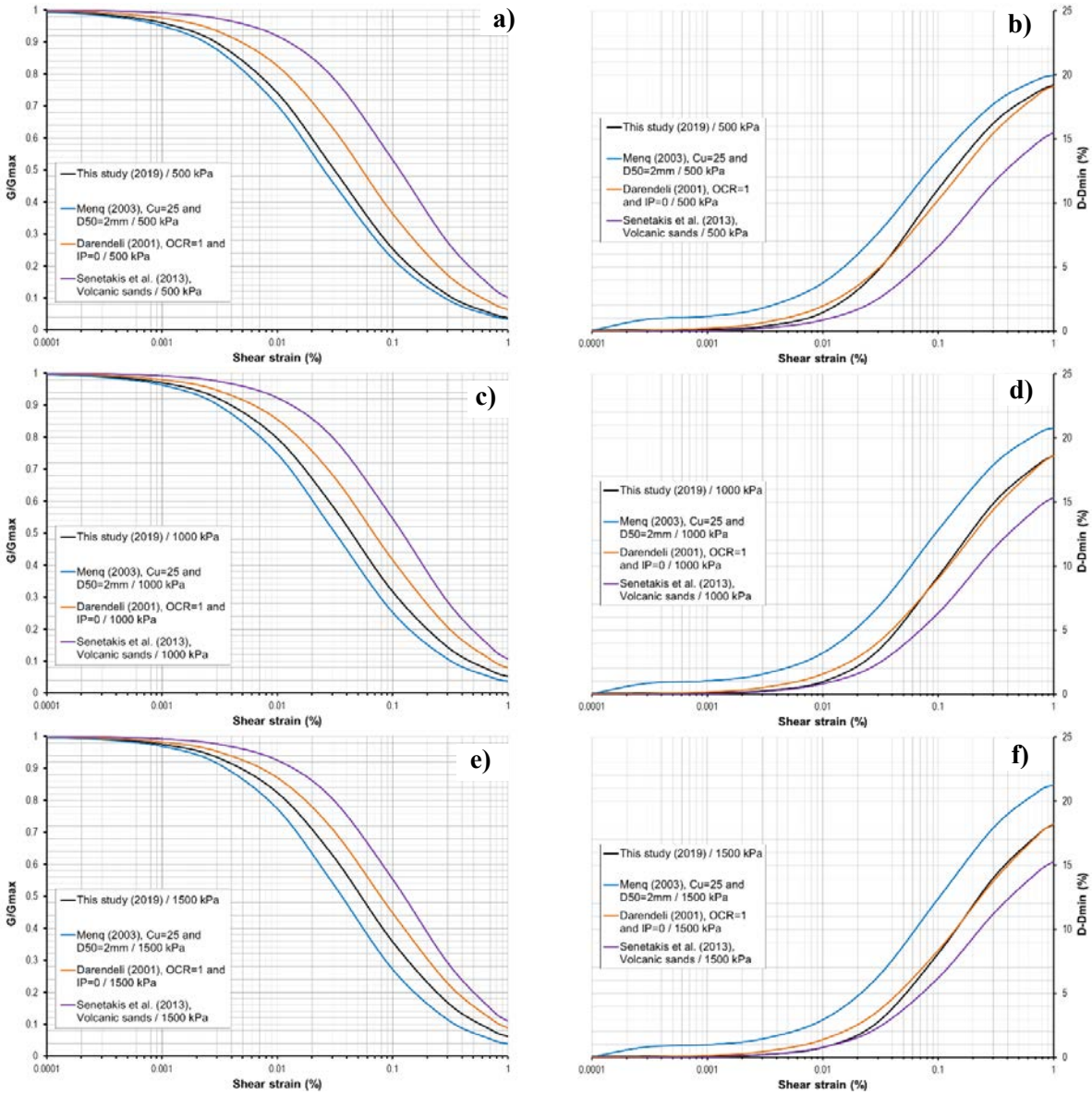

Figure 10: Design G/G_{max}-log(γ) (a, c and e), $(D-D_{min})$-log(γ) (b, d and f) curves for LO and MW proposed in this study, and comparison with corresponding curves proposed by Menq (2003), Darendeli (2001), and Senetakis et al. (2013)

Comparison between this study curves and moraines, tailings and structural fill test results

Figure 11 shows the curves proposed in this paper with RC and TS test results of natural and anthropogenic materials like moraine soil (MO), tailings (TL), and structural fill (SF), which are frequently used in the mining industry. Representative samples of those materials collected from different mining projects were tested in the Anddes geotechnical laboratory in Lima.

Table 3 shows the properties of moraine soil, tailings, and structural fill used in this comparison.

Table 3: Summary of properties of natural and anthropogenic materials

Material	Sample	USCS[1]	Y_d[2] (g/cm³)	e[3]	Gs[4]	G[5] (%)	S[6] (%)	F[7] (%)	LL[8] (%)	LP[9] (%)	IP[10] (%)	W[11] (%)
Moraine soil	MO_01	ML	1.72	0.59	2.72	5	45	50	NP	NP	NP	20
Tailing	TL_01	SM	1.79	0.87	3.34	0	70	30	NP	NP	NP	5
Structural fill	SF_01	SP-SM	1.78	0.70	2.99	30	60	10	NP	NP	NP	5

Notes: 1) Unified Soil Classification System, 2) Dry unit weight, 3) Void ratio at 1 atmosphere of confining pressure, 4) Specific gravity, 5) Gravel content, 6) Sand content, 7) Fines content, 8) Liquid limit, 9) Plastic limit, 10) Plasticity index and 11) Water content.

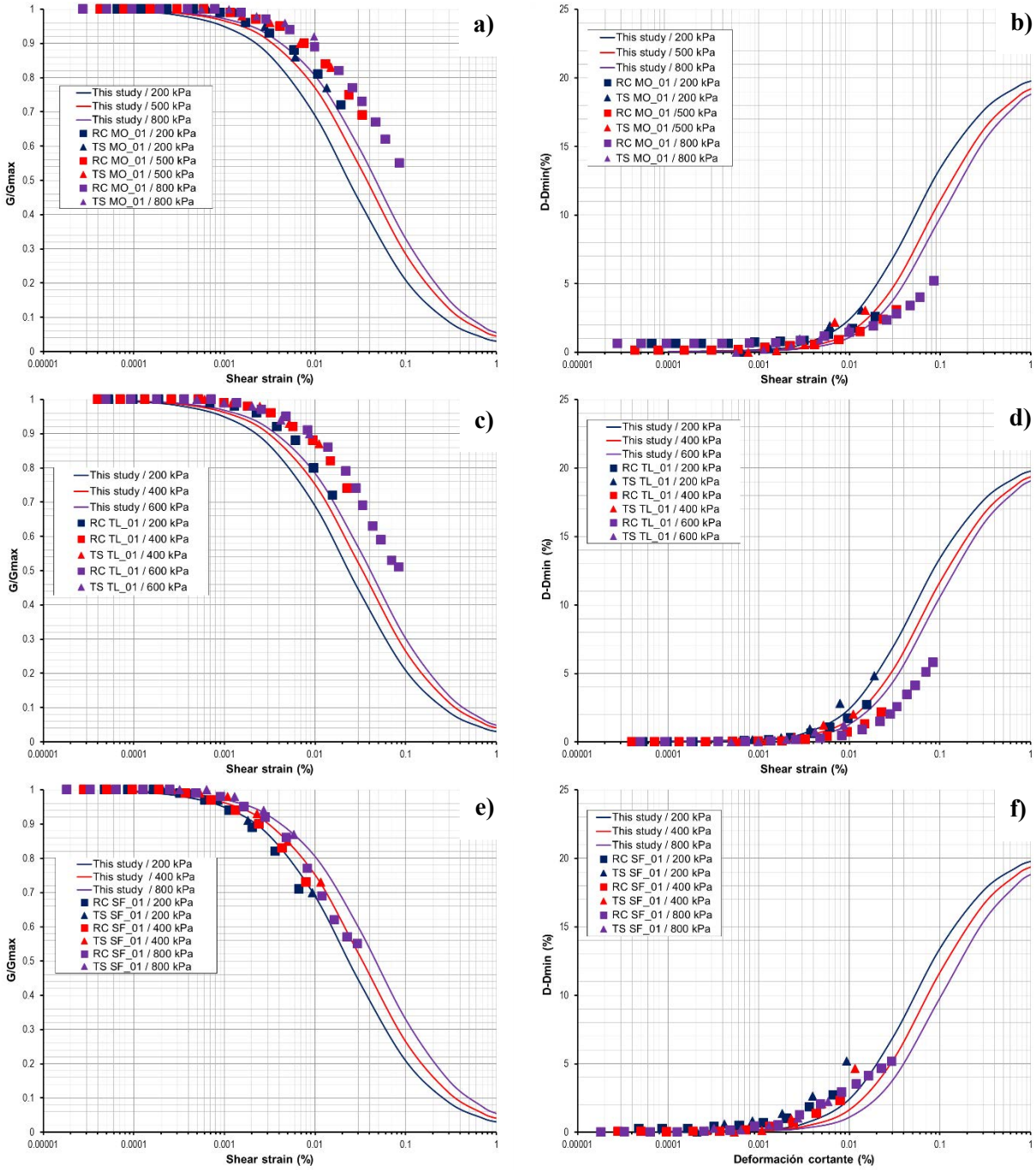

Figure 11: Normalized shear modulus and damping ratio versus shear strain for (a and b) moraine soil, (c and d) tailings, (e and f) structural fill and curves for LO and MW (this study)

Based on the comparison shown in Figure 11, we can conclude that:

- The curves proposed in this study underestimate the RC and TS test results of moraine soil and tailings G/G_{max}-log(γ) curves at all confining pressures. The D-D_{min}-log(γ) curves proposed in this study are in good agreement at 200 and 500 kPa with moraine soil and at 200 to 400 kPa with tailings.
- At 800 kPa the curves proposed in this study overestimate the RC and TS test results of moraine soil and tailings after 0.01% shear strain. Good agreement between G/G_{max}-log(γ) structural fill curves and the curves proposed in this study at all confining pressures is observed. For D-D_{min}-log(γ) curves an underestimating of the curves proposed in this study after 0.001% shear strain is observed.

Conclusion

Little is known about the dynamic properties of ROM leached ore and mine waste materials due to the maximum particle size allowed by commercial testing devices. However, the homothetic technique is an excellent tool to test these materials at scale in standard devices, as shown by the similar shear wave velocity values obtained in the field by geophysical tests and RCTS tests in leach ore and mine waste materials.

Beyond Parra et al. (2016), there are no curves in the literature that represent at the same time the dynamic behaviour of normalized shear modulus and the damping ratio of LO and MW; however, sometimes Menq's (2003) curves are in good agreement with normalized shear modulus but not with the damping ratio.

This paper shows that the curves (G/G_{max}-log(γ) and D-D_{min}-log(γ)) proposed in this study are in good agreement with the structural fill (SP-SM) curve since this material is coarser than moraine soil (ML) and tailings (SM).

The author proposes G/G_{max}-log(γ) and D-D_{min}-log(γ) as a function of mean effective confining pressure (Hardin and Drnevich, 1972; Tanaka et al., 1987; Darendeli, 2001; Menq, 2003; Zhang et al., 2005; Senetakis et al., 2013; etc.). This is due to the limited information about LO ore and MW in terms of maximum particle size, different grain size distribution, mineralogical variation, etc.

The G/G_{max}-log(γ) and D-D_{min}-log(γ) curves proposed in this paper for LO and MW materials may be taken as a preliminary reference for seismic response and rigorous numerical dynamic analysis of heap leach pads and mine waste rock dumps facilities. For detailed engineering and updated geotechnical assessment of these materials, specific cyclic testing (RCTS, CTX, centrifuge test, etc.) on representative samples is required to confirm their dynamic properties.

The authors suggests that it is necessary to do more dynamic testing (RCTS and CTX) to confirm or adjust the curves proposed in this paper. These tests should control for other parameters such as mineralogy,

mining, and preparation (blasting and/or crushing), and utilize larger devices for analyzing Cu and particle size in a broader range and under more significant confining pressures. It must be mentioned that in large slurry tailings facilities, waste rock is used as the main source of the material for the construction of the containing dam. Therefore, the proposed curves may also be used as a preliminary model for assessing dynamic behaviour.

References

Besio, G. 2012. *Uso del método de curvas homotéticas en la representación de ensayos monotónicos y cíclicos en suelos grueso.* Tesis de Ingeniero Civil, Universidad de Chile, Santiago de Chile.

Darendeli, M. 2001. Developing of a new family of normalized modulus reduction and material damping curves, PhD dissertation, University of Texas at Austin, Austin, Texas.

De la Hoz, K. 2007. *Estimación de los parámetros de Resistencia al corte en suelos granulares gruesos*. Tesis de Ingeniero Civil y Magister, Universidad de Chile, Santiago de Chile.

Dorador, L. 2010. *Análisis experimental de las metodologías de curvas homotéticas y corte en la evaluación de propiedades geotécnicas de suelos gruesos*. Tesis de Ingeniero Civil y Magister, Universidad de Chile, Santiago de Chile.

Hardin, B. and V. Drenevich. 1972. Shear modulus and damping in soils design equations and curves. ASCE, *Journal of the Soil Mechanics and Foundations Division*: 606–624.

Hawley, M. and J. Cunning. 2017. *Guidelines for Mine Waste Dump and Stockpile Design*. New York: CRC Press.

Marachi, D., C. Chan and H. Seed. 1972. Evaluation of properties of rock fill materials. *Journal of the Soil Mechanics and Foundations Division* 98: 95–114.

Menq, F. 2003. Dynamic properties of sandy and gravelly soils. PhD dissertation, University of Texas at Austin.

Parra, D., P. Reyes, A. Keene, K. Stokoe, H. Jaffal and C. El Mohtar. 2016. On the dynamic properties of leached ore and mine waste. In *Proceedings of Heap Leach Mining Solutions 2016*, Lima. Peru. Published by InfoMine, Vancouver: 317–332.

Rollins, K., M. Evans, N. Diehl and W. Daily. 1998. Shear modulus and damping relationship for gravels, *Journal of Geotechnical and Environmental Engineering* 124(5): 69–81.

Seed, H., R. Wong, I. Idriss and K. Tokimatsu, K. 1986. Moduli and damping factors for dynamic analyses of cohesionless soil, *Journal of Geotechnical Engineering,* ASCE: 112:1016–1032.

Seed, H. and I. Idriss. 1970. Soil moduli and damping factors for dynamic response analyses, Report EERC 70-10, Earthquake Engineering Research Center, University of California, Berkley.

Senetakis, K., A. Anastasiadis and K. Pitilakis. 2013. Normalized shear modulus reduction and damping ratio curves of quartz sand and rhyolitic crushed rock. *Soil and Foundations,* The Japanese Geotechnical Society: 879–893.

Varadarajan, A., K. Sharma, K. Venkatachalam and A. Gupta. 2003. Testing and modelling two rock fill materials. *Journal of Geotechnical and Geoenvironmental Engineering* 129: 206–218.

Verdugo, R. and K. De la Hoz. 2006. *Caracterización geomecánica de suelos granulares grueso. Revista Internacional de Desastres Naturales Accidentes e Infraestructuras Civil* 6: 199–2006.

Vucetic, M. and R. Dobry. 1991. Effect of soil plasticity on cyclic response. *Journal of Geotechnical Engineering* 117(1): 89–107.

Zhang, J., R. Andrus and C. Juang. 2005. Normalized shear modulus and material damping ratio relationships. *Journal of Geotechnical and Geonvironmental Engineering* 31: 453–464.

Bibliography

Golder Associates Ltd. 1987. Regional study of coal mine waste dumps in British Columbia. Stage II, report prepared for Canadian British Columbia Mineral Development Agreement: 862–1231.

Proceedings of Tailings and Mine Waste 2019
November 17–20, 2019, Vancouver, Canada
Published by the University of British Columbia Press, 2019

Material-Specific Intrinsic Oxidation Rates from Custom Laboratory Oxygen Consumption Testing

D. Morgan Warren, Golder Associates Inc., USA
Jacob S. Waples, HydroGeoLogica Inc., USA
Matthew Cashimer, Golder Associates Inc., USA

Abstract

The rate of oxygen consumption provides an indication as to sulphide oxidation rates, which are important for understanding the timing and magnitude of potential acid rock drainage (ARD). The rate of oxygen consumption may be used to calculate a material's intrinsic oxidation rate (IOR), which represents the combination of chemical and microbial processes driving the oxidation of sulphides within a material. Common practice for assessing ARD potential is to use literature values for laboratory measured sulphide oxidation, but these values are usually based on ideal pyrite surfaces, or rates from humidity cells tests, which are more variable and can be affected by factors. In practice, an IOR is needed for a bulk material, such as tailings or waste rock, which will have other minerals present as well as varying amounts of moisture, organic matter, and microbial activity.

We present a time- and cost-efficient method that has been used to estimate order of magnitude IOR values, based on oxygen consumption, of tailings. The laboratory method includes measurement of oxygen and temperature for a relatively small sample over one to seven days and interpretation of results. While the method is relatively simple by design, and consequently has some inherent limitations, it has produced replicable results that are consistent with material properties, other geochemical testing, and literature values. These estimated IOR values have been used as inputs for geochemical modelling and assessments to assist mine operators in making decisions for waste material management.

Introduction

Understanding the environmental behavior of mine materials during weathering is important for planning aspects of the mine life cycle such as permitting and closure. This is particularly true for sulphide-containing mine wastes. Sulphide oxidation produces acidity, and in the absence of sufficient neutralization potential, acid rock drainage (ARD) may develop. Understanding the rate of sulphide oxidation helps in predictions as to the potential, timing, and magnitude of ARD issues.

Typically, an understanding of the overall ARD potential is generated through a combination of laboratory testing and predictive geochemical modelling with results of the laboratory testing used as inputs to the geochemical modelling. A typical laboratory testing program is phased, starting with static acid-base accounting (ABA), elemental content and mineralogical content, and then proceeding on to short-term leach testing, and kinetic testing (e.g., humidity cell tests [HCT]). With the exception of the HCTs, the goal of most geochemical characterization tests is to provide an estimate of a material's overall potential to generate acidity or potential to neutralize acidity (NP) based on its bulk composition. These tests do not provide sulphide oxidation rates or acid production (AP) rates that are useful inputs for modeling to estimate the generation, timing, and magnitude of potential ARD.

The HCT does provide an indication as to sulphide oxidation rates, based on sulphate release. However, HCT-based rates may not be an accurate reflection of the rate of sulphide oxidation due to other sources and sinks of sulphate in the HCT sample (e.g., dissolution of sulphate minerals like gypsum and precipitation of secondary hydrous sulphate minerals such as jarosite or schwertmannite). Sulphate release rates may also be affected by conditions in the HCT, such as varying moisture content with time, incomplete rinsing, and secondary mineral precipitation. In addition, selecting an appropriate time period over which to calculate sulphate release is complicated as release rates are seldom constant.

An alternative approach is to estimate the rate of sulphide oxidation through the direct measurement of the amount of oxygen (O_2) consumed by a sample. If we assume the primary reaction governing sulphide oxidation is accurately reflected in Equation 1 (e.g., Nordstrom and Alpers, 1999), then measuring the rate and amount of consumed oxygen should provide a reasonable sulphide oxidation rate or alternative to an AP estimate relative to using sulphate production rates and estimates based on the total sulphur content.

$$FeS_2 + \frac{15}{4}O_2 + \frac{7}{2}H_2O \rightarrow Fe(OH)_3 + 2SO_4^{2-} + 4H^+ \quad (1)$$

There are many factors contributing to the reactivity of a material and the sulfide oxidation rate beyond the simple reaction shown in Equation 1, such as sulphide content, sulphide mineral form and surface area, moisture content, content and exposure of sulphide and non-sulphide minerals, porosity, organic matter content, pH and ferric iron concentrations, temperature, oxygen availability and transport, and the microbial populations. The concept of an intrinsic oxidation rate (IOR) is used herein to refer to the collective effect of all these factors on the rate of O_2 consumption in the material (Gibson et al., 1994; Lottermoser, 2010). The IOR of a material is an assumed overall oxidation rate accounting for the applicable factors, rather than isolating the particular components. It is as the oxidation rate would appear in the field and is generally described by O_2 loss.

The IOR is typically presented in units of kilograms of oxygen consumed per cubic meter of material per second ($kg(O_2)m^{-3}s^{-1}$) (Ritchie, 1994; Lottermoser, 2010) and has commonly been used to describe the

rate of a bulk material's oxidation rate in mine wastes by other practitioners and researchers in the field of mine waste management (e.g., Gibson et al., 1994; Lottermoser, 2010). As such the IOR is used herein to describe the amount of O_2 consumed by a sample of sulphide-containing mine waste.

The method we present below provides a relatively cost and time-efficient procedure for obtaining an order of magnitude IOR for different types of mine wastes sufficient for use in initial studies and ARD evaluations. By design, it is intended to be simple with an understanding of its limitations and potential drawbacks. Moreover, the method is intended to be used and interpreted in the context of a complete geochemical characterization program. Following the description of the method, we provide results for using this method on several type of tailings samples.

Oxygen consumption testing

Background and testing overview

Estimating sulphide oxidation by oxygen consumption testing (OCT) in a container has been performed by others since the late 1990s (e.g., Eidsa et al., 1997; Andersen et al., 1999; Hollings et al., 2001; Jerz and Rimstidt, 2004; Elberling, 2005; Schmieder et al., 2012). Typically, there are three different methods for measuring the gas content within a sealed container:

1. electrochemical sensor;
2. gas chromatograph; and
3. pressure differences over time.

Golder's method uses the first option, an electrochemical sensor, and was chosen for ease of use and cost as this method was designed to be easily implemented.

In brief, the method used in this study used an airtight chamber (see Figure 1) with an electrochemical sensor installed in the lid. The airtight chamber contained a known amount of sample and known amount of headspace. Oxygen is assumed to be consumed according to Equation 1 and the change in O_2 is measured at regular intervals. Because the rate of oxygen consumption is assumed to be governed by Equation 1, and thus proportional to the mass of sulphide minerals present (e.g., pyrite), the IOR is derived from the stoichiometric relationship between O_2 and pyrite in Equation 1. The testing proceeds until sufficient O_2 has been consumed for IOR calculations. An estimate of the required duration is typically inferred from the total sulphur content. Along with measuring the amount of consumed oxygen within the chamber, the ambient temperature and oxygen content is measured outside the chamber in the testing area as a control.

Assumptions and limitations

The test method described herein is not without its limitations, which need to be considered for data interpretation and to understand the practicalities of applying the results to understanding the environmental

behavior of sulphide-containing mine wastes. As discussed above, this method was designed to be cost- and time-efficient and was not designed to replicate the level of precision in a laboratory. Assumptions include the following:

- All sulphides are present as pyrite: Although mineral content determination is recommended prior to performing this test work, it is possible there could be trace amounts of other sulphide minerals consuming O_2.
- All decreases in O_2 are due to consumption by pyrite oxidation: There could be microbial populations respiring the O_2 to form CO_2 within the sample or other O_2 consuming reactions; these are not taken into account in the IOR calculations.
- Changes in pressure can be ignored: The internal pressure in the vessel will change as oxygen is consumed. The effect of changing pressure on the measurement of oxygen within the chamber is not taken into account.
- Carbon dioxide gas production can be ignored: As acid generation occurs, subsequent neutralization by carbonates may produce carbon dioxide gas. The method does not measure the production of carbon dioxide gas, which may subsequently affect the pressure in the vessel and measurement of oxygen.
- The oxidation rate is constant for the evaluated period of the test: Changes in sulphide oxidation rates are possible in response to changes factors such as pH, oxygen availability, sulphide mineral availability, and/or microbial activity. Generally, a consistent rate of oxygen depletion occurred throughout the testing period, and a period of relatively oxygen depletion was selected for determination of the IOR.

Methods

Testing chamber construction

The OCT testing chamber consisted of a wide-mouth threaded glass mason jar with a plastic lined metal lid and rubber gasket capable of making an airtight seal (see Figure 1). One Teledyne Type R-22 oxygen sensor was inserted through the lid approximately halfway the thickness of the sensor. Silicone sealant was applied around the sensor on both sides of the lid for an airtight seal. A thin coat of petroleum jelly was placed on the exterior chamber threads to promote an airtight seal during testing. During procedure development, testing of the silicone and the petroleum jelly were performed to confirm that these materials did not consume oxygen or off gas such that oxygen measurements were affected. The ambient environment of the testing area was monitored with an additional Teledyne R-22 oxygen sensor and one type K thermocouple wire to record the temperature. The temperature inside the chamber was not measured. Although sulphide oxidation is exothermic and will cause temperature increases, because the sulphide contents were relatively

low (median sulphide content of 0.63 weight percent [wt. %] for the 16 samples), intra-test changes in temperature, if any, were not expected to have been material for the calculated oxygen depletion rates. The chamber sensor, ambient sensor, and ambient thermocouple were each connected to a Campbell Scientific CR1000 datalogger which collected readings every minute.

Figure 1: Example testing chamber

Sample preparation

Each oxygen consumption test (OCT) consisted of approximately 200 +/– 0.1 g of tailings. The volume of each testing chamber was measured to within +/– 0.01 mL in order to estimate the headspace with ambient air and mass of oxygen in the test chamber. The tailings were loosely pressed into the chamber with a flat surface. A flat and relatively smooth surface was important for interpretation of results. The sample generally filled approximately one-third of the chamber (a height of approximately ¾ of an inch); minimal headspace was desired to maximize the ability to measure a change in oxygen; however, some headspace was required and the sample needed to be sufficiently below the sensor to avoid interference with the sensor.

Samples

Sixteen samples, including four types of tailings, were selected for OCT, including:

- Underflow sands (nine samples): Tailings produced by cyclone of whole tailings into the overflow and underflow (sand) fractions.
- Whole tailings (three grain size types, seven samples): Whole tailings samples were collected from active and closed tailings impoundments. Whole tailings were spigotted, resulting in grain size fractionation. As such, whole tailings samples were grouped into three different categories based on the dominant grain size fraction: coarse, intermediate, and fine grained.

Subsamples of the tailings were sent for additional testing to support interpretation of test results, which included moisture content (ASTM D2216), specific gravity (ASTM D854), and ABA (e.g., sulphur speciation, carbon speciation, NP) (Sobek et al., 1978; Lawrence and Wang, 1997). Each sample was also submitted for HCTs (ASTM D5744) such that there were HCT-Derived IOR values available for comparison to the OCT method. Results of this testing are summarized in Table 1.

Table 1: Characterization results, pre-oxygen consumption testing

Sample ID	Tailings type	Total sulphur Wt. %	Sulphide sulphur Wt. %	Neutralization potential t $CaCO_3$/kt	Paste pH	Moisture %
Sample 1	UF sands	1.19	1.14	13	8.1	5.5
Sample 2	UF sands	0.35	0.17	17	8.1	3.8
Sample 3	UF sands	0.69	0.52	18	8.2	5.2
Sample 4	UF sands	0.65	0.48	22	8.2	7.4
Sample 5	WT coarse	0.98	0.74	73	7.7	9.9
Sample 6	WT intermediate	1.2	0.94	34	8.3	6
Sample 7	UF sands	4.49	3.48	2	4	4.4
Sample 8	UF sands/WT Int.	0.98	0.78	15	8.3	11.3
Sample 9	Underflow sands	0.58	0.43	12	8.5	6.8
Sample 10	Underflow sands	0.12	0.1	21	8.1	6.5
Sample 11	WT Intermediate	2.7	1.75	5	5.4	10.9
Sample 12	WT Intermediate	0.62	0.42	29	8	8.2
Sample 13	WT Fine	1.27	0.47	20	7.7	24.6
Sample 14	WT Coarse	4.37	3.3	3	3.9	6.9
Sample 15	UF Sands	0.62	0.24	6	4.3	8.5
Sample 17	UF Sands	1.35	1.21	18	8.1	12.6

UF = Underflow; WT = Whole tailings

Results

Graphical results of the 16 OCT trial tests are presented in Figure 2 for samples 1 through 8 and Figure 3 for samples 9 through 17. Rates of oxygen consumption were calculated by fitting a linear regression to the

slope of the natural logarithm of the oxygen concentration ($\ln(O_2)$). For each test, the rate of oxygen consumption was calculated for a selected time period that best represented a linear or near-linear relationship between $\ln(O_2)$ and time. In general, a linear or near-linear response was observed approximately 5 hours into testing. The rate of oxygen consumption was converted to an IOR in units of mass O_2 consumption rate per volume of tailings over time ($kg(O_2)m^{-3}s^{-1}$) by calculating the density of oxygen in the headspace of each container in combination with a known mass and volume of tailings in each test. The derived OCT IORs are summarized in Table 2.

Table 2: Test details and calculated IOR values

Sample ID	OCT test duration hr	OCT IOR (x 10^{-8}) $kg(O_2)m^{-3}s^{-1}$	Replicate OCT IOR (x 10^{-8}) $kg(O_2)m^{-3}s^{-1}$	RPD %	HCT cycles	HCT leachate pH	HCT-derived IOR (x 10^{-8}) $kg(O_2)m^{-3}s^{-1}$
Sample 1	92.8	2.24	2.96	27.7	81	7.7	2.74
Sample 2	92.8	2.84	3.25	13.5	31	8.4	0.56
Sample 3	243.3	2.53	2.48	2.0	57	7.7	0.83
Sample 4	243.3	3.06	2.89	5.7	31	8.1	1.55
Sample 5	144.5	3.72	2.67	32.9	81	7.5	13.85
Sample 6	144.5	8.14	8.57	5.1	81	8.0	3.35
Sample 7	95.4	8.24	7.49	9.5	57	2.8	132.71
Sample 8	95.4	3.18	3.27	2.8	65	7.9	2.36
Sample 9	165.9	3.02	2.92	3.4	57	7.4	2.57
Sample 10	165.9	6.60	6.74	2.1	81	3.0	36.11
Sample 11	262.9	10.79	7.59	34.8	81	4.8	6.70
Sample 12	262.9	2.64	2.66	0.8	57	7.6	1.09
Sample 13	172.6	3.96	2.66	39.3	65	7.5	27.15
Sample 14	210.1	13.17	13.91	5.5	57	2.5	118.14
Sample 15	210.1	4.69	4.15	12.2	31	4.4	3.41
Sample 17	187.1	4.23	1.32	104.9	65	7.8	2.04

For comparison, HCT-derived IORs were calculated from weekly sulphate production rates. The long-term, steady-state sulphate production rate was taken to be equal to the arithmetic mean of the last 5 cycles of weekly testing in the HCTs. Sulphate production rates were then converted to IOR values using the stoichiometry in Equation 1. Table 2 presents the number of weekly cycles the HCTs had been running at the time the sulphate production rate was calculated along with the HCT-derived IOR.

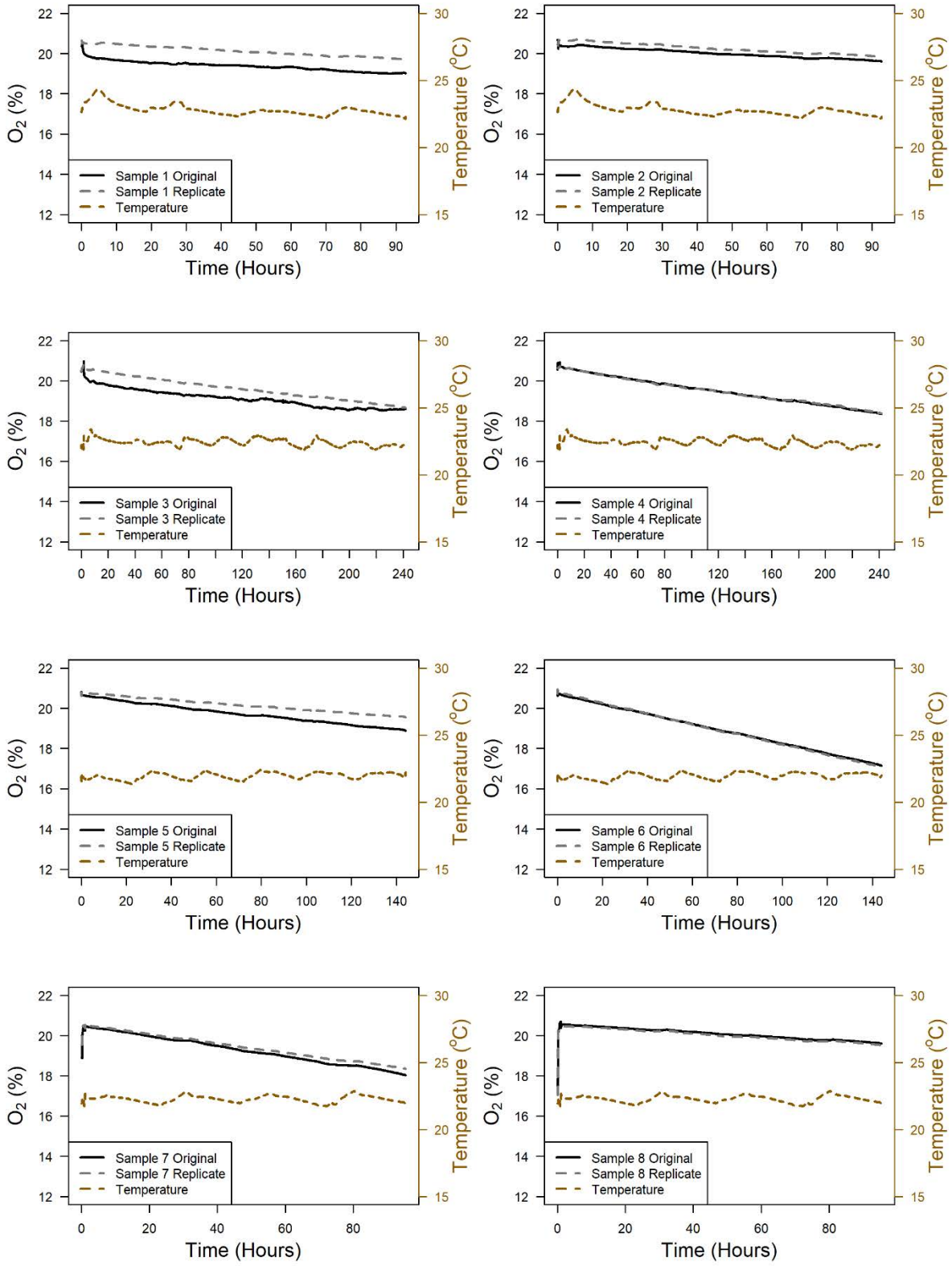

Figure 2: Timeseries of O_2 and temperature for samples 1 through 8

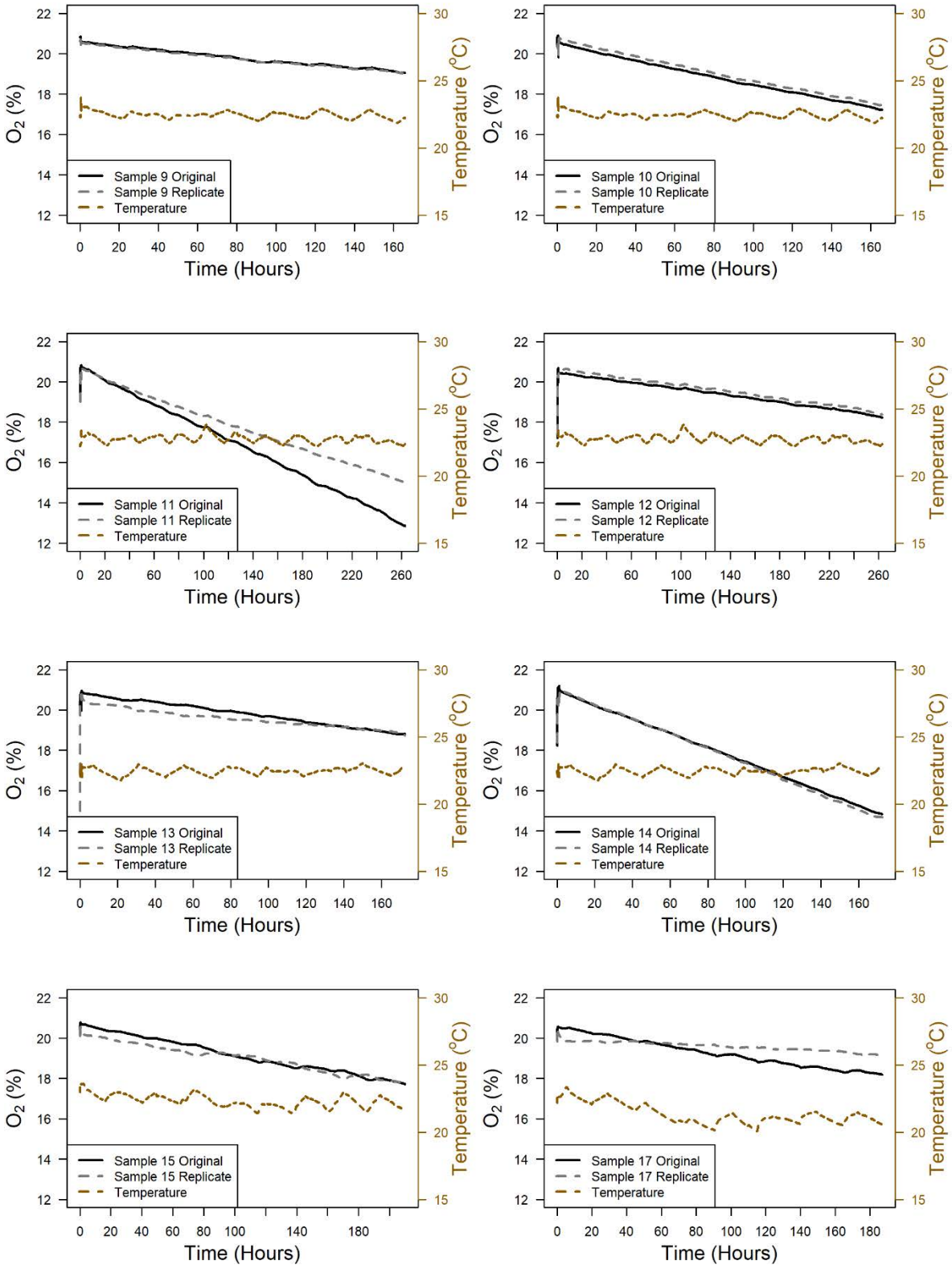

Figure 3: Timeseries of O_2 and temperature for samples 9 through 17

The OCT oxygen consumption rates ranged from 2.36×10^{-8} to 1.35×10^{-7} $kg(O_2)m^{-3}s^{-1}$, with a geometric mean of 4.17×10^{-8} $kg(O_2)m^{-3}s^{-1}$ and the HCT-derived rates ranged from 5.61×10^{-9} to 1.33×10^{-6} $kg(O_2)m^{-3}s^{-1}$, with a geometric mean of 5.34×10^{-8} $kg(O_2)m^{-3}s^{-1}$. In calculating the OCT IORs for the original and replicate samples, the same testing time interval was used. In general, the OCT repeatability was good, with 11 of the 16 trials having a relative percent difference (RPD) less than 15% and all but two had RPDs less than 35%. Both of the samples with poorer reproducibility had higher moisture content than any of the other samples as well as one of them being an older whole tailings sample (deposited more than 20 years ago) that may have had greater heterogeneity.

Discussion

Figure 4A presents the IOR versus total sulphur content by material type (UF Sands, WT Intermediate, WT Coarse, and WT Fine). The oxygen consumption rates show an overall increasing trend with increasing total sulphur, which is expected because oxygen consumption is related to the pyrite oxidation reaction. However, at the lower total sulphur contents, there appeared to be a baseline reaction rate range of approximately 2×10^{-8} to 3×10^{-8} $kg(O_2)m^{-3}s^{-1}$ up to a total sulphur content of approximately 1 wt. %. At total sulphur values higher than 1 wt. %, the IOR increased steadily with increasing total sulphur up to the maximum rate observed in this study of 1.35×10^{-7} $kg(O_2)m^{-3}s^{-1}$, corresponding to a total sulphur content of 4.37 wt. %. Figure 4C presents the OCT IOR compared to the ABA paste pH. Good agreement is also observed here as the higher IORs are observed for the lower paste pH samples, which is expected because pyrite oxidation rates are faster under acidic conditions.

Figure 4B compares the HCT-derived IORs with the OCT IORs and Figure 4D presents the HCT-derived IORs versus HCT leachate pH. General trends are similar for OCT and HCT-derived IORs, with higher rates for acidic and higher-sulphide materials. In general, the OCT IORs promoted a higher degree of reproducibility and consistency than the HCT-derived IORs, with the OCT IORs spanning one degree of magnitude and HCT-derived IORs spanning three orders of magnitude. The greater variability of the HCT-derived rates may be a function of the HCT method used to calculate the rates. The HCTs include weekly drying, saturating, and flushing of the sample. These fluctuations in moisture content are more pronounced, and may, therefore, affect sulphide oxidation rates more significantly. Alternatively, the greater variability in the HCT-derived rates may be due to the longer time period over which the rates are calculated. The OCT procedure is focused on determining the IOR, as opposed to the HCT which may have many objectives (e.g., metals loading rates, determining propensity for acid generation, etc.). As such, this relatively fast, inexpensive, and simple method can be used to supplement HCTs, providing more reliable information for modeling and evaluations of sulphide oxidation.

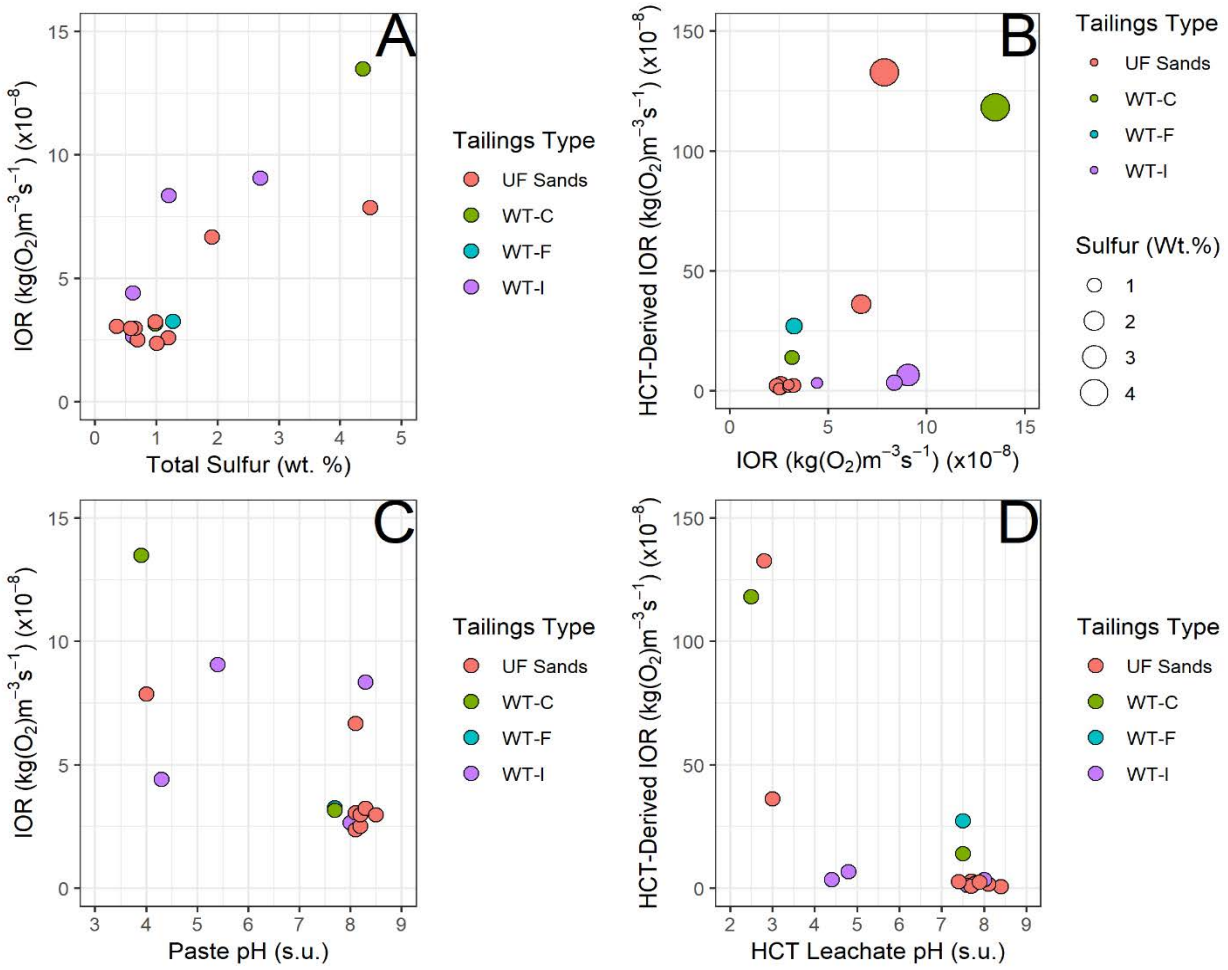

Figure 4: A: IOR versus total sulphur, B: HCT-derived IOR versus IOR, C: IOR versus paste pH, and D: HCT-derived IOR versus HCT leachate pH

Conclusions

This study presents the results of a time- and cost-efficient method for evaluating the sulphide oxidation rate of sulphide-bearing mine wastes in terms of an order of magnitude IOR. The OCT method was applied to 16 tailings samples, which also had comparable HCT-derived IOR values. Comparing the two IOR methods revealed the OCT IORs are more consistent and reproducible than the HCT-derived IORs. Further comparison to paste pH and total sulphur values indicate expected trends with higher rates associated with lower paste pH values and higher values of total sulphur.

The method presented is intended to be cost- and time-efficient to estimate order of magnitude IOR value in order to complement other geochemical characterization programs for a more complete understanding of the weathering behavior of mine waste and to support modeling and ARD evaluations.

References

Andersen, M.S., F. Larsen and D. Postma. 2001. Pyrite oxidation in unsaturated aquifer sediments. Reaction stoichiometry and rate of oxidation. *Environmental Science and Technology* 35(20): 4074–4079.

Andersen, M.E., J.M. Scharer and R.V. Nicholson. 1999. The Oxygen Consumption Method (OCM): A new technique for quantifying sulfide oxidation rates in waste rock. In *Proceedings of Mining and the Environment II,* September 1999, Sudbury, Canada.

ASTM International. 2018. D5744-18 Standard test method for laboratory weathering of solid materials using a humidity cell.

Eidsa, G., T. Briseid and H. Ese. 1997. Pyrite oxidation measured by oxygen consumption and carbon dioxide production in laboratory respirometer tests. In *Proceedings of the 4th International Conference on Acid Rock Drainage,* May 31–June 6, Vancouver, Canada: 321–331.

Elberling B. 2005. Temperature and oxygen control on pyrite oxidation in frozen mine tailings. *Cold Regions Science and Technology* 41(2): 121–133.

Gibson, D.K., G. Pantelis and A.I.M. Ritchie. 1994. The relevance of the intrinsic oxidation rate to the evolution of polluted drainage from a pyritic waste dump. In *Proceedings of the American Society of Mining and Reclamation:* 258–264.

Hollings, P., M.J. Hendry, R.V. Nicholson and A. Kirkland. 2001. Quantification of oxygen consumption and sulphate release rates for waste rock piles using kinetic cells: Cluff Lake uranium mine, northern Saskatchewan, Canada. *Applied Geochemistry* 16: 1215–1230.

Jerz, Jeanette K. and J.D. Rimstidt. 2004. Pyrite oxidation in moist air. *Geochimica et Cosmochimica Acta* 68(4): 701–714.

Lawrence, R.W. and Y. Wang. 1996. Determination of neutralization potential for acid rock drainage prediction, MEND Project Report 1.16.3, MEND, Ottawa, Ontario.

Lottermoser, B.G. 2010. *Mine Wastes*, third edition. Berlin, Germany: Springer-Verlag.

Nordstrom, D.K. and C.N. Alpers. 1999. Geochemistry of acid mine waters. In *The Environmental Geochemistry of Mineral Deposits,* G.S. Plumlee and M.J. Logsdon (editors). Rev. Econ. Geol. V. 6A. Society of Economic Geologists, Littleton, Colorado, USA.

Ritchie, A.I.M. 1994. The waste-rock environment. In J.L. Jambor and D.W. Blowes (editors), *Environmental Geochemistry of Sulfide Mine-Wastes,* 22. Mineralogical Association of Canada, Nepean: 133–161 (short course handbook).

Schmieder, P.J., J.R. Taylor and N. Bourgeot. 2012. Oxygen consumption techniques to quantify acidity generation rates. 1st International acid and metalliferous drainage workshop in China. December 2012, Beijing, China.

Sobek, Andrew A., William A. Schuller, John R. Freeman and Richard M. Smith. 1978. Field and laboratory methods applicable to overburdens and mine soils. United States Environmental Protection Agency, Industrial Environmental Research Laboratory, Cincinnati, OH, EPA-600/2-78-054: 218.

Proceedings of Tailings and Mine Waste 2019
November 17–20, 2019, Vancouver, Canada
Published by the University of British Columbia Press, 2019

Effects of Shear on Dewatering and Compressibility of Treated Oil Sands Tailings

Scott E. Webster, Coanda Research & Development Corp., Canada
Tayfun Aydin, Coanda Research & Development Corp., Canada
Clara Gomez, Coanda Research & Development Corp., Canada
Amarebh Sorta, Coanda Research & Development Corp., Canada
Babak Derakhshandeh, Suncor Energy, Canada
Abu Junaid, Canadian Natural Resources Ltd, Canada
Reza Moussavi Nik, Imperial Oil, Canada
Givemore Sakuhuni, Imperial Oil, Canada

Abstract

The ultimate goal of treating oil sands tailings is to develop a reclaimable landscape within a reasonable time frame, with dewatering and consolidation being two of the most important aspects of this objective. Among several technologies proposed for dewatering of tailings, the flocculation process involves the addition of a polymeric flocculant to the raw tailings stream, which is typically followed by pipeline transport to deposition sites. Treated tailings experience a range of shear conditions during transport and deposition. It is generally presumed that shearing adversely affects the water release and compressibility of treated tailings. Accordingly, shear rate is considered a constraint when designing processing equipment, pipelines, and deposition methods used in tailings treatment facilities. However, despite its importance, there is a lack of knowledge on the effects of shearing on dewatering and long-term consolidation characteristics of treated tailings. Also, the impact of processing variables such as flocculant type, dosage, and mixing conditions on the shear-dewatering relationship is not fully understood.

This study explores the relationship between the applied shear and performance metrics. Fluid fine tailings (FFT) and thickened tailings (TT) were flocculated under different dosages using an inline dynamic mixer with a partially hydrolyzed polyacrylamide (HPAM) from SNF and XUR polymer from Dow. Treated tailings were then sheared in a Couette shear device under conditions mimicking pipeline transport scenarios expected in the field operations. Measurements were made on both unsheared and sheared materials to assess their short-term dewatering, 6-month settling, and geotechnical characteristics. Overall, substantial shear was found to degrade material strength and immediate dewatering properties, while some amount of shear, depending on the material, appeared to improve consolidation in short single-drainage

settling columns, consistent with some previous studies. Large-strain consolidation and seepage-induced consolidation geotechnical tests suggested that the material subjected to low amounts of shear consolidated slightly more rapidly at higher void ratios than material exposed to higher shear.

Introduction

Flocculation is a common technique used in various tailings treatment technologies. During the process of flocculation, fine particles form larger aggregates, bonding with each other and, usually, a polymeric additive (Wang et al., 2014). The formation process of these aggregates defines their strength, which is a result of interplay between the floc aggregation and breakage. During the rapid initial floc formation, aggregation dominates over breakage. However, the breakage becomes more important as aggregates get larger, until floc sizes reach an equilibrium for a given shear experience. The rate of aggregation depends on the rate of collisions and the fraction of collisions resulting in particle attachment, and is countered by the rate of breakage. The net balance between these two rates is the rate of floc growth (Jarvis et al., 2005).

Assuming there is a direct relationship between the floc size at the final deposition point and the objective of a given tailings treatment application, knowledge of the rate of floc growth would be invaluable for the design of the treatment process. Given the changes occurring in the material properties of the flocculated tailings and the variance in the shear conditions it experiences along a transportation line, it is not practical to pursue an explicit understanding of all the details of floc growth and breakup. Instead, an alternative approach could focus on quantification of the relevant shear experiences for the treated tailings, and determination of the effects on key performance indicators. This is the approach explored in this paper.

Flocculated materials such as treated tailings are inhomogeneous systems with large flocs, making them unsuitable for shearing in commercial narrow gap rheometers. This is one reason why these systems have not been studied in detail. Some investigations have been performed on the effects of shearing on flocculated clay suspensions. Several studies showed that “gentle” shearing improved dewatering and consolidation of clay suspensions (Terzaghi et al., 1996; G. Channell, 1999; Channell et al., 2000; Johnson et al., 2000), while others showed the opposite behaviour at high shear rates (Comings et al., 1954; Scott, 1968; Vesilind and Jones, 1993). These studies did not quantify the effects of shearing or the magnitude of the applied shear.

A more recent study by Gladman et al. (2005) used 10 wt% calcite suspensions flocculated with a high molecular weight polymer. By applying shear rates ranging from 1 s^{-1} to 20 s^{-1}, they found a critical shear rate at which the effects of shear on hindered settling and compressibility of suspensions changed from beneficial to detrimental. They used a wide gap Couette geometry to accommodate floc sizes. Given the non-uniform shear distribution in the gap, the reported shear rates were approximations of the average shear calculated from a rheological model.

Using a large Couette geometry, specifically designed to provide uniform shear distribution under certain limitations while accommodating flocs, Derakhshandeh et al. (2016) studied the effects of shearing on dewatering of ~31 wt% FFT suspensions treated with three different flocculants. The shear rates were estimated to be between ~10 s^{-1} to ~70 s^{-1}. It was found that the shearing generally increased the long-term water release of the samples, while slightly negatively impacting the short-term water release and yield characteristics.

The overall objective of this study was to understand the effects of selected shearing conditions on short- and long-term water release, and compressibility of FFT and TT using two polymers; a partially hydrolyzed polyacrylamide (HPAM) from SNF and XUR polymer from Dow.

Methodology

Treatment of both FFT and TT samples involved two steps: sample characterization and flocculation. Raw tailings were characterized via measurements of the solids content (measured by halogen moisture analyzer), methylene blue index (MBI, measured by halo-titration), density, rheology, pH, and conductivity. These properties are shown in Table 1. The flocculation was performed either using a bench-top mixer for initial investigatory experiments (to determine an appropriate dose for larger batches) or, for the most part of the study, a dynamic in-line mixer used for producing the materials evaluated in the main analysis.

Table 1: Material properties for raw FFT and TT

Tailings type	Process scale	Solids Content	MBI	Density	Bingham yield	Bingham consistency	pH	Conduct.
(–)	**(–)**	**(wt%)**	**(meq / 100 g)**	**(kg/m³)**	**(Pa)**	**(Pa·s)**	**–**	**(mS/cm)**
FFT	Bench	28.8	7.2	1,190	1.9	0.0078	7.2	1.03
FFT	5” inline	26.9	7.5	1,183	1.1	0.0070	7.3	1.18
FFT	5” inline	29.8	7.4	1,198	1.7	0.0073	7.5	0.97
TT (*)	Bench	41.8	5.1	1,353	3.0	0.0173	8.4	0.80
TT (*)	5” inline	41.5	5.5	1,338	2.6	0.0125	8.2	0.70
TT (*)	5” inline	42.1	4.9	1,330	2.6	0.0159	8.4	0.67

(*) Thickened tailings were previously flocculated in a commercial thickener and came from the thickener underflow

The primary piping and frame for the inline flocculation test apparatus is shown in Figure 1. Larger tanks were dedicated to storage and preparation of raw tailings while smaller tanks were dedicated to polymer preparation. Mechanical mixers and external recirculation loops were employed in the preparation tanks to ensure uniform material composition. Progressive cavity pumps were used for the delivery of raw tailings and polymer. The flow rates of each stream were measured using Endress and Hauser

electromagnetic flow meters. Flow rates were actively controlled using the computer connected to the DAQ (data acquisition) system which constantly monitored the flow meters and controlled the delivery pumps.

Figure 1: Flocculation facility primary piping and tank support frame

The tailings were mixed with the polymer using a 127 mm inline dynamic mixer designed with a 15.9 mm diameter shaft and two pitched blade turbine impellers with 89 mm diameters. The tailings flow rate was 100 L/min with 0.4 wt% polymer added as necessary to achieve the desired dosage. Samples were collected approximately 4 m downstream of the mixer after travelling through piping and hose with 0.0762 m diameter.

Optimal mixing conditions in the dynamic mixer (between 1,400 and 4,100 RPM) were determined after a series of three tests at different mixer speeds using the dosage determined during the bench tests, which are described in the next section. The best material was selected based on visual observation, initial settling, and initial water release results. This material looked sufficiently mixed and had the largest floc structures with minimum exposure to shear in excess of the mixing required to produce well flocculated material. Additional tests were performed at the ideal mixing speed but with 50% higher and lower dosages to study the influence of polymer dosage on the shearing effects.

Following the flocculation of FFT and TT, treated samples were sheared using the same Couette device from the previous study (Derakhshandeh et al., 2016). The rotating bob and the outer cylinder have diameters of 285 mm and 314 mm diameters, respectively. 8 mm thick baffles are installed along both the bob and outer cylinder walls. While the design intent of the Couette device is to apply a known and uniform

amount of shear to the treated material (Derakhshandeh et al., 2016), it is acknowledged that this is an idealized flow configuration within the device and is subject to some operational limitations. Non-idealized flow conditions arise partly due to the transition from a laminar to a turbulent flow configuration at increased speeds depending on the apparent viscosity of the samples. Using a stationary outer cylinder with a rotating bob, the transitional Reynolds number is around 125 for Newtonian fluids (Andereck et al., 1986). Even for a laminar flow in the Couette device, the shear rate applied to the material changes due to the changes in the wall boundary conditions; as the bob rotates the fluid shearing occurs in a gap varying from between the baffles to the distance between the cylinder and bob walls. This variance can reduce the intended shear rate by roughly a factor of 2. It should be noted that designing a shearing device to uniformly shear tailings samples with different non-Newtonian properties, floc sizes and dewatering properties is nearly impossible. Therefore, the existing apparatus was used as an approximate means of shearing the various tailings samples used in this study.

The shearing conditions used for Couette testing were selected based on slightly different rationales for the FFT and TT. For the flocculated FFT, low and high shear conditions were based on the nominal laminar flow shear rate at the pipe wall expected for high and low flow field conditions. The high shear condition for TT was based on a turbulent shear environment expected in a field pipeline. The low shear condition for TT was chosen to provide a laminar environment for contrast to the turbulent high shear condition. All the shear times were selected to match residence times in field pipeline scenarios. The conditions are detailed in Table 2.

Table 2: Couette shear conditions for FFT and TT

Flocculated material	Shear condition	Shear rate	Shear time	Link to field scale pipe flow
(–)	**(–)**	**(s^{-1})**	**(min)**	**(–)**
FFT	Unsheared	0	0	N/A
FFT	Low	17	3	Laminar wall shear
FFT	High	86	30	Laminar wall shear
TT	Unsheared	0	0	N/A
TT	Low	17	3.7	Laminar wall shear
TT	High	200	2.8	Turbulent bulk shear rate

Data and discussion

Dewatering, strength, and settling column results

Flocculated material samples produced in the bench mixer were evaluated to determine the optimal dosages

based on capillary suction time (CST) and 7-day water release measurements performed in 500 mL graduated cylinders. For the FFT, dosages of 900 and 950 g/t (solids) were selected for HPAM and XUR polymers, respectively, while for the TT, reflocculation dosages of 300 and 250 g/t were selected, again for HPAM and XUR polymers. While it may have been possible to select the same dosage for the two polymers and achieve similar results mostly on short-term dewatering performance, the dosage may not have been optimum in actuality with respect to long-term dewatering, strength, or settling performance as will be seen from the results. Hence a direct comparison of the performance of the polymers was not possible and was not a goal of this study.

The dosages selected in the bench tests were then used to produce larger quantities of material with the inline dynamic mixer using the strategy described above, along with the 50% under- and over-dosed samples. In general, high shear conditions seem to have caused deterioration in dewatering and strength of the HPAM treated FFT while achieving higher solids consolidation over time. Figure 2 presents the immediate CST and peak yield stress results along with the six-month settling results (2 L graduated cylinders) for the FFT samples. For the optimally dosed HPAM samples, we see that the low shear condition did not substantially degrade (increase) the CST result, but that the high shear condition caused a substantial increase, indicating a loss of immediate dewatering potential. The yield stress results were as expected, with shear causing floc breakdown proportional to the amount of shear experienced. The settling column results were interesting, with higher solids content achieved after six months for the sheared samples, with the high shear case having the best results: 45 wt% solids vs 40 wt% for the unsheared sample. The high shear column eventually surpassed the other two columns after a few days of settling. For the HPAM treated FFT samples, the under- and over-dosed samples displayed relatively similar behaviour with some expected differences in the CST and yield results. The column results for the underdosed material were fairly good, actually surpassing or matching the optimal case for the unsheared and low-shear conditions but falling short of the high-shear optimal dose result. In general, these results suggest that for HPAM treated FFT, moderate or high shear could have a beneficial effect on the overall results in some deposition scenarios. This might not be the case if the process relied on immediate dewatering or material strength.

The XUR treated FFT samples demonstrated similar trends as the HPAM treated samples with the exception of the settling data. The results are shown in Figure 2. The CST trends were similar to the HPAM results, as were the yield stress outcomes, except the absolute magnitudes of yield stress were much lower, as expected for this polymer. The settling column results were different, with the low shear condition having the best long-term results for all three polymer dosages. The high shear condition was worse than the unsheared sample for the underdosed material, but better than the unsheared results for the optimal and overdosed columns. The settling curve for the unsheared and low-shear samples shows a quick rise to the steady state value, but the high shear column settled much more slowly and took around three months to

approach the performance of the other columns. Notably, the best settling column result for this material was from the overdosed condition. Perhaps the "optimal" dose selected here was not truly the optimum, but it appears that good performance is achievable for this material over a wide range of dosage levels, with the underdosed sample also providing good settling column performance. High shear conditions appeared to be detrimental to XUR treated samples, but high shear might lead to better results than the unsheared condition, if a much longer settling period could be tolerated.

In general, low shear conditions produced better dewatering, material strength and settling for HPAM treated materials over high sheared conditions. Figure 3 shows the CST, yield stress, and settling column results for the thickened tailings (TT). For the HPAM treated material, we once again saw minimal impact on CST for the low shear condition, but an increase in CST (decrease in dewatering) for the highly sheared samples. The yield stress values declined with shear for the optimally dosed material, as expected, but the overdosed samples actually increased in yield stress after low shear, while maintaining a significant decrease for the high shear scenario. The low-shear HPAM treated TT had the highest six-month settling column solids results at around 57 wt% vs 54 wt% for the unsheared column. The under/overdosed column results had similar trends. Again, we have found that some shear can be beneficial in certain scenarios.

The XUR treated TT materials displayed an unusual CST characteristic. The results for the unsheared sample were moderate, but deteriorated for the low-shear case. However, the high-shear data was somewhat improved over the low-shear condition. This behaviour was observed for all three dosage levels, suggesting that it is a real phenomenon, and not just an anomalous sample. The XUR + TT yield stress results were low, as expected for this polymer. The XUR treated TT settling column results were fairly similar for all dosage and shear levels at around 56 wt%, with the high-shear, overdosed sample higher by a few wt%. The optimum dose settling curves shown in Figure 3 show a slower rise to the maximum solids, taking several months to stabilize. In this case the unsheared sample settled the fastest.

Consolidation testing results

Large-strain consolidation (LSC) and seepage-induced consolidation (SIC) tests were performed on the low and high shear samples described above. The LSC tests involved a step loading of a sample, allowing complete consolidation at each stage, followed by a permeability measurement. Details of the test methodology can be found in Pollock (1988). The SIC testing involves an application of seepage loading of a sample through a use of flow pump followed by one or more loading steps. Permeability at the end of each loading step is measured using a flow pump and consolidation parameters are calculated from measured data and using a numerical tool based on large-strain consolidation theory (Abu-Hejleh et al., 1996). Despite the differences in LSC and SIC testing methodologies, the results are expected to be similar.

Figure 4 shows the compressibility and permeability results obtained from the tests. Generally, there is no substantial differences between low and high sheared samples in terms of compressibility. Low sheared samples have the similar or slightly higher permeability compared to the high sheared samples (in particular, at higher void ratios). Both the LSC and SIC provided similar results except for the HPAM-treated FFT samples, where the SIC results suggested higher compressibility and permeability than the LSC data. Looking again at the LSC data in Figure 4, all but the TT-XUR results have either slightly better permeability or compressibility at higher void ratios for the low-shear samples.

Conclusion

Samples of fluid fine tailings and thickened tailings from Alberta oil sands mines were treated with two polymer flocculants and then subjected to varying levels of shear. Increasing shear was found to degrade material strength and immediate dewatering properties, while some amount of shear, depending on the material, appeared to improve consolidation in short single-drainage settling columns, consistent with some previous studies. Large-strain consolidation and seepage-induced consolidation geotechnical tests were somewhat less conclusive about possible improvements in consolidation properties for sheared material, but the results generally suggested that material subjected to low amounts of shear consolidated slightly more rapidly at higher void ratios than more highly sheared material. Unsheared samples were not evaluated in the geotechnical testing.

The optimal amount of shear likely depends on the specific deposition or processing strategy selected for final tailings disposal. Certain methods such as filtration could be less tolerant to shear, but deep deposits might benefit from some shear experienced in pipelines downstream of the flocculation process. Generally, we did not see evidence that shear caused long-term deterioration of consolidation performance, which should help alleviate concerns regarding floc damage during post-treatment processing and transport.

Future work should include attempts to deepen the understanding of the actual amount of shear experienced in specific field deposition strategies and the commensurate effects on the floc structure of the tailings. Additional data from more samples would improve confidence in the repeatability of the geotechnical compressibility and permeability results. The behaviour of the XUR-treated TT in particular was somewhat unusual and could benefit from further study, showing a decrease in immediate dewatering for low shear, but then an improvement under high shear conditions. This was also the only material which did not exhibit superior performance for the low-shear sample in the geotechnical tests; instead, the results were the same for both shear cases.

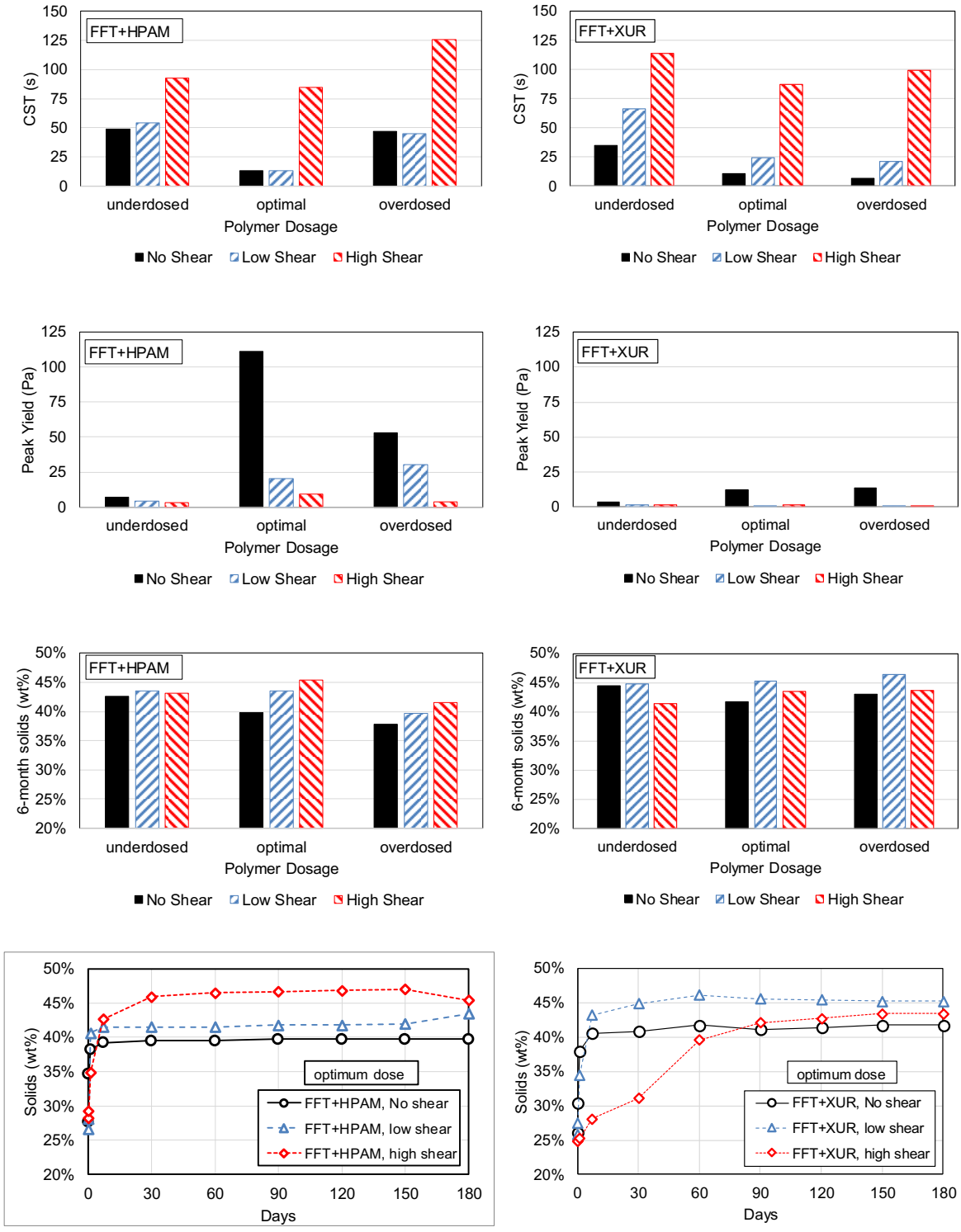

Figure 2: CST, yield stress and settling column results for FFT. Optimal dose column settling traces shown as example

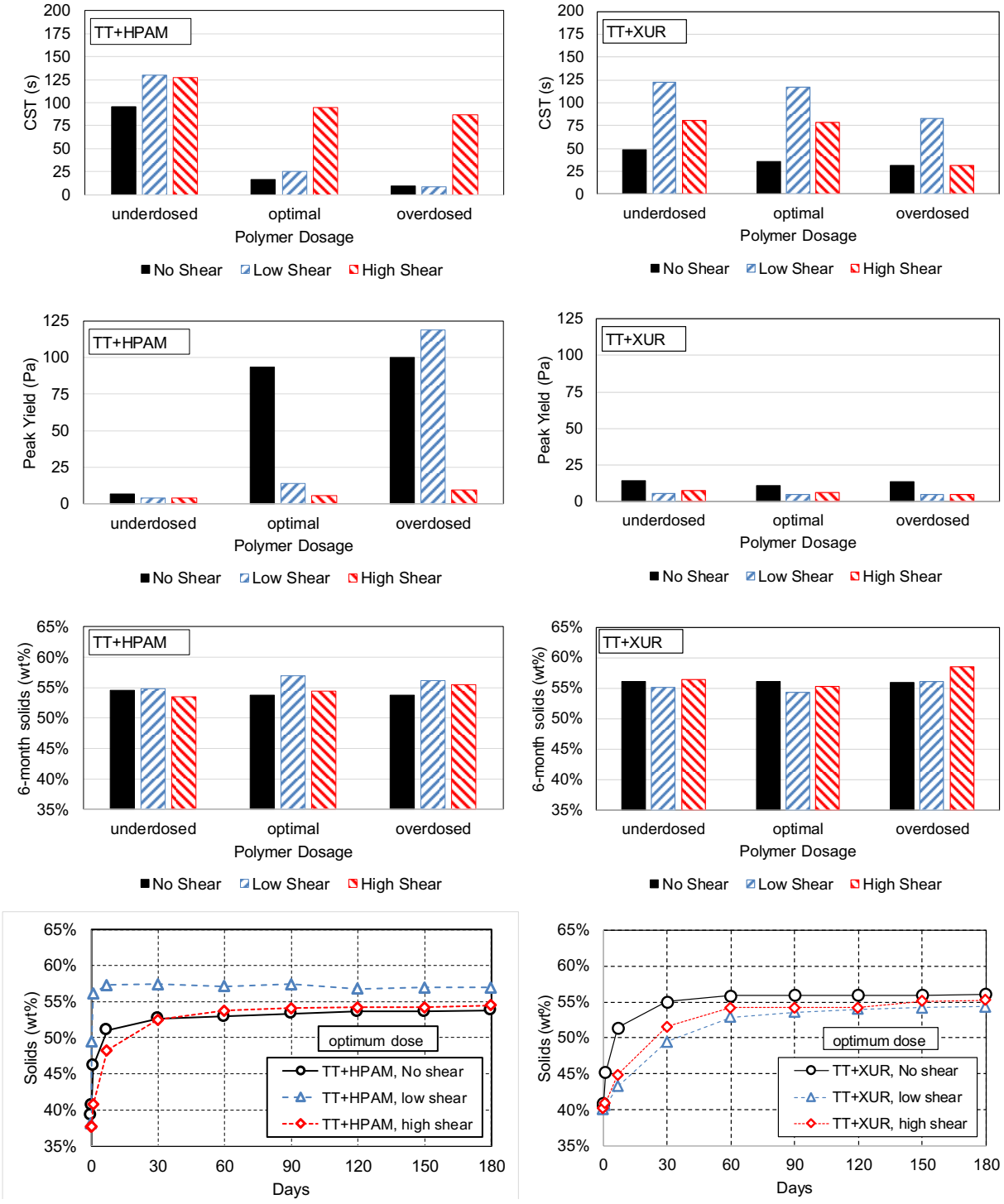

Figure 3: CST, yield stress and settling column results for TT. Optimal dose column settling traces shown as example

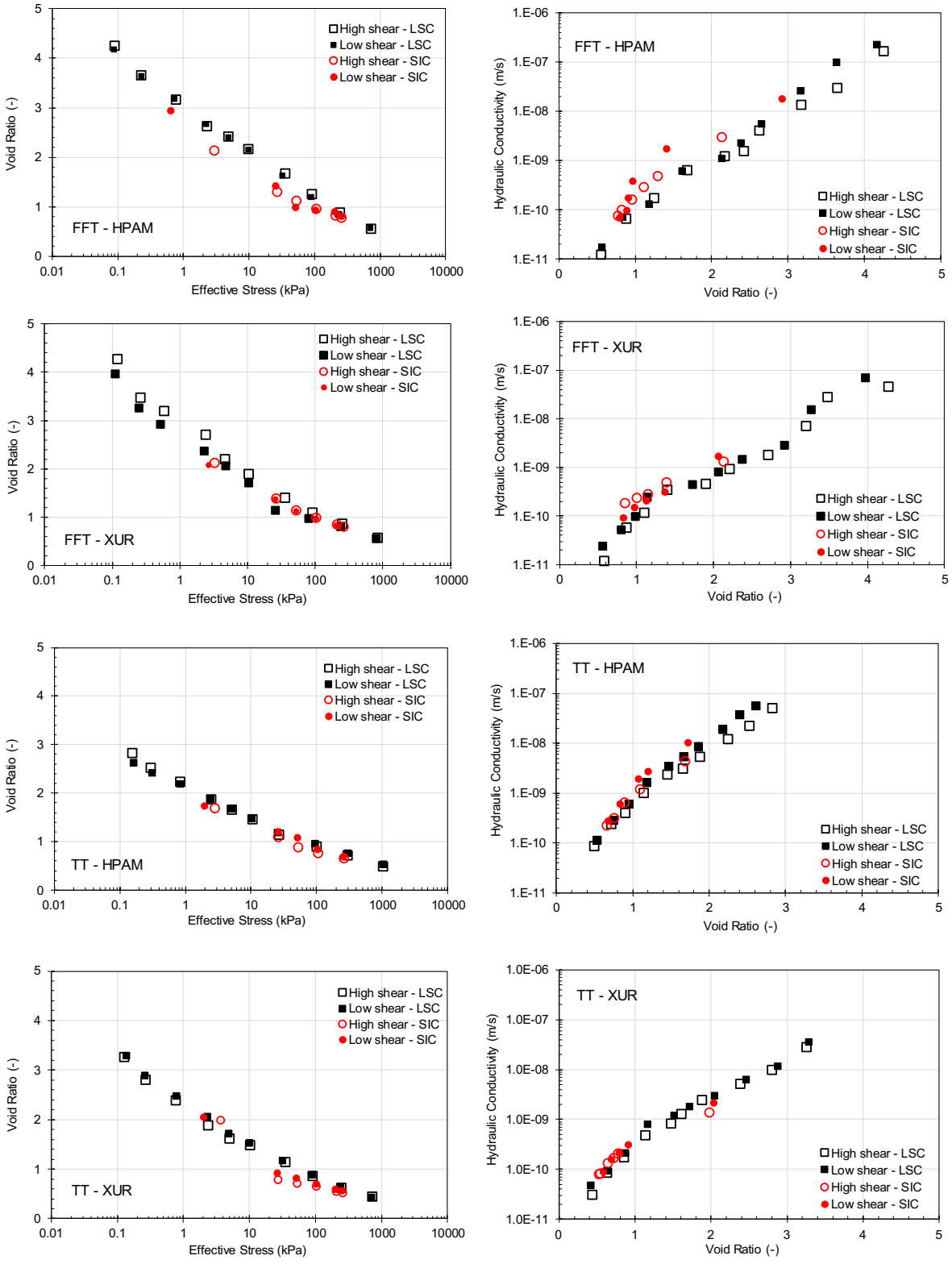

Figure 4: Compressibility and permeability results from LSC and SIC studies on the sheared tailings samples

Bibliography

Abu-Hejleh, A.N., D. Znidarcic and B.L. Barnes. 1996. Consolidation characteristics of phosphatic clays. *Journal of Geotechnical Engineering* 122(4): 295–301.

Andereck, C.D., S.S. Liu and H.L. Swinney. 1986. Flow regimes in a circular Couette system with independently rotating cylinders. *Journal of Fluid Mechanics* 164: 155–183.

Channell, G.M. 1999. *Mechanics of aggredated alumina suspensions: Behavior under shear and compression.* PhD dissertation, University of Illinois at Urbana-Champaign.

Channell, K., K.T. Miller and C.F. Zukoski. 2000. Effects of microstructure on the compressive yield stress. *AIChE Journal:* 72–78.

Comings, E.W., C.E. Pruiss and C. DeBord. 1954. Continuous settling and thickening. *Ind. Eng. Chem.:* 1164–1172.

Derakhshandeh, B., A. Junaid and G. Freeman. 2016. Effects of shearing and shearing time on dewatering and yield characteristics of oil sands flocculated fine tailings. 5th International Oil Sands Tailings Conference. Lake Louise, Alberta.

Gladman, B., S. De Kretser, M. Rudman and P. Scales. 2005. Effect of shear on particulate suspension dewatering. *Trans IChemE Part A:* 1–4.

Jarvis, P., B. Jefferson, J. Gregory and S.A. Parsons. 2005. A review of floc strength and breakage. *Water Research* 39: 3121–3137.

Johnson, S., P. Scales, D. Dixon and M. Pascoe. 2000. Use of a super thickener device to concentrate potable water sludge. *Water Research:* 288–294.

Pollock, G.W. 1988. *Large Strain Consolidation of Oil Sand Tailings Sludge.* Edmonton: University of Alberta.

Scott, K.J. 1968. Experimental study of continuous thickening of a flocculated silica slurry. *Industrial & Engineering Chemistry Fundamentals:* 582–595.

Terzaghi, K., R.B. Peck and G. Mesri. 1996. *Soil mechanics in engineering practice.* New York: John Wiley & Sons Inc.

Vesilind, P. and G. Jones. 1993. Channelling in batch thickening. *Water Science and Technology:* 59–65.

Wang, C., D. Harbottle, Q. Liu and Z. Xu. 2014. Current state of fine mineral tailings treatment: A critical review on theory and practice. *Minerals Engineering* 58: 113–131.

Proceedings of Tailings and Mine Waste 2019
November 17–20, 2019, Vancouver, Canada
Published by the University of British Columbia, 2019

An Overview of Seepage Control Measures in In-Pit Dams with a Design Example from Alberta Oil Sands

Pathma Wedage, Wood Environment & Infrastructure Solutions, Canada
Yang Li, Wood Environment & Infrastructure Solutions, Canada
Mickey Davachi, Wood Environment & Infrastructure Solutions, Canada

Abstract

Mining dams are typically constructed in stages over the lifespan of a mine, and in most situations, they are required to function as dams while being constructed. These dams are either constructed out-of-pit or in-pit to store fluids and semi-solid waste generated from the processing of ore. The operating life span of an in-pit dam varies from a few years to several decades before the structure can be decommissioned. The in-pit dams are constructed using overburden waste materials and the coarser fractions of oil sand tailings, with minimal use of imported materials. In the Alberta oil sands, the in-pit dams could be up to about 100 m in height, a few kilometers in length, and up to 3 km in base width. Due to the exceptionally large material volumes involved, non-traditional design methods are used to meet construction requirements and save costs. One design method involves designing dams with internal drainage systems, where tailings sand, petroleum coke, or glacial outwash sand are used to construct the internal filter drain. A second approach relies on hydraulically placed fine tailings on the upstream slope of the dam constructed of cohesive fills, or to construct the dam primarily using tailing sand. A third approach involves overbuilding of the dam to reduce the risk of hydraulic fracture and to achieve low hydraulic gradients.

The first part of this paper presents an overview of recently implemented seepage control design methods for in-pit dams from the authors' experience. The second part of this paper presents a design example illustrating the key steps that are followed in the design of an internal seepage control system for an overburden filled in-pit dam.

Introduction

In Alberta, the active mining footprint of oil sands is about 900 km^2, which is about 20% of the oil sands reserves in the region (CAPP, 2019). The oil sands on the higher ground away from the Athabasca River are recovered in-situ by the drilling of wells. The overburden soil cover in the areas dedicated to open-pit mines varies from about 30 m closer to the river to a maximum up to 90 m in other areas. The typical

maximum thickness of oil sand ore is about 60 m. When oil sands are mined using surface mining techniques, the raw oil known as bitumen is extracted from the sand using water-based processes and the bitumen is upgraded into crude oil. The material remaining after the extraction processes consists of a mixture of water, sand, clay, fine silts and residual bitumen, which is known as tailings. Tailings are pumped by pipelines and stored in various tailings storage facilities located on-site. There are at least 25 major tailings storage facilities in the active oil sands mines. Many of these storage facilities are constructed as internal (in-pit) tailings storage facilities constructed within mined out areas of the pits and, a few are constructed as external (out-of-pit) constructed over the original landscape. The first use of these storage facilities is to provide safe containment to the tailings until reclamation, with the second use as a source of recycled water to feed the oil sand extraction process. The containments to the tailings are provided by engineered dams and/or in-situ pit walls depending on the layout of the storage facility. The in-pit dams are constructed using overburden waste materials and the coarser fractions of oil sand tailings, with minimal use of imported materials.

The dams are licensed and regulated through Alberta Environment and Parks and the Alberta Energy Regulator. The designs comply with the Alberta Dam Safety Regulations and guidelines of the Canadian Dam Association (CDA). The dams are typically constructed in stages over the lifespan of a mine and in most situations, are required to function as dams while they are being constructed. The operating life span of an in-pit dam varies from a few years to several decades before the structure can be decommissioned. In some cases, the in-pit dams may be required to function for many years after the mine closure. Occasionally, the in-pit dams are designed to accommodate reverse flow during the operating life of the dam due to the changes in upstream and downstream conditions and the operating levels over time. The design, construction, and operation of these structures rely on instrumentation monitoring, and "the observational method" is used to continuously review and change any practices if necessary.

This paper presents an overview of recently implemented seepage control design methods for in-pit dams in Alberta and a design example illustrating the key steps that are followed in the design of an internal seepage control system for an overburden filled in-pit dam.

Geological setting for in-pit dams

The general geological profile in the oil sand leases typically comprises Pleistocene deposits with some thin Holocene cover, underlain by the Cretaceous Clearwater Formation and McMurray Formation. The McMurray Formation is underlain by Devonian Limestone. The McMurray Formation strata typically comprise oil sand, water sand and muds deposited in marine, estuarine, and continental environments which extend up to about 150 m below pre-mining ground surface. The estuarine sequence, and in some areas both the estuarine and the marine sequences of the McMurray Formation contain the recoverable oil sand.

The fluvial sequence in the lower portion of the McMurray Formation contains the most relevant strata for the in-pit dam system, which include the continental pond muds and water-bearing fluvial sand. The pond muds are generally characterized as over-consolidated, high plastic, slickensided and/or pre-sheared clays. The most significant hydro-geological feature for seepage considerations beneath in-pit dams is the basal aquifer in the water sand. The water sand is typically encountered below the pond muds, and in some places interbedded with the pond muds.

Factors affecting cross-sectional details of in-pit dams

The design slopes of in-pit dams are mainly controlled by the geotechnical characteristics of the foundation materials and various fill zones, dam height, and the operating pond conditions. The dam consequence classification and the ability or inability to implement remedial measures in a timely manner, if less than expected performance conditions develop, also play a role in the selection of the design slopes.

Common to most in-pit structures located in oil sand mines, the weakest foundation unit governing the design of in-pit dams is the pond muds within the Lower McMurray sequence. In general, the Lower McMurray deposits are neither mined nor used as construction materials. The pond muds are generally characterized as over-consolidated, high plastic, slickensided and/or pre-sheared clays. The designs are based on C'=0 kPa and ϕ' residual ranging between 9 and 11 deg along sub-horizontal beddings of the pond muds. Where pond muds are absent, underlying Paleosol and/or weaker facies of Devonian Formation govern the designs. The design parameters for these units are C'=0 kPa and ϕ' residual ranging between 10 and 13 deg.

The different types of overburden material that will be used in the construction of an in-pit dam are selected based on the availability of material within an economic haul distance and generally grouped into various specifications. The high specification material is intended for the low hydraulic conductivity and integrity in the central "core" of the structure. This zone consists of a clayey silty sand-based mixture of Kcw and lean oil sands and is placed and compacted in lift thickness in the range of 0.3 to 1 m using fully loaded heavy haulers (up to 400 tons), with specified degree of compaction exceeding 97% of Standard Proctor Maximum Dry Density over the entire lift thickness. The construction of high specification zones would be done in a manner to ensure that the material will be delivered to the site and compacted in an unfrozen state. The inter-lift surfaces are cleaned to minimize the occurrence of potential defects (sliding layers and preferential seepage pathways), and the freeze-thaw affected zones are removed before construction begins in a given year after winter months. The high specification zones are typically supported by fills constructed of lower-quality overburden or waste material. In the terminology of water dams, these outer zones are referred to as "shells." Allowable materials in the low specification zones include the fills which can be placed in up to 2 m thick lifts and trafficable under heavy haul truck traffic. Suitable fills

include Pleistocene, Clearwater, Upper McMurray, and Middle McMurray. Because of the collective characteristics of the exterior low specification zones within the dam structure and the presence of relatively weak foundation clays, the external slopes of the in-pit dams are required to be 5H:1V or flatter to meet the applicable stability design criteria.

Another factor that affects the cross-sectional dimensions of an in-pit dam structure is the operational needs for having infrastructure corridors and haul road surfaces over the crest or on the exterior slopes of the structure.

An overview of seepage control approaches

In-pit dams are constructed to facilitate mining while providing containment to tailings on the already mined out parts of a mine pit. Once the mining is completed, and tailings are placed on both sides of the in-pit structures, the structure is no longer required to function as a dam. Most often, in-pit dams fall in the "significant" consequence of failure category as per CDA 2013/2014 classification. As part of the owner's own risk management plan, considering economic and reputation reasons, the in-pit structures are typically are designed, constructed and operated considering a higher risk category than that is predicted by the CDA classification. The operating life span of an in-pit structure as a dam can be a few years to a few decades. Due to their extremely wide cross-sections and the relatively short operating timeframe, the wetting front from the tailings pond may not likely reach the central high specification "core" zone during the operating life of the structure. It is also important to recognize the generally positive benefit of the large cross-sectional geometry, particularly when considering seepage related failure modes such as piping, overtopping, slope instability or unraveling of the downstream slope. However, industry acceptable means of seepage control measures are incorporated in the current designs to handle seepage flows from hypothetical worst-case scenarios involving cracks/defects though the dam core, and seepage through foundation and abutments.

Seepage control through dam fills

Overburden filled dams with internal filter drains

One of the design approaches for the overburden filled in-pit dam structures is designing the dam with an internal seepage control system that includes a sand chimney filter with a system of collector pipes and offtake pipes or other means of seepage removal mechanisms such as sump pump systems. The seepage collected into external open sumps or internal gravel sumps is pumped back to the tailings pond, as required to maintain the downstream conditions or the phreatic lines within acceptable levels. Typically, tailings sand or overburden sand (Pf sand) of the desired specification is being used for the chimney with High-Density Poly-Ethelene (HDPE) pipes being used as the drain pipes.

The dams are designed based on the assumption that the compacted high specification zones provide the primary structural stability and seepage control. The sand chimney provides defense against seepage and/or runoff water eroding the high specification zone (i.e. defense against piping) if a continuous seepage path through the compacted high specification zone did develop. The drainage system is designed to handle a worst-case scenario that includes upstream cracking as well as construction defects. A generic cross-section of an overburden filled dam structure with an internal drainage system is shown in Figure 1.

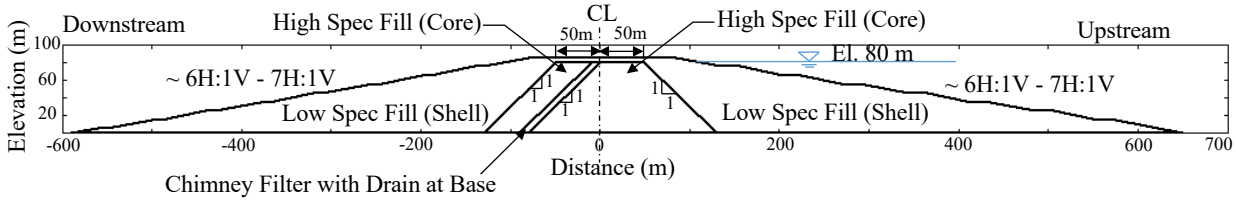

Figure 1: A generic cross-section of an overburden filled dam

Tailings sand or upstream beaches

Another design approach for in-pit dam structures is to construct the dam structure primarily using hydraulically placed tailing sand. These dams are constructed as compacted sand cells, with each sand pour ranging from 3 to 5 m in lift height, followed by the formation of upstream beaches. Internal drainage pipes are installed to handle construction water such that the downstream slope could be kept free of seepage and the phreatic line is maintained sufficiently low to achieve the desired compaction to the cell sand. In some instances, a dam originally designed as an overburden filled structure is modified to a tailings sand structure as the construction progresses to accommodate available materials or vice versa.

Other

The third category of the structures is the in-pit structures constructed strictly using overburden fills, designed for relatively short operating life. Example structures are Syncrude's Highway berm (Cameron and Fong, 2001) and South West Dam (Cameron et al., 2001). These structures do not have conventional clay cores or internal filters but include various compacted and uncompacted fill zones. These structures are built on uncontrolled fills such as dragline rejects existing on the pit floor that is typically not removed. The design against piping relies on limiting the overall seepage gradients through the fills, foundations units and at abutments as suggested in Lane (1935). The design against hydraulic fracturing risk of the fills is achieved by performing hydraulic fracture checks as outlined in Barlow et al. (1998), assuming water or heavy fluids consisting of fines tailings would be in direct contact with the upstream slope of the structure. In reality, the sand and/or composite tailings within the containment pond are not capable of propagating or sustaining cracks, hence provide protection against hydraulic fracture.

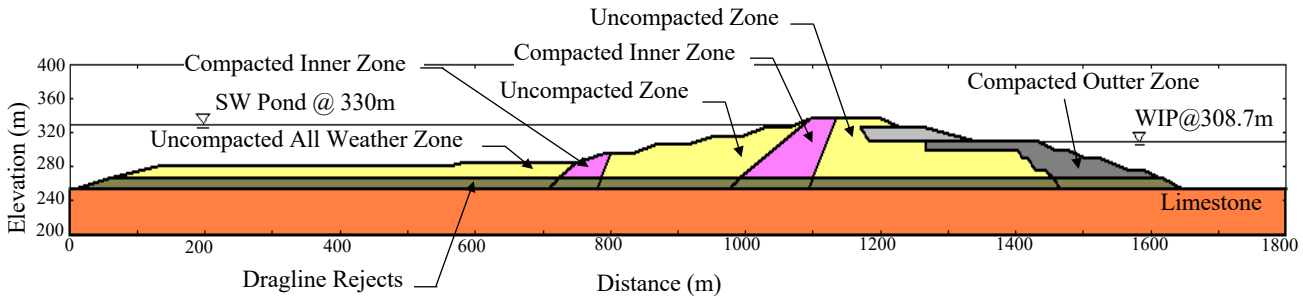

Figure 2: A generic cross-section of Southwest Dam (from Cameron and Fong, 2001)

Seepage control at abutments

The mechanisms that can form zones of preferential seepage and internal erosion at the abutments include formation of a colluvial apron, poor compaction of fill at the pit wall contact, cracking of dam fills from differential settlement, formation of stress relief fractures at the pit wall, and occurrence of pervious layers within the McMurray Formation pit wall.

Several design measures are adopted in in-pit dams to mitigate cracking and seepage concerns at the abutments. To reduce the potential for cracking of the in-situ pit wall due to stress relief from mining, and to reduce the potential for cracking of the dam fill due to differential settlement, the pit walls at the dam core contact are designed to flatter slopes (a higher factor of safety) than elsewhere. The flatter pit wall slopes also facilitate achieving the specified compaction of the dam core fills against the pit wall with mine equipment. The pit walls are constantly monitored using instrumentation, as the mining approaches the final design limits, an alteration to the designs are made if monitoring indicates the potential for cracking.

Surface preparation at the abutments is carried out to remove loose, disturbed or cracked material to provide a competent base and slope face for fill placement. The pit wall slopes at the core contact are trimmed to the design slope using dozer trim, rather than following a cut and fill trim followed in elsewhere. The core and the sand chimney are widened and keyed into the final pit wall slopes to remove the disturbed zones. These design features enhance drainage, crack stopping and filtering capabilities at the contact between the fills and the in-situ pit wall if a zone affected by wetting/drying and freeze/thaw processes remained below the clean-up zone.

Compacted flares are constructed on the upstream and downstream sides of abutments. The design purpose of these would be to increase the length of the seepage path, thereby reducing the seepage gradients and the piping potential.

Seepage control at pit floor

The water sand in the Middle and Lower McMurray forms an aquifer that would be de-pressurized to allow mining of the lower benches, as required. This sand aquifer could provide a seepage path between the tailings pond and the downstream section of the dam potentially causing uplift pore pressures to rise above the base of feed in the downstream dam slopes, or seepage discharge and piping in the toe region. One of the ways to mitigate the uplift pressures on the downstream side of the in-pit dams is to continue to operate depressurization wells during the operational phase of the tailings pond until the downstream side is in-filled with sufficient tailings.

In some instances, the mining plan allows the placement of an overburden waste cover over the entire footprint of the pond prior to the placement of any tailings. In other situations, compacted clay fills are placed over the areas where the water sand is exposed or within a few meters below the pit floor. In addition, a layer of compacted fill liner is constructed within the dam footprint where the low permeable in-situ cover over water sand and/or limestone is insufficient. The compacted fill liner is typically a clayey, silty, sand-based bituminous fill (commonly referred to as the base seal).

A design example for an overburden filled in-pit dam

When designing an in-pit dam with a system of internal filter drains, the upstream slope of the dam is conservatively assumed to be exposed to water or pond fluid. The blinding effects of the tailings on the upstream slope or the footprint of the tailings containment area are not relied on to allow flexibility for the tailings operations. Worst-case scenarios are modeled by introducing continuous horizontal defects and/or vertical cracks through the High Specification zone. Chimney filter is sized to intercept and drain seepage from the most adverse “worst case” scenario involving defects or cracks without head build up over permissible levels. The permissible levels are defined considering downstream hydraulic fracture protection, downstream stability, and overall hydraulic gradients. The drain pipes are designed to provide 5 to 10 times higher capacity to discharge the flows resulting from the modeled worst cases. The example presented in this paper applies to a tailing pond with a normal operating pond level of 80 m above the base of pit. The main seepage control elements include; a compacted core, a 10 m or a 15 m wide inclined sand chimney, a perforated collector drain pipe at the base of the chimney, and a system of offtake pipes extending to the downstream toe.

2D and 3D Seepage modelling

The general objective of the seepage modeling is to estimate the seepage quantities to the seepage collection system, to estimate the position of the phreatic line with time, to estimate exit gradients, and to study the sensitivity of these quantities to variations in assumed material parameters and boundary conditions.

Transient seepage analysis tools are used to assess the progression of the wetting front through the overburden fill section over the pond operation period, which could be used to select the instrumentation alert levels.

The two-dimensional steady-state seepage modeling is carried out to determine the potential seepage flow rates that would develop if one or more horizontal defects were present in the dam core. These could include continuous or mostly-continuous layers of rubble or frozen material, or zones of poorly compacted material, any of which would result in higher conductivity. The defects are modeled as through-going high pervious layers within the core, each with a transmissivity equivalent to 1 cm to 10 cm thick gravel layers, or 50 to 75 cm thick sand layers. The sensitivity of the calculated flow and the head build-up within the chimney to the hydraulic conductivity of the chimney is checked by varying the hydraulic conductivity of the chimney within the expected range. Figure 3 illustrates the sensitivity of the flow into the drain pipe and the piezometric elevation within the chimney versus the chimney width and permeability, for the dam configuration shown in Figure 1. As seen from this chart, if the hydraulic conductivity of the chimney is 4×10^{-4} cm/s or higher, the capacity of the 10 m wide chimney is sufficient to safely transfer the seepage water into the drainpipe due to the assumed worst-case involving several horizontal defects. Similarly, if the hydraulic conductivity of the chimney is 3×10^{-4} cm/s or higher, the capacity of a 15 m wide chimney is sufficient to safely transfer the seepage water into the drainpipe due to the assumed worst-case involving horizontal defects. For sizing the drain pipes, the estimated unit flows into the drainpipe based on the horizontal defect model can be used.

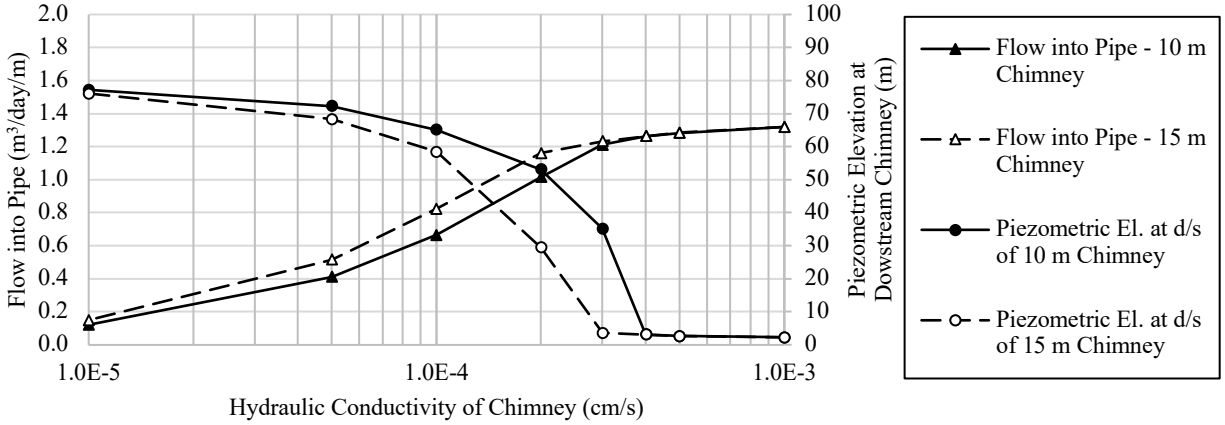

Figure 3: Results of 2-dimensional seepage sensitivity models

The second modeling step is to undertake a three-dimensional seepage model to estimate the flow quantities, distribution of hydraulic head within the chimney and sensitivity of the flow to chimney permeability resulting from a through-going vertical crack. Figure 4 presents the 3D model geometry and the boundary conditions corresponding to the dam configuration illustrated in Figure 1.

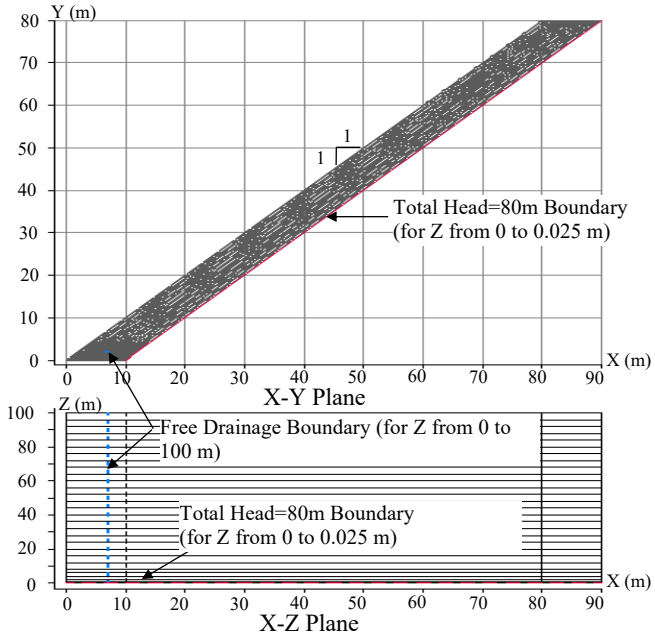

Figure 4: An example of a 3-dimensional seepage model geometry

The model includes a 10 m wide sand chimney and a perforated collector pipe. The collector pipe is modeled as a perfect drain. At the location of the proposed collector pipe, a free seepage boundary condition is assumed. Some general guidance on selecting crack dimensions are provided in Sherard (1973 and 1985). Utilizing the symmetry of flow on either side of the crack, only one side of the chimney is modeled. Accordingly, for an assumed 50 mm crack, a 25 mm wide zone at the upstream side of the chimney would be exposed to the pond head, whereas the remainder of the upstream side of the chimney is not exposed to any head boundary. The model extends to a significant distance along the chimney (in the z-direction). Crack widths ranging from 5 to 50 mm crack are examined. Based on the authors' experience, the flows resulting from the modeled cracks are less sensitive to minor variations in the crack width, but more sensitive to the discharge capacity of the chimney.

Figure 5 shows the positions of the phreatic line (saturated/unsaturated zone boundaries), and the pressure head contours at the "crack" and, at various distances away from the crack for the assumed 50 mm wide crack. From Figure 5, the maximum pressure on the downstream face of the chimney is 320 kPa (32 m), which occurs at an approximate elevation of 25 m. The corresponding total head on the downstream face of the chimney at El. 25 m is El. 57 m. About 10 m away from the modeled crack, the pressure head is less than 24 m with a corresponding total head on the downstream face of the chimney at El. 25 m is El. 49 m.

The model allows the designer to estimate the extent of the zone influenced by an assumed vertical crack. These pressures are checked against the maximum allowable pressures from the hydraulic fracture considerations as outlined in Barlow et al. (1998), to confirm the acceptance of the chimney drain sizing

and/or the downstream fill cover thickness and specifications. Additionally, the estimated flow into the drainpipe resulting from the model can be used as a guidance to select the sizing of the drain pipes.

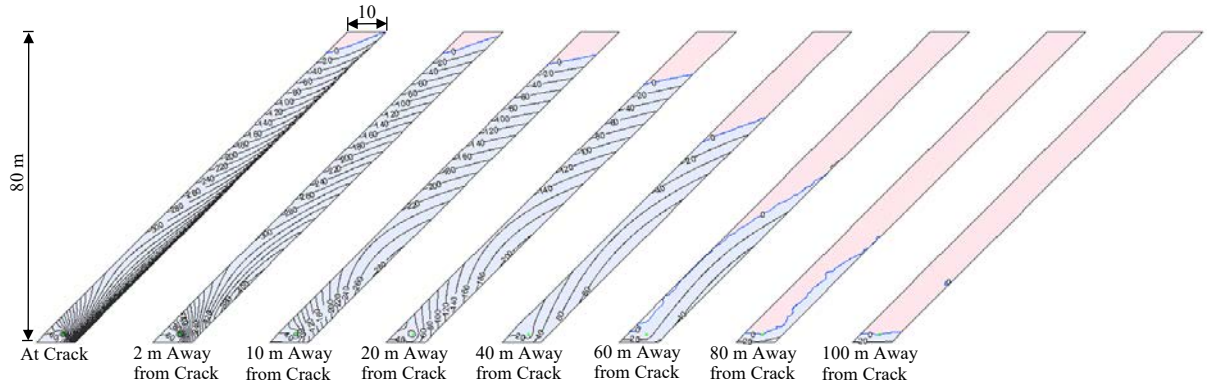

Figure 5: Results of a 3-dimensional seepage model

Design principles for granular filter drains

The two primary functions required from the filters and drains are "retention" requirement and "permeability" requirement. In the interest of preventing internal erosion due to concentrated leaks, a filter should be constructed with permeability close to the adjacent upstream fill. In this instance, high pore pressures can develop, and seepage that enters the filter system may not readily be transferred out. Conversely, if the filter is too coarse relative to the adjacent upstream fill or segregated with coarser zones near the interface it may let the excessive movement of the upstream fill material into the filter. The ideal filter material should not segregate, not change in gradation with time, be non-cohesive, be internally stable, and should have the ability to control and seal a concentrated leak (ICOLD, 1994). A comprehensive review of available methods for designing filters is documented in Fell et al., 2005. It is noted that the procedures developed by Sherard et al. (1984) and Sherard and Dunnigan (1989) have become the most widely adopted in the industry including USBR (1987), USDA-SCS (1994), ICOLD (1994) and USSD (2011). The filter criteria for material types that are applicable for in-pit overburden filled dams adopted from Sherard's contributions are summarized in Table 1 below. These criteria do not include specific reference to limiting the fines content. However, some limitations on fines content and nature such as that required by the USBR (1977) appear to be implied by the additional notes.

The typical gradation sizes of the base materials for the overburden filled dams and the materials considered for the filters in Alberta oil sands are shown in Figure 6. From the gradation envelopes presented in Figure 6; the d_{85} of the Base soil is in the range of 0.1 and 0.3 mm, the D_{15} of the Pf sand is in the range of 0.1 and 0.4 mm, and the D_{15} of the tailings sand is less than 0.13 mm. From Table 1, for a base soil with d_{85} in the range of 0.1 – 0.5 mm (Soil Category 2), the D_{15} of the filter should be less than 0.7 mm. As such, the retention criterion is satisfied by both the Pf sand and tailings sand filters.

Table 1: Filter criteria (based on Sherard and Dunnigan, 1989)

Base soil category	Percent finer than #200 sieve[1]	Filter criteria[2]
1	Fine silts and clays: more than 85% finer	$D_{15} \leq 9 \times d_{85}$, if less than 0.2 mm use 0.2 mm
2	Sands, silts, clays, and silty and clayey sands: 40 to 85% finer	$D_{15} \leq 0.7$ mm
3	Sands and gravels: less than 15% finer	$D_{15} \leq 4 \times d_{85}$ mm[3]

Notes

1. Category designation for soil containing particles larger than the #4 sieve (4.75 mm) is determined from a gradation curve of the base soil which has been adjusted to 100% passing the No. 4 (4.75 mm) sieve.
2. Filters are to have a maximum particle size of 75mm (3 inches) and a maximum of 5% passing the No. 200 (0.075 mm) sieve with the plasticity index (PI) of the fines equal to zero. To ensure sufficient permeability, filters are to have a D_{15} size equal to or greater than $4 \times d_{15}$ but no smaller than 0.1 mm.
3. The d_{85} may be determined from the original gradation curve of the base soil without adjustment for particles larger than 4.75mm.

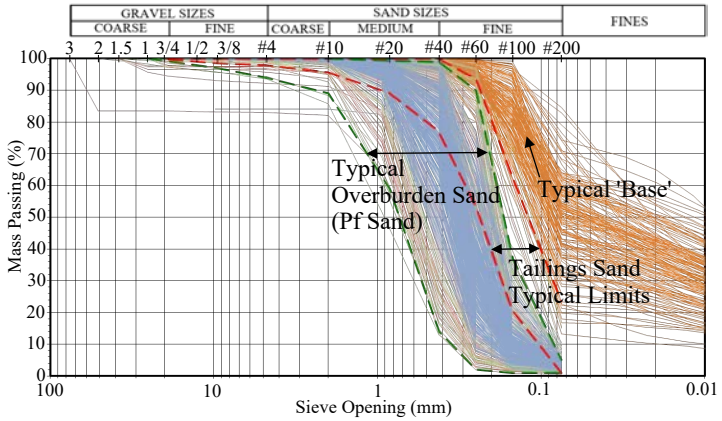

Figure 6: Typical gradations of base and filter materials

The permeability is checked using the Terzaghi relationship ($D_{15}/d_{15}>4$), to ensure a ratio of permeability about 15 to 20 times between the filter and the adjacent core material. From the gradation envelopes presented in Figure 6, the d_{15} of the Base soil is less than 0.01 mm, the D_{15} of the Pf sand is in the range of 0.1 and 0.4 mm, and the D_{15}/d_{15} is 10 or higher for the Pf sand, thus satisfying the Permeability Criteria. In the case of a tailings sand filter, the D_{15} of the tailings sand would have to be restricted to be greater than 0.1 mm. Therefore, while Pf sand, in general, satisfies the permeability criterion, only a selective portion of tailings sand can be accepted for the chimney filter ($D_{15} > 0.1$ mm). Also, site-specific correlations among hydraulic conductivity, fines content, and the void ratio are developed, and limits on the acceptable grain size distributions are included in the design specifications.

The third aspect that needs to be fulfilled by the internal drainage system is the discharge capacity of the chimney, which is normally checked through rigorous modeling involving horizontal defects and vertical cracks as described in the preceding paragraphs.

The additional considerations on the chimney material are the specification of a maximum size of 75 mm, a limit on the minimum D_{10} and maximum D_{90} to minimize segregation during placement (alternatively, a uniformity coefficient D_{60}/D_{10} of 6 or less), and that the material shall be cohesionless to be able to "selfheal" by collapse. Sherard and Dunnigan (1989) have reported that filters containing appropriate quantities of fine sand will reliably control and seal concentrated leaks through the "base" if the D_{15} is less than 0.5 mm, which is the case with both the Pf sand and tailings sand.

Design procedures for drain pipes

The Drain pipes should be able to handle the calculated seepage flows with an adequate factor of safety on the flow capacity, the grades of the pipes should be sufficiently large to prevent siltation and the drain pipes should have adequate margin of safety against structural failure under the static loading of the fill above them.

The drain pipes are installed near the base of the chimney filter such that the seepage water is collected and removed from the chimney efficiently. The fill height above the drain pipes can be up to 100 m for in-pit dams. Flexible HDPE pipes are designed using performance criteria, which include consideration of wall deflections, wall buckling, pipe stresses, and pipe strains. The integrity and structural performance of the internal drain pipes depend on the type of pipe, type and placement specifications of fill surrounding the pipe, and the depth of burial.

In the assessment of the integrity of the buried drain pipes, guidelines provided in the *Handbook of Polyethylene Pipes* (Plastic Pipe Institute, 2019) and FEMA (2007) are followed to develop the performance criteria. The performance criteria are checked using the commercially available software that allows modelling of soil-structure interaction problems. Based on the authors' experience, HDPE pipes with DR11 to DR9 designation meet the performance (pipe deflections, wall buckling, stresses, and strains) criteria for burial depths ranging from 80 to 100 m. The acceptable performance is highly dependent on the required degrees of compaction within the pipe bedding below the pipe, the haunch zones, and the pipe backfill zones to the sides of the pipe, hence requiring stringent construction quality control during installation.

Conclusion

This paper presents an overview of recently implemented seepage control design methods for in-pit dams in Alberta, and the key considerations and a design example illustrating the main steps that are followed in the design of an internal seepage control system for an overburden filled in-pit dam. The use of two-dimensional and three-dimensional seepage modelling to evaluate the seepage flow conditions and to design the seepage control elements have been illustrated through the example.

References

Barlow, P.J., P. Lach, E. McRoberts and R. Cameron. 1998. Hydraulic fracture involving MFT. In *Proceedings of the 51st Canadian Geotechnical Conference,* Canadian Geotechnical Society, Edmonton, Alberta Canada, 1: 403–412.

Cameron, R. and V. Fong. 2001. Performance of a quasi-homogeneous earth-fill dam retaining 35m of tailings fluid with no filters or clay core: Syncrude's highway berm. In *Proceedings of the 54th Canadian Geotechnical Conference,* Canadian Geotechnical Society, Calgary, Alberta, Canada 1: 297–304.

Cameron, R., W. Mimura, V. Fong and L. Lussier. 2001. Detailed construction procedures and considerations in Syncrude's quasi-homogeneous earth-fill dams. In *Proceedings of the 54th Canadian Geotechnical Conference,* Canadian Geotechnical Society, Calgary, Alberta, Canada 1: 235–243.

Canadian Dam Association (CDA). 2013. Dam safety guidelines.

Canadian Dam Association (CDA). 2014. Application of dam safety guidelines to mining dams. Technical bulletin.

CAPP. 2019. Canadian Association of Petroleum Producers. Canadian oil and natural gas. Accessed September 13, 2019 from https://www.capp.ca/canadian-oil-and-natural-gas.

Fell, R., P. MacGregor, D. Stapledon and G. Bell. 2005. *Geotechnical Engineering of Dams.* CRC Press.

FEMA P-676. 2007. Technical manual: Plastic Pipe used in embankment dams, best practices for design, construction, problem identification and evaluation, inspection, maintenance, renovation, and repair. Federal Emergency Management Agency.

ICOLD. 1994. Embankment dams granular filters and drains: Review and recommendations. International Commission on Large Dams, Committee on Materials for Fill Dams, Paris. Bulletin 95.

Lane, E.W. 1935. Security from under-seepage masonry dams on earth foundations*. Transactions of American Society of Civil Engineers* 100: 1257–1935.

Plastic Pipe Institute. 2019. *Handbook of Polyethylene Pipe,* second edition. Design of PE Piping Systems, Chapter 6.

Sherard, J.L. 1973. *Embankment Dam Cracking. Embankment Dam Engineering,* Casagrande volume. New York: John Wiley & Sons: 272–353.

Sherard, J.L., L.P. Dunnigan and J.R. Talbot. 1984. Filters for silts and clays. *Journal of Geotechnical Engineering, ASCE,* June: 684–700.

Sherard, J.L. 1985. Hydraulic fracturing in embankment dams. symposium on seepage and leakage from dams and impoundments, *ASCE,* May: 115–141.

Sherard, J.L. and L.P. Dunnigan. 1989. Critical filters for impervious soils. *Journal of Geotechnical Engineering, ASCE,* July: 927–947.

US Society on Dams (USSD). 2011. Materials for embankment dams.

USBR. 1977. Design of small dams. United States Department of Interior, Bureau of Reclamation, Denver.

USBR. 1987. Embankment dam instrumentation manual. United States Department of Interior, Bureau of Reclamation, Denver.

USDA-SCS. 1994. Gradation design of sand and gravel filters, Part 623, Chapter 26 of *National Engineering Handbook.* United States Department of Agriculture, Soil Conservation Service.

Proceedings of Tailings and Mine Waste 2019
November 17–20, 2019, Vancouver, Canada
Published by the University of British Columbia, 2019

Cycloned Copper Tailings Sands: Practical Methods for Benchmarking Design Parameters

Jared Whitehead, Klohn Crippen Berger Ltd, Canada
Andrew Witte, Klohn Crippen Berger Ltd, Canada

Abstract

British Columbia (BC) has a history of successful design, construction, operation, and closure of major tailings dams composed of cycloned tailings sand. Fundamental to this success is a solid understanding of the engineering properties of cycloned sand, such as relative density, void ratio, strength, and permeability. The two main cycloned sand material parameters typically used in design analyses are strength, often represented by a friction angle and unit weight, and hydraulic conductivity. However, controlling these parameters through direct field measurement is not always straightforward. This paper provides insight into the link between design parameters and quality control (QC) testing programs to inform future engineering designs.

Introduction

Modern copper mining in BC (and around the world) is focusing on development and/or expansion of massive, relatively low-grade, porphyry ore deposits. Such operations are typically only viable at low production costs which makes using the tailings stream as a construction material source for tailings facility development very attractive. The recent worldwide focus on tailings facility design and dam safety in the wake of recent dam failures (e.g., Mount Polley in 2014, Samarco in 2015, Brumadinho in 2019) has placed increased emphasis on responsible tailings management; namely on identifying critical controls to mitigate high consequence risks or failure modes of the facility (MAC, 2017). Measuring and monitoring the construction and performance of a tailings facility against the design assumptions is critical for assuring the integrity of the facility.

Consistent with the engineering design process, QC testing is performed in parallel with performance monitoring (e.g., instrumentation) to confirm that construction is in accordance with the relevant specifications and standards, and that the design intent has been satisfied. QC testing is a typical critical control for a cycloned sand tailings dam and this paper presents field and laboratory testing data for two cycloned sand tailings dams in BC in relation to engineering design parameters. Published cycloned sand

data from other sites are also studied for comparison. Of equal importance to understanding these design parameters is the influence of stress state on sand behaviour under shear (e.g., whether it will exhibit contractive or dilative behaviour). At the time this paper was written, laboratory testing was in progress to define critical state parameters for copper cycloned sands which will be presented in a follow up paper.

British Columbia subject sites

Two mine sites in BC are considered for this study: the Copper Mountain Mine near Princeton, BC and a copper mine at an undisclosed location in BC (Site A). Both sites utilize conventional slurry tailings deposition with single-stage cycloning to produce dam fill material that is deposited directly onto the embankment slopes without additional mechanical compaction. Both tailings facilities consist of homogeneous cycloned sand embankments over earthfill starter dams and underdrainage systems. Details of each facility are summarized in Table 1.

Table 1: Summary of cycloned sand dams studied

Mine site	Location	Embankment name	Approx. crest to toe height (2018)	Downstream slope	Construction type
Copper Mountain Mine	Princeton, BC	East Dam	150 m	2.5H:1V	Modified centerline, starter dam, no core
		West Dam	150 m	2.5H:1V	Modified centerline, starter dam, no core
Site A	Undisclosed location, BC	Embankment 1	120 m	2.5H:1V	Modified centerline, starter dam, no core
		Embankment 2	10 m	10H:1V to 25H:1V	Modified upstream, no core

Copper Mountain Mine's East and West Dams feature direct deposition on moderate slopes and are currently under construction (as of 2019). Embankment 2 at Site A is currently under construction (as of 2019) and features direct deposition on a very flat slope that is located several hundred meters upstream of Embankment 1. Embankment 1 construction was completed to its ultimate elevation in 2011.

Tailings and cycloned sand index properties

The index properties of copper tailings materials are a function of the ore type/parent rock and the processes used to extract the ore (e.g., ore crushing/grinding sequences, flotation, single or double-stage cycloning). In general, the solids in hard rock mine tailings are quite angular due to the grinding process (Garga and McKay, 1984). This is visible in the magnified Scanning Electron Microscope (SEM) images of the cycloned sand produced at the subject sites (Figure 1). The angularity of the particles has a significant effect on the strength and hydraulic properties of the material as compared to materials formed and deposited by natural processes (e.g., long-term physical and chemical weathering processes). Even the fine particles within the tailings are angular, allowing more open pore spaces to form and water to flow more freely than in natural soils of similar gradation. The SEM images do not reveal evidence that suggests particle crushing occurred (at stresses up to 1,500 kPa) although particle crushing could occur under higher stresses which could have a significant influence on strength and permeability behaviour of the cyclone sand.

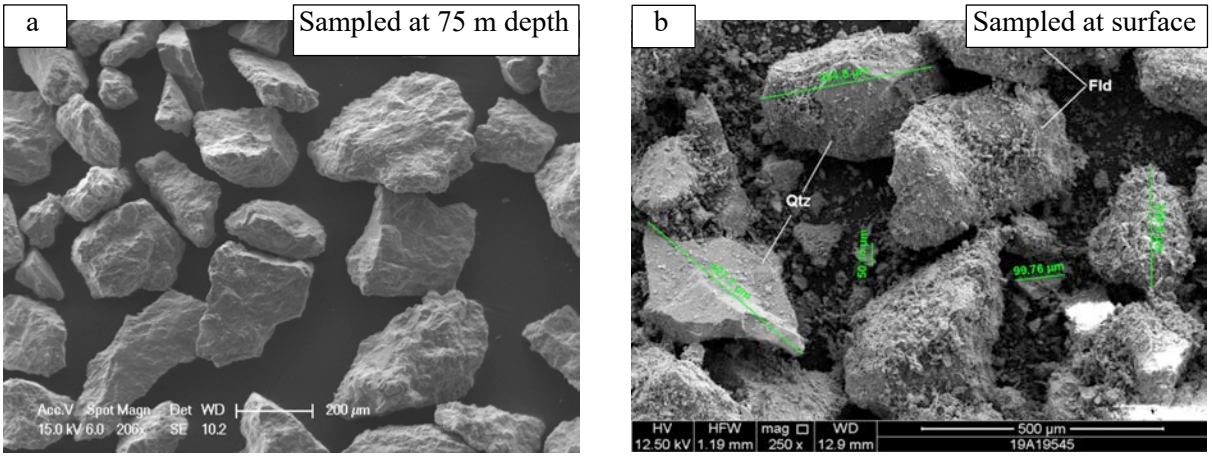

Figure 1: SEM photos of cycloned sand from a) Copper Mountain Mine and b) Site A

Cycloned sand is produced via centrifugal mechanical devices (cyclones) that separate a tailings feed into a coarse portion (underflow sands) used for dam construction and a fine portion (overflow slimes) discharged to the interior of the tailings impoundment. Particle size distribution bands of in-situ cycloned sands from the subject sites are plotted with published copper cycloned sand gradations from Garga and McKay (1984) and Valenzuela (2016) in Figure 2. Typical gradations Fraser River Sand are also provided for reference.

A relatively "clean" sand can generally be produced from cycloning operations if the input tailings feed is no more than 60% finer than the No. 200 sieve or 0.074 mm (Lighthall et al., 1989). This claim is supported by the gradation curves from the subject sites cycloned sand in Figure 2. Table 2 summarizes some index properties of cycloned sand from the subject sites, as well as some other published reference data.

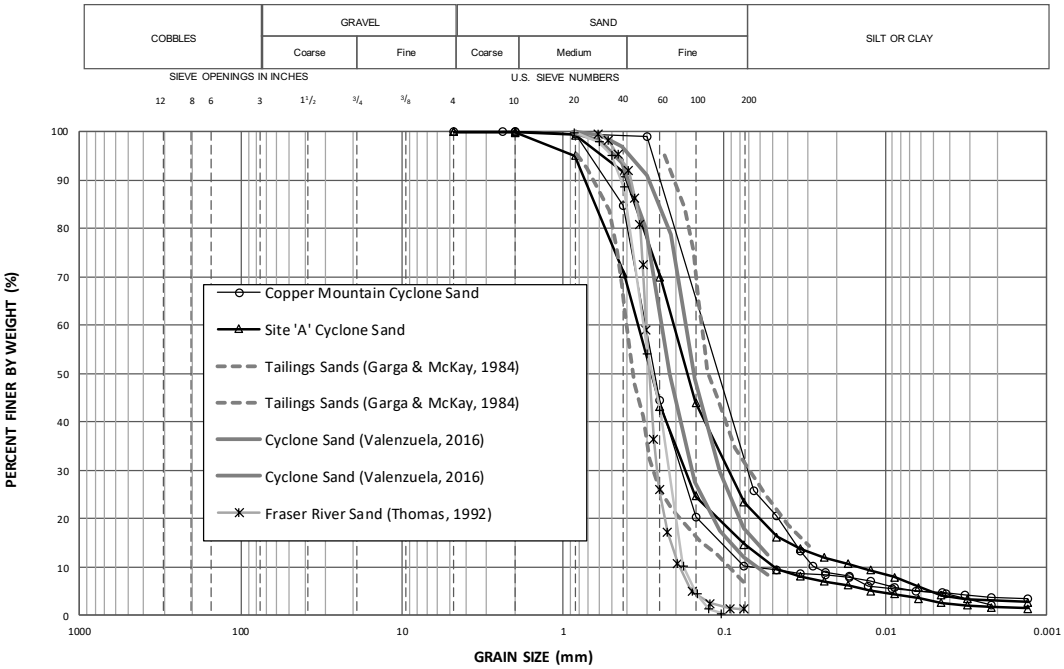

Figure 2: Particle size distributions of cycloned copper tailings sand materials

Table 2: Summary of cycloned sand index properties

Site/Reference	Ore type	Specific gravity	Tailings feed	Cyclone sand			
			Mean fines content[1]	Mean fines content[1]	Range of in-situ void ratios[2]	Range of in-situ relative density	ϕ_p' [3]
Site A (2013–2019)	Cu, Mo Porphyry	2.76	45% (126 tests)	16% (785 tests)	0.5 to 0.9 (Mean = 0.7) (216 tests on uncompacted cycloned sand)	26% to 100% (Mean = 67%) (216 tests on uncompacted cycloned sand)	33°–39°
Copper Mountain (2014–2018)	Cu, Au, Ag Porphyry	2.83	45% (1,262 tests)	14% (8,710 tests)	0.6 to 0.9 (Mean = 0.8) (388 tests on uncompacted cycloned sand)	22% to 100% (Mean = 60%) (388 tests on uncompacted cycloned sand)	35°–40°
Unpublished copper mine	Cu, Mo Porphyry	2.65	40%	12%	0.4 to 0.6 (Mean = 0.5) (690 tests on compacted cycloned sand)	–	36°–38°
HVC – Trojan (Lighthall et al., 1989)	Cu, Mo Porphyry	–	45%	5%–10%	–	7%–67% (Compacted)	–
Gibraltar (Lighthall et al., 1989)	Cu, Mo Porphyry	–	45%–50%	10%	–	35%–53% (No compaction)	–
Brenda (Lighthall et al., 1989)	Cu, Mo Porphyry	2.70	45%	<5%	–	23%–57%% (No compaction) 41%–63% (Compacted)	–

Notes:

1. Fines content is defined as the percent finer than 0.074 mm (by weight) and is determined by No. 200 Wash Sieve tests. Values presented are arithmetic mean.
2. Void ratio determined from nuclear densometer testing performed 300 mm below surface.
3. ϕ_p'= peak drained friction angle (from drained and undrained triaxial testing – refer to Section 4.2).
4. Fines content and void ratio for Site A (2013–2019) and Copper Mountain (2014–2018) are based on annual construction summary reports and sampling databases.

Quality control of design parameters

The following key design parameters, to be verified in-situ by QC testing, are commonly employed for the design of cycloned sand dams:

- *Dry unit weight* and *frictional strength*, which govern shear resistance for slope stability; and
- *Hydraulic conductivity*, which is critical in providing a well-drained downstream shell to maintain a low phreatic surface.

This section summarizes the result of several years of field and laboratory testing at the subject sites. The following physical properties are measured by the QC field and laboratory tests on cyclone sand:

- In-place *dry density* as a measure of in-situ unit weight and strength state;
- *Peak secant friction angle* as a measure of frictional strength for a given density and stress state;
- In-place *hydraulic conductivity*, as a measure of the draining capability of the sand; and
- *Particle size distribution* and the *fines content* as they relate to hydraulic conductivity.

Dry unit weight

Field moist density and field moisture content of the cycloned sand can be measured using a nuclear densometer, from which dry density can be calculated. For geotechnical analysis, the unit weight above the water table should not be specified as the dry unit weight since the cyclone sand in the field is rarely completely dry and usually has some residual moisture content. This is an important distinction that requires care and attention by the designer. However, dry unit weight is a common design parameter and is relatively easy to measure.

The in-situ strength state of the cyclone sand can be correlated to its relative density[1], which in turn can be correlated to the void ratio using dry density and specific gravity[1]. These parameters are particularly useful to the designer when they are measured over time, to compare historic densities with current densities and determine the degree and rate of consolidation.

Due to size limitations of the moisture-density nuclear gauge, in-place density and moisture content can only be measured up to 300 millimeters (mm) depth below surface, and therefore, the readings can be significantly influenced by heavy traffic and/or over-wet surfaces (e.g., equipment and/or water ponding on the dam surface) and will not be representative of the soil state at depth. A profile of the change in density

[1] Void ratio $e = \frac{G\gamma_w}{\gamma_d} - 1$, where G = specific gravity, γ_w = density of water, and γ_d = dry density.
Relative density $D_r = \frac{e_{max} - e}{e_{max} - e_{min}} \times 100\%$, where e_{max} = maximum void ratio (from maximum index density test), e_{min} = minimum void ratio (from minimum index density test).

with depth can be estimated by excavating safe test trenches, and performing tests at selected depths, typically as deep as 5 meters (m) from surface. For large dams, longer profiles of densities can be developed using Cone Penetration Testing (CPT) and empirical void ratio correlations. The CPT has been used extensively to determine the density and bearing capacity of cycloned sand and tailings materials, and subsequently assess the soil state and benchmark the design assumptions. It is particularly useful when investigating consolidation of the cyclone sand over time and selecting parameters for laboratory testing (e.g., triaxial, direct simple shear or oedometer tests).

Nuclear densometers measure moisture content using an indirect method that requires calibration. Typical units use a millicurie (mCi) americium-241: beryllium neutron source to measure the hydrogen content (i.e., the water content) of the soil (Troxler, 2006), which is sensitive to the depth of measurement. The authors' experience at the subject sites suggests that field moisture typically underestimates the laboratory moisture content of the soil (following a linear relationship, illustrated in Figure 3a), resulting in an overestimate of dry density. This underestimation can be attributed to partial drying of the sand surface prior to testing. Best practice is to take a sample at each test location to determine the laboratory moisture content which can be used to correct the field dry density.

Field dry density measurements

Figure 3b shows the variation of the field dry density and laboratory moisture content for the subject sites. Unpublished data from a compacted cycloned sand dam constructed using hydraulic cells is also presented, which exhibits higher dry densities and moisture contents compared to the subject sites. These higher dry densities reflect the additional compaction achieved from the application of hydraulic cell placement methods. The higher range of dry densities (greater than 1,800 kilograms per cubic meter [kg/m^3]) observed at the subject sites are attributed to heavy equipment traffic compacting the cycloned sand on or near the dam crests. Conversely, the lower range of densities (less than 1,500 kg/m^3) resulted from tests completed on freshly deposited sand which was still draining and consolidating at the time of testing. There is no evidence at the subject sites that dry density varies with location on the dam (crest, slope, and toe) for uncompacted, directly deposited cycloned sand near surface and at shallow depths (less than 5 m). Density profiles developed from CPT profiles at depth may reveal differences at different locations at the crest, slope and toe, due to the additional consolidation under the varied vertical stresses.

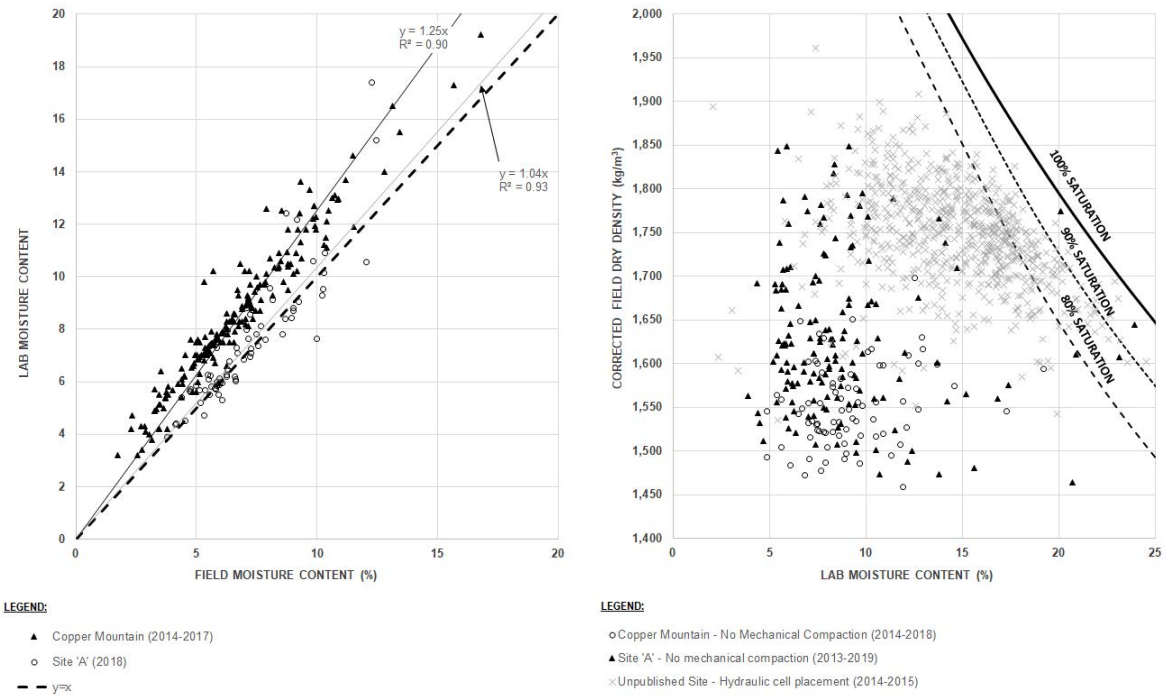

a) **b)**

Figure 3: a) Field vs lab moisture content; b) Corrected field dry density vs lab moisture content

Calculated void ratio and relative density

The mean "void ratio" calculated from the corrected field dry densities (at surface) and mean laboratory specific gravity are plotted against the field moisture content and relative density for the subject sites and for an unpublished database from compacted cycloned sand dam in Figure 4. A void ratio in the context of this paper is one that represents the soil state before it is consolidated under an additional overburden stress (i.e., buried by subsequent cyclone sand deposition). Like Figure 3b, the unpublished data from the compacted sand dam exhibits lower void ratio (typically between 0.4 and 0.6) due to the hydraulic cell placement method and mechanical compaction. Uncompacted sand at the subject sites exhibit significant scatter in void ratio as there is no control over the degree of compaction.

However, the cycloned sand produced at these sites have consistently met the respective design relative density (discussed below) requirements for sand placed directly on the slope. The variations observed in void ratio and moisture content between the three sites is also due to the differences in specific gravity as illustrated in Table 2.

.

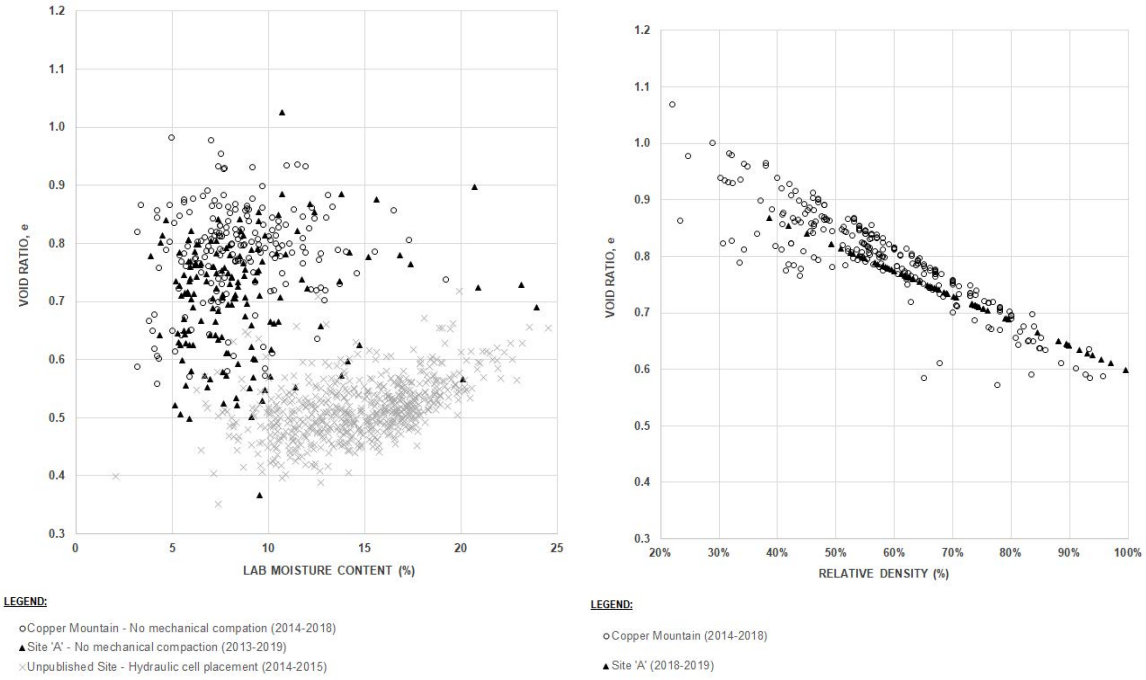

Figure 4: Void ratio versus field moisture content and relative density

Relative density is a measure of in-place density in relation to loosest and densest states that the cyclone sand can attain. It can be calculated from field and laboratory measurements using specific gravity (ASTM D854), maximum and minimum index dry density (ASTM D4253 and D4254, respectively) and the measured dry density void ratio as discussed above (refer to footnote 1). Void ratio is plotted against relative density for the subject sites in Figure 4. The scatter observed for Copper Mountain is due to the use of different maximum and minimum index dry densities at different construction phases. The results for Site A follow a linear trend as they are based on one field program and one maximum and one minimum index dry density laboratory test. If more tests on maximum and minimum index dry densities are done for Site A, a similar scatter as seen for Copper Mountain is expected. The results from Site A show nearly all measurements above 50% relative density and the results from Copper Mountain show about two thirds of the measurements are above 50% relative density. The mean void ratio for Site A (about 0.7) is lower than that for Copper Mountain (about 0.8). These differences are attributed to the direct deposition on the significantly flatter slopes and at lower solids content[2] (targeting ~70%) at the Site A Embankment 2 compared to the more moderate slopes and higher solids content (targeting >75%) at Copper Mountain's East and West Dams, and the subsequently greater impact of gravitational drainage through the sand and consolidation on the flatter slopes.

[2] Solids content is the ratio of the weight of the solids to the total weight of the slurry, expressed as a percentage.

Friction angle

Monotonic triaxial compression testing can be used to benchmark the strength values used in design based on the relative densities measured in the field. Reconstituted specimens can be prepared to a target initial dry density/void ratio (based on a representative value from field density testing), saturated and consolidated to simulate the expected loading and drainage conditions for current and future dam raises. In addition to deriving a friction angle at failure, results from the triaxial test can be used to assess the void ratio and consolidation stress relationship. Figure 5 summarizes peak secant friction angle[3] (ranging from 36° to 41°) with consolidated void ratio (ranging from 0.6 to 0.8) from undrained triaxial testing of cycloned sand from the subject sites; the results are generally fines content independent for sand with less than 20% fines. Figure 5 also presents the results of isotropically and anisotropically (k_o) consolidated triaxial tests that suggests that friction angle of cycloned sand is independent of the consolidation stress path. These tests on relatively loose specimens of saturated cycloned sand exhibit an initial contractive behaviour in shear but show dilative behaviour as they approach the phase transformation line. This illustrates the importance of maintaining unsaturated conditions in the cycloned sand dam shells in the field.

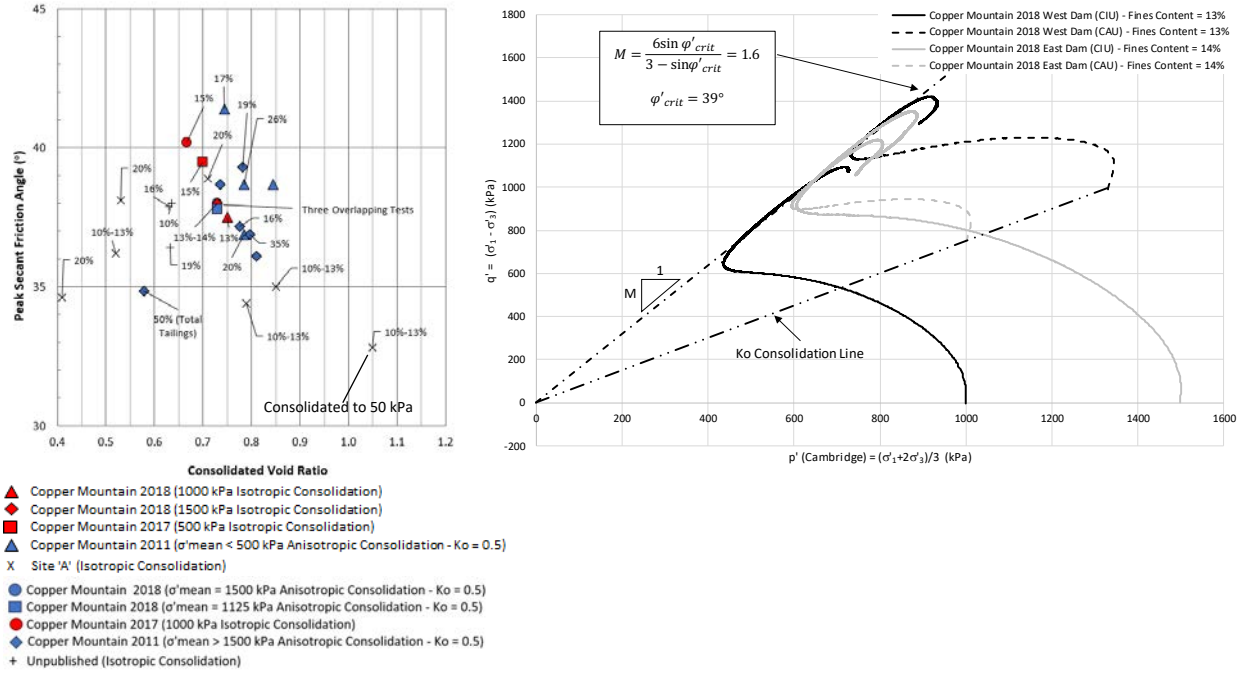

Figure 5: Consolidated undrained triaxial test results for copper cycloned sand consolidated to between 250 kPa and 2,000 kPa). Data labels show fines content. Not all samples had an associated gradation test

[3] Peak secant friction angle is calculated using the following relationship: $M = \frac{6sin\ \varphi'_{crit}}{3-sin\varphi'_{crit}}$ where M = slope of inclination of triaxial failure envelope (at maximum obliquity) on 'p-q' plot. A cohesion intercept of zero is assumed.

Busslinger et al. (2013) observed similar results for copper-gold cycloned sand under high stresses from undrained triaxial tests (i.e., average peak secant friction angle of 38° for samples compacted to 103% of the standard Proctor maximum dry density). Empirical correlations with CPTs performed at Copper Mountain Mine estimated relative densities between 40% and 60% and friction angles greater than 35° for the cycloned sand, which agree with the results of the triaxial testing in Figure 5.

Thomas (1992) tested Fraser River sands under similar conditions to those discussed above and reported that the average mobilized friction angle (at maximum obliquity) of Fraser River sand ranges from approximately 32° to 36° and is independent of relative density, confining stress, anisotropy and mode of loading. Notwithstanding, relative density and confining stress will have a strong influence on whether the sand will exhibit a contractive or dilative behaviour when saturated. A connection is made with these results and copper cycloned sands given their similar gradation envelopes (refer to Figure 2), although cycloned sands exhibit slightly higher peak secant friction angles, likely due to the angularity of the particles (Figure 2). This observation is in general agreement with the work of Mittal and Morgenstern (1975) on highly angular Brenda tailings sand and more sub-rounded Ottawa Sand for triaxial tests performed on these materials at similar densities and stress levels.

Hydraulic conductivity

The hydraulic conductivity of cycloned sand is a measure of its draining capability. Conventional cycloned sand dams generally rely on drained conditions in the downstream sand shell (usually promoted by underdrainage systems) and require several orders of magnitude difference in hydraulic conductivity between the upstream stored tailings and the cycloned sand to achieve this. Vick (1990) shows that the greater the contrast in permeability between cycloned sands and upstream tailings, the lower the phreatic level that will be maintained. Large above-water tailings beaches are often incorporated into the design of sand dams to distance the free-water pond from the sand shell, reduce overall seepage gradients, and, together with an extensive underdrainage system, promote low phreatic levels beneath the downstream shell to improve stability.

Estimates of seepage rates and phreatic surface levels used to inform design decision (i.e., seepage control measures) are sensitive to the assumed or modeled hydraulic conductivity values and assumed anisotropies. Hydraulic conductivity can be estimated using empirical correlations, in-situ tests and/or laboratory tests as discussed in the following sections.

Empirical correlations

The hydraulic conductivity of sand can be estimated using the relationship proposed by Hazen (1911):

$$k = 0.01 \times D_{10}^2$$

where D_{10} (the particle size for which 10% is finer by mass, in mm) is selected from the particle size distribution derived from hydrometer tests (ASTM D6913).

In-situ tests

In-situ hydraulic conductivity can be estimated in the field using constant head techniques using either a Guelph Permeameter (Eijkelkamp, 2011) or Double-Ring Infiltrometer (Ahuja et al., 1976; Fatehnia et al., 2016). These methods are practical for estimating the infiltration rate of silty sands (such as copper cycloned sand) with hydraulic conductivities on the order of 10^{-5} to 10^{-6} meters per second (m/s), but constant heads may be more difficult to maintain for more free-draining sands, based on the authors' experience. Falling head techniques may be more appropriate for such conditions, but require more complicated analyses to interpret the results.

Hydraulic conductivities measured using the Guelph Permeameter and the Double Ring Infiltrometer at the subject sites are plotted against D_{10} in Figure 6a and against fines content in Figure 6b. Typical measurements for Fraser River Sand are also shown in Figure 6a and Figure 6b for reference (Thomas, 1992; Northcutt and Wijewickreme, 2013; Neilson-Welch and Smith, 2001). In-situ saturated hydraulic conductivity does not appear to vary significantly with moderate changes in D_{10} or fines content, within the expected uncertainties associated with such measurements. These results suggest that for the given range of measured hydraulic conductivities of copper cycloned sands, using D_{10} and fines content as the sole metric for estimating hydraulic conductivity may not be appropriate and should be supplemented with in-situ testing to verify the design hydraulic conductivity.

Laboratory permeability testing

Laboratory permeameter testing is a useful control test to benchmark field measurements. Permeameter testing was performed on reconstituted samples of cycloned sand from Copper Mountain with fines contents between 15% and 30%. The tests were conducted under constant head conditions in accordance with ASTM D2434 using three different hydraulic gradients (0.3, 1.0, and 2.0). The test specimens were prepared by moist tamping to a target initial void ratio of 0.75 to simulate consolidated field conditions at over 100 kilopascals (kPa) (based on previous triaxial testing) and flushed with CO_2 to improve overall saturation of the sample. The 20% fines specimen was re-prepared and tested at a lower void ratio of 0.70 to assess the influence of reduced void ratio on hydraulic conductivity (i.e., to simulate increased burial depth).

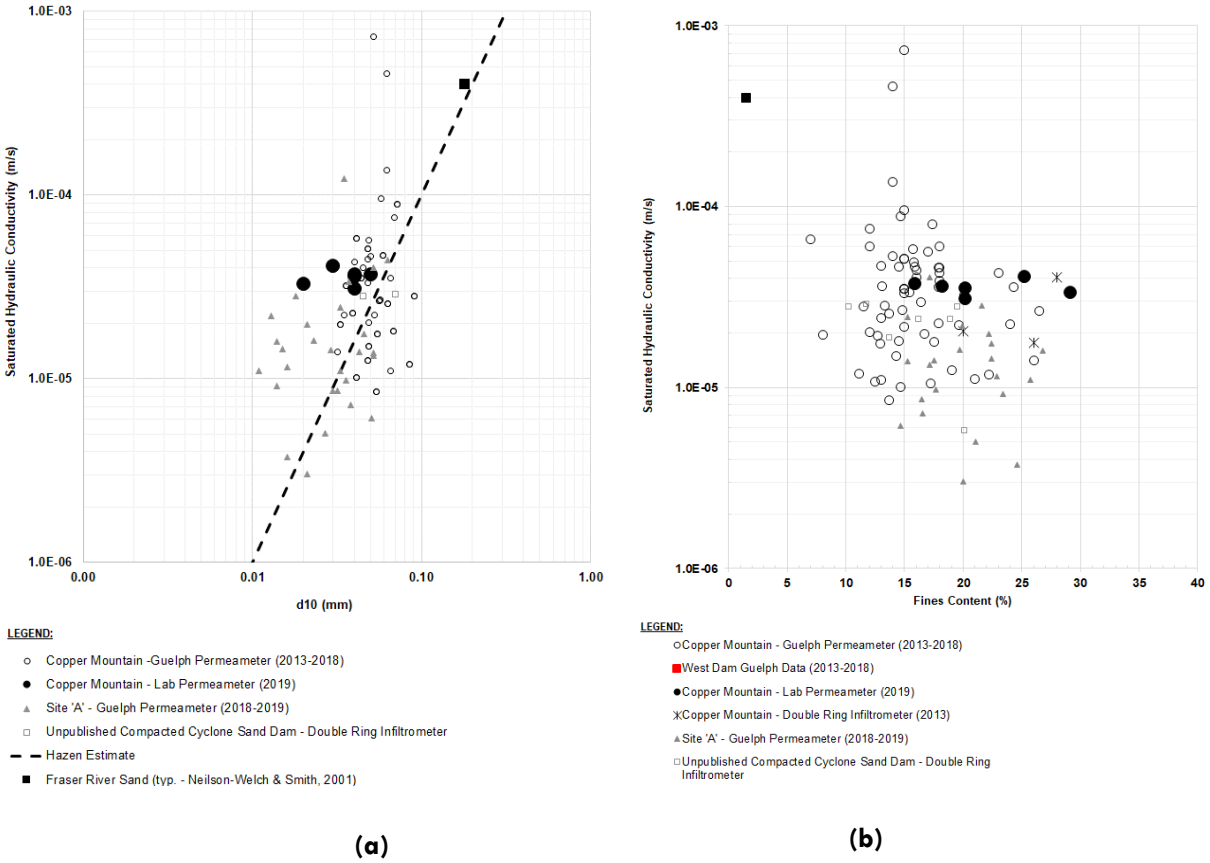

(a) (b)

Figure 6: Comparison of in-situ hydraulic conductivity measured with a Guelph Permeameter to D_{10} (Hazen's equation) and fines content

Details of the samples and test results are listed in Table 3. The percentage of material finer than 74 microns (fines), 44 microns (visible particles), and 2 microns (clay-sized) is also provided in listed in Table 3. For reference, Site A cycloned sand with fines content up to 30% had between 3% and 4% clay-sized particles. The percentage of clay-sized material is likely to be the primary controller on the permeability of the sand however it is not readily determined in the field without the hydrometer test; rather standard practice is to use fines content as a proxy for hydraulic conductivity. The laboratory permeameter results are also plotted on Figure 6b for comparison with the in-situ test results.

Table 3: Index properties of permeameter samples

Property	Units	Target fines content					
		15%	18%	20%	25%	30%	20%
Percent finer than 0.074 mm (no. 200 sieve)	%	15.9	18.2	20.2	25.2	29.1	20.2
Percent finer than 0.044 mm (no. 325 sieve)	%	9.8	10.6	11.0	13.9	15.2	11.0
Percent finer than 0.002 mm (clay sized)	%	3.6	3.8	3.5	3.6	3.6	3.5
D_{10} [1]	mm	0.05	0.04	0.04	0.03	0.02	0.04
Initial void ratio [2]	–	0.75	0.75	0.75	0.75	0.75	0.70
Initial moisture content	%	13.9	14.5	14.5	14.5	14.0	13.9
Hydraulic conductivity measured by lab permeameter	m/s	3.7×10^{-5}	3.7×10^{-5}	3.6×10^{-5}	4.1×10^{-5}	3.3×10^{-5}	3.1×10^{-5}
Hydraulic conductivity calculated based on D_{10} [3]	m/s	2.5×10^{-5}	1.6×10^{-5}	1.6×10^{-5}	0.9×10^{-5}	0.4×10^{-5}	1.6×10^{-5}

Notes:
1. D_{10} is the particle size at which 10% of the sample's mass is comprised of particles with a diameter less than this value.
2. Void ratio, e was calculated using a mean specific gravity of 2.8 based on site testing.
3. Hydraulic Conductivity, k, is estimated using Hazen's equation where $k = 0.01\times D_{10}^2$.

Discussion of hydraulic conductivity

Considering the level of uncertainty associated with the measurement techniques, the variations observed in hydraulic conductivity do not appear to correlate with fines content (% finer than 74 microns) when fines content is less than 20%. This agrees with the work of Valenzuela (2016), who observed more marked changes in hydraulic conductivity with fines contents exceeding about 30%. Valenzuela (2016) suggests that this could be attributed to a change in the structure of the soil skeleton "since coarse grains would not all be in contact and fines would then not only fill the spaces left by the skeleton of coarse grains but would also partly replace the grain-to grain-contact".

Neilson-Welch and Smith (2001) performed slug tests on Fraser River Sand with variable fines contents and demonstrated a consistent hydraulic conductivity in the order of 10^{-4} m/s in these materials. The clay content of Fraser River Sand was not published but is expected to be negligible based on sieve analysis results (refer to Figure 1). A connection is made with these results and copper cycloned sands given

their similar gradation envelopes (refer to Figure 1), although cycloned sands exhibit slightly lower hydraulic conductivities, likely due to the higher fines and slightly higher clay content.

Although the data presented herein is limited to low clay content sands (less than 4%), it suggests that cycloned sand with less than 20% fines and less than 5% clay-sized particles should have a hydraulic conductivity within the range of 10^{-5} to 10^{-4} m/s. This is in general agreement with the work of Vick (1990) and Qiu and Sego (2001). The authors suggest that practitioners consider adding a clay-sized particle acceptance criterion to hydraulic conductivity QC testing programs.

Conclusion

This paper assembled the results of numerous laboratory and field testing programs conducted at two major copper cycloned sand tailings dams in BC for the purpose of illustrating the link between design parameters and QC testing to inform future engineering designs. The key conclusions from this study are:

1. Relative density testing indicates that cycloned sand placed with direct hydraulic deposition onto the dam slope yields a relative density between about 40% and 70% without compactive effort, which is acceptable for homogeneous sand dams without internal deformation sensitive elements such as seepage barriers or filters. Such relative densities are likely not acceptable when considering the dynamic behaviour of the cycloned sand if it were saturated. This highlights the importance of an extensive underdrainage system for dams constructed in this manner.
2. The peak secant friction angle ranges from 36° (40% initial relative density) to 41° (60% initial relative density), and averages 38° at an initial relative density of 50% due to the increased angularity generated by grinding processes. For the expected range of relative density (50% to 90%) and void ratio (0.5 to 0.9) for cycloned sand, these values are generally higher than those assumed for design. Thus, cyclone sand placed without mechanical compaction (i.e., without a compaction specification) can still meet the design intent provided it is well drained (i.e., unsaturated) to eliminate the potential for contractive behaviour.
3. The frictional strength of cycloned sand measured using undrained triaxial testings appears to be consolidation stress path and fines content independent for fines contents up to 20%.
4. Considering the level of uncertainty associated with field and laboratory measurement techniques, the hydraulic conductivity of cycloned sand ranges from 10^{-5} to 10^{-4} m/s and appears to be fines content independent for fines contents up to 20%.
5. For QC testing to be considered a critical control, the field and laboratory programs should target direct measurement of the key design parameters rather than relying on proxy values

like field dry density (for frictional strength) or fines content (for hydraulic conductivity). Rather, routine QC testing should include:

- Advanced laboratory testing of static and dynamic soil properties including determination of a critical state line and state parameter to assess contractive and dilative behaviour of the cycloned sand.
- Field measurement of hydraulic conductivity paired with laboratory permeability and hydrometer testing (all on the same sample) to identify the particle size(s) that control hydraulic conductivity of the cyclone sand at each site.
- SEM imaging to establish changes in the soil skeleton with different gradations and stress levels.
- Further verification of field and laboratory measurements with regular CPT campaigns.

Acknowledgements

The authors wish to thank Mr. Bill Chin of Klohn Crippen Berger Ltd for his input and review of this paper. The authors also wish to thank Copper Mountain Mine for granting the publication of quality control data from their tailings facility.

References

Ahuja, Lajpat R., S.A. El-Swaify and Ausafur Rahman. 1976. Measuring hydrologic properties of soil with a double-ring infiltrometer and multiple-depth tensiometers 1. *Soil Science Society of America Journal* 40(4): 494–499.

Busslinger, M., H. Plewes and G. Parkinson. 2013. Testing of cyclone sand tailings at high stresses. Geo-Montreal 2013.

Eijkelkamp, 2011. Operating instructions. 09.07 Guelph Permeameter, 11/2011, accessed 08/04/2019 from https://www.eijkelkamp.com/download.php?file=b2082939.pdf

Fatehnia, M., K. Tawfiq and M. Ye. 2016. Estimation of saturated hydraulic conductivity from double-ring infiltrometer measurements. *European Journal of Soil Science* 67(2): 135–147.

Garga, Vinod K. and Larry D. McKay. 1984. Cyclic triaxial strength of mine tailings. *Journal of Geotechnical Engineering* 110(8): 1091–1105.

Hazen, Allen. 1911. Discussion: Dams on sand foundations. *Transactions, American Society of Civil Engineers* 73(11).

Mining Association of Canada (MAC). 2017. *A Guide to the Management of Tailings Facilities*, third edition.

Mittal, Hari K., and Norbert R. Morgenstern. 1975. Parameters for the design of tailings dams. *Canadian Geotechnical Journal* 12(2): 235–261.

Neilson-Welch, Laurie, and Leslie Smith. 2001. Saline water intrusion adjacent to the Fraser River, Richmond, British Columbia. *Canadian Geotechnical Journal* 38(1): 67–82.

Northcutt, Sheri and Dharma Wijewickreme. 2013. Effect of particle fabric on the coefficient of lateral earth pressure observed during one-dimensional compression of sand. *Canadian Geotechnical Journal* 50(5): 457–466.

Lighthall, P.C., Bryan D. Watts and Steve Rice. 1989. Deposition methods for construction of hydraulic fill tailings dams. *Geotechnical Aspects of Tailings Disposal and Acid Mine Drainage*.

Thomas, Joyis. 1992. Static, cyclic and post liquefaction undrained behaviour of Fraser River sand. PhD dissertation, University of British Columbia. Retrieved from https://open.library.ubc.ca/collections/ubctheses/831/items/1.0050443

Valenzuela, Luis. 2016. Design, construction, operation and the effect of fines content and permeability on the seismic performance of tailings sand dams in Chile. *Obras y Proyectos* 19: 6–22.

Vick, Steven G. 1990. *Planning, Design, and Analysis of Tailings Dams*. Canada: BiTech Publishers Ltd.

Bibliography

Barrera, Sergio, Luis Valenzuela and Jose Campaña. 2011. Sand tailings dams: design, construction and operation. In *Proceedings of Tailings and Mine Waste, 2011.*

Proceedings of Tailings and Mine Waste 2019
November 17–20, 2019, Vancouver, Canada
Published by the University of British Columbia, 2019

Obstacles to Effective Mine Closure, Rehabilitation, and Relinquishment

David J. Williams, The University of Queensland, Australia

Abstract

The mining industry's social and financial licences to operate are under increasing and high threat. There is a risk that the industry's control of its destiny will be taken away due to a community-wide "lack of trust", which is in turn due to past poor performance. In the aftermath of recent high profile tailings dam failures, the design of tailings dams has become more conservative and more regulated – "the tail is now wagging the dog". Waste rock dumps continue to generate poor quality seepage, and the conventional end dumping of waste rock makes the ultimate closure and rehabilitation of such dumps challenging. There is a lack of guidance on the closure and rehabilitation of open pits.

Mine relinquishment carries a requirement for "stability in perpetuity", a far more stringent requirement than is placed on any other infrastructure, which is extremely challenging to achieve. The "elephant in the room", and possibly the biggest challenge to rehabilitation and ultimately achieving mine relinquishment, is the mining industry's application of net present value accounting with a high discount factor. It delays expenditure, discounts future costs, results in escalating impacts over time, discourages rehabilitation, and prevents relinquishment. Regulators also focus on cost.

Mine closure and ultimate relinquishment need to be genuinely front of mind from the planning of a mining project, and throughout operations to rehabilitation and ongoing maintenance. The way a mining project is developed and operated affects dramatically its potential impacts, and much can be done throughout its development and operation to minimize these. Conventional open pit mining, waste rock and tailings management practices need to be challenged. What may initially minimize capital and operating costs can lead to inflated closure, rehabilitation, and ongoing maintenance costs. Wastes should be seen as a potential "closure resource", providing materials potentially suitable for rehabilitation purposes. Conditions imposed in an environmental authority, aimed at containment, can exacerbate impacts, and can be counter to closure. There is a divergence between the mining industry's discounting of future closure expenditure and the government's application of consumer price index-based increases to closure costs. The obstacles to mine operations facilitating mine closure, rehabilitation, and relinquishment are discussed.

Introduction

Mining is governed by boom and bust cycles, which mining companies perpetuate to a degree greater than any other industry. The demand for a given commodity ultimately drives up its price, and prompts exploration for more supply. New ore body discoveries over a period of years lead to the development of large new mines, which then increase supply over demand, driving down the price (causing a bust). Less efficient mines may be forced to close, and ongoing mines deplete reserves, leading to a loss of supply and dwindling stockpiles. This then causes the price to recover, leading to some closed mines being re-opened. However, this fails to meet demand, causing the price to rise further, leading to another boom. The total costs of finding, mining, and processing the commodity, plus the costs of failed projects and mine closures, are not fully accounted for.

Many companies are caught with limited production when commodity prices are high. Typically, a 1% under-supply results in about a 10% increase in price, and the reverse is also true. Mining companies caught out by an over-supply exacerbate this by producing more commodity to lower production costs and maintain or increase market share, which creates a spiralling slump in prices until the demand-supply returns towards a balance. Prices then increase, setting off the next boom in production, and the inevitable bust to follow.

Mining projects can last from as little as a couple of years to well over 100 years. However, the net present value (NPV) accounting approach is universally applied irrespective of project duration, with an associated high discount factor several times the consumer price index. The discount factor typically ranges from 6%, which is applied at low points of the mining cycle when the industry is short of cash flow and is risk averse, to 10%, which is applied during boom times to justify new projects when commodity prices are high. There is also an aspiration to achieve an internal rate of return of say 15%, which is unrealistic, even in the short term. Mining project costs deflate during low points of the cycle and inflate during high points, as mining companies collectively struggle to expand, and consultant, supplier, and contractor costs escalate. When applied to a short-term operation, the effect of discounting is small, while for a very long-term operation discounting has a huge effect. In any case, the mentality of discounting future costs back to present day costs persists. It has enshrined a short-term approach to open pit slopes, and to the handling of mining and mineral processing wastes.

Geotechnical closure risks and challenges

The geotechnical closure risks and challenges for conventional large-scale open pits, waste rock dumps, and tailings dams, and how these are impacted by the conventional approaches to open pit mining and the handling of mining and processing wastes, are discussed in the following sections.

Open pits

Open pits are constructed with walls as steep as can safely be constructed, to minimize the stripping of overburden. Geotechnical closure risks and challenges faced by open pits include pit wall instability, both geotechnical and erosional, and poor water quality (Figure 1). Pit water is typically saline due to net evaporation and may be acidic if sulphide minerals in the pit walls are exposed to the environment. As sulphide minerals oxidize, the oxidation products may tend to seal the unoxidized sulphides. Pit water quality will become increasingly poor in a dry climate, although the pit may remain a "sink", due to net evaporation maintaining the pit water level below the surrounding groundwater level as it recovers post-mining. In a wet climate, or when additional mine-affected water is diverted to the pit, the pit water may rise above the surrounding groundwater level, and may become a source of poor quality water.

Figure 1: Open pit geotechnical and erosional instability and poor pit water quality

Few open pits have been successfully rehabilitated, with post-closure treatments often limited to bunding and fencing (Figure 2a), with occasional pit backfilling and the establishment of pit lakes (Figure 2b). There may also be a requirement to flatten the pit slopes within the weathered zone to a nominal 45° to maintain geotechnical stability. This would also require that any waste rock dumps, bunding and fencing be kept well back from the potential degrading or flattening of the pit slopes.

(a) **(b)**

Figure 2: Post-closure treatment of open pits:
(a) bunding and fencing, and (b) backfilling and pit lake

Waste rock dumps

The conventional approach of end-dumping waste rock as close as possible to the point of egress from the open pit, then pushing out the dump lift until it becomes cheaper to go up, inverts the ground profile, exposing potentially contaminating waste rock on the top and far side of the dump (Figure 3). When the horizontal haul distance exceeds about five times the lift height it becomes cheaper to establish another lift. End-dumping waste rock produces "oxidation reactors" (Figure 4), comprising a base rubble zone formed by the ravelling of boulders, alternating but discontinuous coarse and fine-grained angle of repose layers, and a haul truck-compacted trafficked surface on the tops of each lift. The base rubble zone allows the ready ingress of oxygen, which passes up the coarse-grained angle of repose layers from which it diffuses into adjoining fine-grained angle of repose layers. Oxidation is dominant in the fine-grained layers, which present the highest surface area to volume ratio, and these layers store the most water, until breakthrough seepage occurs.

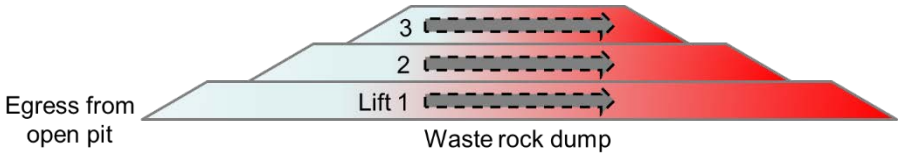

Figure 3: Conventional waste rock dump construction

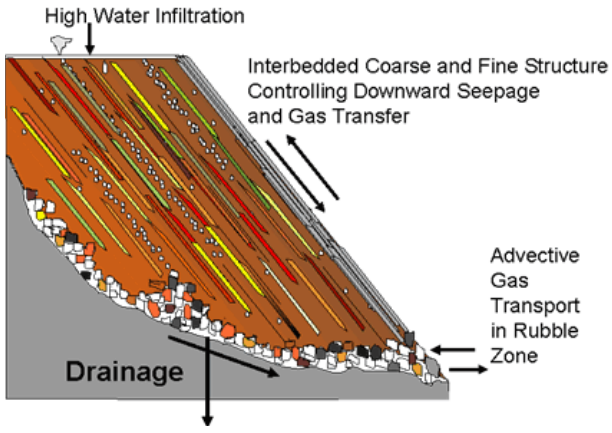

Figure 4: Conventional waste rock dump construction (GARD Guide, 2009)

The geotechnical closure risks and challenges faced by conventional waste rock dumps include geotechnical slope instability; erosional instability, particularly in a dry climate if the slope is flattened and topsoiled; differential settlement, affecting slope profile and drainage; spontaneous combustion of high sulphide waste rock or coal reject; and poor seepage water quality. Waste rock dumps may generate poor quality rainfall runoff. Seepage from conventional waste rock dumps may be saline if the waste rock releases salinity, and may be acidic if sulphide minerals are present within the waste rock.

Seepage from a waste rock dump will be lagged in time due to the waste rock initially being relatively dry, requiring that it be wet-up by rainfall infiltration sufficiently for the storage capacity of the dump to be exceeded and its unsaturated hydraulic conductivity to be overcome. The generation of acidic seepage may be lagged geochemically by any neutralization capacity within the waste rock. Seepage may emerge at topographic low points around the toe of the waste rock dump, and may infiltrate to a groundwater resource.

Few waste rock dumps have been successfully rehabilitated, which at best involves encapsulation of potentially acid-forming (PAF) waste rock by non-acid-forming (NAF) or acid-neutralizing capacity (ANC) waste rock (Figure 5), and covers (designed according to the climate-based guidelines for covers over mine wastes given in the GARD Guide, 2009; Figure 6). Covers for the tops of waste rock dumps are either rainfall-shedding for rainfall infiltration control in wet climates, or store-and-release in dry climates.

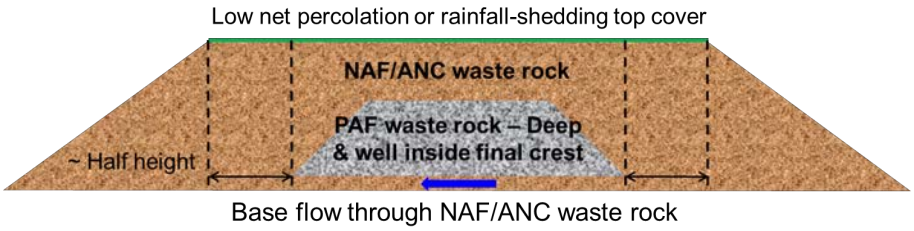

Figure 5: Encapsulation of PAF waste rock by NAF or ANC waste rock

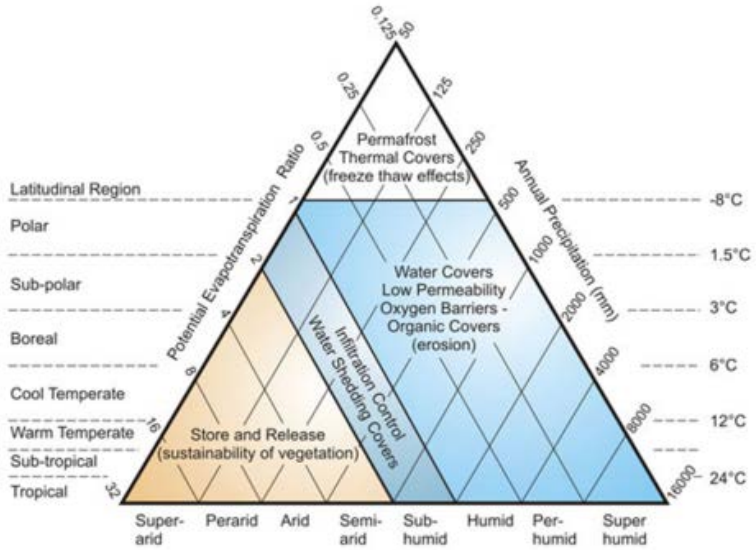

Figure 6: Climate-based guidelines for covers over mine wastes (GARD Guide, 2009)

Tailings dams

There is a commonly held perception, supported by the NPV accounting approach with a high discount factor, that transporting tailings as a slurry, using an inexpensive and robust centrifugal pump, to a surface dam is the most economic. Further, tailings dams are raised in a series of lifts to delay design and

construction costs, and their footprints are also limited, resulting in high rates of rise, and possible under-consolidation and limited desiccation of the tailings, which remain loose and water-entrained.

While the tailings dam is "designed", the management of tailings deposition may not be optimized. Initially, capital and operating expenditure are minimized. However, costs inevitably rise over time as the height and length of the tailings dam increase. Reduced capital costs are absorbed by ever-increasing operating costs. In terrain of low topographic relief, such as in Australia, escalating dam construction costs limit the economic height of tailings storages, forcing new sites to be developed.

Dewatering tailings to a paste or by filtration is perceived to be too expensive, particularly when discounted, and is often rejected as an option. The reduced storage volume occupied by tailings paste or filter cake, and the relative ease of capping dewatered tailings are discounted, as is potential for a higher-level future land use. The cost of rehabilitating the resulting soft and wet tailings is also discounted and not considered to be significant. The potential future "value" post-closure is also typically not considered.

The geotechnical closure risks and challenges faced by conventional surface tailings storage facilities include the geotechnical instability of the dam; erosional instability of the outer slope of the dam, particularly in a dry climate if the slope is flattened and topsoiled; differential settlement of the tailings, affecting their profile and drainage; and poor runoff and seepage water quality. Tailings are expected to drain down on the cessation of deposition, but may be recharged by high rainfall if this is not discharged via a spillway.

Tailings runoff and seepage may be saline (particularly if saline process water is used), acidic, or alkaline. Runoff and seepage volumes may be highest during tailings deposition or following periods (both during operations and post-closure) of heavy rainfall unless excess ponded water can be removed, either by pumping or via a spillway. Runoff and/or seepage of poor quality may initially be lagged due to neutralizing processing chemicals. Runoff will typically affect surface waters. Seepage may emerge at topographic low points around the toe of the tailings dam, and may infiltrate to a groundwater resource.

Few tailings storage facilities have been successfully rehabilitated, due to the difficulty and expense of capping "slurry-like" tailings, particularly at a time when the mine is no longer producing revenue. Where possible, a closure spillway should be provided, preferably cut through natural rock, to limit the recharging of seepage from the tailings (Figure 7, above). To limit the discharge of suspended sediment, a lined sediment pond may be constructed on the tailings storage facility, located just upstream of the spillway (Figure 7, below). Increasingly, the potential for reprocessing tailings, and disposal of the residual tailings in the completed open pit, is being considered.

Figure 7: Tailings dam closure: (above) spillway cut through natural rock, and (below) lined sediment pond located just upstream of spillway

Obstacles to mine closure, rehabilitation, and relinquishment

Obstacles to mine closure, rehabilitation, and relinquishment include NPV accounting with a high discount factor, comfort in "doing what we have always done" and poor community perceptions of the mining industry, and increasing regulatory obstacles. These topics are discussed in the following sections.

Net present value accounting

Infrastructure projects require delivery as soon as possible to enable their use and a return on expenditure, and sustained operation with minimal downtime to maintain revenue. However, mining projects are long-

term and are seen to deliver revenue only through the production of the commodity. Further, infrastructure projects are typically completed at the outset in order to provide value, while mining projects are necessarily incremental, with the progressive expansions of the open pit, the waste rock dumps and the tailings storage facilities, plus water dams for storing process water, and mine-affected water and sediments.

The aim is to minimize the costs of mining and processing to maximize the return from the commodity produced. Mines target high-grade ores to maximize the initial return on expenditure, and rehabilitation is seen as a non-productive cost that must be delayed and minimized. Indeed, mining regulators also see mine rehabilitation simply in cost terms. Rehabilitation is typically left to the end of the operation, when the impacts of mining and processing have escalated, making them difficult to reverse, and the operation is no longer producing revenue to support the cost of rehabilitation.

Net present value accounting with a high discount factor reinforces the short-term approach that limits capital expenditure on mining projects, not only at start-up but also at every expansion. Open pits are cut back and deepened progressively to suit the location of the ore body and its grade, not constrained by the extraction of potentially contaminating waste rock. Waste rock dumps are constructed with the primary aim of minimizing haulage costs, less constrained by the nature of the waste rock being produced and the effective encapsulation of potential contaminating waste rock. Tailings dams are raised progressively, often with too small a footprint to limit the rate of rise of the deposited tailings to enhance densification, and making it difficult to ensure the continuity of different zones in the dams. Over time, costs inevitably increase as options inevitably decrease (Figure 8).

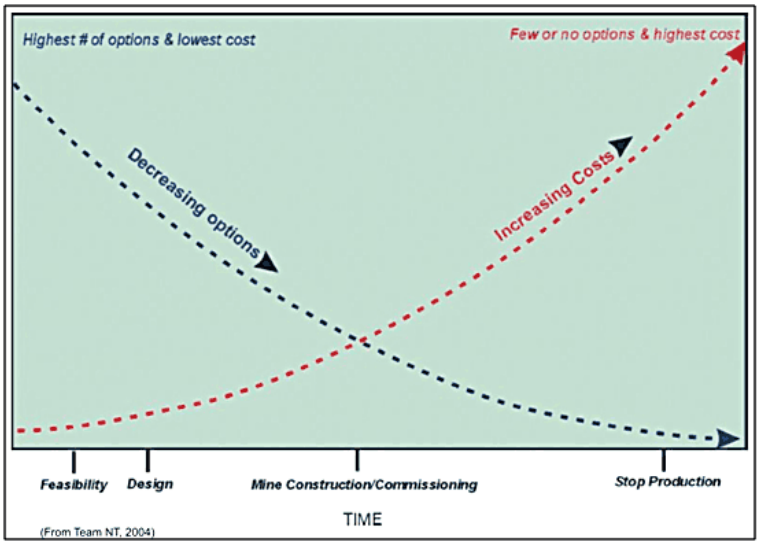

Figure 8: Over time, costs increase as options decrease (GARD Guide, 2009)

Maintaining the status quo and poor community perception

Doing what we have always done will, inevitably, result in similar and predictable poor outcomes.

Conventional large-scale open pit mining and processing has resulted in a legacy of unrehabilitated open pits; waste rock dumps that generate poor quality seepage, erode and look unsightly; and tailings dams that generate poor quality water and dust, erode and cover vast footprints, and whose stability cannot be ensured in perpetuity.

Designing for in perpetuity requires that probable maximum floods and extreme seismic events be catered for. The climate has always varied, and all too often average annual rainfall totals are used as a basis for design. In Australia, "a land ... of droughts and flooding rains" (Dorothea Mackellar, 1908), rainfall totals in any one year typically range from about half to about twice the average. Flood magnitudes and their frequency may increase with the effects of climate change. Estimating the seismic risk in perpetuity (generally taken to be a return interval of 10,000 years) for Australia, a region of low seismic activity and a short period of historical earthquake data, requires considerable projection.

Regulatory obstacles

Mine operators look to regulators to specify rehabilitation requirements, while regulators tend to specify only general goals for the rehabilitation of areas disturbed by mining, such as the following (Queensland Government, 2014):

1. safe to humans and wildlife;
2. non-polluting;
3. stable; and
4. able to sustain an agreed post-mining land use.

In their environmental impacts statement submitted prior to mining activity being approved, mining companies and their consultants tend to focus on the post-mining land use, which is often presumed to be grazing, even if this was not the pre-mining land use and/or it is unsustainable for the site. Only very broad comments are made about how a grazing post-closure land use might be achieved. Whether or not grazing is an appropriate or sustainable post-mining land use is typically not addressed, and conventional mining activities may make a grazing post-mining land use very difficult to achieve, and/or very expensive to achieve, for very marginal future returns. Restoring ecological function may be a more reasonable outcome of mine site rehabilitation in situations where productive land use is not possible, while development, industrial land use, and cropping may be possible post-mining in certain situations.

As trust in the mining industry rehabilitating mines has eroded over time, regulations and bonds have increased. Bonding of mines commenced in about the 1970s and 1980s, generally taking the form of an insurance policy or bank guarantee for the assessed rehabilitation liability. Initially, the rehabilitation liability was set at about $20,000/ha. However, this has risen to between $85,000 and $215,000/ha in recent years, partly due to inflation, but also due to a perception that a higher cost was needed to persuade mining

companies to carry out more rehabilitation. The actual rehabilitation costs could be far lower than the rates set by regulators, if carried out progressively, making use of available and suitable mine waste materials and equipment. Rehabilitation costs could also be reduced by changing the ways mines and processing plants are operated to reduce rehabilitation liabilities.

In Australia, the assessed rehabilitation liability or security deposit has mostly been provided by way of a bank guarantee, the cost of which varies with the financial strength of the mining company. The cost is based on a benchmark such as the London Interbank Offered Rate (LIBOR), plus a premium of around 0.3% per annum of the value, and would be expected to be 1.5 to 3% pa of the security deposit. While this rate is of a similar order to the inflation rate, the bank guarantee and budget to cover the security deposit tie up funds that could be used more productively, and the security deposit could be substantially higher than the actual cost of rehabilitation. The cost of a bank guarantee could range from about AUD1,300 to 6,500/ha per annum.

In Western Australia, and recently in Queensland, the state has required that the bank guarantee amount be paid into a government fund devoted to the rehabilitation of abandoned mines. In other words, it is no longer an insurance cover for the rehabilitation liabilities of existing operations. Further, the Queensland government has set minimum rehabilitation requirements for mines put into "care and maintenance", and is proposing the introduction of a residual risk payment to secure relinquishment, in addition to the rehabilitation of the site. The residual risk cost would provide insurance against the possible future failure of rehabilitation, but its imposition is likely to prove to be a further barrier to mine rehabilitation and relinquishment.

The residual risk (Queensland Government, 2018) has been assessed based on satisfying the operating conditions imposed in an environmental authority. A lack of trust that the environment will be protected during mining operations has resulted in a requirement for zero water and sediment discharge to the environment, which can exacerbate impacts and is not sustainable post-closure. It may also not be possible during flooding events. The requirement for zero water discharge leads to the storage of an excessive and increasing inventory of mine-affected water in surface ponds on site, which will concentrate salinity over time through net evaporation. The collection of sediment in ponds requires regular cleaning of the ponds, which is unsustainable post-closure. Therefore, satisfying the operating conditions is likely to add to, rather than reduce, residual risks post-closure.

Some suggested solutions

The following sections discuss some means of overcoming obstacles to effective mine closure, rehabilitation, and relinquishment, including pit backfilling with wastes, pit lakes, the encapsulation of potentially contaminating waste rock, integrated waste rock and tailings storages, reducing tailings

production, improving operational practices to improve stability, whole-of-mine-life cycle accounting, and re-focussing on post-mining "value" rather than "cost".

Pit backfilling with wastes

Where mineable and/or economic ore reserves would not be sterilized, and a series of open pits is mined at the site, the progressive backfilling of completed pits with mining and/or processing wastes may be both an economic and appropriate method of managing mining and processing wastes. The backfilling of completed pits with waste rock or coarse-grained processing wastes is straightforward and could involve end-dumping from the crest of the pit, as was done at Kidston Gold Mines in North Queensland, Australia in the 1990s (Figure 9). The Kidston pit was 240 m deep and end-dumping durable waste rock from the crest initially formed an angle of repose of 40º, which flattened to 38º as the waste rock settled about 1.5% or 4 m and the toe kicked out about 10 m over a number of weeks after dumping. Scarps up to 1 m high formed in the crest of the waste rock reflected from pit slope benches.

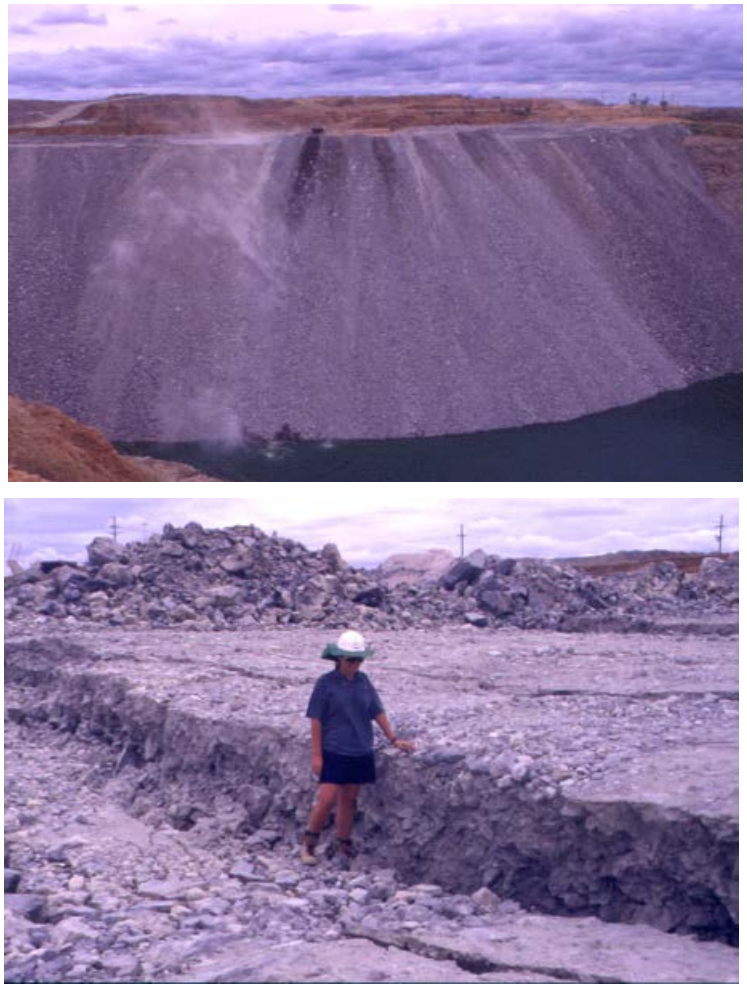

Figure 9: End-dumping waste rock in-pit at Kidston Gold Mines: (above) 240 m high dump face, and (below) scarps up to 1 m high formed at crest reflected from pit slope benches

In some cases, waste rock is trucked down pit ramps to limit the height of dumping and ensure safe dumping, but full-height end-dumping can safely be practiced from a crest edge windrow. The waste rock will self-compact post-backfilling, but to limit the post-backfilling settlement to about 0.3% the last 10 m of waste rock could be paddock-dumped and compacted.

In-pit tailings deposition is increasingly being practiced, particularly as approval for surface tailings dams becomes more difficult, mainly due to opposition from the surrounding community and land users, and from green groups opposed to mining. Typically, the tailings are deposited in-pit at the same slurry or thickened consistency as would be used for surface disposal, particularly for existing mines that previously used surface disposal. However, the V-shape of the pit results in initially very high rates of rise and this, together with the difficulty of dewatering a pit and reduced net evaporation, result in a low settled density and rapid filling of the pit. Continued in-pit disposal of tailings at a slurry consistency results in a wet and soft deposit that is difficult to cover using plant, including where the surface is exposed to desiccation and a thin crust is formed, which is prone to bow-waving. However, water and tailings can be displaced by end-dumping waste rock or by delivering coarse-grained processing wastes such as coarse coal reject or smelter slag hydraulically.

Pit lakes

A completed pit will inevitably collect some water from incident rainfall and runoff, and from groundwater inflows, even in a dry climate. However, in a net evaporative climate, and even in a wet climate, the pit water is likely to be contaminated and net evaporation will concentrate contaminants. In a dry climate, the pit water level will likely remain below the surrounding groundwater level, maintaining the pit as a "sink", while in a wet climate contaminated pit water may become a "source".

In a dry climate, it will likely not be possible to maintain pit water quality by dilution or flushing with clean water, and poor quality pit lake water will likely not be an acceptable post-closure option. A shedding soil cover over waste backfill may be the only means of containing poor quality entrained water. In a wet climate, regular dilution or flushing with clean water may maintain acceptable pit lake water quality. In a marginally net positive water balance climate, an increase in open water due to completed pits may convert the climate to a net negative water balance.

Encapsulation of potentially contaminating waste rock

Increasing attention is paid to the geochemical characterization of waste rock and tailings, particularly for new mining projects, although this may not be continued as mining progresses, perhaps until contaminated seepage emerges. Geochemical characterization is not always matched by the selective placement and encapsulation of potentially acid-forming or otherwise contaminating wastes.

Ideally, inert waste rock, which is more likely to be excavated from the oxidized zone above the

groundwater table, should be used to form the base and sides of a surface waste rock dump, allowing the encapsulation of potentially contaminating waste rock, such as potentially acid-forming sulphidic waste rock, within (Figure 5). Further, potentially contaminating waste rock should ideally be covered with a compacted layer of inert waste rock or soil prior to each wet season, to limit the wetting-up of the potentially contaminating waste rock and so limit potential seepage and the transport of contaminants. However, minimizing haul distance and hence cost dictates dumping as close as possible to the point of egress from the open pit, and the employment of end-dumping from a haul truck over a tip-head as this is more cost-effective than paddock-dumping and dozing.

The conventional end-dumping of potentially contaminating waste rock does not preclude measures to seal the base rubble zone that forms, to avoid it acting as an oxidation reactor. There are three means of achieving this:

1. dozing out the toe of the dump;
2. end-dumping towards a toe bund; or
3. end-dumping onto paddock-dumped inert waste rock to interrupt the base rubble zone.

Potentially contaminating tailings may be deposited and maintained underwater to limit oxidation and the formation of contaminants, provided that the climate and topography allow this, and deposition is planned to achieve it. Where maintaining full saturation is not possible, the most potentially contaminating, usually sulphidic, tailings could be deposited and maintained underwater, while the oxidized tailings may be deposited above water.

Integrated waste rock and tailings storages

Mining and processing essentially separate materials based on their particle size distribution and mineralogy, and the separate waste rock, coarse-grained processing wastes, and tailings streams are conventionally disposed of separately.

There is increasing attention being paid to integrated waste rock and tailings storage. In its simplest form for a surface storage, the weathered and durable waste rock are used to construct a robust earth and rockfill dam, behind which tailings slurry is stored. An extension of this is to dewater the tailings in-plant and place them behind the dam, without or with compaction. Waste rock and tailings can also be "co-located" in a completed pit. In its simplest form, this could involve end-dumping waste rock from one side of the pit, while tailings slurry is deposited from the other side of the pit. An extension of this is to dewater the tailings to recover process water and chemicals, and deposit them by gravity to the pit. There may be little advantage in filtering the tailings, since filtered tailings would be difficult to place in-pit without the cost of transporting them to the pit base.

Reducing tailings production

With the advent of large-scale open pit mining facilitated by large haul trucks and shovels from the 1970s, the entire ore was conventionally crushed and ground for processing. There is increasing attention on the possibility of selectively segregating ore of different size fractions for separate processing, reducing the need for expensive grinding and hence reducing the production of tailings to be disposed of, and hence the cost of tailings disposal.

Improving operational practices to improve stability

Azam and Li (2010) found that for a world inventory of 18,401 mine sites, the average tailings dam failure rate over 100 years to 2010 is 1.2% or 2.2/year, which is more than two orders of magnitude higher than that reported for water retaining dams of 0.01%. Among the causes they identified for this high tailings dam failure rate were construction using mine wastes; sequential dam raises together with an increase in tailings production; a lack of regulations on design criteria, particularly in developing countries; and high maintenance costs post-closure. Clearly, there is scope for the improved design, construction, operation, and closure of tailings dams, as illustrated in Figure 10 (Silva et al., 2008).

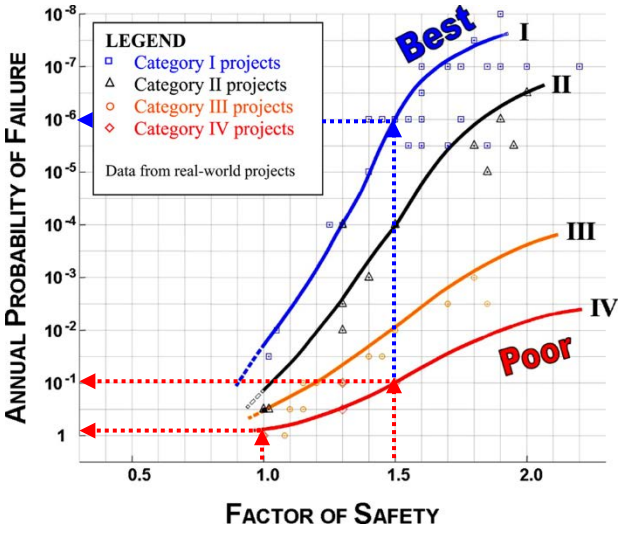

Figure 10: Annual probability of failure versus factor of safety for different levels of design and construction (Silva et al., 2008)

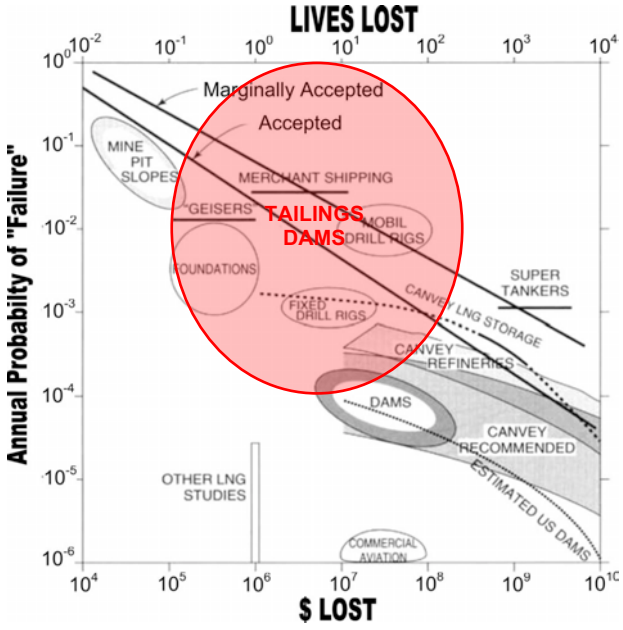

Figure 11: Tolerable levels of risk (Silva et al., 2008)

Figure 10 shows the estimated relationships between the factor of safety (FoS) and the annual probability of failure (P_f) as a function of the standard of design, construction, operation and closure, ranging from poor (representing the worst tailings dams) to best (typical of critical water retaining dams). As shown in Figure 10, for a FoS of 1.5, the P_f reduces from an unacceptable 10^{-1} for poor design,

construction, operation, and closure to an acceptable 10^{-6} for the best design, construction, operation and closure, comparable to the P_f of civil aviation (Figure 10). A FoS of unity would make the failure of a poorly designed and constructed tailings dam almost certain. The high range of P_f for tailings dams, and potential for loss of life and cost, depending on their standard of design, construction, operation and closure, is superimposed on Figure 11.

Whole-of-mine-life cycle accounting

The NPV accounting approach, with a high discount factor, is in part responsible for the high failure rate of tailings dams, and the poor performance of waste rock dumps and pits. It discourages and delays the capital expenditure necessary to ensure a high standard of design, construction, operation and, particularly, closure. This results in escalating impacts over time, which in turn result in escalating operational costs, at the expense of capital. There is clearly an argument for whole-of-mine-life cycle accounting, in which all costs that will incurred over the lifespan of a mine are allowed for. The total cost of an asset is often far greater than the initial capital outlay and can vary significantly between different alternative solutions to a given operational need. Consideration of the costs over the whole life of an asset provides a sound basis for decision-making.

Re-focussing on post-mining "value" rather than "cost"

Both mine operators and regulators focus on the cost of mine site rehabilitation, essentially assuming that the rehabilitated mine site will be unproductive post-closure. In fact, all activities on a mine site involve a cost, which must be allowed for in the assessment of the value of the commodity produced. Due to the focus on the cost of mine site rehabilitation, and the loss of revenue at closure, the initial focus is on attempting to recover rehabilitation costs. This leads to the removal of infrastructure with some scrap value, such as the copper and steel in electricity transmission lines, and building materials. There is a need for a change in the narrative surrounding mine site rehabilitation to re-focus on post-mining "value" rather than "cost", as is illustrated in Table 1.

Table 1: Conventional "cost" versus "value" approach to mine rehabilitation

Conventional cost-based rehabilitation	Value-added rehabilitation
Production rules	Post-closure "value" is identified upfront
Rehabilitation is seen by operator and regulator as a "cost"	Examples include: • Renewable energy (NIMBY) – solar, wind and pumped storage, delivered to grid via mine transmission lines • Agriculture and/or fishery using water dams • Tourism and heritage (older the better)
Operator discounts cost over time, discouraging rehab	
Infrastructure such as power lines are stripped	
Rehabilitation is limited to "smoothing" and "greening"	
Post-closure land use and function are limited	"Value" sets rehabilitation budget
Operator loses social and financial licences to operate	Potential wins for operator, future land user and Government

Conclusion

The mining industry's social and financial licences to operate, and control of its own destiny, will continue to decline unless the obstacles to mine closure, rehabilitation, and relinquishment are tackled. These obstacles include NPV accounting with a high discount factor, comfort in "doing what we have always done" and poor community perceptions of the mining industry, and increasing regulatory obstacles.

Among the suggested means of overcoming obstacles to effective mine closure, rehabilitation, and relinquishment discussed are pit backfilling with wastes, pit lakes, the encapsulation of potentially contaminating waste rock, integrated waste rock and tailings storages, reducing tailings production, improving operational practices to improve stability, whole-of-mine-life cycle accounting, and re-focussing on post-mining "value" rather than "cost".

Mine closure and ultimate relinquishment need to be genuinely front of mind from the planning of a mining project, and throughout operations to rehabilitation and ongoing maintenance. Conventional open pit mining, waste rock and tailings management practices need to be challenged. There is a divergence between the mining industry's discounting of future closure expenditure and the government's application of consumer price index-based increases to closure costs.

References

Azam, S. and Q. Li. 2010. Tailings dam failures: A review of the last one hundred years. *Geotechnical News* 28(4): 50–53.

GARD Guide. 2009. Global Acid Rock Drainage Guide. International Network for Acid Prevention. Retrieved from www.gardguide.com/images/5/5f/TheGlobalAcidRockDrainageGuide.pdf.

Queensland Government. 2014. Guideline for rehabilitation requirements for mining resource activities. Queensland Government. Retrieved from https://environment.des.qld.gov.au/assets/documents/regulation/rs-gl-rehabilitation-requirements-mining.pdf.

Queensland Government. 2018. Managing residual risks in Queensland, discussion paper, part of the Financial Assurance Framework Reform package. Queensland Government. Retrieved from https://environment.des.qld.gov.au/management/pdf/managing-residual-risks-discussion-paper.pdf.

Silva, F., T.W. Lambe and W.A. Marr. 2008. Probability and risk of slope failure. *J Geotech and Geoenv Eng, ASCE*, 134(12): 1691–1699.

Chapter 7
Posters

TAILINGS AND MINE WASTE 2019

Proceedings of Tailings and Mine Waste 2019
November 17–20, 2019, Vancouver, Canada
Published by the University of British Columbia, 2019

Flow Control Layer Used to Reduce Water Percolation in Waste Rock Piles: Performance Evaluation Using a Laboratory Physical Model

Abdeljalil Ait Kouia, UQAT-RIME, Canada
Abdelkabir Maqsoud, UQAT-RIME, Canada
Bruno Bussière, UQAT-RIME, Canada

Abstract

The reclamation of waste rock piles is complex due to their configuration and heterogeneity, and existing mine site reclamation techniques must be adapted for this particular context. Bearing this in mind, an alternative approach is proposed for waste rock piles reclamation. It consists of installing finer material inside and on the top of the waste rock pile. These finer layers, called flow control layers (FCLs), deviate water flowing inside the pile toward the slope of the pile and limit water infiltration into the reactive waste rocks.

In order to better understand the hydrogeological behaviour of this type of system, experiments were performed in a laboratory using a physical model (2.5 m × 0.6 m × 1.5 m). This physical model was equipped with probes to measure volumetric water content. Water was also collected at numerous holes in order to evaluate percolation. A rotation axis allowed for the model to be inclined, and a rain simulator was used to introduce water at the surface of the model. The physical model was tested using different cover layer thicknesses, inclinations, and precipitation rates.

Investigation results showed that the thickness of the FCL had a direct impact on the cover performance. However, the influence of this parameter was less pronounced than the influence of the inclination or the precipitation rate. The precipitation rate had the largest impact on the diversion capacity of the cover. The results of these experiments demonstrated the ability of the FCL to divert water, and enabled the assessment of the influence of critical parameters on water diversion capacity.

Introduction

The extraction or exploitation of mineral resources generates large amounts of solid wastes such as waste rocks and tailings (Aubertin et al., 2002a). These wastes are often stored at the surface, in tailings storage facilities (TSFs) or waste rock storage facilities (WRSFs), or in some cases returned underground as

backfill. When mine wastes contain sulphide minerals, such as pyrite and pyrrhotite, and are exposed to water and atmospheric oxygen, they can oxidize and generate acid. When the amount of acid generated is too great to be neutralized by other minerals in the tailings, acid mine drainage (AMD) is formed (Aubertin et al., 2002b; Blowes et al., 2003).

AMD is one of the most prevalent environmental problems in the mining industry. To control the production of AMD, a variety of waste management options and mine site reclamation strategies are available; for example, oxygen barrier covers or hydraulic barrier covers (Aubertin et al., 2016). Oxygen barrier covers limit the oxygen fluxes that reach underlying acid-generating mine wastes. Different techniques can be used as oxygen barriers, including (Aubertin et al., 2016):

1. water covers;
2. covers with capillary barrier effects; and
3. monolayer covers combined with an elevated water table (EWT).

By contrast, hydraulic barrier covers aim to prevent water infiltration. In humid climates, such barriers can be made with natural and synthetic combined materials (e.g., clay, geosynthetic clay liner, and geomembranes). Store and release covers may also be used to control water infiltration, although they are generally used in arid environments (Zhan et al., 2001; Williams et al., 2003; Bossé et al., 2015).

These reclamation techniques have mainly been used for TSFs. However, due to physical, hydrogeological, and geochemical differences between waste rocks and tailings, reclamation techniques developed for TSFs must be adapted. An alternative approach is proposed to control and reduce water infiltration into waste rock piles by implementing a flow control layer (FCL) inside and on top of WRSFs (Aubertin et al., 2002a; 2005; 2009; Aubertin, 2013; Martin et al., 2005; 2017). These FCLs are transport layers that enable water diversion (Ross, 1990; Steenhuis et al., 1991). Water infiltration is controlled by using capillary barrier effects that divert water to the sides of the pile (Aubertin et al., 2013).

The proposed method was first assessed using numerical modelling, and results indicated that the water accumulating in the FCL could be diverted towards the outside of the pile (Fala et al., 2005; 2013; Broda et al., 2017), leaving the core near its residual volumetric water content. In addition, an experimental waste rock pile (60 m long × 35 m wide × 5–7 m high) was constructed at the Lac Tio mine near Havre-St-Pierre (Quebec) to evaluate the response of the proposed method under field conditions. Results of these investigations suggest that the system can control, at least in part, deep water percolation, and decrease water contamination (Martin et al., 2017; Dubuc, 2018; Dimech et al., 2019).

In order to better understand the hydrogeological behaviour of such a system and better quantify the impact of the main factors of influence, a laboratory-scale instrumented physical model was constructed. This model allowed for the simulation of multiple different cover configurations and test conditions. Tested

configurations were inspired by those in the Lac Tio mine site, and the influence parameters assessed are cover layer thickness, inclinations, and precipitation rates.

Materials and methods

Experimental setup

The laboratory-scale physical model, inspired by the one used by Bussière (1999), was constructed using a custom steel box with a length of 2.5 m, a width of 0.6 m and a height of 1.5 m. The front was made of tempered glass and the top of the box was open to the atmosphere. The setup was equipped with a rotation axis that allowed for control over the model's inclination (up to a maximum slope of 20°). The facade at the bottom of the slope had openings at several strategic locations that were linked to drains. The drains were installed mainly at the height of the interface between the waste rock and sand layer, as well as at each interface between the cover layer (at each three 25-cm-thick sand layers) that will be added during future tests. These drains will be used to recover runoff and lateral diversion water at the interface (Figure 1).

To recover percolation and infiltration water, eight drains were installed at the bottom of the box (Figure 1). These drains were spaced 30 cm apart and between each two drains, a watertight obstacle was installed in order to recover all the water entering the area of each drain and limit any evacuation through preferential flow paths at the base of the box.

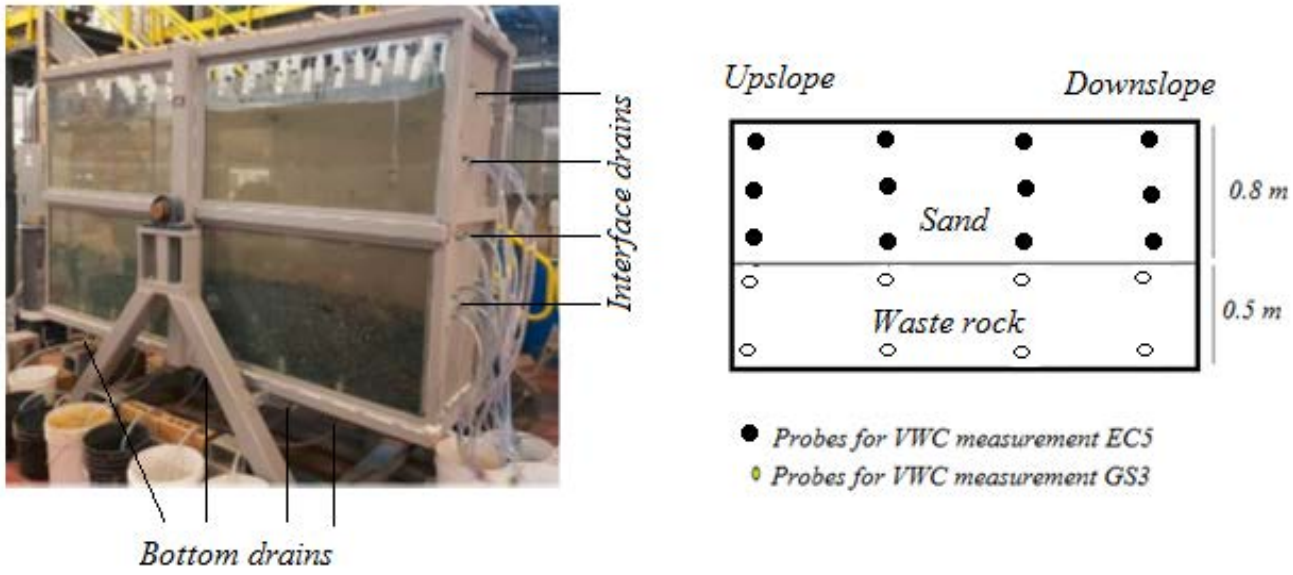

Figure 1: Experimental setup

The experimental setup was equipped with twenty probes to measure volumetric water content (VWC). The probes were installed as follows (Figure 1):

1. Two levels of instrumentation in the waste rocks (at the base and near the interface) for a total of eight GS3 probes.
2. A level of instrumentation in each sand layer, composed of four EC5 probes.

The probes used for volumetric water content were calibrated for each materials (see Ait khouia, 2018).

Material properties and testing methodology

Two materials were used in this study: truncated waste rocks (<50 mm) from the Lac Tio mine, and finer sandy material. These two materials were characterized for their physical and hydrogeological properties. The grain-size distributions of the materials were measured using Sieve Analysis (ASTM D6913-04 2009). However, for the finer particles (lower than 0.425 mm), a Mastersizer Standard Type S laser diffraction particle size analyzer was used (Malvern Instruments – Merkus, 2009). The water-retention curve (WRC) was measured for both materials using the column method (Peregoedova, 2012). The saturated hydraulic conductivity was measured in large columns using both constant- and variable-head methods (Peregoedova, 2012; Kalonji, 2015).

The main characterization results are presented in Figure 2. The D_{10} (diameter at which 10% of particles pass) was ~0.55 and 0.13 mm for the waste rocks and sand, respectively. The D_{60} (diameter at which 60% of particles pass) was ~14.50 and 0.36 mm for the same materials, respectively. These parameters were used to determine the uniformity coefficient ($C_U = D_{60}/D_{10}$) and the curvature coefficient ($C_c = D_{30}^2/(D_{60}\times D_{10})$. The calculated coefficients for the waste rocks were 26.36 and 3.66 for the C_U and C_c, respectively. According to the ASTM soil classification system (based on the Unified Soil Classification System [USCS] system; McCarthy, 2007), the waste rocks correspond to a poorly graded gravel. The sandy material was characterized by a C_U of 2.77 and a C_c of 1.03. According to the ASTM soil classification system, the sandy material is a well graded sand. The air entry values (AEV) estimated from the WRC are 20 cm and 1 cm of water for the sand and waste rocks, respectively. The waste rocks and sand have k_{sat} values of 7.7×10^{-1} cm/s (porosity = 0.28) and 4.3×10^{-3} cm/s (porosity = 0.40), respectively.

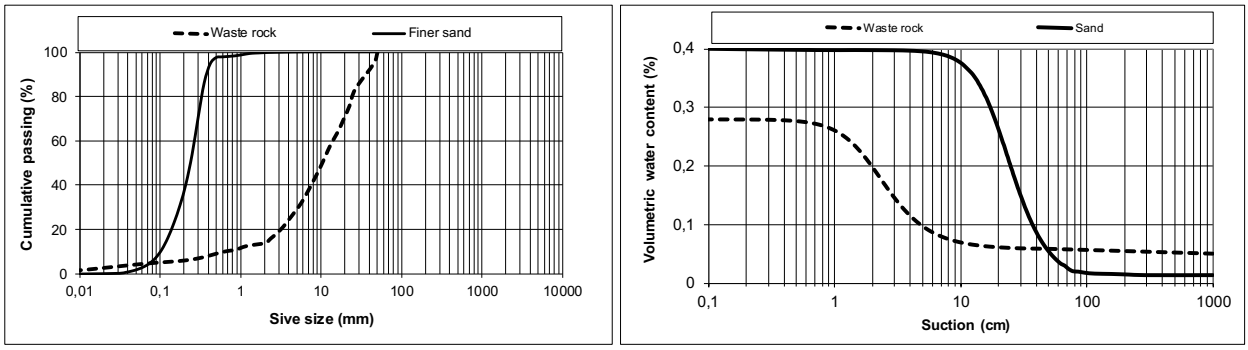

Figure 2: Grain-size distribution and WRC of the materials used in the physical model

In this study, several scenarios were tested in order to evaluate the impact of cover thickness, slope inclination, and precipitation intensity on the hydrogeological behaviour of the FCL. For each scenario, all parameters were kept constant, and only one was varied to highlight its degree of influence.

In the first series of tests, 25 cm of fine sand was used as a cover material. Three inclinations were tested: 3°, 10°, and 20°. For each inclination of the physical model, two different precipitation rates were applied. One rate was equivalent to half the sand's k_{sat}, which was about 77 mm/h, and the other was equivalent to the sand's k_{sat}, which was about 154 mm/h applied for a period of one hour.

In the second series of tests, the thickness of the sand layer was increased to 50 cm; i.e., an additional 25 cm was added. For this configuration of the model, the same scenarios were tested with the same slopes and precipitation rates as for the 25 cm layer.

In the third series of tests, the thickness of the sand layer was further increased by adding an additional 25 cm, thus giving a total thickness of 75 cm for the sand layer. For this new thickness, the same scenarios as in the previous cases were tested. The duration of each series of test was approximately one week (precipitation performed for one hour and drainage period about seven days) and a 48-hour period was left between successive tests to let the system equilibrate.

Results

Hydrogeological behaviour

A total of 18 tests were performed in the laboratory to assess the impacts of the different tested parameters. In this paper, selected results of the physical modeling in the laboratory are presented, highlighting the influence of each parameter evaluated. These results are presented as a graph showing the evolution of the volumetric water content in the model layers. In all figures, the dashed line corresponds to the porosity (assumed to be equal to VWC at saturation), and the solid line corresponds to the layer interface.

Effect of slope

When the physical model was inclined to yield different slopes, different hydrogeological behaviours were observed. Results from tests with a cover thickness of 25 cm and an inclination of 3° and 20° are presented for two locations: near the top and near the bottom of the slope (see Figure 3). In these modellings the precipitation rate used corresponds to 77 mm/h.

In terms of the VWC, the greatest variations were observed in the upper part of the slope when the slope increased from 3° to 20° (Figure 3 – near the top); i.e., from 0.37 to 0.15 over four hours of natural drainage. In contrast, VWCs near the bottom of the slope remained at around 0.33 for both inclinations (saturation estimated at about 0.38), even after two days of free drainage. The VWC in the waste rocks were stable in all tests at a value of about 0.05.

In this case, the sandy layer acted as a water flow control layer that diverted water along the interface between the sandy layer and waste rocks. This water diversion is favoured by the capillary barrier effects created at the interface. Similar results were obtained by Bussière et al. (2003).

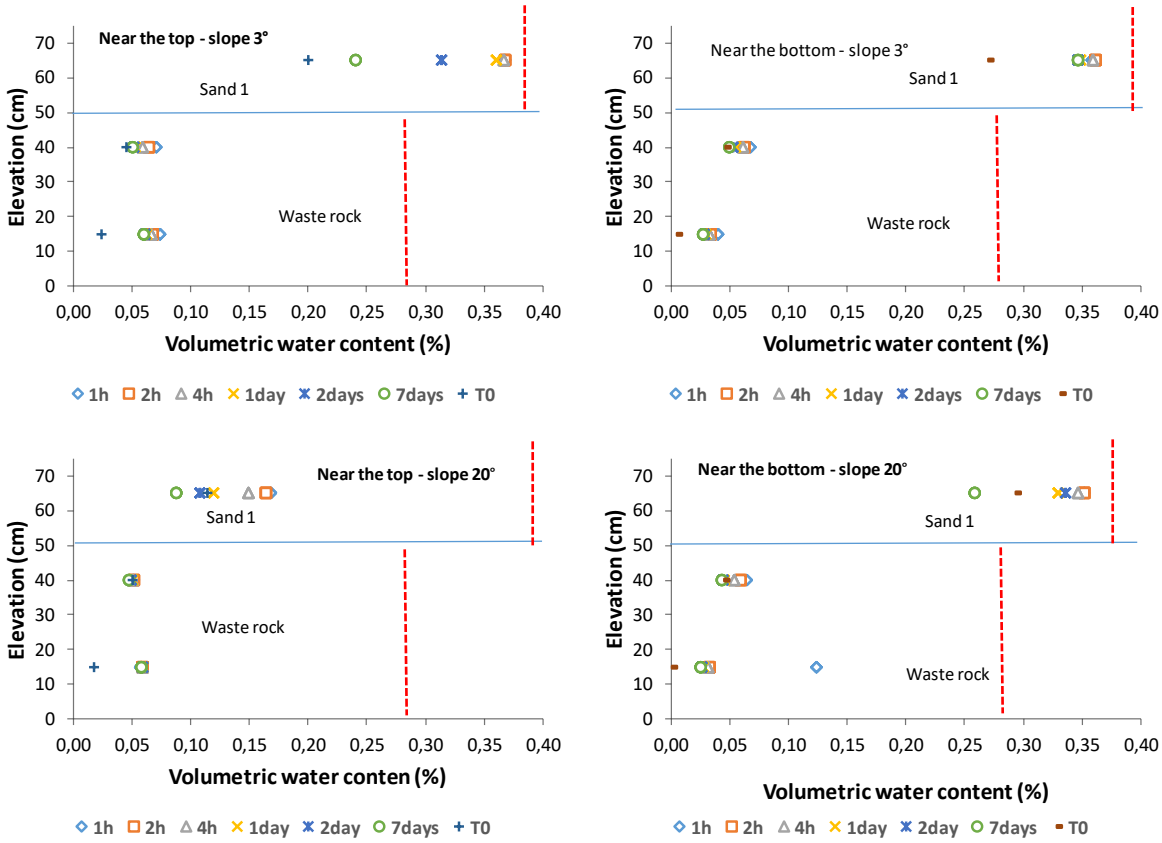

Figure 3: Slope effect on the hydrogeological behaviour for the 77 mm/h precipitation rate and 25 cm thick FCL (dashed line: layer saturation)

Effect of cover thickness

In the case of variation in sand layer thickness, the overall behaviour is similar: the top of the slope drains to a low VWC (about 0.07), while at the bottom of the slope, the VWC remained high, especially in the first layer of the FCL (sand 1) (see Figure 3). The increase in FCL thickness to 50 cm showed the following effects after seven days of drainage and for precipitation rates of 77 mm/h with a slope of 20°:

1. Near the top of the slope, the VWCs are in the same range : 0.09 in sand 1 (25 cm FCL thickness) versus 0.09 and 0.11 respectively in sand 2 and 1 (50 cm FCL thickness).
2. Near the bottom of the slope, the variations in the VWC are greater, with values at 0.12 and 0.26 in sand 2 and 1 respectively in the 50 cm FCL, and the VWC value at about 0.30 for the 25 cm FCL thickness.

In the waste rock layer, VWCs were not greatly affected by changes in the thickness of the FCL.

Precipitation rates effect

Two precipitation rates were used in the experiments. For the precipitation rate of 77 mm/h, one can observe for the 50 cm FCL thickness, in the upper layer (sand 2), VWC values near the top increased to 0.17 in the first few hours, then gradually decreased and stabilized around 0.08 after seven days of natural drainage (Figure 5). Near the bottom, VWC values increased to 0.30 in the first few hours, then gradually decreased and stabilized around 0.12 after seven days of natural drainage. In the lower layer (sand 1), the VWC were higher near the bottom (between 0.36 and 0.30); however, near the top the VWCs remain stable (0.12 and 0.11).

The application of higher precipitation rates (154 mm/h for one hour) had an immediate effect on the VWC, regardless of the inclination or the thickness of FCL. The increase in precipitation rate caused an increase in the VWC over the first few hours of the tests. For the 50 cm FCL thickness, in the upper layer (sand 2), VWC values near the top increased to 0.20 in the first few hours, then gradually decreased and stabilized around 0.08 after four days of natural drainage (Figure 5). Near the bottom, VWC values increased to 0.37 in the first few hours, then gradually decreased and stabilized around 0.12 after seven days of natural drainage.

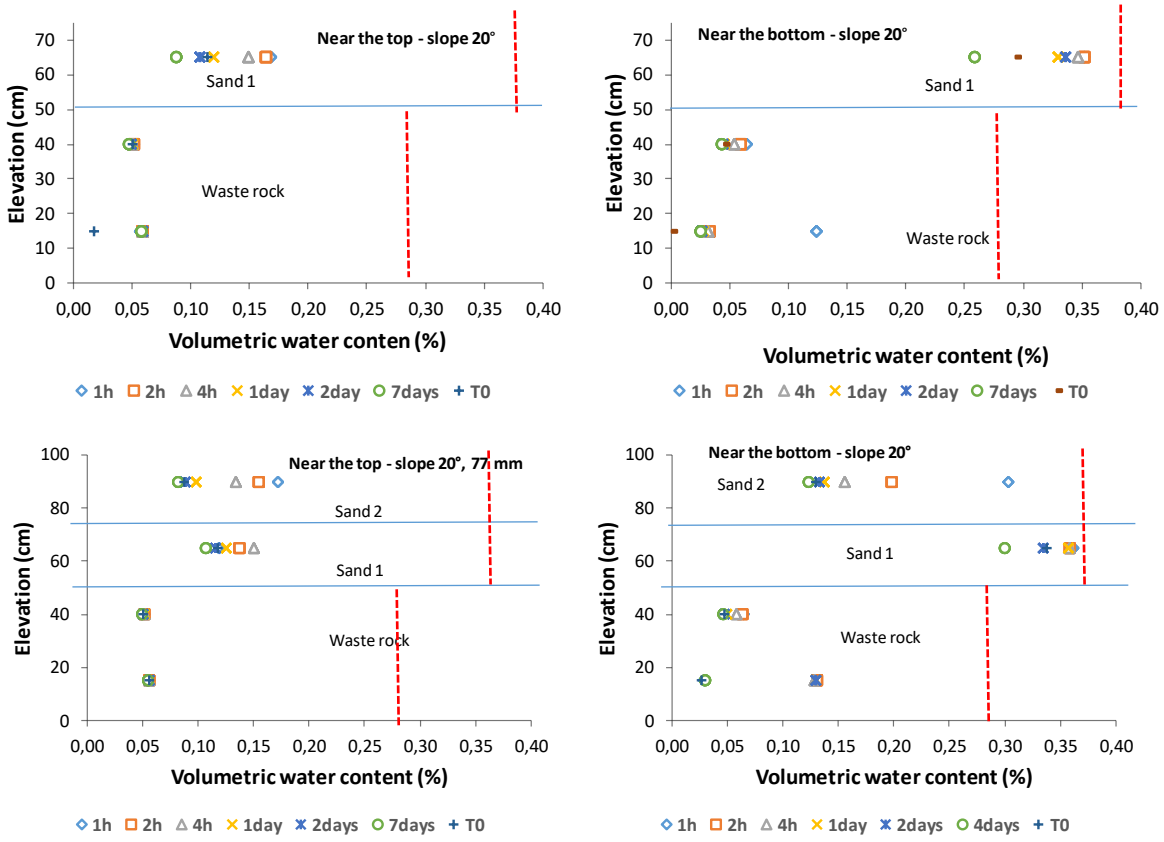

Figure 4: Effect of cover thickness for the precipitation rate of 77 mm/h and 20° inclination (dashed line: layer saturation)

Water diversion capacity

Tests performed using the physical model showed the impacts of inclination, cover thickness, and precipitation rate on the hydrogeological behaviour of the water flow control layer. The hydrogeological behaviour of the cover is closely related to its diversion capacity. In order to evaluate this parameter, percolating water was collected and measured at the bottom of each hole. These results are presented in Figure 6 for six specific cases to highlight the influence of the slope inclination, precipitation rate, and cover thickness.

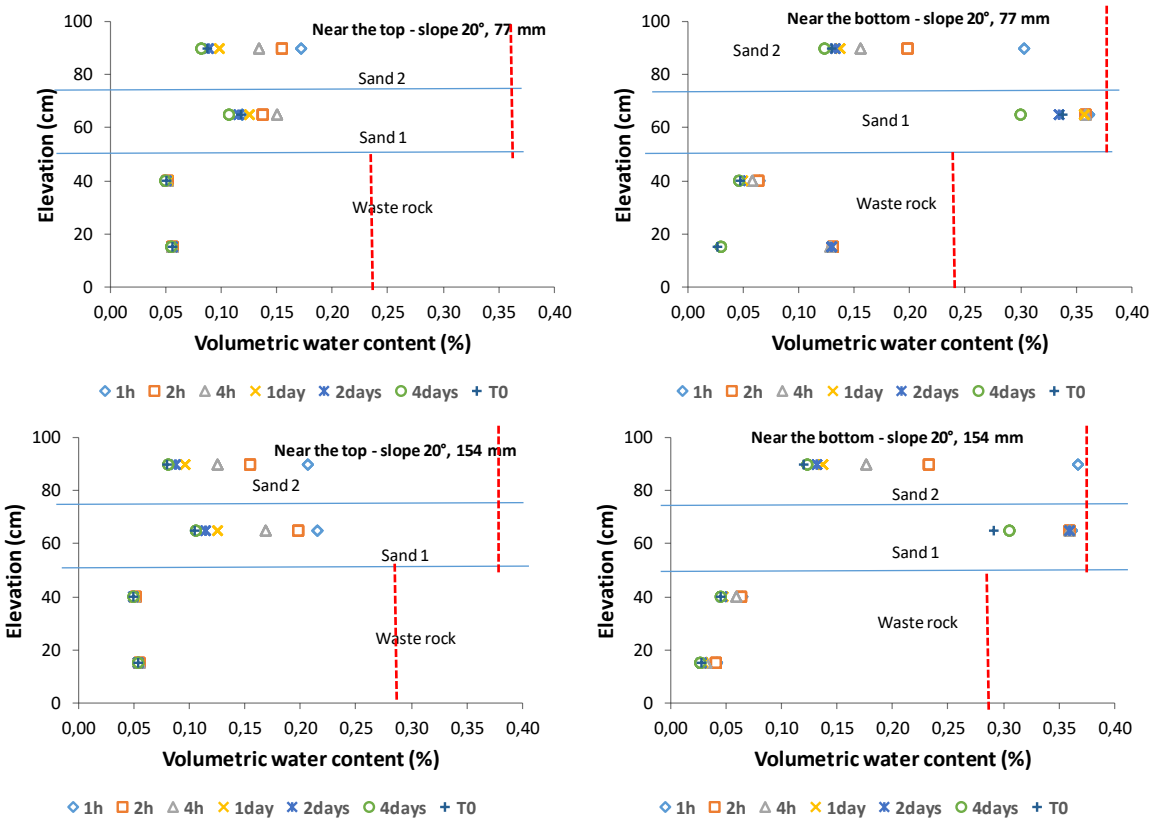

Figure 5: Effect of precipitation rate on volumetric water content for the 20° inclination and 50 cm thick FCL (dashed line: layer saturation)

The collected water volumes were used to evaluate the effective length of the capillary break and to determine the degree of influence of the analyzed parameters on the diversion capacities. In inclined cases of cover systems using capillary barrier effects, water flows down the slope to a point where the degree of saturation is high enough to allow water infiltration (Ross, 1990; Steenhuis et al., 1991). This infiltration point is called the DDL point and the distance between the infiltration point and the top of the slope corresponds to the length of lateral diversion.

Figure 6(a) compares two cases with the same thickness of FCL (25 cm) and the same precipitation rate (77 mm/h) applied for a period of one hour. Inclinations used were 3° and 20° (blue and orange colours). For the inclination of 3°, the water was diverted to hole number 4, where approximately 8% of the total water was recovered. The distance between the top of the slope and this hole is estimated at 120 cm. Increasing the inclination to 20° further increased the amount of water diverted by the system and, therefore, the length of lateral diversion. In this case, the DDL is located at 180 cm. These results are in accordance with those of previous studies (Bussière, 1999; Qian et al., 2009; Sawada et al., 2017).

The thickness of the FCL had the same effect as the inclination, but with a less pronounced intensity. Thus, increasing the thickness of the sandy layer slightly increased the lateral diversion capacity of the

system for the precipitation rate and duration tested. As shown in Figure 6(b), the transition from a thickness of 25 cm to 50 cm increased the length of lateral diversion from 60 cm to 90 cm. The same behaviour was observed by Qian et al. (2010) and Sawada et al. (2017).

The precipitation rate had an inverse effect on the diversion capacity of the cover system. The increase in the recharge rate led to a reduction in diversion capacity. The results of these tests, shown in Figure 6(c), indicated that the length of lateral diversion decreased from 150 cm to 90 cm when precipitation was increased from 77 mm to 154 mm per hour. The same behaviour was shown in the work of Bussière (1999), Qian et al. (2010) and Sawada et al. (2017).

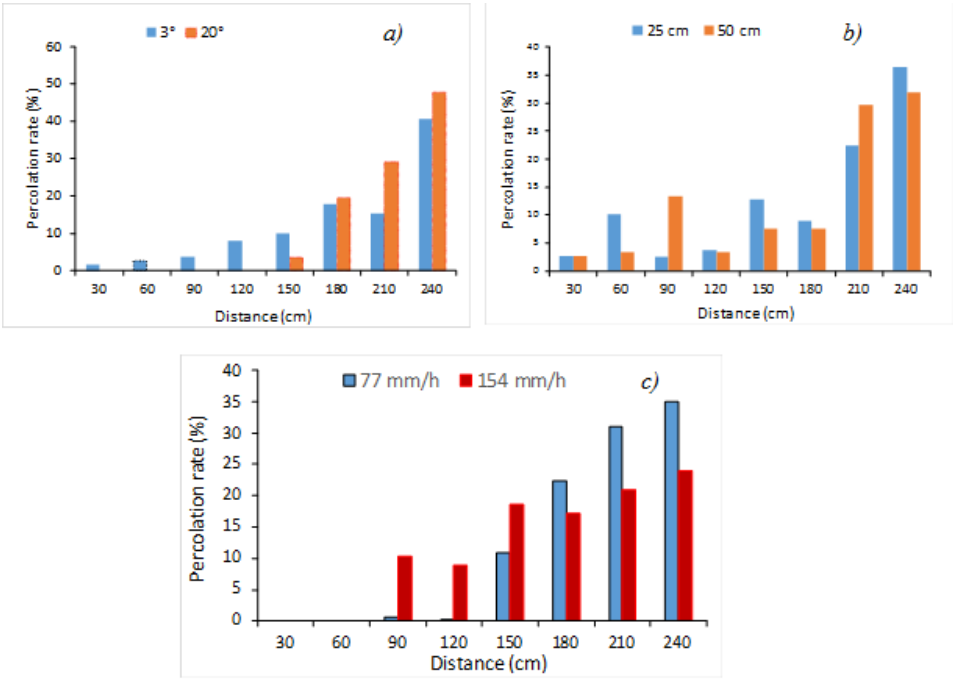

Figure 6: Assessment of water percolation rate as a function of: a) inclination; b) FCL thickness; and c) precipitation rate

Conclusion

The purpose of this study was to better understand the ability of a FCL to divert water using capillary barrier effects created between waste rock and sandy materials. The hydrogeological behaviour was evaluated using an original laboratory physical model that enabled control over the parameters governing the length of lateral diversion in waste rock pile covers. The FCL, made of a fine sand, was tested using different slopes (3°, 10°, and 20°), different cover layer thicknesses (25, 50, and 75 cm), and two precipitation rates.

The results of the tests performed in this study made it possible to estimate the degree of influence of the tested parameters. In our study, the thickness of the FCL had a direct impact on the performance of the capillary barrier. However, the impact of cover thickness was less pronounced than that of the inclination

or the precipitation rate. Increasing the inclination of the cover system had a major effect on the lateral diversion capacity of the cover. A steeper slope further increased the amount of water being diverted laterally by the capillary barrier and, therefore, the effective length of the capillary break. However, precipitation intensity was the most important parameter influencing lateral diversion capacity. When the rate of precipitation was increased, the amount of water infiltrating into the waste rocks increased significantly. This effect is due to the difference in the materials' hydrogeological properties, which controls the strength of the capillary barrier effects created along the interface of the two materials. The evaluation of the length of lateral diversion using the water percolation at the various orifices showed that the precipitation rate applied has a direct impact on the diversion capacity of the system. The greater the recharge rate, the lower the diversion capacity and lateral diversion length.

Numerical simulations are in progress to simulate the different tests performed in the laboratory. The demonstration that a numerical model can reproduce the behaviour of the FCL tested, which will allow larger-scale extrapolations.

Acknowledgements

This project was funded by the NSERC UQAT Industrial Chair on mine site reclamation. The authors would like to thank the industrial partners of the Chair and NSERC for their support.

References

Ait khouia, A. 2018. *Évaluation de la capacité de déviation latérale de la couche de contrôle des écoulements d'eau dans un modèle physique au laboratoire.* Masters' thesis, Polytechnique, Montreal, Quebec, Canada.

Aubertin, M. 2013. Waste rock disposal to improve the geotechnical and geochemical stability of piles. 23rd World Mining Congress, Montreal, Quebec, Canada.

Aubertin, M., O. Fala, B. Bussière, V. Martin, D. Campos, A. Gamache-Rochette, M. Chouteau, M. and R.P. Chapuis. 2002a. *Analyse des écoulements de l'eau en conditions non saturées dans les haldes à stériles. Symposium Rouyn-Noranda QC, Canada*.

Aubertin, M., L. Bernier and B. Bussière. 2002b. *Environnement et gestion des rejets miniers (ressource électronique): manuel sur cédérom. Mont-Royal, Québec: Presses Internationales Polytechnique*.

Aubertin, M., O. Fala, J. Molson, A. Gamache-Rochette, B. Lahmira, V. Martin, R. Lefebvre, B. Bussière, R.P. Chapuis and M. Chouteau. 2005. *Évaluation du comportement hydrogéologique et géochimique des haldes à stériles. In Proceedings of the Symposium sur l'Environnement et les Mines,* Rouyn-Noranda, CD-Rom, CIM.

Aubertin, M., E. Cifuentes, S. Apithy, B. Bussière, J. Molson and R.P. Chapuis. 2009. Analyses of water diversion along inclined covers with capillary barrier effects. *Canadian Geotechnical Journal* 46: 1146–1164.

Aubertin, M., M. James, M. Maknoon and B. Bussière. 2013. *Recommandations pour améliorer le comportement hydrogéotechnique des haldes à stériles.* GeoMontreal 2013, Can Geotechnical Society, Montreal, Quebec, Canada.

Aubertin, M., B. Bussière, T. Pabst, M. James and M. Mbonimpa. 2016. Review of reclamation techniques for acid generating mine wastes upon closure of disposal sites. Geo-Chicago: Sustainability, Energy and the Geoenvironment, August 14–18, Chicago.

Blowes, D.W., C.J. Ptacek, J.L. Jambor and C.G. Weisener. 2003. The geochemistry of acid mine drainage. In *Environmental Geochemistry* (edited by B.S. Lollar) *Vol. 9: Treatise on Geochemistry* (edited by H.D. Holland and K.K. Turekian). Oxford: Elsevier-Pergamon: 149–204.

Bossé, B., B. Bussière, R. Hakkou, A. Maqsoud and M. Benzaazoua. 2015. Field experimental cells to assess the hydrogeological behaviour of store-and-release covers made with phosphate mine waste. *Canadian Geotechnical Journal* 52(9): 1255–1269.

Broda, S., M. Aubertin, D. Blessent, E. Hirthe and T. Graf. 2017. Improving control of contamination from waste rock piles. *Environmental Geotechnics* 4(4): 274–283.

Bussière, B. 1999. *Étude du comportement hydrique de couverture avec effets de barrière capillaire inclinées à l'aide de modélisation physiques et numériques. Thèse de doctorat, Département de Génie minéral, École polytechnique de Montréal,* 393 pages.

Bussière, B., M. Aubertin and R.P. Chapuis. 2003. The behaviour of inclined covers used as oxygen barriers. *Canadian Geotechnical Journal* 40(3): 512–535.

Dimech, A., M. Chouteau, M. Aubertin, B. Bussière, V. Martin and B. Plante. 2019. Three-dimensional time-lapse geoelectrical monitoring of water infiltration in an experimental mine waste rock pile. *Vadose Zone Journal* doi:10.2136/vzj2018.05.0098

Dubuc, J. 2018. *Étude des propriétés hydrogéologiques d'une couche de contrôle des écoulements (CCE) placée à la surface de la halde expérimentale construite à la mine du lac Tio.* Masters' thesis, Polytechnique, Montreal.

Fala, O., J.W. Molson, M. Aubertin and B. Bussiere. 2005. Numerical modelling of flow and capillary barrier effects in unsaturated waste rock piles. *Mine Water and the Environment* 24(4): 172–185.

Fala, O., J. Molson, M. Aubertin, I. Dawood, B. Bussière and R.P. Chapuis. 2013. A numerical modelling approach to assess long-term unsaturated flow and geochemical transport in a waste rock pile. *International Journal of Mining, Reclamation and Environment* 27(1): 38–55.

Kalonji, A.K. 2015. *Restauration de sites miniers: Étude du comportement hydrogéologique de couvertures avec effets de barrière capillaire faites de matériaux miniers: Éditions universitaires Européennes.*

Martin, V., B. Bussière, B. Plante, T. Pabst, M. Aubertin, F. Medina, M.-L. Bréard Lanoix, A. Dimech et al. 2017. Controlling water infiltration in waste rock piles: Design, construction, and monitoring of a large-scale in-situ pilot test pile. GeoOttawa, Can Geotechnical Society, Montreal, Quebec, Canada.

Martin, V., M. Aubertin, G. Zhan, B. Bussière and R.P. Chapuis. 2005. *An Investigation into the Hydrological Behaviour of Exposed and Covered Waste Rock Dumps*. SME Preprint 05–109, 10 pp.

McCarthy, D.F. 2007. *Essentials of Soil Mechanics and Foundations: Basic Geotechnics.* 7th edition, 850 pp.

Merkus, H.G., 2009. *Particle Size Measurement, Fundamentals, Practice, Quality.* Springer.

Morris, C.E. and J.C. Stormont. 1997. Capillary barriers and subtitle D covers: Estimating equivalency. *Journal of Environmental Engineering* 123(1): 3–10.

Peregoedova, A. 2012. *Étude expérimentale des propriétés hydrogéologiques des roches stériles à une échelle intermédiaire de laboratoire. École Polytechnique de Montréal.*

Qian, T., L. Huo and D. Zhao. 2010. Laboratory investigation into factors affecting performance of capillary barrier system in unsaturated soil. *Water, Air, and Soil Pollution* 206(1–4): 295–306.

Ross, B. 1990. The diversion capacity of capillary barriers. *Water Resources Research* 26(10): 2625–2629.

Sawada, M., M. Mimura and M. Yoshimura. 2017. Infiltration control using capillary barriers for conservation of historical tumulus mounds. *Japanese Geotechnical Society Special Publication* 5(2): 5–10.

Steenhuis, T.S., J. Parlange and K.J.S. Kung. 1991. Comment on "The diversion capacity of capillary barriers" by Benjamin Ross. *Water Resources Research* 27(8): 2155–2156.

Williams, D., N. Currey, P. Ritchie and G. Wilson. 2003. Kidston waste rock dump design and "store and release" cover performance seven years on. In 6th International Conference on Acid Rock Drainage. The Australasian Institute of Mining and Metallurgy (AusIMM): 419–426.

Zhan, G., M. Aubertin, A. Mayer, K. Burke and J. McMullen. 2001. Capillary cover design for leach pad closure. Transaction-Society for Mining Metallurgy and Exploration Incorporated, 310: 104–110.

Proceedings of Tailings and Mine Waste 2019
November 17–20, 2019, Vancouver, Canada
Published by the University of British Columbia, 2019

Governance Implications for the Post-Closure Protection of Tailings Facilities in Violent Landscapes in Ghana

Kofi Kwakye Ameyaw, University of Ghana, Ghana

Abstract

This paper explores opportunities for promoting inclusiveness to safeguard the integrity and security of decommissioned and closed tailings facilities, and to protect life and property in violent and resistant mining landscapes in Ghana.

The general objective of the study was to establish a participatory framework for guaranteeing the permanence, integrity, and security of decommissioned and closed tailings facilities, and to guard against unforeseen breaches and their associated repercussions. Specifically, the fivefold objectives were to study the existing policy, legislative, and institutional framework for managing decommissioned and closed tailings facilities in Ghana. The study also aimed to:

- Interrogate the status of available safeguards for protecting decommissioned and closed tailings facilities.
- Identify the factors that threaten the security and integrity of decommissioned and closed tailings facilities.
- Investigate the possible causes of these factors.
- Examine the level of public awareness and consciousness about these factors and the effectiveness or otherwise of existing mechanisms for mitigating them.
- Build a consensus of relevant key stakeholders on the most appropriate option for guaranteeing the permanence, security, and integrity of decommissioned and closed tailings facilities.

The methodology used for data collection included the organization of community durbars ((inaugural celebrations) in selected mining communities, the use of questionnaires and interview guides, personal communication with selected members of the mining industry, and inspection of selected decommissioned and closed tailings facilities.

The results of the study indicated that there are prescribed safeguards to ensure the safety of decommissioned and closed tailings facilities. However, there are uncertainties about their effectiveness in offering permanent protection and security against possible human encroachment due to performance gaps

in monitoring to control anthropogenic threats, and due to ignorance about the inherent dangers of tailings facility breaches. The situation therefore warrants proactiveness on the part of all concerned authorities and relevant stakeholders to come up with the most appropriate interventions. The timely implementation of these interventions may help to avert what could be described as a potential environmental timebomb.

On the whole, the volatility of the prevailing situation provides incentives for all key relevant stakeholders to recognize the urgent need for the national security apparatus to maintain the security and integrity of decommissioned and closed tailings facilities. This should be a top priority concern.

Introduction/background

The mining industry in Ghana accounts for 5% of the country's GDP, and minerals make up 37% of the country's total exports. The main focus of Ghana's mining and minerals development industry remains focused on gold. Ghana is also a major producer of bauxite, manganese, and diamonds. Ghana has large-scale mining companies producing gold, diamonds, bauxite, and manganese, and there are also registered small mining groups and mine support service companies.

Observations from the Commission for Human Rights and Administrative Justice (CHRAJ, 2009) clearly show that since the beginning of the gold boom in Ghana, rampant cases of violation of human rights have occurred among the people living in mining areas, especially gold mining communities. The violations of human rights and degradation of the environment are a bone of contention between the host communities and gold mining companies, and they have been decried by community leaders and civil society organizations.

The causes and effects of violence on the Ghanaian mining landscape

Notwithstanding the significant contribution of the mining sector to socio-economic development, the mining landscape in Ghana has been characterized by violence in recent years. For instance, it was reported by the Ghana National Coalition on Mining in 2010 that:

> "The loss of farmlands, clean environment, housing and fresh water, coupled with uncontained alternative sources of livelihood, prompt most communities on the fringes of mines to logically protest."

The deprivation of property that some community members have suffered time and time again has generated considerable social and legal resistance. Sometimes this dissent manifests itself in firm but peaceful protests and demonstrations against both company and government officials.

It was alleged that all mining companies, in addition to their own private security, utilize state security personnel (especially the police and military) to protect their property and concessions. These security

forces sometimes use violent and forceful means to terminate demonstrations, resulting in loss of life, injuries, and terror.

The Human Rights Clinic (HRC's) visit to Tarkwa confirmed that violence has been, and is still being, inflicted upon community members.

Problem statement

Against the background of such a violent mining landscape, and the potential danger that can be posed by tailings in such a vulnerable landscape, security-related questions arise, such as the kind of institutional as well as policy and legislative framework in place for containing such volatile situations and their efficiency or otherwise in doing so; the status of available safeguards for protecting tailings storage facilities; and the causes of threats to or conflicts over the security and integrity of decommissioned and closed tailings storage facilities. Other issues of similarly genuine concern relate to the level of public consciousness of the threats as well as the effectiveness or otherwise of existing mechanisms for mitigating them. This is a violent mining terrain in which there are potential threats to closed and decommissioned mines and tailings storage facilities (TSF).

General objective

The general objective of the research was to establish a participatory framework for guaranteeing the permanence, integrity, and security of closed and decommissioned TSFs to guard against breaches and their associated repercussions.

Specific objectives

The five-fold specific objectives of the research were to achieve the following;

- Study the existing policy, legislative, and institutional framework for managing tailings storage facilities in Ghana.
- Interrogate the status of available safeguards for protecting closed and decommissioned tailings storage facilities.
- Identify and investigate the factors that threaten the security and integrity of closed and decommissioned tailings storage facilities.
- Examine the level of public awareness of the threats and the effectiveness or otherwise of the mitigating mechanisms.
- Explore the possibility of building a consensus of relevant key stakeholders on the most appropriate options for guaranteeing the permanence, security, and integrity of decommissioned and closed tailings storage facilities.

Definition of tailings material and tailings storage facilities

Tailings from the mining and extractive industries are most commonly fine-grained or finely ground materials left over from the extraction, beneficiation, or concentration processes. Most of these processes are water-based, and consequently tailings are usually produced, transported, and discharged into a tailings storage facility as slurry.

Tailings are typically chemically similar to the parent material, but have been subjected in some way to physical and/or chemical separation processes, such as crushing and grinding, flotation, cyanidation, or acid leaching, which can have significant influences on their properties and behaviour. In addition, the presence of process reagents, the evaporation of water, weathering and access to oxygen after deposition may alter its physical and chemical properties and risk profile.

A tailings storage facility will therefore have components that require careful management. Typical adverse characteristics of tailings can include:

- remnant cyanide;
- radioactivity;
- alkalinity (high pH) or acidity (low pH);
- sulphides, which may generate acid and consequently mobilize heavy metals;
- elevated arsenic levels;
- highly saline pore water;
- release of toxic gases; and
- colloidal clays (which are not adverse chemically, but have a deleterious effect on settling and strength characteristics).

Similarly, tailings that segregate after deposition may result in slimes ponds that have particularly adverse physical characteristics for long-term stability.

Tailings storage facilities are built structures used to confine tailings. A tailings storage facility includes the dam or other structure and associated tailings delivery infrastructure. The term refers to the overall facility, and may include one or more tailings dams.

The primary purpose of a tailings storage facility is to safely contain tailings to achieve solid sedimentation and consolidation, and to facilitate water recovery or removal without impacting on the environment. The nature of tailings storage facility design and operation is fundamentally different from a water dam in the way water is managed and in rehabilitation and closure. A tailings storage facility should not be used for the storage of water. Where a tailings storage facility is to permanently hold water (such as where sub-aqueous tailings disposal is proposed) the design of the tailings storage facility should also be consistent with standards used for water reservoirs.

Methodology

Description of the study area

The study was limited to the four political regions of Ghana that are known for being rich in various minerals and consequently have the highest concentration of mining operations, namely Ashanti, Western, Western North, and Eastern Regions. The specific locations and the extent of mineral endowment are depicted on the map of Ghana below.

Minerals map of Ghana

NAME	LOCATION(S) OF MINERALS
KUMASI	ASHANTI REGION
TAKORADI	WESTERN / WESTERN NORTH REGION
KOFORIDA	EASTERN REGION

Figure 1: Location of study sites in Ghana

Methods used for data collection

Data for the study was collected through the methods listed below.

1. The use of questionnaires.
2. Personal communication with selected key stakeholders.
3. The use of interview guides for focal group discussions in selected communities.
4. Field inspection of selected previously mined terrains.

The combination of methods provided an opportunity to assemble comprehensive data that could be analyzed to show the realities of the situations on the ground.

Focal group work

Figure 2: Personal communication with key personnel of relevant state regulatory institutions and mining companies

In an effort to understand the dynamics of the management of closed tailings storage facilities, the authors made a conscious effort to engage key management personnel of Environmental Protection Agency (EPA), Minerals Commission and a selected mining company to find out more about field practicalities involved

in the management of tailings storage facilities in general, but with specific reference to closed and decommissioned tailings storage facilities.

Results/findings

Data was collected from a total of 297 respondents, of which 12 belonged to different institutions and the remaining 285 were from nine different mining endemic communities

Institutional policy and legislative framework for managing decommissioned and closed tailings storage facilities in Ghana

The EPA and the Minerals Commission were identified as the statutory regulatory institutions which have direct responsibilities for the post-closure protection management of tailings storage facilities. The EPA is confronted with challenges in the execution of its mandate. These include financial, logistical, and technical personnel constraints, as well as inadequate information flow and institutional role conflicts.

The status of existing safeguards for protecting the integrity of tailings storage facilities

The EPA has a manual of safeguards guiding the security and integrity of tailings storage facilities. The results of the study showed that the existing safeguards conform with international best practices for managing tailings storage facilities.

Potential sources of conflicts in the study area

There are conflicts actors, conflict manifestations, and mitigation actions for complementary management.

Potential threats to sustainable mining industry in the study area

The study identified threats within the study area that are not necessarily related to the management of closed and decommissioned tailings storage facilities.

Figure 3: Evidence of vandalization of the property of a local company by aggrieved company workers

Public or community consciousness and awareness of threats to closed tailings facilities

The public or community awareness or consciousness level of factors that threaten the security of tailings storage facilities was different in different communities, and generally calls for intensive sensitization.

Respondents' opinion about multiple stakeholders participation for protecting closed and decommissioned tailings storage facilities

Respondents were unanimous about the participation of multiple stakeholders in the post-closure management and protection of tailings storage facilities. However they expressed a need to approach this with caution in order to guard against abuses or excesses.

Conclusions

- There is a policy, institutional and legislative framework in place in Ghana for managing closed and decommissioned tailings storage facilities.
- The mandated state regulatory institutions are however challenged in the execution of their mandates by financial, logistical, and technical staff constraints, as well as by institutional role conflicts.
- Generally, the governance aspects of closed TSF are exclusively handled by the EPA, the Minerals Commission, and concerned mining companies within the framework of relevant laws and regulations, without the active or formal participation of any other stakeholders.
- As far as the mining industry is concerned, tailings dams have the highest environmental risk. The selected mining company that was questioned was found to have entered into a reclamation security agreement with the EPA that stipulates seven or three years post-closure monitoring before relinquishment, depending on whether there are acid rock drainage (ARD) challenges.
- There are also a number of existing collaborating institutions as well as other community-based organizations that could play roles in the protection and management of closed TSFs.
- Even though a number of conflict resolution mechanisms were identified in the study area, the respondents appeared to be uncertain of their effectiveness in addressing conflicts and threats to the security and integrity of TSFs in the study area.
- There is an non-deterrent legal sanction system that is counter-productive to law enforcement and therefore is a source of concern to affected mining-related regulatory institutions.
- There are relevant standard safeguards for managing TSFs in Ghana, but these are not known to other state regulatory institutions apart from the EPA and the Mineral Commission, which have the professional expertise and legal mandate for the post-closure management of TSFs.

- Conflicts and threats are evident in the studied mining terrain and these have a tremendous potential to either escalate into violence or undermine the integrity and security of closed and decommissioned TSFs.
- There was evidence of vandalization of mining company properties by an angry mob, but the reasons were unrelated to post-closure management protection of TSFs.
- The principal actors in the conflict are predominantly the mining companies and mining communities, and the conflict frequently is related to the violation of the latter's human rights by the former.
- The manifestations of the conflicts are counterproductive to the sustainability of the mining industry because the characteristic communal uprising, agitations, and roadblocks slow down the business processes of the mining companies and hence undermine their financial viability.
- The phenomena of speculative farming and settlement within legitimate mining concessions by mining communities in anticipation of monetary compensation, and communal resistance to planned resettlement schemes, are very frustrating to the mining industry.
- The use of government military personnel to protect mining concessions against communal incursions was seen as a serious concern by the mining communities.
- The knowledge base of mining communities about closed TSFs, procedures for storing the tailings, and management of TSFs after closure, was generally limited because they are not involved in the protection or management of TSFs at any stage.
- However, all three mining communities within the catchment areas of the selected mining companies were knowledgeable about almost all factors that were investigated, and they attributed the source of knowledge to their management of the mining company in question.
- Fortunately, there is consensus among all respondents that multiple stakeholders should be involved in the post-closure protection and management of tailings storage facilities.
- Respondents were however cautious about possible excesses that may be triggered by various reasons, and therefore advocate for a conscious and deliberate effort by powers to harmonize the roles of multi stakeholders in the post-closure protection and management of TSFs, so as to address all possible performance gaps, avoidable excesses, and role conflicts.
- Different respondents operate within the confines of their professional or technical obligations, which provide permanent incentives for them to remain committed to the post-closure protection and management of TSFs.

Recommendations

Against the background of the research findings, the following recommendations are made:

- The capacities of technical staff of state regulatory institutions, namely the EPA and the Minerals Commission, should be built up, so as to improve their competencies and skills for undertaking post-closure protection and management of TSFs. They should be provided with adequate funds and logistics to be able to address all identifiable performance gaps.
- A nation-wide assessment of all TSFs closed within the last two years should be commissioned jointly by the Ministry of Lands and Natural Resources, the Ministry of Environment, Land Science and Technology, and the Ministry of Local Government and National Security to assess their conditions, the threats that they are exposed to, and the extent of risk they pose to both life and property, with a view to advising the central government on how best to safeguard the security and integrity of closed TSFs in a conflict-prone environment.
- A comprehensive capacity building program should be organized for identifiable institutional and community-based stakeholders engaged in conflict resolution in mining communities to enhance their capacities, competencies, and skills in conflict resolution.
- The Ghana Chamber of Mines should encourage its members operating in the study area and all other known conflict zones to subscribe to the position statement published in 2016 by the International Council on Mining and Metals (ICMM), which addresses key areas of governance of tailings dams to prevent their catastrophic failure.
- The EPA and the Minerals Commission should engage multi-disciplinary experts to design a harmonized structure, environmental guidelines, and training program for multiple stakeholder participation in the post-closure protection and management of TSFs to conform with international best practice.

References

CHRAJ (Commission for Human Rights and Administrative Justice). 2009. The state of human rights in mining communities in Ghana.

MESTI. 1994. Environmental Protection Act (Act 490)

MESTI. 1999. Environmental Assessment Regulations.

MLNR . 1999. Forestry Commission Act, (Act 571)

MLNR. 1993. Minerals Commission Act, Act 450.

MLNR. 2006. Minerals and Minerals and Mining Act, an act to revise and consolidated the law relating to minerals and mining and to provide for connected purposes,

MLNR. 2012. Compensation and resettlement regulations, 2012(L12175).

MLNR. 2012. Minerals and mining (health, safety and technical) regulations 2012 (LI2182).

Bibliography

Chirano Gold Mines Ltd. 2015. Reclamation security Agreement signed between the Environmental Protection Agency of the Republic of Ghana.

EPA. 1994. Ghana's mining and environmental guidelines.

EPA. 2001. Environmental guidelines for mining in production forest reserves in Ghana.

EPA. 1999. Environmental assessment regulations 1999 LI (1652). Environmental Regulations.

EPA. 1997. Operational guidelines for mineral exploration in forest resources for selected companies.

Newmont. 2019. Tailings, waste and emissions.

UN. 2014. Safety guidelines and good practices for tailings management facilities.

Victoria State Government. 2017. Technical guideline. Design and management of a tailings storage facility. Retrieved from https://earthresources.vic.gov.au/__data/assets/pdf_file/0010/463681/Guidelines-for-design-and-management-of-tailings-storage-facilities.pdf

List of acronyms

CHRAJ	Commission for Human Rights and Administrative Justice
EPA	Environmental Protection Agency
ICMM	International Council on Mining and Metals
MESTI	Ministry of Environment, Land Science and Technology
MLNR	Ministry of Lands and Natural Resources
TSF	Tailings Storage Facility

Proceedings of Tailings and Mine Waste 2019
November 17–20, 2019, Vancouver, Canada
Published by the University of British Columbia, 2019

Lime in Oil Sand Bitumen Extraction and Tailings Processes

S. Arnipally, Apex Engineering Inc., Canada
A. Tang, Apex Engineering Inc., Canada
G. Halferdahl, Consultant, Canada
J.D. Scott, University of Alberta, Canada
B. Ozum, Apex Engineering Inc., Canada

Abstract

Bitumen is produced from Athabasca oil sand deposits in northeastern Alberta at a rate of more than 1.3×10^6 barrels/day by surface mining followed by water-based extraction. Developed in the 1930s, the Clark hot water extraction (CHWE) process with caustic (NaOH) as an extraction process aid, is used at all oil sands plants. While this process provides acceptable bitumen recovery, it also creates serious operational, environmental, and long-term sustainability challenges. The CHWE process heavily disperses the tightly packed fine-grained clays present in the ore, producing about 2 m^3 of problematic fluid fine tailings (FFT) per barrel of bitumen, which is difficult to dewater and reliably incorporate into a reclaimed landscape. Continuous caustic use in extraction and reusing process water multiple times, combined with a zero-discharge water strategy and the salts present in the ore, has resulted in a detrimental steady increase in the sodium (Na^+) concentration in process water. The entire chemical environment established with caustic gradually impairs bitumen recovery, resulting in higher costs and requiring more time to establish acceptable reclaimed landscapes.

These challenges can be minimized with the relatively simple substitution of lime (CaO) for caustic (NaOH), while achieving at least equivalent, if not better, bitumen recovery. CaO can also be used in tailings processes, such as treating whole tailings, making non-segregating tailings (NST) with lime instead of gypsum or flocculants, and dewatering the huge legacy caustic-FFT inventory of over 10^9 m^3. Recent data comparing CaO and NaOH on bitumen recovery, process water chemistry and tailings characteristics, such as clay dispersion and bitumen-process water contact angles, are presented.

Introduction

The oil sand resources present in Northern Alberta are one of the world's vast hydrocarbon deposits. They extend over 77,000 km^2 and are distributed in three principle regions: Athabasca, Cold Lake, and Peace River. The estimated bitumen volume in-place and ultimate potential for recovery are 270×10^9 m^3 (1.6×10^{12}

bbl) and 50×10^9 m^3 (300×10^9 bbl), respectively. Where the overburden thickness is less than about 75 m, the McMurray Formation is surface mineable, with in-place bitumen of about 24×10^9 m^3 (144×10^9 bbl). Since the 1990s, commercial bitumen recovery from greater depths has employed thermal steam assisted recovery processes, such as steam assisted gravity drainage (SAGD), and cyclic steam stimulation (CSS).

Today, more than 1.3×10^6 bbl/d of bitumen is produced from Athabasca oil sand by surface mining followed by water-based extraction. The Clark hot water extraction (CHWE) process of the 1930s, or some version thereof, uses caustic (NaOH) as an extraction process aid and is the standard process at all oil sands plants (Chalaturnyk et al., 2002). NaOH increases the pH, reduces the water surface (γ_W) and bitumen-water interfacial ($\gamma_{B/W}$) tensions, and increases the repulsive forces in the water film between bitumen and sand, enabling the liberation and recovery of bitumen (Kasperski, 2001).

At the same time as γ_W and $\gamma_{B/W}$ are reduced enabling bitumen liberation from the ore, clays present in the ore are heavily dispersed, producing what is referred to as fluid fine tailings (FFT), a thick fluid with yogurt-like consistency that is difficult to dewater and incorporate in a reclaimed landscape. At the same time, reducing $\gamma_{B/W}$ slows down the coalescence and aeration kinetics of bitumen droplets (the second and third parts of bitumen extraction), which reduces the overall efficiency of the bitumen recovery process, leading to larger process vessels and increased capital and operating costs. Further, the reduction of γ_W and $\gamma_{B/W}$ promotes the stability of the produced extraction froth (typically 30% bitumen, 60% water and 10% solids of mostly fines <45 μm size), making it more difficult to clean up. Because oil sand plants operate with a zero-discharge strategy, water recovered from tailings is reused in the extraction process many times. This water reuse and continuous caustic use in extraction results in a steady increase in process water Na^+ concentration, also contributing to operational, environmental, and long-term sustainability challenges.

While the CHWE process enables bitumen recovery, it produces fluid fine tailings (nominally 33 weight % solids or about 84 % volume water) with a stable structure, which will remain in a fluid state and present a serious environmental liability for centuries (Kasperski, 1992; McKinnon, 1989). The bi-wetted nature of the FFT clay particles, especially kaolinite clays less than 0.2 μm in size, and the steady increase in process water Na^+ concentration also promote the stable structure of FFT (Levine, 1993; Kotlyar et al., 1995 and 1998; Johnston, 2010; Jiang et al., 2007 and 2008).

Even though the CHWE process is used as a standard process to produce bitumen, it is the source of serious operational, tailings management, water chemistry, environmental, long-term sustainability, and mine closure challenges. The oil sand industry, government and regulatory authorities are aware of these challenges and have committed extensive efforts to develop novel technologies to address these challenges but with limited success. Because oil sand tailings and bitumen froth are both produced in the extraction

plant, solutions to tailings and extraction efficiency challenges should be sought together in the extraction plant.

Efforts to develop novel bitumen extraction processes

The oil sand industry has invested in the development of better bitumen extraction and tailings management processes. In extraction, low-energy (less than the traditional CHWE process at 80°C) and non-caustic bitumen extraction processes that reduce tailings (i.e., FFT-make) and process water chemistry challenges caused by the CHWE processes (Mankowski et al., 1999; Siy et al., 2001), have been studied. Also, the use of cyclones and thickeners was implemented to improve tailings and recycle the warmest possible water to reduce thermal energy use. Non-additive extraction processes were commercially implemented at Albian Sands' Muskeg River Mine and Syncrude Canada Ltd.'s Aurora North Mine plants. However, these non-additive processes produced lower than expected bitumen recoveries, and both plants were converted to the CHWE process with NaOH.

Acidic bitumen extraction and separation of bitumen from oil sand with cyclones and thermal cracking (AOSTRA Taciuk process) were tested in pilot-scale facilities, but neither was ultimately adopted commercially.

Development of novel extraction processes is needed to address the above referenced challenges; the success of such efforts will improve profitability and reduce environmental and long-term sustainability challenges of oil sand plants.

Efforts to develop new tailings management processes

Since the first commercial oil sands plant started to produce bitumen using the CHWE process in 1967, oil sands operators have experienced a steady increase in the inventory of FFT and the process water concentrations of sodium (Na^+). The excessive and unnecessary dispersion of clays in NaOH extraction process slurry is the source of the existing FFT inventory, and its growth and was first cautioned about by Dr. K.A. Clark, the inventor of the CHWE process, in his 1939 publication.

To address the FFT problem (production rate and volume), composite tailings (CT) was introduced in 1990s (Caughill et al., 1993). While it was initially heralded as a great success, it has proven to be problematic for a number of reasons. It uses hydro-cyclones to separate whole tailings into an underflow (about 63 wt. % solids and more than 93 wt. % sand) and an overflow (about 12 wt. % solids and more than half of these solids are less than 44 μm diameter or fines), followed by treating a blend of underflow and legacy FFT with gypsum ($CaSO_4$). Recently, Suncor Energy Inc. has ended CT production, perhaps due to a new understanding of the impact of the sodium absorption ration (SAR). It was experimentally observed that with SAR values of oil sand ore-water slurries larger than about 7, Na^+ occupies the adsorption sites

on the clay, resulting in heavy dispersion of clays; therefore, the needed increase in the yield stress of the fines-water slurry (to prevent fines segregation from sand) does not occur. SAR values of many oil sand tailings are greater than 20; therefore, the calcium in gypsum is not effective in preventing fines segregation (Miller et al., 2010; Dawson et al., 1999).

Additionally, the fines balance issue as it relates to ore and CT production has become better understood. Depending on the concentration of fines in the incoming ore and the sand to fines (SFR) of the CT made, there is about as much FFT made from the CT overflow as used in the CT process, leading to no net benefit in making CT from the perspective of reducing the FFT inventory. Also, the continuous accumulation of Ca^{2+} and SO_4^{2-} ions from gypsum use, detrimentally affects the recycled release water chemistry, potentially promoting scaling in process pipes and valves, and may also cause H_2S emissions from the tailing ponds through anaerobic reduction of SO_4^{2-} with the unrecovered hydrocarbons in the tailings.

Other methods developed to address the FFT inventory problem include tailings reduction operations (TRO), atmospheric drying of FFT, in-line thickening of FFT with flocculants, capping FFT with petroleum coke produced when the produced bitumen is upgraded, and scroll centrifuging and pressure filtering FFT, with various flocculants, including CaO as coagulant. None of the field trials of these processes has generated sufficient confidence for full-scale commercial implementation. High capital and operating costs are likely major challenges associated with these methods.

Clearly, a reliable, robust, and cost-effective method that is environmentally sensitive is needed that addresses extraction, tailings, and closure perspectives simultaneously.

CaO in extraction and tailings processes

Our research focused on using benefits of lime (CaO) chemistry, which increases pH and provides Ca^{2+} ions in aqueous environments. These characteristics make CaO as additives for bitumen extraction, tailings management and dewatering of existing FFT inventory in simple, cost effective and environmentally friendly manners. Our philosophy to reduce environmental impacts and to improve long-term sustainability of oil sand plants is based on the development and adaptation of the following principles:

1. Reduce or eliminate the unnecessary (from a bitumen recovery perspective) and detrimental dispersion of clay particles in the extraction process slurry.
2. Recombine and properly place coarse and fine tailings fractions together as non-segregating materials (make a sedimentary deposit similar to the original ore minus the hydrocarbons).
3. Convert Na-Clay to Ca-Clay before implementation of any FFT dewatering technology.
4. Reduce or eliminate the steady increase in Na^+ concentration in process affected water.

To achieve these fundamental objectives, our research shows that the following processes, all based on the use of CaO, could have great impact on profitability, reduction of environmental and long-term sustainability challenges of oil sand plants:

1. bitumen extraction processing at about 150–450 mg-CaO/kg-ore;
2. whole tailings treatment at about 800–1,500 g-CaO/m^3-whole tailings;
3. making non-segregating tailings (NST) from a blend of whole tailings cyclone underflow and either tailings thickener underflow or legacy FFT at about 800–1,100 g-CaO/m^3-NST; and
4. dewatering of legacy FFT (produced by CHWE extraction process), at more than 3,000 g-CaO/m^3-FFT.

Bitumen extraction with CaO instead of NaOH

Bitumen extraction in ore-water slurry-based systems involves three fundamental processes or steps, as depicted in Figure 1:

1. bitumen liberation from oil sand ore matrix;
2. coalescence of small liberated bitumen droplets to form larger droplets; and,
3. aeration of larger bitumen droplets with air to promote floatation and allow skimming off a bituminous froth for further processing (Ozum et al., 2014a).

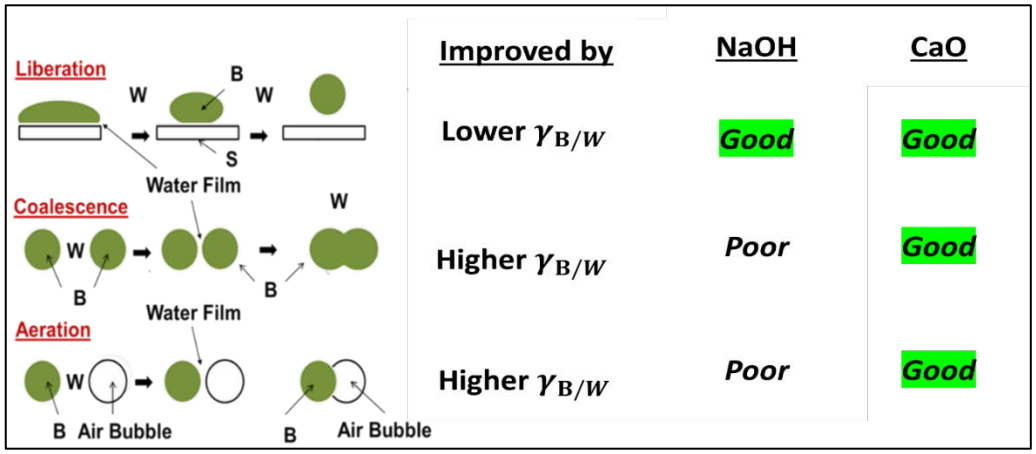

Figure 1: Role of bitumen-water IFT on the efficiency of bitumen extraction

When CaO is used as an extraction process additive replacing NaOH of the CHWE process, it increases the pH of the ore-water slurry and promotes bitumen liberation from the ore by a similar mechanism as the CHWE process, while Ca^{2+} ions simultaneously react with all the active species in the ore-water slurry. The following major reactions take place in oil sand ore-water slurry systems with lime:

$$CaO + H_2O \rightarrow Ca(OH)_2 \leftrightarrow Ca^{2+} + 2OH^- \quad (1)$$

$$Ca(OH)_2 + NaHCO_3 \rightarrow \underline{CaCO_3} + NaOH + H_2O \quad (2)$$

$$Ca(OH)_2 + Ca(HCO_3)_2 \rightarrow 2\underline{CaCO_3} + 2H_2O \quad (3)$$

$$Bitumen^- + Ca^{2+} + Clay^- \rightarrow Bitumen - Ca - Clay \quad (4)$$

$$Ca(OH)_2 + 2Clay - Na \rightarrow Clay - Ca - Clay + 2NaOH \quad (5)$$

$$Ca(OH)_2 + 2Nap - H \rightarrow \underline{(Nap)_2 - Ca} + 2H_2O \quad (6)$$

The excess *Ca(OH)₂* in tailings and/or release water reacts with atmospheric CO_2:

$$Ca(OH)_2 + CO_2 \rightarrow \underline{CaCO_3} + H_2O \quad (7)$$

$$CaCO_3 + CO_2 + H_2O \rightarrow Ca(HCO_3)_2 \quad (8)$$

Our research finds that at about 50ºC, using CaO as an extraction process aid at under about 400 mg-CaO/kg-ore, clays and bitumen do not bind together, and therefore, lime does not reduce bitumen recovery (Reaction 4), different than the claims made by using $CaCl_2$ as a process aid (Liu et al., 2005; Masliyah et al., 2004). Our observations show that CaO increases bitumen recovery efficiency and froth formation kinetics by suppressing surfactant activities of water soluble naphthenates (Reaction 6) and beneficially increasing $\gamma_{B/W}$ in the extraction slurry. Increasing $\gamma_{B/W}$ accelerates bitumen droplet coalescence and aeration steps as shown in Figure 1 (Pan et al., 2012; Pan and Yoon, 2010). CaO suppresses silt-clay size particle dispersion by coagulation (Reaction 5) and increasing γ_W also by Reaction 6. Increasing γ_W and $\gamma_{B/W}$ in the extraction process slurry potentially reduces the emulsion stability of the bitumen froth, thereby potentially improving the efficiency of froth treatment. Elimination of a steady increase in process water Na^+ concentration caused by caustic in the CHWE process also helps all of the above listed challenges of oil sand plants.

Our in-house research as well as third-party verification tests performed by Shell Canada Ltd. and by NAIT (as requested by COSIA TEPA) provided encouraging results indicating that CaO is a much superior extraction process aid compared to NaOH (Ozum and Scott, 2010 a, b; Ozum et al., 2012; Ozum et al., 2014 a, b; COSIA, 2014).

The fundamental difference between CaO and NaOH in extraction is that CaO increases while NaOH decreases the $\gamma_{B/W}$. For faster bitumen extraction process kinetics and higher bitumen recovery efficiencies, $\gamma_{B/W}$ must be increased, not decreased. Floatation technology used in mineral processing is based on alteration of the mineral surfaces from hydrophilic (water wet) to hydrophobic (oil wet) to promote floatation, since air is also hydrophobic (oil wet). However, oil sand extraction with *NaOH* makes bitumen surface more hydrophilic. Lime reverses this contradiction and thereby improves bitumen extraction.

We continued performing extraction tests to compare performance NaOH and CaO as extraction process additives on normal-grade and low-grade ore samples. Extraction tests were made using a Denver Flotation apparatus at 800 rpm disperser rotating speed and 50°C slurry temperature. Bitumen recovery efficiency, process water chemistry, bitumen-water contact angle, standpipe settling and dispersive and non-dispersive hydrometer tests on –45 μm (–325 mesh) size fraction of the tailings were made.

Test results presented in Tables 1 and 2 show that both CaO and NaOH provided comparable bitumen recovery efficiency on normal and low grade ore, while CaO provided higher bitumen recovery on low grade (high fines) ore. CaO additive performed better than NaOH by maintaining the integrity of the process water chemistry; suppressing an increase in process water Na^+ concentration and SAR value.

Table 1: Comparison of bitumen extraction efficiency using *NaOH* and *CaO*

	Dosage (ppm)	Bitumen recovery (%)		Contact angle	
		Low grade	**Normal grade**	**Low grade**	**Normal grade**
NaOH	200	83	99	62°	88°
CaO	300	88	99	74°	105°
CaO	400	91	(–)	82°	(–)

Table 2: Process water chemistry, low and normal grade ores with *NaOH* and *CaO*

		pH	Na^+	Ca^{2+}	Cl^-	SO_4^{2-}	SAR
			mg/L	mg/L	mg/L	mg/L	
Low grade	no additive	7.8	319	14	166	201	20
	200 ppm *NaOH*	8.8	450	3	213	228	56
	300 ppm CaO	8.7	392	4	200	221	46
	400 ppm CaO	8.9	337	7	224	229	31
Normal grade	0 additive	7.8	319	14	166	201	20
	200 ppm *NaOH*	8.8	367	5	178	255	32
	300 ppm CaO	8.8	321	9	173	233	27

Contact angle measurements, depicted in Figure 2, show that CaO increases the bitumen-water contact angle more effectively compared to NaOH in both normal and low-grade ores. This observation supports that the bitumen-water interface is less water wet with CaO extraction compared to that of NaOH; which results in faster extraction process kinetics and higher bitumen recovery efficiency with CaO.

Standpipe settling tests show that CaO suppresses silt-clay size particle dispersion compared to NaOH, seen in Figure 3. Therefore, CaO in extraction would reduce FFT production compared to NaOH.

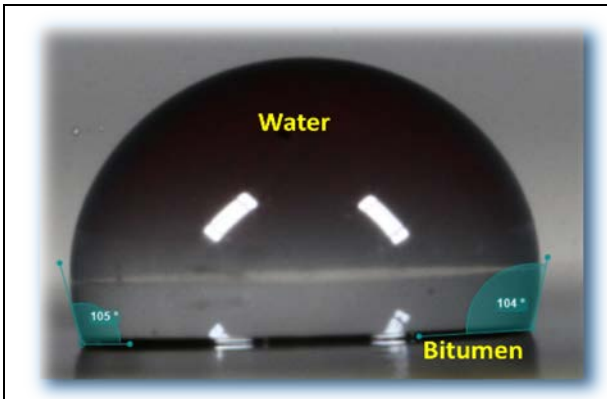

Figure 2: Bitumen-water contact angle

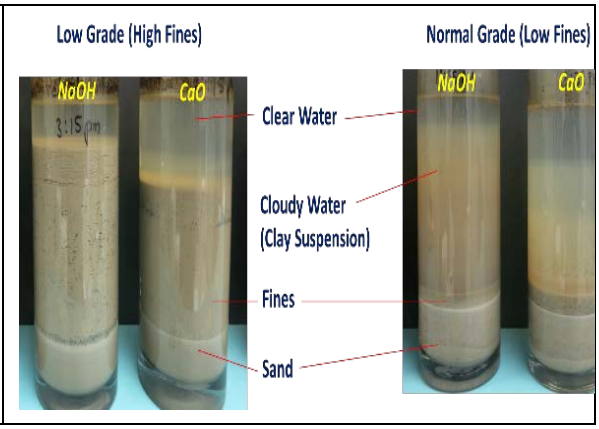

Figure 3: Tailings after 30 days of settling

Dispersive and non-dispersive hydrometer tests were made on –45 µm (–325 mesh) fraction of the low-grade ore extraction tailings produced by either NaOH or CaO as extraction process aids. The hydrometer results, presented in Figure 4, reinforce that NaOH promotes excessive dispersion of silt and clay size particles, thereby potentially making more FFT than that made with CaO.

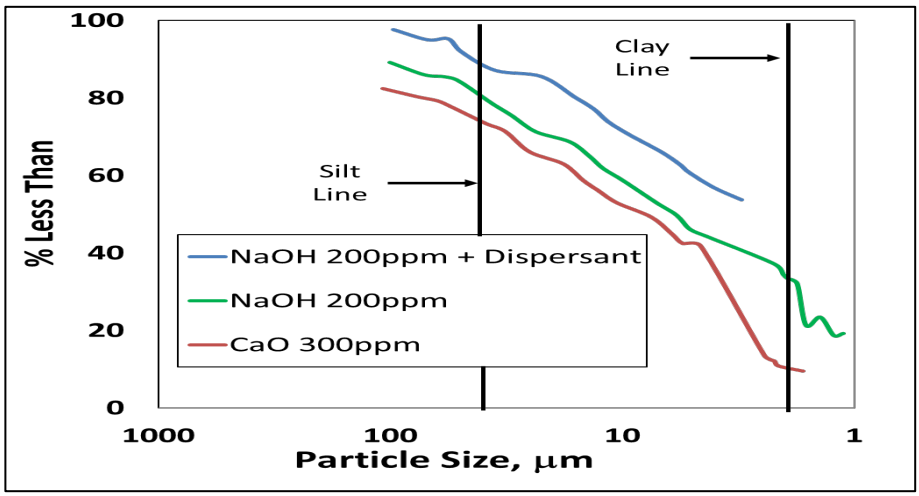

Figure 4: Hydrometer tests on extraction fines from low grade ore

Tailings processes using CaO

Lime has been used to improve the geotechnical properties of soils for decades; we focused on lime use in oil sand tailings processes because of its chemistry, discussed in the section on lime in extraction.

Together with Shell Canada, Canadian Natural Resources and Alberta Energy Research Institute, we investigated NST production by treating a blend of whole tailings cyclone underflow (about 59%–63% solids, 3%–7% fines) and tailings thickener underflow (about 35%–40% solids; over 50% fines) with CaO; the results of these tests are summarized in seven reports (Scott et al., 2007; Apex, 2004–2005). Laboratory test results were promising; however, pilot-scale tests were discontinued because of lower than expected thickener underflow solids contents produced in the commercial plant. Highlights of this work are that it is possible to produce NST with lower solids contents than the CT process (with gypsum) using CaO dosages of about 600–800 g–CaO/m^3-NST, and the produced NST had a higher hydraulic conductivity than CT, and the process maintains the integrity of released process water for recycling to the extraction process. Recent tests made on NST production showed that the CaO dosage needed to prevent segregation in NST has increased by about 10–15% over the last decade or so and is attributed to the steady increase in process water Na^+ concentration with ongoing caustic use.

Whole tailings treatment with CaO has been studied for direct deposition of the whole tailings, to improve tailings thicker performance and simultaneously improve water chemistry of the tailings thicker overflow for its recycling to the extraction process (Ozum et al., 2004; Hamza et al., 1996; Kessick, 1983; Lane, 1983). When whole tailings are treated with CaO at about 900 to 1,300 g-CaO/m^3 whole tailings, the emulsion structure of the tailings is destabilized, promoting the release of unrecovered bitumen. Depending on the process objectives, the released bitumen could be removed from the whole tailings, the tailings cyclone underflow or overflow by a flotation process, as depicted in Figure 5. Whole tailing treatment with CaO and recycling tailings thickener overflow to the extraction process would potentially provide benefits to the long-term overall performance of oil sand plants.

Our work shows that the existing FFT inventory can be significantly dewatered by CaO treatment with more than 3,000 g-CaO/kg-FFT dosages, replacing costly polymeric flocculants, before the implementation of any commonly used dewatering technologies, including centrifuging and pressure filtering (Arnipally et al., 2018; Tate et al., 2017). Other options are to treat the water layer of an existing FFT impoundment (pond) with CaO at about 600–1,000 g-*CaO*/m^3-water before reusing it in extraction, or treat a layer of aged FFT with CaO with over 3,000 g-CaO/m^3 FFT dosages.

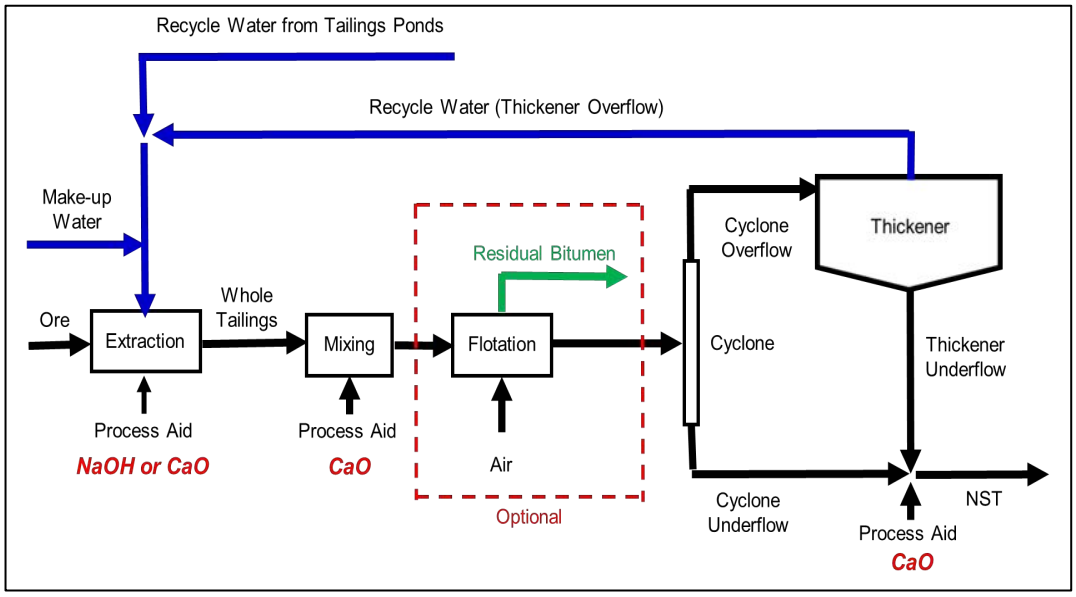

Figure 5: Whole tailings treatment with CaO

Conclusion

Existing environmental and long-term sustainability challenges of the oil sand plants could be alleviated by using CaO as additives for bitumen extraction, NST production, whole tailings treatment and FFT dewatering processes. Using CaO as an extraction additive offers a new paradigm for the oil sand plants; it would improve bitumen extraction efficiency and profitability and reduce currently experienced environmental, water chemistry, mine closure, and long-term challenges.

References

Apex Engineering Inc. 2004–2005. Seven reports, NST production from Albian Sands Muskeg River Mine tailings material using CaO additive, produced for Shell Canada Ltd., Canadian Natural Resources Limited and Alberta Energy Research Institute, Apex Engineering Inc., Edmonton, AB, Canada.

Arnipally, S., Burden, J.D. Scott and B. Ozum. 2018. Lime as an additive for oil sands ore-water slurry based bitumen extraction, tailings disposal and fluid fine tailings dewatering processes, Tailings and Mine Waste 2018, Sept. 30 – Oct. 2, Keystone, CO, USA.

Caughill, D.L., N.R. Morgenstern and J.D. Scott. 1993. Geotechnics of nonsegregating oil sands tailings, *Can. Geotechnical Journal* 30(5): 801–811.

Chalaturnyk, R.J., J.D. Scott and B. Ozum. 2002. Management of oil sands tailings, *Petroleum Science and Technology* 20: 9–10, 1025–1046.

COSIA. 2014. Apex project report, by B. Zhao and H. Mian, a slides presentation package produced by NAIT-NARCOSS, January 31, Calgary, Alberta, Canada.

Dawson, R.F., D.C. Sego and G.W. Pollock. 1999. Freeze-thaw dewatering of oil sands fine tails. *Canadian Geotechnical Journal* 36: 587–598.

Hamza, H.A., D.J. Stanonick and M.A. Kessick. 1996. Flocculation of lime-treated oil sands tailings, *Fuel* 75(3): 280–284.

Jiang, T., G.J. Hirasaki, C.A. Miller, K. Moran and M. Fleury. 2007. Diluted bitumen water-in-oil emulsion stability and characterization by nuclear magnetic resonance (NMR) measurements. *Energy & Fuels* 21(3): 1325–1336.

Jiang, T. G.J. Hirasaki, C.A. Miller and K. Moran. 2008. Using silicate and pH control for removal of the rag layer containing clay solids formed during demulsification, *Energy & Fuels* 22: 4158–4164.

Johnston, C.T. 2010. Probing the nanoscale architecture of clay minerals, *Clay Minerals* 45: 245–279.

Kasperski, K.L. 2001. Review of research on aqueous extraction of bitumen from mined oil sands, Natural Resources Canada, Western Research Centre, Division Report, CWRC 01–17.

Kasperski, K.L. 1992. A review of properties and treatment of oil sands tailings, *AOSTRA Journal of Research* 8:11–53.

Kotlyar, L.S., B.D. Sparks, J.R. Woods, C.E. Capes and R. Schutte. 1995, Biwetted ultrafine solids and structure formation in oil sands fine tailings, *Fuel* 74, 6: 1146–1149.

Kotlyar, L., B. Sparks, J. Woods, S. Raymond, Y. Le Page and W. Shelfantook. 1998. Distribution and types of solids associated with bitumen. *Pet. Sci. Technol.* 16(1 and 2): 1–19.

Lane, S. 1983. Lime coagulation and stabilization of total oilsands tailings, Petroleum Society of Canada, PETSOC-83-34-33, Annual Technical Meeting, May 10–13, Banff, Alberta, Canada.

Levine, S. 1993. Mathematical modelling of the microstructure present in oil sands fine tailings, Oil Sands – Our Petroleum Future Conference, April 4–7, Edmonton, Alberta, Canada.

Liu, J., Z. Xu and J. Masliyah. 2005. Interaction forces in bitumen extraction from oil sands, *Journal of Colloid and Interface Science* 287: 507–520.

Mankowski, P., S. Ng, R. Siy, J. Spence and P. Stapleton. 1999. Syncrude's low energy extraction process: Commercial implementation, Paper 11, *Proceedings,* Third Annual Meeting of the Canadian Mineral Processors, January 20, Ottawa, Ontario, Canada.

Masliyah, J., Z.J. Zhou, Z. Xu, J. Czarnecki and H. Hamza. 2004. Understanding water-based bitumen extraction from Athabasca oil sands, *Can. J. Chem. Eng.* 82: 628–654.

McKinnon, M.D. 1989. Development of the tailings pond at Syncrude's oil sands plant, *AOSTRA Journal of Research* 5: 109–133.

Miller, W.G., J.D. Scott and D.C. Sego. 2010. Influence of the extraction process on the characteristics of oil sands fine tailings, *CIM Journal* 1(2): 93–112.

Ozum, B., J. Rick, R.J. Chalaturnyk and J.D. Scott. 2004. Production of nonsegregating slurry from whole tailings, CIM Edmonton 2004 Conference, May 9–12, Edmonton, Alberta, Canada.

Ozum, B. and J.D. Scott. 2010a. Methods to reduce production of oil sands mature fine tailings, GEO2010 – 63rd Canadian Geotechnical Conference, September 12–26, Calgary, Alberta, Canada.

Ozum, B. and J.D. Scott. 2010b. Methods to reduce production of oil sands fluid tailings, 2nd International Oil Sands Tailings Conference, December 5–8, Edmonton, Alberta, Canada.

Ozum, B., N.A. Romaniuk, A. Sorta and J.D. Scott. 2012. Oil sands mature fine tailings and bitumen extraction, IOSTC-2012, December 2–5, Edmonton, Alberta, Canada.

Ozum, B., N. Romaniuk, A. Sorta, B. Feland and J.D. Scott. 2014a. Integrating oil sands bitumen extraction processes and nonsegregating tailings production, Tailings and Mine Waste 2014 Conference, October 6–8, Keystone, Colorado, USA.

Ozum, B., N. Romaniuk, A. Sorta, B. Feland and J.D. Scott. 2014b. A paradigm change needed in oil sands industry: CaO as additives for bitumen extraction and nonsegregating tailings production processes, SPE 170174-MS, SPE Heavy Oil Conference-Canada, June 10–12, Calgary, Alberta, Canada.

Pan, L. and R.H. Yoon. 2010. Hydrophobic forces in wetting films, *Faraday Discussion* 146: 325–340.

Pan, L., S. Jung and R.H. Yoon. 2012. A fundamental study on the role of collector in the kinetics of bubble-particle interaction, *International Journal of Mineral Processing* 106–109, 37–41.

Scott, J.D., R. Donahue, J.G. Blum, T.G. Paradis, B. Komishke and B. Ozum. 2007. Production of nonsegregating tailings with CaO or CaO and CO2 for improved recycle water quality, CONRAD's Water Usage Workshop, November 21 and 22, Calgary, Alberta, Canada.

Siy, R., J. Spence, K. Sury and G. Allcock. 2001. Cold dense slurrying process for extracting bitumen from oil sand, Canadian patent, CA 2, 217, 623, August 7, 2001.

Tate, M., J. Fox, J. Leikam and Nikolas Romaniuk. 2017. Use of calcium hydroxide as a coagulant to improve oil sands tailings treatment. Tailings and Mine Waste 2014 Conference, November 8, Banff, Alberta, Canada.

Proceedings of Tailings and Mine Waste 2019
November 17–20, 2019, Vancouver, Canada
Published by the University of British Columbia, 2019

Projecting Changes to Future Extreme Precipitation Events for the Design of Tailings Facilities

Stephen Clark, Klohn Crippen Berger, Canada
Mary-Jane Piggott, Klohn Crippen Berger, Canada

Abstract

Tailings storage facilities (TSFs) in British Columbia (BC) are designed to withstand a range of large and statistically infrequent rainfall and snowmelt events. Estimating the rainfall and subsequent runoff from these events generally relies on limited periods of on-site rainfall records that are supplemented by regional data. The result is the development of intensity-duration-frequency (IDF) curves that describe the relationship between rainfall intensity, rainfall duration, and return period. These curves are then used in the design of water management elements associated with the TSF.

While TSFs have a limited operational life, their design life extends beyond this into closure. From published data and studies, a warming climate in BC will result in an increase in intensity and frequency of future extreme rainfall events. This will affect IDF curves, which in turn may affect the required size of water management structures such as diversions and spillways. The closure plan/design for each TSF is unique, but in all cases there are water management elements. Development of a closure plan for TSFs should therefore take into consideration the impact of future climate scenarios.

In this paper, projected changes in extreme rainfall are estimated for several mine sites in BC using four different methods. These methods include reviewing trends in historical data; reviewing trends in data from downscaled (i.e., modelled) future climate scenarios; using the IDF_CC Tool developed by the University of Waterloo; and scaling based on estimated increases in atmospheric moisture-holding capacity (i.e., Clausius-Clapeyron scaling). The expected change and estimated confidence limits from each method are compared to evaluate their relative merits.

Results of the comparison indicate that there is little or no benefit in using site-specific rainfall data that spans only a short period of record. Most historical datasets, particularly those with a period of record of less than 50 years, are only marginally adequate for estimating 1,000-year return period events, and simply do not contain enough data to project future changes of such events. Based on the observed level of uncertainty involved in the climate change projections, more emphasis should be placed on obtaining consistent and reliable estimates than site-specific ones.

Clausius-Clapeyron scaling was found to be the most consistent and reliable method for projecting future changes to maximum precipitation. For an increase in average annual temperatures of 3.1°C in BC from historical levels to the end of the 21st century, Clausius-Clapeyron scaling estimates a 25% increase in extreme rainfall magnitudes. A downscaled future climate scenario is appropriate for estimating future changes to secondary flood-affecting factors such as snow accumulation, evaporation, and soil moisture.

Introduction

Tailings storage facilities (TSFs) in British Columbia (BC) are designed to withstand large and statistically infrequent rainfall and snowmelt events as prescribed by the Health, Safety and Reclamation Code for Mines in BC (MEM, 2017). When designing the water management system associated with conventional TSF dams, consideration is given to two things: the volume of runoff to be managed within the dam impoundment; and the peak flow rate to be catered for by the conveyance structures associated with the facility (e.g., ditches, culverts and spillways).

Generally speaking, the inflow design flood selected for a TSF is based on the CDA (2013) consequence classification of the dam and whether the facility is in a state of Operation, Closure – Active Care, or Closure – Passive Care (CDA, 2014). Design floods for TSFs in BC range from 1/3 between the 1,000-year return period flood and Probable Maximum Flood (PMF) for Significant Consequence facilities to the PMF for Extreme Consequence facilities.

Operating TSFs are typically designed to store the design volume without release of water and the duration of the design flood can range from 72 hours, the minimum required by law in BC, to 30 days. Design floods adopted for diversion structures and closure spillways associated with a TSF are commonly less than 24 hours in duration because peak flow rate, rather than total runoff volume, is the parameter of interest.

Over the period 1900 to 2009, global temperature rose by approximately 1°C and the magnitude of extreme 24-hour rainfall events increased at an average rate of between 5.9% and 7.7% per degree Celsius globally (Westra et al., 2013). Global temperatures have risen an additional 0.3°C between 2009 and 2018 and, under a moderate emissions scenario, are projected to reach 2.5°C above pre-1900 levels by the end of the 21st century[1]. The associated effects on future extreme rainfall will undoubtedly have a significant impact on the design of many TSFs, and particularly on the design of closure spillways, diversion channels and cover systems. The effects of climate change will be different for Operation versus Closure time periods, for spring versus summer storms, and for short-duration versus long-duration flood events.

[1] IPCC, 2014. Reflects the median of emissions scenarios RCP 4.5.

Climate change projections

The Intergovernmental Panel on Climate Change (IPCC) has released several emission scenario reports. The most recent of these is the Fifth Assessment Report (AR5) (PCIC, 2014), which outlines a range of Representative Concentration Pathways (RCPs), which are projections of future atmospheric greenhouse gas (GHG) concentrations that are used to estimate changes to the Earth's climate. The RCP 2.6 scenario assumes that GHG emission rates peak between 2010 and 2020 and is the "Low Emissions" scenario (Meinshausen et al., 2011). The RCP 8.5 scenario assumes that GHG emission rates continue to rise throughout the remainder of the 21st century and is the "High Emissions" scenario. GHG emissions in RCP 4.5 scenario peaks around 2040 and is a "Moderate Emissions" scenario.

The RCP scenarios replace the Special Report on Emissions Scenarios (SRES) emissions scenarios from the earlier Fourth Assessment Report (AR4). The next Assessment Report, AR6, is expected by 2022.

Global climate models (GCMs) are being used to estimate changes to global climate under these Assessment Report emissions scenarios. GCMs are limited to coarse spatial resolutions and large timesteps that give changes over monthly or seasonal timescales only. Downscaling the outputs of GCMs to finer resolutions and shorter timescales is used to estimate changes to daily climate data in small regions. The Pacific Climate Impacts Consortium (PCIC), based in University of Victoria, BC, developed a statistical downscaling method, and Environment and Climate Change Canada (ECCC) provides access to the downscaled climate data (PCIC, 2019; ECCC, 2019). This downscaled climate data includes numerous timeseries (i.e., one for each GCM) of gridded daily precipitation and minimum and maximum daily temperature for the 1950 to 2100 period.

Available methods for projecting future changes to extreme precipitation

Method 1 – Trends in historical data

For legislated flood assessments, Engineers and Geoscientists BC (EGBC) recommends examining historical records for trends of increasing flood or precipitation magnitudes (2018). The trends can be used to estimate a percentage increase from historical IDF values to future IDF values. A nominal increase of 10% to flood flows is recommended in the absence of a statistically significant trend, while an increase of 20% is suggested for small drainage basins with limited information. However, historical trends are not necessarily indicative of the future rate of climate changes and they generally rely on too short of a record to project changes that will occur over the course of the 21st century.

Method 2 – Trends in downscaled climate scenarios

The increasing availability of downscaled future climate data provides an opportunity to address these limitations of historical data. ICOLD (2016) discusses the use of downscaled climate data for hydrologic

modelling of future climate conditions for dams. The downscaled future climate data available from Environment Canada can be used to estimate trends by the same general method as proposed by EGBC. The long record period (1950 to 2100) of downscaled data eliminates the need for extrapolation, and the availability of multiple sets of downscaled data limits the effect that data outliers can have on trend lines. Drawbacks of this approach include the still somewhat limited availability of data, and the uncertain level of accuracy of climate models and downscaling techniques.

Method 3 – IDF_CC Tool, version 3.5

Dr. Simonovic and a research team at University of Waterloo have developed the web-based IDF_CC Tool, version 3.5, which allows users to generate IDF tables based on these downscaled future climate data sets (FIDS, 2018). The program uses the downscaled data to transpose historical Environment Canada IDF tables to a given site and adjust them to future climate projections. The program includes the estimation of IDF tables for both gauged and ungauged sites and was recommended by APEGBC (2016) for use on BC Ministry of Transportation and Infrastructure (BC MoTI) projects.

Method 4 – Clausius-Clapeyron scaling

A benchmark for checking the reasonableness of climate change projections is Clausius-Clapeyron scaling. The Clausius-Clapeyron relationship relates air temperature to its moisture holding capacity; 1°C warmer air can store approximately 7% more moisture. Clausius-Clapeyron scaling (C-C Scaling) assumes that there is a direct translation from increase in air moisture holding capacity to increase in the magnitude of extreme rainfall events. This has been a reasonable predictor of the observed global rate of change to maximum daily rainfall from 1900 to 2009 (Westra et al., 2013) and is a recommended method for adjusting both frequent storm event (Zhang et al., 2017) and PMP event (Kunkel et al., 2013) magnitude to future climates.

In a presentation about the "Challenges in understanding and projecting changes in extreme precipitation", Zwiers (2017) discusses the relative merits and uncertainties of C-C Scaling versus using historical or modelled climate data.

Extreme daily precipitation projections

As noted in the preceding text, the need to include the potential impact of climate change in the design of water management structures and TSFs means that engineers must identify an appropriate method to estimate future changes to extreme precipitation.

Methodology

To determine the potential variability in results using the methods available, we examined the results from

the four methods described above at three remote sites in interior BC, one in each of the following regions:

1. East Kootenays (Southeast BC)
2. Bulkley-Nechako (Central BC)
3. Thompson-Nicola (South Central BC)

The details of how each of the four methods were applied are described below. In this assessment, methods 1, 2 and 4 adopted the historical baseline period from 1971 to 2000. For Method 3, the historical baseline used was the Environment Canada IDF curves, which were last updated in 2012. For all methods, three future periods were considered: 2011 to 2040; 2041 to 2070; and 2071 to 2100 [(2)].

Method 1 – Trends in historical data

In assessing Method 1, three climate stations in close proximity to each site and with the longest period of record were used. For the three regions considered, the periods of record ranged from 37 years to over 100 years. Trends in annual maximum precipitation were calculated using the Thiel-Sen approach to estimate trend slope as outlined in Zhang et al. (2000), and the Mann-Kendall test to estimate statistical significance. The "zyp" R package[3] prepared by Bronaugh and Werner (2019) and available from the PCIC website was used for these calculations. Where trends were found to be statistically significant, the trend (in % increase per °C warming) was projected into the future based on RCP 4.5 "Moderate Emissions" scenario temperature changes. Future temperature projections were downloaded from ECCC (2019). The minimum, maximum and median trends from the three sites are reported here.

Method 2 – Trends in downscaled climate scenarios

For Method 2, daily precipitation for the RCP 4.5 "Moderate Emissions" scenario was downloaded from ECCC (2019) and included results from 24 different GCMs. Trends in extreme precipitation were calculated using the Thiel-Sen approach and Mann-Kendall test for each GCM, in the same way as Method 1. A linear trend was fit over the period 1970 to 2100. The median, 10th percentile and 90th percentile estimated precipitation changes are reported here.

Method 3 – IDF_CC Tool, version 3.5

Unlike the other methods, which estimate only a percentage increase in IDF values, Method 3 produces IDF tables. Therefore, the projected future rainfall depths for the 5-year 24-hour storm under the RCP 4.5 "Moderate Emissions" scenario were compared to the historical Environment Canada IDF values. The

[2] Method 3, IDF_CC Tool, requires a 50-year period between 2006 and 2100 to calculate future IDF tables. Therefore, the results of this method actually correspond with the future periods 2006 to 2056, 2030 to 2080, and 2050 to 2100.
[3] R is an open source programming language that is used primarily for statistics and for which custom modules can be added. The "zyp" module was prepared by staff at PCIC for the purpose of fitting trends to climate data.

median, 25th percentile and 75th percentile estimated precipitation changes are reported here.

Method 4 – Clausius-Clapeyron scaling

Method 4 estimated the future temperature increases based on median, minimum and maximum projected temperature changes under the RCP 4.5 "Moderate Emissions" scenario. Temperature data was downloaded from ECCC (2019). Changes to precipitation were calculated simply as a 7% increase per degree Celsius of warming. Changes based on the minimum, maximum and median projected future warming are presented here.

Results

The projected changes to extreme daily precipitation using each of the four methods are presented on Figure 1 for the East Kootenay region, Figure 2 for the Bulkley-Nechako region, and Figure 3 for the Thompson-Nicola Region.

Method 1 – Trends in historical data

Table 1 summarizes the historical climate station data used in Method 1 for each of the three regions. Included are the period of record of each station, the estimated linear trend reported as a percent change over a 100-year period, and the statistical significance of the trend.

Projections based on trends in historical data resulted in somewhat scattered estimates for each of three sites, and for seven out of nine stations analysed resulted in statistically insignificant trends. The most dramatic positive and negative trends (and also the only statistically significant trends) were found to occur at the Fort St James and Prince George stations, respectively. It is interesting to note this variability despite the stations being only 100 km apart and both having long periods of record. By comparison, the three stations in the East Kootenays region had very similar trends, despite two of the three stations having record lengths of less than 40 years. In the Thompson-Nicola region, the fitted trends showed larger precipitation increases at Hope, a relatively wet climate, than at Lytton and Kamloops, which have drier climates.

An average increase in precipitation of 6% over the past 100-years was found to occur across the stations considered. It should, however, be noted that the amount of scatter in the results suggests that the trend estimates from any individual station can be unreliable, even those with long periods of record. The level of scatter was considerably reduced by using the Thiel-Sen approach (in R) to estimate trend slopes, as opposed to the ordinary least squares method (in Excel), because it better screens data outliers.

The 20% increase in runoff recommended by EGBC (2018) for small catchments seems reasonable when compared to estimates using methods 1, 2 and 3.

Table 1: Trends in historical maximum daily precipitation data

Region	Climate station	Station ID(s)	Period of record (no. of complete years)	Estimated trend (% change over 100 years)[1]	Statistically significant?[2]	Projected change from 1985 to 2085[3]
East Kootenay	Fernie	1152850	1914 to 2018 (105)	11%	No (P = 0.43)	29%
	Sparwood	1157630	1980 to 2018 (39)	7%	No (P = 0.88)	19%
	Fording River Cominco	1152899	1971 to 2007 (37)	7%	No (P = 0.88)	18%
Bulkley-Nechako	Prince George	1096436, 1096450, 1096453	1916 to 2017 (102)	–17%	Yes (P = 0.02)	–45%
	Fort St James	1092970	1900 to 2009 (110)	29%	Yes (P = 0.01)	76%
	Smithers	1077500	1943 to 2017 (75)	–8%	No (P = 0.66)	–21%
Thompson-Nicola	Kamloops	1163779, 1163780, 1163781	1914 to 2018 (105)	0%	No (P = 0.91)	0%
	Lytton	1114740, 1114741, 1114739, 1114738	1945 to 2016 (66)	7%	No (P = 0.89)	17%
	Hope	1113540, 1113539, 1113541, 1113542	1938 to 2018 (81)	22%	No (P = 0.23)	56%
Average:				**6%**	**–**	**17%**

1. Based on the Thiel-Sen approach for estimating trend slope, calculating using the 'zyp' R package created by Bronaugh and Werner (2019).
2. Based on the Mann-Kendall test for significance where P-value < 0.05 is a statistically significant trend.
3. Based on estimated station trend, scaled from a change in global average temperature of 1.2°C over the past 100 years (NASA, 2019), to a median projected change in temperature between 1985 and 2085 of 3.1°C for the RCP 4.5 "Moderate Emissions" scenario.

Method 2 – Trends in downscaled climate scenarios

For all three sites the downscaled climate data indicates modest upward trends in precipitation intensity: 11% for the East Kootenays site, 14% for the Bulkley-Nechako site, and 10% for the Thompson-Nicola site between 1985 and 2085. The amount of scatter in the data is far less than in Method 1, which gives a higher level of confidence in the results.

However, these estimated changes for three sites in interior BC are consistently less than estimates using the benchmark case, Method 4.

Method 3 – IDF_CC Tool, version 3.5

The IDF_CC Tool results for all sites estimated the largest increase between the historical and the 2011 to 2040 period, with little or no increases beyond then. The ensemble median for each of the three sites and all three time periods was an increase of 18% to 28% above historical levels.

Method 4 – Clausius-Clapeyron scaling

For all three sites the benchmark method estimates increases in precipitation intensity of 9% for the 2011–2040 period, 18% for the 2041–2070 period, and 24% for the 2071–2100 period. For all three sites and each of the three time periods except one, the best estimate using C-C scaling was within 4% of the median of all four methods. It could be argued that at all three sites Method 4 provided the most reliable and conservative estimates of future changes in extreme precipitation.

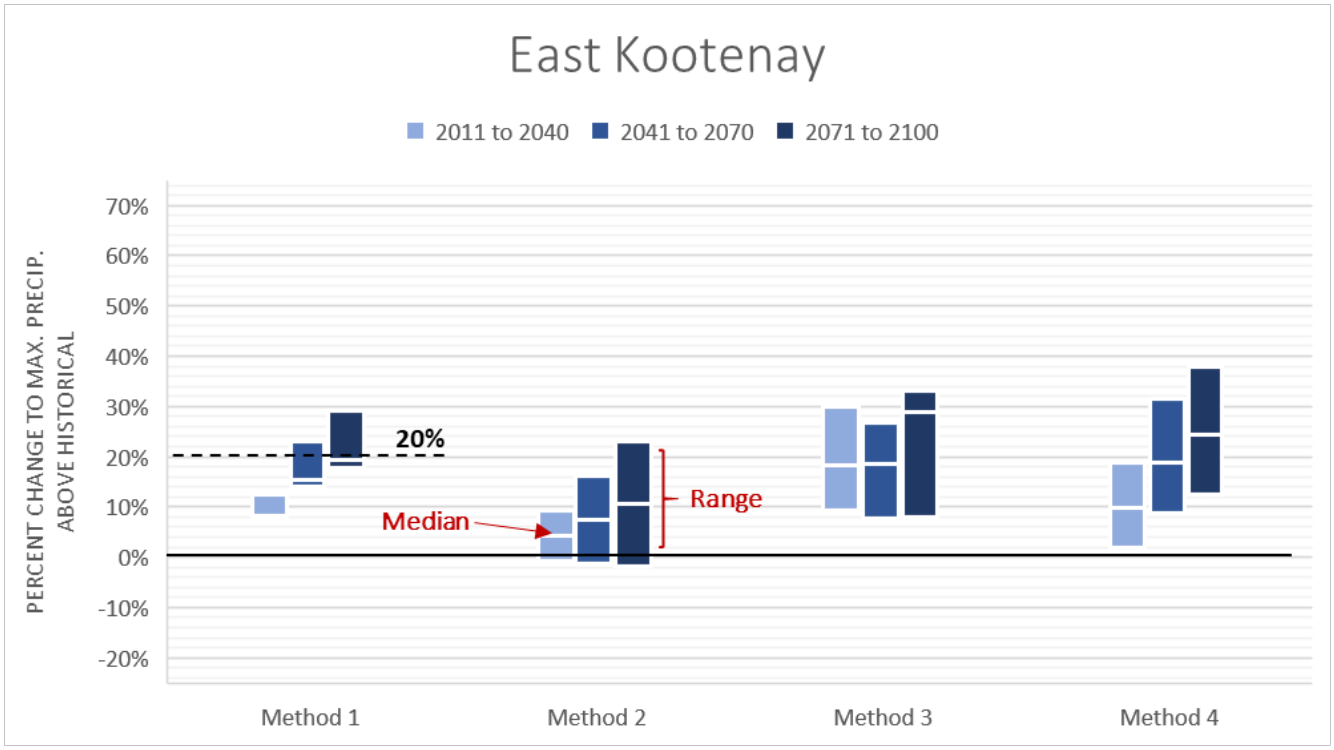

Figure 1 Projected changes to extreme daily precipitation in East Kootenay region

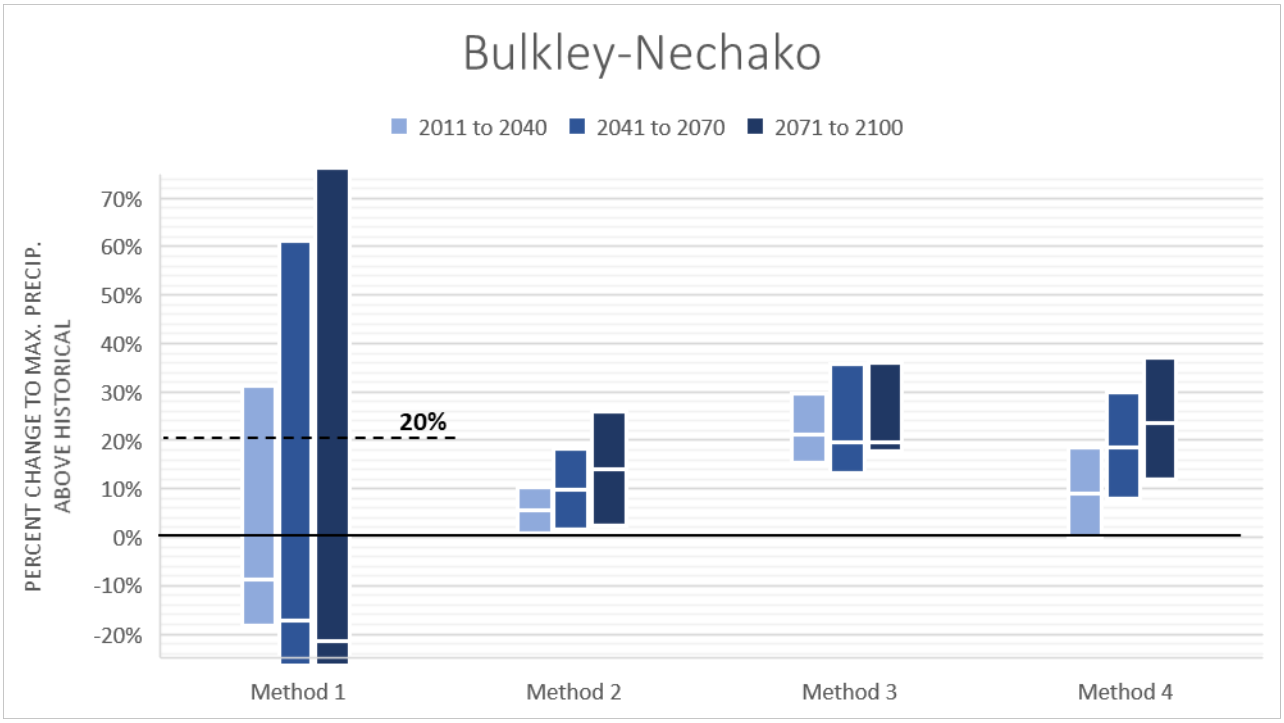

Figure 2: Projected changes to extreme daily precipitation in Bulkley-Nechako region

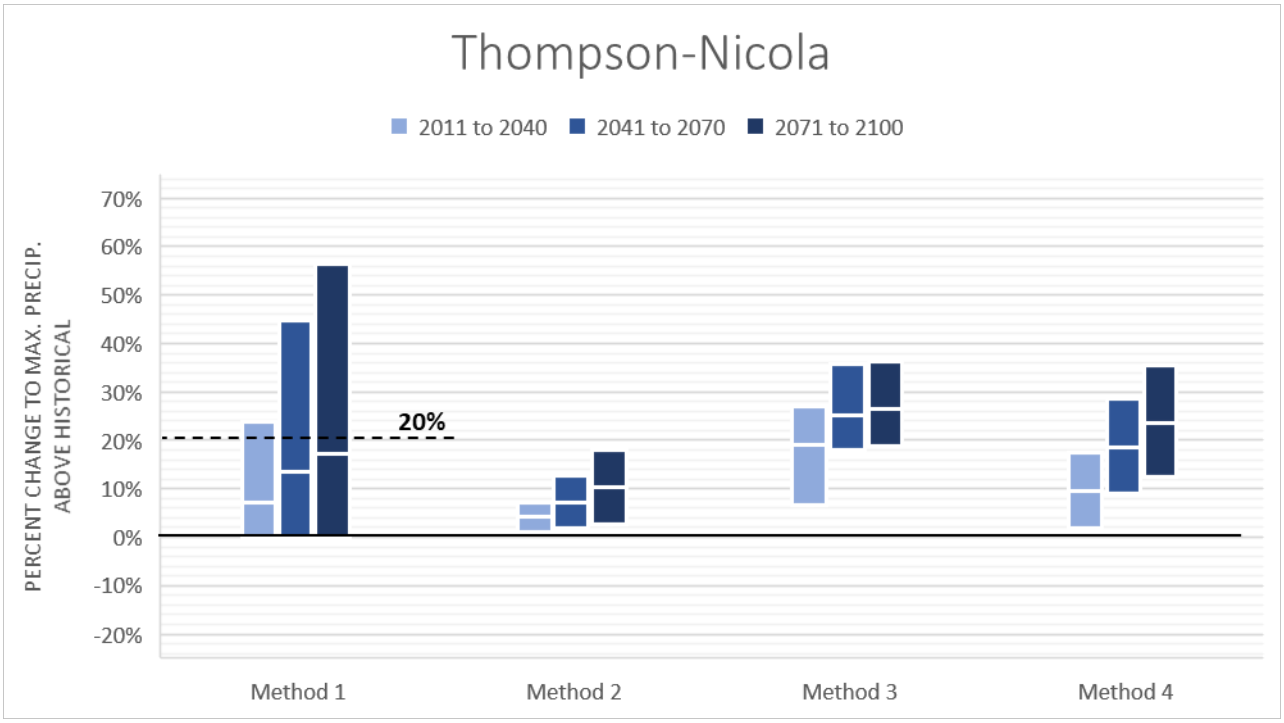

Figure 3: Projected changes to extreme daily precipitation in the Thompson-Nicola region

Extreme multi-day precipitation projections

The above results were for the 24-hour (1-day) maximum precipitation only. To assess the potential impacts to longer duration events (7 to 30 days), the trends in downscaled climate data (Method 2), was used. The results for all three durations at each of the three sites for the period from 1985 to 2085 were then compared. As can be seen in Table 2, the estimated change in 7-day and 30-day precipitation at each site was very similar to the estimated change in 1-day precipitation. This result supports the applicability of the IDF_CC tool or C-C scaling to events longer than a 1-day duration, which they are primarily used for.

Table 2: Trends in 1-day to 30-day downscaled precipitation

Event	Median percent Increase from 1975 to 2085		
	East Kootenays	Bulkley-Nechako	Thompson-Nicola
1-day precipitation	11%	14%	10%
7-day precipitation	10%	13%	10%
30-day precipitation	10%	13%	12%

Conclusion

Several general observations can be made in relation to the four methods for estimating changes to maximum daily precipitation in future climate.

Projections based on trends in historical data (Method 1) is of somewhat limited value due to the scatter in estimated trends from station to station, and the magnification of this scatter when results are projected into the future. However, the flat 20% increase in runoff recommended by EGBC for small catchment areas is comparable to projected precipitation changes for the latter half of the 21st century under "Moderate Emissions" scenario RCP 4.5 by methods 2, 3, and 4.

Trends in downscaled climate scenarios (Method 2) can be used to estimate trends in multi-day precipitation events, spring snowpack, rain-on-snow events, and evaporation through the use of hydrologic models. This provides valuable information for designing TSF storage requirements along with projecting future water balance deficits or surpluses. The results should be based on average trends from a large number of GCMs and compared to a benchmark like Method 4, to reduce uncertainty in the results.

For all three sites, and each of the three time periods except one, the best estimate of changes to extreme daily precipitation using C-C scaling (Method 4) was within 4 percentage points of the median of all four methods. This method is not affected by limited historical measurements, availability of modelled climate data, or errors/limitations in modelled climate data, and appears to be appropriate for precipitation events ranging from 1 day to 30 days, based on the three sites reviewed by this paper.

With the level of uncertainty currently involved in climate change projections, perhaps more emphasis should be placed on consistent estimates than site-specific ones.

References

Association of Professional Engineers British Columbia (APEGBC). 2016. APEGBC professional practice guidelines – Developing climate change-resilient designs for highway infrastructure in British Columbia (interim), V1.0, December.

Bronaugh, D. and A. Werner. 2019. Package "zyp'": Zhang + Yue-Pilon Trends Package for R. Comprehensive R Archive Network. Accessed July 16, 2019, from http://cran.r-project.org/web/packages/zyp/index.html

Canadian Dam Association (CDA). 2013. *Dam Safety Guidelines 2007* (2013 edition).

Engineers and Geoscientists British Columbia (EGBC). 2018. Legislated flood assessments in a changing climate in BC. August 28.

Environment and Climate Change Canada (ECCC). 2019. Climate data for a resilient Canada, Version 1.6.1. Accessed August 30, 2019, from https://climatedata.ca/

Facility for Intelligent Decision Support (FIDS). 2018. IDF_CC Tool 3.5. Accessed July 14, 2019, from https://www.idf-cc-uwo.ca/home

International Commission on Large Dams (ICOLD). 2016. Global climate change, dams, reservoirs and related water resources. V12. Final. November.

IPCC. 2014. Climate change 2014: Synthesis report. Contribution of Working Groups I, II and III to the Fifth Assessment Report of the Intergovernmental Panel on Climate Change. Core writing team, R.K. Pachauri and L.A. Meyer (editors). IPCC, Geneva, Switzerland, 151 pp.

Kunkel, K.E., T.R. Karl, D.R. Easterling, K. Redmond, J. Young, X. Yin and P. Hennon. 2013. Probable maximum precipitation and climate change. *Geophysical Research Letters* 40(7): 1402–1408.

Meinshausen, M., S.J. Smith, K.Calvin, J.S. Daniel, M.L.T. Kainuma, J.-F. Lamarque, K. Matsumoto et al. 2011. The RCP greenhouse gas concentrations and their extensions from 1765 to 2300. *Climatic Change* 109(1–2): 213–241.

Ministry of Energy and Mines (MEM). 2017. Health, safety and reclamation code for mines in British Columbia.

NASA. 2019. Global climate change – vital signs of the planet: Global temperature time series 1884 to 2018. Accessed July 15, 2019, from https://climate.nasa.gov/vital-signs/global-temperature/.

PCIC. 2019. Statistically downscaled climate scenarios. Method: BCCAQ v2. Published February, 2019. Retrieved from https://data.pacificclimate.org/portal/downscaled_gcms/map/

Westra, S., L.V. Alexander and F.W. Zwiers. 2013. Global increasing trends in annual maximum daily precipitation. *J. Clim.* 26: 3904–3918.

Zhang, X., Vincent, L.A., Hogg,W.D. and Niitsoo, A., 2000. Temperature and Precipitation Trends in Canada during the 20th Century. *Atmosphere-Ocean* 38(3): 395–429.

Zhang, X., F. W. Zwiers, G. Li, H. Wan, A. Cannon. 2017. Complexity in estimating past and future extreme short-duration rainfall. *Nature Geoscience* 10, 255–259.

Zwiers, F. 2017. Challenges in understanding and projecting changes in extreme precipitation. National Research Council, January 18. Available at https://www.pacificclimate.org/sites/default/files/publications/1701-jan-18-nrc-zwiers.pdf

Bibliography

Canadian Dam Association (CDA). 2014. Technical bulletin: Application of dam safety guidelines to mining dams.

Taylor, K.E., R.J. Stouffer and G.A. Meehl. 2012: An overview of CMIP5 and the experiment design. *Bulletin of the American Meteorological Society* 93: 485–498. doi: 10.1175/BAMS-D-11-00094.1.

Proceedings of Tailings and Mine Waste 2019
November 17–20, 2019, Vancouver, Canada
Published by the University of British Columbia Press, 2019

The Value of Detailed Topographic Surveys for Consequence Classifications Using Dam Breach Assessments

Alexandra Halliday, Golder, Chile

Abstract

Many national and international guidelines require the design of the Tailings Storage Facility (TSF) to increase in rigour and robustness as the consequence classification of a facility is increased. The outcomes of a Dam Breach Assessment (DBA) are a key input when selecting an appropriate consequence classification for a TSF. A low-resolution and free-sourced topography used in a DBA could result in larger impact areas and as such, a higher consequence classification. This may result in the design and construction budget being incorrectly allocated to mitigate failure modes in areas that may not be necessary given the potential consequences indicated by the DBA. The impact of using the "preliminary" results of a DBA can be significant if they govern the consequence classification.

The quality of topographic survey can have a significant impact on the outcome of a DBA. Often TSFs are constructed and operated in remote locations, outside of the range of high-resolution free-sourced surveys – unlike in metropolitan areas where free-sourced surveys are often of high-quality, with dense survey points resulting in a high-resolution and detailed topography.

Low-resolution topographic surveys can miss critical changes in elevation that can cause terrain features to deviate from their actual conditions. Low-resolution topographies can result in steeper slopes or sharper valleys through the interpolation of survey points that are over 20 m apart. This interpolation, over the potential runout distance of a DBA (often in excess of 1,000 m), can result in significant accumulated changes to the terrain. This change in terrain can result in higher breach velocities and as such longer runout distances, causing the impact of the dam breach to be greater.

Detailed topographic surveys will be required during the TSF design, but the extent of this survey is generally limited to the main mining infrastructure, with the survey downstream of the TSF often obtained with lower quality. This paper aims to provide a set of decision criteria to assist mine owners to decide on what stage to invest in a detailed topographic survey downstream of the TSF, and to show the value that detailed surveys add to both design criteria and emergency response planning.

Introduction

Many national and international guidelines require the design of the Tailings Storage Facility (TSF) to increase in rigour and robustness as the consequence classification of a facility is increased. The outcomes of a Dam Breach Assessment (DBA) are a key input when selecting an appropriate consequence classification for a TSF. A consequence classification is generally assigned to a TSF early in the design process, like the pre-feasibility or scoping phases of engineering studies. During such phases of design, it is unlikely that detailed topographic surveys outside of the main mining infrastructure and downstream of the TSF will be available.

In highly populated metropolitan areas, the quality of free-sourced surveys is often high, whereas in regional or remote areas with low populations free-sourced surveys are usually of much lower quality. TSFs are usually constructed in remote areas, resulting in the need to purchase site-specific topographic surveys of the TSF area and mining infrastructure to obtain detailed topography. As a result, DBAs undertaken in the early phases of design are often done by using free-sourced and low-quality topographic surveys.

For the purposes of this paper, a detailed or high-resolution topographic survey is classified as a survey with a point density of at least one point every 5 m. A low-resolution topographic survey is a survey which has a point density of one point every 20 m or more.

A detailed topographic survey is often overlooked as a critical input in DBA. A detailed topographic survey can pick up sudden changes in the terrain elevation that may be missed with a free-sourced survey. Changes to the elevation points could cause the natural slope of the site to be increased or decreased, or the width of valleys to be narrowed or widened, all of which can significantly vary the outcomes of a DBA. The consequence classification of a TSF and the emergency planning procedures are often governed by the outcomes of a DBA, and many of the proceeding design criteria are dependent on this classification. The impact of using the "preliminary" results of a DBA can be significant if they govern the consequence classification. Designing conservatively is not an unsafe or poor choice considering the recent TSF failures around the world, but an issue arises if the consequence classification assigned is lower than needed, and the design must be adjusted at a later phase of design to increase the robustness of the facility accordingly.

Occasionally, regardless of the outcomes of the DBA there will be overarching factors that will govern the consequence classification, and as such it may not be necessary to invest in a detailed topographic survey at such an early stage of the design studies. Detailed topographic surveys are, however, critical in developing emergency response and evacuation procedures.

The social implications of using preliminary results for early community engagement is another significant consideration. Preliminary results obtained using low-resolution topographic surveys may suggest that certain homes, businesses, or sensitive environmental receptors are in the potential inundation area. If the inundation is adjusted once a detailed topographic survey is obtained and the community needs

to be readvised of the risks in the event of a failure, this can result in a lack of trust in the mine owner from the community.

Even DBAs that were undertaken using a detailed, site-specific topographic survey in the preliminary phases of design should be re-evaluated during later stages of design. In the preliminary phases the key design considerations, for example, the dam construction material, the dam construction method, or the dam alignment are less certain, and may be subject to change during the detailed engineering phase. It is essential that the assumptions used when undertaking the DBA are still relevant during later stages of engineering studies and confirm if any design changes could alter the results of the DBA.

ANCOLD consequence classifications

The Australian National Committee on Large Dams (ANCOLD) provides a guideline for the management, design, and operation of TSFs (ANCOLD, 2012). The guideline stipulates that each TSF must be allocated a consequence classification. The consequence classification aims to categorize each facility based on the potential population at risk and the damage that may occur after a failure, and provide design criteria that aim to reduce the likelihood of a failure occurring, thus seeking to reduce the overall "risk" component of the TSF.

The consequence classification is derived from a combination of the population at risk, and the most significant potential severity of damage (Table 1). The potential damage types described in the ANCOLD guideline are presented in Table 2. To designate a consequence classification to a TSF, each of the eight damage types (seven damage types and the population at risk) needs to be ranked as minor, medium, major or catastrophic in accordance with the descriptions. The damage type with the highest rating will govern the final consequence classification. For example, if seven damage types are rated as minor and one is rated as catastrophic, the overall rating of the "severity of damage and loss" will be classified as catastrophic.

Table 1: Overview of the ANCOLD guideline for consequence classification (after ANCOLD, 2012)

Population at risk	Severity of damage and loss			
	Minor	Medium	Major	Catastrophic
<1	Very Low	Low	Significant	High C
>1 to 10	Significant (Note 2)	Significant (Note 2)	High C	High B
>10 to 100	High C	High C	High B	High A
>100 to 1,000	(Note 1)	High B	High A	Extreme
>1,000		(Note 1)	Extreme	Extreme

Note 1. With a PAR in excess of 100, it is unlikely damage will be minor. Similarly, with a PAR in excess of 1,000 it is unlikely damage will be classified as medium.
Note 2. Change to "High C" where there is the potential of one or more lives being lost. The potential for loss of life is determined by the characteristics of the flood area, particularly the depth and velocity of flow.

Table 2: Overview of the ANCOLD guideline damage types, with relationship to DBA importance (after ANCOLD, 2012)

Damage type	Minor	Medium	Major	Catastrophic
Infrastructure (dam, houses, commerce, farms, community)	<$10 M	$10 M–$100 M	$100 M–$1 B	>$1 B
Business importance	Some restrictions	Significant impacts	Severe to crippling	Business dissolution, bankruptcy
Public health	<100 people affected	100–1,000 people affected	<1,000 people affected for more than one month	>10,000 people affected for over one year
Social dislocation	<100 person or <20 business months	100–1,000 person months or 20 – 20,000 business months	>1,000 person months or >200 business months	>10,000 person months or numerous business failures
Impact area	<1 km^2	<5 km^2	<20 km^2	> 20 km^2
Impact duration	<1 (wet) year	<5 years	<20 years	> 20 years
Impact on natural environment	Damage limited to items of low conservation value (e.g., degraded or cleared land, ephemeral streams, non-endangered flora and fauna) Remediation possible	Significant effects on rural land and local flora and fauna. Limited effects on: **A.** Item(s) of local and state natural heritage. **B.** Native flora and fauna within forestry, aquatic and conservation reserves, or recognized habitat corridors, wetlands or fish breeding areas	Extensive rural effects. Significant effects on river system and areas A and B. Limited effects on: **C.** Item(s) of national or world natural heritage. **D.** Native flora and fauna within national parks, recognized wilderness areas, RAMSAR wetlands and nationally protected aquatic reserves. Remediation difficult.	Extensively affects areas **A and B.** Significantly affects areas **C and D.** Remediation involves significantly altered ecosystems.

The impacts of DBA on consequence classifications

Potential damages that could occur following a dam failure have been categorized into seven damage types, some damage types are directly related to the outcomes of a DBA, others are indirectly impacted by the results of a DBA. For the purposes of this paper, the potential damages have been ranked as one of the following three:

- Not impacted – the damage type is not impacted by the results of a DBA.
- Potentially impacted – the damage type may be impacted by the results of a DBA in some circumstances.
- Directly impacted – the damage type is directly impacted by the results of the DBA.

A summary of the damage ratings is presented in Table 3.

Table 3: The impact of the results of a DBA on each damage type specified in ANCOLD

Damage type	Impact of DBA in classifying damage
Infrastructure (dam, houses, commerce, farms, community)	Potentially impacted
Business importance	Potentially impacted
Public health	Potentially impacted
Social dislocation	Potentially impacted
Impact area	Directly impacted
Impact duration	Directly impacted
Impact on natural environment	Potentially impacted

The impacts of topographic quality on DBAs

A simulation of a hypothetical dam breach was duplicated at the same location using two different topographic survey qualities: a high-resolution site-specific topography and a low-resolution free-sourced topography. All other assessment conditions, including the breach hydrograph, flow rheology, and surface roughness coefficients were constant for the two simulations, which were undertaken using FLO-2D. The topographic survey used for the assessment has been taken from an area with a narrow valley terrain, the total length of the valley in the survey is approximately two kilometres, and the dam has been hypothetically placed in the upper portion of the valley (Figure 1). The release of materials from the dam was assumed to be tailings, and as such, the breach hydrograph was assigned a sediment concentration that varied over time to simulate an initial release of water, followed by tailings combined with the dam construction material that is released during the hypothetical failure.

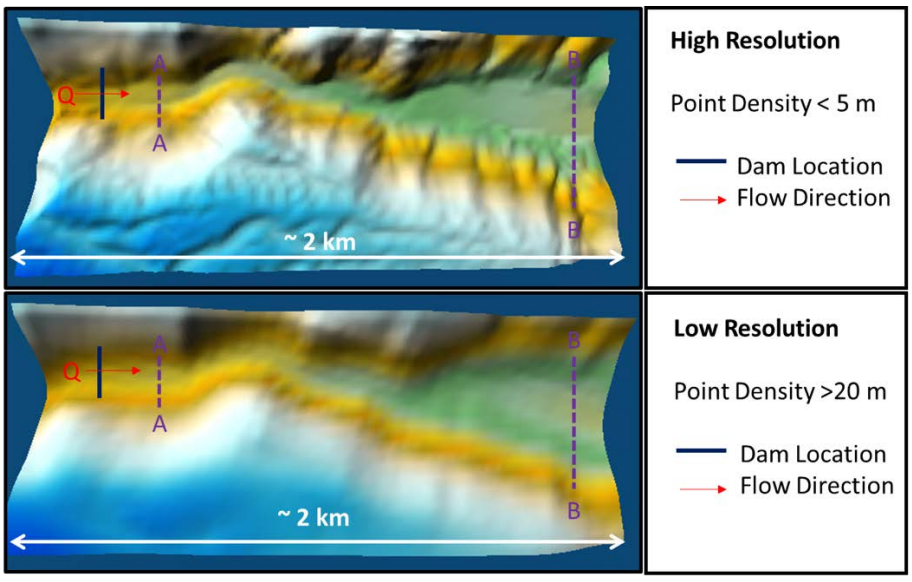

Figure 1: Differences between the high-resolution and low-resolution topographies used to the comparison assessment

As shown in Figure 1, the two topographies can be considered visually similar; however, the low-resolution topography did not interpolate the key changes in the natural terrain that have had an impact on the outcomes of the DBA. As demonstrated in Figure 2, close to the dam breach (Section A-A) the high-resolution topography has a narrower valley with a width of ~57 m, whereas the low-resolution topography has a width of ~12 m greater with a total width of ~75 m. Close to the model boundary (Section B-B), the low-resolution topography has a narrower valley with a width of ~142 m, whereas the high-resolution topography had a valley width of ~252 m (a total difference of ~110 m).

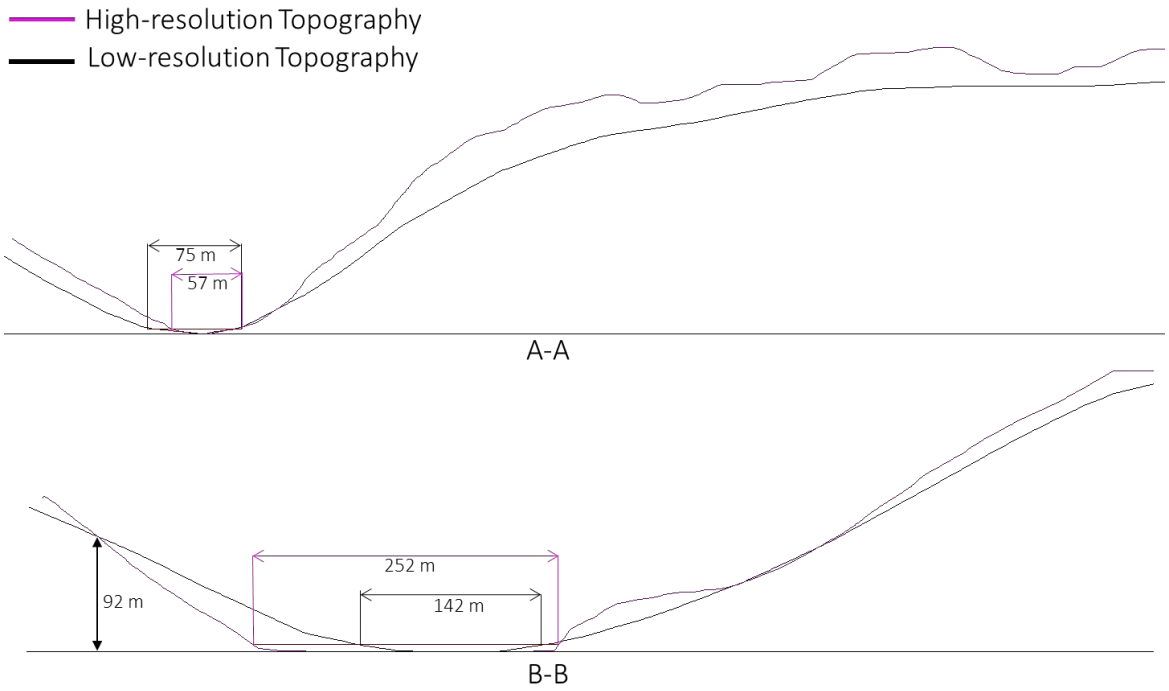

Figure 2: Changes in valley width due to topography resolution

These two changes in the valley dimensions presented in Figure 2 have impacted the results of the DBA. The flow patterns observed are seen in the results for both the high-resolution and low-resolution model simulations. For example, the decrease in surface water depth as the flow moves downstream of the breach is observed in both the low-resolution and high-resolution topography. Similarly, the high velocity zones for both topographies are also consistent. However, there are significant differences in the numerical results of these models, with different velocities, flow depths, runout distances, and inundation areas observed between the two topographic resolutions.

The low-resolution topography resulted in a lower maximum velocity in the first portion of the valley of ~5 m/s, and a higher maximum velocity in the last portion of the valley of ~2 m/s. The high-resolution topography resulted in a higher maximum velocity in the first portion of the valley of ~6 m/s, and a lower maximum velocity in the last portion of the valley of ~1 m/s.

The low-resolution topography resulted in a smaller overall wetted area with a depth of greater than 0.15 m within the computational domain of ~119,225 m^2. It was observed that there was likely more flow beyond the model domain at the end of the 10-hour simulation (as the flow mass had exited the outflow elements). The high-resolution topography resulted in a larger wetted area within the computational domain of ~196,900 m^2 (~60% greater). However, it was observed that the flow mass had finished flowing, mostly within the domain, at the end of the 10-hour simulation.

The maximum flow depth that occurred during the simulation was similar, but slightly higher for the low-resolution topography at 11.5 m, and lower for high-resolution topography at 9.5 m.

The maximum depth of flow at the end of 10-hour simulation was ~8.0 m for the low-resolution topography and ~3.8 m for the high-resolution topography. The low-resolution topography had a narrow distribution of flow and a depth of less than 0.9 m at the model boundary. The maximum flow depth was more widely distributed for the high-resolution and at the model boundary had a depth of less than 0.5 m, (Figure 3 top).

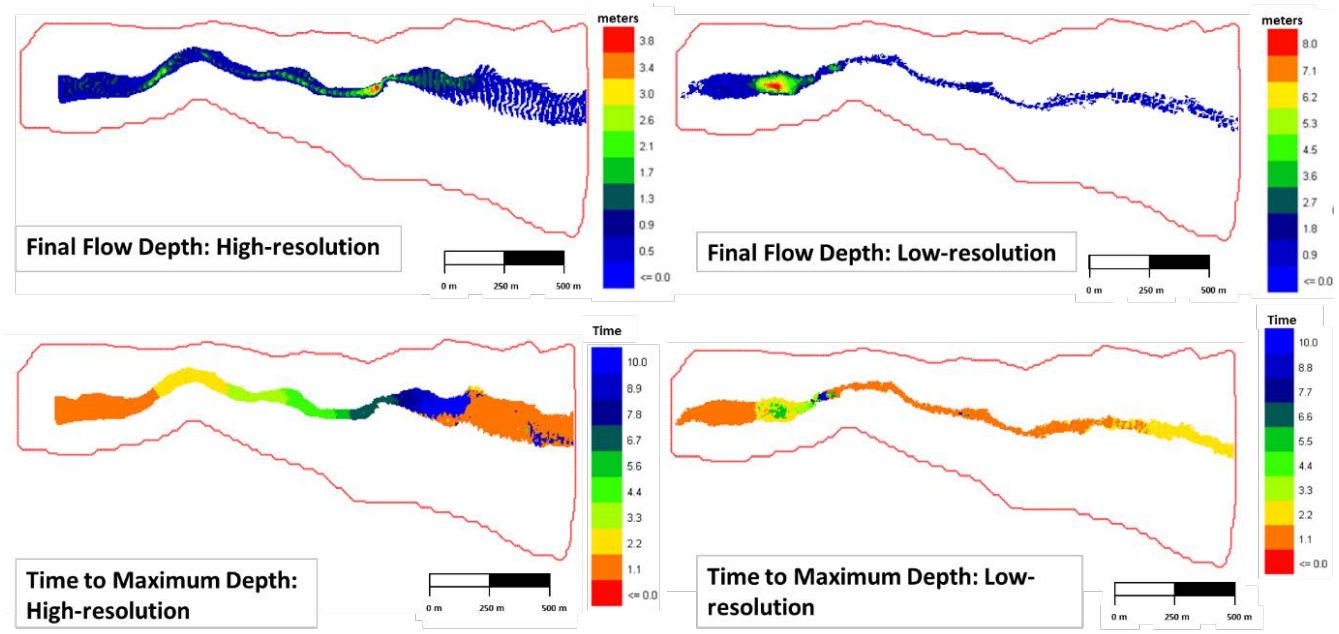

Figure 3: Results of the final flow depth and time for the flood to reach a depth of 60 cm (both topographies)

The surface water elevation of the flow was comparable in terms of distance for flow to reduce. However, the width of the impact was significantly reduced for low-resolution topography.

It took ~1.1 hours for a small depth of flow to reach the model boundary in the low-resolution topography (likely the initial water breach); the main body then took ~2.2-hours to reach the model boundary, in accordance with the maximum depth of flood occurring at the boundary. The high-resolution topography showed a similar pattern. The time for this smaller "initial water breach" to reach the boundary

was ~1.1 hours, with the main flood mass following behind, as observed with the high-resolution topography, but taking a total time to reach the model boundary of ~10 hours (Figure 3 bottom).

With all parameters and inputs constant except for the topographic quality, these differences can be attributed to the interpolated elevation between the two topographies (Figure 2). The low-resolution topography has a wider valley in the first portion of the valley and a much narrower valley in the end portion of the valley, resulting in higher flowing velocities and larger runout distances. The high-resolution topography has more points to capture the sharp change in elevation, resulting in a wider valley, with lower velocities, flow depths, and runout distances. Detailed assessment conditions and results are presented in the paper "Impacts of topographic quality on dam breach assessments" (Halliday and Arenas, 2019).

Design criteria

The design criteria of a TSF are allocated based on the consequence classification of a TSF. These design criteria can significantly increase the size, construction method, and additional facilities required for a TSF, such as spillways and geosynthetic liners. The following six design elements are all governed by the consequence classification of a facility:

- the minimum extreme storm storage;
- the contingency freeboards;
- the wet season water storage allowance;
- the minimum design floods for spillway design and wave-freeboard allowance during the operation phase;
- earthquake loadings (annual exceedance probabilities); and
- the frequency of inspections.

Investing in a high-resolution site-specific survey early for a DBA and deriving a corresponding consequence classification can have a significant impact on the level of design contingencies required for a facility.

Emergency procedures

It is important that mine owners and their consultants (internal and external) have a high level of confidence in the DBA results before emergency response planning and procedures are developed. If a preliminary DBA has been developed in the early stages of design with a low-resolution topography, those responsible for developing the emergency procedures should consider if the DBA should be updated using a high-resolution topographic survey prior to developing them. The safety of the mine employees and the surrounding communities should be the primary concern in the unfortunate event of a TSF failure, and the

type and effectiveness of emergency evacuation procedures is often governed by the outcomes of a DBA. The study presented earlier in this paper shows that the inundation area was approximately 60% higher for the high-resolution topography. In certain circumstances, using a low-resolution topography may result in a portion of the community being advised that they are in the "safe" zone, whereas using a high-resolution could have contradicted that information. There are circumstances and instances when a high-resolution survey may not impact the outcomes of a DBA. These circumstances are discussed in further detail in the following section.

Decision criteria

A detailed topographic survey for use in a DBA is a crucial investment for a TSF. They are critical in developing an appropriate consequence classification, but also in providing accurate outflow times, distances, and inundation areas for emergency evacuation procedures. In the early phases of design, investing in a detailed topographic survey downstream of the TSF may seem like an unnecessary and costly exercise. There are occasions when mine owners do not need to invest in detailed topographic surveys until later phases of the design, and conversely, there are occasions when investing in the detailed topographic survey could save mine owners significantly and it is therefore economically beneficial to invest early. A set of decision criteria, which aim to assist mine owners and designers on if and when to commit to investing in detailed topographic survey, is presented in Figure 4.

Conclusion

The consequence classification of a TSF can be heavily impacted by the results of a DBA. If a low-resolution or free-sourced topographic survey is used to assess the impacts of a potential breach of a TSF, the corresponding consequence classification may be grossly over-estimated or under-estimated. Such an over- or under-estimation in consequence classification could lead to the over-design of facilities that is not detrimental to a TSF. However, it is critical that designers understand and consider all factors that have an impact on their design and make a conscious choice to design for those risks accordingly. This allows for the correct allocation of funding, resources, and time. Additional funding that may be used to overbuild a facility could have been more appropriately allocated to emergency response plans, evacuation procedures, and instrumental monitoring equipment such as the installation of vibrating monitoring piezometers or remote monitoring cameras to provide real-time monitoring of potential deformations.

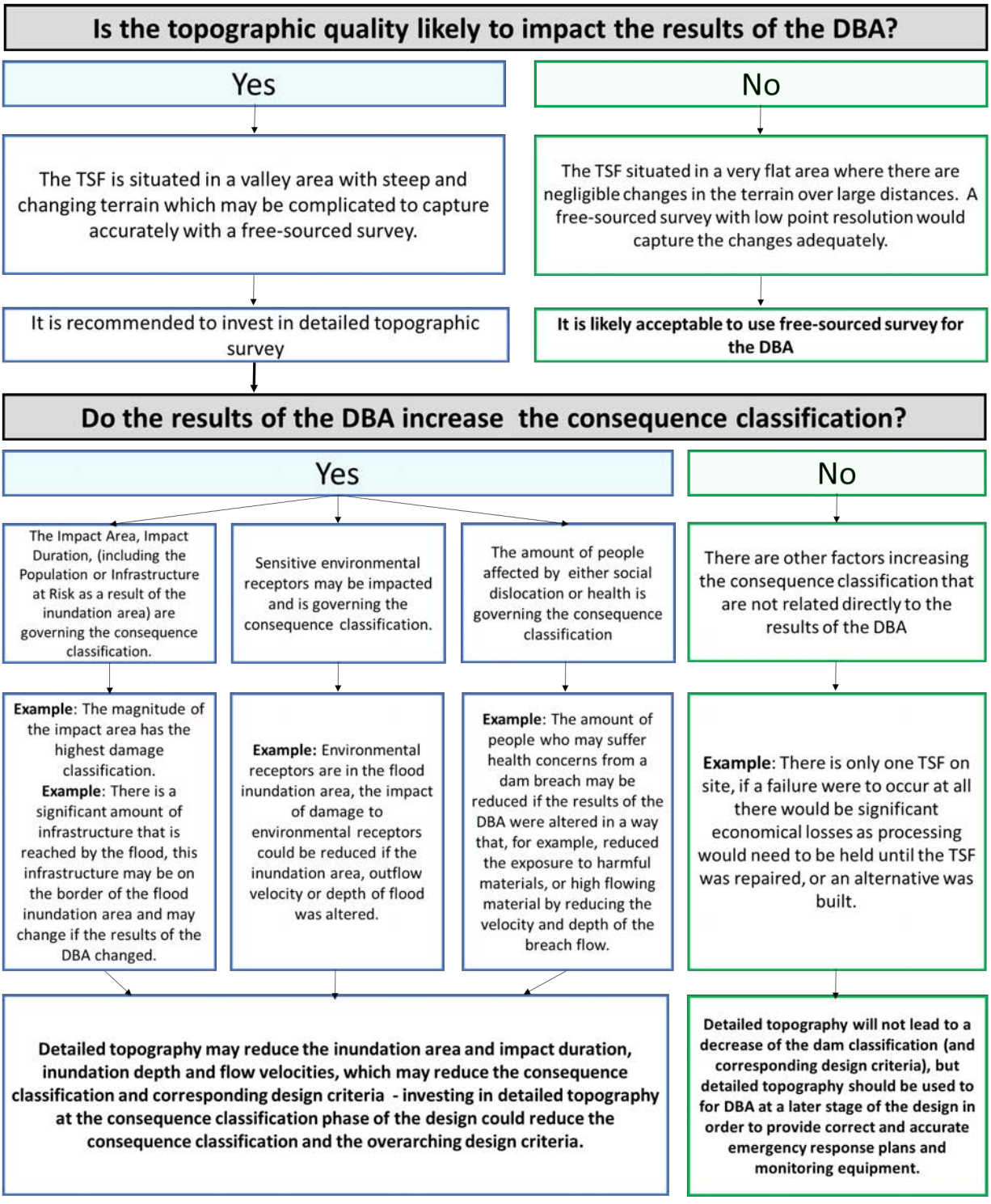

Figure 4: Decision criteria for assisting in what phase of the design to invest in detailed topographic survey

Community engagement should be considered at a phase of design that allows mine owners to provide the most accurate results of inundation areas and corresponding evacuation protocols. This aims to avoid

the unnecessary social implications that can arise if the results of a preliminary DBA change when undertaken using a detailed topographic survey.

Many DBA softwares require the interpolation of the elevation of the topography within the software to generate a mesh. The individual grid size of the mesh size can generally be selected, and a smaller mesh will better capture the changes in natural topography, much the same way a detailed survey would. The implications of opting to use a large grid square for DBA to reduce the run time should be considered when undertaking DBAs. There will be occasions when a small grid square is not feasible; for example, when considering DBAs with large runout distances or areas.

Mine owners and designers should be aware of the risks, both economical and safety-related, associated with using low-resolution topographies for DBAs.

References

Australian National Committee on Large Dams Incorporated (ANCOLD). 2012. *Guidelines on Tailings Dams: Planning, Design, Construction, Operation and Closure.*

Halliday, A. and A. Arenas. 2019. The impacts of topographic quality on dam breach assessments. In *Proceedings of the Tailings 2019 Conference,* Santiago, Chile.

Proceedings of Tailings and Mine Waste 2019
November 17–20, 2019, Vancouver, Canada
Published by the University of British Columbia, 2019

Considerations of Tailings Storage Facilities Design over Soft Soils – Case Study

Waldo Huallanca, Anddes, Peru
Myzael Valdivia, Anddes, Peru
Miguel Regalado, Anddes, Peru
Rolando Rojas, Anddes, Peru

Abstract

Construction of new mining projects over little-explored and complex geological formation areas have become more frequent. Such is the case when foundations consist of soft materials, on which important structures will be constructed. These new structures could have a high potential environmental or economic impact, such as tailings storage facilities (TSF). Over the last years, TSF failures have been reported due to the presence of soft soils in the foundation; this is the case of the well-documented Mount Polley case. Hence, a safe geotechnical TSF design over soft soils is an engineering challenge. This paper describes a case study called TSF N4 located in the Andes. The original design and analysis were conducted without taking into account the significance of soft soils in the foundation. The importance of soft soil behaviour was identified after an independent dam safety review (following the guidelines of the Canadian Dam Association [CDA]) for TSF N4.

For the case study, an associated geotechnical risk, due to potential soft soil undrained behaviour, was identified, relating to stability problems in the current condition and also in regard to future raises of the TSF N4. In order to define the soft soil foundation behaviour, geotechnical site and laboratory programs were conducted to enable an adequate description of the geotechnical parameters that influence the overall analyses. Finally, a redesign of TSF N4 was performed with different construction stages to allow adequate consolidation of the foundation soil and ensure excess pore pressure dissipation, in order to avoid failure due to the undrained behaviour of the foundation. Stabilization countermeasures were proposed along the toe of the dam in order to increase the short-term static condition factor of safety and reduce the risk associated with soft soils.

Introduction

TSF failures have been reported due to the presence of soft soils (weak layers) in the foundation; that is the

case with the well-documented Mount Polley failure in British Columbia, Canada, in 2014 (Morgenstern et al., 2015). The Los Frailes failure in Aznalcóllar, Spain, in 1998 (Alonso and Gens, 2006) is not as well reported; however, the evidence suggests a foundation failure due to a soil that lost its mechanical integrity. The recent failure of Saddle Dam D at the Xe-Pian Xe-Namnoy hydroelectric power project in Laos (2018) was related to the high permeability of the foundation, which enabled internal erosion and caused a softening of the foundation (Schleiss et al., 2019).

The mining industry continues to develop, and this allows mining companies to have better opportunities for precious metal extraction. However, this has led to new challenges for the civil and geotechnical design of earth and rockfill structures. One of the major new challenges involves the design of facilities to be built on soft soils, basically because there are few possibilities of finding firm or dense soil, or sound rock, in the majority of mining projects located in the South America Andes (Lupo, 2005). Despite this, engineering in this part of the world has been able to deal with these problems and appropriately design mining facilities (Reyes et al., 2015; Mantilla and Negrón, 2016).

However, current designs have usually been based on criteria used by international practitioners, as well as best practices and lessons learned from complex cases that were not designed or constructed appropriately and, in consequence, failed, such as the case of the well-known Mount Polley TSF.

According to the Mount Polley report (Morgenstern et al., 2015), the north side of the dam failed due to the presence of a compressible and glaciolacustrine soil (GLU) that was susceptible to an undrained failure that was not considered in the original design of the TSF. This was related to the fact that material presented overconsolidated behaviour prior to the construction of the dam, but then changed to normally consolidated behaviour due to the loads applied during the construction, which caused the undrained behaviour of the GLU soil.

The present study describes a case study named TSF N4 located in the Andes, where researchers studied how the design criteria for the stability of the dam was modified over the years, based on the observations of different specialists. These findings and recommendations could come from the designer of the dam or the dam safety reviewer, among others, showing that points of view can vary according to varied experiences and based on the risks associated with the structure. This study focusses on the behaviour of a tailings dam founded on soft soil, similar to the case of the Mount Polley TSF.

Case study geotechnical overview and analysis

Stage design

The case study presented in this paper is a 35 m-high TSF with a global downstream slope of 1V:2H, as shown in Figure 1. The TSF was founded on soft soil and is currently in its penultimate configuration. The

TSF embankment is composed of structural fill and was built by means of centerline raises, with a pumping system that keeps the beach as far as 100 m from the crest.

This was the sequence of the dam's construction during its operational stage:

- The original tailings dam design was carried out by Consultant A at the end of the nineties. The starter dam was formed from mine waste (hereinafter rockfill), and presented early complications related to its stability. Therefore, in 2000 the same Consultant A amended the design to increase stability. In the first half of 2001 the construction of the first buttress (stabilization berm) was completed. In 2004, Consultant B was commissioned to perform a geotechnical analysis and design the dam's raises by means of the downstream method using mine waste. The first had an elevation of 3,437.60 masl, while the second had an elevation of 3,440.60 masl. Between 2007 and 2008, the same consultant designed a raise of 1 m using the centerline method, up to an elevation of 3,441.60 masl.
- In 2011, the same consultant engineered another dam raise by means of the centerline method, up to an elevation of 3,455 masl. This included a considerable volume of replacement of improper material with rockfill located at the toe of the dam. A year later, Consultant B engineered another dam raise to an elevation of 3,443.8 masl (i.e., 2 m higher) using the centerline method, incorporating a gabion wall covered by a geomembrane.
- Since 2014, Anddes has been the designer of the tailings dam. Its first challenge was to develop the engineering up to 3,446 masl, in three phases: the first entailed construction of a reinforced soil wall on the crest, the second and third phases were the sequential construction of a structural fill buttress along the toe of the dam. In addition, Anddes wished to place a filter material between the downstream slope and the proposed buttress.
- In 2015, Anddes carried out the update of the tailings dam design for the raise up to 3,449 masl. This was supported by a robust geotechnical site investigation program that included field and laboratory tests. The results of the analyses and subsequent geotechnical design considered constructing buttresses additional to those recommended and built in previous stages along the toe and abutments of the tailings dam. Also that year, an integrated hydraulic and hydrologic test was carried out that included a water balance. Finally, between 2017 and 2018, Anddes designed engineering for the raise of the dam up to 3,452 and 3,455 masl, which included the construction of additional or superimposed buttresses.

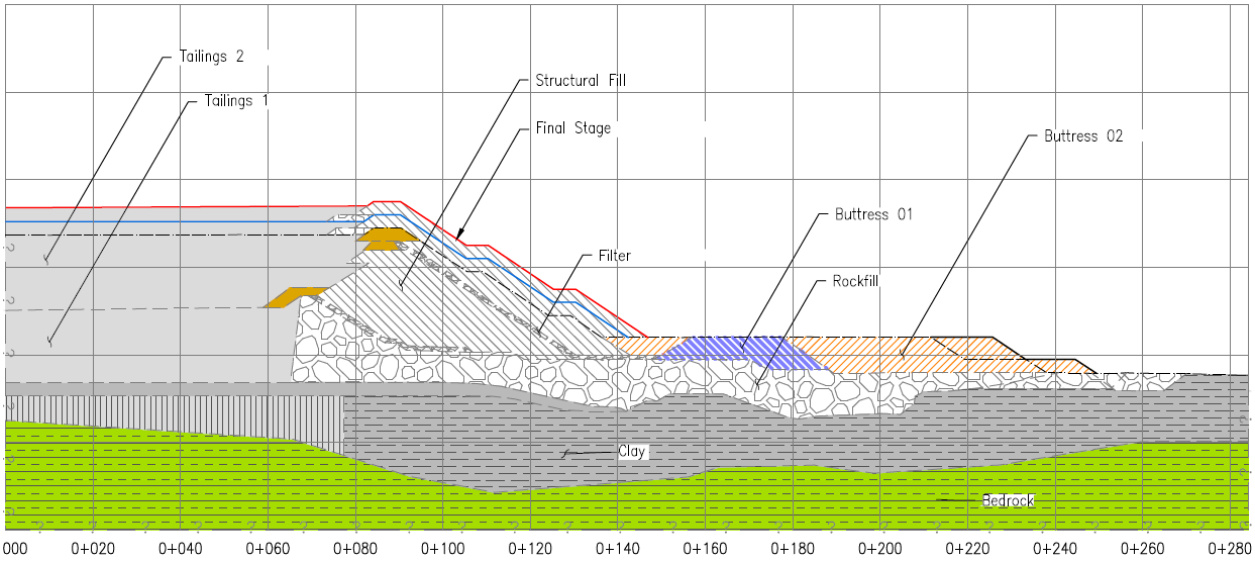

Figure 1: Typical cross section

Dam safety review

The owner of TSF N4 commissioned an independent consulting company (ICC) to perform a dam safety review (DSR). The ICC made several recommendations to bring the tailings storage facility into alignment with CDA dam safety guidelines. Included in the recommendations were that the designers should perform a dam break analysis, review the previous stability analyses, and evaluate a deep foundation failure of the underlying clay.

Following the recommendations, the Owner commissioned a new designer to perform both studies, and invited the ICC to make a site visit to the mine. ICC visited the site 6 months after the DSR was completed.

Dam break analysis and dam failure consequence classification

The analysis was carried out evaluating a potential breach and the resulting inundation area using Flo-2D software and the rheological properties of tailings. Empirical relationships were used to estimate the size and type of potential breach under several scenarios, and the results for affected areas based upon a dam failure at the current and final dam elevation. Both scenarios assumed that the embankment would fail under an extreme storm event (rainy day scenario, according to CDA), a percentage of the tailings would be mobilized, and the resulting solids content of the released slurry varied from 50% to 60% by weight. Figure 2 shows the highest risk area below the dam at the current case time scenario (current dam elevation and 50% solids content), and Figure 3 shows the highest risk area below the dam in the worst scenario (final dam elevation and 60% solid content). This worst case scenario considered a concrete wall approximately 1,500 m downstream of the TSF.

Figure 2: Highest risk area below the dam – 60% solids content

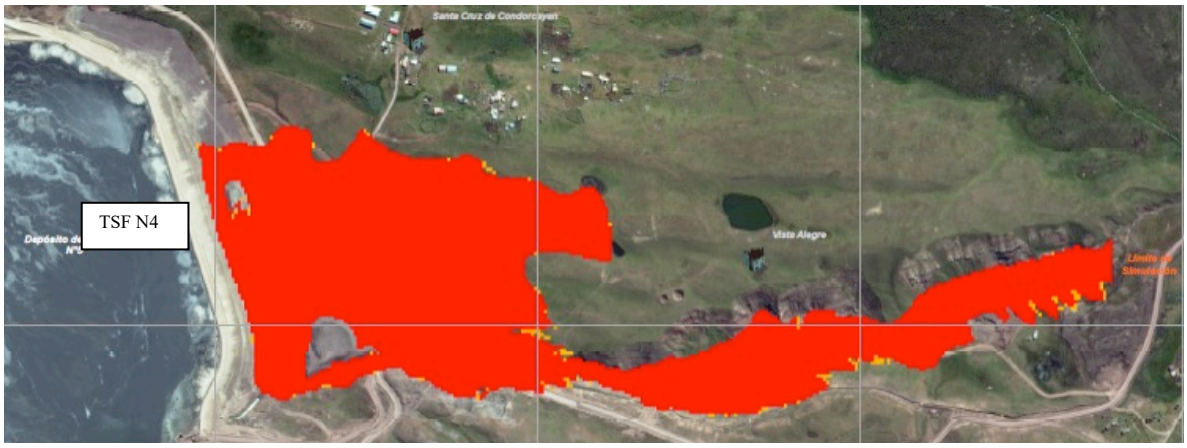

Figure 3: Highest risk area below the dam – 50% solids content

Based on the potential inundation map and considering the associated risks, TSF N4 would be classified as either as a low or significant consequence (CDA, 2014). The likelihood of any loss of life is virtually zero (all structures are far from the risk area), and the environmental impacts would be limited to the natural lagoon immediately downstream of the dam. Economic impacts would be limited to the mine owner.

The updated CDA mining dam guidelines for a significant consequence dam classification require that the facility safely handle a design flood and earthquake for a return period of between 100 and 1,000 years (CDA, 2014).

In addition to the CDA requirements for a significant consequence dam classification, an emergency response plan must be developed for the whole TSF.

Table 1: Target levels for flood hazards, standards based assessments, for construction, operation, and transition phases (CDA, 2014)

Dam classification	Annual exceedance probability – floods
Low	1/100
Significant	**Between 1/100 and 1/1,000**
High	1/3 Between 1/1,000 and PMF
Very High	2/3 Between 1/1,000 and PMF
Extreme	PMF

Table 2: Target levels for earthquake hazards, standards based assessments, for construction, operation, and transition phases (CDA, 2014)

Dam classification	Annual exceedance probability – earthquakes
Low	1/100 AEP
Significant	**Between 1/100 and 1/1,000**
High	1/2,475
Very High	1/2 Between 1/2,475 and 1/10,000 or MCE
Extreme	1/10,000 or MCE

Design criteria

According to the CDA (2014) the consequence dam classification is significant for an annual exceedance probability between 1/100 and 1/100 for earthquake and flood. The seismic study concluded that an operational basis earthquake (OBE) with a return period of 475 years would produce a maximum ground acceleration of 0.272g. The maximum considered earthquake (MCE) (2,475 years return period) would produce a maximum ground acceleration of 0.457g. Both of these were estimated via a probabilistic seismic hazard methodology. The MCE peak ground acceleration (PGA) was estimated using the IBC (International Building Code) and ICOLD (International Commission on Large Dams) methodologies as 0.416 and 0.558g, respectively. The re-evaluated stability analyses were completed using the OBE PGA, reduced by the method developed by Bray and Travasarou (2009), to 0.11g. In general, the procedures used to develop seismic parameters are reasonable, and are consistent with standard practices.

Geotechnical site investigation program and geotechnical parameters

The tailings storage facility was characterized by means of a comprehensive and extensive quantity of geotechnical site investigations. They were carried out in 40 test pits, 10 geotechnical boreholes, and 11 seismic piezocone tests with pore pressure measurement (SCPTu) during different geotechnical site campaigns.

Both drained and undrained behaviours were taken into account by means of a series of consolidated drained, unconsolidated drained compression triaxial tests and consolidation tests of undisturbed and

remolded specimens of the involved materials. For a better characterization, a geophysical survey program was carried out including the dam, tailings impoundment, and foundation. From these valuable geotechnical investigations, the materials involved in the analyses were appropriately characterized.

Table 3 shows the geotechnical properties of the materials.

Table 3: Geotechnical properties of the materials used in the stability analyses

Material	Total unit weight (kN/m³)	Saturated unit weight (kN/m³)	Effective stress parameters		Total stress parameters	
			c' (kPa)	ϕ' (°)	c (kPa)	ϕ (°)
Rockfill	20	21	0	37	–	–
Mine waste	20	21	0	36	–	–
Structural fill	20	21	0	37	–	–
Filter	20	21	0	36	–	–
Buttress mine waste	20	21	0	37	–	–
Tailings 1	21	22.5	0	27	5	20
Tailings 2	18	20	0	24	20	–
Clay	17.5	18	20	20	0.2*σ'_n	–
Silt	18	20	0	16	–	–
Rock	22	24	150	30	–	–

Geotechnical historical analyses

The geotechnical model used in the majority of stability analyses by the different consultants included the outcrop rock and clayey and silty foundation materials underlying the rockfill and dike, an ancient tailings stratum below the dam, a drainage material between the existing rockfill and dike, a stability berm (buttress), and the tailings impoundment. Figure 1 presents the configuration of the critical section.

The tailings dam was originally designed at the end of the nineties by Consultant A. The dam was primarily made from mine waste, with an elevation of 3,435.60 masl. However, the stability analyses of the structure were not provided by the owner.

In 2003, Consultant B took over the design of the dam, and in 2004, 2D slope stability analyses of the dam raises were carried out in two stages: the first stage considered a raise from 3,435.6 to 3,437.6 masl, and the second stage, from 3,437.6 masl to 3,440.6 masl. The raises were proposed with the downstream method, using mine waste and including a stability berm along the toe of the dam.

The factor of safety (FS) obtained for the first stage in the short-term static condition, was equal to 1.27. The design used a clayey foundation in an undrained condition; however, no consolidation analysis was performed to estimate the time at which the clayey foundation would be in an undrained condition.

The raise also took into account a considerable displacement of the new dam crest relative to the previous one, where the toe upstream of the raise would rest on the upper part of the existing slope, in order to guarantee the construction on a suitable support. The second stage was similar, with a FS of 1.89, 1.12 and 1.16, under long-term static, pseudo-static, and post-earthquake conditions, respectively. The design did not consider the short-term stability design of the dam for this second stage.

The pseudo-static design was performed using a seismic coefficient equal to 0.13 obtained over a return period of 150 years, bearing in mind the seismic hazard assessment study by Castillo and Alva (1993) with a PGA of 0.26g for Class B soil. The seismic coefficient was calculated considering 50% of the PGA.

Between 2007 and 2008, Consultant B designed a raise from 3,440.60 to 3,441.60 masl using the centerline method. In 2011, the raise dam engineering was carried out using the centerline method from 3,441.60 to 3,455.00 masl. The design included the replacement of inadequate foundation material (soft clays) located in the toe of the dam. The results of the slope stability analyses yielded safety factors under long-term static and pseudo-static conditions equal to 1.68 and 1.09, respectively. Again, the design did not consider the short-term static analysis associated with the undrained condition of the clayey foundation.

For design purposes, the seismic hazard assessment study was updated in 2009, resulting in PGA values of 0.25g in Class B soil and 0.37g in Class C for a 475-years return period. Also, a seismic coefficient of 0.13 was set, similar to the one used in the 2004 design. The seismic coefficient was obtained considering 50% of the PGA.

In 2012, consultant B designed the last raise of the dam to 3,443.80 masl using the centerline method.

In 2014, a dam safety review (DSR) was carried out, mainly making observations about the parameters of the clayey foundation, determining that the tailings dam did not present suitable static stability conditions, and ignoring the undrained condition; therefore, further research was recommended for the TSF foundation. Safety factors obtained during the DSR in the short-term static condition presented FS equal to 1.2, less than the FS required.

In 2015, Anddes carried out an update of the geotechnical parameters according to the DSR recommendations. The geotechnical site investigations determined that the clayey foundation behaves undrained during static conditions when subjected to rapid loading, and subsequent designs viewed this condition as critical. The design of the raise of the dam was verified from 3,444.80 to 3,446.00 masl, in three construction phases. The first one consisted of the construction of a reinforced soil wall at the crest, while the second and third ones consisted of the sequential construction of a structural fill buttress along the entire toe of the dam. For the design, consolidation analyses were carried out to estimate the time it would take for the clay to reach 90% of consolidation and, consequently, determine the time at which it will present undrained resistance. From this, the construction sequence of three stages indicated above was carried out in order to guarantee the stability of the structure, particularly for short-term stability control.

The results of the FS obtained under short-term static, long-term static, pseudo-static, and post-earthquake conditions were 1.41, 1.53, 1.00, and 1.34 for each condition of Phase 3, respectively.

The seismic hazard assessment study was updated in 2015 by Anddes with a PGA value of 0.27g in rock (type B) and a 475-years return period. Also, a seismic coefficient of 0.11 was determined by the method of Bray and Travasarou (2009), associated with an allowable displacement of 100 cm.

By the end of 2015, Anddes had carried out the design of the dam raise from 3,446 to 3,449 masl. The design was carried out in a sequence of two stages, using additional buttresses to those raised to 3,446 masl to guarantee short-term stability due to the undrained resistance of the clayey foundation. The FS obtained on the short-term static, long-term static, and pseudo-static were 1.38, 1.51 and 1.04, respectively.

In 2018, Anddes carried out the subsequent design for the raises to 3,452 and 3,455 masl, using the previous criteria for the short-term static design, which was the critical factor for the structure, according to the DSR. Currently, the dam crest is located at 3,449 masl, with future expected raises to 3,452 masl by 2022, and 3,455 masl by 2025.

Table 4 presents the FS obtained in the dam by the different consultants for each one of its raises. Figures 4, 5, 6, and 7 present the FS under short-term static, long-term static, pseudo-static, and post-earthquake conditions, respectively.

Table 4: Summary of factor of safety results obtained by the different consultants

Consultant	Date		Dam crest	Factor of safety (FS)			
	From	Until	(masl)	Short-term	Long-term	Pseudo-static	Post-earthquake
Anddes	July 21	July 24	3,455	1.30	1.64	1.00	–
	Oct. 18	July 21	3,452	1.35	1.71	1.04	–
	Oct. 16	Oct. 18	3,449	1.38	1.51	0.98	1.34
	Nov. 15	Oct. 16	3,446	1.41	1.53	1.07	–
Consultant B	July 07	July 10	3,441.60	–	–	–	–
	July 05	Jul-07	3,440.60	–	1.86	1.12	1.16
	July 04	Jul-05	3,437.60	1.27	–	–	–

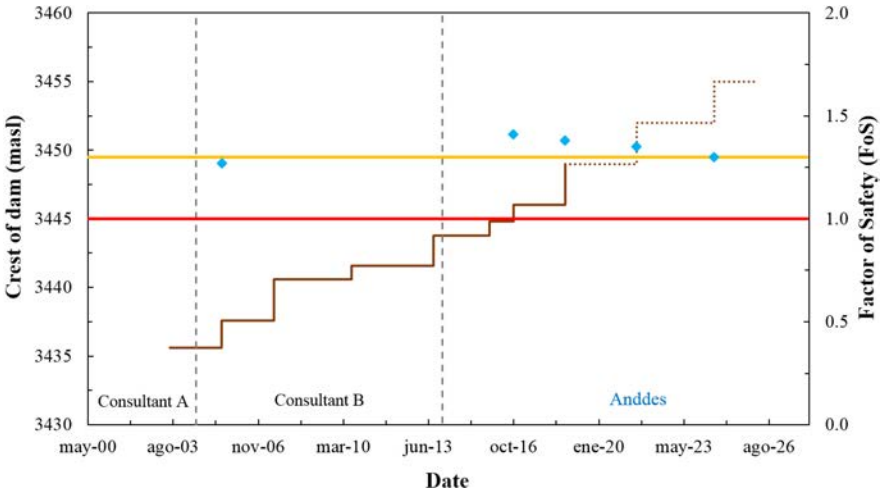

Figure 4: Time history of short-term static factor of safety

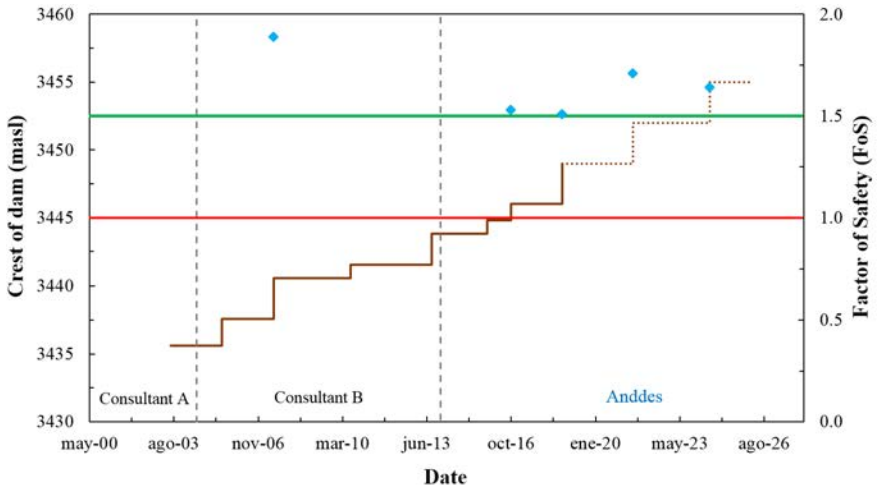

Figure 5: Time history of long-term static factor of safety

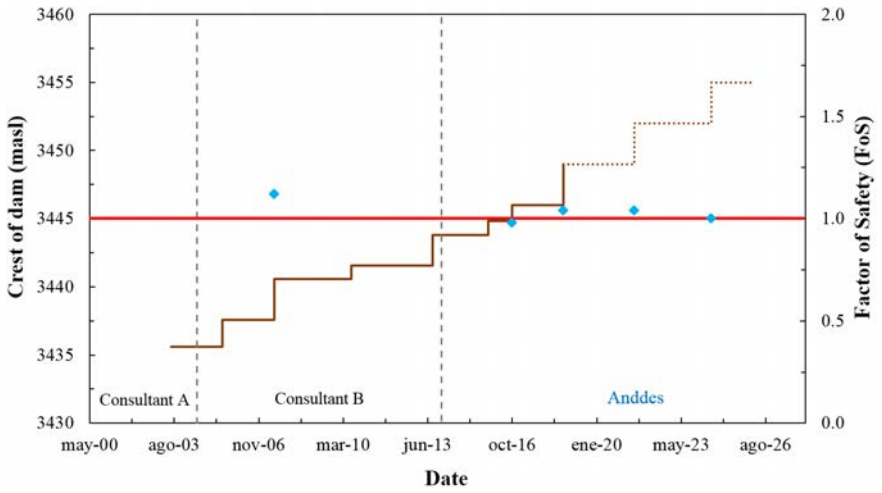

Figure 6: Time history of pseudo-static factor of safety

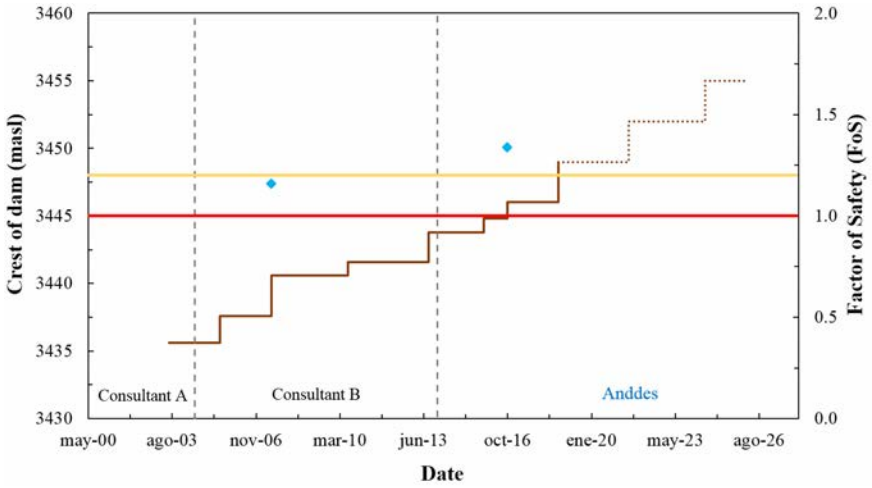

Figure 7: Time history of post-earthquake factor of safety

It is important to consider the role of DSR studies, because they allow the review of aspects of design or construction that consultants did not take into account during the design of a dam, and which could generate new risks in the future. This is the case for this dam, where previous studies reviewed by Anddes did not include the short-term condition for slope stability. The risks involved would have been similar to those in the Mount Polley tailings dam. Although it was not verified, it might be that Consultant B's design in 2011 would have determined a short-term failure, so it is vital to carry out controls in the engineering of high-risk structures such as tailings dams.

A DSR is not the only factor that has an important role in dam safety. The EoR (Engineer of Record) and the Independent Geotechnical Review Board (IGRB) also play an important role, as do management control and operation of the dam according to international standards such as those proposed by the Mining Association of Canada (MAC). The effective participation of each specialist will facilitate adequate control of dam safety.

Finally, the DSR carried out immediately after the failure of the Mount Polley dam identified a foundation failure mechanism in the undrained condition for the short-term stability analysis. In addition, the increase of the undrained resistance of the soil during the consolidation time was taken into account in the design, which allowed a stability analysis to be carried out according to the construction stages, which are presented in the following section.

Design over soft foundation by staged construction

The design should consider the construction stages and the changes in the geotechnical aspects (change of drained and undrained resistance, and generation of pore pressure excess, among others) that occur due to the increase or decrease of loading applied to soft soils. This will guarantee short-term stability, due to the undrained resistance of soft soils. The following criteria should be considered for the geotechnical

evaluation:

- Sufficient quality geotechnical site investigations should be performed to adequately define the geological origin, the foundation surface profile, the soft soil extension or other material, and the variation of water levels.
- Also, geotechnical site investigations should include SCPTu tests, permeability tests, and unaltered samples. SCPTu tests can establish the clay-like or sand-like behaviour type of soils for evaluation of liquefaction potential, the estimation of over-consolidation ratio, and the estimation of normally consolidated areas (critical for stability).
- Uncertainty in the geotechnical characterization can be reduced with an extensive laboratory program that includes the characterization of the resistance of the material with triaxial compression tests (CU, CD, and UU) at an adequate deformation rate (lower than 2%/h for clays) according to the type of soil. Likewise, consolidation and permeability tests can estimate the soil compressibility, the time to dissipate the excess of pore pressures, and the over-consolidation ratio.
- Resonant column and torsional shear tests are important in order to determine the seismic coefficient for slope stability analysis in the pseudo-static condition, and to assess the dynamic response of soft soils.
- Structures founded on soft soils usually have short-term static stability issues due to the soil's undrained behaviour, resulting in the need to incorporate stability buttresses at the toe of the dam or to construct gravel columns in the foundation.
- The design of the stability buttresses should take into consideration the foundation undrained resistance, as well as estimate the consolidation time previous to the construction of the next stage.
- After the construction of the buttress, a partial or total stage of the dam could be raised, depending on the results of FS in the short-term static condition. It is necessary to consider that a subsequent raise will activate an undrained zone on the foundation of the dam. Also, at the commencement of this construction stage, the previous undrained area under the buttress will have a drained behaviour.
- Subsequent stages of raises should guarantee the drained behaviour of the foundation. For this reason, the consolidation time of the previous stage should be estimated. A new raise will usually be subject to the aforementioned: designed with buttresses along the toe of the dam.
- On the other hand, computational programs should be used to estimate the undrained resistance of the soil and also the FS in the short-term static condition, without considering the loading introduced in the stage. A user-friendly limit equilibrium software has been used by Anddes, since it allows the user to deactivate loadings that increase soil resistance; however, this increase would occur after the consolidation of the material.

Conclusions

The following conclusions can be inferred from all of the above mentioned:

The foundation failure mechanism is an important factor to consider, according to previous case histories of failure such as Los Frailes, Mount Polley, and Xe-Pian Xe-Namnoy, which were among other tailings storage facilities whose designs did not foresee issues related to the underlying foundation. This aspect should be addressed ,whether detected during the design phase, or during the operational phase.

The presence of weak layers in the foundation could lead to an undrained condition failure; therefore, it is vital to determine their existence and main geotechnical characteristics, given that their behaviour needs to be evaluated carefully, taking into consideration their complexities and critical conditions.

For the case study presented in this paper, prior to the development of the dam safety review the short-term slope stability condition was not adequately taken into account. But after this review it was appropriately considered, which led to taking countermeasures such as the construction of the stabilization berm that improved the stability conditions and ensured the physical integrity of the tailings storage facility.

It is also suggested that the dam safety review, EoR, and audits, should be done by companies or professionals who have great and verified experienced in these matters.

The design carried out for the short-term static condition considered the limit equilibrium method analysis and the estimation of times by means of one-dimensional consolidation. It is recommended to perform a numerical modeling using the finite element method, which permits the user to determine the consolidation times, the associated pore pressure dissipations, and the undrained resistance of the clayey foundation, to obtain factors of safety and compare them with the results presented in the current research.

Acknowledgements

The authors would like to thank Anddes professionals for their continuous support, guidance and collaboration in this research.

References

Alonso, E.E. and A. Gens. 2006. Aznalcóllar dam failure. Part 1: Field observations and material properties. *Geotechnique* 56(3): 165–183.

Boswell, J. and J. Sobkowicz. 2018. Leading versus lagging indicators of tailings dam integrity. In *Proceedings of the Tailings and Mine Waste Conference*, Colorado, USA, September 30 – October 2: 51–62.

Bray J. and T. Travasarou. 2009. Pseudostatic coefficient for use in simplified seismic slope stability evaluation. *ASCE; Journal of Geotechnical and Geoenvironmental Engineering* 135(9).

Canadian Dam Association (CDA). 2014. Application of dam safety guidelines to mining dams.

Castillo, J. and J. Alva. 1993. *Peligro Sísmico en el Perú. VII Congreso Nacional de Mecánica de Suelo e Ingeniería de Cimentaciones. Lima, Diciembre*.

Lupo, J.F. 2005. Heap leach facility liner design. In *Proceedings of the North American Geosynthetics Society (NAGS) GRI19 Conference,* Las Vegas.

Mantilla, H. and J. Negrón. 2016. Total and differential settlement of a heap leach pad founded on an existing mine waste dump. In *Proceedings of Heap Leach Mining Solutions,* Lima, Peru, October 18–20.

Morgenstern, N.R., S. Vick and D. van Zyl. 2015. Report on Mount Polley tailings storage facility breach, Independent Expert Engineering Investigation and Review Panel, Province of British Columbia. Available at https://www.mountpolleyreviewpanel.ca/sites/default/files/report/ReportonMountPolleyTailingsStorageFacilityBreach.pdf

Reyes A., M. Valdivia, E. Tapia and L. Salas. 2015. 1-D Seismic response analysis for seismic permanent displacements estimation on a heap leach pad. In *Proceedings of Heap Leach Solutions,* Reno, Nevada, USA, September 14–16.

Schleiss A., J. Torunier and A. Chraibi. 2019. Failure of saddle dam D final report, Independent Expert Panel (IEP).

WISE Uranium Project. 2018. Chronology of major tailings dam failures. Last updated 2 Oct 2019. Retrieved from http://www.wise-uranium.org/mdaf.html

Proceedings of Tailings and Mine Waste 2019
November 17–20, 2019, Vancouver, Canada
Published by the University of British Columbia, 2019

Probabilistic Assessment of the Seismic Pseudostatic Coefficient in Mining Projects

Jorge Macedo, Georgia Institute of Technology, USA
Gabriel Candia, University of Desarrollo, Chile

Abstract

Pseudostatic slope stability procedures, wherein a horizontal seismic coefficient is applied to a potential sliding mass in a conventional slope limit equilibrium analysis, are often employed in mining projects to evaluate the seismic performance of geotechnical infrastructure. However, they are limited unless the parameters used in the analysis accurately reflect the potential seismic demand and its impact on the seismic performance of the geotechnical system being designed.

This paper proposes a performance-based probabilistic procedure to estimate the pseudostatic coefficient in a rational and transparent manner. The proposed procedure estimates a pseudostatic coefficient, which is consistent with the maximum allowable level of seismic-induced displacements that the geotechnical structure can sustain, the properties of the sliding mass, and the seismic demand at the site of the project. In addition, the calculated pseudostatic coefficient can be directly associated with a return period or hazard design level. The proposed procedure is applicable for a wide range of geotechnical systems in mining projects shaken by shallow crustal earthquakes along active margins, as well as for subduction zone earthquakes. An illustrative example for the application of the procedure for the stability evaluation of a tailings dam, in the context of a mining project, is shared.

Introduction

The assessment of the seismic stability of geotechnical systems in mining projects is typically performed by: (a) traditional pseudostatic slope stability analyses; (b) Newmark-based slope displacement analyses; and (c) advanced finite elements or finite differences numerical analyses. Although robust numerical analyses, i.e., method (c), are increasingly used in the industry, methods (a) and (b) are preferred in engineering practice in the seismic design of geotechnical systems in the context of mining projects, at least in the preliminary design stages.

Pseudostatic slope stability procedures, wherein a horizontal seismic coefficient is applied to a potential sliding mass in a conventional slope limit equilibrium analysis, are often employed in mining

projects to evaluate the seismic performance of geotechnical structures such as tailings dams, heap leach pads, stockpiles, etc. Pseudostatic slope stability procedures can be employed in a straightforward manner, and thus, their use in engineering practice is appealing. They have the benefit of accumulated experience, reduced cost, and user-friendliness, since they merely require the estimation of a Factor of Safety (FS) against seismic "failure" (Papadimitriou et al., 2014). However, they are limited unless the parameters used in the analysis accurately reflect the potential seismic demand and its impact on the seismic performance of the geotechnical system being designed. As discussed in Bray and Travasarou (2009), and Macedo et al. (2018), the seismic coefficient that is employed in a pseudostatic slope stability analysis should be selected in a rational manner if this procedure is to form a sound basis for a seismic slope stability assessment. The selection of the seismic coefficient employed in the analysis is often based on precedence, regulatory design guidance, engineering judgment, and comfort level of the designer, without due consideration of the seismic displacement that constitutes satisfactory performance for each particular project, and without incorporating the vastly different seismic exposure for sites around the world.

Recent studies relate the selection of the seismic coefficient to be used in pseudostatic slope stability analysis to the allowable displacement that an earth/waste system can sustain during an earthquake (e.g., Bray and Travasarou, 2009; Papadimitriou et al., 2014). Although these efforts provide a rational basis for selecting the seismic coefficient based on the allowable level of displacement, they are not formulated in a rigorous probabilistic framework (e.g., they do not consider the entire seismic hazard curve in the selection of the seismic coefficient), and they are not hazard consistent.

This paper proposes a performance-based probabilistic procedure to estimate the pseudostatic coefficient in a rational and transparent manner, which can incorporate the hazard level (i.e., return period) directly in the estimation of the pseudostatic coefficient in the context of a mining project.

Pseudostatic slope stability analysis

As described in Bray and Travasarou (2009), in a pseudostatic slope stability analysis, a FS is computed using a static limit equilibrium method in which a horizontal earthquake-induced inertial force is applied to the potential sliding mass. This pseudostatic force represents the destabilizing effects of the earthquake shaking and is expressed as the product of a seismic coefficient (k) and the weight (W) of the potential sliding mass (see Figure 1). The pseudostatic analysis also requires the use of appropriate material dynamic strengths (S). If the calculated FS is above a specified minimum value, the earth structure or natural slope is considered to be safe. The limit equilibrium method should satisfy all three conditions of equilibrium to ensure that a reliable FS is calculated (Duncan and Wright, 2005).

The design seismic coefficient and acceptable minimum FS are often selected based on precedence. Several combinations of seismic coefficient and FS are listed in Table 1. Seismic coefficient values often

range from 0.1 to 0.2 with factors of safety from 1.0 to 1.5. The basis for these combinations of values is not always clear, and usually are based on satisfactory performance observed in similar projects.

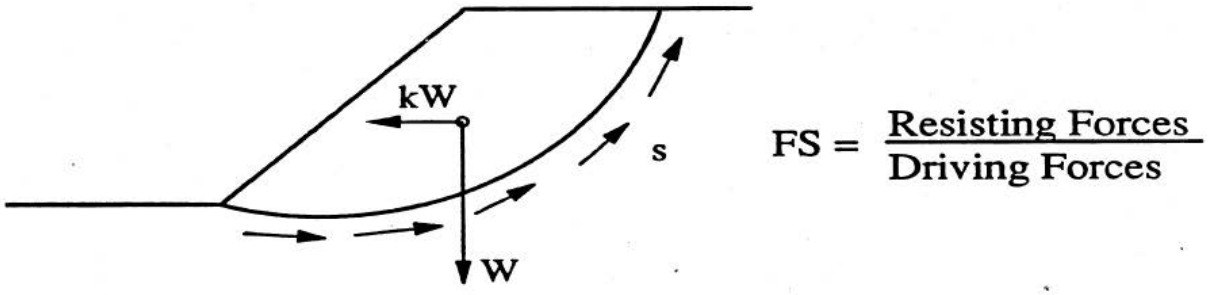

Figure 1: Schematic representation of a pseudostatic slope stability analysis. FS is the safety factor

Table 1: Seismic coefficients used previously
(e.g., Seed and Martin, 1966; Seed et al., 1978; Seed, 1979; Seed, 1981)

Dam	Country	Seismic coefficient	Factor of safety
Aviemore	New Zealand	0.10	1.50
Bersemisnoi	Canada	0.10	1.25
Digma	Chile	0.10	1.15
Globocica	Yugoslavia	0.10	1.00
Karamauri	Turkey	0.10	1.20
Kisenyama	Japan	0.12	1.15
Mica	Canada	0.10	1.25
Netzahualcovote	Mexico	0.15	1.36
Oroville	USA	0.10	1.20
Paloma	Chile	0.12 and 0.20	1.25 and 1.10
Ramganga	India	0.12	1.20
Tercan	Turkey	0.15	1.20
Yeso	Chile	0.12	1.50

Critical design issue

Before further discussing the performance-based pseudostatic slope displacement procedure, it is imperative that a key design issue be addressed. In the evaluation of the seismic performance of a geotechnical system or natural slope, the engineer should first assess if there are materials in the geotechnical system or its foundation that can lose significant strength as a result of cyclic loading (e.g., soil liquefaction). If this is the case, this should be the primary focus of the evaluation, because large displacement flow slides are possible. There is abundant research on this topic, and it is not the focus of this study. This study addresses the seismic performance of geotechnical systems wherein flow slides are not likely (i.e., the post-liquefaction slope stability FS is greater than one).

Probabilistic evaluation of the pseudostatic coefficient

In this section we discuss the proposed framework for the probabilistic estimation of the pseudostatic coefficient. The proposed framework is based on the concept of a displacement hazard curve (DHC), which provides the annual rate of exceedance for different levels of seismically-induce slope displacements. DHCs are typically estimated using Newmark-based models for the evaluation of seismically induced displacements (D).

Estimation of seismic-induced displacement hazard curves

The estimation of a displacement hazard curve needs the formulation of robust probabilistic procedures for the estimation of D. These procedures are typically based on seismic sliding block displacement analysis, and can be broadly categorized as:

1. Procedures to estimate D considering rigid sliding blocks, neglecting the dynamic response of the sliding mass (e.g., Saygili and Rathje, 2008; Jibson, 2007; Watson-Lamprey and Abrahamson, 2006).
2. Procedures to estimate D considering a decoupled approximation for the dynamic response of the slope. This approximation assumes no relative displacements during the seismic response analysis, whose results are then used to calculate the seismically induced permanent displacement (e.g., Rathje and Antonakos, 2011).
3. Procedures to estimate D based on fully coupled stick-slip sliding blocks, which capture the simultaneous occurrence of the nonlinear dynamic response of the potential sliding mass and the effects of periodic sliding episodes (e.g., Bray and Travasarou, 2007; Bray et al., 2018; Bray and Macedo, 2019).

The rigid sliding block analyses should not be used except in those few cases wherein the potential sliding mass is shallow and stiff, or for regional screening assessments when there is insufficient information to characterize the actual fundamental period of the potential sliding mass. Regarding the procedures 2) and 3) above, due to the inherent limitations of the decoupled approximation, fully coupled stick-slip sliding block analyses are preferred (Rathje and Bray, 1999; Rathje and Bray, 2000). Alternatively, the procedures to estimate D can be also categorized by its applicability to different tectonic settings. Most procedures have been developed for tectonic settings consistent with shallow crustal seismicity (e.g., California). Whereas, we are aware of only one robust procedure developed by Bray et al. (2018) for subduction settings.

Using a seismic displacement model, and the intensity measure (*IM*) hazard information a DHC can be estimated. For example, for the case of D models that use one IM (e.g., as in the Bray and Travasarou, 2007; Bray et al., 2018; and Bray and Macedo, 2019 models), a DHC can be estimated from Equation 1 (Macedo et al., 2018):

$$\lambda_d = \sum_{i=1}^{nky} \sum_{j=1}^{nts} \int_0^{\infty} P\,(D > d|IM, k_{yi}, T_{sj}) \Delta\lambda(IM) d(IM) w_{ij} \quad (1)$$

where IM is the intensity measure considered in the D model, k_y and T_s are properties of the slope system, defined as the yield coefficient and the period of the sliding mass respectively (for a detailed explanation of these properties refer to Macedo et al., 2018). The term $P\left(D > d\middle|IM, k_{yi}, T_{sj}\right)$ in equation 1 is the conditional probability the displacement "*d*" level is exceeded given *IM,* k_{yi} and T_{sj}, and $\Delta\lambda(IM)$ is the annual probability of occurrence of *IM*. The uncertainties of k_y and T_s are treated as epistemic in a logic tree scheme, in which *nky* values for k_y are defined with weighting factors wky_i (*i*=1: *nky*) and *nts* values for T_s are defined with weighting factors wts_j (*j*=1: *nts*). The weighting factor for each combination of k_y and T_s is defined as w_{ij}. k_y and T_s may be considered to be represented by an adequate distribution to assign their alternative values and weighting factors.

Figure 2 shows an example of displacement hazard curves estimated by Macedo et al. (2018) for a project site with contribution from different tectonic settings (i.e., subduction interface, subduction intraslab, and shallow crustal). Such scenario is typically found in mining projects in South America (e.g., Peru and Chile).

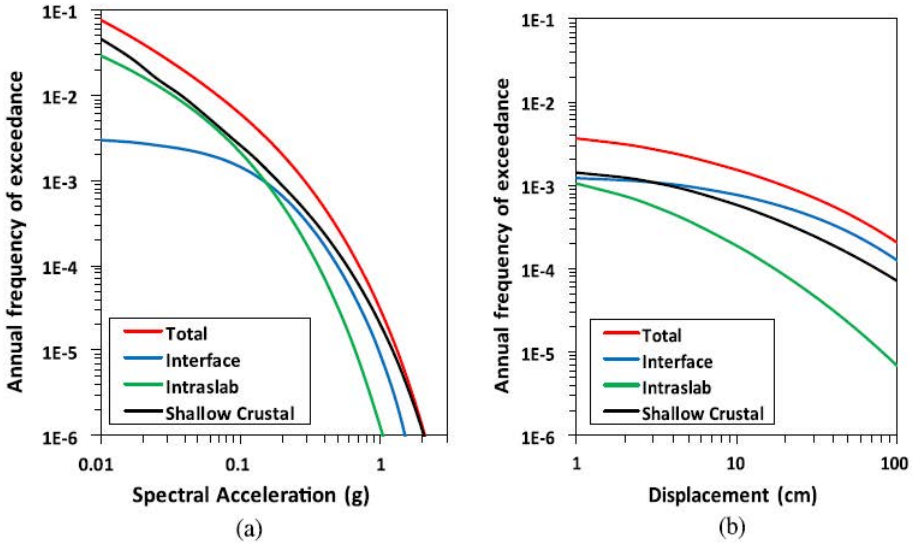

Figure 2: Illustration of DHC estimated in an area with contribution from different tectonic settings: a) IM hazard curves; b) D hazard curves. Notice how a traditional PSHA shows that the shallow crustal seismic sources contribute more to the hazard, whereas the D hazard curves show that the interface actually contributes more to the hazard

Results from a typical probabilistic hazard assessment (PSHA), show that the seismic sources that contribute the most to the hazard are shallow crustal seismic sources – Figure 2(a). However, a DHC – Figure 2(b) – shows that the interface seismic sources actually contribute the most to the displacement hazard. Engineers design for engineering demand parameters such as D not for intensity measures such as a spectral acceleration. Thus it will be misleading to base the seismic design on only PSHA results. In this particular example a DHC is better suited for making decisions. Thus a connection between a DHC and the selected pseudostatic coefficient is desired. Indeed, in this study the concept of a DHC is the cornerstone of the proposed procedure for the probabilistic estimation of a pseudostatic coefficient as explained in the following.

Proposed procedure

The proposed procedure for the estimation of a performance-based, hazard-consistent pseudostatic coefficient can be divided in seven steps:

1. In consultation with the client and regulators define the allowable level of seismic slope displacement of the geotechnical system to achieve the desired performance level.
2. Select an appropriate hazard design level (i.e., a return period) for the allowable seismic slope displacement. Several values may be selected, each with their respective hazard design level.
3. Develop a logic tree for the ground motion models used in the PSHA evaluation and another logic tree for alternative D models.

4. Develop a best estimate of the fundamental period of the sliding mass (T_s), and develop a logic tree for alternative values of T_s. The logic tree and its weights can be developed by considering an underlain distribution for T_s, which is typically a lognormal distribution (Macedo et al., 2018).
5. Assume an initial mean value of the system's yield coefficient (k_y). The uncertainty of k_y could also be modeled using an appropriate coefficient of variation value for this variable to build a logic tree with alternative values and weights.
6. Calculate an initial DHC following the procedures described in the "Estimation of seismic-induced displacement hazard curves" section.
7. Iterate using different values of k_y to recalculate D hazard curves until this curve passes through the intersection of the horizontal line that goes through the selected return period in Step 2 and the vertical line that goes through the tolerable level of seismic displacement defined in Step 1. The procedure has to be repeated for each of the branches that result from the combination of the IM and D logic trees. The corresponding k_y values are realizations of the pseudostatic seismic coefficient (k) compatible with the tolerable level of seismic slope displacement and the specified return period.

An illustrative scheme of the proposed procedure is shown in Figure 3. The proposed procedure has been implemented in a MATLAB graphical user interface (GUI). The GUI also offers embedded PSHA capabilities, a suite of D models, and an automated generation of logic trees. All these features make straightforward the implementation of the proposed procedure in the seismic design/evaluation of geotechnical infrastructure in mining projects.

Illustrative example

This example uses the proposed procedure in the seismic evaluation of a tailings dam, which is a geotechnical structure often used in mining projects to deposit the waste residuals after the mineral processing. Figure 4 shows the geometry considered for the dam, which is similar to the geometry considered by Bray and Travasarou (2007) and Macedo et al. (2018) when showing examples for the application of D models.

The best estimates for Ts and k_y are reported as 0.33 s and 0.14 respectively. Ts is estimated from measured shear wave velocities, which have a best estimate of 400 m/s. k_y is estimated from a pseudostatic slope stability analyses performed with the total stress strength properties of C=14 kPa and ϕ= 21° based on triaxial compression tests. Additionally, covariance values of 0.25 and 0.15 are considered for Ts and k_y respectively, which are in the medium range of the ranges provided by Macedo et al. (2018). These coefficients of variation values are used to build logic trees for alternative values in k_y and T_s.

The tailings dam is hypothetically placed in the Peruvian Andes, where most mining projects are actually located, at coordinates: S11.92°W76°. Thus, the tailings dam will be potentially affected by seismic sources in the subduction interface, subduction intraslab and shallow crustal tectonic settings.

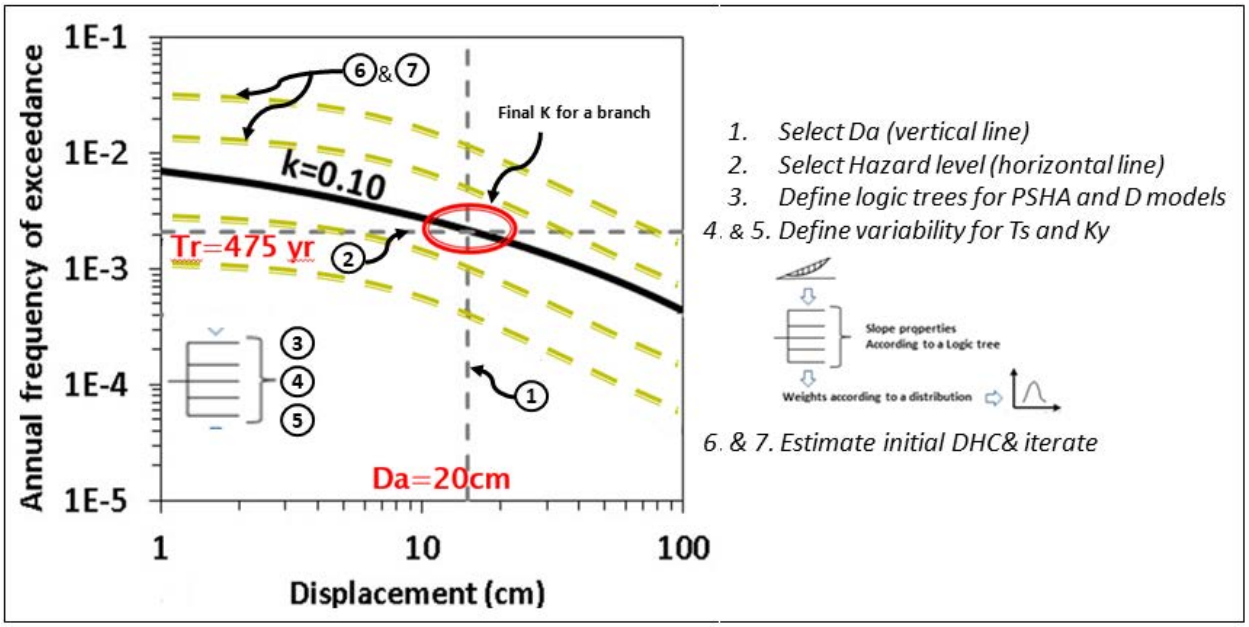

Figure 3: Schematic description of the proposed procedure. Da is the allowable level of displacements (20 cm in the illustration), the hazard level is indicated by the horizontal line (with a return period of 475 years), k is the estimated pseudostatic coefficient after iterations

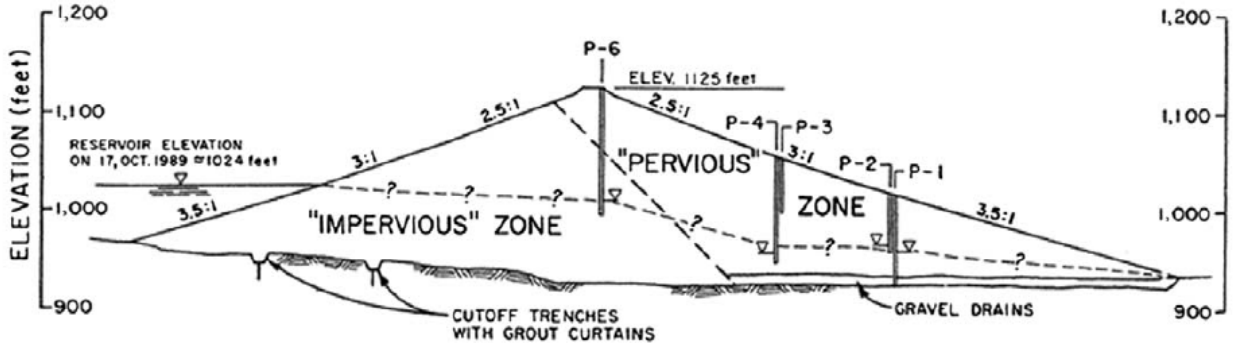

Figure 4: Cross section of the hypothetical tailings dam used in illustrative example (adapted from Bray and Travasarou, 2007 and Macedo et al., 2018)

Figure 5(a) shows the seismic sources for Peru provided by Sencico (2016), the official agency for seismic hazard assessment, along with the location of the evaluation point. The geometry of seismic sources and seismicity parameters for Peru are available in the implemented GUI. Figure 5(b) shows the Sa(T=0.5s) hazard curve (i.e., the spectral acceleration at the degraded period of the system as required in the Bray et al., 2018, and Bray and Macedo, 2019 slope displacement models). Notice from Figure 5(b) the contribution

of different source mechanism to the total hazard, which is dominated in this case by intermediate depth 'intraslab' events.

We define a logic tree with five alternative seismic hazard models; each branch corresponds to a different combination of GMM. We adopted the logic tree defined by Sencico (2016) for Peru, which considers five GMMs for subduction sources, and one GMM for shallow crustal sources; all branches have equal weights in the logic tree structure. For the slope system parameters, we consider five k_y values and five T_s values, sampled independently from their corresponding PDFs. Finally, we define two sets of alternative displacement models, with equal weights of 0.5: the first set uses the Bray et al. (2018) D model for subduction earthquakes and the Bray and Travasarou (2007) D model for shallow crustal earthquakes, while the second set uses the Bray et al. (2018) D model for subduction earthquakes and Rathje and Antonakos (2011) D model for shallow crustal earthquakes. Notice that the Bray et al. (2018) D model is, to date, the only existing model developed for subduction sources. In summary, the resulting logic tree, shown in Figure 6, has 250 branches that combine five GMM models, 25 sets of slope parameters, and two slope displacement models.

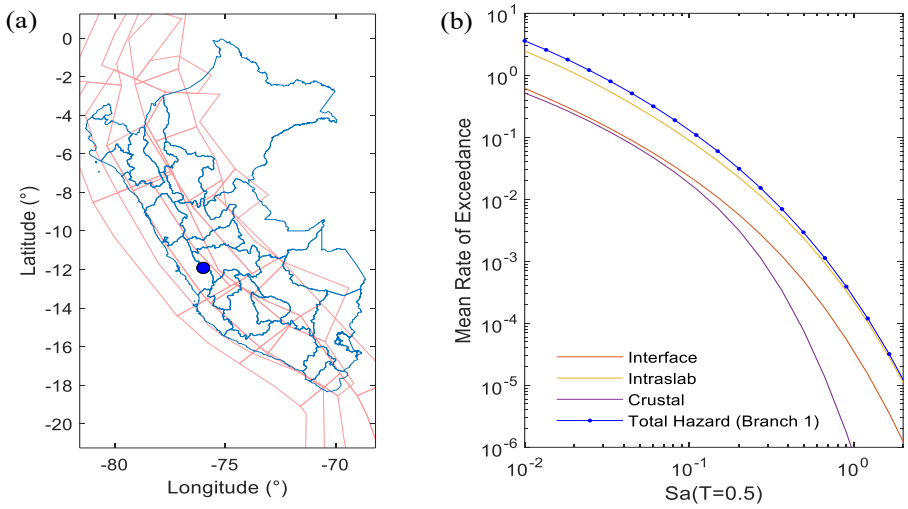

Figure 5: (a) SENCICO's (2016) seismic source model and site location; and (b) spectral acceleration hazard curves at the degraded period of 0.5 s based on one branch of the logic tree

Using the inputs defined above, we perform the probabilistic evaluation of the pseudostatic coefficient. First we will consider a tolerable seismically-induced displacement (Dt) of 15 cm, and a return period of 475 years, which is typically required by the local regulators in Peru (Ministerio de energia y minas, 1997). In addition, we will consider a return period of 2475 years. Then we proceed with the evaluation of DHCs (i.e., Equation 1), assuming an initial value for k_y, and performing iterations until the resulting curve passes through the intersection of the horizontal line that defines the return period and the vertical line that defines

Dt. The final k_y value is the pseudostatic coefficient, which is consistent with Dt and the selected return period.

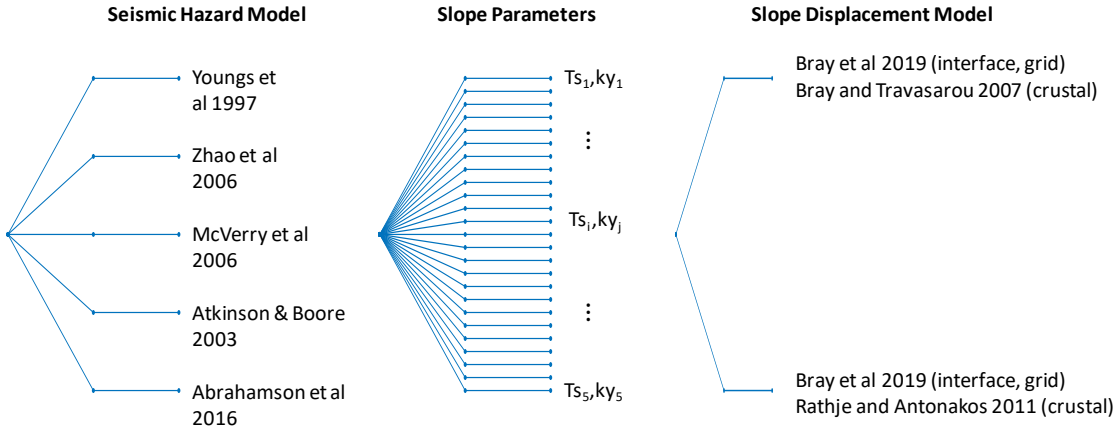

Figure 6: Logic tree definition within the proposed platform for the illustrative example

This procedure can be repeated for each of the branches that result from the combination of the IM and D logic trees (Figure 6). Figure 7 illustrates the results for one of the logic tree branches, which provide pseudostatic seismic coefficients of 0.10 for a return period of 475 years and a pseudostatic seismic coefficient of 0.27 for a return period of 2475 years. These pseudostatic coefficients can be used in posterior slope stability analyses to estimate the safety factor. For example, if the pseudostatic coefficient of 0.10 (consistent with 475 years of return period) is used and a safety factor greater than 1 is calculated, then the conclusion is that the expected amount of seismically-induced displacements is lesser than 15 cm (the considered level of tolerable displacements). On the other hand, if the pseudostatic coefficient of 0.27 is used and a safety factor lesser than 1 is obtained, then the conclusion is the expected amount of seismically-induced displacements is higher than 15 cm (the considered level of tolerable displacements).

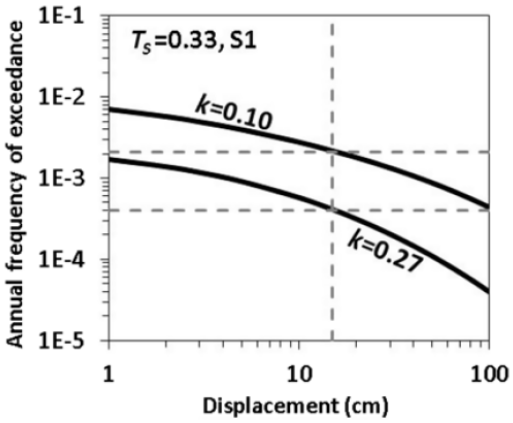

Figure 7: Estimation of the pseudostatic coefficient, using the proposed procedure in this study, for the tailings dam considered in the illustrative example

Conclusion

Pseudostatic slope stability evaluations can be limited unless the parameters used in the analyses reflect the potential seismic demand and its impact on the seismic performance of the geotechnical system being evaluated or designed. The seismic coefficient to be employed in a pseudostatic slope stability analysis should be selected in a rational manner if this procedure is to form a sound basis for a seismic slope stability assessment. The selection of the seismic coefficient employed in the analysis is often based on precedence, regulatory design guidance, and engineering judgment, without due consideration of the seismicity, the seismic sources governing the site where the analyses are performed, and the properties of the system being evaluated. In this study we have proposed a probabilistic procedure for the rational selection of the pseudostatic coefficient to be used in slope stability analyses. The procedure has its cornerstone on the evaluation of displacement hazard curves and it is informed by: 1) the maximum level of seismically-induced displacements that the structure can tolerate; 2) the hazard design level at the evaluation site; and 3) the properties of the sliding mass. The procedure has been formulated to be applied on different tectonic settings such as subduction earthquake zones, as well as shallow crustal earthquake zones. Importantly, the proposed procedure can be applied in a straightforward manner in the context of mining projects, through a graphical user interface provided by the authors at https://github.com/gacandia/SeismicHazard.

References

Bray, J.D. and J.L. Macedo. 2019. Procedure for estimating shear-induced seismic slope displacement for shallow crustal earthquakes. *Journal of Geotechnical and Geoenvironmental engineering*.

Bray, J.D. and T. Travasarou. 2007. Simplified procedure for estimating earthquake-induced deviatoric slope displacements. *Journal of Geotechnical and Geoenvironmental Engineering* 133(4): 381–392.

Bray, J.D. and T. Travasarou. 2009. Pseudostatic coefficient for use in simplified seismic slope stability evaluation. *Journal of Geotechnical and Geoenvironmental Engineering* 135(9): 1336–1340.

Bray, J.D., J.L. Macedo and T. Travasarou. 2018. Simplified procedure for estimating seismic slope deviatoric displacements in subduction zones. *Journal of Geotechnical and Geoenvironmental Engineering*. Accepted for publication.

Duncan, J.M. and S.G. Wright. 2005. *Soil Strength and Slope Stability*. New Jersey: John Wiley & Sons, Inc.

Jibson, Randall W. 2007. Regression models for estimating coseismic landslide displacement. *Engineering Geology* 91(2–4): 209–218.

Macedo, J., J.D. Bray, N. Abrahamson and T. Travasarou. 2018. Performance-based probabilistic seismic slope displacement procedure. *Earthquake Spectra.* 35(2): 673–695.

Minsterio de energía y minas. 1997. *Guía ambiental para la estabilidad de taludes de depósitos de desechos sólidos de mina.*

Papadimitriou, A.G., G.D. Bouckovalas and K. Andrianopoulos. 2014. Methodology for estimating seismic coefficients for performance-based design of earth dams and tall embankments. *Soil Dynamics Earthquake Engineering* 56: 57–73.

Rathje, E.M. and G. Antonakos. 2011. A unified model for predicting earthquake-induced sliding displacements of rigid and flexible slopes. *Engineering Geolog*. 122(1):51–60.

Rathje, Ellen M. and J.D. Bray. 1999. An examination of simplified earthquake induced displacement procedures for earth structures. *Canadian Geotechnical Journal*. 36(1): 72–87. doi:10.1139/t98-076.

Rathje, E.M. and J.D. Bray. 2000. Nonlinear coupled seismic sliding analysis of earth structures. *Journal of Geotechnical and Geoenvironmental Engineering* 126(11): 1002–1014.

Saygili, G. and E.M. Rathje. 2008. Empirical predictive models for earthquake-induced sliding displacements of slopes. *Journal of Geotechnical and Geoenvironmental Engineering* 134(6): 790–803.

Seed, Harry. 1979. Considerations in the earthquake-resistant design of earth and rockfill dams. *Geotechnique* 29(3): 215–263.

Seed, H. Bolton. 1981. Earthquake-resistant design of earth dams. *Proceedings of First International Conference on Recent Advances in Geotechnical Earthquake Engineering and Soil Dynamics*, Univ. of Missouri-Rolla, MO, April 26 – May 3.

Seed, H. Bolton and G.R. Martin. 1966. The seismic coefficient in earth dam design. *J. Soil Mechanics and Foundation Div. ASCE*. 92(3): 25-58.

Seed, H. Bolton, Makdisi FI, DeAlba P. (1978). Performance of earth dams during earthquakes. *J. Soil Mechanics and Foundation Div., ASCE.* 104(7): 967–994.

Sencico. 2016. *Actualización del programa de cómputo orientado a la determinación del Peligro Sísmico en el país. Servicio Nacional de Capacitación para la Industria de la Construcción.* Lima, Peru.

Watson-Lamprey, J. and N. Abrahamson. 2006. Selection of ground motion time series and limits on scaling. *Soil Dynamics and Earthquake Engineering* 26(5): 477–482.

Proceedings of Tailings and Mine Waste 2019
November 17–20, 2019, Vancouver, Canada
Published by the University of British Columbia, 2019

Tailings Slurry Thickening Using Super Absorbent Polymers and Parameters Affecting the Absorbency

Khadija El Mahboub, Université du Québec en Abitibi-Témiscamingue/RIME, Canada
Tikou Belem, Université du Québec en Abitibi-Témiscamingue/RIME, Canada
Mamert Mbonimpa, Université du Québec en Abitibi-Témiscamingue/RIME, Canada
Abdelkabir Maqsoud, Université du Québec en Abitibi-Témiscamingue/RIME, Canada
Nor el hoda Addi, Université du Québec en Abitibi-Témiscamingue/RIME, Canada
Cyrille Ngandu Kabamba, Université du Québec en Abitibi-Témiscamingue/RIME, Canada
Lotiyé Élysée Poudama, Université du Québec en Abitibi-Témiscamingue/RIME, Canada
Jean-François Lemay, Collège Shawinigan/CNETE, Canada

Abstract

This paper introduces a new alternative method for mine tailings slurries thickening, which consists of using super absorbent polymers (SAPs), exploiting their high water absorption and retention capacities. The factors affecting this dewatering process are also assessed and discussed. In this context, several experimental tests were conducted using two different types of SAP (SAP 1 and 2) to evaluate their potential for the densification of four types of tailings slurry with two addition methods (indirect and direct) of the SAPs. Two initial solid mass concentrations of 40 and 50% were investigated. The tested SAP dosages were in the range of 6–29 kg dry PSA/m^3 of tailings slurry. The SAP 1 displayed a greater water absorbency than the SAP 2.

The results indicate that a final solid concentration $C_{w\%final}$ of 70–82% can be achieved at dosages of 10–29 kg/m^3. The effectiveness of this SAP dewatering process was affected by several factors, including: the type of SAP and its dosage, the mineralogical and physical properties of the tailings slurry as well as its initial solid content, the pore water chemistry, the SAP residence time (RT), and their addition method (direct or indirect).

Introduction

Mineral processing plants generate large amounts of tailings. These tailings are the residual finely ground (1–600 µm) rock produced after the economical ore has been extracted, and process water (Edraki et al., 2014). This large volume of produced tailings is generally deposited on the surface as a slurry in tailings

storage facilities (TSF), with solid content ranging between 25 and 45% (Bussière, 2007). This conventional deposition method, which seems to be simple and inexpensive, can lead to excessively costly and occasionally disastrous issues, mainly acid mine drainage and tailings dam failure. Such problems are inherently linked to poor tailings management, especially poor mine water management. Considering the potentially devastating socioeconomic and environmental consequences of poor tailings management, it seems crucial to reconsider alternative approaches for tailings management rather than the conventional one. Densifying tailings prior to deposition (thickened, paste, and filtered) is one of several alternative methods for good management practices for tailings deposition.

The main densifying equipment currently used to enhance water recovery from the tailings slurries are hydrocyclones, conventional thickeners, high-capacity thickeners, and disc filter, or filter press. These tailings management approaches significantly reduce the environmental footprint as a result of improved tailings slurry density, thus ensuring their chemical and mechanical stability. However, these dewatering technologies are expensive and do not always reach the intended target in terms of solid mass concentration. That is because of the finely ground mineral ore associated with the new ore grinding processes for maximum recovery of valuable minerals from mined ore. This may adversely affect the overall stability of the TSF. Therefore, significant research efforts are required to find more efficient and cost-effective methods for the densification.

The high water absorption abilities of super absorbent polymers (SAPs) offer new possibilities for an effective and non-mechanized thickening process. Masuda and Iwata (1990) were the first to demonstrate the superior effectiveness of using SAPs for fine coal dewatering. Further studies confirmed the high water absorption ability of the SAPs, while promoting lower moisture content of fine coal (Peer and Venter, 2003; Roshani et al., 2017). Kuai et al. (2000) also reported that SAP-based sewage sludge thickening was able to reduce the water content by 91%. Farkish and Fall (2013) pointed out the superior performance of SAPs in rapidly dewatering mature fine tailings (MFT). Joseph-Soly et al. (2016) investigated the feasibility and efficiency of using the SAPs for dewatering and densification of fine-grained nickel laterite slurries. They found that a dosage of 2–3 wt.% showed an increase in the sediment consolidation from 20–25 wt.% to 40–55 wt.% within 8 hours by indirect contact between the SAPs and the slurries. Joseph-Soly et al. (2019) also demonstrated the potential for using SAP in rapid dewatering of fine sulphide minerals slurries, especially pyrite and chalcopyrite, to produce a dense sediment consolidation up to 82 wt.% from the slurries, with a solids content in the range of 8–30 wt.% within 30 minutes by indirect contact between the slurries and SAP at dosages lower than 3 wt.%. Therefore, this new SAP-based dewatering process is a promising approach that opens the door to different mining industry applications.

The SAPs are capable of absorbing and retaining large amounts of water relative to their own mass (Zohuriaan-Mehr and Kabiri, 2008). They are hydrophilic materials that entrap water molecules of aqueous

solution via capillary and osmosis forces in their macro-porous structure (Zohuriaan-Mehr and Kabiri, 2008). The number of cross-links between the polymer chains will dictate the amount of water absorbed by the SAPs (Buchholz and Graham, 1998). As the number of cross-links increases, the expansion of the polymer chains decreases, thus leading to reduced absorbency (Radwan et al., 2017).

The main objective of this study is to conduct an efficient experimental program using the SAP characteristics to enhance dewatering of four different types of tailings slurry, while investigating the parameters affecting the absorption capacity of the SAPs. To date, no attempt has been made to use SAPs for the thickening and densification of real mine tailings, which are very complex materials. Hence, addressing this research project allows for a better understanding of the SAP's behaviour within the tailings slurry, and for a consideration of the feasibility and efficiency of this dewatering process.

Materials and methods

Materials

Tailings samples

In this study, four tailings were sampled from different mining companies in the Abitibi-Témiscamingue region in Quebec, Canada (tailings A, B, C, and D) and stored separately in plastic barrels. The collected tailings were manually homogenized in the laboratory, and subsamples were taken for various characterizations: physical, mineralogical, and chemical characterizations. The relative density (D_R) of the tailings was determined using a helium pycnometer. The values of the initial solid content ($C_{w\%\text{-initial}}$) of the tailings and their relative density are tabulated in Table 1. The particle size distribution (PSD) of tailings was carried out using a Malvern Mastersizer S2000 laser particle size analyzer. The mineralogical composition was determined by X-ray diffraction (XRD) using a Bruker AXS Advance D8. The chemical composition of mine waters was determined by inductively coupled plasma atomic emission spectroscopy (ICP-AES). The tailings slurries were prepared by adding mine waters to the tailings to reach solid contents of about 40 and 50%.

Table 1: Solid contents and relative densities of the mine tailings samples

Parameter	Tailing A	Tailing B	Tailing C	Tailing D
$C_{w-initial}$ (%)	80.6	79.8	83	78.9
D_R	2.77	2.90	3.10	2.74

The resulting gradation parameters of the tailings are summarized in table 2, where D_x is the diameter of x percent passing. As this table illustrates, based on the values of $P_{20\mu m}$ (cumulative percent of the particles of diameter lower than 20 μm), the tailings A and B show a higher content of very fine particles

with a percentage of 43% and 48%, respectively. The tailings from mines C and D present a lower amount of very fine particles with percentages of 35% and 38%, respectively. The results of mineralogical analysis show that the mine A tailings contain a high amount of albite (42.3%) and quartz (24.4%). Tailings B are dominated by quartz (47.8%) and chlorite (22.1%). Tailings C contain also a high amount of quartz (72.7%) and sulphide (~20% pyrite). Tailings D are abundant with albite (59.6%) and quartz (20.1%).

Table 2: Tailings samples gradation parameters

Parameter	Tailing A	Tailing B	Tailing C	Tailing D
D_{10} (µm)	3.4	1.9	5.3	3.4
D_{30} (µm)	11.1	3.8	16.3	13.5
D_{50} (µm)	25.0	5.8	33.9	35.3
D_{60} (µm)	36.3	7.1	46.7	54.2
D_{90} (µm)	123.2	15.2	133.5	182.9
C_U	10.7	3.8	8.8	16.1
C_c	1.0	1.1	1.1	1.0
$P_{20µm}$ (%)	43.0	48.0	35.0	38.0

Superabsorbent polymers

Two types of synthetic, cross-linked, and negatively charged SAPs were investigated. These SAPs were provided by two different companies. The first type (SAP 1) is commercially named SAG-MD6K (from Recyc PHP Inc., Drummondville, Canada). The second type (SAP 2) is called APROMUD-G300 (from the supplier APROTEK, S.A.R.L., France). The negative charge on these SAPs is neutralized by adsorbed Na^+ at different concentrations. The concentrations of Na^+ were determined by microwave plasma atomic emission spectroscopy (MP-AES). The Fourier Transform Infrared Spectroscopy (FTIR) analysis was conducted to identify the chemical composition of these SAPs. The obtained spectra indicated that SAP 1 and 2 are chemically distinct. The SAP 1 corresponds to Cobalt thiocyanate Tosylmethyl isocyanides Nitrous oxide gas (172 ppm of adsorbed Na^+). The SAP 2 corresponds to Poly (acrylonitrile) 1, 6-Dicyanohexane Cyclohexane (135 ppm of adsorbed Na^+).

The PSD of the two SAP samples in the dry state was characterized in a Malvern Mastersizer 3000 laser particle size analyzer using dry dispersion. The main parameters deduced from the grain size distribution of the SAPs are summarized in Table 3.

Table 3: Physical properties of the SAP used

Parameter	SAP 1	SAP 2
D_{10} (μm)	297	240
D_{50} (μm)	501	505
D_{60} (μm)	550	550
C_U	1.9	2.3
Span	1.06	1.4
S.S.A. (m^2/g)	0.0812	0.2606

It should be mentioned that SAP 1 and 2 have a similar grain size distribution; however, the D_{10} are different (SAP 2 has the smallest one). Therefore, SAP 2 included the highest amount of fine particles (fewer than 240 μm). Based on both their low coefficient of uniformity C_U (= D_{60}/D_{10}) < 6 and Span values, the two SAPs have a narrow and uniform PSD. But, the grain size of the SAP 1 seems to be more uniformly and narrowly distributed than that of the SAP 2. That is because of its narrow Span of 1.06 compared to that of SAP 1 (= 1.4). The specific surface area (S.S.A.) of the SAP 2 is three times higher than that of SAP 1 (see Table 3).

Methods

SAP dosages

In this study, the SAP dosages (D_{vSAP}) are defined as the ratio of the dry mass of SAP (M_{SAP}) to the volume of the tailings slurry (V_{slurry}) as follows (Sahi et al., 2017):

$$D_{vSAP} = \frac{M_{SAP}}{V_{slurry}} = \rho_{slurry}\left(\frac{M_{SAP}}{M_{slurry}}\right)$$

Where:

ρ_{slurry} = tailings slurry density (in g/cm^3, kg/m^3 or t/m^3)

M_{slurry} = the mass of the tailings slurry (g, kg or t).

Here D_{vSAP} is expressed in kg of dry SAP/m^3 of tailings slurry (kg/m^3). In this study, the SAP dosage ranged from 0 to 25 kg/m^3. In addition, the target final $C_{w\%-final-target}$ was set at 70%.

Tailings slurry dewatering using the indirect addition method of SAP

In this experiment, a wet geotextile bag is filled with a known mass of SAP and is submerged into rectangular containers containing tailings slurries with varying $C_{w\%-intial}$ (40 and 50%). Different RT (ranging from 5 minutes to 72 hours) are investigated. The containers are covered with lids. Once the required contact time has elapsed, the bag is removed and suspended for 20 minutes over the container to

ensure that the excess free water returns back to the dewatered tailings. The thin layer of mine tailings covering the swollen geotextile bags is removed and placed into containers, using a spatula. The resulting thickened tailings is then weighed and oven dried (60°C). After three days of drying, the sample is removed and reweighed to calculate the gravimetric water content (w) and the corresponding solid mass concentration (C_w).

Tailings slurry dewatering using the direct addition method of SAP

The first step in this experiment is to prepare a known mass of tailings slurry at two different solid mass concentrations $C_{w–initial}$ (40 and 50%). After that, a fixed mass of SAP is directly placed into a Kitchen Aid mixer bowl (475 watts with four speeds) that contains the tailings slurry. The SAP-tailings slurry mixture is then kneaded at a low speed (speed 1) for 7 minutes and stored in sealed plastic containers. At specific time intervals, the slump of the obtained mixture (SAP-based thickened tailings) is measured using the small Abrams cone (150 mm height). Subsequently, the solid mass concentration (C_w) of the SAP-based thickened tailings is calculated from a statistical regression model relating the solid mass concentration of mine tailings without SAP (C_w), to the corresponding slump (s) value as follows:

$$C_w(\%) = a + b \times s(cm) + c \times s(cm)^2$$

Where:

a, b and c are constants dependent upon the type of tailings, as listed in Table 4.

Table 4: Regression parameters for the different tailings studied

Tailing type	Parameters		
	a	*b*	*c*
Tailing A	0.816793	–0.005397	–0.00015
Tailing B	0.8163	–0.014749	0.000171
Tailing C	0.835965	–0.008358	0.000038
Tailings D	0.791295	0.002289	–0.000439

Results

Tailings slurry thickening using in-geotextile bag SAPs (indirect method)

Figure 1a presents the change over elapsed time in the final solid mass concentration $C_{w\%–final}$ of tailing A slurry at $C_{w\%–initial}$ of 50%. Three different dosages of SAP 1 (9, 10, and 12 kg/m^3) were investigated using the indirect addition method. It can be seen that for D_{vSAP} of 9 kg/m^3, $C_{w\%–final}$ reached 61.7% in about 20 minutes. Hence, the dewatering was rapid, with approximately 95% taking place within 5 minutes. The increase in the SAP 1 dosage from 9 to 12 kg/m^3 resulted in a $C_{w\%–final}$ of 71.7%, hence more than 16% increase in the final solid content. From Figure 1(a), it can be observed that the target final solids content

$C_{w\%–final}$ (≥ 70%) can be achieved with a D_{vSAP} ≥ 12 kg SAP/m^3 tailings slurry after a short RT (~ 10 min).

Figure 1(b) presents the results of tailing A slurry dewatering from initial solid mass concentrations $C_{w–initial}$ of 40 and 50%. Different SAP dosages were investigated (from 6 to 18 kg/m^3), using the indirect addition method for a RT of 72 hours. From Figure 1(b) it can be observed that the factors influencing the SAP thickening process are primarily the $C_{w\%–intial}$ of the tailings slurry, the type of SAP used, and the SAP dosage. Indeed, from $C_{w\%–initial}$ = 40%, the use of SAP 1 at low dosages in the range 8–12 kg SAP/m^3 tailings slurry allowed reaching $C_{w\%–final}$ in the range 57%–68%. This $C_{w\%–final}$ are below the target final solid content $C_{w\%–final–target}$ of 70% (or more).

However, it was possible to exceed this target and obtain $C_{w\%–final}$ in the range of 70–75%, from an initial $C_{w\%–initial}$ of 50% with SAP 1 and using the same range of SAP dosage. It can be seen that using SAP 2 at D_{vSAP} of 12 kg/m^3 yielded thickened tailings at $C_{w\%–final}$ of 74.6% from tailings slurry having a $C_{w\%–initial}$ of 50%. From tailings with $C_{w\%.–intial}$ of 40% a dosage D_{VSAP} of 16 kg/m^3 was required to achieve the same $C_{w\%–final}$. Hence, it can be concluded that the dewatering efficiency is increased when the initial solid mass concentration $C_{w\%–initial}$ of the tailings slurry is increased. The higher the $C_{w\%–initial}$, the lower the SAP dosage.

Furthermore, it can be observed that for $C_{w\%–intial}$ of 50% at D_{vSAP} in the range of 6–12 kg/m^3, the achieved $C_{w\%–final}$ was in the range of 64.4–75.5% using SAP 1 versus in the range of 63.4–74.6 when SAP 2 is used. Thus, SAP 2 has a slightly lower water absorption capacity than SAP 1 at lower dosages (D_{vSAP} ≤ 12 kg/m^3 for $C_{w\%–initial}$ of 50% and D_{vSAP} ≤ 14 kg/m^3 for $C_{w\%–initial}$ of 40%). That could be attributed to both the high negative charge of the SAP 1 (as a result of a high concentration of adsorbed Na^+ on its surface) and a lower content of fine grains compared with SAP 2. Indeed, the electrostatic repulsion between the negatively charged groups increases with increasing the concentration of adsorbed cations (Bhardwaj et al., 2007). As a result, the osmotic pressure within the SAP 1 hydrogel increases. That leads to an uncoil SAP 1 chains to attract more water molecules (Yu et al., 2011).

Furthermore, the smaller the SAP grain size, the larger the amount of water absorbed (Zohuriaan-Mehr and Kabiri, 2008). However, the obtained $C_{w\%–final}$ using SAP 1 and 2 were similar at higher dosages (D_{vSAP} ≥ 14 kg/m^3 for $C_{w\%–initial}$ of 50% and D_{vSAP} ≥ 16 kg/m^3 for $C_{w\%–initial}$ of 40%). The highest $C_{w\%–final}$ achieved was about 76% (corresponding to an increase of 52% and 90% from tailings slurry with $C_{w\%–initial}$ of 50 and 40%, respectively) at a dosage of 16 kg/m^3 for $C_{w\%–initial}$ of 50% versus 18 kg/ m^3 for $C_{w\%–intial}$ of 40%.

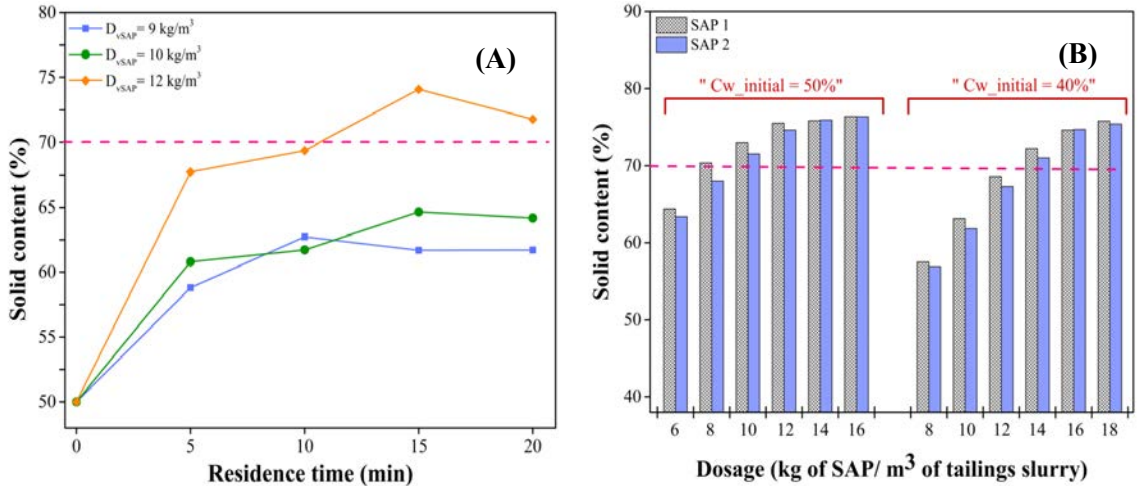

Figure 1: Variation in solid content: (a) as a function of RT in tailing A slurry ($C_{w\%\text{-initial}}$ = 50%) using the indirect addition of SAP 1; (b) as a function of SAP 1 and 2 dosages in tailing A slurry ($C_{w\%\text{–initial}}$ = 40 and 50%)using the indirect addition method (RT = 72 h)

Effect of addition method (direct and indirect) on SAP-based dewatering process

From Figure 2, it can be generally observed that the final solid content of the tailings thickened by the direct addition method was substantially lower than that obtained with SAP 1 geotextile bags. Indeed, it was possible to dewater tailing A slurry from $C_{w\%\text{–initial}}$ of 50% to $C_{w\%\text{–final}}$ of 75% using the indirect addition of SAP 1 at a dosage of 12 kg/m^3 compared to just about 70% with the direct method. This can be explained by the reduced absorbency of the SAP in direct contact with tailings slurry. Indeed, when the direct addition method is adopted, the tailings particles adhere on the swollen polymer grains. The amount of absorbed water then reduces owing to the confining pressure imposed by the tailings particles on these swollen polymer grains. This causes the release of a certain amount of water from these swollen SAPs.

It was found that the confinement increases as thickened material particles become finer (Buchholz and Graham, 1998; Bhardwaj et al., 2007). From Figure 2(a), it can be observed that for tailing A slurry with $C_{w\%\text{–initial}}$ of 40%, a $C_{w\%\text{–final}}$ of about 72% was achieved at a dosage of 14 kg/m^3 in the indirect addition method, versus 20 kg/m^3 using the direct method. Thus, the same degree of dewatering can be achieved for both SAP dewatering methods (direct and indirect) but with much higher SAP dosages in the direct method. Hence, increasing the SAP dosage increases the water absorption capacity of the SAP in the tailings slurry-SAP mixtures. This can be ascribed to the fact that increasing the number of swollen SAP gels (as a result of increased dosage) gives rise to greater resistance to external forces applied by the tailings particles. Consequently, the amount of water retained by the swollen SAP increases (Bhardwaj et al., 2007).

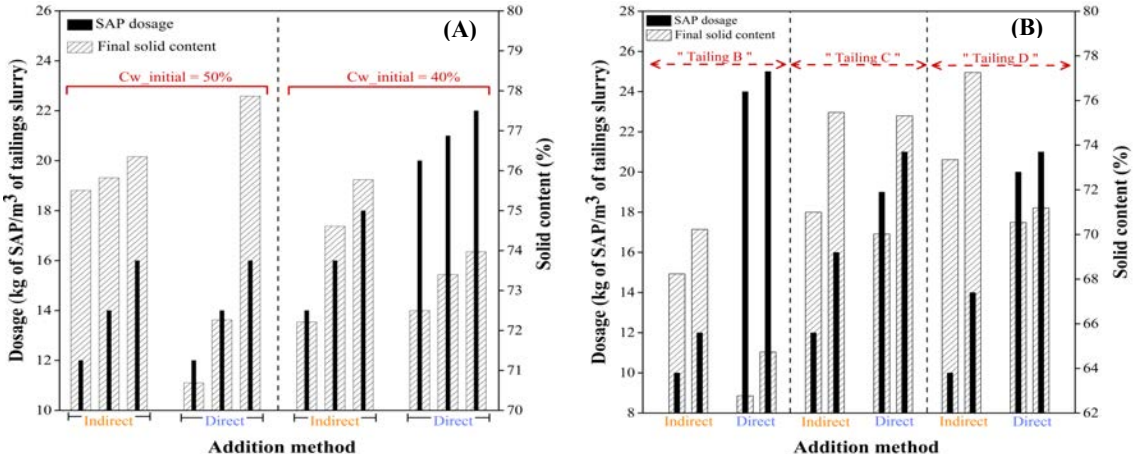

Figure 2: SAP dosages required to achieve the targeted final solid content ($C_{w\%-final} \geq 70\%$) from: (a) tailing A slurry ($C_{w\%-intial} = 50\%$) using both SAP 1 addition methods (direct and indirect); (b) from tailing B, C and D slurries ($C_{w\%-intial} = 50\%$) using both SAP 1 addition methods (RT = 72 hours)

The magnitude of the difference in SAP absorbency between the two SAP dewatering methods (indirect and direct) depends on the type of tailings and their initial solid mass concentration. As shown in Figure 2a, this difference was more pronounced with an initial solids content of the tailing A slurry $C_{w\%-initial}$ of 40% than with $C_{w\%-initial}$ of 50%. This difference was also more amplified in the tailing B slurry than in the other tailings types. This is displayed in Figure 2(b), where moving from the indirect to the direct dewatering method of the tailing B slurry at $C_{w\%-initial}$ of 50% led to a decrease of 11% in final solid content. This decrease was also observed when using a SAP dosage twice as high as that in the indirect method. These results indicate that the swollen SAP displayed a lesser ability to retain its water in tailing B slurry than in the other tailings slurries. This could be somewhat rationalized in terms of difference in particle size distribution. The tailing B contains the highest amount of fine particles. That may foster greater confining pressure to the swollen SAP compared to the other types of tailings.

Discussion

Effect of mine water ionic strength on SAP absorbency

The effect of the ionic strength on the water absorption capacity of SAP 1 at a dosage of 1 g/500 ml was assessed. Three different tailings supernatant waters were considered: tailing A supernatant (S-tailing A), tailing B supernatant (S-tailing B), and tailing C supernatant (S-tailing C). A dimensionless factor f was used to compare and measure the sensitivity of the SAP in each medium (Parvathy and Jyothi, 2012):

$$f = 1 - \frac{Q_{SAP-medium}}{Q_{SAP-distilled\_water}}$$

The calculated values of f ($0 < f < 1$) indicate that the absorbency of the SAP was much lower in the supernatant water than in distilled water. In agreement with the literature (Sadeghi et al., 2013; Sophia et al., 2016), the SAP water absorption capacity decreased as the supernatant ionic strength increased (Figure 3). That can be ascribed to the combined effect of the charge screening of monovalent cations and complex formation between the charged groups of the SAP and multivalent cations of the external medium. As a consequence, the differential osmotic pressure between the SAP and mine water is reduced. The electrostatic repulsions between the charged groups is diminished. Water absorbency is then decreased. This subsequent decrease is more pronounced as the multivalent cations concentration increases due to their complexing ability, which gives rise to an additional crosslinking of the SAP network. Considering the test results obtained in September 2018 (Figure 3), the highest f value (corresponding to the lower absorbency) was obtained with tailing C supernatant water having the highest ionic strength. Based on the f values, the tailings supernatants were classified in decreasing order of SAP compatibility as follows: S-tailing A > S-tailing B > S-tailing C.

It was found that the ionic strength of the tailings supernatant waters obtained in September 2018 were dramatically altered in February 2019. The calculated f values in September 2018 with S-tailing A, S-tailing B and S-tailing C were 0.78, 0.84 and 0.87, respectively. Whereas the f values calculated in February 2019 were 0.85, 0.11 and 0.22, respectively. Thus, with S-tailing B and S-tailing C, the f value decreased considerably, by 87 and 74% respectively, while an increase in the f value by 10% was observed with S-tailing A. Consequently, the tailings supernatants were classified in decreasing order of SAP compatibility as follows: S-tailing B > S-tailing C > S-tailing A. This is because the lower the f value, the greater the absorption capacity of the SAP. These findings highlighted that the SAP thickening process is very challenging. This is due to the dependency of the SAP efficiency on the pore water chemistry of the thickened tailings system, which varies widely over time.

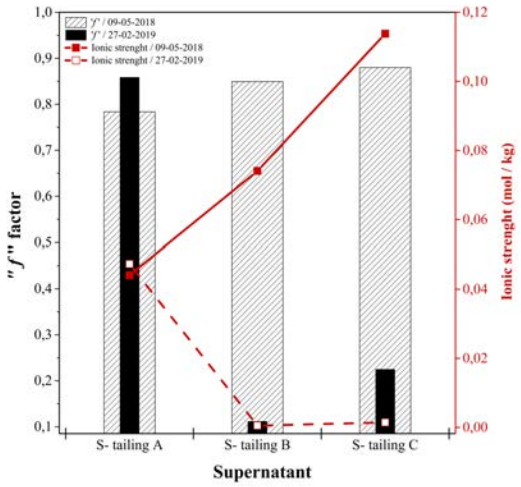

Figure 3: SAP 1 sensitivity towards three tailings supernatants with different ionic strengths

SAP compatibility by indirect contact with the four thickened tailings

Figure 4 demonstrates the major effect of SAP dosage on the SAP thickening process by indirect contact between SAP 1 and tailings slurries with $C_{w\%-initial}$ of 50%. For all four types of tailings, the final solid content of the thickened tailings increased when the SAP dosage was increased. Such final solids content showed a tendency to level out at higher dosages depending on the type of tailings. For that reason, the use of SAP at optimum dosages is fundamental not only to thicken the tailings slurries to a final solid content exceeding 70%, but also to ensure the economic viability of this non-conventional thickening process. The tailing D slurry was the first to achieve the minimum target final solids content (set at 70 %) at the lowest SAP 1 dosage of 8.4 kg/m^3. The tailings that followed were respectively tailings A, C, and B at SAP 1 dosages of 10.6, 11.8, and 11.9 kg/m^3, respectively. Thus, when the geotextile bags method is adopted, the tailings slurries can be classified in decreasing order of SAP 1 compatibility as follows: Tailing D > Tailing A > Tailing C > Tailing B.

These observations indicate that the SAP behaved in an unexpected manner, when indirectly mixed with tailings slurries. Indeed, the contact between the SAP and tailings particles is somewhat limited when the indirect method is used. As a consequence, the pore water quality should be the main factor controlling the water absorption capacity of SAP rather than tailings properties. Based on the ionic strength *(I)* values of the tailings pore water, the SAP water absorption capacity and the concomitant thickening using the indirect method should be decreased in the following tailings order: Tailing B ($I = 5.1\times10^{-4}$ mol/kg) > Tailing C ($I = 1.5\times10^{-3}$ mol/kg) > Tailing D ($I = 3.2\times10^{-2}$ mol/kg) > Tailing A ($I = 4.7\times10^{-2}$ mol/kg).

This is a much more abrupt SAP behaviour change in the indirect method than expected, which was high “dewaterability”, particularly for the tailing B having the lowest ionic strength. These findings demonstrate that SAP dewatering behaviour could be particularly related to the particles surface charge. That depends on the mineralogical properties of the thickened tailings. It has been reported that the presence of certain clay minerals in the thickened materials negatively impacts the SAP water absorption capacity, even in the case of the indirect addition method (Anastassakis, 2005; Sophia et al., 2016). This was explained by an increase in negative charge on the surface of thickened material particles. Indeed, the interaction between SAP and particles increases with an increase in their negative surface charge. As a result, the interaction between SAP and water decreases. Hence, further measurements of the Zeta-potential of the tailings slurries are certainly needed to confirm this hypothesis.

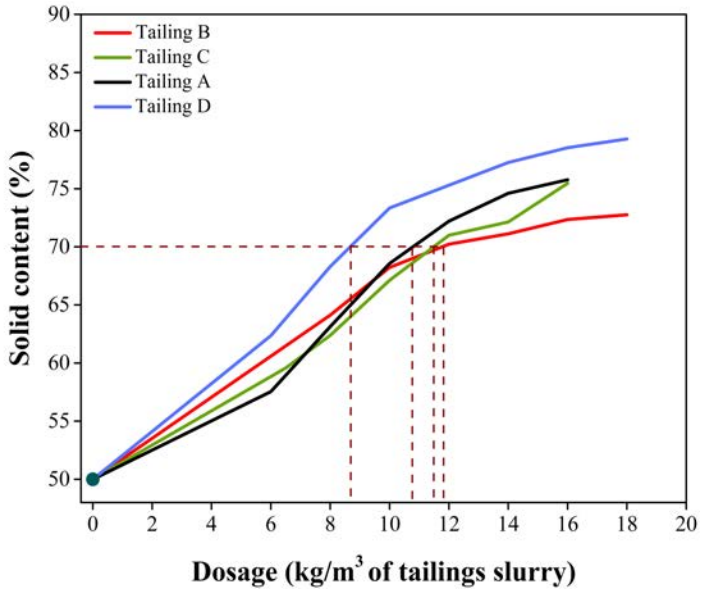

Figure 4: SAP dosages required to achieve the targeted final solid content (set at 70%) from a $C_{w\%-initial}$ of 50% for the four types of tailings using the indirect addition of SAP1(RT = 72 h)

Conclusion

The finding emerging from this study shows that the SAP dewatering method should be a promising alternative for rapid densification of tailings slurries that are dedicated to being deposited on the surface or returned underground in the form of cemented paste backfill. While taking into account the main parameters affecting SAP absorbency, it was clear from the results that for all tailings slurries investigated, rapid and significant dewatering can be achieved within 15 minutes. This results in a final solid mass concentration greater than 70% by the indirect or the direct addition method of SAP at optimum dosages. The indirect method shows generally the best performance, particularly with regard to SAP dosages. The dewatering rate increases with increasing the initial solid mass concentration of the tailings slurries.

Furthermore, the SAP water absorbency and concomitant dewatering rate decreases with an increase in the supernatant water ionic strength. The type of SAP and more specifically its grain size and the concentration of the adsorbed cation (ex. Na^+), has an effect on the SAP water absorption capacity. In addition, the particles surface charge of the tailings to be thickened seems to be the dominant factor controlling the amount of water absorbed by the SAP. However, the direct method does not seem to offer an alternative to the current tailings management practices, mainly because of water that remains in the SAP-tailings mixtures (entrapped within the polymers), over which there is no control, especially in the long term. The SAP dewatering process must then be subjected to a cost-effective assessment, so that it can be applied both in primary (thickening) and secondary (filtering) dewatering treatments.

References

Anastassakis, G.N. 2005. Physicochemical factors affecting flocculation of pre-reduced nickeliferous laterite suspension. *Sep. Purif. Technol.* 45(1): 16–24.

Bhardwaj, A., I. Shainberg, D. Goldstein and D. Warrington. 2007. Water retention and hydraulic conductivity of cross-linked polyacrylamides in sandy soils. *Soil Sci. Soc. Am.* 71(2): 406–412.

Buchholz, F.L. and A.T. Graham. 1998. *Modern superabsorbent polymer technology*. New York: John Wiley & Sons, 1998.

Bussière, B. 2007. Colloquium 2004. Hydrogeotechnical properties of hard rock tailings from metal mines and emerging geoenvironmental disposal approaches. *Canadian Geotechnical Journal* 44(9): 1019–1052.

Edraki, M., T. Baumgartl, E. Manlapig, D. Bradshaw, D.M. Franks and C.J. Moran. 2014. Designing mine tailings for better environmental, social and economic outcomes: a review of alternative approaches. *Clean Prod.* 84: 411–420.

Farkish, A. and M. Fall. 2013. Rapid dewatering of oil sand mature fine tailings using super absorbent polymer (SAP). *Miner. Eng*. 50: 38–47

Joseph-Soly, S., A. Nosrati and J. Addai-Mensah. 2016. Improved dewatering of nickel laterite ore slurries using superabsorbent polymers. *Adv. Powder Technol.* 27(6): 2308–2316.

Joseph-Soly, S., A. Nosrati, W. Skinner and J. Addai-Mensah. 2019. Superabsorbent-mediated dewaterability of fine hydrophobic sulphide mineral slurries. *Sep. Sci. Technol*. 1–15.

Sadeghi, Mohammad, Hossein Sadeghi, Sahar Mirdarikvande, Farnosha Khani, Anahita Godarzi and Hadis Shasavari. 2013. Investigation swelling behavior of a novel alginate based composite hydrogel in various salinity solutions. *Bulletin of Environment, Pharmacology and Life Sciences* 3(3): 54–58.

Kuai, L., F. Doulami and W. Verstraete. 2000. Sludge treatment and reuse as soil conditioner for small rural communities. *Bioresour. Technol.* 73(3): 213–219.

Masuda, K. and H. Iwata. 1990. Dewatering of particulate materials utilizing highly water-absorptive polymer. *Powder Technol*. 63(2): 113–119.

Peer, F. and T. Venter. 2003. Dewatering of coal fines using a super absorbent polymer. *S. Afr. I. Min. Metall.* 103(6): 403–409.

Radwan, M. A., O.H. Al-Sweasy and H.A. Elazab. 2017. Preparation of hydrogel based on acryl amide and investigation of different factors affecting rate and amount of absorbed water. *Agric. Sci.* 8(2): 161.

Roshani, A., M. Fall and K. Kennedy. 2017. Impact of drying on geo-environmental properties of mature fine tailings pre-dewatered with super absorbent polymer. *Nt. J. Environ. Sci. Te.* 14(3): 453–462.

Sahi, A., T. Belem, A. Maqsoud and M. Mbonimpa. 2017. Preliminary assessment of tailings pulp thickening using super absorbent polymers. *Proceedings of the Canadian Geotechnical Conference*, GeoOttawa2017, Ottawa, Canada (paper 832).

Yu, J., I. Shainberg, Y. Yan, J. Shi, G. Levy and Mamedov, A. 2011. Superabsorbents and semiarid soil properties affecting water absorption. *Soil. Sci. Soc. Am,* 75(6): 2305–2313.

Zohuriaan-Mehr, M.J. and K. Kabiri. 2008. Superabsorbent polymer materials: A review. *Iran Polym.* 17(6): 451.

Proceedings of Tailings and Mine Waste 2019
November 17–20, 2019, Vancouver, Canada
Published by the University of British Columbia, 2019

Comparative Analysis of the Post-Liquefaction Shear Strength of Cyclone Tailings based on SCPTu and Laboratory Testing

Brahian Román, Klohn Crippen Berger, Peru
Héctor Barriga, Klohn Crippen Berger, Peru
Abel Najarro, Klohn Crippen Berger, Peru

Abstract

There have been many cases of flow failure of sand tailings dams triggered by liquefaction in the last 20 years. Currently, there is a need to assess the stability of tailings dams constructed in the past against flow failure, since their design and construction quality is unknown, and did not follow safety guidelines. In engineering practice, it is common practice to ensure the safety of dams against flow failure by carrying out post-liquefaction stability and deformation analyses. However, this procedure requires an appropriate estimation of the post-liquefaction shear strength, which is a difficult task due to the high level of uncertainty involved and the lack of understanding of its mobilization mechanism and controlling factors. This paper examines the engineering evaluation of the post-liquefaction shear strength for the stability analysis of an existing non-plastic cyclone tailings dam located in an area of great seismic activity in Peru. The purpose is to compare methods based on in-situ and laboratory testing, aiming to provide insight on how to deal with the uncertainty and limitations of the evaluation of post-liquefaction shear strength from the practitioner viewpoint.

The research took a case study approach, which consisted of the revision and diagnosis of the activities of geotechnical exploration and design conducted for one project, discussion of issues and limitations found, and evaluation of implications on similar projects. The diagnosis comprised a literature review and interviews to establish factors controlling the post-liquefaction shear strength, as well as limitations in the methodologies for its estimation.

The results indicate that the post-liquefaction shear strength obtained through in-situ testing is more conservative than values obtained from laboratory testing for this particular project. Furthermore, several key weaknesses in the evaluation of the post-liquefaction shear strength were found. These key weaknesses included poor strain-rate application in undrained monotonic tests, sample disturbance effects during sampling and laboratory preparation, and lack of strain-softening response in post-cyclic

monotonic tests for the laboratory-based approach. For the approach based on in-situ testing, the main issues found were the lack of accurate data in fines correction factors, and great scattering in the result obtained. Some considerations to address such limitations are provided.

Introduction

There have been many cases of flow failure in tailing dams triggered by liquefaction in the last 20 years around the world (Blight, 2010). Davies et al. (2002) highlight the need to prevent structural tailings from behaving in a contractive way under any shear mode, even in areas that are not prone to earthquakes. Currently, there is a need to raise tailings dam to increasingly higher heights as ore demand increases. According to critical state theory, this increases the susceptibility to the strain-softening response that is required for flow failure. Hence, it is important to assess susceptibility to flow failure of the foundation or of dams constructed with tailings. Ishihara (1993) suggested a flowchart for the analysis of problems in soils undergoing liquefaction. For sloping ground such as embankments or dams, it is necessary to carry out a post-liquefaction stability analysis to estimate the likelihood of flow failure.

According to Finn (1998), the post-liquefaction stability of embankments can be evaluated by determining the shear strength of the post-liquefaction soils (residual shear strength or steady state shear strength), and then conducting a stability analysis incorporating these strengths to determine the factor of safety of the soil structure in its original configuration. The key aspect of this procedure is the appropriate estimation of the residual shear strength of the soil, hereafter referred as post-liquefaction shear strength. However, the estimation of the post-liquefaction shear strength is one of the most difficult issues in recent geotechnical engineering, since there are many factors of uncertainty and its mobilization mechanism cannot be reproduced accurately in the laboratory (Kramer, 2008).

Therefore, the selection of an appropriate value of the post-liquefaction shear strength is very complex and requires suitable engineering judgment. This paper examines the engineering evaluation of the post-liquefaction shear strength for the stability analysis of an existing cyclone tailings dam located in an area of great seismic activity in Peru. The case study approach was used for the research, which consisted of the revision and diagnosis of the activities of geotechnical exploration and design conducted for one tailings dam design project, discussion of issues and limitations found, and evaluation of implications for similar projects.

Objectives

The goal of this study is to provide insight into how to deal with the uncertainty and limitations of the evaluation of post-liquefaction shear strength for practical applications, while answering the following research questions:

- What is the current state-of-practice in the evaluation of post-liquefaction shear strength?
- What are the factors controlling post-liquefaction shear strength and how does it mobilize?
- What are the main sources of uncertainty and limitations in its evaluation for this particular project?
- How can these sources be addressed for practical applications?

Theoretical framework

Castro et al. (1992) stated that since soil density increases with increasing effective stress, and post-liquefaction shear strength increases with increasing density, then the post-liquefaction shear strength should increase with increasing pre-earthquake effective confining stress ($\frac{S_{us}}{\sigma_o'}$). This concept enables the widespread use of normalized ratios for post-liquefaction stability analysis in engineering practice. Current state-of-practice in the estimation of post-liquefaction shear strength includes two main approaches: one based on in-situ testing using data from back-analysis of real flow failures, and the other based on laboratory element tests.

Post-liquefaction shear strength based on in-situ testing

Seed and Harder (1990) were the first to relate in-situ testing (N_{60} from SPT) to the shear strength obtained by back-analysis of real flow failures. Subsequently, Olson and Stark (2002), Idriss and Boulanger (2008), and Robertson (2010) applied this idea for CPT testing as well. The Olson and Stark (2002) approach has a database of 33 cases of real flow failure, and included the kinetics of failure in its formulation. They found no effect from fines on the post-liquefaction shear strength. However, Idriss and Boulanger (2008) used the data and methodology of Olson and Stark (2002) and incorporated correction factors due to the fines content being similar to those proposed by Tokimatsu and Seed (1987). The reasoning behind this is that for a certain relative density, an increase in fine contents causes a reduction in penetration resistance.

Finally, Robertson (2010) expanded the database of real flow failures to 36 and included concepts of critical state soil mechanics. According to Robertson (2010), flow failure can occur only in soils with a normalized CPT tip resistance of less than 70 MPa. This value corresponds to a state parameter (ψ) of approximately –0.05, consistent with the findings of Jefferies and Been (2006), who stated that soils with $\psi > -0.05$ are susceptible to strain-softening and post-liquefaction shear strength mobilization. Table 1 shows a summary of these approaches.

Table 1: Studies of post-liquefaction shear strength based on CPT and flow slide field case studies (adapted from National Academy of Science report, 2016)

Source	Remarks	Equation for S_u/σ_0' ratio	Upper limit for strain-softening behaviour
Olson and Stark (2002)	Found no influence of fines content	$0.03 + 0.0143(q_{c1}) \pm 0.03$	$q_{c1} \leq 6.5\ MPa$
Idriss and Boulanger (2008)	Includes correction factors for fines content	$\exp\left(\frac{q_{c1Ncs-Sr}}{24,5} - \left(\frac{q_{c1Ncs-Sr}}{61.7}\right)^2 - \left(\frac{q_{c1Ncs-Sr}}{106}\right)^3 - 4.42\right)$* $\exp\left(\frac{q_{c1Ncs-Sr}}{24,5} - \left(\frac{q_{c1Ncs-Sr}}{61.7}\right)^2 - \left(\frac{q_{c1Ncs-Sr}}{106}\right)^3 - 4.42\right) \times \left(1 + exp\left(\frac{q_{c1Ncs-Sr}}{11.1} - 9.82\right)\right)$**	No upper limit is provided
Robertson (2010)	Suggests a minimum S_u/σ' ratio of 0.03 and 1 kPa for shallow deposits	$\frac{\left[0.02199 - 0.0003124Q_{tn,cs}\right]}{\left[1 - 0.02676Q_{tn,cs} + 0.0001783\left(Q_{tn,cs}\right)^2\right]}$	$Q_{tn,cs} \leq 7\ MPa$

Where:

σ'_o: Pre-earthquake effective stress

q_{c1}: Normalized cone tip resistance (Olson and Stark, 2002)

$q_{c1Ncs-Sr}$: Clean-sand corrected normalized cone tip resistance (Idriss and Boulanger, 2008)

$Q_{tn,cs}$: Clean-sand equivalent cone tip resistance (Robertson, 2010)

Notes:

*: For cases where void ratio redistribution is negligible

**: For cases where void ratio redistribution is not negligible

Post-liquefaction shear strength based on laboratory testing

Post-liquefaction shear strengths are obtained from laboratory element tests (triaxial, stacked shear ring, direct simple shear) by using classical steady state theory. Recently, Fourie and Reid (2018) developed a new type of stress path, named constant shear drained in direct simple shear, to trigger flow failure resembling the static liquefaction failure of the Fundão tailings dam in 2015. According to this theory, only soils showing strain-softening response in undrained tests are susceptible to flow failure, and the post-liquefaction shear strength is the shear strength mobilized at large strains. In practice, this can be estimated by the following formula:

$$\frac{s_{us}}{\sigma_0'} = \left(\frac{q}{2}\right) \times \left(\frac{1}{\sigma_o'}\right) \quad (1)$$

Where:

q: Deviator stress at large strains

σ'_o: Pre-earthquake effective stress

Many researchers have proposed post-liquefaction ratios for the steady strength condition in undrained monotonic triaxial and post-cyclic monotonic tests. Many researchers have proposed unique post-liquefaction shear strength ratios for the steady state condition. For example, Pillai and Salgado (1994) carried out undrained monotonic tests in frozen samples of sands from Duncan Dam in Canada, obtaining a constant value of 0.21. The CANLEX project (Wride et al., 2000) carried out a comprehensive set of laboratory and in-situ testing for liquefaction evaluation in tailings and natural sands, highlighting the need to avoid the use of conventional sampling techniques to estimate in-situ density due to large disturbances. Sampling using double-tube coring and frozen techniques are recommended for preserving the original fabric of granular soils.

Factors controlling the post-liquefaction shear strength

Classical steady state theory dictates that the post-liquefaction shear strength "is the shear strength mobilized at large shear strains, constant effective stresses, constant volume and constant shear rate" (Poulos, 1981). Ishihara (1993) obtained experimental evidence of the existence of the steady state in triaxial testing for clean sands. According to Verdugo (1992), at the steady state all fabric effects are erased so that the post-liquefaction shear strength is solely dependent on void ratio. Nevertheless, further research found that the mechanism of post-liquefaction shear strength in the laboratory is also dependent on other factors, such as the strain rate of monotonic loading (Yamamuro and Lade, 1998), fines content, particle crushing (Yu, 2017) starting from 1,000 kPa, plasticity and mineralogy, and sensitivity in fine-grained soils.

Furthermore, the mobilization of the post-liquefaction shear strength in the field is even more complex due to factors that cannot be reproduced accurately in the laboratory, such as particle rearrangement, which may trigger flow failure by creating a contractive layer of fines within a dilative stratum (NRC, 1985), especially in soils with high levels of non-plastic silt as fine tailings. In addition, the post-liquefaction shear strength is not a soil property, but a system characteristic (Boulanger, 2016).

Case study

Dam section scheme

This case study consisted of a stability analysis of an existing 30 m high downstream tailings dam located in the highest seismic area of Peru. The existing tailings dam was constructed using coarse cyclone tailings (downstream method) over a closed upstream tailings dam (Figure 1). Flow failure is likely to take place on the upstream tailings dam working as a foundation, since these types of dams are prone to liquefaction. To evaluate the post-liquefaction shear strength, a in-situ and laboratory testing was carried out including seismic piezocone (SCPTu), triaxial CU, direct simple shear (DSS) and subsequent undrained post-cyclic monotonic tests.

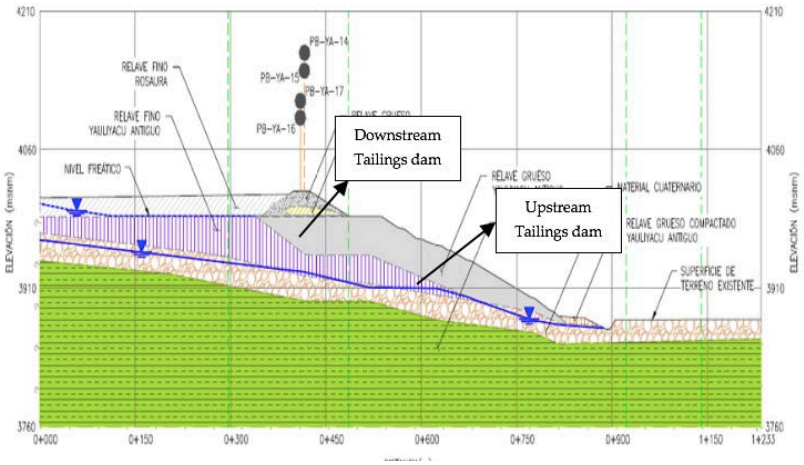

Figure 1: Cross-section of the downstream and upstream tailings dam

Failure consequence and classification

The downstream tailings dam was classified as of Significant consequence according to Canadian Dam Association (CDA) guidelines. Therefore, the annual exceedance probability for seismic design was considered for a 500 years of return period, which was established as the Operating Basis Earthquake (OBE), which is also in agreement with the Peruvian guidelines for seismic design, which gave a 0.40 g of peak ground acceleration.

Tailings characteristics

Index properties

Figure 2 shows the particle size distribution of samples obtained from the SCPTu testing at different depths. The amount of fines increase with depth shows up to 90% of material passing sieve N°200 for 56 m of depth. Figure 3 summarizes some index properties at different depths obtained from sampling of the SCPTu sounding. Moisture and plasticity increase with depth as well, although the plasticity indexes were low, so tailings were classified based on the SUCS system as SM (silty sand) and CL (low plasticity clay).

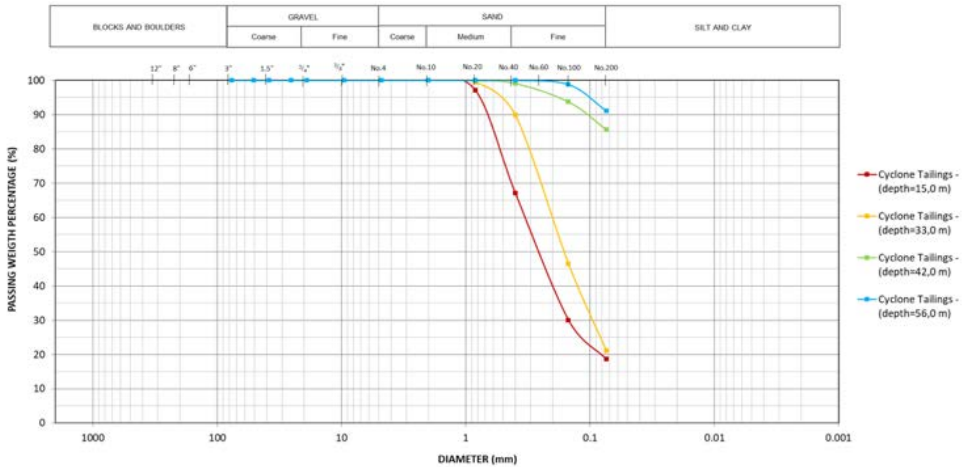

Figure 2: Particle size distribution of cyclone tailings

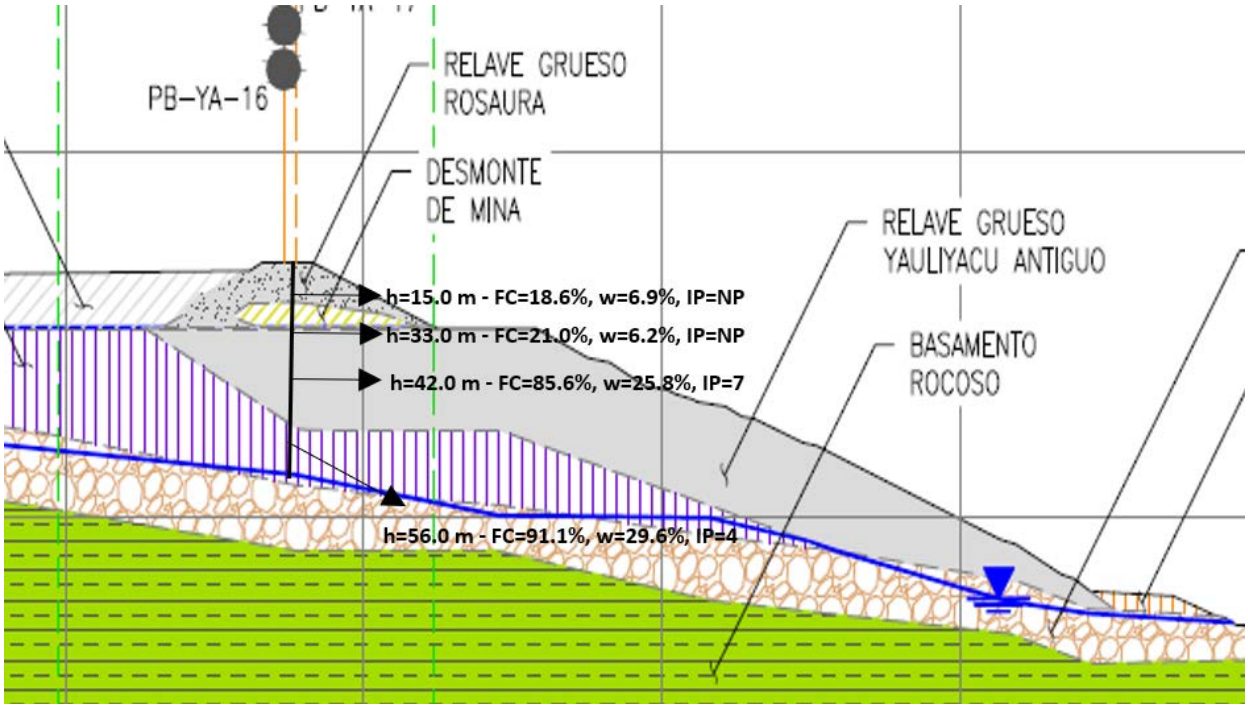

Figure 3: Summary of index properties at different depths

SCPTu investigations

Results from the SCPTu testing are shown in Figure 4, including the cone tip resistance with upper limits for the strain-softening response according to Table 1 (the lower value will be susceptible to flow liquefaction), dynamic excess of pore water pressure, sleeve friction, state parameter, liquefaction triggering analysis, and soil density. Most values of cone tip resistance are above 5 MPa, with almost null dynamic excess of pore water pressure, indicating stiff tailings throughout the testing depth except for two layers. One of these layers is between 41 m and 46.5 m where the cone tip resistance is greatly reduced and soil behaviour tends to be undrained (high values of dynamic pore water pressure) suggesting a lens of fine tailings.

The second layer can be seen starting from 53 m depth (overflow of upstream tailings dam working as foundation) showing similarly low values of cone tip resistance and high dynamic pore water pressure excess. Liquefaction can be triggered only in these two layers due to their level of saturation, as shown in the dynamic excess of pore water pressure. Deterministic liquefaction-triggering analysis was conducted only for the two layers mentioned above. The methodology of the National Centre for Earthquake Engineering Research (NCEER) was used to estimate the cyclic resistance ratio (CRR). The cyclic shear stress ratio (CSR) was obtained from the simplified model proposed by Seed and Harder (1990). Further, these two layers are fully contractive and will undergo flow liquefaction and shear strength reduction in

case of the OBE. Soil densities were estimated from correlations based on friction ratio and tip resistance proposed by Robertson and Cabal (2010).

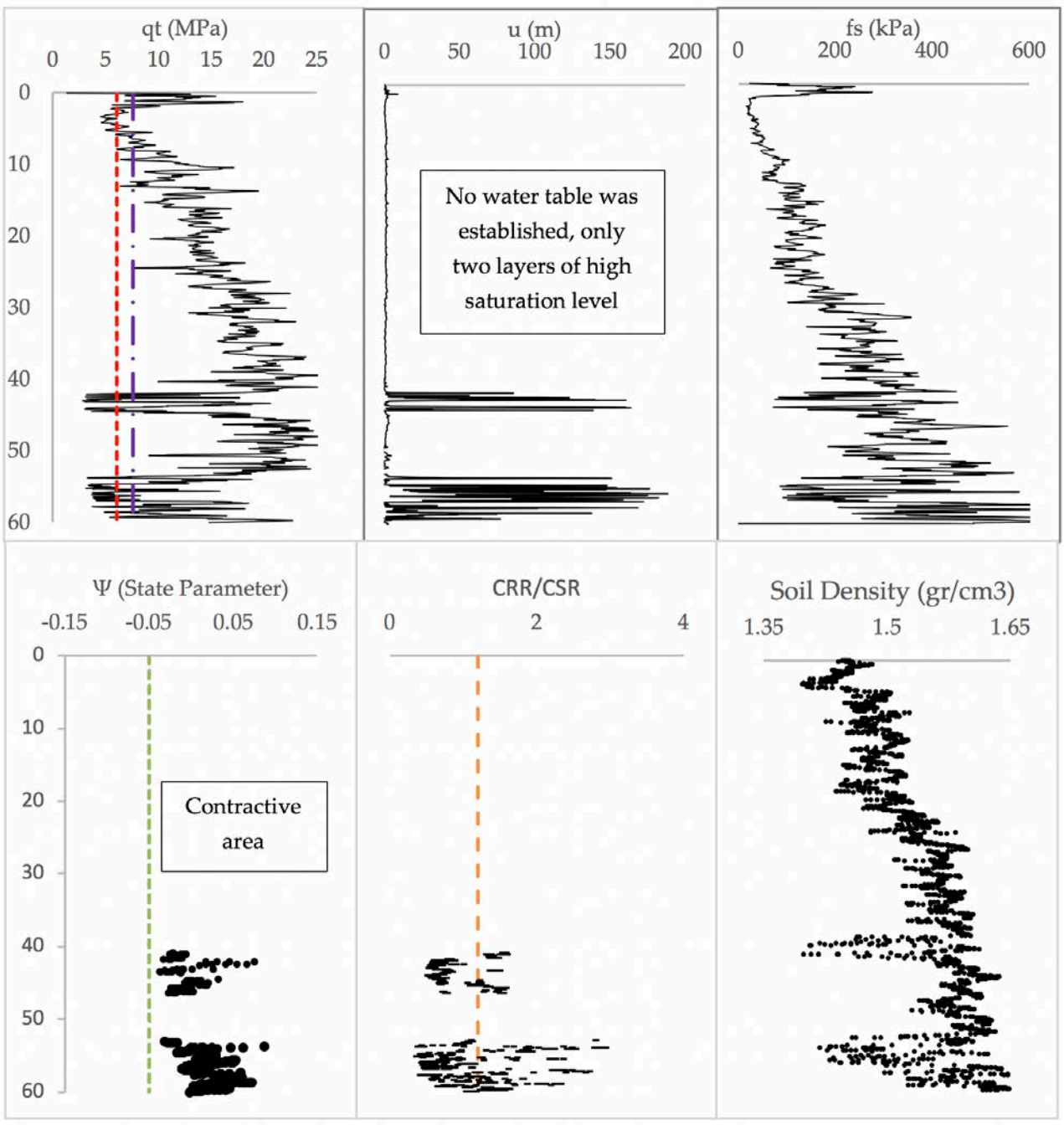

Figure 4: SCPTu and parameters results

Laboratory testing

Triaxial compression CU

Three undrained triaxial compression tests were conducted on disturbed samples of tailings obtained from the closed upstream tailings dam at a depth of 42 m depth (see Figure 5). These tailings are classified as CL based on the Soil Unified Classification System (SUCS) standards, with 85.6% of fines content. The triaxial sample was setup with a 70 mm diameter and a height of 150 mm. The effective confining stress applied ranged from 400 kPa to 800 kPa. Tests were finished upon achieving 15% of axial strain. The moist-tamping method was selected for specimen preparation since it provides a wider range of densities. The target density was 1.4gr/cm^3 of dry density. Densities after consolidation varied between 1.512 to 1.655 gr/cm^3.

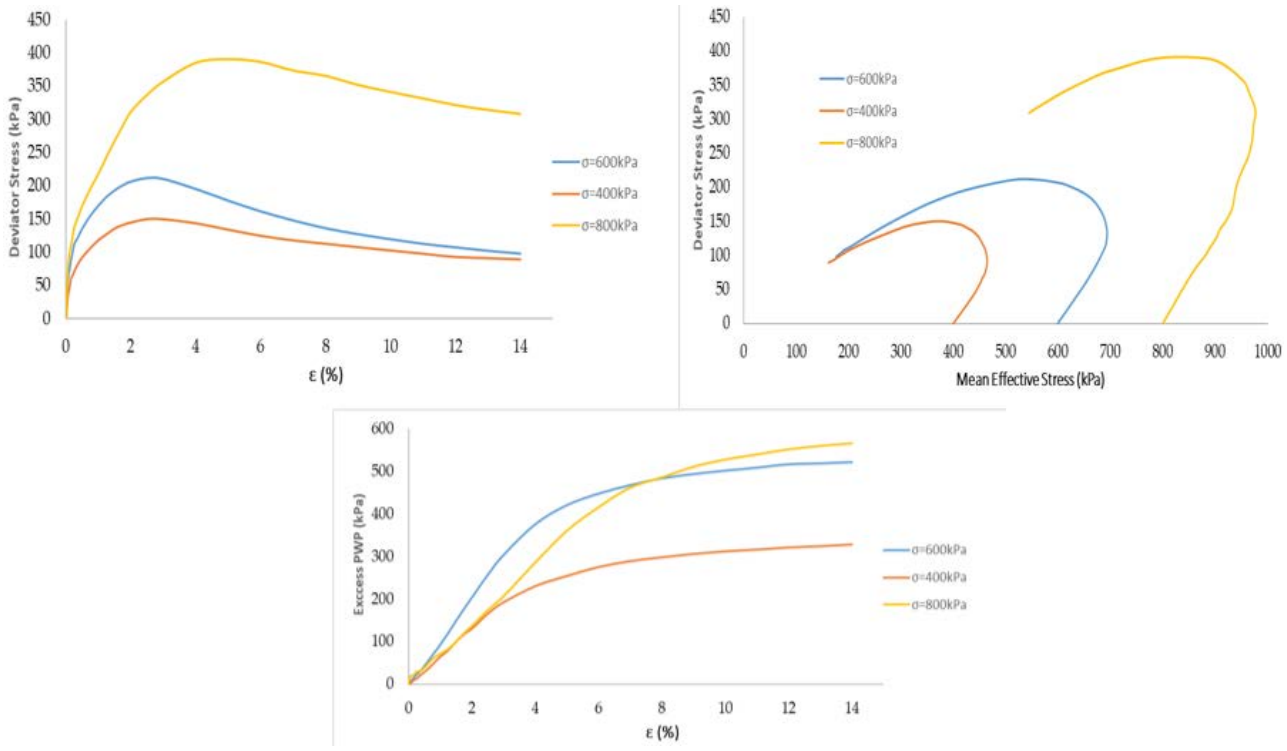

Figure 5: Undrained triaxial compression tests results

As shown in Figure 1, the three samples presented strain-softening response even at the lowest confining stress applied. However, only the tests at 400 kPA and 600 kPA seem to have reached a steady state condition at about 14% of axial strain, whereas the test at 800 kPA presents a deviator stress far above the ultimate steady state despite its similar density. This anomaly could be explained by two reasons, such as changes in void ratio during sample preparation and saturation, and low level of axial strain (only 14% was used). The post-liquefaction shear strength was estimated from Equation (1) based

on the concepts of critical state soil mechanics for the tests at 400 kPA and 600 kPA, only obtaining a ratio $\frac{S_{us}}{\sigma'_o}$ = 0.10 where σ'_0 is the pre-earthquake effective confining stress.

Direct simple shear (DSS) and post-cyclic monotonic testing

Three cyclic simple shear (DSS) and monotonic post-cyclic tests were conducted in disturbed tailings obtained from sampling during the SCPTu of the closed upstream tailings dam at 56 m depth (see Figure 2). All of the DSS testing was carried out using the Berkeley bi-directional simple shear device developed by Boulanger (2016), which includes a sealed chamber enabling truly undrained shearing. The sample was reconstituted using the moist-tamping method of sample preparation to 1.5gr/cm^3 of density at 500 kPa of confining stress. All cyclic loading was stress-controlled applying uniform cyclic stress ratios, CSR = τ_{cyc}/σ'_{vc} of 0.158 to 0.243, until a shear strain of 5% in double amplitude was achieved (failure criteria according to Ishihara, 1993). The results of one test are shown in Figure 6. This shows a cyclic softening and large vertical strains after 51 uniform sinusoidal cycles where liquefaction failure criteria strain was achieved for an excess pore water pressure ratio (r_u[1]) of 0.49 respectively.

Although a zero effective stress condition is never reached (initial liquefaction), the large strains induced and the stress reversal occurring during the test allow us to conclude that cyclic liquefaction took place. After the application of the cyclic shear loading, the specimens were subjected to monotonic shear loading without allowing reconsolidation, which replicates the conditions of flow failure following an earthquake. In this case, a strain-hardening response was obtained despite the fact that the soil underwent large deformation as a result of pore water pressure increment.

By applying equation (1) to the three test results, an average undrained ratio $\frac{S_{us}}{\sigma'_o}$ = 0.23 was obtained with a strain-hardening response in all of them. However, only soils showing strain-softening behaviour mobilize the post-liquefaction shear strength and undergo flow failure. The following possibilities may explain this phenomenon:

- As pointed out by Yamamuro and Lade (1998), the strain rate of the monotonic loading (both in triaxial and post-cyclic) affects the stress-strain behaviour in undrained testing. They suggest the application of 0.01%/min or lower for tests focussing on the estimation of steady-state shear strength. The three post-cyclic monotonic tests were conducted at a relatively high strain rate (0.25%/min), and therefore the post-liquefaction shear strength is not conservative.

[1] r_u is defined as the relationship between the pore water pressure excess and the effective confining stress.

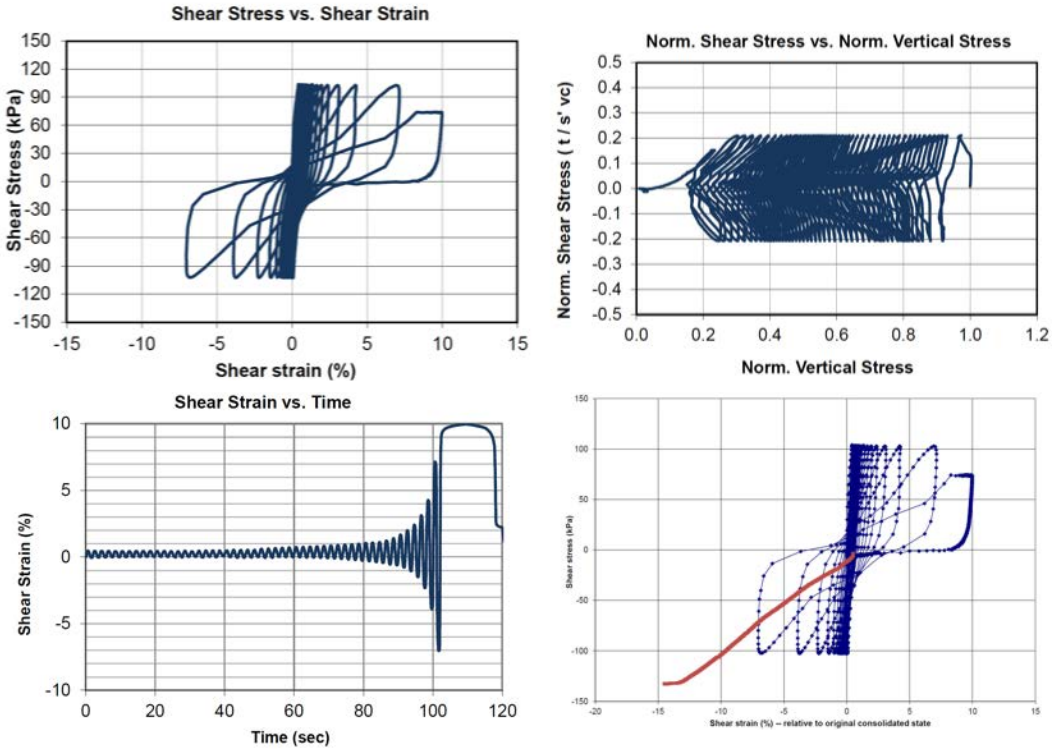

Figure 6: Cyclic test results for n tailings (ρ_d = 1.5 gr/cm3 - τ_{cyc}/σ'_o = 0.209 – r_u = 0.49)

- Lack of application of the initial static shear stress as done in cyclic triaxial testing by Ishihara et al. (1991), in which the same strain-softening response is obtained in both static and cyclic loading (Figure 7). This is important for cases with high static bias, such as in slopes.

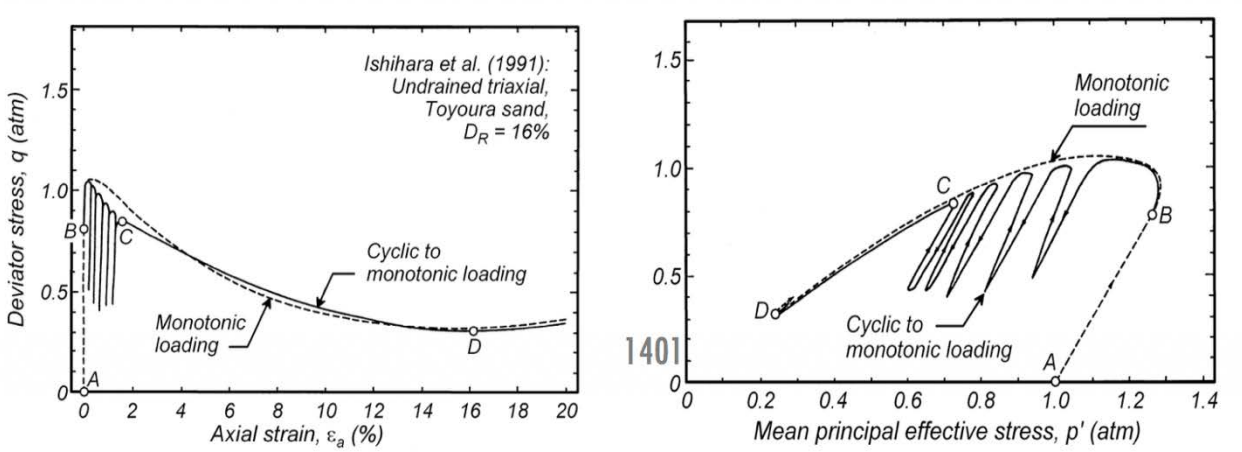

Figure 7: Undrained behaviour of Toyoura sand in monotonic loading versus cyclic-to-monotonic loading (Ishihara et al., 1991)

- Yasuda (1995) suggested that high post-cyclic shear strengths may be related to the excess pore water pressure generated in the cyclic loading. After conducting post-cyclic monotonic tests in

torsional hollow cylinder apparatus, he concluded that lower shear strength is obtained with higher r_u values during the undrained cyclic loading. The three DSS tests conducted for this case study did not reach the initial liquefaction ($r_u = 1$) defined by Seed and Harder (1990), only achieving 0.48, 0.30 and 0.49 of excess pore pressure respectively. These low r_u values are common in dilatant specimens, which does not represent the contractive condition of the tailings found on the field according to the SCPTu tests. Hence, it is very likely that the density and confining stress established for DSS testing did not reflect field conditions; a higher stress confining stress would probably generate post-cyclic contractive behaviour. To avoid this, it is recommended that a realistic state parameter (ψ) is used when establishing laboratory testing conditions.

Comparison of in-situ and laboratory results for post-liquefaction shear strength

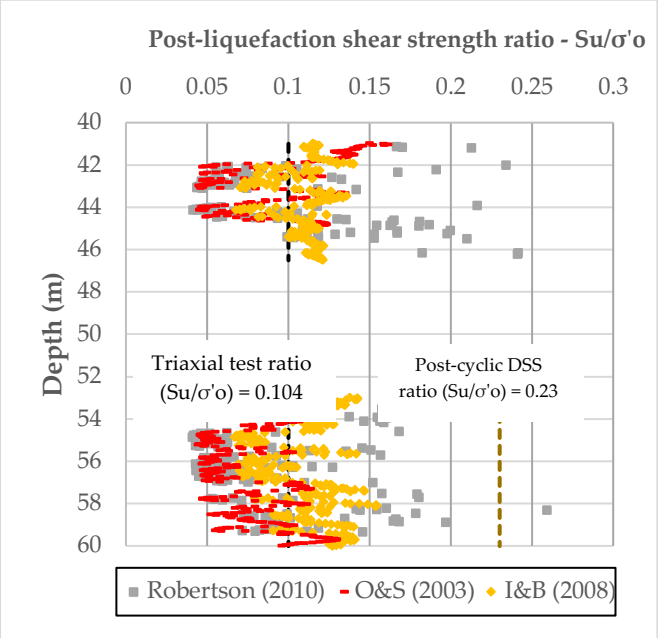

Figure 8: Post-liquefaction shear strength of case study

Figure 8 Shows the undrained ratios $\frac{S_{us}}{\sigma'_o}$ obtained from in-situ testing applying the methodologies suggested by Robertson (2010), the average value of Olson and Stark (2002), and Idriss and Boulanger (2008) corrected for 85% and 90% of fines content. As seen in Figure 8, Olson and Stark (2002) and Robertson (2010) are more conservative, but Idriss and Boulanger (2008) shows less scattering. Robertson (2010) provides higher values when the normalized tip resistance approaches the upper limit for the strain softening response (7 mPA). Laboratory-based results from the post-cyclic tests are much higher than all the results obtained, representing an upper bound for tailings, whereas the ratio estimated from undrained triaxial testing is more conservative.

Dealing with uncertainty and limitations in the engineering evaluation

There are many factors controlling the post-liquefaction shear strength that are not included in any methodology for its estimation. Furthermore, there is a great deal of uncertainty associated with the parameters obtained from in-situ and laboratory testing with a limited number of case studies. These contribute to the high level of uncertainty when establishing a post-liquefaction shear strength value for design and mitigation measures. The best way to address such limitations is by using conservative values and following some recommendations such as:

- The selection of a representative post-liquefaction shear strength value for layers with a high level of scattering should be defined following a volume criterion. According to Jefferies (2014), the loosest 10% (by volume) of any stratum controls the overall behaviour of the stratum. For the case study in this paper, the lowest value of the three methodologies was 0.03 for Robertson (2010), 0.04 for Olson and Stark (2002), and 0.07 for Idriss and Boulanger (2008) as worst-case scenarios.
- Laboratory-based results are generally higher, as for the present case study. This is in agreement with Castro et al. (1992) who studied silty sands from the failed Lower San Fernando dam by means of triaxial testing, and stated that conservative to very conservative interpretation of the laboratory test data was necessary to provide a reasonable level of agreement with the field strength estimated from the observations. As shown, the results of the triaxial test are twice the results obtained through methodologies based on in-situ testing. It is suggested that the results from laboratory testing be used as upper bound limits.
- All results obtained must be validated through a literature review and expert judgment. Olson and Stark (2003) conducted a comparative analysis between ratios obtained for granular soils in laboratory tests and ratios obtained by Olson (2001) from historic cases. According to this study, laboratory-based post-liquefaction ratios ranged from 0.02 to 0.22 over a wide range of effective stresses, while back-calculated post-liquefaction ratios varied from 0.03 to 0.10. The results of the present case study fall within the ranges mentioned.
- The influence of non-plastic fines content for in-situ evaluation of post-liquefaction shear strength using CPT is still controversial. Olson and Stark (2003) and Robertson (2010) stated that fines content have no effect on the post-liquefaction shear strength, whereas Idriss and Boulanger (2008) and Viles et al. (2018) found that the tip resistance of CPT testing in soils with the same state decreases as function of fines content, which will impact on the estimation of the post-liquefaction shear strength. The only way of addressing this contradiction is by determining through sampling the actual non-plastic fines content and, if the amount of fines is high (above 50%), use the worst-

case scenario of post-liquefaction shear strengths for stability analysis to account for the uncertainty of the fines content effect.

Conclusion

This paper aimed to answer four research questions described in the introduction. The main conclusions are:

- Current state-of-practice in the evaluation of post-liquefaction shear strength involves approaches based on in-situ testing and laboratory testing. The former uses correlations from real flow failures, and the latter applies the concepts of the steady state theory. Three methodologies are more reliable for the approach based on in-situ testing: Olson and Stark (2002), Idriss and Boulanger (2008), and Robertson (2010).
- Methodologies proposed by Olson and Stark (2002) and Robertson (2010) provide upper limits for strain-softening that are very helpful, as soils with this type of behaviour are susceptible to flow failure. These values can be validated through in-situ estimation of the state parameter (ψ) from CPT correlations.
- For this case study, Olson and Stark (2002) and Robertson (2010) provide more conservative results, while Idriss and Boulanger (2008) shows higher values and is strongly dependent on correction factors for fines content.
- The effects of non-plastic fines on the post-liquefaction shear strength evaluation using CPT is yet to be clarified. It is necessary to account for this uncertainty in engineering applications. The authors suggest conducting sampling from contractive tailings, aiming to establish the real fines content and, if fines are high (above 50%), use the worst-case scenario of post-liquefaction shear strengths for stability analysis to account for the uncertainty of the fines content effect.
- Classic steady state theory dictates that the post-liquefaction shear strength is the shear strength mobilized at large strains in undrained condition. However, recent research shows that there are many other factors affecting the mobilization mechanism such as strain rate, particle crushing, plasticity, grain size, permeability of overlying confining layers.
- The factors mentioned above are not included in the approaches for the estimation of the post-liquefaction shear strength of this case study. In addition, there are uncertainties in the parameters obtained from in-situ and laboratory testing and scattering in the results from the methodologies. These constitute the main sources of uncertainty and limitations in the estimation of the post-liquefaction shear strength.

- To address such limitations, conservatism and engineering judgment should be applied, paying attention to factors that can be controlled, such as the shear mode and strain rate in laboratory testing. Undrained triaxial testing and DSS post-cyclic monotonic testing should be conducted at low strain rates when the goal is to evaluate the post-liquefaction behaviour. 0.005%/min to 0.01%/min will provide more conservative results.
- Laboratory testing should resemble the in-situ state conditions (density and effective confining stress) of the soils. For this case study, the DSS showed strain-hardening behaviour that did not replicate the contractive state of tailings at a depth of 56 m, established through CPT testing (ψ>-0.05). In addition, post-cyclic monotonic tests should be conducted with an initial static shear stress when tailings are part of sloping ground.
- Results must be validated through expert judgment and literature review. The database presented by Olson and Stark (2003) can be used as a first screening since it encompasses case studies from several types of materials (including tailings).

References

Blight, G. 2010. *Geotechnical Engineering for Mine Waste Storage Facilities*. The Netherlands: CRC Press/Balkema.

Boulanger, I. 2016. Liquefaction-induced flow slides governed by residual shear strength of liquefied soil. US-NZ-Japan International Workshop, November 2–4, 2016, Berkeley, California.

Castro, G., R.B. Seed, T.O. Keller and H.B. Seed. 1992. Steady state strength analysis of lower San Fernando dam slide. *Journal of Geotechnical Engineering* 118(3).

Davies, M.P., E.C. McRoberts and T.E. Martin. 2002. Static liquefaction of tailings – Fundamentals and case histories. In *Proceedings of Tailings Dams 2002,* ASDO/USCOLD, Las Vegas, Nevada.

Finn, L.W. 1998. Estimating post-liquefaction displacements in embankments dams and prioritizing remediation measures. In *Proceedings of the 4th International Conference on Case Histories in Geotechnical Engineering*, St. Louis, Missouri.

Idriss, I. M. and R. Boulanger. 2008. *Soil Liquefaction during earthquakes*, Earthquake Engineering Research Institute, California.

Ishihara, K. 1993. Liquefaction and flow failure during earthquakes. *Geotechnique* 43(3): 351–415.

Ishihara, K., R.L. Verdugo and A.A. Acacio. 1991. Characterization of cyclic behavior of sand and post-seismic stability analyses. In *Proceedings of the 9th Asian Regional Conference on Soil Mechanics and Foundation Engineering,* Bangkok, Thailand, 2: 45–70.

Jefferies, M.G. and K. Been. 2006. *Soil Liquefaction – A Critical State Approach*. London: Taylor and Francis.

Jefferies, M.G. 2014. Geotechnical evaluation of the Ocroyoc dam. Technical report, Golder Associates.

Kramer, S. 2008. Evaluation of liquefaction hazards in Washington State, Washington State Transportation Center (TRAC), US Department of Transportation Federal Highway Administration.

NRC (National Research Council). 1985. Committee on earthquake engineering liquefaction of soils during earthquakes. Washington, USA.

Olson, S. M. and T.D. Stark. 2002. Liquefied strength ratio from liquefaction flow failure case histories. *Canadian Geotechnical Journal* 39(3): 639–647.

Olson, S.M. and T.D. Stark. 2003. Yield strength ratio and liquefaction analysis of slopes and embankments. *Canadian Geotechnical Journal* 129(8): 629–647.

Olson, S. 2001. Liquefaction analysis of level and sloping ground using field case histories and penetration resistance. PhD thesis, University of Illinois.

Pillai, V.S. and F.M. Salgado. 1994. Post-liquefaction stability and deformation analysis of Duncan dam. *Canadian Geotechnical Journal* 31(6): 967–978.

Poulos, S. J. 1981. The steady state of deformation. *Journal of Geotechnical Engineering* 107 (GT5): 553–562.

Robertson, P.K. 2010. Evaluation of flow liquefaction and liquefied strength using the cone penetration test. *Journal of Geotechnical and Geoenvironmental Engineering* 136: 6.

P.K. Robertson and K.L. Cabal. 2010. Estimating soil unit weight from CPT. 2nd International Symposium on Cone Penetration Testing, Huntington Beach, CA, USA, May 2010.

Seed, H.B. and I.M. Idriss. 1971. Simplified procedure for evaluating soil liquefaction potential. *Journal of the Soil Mechanics and Foundations Division,* ASCE, 97(9): 1249–1273.

Seed, H.B. and L.F. Harder, Jr. 1990. SPT-Based analysis of cyclic pore pressure generation and undrained residual strength. In *Proceedings of H.B. Seed Memorial Symposium*, 2: 351–376. Bi-Tech Publishing Ltd.

Tokimatsu, Kohji and H.B. Seed. 1987. Evaluation of settlements in sands due to earthquake shaking. *Journal of Geotechnical Engineering*, 113(8): 896–906.

Verdugo, R. 1992. Characterization of sandy soils under large deformations, PhD thesis, Tokyo University, Japan.

Wride, C.E. (Fear), P.K. Robertson, K.W. Biggar, R.G. Campanella, B.A. Hofmann, J.M.O. Hughes, A. Küpper, D.J. Woeller, J. Yamamuro and P. Lade. 2000. Interpretation of in situ test results from the CANLEX sites. *Can. Geotech. J.* 37: 505–529.

Yamamuro, J. and P. Lade. 1998. Steady state concepts and static liquefaction of sands. *Journal of Geotechnical and Ge-environmental Engineering* 124(9): 868–877.

Yasuda, S. 1995. Undrained deformation and liquefaction of sand under cyclic stresses. *Soils and Foundations*, 15(1).

Yu, F.W. 2017. Particle breakage and the critical state of sands. *Geotechnique* 67(8): 713–719.

Proceedings of Tailings and Mine Waste 2019
November 17–20, 2019, Vancouver, Canada
Published by the University of British Columbia, 2019

Development of a Novel Flocculant for Oil Sands Tailings

Lizbeth Rostro, Dow, USA
Orlando Castellanos Diaz, Dow, Canada
Paul A. Gillis, Dow, USA
Wu Chen, Dow, USA
Jason Tubbs, Dow, USA

Abstract

For the past six years, Dow has developed a novel flocculant (XUR) to enhance the dewatering and consolidation of fluid fine tailings (FFT) while providing a sustainable solution. New insights regarding testing and evaluation methods for tailings consolidation were found during the development of the flocculant. These changes in perspective allowed significant reductions in XUR flocculant dosage compared to those obtained with traditional test methods. Laboratory and field testing have demonstrated superior and robust performance of XUR for: a) dewatering of FFT and achieving water quality which allows water recirculation and efficient tailings ponds management; and b) consolidating of solids and achieving good geomechanical properties, which provide the ideal conditions for land reclamation. Most importantly, the field tests have validated XUR's performance and the test methods that have been developed.

Introduction

Oil sands mining operations generate substantial volumes of FFT which require tailings ponds for management and associated operational costs. The FFT is comprised of a stable colloidal suspension that is resistant to consolidation. Without treatment, these streams cease dewatering past a solids content of 30 to 40% by weight (wt%). Flocculants are commonly used to increase consolidation. Dow has developed a XUR to enable the dewatering and enhance the consolidation of FFT in tailings ponds while providing a sustainable solution. The flocculant development efforts have produced new insight regarding testing and evaluation methods for tailings consolidation.

Driven by different interactions between the XUR flocculant and the suspended particles as compared to commonly used flocculants, the evaluation methods had to be reconsidered. Changes in the test methods

led to significant improvements in the treatment strategy for the use of XUR. Specifically, the use of filtration tests such as capillary suction time (CST), gravity drainage test through a screen or permeability (cake resistance) tests and short-term settling/consolidation tests (<24 hours) were re-examined. It was determined that long-term gravity consolidation tests (>1,000 hours) were more relevant to the application of this product in depositional consolidation methods. The performance of a product is measured by the water release as it rises through the treated tailings and more accurately simulates field conditions. The laboratory methods should be relevant to the ultimate goal in the field – multi-year dewatering/consolidation and soil remediation. These changes in perspective allowed significant reductions in XUR flocculant dosage compared to the more traditional test methods. Finally, treatment with XUR was demonstrated to have a smaller environmental impact with less water use for treatment, more efficient use of deposit volumes, and the ability to treat to trafficable conditions, all while using treatment strategies that are less energy intensive (e.g. in-line flocculation).

Evolution of laboratory techniques

There are a variety of test methods used to evaluate the effectiveness of flocculants to treat tailings. Initially, Dow took the conventional approach and focused on performance measurements that could be completed within 20 hours. This simplified the testing schedule. New experiments were designed each day based on the proceeding day's results and allowed hundreds of formulations, dosages, and processing parameters to be screened each month. A key performance indicator was the settling rate, measured by monitoring the mudline in a settling chamber and calculating the solids content under the mudline. Although this test mimics the initial separation process when a treated FFT is deposited in the pond, the critical issue was whether the short-term settling observed in a laboratory correlated with long-term consolidation in the field.

After conducting several hundred settling tests, a number of key parameters were identified. First, it was determined that the settling chamber diameter needed to be large enough so that wall effects did not influence the results. Dow found that 5-gallon graduated cylinders (12-inch diameter) were adequately sized to prevent this effect. It was also observed that early assessment of performance (<24 hours) was not always predictive of long-term settling performance, as some treatments initially dewater rapidly but then plateau at a lower final solids content. In order to best judge performance, settling times greater than 1,000 hours were required (Kuvadia et al., 2017). This issue is illustrated in Figure 1, which contains settling curves of a FFT sample treated with three XUR dosage levels. The solids content was monitored for ~4,000 hours. The time scale along the x-axis is logarithmic to better illustrate settling behaviours. At 20 hours, the lowest (worst) dewatering performance was found in the low dosage treatment (red solid line). However, after 100 hours, this sample showed the best performance. At 3,000 hours, the slope of this sample continued to rise, indicating even better future dewatering results.

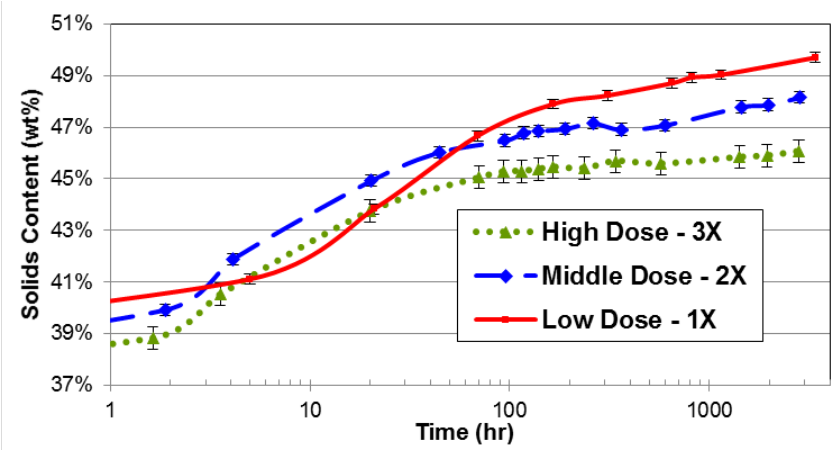

Figure 1: Effect of settling time on measuring consolidation performance

There are two main reasons why longer settling performance are important. First, a longer test is more representative of the long residence time that treated tailings will experience at the deposition site. Second, there are theoretical mechanisms that suggest that initial settling rates could be inversely related to longer term settling capability. For example, short-term settling rate increases with larger floc sizes. However, larger flocs trap water inside them and diminish the long-term dewatering ability. An amendment that creates large flocs will initially dewater rapidly but then stop dewatering. An additive, such as XUR, that forms small flocs, will start slowly, but then reach significantly higher solids levels with time.

Other laboratory techniques were used during the evaluation of XUR's performance. One such method is the CST. This method, which is commonly used in the industry to screen sludge treatments, was found to be ineffective for XUR treatment optimization in remediation processes that are not filtration based (Mayer, 2006). The test lasts a few seconds to a few minutes, closely mimicking the mechanism of an initial gravity filtration process. This method has good representation of the initial filtration rate and favours large flocs, which allows fast initial water drainage. However, the long-term dewatering and consolidation effects are not detected since the test only lasts a few minutes. We conclude that CST should only be used as a tool for gravity filtration process, and not as a tool for flocculant screening in thickening, in-line flocculation, or centrifugation processes.

XUR performance robustness

The superior performance of XUR in dewatering of FFT led to the evaluation of XUR at different process scales. Figure 2 shows a timeline of laboratory and field tests done with XUR. Initially, high throughput testing was used to screen a broad range of amendments to identify the best flocculants using FFTs with a wide range of properties (Mohler et al., 2012). Subsequently, mixing flow loops (Mohler et al., 2014) and once-through units (Gillis et al., 2013) were designed, built, and used internally to optimise the treatment

conditions (i.e. mixing intensities and dosages). Together with an upgrade to 5-gallon containers, Dow's testing capabilities resulted in the ability to optimise the treatment conditions used in a number of field tests (Figure 2) (Kuvadia et al., 2017). As a result, the dosage was optimised to 350 parts per million (ppm) while only requiring pipeline mixing to achieve good dewatering (Rostro et al., 2018). Further studies showed the resilience of XUR at 350 ppm with a large number of FFT sources ranging in clay content and initial solids content (Kuvadia et al., 2017).

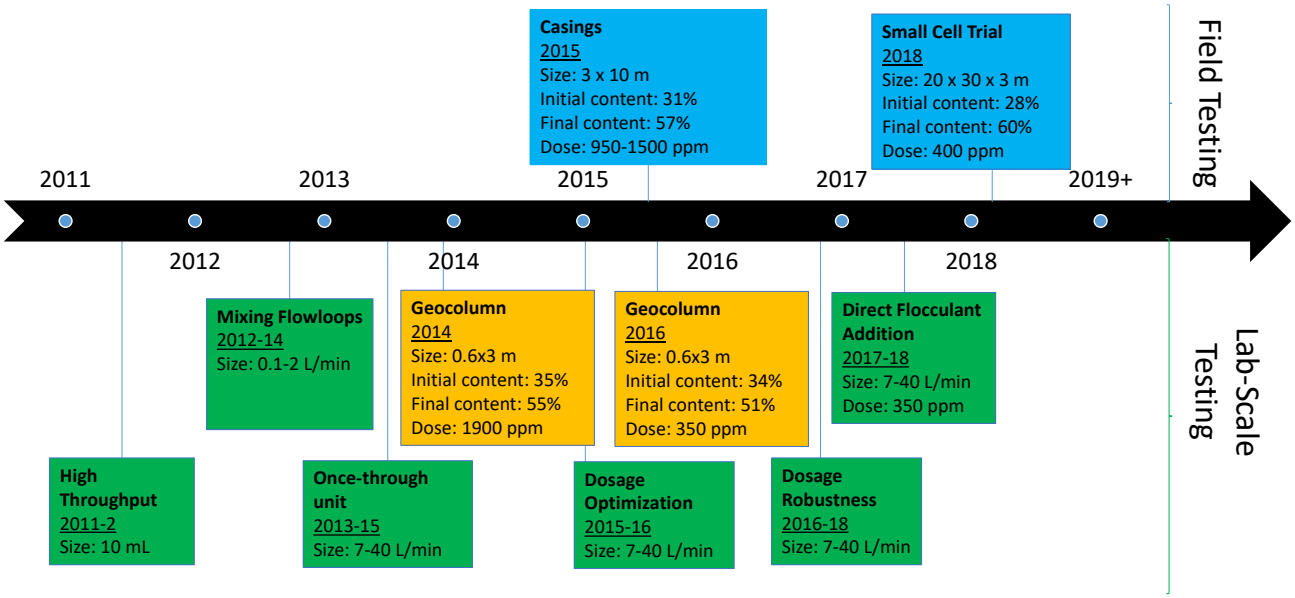

Figure 2: Timeline of XUR laboratory and field testing (green: internal laboratory work; orange: laboratory work by mine operator; blue: field work by mine operator)

Upon dosage optimization to 350 ppm at the laboratory scale, the efforts shifted to showcase the performance of XUR at larger scales and under conditions that more closely mimic a full-scale process. In 2014, 3 metre (m) tall geocolumns were filled by a mine operator with XUR treated tailings at 1,900 ppm. The fill was completed using Dow's flocculation rig, which was comprised of two pump systems (one for FFT and one for XUR solution) and a static mixer. The geocolumn was equipped with pressure transducers to monitor the pore pressure dissipation and was marked along the height of the column, which enabled the ability to determine the solids content under the mudline. The geocolumn was monitored for about a year before decommissioning. At this time long-term laboratory studies had not been conducted and as a result, the optimised treatment conditions for the trial were at the higher dosage (Poindexter et al., 2015). In 2016, another geocolumn (GC5) was filled with FFT treated with XUR at the optimised dosage of 350 ppm. Table 1 details the comparative results of both geocolumns filled with XUR treated tailings and one filled with partially Hydrolysed Poly-AcrylaMide (HPAM) treated tailings (discussed later in the report). Although the FFT sources used to fill GC2 and GC5 were different, it is important to note the similarities in performance even at the drastically different treatment rates. The results show that the dewatering

performance was comparable between the XUR treatment at 1,900 ppm and 350 ppm with a degree of settlement of 99% and 98%, respectively. In addition, the pore pressure dissipation monitored in the geocolumn confirmed that regardless of the dosage with XUR, the pore pressure is completely dissipated. The final solids content of the GeoColumns (GCs) are different; however, the GC2 settled for more than two years while GC1 was decommissioned after significantly less settling time. These findings confirm the validity of the laboratory techniques developed and showcase the robustness of XUR and the significant tolerance to dosage changes.

Table 1: Comparison of geocolumn performance between HPAM and XUR (Stianson et al., 2016b)

	GC1	GC2	GC5
Treatment type	HPAM	XUR	XUR
Dosage	1,000 ppm	1,900 ppm	350 ppm
Final solids content	47 wt.%	57 wt.%	51 wt.%
Degree of settlement (%)	88	99	98
Degree of pore-water pressure dissipation (%)	65	100	100

A similar study to those of the geocolumns was performed in the field using cement casings with a 3 m diameter and 10 m height. Given the larger size relative to the geocolumns, these casings represent a step closer to the field scale. The XUR casing was filled at 10 gallons per minute (gpm) using Dow's flocculation rig. The treatment conditions at this time (before the low dosage optimization) were optimised to 1,500 ppm, a 21% reduction in dosage compared to the previous years' work. The dewatering performance was compared across all filled casings (Stianson et al., 2016a). In particular the FFT treated with XUR reached 57 wt% after 180 days (Stianson et al., 2016a). The casings have been in place for nearly four years and have continued to consolidate over time. Although the casing performance is no longer tracked on a continuous basis, the solids content of the XUR filled casing now exceeds 60 wt%. Table 2 details the comparative performance for a given time. The HPAM performance will be detailed later in the "Tailings treatment robustness of XUR vs. polyacrylamides" section of this paper.

Table 2: Data comparing HPAM and XUR from the casing pilot study. All data collected within the same timeframe – 180 days (Stianson et al., 2016a)

	Casing 1	Casing 2	Casing 3	Casing 8
Treatment type	none	HPAM	XUR	HPAM – Centrifuge
Dosage (ppm)	–	950	1,500	1,200
Start solids content	35 wt.%	32 wt.%	31 wt.%	45 wt.%
Final solids content	44 wt.%	50 wt.%	57 wt.%	46 wt.%

Lastly, based on the encouraging results from GC5, a 1,500 cubic metre (m^3) deposit was filled with FFT in 2018. The deposit was 20 m x 30 m x 3 m in size and was filled with XUR treated FFT at 400 ppm. The target dosage was 350 ppm, but due to process limitations 400 ppm was the lowest attainable treatment rate. The deposit was filled in about eight hours using existing onsite equipment. The deposit was equipped with wire logging to monitor pore pressure dissipation, temperature and mudline changes. In addition, samples were taken during the trial for lab monitoring and evaluation. Preliminary results show that the solids content at the bottom of the deposit had reached 64 wt% in under eight months. It is expected that the solids content of tailings will increase as the height/self-weight of the deposit increases. Under these conditions the treated material will be at even higher solids content and allow for the tailings ponds to be remediated without further treatment or earthworks.

In addition to the effectiveness of XUR and its scalability to field performance, perhaps the other important characteristic of an amendment for dewatering FFT is its robustness to variability in operation conditions. Robustness is critical due to the variability in mineral deposits and the resulting variation in clay content and other FFT properties. The greater the ability of the process to handle FFT variation, the fewer the interventions needed to operate a continuous process.

The effect of dosage and mixing on XUR's performance have been reported previously (Kuvadia et al., 2017; Rostro et al., 2018). At the early stages of the XUR development, when dosages were high (>1,200 ppm), the use of dynamic mixing was required to achieve good mixing and to have an effective interaction between the flocculant and the fines in the FFT. As the treatment dosage decreased, it was determined that dynamic mixing was no longer required (Rostro et al., 2018). Moreover, the treated FFT was found to be tolerant to intense mixing intensities as this did not seem to affect long-term dewatering performance or the quality of the release water (Poindexter et al., 2016).

Furthermore, Dow tested XUR's robustness by treating a wide variety of FFT with a broad range of properties. These samples varied in clay content (MBI values from 7 to 11) and initial solids content (32 to 41 wt%). Over 40 different FFTs were evaluated. Figure 5 shows the performance of three treated samples showing variation of initial solid content and clay content. XUR was found to provide significant dewatering at moderate (<500 ppm) dosages in all of the samples tested (Kuvadia et al., 2017).

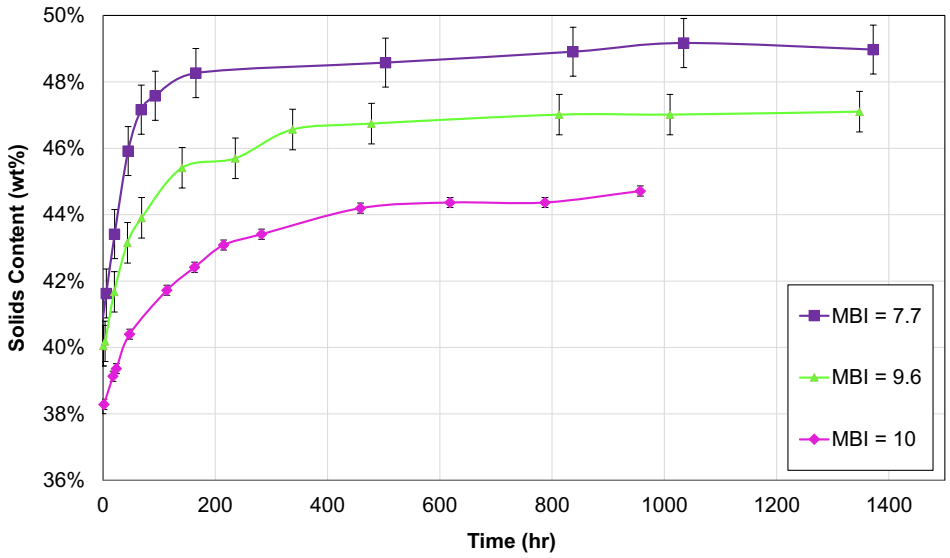

Figure 5: Strong performance of XUR across a wide range of FFTs (variable initial solids content and clay content) (Kuvadia et al., 2017)

Tailings treatment robustness of XUR vs. polyacrylamides

In addition to its performance and robustness, another critical characteristic of XUR is its superior effectiveness compared to alternative flocculants. Currently, HPAM is the incumbent amendment in the industry. In general, HPAM forms large flocs and will often show initial higher dewatering rates whereas XUR forms small flocs which typically generate slower responses but with ultimate higher dewatering performance. Due to this difference, one could be misled and make incorrect conclusions when evaluating performance solely based on test methods such as CST or short-term dewatering analysis.

One study comparing XUR with HPAM was the geocolumn work, introduced earlier. The dewatering performance as well as deposition characteristics are summarised in Table 1 (Poindexter et al., 2015). As can be seen, the dewatering performance during this time showed the superior ability of XUR (GC2) to flocculate FFT compared to HPAM (GC1). Here, the same FFT source was used for both geocolumns enabling a direct performance comparison. The solids content attained by XUR was 10 wt% higher than that by HPAM. Also, HPAM was not able to completely dissipate the pore pressure in the deposit and only reached 65% dissipation. Even when comparing HPAM's performance to XUR at the low dosage, XUR's overall performance is superior in its ability to dewater. This is showcased by the higher solids content and the poor pressure dissipation. Additional information and images can be found elsewhere (Poindexter et al., 2015).

Field-scale tests have also been used to compare XUR and HPAM. Table 2 shows the dewatering performance comparison from the casings fill in 2015 with XUR, HPAM, and centrifuge cake treated with HPAM. All casings detailed in Table 2 were filled with a homogenised FFT sample. The first casing

performed the poorest and was the control experiment with no amendment. The best dewatering performance (highest solids content) was attained from Casing 3 which was filled with XUR treated tailings. This performance was superior to the HPAM treatment (Casing 2) which only reached 50 wt% solids compared to 57 wt% from XUR. Additionally, the centrifuge cake samples attained from using HPAM only reached 46 wt%. With this performance XUR outperformed the HPAM treatment when comparing both in-line flocculation and centrifuge treatment. In summary, all evaluations in the field comparing XUR and HPAM have shown higher final solids content when XUR was used.

Another important performance indicator is the water quality released from the treated FFT. In the geocolumn work of 2014, the mine operator retrieved water and gas samples for analysis. As shown in Figure 6, the quality of the water is quite different between the two treatments. The release water from HPAM is brown in color compared to the clear water from XUR. The brown color is attributed to residual fines that HPAM is unable to capture. A summary of additional analytical results is presented in Table 3.

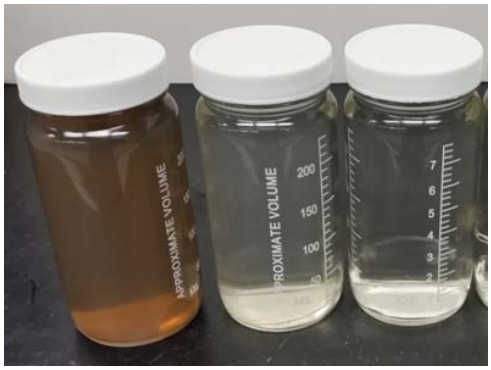

Figure 6: Release water from GC1 (HPAM, left) and GC2 (XUR, middle and right)

Table 3: Comparison of water quality from geocolumns between HPAM and XUR. Values are average across column taken at 400 days at 25°C (*data after 1,000 days)

	GC1	GC2	GC5	GC11
Treatment type	HPAM (1,000 ppm)	XUR (1,900 ppm)	XUR (350 ppm)	None
pH	8.7	8.5	9.1	9.1
Total dissolved solids (mg/L)	1,400	1,400	1,400	1,300
Total suspended solids (mg/L)	300	80	<10	n/a
Turbidity (NTU)	200	0	120	200
Dissolved oxygen (mg/L)	5.2	3.8	5.2	1.5
Naphthenic acids (mg/L)	6.5*	9.0*	11	6.5

In general, the results showed limited variation between geocolumns. The pH, dissolved oxygen, and oxidative-reductive potential increased over time for all the water samples, which indicates changes in

oxidative environment. This trend is favourable as oxidizing conditions are more supportive of aquatic life. The total suspended solids (TSS) and turbidity decreased over time for all columns, with the untreated sample being the slowest and those treated with XUR being the fastest. For instance, GC5 yielded values below 100 nephelometric turbidity units (NTU) and 10 milligrams per litre (mg/L) TSS within a couple of months, while HPAM took more than a year to reach similar values. Minor differences in metal concentrations (such as arsenic, copper, cadmium, chromium of selenium) were observed within the geocolumns.

Although naphthenic acid values for XUR treated material were, in general, higher than other geocolumns, all values were below typical reported tailings water concentration. Some naphthenic acid degradation was seen on the older samples for both HPAM- and XUR-treated release water. This degradation towards lower molecular weight compounds reduces the toxicity of water. Eco-toxicity tests with *Ceriodaphnia dubia* (a regional water flea species) and rainbow trout were also conducted. No trout mortality was detected in any of the columns. There was, however, high toxicity towards *dubia* in all columns, with the column with no treatment being the most toxic. The use of XUR seems to indicate lower levels of toxicity as the dosage is increased. Further analysis is necessary to provide definitive conclusions.

Finally, qualitative gas analysis suggested potential emissions of residual hydrocarbons (such as pentane) and of gases generated by microbial activity (after DNA sequencing). Hydrocarbon, CO_2, and methane emissions exceeded those of ambient conditions, especially after agitation of samples. Note that gas testing results were affected by air entrainment during the monitoring of the geocolumns.

Environmental and performance benefits of XUR

It is clear from the data that the use of flocculants in tailings ponds will have a significant effect on tailings pond management, water quality, and utility requirements for mine ore processing. At the beginning of the treatment process, the flocculant is typically hydrated, which requires a hydration facility that uses energy and requires maintenance. Once treated, the dewatering performance impacts the volume of the depositional pond and how much water can be recycled back into the process. With higher dewatering performance the solids reach higher consolidation, the volume of the pond decreases, and there is more volume of water removed for recycling. Also, with the higher water quality the resources required for recyclability are lowered. The surface area of the pond, together with the water quality, impacts potential greenhouse gas emissions via evaporation of hydrocarbons or chemical reaction catalyzed by ultra-violet (UV) light. This area is also exposed to migratory wildlife that can be impacted by the water surface properties and toxicity. While the specific benefits of XUR to a particular tailings pond depends on the pond and process characteristics, Table 4 provides a quantitative account of those benefits.

Table 4: Impact of XUR on sustainable tailings pond management relative to current treatment options

XUR performance	Description	Utilities water treatment	Water resources	Pond remediation/ reclamation	Land disturbance	GHG emissions	Wildlife disturbance	Occupational safety	CAPEX and OPEX
Absolute water release	Increase in release water volume due to the higher solids content attained. Enables the ability to recycle more water.		■						■
Settling performance	Higher solid content of the treated tailings results in a more compact (smaller) deposit. Better conditions for reclamation and significantly lower cost for reclamation and earthworks.			■	■				■
Water quality – solid content	Greater ability to capture fines and thus lower solids content in the release water. Less stress on water treatment facilities (lower cost) and better recyclability, less water intake. Less maintenance implies less manpower exposure and lower safety risks.	■	■					■	■
Water quality – composition	No changes in water toxicity, hydrocarbon content, nor mineral content of water. No additional divalent content reduces water treatment requirements and costs. Lower hydrocarbon content and exposed area (smaller pond size) reduces GHG emissions. Positive toxicity implies minimal impact on migratory wildlife.	■		■		■	■	■	■
Dosage optimization	Reduced dosage for treating ponds (300–500 ppm) requiring less process water for hydration, slower pond growth, and potential lower costs on earthwork (pumps, pipes, etc.).		■		■				■
Robust performance	Same dosage applied to a variety of FFTs with no impact on consolidation or water quality. Can be used in existing infrastructure.		■					■	■

Tailings remediation with XUR in powder form

Recent developments have shown that XUR can be used to flocculate FFT without the need to hydrate the flocculant prior to treatment. This means that XUR powder can be added directly into the FFT before it is deposited for remediation. The performance attributes described for XUR in the aqueous form have been shown to translate to the treatment with the dry form of XUR. As such, the treatment can be done by using XUR directly at dosages of 350 ppm with high quality release water and superior dewatering performance. As shown in Figure 8, the dewatering capability is nearly identical with either treatment strategy. In turn, this new process eliminates the need for the flocculant hydration step, and most importantly it eliminates

the need for adding water to the FFT. Therefore, the deposit volume requirements are reduced even further. Ultimately, this development will reduce the capital and operation cost for tailings management.

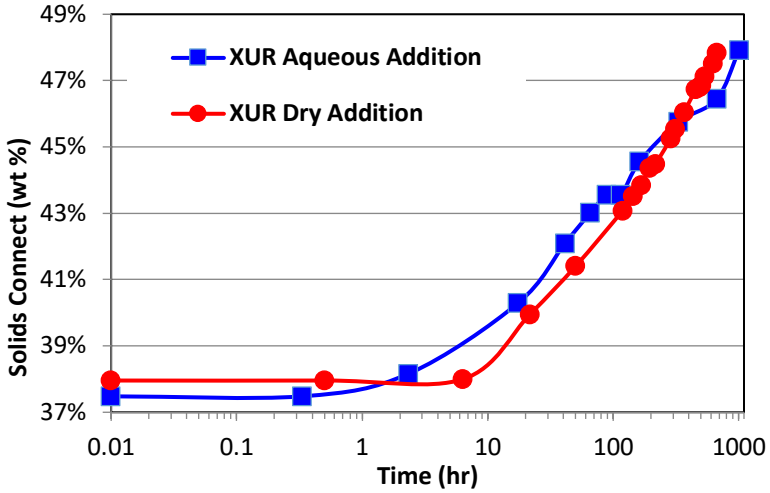

Figure 8: Dewatering performance of XUR treated tailings by method of aqueous XUR solution addition or XUR dry powder addition

Conclusion

In summary, significant progress was made to understand the test conditions for the development of a novel flocculant for the remediation of oil sands tailings. These findings resulted in the optimization of the treatment strategy with XUR. The use of short-term tests such as CST and overnight settling analysis were found to be unsuitable for evaluating XUR, and limited the ability to fully capture the effectiveness of XUR. The excellent performance obtained from XUR led to a number of field tests. In these tests, the novel flocculant showcased the ability to treat at dosages as low as 350 ppm, while releasing high-quality water and obtaining higher solids content compared to HPAM. Solid content surpassed the 60 wt% mark at field scale.

From a sustainability perspective, the lower dosage combined with the ability to use the flocculant in the dry form significantly decreases the impact on the water requirements for remediation. Furthermore, the high-quality water that is released will require less water treatment for recycling the water in the process. In addition, the lower dosages will require less depositional volume, and the consolidation attained will also result in lower volume requirements for the ponds. The treatment using XUR will have a smaller impact on the land disturbance, also reducing costs and improving occupational hazard exposure. Moreover, due to the ability of XUR to obtain higher solids content (surpassing 60 wt%) the tailings ponds can be remediated with potentially minimal surface treatment and no bulk treatment or handling before capping. Lastly, it is expected that dry powder addition of XUR will provide a better sustainable and environmentally conscious solution without impacting dewatering performance.

References

Gillis, Paul, Jason Moore, Michael Poindexter, Cole Witham, Wu Chen, Harpreet Singh, Carol Mohler and Jesus Atias. 2013. The effects of in-line static mixer flow loop operational parameters on flocculant performance in mature fine tailings (MFT) samples. Tailings and Mine Waste, Banff, Alberta.

Kuvadia, Zubin, Michael Poindexter, Paul Gillis, Lizbeth Rostro, Wu Chen and Jason Tubbs. 2017. Statistical data mining approach to improve understanding of flocculant dewatering of fluid fine tailings. Tailings and Mine Waste, Banff, Alberta.

Mayer, E. 2006. Laboratory testing protocols used for biosolids dewatering. *Filtration* 6(3): 193–199.

Mohler, C. E., M.K. Poindexter, J. Atias, W. Chen, and C.A. Witham. 2012. Development of flocculants for oil sands tailings using high-throughput techniques. International Oil Sands Tailings Conference, Edmonton, Alberta.

Mohler, C., M. Poindexter, C. Acevedo, T. Sanders Jr., G. Meyers, C. Reinhardt, W. Chen, H. Singh and J. Atias. 2014. Clay-flocculant interactions in developing next generation flocculants for oil sands fluid fine tailings management. Fourth International Oil Sands Tailings Conference, Lake Louise, Alberta: 437–445.

Poindexter, M., P. Gillis, J. Moore, J. Tubbs, R. Mahood and G. Freeman. 2015. Geotechnical column evaluation of new flocculant technology for dewatering oil sands mature fine tailings. *Tailings and Mine Waste Conference,* October 25–28, Vancouver, British Columbia: 490–499.

Poindexter, Michael, Paul Gillis, Jason Moore, Lizbeth Rostro, Wu Chen and Jason Tubbs. 2016. Optimization of new flocculant technology for dewatering oil sands mature fine tailings. Fifth International Oil Sands Tailings Conference, December 4–7, Lake Louise, Alberta.

Rostro, L., P.A. Gillis, W. Chen, J. Tubbs, and M. Poindexter. 2018. Robust low dosage treatment across multiple oil sands fluid fine tailings samples using an amendment. International Oil Sands Tailings Conference, Edmonton, Alberta.

Stianson, J., R. Mahood, D. Thomas, J. Song and L. Li. 2016a. A Shell tailings consolidation casing experimental pilot project (TCCEPP). International Oil Sands Tailings Conference*,* December 4–7, Lake Louise, Alberta: 432–441.

Stianson, J., R. Mahood, D.G. Fredlund, and J. Sun. 2016b. Large-strain consolidation modeling to determine representative tailings consolidation properties from two meso-scale column tests. Fifth International Oil Sands Tailings Conference. December 4–7, Lake Louise, Alberta: 40–50.

Chapter 8

Additional Paper

TAILINGS AND MINE WASTE 2019

Proceedings of Tailings and Mine Waste 2019
November 17–20, 2019, Vancouver, Canada
Published by the University of British Columbia

Laboratory and CPT_U Characterization of Samarco Sand Tailings

Richard Dawson, Stantec Consulting Ltd, Canada
Andrew Burgin, Stantec Consulting Ltd, Canada
Mathieu Wacowich, Stantec Consulting Ltd, Canada
Jose Bernardo, Samarco Mineracao SA, Brazil
Analisa Vasconcelos, Samarco Mineracao SA, Brazil

Abstract

Samarco was founded in 1977 as a fully integrated iron ore mining and processing company. Iron ore pellets are the main product, with sales to the international steel industry. Following the Fundão dam failure on November 5, 2015, in Brazil, Samarco ceased operations in order to focus on environmental remediation and tailings dam safety measures. Samarco then embarked on a multi-faceted program to ensure that these water and tailings containment structures complied with best practices in tailings dam safety management, and in March of 2016, Stantec was retained to assist in this regard. There are two remaining sand tailings structures at Samarco. Laboratory testing of Samarco tailings sand over a wide stress range shows that the critical state line (CSL) is curved in e vs log(p') space. Very loose samples are extremely brittle. The link between laboratory and field behaviour was investigated by measuring shear wave velocity in the lab using bender elements and converting compressibility and CSL lines to equivalent $Q_{tn,cs}$ using a published relationship. This shows a gradual increase in "equivalent" $Q_{tn,cs}$ with depth indicating that the liquefied shear strength should also increase with higher effective stress conditions.

Introduction

Samarco was founded in 1977 as a fully integrated iron ore mining and processing company. Iron ore pellets are the main product with sales to the international steel industry. The company has two operating units: Germano, near Mariana (MG), where iron ore extraction and beneficiation occur, and Ubu, in Anchieta (ES), where four pelletizing plants are located. The units are interconnected by three 400-kilometer-long pipelines, which run through 25 municipalities of the two states.

Iron ore processing at Samarco's Germano mining and processing complex results in two distinct kinds of tailings, hydraulically transported as two separate slurry streams to the tailings containment areas.

There is a coarse "sand" tailing consisting of silt and sand sized particles that form a drainable beach deposit, and a fine "slimes" tailings that displays clay-like behaviour and settles slowly from suspension to form a weak, cohesive deposit. Safe storage and containment for each of these materials is key to the geotechnical integrity of the tailing's structures.

Following the Fundão dam failure on November 5, 2015, Samarco ceased operations in order to focus on environmental remediation and tailings dam safety measures. Figure 1 shows a satellite image of Samarco's Germano site. There are two existing tailings structures at the Germano mine site:

- The Germano main dam (GMD) complex was the first area developed to contain tailings for the mining operation, and was in operation between 1976 and 2016. It is in the valley south of the Fundão basin and upstream from the Santarém reservoir. There is a large starter dam halfway up the valley with upstream raises from its crest, and a lower structure consisting entirely of well drained tailings sand also placed in an upstream fashion. This lower structure is tightly wedged into the valley walls near the toe and contains a rock drain all along its length. The overall GMD structure is 165 m high with 3H:1V downstream slopes and contains about 150 million m^3 of tailings.

Figure 1: Samarco's Germano site

- The Germano Pit (GP) tailings facility is contained within the mined-out Germano Pit and was operated between 2001 to 2015 as a tailings sand (no slimes) storage area, surrounded on three sides by the pit itself. The dam structure at the pit outlet is about 50 m high with 3H:1V downstream slopes. The GP storage is much smaller than GMD and contains about 20 million m^3 of sand.

After ceasing operations in late 2015, Samarco embarked on a multi-faceted program to ensure that both structures complied with best practices in tailings dam safety management, and in March 2016 Stantec was retained to assist in this regard. Both Samarco structures employed upstream construction for dam raising, and both structures contain underdrains in the toe regions that control drainage conditions. There are no fluids currently impounded behind these structures.

The purpose of this paper is to present the results from detailed laboratory and field evaluations carried out to characterize tailings sand geotechnical properties for Samarco tailings sand. Findings from this work have been used to evaluate dam safety. The work builds on the findings from the Fundão Tailings Dam Review Panel (2016) report.

Laboratory test program

a)

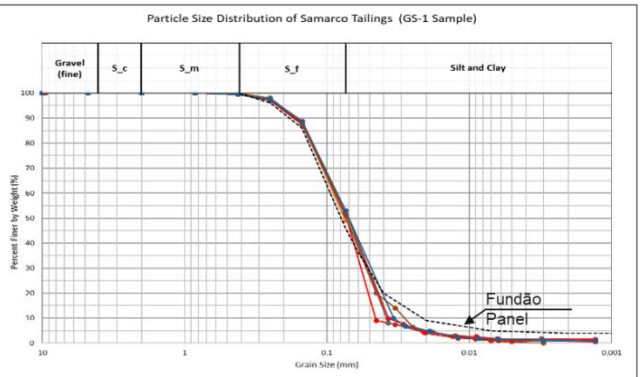

b)

Sample ID	% Fines (<74µm)	D_{10} (mm)	Specific Gravity, G_s	Relative Density	
				e_{max}	e_{min}
GS1	52 (49 – 53) (8 tests)	0.029 – 0.045 (6 tests)	2.94 (2.91 - 2.98) (5 tests)	0.85	0.40

c)

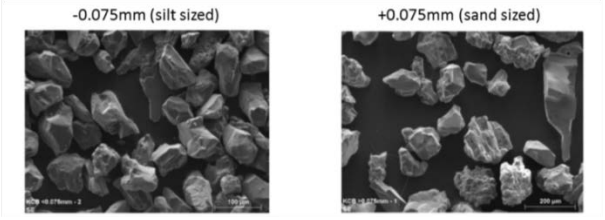

Figure 2: Samarco tailings sand properties: a) grain size distributions, b) index properties, c) scanning electron micrographs from Fundão Panel report

Laboratory tests were carried out in 2018 with "typical" Samarco tailings sand sampled from the Germano Pit tailings facility. Figure 2 shows the grain size distribution for the sample material compared with the tailings sand tested during the Fundão Tailings Dam Review Panel (2016) program. Grain sizes for the two sets of silty sand samples are similar, with about 50% fines. The scanning electron micrographs (SEM) in Figure 1(c) (from the Fundão Panel report) show that the individual grains are sub-angular and blocky; both silt-size and sand-sized particles have similar grain shapes.

Compressibility

Figure 3 shows a series of consolidation tests carried out in a conventional oedometer apparatus up to a maximum vertical effective stress of 6 MPa and with initial void ratio varying between 0.59 and 0.84. All the tests are curvilinear in e versus σv' space and roughly parallel to one another.

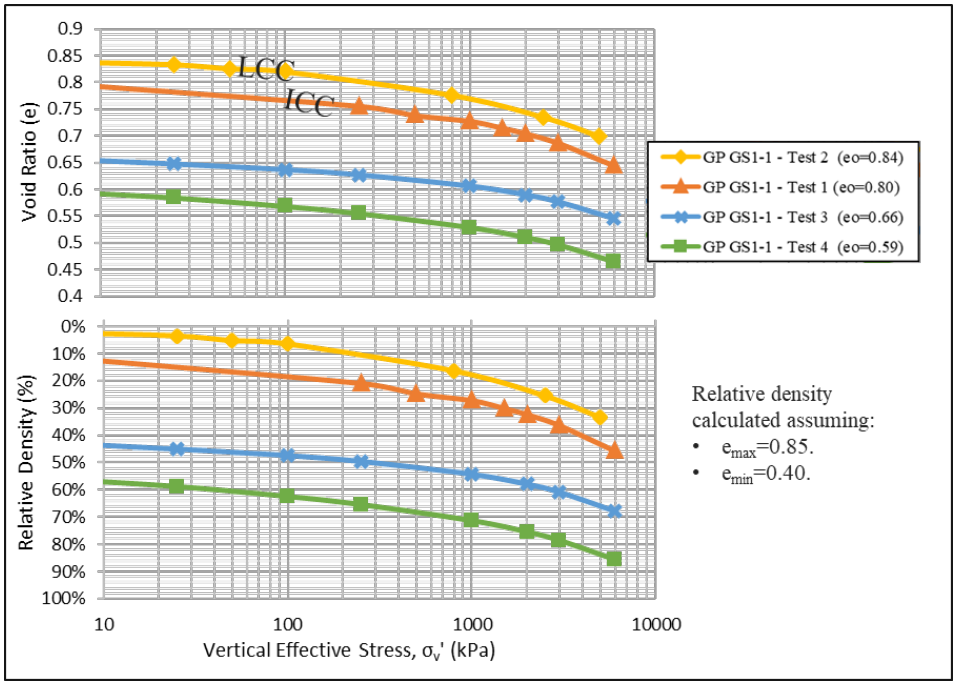

Figure 3: Samarco tailings sand compressibility from oedometer tests

The loosest test with initial void ratio equal to 0.84 is labelled as a limited compression curve (LCC) following terminology used by Robertson (2018). The LCC is a very loose sand with an initial density at the maximum void ratio (i.e., 0% relative density). The line labelled as ICC represents compressibility for a loose sand with 10% initial relative density. These are reference compressibility lines for tailings sand behaviour loose of the critical state condition.

Critical state line

Determination of the CSL over a range of higher stress initial consolidation conditions was a focus for the testing program. These tests were carried out with triaxial testing equipment specially equipped for consolidating at high cell pressures. The testing included nine isotropic triaxial (three drained and six undrained) and one an-isotopically consolidated undrained test. Void ratios after shearing were determined by freezing the sample prior to removing it from the test apparatus and measuring moisture content of the frozen material; this method avoids some of the pitfalls associated with determining accurate void ratio.

Figure 4 shows the "best fit" CSL (mean effective stress versus relative density) determined for Samarco tailings sand from the testing program compared with two other sandy materials (Robertson,

2018); these were selected because of their curvilinear behaviour at higher stress. Curvature of the CSL in sands at high stresses indicates onset of particle crushing. The figure also shows Samarco sand CSL derived by the Fundão Tailings Dam Review Panel (2016) program for reference. The critical state friction angle is 32°. Key points are noted as follows:

- Three curves (including the CSL in this paper) are curvilinear over a larger stress range. These curves are relatively flat at low stresses and steepen at about 20 to 30% relative density.
- The two Samarco tailings sand CSLs (this paper and the Fundão Panel's) are similar for mean effective stress (p') in the 100 to 1,000 kPa range.
- The CSL for the work carried out for this paper is represented by a power curve relationship. The laboratory data did not provide good CSL definition at low stresses and the curve is shown as dashed less than 100 kPa.

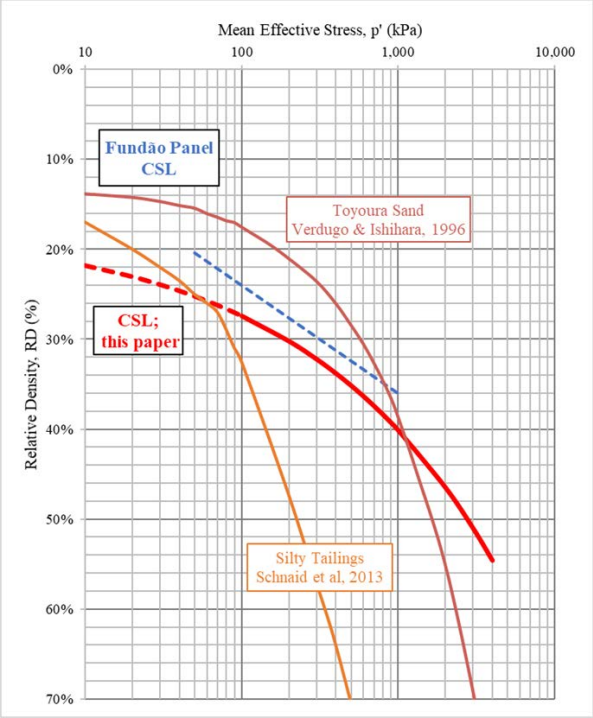

Figure 4: Critical state line for Samarco sand tailings and other sand-like soils

Critical state soil mechanics principles indicate that the large-strain strength ratio of a soil is independent of the initial stress conditions, provided that the CLS and compressibility lines are parallel. The large-strain strength ratio may decrease if the slope of the compressibility line steepens and converges towards the CSL at high stresses. This phenomenon is explored further through evaluation of strain weakening response at different stress levels.

Brittleness

Figure 5 shows a summary of the stress/strain and stress paths (in p'-q space) for five contractant undrained triaxial tests. All tests show a marked strain weakening response at 1 to 2% strain, which is typical for sands susceptible to flow liquefaction. The liquefied shear strength ($Su_{(liq)}$) is the shear strength mobilized at large deformations in a saturated soil after triggering of a strain softening response. The inset table in Figure 5 shows the Brittleness Index (IB) and the large-strain undrained strength ratio ($Su_{(liq)}/\sigma v'$).

The Brittleness Index (IB) is a measure of this strain weakening response strength loss from peak to residual defined as:

$$I_B = (q_{max}-q_{min})/q_{max}$$

Test ID	e_{final}	P_0' (kPa)	I_B	S_u/σ_v'
1. CIU_200kPa	0.72	200	0.33	0.30
2. CIU_700kPa	0.73	700	0.96	0.01
3. CIU_1200kPa	0.85	1,200	0.87	0.02
4. CIU_2500kPa	0.74	2,500	0.50	0.10
5. CAU_2500kPa	0.69	3,333	0.32	0.21

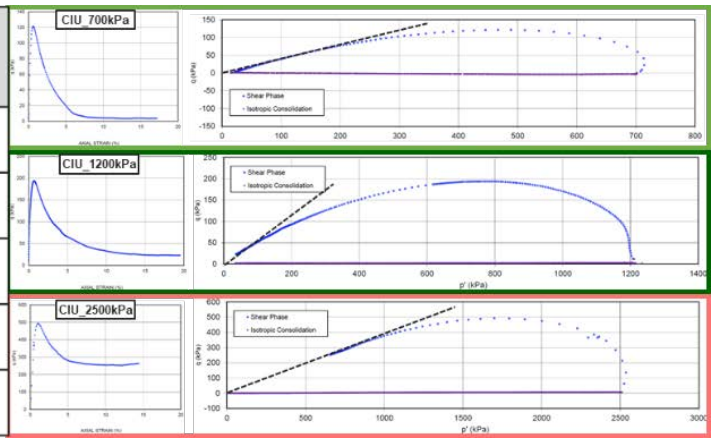

Figure 5: Brittle behaviour from Samarco sand triaxial tests

Sadrekarimi and Olson (2011) provide important insights about laboratory testing for CSL and brittle behaviour of sandy soils. They have observed unique relationships between sand brittleness and critical strength ratio (σ'_c/σ'_{cs}) that is independent of sand type, mode of shear, fabric, and particle damage. Figure 6 presents their data shown in two different formats, indicating that the critical strength ratio increases with decreasing brittleness (left-hand graph), and that brittleness increases with increasing σ'_c/σ'_{cs} (right-hand graph).

Figure 6 also shows the Samarco tailings sand contractant test data plotted against the Sadrekaremi and Olson (2011) relationships. Most of the Samarco tailings sand tests data fits the trends. Robertson (2018) has examined these trends with respect to liquefaction behaviour at high stresses and noted that most liquefaction flow failures occur at brittleness index values greater than 0.4, which corresponds to $Su_{(liq)}/\sigma'_{va}<0.1$.

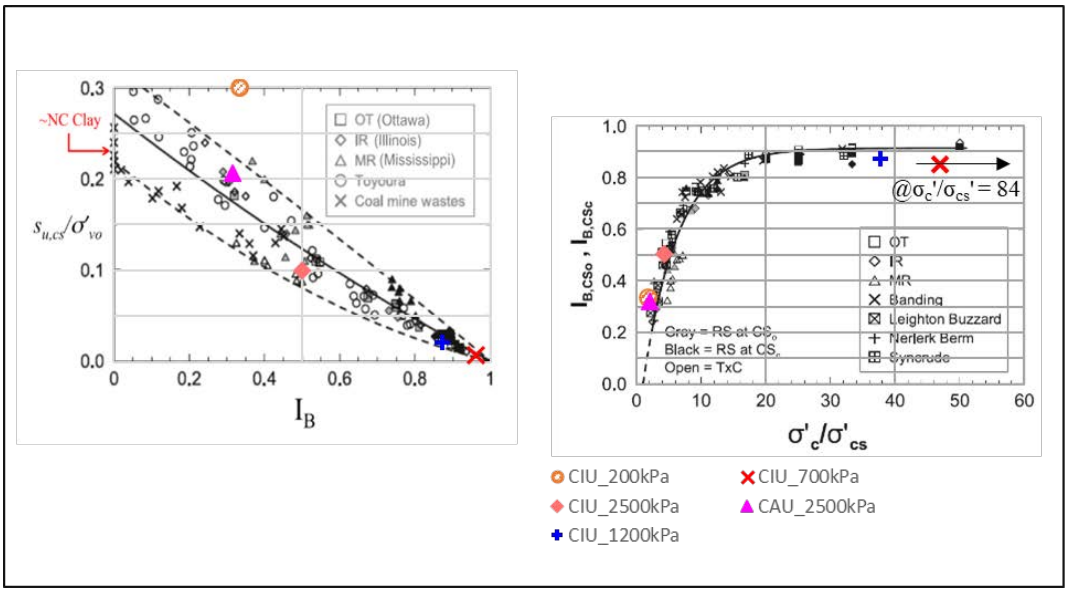

Figure 6: Brittle behaviour of sandy soils

Loose samples of Samarco tailings sand show markedly less brittle behaviour at po' >2,500, corresponding to a critical strength ratio of about 4 between the LCC and CSL (see Figure 6), which shows that the large-strain strength ratio ($Su_{(liq)}/\sigma v'$) decreases at high stresses.

Shear wave velocity measurement

Shear wave velocity (Vs) is a small-strain response. In tailings sands it is related to relative density, effective stress, state, stress history, and mineralogy. It can be measured in the laboratory using bender elements. Cunning et al (1995) provide a framework for normalizing lab derived Vs data based on a relationship between normalized shear wave velocity (V_{S1}) and void ratio, where V_{S1} is defined as:

$$V_{S1} = V_S(P_{atm}/\sigma_v')^{0.25}$$

Where:

P_{atm} = atmospheric pressure

σ_v' = vertical effective stress

The procedure adjusts for variable effective stress conditions so that the normalized data for saturated samples typically fit a straight-line relationship. Robertson (2017) and others have observed that unsaturated test samples display a different relationship due to effects of soil suction on the shear wave velocity measurements.

Figure 7 shows test results from bender element testing of Samarco tailings sand. The saturated data derived from triaxial tests defines a straight-line relationship between V_{S1}. Figure 7 also shows normalized data from the Fundão Panel report for comparison; this data appears to fit a slightly different trend. The

unsaturated Samarco tailings sand data lies above the saturated data separated by V_{S1} values of about 100 m/s.

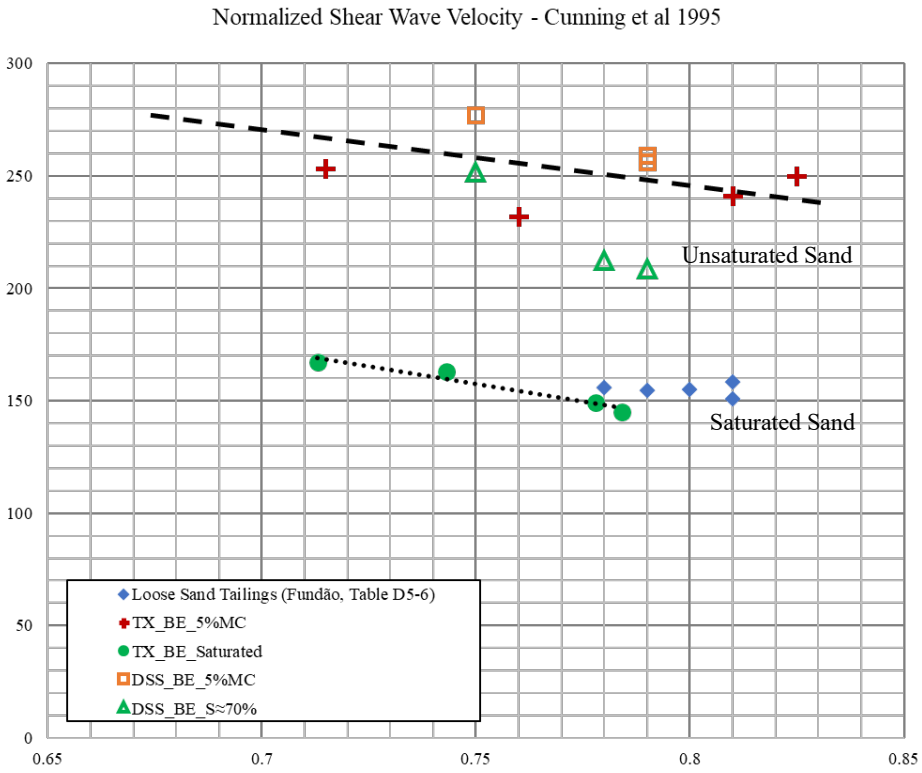

Figure 7: Normalized shear wave velocity versus void ratio

Cone penetration testing

Samarco has carried out over 100 CPTu soundings at their two tailings facilities. Cone penetration testing is the main investigation method for soil type behaviour at these facilities. It is also used to supplement piezometer data for monitoring water table conditions.

Figure 8 shows penetration test data for GP and GMD plotted on the Robertson (2016) modified, normalized soil behaviour type (mod. SBTn) chart. The data was screened to remove values above the water table (i.e., unsaturated sand) and to exclude clay-type material (I_B<22). Robertson (2010) indicates that Q_{tn},cs = 70 represents a conservative boundary between contractant and dilatant response. Robertson's (2010) evaluation of Class A (most reliable case history data) flow liquefaction case history data for the mean +1 standard deviation (i.e., about 70 of normalized tip resistance values from interpreted failure zone plots at Q_{tn},cs <70). Most of the CPTu profile data for Samarco sand tailings deposits classifies as transitional contractive material (TC in Figure 8). The histograms for saturated tailings sand from both deposits show remarkably similar normalized penetration resistance (Q_{tn},cs) statistics with mean values of 59 and standard deviation of about 10.

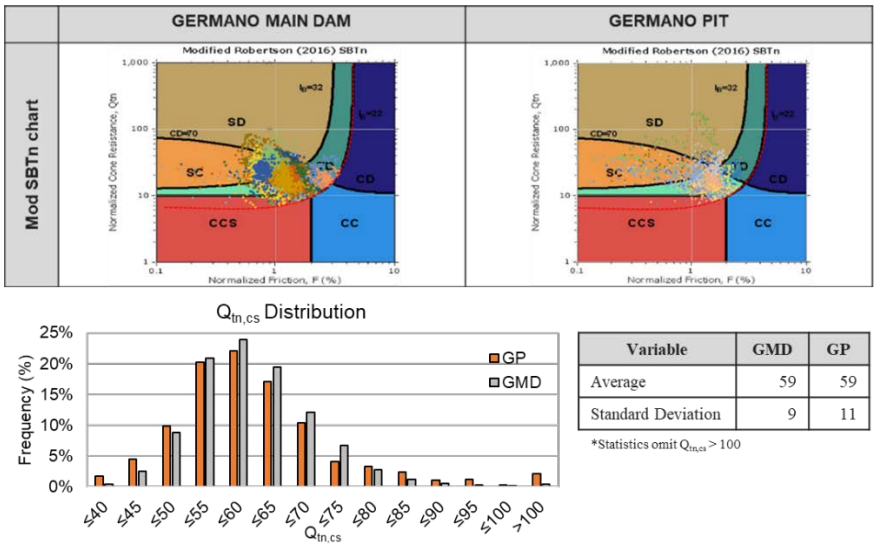

Variable	GMD	GP
Average	59	59
Standard Deviation	9	11

*Statistics omit $Q_{tn,cs} > 100$

Figure 8: CPTu soil behaviour type (modified SBTn, Robertson, 2016) for saturated Samarco tailings sand

Figure 9 shows two representative profiles of normalized tip resistance with depth for the sand tailings deposits at Samarco. The left-hand plot shows dilatant sands/silts above the historic water table and contractant sand-like material below. Since deposition ceased the water table has drained down by 20 m, and there is an unsaturated fringe zone of contractant material above the currently saturated sand tailings. The right-hand profile shows dilatant sand tailings above a blanket drain; downwards drainage has provided conditions favouring a more densified (i.e., dilatant) deposit. This type of well drained deposit, sometimes referred to as a sand stack, forms the downstream structural containment for both GP and GMD structures at Samarco.

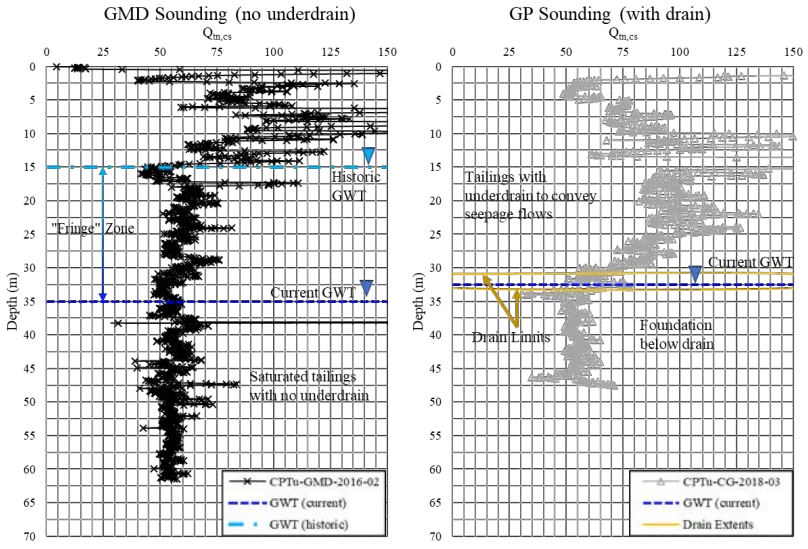

Figure 9: Representative $Q_{tn,cs}$ profiles with depth

Shear wave velocity can be measured in the laboratory and the field, permitting correlations tied to a site-specific critical state framework. Seismic CPTu soundings were carried out at Samarco, but results did not provide adequate resolution needed for these evaluations. The CPTu profiles measured every 5 cm show that Q_{tn},cs varies by 5-1- units over 1 m depth in many profiles. Robertson (2015) proposes the following relationship for young, unbonded silica based soils:

$$Vs_{1} = (Q_{tn},cs\ \alpha_{vs}/K_c)^{0.5}\ m/s$$

or

$$Q_{tn},cs = (K_{c/}\ \alpha_{vs})(V_{s1})^2$$

Where

$$\alpha vs/Kc = 360 \text{ for } 50< Qtn,cs<160$$

Figure 10 shows a typical profile illustrating "equivalent" Vs1 profile converted from Q_{tn},cs using the Robertson (2015) equations. The CSL from the laboratory test work, also expressed in Vs1 units, is also plotted on this figure, showing mostly dilatant sand above the water table (with a contractant fringe zone) and mostly contractant material below the water table. This behaviour mirrors the conditions shown in Figure 9 where Q_{tn},cs = 70 provides the boundary between dilatant and contractant behaviour. The difference is that the boundary, expressed using the measured CSL converted to V_{s1}, is not constant with depth (i.e., the contractant boundary expressed in V_{s1} units increases with vertical effective stress).

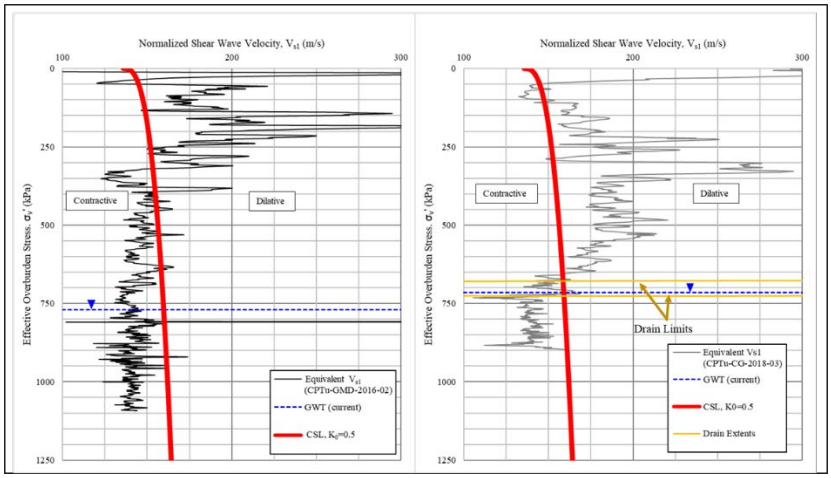

Figure 10: Equivalent normalized shear wave velocity versus effective overburden stress (same soundings as Figure 9)

Critical state framework

Shear wave velocities measured in the laboratory provide a means to compare laboratory compressibility and CSL relationships with field data derived from CPTu profiles. In this way, a site-specific boundary for

delineating contractant/dilatant behaviour is realized, and estimates of liquefied shear strength may be obtained.

Figure 11 shows two plots containing profiles from each tailing's facility (GMD and GP), using the same data as in Figure 7. Compressibility lines (ICC and LCC) and critical state lines (CSL) are superimposed on these plots using the e vs Vs_1 and Q_{tn},cs vs Vs_1 relationship described in this paper. Key points are noted:

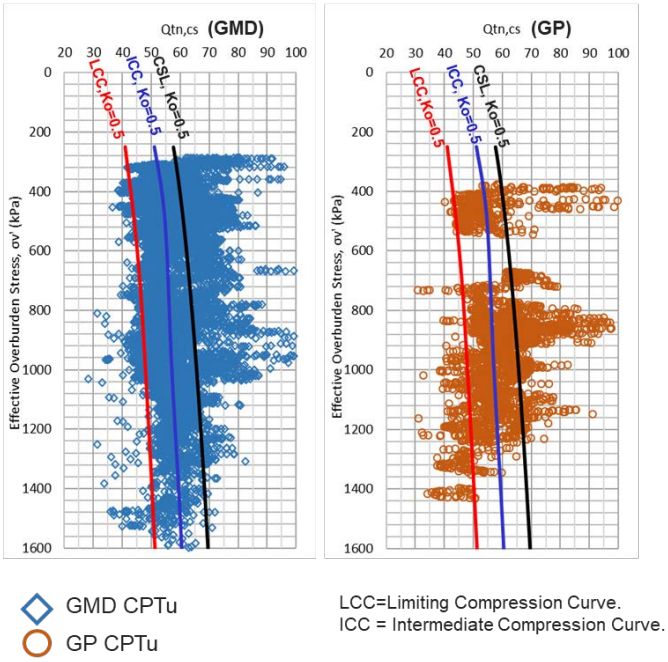

Figure 11: GMD and GP Qtn,cs profile with superimposed "equivalent" compressibility and CSL lines

- The CSL lines at Ko = 0.5 in both plots increase gradually with increasing vertical effective stress from about Q_{tn},cs =60 to Q_{tn},cs =70, confirming that the latter value is a conservative contractive/dilatant boundary over a wide range of stress conditions.
- The LCC at K_o = 0.5 envelopes most (over 90%) of the contractant CPTu data, and also shows increasing Qtn,cs with increasing vertical effective stress.
- The ICC at Ko = 0.5 is situated about half-way between the LCC and CSL lines and envelopes about 50 to 60% of the contractant data from the CPTu profiles.

The relationships shown in Figure 11 derived from the laboratory data (LCC, ICC, and CSL lines) indicate that the "equivalent" Q_{tn},cs increases with effective overburden pressure. This is an artifact of the gradual convergence between the compressibility lines and the CSL from lab testing.

Jeffries and Been (2016) and Robertson (2010) propose relationships between Qtn,cs and liquefied strength ratio (Su/σv') that provide conservative estimates to flow liquefaction case histories. The reference

compressibility lines (LCC and ICC) in Figure 10 show a gradual increase in Q_{tn},cs with depth, indicating that the liquefied shear strength also increases under increasing effective stress conditions.

Conclusions

- Laboratory testing of Samarco tailings sand over a wide stress range shows that the CSL is curved in e vs log(p') space. The rate of change in brittle behaviour corresponds with trends established by Sadrekarimi and Olson (2011), indicating a gradual decrease in brittleness and increase in liquefied strength ratio with depth. Saturated Samarco tailings sand profiles to show a contractant response using conventional normalized tip resistance relationships with mean Q_{tn},cs = 60 and standard deviation of 10.
- The CSL was not well defined at low stresses (p´<100 kPa) but our "best estimate" suggests it is fairly flat, indicating that the liquefied shear strength is very sensitive to shallow loading conditions. Laboratory tests consolidated with initial void ratio near the minimum Relative Density (i.e., very loose) are extremely brittle.
- The link between laboratory and field behaviour was investigated by measuring shear wave velocity in the lab using bender elements and converting compressibility and CSL lines to equivalent Q_{tn},cs using a published relationship. There is a compelling trend of increasing "equivalent" Q_{tn},cs with depth, indicating that the liquefied shear strength should also increase accordingly.

References

Cunning, J.C., P.K. Robertson and D.C. Sego. 1995. Shear wave velocity to evaluate in situ state of cohesionless soils. *Canadian Geotechnical Journal* 32: 848-858.

Fundão Tailings Dam Review Panel. 2016. Report on the immediate causes of the failure of the Fundão dam.

Jeffries, M.G. and K. Been. 2016. *Soil Liquefaction – A Critical State Approach.* Taylor & Francis, London.

Robertson, P.K. 2010. Evaluation of flow liquefaction and liquefied strength using the cone penetration test. *Journal of Geotechnical Geoenvironmental Engineering*, ASCE 136(6).

Robertson, P.K. 2015. Comparing CPT and Vs liquefaction triggering methods. *Journal of Geotechnical Geoenvironmental Engineering*, ASCE 141(9).

Robertson, P.K. 2016. Cone penetration test (CPT) soil behaviour type (SBT) classification system – An update. *Canadian Geotechnical Journal* 53: 1920–1927.

Robertson, P.K. 2017. Evaluation of flow liquefaction: Influence of high stresses. In *Proceedings of the 3rd International Conference in Earthquake Engineering,* Vancouver, British Columbia, Canada.

Robertson, P.K. 2018. Evaluation of liquefaction in tailings and mine waste: An update. Retrieved from https://www.cpt-robertson.com/PublicationsPDF/Robertson%20T%26M%202018%20Final.pdf (accessed October 7, 2019).

Robertson, P.K., A.J.P. Viana da Fonseca, B. Ulrich and J. Coffin. 2017. Characterization of unsaturated mine waste: A case history. *Canadian Geotechnical Journal* 54: 1752-1761.

Sadrekarimi, A. and S. Olson. 2011. Yield strength ratios, critical strength ratios, and brittleness of sandy soils from laboratory tests. *Canadian Geotechnical Journal* 48: 493-510.

Bibliography

Been, K., M.G. Jefferies and J. Hachey. 1991. The critical state of sands. *Geotechnique* 4(3): 365-381.

Olson, S. and T. Stark. 2002. Liquefied strength ratio from liquefaction flow failure case histories. *Canadian Geotechnical Journal* 39: 629–647.

Sadrekarimi, Abouzar. 2014. Effect of the mode of shear on static liquefaction analysis. *Journal of Geotechnical Geoenvironmental Engineering*, ASCE 140(12).

Schaid, F., J. Bedin, A.J.P. Viana de Fonseca and L. Moura Costa Filho. 2013. Stiffness and strength governing the static liquefaction of tailings. *Journal of Geotechnical and Geoenvironmental Engineering*, ASCE.

Verdugo, R. and K. Ishihara. 1996. The steady state of sandy soils. *Soils and Foundation*, Japanese Geotechnical Society 36(2): 81–91.

Chapter 9

Author Index

TAILINGS AND MINE WASTE 2019

Author Index